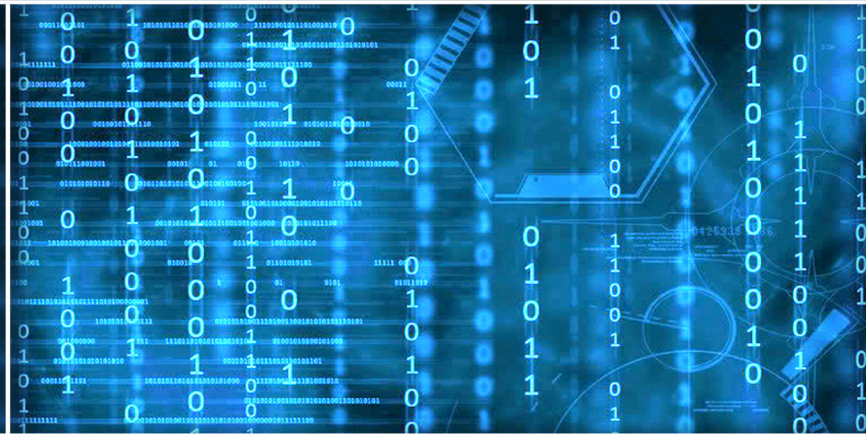


Volume 11 Issue 10

October 2020



ISSN 2156-5570(Online)

ISSN 2158-107X(Print)



Editorial Preface

From the Desk of Managing Editor...

It may be difficult to imagine that almost half a century ago we used computers far less sophisticated than current home desktop computers to put a man on the moon. In that 50 year span, the field of computer science has exploded.

Computer science has opened new avenues for thought and experimentation. What began as a way to simplify the calculation process has given birth to technology once only imagined by the human mind. The ability to communicate and share ideas even though collaborators are half a world away and exploration of not just the stars above but the internal workings of the human genome are some of the ways that this field has moved at an exponential pace.

At the International Journal of Advanced Computer Science and Applications it is our mission to provide an outlet for quality research. We want to promote universal access and opportunities for the international scientific community to share and disseminate scientific and technical information.

We believe in spreading knowledge of computer science and its applications to all classes of audiences. That is why we deliver up-to-date, authoritative coverage and offer open access of all our articles. Our archives have served as a place to provoke philosophical, theoretical, and empirical ideas from some of the finest minds in the field.

We utilize the talents and experience of editor and reviewers working at Universities and Institutions from around the world. We would like to express our gratitude to all authors, whose research results have been published in our journal, as well as our referees for their in-depth evaluations. Our high standards are maintained through a double blind review process.

We hope that this edition of IJACSA inspires and entices you to submit your own contributions in upcoming issues. Thank you for sharing wisdom.

Thank you for Sharing Wisdom!

Managing Editor
IJACSA
Volume 11 Issue 10 October 2020
ISSN 2156-5570 (Online)
ISSN 2158-107X (Print)
©2013 The Science and Information (SAI) Organization

Editorial Board

Editor-in-Chief

Dr. Kohei Arai - Saga University

Domains of Research: Technology Trends, Computer Vision, Decision Making, Information Retrieval, Networking, Simulation

Associate Editors

Chao-Tung Yang

Department of Computer Science, Tunghai University, Taiwan

Domain of Research: Software Engineering and Quality, High Performance Computing, Parallel and Distributed Computing, Parallel Computing

Elena SCUTELNICU

"Dunarea de Jos" University of Galati, Romania

Domain of Research: e-Learning, e-Learning Tools, Simulation

Krassen Stefanov

Professor at Sofia University St. Kliment Ohridski, Bulgaria

Domains of Research: e-Learning, Agents and Multi-agent Systems, Artificial Intelligence, Big Data, Cloud Computing, Data Retrieval and Data Mining, Distributed Systems, e-Learning Organisational Issues, e-Learning Tools, Educational Systems Design, Human Computer Interaction, Internet Security, Knowledge Engineering and Mining, Knowledge Representation, Ontology Engineering, Social Computing, Web-based Learning Communities, Wireless/ Mobile Applications

Maria-Angeles Grado-Caffaro

Scientific Consultant, Italy

Domain of Research: Electronics, Sensing and Sensor Networks

Mohd Helmy Abd Wahab

Universiti Tun Hussein Onn Malaysia

Domain of Research: Intelligent Systems, Data Mining, Databases

T. V. Prasad

Lingaya's University, India

Domain of Research: Intelligent Systems, Bioinformatics, Image Processing, Knowledge Representation, Natural Language Processing, Robotics

CONTENTS

Paper 1: Performance Analysis for Mining Images of Deep Web

Authors: Ily Amalina Ahmad Sabri, Mustafa Man

PAGE 1 – 7

Paper 2: Alzheimer's Disease Detection using Neighborhood Components Analysis and Feature Selection

Authors: Mohamed Maher Ben Ismail, Reema Alabdullatif, Ouiem Bchir

PAGE 8 – 16

Paper 3: Support Kernel Classification: A New Kernel-Based Approach

Authors: Ouiem Bchir, Mohamed M. Ben Ismail, Sara Algarni

PAGE 17 – 26

Paper 4: e-Lifestyle Confirmatory of Consumer Generation Z

Authors: Tony Wijaya, Arum Darmawati, Andreas M Kuncoro

PAGE 27 – 33

Paper 5: A Novel Chaotic System for Text Encryption Optimized with Genetic Algorithm

Authors: Unnikrishnan Menon, Anirudh Rajiv Menon, Atharva Hudlikar

PAGE 34 – 40

Paper 6: Optimizing the C4.5 Decision Tree Algorithm using MSD-Splitting

Authors: Patrick Rim, Erin Liu

PAGE 41 – 47

Paper 7: Extraction of Keywords for Retrieval from Paper Documents and Drawings based on the Method of Determining the Importance of Knowledge by the Analytic Hierarchy Process: AHP

Authors: Kohei Arai

PAGE 48 – 55

Paper 8: Data Retrieval Method based on Physical Meaning and its Application for Prediction of Linear Precipitation Zone with Remote Sensing Satellite Data and Open Data

Authors: Kohei Arai

PAGE 56 – 65

Paper 9: Ranking Beauty Clinics in Riyadh using Lexicon-Based Sentiment Analysis and Multiattribute-Utility Theory

Authors: Zuhaira M. Zain, Aya A. Alhajji, Norah S. Alotaibi, Najwa B. Almutairi, Alaa D. Aldawas, Muneerah M. Almazrui, Atheer M. Alhammad

PAGE 66 – 75

Paper 10: Blockchain Network Model to Improve Supply Chain Visibility based on Smart Contract

Authors: Arwa Mukhtar, Awanis Romli, Noorhuzaimi Karimah Mohd

PAGE 76 – 82

Paper 11: Development of Relay Selection Method for Audio Transmission in Cooperative Ad Hoc Networks

Authors: Usha Padma, H.V.Kumaraswamy, S.Ravishankar

PAGE 83 – 89

Paper 12: KadOLSR: An Efficient P2P Overlay for Mobile Ad Hoc Networks

Authors: Mohammad Al Mojamed

PAGE 90 – 96

Paper 13: Identification of Student-Teachers Groups' Needs in Physical Education and Sport for Designing an Open Distance Learning on the Model of Small Private Online Courses

Authors: Mostafa HAMSE, Said LOTFI, Mohammed TALBI

PAGE 97 – 105

Paper 14: A Classification Javanese Letters Model using a Convolutional Neural Network with KERAS Framework

Authors: Yulius Harjoseputro

PAGE 106 – 111

Paper 15: Debris Run-Out Modeling Without Site-Specific Data

Authors: NMT De Silva, Prasad Wimalaratne

PAGE 112 – 116

Paper 16: Improved Selected Mapping Technique for Reduction of PAPR in OFDM Systems

Authors: Saruti Gupta, Ashish Goel

PAGE 117 – 122

Paper 17: Efficient DWT based Fusion Algorithm for Improving Contrast and Edge Preservation

Authors: Sumanth Kumar Panguluri, Laavanya Mohan

PAGE 123 – 131

Paper 18: A Comparison of Classification Models to Detect Cyberbullying in the Peruvian Spanish Language on Twitter

Authors: Ximena M. Cuzcano, Victor H. Ayma

PAGE 132 – 138

Paper 19: An Investigative Study of Genetic Algorithms to Solve the DNA Assembly Optimization Problem

Authors: Hachemi Bennaceur, Meznah Almutairy, Nora Alqhtani

PAGE 139 – 150

Paper 20: A Planar Antenna on Flexible Substrate for Future 5G Energy Harvesting in Malaysia

Authors: A. K. M. Zakir Hossain, Nurulhalim Bin Hassim, S. M. Kayser Azam, Md Shazzadul Islam, Mohammad Kamrul Hasan

PAGE 151 – 155

Paper 21: Rule-based Text Normalization for Malay Social Media Texts

Authors: Siti Noor Allia Noor Ariffin, Sabrina Tiun

PAGE 156 – 162

Paper 22: Distributed Beam Forming Techniques for Dual-hop Decode-and-Forward based Cooperative Relay Networks

Authors: Zahoor Ahmed, Zuhaibuddin Bhutto, Syed Muhammad Shehram Shah, Ramesh Kumar, Ayaz Hussain

PAGE 163 – 168

Paper 23: An M/M/1 Preemptive Queue based Priority MAC Protocol for WBSN to Transmit Pilgrims' Data

Authors: Shah Murtaza Rashid Al Masud, Mahmood ul Hassan, Khalid Mahmood, Muhammad Akram

PAGE 169 – 178

Paper 24: Hybridized Machine Learning based Fractal Analysis Techniques for Breast Cancer Classification

Authors: Munmun Swain, Sumitra Kisan, Jyotir Moy Chatterjee, Mahadevan Supramaniam, Sachi Nandan Mohanty, NZ Jhanjhi, Azween Abdullah

PAGE 179 – 184

Paper 25: Detection of Anomalous In-Memory Process based on DLL Sequence

Authors: Binayak Panda, Satya Narayan Tripathy

PAGE 185 – 194

Paper 26: Implementation of Random Direction-3D Mobility Model to Achieve Better QoS Support in MANET

Authors: Munsifa Firdaus Khan, Indrani Das

PAGE 195 – 203

Paper 27: An Empirical Analysis of BERT Embedding for Automated Essay Scoring

Authors: Majdi Beseiso, Saleh Alzahrani

PAGE 204 – 210

Paper 28: Tracking Coronavirus Pandemic Diseases using Social Media: A Machine Learning Approach

Authors: Nuha Noha Fakhry, Evan Asfoura, Gamal Kassam

PAGE 211 – 219

Paper 29: Modified K-nearest Neighbor Algorithm with Variant K Values

Authors: Kalyani C. Waghmare, Balwant A. Sonkamble

PAGE 220 – 224

Paper 30: Binary Operating Antenna Array Elements by using Hausdorff and Euclidean Metric Distance

Authors: Elson Agastra, Julian Imami, Olimpjon Shurdi

PAGE 225 – 230

Paper 31: Environmental Sustainability Coding Techniques for Cloud Computing

Authors: Shakeel Ahmed

PAGE 231 – 237

Paper 32: High Priority Requests in Grid Environment

Authors: Tariq Alwadan, Salah Alghyaline, Azmi Alazzam

PAGE 238 – 242

Paper 33: A Hybrid Approach for Single Channel Speech Enhancement using Deep Neural Network and Harmonic Regeneration Noise Reduction

Authors: Norezmi Jamal, N. Fuad, MNAH. Shaabani

PAGE 243 – 248

Paper 34: Improving the Performance of Various Privacy Preserving Databases using Hybrid Geometric Data Perturbation Classification Model

Authors: Sk. Mohammed Gouse, G.Krishna Mohan

PAGE 249 – 257

Paper 35: High-Level Description of Robot Architecture

Authors: Sabah Al-Fedaghi, Manar AlSaraf

PAGE 258 – 267

Paper 36: Enhancing Acceptance Test Driven Development Model with Combinatorial Logic

Authors: Subhash Tatale, V. Chandra Prakash

PAGE 268 – 278

Paper 37: A Comprehensive Study of Blockchain Services: Future of Cryptography

Authors: Sathya AR, Barnali Gupta Banik

PAGE 279 – 288

Paper 38: Prototyping with Raspberry Pi in Healthcare Domain

Authors: Hari Kishan Kondaveeti, Sruti Raman, Praveen Raj

PAGE 289 – 303

Paper 39: Effect of Route Length and Signal Attenuation on Energy Consumption in V2V Communication

Authors: Mahmoud Zaki Iskandarani

PAGE 304 – 309

Paper 40: Handwritten Numeric Image Classification with Quantum Neural Network using Quantum Computer Circuit Simulator

Authors: Achmad Benny Mutiara, Muhammad Amir Slamet, Rina Refianti, Yusuf Sutanto

PAGE 310 – 319

Paper 41: A Novel Approach to Mammogram Classification using Spatio-Temporal and Texture Feature Extraction using Dictionary based Sparse Representation Classifier

Authors: Vaishali D. Shinde, B. Thirumala Rao

PAGE 320 – 332

Paper 42: A Hybrid POS Tagger for Khasi, an Under Resourced Language

Authors: Medari Janai Tham

PAGE 333 – 342

Paper 43: Robust Drowsiness Detection for Vehicle Driver using Deep Convolutional Neural Network

Authors: A F M Saifuddin Saif, Zainal Rasyid Mahayuddin

PAGE 343 – 350

Paper 44: Towards a Multi-Agent based Network Intrusion Detection System for a Fleet of Drones

Authors: Said OUIAZZANE, Fatimazahra BARRAMOU, Malika ADDOU

PAGE 351 – 362

Paper 45: MSTD: Moroccan Sentiment Twitter Dataset

Authors: Soukaina MIHI, Brahim AIT BEN ALI, Ismail EL BAZI, Sara AREZKI, Nabil LAACHFOUBI

PAGE 363 – 372

Paper 46: Load Balancing Problem on Hyper Hexa Cell Interconnection Network

Authors: Aryaf Al-Adwan, Basel A. Mahafzah, Anaam Aladwan

PAGE 373 – 379

Paper 47: Attribute-based Encryption for Fine-Grained Access Control on Secure Hybrid Clouds

Authors: Sridhar Reddy Vulapula, Srinivas Malladi

PAGE 380 – 387

Paper 48: Gabor Capsule Network for Plant Disease Detection

Authors: Patrick Mensah Kwabena, Benjamin Asubam Weyori, Ayidzoe Abra Mighty

PAGE 388 – 395

Paper 49: Comparison Performance of Lymphocyte Classification for Various Datasets using Deep Learning

Authors: Syadia Nabilah Mohd Safuan, Mohd Razali Md Tomari, Wan Nurshazwani Wan Zakaria, Nor Surayahani Suriani

PAGE 396 – 402

Paper 50: Supervised Hyperspectral Image Classification using SVM and Linear Discriminant Analysis

Authors: Shambulinga M, G. Sadashivappa

PAGE 403 – 409

Paper 51: Manar: An Arabic Game-based Application Aimed for Teaching Cybersecurity using Image Processing

Authors: Afnan Alsadhan, Asma Alotaibi, Lulu Altamran, Majd Almalki, Moneera Alfulaij, Tarfa Almoneef

PAGE 410 – 416

Paper 52: A Machine Learning Approach to Identifying Students at Risk of Dropout: A Case Study

Authors: Roderick Lottering, Robert Hans, Manoj Lall

PAGE 417 – 422

Paper 53: Customized BERT with Convolution Model: A New Heuristic Enabled Encoder for Twitter Sentiment Analysis

Authors: Fatima-ezzahra LAGRARI, Youssfi ELKETTANI

PAGE 423 – 431

Paper 54: Empirical Oversampling Threshold Strategy for Machine Learning Performance Optimisation in Insurance Fraud Detection

Authors: Bouzgarne Itri, Youssfi Mohamed, Bouattane Omar, Qbadou Mohamed

PAGE 432 – 437

Paper 55: Design of an Electro-Stimulator Controlled by Bluetooth for the Improvement of Muscular Atrophy

Authors: Paul Portilla Achata, Raúl Sulla Torres, Juan Carlos Copa Pineda, Agueda Muñoz del Carpio Toia, Jose Sulla-Torres

PAGE 438 – 445

Paper 56: Dual Annular Ring Coupled Stacked Psi Shape Patch Antenna for Wireless Applications

Authors: K. Mahesh Babu, T.V. Rama Krishna

PAGE 446 – 453

Paper 57: Secure Communication across the Internet by Encrypting the Data using Cryptography and Image Steganography

Authors: P Rajesh, Mansoor Alam, Mansour Tahernehzadi, T Ravi Kumar, Vikram Phaneendra Rajesh

PAGE 454 – 458

Paper 58: White Blood Cells Detection using YOLOv3 with CNN Feature Extraction Models

Authors: Nurasyeera Rohaziat, Mohd Razali Md Tomari, Wan Nurshazwani Wan Zakaria, Nurmiza Othman

PAGE 459 – 467

Paper 59: A Novel Solution for Distributed Database Problems

Authors: Bishoy Sameeh Matta Sawiris, Manal A. Abdel-Fattah

PAGE 468 – 474

Paper 60: Secure Software Defined Networks Controller Storage using Intel Software Guard Extensions

Authors: Qasmaoui Youssef, Maleh Yassine, Abdelkrim Haqiq

PAGE 475 – 481

Paper 61: Dynamics of Organizational Change

Authors: Maximo Flores-Cabezas, Desiree Flores-Moya, Brian Meneses-Claudio

PAGE 482 – 494

Paper 62: Impact of Change in Business IT Alignment: Evaluation with CBITA Tool

Authors: Imgharene Kawtar, Doumi Karim, Baina Salah

PAGE 495 – 504

Paper 63: Enhancing VoIP BW Utilization over ITTP Protocol

Authors: AbdelRahman H. Hussein, Mahran Al-Zyoud, Kholoud Nairoukh, Sumaya N. Al-Khatib

PAGE 505 – 510

Paper 64: High-Security Image Steganography Technique using XNOR Operation and Fibonacci Algorithm

Authors: Ali Abdulzahra Almayyahi, Rossilawati Sulaiman, Faizan Qamar, Abdulwahhab Essa Hamzah

PAGE 511 – 522

Paper 65: Very Deep Neural Networks for Extracting MITE Families Features and Classifying them based on DNA Scalograms

Authors: Mael SALAH JRAD, Afef ELLOUMI OUESLATI, Zied LACHIRI

PAGE 523 – 532

Paper 66: The Prediction of Outpatient No-Show Visits by using Deep Neural Network from Large Data

Authors: Riyadh Alshammari, Tahani Daghistani, Abdulwahhab Alshammari

PAGE 533 – 539

Paper 67: Virtual Simulation for Entertainment using Genetic Information

Authors: Jin Woo Kim, Hun Lim, Taeho You, Mee Young Sung

PAGE 540 – 545

Paper 68: Level of Depression in Positive Patients for COVID-19 in the Puente Piedra District of North Lima, 2020

Authors: Rosa Perez-Siguas, Eduardo Matta-Solis, Hernan Matta-Solis, Anika Remuzgo-Artezano, Lourdes Matta-Zamudio, Melissa Yauri-Machaca

PAGE 546 – 551

Paper 69: Blockchain and Internet of Things for Business Process Management: Theory, Challenges, and Key Success Factors

Authors: Mabrook S. Al-Rakhami, Majed Al-Mashari

PAGE 552 – 562

Paper 70: A Trust-Based Collaborative Filtering Approach to Design Recommender Systems

Authors: Vineet K. Sejwal, Muhammad Abulaish

PAGE 563 – 573

Paper 71: A Game-Based Learning Approach to Improve Students' Spelling in Thai

Authors: Krittiya Saksrisathaporn

PAGE 574 – 579

Paper 72: Physical Parameter Estimation of Linear Voltage Regulators using Model-based Approach
Authors: Ng Len Luet, Mohd Hairi Mohd Zaman, Asraf Mohamed Moubark, M Marzuki Mustafa
PAGE 580 – 589

Paper 73: Artificial Bee Colony Algorithm Optimization for Video Summarization on VSUMM Dataset
Authors: Vinsent Paramanatham, S. SureshKumar
PAGE 590 – 596

Paper 74: Continuous Human Activity Recognition in Logistics from Inertial Sensor Data using Temporal Convolutions in CNN
Authors: Abbas Shah Syed, Zafi Sherhan Syed, Areez Khalil Memon
PAGE 597 – 602

Paper 75: Design of Multi-View Graph Embedding for Features Selection and Remotely Sensing Signal Classification
Authors: Abdullah Alhumaidi Alotaibi, Sattam Alotaibi
PAGE 603 – 608

Paper 76: How Images Defects in Street Scenes Affect the Performance of Semantic Segmentation Algorithms
Authors: Hoda Imam, Bassem A. Abdullah, Hossam E. Abd El Munim
PAGE 609 – 618

Paper 77: Emotion Analysis of Arabic Tweets during COVID-19 Pandemic in Saudi Arabia
Authors: Huda Alhazmi, Manal Alharbi
PAGE 619 – 625

Paper 78: HPSOGWO: A Hybrid Algorithm for Scientific Workflow Scheduling in Cloud Computing
Authors: Neeraj Arora, Rohitash Kumar Banyal
PAGE 626 – 635

Paper 79: Evaluating the Effect of Multiple Filters in Automatic Language Identification without Lexical Knowledge
Authors: Guan-Lip Soon, Nur-Hana Samsudin, Dennis Lim
PAGE 636 – 645

Paper 80: Classification of Common and Uncommon Tones by P300 Feature Extraction and Identification of Accurate P300 Wave by Machine Learning Algorithms
Authors: Rafia Akhter, Kehinde Lawal, Md. Tanvir Rahman, Shamim Ahmed Mazumder
PAGE 646 – 652

Paper 81: A Perception Centered Self-Driving System without HD Maps
Authors: Alan Sun
PAGE 653 – 661

Paper 82: Static vs. Dynamic Modelling of Acoustic Speech Features for Detection of Dementia
Authors: Muhammad Shehram Shah Syed, Zafi Sherhan Syed, Elena Pirogova, Margaret Lech
PAGE 662 – 667

Paper 83: Multi-Objective Evolutionary Programming for Developing Recommender Systems based on Collaborative Filtering
Authors: Edward Hinojosa-Cardenas, Edgar Sarmiento-Calisaya, Cesar A. Martinez-Salinas, Lehi Quincho-Mamani, Jair F. Huaman-Canqui
PAGE 668 – 676

Paper 84: Face Verification across Aging using Deep Learning with Histogram of Oriented Gradients

Authors: Areeg Mohammed Osman, Serestina Viriri

PAGE 677 – 683

Paper 85: Multi-Target Energy Disaggregation using Convolutional Neural Networks

Authors: Mohammed Ayub, El-Sayed M. El-Alfy

PAGE 684 – 693

Paper 86: Multi-Label Arabic Text Classification: An Overview

Authors: Nawal Aljedani, Reem Alotaibi, Mounira Taileb

PAGE 694 – 706

Paper 87: Census Estimation using Histogram Representation of 3D Surfaces: A Case Study Focusing on the Karak Region

Authors: Subhieh El-Salhi, Safaa Al-Haj Saleh, Frans Coenen

PAGE 707 – 718

Paper 88: Novel Control Scheme for Prosthetic Hands through Spatial Understanding

Authors: Yunan He, Osamu Fukuda, Nobuhiko Yamaguchi, Hiroshi Okumura, Kohei Arai

PAGE 719 – 725

Paper 89: Deep Acoustic Embeddings for Identifying Parkinsonian Speech

Authors: Zafi Sherhan Syed, Sajjad Ali Memon, Abdul Latif Memon

PAGE 726 – 734

Performance Analysis for Mining Images of Deep Web

Ily Amalina Ahmad Sabri¹, Mustafa Man²

Faculty of Ocean Engineering Technology and Informatics
Universiti Malaysia Terengganu
Terengganu, Malaysia

Abstract—In this paper, advancing web scale knowledge extraction and alignment by integrating few sources has been considered by exploring different methods of aggregation and attention in order to focus on image information. An improved model, namely, Wrapper Extraction of Image using DOM and JSON (WEIDJ) has been proposed to extract images and the related information in fastest way. Several models, such as Document Object Model (DOM), Wrapper using Hybrid DOM and JSON (WHDJ), WEIDJ and WEIDJ (no-rules) are been discussed. The experimental results on real world websites demonstrate that our models outperform others, such as Document Object Model (DOM), Wrapper using Hybrid DOM and JSON (WHDJ) in terms of mining in a higher volume of web data from a various types of image format and taking the consideration of web data extraction from deep web.

Keywords—Data extraction; Document Object Model; web data extraction; Wrapper using Hybrid DOM and JSON; Wrapper Extraction of Image using DOM and JSON

I. INTRODUCTION

As web sites are getting more complicated, the construction of efficient web information extraction systems becomes vital. A common arising issue in data extraction is the difficulties in locating the important segments, which contained the information being searched in a page. People always view a web page as different semantic objects rather than single objects. Some research efforts showed that the spatial and visual cues can help the users to unconsciously divide the web page into several semantic parts. Many recent works [1, 2] tried to extract the structured information from web pages using visual segmentations.

Deep web is known to contain more valuable informations compared to surface webs. Due to its complexities, deep web requires more efforts and the process may be time consuming. In addition, most of the web pages in deep web are generated only for visualizations, and the available data are not possible for exchange nor extraction. Thus, extraction process of deep web is crucial. Normally, each web page within a deep web, has similar characteristics; they share the same structures and templates. They are also encoded in a consistent way across all the pages. However, due to certain complexity issues, there are several deep web which are incompatible with the standards extraction process.

The primary drawback of the existing data extraction methods is the large volume of images to be extracted, making the process to be consuming. After the problem has been

identified, the extraction process must be defined using the algorithms, either in pseudo code or flowchart to ensure the inputs, processes and outputs that will be involved in extraction process. The input is user's admittances such as web address. The process of image's extraction involves the construction of HTML documents into tree structures, finding the tags, checking of the images by segmentations and representation of the data in JSON format. The outputs are the extracted images and their related information, represented in tabular format.

There are some discussions of algorithms for data classifications, data extraction and data integration used in machine learning. They are also being used as the base algorithms in some data extractor systems. Researchers designed various models of algorithms to detect more extracted web contents and to increase the performance of extracting information. Besides that time processing for extracting data can be decreased.

Umamageswari, Kalpana [3] proposed Boyer Moore String Pattern Matching Algorithm. This algorithm was used to find patterns in the extracted data. The patterns were aligned with texts and then checked either it matched the opposing character of texts. The algorithm outperformed the efficiencies of other existing pattern matching methods.

Polynomial algorithm was proposed by Pouramini, Khaje Hassani [4] in their extraction algorithms. The page element was checked by traversing of the DOM tree in mixed approach; bottom up and top down. This polynomial algorithm nevertheless was only applicable for visible pages and cannot be applied for the whole web pages.

Heuristic algorithm was proposed for automatic navigation and information extraction from Scientific Publishers' Website [5]. It didn't require the processing of the entire DOM tree to identify the locations of attribute value pairs but it required linear time since it did not involve complex pattern matching or string alignment algorithms. Although the execution time was really reduced but it didn't work well in case of different domains such as structured journal pages linked to single publishers' websites.

Raza and Gulwani [6] discussed a predictive program synthesis algorithm for texts and web data extraction. The program synthesis technique for data extraction tasks included a general form of DSLs' extraction, a synthesis algorithm designed in a domain-parametric fashion, as well as concrete

DSLs and algorithm instantiations in the practical application domains of texts and webs extraction. Nonetheless, this predictive synthesis cannot be applied to other practical application domains such as richly formatted documents such as XML-based formats (DOCX, ODF, PPTX, etc.).

A method has been proposed to deal with deep web based on visual recognition combined with DOM analysis [7]. VRDE was proposed to solve the problems of DOM structures inefficiencies when dealing with large volumes of images and multi web pages [8]. The limitation of this research work was the presence of its noisy information which cannot be removed completely.

Manjaramkar and Lokhande [9] proposed DEPTA. This research extracted all the data based on the data mining regions, record extractions and record alignments. The proposed system used two major steps: the first step was the recognition of data regions inside the input web pages, following by its extraction. Second step was the arrangement of extracted data in structured formats. The tag substrings in record segmentation modules were examined and if there were any repetitions of tags, only one tag was selected. Partial tree alignment approach was based on tree matching, which means placing those records field in a couple of records that can be organized and liberated to other data field.

Kamanwar and Kale [10] agreed that Web Data Extraction is the process of extracting user's required information from web pages. Nowadays, the extractor is used to extract information because web page is an ocean of data which makes browsing information as a very complicated task. Normally the contents of web documents are unstructured. Web data extraction is defined as a process which use tool and wrappers as mediums to extract information from web documents in HTML format. The noisy information such as tags, advertisements, and banner will be removed by wrapper.

Fang [11] has proposed STEM to extract sequences of identifiers from the tag path of web pages. Then a suffix tree is built on top of these sequences and four refining filters are proposed to screen out the region which contains unnecessary information.

Pouramini, Khaje Hassani [4] proposed Handle-based Wrapper by using DOM tree approach. This research worked on text features as handles to extract data records from web pages such as textual delimiters, keywords, consents or text patterns. Polynomial algorithm has been proposed to check against the page elements in two situations; mixed bottom up and top-down traverse DOM-tree. Yet, the extraction process can only be performed on the visible parts, and not on the whole page, thus limits its further applications.

TANGO was presented by Jiménez and Corchuelo [12], aimed to learn rules for a precise and recallability extraction of information from semi-structured web documents. The high precision and recallability are pre-requisites in the context of Enterprise Systems Integration. It relies on an open catalogue of features that helps to map the input documents into a knowledge base in which every DOM node is represented by means of HTML, DOM, CSS, relational, and user-defined features.

II. RESEARCH METHOD

Wrappers are tools developed using specific techniques or models to be used for image's extraction from web. The wrapper is divided into two main parts. The first part involves the process of the insertion "URL" of web page. It involves the parsing of the HTML web page and storing them as Document Object Model (DOM) tree. The conversion from HTML web pages to DOM tree structure is important to understand the structure of HTML pages in tree environment. This method is useful in gauging the structure of data, whether it is structured, semi-structured or unstructured. The second part is related to the extraction techniques. The wrapper applies the extraction techniques; DOM, hybrid model of DOM and JSON (WHDJ) and hybrid model of DOM, JSON and visual segmentation (WEIDJ).

JSON is a syntax for storing and exchanging data. The advantage of JSON is an open-standard format that uses human readable text to transmit data objects [13]. The growing popularity of the JSON format has fueled increased interest in loading and processing JSON data within analytical data processing systems [14].

A JSON object is a key-value data format that is typically rendered in curly braces. When working with JSON, JSON objects can be represented in a *.json file*, but they can also exist as a JSON object or string within the context of a program. JSON may be coded with lots of lines, this shows that the format is generally set up with two curly braces (or curly brackets) that look like this { } on either end of it, and with key-value pairs populating the space between. Most data used in JSON ends up being encapsulated in a JSON object.

Key-value pairs have a colon between them as in "key": "value". Each key-value pair is separated by a comma, so the middle of a JSON looks like this: "key": "value", "key": "value", "key": "value". Fig. 1 shows the sample of output using JSON approach in key-value pairs.

A. DOM Tree

The Document Object Model (DOM) is a programming API for HTML and XML documents. People can create and build documents using DOM [15]. Besides that this model can be used to manipulate elements and contents of HTML and XML documents such as add, modify or delete [13, 16].

Page level data extraction system is developed using DOM Tree by Narawade, Prabhakar [17]. There are two types of technique for data extraction; online and offline. There are three stages involves; web page renderers, section selectors, and pattern generators. A web page renderer will accept a *url* as inputs from users. After that the web page will be displayed in web browser. Then, DOM tree structure will be applied for content extraction and its representation in structured formats. The section selector acts to divide web pages into different sections that enable user to select particular record or whole data section. The system will dynamically extract the contents from the different structured web pages such as blogs, forums, articles, etc. Pattern generator creates relatively absolute patterns based on the origin of selected data regions.



Fig. 1. Output Presentation of JSON.

B. Wrapper using Hybrid DOM and JSON (WHDJ)

This section describes the extraction techniques of web data using hybrid DOM and JSON approaches. Images are extracted by converting HTML documents into tree structure and the engine will try to find the location of tags for each image. Then, JSON approach will be applied in order to retrieve and transform image's information into an array.

C. Wrapper Extraction of Image using DOM and JSON (WEIDJ)

Finding and extracting the complete images from web pages without failure is complex since a special operation is needed to find tags and extract all images without missing any values. This study presents Wrapper Extraction of Image using DOM and JSON (WEIDJ) [13]. This method can solve this problem by converting the HTML documents to a tree structure and composing web pages into several sections based on visual segmentations as shown in Fig. 1. Then, the engine will try to find tags for each image. This approach also considers certain rules to be filtered before the image extraction process. The rules will encompass the filtering of noise information, repetitive image filenames and non-related images to the website or web page. After the process of filtering noise information, the extracted images will be transformed into structured format also known as tabular form. The image's filenames will be indexed before storing them into multimedia database.

D. WEIDJ No-Rules

This method has same flows to WEIDJ model but WEIDJ no-rules will retrieved images without filtering noise images nor considering the repetition of file images. However, the performance of extraction process in terms of extraction time is still the best compared to DOM and WHDJ.

Fig. 2 shows an example on visual segmentation of layout structure for www.wwf.org.my. A visual segmentation is developed using each leaf node as an object. Visual segmentation is proposed because it is easier to be understood as compared to texting in details. This segmentation is important to check the availability of required information in each block. During the experimental works, problems of data extraction have been detected. There are certain images that cannot be extracted. As the solution, the availability of images in each block should be checked. The advantage of structuring partition is it can provide a user friendly view for the web page [13].

At this level, all suitable visual blocks contained in the current web page will be recognized. Basically, every node in the DOM tree can be presented as a visual block but nodes such as <TABLE> and <P> are not suitable to be represented as a single visual block. Several rules in extracting the visual blocks are as below[13]:

- Tags cue such as <hr> usually displayed as a horizontal rule in visual browser. If each DOM node contains this tag, the section will be divided.
- If a DOM node has different background colour from one of its child node, it will not be divided into any segments.

When appropriate blocks are extracted, the rest of invalid nodes will be ignored. Separator can be used as indicator to divide different section within a page. These visual blocks segmentation is applied to check every single multimedia element so that all required information can be retrieved [13].

The advantages of this proposed wrapper is user can automatically select all images to store in single multimedia database or select by manually. Fig. 3 and Fig. 4 show the examples of selecting images either by automatically or manually.



Fig. 2. Layout Structure and Visual Segmentation of WWF Web Page.

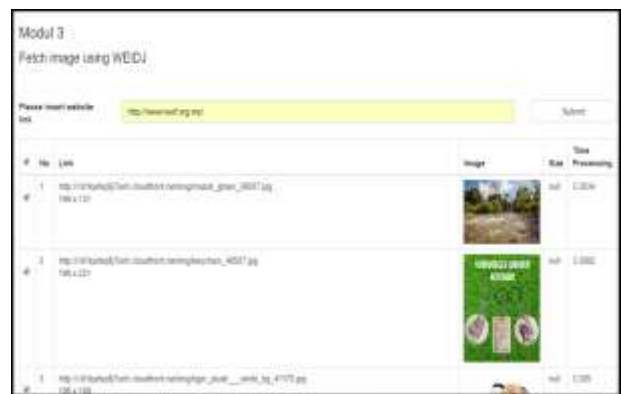


Fig. 3. Select Images with Automatic Selection.



Fig. 4. Select Images with Manual Selection.



Fig. 5. Biodiversity Dataset.

III. RESULTS AND DISCUSSIONS

The rapid development of computer and technologies has increased the usage of web. Deep web is a part of webs. It contains various useful information, which are beneficial to public users. The contents is dynamically generated from various data sources. The numbers of web pages for deep web is extremely large. Thus extraction of images from deep webs is very complicated and time consuming.

The dataset called Science and Technology Resources on the Internet, “Biodiversity Web Resources” has been selected, which consists of 43 online databases [18] as shown in Fig. 4 and Setiu Wetlands web page, namely, WWF-Malaysia [13]. The benchmark of datasets that have been applied in this experimental work are from [18] [19] for instant dataset. A web page, WWF- Malaysia was used for the testing of real datasets as shown in Fig. 5. The two categories of these datasets are dense. The overall characteristics of these benchmark dataset are tabulated in Table I.

The overall characteristics of these benchmark dataset are tabulated in Table I. There are three domain that have been selected; General Biodiversity and Endangered Species Information, Databases and Datasets: Broad Scope and Databases and Datasets: Narrow Scope. There are seventeen uniform resource locators that have been used in mining images from deep web.

WWF stands for World Wide Fund for Nature. It was formerly known as the World Wildlife Fund but the name was later changed to indicate it also deals with environmental issues rather than wildlife alone [16]. Fig. 6 shows main page for WWF website that contains images, text, symbol logo and others.

Data storage and data extraction industries are the basis of large data analysis and mining. The storage and extraction big data is relatively simple but become complicated when dealing with large volumes of data. Web page contains many valuable information. The extraction of semi-structured data, especially those involving large images, is limited by its long execution times. For this reason, crawlers play important role to solve this problem. In this research, experiments were performed based on extracting images from the whole website.

TABLE I. CHARACTERISTICS OF INSTANT DATASET

URL	Uniform Resource Locator (URL)	
General Biodiversity and Endangered Species Information		Domain
1	http://www.amnh.org/	American Museum of Natural History (AMNH) Hall of Biodiversity
2	http://ocean.si.edu/	Ocean Portal: Smithsonian Institution
3	http://www.iucn.org/	International Union for Conservation of Nature
4	http://www.endangeredspeciesinternational.org	Endangered Species International
5	http://www.wwf.my	World Wide Fund for Nature
Databases and Datasets: Broad Scope		Domain
6	http://www.gbif.org/	Global Biodiversity Information Facility (GBIF)
7	http://www.unep-wcmc.org/	UN Environment Programme: World Conservation Monitoring Centre (UNEP-WCMC)
8	http://www.natureserve.org/	NatureServ
9	http://www.organismnames.com/query.htm	Index of Organism Names: ION
10	http://www.catalogueoflife.org/col/search/all	Catalogue of Life
11	http://animaldiversity.ummz.umich.edu/site/index.HTML	Animal Diversity Web
Databases and Datasets: Narrow Scope		Domain
14	http://bugguide.net/node/view/15740	BugGuide.Net
15	http://www.amphibiaweb.org/	AmphibiaWeb
16	http://www.reefbase.org/	ReefBase
17	http://primate.lit.library.wisc.edu/	PrimateLit



Fig. 6. World Wide Fund for Nature (WWF) Web Page.

Normally, information in deep web is presented in “divs” sections. In the experiment, 30 pages or URLs have been selected randomly from the same website. The time taken for extraction of one page to another page was calculated. From the deep web result page, this research shows that WEIDJ is efficient because it can retrieve and extract semi-structured data from level of pages. The result shows that this model is very effective and can be used to extract the data quickly and accurately. The problems related to extraction’s efficiencies and accuracies of different deep web page heterogeneity have been solved. The interference of web page noise [7] to data extraction also can be removed completely.

Fig. 7 shows the results of the crawl, the abscissa represents the number of pages extracted and the vertical axis represents the total time taken to extract the corresponding pages of WWF.

Table II shows the result of experimental of image extraction for web crawler. There are seven benchmarks that have been considered in this experimentation such as; ‘Link Found’, ‘Img found’, ‘Img retrieved’, ‘Img filtered’, and ‘Time’. The analysis shows that the total of link found is in within range between three models but the findings of image retrieved is different between these models. Due to their genericities, the existing unsupervised approaches have significant drawbacks. The proposed alternative technique is more suitable especially to be applied in real life scenarios and offers several advantages WEIDJ are enabling to mix different types of images. As we know, there are various type of images that can be found in web pages such as TIFF (also known as TIF, file ending with .tif), JPEG (also known as JPG, file ending with .jpg), GIF (file ending with .gif), PNG (file

ending with .png) and raw image files. Types of recognizers for each image is very important as the extraction process can be improved using the structural features of data. Fig. 8 shows types of image that can be retrieved by WEIDJ model.

Fig. 9 shows the output for data extraction by corresponding page. The extraction time will be calculated from the beginning of the extracted page to the next page [16].

The description of targeted images allows user to avoid the extraction of unnecessary images such as logos and buttons. Fig. 10 shows the example of images that have been extracted by WHDJ approach. This approach will ensure the extraction of useful information and all the noisy information and images will be neglected.

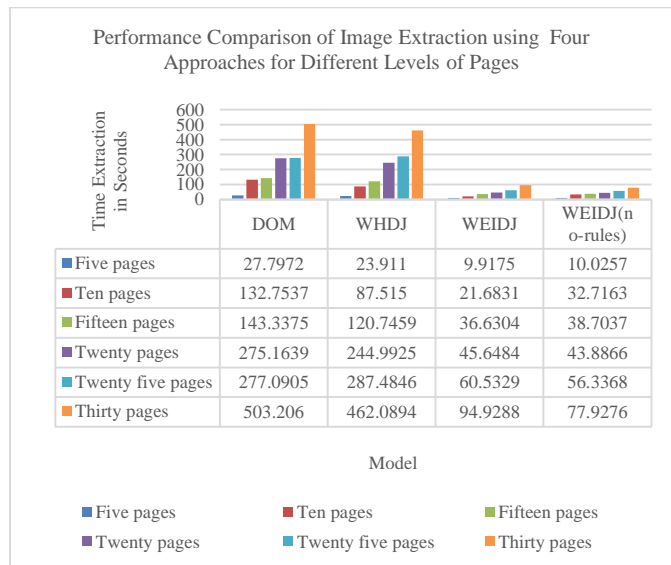


Fig. 7. The Extracted Pages of WWF Website.

```

if(empty($imagetype)) return false;
switch($imagetype)
{
    case 'image/bmp': return '.bmp';
    case 'image/cis-cod': return '.cod';
    case 'image/gif': return '.gif';
    case 'image/ief': return '.ief';
    case 'image/jpeg': return '.jpg';
    case 'image/jpg': return '.jpg';
    case 'image/pipeg': return '.jfile';
    case 'image/tiff': return '.tif';
    case 'image/x-cmu-raster': return '.ras';
    case 'image/x-cmx': return '.cmx';
    case 'image/x-icon': return '.ico';
    case 'image/x-portable-anymap': return '.pnm';
    case 'image/x-portable-bitmap': return '.pbm';
    case 'image/x-portable-graymap': return '.pgm';
    case 'image/x-portable-pixmap': return '.ppm';
    case 'image/x-rgb': return '.rgb';
    case 'image/x-xbitmap': return '.xbm';
    case 'image/x-xpixmap': return '.xpm';
    case 'image/x-xwindowdump': return '.xwd';
    case 'image/png': return '.png';
    case 'image/x-jpe': return '.jpe';
    case 'image/x-freehand': return '.fh';
    default: return false;
}
    
```

Fig. 8. Types of Image.

TABLE II. IMAGE EXTRACTION BY WEB PAGES FOR BENCHMARK

General Biodiversity and Endangered Species Information																	
Model	DOM					WHDJ					WEIDJ					WEIDJ(no-rules)	
Benchmark	Link Found	Img found	Img retrieved	Img filtered	Time	Link Found	Img found	Img retrieved	Img filtered	Time	Link Found	Img found	Img retrieved	Img filtered	Time	Img retrieved	Time
amnh.org	132	4881	2125	2756	10556.2238	132	4013	2028	1985	8778.3747	132	1521	1385	136	457.7495	4934	475.1597
ocean.si.edu	97	1966	1610	356	2319.4244	97	1705	1505	200	2076.7548	96	836	803	33	312.985	2011	329.4163
iucn.org	96	999	811	188	1979.6851	96	707	596	111	1625.4596	96	340	310	30	308.6347	2008	278.9528
endangeredspeciesinternational.org	6	77	44	33	150.9678	6	59	44	15	91.347	30	262	102	160	26.4048	411	25.9593
wwf.org.my	142	1803	1374	429	1900.9394	142	1626	1370	256	1385.7157	143	1311	1059	251	318.2913	1899	285.2288

DATABASES AND DATASETS: BROAD SCOPE

Benchmark	Link Found	Img found	Img retrieved	Img filtered	Time	Link Found	Img found	Img retrieved	Img filtered	Time	Link Found	Img found	Img retrieved	Img filtered	Time	Img retrieved	Time
http://www.gbif.org/	62	342	106	236	545.4321	62	205	101	104	361.3751	62	143	107	36	147.4583	603/357	142.1595
http://www.unep-wcmc.org/	30	310	227	83	695.9005	30	247	216	31	573.0375	30	195	189	6	129.1575	312/304	114.6983
http://www.natureserve.org/	63	767	557	210	929.8449	63	626	498	128	791.9172	64	347	274	73	77.2083	822/802	97.894
http://www.organismnames.com/query.htm	21	270	113	157	377.3488	21	223	111	112	304.9616	34	282	280	2	35.9359	2145/720	50.1937
http://www.catalogueoflife.org/col/search/all	33	314	8	306	363.7471	33	316	80	236	371.8078	43	130	228	229	65.0781	1896/509	62.099
http://animaldiversity.ummz.umich.edu/site/index.html	79	631	589	42	1020.3173	79	510	474	36	757.0506	79	383	257	126	163.663	125	108.732
http://www.theplantlist.org/	32	606	266	340	700.2953	32	457	219	238	528.9477	32	220	115	105	42.9643	942/598	53.3552
http://www.iucnredlist.org/	92	4536	3290	1246	8610.6563	92	4081	3280	801	6222.5125	95	2760	2551	209	432.0595	4614/4591	440.4091
http://www.itis.gov/	39	465	108	357	1253.9414	39	167	107	60	559.0691	40	70	32	38	78.4108	479	70.2567
http://www.consbio.org/	39	374	231	143	204.4485	39	342	215	127	290.8351	40	141	131	13	96.2886	383	107.2494

DATABASES AND DATASETS: NARROW SCOPE

Databases and Datasets: Narrow Scope																	
Model	DOM					WHDJ					WEIDJ					WEIDJ(no-rules)	
Benchmark	Link Found	Img found	Img retrieved	Img filtered	Time	Link Found	Img found	Img retrieved	Img filtered	Time	Link Found	Img found	Img retrieved	Img filtered	Time	Img retrieved	Time
http://bugguide.net/node/view/15740	83	5100	4695	338	9843.5567	58	1218	1018	200	2561.8086	88	5292	3914	1317	1040.6848	8632/5100	1396.5794
http://www.amphibiaweb.org/	9	127	50	77	167.6131	9	27	21	6	55.1403	3	77	69	8	4.6227	158/79	6.6687
http://www.reefbase.org/	95	5276	119	5157	4071.2581	95	1196	119	1077	757.0451	99	206	133	73	178.8349	5478/5532	173.0226
http://primatelit.library.wisc.edu/	7	15	5	10	45.5	7	15	5	10	44.6401	12	29	14	15	34.7044	29/14	39.8865



Fig. 9. Extracting 5 Pages.



Fig. 10. Example of Noisy Images.

IV. CONCLUSION

The World Wide Web contains large unstructured and semi-structured data. Researchers are welcomed to develop and implement various techniques to extract data from web sources due to the need for structured information. A wide range of web data extraction in several fields has been developed and continues to be proliferated. In this paper, WEIDJ as the best approaches among several models; DOM and WHDJ have been discussed. This wrapper provides three different level of extraction for DOM, WHDJ and WEIDJ. This paper discusses about extracting images for deep web using DOM, WHDJ and WEIDJ models. It is easy for human to extract images by just entering the data (web URL for extraction) without any needs to be informed of the instructions involved during the extraction process. The proposed method has numbers of advantages over previous extraction based techniques. In the first part of this paper, the applications of web data extraction systems to real world scenario were reviewed. The focus is how the application can work in practices and classify two models: DOM and JSON that have been applied by discussing several models. A simple implementation was provided in extracting multimedia data focusing on image using several websites. In future work, we plan to extend our approach to extract data from multi-web page. The performance of image extraction will influence the time for extraction process. Proposed technique gives good result in time processing in extracting data. The impact of the study for the nation building is the extraction of image that can be used for other purposes.

ACKNOWLEDGMENT

I sincerely thank all those who helped me in completing this task especially Basiswa Universiti Malaysia Terengganu (BUMT).

REFERENCES

- [1] Malhotra, P. and S.K. Malik. Web page segmentation towards information extraction for web semantics. in International Conference on Innovative Computing and Communications. 2019. Springer.
- [2] Gulati, P. and M. Yadav, A novel approach for extracting pertinent keywords for web image annotation using semantic distance and euclidean distance, in Software Engineering. 2019, Springer. pp. 173-183.
- [3] Umamageswari, B., R. Kalpana, and V. Archana, Web Data Extraction System using Boyer Moore String Pattern Matching Algorithm. 2018.
- [4] Pouramini, A., S. Khaje Hassani, and S. Nasiri, Data extraction using content based handles. Journal of AI and Data Mining, 2017.
- [5] Kumaresan, U. and K. Ramanujam, Web Data Extraction from Scientific Publishers' Website Using Heuristic Algorithm, 2017.
- [6] Raza, M. and S. Gulwani, Automated Data Extraction using Predictive Program Synthesis. 2017.
- [7] Cai, Z., et al., A Vision Recognition Based Method for Web Data Extraction, 2017.
- [8] Cai, D., et al., VIPS: a vision-based page segmentation algorithm. 2003, Microsoft Technical Report, MSR-TR-2003-79.
- [9] Manjaramkar, A. and R.L. Lokhande. DEPTA: An efficient technique for web data extraction and alignment. in Advances in Computing, Communications and Informatics (ICACCI), International Conference on. 2016. IEEE.
- [10] Kamanwar, N. and S. Kale. Web data extraction techniques: A review. in Futuristic Trends in Research and Innovation for Social Welfare (Startup Conclave), World Conference, 2016. IEEE.
- [11] Fang, Y.X., et al., STEM: A suffix tree-based method for web data records extraction. Knowledge and Information Systems, 2018. vol. 55(2), pp. 305-331.
- [12] Jiménez, P. and R. Corchuelo, On learning web information extraction rules with TANGO. Information Systems, 2016. vol. 62, pp. 74-103.
- [13] Sabri, I.A.A. and M. Man, Improving performance of DOM in semi-structured data extraction using WEIDJ model. Indonesian Journal of Electrical Engineering and Computer Science, 2018. vol. 9(3), pp. 752-763.
- [14] Li, Y.N., et al., Mison: A Fast JSON Parser for Data Analytics. Proceedings of the Vldb Endowment, 2017. vol. 10(10), pp. 1118-1129.
- [15] Sabri, I.A.A. and m. Man, A performance of comparative study for semi-structured web data extraction model. International Journal of Electrical and Computer Engineering (IJECE), 2019. vol. 9(6), pp. 5463-5470.
- [16] Sabri, I.A.A., et al. Web data extraction approach for deep web using WEIDJ. in 16th International Learning & Technology Conference 2019. Riyadh, Saudi Arabia: Elsevier.
- [17] Narawade, S.M., et al., A web based data extraction using hierarchical (DOM) tree approach. International Journal for Innovative Research in Science and Technology, 2016. vol. 2(11), pp. 255-257.
- [18] Sabri, I.A.A. and M. Man, Improving performance of DOM in semi-structured data extraction using WEIDJ model. Indonesian Journal of Electrical Engineering and Computer Science, 2018. vol. 9(3), pp. 752-763.
- [19] Creech, J. Biodiversity web resources. Science and Technology Resources on the Internet 2012 [cited 2017 31 May 2017]; Available from: <http://www.istl.org/12-fall/internet.html>.

Alzheimer's Disease Detection using Neighborhood Components Analysis and Feature Selection

Mohamed Maher Ben Ismail¹, Reema Alabdullatif², Ouiem Bchir³
College of Computer and Information Sciences, King Saud University, Riyadh, KSA

Abstract—In this paper, we propose a Computer Aided Diagnosis (CAD) system in order to assist the physicians in the early detection of Alzheimer's Disease (AD) and ensure an effective diagnosis. The proposed framework is designed to be fully-automated upon the capture of the brain structure using Magnetic Resonance Imaging (MRI) scanners. The Voxel-Based Morphometry (VBM) analysis is a key element in the proposed detection process as it is intended to investigate the Gray Matter (GM) tissues in the captured MRI images. In other words, the feature extraction phase consists in encoding the voxel properties in the MRI images into numerical vectors. The resulting feature vectors are then fed into a Neighborhood Component Analysis and Feature Selection (NCFS) algorithm coupled with K-Nearest Neighbor (KNN) algorithm in order to learn a classification model able to recognize AD cases. The feature selection based on NCFS algorithm improved the overall classification performance.

Keywords—Alzheimer detection; classification; feature selection

I. INTRODUCTION

Alzheimer's Disease (AD) is an irreversible and progressive disorder that affects the brain of some elderly people. It destroys the memory and thinking skills and, eventually, the ability to perform simple tasks. Among older adults, it is the most common cause of dementia accounting for 60% to 80% of the cases. AD is ranked as the sixth cause of death in the United States, and moving to be in the third position based on recent statistic of the Alzheimer's Association [3]. In fact, the number of cases has drastically increased during the last 15 years. Currently, around 5 million Americans are diagnosed with AD and their number is expected to rise almost three-folds this number by 2050 as reported by the Alzheimer's Association [4]. According to the Saudi Alzheimer's Disease Association [3], there are 130,000 patients diagnosed with the disease in the kingdom. However, given the social norms and the lack of care systems in rural areas, these numbers represent probably a proportion of the actual cases.

Typically, dementia patients lose their cognitive functioning abilities such as thinking and remembering as well as their behavioral abilities. For the severe cases, AD patients become completely dependent on others in their basic daily activities. Besides, the serious physical and mental responsibilities that need to be taken by a caregiver, who is usually a family member, financial obligations are induced as well. In fact, The Alzheimer's Association [3] claims that AD's cost exceeds quarter of a trillion dollars nationwide.

Although Alzheimer's has no cure at the time being, clinical trials are still undergoing to develop medicines able to cure this disease. In fact, there are treatments which slow or delay the symptoms and maintain the mental function of the patients as reported by The National Institute on Aging [29]. For that, early diagnosis benefits the patients to sort out their life plans, financial situations as well as any legal issues while they are capable to do so mentally. Furthermore, on a nation level, upon early diagnosis, trillions of dollars could be saved on medical and care costs. However, AD cannot be definitely diagnosed except through autopsy using a microscope to examine the brain tissues. On the other hand, clinical assessment is performed to rule out other causes of dementia through appropriate tests as shown in Web MD [35]. One should note that more accurate diagnosis is made possible through the identification of AD biomarkers which can help in detecting it even before clinical symptoms are reported on patients. Namely, neuroimaging is an example of biomarkers that can capture changes in the brain without any invasive procedure as introduced in [11].

Several researchers around the globe took the interest in designing Computer Aided Diagnosis (CAD) systems to assist in the early detection of this serious disease and assure an effective diagnosis [1]. In particular, image based approaches have been coupled with machine learning techniques to address the AD detection challenge. These efforts have yielded promising results and have exhibited noticeable margin for improvement. Despite these efforts, the choice of the appropriate features and ML techniques remains a challenging open problem with a considerable room for improvement. In other words, the selection of (i) the appropriate visual descriptors used to encode the visual properties of the dataset and (ii) the supervised learning algorithm to map these resulting feature vectors into the positive or negative classes, can be investigated to improve the overall CAD performance. Such CAD system can be used in hospitals to assist doctors and radiologists in the interpretation of the relevant medical images. This would increase the accuracy of the clinical diagnosis.

In this paper, we propose to use standard features used to encode the biomarkers along with the Neighborhood Component Analysis and Feature Selection (NCFS) introduced in [15] as classification algorithm to improve the AD detection rate. More precisely, we intend to extract whole-brain atrophy features from structural MRI obtained from ADNI then apply the supervised NCAFS classifier to select a relevant subset of the highly-dimensional features to use it in k-nearest neighbor classification.

The rest the paper is organized as follows: Section II introduces the background of this work, Section III discusses an overview of the CAD researches in AD, Section IV describes our classification framework, and a summary and conclusion are presented in Section V.

II. RELATED WORKS

Different approaches and different classification methods are being investigated to introduce a reliable classification system that can detect AD in an automatic manner. Moreover, as the features that are extracted from such medical images are usually high-dimensional, suitable selection and reduction methods have been adopted to enhance the classification performance, address the curse of dimensionality, and reduce the time complexity.

In particular, the features extracted from structural images have been exploited in the design AD detections systems. Namely, the voxel-wise measures were commonly used when the intensities of the voxels were used as features. The voxels of choice are usually selected from the regions that exhibit differences between groups either found automatically by VBM or by prior knowledge of the anatomical regions affected by AD. For the later, pre-defined anatomically labeled atlases are used to locate those regions in the MR images. The authors in [9] relied on prior knowledge acquired by selecting 9 regions for which the voxels intensities were provided. Most of the selected regions were located in medial temporal lobe as its atrophy is considered a key biomarker. The number of features was then significantly reduced by pruning a Random Forest. To minimize the overfitting caused by the fact that the data includes more features than samples, multiple SVM classifiers were trained with random subsets from the pruned features and their dichotomic outcomes were averaged to create a classification index. On the other hand, the ROIs were specified on the basis of VBM analysis as outlined by the researchers in [5]. Accordingly, voxel values from the regions with decreased Gray Matter (GM) volume were used as raw features. The number of features was then reduced statistically using a probability distribution function that created a histogram of the intensity values. The optimal number of bins in the histograms was selected based on Fisher criterion maximization. As in [9], an SVM with linear kernel was used for the classification.

A feature extraction approach, similar to the one proposed in [6], was outlined in [7] along with a feature ranking method as feature selection approach. The approach aims to measure the relevance and the discriminative power of the visual features using a statistical t-test. A subset containing the top ranked features was then fed into a linear SVM learner for the classification task. The framework outlined in [23] relied also on the voxel values of GM map. However, the voxels of the whole GM tissue were acquired instead of specific ROIs. For those features, bottom-up hierarchical clustering was conducted to build a tree that illustrates the structural relationships among them. Then, the relationships captured by the tree were imposed on a sparse learning to determine the informative features. More than one brain tissue was incorporated in the development of the system introduced in [21]. Specifically, voxel intensities in both GM and white

matter (WM) maps were saved as raw features followed by reduction by means of the statistical model Partial Least Square (PLS). PLS is similar to the famous Principal Component Analysis (PCA). However, it takes the class labels into account. Combining the features resulted in a slightly better performance when coupled with a linear SVM compared to GM based performance. The Regularized Logistic Regression (RLR) was adopted by the researchers in [8] to directly operate on the density map of GM instead of performing the reduction and classification at two steps in the voxel space. Scores were assigned by the RLR classifier based on conditional probabilities metrics that captures the similarity of the anatomical patterns found in a given individual to those in AD patients.

Instead of handling voxel values, the authors in [12] processed features further to obtain better visual data representation. Specifically, after VBM analysis, GM map generation and ROIs selection respectively, the texture features were extracted. Namely, the Gray Level Co-occurrence Matrix (GLCM) and Gabor filters were used for the texture feature extraction. On the other hand, an SVM Recursive Feature Elimination (SVM-RFE) was used along with a covariance metric to remove redundant data and consider the relevant features only. Thu SVM-RFE discarded the least significant features for classification in a backward sequential selection manner while the covariance was used to measure the correlation between the features. The measure of the cortical thickness was adopted in [10]. It was obtained by measuring the distances between the vertices on the meshes of the inner and the outer cortical surfaces. The feature vector of each subject encoding the thicknesses information was then transformed to the frequency space to remove noise. To accomplish that, a Manifold Harmonic Transform with eigen functions of the Laplace–Beltrami operator as the basis function of the transform was used. A cut-off to a certain number of eigenvectors was made which filtered the high frequency components while preserving the discriminating low frequency data. Principal Component Analysis (PCA) was then used followed by Linear Discriminant Analysis to transform the feature vectors into points in LDA space then find the axis that best separates the groups. In [13], the features were constructed as an ensemble of the following: the average cortical thickness values, the standard deviation in cortical thickness, the total surface area of the cortex, the volumes of cortical and WM ROIs. Note that a Logistic Regression with stability selection introduced in [24] yielded the best results when couple with a random forest classifier. Beside voxel values and cortical thickness, other methods have been explored in this area as well. Namely, the researchers in [17] experimented the Wavelet coefficients obtained using a Two-dimensional Discrete Wavelet Transform (2D-DWT) along with Haar wavelet function of level 3. On the other hand, the Principal Component Analysis (PCA) was adopted as a dimensionality reduction technique and the Normalized Mutual Information Feature Selection (NMIFS) that is derived from the minimum Redundancy Maximum Relevance (mRMR) was used as feature selection. Circular Harmonic Functions (CHFs) were utilized in [2] to extract local features of hippocampus and posterior cingulate cortex (PCC) from each slice of the 3D MRI. Those two ROIs

were selected for the noticeable harm the disease imposes on them. As depicted in [30], the features obtained from each ROI were then quantized using the bag-of-visual words approach by representing them as a histogram of occurrence of quantized visual features. The histograms of both ROIs were then combined in a single vector creating a signature for each subject. PCA was used for dimensionality reduction and the resulting features were finally fed into an SVM with the Radial Basis Function (RBF) as a kernel. Another approach introduced by the researchers consisted in fusing the features extracted from different modalities prior to learning the classification models. This was intended to exploit the complementary information provided by the different features to better capture the classes properties. Recently, the performance of deep learning on MRI and PET images was investigated in [22]. Automatic extraction of multi-level features was conducted by cascaded convolutional neural networks (CNN) on images from both modalities. The fully connected layer of the network was then followed by a softmax layer to perform the classification.

In [18], the authors investigated the connectivity of the hippocampus, precuneus and primary visual cortex and correlated each with the voxels of the brain. Sixteen AD patients and sixteen healthy controls were considered for this research. It was revealed that AD patients showed greater FC in left hippocampus with right insula. In [34], four seeds, right and left hippocampi and isthmus of the cingulate cortices (ICCs), which are parts within DMN were selected in a multi-class classification among them 10 AD, and 12 HC subjects. Pearson correlation coefficients were calculated between all possible pairs of the ROIs resulting in a 6-dimensional feature vectors. Then, to maximize the group differences and reduce noise, regularized LDA was applied to map the features into a one-dimensional sub-space. Finally, a decision tree was constructed and the classification was performed using AdaBoost ensemble learning.

For ICA, the researchers in [31-32] experimented 8 different types of FC measures and their variations to define the connections mostly related to the disease and might deliver better classification performance. Among these measures, matrices that record the connections between components obtained from ICA, the dynamics of these matrices found via a sliding window, and the graph properties of the matrices were used. For classification, Elastic net logistic regression was deployed to evaluate those measures individually. The FC dynamics variation outperformed the other measures. On the other hand, a new metric derived directly from the rs-fMRI signal instead of FC measure was depicted in [20]. ICA was conducted to decompose the signals acquired from 15 AD and 15 healthy elderlies into their spatial components and their weights of time-courses. Then, a goodness-of-fit (GoF) calculation, template matching and SVM classification were applied to identify the neuronal components among the decomposed ones. Next, a brain activity map was constructed based on these components by computations involving the BOLD signals amplitudes and their standard deviations. Hippocampus and accumbens were selected separately as part of several experiments to train a linear SVM model. The rs-fMRI data obtained from ADNI as used to classify 20 healthy

subjects and 20 patients with AD in [19] using a linear SVM model. The automated anatomical labeling (AAL) atlas, a software package and digital atlas of the human brain, was used to divide the whole brain into 90 distinct regions and construct a graph with the regions as nodes. The signal of each node was computed by averaging the time series of voxels in each region to represent them and Pearson's correlation coefficients were employed to define the edges of the functional connectivity network. Graph metrics were then computed and used as discriminative features after selecting the optimal subset via Fisher score feature selection algorithm.

III. PROPOSED METHOD

This research is intended to design and implement a reliable CAD system for automatic detection of Alzheimer's disease (AD) based on MR images. Specifically, typical features are extracted to encode the visual properties of the patient MRI image. Then, the mapping between these features and the pre-defined class values (AD or Not-AD) is learned in a supervised manner. In other word, a supervised learning task is carried out by training a classification model using the annotated features extracted from the MR images. The resulting model is then intended to predict the class label of any unannotated MRI image features. Typically, the available data is divided into training and testing sets. Each image from the training set is then processed to extract a new representation vector that encapsulates its visual properties. Thus, a matrix containing all the training vectors is then fed into the classification algorithm along with their corresponding labels to learn a model for this specific problem. The system is evaluated with the testing set by comparing the labels predicted by the learned model with the ground truth labels. Though feature selection is not typically a key element, it is considered an important step in cases of high-dimensional vectors as in AD classification problems.

NCFS is an embedded feature selection method which aims to find a weighting vector w for the features. In fact, the optimal weight vector is the one that maximizes the leave-one-out classification of nearest neighbor algorithm based on a gradient ascent technique. Let $T = \{(x_1, y_1), \dots, (x_i, y_i), \dots, (x_N, y_N)\}$ be a set of N training samples where x_i is a d -dimensional feature vector and $y_i \in \{1, \dots, C\}$ is its corresponding class label. The weighted distance between two samples x_i and x_j is obtained using:

$$D_w(x_i, x_j) = \sum_{l=1}^d w_l^2 |x_{il} - x_{jl}| \quad (1)$$

where w_l is the weight of the l^{th} feature in the vectors of the sample points. The Gradient ascent algorithm relies on differentiable functions to find the optimal solution. However, the function for selecting the nearest neighbors as a reference point for classification is non-differentiable, thus a probability distribution is used as an approximation to select the reference point. Equation (2) calculates the probability that x_i selects x_j as the reference point.

$$p_{ij} = \begin{cases} \frac{k(D_w(x_i, x_j))}{\sum_{m \neq i} k(D_w(x_i, x_m))} & \text{if } i \neq j \\ 0, & \text{if } i = j \end{cases} \quad (2)$$

where $\kappa(z) = \exp(-z/\sigma)$ is a kernel function and σ is the kernel width which is a parameter between 0 till $+\infty$ that affect the selection probability of each point in the set; i.e. if $\sigma \rightarrow 0$ only nearest neighbors can be selected and if $\sigma \rightarrow +\infty$ all the samples have the same chance.

The probability that a sample x_i is correctly classified can be calculated as:

$$p_i = \sum_j y_{ij} p_{ij} \quad (3)$$

with $y_{ij} = 1$ iff $y_i = y_j$ and $y_{ij} = 0$ otherwise.

The approximate leave-one-out classification accuracy can be found for a particular weighting vector as follows:

$$\xi(w) = \frac{1}{N} \sum_i p_i = \frac{1}{N} \sum_i \sum_j y_{ij} p_{ij} \quad (4)$$

A regularization parameter $\lambda > 0$ that can be tuned via cross validation is also included in the object function to reduce overfitting and accomplishing the feature selection by driving many of the weights in w to 0:

The regularization term formulated as:

$$\xi(w) = \sum_i \sum_j y_{ij} p_{ij} - \lambda \sum_{l=1}^d w_l^2 \quad (5)$$

The derivative of the object function $\xi(w)$ with respect to w_l is computed as:

$$\begin{aligned} \frac{\partial \xi(w)}{\partial w_l} &= \sum_i \sum_j y_{ij} \left[\frac{2}{\sigma} p_{ij} \left(\sum_{m \neq i} p_{im} |x_{il} - x_{ml}| - |x_{il} - x_{jl}| \right) w_l \right] - 2\lambda w_l \\ &= \frac{2}{\sigma} \sum_i \left(p_i \sum_{m \neq i} p_{im} |x_{il} - x_{ml}| - \sum_j y_{ij} p_{ij} |x_{il} - x_{jl}| \right) w_l - 2\lambda w_l \\ &= 2 \left(\frac{1}{\sigma} \sum_i (p_i \sum_{m \neq i} p_{im} |x_{il} - x_{ml}| - \sum_j y_{ij} p_{ij} |x_{il} - x_{jl}|) - \lambda \right) w_l \quad (6) \end{aligned}$$

This derivative of the objective function yields the update equation for the gradient ascent. Algorithm 1 is a pseudocode of the neighborhood component feature selection procedure.

Algorithm 1: Neighborhood Component Feature Selection

```

NCFS( $T, \alpha, \sigma, \lambda, \eta$ )  $\triangleleft T$ : training set,  $\alpha$ : initial step length,  $\sigma$ : kernel width,  $\lambda$ : regularization parameter,  $\eta$ : small positive constant;
Initialization:  $w^{(0)} = (1, 1, \dots, 1)$ ,  $\epsilon^{(t)} = -\infty$ ,  $t = 0$ 
repeat
for  $i = 1, \dots, N$  do
Compute  $p_{ij}$  and  $p_i$  using  $w^{(t)}$  according to (2) and (3)
for  $l = 1, \dots, d$  do
 $\Delta_l = 2 \left( \frac{1}{\sigma} \sum_i (p_i \sum_{m \neq i} p_{im} |x_{il} - x_{ml}| - \sum_j y_{ij} p_{ij} |x_{il} - x_{jl}|) - \lambda \right) w_l^{(t)}$ 
 $t = t + 1$ 
 $w^{(t)} = w^{(t-1)} + \alpha \Delta$ 
 $\epsilon^{(t)} = \xi(w^{(t-1)})$ 
If  $\epsilon^{(t)} > \epsilon^{(t-1)}$  then
 $\alpha = 1.01\alpha$ 
else
 $\alpha = 0.4\alpha$ 
until  $|\epsilon^{(t)} - \epsilon^{(t-1)}| < \eta$ 
 $w = w^{(t)}$ 
return  $w$ 

```

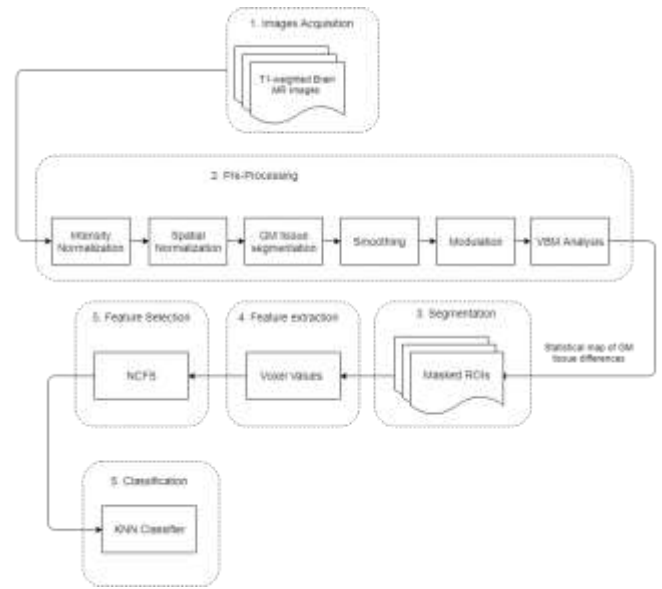


Fig. 1. Detailed Schema of the Proposed CAD System.

Fig. 1 depicts the main components of the proposed system.

This research relies on the images acquired using structural MRI for their ability to produce high resolution images without any injected substance as well as their potential to capture the structure of brain. The atrophies that are a key symptom of AD pathology can be detected using this modality. The T1-weighted sequence is generally used for AD scans as stated in [14] and so will be the images in this framework. Before employing the images in creating a classification model, pre-processing steps need to be carried out. T1-weighted images might exhibit non-uniform intensities throughout the brain caused by a low-frequency smooth signal known as bias field. Bias field is introduced to the scans due to the heterogeneous magnetic field of MRI scanners. This affects the images by blurring them and consequently reducing their high frequency content such as edges besides changing the gray level distribution of tissues from the same class as proved in [27]. Therefore, MR images were corrected for this flaw prior to subsequent processing. Fig. 2 shows the bias field effect on the MR images. N4 intensity normalization method outlined in [33] as a variant of N3 algorithm known for bias correction in medical images, was also used for this purpose as suggested by ADNI. However, in order to produce precise statistics, images need to be aligned to reduce the variability between individuals since people have different sized and shaped brain structures. Spatial normalization (or registration) is the method that achieves that by transforming MR image of each individual to a reference frame called template.

This process is guided by an atlas which locates the position of the different anatomical regions in the template space. Namely, we relied on the MNI templates provided by The Montreal Neurological Institute [28]. Specifically, we adopted their ICBM152 standard from The McConnell Brain Imaging Centre [27]. After the pre-processing phase suggested in [25-26], instead of pre-selecting ROIs from GM tissue to

extract their features, a whole brain analysis is performed to find all the areas that are different between AD patients and healthy elderlies. Following VBM analysis and highlighting the areas that differ between the two groups, these areas are selected as ROIs. The considered features are the voxel values (or intensities) belonging to these ROIs. The algorithm NCFS is then applied to the training set to rank the extracted features according to their amount of positive influence on a *KNN* classifier in a leave-one-out classification. A subset containing the highly ranked features will then be selected as the representing features to be used while training the classification model.

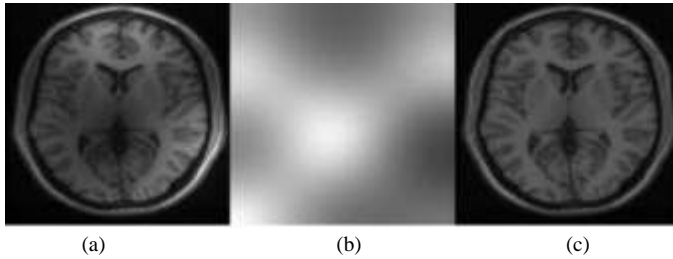


Fig. 2. (a) Bias Field effect on a Slice of MR Image (b) Bias Field Frequency (c) Corrected Image.

IV. EXPERIMENTS

We conducted our experiments on a collection MRI images which includes 100 AD cases versus 100 healthy instances. This dataset was provided by the Alzheimer's Disease Neuroimaging Initiative (ADNI 2020). In particular, we compared the classification performance obtained using various classification methods. Specifically, some of the learned models were built using the original set of features, while others were built after some feature selection. Namely, the algorithms we used in these experiments are *KNN* classifier and *SVM* classifier (with two kernels: linear and RBF). The rationales behind this choice are: (i) *NCFS* is based on ranking the feature relevance according to their contribution in maximizing *KNN* classification performance. In other words, we intended to investigate whether selecting the top ranked features improves the performance of Alzheimer's disease detection. (ii) *SVM* is widely used in related CAD systems and testing it on the designed features would provide a better perception on the validity of the proposed system compared to state of the art solutions. Furthermore, two other existing methods were tested on the same dataset and environment in order to provide a good

ground for comparison. Specifically, the first method is based on *PCA* features reduction while the other relies on *t*-tests to sort the features and select the optimal ones.

A. VBM Analysis

After preprocessing the data, the gray matter tissue maps were analyzed with *VBM* to detect the atrophy regions that differentiated *AD* from *HC* group. For this particular analysis of the selected samples from *AD* and *HC* groups, three significant clusters which include different number of voxels were obtained. Fig. 3 illustrates the locations of these clusters while Table I provides their details. The values of the voxels belonging to the resulting clusters were then extracted from each sample then combined into one feature vector. This means that the feature vector is a concatenation of the voxels values from the three clusters per sample. In the following, we refer to this vector as raw features.

B. Optimization of SVM Hyper-Parameters

As depicted in [16], the *SVM* models rely on finding the optimal hyperplane which maximizes the margin between two classes. The optimization process is formulated using an objective function and resolved using typical mathematical optimization methods. This function is controlled by the parameters known as hyperparameters. Their settings affect the performance of the learning process. Therefore, these parameters need to be tuned to find the set of values which is optimal for solving a specific learning problem. Two kernels were investigated in this project. Namely, we used the linear and RBF kernels. For RBF kernel, a couple of parameters need to be optimized: the cost or regularization term and gamma or kernel width. The cost controls the trade-off between the misclassifications of training samples and width of the margin while the gamma controls the tradeoff between under-fitting loss and over-fitting loss. Both parameters were optimized in this work using Bayesian optimizer with 10-fold cross validation for every different set of features.

C. Optimization of Lambda in NCFS

A tuning via cross validation was conducted on a range of value starting from zero, where no regularization was enforced, to optimize the regularization parameter lambda. In each fold, the lambda values were used and the loss was assessed with Mean Squared Error (MSE). Fig. 4 reports the effect of choosing the appropriate regularization value showing the worst performance when the value was set to zero and an improved performance by more than 10% with 0.018.

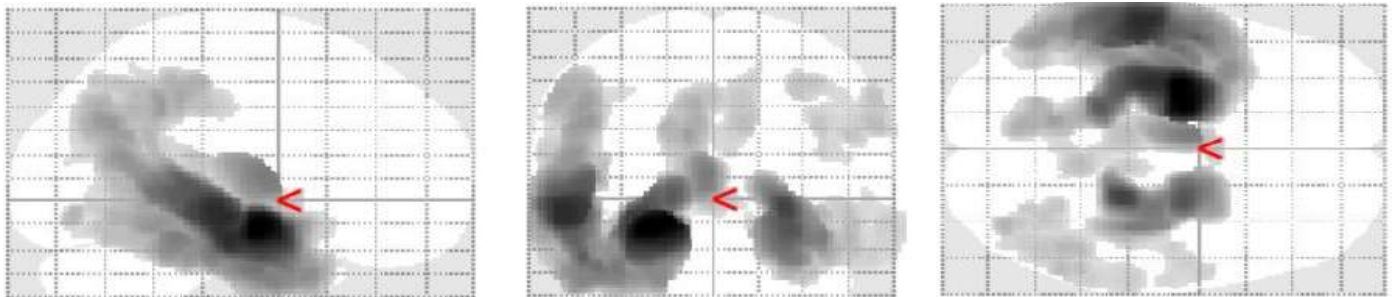


Fig. 3. Glass view of Atrophy Clusters Highlighted by VBM Analysis where $k = 1400$.

TABLE I. ATROPHY CLUSTERS INFO WHERE K = 1400

Cluster ID	MNI coordinates	K_E (voxels quantity)	T-value (peak-level)
1	-26, -9, -14	36607	14.51
2	24, -32, -6	8748	11.46
3	59, -56, 30	1824	6.35

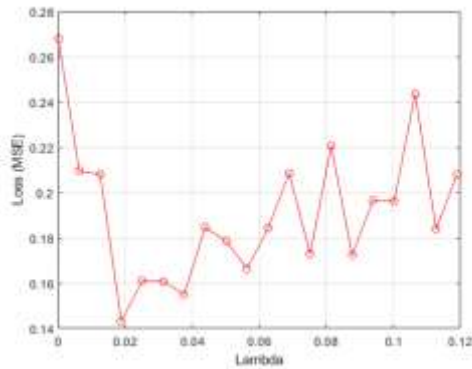


Fig. 4. Loss Results of Tuning the NCFS Regularization Parameter Lambda Measured by MSE.

D. Feature Weighting using NCFS

After optimizing NCFS parameters, the best value was used in the algorithm to rank the raw features. Then, to reduce the dimensionality of the ranked features, a threshold (or cutoff) was determined by iteratively adjusting the number of selected features and feed them to an SVM classifier where its performance is evaluated with 10-fold cross validation. The adjustment started by taking a wider range of values and large step size in order to have a rough estimation where the optimal number is located. After that, in the span that had the highest accuracy, a second adjustment was repeated within its bound with smaller step size as shown in Fig. 5.

E. T-Test based Feature Ranking

As previously mentioned, another type of feature selection was tested in this work. The raw features were ranked using T-test method according to their T-values. For selecting the optimal number of features, the same method used with NCFS features was applied here. The corresponding results are reported in Fig. 6. Though the authors in [7] proposed using fisher criterion to automatically determine the threshold, following our method in determining it won't have major effect as their classification model is also SVM which we use in the evaluation of the optimal number.

F. Features Reduction using PCA

The high dimensionality of raw features was reduced using PCA method. PCA was chosen in our comparative analysis for its effectiveness in significantly reducing the number of features and also being compared to t-test features. Similar to the previous work, using 10-fold cross validation, the orthogonal principal components of the raw features and training samples were extracted in every fold to train the models. The number of components was equal to the number of training samples and they were used directly as the features;

that resulted in a vector with 200 dimensions in our case. However, to improve the PCA performance we only selected the components that retained 95% of data information which further reduced the dimensions to only 75. The improvement in classification is described in Table II.

G. Results obtained using SVM Models

In our experiments, every feature set was used to train and test three classification models. More specifically, we used KNN along with a linear-kernel SVM and a Gaussian RBF SVM. First, we present the results obtained using SVM classifiers.

Table III reports the accuracy, sensitivity, specificity and AUC measures attained using the two SVM classifiers associated with the considered features. As it can be seen, linear SVM yielded noticeably higher accuracy. In particular, it resulted in a 4.5% increase for the raw features while the others did not exhibit large differences in their accuracies as they did not go above 1%. On the other hand, from the sensitivity perspective, which is considered an important measure in this study and the medical field in general, SVM with RBF kernel attained 4.5% improvement in the classification of AD patients with the t-test features compared to the linear kernel. NCFS and PCA features remained rather consistent across the two models but giving better overall performance with the linear kernel. Raw and PCA features scored the highest accuracy among the other features in the linear model and PCA in the RBF model.

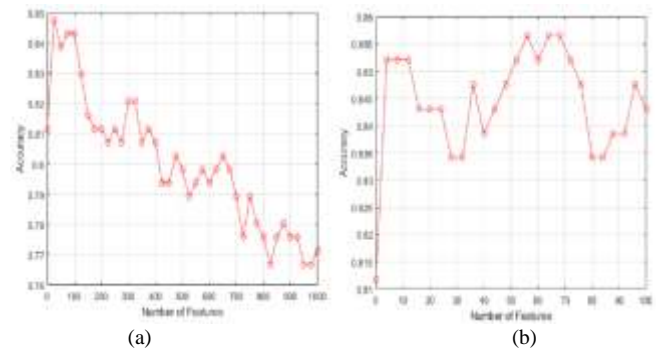


Fig. 5. The Accuracies from Training an SVM Model with NCFS Features of different Dimensions. (a) The First Adjustment Results with Higher Range and Step Size (b) The Second Adjustment within the Bound of the Highest Accuracy Span and Small Step Size.

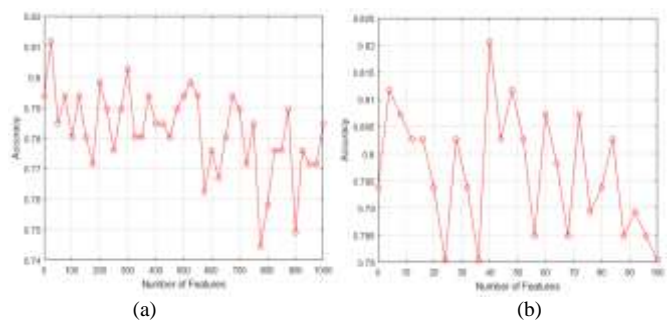


Fig. 6. The Accuracies from Training an SVM Model with T-Test Features of different Dimensions. (a) The First Adjustment Results with Higher Range and Step Size (b) The Second Adjustment within the Bound of the Highest Accuracy Span and Small Step Size; Threshold = 40.

TABLE II. DIFFERENCES IN CLASSIFICATION RESULTS OF PCA WITH ALL THE COMPONENTS AND THE COMPONENTS WITH 95% PRESERVE

Features	Linear SVM			
	Acc %	Sen %	Spe %	AUC %
PCA-All	77.58	73.15	81.74	85.83
PCA	87.00	83.33	90.43	92.38

TABLE III. CLASSIFICATION RESULTS OF SVM MODELS ON EACH TYPE OF FEATURE

Features	Linear SVM				RBF SVM			
	Acc %	Sen %	Spe %	AUC %	Acc %	Sen %	Spe %	AUC %
Raw	87.0	87.0	86.9	93.3	82.5	78.7	86.0	91.2
NCFS	84.3	82.4	86.0	91.5	83.8	79.6	87.8	90.2
T-test	81.6	75.0	87.8	88.7	82.5	79.6	85.2	85.0
PCA	87.0	83.3	90.4	92.3	86.1	82.4	89.5	91.7

Fig. 7 and Fig. 8 depict the ROC curves produced by plotting the true and false positive rates from each classifier. The higher the curve is, the larger AUC value which measures the area under this curve and the better the classifier. T-test features showed the least AUC values with RBF kernel which can be perceived in how low its curve is in Fig. 8 compared to the other curves. The unexpected performance of the raw features can be attributed to two facts. The first one is that these features are a result of a statistical analysis that discriminates between the two groups. This yields a fair separability between the data instances from the two classes. The second fact is that kernel SVM is a powerful classifier when the hyperparameters are optimized and can handle efficiently highly dimensional data.

H. Results Obtained using KNN

The classification results obtained using KNN yielded different but predictable results. The Manhattan distance (or city block) was used as the distance metric to decide the nearest neighbors of any given sample. As it can be seen in Table IV, the number of neighbors K was set to be 3, 5 and 7 respectively to assess its effect on the performance. NCFS features resulted in the highest performance measures and ROC curve, followed by t-test features as confirmed by Fig. 9. As NCFS ranked the features based on their contribution in maximizing KNN classification, this had an advantage of giving it a classification power similar to SVM classifier. Unfortunately, the sensitivity dropped by about 5% compared to SVM results. This means that more AD instances were misclassified in all number of neighbors variations and could indicate that the initial features weren't discriminative enough. Likewise, the performance with raw features declined in this round in all the three settings. Unlike SVM, KNN doesn't have the ability to deal with the high dimensionality in data which in turn affected the distance by the irrelevant features.

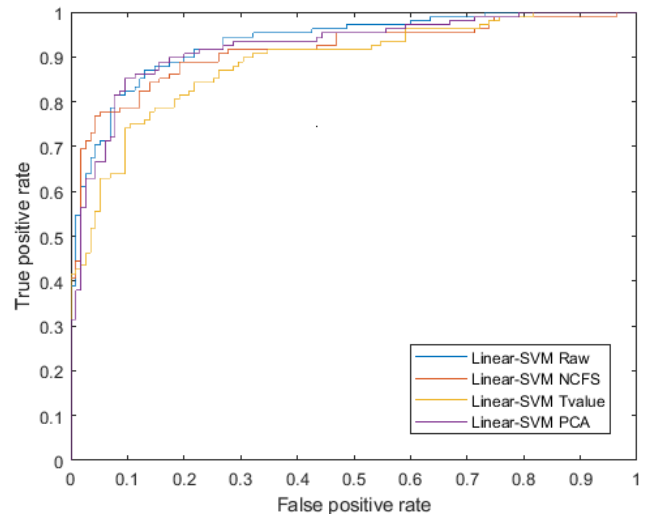


Fig. 7. ROC Curves for Linear SVM Classifications with the different Features Types.

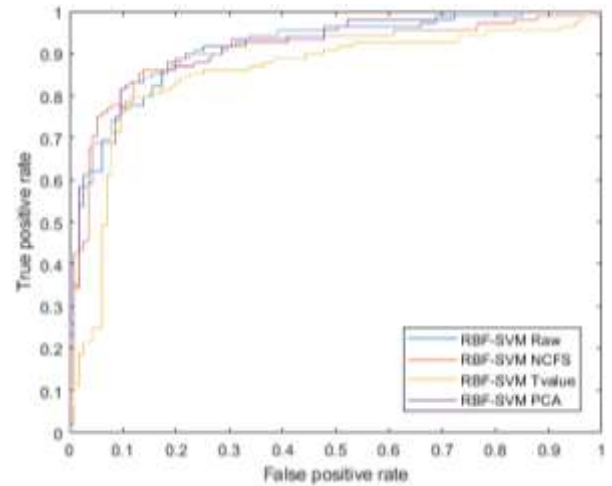


Fig. 8. ROC Curves for RBF-SVM Classifications with the different Features Types.

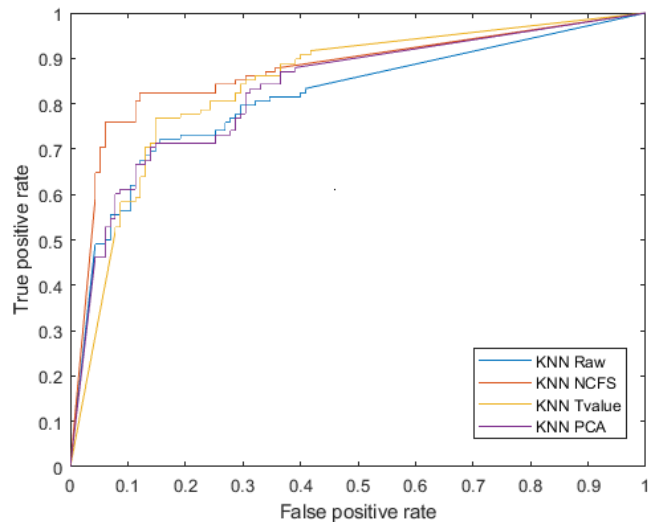


Fig. 9. ROC Curves for KNN Classifications with the different Features Types.

TABLE IV. CLASSIFICATION RESULTS OF KNN MODELS ON EACH TYPE OF FEATURE WITH DIFFERENT NUMBER OF NEIGHBORS K

Features	K = 3				K = 5				K = 7			
	Acc %	Sen %	Spe %	AUC %	Acc %	Sen %	Spe %	AUC %	Acc %	Sen %	Spe %	AUC %
Raw	78.5	72.2	84.4	81.4	78.0	66.7	88.7	83.9	78.9	68.5	88.7	85.0
NCFS	83.0	76.9	88.7	87.2	81.6	77.8	85.2	88.6	83.0	78.7	87.0	89.2
T-test	80.3	76.9	83.5	84.4	80.7	75.9	85.2	86.8	82.5	76.9	87.8	87.8
PCA	77.6	66.7	87.8	83.1	79.8	69.4	89.6	85.0	80.3	70.4	89.6	85.3

V. CONCLUSIONS

In this paper, we proposed a fully-automated CAD system able to detect AD cases. A detailed description of the different component of the proposed system was provided. In particular, the Neighborhood Component Analysis and Feature Selection (NCFS) approach was combined with K-Nearest Neighbor (KNN) as the supervised learning algorithm intended to perform feature selection and AD detection. The obtained results confirmed the effectiveness of the proposed unsupervised learning approach as well as the discriminative power of the features used to encode the image visual properties.

ACKNOWLEDGMENT

This work was supported by the Research Center of the College of Computer and Information Sciences at King Saud University, Riyadh, Saudi Arabia. The authors are grateful for this support.

REFERENCES

[1] Abásolo, D., Hornero, R. and Espino, P. (2009) Approximate Entropy of EEG Background Activity in Alzheimer's Disease Patients, *Intelligent Automation & Soft Computing*, 15(4), 591-603.

[2] Ahmed, O. B., Mizotin, M., Benois-Pineau, J., Allard, M., Catheline, G. and Amar, C. B. (2015) "Alzheimer's disease diagnosis on structural MR images using circular harmonic functions descriptors on hippocampus and posterior cingulate cortex," *Computerized Medical Imaging and Graphics*, 44, 13-25.

[3] Alzheimer's Association 2020. Available: <https://www.alz.org/alzheimers-dementia/what-is-Alzheimers>.

[4] Alzheimer's Association, 2019. Available: <https://www.alz.org/alzheimers-dementia/facts-figures>.

[5] Beheshti, I. and Demirel, H. (2015). "Probability distribution function-based classification of structural MRI for the detection of Alzheimer's disease," *Computers in Biology and Medicine*, 64, 208-216.

[6] Beheshti, I. and Demirel, H. (2016). "Feature-ranking-based Alzheimer's disease classification from structural MRI," *Magnetic resonance imaging*, 34(3), 252-263.

[7] Casanova, R., Hsu, F., Sink, K., Rapp, S., Williamson, J. and Resnick, S. (2013). "Alzheimer's disease risk assessment using large-scale machine learning methods," *PLOS ONE*, 8(11).

[8] Chincarini, A., Bosco, P., Calvini, P., Gemme, G., Esposito, M., Olivieri, C., Rei, L., Squarcia, S., Rodriguez, G., Bellotti R. (2011). "Local MRI analysis approach in the diagnosis of early and prodromal Alzheimer's disease," *Neuroimage*, 58(2), 469-480.

[9] Cho, Y., Seong, J.-K., Jeong, Y. and Shin, S. Y. (2012). "Individual subject classification for Alzheimer's disease based on incremental learning using a spatial frequency representation of cortical thickness data," *Neuroimage*, 59(3), 2217-2230.

[10] Craig-Schapiro, R., Fagan, A. M. and Holtzman, D. M. (2009). "Biomarkers of Alzheimer's disease," *Neurobiology of Disease*, 35, 128 - 140.

[11] Ding, Y., Zhang, C., Lan, T., Qin, Z. Zhang, X. and Wang, W. (2015). "Classification of Alzheimer's disease based on the combination of morphometric feature and texture feature," in *IEEE International Conference on Bioinformatics and Biomedicine (BIBM)*, Washington, DC.

[12] Dubey, R., Zhou, J., Wang, Y., Thompson, P. M. and Ye, J. (2014). "Analysis of sampling techniques for imbalanced data: An n= 648 ADNI study," *NeuroImage*, 87, 220-241.

[13] Frisoni, G. B., Fox, N. C., Jack Jr, C. R., Scheltens, P. and Thompson, P. M. (2010). "The clinical use of structural MRI in Alzheimer disease," *Nature Reviews Neurology*, 6(2), 67.

[14] Goldberger, J., Hinton, G. E., Roweis, S. T. and Salakhutdinov, R. R. (2005). "Neighbourhood components analysis," *Advances in neural information processing systems*, 513--520.

[15] Han, F., Lei, M., Zhao, W., and Yang, J. (2012). *New Support Vector Machine for Imbalance Data Classification*. *Intelligent Automation & Soft Computing*, 18(6), 679-686.

[16] Herrera, L. J., Rojas, I., Pomares, H., Guillén, A., Valenzuela, O. and Baños, O. (2013). "Classification of MRI Images for Alzheimer's Disease Detection," in *International Conference on Social Computing*, Alexandria, VA, USA.

[17] Kenny, E. R., Blamire, A. M., Firbank, M. J. and John, T. (2011). "Functional connectivity in cortical regions in dementia with Lewy bodies and Alzheimer's disease," *a journal of neurology*, 135, 569-81.

[18] Khazae, A., Ebrahimzadeh, A. and Babajani-Feremi, A. (2015). "Identifying patients with Alzheimer's disease using resting-state fMRI and graph theory," *Clinical Neurophysiology*, 126, 2132-2141.

[19] Kazemifar, S., Manning, K. Y., Rajakumar, N., Gómez, F. A., Soddu, A., Borrie, M. J., Menon, R. S. and Bartha, R. (2017). "Spontaneous low frequency BOLD signal variations from resting-state fMRI are decreased in Alzheimer disease," *PLoS One*, 12(6).

[20] Khedher, L., Ramirez, J., Gorriz, J. M., Brahim, A. and Segovia, F. (2015). "Early diagnosis of Alzheimer's disease based on partial least squares, principal component analysis and support vector machine using segmented MRI images," *Neurocomputing*, 151, 139-150.

[21] Liu, M., Cheng, D., Wang, K. and Wang, Y. (2018). "Multi-Modality Cascaded Convolutional Neural Networks for Alzheimer's Disease Diagnosis," *Neuroinformatics*, 16(3), 295-308.

[22] Liu, M., Zhang, D. and Shen, D. (2013). "Identifying informative imaging biomarkers via tree structured sparse learning for AD diagnosis," *Neuroinformatics*, 12(3), 381-394.

[23] Meinshausen, N. and Bühlmann, P. (2010). "Stability selection," *Journal of the Royal Statistical Society: Series B (Statistical Methodology)*, 72(4), 417-473.

[24] Mikl, M., Marecek, R., Hlustik, P., Pavlicova, M., Drastich, A., Chlebus, P., Brazdil, M. and Krupa, P. (2008). "Effects of spatial smoothing on fMRI group inferences," *Magnetic resonance imaging*, 26(4), 490-503.

[25] Poldrack, R. A., Mumford, J. A. and Nichols, T. E. (2011). "Spatial normalization," in *Handbook of Functional MRI Data Analysis*, Cambridge University Press, 53-69.

[26] Poldrack, RA. 2007. Region of interest analysis for fMRI. *Soc Cogn Affect Neurosci*, 2(1), 67-70.

[27] The McConnell Brain Imaging Centre (2020), Available: <http://www.bic.mni.mcgill.ca/ServicesAtlases/ICBM152Nlin2009>.

[28] The Montreal Neurological Institute (2020). "Montreal Neurological Institute and Hospital,". Available: <https://www.mcgill.ca/neuro/>.

- [29] The National Institute on Aging, 2020. Available: <https://www.nia.nih.gov/health/alzheimers/treatment>.
- [30] The Saudi Alzheimer's Disease Association, 2020. http://alz.org.sa/?page_id=2187.
- [31] Tustison, N. J., Avants, B. B., Cook, P. A., Zheng, Y., Egan, A., Yushkevich, P. A. and Gee, J. C. (2010). "N4ITK: improved N3 bias correction," *IEEE transactions on medical imaging*, 29(6), 1310-1320.
- [32] Urka, G., Dance, C., Fan, L., Willamowski, J. and Bray, C. (2004). "visual categorization with bags of keypoints," In: *ECCV workshop on statistical learning in computer vision*, 1, 1-22.
- [33] Vos, F. d., Koini, M., Schouten, T. M., Seiler, S., Grond, J. v. d., Lechner, A., Schmidt, R., Rooij, M. d. and Rombouts, S. A. (2018). "A comprehensive analysis of resting state fMRI measures to classify individual patients with Alzheimer's disease," *NeuroImage*, 167, 62-72.
- [34] Wang, Z., Zheng, Y., Zhu, D. C., Bozoki, A. C. and Li, T. (2018). "Classification of Alzheimer's Disease, Mild Cognitive Impairment and Normal Control Subjects Using Resting-State fMRI Based Network Connectivity Analysis," *IEEE Journal of Translational Engineering in Health and Medicine*, 6, 1-9.
- [35] Web MD, 2020. Available: <https://www.webmd.com/alzheimers/guide/making-diagnosis-tests#1>.

Support Kernel Classification: A New Kernel-Based Approach

Ouiem Bchir¹, Mohamed M. Ben Ismail^{2*}, Sara Algarni³
College of Computer and Information Sciences, King Saud University, Riyadh, KSA

Abstract—In this paper, we introduce a new classification approach that learns class dependent Gaussian kernels and the belongingness likelihood of the data points with respect to each class. The proposed Support Kernel Classification (SKC) is designed to characterize and discriminate between the data instances from the different classes. It relies on the maximization of the intra-class distances and the minimization of the inter-class distances to learn the optimal Gaussian parameters. In fact, a novel objective function is proposed to model each class using one Gaussian function. The experiments conducted using synthetic datasets demonstrated the effectiveness of the proposed algorithm. Moreover, the results obtained using real datasets proved that the proposed classifier outperforms the relevant state of the art approaches.

Keywords—Supervised learning; classification; kernel based learning

I. INTRODUCTION

Classification finds applications in many real-world problems related to different fields. Such applications include, for example, analyzing customer data in the areas of commerce [1-2], detecting fraud to benefit industry and government [3], improving the learning process in education [4], predicting the climate for crop production [5], and assisting doctors in detecting anomalies in the healthcare [6]. In order to solve these classifications problems, many approaches have been reported in the literature [7]. However, most approaches assume that the different categories can be separated using linear boundaries, and thus, they are effective when the data has a simple geometric characteristic with well-separated categories.

Kernel-based approaches [8] have been proposed as an alternative solution. They map the data into a new feature space in such a way that categorizing classes with complex boundaries can be reduced to a simple categorization problem in the new feature space. Nevertheless, the choice of an optimal kernel that allows separating linearly the different categories of the data is a challenging problem [9]. The most common used kernel is the Gaussian kernel due to its statistical and geometrical proprieties [10]. However, it is sensitive to the choice of the Gaussian parameters. An exhaustive search of these parameters requires training the classifier many times to consider different possible values. In addition to the problems related to the selection of the set of possible values, and to the time complexity, the exhaustive search may also lead to an over-fitting problem. In fact, the Gaussian parameters are selected based on the value of a criterion function that is computed on the training data [11-

13]. Moreover, a global parameter over the entire data may be inappropriate when the different categories have large characteristics variations.

In this paper, we propose a novel classification algorithm named the Support Kernel Classifier (SKC). It categorizes the data by learning a Gaussian kernel for each category. SKC is designed to learn the Gaussian parameters from the intrinsic geometric characteristics of the data. More specifically, the kernel parameters are learned by minimizing the intra-class distances and maximizing the inter-class distances simultaneously. Moreover, the proposed classifier learns the probability of each data point to belong to each class. In fact, it does not use crisp assignment where an instance belongs or not to a class, but rather learns its likelihood to belong to it. This is intended to better describe the data. Besides, it allows avoiding the over-fitting problem.

The rest of the report is as follows: In Section II, we present the related works. Section III describes the proposed approach. The experimental results and analysis are outlined in Section IV. Finally, we conclude the report and highlight the future works in Section V.

II. RELATED WORKS

In this review, we focus on the main classification approaches based on the Gaussian kernel. More specifically, we focus on the approaches that learn the Gaussian parameters such as the support vector machine [15], the Gaussian mixture [16], and the radial basis function neural network [17].

A. Parameters Selection for the Support Vector Machine

The typical SVM [15] algorithm was extended by mapping the input data vectors into high-dimensional feature space [18]. This mapping can be obtained by using a kernel function $K(x_i, x_j)$ [19]. Thus, the SVM discriminant function becomes:

$$g(x) = \sum_{i \in SV} \alpha_i K(x_i, x_j) + b \quad (1)$$

Although any kernel function can be used, the Gaussian kernel is widely used. It is defined as:

$$K(x_i, x_j) = \exp\left(-\frac{\|x_i - x_j\|^2}{2\sigma^2}\right) \quad (2)$$

The choice of the Gaussian parameter, σ , affects the SVM performance. As shown in Fig. 1, when σ is too small, the discriminant function surrounds each data point, which may lead to an over-fitting problem. Yet, if σ is too large, the discriminant function surrounds all points, which yields mapping all points into a single one [20].

*Corresponding Author

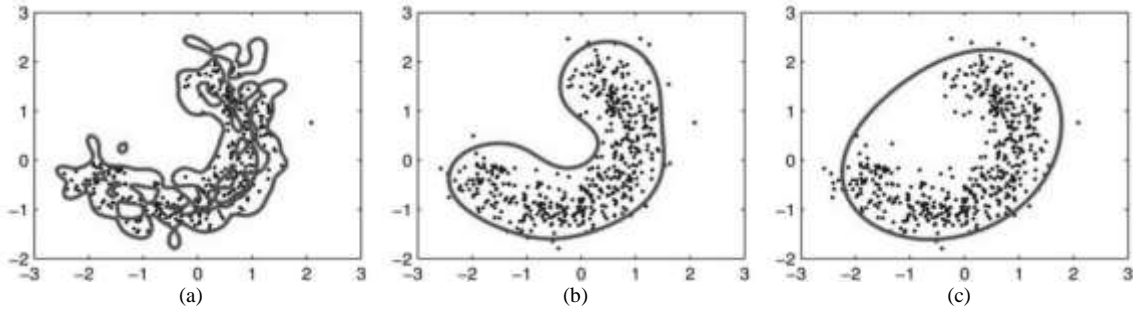


Fig. 1. Hyperplane Affected by the Value of σ : (a) $\sigma=0.1$, (b) $\sigma=2.6$ and (c) $\sigma=10$ [20].

Since the value of the Gaussian parameter has a large impact on the SVM classification results, several attempts have been proposed in the literature to determine this parameter.

The authors in [21] proposed a Gaussian parameters selection approach for a the outlier detection problem. They used the dual function as a criterion to find the optimal kernel parameters. In particular, the introduced the criterion [21]:

$$\max \sum_{i=1}^n \alpha_i K(x_i, x_i) - \sum_{i,j} \alpha_i \alpha_j K(x_i, x_j) \quad (3)$$

Similarly, the authors in [20] used a dual function as an extension of the criterion in (3). They proposed the following objective function:

$$\max \sum_{i=1}^n \alpha_i K(x_i, x_i) - \max \sum_{i,j} \alpha_i \alpha_j K(x_i, x_j) \quad (4)$$

Inspired by the “Fisher linear discrimination” (FLD) [11], the authors in [22] proposed to find the Gaussian parameters using an objective function that minimizes the intra-class distances and maximizes the inter-class distances. The proposed criterion was defined as:

$$f(\sigma) = \frac{s_1^2 + s_2^2}{\|m_1 - m_2\|^2} \quad (5)$$

Where m_1 and m_2 are the mean of the two classes while s_1^2 and s_2^2 are the coincidences of two classes defined as:

$$s_k^2 = N_k - \frac{1}{N_k} \sum_{i=1}^{N_k} \sum_{j=1}^{N_k} K(x_{ki}, x_{kj}) \quad k = \{1,2\} \quad (6)$$

The authors in [23] proposed an approach to learn the Gaussian parameters based on maximizing the “kernel target alignment” (KTA) objective function [12]. KTA maximizes the intra-class similarities and minimizes the intra-class similarities using given the following expression:

$$A(K, y) = \frac{\langle K, y \rangle_F}{\sqrt{\langle K, K \rangle_F \langle y, y \rangle_F}} \quad (7)$$

where $K: x^2 \rightarrow [-1, +1]$ and $y \in \{-1, +1\}^m$. Note that $\langle K, y \rangle_F$ is the difference between the intra-class similarities and the intra-class similarities as defined below:

$$\langle K, y \rangle_F = \sum_{y_i=y_j} k(x_i, x_j) - \sum_{y_i \neq y_j} k(x_i, x_j) \quad (8)$$

where $k(x_i, x_j)$ is the Gaussian kernel function. The optimal σ is obtained by maximizing the following objective function:

$$\begin{aligned} \sigma_{opt} = & \\ \text{argmax} & \left(\sum_{y_i=y_j} \exp\left(-\frac{\|x_i-x_j\|^2}{\sigma^2}\right) - \right. \\ & \left. \sum_{y_i \neq y_j} \exp\left(-\frac{\|x_i-x_j\|^2}{\sigma^2}\right) \right) \end{aligned} \quad (9)$$

The optimization problem formulated in (9) is solved by computing the partial derivative and setting it to zero. Thus,

$$\begin{aligned} \frac{\partial \langle K, y \rangle_F}{\partial \sigma} = & \frac{1}{\sigma^3} \left(\sum_{y_i=y_j} \|x_i - x_j\|^2 \exp\left(-\frac{\|x_i-x_j\|^2}{\sigma^2}\right) - \right. \\ & \left. \sum_{y_i \neq y_j} \|x_i - x_j\|^2 \exp\left(-\frac{\|x_i-x_j\|^2}{\sigma^2}\right) \right) \end{aligned} \quad (10)$$

For the SVM-based approaches, various criterion have been proposed to select the optimal Gaussian parameters [20][21][22]. These approaches are similar to the exhaustive search. Yet, the approach in [31] learns the Gaussian parameter by maximizing the intra-class similarities and minimizing the intra-class similarities. However, this approach is suitable for the two-class problems only.

B. Parameters Selection for the Gaussian Mixture Models

Typical Gaussian Mixture Model (GMM) classifier [16] relies on Bayesian framework, Gaussian probabilistic modelling and the expectation maximization (EM) algorithm [13]. In particular, it assumes that the data can be modelled as a mixture of a finite number of Gaussian functions. GMMs compute the probability density functions (PDF), $P(X | C_i)$ [24], for the data instance X given the class C_i . Then, they classify the test instances using the Bayes’ rule [25] using these PDFs as:

$$P(C_i|X) = P(X|C_i) \cdot \frac{P(C_i)}{P(X)} \quad (11)$$

where $P(C_i)$ is the class i prior probability and $P(X)$ serves as a normalization term. Note that the GMM assumes that the probability density functions, $P(X | C_i)$, are a weighted sum of multiple Gaussians as:

$$P(X|C_i) = \sum_{k=1}^{NG} w_k G_k \quad (12)$$

In (12), NG is the number of Gaussians and w_k is the weight associated with the k^{th} Gaussian G_k constrained to:

$$\sum_{k=1}^{NG} w_k = 1 \quad (13)$$

The k^{th} Gaussian G_k is formulated as:

$$G_k = \frac{1}{(2\pi)^{n/2} |S_k|^{1/2}} \cdot e^{-1/2(x-M_k)^T S_k^{-1}(x-M_k)} \quad (14)$$

where M_k and S_k are the mean and the covariance, respectively. The *GMMs* can be defined through three parameters. Namely, the set of mean, $\{M_k\}$, the set of covariances, $\{S_k\}$, and the weights, $\{w_k\}$ represent the model parameters. The *EM* [13] is the iterative optimization approach typically used to estimate these parameters.

In order to estimate the three parameters M_k , S_k , and w_k , the Maximum Likelihood Estimation (*MLE*) algorithm [26] can be used.

Let $\{x_i\}_{i \in \{1,2,\dots,N\}}$ be a set of data points and let $P_c(x_i|\Theta_c)$ be the conditional probability of x_i belonging to cluster c defined by $\Theta_c = \{M_c, S_c\}$ where M_c is the centroid of the cluster and S_c its covariance matrix. One should note that the set of mean $\{M_k\}$ is initialized using the *K*-means clustering algorithm [14].

GMM [24] defines the total probability distribution of x_i as:

$$P_{\text{total}}(x_i) = \sum_{c=1}^C A_c P_c(x_i|\Theta_c) \quad (15)$$

where C is the number of clusters and A_c which represents the ratio of the number of data instances in the cluster c is computed as:

$$A_c = \frac{N_c}{N} \quad (16)$$

with N_c the number of instances assigned to the cluster c . *GMM* [27] optimizes the log-likelihood of the total probability distribution of x_i below

$$G = \sum_{i=1}^N \log P_{\text{total}}(x_i) \quad (17)$$

The probability that the instance x_i belongs to cluster c , is defined as:

$$w_{ic} = \frac{A_c P_c(x_i|\Theta_c)}{P_{\text{total}}(x_i)} \quad (18)$$

In fact, w_{ic} is considered as the membership of the data instance x_i to the cluster c such that:

$$\sum_{c=1}^C w_{ic} = 1 \quad (19)$$

The number of data points assigned to cluster c can be expressed as

$$N_c = \sum_{i=1}^N w_{ic} \quad (20)$$

The covariance matrix, S_c , is then defined as

$$S_c = \left(\frac{1}{N_c}\right) \sum_{i=1}^N w_{ic} (x_i - M_c) (x_i - M_c)' \quad (21)$$

with

$$M_c = \left(\frac{1}{N_c}\right) \sum_{i=1}^N w_{ic} x_i \quad (22)$$

Similarly to the *MLE* [35] approach, the maximum a posterior (*MAP*) approach [28] computes the *GMM* parameters M_k , S_k , and w_k . However, it estimates $\Theta_c =$

$\{M_c, S_c\}$ by maximizing the posterior probability function not the likelihood function. More specifically, *MAP* finds Θ_c that maximizes:

$$L_{MAP} = \prod_{i=0}^N P(\theta_c|x_i) \quad (23)$$

MAP assumes that θ_c is a random variable with a distribution. In fact, it relies on the equation:

$$P(\theta_c, x_i) = P(\theta_c|x_i)P(\theta_c) \quad (24)$$

Note $P_c(x_i|\Theta_c)$ represents the conditional probability that an instance x_i belongs to a cluster c defined by $\Theta_c = \{M_c, S_c\}$. Where M_c is the centroid of the cluster and S_c is its covariance matrix. For each mixture i in the prior model, *MAP* [28] defines the posterior probability $P_c(\Theta_c|x_i)$ as:

$$P(\theta_c|x_i) = \frac{P(x_i|\theta_c)P(\theta_c)}{P(x_i)} \quad (25)$$

The optimal θ_c is a random variable defined by:

$$\theta_c = \arg \max_{\theta_c} \prod_{x_i} P(\theta_c|x_i) \quad (26)$$

Since $P(x_i)$ is not dependent of θ_c , one can write

$$\theta_c = \arg \max_{\theta_c} \prod_{x_i} P(x_i|\theta_c)P(\theta_c) \quad (27)$$

This yields

$$\theta_c = \arg \max_{\theta_c} \sum_{x_i} \log P(x_i|\theta_c) + \log(P(\theta_c)) \quad (28)$$

If X follows a normal distribution $N(\mu, \sigma)$, where μ is random and σ^2 is fixed. Then,

$$P(x_i|\theta_c)P(\theta_c) = \left[\frac{1}{\sigma\sqrt{2\pi}} \exp\left\{-\frac{(x_i-\mu)^2}{2\sigma^2}\right\} \right] \times \left[\frac{1}{\sigma_0\sqrt{2\pi}} \exp\left\{-\frac{(\mu-\mu_0)^2}{2\sigma_0^2}\right\} \right] \quad (29)$$

This gives

$$f(x|\mu)\pi(\mu) = \frac{1}{2\pi\sigma\sigma_0} \exp\left\{-\frac{1}{2\sigma^2\sigma_0^2} [\sigma_0^2(x_i - \mu)^2 + \sigma^2(\mu - \mu_0)^2]\right\} \quad (30)$$

As it can be seen, $P(x|\theta_c)P(\theta_c)$ is proportional to

$$\exp\left\{-\frac{1}{2\sigma^{*2}}(\mu - \mu^*)^2\right\} \quad (31)$$

where

$$\mu^* = \frac{\sigma_0^2}{\sigma^2 + \sigma_0^2} x + \frac{\sigma^2}{\sigma^2 + \sigma_0^2} \mu_0 \quad (32)$$

and

$$\sigma^{*2} = \frac{\sigma^2\sigma_0^2}{\sigma^2 + \sigma_0^2} = \left(\frac{1}{\sigma^2} + \frac{1}{\sigma_0^2}\right)^{-1} \quad (33)$$

Consequently, it follows a normal distribution with μ^* and σ^{*2} as parameters.

One can claim that *MLE* [26] and *MAP* [38] are efficient approaches that provide interpretable results. However, *MLE* [36] based solutions are prone to over-fitting [33]. On the other hand, *MAP* [28] addresses the over-fitting problem through the assumption that the parameters of the Gaussian distribution that fits the data are known.

C. Parameters Selection for Radial basis Function Network (RBFN)

The Radial Basis Function Network (RBFN) is a particular neural network where the Gaussian distribution is used as activation functions [29]. Besides, the network output is a combination of Gaussian functions of the inputs:

$$O_d(x) = w_0 + \sum_{i=0}^m w_i * G(x, \mu, \sigma) \quad (34)$$

where $O_d(x)$ is the output corresponding to the input x , w_i are the weights, and $G(x, \mu, \sigma)$ is the Gaussian function characterized by the parameters μ and σ . Figure 2 displays the architecture of a RBFN.

Training the RBFN involves learning the optimal weights w_0, w_1, \dots, w_n . These weights are learned using gradient descent. Therefore, the iterative learning process requires deriving the training error, which is defined as:

$$E = \frac{1}{2} \sum_d (t_d - O_d)^2 \quad (35)$$

where t_d is the target label and O_d is the output label.

The authors in [31] used the Gradient descent to learn iteratively the Gaussian parameters. Let $V = [\mu \ \sigma \ w]$ be the vector including the mean μ , the standard deviations σ , and the set of weights w respectively. The update equation of V is defined as follows:

$$V^{new} = V^{old} + \alpha \frac{\partial \varepsilon}{\partial V} \quad (36)$$

where α is the learning rate.

In [32], the researchers proposed the learning of the Gaussian parameters based on the intra-class and inter-class structures in the training data. Specifically, the mean C^k of each class k is computed. Then, the distance d_k is defined as the distance between the mean C^k and furthest sample P belonging to the class k based on the distance.

$$d_k = \|P^k - C^k\| \quad (37)$$

The second step consists in computing the distance between each mean and the closest mean to it.

$$d_c(k) = \operatorname{argmin}(d_c(k, j)) \quad j = 1, \dots, s, j \neq k \quad (38)$$

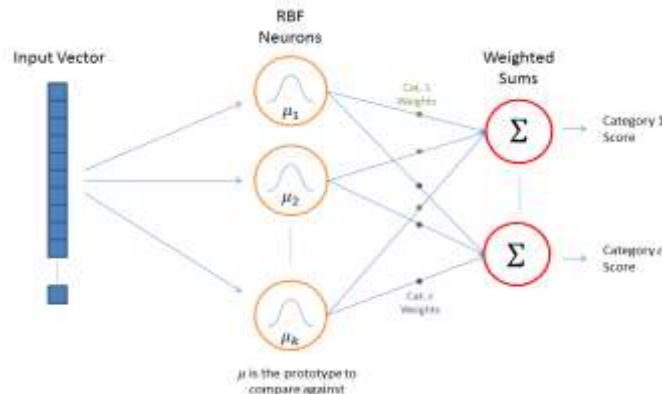


Fig. 2. Radial basis Function Network Architecture [30].

Given a confidence parameter β , the width of class k , σ_w^k is:

$$\sigma_w^k = \frac{d_k}{\sqrt{\ln \beta}} \quad (39)$$

The overlap between class k and class l (σ_B^k) is:

$$\sigma_B^k = \eta \times d_{\min}(k, l) \quad (40)$$

where η is a factor that controls the overlap between the classes. The Gaussian parameter, σ , with respect to class k , is defined in [32] as the largest value between σ_w^k and σ_B^k :

$$\sigma^k = \max(\sigma_B^k, \sigma_w^k) \quad (41)$$

As the choice of η is not straightforward, the authors in [32] suggested the following approximation:

$$\eta \approx \frac{\sum_{i=1}^c \frac{d_k}{\sqrt{\ln \beta}}}{\sum_{k=1}^c d_{\min}(k, l)} \quad (42)$$

The value of the Gaussian parameter, σ , is then updated using gradient descent by deriving the training error defined in (35).

These approaches may be prone to local minima. The approach in [20] tries to avoid the problem by suggesting a way to initialize the parameter based on the intra- and inter-class similarities. However, the suggested approach requires the estimation of other parameters.

III. THE PROPOSED SUPPORT KERNEL CLASSIFICATION

Kernel classification approaches are intended to categorize the data by mapping it into a new feature space. This mapping reduces the complex classification task to a simpler problem in the new feature space. The Gaussian kernel function is commonly used due to its analytical characteristics. However, the performance of the Gaussian kernel based classifiers depends on the setting of the Gaussian parameters. In this work, we propose a new kernel-based classification approach where each class is modeled using a Gaussian function. The optimal Gaussian parameters are learned by optimizing a novel objective functions.

Let a Gaussian function be defined as:

$$G_{ijk} = \exp\left(-\frac{e_{jk}^2}{\sigma_i^2}\right) \quad (43)$$

where σ_i is the scaling parameter, and e_{jk}^2 represents the distance between the data points x_j and x_k . In this work, we use the squared Euclidian distance defined as:

$$e_{jk}^2 = |x_j - x_k|^2 = (x_j - x_k)(x_j - x_k)^T \quad (44)$$

The optimal set of Gaussian parameters $\{\sigma_i\}$ is obtained by minimizing the intra-class distances and maximizing the inter-class distances. More specifically, the proposed approach formulates and minimizes the intra-class distances as follows:

$$J_i^{intra} = \sum_{j=1}^{N_{train}} \sum_{k=1}^{N_{train}} p_{ij}^m p_{ik}^m \left(1 - \exp\left(-\frac{e_{jk}^2}{\sigma_i^2}\right)\right) + K \sigma_i^2 \quad (45)$$

Similarly, it maximizes the inter-class distances below:

$$J_i^{inter} = \sum_{j=1}^{N_{train}} \sum_{k=1}^{N_{train}} \left(p_{ij}^m (1 - p_{ik}^m) + p_{ik}^m (1 - p_{ij}^m) \right) \left(1 - \exp\left(-\frac{e_{jk}^2}{\sigma_i^2}\right) \right) + K \sigma_i^2 \quad (46)$$

In (45) and (46), N_{train} represents the number of observations in the training set $\{x_j\}_{j=1, \dots, N_{train}}$, $m \in]1, \infty)$ is a constant that determines the degree of overlapping between classes, $K \sigma_i^2$ represents a regularization term, and p_{ij} expresses the likelihood that the observation x_j belongs to the class i . Note that p_{ij} satisfies:

$$0 \leq p_{ij} \leq 1 \text{ and } \sum_{i=1}^C p_{ij} = 1 \text{ for } j \in \{1, \dots, N_{train}\} \quad (47)$$

where C is the number of classes. Notice that the regularization term is integrated in (45) in order to avoid the trivial solution of large scaling parameter, σ_i , which would map all data instances into one single point. On the other hand, the regularization term in (47) is intended to avoid the trivial solution of a scaling parameter equal to zero. Besides, K allows ensures the tradeoff between the minimization of J_i^{intra} and the maximization of J_i^{inter} . Note that K is also learned through the optimization of J_i^{intra} and J_i^{inter} .

The distance, r_{jk} , between the data points x_j and x_k , in the new feature space is defined as:

$$r_{jk} = 1 - \exp\left(-\frac{e_{jk}^2}{\sigma_i^2}\right) \quad (48)$$

The Gaussian parameters $\{\sigma_i\}$ are defined with respect to each class in order to better handle the distribution and the geometric characteristics of each class. The proposed approach learns the scaling parameter σ_i for each class and the likelihood for each observation x_i to belong to class i using the given the training set. Moreover, the objective functions J_i^{intra} and J_i^{inter} are based on the relational distances between pairs of data instances rather than the distance between the data instances and the classes. This relaxes the assumption that each class fits a spherical shape [34]. In fact, the objective functions J_i^{intra} and J_i^{inter} do not use the class means/centroids. In the proposed approach, the mean is used only in the testing phase. It is computed after learning $\{\sigma_i, p_{ij}\}$ of each class i .

A. Optimization with Respect to p_{ij}

In order to optimize J_i^{intra} and J_i^{inter} with respect to p_{ij} , we use the relational dual described in [35]. It defines the relation between the relational distance $\{r_{jk}\}$ and the distance between point x_j and class i , d_{ij} , using the probabilities $\{p_{ij}\}$ as follows:

$$d_{ij} = \sum_{j=1}^{N_{train}} e_{jk} \frac{p_{ij}^m}{\sum_{v=1}^{N_{train}} p_{iv}^m} - \frac{1}{2} \sum_{j=1}^{N_{train}} \sum_{q=1}^{N_{train}} \frac{p_{ij}^m e_{jq} p_{iq}^m}{(\sum_{v=1}^{N_{train}} p_{iv}^m)^2} \quad (49)$$

Using the relational dual, we rewrite (45) and (46) and obtain the following set of equations system:

$$\begin{cases} J_i^{intra} = \sum_{j=1}^{N_{train}} p_{ij}^m d_{ij} + K \sigma_i^2 \\ J_i^{inter} = \sum_{j=1}^{N_{train}} (1 - p_{ij}^m) d_{ij} + K \sigma_i^2 \end{cases} \quad (50)$$

In order to optimize J_i^{intra} and J_i^{inter} with respect to p_{ij} , subject to the constraint in (47), we use the language multipliers to obtain:

$$\begin{cases} J_i^{intra} = \sum_{j=1}^{N_{train}} p_{ij}^m d_{ij} + K \sigma_i^2 - \lambda_i (\sum_{i=1}^C p_{ij} - 1) \\ J_i^{inter} = \sum_{j=1}^{N_{train}} (1 - p_{ij}^m) d_{ij} + K \sigma_i^2 - \lambda_i (\sum_{i=1}^C p_{ij} - 1) \end{cases} \quad (51)$$

where d_{ij} is as defined in (49) and λ_i is the Lagrange multiplier variable. Setting the derivatives with respect to p_{ij} of the set of equations in (51) to zero yields:

$$m p_{ij}^{m-1} d_{ij} - \lambda_i = 0. \quad (52)$$

Thus,

$$p_{ij} = \left(\frac{\lambda_i}{m d_{ij}} \right)^{\frac{1}{m-1}} \quad (53)$$

and,

$$\left(\frac{\lambda_i}{m} \right)^{\frac{1}{m-1}} \sum_{i=1}^C \left(\frac{1}{d_{ij}} \right)^{\frac{1}{m-1}} = 1 \quad (54)$$

This results in

$$\lambda_i^{\frac{1}{m-1}} = \frac{m^{\frac{1}{m-1}}}{\sum_{i=1}^C \left(\frac{1}{d_{ij}} \right)^{\frac{1}{m-1}}} \quad (55)$$

and,

$$p_{ij} = \frac{\left(\frac{1}{d_{ij}} \right)^{\frac{1}{m-1}}}{\sum_{k=1}^C \left(\frac{1}{d_{kj}} \right)^{\frac{1}{m-1}}} \quad (56)$$

B. Optimization with Respect to σ_i

In order to optimize J_i^{intra} and J_i^{inter} with respect to σ_i , we derive J_i^{intra} and J_i^{inter} with respect to σ_i^2 and set the derivatives to zero. First, we set the derivative of J_i^{intra} to zero and to obtain:

$$\frac{\partial J_i^{intra}}{\partial \sigma_i^2} = - \sum_{j=1}^{N_{train}} \sum_{k=1}^{N_{train}} p_{ij}^m p_{ik}^m \frac{e_{jk}^2}{\sigma_i^4} \exp\left(-\frac{e_{jk}^2}{\sigma_i^2}\right) + K = 0 \quad (57)$$

which yields:

$$K = \sum_{j=1}^{N_{train}} \sum_{k=1}^{N_{train}} p_{ij}^m p_{ik}^m \frac{e_{jk}^2}{\sigma_i^4} \exp\left(-\frac{e_{jk}^2}{\sigma_i^2}\right) \quad (58)$$

Substituting (58) in (46) gives

$$\begin{aligned} J_i^{inter} &= \sum_{j=1}^{N_{train}} \sum_{k=1}^{N_{train}} \left(p_{ij}^m (1 - p_{ik}^m) + p_{ik}^m (1 - p_{ij}^m) \right) \left(1 - \exp\left(-\frac{e_{jk}^2}{\sigma_i^2}\right) \right) \\ &+ \frac{1}{\sigma_i^2} \sum_{j=1}^{N_{train}} \sum_{k=1}^{N_{train}} p_{ij}^m p_{ik}^m e_{jk}^2 \exp\left(-\frac{e_{jk}^2}{\sigma_i^2}\right) \end{aligned} \quad (59)$$

The derivative of (59) with respect to σ_i^2 can be written as:

$$\frac{\partial J_i^{inter}}{\partial \sigma_i^2} =$$

$$\begin{aligned}
 & -\frac{1}{\sigma_i^4} \sum_{j=1}^{N_{train}} \left(p_{ij}^m (1 - p_{ik}^m) + p_{ik}^m (1 - p_{ij}^m) \right) e_{jk}^2 \exp\left(-\frac{e_{jk}^2}{\sigma_i^2}\right) \\
 & -\frac{1}{\sigma_i^4} \sum_{j=1}^{N_{train}} \sum_{k=1}^{N_{train}} p_{ij}^m p_{ik}^m e_{jk}^2 \exp\left(-\frac{e_{jk}^2}{\sigma_i^2}\right) \\
 & + \frac{1}{\sigma_i^6} \sum_{j=1}^{N_{train}} \sum_{k=1}^{N_{train}} p_{ij}^m p_{ik}^m (e_{jk}^2)^2 \exp\left(-\frac{e_{jk}^2}{\sigma_i^2}\right) \quad (60)
 \end{aligned}$$

Which results in:

$$\sigma_i^2 = \frac{T_1^i}{T_2^i} \quad (61)$$

where

$$T_1^i = \sum_{j=1}^{N_{train}} \sum_{k=1}^{N_{train}} p_{ij}^m p_{ik}^m (e_{jk}^2)^2 \exp\left(-\frac{e_{jk}^2}{\sigma_i^2}\right) \quad (62)$$

and

$$T_2^i = \sum_{j=1}^{N_{train}} \sum_{k=1}^{N_{train}} (p_{ij}^m + p_{ik}^m - p_{ij}^m p_{ik}^m) e_{jk}^2 \exp\left(-\frac{e_{jk}^2}{\sigma_i^2}\right) \quad (63)$$

Based on an iterative optimization approach and the assumption that σ_i and p_{ij} do not change significantly from one iteration to another, we σ_i , and p_{ij} can be updated alternatively using (61), and (56), respectively. Once σ_i and $\{p_{ij}\}$ are optimized with respect to each class i , we define the prototype for each category. Then, it can be used during the testing phase in order to predict the class value for any unlabeled data point. Along with the standard deviation σ_i , we propose to use the mean μ_i of each class i as its prototype. Specifically, we define it as:

$$\mu_i = \frac{\sum_{j=1}^{N_{train}} p_{ij}^m d_{ij}}{\sum_{j=1}^{N_{train}} p_{ij}^m} \quad (64)$$

where d_{ij} is as defined in (49). The proposed training algorithm is depicted below:

Algorithm 1: SKC training phase

Input: training set $\{x_j\}_{j=1, \dots, N_{train}}$

Output: $\{\mu_i, \sigma_i\}_{i=1, \dots, C}$

- 1- Initialize the probability according to the class labels such that $p_{ij} = 1$ if x_j belongs to class i , and 0 otherwise.
- 2- Initialize $\sigma_i^{(0)}$ to 1.
- 3- Set ε to 10^{-5} .

Repeat

- 1- Compute $d_{ij}^{(t)}$ using (49)
- 2- Compute $\sigma_i^{2(t)}$ using (51)
- 3- Compute $p_{ij}^{(t)}$ using (56)

Until $\|\sigma_i^t - \sigma_i^{t-1}\| < \varepsilon$ & $t \leq 100$

Compute μ_i using (64).

The set of Gaussian parameters $\{\mu_i, \sigma_i\}_{i=1, \dots, C}$ defines the model with respect to each class i .

Using the learned models from the training set, we classify the unlabeled data point x_j using

$$\text{class}(x_j) = \arg \max_i (q_{ij}) \quad (65)$$

where

$$q_{ij} = 1 - \exp\left(-\frac{\|x_j - \mu_i\|^2}{\sigma_i^2}\right) \quad (66)$$

The latter equation (66) represents the distance between the test data point x_j and the center μ_i as defined in (48). Note that the parameters $\{\mu_i, \sigma_i\}$ were learned during the training phase. The proposed SKC testing algorithm is detailed below:

Algorithm 2: SKC testing phase

Input: $\{\mu_i, \sigma_i\}_{i=1, \dots, C}$, an unknown observation x_j

Output: class value of (x_j)

- 1- Compute $\{q_{ij}\}$ using (66)
- 2- Predict the class value of (x_j) using (65)

IV. EXPERIMENTS

In order to assess the performance of the proposed approach, we conducted several experiments using both synthetic and real datasets. The synthetic datasets are 2-D datasets generated to represent different geometric characteristics. They were used to illustrate visually how the proposed classifier categorizes them. Moreover, they were intended to analyze and interpret the learned Gaussian parameters. Besides, the proposed approach was evaluated using real benchmark datasets. Specifically, 10 data sets from the UCI repository [46] were used to analyze the performance of the proposed approach. Namely, these datasets are: Handwritten Digits [36], Mammographic Mass [37], E.coli [38], and Haberman's Survival [39], Frogs MFCCs [40], Blood Transfusion Service Center [41], HCC Survival [42], Adolescent Autistic Spectrum Disorder Screening [43], Libras Movement [44], and Seeds of wheat [45] data sets. Table I summarizes the considered real datasets.

A. Experiments using Synthetic Datasets

In order to show that SKC succeeds to learn the optimal Gaussian parameters for each class, and simultaneously classifies accurately the data instances. Therefore, we set the fuzzifier m to 2, and the maximum number of iterations to 100. Then, we run SKC on the synthetic 2-D datasets in Fig. 3. As it can be seen, the datasets include 3 classes with the same intrinsic characteristics. However, class 1 and class 2 exhibit low inter-class distances, while they show large inter-class distances with class 3. SKC classifies correctly data set 1 as shown in Fig. 3(b). It learns two similar Gaussian parameters for class 1 and class 2 ($\sigma_1 = 0.0002$ and $\sigma_2 = 0.0001$), and a larger Gaussian parameter ($\sigma_3 = 0.0050$) for class 3. Indeed, σ_1 is not too large so that points from class 2 get assigned to class 1. Similarly, σ_2 is not too large so that points from class 1 are not labeled as class 2. On the other hand, σ_3 is relatively larger because its intra-class distances are larger.

TABLE I. CHARACTERISTICS OF THE 10 REAL DATASETS

Name	N° of elements	Feature size	N° of categories	Categories
Handwritten Digits [36]	7494	17	10	Digit numbers from 0 to 9
Mammographic Mass [37]	961	6	2	Benign malignant
E.coli [38]	336	8	8	Protein localization sites
Haberman's Survival [39]	306	4	2	5 years < 5 years
Frogs MFCCs [40]	7195	22	4	Bufoinae Dendrobatida Hylidae Leptodactylida
Blood Transfusion Service Center [41]	748	5	2	Donating Not donating
HCC Survival [42]	165	50	2	Survives Dies
Adolescent Autistic Spectrum Disorder Screening [43]	104	64	2	ASD Not ASD
Libras Movement [44]	135	91	15	Hand movement types
Seeds of wheat [45]	210	8	3	Kama, Rosa Canadian

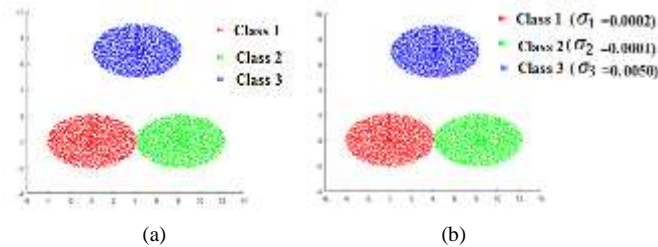


Fig. 3. Classifying Synthetic Dataset using SKC. (a) The Synthetic Dataset, (b) The Classification Result Obtained using SKC. The Learned Gaussian Parameters are: $\sigma_1 = 0.0002$, $\sigma_2 = 0.0001$ and $\sigma_3 = 0.005$.

The Gaussian Mixture Models (*GMM*) based classification [16] is the most similar approach to *SKC* because it learns a Gaussian mixture for each class. Therefore, we compare the classification results obtained using *SKC* and to those achieved using *GMM* on various different datasets.

As shown in Fig. 4(a), the dataset includes has three classes where class 1 and 2 have similar size and density while class 3 which is larger and less dense. *SKC* succeeds to learn the optimal Gaussian parameters for each class ($\sigma_1 = 3.35 \cdot 10^{-04}$, $\sigma_2 = 8.07 \cdot 10^{-04}$, and $\sigma_3 = 9.31 \cdot 10^{-01}$), and classifies accurately dataset 2 as shown in Figure 4-(b). In fact, the classification problem gets easier if the classes have similar volume and density. Such performance is attained through the Gaussian parameters learned by *SKC* where a larger σ_3 allows shrinking class 3 so it is less sparse and has a comparable volume to class 1 and class 2. Since class 1 and class 2 have

comparable intra/inter class distances, similar Gaussian parameters are learned by *SKC*. On the other hand, s reported in Fig. 4(c), *GMM* is not able to classify accurately dataset 2.

Another synthetic dataset is shown in Fig. 5(a). As one can notice, despite the good classification results obtained using *SKC*, some border points are misclassified as reported in Fig. 5(b). On the other hand, as shown in Fig. 5(c), *GMM* yields poor classification results because it learns larger a Gaussian parameter for class 1 compared to class 2 which results in similar density and volume for both classes.

Fig. 6 reports the classification results obtained by *SKC* and *GMM* using a different synthetic dataset. Although the inter-class distances are too small for the border points, *SKC* classifies correctly this dataset as displayed in Fig. 6(b). In fact, *SKC* learns double the value of σ_2 for class 1 to shrink it more than class 2. This yields a considerable separation between both classes. On the other hand, as reported in Figure 6-(b), *GMM* misclassifies the border points which degrades the overall classification performance.

Similarly, for the synthetic dataset in Fig. 7, both classifiers misclassify some border points from class 2 which the inter-class distances with class 1 is lower than the intra-class distance. In particular, *SKC* learns similar Gaussian parameters for class 1 and class 2, cannot discriminate accurately between the border points. Whereas, some of the points from class 2 that are misclassified by *GMM* have relatively large inter-class distance with class 1.

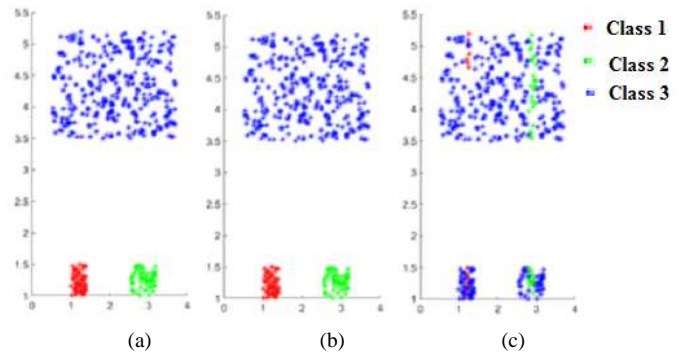


Fig. 4. Classification Results Obtained using SKC and GMM. (a) The Synthetic Dataset, (b) SKC Classification Results with $\sigma_1 = 3.35 \cdot 10^{-04}$, $\sigma_2 = 8.07 \cdot 10^{-04}$, and $\sigma_3 = 9.31 \cdot 10^{-01}$, and (c) GMM Classification Results.

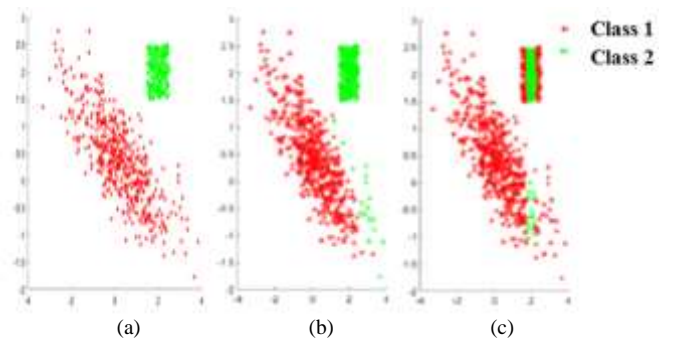


Fig. 5. Classification Results Obtained using SKC and GMM.(a) The Synthetic Dataset, (b) SKC Classification Results with $\sigma_1 = 7.62 \cdot 10^{-02}$, and $\sigma_2 = 8.82 \cdot 10^{-04}$, and (c) GMM Classification Results.

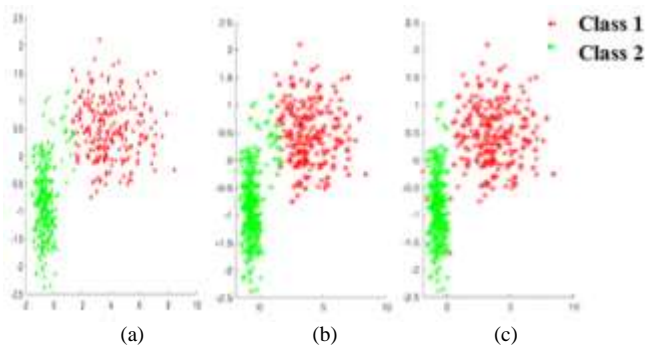


Fig. 6. Classification Results Obtained using SKC and GMM. (a) The Synthetic Dataset, (b) SKC Classification Results with $\sigma_1 = 5.11 \cdot 10^{-03}$, and $\sigma_2 = 2.29 \cdot 10^{-03}$, and (c) GMM Classification Results.

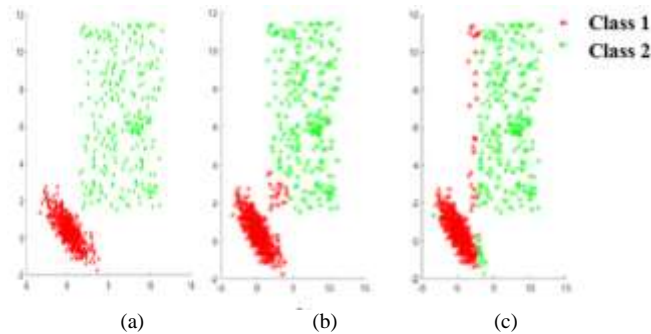


Fig. 7. Classification Results Obtained using SKC and GMM. (a) The Synthetic Dataset, (b) SKC Classification Results with $\sigma_1 = 2.45 \cdot 10^{-05}$, and $\sigma_2 = 3.88 \cdot 10^{-05}$, and (c) GMM Classification Results.

Based on the comparison of the classification results obtained by *SKC* and *GMM* using the different synthetic datasets, one can claim that the learning of the optimal Gaussian parameters using the intra-class and the inter-class characteristics of each dataset, makes *SKC* outperform *GMM*. Besides, in case of large volume variations for the different classes, *GMM* misclassifies a considerable proportion of the dataset. In fact, *GMM* does not include the inter-class distance in the learning process of the Gaussian parameters of the large classes. This yields the misclassification of some points from the other near classes. Moreover, *GMM* fails to classify the border points when the two classes are too close. This can be attributed to the fact that it learns the Gaussian parameters based on the intra-class distances only.

B. Experiments using Real Dataset

In this section, we report the classification results of the benchmark datasets from the UCI repository [46]. The classification task was conducted using the proposed *SKC*, the Gaussian Mixture Model classifier (*GMM*) [16], the *K*-nearest Neighbour classifier (*KNN*) [47], the kernel Support Vector machine (*SVM*) with Gaussian kernel [18], and the Naïve Bayes approach [19]. Note that for *KNN* we set three different values of *K* ($K=1$, $K=3$, and $K=5$). For the Gaussian kernel *SVM* we varied the Gaussian parameter by setting 6 different values (10^{-5} , 10^{-4} , 10^{-3} , 10^{-2} , 10^{-1} , and 1). For *SKC*, we set the fuzzifier *m* to 2, and the maximum number of iterations to 100.

We adopted a 10-folds cross validation approach, along with the accuracy, the sensitivity, and the specificity as performance measures to report the classification performance. Thus, Tables II and III show the average scores over the 10 training iterations. Moreover, a t-test was conducted to evaluate the statistical significance of the obtained results. In Tables II and III, the best results are shown in red. On the other hand, the green color represents the results that are not significantly different according to the t-test. As it can be seen, *SKC* overtakes all classifiers on Handwritten Digits [36] and Mammographic Mass [37] datasets. Moreover, it yields the best performances on the remaining 7 data sets.

Similarly, *SKC* outperforms *KNN* [47] on Handwritten Digits [46] and Mammographic Mass [47] data sets. However, it yields the same performance attainment on the other datasets. Even though *KNN* does not use the Gaussian kernel, it uses the local characteristics of the data by labelling the unknown instances based on their neighbouring points in the training set. Moreover, it requires a prior setting of the number of neighbours (*K*).

TABLE II. PERFORMANCES MEASURES OBTAINED USING THE DIFFERENT CLASSIFIERS ON HANDWRITTEN DIGITS, MAMMOGRAPHIC MASS, E.COLI, AND HABERMAN'S SURVIVAL, AND FROGS MFCCS DATASETS

		Accuracy	Sensitivity	Specificity	t-test
Handwritten Digits	<i>SKC</i>	0.84	0.91	0.99	
	<i>GMM</i>	0.47	0.45	0.99	1
	<i>KNN</i>	0.78	0.78	1	1
	<i>SVM</i>	0.16	0.17	0.89	1
	<i>NB</i>	0.83	0.83	0.98	1
Mammographic Mass	<i>SKC</i>	0.78	0.79	0.85	
	<i>GMM</i>	0.76	0.73	0.8	1
	<i>KNN</i>	0.77	0.77	0.77	1
	<i>SVM</i>	0.53	0.56	0.48	1
	<i>NB</i>	0.76	0.71	0.73	1
E.coli	<i>SKC</i>	0.82	0.94	0.98	
	<i>GMM</i>	0.55	0.63	0.94	0
	<i>KNN</i>	0.72	0.83	0.95	1
	<i>SVM</i>	0.7	0.89	0.95	1
	<i>NB</i>	0.75	0.87	0.95	1
Haberman's Survival	<i>SKC</i>	0.71	0.77	0.77	
	<i>GMM</i>	0.49	0.38	0.54	1
	<i>KNN</i>	0.61	0.65	0.51	1
	<i>SVM</i>	0.62	0.75	0.26	1
	<i>NB</i>	0.62	0.69	0.42	0
Frogs MFCCs	<i>SKC</i>	0.76	0.96	1	
	<i>GMM</i>	0.4	0.48	1	1
	<i>KNN</i>	0.69	0.77	1	0
	<i>SVM</i>	0.23	0.88	1	1
	<i>NB</i>	0.72	0.8	1	1

TABLE III. PERFORMANCES MEASURES OBTAINED USING THE DIFFERENT CLASSIFIERS ON BLOOD TRANSFUSION SERVICE CENTER, HCC SURVIVAL, ADOLESCENT AUTISTIC SPECTRUM DISORDER SCREENING, LIBRAS MOVEMENT, AND SEEDS OF WHEAT DATASETS

		Accuracy	Sensitivity	Specificity	t-test
Blood Transfusion Service Center	SKC	0.68	0.75	0.72	
	GMM	0.46	0.38	0.71	1
	KNN	0.53	0.51	0.6	0
	SVM	0.64	0.74	0.34	1
	NB	0.66	0.73	0.43	0
HCC Survival	SKC	0.58	0.48	0.65	
	GMM	0.49	0.6	0.43	1
	KNN	0.52	0.53	0.51	0
	SVM	0.58	0.23	0.55	1
	NB	0.55	0.44	0.62	0
Adolescent Autistic Spectrum Disorder Screening	SKC	0.99	0.98	1	
	GMM	0.81	0.67	0.9	0
	KNN	0.85	0.74	0.92	0
	SVM	0.64	0.53	0.7	1
	NB	0.9	0.8	0.96	1
Libras Movement	SKC	0.72	0.78	1	
	GMM	0.41	0.39	0.98	1
	KNN	0.62	0.64	0.99	0
	SVM	0.18	0.43	0.96	0
	NB	0.67	0.67	0.99	0
Seeds of wheat	SKC	0.9	0.86	0.93	
	GMM	0.89	0.85	0.91	0
	KNN	0.9	0.84	0.92	0
	SVM	0.9	0.89	0.99	0
	NB	0.89	0.83	0.93	0

In addition SKC yields the same results as SVM [18] on HCC survival [42] and Seeds of wheat [45], while it beats SVM [18] on the remaining datasets. In fact, although Kernel SVM [18] relies on the inter-class distances through the learning the optimal hyperplanes that guarantee the best inter-class margin, it uses one global sigma for all the data in the original features space. In other words, it assumes that all classes follow the same distributions.

Also, one can see that SKC attains similar results as NB [19] on Haberman's survival [39], Blood Transfusion Service Center [41], HCC survival [42], Libras movement and Seeds of wheat [45]. On the other hand, it outperforms NB [19] on the remaining 5 datasets. This results can be attributed to the fact that NB [19] learns a sigma for each feature with respect to each class. Therefore, if the features are not independent it fails to discover the correct structure of the data. Moreover, NB doesn't take into consideration the inter-class distances.

SKC yields similar performance to GMM [16] on E.coli [38], Adolescent Autistic Spectrum Disorder Screening [43], and Seeds of wheat [45] data sets. It overtakes GMM [16] on

the 7 other data sets. Even though, GMM learns a Gaussian parameter with respect to each feature and the corresponding covariance matrix, it does not take into consideration the inter-class dissimilarities. Therefore, the Gaussians parameters are learned based on the intra-class distances only.

V. CONCLUSIONS

Despite the researchers' efforts to address the supervised learning challenges, most of the classification algorithms exhibit some limitations. The classification task is even more acute when the data classes show different distribution characteristics. Kernel-based classifiers were introduced to overcome this problem through the mapping of the data into a new feature space using a specific kernel function. This mapping is intended to obtain better separation between the data classes and simplify the classification task. Even though the Gaussian function proved to yield reasonable classification accuracy, its performance depends on the choice of its parameters' values. Moreover, if the data include highly variant classes in terms of size, density, and shape, the data mapping into a new feature space using one global Gaussian is not effective. Typically, the tuning of the Gaussian parameters is done through some search strategy that is intended to optimize a predefined criterion function. In this paper, we proposed a new classification algorithm that learns a Gaussian function for each data class. The proposed Support Kernel Classification (SKC) is designed to characterize and separate the data instances from the different classes. It relies on the maximization of the intra-class distances and the minimization of the inter-class distances to learn the optimal Gaussian parameters. In fact, a novel objective function is optimized to model each class using one Gaussian function. The experiments conducted using synthetic datasets demonstrated the effectiveness of the proposed algorithm. Moreover, the results obtained using real datasets proved that the proposed classifier outperforms the relevant state of the art approaches.

ACKNOWLEDGMENT

This work was supported by the Research Center of the College of Computer and Information Sciences at King Saud University, Riyadh, Saudi Arabia. The authors are grateful for this support.

REFERENCES

- [1] G. P. Zhang, "Neural networks for classification: a survey," IEEE Trans. Syst. Man Cybern. Part C (Applications Rev.), vol. 30, no. 4, pp. 451–462, 2000.
- [2] D. L. García, À. Nebot, and A. Vellido, "Intelligent data analysis approaches to churn as a business problem: a survey," Knowl. Inf. Syst., vol. 51, no. 3, pp. 719–774, 2017.
- [3] A. Abdallah, M. A. Maarof, and A. Zainal, "Fraud detection system: A survey," Journal of Network and Computer Applications, vol. 68, pp. 90–113, 2016.
- [4] C. Angeli, et al., "Data mining in educational technology classroom research: Can it make a contribution?," Comput. Educ., vol. 113, pp. 226–242, 2017.
- [5] N. Gandhi and L. J. Armstrong, "A review of the application of data mining techniques for decision making in agriculture," in Int. Conf. on Contemporary Computing and Informatics, 2016, pp. 1–6.
- [6] W. Sun, et al., "A survey of data mining technology on electronic medical records," in e-Health Networking, Applications and Services (Healthcom), IEEE 19th International Conference on, 2017, pp. 1–6.

- [7] J. Han and M. Kamber, *Data Mining: Concepts and Techniques*, vol. 12, 2011.
- [8] D. Tien Bui, T. A. Tuan, H. Klempe, B. Pradhan, and I. Revhaug, "Spatial prediction models for shallow landslide hazards: a comparative assessment of the efficacy of support vector machines, artificial neural networks, kernel logistic regression, and logistic model tree," *Landslides*, vol. 13, no. 2, pp. 361–378, 2016.
- [9] M. E. Abbasnejad, D. Ramachandram, and R. Mandava, "A survey of the state of the art in learning the kernels," *Knowl. Inf. Syst.*, vol. 31, no. 2, pp. 193–221, 2012.
- [10] M. Tian and W. Wang, "An efficient Gaussian kernel optimization based on centered kernel polarization criterion," *Inf. Sci. (Ny.)*, vol. 322, pp. 133–149, 2015.
- [11] K. Fukunaga, *Introduction to Statistical Pattern Recognition*, vol. 22, 1990.
- [12] N. Cristianini, J. Kandola, A. Elisseeff, and J. Shawe-Taylor, "On kernel-target alignment," *Adv. Neural Inf. Process. Syst.* 14, pp. 367–373, 2002.
- [13] A. P. Dempster, et al., "Maximum Likelihood from Incomplete Data via the EM Algorithm," *J. R. Stat. Soc. Ser. B*, vol. 39, no. 1, pp. 1–38, 1977.
- [14] J. MacQueen, "Some methods for classification and analysis of multivariate observations," *Proc. fifth Berkeley Symp. ...*, vol. 233, no. 233, pp. 281–297, 1967.
- [15] C. Cortes and V. Vapnik, "Support-Vector Networks," *Mach. Learn.*, vol. 20, no. 3, pp. 273–297, 1995.
- [16] R. O. Duda and P. E. Hart, *Pattern Classification and Scene Analysis*, vol. 7, 1973.
- [17] D. S. Broomhead and D. Lowe, "Radial basis functions, multi-variable functional interpolation and adaptive networks," 1988.
- [18] K. R. Müller, et al., "An introduction to kernel-based learning algorithms," *IEEE Transactions on Neural Networks*, vol. 12, no. 2, pp. 181–201, 2001.
- [19] M. A. Aizerman, E. A. Braverman, and L. Rozonoer, "Theoretical foundations of the potential function method in pattern recognition learning," *Autom. Remote Control*, vol. 25, pp. 821–837, 1964.
- [20] Y. Xiao, H. Wang, and W. Xu, "Parameter selection of gaussian kernel for one-class SVM," *IEEE Trans. Cybern.*, vol. 45, no. 5, pp. 927–939, 2015.
- [21] D. Kakde, et al., "Peak criterion for choosing Gaussian kernel bandwidth in Support Vector Data Description," in *IEEE Int Conf on Prognostics and Health Management, ICPHM, 2017*, pp. 32–39.
- [22] W. Wang, Z. Xu, W. Lu, and X. Zhang, "Determination of the spread parameter in the Gaussian kernel for classification and regression," *Neurocomputing*, vol. 55, no. 3–4, pp. 643–663, 2003.
- [23] S. Zhong, D. Chen, Q. Xu, and T. Chen, "Optimizing the Gaussian kernel function with the formulated kernel target alignment criterion for two-class pattern classification," *Pattern Recognit.*, vol. 46, no. 7, pp. 2045–2054, 2013.
- [24] G. McLachlan and D. Peel, "Mixtures of factor analyzers," *Finite Mix. Model.*, pp. 238–256, 2000.
- [25] H. Jeffreys, "Scientific Inference," *Library (Lond.)*, vol. 2, 1931.
- [26] J. Pfanzagl and H. R., *Parametric Statistical Theory*. Walter de Gruyter, 1994.
- [27] A. Ortiz-Rosario, H. Adeli, and J. A. Buford, "MUSIC-Expected maximization gaussian mixture methodology for clustering and detection of task-related neuronal firing rates," *Behav. Brain Res.*, vol. 317, pp. 226–236, 2017.
- [28] C. P. Robert, *The Bayesian Choice: From Decision-Theoretic Foundations to Computational Implementation*, vol. 91, no. 433, 2007.
- [29] D. Broomhead, D. S. and Lowe, "Multivariable Functional Interpolation and Adaptive Networks," *Complex Syst.*, vol. 2, pp. 321–355, 1988.
- [30] C. McCormick, "Radial Basis Function Network (RBFN) Tutorial," 2013. [Online]. Available: <http://mccormickml.com/2013/08/15/radial-basis-function-network-rbfn-tutorial/>. [Accessed: 17-Apr-2018].
- [31] L. W. Kang, et al., "A new neural network model for the state-of-charge estimation in the battery degradation process," *Appl. Energy*, vol. 121, pp. 20–27, 2014.
- [32] M. J. Er, S. Wu, J. Lu, and H. L. Toh, "Face recognition with radial basis function (RBF) neural networks," *IEEE Trans. Neural Networks*, vol. 13, no. 3, pp. 697–710, 2002.
- [33] C. K. I. Williams and C. E. Rasmussen, "Gaussian processes for machine learning.," *Gaussian Processes for Machine Learning*, 2006.
- [34] O. Bchir, et al., "Fuzzy clustering with learnable cluster-dependent kernels," *Pattern Anal. Appl.*, 2016.
- [35] R. J. Hathaway, et al., "Relational duals of the c-means clustering algorithms," *Pattern Recognit.*, 1989.
- [36] F. Alimoglu, "Combining multiple classifiers for pen-based handwritten digit recognition," *Institute of Graduate Studies in Science and Engineering, Bogazici University*, 1996.
- [37] M. Elter, R. Schulz-Wendtlund, and T. Wittenberg, "The prediction of breast cancer biopsy outcomes using two CAD approaches that both emphasize an intelligible decision process," *Med. Phys.*, 2007.
- [38] P. Horton and K. Nakai, "A probabilistic classification system for predicting the cellular localization sites of proteins," *Int. Conf. Intell. Syst. Mol. Biol.*, 1996.
- [39] D. DeCoste, "Anytime Query-Tuned Kernel Machines via Cholesky Factorization," in *SDM, 2003*.
- [40] J. G. Colonna, M. Cristo, M. Salvatierra, and E. F. Nakamura, "An incremental technique for real-time bioacoustic signal segmentation," *Expert Syst. Appl.*, 2008.
- [41] I. C. Yeh, K. J. Yang, and T. M. Ting, "Knowledge discovery on RFM model using Bernoulli sequence," *Expert Syst. Appl.*, 2009.
- [42] M. S. Santos, P. H. Abreu, P. J. García-Laencina, A. Simão, and A. Carvalho, "A new cluster-based oversampling method for improving survival prediction of hepatocellular carcinoma patients," *J. Biomed. Inform.*, 2015.
- [43] F. Thabtah and Fadi, "Autism Spectrum Disorder screening: Machine learning adaptation and DSM-5 fulfillment," in *Proceedings of the 1st International Conference on Medical and Health Informatics 2017 - ICMHI '17, 2017*.
- [44] D. B. Dias, R. C. B. Madeo, T. Rocha, H. H. Biscaro, and S. M. Peres, "Hand movement recognition for Brazilian Sign Language: A study Using distance-based neural networks," in *Proceedings of the International Joint Conference on Neural Networks, 2009*.
- [45] M. Charytanowicz, J. Niewczas, P. Kulczycki, P. A. Kowalski, S. Łukasik, and S. Zak, "Complete gradient clustering algorithm for features analysis of X-ray images," *Adv. Intell. Soft Comput.*, 2010.
- [46] D. Dheeru and E. Karra Taniskidou, "{UCI} Machine Learning Repository." 2017.
- [47] J. M. Keller, M. R. Gray, and J. A. Givens, "A fuzzy k-nearest neighbor algorithm," *IEEE Trans. Syst. Man. Cybern.*, no. 4, pp. 580–585, 1985.

e-Lifestyle Confirmatory of Consumer Generation Z

Tony Wijaya¹, Arum Darmawati², Andreas M Kuncoro³
Faculty of Economy, Universitas Negeri Yogyakarta
Yogyakarta, Indonesia

Abstract—The development of information technology has changed daily life patterns that tend towards digital. Differences across generations will result in understanding different behaviors and lifestyles, which are a challenge in this research. Lifestyle is needed in determining market segments of consumer behavior. Lifestyle understanding in Generation Z is expected to provide valuable information in various fields of socio-economic life. These findings are expected to provide an overview for marketers targeting the market in this segment. Understanding lifestyles can be an ingredient in developing marketing strategies according to the intended segment, especially Generation Z, which has identified a lifestyle following information technology or digital development. The research aimed to confirm e-lifestyle factors among Generation Z, especially university students, as members of the academic environment's dominant academic community. Specifically, the aim is to identify the pattern of e-lifestyle formation in Generation Z, especially among students and the information or social media used by Generation Z. This type of research is a survey. This research was initiated through empirical field observations. The study population used in this study was university students in Yogyakarta-Indonesia. The sampling technique uses a simple random sampling technique. The data used are primary: the response given by research subjects related to e-lifestyle factors. Data was collected through a survey using a questionnaire. The data analysis technique in this study uses a Confirmatory Factor Analysis (CFA). The results showed that the motives that became the basis of e-lifestyle in the Z generation corresponded to four factors, namely, e-activities, e-interests, e-opinions, and e-values. Information or social media are often used by Generation Z, namely, Instagram, Youtube, Line, Facebook, Twitter, Discard, Pinterest, Spotify, and Telegram. The purpose of using the information or social media is communication, entertainment, consumption or shopping, and community activities.

Keywords—*e-Lifestyle; consumer; Generation Z; social media; information technology*

I. INTRODUCTION

The development of the internet in Indonesia is developing and encouraging digital media in communication or other purposes. Data from the Ministry of Communication and Information of the Republic of Indonesia shows that internet users in Indonesia in 2019 have reached 54 percent or 143 million of Indonesia's 265 million inhabitants. Of these internet users, 80 percent are teenagers aged 15-19 years. For Facebook users, Indonesia is ranked 4th in the world. In one minute, there were 3.3 million information uploaded on Facebook and 2.9 million information spread on WhatsApp every minute from this data. This result is based on UNESCO research concludes that 4 out of 10 Indonesians are active on social media such as Facebook and WhatsApp [1].

Communication technology has facilitated daily life and communication [2] and changing ways and patterns of life that impact product utilization [3]. According to [4], understanding lifestyles is useful in delivering products appropriate to the target segment, especially as a basis for compiling information technology-based marketing on products. Understanding digital-oriented lifestyles (e-lifestyle) helps understand segments of products to be marketed through digital media. For example, [3] uses a digital-oriented lifestyle (e-lifestyle) in analyzing the adoption process of using information technology in banking. [5] managed to identify the avoidance of advertisements in terms of digital lifestyle (e-lifestyle), and [6] examined the relationship of e-lifestyle with perceived corporate identity, consumer satisfaction, and loyalty of cellular service users.

The Indonesian Internet Service Providers Association in 2017 shows that based on age group, 49.52 percent of internet users in Indonesia aged 19 to 34 years who produce new professions in the digital world, that digital-oriented lifestyle is the majority in the Z generation group. This generation has different characteristics and characteristics from the previous generation, but information about the generation is minimal [7]. Generational understanding is essential because generational boundaries have different ways of thinking, decision making, and behavior that cause problems when there are gaps in understanding across generations. Communication is an essential part of this generation [8], so understanding this generation's lifestyle is essential in the educational, social, and economic context.

Generation Z is the generation after 1995, which is also called i-generation or post-millennial. Different terms refer to this generation, such as i-Generation, technology generation, online generation, Post Millennials, and Facebook Generation [8]. The differences in each generation bring significant and significant differences in the segmentation of consumer behavior. According to Forrester Research, Generation Z consumes more online media than offline media and spends 3.9 hours a week watching shows online, compared to all US adults who only spend 1.6 hours a week. According to The Cassandra Intelligence Group Report that studies the habits of Generation Z, more than a third of Generation Z uses tablets or gadgets regularly, 70% of ages 10 to 13 carry mobile devices, and 65% use mobile applications.

Generation Z has similarities to generation Y and can apply all activities at once by only using technology. This generation spends much time dealing with cyberspace. This generation is familiar with technology and familiar with digital technology and communication. Experts highlight the fact that Generation Z can adapt well to the real and virtual

worlds. This generation can easily switch between two real and virtual because they have the assumption of complementing one another [9]. The consequence of this condition is that part of Generation Z can easily find and explore the information they need. This generation also quickly shares information with others. The communication processing between these generations is sustainable because it uses various communication devices or social media. This generation is an active social media user with many contacts and has daily relationships through social media channels [10]. Generation Z uses various mobile devices and likes to assess the reality and the environment around them. This generation embodies their opinions and attitudes using Twitter, blogs, and internet forums and likes to share photos (Instagram, Pinterest, Snapchat) and films (YouTube, Instagram, Snapchat). Generation Z not only uses Internet content, but they also create and control it [11]. Lifestyle understanding in this group and the media are essential information for all interested parties in designing appropriate communication for this generation.

Lifestyle is an important factor considered in predicting consumer behavior. Lifestyle is a living pattern people who spend time and money on specific activities and are contemporary and comprehensive [12]. Lifestyle describes the whole person who interacts with their environment. Compared to relatively stable values, lifestyles tend to change more quickly. Lifestyle is needed in determining market segments of consumer behavior [13]. Author in [14] stated that lifestyle segmentation measures human activities based on individual patterns of spending time, interests, and points of view of themselves and others according to underlying characteristics, such as income, education, and residence. In predicting consumer behavior, experts argue that individual lifestyles will determine individual consumption behavior. Lifestyle understanding in Generation Z is expected to provide valuable information in various fields of socio-economic life. Building and validating an electronic lifestyle scale that can describe a more holistic lifestyle for online marketers have received researchers' attention in several countries, such as [15] in Malaysia, [16] in Turkey, and [17] in India. e-Lifestyle is the main focus of this research. In principle, the formulation of the problem is based on confirmation of e-lifestyle factors.

II. LITERATURE REVIEW

A. e-Lifestyle

In the digital age, [18] uses Kelly's construction theory to build a lifestyle scale in the domain of IT adoption. In contrast, [19] uses the theory of human motivation and the value of hope to build a lifestyle instrument for hospitality consumers. Personal construction theory emphasizes human capacity and emotional experience, stating that individuals engage in certain behaviors due to a series of natural consequences [20]. Human motivation theory states that motivation largely contributes to certain behaviors, such as motivation from basic needs, food, hobbies, goals, circumstances, or ideals [19]. Expectancy value theory, which Fishbein developed in the 1970s [21], suggests that people orient themselves to the world following the expectations or beliefs and evaluations of each individual.

In [22], argues that lifestyle is a set of behaviors initiated by motivation, which develops by interacting with environmental conditions and shapes by choices, conditions, cognition, and beliefs. Human motivation theory, expectancy-value theory, and unique construction theory all originate from sociology and psychology. Therefore, from a sociological perspective, lifestyles are motivated by external stimulants [22]. From a psychological standpoint, [22] suggests that the internal trust initiates lifestyle. The AIO study considers lifestyle as a series of behaviors that reflect individual psychological considerations and sociological consequences. Based on the literature review above, theories related to lifestyle are generally agreed that human behavior can be predicted and explained by the function of psychological and sociological variables.

Psychological and sociological constructions can predict e-lifestyles. This study uses four constructs that are electronic activities (e-activities), electronic interests (e-interests), electronic opinions, (e- opinion) and electronic values (e-values) to evaluate lifestyle. Lifestyle is a series of behaviors that reflect an individual's psychological problems (internal beliefs) and sociological consequences (external stimuli). This research operationalizes digital or electronic activities as "observable actions" in using services or products supported by information technology, electronic interest as logical tendencies to use services or products supported by information technology, electronic opinion as "fundamental responses" on issues of services or products supported by information technology, and electronic value as basic beliefs about services or products supported by information technology. Specifically, the first three constructs of activities-e, e-opinion, e-interest are based on AIO [14], while, the e-value construct is drawn from the LOV, VALS, and RVS studies [23], [24], [25], [26] designed the lifestyle of 27-item internet users, [27] made 30 statement items to assess the lifestyle of internet users, [28] proposes a 38-item assessment of lifestyle-related to internet use by internet buyers, [29] expanding and replicating the work of [30], [25] adopted 56-item China-VALS to survey consumer lifestyles in the mobile market. Several researchers have tested the e-lifestyle construct, such as [16], which measures it based on factors of interest, entertainment, sociability, perceived importance, concern, and novelty. Author in [17] also tested e-lifestyle constructs using the subject of shoppers in India. Previous studies have not examined the Z generation group, which is the dominant part of the digital era segment.

B. Generation Z and behaviour

The emergence of theories about generation gave birth to groups of generations X, Y, and Z. Several researchers have tried to understand generational characteristics and study generational differences between groups [31], [32], [33]. Some authors like William Strauss and Neil Howe describe the demographic group with the birth year beginning after the 1980s as the millennial generation written in *Generations; The History of America's Future, 1584 to 2069*. This generation is referred to as the Y generation, a continuation of the baby boomer generation or generation X. The change of generation from generation X to Y generation carries significant and significant implications, especially in marketing. Some

literature states that this group numbered more than three times the number of previous generations. Gen Y is a unique consumer group in decision making, and its behavior is heavily influenced by media technology and information. Marketers need to identify consumer behavior in this group and the media that influence it as a basis for the preparation of segmentation, targeting, and positioning. According to [34], generation Y is more individualistic but cares about social responses, more educated, intelligent in technology, updated information, and more structured in certain groups. Many companies use event marketing to attract generation Y by involving the activities of this group community. Author in [35] shows that generation Y loves electronic media such as television and the Internet, and the majority respond to advertisements based on billboard media and shared community media. These behaviors need to be taken into consideration for companies in determining the appropriate media for this generation.

Generation X is a generation before 1980. The generation born between 1980-1995 is called the Y generation, called the millennial generation, and after 1995 is called the Z generation, called i-generation or post-millennial. The differences in each generation bring significant and significant differences in the segmentation of consumer behavior. According to Forrester, Generation Z consumes more online media than offline media and spends 3.9 hours a week watching shows online, compared to all US adults who only spend 1.6 hours a week. According to The Cassandra Intelligence Group Report that studies the habits of Generation Z, more than a third of Generation Z uses tablets or gadgets regularly, 70% of ages 10 to 13 carry mobile devices, and 65% use mobile applications.

Generation Z has similarities to generation Y and can apply all activities at once by only using technology. This generation spends much time dealing with cyberspace. For example, this group also has a high dependence on smartphones [36]. This generation is familiar with technology and familiar with digital technology and communication. Understanding consumer behavior in this group and the media that influence it considers marketers to design appropriate marketing communications. Socially, Generation Z values peer groups more and prefers social media in cyberspace. This group is more imaginative, confident, optimistic, and more lateral. Generation Z likes involvement and efforts to build relationships. Generation Z has similarities with Generation Y because it is a continuation of Generation Y, preferring social media in communication and self-expression. Generation Z tends to focus on innovation. This generation was born in the era of internet technology and is instant like touch screen media. Technological innovations become the hope for this group to provide comfort for them. This generation is classified as a generation with free choices on products that tend to be influencers for family consumption.

Generation Z has more power than previous generations to redefine production and consumption [37]. Generation z group is a generation group that is closely related to socially and technologically [38]. Generation Z stands out from the rest of

the generation in at least one aspect that this group has never seen without the Internet [39]. Regarding the behavior of Generation Z, marketers need to involve this generation in building brand equity such as various marketing activities that involve the group directly and build networks for this group through digital social media so that this group feels part of the company. Generation Z customers are highly customized online, and app shoppers. As Generation Z's purchasing power grows, marketers need to understand how their consumers behave [37]. Marketers must adapt related to the way in sharing information on brands and products that tend to be mobile compared to print media. Marketers can also use digital media to communicate family products through this generation according to their role as influencers for family purchases.

III. DESIGN METHODOLOGY

This type of research is a survey. This research was initiated through empirical field observations, also added with environmental data. The research population used in this study is the Z generation of consumers. This study sample is a group of students who fall into the Z generation category born after 1995. The sampling technique uses convenience sampling techniques. The data used are primary; that is, the response provided by research subjects related to e-lifestyle. Samples were collected from as many as 427 respondents and met the criteria for analysis. Data was collected through a survey using a closed and open questionnaire. A closed questionnaire was used to identify the e-lifestyle of the respondents using a Likert scale. An open questionnaire is used to explore information about the factors of respondents using information and communication technology. This study's variables are interdependent, namely e-lifestyle variables consisting of four constructs; e-activities, e-interest, e-opinions, and e-values. The indicators of the four constructs as follows in Table I [24] [43].

A. Data Normality Test

Data normality can be observed through skewness and kurtosis values. Observation can be done by paying attention to the value of z or z value. Data is said to be normal if it has a critical value below the z value. The z value for the probability of 1% is ± 2.58 . Based on the normality test data, it is known that all data derived from e-lifestyle variable data have a critical ratio or critical value below ± 2.58 .

TABLE I. E-LIFESTYLE CONSTRUCTS

e-Activities	e-Interests	e-Opinions	e-Values
Work	Family	Themselves	Respected
Hobbies	Home	Social issues	Accomplishment
Social events	Job	Politics	Fullfilment
Vocation	Community	Business	Relationships with others
Entertainment	Recreation	Economics	Expectation
Club	Fashion	Education	Prejudices
membership	Food	Production	Hopes
Community	Media	Future	Demands
Shopping	Achievements	Culture	
Sports			

Sources: Adapted from [24] [43]

B. Test Instrument

According to [40], validity indicates the accuracy and accuracy of measuring instruments in carrying out their measurement functions. A validity test using factor analysis was performed. The test results show that the KMO value of 0.550 is higher than 0.5 [41], which indicates that the number of samples has fulfilled the sample adequacy rules for further analysis. Validity analysis shows that there are three invalid items with extraction values less than 0.4 [42].

Reliability testing is related to the problem of trust in the instrument. An instrument can have a high level of confidence if testing the instrument shows permanent results. Thus, the instrument reliability problem is related to the problem of the accuracy of the results. This study's reliability analysis uses Cronbach Alpha to identify how well the questionnaire's items are related to one another. The Alpha coefficient obtained ranges from 0.729 to 0.823 greater than 0.7 [42].

C. Data Analysis Techniques

Data analysis techniques in this study used factor analysis techniques. The factors formed in the analysis are based on the concept of confirmation using CFA.

IV. RESULT AND DISCUSSION

A. Result

Factor analysis can group or reduce the number of similar questions to provide information on whether several questions in one attribute measure the same domain or not. If the same will become one group and, if not, will be separated. The extraction results of the communalities in the variables are presented in Table II. Communality is a measure of the percentage of variation in variables explained by factors. The extreme value of communality is between 0.0 and 1.0. Estimation of 1.0 means that the variables' variance correlates perfectly with other variables due to several shared factors. For example, ea1 (factor 1) is 0.444, which means a factor 1 question or item shows a 44.4% level of equality with other variables caused by several shared factors. In comparison, the remaining 55.6% is the uniqueness of that variable, influenced by other factors.

The rotation factor method used is the varimax rotation method, where the results can be seen after six iterations, from Table III, known variable e-lifestyle factors grouping. The results of the rotation factors in Table III confirm four dimensions. Dimension 1 is an e-activities factor; dimension 2 is an e-interests factor; dimension 3 is an e-opinions factor. Dimension 4 is the e-values factor. The results of the rotation component matrix are as follows in Table III.

TABLE II. COMMUNALITIES

Communalities	
	Extraction
ea1	.444
ea2	.476
ea3	.475
ea4	.491
ea5	.496
ea6	.443
ea7	.520
ea8	.508
ea9	.532
ea10	.520
ei1	.495
ei2	.497
ei3	.623
ei4	.650
ei5	.732
ei6	.695
ei7	.706
ei8	.787
ei9	.776
ei10	.624
ei11	.148
ei12	.106
eo1	.492
eo2	.169
eo3	.552
eo4	.560
eo5	.563
eo6	.582
eo7	.638
eo8	.644
eo9	.595
eo10	.526
eo11	.586
eo12	.649
ev1	.676
ev2	.711
ev3	.728
ev4	.629
ev5	.587
ev6	.588
ev7	.551
ev8	.416
ev9	.465
ev10	.478

Extraction Method: Principal Component Analysis.

Sources: Data Processed

TABLE III. COMPONENT MATRIX

Component Matrix ^a				
	Component			
	1	2	3	4
ea1			.631	
ea2			.523	
ea3			.518	
ea4			.609	
ea5			.425	
ea6			.568	
ea7			.643	
ea8			.635	
ea9			.634	
ea10			.443	
ei1		.673		
ei2		.674		
ei3		.749		
ei4		.773		
ei5		.825		
ei6		.818		
ei7		.829		
ei8		.872		
ei9		.862		
ei10		.783		
eo1	.456			
eo2	.392			
eo3	.408			
eo4	.462			
eo5	.507			
eo6	.602			
eo7	.592			
eo8	.631			
eo9	.599			
eo10	.612			
ev1				.402
ev2				.449
ev3				.842
ev4				.786
ev5				.512
ev6				.453
ev7				.473
ev8				.525
ev9				.629
ev10				.610
Extraction Method: Principal Component Analysis.				
a. 4 components extracted.				

Sources: Data Processed

B. Qualitative Analysis

Qualitative analysis is used to identify the factors of respondents using information and communication technology. In general, students use information and communication technology daily with considerations, namely:

1) *Social media communication*: Students use information and communication technology intending to communicate actively or passively in social media. Some excerpts from student opinions are as follows:

"... to see info from Instxxxxm ..."
 "... everyday for Youxxbe access ..."
 "... look for trends or those that are viral ..."
 '... make it exist..update in ..."

The communication carried out also aims to update/upload information from individual activities, a form of self-actualization. Some excerpts from student opinions are as follows:

"... to upload photos ... videos of precious moments ..."
 "... self-actualization ... seen ... seeing ..."

Information about social media that are often used by Generation Z with the highest to lowest ranking; Instagram, YouTube, Line, Facebook, Twitter, Discard, Pinterest, Spotify, and Telegram. Some excerpts from student opinions are as follows:

"... info on Instagram ..."
 "..Video..youtube .."
 "..Chat use the line ..."
 "..Update..info..facebook .."
 "... communication ... news friends ... Twitter .."
 "... discard ..."
 "... Pinterest ..."
 "..Spotify ... sometimes telegrams ..."

2) *Entertainment*: Students use information and communication technology with the aim of entertainment. Some excerpts from student opinions are as follows:

"... listen to music ..."
 "... watch..movie .."
 "..Game .."
 "... Information of fashion ..."

3) *Shopping or consumption*: Students use information and communication technology with the aim of consumption/shopping. Some excerpts from student opinions are as follows:

".. make buying goods ... online ..."
 "... the need to see products that are more trendy ..."
 "... transactions to buy goods ..."
 "... order goods ..."

4) *Community or hobby*: Students use information and communication technology as a means to form a community or a shared hobby. Some excerpts from student opinions are as follows:

"..For a group of hobbies ..."
 "... community ... the same ..."

C. Discussion

Generation Z is a generation close to technology [37] and cannot be separated from the internet [38]. Generation Z has a lifestyle supported by various mobile devices and likes to assess the reality and the surrounding environment. These findings are also consistent with the findings that most of this generation uses technology for communication, entertainment, hobbies, and consumption purposes. Information media is used as a medium to find information. This generation embodies their opinions and attitudes using media such as Twitter, blogs, and internet forums and likes to share photos (Instagram, Pinterest, Snapchat) and films (YouTube, Instagram, Snapchat) as part of communication. This generation not only uses Internet content but is also involved in creating and controlling information technology. Author in [39] explains that four constructs can be used in measuring e-lifestyle combined from AIO, VALS, ROV, and LOV, namely; e-activities, e-interests, e-opinions, and e-values. Digital-oriented lifestyles can be identified through a) e-activities in the form of actions that can be observed in using services or products supported by information technology including work, hobbies, social activities, entertainment, sports, b) e-interest in the form of logical tendencies in using services or products supported by information technology include work demands, family, community, and available media factors, c) e-opinion as a fundamental response to the problems of services or products supported by information technology including social, economic, political and educational needs, and d) e-values in the form of fundamental beliefs about services or products supported by information technology including expectations, needs, relationships with fellow individuals, and requests.

Following the construct combined from AIO, VALS, ROV, and LOV, Generation Z has a lifestyle following e-lifestyle. This study's results follow the validation of [44], who used the formative first-order and second-order hierarchical latent constructs. The finding of this research confirmation contributes to the body of knowledge regarding e-lifestyle measurement in Generation Z. According to the Z generation group, which is consistent with the use of digital technology, e-lifestyle shows the form of activities that this generation does daily. Generation Z's lifestyle relies heavily on digital devices, internet services available, and innovative digital products for entertainment, interpersonal relationships, social networking, economic transactions, and the overall gathering of information and knowledge [45].

V. CONCLUSION

Based on the results of the analysis and discussion, it can be concluded that motives of e-lifestyle in Generation Z, primarily among students, are formed in four factors: e-activities, e-interests, e-opinions, and e-values. Digital-oriented lifestyles can be identified through e-activities in the form of actions that can be observed using services or products supported by information technology, including work, hobbies, social activities, entertainment, and sports. e-Interest in the form of logical tendencies in using services or products supported by information technology include work demands, family, community, and available media factors, e-

opinion as a fundamental response to the problems of services or products supported by information technology including social, economic, political and educational needs, and e-values in the form of fundamental beliefs about services or products supported by information technology including expectations, needs, relationships with fellow individuals, and requests. Information or social media are often used by Generation Z, namely Instagram, Youtube, Line, Facebook, Twitter, Discard, Pinterest, Spotify, and Telegram. Using information or social media is communication, entertainment, consumption or shopping, and community or hobby activities. The findings are generally expected to be used as materials for planning strategies related to lifestyles in the digital age and patterns of shaping behavior from e-lifestyle to be a part of consumer education and socialization. According to the media, socialization and education activities can use digital or media information technology often used by Generation Z.

This research does not classify the gender aspects of the subject or Generation Z, even though it is likely that there will be differences in behavior by gender [46]. Future studies can consider gender aspects in analyzing e-lifestyle in this generation. Another possibility is that this generation group will adapt quickly to possible future behavior changes, so the longitudinal analysis is needed. Besides, further research can consider other e-lifestyle measurement models such as LOV, and RVS studies [23] [24].

ACKNOWLEDGMENT

The authors would like to thank Institute of Research and Community Service-UNY which funded this research.

REFERENCES

- [1] www.kominfo.go.id.
- [2] Hassan, S, H, Thurasamy, T, R, and Lio, W, Y, "E-lifestyle, customer satisfaction and loyalty among mobile subscribers in Thailand," *International Review of Management and Marketing*, Vol 7 (1), 354-362, 2017.
- [3] Yu, C, S, "Using E-lifestyle to Analyze Mobile Banking Adopters and non-Adopters," *Journal of Global Information Technology Management*, Vol 18, pp.188-213, 2015.
- [4] Chen, T.Y, and He, Q.Y, "Applying decision tree techniques to segmentation bases for e-marketing," *Management Science Research*, 3(1), pp.1-25, 2006.
- [5] Koshksaray, A, A, Franklin, D, and Hanzae, K, H, "The relationship between e-lifestyle and internet advertising avoidance," *Australasian Marketing Journal*. Vol 23. No 1.2015.
- [6] Hassan, S, H., Yee, L, W, and Thurasamy, R, "Consumer e-lifestyle, perceived corporate identity, customer satisfaction and loyalty among young mobile service subscribers: A cross cultural examination of Indonesia-Malaysia-Thailand growth triangle (IMT-GT)". *International Journal of Management and Applied Science Journal*. Vol 2.(7), 2016.
- [7] Singh, A, P, and Dangmai, J, "Understanding the generation Z: The future workforce," *South-Asian Journal of Multidisciplinary Studies*. Vol 3. No 3, 2016.
- [8] Dolot, A, "The characteristic of generation Z," *E-mentor*. Vol 2. No 74, 2019.
- [9] Żarczyńska-Dobiesz, A, & Chomałowska, B, "Pokolenie Z na rynku pracy – wyzwania dla zarządzania zasobami ludzkimi," *Prace Naukowe Uniwersytetu Ekonomicznego we Wrocławiu*, Vol 350, pp.405–415, 2014.
- [10] Csobanka, Z.E, "The Z Generation," *Acta Technologica Dubnicae*, Vol 6(2), pp.63–76, 2016.
- [11] Hardey, M, "Generation C: Content, creation, connections and choice," *International Journal of Market Research*, Vol 53(6), pp.749–770, 2011.

- [12] Engel, J.F, Roger, D.B, and Paul, W. M, Consumer behavior. International Edition, Forth Worth : Dreyden Press, 2000.
- [13] Suprpto, B, and Wijaya, T, "Intention of Indonesians consumers on buying organic food," International Journal of Trade, Economics, and Finance, Vol 3. No 2, 2012.
- [14] Plummer, J.T, "The concept and application of life style segmentation," Journal of Marketing, Vol. 38 No. 1, pp. 33-7, 1974.
- [15] Ahmad, N, Omar, A, and Ramayah, T, "Examining the validity and reliability of e-lifestyles scale in the Malaysian context: Preliminary results". In 3rd International Conference on Technology and Operations Management (ICTOM2012), 4th-6th July 2012.
- [16] Mendi, B, and Mendi, O, "Evaluation of Validity and Reliability of the Turkish Version of the E-lifestyle Instrument," Journal of Yaşar University. Vol 10 No. 4, pp. 6624-6632, 2015.
- [17] Pandey, S, and Chawla, D, "E-lifestyles of Indian online shoppers: A scale validation," Journal of Retailing and Consumer Services, Vol. 21 Issue 6, pp. 1068-1074, 2014.
- [18] Malhotra, Y, "Bringing the adopter back into the adoption process: a personal construction framework of information technology adoption," The Journal of High Technology Management Research, Vol. 10 No. 1, pp. 79-104, 1999.
- [19] Lin, F.Y, An analysis of hospitality consumer lifestyles in the United States" PhD dissertation, Texas Tech University, Lubbock, TX, 2003.
- [20] Neimeyer, R.A, and Neimeyer, G.J, Advances in Personal Construct Psychology, 5th ed., Praeger, New York, NY, 2002.
- [21] Ajzen, I, and Fishbein, M, Understanding attitude and predicting social behavior. Englewood Cliff, New York : Prentice Hall, 1980.
- [22] Walters, G.D, Lifestyle Theory: Past, Present, and Future, Nova Science Publishers, Commack, NY, 2006.
- [23] Roy, S, and Goswami, P, "Structural equation modeling of value-psychographic trait-clothing purchase behavior: a study on the urban college-goers of India", Young Consumers, Vol. 8 No. 4, pp. 269-277, 2007.
- [24] Harcar, T, and Kaynak, E, Lifestyle orientation of rural US and Canadian consumers, Asia Pacific Journal of Marketing and Logistics, Vol. 20 No. 4, pp. 433-454, 2008.
- [25] Zhu, H, Wang, Q, Yan, L, and Wu, G, "Are consumers what they consume? Linking lifestyle segmentation to product attributes: an exploratory study of the Chinese mobile phone market," Journal of Marketing Management, Vol. 25 No. 3. 295-314, 2009.
- [26] Kim, K.H, Park, J.Y, Kim, D.Y, and Moon, H.I, "Internet user lifestyle: its impact on the effectiveness of internet advertising in Korea", Conference, American Academy of Advertising, Salt Lake City, UT, USA, 2001.
- [27] Yang, K.C.C, "A comparison of attitudes towards internet advertising among lifestyle segments in Taiwan," Journal of Marketing Communications, Vol. 10 No. 1, pp. 195-212, 2004.
- [28] Brengman, M., Genuens, M., Weijters, B, Smith, S.M, and Swinyard, W.R, "Segmenting internet shoppers based on their web-usage-related lifestyles: a cross-cultural validation," Journal of Business Research, Vol. 58, pp. 79-88, 2005.
- [29] Allred, C.R, Smith, S.M, and Swinyard, W.R, "E-shopping lovers and fearful conservatives: a market segmentation analysis," International Journal of Retail & Distribution Management, Vol. 34 No. 4, pp. 308-33, 2006.
- [30] Swinyard, W.R, and Smith, S.M, "Why people (don't) shop online: a lifestyle study of the internet consumer," Psychology & Marketing, Vol. 20 No. 7, pp. 567-97, 2003.
- [31] Lazanyi, K, and Bilan, Y, "Generation Z on the labourmarket-do they trust others within their workplace?" Polish Journal of Management Studies. Vol. 16 No. 1, pp. 78-93, 2017.
- [32] Lanier, K, "5 Things HR professionals need to know about generation Z: thought leaders share their views on the HR profession and its direction for the future," Strategic HR Review. Vol. 16 No. 6, pp. 288-290, 2017.
- [33] Grow, J.M, and Yang, S, "Generation-Z enters the advertising workplace: expectations through a gendered lens," Journal of Advertising Education. Vol. 22 No. 1, pp. 7-22, 2018.
- [34] Syrett, M, and Lammiman, J, "Advertising and millennials," Young Consumers. Vol 5. No 4. 62-73, 2004.
- [35] Valentine, D, B, and Powers, T, L, "Generation Y values and lifestyle segments," Journal of Consumer Marketing, Vol. 30 No. 7, pp. 597-606, 2013. <https://doi.org/10.1108/JCM-07-2013-0650>.
- [36] Bukhori, B, Said, H., Wijaya, T., and Nor, F. M. "The Effect of Smartphone Addiction, Achievement Motivation, and Textbook Reading Intensity on Students' Academic Achievement," iJIM. Vol. 13, No. 9, 2019. doi.org/10.3991/ijim.v13i09.9566.
- [37] Priporas, C-V, Stylos, N, and Fotiadis, A, K, "Generation Z consumers' expectations of interactions in smart retailing: A future agenda," Computers in Human Behavior. Vol 77. 2017.
- [38] Turner, A, "Generation Z: Technology and Social Interest," The Journal of Individual Psychology Vol 71 No. 2, pp. 103-113, 2015. [doi:10.1353/jip.2015.0021](https://doi.org/10.1353/jip.2015.0021).
- [39] Chillakuri, B, "Understanding Generation Z expectations for effective onboarding," Journal of Organizational Change Management, Vol. ahead-of-print No. ahead-of-print., 2020. <https://doi.org/10.1108/JOCM-02-2020-0058>.
- [40] Sekaran, U, Research methods for business: Skill-building approach, Fourth Ed, New York : John Wiley & Sons Inc, 2003.
- [41] Gie, Y, A, and Pearce, S, "A beginner's guide to factor analysis: Focusing on exploratory factor analysis," Tutor Quant Methods Psychol. Vol 9, pp. 79-94, 2013.
- [42] Hair, J.F, Black, B, Babin, B, Anderson, R, E, and Tatham, R. L, Multivariate data analysis, 6th Ed, New Jersey: Prentice Hall International, Inc, 2006.
- [43] Yu, C, S, "Construction and validation of an E-lifestyle instrument," Internet Research, Vol 21(3), pp.214-235, 2011.
- [44] Hassan, S, H, Ramayah, T, Mohamed, O, and Maghsoudi, A, "E-lifestyle conceptualization: Measurement model validation using variance based structural equation modeling (SEM-PLS)," Modern Applied Science, Vol 9 (2), pp.319-332, 2015.
- [45] Hoque, A. S. M. M, "Digital device addiction effect on lifestyle of generation Z in Bangladesh," Asian People Journal (APJ), 1(2), pp.21-44, 2018.
- [46] Kraljević, R, and Filipović, Z, "Gender Differences and Consumer Behavior of Millennials", Acta Economica Et Turistica, Vol 3 No. 1, pp. 5-13. 2017. [doi: https://doi.org/10.1515/aet-2017-0002](https://doi.org/10.1515/aet-2017-0002).

A Novel Chaotic System for Text Encryption Optimized with Genetic Algorithm

Unnikrishnan Menon¹, Atharva Hudlikar³
School of Electrical and Electronics Engineering
Vellore Institute of Technology
Vellore, India

Anirudh Rajiv Menon²
School of Electronics Engineering
Vellore Institute of Technology
Vellore, India

Abstract—With meteoric developments in communication systems and data storage technologies, the need for secure data transmission is more crucial than ever. The level of security provided by any cryptosystem relies on the sensitivity of the private key, size of the key space as well as the trapdoor function being used. In order to satisfy the aforementioned constraints, there has been a growing interest over the past few years, in studying the behavior of chaotic systems and their applications in various fields such as data encryption due to characteristics like randomness, unpredictability and sensitivity of the generated sequence to the initial value and its parameters. This paper utilizes a novel 2D chaotic function that displays a uniform bifurcation over a large range of parameters and exhibits high levels of chaotic behavior to generate a random sequence that is used to encrypt the input data. The proposed method uses a genetic algorithm to optimize the parameters of the map to enhance security for any given textual data. Various analyses demonstrate an adequately large key space and the existence of multiple global optima indicating the necessity of the proposed system and the security provided by it.

Keywords—Chaotic map; genetic algorithm; encryption; bifurcation diagram; Lyapunov exponent

I. INTRODUCTION

The Internet is utilized primarily for transmission of data. However, while we take advantage of the Internet's capabilities, unauthorized individuals have the chance to intercept our information and then visit, copy, and destroy it. Therefore, the security and protection of data and information becomes a hot problem studied by experts and enthusiasts alike.

Many encryption systems have gained popularity and momentum over time that have proven to be effective for secure transmission of data. Around 1974, an IBM team developed the Data Encryption Standard (DES) and it was adopted as a national standard in 1977 [1]. Since that time, many cryptanalysts have attempted to find shortcuts for breaking the system. [2]. In 2001, as the outcome of a public competition, Rijndael was announced as the Advanced Encryption Standard (AES) by the US National Institute of Standards and Technology (NIST). Today, the AES is one of the most widely used encryption primitives [3]. Many such algorithms have been used in the past few decades. However, when these algorithms were utilized years ago, the digital technologies were quite different from now and the magnitude of the challenges was lower [4]. For instance, AES suffer from

some drawbacks such as, long encryption and decryption time, and patterns appearance in the ciphered image [5].

The theory of dynamical systems and chaos have shown significant scope for research and applications in the field of cryptography [6]. The property of high sensitivity exhibited by a chaotic system with respect to its initial conditions and parameters implies strong cryptographic qualities, and its random-like behavior and unstable orbits with long periods, are quite beneficial to cryptosystems making them resilient to brute force attacks.

Chaos-based ciphers have shown exceptional properties in aspects of security, complexity, speed, and computing power. This is because chaotic maps have many attributes that translate to an efficient cryptographic property. They display an ergodic nature, which means that these systems cannot be broken down to a simplified expression. This adds to the confusion factor of the encryption system. They are also sensitive to initial control parameters. This ensures that the plaintext and/or secret key cannot be obtained easily. A small deviation in the input can cause a large change in the output. Chaotic maps exhibit structure complexity and deterministic dynamics, which allows the cryptographic process to be simple, yet allow for a highly complex encryption and a pseudo-random behavior, respectively [7].

This paper utilizes and proposes a 2D hybrid chaotic map with desirable properties, such as those mentioned above, to generate pseudo-random sequences for text encryption purposes. The proposed map is extremely sensitive to the values of the parameters (taken as the key for encryption) and will therefore return vastly different sequences for minutely dissimilar keys. Hence there arises a need to find optimal key values for a given plaintext.

This problem can be tackled using Genetic Algorithms. As compared to the traditional optimization methods, Genetic Algorithms are robust, global and can be applied generally without making any domain-specific changes. It can be used not only for general, but also for indifferent and unconventional optimization problems [8, 9].

Many genetic algorithm models have been introduced by researchers largely working from an experimental perspective. Most of these studies are application oriented and are typically interested in using them as optimization tools. Researchers have also been improving systems by hybridizing them with genetic algorithms. For instance, a heuristic modified method

based on the genetic algorithm for solving constrained optimization problems was introduced in 2009 [10].

In its most generic usage, Genetic Algorithms work by creating a population of agents at every iteration with randomly assigned parameters. These agents are then evaluated based on their performance in the given environment and the best performing agents are carried forward to the next generation of agents. These algorithms encode a potential solution to a specific problem on a simple chromosome-like data structure and apply recombination operators to these structures to preserve critical information. Genetic algorithms are often viewed as function optimizers, although the range of problems to which they have been applied is quite broad [11,12].

This paper explores how genetic algorithms can optimize the key that is used by the proposed chaotic map to generate a pseudo random sequence, favorable for the encryption of a given plaintext.

II. OPTIMIZATION USING GENETIC ALGORITHM

Genetic algorithms are random heuristic search operations that are developed to imitate the mechanics of natural selection and genetics.

These are population-based search algorithms in which the individuals in the population represent samples from the set of all possibilities.

Genetic algorithms operate on string structures, analogous to biological systems, which are evolving in time according to the rule of survival of the fittest by using a randomized yet structured information exchange. The success of the winning individuals is normally dependent on their genes and is calculated using a fitness function that determines how well an individual performed from the moment it spawned, till termination. A percentage of the best individuals are then chosen which show the most promising fitness values. These individuals are then made to reproduce with each other to spread their genes in the subsequent generations of offspring. The individuals evolve over time to form even better gene variants by sharing and mixing their information about the domain of operation. The genetic algorithm simulates this process and calculates the optimum of objective functions [13].

This paper presents a new functional genetic algorithm optimization methodology that is applied to find out the best set of parameters for the proposed 2D chaotic map during the encryption process. This optimization technique ensures that, given the plaintext, the secret key generated will be the one that always ensures maximum confusion and diffusion attributes in the ciphertext thereby enhancing the security of confidential data. In the proposed chaotic map, the coefficients 'a' and 'b' need to be fine-tuned dynamically depending on the plaintext. Thus, these 2 coefficients of the chaotic map serve as chromosomes in the genetic algorithm.

The genetic algorithm implemented mainly involves the following 4 major steps:

A. Evaluation of Fitness

This is done using an objective function that summarizes, as a single figure of merit, how close a given design solution is to achieving the set target. This figure directly indicates how well an individual has performed in the current generation with respect to other individuals belonging to the same generation. The individuals are evolved till a point where certain desirable threshold conditions pertaining to fitness are met.

B. Selection

Fitness Proportionate Selection is applied to the parent generation. Every individual can become a parent with a probability which is proportional to its fitness. This implies that individuals with larger fitness values have a higher chance of mating and propagating their superior features to the next generation. This strategy applies a selection pressure to the more fit individuals in the population, evolving better off spring over time. The proposed algorithm considers only the top 20% of the individuals in a generation and rejects the rest.

C. Crossover

This step is analogous to biological reproduction. Parts of the selected parents' chromosomes are copied and pasted to generate one or more offspring. A random crossover point is selected and sections of the two parents from left and right of the crossover point are swapped to get new off-springs.

D. Mutation

The mutation operation in a genetic algorithm is mainly responsible for exploration of search space. Certain chromosomes in the offspring's DNA are chosen and randomly replaced with variations. This ensures that the new offspring produced are not simply a mere reflection of their previous generation but rather have their own unique features that could potentially lead to better fitness values. In this case, mutation operation is carried out by tweaking the values of the coefficients 'a' and 'b' using a relatively small step value which may be either positive or negative.

The evolutionary process terminates when a generation of individuals carries majority of genomes satisfying the desired threshold.

III. ASSOCIATED CHAOTIC FUNCTIONS

The following maps have played a key role in the conceptualization of the proposed 2D chaotic system:

A. Circle Map

This is a one-dimensional chaotic map that, for certain values of Ω and K , behaves in a chaotic manner [14]. This can mathematically be expressed as:

$$\theta_{n+1} = \theta_n + \Omega - \frac{K}{2\pi} \sin(2\pi(\theta_n)) \text{ mod } 1 \quad (1)$$

The circle map is an integral part of the proposed chaotic system whose initial conditions and parameter ranges have been defined in Section IV(c).

B. Hénon Map

In 1976, Hénon published literature detailing a 2D chaotic map which could be used as a reduced approach to study the dynamics of the Lorenz system [15, 16]. The Hénon map is mathematically defined by equations (2) and (3):

$$x_{n+1} = 1 - ax_n + y_n \quad (2)$$

$$y_{n+1} = bx_n \quad (3)$$

IV. PROPOSED CHAOTIC MAP

The proposed hybrid chaotic map is a 2D map which combines 2 different chaotic maps non-linearly. The maps used are Circle Map and Hénon Map. Equations (4) and (5) define this system as given below:

$$x(i+1) = C(a, b, y(i)) \text{ mod } 1 \quad (4)$$

$$y(i+1) = H(a, x(i)) \quad (5)$$

where $C(a, b, y(i))$ is the Circle Map as a function of a and b (the two parameters of the map), $H(a, x(i))$ is the chaotic dimension of the Hénon Map as a function of a . The system equation hence becomes:

$$x(i+1) = x(i) + d + (a \sin(2\pi y(i))) \text{ mod } 1 \quad (6)$$

$$y(i+1) = 1 - ax(i)^2 + y(i) \quad (7)$$

A. Bifurcation Diagram

A bifurcation diagram depicts the values approached asymptotically by a system with respect to its parameters [17]. The map shows the distribution of values taken by the system over a range of the parameters across numerous iterations.

The bifurcation diagram for the proposed system between dimension x and parameter a is shown:

Additionally, a bifurcation diagram was generated between dimension x and the second parameter b .

Fig. 1 and 2 show that for all depicted points of a and b , the map approaches almost all values in the normalized range, resulting in densely populated bifurcation diagrams. Thus, for a and b values taken over a large range, a uniform chaos is exhibited by the map. From the bifurcation diagrams, the ranges of a and b useful for the purpose of this paper are (1,4) and (0,4) respectively.

B. Lyapunov Exponent

Lyapunov exponents are used to check whether a system exhibits chaotic behavior. Equation (8) defines a mathematical expression for Lyapunov Exponent and is used to visualize the rate of divergence of a pair of orbits that were initially infinitesimally close [18]. It also infers a sensitivity to a variation in the initial conditions.

$$L_y(f(x)) = \lim_{n \rightarrow \infty} \left(\frac{1}{n} \sum_{i=0}^{n-1} \ln |f'_i(x)| \right) \quad (8)$$

where $f'_i(x)$ is the derivative of the i^{th} iterate $f_i(x)$.

A constantly positive value of Lyapunov exponent implies an unstable or chaotic orbit. For the proposed 2D chaotic system, L_x and L_y are the Lyapunov exponents for the x and y

dimensions, respectively. A system is chaotic if at least one of the Lyapunov exponents remains positive.

For the proposed map, both dimensions exhibit positive Lyapunov exponents across 2000 iterations with values around 4 for both dimensions implying that both dimensions of the map are chaotic in nature as shown in Fig. 3. The first 500 iterations have been ignored to avoid the influence of initial state.

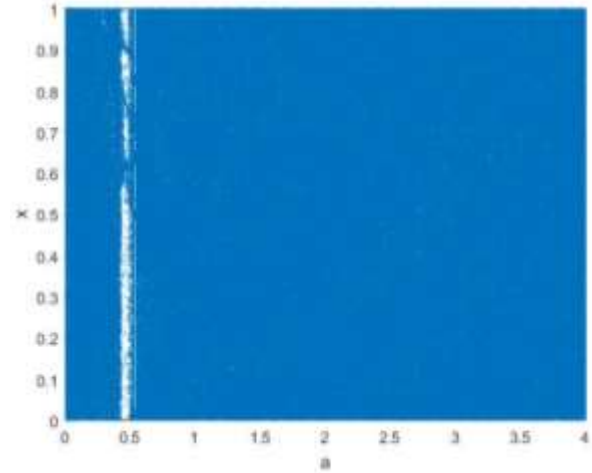


Fig. 1. Bifurcation Diagram of x Dimension vs. Coefficient a .

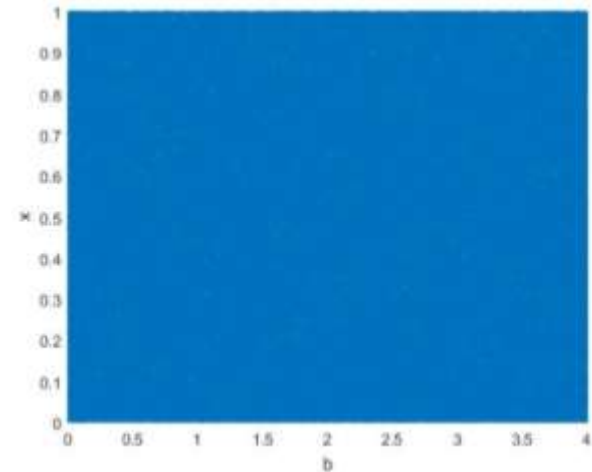


Fig. 2. Bifurcation Diagram of x Dimension vs. Coefficient b .

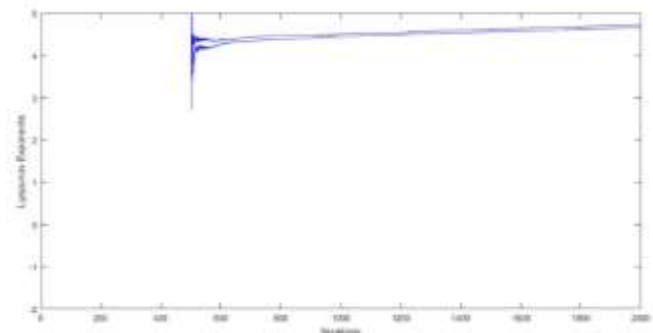


Fig. 3. Lyapunov Exponents for x and y Dimensions.

C. Selecting Initial Value of Chaotic Map

The initial x and y dimension values x_0 and y_0 respectively, of the chaotic map have been set as follows:

$$x_0 = \frac{P_{avg}}{P_{max}} \quad (9)$$

$$y_0 = 1 - x_0 \quad (10)$$

where the average and sum of ASCII values of plaintext are represented by P_{avg} and P_{max} .

This allows for a different initial value for the x and y dimensions and hence a completely different pseudo random sequence for every plaintext.

V. PROPOSED ALGORITHM

A. Key Generation

The key to be generated is the set of parameters (a and b) required by the chaotic map. The key is optimized for the given confidential data using a genetic algorithm Fig. 4.

1) An initial population of (a, b) pairs is generated with each pair having random a and b values selected from the ranges defined in Section IV.

2) Encryption of plaintext is done with each of these pairs (encryption procedure explained in section V(b)).

3) The fitness function for each (a, b) pair is calculated using the Jaccard index of similarity [19]. It is a statistic used for gauging the similarity between 2 sets and is defined as the size of the intersection divided by the size of the union of the sample sets as shown in equation (11):

$$J(A, B) = \frac{A \cap B}{A \cup B} \quad (11)$$

The above equation returns a score from 0 – 100. Where 0 means no similarity at all and 100 implies that both sets are the same. The fitness function taken for the proposed algorithm is:

$$F(\text{genome}) = 100 - J(P, E) \quad (12)$$

where F is the fitness function of the particular genome, P is the set of ascii values of the plain text and E is the ascii set of the encrypted cipher text obtained on encrypting the original text with the a and b values of that genome.

4) Once the fitness of each key pair in the population is calculated, the top 20% of the population are promoted (selection).

5) A pair of offsprings are generated for every set of parents randomly selected from the promoted/selected set,

where the a and b values of both parents are used to form different combinations of possible key values resulting in the formation of offsprings.

6) The selected parents and offspring are then made to undergo mutation where their (a, b) are modified in small random steps with a probability of 0.1

7) The mutated set now becomes the next generation.

8) The process is repeated for every subsequent generation till a desired fitness value of at least 95% is observed for more than 50% of the individuals belonging to that generation.

9) The optimal key is the genome with the best fitness function once the threshold conditions have been met.

10) The final encryption is done with the optimised (a, b) values.

B. Encryption

1) The initial values of the x and y dimensions are taken as shown in section IV(c).

2) For a given (a, b) pair, pseudorandom sequences of floating point values, for each dimension of the map i.e. x and y , of length equal to size of plaintext are obtained by iterating the chaotic map.

3) The arrays of floating point values are each sorted in decreasing order.

4) Each element in the original arrays is replaced with the index at which that floating point element appears in the corresponding sorted arrays. This gives rise to two pseudo random arrays of integer values, S_x and S_y .

5) The final key array will contain values picked from S_y occurring at the indices represented by the values of S_x .

6) The ciphertext is obtained by performing bitwise-XOR operation between the pseudorandom sequence and the plaintext.

C. Decryption

1) The key required for decryption consists of the optimized (a, b) along with the initial x and y values used in the encryption phase.

2) The final pseudorandom array is generated using the same procedure followed in the encryption step using the aforementioned key.

3) The plaintext is retrieved by performing bitwise-XOR operation between the pseudorandom sequence obtained in the previous step and the ciphertext.

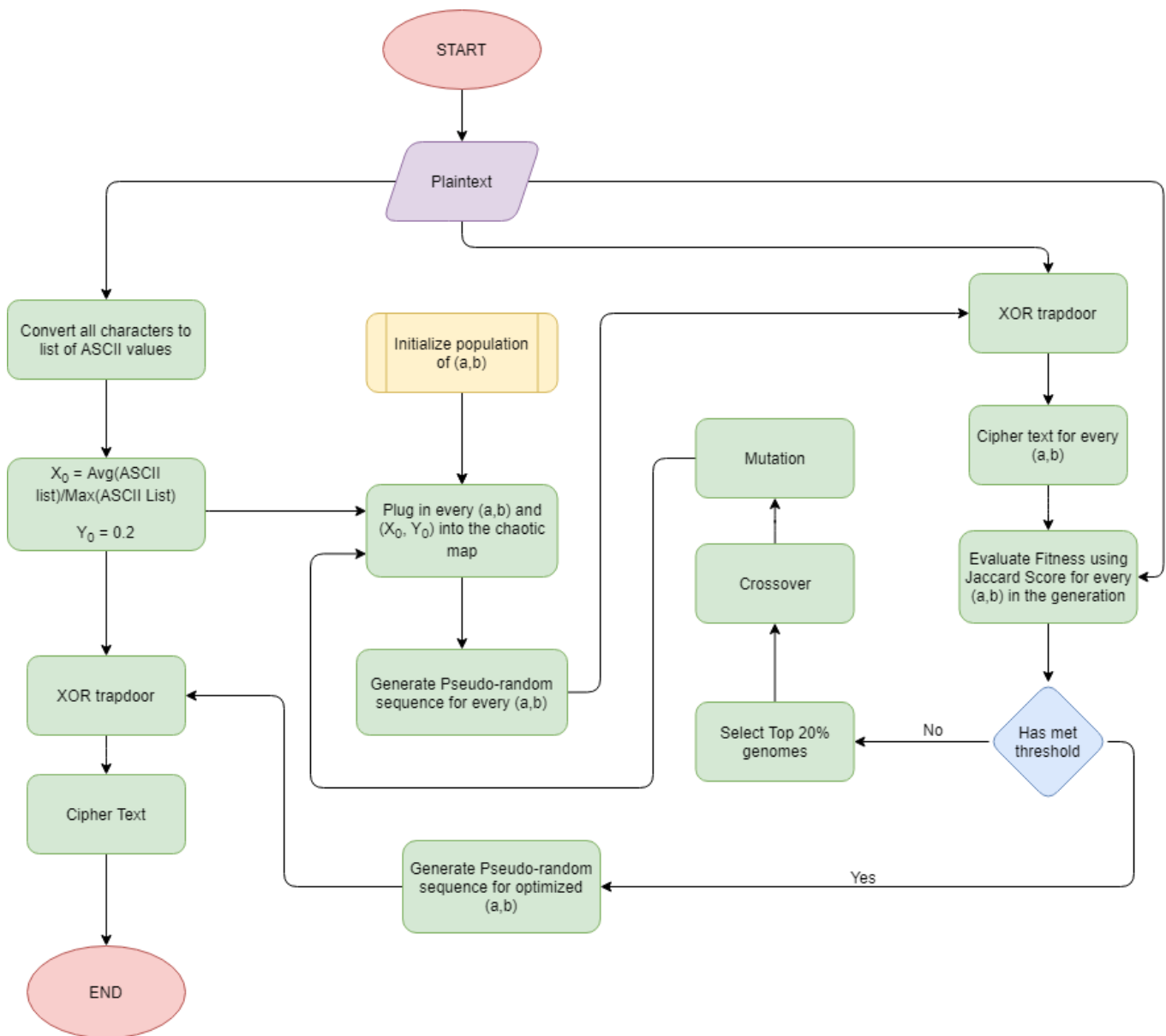


Fig. 4. Flow Diagram of Proposed Algorithm.

VI. EXPERIMENTAL ANALYSIS

The proposed algorithm was evolved and tested upon multiple plaintext data samples of varying lengths.

The genetic algorithm was deployed for each sample plaintext. The different possibilities of the coefficients (a, b) along with their corresponding fitness values for every genome spawning across all generations were recorded.

For visualization, 2D plots of the data were prepared, where the coefficients a and b were plotted on the x and y

axes, respectively. The fitness scores of every agent have been graphed as a color scale plot.

Fig. 5 shows that there exist a variety of (a, b) pairs with differing fitness values. While the average fitness demonstrated by an (a, b) pair increases with the length of the plaintext, there clearly exists a set of (a, b) pairs which show maximum fitness scores. This implies that for smaller plaintexts, an extremely minute alteration from the optimum in the values of (a, b) can lead to subpar encryption, thus reinforcing the proposed approach.

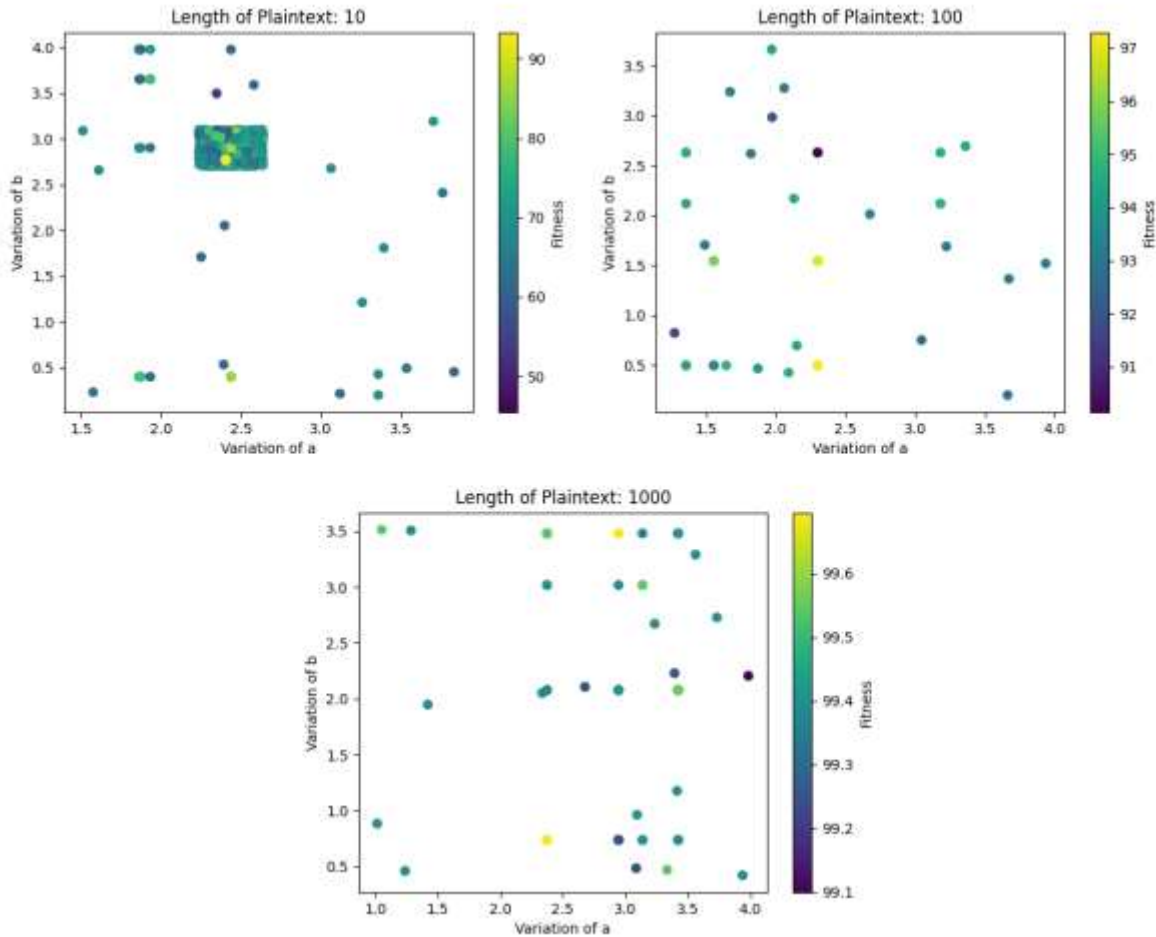


Fig. 5. Variation of Fitness Values for Individuals with different Coefficients for Fixed Plaintext Size.

Additionally, a secondary analysis was performed to study how changing the length of plaintext affects the number of generations till termination as well as the maximum fitness scores achieved. Table 1 depicts these variations. The population size for each generation was fixed to be 20 individuals. Note that upon increasing the population parameter, the range of variations covered by individuals in each generation increases significantly, thereby reducing the number of generations required and hence converging to the optimum set of parameters in a shorter runtime. All codes relevant to the analysis presented in this paper have been compiled into a GitHub repository [20].

TABLE I. EFFECT OF PLAINTTEXT LENGTH ON EVOLUTION ATTRIBUTES

S.No.	Length of Plaintext	No. of Generations	Max Fitness
1.	10	234	92.8571
2.	50	4	94.5946
3.	100	6	97.2603
4.	300	5	98.9744
5.	700	2	99.3658
6.	1000	4	99.7037

VII. KEY SPACE ANALYSIS

The key space of any cryptosystem should be very large to provide an extremely vast range of possible key combinations for an attacker to access the plaintext. For the proposed system, the keys being used for decryption are the a and b parameters along with the x_0 and y_0 initial values with selected ranges $(1,4)$, $(0.1,4)$, $(0,1)$ and $(0,1)$ respectively. Both a and b show a precision of 10^{-15} , i.e. a variation in their values by an amount as small as 10^{-15} will not allow decryption to occur, while the precisions shown by both x_0 and y_0 are 10^{-16} . Thus, the size of the entire possible key space is:

$$3 \times 10^{15} \times 3.9 \times 10^{15} \times 1 \times 10^{16} \times 1 \times 10^{16} \\ = 1.17 \times 10^{63} \gg 2^{128}$$

As a result, the key space provided by the proposed algorithm is large enough to resist brute force attacks.

VIII. FUTURE SCOPE

This paper presents the idea of using genetic algorithms to obtain optimized values of the parameters that are used in the chaotic function. As a proof of concept, we have used a basic XOR trapdoor. The proposed system can be further upgraded

by implementing a more complex trapdoor or by using this algorithm as an optimizing precursor to existing algorithms such as AES, DES, 3DES, RSA, etc. Further work can be done in selecting an improved class of genetic algorithms that can produce better results.

IX. CONCLUSION

This paper inspects a method that makes use of concepts stemming from genetic algorithms to optimize a novel 2D hybrid chaotic map. The proposed map demonstrates uniform chaotic behavior for a wide range of key parameters thereby allowing the genetic algorithm to explore various key possibilities resulting in optimal encryption for every plaintext. This technique can be used to generate keys for other established encryption schemes as well that use bit operations in the trapdoor function. The key generation system proposed in this paper is also resistant to brute force attacks thereby ensuring that it takes an infeasible amount of time and key permutations for an unauthorized interceptor to gain access owing to the large key space. The method introduced in this paper enhances the security by increasing the entropy in the key using algorithms that are analogous to evolutionary trends observed in nature.

REFERENCES

- [1] Coppersmith, D. (1994). The Data Encryption Standard (DES) and its strength against attacks. IBM journal of research and development, 38(3), 243-250.
- [2] Biham, E., & Shamir, A. (1991). Differential cryptanalysis of DES-like cryptosystems. Journal of CRYPTOLOGY, 4(1), 3-72.
- [3] Osvik, D. A., Bos, J. W., Stefan, D., & Canright, D. (2010, February). Fast software AES encryption. In International Workshop on Fast Software Encryption (pp. 75-93). Springer, Berlin, Heidelberg.
- [4] Dawood, O., & Hammadi, O. (2017). An Analytical Study for Some Drawbacks and Weakness Points of the AES Cipher (Rijndael Algorithm). Qalaai Zanist Journal, 2(2), 111-118.
- [5] Huang, C. W., Yen, C. L., Chiang, C. H., Chang, K. H., & Chang, C. J. (2010, August). The five modes AES applications in sounds and images. In 2010 Sixth International Conference on Information Assurance and Security (pp. 28-31). IEEE.
- [6] Schmitz, R. (2001). Use of chaotic dynamical systems in cryptography. Journal of the Franklin Institute, 338(4), 429-441.
- [7] Kocarev, L. (2001). Chaos-based cryptography: a brief overview. IEEE Circuits and Systems Magazine, 1(3), 6-21.
- [8] D'addona, D. M., & Teti, R. (2013). Genetic algorithm-based optimization of cutting parameters in turning processes. Procedia Cirp, 7, 323-328.
- [9] Hui, W. J., & Xi, Y. G. (1996). Operation mechanism analysis of genetic algorithm. Control Theory Appl, 13(3), 297-303.
- [10] Tsoulos, I. G. (2009). Solving constrained optimization problems using a novel genetic algorithm. Applied Mathematics and Computation, 208(1), 273-283.
- [11] Whitley, D. (1994). A genetic algorithm tutorial. Statistics and computing, 4(2), 65-85.
- [12] Michalewicz, Z. (2013). Genetic algorithms+ data structures= evolution programs. Springer Science & Business Media.
- [13] Haldurai, L., Madhubala, T., & Rajalakshmi, R. (2016). A study on genetic algorithm and its applications. International Journal of Computer Sciences and Engineering, 4(10), 2347-2693.
- [14] Khan, M., & Masood, F. (2019). A novel chaotic image encryption technique based on multiple discrete dynamical maps. Multimedia Tools and Applications, 78(18), 26203-26222.
- [15] Hénon, M. (1976). A two-dimensional mapping with a strange attractor. In The Theory of Chaotic Attractors (pp. 94-102). Springer, New York, NY.
- [16] Wen, H. (2014). A review of the Hénon map and its physical interpretations. School of Physics Georgia Institute of Technology, Atlanta, GA, 30332-0430.
- [17] Hale, J. K., & Koçak, H. (2012). Dynamics and bifurcations (Vol. 3). Springer Science & Business Media.
- [18] Wolf, A., Swift, J. B., Swinney, H. L., & Vastano, J. A. (1985). Determining Lyapunov exponents from a time series. Physica D: Nonlinear Phenomena, 16(3), 285-317.
- [19] Ivchenko, G. I., & Honov, S. A. (1998). On the jaccard similarity test. Journal of Mathematical Sciences, 88(6), 789-794.
- [20] Menon, A., Menon, U., & Hudlikar, A. (2020, August). Chaotic Genesis. Retrieved from https://github.com/axe76/Chaotic_Genesis.

Optimizing the C4.5 Decision Tree Algorithm using MSD-Splitting

Patrick Rim¹
California Institute of Technology
Pasadena, CA 91125, USA

Erin Liu²
Troy High School
Fullerton, CA 92831, USA

Abstract—We propose an optimization of Dr. Ross Quinlan’s C4.5 decision tree algorithm, used for data mining and classification. We will show that by discretizing and binning a data set’s continuous attributes into four groups using our novel technique called MSD-Splitting, we can significantly improve both the algorithm’s accuracy and efficiency, especially when applied to large data sets. We applied both the standard C4.5 algorithm and our optimized C4.5 algorithm to two data sets obtained from UC Irvine’s Machine Learning Repository: Census Income and Heart Disease. In our initial model, we discretized continuous attributes by splitting them into two groups at the point with the minimum expected information requirement, in accordance with the standard C4.5 algorithm. Using five-fold cross-validation, we calculated the average accuracy of our initial model for each data set. Our initial model yielded a 75.72% average accuracy across both data sets. The average execution time of our initial model was 1,541.57 s for the Census Income data set and 50.54 s for the Heart Disease data set. We then optimized our model by applying MSD-Splitting, which discretizes continuous attributes by splitting them into four groups using the mean and the two values one standard deviation away from the mean as split points. The accuracy of our model improved by an average of 5.11% across both data sets, while the average execution time reduced by an average of 96.72% for the larger Census Income data set and 46.38% for the Heart Disease data set.

Keywords—C4.5 Algorithm; decision tree; data mining; machine learning; classification

I. INTRODUCTION

In machine learning, classification is a type of supervised learning with many useful applications, from catching spam emails [1] to categorizing tumor scans [2]. Classification problems analyze data sets containing a collection of records that each have a set of attributes and a class label. The task is to create a model that maps each record’s attribute set onto its class label. A classification model can be used for descriptive purposes by summarizing the attributes in a data set that correlate with a specific class label [3]. It can also be used for predictive purposes by classifying new records with unknown class labels [3].

There are many different ways to create a classification model based on a data set, but they all follow a similar approach. First, the data set must be split into a set of training data and a set of testing data. The training data is composed of records where the class label is included [4]. Each classification technique applies a different learning algorithm to the training data in order to build the classification model. Once the model is constructed, it is then applied to the testing data, which is composed of records where the class label is

removed [4]. The accuracy of the model can then be calculated by comparing the class labels predicted by the model to the actual class labels of the testing data.

There are two general types of attributes in a data set. Discrete attributes are composed of values from a finite or countably infinite set, such as the set of natural numbers or non-numeric values [5]. Continuous attributes are composed of values from an uncountably infinite set, such as the set of real numbers, which includes all decimal values [5]. Many learning algorithms can only use discrete attributes [6]. Thus, these algorithms must employ different methods to discretize continuous attributes. One such algorithm, the C4.5 decision tree algorithm, splits continuous attributes into two groups at a split point that minimizes the expected information requirement [7]. In order to do this, the C4.5 algorithm calculates the expected information requirement for each possible split point. However, this method is inefficient and can consume large amounts of time, especially when applied to large data sets [8].

In this paper, we propose an optimization of the C4.5 decision tree algorithm that discretizes continuous attributes using our novel technique called MSD-Splitting. We will show that our optimization significantly improves both the accuracy and efficiency of the C4.5 algorithm. This paper is structured as follows: Section 2 describes relevant related work. Section 3 details the steps of the standard C4.5 decision tree algorithm. Section 4 describes MSD-Splitting and how it optimizes the C4.5 algorithm. In Section 5, we discuss and compare the results of the standard C4.5 algorithm and our optimized C4.5 algorithm when applied to two different data sets. In Section 6, we summarize our findings and present our conclusion.

II. RELATED WORK

There has been an extensive amount of work done on the Census Income and Heart Disease data sets from UC Irvine’s Machine Learning Repository using various approaches. One work done by Chakrabarty and Biswas [9] applies the Gradient Booster Classifier Model to the Census Income data set and calculates its accuracy. Another work done by Hedeshi and Abadeh [10] applies a fuzzy-boosting PSO approach to the Heart Disease data set to detect coronary artery disease.

There has also been an extensive amount of work done on the C4.5 decision tree algorithm, including the calculation of its accuracy and efficiency when applied to various data sets. For instance, a work done by Budiman et al. [11] calculates the accuracy of the C4.5 algorithm when applied to a student

data set. Another work done by Chauhan and Chauhan [12] calculates the accuracy of the C4.5 algorithm when applied to data sets of various sizes, as well as data sets containing noisy or missing data. Hssina, Merbouha, Ezzikouri, and Erritali [13] calculated the efficiency of the C4.5 algorithm when applied to a data set describing weather by measuring execution time. However, none of these works offer an optimization of the C4.5 algorithm.

There are works done that do offer an optimization to either the accuracy or the efficiency of the C4.5 algorithm. A work done by Muslim, Nurzahputra, and Prasetyo [14] shows that the accuracy of the C4.5 algorithm can be improved by using the Split Feature Reduction Model and Bagging Ensemble. Agrawal and Gupta [8] showed that applying L'Hospital's Rule to the C4.5 algorithm improves its efficiency. Another work done by Yang and Chen [15] proposes a novel algorithm called Taiga that improves the efficiency of the C4.5 algorithm. However, these works do not offer an improvement to both the accuracy and efficiency of the C4.5 algorithm.

For this reason, we applied our novel technique of MSD-Splitting to the C4.5 algorithm in order to improve both the accuracy and efficiency of the algorithm. The efficiency of our optimized C4.5 algorithm improves from the efficiency of the standard C4.5 algorithm to a greater degree when applied to larger data sets. Since we created the technique of MSD-Splitting, there is currently no work in the literature that references it.

III. C4.5 DECISION TREE ALGORITHM

Decision tree induction is a common classification technique used to build models [16]. The learning algorithms that decision trees use differ in the methods that they employ to select the attribute that is used to split the records at a given point in the tree. Dr. Ross Quinlan was instrumental in the development of decision tree learning algorithms, inventing the widespread ID3 and C4.5 algorithms [17][18]. These two algorithms both select attributes using a concept called information gain [17][18]. We will now describe the steps of the standard C4.5 algorithm.

A. Information Gain

To determine which attribute to use to split the records in a given node, which is a point on the decision tree, information gain is calculated for all of the attributes, and the one with the highest information gain is selected [19]. Information gain is the expected drop in entropy after the records in a node are split using a certain attribute [19]. In other words, it is a measure of how much information the model gains from splitting the records in a node using a certain attribute. Information gain is calculated using the following formula [19]:

$$\text{Gain}(A) = \text{Entropy}(D) - \text{Entropy}_A(D) \quad (1)$$

where A is a given attribute in a data set D .

Entropy, which is the expected information needed to classify a record in a given node, is calculated using the following formula [19]:

$$\text{Entropy}(D) = - \sum_{i=1}^m p_i \log_2(p_i) \quad (2)$$

where m is the total number of classes and p_i is the probability that any given record in the node belongs to the class i .

Entropy_A, which is the information needed to classify the records in a given node after it is partitioned using a certain attribute, is calculated using the following formula [19]:

$$\text{Entropy}_A(D) = \sum_{j=1}^n p_j \cdot \text{Entropy}(D_j) \quad (3)$$

where n is the number of partitions, p_j is the probability that any given record in the node is in partition j , and D_j is the subset of records that are in partition j .

B. Gain Ratio

In Quinlan's ID3 algorithm, information gain was used exclusively to select splitting attributes [17]. However, the attribute selection method of using the highest information gain has an inherent bias towards attributes that have a larger number of different values, because these attributes will produce a larger number of outcomes to be summed when chosen as the splitting attribute [18]. Due to this issue, Quinlan invented the C4.5 algorithm, a successor of the ID3 algorithm, which optimizes the information gain calculation process [18]. In the C4.5 algorithm, the information gain calculation is normalized to account for the number of outcomes a particular attribute will produce [18]. This normalized attribute selection measure is known as gain ratio. Gain ratio is the ratio of the information gain of a certain attribute to its split information [20]. It is calculated using the following formula [20]:

$$\text{GainRatio}(A) = \text{Gain}(A) / \text{SplitInfo}(A) \quad (4)$$

where A is a given attribute in a data set D .

SplitInfo, which is used to normalize the information gain calculation, is calculated using the following formula [20]:

$$\text{SplitInfo}(A) = - \sum_{j=1}^n p_j \log_2(p_j) \quad (5)$$

where n is the number of partitions and p_j is the probability that any given record in the node is in partition j . Since SplitInfo increases as the number of partitions increases, it normalizes the information gain of attributes with a large number of partitions.

C. Splitting Continuous Attributes

As mentioned previously, the C4.5 algorithm can only use discrete attributes to classify a data set [6]. The C4.5 algorithm divides records based on discrete attributes by creating branches on the decision tree for each distinct value [18]. However, this is difficult with continuous attributes as there may be too many distinct values. Creating a branch on the decision tree for each distinct value can lead to overfitting, an error where a model is too specific to a particular set of data, causing it to perform poorly when given new, unseen data [21]. The standard C4.5 algorithm addresses this problem by splitting continuous attributes into two groups at an ideal split point [18]. The set of possible split points is given by the set of the midpoints between any two adjacent values in the attribute. The ideal split point for a given continuous attribute is the point

with the minimum expected information requirement [7]. The expected information requirement calculation is equivalent to the Entropy_A calculation [19].

D. Decision Tree Building

Building the decision tree is a recursive process, as shown in Fig. 1. First, all of the records in the training data are placed in the top node, or the root node, of the decision tree. The attribute with the highest gain ratio is chosen as the first splitting attribute [22]. Once the data set is split into different nodes based on the first attribute, each node is then split based on the attribute with the highest gain ratio when applied to the data in the node. Each node is given a majority label based on the class label of the majority of the records in the node [22]. This process is continued until one of the three stopping conditions is met: 1) all of the records in the node belong to the same class; 2) the node is empty; 3) none of the attributes provide any further information gain [22]. Once a stopping condition is met, the final node is considered a leaf and is given a class label [22]. Once every record in the data set is placed into a leaf, the decision tree building process is complete.

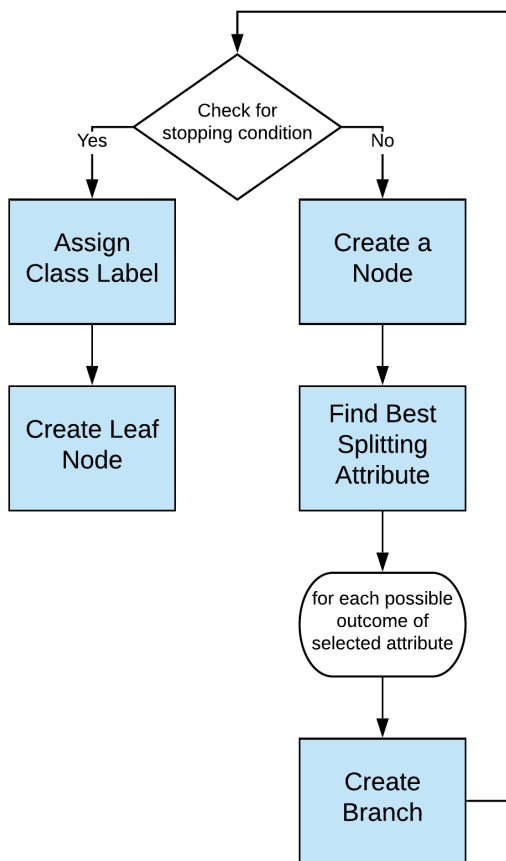


Fig. 1. Flowchart of the Recursive C4.5 Decision Tree Building Algorithm.

As an example, Fig. 2 shows the top two levels of our decision tree for the Heart Disease data set. Our model calculated that the ‘Chest Pain’ attribute yielded the highest gain ratio for the root node, which is why it was chosen as the

first splitting attribute. Then, we can see that four new nodes were created based on the values of the ‘Chest Pain’ attribute. We can also see that for each node, our model chose different attributes as the next splitting attribute. These attributes were chosen because they yielded the highest gain ratio for their respective nodes.

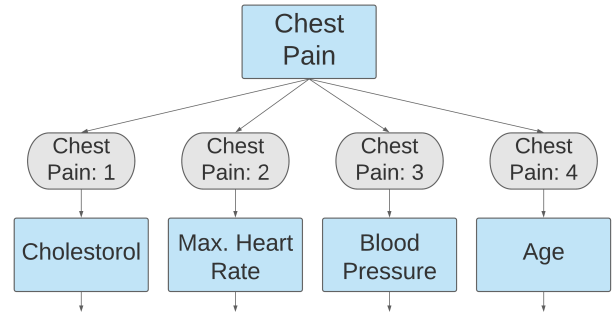


Fig. 2. Our Decision Tree for the Heart Disease Data Set.

Fig. 3 shows a segment of the bottom end of a generic decision tree. Leaves are created when one of the stopping conditions is met. They can be created on different levels of the decision tree.

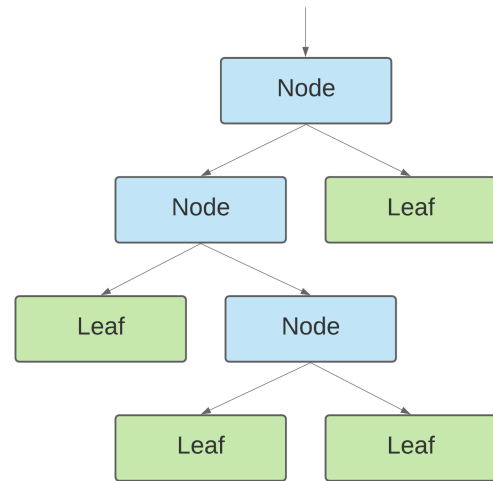


Fig. 3. Generic Diagram of Decision Tree Leaves.

In practice, the records in a leaf are not always guaranteed to have the same class label. For instance, the records in a leaf may still consist of different class labels while none of the attributes provide further information gain. In this case, the leaf is labeled with the class label of the majority of the records in the leaf [22].

E. Classifying New Data

Once the decision tree is built, it can be used to classify new, unclassified data [16]. Each new record is passed through the tree and branched at each node based on its attribute values until it is finally classified into a leaf [23]. The record is then labeled with the class label of the leaf. If the record reaches a

node that does not contain a branch for the record's attribute value, the record is labeled with the majority label of the node [22].

IV. MSD-SPLITTING

We will now describe MSD-Splitting and how it improves the accuracy and efficiency of the C4.5 algorithm. MSD-Splitting is short for Mean and Standard Deviation Splitting. The mean (μ) of an attribute is the average of its values. It is calculated using the following formula [24]:

$$\mu = \frac{\sum_{i=1}^n x_i}{n} \quad (6)$$

where x_i is the i -th value and n is the total number of values in the attribute.

The standard deviation (σ) of an attribute is a measure of the dispersion of its values. It is calculated using the following formula [25]:

$$\sigma = \sqrt{\frac{\sum_{i=1}^n (x_i - \mu)^2}{n}} \quad (7)$$

where x_i is the i -th value, μ is the mean, and n is the total number of values in the attribute.

Thus, we can write the two values that are one standard deviation away from the mean as

$$\mu - \sigma, \mu + \sigma$$

where μ is the mean and σ is the standard deviation of the attribute.

Standard deviation is important because it measures the typical dispersion of the values in the attribute [25]. Thus, values within one standard deviation away from the mean can be considered to have a lower than typical deviation, while values more than one standard deviation away from the mean can be considered to have a higher than typical deviation.

MSD-Splitting splits each continuous attribute into four groups, using its mean (μ) and the values one standard deviation away from the mean ($\mu - \sigma$, $\mu + \sigma$) as logical split points. A value x in the attribute is binned into one of four groups, which are defined as follows:

- 1) $x < \mu - \sigma$: below mean, high deviation
- 2) $\mu - \sigma \leq x < \mu$: below mean, low deviation
- 3) $\mu \leq x < \mu + \sigma$: above/at mean, low deviation
- 4) $x \geq \mu + \sigma$: above mean, high deviation

The values in each of these four groups are estimated to share a similar deviation and to be closely related to each other. The four groups are labeled on the graph of a normal distribution in Fig. 4.

A. Application to the C4.5 Algorithm

The standard C4.5 algorithm splits continuous attributes into two groups by choosing one split point with the minimum expected information requirement [7]. However, this process is often inaccurate and inefficient. The two groups will likely provide little information gain because the values in each of the two groups are not likely to be closely related to each other. Attributes with low information gain are detrimental to

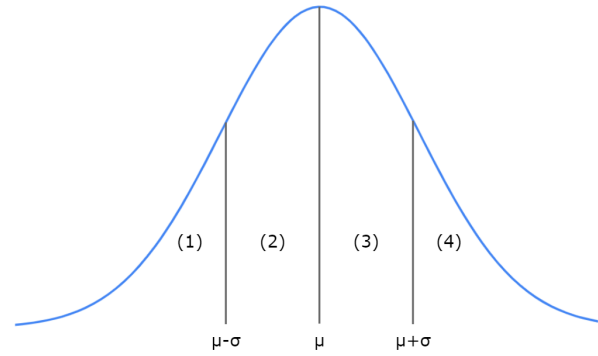


Fig. 4. Four Groups Created by MSD-Splitting on the Graph of a Normal Distribution.

the overall accuracy of the model [26]. Furthermore, iterating through every possible split point in a large data set and calculating the expected information requirement for each point can consume large amounts of time [8].

Our optimized C4.5 algorithm instead splits continuous attributes using MSD-Splitting. By doing so, we improve both the accuracy and efficiency of the C4.5 algorithm.

B. Effect on Accuracy

Increasing the number of groups into which the values are binned means that the values in each group will generally be more closely related to each other [27]. Splitting continuous attributes using MSD-Splitting doubles the number of groups from two to four. The values in each of the four groups are likely to be more closely related to each other than the values in each of the two groups created by the standard C4.5 algorithm. It is then likely that the discretized attributes will provide higher information gain when it is discretized using MSD-Splitting rather than using the standard C4.5 algorithm's method. Attributes with higher information gain improve the overall accuracy of the classification model [26].

Furthermore, since the groups are created using logical split points that group values with low deviation together and values with high deviation together, we estimate that the values in each group will be even more closely related to each other. Thus, the discretized attributes are even more likely to provide higher information gain [28], improving the overall accuracy of the model.

C. Effect on Efficiency

Discretizing continuous attributes using MSD-Splitting can significantly improve the efficiency of the C4.5 algorithm, especially when it is applied to large data sets. The standard C4.5 algorithm iterates through each possible split point and calculates its expected information requirement. The expected information requirement calculation, which is equivalent to Equation 3, has a linear time complexity [29]. Then, running this calculation for every possible split point has a quadratic time complexity, or a time complexity of $O(n^2)$. On the other hand, finding the split points for the MSD-Splitting method only requires the calculation of the attribute's mean and standard deviation, which has a linear time complexity, or

TABLE I. ACCURACY OF INITIAL AND OPTIMIZED MODELS

Data Set Group	Accuracy of Initial Model (%)	Accuracy of Optimized Model (%)	% Change
Census Income_1234_test5	78.64	80.49	+2.35%
Census Income_1235_test4	78.46	81.28	+3.59%
Census Income_1245_test3	79.84	81.57	+2.17%
Census Income_1345_test2	78.13	81.20	+3.93%
Census Income_2345_test1	79.16	81.94	+3.51%
Census Income Average	78.85	81.30	+3.11%
Heart Disease_1234_test5	67.21	73.77	+9.76%
Heart Disease_1235_test4	73.77	78.69	+6.67%
Heart Disease_1245_test3	80.33	81.97	+2.04%
Heart Disease_1345_test2	63.33	66.67	+5.27%
Heart Disease_2345_test1	78.33	88.33	+12.77%
Heart Disease Average	72.59	77.89	+7.29%
Overall Average	75.72	79.59	+5.11%

TABLE II. EXECUTION TIME OF INITIAL AND OPTIMIZED MODELS

Data Set Group	Exec Time of Initial Model (s)	Exec Time of Optimized Model (s)	% Change
Census Income_1234_test5	1567.50	48.40	-96.91%
Census Income_1235_test4	1575.55	50.98	-96.76%
Census Income_1245_test3	1569.91	48.74	-96.90%
Census Income_1345_test2	1456.98	53.30	-96.34%
Census Income_2345_test1	1537.94	51.30	-96.66%
Census Income Average	1541.57	50.54	-96.72%
Heart Disease_1234_test5	0.04379	0.02660	-39.25%
Heart Disease_1235_test4	0.03903	0.01905	-51.20%
Heart Disease_1245_test3	0.04052	0.02186	-46.06%
Heart Disease_1345_test2	0.03790	0.01968	-48.09%
Heart Disease_2345_test1	0.04137	0.02146	-48.12%
Heart Disease Average	0.04052	0.02173	-46.38%

a time complexity of $O(n)$. Since $O(n)$ is more efficient than $O(n^2)$, we can see that MSD-Splitting improves the efficiency of the C4.5 algorithm. The improvement in efficiency will be greater for larger data sets due to the quadratic time complexity of the standard C4.5 algorithm's method of finding the ideal split point, which grows at a faster rate as the number of values and possible split points increases [30].

V. EXPERIMENTAL RESULTS

We ran both the standard C4.5 algorithm and our optimized C4.5 algorithm with MSD-Splitting on two data sets obtained from UC Irvine's Machine Learning Repository: Census Income, used to predict whether a person's income exceeds \$50,000 per year, and Heart Disease, used to predict whether a person has heart disease [31]. The Census Income data set contains 48,842 records and 14 attributes, while the Heart Disease data set contains 303 records and 76 attributes. We worked with the commonly used Cleveland subset of the Heart Disease data set with 14 attributes. In our initial model, we applied the standard C4.5 algorithm to both data sets, splitting continuous attributes by minimizing the expected information requirement. In our optimized model, we applied our optimized C4.5 algorithm with MSD-Splitting. We then calculated the accuracy and efficiency of our initial and optimized models.

A. Accuracy

To calculate the accuracy of our two models, we split both data sets into five groups and performed five-fold cross-validation for each data set where we ran both models on each data set five times, using one of the groups as the testing data and the other four groups as the training data for each trial [32]. The first trial used the first group of the data set as the testing data, the second trial used the second group as the testing data, and so on. We then averaged the results of each of the five trials to obtain the accuracy of our two models for each data set.

Table I displays the accuracy of our initial and optimized models applied to the Census Income and Heart Disease data sets. The table also displays the % change in accuracy between our two models for each data set.

B. Efficiency

To calculate the efficiency of our two models, we measured the average execution time of both models for each data set, where a low execution time equals high efficiency and a high execution time equals low efficiency. We calculated average execution time using the same five-fold cross-validation technique that we used to calculate the accuracy of our two models.

Table II displays the execution time of our initial and optimized models applied to the Census Income and Heart Disease data sets. The table also displays the % change in execution time between our two models for each data set.

Since the Census Income data set is significantly larger than the Heart Disease data set, the difference between the execution time of our initial model and our optimized model is significantly greater for the Census Income data set than for the Heart Disease data set. This is due to the behavior of the previously mentioned quadratic time complexity of our initial model [30]. In order to account for the different sizes of the data sets, we must compare the efficiency of our two models separately for each data set. Since the overall average execution time and the overall average % change in execution time between our two models do not provide any meaningful information, we chose not to display this information.

C. Discussion

We can see that the overall average accuracy of our initial model is 75.72%, while the overall average accuracy of our optimized model is 79.59%. We can calculate that our optimized model has a 5.11% increase in accuracy from our initial model. Since the only portion of the C4.5 algorithm that was changed between our two models was the method of splitting continuous attributes, we can conclude that splitting continuous attributes using MSD-Splitting rather than by minimizing the expected information requirement increases the accuracy of the C4.5 algorithm.

Our optimized model has a 96.72% decrease in execution time from our initial model when applied to the Census Income data set, compared to a smaller 46.38% decrease when applied to the Heart Disease data set.

Since the execution time of the standard C4.5 algorithm's method of finding the ideal split point increases quadratically with the number of values and possible split points, our initial model takes significantly longer to run when applied to data sets that have continuous attributes with many distinct values. Larger data sets tend to have more distinct values in their continuous attributes than smaller data sets. Thus, our initial model has a longer execution time when applied to larger data sets. While the execution time of the standard C4.5 algorithm's method of finding the ideal split point increases quadratically, the execution time of our optimized C4.5 algorithm's method of finding the split points only increases linearly. This explains why the efficiency of our optimized model improves from the efficiency of our initial model to a greater degree when applied to the larger Census Income data set than when it is applied to the smaller Heart Disease data set.

Again, since the only portion of the C4.5 algorithm that was changed between models was the method of splitting continuous attributes, we can conclude that splitting continuous attributes using MSD-Splitting rather than by minimizing the expected information requirement increases the efficiency of the C4.5 algorithm, especially when applied to larger data sets.

VI. CONCLUSION

In this paper, we described our novel technique of MSD-Splitting and how it improves the accuracy and efficiency of the

C4.5 decision tree algorithm. In our initial model, we applied the standard C4.5 algorithm to two different data sets. Then, in our optimized model, we applied our optimized C4.5 algorithm with MSD-Splitting to the same two data sets. After calculating the accuracy and efficiency of our initial and optimized models, we can conclude that splitting continuous attributes using MSD-Splitting significantly improves the accuracy of the C4.5 algorithm. We can also conclude that MSD-Splitting significantly improves the efficiency of the C4.5 algorithm, especially when applied to large data sets. This is because the execution time of the standard C4.5 algorithm has a quadratic time complexity, while our optimized C4.5 algorithm with MSD-Splitting has a more efficient linear time complexity. Since the increase in execution time of the standard C4.5 algorithm grows faster as the size of the data set increases, our optimized C4.5 algorithm will have an even greater improvement in efficiency from the standard C4.5 algorithm when applied to data sets that are even larger than the ones that we used. For this reason, we believe that our optimized C4.5 algorithm with MSD-Splitting is ideal for classification tasks involving extremely large data sets.

Classifying data sets is critically important in the increasingly consequential fields of data mining and machine learning. As the amount of data that we create grows exponentially [33], we must be able to extract and interpret useful information from this data as accurately and efficiently as possible. By optimizing the widespread C4.5 decision tree algorithm, we refine and expedite the data classification process.

ACKNOWLEDGMENT

This research was conducted at California State University, Fullerton. We would like to thank our research supervisor Dr. Shawn X. Wang, professor of computer science at California State University, Fullerton, for providing invaluable guidance and support.

REFERENCES

- [1] E. G. Dada, J. S. Bassi, H. Chiroma, S. M. Abdulhamid, A. O. Adetunmbi, and O. E. Ajibuwa, "Machine learning for email spam filtering: review, approaches and open research problems," *Heliyon*, vol. 5, no. 6, Jun. 2019.
- [2] T. T. Tang, J. A. Zawaski, K. N. Francis, A. A. Qutub, and M. W. Gaber, "Image-based Classification of Tumor Type and Growth Rate using Machine Learning: a preclinical study," *Scientific Reports*, vol. 9, no. 1, Aug. 2019.
- [3] J. L. Rastrollo-Guerrero, J. A. Gómez-Pulido, and A. Durán-Domínguez, "Analyzing and Predicting Students' Performance by Means of Machine Learning: A Review," *Applied Sciences*, vol. 10, no. 3, p. 1042, Feb. 2020.
- [4] M. A. Shafique and E. Hato, "Formation of Training and Testing Datasets, for Transportation Mode Identification," *Journal of Traffic and Logistics Engineering*, vol. 3, no. 1, Jun. 2015.
- [5] J. Han, M. Kamber, and J. Pei, "2 - Getting to Know Your Data," in *Data Mining*, 3rd ed., Morgan Kaufmann, 2012, pp. 39–82.
- [6] U. M. Fayyad and K. B. Irani, "On the handling of continuous-valued attributes in decision tree generation," *Machine Learning*, vol. 8, no. 1, pp. 87–102, 1992.
- [7] J. R. Quinlan, "Improved Use of Continuous Attributes in C4.5," *Journal of Artificial Intelligence Research*, vol. 4, pp. 77–90, Mar. 1996.
- [8] G. L. Agrawal and H. Gupta, "Optimization of C4.5 Decision Tree Algorithm for Data Mining Application," *International Journal of Emerging Technology and Advanced Engineering*, vol. 3, no. 3, Mar. 2013.

- [9] N. Chakrabarty and S. Biswas, "A Statistical Approach to Adult Census Income Level Prediction," *2018 International Conference on Advances in Computing, Communication Control and Networking (ICACCCN)*, Oct. 2018.
- [10] N. G. Hedeshi and M. S. Abadeh, "Coronary Artery Disease Detection Using a Fuzzy-Boosting PSO Approach," *Computational Intelligence and Neuroscience*, pp. 1–12, Apr. 2014.
- [11] E. H. Budiman, H. H. Haviluddin, N. H. Dengan, A. H. Kridalaksana, M. H. Wati, and Purnawansyah, "Performance of Decision Tree C4.5 Algorithm in Student Academic Evaluation," *Lecture Notes in Electrical Engineering*, Feb. 2018.
- [12] H. Chauhan and A. Chauhan, "Implementation of decision tree algorithm c4.5," *International Journal of Scientific and Research Publications*, vol. 3, no. 10, Oct. 2013.
- [13] B. Hssina, A. Merbouha, H. Ezzikouri, and M. Erritali, "A comparative study of decision tree ID3 and C4.5," *International Journal of Advanced Computer Science and Applications (IJACSA), Special Issue on Advances in Vehicular Ad Hoc Networking and Applications*, Jun. 2014.
- [14] M. A. Muslim, A. Nurzahputra, and B. Prasetyo, "Improving accuracy of C4.5 algorithm using split feature reduction model and bagging ensemble for credit card risk prediction," *2018 International Conference on Information and Communications Technology (ICOIACT)*, Mar. 2018.
- [15] Y. Yang and W. Chen, "Taiga: performance optimization of the C4.5 decision tree construction algorithm," *Tsinghua Science and Technology*, vol. 21, no. 4, pp. 415–425, Aug. 2016.
- [16] R. H. A. Alsagheer, A. F. H. Alharan, and A. S. A. Al-Haboobi, "Popular Decision Tree Algorithms of Data Mining Techniques: A Review," *International Journal of Computer Science and Mobile Computing*, vol. 6, no. 6, pp. 133–142, Jun. 2017.
- [17] J. R. Quinlan, "Induction of decision trees," *Machine Learning*, vol. 1, no. 1, pp. 81–106, Mar. 1986.
- [18] S. L. Salzberg, "C4.5: Programs for Machine Learning by J. Ross Quinlan. Morgan Kaufmann Publishers, Inc., 1993," *Machine Learning*, vol. 16, no. 3, pp. 235–240, Sep. 1994.
- [19] S. Singh and P. Gupta, "Comparative Study ID3, CART, and C4.5 Decision Tree Algorithm: A Survey," *International Journal of Advanced Information Science and Technology (IJAIST)*, vol. 27, Jul. 2014.
- [20] A. Rizka, S. Efendi, and P. Sirait, "Gain ratio in weighting attributes on simple additive weighting," *IOP Conference Series: Materials Science and Engineering*, Oct. 2018.
- [21] R. Jothikumar and B. R. V. Siva, "C4.5 classification algorithm with back-track pruning for accurate prediction of heart disease," *Biomedical Research*, 2016.
- [22] P. Tan, M. Steinbach, A. Karpatne, and V. Kumar, "Chapter 4: Classification: Basic Concepts, Decision Trees, and Model Evaluation," in *Introduction to Data Mining*, Pearson Addison-Wesley, 2006.
- [23] H. Sharma and S. Kumar, "A Survey on Decision Tree Algorithms of Classification in Data Mining," *International Journal of Science and Research (IJSR)*, vol. 5, no. 4, pp. 2094–2097, Apr. 2016.
- [24] H. Hassani, M. Ghodsi, and G. Howell, "A note on standard deviation and standard error," *Teaching Mathematics and its Applications*, May 2010.
- [25] P. J. Barde and M. P. Barde, "What to use to express the variability of data: Standard deviation or standard error of mean?," *Perspectives in Clinical Research*, vol. 3, no. 3, pp. 113–116, 2012.
- [26] D. Rajeshingo and J. P. A. Jebamalar, "Accuracy Improvement of C4.5 using K means Clustering," *International Journal of Science and Research (IJSR)*, 2015, ISSN 2319-7064.
- [27] D. G. Altman and P. G. Royston, "The cost of dichotomising continuous variables," *BMJ Statistics Notes*, May 2006.
- [28] H. Dag, K. E. Sayin, I. Yenidogan, S. Albayrak, and C. Acar, "Comparison of feature selection algorithms for medical data," *2012 International Symposium on Innovations in Intelligent Systems and Applications*, Jul. 2012.
- [29] J. Su and H. Zhang, "A Fast Decision Tree Learning Algorithm," *AAAI'06: Proceedings of the 21st national conference on Artificial intelligence*, vol. 1, pp. 500–505, Jul. 2006.
- [30] E. A. Graf, J. H. Fife, H. Howell, and E. Marquez, "The Development of a Quadratic Functions Learning Progression and Associated Task Shells," *ETS Research Report Series*, vol. 2018, no. 1, pp. 1–28, Dec. 2018.
- [31] B. Becker and R. Detrano, *UCI Machine Learning Repository*, 1996. [Online]. Available: <http://archive.ics.uci.edu/ml>.
- [32] R. Kohavi, "A study of cross-validation and bootstrap for accuracy estimation and model selection," *IJCAI'95: Proceedings of the 14th international joint conference on Artificial intelligence*, vol. 2, pp. 1137–1143, Aug. 1995.
- [33] R. Devakunchari, "Analysis on big data over the years," *International Journal of Scientific and Research Publications*, vol. 4, no. 1, Jan. 2014.

Extraction of Keywords for Retrieval from Paper Documents and Drawings based on the Method of Determining the Importance of Knowledge by the Analytic Hierarchy Process: AHP

Kohei Arai
Saga University, Saga city
Japan

Abstract—Extraction method of keywords for retrieval from paper documents and drawings based on the method of determining the importance of knowledge by the Analytic Hierarchy Process: AHP method is proposed. The method allows distinguish the documents into three categories, letter, form and drawing types of documents, then the most appropriate knowledge about keyword for retrievals, font size, location, frequency of the words etc. are selected for each document type. Production rules are created with more than five of the knowledge on keywords for retrievals. Traditional production system employs isolated knowledge so that it is not easy to take overall suitability of the knowledge. In order to overcome this situation, AHP is employed in the proposed system. Through experiments with 100 documents and diagrams, 98% success rate is achieved, and it is found that appropriate candidates for keywords with likelihood or certainty factor can be extracted with the proposed system. The proposed production system shows 50% of improvement on success rate of the keywords extraction from documents and diagrams compared to the existing production system without AHP.

Keywords—AHP method; extraction keywords; production rule system; document/diagram recognitions; certainty factor

I. INTRODUCTION

Currently, iDC (internet Data Center) development is in progress, which manages a large amount of printed media such as paper and handwritten documents, drawings, etc. in a database so that they can be searched and published on electronic media etc. [1]. Generally, for paper media documents, the operator inserts the search keyword as a handwritten page, converts this page into an electronic medium with a scanner, and registers it.

Regarding the automatic generation of keywords from paper documents etc., the documents are limited to business documents, and are roughly classified into letters and form documents. In the former case, search keywords are used by using the knowledge of the position of the title character string in the layout. It has been proposed that the operator manually extract the data in the form of a table document, etc. [2]-[5]. On the other hand, the method of extracting the search keyword from the digital document after conversion to the electronic medium is as follows: (1) layout related to the position of the document title, (2) character font type, size, (3)

appearance frequency, (4) character. There are methods [6]-[12] that use knowledge about the part of speech and importance of the words in the sequence. A method has also been proposed in which a semantic tag is added to a word to associate it with an ontology class and attribute items and to make it a keyword [13].

In this paper, the author classifies paper documents into letters, forms, and drawings, and propose a keyword extraction method for them. That is, a method of converting an image obtained by a scanner into HTML format, extracting layout information, decomposing words in a character string into parts of speech, and extracting a search keyword by using position, font size, and appearance frequency as knowledge. Is proposed. At this time, the importance of these knowledge varies depending on the document format, and in order to take this into account, the hierarchical analysis method (Analytic Hierarchy Process: AHP) [14] is used. Introducing a decision-making method with AHP to grasp a large amount of knowledge in a production system as a knowledge-based system [15] and constructed a system for extracting search keywords from paper documents, etc., and using real documents and drawings. As a result of testing, it was confirmed that the search keyword could be extracted efficiently, so the author reports here.

The next section describes the related research works on extraction method followed by the proposed method for extraction of keywords. After that some experiments are described followed by conclusion with some discussions together with future research works.

II. RELATED RESEARCH WORKS

Method for real time text extraction of digital manga comic is proposed [17]. On the other hand, extraction of line features from multifidus muscle of CT scanned images with morphological filter together with wavelet multi resolution analysis is proposed [18]. Meanwhile, method for extraction product information from TV commercial is proposed [19] together with text extraction from TV commercial using blob extraction method [20].

Eye-based human-computer interaction allowing phoning, reading e-book/e-comic/e-learning, Internet browsing and TV

information extraction is proposed [21]. Also, method for automatic e-comic scene frame extraction for reading comic on mobile devices is proposed [22] together with method for information extraction from Japan TV commercial [23]. Furthermore, automatic information extraction from on-air TV commercial contents is proposed and well reported [24].

III. PROPOSED METHOD

A. Basic Ideas of the Proposed Method

In the conventional method, first, an operator extracts a keyword for search based on knowledge and experience, writes the keyword on a separate sheet, attaches it to a target paper medium document, etc., and converts it into an image file by a scanner or the like. After that, character recognition is performed. The target paper media document etc. is registered in the database as an image file or in a text file format after recognition. At that time, a keyword is added as a result of recognizing the handwritten character entered on the keyword form. In addition, the attribute information for retrieval is made into a database as metadata. This method involves operator work, is inefficient, and has the problem that the validity and integrity of keywords based on the subjectivity of the operator cannot be maintained.

The proposed method minimizes the intervention of the operator and is designed so that the keywords for retrieval are automatically extracted from the documents, drawings, etc. existing on paper media, the database is constructed, and the retrieval is possible. First, convert a paper medium document into an image file with a scanner etc., classify the document into letters, forms and drawings according to a uniquely developed program, extract layout and font size information, and perform character recognition. Convert to HTML format by using the result (text format). After that, the text format sentences are converted into "divided" sentences using morphological analysis software [11], [12] ChaSen, and parts of speech are given to the words. ChaSen is a free Japanese morphological analyzer released from Nara Institute of Science and Technology Graduate School of Natural Language Processing on February 19, 1997. It analyzes the input Japanese, decomposes it into words, and returns the reading and part of speech of the words. ChaSen can also be used for full-text search, addition of phonetic alphabets, and extraction of specific parts of speech.

Next, the position of the character string, the font size, and the frequency of appearance of words are checked from the file after HTML conversion, and the most suitable keyword for the document etc. is extracted by the production system. At that time, in the knowledge base system, AHP is used in order to consider that the importance of these knowledge differs depending on the document format.

B. Document Format

The author selected 100 types of target documents (letter format: 35, form format: 35, drawing format: 30) including paper media business documents and drawings. Drawings can be identified using the number of characters as an index, and the form format that includes many tables has many line segments such as ruled lines and many characters, and the letter format has few line segments and many characters,

making the document 3 It can be easily classified into any of the types.

In the case of letter format documents, the document title is often used as a search keyword, and the position where it appears, and the font size are important. Next to them, the appearance frequency of the relevant keyword is important. Also, in form-based documents, titles often appear in the table, the position where the document title appears and the frequency of its appearance are important, and the font size is not so important. On the other hand, in the case of drawings, the position of the document title is the most important, the font size is not so important, and the appearance frequency is not so important because the number of characters is small. In other words, the importance of knowledge when extracting search keywords differs depending on the document format.

C. Optimal Knowledge Importance Setting for Document Format

Based on the AHP, we examined the method of considering knowledge importance in advance. We optimized the setting of the importance level of the knowledge keyword based on the target document and 100 document formats described above and estimated the evaluation items required for this in advance. AHP is a problem-solving decision-making method that makes good use of subjective judgment and system approach in problem analysis. When one answer must be extracted from intricately entangled elements, there is a risk of overlooking an important element if it is divided too simply, and it is difficult to flexibly use it with an overly complicated method. Become. Therefore, AHP was born as a method for incorporating many elements in a well-balanced manner and making decisions.

AHP expresses the elements related to decisions in a hierarchical structure. Based on a certain criterion, the evaluation of options is judged hierarchically, and finally all layers are integrated to decide. This procedure is shown below.

1) *Extraction of elements of evaluation items and hierarchy of knowledge for decision making:* One element of the purpose of decision making, multiple elements of evaluation items for objective evaluation, and multiple alternatives for the purpose are prepared. In this paper, we set the importance of knowledge (weighting factor) as the purpose, the font size, the position of the character string and the appearance frequency as the evaluation item elements, and the size of these evaluation item elements as the alternatives. The top layer is the target element, the evaluation layer is the evaluation element for decision making, and the bottom layer is an alternative plan.

2) *Evaluation of the degree of influence of elements in the evaluation layer:* The target document is presented to 10 subjects, and the optimum word is selected as a search keyword, and the knowledge used when selecting the keyword, that is, the degree of influence of the evaluation item element (importance) I got a score from 0 to 1.

3) *One-to-one comparison between elements in each hierarchy:* Select a pair for each layer and perform a one-to-one comparison. If there are n comparison elements in the hierarchy, then $n(n-1) / 2$ one-to-one comparisons will be

performed. The elements in the same hierarchy are compared using a one-to-one comparison table, and the one-to-one comparison matrix shown in Table 1 is created. After that, a one-to-one comparison of the evaluation item hierarchy is performed, and the relative importance between the elements is calculated.

4) *Calculating importance between elements in each hierarchy:* Appendix 1 shows the algorithm for obtaining the weighting factors between elements in each layer.

5) *Consistency check in one-to-one comparison:* In the one-to-one comparison, the inconsistency of the results occurs as the number of elements increases. Therefore, it is necessary to check this consistency. This method is shown in Appendix 2.

6) *Calculating relative importance of the entire hierarchy and determining alternatives:* A one-to-one comparison between the objective evaluation items and each alternative is made. Then, using the weighting factors found at each layer, the optimal alternative is found from the alternatives.

TABLE I. ONE-TO-ONE COMPARISON ON THE EVALUATION ITEM LAYER

	Font Size	Y Position	X Position	Frequenc y	Relative Importance
Font Size	1	2	3	4	0.47
Y Position	1/2	1	2	3	0.28
X Position	1/3	1/2	1	2	0.16
Frequency	1/4	1/3	1/2	1	0.09

D. Construction of Knowledge Base for Search Keyword Extraction

Build a production system for extracting search keywords based on AHP in advance. In this section, we will take up the example of a target document in the “drawing format”, which has not been tried so far, and show how to determine the importance and certainty of knowledge based on AHP. Fig. 1 shows an example of the target document. As illustrated, the characteristic of drawing-format documents is that the number of line segments is large and the number of characters is small. The top layer of the AHP is the purpose, the importance (weighting coefficient), and the evaluation items of the middle layer are the font size, vertical and horizontal position, and appearance frequency. Also, the alternatives of the bottom layer are of high and low importance.

1) *Evaluation items (knowledge about keyword candidates):* In order to extract keyword candidates from the extracted multiple character areas, the following knowledge is effective. (1) Keywords are larger than other characters (Fontsize). (2) The positions with keywords are often left, middle, right (X Position) and vertical (Y Position) in the drawing. (3) Keywords appear frequently in the drawing (Frequency). The evaluation item values (Fontsize, Y Position, X Position, Frequency) of these knowledges are extracted as follows.

a) *Regarding font size (Fontsize) and position information (Y Position, X Position),* the target document was read by a scanner, and converted into HTML language as layout information and extracted by a unique program.

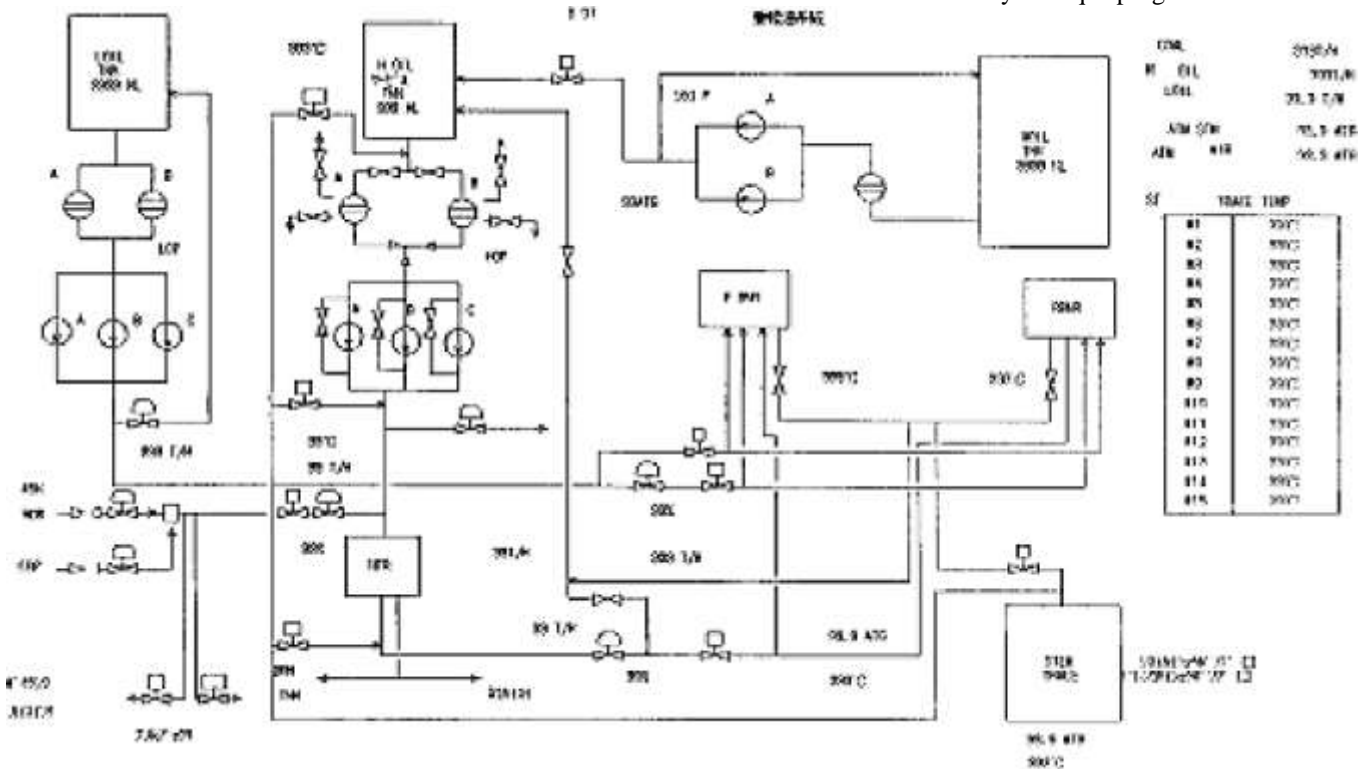


Fig. 1. An Example of the Drawing Diagram Documents.

b) The frequency was extracted by character recognition, converting it to text, and then using the morphological analysis software ChaSen described above to examine the frequency of the "divided words".

2) Impact of evaluation items: The target document in the drawing format was presented to 10 subjects, and the importance or impact of the evaluation items shown in 1) was specified in a 10-point scale from 0 to 1, and the font size : 0.98, frequency of occurrence: 0.98, vertical position: 0.694, horizontal position: 0.23 were found to be the average degree of influence.

3) Knowledge base design: Knowledge of the proposed method is expressed in the form of the production rule "IF then THEN". As for the knowledge of the proposed method, the evaluation item state of the evaluation item such as "the size of Fontsize" was described in the condition part, and the keyword part was described in the consequent part. That is, "IF Fontsize is Big THEN is a keyword in confidence CF". At this time, the evaluation item to be used is to obtain the certainty factor in consideration of the relative importance determined in advance according to each document format. Also, in the knowledge of the proposed method, only the form of logical sum is used in which multiple knowledges with unequal condition parts derive the same consequent part.

4) Certainty factor: One of the features of the production system is that it makes it possible to handle uncertain knowledge by imposing a weighting factor called certainty factor on each knowledge. In this paper, the certainty factor is defined as an index that expresses the degree to which the consequent part can be derived by the condition part in a certain knowledge rule. The range of this value is ± 1 , and when 0 means that the conditional part is not taken into consideration when deriving the consequent part. Negative means a degree of negative consequent derivation, and positive means a degree to support consequent derivation. At this time, the certainty factor was obtained based on the relative importance obtained by AHP. Fig. 2 shows the process steps from knowledge representation and input of the target document to determination of certainty factor. The procedure is shown below.

a) To determine the certainty factor, the purpose of the uppermost layer of the AHP hierarchical structure was to calculate the importance of knowledge, and the evaluation items were Fontsize, X Position, Y Position, and Frequency. In the alternative layer, which is the lowest layer, Big is used when the Fontsize is large, Y Position and X Position are close to the place where importance is considered, and when there is a lot of Frequency in each evaluation item, and Small is used.

Regarding X Position and Y Position, to determine which position in the layout of the character string is important, the document is divided into 5 parts vertically and horizontally, and the positions are A (the end) and B. It is represented by a fuzzy set with (somewhat end), C (middle), D (somewhat end), and E (most end). Fig. 3 shows the membership function. Also, by using the knowledge that the position of a

keyword in the target document is often left, right, upper, or lower in the drawing, A or C or E> for each of the position importance evaluation items, X Position, and Y Position. B or D.

E. Example of Calculation Result of Relative Importance by AHP of Target Document in Letter Format

Table 1 shows the weighting factors (relative importance) of the evaluation items calculated by one-to-one comparison based on AHP. In the case of letter format, 10 subjects were judged to be important for keyword selection in the order of font size, vertical position, horizontal position, and appearance frequency. Therefore, the one-to-one comparison table (matrix) of the evaluation item hierarchy is arranged in the order of Fontsize, Y Position, X Position, and Frequency, and their order numbers are the matrix elements in the first row. Since the element (i, j) of this matrix is the reciprocal of the element (j, i), all elements are obtained as shown in Table 1. This matrix can be used to determine A in Eq. (1), and the eigenvalues and eigenvectors for this can be found to calculate the relative importance in Table 1.

Tables 2 to 5 show the one-to-one comparison results of each alternative for each evaluation item.

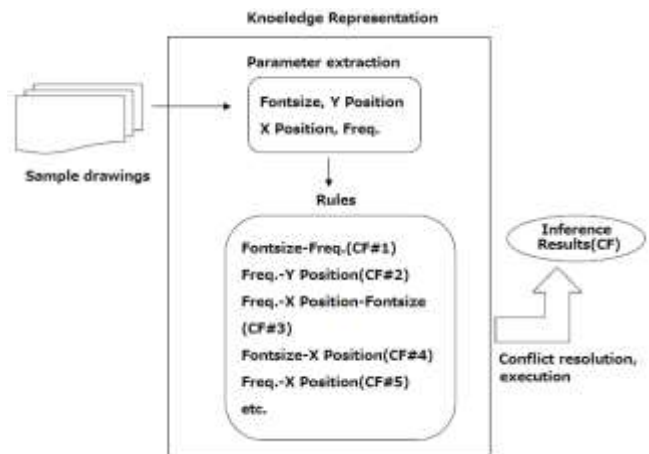


Fig. 2. Process Flow of the Proposed Method and the Relation between Confidential Factors and Knowledge Representations.

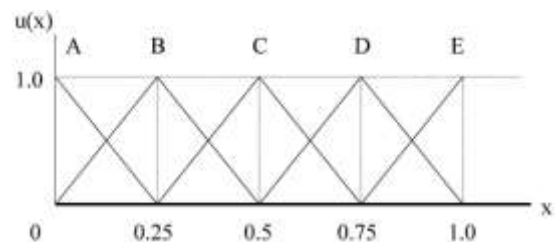


Fig. 3. Membership Function of the Fuzziness on the Location at which the Keywords for Document Retrievals Appear.

TABLE II. ONE-TO-ONE COMPARISON ON THE ALTERNATIVES ON "FONT SIZE"

	Big	Small	Relative Importance
Big	1	9	0.9
Small	1/9	1	0.1

TABLE III. ONE-TO-ONE COMPARISON ON THE ALTERNATIVES ON "Y POSITION"

	Big	Small	Relative Importance
Big	1	6	0.85
Small	1/6	1	0.15

TABLE IV. ONE-TO-ONE COMPARISON ON THE ALTERNATIVES ON "X POSITION"

	Big	Small	Relative Importance
Big	1	4	0.8
Small	1/4	1	0.2

TABLE V. ONE-TO-ONE COMPARISON ON THE ALTERNATIVES ON "FREQUENCY"

	Big	Small	Relative Importance
Big	1	2	0.67
Small	1/2	1	0.33

The maximum relative importance of the evaluation items is 0.47, and the number of subjects is 10. Therefore, if you multiply the relative importance by 20 and make it an integer, the integer values for the evaluation items of Fontsize, Y Position, X Position, and Frequency are It becomes 9, 6, 4, and 2. The one-to-one comparison matrix for the alternative is a 2x2 matrix because there are two alternatives (the evaluation items are large or small). Therefore, the font size of the maximum relative importance is 1: 9 for "large" compared to "small", and the results shown in Table 2 are obtained. The results shown in Tables 3 to 5 are obtained for other evaluation items as well. The relative importance of Tables 2 to 5 can be obtained by the same method as the relative importance of Table 1.

In addition, by checking the consistency of the one-to-one comparison result (calculating the Consistency Index: CI) by the method shown in Appendix 2, it was confirmed that the consistency was found in all cases from Tables 1 to 5 below 0.1. it can. Therefore, although the number of subjects is as small as 10, the results of these one-to-one comparisons are reliable.

Table 6 shows the result obtained by multiplying the weighting factors of the evaluation items in Table 1 by each alternative, adding their values, and integrating.

This shows that the relative importance is 0.85 when all the evaluation items are the Big, and the relative importance is 0.15 when all the evaluation items are the Smallest. Based on Tables 1 to 5, the confidence level of all knowledge is determined as shown in Fig. 4. This is a calculation example of the certainty factor when the font size is large, the horizontal position is large, the vertical position is small, and the appearance frequency is large.

Based on the confidence factor synthesis method [16], the certainty factor was synthesized by the logical sum of two pieces of knowledge. The specific method is shown in Appendix 3.

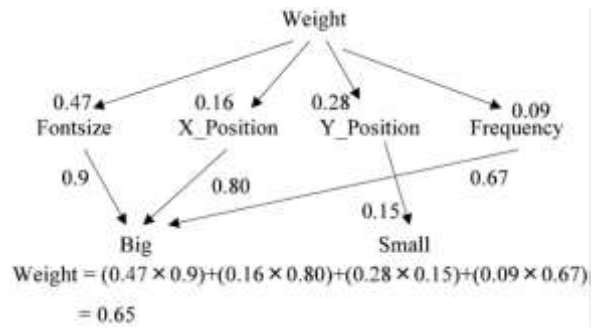


Fig. 4. An Example of the Confidential Factor Determination (In the case that Big: Font Size, Small: Y Position, Big: X Position, Big: Frequency).

TABLE VI. THE ESTIMATED PRIORITIES OF THE ALTERNATIVES

	Font Size	Y Position	X Position	Frequency	Relative Importance
Big	$0.9 \times 0.47 = 0.42$	$0.85 \times 0.28 = 0.24$	$0.8 \times 0.16 = 0.13$	$0.67 \times 0.09 = 0.06$	0.85
Small	$0.1 \times 0.47 = 0.05$	$0.15 \times 0.28 = 0.04$	$0.2 \times 0.16 = 0.03$	$0.33 \times 0.09 = 0.03$	0.15

In Fig. 5, if there are multiple matching knowledge rules in the knowledge base, knowledge conflicts are avoided by selecting and executing the one with the most detailed knowledge condition part. Then, the certainty factor of the keyword and the keyword candidate are output.

If this certainty factor exceeds a certain threshold (0.96 in this paper), keyword candidates are automatically adopted. Otherwise, the certainty factor and keyword candidates are presented to the operator for selection. And register the determined keywords in the database.

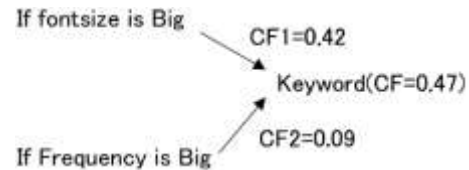


Fig. 5. An Example of Synthesizing Two Confidential Factor into One.

IV. PROPOSED METHOD

A. Evaluation of the Proposed Method and the Conventional Method

The proposed system was evaluated by comparison with the subjective evaluation. The evaluation was performed using 100 types of target documents according to the following procedure for 10 subjects.

- 1) The subject is presented with the target document and asked to select what seems to be a keyword. In addition, for all keyword candidates, the importance (selectivity) was evaluated from 0 to 1 in 1/8 steps.
- 2) Select a keyword based on the proposed method. In addition, the importance (selectivity) was evaluated for all of the keyword candidates.
- 3) The keywords extracted in steps (1) and (2) are compared and the matching rate of the keywords is obtained.

Meanwhile, evaluation of conventional methods is also performed. Similarly, the author selected keywords from 100 target documents, if the importance of all knowledge (evaluation items) was the same and compared them with the keywords selected based on the subjectivity of 10 subject and evaluated the concordance rate.

B. Evaluation Results

Fig.6 shows an example of the keyword matching rate. The results selected by the proposed system as keyword candidates are shown in the left column, and the results selected by the subjects are shown in the right column. Furthermore, at this time, the importance of the keyword candidates selected based on the font size, vertical position, horizontal position, and appearance frequency selected as the evaluation items (parameters), the keyword candidates and the certainty factors determined based on AHP, and the final importance.

Extracted Results			Original Documents		
word	count	Sel.Ratio	word	count	Sel.Ratio
重軽油系統rank1	8	1.000	重軽油系統	8	1.000
重軽油系統	8	1.000			
フムジョウキ2	3	0.375			
フムジョウキ3	1	0.125			
フムジョウキ	4	0.500	ドレソユカイシュウポンプ	2	0.250
ドレソユカイシュウポンプrank2	2	0.250			
ドレソユカイシュウポンプ	2	0.250	ソスイカイシュウポンプ	2	0.250
ソスイカイシュウポンプrank2	2	0.250			
ソスイカイシュウポンプ	2	0.250	LGIL	2	0.250
サービスrank2	2	0.250			
サービス	3	0.375	サービス	1	0.125
ATMrank2	1	0.125	TRACE TEMP	1	0.125
TRACE TEMPrank2	1	0.125	THK	1	0.125

Fig. 6. Shows an Example of the Keyword Matching Rate.

Character string ranked by each parameter

The screenshot shows a 'Text Viewer' window with four panes, each displaying a list of character strings ranked by a specific parameter:

- Font Size (0.41):** Lists strings like '重軽油系統', 'ATM', 'HDP', 'CBP', etc., ranked by their font size.
- Y-Position (0.23):** Lists strings like 'R', '重軽油系統', '重軽油系統', etc., ranked by their vertical position.
- X-Position (0.29):** Lists strings like '重軽油系統', 'B', 'A', etc., ranked by their horizontal position.
- Frequency (0.12):** Lists strings like '重軽油系統', '重軽油系統', etc., ranked by their frequency.

Below the panes is a 'Keyword List' with a 'Rank' column. The top of the list is labeled 'Higher importance' and the bottom 'Lower importance'. The list includes '重軽油系統' (rank 1), 'B', 'C', 'A', '重軽油系統', etc.

To the right, there is a 'Choice Word' section with a 'RESULT' display showing '重軽油系統' and '信頼度 0.761'. Below this is a 'Choice' button and a list of sample images.

Comprehensively ranked string

Fig. 7. An Example of the Knowledge Priority Determination (Objective Document is the Drawing Diagram Document of Fig. 1).

V. CONCLUSION

In the case of a document (2%) in which the keyword size, the position of the keyword candidate in the document, and the frequency of occurrence are exactly the same among the 100 types of target documents (2%), the operator selects the keyword candidate and the importance level. (Confidence factor) had to be presented to make a decision, but it was confirmed that the keywords of the remaining majority (98%) of the target documents could be automatically extracted.

When the importance of knowledge evaluation items (Fontsize, Y Position, X Position, Frequency) is all equal without estimating the certainty factor by AHP proposed in this paper, the font size and appearance frequency of specific keyword candidates are considered. If it is different from other candidates, the keyword can be extracted correctly, but, knowledge about the appearance position of the keyword does not work effectively, and as a result, only 75% can automatically extract the keyword. In the end, it was found that the effect of the confidence evaluation by AHP was about 1.5 times higher in success rate.

This has a great effect of automatically identifying the target document in advance in the letter format, the form format, and the drawing format, and using the importance level of the knowledge relating to the keyword candidate selection suitable for each format. This is because it is possible to grasp the whole thing and make a comprehensive judgment.

VI. FUTURE RESEARCH WORKS

Further experiments are required for the validity check of the proposed method for automatic letter document keyword extractions.

ACKNOWLEDGMENT

The author, also, would like to thank Professor Dr. Hiroshi Okumura and Professor Dr. Osamu Fukuda for their valuable discussions.

REFERENCES

- [1] iDC home page: <http://www.idcinit.com/>.
- [2] iOffice home page: <http://software.fujitsu.com/jp/ioffice/index.html>.
- [3] AIST home page: <http://www.carc.aist.go.jp/nlwww/~y.matsuo/keywaord-extraction/DDD/>.
- [4] Gengokk home page: <http://www.gengokk.co.jp/jyuuyou.htm>.
- [5] [http://H. Sakai, K. Ohtake and S. Masuyama, On retrieval support system by suggesting terms to a user, Proc. of NTCIR WS-2, pp.222-226, 2001.](http://H.Sakai,K.OhtakeandS.Masuyama,Onretrievalsupportsystembysuggestingtermstoauser,Proc.ofNTCIRWS-2,pp.222-226,2001.)
- [6] Fujii Home page: <http://software.ssri.co.jp/fuji/tsproinfo.html>.
- [7] H. Fujii and B. Croft: "A comparison of indexing techniques for Japanese text retrieval", Proc. of SIGIR'93, pp.237-246 (1993).
- [8] S. Ananiadou: "A methodology for automatic term recognition", Proc. of COLING'94, pp.1034-1038 (1994).
- [9] K. Kageura and B. Umno: "Methods of automatic term recognition: a review", Terminology, Vol.3, No.2, pp.259-289 (1996).
- [10] H. Nakagawa and T. Mori: "Nested collocation and compound noun for term recognition", Proc. OF COMPTERM'98, pp.64-70 (1998).
- [11] Nara Institute of Science and Technology Homepage: <http://chasen.aist-nara.ac.jp/>.
- [12] SJIT version dictionary source file <http://chasen.aist-nara.ac.jp/stable/ipadic.win/>.

- [13] Masaki Matsudaira, Toshio Ueda, Hiroyuki Onuma, Masamune Fuchigami, Yukihiko Morita: "Keyword Extraction from Documents and Collection of Related Information", AI Conference, SIG-SWO-A303-02, pp.02-01-02-06 (2002).
- [14] Thomas L. Saaty: Decision making for leaders: The analytic hierarchy process for decisions in a complex world 1999/2000 Edition (2000).
- [15] Yuichiro Anzai: "Production Systems and Artificial Intelligence Research —Toward the Problem of Knowledge Acquisition", Computer Software, Vol.1, No.3, pp.2-12 (1984).
- [16] Buchanan, B.G., and E.H. Shortliffe: Rule-based expert systems: The MYCIN experiments of the Stanford Heuristic Programming Project, Reading, MA, Addison- Wesley (1984).
- [17] Kohei Arai, Tolle Herman, Method for real time text extraction of digital manga comic, International Journal of Image Processing, 4, 6, 669-676, 2011.
- [18] Kohei Arai, Yuichiro Eguchi and Yoichiro Kitajima, Extraction of line features from multifidus muscle of CT scanned images with morphological filter together with wavelet multi resolution analysis, International Journal of Advanced Computer Science and Applications, 2, 8, 60-66, 2011.
- [19] Kohei Arai and Tolle Herman, Method for extraction product information from TV commercial, International Journal of Advanced Computer Science and Applications, 2, 8, 125-131, 2011.
- [20] Kohei Arai and Tolle Herman, Text extraction from TV commercial using blob extraction method. International Journal of Research and Review of Computer Science, 2, 3, 895-899, 2011.
- [21] Kohei Arai, Ronny Mardiyanto, Eye-based human-computer interaction allowing phoning, reading e-book/e-comic/e-learning, Internet browsing and TV information extraction, International Journal of Advanced Computer Science and Applications, 2, 12, 26-32, 2011.
- [22] Kohei Arai and Tolle Herman, Method for automatic e-comic scene frame extraction for reading comic on mobile devices, Proceedings of the Information Technology for Next Generation (ITNG2010) 2010.
- [23] Kohei Arai, T.Herman, Method for information extraction from Japan TV commercial, Proceedings of the 260th conference in Saga of Image and Electronics Engineering Society of Japan, 19-25, 2012.
- [24] Kohei Arai, T.Herman, Automatic information extraction from on-air TV commercial contents, Proceedings of the International Conference on Convergence Content 2012, 171-172, 2012.
- [25] T.L.Saaty:"The Analytic Hierarchy Process," McGrawHill, 1980.

APPENDIX

1) Algorithm for obtaining weighting factors between elements in each layer: Let $A = a_{ij}$ be the one-to-one comparison matrix of the elements A_1, A_2, \dots, A_n . If the weighting factor w to be obtained is given by w_1, w_2, \dots, w_n when A is known, A becomes as shown in Eq. (1).

$$A = [a_{ij}] = \begin{bmatrix} w_1/w_1 & - & w_1/w_n \\ | & | & | \\ w_n/w_1 & - & w_n/w_n \end{bmatrix} \quad (1)$$

At this time, a_{ij} is ideally as follows,

$$a_{ij} = w_i/w_j, a_{ji}=1/a_{ij}$$

$$w = \begin{bmatrix} w_1 \\ | \\ w_n \end{bmatrix}, i, j = 1, 2, \dots, n \quad (2)$$

At this time, if $a_{ij} \times a_{jk} = a_{ik}$ holds for i, j , and k , it can be said that the decision-makers' judgments are perfectly consistent. Next, multiplying Eq. (1) by w from the right yields Eq. (3).

$$Aw = \begin{bmatrix} w_1 & - & w_1 \\ w_1 & | & w_n \\ w_n & - & w_n \\ w_1 & | & w_n \end{bmatrix} \begin{bmatrix} w_1 \\ | \\ w_n \end{bmatrix} = n \begin{bmatrix} w_1 \\ | \\ w_n \end{bmatrix} \quad (3)$$

Then,

$$Aw = nw \quad (4)$$

Equation (4) is obtained as a solution to the eigenvalue problem as follows,

$$(A-nI)w=0 \tag{5}$$

At this time, n must be the eigenvalue of A for $w = 0$. When n becomes the eigenvalue of A , w becomes the eigenvector of A . Also, from rank $(A) = 1$, the eigenvalues λ_i ($i = 1, 2, \dots, n$) except for 0 are given the maximum eigenvalue λ_{max} , and other eigenvalues $\lambda_i = 0$. Since the sum of the main diagonal elements of A is n , λ_{max} satisfies $\lambda_{max} = n$. Therefore, w is the eigenvector normalized to λ_{max} of A . In other words, it can be said that they are completely consistent. However, it is extremely difficult for the decision maker to decide the matrix A that gives the same weighting coefficient as w . Therefore, when the one-to-one comparison matrix obtained from the decision maker is A' and the weighting coefficient obtained from the one-to-one comparison matrix is W' , Eq. (4) is replaced as Eq. (6).

$$A'W' = \lambda'_{max} W' \tag{6}$$

Therefore, W' is the normalized eigenvector for the maximum eigenvalue λ'_{max} of A' .

2) *Method of consistency check in one-to-one comparison:* When an inconsistency occurs in an n -by- n one-to-one comparison matrix, the maximum eigenvalue λ'_{max} becomes larger than n . This is called Satty's theorem [25] and is expressed by Eq. (7).

$$\lambda'_{max} = n + \sum_{i=1}^n \sum_{j=j+1}^n (W_j a_{ij} - W'_i)^2 / W'_i W'_j a_j n \tag{7}$$

From Eq. (7), it is found that λ'_{max} always satisfies $\lambda'_{max} \geq n$. Therefore, *C.I.* (Consistency Index) is defined as an index of consistency check for one-to-one comparison. *C.I.* is expressed by Eq. (8).

$$C.I. = \frac{\lambda'_{max} - n}{n - 1} \tag{8}$$

Consistency increases as *C.I.* = 0 approaches, and conversely decreases with distance from 0. Generally, if *C.I.* is 0.1 or less, it is said that there is consistency.

3) *Confidence synthesis method:* The *CF* that combines CF_1 and CF_2 when deriving the same consequent part is as follows,

$$CF(CF_1, CF_2) = \begin{cases} CF_1 + CF_2 - (CF_1 * CF_2) & CF_1 > 0 \text{ and } CF_2 > 0 \\ CF_1 + CF_2 + (CF_1 * CF_2) & CF_1 < 0 \text{ or } CF_2 < 0 \\ \frac{(CF_1 + CF_2)}{1 - \min(|CF_1|, |CF_2|)} & \text{other} \end{cases} \tag{9}$$

AUTHOR'S PROFILE

Kohei Arai, He received BS, MS and PhD degrees in 1972, 1974 and 1982, respectively. He was with The Institute for Industrial Science and Technology of the University of Tokyo from April 1974 to December 1978 also was with National Space Development Agency of Japan from January, 1979 to March, 1990. During from 1985 to 1987, he was with Canada Centre for Remote Sensing as a Post Doctoral Fellow of National Science and Engineering Research Council of Canada. He moved to Saga University as a Professor in Department of Information Science on April 1990. He was a councilor for the Aeronautics and Space related to the Technology Committee of the Ministry of Science and Technology during from 1998 to 2000. He was a councilor of Saga University for 2002 and 2003. He also was an executive councilor for the Remote Sensing Society of Japan for 2003 to 2005. He is a Science Council of Japan Special Member since 2012. He is an Adjunct Professor of University of Arizona, USA since 1998. He also is Vice Chairman of the Science Commission "A" of ICSU/COSPAR since 2008 then he is now award committee member of ICSU/COSPAR. He wrote 55 books and published 620 journal papers as well as 450 conference papers. He received 66 of awards including ICSU/COSPAR Vikram Sarabhai Medal in 2016, and Science award of Ministry of Mister of Education of Japan in 2015. He is now Editor-in-Chief of IJACSA and IJISA. <http://teagis.ip.is.saga-u.ac.jp/index.html>

Data Retrieval Method based on Physical Meaning and its Application for Prediction of Linear Precipitation Zone with Remote Sensing Satellite Data and Open Data

Kohei Arai

Faculty of Science and Engineering
Saga University, Saga City, Japan

Abstract—Data retrieval method based on physical meaning is proposed together with its application for prediction of linear precipitation zone with remote sensing satellite data and open data. The linear precipitation zone causes extremely severe storm and flood damage, landslide, and so on. Linear precipitation zone is formed in the case that the warm, moist air must continuously flow in, the force to lift this air up and it is often in collisions with mountain slopes or cold fronts, the atmospheric conditions are unstable, and there is a certain direction of wind above the sky. These conditions can be monitored by remote sensing satellite data. The proposed method is intended to attempt for prediction of the linear precipitation zone for disaster mitigation. There are water vapor data, cloud liquid data, cloud fraction data, and upper atmospheric wind data derived from the remote sensing satellite-based mission instruments. Through experiment in the case of the linear precipitation zone which was occurred in northern Kyushu, Japan in the begging of July 2020, a possibility to detect the linear precipitation zone was confirmed. Also, flooding damages and other disasters occurred in the northern Kyushu, in same time period caused by the detected linear precipitation zone is detected with Sentinel-1 of SAR data.

Keywords—Linear precipitation zone; remote sensing satellite data; water vapor; cloud liquid; upper atmospheric wind; disaster mitigation

I. INTRODUCTION

Big Data Analysis: BDA (Data Science) is getting more important for Artificial Intelligence: AI research and applications. In the BDA, Storage & Management, Data collection, Data cleaning, Data retrieval, Data analysis, Data visualization, Data integration, Data language are important components. Data retrieval is a technology for extracting knowledge by comprehensively applying data analysis techniques such as statistics, pattern recognition, and artificial intelligence to a large amount of data. It often implies the expectation that heuristic knowledge acquisition is possible, which is difficult to imagine from the usual way of handling data. Data retrieval and analysis are key issues for remote sensing satellite data analysis. Essentially, remote sensing satellite data is big data and it is not easy to retrieve most appropriate data set for a variety research purpose.

Not to be confused with data extraction (which will be covered later), data retrieval is the process of discovering

insights within a database as opposed to extracting data from web pages into databases. The aim of data retrieval is to make predictions and decisions on the data your business has at hand. IBM SPSS Modeler is the famous software tool for data retrieval followed by Oracle data retrieval. Also, Teradata, Kaggle are getting more popular. On the other hand, while data retrieval is all about sifting through data in search of previously unrecognized patterns, data analysis is about breaking that data down and assessing the impact of those patterns overtime. Analytics is about asking specific questions and finding the answers in big data. The conventional data retrieval methods are concentrated on statistical properties of the data without physical meaning of the data.

In this paper, a data retrieval method utilizing not only statistical properties but also physical meaning of the data in concern is proposed. Also, one of the applications of the proposed method of a data retrieval for remote sensing satellite big data retrieval is shown. There are some remote sensing big data platforms which provide a variety of discipline. For instance, Microsoft and the United States Ocean Atmosphere Agency (NOAA), a joint R & D agreement to develop the best way to extract data from internal systems. This will allow Microsoft to provide weather, water, and oceans provided by NOAA scientists and weather data hosted on Azure cloud platform. In order to extract most appropriate data, not only discipline by discipline and data type by data type, but also physical meaning by physical meaning of the data-based retrieval method is highly required. Therefore, relation among discipline, data type and physical meaning of the data has to be created and use it in the data retrieval is to be established.

In this paper, NOAA provided remote sensing big data platform JAXA's remote sensing data portal, and ESA's remote sensing satellite data portal are used, the most significant issue is how to choose most appropriate dataset, namely, data retrieval. The proposed method is based on the relation among discipline, data type, and physical meaning. Also, one of the applications is presented here, that is prediction of linear precipitation zone. All the linear precipitating some related remote sensing satellite data are chosen from the platform based on a physical meaning.

In the following section, the research background together with related research and the proposed prediction method is

described followed by experiment together with experimental results. After that, concluding remarks and some discussions are described.

II. RESEARCH BACKGROUND

As for the data retrieval methods, knowledge discovery in databases is overviewed [1]. Principles of data retrieval is introduced, mainly the theoretical background of each data retrieval method [2]. Data retrieval as of concepts and techniques are well reported [3]. It is the Encyclopedia book with everything. Data retrieval as practical machine learning tools and techniques is published as tutorials on how to use different techniques and free tools Weka [4]. Also, "Basics of Data Retrieval" is published [5]. This is the book for beginners who can get a bird's-eye view of the whole. On the other hand, "Data Retrieval" is published of details on association rule extraction [6].

Meanwhile, as for the mid-latitude linear precipitation zone is classified as follows according to the internal structure. (1) Squall line type, (2) Back building type, and (3) Back and side building type. The linear precipitation zone is a phenomenon in which cumulonimbus clouds that because heavy rainfall is arranged in a row. It is characterized by a long range of 50 to 200 kilometers and a width of 20 to 50 kilometers, which lasts for hours. Guerrilla heavy rains that bring local heavy rains are generated by a single cumulonimbus cloud and can be set within about an hour in a narrow area of about 10 km square. The linear precipitation zone is like a guerrilla rainstorm procession. This phenomenon has been known since the 1990s, but it has been attracting attention due to a series of damages in recent years. How do linear precipitation zones occur? "The four basic conditions are likely to occur," explains Hiroshi Tsuguchi, a researcher at the Meteorological Research Institute, Japan Meteorological Agency.

First, the warm, moist air must continuously flow in. This becomes the "seed" of the cloud, which is an aggregate of fine water particles. Second, it then requires the force to lift this air up, often in collisions with mountain slopes or cold fronts. Third, the atmospheric conditions are unstable. Warm and moist air forms clouds at a certain height, but cumulonimbus clouds that can reach altitudes of 10,000 meters or more require cold air over thousands of meters and an environment where convection creates a strong updraft. Finally, there is a certain direction of wind above the sky. If these conditions are met, the generated cumulonimbus will be swept away by the wind, and moist air will be immediately supplied behind it, creating new cumulonimbus one after another. Repeatedly like a belt conveyor, a "back-building (backward formation) phenomenon" occurs and cumulonimbus clouds line up in a straight line, causing heavy rainfall directly below.

Local heavy rainfall has been increasing in the statistics of the past 40 years, and there is a possibility that global warming is affecting it. On the other hand, the linear precipitation zone tends to be flat, and there is no change in rainfall or precipitation range, and it is unclear how it relates to global warming. Even if anyone tries to predict the occurrence by simulation analysis of observation data, the underlying real-time data is insufficient. The surface data is relatively rich in the Japan Meteorological Agency's Amedas (Regional

Meteorological Observation System), but cumulonimbus clouds and linear precipitation zones are three-dimensional. The radar and satellite observation networks that search the sky are low in density and lack enough accuracy, making it difficult to grasp three-dimensionally.

Linear precipitation zone is formed in the case that the warm, moist air must continuously flow in, the force to lift this air up and it is often in collisions with mountain slopes or cold fronts, the atmospheric conditions are unstable, and there is a certain direction of wind above the sky. These conditions can be monitored by remote sensing satellite data. The proposed method is intended to attempt for prediction of the linear precipitation zone for disaster mitigation. There are water vapor data, cloud liquid data, cloud fraction data, and upper atmospheric wind data derived from the remote sensing satellite-based mission instruments.

III. RELATED RESEARCH WORKS

As for the disaster mitigation by remote sensing satellite data, four dimensional GIS and its application to disaster monitoring with satellite remote sensing data is proposed [7]. An expectation to remote sensing for disaster management is also mentioned [8]. GIS and application of remote sensing to disaster management and monitoring is proposed [9]. The current status on disaster monitoring with satellites in Japan is announced [10]. An expectation on remote sensing technology for disaster management and response is proposed [11]. On the other hand, disaster monitoring with ASTER onboard Terra satellite is attempted [12]. Clearing house for disaster management is proposed [13]. ICT technology for disaster mitigation is proposed together with Tsunami warning system [14]. Meanwhile, cellular automata for traffic modelling and simulation in a situation of evacuation from disaster areas is published [15].

New approach of prediction of Sidoarjo hot mudflow disaster area based on probabilistic Cellular Automata: CA is proposed [16]. Sensor network for landslide monitoring with laser ranging system avoiding rainfall influence on laser ranging by means of time diversity and satellite imagery data-based landslide disaster relief is proposed and well reported [17]. Visualization of 5D assimilation data for meteorological forecasting and its related disaster mitigation utilizing VIS5D of software tool is proposed [18]. On the other hand, disaster relief with satellite based synthetic aperture radar data is conducted [19]. Also, Sentinel 1A SAR data analysis for disaster mitigation in Kyushu is reported [20]. Flooding and oil spill disaster relief using Sentinel of remote sensing satellite data is well reported [21]. Convolutional neural network considering physical processes and its application to disaster detection is proposed and validated [22].

IV. PROPOSED DATA RETRIEVAL METHOD

NOAA, NASA has the pathfinder program. It is identified four long time-series data sets from existing archives for reprocessing: the Advanced Very High Resolution Radiometer (AVHRR) data, the TIROS Operation Vertical Sounder (TOVS) data, Geostationary Operational Environmental Satellite (GOES) data, and Special Sensor Microwave/Imager (SSM/I) data. The following snapshot of the first project

processed by the Pathfinder Program -- development of the AVHRR Land and Polar data sets -- foreshadows challenges in scale and logistics that will continue to be hurdles of EOS-era data streams.

JAXA has a G-Portal. It is a portal system allowing users to search (satellite/sensor/physical quantity), and download products acquired by JAXA's Earth observation satellite. As for the physical quantity, There are Amount of Precipitation, Precipitation Classification, Particle Size Distribution, Cloud Mask/Classification/Flag, Cloud Phase, Cloud Partial Effective Radius/Shape, Cloud Liquid Water Content/Cloud Ice Water Content, Elements Of Cloud Top (Temperature/Atmospheric Pressure/Attitude), Classified Cloud Fraction, Water Cloud Optical Thickness, Ice Cloud Optical Thickness, Cloud Extinction Coefficient, Doppler Velocity in the atmosphere related subject, for instance.

ESA has The Copernicus Data Hubs (Open Access Hub, Collaborative Data Hub, International Access Hub, Copernicus Services Data Hub). These are ESA online portals, which make Sentinel data available to individuals and entities worldwide. The portals allow the searching for Sentinel data and the download of Sentinel data, selected by the user.

From these remote sensing satellite data portal sites, it is possible to choose and download the data for the specific purpose if users have a knowledge about relation among discipline, data type, and physical meaning of the data. The proposed data retrieval method allows choosing appropriate data from the portal by using the relation. In other word, the proposed method provides the relation (knowledge). If users specify keywords, then the method provides appropriate remote sensing satellite data.

V. ONE OF THE APPLICATIONS OF THE PROPOSED DATA RETRIEVAL METHOD FOR LINEAR PRECIPITATION ZONE DETECTION

By using the proposed retrieval method with the keyword of "Line Precipitation Zone in Kyushu, Japan in July 2020", then the remote sensing satellite data of MTSAT, AMSR, Rain Radar, Sentinel-1 SAR and the open data of Meteorological map, Topographic map data are provided because the proposed method has relation information among discipline, data type, and physical meaning of the data as well as subject (the keyword).

A. Line Precipitation Zone

Due to the effect of warm and moist air flowing from the night of July 3 2020 toward the low pressure and the rainy season front, the station was in the Satsuma and Osumi regions of Kagoshima prefecture from the night of the 4th of July 2020 to the morning of the 4th of July 2020, and in the southern part of Kumamoto from the morning of the 4th of July 2020 to the morning.

Due to severe local rain, the Japan Meteorological Agency announced a heavy rain special warning to Kumamoto and Kagoshima prefectures at 4:50 on the 4th of July 2020. It is possible that a linear precipitation zone with developed rain clouds formed in these areas. Fig.1 shows MTSAT

(Gestational meteorological satellite) images of Japanese vicinity, weather (atmospheric pressure) map of Japanese vicinity, and rain cloud radar images of middle of Kyushu which are acquired during from June 28 to July 12, 2020. From the evening of the 5th of July 2020 to the morning of the 6th of July 2020, it was raining locally in Satsuma and Osumi, Kagoshima Prefecture, and it was a record heavy rain in Kanaya city.

From 6th to 8th of July 2020, due to the stagnant front, it was raining locally in Nagasaki prefecture, Saga prefecture, Fukuoka prefecture Chikugo region, Oita prefecture and northern Kumamoto prefecture. From 7 minutes to 11:40 on the 7th of July 2020, a heavy rain special warning was announced in Nagasaki, Saga and Fukuoka prefectures. On the 8th of July 2020, there was heavy rain from the Tokai region to the Koshin region, Gifu prefecture at 6:30 on the 8th of July 2020, and a heavy rain special warning was announced to Nagano prefecture at 6:43 on the same day.

The Kuma River system that flows through Kumamoto Prefecture was inundated and destroyed at 13 locations in Yatsushiro City, Ashikita Town, Kuma Village, Hitoyoshi City, and Sagara Village, and about 1060 hectares were flooded. At Senjuen, a nursing home for the elderly in Kuma, 14 people died in a submerged facility. According to the Geographical Survey Institute's inundation map, the inundation depth in the Kuma-murato district, where Senjuen is located, reached a maximum of 9 meters. In Hitoyoshi City, a wide area of the city was flooded, and in the center of Sakamoto Town, Yatsushiro City, heavy damage such as driftwood and earth and sand flowing into the housing. In addition, Ashikita (died by a landslide in the Tagawa district, flooded at Sashiki station) and Tsunagi-cho (died by a landslide in the Fukuhama district) have also been damaged.

In Omuta City, Fukuoka Prefecture, 252 mm of "rainfall that we have never experienced" in 3 hours from 3:00 pm on July 6th in 2020 was observed. A large amount of water flowed through the Suwa River (Sekigawa), but no flooding occurred. However, the amount of rainfall exceeded the capacity of Mikawa Pumping Station (Mikawa-cho, Saitama City), causing inland water flooding. Road flooding also occurred in Arao City, Kumamoto Prefecture. The Chikugo River flooded in parts of Oita prefecture in the upper reaches and Fukuoka prefecture in the middle reaches. Damage caused by flooding and flooding in Kurume City, Fukuoka Prefecture, and damage by inland flooding in Omuta City, Fukuoka Prefecture.

In addition, the Oita River in Yufu City, Oita Prefecture, caused an overflow in Shonai Town Higashichoho (around Onoya Station) and Hazama Town Shitaichi (around Tenjinbashi), causing Oita River tributaries (Hanaino River, Kurokawa, etc.) in various parts of the city. Due to frequent floods, debris flows, and sediment disasters, information on the occurrence of disasters was provided. In the Oita River, the water levels at the Dojiri Observatory in Yufu City and the Fuuchi Ohashi Observatory in Oita City, which are directly controlled by the national government, were the highest ever recorded.

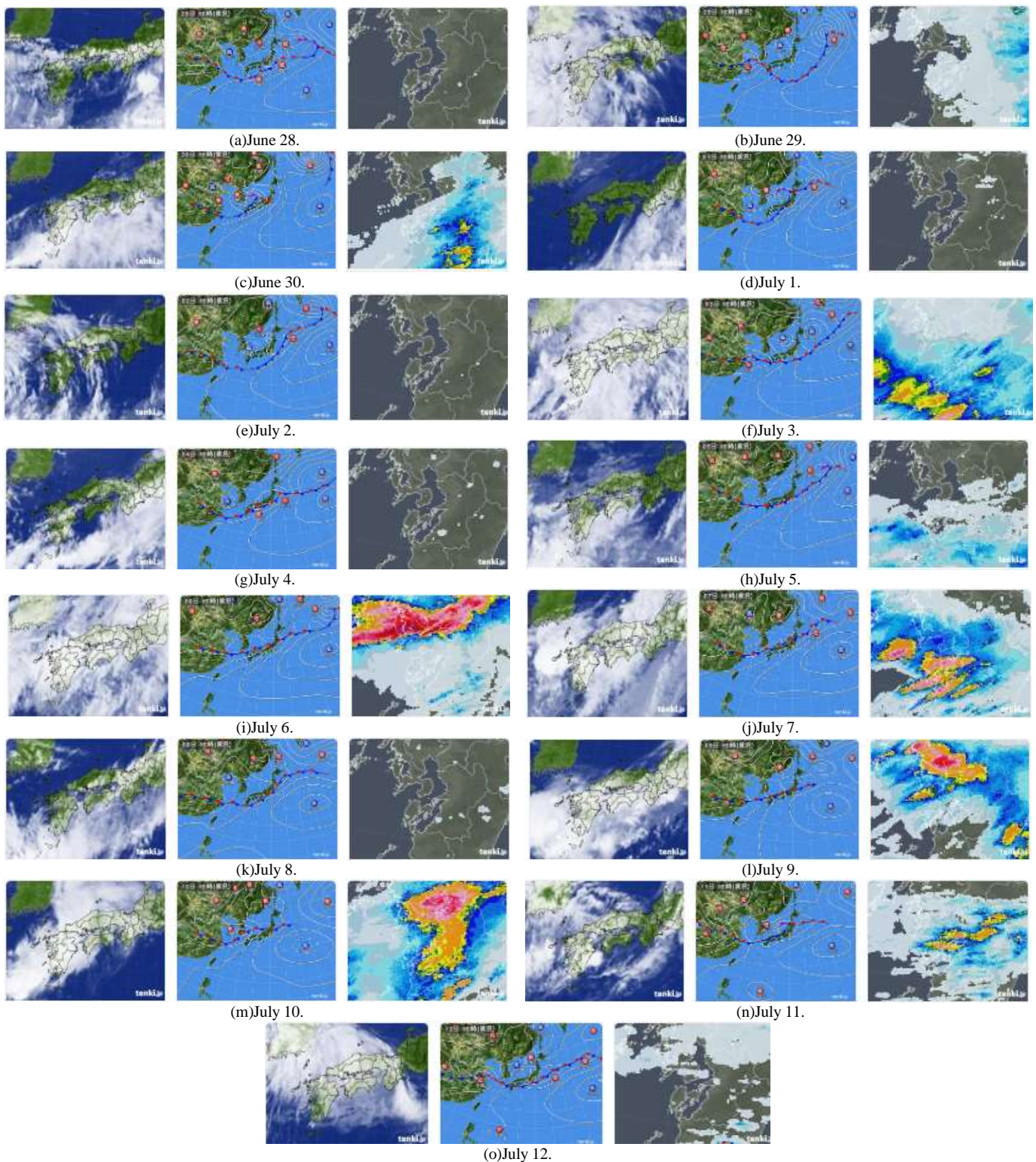


Fig. 1. MTSAT (Gestational Meteorological Satellite) Images of Japanese Vicinity, Weather (Atmospheric Pressure) Map of Japanese Vicinity, and Rain cloud Radar Images of Middle of Kyushu which are acquired during from June 28 to July 12 2020.

The linear precipitation zone is "created by passing or stagnating at almost the same place for several hours by an organized group of cumulonimbus clouds formed by rows of developed rain clouds (cumulonimbus) that occur one after another. A linear stretch of about 50-300 km, a width of about

20-50 km with strong precipitation rain (a forecast term used by the Meteorological Agency in weather forecasts, etc.). It has been pointed out in the 1990s that a linear precipitation area is often seen in Japan when a heavy rainfall occurs. Meteorological Research Institute Tsuguchi and Kato (2014)

[23] objectively extracted the case of heavy rainfall in Japan from April to November 1995-2009 and statistically analyzed the shape of the precipitation area. As a result, it was revealed that the linear precipitation zone occurred in about two-thirds of the cases, except for typhoons.

The entity of the linear precipitation zone is an aggregate of multiple cumulonimbus clouds and is considered to be a kind of meso-convective system. There are also cases with a hierarchical structure of "linear precipitation zone-cumulonimbus group-cumulonimbus".

It seems to be the cause of localized heavy rain. According to an analysis of radar observations by the Meteorological Research Institute of the Japan Meteorological Agency, about 60% (168) of the 261 heavy rains other than typhoons that occurred between 1995 and 2006 were attributed to the linear precipitation zone. It occurs all over Japan and is common in Kyushu and Shikoku. Although the generation mechanism has not been fully clarified, four conditions that are likely to occur are "inflow of warm and moist air that is the source of clouds" "rises due to collision of the air with mountains and cold fronts" "cumulative cloud "Stable atmospheric conditions" and "wind in a certain direction generated by cumulonimbus" are mentioned.

Heavy rains in the northern part of Kyushu caused a developed linear precipitation zone with an altitude of 18,000 meters around Asakura City in Fukuoka Prefecture and Hita City in Oita Prefecture. In Asakura City, the amount of rainfall per hour exceeded 100 mm, and the amount of 24-hour rainfall reached 545.5 mm, the highest ever, with heavy rain continuing.

In recent years, heavy rainfall due to the linear precipitation zone has been occurring in various places. When Tsuguchi et al. analyzed radar observation data for 261 heavy rains other than typhoons that occurred between 1995 and 2009, two-thirds of the 168 cases were due to the linear precipitation zone.

It often leads to large-scale disasters. The 1982 heavy rainfall in Nagasaki recorded the highest hourly rainfall of 187 mm in Japan's observation history, the Tokai heavy rain in 2000 flooded about 70,000 houses, the Hiroshima heavy rain in 2014, and the 15 years in 2015. Heavy rains in Kanto and Tohoku occurred. The linear precipitation zone is also believed to be the cause of the 1957 Isahaya heavy rain, which resulted in 722 dead and missing.

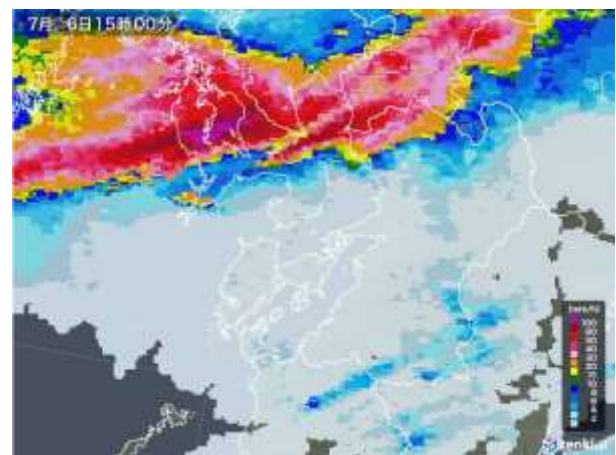
B. Phenomena of the Line Precipitation Zone

One of the causes of the heavy rain this time is that the rainy season front has stagnated from western Japan to eastern Japan for a long time. This is probably because the surface temperature of the Indian Ocean is higher than normal. Due to the high sea surface temperature in the Indian Ocean, updrafts are more likely to occur, and the elevated atmosphere is more likely to descend in the ocean east of the Philippines. For this reason, it seems that the Pacific High goes over to the southwest rather than the north side, making it difficult for the Baiu front to move north, making it easier to stay in the Japanese archipelago.

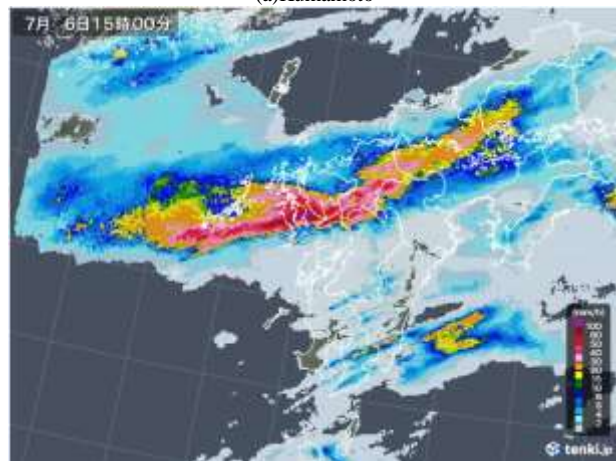
The other is that a large amount of warm and moist air, which is the source of rain clouds, flows in one after another. This is probably due to the westerly meandering. On the west side of Japan (near the Yellow Sea), westerly winds meander to the south, forming a western valley where the air pressure drops, and it is easy for moist air around the Pacific high pressure to flow into the Japanese archipelago.

Therefore, not only rain cloud radar images, but also water vapor, cloud fraction, cloud liquid data have to be investigated. Fig.2 shows rain cloud radar images of Kumamoto, Kyushu, Japan which are acquired on July 6 2020 (most severe rainfall). It looks like a linear precipitation zone over the northern Kyushu, Japan. It was heavy rain continuously for more than 10 hours on July 6 2020.

The basic idea of the proposed method is based on the satellite-based water vapor, cloud fraction, cloud liquid data derived from the mission instrument data of microwave radiometer (Advanced Microwave Scanning Radiometer: AMSR). Estimate moisture supply to the Baiu front from the water vapor data, also estimate cloud amount from the cloud fraction data, as well as estimate cloud liquid amount from the cloud water content data. Then a cause of linear precipitation zone can be estimated.



(a)Kumamoto



(b)Kyushu

Fig. 2. Rain cloud Radar Images of Kumamoto, Kyushu, Japan which are Acquired on July 6 2020 (Most Severe Rainfall).

C. Causes of the Linear Precipitation Zone

Fig. 3, 4, and 5 show the weekly averages of water vapor, cloud water content, and cloud fraction of the Japanese vicinity derived from AMSR during from June 26 to July 11, 2020, respectively. From the South-West (South China Sea), there is a strong moisture (more than 60 mm) supply to the Baiu front situated in Japanese vicinity as shown in Fig.3 (b) and (c). As shown in Fig. 6, Baiu front is situated along with the Japanese island. Therefore, southern part of Baiu front had a severely strong heavy rain as shown in Fig.1 (i), for instance. Just before the line precipitation zone was formed (June 26 to July 3, 2020), there was strong moisture supply. This is one of causes of the severe heavy rainfall in the Japanese vicinity during from July 4 to July 11, 2020.

On the other hand, cloud water content was more than 1000 g/m² during from July 4 to July 11, 2020 as shown in Fig. 4. (a).

This is another cause of the heavy rainfall. Cloud patterns are same as Fig. 5 of cloud fraction correspondingly. These continuous heavy moisture supply and high cloud water content for more than two weeks (during from June 16 to July 11) are causes of the line precipitation zone and severe heavy rainfall during the period.

The rainy season front is stagnant, and local heavy rain continued July 7th in northern Kyushu. Oita flooded the Chikugo River, a first-class river that flows across Fukuoka Prefecture, causing major flooding and flooding in Omuta City.

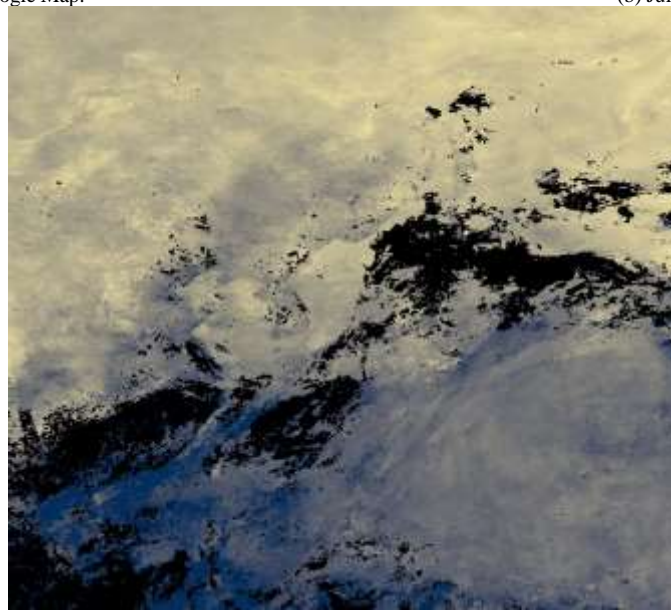
Through checking the sky condition at Omuta City at around 8:00 am on July 7, it was said that the entire area of Kamiyashiki-cho, Omuta City had already been flooded over a wide area. There were fire engines and multiple passenger cars that had already been flooded to the waist level of adults and were stuck in the water.



(a) Google Map.



(b) July 4 – 11.



(c) June 26 – July 3

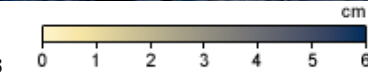


Fig. 3. Water Vapor.

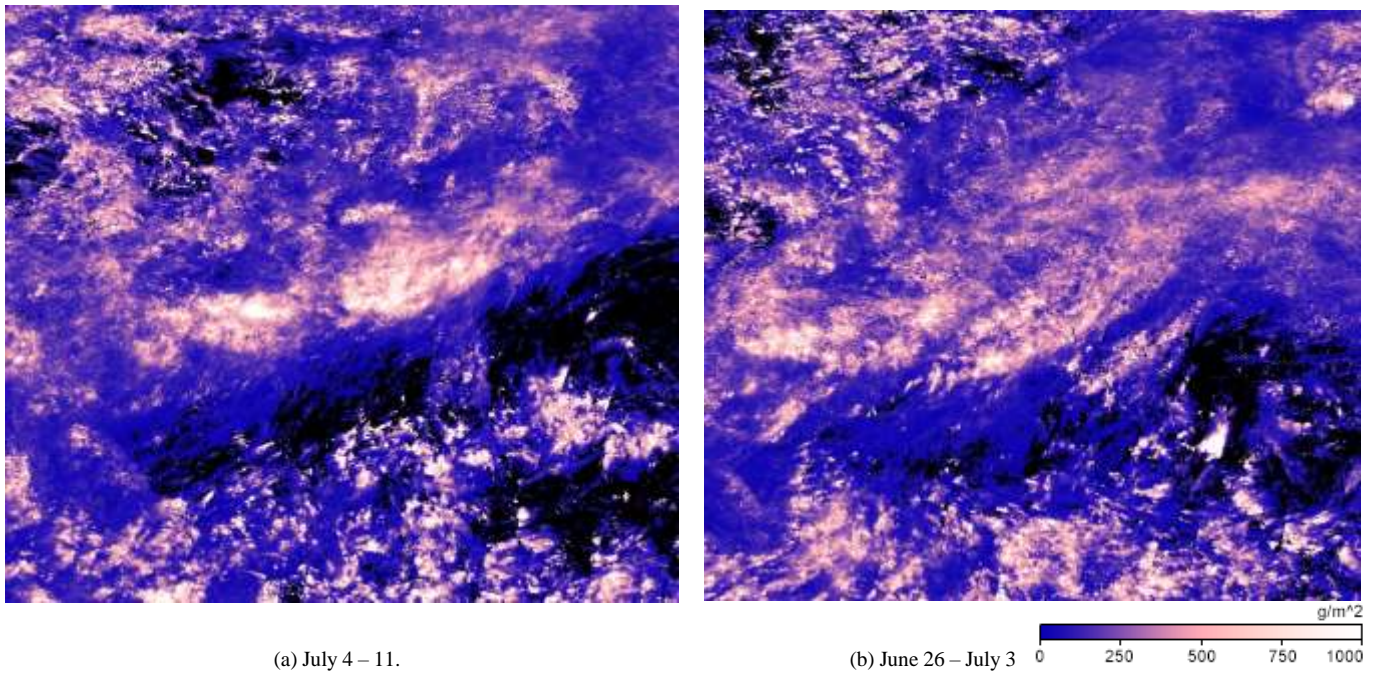


Fig. 4. Cloud Liquid.

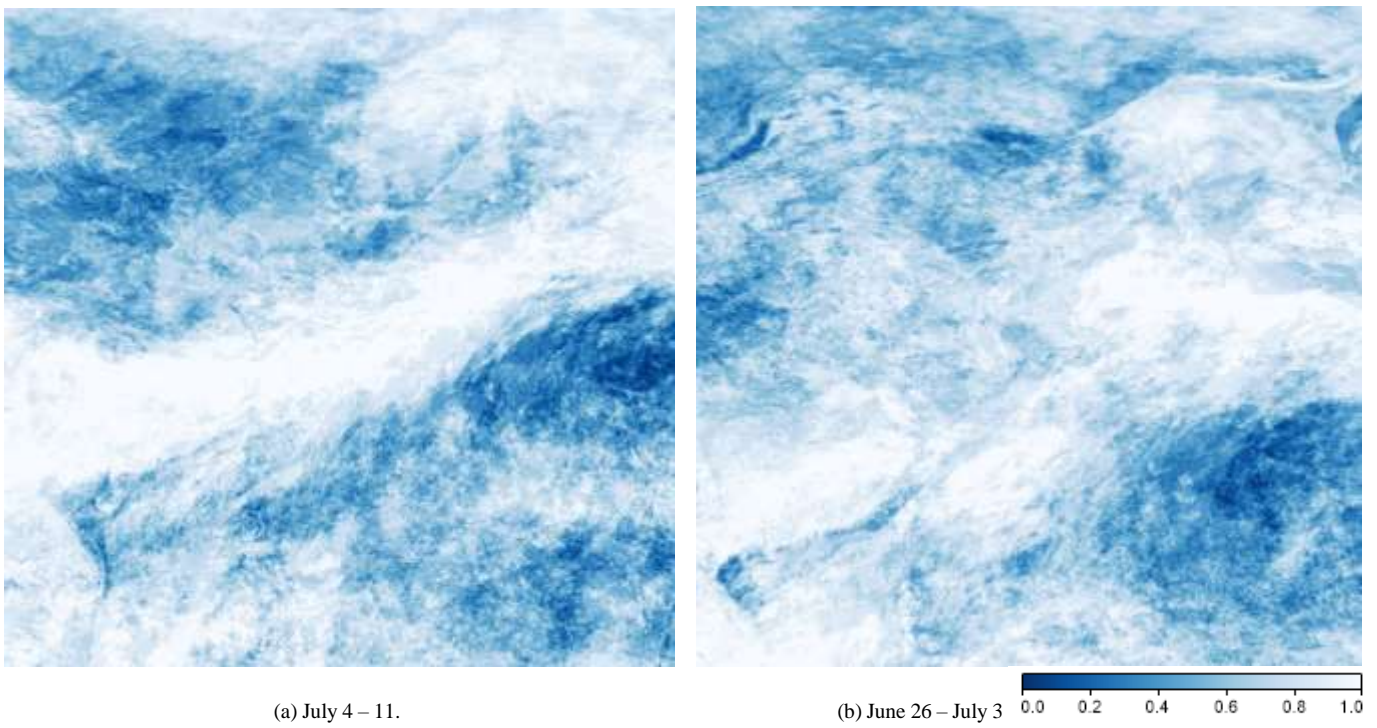


Fig. 5. Cloud Fraction.

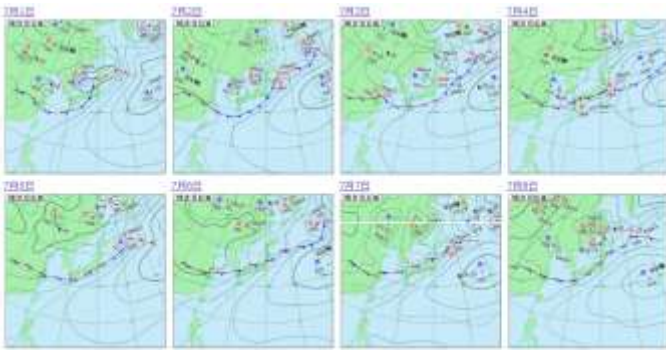
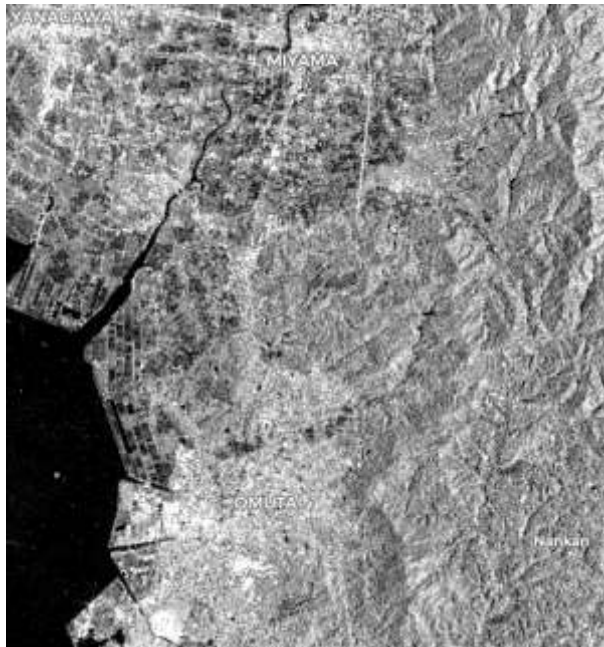


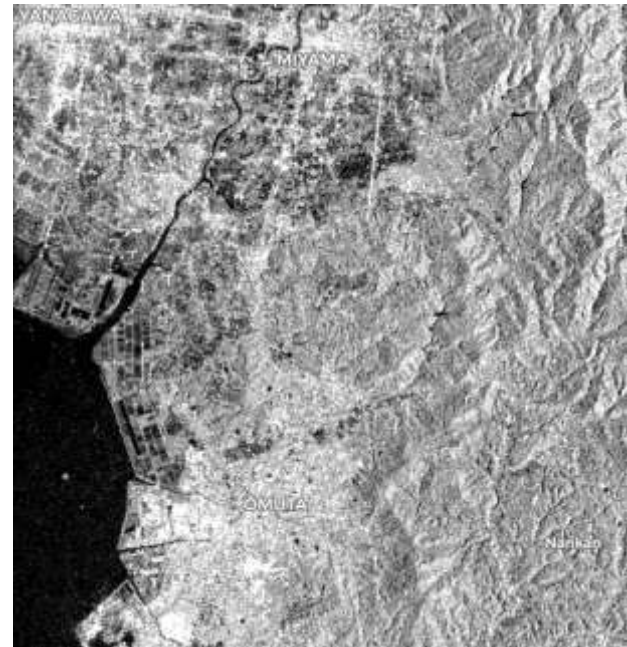
Fig. 6. Situation of Baiu front on July 1 to 8 2020.

D. Line Precipitation Zone of Flood Area Detection

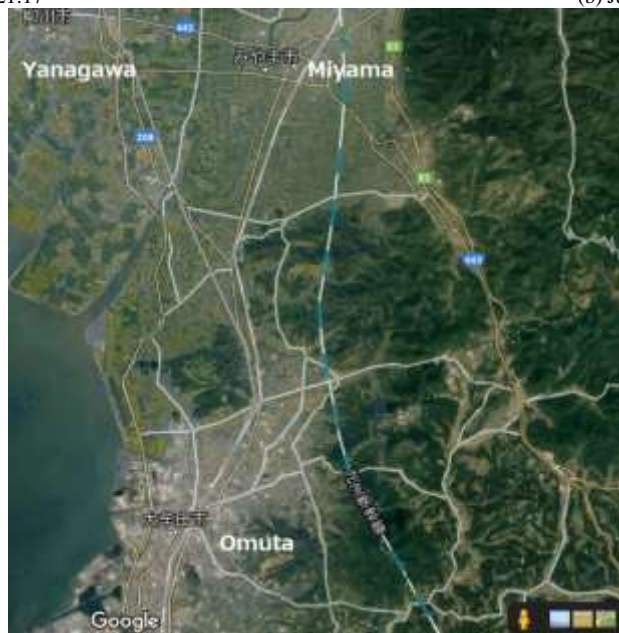
Flood areas due to the line precipitation zone which was occurred during July 4 to July 10, 2020 were detected in the northern Kyushu, Japan with Sentinel-1 of SAR data. Fig.7 shows the detected flood areas. Fig.7 (a) shows Sentinel-1 of SAR imagery data of Omuta and its surroundings which is acquired on July 4, 2020 while Fig.7 (b) shows that acquired on July 10, 2020. By comparing both, it can do done to find the flood areas. The intensity of SAR imagery data indicates the backscattering cross section of the ground surface. The dark areas in the July 10 image comparing to that of July 4 imply the flood areas. In particular, the southern portion of Miyama city, there is the relatively large wide flood areas.



(a) July 4, 21:17



(b) July 10, 21:16.



(c) Google Map.

Fig. 7. Line Precipitation Zone of Flood Area Detection (Omuta City, Japan).

VI. CONCLUSION

It is found that the proposed retrieval method allows retrieval of the appropriate remote sensing satellite data with the keyword of research purpose, location and time information. One of the applications of the proposed method for the following example, (1) Keyword: "Line Precipitation Zone in Kyushu, Japan in July 2020", (2) the remote sensing satellite data of MTSAT, AMSR, Rain Radar, Sentinel-1 SAR and the open data of Meteorological map, Topographic map data as the retrieval result.

This is because of the proposed method has relation between research purpose (keyword) and the information of discipline, data type, and physical meaning of the data.

Prediction of linear precipitation zone with remote sensing satellite data is capable with the proposed method. The linear precipitation zone causes extremely severe storm and flood damage, landslide, and so on. Linear precipitation zone is formed in the case that the warm, moist air must continuously flow in, the force to lift this air up and it is often in collisions with mountain slopes or cold fronts, the atmospheric conditions are unstable, and there is a certain direction of wind above the sky. These conditions can be monitored by remote sensing satellite data.

The proposed method is intended to attempt for prediction of the linear precipitation zone for disaster mitigation. There are water vapor data, cloud liquid data, cloud fraction data, and upper atmospheric wind data derived from the remote sensing satellite-based mission instruments. Through experiment in the case of the linear precipitation zone which was occurred in northern Kyushu, Japan in the begging of July 2020, a possibility to detect the linear precipitation zone was confirmed. Also, flooding damages and other disasters occurred in the northern Kyushu, in same time period caused by the detected linear precipitation zone is detected with Sentinel-1 of SAR data.

Currently, the proposed method has a relation information between research purposes and the related remote sensing satellite data. This is the limitation of the proposed method.

VII. FUTURE RESEARCH WORKS

Further experimental studies are required for the validation of the proposed method. Also, applicability of the proposed method must be confirmed through further experiments. Furthermore, the relation information must be expanded to the other research fields. Then the proposed method can be applicable to the other research fields.

ACKNOWLEDGMENT

The author would like to thank Professor Dr. Hiroshi Okumura and Professor Dr. Osamu Fukuda for their valuable discussions.

REFERENCES

- [1] W. Frawley and G. Piatetsky-Shapiro and C. Matheus, Knowledge Discovery in Databases: An Overview. AI Magazine, Fall 1992, pp. 213-228.
- [2] D. Hand, H. Mannila, P. Smyth: Principles of Data Retrieval. MIT Press, Cambridge, MA, 2001. ISBN 0-262-08290-X (mainly the theoretical background of each data retrieval method).
- [3] Jiawei Han and Micheline Kamber "Data Retrieval: Concepts and Techniques," Morgan Kaufmann, second edition, 2006, ISBN 978-1558609013 (Encyclopedia book with everything).
- [4] Ian H. Witten and Eibe Frank, "Data Retrieval: Practical Machine Learning Tools and Techniques," Elsevier, second edition, 2005, ISBN 978-0120884070 (Tutorials on how to use different techniques and free tools Weka).
- [5] Hiroshi Motoda, Shusaku Tsumoto, Takahira Yamaguchi, Masayuki Numao "Basics of Data Retrieval" Ohmsha, 2006, ISBN 978-4274203480 (Book for beginners who can get a bird's-eye view of the whole).
- [6] Takeshi Fukuda, Yasuhiko Morimoto, Go Tokuyama "Data Retrieval" Kyoritsu Shuppan, 2001.9, ISBN 4-320-12002-7 (Details on association rule extraction).
- [7] Kohei Arai, Four Dimensional GIS and Its Application to Disaster Monitoring with Satellite Remote Sensing Data, Proceedings of the Conference on GIS and Application of Remote Sensing to Disaster Management, 132-137(1997).
- [8] Kohei Arai, An Expectation to Remote Sensing for Disaster Management, Proceedings of the United nation and Japan-US Science/Technology and Space Application Program Joint Symposium on Disaster Management, (1997).
- [9] Kohei Arai, The Conference on GIS and Application of Remote Sensing to Disaster Management Four Dimensional GIS and Its Application to Disaster Monitoring with Satellite Remote Sensing Data, Proceedings of the Conference on GIS and Application of Remote Sensing to Disaster Management, 132-137 Greenbelt, Merryland, U.S.A., 1997.
- [10] Kohei Arai, The Current Status on Disaster Monitoring with Satellites in Japan, Proc. of the Committee on Earth Observation Satellites/Working Group on Information Systems and Services/Task Team 19 Meeting, Greenbelt, Merryland, U.S.A., 1997.
- [11] Kohei Arai, An Expectation on Remote Sensing Technology for Disaster Management and Response, United Naciones Proceedings Series, Edt.Y.Ogawa and Kohei Arai, No.28, p.11, 1998.
- [12] Kohei Arai, Disaster monitoring with ASTER onboard Terra satellite, Proceedings of the Japan-US Science, Technology and Space Application Program Workshop, Hiro, Hawaii, (2000).
- [13] Kohei Arai, Clearing house for disaster management, Proceedings of the Japan-US Science, Technology and Space Application Program Workshop, Hiro, Hawaii, Nov.15, (2000).
- [14] Kohei Arai, ICT technology for disaster mitigation,-Tsunami warning system-, Proceedings of the 1st International Workshop on Knowledge Cluster Systems, 2007.
- [15] Kohei Arai, Tri Harsono, Achmad Basuki, Cellular automata for traffic modelling and simulation in a situation of evacuation from disaster areas, Cellular Automata-Simplicity Behind Complexity, Edt. Aiejandro Salcido, ISDN: 978-953-307-230-2, InTech Publishing Co.Ltd., 193-218, 2011.
- [16] Kohei Achmad Basuki, New Approach of Prediction of Sidoarjo Hot Mudflow Disaster Area Based on Probabilistic Cellular Automata, Geoinformatica - An International Journal (GIJ), 1, 1, 1-11, 2011.
- [17] Kohei Arai, Sensor network for landslide monitoring with laser ranging system avoiding rainfall influence on laser ranging by means of time diversity and satellite imagery data based landslide disaster relief, International Journal of Applied Sciences, 3, 1, 1-12, 2012.

AUTHOR'S PROFILE

- [18] Kohei Arai, Visualization of 5D assimilation data for meteorological forecasting and its related disaster mitigation utilizing VIS5D of software tool, International Journal of Advanced Research in Artificial Intelligence, 2, 9, 24-29, 2013.
- [19] Kohei Arai, Hiroshi Okumura, Shogo Kajiki, Disaster relief with satellite based synthetic aperture radar data, Proceedings of the SAI Future Technology Conference 2017, No.521, 1026-1029, in Vancouver, 2017.
- [20] Kohei Arai, Sentinel 1A SAR Data Analysis for Disaster Mitigation in Kyushu, Kyushu Branch of the Japanese Society on Remote Sensing, Special Lecture for Young Engineers on Remote Sensing, Nagasaki University, 2018.
- [21] Kohei Arai, Flooding and oil spill disaster relief using Sentinel of remote sensing satellite data, International Journal of Advanced Computer Science and Applications IJACSA, 10, 12, 290-297, 2019.
- [22] Kohei Arai, Convolutional neural network considering physical processes and its application to disaster detection, International Journal of Advanced Computer Science and Applications IJACSA, 10, 12, 105-111, 2019.
- [23] Tsuguti, H. and T. Kato, 2014: Contributing Factors of the Heavy Rainfall Event at Amami-Oshima Island, Japan, on 20 October 2010. JMSJ , 92 , 163-183.

Kohei Arai, He received BS, MS and PhD degrees in 1972, 1974 and 1982, respectively. He was with The Institute for Industrial Science and Technology of the University of Tokyo from April 1974 to December 1978 also was with National Space Development Agency of Japan from January, 1979 to March, 1990. During from 1985 to 1987, he was with Canada Centre for Remote Sensing as a Post Doctoral Fellow of National Science and Engineering Research Council of Canada. He moved to Saga University as a Professor in Department of Information Science on April 1990. He was a councilor for the Aeronautics and Space related to the Technology Committee of the Ministry of Science and Technology during from 1998 to 2000. He was a councilor of Saga University for 2002 and 2003. He also was an executive councilor for the Remote Sensing Society of Japan for 2003 to 2005. He is a Science Council of Japan Special Member since 2012. He is an Adjunct Professor of University of Arizona, USA since 1998. He also is Vice Chairman of the Science Commission "A" of ICSU/COSPAR since 2008 then he is now award committee member of ICSU/COSPAR. He wrote 55 books and published 620 journal papers as well as 450 conference papers. He received 66 of awards including ICSU/COSPAR Vikram Sarabhai Medal in 2016, and Science award of Ministry of Mister of Education of Japan in 2015. He is now Editor-in-Chief of IJACSA and IJISA.<http://teagis.ip.is.saga-u.ac.jp/index.html>

Ranking Beauty Clinics in Riyadh using Lexicon-Based Sentiment Analysis and Multiattribute-Utility Theory

Zuhaira M. Zain^{1*}, Aya A. Alhajji², Norah S. Alotaibi³, Najwa B. Almutairi⁴
Alaa D. Aldawas⁵, Muneerah M. Almazrui⁶, Atheer M. Alhammad⁷

Information Systems Department
College of Computer and Information Sciences
Princess Nourah Bint Abdulrahman University
Riyadh, Saudi Arabia

Abstract—In recent years, the amount of beauty-related user-created content has steadily increased. Digital beauty-clinic reviews have major impact on user preferences. In supporting user selection decisions, ranking beauty clinics via online reviews is a valuable study subject, although research on this problem is still fairly limited. Sentiment analysis is a very important subject in the research community to evaluate a predefined sentiment from online texts written in a natural language on a particular topic. Recently, research on sentiment analysis for the Arabic language has become popular, since the language has become the fastest-growing language on the web. However, most sentiment-analysis tools are designed for the Modern Standard Arabic language, which is not widely used on social-media platforms. Moreover, the number of lexicons designed to handle the informal Arabic language is restricted, especially in the beauty-clinic-related domain. Besides, numerous sentiment-analysis studies have concentrated on improving the accuracy of sentiment classifiers. Studies about choosing the right company or product on the basis of the results of sentiment analysis are still missing. In decision-analysis domain, the multiattribute-utility theory has been extensively used in selecting the best option among a set of alternatives. Thus, this research aims to propose a systematic methodology that can develop a beauty-clinic-domain-related sentiment lexicon in Saudi dialect, perform sentiment analysis on online reviews of 10 beauty clinics in Riyadh based on the built lexicon, and feed the lexicon-based sentiment analysis results to the multiattribute-utility theory method to evaluate and rank the beauty clinics. Results showed that the Abdelazim Bassam Clinic is Riyadh's best beauty clinic on the basis of the proposed method. The research not only impacts data analysts regarding how to rate beauty clinics on the basis of lexicon-based sentiment-analysis results, but also directs users toward selecting the best beauty clinic.

Keywords—Arabic language; beauty clinics; ranking; Lexicon-based; machine learning; sentiment analysis; multiattribute-utility theory

I. INTRODUCTION

The number of women who undergo cosmetic procedures in Saudi Arabia has grown significantly over the last few years. Liposuction, laser hair removal, Botox, and filler treatments are all classified as cosmetic procedures. Exposure to cosmetic procedures has increased in Saudi Arabia due to

media penetration, ever-changing beauty standards, the popularity of the fashion and film industries, per capita income growth, reduced prices for cosmetics, and increasing obesity, thereby generating a high demand for cosmetic treatment in Saudi Arabia [1]. This demonstrates that cosmetic procedures are becoming a trend in Saudi Arabia not only for women, but also for men to some extent; one study showed that 90.5% of clients are female and 9.5% of them are male. Therefore, the number of beauty clinics has also relatively increased [2]. However, according to the Saudi Press Agency [3], many beauty clinics took advantage of this trend in an unpleasant way that resulted in many distortions and legal problems, especially related to unlicensed cosmetic surgeries carried out in beauty salons and unlicensed beauty clinics that used untrusted medical devices. This phenomenon is a growing concern for Saudi women when choosing an appropriate clinic, as there is no clear study or analysis of beauty clinics in Saudi Arabia, especially in Riyadh.

Currently, with the advent and rapid growth of social-media apps, people have begun revealing their views and opinions on, for example, goods, social issues, and policies on the Internet, which has increased the number of user-generated reviews containing rich opinions and sentiment information. Opinion mining, often referred to as sentiment analysis, is a research field that seeks to examine individual perceptions or opinions toward entities such as topics, people, problems, organizations, or events. Sentiment analysis (SA) is a way of classifying text into positive, negative, or neutral sentiments that deal with subjective statements. SA is common because people tend to take advice from other people when making successful investments. It also allows for suppliers to provide insight into the success of their products or services [4].

One of the most commonly utilized techniques is lexicon-based SA. Using this technique, sentiment is classified on the basis of sentiment lexicons. Sentiment lexicons are series of terms correlated with positive- or negative-sentiment orientation [5,6]. They are also called polar or opinion terms. There were several studies performed that built sentiment lexicons for the Modern Standard Arabic language [7–10]. However, they are not relevant to views or comments extracted from social-media platforms, which mostly use the

*Corresponding Author

informal Arabic language. The informal Arabic language ignores standard rules of spelling and grammar. Furthermore, it can vary from one region to another because each region has its own dialect. Several studies developed informal Arabic lexicons in the Lebanese [11], Algerian [12], and Saudi dialects [13,14], but they might not be relevant to the beauty-clinic-related context. In addition, most sentiment-analysis studies focused on improving accuracy. There is still a lack of studies providing information on how to select the best product or organization on the basis of sentiment-analysis results.

There is an established method called multicriteria decision making (MCDM) that can help decision-makers to make decision on a set of alternatives. Some well-known MCDM techniques include multiattribute-utility theory (MAUT) [15], VlseKriterijumska Optimizacija I Kaompromisno Resenje (VIKOR) [16], analytic hierarchy process (AHP) [17], and Technique for Order Preference by Similarity to the Ideal Solution (TOPSIS) [18]. Research on MCDM has shown that it is challenging to determine which technique is better because no technique can be the best among the existing techniques [19,20]. However, because of its simplicity, MAUT was commonly used [21–23]. MAUT is a well-established form of decision analysis that explicitly discusses how an alternative can be chosen from a collection of alternatives. This approach allows for the decision maker to separately assess alternatives for each attribute. The decision maker allocates relative weights to different attributes. Then, a formal model is used to combine and aggregate values and weights to produce a global assessment of each alternative [15]. A few examples of successful MAUT applications include its recent use to rank a number of bridges [24], select iron and steel suppliers [25], and identify attributes for inclusion in the framework of an education recommendation system [26]. Nevertheless, to the best of our knowledge, it has not been used to analyze decisions based on sentiment analysis results.

To tackle the aforementioned drawbacks, this study proposes a research method that can build a beauty-clinic-domain-related sentiment lexicon in Saudi dialect, conduct sentiment analysis based on the developed lexicon and pass the results to the multiattribute-utility theory method to assess and rank the beauty clinics. This study facilitates potential clients in selecting an experienced and reputable beauty clinic based on reviews from other people with previous experience in cosmetic procedures by extracting their opinions from Twitter, which is one of the most famous social-media platforms where people express their views. The key contributions of this study are as follows:

- A new sentiment lexicon was built for the informal Arabic language (Saudi dialect) from the Twitter accounts of 10 beauty clinics in Riyadh using a manual approach to address the irrelevant sentiment-lexicon problem;
- Online reviews from the Twitter accounts of 10 beauty clinics were preprocessed by performing tokenization,

normalization, cleaning, stemming, and stop-words removal; and classified into sentiment using the newly built sentiment-lexicon;

- The performance of the 10 beauty clinics was evaluated by applying multiattribute-utility theory using the results of lexicon-based sentiment analysis as inputs to show their ranking.

The remainder of this study is structured as follows: Section 2 outlines previous work related to the study; Section 3 elaborates on the methodology used for the research; Section 4 introduces the findings of the study; Section 5 addresses the sensitivity analyses; lastly, Section 6 provides the study conclusions.

II. RELATED WORK

A. Sentiment Lexicon

A sentiment lexicon is one of the most useful means for carrying out sentiment-analysis research for any language. It is an essential tool for both unsupervised (lexicon-based) and supervised (machine-learning) classifiers. It is used by many researchers to generate unsupervised sentiment models or training features in supervised approaches to train machine-learning algorithms. A sentiment lexicon is a set of opinion words or polar terms correlated on the basis of their orientation, i.e., positive, negative, or neutral. The sources and approaches applied to non-English sentiment-lexicon development are graphically illustrated in Fig. 1. For further information on each method, readers may refer to the work of Kaity and Balakrishnan [27].

Al-Twairesh et al. [28] used a translation-based approach to generate comprehensive Arabic sentiment lexicons (AraSenti-Trans) employing the MADAMIRA tool [29], which recognizes Arabic terms in tweets and eliminates tweets containing non-Arabic terms and dialects. They applied two lexicons constructed by Hu and Liu [30], and Wilson et al. [31] as sentiment-orientation tools after preprocessing. They used MADAMIRA's English glossary to determine word polarity upon comparing both lexicons in [30] and [31]. They also applied a frequency-based approach to build the AraSenti-PMI lexicon by adopting the pointwise-mutual-information (PMI) measure to differentiate words as either positive or negative in a corpus. Mahyoub et al. [32] used a relationship-based approach by introducing an algorithm that assigns sentiment scores to Arabic WordNet entries for Arabic sentiment-lexicon construction. Using synset relationships, a semisupervised-learning algorithm was applied to enhance the number of terms in Arabic WordNet. Badaro et al. [7] used a merger-based approach to combine four existing sentiment lexicons (Standard Arabic Morphological Analyzer [33], English WordNet, English SentiWordNet [34,35], and Arabic WordNet [36]) into a new Arabic sentiment lexicon (ArSenL). However, these lexicons were built for standard Arabic, which is not relevant to the language used on social media, i.e., informal Arabic.

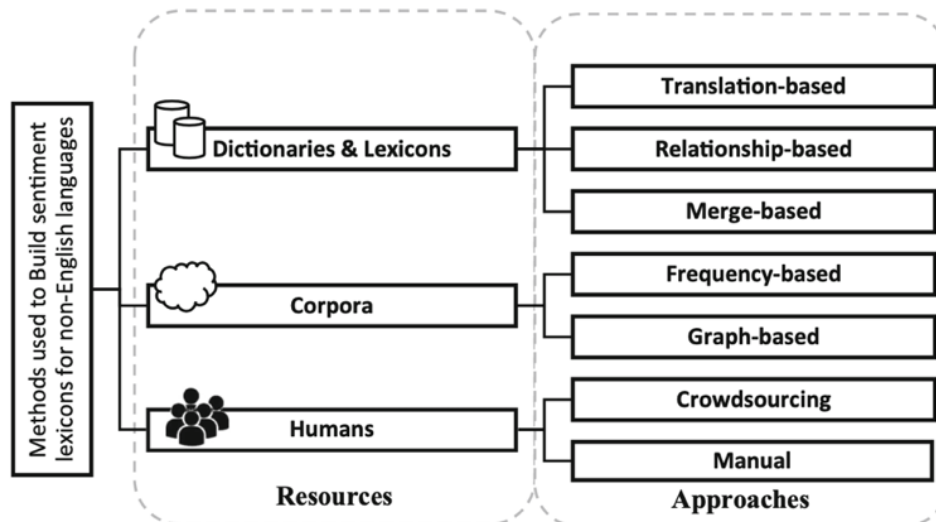


Fig. 1. Resources and Approaches applied to non-English Sentiment-Lexicon Development [27].

Duwairi et al. [37] adopted a crowdsourcing approach to build three sentiment lexicons: a lexicon mapping the Jordanian dialect to Modern Standard Arabic (MSA), a lexicon mapping Arabizi terms to MSA, and an emoticon lexicon. Abdul-Mageed et al. [38] applied a manual approach to develop a 3982 adjective sentiment lexicon as part of the SAMAR system built in MSA and Arabic dialects to examine Arabic subjectivity and sentiments. Al-Ghaith [14] built the SaudiSentiPlus sentiment lexicon containing 7139 Saudi dialect terms by first using an automatic translation of English sentiment lexicons previously generated by [30] and [39]. He then manually extracted all Saudi dialect terms from Twitter sentiment data. However, the lexicons may not be applicable to the beauty-clinic-related context. Despite it being considered time-consuming and costly, many researchers still use a manual approach, particularly those studying sentiment analysis in languages lacking lexical resources.

B. Sentiment Analysis

Sentiment analysis is computational analysis of sentiments, opinions, and emotions in a text related to a specific subject [6]. It assists in attaining many objectives, such as observing public sentiments toward political movements, measuring customer satisfaction [40], establishing market intelligence [41], and predicting sales for a product. Therefore, researchers took advantage of SA and developed it for various purposes in different fields and languages [42,43]. There are four sentiment-analysis tasks: sentiment classification, subjective classification, opinion-spam detection, and review usefulness. SA classification can be done on three levels: the document level, which attempts to show the polarity of an entire document opinion focusing on a single topic (e.g., product or place) from a single opinion holder; the sentence level, which assumes the sentence is a distinct unit that comprises only an opinion; and the feature level, also called the entity level, which seeks to assign polarity to multiple reviews using extracted features [44–48]. These processes can be completed by applying three main techniques: a lexicon-based, machine-learning, or hybrid technique [49]. The lexicon-based technique counts and

weighs sentiment-related words to enable the adoption of a lexicon to perform sentiment analysis. The machine-learning (ML) technique predicts the polarity of a large number of posts using training datasets or annotated corpora. The hybrid technique combines the lexicon-based and machine-learning techniques, whereby the lexicon-based classifier builds a dataset by labeling each tweet on the basis of a sentiment lexicon, and the machine-learning-based classifier is trained and tested using the dataset generated from the lexicon-based approach [49,50].

1) *Lexicon-Based approach*: A lexicon-based approach, known as the dual-polarity algorithm, was developed by El-Beltagy and Ali [51] to determine the weights of Egyptian dialect sentiment lexicon terms, achieving 70% accuracy. Abdulla et al. [52] constructed a lexicon-based sentiment-analysis method by considering negation and intensification to measure text polarity. They applied a basic lexicon-based approach on an Arabic corpus collected from Twitter and Yahoo!-Maktoob by calculating positive and negative terms in a given text, and then they categorized the sentences using a larger category. Applying various lexicon scalability stages, they achieved 70.05% accuracy. Ayyoub et al. [8] developed a sentiment lexicon of approximately 120,000 Arabic terms extracted from Twitter, and developed a lexicon-based sentiment-analysis method using a predicate calculus. Their proposed method demonstrated better predictive accuracy (86.89%) compared to that of the keyword-based method. Assiri et al. [10] built a Saudi dialect lexicon manually that includes 14,000 sentiment words. They then built a weighted lexicon-based classifier. Their proposed classifier removed associations between polarity and nonpolarity terms for a dataset, and then weighted these terms by using their associations. They applied new rules for processing certain linguistic features such as negation and supplication. Their enhanced lexicon-based sentiment-analysis classifier achieved 81% accuracy.

2) *Machine-Learning approach*: Hodeghatta [53] conducted sentiment analysis using the naïve Bayes and MaxEnt algorithms to categorize Twitter messages related to Hollywood movies as positive, negative, and cognitive sentiments across various regions of various countries. The classifiers were tested for both unigrams and bigrams. The MaxEnt classifier with unigrams achieved the highest accuracy of 84%. Jokhio et al. [54] determined the sentiment polarity (positive, negative, or neutral) of English tweets related to plastic-surgery treatments in the United States using a naïve Bayes algorithm. The experimental results demonstrate the importance of the suggested method, which may allow potential groups of people who want to have plastic-surgery treatments to make better decisions. Recently, Naseem et al. [55–57] proposed Deep Intelligent Contextual Embedding (DICE) [55], Hybrid Words Representation [56] and Transformer-based Deep Intelligent Contextual Embedding (DICET) [57] models to improve tweet quality by considering polysemy, syntax, semantics, and out of vocabulary (OOV) words; and handling the noise within the textual context. The evaluation of the models executed on airline-related datasets indicated that their proposed models improved the accuracy for tweets classification with an average accuracy of 93.5%, 94.2%, and 94.6%, respectively. The results verified that their models can successfully handle low-quality data and language complexities. However, these studies only considered tweets written in the English language.

3) *Hybrid approach (Lexicon-Based + ML)*: Yoo and Nam [58] proposed a hybrid approach to Korean sentiment analysis, where a lexicon-based classifier was used to locally parse sentiment components to identify opinions, while a naïve Bayes classifier was used to categorize the text in a dictionary by training the MUSE (Multilingual Sentiment Lexica and Sentiment-Annotated Corpora) opinion corpus. Aldayel and Azmi [59] combined a lexicon-based technique and a machine-learning-based algorithm to detect the polarities of Arabic tweets. Through this approach, the lexical-based classifier was used to label the training data from a manually built sentiment lexicon. The output of the lexicon-based classifier was adopted as training data for the support-vector-machine (SVM) classifier.

However, all aforementioned studies [8,10,51–59] solely focused on how to improve the accuracy or performance of the sentiment classifier, which is not the main focus in this study. There is still a lack of studies providing information on how to select the best product or organization on the basis of sentiment-analysis results.

C. Multiattribute-Utility Theory

Multiattribute-utility theory (MAUT) is a well-established decision-analysis approach that discusses precisely how to choose an alternative from a set of alternatives. Although the functional implementation of the multiattribute-utility technique can differ, the process involves the following steps [15]:

1) Identifying alternatives and value-relevant attributes: The first process is to define the alternatives available and their most important attributes.

2) Separately assessing each alternative in terms of each attribute: Each alternative is assessed in terms of each attribute set out in Step 1.

3) Allocating relative weights to attributes: The weights for each attribute are allocated using a direct-rating method. The total rating for each attribute is calculated and transformed into weights using the following formula:

$$w_i = \frac{w'_i}{\sum_{i=1}^n w'_i} \quad (1)$$

where w_i is the weight for each attribute, and w'_i is the relative importance rating score for each attribute. Thus, individual weights are obtained that sum to 1 for each attribute, as is conventional in the MAUT [15].

4) Aggregating attribute weights and single-attribute assessments of alternatives for a global assessment of alternatives: Weights and single-attribute values or functions are aggregated by adopting the weighted linear additive preference function [15] shown in (2).

$$v(A) = \sum_{i=1}^n w_i v_i(A_i), \quad (2)$$

where $v_i(A_i)$ is the value of alternative A in terms of the i -th attribute, w_i is the importance weight of the i -th attribute, and n is the number of different attributes [15].

5) Conducting sensitivity analyses and offering recommendations: In the previous step, multiattribute utilities are determined for all alternatives. The best alternative should be that with the highest multiattribute utility. Sensitivity analyses are carried out in the last stage of the process to determine the stability of the results. The effect of various values and weights on the multiattribute utility of the available alternatives can then be calculated. Different values and weights can be obtained using various methods of elicitation. For instance, both the direct-rating method and the bisection approach may be applied to obtain values. Thus, multiattribute utilities are measured twice: once using the values calculated using the direct-rating method, and then using the values calculated using the bisecting tool. Then, the resulting multiattribute utility for the available alternatives can be evaluated, and the stability of the results can be calculated. An alternative way of understanding the robustness of the results is to apply a different weighting method. For instance, the equal-weight method can be adopted. This method simplifies the selection process by avoiding information on the relative importance of each attribute [60,61]. This means that the approach assumes that all attributes are of equal weight. For instance, for four attributes, the weight of each attribute would be $1/4 = 0.25$. The total value for each alternative is attained by summing the values in terms of each attribute. The rank-reciprocal rule and rank-sum weighting techniques can also be used to assign weights [15].

III. METHODS

The research methodology of this study, as depicted in Fig. 2, comprises six phases: (1) collecting data, (2) constructing sentiment lexicon, (3) preprocessing, (4) classifying tweets, (5) developing classification models, and (6) ranking beauty clinics. The details of each phase are outlined in the subsections.

A. Phase 1: Collecting Data

In this phase, data were collected using the Twitter application programming interface (API), which is an interface for researchers to collect data from a given social-media service. Opinions were aggregated using the *Tweepy* library by searching for tweets related to the 10 selected beauty clinics (Panorama, Pearl, Alzallal, Obagi, Abas, Derma, Kesaaee, AbdelAzim Bassam, Adma, and The Clinic). These beauty clinics are the most popular in Riyadh. The overall number of aggregated tweets was 780.

B. Phase 2: Constructing Sentiment Lexicon

A sentiment lexicon is a table where each word is associated with its polarity, which indicates each word's orientation (positive, neutral, or negative). In this phase, an informal Arabic sentiment lexicon in the Saudi dialect was built by manually extracting sentiment words from the collected dataset. Each sentiment word was assigned its polarity. Afterward, the lexicon was used to assign polarity to each tweet using its score.

As this project was conducted in the informal Arabic language, many tweets contained emoji. Since most emoji change the meaning of sentences, an emoji lexicon was also built. A function from the Python library called *extract_emojis()* was used to find the emoji in our dataset.

In order to simplify the classification process in Phase 4, the lexicon was separated into four groups: positive- and

negative-word lexicons, and positive- and negative-emoji lexicons. Each of these lexicons was stored in a different list.

C. Phase 3: Preprocessing Data

In this phase, the dataset was preprocessed using the following techniques:

- **Tokenization:** Data were transformed from the sentence level to the word level by dividing the text into a set of meaningful tokens using the *codecs* and *nlk* libraries, and the *word_tokenize()* function.
- **Text cleaning:** All non-Arabic words, special Twitter characters, and usernames (for example, # and @), and irrelevant information (for example, universal resource locators (URLs)) were removed. In addition, retweets were eliminated.
- **Text normalization and eliminating repeated letters:** In this step, some Arabic letters were transformed into general letters, such as unifying the letter *alif* by replacing \aleph , \aleph , and \aleph with \aleph . In addition, repeated letters such as *مرررة* and *مرة* were removed. This process was done using the *re*, *sys*, *string*, and *argparse* libraries.
- **Stop-word removal:** Words with no meaning or that do not hold information and have no effect on the output, such as conjunctions, articles, and prepositions, including *في*/fi (in), *من*/min (of), and *على*/ala (on), were removed. The stop-word list was imported from the *nlk* corpus, which contains MSA stop words. Forty-nine new informal Arabic stop words were added to the list.
- **Text stemming:** Numerous Arabic words have a similar stem. For example, *يكره*/yakrah (he hates), *تكره*/takrah (she hates), *اكره*/akrah (I hate), *يكرهون*/yakrahon (they hate) all originate from *كره*/kurh (hate); thus, all words were replaced with their *كره*/kurh (hate) stem using the *nlk ISRIStemmer* to eliminate redundant terms.

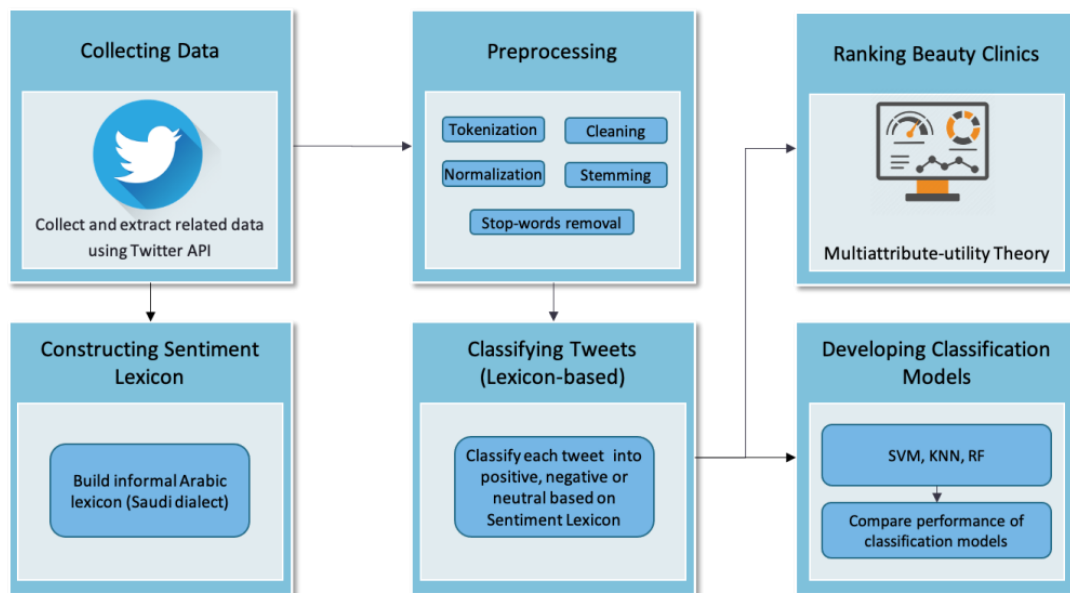


Fig. 2. Research Methodology.

D. Phase 4: Classifying Tweets

Algorithm 1 [59] was applied to classify the preprocessed unannotated tweets as positive, negative, or neutral. The algorithm takes the dataset containing tweets and tokenizes it; then, it checks each token's score from the built lexicon and adds it for each sentence. If the overall score for the tweet is greater than zero, a positive label is assigned; otherwise, a negative label is assigned.

Algorithm 1

```
Input: preprocessed unannotated tweets
Output: set of classified and annotated tweets along with their sentiment
(positive or negative), and a set of unclassified tweets (corresponding to
neutral sentiment).
Begin
For each tweet  $t$  in training set do
 $W =$  tokenize tweet  $t$  into a list of words  $w_1, w_2, \dots$  and
emoji  $e_1, e_2, \dots$ 
score = 0
For each  $w_i, e_i$  in  $W$  do
Stem  $w_i, e_i$ 
If ( $w_i$  is in Lexicon) score = score + positivity_degree( $w_i$ )
Else If ( $e_i$  is in Lexicon) score = score + positivity_degree( $e_i$ )
End for
If (score > 0) return POSITIVE
Else return score < 0 ? NEGATIVE:NEUTRAL
End
```

In order to refer to our four lexicon groups, a function called *tweets_polarity* was created to determine the polarity of each tweet. This function takes one parameter (i.e., a tweet) and returns its polarity. At first, each tweet is tokenized and stored into a tokenized-tweet list, W . Second, the *score* variable is set to zero. Third, a *for* loop is created to run through each word and emoji in W . The body of the *for* loop contains an *if* condition to check if the word belongs to a certain lexicon; for example, if the word belongs to the positive-word lexicon, the *score* variable is increased by one. Fourth, another *if* condition enables determining the polarity value using the *score* variable; for example, if the *score* variable was greater than zero, the polarity was set to positive.

A *for* loop was created to run through each entry in the tweet list, followed by storing the value of that entry as a variable and passing it along to the *tweets_polarity* function before calling it. This function is supposed to return the polarity value for a tweet each time it is called. Lastly, the tweets and their polarity values were saved to a dataset. This dataset was used in Phase 5 to train and test three machine-learning classifiers. It was also used in Phase 6 to calculate the total score and rank the beauty clinics.

E. Phase 5: Developing Classification Model

In this phase, classification models were built on the basis of three popular classifiers: random forest (RF), support vector machine (SVM), and K-nearest neighbor (KNN). The models were trained and tested using Python. The dataset generated from Phase 4 was divided into training and testing sets in a 70:30 ratio. All three classifiers were set to their default values. Next, the performance of the models was compared on the basis of their accuracy.

F. Phase 6: Ranking Beauty Clinics

In this phase, the multiattribute-utility theory technique was applied in the following steps:

1) Identifying alternatives and value-relevant attributes: In this study, we evaluated the 10 most popular beauty clinics in Riyadh on the basis of three attributes generated from lexicon-based sentiment analysis: positive, negative, and neutral tweets.

2) Separately assessing each alternative in terms of each attribute: The 10 beauty clinics were evaluated using the three attributes generated from the lexicon-based sentiment analysis as a function of the total count of positive, negative, and neutral tweets.

3) Allocating relative weights to the attributes: The weights for each attribute were assigned using the direct-rating method. An online questionnaire was designed where the decision makers (beauty-clinic users) were invited to rate the relative importance of the three attributes on a five-point Likert scale, where 1 denotes the least and 5 denotes the most important attribute. The total rating for each attribute was computed and transformed into weights using (1).

4) Aggregating the weights of attributes and the single-attribute assessments of alternatives to calculate the global assessment of alternatives: Weights and single-attribute values were aggregated using (2).

5) Running sensitivity analyses and generating recommendations: The alternatives were ranked on the basis of the aggregation score obtained in Step 4. The alternative with the highest aggregation score was assigned the highest rank; the alternative with the lowest score was assigned the lowest rank. The alternative with the highest score was considered the most preferred. Sensitivity analyses were run to evaluate the stability of the results. In this study, two sensitivity analyses were conducted: (1) using only the single attribute with the highest weight, and (2) using equal weight. In the first, alternatives were ranked on the basis of the rating score for the attribute with the highest weight. In the second, since we used the equal-weight technique, the weight for each attribute was 0.33. The global value for each alternative was computed, and the alternatives were ranked on the basis of their global score. The ranking results using these techniques were compared with the result using the proposed technique.

In order to direct us in the presentation of the results of our analysis, the six following research questions were raised:

- RQ1: What is the structure of the built sentiment lexicon?
- RQ2: What is the total number of positive, negative, and neutral tweets for each beauty clinic?
- RQ3: Which ML classifiers perform best?
- RQ4: Which clinic is the most preferred by clients?
- RQ5: What is the impact of using the single-attribute utility?

- RQ6: What is the impact of using different weighting methods?

IV. RESULTS

A. RQ1 Answer: Structure of Sentiment Lexicon

The sentiment lexicon generated from the 780 tweets collected in this study consisted of 658 sentiment words: 276 negative, 276 positive, and 106 neutral words. Table 1 shows a sample of the informal Arabic word lexicon.

It also consisted of 150 sentiment emoji: 72 positive, 54 negative, and 24 neutral emoji. Table 2 presents an example of the emoji lexicon. Since neutral words and emoji were assigned a polarity of zero, they were not inserted into the lexicon list.

B. RQ2 Answer: Total Number of Positive, Negative, and Neutral Tweets for each Beauty Clinic

We were unable to present the results of tweet classification because we are bound to Twitter’s privacy policy that prevents the publication of the original tweets that were collected. Table 3 portrays the number of tweets for each beauty clinic that were classified as positive, negative, or neutral. The total count of positive, negative, and neutral tweets was considered as the rating score for each clinic in terms of each attribute.

C. RQ3 Answer: Best ML Classifier

Table 4 demonstrates that SVM outperformed RF and KNN in classifying the tweets as positive, negative, or neutral sentiments with 72.1% accuracy. This result was expected, and it was deemed acceptable for the small size of the training dataset. It may have achieved better performance if we had increased the size of the training dataset.

D. RQ4 Answer: Most Preferred Beauty Clinic

Table 5 shows the total relative importance of each attribute as rated by 46 beauty-clinic users. The weights for each attribute were calculated by using (1). Positive tweets had the highest weight value (0.5), followed by neutral tweets (0.4) and negative tweets (0.1). These weight values were used to aggregate the rating score for each beauty clinic.

Table 6 demonstrates the total rating score for each beauty clinic that was computed using (2). The global scores for each beauty clinic were sorted in descending order, and a bar graph was plotted to show the rank.

TABLE I. SAMPLE OF INFORMAL ARABIC WORD LEXICON

Word	Polarity	Word	Polarity
تهيل/t'habel (amazing/female form)	1	مقرف/mogref (disgusting)	-1
يهيل/yhabel (amazing/male form)	1	زفت/zift (bad)	-1
يخفق/ykhageg (outstanding)	1	زحمة/zahma (crowded)	-1
راهب/raheeb (awesome)	1	بعيد/baeed (far)	-1
احسن/ahsan (better/best)	1	سيئ/saye' (bad)	-1
افضل/afdhal (better/best)	1	سيء/saye' (bad)	-1

TABLE II. SAMPLE OF EMOJI LEXICON

Emoji	Polarity	Emoji	Polarity
👍	1	😞	-1
❤️	1	😡	-1
😄	1	❤️	-1
👉	1	👎	-1
♥️	1	😞	-1
👍	1	😞	-1

TABLE III. TWEET CLASSIFICATION

Clinic	Positive Tweets, x_1	Negative Tweets, x_2	Neutral Tweets, x_3	Total Tweets
Panorama Clinic, A_1	8	45	43	96
Pearl Clinic, A_2	3	12	19	34
Alzallal Clinic, A_3	10	18	35	63
Obagi Clinic, A_4	6	6	22	34
Abas Clinic, A_5	23	18	77	118
Derma Clinic, A_6	36	28	98	162
Kesaaee Clinic, A_7	20	7	26	53
AbdelAzim Bassam, A_8	63	18	78	159
Adma Clinic, A_9	4	3	2	9
The Clinic, A_{10}	26	4	22	52
Total, $v_i(A)$	199	159	422	780

TABLE IV. ACCURACY OF MACHINE-LEARNING CLASSIFIERS

Classifier	Accuracy (%)
Random forest (RF)	67.2
Support vector machine (SVM)	72.1
K-nearest neighbor (KNN)	67.2

TABLE V. WEIGHTS FOR EACH ATTRIBUTE

	Positive Tweets	Negative Tweets	Neutral Tweets	Total
Total relative importance rating score	226	46	180	452
w_i	$226/452 = 0.5$	$46/452 = 0.1$	$180/452 = 0.4$	1

TABLE VI. TOTAL AGGREGATION SCORE FOR BEAUTY CLINICS

Clinic	$w_1v_1(A_i)$	$w_2v_2(A_i)$	$w_3v_3(A_i)$	$v(A_i)$
Panorama Clinic, A_1	4	4.5	17.2	25.7
Pearl Clinic, A_2	1.5	1.2	7.6	10.3
Alzallal Clinic, A_3	5	1.8	14	20.8
Obagi Clinic, A_4	3	0.6	8.8	12.4
Abas Clinic, A_5	11.5	1.8	30.8	44.1
Derma Clinic, A_6	18	2.8	39.2	60.0
Kesaaee Clinic, A_7	10	0.7	10.4	21.1
AbdelAzim Bassam, A_8	31.5	1.8	31.2	64.5
Adma Clinic, A_9	2	0.3	0.8	3.1
The Clinic, A_{10}	13	0.4	8.8	22.2

Fig. 3 illustrates the ranking of the 10 Riyadh beauty clinics. AbdelAzim Bassam Clinic was found to be the most preferred among all beauty clinics investigated in this study on the basis of its rank.

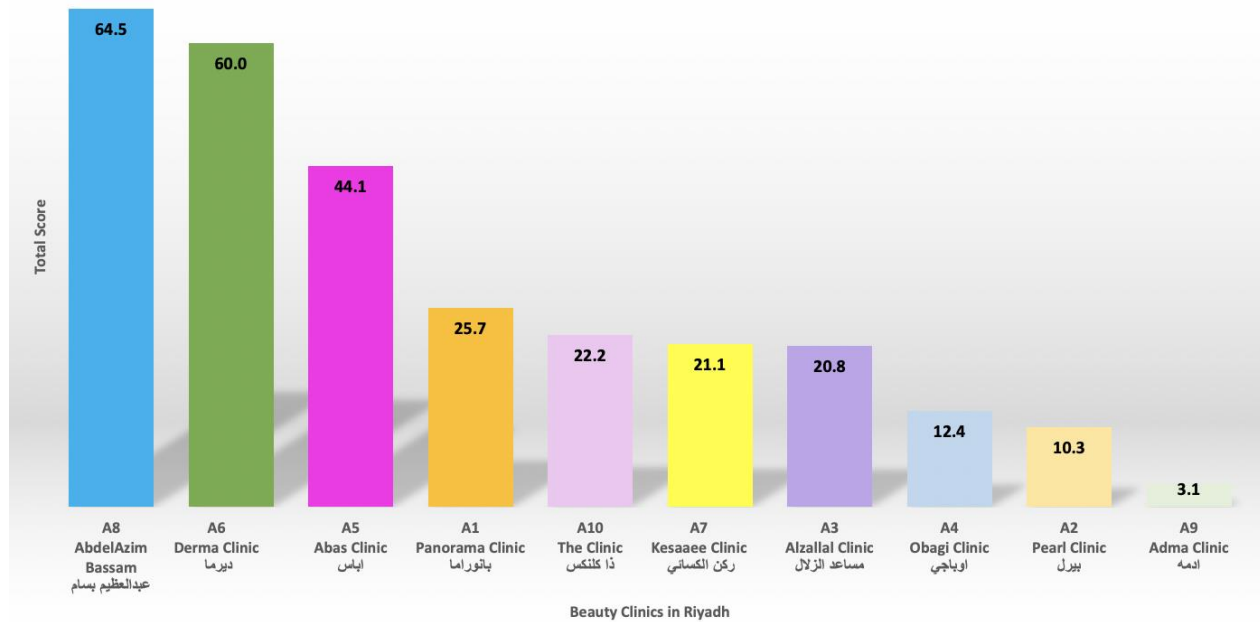


Fig. 3. Ranking of Riyadh's Beauty Clinics

V. DISCUSSION

A. RQ5 Answer: Impact of using the Single-Attribute Utility

Table 7 presents the results of the first sensitivity analysis that was conducted using a single attribute. Results showed that the existing ranking of the alternatives changed for five pairs of alternatives: A_1-A_3 , A_1-A_7 , A_1-A_9 , A_2-A_9 , and A_5-A_{10} . Despite these changes in the ranking of some pairs of alternatives, the first-ranked alternative remained unaffected.

B. RQ6 Answer: Impact of using Different Weighting Methods

Table 8 displays the results of the second sensitivity analysis that was conducted using equal weight. Results showed that the existing ranking of the alternatives changed for five pairs of alternatives: A_2-A_4 , A_3-A_7 , A_3-A_{10} , A_6-A_8 , and A_7-A_{10} . The impact of using equal weight was more critical because it affected the first-ranked alternative.

TABLE VII. SENSITIVITY ANALYSIS USING A SINGLE ATTRIBUTE

Method	Ranking
Proposed (multiattribute utility)	$A_8 > A_6 > A_5 > A_1 > A_{10} > A_7 > A_3 > A_4 > A_2 > A_9$
Single-attribute utility (positive tweets)	$A_8 > A_6 > A_{10} > A_5 > A_7 > A_3 > A_1 > A_4 > A_9 > A_2$

TABLE VIII. SENSITIVITY ANALYSIS USING EQUAL WEIGHT

Method	Ranking
Proposed (relative importance)	$A_8 > A_6 > A_5 > A_1 > A_{10} > A_7 > A_3 > A_4 > A_2 > A_9$
Equal weight (0.33)	$A_6 > A_8 > A_5 > A_1 > A_3 > A_7 > A_{10} > A_2 > A_4 > A_9$

C. Validity Threats

There were three threats to validity considered in this study: threats to construct, internal, and external validity.

Threats to construct validity were related to the performance measure used in this study. Machine-learning performance was measured on the basis of accuracy. Many other performance metrics can be used, such as F-measure, sensitivity, and precision. However, accuracy is widely used by many researchers when measuring the performance of lexicon-based or machine-learning classifiers in sentiment-analysis research.

Threats to internal validity were related to uncontrolled internal factors that might have influenced the experiment results. These internal factors would have occurred during method implementation. In order to minimize these threats, we first used a standard lexicon-based algorithm proposed by [59] to build the training dataset. Second, we chose three well-known classifiers provided by scikit-learn libraries [62] (RF, SVM, and KNN) to train and test the tweet dataset. We applied default settings for all three classifiers. Third, the formula used for MAUT was taken from an established resource [15].

Threats to external validity were related to the possibility of generalizing the results of this study. One possible factor was the use of a dataset from 10 beauty clinics in Riyadh. This dataset was very limited and domain-specific. However, this study focused on evaluating 10 beauty clinics in Riyadh; thus, the best way to reduce this threat was to select the Twitter accounts of the 10 most popular beauty clinics in Riyadh. Another possible factor constituted the methods used for sensitivity analysis. In this study, we ran sensitivity analyses using the single-attribute evaluation technique and the equal-weight method. There are various other methods that can be used, such as VIKOR, AHP, TOPSIS, and the rank-sum

weighting method. However, the methods used in this analysis are among numerous suggested in the literature, and they are commonly used because of their simplicity.

VI. CONCLUSION

In this study, a novel method for ranking beauty clinics in Riyadh was proposed. It started with data collection from 10 beauty clinics in Riyadh using the Twitter API. The dataset was manually transformed into a sentiment lexicon. Then, data were preprocessed by applying tokenization, cleaning, normalization, stop-word removal, and stemming techniques. Next, preprocessed tweets were classified as positive, negative, or neutral using a lexicon-based approach. Lastly, the rating score for each beauty clinic was computed using multiattribute-utility theory to rank the beauty clinics.

Results showed that Abdelazim Bassam Clinic is Riyadh's best beauty clinic on the basis of the proposed method. This study will impact clients when choosing the best beauty clinic. Moreover, it can assist beauty-clinic owners in understanding how they are faring with their clients, as it gives them a better picture of how they stack up against their competitors, thereby providing them with an opportunity to improve their services. Furthermore, this study provides data analysts with an example of how to rate beauty clinics by using lexicon-based sentiment-analysis results.

In the future, we will increase the number of words and emoji in our sentiment lexicon. Furthermore, we will combine some machine-learning algorithms and evaluate their performance in classifying tweets as a function of their polarity. An aspect-based sentiment analysis will be applied to obtain additional attributes to evaluate the performance of beauty clinics.

REFERENCES

- [1] Technavio Research, "Global Cosmetic Surgery Market 2019-2023| Evolving Opportunities with ALLERGAN and Bausch Health| Technavio," 2019.
- [2] S. E. Alharethy, "Trends and demographic characteristics of Saudi cosmetic surgery patients," *Saudi Medical Journal*. vol. 38, no. 7, pp. 738–741, 2017, doi: 10.15537/smj.2017.7.18528.
- [3] Saudi Press, "Medicine and health prohibit a medical device used in a beauty clinic," 2017.
- [4] M. T. Khan, M. Durrani, A. Ali, I. Inayat, S. Khalid, and K. H. Khan, "Sentiment analysis and the complex natural language," *Complex Adaptive Systems Modeling*. vol. 4, no. 1. Springer, Dec. 01, 2016, doi: 10.1186/s40294-016-0016-9.
- [5] S. Ahire, "A survey of sentiment lexicons," 2015, [Online]. Available: <https://www.semanticscholar.org/paper/A-Survey-of-Sentiment-Lexicons-Ahire/2522de6022acf2bc7d5c12a9467d4c41f6358920>.
- [6] W. Medhat, A. Hassan, and H. Korashy, "Sentiment analysis algorithms and applications: a survey," *Ain Shams Engineering Journal*. vol. 5, no. 4, pp. 1093–1113, Dec. 2014, doi: 10.1016/j.asej.2014.04.011.
- [7] G. Badaro, R. Baly, H. Hajj, N. Habash, and W. El-Hajj, "A large scale Arabic sentiment lexicon for Arabic opinion mining," in *Proceedings of the EMNLP 2014 Workshop on Arabic Natural Language Processing (ANLP)*, 2014, pp. 165–173.
- [8] M. al Ayyoub, S. B. Essa, and I. Alsmadi, "Lexicon-based sentiment analysis of Arabic tweets," *International Journal of Social Network Mining*. vol. 2, no. 2, p. 101, 2015, doi: 10.1504/IJSNM.2015.072280.
- [9] R. Eskander and O. Rambow, "SLSA: A sentiment lexicon for standard Arabic," in *Proceedings of the 2015 Conference on Empirical Methods in Natural Language Processing*, 2015, pp. 2545–2550.
- [10] A. Assiri, A. Emam, and H. Al-Dossari, "Towards enhancement of a lexicon-based approach for Saudi dialect sentiment analysis," *Journal of Information Science*. vol. 44, no. 2, pp. 184–202, Apr. 2018, doi: 10.1177/0165551516688143.
- [11] T. Tobaili, M. Fernandez, H. Alani, S. Sharafeddine, H. Hajj, and G. Glavaš, "Senzi: A sentiment analysis lexicon for the latinised Arabic (Arabizi)," in *International Conference Recent Advances in Natural Language Processing, RANLP*, 2019, vol. 2019-September, pp. 1203–1211, doi: 10.26615/978-954-452-056-4_138.
- [12] M. H. Mataoui, O. Zelmati, and M. Boumechache, "A proposed lexicon-based sentiment analysis approach for the vernacular Algerian Arabic," *Res. Comput. Sci*. vol. 110, 2016.
- [13] S. M. Mohammad, M. Salameh, and S. Kiritchenko, "Sentiment lexicons for Arabic social media," in *10th Annual International Conference on Language Resources and Evaluation*, 2016, pp. 33–37, [Online]. Available: <http://www.saifmohammad.com/WebPages/ArabicSA.html>.
- [14] W. Al-Ghaith, "Developing lexicon-based algorithms and sentiment lexicon for sentiment analysis of Saudi dialect tweets," *International Journal of Advanced Computer Science and Applications*. vol. 10, no. 11, 2019, doi: 10.14569/IJACSA.2019.0101112.
- [15] D. von Winterfeldt and W. Edwards, *Decision analysis and behavioral research*. Cambridge: Cambridge University Press, 1986.
- [16] S. Opricovic and G.-H. Tzeng, "Multicriteria planning of post-earthquake sustainable reconstruction," *Computer-Aided Civil and Infrastructure Engineering*. vol. 17, pp. 211–220, 2002.
- [17] T. L. Saaty, "How to make a decision: the analytic hierarchy process," *European Journal of Operational Research*. vol. 48, pp. 9–26, 1990.
- [18] C.-L. Hwang, Y.-J. Lai, and T.-Y. Liu, "A new approach for multiple objective decision making," *Computers Ops Res*. vol. 20, no. 8, pp. 889–899, 1993.
- [19] M. Qaradaghi and J. P. Deason, "Analysis of MCDM methods output coherence in oil and gas portfolio prioritization," *Journal of Petroleum Exploration and Production Technology*. vol. 8, no. 2, pp. 617–640, Jun. 2018, doi: 10.1007/s13202-017-0344-0.
- [20] I. Siksnelyte-Butkiene, E. K. Zavadskas, and D. Streimikiene, "Multi-criteria decision-making (MCDM) for the assessment of renewable energy technologies in a household: A review," *Energies*. vol. 13, no. 5. MDPI AG, Mar. 01, 2020, doi: 10.3390/en13051164.
- [21] M. Velasquez and P. T. Hester, "An analysis of multi-criteria decision making methods," 2013.
- [22] M. Cinelli, S. R. Coles, and K. Kirwan, "Analysis of the potentials of multi criteria decision analysis methods to conduct sustainability assessment," *Ecological Indicators*. vol. 46. Elsevier, pp. 138–148, 2014, doi: 10.1016/j.ecolind.2014.06.011.
- [23] H. Koornneef, W. J. C. Verhagen, and R. Curran, "A multi-criteria decision making framework for aircraft dispatch assessment," in *Advances in Transdisciplinary Engineering*, 2017, vol. 5, pp. 11–20, doi: 10.3233/978-1-61499-779-5-11.
- [24] Z. A. Bukhsh, I. Stipanovic, and A. G. Doree, "Multi-year maintenance planning framework using multi-attribute utility theory and genetic algorithms," *European Transport Research Review*. vol. 12, no. 3, 2020, doi: <https://doi.org/10.1007/s41109-019-0237-x>.
- [25] Z. Ma, J. Zhu, and S. Zhang, "Probabilistic-based expressions in behavioral multi-attribute decision making considering pre-evaluation," *Fuzzy Optimization and Decision Making*. 2020, doi: 10.1007/s10700-020-09335-8.
- [26] M. Maravanyika and N. Dlodlo, "Selecting attributes for inclusion in an educational recommender system using the multi-attribute utility theory," in *Communications in Computer and Information Science*, 2018, vol. 942, pp. 239–252, doi: 10.1007/978-3-030-01535-0_18.
- [27] M. Kaity and V. Balakrishnan, "Sentiment lexicons and non-English languages: a survey," *Knowledge and Information Systems*. 2020, doi: 10.1007/s10115-020-01497-6.
- [28] N. Al-Twairesh, H. Al-Khalifa, and A. Al-Salman, "AraSenTi: large-scale twitter-specific Arabic sentiment lexicons," in *Proceedings of the 54th Annual Meeting of the Association for Computational Linguistics*, 2016, pp. 697–705.

- [29] A. Pasha et al., "MADAMIRA: a fast, comprehensive tool for morphological analysis and disambiguation of Arabic," in Proceedings of the Ninth International Conference on Language Resources and Evaluation (LREC'14), 2014, pp. 1094–1101, [Online]. Available: http://www.lrec-conf.org/proceedings/lrec2014/pdf/593_Paper.pdf.
- [30] M. Hu and B. Liu, "Mining and summarizing customer reviews," in Proceedings of the Tenth ACM SIGKDD International Conference on Knowledge Discovery and Data Mining, 2004, pp. 168–177, doi: 10.1145/1014052.1014073.
- [31] T. Wilson, J. Wiebe, and P. Hoffmann, "Recognizing contextual polarity in phrase-level sentiment analysis," in Proceedings of Human Language Technology Conference and Conference on Empirical Methods in Natural Language Processing, 2005, pp. 347–354, [Online]. Available: <https://www.aclweb.org/anthology/H05-1044.pdf>.
- [32] F. H. H. Mahyoub, M. A. Siddiqui, and M. Y. Dahab, "Building an Arabic sentiment lexicon using semi-supervised learning," Journal of King Saud University - Computer and Information Sciences. vol. 26, no. 4, pp. 417–424, 2014, doi: 10.1016/j.jksuci.2014.06.003.
- [33] M. Maamouri, D. Graff, B. Bouziri, S. Krouna, A. Bies, and S. Kulick, "LDC standard Arabic morphological analyzer (SAMA) version 3.1," Philadelphia, 2010. [Online]. Available: <https://catalog.ldc.upenn.edu/>.
- [34] A. Esuli and F. Sebastiani, "SentiWordNet: a high-coverage lexical resource for opinion mining *," Italy, 2007. [Online]. Available: <http://nmis.isti.cnr.it/sebastiani/Publications/2007TR02.pdf>.
- [35] S. Baccianella, A. Esuli, and F. Sebastiani, "SENTIWORDNET 3.0: an enhanced lexical resource for sentiment analysis and opinion mining," 2010, [Online]. Available: http://www.lrec-conf.org/proceedings/lrec2010/pdf/769_Paper.pdf.
- [36] C. Fellbaum et al., "Introducing the Arabic wordnet project," in Proceedings of the 3rd Global Wordnet Conference, P. Sojka, K.-S. Choi, C. Fellbaum, and P. T. J. M. Vossen, Eds. Jeju Island, Korea, 2006.
- [37] R. M. Duwairi, R. Marji, N. Sha'Ban, and S. Rushaidat, "Sentiment analysis in Arabic tweets," 2014, doi: 10.1109/IACS.2014.6841964.
- [38] M. Abdul-Mageed, M. Diab, and S. Kübler, "SAMAR: subjectivity and sentiment analysis for Arabic social media," Computer Speech and Language. vol. 28, no. 1, pp. 20–37, 2014, doi: 10.1016/j.csl.2013.03.001.
- [39] B. Liu, M. Hu, and J. Cheng, "Opinion observer: analyzing and comparing opinions on the web," 2005, doi: 10.1145/1060745.1060797.
- [40] D. Kang and Y. Park, "Review-based measurement of customer satisfaction in mobile service: sentiment analysis and VIKOR approach," Expert Systems with Applications. vol. 41, no. 4 PART 1, pp. 1041–1050, 2014, doi: 10.1016/j.eswa.2013.07.101.
- [41] Y. M. Li and T. Y. Li, "Deriving market intelligence from microblogs," Decision Support Systems. vol. 55, no. 1, pp. 206–217, Apr. 2013, doi: 10.1016/j.dss.2013.01.023.
- [42] I. Chaturvedi, E. Cambria, R. E. Welsch, and F. Herrera, "Distinguishing between facts and opinions for sentiment analysis: survey and challenges," Information Fusion. vol. 44, pp. 65–77, Nov. 2018, doi: 10.1016/j.inffus.2017.12.006.
- [43] A. Kaur and V. Gupta, "A survey on sentiment analysis and opinion mining techniques," Journal of Emerging Technologies in Web Intelligence. vol. 5, no. 4, pp. 367–371, Nov. 2013, doi: 10.4304/jetwi.5.4.367-371.
- [44] M. Korayem, D. Crandall, and M. Abdul-Mageed, "Subjectivity and sentiment analysis of Arabic: A Survey," in Communications in Computer and Information Science, 2012, vol. 322, pp. 128–139, doi: 10.1007/978-3-642-35326-0_14.
- [45] H. P. Patil and M. Atique, "Sentiment analysis for social media: a survey," in 2015 2nd International Conference on Information Science and Security (ICISS), 2015, pp. 1–4, doi: 10.1109/ICISSEC.2015.7371033.
- [46] V. S. Jagtap and K. Pawar, "Analysis of different approaches to sentence-level sentiment classification," International Journal of Scientific Engineering and Technology. vol. 2, no. 3, pp. 164–170, 2013.
- [47] A. D'Andrea, F. Ferri, and P. Grifoni, "Approaches, tools and applications for sentiment analysis implementation," International Journal of Computer Applications. vol. 125, no. 3, pp. 975–8887, 2015.
- [48] A. B. Pawar, M. A. Jawale, and D. N. Kyatanavar, "Fundamentals of sentiment analysis: Concepts and methodology," in Studies in Computational Intelligence, vol. 639, Springer Verlag, 2016, pp. 25–48.
- [49] E. Aydoğan and M. A. Akcayol, "A comprehensive survey for sentiment analysis tasks using machine learning techniques," in 2016 International Symposium on Innovations in Intelligent Systems and Applications (INISTA), 2016, pp. 9–19, doi: 10.1109/INISTA.2016.7571856.
- [50] Y. Jararweh, M. Al-Ayyoub, and E. Benkhelifa, "Advanced Arabic natural language processing (ANLP) and its applications: introduction to the special issue," Information Processing and Management. vol. 56, no. 2, Elsevier Ltd, pp. 259–261, Mar. 01, 2019, doi: 10.1016/j.ipm.2018.09.003.
- [51] S. R. El-Beltagy and A. Ali, "Open issues in the sentiment analysis of Arabic social media: A case study," in 2013 9th International Conference on Innovations in Information Technology, IIT 2013, 2013, pp. 215–220, doi: 10.1109/Innovations.2013.6544421.
- [52] N. A. Abdulla, N. A. Ahmed, M. A. Shehab, M. Al-Ayyoub, M. N. Al-Kabi, and S. Al-rifai, "Towards improving the lexicon-based approach for arabic sentiment analysis," International Journal of Information Technology and Web Engineering. vol. 9, no. 3, pp. 55–71, Jul. 2014, doi: 10.4018/ijitwe.2014070104.
- [53] U. R. Hodeghatta, "Sentiment analysis of Hollywood movies on twitter," in Proceedings of the 2013 IEEE/ACM International Conference on Advances in Social Networks Analysis and Mining, ASONAM 2013, 2013, pp. 1401–1404, doi: 10.1145/2492517.2500290.
- [54] M. Jokhio, N. A. Mahoto, S. Jokhio, and M. S. Jokhio, "Detecting tweet-based sentiment polarity of plastic surgery treatment," Mehran University Research Journal of Engineering and Technology. vol. 34, no. 4, pp. 403–412, 2015, [Online]. Available: <https://www.researchgate.net/publication/283264994>.
- [55] U. Naseem and K. Musial, "DICE: deep intelligent contextual embedding for twitter sentiment analysis," in Proceedings of the International Conference on Document Analysis and Recognition, ICDAR, Sep. 2019, pp. 953–958, doi: 10.1109/ICDAR.2019.00157.
- [56] U. Naseem, S. K. Khan, I. Razzak, and I. A. Hameed, "Hybrid words representation for airlines sentiment analysis," in Lecture Notes in Computer Science (including subseries Lecture Notes in Artificial Intelligence and Lecture Notes in Bioinformatics), 2019, vol. 11919 LNAI, pp. 381–392, doi: 10.1007/978-3-030-35288-2_31.
- [57] U. Naseem, I. Razzak, K. Musial, and M. Imran, "Transformer based deep intelligent contextual embedding for twitter sentiment analysis," Future Generation Computer Systems. vol. 113, pp. 58–69, Dec. 2020, doi: 10.1016/j.future.2020.06.050.
- [58] G. Yoo and J. Nam, "A hybrid approach to sentiment analysis enhanced by sentiment lexicons and polarity shifting devices," in The 13th Workshop on Asian Language Resources, 2018, pp. 21–28, [Online]. Available: <https://hal.archives-ouvertes.fr/hal-01795217>.
- [59] H. K. Aldayel and A. M. Azmi, "Arabic tweets sentiment analysis - a hybrid scheme," Journal of Information Science. vol. 42, no. 6, pp. 782–797, 2015, doi: 10.1177/0165551515610513.
- [60] J. Jia, G. W. Fischer, and J. S. Dyer, "Attribute weighting methods and decision quality in the presence of response error: a simulation study the full cost of electricity view project," Journal of Behavioral Decision Making. 1998, doi: 10.1002/(SICI)1099-0771(199806)11:23.0.CO;2-K.
- [61] J. R. Bettman, M. F. Luce, and J. W. Payne, "Constructive consumer choice processes," Journal of Consumer Research. vol. 25, no. 3, pp. 187–217, 1998, doi: 10.1086/209535.
- [62] F. Pedregosa et al., "Scikit-learn: machine learning in Python," Journal of Machine Learning Research. vol. 12, pp. 2825–2830, 2011.

Blockchain Network Model to Improve Supply Chain Visibility based on Smart Contract

Arwa Mukhtar¹, Awanis Romli², Noorhuzaimi Karimah Mohd³
Faculty of Computing, Universiti Malaysia Pahang
Kuantan, Malaysia

Abstract—Due to the increasing complexity of supply chains over the past years, many factors significantly contribute to lowering the supply chains performance. Poor visibility is one of the major challenging factors that lowers supply chains performance. This paper proposes a Blockchain-based supply chain network model to improve the supply chain visibility. The model focuses in improving the visibility measurements properties: information sharing, traceability, and inventory visibility. The proposed model consists of information sharing, traceability, and inventory visibility platforms based on Blockchain technology smart contract. The model built with Hyperledger platform and extend the Hyperledger Composer Supply Chain Network (HCSC) model. The research is designed to three main phases. First phase: the preliminary phase which is the literature review phase to identify the existing challenges in the domain. The second phase: the design and implementation phase which is the development steps of the proposed research model. The third phase: the evaluation phase which represent the performance evaluation of the proposed model and the comparisons between the proposed model and the existing models. In the evaluation performance, the common performance metrics Lead time and average inventory levels will be compared in the proposed model, Cloud-based information system, and the traditional supply chain. These proposed platforms offer an end-to-end visibility of products, orders, and stock levels for supply chain practitioners and customers within supply chain networks. Which helps managers' access key information that support critical business decisions and offers essential criteria for competitiveness and therefore, enhance supply chain performance.

Keywords—Supply chain management; supply chain visibility; blockchain; smart contract; information sharing; traceability; inventory visibility

I. INTRODUCTION

Given the globalization and expansion in the supply chain operations, the complexity of chain operations have been increased [1-4]. Due to the decentralized nature of the supply chain, firms are unable to identify the origins of problems that arises within their supply chain flow [5]. For instance, the recall of millions of toys in Mattel (an American multinational toy manufacturing company) in 2015. The firm loss was over \$110 million for product return due to unauthorized paints in its product from an unauthorized supplier. Furthermore, more importantly though in health and food supply chain. Where demand uncertainties and long lead-times of medical supplies and drugs are critical to the whole process specially in health and food safety issues [6]. Moreover, lack of visibility is still a challenging issue for supply chain executives especially in

increasingly complex environment [3, 7, 8]. Improving the visibility level in the supply chain is essential not only to gain access to key decision-making information [9], but also to facilitate more transparency and traceability within the supply chain network [10]. Moreover, in terms of inventory management, the visibility of product inventory reduces the stock repetition, the out of stock situations, and the inventory cost [3]. Overall, the poor visibility hinders efficient supply chain performance [8]. As a consequence, it is critical for firms that experiences such problems caused by poor visibility to adopt new innovative technologies and business models to overcome these challenges [11].

Recently, leading-edge firms using Blockchain technology to optimize their business processes, velocity, throughput, latency, compliance, cost-effective, provenance awareness, and building trust [12]. Blockchain technology has been used to enhance cost effectiveness and security of supply chain transactions [13], physical distribution visibility and shipment tracking [14], risk management [15]. Moreover, recent studies have been employed Blockchain technology to enhance supply chain visibility [16, 17]. Blockchain technology appears as a good fit for digital supply chain integration because of its ledger, security and smart contract platforms, as well as software connectors [13, 18]. Moreover, the technology offers tools to build a cost-effective and flexible digital supply chain network [19]. Thus, it is the right solution to solve core problems in supply chain like transparency, traceability, and poor visibility [17].

Therefore, in this paper, a Blockchain-based supply chain model is proposed to improve supply chain visibility using Blockchain smart contract. Smart Contracts can improve supply chain visibility of assets, orders, and inventory levels, therefore improves information sharing, order traceability and improve inventory visibility.

This paper is organized as follows: Section 2 introduces Blockchain technology and reviews the related literature of the technology. Section 3 reviews the supply chain visibility and explains how Blockchain technology can help improving the supply chain visibility. Section 4 describes the research agenda. While section 5 includes the description of the proposed model and its components. section 6 describes the evaluation phase of the proposed model. Finally, section 7 concludes the paper.

II. BLOCKCHAIN TECHNOLOGY

Blockchain technology was introduced as the core technology of Bitcoin, which is the first electronic payment

system based on a decentralized peer-to-peer network [20]. Blockchain is a digital, shared, immutable, decentralized ledger technology that facilitates sharing transaction records between parties and grouped them into blocks chained to each other [13, 21]. These transactions records are stored in a shared, decentralized ledger without the need of any third-party intermediary [22, 23]. Figure 1 shows the process of building the blocks.

Recently, beyond the Bitcoin, this emerging technology is used in many sectors such as in food manufacturing [24], environmental solution [25], energy sector [26], and supply chain [27]. In the last few years Blockchain technology has been utilized for non-financial applications [28]. Therefore, multiple Blockchain platforms have been developed [29, 30]. Hyperledger, is an open source permissioned Blockchain (Hyperledger Project,2015). While Bitcoin, Ethereum, Litecoin are examples of cryptocurrencies applications of public Blockchain [31].

Recent research communities have examined different aspects of Blockchain and its implication to the entire enterprises ecosystems. Many related perspectives has been investigated such as: security [15], privacy [32], data management Banerjee et al. (2017), identity management [33] and other majors explored and future research directions has been revealed apparently.

In supply chain context, Blockchain promotes the availability of information about the product to all the participating parties in the Blockchain network which offers an enhanced visibility throughout the product life cycle [15]. The registered transfer of goods and any change in the process products details will be documented in a decentralized database. This information availability ensures efficient transactions, efficient recalls in addition to the assurance of food safety and prevention of counterfeits [16]. The tracking and traceability system that Blockchain offers serves supply chains as a secure, transparent and traceable platform that facilitates tracking the materials and determine the provenance or origins of a product from its original to the end customers [34-36]. Since tracking and authenticating the product provenance or origins is critical to the food supply chain [37].

In the same context, both literature review and the practice revealed that using new emerging technologies such as Blockchain technology for the visibility issue seems promising [14, 16-18, 30]. Attention is being given to the benefits that Blockchain can offer for the supply chain, which lead the researchers to emphasis more on the potential capabilities of Blockchain in resolving supply chain challenges. Although prior studies developed different Blockchain-based solutions to increase the supply chains visibility [14, 16-18, 30], according to Dolgui, Ivanov [38], “There is still a lack of scientific methodology to Blockchain-driven design of the smart contracts in the supply chain.”. In line with the literature review findings of Queiroz, Telles [39], “Smart contracts will contribute to several SCM improvements such as improved responsiveness, lead-time reduction, transaction costs reduction, increased visibility and more trust, security and transparency in the network”.

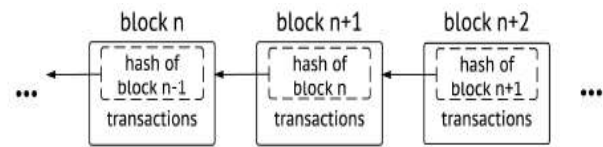


Fig. 1. The Building Blocks Process [23].

Therefore, the proposed HCSC-POS model in this paper differs from alternative models in using Blockchain smart contracts to increase the visibility measurements: information sharing, orders tracking and inventory visibility and aims to fill this gap in the literature.

III. SUPPLY CHAIN VISIBILITY

Supply chain visibility has different definitions in the literature [40]. Visibility in the supply chain refers to the ability of supply chain parties to access timely and accurate key information [7]. In the work of Simatupang and Sridharan [41], the authors defined supply chain visibility as: “The ability to trace the points of origin of materials used in a product”. It is widely agreed that the limited visibility that companies have over their supply significantly contributes to lowering the performance of supply chains [3, 7, 16]. Since poor visibility on supply chains has negative effects such as long lead times [42], counterfeiting [16], stock-outs situations [43], bullwhip-effect[44] and high inventory cost. Although several efforts have been made in the area to improve the poor visibility issue[5], still poor visibility is a major challenge and has negative effects on supply chain networks performance [8, 30, 45]. Table 1 summarizes some of the existing models that have been proposed for the poor visibility issue.

Reviewing the existing models that have been proposed to increase the supply chain visibility in Table 1 shows that recent models tend to utilize new emerging technologies such as FRID tags in [49], Cloud computing in [6], and Blockchain technology for the poor visibility issue supply chain in [14, 16, 30, 45-48]. However, these models suffer from technological limitations in the technology adoption. For example, some of the presented solutions built their models on public Blockchain such as [14, 48]. In this case, the limitations of public Blockchain apply to these models such as: technical difficulties faced by miners (the network participants in Blockchain public networks) and the rapidly growth of blocks size.

TABLE I. SUPPLY CHAIN VISIBILITY EXISTING MODELS

Author	Year	Solution
[6]	2018	Cloud-based information sharing
[30]	2018	Hybrid private/public ledger based on Blockchain
[3]	2018	Supplier Development
[46]	2018	A decentralized information sharing approach
[47]	2018	HACCP, Blockchain and IoT traceability system
[45]	2018	Blockchain-based food traceability system
[16]	2017	Distributed data-driven application
[14]	2017	Online shipment tracking framework
[48]	2017	Information sharing Blockchain scheme
[49]	2016	Automatic identification (Auto-ID) technologies
[40]	2016	Suppliers selection

Although number of studies addressed the importance of supply chain visibility, there is a lack of common effective evaluation metrics to measure supply chain visibility [7, 43]. Visibility measurement is the degree of information sharing within the supply chain [10]. Some scholars in the relevant literature such as [50] and [51] emphasized on the traceability to measure the supply chain visibility. While another stream of visibility measurement work such as [52] pointed to the inventory visibility as a critical measure for supply chain visibility. Additionally, many studies have been proposed to improve the performance of the supply chain. However, the performance still needs to improve. Due to the increasing complexity of supply chains over the past years, many factors significantly contributes to lowering the performance of supply chains [8, 53] such factors as:

- Lack of information sharing [6].
- Poor demand and inventory visibility [8].
- Inventory information inaccuracy [54].
- Information leakage [55].
- Out-of-stock situation [54].
- Poor visibility [3], among others.

Likewise, several models have been developed to improve the visibility of supply chains. However, poor visibility is still a major challenge in complex supply chain network which lowers the supply chains performance [3, 8, 30]. Additionally, poor visibility has negative effects such as counterfeiting [16], stock-outs [43], and bullwhip-effect [7, 44]. Furthermore, this issue is considered as an obstacle to efficient SCPM [8]. Therefore, increasing supply chain visibility helps in improving the business performance since the visibility feature provides an access to accurate information that is necessary for decision-making [14]. As a consequence, a higher level of production, facilitate order traceability, and inventory information visibility will be obtained [6, 10].

Failing short to consider the poor visibility issue leads to inefficient business processes due to lack of information sharing, un seen supply and demand forecast, inventory inaccuracy. As a consequent, leads to low supply chain performance. Therefore, this study is an attempt to fill this gap by proposing supply chain network model based on Blockchain technology smart contract to increase the visibility measurement properties (information sharing, traceability, and inventory visibility).

IV. RESEARCH AGENDA

The author extensively reviews the potential of the appropriate technology for the poor visibility issue in supply chain. Arguably, it is largely agreed between academia and practitioners that the adoption of Blockchain technology is promising for information sharing, traceability and inventory visibility in supply chain [14, 16, 17]. Therefore, based on the reviewed literature recommendations, in this research a supply chain network model is proposed based on Blockchain technology smart contract to improve the visibility in supply chain networks. The proposed model uses the Blockchain

smart contract to increase the information sharing; orders traceability; and inventory visibility within a supply chains network.

As the proposed model focuses on improving the visibility in term of improvement in information sharing, traceability and inventory visibility, this research work was designed to include three main phases in order to achieve this aim as depicted in Figure 2.

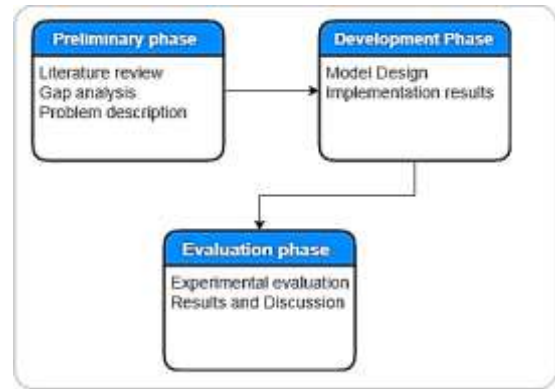


Fig. 2. Research Design.

The first phase: the preliminary phase which illustrates how the researcher identified the existing challenges in supply chain domain, influencing factors, knowledge gap, research problem, and the most appropriate technology to solve the specified research problem. In this phase, the supply chain management literature has been studied to explore these issues. This extensive literature review highlights the current existing challenges in the area and the existing knowledge gap. The second phase: the design and implementation phase where the development steps of the research model are proposed. The third phase: the evaluation phase which finalizes the research design. This phase aims to evaluate the proposed model in terms of improving the supply chain visibility. It represents the experimental evaluation results and the comparison results between the proposed (HCSC-POS) model, Cloud-based model and the traditional supply chain model.

V. THE PROPOSED MODEL

The proposed model is a Blockchain network model (HCSC-POS) improving the visibility in term of improvement in information sharing, traceability and inventory visibility. The proposed model is an extension and built based on Hyperledger Composer Supply Chain Network (HCSC) model which is an implementation of Blockchain platform “Hyperledger Composer” for the supply chains.

The proposed network model consists of three main layers: the business layer, Blockchain layer, and data layer. The first layer is the supply chain business layer which contains four-echelon supply chain trading participants:(Supplier, Manufacturer, Distributor, Retailer) and Customer. Herein, the supply chain participants are connected in a permissioned distributed immutable ledger built on top of HCSC network. Communication between network participants are in collaborative manner between upstream and downstream participants as shown in Figure 3. The second layer is the

Blockchain layer. Wherein, this layer contains the necessary components and features to connect to the Blockchain such as the smart contract and the access control rules. This is the middle layer that connect the business layer with the data layer. The third layer is the data layer. This layer contains the data structure used in the proposed (HCSC-POS) network model. It contains the supply chain participants data, assets data, transactions and events data.

The supply chain network participants trading on a single asset, a product or “Commodity” and six transactions (InitiatePO ViewCommodity Order_Tracking TransferCommodity SetupDemo viewStock). In addition to three main events: StockLevels ProductDetails TrackOrders. The data structure of the proposed HCSC-POS network model consists of three main executable transaction processor functions that represent the smart contract. The subsequent sections will describe the structure and design of the transaction processor functions in details.

A. ViewCommodity Transaction

To achieve product visibility into the proposed (HCSC-POS) network model, the ViewCommodity transaction aims to share product information between HCSC-POS network participants. Throughout the following steps, network participants are able to view products, products origin, and the environmental profile of a product:

- Step1: the product owner posts to the Blockchain the following:
- Product details (tradingSymbol, name, description, origin, quantity, unitPrice, totalPrice, Environmental_Profile, SaftyStock, StockLevelNotification, purchaseOrder, owner, issuer of purchase order), Product origin, Environmental profile.
- Step 2: the issuer/buyer submits ViewCommodity transaction uses the tradingSymbol of the desired product.
- Step 3: If the transaction is successful, the issuer/buyer is provided with full visibility of product details, origin and the environmental profile as Figure 4 shows the flow of information between network participants when submitting ViewCommodity transaction.

Herein, product information is accessible to relevant parties in HCSC-POS network. Customers are now aware of the product origin, and the environmental profile of the product before they buy or place a purchase order of this product.

B. Order_Tracking Transaction

Tracking orders transaction gives the ability to track an order location and status by the order issuer. When a supplier purchases a product, the order status changes to “initiated” purchase order. After confirming the purchase order, the order status changes to “Confirmed” and the order will be added to the ledger. Then, the vendor performs a TransferCommodity transaction to transfer the ordered product ownership from product owner to the new product owner. The steps followed in order tracking are as follows and shown in Figure 5:

- Step1: The vendor posts to the ledger the current status of the order, “Trace” values and order information.
- Step2: The unique orderId property is submitted to Order_Tracking transaction by the orderer.
- Step3: The associated event 'TrackOrders' pushes Trace values, order information and the current order status which promotes orders traceability.

The execution of Order_Tracking transaction pushes the trace information (timestamp, shipperLocation, and Trader company) to the assets registry. The transaction emits event 'TrackOrders' which locates the order tracking information as depicted in Figure 5.

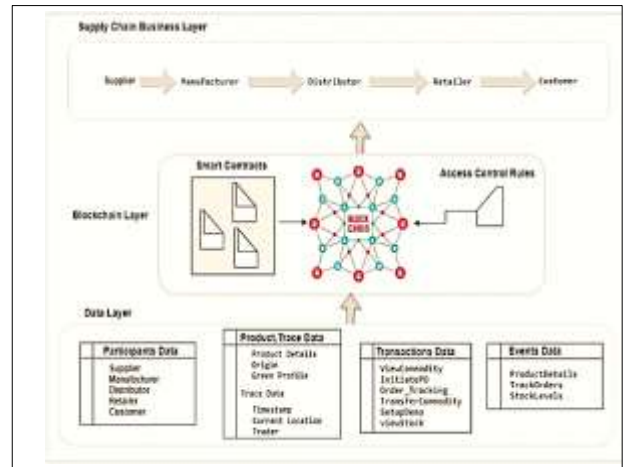


Fig. 3. The Proposed (HCSC-POS) Network Model.

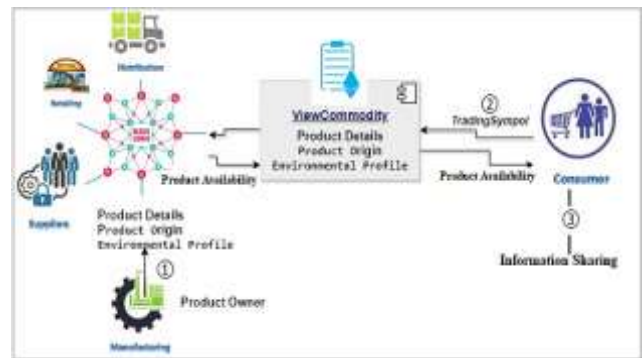


Fig. 4. Transaction View Commodity Flow.

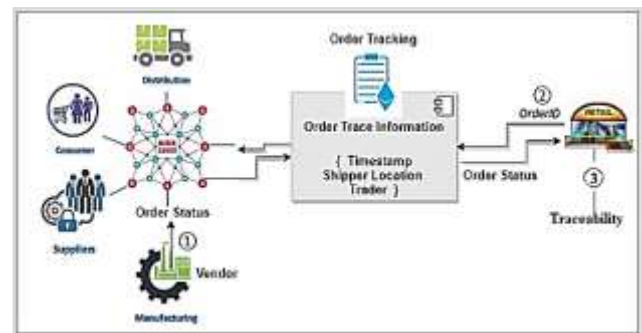


Fig. 5. Transaction Order Tracking Flow.

C. ViewStock Transaction

In order to manage the inventory of the supply chain participants in HCSC-POS network model, the viewStock transaction queries the available quantity in stock for certain products using the tradingSymbol identifier. Then calculates the safety stock based on DailySalesUnits, and leadtime values. The safety stock in HCSC-POS network model is calculated based on the standard safety stocks equation in supply chain inventory theory is adopted from [56]:

$$\text{SafetyStock} = (\text{MaximumDailyUsage} \times \text{MaximumLeadTime}) - (\text{AverageDailyUsage} \times \text{AverageLeadTime}) \quad (1)$$

The transaction compares the stock quantity with the safety stock value. If the safety stock level is reached, automatically notify the participant to place a purchase order for that product. Afterward, the product ownership will be changed to the new owner of the product accordingly.

- Step1: Calculates the safety stock.
- Step2: Check product quantity in stock using product tradingSymbol.

Step3: If product quantity reached the safety stock level, emit event StockLevels and notify product owner by notification message: "Product quantity is less than the safety stock levels "to place purchase order for this product and change the product ownership to the new owner of the product accordingly. Otherwise, if product quantity not reached the safety stock level yet, notification message: "Product quantity within safety stock levels "Figure 6 shows the flow of viewStock transaction.

Product quantity always updated with the most recent, current and available quantity in the stock. This is especially true after performing a purchase order and deduce the ordered quantity from the available quantity in the stock.

Comparison between the updated quantity in stock and the SaftyStock value, if the available quantity is less than or equals to the safety stock, a stock level notification message will be pushed to notify the vendor with "This product has reached the safety stock levels" notification message. Event 'StockLevels' emits and posts Product, oldQty, newQty, SaftyStock to the ledger. This event allows full visibility on information related to inventory levels.

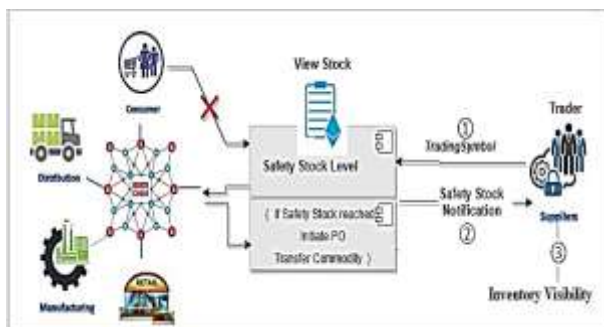


Fig. 6. Transaction viewStock Flow.

VI. PERFORMANCE EVALUATION

In the evaluation phase, performance evaluation will be conducted. The goal is to evaluate the visibility improvement in the proposed HCSC-POS model in terms of information sharing, traceability and inventory visibility.

Therefore, the proposed model will be compared to Cloud-based information system in Gonul Kochan, Nowicki [6], and the traditional supply chain in term of reduction in lead times and inventory levels. Lead time and average inventory levels are common performance metrics that are reduced when visibility is improved in the supply chain [43]. These performance metrics were used in [6] to evaluate the performance of the proposed model. This process is shown at Figure 7.

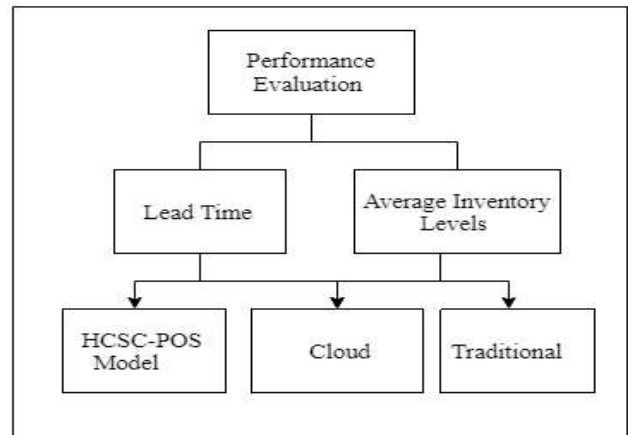


Fig. 7. Performance Evaluation.

In the first comparison, HCSC-POS network model will be compared against the cloud-based information system and the traditional supply chain model, whereby the lead time in HCSC-POS model is compared to the lead time in each model. The second part of the comparison will compare the average inventory levels in HCSC-POS, cloud-based, and the traditional supply chain model as shown in Figure 7. The goal is to evaluate the proposed HCSC-POS model in terms of improving the supply chain visibility bases on the specified common performance metrics.

VII. CONCLUSION

Poor visibility is a major challenge in supply chain networks as it is considered as an obstacle to efficient supply chain performance. Although prior studies have dealt with the issue, however, still poor visibility under an increasingly complex supply chain networks environment a major challenge for supply chain executives. Additionally, although new emerging technologies significantly contribute to overcome the poor visibility issue. Still, some limitations have been reported in the adoption of these technologies.

This paper proposes supply chain network model to improve the supply chain visibility using Blockchain technology smart contract. The proposed model focuses on improving the visibility in term of improvement in the visibility measurement properties: information sharing, traceability and inventory visibility. The information sharing

and traceability platform offer an end-to-end visibility of products provenance, orders statuses, raw material origins, and identifying green products which facilitates the access to key information in the supply chain network that is necessary for decision making. The ability to track orders provides accessibility to trace information. While inventory visibility enables supply chain participant to better control over their inventory by providing accurate inventory updates. As a result, preventing stock repetition, preventing out of stock situation, and bullwhip-effect and reducing the lead times and safety stock level which is accordingly reduces the inventory cost. The benefits that offered by the proposed model are essential criteria for competitiveness, necessary to support critical business decisions, and overall leads to supply chain performance improvements. Future researches could extend HCSC-POS model to include assessment of more performance metric measurements. Additionally, quantifying the visibility and including the sustainability dimensions (environmental, social, and financial) in the HCSC-POS model to solve environmental challenges could be fruitful research areas.

ACKNOWLEDGMENT

The research reported in this study is conducted by the researchers at Universiti Malaysia Pahang (UMP), it is funded by RDU1903111 and PGRS1903188 grants. The researchers would like to thank UMP for supporting this research.

REFERENCES

- [1] Hofmann, H., et al., Sustainability-related supply chain risks: conceptualization and management. *Business Strategy and the Environment*, 2014. 23(3): p. 160-172.
- [2] Giannakis, M. and T. Papadopoulos, Supply chain sustainability: A risk management approach. *International Journal of Production Economics*, 2016. 171: p. 455-470.
- [3] Pradhan, S.K. and S. Routroy, Improving supply chain performance by Supplier Development program through enhanced visibility. *Materials Today: Proceedings*, 2018. 5(2): p. 3629-3638.
- [4] Rostamzadeh, R., et al., Evaluation of sustainable supply chain risk management using an integrated fuzzy TOPSIS- CRITIC approach. *Journal of Cleaner Production*, 2018. 175: p. 651-669.
- [5] Swift, C., V.D.R. Guide Jr, and S. Muthulingam, Does supply chain visibility affect operating performance? Evidence from conflict minerals disclosures. *Journal of Operations Management*, 2019.
- [6] Gonul Kochan, C., et al., Impact of cloud-based information sharing on hospital supply chain performance: A system dynamics framework. *International Journal of Production Economics*, 2018. 195: p. 168-185.
- [7] Somapa, S., M. Cools, and W. Dullaert, Characterizing supply chain visibility—a literature review. *The International Journal of Logistics Management*, 2018. 29(1): p. 308-339.
- [8] Dweekat, A.J., G. Hwang, and J. Park, A supply chain performance measurement approach using the internet of things: Toward more practical SCPMS. *Industrial Management & Data Systems*, 2017. 117(2): p. 267-286.
- [9] Messina, D., A.C. Barros, and A. Lucas, How much visibility has a company over its supply chain? A diagnostic metric to assess supply chain visibility. 2018.
- [10] Francisco, K. and D. Swanson, The Supply Chain Has No Clothes: Technology Adoption of Blockchain for Supply Chain Transparency. *Logistics*, 2018. 2(1): p. 2.
- [11] Lehmacher, W., et al. Impact of the Fourth Industrial Revolution on Supply Chains. in *World Economic Forum*, Geneva, Switzerland, REF. 2017.
- [12] Morris, V., et al., Developing a Blockchain Business Network with Hyperledger Composer using the IBM Blockchain Platform Starter Plan. *International Technical Support Organization*, 2018.
- [13] Korpela, K., J. Hallikas, and T. Dahlberg, Digital supply chain transformation toward blockchain integration. in *proceedings of the 50th Hawaii international conference on system sciences*. 2017.
- [14] Wu, H., et al., A Distributed Ledger for Supply Chain Physical Distribution Visibility. *Information*, 2017. 8(4): p. 137.
- [15] Kshetri, N., 1 Blockchain's roles in meeting key supply chain management objectives. *International Journal of Information Management*, 2018. 39: p. 80-89.
- [16] Madhwal, Y. and P.B. Panfilov, Blockchain and Supply Chain Management: Aircrafts'parts'business Case. *Annals of Daam and Proceedings*, 2017. 28.
- [17] Min, H., Blockchain technology for enhancing supply chain resilience. *Business Horizons*, 2019. 62(1): p. 35-45.
- [18] Pournader, M., et al., Blockchain applications in supply chains, transport and logistics: a systematic review of the literature. *International Journal of Production Research*, 2019: p. 1-19.
- [19] Saberi, S., et al., Blockchain technology and its relationships to sustainable supply chain management. *International Journal of Production Research*, 2019. 57(7): p. 2117-2135.
- [20] Nakamoto, S., Bitcoin: A peer-to-peer electronic cash system. 2008.
- [21] Risius, M. and K. Spohrer, A Blockchain Research Framework What We (don't) Know, Where We Go from Here, and How We Will Get There. *Business & Information Systems Engineering*, 2017. 59(6): p. 385-409.
- [22] Kamble, S., A. Gunasekaran, and H. Arha, Understanding the Blockchain technology adoption in supply chains-Indian context. *International Journal of Production Research*, 2019. 57(7): p. 2009-2033.
- [23] Christidis, K. and M. Devetsikiotis, Blockchains and smart contracts for the internet of things. *Ieee Access*, 2016. 4: p. 2292-2303.
- [24] Bünger, M. Blockchain for industrial enterprises: Hype, reality, obstacles and outlook. 2017 30-05-2018]; Available from: <https://internetofthingsagenda.techtarget.com/blog/IoT-Agenda/Blockchain-for-industrial-enterprises-Hype-reality-obstacles-and-outlook>.
- [25] Imbault, F., et al., The green blockchain Managing decentralized energy production and consumption. 2017 1st Ieee International Conference on Environment and Electrical Engineering and 2017 17th Ieee Industrial and Commercial Power Systems Europe (Eeeic / I&Cps Europe), 2017.
- [26] Dabbs, A. What blockchain can do for the environment. 2017 20-05-2018]; Available from: <https://www.greenbiz.com/users/alistair-dabbs>.
- [27] Li, Z., et al. A Hybrid Blockchain Ledger for Supply Chain Visibility. in 2018 17th International Symposium on Parallel and Distributed Computing (ISPDC). 2018. IEEE.
- [28] Kouhizadeh, M. and J. Sarkis, Blockchain practices, potentials, and perspectives in greening supply chains. *Sustainability*, 2018. 10(10): p. 3652.
- [29] Plant, L., Implications of open source blockchain for increasing efficiency and transparency of the digital content supply chain in the australian telecommunications and media industry. *Australian Journal of Telecommunications and the Digital Economy*, 2017. 5(3): p. 15.
- [30] Li, Z., et al., A Hybrid Blockchain Ledger for Supply Chain Visibility. 2018: p. 118-125.
- [31] Casino, F., T.K. Dasaklis, and C. Patsakis, A systematic literature review of blockchain-based applications: Current status, classification and open issues. *Telematics and Informatics*, 2019. 36: p. 55-81.
- [32] Zyskind, G., O. Nathan, and A. Pentland, Decentralizing Privacy: Using Blockchain to Protect Personal Data. 2015 Ieee Security and Privacy Workshops (Spw), 2015: p. 180-184.
- [33] Kosba, A., et al. Hawk: The blockchain model of cryptography and privacy-preserving smart contracts. in *Security and Privacy (SP)*, 2016 IEEE Symposium on. 2016. IEEE.
- [34] Tian, F. An agri-food supply chain traceability system for China based on RFID & blockchain technology. in *Service Systems and Service Management (ICSSSM)*, 2016 13th International Conference on. 2016. IEEE.
- [35] Kshetri, N., Can blockchain strengthen the internet of things? *IT professional*, 2017. 19(4): p. 68-72.

- [36] Omran, Y., et al., Blockchain-driven supply chain finance: Towards a conceptual framework from a buyer perspective. 2017.
- [37] Galvez, J.F., J. Mejuto, and J. Simal-Gandara, Future challenges on the use of blockchain for food traceability analysis. *TrAC Trends in Analytical Chemistry*, 2018. 107: p. 222-232.
- [38] Dolgui, A., et al., Blockchain-oriented dynamic modelling of smart contract design and execution in the supply chain. *International Journal of Production Research*, 2019: p. 1-16.
- [39] Queiroz, M.M., R. Telles, and S.H. Bonilla, Blockchain and supply chain management integration: A systematic review of the literature. *Supply Chain Management: An International Journal*, 2019.
- [40] Yousefi, S., H. Mahmoudzadeh, and M. Jahangoshai Rezaee, Using supply chain visibility and cost for supplier selection: a mathematical model. *International Journal of Management Science and Engineering Management*, 2017. 12(3): p. 196-205.
- [41] Simatupang, T.M. and R. Sridharan. A characterization of information sharing in supply chains. in *ORSNZ Conference University of Canterbury, New Zealand*. 2001.
- [42] Apiyo, R. and D. Kiarie, Role of ICT tools in supply chain performance. *International Journal of Supply Chain Management*, 2018. 3(1): p. 17-26.
- [43] Caridi, M., et al., Measuring visibility to improve supply chain performance: a quantitative approach. *Benchmarking: An International Journal*, 2010. 17(4): p. 593-615.
- [44] Barratt, M. and R. Barratt, Exploring internal and external supply chain linkages: Evidence from the field. *Journal of Operations Management*, 2011. 29(5): p. 514-528.
- [45] Mohan, T., Improve Food Supply Chain Traceability using Blockchain. 2018, The Pennsylvania State University.
- [46] Imeri, A. and D. Khadraoui. The security and traceability of shared information in the process of transportation of dangerous goods. in *New Technologies, Mobility and Security (NTMS), 2018 9th IFIP International Conference on*. 2018. IEEE.
- [47] Tian, F., An information System for Food Safety Monitoring in Supply Chains based on HACCP, Blockchain and Internet of Things. 2018, WU Vienna University of Economics and Business.
- [48] Nakasumi, M. Information sharing for supply chain management based on block chain technology. in *2017 IEEE 19th Conference on Business Informatics (CBI)*. 2017. IEEE.
- [49] Papert, M., P. Rimpler, and A. Pflaum, Enhancing supply chain visibility in a pharmaceutical supply chain: Solutions based on automatic identification technology. *International Journal of Physical Distribution & Logistics Management*, 2016. 46(9): p. 859-884.
- [50] Mattoli, V., et al., Flexible tag datalogger for food logistics. *Sensors and Actuators A: Physical*, 2010. 162(2): p. 316-323.
- [51] Amr, M., et al. Merging supply chain and Blockchain technologies. in *The International Maritime Transport and Logistics Conference, Marlog*. 2019.
- [52] Zhang, A.N., M. Goh, and F. Meng, Conceptual modelling for supply chain inventory visibility. *International Journal of Production Economics*, 2011. 133(2): p. 578-585.
- [53] Lima-Junior, F.R. and L.C.R. Carpinetti, Quantitative models for supply chain performance evaluation: A literature review. *Computers & Industrial Engineering*, 2017. 113: p. 333-346.
- [54] Cui, L., et al., Investigation of RFID investment in a single retailer two-supplier supply chain with random demand to decrease inventory inaccuracy. *Journal of cleaner production*, 2017. 142: p. 2028-2044.
- [55] Hassan, A.Y. and H.H. Nasereddin, Information Sharing Characteristics In Supply Chain Management. *EPH-International Journal of Business & Management Science (ISSN: 2208-2190)*, 2018. 4(1): p. 01-09.
- [56] Chan, F., S. Routroy, and R. Kodali, Differential evolution algorithm for supply chain inventory planning. *Journal of Manufacturing Technology Management*, 2005.

Development of Relay Selection Method for Audio Transmission in Cooperative Ad Hoc Networks

Usha Padma¹, H.V. Kumaraswamy²

Dept of TCE, RVCE
Bengaluru, India

S. Ravishankar³

Dept of ECE, RVCE
Bengaluru, India

Abstract—The quality of service parameters, such as Latency and Bit error rate for audio transmission in IEEE 802.11b Wireless ad hoc network are analyzed in this paper. The issue addressed here is that the quality of the audio, when transmitted directly from source to destination in ad hoc network is low. This can be improved by incorporating a relay between source and destination, where the relay uses decode and forward technique before forwarding the information to the destination. Destination applies Maximal ratio combining (MRC), to combine the signal received from the source and the relay. This concept is called Cooperative communication. A location aware channel estimation based relay selection strategy is proposed in this paper for a wireless ad hoc network. Audio is transmitted using 16 QAM modulation scheme over a Rayleigh fading channel in the presence of additive white Gaussian noise (AWGN). This paper focusses on the relay selection method for audio transmission in cooperative ad hoc networks where best relay is selected based on the average channel strength supported between the source and the destination. Audio quality at the destination is observed for the cases of relay presence and relay absence. Results showed that the measured audio quality with the presence of relay was far better than the measured quality in the absence of relay which stresses the importance of cooperative communication.

Keywords—Cooperative communication; channel strength; ad hoc networks; maximal ratio combining; IEEE 802.11b; G.711 Codec; Mean Opinion Score (MOS)

I. INTRODUCTION

The connectivity of ad hoc networks have been extensively studied over few years, from local observations, to global network properties. Fading is one of the major issue of wireless communication (WC) and broadcasting behaviour of ad hoc networks plays a key role in transmission of data. Cooperative communication uses a suitable relay node that helps the source node to forward data to destination node and also increases the stability by cooperative spatial diversity. One of the resources used to provide cooperative communication is relay [1]. Even though employing a relay increases the number of transmissions to three times that of a direct communication, it can considerably improve the signal to noise ratio between the source and destination, thereby improving the channel strength to significantly improve the quality of end-to-end communication. The disadvantage of cooperative communication is that the overheads incurred in channel access are more as each relay has to contend to access the channel, when compared to conventional IEEE 802.11 Distributed coordination function (DCF). There is a need to design the MAC protocol as per the requirement of

Cooperative communication. A MAC protocol CoopMAC was developed for WLAN in [2], where users with low data rate maintained a CoopTable, of helper nodes with high data rates to help them in forwarding their data. Relay enabled MAC protocol was developed for wireless ad hoc network in [3], where the source selected the relay based on the channel conditions collected and advertised by the relay. A cross layer triple-busy-tone MAC protocol was designed [4] for wireless networks, where not only control and data frames are protected by busy tones, but also the data forwarded by the relay are protected by busy tone to avoid collisions in the network. A network coding aware MAC protocol was proposed [5] in which the relay delivers its own data, while relaying the data from the source simultaneously. A distributed MAC protocol was proposed [6] to maximize the lifespan of Wireless sensor networks by considering the channel state information and residual energy level in sensor nodes. A vehicular cooperative MAC protocol was designed for gateway downloading scenarios in vehicular networks, where all vehicles are considered to be interested in the information that is alike [7]. A MAC protocol by name CD-MAC was designed [8] to allow the relay to transmit its own data along with source data simultaneously using space-time coding. A distributed cooperative MAC was designed for wireless networks [9] by exploring the concepts such as cooperation region, thereby identifying the benefits of cooperative transmissions. In order to improvise the lifespan of the mobile ad hoc networks, a distributed energy adaptive location aware MAC [10] protocol was designed, where the relay was selected based on the location information and amount of remaining energy.

Work focussing on Call signalling protocols and types of codec, for Voice over IP are presented in [15],[16], [17]. Quality of the ongoing Voice over IP calls were analyzed in [18]. It was also found that, addition of a single call in cell degraded the quality of the calls in progress. Quality of service parameters such as delay, loss rate, jitter and R score were proposed in [19],[20],[21]. To improve performance of voice data, performance optimization schemes such as header compression, label based forwarding and packet aggregation are proposed for a wireless mesh network [22]. Delay components that contributes towards the calculation of end-to-end delay for voice type of data are presented in [22].

G.711, G.729 and G.723 VoIP codecs were evaluated in terms of various Quality of service (QOS) parameters over Wi-Fi networks [11] and authors concluded that G.711 showed better performance. Authors developed an analytical

model and analyzed the quality of voice using G.711 codec over wireless mesh networks [12], where the maximum mean opinion score attained was 3.3 for a single hop. Quality of VoIP calls were evaluated for three codecs, G.711, G.729 and G.723.1 over MANET in an indoor environment [23]. G.711 codec provided the highest MOS of 4 among all the codecs considered for evaluation.

Cooperative MAC protocols reviewed so far focus on the enhancement of throughput and energy efficiency or Network lifespan for transmission of data. Since most of researches have focussed only on transmission of normal data in cooperative ad hoc networks, there is a need to analyze the performance of voice data in cooperative ad hoc networks. Therefore in this paper, we have focussed on transmission of audio information over a cooperative ad hoc network by modifying the MAC protocol, to select the relay in a distributed manner by estimating the mean channel capacity. As per the literature review, we found that G.711 codec performed best in terms of MOS and therefore we chose the same codec in our simulation. We considered a fixed ad hoc network, where nodes were deployed randomly. We developed a mathematical model to select a suitable relay based on mean channel estimation. We also modified the existing MAC protocol to include the location information of the source and destination in the control frames and developed a new control frame to announce the selected relay in a decentralized manner. Results are used to determine the performance of the network in the absence and presence of the relay node.

The remaining sections of the paper is organized as follows. System model and Assumptions are presented in Section 2. Section 3 explains the distributed relay selection based MAC protocol. In Section 4, we elaborate the relay selection which is based on channel estimation. Details about the modifications carried out at MAC layer are presented in Section 5. Section 6 details about the Audio codec specifications and the formulae used for measurement of audio quality. Performance analysis of the proposed relay selection method and conclusion drawn are explained in Section 7.

II. SYSTEM MODEL AND ASSUMPTIONS

We considered static wireless ad hoc network consisting of one source, n relays and one destination node. We assume that the reader has the knowledge of IEEE 802.11b Medium access control protocol, which supports a maximum data rate of 11 Mbps. Every node is equipped with a single antenna and constrained to half duplex mode of communication. All the nodes that are randomly distributed in the network use the proposed MAC protocol. Nodes willing to transmit information will contend to access the channel using CSMA/CA. It is also assumed that all the nodes use the same transmission power.

A. Physical Layer

Propagation model considered at this layer is slow faded Rayleigh channel and path loss depends on the distance travelled by the information. Received signal power R_p is computed at the destination and the relays by considering the transmitted power T_p , the distance travelled by the packets d

and attenuation constant α . Power spectral density of the noise (N_0), is fixed to -60dBm. Channel capacity is computed by considering the received signal power to noise power and the bandwidth. Decode and forward scheme is used at the relay, where signal broadcasted by source in phase 1 is decoded at the relay node. After decoding, the re-encoded data by the selected relay node is broadcasted to destination in phase 2. MRC is used at the receiver to maximize the signal power by combining the information received from the relay and the source. 16-QAM modulation is used at this layer to attain the required data rate.

Let h_{sr} , h_{sd} and h_{rd} represent the gain of the channel from source to relay, from source to destination and relay to destination respectively. The concept of cooperation is modeled in two phases. Source broadcasts information to destination in first phase. All nodes that are in the transmission range of source will overhear the information broadcasted by the source. Signal received from the source to relay and relay to destination are represented as y_{sr} and y_{rd} respectively.

$$y_{sr} = \sqrt{P_s} h_{sr} x + \eta_{sr} \quad (1)$$

Where P_s represents the power transmitted at the source and information symbol transmitted by the source is represented by x . In phase two, with decode & forward protocol, the node which decodes the symbols of the received information from the source will become the relay node, only that relay node can retransmit the information with power P_r to the destination.

$$y_{rd} = \sqrt{P_r} h_{rd} x + \eta_{rd} \quad (2)$$

Where P_r represents the power transmitted at the relay. It is assumed that the Channel gains h_{rd} and h_{sd} are known at the destination and also they are independent of each other. Destination, upon receiving signal from the source and the relay, detects the transmitted symbol with the awareness of channel gains h_{rd} and h_{sd} , respectively. Destination performs MRC to maximize the SNR and minimize the bit error rate. Signals received from source and relay are combined at the destination, which is represented as:

$$y = m_1 y_{sd} + m_2 y_{rd} \quad (3)$$

Where m_1 and m_2 are represented as:

$$m_1 = \frac{\sqrt{P_s} h_{sd}}{N_0} \quad (4)$$

$$m_2 = \frac{\sqrt{P_r} h_{rd}}{N_0} \quad (5)$$

m_1 and m_2 are used for maximizing the SNR at the MRC output of destination. After performing MRC at the destination, SNR at the destination is given by:

$$\gamma = \frac{P_s |h_{sd}|^2 + P_r |h_{rd}|^2}{N_0} \quad (6)$$

B. MAC Layer

At this layer we have assumed that all the transmitted control packets are successfully decoded by all the other nodes that are present in the transmission range. Both the control and data packets are broadcasted with a constant rate and same transmission power is used for both types of packets.

For successful decoding of the control packets, this assumption is necessary. For decoding of the data packets, we have fixed the threshold for number of errors. If the number of errors are less than the threshold, data packets are accepted or else they will be rejected.

III. DISTRIBUTED RELAY SELECTION BASED MAC PROTOCOL

With the intention of improving the audio/voice quality over wireless ad hoc networks, we present a novel MAC protocol, where the relay is selected in a distributed manner.

When a relay is involved, there is a need to extend the reservation of the channel in terms of time and space, so that the relay can coordinate with the source and destination.

Aside from the Control frames such as ACK, RTS and CTS, new control frames are needed for relaying the information in the network. In this MAC protocol, a new control frame is used to assist the source, i.e., Ready-To-Forward (RTF). The RTF frame is used for announcing the selected suitable relay in a decentralized manner, where RTF is broadcasted by the winning relay to announce its selection to source, destination and other lost relays. Here, Suitable helper node (relay) means the one that relays the information with maximum mean channel capacity which is explained in section V. Time required for transmission of RTF, ACK, RTS and CTS frames are T_{RTF} , T_{ACK} , T_{RTS} and T_{CTS} , respectively.

Fig. 1, 2 and 3 shows the methodology in the form of flowcharts. Fig. 1 gives the procedure which can be used by the Source node, Fig. 2 represents the procedure to be followed at the relay node and similarly, Fig. 3 represents the methodology at the Receiving node.

A. Methodology at the Source Node

The flowchart shown in Fig. 1 provides the methodology which can be used by the source node. It is required to sense the channel, to check if the channel is idle.

Whenever the source has the data to transmit, it checks for the idleness of the channel by sensing the channel. If it finds the channel idle for a DIFS time, source node selects a Backoff timer (BT) randomly between Zero and CW. As soon as the BT reaches 0, source broadcasts RTS in the Network. Here RTS includes the information about the location of the source. NAV present in the RTS, will provide information about duration for which the source wants to hold the channel, because of which other nodes will refrain themselves from using the channel for a period of NAV. Source node has to

wait for a duration of back off time, if the channel is found to be busy.

If CTS is not received by the source before the expiry of $T_{RTS} + SIFS + T_{CTS}$, Source performs retransmission of RTS. If source receives CTS before the expiry of $T_{RTS} + SIFS + T_{CTS}$, then source node waits for another $SIFS + T_{min\ Backoff} + T_{RTF}$, where $T_{min\ Backoff}$ is the minimum backoff counter set by the winning relay. If source does not receive RTF before the expiry of $SIFS + T_{min\ Backoff} + T_{RTF}$, it means no suitable relay exists. Then, source broadcasts data directly to the destination with the available channel capacity between the source and the destination. If RTF is received at the source, then the source originates a communication cooperatively with the winning relay to the destination by transmitting the data on the channel.

If the source receives the Acknowledgement within $Transmission\ delay_{Source} + Transmission\ delay_{Relay} + Propagation\ delay_{SR} + Propagation\ delay_{RD} + 2SIFS + T_{ACK}$, transmission is declared to be successful, otherwise source assumes that collision has occurred and begins a backoff timer randomly similar to that of DCF.

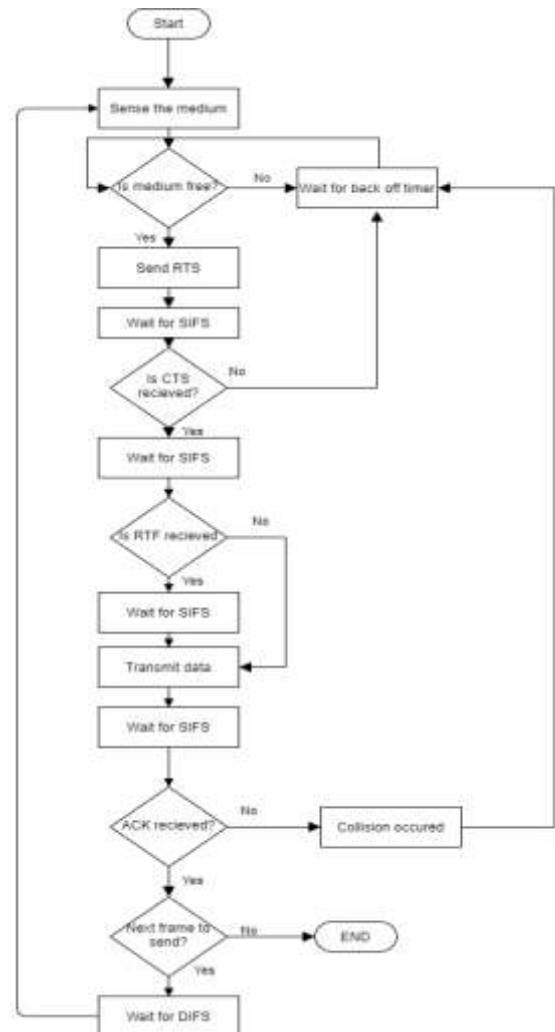


Fig. 1. Methodology to be used at Source.

B. Methodology at the Destination Node

Initially the destination node is in idle state as shown in Fig. 2. If the RTS from the source is received at the destination, Destination node computes the channel capacity available between itself and the source node.

Destination node generates a CTS packet, where the CTS includes the channel capacity provided between the destination & the source, information about the location of the destination apart from NAV and destination MAC address.

If the destination does not receive RTS, then it is forced to wait for the duration of time specified in back off timer. After broadcasting CTS, Destination waits to receive RTF from the winning relay.

C. Methodology at the Relay Node

If the destination does not receive RTF within $SIFS + T_{min}^{Backoff} + T_{RTF}$, it thinks that no suitable relay exists and waits for the direct transmission of data from the source.

Otherwise, the destination node waits for the data from both the winning relay and the source. Upon receiving the data, the destination performs MRC and then extracts the information. If destination decodes and extracts original data correctly, it broadcasts the ACK. Or else, it lets the source to timeout and make a retransmission of the same data.

All the nodes other than source and destination compute to take the position of the relay node in the networks. All these nodes will be in idle state as shown in Fig. 3. If the RTS is received from source, all these nodes will wait to receive CTS from destination node. If they haven't received either of them then they goes back to idle state. Once the CTS is received, all these nodes will compute the channel capacity supported (C_1) between themselves and the source node. Similarly, all these nodes will compute the channel capacity (C_2) supported between themselves and the destination. All these nodes will compute the average of C_1 and C_2 respectively and checks if the computed average channel capacity is greater than that supported between source and destination. Every node whose average channel capacity is greater than C will compute their backoff timer value, which is explained in the Section V.

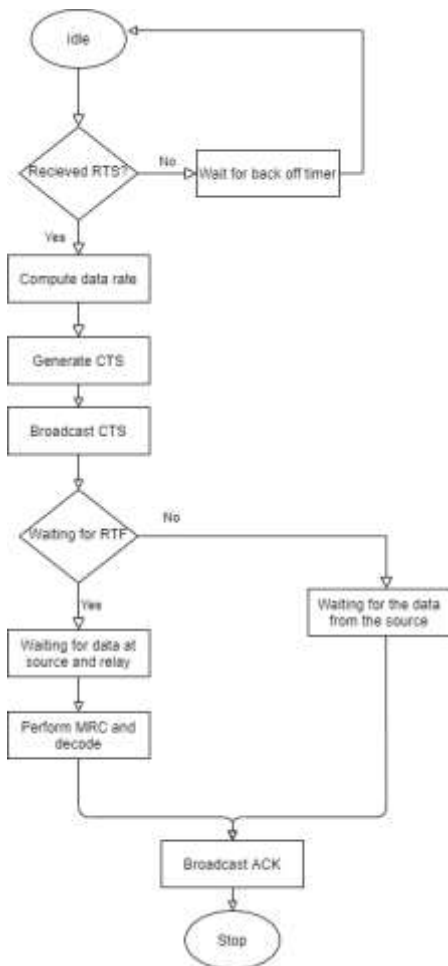


Fig. 2. Methodology to be used at Destination.

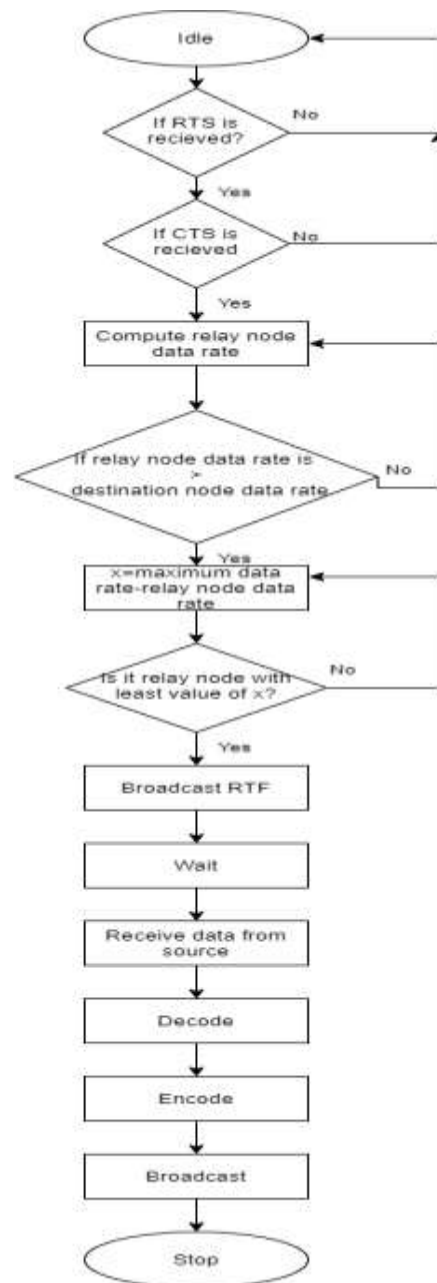


Fig. 3. Methodology to be used at the Relay Node.

Node with the least backoff value will backoff earlier and broadcasts the RTF first. This node will be chosen as the relay in the network. Upon hearing to the RTF, other nodes will stop contending and sets their timer value to the one received in RTF. After the expiry of SIFS, winning relay node waits for the data to arrive from source node. Received data packets at the relay are decoded, re-encoded and broadcasted to the destination.

IV. MODIFICATIONS AT THE MAC LAYER

CSMA/CA DCF is used at MAC Layer to facilitate cooperative communication. Few modifications are proposed to the frame formats of existing RTS and CTS. RTF is the new frame developed, which is broadcasted by the winning relay node. The winning relay node selected in a distributed manner is the one which is used to cooperate between the source and destination.

A. Modified RTS Frame

Modified RTS frame format is as shown in Fig. 4. Source node broadcasts the RTS in the network. FCS field is not used in our work.

In order to incorporate the location information of the source, two bytes are included between FCS and destination MAC address. These two bytes carry the X-Y coordinates of the source. X-Y coordinates of the source provides the location information of the source.

B. Modified CTS Frame

Fig. 5 shows the modified CTS frame. Destination broadcasts the CTS in response to the RTS broadcasted by the source. X-Y coordinates of the destination are carried in the last two bytes of the CTS frame. Four bytes are included between the destination location information and destination MAC address of the CTS frame to carry the data rate supported between the source node and destination node.

C. RTF Frame

All nodes in the network will receive a copy of both CTS and RTS. Location information of source is available in RTS and location information of destination is available in CTS. Every node in the network other than source and destination are also aware of their location information. All the nodes can compute the data rate supported between themselves and destination, also between themselves and source. Euclidean distance between the nodes, transmitted power, channel attenuation constant and Rayleigh fading coefficients are considered in computing the data rate in the network. Nodes located at different positions with varying fading coefficients provide different Signal to Noise ratio, which in turn results in different supported data rates. As the data rate supported between source and destination is included in CTS, all nodes willing to help the source can compare their computed data rate with the one received in CTS. Using the eqs. (7) and (8), which is explained in Section V, a node that is willing to cooperate as a relay will be selected as suitable relay node. The node which is selected as relay node should broadcast RTF frame in the network. Frame format of RTF frame is as shown in the Fig. 6.

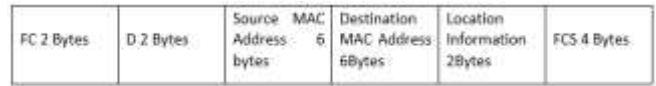


Fig. 4. Modified RTS Frame.



Fig. 5. Modified CTS Frame



Fig. 6. RTF Frame.

V. CHANNEL ESTIMATION BASED RELAY SELECTION

Performance of MAC protocol will be affected significantly by the selection of suitable relay in distributed manner. We assume that the condition of the channel is not variant during one transmission session. Suitable relay selection based on the instantaneous location may be more appropriate than relay selection based on instantaneous channel condition in a wireless ad hoc network. We propose a location aware channel estimation based relay selection strategy, where location information are included in the handshaking packets. Localization algorithms or GPS can be used to obtain the location information of the wireless devices. Location information of the source node and destination node are included in RTS and CTS respectively. Every node willing to become relay will learn about the location information through RTS and CTS that are broadcasted in the network. CTS frame also carries the channel capacity(C) supported between destination and source nodes. As the nodes willing to become relay nodes are aware of their own location information, every node can compute the distance between themselves and the source. Received signal power at the relay node is based on the distance travelled, transmitted power at the source and channel attenuation constant. Possible Channel capacity between relay and source(C_1) is computed using Bandwidth and Signal power to Noise power ratio. Similarly possible Channel capacity between destination and relay(C_2) is also computed. C_{Mean} is computed at each relay node, where C_{Mean} is given by:

$$C_{Mean} = (C_1 + C_2)/2. \quad (7)$$

If C_{Mean} is greater than C, then highest channel capacity is computed as:

$$D = \text{Maximum Channel capacity} - C_{Mean} \quad (8)$$

Where maximum channel capacity for IEEE 802.11b is 11Mbps. The relay with minimum value of D become the winning relay which will backoff first and broadcasts RTF in the network. This is a completely distributed strategy where every relay node makes its decision independently.

VI. AUDIO CODEC

ITU-T defines all its audio codecs with certain specified characteristics and operation methodologies. For G.711 audio codec, ITU-T defined the specifications as 8kHz sampling

frequency, each packet size of 20 ms, speed of 64 kbps, and maximum size of the payload to be 160 bytes.

Initially, after the audio signal matching specifications in .wav format is accepted at the application layer, it has been sampled at the rate of 8 kHz. The samples so received are modulated using Additive Differential Pulse Code Modulation as per ITU-T standards of G.711 codec. This modulated signal is then Huffman encoded and sent to the physical layer for further physical transmission after 16 QAM modulation.

At the receiver end, the QAM demodulation is performed at the physical layer and then sent to MAC layer. Datagrams received are then Huffman decoded and then converted back to original samples at the application layer.

E-model is the suitable method for evaluating the quality of voice, which is defined by ITU-T [13][14]. R Factor defined by E-model, provides the overall measurement of quality of voice, which is given by:

$$R=R_0-I_s-I_d-I_e + AF \tag{9}$$

R_0 represents the quality of the voice in the absence of distortion which is considered to be equal to 100 in our work, I_s represents impairments due to packet loss, I_d represents impairments due to delay and jitter and impairments due to encoding are represented by I_e . AF represents the advantage factor which can be tolerated by the user. AF is chosen to be 5 for ad hoc networks and impairments due to jitter is not considered in our work.

One of the approaches to translate the ratings of R factor into an overall measurement from which the quality of the speech can be judged is MOS.

$$MOS = 1 + (0.035 * R) + (7 * 10^{-6} * R * (R - 60) * (100 - R)) \tag{10}$$

MOS value ranges from 1 to 5, where 4 and above 4 is considered to provide better quality of conversational voice [12].

Total delay incurred in transmission of audio in a cooperative ad hoc network includes packetization delay (P_d) at the source, transmission delay from source to link (T_s), transmission delay from relay to link (T_r), propagation delay from the source to the relay (P_{sr}), propagation delay from the relay to the destination (P_{rd}), processing delay for each bit at the relay (B_p) plus 3*SIFS. Processing delay for each bit at the relay is considered to be 0.1µsec.

Total enr-to-end latency in one direction from source to destination $Total_{Delay}$ is:

$$Total_{Delay} = P_d + T_s + T_r + P_{sr} + P_{rd} + B_p + 3 * SIFS \tag{11}$$

VII. PERFORMANCE EVALUATION AND CONCLUSION

A distributed relay selection algorithm based on mean channel capacity is developed for a cooperative ad hoc network for transmission of Audio signals. Rayleigh fading channel is considered with AWGN for transmission of audio information is in this work. Existing 802.11b is modified for inclusion of location information in RTS and CTS, and data rate in CTS. New frame RTF is generated for announcing the selected relay in a distributed manner. Above mentioned

algorithm is simulated using MATLAB 2018. The proposed MAC protocol is evaluated by comparing it with IEEE 802.11b DCF. Since main purpose of this protocol is to improve the quality of audio when transmitted over a cooperative ad hoc network, System performance is analyzed by computing Throughput, Packet delivery ratio and Mean Opinion Score (MOS). Parameters used in our work for simulation are listed in Table I.

We considered four cases to analyze the performance of the network. In case 1, Audio quality was observed at the destination in the absence of relay. In case 2, we selected the relay which supported maximum Channel capacity between itself and the source. In case 3, we selected the relay which supported maximum Channel capacity between itself and the destination. In case 4, we selected the relay with mean channel capacity, which is explained in Section V.

Fig. 7 shows the positioning of the nodes with 20 nodes deployed in the network. Node 10 is chosen to be the source and node 11 is chosen to be the destination. In case 2, node 5 is chosen as the relay and in case 3, node 17 is chosen as the relay node. Whereas in case 4 as per the relay selection method, node 15 is chosen as the relay node. Performance analysis of the system is depicted in Table II. The Total end-to-end delay incurred by the packet from source-to relay & from relay to destination is 20.286 msec in case 4.

TABLE I. PAREMETERS CONSIDERED FOR SIMULATION

Parameter	Value
Area	250 x 250 m ²
Bandwidth	20MHz
Data Rate	11 Mbps(Maximum)
Transmitting Signal Power	10 dB
Noise PSD	-60dBm
SIFS	10µsecs
DIFS	50µses
Attenuation Constant (α)	3
Audio Codec	ITU G.711
G.711 Operating Speed	64kbps
Audio signal Sampling Rate	8.192KHz
Modulation technique used by Codec	Adaptive Differential Pulse Code Modulation
Modulation technique used at Physical Layer	16 QAM
Channel Type	Rayleigh Fading Channel

TABLE II. PERFORMANCE ANALYSIS

	No. of Packets sent	No. of Packets lost	Packet Delivery Ratio	Throughput (kbps)	MOS
Case 1	109	42	0.6146	5.0981*10 ⁴	3.1250
Case 2	109	29	0.7339	1.3637*10 ⁴	3.8643
Case 3	109	26	0.7615	1.6437*10 ⁴	3.9856
Case 4	109	22	0.7981	6.5728*10 ⁴	4.1321

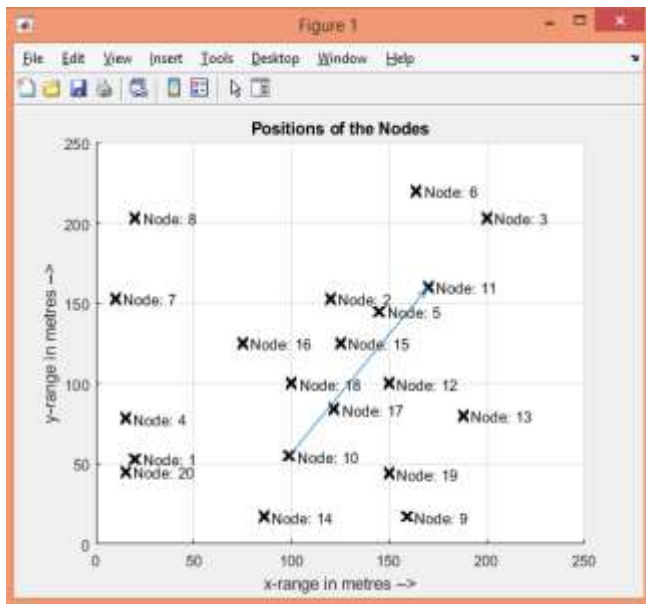


Fig. 7. Positioning of Nodes with Node 10 as Source and Node 11 as Destination.

160 bytes of data are transmitted in one frame. For decoding of the data packets, we have fixed the threshold for number of errors as 604. The threshold for number of errors was fixed by averaging the number of error bits for ten transmissions. If the number of errors are less than the threshold, data packets are accepted or else they are rejected.

We demonstrated that the proposed MAC protocol for distributed relay selection in cooperative ad hoc network can significantly improve the quality of the audio received at the destination when compared with the normal wireless ad hoc network and 802.11 DCF. We also proposed a mathematical model to select the relay based on mean channel estimation. In our future work, we would like to work on transmission of video over cooperative ad hoc networks. This work can also be extended by considering the hidden node problem and exposed node problem in ad hoc networks.

REFERENCES

- [1] N. Laneman, D.N.C. Tse, and G.W. Wornell, "Cooperative Diversity in Wireless Networks: Efficient Protocols and Outage Behaviour," IEEE Trans. Information Theory, vol. 50, no. 12, pp. 3062-3080, Dec. 2004.
- [2] P. Liu, Z. Tao, S. Narayanan, T. Korakis, and S.S. Panwar, "CoopMAC: A Cooperative MAC for Wireless LANs," IEEE J. Selected Areas in Comm., vol. 25, no. 2, pp. 340-354, Feb. 2007.
- [3] H. Zhu and G. Cao, "rDCF: A Relay-Enabled Medium Access Control Protocol for Wireless Ad Hoc Networks," IEEE Trans. Mobile Computing, vol. 5, no. 9, pp. 1201-1214, Sept. 2006.
- [4] H. Shan, P. Wang, W. Zhuang, and Z. Wang, "Cross-Layer Cooperative Triple Busy Tone Multiple Access for Wireless Networks," Proc. IEEE GLOBECOM, pp. 1-5, Dec. 2008.
- [5] X. Wang, J. Li, and M. Guizani, "NCAC-MAC: Network Coding Aware Cooperative Medium Access Control for Wireless Networks," Proc.

- IEEE Wireless Comm. and Networking Conf. (WCNC '12), pp. 1646-1651, Apr. 2012.
- [6] C. Zhai, J. Liu, L. Zheng, and H. Xu, "Lifetime Maximization via a New Cooperative MAC Protocol in Wireless Sensor Networks," Proc. IEEE GLOBECOM, pp. 1-6, Dec. 2009.
- [7] J. Zhang, Q. Zhang, and W. Jia, "VC-MAC: A Cooperative MAC Protocol in Vehicular Networks," IEEE Trans. Vehicular Technology, vol. 58, no. 3, pp. 1561-1571, Mar. 2009.
- [8] S. Moh and C. Yu, "A Cooperative Diversity-Based Robust MAC Protocol in Wireless Ad Hoc Networks," IEEE Trans. Parallel and Distributed Systems, vol. 22, no. 3, pp. 353-363, Mar. 2011.
- [9] H. Shan, H. Cheng, and W. Zhuang, "Cross-Layer Cooperative MAC Protocol Distributed Wireless Networks," IEEE Trans. Wireless Comm., vol. 10, no. 8, pp. 2603-2615, Aug. 2011.
- [10] Xiaoyan Wang, Jie Li, "Improving the Network Lifetime of MANETs through Cooperative MAC Protocol Design", IEEE Transactions on Parallel and Distributed Systems, vol. 26, no. 4, pp.1010-1020, April 2015.
- [11] Shreekanth Gurrapu, Saurabh Mehta and Shraddha Panbude, "Comparative study for performance Analysis of voip codecs over wlan in nonmobility Scenarios", International Journal of Information Technology, Modeling and Computing (IJITMC), Vol. 4, No.4, November 2016.
- [12] Amit Chhabra, Gurpal Singh, "Performance Evaluation and Delay Modelling of VoIP Traffic over 802.11 Wireless Mesh Network", International Journal of Computer Applications (0975 – 8887), Volume 21– No.9, May 2011.
- [13] Leandro Carvalho, Edjair Mota, Regeane Aguiar Anderson Barreto, "An E-Model Implementation for Speech Quality Evaluation in VoIP Systems", IEEE Symposium Computers and Communications (ISCC 2005), pp. 1530-1536, IEEE, 2005.
- [14] L. Ding and R.A. Goubran, "Speech quality prediction in VoIP using the extended E-model", IEEE GLOBECOM 2003, pp. 3974-3978, 2003.
- [15] H. Schulzrinne, J. Rosenberg, "Internet Telephony: Architecture and Protocols- an IETF Perspective", Computer Networks and ISDN Systems, Vol.31, pp. 237-255, Feb. 1999.
- [16] Bur Goode, Senior Member, "Voice Over Internet Protocol (VoIP)", Proceedings of the IEEE, Vol.90, No.9, Sep 2002.
- [17] Trad, F. Munir, H. Afifi, "Capacity Evaluation of VoIP in IEEE 802.11e WLAN Environment", IEEE CCNC Proceedings, Sep 2002.
- [18] S. Garg, M. Kappes, "Can I Add a VoIP Call?", Proc. Of IEEE ICC'03, Vol. 2, May 2003.
- [19] X. Wang, A. Patil, W. Wang, "VoIP over Wireless Mesh Networks: Challenges and Approaches", WICON'06: Proceedings of the 2nd Annual International Workshop on Wireless Internet, New York, USA 2006.
- [20] H.Y. Wei, K. Kim, A. Kashyap, S. Ganguly, "On Admission of VoIP Calls Over Wireless Mesh Network", Proceedings of IEEE ICC, 2006.
- [21] K. Kyungtae, H. Sangjin, "VoMESH: Voice Over Wireless Mesh Networks", Proc of IEEE Wireless Communications and Networking Conference, Las Vegas, USA, 2006.
- [22] S. Ganguly et al., "Performance Evaluation for Deploying VoIP Services In Mesh Networks", IEEE Journal on Selected Areas in Communication, 2006, pp 2147-2158.
- [23] Lina Abou Haibeh, Nadir Hakem, Ousama Abu Safia, "Performance Evaluation of VoIP Calls Over MANET for Different Voice Codecs", IEEE 7th Annual Computing and Communication Workshop and Conference, 2 March 2017.

KadOLSR: An Efficient P2P Overlay for Mobile Ad Hoc Networks

Mohammad Al Mojamed

Computer Science Department, Computing College
Umm al-qura University, Al-qunfudah, Saudi Arabia

Abstract—P2P and MANET are self-organized, decentralized, and dynamic networks. Although both networks have common characteristics, they are used for different purposes and operate at different layers. P2P provides the ability for peers to store and locate services in the network, while MANET provides an underlying routing capability to reach other mobile nodes. Thus, P2P and MANET could complement each other. However, P2P is originally designed to operate over the Internet, which provides rich routing capabilities compared to MANET. Therefore, deploying P2P over MANET must come with careful consideration of how to adjust P2P approaches to better suit MANET. In this paper, a novel system called KadOLSR is proposed to better develop an efficient P2P over MANET. The structure of the well-known Kademlia is used along with the OLSR. KadOLSR optimizes the similarities between P2P and MANET to reduce overlay management communication overhead and hence deploys a lightweight and efficient P2P over MANET. The network layer routing information is shared with the overlay to achieve the optimization. A cross-layer channel is constructed between the network layer and the overlay layer to exchange relevant routing information. The proposed system is designed, and its performance is evaluated using a network simulator. The performance of KadOLSR is also compared to one of the recent P2P for MANET systems. The simulation results show that KadOLSR performs well across all different network sizes and mobility speeds.

Keywords—Peer-To-Peer P2P; Mobile ad hoc Networks MANET; cross layering; Kademlia; Optimized Link State Routing OLSR; KadOLSR

I. INTRODUCTION

Peer-To-Peer (P2P) networks are used to overcome the limitations of the centralization issue when sharing resources through constructing decentralized networks. Originally, P2P was used for file sharing. It was then used in other fields such as distributed computing and streaming. P2P in general can be classified into two categories: unstructured overlays and structured overlays [1]. In the former category, no structure is followed by peers when forming the overlay. Flooding and random walk are among the techniques used to locate services within the overlay. The latter category employs a sort of organization when forming the overlay to provide a search strategy for locating network services. Overlays are therefore constructed as a multi-dimensional grid, ring, or mesh.

A mobile ad hoc network (MANET) is a self-organized and distributed network that consists of mobile nodes which collaborate with each other to provide communication among themselves in an infrastructureless network [2]. Routing

protocols in MANET can be classified in general into reactive, proactive, and hybrid MANET routing. In the proactive approach, each mobile node maintains routing entries to other nodes in advance of their usage. The second approach is mainly based on working on-demand. Routes to other nodes are fetched once they are needed. The hybrid approach combines both reactive and proactive routing. The reactive technique is used to find far away nodes, whereas the proactive technique is used to maintain routes to close nodes.

P2P and MANET are self-organized, decentralized, and dynamic networks. Although both networks have common characteristics, they are used for different purposes and operate at different layers. P2P provides the ability for peers to store and locate services in the network, while MANET provides an underlying routing capability to reach other mobile nodes. Thus, P2P and MANET could complement each other. However, P2P was initially deployed over the Internet, which provides rich routing capabilities compared to MANET. Therefore, deploying P2P over MANET must come with careful consideration of how to adjust P2P approaches to better suit an environment like MANET.

In this paper, we propose a novel combination of the P2P approach and the MANET routing protocol to better develop an efficient P2P over MANET system. The structure of the well-known and most widely used overlay system [3] [4] [5], Kademlia [6], is used, along with a proactive routing protocol, OLSR [7]. However, the proposed system, KadOLSR, optimizes similarities between MANET and P2P to reduce overlay management communication overhead, and hence deploys a lightweight and efficient P2P over MANET. The underlay routing information is made available for overlay in order to achieve the optimization. A cross-layer path is constructed between the network layer and the overlay layer to exchange relevant routing information. The proposed system is designed, and its performance is evaluated using a network simulator. The performance of KadOLSR is also compared to one of the recent P2P for MANET systems.

The rest of the paper is organized as follows: Section II reviews the work related to deploying P2P overlays over MANET. It also highlights the adopted overlay and underlay. Section III introduces the proposed system, KadOLSR. The proposed system is then evaluated in Section IV. The experimental setups and performance metrics are also presented in this section. Finally, Section V concludes the paper.

II. BACKGROUND

A. Related Works

Several systems have been proposed and published in the literature in the past decade to enhance the performance of P2P networks over isolated MANETs. Different deployment strategies, different overlay systems, and different underlay protocols were used to propose efficient combinations of P2P and MANET [1].

Authors in [8] proposed the MACARON P2P overlay for MANET. The proposed system does not use the DHT design. Instead, it uses an unstructured name-location based design to create the overlay. For the underlying MANET routing, MACARON depends on a proactive protocol where it uses OLSR. MACARON builds a cross layer channel to reduce the overlay routing overhead. The routing updates in the underlying network are made available for the overlay through the cross-layer channel. Each node in MACARON is required to maintain $O(\sqrt{n})$ routing entries, where n is the network size. Moreover, it uses landmark nodes to facilitate overlay routing, where the network should have at most $O(\sqrt{n})$ landmark nodes.

The performance of structured P2P systems over MANET was analyzed in [9]. The paper follows the straight layering approach, where the overlay protocols were deployed as they are on top of the underlying networks. The performance of the ring-based Chord and Tree-based Kademlia were tested, with a focus on scenarios of MANET networks that have low mobility and low churn conditions. Both overlays were deployed over the underlying network, which relies on the AODV as the routing protocol. The paper concluded that layered Chord and Kademlia performs reasonably well with small network sizes. However, overlay performance degraded as the network sizes increased due to the heavy overlay maintenance overhead.

The work in [10] proposed an unstructured P2P overlay for MANET that uses underlay characteristics to make sure that the overlay matches the underlay as closely as possible. The system is based on maintaining physically closest peer neighbors. Each peer maintains a list of physical neighbors that contains a neighbor's IP address, physical distance, and overlay maintenance state. The system floods the network with neighbor request and reply messages and hello maintenance and reply messages for overlay creation and maintenance. The input language of the UPPAAL model checker was used to model the proposed structure.

OneHopOverlay4MANET [11] [12] [13] proposed a one logical hop overlay system that is based on the distributed hash table. It builds an overlay similar to that of the EpiChord P2P system. However, the system constructs a cross-layer path between itself and the MANET routing that is used to reduce overlay management optimizing of the existing underlay routing information. Similar to EpiChord and Chord, OneHopOverlay4MANET maintains successor and predecessor lists to guarantee overlay performance. Furthermore, the system depends heavily on a cache that each peer maintains. The cache is mainly populated through underlay routing information.

3D-Overlay was proposed by [14]; it builds a structured P2P overlay for MANET based on three-dimensional logical space. Each peer is assigned an overlay identifier in the form of three entries $\{x|y|z\}$ depending on its location in the three rectangular coordinates. Thus, physical relationships among nodes in the network are considered at the overlay level. 3D-Overlay peers exchange periodic probe messages to maintain the overlay. The system also gives a weight to each link between peers in terms of the number of hops using the underlay routing information provided by the OLSR routing protocol.

MA-SP2P [15] constructs a minimum spanning tree that can be used to build the overlay. A peer minimum spanning tree consists of the peer itself and up to two logical hops neighbors. The overall logical ID space is then disseminated between peers, so that each peer is responsible for a part of the ID space. Each portion of the ID space is a contiguous identifier that is limited with an upper end value and a lower end value. Each of the upper end values and lower end values of a peer's portion should point to a neighbor that has a part of the ID space greater than and lower than the current peer limits, respectively. MA-SP2P depends on exchanging probe messages among peers to maintain the constructed overlay.

The Chord P2P system was deployed on MANET by [16]. The work focused on converging separated Chord rings in MANET. A cross-layer path was used to send underlay routing information of physical neighbors to the overlay. The Chord system was modified to include a new table called the Chord Neighbor Table (CNT). It is used to maintain information about physical neighbors to find any neighboring peers that belong to a different Chord ring. Once a new ring is identified, the system converges it to the existing overlay ring.

Not only were P2P systems used at the application layer to locate services and resources, they were also used in some works to enhance underlay routing. The authors of [17] proposed a KDSR, which is an underlay integration to enhance routing in MANET. It is an integration of Kademlia P2P and the DSR routing protocol. Each node in the proposed system is required to maintain k -bucket routing tables, similar to the original Kademlia, with some changes of the stored contents to better suit MANET. Similar to DSR, the KDSR maintains a cache route table. Kademlia's strategies of updating k -bucket entries are also used to populate the DSR cache route repository.

B. Kademlia

Kademlia is a structured P2P overlay which is based on distributed hash table. It uses 160-bit address space. A hash function is used to allocate a 160-bit identifier for each key and peer in the overlay. Based on its allocated identifier, an object is placed on peers with the closest identifiers on the logical overlay. The notation of exclusive OR (XOR) is used by Kademlia to find out the distance between identifiers. It constructs an overlay as a tree-like topology based on the peers' bitwise XOR. This is to highlight the importance of the differences at a higher order bit compared to the differences at a lower order bit. It is due to the fact that a difference at a higher order bit is a larger distance on the tree-like topology. A Kademlia binary tree is shown in Fig. 1 for peer 1011.

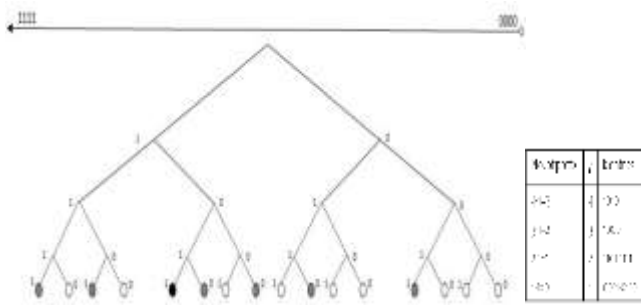


Fig. 1. A Binary Tree for Peer 1011.

A Kademlia peer stores and maintains a list for each bit of its identifier. Such lists are known as buckets. A list is the distance to a particular Kademlia peer or Kademlia subtree of peers. A bucket or list maintains multiple entries to a subtree of the logical space up to a configuration parameter k . In the i^{th} list of a peer, it should store addresses to peers with $i-1$ bits matching the identifier prefix, I [1 , maximum bit of the address space]. The entries of a bucket are stored based on the last seen time. Fig. 1 shows an example of a binary tree for peer 1011, along with its bucket.

Kademlia uses concurrent lookup to find a key on the overlay. For a lookup, firstly a peer finds the L closest peers in its tree. L is a configuration parameter known as the concurrency parameter. It then sends parallel queries to the chosen L peers. The initiator of the queries then uses the received replies to fire another set of queries until it finds the destination.

C. OLSR

OLSR is a proactive MANET link state-based routing protocol that depends on the periodic exchange of management messages among all participating nodes to maintain routing tables. Each node is responsible for diffusing partial link states to others. However, OLSR minimizes the volume of control messages by adopting the MultiPoint Relaying (MPR) strategy. In the MPR strategy, each OLSR node selects a set of neighboring nodes as its MPRs to transmit its control traffic. In order to select MPRs, an OLSR node gathers information about its neighbors, which can be up to 2-hops away. The node then selects a minimum number of 1-hop neighbors as its MPRs, ensuring that all of its 2-hops neighbors can be reached through at least one of the selected MPRs.

OLSR also uses Hello and Topology Control messages to build routing tables. Hello messages are broadcast to neighbors only with the purpose of spreading the link states and physical neighbors of the current node. On the other hand, Topology Control messages are used to diffuse link states throughout the network. They are created and forwarded by MPRs only to minimize routing overhead.

III. PROPOSED SYSTEM

To deploy an efficient P2P overlay over an ad hoc network, the overlay must be aware of the underlying network and better optimize existing routing knowledge.

In our proposed system, we opt for the reduction of overlay management overhead via constructing a cross-layer channel between the network layer that operates the OLSR routing protocol and a modified Kademlia that resides at the application layer. Fig. 2 illustrates the structure of the proposed system.

KadOLSR is designed to meet the following needs:

- Effective deployment of P2P over MANET by building an overlay that can achieve a higher success ratio with minimum latency.
- Optimizing existing underlay routing information for overlay management.
- Avoiding duplicated routing in overlay routing and underlay routing.
- Keeping P2P management traffic at minimum on a scarce environment such as MANET.

The proposed system uses two independent routings. The first is the underlay routing, which is carried out using the OLSR protocol to construct routes among participating mobile nodes. The second routing is carried out at the overlay level using Kademlia to locate shared and distributed objects or keys in the network. However, the underlay routing information is optimized in the proposed system to reduce the overlay routing load to a minimum level.

The proposed system makes use of MANET's proactive routing protocol, which maintains routing entries for each of the available MANET nodes in advance. Thus, the underlay is not required to carry out any specific routing procedure to satisfy the overlay's needs. The OLSR is modified to fire notifications to the cross-layer channel regularly or when changes occur in the routing table. Fired notifications are the IP addresses for each routing entry that the current node is aware of along with a timestamp for each passed IP address.

From the perspective of the overlay, each peer in the proposed system is required to subscribe to the cross-layer notification board in order to receive fired underlay routing notifications. Once the underlay fires routing information, the overlay will be able to receive such notifications, which will be used to update overlay routing tables.

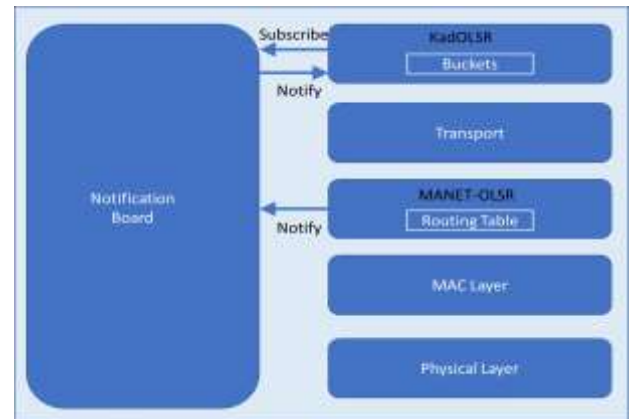


Fig. 2. KadOLSR Structure.

The traditional Kademlia namespace is organized as a complete binary tree. A peer can choose a random value of the used namespace or can calculate its own identifier using a hash function. In the proposed system, each peer is assigned an overlay identifier based on its IP address. A hash function such as SHA-1 can be used to generate the overlay ID.

A peer hashes each received IP address from the notification board and places it in the appropriate bucket. Since the underlay is proactive and maintains the routing table for all of the nodes in the network, the overlay will have a complete view of the existing peers. On the other hand, as a node joins the MANET network, it will exchange underlay routing messages with other participating nodes in order to build its routing table. This, however, would result in its IP address being inserted into other nodes' routing tables. Consequently, other mobile nodes would send routing notifications to their upper overlays that contain the IP address of the joining peer. Thus, other peers would notice the existence of the current joining peer.

IV. PERFORMANCE EVALUATION FOR KADOLSR

A. Simulation Setups and Performance Metrics

The proposed system is evaluated in this section. The OMNeT++ [18] simulation library and framework are used to evaluate the performance of KadOLSR. OMNeT++ is a component-based C++ for building network simulators. The INET framework [19] and the Overlay Network Simulation framework OverSim [20] were used to simulate the underlay and the overlay, respectively. INET supports communication networks, including wireless networks, wired networks, sensor networks, and mobile ad hoc networks. OverSim is another simulation framework for OMNeT++ for P2P networks. It provides implementations for several structured and unstructured P2P protocols. The simulated scenarios are repeated 10 times, and the plotted result is the average of the 10 repetitions. Table I shows the parameters that were used. Each network is given around 60s at the beginning of a simulation to stabilize. Then, the measurement is taken for 1000 s. The Random Way Point mobility model is the mobility model that we used. Two scenarios of lookup frequency were used, where each node fires a lookup every 10s and 60s.

For evaluating the proposed system, the following performance metrics were considered:

- Packet delivery ratio (PDR): the ratio of the answered key lookups to the overall sent key lookups.
- End-To-End delay: the average time that a node requires in order to determine the issued key lookups. It starts from the time that the key lookup is sent until the time at which the node receives the answer for the query.
- Traffic load: the total traffic that was released in the network, including underlay routing protocol traffic and overlay traffic.

B. Results and Discussion

The performance of the proposed system in terms of managing to solve key lookups is shown in Fig. 3 and Fig. 4.

Fig. 3 shows the success ratio as a function of network sizes for nodes moving at 3 m/s and sending random key lookups every 60s. Overall, both systems, layered Kademlia and KadOLSR, achieve good performance for networks consisting of 80 nodes and less. However, as more nodes participate in the network, the performance of the layered Kademlia deteriorates and decreases to around 80%, while the KadOLSR achieves 95% and more.

This can be seen as the result of collisions as more traffic is released in the network with a larger number of nodes. Moreover, Kademlia builds and populates its routing buckets gradually using a pinging mechanism, which results in a higher volume of traffic that affects the success ratio. However, KadOLSR optimizes MANET routing information to populate the overlay, causing less traffic in the network and hence, better performance.

Decreasing the lookup frequency (to 10s) involves generating extra traffic in the network, even though KadOLSR maintains better performance compared to the layered approach, as can be seen in Fig. 4. The figure also shows that as mobile nodes move faster, a reduction can be seen in the packet delivery ratio for both systems. This is expected, as frequent changes in the topology cause more traffic and a disruption in the routing efficiency.

TABLE I. SIMULATION PARAMETERS

Parameter	Value
Simulator	OMNeT++ with INET and OverSim Frameworks
Mobility model	Random Waypoint Model
Mobility pause time	Random between 1 and 50 s
Network size	40, 60, 80, 100, 120, 140
Mobility speed	1, 2, 3, 4, 5 m/s
Repetition	10
Lookup frequency	10, 60 s
Kademlia k	8
Kademlia S	4
Kademlia b	1
Transmission range	250 m
Topology size	1000 m x 1000 m
Simulation time	1000 s
Stabilization time	60 s

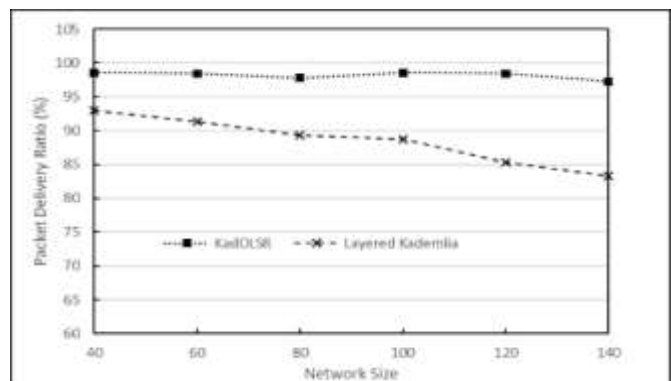


Fig. 3. Packet Delivery Ratio with 60 s Lookup Frequency and 3 m/s Speed.

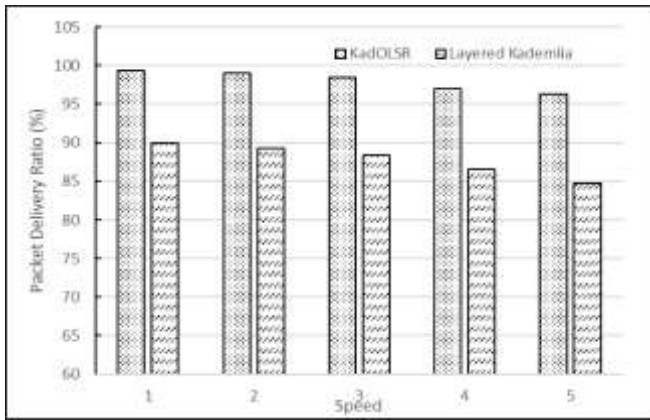


Fig. 4. Packet Delivery Ratio with 10 s Lookup Frequency and 100 Mobile Nodes.

The average time of the end-to-end delay is shown in Fig. 5 and Fig. 6. The result shown is the average delay for those key lookup queries that overlays managed to solve.

The delay is affected mainly by two factors. The first is the availability of the address for a peer, which stores the key, at current overlay buckets, and the second is the efficiency of the underlay routing protocols to route the query. Node mobility speed and network size negatively affect the end-to-end delay, as shown in the figures. This is a result of the extra traffic that is introduced to the network and hence, possible collisions, as more nodes are added to the network or the node speed increases. Overall, both layered and cross-layered systems achieve similar results; nevertheless, KadOLSR manages to solve key lookups in less time in the largest simulated scenario, as displayed in Fig. 6. This is, however, achieved while maintaining a higher success rate, as presented previously in Fig. 3.

The total released traffic in the network is depicted in Fig. 7 and Fig. 8. This includes both overlay and underlay traffic and is measured as the total sent traffic from the network layer for all participating nodes.

KadOLSR outperforms the layered Kademlia in both presented scenarios. The reduction of KadOLSR traffic is the result of using a cross-layering mechanism to feed the overlay using underlay routing information and therefore cut the overlay management load. Fig. 8 shows how the network load for the layered approach increases as the number of nodes increases. The layered approach yields its worst performance with a network size of 140 nodes, where it generates about 90,000 extra packets compared to the proposed approach. Such communication overhead would increase the chance of collisions and hence retransmission, which results in performance degradation, as shown in the previous figures.

The performance of KadOLSR is compared against Layered Kademlia and OneHopOverlay4MANET [11] in terms of success rate, discovery delay, and network load, as shown in the following figures. In terms of the lookup success ratio, Fig. 9 shows that KadOLSR performance was the best in an intensive scenario where each node was moving at 5 m/s and each node sent a lookup query every 10 seconds.

The layered Kademlia gives a competitive result when the size of the network is less than 100 nodes. However, for a network consisting of more than 100 nodes, both cross-layered systems, KadOLSR and OneHopOverlay4MANET, manage to maintain good performance. This is achieved because of relying on the cross-layer channel technique to build overlay routing tables at minimum cost.

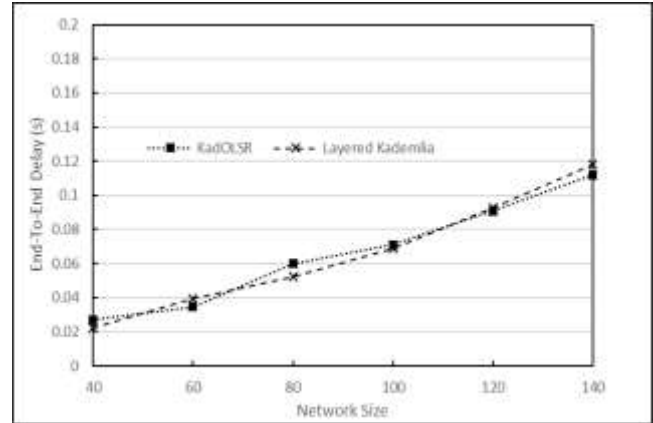


Fig. 5. End-To-End Delay with 60 s Lookup Frequency and 1m/s Speed.

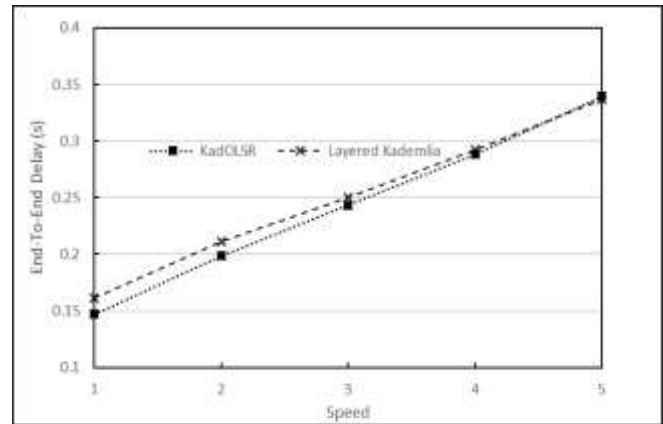


Fig. 6. End-To-End Delay with 10 s Lookup Frequency and 140 Mobile Nodes.

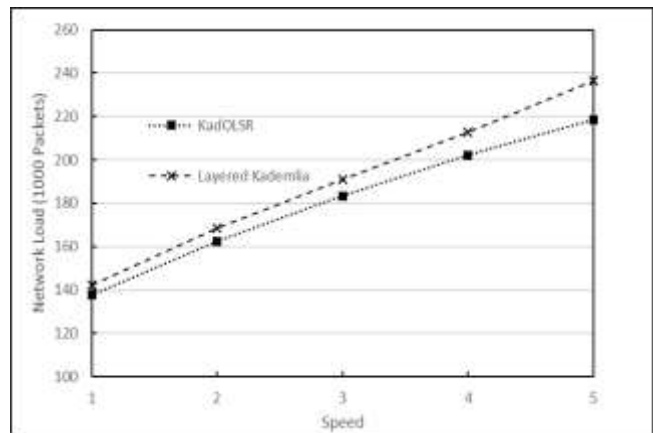


Fig. 7. Network Load with 60 s Lookup Frequency and 120 Mobile Nodes.

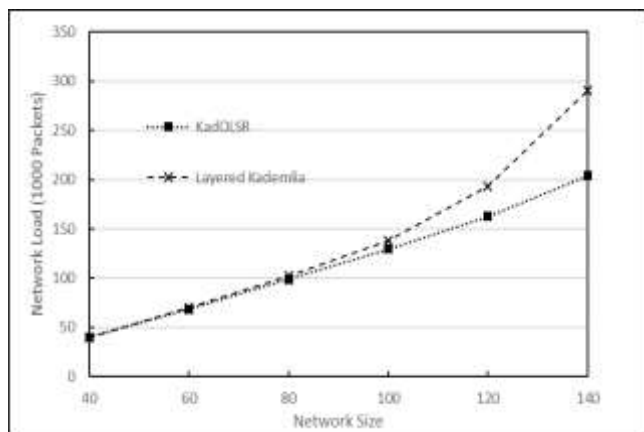


Fig. 8. Network Load with 10 s Lookup Frequency and 2 m/s Speed.

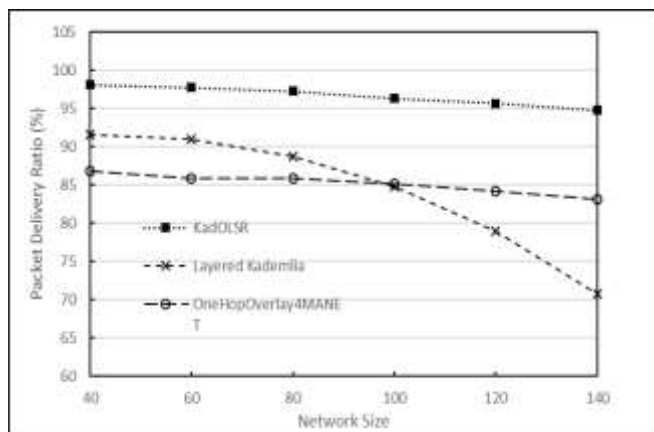


Fig. 9. Packet Delivery Ratio with 10 s Lookup Frequency and 5 m/s Speed.

Regarding the discovery delay, Fig. 10 shows that a slight increase of the average end-to-end delay was experienced by the proposed system. An obvious reason for the increase is that KadOLSR achieves the best performance in terms of the delivery ratio, meaning that the system manages to solve most of the issued lookup queries, including those which were resolved using a higher delay. Thus, average experienced delay is slightly higher.

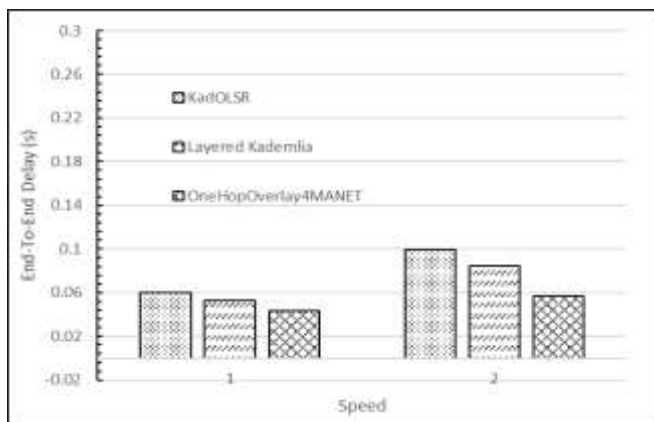


Fig. 10. End-To-End Delay with 60 s Lookup Frequency and 80 Mobile Nodes.

A similar trend to the success ratio appears in the traffic load as Fig. 11 shows, where layered Kademia traffic increases dramatically for 100 nodes and higher network size. This is a result of the pinging mechanism that Kademia used to maintain overlay entries. Moreover, the KadOLSR network's traffic was the smallest among all the compared systems; its total released traffic was kept under 300 k packets for the largest network.

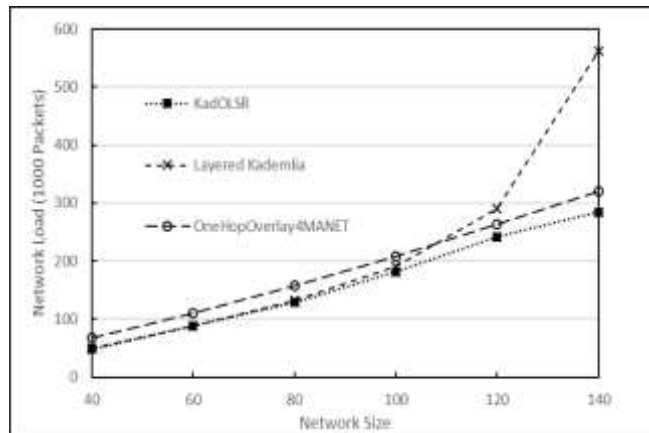


Fig. 11. Network Load with 10 s Lookup Frequency and 5 m/s Speed.

V. CONCLUSION

This paper proposed a novel optimized P2P system for MANET using a Kademia overlay and OLSR for the MANET underlay. The proposed system, KadOLSR, uses a cross-layering technique to reuse underlay routing information for overlay routing management. The proposed system was evaluated in a simulation environment. Its performance was compared to the layered Kademia over OLSR and one of the recent P2P overlay systems for MANET, OneHopOverlay4MANET. The simulation results show that KadOLSR performs well across all different network sizes and mobility speeds. The other two overlays give a reasonable performance for networks consisting of less than 100 nodes. However, as network size increases, the two overlay's performance deteriorates. The use of cross-layering allows the proposed system to reduce the overlay management communication load, which was reflected in good performance in solving key lookup queries. For future work, a plan is made to deploy the proposed system over reactive MANET routing protocols to find out how the cross-layering technique would help maintaining the overlay over reactive MANET.

REFERENCES

- [1] M. al Mojamed and M. Kolberg, "Structured Peer-to-Peer overlay deployment on MANET: A survey," *Computer Networks*, Elsevier, vol. 96, pp. 29–47, 2016.
- [2] Y. Jahir, M. Atiquzaman, H. Refai, A. Paranjothi, and P. G. LoPresti, "Routing protocols and architecture for Disaster Area Network: A survey," *Ad Hoc Networks*, vol. 82, pp. 1–14, Jan. 2019, doi: 10.1016/j.adhoc.2018.08.005.
- [3] A. Delgado Peris, J. M. Hernández, and E. Huedo, "Evaluation of alternatives for the broadcast operation in Kademia under churn," *Peer-to-Peer Networking and Applications*, vol. 9, no. 2, pp. 313–327, 2016, doi: 10.1007/s12083-015-0338-y.

- [4] R. Pecori, "S-Kademlia: A trust and reputation method to mitigate a Sybil attack in Kademlia," *Computer Networks*, vol. 94, pp. 205–218, 2016, doi: 10.1016/j.comnet.2015.11.010.
- [5] M. al Mojamed and A. Al-Shehri, "Performance evaluation of Kademlia in mobile ad hoc networks," *International Conference on Ubiquitous and Future Networks, ICUFN*, pp. 458–463, July 2018, doi: 10.1109/ICUFN.2018.8436723.
- [6] P. Maymounkov and D. Mazieres, "Kademlia: A peer-to-peer information system based on the xor metric," *Peer-to-Peer Systems*, pp. 53–65, 2002.
- [7] T. Clausen et al., "Optimized Link State Routing Protocol (OLSR)." Accessed: Sep. 19, 2020. [Online]. Available: <https://hal.inria.fr/inria-00471712>.
- [8] B. Deokate, C. Lal, D. Trcek, and M. Conti, "Mobility-aware cross-layer routing for peer-to-peer networks R," vol. 73, pp. 209–226, 2019, doi: 10.1016/j.compeleceng.2018.11.014.
- [9] A. Sewak, M. Pandey, and M. Gore, "Performance evaluation of Peer-to-Peer structured overlays over mobile ad hoc networks having low dynamism," in *Lecture Notes in Computer Science*, vol. 10026, LNCS, 2016, pp. 208–223.
- [10] Y. Hammal, M. Seddiki, M. Benchaiba, and A. Abdelli, "Formal specification and analysis of a cross-layer overlay P2P construction protocol over MANETs," in *2017 IEEE Wireless Communications and Networking Conference (WCNC)*, 2017, pp. 1–6, doi: 10.1109/WCNC.2017.7925622.
- [11] M. al Mojamed and M. Kolberg, "Design and evaluation of a peer-to-peer MANET crosslayer approach: OneHopOverlay4MANET," *Peer-to-Peer Networking and Applications*, 2017, doi: 10.1007/s12083-015-0413-4.
- [12] M. al Mojamed and M. Kolberg, "OnehopMANET: One-hop structured P2P over mobile ad hoc networks," *2014 Eighth International Conference on Next Generation Mobile Apps, Services and Technologies IEEE(NGMAST)*, pp. 159–163, 2014, doi: 10.1109/NGMAST.2014.25.
- [13] M. al Mojamed and M. Kolberg, "Performance evaluation of OnehopMANET," in *Science and Information Conference IEEE(SAI)*, 2015, pp. 1028–1032.
- [14] S. a. Abid, M. Othman, and N. Shah, "3D P2P overlay over MANETs," *Computer Networks*, vol. 64, pp. 89–111, 2014, doi: 10.1016/j.comnet.2014.02.006.
- [15] N. Shah, D. Qian, and R. Wang, "MANET adaptive structured P2P overlay," *Peer-to-Peer Networking and Applications*, vol. 5, no. 2, pp. 143–160, 2012, doi: 10.1007/s12083-011-0115-5.
- [16] J. Qing Mei, H. Ji, and T. Li, "Cross-layer optimized Chord protocol for separated ring convergence in MANET," *Journal of China Universities of Posts and Telecommunications*, vol. 16, no. 4, pp. 84–90, Aug. 2009, doi: 10.1016/S1005-8885(08)60253-8.
- [17] B. Zhao, Y. Wen, and H. Zhao, "KDSR: An efficient DHT-based routing protocol for mobile ad hoc networks," *2009 Ninth International Conference on Hybrid Intelligent Systems*, vol. 2, pp. 245–249, 2009, doi: 10.1109/HIS.2009.160.
- [18] "OMNeT++ Discrete Event Simulator." <https://omnetpp.org/> (accessed Apr. 07, 2020).
- [19] "INET Framework - INET Framework." <https://inet.omnetpp.org/> (accessed May 07, 2020).
- [20] "The OverSim P2P Simulator." <http://www.oversim.org/> (accessed Sep. 07, 2020).

Identification of Student-Teachers Groups' Needs in Physical Education and Sport for Designing an Open Distance Learning on the Model of Small Private Online Courses

Mostafa HAMSE¹, Mohammed TALBI³

Laboratory of Analytical Chemistry and Physio Chemistry of Materials, Observatory of Research in Didactics and University Pedagogy, Faculty of Sciences Ben M'SIK Hassan II University, Casablanca, Morocco

Said LOTFI²

Multidisciplinary Laboratory in Education Sciences and Training Engineering, Normal Superior School (ENS) Hassan II University, Casablanca, Morocco

Abstract—Currently, there are witnessing several distance-learning offerings: FOAD (Open Distance Learning) MOOCs (Massive Open Online Course) and SPOCS (Small Private Online Courses) in various intervention sectors including education and training. However, little research has dealt with analyzing the needs of participants before implementing SPOCS in higher education. This study aims to identify needs in order to design and guide a technopedagogical device in SPOCS' form for teacher training. The results showed that more than 70% of interviewees declared that SPOC reduces participants' travel time, 87% aimed at developing professional competence in planning learning, 77% wanted students' evaluation and more than 60% wanted to know the disciplinary knowledge relating to physical and sporting activities (PSA) and their Learning activities' management. In addition, 64.3% of participants preferred, as device's form and design, the four modalities at the same time: text structured in title, video capsules, images and sound recording. In terms of educational tutoring, more than 75% of participants declared their need to understand certain concepts in the course. These results will guide us to focus attention on three basic professional skills: planning, management and evaluation of learning as a priority training module in the envisaged SPOC with technical and pedagogical support both audiovisual and textual.

Keywords—Needs; physical education and sport; professional training; SPOC; teachers

I. INTRODUCTION

Several descriptive studies have shown that information and communication technologies (ICT) are experiencing remarkable expansion in various sectors of society: economic, political, social, cultural and the education and training sector (Traoré, 2008; Redecker et al., 2009; Biaz et al., 2009; Maddux et al., 2012; Collin, et al., 2013; Ait Kaikai, 2014) [1]–[6]. Information and Communication (ICT) is defined by (UNESCO 2006) [7] as a form of technology used to transmit, store, create, share or exchange information. This broad definition of ICT includes technologies such as: radio, television, video, DVD, telephone (both landline and mobile), satellite systems, computer and network hardware and software, and associated equipment and services technologies,

such as video, in addition to the equipment and services associated with these technologies, such as videoconferencing and electronic mail.

In this regard, in Morocco, the strategic vision of the 2015-2030 reform continues to proclaim capital importance to the integration of ICTs for the development and promotion of digital-based education and training through the implementation of adapted, scalable, open and innovative systems. In addition, and with the aim of strengthening the integration of educational technologies to improve the quality of learning and to promote the transition from a knowledge-consuming society to a society that produces and disseminates it, the Superior Council of the Education, Training and Scientific Research (CETSR) [8] recommends developing a national program, aiming to complete the equipment of educational establishments with educational technologies, multimedia rooms and audiovisual equipment, to connect them to the network internet and to equip school libraries and university research structures with the necessary digital resources, medium-term integration of ICT as the main subject in initial and continuing training of all educational actors and the development and promotion of distance learning as a complement to face-to-face courses. Otherwise, some studies have concluded that, the lack of teachers' training (initial or / and continuous) in terms of digital tools' use, the deficiency in the educational exploitation of ICT and individual factors are the main obstacles linked to the integration of ICT in Morocco's classroom (El Ouidadi et al. (2011) [9]. Nevertheless, the operationalization of these recommendations requires on part of all actors intervening in the field of education and training a specific mobilization based on collaborative work which highlights an administrative will, an educational and multimedia design in order to carry out this quest to integration ICT in education and training in Morocco.

In this context, the professional training of future teachers of Physical and Sports Education (PSE) at the Regional Center of Education and Training Professions (RCETP) Casablanca-Settat, adhered to this vision by taking advantage of the

structuring characteristics, organization and adaptation offered by Open and Distance Learning (ODL) to offer them an ODL on the model of SPOCs (Small Private Online Courses) for completing, on the one hand, their initial training in face to face, and on the other hand, for further developing their professional teaching skills [10]. However, recourse to the use of this distance training device in vocational training requires a particular educational, multimedia and organizational design [11]. Therefore, we refer in the design of our SPOC to training engineering by referring to the ADDIE Model (Analysis, Design, Development-Implementation and Evaluation) which is very well known worldwide in training engineering and ODL design. This model is presented in 4 steps: Analysis, Design, Realization and Evaluation [12]. In this engineering, the analysis of training needs represents an essential key to the training design, because it provides the elements of orientation, planning and strategy, which are necessary for the formulation of effective learning objectives that contribute to a best performance [13].

In this study, we focus on the first step reserved for the participants' needs analysis for the establishment of an ODL device based on SPOCs envisaged.

The objective of this study is to identify the student-teachers groups' needs in terms of skills, design and educational tutoring, to guide a future design of this technopedagogical device.

II. THEORETICAL BACKGROUND

A. ICT and its uses

The Organization for Economic Co-operation and Development (OECD) (2001, 2006) [14]-[15] stresses the economic importance and impact of ICT in developed countries and stresses the need for these countries to train a workforce with the skills necessary to use ICTs to increase productivity, as well that the need for young people to develop ICT skills for possible preparation for adult life. In this regard, many researches have concluded that, ICT has become an essential way in improving the quality of learning. Indeed, for Basque et al., 2003; Mastafi (2013) [16]-[17] these technologies, when combined and interconnected, make it possible to search for, store, process and disseminate an impressive amount of information, in the form of different data types (text, sound, images, simulations, etc.), and can be used to exchange, communicate, collaborate, cooperate, produce, create and publish. In addition, the integration of ICT brings several benefits such as flexibility, accessibility, increased exchanges and interactions between various actors (Karsenti, 2003; Nafidi et al., 2015) [18]-[19]. ICTs delocalize, in time and space, the exchanges between teachers and learners, and thereby diversify learning activities and teaching and learning methods (Peraya, 2006; Depover et al., 2007) [20]-[21]. Likewise, Cleary et al. [22] analyzed determining factors of ICT's integration in the classroom and They distinguished five factors which favor this integration and which have a positive impact on students' academic results: Training, environmental context, individual variables, the importance of a community and a human support network and the time that one is willing to devote for it.

On the other hand, it's observed in recent years an ICT explosion and a diversity of distance learning platforms, MOOCs (Delpeyroux et al., 2015) [23], the appearance of mobile devices such as smartphones, tablets and other mobile devices and the social media revolution like Facebook, Viadeo, LinkedIn, Twitter, have become very effective means to allow learners who have not had the chance to register in one of the best universities in the world to take advantage of distance course content to learn and improve their knowledge (Riyami 2018) [24]. In short, ICT has opened up new horizons and has enabled a vital development of this type of education [25]. However, the successful integration of ICT into education requires that teachers be well equipped with the methods necessary for a rational and effective use of these technologies in the teaching-learning process (Ahaji, 2012) [26]. Otherwise, ICT is also of great interest to teachers. Indeed, the study conducted by Neema-Abooki and Nakintu (2015) [27] reveals that it is urgent that teachers have sufficient knowledge of ICT to have a competitive advantage in the world of education today. Thus (Sumande, 2016) [28] stipulates that distance education and learning in the 21st century requires both teachers and students to have a little mastery of ICT because this is due to modern teaching methodologies introduced in distance education. Similarly, for Sandholts, Ringstaff and Dwyer (1997), ICTs trigger change in teaching methods and could even pretend to facilitate the transition from the traditional method to the new method of learning using knowledge-building situations [29]. Similarly, these ICTs offer teachers several opportunities that can complement and reinforce their face-to-face lessons. Guay (2001) [30] proposes a taxonomy of four educational activities favored by ICT: demonstration, simulation, exercise and communication activities. In this perspective, they would contribute to the development of distance education and increased access to different international networks and online resources [31].

B. ICT and Classroom's Integration

According to Mc Gorry [32], the use of ICT can encourage distance education by overcoming the problems linked to cost, to the reduction of the number of teachers. However, these strengths of ICT for teachers remain dependent on their motivation and acceptance of change. For their part, Aziz Rasmy and Thierry Karsenti [33], according to their study on the motivation of teachers in the context of continuous professional development linked to the integration of technologies, note that the feeling of lack of ICT skills pushes teachers to resist change and commitments in carrying out their various tasks. Martine Leclerc (2007) [34] concludes in her study on the profiles of teachers facing the integration of ICT that those who resist "fiercely ICT integration" have a very negative representation. In fact, not only are they not convinced of the educational benefits of ICT, but they consider that these technologies have no benefit and constitute an "unnecessary burden for the teacher".

In this context, the integration of ICT is a systemic process (Depover and Strebelle, 1997) [35]. The adoption of ICT by teachers represents the ultimate outcome of this process, but also an immense challenge (Hutchison and Reinking, 2011; Karsenti and Collin, 2013; Livingstone 2012) [36]-[37]-[38],

despite the ubiquity of technologies in our society (Ertmer and Ottenbreit-Leftwich, 2010; Thibert, 2012). Indeed, for a sustainable and effective integration of ICT in the classroom, it is necessary to follow a multidimensional approach focused on technological equipment, integration content and teacher training. In this sense, Biaz et al. [3] studied the integration of ICT in the work of teachers and stressed the importance of teacher training in the optimal use of ICT for improving the quality of teaching and learning ease of students. Thus, Bibeau in 2007 [39] studied on his side the conditions that can act on the integration of ICT's success in education in general and concluded that ICT improves the motivation of students and allows the development of operations higher order cognitive. This has been confirmed by Labrique [40] that these digital tools can facilitate the rapid acquisition of high-level skills. Nevertheless, and despite these conditions, the integration of ICT is faced with other difficulties, among others, the low confidence of teachers in the effectiveness of ICT for teaching and for student's learning. Like Tardif (1998) [41] and Lebrun (2002) [42], teachers would need to know the relevance of integrating ICT for their teaching a better learning.

C. Barriers of ICT's Integration

The difficulties or obstacles linked to the integration of ICT by teachers seem to come from several sources that can be grouped into two main categories: external factors (linked to school, society, etc.) and internal factors (linked to the teacher or teaching) (Karsenti and Gauthier 2006) [43]. For these authors, the equipment of establishments presents a main external obstacle. For Ertmer, P. (1999) [44], the non-use of ICT by teachers is due to internal factors, in this case, their attitudes, beliefs, practices and resistance to change. Thus, Pelgrum, WJ (2001) [45] mentions, as internal and immaterial obstacles, the insufficient knowledge and skills of teachers in the field of ICT, the difficulty of integrating the use of ICT in teaching and the insufficient time of teachers. Similarly, the British Educational Communications and Technology Agency (BECTA, 2005) [46] and the OECD (2004) [9] emphasize that when the school culture is inadequate, it slows down the integration of ICT by teachers. The internal factors blocking the integration of ICT by teachers are lack of time, poor feeling of technopedagogical competence or self-efficacy, anxiety, difficulties related to class management and motivation or attitudes towards the use of ICT.

However, it should be noted that these barriers revealed by the research literature are structural only in relation to the school and the teacher, while there are other functional obstacles which are mentioned in the literature, namely class management skills, weak administrative support, poor school funding and inadequacy with the school curriculum (Al-Alwani, 2005; Balanskat et al. 2006; Becta, 2004; Beggs, 2000; Gomes, 2005; Lazaros and Rogers, 2006; Schoepp, 2005) [47]-[48]-[49]-[50]-[51]-[52]-[53].

III. METHODS

A. Sample

Our sample is made up of 70 student teachers, including 19 students in vocational training, all of whom are in

vocational training at the Regional Center for Education and Training Professions Casablanca-Settat (RCETP), during the 2018/2019 period, Physical and Sports Education (EPS) intended for teaching at the middle and qualifying school. It is divided into two groups:

A group with hybrid training: formed by 44 student-teachers (62.9%) whom we called hybrid in reference to the nature of the ODL received. They undergo a dual initial training: face-to-face at RCETP and online training through an ODL-SPOC device called FP@STAPS, hosted on a MOODLE Version 3.2 platform, a Learning Management System which used to create and distribute dynamic interactive online courses [54]. - A group with distant training formed by 26 student-teachers of the 2017 training promotion who practice their profession in practice and undergo face-to-face training at RCETP spread over 4 weeks of reception, training and evaluation.

B. Measuring Instruments

In the present survey, we administered a questionnaire to two groups in our sample, in order to collect the following parameters:

- Perceptions of SPOCs' interest.
- The professional skills expected from the FP@STAPS system.
- Design needs for training content, and educational tutoring.

This questionnaire composed of closed questions of dichotomous type and multiple choice.

C. Data Analysis

The data are analyzed by ANOVA I, Khi 2 ($p < 0.05$) by comparing the variables' frequencies, and we examined the effect of the group on the following variables: the perceptions' scale of SPOCs, professional skills targeted by student-teachers, expected forms of FP@STAPS content and educational tutoring needs, with the significance level defined at $p < 0.05$. The data was processed with SPSS software.

IV. RESULTS

The results on the SPOCs' perceptions of trainees are presented in Table I, the professional skills expected by the participants are presented in Table II, and for the design (or form) needs of FP@STAPS and educational tutoring are presented respectively in Tables III and IV.

A. Perceived Interest in SPOCs

Analysis of data relating to student-professors' perceptions of SPOC, shows that 77.1% of those interviewed showed the importance of SPOC, including the reduction in travel time of participants, the decrease in contacts with learners (30.0%), individualized follow-up through a SPOC (21.4%); the feasibility of a face-to-face course compared to a SPOC (10.0%). Furthermore, the analysis of the data presented in Table I does not indicate any significant difference between the groups in all the parameters of the SPOCs' interest perception.

B. Professional Skills Related PES Teaching Expected by Students via an ODL-SPOC “FP@STAPS”

From Table II, we can notice that all of the student-teachers do not perceive that SPOCs allow the development of the following professional skills: planning of learning, evaluation of students, design of a training plan, disciplinary knowledge relating to physical and sports activities (PSA).

However, the learning management skill is the only skill perceived to be developed by the SPOCs by 62.9% of student-teachers. Our results showed that there is no significant difference between the two groups.

C. Design (or form) needs of “FP@STAPS”

The form of content preferred by the students towards FP@STAPS device varies between text structured in titles, video sequences, images and sound recording. In fact, 64.3%

of student-teachers prefer the four modalities at the same time (Table III). No significant difference was observed between the two groups at this level.

D. Needs Related to Educational Tutoring

The educational tutoring needs expressed by student-teachers relate to: the explanation of certain course concepts (77.1%), resolution of technical problems related to the platform (68.6%), highlighting the activities’ objectives (38.6%), and works’ assessment (34.3%).

It is also noted that the dependence of all the needs related to educational tutoring and student-teachers’ group type is statistically insignificant. However, we have noticed that the hybrid group needs significantly more explanation of objectives than the distant group.

TABLE I. PERCEPTION OF SPOCs’ INTEREST IN TWO GROUPS (HYBRID AND DISTANT). THE DATA ARE PRESENTED IN FREQUENCIES AND PERCENTAGES AND COMPARED BY THE CHI-SQUARE TEST

		Group						Chi-square test 2		
		Hybrid		Distanced		Total		Khi2	dll	p
		N	%	N	%	N	%			
SPOC is easier than a face-to-face course at RCETP	By no means agree	1	1.4%	2	2.9%	3	4.3%	4.902	4	0.297
	Little agree	11	15.7%	3	4.3%	14	20.0%			
	Moderately agree	23	32.9%	11	15.7%	34	48.6%			
	Somewhat agree	7	10.0%	8	11.4%	15	21.4%			
	Totally agree	2	2.9%	2	2.9%	4	5.7%			
The SPOC allows individualized follow-up and teaching	By no means agree	0	0.0%	1	1.4%	1	1.4%	6.829	4	0.145
	Little agree	1	1.4%	2	2.9%	3	4.3%			
	Moderately agree	12	17.1%	8	11.4%	20	28.6%			
	Somewhat agree	18	25.7%	13	18.6%	31	44.3%			
	Totally agree	13	18.6%	2	2.9%	15	21.4%			
The SPOC reduces the participants’ travel time	By no means agree	2	2.9%	2	2.9%	4	5.7%	3.214	3	0.360
	Little agree	0	0.0%	0	0.0%	0	0.0%			
	Moderately agree	3	4.3%	0	0.0%	3	4.3%			
	Somewhat agree	7	10.0%	2	2.9%	9	12.9%			
	Totally agree	32	45.7%	22	31.4%	54	77.1%			
In a face-to-face course,I am more often in contact with other learners compared to a SPOC	By no means agree	1	1.4%	0	0.0%	1	1.4%	3.673	4	0.452
	Little agree	5	7.1%	4	5.7%	9	12.9%			
	Moderately agree	12	17.1%	3	4.3%	15	21.4%			
	Somewhat agree	15	21.4%	9	12.9%	24	34.3%			
	Totally agree	11	15.7%	10	14.3%	21	30.0%			
The face to face course at RCETP is more prestigious than a SPOC	By no means agree	1	1.4%	3	4.3%	4	5.7%	4.309	4	0.366
	Little agree	4	5.7%	2	2.9%	6	8.6%			
	Moderately agree	22	31.4%	12	17.1%	34	48.6%			
	Somewhat agree	11	15.7%	8	11.4%	19	27.1%			
	Totally agree	6	8.6%	1	1.4%	7	10.0%			

TABLE II. THE PROFESSIONAL SKILLS TARGETED BY SPOCS ACCORDING TO STUDENT-TEACHERS. DATA ARE PRESENTED IN FREQUENCIES AND PERCENTAGES AND COMPARED BY THE CHI-SQUARE TEST

		Group						Chi-square test 2		
		Hybrid		Distanced		Total				
		N	%	N	%	N	%	Khi2	dll	p
Learnings' planning	By no means agree	4	5.7%	5	7.1%	9	12.9%	1.500	1	0.221
	Little agree	40	57.1%	21	30.0%	61	87.1%			
	Moderately agree	0	0.0%	0	0.0%	0	0.0%			
	Somewhat agree	0	0.0%	0	0.0%	0	0.0%			
	Totally agree	0	0.0%	0	0.0%	0	0.0%			
Managing learning activities	By no means agree	0	0.0%	5	7.1%	5	7.1%	70.000	2	0.000
	Little agree	0	0.0%	21	30.0%	21	30.0%			
	Moderately agree	0	0.0%	0	0.0%	0	0.0%			
	Somewhat agree	44	62.9%	0	0.0%	44	62.9%			
	Totally agree	0	0.0%	0	0.0%	0	0.0%			
Evaluating students	By no means agree	10	14.3%	6	8.6%	16	22.9%	0.001	1	0.973
	Little agree	34	48.6%	20	28.6%	54	77.1%			
	Moderately agree	0	0.0%	0	0.0%	0	0.0%			
	Somewhat agree	0	0.0%	0	0.0%	0	0.0%			
	Totally agree	0	0.0%	0	0.0%	0	0.0%			
Knowing the disciplinary knowledge of PSA	By no means agree	11	15.7%	12	17.1%	23	32.9%	3.315	1	0.069
	Little agree	33	47.1%	14	20.0%	47	77.1%			
	Moderately agree	0	0.0%	0	0.0%	0	0.0%			
	Somewhat agree	0	0.0%	0	0.0%	0	0.0%			
	Totally agree	0	0.0%	0	0.0%	0	0.0%			
Design a school team training plan	By no means agree	12	17.1%	10	14.3%	22	31.4%	0.949	1	0.330
	Little agree	32	45.7%	16	22.9%	48	68.6%			
	Moderately agree	0	0.0%	0	0.0%	0	0.0%			
	Somewhat agree	0	0.0%	0	0.0%	0	0.0%			
	Totally agree	0	0.0%	0	0.0%	0	0.0%			
Organizing a school sport's event	By no means agree	15	21.4%	15	21.4%	30	42.9%	3.717	1	0.054
	Little agree	29	41.4%	11	15.7%	40	57.1%			
	Moderately agree	0	0.0%	0	0.0%	0	0.0%			
	Somewhat agree	0	0.0%	0	0.0%	0	0.0%			
	Totally agree	0	0.0%	0	0.0%	0	0.0%			
Assume an arbitration task in an optional sport	By no means agree	22	31.4%	15	21.4%	37	52.9%	0.388	1	0.533
	Little agree	22	31.4%	11	15.7%	33	47.1%			
	Moderately agree	0	0.0%	0	0.0%	0	0.0%			
	Somewhat agree	0	0.0%	0	0.0%	0	0.0%			
	Totally agree	0	0.0%	0	0.0%	0	0.0%			
Contributing to the sports students' orientation.	By no means agree	20	28.6%	20	28.6%	40	57.1%	6.608	1	0.010
	Little agree	24	34.3%	6	8.6%	30	42.9%			
	Moderately agree	0	0.0%	0	0.0%	0	0.0%			
	Somewhat agree	0	0.0%	0	0.0%	0	0.0%			
	Totally agree	0	0.0%	0	0.0%	0	0.0%			
Online Learning	By no means agree	19	27.1%	13	18.6%	32	45.7%	0.306	1	0.580
	Little agree	25	35.7%	13	18.6%	38	54.3%			
	Moderately agree	0	0.0%	0	0.0%	0	0.0%			
	Somewhat agree	0	0.0%	0	0.0%	0	0.0%			
	Totally agree	0	0.0%	0	0.0%	0	0.0%			
Other	By no means agree	41	58.6%	25	35.7%	66	94.3%	0.268	1	0.605
	Little agree	3	4.3%	1	1.4%	4	5.7%			
	Moderately agree	0	0.0%	0	0.0%	0	0.0%			
	Somewhat agree	0	0.0%	0	0.0%	0	0.0%			
	Totally agree	0	0.0%	0	0.0%	0	0.0%			

TABLE III. DESIGN'S PARAMETERS EXPECTED FROM THE FP@STAPS DEVICE

		Group						Chi-square test 2		
		Hybrid		Distanced		Total				
		N	%	N	%	N	%	Khi 2	dll	p
Explain some concepts in the course	Non	10	14,3%	6	8,6%	16	22,9%	0.001	1	0.973
	Oui	34	48,6%	20	28,6%	54	77,1%			
Highlight the educational activities' objectives	Non	18	25,7%	25	35,7%	43	61,4%	21.051	1	0.000
	Oui	26	37,1%	1	1,4%	27	38,6%			
To help solving technical problems	Non	13	18,6%	9	12,9%	22	31,4%	0.195	1	0.659
	Oui	31	44,3%	17	24,3%	48	68,6%			
To help resolving conflicts within the group	Non	31	44,3%	21	30,0%	52	74,3%	0.910	1	0.340
	Oui	13	18,6%	5	7,1%	18	25,7%			
To give works' assessment	Non	31	44,3%	15	21,4%	46	65,7%	1.181	1	0.277
	Oui	13	18,6%	11	15,7%	24	34,3%			
Other	Non	43	61,4%	25	35,7%	68	97,1%	0.146	1	0.703
	Oui	1	1,4%	1	1,4%	2	2,9%			

TABLE IV. EDUCATIONAL TUTORING NEEDS

Expected forms of FP@STAPS content	Group						Chi-square test 2		
	Hybrid		Distanced		Total				
	N	%	N	%	N	%	Khi 2	dll	p
Text form structured in title and subtitle	1	1,4%	2	2,9%	3	4,3%			
Video sequences (capsules)	8	11,4%	4	5,7%	12	17,1%			
Images and course diagrams	5	7,1%	5	7,1%	10	14,3%	2.182	3	0.535
The four modalities at the same time	30	42,9%	15	21,4%	45	64,3%			
Sound recording	0	0,0%	0	0,0%	0	0,0%			

V. DISCUSSION

The aim of our study is to identify the training needs of PES student-teachers for a SPOC (FP@STAPS), in terms of perception, design and educational tutoring. The interest of our study is to orient the design and technopedagogical piloting of this training device. For this, we compared two training groups: hybrid and distant. The first result of our study showed that all of the student-teachers declare that SPOC reduces student travel time and allows for individualized monitoring and teaching. These declarations show the positive attitude of student-teachers towards SPOCs, which can be explained by their predispositions to get involved for a good integration of these types of device in training. In this regard, some researchers have found that the key to the pedagogical integration of educational technologies lies above all in positive attitudes towards ICT (Player-Koro, 2007) [55]. Similarly, the positive representation of teachers vis-à-vis the introduction of ICT in the educational environment is certainly influenced by the progressive integration of technology in everyday life (Biaz, 2009) [3]. In addition, these positive statements regarding SPOCs lie in its spatio-temporal flexibility by allowing distant people to follow training courses without having to travel [56], as well as the diversity of teaching methods. This flexibility of the educational

sequences, the articulation between training time, working time and leisure time, the pace of progression and acquisition of skills and the ability offered to each to have control of his own course of training (Blandin, Fage, Haeuw, Hellouin, Peyrondet and Primois, 2002) [57]. However, faced with these advantages of the SPOCs concerning spatio-temporal autonomy and the individualization of learning, there are challenges linked to achieving the objectives expected by these devices, in this case the low persistence rate. Indeed, the traditionally low persistence rates of ODL learners have been a subject of concern and study for many years (Scalese, 2001) [58]. Research on the factors related to abandonment or persistence has allowed some progress on this aspect of ODL (Bourdages & Delmotte, 2001). [59] Indeed, the abandonment of studies in distance education institutions is linked to a multitude of variables, linked both to demographic factors (age, sex, civil status, ethnic or social origin, etc.) Bourdages (1996) [60], environmental factors (family, job, material or geographic conditions, life changes, etc. (Woodley and Parlett, 1983; Billings, 1988; Powell, Conway and Ross et al., 1990) [61]-[62]-[63] and educational factors such as lessons, teaching aid, assignments, feedback, etc. (Roberts, 1984; Rekkedal, 1985; Taylor, 1986; Sweet, 1986; Sung, 1986; Garrison, 1987; Ritchie and Newby, 1989) [64]-[65]-[65]-[66]-[67]-[68]-[69]-[70]. However, almost a third of student-

teachers preferred a face-to-face course at RCETP than a SPOC when about 50% are unable to make this comparison. Indecision and concern about seeing the evidence of The beneficial contribution of ICT before using it themselves are the explanatory factors for this fact (Villeneuve, 2011) [71].

Faced with these findings, we suggest capitalizing on these positive representations of student teachers with regard to SPOCs, by providing close support and monitoring through quality educational tutoring reducing the dropout rate.

Our results also showed a dominance of three main skills expected by student-teachers of the SPOC: learnings' planning with dominance of hybrid group compared to distant group (50.1% vs 30%). This fact could be explained by the increased need for student-teachers in face-to-face training, for this planning skill. It therefore constitutes, on the one hand, the trigger for their teaching-learning act, and on the other hand the element design of learning sessions during teaching placements. The competence of student's assessment, and according to the results observed, shows the importance of this axis of evaluation for student-teachers. This observation can be interpreted by the difficulty that student teachers find in an assessment. Indeed, the great difficulty in PSE to have an objective assessment is the definition of the assessment's criteria and standards (David, 2000; MacDonald & Brooker, 1997) [72]-[73]. Added to this is the difficulty of judging heterogeneous school populations with the same evaluative framework, in very diverse material and human teaching contexts and in physical and sports activities whose differences in internal logic cannot be erased. Teachers show an attitude of doubt to the observables' choice, benchmarks and criteria that they would like relevant (Brau-Antony, 2000; David, 2000) [74]-[72]. The professional training competence for school teams (68.6%) reflects its usefulness in the teaching task at the level of SSA (School Sports Association) sessions preparing students for school sports games. The future training content of our planned FP@STAPS system will integrate these skills into the teaching content. In addition, the finding of a statistically significant relationship of dependence between the type of group: hybrid or distant and the two skills, namely the management of learning activities and the contribution to the orientation of sports students, showed the interest given by student teachers to these two skills, which have a direct link with their daily practice.

The form and design of the SPOC (FP @ STAPS) expected by the majority of student teachers in our sample is the mixed integration of textual, pictorial and audiovisual media. This choice can be justified by the need to personalize the training path and the choice of supports (Chovino and Dallaire, 2018) [75], and by the different learners' learning styles that must be taken into account in FP@STAPS's design.

This observation requires us to integrate into our system diagrams and synthetic video capsules to respond to the visual learning style of trainees, facilitate memorization and ensure design's simple and effective ergonomics.

The need for educational tutoring mainly relates to the explanation of certain course concepts and technical problems related to the platform. This means the need to be welcomed and supported in their learning processes by facilitating the

transfer of knowledge and helping them in the personal process of learning and assimilating their knowledge (Berrouk & Jaillet, 2013; Denis, 2003; Racette, Poellhuber, & Bourdages, 2017) [76]-[77]-[78]. Thus, two thirds of the student-teachers interviewed expressed their need for help in solving possible technical problems, which can be interpreted by the non-familiarization of student teachers with this kind of distance training via a platform comprising previously unimaginable features. This technical aid joins the nine tutorial functions proposed by Glikman (2002) [79], including help in using the tools and software of the platform. However, we found that three quarter of student-teachers refuse to resolve conflicts within the group, this result can be understood by their perceptions expressed beforehand towards the contribution of SPOCs in the individualized teaching of learners and subsequently, they do not favor collaborative work which can be a source of conflict within the class group. This statement goes against the words of (De Lièvre, Depover, Quintin, & Decamps, 2003) [80] which highlights the tutorial function of supporting learners and setting up a climate of collaborative trust in groups of learners. In addition, the majority of student-teachers do not accept their work's online evaluation, because for them, it is an optional act and not compulsory. This surprising result, thwarts the results of certain works that have distinguished the evaluative function as essential tasks of tutors [81].

In general, the results shown in this fourth axis concerning the need for student teachers for pedagogical tutoring illustrate the technopedagogical need for student teachers which could be explained by, on the one hand, the interest accorded to training content and on the other hand to the technical inexperience of student-teachers in this kind of online training, which would push us as a pedagogical tutor of FP@STAPS to provide suitable technopedagogical help which confirms the different functions of the tutor online: disciplinary, methodological and technical, which are further explained in the words of Marie Micholet (2018) [82]. In addition, our main concern is to go beyond the framework of a single transmission of knowledge towards close support likely to ensure the motivation of student teachers to follow our online training. It should be noted that our present study is a first step to conceive FP@STAPS envisaged. It was limited to identifying needs of technopedagogical order and did not target the learners' psychological dimension.

VI. CONCLUSION

Our study identified the student-teachers' needs for the design of a distance learning device based on the SPOC model "FP@STAPS". These needs are articulated in four axes: perception of interest of the SPOC, the needs in professional skills, the form of the SPOC and the educational tutoring. Similarly, our work underlined the importance of the courses' planning and evaluation, mixed multimedia supports: text, video capsules, images and audio files and educational tutoring.

The student teachers asked for their need for technopedagogical help relating to the resolution of the platform's technical problems used and educational objectives' clarification. These conclusions will serve us in the future

stage of designing the device to plan a training module reserved for basic professional skills in PSE: planning, management and evaluation in PSE. By integrating various digital resources into our platform, and a appropriate tutoring mode, we will respond on the one hand, to the students' different learning styles and on the other hand, support the student-teachers while awaiting the educational objectives.

Future research axes will determine student-teachers' learning styles to have other precise data that will allow us to tailor-make our online distance training, by questioning a larger sample concerning several training centers in Morocco.

ACKNOWLEDGMENT

The authors would like to thank the director of RCETP Casablanca-Settat and PES student-teachers who enthusiastically participated in the different phases of our study.

REFERENCES

- [1] Traoré D. Quel avenir pour l'usage pédagogique des TIC en Afrique subsaharienne? Cas de cinq pays membres du ROCARE. ICT Chang Mindsets Educ L'éducation À L'aide TIC Bamenda Cameroon Langaa. 2008.
- [2] Redecker, C., Ala-Mutka, K., Bacigalupo, M., Ferrari, A. & Punie, Y. (2009). Learning 2.0: the impact of web 2.0 innovations on education and training in Europe. Séville, Espagne : Institute for Prospective Technological Studies.
- [3] Biaz A, Bennamara A, Khyati A, Talbi M. Intégration des technologies de l'information et de la communication dans le travail enseignant, état des lieux et perspectives. EpiNet Rev Électronique L'EPI. 2009;120.
- [4] Maddux CD, Johnson DL. External validity and research in information technology in education. Taylor & Francis; 2012.
- [5] Collin S, Karsenti T. Usages des technologies en éducation: analyse des enjeux socioculturels. Éducation Francoph. 2013;41(1):192-210.
- [6] Kaikai HA. Appropriation des Technologies de l'Information et de la Communication au sein de l'Université marocaine: Perceptions des étudiants. Rev FRANTICE. 2014;(8).
- [7] Using ICT to develop literacy. Bangkok: UNESCO; 2006.
- [8] Conseil Supérieur de l'Éducation, de la Formation et de la Recherche Scientifique « Vision stratégique de la réforme 2015-2030, Levier 12; Article 77 pp : 43.
- [9] El Ouidadi O, Lakdim A, Essafi K, Sendide K. Contribution à l'évaluation de l'impact de l'intégration des TICE dans l'enseignement et l'apprentissage: exemple de la division cellulaire (mitose) en deuxième année de baccalauréat sciences expérimentales. Rev Électronique L'EPI Paris. 2011.
- [10] Unité Centrale de la Formation des Cadres; Curriculum d'éducation physique et sportive ; Filière de Qualification des Professeurs du Secondaire Qualifiant -Juillet 2012-.
- [11] Drissi MM, Mohammed T, Mohamed K. La formation à distance, un système complexe et compliqué (Du triangle au tétraèdre pédagogique). sept 2006 [cité 4 oct 2018];(83). Disponible sur: <https://www.epi.asso.fr/revue/articles/a0609b.htm>.
- [12] Parmentier C. L'ingénierie de formation: outils et méthodes. Paris: Ed. d'Organisation; 2008.
- [13] Félix, Y. (2010). Analyse des besoins technologiques des apprenants à distance à la Télé-université (Doctoral dissertation, Télé-université).
- [14] Organization for Economic Co-operation and Development [OECD] (2001). The well-being of nations: The role of human and social capital. Paris: OECD.
- [15] OCDE (2004). OECD survey of upper secondary schools - Technical report. OCDE.
- [16] Basque J, Lundgren-Cayrol K. Une Typologie Des Typologies Des Usages Des « Tic » En Éducation. 2003;35.
- [17] Mastafi M. Intégration et usages des TIC dans le système éducatif marocain: Attitudes des enseignants de l'enseignement primaire et secondaire. 2013.
- [18] Karsenti T. Favoriser la motivation et la réussite en contexte scolaire: Les TIC feront-elles mouche. Vie Pédagogique. 2003;127:27-32.
- [19] Nafidi Y, Alami A, Zaki M, Afkar H. Open and Distance Learning in the Initial Education of Trainee Teachers. Int J Educ. 2015;13.
- [20] Peraya D. La formation à distance: un dispositif de formation et de communication médiatisées. Une approche des processus de médiatisation et de médiation. Calidoscôpio. 2006;4(3):200-204.
- [21] Depover C, Karsenti T, Komis V. Enseigner avec les technologies: favoriser les apprentissages, développer des compétences. PUQ; 2007.
- [22] Cleary, Christopher, Abdeljalil Akkari, and Diego Corti. "L'intégration des TIC dans l'enseignement secondaire." Formation et pratiques d'enseignement en questions 7 (2008): 29-49.
- [23] Delpeyroux S, Bachelet R. Intégrer un MOOC dans un cursus de formation initiale. :10.
- [24] Riyami B. Analyse des effets des TIC sur l'enseignement supérieur au Maroc dans un contexte de formation en collaboration avec une université française. 2018;168.
- [25] Depover, C., & Orivel, F. (2012). Les pays en développement à l'ère de l'e-learning. Institut international de planification de l'éducation (Unesco).
- [26] Ahaji K, Zahim S, Badda B. Soubassements théoriques pour guider l'intégration réussie des TICE. EpNet Rev Electron L'EPI. 2012;142.
- [27] Neema-Abooki PA, Neema-Abooki NR. Usability of Computers in Teaching and Learning at Tertiary-level Institutions in Uganda. Afr J Teach Educ. 2015;4(1).
- [28] Sumande CT, Castolo CL, Comendador BEV. The ICT level of confidence of course specialists in distance education: The Polytechnic University of the Philippines experience. Turk Online J Distance Educ. 2016;17(4).
- [29] Haymore Sandholtz J, Ringstaff C, OWYER DC. La classe branchée. Enseigner À L'ère Technol Paris CNDP Titre Orig Teach Technol Creat Stud-Centered Classr. 1997.
- [30] Guay P-J. Les TIC et l'enseignement: un tour d'horizon. Bull Clic. 2001;41:2-5.
- [31] Organisation des Nations Unies pour l'éducation, la science et la culture. (2003). Développements récents et perspectives de l'enseignement supérieur en Afrique subsaharienne au 21e siècle. Paris : Auteur.
- [32] McGorry SY. Online, but on target? Internet-based MBA courses: A case study. Internet High Educ. 2002;5(2):167-175.
- [33] Rasmy A, Karsenti T. Les déterminants de la motivation des enseignants en contexte de développement professionnel continu lié à l'intégration des technologies. Rev Int Technol En Pédagogie Univ J Technol High Educ. 2016;13(1):17-35.
- [34] Leclerc M. Un nouveau regard sur les profils des enseignants à l'égard de l'intégration des TIC. Can J Learn Technol Rev Can L'apprentissage Technol. 2007;33(2).
- [35] Depover C, Strebelle A. Un modèle et une stratégie d'intervention en matière d'introduction des TIC dans le processus éducatif. IRDP; 1997.
- [36] Hutchison A, Reinking D. Teachers' perceptions of integrating information and communication technologies into literacy instruction: A national survey in the United States. Read Res Q. 2011;46(4):312-333.
- [37] Karsenti, T. et Collin, S. (2013). TIC et éducation : avantages, défis et perspectives futures. Éducation et francophonie, 41(1), Numéro thématique.
- [38] Livingstone S. Critical reflections on the benefits of ICT in education. Oxf Rev Educ. févr 2012;38(1):9-24.
- [39] Bibeau R. Les technologies de l'information et de la communication peuvent contribuer à améliorer les résultats scolaires des élèves. Rev L'EPI. 2007;94.
- [40] Labrique S, Grenier D, Labrique F. Entre savoir et savoir-être, du rôle des TIC dans le processus d'apprentissage du génie électrique: compte rendu d'innovation. Didask Paris. 2004.

- [41] Tardif, J., Intégrer les nouvelles technologies de l'information. Quel cadre pédagogique ? Paris : ESF Editeur. Collection "Pratiques et enjeux pédagogiques". 1998.
- [42] Leburun M., Des technologies pour enseigner et apprendre, Paris, De Boeck Université, 2002.
- [43] Karsenti, Thierry, and Clermont Gauthier. "Les TIC bouleversent-elles réellement le travail des enseignants." *Formation et profession* 12.3 (2006): 2-4.
- [44] Ertmer PA. Addressing first-and second-order barriers to change: Strategies for technology integration. *Educ Technol Res Dev*. 1999;47(4):47-61.
- [45] Pelgrum WJ. Obstacles to the integration of ICT in education: results from a worldwide educational assessment. *Comput Educ*. 2001;37(2):163-178.
- [46] BECTA (2005). What the research says about barriers to the use of ICT in teaching. Becta ICT Research.
- [47] Al-Alwani AES. Barriers to integrating information technology in Saudi Arabia science education. University of Kansas; 2005.
- [48] Balanskat A, Blamire R, Kefala S, others. A review of studies of ICT impact on schools in Europe. *Eur Sch*. 2006.
- [49] Becta A. A review of the research literature on barriers to the uptake of ICT by teachers. Lond UK BECTA Httppublications Becta Org Ukdisplay Cfm. 2004.
- [50] Beggs TA. Influences and Barriers to the Adoption of Instructional Technology. 2000.
- [51] Gomes C. Integration of ICT in science teaching: A study performed in Azores, Portugal. *Recent Res Dev Learn Technol*. 2005;13(3):63-71.
- [52] Lazaros EJ, Rogers GE. Critical Problems Facing Technology Education: Perceptions of Indiana Teachers. *J Ind Teach Educ*. 2006;43(2):45-69.
- [53] Schoepp K. Barriers to technology integration in a technology-rich environment. *Learn Teach High Educ Gulf Perspect*. 2005;2(1):1-24.
- [54] Moodle H. Moodle. West Perth Aust Moodle HQ. 2018.
- [55] Player-Koro C. Why teachers make use of ICT in education. In: *Arbetspaper presenterat vid 10th Pre-Conference of Junior Researchers of Earli*, 27-28 augusti, Budapest, Ungern. 2007.
- [56] Mustapha A. Formation à distance: dispositif et gestion-. *Télévision Interactive*, Rabat, Maroc; 2005.
- [57] Blandin B, Fage C, Haeuw F, Hellouin V, Peyrondet J, Primois C. Le BA BA de la FOAD. In: *Forum Français de la Formation à distance*. 2002.
- [58] Scalse ER. What Can a College Distance Education Program Do To Increase Persistence and Decrease Attrition?. *J Instr Deliv Syst*. 2001;15(3):16-20.
- [59] Bourdages L, Delmotte C. La persistance aux études universitaires à distance. *Int J E-Learn Distance Educ Int E-Learn Form À Distance*. 2007;16(2):23-36.
- [60] Bourdages L. La persistance et la non-persistance aux études universitaires sur campus et en formation à distance. *Distances*. 1996;1(1):51-68.
- [61] Woodley A, Parlett M. Student drop-out. *Teach Distance*. 1983;24:2-23.
- [62] Billings, D.M. (1988). A conceptual model of nontraditional undergraduate student attrition. *Review of Educational Research*, 55, 485-540.
- [63] Powell R, Conway C, Ross L. Effects of student predisposing characteristics on student success. *Int J E-Learn Distance Educ Int E-Learn Form À Distance*. 1990;5(1):5-19.
- [64] Roberts D. Ways and means of reducing early student drop-out rates. *Distance Educ*. 1984;5(1):50-71.
- [65] Rekkedal T. Introducing the Personal Tutor/Counsellor in the System of Distance Education. *Project Report 2*. ERIC; 1985.
- [66] Taylor JC. Student persistence in distance education: a cross-cultural multi-institutional perspective. *Distance Educ*. 1986;7(1):68-91.
- [67] Sweet R. Student dropout in distance education: An application of Tinto's model. *Distance Educ*. 1986;7(2):201-213.
- [68] Sung N. Perceptions of program and learning environment as determinants of persistence and poststudy attitudes in adult distance learning. University Microfilms; 1986.
- [69] Garrison DR. Researching dropout in distance education. *Distance Educ*. 1987;8(1):95-101.
- [70] Ritchie H, Newby TJ. Instruction: Classroom lecture/discussion vs. live televised instruction: A comparison of effects on student performance, attitude, and interaction. *Am J Distance Educ*. 1989;3(3):36-45.
- [71] Villeneuve SP. L'évaluation de la compétence professionnelle des futurs maitres du Québec à intégrer les technologies de l'information et des communications (TIC): maîtrise et usages. 2011.
- [72] David B. Éducation physique et sportive: la certification au baccalauréat. Institut national de recherche pédagogique; 2000.
- [73] Macdonald D, Brooker R. Assessment issues in a performance-based subject: A case study of physical education. *Stud Educ Eval*. 1997;23(1):83-102.
- [74] Brau-Antony S. Étude des référentiels d'évaluation: l'exemple du volley-ball. *L'Education Phys Sport Certif Au Bac*. 2000;57-76.
- [75] Chovino, L. et Dallaire, F. (2018). Guide sur la personnalisation des apprentissages en formation à distance pancanadienne francophone. Montréal, QC: REFAD.
- [76] Berrouk S, Jaillet A. Les fonctions tutorales: pour un déséquilibre dynamique. *Distances Médiations Savoirs Distance Mediat Knowl*. 2013;1(2).
- [77] Denis B. Quels rôles et quelle formation pour les tuteurs intervenant dans des dispositifs de formation à distance? *Distances Savoirs*. 2003;1(1):19-46.
- [78] Racette N, Poellhuber B, Bourdages-Sylvain M-P. Quelles sont les caractéristiques de l'emploi et du travail des tuteurs en formation ouverte et à distance? *Distances Médiations Savoirs Distance Mediat Knowl*. 2017;(18).
- [79] Glikman V. Des cours par correspondance au" e-learning"[From correspondence courses to" e-learning"]. Paris Press Univ Fr. 2002.
- [80] De Lièvre B, Quintin J. et Decamps S. 2003. In: Les représentations a priori et a posteriori du tutorat à distance Conférence EIAH. 2003. p. 115-126.
- [81] De Lièvre B, Depover C, Quintin J-J, Decamps S. Les représentations a priori et a posteriori qu'ont les apprenants du rôle du tuteur dans une formation à distance. In 2003.
- [82] Marie Micholet. Un tutorat transversal à distance et en ligne pour l'université. Linguistique. Université Paul Valéry - Montpellier III, 2018. Français. ffnnt : 2018MON30031ff. fftel-02019880f.

A Classification Javanese Letters Model using a Convolutional Neural Network with KERAS Framework

Yulius Harjoseputro

Department of Informatics
Universitas Atma Jaya Yogyakarta
Yogyakarta, Indonesia

Abstract—One of the essential things in research engaged in the field of Computer Vision is image classification, wherein previous studies models were used to classify an image. Javanese Letters, in this case, is a basis of a sentence that uses the Javanese language. The problem is that Javanese sentences are often found in Yogyakarta, especially the use of name tourist attractions, making it difficult for tourists to translate these Javanese sentences. Therefore, in this study, we try to create a Javanese character classification model hoping that this model will later be used as a basis for developing research into the next stage. One of the most popular methods lately for dealing with image classification problems is to use Deep Learning techniques, namely using the Convolutional Neural Network (CNN) method using the KERAS framework. The simplicity of the training model and dataset used in this work brings the advantage of computation weight and time. The model has an accuracy of 86.68% using 1000 datasets and conducted for 50 epochs based on the results. The average inference time with the same specification mentioned above is 0.57 seconds, and again the fast inference time is because of the simplicity of the model and dataset toolbar. This model's advantages with fast and light computation time bring the possibility to use this model on devices with limited computation resources such as mobile devices, familiar web server interface, and internet-of-things devices.

Keywords—Javanese letters; deep learning; convolutional neural network; epoch; framework KERAS

I. INTRODUCTION

Indonesia is a country that has a variety of cultures; one of the cultures heritages that must preserve is the Javanese letters [1], [2]. Javanese letter is an ancient Javanese character, used since the 17th century [3]. Because the Javanese letters are considered a Javanese style, some researchers raised this topic for their research [1], [4]–[7]. One of the researchers who raised the Javanese letters' issue was the one conducted by Widiarti and Wastu in 2009. The Javanese letters' application was widely available in Indonesia, especially in the province of Yogyakarta Special Region. For example, use in street name, menu names in restaurants around the Sultan's Palace, electronic media [8], and many others. The city of Yogyakarta is also known as one of the towns of Tourism, and not a few tourists who visit Yogyakarta every year. Even Javanese letters' application is often found in tourist destinations that tourists usually visit, for example, in the Palace, North and

South Square, Malioboro, and many others. Therefore, in this study, we try to create a Javanese character classification model hoping that this model will later be used as a basis for developing research into the next stage.

This research is significantly related to digital images, and image classification [9], especially in this case, is the Javanese letters' image. Digital painting is now a necessity for many people for various purposes. It can see from the importance of digital images in various fields of science and entertainment. One function of the image, in this case, is to obtain important information contained in the picture, where the extraction of data from an image is the primary goal of Computer Vision [10]. The extraction results can be processed again to get the classification results from the image. The idea of image classification is to give a computer input from a collection of numbers processed from the image. It will produce a number that represents the category of the image.

Image classification alone is not enough, in this case, to get the processing results from that image. There needs to be a technology that can support making the image classification results better, seen from its accuracy and computation time. Therefore, several studies have emerged that use techniques from Deep Learning. Deep Learning is one of the sub-areas of Machine Learning, where the algorithm used is inspired by how the human brain works. In recent years Deep Learning has shown exceptional performance, mostly influenced by more reliable computational factors, large datasets, and techniques for training deeper networks.

One method of deep learning is the CNN method, inspired by the human brain [11] and uses image input as an assumption. Convolutional Neural Network (CNN), in the next few decades, will have many breakthroughs in various fields related to pattern recognition; from image processing to sound detection, the most useful aspect of CNN is reducing the number of parameters in artificial neural networks. This led the researchers to complete complex tasks, which could not be solved using artificial neural network methods [12]. CNN is an algorithm of deep learning, development of Multi-Layer Perception (MLP), designed to manage data in the form of grids, two-dimensional images such as images sounds [13].

This network has a particular layer called the convolution layer, wherein this layer, an inserted image will be processed

based on a predetermined filter. Each of these layers will produce a pattern of several parts of the image, which will be easier to classify later. This technique can make the image learning function more efficient to implement. Several annual competitions carried out to enhance research in the field of Computer Vision, including each year, state of the art methods have emerged to win this competition, for example, GoogLeNet [14], AlexNet [15], and ResNet [16]. Besides, many studies have attempted to overcome this problem using a Convolution Neural Network (CNN) because of its ability to provide high character detection [6]. Some uses of the CNN method in its application, especially to recognize the character carried out by Harjoseputro in 2018. His research has succeeded in classifying the Javanese letters with an accuracy of 85% [9]. As for research on the character of Arabic handwriting[17], this study has successfully implemented deep learning and produced accuracy for each AIA9k and AHCD database of 94.8% and 97.6%.

Therefore, the writer thinks that how the Javanese letters are to decorate in tourist attractions, where the visitors, mostly tourists, do not understand the Javanese letters' meaning. In this case, the author would like to conduct research to create Javanese letters using the Convolutional Neural Network method using the Hard Framework. In this case, hard is the high-level neural network API developed in Python, focusing on the goal of accelerating the research or trial process. In this case, the KERAS framework is that there is a built-in function suitable for this Convolutional Neural Network method. Also, with this Hard framework can run the same source code using the CPU or GPU smoothly.

II. THE MATERIAL AND METHOD

Before discussing the methods used in this research, it is better to know any theory or material about the research topic carried out.

A. Deep Learning

Deep Learning is one area of Machine Learning [9], [17], which utilizes artificial neural networks to implement problems with large datasets. Also, it is a technology that is inspired by the functioning of the human brain. Besides, artificial neuron networks automatically analyze large data sets to find underlying patterns without human intervention. Deep learning identifies unstructured data patterns, such as pictures, sounds, videos, and text [11]. Deep Learning techniques provide a robust architecture for Supervised Learning. By adding more layers, the learning model can better represent labeled image data. Three fundamental reasons underlying the popularity of deep learning today are increased hardware capabilities for computational processing, increased size of data used to train networks, and the growing development of research related to machine learning and data processing. Some deep learning areas include computer vision, speech recognition, natural language processing, and other related fields. In Fig. 1, the following is an overview of the scope of deep learning.

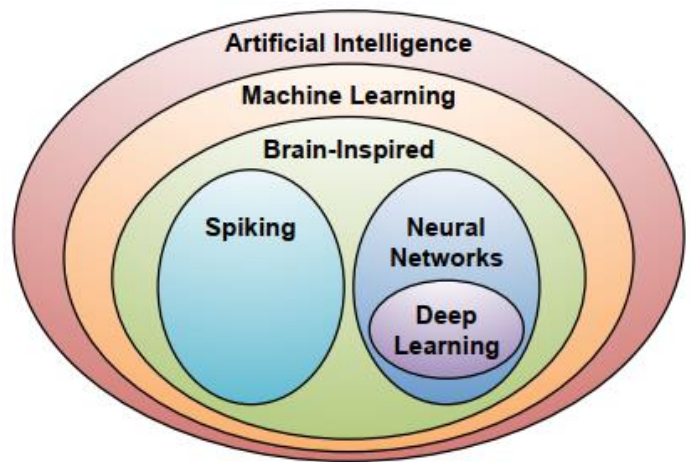


Fig. 1. Deep Learning Scope [18].

B. Convolutional Neural Network

In this Deep Learning technique, one of them is the CNN or Convolutional Neural Network method. This method is a development of the Multilayer Perceptron (MLP), designed to process two-dimensional data. CNN is included in the type of Deep Neural Network because of the high network depth and widely applied to image data [19]. Besides, this CNN method can be excellent in finding useful features in the image to the next layer to form a non-linear hypothesis that can increase a model's complexity. However, completing this method requires a reasonably elaborate model, so it will certainly require quite a long training time. Therefore, when using this CNN method, GPU is very much recommended to speed up the training process [7]. In Fig. 2, the following is the architecture in the Multilayer Perceptron, which has several x layers, shown in red and blue squares with each layer containing y neurons shown in white circles. MLP accepts one-dimensional input data and propagates the data on the network to produce output. Each relationship between neurons on two adjacent layers has a one-dimensional weight parameter that determines the model's quality. Every input data in the segment is carried out linearly with the actual weight value. Then the computational results will be transformed using a non-linear operation called the activation function [19].

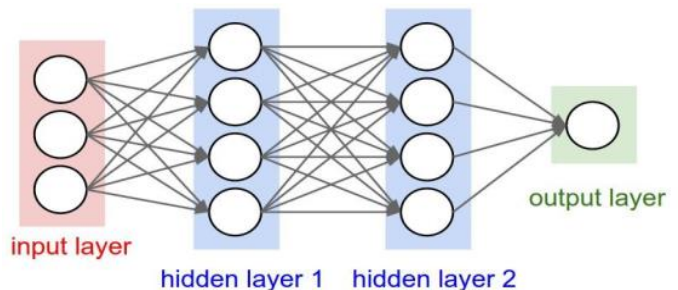


Fig. 2. Perceptron Multilayer Architecture [20].

Convolutional Neural Network (CNN) has several architecture layers, including the convolution layer, pooling layer, full connected layer, and loss layer. Each of these layers has a role in doing the process of managing two-dimensional data. The convolution layer is to carry out convolution operations at the output of the previous layer. This layer is the primary process that underlies a CNN. Convolution is a mathematical term used to apply a function to the output of other functions. The purpose of convolution in an image is to extract features from an input image. The convolution will produce a linear transformation of the input data according to the input data's information. The convolution layer is a system that studies the workings of the visual cortex of the brain and to study filters of the inserted images [13].

C. Tensorflow and Keras Framework

TensorFlow is a software library that has an open-source source for performing numerical calculations using data flow graphs. TensorFlow is created and developed by the Google Brain team and researches Google's intelligence engine for Machine Learning and Deep Learning. Also, TensorFlow is designed for large scale distributed training and inference. The distributed TensorFlow architecture contains a master service with kernel implementation. Tensorflow is designed to be used both in research, development, and production systems. Besides, TensorFlow can run on a single CPU and GPU system and an extensive distributed system with hundreds of nodes used; in its development, TensorFlow has been used to support various algorithms, including in the training process and inference for various Deep Neural Network models. Tensorflow is also the most famous library of data science with many community development and support [21].

Keras is a High-Level Neural Network API that can be run on machine learning frameworks such as Tensorflow, CNTK, or Theano. Hard is built using the python programming language. Keras also provides an API [22] that makes it easy for users to build ANN architecture. Hard has several applications, which are deep learning models that are used together with pre-trained weights. These models can be used to predict, perform feature extraction, or fine-tuning. These models include *Xception*, *VGG16*, *VGG19*, *ResNet50*, *InceptionV3*, *InceptionResNetV2*, *MobileNet*, *DenseNet* & *NasNet* [21].

D. Javanese Letters Dataset

This dataset contains images of all existing Javanese characters, namely, 20 Javanese characters, including HA, NA, CA, RA, KA, DA, TA, SA, WA, LA, PA, DHA, JA, YES, YES, MA, GA, BA, THA, NGA, each measuring 32 X 32 pixels taken from various repositories available on the website. Javanese script that is meant not included with his partner. The dataset used is not noisy, which means that it does not require this study's data set's cleansing process. The overall dataset has 1000 training images and 100 test images collected through a repository on the website. The following is an illustration of the image in the Javanese script dataset that will be used can be seen in Fig. 3.

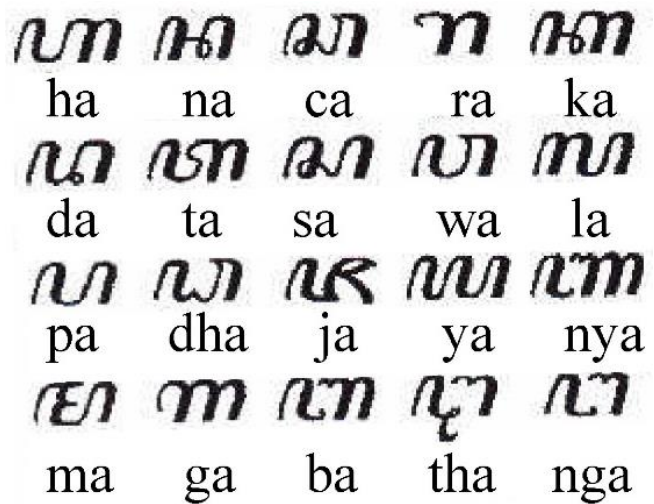


Fig. 3. Sample of Javanese Letter (Source from Google.com).

E. Proposed Javanese Letters Training Model

This work's primary goal is to create the Javanese language alphabet classifier based on the image dataset. The Javanese letters consist of 20 main characters known as Ha-Na Ca-Ra-Ka. The name Ha-Na-Ca-Ra-Ka comes from the first five letters of the Javanese letters [23]. The original data used to train the model uses the set data of the Javanese language alphabet image shown in Fig. 4, with most is a photo of the handwritten alphabet. The image's uses as the primary data in this work will lead to selecting the method to classify the Javanese language alphabet to purposes of the algorithm that suits it. Many machine learning algorithms work for image data types classification with many different approaches such as Support Vector Machine, Bayesian method, and a various number of Neural Network method like Deep Learning.

The Deep Learning approach currently is the most algorithm used for image recognition and classifier. Deep learning is just like the standard Neural Network method but with many layers on its network that makes Deep Learning powerful because of its feature extraction approach that can deal with various object patterns on the image. The current state-of-the-art Deep Learning layers model for image recognition and classifier is called Convolutional Neural Network (CNN). CNN uses some convolution layer stack instead of a fully connected layer to extract the images' feature. Convolution layer on CNN will perform better for feature extraction from the picture because it will use a filter that will learn and adapt to minimize training loss using the Back Propagation or Stochastic Gradient Descent (SGD) technique. The advance of CNN to work with image data objects will be used and adapted to train the Javanese language alphabet dataset.

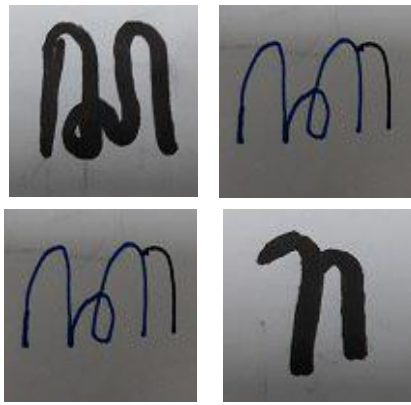


Fig. 4. Sample of Javanese Language Image used in the Dataset.

F. The Convolutional Model

One of the CNN model keys is using the right number and position of the convolution layer stacked to do the feature extraction from the image. Complex image objects like animals, people, or vehicles usually need more than 20 layers of convolution to get the right feature, pattern, and edge detection from the object. Although CNN has an excellent feature extraction result, the uses of so many convolution layers will slowly cost the computation process and time to train the model; also, many image datasets for training are needed. Some standard CNN model with 10 class objects with a lot of complexity usually needs many hours to feed the dataset into the model, even using parallel computation method with GPU or multi-threaded server CPU.

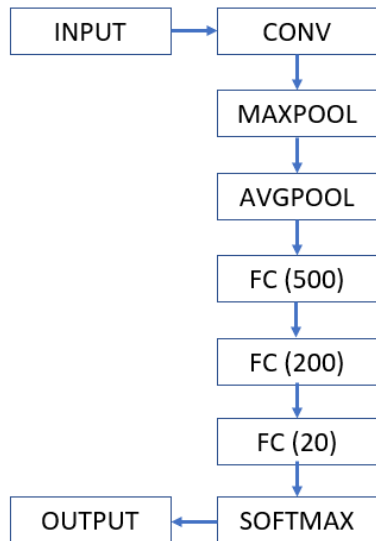


Fig. 5. Architectural Research Model.

The architectural model developed in this study can see in Fig. 5, which includes input with an image size of 32x32 and then continued with the usual convolution layer and the MaxPooling layer. The results of the operation of all these layers then added to the AvgPooling layer. Then the results of this pooling layer will be finalized with the fully connected layer with the number of neurons 500, 200, and 20. ReLU activates each of these Fully Connected layers. After that we

use Softmax, which is a function to take vector input and distribute the output probability.

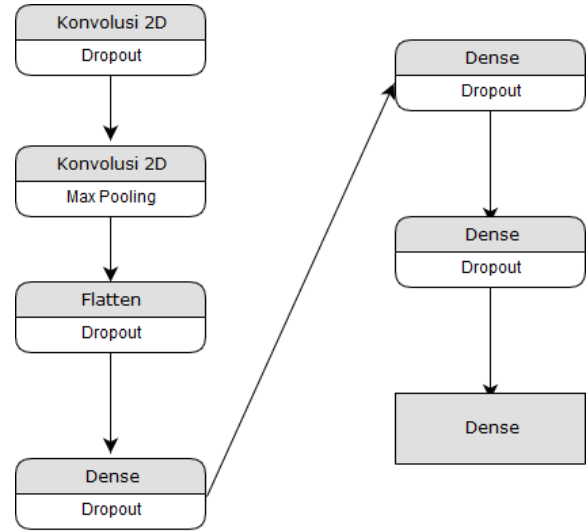


Fig. 6. The Layers in the Training Process.

The Javanese script image will be processed using seven network layers. Each operation will be carried out, such as the convolution process, the max-pooling process, the dense process, the flatten process, and the dropout process depicted in the diagram in Fig. 6.

Cases in this work are different from standard image classification—the difference in this work caused by the image data used on the dataset. Every image on the dataset only contains written Javanese alphabet objects with a simple edge or image feature, not as complex as the animal image object. The alphabet object class also only had a more straightforward form and pattern. As shown in Fig. 4, the image dataset of the Javanese language used in this work is a simple image containing one alphabet for each image class with a mostly white and clean background. The difference for each class is only the writing style and some lighting noise. The size and quality of the dataset will be small. Applying the complex convolution layer used in public image classifying wouldn't suit the alphabet data image used in this work. It will cause failed feature extraction and overfitting models because of the burdensome extraction process. The solution to the problem, the small custom size of Convolutional Neural Network with sequential layer, will be used in this work; this approach also benefits from computational cost and time. Finally, other activation layers and different coats will be combined to get the right learning and fine-tuned models.

After selecting the final sequential layer, we decided to use CNN based deep learning network with a combination of convolution layer, dense layer, and some activation function and downsampling layer to train the dataset. The final system will consist of two convolution layers and two Dense layers with Rectified Linear Unit (ReLU) activation function, Flatten layer between them, Dropout process after each segment, and final dense layer a Softmax activation function. The whole sequential layer of the model is shown in Table I.

TABLE I. MODEL SUMMARY

Layer ^(a)	Output Shape ^(b)	Parameter
Convolution 2D (ReLU activation)	(None, 32, 32, 32)	320
Dropout	(None, 32, 32, 32)	0
Convolution 2D (ReLU activation)	(None, 32, 32, 32)	9248
Max Pooling	(None, 32, 16, 16)	0
Flatten	(None, 8192)	0
Dropout	(None, 8192)	0
Dense (ReLU activation)	(None, 500)	4096500
Dropout	(None, 500)	0
Dense (ReLU activation)	(None, 200)	100200
Dropout	(None, 200)	0
Dense (Softmax activation)	(None, 20)	4020
Total Parameter :		4210288

Layer listed on a sequential order

"None" on the first column shape means the batch size

Based on Table I, there will be 11 layers with 4210288 parameters used for training to get the final output model for the inferences process. The first two convolutional layers function as many other CNN model worked as the primary feature extraction. Due to the type of object on the image is a simple alphabet pattern, so we only use two convolutional layers with the ReLU activation function applied for each output of the layers. The next Flatten layer is to reshape the convolutional layers' output to have a more simplified linear shape to ease the classification. The following dense layers with the ReLU activation function will work like a fully connected layer and merge the output shape. The final dense layers with Softmax activation function used to convert the final output shape result to match the number of the class used in this classification (20 classes). The Dense layers in this model are like other traditional non-fully convolutional neural network layers, which serve the purpose of doing actual classification from the result convolution layer.

III. RESULT AND DISCUSSION

The CNN model adapted for classifying the Javanese language image in this work was evaluated and tested with 20 classes of Javanese language alphabet. The dataset contains 50 image data, with 80% of it used for training the model and 20% for testing the model. The training and testing process was done only with 2.7 GHz Intel i5-6198DU CPU, 8 GB of memory. The specification mentioned for the training and testing process is just a regular notebook specification without GPU acceleration. Using that specification proves that the adapted model did not need a vast resource of computation and capable of being adjusted on the devices with limited computation resources. Training and testing process of the adapted CNN layers are running with Keras framework with Theano backend on Python programming language.

As shown in Fig. 7, the proposed model evaluated the provided training and testing dataset; some metrics were recorded during the training and testing process. We record the time needed to finish the training per sequent of the epoch and the practice's final loss result during the training process. One epoch means feeding the whole image dataset to the network once. The right number of epochs will be needed to

get the optimum model accuracy. The model accuracy also will be recorded during the testing process; this approach is needed to decide which final model will have the best accuracy.

```
def create_model(ep_model):  
    epochs = ep_model  
    lrate = 0.01  
    decay = lrate / epochs  
  
    model_javanese = Sequential()  
    model_javanese.add(Conv2D(32, (3, 3), input_shape=(1, 32, 32),  
activation='relu', padding='same'))  
    model_javanese.add(Dropout(0.2))  
    model_javanese.add(Conv2D(32, (3, 3), activation='relu',  
padding='same'))  
    model_javanese.add(MaxPooling2D(pool_size=(2, 2)))  
    model_javanese.add(Flatten())  
    model_javanese.add(Dropout(0.2))  
    model_javanese.add(Dense(500, activation='relu',  
kernel_constraint=maxnorm(3)))  
    model_javanese.add(Dropout(0.2))  
    model_javanese.add(Dense(200, activation='relu',  
kernel_constraint=maxnorm(3)))  
    model_javanese.add(Dropout(0.2))  
    model_javanese.add(Dense(20, activation='softmax'))  
    model_javanese.compile(loss='categorical_crossentropy',  
optimizer='adadelta', metrics=['accuracy'])  
    return model_javanese
```

Fig. 7. Sample Code for Create Model.

The final training and testing metrics show in Table II and Table III. The training process's total time in Table II shows linear results based on the number of epochs. The training process time gets longer to finish, and the loss value gets smaller for every more significant number of epochs. The training time gets more prolonged because of the more computation process needed for each more significant epoch. The average time needed for training the dataset per epoch is around 12.194 seconds. Based on the result, the training process time with only 12.194 seconds average per epoch is pretty much fast than other many CNN training processes, even with no accelerated hardware used. The light computation process mainly happens because of the simple model, with only 11 layers of computation assigned in this model. Although only using a simple model for training the model, the final result shows a fair number of accuracies. Table II shows various accuracy results for each model with different epoch numbers of training. The more significant number of epochs will result in better accuracy, shown on the resulting model with 5 to 50 epochs. After that, the 75 epoch results show that the accuracy gets the saturation point reduced. Overly high epoch on training may cause overfitting, which leads to stagnant or decreasing accuracy like what happens on these experimental results, so finding the epoch's right number is essential. Our model from the training also shows fast inference time when doing the classification. The average inference time with the same specification mentioned above is 0.57 seconds, and again the fast inference time is because of the simplicity of the model and dataset toolbar.

TABLE II. TIME REQUIRED FOR MODEL TRAINING

Epoch	Time (s)	Loss
5	65.04	2.566
10	123.13	1.4490
25	301.51	0.5596
50	639.85	0.3237
75	949.68	0.2882

TABLE III. TESTING THE ACCURACY FOR MODEL TRAINING

Epoch	Accuracy ^(c)
5	26.74%
10	57.44%
25	75.60%
50	86.68%
75	82.12%

Accuracy based on the selected 1000 images testing dataset

As shown in Table III, the overall result shows that the Javanese language image classifier can perform reasonably well with the proposed model based on the Convolutional Neural Network layers. The simplicity of the training model and dataset used in this work brings the advantage of computation weight and time. Although it had a simple model and dataset, the model's accuracy result is fair, with around 86.68% accuracy on a 50 training epoch model. This model's advantages with fast and light computation time bring the possibility to use this model on devices with limited computation resources such as mobile devices, familiar web server interface, and internet-of-things devices.

IV. CONCLUSIONS

In this study, five trials have been carried out, starting from at least five epochs, and the most are 75 epochs. From the five trials for the training time, it can be concluded that the more number of epochs conducted, the time needed for training is also longer with an increase in time by two times per trial. While the accuracy also has varying results, in epochs 5 to 50, the accuracy level increases. Whereas at 75 epochs, the level of accuracy has decreased by approximately 4%.

This study's results are a model with the best accuracy and time of 86.68% and 639.85 seconds using 1000 datasets and 50 epochs. Meanwhile, the smallest accuracy obtained in this study was 26.74% with five epochs.

This model's advantage is that the computation time is fast. The accuracy is relatively high, making it suitable for further development, especially implementing this model to a system that can recognize Javanese characters using a mobile or web platform.

REFERENCES

[1] A. Setiawan, A. S. Prabowo, dan E. Y. Puspaningrum, "Handwriting Character Recognition Javanese Letters Based on Artificial Neural Network," *Int. J. Comput. Netw. Secur. Inf. Syst. Vol.*, vol. 1, no. 1, hal. 39–42, 2019.

[2] G. H. Wibowo, R. Sigit, dan A. Barakbah, "Javanese Character Feature Extraction Based on Shape Energy," *Emit. Int. J. Eng. Technol.*, vol. 5, no. 1, hal. 154–169, 2017.

[3] M. L. Afakh, A. Risnumawan, M. E. Anggraeni, M. N. Tamara, dan E. S. Ningrum, "Aksara jawa text detection in scene images using convolutional neural network," in *Proceedings - International Electronics Symposium on Knowledge Creation and Intelligent Computing, IES-KCIC 2017*, 2017, hal. 77–82.

[4] A. R. Widiarti dan P. N. Wastu, "Javanese character recognition using Hidden Markov Model," *World Acad. Sci. Eng. Technol.*, vol. 57, no. September 2009, hal. 261–264, 2009.

[5] G. S. Budhi dan R. Adipranata, "Handwritten Javanese Character Recognition Using Several Artificial Neural Network Methods," *J. ICT Res. Appl.*, vol. 8, no. 3, hal. 195–212, 2015.

[6] Y. Harjoseputro, Y. D. Handarkho, dan H. T. R. Adie, "The Javanese Letters Classifier With Mobile Client-Server Architecture And Convolution Neural Network Method," *Int. J. Interact. Mob. Technol.*, vol. 13, no. 12, hal. 67–80, 2019.

[7] C. K. Dewa, A. L. Fadhilah, dan A. Afiahayati, "Convolutional Neural Networks for Handwritten Javanese Character Recognition," *IJCCS (Indonesian J. Comput. Cybern. Syst.)*, vol. 12, no. 1, hal. 83–94, 2018.

[8] A. P. Ardhana, D. E. Cahyani, dan Winarno, "Classification of Javanese Language Level on Articles Using Multinomial Naive Bayes and N-Gram Methods," *J. Phys. Conf. Ser.*, vol. 1306, no. 1, hal. 1–9, 2019.

[9] Y. Harjoseputro, "Classifying Javanese Letters with Convolutional Neural Network (CNN) Method," 2018, no. 1, hal. 52–59.

[10] S. J. D. Prince, "Computer vision: models, learning and inference," in Cambridge University Press, 2012.

[11] K. Chauhan dan S. Ram, "Image Classification with Deep Learning and Comparison between Different Convolutional Neural Network Structures using Tensorflow and Keras," *Int. J. Adv. Eng. Res. Dev.*, vol. 5, no. 02, hal. 533–538, 2018.

[12] S. Albawi, T. A. Mohammed, dan S. Al-Zawi, "Understanding of a convolutional neural network," *Proc. 2017 Int. Conf. Eng. Technol. ICET 2017*, vol. 2018-Janua, no. April 2018, hal. 1–6, 2018.

[13] Tutut Furi Kusumaningrum, "Implementasi Convolution Neural Network (CNN) Untuk Klasifikasi Jamur Konsumsi Di Indonesia Menggunakan Keras," *Univ. Islam Indones. Yogyakarta*, vol. 10, no. 2, hal. 1–15, 2018.

[14] C. Szegedy et al., "Going Deeper with Convolutions," in *Designing and Tracking Knowledge Management Metrics*, 2015, hal. 1–9.

[15] A. Krizhevsky, I. Sutskever, dan G. E. Hinton, "ImageNet Classification with Deep Convolutional Neural Networks," *Adv. neural Inf. Process. Syst.*, hal. 1097–1105, 2012.

[16] K. He, X. Zhang, S. Ren, dan J. Sun, "Deep residual learning for image recognition," in *Proceedings of the IEEE Computer Society Conference on Computer Vision and Pattern Recognition*, 2016, vol. 2016-Decem, hal. 770–778.

[17] K. Younis dan A. Khateeb, "Arabic Hand-Written Character Recognition Based on Deep Convolutional Neural Networks," *Jordanian J. Comput. Inf. Technol.*, vol. 3, no. 3, hal. 186, 2017.

[18] V. Sze, Y.-H. Chen, T.-J. Yang, dan J. S. Emer, "Efficient Processing of Deep Neural Networks: A Tutorial and Survey," *Proc. IEEE*, vol. 105, no. 12, hal. 2295–2329, 2017.

[19] W. S. E. Putra, A. Y. Wijaya, dan R. Soelaiman, "Klasifikasi Citra Menggunakan Convolutional Neural Network (CNN) pada Caltech 101," *J. Tek. ITS*, vol. 5, no. 1, hal. A65–A69, 2016.

[20] A. Dutt dan A. Dutt, "Handwritten Digit Recognition Using Deep Learning," vol. 6, no. 7, hal. 990–997, 2017.

[21] G. Nguyen et al., "Machine Learning and Deep Learning frameworks and libraries for large-scale data mining: a survey," *Artif. Intell. Rev.*, vol. 52, no. 1, hal. 77–124, 2019.

[22] A. A. Kristanto, Y. Harjoseputro, dan J. E. Samodra, "Implementasi Golang dan New Simple Queue pada Sistem Sandbox Pihak Ketiga Berbasis REST API," *J. RESTI (Rekayasa Sist. dan Teknol. Informasi)*, vol. 4, no. 4, hal. 745–750, 2020.

[23] Y. Sugianela dan N. Suciati, "Javanese Document Image Recognition Using Multiclass Support Vector Machine," *CommIT (Communication Inf. Technol. J.)*, vol. 13, no. 1, hal. 25, 2019.

Debris Run-Out Modeling Without Site-Specific Data

NMT De Silva¹, Prasad Wimalaratne²

University of Kelaniya, Sri-Lanka¹
University of Colombo School of Computing, Sri-Lanka²

Abstract—Recent population growth and actions near hilly areas increase the vulnerability of occurring landslides. The effects of climate change further increase the likelihood of landslide danger. Therefore, accurate analysis of unstable slope behavior is crucial to prevent loss of life and destruction to property. Predicting landslide flow path is essential in identifying the route of debris, and it is essential necessary component in hazard mapping. However, current methodologies of determining the flow direction of landslides require costly site-specific data such as surface soil type, categories of underground soil layers, and other related field characteristics. This paper demonstrates an approach to predict the flow direction without site-specific data, taking a large landslide incident in Sri Lanka at Araranyaka region in the district of Kegalle as a case study. Spreading area assessment was based on deterministic eight-node (D8) and Multiple Direction Flow (MDF) flow directional algorithms. Results acquired by the model were compared with the real Aranayaka landslide data set and the landslide hazard map of the area. Debris paths generated from the proof of concept software tool using the D8 algorithm showed greater than 76% agreement, and MDF showed greater than 87% agreement with the actual flow paths and other related statistics such as maximum width of the slide, run-out distance, and slip surface area.

Keywords—Landslide flow path; route of debris; hazard mapping; D8 Algorithm; multiple direction flow algorithm

I. INTRODUCTION

A landslide is widespread in earth motion when the slope changes from a steady to an unsteady state. It happens due to geological, morphological causes, or human activities. There are many categories of landslides, namely Rock Slides, Earth Flows, Debris Slides, Debris Flows, and Rock Falls [1].

Rainfall is a major initiating factor for most landslides in Sri Lanka [2]. During heavy rains, water penetrates the top layer of soil into the deep layers of the earth beneath them, filling the ground's empty pores. When the water in the pores reaches saturation, it causes an internal pressure, called the "pore pressure of water," and in most cases, it causes a landslide.

Predicting a landslide flow path is very important for determining the flow path and the sedimentation area. It is also vital for mapping the hazards of landslides, early warnings, evacuation, and mitigation. Hence flow direction is a prime component in risk assessment and measures to eliminate rapid landslides [3].

When dispensing early warnings, it is impossible to visit every site before issuing of warning. Even without site-specific information, if there is a method that can be used to get an idea

of the landslide-prone area, accordingly, the landslide's flow path can be predicted, and evacuation paths can be decided. Instructing people as per prediction will reduce the possible damages to lives during the landslide. Therefore, this work can be used to get an idea about the elevation and possible flow paths of a site prior to visiting without expensive site-specific data.

II. LITERATURE REVIEW

Many research works have been carried out globally to predict, mitigate, and manage these disasters and do better decision-making. The following are some attempts done by people worldwide to predict landslide initiation points, flow path, and run-out distance.

The paper by Gomes et al. [4] elaborates on how to combine spatial models for landslides and flows prediction. A map has been constructed with landslides starting points, flows size, and run-out distance of mass movements in Quitite and Papagaio in Rio de Janeiro city, Brazil, using this combined model. In this study, the landslide model (SHALSTAB) was combined with the debris-flow simulation model (FLO-2D).

In 2020, Zhao et al. came up with landslide run-out modeling method [5] with the integration of Gaussian process emulation and open-source simulation tool r.avaflo. The developed model is then tested with the landslide that happened in Bondo in 2017.

Tesfahunegn Abera Gebreslassie carried out dynamic simulations of landslide run-out for his master's research using DAN3D and BING models [6]. Finneidfjord quick-clay landslide has been taken as the case study to stimulate the above models. DAN3D and BING models require terrain models of the path and the mass at the release area, shear strength, and the dynamic viscosity as inputs and calculate the run-out distance and the flow velocity. This study shows that the run-out distance is higher using DAN3D than the BING model; however, DAN3D uses ten times execution time than the BING model.

"Linking rainfall-induced landslides with debris flows runoff patterns towards catchment scale hazard assessment", a paper by LinfengFan et al. [7] described a methodology to predict landslide pathways with the integration of the novel Landslide Hydro-mechanical Triggering (LHT) model. The obtained result is compared with the continuum-based model RAMMS, which showed a reasonable agreement.

In 2016, a paper presented by Formetta et al. came up with a methodology to systemically calibrate, verify, and compare different models and select the models whose behavior is the most reliable for a particular case study. This approach

integrates the hydrological model package (NewAge-JGrass) and other components, such as the uDig open-source geographic information system, physically based landslide susceptibility model, parameter calibration algorithm, and a model for pixel-by-pixel comparison of modeled and actual landslide [8]. The procedure was applied in a test case on the Salerno–Reggio Calabria highway landslide with adequate performance. This integrated method would be useful for landslide early warning systems and decision-makers dealing with risk management assessments.

Syah et al. have presented a paper describing a numerical analysis of landslide movements [9]. For this paper, erosion and deposition along the flow path have taken into consideration, and the model has tested with landslides, which were previously attempted by Egashira et al. [10], McDougall and Hungr [11], and Blanc [12]. The result achieved by this study showed more accurate predictions than previous attempts.

Landslide run-out analysis — current practice and challenges by Scott McDougall, presented a useful review of tools and methods that have been developed, challenges faced by researchers, challenges solved by researchers, simulation of debris flows, and potential future works [13].

The above literature related to landslide flow path modeling required expensive fieldwork at landslide incurred or landslide-prone sites. The proposed methodology can be used to get an idea of the landslide flow path even without site-specific information. This work can also be used as a tool for geologists to get an idea about the elevation and possible flow paths and other related statistics of a site before visiting for investigations.

III. DESIGN AND IMPLEMENTATION

The development of the model is done using MATLAB R2017. MATLAB image processing toolbox is used for the analysis of Digital Elevation Models (DEMs). The developed tool followed an object-oriented programming (OOP) approach to build flow directions and stream networks. Fig. 1 shows the methodology carried out.

A. Data Pre-Processing

Contour data formatted as shape file was obtained from the Sri Lanka Survey Department. These files were converted to ASCII format, which is a convenient format to MATLAB. The conversion is done by using the inbuilt functions of ArcGIS software.

B. Generate DEM using ASCII Data

DEM is widely used in various hydrological modeling. It can be joint with other data sets, such as rainfall data and penetration capability for practical use.

A 10m resolution contour data was used to obtain DEM of Aranayaka Landslide area. DEM file is created as a grid object which contains a numerical matrix and information on georeferencing. Grid object is associated with datasets such as flow accumulation grids, gradient grids. Created DEM has a projected coordinate system and that elevation and horizontal coordinates are in meter units.

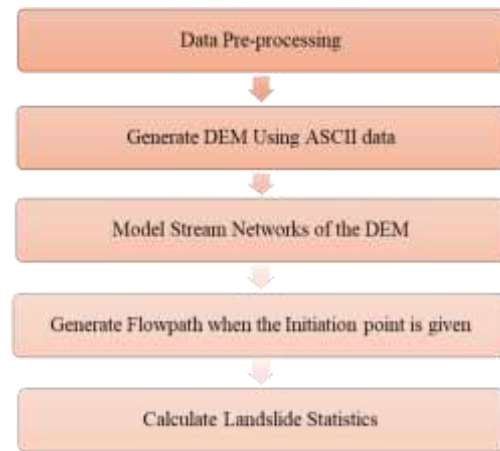


Fig. 1. Design Methodology.

The 2D-Euclidean distance between the two cells determines the physical location of each DEM cell. Euclidian distance (d_{ij}) defined as squared distances between two vectors, is the sum of squared differences in their coordinates (x_i, x_j and y_i, y_j), as shown in (1) [14].

$$d_{ij} = \sqrt{[(x_i - x_j)^2 + (y_i - y_j)^2]} \quad (1)$$

C. Model Stream Networks of the DEM

Based on a digital elevation model's flow direction, an instance of a stream object is created, which encapsulates the information on a stream network's geometry and connectivity.

D. Generate Flow Path when the Initiation Point is given

The debris flow run-out algorithms control the movement's direction from one cell to its eight neighboring cells. Single Directional Flow (SDF) and Multiple Directional Flow (MDF) algorithms were implemented, so the flow path's accuracy and other calculated statistics can be compared for better decision-making.

The D8 SDF algorithm is one of the primary and well-known algorithms that lead flow from each cell to one of eight adjacent neighbors centered on the slope's incline. To calculate the primary flow, the slope (S_{ij}) direction to each neighboring cell has to be calculated and set the direction for the largest S_{ij} [15].

$$S_{ij} = \frac{Z_i - Z_j}{d_{ij}} \quad (2)$$

The MDF algorithm divides and releases in each cell in several directions to all cells on a weighted slope basis. The slope gradients, slope lengths, and two weights are used to direct the center cell flow to each downslope cell in a 3 x 3 moving window. Every cell receives a portion of the release from each upslope cell, and hence, the upslope supporting area of the receiving cell is a collection of fractional contributions from many different cells [16]. In this study, both D8 and MDF algorithms are developed and tested.

E. Calculate Landslide Statistics

Finally, the landslide statistics such as landslide area, run-out distance, landslide crown, maximum width, and length of the main body were generated. The initiation points of the landslide are the primary user input to calculate the above statistics. These statistics were produced using flow paths generated from different flow routing algorithms.

Multiple points were selected from the D8, and MDF generated the landslide's main body for the calculations. As shown in Fig. 2 and Fig. 3, the initiation points and a point in the main body's toe were selected, and Euclidian distance between these points of the flow paths was calculated. From that, total main body area, crown width and maximum width is derived. All these statistics are calculated for both SDF and MDF flow paths.

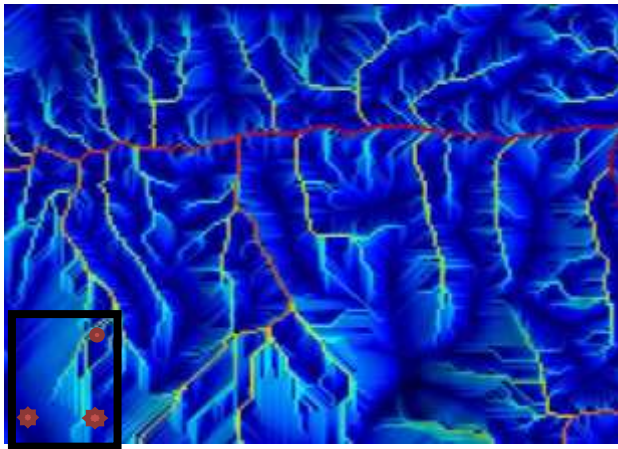


Fig. 2. Selected Points from the main Body of the Landslide (MDF).

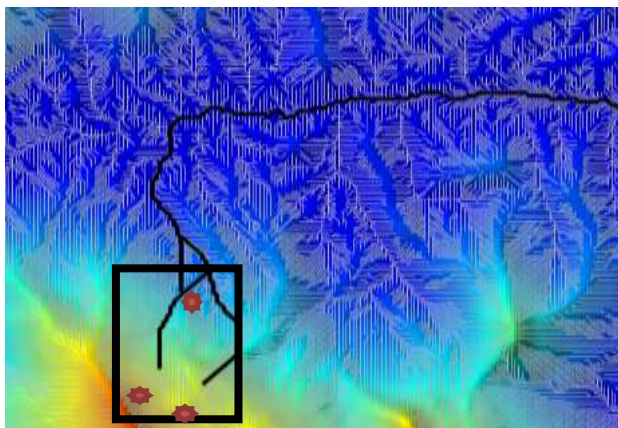


Fig. 3. Selected Points from the main Body of the Landslide (SDF).

IV. EVALUATION

The developed model was evaluated using Aranayaka post landslide data such as drone images after the disaster, actual flow path, length of the landslide and flow volume. These statistics were taken as the baseline for the evaluation criteria and the accuracy of the generated statistics of this research was tested for compatibility and for deviations.

After creating all the available streams of the landslide area, the flow path is predicted with the given landslide

initiation point. Afterward, the actual boundary created with ARCGIS was placed on top of the generated model to check for closeness. Fig. 4 shows the procedure carried out in the evaluation process.

A. Identify the Actual Flow Path using Drone Images

Unmanned Aerial Vehicles (UAV) is a technology used in worthwhile to capture images with Global Positioning System (GPS). Using drones for mapping is a fast, lost cost, safe and accurate method. The image processing methods can be used to pool the images and develop orthophoto from many different photos. Also, it helps to visualize the 3D image of the landslide.

DJI Panthom IV drone was used to collect material. "DGI Pro" and "Drone deploy" software were used to control the drone and Google Earth was taken as the base map. The flying path was manually set and continuous photos were taken during the mission. The drone captured multiple photos of each distinct feature, from multiple angles. Sufficient image overlap should be identified for better map detail and for efficient processing. In this case, 55%-65% image overlaps were preserved throughout the task. Altogether 577 images were taken to cover the entire landslide area.

Agisoft Photo scanner software was used to generate of 3D model and Digital Elevation Model (DEM). It is image processing software that automatically builds professional quality textured 3D models from a robust alignment of still images. Fig. 5 shows the generated DEM for Aranayaka landslide using drone images. The contours were produced from the generated DEM after the landslide, and contours prior to the landslide were obtained from secondary sources.

B. Plot the Actual flow Path in the Location of the Landslide using GIS

The goal is to verify the flow path of the Aranayaka Landslide generated by the model. For this purpose, the landslide flow path generated by drone images was plotted in the Aranayaka map by georeferencing Using ArcGIS. To map the landslide flow path, contour data of the studied area was taken from Sri Lanka Survey Department.

For evaluation of the carried-out work, Aranayaka landslide data were taken from the National Building Research Organisation (NBRO), which is designated as the leading national point for landslide managing in Sri Lanka. Using the data obtained from NBRO, the Aranayaka landslide area's actual boundary is generated on top of the contour map as shown in Fig. 6. The produced boundary is used to evaluate the model generated from MATLAB.

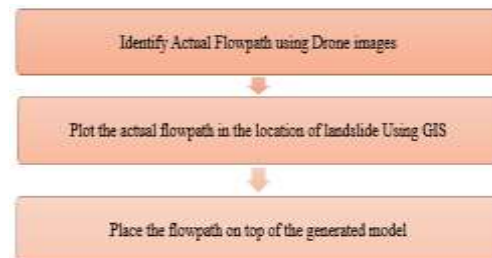


Fig. 4. Evaluation Methodology.



Fig. 5. DEM Created using Drone Images.

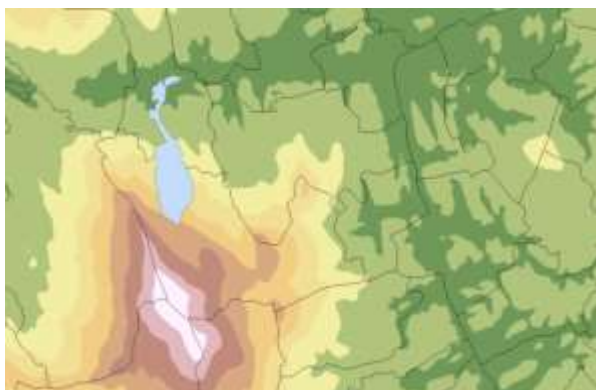


Fig. 6. Actual Landslide Flow Path Mapped in DEM.

C. Place the Flow Path on Top of the Generated Model

The actual landslide flow path mapped from ARCGIS in the previous step was placed on top of the model generated SDF and MDF flow paths by georeferencing as shown in Fig. 7 and Fig. 8.

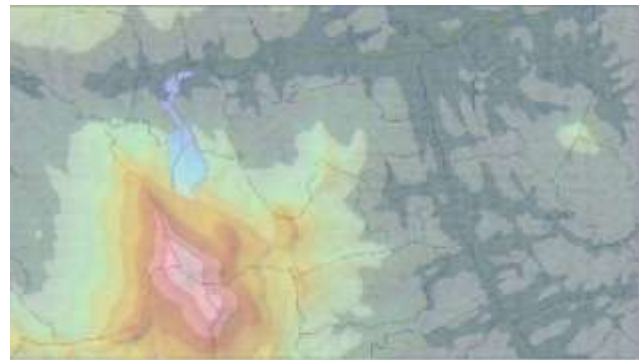


Fig. 7. Actual Landslide Flow Path Placed on the flow Path Generated from SDF.

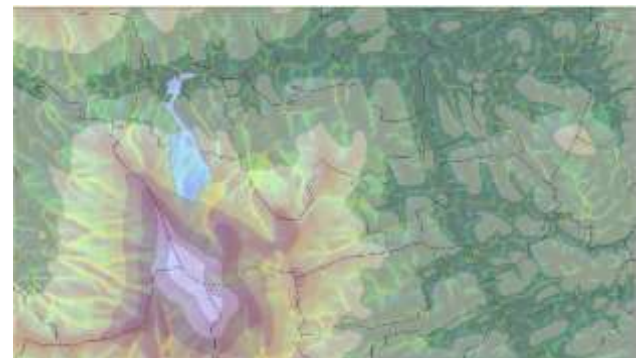


Fig. 8. Actual Landslide Flow Path Placed on the flow Path Generated from MDF.

V. RESULTS

Based on the result of different simulations, it is observed that both SDF and MDF flow paths fit inside the actual landslide boundary when the initiation points are given, and flow directions are also in the proper direction of the actual landslide.

Real landslide statistics were obtained from NBRO as per their detailed analysis and investigation carried at the actual landslide site area. These actual statistics and statistics generated from SDF and MDF are shown in the Table I.

Among the generated statistics, maximum width, length of the main body and flow length are critical indicators to identify the spreading area. So, people of the predicted perimeter can be alarmed to evacuate because the area is identified as high risk and landslide-prone. Also, safe evacuation paths can be determined by examining the predicted flow path of the landslide. Hence the lives of people will not be damaged during the evacuation process.

Table II shows the comparison SDF and MDF results deviation from actual landslide statistics. MDF algorithm produced the length of the main body of Aranayaka landslide as 1.29 Km, which is very close to the length of the main body of 1.26 Km. Also, MDF calculated the maximum width of the landslide deviates only 2.3% from the actual Aranayaka data. Both D8 and MDF algorithms generate a flow length of 1.925 Km, which has a 15.1% of deviation from the actual flow length. As per the results, a more accurate flow path and statistics can be generated using MDF compared to SDF.

TABLE I. COMPARISON OF RESULTS

	Actual	SDF	MDF
Area of Main Landslide Body	0.56Km ²	0.429 Km ²	0.488 Km ²
Landslide crown	345.45m	329.8m	325.57m
Maximum Width	600.07m	535.3m	619.9m
Length of the main body	1.26Km	1.02Km	1.29Km
Flow length	2.268Km	1.925Km	1.925Km

TABLE II. PERCENTAGE OF DEVIATION FROM THE ACTUAL STATISTIC

	SDF Deviation (%)	MDF Deviation (%)
Main Landslide Body	23.3	12.75
Landslide crown	4.5	5.7
Maximum Width	10.7	3.3
Length of the main body	25.8	2.3
Flow length	15.1	15.1

VI. CONCLUSION AND FUTURE WORK

The landslide flow paths and statistics predicted by the Proof of concept prototype shows good agreement with the actual landslide data collected for the selected case study. However, the MDF algorithm produced more fitting flow paths and relevant statistics for the selected landslide.

Deviation of the generated flow paths and other statistics would have caused due to the unavailability of site-specific data such as soil condition, soil type, spreading velocity, the volume of the slip surface, gravity, and other forces.

Even without knowing any of the site-specific data, this tool can be used and predict results with more than 87% accuracy with the landslide-prone area's contour data as the only input. When compare the implemented tool with the other flow path based tools such as FLOW-R, RAMMS, and DAN3D, all of these tools require site-specific data, which may difficult to collect from all landslide-prone sites prior to a landslide.

This study has been mainly based on Aranayaka Landslide area. This model can be expanded to fit with most of the Sri Lankan landslide context with additional work. Then it will give immense help to reduce the impact of a landslide as the flow path can be determined prior and evacuation paths can be decided accordingly before the disastrous situations. Also, other than used SDF and MDF algorithms, there are many more flow routing algorithms available. These algorithms also can be implemented and integrated with this model to compare the results for higher accuracy.

When calculating the run-out distance and spreading of the landslide, geotechnical information about the landslide is essential. Therefore, the implemented tool can be extended by integrating site-specific geology-related knowledge, checking for results produced with site-specific data and without site-specific data, and testing for accuracy of predictions.

REFERENCES

- [1] US Department of the Interior, "Landslide Types and Processes," July 2004. [Online]. Available: <https://pubs.usgs.gov/fs/2004/3072/fs-2004-3072.html>. [Accessed 20th September 2020].
- [2] Nawagamuwa U.P., Perera L.P. (2017) Recommending Rainfall Thresholds for Landslides in Sri Lanka, Advancing Culture of Living with Landslides. WLF 2017.
- [3] Eranga Dulanjalee ,Landslide Flow Path Assessment for Susceptibility Mapping at a Regional Scale , 8th Annual NBRO Symposium,January 2018.
- [4] Roberto Arnaldo Trancoso Gomes, Renato Fontes, Osmar Abílio de Carvalho Júnior, Nelson Ferreira and Euripedes Vargas do Amaral, "Combining Spatial Models for Shallow Landslides and Debris-Flows Prediction," Remote Sensing, no. 5, pp. 2219-2237, 2013.
- [5] Zhao, H., Amann, F. and Kowalski, J., 2020. Emulator-based global sensitivity analysis for flow-like landslide run-out models. arXiv preprint arXiv:2010.04056.
- [6] T. A. Gebresslassie, "Dynamic simulations of landslide run-out in cohesive Soils," Oslo, 2015.
- [7] Fan, L., Lehmann, P., McArdeell, B. and Or, D., 2017. Linking rainfall-induced landslides with debris flows runoff patterns towards catchment scale hazard assessment. *Geomorphology*, 280, pp.1-15.
- [8] Giuseppe Formetta, Giovanna Capparelli, and Pasqua, "Evaluating performance of simplified physically-based models for shallow landslide susceptibility," *Hydrol. Earth System*, no. 20, p. 4585-4603, 2016.
- [9] Syah, A., Fathani, T.F. and Faris, F., 2019. A Numerical Analysis of Landslide Movements Considering the Erosion and Deposition along the Flow Path. In *Journal of the Civil Engineering Forum* (Vol. 5, No. 3, p. 187).
- [10] Egashira, S., Itoh, T. and Takeuchi, H. (2001) 'Transition mechanism of debris flows over rigid bed to over erodible bed', *Physics and Chemistry of the Earth, Part B: Hydrology, Oceans and Atmosphere*. Elsevier, 26(2), pp. 169-174.
- [11] McDougall, S. and Hungr, O. (2005) 'Dynamic modelling of entrainment in rapid landslides', *Canadian Geotechnical Journal*. NRC Research Press, 42(5), pp. 1437-1448.
- [12] Blanc, T. (2008) Numerical simulation of debris flows with the 2D-SPH depth integrated model. na.
- [13] S. McDougall, "Landslide run-out analysis — current practice and challenges," *Canadian Geotechnical Colloquium*, vol. 57, pp. 605-620, 2017.
- [14] P.Barrett, Paul Barrett, Wikimedia Foundation, Inc, [Online]. Available: <http://www.pbarrett.net/techpapers/euclid.pdf>. [Accessed 1st July 2020].
- [15] M. Cooper, "Depth Recovery through Linear Algebra," in *Line Drawing Interpretation*, Springer Science & Business Media., p. 118.
- [16] P. Quinn, K. Beven, P. Chevallier And O. Planchon, "The Prediction Of Hillslope Flow Paths For Distributed Hydrological Modelling Using Digital Terrain Models," *Hydrological Processes*, Vol. Vol. 5, Pp. 59-79, 1991.

Improved Selected Mapping Technique for Reduction of PAPR in OFDM Systems

Saruti Gupta¹, Dr. Ashish Goel²

Department of Electronics and Comm. Engg, JIIT, Noida, India

Abstract—High peak to average power ratio (PAPR) is a limiting factor towards the performance of an OFDM system. Selected Mapping (SLM) is a popular peak to average power ratio (PAPR) reduction scheme used with the OFDM systems. In this technique, U set of candidate sequences are generated that leads to improvement in the PAPR reduction ability of the OFDM systems. The major concern of the conventional SLM is that as the number of candidates is increased, there is a proportional rise in the inverse fast Fourier transforms (IFFT) computations of the systems. In our article we have proposed a scheme in which we increase the number of candidate sequence as $(U+U^2/4)$ that leads to improved PAPR performance of the OFDM systems without any equivalent rise in the IFFT computations. It has been demonstrated that both the simulation and analytical results are well-approximated in our proposed schemes. We also estimate the threshold value of PAPR at a fixed value of complementary cumulative distribution function (CCDF) for different number of subcarriers and candidate sequences. Results demonstrate that our proposed scheme outperforms in terms of PAPR reduction ability of the OFDM signal and obtains effective PAPR threshold values with negligible loss in BER performance of the system.

Keywords—Orthogonal Frequency Division Multiplexing (OFDM); Peak to Average Power Ratio (PAPR); Selected Mapping (SLM); Complementary Cumulative Distribution Function (CCDF); PAPR threshold

I. INTRODUCTION

Orthogonal frequency Division Multiplexing (OFDM) is a high speed multicarrier modulation scheme that is widely used in many of the wireless application standards such as Digital Video Broadcasting (DVB) [1], IEEE 802.11a and IEEE 802.16d based Wimax broadband access [2]. The key advantages of the OFDM system are increased data rate, high spectral efficiency and resistance against multipath fading effects [3]. High peak-to-average power ratio (PAPR) of the OFDM signal is one of the main disadvantages of the OFDM system that requires large range linear amplifiers in order to limit the non-linear distortions of the OFDM signals. To overcome these problem different categories of PAPR reduction techniques have been proposed. Signal distortion techniques such as clipping [4], clipping and filtering [5] and companding [6] have been proposed. Various Signal scrambling schemes includes coding [7], selective mapping (SLM) [8], partial transmit sequence (PTS) [9], active constellation extension (ACE) [10], tone Reservation (TR) [11] and tone injection (TI) [12]. Selective Mapping (SLM) is a well-known PAPR reduction technique, where the input data blocks are multiplied with random phase vector to yield a set of U independent data sequences. The time-domain candidate

sequences are obtained after applying the inverse fast Fourier transform (IFFT), and out of them the one with the lowest PAPR value is chosen and transmitted towards the receiver side. With increase in number of candidates the PAPR reduction ability of the OFDM signal can be improved but this leads to equivalent rise in IFFT computations. The major concern in the conventional SLM-OFDM system is to reduce the PAPR value of the OFDM signals by increasing the number of candidates without any proportional rise in the number of IFFT's. In the literature [13-17] many PAPR reduction techniques have been proposed for enhancing the number of candidate sequences in the SLM-OFDM system. These techniques aim to increase the candidate sequence of considering effects of bit redundancy and computational complexity of the SLM-OFDM system.

In [13] Shapiro-Rudin sequence set are used as phase sequence for the SLM system in order to improve PAPR performance of the OFDM signals but these may not be the best determinate phase sequence set for SLM technique. In [14] an improved SLM scheme is designed in which U^2 number of candidates are generated by using the real parts and imaginary parts of the data. In [15] GreenOFDM Algorithm is proposed to improve the PAPR reduction capability of the OFDM signals with the same number of IFFT computations as in conventional SLM-OFDM. In this scheme the number of candidates is increased by dividing the input data into two groups each containing $U/2$ candidates and finally merging to generate $(U^2/4)$ set of candidates. A variant of GreenOFDM Algorithm is suggested in [16] where the weighting factor α is used to generate the number of candidates. In [17] authors use the PSK modulated signal sequences, orthogonal phase factor sets and deformation parameter set to increase the number of candidate signals thereby improving the PAPR performance of the OFDM system. Another variant of GreenOFDM Algorithm is proposed in [18] where number of candidate sequences is increased to U^2 , in comparison to those in GreenOFDM Algorithm.

In contrast to the previous schemes, we have addressed more combination of candidate sequence to be generated with the same IFFT computations as in conventional SLM scheme. In our proposed scheme we have increased the number of candidate sequence as $(U + U^2/4)$ that leads to improved PAPR performance of the OFDM systems without any proportional rise in the IFFT computations of the system. Here, we also study the effects for different number of subcarriers and candidate sequences to estimate the threshold value of PAPR at a fixed value of CCDF. The paper is organized as follows. In Section II conventional SLM- OFDM is discussed.

Section III gives the details about the GreenOFDM technique, Algorithm of our proposed scheme and the effects of PAPR threshold. Section IV provides both the simulation and analytical results for our proposed schemes in terms of PAPR threshold performance and BER degradations. The conclusions are provided in Section V.

II. CONVENTIONAL SLM-OFDM

In an OFDM system, the input data block $X = [X_0, X_1, \dots, X_{N-1}]$ is complex modulated using M-ary quadrature phase shift keying over N orthogonal sub-carriers during parallel transmissions. The time domain OFDM sequence is then generated by using LN - point IFFT to the complex modulated OFDM symbols and is given as.

$$x(n) = \frac{1}{\sqrt{N}} \sum_{k=0}^{LN-1} X(k) \exp\left(\frac{j2\pi nk}{LN}\right), \quad 0 \leq n \leq LN-1 \quad (1)$$

where $j = \sqrt{-1}$ and $L = \text{Oversampling factor}$. For $L=4$, the PAPR results are well-approximated to the analog symbols. Larger value of L leads to rise in computational complexity rather than any gain for approximation of results.

The ratio of the peak power and the mean power represents the PAPR of the OFDM signal $x(n)$ and is expressed as.

$$PAPR = \frac{\max_{n \in \{0, LN-1\}} \{|x(n)|^2\}}{E\{|x(n)|^2\}} \quad (2)$$

where $E\{\cdot\}$ is the expectation operator.

Cumulative distribution function (CCDF) [19] is used to estimate the PAPR of the OFDM signals and is expressed as the probability that the PAPR of an OFDM signal exceeds a specific threshold value of PAPR (γ_0) that is given by.

$$CCDF(\gamma_0) = \text{Prob}\{PAPR > \gamma_0\} \quad (3)$$

The semi-empirical approximation for the CCDF of the OFDM signal as given in [20] can be expressed as.

$$CCDF_{OFDM}(\gamma_0) \approx 1 - (1 - e^{-\gamma_0})^{2.8N} \quad (4)$$

Fig. 1 shows the block diagram of conventional SLM-OFDM system. In this technique, U candidates sequences are produced by element wise multiplication of modulated data block $X(k)$ with the random phase vector sequence $B_u(k)$ where $0 \leq u \leq U-1$.

The pseudo random noise sequence $B_u(k)$ consists of the set of phase factors $\beta_u(k)$ with $|\beta_u(k)|=1$. The candidate sequences are then presented by.

$$X_u(k) = X(k)\beta_u(k) \quad 0 \leq u \leq U-1 \quad (5)$$

The time domain candidate symbol sequence generated using LN - point inverse fast Fourier transform (IFFT) can be expressed as.

$$x_u[n] = \text{IFFT}\{X_u(k)\} \quad (6)$$

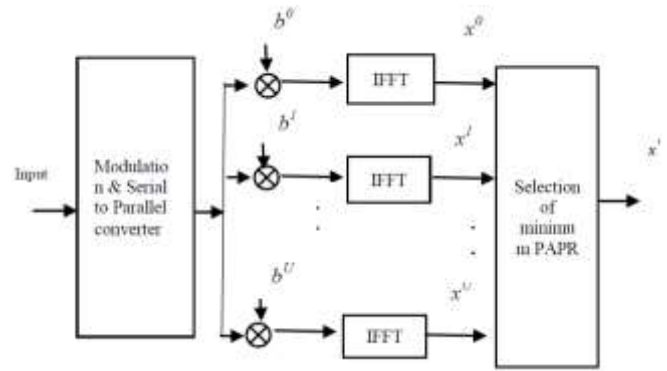


Fig. 1. Block Diagram of Conventional SLM-OFDM System.

Among these U candidate sequences, the one with the minimal PAPR value is selected for transmission and satisfies the following:

$$x^{j_0} = \arg \min\{x_u[n]\} \quad (7)$$

where j_0 is the index of the phase set which provides the minimal PAPR value of the OFDM signal and is selected for transmission.

The semi-empirical approximation for the CCDF of the SLM-OFDM signal is analyzed as.

$$CCDF_{SLM}(\gamma_0) \approx \left(1 - (1 - e^{-\gamma_0})^{2.8N}\right)^{C_{in}} \quad (8)$$

where $C_{in} = U$ represents the number of candidate signal generated by SLM-OFDM system.

It can be seen that the value of the CCDF decreases with increase in number of candidates in the SLM scheme but leads to rise in number of IFFT computations [21]. In order to improve the PAPR reduction capability of the OFDM signals the number of candidates in the SLM scheme should be increased in a manner that it should not affect number of IFFT's in the system. Therefore, this motivates us to design an algorithm that aims to reduce the PAPR of the OFDM signals by the increasing the number of candidates in the SLM scheme without any proportional rise in IFFT computations of the system.

III. PROPOSED SCHEME

A. Existing Green-OFDM Algorithm

Green-OFDM [15] was proposed to overcome the limitation of SLM-OFDM systems by increasing the number of candidates that results in improvement in the PAPR reduction ability of the OFDM signals. In this scheme the input data is split into two parts each containing $U/2$ candidate. Here the phase vectors for the two input segments are chosen as $\{\beta_{g1}(k)\} \in \{\pm 1\}$ and $\{\beta_{g2}(k)\} \in \{\pm j\}$ to ensure that they do not cancel out the subcarriers of the two segments and maintain the orthogonality among the subcarriers.

These input data segments are expressed in terms of multiplication with the random phase sequences $\beta_{g1}(k)$ and $\beta_{g2}(k)$ as.

$$X_{g_1}(k) = X(k)\beta_{g_1}(k) \quad 0 \leq g_1 \leq \frac{U}{2} - 1 \quad (9)$$

$$X_{g_2}(k) = X(k)\beta_{g_2}(k) \quad \frac{U}{2} \leq g_2 \leq U - 1 \quad (10)$$

Then IFFT is applied to each part of the input data segments that is expressed as:

$$x_{g_1}[l] = IFFT\{X_{g_1}(k), \beta_{g_1}(k)\} \quad (11)$$

$$x_{g_2}[m] = IFFT\{X_{g_2}(k), \beta_{g_2}(k)\} \quad (12)$$

Finally these are added together to generate $(U^2/4)$ candidates as given by.

$$x_{g_1,g_2}[n] = x_{g_1}[l] + x_{g_2}[m] \quad (13)$$

In order to preserve the Euclidean distance the sequence $x_{g_1,g_2}[n]$ is normalized as.

$$x_{g_1,g_2}[n] = \frac{x_{g_1}[l] + x_{g_2}[m]}{\sqrt{2}} \quad (14)$$

Instead of U candidates offered in conventional SLM scheme, here $(U^2/4)$ set of independent candidates are generated and among these the one with the minimum PAPR value is selected for transmission.

The semi-empirical approximation for the CCDF of the Green-OFDM signal using $C_{in}=(U^2/4)$ is then evaluated as:

$$CCDF_{GreenSLM}(\gamma_0) \approx \left(1 - (1 - e^{-\gamma_0})^{2.8N}\right)^{C_{in}} \quad (15)$$

B. Proposed Algorithm

In our proposed design, a variant of GreenOFDM is designed where more possible combination of candidates are generated for a given value of U candidate sequence. Here, we have utilized two segment parts, $x_u[n]$ consisting of set of U candidates and the other segment $x_{g_1,g_2}(k)$ containing $(U^2/4)$ set of candidates retaining the orthogonality between the two segment parts. The first input data segment is multiplied with $\beta_u(k) \in \{\pm 1\}$ and the other data segment is rotated by $\{\beta_{g_1}(k)\} \in \{\pm 1\}$ and $\{\beta_{g_2}(k)\} \in \{\pm j\}$ ensuring the orthogonality among subcarriers for the entire segments. After applying IFFT to these data segments the time domain sequences $x_{g_1,g_2}[n]$ and $x_u[n]$ are finally merged to obtain $\{x_{u,g_1,g_2}[n]\}$. The first segment produces U candidate sequence and the second group generates $U^2/4$ candidate combinations.

Therefore, the number of candidate sequence equal to $(U+U^2/4)$ is generated. Among these the one that satisfies the criteria of minimum PAPR that corresponds to optimal phase vector is selected for transmission. The corresponding transmitted sequence is then presented as.

$$x' = \operatorname{argmin} \{x_{u,g_1,g_2}[n]\} \quad (16)$$

The proposed scheme is described in Algorithm 1 as follows:

Algorithm 1

```

1: Begin
2: Set it= maximum iteration
3: For z=1:it
4: Compute  $X(k), \beta_u(k)$  where  $\beta_u(k) \in \{\pm 1\}$ 
5: Assume  $PAPR_{\min}=t$ 
6: For u=0:U-1
7:  $X_u(k) = \{X(k), \beta_u(k)\}$ 
8:  $x_u[n] = IFFT\{X_u(k)\}$ 
9: If  $PAPR\{x_u[n]\} < PAPR_{\min}$ 
10: Initialize  $PAPR_{\min} = PAPR\{x_u[n]\}$ 
11: End if
12: End For
13: Compute
     $x_{g_1}[l] = IFFT\{X_{g_1}(k), \beta_{g_1}(k)\}, x_{g_2}[m] = IFFT\{X_{g_2}(k), \beta_{g_2}(k)\}$ 
    where  $\beta_{g_1}(k) \in \{\pm 1\}, \beta_{g_2}(k) \in \{\pm j\}$ 
14: Assume  $\min PAPR=t$ 
15: For  $g_1=0 : U/2 - 1$ 
16: For  $g_2=U/2 : U - 1$ 
17:  $x_{g_1,g_2}[n] = \frac{x_{g_1}[l] + x_{g_2}[m]}{\sqrt{2}}$ 
18: If  $PAPR\{x_{g_1,g_2}[n]\} < \min PAPR$ 
19: Initialize  $\min PAPR = PAPR\{x_{g_1,g_2}[n]\}$ 
20: End if
21: End For
22: Combining symbol candidates  $x_{g_1,g_2}[n]$  and  $x_u[n]$ 
23: Evaluate the minimal PAPR
24:  $\operatorname{Minima}\{PAPR_{\min}, \min PAPR\}$ 
25: Transmit Symbol candidate  $x' = \operatorname{argmin}\{x_{u,g_1,g_2}[n]\}$ 
26: End For
27: End

```

In our proposed scheme the number of candidates generated C_{in} is equal to $(U+U^2/4)$ with same number of IFFT computations as in conventional SLM scheme. This would result in a better CCDF value that would yield good PAPR performance of the designed system. The semi-empirical approximation for the CCDF of the proposed algorithm is then evaluated as.

$$CCDF_{proposed}(\gamma_0) \approx \left(1 - (1 - e^{-\gamma_0})^{2.8N}\right)^{C_{in}} \quad (17)$$

C. PAPR Threshold Parameter

To study the effects for different values of subcarriers and candidate sequences in our proposed scheme we estimate the threshold value of PAPR γ_0 at a fixed value of $CCDF(\gamma_0) = c_f$.

The expressions in (17) are rearranged to obtain the following equations of thresholds as follows:

$$\gamma_{0(OFDM)} \approx -\log \left(1 - \left(1 - c_f \right)^{\frac{1}{2.8N}} \right) \quad (18)$$

$$\gamma_{0(Proposed)} \approx -\log \left(1 - \left(1 - c_f^{1/C_{in}} \right)^{\frac{1}{2.8N}} \right) \quad (19)$$

In the above expressions the value of number of candidates C_{in} for SLM, GreenOFDM and proposed scheme is considered as U , $U^2/4$ and $(U + U^2/4)$. Thus, it can be noted here that the PAPR performance of the designed system at a given CCDF can also be analyzed from the number of candidates and the subcarriers.

IV. SIMULATION RESULTS

Using various computer simulations we demonstrate the PAPR performance, effects of the PAPR threshold for different values of subcarriers and sub-bands at a fixed value of $CCDF=10^{-3}$, and the BER performance of our proposed scheme with the conventional SLM and the existing GreenOFDM schemes. Simulations are carried on 10000 QPSK modulated OFDM symbols for oversampling factor $L=4$, subcarriers $N=64$ and candidate sequence $U=8$. We have used AWGN channel and 3-tap Stanford University Interim (SUI) 5-multipath fading channel having average path gains [0 dB, -5 dB, -10 dB], and path delays [0 μ s, 4 μ s, 10 μ s] are considered for receiver side effects under perfect side information(PSI) condition in our proposed scheme.

In Fig. 2, we have evaluated the CCDF of PAPR for our proposed scheme and compared the performance with OFDM, conventional SLM and GreenOFDM technique. Theoretical CCDF of PAPR is the upper bound of the PAPR performance and simulation results will never exceed these values. It is studied from the graph that the simulated results and analytical curves evaluated from expressions (17) are well approximated for our proposed scheme. In our proposed scheme the number of candidates $C_{in}=U+U^2/4$ results a decrease in the $CCDF(\gamma_0)$ value with same number of IFFT computations as required in the conventional SLM and hence improves the PAPR performance of our designed system. It is observed from the graph that at a given $CCDF=10^{-3}$ the PAPR reduction ability of the proposed scheme outperforms the OFDM system by 3.9dB, conventional SLM by 0.6dB and the GreenOFDM by 0.2dB.

Fig. 3 presents the PAPR thresholds $\gamma_0[dB]$ for different values of subcarriers N ranging from 64 to 1024 at a fixed value of $CCDF(\gamma_0) = 10^{-3}$ in our proposed scheme. The PAPR thresholds $\gamma_0[dB]$ are evaluated for candidate sequence $U=4,8,16$ and 32 in our proposed scheme for different subcarriers.

It is seen that the value of PAPR threshold $\gamma_0[dB]$ increases for increasing values of subcarriers N . It is observed that for a fixed value of $CCDF(\gamma_0)=10^{-3}$, the value of $\gamma_0[dB]$

decreases as the candidate sequence U is increased from 4 to 32 in our proposed scheme. It is studied from the graph that the simulated results and analytical curves evaluated from expressions (19) are well approximated for our proposed scheme.

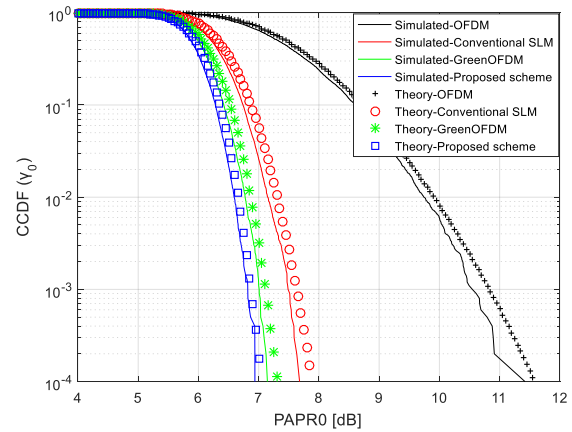


Fig. 2. PAPR Performance of Proposed Scheme and the Existing Schemes for Simulated and Approximate Results.

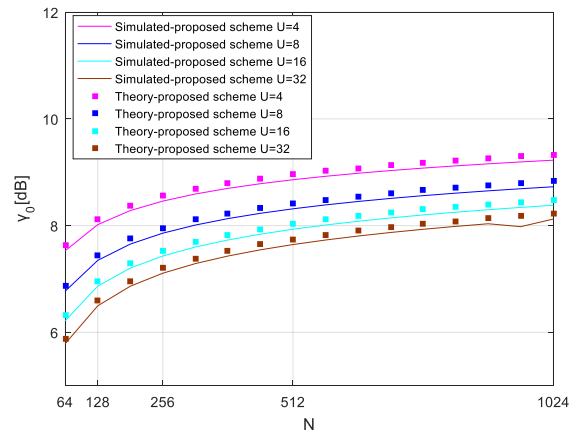


Fig. 3. $\gamma_0[dB]$ Versus N at a Fixed $CCDF(\gamma_0) = 10^{-3}$ for Proposed Scheme with $U=4,8,16$ and 32 with Simulated and Approximate Results.

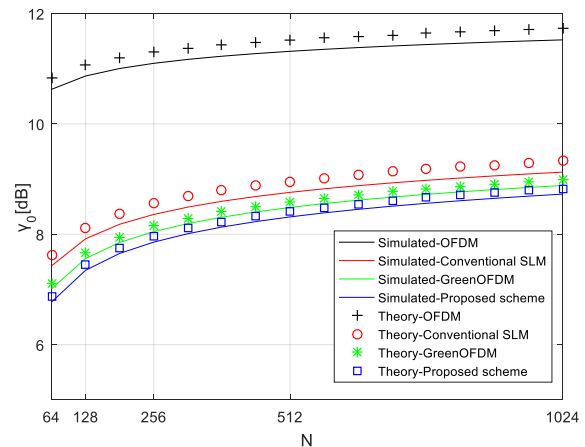


Fig. 4. $\gamma_0[dB]$ Versus N at a Fixed $CCDF(\gamma_0) = 10^{-3}$ for Proposed Scheme and the Existing Schemes with Simulated and Approximate Results.

In Fig. 4, we plot PAPR thresholds $\gamma_0[dB]$ for different number of subcarriers at a fixed value of $CCDF(\gamma_0) = 10^{-3}$ and $U=8$ for our proposed scheme and compared the performance with the OFDM, conventional SLM and Green-OFDM schemes. It is seen that the value of PAPR thresholds $\gamma_0[dB]$ increases for increasing values of subcarriers N . It is studied from these curves that the simulated results and analytical curves evaluated from expression (19) are well approximated for our proposed scheme. It is noticed that at a given $CCDF=10^{-3}$ the PAPR reduction ability of the proposed scheme outperforms the OFDM system by 3.9dB, conventional SLM by 0.6dB and the GreenOFDM by 0.2dB. Therefore, in our proposed scheme at a given $CCDF(\gamma_0) = 10^{-3}$ the value of $\gamma_0[dB]$ is lower as compared to that in OFDM, conventional SLM and GreenOFDM schemes.

Table I presents that the simulation results for different number of candidates U at subcarriers $N=64$ and their comparative analysis of the PAPR performance of our proposed scheme with some of the existing schemes. It is noted that for $U=4$ the PAPR value at $CCDF=10^{-3}$ for the proposed scheme, GreenOFDM [15] and conventional SLM is 7.59 dB, 8.72 dB and 8.35 dB. It is found from the results that for $U=8$ at $CCDF=10^{-3}$ the proposed scheme outperforms the GreenOFDM[15] and conventional SLM by 0.19 dB and 0.58 dB. In the proposed scheme for $U=16$ the PAPR performance gap at $CCDF=10^{-3}$ with GreenOFDM [15] and conventional SLM equals to 0.10 dB and 0.75 dB.

It is also noted that for $U=32$ the PAPR value at $CCDF=10^{-3}$ for the proposed scheme, GreenOFDM [15] and conventional SLM is 5.80 dB, 5.86 dB and 6.56 dB. The PAPR performance gap with the existing schemes reduces for higher values of candidate set. However, the higher value of U leads to more number of IFFT computations and increases the computational complexity of the system. Therefore, it is found that the proposed scheme offers a good PAPR performance with same number of IFFT computations in comparison to the existing schemes.

The BER performance of our proposed scheme, OFDM and conventional SLM over the AWGN and Rayleigh fading channel are presented in Fig. 5. It is studied from the graph that the multipath fading channel offers high BER distortions than the AWGN channel. It is noticed from the curves that under PSI condition our proposed scheme offers negligible loss in the BER performance when compared to OFDM system and the conventional SLM scheme over the AWGN and Rayleigh fading channel.

TABLE I. COMPARATIVE ANALYSIS OF THE PAPR PERFORMANCE OF PROPOSED SCHEME WITH EXISTING SCHEMES

Number of Candidate (U)	PAPR(dB) at CCDF (10^{-3})		
	Conventional SLM	GreenOFDM	Proposed Scheme
4	8.35	8.72	7.59
8	7.41	7.02	6.83
16	6.98	6.33	6.23
32	6.56	5.86	5.80

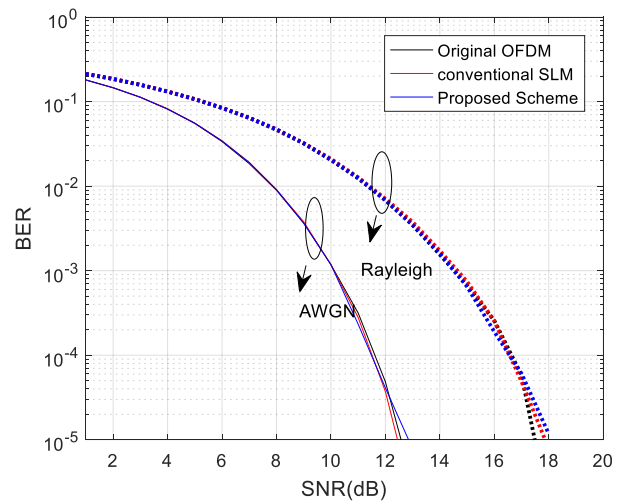


Fig. 5. BER Performance of the Proposed Scheme over AWGN and Rayleigh Fading Channels.

V. CONCLUSION

Our article aims to generate more set of candidate sequence that achieves effective PAPR performance of the OFDM signal without any equivalent rise in the IFFT computations. It has been demonstrated that the simulation and analytical results are well-approximated for our proposed schemes. Effects of subcarriers and candidates sequence on PAPR threshold are studied in our proposed scheme. The receiver side of our proposed scheme under PSI condition offers negligible loss in BER performance of the system as compared to OFDM system. Thus, the proposed scheme outperforms well in terms of PAPR reduction capability of the OFDM signal in comparison to that to the performance in OFDM, conventional SLM and Green-OFDM system using the same number of IFFT's.

REFERENCES

- [1] Y. Wu and W. Y. Zou, "Orthogonal frequency division multiplexing: A multi-carrier modulation scheme", IEEE Trans. Consumer Electronics, vol. 41, no. 3, pp. 392-399, August 1995.
- [2] W. Y. Zou and Y. Wu, "COFDM: An overview," IEEE Trans. Broadcasting, vol. 41, no. 1, pp. 1-8, Mar. 1995.
- [3] T. Jiang and Y. Wu, "An overview: Peak-to-average power ratio reduction techniques for OFDM signals," IEEE Trans. Broadcast., vol. 54, no. 2, pp. 257-268, June 2008.
- [4] K R Panta, J. Armstrong, "Effects of clipping on the error performance of OFDM in frquency selective fading channel Wireless Communications" IEEE Transactions on Wireless Comm., vol. 3, no. 2, pp. 668-671, March 2004.
- [5] X. Li and L. J. Cimini, Jr, "Effects of clipping and filtering on the performance of OFDM," IEEE Communications Letters, vol. 2, no. 5, pp.131-133, May 1998.
- [6] T. Jiang and G. X. Zhu, "Nonlinear companding transform for reducing peak-to-average power ratio of OFDM signals," IEEE Trans. Broadcasting, vol. 50, no. 3, pp. 342-346, Sep. 2004.
- [7] T. Jiang and G. Zhu, "Complement block coding for reduction in peak-to-average power ratio of OFDM signals," IEEE Communications Magazine, vol. 43, no. 9, pp. S17-S22, Sep. 2005.
- [8] R. W. Bauml, R. F. H. Fisher, and J. B. Huber, "Reducing the Peak-to-Average Power Ratio of Multicarrier Modulation by Selected Mapping,"IEEE Electron. Lett., vol. 32, no. 22, pp. 2056-2057, Oct.1996.

- [9] S. H. Muller and J. B. Huber, "OFDM with reduced peak-to-average power ratio by optimum combination of partial transmit sequences," *IEEE Electron. Lett.*, vol. 33, no. 5, pp. 36–69, Feb. 1997.
- [10] B.S. Krongold and D.L. Jones, "Peak Power Reduction via Active Constellation Extension," *IEEE Trans. Broadcast.*, vol. 49, no. 3, pp. 258–268, Sep. 2003.
- [11] J. Tellado, "Multicarrier Transmission with low PAR." Ph.D.thesis, Stanford University, CA, 1998.
- [12] S.H.Han, J.M.Cioffi, J.H.Lee, "Tone injection with hexagonal constellation for peak-to-average power ratio reduction in OFDM," *IEEE Commun. Lett.*, vol. 10, no. 9, pp. 646–648, Sept. 2006.
- [13] N. Ohkubo and T. Ohtsuki, "Design Criteria for Phase Sequences in Selected Mapping," *IEICE Trans. Commun.*, vol. E86-B, no. 9, pp. 2628–2636, Sep. 2003.
- [14] Fische R.F.H.: 'Widely-linear selected mapping for peak-to-average power ratio reduction in OFDM', *Electron. Lett.*, 2007,43,(14),pp.766-767.
- [15] J.G. Mestdagh, J.L. Gulfo Monsalve and J-M. Brossier. "GreenOFDM: a new selected mapping method for OFDM PAPR reduction". *Electronics Letters*, vol. 54, no. 7, pp. 449-450, 2018.
- [16] D. Yu and Y. Wan, "A New Method for Reducing PAPR in OFDM System Based on GreenOFDM". 10th International Conference on Communications, Circuits and Systems (ICCCAS). pp. 227-231, Chengdu, China, 2018.
- [17] Z. Zhou, L. Wang and C. Hu. "Improved SLM Scheme for Reducing the PAPR of QAM OFDM Signals". 2019 IEEE 2nd International Conference on Electronics Technology (ICET). pp.28-33, May 2019.
- [18] Jorge Luis Gulfo Monsalve, Laurent Ros, Jean-Marc Brossier, Denis Mestdagh An improved GreenOFDM scheme for PAPR reduction.
- [19] Wang Y, Wang LH, Ge JH, Ai B. An efficient non linear companding transform for reducing PAPR of OFDM signals *IEEE Transactions on Broadcasting*. 2012 Dec ;58(4):677-684.
- [20] Ochiai, H., and Imai, H.: 'On the distribution of the peak-to-average power ratio in OFDM signals', *Trans. Commun.*, 2001, 49, (2), pp. 282–289.
- [21] Breiling H, Muller-Weinfurtner S H, Huber J B. SLM peak-power reduction without explicit side information[J]. *IEEE Communications Letters*, 2001, 5(6):239-241.

Efficient DWT based Fusion Algorithm for Improving Contrast and Edge Preservation

Sumanth Kumar Panguluri^{1*}, Laavanya Mohan²

Department of Electronics and Communication Engineering

Vignan's Foundation for Science, Technology and Research, Vadlamudi, Guntur, Andhra Pradesh, 522213, India

Abstract—The main principle of infrared (IR) image is that it captures thermal radiation of light. The objects that are captured in low light, fog, and snow conditions can be detected clearly in IR image. But the major drawback of IR image is that it provides poor resolution and low texture information. Due to that humans are unable to understand overall scene information present in IR image. Nowadays for the detection of objects in poor weather conditions with improved texture information, the result of visible (VI) and IR image fusion is used. It is mostly used in military, surveillance, and remote sensing applications. The efficient DWT based fusion algorithm for improving contrast and edge preservation is presented in this paper. First morphology hat transform is applied on source images for improving contrast. DWT on decomposition produces low frequency and high frequency sub-bands. A novel mean weighted fusion rule is introduced in this paper for fusing low frequency sub-bands. Its aim is to improve the visual quality of final fused image. The max fusion rule has used for fusing high frequency sub-bands to improve edge information. The final fused image is reconstructed by using IDWT. In this paper, the proposed fusion algorithm has produced improved results both subjectively and as well as objectively when compared to existing fusion methods.

Keywords—Visible image; infrared image; Discrete Wavelet Transform (DWT); Inverse Discrete Wavelet Transform (IDWT); novel mean-weighted fusion rule; max fusion rule

I. INTRODUCTION

Digital image processing is a significant and very useful research area, which plays a vital role in day today life of humans. The usage of it has been increased exponentially in the last decades. It is applied in wide range of applications such as medical [1], [2], [3], security [4], etc. This paper presents latest research area work of digital image processing.

Nowadays improving scene information for better human observation that is captured during bad weather conditions is playing a significant role in many vital applications like remote sensing [5], military [6], and surveillance [7]. This can be done by using VI and IR image fusion. Presently a lot of research is going on VI and IR image fusion [8]. The main motive of researchers is to improve the result of VI and IR image fusion. The IR camera sensor is used for capturing IR images. The basic principle of the IR camera sensor is that it captures thermal radiation of light. The VI camera sensor is used for capturing VI images. The basic principle of VI camera sensor is that it captures reflection of light. The object information details are better provided in the IR image irrespective of weather conditions. But the drawback of IR image is that it provides poor spatial resolution. The

background details such as textures are provided well in VI image due to high spatial resolution. The disadvantage of VI image is that object details are not seen properly in bad weather conditions such as low light, fog, and snow. The fusion of these both images will produce a single image. It provides better scene information such as good object details and as well as better background information in single image.

Traditionally fusion process can be implemented in two ways:

- Fusion in spatial domain.
- Fusion in transform domain.

The fusion methods in spatial domain are weighted average [9] and PCA [10] fusion. These methods don't require any transforms. They are applied directly to pixels. Advantages of these methods are, fusion can be done in a fast manner and computational complexity of fusion algorithm is less. The main drawbacks of these methods are:

- They produce blurred results after fusion.
- Spatial distortions and spectral degradations are produced in the final fusion result.

The fusion in transform domain mainly comprises of three steps:

- First transform is applied on source images. On decomposition it produces low frequency and high frequency sub-images.
- Fusion rules are applied.
- Inverse transform is applied for reconstructing fused image.

The main advantage of fusion methods in transform domain is that high quality fused images are produced compared to fusion methods in spatial domain. Nowadays so, many transform domain fusion methods have been developed. The transforms that are used in these methods are Discrete Wavelet Transform [11], Laplacian pyramid transform [12], Contour-let transform [13], and Dual-tree complex wavelet transform [14].

An efficient DWT based fusion algorithm for improving contrast and edge information is presented in this paper. Its motive is to achieve both better contrast and rich texture information resultant fused image.

*Corresponding Author

II. RELATED WORKS

Habeeb et al. [15] have developed a DWT based fusion algorithm. Here source images used are VI and IR images. In this algorithm sharpen filter has been proposed. Here sharpen filter has been used for improving the contrast and edge enhancement of the IR image. DWT on decomposition produces both detailed and approximation coefficients. For merging both detailed and approximation coefficients weighted averaging rule has been used. The fused image is reconstructed using IDWT. Mainly this algorithm has been developed for highlighting edges and fine details of output resultant fused image. The limitation of this method is that the resultant fused image shows less visible feature information.

Habeeb et al. [16] have introduced the fusion algorithm for combining multi-modal images in the spatial domain. The modalities chosen are VI and IR images. First PCA is applied to both source images for reducing dimensionality. Enhancement of infrared image is done by using a 3×3 sharpen filter. Similarly, for enhancing the visible image histogram equalization method is used. Finally, weighted average rule is used for fusing the output of sharpen filter and histogram equalization. This algorithm achieved better results than traditional methods results. But the main drawback of this fusion algorithm is that it produced a blurred result.

Xu and Su [17] have proposed a DWT based enhanced fusion method. On DWT decomposition detailed and approximation coefficients are produced. The approximation coefficients of the IR image are modified using a stretching mechanism for improving contrast. The simple average scheme has been used for combining approximation coefficients. Max-fusion rule was used to combine detailed-coefficients. The fused image is reconstructed using IDWT. This method had produced a better result when compared to similar methods results. The limitation of this method is complexity of fusion method is more. More number of decomposition levels was used to get satisfactory results.

S. Panguluri and L. Mohan [18] have developed VI and IR image fusion algorithm using DWT and unsharp masking. On DWT decomposition detailed and approximation coefficients are produced. The unsharp masking technique was applied to the approximation-coefficients. Later average fusion rule was used for fusing output coefficients generated after unsharp masking. Max fusion rule was used for fusing detailed-coefficients. The resultant fused image had been reconstructed with IDWT. This algorithm has produced high contrast and edge informative resultant fused image. The drawback of the algorithm is that edge improvement of the fused image have done partially only.

Zhan et al. [19] have developed a fusion scheme based on DWT for fusing IR and VI images. Mainly DWT is used for producing both detailed and approximation coefficients. Regional energy-based rule was used for fusing approximation coefficients. Weighted sum and difference of neighboring coefficients based fused strategy was used to integrate detailed coefficients. This fusion technique had produced better target information in the resultant fused image compared to similar research techniques. The limitation of this fusion scheme is

that it produced poor background textures in the resultant fused image.

Han et al. [20] have presented VI and IR image fusion method using discrete wavelet transform. For fusing detailed coefficients weighted average rule based on feature selection has been used. Absolute selection value rule was used for fusing approximation-coefficients. This method is producing superior results compared with traditional methods. The problem of this method is that it produced poor illumination fused image.

Shah et al. [21] have introduced an IR & VI image fusion mechanism based on DWT. Here detailed and approximation coefficients are produced by combining curvelet and DWT. The fusion strategy used for combining detailed and approximation coefficients is the mean-max rule. The proposed method fused image obtained better contrast and good sharpness when compared to similar work. The drawback of this method is that for producing a fused image it has used two multi-scale transforms.

Zhan and Zhuang [22] have proposed an IR & VI image fusion algorithm using three stages of the discrete wavelet transform. Mainly different fusion rules were in three different stages. The resultant fused image has achieved more contrast and good sharpness when compared to similar work mechanisms. The limitation of this method is the complexity of the fusion algorithm is more. Since more number of fusion strategies have been used in the fusion algorithm for getting a good result.

The motive of all the above methods is to improve contrast and enhance the edge information of the resultant fused image. If the contrast and texture information of the fused image is more, then the detection of objects becomes easy and also overall scene information can be better understood by humans. To achieve both better contrast and rich texture information of the resultant fused image, the above methods face many problems.

Most of the problems faced are:

- In the fusion method, edge improvement of the fused image is done partially only.
- An obtained fused image contains less visible feature information.
- More number of decomposition levels are required for getting satisfactory results. It increases the complexity of the fusion algorithm. It also increases computational time.
- Two different multi-scale transforms are used in the fusion algorithm. This increases the complexity of the fusion algorithm.
- Multiple stages of discrete wavelet transform and more number of different fusion rules has been used in the fusion algorithm. This increases the complexity of the fusion algorithm.

The aim of this paper is to achieve both better contrast and rich texture information resultant fused image. At the same

time reducing the above-mentioned problems. This paper introduces an efficient DWT based fusion algorithm. Mainly in this method morphology hat transform has used for improving contrast. A new fusion rule "Novel mean-weighted fusion rule" is introduced for improving quality of final fused image. Single level decomposition of DWT is used in this method in order to reduce the complexity problem.

III. PROPOSED METHOD

An efficient DWT based fusion algorithm for improving contrast and edge preservation has been presented. First source images are resized into 256×256 . Morphology hat transform is applied to both resized images to improve contrast. DWT on decomposition will produce both detailed and approximation coefficients. A novel mean-weighted fusion rule is introduced for integrating approximation coefficients. Detailed-coefficients are integrated using max fusion rule. The resultant fused image is reconstructed using IDWT. The proposed algorithm block diagram is shown in Fig. 1.

A. Morphology Hat Transform

Morphology hat transform is a contrast enhancement technique. As shown in Fig. 1, morphology hat transform is applied to both resized images to improve contrast. It is a combination of two transforms. They are top-hat transform and bottom-hat transform. The purpose of the top-hat transform is to highlight brightness information and bottom-hat transform purpose is to highlight darkness information.

Top-hat transform can be defined in such a way that difference between the original image and its opening image. The expression for top-hat transform is given by

$$TH(x, y) = f(x, y) - f_{OP}(x, y) \quad (1)$$

$$f_{OP}(x, y) = f \circ s \quad (2)$$

Where "TH(x,y)" indicates top-hat transform image, "f(x,y)" indicates original image, "f_{OP}(x,y)" indicates opening of "f(x,y)" by structuring element "s".

Bottom-hat transform can be defined in such a way that subtracting the original image from its closing image. The expression for bottom-hat transform is given by

$$BH(x, y) = f_{CL}(x, y) - f(x, y) \quad (3)$$

$$f_{CL}(x, y) = f \bullet s \quad (4)$$

Where "BH(x,y)" indicates bottom-hat transform image, "f(x,y)" indicates original image, "f_{CL}(x,y)" indicates closing of "f(x,y)" by structuring element "s".

The final expression for the morphology hat transform is given by

$$MH(x, y) = f(x, y) + TH(x, y) + BH(x, y) \quad (5)$$

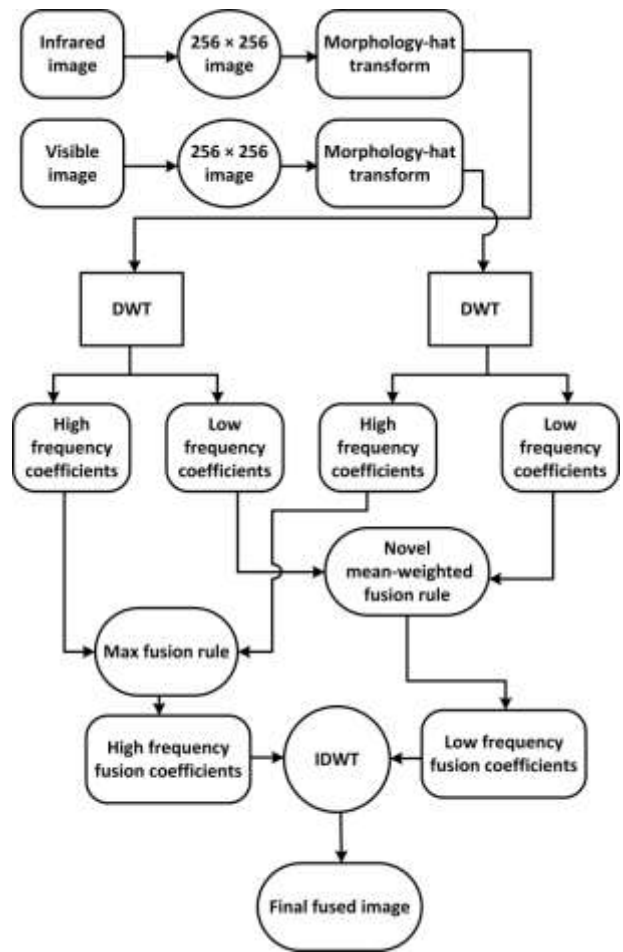


Fig. 1. Block Diagram of the Proposed Algorithm.

Where "MH(x,y)" indicates morphology hat transform image, "f(x,y)" indicates the original image, "TH(x,y)" indicates top hat transform image and "BH(x,y)" indicates bottom hat transform image.

B. DWT

DWT is an efficient multi-scale transform. As shown in Fig. 1, DWT is applied to the output of morphology-hat transform images of both source images. On decomposition, it produces four sub-band images. They are "LL, LH, HL and HH" sub-band images. "LL" sub-band image represents approximation coefficients. It provides average information. The "LH, HL, and HH" sub-band images represent detailed coefficients and they provide edge information. The main advantage of using DWT is that it removes spatial distortions and spectral degradations in the final fused image.

C. Fusion Strategy for Low-Frequency Coefficients

As shown in Fig. 1, "Novel mean-weighted fusion rule" is used to integrate approximation coefficients. Generally, approximation coefficients contain average or smoothening information. Let "F_{L1}(U,V)" represents low-frequency coefficients produced after morphological hat transform of IR image. "F_{L2}(U,V)" represents low-frequency coefficients produced after morphological hat transform of VI image.

The formula for novel mean-weighted fusion rule is given by.

$$F_{MW}(U, V) = W1 * F_{L1}(U, V) + W2 * F_{L2}(U, V) \quad (6)$$

Here W1, W2 represents weights.

The process for the generation of weights for novel mean-weighted fusion rule is shown in Fig. 2. First IR and VI images are resized into 256×256 . Let "X" represents the resized IR image and "Y" represents the resized VI image. Sharpen filter is applied to the output of the resized image of the IR image.

The 3×3 sharpen filter used here is shown in Fig. 3. The output of the sharpen filter is indicated by "S(X)". The use of the sharpen filter is to highlight the fine details and edges of the IR image.

Histogram equalization is applied to the output of the resized image of VI images. The output of histogram equalization is indicated by "H(Y)". The main principle of histogram equalization is to make all the grey levels participate in image information. So, that high contrast image is produced at the output of histogram equalization.

The formula for calculation of weight "W1" is given by

$$W1 = \frac{[mean(S(X))]}{[mean(S(X)) + mean(H(Y))]} \quad (7)$$

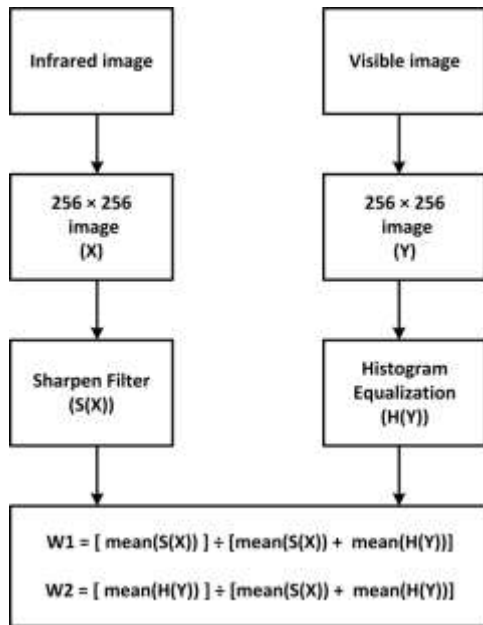


Fig. 2. Block Diagram for Generation of Weights for Novel mean-Weighted Fusion Rule.

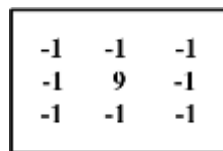


Fig. 3. 3×3 Sharpen Filter1.

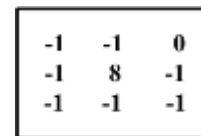


Fig. 4. 3×3 Sharpen Filter2.

The formula for calculation of weight "W2" is given by

$$W2 = \frac{[mean(H(Y))]}{[mean(S(X)) + mean(H(Y))]} \quad (8)$$

The novel mean-weighted fusion rule is mainly used to enhance brightness and improve the sharpness of edges of original images. So, that clarity of resultant fused image increases.

D. Fusion Strategy for High-frequency Coefficients

As shown in Fig. 1, "Max fusion rule" is used for integrating detailed-coefficients. Mainly detailed-coefficients purpose is represent edge information. Edge information reflects textures of original images. Let " $F_{H1}(U, V)$ " represents detailed coefficients produced after morphological hat transform of IR image and " $F_{H2}(U, V)$ " represents detailed coefficients produced after morphological hat transform of VI image.

The formula for max fusion rule is given by

$$F_{Max}(U, V) = \max[(F_{H1}(U, V), (F_{H2}(U, V)))] \quad (9)$$

The purpose of max fusion rule is to highlight edge information of fused image. So, that it helps to improve textures of the final fused image.

IV. EXPERIMENTAL RESULTS AND ANALYSIS

A. Software and Hardware Details

The Mat-lab 2019b software has used for developing fusion algorithm. The features of the computer that is used for developing fusion algorithm are corei5 processor, 4GB RAM and 1TB hard disk.

B. Comparison Methods for Evaluating the Proposed Method

In this paper proposed method fused image is compared with four existing similar work methods fused images.

The methods are:

- Sharpen Filter method [15].
- PCA method [16].
- Enhanced Contrast method [17].
- Unsharp Masking method [18].

The above four methods are implemented in this paper.

1) *Experimental process of sharpen filter method:* First source images (VI, IR) are resized into 256×256 . For enhancing edge information, a sharpened filter is applied to the IR image in the spatial domain. The 3×3 sharpen filter that has used in this method is shown in Fig. 4.

Applying DWT produces both detailed and approximation coefficients. "Weighted average strategy" has used for integrating both detailed coefficients and approximation coefficients. Finally on applying IDWT produces the final fused image.

2) *Experimental process of PCA method:* First source images (VI, IR) are resized into 256×256 . PCA is applied to both the source images for reducing dimensionality reduction. Sharpen filter has applied to the output of PCA of IR image to highlight edge information. The 3×3 sharpen filter that has used in this method is shown in Fig. 5.

0	-1	-1
-1	9	-1
-1	-2	-1

Fig. 5. 3×3 Sharpen Filter3.

For improving contrast histogram-equalization has applied to the output of PCA of VI image. "Weighted average strategy" has used for integrating the output of sharpening filter and histogram equalization output. The output of weighted average fusion produces a resultant fused image.

3) *Experimental process of enhanced contrast method:* First source images (VI, IR) are resized into 256×256 . Applying DWT produces both detailed and approximation coefficients. "Simple average strategy" has used for integrating approximation coefficients. "Max fusion strategy"

has used for integrating detailed coefficients. Finally on applying IDWT produces resultant fused image.

4) *Experimental process of unsharp masking method:* First source images (VI, IR) are resized into 256×256 . Applying DWT produces both detailed and approximation coefficients. Here unsharp masking has applied to approximation coefficients produced after DWT decomposition. "Average fusion rule" has used for integrating the result of unsharp masking of both approximation coefficients. "Max fusion strategy" has used for integrating detailed coefficients. Finally on applying IDWT produces the final fused image.

C. Subjective Analysis of Results

Subjective analysis of results is mainly used for evaluating the proposed method resultant fused image with comparison methods resultant fused images. TNO image fusion dataset [24] source images (VI, IR) are used in this paper for verifying the working of proposed fusion algorithm. Mainly four sets of source (VI, IR) images are used in this paper. And they are shown in Fig. 6 to 9.

Here Fig. 6 shows the fused results of "soldier image". It gives clear information that the military man and trees are not properly identified in sharpen filter method fused image, PCA method fused image, enhanced contrast method fused image and unsharp masking method fused image due to low contrast and poor texture information. Whereas in the proposed method fused image the military man and trees details are clearly identified. Mainly because the proposed method resultant fused image is providing more contrast and rich texture information.

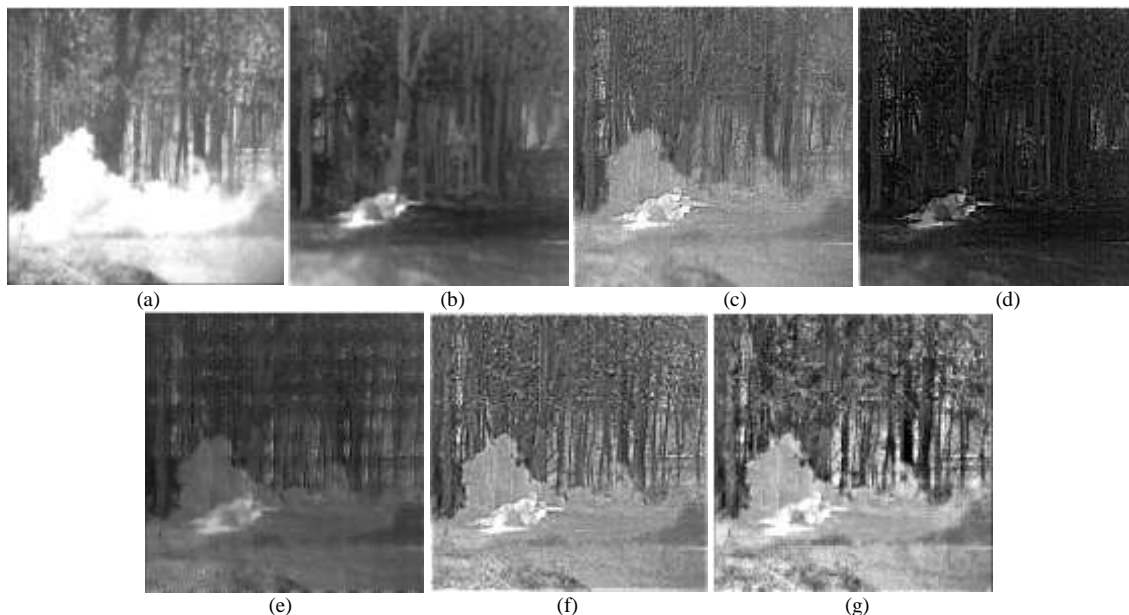


Fig. 6. The Fused Results of "Soldier Image": (a) VI Image, (b) IR Image, (c) Sharpen Filter Method Fused Image, (d) PCA Method Fused Image, (e) Enhanced Contrast Method Fused Image, (f) Unsharp Masking Method Fused Image, (g) Proposed Method Fused Image.

Here Fig. 7 shows the fused results of "traffic image". Due to poor brightness letters on the name board are not visualized clearly in other methods resultant fused images. Whereas in the proposed method fused image letters on the name board are clearly identified due to more brightness.

Here Fig. 8 shows the fused results of the "two-person image". House, two persons and board are observed clearly in the proposed method resultant fused image when compared to other methods resultant fused images. It is because of two reasons. The first one is that the proposed method resultant

fused image is having high contrast when compared to other methods resultant fused images. The second one is that texture information is highly improved in the proposed method resultant fused image.

Here Fig. 9 shows the fused results of "soldier in trench image". Solider and trench details are identified clearly in the proposed method resultant fused image when compared to other methods resultant fused images. It is because the contrast is high and also texture information is more in the proposed method resultant fused image.

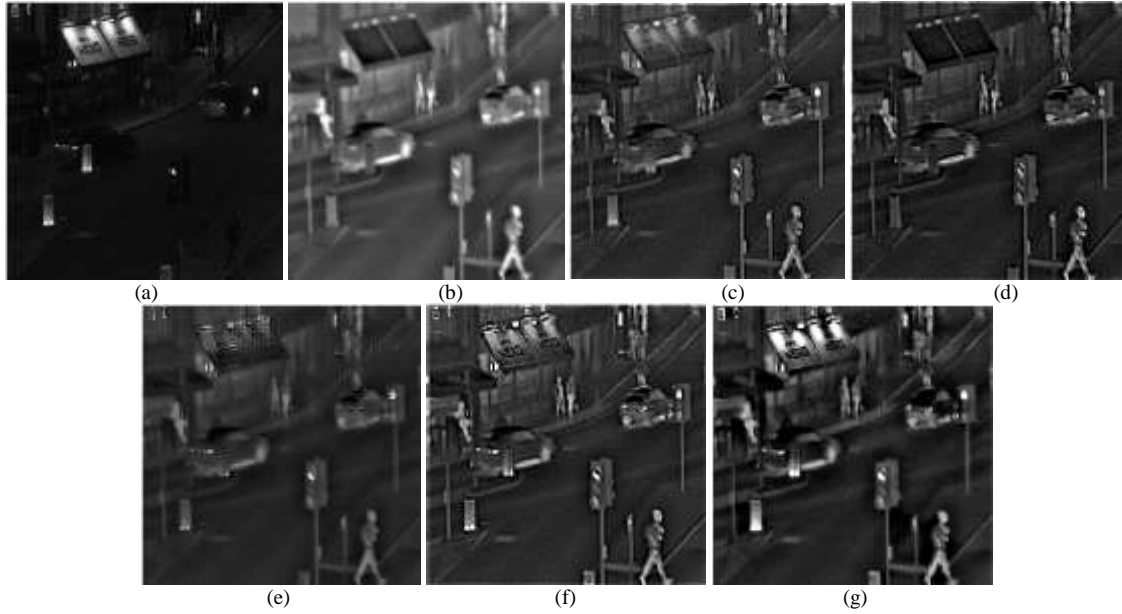


Fig. 7. The Fused Results of "Traffic Image": (a) VI Image, (b) IR Image, (c) Sharpen Filter Method Fused Image, (d) PCA Method Fused Image, (e) Enhanced Contrast Method Fused Image, (f) Unsharp Masking Method Fused Image, (g) Proposed Method Fused Image.

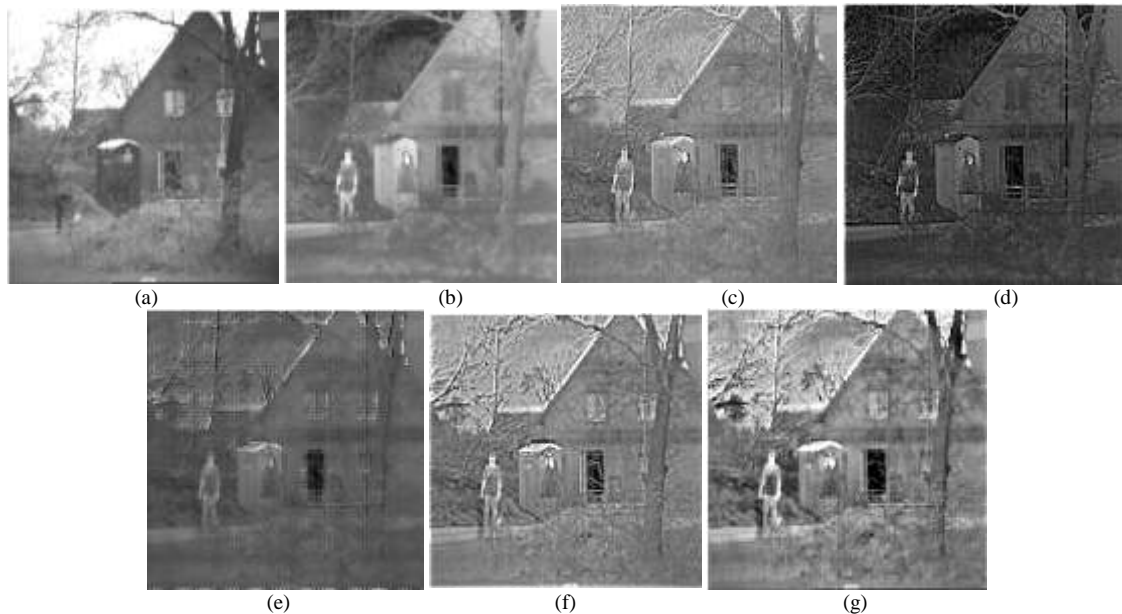


Fig. 8. The Fused Results of "Two Person Image": (a) VI Image, (b) IR Image, (c) Sharpen Filter Method Fused Image, (d) PCA Method Fused Image, (e) Enhanced Contrast Method Fused Image, (f) Unsharp Masking Method Fused Image, (g) Proposed Method Fused Image.

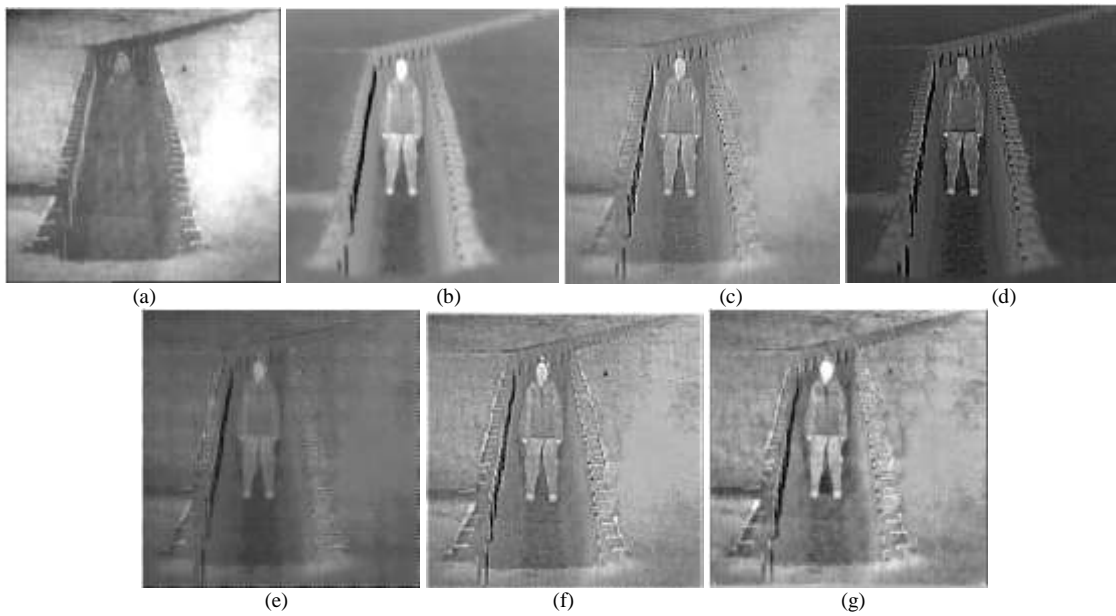


Fig. 9. The Fused Results of "Soldier in Trench Image": (a) VI Image, (b) IR Image, (c) Sharpen Filter Method Fused Image, (d) PCA Method Fused Image, (e) Enhanced Contrast Method Fused Image, (f) Unsharp Masking Method Fused Image, (g) Proposed Method Fused Image.

D. Objective Analysis of Results

Objective analysis of results gives accurate information for evaluating the proposed method resultant fused image with comparison methods resultant fused images. Performance metrics used for experimentation are mean, standard deviation, entropy, mean gradient, spatial frequency, QAB/F and visual information fidelity.

1) *Mean*: Mean metric gives average value of brightness information of the fused image. It is calculated by.

$$\mu = \frac{1}{P \times Q} \sum_{x=1}^P \sum_{y=1}^Q G(x, y) \quad (10)$$

2) *Standard deviation*: Standard deviation metric gives contrast details of the fused image. The value of standard deviation is high means, it represents more contrast. More contrast means, better visualization of fused image. The formula for standard deviation is given by

$$STD = \sqrt{\frac{1}{P \times Q} \sum_{x=1}^P \sum_{y=1}^Q (G(x, y) - \mu)^2} \quad (11)$$

3) *Entropy*: Entropy metric represents the amount of information and texture richness present in the fused image. The value of entropy is more means, the fused image contains more information and textures. It is calculated by.

$$E = - \sum_{i=0}^{L-1} h(i) \log h(i) \quad (12)$$

4) *Mean gradient*: The mean gradient metric represents the amount of edge information preserved in the fused image. The value of the mean gradient is more means, the fused

image contains more edge preservation information. It is calculated by.

$$MG = \frac{1}{(P-1)(Q-1)} \sum_{x=1}^{P-1} \sum_{y=1}^{Q-1} \sqrt{A} \quad (13)$$

$$A = \frac{[G(x, y) - G(x-1, y)]^2 + [G(x, y) - G(x, y-1)]^2}{2} \quad (14)$$

5) *Spatial frequency*: The spatial frequency metric gives the activity level information in the fused image. The value of spatial frequency is more means, the fused image provides better overall scene information. It is calculated by.

$$SF = \sqrt{RF^2 + CF^2} \quad (15)$$

$$RF = \sqrt{\frac{1}{P \times Q} \sum_{x=0}^{P-1} \sum_{y=1}^{Q-1} [G(x, y) - G(x, y-1)]^2} \quad (16)$$

$$CF = \sqrt{\frac{1}{P \times Q} \sum_{x=0}^{P-1} \sum_{y=1}^{Q-1} [G(x, y) - G(x-1, y)]^2} \quad (17)$$

6) *Visual information fidelity*: The visual information fidelity (VIF) metric is mainly used for assessing image quality [23]. If its value is more means, the fused image provides better visual quality.

7) $Q^{AB/F}$: It measures edge information of fused image which is transferred from source images [8]. If QAB/F value is more means, the fused image provides better visual quality. It is calculated by.

$$Q^{AB/F} = \frac{\sum_{x=1}^P \sum_{y=1}^Q Q^{AF(x,y)w^A(x,y)} + Q^{BF(x,y)w^B(x,y)}}{\sum_{x=1}^P \sum_{y=1}^Q (w^A(x,y) + w^B(x,y))} \quad (18)$$

$$Q^{XF}(x, y) = Q_g^{XF}(x, y) * Q_a^{XF}(x, y) \quad (19)$$

Tables I to IV, shows a comparison of fused results for different images. Table I, shows a comparison of fused results for "soldier image". Table II, shows a comparison of fused results for "traffic image". Table III, shows a comparison of fused results for "two-person image". And Table IV shows a comparison of fused results for "soldier in trench image". From Tables I to IV, it can be observed that the proposed method resultant fused image got better values with respect to mean, standard deviation, entropy, mean gradient, spatial frequency, QAB/F and visual information fidelity when

compared with sharpen filter, PCA, enhanced contrast and unsharp masking method fused images. Better values are highlighted in bold. The above results indicate clearly that the proposed method resultant fused image has more contrast, abundant information, and rich texture information.

Table V shows average values comparison of fused results for all images. The proposed method resultant fused image got better values with respect to mean, standard deviation, entropy, mean gradient, spatial frequency, QAB/F and visual information fidelity when compared to other methods resultant fused images. Better values are highlighted in bold.

TABLE I. COMPARISON OF FUSED RESULTS FOR "SOLDIER IMAGE"

Method	Metrics						
	Mean	Standard Deviation	Entropy	Mean gradient	Spatial frequency	Visual information fidelity	Q ^{AB/F}
Sharpen filter	124.0698	40.5652	7.2105	16.9310	31.4599	0.2224	0.3419
PCA	43.2393	34.1662	6.5312	18.3565	36.8269	0.1572	0.0801
Enhanced Contrast	76.9080	33.4912	6.7980	19.4072	38.2319	0.2020	0.2900
Unsharp Masking	125.3929	44.2200	7.3553	16.5040	33.8773	0.2337	0.3017
Proposed	126.6302	54.9712	7.6595	21.2282	39.9982	0.2868	0.3915

TABLE II. COMPARISON OF FUSED RESULTS FOR "TRAFFIC IMAGE"

Method	Metrics						
	Mean	Standard Deviation	Entropy	Mean Gradient	Spatial frequency	Visual information fidelity	Q ^{AB/F}
Sharpen filter	59.5920	31.3472	6.4518	10.5824	24.4383	0.3105	0.4206
PCA	43.0666	30.4120	6.3542	11.1434	25.3689	0.1113	0.2086
Enhanced Contrast	45.0016	21.4406	5.8698	8.2988	27.9744	0.2706	0.3230
Unsharp Masking	53.5542	34.4583	6.4867	10.0918	28.7333	0.3061	0.4097
Proposed	60.4746	42.1035	6.6095	11.8961	31.5769	0.3511	0.4754

TABLE III. COMPARISON OF FUSED RESULTS FOR "TWO PERSON IMAGE"

Method	Metrics						
	Mean	Standard Deviation	Entropy	Mean Gradient	Spatial frequency	Visual information fidelity	Q ^{AB/F}
Sharpen filter	134.9493	33.4370	6.7858	15.4056	31.7258	0.2227	0.3574
PCA	66.7068	36.1359	6.6406	16.5647	37.0675	0.1113	0.0339
Enhanced Contrast	94.7685	25.6222	6.2880	17.2837	34.4049	0.1897	0.2881
Unsharp Masking	135.7702	39.9744	6.9771	15.6680	35.8205	0.2233	0.3015
Proposed	134.1056	43.4814	7.2571	18.8569	38.4685	0.2559	0.3823

TABLE IV. COMPARISON OF FUSED RESULTS FOR "SOLDIER IN TRENCH IMAGE"

Method	Metrics						
	Mean	Standard Deviation	Entropy	Mean gradient	Spatial frequency	Visual information fidelity	Q ^{AB/F}
Sharpen filter	147.9086	31.2237	6.7472	9.9293	26.4840	0.2894	0.3488
PCA	69.4152	30.6458	6.0319	10.6731	28.8537	0.1225	0.0419
Enhanced Contrast	101.9884	27.6724	6.2395	13.3696	25.3931	0.2448	0.3279
Unsharp Masking	147.9915	33.4422	6.8864	10.8619	26.5583	0.3192	0.3485
Proposed	148.0603	34.2963	7.0449	13.6658	29.3711	0.3644	0.4516

TABLE VI. AVERAGE VALUES COMPARISON OF FUSED RESULTS FOR ALL IMAGES

Method	Metrics						
	Mean	Standard Deviation	Entropy	Mean gradient	Spatial frequency	Visual information fidelity	$Q^{AB/F}$
Sharpen filter	116.6299	34.1432	6.7988	13.2120	28.5270	0.2612	0.3671
PCA	55.6069	32.8399	6.3894	14.1844	32.0292	0.1256	0.0911
Enhanced Contrast	79.6666	27.0566	6.2988	14.5898	31.5010	0.2260	0.3072
Unsharp Masking	115.6772	38.0237	6.9263	13.2814	31.2473	0.2706	0.3403
Proposed	117.3176	43.7131	7.1427	16.4117	34.8536	0.3145	0.4252

V. CONCLUSIONS AND FUTURE WORK

This paper introduces an efficient DWT based fusion algorithm for improving contrast and edge preservation. Mainly in this algorithm morphology hat transform is used for improving contrast. For improving brightness and edge information of fused image a new fusion rule "Novel mean-weighted fusion rule" is used for fusing approximation coefficients. Single level decomposition of DWT is used in algorithm in order to reduce the complexity problem.

Here proposed method fused image is compared with four existing similar work methods:

The methods are

- 1) Sharpen Filter method.
- 2) PCA method.
- 3) Enhanced Contrast method.
- 4) Unsharp Masking method.

The above four methods are implemented in this paper. Here four sets of source (VI, IR) images are used for verifying the performance of proposed method. The experimental results clearly shows that our proposed method has produced improved results when compared to similar existing techniques both subjectively as well as objectively.

In future the above work can be extended by introducing deep learning concepts for improving the quality of fused image.

REFERENCES

- [1] P. Kaur, P. Sharma, and A. Palmia, "Fuzzy clustering-based image segmentation techniques used to segment magnetic resonance imaging/computed tomography scan brain tissues: Comparative analysis," International Journal of Imaging Systems and Technology, May 2020.
- [2] P. Kaur, and T. Chaira, "A novel fuzzy approach for segmenting medical images," Soft Computing, pp. 1–11, Oct 2020.
- [3] P. Kaur, "Intuitionistic fuzzy sets based credibilistic fuzzy C-means clustering for medical image segmentation," International journal of information technology, vol. 9, no. 4, pp. 345-351, 2017.
- [4] L. D. Griffin, M. Caldwell, J. T. Andrews, and H. Bohler, "'unexpected item in the bagging area': Anomaly detection in x-ray security images," IEEE Transactions on Information Forensics and Security, vol. 14, no. 6, pp. 1539-1553, 2018.
- [5] H. Li, W. Ding, X. Cao, and C. Liu, "Image registration and fusion of visible and infrared integrated camera for medium-altitude unmanned aerial vehicle remote sensing," Remote Sensing, vol. 9, no. 5, pp. 441, 2017.
- [6] A. C. Muller, and S. Narayanan, "Cognitively-engineered multisensor image fusion for military applications," Information Fusion, vol. 10, no. 2, pp. 137–149, 2009.
- [7] N. Paramanandham, and K. Rajendiran, "Multi sensor image fusion for surveillance applications using hybrid image fusion algorithm" Multimedia Tools and Applications, vol. 77, no. 10, pp. 12405–12436, 2018.
- [8] J. Ma, Y. Ma, and C. Li, "Infrared and visible image fusion methods and applications: A survey," Information Fusion, vol. 45, pp. 153–178, 2019.
- [9] X. Li, and S. Y. Qin, "Efficient fusion for infrared and visible images based on compressive sensing principle," IET Image Processing, vol. 5, no. 2, pp. 141–147, 2011.
- [10] H. Li, L. Liu, W. Huang, and C. Yue, "An improved fusion algorithm for infrared and visible images based on multi-scale transform," Infrared Physics & Technology, vol. 74, pp. 28–3, 2016.
- [11] H. Li, B. S. Manjunath, and S. K. Mitra, "Multisensor image fusion using the wavelet transform," Graphical models and image processing, vol. 57, no. 3, pp. 235–245, 1995.
- [12] D. M. Bulanon, T. F. Burks, and V. Alchanatis, "Image fusion of visible and thermal images for fruit detection," Biosystems engineering, vol. 103, no. 1, pp. 12–22, 2009.
- [13] J. Cai, Q. Cheng, M. Peng, and Y. Song, "Fusion of infrared and visible images based on nonsubsampling contourlet transform and sparse K-SVD dictionary learning," Infrared Physics & Technology, vol. 82, pp. 85–95, 2017.
- [14] N. Aishwarya, and C. B. Thangammal, "Visible and infrared image fusion using DTCWT and adaptive combined clustered dictionary," Infrared Physics & Technology, vol. 93, pp. 300–309, 2018.
- [15] N. J. Habeeb, S. H. Omran, and D. A. Radih, "Contrast Enhancement for Visible-Infrared Image Using Image Fusion and Sharpen Filters," in 2018 International Conference on Advanced Science and Engineering (ICOASE). IEEE, pp. 64-69, 2018, October.
- [16] N. J. Habeeb, A. Al-Taei, and M. Fadhil-Ibrahim, "Contrast Enhancement for Multi-Modality Image Fusion in Spatial Domain," Journal of Theoretical and Applied Information Technology, vol. 96, no. 20, pp. 6926–6936, 2018.
- [17] F. Xu, and S. Su, "An enhanced infrared and visible image fusion method based on wavelet transform," in 2013 5th International Conference on Intelligent Human-Machine Systems and Cybernetics. IEEE, vol. 2, pp. 453-456, 2013, August.
- [18] S. Panguluri, and L. Mohan, "Discrete Wavelet Transform Based Image Fusion Using Unsharp Masking," Periodica Polytechnica Electrical Engineering and Computer Science, vol. 64, no. 2, pp. 211-220, 2020.
- [19] L. Zhan, Y. Zhuang, and L. Huang, "Infrared and visible images fusion method based on discrete wavelet transform," Journal of Computers, vol. 28, no. 2, pp. 57–71, 2017.
- [20] X. Han, L. li Zhang, L. yao Du, K. wei Huan, and X. guang Shi, "Fusion of infrared and visible images based on discrete wavelet transform," in Selected Papers of the Photoelectronic Technology Committee Conferences held June–July 2015. International Society for Optics and Photonics, vol. 9795, pp. 97951O, 2015, November.
- [21] P. Shah, S. N. Merchant, U. B. Desai, "Fusion of surveillance images in infrared and visible band using curvelet, wavelet and wavelet packet transform," International Journal of Wavelets, Multiresolution and Information Processing, vol. 8, no. 02, pp. 271-292, 2010.
- [22] L. Zhan, and Y. Zhuang, "Infrared and visible image fusion method based on three stages of discrete wavelet transform," Int. J. Hybrid Inf. Technol, vol. 9, pp. 407-418, 2016.
- [23] Y. Han, Y. Cai, Y. Cao, and X. Xu, "A new image fusion performance metric based on visual information fidelity," Inform. Fus, vol. 14, no. 2, pp. 127–135, 2013.
- [24] Toet, A. "TNO Image fusion dataset," Figshare. data, 2014.

A Comparison of Classification Models to Detect Cyberbullying in the Peruvian Spanish Language on Twitter

Ximena M. Cuzcano¹, Victor H. Ayma²

Systems Engineering Department, University of Lima, Lima 15023, Peru

Abstract—Cyberbullying is a social problem in which bullies' actions are more harmful than in traditional forms of bullying as they have the power to repeatedly humiliate the victim in front of an entire community through social media. Nowadays, multiple works aim at detecting acts of cyberbullying via the analysis of texts in social media publications written in one or more languages; however, few investigations target the cyberbullying detection in the Spanish language. In this work, we aim to compare four traditional supervised machine learning methods performances in detecting cyberbullying via the identification of four cyberbullying-related categories on Twitter posts written in the Peruvian Spanish language. Specifically, we trained and tested the Naive Bayes, Multinomial Logistic Regression, Support Vector Machines, and Random Forest classifiers upon a manually annotated dataset with the help of human participants. The results indicate that the best performing classifier for the cyberbullying detection task was the Support Vector Machine classifier.

Keywords—Cyberbullying detection; machine learning; natural language processing; feature extraction

I. INTRODUCTION

Harassment in social networking sites, better known as cyber bullying, has silently impacted many people in recent years. The most prominent acts of virtual harassment occur through rumors, insults, threats, humiliation, and sexual harassment [1]. A survey conducted in 28 countries across the world revealed that 17% of young people experience cyberbullying before the age of 25 [2]. In Europe, 13-15-year-olds are more likely to be bullied online [3]. On the other hand, the Asia-Pacific countries present around 53% of cyberbullying experiences on social networks, followed by the Middle East and Africa with 39% [2]. Regionally in America, 59% of United States adolescents have experienced some form of cyberbullying [4]. Meanwhile, Latin America experiences the highest amount (76%) of cyberbullying on social media platforms [2]. In Peru, a study revealed that at least 58% of kids between 8-12 years old are prone to online harassment [5].

Despite the efforts to prevent cyberbullying events and mitigate its effects [6, 7], the problem coexists with a generation that is always connected to different social media platforms through the Internet, using a computer or mobile phone, where they interact between groups [8]. Moreover, the use of popular social network platforms, such as Twitter, which offer tweet posting anonymity, encourage harassing behaviors with more frequency and cruelty [9], negatively affecting the

self-esteem of the victims. Hence, automatic cyberbullying detection becomes important.

Currently, typical cyberbullying detection approaches employ text analysis subtasks such as pre-processing, feature extraction, feature selection, and classification to identify online harassing events. Despite such a well-defined pipeline, there exist very few works in the literature aiming at detecting cyberbullying in textual data from social media written in other languages different from the English language [10-13]. Furthermore, there are a limited number of works trying to solve the automatic cyberbullying detection problem in Spanish languages [14-17].

In this work, we propose to compare four machine learning algorithms for detecting cyberbullying on Twitter textual data written in the Peruvian Spanish language. To reach our goal, we have built an annotated text messages dataset from Twitter written in Peruvian Spanish. The dataset was validated with the help of human participants through an online service specially created to verify and annotate the offensive content according to no harassment, direct harassment, hate speech, and sexual harassment [18,19]. Then, we have used Natural Language Processing (NLP) techniques for pre-processing and subsequent feature extraction. Finally, we have trained and assessed the performances of a Naive Bayes (NB), Random Forest (RF), Support Vector Machine (SVM), and Multinomial Logistic Regression (MLR) classifiers.

The rest of the paper is structured as follows. The next section presents the related works aiming to automatically detect cyberbullying in social media. Section III describes our methodology to perform the automatic detection of cyberbullying events on Twitter. Section IV provides details of the experimental procedure adopted to perform classifiers' performance comparison as well as presents and discusses the experimental results. Finally, Section V summarizes our research findings along with suggestions for potential future work.

II. RELATED WORKS

In recent years, automatic cyberbullying detection in social media has attracted the attention of the scientific community. The early works of Dinakar et al. [19] and Yin et al. [20] demonstrate the researchers' interest in detecting cyberbullying events in social media textual data using supervised machine learning tools. In 2016, Di Capua et al. [21] explored ways of combining semantic, syntactic, sentiment, and social features

within the machine learning pipeline to detect cyberbullying on large data streams from YouTube, Twitter, and Formspring. Chatzakou et al. [22] studied text features, user features, and network-based features to find the set of features that best distinguish bullies and aggressors, thus, detecting bullying and aggressive behavior on Twitter. Later, Davison et al., [23] aimed to identify different types of cyberbullying on Twitter data via a multiclass classifier. Park and Fung [10] employed traditional supervised classifiers and neural network-based models to identify sexist and racist posts on Twitter. Chen et al. [11] aimed to find the best suited supervised classifier at detecting harassment in manually labeled social media comments from Twitter and Facebook. Most recently, Lee et al. [12] investigated the efficacy of traditional machine learning and neural networks-based models at detecting abusive language on a Twitter dataset. Hani et al. [13] extended the work of Reynolds et al. [24] at detecting cyberbullying events in text messages from Formspring.me by introducing a set of new classifiers. Such a group of works exposes the scientific efforts made to detect cyberbullying from textual data written in the English language.

However, the cyberbullying issue is common across countries and languages. In this sense, Ptaszynski et al. [25] developed a systematic approach upon machine learning techniques to automatically detect cyberbullying entries in the Japanese language. Van Hee et al. [26] trained an SVM classifier in a Dutch text messages dataset collected from Ask.fm social network to identify seven cyberbullying-related categories, thus, detecting cyberbullying events. Similarly, Del Vigna et al. [27] assessed the SVM and a neural network-based classifier on the task of hate speech recognition upon a manually annotated Italian corpus of Facebook. Özel et al. [28] considered a feature selection stage within the machine learning pipeline, to detect cyberbullying in Turkish text messages using labeled data from Instagram and Twitter. Haidar et al. [29] presented a machine learning-based approach to detect cyberbullying in the Arabic language from Twitter textual data collected across the Middle East Region countries. Furthermore, Mouheb et al. [30] presented a real-time cyberbullying detection system in Twitter streams that classify bullying messages according to the offensive strength. On the other hand, Bai et al. [31] focused on detecting offensive speech in German social media through a binary classification scheme that considers traditional supervised classifiers and neural networks models. Most recently, Nurrahmi and Nurjanah [32] employed text processing and machine learning techniques to detect bullies from the automatic analysis of Twitter posts written in the Indonesian language. Also, Febriana and Budiarto [33] constructed a dataset of Twitter posts collected during the presidential election period in Indonesia to promote the detection of hateful speech and tested its usefulness by submitting it to a basic sentiment analysis model. Win [34] used the SVM algorithm on a set of textual data collected from Facebook in the Myanmar language to discriminate bullying messages.

In a different direction, some authors have addressed the cyberbullying detection task through the implementation of multilingual cyberbullying detection platforms. For instance, Unsvåg and Gambäck [35] conducted experiments on Twitter

text messages written in English, Portuguese, and German languages to measure the effects of including Twitter user's features on the hate speech classification task. The authors observed that tweets with similar content written in different languages hinder the classifiers' performances. Pawar and Raje [36] modeled linguistic patterns upon a hand-labeled bilingual (Hindi and Marathi languages) dataset using Machine Learning and Natural Language Processing techniques to detect cyberbullying in Twitter and Internet forums. Moreover, Steimel et al. [37] experimented with a general cyberbullying detection model across multiple languages (English and German) with data collected from Twitter. Their findings showed that multilingual classifier optimization is not possible even in environments that use comparable datasets.

Despite the efforts to tackle cyberbullying detection in social media, the works aiming at detecting offensive behavior in the Spanish language are yet scarce. For instance, Gómez-Adorno et al. [14] addressed the detection task as a binary classification problem, employing supervised Machine Learning models to detect aggressive tweets, a cyberbullying-related topic, in a Mexican-Spanish language dataset proposed in the 2018 edition of MEX-A3T contest. Similarly, Molina-González et al. [15] proposed an ensemble of supervised classifiers to identify offensive messages on the 2019 edition of MEX-A3T. Gutiérrez-Esparza et al. [16] developed a classification model to detect cyberbullying events (i.e., racism, violence based on sexual orientation, and violence against women) on a Mexican-Spanish textual dataset collected from Facebook. The authors highlight the participation of school professors and psychologists, with experience in evaluation and intervention in cases of bullying, during the annotation process. Finally, in a more recent study, López-Martínez et al. [17] proposed an online-tool capable of detecting cyberbullying from tweets written in Spanish. The authors combined Open Source Intelligence tools with Natural Language Processing techniques to compile information from the victim's Twitter account and analyzed tweets from every follower.

III. METHODOLOGY

Currently, there exist several works focused on detecting cyberbullying in social media. However, the vast majority focuses on text analysis in the English language due to the availability of resources for text analysis, including textual datasets. Such a lack of works aiming for cyberbullying detection in other languages is primarily due to language variants and its grammar complexity. Language variants are specific to a region and vary according to demographic and social factors, such as the appearance of words according to the dialect, idioms, and colloquialisms [16,38]. Language grammar complexity, on the other hand, is attributed to morphology and syntax rules, such as gender and number derivations, verb conjugations, enclitic forms, superlatives, and diminutives suffixes, among others [39]. Therefore, it is paramount to consider both aspects when acquiring textual data intended to model cyberbullying in social media.

In this work, we propose the automatic detection of cyberbullying through the identification of its four categories in an analysis of Spanish tweets collected from Twitter users

resident in Peru. Our method combines Natural Language Processing (NLP) and Machine Learning (ML) techniques to establish a correspondence between the users' tweets and the types of cyberbullying, namely, no harassment, direct harassment, hate speech, and sexual harassment [18,19]. A class label is assigned to a tweet according to the conventional four-stage classification scheme, as shown in Fig.1 the Dataset Collection stage gathers a set of tweets from Peruvian Twitter users; the Pre-Processing stage improves the data quality by removing inconsistencies from the tweets; the Feature Extraction stage obtains a compact representation (x) of a tweet; finally, the Model Selection Stage choose the best-suited classifier to solve the automatic cyberbullying detection problem via a classifiers' performance comparison.

A. Dataset Collection

In this work, we have constructed and made publicly available¹ a dataset consisting of a collection of 10,096 tweets in Spanish from comments and interactions between Peruvian Twitter users with the help of the Streaming API² tool. We collected the dataset during August 2019 and January 2020 from users with an age range between 14 and 60 years old. To ensure class discriminability among tweets, we included common words, jargons relative to Peruvian people, and offensive words during the tweet retrieval process. Furthermore, we have added a geographical delimitation filter after the tweets retrieval process to ensure that the collected tweets belong to Peruvian users only. The filter is part of the Streaming API tool, which is composed of delimiting quadrants with the latitude and longitude coordinates of the different regions of Peru.

The collected tweets were labeled with the help of human participants, who were mostly undergraduate students from the last year of Psychology, Communications, and Law schools from different universities in Peru. The participants evaluated a set of twenty randomly selected tweets via a website specially created to guarantee anonymous sessions not to reveal the participant' identities. In one session, a participant assigns a class label to each tweet from the set of twenty tweets according to the four cyberbullying categories. Moreover, we made cyberbullying categories definitions available throughout the labeling process, and we also ensured that a tweet gets evaluated by at least three different participants to avoid labeling conflicts [40].

Finally, after applying the region based filtering and tweet labeling processes, we obtained a dataset comprised of 10,096 tweets, which class distribution corresponds to 5122, 2127, 1000, and 1847 observations for the no harassment, direct harassment, hate speech, and sexual harassment, respectively.

B. Pre-Processing

In this stage, we performed a set of transformations over the original tweets in the dataset to enhance data quality and facilitate its processing for further analysis. In this sense, we first removed symbols, hash tags, mentions, digits, emoticons, and web links from the dataset. Then, we eliminated repetitive

characters, using regular expressions, to correct spelling errors except for the consecutive characters r, l, c, and e, because they represent single sound letters, e.g., "aburrido", "llamada", "acción", "reenviar". Then, we converted all the tweets to lowercase to standardize the data. After that, we applied a word tokenization technique overall the tweets to translate the Peruvian jargon to words with the closest meaning in the Spanish dictionary, e.g., "yapa" to "extra" or "monse" to "aburrido". Finally, we eliminated the stopwords, such as y, a, pero, que, tu, among others, because they often are irrelevant to the tweets analysis in further steps.

C. Feature Extraction

The feature extraction stage aims at establishing relationships between words in a tweet that might help discriminate the intent of abuse. Therefore, here, we used a set of techniques oriented to the semantic and syntactic analysis among words, whose objectives are to relate groups of words to establish the intention and context in which they were used. To perform the semantic analysis, we used stemming and lemmatization techniques implemented with a neutral Spanish dictionary in the Snowball Stemmer³ and Spacy⁴ tools, respectively. On the other hand, we based the syntactic analysis on the n-gram technique, specifically in its bi-gram and tri-gram variants, using the nltk⁵ library. It is worth mentioning that we applied these techniques before the stopwords removal in the pre-processing stage to maintain the context of the message, e.g., "no eres tonto" is different from "eres tonto". Subsequently, we used the TF-IDF statistical measure to obtain numerical representations of the tweets and the frequency of their words, allowing us to know the degree of importance of a feature. Specifically, we complemented the stemming and lemmatization semantic representation techniques with the TF-IDF technique, and the bi-grams and tri-grams syntactic feature extraction techniques with the TF-IDF method.

D. Model Selection

The model selection stage's purpose is to select the best-suited classifier in detecting the four types of cyberbullying from tweets posted in the Peruvian Spanish language. Hence, we conducted a performance comparison among the most common supervised algorithms for text classification problems. Specifically, we trained a Naive Bayes (NB), Multinomial Logistic Regression (MLR), and Random Forest (RF) classifiers, which are suitable when working with a large number of features [41-43]. We also trained a Support Vector Machine (SVM) classifier, which has proven to behave well in text classification tasks with small class samples [44]. Such models were implemented using the Scikit-Learn⁶ library for Python and were set to work upon their by default parameters.

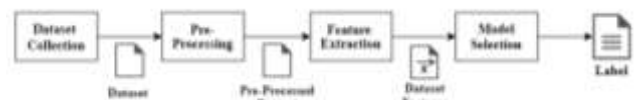


Fig. 1. Overview of our Methodology.

¹ Available in: https://github.com/ximenamar/sp_tweets_cyberbullying

² Available in: <https://developer.twitter.com/en/docs/tweets/filter-realtime/api-reference/post-statuses-filter>

³ Available in: <https://snowballstem.org/download.html>

⁴ Available in: <https://spacy.io/api/lemmatizer>

⁵ Available in: <http://www.nltk.org/api/nltk.html?highlight=ngram>

⁶ Available in: <https://scikit-learn.org/stable/>

IV. RESULT ANALYSIS

In order to assess the performances of the four classification algorithms on the cyberbullying detection task over Twitter textual data written in Peruvian Spanish language, we performed a dataset partitioning into a training and testing sets according to a 70% and 30% proportions, respectively. Moreover, we include data under-sampling scheme in our experiments to examine whether the data balancing improves the classifiers' performances. Specifically, we randomly selected data from the majority classes to compensate for such imbalance. In this way, we evaluate the classifiers' performances based on 10-fold cross-validation procedure over two datasets: an imbalanced dataset, which maintains the original class distribution, and a balanced dataset, which contains approximately four thousand observations equally distributed among the classes. Finally, we assessed the classifiers based on the average of the accuracy, precision, recall, and F1-Score performance metrics. Next, we report and discuss the results obtained from such experimental procedure.

A. Classifiers' Assessment on the Imbalanced Dataset

TABLE I summarizes the classifiers' performance scores on detecting the cyberbullying in an imbalanced dataset. The performance metrics correspond to the average and the standard deviation (in parentheses below the average score) of

the accuracy, precision, recall, and F1-score, respectively, for the semantic (Stemming and Lemmatization) and syntactic (Bi-grams and Tri-grams) data representations schemes combined with the TF-IDF.

In general, the results indicate that the classifiers using the semantic schemes to represent the textual data performed significantly better compared to their syntactic-based counterparts. We attribute this behavior to Spanish language properties, such as the use of proper nouns next to potentially relevant words. While semantic schemes for textual data representation consider the relevance of a word via its occurrence throughout the dataset, the syntactic schemes ponder the appearance of compositions of words, reducing their representatively in the dataset.

Further analysis of the classifiers' performances based on semantic schemes reveals that the stemming-based classifiers performed slightly better than lemmatization-based classifiers; these differences in the results are due to the feature extraction techniques principles. Whereas stemming removes affixes and suffixes to obtain word roots, lemmatization transforms words into their dictionary form, which turns the classification of textual data a challenging task, especially in languages with complex morphology [45].

TABLE I. CLASSIFIERS' PERFORMANCE METRICS ON A IMBALANCED DATASET

Performance Metrics	Models	Feature Extraction Schemes			
		Stemming & TF-IDF	Lemmatization & TF-IDF	Bi-grams & TF-IDF	Tri-grams & TF-IDF
Accuracy	NB	0.674 (+/-0.003)	0.667 (+/-0.006)	0.630 (+/-0.006)	0.622 (+/-0.006)
	RF	0.797 (+/-0.002)	0.792 (+/-0.007)	0.751 (+/-0.005)	0.722 (+/-0.001)
	SVM	0.792 (+/-0.003)	0.793 (+/-0.007)	0.753 (+/-0.007)	0.710 (+/-0.004)
	MLR	0.764 (+/-0.007)	0.750 (+/-0.008)	0.678 (+/-0.007)	0.628 (+/-0.005)
Precision	NB	0.834 (+/-0.139)	0.838 (+/-0.148)	0.626 (+/-0.386)	0.629 (+/-0.392)
	RF	0.814 (+/-0.111)	0.819 (+/-0.097)	0.820 (+/-0.119)	0.850 (+/-0.130)
	SVM	0.801 (+/-0.087)	0.817 (+/-0.100)	0.838 (+/-0.109)	0.871 (+/-0.124)
	MLR	0.822 (+/-0.111)	0.818 (+/-0.117)	0.835 (+/-0.153)	0.855 (+/-0.156)
Recall	NB	0.370 (+/-0.361)	0.348 (+/-0.369)	0.281 (+/-0.415)	0.272 (+/-0.419)
	RF	0.712 (+/-0.155)	0.694 (+/-0.181)	0.571 (+/-0.285)	0.495 (+/-0.322)
	SVM	0.715 (+/-0.169)	0.710 (+/-0.173)	0.581 (+/-0.281)	0.491 (+/-0.330)
	MLR	0.603 (+/-0.222)	0.598 (+/-0.255)	0.382 (+/-0.362)	0.277 (+/-0.415)
F1-Score	NB	0.402 (+/-0.234)	0.368 (+/-0.245)	0.252 (+/-0.304)	0.232 (+/-0.3021)
	RF	0.752 (+/-0.113)	0.739 (+/-0.119)	0.627 (+/-0.191)	0.552 (+/-0.225)
	SVM	0.748 (+/-0.119)	0.750 (+/-0.120)	0.642 (+/-0.186)	0.545 (+/-0.236)
	MLR	0.669 (+/-0.134)	0.664 (+/-0.156)	0.410 (+/-0.263)	0.245 (+/-0.303)

Despite the unbalanced characteristic of the dataset, a classifier-based analysis exhibits the SVM and RF models as the best two performing classifiers, with small differences in scores for both classifiers. Regarding the average scores to all the metrics, the SVM obtained the best scores in most of the evaluated cases, whereas the RF obtained the lowest standard deviation values. We attribute these behaviors to the classifiers' training characteristics. On the one hand, the SVM classifier defines a decision surface based on the most representative samples within the training set, which battles the imbalance. On the other hand, the RF classifier bootstrap characteristic randomly selects a subset of training samples to build a tree within the forest; however, the training subsets are majority different among trees in the forest, thus overcoming the imbalance on the dataset.

B. Classifiers' Assessment on the Balanced Dataset

Similar to TABLE I, Opresents the classifiers' performance scores obtained from their execution on a balanced dataset. The results reinforce the classifiers' performance behavior elicited from the feature-based analysis on an imbalanced dataset.

In a classifier-based analysis, however, the results show that in general, the SVM classifier performed better than the rest of classifiers, closely followed by the RF classifier. In a classifier-based analysis, however, the results show that in general, the SVM classifier performed better than the rest of classifiers, closely followed by the RF classifier. We believe that this is due to the linear kernel used during the SVM training, which makes the SVM performs better in tasks with high-dimensional feature spaces [46], such text classification for cyber bullying detection.

TABLE II. CLASSIFIERS' PERFORMANCE METRICS ON A BALANCED DATASET

Performance Metrics	Models	Feature Extraction Schemes			
		Stemming & TFIDF	Lemmatization & TFIDF	Bi-grams & TFIDF	Tri-grams & TFIDF
Accuracy	NB	0.761 (+/-0.008)	0.763 (+/-0.008)	0.651 (+/-0.006)	0.467 (+/-0.020)
	RF	0.797 (+/-0.009)	0.786 (+/-0.008)	0.621 (+/-0.013)	0.539 (+/-0.009)
	SVM	0.805 (+/-0.007)	0.805 (+/-0.009)	0.689 (+/-0.013)	0.612 (+/-0.015)
	MLR	0.795 (+/-0.010)	0.791 (+/-0.008)	0.672 (+/-0.009)	0.609 (+/-0.015)
Precision	NB	0.760 (+/-0.110)	0.750 (+/-0.020)	0.648 (+/-0.038)	0.625 (+/-0.179)
	RF	0.815 (+/-0.088)	0.808 (+/-0.109)	0.680 (+/-0.179)	0.673 (+/-0.213)
	SVM	0.811 (+/-0.072)	0.802 (+/-0.081)	0.675 (+/-0.116)	0.665 (+/-0.187)
	MLR	0.809 (+/-0.091)	0.795 (+/-0.083)	0.691 (+/-0.137)	0.687 (+/-0.193)
Recall	NB	0.766 (+/-0.117)	0.756 (+/-0.098)	0.649 (+/-0.168)	0.476 (+/-0.316)
	RF	0.799 (+/-0.103)	0.781 (+/-0.125)	0.627 (+/-0.113)	0.528 (+/-0.261)
	SVM	0.806 (+/-0.088)	0.796 (+/-0.074)	0.661 (+/-0.122)	0.570 (+/-0.187)
	MLR	0.794 (+/-0.091)	0.783 (+/-0.107)	0.659 (+/-0.151)	0.564 (+/-0.216)
F1-Score	NB	0.758 (+/-0.058)	0.748 (+/-0.065)	0.634 (+/-0.062)	0.428 (+/-0.136)
	RF	0.798 (+/-0.053)	0.780 (+/-0.061)	0.636 (+/-0.114)	0.522 (+/-0.163)
	SVM	0.805 (+/-0.064)	0.796 (+/-0.070)	0.662 (+/-0.104)	0.575 (+/-0.119)
	MLR	0.795 (+/-0.056)	0.782 (+/-0.065)	0.659 (+/-0.113)	0.568 (+/-0.117)

VI. CONCLUSIONS AND FUTURE WORK

In this work, we have proposed a machine learning classifiers' comparison to detect cyberbullying on Twitter posts written in the Peruvian Spanish language. The classifiers were trained upon a set of text messages collected from Twitter users resident in Peru. Moreover, the dataset content was validated by matter-related participants, i.e., psychologists, sociologists, among others, through a web application. We conducted experiments over imbalanced and balanced versions of the dataset using feature extraction schemes, which involve the combination of semantic and syntactic techniques from the Natural Language Processing field.

The experimental analysis demonstrated that semantic-based schemes for text representation are better than syntactic-based schemes. Moreover, classifiers working upon stemming features showed superior from those using lemmatization features. Furthermore, the Support Vector Machine classifier has shown a consistent performance among the feature extraction schemes despite the different performances showed by the classifiers in both datasets, obtaining superior results in the balanced dataset.

In our experiments, we relied on a pre-processing scheme based on traditional text processing techniques, such as the removal of repetitive characters, emoticons, stop words, and so on, to ease the classifiers' training. However, it would be interesting to assess the classifiers' performances over tweets that include emoticon characters as they are often used to reinforce emotions in text messages.

Finally, in this work, we have translated common jargons in Peruvian Spanish language to their dictionary equivalent, so to be part of the training process. However, it would be interesting to include jargon into a pre-defined Spanish language lexicon and assess the classifiers' performances

REFERENCES

- [1] J. L. Pedreira Massa and H. S. Basile, "El acoso moral entre pares (bullying)," *Construção psicopedagógica*, 2011, vol. 19, no. 19, pp. 8–33.
- [2] M. Newall, "Global views of cyberbullying," 2018. [Online]. Available: <https://www.ipsos.com/en/global-views-cyberbullying>.
- [3] V. Dalla Pozza, A. Di Pietro, S. Morel, and E. Psaila, "Cyberbullying among young people," 2016. [Online]. Available: [https://www.europarl.europa.eu/RegData/etudes/STUD/2016/571367/IPOL_STU\(2016\)571367_EN.pdf](https://www.europarl.europa.eu/RegData/etudes/STUD/2016/571367/IPOL_STU(2016)571367_EN.pdf).
- [4] M. Anderson, "A majority of teens have experienced some form of cyberbullying," 2018. [Online]. Available: <https://www.pewresearch.org/internet/2018/09/27/a-majority-of-teens-have-experienced-some-form-of-cyberbullying/>.
- [5] DQ Insitute, "The 2018 DQ impact report," 2018. [Online]. Available: https://www.dqinstitute.org/2018DQ_Impact_Report/#Cyber-Pandemic.
- [6] J. Vitak, K. Chadha, L. Steiner, and Z. Ashktorab, "Identifying women's experiences with and strategies for mitigating negative effects of online harassment," in *Proceedings of the 2017 ACM Conference on Computer Supported Cooperative Work and Social Computing (CSCW '17)*, 2017, pp. 1231–1245.
- [7] M. Fan, L. Yu, and L. Bowler, "Feelbook: A social media app for teens designed to foster positive online behavior and prevent cyberbullying," in *Proceedings of the 2016 CHI Conference Extended Abstracts on Human Factors in Computing Systems (CHI EA '16)*, 2016, pp. 1187–1192.
- [8] B. Belsey, "Cyberbullying: An emerging threat to the "always on" generation," 2006. [Online]. Available: <http://www.billbelsey.com/?p=1827>.
- [9] J. Suler, "The online disinhibition effect," *Cyberpsychology & behavior*, 2004, vol. 7, no. 3, pp. 321–326.
- [10] J. H. Park and P. Fung, "One-step and two-step classification for abusive language detection on twitter," in *Proceedings of the First Workshop on Abusive Language Online*, 2017, pp. 41–45.
- [11] J. Chen, S. Yan, and K.-C. Wong, "Aggressivity detection on social network comments," in *Proceedings of the 2017 International Conference on Intelligent Systems, Metaheuristics & Swarm Intelligence (ISMSI '17)*, 2017, pp. 103–107.
- [12] Y. Lee, S. Yoon, and K. Jung, "Comparative studies of detecting abusive language on twitter," in *Proceedings of the 2nd Workshop on Abusive Language Online (ALW2)*, 2018, pp. 101–106.
- [13] J. Hani, M. Nashaat, M. Ahmed, Z. Emad, E. Amer, and A. Mohammed, "Social media cyberbullying detection using machine learning," *International Journal of Advanced Computer Science and Applications*, 2019, pp. 703–707.
- [14] H. Gómez-Adorno, G. B. Enguix, G. E. Sierra, O. Sánchez, and D. Quezada, "A machine learning approach for detecting aggressive tweets in spanish," in *Proceedings of the Third Workshop on Evaluation of Human Language Technologies for Iberian Languages (IberEval 2018)*, 2018, pp. 102–107.
- [15] M. D. Molina-González, F. M. Plaza-del-Arco, M. T. Martín-Valdivia, and L. A. Ureña-López, "Ensemble learning to detect aggressiveness in mexican spanish tweets," in *Proceedings of the First Workshop for Iberian Languages Evaluation Forum (IberLEF 2019)*, 2019, pp. 495–501.
- [16] G. O. Gutiérrez-Esparza, M. Vallejo-Allende, and J. Hernández-Torruco, "Classification of cyber-aggression cases applying machine learning," *Applied Science*, 2019, vol. 9, no. 9, Article ID 1828.
- [17] A. López-Martínez, J. A. García-Díaz, R. Valencia-García, and A. Ruiz-Martínez, "CyberDect. A novel approach for cyberbullying detection on twitter," *International Conference on Technologies and Innovation*, Spring, Cham, 2019, pp. 109–121.
- [18] J. Golbeck, Z. Ashktorab R. O. Banjo, A. Berlinger, S. Bhagwan, C. Buntain, P. Cheakalos, A. A. Geller, Q. Gergory, R. K. Gnanasekaran, et al., "A large labeled corpus for online harassment research," in *Proceedings of the 2017 ACM on Web Science Conference (WebSci)*, 2017, pp. 229–233.
- [19] K. Dinakar, R. Reichart, and H. Lieberman, "Modeling the detection of textual cyberbullying," *Proc. Fifth International AAAI Conference on Weblogs and Social Media (SWM '11)*, 2011, pp. 11–17.
- [20] D. Yin, Z. Xue, L. Hong, and B. Davison, "Detection of harassment on Web 2.0," in *Proceedings of the Content Analysis in the WEB 2.0*, 2009, vol. 2, pp. 1–7.
- [21] M. Di Capua, E. Di Nardo, and A. Petrosino, "Unsupervised cyber bullying detection in social networks," 2016 23rd International Conference on Pattern Recognition (ICPR), 2016, pp. 432–437.
- [22] D. Chatzakou, N. Kourtellis, J. Blackburn, E. D. Cristofaro, G. Stringhini, and A. Vakali, "Mean birds: Detecting aggressors and bullies on twitter," in *Proceedings of the 2017 ACM on Web Science Conference (WebSci '17)*, 2017, pp. 13–22.
- [23] T. Davidson, D. Warmesley, M. Macy, and I. Weber, "Automated hate speech detection and the problem of offensive language," in *Proceedings of the Eleventh International AAAI Conference on Web and Social Media (ICWSM 2017)*, 2017, pp. 1–4.
- [24] K. Reynolds, A. Kontostathis and L. Edwards, "Using machine learning to detect cyberbullying," 2011 10th International Conference on Machine Learning and Applications and Workshops, 2011, pp. 241–244.
- [25] M. Ptaszynski, P. Dybala, T. Matsuba, F. Masui, R. Rzepka, and K. Araki, "Machine learning and affect analysis against cyber-bullying," in *Proceedings of the Linguistic And Cognitive Approaches To Dialog Agents*, 2010, pp. 7–16.
- [26] C. Van Hee, B. Verhoeven, E. Lefever, G. D. Pauw, W. Daelemans, and V. Hoste, "Detection and fine-grained classification of cyberbullying events," *International Conference Recent Advances in Natural Language Processing (RANLP)*, 2015, pp. 672–680.

- [27] F. Del Vigna, A. Cimino, F. Dell'Orletta, M. Petrocchi, and M. Tesconi, "Hate me hate me not: Hate speech detection on facebook," in Proceedings of the First Italian Conference on Cybersecurity (ITASEC17), 2017, pp. 86–95.
- [28] S. A. Özel, E. Saraç, S. Akdemir and H. Aksu, "Detection of cyberbullying on social media messages in Turkish," 2017 International Conference on Computer Science and Engineering (UBMK), 2017, pp. 366–370.
- [29] B. Haidar, M. Chamoun, and A. Serhrouchni, "Multilingual cyberbullying detection system: Detecting cyberbullying in Arabic content," 2017 1st Cyber Security in Networking Conference (CSNet), 2017, pp. 1–8.
- [30] D. Mouheb, M. H. Abushamleh, M. H. Abushamleh, Z. A. Aghbari and I. Kamel, "Real-time detection of cyberbullying in Arabic twitter streams," 2019 10th IFIP International Conference on New Technologies, Mobility and Security (NTMS), 2019, pp. 1–5.
- [31] X. Bai, F. Merenda, C. Zaghi, T. Caselli, and M. Nissim, "Rug at germeval: Detecting offensive speech in German social media," in Proceedings of the GermEval 2018 Workshop, 2018, pp. 63–70.
- [32] H. Nurrahmi and D. Nurjanah, "Indonesian twitter cyberbullying detection using text classification and user credibility," 2018 International Conference on Information and Communications Technology (ICOIACT), 2018, pp. 543–548.
- [33] T. Febriana and A. Budiarto, "Twitter dataset for hate speech and cyberbullying detection in indonesian language," 2019 International Conference on Information Management and Technology (ICIMTech), 2019, pp. 379–382.
- [34] Y. Win, "Classification using support vector machine to detect cyberbullying in social media for Myanmar language," 2019 IEEE International Conference on Consumer Electronics - Asia (ICCE-Asia), 2019, pp. 122–125.
- [35] F. Unsvåg and E. Gambäck, "The effects of user features on twitter hate speech detection," in Proceedings of the 2nd Workshop on Abusive Language Online (ALW2), 2018, pp. 75–85.
- [36] R. Pawar and R. R. Raje, "Multilingual cyberbullying detection system," 2019 IEEE International Conference on Electro Information Technology (EIT), 2019, pp. 040–044.
- [37] K. Steimel, D. Dakota, Y. Chen, and S. Kübler, "Investigating multilingual abusive language detection: A cautionary tale," in Proceedings of the International Conference on Recent Advances in Natural Language Processing (RANLP 2019), 2019, pp. 1151–1160.
- [38] S. Dhuliawala, D. Kanojia, and P. Bhattacharyya, "SlangNet: A wordNet like resource for english slang," Language Resources and Evaluation Conference (LREC 2016), 2016, pp. 4329–4332.
- [39] S. Rodríguez and J. Carretero, "A formal approach to spanish morphology: the coes tools," Procesamiento del Lenguaje Natural, 1996, vol. 19, pp. 118–127.
- [40] S. R. Bowman, G. Angeli, C. Potts, and C. D. Manning, "A large annotated corpus for learning natural language inference," in Proceedings of the 2015 Conference on Empirical Methods in Natural Language Processing, 2015, pp. 632–642.
- [41] L. Breiman, "Random forests," Machine Learning, 2001, vol. 45, pp. 5–32.
- [42] J. Abellán and J. G. Castellano, "Improving the naive bayes classifier via a quick variable selection method using maximum of entropy," Entropy, 2017, vol. 19, no. 6, p. 247.
- [43] D. W. Hosmer and S. Lemeshow, "Applied logistic regression," New York: Wiley, 2000.
- [44] A. C. Gay Thomé, "SVM classifiers – concepts and applications to character recognition," in Advances in Character Recognition, Xiaoqing Ding, IntechOpen, 2012.
- [45] V. Balakrishnan and E. Lloyd-Yemoh, "Stemming and lemmatization: A comparison of retrieval performances," in Proceedings of SCEI Seoul Conferences, 2014, pp. 174–179.
- [46] S. M. Erfani, S. Rajasegarar, S. Karunasekera, and C. Leckie, "High-dimensional and large-scale anomaly detection using a linear one-class SVM with deep learning," Pattern Recognition, 2016, vol. 58, pp. 121–134.

An Investigative Study of Genetic Algorithms to Solve the DNA Assembly Optimization Problem

Hachemi Bennaceur¹, Meznah Almutairy², Nora Alqhtani³
Faculty of Computer and Information Sciences, Computer Science Department
Al Imam Mohammad Ibn Saud Islamic University (IMSIU)
Riyadh, Saudi Arabia

Abstract—This paper aims to highlight the motivations for investigating genetic algorithms to solve the DNA Fragments Assembly problem (DNA_FA). DNA_FA is an optimization problem that attempts to reconstruct the original DNA sequence by finding the shortest DNA sequence from a given set of fragments. We showed that the DNA_FA optimization problem is a special case of the two well-known optimization problems: The Traveling Salesman Problem (TSP) and the Quadratic Assignment Problem (QAP). TSP and QAP are important problems in the field of combinatorial optimization and for which there exists an abundant literature. Genetic Algorithms (GA) applied to these problems have led to very satisfactory results in practice. In the perspective of designing efficient genetic algorithms to solve DNA_FA we showed the existence of a polynomial-time reduction of DNA_FA into TSP and QAP enabling us to point out some technical similarities in terms of solutions and search space complexity. We then conceptually designed a genetic algorithm platform for solving the DNA_FA problem inspired from the existing efficient genetic algorithms in the literature solving TSP and QAP problems. This platform offers several ingredients enabling us to create several variants of GA solvers for the DNA assembly optimization problems.

Keywords—Genetic Algorithms; Traveling Salesman Problem; Quadratic Assignment Problem; DNA fragments assembly problem

I. INTRODUCTION

The DNA fragment assembly problem attempts to reconstruct the original DNA sequence by finding the shortest DNA sequence from a large number of fragments [1]. DNA_FA is a hard optimization problem due to its high complexity, the larger the sequence, the larger the fragments set input and consequently the higher and harder computation [2]. Metaheuristics have been shown to be the best alternative techniques to solve this problem. Especially, the DNA_FA problem was tackled with some metaheuristic algorithms such as Genetic Algorithms [3], Tabu Search [4], Simulated Annealing [5], Particle Swarm Optimization [6], and Ant Colony Optimization [7].

The famous Traveling Salesman Problem (TSP) and the Quadratic Assignment Problem (QAP) are two important problems in the field of combinatorial optimization and for which there exists an abundant literature. Genetic Algorithms applied to these problems have led to very satisfactory results in practice [8],[9],[10].

Our main contributions are: first, we presented a formal proof of the existence of a polynomial-time reduction of

DNA_FA into TSP and QAP enabling us to point out some technical similarities in terms of solutions and search space complexity. Particularly, we have theoretically demonstrated that all these three optimization problems have a similar topological structure and they need to explore a search space of solutions with a same complexity to find an optimal solution. Notice that although many works mentioned the relationship between DNA_FA with the TSP problem, but to the best of our knowledge none provided a formal demonstration enabling to take advantages from the existent solvers of TSP and QAP problems to treat efficiently the DNA_FA problem. For this purpose, we revisited the relationship and the similarities between DNA_FA and TSP and established a new relationship and similarities between DNA_FA and QAP. Second, as the TSP and QAP problems were solved efficiently using GA algorithms, we believe it is worth to exploit these similarities in order to deeply investigate the use of GA algorithms for solving the DNA_FA problem. Based on these facts, we proposed a genetic algorithm platform including main GA concepts and tools (selection, crossover, mutation, ...) enabling us to design several variants of GA solvers for the DNA_FA. The platform regroups the best GA concepts inspired from the existing efficient genetic algorithms in the literature solving TSP and QAP problems such that when they are used synergistically, we lead to efficient GA solvers. Few research works based on GA have been developed to solve the DNA_FA problem; the more recent GA algorithm used a basic schema with traditional simple GA concepts [11]. We think there is ample room for improvements by integrating the more recent advanced GA concepts used for solving TSP and QAP problems.

The remaining sections of the paper are structured as follows. The related work is discussed in Section II. Section III presents the DNA_FA, TSP, and QAP problems formally and provides formal proof of the equivalence between these three problems. In Section IV the existing GA solutions to solve the DNA_FA problem, TSP, and QAP are presented and discuss these solutions in Section V. Finally, we proposed, in section VI a GA platform for designing efficient GA solvers for the DNA_FA problem.

II. RELATED WORK

Through research in the previous literature, we found some studies that indicated a relationship between TSP and DNA_FA problem [12],[13],[14]. In 1995 Parsons et al. [12]

noticed the similarity between DNA_FA and TSP but they argued that the mapping is not easy for some issues; some of these issues are (i) the DNA_FA problem is a maximization problem where the TSP is a minimization problem, and (ii) the TSP seeks to find a Hamiltonian circuit where the DNA_FA seeks to find a Hamiltonian path. In 2013 Mallén and Fernández [15] tried to overcome these issues by adding a dummy city with zero distance to all the other cities to form an open Hamiltonian path instead of a Hamiltonian circuit. Also, they multiplied the objective function by (-1) to convert the maximization into minimization.

There are many studies mentioned the relationship between TSP and QAP [16],[17],[18],[19]. However, no study has formally shown the relationship between the DNA_FA problem with the TSP and QAP problems. Moreover, no study has explored the numerous similarities between the DNA_FA problem with the TSP and QAP problems to take advantage of the many efficient techniques developed for these two problems in order to solve the DNA_FA problem.

Few genetic algorithms have been developed to solve the DNA_FA problem (see section IV for more details), compared to what have been developed for the TSP and QAP problems [9], [10], [20],[21], [22]. Moreover, these GA algorithms did not exploit the recent progress performed in the context of TSP and QAP problems. For instance, if we consider the crossover operator which is the main concept of GA algorithms, recently many modern crossover types (e.g. the Sequential Constructive Crossover) have been designed and successively tested for the TSP and QAP problems that have yielded to better performances. Due to the numerous similarities with the TSP and QAP problems shown in this paper, we believe and expect that well-designed GA solvers inspired from existing GA for these two problems would produce similar performance for DNA_FA problem. Unfortunately, no work investigated deeply these similarities in order to exploit the more advanced genetic algorithms designed for TSP and QAP for solving the DNA_FA problem. For this purpose, it is worth to investigate how these advanced operators originally designed for the TSP and QAP behave when they are applied to the DNA_FA problem.

III. DNA_FA VERSUS TSP AND QAP

In this section we describe the optimization problems DNA_FA, TSP and QAP, then we provide formal proofs showing the existence of polynomial-time reductions of the DNA_FA problem into the TSP and QAP problems respectively.

A. DNA_FA Problem

Given a set of DNA fragments drawn from a finite alphabet $\{A, T, C, G\}$, Adenine (A), Thymine (T), Guanine (G), and Cytosine (C). The goal of the DNA_FA problem is to find the shortest superstring sequence covering all fragments that is a superset of all input fragments. Intuitively, the goal is to find an optimal permutation of the fragments maximizing the number of overlaps between the fragments.

Formally, given a set of n fragments $F = \{f_1, f_2, \dots, f_n\}$, drawn from a finite alphabet $\Sigma = \{A, C, G, T\}$, the problem consists in finding an optimal permutation of the fragments

$F' = \langle f'_1, f'_2, \dots, f'_n \rangle$ that maximizes the number of overlaps between every pair of two consecutive fragments and thus minimizes the length of F' .

$$\text{MAX}_{\langle f'_1, f'_2, \dots, f'_n \rangle} \left(\sum \text{overlapping}(f'_i, f'_{i+1}) \right)$$

$$\text{where } 1 \leq i \leq n - 1 \quad (1)$$

B. TSP Problem

Given a set of n cities along with the distance information between every pair of those cities, the goal of the Travelling Salesman Problem is to find the shortest tour that visits all cities once and returns to the starting city.

The TSP problem can be modeled as follows. Let $\langle x_1, x_2, \dots, x_n \rangle$ refers to a tour, the goal is to find the lowest cost tour such that.

$$\text{MIN}_{\langle x_1, x_2, \dots, x_n \rangle} \sum_{i=1}^{n-1} d_{(i)(i+1)} + d_{(n)(1)} \quad (2)$$

where $d_{(i)(i+1)}$ is the distance between city x_i and city x_{i+1} , and $d_{(n)(1)}$ is the distance between city x_n and the starting city x_1 .

C. QAP Problem

Given two sets of equal size “facilities” and “locations”, for each pair of locations, a distance is specified and for each pair of facilities a weight or a flow is specified. The problem is to assign all facilities to different locations with the goal is to minimize the total distances weighted by the corresponding flows.

Formally, given two sets P (“facilities”) and L (“locations”), with a weight function $w: P \times P \rightarrow \mathbb{R}$ and a distance function $d: L \times L \rightarrow \mathbb{R}$. The goal is to find the assignment $f: P \rightarrow L$ such that the cost function (the distance multiplied by the weight) is minimized:

$$\text{MIN}_f \sum_{a,b \in P} w(a,b) \times d(f(a), f(b)) \quad (3)$$

$$\{\displaystyle \sum_{a,b \in P} w(a,b) \cdot d(f(a), f(b))\}$$

D. Polynomial Reduction of DNA_FA into TSP and QAP

Notice that although many works mentioned the relationship between DNA_FA with the TSP problem [12], [13], [14], but to the best of our knowledge none provided a formal demonstration enabling to take advantages from the existent solvers of TSP and QAP problems to treat efficiently the DNA_FA problem. For this purpose, we revisited the relationship and the similarities between DNA_FA and TSP presented in [15] and established a new relationship and similarities between DNA_FA and QAP. Namely, we showed that DNA_FA is a special case of TSP and QAP problems.

The DNA_FA problem can be represented as a directed complete weighted graph $G = (V, E)$ where V represents the set of fragments and E is the set of edges. The weight of an arc of G expresses the overlap cost between the two corresponding fragments and it is set to zero if there is no overlap. An optimal solution of DNA_FA corresponds to a Hamiltonian path in G . DNA_FA can be easily transformed into a TSP problem. Let's consider $G' = (V \cup \{s\}, E \cup E')$ the complete graph G of DNA_FA augmented by the virtual

vertex s connected to every vertex of V . For each vertex v of V , two arcs $(s,v) \in E'$ and $(v,s) \in E'$ with zero weights are added to G . We can easily see that the problem of finding a Hamiltonian path in G amounts to find an optimal solution to the TSP represented by the graph G' . Hence, DNA_FA is a special case of the TSP problem.

Regarding the QAP, we established a new relationship between the DNA_FA problem and the QAP, we showed that DNA_FA is a special case of QAP problem as follows. Let us consider the set of fragments of the problem as a set of n facilities and the possible positions of each fragment in the solution sequence as a set of n locations. Taking into account the distance between a pair of locations as the overlap cost between their corresponding fragments, and set the flow equal to 1 for every pair of facilities, we can see that finding the optimal permutation assigning to each location exactly one facility so as to minimize the total cost (the distances multiplied by the weight) amounts to find an optimal solution to the associate DNA_FA problem. Thus, clearly DNA_FA is a special case of the QAP problem.

As the famous TSP and QAP problems are NP-Hard [23], it follows automatically from this demonstration DNA_FA is also NP-hard.

In the perspective of designing an effective and robust genetic algorithm platform for solving DNA_FA, Table I. points out some technical similarities in order to get out the most profit from the efficient genetic algorithms designed to solve TSP and QAP problems.

From Table I, we can see that the three optimization problems need to explore a same size search space to find an optimal solution.

TABLE I. TECHNICAL SIMILARITIES BETWEEN DNA-FA, TSP, AND QAP

Characteristics	DNA_FA	TSP	QAP
Variables	Fragments	Cities	Facilities, locations
Constraints	Every fragment must be present in the final sequence. No duplicate fragment is allowed.	Every city should be present in the tour. No duplicate city is allowed.	Every facility should be assigned to one location. No duplicate facility or location is allowed.
Objective Function	Find an optimal permutation of the fragments in which the length of the sequence is minimized.	Find an optimal permutation of cities (an optimal tour) in which the total cost of the tour is minimized.	Find an optimal permutation of facilities (assignment of facilities to locations) in which the cost of the assignment is minimized.
Feasible solution	A sequence that contains all the fragments.	A tour that visits all cities once.	An assignment of each facility to one location
Complexity	NP-hard	NP-hard	NP-hard

IV. GENETIC ALGORITHM (GA) SOLUTIONS

Basic genetic algorithm schema contains various concepts such as population encoding, population initialization, fitness function, selection, crossover, mutation and replacement operators, and stopping conditions.

Each concept has its importance in the algorithm; for instance, encoding the population represents a feasible solution of the problem. Basically, the type of the problem determines the appropriate encoding type (e.g., in the TSP a tour (individual) is usually encoded as a sequence of integers, where each integer represents a city). The initial population may influence the overall behavior of finding solutions. Getting a good initial population can strongly influence the performance of the search. The fitness function is used to evaluate the quality of each individual within the population. The fitness function has to be designed to accurately assess the individual's quality in order to select the best and the fittest individuals for crossover and mutation operations. Selection is the operation where the parents (individuals) are selected from the population according to the fitness function for crossover and mutation operations. The purpose of selection is to ensure that the fitter individuals in the population will be maintained so that the offspring produced has a higher fitness. The crossover operator plays the most crucial role in GA as it aims to explore the huge search space of the problem. Traditionally, it is a binary operation taking two individuals as parents to create new offspring. Recently, the crossover operator has been generalized to take more than two parents to generate new offspring. This type of crossover is called Multi-Parents Crossover (MPX) [24]. The mutation operator aims to ensure diversity in the population by allowing a certain change in the individual, which helps to escape local optima. The replacement allows individuals from the current generation to be replaced by a better newly generated offspring. The stopping condition is a vital operator; it is necessary to identify a tradeoff between the algorithm stopping criteria and the algorithm performance.

The fundamental concept behind GAs is inspired by natural evolution, where the GA operators evolve generations of potential solutions of a given problem. More in detail, the GA initiates a population of possible solutions (i.e., individuals) after defining the appropriate solution encoding. Then, calculates the fitness for each individual within the population using the fitness function. The selection operator then selects individuals (parents) based on their fitness to produce a new offspring by carrying out the crossover and mutation operations. The new offspring will inherit the parent's characteristics and will be added to the next generation via a replacement strategy. This process keeps on iterating until the stopping condition is reached, and hence the solution with the best fitness value is returned. The GA procedure is illustrated in Fig. 1.

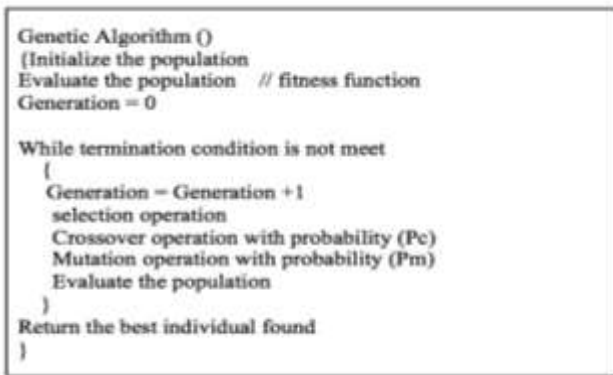


Fig. 1. GA Procedure.

A. GA solutions for the DNA_FA problem

Here we review the previous works using genetic algorithms for the DNA_FA. As aforementioned, the DNA_FA problem reconstructs the original DNA from a large number of fragments. To illustrate the problem, consider the following example:

An input of five fragments could look like:

TCGG, GCAG, ATCG, CAGC, GATC.

Two possible final sequences involving all input fragments are:

CAGCAGATCGG (length = 11)

GATCGGCAGC (length = 10)

The latter sequence is better since its length is 10, compared to 11 for the former sequence.

In order to deal with this problem, let us introduce the following terms:

Prefix: A substring comprising the first n characters of fragment f .

Suffix: A substring comprising the last n characters of fragment f .

Overlap (w): Common sequence between the suffix of one fragment and the prefix of another fragment.

Contig: overlapped fragments without gaps.

By applying the overlapping measure to the above example, we found that w (GCAG, CAGC) = 3 whereas w (CAGC, GCAG) = 2. This means that these two fragments can be represented in a sequence of 5 letters (4+4-3): GCAGC, which is better the other sequence of length 6: CAGCAG.

The overlaps between fragments can be represented as a directed weighted complete graph. The set V of nodes in this graph corresponds to the set of fragments. A directed edge from fragment a to a different fragment b with weight $t \geq 0$ exists if the suffix of a with t characters is a prefix of b .

Table II shows the overlap (w) matrix for the aforementioned example, the symbol (-) means there is no edge.

TABLE II. THE OVERLAP MATRIX

w	TCGG	GCAG	ATCG	CAGC	GATC
TCGG	-	1	0	0	1
GCAG	0	-	0	3	1
ATCG	3	1	-	0	1
CAGC	0	2	0	-	0
GATC	2	0	3	1	-

Once the overlap weighted directed complete graph is built as a pre-processing step, the DNA fragments assembly problem can be transformed into the problem of finding a Hamiltonian path that goes through every vertex (i.e. a complete order of the fragments). The quality of each path (i.e. sequence of fragments) is measured by the sum of the weights of its edges, which represents the total overlaps between fragments.

There were relatively few historical studies in the area of DNA fragments assembly using genetic algorithms. Some preliminary works were carried out in the early 1990s [3], [12]. In later works GA algorithms were enhanced by combining them with other searching metaheuristics in order to achieve better results. For instance [25] proposed a method named SAX, it combines GA algorithm enhanced with the simulated annealing metaheuristic to solve the DNA-FA. SAX implemented a greedy approach to generate the initial population, the order crossover (OX) operator, and the inversion mutation operator. SAX enhanced the GA approach with the simulated annealing metaheuristic to escape local optima. The proposed method was able to achieve relatively better overlapping scores on different datasets that reach the size of 400k bp (characters). However, the drawback of this GA solver is its high computational time. The authors in [26] examined different types of the population initialization including random initialization, 2-opt heuristics, and greedy methods. The crossover operators implemented in this study were the Cycle crossover (CX), Edge Recombination (ERX), Order crossover OX, and Partial Mapped crossover (PMX). According to their results, when using the 2-opt to initialize the population, the quality of the solution is improved without a significant increase in the overall execution time, regardless of the type of the applied crossover.

Another work using GA approach is presented in [27], it combines different GA variations in different ways: (1) Recentering-Restarting GA (RRGA) in order to avoid getting stuck on local optima, (2) Island Model GA (RRGA+IM) which divides the population into multiple islands. And finally, (3) GA which uses Ring Species (RRGA+RS), where the population is treated as a ring. The first and last individuals of the population are considered adjacent. They used two methods to initialize the population; the identity permutation and the 2-opt heuristic method proposed in [26]. The PMX crossover and swap mutation operators are implemented for all GA variations. These methods proved to be better since it records more overlapping score for all the tested datasets than the results obtained in [25]. However, among these three methods (RRGA, RRGA+IM, RRGA+RS) there is not a dominatrix; they all have the same convergence

performance. For that reason, some restarting strategies were implemented in the next work [28] in order to distinguish the performance of the above three GA variations. These strategies include dynamic restart where the search restarts after convergence, forcing initial restart where the search is forced to restart again in order to escape local optima. The experimental results showed that the RRGGA has better convergence performance than RRGGA+IM and RRGGA+RS. In [29] the authors used RRGGA along with the Power Aware Local Search (PALS) as a genetic operator and the 2-opt heuristic for initializing the population. Three types of experiments were performed with the objective function is minimizing the number of contigs and maximizing the overlap score. In the first experiment, PALS was used as a genetic operator, in the second experiment PALS is used after executing the GA. Whereas, in the last experiment, PALS was used as a genetic operator and utilized after GA execution as well. The results show that the first experiment using PALS as a genetic operator performs better than the other two experiments.

Despite the importance of the DNA fragments assembly problem, most of the previously mentioned studies ignore reporting the accuracy of their works (the degree to which the assembler covers the reference genome). However, there are some studies that assessed the accuracy as in [11]. In contrast with previous works that focused on maximizing the overlapping score as a fitness function, in [11] the fitness function is defined to minimize the total length of a scaffold (the sum of the length of the contigs), and the number of contigs on the scaffold. The basic one-point order crossover has been implemented in this study. They assessed the accuracy and measured how the assembler actually covers the reference genome. In the next work [30] some improvements have been applied; the first one is to merge any two contigs that have overlapped between them longer than the length of the fragment. The other improvement is a post-processing step to merge each left chaff contigs into the appropriate location on long contigs (chaff means a contig of length shorter than 3–4 times the fragment length). The experimental results showed that the algorithm found a single correct contig identical to the reference in over 95% of 200 runs for most instances and decreases to 87.5% for the largest instances. However, as they mentioned, the main drawback of their method is the higher computational time.

Table III shows genetic algorithm performances in terms of the overlapping score for the DNA_FA problem. The first column represents the datasets used mainly in the literature with its mean fragment's length and sequence length (within brackets), obtained from the National Center for Biotechnology Information NCBI¹. The first 10 datasets were fragmented (i.e., cutting the original sequence into fragments) using a tool called GenFrag and denoted by the dataset name-the coverage. These datasets are obtained from four

sequences, ranging in length from 3 to 77 thousand bp. The "Acin" datasets fragmented using a different tool called DNAGen; the "Acin" sequences are longer (except "Acin1", which is the smallest one in this table) and more difficult since they contain longer and more fragments). The "Acin" datasets are obtained from six sequences, ranging in length from 2 to 426 thousand bp. The rest columns are the references with the used method name (reference, method name), and for each method the sum of the generated overlapping score for each dataset is recorded. The symbol (-) means that this reference has not applied this method to the corresponding dataset. We considered in this table only references that report the overlapping score for their work.

From Table III, SAX presents competitive results for the small datasets. RRGGA_RS was more performant for the long datasets ("Acin") comparing with the other methods, namely, it obtained more overlapping scores for three out of six "Acin" datasets. RRGGA_IM gave satisfying results for eight out of sixteen reported datasets. GA2o is outperformed by the two other methods on the tested datasets.

In view of all that has been mentioned so far, such studies suffer from a lack of efficiently dealing with the accuracy, the time and space complexities. While DNA fragments assembly is a growing field, although GA gave very satisfactory results for similar hard optimization problems TSP and QAP, research works based on genetic algorithms for DNA assembly remains relatively poor. From reviewing and studying the previous related works of the GA, we can see that there are different ways to initialize and to represent the population. Also, it is obvious that the type of crossover affects the produced results in terms of solution quality and computational time. However, combining the GA with other good metaheuristics algorithms could improve the solution quality.

B. GA Solutions for TSP and QAP

This section reviews GA algorithms designed to solve the TSP and QAP problems, and their associated experimental results. This review is not exhaustive, we considered only more recent GA algorithms designed with advanced concepts.

GA design mainly begins with encoding the population. Different types of encoding were used for the optimization problems TSP and QAP. Most works of the wide literatures used the identity permutation such as for TSP in [10] [31] and QAP in [9]. Another advanced types of population encoding were used for TSP such as value encoding [20], and real number encoding [21].

The common strategies of generating of initial populations are the random generation as investigated for TSP in [21] and the greedy procedure as in [21]. Recently more advanced strategies have been designed; the Multi-Agent Reinforcement Learning (MARL) was proposed in [31] for solving TSP problems. The sequential sampling method has been implemented in [9] for solving QAP problem in order to improve the GA algorithm and to speed up the convergence.

¹ The National Center for Biotechnology Information (NCBI) is part of the United States National Library of Medicine (NLM), a branch of the National Institutes of Health (NIH). The NCBI houses a series of databases relevant to biotechnology and biomedicine and is an important resource for bioinformatics tools and services. Major databases include GenBank for DNA sequences. <https://www.ncbi.nlm.nih.gov/guide/>.

TABLE III. THE OVERLAPPING SCORE GENERATED BY THE GA FOR THE DNA FRAGMENTS ASSEMBLY PROBLEM. (* INDICATES THAT THE REFERENCE IMPLEMENTED MORE THAN FOUR METHODS, THE TABLE DISPLAYS THE RESULT OF THE BETTER ONE)

Dataset	(reference, method)				
Dataset (fragment length, sequence length)	([25],SAX)	([26], GA2o*)	([27],RRGA)	([27],RRGA_RS)	([27],RRGA_IM)
x60189-4 (395, 3835)	11478	-	11478	11478	11478
x60189-5 (286, 3835)	14027	13988.20	14161	14161	14161
x60189-6 (343, 3835)	18301	18293.03	18301	18301	18184
x60189-7 (387, 3835)	21268	21221	21228	21257	21218
m15421-5 (398, 10089)	38726	37967.13	38675	38668	38667
m15421-6 (350, 10089)	48048	-	48034	48048	48052
m15421-7 (383, 10089)	55072	53041.89	55094	55020	54986
j02459-7 (405, 20000)	115301	109513.62	116198	116110	116336
bx842596-4 (708, 77292)	223029	-	227151	227090	227171
bx842596-7 (703, 77292)	417680	-	441893	441867	442100
Acin1 (182, 2170)	46865	-	47436	47450	47437
Acin2 (1002, 147200)	144567	-	151285	151253	151243
Acin3 (1001, 200741)	155789	-	167035	166882	167214
Acin5 (1003, 329958)	145880	-	163061	163066	163027
Acin7 (1003, 426840)	157032	-	179835	179932	179886
Acin9 (1003, 156305)	314354	-	342936	342949	342965

The selection operator can have an impact on the overall performance of the GA algorithm [21]. The roulette wheel is the common selection operator used for optimization problems [20],[31],[32] [21], the tournament selection was implemented for TSP [22], and the stochastic remainder selection was used for QAP [33]. More recently in [21], a greedy method was designed as a selection operator for TSP.

The crossover operator is the main operator of GA as it plays a crucial role to explore efficiently the search space of the optimization problem. Hence, several advanced crossover operators have been designed for solving TSP as well as QAP using GA algorithms. The parents' characteristics are mainly inherited by crossover operators. The Sequential Constructive Crossover SCX is an intelligent crossover designed by Ahmed [10] to solve the TSP. A comparative study between SCX, ERX and generalized N-point crossover (GNX) for some benchmark TSPLIB² instances found SCX outperforms ERX and GNX in term of the solution quality. Most recently, a modified version of sequential constructive crossover, named greedy SCX (GSCX) was proposed for solving TSP [34]. The reverse greedy sequential constructive crossover (RGSCX) and the comprehensive sequential constructive crossover (CSCX) are two new crossover operators enhancing SCX for solving TSP [35].

The encouraging results obtained using SCX proved its effectiveness to solve the TSP problem. Wherefore, Ahmed [33] investigated its effectiveness for the QAP problem. He compared SCX with one-point crossover (OPX) and swap

path crossover (SPX), and concluded that SCX was better in terms of solution quality. An Improved Genetic Algorithm (IGA) adapting and implementing SCX with the combined mutation for finding effective solution to the QAP was proposed in [9]. The performance of IGA using the adaptive and exchange mutation was evaluated on some QAPLIB instances and compared to a simple GA algorithm. The results showed that the IGA was better in terms of solution quality. The gaps with the best-known solutions were improved by 0.83% to 5.82% over the simple GA. However, the IGA takes longer time than the simple GA. SCX was also applied successfully for solving QAP with a combination of sequential sampling and random algorithms to generate the initial population [36]. Notice as well, the multi-point crossover implemented in [31] showed satisfying performance for solving TSP problems relatively to the classical crossover operators.

Another types of advanced crossover operators were designed in [32] to solve the QAP relying on the idea of a frequency model. Three crossover operators were introduced for enhancing GA, namely, the Highest Frequency crossover (HFX), the Greedy HFX (GHFX), and the Highest Frequency Minimum Cost crossover (HFMCX). The authors presented a detailed comparative study between One Point crossover, Swap Path crossover, SCX, and the new three crossover operators. The experimental results showed that the frequency models were better in term of computational time, precisely, HFX and GHFX were faster by 2 and 1.5 times than SCX, respectively. However, in term of solution quality all crossover operators found good near-optimal solutions on the tested benchmarks.

In order to compare the effectiveness of different types of crossover operators for solving the QAP using GA algorithm,

² The TSPLIB is a library of samples for the TSP and other problem such as Hamiltonian cycle problem, Sequential ordering problem, and Capacitated vehicle routing problem. <http://comopt.ifi.uni-heidelberg.de/software/TSPLIB95/>.

Misevicius and Kilda [37] implemented twelve different crossover operators; including the uniform like crossover (ULX) and its modifications (the randomized ULX crossover (RULX), the ULX crossover combined with repair procedure (RX), the block crossover (BX), the uniform partially-mapped crossover (UPMX), the distance preserving crossover (DPX), the cycle crossover, the swap path crossover, the one point crossover, the order-based crossover, the cohesive crossover (COHX), and, finally, the multi-parent crossover (MPX). The comparison showed that the multi-parents' crossover led to better performances.

Various types of mutation have been investigated for the TSP and QAP problems, including the Exchange Mutation [31],[21],[22], the Reciprocal Exchange Mutation[10]. The principle of these two mutation operators is similar to the Swap Mutation, which randomly selects two positions in the individual and swap the corresponding values. More advanced mutation operators have been designed for the TSP and QAP problems such as the interchange mutation in [20], and the inversion mutation in [22] which it selects two positions within an individual and then inverts the substring between these two positions. The adaptive and combined mutation operators were proposed for solving QAP in [36]. The adaptive mutation assigns highest probability values for the fittest individuals; therefore, all individuals will not have the same likelihood of mutation. Whereas, the combined mutation combines more than one type of mutation operators.

Table IV shows the results obtained for TSP in terms of the tour cost for some TSPLIB instances. The rows correspond to the results obtained for a problem instance by different

types of crossover operators. The first column represents the dataset and its best-known solution (within parentheses), (e.g., bayg29 means the instance named "bayg" with 29 cities and the best-known solution 1610). The remaining columns display for each reference the name of the GA crossover operator as well as the obtained solution (tour cost). The symbol (-) means this crossover type has not been applied in this reference to the corresponding dataset. The table clearly shows that the Sequential Constructive Crossover (SCX) and the Smart Multi-Point Crossover (SMX) achieved better solutions for the tested datasets.

Table V shows the results obtained for solving the QAP problem in terms of the solution quality, which measured by the percentage of deviation (excess%) of average solution value over the best-known solution value reported in QAPLIB. The lower the percentage the better the solution quality. The datasets used for the QAP were obtained from the QAPLIB [38], which is a library with instances size varies from 12 to 256 facilities (or locations). The table displays in the first column the names and the sizes of datasets (e.g., "tai20a" means the dataset named tai contains 20 facilities or locations; the character "a" means random instances, and the character "b" as in "tai20b" means real-life like instances) [38]. The remaining columns represent for each reference the name of the GA crossover operator types as well as the obtained solutions. The symbol (-) means this crossover type has not been applied in this reference to the corresponding dataset. From this table we can notice that the multi-parents' crossover (MPX) followed by the Sequential Constructive Crossover (SCX) dominate the other crossover types.

TABLE IV. THE IMPACT OF GA CROSSOVER OPERATORS ON THE RESULTING TOURS OF TSP USING DIFFERENT DATASETS (TSPLIB INSTANCES)

TSPLIB instances	Ref [10]	Ref [31]	Ref [21]	Ref [34]	Ref [35]	Ref [35]
	SCX	SMX	PMX	GSCX	RGSCX	CSCX
bayg29 (1610)	1610	-	-	1634	-	-
Ftv33 (1286)	-	-	-	1380	1396	1341
Ftv35 (1473)	-	-	-	1531	1583	1499
Ftv38 (1530)	-	-	-	1613	1672	1550
P43 (5620)	-	-	-	5631	5625	5627
Ftv44 (1613)	-	-	-	1706	1627	1613
Ftv47 (1776)	-	-	-	1846	1919	1833
Ry48p (14422)	-	-	-	15469	15293	14983
att48 (33522)	-	33522	33523.06	-	-	-
eil51 (426)	426	426	-	436	-	-
berlin 52 (7542)	7542	7542	-	7926	-	-
eil76 (538)	538	538	-	-	-	-
pr76 (108159)	108159	108159	-	116844	-	-
kroa100 (21282)	21282	21282	-	-	-	-
eil101 (629)	629	629	-	-	-	-
lin105 (14379)	14379	14379	-	15921	-	-
bier127 (118282)	-	118678	-	-	-	-

TABLE V. THE IMPACT OF GA CROSSOVER OPERATORS ON THE RESULTING SOLUTION QUALITY OF QAP USING DIFFERENT DATASETS (QALIP INSTANCES). (** INDICATES THAT THE REFERENCE IMPLEMENTED 12 DIFFERENT TYPES OF CROSSOVER OPERATORS, THE TABLE DISPLAYED THE BEST OBTAINED RESULT).

QALIP instances	Ref [32]			Ref [33]			Ref [37]**	Ref [36]
	HFX	GHFX	HFM CX	OPX	SPX	SCX	MPX	SCX
Tai20a	6.81	5.59	4.82	6.57	5.59	4.50	0.246	1.20
Tai20b	8.45	8.31	7.67	8.73	9.12	6.56	0.000	0.44
Tai25a	6.18	5.82	5.33	5.01	5.61	4.58	0.150	1.71
Tai25b	10.05	10.73	7.45	12.92	15.42	5.24	0.000	0.14
Tai30a	6.11	6.12	5.66	5.16	5.49	4.29	0.035	2.30
Tai30b	11.32	10.04	9.05	13.4	10.55	8.78	0.001	0.18
Tai35a	5.78	5.21	5.71	4.92	5.35	4.95	0.194	2.42
Tai35b	8.45	7.11	6.02	7.49	6.76	5.00	0.019	0.33
Tai40a	7.44	6.23	4.23	4.97	5.76	4.53	0.374	2.48
Tai40b	9.22	10.52	8.11	9.44	11.57	7.30	0.000	0.03
Tai50a	7.13	5.47	5.46	5.00	4.91	4.51	0.583	3.07
Tai50b	8.15	8.43	5.28	7.46	6.68	5.60	0.014	0.56
Tai60a	6.73	6.00	5.74	4.89	4.60	4.54	0.572	3.28
Tai60b	7.83	7.11	5.11	6.95	8.14	5.12	0.010	0.34
Tai80a	5.41	4.55	4.02	4.32	3.83	4.35	0.218	3.41
Tai80b	7.05	6.41	5.39	6.15	6.07	6.63	0.016	2.17
Tai100a	5.49	5.04	3.65	4.04	3.22	4.02	0.108	2.92
Tai100b	8.34	7.09	5.23	9.33	5.39	5.08	0.064	0.95
Tai150b	-	-	-	-	-	-	0.241	1.81

From the literature review we noticed that the TSP and QAP problems have been treated with various GA designs, including different advanced GA concepts. The SCX crossover emerges from the lot as it is shown experimentally to be the most performant crossover for the TSP and QAP problems. We also noticed that the exchange mutation operator is mostly used for TSP in the literature. The datasets used for the TSP were obtained from the TSPLIB, which is a library of instances of the TSP and related problems from various sources and of various types with number of cities varies from 14 to more than 33k cities.

The QAP literature review included other types of performant crossover operators; as the frequency models and the multi-parents' crossover.

V. DISCUSSION

In the light of what has been studied and reviewed so far, we noticed that GA algorithms applied to the TSP and QAP problems have led to very satisfactory performances in practice. We likewise noticed that some advanced types of genetic algorithm operators have been widely used for the two problems, and their effectiveness has been investigated to solve these two problems. Unfortunately, these advanced GA operators have not yet been exploited for solving the DNA_FA problem. The similarities between DNA_FA and these two problems pointed out in this paper are strong indicators of the benefit that the use of the advanced GA algorithms can bring to solve the DNA_FA problem. That is

why it is worth to design GA platform including advanced GA operators and to investigate its effectiveness for solving the DNA_FA problem.

More in detail, we have noticed that the most efficient crossover operators SCX, frequency model and the multi-parent crossovers have not been adapted and exploited for the DNA_FA problem. Likewise, the 2-opt heuristics for initializing the population was used few times for the DNA_FA problem. Regarding the mutation operators, the Adaptive and Combined mutation designed for the TSP and QAP problems can be exploited for the DNA_FA problem.

In order to design GA platform including advanced GA operators, Table VI summarizes the main GA operators and their values and Table VII shows the used GA operators so far for each problem (DNA_FA, TSP, QAP). As well as the different GA parameters tunings: such as the population size, the crossover and mutation probabilities, the number of generations, and the number of runs. Defining a proper setting for GA parameters can drastically improve the algorithm performance. However, it is not an easy task, generally the parameters are set experimentally, and Table VII supplies some GA parameter settings for the three optimization problems. From Table VII, we can clearly see the advanced operators that have not been adapted and implemented so far for the DNA_FA problem.

VI. GA PLATFORM TO SOLVE THE DNA_FA PROBLEM

Our GA platform design to solve the DNA_FA problem is inspired from the efficient GA approaches developed for the TSP and QAP problems. The GA platform gathers several advanced GA operators and tools which have shown their effectiveness in the TSP and QAP contexts. The GA platform contains the best advanced GA tools for our problem DNA_FA and one could build many variants of GA algorithms for solving it by integrating in different and judicious ways the ingredients of this platform.

A. The Flowchart of the GA Platform

Fig. 2 presents the flowchart of our GA platform to solve the DNA_FA problem.

B. The GA Concepts of the Designed Platform

1) *Initial population*: Our GA platform design includes the random, the greedy and the 2-opt heuristics strategies

which yielded to good performances as shown in [27][28][29]. The previous works showed that the computational time when using the 2-opt and greedy initialization strategies was better than when using the random way.

2) *Fitness function*: As the fitness function is repeatedly applied to each individual of each generation it should be relatively easy to compute and should also give an accurate evaluation of the quality of each individual. We reported two related fitness functions from the literature. The first one is a simple fitness function that sums the overlap for each of the adjacent fragment's pairs, as expressed by the formula (4) in [3].

$$F1 = \sum_{i=1}^{n-1} w[i, i + 1] \quad (4)$$

where $w[i, i + 1]$ is the overlap between fragment i and fragment $i + 1$. This function attempts to maximize the value F1.

TABLE VI. GA OPERATORS AND THEIR VALUES

GA operator	values
Population encoding	Integer encoding, value encoding.
Population initialization	Random initialization, greedy initialization, 2-opt heuristics initialization, and sequential sampling initialization.
Crossover operator	Multi-parents crossover, order crossover, cycle crossover, edge recombination crossover, partial mapped crossover, sequential constructive crossover, greedy sequential constructive crossover, reverse greedy sequential constructive crossover, comprehensive sequential constructive crossover, one-point crossover, highest frequency crossover, greedy highest frequency crossover, highest frequency minimum cost crossover, uniform like crossover, randomized uniform like crossover, block crossover, uniform partially mapped crossover, distance preserving crossover, cohesive crossover, and smart multi-point crossover.
Mutation operator	Inversion mutation, swap mutation, reciprocal mutation, exchange mutation, interchange mutation, combined mutation, and adaptive mutation.
Selection operator	Roulette wheel selection, tournament selection, greedy selection, and stochastic reminder selection.
Stopping condition	Number of generations, CPU time, no improvement for number of iterations.

TABLE VII. THE EXISTING GA DESIGN AND EXPERIMENTAL SETTINGS FOR DNA_FA, TSP AND QAP

GA design and experimental settings	DNA_FA	TSP	QAP
Population encoding	Integer number (sequence of integer numbers, each of which represents a city to be visited)	integer numbers, value encoding (sequence of some values such as real numbers, characters, each of which represents a city to be visited)	Integer numbers
Population initialization	Random, greedy, 2-opt heuristics	Random, greedy, MARL	Sequential sampling, random
Population size	Varies from 11 to 2500 Individuals.	Varies from 20 to 200 individuals.	Varies from 30 to 200 individuals.
Selection	Tournament.	Roulette wheel, tournament, greedy.	Roulette wheel, stochastic reminder selection.
Crossover	OX, ER, PMX, one-point order. CX	SCX, ERX, GNX, PMX, smart multi point crossover, order insert crossover.	SCX, OPX, SPX, HFX, GHFX, HFMCX, MPX.
Mutation	Inversion mutation, swap mutation	Reciprocal mutation, exchange mutation, interchange mutation, inversion mutation	Reciprocal exchange mutation, combined mutation, adaptive mutation, swap mutation
Crossover probability	Varies from (60% to 100%)	Varies from (90% to 100%)	100%
Mutation probability	2%	Varies from (1% to 20%)	Varies from (5% to 15%)
Stopping condition	No improvement for number of iterations.	Optimal rout, number of generations.	Number of generations, CPU time.
Number of runs	From 5 runs to 30 runs	From 10 runs to 30 runs.	20 runs.
Number of generations	Varying from (1 K to 512 K) generations	Varying from (20 to 10k) generations.	Varying from (5000 to 10k) generations.

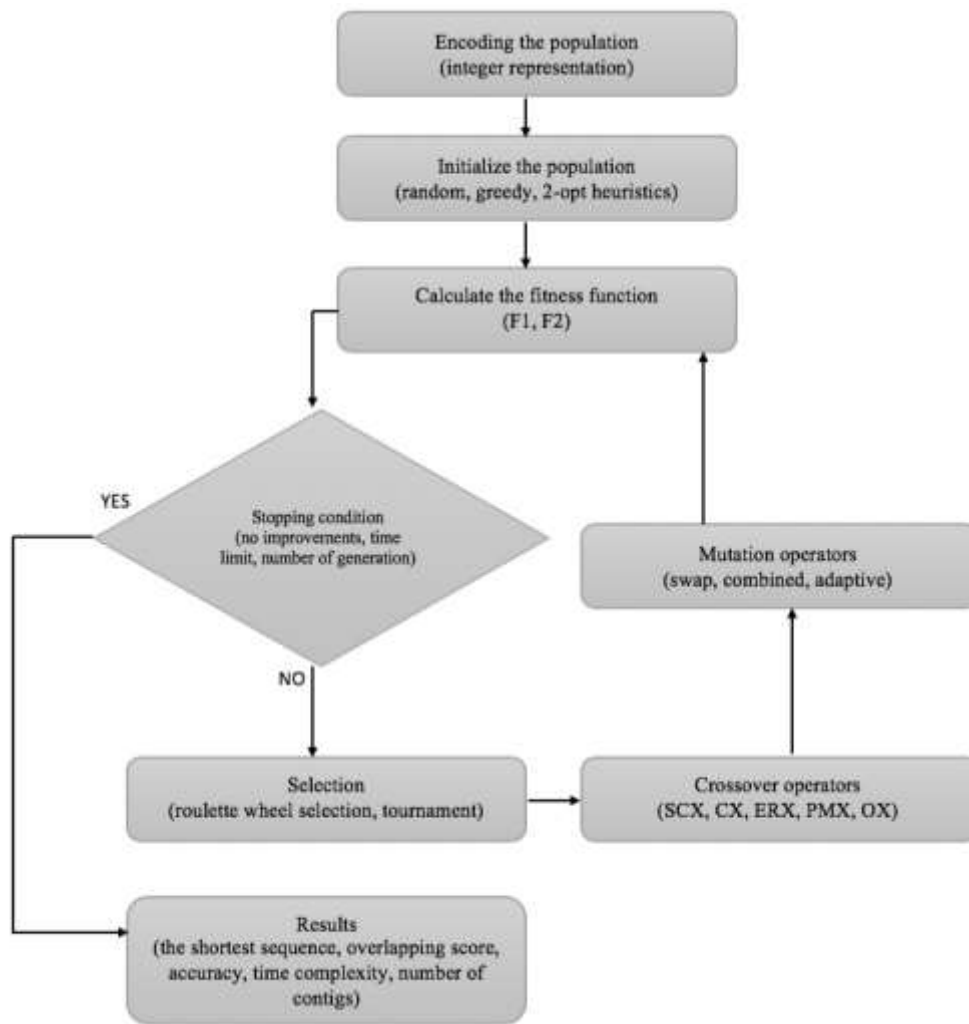


Fig. 2. GA Platform Design for the DNA Fragments Assembly Problem.

The second fitness function F2 is expressed by the formula (5) in [3].

$$F2 = \sum_{i=1}^n \sum_{j=1}^n |i - j| * w[i, j] \quad (5)$$

The fitness function F2 considers the overlap between adjacent fragments and the overlap between non-adjacent fragments as well. However, the complexities of F1 and F2 are different, F1 takes $O(n)$ where F2 is of $O(n^2)$ because all pairs of fragments must be considered [3]. These two fitness functions are included in the platform.

3) *Selection operator*: Several selection operators were used for these three problems as shown in Table VI (e.g., roulette wheel selection, rank selection, elitist selection, and tournament selection). As roulette wheel selection widely used and consumes least amount of time, and tournament selection can maintain diversity by giving an equal chance to all the individuals to compete [39]; The roulette wheel selection and the tournament selection are selected to be added to the platform.

4) *Crossover operator*: Several crossover operators SCX, CX, PMX, ERX, and Order Crossover are candidate to be

included in the platform. A special attention should be given to the SCX crossover as it was one of the best operators for the TSP and QAP problems and we predict same performance in the DNA_FA context.

5) *Mutation operator*: The swap mutation operator with its variants were widely used for DNA_FA, TSP, and QAP. Combined and adaptive mutation was designed for the QAP problem. The last one seems more suitable as it was performant for the QAP problem.

VII. CONCLUSION

This paper aims to show why it is worth to investigate genetic algorithms for solving the DNA fragment assembly problem. We have provided a simple formal proof showing the relationship between this problem and the famous TSP and QAP problems enabling us to extract some similarities between these three optimization problems. TSP and QAP have been solved efficiently using GA algorithms designed with advanced GA operators and tools. For this reason, we exploited the extracted similarities between the DNA_FA problem and the TSP and QAP problems to design an efficient GA platform integrating several advanced operators used for

TSP and QAP. Our future work is to implement the designed GA platform and to conduct comprehensive experiments in order to get the best combination of integrating the different operators of GA to build a robust solver for the DNA_FA problem.

REFERENCES

- [1] G. Luque and E. Alba, "Metaheuristics for the DNA Fragment Assembly Problem," 2005, doi: 10.5019/j.ijcir.2005.28.
- [2] Pavel A. Pevzner, *Computational Molecular Biology An Algorithmic Approach*. The MIT Press, 2000.
- [3] R. J. Parsons, S. Forrest, and C. Burks, "Genetic Algorithms for DNA Sequence Assembly," *Proc. Int. Conf. Intell. Syst. Mol. Biol.*, vol. 1, pp. 310–318, 1993.
- [4] J. Błażewicz, P. Formanowicz, M. Kasprzak, W. T. Markiewicz, and J. Węglarz, "Tabu search for DNA sequencing with false negatives and false positives," *Eur. J. Oper. Res.*, vol. 125, no. 2, pp. 257–265, Sep. 2000, doi: 10.1016/S0377-2217(99)00456-7.
- [5] G. Minetti and E. Alba, "Metaheuristic assemblers of DNA strands: Noiseless and noisy cases," in *IEEE Congress on Evolutionary Computation*, Jul. 2010, pp. 1–8, doi: 10.1109/CEC.2010.5586524.
- [6] K. Huang, J. Chen, and C. Yang, "A Hybrid PSO-Based Algorithm for Solving DNA Fragment Assembly Problem," in *2012 Third International Conference on Innovations in Bio-Inspired Computing and Applications*, Sep. 2012, pp. 223–228, doi: 10.1109/IBICA.2012.8.
- [7] C. Blum, M. Y. Vallès, and M. J. Blesa, "An ant colony optimization algorithm for DNA sequencing by hybridization," *Comput. Oper. Res.*, vol. 35, no. 11, pp. 3620–3635, Nov. 2008, doi: 10.1016/j.cor.2007.03.007.
- [8] A. Hussain, Y. S. Muhammad, M. Nauman Sajid, I. Hussain, A. Mohamud Shoukry, and S. Gani, "Genetic Algorithm for Traveling Salesman Problem with Modified Cycle Crossover Operator," *Comput. Intell. Neurosci.*, vol. 2017, pp. 1–7, 2017, doi: 10.1155/2017/7430125.
- [9] Z. H. Ahmed, "An improved genetic algorithm using adaptive mutation operator for the quadratic assignment problem," in *2015 38th International Conference on Telecommunications and Signal Processing (TSP)*, Jul. 2015, pp. 1–5, doi: 10.1109/TSP.2015.7296481.
- [10] Z. H. Ahmed, "Genetic Algorithm for The Traveling Salesman Problem Using Sequential Constructive Crossover," 2010.
- [11] D. Bucur, "De Novo DNA Assembly with a Genetic Algorithm Finds Accurate Genomes Even with Suboptimal Fitness," in *Applications of Evolutionary Computation*, vol. 10199, G. Squillero and K. Sim, Eds. Cham: Springer International Publishing, 2017, pp. 67–82.
- [12] R. J. Parsons, S. Forrest, and C. Burks, "Genetic algorithms, operators, and DNA fragment assembly," *Mach. Learn.*, vol. 21, no. 1–2, pp. 11–33, 1995, doi: 10.1007/BF00993377.
- [13] A. B. Ezzeddine, S. Kasala, and P. Navrat, "Applying the Firefly Approach To The Dna Fragments Assembly Problem," p. 13.
- [14] W. Wetcharaporn, N. Chaiyaratana, and S. Tongshima, "DNA Fragment Assembly by Ant Colony and Nearest Neighbour Heuristics," in *Artificial Intelligence and Soft Computing – ICAISC 2006*, vol. 4029, L. Rutkowski, R. Tadeusiewicz, L. A. Zadeh, and J. M. Żurada, Eds. Berlin, Heidelberg: Springer Berlin Heidelberg, 2006, pp. 1008–1017.
- [15] G. M. Mallén-Fullerton and G. Fernández-Anaya, "DNA fragment assembly using optimization," in *2013 IEEE Congress on Evolutionary Computation*, Jun. 2013, pp. 1570–1577, doi: 10.1109/CEC.2013.6557749.
- [16] E. Çela, *The Quadratic Assignment Problem*, vol. 1. Boston, MA: Springer US, 1998.
- [17] E. Çela, "Problem Statement and Complexity Aspects," in *The Quadratic Assignment Problem*, vol. 1, Boston, MA: Springer US, 1998, pp. 1–25.
- [18] E. Çela, V. G. Deineko, and G. J. Woeginger, "The multi-stripe travelling salesman problem," *Ann. Oper. Res.*, vol. 259, no. 1, pp. 21–34, 2017, doi: 10.1007/s10479-017-2513-4.
- [19] R. E. Burkard, E. Çela, P. M. Pardalos, and L. S. Pitsoulis, *The Quadratic Assignment Problem*.
- [20] S. S. Juneja, P. Saraswat, K. Singh, J. Sharma, R. Majumdar, and S. Chowdhary, "Travelling Salesman Problem Optimization Using Genetic Algorithm," in *2019 Amity International Conference on Artificial Intelligence (AICAI)*, Feb. 2019, pp. 264–268, doi: 10.1109/AICAI.2019.8701246.
- [21] W. Xueyuan, "Research on Solution of TSP Based on Improved Genetic Algorithm," in *2018 International Conference on Engineering Simulation and Intelligent Control (ESAIC)*, Aug. 2018, pp. 78–82, doi: 10.1109/ESAIC.2018.00025.
- [22] R. Liu and Y. Wang, "Research on TSP Solution Based on Genetic Algorithm," in *2019 IEEE/ACIS 18th International Conference on Computer and Information Science (ICIS)*, Jun. 2019, pp. 230–235, doi: 10.1109/ICIS46139.2019.8940186.
- [23] S. Sahni and T. Gonzalez, "P-Complete Approximation Problems," *J. ACM JACM*, vol. 23, no. 3, pp. 555–565, Jul. 1976, doi: 10.1145/321958.321975.
- [24] Alfonsas Misevičius, Dalius Rubliauskas, "Performance of Hybrid Genetic Algorithm for The Grey Pattern Problem," *Information technology and control*, 2005.
- [25] G. Minetti, G. Leguizamón, and E. Alba, "SAX: a new and efficient assembler for solving DNA Fragment Assembly Problem," p. 12, 2012.
- [26] G. Minetti, E. Alba, and G. Luque, "Seeding strategies and recombination operators for solving the DNA fragment assembly problem," *Inf. Process. Lett.*, vol. 108, no. 3, pp. 94–100, Oct. 2008, doi: 10.1016/j.ipl.2008.04.005.
- [27] J. Hughes, S. Houghten, G. M. Mallén-Fullerton, and D. Ashlock, "Recentering and Restarting Genetic Algorithm variations for DNA Fragment Assembly," in *2014 IEEE Conference on Computational Intelligence in Bioinformatics and Computational Biology*, May 2014, pp. 1–8, doi: 10.1109/CIBCB.2014.6845500.
- [28] J. A. Hughes, S. Houghten, and D. Ashlock, "Restarting and recentering genetic algorithm variations for DNA fragment assembly: The necessity of a multi-strategy approach," *Biosystems*, vol. 150, pp. 35–45, Dec. 2016, doi: 10.1016/j.biosystems.2016.08.001.
- [29] Uzma and Z. Halim, "Optimizing the DNA fragment assembly using metaheuristic-based overlap layout consensus approach," *Appl. Soft Comput.*, vol. 92, p. 106256, Jul. 2020, doi: 10.1016/j.asoc.2020.106256.
- [30] D. Bucur, "A stochastic de novo assembly algorithm for viral-sized genomes obtains correct genomes and builds consensus," *Inf. Sci.*, vol. 420, pp. 184–199, Dec. 2017, doi: 10.1016/j.ins.2017.07.039.
- [31] M. M. Alipour, S. N. Razavi, M. R. Feizi Derakhshi, and M. A. Balafar, "A hybrid algorithm using a genetic algorithm and multiagent reinforcement learning heuristic to solve the traveling salesman problem," *Neural Comput. Appl.*, vol. 30, no. 9, pp. 2935–2951, Nov. 2018, doi: 10.1007/s00521-017-2880-4.
- [32] H. Bennaceur and Z. Ahmed, "Frequency model based crossover operators for genetic algorithms applied to the quadratic assignment problem," *Int Arab J Inf Technol*, vol. 14, pp. 138–145, 2017.
- [33] Z. H. Ahmed, "A Simple Genetic Algorithm using Sequential Constructive Crossover for the Quadratic Assignment Problem," vol. 73, p. 4, 2014.
- [34] Zakir Hussain Ahmed, "Solving the Traveling Salesman Problem using Greedy Sequential Constructive Crossover in a Genetic Algorithm," February 2020.
- [35] Zakir Hussain Ahmed, "Genetic Algorithm with Comprehensive Sequential Constructive Crossover for the Travelling Salesman Problem," *IJACSA Int. J. Adv. Comput. Sci. Appl.* Vol 11 No 5, 2020.
- [36] Z. H. Ahmed, H. Bennaceur, M. H. Vulla, and F. Altukhaim, "A Hybrid Genetic Algorithm for the Quadratic Assignment Problem," p. 7.
- [37] A. Misevičius and B. Kilda, "Comparison of Crossover Operators for The Quadratic Assignment Problem," 2015, doi: 10.5755/j01.itc.34.2.11999.
- [38] R. E. Burkard, S. Karisch, and F. Rendl, "QAPLIB-A quadratic assignment problem library," *Eur. J. Oper. Res.*, vol. 55, no. 1, pp. 115–119, Nov. 1991, doi: 10.1016/0377-2217(91)90197-4.
- [39] N. Saini, "Review of Selection Methods in Genetic Algorithms," *Int. J. Eng. Comput. Sci.*, vol. 6, no. 12, Art. no. 12, Dec. 2017.

APPENDIX

TABLE VIII. SYMBOLS AND NOTATIONS

Symbol	Refer to
DNA_FA	DNA Fragments Assembly problem.
TSP	Traveling Salesman Problem.
QAP	Quadratic Assignment Problem.
GA	Genetic Algorithms.
A	Adenine (A).
T	Thymine (T).
G	Guanine (G).
C	Cytosine (C).
MPX	Multi-Parents Crossover.
OX	order crossover.
CX	Cycle Crossover.
ERX	Edge Recombination Crossover.
PMX	Partial Mapped crossover.
SCX	Sequential Constructive Crossover.
GSCX	Greedy Sequential Constructive Crossover.
RGSCX	Reverse Greedy Sequential Constructive Crossover.
CSCX	Comprehensive Sequential Constructive Crossover.
OPX	One-Point Crossover.
HFX	Highest Frequency Crossover.
GHFX	Greedy Highest Frequency Crossover.
HFMCX	Highest Frequency Minimum Cost Crossover.
ULX	Uniform Like Crossover.
RULX	Randomized Uniform Like Crossover.
BX	Block Crossover.
UPMX	Uniform Partially Mapped Crossover.
DPX	Distance Preserving Crossover.
COHX	Cohesive Crossover.
SMX	Smart Multi-Point Crossover.
MARL	Multi-Agent Reinforcement Learning.
RRGA	Recentering-Restarting Genetic Algorithm.
RRGA+IM	Island Model Genetic Algorithm.
RRGA+RS	Ring Species Genetic Algorithm.
PALS	Power Aware Local Search.
NCBI	The National Center for Biotechnology Information.
TSPLIB	TSP library.
QAPLIB	QAP library.

A Planar Antenna on Flexible Substrate for Future 5G Energy Harvesting in Malaysia

A. K. M. Zakir Hossain¹, Nurulhalim Bin Hassim²

S. M. Kayser Azam³, Md Shazzadul Islam⁴, Mohammad Kamrul Hasan⁵

Centre for Telecommunication Research and Innovation (CeTRI), Fakulti Teknologi Kejuruteraan Elektrik and Elektronik (FTKKE), Universiti Teknikal Malaysia Melaka (UTeM), Melaka, Malaysia^{1,2}

Department of Electrical and Computer Engineering, International Islamic University Malaysia, Kuala Lumpur, Malaysia^{3,4}

Center for Cyber Security, Faculty of Information Science and Technology, The National University of Malaysia Kuala Lumpur, Malaysia⁵

Abstract—This article presents a planar monopole antenna on flexible substrate for middle band 5G (3.5 GHz) application in Malaysia. The antenna has been designed and optimized for its gain and efficiency with an improved performance in contrast of flexible substrate-based other antennas. The antenna resonates at 3.53 GHz and it has a -10dB bandwidth of 545 MHz. The bending effects of this antenna on the S-parameter and gain have also been investigated. The antenna is able to suppress all the other frequency bands until 20 GHz. The designed antenna has been utilized with a newly designed rectifier to act as an rectenna at 3.5 GHz for RF energy harvesting applications. A reasonable amount of DC output voltage of 930 mV, and a Power Conversion Efficiency of 43.5% have been obtained while 0 dBm RF input power is delivered to the rectifier input terminal. Apart from the utilization as an energy harvester being connected with the proposed rectifier, the designed antenna on flexible substrate can also be employed to biomedical and sensor applications.

Keywords—Planar monopole; flexible substrate; 3G; bending effect; rectenna; RF rectifier; energy harvesting

I. INTRODUCTION

According to the recent allocation of 5G by Malaysian Communications and Multimedia Commission (MCMC) for mobile broadband services, three different frequency bands of 700 MHz, 3.5G Hz, and 26/28 GHz are going to be utilized for future 5G applications [1]. The end users are expecting a shuttle change in the wireless telephony and access to the internet with the possible implementation of 5G which will enable many precise and automated applications such as IOT, biomedical sensing, energy harvesting, automated agriculture etc. [2]. Expecting a paradigm shift, all these applications are in the pipeline for the researchers to explore further by utilizing the power of 5G. Since an antenna is the main getaway for any radio frequency (RF) to any device, it will play a major role in the successful establishment of 5G. Also, an antenna is the frontline component to improve the energy harvesting for 5G.

Antennas on rigid substrates (PCB) are comparatively better in gain performance. However, for the applications like wearable biomedical devices/body area network (BAN) devices, microwave sensing devices, rigid antennas are not fully suitable because of their inflexibility. In [3], a dipole rectenna is proposed on the flexible substrate for the energy

harvesting application [3]. An array is designed for the rectenna to harvest the RF energy from 7 GHz to 12 GHz frequency band. However, the dimension of the antenna is large in size. A planar double monopole antenna on the paper substrate is proposed in [4] for RF energy harvesting within the 2.45 GHz ISM band. The antenna exhibits a good gain of 4dBi; however, the antenna dimension is very large around $(60 \times 30 \text{ mm}^2)$. A planar slotted-ring antenna is proposed in [5] which also works for 2.45 GHz ISM band. The antenna is realized on the transparent polyethylene terephthalate (PET) substrate which has a dimension of $27.2 \times 25.5 \text{ mm}^2$ with a 2.4 dBi directive gain. Recently, a CPW-fed monopole antenna is proposed on the PET substrate in [6] for energy harvesting applications with the future 5G network at 3.5 GHz. The antenna exhibits a good efficiency at 3.5 GHz yet suffers with a low realized gain of 1.51 dBi.

As important as the antennas, the rectifiers are also the essential part of the RF energy harvesting system. In [7] the authors have proposed an antenna-rectifier (rectenna) from 900 MHz to 3GHz having band notches at ISM and WLAN applications. The antenna has been designed on a thin flexible and transparent substrate named poly-methyl methacrylate (PMM) and the structure is circular loop in nature. The operating frequencies are 940 MHz, 1.86 GHz, 2.14 GHz, and 2.49 GHz respectively for different application such as GSM (900 and 1800) and LAN. Still, the dimensions are large and the results show that the antenna works well in the lower frequency due to the largeness of the structure. In [8] the authors have utilized a spiral antenna for energy harvesting at GSM 1800 (1.7 GHz to 1.9 GHz) with a RF/DC converter (a voltage doubler) with a Schottky diode HSMS2850. Due to the larger size of the antenna ($800 \times 900 \text{ mm}^2$), the realized measured gain is comparatively high around 7dBi. However, the efficiency of the whole rectenna system is very low as 0.6%. Recently another planar microstrip DGS antenna has been proposed in [9] to harvest the RF energy between 1 GHz to 5 GHz. The antenna as has a decent size of $45 \times 41 \text{ mm}^2$. However, the proposed antenna has a small realized gain of only 2.7 dBi.

In this work, a monopole antenna has been designed and integrated with a new rectifier to improve the antenna gain and the power conversion efficiency (PCE) without any distinct impedance network between the antenna and the rectifier.

This research is partially sponsored by the Center for Research and Innovation (CRIM), Universiti Teknikal Malaysia Melaka (UTeM), Melaka, Malaysia

Until 20 GHz, no resonance is offered by the designed antenna which contributes to reduce the obligatory use of output filter for the rectenna. Antenna design is described in Section II, and rectifier design is explained in Section III. The overall performance analysis of the proposed rectenna is discussed in Section IV.

II. ANTENNA DESIGN

The antenna designed here is a keyhole-shaped microstrip planar antenna with partial ground plane. The substrate used here is Kapton HN with a dielectric constant of $\epsilon_r = 3.5$, height (h) of 0.125 mm and the loss tangent ($\tan \delta$) of 0.001. The full 3-D simulator CST MWS 2019 has been used for the design and simulation. Fig. 1 shows the design structure of the antenna.

The antenna design steps can be seen from Fig. 2. At first, a rectangular patch has been designed with $6.8 \times 6.8 \text{ mm}^2$ dimension. After that, a circular patch is modeled and centered at the middle point of the top arm of the rectangle with a radius of 6 mm to make it as a keyhole shape. A feedline of 12.8 mm length is then connected to make it a microstrip feedline. The ground plane is reduced to 9 mm length with the same width of the total antenna structure to make the partial ground plane (PGP) structure. The final dimension of the antenna is $27.4 \times 15.6 \text{ mm}^2$.

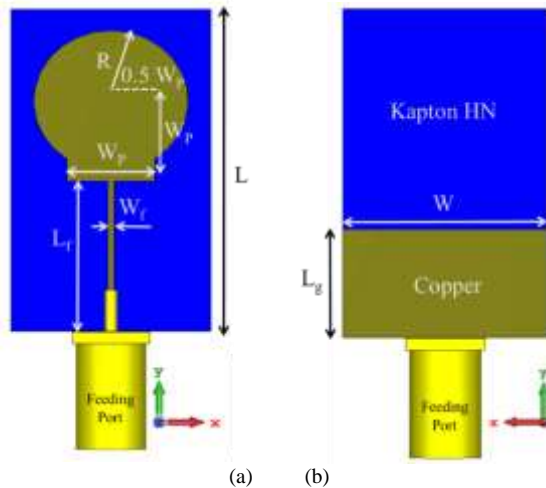


Fig. 1. Planar Keyhole-Shaped Antenna Design (a) front view and (b) back view ($L = 27.4 \text{ mm}$, $W = 15.6 \text{ mm}$, $L_f = 12.8 \text{ mm}$, $L_g = 9 \text{ mm}$, $W_p = 6.8 \text{ mm}$, $R = 6 \text{ mm}$, and $W_f = 0.5 \text{ mm}$).

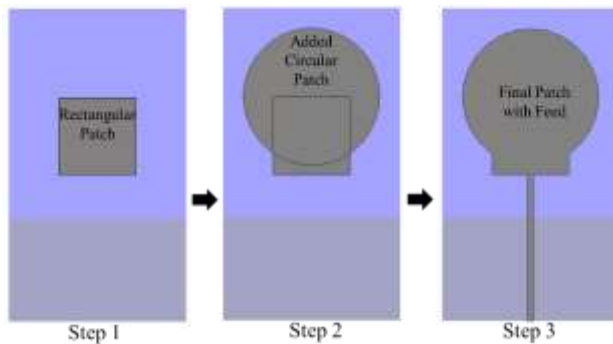


Fig. 2. Three Steps of the Antenna Design.

The antenna dimensions have been estimated by the equations as follows [10], [11]:

$$\epsilon_{eff} = \frac{\epsilon_r + 1}{2} + \frac{\epsilon_r - 1}{2} \left[1 + 12 \frac{h}{W_p} \right]^{-\frac{1}{2}} \quad (1)$$

$$L_{eff} = \frac{c}{2 f_r \sqrt{\epsilon_{eff}}} \quad (2)$$

$$\Delta L = 0.412 h \frac{(\epsilon_{eff} + 0.3) \left(\frac{W_p}{h} + 0.264 \right)}{(\epsilon_{eff} - 0.258) \left(\frac{W_p}{h} + 0.8 \right)} \quad (3)$$

$$L_p = L_{eff} - 2\Delta L \quad (4)$$

Where, ϵ_e is the effective dielectric constant, L_e is the effective length of the patch, C_0 is the speed of the light at vacuum, and f_c is the resonant/center frequency. Length (L_g) and width (W_g) of the PGP have been calculated from (5) and (6), respectively.

$$L_g = 6h + L_p \quad (5)$$

$$W = W_g = 6h + W_p \quad (6)$$

The radius (r) of the circular patch has been approximated by (7) and (8) as follows [12]:

$$r = \frac{F}{\left\{ 1 + \frac{2h}{\pi \epsilon_r F} \left[\ln \left(\frac{\pi F}{2h} \right) + 1.7726 \right] \right\}^{\frac{1}{2}}} \quad (7)$$

$$F = \frac{8.791 \times 10^9}{f_c \sqrt{\epsilon_r}} \quad (8)$$

III. RECTIFIER DESIGN

Conventionally, an RF rectifier is connected to the antenna through an impedance matching network which sometimes adds more loss of the input RF signal coming from the antenna. Thus, the overall PCE can be decreased. To avoid such a possibility of losing some PCE, a voltage doubler topology-based new RF rectifier has been proposed in this work which omits the need of the impedance matching network between the rectifier and the antenna to construct the complete rectenna circuit. Fig. 3(a) demonstrates a topological circuit of the rectenna, and Fig. 3(b) shows the final layout of the proposed rectifier.

Two Schottky diodes with the model of SMS7630-079LF, and two capacitors of 1000 pF have been utilized to construct the voltage doubler circuit. The core of the proposed rectifier has been designed with transmission lines of 1.14 times higher impedance than that of the RF feedline. To avoid sudden rise of impedance after the feedline which can be potentially threatening to increase the return loss [13], [14], a tapered transmission line has been employed from lower to higher impedance. As depicted in Fig. 3(b), Tapered Line 1 of about $\lambda/60$ length is connected between the feedline and the rectifier core. On the other hand, to serve the purpose of DC feed, a longer tapered line has been connected between the rectifier core and the output terminal. As seen in Fig. 3(b), Tapered Line 2 of about $\lambda/12$ length has been utilized to perform like the DC feed. Because the rectifier output terminal needs to block the RF signal as much as possible, Tapered Line 2 is

ended with 2 times higher impedance line than that of the RF feedline. In other words, impedance of the output DC line is 1.75 times higher than that of transmission lines of the rectifier core. Such a gradual rise of impedance at the two terminals of the rectifier core provides more stability while the rectification process is performed. As a result, a better PCE can be achieved by the following equation:

$$PCE = \frac{P_{DC}}{P_{RF}} \times 100 (\%) \quad (10)$$

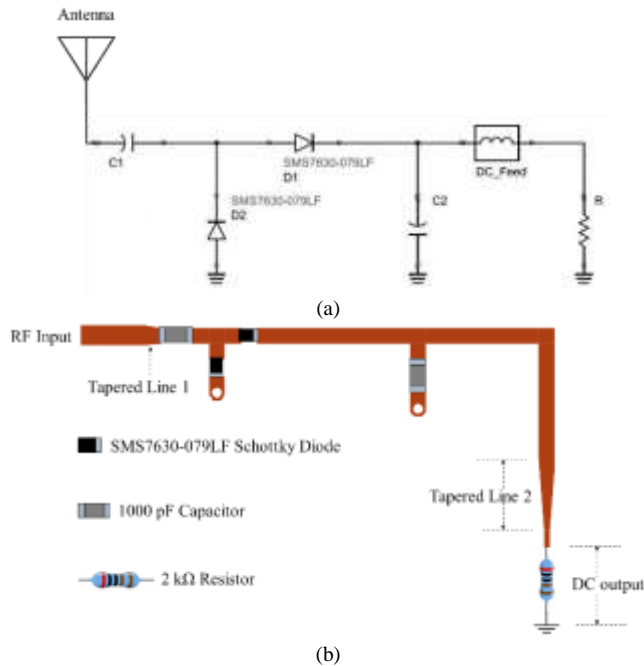


Fig. 3. Proposed Rectifier (a) Topological Circuit of the Rectenna (b) Final Layout.

The rectifier has been designed and simulated by utilizing manufacturers’ spice models with the design tool-kit and electromagnetic simulator of Advanced Design System (ADS) 2017. The design, optimization and simulation have been performed by considering the DC load resistor as 2 kΩ, and the center frequency as 3.5 GHz.

IV. RESULTS AND DISCUSSIONS

A. Antenna

Fig. 4 shows the S-parameter (S_{11}) and VSWR responses of the designed planer antenna. Fig 4(a) depicts a wide-span response of the designed antenna until 20 GHz. It is seen that the antenna has resonance only at 3.53 GHz between 1 GHz and 20 GHz. It clearly demonstrates that other frequency bands are suppressed by the designed antenna. Fig 5(b) shows the exploded view of the S_{11} response of the antenna between 3 GHz and 4 GHz. It is seen that the antenna has the S_{11} value as low as -22.5 dB at 3.53 GHz and the -10 dB bandwidth (BW) is around 545 MHz. To justify the resonance further, Fig. 5(c) also shows the VSWR response of the antenna. As expected, it also shows that the value is below 2 for the entire BW of the antenna.

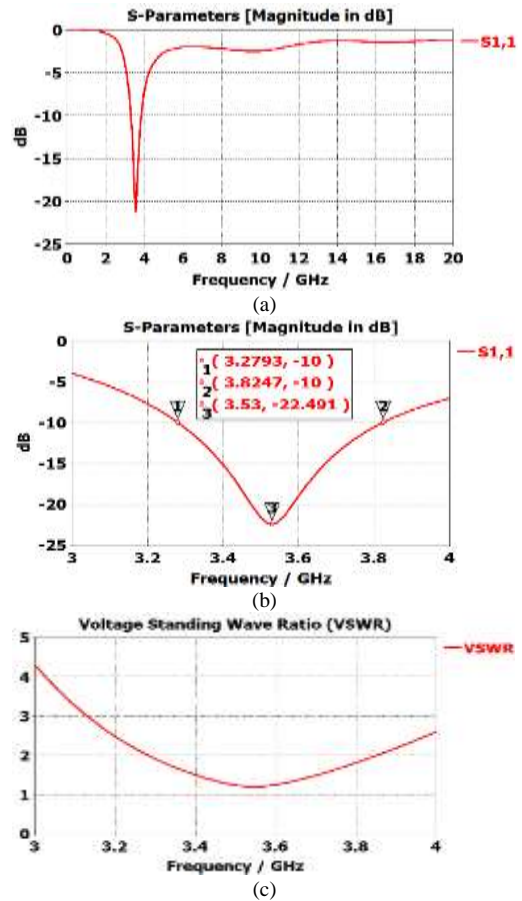


Fig. 4. Impedance Matching Responses of the Designed Antenna (a) S_{11} in Wide-Span (b) S_{11} in Narrow-Span (c) VSWR.

After the impedance matching quality of the antenna is observed, the next step is to check the radiation properties of the antenna. Fig. 5 presents a 3D and a 2D polar plot of the radiation pattern of the antenna, the realized gain, and the radiation efficiency of the antenna. As Fig. 5(a) illustrates the 3D radiation pattern of the antenna, it can be seen that the pattern is omni-directional with a maximum realized gain of 2.07dB at the center frequency of 3.53 GHz. The omni-directional radiation pattern can also be understood by looking at the E-plane and the H-plane responses of the antenna according to the 2D polar pattern depicted in Fig. 5(b). Because the E-plane exhibits nearly a circular while the H-plane exhibits a bidirectional 2D patterns, the designed antenna offers a typical monopole omni-directional radiation pattern which is not just the most effective radiation for ambient RF energy harvesting but also efficient for many other applications like biomedical and sensor-based systems.

Fig. 6(c) shows realized gain of the antenna from 3~4 GHz. The maximum realized gain is 2.07 dB. Fig. 6(d) reveals the radiation efficiency of the antenna. The efficiency is very high throughout the whole bandwidth by reaching to 99.5%, and it never goes below 98%. Thus, these radiation parameters justify the quality of the designed antenna on the flexible substrate. To assess the antenna flexibility, the investigations on its bending ability has been performed. Here, two bent conditions with an angle of 90° have been investigated using

CST MWS: bending along width (Fig. 7(a)), and bending along length (Fig. 7(b)).

Fig. 6(c) summarizes the S_{11} response and Fig. 6(d) summarizes the realized gain of the antenna for no bending, width-wise bending, and length-wise bending conditions. From the S_{11} response for different bending conditions, it is seen that there is no change in the response for the length-wise bending, and it is fully overlapped with the response of the unbent condition. However, the width-wise bending condition gives a visible shift in the resonance, and a loss of S_{11} value but it is still below -17 dB while resonating around 3.51GHz. Once again, it can be understood that the design is stable in terms of impedance matching. Fig. 6(d) presents the realized gain for different bending conditions. Here, the realized gain is dissimilar to the unbent condition (2.07 dB). For length-wise bending and width-wise bending, the realized gain drops to 1.96 dB and 1.84 dB, respectively. Nevertheless, such a range of realized gain is decently remarkable compared with other flexible antennas.

B. Rectifier

Because of the two tapered lines used at both terminals of the rectifier core, there have been some significant effects on the return loss, output DC voltage, and PCE of the rectifier. In Fig. 7, the minimum return loss is observed as -28.91 dB at 3.5 GHz, and the -10 dB bandwidth is seen as 80 MHz which fits in the 5G band of Malaysia (100 MHz BW at 3.5 GHz center frequency).

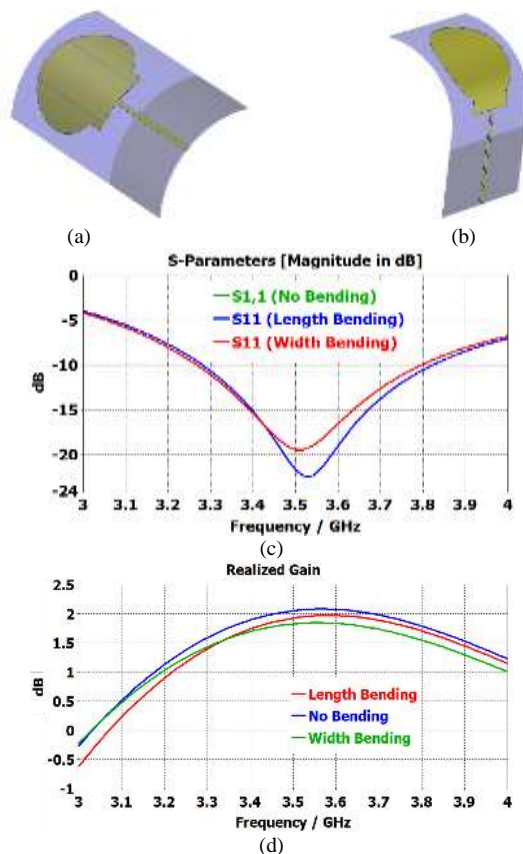


Fig. 6. Antenna in Flexibility (a) width-wise Bending (b) Length-wise Bending (c) effects on S_{11} (d) effects on Realized Gain Response.

In terms of different RF power delivered to the input terminal of the rectifier, changes of output DC voltage (V_{out}) and PCE have been presented in Fig. 8.

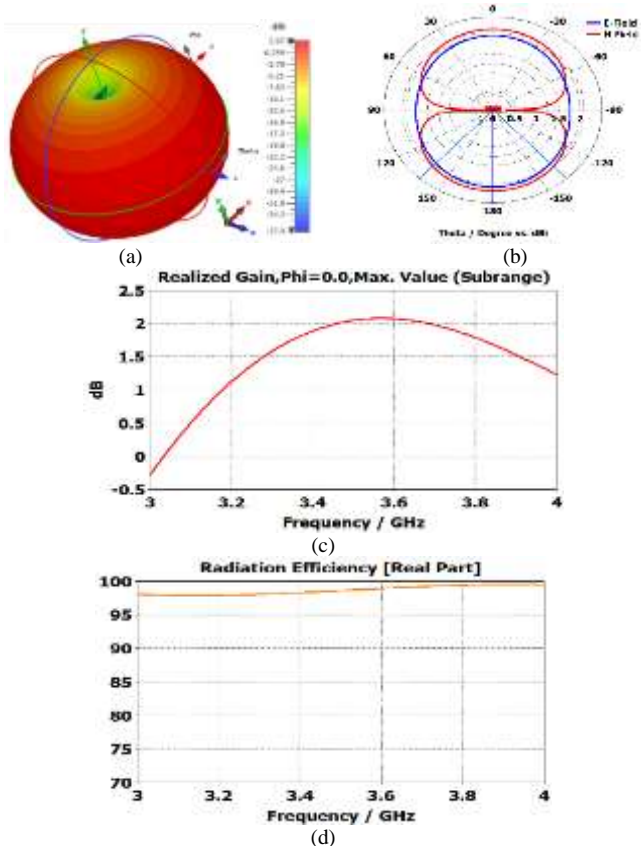


Fig. 5. Radiation properties (a) 3D pattern (b) 2D polar pattern (c) realized gain (d) radiation efficiency

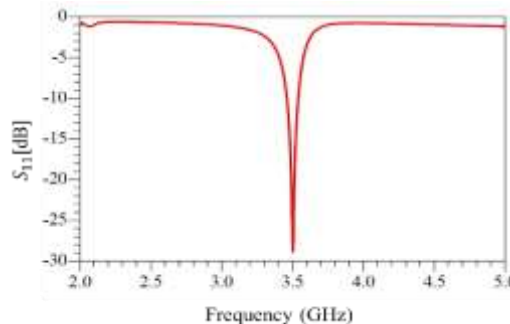


Fig. 7. Impedance Matching in S_{11} of the Proposed Rectifier.

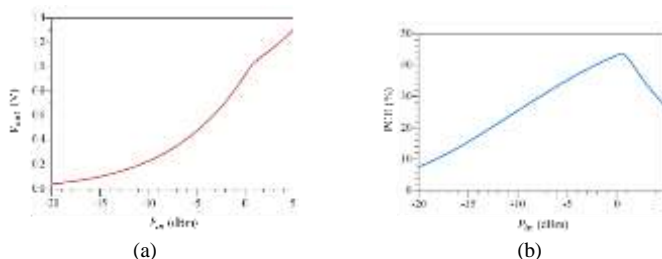


Fig. 8. Rectifier Response with different RF Power from Antenna (a) V_{out} Change (b) PCE Change.

REFERENCES

According to Fig. 8(a), output DC voltage varies from 100 mV to 930 mV while the RF power delivered to the input varies from -15 dBm to 0 dBm. For the same variation of RF power, PCE of the rectifier varies from 15.3% to 43.5%. The highest PCE (43.65%) is obtained when 0.5 dBm RF power is delivered to the rectifier from the antenna. Although PCE starts decreasing with the increase of RF power, the output DC voltage continues to increase. However, most of the energy harvesting and sensor-based systems are not surrounded by high RF power in the environment. Therefore, it is better to achieve higher PCE for the lower RF power which is a remarkable aspect of the proposed rectifier.

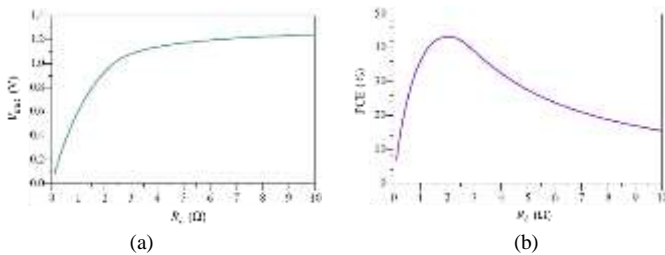


Fig. 9. Effects of Load Variation on (a) V_{out} and (b) PCE for 0 dBm RF.

Although the proposed rectifier is designed with 2 k Ω load resistor, load variation and its effects on output DC voltage and PCE are important to observe as illustrated in Fig. 9.

Output DC voltage remains quite stable (930~1242 mV) within the range of 2~10 k Ω load variation when the antenna delivers 0 dBm RF power to the rectifier. PCE gradually decreases with the increase of load resistances; yet PCE does not go below 15.45% even if the load resistance is increased to 10 k Ω . The proposed rectifier occupies a small area of 29.6 \times 13.6 mm².

V. CONCLUSIONS

A planar keyhole-shaped monopole antenna with partial ground plane has been designed, and its performance has been analyzed for 3.5 GHz. An omni-directional radiation pattern has been found which is suitable for the RF energy harvesting systems. The designed antenna has the maximum realized gain of 2.07 dBi and the maximum efficiency of 99.5%. A new RF rectifier has been introduced and then the antenna is integrated with it to construct a rectenna for the energy harvesting system. The proposed rectifier has the highest PCE of 43.65% when 0.5 dBm RF power is delivered from the antenna. Apart from the 5G applicability, the designed antenna with the proposed rectifier can be efficiently applied in energy harvesting, biomedical and sensor-based systems.

ACKNOWLEDGMENT

This research is done in collaboration with, Universiti Teknikal Malaysia Melaka (UTeM), Melaka, Malaysia; Department of Electronics and Computer Engineering (ECE), International Islamic University Malaysia (IIUM) and Faculty of Information Science and Technology, University Kebangsaan Malaysia (UKM).

[1] The Malaysian Communications and Multimedia Commission, "Final Report on Allocation of Spectrum Bands for Mobile Broadband Service in Malaysia" Jan 2020. Last accessed Sept 2020. Available at https://www.mcmc.gov.my/skmmgovmy/media/General/pdf/Final-Report_Allocation-of-Spectrum-Bands-for-Mobile-Broadband-Service-In-Malaysia_20191231.pdf

[2] M. S. Islam, M. I. Ibrahimy, S. M. A. Motakabber, A. K. M. Z. Hossain, and S. M. K. Azam, "A wideband millimeter-wave printable antenna on flexible substrate for breast cancer imaging," presented at the 2019 7th International Conference on Mechatronics Engineering (ICOM), Putrajaya, 2019, Accessed: Dec. 23, 2019. [Online]. Available: <http://www.iium.edu.my/icom/programme.pdf>.

[3] K. D. Song, T. B. Stout, S. Yang, J. Kim, and S. H. Choi, "Energy harvesting of dipole rectenna for airship applications," in *Nanosensors, Microsensors, and Biosensors and Systems* 2007, Apr. 2007, vol. 6528, p. 65280K, doi: 10.1117/12.721765.

[4] I. Kharrat, P. Xavier, T.-P. Vuong, and G. E. P. Tourtollot, "Compact Rectenna Design for Lossy Paper Substrate at 2.45 GHz," *Progress In Electromagnetics Research*, vol. 62, pp. 61–70, 2016, doi: 10.2528/PIERC15093005.

[5] H. Dong, X. Hou, Q. Zhang, and F. Wang, "Flexible slot-ring antenna for RF wireless energy harvesting," in *2018 International Workshop on Antenna Technology (iWAT)*, Mar. 2018, pp. 1–4, doi: 10.1109/iWAT.2018.8379233.

[6] S. M. K. Azam, M. S. Islam, A. K. M. Z. Hossain, and M. Othman, "Monopole Antenna on Transparent Substrate and Rectifier for Energy Harvesting Applications in 5G," *International Journal of Advanced Computer Science and Applications (IJACSA)*, vol. 11, no. 8, Art. no. 8, 31 2020, doi: 10.14569/IJACSA.2020.0110812.

[7] S. Bellal, H. Takhedmit, and L. Cirio, "Design and experiments of transparent rectennas for wireless power harvesting," in *2016 IEEE Wireless Power Transfer Conference (WPTC)*, 2016, pp. 1–4.

[8] Bouchouicha, D., Dupont, F., Latrach, M., & Ventura, L. (2010). Ambient RF energy harvesting. *Renewable Energy and Power Quality Journal*, 1(8), 1309-1313. doi:10.24084/repqj08.652.

[9] Pandey, R., Shankwar, A. K., & Singh, A. (2020). Defected ground structured wideband antenna for RF energy harvesting. Paper presented at the Proceedings of the 4th International Conference on Trends in Electronics and Informatics, ICOEI 2020, 288-291. doi:10.1109/ICOEI48184.2020.9142951.

[10] M. S. Islam, M. I. Ibrahimy, S. M. A. Motakabber, A. K. M. Z. Hossain, and S. M. K. Azam, "Microstrip patch antenna with defected ground structure for biomedical application," *Bulletin of Electrical Engineering and Informatics*, vol. 8, no. 2, pp. 586–595, Jun. 2019, doi: 10.11591/eei.v8i2.1495.

[11] M. S. Islam, M. I. Ibrahimy, S. M. A. Motakabber, and A. K. M. Z. Hossain, "A Rectangular Inset-Fed Patch Antenna with Defected Ground Structure for ISM Band," in *2018 7th International Conference on Computer and Communication Engineering (ICCCCE)*, Sep. 2018, pp. 104–108, doi: 10.1109/ICCCCE.2018.8539260.

[12] C. A. Balanis, *Antenna Theory: Analysis and Design*. John Wiley & Sons, 2016.

[13] S. M. K. Azam, M. I. Ibrahimy, S. M. A. Motakabber, and A. K. M. Z. Hossain, "Plans for Planar: Phase-Noise Reduction Techniques in Voltage-Controlled Oscillators," *IEEE Microwave Magazine*, vol. 20, no. 11, pp. 92–108, Nov. 2019, doi: 10.1109/MMM.2019.2935364.

[14] S. M. K. Azam, M. I. Ibrahimy, S. M. A. Motakabber, A. K. M. Z. Hossain, and M. S. Islam, "A miniaturized hairpin resonator for the high selectivity of WLAN bandwidth," *Bulletin of Electrical Engineering and Informatics*, vol. 8, no. 3, pp. 916–922, Sep. 2019, doi: 10.11591/eei.v8i3.1496.

Rule-based Text Normalization for Malay Social Media Texts

Siti Noor Allia Noor Ariffin¹, Sabrina Tiun²
Faculty of Information Science and Technology
Universiti Kebangsaan Malaysia, Bangi
Selangor, Malaysia

Abstract—Malay social media text is a text written on social media networks like Twitter. Commonly, this text comprises non-standard words, filled with dialects, foreign languages, word abbreviations, grammatical neglect, spelling errors, and many more. It is well known that this type of text is difficult to process due to its high noise and distinct text structure. Such problems can be resolved using rigorous text normalization, which is critical before any technique can be implemented and evaluated on social media text. In this paper, an improved normalization method towards Malay social media text was proposed by converting non-standard Malay words using a rule-based model. The method normalizes common language words often used by Malaysian users, such as non-standard Malay (like dialect and slangs), Romanized Arabic, and English words. Thus, a Malay text normalizer was proposed using a set of rules that extend across different domains of natural language processing (NLP) and is expected to address the challenges of processing Malay social media text. This study implements the proposed Malay text normalizer in a Part-of-Speech (POS) tagging application to evaluate the normalizer's performance. The implementation demonstrates a substantial improvement in the POS tagging efficiency over several pre-processing stages, with an improvement of accuracy up to 31.8%. The increase of accuracy in the POS tagging indicates two main points. First, the Malay text normalizer's rules improve the performance of a Malay text normalizer on social media text. Second, our proposed Malay text normalizer has successfully improved the POS tagging percentage and demonstrates the importance of normalized pre-processing in any NLP application.

Keywords—Malay normalization; Malay text normalization; informal Malay text; Malay tweets; rule-based normalizer

I. INTRODUCTION

Twitter is among the most influential social networks globally after Facebook, and it is expected to remain a common choice for years to come [1]. Twitter is a micro-blogging and social networking service that enables registered users to write, read, and share a short text with other users. A short text, called tweet writing, is limited to only 280 letters [2][3]. This restriction leads users to engage more creatively using a non-standard way of writing. For example, slang, abbreviations, emoticons, and shortcuts are [4] used to satisfy the criteria for a limited number of characters permitted by tweets. According to the study published by [1], from the first quarter of 2010 to the fourth quarter of 2018, there were 1,318 million users worldwide active monthly on Twitter accounts. These statistics clearly show that Twitter has an extensive social media text

database (or texts written in colloquial or non-standard language).

Studies on the normalization of Malay social media texts are still lacking and needs improvement from various aspects. Besides, current normalization techniques are unable to normalize nearly the entire vocabulary of Malay social media content. One way to improve the quality of language processing on social media data is by using normalization methods that can automatically convert non-standard terms to its corresponding standard token [5]. Therefore, the goals of this study are to propose an improved normalization technique that can normalize Malay social media texts by converting and mapping non-standard Malay words to its corresponding standard Malay word form. This technique includes converting shorten and typographical words of Romanized Arabic and English words. The method helps to boost the efficiency of any NLP applications such as Machine Translation, Named Entity Recognition, POS Tagging, and more [6].

Designing an automated Malay text normalizer without human intervention seems to be a challenging job. Therefore, this study decides to develop a Malay text normalizer based on a set of rules, as mentioned in Section III. The critical challenge in developing text normalization for Malay social media text is building a repository that contains all non-standard word variations present in a training corpus. The repository was built from an extensive collection of Malay tweets. This study extracts the Malay tweets data manually from the Malaysian Twitter account like [9]. The data extracted are carefully selected to only tweets written using non-standard Malay language to ensure that the data used is appropriate and aligned with the objective of this study. However, due to time restriction, this study only managed to collect 1,791 tweets, and the total number of words in the data collection is only 38,714 words. The built-in repository includes 2,848 non-standard word variants that are mapped into 1,292 standard forms [7]. The most massive non-standard word variants in this category refer to the term 'beritahu' with 16 variants.

The performance of this proposed Malay text normalizer is evaluated based on an application-based method. This study adopts the approach of evaluating a text normalizer like [8]. The author in [8] evaluates a text normalization technique of English text based on the performance of a spell checkers. Whereas, for the Malay text normalizer, the performance of the POS tagging is used instead. POS is the method of tagging a word with its corresponding tags. This POS tagging

application's performance is evaluated based on the same evaluation method of [9].

This study presents the first attempt to produce a text normalizer for Malay social media content. The technique proposed consists of three steps: (i) pre-process tweets, (ii) detect non-standard words, and (iii) correct it using Malay text normalizer. This paper's organization shall be as follows: Section II presents the related works; Section III presents the method; Section IV presents the evaluation and results; and finally, the conclusion present in Section V.

II. RELATED WORK

Social media text is challenging to read since much of the content in this area appears in dialects, slangs, abbreviations, and foreign languages. This study utilized a corpus of data from Malay's Twitter users in Malaysia. The data in this corpus must be pre-processed to remove any unnecessary sign or language mistake. The pre-processing phase is a critical step that must be completed by each researcher to be able to process their work computationally. According to [10], their study findings revealed that 17 pre-processing techniques were used to process text data from the Malay language. These techniques of pre-processing include capitalization, tokenization, spelling correction, and more. According to [10], the Sabah dialect study by [11] is the Malay text-based analysis using the most pre-processing technique. The authors in [11]'s used 7 of the 17 pre-processing techniques identified by [10]. Meanwhile, studies by [12] and [13] were using the entire six pre-processing techniques. Both studies of [12] and [13] use the same pre-processing techniques, such as stop words, tokenization, spelling correction, punctuation removal, and non-word removal.

Additionally, the studies conducted by [14], [15], [16], and [17] are using only four pre-processing techniques [10]. The authors in [14]'s used pre-processing methods such as capitalization, spam elimination, emoticon elimination, and symbol removal. [15]'s analysis used capitalization methods, selecting only tweets written or containing the language of analysis, filtering tweets that did not suit the report's features, and selecting only tweets that could be encoded and decoded. Besides, the study by [16] used pre-processing techniques such as the removal of stop words, diacritical removal, repeated removal of letters, and the removal of specific markers from social media. Lastly, [17] research used techniques for stop word elimination, tokenization, elimination of punctuation, and removal of multiple phrases.

Nevertheless, according to [18], pre-processing of data can only be achieved using eight basic techniques: (i) transforming upper case letters, (ii) eliminating punctuation, (iii) deleting words, (iv) neutralizing text, (v) correcting spelling errors, (vi) tokenizing, (vii) stemming, and (viii) lemmatizing. Furthermore, a study of social media text was conducted by [19] using eight normalization techniques to neutralize texts containing dialects and other grammatical errors. This social media text study by [19] focused on the Indonesian language; however, this study also considers other language families, like Malay. Table I shows the overall pre-processing techniques performed by [19].

TABLE I. LIST OF NORMALIZATION TECHNIQUES USED BY [19]

Steps	Pattern	Example	
		Before	After
Convert all tokens to lowercase	ABC → abc	Media	media
Removal of the word <i>-nya</i> and <i>ny</i>	ABCnya → ABC	makanannya	makanan
	ABCny → ABC	kelakarny	kelakar
Separate the word <i>lah</i> , <i>lh</i> dan <i>la</i>	ABClah → ABC lah	jomlah	jom lah
	ABClh → ABC lh	dialh	dia lah
	ABCla → ABC la	lantakla	lantak la
Removal of words with hyphens or 2	ABC-ABC → ABC	bunga-bunga	bunga
	ABC2 → ABC	kucing2	kucing
	ABC ² → ABC	arnab ²	arnab
Removed character repetition	AABBCC → ABC	nakkkkkk	nak
Separate words with several similar words into two groups	ABABABAB → ABAB	hehehehe	hehe
Break together two or more words which offer different meanings	ABAC → AB AC	takapa taknak	tak apa tak nak
Converts typographical terms into actual types of words	AC → ABC	byk	banyak
	ABCX → ABC	cantix	cantik

In summary, considering the pattern of pre-processing techniques set out in Table I, this research has decided to adopt, incorporate and make some improvements to all of these pre-processing techniques to suit the corpus of studies containing the Malay social media texts.

III. METHOD

Throughout this section, the solution to the crucial challenge of normalizing Malay social media text (see Section I) is addressed in detail in the form of a rule-based Malay text normalizer. Therefore, this study constructs a semi-autonomous rule-based model to normalize the Malay social media text effectively. This study's training corpus consists of tweets written in a non-standard Malay language and mixed language. The mixed language mentioned here is a tweet written by mixing the Malay with foreign languages like English or Romanized Arabic. The rule-based Malay text normalizer is designed to normalize only words written in Malay, Romanized Arabic, and English. Other languages will not be normalized. The corpus is first converted into a lower case to reduce the scale of the vocabulary. Normalization procedures and their associated standardized forms are implemented sequentially on the vocabulary list.

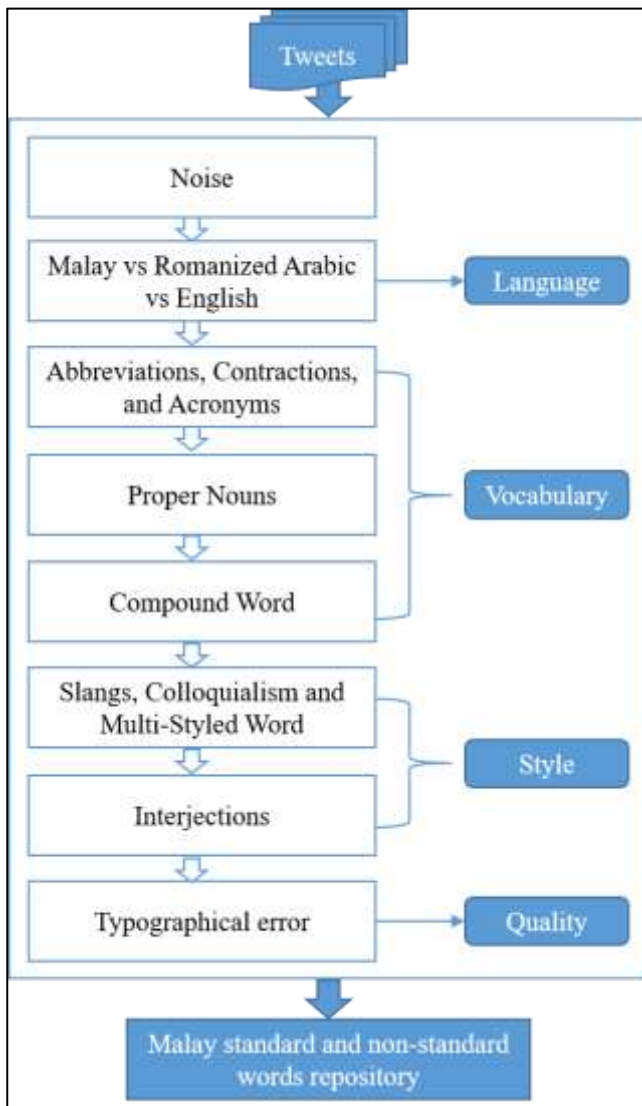


Fig. 1. The Architecture of the Rule-based Malay Text Normalizer.

This study first describes the Malay social media text's challenges and then offers solutions in normalization procedures to these challenges. The challenges are set out, and the rules used to resolve them are listed accordingly to avoid contradictory rules. Fig. 1 demonstrates the Malay text normalizer architecture based on rules that address sequentially specific problems. The rules are constructed while considering the complexities of these difficulties, thereby providing an almost ideal translation of non-standard Malay text into its structured forms.

A. Noise

Noise decides by including all the following in the document: marks, punctuations, or numerals.

1) Any word in the corpus present in Unicode is dropped. Unicode word is a term written using characters in Chinese, Korean, and Japanese.

2) Any web links are omitted from the corpus. Commonly, web links start with HTTP(s) or www.

3) Any link to the user profile that began with the '@' symbol followed by the username will be removed.

4) All punctuation characters, symbols, and numerals are omitted from the corpus.

5) All the standalone letters, multiple white spaces, and white space found in the corpus at the beginning and end sentences are eliminated.

B. Malay vs Romanized Arabic vs English

This study defines terms in Malay, Romanized Arabic, and English. It uses the rules set out in this subsection to pre-normalize terms that correspond to each language.

1) Referring to the source provided by [20] and [21], all non-standard Malay words are replaced with their standard word form.

2) Non-standard Romanized Arabic words are converted by comparison to the source provided by [20] and [21] into their correct standard form.

3) American English is used for standardizing all English words by referring to the [22] sources.

C. Abbreviations, Contractions, and Acronyms

An abbreviation is a shorter type of a sentence or phrase. A contraction is an abbreviation simplified by a word or phrase omitting the internal letters. In contrast, an acronym is an abbreviation formed from the original components of a word or phrase. All abbreviations and subclasses of these are extended to their full forms. The letter 'x' in the corpus, for example, is generally referred to as 'tak'. The letter 'x' is then transformed into its full form 'tak' or written as 'tidak'. The initial letter for Malaysia's currency, 'rm' is also extended to 'ringgit malaysia'.

D. Proper Nouns

According to [23], a proper noun is a noun that designates a being or object, does not take a restrictive modifier, and is usually capitalized. For example, 'Idris' (person), 'Johor' (place), 'Mercy Malaysia' (organization), 'Cat' (animal), and many others. All proper nouns are transformed into lowercase and standard form, as are the other words in the text like 'tranung', 'teganu', and 'ganu' to 'terengganu'.

E. Compound Word

According to [24], a compound word comprises components that are terms or any of the various combinations of words, combining forms or affixes. All compound words will be separated, normalized, or removed to simplify the next computational process. The following transformations occur for the standardization of compound words:

1) Separate words that repeat the same two letters in different groups of words like 'hehehehe' to 'hehe'.

2) Separate, normalize, and eliminate any '-nya' particles from words. For example, 'makanannya' to 'makanan'.

3) Normalize the word '-la/-lah' and distinguish it from the word. For example, 'jomlah' to 'jom lah'.

4) Remove the hyphen (-) and the word after it, and the number 2 from the word. For instance, 'bunga-bunga' to 'bunga', and 'kucing2' to 'kucing'.

5) Separate words combine several words of different meanings into different word groups like ‘taknak’ to ‘tak nak’.

F. Slangs, Colloquialism and Multi-Styled Word

A colloquialism is a word or term used in informal language. In contrast, slang is a colloquialism that is not considered typical in a language but appropriate when used in a social context.

1) Slang is normalized by the rules of the language to which it belongs. This study considered slang to be part of the vocabulary of their respective language.

2) In Malay, colloquialism used for family relationships is translated into their respective formal names. For instance, ‘kak’, ‘akak’, ‘akok’, and ‘kakok’ turn all into ‘kakak’ or ‘mok’ and ‘omak’ to ‘mak’.

G. Interjections

An interjection or exclamation is a word or expression used in a sentence to express an emotion, a feeling, or a pause. An interjection term widely used in social media text in Malaysia is the term ‘haha’. The word ‘haha’ in the interjection is a laughing phrase and found 273 times in the corpus. An interjection word that occurs in Malay social media text is usually derived from the user’s word. The word interjection must, therefore, transformed into a simple type of word. For standardizing interjections, the following transformations occur:

1) Malay expression like ‘adoh’, ‘adoi’, ‘adui’, ‘haduh’, and ‘adeh’ to ‘aduh’.

2) English words such as ‘tq’, ‘thank’, ‘thanks’, and ‘tenkiu’ to ‘thank you’.

H. Typographical Error

The typographical error described in this paper is a typing error, such as the misspelled word [25] that most likely occurred due to finger or hand slips. Any typographical mistake or sometimes shortened to typo will be corrected using a standard list of Malay spell checks.

Words that are not transformed are left unnormalized according to the rule-based mentioned in this section. It reflects the development of this text normalizer for Malay social media text. In the next section, this Malay text normalizer’s performance is evaluated by observing its efficiency on the POS tagging application. Previous studies on the POS tagging application show that utilizing text normalizer before the tagging process can yield a significant increase in the efficiency of POS tagging [7][26][5]. This increase in the performance of the POS tagging application is due to the reduction of unknown words [7], and non-standard words [5] proportion exist in the corpus after applying text normalizer [26]. Applying text normalizer on a corpus significantly impacts POS tagging performance because one of its essential features is context information [5]. A wrongly tagged word may influence the surrounding term and negatively impact the POS tagging application.

IV. EVALUATION AND RESULTS

This study uses a collection of Malay tweets and domain-dependent information such as the one in the standardization repository to evaluate the proposed Malay text normalizer by applying it on POS tagging. Besides, this study also uses the research results from [9] as a benchmark to assess the proposed Malay text normalizer. In [9], they only use necessary pre-processing procedures and yet still achieves a good of POS tagging accuracy. However, by applying more efficient pre-processing, including an efficient Malay text normalizer, the POS tagging better performance is expected. Therefore, this study will attempt to use a new collection of raw Malay tweets called test corpus on several pre-processing stages settings and evaluated the results by observing its performance on the POS tagging application. All text in the test corpus is initially converted to lowercase. Subsequently, the following pre-processing procedure takes place: (1) removal of punctuations; (2) removal of symbols; (3) removal of numerals; (4) lower casing; and (5) normalization of text using Malay text normalizer. Each test corpus from various pre-processing settings will be tagged using the Malay POS tag set by an annotator.

Note that each pre-processing procedure usually reduces the resulting vocabulary (the number of unique words) in the corpus. In [9]’s study, they have used a new collection of Malay tweets as their test corpus. They used this test corpus to evaluate the performance of the POS tagging application. The test corpus was duplicated into two sets of test corpus with the same array of tweets: one set consisting of raw tweets (2,112 tokens) and the other set containing normalized tweets (2,089 tokens). The difference in total token for both sets of test corpus shows that the pre-processing procedure will reduce the corpus’s token size. Fig. 2 presents the results from [9]’s study. To be noted, the work of [9] will be the benchmark of our study.

This study assesses the efficiency of POS tagging using the same method as [9]. This study also uses the original Malay tweet collection of [9] as the test corpus.

Like [9], our proposed Malay text normalizer’s performance was evaluated on the application of POS tagging, following several steps. The first step is by tagging the data in the training corpus manually with its corresponding POS tags by an annotator who is fluent in the language present in the corpus. The POS tags used by the annotator to tag the words are Malay POS tag sets that are designed, particularly for Malay social media text. The tagged (or annotated) training corpus is then used to train the machine learning classifier to determine the POS of the words (or tokens) in the test corpus. The test corpus (from [9]’s work) is duplicated into several sets of test corpus with the same collection of tweets [9][6]. One set of test corpus is kept unnormalized (original array of tweets), and the other test corpus is prepared according to several different pre-processing procedures. These pre-processing are concerning punctuation, symbol, numeral, case, and normalization by text normalizer (see Fig. 3). After that, once again, the annotator will manually test the prediction outcome by matching the POS tags of each term in the test corpus expected by the classifier with its real POS tags of [21].

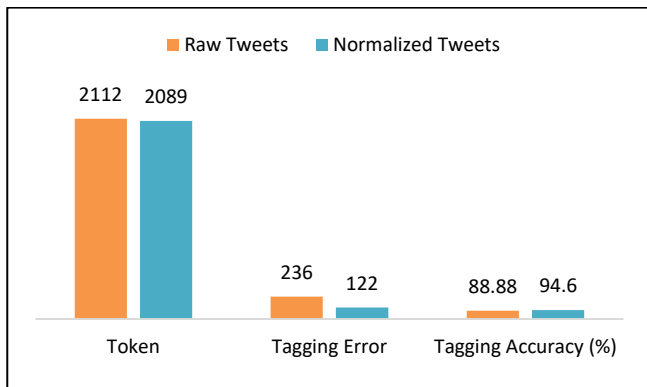


Fig. 2. The Results of [9]’s Malay Text Normalization Applied to the Malay POS Tagging.

The POS tagging efficiency of the test corpus is measured by comparing the number of tokens in the corpus, the number of tokens wrongly tagged by the classifier, and the percentage of POS tagging accuracy. The analysis even adopts and modifies [6]’s methods of assessing the NLP’s performance by noting distinct changes in accuracy and the number of unique words in the various pre-processing procedures.

A. Experimental Results

Fig. 3 shows the POS tagging performance of the test corpus in different pre-processing procedures settings [26]; (i) comparing the token number, (ii) tagging error number, and (iii) tagging accuracy percentage. In Fig. 3, essential pre-processing procedures that seem to improve the POS tagging performance are removing punctuation, lower casing, and normalization (the process by Malay text normalizer). The use of the Malay text normalizer produces the highest impact among all pre-processing by enhancing the performance of POS tagging by up to 97.43%, thereby establishing the importance of normalization as a pre-processing process for the Malay social media text.

Note that this study used the findings of [9] (refer Fig. 2) as the benchmark of this study’s POS tagging performance evaluation. The author in [9] only compared the POS tagging results between their raw and normalized test corpus. Despite using only basic normalization techniques on the normalized test corpus, [9] managed to get a high percentage in POS tagging accuracy with 94.6% (see Fig. 5). Meanwhile, even though this study used the same collection of test corpus as [9], the total number of tokens of both studies’ raw tweets is different (see Fig. 4). Fig. 4 shows that this study has more token in the raw tweets test corpus compared with [9]’s study. The difference in the total token is due to the POS tagger format. QTAG POS tagger used by [9] has some restrictions on the symbols or punctuation allowed in the corpus, which [9] did not mention it clearly in their study. This study’s machine learning tagger did not have any restriction, which leads to more token exist in the corpus.

The POS tagging performance of the raw tweets test corpus between these two studies (see Fig. 4) shows that [9] still managed to achieve POS tagging accuracy above 80% even with a lower total token, the lowest tagging error compared to this study. Meanwhile, in Fig. 5, the results show that this

study achieved the highest POS tagging accuracy of over 97% compared to the [9]’s study and that the tagging error in this study was also the lowest. This comparison clearly shows that the proposed rule-based Malay text normalizer can reduce the proportion of unknown words. ‘Unknown word’ is a word that does not exist in the repository or the training corpus that causes tagging error in the test corpus and better impacts the POS tagging.

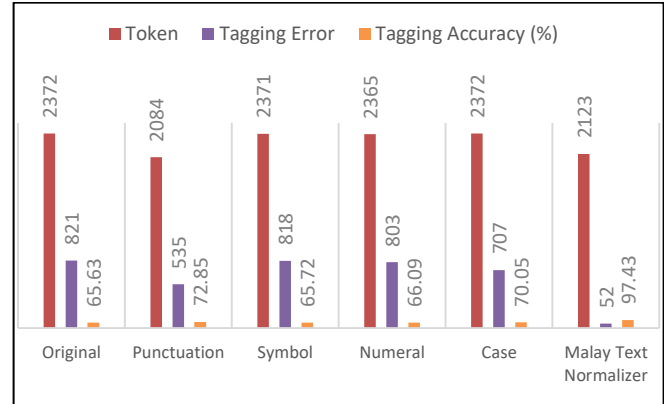


Fig. 3. POS Tagging Application Performance at different Pre-Processing Procedures.

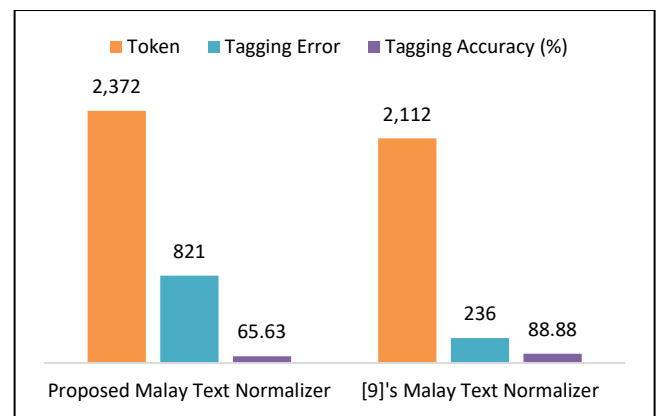


Fig. 4. The POS Tagging Performance of the Proposed Malay Text Normalizer and [9]’s Malay Text Normalizer on Raw Tweets Test Corpus.

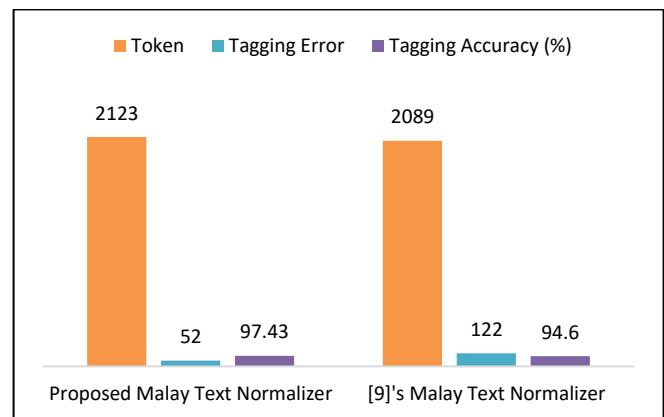


Fig. 5. The POS Tagging Performance of the Proposed Malay Text Normalizer and [9]’s Malay Text Normalizer on Normalized Tweets Test Corpus.

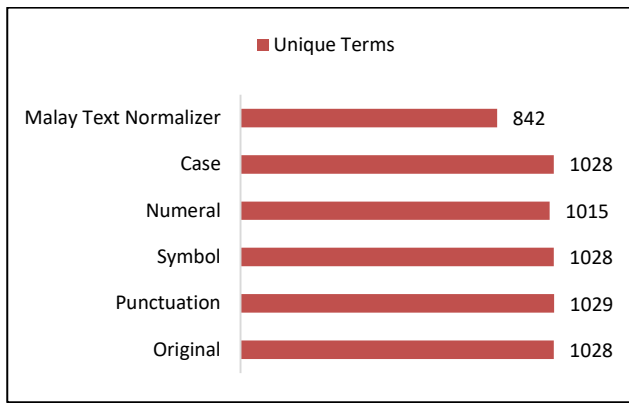


Fig. 6. The Number of unique Terms at different Pre-Processing Procedures.

This study also presents the effect of different pre-processing stages on the test corpus' vocabulary capacity. Initially, the test corpus's vocabulary size is 1,028 terms, which is reduced to 842 terms at the last step. Fig. 6 shows the vocabulary size of the test corpus after each pre-processing procedure. Significant reductions in vocabulary size are observed after applying the Malay text normalizer with a significant reduction of 18% from the original size.

Interestingly, the observed improvements in POS tagging performance are closely associated with reducing unique terms at each pre-processing level. In summary, this study concludes that the normalization of Malay social media text can yield good results in noise reduction, text normalization, and reduction of a unique term, all of which impact enhancing POS tagging efficiency.

V. CONCLUSION

This study aims to propose an improved text normalizer model, particularly for Malay's social media text. The proposed text normalization model converts and maps non-standard words to their corresponding standard word form. This model includes converting the simplified (or abbreviated) and typographical words of Malay, Romanized Arabic, and English.

The text normalizer for Malay social media text was built based on a rule-based approach. In which a repository that stores all non-standard word variants in the corpus was constructed. Besides, an extensive collection of Malay tweets was used as a training corpus consists of 1,791 tweets with 38,714 terms. For assessing the rule-based Malay text normalizer model, an application-based evaluation approach was used. In other words, the proposed Malay text normalizer was applied to POS tagging on social media text. The performance of the POS tagging was used to assess the performance of the proposed Malay text normalizer. In other words, if the POS tagging has improved, it also means that the proposed Malay text normalizer has improved as well.

In this study, experiments on the impact of various pre-processing stages on social media were also conducted: pre-processing punctuation, symbol, numeral, and case. The pre-processing stages with the lowest total number of the unique terms are the best pre-processing stage, and it is recommended to be used to normalize any social media text written in the

Malay language. Thus, from the experiment, the text normalization by the proposed Malay text normalizer is one of the three best pre-processing (the other two are punctuation removal and lower casing).

In general, this study focuses on developing improved normalization techniques based on the modification, addition, and integration of several normalization techniques by previous studies. This study evaluated the Malay tweets collection POS tagging performance by referring to the method used by [9]. Additionally, this POS tagging efficiency can also be measured using the Hidden Markov Model, Maximum Entropy, and Support Vector Machine [27]. Besides, this research also aims to contribute to other language processing modules concentrating on the Malay social media domain, including non-standard words such as the text-to-speech system [5]. This study can be further improved by adding more non-standard Malay tweets collection into the training corpus. We assumed that by increasing the training corpus' size, the POS tagging performance for the proposed Malay text normalizer could also be increased (refer Fig. 5). The tremendous impact of our enhanced rule-based text normalizer model on the performance of an NLP application (POS tagging) proves that it is a reliable tool to normalize Malay social media content.

ACKNOWLEDGMENT

Universiti Kebangsaan Malaysia partially funds this research work under the research grant code: GUP-2020-063.

REFERENCES

- [1] Statista. (2019) The number of social network users in Malaysia from 2017 to 2023 (in millions). Retrieved Feb 20, 2019, from <https://bit.ly/2D33zzt>.
- [2] Meftah, S., & Semmar, N. (2018, May). A neural network model for part-of-speech tagging of social media texts. In Proceedings of the Eleventh International Conference on Language Resources and Evaluation (LREC 2018).
- [3] Kumar, P., & Gruzd, A. (2019, January). Social Media for Informal Learning: a Case of #Twitterstorians. In Proceedings of the 52nd Hawaii International Conference on System Sciences.
- [4] Gupta, B., Negi, M., Vishwakarma, K., Rawat, G., & Badhani, P. (2017). Study of Twitter sentiment analysis using machine learning algorithms on Python. *International Journal of Computer Applications*, 165(9), 0975-8887.
- [5] Li, C., & Liu, Y. (2015, June). Joint POS tagging and text normalization for informal text. In Twenty-Fourth International Joint Conference on Artificial Intelligence.
- [6] Khan, O. A., & Karim, A. (2012, November). A rule-based model for normalization of sms text. In 2012 IEEE 24th International Conference on Tools with Artificial Intelligence (Vol. 1, pp. 634-641). IEEE.
- [7] Derczynski, L., Ritter, A., Clark, S., & Bontcheva, K. (2013, September). Twitter part-of-speech tagging for all: Overcoming sparse and noisy data. In Proceedings of the International Conference Recent Advances in Natural Language Processing RANLP 2013 (pp. 198-206).
- [8] Clark, E., & Araki, K. (2011). Text normalization in social media: progress, problems, and applications for a pre-processing system of casual English. *Procedia-Social and Behavioral Sciences*, 27, 2-11.
- [9] Ariffin, S. N. A. N., & Tiun, S. (2018). Part-of-Speech Tagger for Malay Social Media Texts. *GEMA Online® Journal of Language Studies*, 18(4).
- [10] Bakar, M. F. R. A., Idris, N., Shuib, L., & Khamis, N. (2020). Sentiment Analysis of Noisy Malay Text: State of Art, Challenges, and Future Work. *IEEE Access*, 8, 24687-24696.
- [11] Hijazi, M. H. A., Libin, L., Alfred, R., & Coenen, F. (2016, October). Bias aware lexicon-based Sentiment Analysis of Malay dialect on social

- media data: A study on the Sabah Language. In 2016 2nd International Conference on Science in Information Technology (ICSITech) (pp. 356-361). IEEE.
- [12] Alsaffar, A., & Omar, N. (2014, November). Study on feature selection and machine learning algorithms for Malay sentiment classification. In Proceedings of the 6th International Conference on Information Technology and Multimedia (pp. 270-275). IEEE.5.
- [13] Eshak, M. I., Ahmad, R., & Sarlan, A. (2017, November). A preliminary study on hybrid sentiment model for customer purchase intention analysis in social commerce. In 2017 IEEE conference on big data and analytics (ICBDA) (pp. 61-66). IEEE.
- [14] Shamsudin, N. F., Basiron, H., Saaya, Z., Rahman, A. F. N. A., Zakaria, M. H., & Hassim, N. (2015). Sentiment classification of unstructured data using lexically based techniques. *Jurnal Teknologi*, 77(18).
- [15] Tan, Y. F., Lam, H. S., Azlan, A., & Soo, W. K. (2016, April). Sentiment Analysis for Telco Popularity on Twitter Big Data Using a Novel Malaysian Dictionary. In ICADIWT (pp. 112-125).
- [16] Al-Moslmi, T., Gaber, S., Al-Shabi, A., Albared, M., & Omar, N. (2015). Feature selection methods effects on machine learning approach in Malay sentiment analysis. In Proc. 1st ICRIL-Int. Conf. Inno. Sci. Technol. (IICIST) (pp. 1-2).
- [17] Al-Saffar, A., Awang, S., Tao, H., Omar, N., Al-Saiagh, W., & Albared, M. (2018). Malay sentiment analysis based on combined classification approaches and Senti-lexicon algorithm. *PloS one*, 13(4).
- [18] Kulkarni, A., & Shivananda, A. (2019). Natural language processing recipes. Apress.
- [19] Le, T. A., Moeljadi, D., Miura, Y., & Ohkuma, T. (2016, December). Sentiment analysis for low resource languages: A study on informal Indonesian tweets. In Proceedings of the 12th Workshop on Asian Language Resources (ALR12) (pp. 123-131).
- [20] Dewan Bahasa dan Pustaka. (2005). *Kamus Dewan* (Edisi keempat). Kuala Lumpur: Dewan Bahasa dan Pustaka.
- [21] Othman, A., & Karim, N. S. (2005). *Kamus komprehensif bahasa Melayu*. Penerbit Fajar Bakti.
- [22] Hornby, A. S., & Omar, A. H. (2007). *Oxford Compact Advanced Learner's English-Malay Dictionary*. Oxford Fajar.
- [23] Merriam-Webster. (n.d.). Proper noun. In Merriam-Webster.com dictionary. Retrieved August 3, 2020, from <https://www.merriam-webster.com/dictionary/proper%20noun>.
- [24] Merriam-Webster. (n.d.). Compound. In Merriam-Webster.com dictionary. Retrieved August 3, 2020, from <https://www.merriam-webster.com/dictionary/compound>.
- [25] Merriam-Webster. (n.d.). Typographical error. In Merriam-Webster.com dictionary. Retrieved July 31, 2020, from <https://www.merriam-webster.com/dictionary/typographical%20error>.
- [26] Van der Goot, R., Plank, B., & Nissim, M. (2017). To normalize, or not to normalize: The impact of normalization on part-of-speech tagging. arXiv preprint arXiv:1707.05116.
- [27] Mohamed, H., Omar, N., & Juzaidin, M. (2011). Malay Part of Speech Tagger, A comparative study on Tagging Tools. *Asia-Pacific Journal of Information Technology and Multimedia*. Vol, 4(1), 11-23.

Distributed Beam Forming Techniques for Dual-hop Decode-and-Forward based Cooperative Relay Networks

Zahoor Ahmed¹, Zuhaibuddin Bhutto^{2*}, Syed Muhammad Shehram Shah³, Ramesh Kumar⁴, Ayaz Hussain⁵

Electrical Engineering Department, Balochistan University of Engineering & Technology, Pakistan¹

Computer System Engineering Department, Balochistan University of Engineering & Technology, Pakistan²

Software Engineering Department, Mehran University of Engineering & Technology, Pakistan³

Department of Electronic Engineering, Dawood University of Engineering and Technology, Pakistan⁴

College of Information and Communication Engineering, Sungkyunkwan University, Suwon, Republic of Korea⁵

Abstract—In this paper, it has been proved that the transmission rate can be increased substantially by alleviating co-channel interference by use of beamforming techniques at relay stations. In this setup, the downlink transmission segment is taken into consideration from the Base Station (BS) to two Mobile Stations (MS). The data is transmitted concurrently through two Relay Stations (RS) using the same frequency channel. It is assumed that the RSs use decode-and-forward (DF) strategy. In this technique of beamforming, pre-coding vectors are used at the RS to alleviate co-channel interferences. Due to this strategy, each user will be able to get its own data sans interference. Two pre-coding techniques which incarnate two different transmission protocols have been proposed. Simulations results show that such type of schemas outperforms their counterpart brethren schemas.

Keywords—Beamforming; base station; decode and forward; mobile station; relay station

I. INTRODUCTION

To acquire a higher data rate, MIMO techniques are widely used in most current wireless communication systems. The channel coding or forward error correction (FEC) scheme is an important part of MIMO communication systems if one targets high QoS for mobile users. It is essential to exploit high-performance FEC methods to achieve the performance gains in MIMO based communication systems. The FEC methods like turbo codes and LDPC codes [1-4] promises to come close to the Shannon capacity limit. The harsh channel conditions demand to use FEC schemes with iterative decoding to achieve the performance goals. Turbo codes are one of the coding schemes that are based on the concept of iterative decoding [1-4].

The relay is considered a useful technique to receive, process and retransmit signals in a wireless network. Currently, many wireless systems are using relaying techniques. By use of relays, an extension of coverage areas or hotspot capacity enhancement can be achieved. Initially, the idea of cooperative transmission was presented in [4]. The author in [5] present a cooperative system by sharing the wireless communication network by two users transmitting coherently

using the same codebook. The authors proved that due to this set up the capacity region is increased. A zero force multiuser relaying system having multiple nodes both at source and destination was introduced in [6] and [7], where the channel is orthogonalized between the source and destination pairs by a relay gain allocation. A good variety of relaying protocols has been discussed in [8]. The DF protocol has been found to have numerous advantages as compared to another type of relaying protocols [9].

In this paper, a novel technique of Cooperative Relay (CR) having multiple decode and forward (DF) relays is presented. The focus is made only on downlink transmission. The relays are installed on such a position where the establishment of a healthy link-budget to the BS is ensured. It is supposed that each relay has channel information about the second hop transmission. But this information is limited about the characteristics of their own channel. The information of the channel is gained by the uplink transmission between the mobiles and the relays or by users' feedback. In the second hop, the channel information of their own makes the RS able to reckon pre-coding vectors to annul co-channel interference (CCI) [10-12]. The cancellation or alleviation of CCI is very helpful to get architecture of the receiver for MS.

In this paper, in addition of CCI cancellation, Maximum Ratio Combining (MRC) [13] and Space-Time Codes (STC) [14-18] are also used so that a good diversity gain can be achieved at Mobile Stations. While transmitting cooperatively to the MS, the relays are synchronized to its maximum level. The MRC relay scheme has phase synchronization amongst the transmitting relays. The high degree of synchronization amongst RS is relaxed at the cost of performance degradation by utilization of STC relaying technique. In both scenarios, it has been seen that when transmit is made concurrently to the consumers with the same frequency channel, a superior multiplexing gain is obtained as compared to transmit to the diverse user(s) using disparate channel(s). The simulation results confirmed that the proposed protocols/schemes are more efficient. Particularly the ameliorated transmission rates of both schemes are worth to explore.

*Corresponding Author

The paper has been organized as follows; the system model is discussed in Section II. MRC-relay is elaborated in Section III whereas Section IV discusses the Space-Time-relay protocols. The simulation results are presented in Section V, and the conclusion is given in Section VI.

II. SYSTEM MODEL

The model shown in Fig. 1 is considered. The proposed model comprises a single BS, two MSs and two DF relays. Because of the enormous distance between them, it is assumed that the BS does not have a direct connection with MS.

The relays are fixed at such positions where healthy link-budget from the relays to the base stations is established. Initially, it is supposed that each MS is equipped with a single antenna. The numbers of antennas at BS are presented by B , at RS by R and at MS by 1 and it is assumed that $B \geq R > 1$. Further, it is assumed that the transmission scheme based on OFDM to ensure that the channel between each pair of transmitting and receiving antenna is not frequency selective. The channels between BS and RS are represented by $\mathbf{H}_i \in \mathbb{C}^{R \times B}$ with $i = 1, 2$. The second hop channel between RS_i and MS_j is represented by $\mathbf{h}_{i,j} \in \mathbb{C}^R$, with $(i, j) \in \{1, 2\}^2$. Furthermore, it is assumed that the channel between the nodes is *i.i.d* block fading. Every relay has channel information only about the second hop, *i.e.* RS_1 and RS_2 know only about $\mathbf{h}_{1,1}^H$ and $\mathbf{h}_{2,1}^H$, and $\mathbf{h}_{1,2}^H$ and $\mathbf{h}_{2,2}^H$, respectively. $(\mathbf{h}_{1,1}^H, \mathbf{h}_{2,2}^H)$ represents direct link channel whereas $(\mathbf{h}_{1,2}^H, \mathbf{h}_{2,1}^H)$ represents the cross-link channel. The power constraint at BS is represented by P_{BS} and at RS by P_{RS} . Moreover, Additive White Gaussian Noise (AWGN) is assumed on each link having variance σ_{RS}^2 at RS stations and σ_{MS}^2 at MS station.

The proposed model is a half-duplex relay. The data is transmitted to MS in two phases. In the first phase, the BS transmits the data to two RSs, which is referred to as a broadcast scenario. In the second stage, both relays simultaneously transmit to MS_1 and MS_2 using the same channels. In the proposed scheme, due to the cancellation of CCI, the MS merely receive its own data. In the next section, the cancellation of CCI is done by use of pre-coding vectors will be discussed.

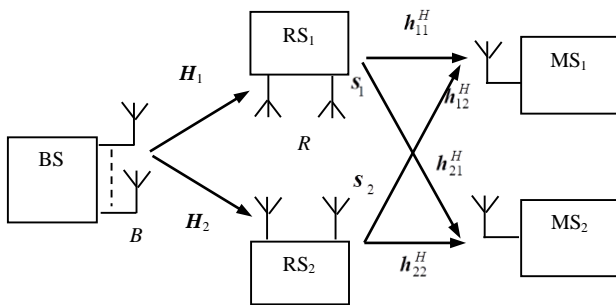


Fig. 1. System Model.

III. MAXIMUM RATIO COMBINING RELAY

One of the main purposes of Maximum Ratio Combining relay is to improve the diversity gain by using the cross-link channel. In order to provide additional array gain, the MRC also synchronizes the phase of each user's signal at the receiver. The symbols which are supposed to transmit to MS_1 and MS_2 are represented by s_1 and s_2 . Primordially, the Base Station transmits the data symbol $\mathcal{S} \in \mathbb{C}^B$ to two relays with $\mathcal{S} = (s_1, s_2)$. Since both relays receive the same information, so it is the multicast scenario. Since it is required that both relays may decode the data perfectly received from BS, so in second hop the maximum transmission rate can be achieved as:

$$R_1 = \max_{\mathcal{R}} \min \left\{ \log_2 \det \left(\mathbf{I}_R + \frac{1}{\sigma_{RS}^2} \cdot \mathbf{H}_1 \cdot \mathbf{A} \cdot \mathbf{H}_1^H \right), \log_2 \det \left(\mathbf{I}_R + \frac{1}{\sigma_{RS}^2} \cdot \mathbf{H}_2 \cdot \mathbf{A} \cdot \mathbf{H}_2^H \right) \right\} \quad (1)$$

with: $\text{tr}(\mathbf{A}) = \text{tr}(\mathbf{s} \cdot \mathbf{s}^H) = P_{BS}$.

When the data received from BS is decoded by the RS, then in the second phase the transmitted signal vectors from RS_1 and RS_2 is written as:

$$\mathbf{x}_1 = s_1 \cdot \mathbf{v}_1 + s_2 \cdot \mathbf{v}_2 \quad (2)$$

and

$$\mathbf{x}_2 = s_1 \cdot \mathbf{v}_3 + s_2 \cdot \mathbf{v}_4 \quad (3)$$

with $\mathbf{v}_k \in \mathbb{C}^R$ ($k = 1, 2, 3, 4$) are the pre-coding vectors having the condition that $\text{tr}(\mathbf{v}_k \cdot \mathbf{v}_k^H) = 1$ in order to satisfy the transmit power constraints. The pre-coding vectors also have to fulfill the condition given below in (4) and (5):

$$\mathbf{h}_{2,1}^H \cdot \mathbf{v}_1 = 0 \quad \mathbf{h}_{1,1}^H \cdot \mathbf{v}_2 = 0 \quad (4)$$

and

$$\mathbf{h}_{2,2}^H \cdot \mathbf{v}_3 = 0 \quad \mathbf{h}_{1,2}^H \cdot \mathbf{v}_4 = 0 \quad (5)$$

Actually, the pre-coding vectors lay in the null space of the corresponding channel. This type of pre-coding vectors is easily formed at RSs because of a large number of antennas while it is comparatively difficult at MSs due low number of antennas. The dimension of kernel space of $\mathbf{h}_{i,j}^H$ is never null for independent and identical distribution AWGN channel $\forall (i, j) \in \{1, 2\}$. By use of these pre-coding vectors, the CCI is annulled and only the specific users receive the transmitted data symbols.

Considering expressions (2) to (5), the received signal at MS_1 and MS_2 is written as:

$$y_1 = (\mathbf{h}_{1,1}^H \cdot \mathbf{v}_1 + \mathbf{h}_{1,2}^H \cdot \mathbf{v}_3) s_1 + n_1 \quad (6)$$

and

$$y_2 = (\mathbf{h}_{1,2}^H \cdot \mathbf{v}_2 + \mathbf{h}_{2,2}^H \cdot \mathbf{v}_4) s_2 + n_2 \quad (7)$$

where n_1 represents AWGN at MS1 and n_2 the noise at MS2. To satisfy the power constraint, the equation $E(s_1 \cdot s_1^* + s_2 \cdot s_2^*) = P_{RS}$ is taken into consideration.

As it is known that each MS has only a single receiving antenna, hence in (6) and (7) the quantities $\mathbf{h}_{i,j}^H \cdot \mathbf{v}_k$, $(i, j) \in \{1, 2\}^2$ and $k = 1, 2, 3, 4$ are complex scalar numbers. For any pre-coding vector \mathbf{v}_k which satisfies equations (2) to (5), the other pre-coding vector $\mathbf{v}_k \cdot e^{j\phi}$ is also an expedient pre-coding vector. Hence the pre-coding vectors are chosen in such a way that the term $\mathbf{h}_{i,j}^H \cdot \mathbf{v}_k$ in (6) and (7) have zero phases all over, i.e.

$$\angle(\mathbf{h}_{1,1}^H \mathbf{v}_1) = \angle(\mathbf{h}_{1,2}^H \mathbf{v}_3) = \angle(\mathbf{h}_{1,2}^H \mathbf{v}_2) = \angle(\mathbf{h}_{2,2}^H \mathbf{v}_4) = 0 \quad (8)$$

It is easy to calculate all these pre-coding vectors. For example, if \mathbf{v}_1^0 is found in the null space of $\mathbf{h}_{2,1}^H$, the final pre-coding vector at RS1 can be computed as:

$$\mathbf{v}_1 = \mathbf{v}_1^0 \cdot \frac{(\mathbf{h}_{1,1}^H \cdot \mathbf{v}_1^0)^*}{|\mathbf{h}_{1,1}^H \cdot \mathbf{v}_1^0|} \quad (9)$$

It is seen that the pre-coding vector in (9) is unique and is independent of the selection of \mathbf{v}_1^0 . By selecting the pre-coding vector \mathbf{v}_1 , the commensurate model of channel model between RS1 and MS1 is given by:

$$\mathbf{h}_{1,1}^H \cdot \mathbf{v}_1 = \mathbf{h}_{1,1}^H \mathbf{v}_1^0 \cdot \frac{(\mathbf{h}_{1,1}^H \cdot \mathbf{v}_1^0)^*}{|\mathbf{h}_{1,1}^H \cdot \mathbf{v}_1^0|} = |\mathbf{h}_{1,1}^H \cdot \mathbf{v}_1^0| = |\mathbf{h}_{1,1}^H \cdot \mathbf{v}_1| \quad (10)$$

From the above equation, it is obvious that the term $\mathbf{h}_{1,1}^H \cdot \mathbf{v}_1$ is a non-negative real number. Following the same procedure, the rest of the pre-coding vectors can be derived. Similarly, the SNR at MS1 and MS2 is computed as:

$$\text{SNR}_{1,\text{MRC}} = \frac{(|\mathbf{h}_{1,1}^H \cdot \mathbf{v}_1| + |\mathbf{h}_{1,2}^H \cdot \mathbf{v}_3|)^2 \cdot E(s_1 \cdot s_1^*)}{\sigma_{\text{MS}}^2} \quad (11)$$

and

$$\text{SNR}_{2,\text{MRC}} = \frac{(|\mathbf{h}_{2,1}^H \cdot \mathbf{v}_1| + |\mathbf{h}_{2,2}^H \cdot \mathbf{v}_4|)^2 \cdot E(s_2 \cdot s_2^*)}{\sigma_{\text{MS}}^2} \quad (12)$$

The maximum achievable rate in the second hop is:

$$R_{2,\text{MRC}} = \log_2(1 + \text{SNR}_{1,\text{MRC}}) + \log_2(1 + \text{SNR}_{2,\text{MRC}}) \quad (13)$$

and the overall transmission rate is given by:

$$R_{\text{MRC}} = \frac{1}{2} \cdot \min(R_1, R_{2,\text{MRC}}) \quad (14)$$

For analyzing the signal's diversity order, Rayleigh fading channel $\mathbf{h}_{i,j} \cong \text{XN}(0, \sigma_{i,j}^2 \cdot \mathbf{I}_R)$, $(i, j) \in \{1, 2\}$ is assumed, where $\sigma_{i,j}^2$ is the variance of the channel. The relationship $\text{tr}(\mathbf{v}_k \cdot \mathbf{v}_k^H) = 1$, for $k \in [1, 4]$, shows that $\mathbf{h}_{i,j}^H \cdot \mathbf{v}_k$ is the linear combination of the complex random normal variable. Due to this isotropic property of complex normal random vectors (9), the term $\mathbf{h}_{i,j}^H \cdot \mathbf{v}_k$ is also a normal random variable with variance $\sigma_{i,j}^2$.

It is observed that second-order diversity can be obtained by the Cooperative Maximum Ratio Combining (CMRC) transmission strategy subject to the condition that the cross-link and direct link are equally robust. Secondly, at the receiver end, the received signals from different relays coherently add up if they have the same phase. In other words, a management to get additional array gain is made. However, for alignment of the phases of different signals, the relays are to be synchronized. It means that a global phase reference for the relay nodes has to be taken into account. The CMRC scheme deals two users at the same time providing maximum transmission rate to each user. This achievement is possible sans additional resources or channel knowledge.

IV. COOPERATIVE SPACE-TIME (CSR) RELAY

Like the CMRC transmission technique, the CST Relay by dint of channel knowledge in the second hop cancels CCI occurring to the MS from the RS side. Additionally, CST Relaying technique is also used to cater to optimal diversity at MS. In such a scenario, it necessary to synchronize the symbol level between relays.

The symbols which are supposed to transmit from BS to MS1 and from BS to MS2 are represented by two successive time slots $\mathcal{X}_1^{(1)}$, $\mathcal{X}_1^{(2)}$, and $\mathcal{X}_2^{(1)}$, $\mathcal{X}_2^{(2)}$ respectively. In the initial phase of the transmission, the BS sends the data to two relays in two successive time slots. In initial hop, the rate of expression all the time shall remain the same as that of Eq. (1).

When decoding of all the four symbols by two relays is finished than in the second phase they start retransmitting to two end users. The phase-II transmission is made in two consecutive time slots.

Equation (15) and (16) denotes the transmitted signals respectively by RS1 and RS2 during the first time slot.

$$\mathbf{x}_1^{(1)} = s_1^{(1)} \cdot \mathbf{v}_1 + s_2^{(1)} \cdot \mathbf{v}_2 \quad (15)$$

and

$$\mathbf{x}_2^{(1)} = s_1^{(2)} \cdot \mathbf{v}_3 + s_2^{(2)} \cdot \mathbf{v}_4 \quad (16)$$

where $\mathbf{v}_k \in \mathbb{C}^R$ ($k = 1, 2, 3, 4$) denote the pre-coding vectors. They satisfy the condition mentioned in (4), (5) and $\text{tr}(\mathbf{v}_k \cdot \mathbf{v}_k^H) = 1$.

Equation (17) and (18) denotes the transmitted signals respectively by RS1 and RS2 during the second time slot.

$$\mathbf{x}_1^{(2)} = (-s_1^{(2)})^* \cdot \mathbf{v}_1 + (-s_2^{(2)})^* \cdot \mathbf{v}_2 \quad (17)$$

and

$$\mathbf{x}_2^{(1)} = (s_1^{(1)})^* \cdot \mathbf{v}_3 + (s_2^{(1)})^* \cdot \mathbf{v}_4. \quad (18)$$

Because of the cancellation of multiuser interference by the pre-coding vector, the received signal at MS1 and MS2 is written as:

$$\mathbf{y}_1 = \begin{bmatrix} \mathbf{h}_{1,1}^H \cdot \mathbf{v}_1 & \mathbf{h}_{1,2}^H \cdot \mathbf{v}_3 \\ (\mathbf{h}_{1,2}^H \cdot \mathbf{v}_3)^* & -(\mathbf{h}_{1,1}^H \cdot \mathbf{v}_1)^* \end{bmatrix} \cdot \mathbf{s}_1 + \mathbf{n}_1 \quad (19)$$

and

$$\mathbf{y}_2 = \begin{bmatrix} \mathbf{h}_{2,1}^H \cdot \mathbf{v}_2 & \mathbf{h}_{2,2}^H \cdot \mathbf{v}_4 \\ (\mathbf{h}_{2,2}^H \cdot \mathbf{v}_4)^* & -(\mathbf{h}_{2,1}^H \cdot \mathbf{v}_2)^* \end{bmatrix} \cdot \mathbf{s}_2 + \mathbf{n}_2 \quad (20)$$

where $\mathbf{y}_i = [y_i^{(1)}, (y_i^{(2)})^*]^T$, $i = 1, 2$ is referred to as the vector of the signal received at MS $_i$, whereas $\mathbf{s}_i = [s_i^{(1)}, s_i^{(2)}]^T$ is known as the vector of the transmitted signal, and $\mathbf{n}_i = [n_i^{(1)}, (n_i^{(2)})^*]^T$ represents the vector of noise at MS $_i$.

Taking into consideration this new approach of CR and following the basic decoding scheme of *Alamouti* code, the SNR received at MS1 and MS2 for each symbol is expressed as:

$$\text{SNR}_{1,\text{STC}} = \frac{\left(|\mathbf{h}_{11}^H \cdot \mathbf{v}_1|^2 + |\mathbf{h}_{12}^H \cdot \mathbf{v}_3|^2 \right) \mathbb{E} \left((s_1^{(1)}) \cdot (s_1^{(1)})^* \right)}{\sigma_{\text{MS}}^2} \quad (21)$$

and

$$\text{SNR}_{2,\text{STC}} = \frac{\left(|\mathbf{h}_{21}^H \cdot \mathbf{v}_2|^2 + |\mathbf{h}_{22}^H \cdot \mathbf{v}_4|^2 \right) \mathbb{E} \left((s_2^{(1)}) \cdot (s_2^{(1)})^* \right)}{\sigma_{\text{MS}}^2} \quad (22)$$

where $\mathbb{E} \left((s_1^{(1)}) \cdot (s_1^{(1)})^* \right) + \mathbb{E} \left((s_2^{(1)}) \cdot (s_2^{(1)})^* \right) = P_{\text{RS}}$. Here, it is assumed that $s_i^{(1)}$ and $s_i^{(2)}$ is equated in power, $i = 1, 2$. In the second hop, the optimal rate of transmission at each time slot is given by:

$$R_{2,\text{STC}} = \log_2 \left(1 + \text{SNR}_{1,\text{STC}} \right) + \log_2 \left(1 + \text{SNR}_{2,\text{STC}} \right) \quad (23)$$

and the overall transmission rate of two hops is given by

$$R_{\text{STC}} = \frac{1}{2} \min \left(R_1, R_{2,\text{STC}} \right) \quad (24)$$

For transmission over the second hop, a Rayleigh fading channel is considered, $\mathbf{h}_{i,j}^H \mathbf{v}_k$ is a Gaussian random variable. From Eq. (21) and (22) it is seen that the received signal will be of second-order diversity having no array gain. If it is compared with the CMRC relay, one can see that the only difference is the synchronization of symbols between the relays, which is not difficult to implement as compared to phase synchronization. The cooperative space-time relay obtains maximum rate sans additional bandwidth and channel knowledge.

V. SIMULATION RESULTS

For performance evaluation, the two proposed relay schemes are compared and simulated with some latest CR schemes available in the literature. For this, the following three types of CR techniques are considered.

A. Zero-Forcing (ZF)

During the second hop, RS $_1$ transmits the data of MS $_1$ and RS $_2$ transmits the data of MS $_2$. To counter the CCI to the cross-link, each relay uses a pre-coding vector. The pre-coding vectors \mathbf{v}_1 and \mathbf{v}_4 are chosen according to (4) and (5). In the second hop, the transmitted signal by the relays is denoted as:

$$\mathbf{x}_1 = s_1 \cdot \mathbf{v}_1, \quad \mathbf{x}_2 = s_2 \cdot \mathbf{v}_4 \quad (25)$$

where $\mathbb{E} \left(s_1 \cdot s_1^* \right) = \mathbb{E} \left(s_2 \cdot s_2^* \right) = P_{\text{RS}}$.

B. Beamforming (BF $_1$) Case-I

In this scenario, the relay station RS $_1$ transmits data to MS $_1$ and the relay station RS $_2$ to MS $_2$. The beamforming vectors RS $_1$ and RS $_2$ are employed on the transmitter side and are chosen as:

$$\mathbf{v}_1 = \frac{\mathbf{h}_{11}}{\|\mathbf{h}_{11}\|}, \quad \mathbf{v}_2 = \frac{\mathbf{h}_{22}}{\|\mathbf{h}_{22}\|} \quad (26)$$

and RS $_1$ and RS $_2$ transmit:

$$\mathbf{x}_1 = s_1 \cdot \mathbf{v}_1, \quad \mathbf{x}_2 = s_2 \cdot \mathbf{v}_2 \quad (27)$$

where $\mathbb{E} \left(s_1 \cdot s_1^* \right) = \mathbb{E} \left(s_2 \cdot s_2^* \right) = P_{\text{RS}}$. In this scenario, the data along with interferences is received by each user.

C. Beamforming (BF $_2$) Case-II

In this scheme, RS $_1$ and RS $_2$ transmit to MS $_1$ and MS $_2$ in time t_1 and t_2 , respectively. At time t_1 , both the relay stations RS $_1$ and RS $_2$ transmit data to MS $_1$ and at time t_2 to MS $_2$. While transmitting the data to end users at time t_1 and t_2 , both the relays RS $_1$ and RS $_2$ go on beamforming. The channels are orthogonal, so there shall be no CCI at the MS receivers.

Fig. 2 shows the transmission schemes amongst different schemes. To have an equitable comparison between diverse transmission scenarios, first, it is required to normalize the rate to a number of the channel used by each relay. The performance of the proposed CMRC, STC and CR are simulated by comparing them with three other schemas discussed above. It is assumed that the channels both at first and second hops are independent and identical distribution

Rayleigh fading channel. Further, it is assumed that $\mathbf{h}_{i,j} \cong \mathcal{CN}(0, \sigma_{i,j}^2 \mathbf{I}_R)$ for $(i, j) \in \{1, 2\}$, where $\sigma_{i,j}^2$ is a variance of the channel. The direct link (DL) is defined as:

$$SNR_{DL} = \frac{P_{RS} \cdot \sigma_{i,j}^2}{\sigma_{MS}^2} \quad (28)$$

and mathematically the cross-link SNRs may be written as:

$$SNR_{CL} = \frac{P_{RS} \cdot \sigma_{i,j}^2}{\sigma_{MS}^2}, \quad (i, j) \in \{1, 2\}, \quad i \neq j \quad (29)$$

Fig. 3 illustrates the average transmission rate of the proposed schemas. For simulation purpose, the SNR of the cross link as 20 (in the first hop) and 10dB (in the second hop) is considered, whereas the SNR of cross-link has been set to vary from zero to 10dB. In first hop, the cross-link SNR is taken as 20dB. Results show that whenever the cross-link is meager, then transmission may be done by beamforming.

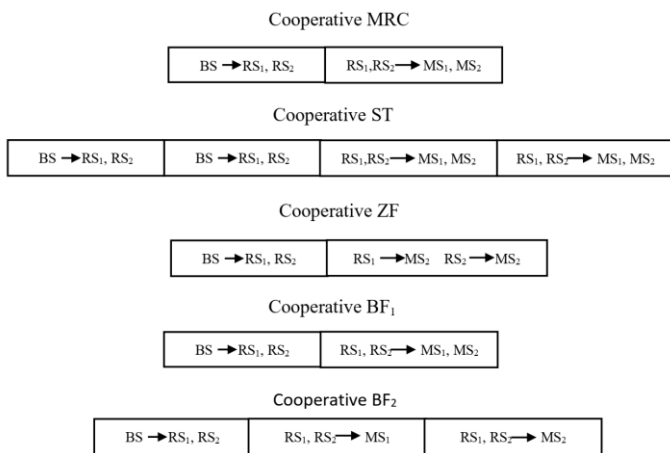


Fig. 2. Relay Protocols Transmission Schemes.

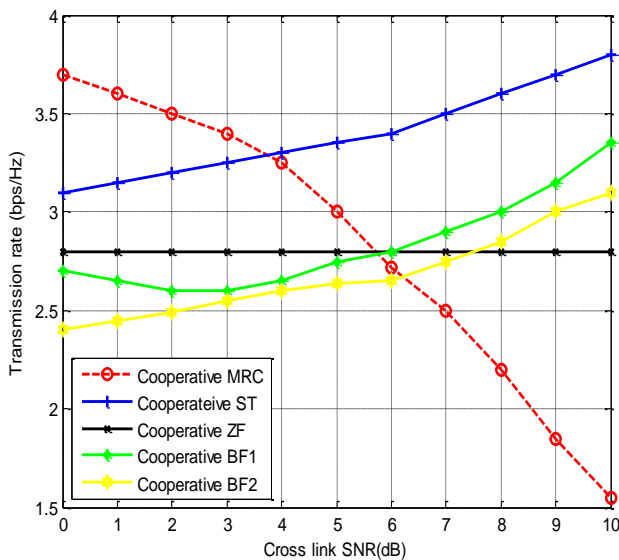


Fig. 3. Transmission Rates vs Cross-Link SNR of some Cooperative Schemes.

It can be proved that the interferences induced in the receiver are weak. Hence in such a scenario, combating to annul the cross-link interference is not incumbent rather it may devour a freedom of one spatial degree at the transmitter.

On the other hand, when the cross-link appears to be stronger, then the cross-talk interference at the receiver may cause critical degradation of performance if interference is not countered. From results, it is seen that the new proposed CMRC schemes outperform others if the cross-link SNR is greater than 4 dB. Whenever cross link-SNR is greater than 7 dB, then the CST scenario gains better transmission rate as compare to ZF, BF₁, and BF₂. Hence it is concluded that whenever the direct link and cross-link come closer to each other, then the new proposed cooperative approaches perform well.

Fig. 4 depicts a scenario presenting the average transmission rate between the cross and direct-links when they are equally powerful. Because of the same multiplexing gain, the average rate of transmission of the expounded schemas and the ZF cooperative relaying strategies resemble to each other. Its mean, the relay nodes transmit to all users in same time and frequency. Whereas in the case of BF₂, the relay nodes transmit to all users using different channels, and as a result loses the multiplexing gain. This scene is observed in the given figure from the narrow slope of BF₂ cooperative relay. In this proposal, where one mobile user is equipped with two relays, hence the received signals get maximum diversity and higher array gains. This tells us the reasons that why BF₂ cooperative relays offer higher transmission rates at lower SNRs.

The impact of noisy channel estimates is considered over the whole system performance. In fact, in this proposed scheme, the purpose of the provision of channel information about the second hop is to suppress the interferences. In this case, it is worth to investigate the impact of imperfect channel information. So, here it is supposed that the relays have noisy channel and hence $\tilde{h}_{i,j}$ is used instead of $h_{i,j}$.

$$\tilde{h}_{i,j} = h_{i,j} + \hat{h}_{i,j} \quad i, j = 1, 2 \quad (30)$$

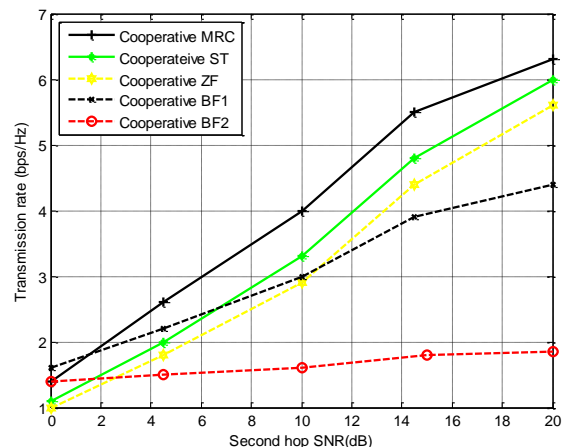


Fig. 4. Transmission Rates vs SNR in the Second Hop of different CR Schemes (1st hop SNR=20 dB, 2nd hop Direct Link SNR=10 dB).

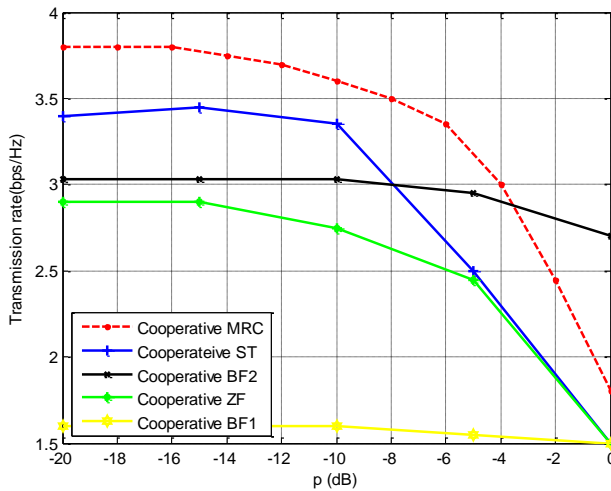


Fig. 5. Transmission Rate of difference Schemes vs the Erroneous Channel State Information at Relays.

Each entry of $\hat{h}_{i,j}$ is modeled as *i.i.d* circularly symmetric zero mean complex normal random variable $\mathbf{h}_{i,j} \cong CN(0, \sigma_{i,j}^2, \mathbf{I}_R)$. To quantify the estimation accuracy the parameter $\rho = \hat{\sigma}_{i,j}^2 / \sigma_{i,j}^2$ is used. Simulation results are given in Fig. 5.

It is known that a set up having interference cancellation capability may also be sophisticated to erroneous channel estimates. The BF2 cooperative relay scheme is unsusceptible to erroneous channel information by virtue of its characteristics that the relay nodes provide services to users through diverse channels. Even in worst in the case where the channel information is not perfect, the relay does not cause interference to other subscribers.

VI. CONCLUSIONS

Two novel CR technique using Decode and Forward strategy is proposed. The proposed techniques have the property that exchange of transmission data or knowledge of channel is not required by the relays and the signal received at each MS is free of interference. In term of spectral efficiency, the CMRC technique outdoes others at the cost of the high level of synchronization between different relaying stations. In case of synchronization problem, some type of cooperative space-timing technique is preferred. When the cross-link is powerful, then the both schemes surmount the conventional ZF and beamforming relay techniques.

The decode and forward strategy is lethargic as compared to other protocols explored in literature. Future work may be extended to use other protocols by countering the emerging problems. The use of spectrum may also be enhanced in future works.

ACKNOWLEDGMENT

This work was supported by the Balochistan University of Engineering and Technology, Khuzdar Pakistan, Research Fund.

REFERENCES

- [1] Sendonaris, E. Erkip and B. Aazhang, "User cooperation diversity-Part I: System Description" IEEE Transaction on communication, vol. 51, no. 2, pp.1927-1938, 2013.
- [2] A. Sendonaris, E. Erkip and B. Aazhang, "User cooperation diversity-Part I: Implementation aspects and performance analysis" IEEE Transaction on communication, vol. 51, no. 1, pp.1939-1948, 2013.
- [3] I. Ali, H. Lee, Y. S. Kil, A. Hussain, S. H. Kim, "Spatially Coupled LDPC Codes For Power Line Communications With Impulsive Noise", IEICE Electronics Express, vol. 15, no. 15, PP. 20180486-20180486, 2018.
- [4] I. Ali, H. Lee, A. Hussain, S. H. Kim, "Protograph-Based Folded Spatially Coupled LDPC Codes for Burst Erasure Channels", IEEE. Wireless Communications, vol. 8, no. 2, pp. 516-519, 2019.
- [5] I. Ali, J. H. kim, S. H. Kim, H. Kwak, J. S. No, "Improving Windowed Decoding of SC LDPC Codes by Effective Decoding Termination, Message Reuse, and Amplification", IEEE Access, vol. 6, pp. 9336-9346, 2017.
- [6] X. Gao, Xianbin, Victor CM, "Leung. A two-hop equalize-and-forward relay scheme in OFDM-based wireless networks over multipath channels" Wiley journal on wireless communications and mobile computing vol. 16, no. 7, pp.778-793, 2015.
- [7] A. Wittneben and I. Hammerstroem, "Multiuser zero forcing relaying with noisy channel state information" IEEE Wireless Communications and Networking Conference. New Orleans, LA, USA, 2005.
- [8] R. U. Nabar, H. Bolcskei and F. Kneubulher, "Fading relay channels: performance limits and space-time signal design" IEEE Journal on Selected Areas in Communications, vol. 22, no. 6, pp.1099-1109, 2004.
- [9] J. N. Laneman, D. N. C. Tse and G. Wornell, "Cooperative diversity in wireless networks: efficient protocols and outage behaviour" IEEE Transaction on Information Theory, vol. 50, no. 12, pp.3062-3080, 2004.
- [10] Z. Bhutto, W. Yoon, "Dual-Hop Cooperative Relaying with Beamforming Under Adaptive Transmission in κ - μ Shadowed Fading Environments". Electronics, vol. 8, no. 658, 2019.
- [11] M. Torabi, D. Haccoun, "Capacity of Amplify-and-Forward Selective Relaying with Adaptive Transmission under Outdated Channel Information", IEEE Trans. Veh. Technol. vol. 60, pp. 2416-2422, 2011.
- [12] M. Torabi, D. Haccoun, J. F. Frigon, "Impact of Outdated Relay Selection on the Capacity of AF Opportunistic Relaying Systems with Adaptive Transmission over Non-Identically Distributed Links", IEEE Trans. Wirel. Commun. vol. 10, pp. 3626-3631, 2011.
- [13] T. Lo. Maximum ratio transmission, "IEEE Transaction Communication", vol. 47, no. 2, pp.1458-1461, 1998.
- [14] S. Alamouti, "A simple transmit diversity technique for wireless communications", IEEE Journal on Selected Areas in Communications, vol. 16, no. 5, pp.1451-1458, 1998.
- [15] H. Phan, H. T. Q. Duong, H. J. Zepernick, L. Shu, "Adaptive Transmission in MIMO AF Relay Networks with Orthogonal Space-Time Block Codes over Nakagami-m Fading", EURASIP Journal of Wireless. Communications and Network., vol. 2011, pp. 1-13, 2012.
- [16] R. Kumar, A. Hussain, A. Azizl, and I. Joe, "Wireless DF Relaying with Beamforming for an Unmanned Aircraft System over κ - μ Fading Channels", Journal of Next Generation Information Technology, vol. 7, no. 3, pp. 26-35, January 2017.
- [17] R. Kumar, A. Azizl, and I. Joe, "Cooperative Dual-Hop Decode-and-Forward Relaying with Beamforming over κ - μ Fading Channels", Journal of Next Generation Information Technology, vol. 7, no. 4, pp. 38-49, July 2018.
- [18] R. Kumar, and I. Joe, "Performance Analysis of Wireless Cooperative Multicast Network using Decode and Forward Relaying", Journal of Next Generation Information Technology, vol. 7, no. 3, pp. 26-35, September 2016.

An M/M/1 Preemptive Queue based Priority MAC Protocol for WBSN to Transmit Pilgrims' Data

Shah Murtaza Rashid Al Masud¹, Mahmood ul Hassan², Khalid Mahmood³, Muhammad Akram⁴

Department of Computer Science, IIC University of Technology, Phnom Penh, Kingdom of Cambodia^{1,2}

Department of Computer Skills, Najran University, Najran, Kingdom of Saudi Arabia²

Department of Information Systems, Tehama Branch, King Khalid University, Abha, Kingdom of Saudi Arabia³

College of Computer Science and Information systems, Najran University, Najran, Kingdom of Saudi Arabia^{1,4}

Abstract—Every year during Hajj in Saudi Arabia and Kumbh Mela in India, many pilgrims suffering from different medical emergencies thus need real-time and fast healthcare services. Quick healthcare can be facilitated by setting up Wireless Body Sensor Network (WBSN) on pilgrims because of its suitability for a wide range of medical applications. However, higher delay, data loss and excessive energy consumption may occur in the network when multiple emergency data aggregate at the coordinator for accessing the data communication channel simultaneously. In this context, for low delay and energy-efficient data transmission, an M/M/1 preemptive queue technique is proposed and minimal backoff period is considered to develop a priority Medium Access Control (MAC) protocol for WBSN. Our proposed MAC is designed based on IEEE802.15.6 standard that supports modified MAC superframe structure for heterogeneous traffic. The proposed priority MAC protocol has been simulated using the Castalia simulator to analyze the results. In the first scenario considering varying nodes, the delay is calculated as 13 ms and 33 ms for the emergency, and the normal medical condition. Besides, for emergency and normal medical condition energy consumption per bit is calculated at around 0.12 μ j and 0.19 μ j. In the second scenario, we consider variation in traffic size. For 16 bytes traffic size, delay of extremely very high critical traffic is 5.8 ms and 14.5 ms for extremely low critical traffic. Similarly, extremely very high critical traffic consumes 0.035 μ j energy per bit, whereas extremely low critical traffic consumes 0.37 μ j. In the third scenario, the delay, data loss rate, average energy consumption and throughput for the proposed priority MAC are analyzed. Result demonstrates our proposed priority MAC protocol outperforms the state-of-the-art protocols.

Keywords—Wireless body sensor network; medium access control protocol; preemptive queue; priority; heterogeneous traffic

I. INTRODUCTION

According to the World Health Organization (WHO), the number of pilgrims from all over the world congregates to perform Hajj is more than two million. During Kumbh Mela in India, around sixty million pilgrims congregate at different four cities. Among many problems during the pilgrimage, pilgrims health monitoring is the most crucial issue. During the expedition, it is essential to identify people with health risk. Once they are detected, it is easy to monitor them and medical help and assistant can easily be provided for them [1-5].

So far, a few tracking and monitoring systems are proposed including, GPS as trackers [6], pilgrim's locator system [7], Hajj Locator for tacking pilgrims in a crowded environment [8]. RFID based location-tracking system [9]; WSNs based intelligent transportation systems (ITS) for facilitating efficient traffic movements [10]. Therefore, the healthcare sectors during Hajj and other religious festivals are looking for advanced Information and Communication Technology (ICT), which will be able to give health care services to pilgrims' in a wide-crowded area. There is a massive demand for deploying a new technology that can monitor and provide a real-time treatment to the pilgrims throughout the whole pilgrimage routine.

Wireless Body Sensor Networks (WBSNs) are offering a quick evolution in patients' healthcare monitoring applications. There are plenty of possibilities where location independent WBSNs are useful for monitoring, diagnosis, and treatment of diseases [11]. The IEEE 802.15.6 standard based WBSN/WBAN facilitates to deal with heterogeneous traffic include emergency and routine medical traffic. However, emergency data is mandatory to transmit ahead of other non-emergency traffic because any delay or data lost during transmission may impede patients' life [11].

Emergency traffic is very unpredictable and may produce regularly and eve randomly. Generally, emergency data are to be transmitted in non-scheduled and contention-free phase. However, normal (regular) medical data are to be sent in contention access period. But, the problem occurs when multiple emergency data aggregate at body coordinator to be transmitted simultaneously in WBAN medium thus results in data collision, data loss, severe delay and energy inefficiency. Hence, for collision-free, low delay and power-efficient data transmission, it is significant to identify the criticality level of emergency traffic to set the priority of emergency traffic. Hence, in this research, we proposed an M/M/1 preemptive queue-based priority MAC protocol to efficiently transmit pilgrims' data to the healthcare station with no delay and an energy-efficient manner. In a preemptive priority queue approach, data with high priority should access the communication channel faster and ahead of low priority data. Besides, for energy-efficient and low delay data transmission, a modified MAC superframe is proposed. Where Exclusive Access Phase (EAP) is fixed for emergency data transmission and Managed Access Phase is allocated for normal medical data transmission in WBSN medium.

The proposed priority MAC protocol has been simulated using Castalia simulator [20] to analyze and validate the results. The performance metrics of the proposed MAC protocol are analyzed and verified with state-of-the-art protocols. Results are compared with the most recent traffic adaptive based MAC protocol (TA-MAC) and traffic priority based channel access technique (TPCAT) protocol. Results demonstrate that delay, data loss rate, and the average energy consumption are relatively low, and the throughput is high during emergency data transmission in a network due to no data retransmission and collision. The main drawback of this research is to consider limited quality of service (QoS) requirement and limited biomedical data for our proposed priority MAC protocol.

The remainder of the paper is organized as follows: In Section 2, the related work is introduced. WBSN traffic classification, prioritization, network management are presented in Section 3. Section 4 shows a discussion for the simulation results. Finally, the paper ends with a conclusion in Section 5.

II. RELATED WORK

This section reviews the literature to analyze different methods, mechanisms, schemes that are available and applied for developing priority MAC protocol for medical applications. The priority MAC protocol must consider heterogeneous traffics. It should deem about different application requirements and the key challenges, including high data rates and prioritization of critical emergency data, low energy consumption, and low delay. The MAC protocol must ensure the timely delivery of medical data in the WBSN medium because any loss of such critical data may jeopardize the life of patients.

For better traffics adaptation and higher energy efficiency, the IEEE802.15.6 standard-based adaptive MAC protocol with modified superframe (A-MAC) is proposed [12]. A novel energy-efficient and lower delay MAC protocol for WBAN by using the radio wake-up mechanism is proposed [13]. IEEE802.15.4 standard-based traffic-aware and reliable MAC for WBAN is offered by [14]. To design the protocol, the authors classified the emergency traffics into different criticality levels based on the threshold value. The superframe is modified and divided into different time slots for channel access. A dynamically allocated time slot for IEEE802.15.4 based MAC superframe is proposed by the authors [15], CAP is divided into four phases. The data is prioritized into four different types, and according to the level of priority data get access to the phases as emergency traffic ET-CAP (Phase 1), on-demand traffic ODT CAP (Phase 2), normal traffic NT-CAP (Phase 3), and non-medical traffic NMT-CAP (Phase 4).

A traffic priority based channel assignment technique (TP-CAT) for critical traffic is proposed by [16], which is based on IEEE802.15.6. The method is developed based on two algorithms include low threshold and high threshold adaptive time slot algorithms. The main goal of TP-CAT is set to low delay data transmission for critical data. Traffic-adaptive

priority MAC protocol (TAP-MAC) is proposed [17] using a modified MAC superframe structure aims to reduce contention in the CAP period; otherwise, the collisions in data transmission channels may increase. Energy-Efficient Traffic Prioritization scheme (EETP) with modified MAC superframe is proposed in [18]. Where traffic is prioritized into four categories according to delay, reliability and criticality constraints [18], besides, both CSMA/CA and TDMA techniques are used to access the channel for non-emergency and life-critical emergency traffic, respectively.

Traffic sensitive WBAN by using TDMA based non-preemptive priority queue method has been proposed by [19]. Three different traffic priority levels, including emergency traffic, on-demand and normal traffic, are being classified and non-preemptive queues method at the WBAN coordinator has been proposed for data transmission in the medium. In this study, similar types of data need to wait for transmitting in the pre-reallocated time slots; as a result, delay and energy consumption both are increased.

Most of the existing protocols, as explained above, are proposed based on the IEEE 802.15.4 and the IEEE 802.15.6 standards that pay attention to a particular class of traffic either high or low. In WBAN, high-priority traffic is usually the lowest load traffic. And low-priority traffic is usually the highest load traffic, hence ignoring both or one of them the MAC superframe may strictly harm the overall transmission, energy consumption, overall delay and network throughput. Different data types reflect the primary motivation of almost all the MAC protocol mentioned above. However, there is a crucial necessity to provide additional importance to handle various emergency data and its criticality levels. The observation on the shortcomings of the current WBSN priority and traffic management protocol has encouraged us to develop a novel traffics' management solution for a network to cope with challenges above including lower delay and lower energy consumption; and higher network throughput.

III. WBSN OPERATION FOR THE PROPOSED PRIORITY MAC PROTOCOL

A. Data Classification and Prioritization

To deal with a normal (regular) medical and emergency event at any moment is much more comfortable, encouraging and less challenging than that of multiple emergency events simultaneously at WBSN coordinator level. Based on our study [1-7], to build a priority MAC protocol in this research, we consider heterogeneous traffic. Besides, emergency data is further classified into twelve different classes based on traffics severity level during the pilgrimage as presented in the following Table I.

Emergency critical data are usually event-triggered traffic and is produced whenever a life-threatening circumstance occurs. Hence, it is to be delivered and transmitted in WBAN medium with no delay, no loss and in a timely and real-time manner. On the other hand, non-critical normal physiological data require periodic monitoring hence does not restrict to strict delay or reliability constraints.

B. Proposed MAC Superframe Structure

The entire communication channel of the IEEE 802.15.6 standard is divided into superframe structures. Each superframe is encircled by a beacon period of equal length. To avoid data collision and simplicity of the research work, we further modify the MAC superframe, which is presented in Fig. 1.

In our proposal, we assign an Exclusive Access Phase (EAP) for emergency traffic that is a combined version of both EAP1 and EAP2. User priority UP₇ is set to ensure its highest level of priority over all sorts of medical data. Emergency medical data are aperiodic and required contention-free access to the channel, which is not scheduled based. Besides, in our proposed mechanism, for on-demand medical data Random Access Period (RAP) is proposed that is a combined version RAP1 and RAP2. And finally, for normal medical or non-medical traffic a scheduled based or query-based Managed Access Period or phase (MAP) is proposed, which is a combined version of both MAP 1 and MAP 2. It can be observed from the above discussion that, in this research, sensor nodes use a priority-aware CSMA/CA access scheme for EAP access phases along with preemptive priority queue model to attain contention-free data communication and nodes allocation.

TABLE I. SEVERITY LEVEL OF DISEASES

Disease	Severity level
Respiratory diseases such as pneumonia, influenza, asthma,	extremely very high critical traffic
Heart attack due to heatstroke or heat attack	Extremely high critical traffic
Diabetes due to blood sugar	Extremely critical traffic
Cardiovascular disease (Heart disease)	Very high critical traffic
Blood pressure	High critical traffic
Gastroenteritis	Critical traffic
Hypertension	Moderately critical traffic
Skin disease, Dry eye	Moderately low critical traffic
High Fever or High Body Temperature	Moderately very low critical traffic
Urinary tract infection (UTI)	Low critical traffic
Diarrhoea and jaundice	Very low critical traffic
Meningococcal	Extremely low critical traffic

In this research, we suppose, emergency data, on-demand data and normal data comprise the highest priority, the medium priority, and the lowest priority respectfully. Also, for collecting emergency data considering different criticality levels, five sensors are to be utilized, followed by one sensor for on-demand data. Normal physiological data are to be collected periodically by the same sensors that are deployed for emergency traffic. Usually, emergency or critical data and normal physiological data can easily be differentiated by their threshold values. Thus, the priority-criticality index for the data is defined by the combination of the highest level of user priority (P₁: emergency data) and different data criticality level (C₁-C₁₂). The index (I) is initiated to identify the criticality stage of emergency data as $I = P_1 C_i$ where $i=1-12$, that ranges from P₁C₁-P₁C₁₂ with WBAN user priority 7. Moreover, the higher the index, the higher the emergency data criticality level. Therefore the emergency traffic with the highest criticality level gets privileged to communicate faster in WBAN medium followed by on-demand traffic (P₂) with WBAN user priority 6, and normal traffic (P₃) with WBAN user priority 5. Body sensors and body coordinator have different activities such as sensors sense, process and transmit data to coordinator; whereas, coordinator collects, processes, sorts, and transmits data for further processing at healthcare centres. The following Table II illustrates the severity (criticality)-priority index table.

C. The Functions of Sensor Nodes and Coordinator

To deal with heterogeneous traffic for the proposed priority MAC protocol, we deploy an M/M/1 preemptive priority queue with different user priority and other classes of traffics. An M/M/1 queue deals with one server and one channel (wireless medium) where both the inter-arrival time and service time are exponentially distributed and arrivals are determined by the Poisson process. Besides, the service time (Backoff process duration) of the M/M/1 priority queue model does not follow any universal probability law and the Poisson process can model the generated traffic in the system. In this proposed model, emergency traffic is classified and prioritized through the severity level of pilgrims' health-related problems. From the numerical analysis, we find that the physiological data with the uppermost priority should not stay at the queue for a long time which reduces the overall delay during communication. Furthermore, for energy-efficient data transmission, we suggest a sleep/idle-wakeup method that decreases unnecessary energy consumption.

The sensor node sensed data and send it to the coordinator node. After receiving data from sensors, the coordinator node compares the sensed data with the pre-defined threshold value to define whether the event is an emergency or not. An emergency event occurs when data exceeds the pre-defined threshold value. Otherwise, data belong to either on-demand (aperiodic) or normal (periodic). The data transmission rate is higher in emergency condition than on-demand or normal state. Once data types are defined, data are sent to the nearest access point through the data communication channel. Emergency data is further classified and send to healthcare stations through dedicated time slot based on the criticality level.

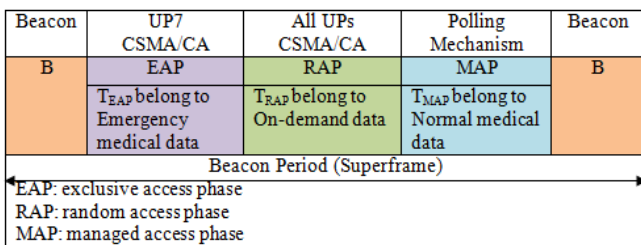


Fig. 1. Proposed MAC Superframe Structure.

TABLE II. SEVERITY (CRITICALITY)-PRIORITY INDEX TABLE

Providing User Priority (UP) according to IEEE802.15.6 standard	Index of Data Priority	Index of Emergency Data Criticality	Criticality-Priority Index Table	Types of Access Phases
UP ₇ for the Emergency medical situation	P ₁ , indicates the highest priority	C _i ={1,2,3,4,5,...,12}	Indices for different emergency data: P ₁ C ₁ ={P ₁ C ₁ , P ₁ C ₂ , P ₁ C ₃ , P ₁ C ₄ , P ₁ C ₅ , P ₁ C ₁₂ }	EAP (EAP1 and EAP2)-Exclusive Access Phase
UP ₆ for high priority medical data	P ₂ , indicates the medium priority	P ₁ C _i = 0		RAP (RAP1 and RAP2)-Random Access Phase
UP ₅ for medical data	P ₃ , indicates the lowest priority	P ₁ C _i = 0		MAP (MAP1 and MAP2)-Managed Access Phase

The following Fig. 2 presents the algorithm that depicts the role of the coordinator node to identify different types of data, e.g. emergency, on-demand or normal. If any data come from body sensor node which is categorized as an emergency and if there is a corresponding level of criticality or emergency type already stored before in the criticality index table, then the status of that particular data traffic will be designated and counted as critical. In our research, we further define and assess the level of criticality of data, as presented in Fig. 3.

- a) If the priority-criticality index value $P_1C_i=P_1C_1$, then the traffic is nominated as extremely very high critical traffic.
- b) If the priority-criticality index value $P_1C_i=P_1C_2$, then the traffic is nominated as extremely high critical traffic.
- c) If the priority-criticality index value $P_1C_i=P_1C_3$, then the traffic is nominated as extremely critical traffic.
- d) If the priority-criticality index value $P_1C_i=P_1C_4$, then the traffic is nominated as very high critical traffic.
- e) And if the priority-criticality index value $P_1C_i=P_1C_5$, then the traffic is nominated as high critical traffic.
- f) If the priority-criticality index value $P_1C_i=P_1C_6$, then the traffic is nominated as extremely critical traffic.
- g) If the priority-criticality index value $P_1C_i=P_1C_7$, then the traffic is nominated as moderately critical traffic.
- h) If the priority-criticality index value $P_1C_i=P_1C_8$, then the traffic is nominated as moderately low critical traffic.
- i) And if the priority-criticality index value $P_1C_i=P_1C_9$, then the traffic is nominated as moderately very low critical traffic.

- j) If the priority-criticality index value $P_1C_i=P_1C_{10}$ then the traffic is nominated as low critical traffic.
- k) And if the priority-criticality index value $P_1C_i=P_1C_{11}$, then the traffic is nominated as very low critical traffic.
- l) If the priority-criticality index value $P_1C_i=P_1C_{12}$, then the traffic is nominated as extremely low critical traffic.

Pseudo code 1: To define heterogeneous physiological data types at coordinator level

Input:

Threshold value for each physiological heterogeneous data/packets/traffic (vital sign): threshold value

Physiological data/packets/traffic are sensed by various sensors: data

Output:

Data types' classification by sensor nodes

Begin

//Sensors sense data from Pilgrims/Patients and send to coordinator/gateway/hub/sink/master node for further processing

1. **if** data exceeds (> or <) threshold value **then**
 Category of data is in emergency condition
 Set the highest priority
 Send data from coordinator to channel as soon as channel is idle for allocation of slots in superframe for data transmission using CSMA/CA access mechanism
 2. **elseif** data exceeds (> or <) or within (<>)threshold value
 (is sensed due to the request received from healthcare station via the body coordinator) **then**
 Category of data is in on-demand scenario
 Set the second highest priority
 Coordinator send data received from sensor to channel for allocation of slots for data transmission using CSMA/CA access mechanism
 3. **elseif** data within (<>) threshold value **then**
 Category of data is in normal scenario
 Set low priority
 Send data from coordinator to channel in allocated time for allocation of slots for data transmission using scheduled access mechanism
 4. **else**
 Repeat step 1
 5. **end if**
- End**

Fig. 2. The Role of the Coordinator to Identify Heterogeneous Traffic.

Pseudo code 2: To handle emergency and non-emergency events along with the criticality levels of emergency data at coordinator node

Input:

T: Traffic that justifies patients'/pilgrims' health status data type

P_1C_i : Priority-criticality (severity) index value

Output:

Emergency events classification based on data criticality level

Begin

// for every arrive data from the sensor node

1. **if** (data type == emergency)&&($P_1C_i = P_1C_1$) **then**
T nominates as extremely very high critical traffic
2. **elseif** (data type == emergency)&&($P_1C_i = P_1C_2$) **then**
T nominates as extremely high critical traffic
3. **elseif** (data type == emergency)&&($P_1C_i = P_1C_3$) **then**
T nominates as extremely critical traffic
4. **elseif** (data type == emergency)&&($P_1C_i = P_1C_4$) **then**
T nominates as very high critical traffic
5. **elseif** (data type == emergency)&&($P_1C_i = P_1C_5$) **then**
T nominates as high critical traffic
6. **elseif** (data type == emergency)&&($P_1C_i = P_1C_6$) **then**
T nominates as critical traffic
7. **elseif** (data type == emergency)&&($P_1C_i = P_1C_7$) **then**
T nominates as moderately critical traffic
8. **elseif** (data type == emergency)&&($P_1C_i = P_1C_8$) **then**
T nominates as moderately low critical traffic
9. **elseif** (data type == emergency)&&($P_1C_i = P_1C_9$) **then**
T nominates as moderately very low critical traffic
10. **elseif** (data type == emergency)&&($P_1C_i = P_1C_{10}$) **then**
T nominates as low critical traffic
11. **elseif** (data type == emergency)&&($P_1C_i = P_1C_{11}$) **then**
T nominates as very low critical traffic
12. **elseif** (data type == emergency)&&($P_1C_i = P_1C_{12}$) **then**
T nominates as extremely low critical traffic
13. **else**
if (data type == on-demand)&&($P_1C_i = 0$) **then**
T nominates as on-demand
14. **end if**
15. **else**
16. **if** (data type == no event or normal)&&($P_1C_i = 0$) **then**
T nominates as normal traffic
17. **end if**
18. **end if**
19. **end**

Fig. 3. The Role of the Coordinator to Deal with Emergency Traffic.

The following Fig. 4 shows the deployment of CSMA/CA mechanism for the proposed model and for that the user priority is set to UP_i where, $i = 5-7$ for normal, on-demand and emergency traffic respectively. The proposed WBAN should handle heterogeneous traffic hence for the transmission of emergency traffic the length of back off counter (BC) must be minimal, otherwise for normal medical data the length of BC can be more. And data is transmitted when the $BC=0$. Moreover, in this emergency data transmission case the contention window (CW) is set to a minimum as $CW=CW_{min}$. for the rest of the cases, the CW is set to CW_{max} . In the case of transmission of the normal medical data, the coordinator needs to wait until the emergency data are all transmitted.

D. Analytical Model of the Proposed Priority MAC Protocol M/M/1 Queue based Preemptive Method

In this research, the overall delay is calculated as the addition of transmission delay and the queue delay. Average data transmission time is considered as the packet transmission delay from the source to the destination node. The queue delay demonstrates the moment when the packet departs or leaves the queue due to not successfully transmission of packets. The service time is being served as the queue delay in our queuing model. We consider the average delay to analysis the performance of our analytical model. The delay can be calculated for extremely very high critical traffic, extremely high critical traffic, extremely critical traffic, very high critical traffic, and high critical traffic as shown in quations (1), (2), (3), (4), and (5), respectively.

$$E(t_{p1c1}) = \frac{\frac{1}{\mu}}{1-\rho_{p1c1}} \tag{1}$$

$$E(t_{p1c2}) = \frac{E(n_{p1c2})}{\lambda p1c2} = \frac{\frac{1}{\mu}}{(1-\rho_{p1c1})(1-\rho_{p1c1}-\rho_{p1c2})} \tag{2}$$

$$E(t_{p1c3}) = \frac{E(n_{p1c3})}{\lambda p1c3} = \frac{\frac{1}{\mu}}{(1-\rho_{p1c1}-\rho_{p1c2})(1-\rho_{p1c1}-\rho_{p1c2}-\rho_{p1c3})} \tag{3}$$

$$E(t_{p1c4}) = \frac{E(n_{p1c4})}{\lambda p1c4} = \frac{\frac{1}{\mu}}{(1-\rho_{p1c1}-\rho_{p1c2}-\rho_{p1c3})(1-\rho_{p1c1}-\rho_{p1c2}-\rho_{p1c3}-\rho_{p1c4})} \tag{4}$$

$$E(t_{p1c5}) = \frac{E(n_{p1c5})}{\lambda p1c5} = \frac{\frac{1}{\mu}}{(1-\rho_{p1c1}-\rho_{p1c2}-\rho_{p1c3}-\rho_{p1c4})(1-\rho_{p1c1}-\rho_{p1c2}-\rho_{p1c3}-\rho_{p1c4}-\rho_{p1c5})} \tag{5}$$

For n different severity level of traffic, the delay can be formulated as follows:

$$E(n_{p1ci}) = \frac{\rho_{p1c1} + \rho_{p1c2} + \rho_{p1c3} + \rho_{p1c4} + \rho_{p1c5}}{1 - \rho_{p1c1} - \rho_{p1c2} - \rho_{p1c3} - \rho_{p1c4} - \rho_{p1c5}} - \frac{\rho_{p1c1} + \rho_{p1c2} + \rho_{p1c3} + \rho_{p1c5}}{1 - \rho_{p1c1} - \rho_{p1c2} - \rho_{p1c3} - \rho_{p1c4}} \\ = \frac{\rho_{p1ci}}{(1 - (\sum_{i=1}^{n-1} \rho_{p1ci})) (1 - (\sum_{i=1}^n \rho_{p1ci}))} \tag{6}$$

And by applying Little's law we get,

$$E(t_{p1ci}) = \frac{E(n_{p1ci})}{\lambda p1ci} = \frac{\frac{1}{\mu}}{(1 - (\sum_{i=1}^{n-1} \rho_{p1ci})) (1 - (\sum_{i=1}^n \rho_{p1ci}))} \tag{7}$$

Over a communication channel, at the destination, throughput is measured as the number of packets correctly received at the destination point in a unit time (the average transmission rate). Kbps is considered as the unit of throughput.

Throughput measures the actual level of network traffic between the transmitting node and receiving nodes. The throughput is calculated as follows.

$$\text{Throughput} = \frac{\sum \text{Packets received}}{\sum \text{Packets generated}} \tag{8}$$

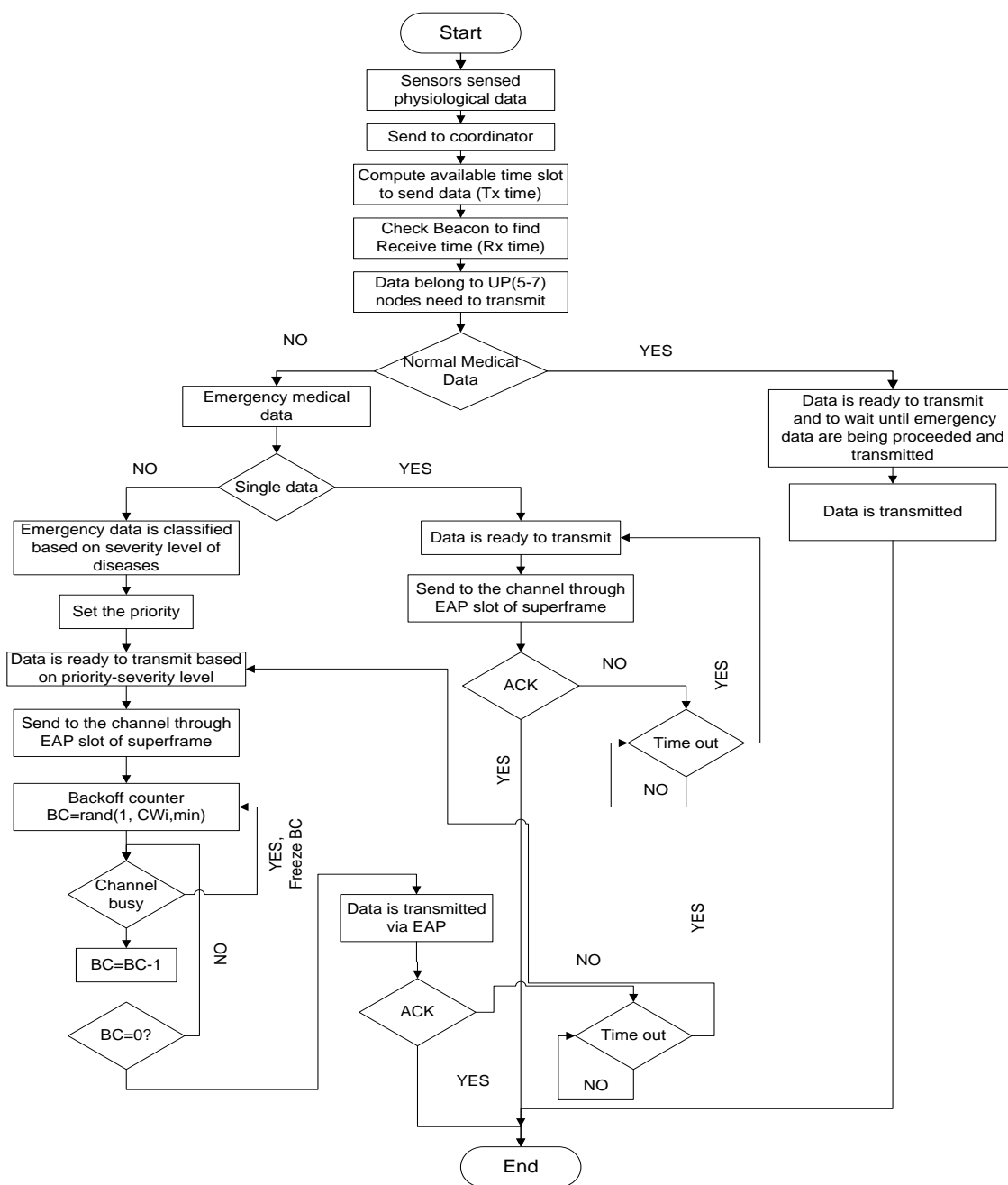


Fig. 4. Operational Flowchart of the Proposed MAC Protocol based on CSMA/CA Mechanism.

Efficient and the low energy consumption is considered as the fundamental requirement of designing MAC protocol for WBAN and its associated networks. The behaviour of wireless network nodes depends on energy consumption and the way to manage it. A network having low traffic consumes less energy than the one with heavy traffic. In this research, the energy consumption of the network is calculated as the cumulative sum of energy consumed by all the sensor nodes. Where energy consumed by a single node is defined as how much remaining energy is subtracting from the initial (preliminary) energy. To systematically and comprehensively evaluate the MAC protocols of WBAN applications, we evaluate energy efficiency by calculating average energy consumption per bit.

At the time of a network simulation run, the energy consumption per bit is calculated as the ratio of the total energy (power) consumption over the total number of bits delivered. Hence, the total energy consumed can be computed as follows.

$$E_{tec} = T_{wakeup} \times P_{wakeup} + T_{tx} \times P_{tx} + T_{rx} \times P_{rx} + T_{sleep} \times P_{sleep} \quad (9)$$

The total dropped packets are considered as the difference between total transmitted packets (data and control) and total received packets (data & control) during the data transmission session. Thus, packet drop ratio at the destination node is calculated and defined as the total number of dropped packets

over total transmitted packets. The the packets dropped loss ratio can be formulated as follows.

$$\text{Packets loss ratio} = \frac{\text{Number of lost packets}}{\text{Number of received packets}} \quad (10)$$

E. Simulation Environment

The proposed protocol is simulated using Castalia simulator. In this simulation, sensors generate heterogeneous medical packets in term of priority and sensitivity.

F. Simulation Parameters

To observe the performance of the proposed priority MAC protocol, various scenarios are considered to implement and evaluate include variation in a number of nodes (network size), and traffic sizes up. Varied network sizes ranging from 1 node to 12 nodes are considered to evaluate the performance of the protocol for different sized network. On the other hand, various traffic sizes ranging from 16 bytes to 127 bytes are supposed to assess the performance of the protocol. Correlated with other simulation environments, these nodes are considered with a transmission range of 5 to 10 meters. The operating frequency is set to be 2.4 GHz ISM band, and the bandwidth of the channel is considered to be 250 kbps. The simulation parameters are summarized in Table III.

TABLE III. SIMULATION PARAMETERS

Parameters	Value
Number of nodes	12
Nodes transmission range	From sensing range to max 5m to 10 m
mMaxBANSize	< 64 nodes
MAC	IEEE 802.15.6
Channel mode	Wireless Model
Superframe size	255 slots
Superframe Duration	122.88 ms
Simulation time or runtime	150 Seconds
Frequency band/ Operating Frequency	2.4 GHz ISM
Channel or Data rates or Bandwidth	Various data rates up to 250 kbps
Area Size	5m x 5m
Packet Size	Variable, up to 512 bytes
macMaxCSMABackoffs	*So far there is no specific unit
Initial energy	1 Joule
Transmission power consumption	12.3 mA
Reception power consumption	14 mA
Idle power consumption	0.4 mA
Beacon size	40 ytes

IV. RESULT AND DISCUSSION

A. Performance Evaluation and Result Discussion

The performance of the priority MAC protocol is analyzed and evaluated for diverse scenarios, and QoS conditions such as delay, energy, throughput, and packets dropped rate considering the variation of sensor nodes in the network and different packet sizes up. We assume a star topology WBAN with a single hop and heterogeneous traffic or data. In our

proposed analytical model for the MAC superframe structure, the length of EAP2, RAP2 and CAP is set to zero. We assume that data can access the channel without RTS/CTS mechanism, and data retransmission may occur if there is any collision. The performance of the MAC model is compared with TA-MAC protocol and TP-CAT protocol, and the simulation results are depicted in the subsequent sub-sections.

B. First Scenario

In the first scenario, delay and energy consumption comparison for urgent and normal traffic under varying nodes for the Proposed Priority MAC Protocol is portrayed.

Fig. 5 illustrates the situation where the network size (the number of nodes) increases for both emergency and normal medical cases from 1 to 12 with the constant packets size 16 Bytes. It has been found that the delay for both normal and emergency medical traffic increases with the increasing number of nodes.

Hence, the increase in overall delay is due to the increased number of nodes and packets generated, thus increased wait, collisions and retransmissions in the network. In the implementation of the proposed priority MAC protocol, we assume there is no data collision and retransmission in the network since we deploy a preemptive priority queue scheme and the modified MAC superframe structure.

Therefore, in the proposed priority MAC protocol deploying technique, the emergency medical traffic proceeds ahead of normal medical traffic and to access the channel faster than normal medical traffic. Hence the delay in emergency traffic is much less than normal medical traffic.

The energy consumption rate for normal medical traffic is higher than that of emergency medical traffic because normal traffic needs to wait more in the network for being transmitted to the communication channel than emergency traffic. If the delay increases in the network drastically for the normal traffic, then there is a more possibility of more energy consumption whereas the level of energy consumption is lower for emergency traffic as presented in Fig. 6.

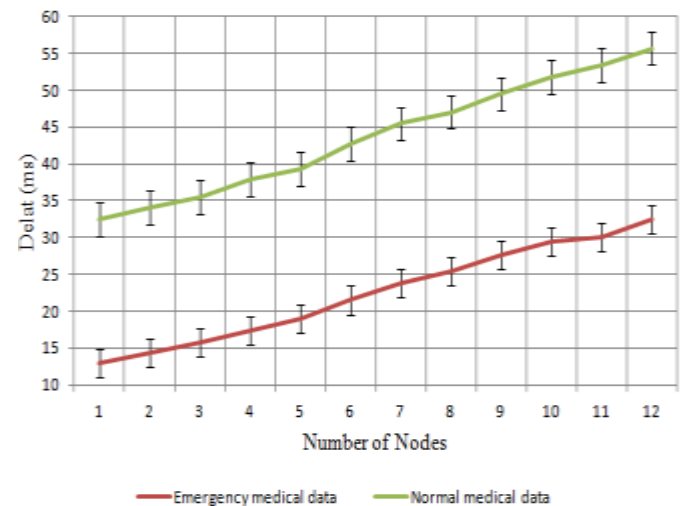


Fig. 5. Delay Assessment for Emergency Medical and Normal Medical Traffics under Varying Sensor Nodes in the Network.

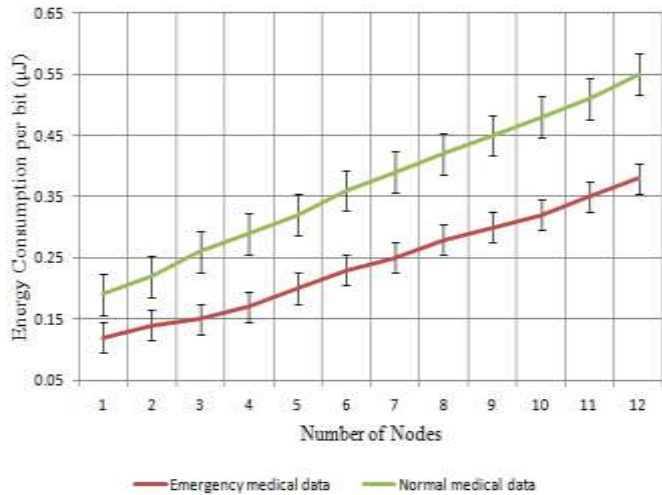


Fig. 6. Energy Consumption Assessment for Emergency Medical and Normal Medical Traffics under Varying Sensor Nodes in the Network.

C. Second Scenario

In the second scenario, the performance analysis of different emergency traffic considering their level of priorities for the proposed priority MAC protocol is presented.

In this section, the performance of different emergency traffic is analyzed based on their priorities and level of criticality. The results are determined considering variation in traffic sizes.

It is observed that at 2.4 GHz frequency band and 250 kbps data rate, the emergency traffic with the highest priority can send data faster than that of lower priority. The results differ with the number of packets sizes up to 127 bytes.

Here, user priority seven is considered for emergency traffic. However, the difference in delay values between P_1C_1 (Extremely very high critical data) extremely very high critical emergency traffic and P_1C_{12} (Extremely Low critical data) extremely low critical traffic under WBAN user priority seven is observed. P_1C_1 extremely very high critical emergency traffic provides less delay than other low critical emergency traffic because P_1C_1 (Extremely very high critical data) gets earlier and more channel opportunities. However, the cumulative delay of 12 emergency data and normal data is equal to the average delay of twelve nodes during the medical normal and emergency events as presented earlier in Fig. 5. The data collision and data retransmission possibility are less since we deploy preemptive priority queue at the MAC level that ensures fast and low delay data communication which is illustrated in Fig. 7.

Also, emergency traffic with the highest critical index P_1C_1 (Extremely very high critical data) consumes less energy than emergency traffic with lower criticality index. Include P_1C_2 (Extremely high critical data), P_1C_3 (Extremely critical data), P_1C_4 (Very high critical data), P_1C_5 (High critical data) and so forth until P_1C_{12} (Extremely low critical data). However, the energy consumption increases for all traffic classes according to packet size up, and the result is illustrated in Fig. 8.

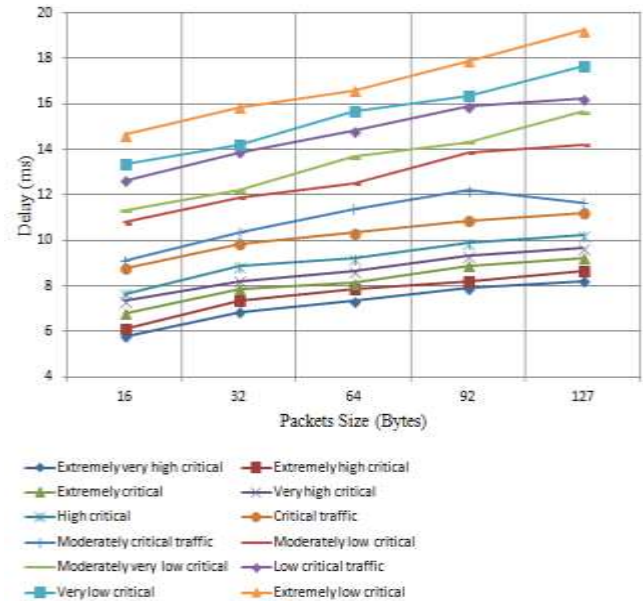


Fig. 7. Average Delay (ms) of Emergency Traffic is Analyzed based on their Priorities and Criticality Level as Compared to Packet Sizes up.

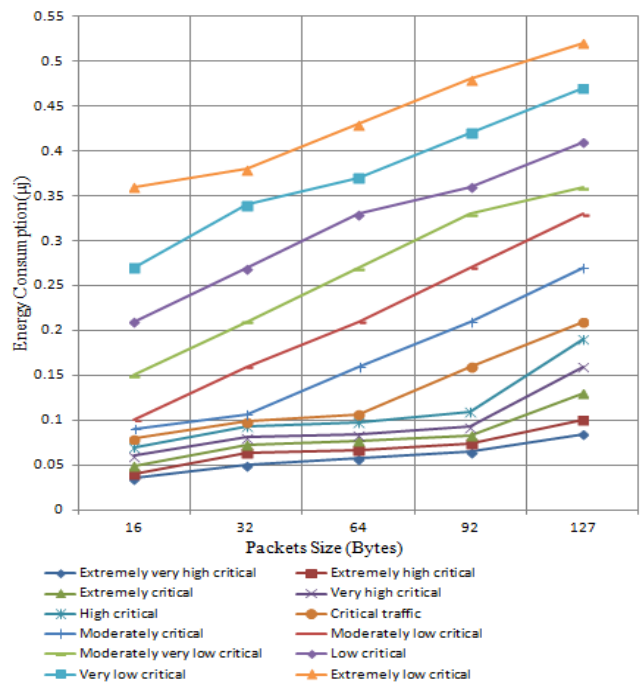


Fig. 8. Overall Energy (Power) Consumption Per Bit (µJ) of Emergency Traffic is Analyzed based on their Priorities Level as Compared to Packet Sizes up.

D. Third Scenario

In the third scenario, the performance analysis and evaluation of proposed priority MAC protocol based on heterogeneous traffic, considering variation in the number of sensor nodes (Network Size) are discussed.

For all the distinct circumstances, we assign the maximum number of sensor nodes as 12 because under 12, the proposed IEEE 802.15.6 priority MAC protocol and other competitive

MAC protocols such as TA-MAC protocol and TP-CAT protocol show performance inconsistency and difference. It is remarkable that for a maximum number of sensor nodes 12, the average delay of the proposed MAC sharply decreases, which is less than TA-MAC protocol and TP-CAT protocol, as shown in Fig. 9.

In a wireless network, an increase in the number of nodes may increase the number of traffic load; hence, collisions, data retransmissions also increase. However, in the proposed priority MAC protocol, the CAP is set to zero. And the EAP phase is fixed for emergency data access, hence, contention in our proposed priority MAC is significantly less than that of the TP-CAT protocol and TA MAC protocol, resulting in a lower number of collisions, and therefore lower energy consumption. Fig. 10 portrays the average power consumption per bit basis.

Fig. 11 shows the overall network throughput of the priority MAC protocol, TA-MAC protocol and TP-CAT protocol. Here, in this research, when the network has increased number of sensor nodes (in our case nodes range 1-12) or traffic load, then the throughput of all three protocols such as priority MAC, TP-CAT protocol and TA-MAC protocol also increases. Our proposed priority MAC protocol shows enhanced throughput over TA-MAC and TP-CAT protocol with the increased number of sensor nodes. Data classification and prioritization mechanism, EAP allocation for emergency data transmission make the priority MAC protocol of this research outperforms TA-MAC and TP-CAT protocol.

In a wireless network, an increase in the number of nodes may increase the amount of traffic load; hence, collisions, data retransmissions also may increase thus results in raising the percentage of packets dropped rate. However, as discussed in earlier sections, in the proposed priority MAC protocol, the CAP is set to zero, and the EAP phase is fixed for emergency data access. Hence, contention and packets retransmission in the proposed priority MAC is significantly less than that of TP-CAT and TA-MAC protocol, resulting in a lower number of collisions. Therefore lower packets dropped rate in our proposed priority MAC protocol. The packet dropped rate is shown in Fig. 12.

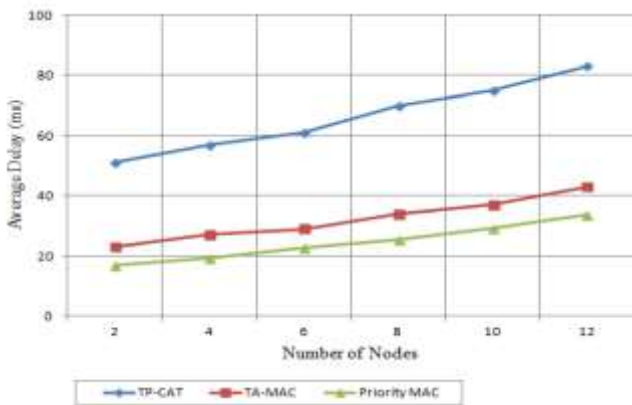


Fig. 9. Average Delay in Millisecond (ms) as Compared to the Number of Nodes.

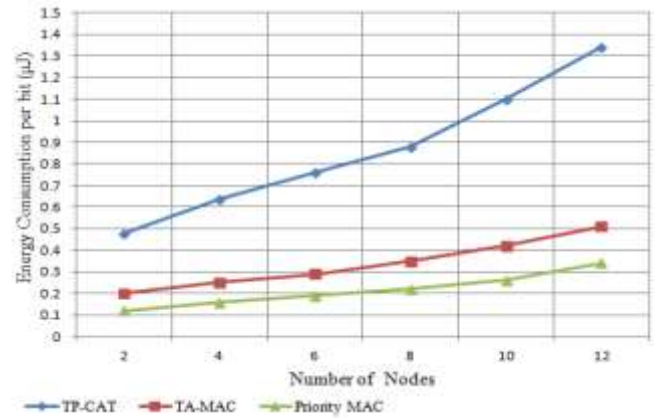


Fig. 10. Average Power (Energy) Consumption Per Bit.

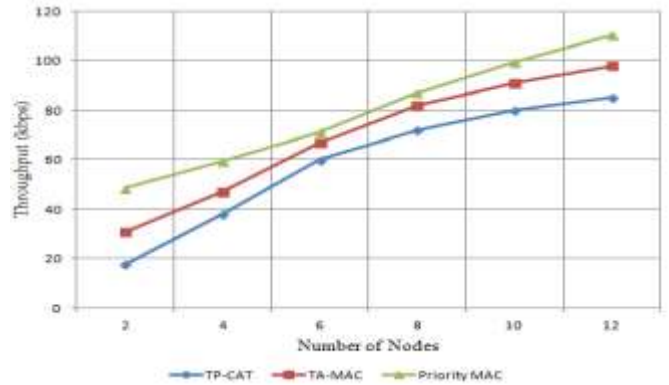


Fig. 11. Overall Network Throughput.

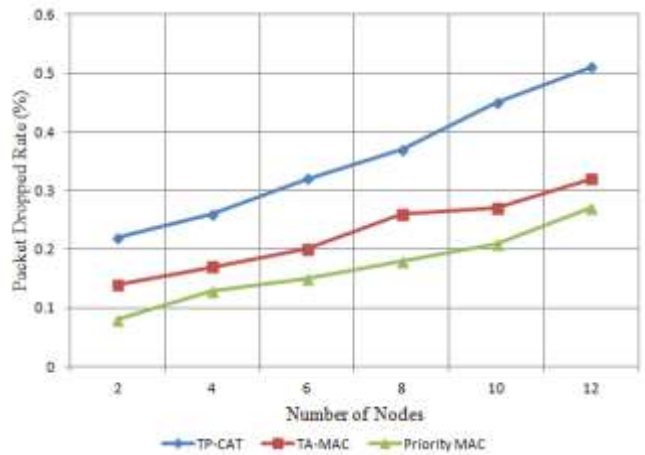


Fig. 12. Packets Dropped Rate (%).

V. CONCLUSION

To monitor pilgrims' health in a real-time manner, several issues are considered in designing an M/M/1 preemptive queue-based priority MAC protocol. First, pilgrims emergencies are categorized and prioritized based on the level of criticality. Second, algorithms are developed to define the role of different sensors and the coordinator. Third, the MAC superframe structure is improved according to the IEEE 802.15.6 standard for fast and collision-free data transmission.

Fourth, to reduce the delay of physiological data transmission, an M/M/1 preemptive priority queue model is proposed and minimal backoff period is considered. Fifth, to improve energy efficiency, sleep and the wake-up mechanism is used. The proposed priority MAC protocol has been simulated using the Castalia simulator. Results are compared with the most recent traffic adaptive based MAC protocol (TA-MAC) and traffic priority based channel access technique (TP-CAT) protocol. Results demonstrate that delay, data loss rate, and the average energy consumption are relatively low. The throughput is high during emergency data transmission in a network due to no data retransmission and collision. Our future plan is to experiment the proposed MAC protocol with non-preemptive priority queue method. And also for broader types of biomedical data with boundless QoS issues.

ACKNOWLEDGMENT

We would like to express our gratitude to IIC University of Technology, Cambodia and Najran University, Saudi Arabia for providing us excellent research environment.

REFERENCES

- [1] WHO report on Hajj: http://www.who.int/csr/ITH_final.pdf.
- [2] MoH KSA guideline on Hajj: <https://www.moh.gov.sa/en/Hajj1432/Awareness/Documents/DlelHaj-E.pdf>.
- [3] Abdullah, A., Jamil, A., & Memish, Z. (2012). Pattern of diseases among visitors to Mina health centers during the Hajj season, 1429H (2008G). *Journal of Infection and Public Health*, 5, 22–34.
- [4] Ahmed, Q. A., Arabi, Y. M., & Memish, Z. A. (2006). Health risks at the Hajj. *Lancet*, 367(9515), 1008–1015. [https://doi.org/10.1016/S0140-6736\(06\)68429-8](https://doi.org/10.1016/S0140-6736(06)68429-8).
- [5] Ahmed, Q. A., Arabi, Y. M., & Memish, Z. A. (2015). Health risk at the Hajj. 6736 (APRIL 2006). [https://doi.org/10.1016/S0140-6736\(06\)68429-8](https://doi.org/10.1016/S0140-6736(06)68429-8).
- [6] Alkar, A.Z and Karaca, M.A., 2009, "An Internet Based Interactive Embedded Data-Acquisition System for Real-Time Applications", *IEEE Transactions on Instrumentation and Measurement*, Vol.58, No.3, pp. 522.
- [7] Aladdein Amro, Qasem Abel-Muti Nijem, 2012 Pilgrims "Hajj" Tracking System (emutawiff)," *Contemporary Engineering Sciences*, Vol.5, No.9, p.p.437-446.
- [8] Jaafar, A.D. ; Aris, M.F.M. ; Ayu, M.A., Hajj Locator: A Hajj pilgrimage tracking framework in crowded ubiquitous environment, *International Conference on Multimedia Computing and Systems (ICMCS)*, 2011, page 1-6, Print ISBN: 978-1-61284-730-6.
- [9] Lionel M.Ni and Dian Zhang ,Michael.R.Souryal,2011, "RFID-Based Localization and Tracking Technologies", *IEEE Wireless Communication*. [8] Teddy Mantoro, Media.A.Ayu, Murni Mahmud, 2012, "Hajj Crowd Tracking in a Pervasive Environment", *International Journal of Mobile Computing and Multimedia Communication*, 4(2), 11-2.
- [10] O. Tayan, 'A Proposed Model for Optimizing the Flow of Pilgrims between Holy Sites During Hajj Using Traffic Congestion Control', *Proceedings of the International Journal of Engineering and Technology*, Publication Date: April 10, 2010.
- [11] L. J. Akinbami, J. E. Moorman, and X. Liu, "Asthma prevalence, health care use, and mortality: United States, 2005-2009.," *National health statistics reports*, no. 32, pp. 1-14, Jan. 2011.
- [12] Yuan, D., Zheng, G., Ma, H., Shang, J., & Li, J. (2019). An Adaptive MAC Protocol Based on IEEE802.15.6 for Wireless Body Area Networks. *Wireless Communications and Mobile Computing*, 2019, 1–9. <https://doi.org/10.1155/2019/3681631>.
- [13] Rismanian Yazdi, F., Hosseinzadeh, M., & Jabbehdari, S. (2019). A Priority-Based MAC Protocol for Energy Consumption and Delay Guaranteed in Wireless Body Area Networks. *Wireless Personal Communications*, (May). <https://doi.org/10.1007/s11277-019-06490-z>.
- [14] Gouda, K. C., Biswal, S. P., Debnath, S., Sahu, S. K., Science, C., Online, F., & Notes, L. (2019). Implementation of Traffic Priority Aware Medium Access Control Protocol for Wireless Body Area Networks. *Springer Link*, 1–7.
- [15] Bhandari, S., & Moh, S. (2019). A Mac Protocol with Dynamic Allocation of Time Slots Based on Traffic Priority in Wireless Body Area Networks. *International Journal of Computer Networks & Communications*, 11(4), 25–41. <https://doi.org/10.5121/ijcnc.2019.11402>.
- [16] Ambigavathi, M., & Sridharan, D. (2018c). Traffic Priority Based Channel Assignment Technique for Critical Data Transmission in Wireless Body Area Network. *Journal of Medical Systems*, 42(11). <https://doi.org/10.1007/s10916-018-1054-y>.
- [17] Henna, S., Sajeel, M., Bashir, F., Asfand-E-Yar, M., & Tauqir, M. (2017). A fair contention access scheme for low-priority traffic in wireless body area networks. *Sensors (Switzerland)*, 17(9). <https://doi.org/10.3390/s17091931>.
- [18] Ullah, F., Abdullah, A. H., Kaiwartya, O., Lloret, J., & Arshad, M. M. (2017). EETP-MAC: energy efficient traffic prioritization for medium access control in wireless body area networks. *Telecommunication Systems*, 1–23. <https://doi.org/10.1007/s11235-017-0349-5>.
- [19] Gündoğdu, K., & Çalhan, A. (2016). An Implementation of Wireless Body Area Networks for Improving Priority Data Transmission Delay. *Journal of Medical Systems*, 40(75).
- [20] Castalia simulator: <http://castalia.npc.nicta.com.au>.

Hybridized Machine Learning based Fractal Analysis Techniques for Breast Cancer Classification

Munmun Swain¹, Sumitra Kisan², Jyotir Moy Chatterjee³
Mahadevan Supramaniam⁴, Sachi Nandan Mohanty⁵, NZ Jhanjhi⁶, Azween Abdullah⁷
Department of CSE, VSSUT Burla, Odisha, India^{1,2}
Department of IT, Lord Buddha Education Foundation, Kathmandu, Nepal³
Research and Innovation Management Center, SEGi University, Malaysia⁴
Department of CSE, ICFAI Foundation of Higher Education University, Hyderabad, India⁵
School of Computer Science and Engineering, SCE, Taylor's University, Malaysia^{6,7}

Abstract—The usefulness of Fractal Analysis (FA) is not limited to a particular area. It is applied in variety of fields and has shown its efficiency towards irregular objects. Fractal dimension is the best measure of the roughness for natural elements and hence, it can be treated as a feature of the natural object. Breast masses are irregular and differs from a malignant tumor to benign; hence breast can be treated as one of the best areas where fractal geometry can be applied. It gives a scope where fractal geometry concept can be used as a feature extraction technique in mammogram. On the other hand, the support vector machine is an emerging technique for classification. The survey shows that few works have done on breast mass classification using support vector machine. In our work two most effective techniques are used in separate operations, FA: Box Count Method (BCM) and Support Vector Machine (SVM) that result well in their fields. Feature extraction is done through Box Count Method. The extracted feature, “fractal dimension”, measures the complexity of the input data set of 42 images. For the next segment, the resulting Fractal Dimensions (FD) are processed under the support vector machine classifier to classify benign and malignant cells. The result analysis shows that the combination of SVM and FD yielded the highest with 98.13% accuracy.

Keywords—Mammography; feature extraction; fractal dimension; box-counting method; classification; support vector machine

I. INTRODUCTION

Now a day's most of the women are suffering from Breast cancer, which is the most valid cause of cancer-related death [1]. As women are not treated in an initial stage in urban areas or under growing cities, the survival rate became very less. Women's breast consist of micro-calcifications, which are tiny calcium that deposited in the breast tissues; it makes a small bright spot in the mammogram. Micro-calcification is very small in size, so it is very difficult to detect (range of 0.05-1mm). Image processing is a tool that is widely spread in the field of medicine, mainly for the diagnose of diseases or disruption of the human body. The anatomical structure of breast cancer can be observed through its medical image which can be taken through high-quality imaging tools such as- X-Ray, Mammography, Thermography, Ultrasonograph, Medical Resonance Image.

Mammography and X-Ray are both treated as standard methods for breast cancer detection but, it is noticed that they are unable to detect the whole mass until it works on a specific size. Due to the high radiation, these methods are not preferable for below the age of 40 [2].

To overcome the above limitations a new tool is introduced known as “Thermograph”. This tool explores the usefulness of non-ionizing, free-radiation, convenient and beneficial. It is useful for a routine check-up to increase the certainty of breast malignant identification. Due to the convenient and non- ionizing feature, it can work for the urban areas.

Breast cancer & clumps show up as thick locales in mammograms. Generous clumps are round, smooth & all around outlined limits while malignant tumors have speculated, irregular, small dot-like, clustered, various in size, and blurry boundaries. The surface contrasts have been seen among benign & malignant clumps with former being generally homogenous & later show heterogeneous surface [3]. Thermograph technique is used to detect the temperature distribution over the entire surface of the breast. Due to the angiogenesis, the temperature of the skin over the tumor surface is more than the surrounding. It is easy to find the anomalous region with the help of an infrared camera [4-5].

Cancerous tumors exhibit arbitrariness related with their development & is ordinarily sporadic & complex fit as a fiddle. Thus FA can give a decent measure to their intricate examples than the conventional Euclidean geometry. A few PC supported strategies have been created to help specialists to improve the proficiency and precision of mammographic screening programs [6-10]. Different fractal-based methods have been utilized by researchers in different fields for fractal dimension estimation in natural objects such as cloud, trees, deserts. Nguyen. and Rangayyan [12] used fractal study for identification of abnormal sections in the mammogram, before testing in infrared camera. In 2010 Tavakal et al. [13] introduced the concept of FA for segmentation and division of breast thermography as Benign (range ≤ 1) or Malignant (> 1).

This paper is organized as follows: Section 1 provides the overall views; Section 2 is dedicated to the related works done in this area and Section 3 represents all the methodologies

which are used. Similarly, Section 4 describes experimental results. Finally, the work is concluded in Section 5.

II. RELATED WORK

Several researchers have introduced different methodologies for extracting features and classifying the mammogram images.

Heriana and Soesanti [15] proposed a method, which takes the image dataset, extracts the features through the fractal algorithm and after successful extraction of data, classification is done using C-means clustering algorithm. The result shows that 64x64 pixel box sizes are more consistent than 32 x 32 pixels. Several methods are developed such as image filtering and local threshold [16], stochastic fractal methods [17], wavelet analysis, fuzzy logic [18] for classification and segmentation. After few years Chang and Chen [22] were able to segment the tumor into malignant and benign type by calculating the Fractal dimension of ultrasound images. Rangayan and Shen [23] used Fourier transformation that detects the cancer affected area. They have used neural network classifier and got 89.21% accuracy in their preliminary analysis stage. Nooden, in 2010 with other researchers used probabilistic neural network for detection of cancerous zones in mammograms [24]. Moldovanu and Moraru [25] tried to highlight the connection between the fractal dimension of breast cancer and the knowledge which is extracted using the k-means algorithm [25]. In 2010, Patel & Sinha [19] developed a strategy for clinical image improvement, in light of the idea of fractal derivative & image processing strategies like segmentation of image with self-similar properties. The paper manages definite aftereffects of programmed recognition of breast cancer mass utilizing self-similar fractal-utilized segmentation. The [14] review shows that the concept of region of interest (ROI) is also one of the interesting techniques for cancerous area identification. After that Nam and Chai [20] used box-counting method to identify the area of established micro-calcification in mammograms and found the zones of cancerous micro-calcification cells. In 2001 also the fractal concept was used by Zheng and Chan to locate tumor cells on mammograms [11]. They have divided the image into the size of 16 x 16 boxes and determined the fractal dimension. They have noticed that the fractal dimensions of the portions, which contain cancer, lies within a certain boundary. Classification of galactograms using fractal properties was also done in 2006 [21]. Similarly in 2014 Netprasat with other authors [26] developed architectural distortion detection using SVM with an accuracy of 91.67%.

Recently Roy and Gogoi [28], presented the two most effective features i.e. fractal geometry and lacunarity on mammograms and thermo-grams. They proved that these features are giving better results than a texture feature. One of the fractal algorithms, the box-counting method was used by Zheng et al. and Rangayyan et al. to detect distorted sites through a mammogram. Similarly, Tavakol [27] introduced a method of fractal study for the fragmentation of breast cancer. Roy et al. [28] used the Hurst co-efficient and lacunarity features for dividing normal and abnormal states in a breast thermogram. He noticed that the value of lacunarity was greater in an abnormal state as compared to that of the normal

state. Sankar & Thomas [29] proposed a methodology to distinguish benign and malignant tumors in breast mammogram. Early prediction of breast cancer is done by Machireddy and others in 2019 [30] to decide if multiresolution FA of voxel utilized dynamic contrast-enhanced magnetic resonance imaging (DCE-MRI) parametric maps can give premature expectation of breast cancer reaction to neoadjuvant chemotherapy (NACT). Le Hoang Son et al. [31] focuses on the recent development over investigates regarding machine learning for big data analytics & other strategies in response to advanced modern computing for different applications. Chatterjee [32], attempted to give a reasonable progressively huge appreciation about the IoT in big data structure near to its different issues, troubles & zeroed in on giving potential game plans by machine learning procedure. Chatterjee [33], talked about various issues relating to bioinformatic data assortments & make different proposition on the right usage of machine learning frameworks for bioinformatics explore. [34], efficiently applied fractal dimension to detect tumor. Not only in gray images, but also in different color model, the fractal concept can be applied this is proved in [35]. It is also seen that the fractal geometry works properly in face shape classification [36].

III. METHODOLOGIES

A. Modified Relative Improved Differential Box Counting Method

The steps for this method are as follows:

1) The image of size $M \times M$ is divided into blocks of size $l \times l$ which cover the entire image surface with boxes of sides $l \times l \times l'$.

Where $l' = l \times G/M$.

G = Number of Gray Intensity Levels.

2) The boxes are assigned with a scale of $l \times l \times l'$ starting the pixel with minimum gray level in the block.

3) Number of boxes in each block is found out as n_r , using Eq.

$$n_r(i, j) = \begin{cases} 1 & MI = MN \\ \text{ceil}\left(\frac{MI}{l'}\right) & MI \neq MN \end{cases} \quad (1)$$

4) Total number of boxes needed to cover whole image is given as N_r using Eq. 1

$$N_r = \sum_{(i,j)} n_r(i, j) \quad (2)$$

5) Different N_r values are calculated for a different scale l .

6) The log of both N_r and scale is taken and a graph is plotted with $\log(N_r)$ in y-axis and $\log(l)$ in x-axis.

7) The best fit line for all the plotted lines, is drawn and the slope of the best fit line is calculated which gives the FD of the image.

B. Support Vector Machine (SVM) Classification

A SVM is a discriminative classifier, which is used for classification purposes. The main objective of the support vector machine is to design a hyperplane margin that classifies all the datasets into some classes respectively. For a flexible classification and visualization, it depends on a margin which must be at maximum distance from both the support vector lines of individual classes. The algorithmic steps are given below:

1. Start with taking input as fractal dimension which is extracted by using fractal geometry.
2. 42 data are structurally lying in a linear fashion before using SVM.
3. Now for classification purpose, we are taking a line, with two equidistant parallel lines to it.
4. Pick a large number (no of repetition or epochs).
5. Pick a number close to 1(the expanding factor (0.99)).
6. Pick a random point.
If point is correctly classified, then take it for classification process.

$$y = \omega^T x + b \quad (3)$$

$$\omega^T x + b < 0 \text{ (comes under class '-1')}$$

$$\omega^T x + b > 0 \text{ (comes under class '+1')}$$

$$\text{For } x \in \mathbb{R}^2$$

$$\omega_1 x_1 + \omega_2 x_2 + b = 0$$

$$y = mx + b \quad (4)$$

$$m = \text{slope}$$

$$b = \text{intercept}$$

7. If the point is not classified move the line towards point split the lines using expanding factor
8. After finding the exact line, we can separate the dataset in to binary classes.

IV. EXPERIMENTAL RESULTS AND DISCUSSION

The medical images are usually noisy and are not in acceptable stage for classification. So a pre-processing technique is used to upgrade the image quality. Fig. 1 shows the overall classification procedure where the fractal geometry technique, Modified Relative Improved Differential Box Counting Method is used for feature extraction. Finally SVM is applied to classify the dataset as Malignant or Benign.

The Breast Cancer dataset is retrieved from 'mammoimage.org' and 'visualsonline.cancer.gov'. This dataset consists of 42 instances and the experiment shows that among 42 instances, 20 cases are benign and 22 are malignant cancer cells. The dataset is separated into two binary classes i.e. 0 and 1, where 0 identifies benign class and 1 identifies the malignant class.

MATLAB R2016a as application software, is used for extracting features of 42 images using fractal dimension estimation method and is displayed in Table I. For the testing purpose, we considered all gray images as input. In this study, the classification testing is done through two approaches and the simulation is done using Scikit-learn open-source framework.

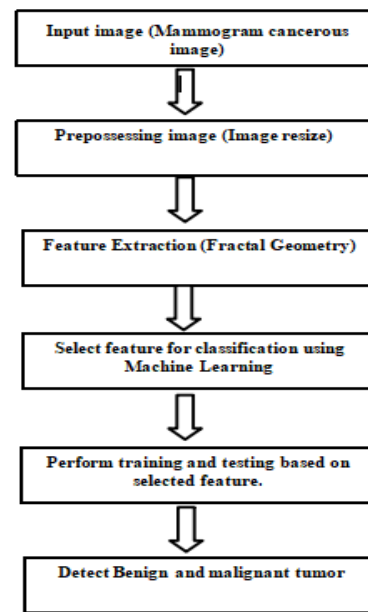


Fig. 1. Framework of Procedure.

First, it is tested by a support vector machine which linearly classifies the dataset into two clusters/classes i.e. Malignant, Benign. The second classification is based on a support vector machine with kernel functions i.e. Polynomial, Radial basis function. In our work more emphasis is given to SVM Linear classifier for classification of the dataset and kernel function is taken for comparison of accuracy for both classifier. The classification is based on SVM as supervised learning and the results obtained shows that 20 images belong to Benign and 22 images come under malignant out of 42 images in a dataset.

If the data are linearly separable, it is easy to use linear support vector machine, but if the data are in high dimensional, it needs non-linear SVM like kernel function to reduce the cost of data. Fig. 1 and Fig. 2 shows the example of an original image and its corresponding micro-calcification extraction, respectively (Fig. 3).

Fig. 4 shows one example of fractal dimension estimation of an image. Fig. 5 displays the linear fashion of malignant and benign training data in SVM classifier. Here x-axis contains a fractal dimension and the y-axis contains error value.

The linear SVM classifier classifies the two classes based on the target values and it is displayed in Fig. 1. Two classes are separated by their individual support vector line and the linear hyperplane margin, which are situated at equal maximum distance between two classes of malignant and benign. In Fig. 6, upper dots identify malignant class and benign class is identified by the lower dots.

We have observed that linear SVM classifiers are efficient and work properly, but the datasets available, are not in a linear fashion. For the non-linear datasets the kernel based SVM classifier plays an important role. A kernel is a method for calculating the dot product in between two vectors and hence, kernel functions are generally called "generalized dot

product". In this paper, we have considered two functions- Radial basis function and Polynomial kernel function and compared the accuracy. The result of Radial basis function and Polynomial kernel are shown in Fig. 7 and Fig. 8, respectively.

The result shows that overall accuracy of classification results in linear classification is 98.13%. Similarly the accuracy of a polynomial function is 96.16% and RBF is 94.74%.

TABLE I. FRACTAL DIMENSION ESTIMATION

Sl. No	Fractal dimension	Error	Target
1	1.693154	1.751434	1
2	1.331064	2.113657	0
3	1.358351	2.063793	0
4	1.358351	2.063793	0
5	1.807444	1.716059	1
6	1.839397	1.688727	1
7	1.505514	1.936841	1
8	1.375962	2.035717	0
9	1.722222	1.740258	1
10	1.752072	1.742001	1
11	1.375297	2.023377	0
12	1.72948	1.737463	1
13	1.587038	1.841367	1
14	1.82948	1.73748	1
15	1.839397	1.688727	1
16	1.839397	1.688727	1
17	1.839433	1.688733	1
18	1.34443	2.079553	0
19	1.352484	2.041328	0
20	1.789989	1.745767	1
21	1.839397	1.688727	1
22	1.313856	2.121255	0
23	1.48806	1.911533	0
24	1.459652	1.910951	0
25	1.360302	2.061959	0
26	1.581077	1.875687	1
27	1.793135	1.709228	1
28	1.839397	1.688727	1
29	1.353005	2.039656	0
30	1.46975	1.951866	0
31	1.426418	1.945996	0
32	1.820102	1.696682	1
33	1.328999	2.073889	0
34	1.39603	2.001665	0
35	1.330272	2.100327	0
36	1.338278	2.09254	0
37	1.839397	1.688727	1
38	1.639982	1.834418	1
39	1.35651	2.06708	0
40	1.839396	1.688727	1
41	1.777638	1.712549	1
42	1.482583	1.911528	0

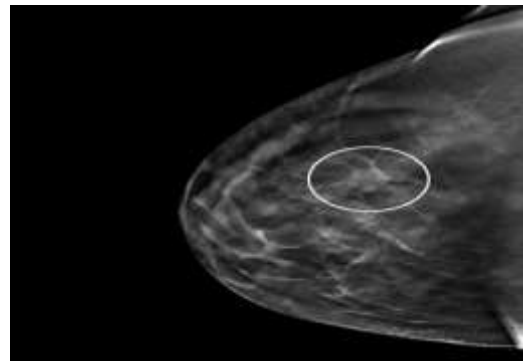


Fig. 2. Original Image.

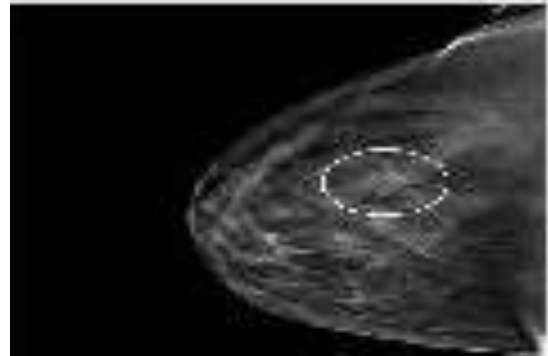


Fig. 3. Extraction of Micro-Calcification.

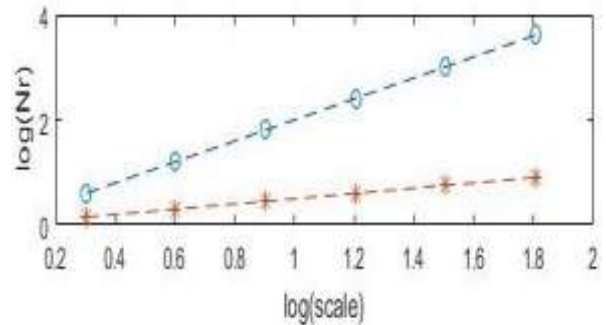


Fig. 4. Fractal Dimensional.

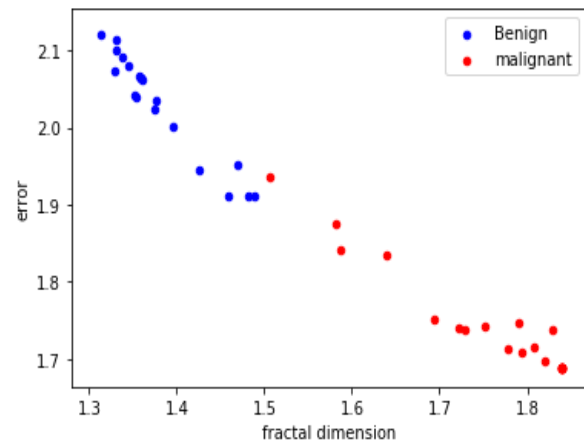


Fig. 5. Trained Dataset.

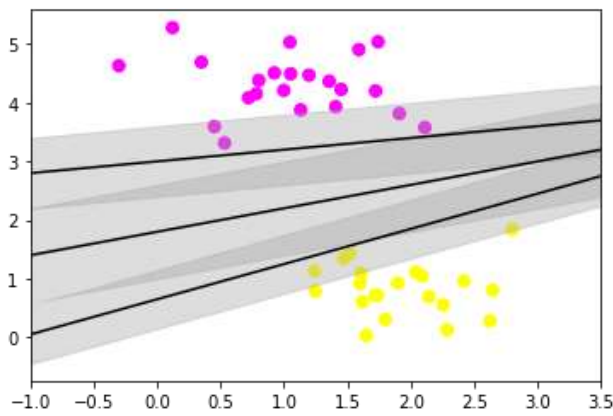


Fig. 6. Classification using LSVM.

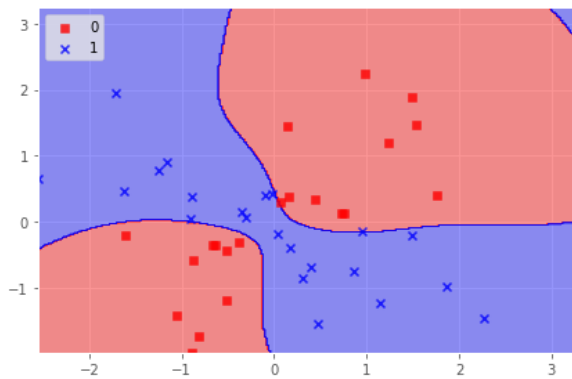


Fig. 7. Radial Basis Function.

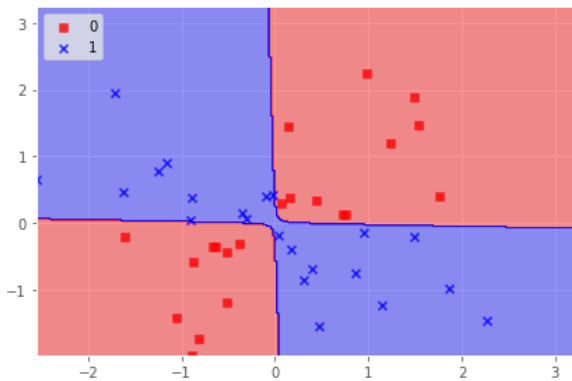


Fig. 8. Polynomial Kernel.

V. CONCLUSION

FA is one of the best ways to represent natural objects. Hence it is the most suitable method for the study and analysis of breast cancer. The analysis of the previous works shows that limited research is done on the classification of breast mass using a machine learning technique. We have hybridized two finest methods i.e. fractal geometry and machine learning to classify the malignant and benign from the breast mammogram images. In our proposed method, we have used the box count technique for the extraction of features (fractal dimension). After analyzing the fractal dimension of each image we set a threshold value that shows if FD is less than

1.5, they come under benign represented as target=0 and those having $FD > 1.5$, comes under malignant class represented as target=1. The support vector machine is used for the classification of the calculated FDs. The procedure is implemented in python with a dataset having 42 images and we got the result with an accuracy of 98.13% in Linear SVM. In this procedure, we have trained 33 images and according to the training dataset 9 images are tested automatically. Kernel SVM is also implemented which provides less accuracy than the LSVM. The result analysis shows that the proposed procedure is somehow noisy for large datasets. So we can extend our work and aim to develop an more efficient technique for the large dataset with less noisy that would give better performance. In future we will try to use multiple machine learning techniques to test the proposed method on a large database to achieve higher accuracy.

REFERENCES

- [1] Gogoi, U. R., Majumdar, G., Bhowmik, M. K., Ghosh, A. K., & Bhattacharjee, D. (2015, September). Breast abnormality detection through statistical feature analysis using infrared thermograms. In 2015 International Symposium on Advanced Computing and Communication (ISACC) (pp. 258-265). IEEE.
- [2] Gogoi, U. R., Bhowmik, M. K., Bhattacharjee, D., Ghosh, A. K., & Majumdar, G. (2016). A study and analysis of hybrid intelligent techniques for breast cancer detection using breast thermograms. In Hybrid Soft Computing Approaches (pp. 329-359). Springer, New Delhi.
- [3] Mu, T., Nandi, A. K., & Rangayyan, R. M. (2008). Classification of breast masses using selected shape, edge-sharpness, and texture features with linear and kernel-based classifiers. *Journal of Digital Imaging*, 21(2), 153-169.
- [4] Araújo, M., Lima, R. C. F., Magnani, F. S., Silva, R. T. N., & Santos, F. G. S. (2008, November). The use of a database as an auxiliary tool in thermographic diagnosis for early detection of breast diseases. In Proceedings of 12th Brazilian Congress of Thermal Sciences and Engineering, Brazil.
- [5] Bhowmik, M. K., Gogoi, U. R., Das, K., Ghosh, A. K., Bhattacharjee, D., & Majumdar, G. (2016, May). Standardization of infrared breast thermogram acquisition protocols and abnormality analysis of breast thermograms. In *Thermosense: Thermal Infrared Applications XXXVIII* (Vol. 9861, p. 986115). International Society for Optics and Photonics.
- [6] Nunes, F. L., Schiabel, H., & Goes, C. E. (2007). Contrast enhancement in dense breast images to aid clustered microcalcifications detection. *Journal of digital imaging*, 20(1), 53-66.
- [7] Rangayyan, R. M., Shen, L., Shen, Y., Desautels, J. L., Bryant, H., Terry, T. J., ... & Rose, M. S. (1997). Improvement of sensitivity of breast cancer diagnosis with adaptive neighborhood contrast enhancement of mammograms. *IEEE transactions on information technology in biomedicine*, 1(3), 161-170.
- [8] Wei, L., Yang, Y., Nishikawa, R. M., Wernick, M. N., & Edwards, A. (2005). Relevance vector machine for automatic detection of clustered microcalcifications. *IEEE transactions on medical imaging*, 24(10), 1278-1285. 9. Strickland, Robin.N., Hahn, Hee.: Wavelet Transforms for Detecting Microcalcifications in Mammograms. *IEEE Transactions on Medical Imaging*, vol.15, no.2, pp. 218-229 (1996).
- [9] Strickland, R. N., & Hahn, H. I. (1996). Wavelet transforms for detecting microcalcifications in mammograms. *IEEE Transactions on Medical Imaging*, 15(2), 218-229.
- [10] Oktem, V., & Jouny, I. (2004, September). Automatic detection of malignant tumors in mammograms. In The 26th Annual International Conference of the IEEE Engineering in Medicine and Biology Society (Vol. 1, pp. 1770-1773). IEEE.
- [11] Zhen, L., & Chan, A. K. (2001). An artificial intelligent algorithm for tumor detection in screening mammogram. *IEEE transactions on medical imaging*, 20(7), 559-567.

- [12] Rangayyan, R. M., & Nguyen, T. M. (2007). Fractal analysis of contours of breast masses in mammograms. *Journal of Digital Imaging*, 20(3), 223-237.
- [13] Etehad Tavakol, M., Lucas, C., Sadri, S., & Ng, E. Y. K. (2010). Analysis of breast thermography using fractal dimension to establish possible difference between malignant and benign patterns. *Journal of Healthcare Engineering*, 1(1), 27-43.
- [14] Ibrahim, A., Mohammed, S., & Ali, H. A. (2018, February). Breast cancer detection and classification using thermography: a review. In *International Conference on Advanced Machine Learning Technologies and Applications* (pp. 496-505). Springer, Cham.
- [15] Heriana, O., & Soesanti, I. (2015, October). Tumor size classification of breast thermal image using fuzzy C-Means algorithm. In *2015 International Conference on Radar, Antenna, Microwave, Electronics and Telecommunications (ICRAMET)* (pp. 98-103). IEEE.
- [16] Melloul, M., & Joskowicz, L. (2002). Segmentation of microcalcification in X-ray mammograms using entropy thresholding. In *CARS 2002 Computer Assisted Radiology and Surgery* (pp. 671-676). Springer, Berlin, Heidelberg.
- [17] Li, H., Liu, K. R., & Lo, S. C. (1997). Fractal modeling and segmentation for the enhancement of microcalcifications in digital mammograms. *IEEE transactions on medical imaging*, 16(6), 785-798.
- [18] Verma, B., & Zakos, J. (2001). A computer-aided diagnosis system for digital mammograms based on fuzzy-neural and feature extraction techniques. *IEEE transactions on information technology in biomedicine*, 5(1), 46-54.
- [19] Patel, B. C., & Sinha, G. R. (2010). Early detection of breast cancer using self-similar fractal method. *International Journal of Computer Applications*, 10(4), 39-43.
- [20] Nam, S. H., & Choi, J. Y. (1998, November). A method of image enhancement and fractal dimension for detection of microcalcifications in mammogram. In *Proceedings of the 20th Annual International Conference of the IEEE Engineering in Medicine and Biology Society. Vol. 20 Biomedical Engineering towards the Year 2000 and Beyond (Cat. No. 98CH36286)* (Vol. 2, pp. 1009-1012). IEEE.
- [21] Kontos, D., Megalooikonomou, V., Javadi, A., Bakic, P. R., & Maidment, A. D. (2006, April). Classification of galactograms using fractal properties of the breast ductal network. In *3rd IEEE International Symposium on Biomedical Imaging: Nano to Macro, 2006.* (pp. 1324-1327). IEEE.
- [22] Chang, R. F., Chen, C. J., Ho, M. F., Chen, D. R., & Moon, W. K. (2004, May). Breast ultrasound image classification using fractal analysis. In *Proceedings. Fourth IEEE Symposium on Bioinformatics and Bioengineering* (pp. 100-107). IEEE.
- [23] Shen, L., Rangayyan, R. M., & Desautels, J. L. (1994). Detection and classification of mammographic calcifications. In *State of the Art in Digital Mammographic Image Analysis* (pp. 198-212).
- [24] Noodeh, A. S., Rabbani, H., Dehnavi, A. M., & Noubari, H. A. (2010, November). Detection of cancerous zones in mammograms using fractal modeling and classification by probabilistic neural network. In *2010 17th Iranian Conference of Biomedical Engineering (ICBME)* (pp. 1-4). IEEE.
- [25] Moldovanu, S., & Moraru, L. (2010, September). Mass detection and classification in breast ultrasound image using K-means clustering algorithm. In *2010 3rd International Symposium on Electrical and Electronics Engineering (ISEEE)* (pp. 197-200). IEEE.
- [26] Netprasat, O., Auephanwiriyakul, S., & Theera-Umpon, N. (2014, July). Architectural distortion detection from mammograms using support vector machine. In *2014 International Joint Conference on Neural Networks (IJCNN)* (pp. 3258-3264). IEEE.
- [27] Etehad Tavakol, M., Lucas, C., Sadri, S., & Ng, E. Y. K. (2010). Analysis of breast thermography using fractal dimension to establish possible difference between malignant and benign patterns. *Journal of Healthcare Engineering*, 1(1), 27-43.
- [28] Roy, A., Gogoi, U. R., Das, D. H., & Bhowmik, M. K. (2017, December). Fractal feature based early breast abnormality prediction. In *2017 IEEE Region 10 Humanitarian Technology Conference (R10-HTC)* (pp. 18-21). IEEE.
- [29] Sankar, D., & Thomas, T. (2009, December). Analysis of mammograms using fractal features. In *2009 World Congress on Nature & Biologically Inspired Computing (NaBIC)* (pp. 936-941). IEEE.
- [30] Machireddy, A., Thibault, G., Tudorica, A., Afzal, A., Mishal, M., Kemmer, K., & Roy, N. (2019). Early prediction of breast cancer therapy response using multiresolution fractal analysis of DCE-MRI parametric maps. *Tomography*, 5(1), 90.
- [31] Tripathy, H. K., Acharya, B. R., Kumar, R., & Chatterjee, J. M. (2019). Machine learning on big data: A developmental approach on societal applications. In *Big Data Processing Using Spark in Cloud* (pp. 143-165). Springer, Singapore.
- [32] Chatterjee, J. M. (2018). IoT with Big Data Framework using Machine Learning Approach. *International Journal of Machine Learning and Networked Collaborative Engineering*, 2(02), 75-85.
- [33] Chatterjee, J. M. (2018). Bioinformatics using machine learning. *Global journal of internet interventions and it fusion [issn: 2582-1385 (online)]*, 1(1).
- [34] Kisan, S., Mishra, S. N. & Mishra, D., Analysis of Tumor using Fractal Dimension. *International Journal of Advance Computing Technique and Applications (IJACTA)*, ISSN: 2321-4546, Vol 5, Issue 1, January- June 2017.
- [35] Kisan, S., Mishra, S. N., Chawda, A. & Nayak, S., "Estimation of Fractal Dimension in Different color model", *IJKDB-8*, IGI Global, 2017.
- [36] Kisan, S., Nayak, S., Chawda, A. & Mishra, S.N., Face Shape Classification based on Modified Relative Improved Differential Box Count Method. *International Journal of Advanced Science and Technology (IJAST)*, 2020, Volume 29, Issue 3, ISSN: 2005-4238, ISSN: 2207-6360 (Online), Page: 3878-3889.

Detection of Anomalous In-Memory Process based on DLL Sequence

Binayak Panda¹, Dr. Satya Narayan Tripathy²

PG. Dept. of Computer Science
Berhampur University, Berhampur
Odisha, India

Abstract—The use of Computer systems to keep track of day to day activities for single-user systems as well as the implementation of business logic in enterprises is the demand of the hour. As it plays a vital role in making available information on one click as well as impacts improvement in business and influences the profit or loss. There is always a possible threat from unauthorized users as well as untrusted or unknown applications. Trivially a host is intended to run with a list of known or trusted applications based on user's preference. Any application beyond the trusted list can be called as untrusted or unknown application, which is not expected to run on that host. Untrusted applications becomes available to a host from sources like websites, emails, external storage devices etc. Such untrusted programs may be malicious or non-malicious in nature but the presence must be detected, as it is not a trusted program from user's view point. All such programs may target the system either to steal valuable information or to decrease the system performance without the knowledge of the user of the system. Antimalware vendors provide support to defend the system from malicious programs. They do not include users trusted program list in to consideration. It is also true that new instances of attacks are found very frequently. Hence there is a need for a system which can be self-defending from anomalous activities on the system with reference to a trusted program list. In this paper design of an "Anomalous In-Memory Process detector based on the use of the DLL (Dynamic Link Library) sequence" is proposed, which does accountability of trusted programs intended to run on a particular host and create a knowledgebase of classes of processes with TF-IDF (Term Frequency-Inverse Document Frequency) multinomial logistic regression based learning approach. This knowledgebase becomes useful to map a suspected In-memory process to a class of processes using loaded DLL's of it. With a cross-validation approach, the suspected process and processes of its predicted class are used to conclude whether it is a trusted, variant of the trusted or untrusted process for that host. Not necessarily the untrusted program is a malware but it may be a program not listed in the trusted program list for the specific host. Hence this work aims to detect anomaly in concern with list of trusted applications based on user's preference by doing a dynamic analysis on In-memory processes.

Keywords—Anomalous In-memory Process; dynamic analysis; DLL hijacking; DLL injection; TF-IDF multinomial logistic regression

I. INTRODUCTION

In the 21st century use of computers is becoming quite obvious in all fields, starting with the banking sector, education sector, health sector, e-commerce, etc. The use of

computers is not only limited to such big domains; but also are extended to be used by individuals in their home's, small offices, and various goods' retail counters to keep track of their day to day activities. Whether large commercial sectors or small retail counters or individual use of computers increases day by day with the availability of Internet facilities.

On the contrary, the risk of the exploitation of data and information kept on computers also increases day by day because of the exposure of computers to the outside world due to internet connectivity. There are intelligent programmers, who somehow put a piece of code (a small program which is unknown or untrusted) on a computer of interest with an intention of either stealing or misusing the data kept on computers or making computers non operable. Such programs are referred to as malware or potentially unwanted application (PUA). There exist many categories of such malware like viruses, worm, spyware, adware, ransomware, etc. The adverse effect of the presence of malware on a computer system scales from a very small impact to an extremely large impact. PUA do not have any specific types as they seem to be normal programs but there may a possible threat due to the presence of them.

Quick heal annual threat report 2019 says that prediction of becoming vicious about ransomware happened to be true in 2018. Only in one month, the ransomware detection reached 2Million in 2018. Also, the prediction about small and medium-sized businesses to be in the red zone became true. Cryptojacking is a new buzzword suppressing ransomware, which is a process of using someone's computer to earn money. The only sign of a computer used for cryptojacking is a little slower computer performance while executing programs. The CPU is targeted up to 100% by cryptojacking which leads to hardware faults slowly. The owner of the compromised computer becomes unaware of being a victim of cryptojacking. The report says about detection of more than 800k cases of cryptojacking in 2018. It also has given information about an Infector named W32.Pioneer.CZ1, which injects the files on to disk and then decrypts the malicious DLL present in the file and drops it to do malicious activities. "Fig. 1" shows the frequency of attack of various malware types per day, per hour, and per minute referring to Quick heal threat report 2019 [1]. Internet security threat report, Symantec 2019 says 69 million events detected in 2018 which is 4 times to cases in 2017. The report also speaks about PUA which is not necessarily harmful but may lead to security risks. The existence of such PUA may also result in Host-

Based exploits. It also says about cases of Cryptojacking and its consequences. The report mentioned about supply chain attacks which target third party software by injecting code into its libraries. These libraries are integrated into larger software projects. Injection of code in to libraries can be understood as DLL injection, which is a possible approach of exploiting a host [2].

The case of infector W32.Pioneer.CZ1, supply chain attack and possibility of threat due to the presence of PUA points out a need of a system for real time detection of host based exploitations. Antimalware vendors do provide support in detecting malicious programs with signature based static analysis but they don't take users preference in to consideration. Hence some unwanted or unknown programs referring to users preferred list left undetected. Such unknown programs may be a malware or PUA, which is a possible threat to that host. These observations motivated to apply multi-class classification approach on known or trusted processes using their respective list of loaded DLL's on a host considering its users preferred list of programs. This knowledge helps in detecting a deviation from known In-memory processes which is either a malfunctioned known process or unknown process or untrusted process using some potentially unwanted DLL or malfunctioned DLL.

The organization of the remaining sections in this paper is as follows: Section 2 speaks about the related works on malware analysis considering In-memory processes and injection of unwanted DLL's. Section 3 speaks about the design of the System in detecting anomalies or deviations with respect to In-memory processes and their respective loaded DLL's. It is about designing an Anomalous In-Memory Process detector based on the use of DLL's, which learns the trusted programs intended to run on a particular host and creates multiple class of them referring their usage of DLL's. With a cross validation approach a suspected process gets validated with processes of a class it is mapped to and gets detected as either trusted or variant of trusted or untrusted for the specific host. Section 4 speaks about the experimental setup for the empirical evaluation of the system. Section 5 describes the concluding remark of the work.

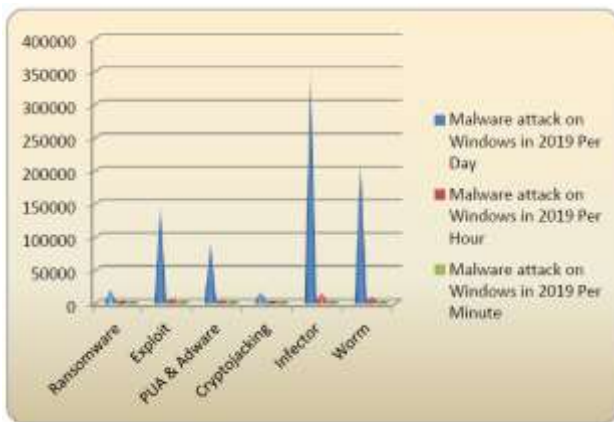


Fig. 1. Malware Attack on Windows in 2019.

II. RELATED WORK

Analysis of the behavior of unknown programs like PUA, malware etc. is becoming truly diversified. Various forms of analysis are done on a system to identify a threat to the information stored on the computer. The analysis can be in the form of identification of untrusted programs available on secondary storage or anomalous In-memory processes. The approaches of analysis can be said as either static or dynamic or hybrid or memory-based [3]. The static analysis considers opcode's, N-gram opcode sequences, control flow graph as features to analyze further without executing the programs. The dynamic analysis considers function calls, API calls, function parameters, instruction traces, and instruction flows as features to analyze further after executing the programs [4]. The hybrid analysis is a combination of static analysis and dynamic analysis [5]. The memory-based analysis is also a kind of dynamic analysis that considers network connection information, changes in registry keys and In-memory processes and there DLL sequences for further analysis during the execution of programs [6, 7, 8]. With run time attributes of benign process using string analysis for anomaly detection in Android operating system is found effective [9]. Studying the behavior of malware is becoming popular with memory forensic techniques for malware injection and hidden processes [10]. DLL injection is a process where the malicious DLL gets injected on to an In-memory process and the control of execution gets transferred to that code block [11]. Reflective DLL injection has also gained popularity where they do malicious activities in memory only without leaving any footprint [12, 13].

A Windows application uses DLL files during runtime to load libraries. It tries to locate the DLL with a hierarchy of searches. First, it tries to find with the given path. But when it fails to locate, it searches at some predefined set of directories. Malware programs breaches this search order to load malicious DLL during run time. In this context, DLL-Side loading is becoming a very popular method for attacking Windows systems [14]. In such cases, the malware payload places the spoofed malicious DLL into a specific location so that the spoofed DLL gets loaded instead of legitimate DLL. Such DLL-Side loading bypasses the signature-based static analysis process. This DLL load order hijacking process to load a malicious DLL in run time can also be referred to as DLL hijacking. A variant of such an approach where a malware launcher loads the malicious DLL compromising a victim processes memory whereby loads the malicious DLL by creating a thread. Such an approach of entry of malicious DLL onto to system is referred to as DLL Injection. With this approach, the program loads unintended DLL's due to the presence of side-loading vulnerability of Windows side-by-side manifests [15].

Typically when malware attacks, it makes available its payload physically on the system storage and gets loaded on to memory to do the malicious activity. In such cases either the traditional static analysis using signature-based detection becomes helpful or the dynamic analysis considering the various run-time behaviors of processes becomes helpful. But Fileless malware has become a new possible attack type, where the malware is not saving the payload on system

storage rather it malfunctions the trusted and legitimate processes of the Operating System. It injects the malicious program directly on to the compromised processes memory without dropping any file to the file system. As no physical file presents the Sandbox detection approach fails. Again as there is no possibility of having a signature, hence the signature detection also fails. Hence the detection complexity becomes too high for Fileless malware. The possibility of investigating Fileless malware is only limited to analysis of the behavior of the system using the snapshots of In-memory processes, which is considered here as Memory based analysis [16]. Information retrieval theory is applied with a dynamic analysis to extract API calls and system calls to classify malicious programs. They are stored in documents on which the TF-IDF weighting approach is applied to get a good accuracy of malware classification [17].

In this paper, a novel approach is proposed considering memory based dynamic analysis of In-memory processes in identifying any deviation from the trusted process list of a particular host. The DLL lists of In-memory processes are taken in to consideration for deciding a suspected process as either trusted or variant of trusted or untrusted for a specific host. The list of trusted in-memory processes are classified in to multiple classes considering the DLL sequences they use at various instances. A suspected process gets mapped in to one of the trusted class of processes based on its DLL sequence. For this multi-class classification DLL lists are formed as attribute vectors with Vector Space Model (VSM), on which TF-IDF multinomial Logistic regression is used to train the system. Objective of training process is to prepare a knowledgebase of classes of processes, which are considered as known or trusted and legitimate processes from the viewpoint of a particular user. This system can take an In-memory process at any random instance of time and do a prediction of its class using the learned knowledge base. The cosine similarity metric is used to cross-validate a suspected process with all the processes of the predicted class before concluding it as either a trusted or variant of a trusted or untrusted process for that specific host. In this work a list of processes are declared as trusted processes from the user's regular use viewpoint. A variant of a trusted process is understood as a process of an updated version application from trusted list. Any other process other than a trusted or a variant of trusted is understood as untrusted.

III. SYSTEM DESIGN

A. System Overview

The anomalous In-memory process detection system can be divided into three parts: data preprocessing, the process class prediction model of the system, and cross-validation of the predictors result. Data preprocessing is about collecting the DLL sequences loaded for all In-memory processes with reference to a given list of trusted applications of the specific host, using Windows Sysinternals Process utilities like Pslist.exe and Listdlls.exe [18]. Pslist.exe shows information about In-memory processes. Listdlls.exe shows the list of DLL's loaded for a specific process at that time instance. A TF-IDF weight matrix gets generated defining weight of each DLL in the collected DLL sequences for the list of In-memory

processes. The said system applies multinomial classification on the data set of In-memory processes to classify them in to multiple classes of processes based on DLL sequences as feature vector. The process class prediction model is trained and tested using the generated data set. For the training and testing phase of the system multinomial Logistic Regression, multinomial Naive Bayes, and Support Vector Classifier (SVM-SVC for multiclass problem) mechanisms are used. The training phase of the model uses the approach of learning the usual activity of a host from In-memory processes and their respective DLL sequences to create the knowledge base of processes as multiple classes. The testing phase of the model uses the knowledge gained in the training phase, to decide accuracy of the system in classifying In-memory processes to their class. Cosine similarity measure is used for Cross Validation of the predictors result. With cosine similarity the DLL sequence of a suspected In-memory process is compared with DLL sequences of processes of the predicted class to verify the similarity of the suspected process and subsequently to say whether the process is a trusted, variant of trusted or untrusted.

B. Data Preprocessing

There are various run time attributes of an In-memory process, which speaks about the behavior of it. Some attributes are process path, process name, process priority, number of threads, number of handles, private virtual memory, path of all the DLL's loaded, etc. In this system, the focus is given on two run time attributes namely path of the process and path of all the DLL's loaded. Pslist.exe is used to collect all the process names and their respective process ids. "Fig. 2" represents a sample output which is a list of elements a.k.a. *In_Memory_Process_List* where each element is a 2-tuple say *Process_tuple (pname,pid)* containing process name and process id for all the In-Memory processes at a particular time instance.

Listdlls.exe is used to collect all the DLL's loaded on to the memory for each element of the *In_Memory_Process_List* at that time instance. "Fig. 3" represents the absolute path of the program corresponding to one of the In-memory process and the absolute path of all its loaded DLL's. There will be a list of such records based on the number of In-memory processes at that time instance. Let that be referred as a Database DLL List a.k.a. *DBDLLList[]*. The algorithmic steps for generating a collection of *DBDLLList's* at various time instances is explained in Algorithm 1 which is a.k.a. *IMPDLLList*.

```
[['Idle 0', 'System 4', 'smss 276', 'csrss 388', 'wininit 440', 'csrss 452', 'smss  
vices 488', 'lsass 512', 'lsass 520', 'winlogon 688', 'svchost 480', 'svchost 740',  
'', 'NlsLang 824', 'svchost 828', 'svchost 860', 'svchost 1090', 'svchost 1032', '  
svchost 1128', 'svchost 1308', 'spoolsv 1496', 'svchost 1532', 'smssvc 1620', '  
svchost 1648', 'svchost 1676', 'smssvc 1720', 'svchost 1892', 'WiFiHost 1028', '  
taskhost 1336', 'explorer 1768', 'lsass 2268', 'GoogleCrashHandler 2288', 'sm  
ssvc 2432', 'Ntfs.sys 2456', 'AgntEx 2968', 'AgntEx 2968', 'svchost 2984', 'SearchIndexe  
r 3036', 'svchost 3224', 'wscntlm 3264', 'WINWORD 3696', 'AcroRd32 1848', 'AcroR  
d32 1428', 'RdrCEF 1940', 'RdrCEF 2756', 'RdrCEF 3884', 'notepad++ 2016', 'chrom  
e 2844', 'chrome 3940', 'chrome 2128', 'chrome 2728', 'chrome 3948', 'chrome 381  
2', 'notepad 732', 'dwm 4032', 'chrome 2420', 'audiocd 1420', 'pythonw 2780', 'p  
ythonw 3648', 'cmd 3496', 'conhost 948', 'pslist 2556']
```

Fig. 2. *In_Memory_Process_List* at a Time Instance.

C. Process Class Prediction Model

The records present in $EncrDBDLLList[]$ are being tokenized using the classical separator blank space. With this an In-memory process P is represented as a text $P_{text} = \{S_0, S_1, S_2, \dots, S_n\}$ where each S_i is considered as a string of the text. Here S_0 represents the process class p_i for an In-memory process. S_1 to S_n represents DLL sequence of that process where each S_i represents dll_i for $1 \leq i \leq n$. Let C is the set of the text representation of m In-memory processes such that $C = \{P_{text}^1, P_{text}^2, P_{text}^3, \dots, P_{text}^m\}$, where each P_{text}^i represents the text representation of i^{th} In-memory process. Further C is split into two lists named as C_{tags} and C_{docs} . Where S_0 will be included in C_{tags} when $S_0 \in P_{text}^i$ and $\forall P_{text}^i \in C$. S_j will be included in C_{docs} when $S_j \in P_{text}^i$ with $1 \leq j \leq n$ and $\forall P_{text}^i \in C$.

The use of VSM is very common in representing textual documents algebraically as vectors in a multidimensional space [19]. The components of such a vector represent the importance of a term in a document. TF-IDF is very popular in evaluating how important a word is in a document. TF-IDF weighting schema is the most popularly used approach in converting textual documents to a VSM [20].

In this context, C_{tags} is the document representing the list of classes of In-memory processes, where existence of more than 3 classes observed. C_{docs} is the list of DLL's for process classes in C_{tags} . C_{docs} is treated as a textual document, which is the list of the text representation of DLL sequences of all In-memory processes. The TF-IDF weighting schema is applied to find out the VSM view of the system for a particular host. Considering TF-IDF over raw frequencies of occurrences of words is to scale down the impact of very frequently occurring words in a document which is empirically less informative than the words of less frequency. C_{docs} is represented by a "Feature-DLL to In-Memory-Process" weight matrix, where the element (i,j) illustrates an association of i^{th} DLL to j^{th} In-memory Process. Using TF-IDF weighting schema, the weight of i^{th} DLL to j^{th} In-Memory Process is denoted as $W_{i,j}$ and defined as given in (1).

$$W_{i,j} = TF_{i,j} \times IDF_i \quad (1)$$

$TF_{i,j}$ in (1) is the L_2 normalized term frequency for i^{th} DLL with respect to the j^{th} In-memory process. The Term Frequency $TF_{i,j}$ is defined as given in (2).

$$TF_{i,j} = \frac{n_{i,j}}{\sqrt{\sum_k (n_{k,j})^2}} \quad (2)$$

Here $n_{i,j}$ is the number of occurrences of i^{th} DLL in j^{th} In-memory Process, and $\sqrt{\sum_k (n_{k,j})^2}$ is the magnitude of the vector representation of DLL's present in the j^{th} In-memory Process.

IDF_i in (1) is the Inverse document frequency for i^{th} DLL in C_{docs} . The Inverse Document Frequency IDF_i is defined as given in (3).

$$IDF_i = \log\left(\frac{|C_{docs}|}{1+|C_{docs}|S_i \in C_{docs}|}\right) \quad (3)$$

Here $|C_{docs}|$ represents the total number of In-memory processes and $|C_{docs}|S_i \in C_{docs}|$ represents the number of In-memory processes in C_{docs} containing the i^{th} DLL i.e. S_i . Using (1) W the weight matrix of C_{docs} is found for the 'Feature-DLL to In-Memory-Process' matrix representation of the system. W is typically a sparse matrix and tells statistically how important a DLL is to an In-memory process in the collection of all the In-memory processes.

Weight matrix W is then split into a training and testing data set with 3:1 ratio with random sample selection. Multinomial logistic regression, multinomial Naïve Bayes, and SVM-SVC (SVC) learning methods are applied on the proposed model. The objective is to choose the classifier which results with highest accuracy in process class prediction by using a DLL sequence as attribute vector. "Fig. 6" shows the functional representation of the model.

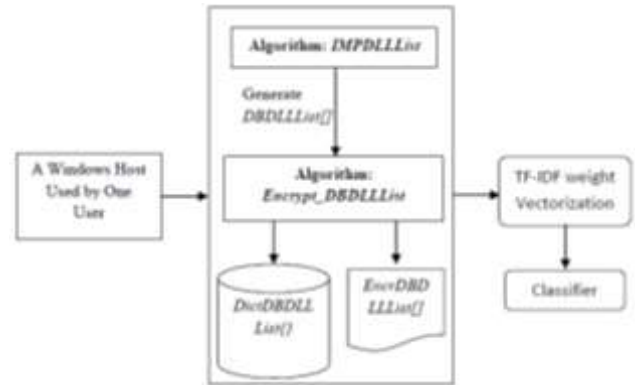


Fig. 6. Process Class Prediction Model.

D. Cross Validation

The cosine similarity measure is used to cross-validate the suspected process with all the processes of the predicted process class. It is used to find the relative closeness of the suspected process with the trusted processes of the predicted class. Cosine Similarity is a similarity distance measure which finds the cosine angle between two vectors u and v , which is defined as given in (4).

$$\cos(\theta) = \frac{u \cdot v}{|u| \cdot |v|} \quad (4)$$

Here $u \cdot v$ is the dot product of two vectors u and v . $|u| \cdot |v|$ represents product of magnitudes of vectors u and v , respectively. Cosine angle as 0° (i.e. Cosine distance measured as 1) between two vectors concludes both are similar where as an angle close to 0° (i.e. Cosine distance measured is close to 1) indicates they are closely similar. What must be the accepted value to consider case of closely similar vectors to case of similar vectors depends on field of application and experiential results? But a larger angle says they are dissimilar.

The proposed system has the objective of detecting anomalous In-memory processes on a specific host with reference to trusted applications list. With VSM and TF-IDF any In-memory process can be represented as a weighted vector considering DLL sequence as attribute vector. Hence any suspected process can be applied on the model to find its

process class. All the processes of the predicted process class can be compared with the suspected process using the Cosine similarity measure. This cosine similarity distance is used to conclude whether the suspected process is to be considered as trusted, variant of trusted or untrusted. The algorithmic steps of cross validation are explained in Algorithm 3 which is a.k.a. *Cross_validate_suspected_process*. The algorithm needs a Suspected_Process information similar to the sample record shown in “Fig. 3”, i.e. in the form of [process_path, dll1_path, dll2_path, ..., dllm_path]. It also refers *EncrDBDLLLList[]* and *DictDBDLLLList{}* which are found during learning stage of model using Algorithm 2 **Encrypt_DBDLLLList**, to encode the Suspected_Process information such that it can be applied on Process Class Prediction Model. β_1 and β_2 are the threshold values for considering cosine distance measure to decide process as a trusted and a variant of some trusted program, respectively.

The Suspected_Process will be a trusted process if the number of processes of the predicted class whose Cosine distance is measured as 1 with the Suspected_Process becomes \geq the threshold β_1 . Here β_1 will be the minimum count for the number of processes of the predicted class whose Cosine distance is measured as 1 with the Suspected_Process. An optimize value for β_1 to be found from experiment for a specific host.

The Suspected_Process will be a variant of some trusted process if the average of Cosine distances measured between the processes of predicted class and the Suspected_Process becomes \geq the threshold β_2 . Here β_2 will be the minimum average cosine distance between the processes of predicted class and the Suspected_Process. An optimize value for β_2 to be found from experiment for a specific host.

The Suspected_Process which fails to qualify the threshold β_1 followed by β_2 will be an untrusted process.

Algorithm 3: *Cross_validate_suspected_process*

Require: *Suspected_Process* Information, *EncrDBDLLLList[]* and *DictDBDLLLList{}* as explained above. β_1 is the threshold to conclude *Suspected_Process* is trusted and β_2 is the threshold to conclude *Suspected_Process* is a variant of some trusted process as explained above.

Ensure: Trusted or A variant of trusted or Untrusted as explained above

1. *encr_process* = Encrypt_DBDLLLList (*Suspected_process* , *DictDBDLLLList{}*)
2. *predict_process_class* = *ProcessClassPredictionModel*(*encr_process*)
3. Initialize *verify_proces_list[]* = NULL
4. *verify_proces_list.append*(*encr_process*)
5. For *p_class* in *EncrDBDLLLList[]*
 If (*p_class*[0] == *predict_process_class*)
 verify_proces_list.append(*p_class*[1..n])
6. *TF_IDF_mtrix* = *tf_idf_vectorizer*(*verify_proces_list[]*)
7. *Cosine_measure[]* = *cosine_similarity*(*TF_IDF_mtrix*[0], *TF_IDF_mtrix*[1..n])
8. If (*count*(*Cosine_measure*[], *value*(‘1’)) $\geq \beta_1$)
 Print (Trusted)

- ```
Else if (average(Cosine_mesure[]) >= β_2)
 Print (A variant of Trusted Application hence
 assumed as trusted)
Else
 Print (Untrusted)
9. End
```

## IV. EXPERIMENTAL SETUP AND EVALUATION

For the experimental setup and evaluation of the proposed system following steps are taken.

- A questionnaire is used to collect the list of application programs with reference to specific users’ interest. It is considered as the trusted application list for this host and any other application is assumed as untrusted. Table I and Table II show a sample list of system processes and trusted processes of the host respectively. Combination of such system processes and processes of the trusted application is considered as the list of trusted processes on which anomalous activity is monitored.
- The Algorithm-1 *IMPDLLLList* is invoked with a fresh installation of the Windows operating system along with all the listed trusted application software’s. The invocation of the algorithm is scheduled depending on use of various application programs time to time. *IMPDLLLList* is invoked aperiodically for approximately 20 times a day for a continuous run of a specific time duration (e.g. 5 hours a day) to generate *DBDLLLList[]*. With the above-said schedule *IMPDLLLList* is invoked for 10 days to generate the final trusted *DBDLLLList[]*, which contained around 10000 records. One record of *DBDLLLList[]* is shown in “Fig. 3.”
- The algorithm *Encrypt\_DBDLLLList* is invoked on the trusted *DBDLLLList[]*, to generate *EncrDBDLLLList[]* and *DictDBDLLLList{}*. The model is trained and tested with training and testing set of 3:1 ratio with random sample selection on these 10000 records.

The proposed model works on a multi-class problem where the In-memory processes of a host are classified into several classes and a suspected process gets predicted to belong to a specific class of the processes. The performance of three classifiers are compared in terms of accuracy, {Micro | Macro | Weighted} Precision, {Micro | Macro | Weighted} Recall and {Micro | Macro | Weighted} F1-score considering the multinomial classification approaches named multinomial Logistic Regression, multinomial Naïve Bayes and SVM-SVC (further referred as SVC in this paper). For a binomial classification case evaluation of performance metrics is done based on positive class and negative class, whereas for a multinomial classification case evaluation of performance metrics is done based on One-vs.-Rest (OvR) classes. For each class in case of multinomial classification the below mentioned basic parameters are found, which are used to evaluate overall performance metrics of the model. The basic parameters referred above are True Positive (TP) — the classifier correctly predicts the class, True Negative (TN) — the classifier correctly predicts which are not of the class,

False Positive (FP) — the classifier incorrectly predicts other classes to be of the class and False Negative (FN) — the classifier incorrectly predicts the class to be of other class. Table III explains pictorially a sample case of three classes in which how TP, FP, FN, and TN for CLASS1 to be considered in a multinomial classification scenario.

In the proposed model the below-given performance metrics are calculated for three multi-classification approaches named as OvR Logistic Regression, OvR Naïve Bayes and OvR SVC. Recall for a class says a fraction of all samples of that class which is predicted correctly, which is evaluated as given in (5). Precision for a class says a fraction of all predicted samples of that class which is predicted correctly, which is evaluated as given in (6). F<sub>1</sub> score of a class will be the harmonic mean of precision and recall of that class, which is evaluated as given (7).

$$recall = \frac{TP}{TP+FN} \tag{5}$$

$$precision = \frac{TP}{TP+FP} \tag{6}$$

$$F_1Score = 2 \times \frac{precision \times recall}{precision + recall} \tag{7}$$

TABLE I. LIST OF SYSTEM PROCESSES TO SUPPORT TRUSTED PROCESSES

| Process name  | Process Path                          |
|---------------|---------------------------------------|
| Cmd           | C:\Windows\System32\cmd.exe           |
| Conhost       | C:\Windows\system32\conhost.exe       |
| Conhost       | C:\Windows\system32\conhost.exe       |
| Csrss         | C:\Windows\system32\csrss.exe         |
| Csrss         | C:\Windows\system32\csrss.exe         |
| Dwm           | C:\Windows\system32\Dwm.exe           |
| Hkcmd         | C:\Windows\System32\hkcmd.exe         |
| Igfxpers      | C:\Windows\System32\igfxpers.exe      |
| Igfxsvc       | C:\Windows\system32\igfxsvc.exe       |
| Igfxtray      | C:\Windows\System32\igfxtray.exe      |
| Lsass         | C:\Windows\system32\lsass.exe         |
| Lsm           | C:\Windows\system32\lsm.exe           |
| SearchIndexer | C:\Windows\system32\SearchIndexer.exe |
| Services      | C:\Windows\system32\services.exe      |
| Smss          | C:\Windows\System32\smss.exe          |
| Spoolsv       | C:\Windows\System32\spoolsv.exe       |
| Svchost       | C:\Windows\system32\svchost.exe       |
| Svchost       | C:\Windows\System32\svchost.exe       |
| Svchost       | C:\Windows\system32\svchost.exe       |
| Svchost       | C:\Windows\system32\svchost.exe       |
| Taskhost      | C:\Windows\system32\taskhost.exe      |
| Wininit       | C:\Windows\system32\wininit.exe       |
| winlogon      | C:\Windows\system32\winlogon.exe      |
| wuauclt       | C:\Windows\system32\wuauclt.exe       |
| WUDFHost      | C:\Windows\System32\WUDFHost.exe      |
| explorer      | C:\Windows\Explorer.EXE               |

TABLE II. A SAMPLE LIST OF TRUSTED PROCESSES OF A HOST

| Process namez | Process Path                                                        |
|---------------|---------------------------------------------------------------------|
| notepad       | C:\Windows\system32\notepad.exe                                     |
| devcpp        | C:\ProgramFiles\Dev-Cpp\devcpp.exe                                  |
| firefox       | C:\ProgramFiles\MozillaFirefox\firefox.exe                          |
| SnippingTool  | C:\Windows\system32\SnippingTool.exe                                |
| notepad++     | C:\ProgramFiles\notepad++\notepad++.exe                             |
| Vlc           | C:\ProgramFiles\VideoLAN\VLC\vlc.exe                                |
| FreeCell      | C:\ProgramFiles\MicrosoftGames\FreeCell\FreeCell.exe                |
| Hearts        | C:\ProgramFiles\MicrosoftGames\hearts\hearts.exe                    |
| Chess         | C:\ProgramFiles\MicrosoftGames\chess\chess.exe                      |
| chrome        | C:\ProgramFiles\Google\Chrome\Application\chrome.exe                |
| EXCEL         | C:\ProgramFiles\MicrosoftOffice\Office12\EXCEL.EXE                  |
| Zoom          | C:\Users\binu\AppData\Roaming\Zoom\bin\Zoom.exe                     |
| AcroRd32      | C:\ProgramFiles\Adobe\AcrobatReaderDC\Reader\AcroRd32.exe           |
| pythonw       | C:\Users\binu\AppData\Local\Programs\Python\Python36-32\pythonw.exe |
| POWERPNT      | C:\ProgramFiles\MicrosoftOffice\Office12\POWERPNT.EXE               |
| WINWORD       | C:\ProgramFiles\MicrosoftOffice\Office12\WINWORD.EXE                |

TABLE III. TP, FP, TN, AND FN FOR CLASS1 IN MULTINOMIAL CASE

| Predicted Class | True Class |         |         |
|-----------------|------------|---------|---------|
|                 | Class 1    | Class 2 | Class 3 |
| Class 1         | TP         | FP      |         |
| Class 2         | FN         |         | TN      |
| Class 3         |            |         |         |

For a multi-class scenario: Micro precision, Micro recall and Micro F<sub>1</sub>Score are calculated globally considering total TP, total FP, and total FN of the model instead of considering individual classes. In such case Accuracy of the model is same as Micro precision, Micro Recall, and Micro F<sub>1</sub>Score measured for the model globally. Macro precision, Macro recall and Macro F<sub>1</sub>Score are calculated considering the precision, recall, and F<sub>1</sub>Score of individual classes and taking the un-weighted mean of the measures. The Weighted precision, weighted recall and Weighted F<sub>1</sub>Score are calculated considering the precision, recall, and F<sub>1</sub>Score of individual classes and taking the weighted mean of the measures. The weight for each class is the total number of samples of that class. Accuracy and all the calculated Micro, Macro and Weighted performance metrics for the considered classifiers on the testing data is shown in Table IV.

The comparison of accuracy for the three classifiers OvR Logistic Regression, OvR Naïve Bayes and OvR SVC is plotted in “Fig. 7”. It has been found that the performance of OvR SVC is better than OvR Naïve Bayes but OvR Logistic Regression is found better than OvR SVC. The comparison of precision, recall and F<sub>1</sub>score for all three classifiers is plotted in “Fig. 8”, “Fig. 9” and “Fig. 10”, respectively. Considering all these metrics, it is found that OvR Logistic Regression

Classifier is most efficient for the model in comparison to other two classifiers. OvR Logistic Regression Classifier outperformed others with accuracy rate as 97% in predicting a process to its class and highest rates in precision, recall and F<sub>1</sub>Score.

To ensure the result of the system in identifying a suspected process as either trusted or variant of a trusted or untrusted, the processes of predicted class for a suspected process need to be cross-validated. Cross-validation of the suspected process is done with processes of predicted class considering cosine distance measure. As the OvR Logistic Regression classifier resulted with higher accuracy over the other two, it is chosen to predict the class of a suspected process at any time instance. As explained in Algorithm 3 Cross\_validate\_suspected\_process, Cosine distance is measured between DLL sequence vector of a suspected process and DLL sequence vectors of all the processes of the predicted class. The calculated list of cosine distance measures are used to reach a conclusion about the suspected In-memory process as either a trusted or a variant of trusted or untrusted type for the specific host. To evaluate the systems performance 300 processes of mixed samples are selected from the considered host. In these samples 200 processes are from trusted process list, 40 processes are from variant of the trusted process list and 60 processes are neither from the trusted list of processes nor from variant of any trusted process. Table V shows the confusion matrix for the 300 processes considered as suspected processes, which are initially applied to process class prediction model and further Cross validated using cosine distance measure. During the Cross validation of suspected process with processes of predicted class the optimized threshold value for  $\beta_1$  and  $\beta_2$  are calculated by several iterations. For the considered host the optimized value for  $\beta_1$  is found as 1, which is the minimum number of processes from the predicted class with cosine distance as 1 to the suspected process. The optimized value for  $\beta_2$  is found as 0.90, which is the average cosine distance of processes from the predicted class to the suspected process. “Fig. 11” speaks about precision and recall of the case study on the preferred host. In all cases, precision is above 95%. Whereas for trusted and untrusted processes recall is more than 93%, but for variant of process it is 84%.

TABLE IV. PERFORMANCE METRICS OF THE 3 MULTINOMIAL CLASSIFIERS

| Performance metrics | OvR Log Reg | OvR Naïve Bayes | OvR SVC |
|---------------------|-------------|-----------------|---------|
| Accuracy            | 0.97        | 0.88            | 0.92    |
| Micro Precision     | 0.97        | 0.88            | 0.92    |
| Micro Recall        | 0.97        | 0.88            | 0.92    |
| Micro F1-score      | 0.97        | 0.88            | 0.92    |
| Macro Precision     | 0.79        | 0.48            | 0.75    |
| Macro Recall        | 0.8         | 0.5             | 0.76    |
| Macro F1-score      | 0.79        | 0.47            | 0.75    |
| Weighted Precision  | 0.95        | 0.7             | 0.9     |
| Weighted Recall     | 0.97        | 0.88            | 0.92    |
| Weighted F1-score   | 0.96        | 0.74            | 0.91    |

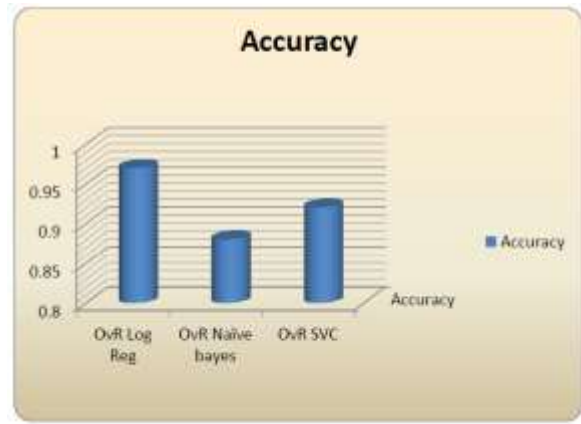


Fig. 7. Accuracy Comparison of the 3 Classifiers.

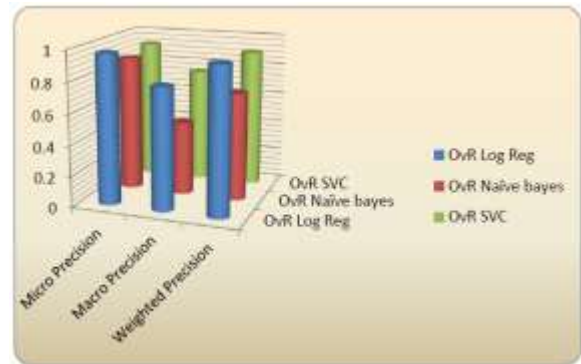


Fig. 8. Precision Comparison of the 3 Classifiers.

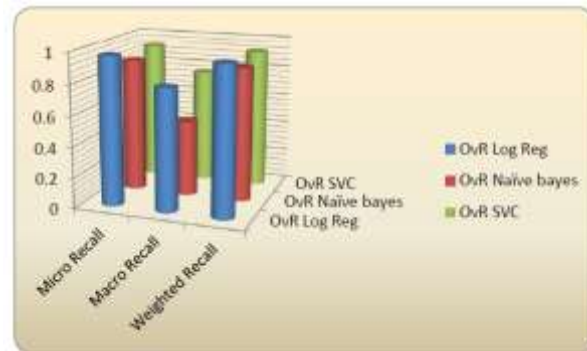


Fig. 9. Recall Comparison of the 3 Classifiers.

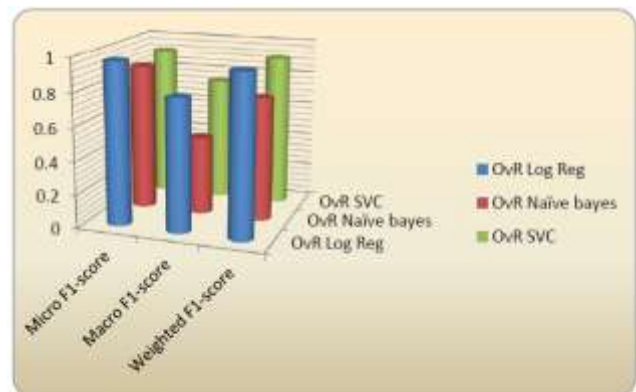


Fig. 10. F<sub>1</sub>Score Comparison of the 3 Classifiers.

TABLE V. A CASE STUDY OF CROSS VALIDATION FOR THE SPECIFIC HOST

| Prediction Cross Validated | Actual Cases applied to Model |                    |           |
|----------------------------|-------------------------------|--------------------|-----------|
|                            | Trusted                       | Variant of Trusted | Untrusted |
| Trusted                    | 191                           | 2                  | 1         |
| Variant of trusted         | 5                             | 38                 | 2         |
| Untrusted                  | 4                             | 0                  | 57        |

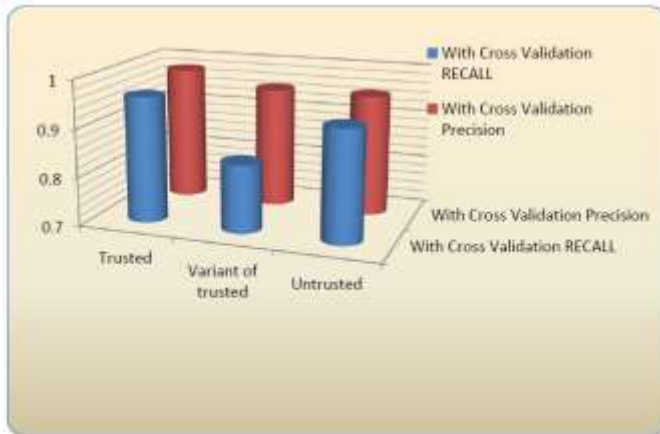


Fig. 11. Recall and Precision after Cross Validation of the Specific Host.

## V. CONCLUSION

The said system considers the trusted process list of a specific host as a multi-class problem considering DLL sequences as attribute vectors for In-memory processes. The objective of the system is to detect any deviation in the In-memory processes of the specific host. The system works in two stages. First stage is the process class prediction model, which is used to predict the class of a suspected process referring its DLL sequence as attribute vector. Second stage is Cross validation of the suspected process with the processes of predicted class. Three different multinomial classification approaches considered during evaluation of the process class prediction model where OvR Logistic Regression is proven to be the best performer compared to others. With OvR Logistic Regression 97% of accuracy and more than 95% of weighted precision, recall, and  $F_1$  score achieved for the model. To identify anomaly or deviation with some In-memory process during Cross validation of the suspected process with processes of the predicted class, use of cosine distance measure is found very effective. The case study during evaluation of system shows precision above 95% for all trusted, variant of trusted and untrusted processes. Recall of variant of trusted process is found as 84% where as 93% for trusted and untrusted processes. These results are quite impressive for finding any deviation with respect to In-memory processes of the host under consideration. An optimized value for threshold's  $\beta_1$  and  $\beta_2$  plays significant role for concluding the suspected process as either trusted or variant of a trusted or untrusted. In the case study using  $\beta_1$  as 1 and  $\beta_2$  as 0.9 shows the best performance on the host under consideration. It is also observed higher  $\beta_1$  moves less occurring trusted processes to a variant of trusted process and higher  $\beta_2$  moves a variant of trusted to untrusted process.

Hence  $\beta_1$  and  $\beta_2$  has impact on false negative cases. A lower value of  $\beta_2$  moves untrusted process to variant of trusted process and variant of trusted to trusted process. Hence  $\beta_2$  has impact on false positive cases. So an optimized value of  $\beta_1$  and  $\beta_2$  has significant impact on the performance of the system. It is also to be understood that the model's performance relies on the agreed list of trusted processes by the user on a specific host. The data collection for the training of process class prediction model is to be done under a proper supervision, as a biased data may result in higher false negatives or higher false positives. This system is found effective with memory based dynamic analysis for detection of anomaly or deviation from its normal operation with reference to known or trusted In-memory processes of a specific host. This system may help to have zero-day detection with respect to the presence of anomalous In-memory processes on a specific host which can be either an unknown program or a PUA or a malware. This system can be extended to find anomalies with In-memory processes considering a group of hosts with possible communication among the hosts. Using an efficient protocol for exchanging information about processes may help in reducing false negative or false positive cases. Analysis of communication cost with expectations in decrease in false positive and false negative cases may be crucial in performance evaluation of the system.

## REFERENCES

- [1] Quick Heal threat report (2019): <https://www.quickheal.co.in/documents/threat-report/QH-Annual-Threat-Report-2019.pdf>.
- [2] Internet Security threat report, Symantec (2019) : <https://docs.broadcom.com/doc/istr-24-2019-en>.
- [3] Sihwail, Rami & Omar, Khairuddin & Zainol Ariffin, Khairul Akram. (2018). A survey on malware analysis techniques: static, dynamic, hybrid, and memory analysis. 8. 1662. 10.18517/ijaseit.8.4-2.6827.
- [4] E. Gandotra, D. Bansal, and S. Sofat, "Malware Analysis and Classification: A Survey," J. Inf. Secur., vol. 05, no. 02, pp. 56–64, 2014.
- [5] P. V. Shijo and A. Salim, "Integrated static and dynamic analysis for malware detection," in Procedia Computer Science, 2015, vol. 46, pp. 804–811.
- [6] Watson, Michael & Shirazi, Syed Noorulhassan & Marnerides, Angelos & Mauthe, Andreas & Hutchison, David. (2015). Malware Detection in Cloud Computing Infrastructures. IEEE Transactions on Dependable and Secure Computing. 13. 1-1. 10.1109/TDSC.2015.2457918.
- [7] R. Mosli, R. Li, B. Yuan, and Y. Pan, "Automated malware detection using artifacts in forensic memory images," in 2016 IEEE Symposium on Technologies for Homeland Security, HST 2016, 2016, pp. 1–6.
- [8] C. Rathnayaka and A. Jamdagni, "An efficient approach for advanced malware analysis using memory forensic technique," Proc. - 16th IEEE Int. Conf. Trust. Secur. Priv. Comput. Commun. 11<sup>th</sup> IEEE Int. Conf. Big Data Sci. Eng. 14th IEEE Int. Conf. Embed. Softw. Syst., pp. 1145–1150, 2017.
- [9] Sanz, Borja & Santos, Igor & Ugarte-Pedrero, Xabier & Laorden, Carlos & Nieves, Javier & Bringas, Pablo. (2014). Anomaly Detection Using String Analysis for Android Malware Detection. 10.1007/978-3-319-01854-6\_48.
- [10] C. W. Tien, J. W. Liao, S. C. Chang, and S. Y. Kuo, (2017) "Memory forensics using virtual machine introspection for Malware analysis," in 2017 IEEE Conference on Dependable and Secure Computing, 2017, pp. 518–519.
- [11] S. Kim, J. Park, K. Lee, I. You, and K. Yim, (2012): "A Brief Survey on Rootkit Techniques in Malicious Codes," J. Internet Serv. Inf. Secur., vol. 3, no. 4, pp. 134–147, 2012.
- [12] Navaki Arefi, Meisam & Alexander, Geoffrey & Rokham, Hooman & Chen, Aokun & Faloutsos, Michalis & Wei, Xuetao & Oliveira, Daniela

- & Crandall, Jedidiah. (2018): FAROS: Illuminating In-memory Injection Attacks via Provenance-Based Whole-System Dynamic Information Flow Tracking. 231-242. 10.1109/DSN.2018.00034.
- [13] A. Hosseini, "Ten Process Injection Techniques: A Technical Survey of Common and Trending Process Injection Techniques," 2017. [Online]. Available: <https://www.endgame.com/blog/technicalblog/ten-process-injection-techniques-technical-survey-common-and-trending-process>.
- [14] Amanda Steward. (2014): FireEye DLL Side-Loading: A Thorn in the Side of the Anti-Virus Industry. Retrieved March 13, 2020.
- [15] Microsoft. (2018, May 31): About Side-by-Side Assemblies. Retrieved March 13, 2020.
- [16] K., Sudhakar & Kumar, Sushil. (2019): An emerging threat Fileless malware: a survey and research challenges. In Cyber Security 3. 1. Publisher: Springer (Biomed Central Ltd.) Dec- 2019 DOI:10.1186/s42400-019-0043-x.
- [17] Cheng, J.Y.C., Tsai, T.S., Yang, C.S., (2013): An information retrieval approach for malware classification based on Windows API calls. Int. Conf. on Machine Learning and Cybernetics, p.1678-1683. <https://doi.org/10.1109/ICMLC.2013.6890868>.
- [18] Windows Sysinternals Process Utilities: <https://docs.microsoft.com/en-us/sysinternals/downloads/process-utilities>.
- [19] Baeza-Yates, R.A., Ribeiro-Neto, B (1999): Modern Information Retrieval. Addison-Wesley Longman Publishing Co., Inc., Boston, MA, USA (1999).
- [20] Salton, G., McGill, M.: Introduction to modern information retrieval. McGraw-Hill New York (1983).

# Implementation of Random Direction-3D Mobility Model to Achieve Better QoS Support in MANET

Munsifa Firdaus Khan<sup>1</sup>, Indrani Das<sup>2</sup>

Department of Computer Science  
Assam University Silchar, Silchar  
Cachar, Assam, India

**Abstract**—Mobile Ad hoc Networks (MANETs) provides changing network topology due to the mobility of nodes. The complexity of the network increases because of dynamic topology of nodes. In a MANET, nodes communicate with each other without the help of any infrastructure. Therefore, achieving QoS in MANET becomes a little difficult. The movement of mobile nodes is represented through mobility models. These models have great impact on QoS in MANET. We have proposed a mobility model which is a 3D implementation of existing Random Direction (RD) mobility model. We have done a simulation on AODV with QoS metrics throughput, delay and PDR, using NS-3 and performed analysis of the proposed mobility models with other 3D mobility models, namely Random Way Point (RWP) and Gauss Markov (GM). It is concluded that our proposed model gives better throughput, delay and PDR for AODV routing protocol in comparing to RWP and GM mobility models. This paper is for students and researchers who are involved in wireless technology and MANET. It will help them to understand how a mobility model impacts the entire network and how its enhancement improves the QoS in MANET.

**Keywords**—Ad Hoc On Demand Distance Vector (AODV); random direction; mobility model; Quality-of-Service (QoS); Mobile Ad Hoc Networks (MANETs); NS-3

## I. INTRODUCTION

In Mobile Ad hoc Networks (MANETs), nodes are mobile, self-configuring and self-deployable. Since it is a wireless network communication between the nodes takes place through radio waves without the support of any central administration [13]. Because of its flexibility, it is used in large areas like military field, emergency operations, commercial field and wireless sensor network. The unique characteristics of MANET like changing node topology, node mobility, absence of base station and limited availability of resources like battery power and bandwidth make routing complex and in return degrades the QoS in MANET. QoS is the performance level of a service provided by a network to the user. QoS parameters like throughput, maximum bandwidth, Packet Delivery Ratio, delay, jitter and Packet Loss Ratio are used to verify the performance level of a network [4][6].

Since in MANET, nodes are mobile, therefore it is vital to utilize a mobility model for simulation [1]. Mobility model helps us to represent the node's position and movement with respect to speed, direction, time and distance. In order to relate to real world scenarios, it is essential to represent mobile nodes with varying velocity and way because in reality a

mobile node does not progress in a direct line with fixed speed and direction. We have designed and implemented a mobility model in 3D by modifying the 2D Random Direction (RD) mobility model. Several works have been done in the enhancement of Random Direction mobility model. We have used standard routing protocol AODV for performance analysis with QoS parameters throughput, delay and PDR. Simulation is done in NS-3. It is analyzed that our proposed model gives better throughput, delay and PDR for AODV routing protocol. With the growing use of wireless networks in all the fields it has become significant to provide secure and better network communication by improving QoS in MANET. This paper is for students, researchers focusing on wireless networks and MANET. It will provide them a basic idea about the impact of mobility model in providing QoS support in MANET. It will also make them understand how a mobility model is important for simulation in MANET.

The rest of the paper is prepared in the consequent way: Section II discusses the related work. Section III gives the brief overview of the existing mobility model. Section IV illustrates the proposed mobility model. Section V discusses the AODV routing protocol. Section VI shows the experimental results and lastly Section VII concludes the paper.

## II. RELATED WORK

Nain et al. [19] considered two variations of Random Direction mobility model with wrap around and with reflection. A simple path-wise relationship has been established for both the models. The authors have shown that if the users are initially uniformly distributed in the movement space with uniform position and direction, then they preserve the uniform distribution for random movement patterns.

Carofiglio et al. [20] proposed a method to improve route efficiency by choosing the most stable path in order to reduce latency and overhead due to route reconstruction. The movement of the node is represented using Random Direction mobility model and the probability of exact and approximate path availability and path duration is derived. The authors also propose an approach to improve the efficiency of the reactive routing protocol.

Gloss et al. [21] shows that the location dependent parameterization of the random direction mobility model can be used to create non-homogeneous mobility scenarios in a very flexible way. In particular the proposed transformation of

traces to RD-LDP parameterizations seems to be a promising approach to gain valuable, realistic mobility models that meet the requirements of stationary simulation techniques. Besides this transformation of traces to RD-LDP parameterizations, scenario creation based on sojourn density or movement guidelines appears to be a valuable method for distinguished simulation studies with non-homogeneous mobility scenarios.

Wu et al. [24] presents space probability distribution functions of the RDM in 3-D and prove it by simulating data. Consequently, the results of this paper are of practical value for performance analysis of Mobile Ad Hoc Network and provide a fundamental basis for the research on some its characteristics, such as, connectivity, average path length, network capacity and so on. Moreover, they provide precise theoretic foundations for derivations, proofs, simulations and applications of Ad Hoc network based on 3-D Random Direction Mobility Model.

Liu et al. [22] enhanced the Random Direction through equipping it with a commonly used, decentralized sense and avoid protocol—sense-and-stop (S&S) to analyze critical networking statistics for the unmanned aircraft system in a 2-D airspace. It is proved that the stationary node distribution in the enhanced model maintains the uniformity regardless of initial distributions. Moreover, it is also shown that the stationary inter-vehicle distance distribution in the enhanced model loses the uniformity.

Junfie et al. [23] introduced two 3-D smooth turn (ST) random mobility models (RMMs) to facilitate the design and evaluation of airborne networks (ANs). Both models are extended from the basic 2D Smooth Turn random mobility model, but differ in motion patterns along the z direction. In particular, the aerial mobility along the z direction is assumed to be independent of the other two dimensions in the z-independent ST RMM, while dependent in the z-dependent ST RMM. The z-independent ST RMM is more suitable for applications with less variation in aerial mobility along the z direction, such as civilian and commercial applications; while the z-dependent ST RMM is suitable for applications involving climbing or descending turns, such as military applications and air shows. Table I gives all the notations and descriptions that are used in this paper.

TABLE I. NOTATIONS AND DESCRIPTIONS

| Notations   | Descriptions                                                                        |
|-------------|-------------------------------------------------------------------------------------|
| $S_t$       | New speed at a fixed time interval t                                                |
| $D_t$       | New direction at a fixed time interval t                                            |
| $P_t$       | New pitch at a fixed time interval t                                                |
| $\tilde{S}$ | Mean speed                                                                          |
| $\tilde{D}$ | Mean direction                                                                      |
| $\tilde{P}$ | Mean pitch                                                                          |
| $Sx_{t-1}$  | Random variable for speed determined from a Gaussian distribution at time (t-1)     |
| $Dx_{t-1}$  | Random variable for direction determined from a Gaussian distribution at time (t-1) |
| $Px_{t-1}$  | Random variable for pitch determined from a Gaussian distribution at time (t-1)     |
| $\Theta$    | Random Direction of a node                                                          |

### III. EXISTING MOBILITY MODELS

#### A. Gauss Markov Mobility Model

It is memory based realistic mobility model proposed by Liang and Haas [15]. Though this model was initially designed for wireless personal communication services (PCS) networks, it is used in MANET for its realistic behavior [10]. At a given time interval 't', the speed and direction of each node are estimated on the basis of the previous value of direction and speed at (t-1)<sup>th</sup> time interval. A tuning parameter,  $\alpha$  is used to determine the degree of randomness for computing previous speed and direction. Therefore, this model imitates the characteristics of temporal dependency. The speed, direction and pitch are measured by the given mathematical formulas [11][12][16][17]:

$$S_t = \alpha S_{t-1} + (1-\alpha)\tilde{S} + \sqrt{(1-\alpha^2)}Sx_{t-1} \quad (1)$$

$$D_t = \alpha D_{t-1} + (1-\alpha)\tilde{D} + \sqrt{(1-\alpha^2)}Dx_{t-1} \quad (2)$$

$$P_t = \alpha P_{t-1} + (1-\alpha)\tilde{P} + \sqrt{(1-\alpha^2)}Px_{t-1} \quad (3)$$

Where  $S_t$ ,  $D_t$  and  $P_t$  are the new speed, direction and pitch at time interval t,  $\tilde{S}$ ,  $\tilde{D}$  and  $\tilde{P}$  are the mean speed, mean direction and mean pitch,  $Sx_{t-1}$ ,  $Dx_{t-1}$  and  $Px_{t-1}$  are random variables and  $\alpha$  is a random variable whose value lie within the range of  $0 < \alpha < 1$ . With the varying values of  $\alpha$ , randomness is determined.

#### B. Random Way Point Mobility Model

This mobility model is often used frequently in Mobile Ad hoc Networks (MANET) as it is simple and easily available in network simulators [12]. It was proposed by Johnson and Maltz [14]. In this model, nodes are initially deployed randomly. Nodes move freely and each node does not depend on the other nodes. This model chooses speed, direction and destination randomly. The working of the model is as follows:

Initially the node selects a particular position within the simulation area and considers it as the destination and starts moving towards it with a constant velocity which is uniformly selected from the interval [minimum\_velocity, maximum\_velocity] [1][11][14]. Upon arriving the selected destination, the node pauses for some time called the pause time and once the pause time finish, then the node begins moving on its way to another destination with a new velocity, which is independent of the previous one [1][10][11][14]. When the pause time is huge and velocity is minimum then the network topology becomes stable, whereas when the pause time is small and the velocity is maximized then the network topology will become highly dynamic. When the pause time is zero and velocity is selected randomly from the interval [minimum\_velocity, maximum\_velocity] then the node becomes continuously movable. In this model, the nodes stops unexpectedly, velocity changes abruptly and destination are selected randomly [12]. This model is memory less [14].

### C. Random Direction-2D Mobility Model

This is a memory less mobility model where the node moves on the basis of a random direction  $d$ . At a specific time period 't', the speed  $v(t)$  of a node is determined as a Gaussian Distribution from the interval [minimum\_speed, maximum\_speed] and an angular direction  $d$  is chosen from the interval  $[0, 2\pi]$ . Considering the node speed, pause time and angular direction, each node moves towards a definite direction until it arrives the boundary of the model. When it arrives the boundary, it pauses, selects a new direction and speed and starts moving towards a new direction [18].

After selection of speed and direction randomly, the velocity of a node in a Random Direction is calculated as:

$$(\text{speed} * \cos\Theta, \text{speed} * \sin\Theta) \quad (4)$$

We have shown in Fig. 1, the rectangular simulation boundary of a simulation area with a node for Random Direction-2D. A node can touch a boundary in the following four ways:

Case I: When a node touches BC of the rectangular boundary as shown in Fig. 1, then it will bounce backwards, i.e. making the value of the X-axis as negative and Y-axis as either positive or negative and Z axis to zero. The direction ( $\Theta$ ) of the node should lie within the range of  $90^0$  to  $270^0$ .

Case II: When a node touches AD of the rectangular boundary as shown in Fig. 1, then it will bounce rightwards, i.e. making the value of the X-axis as positive and Y-axis as either positive or negative and Z axis to zero. The direction ( $\Theta$ ) of the node should lie within the range of  $-90^0$  to  $+90^0$ .

Case III: When a node touches AB of the rectangular boundary as shown in Fig. 1, then it will bounce downwards, i.e. making the value of the X-axis as either positive or negative and Y-axis as negative and Z axis to zero. The direction ( $\Theta$ ) of the node should lie within the range of  $180^0$  to  $360^0$ .

Case IV: When a node touches DC of the rectangular boundary as shown in Fig. 1, then it will bounce upwards i.e. making the value of the X-axis as either positive or negative and Y-axis as positive and Z axis to zero. The direction ( $\Theta$ ) of the node should lie within the range of  $0^0$  to  $180^0$ .

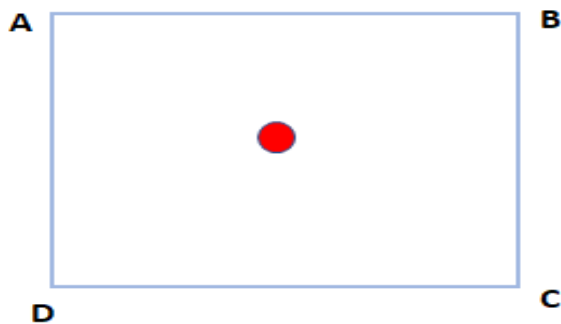


Fig. 1. Rectangular Boundary of the Simulation Area.

### Algorithm 1: Algorithm for Random Direction -2D mobility model

---

|                     |                                                                                                                                                          |
|---------------------|----------------------------------------------------------------------------------------------------------------------------------------------------------|
|                     | <b>Initialize:</b>                                                                                                                                       |
|                     | Set Rectangular Boundary ← value; Speed ← value; pause time ← value;                                                                                     |
| <b>Procedure 1:</b> | Do Initialize ()                                                                                                                                         |
|                     | i. Pick a random value of $\Theta$ between $0$ to $2 * \pi$                                                                                              |
|                     | ii. Call SetDirectionandSpeed().                                                                                                                         |
| <b>Procedure 2:</b> | SetDirectionandSpeed().                                                                                                                                  |
|                     | i. Calculate the velocity using speed and direction using the following formula:                                                                         |
|                     | Velocity= (speed * cos $\Theta$ , speed * sin $\Theta$ , 0);                                                                                             |
|                     | ii. The node in motion reaches the boundary and call the BeginPause().                                                                                   |
|                     | BeginPause()                                                                                                                                             |
|                     | The node pauses for pause time                                                                                                                           |
|                     | i. The node calls ResetSpeedandDirection().                                                                                                              |
| <b>Procedure 3:</b> | ResetSpeedandDirection()                                                                                                                                 |
|                     | i. The node can lie on any of the four sides of the rectangular boundary:                                                                                |
|                     | a. If the node lies on the right side of the rectangular boundary then the direction should be (-, +, 0) so the value of $\Theta$ lie between (90, 270). |
|                     | b. If the node lies on the left side of the rectangular boundary then the direction should be (+, +, 0) so the value of $\Theta$ lie between (-90, +90). |
|                     | c. If the node lies on the top of the rectangular boundary then the direction should be (+, -, 0) so the value of $\Theta$ lie between (180, 360).       |
|                     | d. If the node lies on the bottom of the rectangular boundary then the direction should be (+, +, 0) so the value of $\Theta$ lie between (0, 180).      |
|                     | ii. SetDirectionAndSpeed ()                                                                                                                              |

---

### IV. RANDOM DIRECTION-3D MOBILITY MODEL

This mobility model is a 3D version of the existing Random Direction-2D mobility model where the node moves on the basis of a random direction  $d$ . At a specific time period 't', the speed  $v(t)$  of a node is determined as a Gaussian Distribution from the interval [minimum\_speed, maximum\_speed] and an angular direction  $d$  is chosen from the interval  $[0, 2\pi]$ . Considering the node speed, pause time and angular direction, each node moves towards a definite direction until it arrives the boundary of the model. When it



arrives the boundary, it pauses, selects a new direction and speed and starts moving towards a new direction.

A random point on the surface of a sphere can be calculated using the following steps:

- 1) Choose a random value of  $\Theta$  between 0 and  $2\pi$ .
- 2) Choose a random value of  $z$  between -1 and 1.
- 3) Compute the following:

$$(x, y, z) = (\sqrt{1 - z^2} \cos\theta, \sqrt{1 - z^2} \sin\theta, z)$$

The 3D simulation area of a box and a node is shown in Fig. 2. Here,  $\Theta$  is used to determine the value of direction which lie within the range  $(0^0, 360^0)$  and the value of  $z$  lies within the range  $(-1,1)$ . When a node touches a boundary of the box, then these six cases happens:

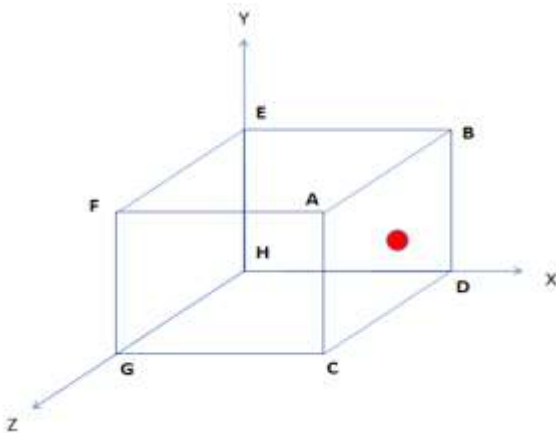


Fig. 2. A 3D Simulation Area.

Case I: When a node touches ABCD wall of the box as shown in Fig. 2, then it will bounce back so that the value of X-axis should be negative irrespective of Y-axis and Z-axis in order to remain within the box. The direction ( $\Theta$ ) of the node should lie within the range of  $90^0$  to  $270^0$  so that Case I holds, such that the values considered for X-axis as negative, Y-axis and Z-axis as either positive or negative and  $z$  lie within the range from  $(-1,1)$ .

Case II: When a node touches EFGH wall of the box as shown in Fig. 2, then it will bounce back so that the value of X-axis should be positive irrespective of Y-axis and Z-axis in order to remain within the box. The direction ( $\Theta$ ) of the node should lie within the range of  $-90^0$  to  $90^0$  so that Case II holds, such that the values considered for X-axis as positive, Y-axis and Z-axis as either positive or negative and  $z$  lie within the range from  $(-1,1)$ .

Case III: When a node touches AB EF wall of the box as shown in Fig. 2, then it will bounce back so that the value of Y-axis should be negative irrespective of X-axis and Z-axis in order to remain within the box. The direction ( $\Theta$ ) of the node should lie within the range of  $180^0$  to  $360^0$  so that Case III holds, such that the values considered for Y-axis as negative, X-axis and Z-axis as either positive or negative and  $z$  lie within the range from  $(-1,1)$ .

Case IV: When a node touches CDGH wall of the box as shown in Fig. 2, then it will bounce back so that the value of Y-axis should be positive irrespective of X-axis and Z-axis in order to remain within the box. The direction ( $\Theta$ ) of the node should lie within the range of  $0^0$  to  $180^0$  so that Case IV holds, such that the values considered for Y-axis as positive, X-axis and Z-axis as either positive or negative and  $z$  lie within the range from  $(-1,1)$ .

Case V: When a node touches ACGF wall of the box as shown in Fig. 2, then it will bounce back so that the value of Z-axis should be negative irrespective of X-axis and Y-axis in order to remain within the box. The direction ( $\Theta$ ) of the node should lie within the range of  $0^0$  to  $360^0$  so that Case V holds, such that the values considered for Z-axis as negative, X-axis and Y-axis as either positive or negative and  $z$  lie within the range from  $(-1,0)$ .

Case VI: When a node touches BDEH wall of the box as shown in Fig. 2, then it will bounce back so that the value of Z-axis should be positive irrespective of X-axis and Y-axis in order to remain within the box. The direction ( $\Theta$ ) of the node should lie within the range of  $0^0$  to  $360^0$  so that Case VI holds, such that the values considered for Z-axis as positive, X-axis and Y-axis as either positive or negative and  $z$  lie within the range from  $(0,1)$ .

The velocity of a node in 3D is determined using the following formula:

$$\text{Velocity} = \text{speed} * (\cos\theta * \sqrt{1 - z^2}, \sin\theta * \sqrt{1 - z^2}, z) \quad (5)$$

The Flowchart of the algorithm for Random Direction-3D mobility model is shown in Fig. 3, Fig. 4 and Fig. 5, respectively.

---

**Algorithm 2: Algorithm for Random Direction -3D mobility model**

---

**Initialize:** Set Rectangular Box Boundary ← value;  
Speed ← value; pause time ← value;

**Procedure 1:** Do Initialize PrivateFunction().

- i. Pick a random value of  $\Theta$  between 0 to  $2 * \pi$  and  $z$  between -1 to 1.
- ii. Call SetDirectionandSpeed Function () .

**Procedure 2:** SetDirectionandSpeedFunction().

- i. Calculate the velocity using speed and direction using the following formula:

$$\text{Velocity} = \text{speed} * (\cos\theta * \sqrt{1 - z^2}, \sin\theta * \sqrt{1 - z^2}, z)$$

- ii. The node in motion reaches the boundary and call the BeginPause Function () .

BeginPause Function () .  
The node pauses for pause time

- iii. The node calls ResetSpeedandDirectionFunction().

---

**Procedure 3:** ResetSpeedandDirectionFunction()

- i. The node can lie on any of the six faces of the box:
  - a) If the node lies on the right side of the box then the direction should be (-, +, +) so the value of  $\Theta$  lies between (90, 270) and  $z$  (-1, 1).
  - b) If the node lies on the left side of the box then the direction should be (+, +, +) so the value of  $\Theta$  lies between (-90, +90) and  $z$  (-1, 1).
  - c) If the node lies on the top side of the box then the direction should be (+, -, +) so the value of  $\Theta$  lies between (180, 360) and  $z$  (-1, 1).
  - d) If the node lies on the bottom side of the box then the direction should be (+, +, -) so the value of  $\Theta$  lies between (0, 180) and  $z$  (-1, 1).
  - e) If the node lies on the Front side of the box then the direction should be (+, +, -) so the value of  $\Theta$  lies between (0, 360) and  $z$  (-1, 0).
  - f) If the node lies on the Back side of the box then the direction should be (+, -, +) so the value of  $\Theta$  lies between (0, 360) and  $z$  (0, 1).
- ii. SetDirectionAndSpeedFunction()

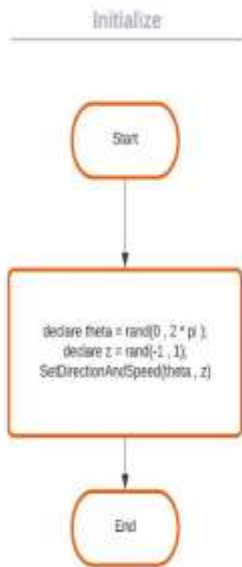


Fig. 3. Flowchart for Procedure 1.

**SetDirectionAndSpeed(theta , z)**

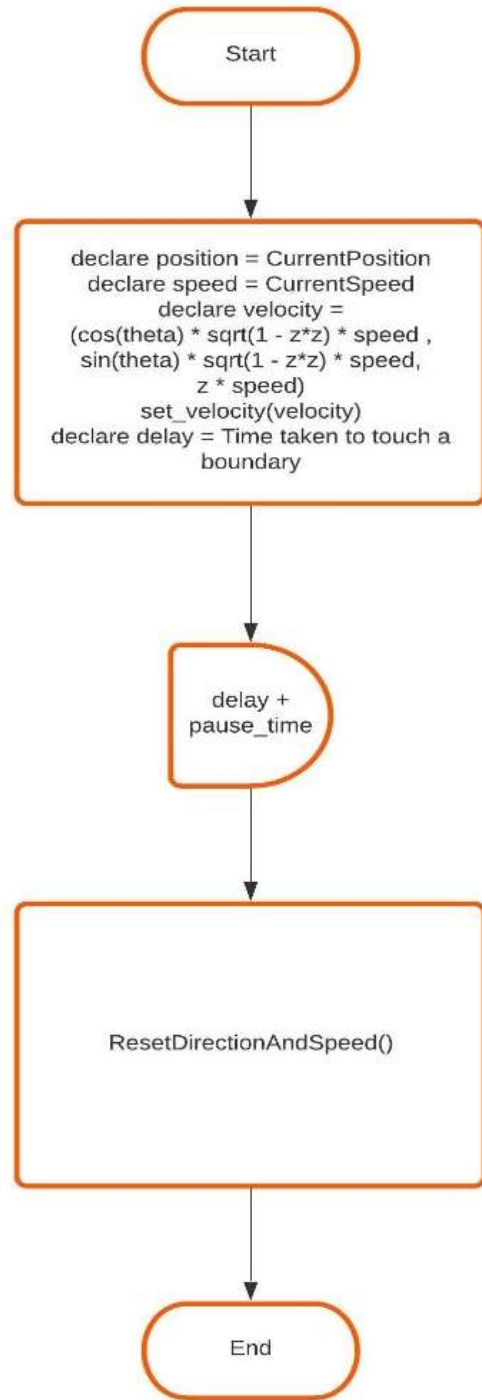


Fig. 4. Flowchart for Procedure 2.

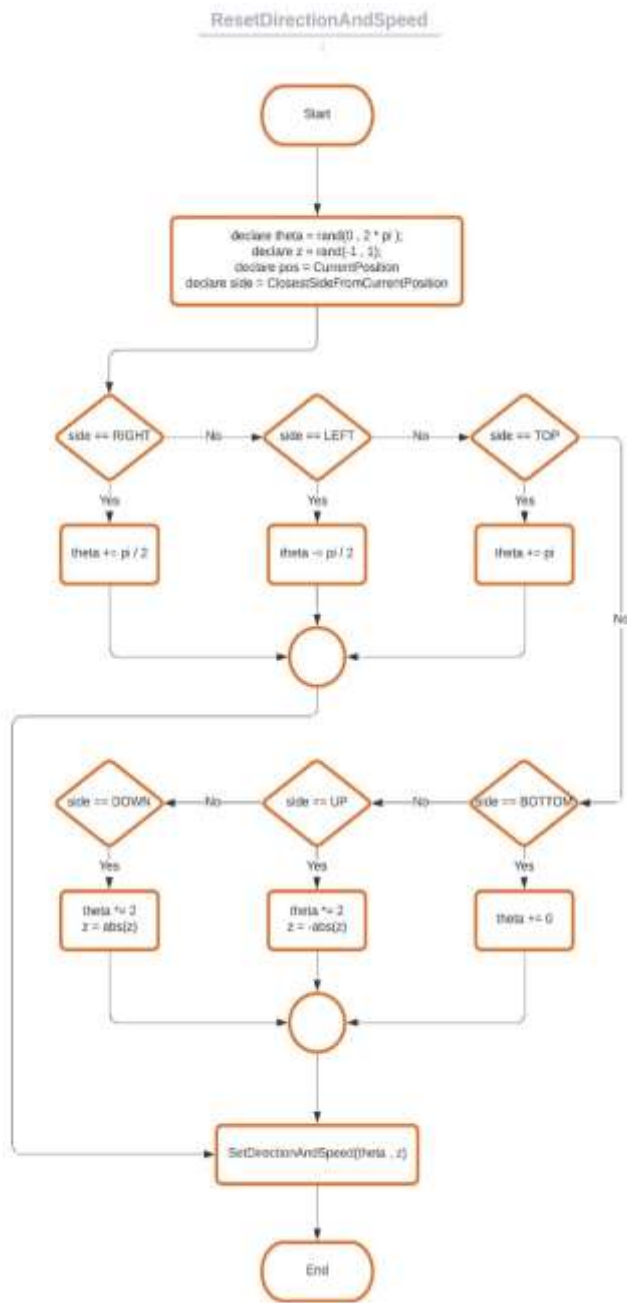


Fig. 5. Flowchart for Procedure 3.

## V. AD HOC ON DEMAND DISTANCE VECTOR ROUTING PROTOCOL

Ad Hoc On Demand Distance Vector (AODV) is a reactive routing protocol where a path is discovered whenever a node wants to exchange information with another node [3][5][7][9][25]. It is one of the most popular and efficient routing protocols. This protocol has minimum space complexity because a path is created on demand and also path information is deleted if not required [3]. It provides loop free paths and is scalable for huge networks [2][3][4]. When a source node wants to exchange information with the destination node and the required path is unavailable, in that case path discovery procedure is initiated and source node

broadcasts a Route Request (RREQ) packets to all the neighbor nodes. When the neighbor nodes receive the RREQ packets, if it has the path to the destination or if it is the destination then it sends a Route Reply (RREP) packet else it broadcast the RREQ packet to its neighbor nodes [8]. A source may receive more than one RREP from its neighbor nodes in that case it selects the path with the least number of hops because all the nodes in MANET are mobile so less hop count will lead to a more stable path. Once the destination receives the RREQ packet a reverse path is created to transmit the RREP packet using that path. Once the path is discovered data can be transferred using that path. When a node does not receive any messages from its corresponding neighbor nodes during path discovery procedure then it considers a path breakage. Due to the mobility of nodes, path breakage is obvious in MANET. Whenever a node detects path failure, then Route Error (RERR) packet is transmitted to its corresponding neighbor nodes so that all the associated nodes gets information about the broken path [3][7][8].

## VI. EXPERIMENT AND RESULTS

### A. Experimental Parameters

We have considered an AODV routing protocol to check the impact of all the 3D mobility models, namely, Gauss Markov, Random Way Point and Random Direction-3D using various group of nodes like 20, 40, 60, 80, 100 and 120 in NS-3. Table II shows all the simulation parameters and values. Table III, Table IV and Table V represent the parameters and corresponding values for Gauss Markov, Random Way Point and Random Direction-3D mobility models. Since, Random Direction and Random Way point mobility models are memoryless mobility models we have considered the value of tuning parameter as zero (means memoryless) in Gauss Markov to keep the similarity with the other mobility models.

TABLE II. EXPERIMENTAL PARAMETERS AND ITS VALUES

| Parameters              | Values                                                  |
|-------------------------|---------------------------------------------------------|
| Number of nodes         | 20,40,60,80,100 and 120.                                |
| Routing Protocol        | AODV                                                    |
| Number of flows         | 10                                                      |
| Transmission Power      | 9.5dBm                                                  |
| Total Simulation Time   | 120 seconds                                             |
| Traffic                 | CBR                                                     |
| Data Rate               | 1024 bps                                                |
| Packet Size             | 512 kbps                                                |
| Propagation Delay Model | Constant Speed Propagation Delay                        |
| Propagation Loss Model  | Friss Propagation Loss                                  |
| Position Allocator      | Random Box<br>X[0,500]<br>Y[0,500]<br>Z[0,500]          |
| Mobility Models         | Gauss Markov, Random Way Point and Random Direction-3D. |

TABLE III. PARAMETERS FOR GAUSS MARKOV MOBILITY MODEL

| Parameters                 | Values                               |
|----------------------------|--------------------------------------|
| Bounds                     | X[0,500], Y[0,500] and Z[0,500]      |
| Time Step                  | 15 seconds                           |
| Tuning Parameter, $\alpha$ | 0.0                                  |
| Mean Velocity              | [0,20]m/s                            |
| Mean Direction             | [0,6.283185307]                      |
| Mean Pitch                 | [0.02, 0.5]                          |
| Normal Velocity            | Mean=0.2, Variance=0.4 and Bound=0.6 |
| Normal Direction           | Mean=0.5, Variance=0.6 and Bound=0.7 |
| Normal Pitch               | Mean=0.3, Variance=0.5 and Bound=0.8 |

TABLE IV. PARAMETERS FOR RANDOM WAY POINT MOBILITY MODEL

| Parameters | Values    |
|------------|-----------|
| Speed      | [0,20]m/s |
| Pause Time | 2 seconds |

TABLE V. PARAMETERS FOR RANDOM DIRECTION-3D MOBILITY MODEL

| Parameters | Values                          |
|------------|---------------------------------|
| Bounds     | X[0,500], Y[0,500] and Z[0,500] |
| Speed      | [0,20]m/s                       |
| Pause Time | 2 seconds                       |

### B. Experimental Results

For experimentation, we have considered parameters like throughput, PDR and delay. We have done a huge number of experiments using different set of nodes like 20, 40, 60, 80, 100 and 120 with our presented mobility model, namely, Random Direction-3D (RD-3D) model and other existing mobility models like Gauss Markov (GM) and Random Way Point (RWP) to check their impact on QoS support in MANET. The experiment is also done to analyze the influence of these mobility models on routing protocol AODV.

1) *Throughput*: It is interpreted as the number of bits transmitted per second during the exchange of information in a network [5]. This parameter is used here as one of the performance measures to check the effect of mobility models in AODV. The higher the throughput values the better is the QoS. The results for throughput of AODV with a different set of nodes and distinct mobility models are shown in Table VI. It is observed in Table VI that the highest throughput obtained for AODV is 54.5994 kbps using Random Direction-3D for 20 nodes, whereas the least is 4.0318 kbps using Gauss Markov for 20 nodes. It is noticed that for 20, 60, 100 and 120 nodes RD-3D gives higher throughput, whereas GM gives lower throughput as shown in Fig. 6. The average throughput for AODV is better using the RD-3D mobility model in compared to GM and RWP mobility models.

a) *Delay*: It is defined as the total time spends by a node during transmission of data to its destination [5]. We have used delay as one of the performance measures to check the

impact of mobility models in AODV. The lower the delay values the better is the QoS. Delay values for AODV are shown in Table VII using a distinct set of nodes and our proposed and existing mobility models. It is observed in Table VII that the highest delay obtained for AODV is 882.2117 seconds using GM mobility models for 120 nodes, whereas the least is 257.0947 seconds using RD-3D for 40 nodes. It is noticed that for all set of nodes except 20 nodes RD-3D gives lower delay values whereas GM gives higher delay values. Moreover, it is also analyzed that the average delay for AODV is lower using the RD-3D mobility model in compared to GM and RWP mobility models as shown in Fig. 7.

b) *Packet-Delivery-Ratio*: It is expressed as the ratio of total number of data transmitted at the destination to the total number of data generated at the source [5]. PDR is used as one of the performance metrics to analyze the effect of the various mobility models using a different set of nodes on AODV as shown in Table VIII. It is observed in Table VIII that the highest PDR obtained for AODV is 0.8942 using RD-3D mobility models for 80 nodes, whereas the least is 0.4911 using RD-3D for 20 nodes. It is noticed that for 60, 80, 100 and 120 set of nodes RD-3D gives higher PDR values, whereas for 20 and 40 nodes, GM gives higher PDR values. Furthermore, it is also analyzed that the PDR for AODV is better using the RD-3D mobility model in compared to GM and RWP mobility models as shown in Fig. 8.

TABLE VI. THROUGHPUT FOR AODV

| Number of nodes | Random Direction-3D | Gauss Markov | Random Way Point |
|-----------------|---------------------|--------------|------------------|
| 20              | 54.5994             | 4.0318       | 17.8825          |
| 40              | 10.9631             | 7.5399       | 16.8110          |
| 60              | 23.6391             | 17.6690      | 16.2925          |
| 80              | 21.4512             | 22.9984      | 20.1144          |
| 100             | 21.3552             | 18.6597      | 21.0392          |
| 120             | 25.4842             | 20.0737      | 17.3983          |

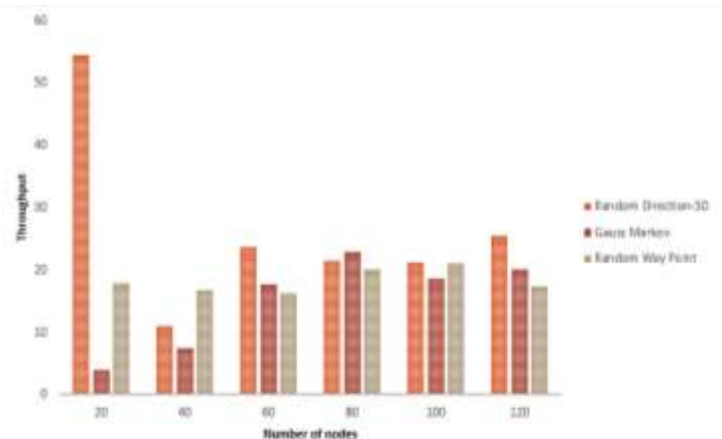


Fig. 6. Throughput for AODV.

TABLE VII. DELAY FOR AODV

| Number of nodes | Random Direction-3D | Gauss Markov | Random Way Point |
|-----------------|---------------------|--------------|------------------|
| 20              | 601.4657            | 848.1105     | 462.6682         |
| 40              | 257.0947            | 494.7951     | 523.2514         |
| 60              | 367.6813            | 586.6404     | 557.2569         |
| 80              | 362.2419            | 777.1103     | 635.3308         |
| 100             | 392.2723            | 859.5799     | 748.4077         |
| 120             | 477.5648            | 882.2117     | 778.2379         |

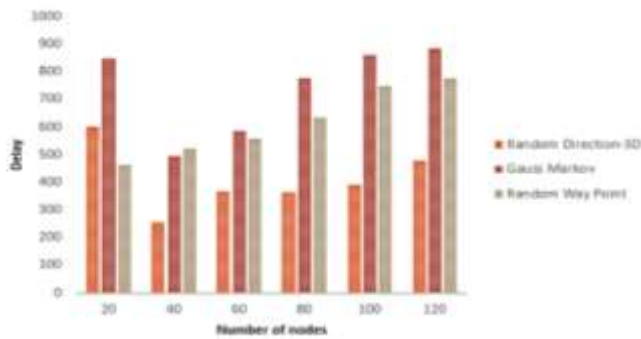


Fig. 7. Delay for AODV.

TABLE VIII. PDR FOR AODV

| Number of nodes | Random Direction-3D | Gauss Markov | Random Way Point |
|-----------------|---------------------|--------------|------------------|
| 20              | 0.4911              | 0.8627       | 0.8220           |
| 40              | 0.8312              | 0.8853       | 0.8799           |
| 60              | 0.8931              | 0.8596       | 0.8541           |
| 80              | 0.8942              | 0.8223       | 0.8384           |
| 100             | 0.8729              | 0.7849       | 0.7654           |
| 120             | 0.8668              | 0.7184       | 0.7128           |

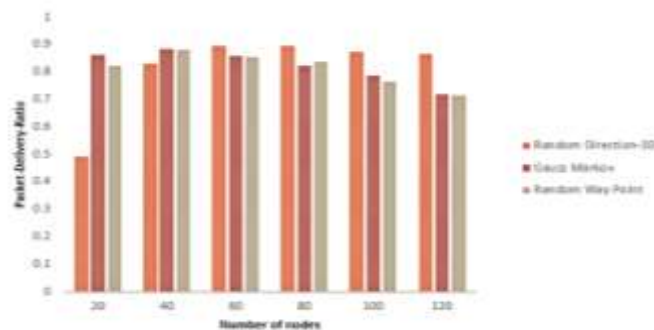


Fig. 8. Packet-Delivery-Ratio for AODV.

## VII. CONCLUSION AND FUTURE WORK

We have designed and implemented a 3D mobility model by modifying the existing 2D Random Direction mobility model. The proposed mobility model is tested in NS-3 on the routing protocol AODV. The impact of the mobility model is observed using performance measures throughput, PDR and delay. We know that the higher values of PDR and throughput

gives better QoS and lower values of delay give better QoS in MANET. It is noticed in Table VI that the RD-3D mobility model gives better throughput in comparison to RWP and GM whereas GM gives the least throughput. One of the reasons for GM giving least throughput is the use of least value of the tuning parameter. Since, we have considered all the memory less mobility models, we have considered the value of tuning parameter of GM as zero. Moreover, it is observed in Table VII that among the three mobility models RD-3D gives the least delay. Furthermore, from Table VIII it is noticed that the average PDR value is better for RD-3D mobility model in comparison to RWP and GM mobility models. It is concluded that the RD-3D mobility model outperforms well in terms of throughput, delay and PDR in comparing to RWP and GM mobility models. Our model can be further analyzed on other routing protocols like DSDV, DSR, AOMDV, etc.

## REFERENCES

- [1] T. Camp, J. Boleng, and V. Davies. "A survey of mobility models for ad hoc network research", *Wireless communications and mobile computing* 2.5, pp. 483-502, 2002.
- [2] P. Landge, A. Nigavekar, "Modified AODV protocol for energy efficient routing in MANET", *Int J Eng Sci Res Technol*, vol. 5(3), pp. 523–529, 2016.
- [3] A.Ahmed, A. Hanan, I. Osman, "AODV routing protocol working process", *Journal of Convergence Information Technology*, vol.10(2), pp. 1-7, 2015.
- [4] M.F. Khan, I. Das, "Effect of Different Propagation Models in Routing Protocols", *International Journal of Engineering and Advanced Technology (IJEAT)*, vol. 9(2), pp.3975-3980, 2019.
- [5] M.F. Khan and I. Das, "An Investigation on Existing Protocols in MANET", *Innovations in Computer Science and Engineering, Lecture Notes in Networks and Systems* 74, pp. 215-224, 2019.
- [6] M.F. Khan and I. Das, "A study on quality-of-service routing protocols in mobile ad hoc networks". In: *2017 international conference on computing and communication technologies for smart nation (IC3TSN)*. IEEE, pp.95–98, 2017.
- [7] P.K. Maurya, G. Sharma, V. Sahu, A. Roberts, M. Srivastava, "An overview of AODV routing protocol", *International Journal of Modern Engineering Research (IJMER)*, vol. 2(3), pp. 728-732, 2012.
- [8] I. Chakeres and M. Elizabeth, "AODV routing protocol implementation design", *24th International Conference on Distributed Computing Systems Workshops, 2004. Proceedings. IEEE, 2004.*
- [9] C. Murthy, B. Manoj, "Ad hoc Wireless Networks: Architectures and Protocols", Prentice Hall PTR, 2004.
- [10] D. A. Guimarães, E. P. Frigieri, and L. J. Sakai. "Influence of node mobility, recharge, and path loss on the optimized lifetime of wireless rechargeable sensor networks." *Ad Hoc Networks* 97, 102025, 2020.
- [11] J. D. M. M. Biomo, T. Kunz, and M. St-Hilaire. "An enhanced Gauss-Markov mobility model for simulations of unmanned aerial ad hoc networks." *2014 7th IFIP Wireless and Mobile Networking Conference (WMNC)*. IEEE, 2014.
- [12] D. Broyles, A. Jabbar and J. P. G. Sterbenz. "Design and analysis of a 3-D gauss-markov mobility model for highly-dynamic airborne networks." *Proceedings of the international telemetering conference (ITC)*, San Diego, CA, 2010.
- [13] J. Broch, D. A. Maltz, D. B. Johnson, Y.C. Hu and J. Jetcheva "A performance comparison of multi-hop wireless ad hoc network routing protocols" *Proceedings of ACM MobiCom*. Vol. 114, 1998.
- [14] D. B. Johnson and D. A. Maltz. "Dynamic source routing in ad hoc wireless networks." *Mobile computing*. Springer, Boston, MA, pp.153-181, 1996.
- [15] B. Liang and J.H. Zygmunt. "Predictive distance-based mobility management for PCS networks." *IEEE INFOCOM'99. Conference on Computer Communications. Proceedings. Eighteenth Annual Joint*

- Conference of the IEEE Computer and Communications Societies. The Future is Now (Cat. No. 99CH36320). Vol. 3. IEEE, 1999.
- [16] L. Ghouti, T. R. Sheltami, and K. S. Alutaibi. "Mobility prediction in mobile ad hoc networks using extreme learning machines." *Procedia Computer Science* 19, pp. 305-312, (2013).
- [17] N. Meghanathan, "Impact of the Gauss-Markov mobility model on network connectivity, lifetime and hop count of routes for mobile ad hoc networks", *Journal of networks*, vol. 5(5), pp.509, 2010.
- [18] <https://www.nsnam.org> (accessed on dated 11/07/2020).
- [19] P. Nain, D. Towsley, B. Liu, and Z. Liu, "Properties of random direction models", In *Proceedings IEEE 24th Annual Joint Conference of the IEEE Computer and Communications Societies*, vol. 3, pp. 1897-1907, March 2005.
- [20] G. Carofiglio, C. F. Chiasserini, M. Garetto and E. Leonardi, "Route stability in MANETs under the random direction mobility model", *IEEE transactions on Mobile Computing*, vol. 8(9), pp. 1167-1179, 2009.
- [21] B. Gloss, M. Scharf and D. Neubauer, "A more realistic random direction mobility model". TD (05), 52, 13-14, 2005.
- [22] M. Liu, Y. Wan, and F. L. Lewis, F. L, " Analysis of the random direction mobility model with a sense-and-avoid protocol", In *2017 IEEE Globecom Workshops GC Workshops*, pp. 1-6, IEEE, December 2017.
- [23] J. Xie, Y. Wan, B. Wang, S. Fu, K. Lu, and J.H. Kim, "A comprehensive 3-dimensional random mobility modeling framework for airborne networks". *IEEE Access*, 6, pp.22849-22862, 2018.
- [24] J. Wu, X. Zhu, and X. Wang, "Anaysis of 3 -D Random Direction Mobility Model for Ad Hoc Network", *6th International Conference on ITS Telecommunications Proceedings*, IEEE, 2006.
- [25] M. F. Khan and I. Das, "Performance Evaluation of Routing Protocols in NS-2 and NS-3 Simulators", *International Journal of Advanced Trends in Computer Science and Engineering*, vol. 9(4), pp.6509-6517, 2020.

# An Empirical Analysis of BERT Embedding for Automated Essay Scoring

Majdi Beseiso<sup>1</sup>

Department of Computer Science  
Al-Balqa Applied University, Alsalt, Jordan

Saleh Alzahrani<sup>2</sup>

Information Systems Department, Al-Imam Mohammad Ibn  
Saud Islamic University, Riyadh, Saudi Arabia

**Abstract**—Automated Essay Scoring (AES) is one of the most challenging problems in Natural Language Processing (NLP). The significant challenges include the length of the essay, the presence of spelling mistakes affecting the quality of the essay and representing essay in terms of relevant features for the efficient scoring of essays. In this work, we present a comparative empirical analysis of Automatic Essay Scoring (AES) models based on combinations of various feature sets. We use 30-manually extracted features, 300-word2vec representation, and 768-word embedding features using BERT model and forms different combinations for evaluating the performance of AES models. We formulate an automated essay scoring problem as a rescaled regression problem and quantized classification problem. We analyzed the performance of AES models for different combinations. We compared them against the existing ensemble approaches in terms of Kappa Statistics and Accuracy for rescaled regression problem and quantized classification problem respectively. A combination of 30-manually extracted features, 300-word2vec representation, and 768-word embedding features using BERT model results up to  $77.2 \pm 1.7$  of Kappa statistics for rescaled regression problem and  $75.2 \pm 1.0$  of accuracy value for Quantized Classification problem using a benchmark dataset consisting of about 12,000 essays divided into eight groups. The reporting results provide directions to the researchers in the field to use manually extracted features along with deep encoded features for developing a more reliable AES model.

**Keywords**—Automated Essay Scoring (AES); BERT; deep learning; neural network; language model

## I. INTRODUCTION

Automated Essay Scoring (AES) involves the use of statistical models for extracting useful features from the essay and assigning grades in the numeric range. It helps to reduce human efforts in manual grading of essays and improve the effectiveness and efficiency of writing assessment. Several models have been proposed for automatic essay scoring in the recent past. Broadly, these models can be further categorized into two classes [1]. The first type of AES models belongs to feature engineering-based models. These models use manually extracted features from an essay in term of number of words, number of grammatical errors, number of unique vocabulary words, term frequency, inverse document frequency, etc. [2-3]. Feature engineering-based models have the benefits of using manually extracted features that can be easily explained and modified to adapt different scoring criteria. However, these model suffer from the limitation of lack of

understanding some cement features leading to low accuracy of the models.

The second type of AES models is called an end to end models. These models are developed using machine learning or deep learning techniques [4, 5] based on some word embedding methods [6, 7]. The word embedding methods represent essay into low dimensional vectors. A dense layer follows the low dimensional vectors for transforming them into a deep encoded vector for further scoring of the essay. End to end models exhibits good performance for extracting semantic features and address the limitation of feature engineering models. However, these models are unable to integrate manually extracted features.

AES engine assigns a score to an essay based upon extracted features from the raw data of essays. The scoring process involves two phases [8]. The first phase consists of collecting the data for scoring by AES engine. The engine is trained based on some holistic rubrics that specify the satisfaction criteria of the essay. The rubrics consider different factors like grammatical errors, spelling mistakes, clarity, organization of the text, and Cohesion of the essay [9]. Kaggle competition has made AES data set available to the public. The second phase involves dividing the essay dataset into two data subsets for training and testing purposes. The training data set is a labelled data set used for developing a trained model of AES engine based upon the selected features of essay dataset. The trained model is further applied to the test data set for assigning them the labels as a score of the essay.

In this paper, we focus on manually extracted features as well as word embedding features of BERT model for analyzing the performance of but language model in automated scoring of essay. We conduct a set of experiments using word-embedding models along with the manually extracted features and compare their performances for automated scoring of essay using a benchmark dataset. The performance of different models is compared in terms of Kappa statistics and accuracy by considering the automatic scoring process as rescaled regression and quantized classification problem, respectively.

Rest of the paper is structured as follows. Section 2 highlights the background of AES and describes the different models developed for efficient AES. Section 3 describes the details of experiments, such as experimental setup, benchmark dataset and performance metrics. It provides comprehensive experimental mythology being following in this work. Section

4 presents results, analyses and compares the results with the existing approaches. Section 5 concludes this paper at the end.

## II. BACKGROUND

AES is considered as one of the most challenging problems in natural language processing (NLP). The significant challenges are the length of the essay, the presence of spelling mistakes affecting the quality of the essay. Several research efforts have been invested in the recent past for automated essay scoring [8, 10]. Initially, these research efforts involve the use of statistical methods based upon bag of words (BOW), use of Logistic regression method, and other probability-based methods. Some researches applied neural networks for automated scoring of essays using the word embedding method [6]. Embedding methods mainly work on characters words or sentences and transform them into n-dimensional vectors by preserving semantic features. It results in a conversion of character data into a sequence of n-dimensional data. The n-dimensional vector can be further used to create the model of different neural networks like LSTM, CNN and GRU [11]. These neural networks are the nonlinear models that are used to score the given essay based upon some scoring rubrics.

Ke et al. (2019) [12], Chen et al. (2010) [13], and Wang et al. (2018) [14] have summarized supervised and unsupervised learning-based embedding methods. In supervised learning methods for automatic scoring of essays, the researches considered AES problem as a regression problem and classification problem. Regression problem involves predicting the score of essay in the given numeric range. Classification problem involves the classification of essay to one of the predefined classes like medium, low and high. In case of regression, researchers use linear regression [15, 16], support vector regression [17, 18], and sequential minimal optimization (SMO, a variant of support vector machines) [19] for automatic scoring of the essays based upon different features. In the case of classification, researchers employed SMO [19], logistic regression [20] and Bayesian network classification [21] for classifying essays to their predefined classes. Many researchers also used neural networks for automated scoring of essays. Taghipour and Ng [22] proposed the first approach based on neural network for scoring essays. They used a series of words as input to convolutional layer and extracted n-gram features from essays. The extracted features represent local text dependencies among words. The extracted features are passed to LSTM layers for capturing long-term dependencies in the words of essay. Further, they concatenated vectors at different time intervals for feeding to a dense layer. Finally, they predicted the score of the essay after training of the model.

The above-cited research work uses different types of features like implicit features or explicit about scoring the essay automatically using different models. The performance of the model is mainly dependent upon the extent to which the extracted feature represents the given essay. Some researchers focused on manually extracted features, word2vec feature representation or embedding representation. In this work, we believe and hypothesize that both manually extracted features and deep-encoded features can contribute to enhancing the

performance of AES models. Therefore, we conducted a comprehensive set of experiments in this work to evaluate word embedding in combination with manually extracted features and word2vec features.

## III. EXPERIMENTS

This section describes a comprehensive set of experiments conducted in this work to evaluate the performance of word embedding in combination with manually extracted features and word2vec features. It presents for experimental methodology by explaining different proposed in this work. Benchmark data set is used for comparing the performance of different models based upon different feature sets. This section also defines the set of performance metrics used to measure the performance of different models in this work.

### A. Experimental Methodology

To conduct a comprehensive set of experiments, we followed the experimental methodology presented in Fig. 1. The proposed methodology consists of four modules, namely, essay raw data collection, feature extraction, scoring engine, and performance evaluation.

Raw data collection module collects the raw data of essays from the database and feeds into the feature extraction module. The feature extraction module can employ different types of methods for extracting relevant features that preserve the semantics of the essay. The features can be extracted manually, word2vec representation or by using the word embedding method. In this work, we focus on measuring the performance of AES models based upon different combinations of manually extracted features, word2vec representations, and word embedding using BERT model. We use 30 manually extracted features, 300-dimensional word2vec representation, and 768-word embedding features using BERT model and forms different combinations for evaluating the performance of AES models. Table I. summarizes manually extracted used in this work.

The different combinations of manually extracted features, word2vec representation and word embedding features are provided as input to AES engine for scoring the test essay data set after training of AES model based on training essay data set. The performance evaluation module analyses the performance of AES models based upon different combinations of manually extracted features, word2vec representation and word embedding features as presented in Fig. 1. Here, we fine-tuned the BERT model using different hyper-parameters. The optimal values used in this set of experiments are presented in Table II.

### B. Benchmark Dataset

Most AES related research work used the Automated Student Assessment Prize (ASAP) dataset for evaluating AES models [1, 2, 3,]. This data set contains about 12,000 essays divided into eight groups. Essays in the data set are not assigned in the normalized score range. We assign scores that range from [2 - 12] to [10 - 60]. Essays in the data set also have a variable length ranging from 120 tokens to 500 tokens. Sentences have a length from 120 to 500 tokens. Each group of the data set contains about 700 to 1800 items.



To use the available data as benchmark dataset in our experiments, we normalize the essays score in the range of 0 to 10 by applying independent transformation for essay group. The resultant distribution of the scores in the data set is not uniform but seems like the normal distribution. Since the current work involved the comparison of the performance of the AES model in scoring rescaled regression problem and Quantized Classification problem, so we distributed dataset into three subgroups by approximating two quartile cut points. Each subgroup is replaced with its number in ascending order

for obtaining a discrete score of 0, 1, or 2 effectively. We use 3-quantile subgroups discretization to produce far from equally populated subgroups due to skewed score frequencies in our experiments. A complete dataset has the frequencies per 3-subgroups in classification problem as presented in Table III.

In this work, we use this dataset as a benchmark dataset for evaluating the performance of different models based upon different combinations of manually extracted features, word2vec representation and word embedding features.

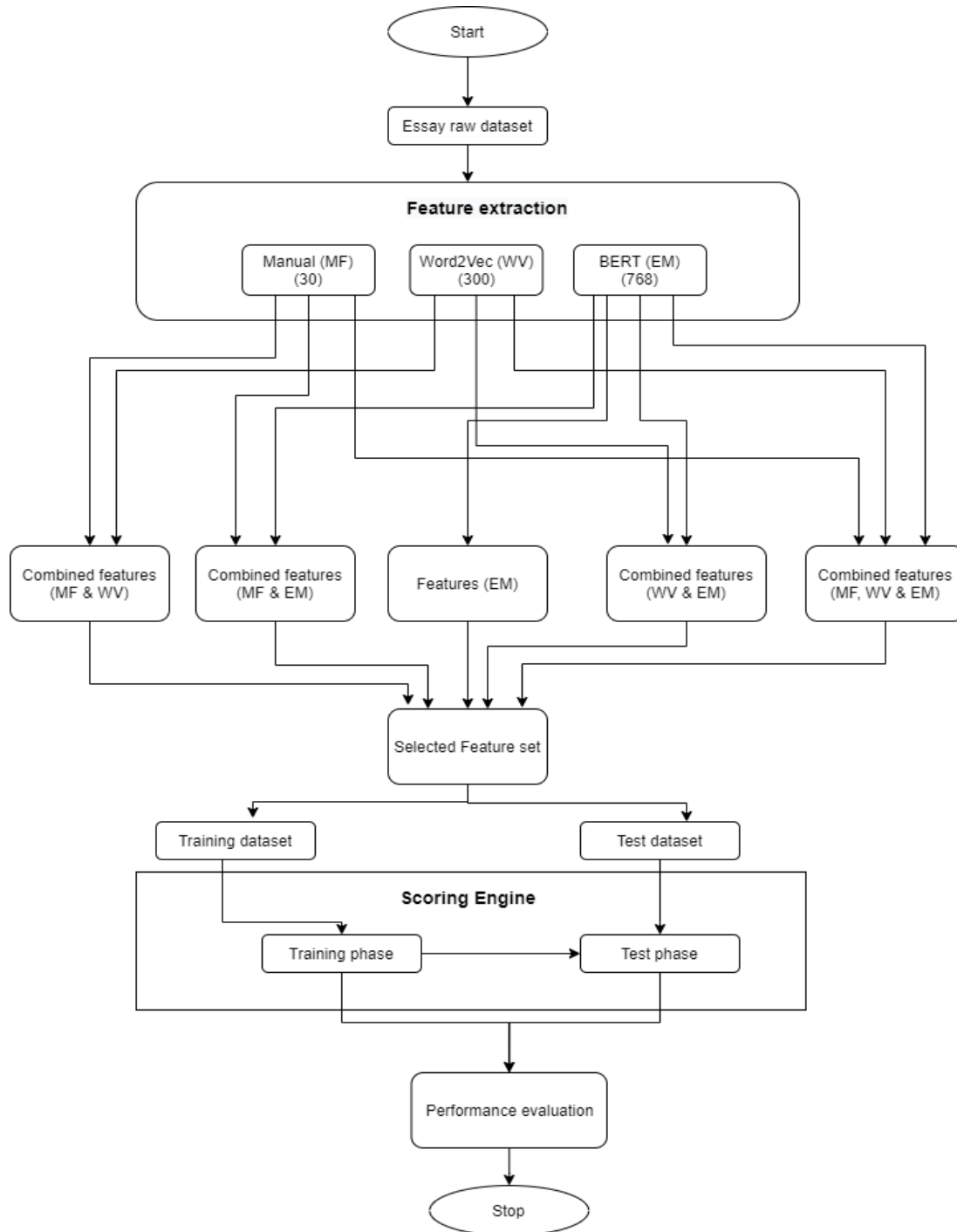


Fig. 1. Experimental Methodology.

TABLE I. SUMMARY OF MANUALLY EXTRACTED FEATURES

| Features                                                         | Description                                                                                                      |
|------------------------------------------------------------------|------------------------------------------------------------------------------------------------------------------|
| Similarity                                                       | A similarity measure between 8 manually selected group representatives and the group essays                      |
| word count, token count, unique token count                      | Essay text aggregates                                                                                            |
| nostop count                                                     | Total number of nostop tokens                                                                                    |
| sentence count                                                   | Total number of sentences                                                                                        |
| ner count                                                        | Total number of named entities                                                                                   |
| Comma count, question count, exclamation count, quotation count  | Total number of punctuation entities                                                                             |
| organization, caps, person, location, money, time, date, percent | Anonymized entities that were mentioned in the original essay, but were obfuscated before publishing the dataset |
| noun, adj, pron, verb, cconj, adv, det, proppn, num, part, intj  | Linguistic entities                                                                                              |

TABLE II. HYPER-PARAMETERS OF BERT MODEL

|                        |                                                                              |
|------------------------|------------------------------------------------------------------------------|
| Batch size             | 16                                                                           |
| Optimizer              | Adam                                                                         |
| Learning rate          | 1e-4                                                                         |
| Dropout                | 0.7                                                                          |
| Model Capacity         | 4 (128 and 64 hidden units)                                                  |
| Loss                   | MSE/Categorical Cross entropy                                                |
| Epochs                 | 200 (reported for the model with best validation loss)                       |
| K-fold                 | 10                                                                           |
| Cross-Validation Steps | 5                                                                            |
| BERT model             | BERT-Base, Uncased: 12-layer, 768-hidden, 12-heads, 110M parameters [7], [8] |

TABLE III. FREQUENCIES PER 3-SUBGROUPS IN A CLASSIFICATION PROBLEM

| label     | 0    | 1    | 2    |
|-----------|------|------|------|
| Frequency | 15.6 | 34.5 | 49.9 |

### C. Performance Metrics

This section describes the performance metrics used for measuring the performance of AES models. The most widely used performance evaluation metric is the Kappa statistics, specifically for regression problems. Kappa statistic is an agreement metric whose value ranges from 0 to 1. Kappa statistics can be computed using Equation 1 [8].

$$k = \frac{p_o - p_e}{1 - p_e} \quad (1)$$

Where,  $p_o$  represents the observed exact agreement among AES models and  $p_e$  represents the hypothetical probability of chance agreement.  $K=1$  indicates that models agree and  $K=0$  indicates total disagreement of AES models. In the case of the classification problem, we measure the performance in terms of accuracy of the AES model. WE computed accuracy from a

confusion matrix that gives the number of essays assigned correct score label as expected.

## IV. RESULTS AND DISCUSSION

This section presents the experimental results obtained in this work based on given benchmark dataset using different AES models. For a comprehensive comparison of AES models, we use baseline performance as the performance of a combination of 30-manually extracted features and 300-word2vec [23] features reported in the study [24]. In [24], the authors used 330-features and neural network for automated scoring of essays. Furthermore, we use 768 word-embedding features of BERT model. We use combinations of three feature sets to evaluate the performance of AES models. The performance of different models in terms of Kappa statistics and accuracy for the rescaled regression problem and Quantized Classification problem is presented in Table IV.

The values presented for reference model [1] in Table I utilized the 5-fold cross-validation method based on 80% of the dataset in their experiments. The authors of the study [1] have not reported standard deviation estimates. They only reported mean values of Kappa statistic metric. Whereas, in our experiments, we used 90% of benchmark essay dataset. We conducted experiments using 10-fold cross-validation. We presented these results as mean and standard deviation values of Kappa statistics and accuracy for five iterations in our experiments.

In these experiments, we also plotted learning curves for regression and classicization tasks considered in this work based on different feature sets in terms of Mean Squared Error (MSE) and accuracy, respectively. Fig. 2 presents the learning curves obtained in this set of experiments.

It can be observed from Table IV that performance of AES model based on a combination of use 30 manually extracted features, 300 feature dimensional word2vec representation, and 768-word embedding features using BERT model has reported better performance in comparison to the other feature combinations. This model has reported kappa statistics value of  $77.2 \pm 1.7$  for rescaled regression problems and accuracy of  $75.2 \pm 1.0$  for Quantized classification problem. Fig. 3 presents the confusion matrix for the rescaled regression problem based on MF+MV+EM features in this work.

Fig. 4 presents the confusion matrix for the quantized classification problem based on MF + MV + EM features in this work. It can be noted from Table IV that BERT word embedding model has reported the similar performance that of 30-manually extracted features and 300-word2vec features. In the case of BERT embedding, regression problem has better values of Kappa statistics than that of MF-WV combination. In contrast, slightly lower value of accuracy has been reported by BERT embedding for classification problem than that of MF-WV combination. It has been observed that both manual features and Word2Vec embedding methods individually score about 66-67% of accuracy on the quantized classification task. It can also be noticed that WV-EM embedding combination has reported similar performance with minor variation in comparison to MF-WV combination. Such kind of behaviour may be due to the bigger input

dimension size whilst preserving the same model capacity. Small dataset size and curse of dimensionality can be a significant cause of the decreased accuracy of the results. It can also be noted that ME-EM embedding combination of features has reported better-rescaled regression and quantized

classification results in comparison to the results reported in [1]. It is worth mentioning that the authors of the study [1] have used an ensemble of LSTM based encoders and XGboost, whereas we employed only a shallow 2-hidden layers feed-forward network.

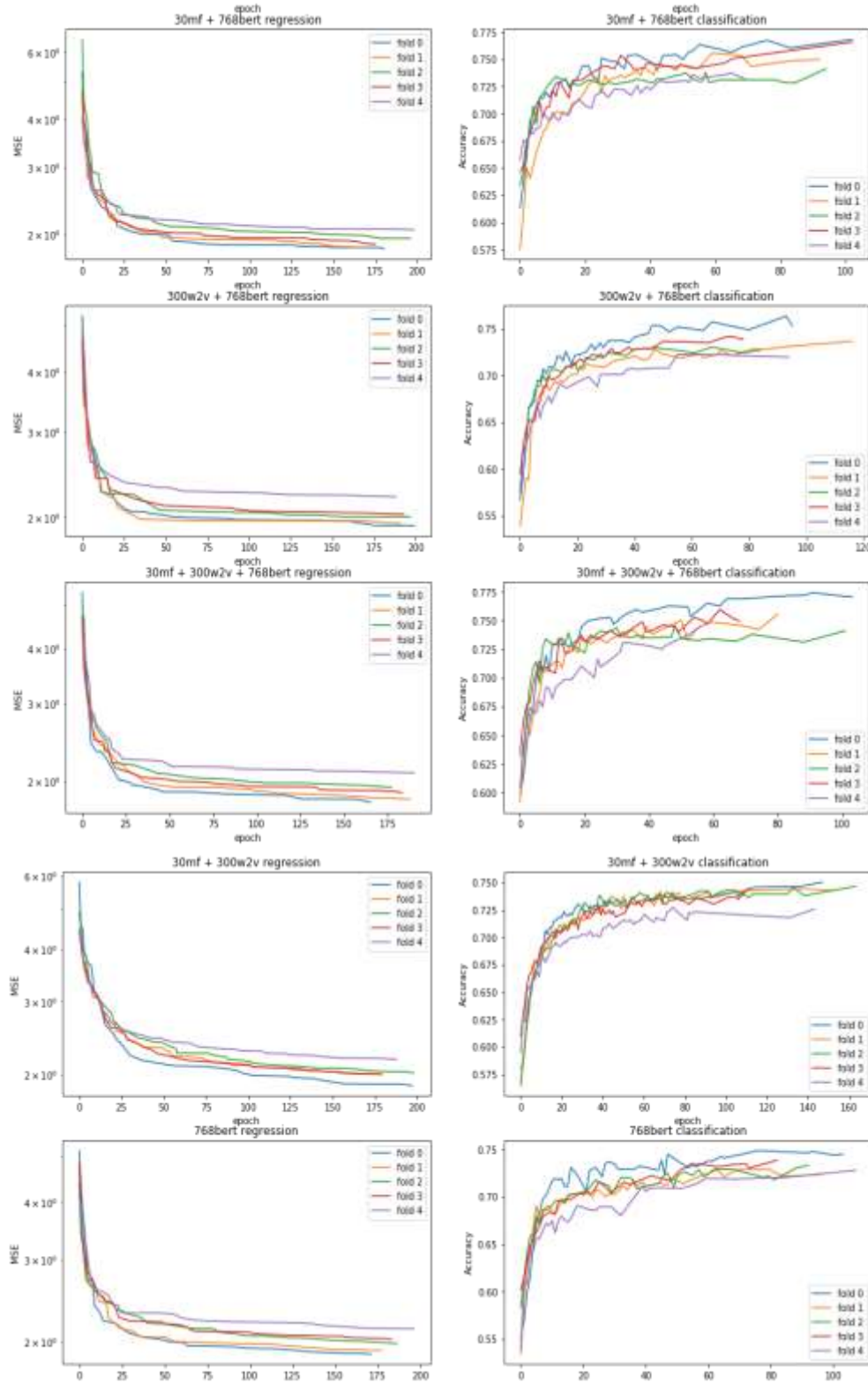


Fig. 2. Learning Curves.

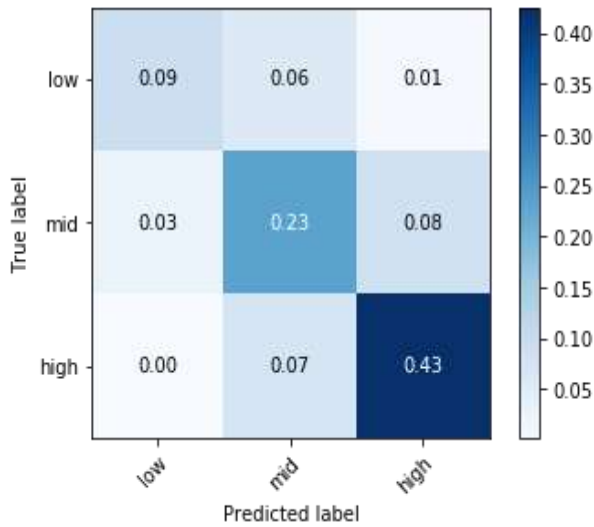


Fig. 3. Confusion Matrix for Rescaled Regression Problem based on MF+MV+EM Features.

TABLE IV. COMPARATIVE PERFORMANCE EVALUATION RESULTS OF AES MODELS

| Model                   | Problem                  | Parameters (%) |            |
|-------------------------|--------------------------|----------------|------------|
|                         |                          | Parameter      | Value      |
| TSLF-ALL [1]            | Rescaled Regression      | Kappa Score    | 77.3       |
| 30mf + 300w2v           | Rescaled Regression      | Kappa Score    | 74.7 ± 1.5 |
|                         | Quantized Classification | Accuracy       | 74.2 ± 0.9 |
| 768bert                 | Rescaled Regression      | Kappa Score    | 76.0 ± 1.6 |
|                         | Quantized Classification | Accuracy       | 73.3 ± 0.8 |
| 30mf + 768bert          | Rescaled Regression      | Kappa Score    | 77.0 ± 1.4 |
|                         | Quantized Classification | Accuracy       | 75.1 ± 1.4 |
| 300w2v + 768bert        | Rescaled Regression      | Kappa Score    | 74.8 ± 1.7 |
|                         | Quantized Classification | Accuracy       | 73.5 ± 1.2 |
| 30mf + 300w2v + 768bert | Rescaled Regression      | Kappa Score    | 77.2 ± 1.7 |
|                         | Quantized Classification | Accuracy       | 75.2 ± 1.0 |

Nadeem et al. [25] also used BERT embedding for AES. But, they only reported results for the first and second essay groups. Their results are even worse than the results of the AES model based on MF features. They were only able to improve results slightly by using a combination of both feature inputs.

It can be observed from Table IV that the performance of all combinations in case of a rescaled regression problem is better in comparison to the corresponding quantized classification problem. This can happen because a Kappa statistic score is capable of tolerating deviations from a ground truth label and scoring near predictions to some degree. Whereas, accuracy does count only exact category equality.

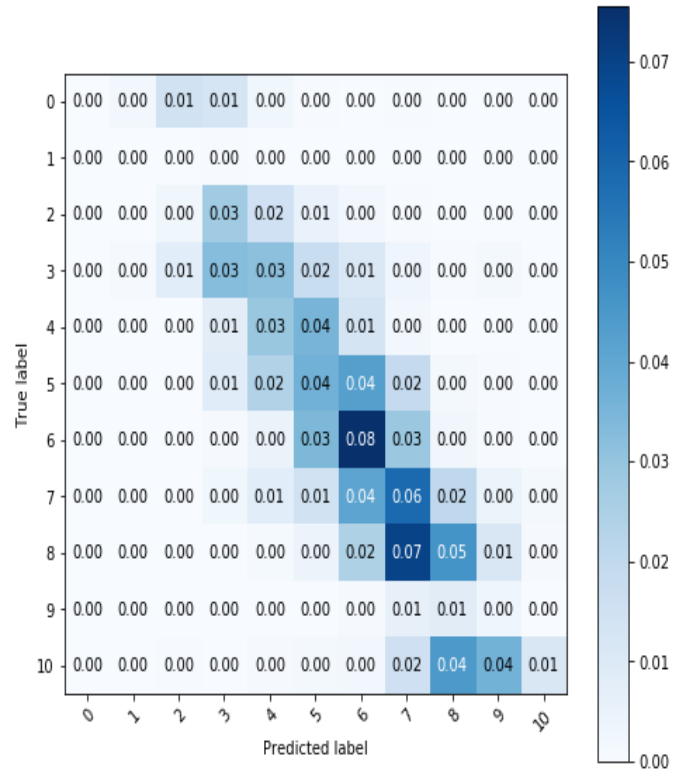


Fig. 4. Confusion Matrix for Quantized Problem based on MF+MV+EM Features Classification.

## V. CONCLUSION

Despite many challenges, researchers are investing continuous efforts in developing efficient and effective AES using different features of essays. In this paper, we demonstrated a comparative empirical analysis of AES models based on different combinations of various features, namely, manually extracted features, word2vec representation and word embedding using BERT model. The reporting results support our hypothesis that both manually extracted features and deep-encoded features contribute to enhancing the performance of AES models. A combination of manually extracted features, word2vec representation and word embedding using BERT model leads to better performance in comparison to other feature combinations as well as the existing ensemble-based approaches. This combination of features resulted up to 77.2 ± 1.7 of Kappa statistics for rescaled regression problem and 75.2 ± 1.0 of accuracy value for Quantized Classification problem using a benchmark dataset consisting of about 12,000 essays divided into eight groups.

In this paper, we mainly contributed to explaining and comparing AES models based on combinations of various feature sets. We conclude that both manually extracted features and deep-encoded features contribute to enhancing the performance of AES models, makes AES models more reliable than human beings and helps in saving time and money for scoring essays.

REFERENCES

- [1] Liu, Jiawei, Yang Xu, and Yaguang Zhu. "Automated essay scoring based on two-stage learning." arXiv preprint arXiv:1901.07744 (2019).
- [2] Yannakoudakis, Helen, Ted Briscoe, and Ben Medlock. "A new dataset and method for automatically grading ESOL texts." Proceedings of the 49th annual meeting of the association for computational linguistics: human language technologies. 2011.
- [3] Chen, Hongbo, Jungang Xu, and Ben He. "Automated essay scoring by capturing relative writing quality." *The Computer Journal* 57.9 (2014): 1318-1330.
- [4] Taghipour, Kaveh, and Hwee Tou Ng. "A neural approach to automated essay scoring." Proceedings of the 2016 conference on empirical methods in natural language processing. 2016.
- [5] Alikaniotis, Dimitrios, Helen Yannakoudakis, and Marek Rei. "Automatic text scoring using neural networks." arXiv preprint arXiv:1606.04289 (2016).
- [6] Mikolov, Tomas, et al. "Distributed representations of words and phrases and their compositionality." *Advances in neural information processing systems*. 2013.
- [7] Pennington, Jeffrey, Richard Socher, and Christopher D. Manning. "Glove: Global vectors for word representation." Proceedings of the 2014 conference on empirical methods in natural language processing (EMNLP). 2014.
- [8] Rodriguez, Pedro Uria, Amir Jafari, and Christopher M. Ormerod. "Language models and Automated Essay Scoring." arXiv preprint arXiv:1909.09482 (2019).
- [9] Arter, Judith. "Rubrics, Scoring Guides, and Performance Criteria: Classroom Tools for Assessing and Improving Student Learning." (2000).
- [10] Page, Ellis B. "The imminence of... grading essays by computer." *The Phi Delta Kappan* 47.5 (1966): 238-243.
- [11] Bahdanau, Dzmitry, Kyunghyun Cho, and Yoshua Bengio. "Neural machine translation by jointly learning to align and translate." arXiv preprint arXiv:1409.0473 (2014).
- [12] Ke, Zixuan, and Vincent Ng. "Automated Essay Scoring: A Survey of the State of the Art." *IJCAI* (2019): 6300-6308.
- [13] Chen, Yen-Yu, et al. "An unsupervised automated essay-scoring system." *IEEE Intelligent systems* 25.5 (2010): 61-67.
- [14] Wang, Yucheng, et al. "Automatic essay scoring incorporating rating schema via reinforcement learning." Proceedings of the 2018 Conference on Empirical Methods in Natural Language Processing. 2018.
- [15] Landauer, Thomas K. "Automated scoring and annotation of essays with the Intelligent Essay Assessor." *Automated essay scoring: A cross-disciplinary perspective* (2003).
- [16] Miltsakaki, Eleni, and Karen Kukich. "Evaluation of text coherence for electronic essay scoring systems." *Natural Language Engineering* 10 (1) (2004): 25.
- [17] Persing, Isaac, and Vincent Ng. "Modeling argument strength in student essays." Proceedings of the 53rd Annual Meeting of the Association for Computational Linguistics and the 7th International Joint Conference on Natural Language Processing (Volume 1: Long Papers). 2015.
- [18] Cozma, Mădălina, Andrei M. Butnaru, and Radu Tudor Ionescu. "Automated essay scoring with string kernels and word embeddings." arXiv preprint arXiv:1804.07954 (2018).
- [19] Vajjala, Sowmya. "Automated assessment of non-native learner essays: Investigating the role of linguistic features." *International Journal of Artificial Intelligence in Education* 28.1 (2018): 79-105.
- [20] Nguyen, Huy V., and Diane J. Litman. "Argument Mining for Improving the Automated Scoring of Persuasive Essays." *AAAI*. Vol. 18. 2018.
- [21] Rudner, Lawrence M., and Tahung Liang. "Automated essay scoring using Bayes' theorem." *The Journal of Technology, Learning and Assessment* 1.2 (2002).
- [22] Taghipour, Kaveh, and Hwee Tou Ng. "A neural approach to automated essay scoring." Proceedings of the 2016 conference on empirical methods in natural language processing. 2016.
- [23] Mikolov, Tomas, et al. "Efficient estimation of word representations in vector space." arXiv preprint arXiv:1301.3781 (2013).
- [24] Turanga1, "Automated students assessment and essay generator", 2012. Online available: <https://github.com/Turanga1/Automated-Essay-Scoring>. Last accessed on September 13, 2020.
- [25] Nadeem, Farah, et al. "Automated Essay Scoring with Discourse-Aware Neural Models." Proceedings of the Fourteenth Workshop on Innovative Use of NLP for Building Educational Applications. 2019.

# Tracking Coronavirus Pandemic Diseases using Social Media: A Machine Learning Approach

Nuha Noha Fakhry<sup>1</sup>, Gamal Kassam<sup>3</sup>  
Business Informatics  
German University in Cairo, Cairo, Egypt

Evan Asfoura<sup>2</sup>  
Marketing Department, College of Business  
Dar Al Uloom University, Riyadh, Saudi Arabia

**Abstract**—With the increasing use of social media, a growing need exists for systems that can extract useful information from huge amounts of data. While, People post personal data interactively, an outbreak of an epidemic event can be noticed from these data. The issue of detecting the route of pandemic diseases is addressed. The main objective of this research work is to use a dual machine learning approach to evaluate current and future data of Covid-19 cases based on published social media information in specific geographical region and show how the disease spreads geographically over the time. The dual machine learning approach used based on traditional data mining methods to estimate disease cases found in social media related to specific geographical region. On other hand, sentiment analysis is conducted to assess the public perception of the disease awareness on the same region.

**Keywords**—Pandemic diseases; outbreak detection; social media; sentiment analysis; machine learning; text mining; geo-located data; CRISP-DM

## I. INTRODUCTION

Nowadays, a lot of factors are responsible for the emergence of infectious diseases such as SARS or avian influenza, which leads to more health challenges worldwide, to avoid these concerns government and global health leaders worked together and revised the IHR. The IHR provides the framework and regulations to detect and respond to outbreak diseases [1]. In 2007, All countries that had knowledge about an outbreak of a disease with an international concern had to report it to the WHO within 24 hours of notice to help in the containment of the disease and to be timely efficient regardless of the location that the disease spread in. However, this information may not be sufficient enough to respond to any disease outbreak [2].

New technologies lately that are internet related, change the way people access or find out about health information. Official health authorities do not fully control the information related to a certain new epidemic disease as journalists and the general public are now in direct contact with raw data. Social media allows reporting mechanisms that makes it easier for the public to access it [1]. Social media such as Twitter and Facebook are increasingly being used as tools for real-time knowledge discovery relating to social events, emerging threats, epidemics, and even product trends [3]. For example, real time analysis of Twitter users' tweet content can be or is being used to detect earthquakes and provide warnings [4], to identify needs (e.g., medical emergencies, food and water shortages) during recovery from natural disasters such as the

Haiti Earthquake [5], and to track emergence of specific syndromic characteristics of influenza-like illness [6], and collect epidemic related tweets [4]. The role of social media in the biomedical domain has become significant in recent years [3, 7]. Researchers and physicians have utilized social media data to communicate and share information between patients and health care decision makers [3], and to develop large scale, dynamic disease surveillance systems [7] and mining biomedical and health-related information [4]. An immediate and direct use of social media in the biomedical domain is a mean for patients and professionals to communicate and exchange information. Web 2.0 along with ubiquitous mobile computing devices allows individuals to dynamically and seamlessly interact with each other in real time, regardless of their locations. PatientsLikeMe is a social network for patients that improves lives and a real-time research platform that advances medicine. On PatientsLikeMe's network, patients connect with others who have the same disease or condition, allowing them to track and share their own experiences. Eijk et al. illustrated the use of OHCs for ParkinsonNet, a social network for Parkinson disease patients whose participants (both patients and professionals) use various types of OHCs to deliver patient-centered care [8]. Merolli et al. explored different ways that chronic disease sufferers engage in social media in order to better tailor these online interventions to individually support patients in specific groups [9]. Additionally, Twitter, Facebook, and other social blogging services provide conduits for patients and medical practitioners to collaborate, exchange, and disseminate information through official broadcasting channels/webpages or discussion groups [10]. Most popular social media providers such as Twitter and Facebook allow their posts to be geo-located. These properties provide researchers in the healthcare community the ability to monitor the medical related emergencies. In late 2019, a novel coronavirus was identified (COVID-19). This is likely the third time in three decades that a zoonotic coronavirus has jumped from infecting animals to humans. As of today, 213 have died and 9809 have been infected in China with the center of the outbreak being located in Wuhan but now having spread, with confirmed cases in twenty-two other countries. While the fatality rate of COVID-19 is less than other recent respiratory virus outbreaks, it remains much higher than other commonly encountered causes of respiratory infection but its full impact is yet undetermined. The WHO has now declared the coronavirus outbreak to be a public-health emergency of international concern [11].

The aim of this work is to be able to track pandemic diseases using machine learning techniques, text mining and sentiment analysis through social media platforms. The solution will follow the CRISP-DM process which provides a structured approach to planning a data science project, it'll be explained in detail in the methodology section. This paper is organized as follows, the first section discusses machine learning and its techniques. The second section includes an introduction to sentiment analysis and how it could be achieved. The third and last section discusses the role that social media plays in public health.

## II. BACKGROUND

There are many Challenges and opportunities of Social media in the Public health is known to be 'the science and art of preventing disease, prolonging life and promoting health through the organized efforts and informed choices of society, organizations, public and private, communities and individuals. Information is the main source to the public health while health data is the foundation. The timelines of health data controls and limits the actionable information of the public health as the conventional route of the data goes all the way from the patient's self-report to the doctor, diagnosis is confirmed and then data goes from the doctor or the facility to the public health authority. Health data that are present on social media differ from the mentioned conventional route by excluding the 'middleman'. Unfortunately, the middle man has an important role. They confirm information about the population and send them to the authorities they serve in order to increase the level of confidence of the information. Governmental actions or interventions are dependent on this confidence. Back in 2009, in the outbreak of H1N1 and Haiti cholera the public health officials realized that social media has the ability to indicate the trends of disease outbreak faster and with higher quality in comparison with traditional methods of public health reporting. Mining online data, searching the behavior of the internet data and social network data began from researchers and practitioners. The purpose was to help in predicting a variety of social, economic, behavioral and health-related events. Majority of the work was on predicting aggregate properties, like the commonness of occasional influenza in a given area, country or a city (e.g. Google Flu Trends, Monitoring Dengue activity using Internet search [12, 13].

There are also challenges that face social media in disease surveillance. The most asked question is how to make sure of the verification of the information coming from social media, as the verification of such large noisy data is considered a big challenge. Public health officials integrate information coming from social media as it could add additional advantages to their surveillance responsibilities [14]. However, analyzing social media data can be done through verifying and comparing them with other sources, which will help in identifying rumors early. A challenge concerning this issue, the spread of rumors across multiple social media platforms or a malicious actor spamming the system with false information, this makes validation more difficult. To overcome these issues many systems verify the messages by reviewing them through a moderator, reports to be labeled clearly as community contributions and enable user's feedback and corroboration of

submissions, this was proven to be successful by Wikipedia. In general, social media is considered to be a two-way information exchange as the crowd can see and evaluate the quality of information published by other users. Many challenges exist in mining the social media. First, data that consists of text might be hard to analyze as harvested data (e.g. a tweet) may not contain complete information and meaning that helps in the classification process. Also, coding for geographic origins may have certain limitations, accounts on social networking sites may not contain geographic information so visible geographic information won't be accessible [15]. So it's better to use data mining sources that track IP addresses or use techniques to monitor social media activity on mobile phones. The majority of new mobile phones have Global Positioning Systems (GPS) or monitoring chips that can easily be attached to independent devices. This technology can track the location of the device needed to be tracked, but also as a challenge users may now allow to share this information for public use. As social media platforms are in constant growth, the attention should be focused on the potential demographic biases coming from users of any service. Moreover, overfitting is a famous issue in machine learning, it's a used methodology in mining large data sets like those extracted from social media. Constructing models that fit many data points coming from social media is easy in order to calculate statistics from public health sources (e.g. disease incidence curves), predictability of these models should be tested. This issue can also be addressed by avoiding using data coming from official sources in the process of developing the models. For example, in article [16], sentiments about vaccinations were extracted by performing fraction classification on the data manually, then machine learning algorithms are applied on the trained on human-labeled data in order to evaluate all of the remaining data in the data set. After developing the fully labeled data set, correlation was done against the estimates of the CDC regarding H1N1 vaccination rates per geographic region, estimating the strong correlation between sentiments and vaccination rates (in a certain direction, e.g. regions with more positive sentiment had higher vaccination coverage).

This work aims to cover the lake of the previous researches in machine learning field using Twitter as a social media platform in order to respond to the pandemic crisis happening right now worldwide, no articles were found to have used machine learning techniques in applying it for detecting people that have symptoms related to the novel Coronavirus. Social media platforms are considered to be a huge source of data especially that it provides real-time data. There was a gap, no articles used Social media platforms in order to detect illness and make future predictions in order to support hospitals nowadays. Article [8] presented an automatic detection model for Coronavirus from X-ray images utilizing transfer learning with convolutional neural networks. Another article [17] used machine learning methods in order to classify Coronavirus using CT Images, this is more of a diagnostic solution.

In order to solve the problem and also accomplish the mentioned opportunities in the introductory chapter in section 1.3, a model was built. Extracting data from Twitter which is a

popular social media platform and classifying them using machine learning techniques. A CRISP DM approach was used.

### III. RESEARCH METHODOLOGY

The model used in this Paper follows the same framework in Fig. 1. The model begins with the data extraction phase from any social media platform then the data extracted follows two paths.

The first path includes a couple of data preprocessing and tagging techniques then a classification algorithm should be applied to the preprocessed data. The results should be visualized in order to observe patterns that will lead to the outbreak prediction or tracking. The second path is related to the process of sentiment analysis. The data extracted should undergo the same preprocessing steps, perform sentiment analysis on the extracted data using a machine learning approach and finally assess the statistics and visualize them

This model help to raise awareness about how the Coronavirus is spreading in a statistical manner all over the United States. This will be achieved by extracting twitter data about the virus and trying to detect from the text if someone is sick or tested positive for the virus. The classified data will help hospitals to expect a certain amount of cases per day and be prepared for the future predictions made. Also, sentiment analysis using machine learning was made in order to analyze people's consent about the pandemic. A Quantitative method is used as it will maximize the results of our findings, as well as facilitating predictions which is one of the important goals of this paper. Also, quantitative research involves assigning numbers to variables which are used later in extracting statistical information related to these variables as well as exploring the relationship between them that can be used to compare the variables to real time data.

The work's solution follows a CRISP-DM approach as mentioned in the introduction. The process life cycle follows six phases. The first phase is business understanding, this phase is related to the business point of view and understanding the target of the work and how to get there through designing a plan to accomplish the objectives. The second phase is data understanding, this phase is concerned with collecting the data, getting familiar with it and discovering interesting patterns. The third phase is data preparation, this phase includes processes that are applied on the data to form the final dataset that enters the model for example, data cleaning, generating new attributes and so on. The fourth phase is the modeling, in this phase a couple of approaches are applied as some problems in data mining have more than one solution approach. The fifth phase is evaluation, in this stage one of the approaches implemented in the modeling phase wins as it ensures high quality but before going to the final phase this model should be evaluated to be sure it achieves the work's objectives. The sixth and final phase is deployment, this phase doesn't mean that an end for the work is reached as the information gained has to be visualized in a way that whoever is going to use it will be able to understand it. It's important to decide on what actions will be done in order to make use of the implemented model. [18].

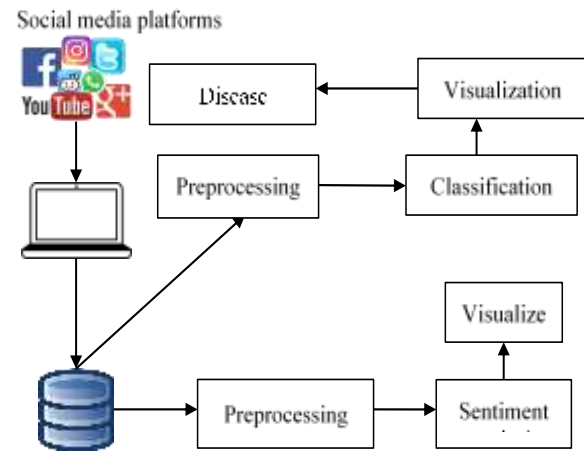


Fig. 1. Conceptual Design.

Some external software components will be used in this work which are of great use in the machine learning, text mining and sentiment analysis fields. Twitter API account is used to give access in gathering tweets from Twitter. As well as R, which is a free software under the GNU-license that allows us to perform a variety of different computations and visualizations on data. In a way it's quite similar to MATLAB. R contains a lot of different mathematical functions for dealing with time series, such as the possibility to automatically compute the autocorrelation function of a time series and visualize it in a compelling manner. All plots of time series data in this work have been created using R, Lastly RapidMiner which is a data science software platform developed by the company of the same name that provides an integrated environment for data preparation, machine learning, deep learning, text mining, and predictive analytics. It is used for business and commercial applications as well as for research, education, training, rapid prototyping, and application development and supports all steps of the machine learning process including data preparation, results visualization, model validation and optimization. Extensions were added to RapidMiner to be used in this work: MeaningCloud text analytics, Text analysis by AYLIEN, Rosette text analytics, text processing and finally WordNet extension. Using these tools will help us gather the data that'll support this work as well as understanding the data and exploring the hidden patterns to be able to provide useful information that people, hospitals and States will benefit from.

### IV. IMPLEMENTATION

This work follows the CRISP-DM phases which are discussed in the methodology section. This section will provide the detailed procedures followed in the work that helped in reaching the stated goals and solving the problems mentioned in the introduction.

#### A. Business Understanding

This part includes the objectives and goals of the work to be able to identify the problems related to data mining as well as the opportunities that this work should handle. The problems are how to extract tweets from Twitter and be able to classify them based on whether a person is sick or not and also after the classification of the tweets they should be



compared to real world data in order to compare the results and measure their accuracy. If these two problems are solved, a couple of opportunities will arise, the first one is if the data is correlated with the real-world data this will be faster in tracking the disease and be able to help people, hospitals or countries allocate the needed resources for the current crisis. Also, future predictions can be made from patterns extracted from the data and lastly, the data gathered can be used to measure the sentiment of people and see how they're reacting towards the crisis and whether they need mental health support or not.

**B. Data Understanding**

The data used in this work were tweets posted during the Coronavirus crisis event. Twitter API makes it simple to gather data from twitter using keywords, language, geolocation and more. In order to gather data from Twitter API, a simple code was written in R to support the gathering process. Several data sets are gathered during the month of June in the year 2020. After the data is gathered it's being stored in an excel sheet which is going to act as the database for simplicity. As soon as the data is stored the preprocessing and tagging begins and also sentiment analysis will be performed to classify positive and negative tweets. The main objective is to perform naive bayes analysis to be able to predict from the tweet if someone is actually sick or tested positive for the Coronavirus, also the keywords that influenced the classification and finally comparing the accuracy of the classifiers together. A lot of tweets are somehow dependent on the history for example if someone tweeted "I'm very sick right now" this would be classified as a sick person tweet even if the user's history indicated that he suffers from cancer as i won't be considering the history of tweets as it requires a more sophisticated system.

In the initial approach section random tweets were extracted from all around the world from R related to Coronavirus using specific keywords. The first search query contained the keyword "Corona". The second search query contained "cough OR fever OR tiredness". Finally the third search query contained "corona AND tested AND positive". Using data from all around the world was too general so instead data was extracted only from the 51 states in America. This was achieved by using a library in R that supports twitter API which is called (twitterR), this library had a function that helped in extracting tweets using geocode. It took four arguments which were latitude, longitude, a number that represents the area of a circle and the fourth argument was either Km or miles which depends on the area of the circle. Twitter then responds with data that has been geotagged only in this location. Unfortunately, when searching in a specific circle of radius it might as well include tweets from another state around the area so this tweet may appear twice in the data while searching in two different circles, to avoid this each tweet's individual id is checked and duplicates are removed.

This work focuses mainly on the spread of Coronavirus in the United States of America. A classifier cannot be used by multiple languages so in order to achieve this, tweets in English language were only extracted. The (twitterR) library in R has a function that supports extracting tweets in a specific

language only. The positions of the extracted data from the United States are present in Table I.

**C. Rate Limiting of the Extracted Twitter Data**

If the premium account is not purchased in Twitter API, unlimited requests cannot be made so a limit does exist. The limit is restricted to 180 GET requests per 15 minutes per user.

**D. Description of the Tagging Process**

The twitter search API was used in order to extract the training dataset, tweets in English were extracted as many as possible by the process mentioned earlier in the description phase. Data was collected by searching for tweets using the keywords in section regional concerns as well as the specified tagged geo locations that were mentioned in the last section. The data was then stored in an xlsx format to be supported by RapidMiner.

Once the tweets were stored the tagging process started. Tweets that indicated that someone has tested positive for the virus or had symptoms were tagged as relevant, meaning that the label column was set to True while tweets that didn't indicate any of the cases were labeled False. It's important to put into consideration that all tweets that indicated the sickness of someone is classified as True, in other words if a mother tweeted that her son is sick or wishing someone to feel better, it will be classified as True.

In this work, only illnesses that had symptoms like fever, diarrhea, fever, tiredness and so on were considered to be relevant while tweets about broken bones and cancer were considered to be irrelevant. Also a lot of tweets depend on the history of the user, for example a tweet with the text "I feel so sick right now" will be considered as relevant but if we checked the history of the user this sickness might be related to cancer. This wasn't handled in the work as it'll require a more sophisticated system. Check Table II and Table III for more examples of the tweets.

TABLE I. THE POSITIONS OF THE STATES

| State         | Latitude  | Longitude   | Radius |
|---------------|-----------|-------------|--------|
| New York      | 40.712776 | -74.005974  | 250Km  |
| Washington    | 47.751076 | -120.740135 | 250Km  |
| New Jersey    | 40.058323 | -74.405663  | 250Km  |
| California    | 36.778259 | -119.417931 | 250Km  |
| Florida       | 27.664827 | -81.515755  | 250Km  |
| Louisiana     | 30.984299 | -91.962334  | 250Km  |
| Illinois      | 40.633125 | -89.398529  | 250Km  |
| Massachusetts | 42.407211 | -71.382439  | 250Km  |

TABLE II. EXAMPLES OF TWEETS THAT BELONG TO THE TRUE CLASS

| Tweet                                                                                                                                                                                         | Label |
|-----------------------------------------------------------------------------------------------------------------------------------------------------------------------------------------------|-------|
| if you have been going to frosty factory GO GET TESTED FOR CORONA 6 people have already tested positive from using the same microphone for karaoke. get tested or stay the hell away from me. | True  |
| hehe... someone ah the blm protest has tested positive for corona ??????????????????gonna order a test tomorrow uhm                                                                           | True  |

TABLE III. EXAMPLES OF TWEETS THAT BELONG TO THE FALSE CLASS

| Tweet                                                                                                                                           | Label |
|-------------------------------------------------------------------------------------------------------------------------------------------------|-------|
| RT @Plat4omLive: common symptoms of COVID-19 include: fever dry cough tiredness Some Less common symptoms include: aches and pains sore throats | False |
| RT @HigherHealthSA: #MythBuster No. 4. Being able to hold your breath for prolonged periods of time does not mean you're #Covid19 free! The...  | False |

### E. Modeling and Evaluation

This section basically explains how the first steps were taken into the prwork and resulted in the final implementation of the model. All the steps are previewed below alongside the tools and everything used to get to the results.

### F. Initial Implementation of the Model

To begin with, 200 samples of tweets were extracted worldwide not from a certain state or country. They were tested using the Naive Bayes classifier in RapidMiner, it was chosen as a result of its popularity in text classification. First of all the data was extracted from R and all the preprocessing has been applied, especially tokenization and Lowercase Tokens as the Naive Bayes classifier cannot work with strings directly it has to be converted to vectors that includes individual words. As for the model created in RapidMiner the input dataset which is the 200 tweets is split into two parts, 10% to be labelled and act as a training dataset and the other 90% acts as the testing dataset. When the data enters the model it'll output the classification prediction for the unlabeled data and the accuracy of the classifier. The output data was the text field which contained the text in the tweet as well as the label field which specifies whether someone is sick or has tested positive for Coronavirus or not, this field is binary either true or false. Other fields like Retweet count and the date were also present.

The first attempt resulted in a 100% accuracy, 100% class precision and a 100% class recall as shown in Table IV.

### G. Continued Implementation of the Model

Since the Naive Bayes classifier gave extraordinary results while working with a small dataset of 200 tweets, the next step was to try a larger dataset of 1000 tweets. The same criterion was followed in testing this amount of data except that the majority of the data were categorized to be False, i.e. indicating that people don't have Coronavirus nor the symptoms.

The results were great, the classifier gave an accuracy of 96.59% which is of course less accurate but still it's perfect. The rest of the results are present below in Table V.

To make sure that the right classifier was used, another popular classifier which is the SVM as it's also known to give decent results regarding text classification. The same experiment applied on the 200 tweets dataset on the Naive Bayes classifier was done once more but using the SVM as a classifier with the same dataset. The results were so far from good compared to the Naive Bayes classifier. SVM achieved 75% accuracy as shown in Table VI.

TABLE IV. PERFORMANCE VECTOR FOR 200 TWEETS USING NAIVE BAYES

|              | True True | True False | Class Precision |
|--------------|-----------|------------|-----------------|
| Pred. True   | 9         | 0          | 100%            |
| Pred. False  | 0         | 10         | 100%            |
| Class recall | 100%      | 100%       |                 |

TABLE V. PERFORMANCE VECTOR FOR 1000 TWEETS USING NAIVE BAYES

|              | True True | True False | Class Precision |
|--------------|-----------|------------|-----------------|
| Pred. False  | 51        | 0          | 100%            |
| Pred. True   | 3         | 34         | 91.89%          |
| Class recall | 94.4%     | 100%       |                 |

TABLE VI. PERFORMANCE VECTOR FOR 200 TWEETS USING SVM

|              | True True | True False | Class Precision |
|--------------|-----------|------------|-----------------|
| Pred. False  | 8         | 2          | 80%             |
| Pred. True   | 1         | 6          | 85.71%          |
| Class recall | 88.89%    | 75%        |                 |

Based on the results, the rest of the work will be handled using the Naive Bayes classifier as it shows better accuracy results of 96.59% especially in classifying the minority class. Final implementation of the model.

The process executed in this phase was performed using the model in Fig 2. The first step is collecting the data from twitter from the 51 states in the United States over 7 days from the 18th of June 2020 till the 25th of June 2020 using the same keywords mentioned in the data collection section. The first step is to split the data into testing and training datasets. Data preprocessing is the next step to be executed in order to remove noisy data and convert it to a suitable format. Furthermore, performing building and testing of the model using Naive Bayes algorithms. Furthermore, the classification algorithm from RapidMiner is applied on the preprocessed data.

The training phase is very important, it plays a role in identifying patterns in the dataset in order to build an accurate model. A part of the classification training process one of the attributes should be assigned to act as a label column. This column is used to train the model and predict the positive tweets which is our aim. Basically, after selecting the label class and its value, it's used in calculating conditional probability based on the other attributes given in the same row.

After applying the model on the data from each State, the output should include the category of which the text is classified whether it's true or false as shown in Fig 3.

After the data is classified to their category it enters another model in order to output the word frequency in the total document, in the True class and in the False class. This will help us fig. out which words occur more in the True class which can be used later on as keywords in our search queries. Check Fig 4 and Table VII these are the words frequencies from one of the datasets of Ohio tweets.

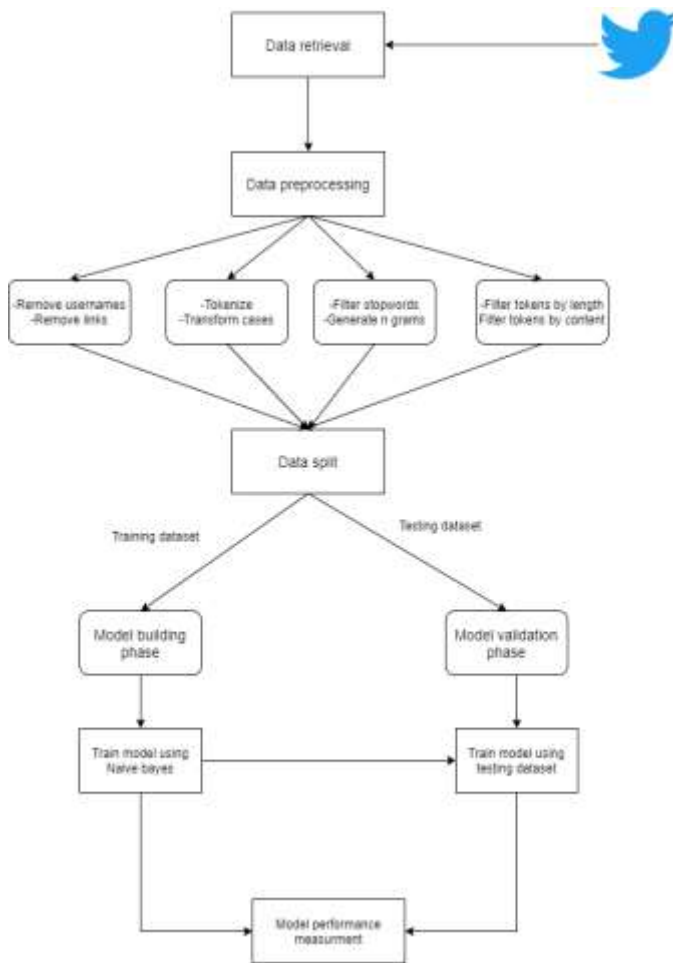


Fig. 2. Classification Model.

| ItemId | id       | label | preprocessed | tokenized | filtered | vector | classification | error |
|--------|----------|-------|--------------|-----------|----------|--------|----------------|-------|
| 1      | 11111111 | True  |              |           |          |        |                |       |
| 2      | 11111111 | True  |              |           |          |        |                |       |
| 3      | 11111111 | True  |              |           |          |        |                |       |
| 4      | 11111111 | True  |              |           |          |        |                |       |
| 5      | 11111111 | True  |              |           |          |        |                |       |
| 6      | 11111111 | True  |              |           |          |        |                |       |
| 7      | 11111111 | True  |              |           |          |        |                |       |
| 8      | 11111111 | True  |              |           |          |        |                |       |
| 9      | 11111111 | True  |              |           |          |        |                |       |
| 10     | 11111111 | True  |              |           |          |        |                |       |
| 11     | 11111111 | True  |              |           |          |        |                |       |
| 12     | 11111111 | True  |              |           |          |        |                |       |
| 13     | 11111111 | True  |              |           |          |        |                |       |
| 14     | 11111111 | True  |              |           |          |        |                |       |
| 15     | 11111111 | True  |              |           |          |        |                |       |
| 16     | 11111111 | True  |              |           |          |        |                |       |
| 17     | 11111111 | True  |              |           |          |        |                |       |
| 18     | 11111111 | True  |              |           |          |        |                |       |

Fig. 3. Data Output in RapidMiner.



Fig. 4. Ohio Word List.

TABLE VII. TOP 5 WORDS IN THE DATASET OF OHIO

| Word         | In documents | Total | Class (true) | Class (false) |
|--------------|--------------|-------|--------------|---------------|
| Corona       | 111          | 110   | 104          | 7             |
| Cough        | 43           | 27    | 39           | 4             |
| Corona virus | 23           | 23    | 21           | 2             |
| Virus        | 23           | 23    | 21           | 2             |
| Fever        | 21           | 21    | 18           | 3             |

Another process added to the model is extracting the influence words from the class True based on multiple things. Retweet count, weight by correlation, weight by Gini index, weight by information gain and finally weight by information gain ratio as shown in Fig 5 The Retweet count is considered to be important in this case as the more retweets a tweet gets, the more important the tweets is. These different weights are then applied and their average is taken. Table VIII contains the top 3 influence words in the Ohio dataset.

1) *K. Sentiment analysis of tweets:* This part will include the explanation of the model that exists in Fig 6. Five-fold cross-validation was used, the main process was repeated 5 times but with different training and testing sets each time. This process was carried out in RapidMiner as shown in Fig 7. First, the data were split into two sets. 90% of the tweets were classified as the testing set, while the remaining 10% were for the training set. From the training data, all the n-grams were extracted. The training and testing datasets were converted into their corresponding feature vectors. A feature vector would always be 0 if the n-gram did not occur in the tweet. If it occurred in the tweet it will have the value of 1 (present) or the frequency, this depends on the configurations used. The training vectors were used to train a classifier. This classifier was the Naive Bayes, it would then classify the testing dataset into positive or negative. The label assigned to a tweet was compared to the actual class to see if they are the same. The statistics of the output data were saved for visualizations. The statistics of interest are the accuracy value, the confusion matrix and the classified tweets.

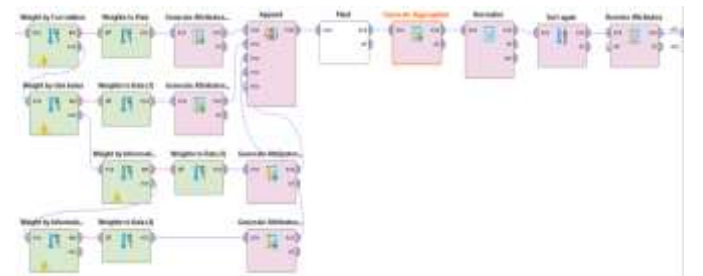


Fig. 5. Determining Influence in RapidMiner.

TABLE VIII. TOP 3 INFLUENCE WORDS IN OHIO DATASET

| Attribute | Importance |
|-----------|------------|
| Fever     | 1          |
| Corona    | 0.934      |
| Cough     | 0.924      |

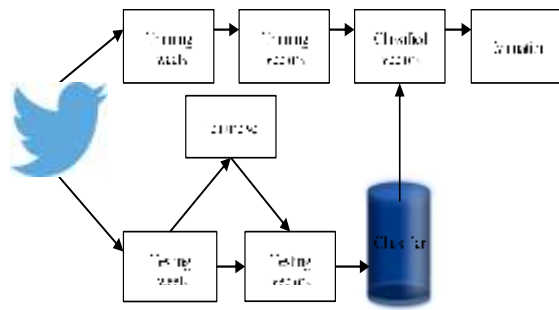


Fig. 6. Process of Sentiment Analysis.

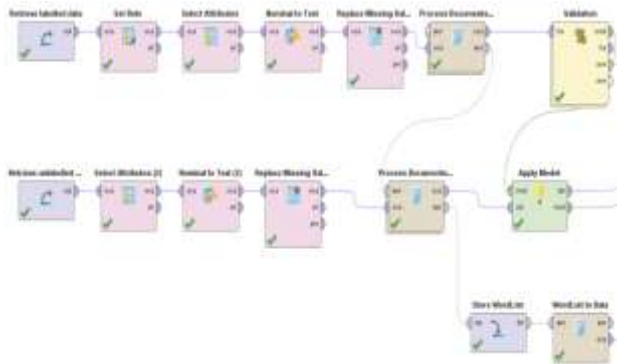


Fig. 7. Sentiment Process in RapidMiner.

a) *Deployment*: As mentioned previously in the business understanding phase, the objectives of this work is to extract tweets from Twitter related to the novel coronavirus and classify them based on True (sick) or False (not sick) then compare them with real world data and measure the correlation. Based on the results predictions were made and also sentiment analysis and people’s consent were measured. In the model implementation, keywords that affected the classification were extracted in each State as well as statistical numbers in each State in America and visualizations will be discussed in the results section.

b) *Time series*: In order to evaluate the results and be able to compare it to real world data, it’s better to see the data in a time series format. Two types of time series were used, the first was daily values and the second was weekly values.

To get a better understanding of the output data, the known number of positive tweets per day has to be recorded so it can be known if the data recorded was more or less than expected and use these numbers in many different applications. An example for one application, to support hospitals and their staff of how many cases per day to expect.

To model the time series, a package called the prophet was used in R to forecast. It’s a procedure for forecasting time series data based on an additive model where non-linear trends are fit with yearly, weekly, and daily seasonality.

## V. RESULTS

The total positive tweets collected are 240,331 during the period of 17-06-2020 till 23-06-2020. This means that around 34,333 tweets were collected per day. After applying the Naive Bayes classifier on our data a plot chart was made to

visualize the positive tweets gathered over each day as shown in Fig 8 alongside with the same plot chart but with the cumulative numbers in order to visualize the increases and decreases in the number of cases in Fig 9

After collecting data from each state in the United States. The positive numbers were visualized on the map in Fig 10. The darker the color gets on the map the higher the number.

As a result of having 51 states, the visualization for each one cannot be included in this paper but as an example positive numbers for both California and New York will be visualized and discussing their results in Fig 11 and Fig 12. In California no certain pattern was noticed over the days. The first day 17-06-2020 was a 4Wednesday and it had 4,108 positive cases then numbers kept increasing and decreasing but in the last two days they kept increasing with a high percentage to reach 5,545 and finally the peak which is 7,73. This pattern could be observed better if data for another week was extracted and be able to compare them and observe if they have the same pattern.

The New York numbers were a lot less than those of California. In total they were 4,898. It reached its peak on Friday the 19th by scoring 916 positive cases. It started decreasing till the last day to reach 627 positive cases. As stated that the numbers of the two states are very different from each other, they do not follow the same pattern so each State has to be visualized separately in order to get accurate results.

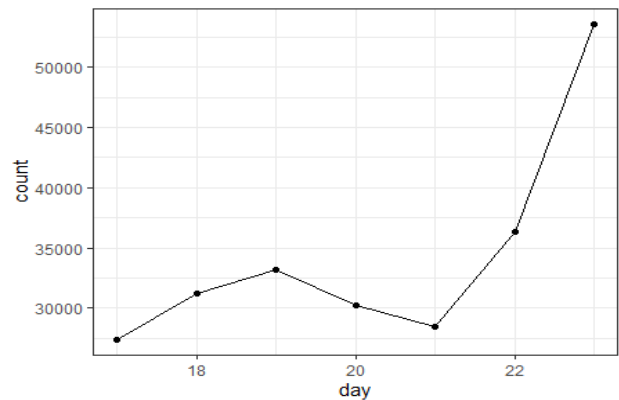


Fig. 8. Positive Tweets in the United States.

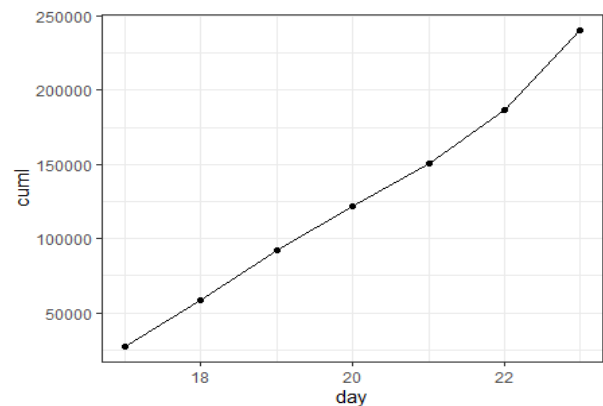


Fig. 9. Cumulative Positive Tweets in the United States.

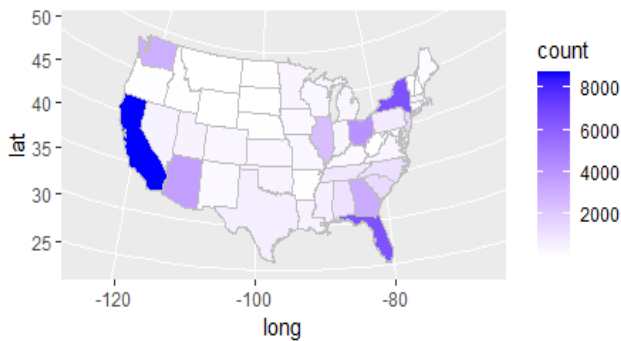


Fig. 10. Cases in Every State.

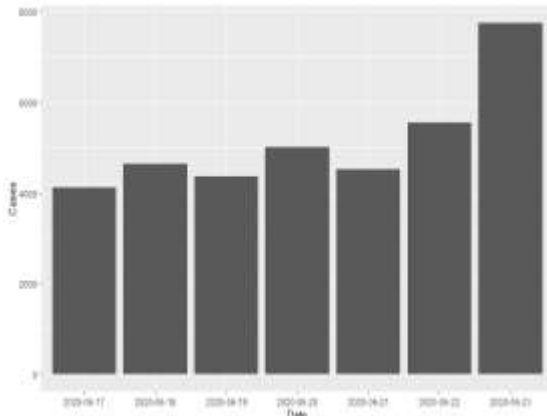


Fig. 11. Cases in California.

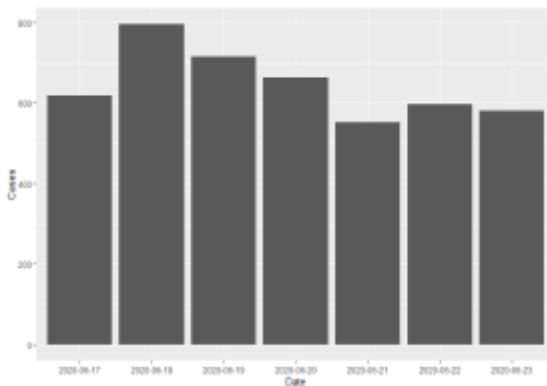


Fig. 12. Cases in New York.

## VI. CONCLUSION

In this paper, a model was designed in order to indicate if someone is sick or has tested positive for Coronavirus through twitter during a given day. To achieve this machine learning algorithms were used alongside statistics. The Naive Bayes classifier showed promising results in classifying the data accurately by achieving 96.59% accuracy after the preprocessing steps have been applied.

In order to be able to compare the classified tweets with real world data, Johns Hopkins dashboard was used to get the real data and compare them with each other. Both data were highly correlated.

The model also analyzed the word frequency to output the most frequent words that occurred in the True class and in the False class. Furthermore, influence words were extracted by calculating their weight by correlation, weight by Gini index and weight by information gain. The extracted influence words can therefore be used in search queries.

The performance for the predictions wasn't tested as mentioned before. The package used for this process was Prophet created in R-code. Hopefully, the performance of this predictor will give good results as our data is very close to being accurate.

The divergence between real cases and public sentiment could indicate many possible problems like public over- or underestimating of threats caused by diseases, because lack of the public media to reach and inform people properly to improve their awareness. It could also indicate lack of public healthcare infrastructures or deficiency of protection measures conducted by public authorities. Anyway, these new kinds of significant information can help decision maker in different application domains.

## ACKNOWLEDGMENT

The researchers extend their thanks and gratitude to the Deanship of Graduate Studies and Scientific Research at Dar Al Uloom University for their support and funding of this study.

Also, the researchers extend their thanks to the German University in Cairo (GUC).

## REFERENCES

- [1] C. Paquet, D. Coulombier, R. Kaiser, & N. Ciotti. (2006). Epidemic intelligence: a new framework for strengthening disease surveillance in Europe. *Euro Surveill*, 11(12), 212-214.
- [2] M. Tsytarau, & T. Palpanas, (2012). Survey on mining subjective data on the web. *Data Mining and Knowledge Discovery*, 24(3), 478-514.
- [3] C. Tucker, & H. Kim, (2011). Predicting emerging product design trend by mining publicly available customer review data. In *DS 68-6: Proceedings of the 18th International Conference on Engineering Design (ICED 11)*, Impacting Society through Engineering Design, Vol. 6: Design Information and Knowledge, Lyngby/Copenhagen, Denmark, 15.-19.08. 2011.
- [4] T. Sakaki, M. Okazaki, & Y. Matsuo, (2010, April). Earthquake shakes Twitter users: real-time event detection by social sensors. In *Proceedings of the 19th international conference on World wide web* (pp. 851-860).
- [5] A> P. Rajan, & S. Suresh, (2015). Application of Retail Analytics Using Association Rule Mining in Data Mining Techniques with Respect to Retail Supermarket. *IJEMR*, 5(1).
- [6] N. Collier & S. Doan, (2011, November). Syndromic classification of twitter mesges. In *International Conference on Electronic Healthcare* (pp. 186-195). Springer, Berlin, Heidelberg.
- [7] S. Tuarob & C. S. Tucker, (2013, August). Fad or here to stay: Predicting product market adoption and longevity using large scale, social media data. In *ASME 2013 International Design Engineering Technical Conferences and Computers and Information in Engineering Conference*. American Society of Mechanical Engineers Digital Collection.
- [8] Van der Eijk, M., Faber, M. J., Aarts, J. W., Kremer, J. A., Munneke, M., & Bloem, B. R. (2013). Using online health communities to deliver patient-centered care to people with chronic conditions. *Journal of medical Internet research*, 15(6), e115.
- [9] L. F. Lopes, J. Zamite, B. Tavares, F. Couto, F. Silva & M. J. Silva, (2009, September). Automated social network epidemic data collector. In *INForum informatics symposium*. Lisboa.

- [10] B. W. Hesse, D. Hansen, T. Finholt, S. Munson, W. Kellogg & J. C. Thomas. (2010). Social participation in health 2.0. *Computer*, 43(11), 45-52.
- [11] J. B. Long, & J. M. Ehrenfeld, (2020). The Role of Augmented Intelligence (AI) in Detecting and Preventing the Spread of Novel Coronavirus.
- [12] Google flu trends: 'how does this work?' <http://www.google.org/flutrends/about/how.html> Accessed: 2-24-2020.
- [13] L. C. Madoff, D. N. Fisman & T. Kass-Hout (2011). A new approach to monitoring dengue activity. *PLoS neglected tropical diseases*, 5(5). [kasshout/edemocracy-egypts-18-day-revolution](https://doi.org/10.1371/journal.pntd.1000184). Accessed: 2-24-2020.
- [14] SentiWordNet. <http://sentiwordnet.isti.cnr.it/>. Accessed: 2-24-2020.
- [15] S. J. Lee & K. Siau. (2001). A review of data mining techniques. *Industrial Management & Data Systems*.
- [16] K. Wilson & J. S. Brownstein, (2009). Early detection of disease outbreaks using the Internet. *Cmaj*, 180(8), 829-831.
- [17] M. Barstugan, U. Ozkaya & S. Ozturk. (2020). Coronavirus (covid-19) classification using ct images by machine learning methods. *arXiv preprint arXiv:2003.09424*.
- [18] J. Wirth, R., & Hipp (2000, April). CRISP-DM: Towards a standard process model for data mining. In *Proceedings of the 4th international conference on the practical applications of knowledge discovery and data mining* (pp. 29-39). London, UK: Springer-Verlag.

# Modified K-nearest Neighbor Algorithm with Variant K Values

Kalyani C. Waghmare<sup>1</sup>, Balwant A. Sonkamble<sup>2</sup>

Department of Computer Engineering  
Pune Institute of Computer Technology, Pune, India

**Abstract**—In Machine Learning K-nearest Neighbor is a renowned supervised learning method. The traditional KNN has the unlike requirement of specifying ‘K’ value in advance for all test samples. The earlier solutions of predicting ‘K’ values are mainly focused on finding optimal-k-values for all samples. The time complexity to obtain the optimal-k-values in the previous method is too high. In this paper, a Modified K-Nearest Neighbor algorithm with Variant K is proposed. The KNN algorithm is divided in the training and testing phase to find K value for every test sample. To get the optimal K value the data is trained for various K values with Min-Heap data structure of 2\*K size. K values are decided based on the percentage of training data considered from every class. The Indian Classical Music is considered as a case study to classify it in different Ragas. The Pitch Class Distribution features are input to the proposed algorithm. It is observed that the use of Min-Heap has reduced the space complexity nonetheless Accuracy and F1-score for the proposed method are increased than traditional KNN algorithm as well as Support Vector Machine, Decision Tree Classifier for Self-Generated Dataset and Comp-Music Dataset.

**Keywords**—Classification; K-nearest Neighbor (KNN) classification algorithm; Indian Classical Music; Performance measures; Heap data structure

## I. INTRODUCTION

The K-nearest neighbors is a simple and effective classification algorithm. The most important advantage is that the classification results can be easily interpreted. Despite all these advantages, it has shortcomings like high computational cost, large memory requirement, and equal-weighted features and in last deciding appropriate value of the input parameter K [1]. There are many variants of the KNN algorithm proposed to overcome these shortcomings. In [2, 3] the author proposed a weighted KNN. In [2] first learns weights for different attributes and according to the weights assigned, each attribute would affect the process of classification that much only. In [3] inverse of Euclidean distance is considered as the weight for load forecasting. In [4] various distance functions are implemented with KNN on a medical dataset with different types of attributes. In [5] authors used various pitch distributions as feature set for KNN with different distance functions in Raga Identification.

In [6] authors pointed out that traditional KNN has limitations to solve few problems like imbalance, noisy, sparse dataset. The authors proposed Hybrid KNN (HBKNN) to sort out these problems.

In KNN variations the researchers combined KNN with K-means clustering algorithm to reduce the computation complexity. In [7] authors applied this approach to improve accuracy in air quality assessment. This approach worked well for Big data as well in [8].

The basic assumption of the standard KNN is fixed K value for all data points to classify. However, many datasets have uneven distributions of data points, or even experts also not able to predict optimal K value. So many researchers proposed various methods for predicting k value. In [9] authors proposed a local mean representation-based k-nearest neighbor classifier (LMRKNN) method. In this method the representation-based distances calculated by the categorical k-local mean vectors instead of the simple majority vote for making the classification decision. The LMRKNN is outperformed on many real datasets downloaded from the University of California, Irvine (UCI), and Knowledge Extraction based on Evolutionary Learning (KEEL) repositories than traditional KNN. In [10] authors proposed an algorithm called Adaptive K-nearest neighbor (AdaKNN) algorithm which uses the density and distribution of the neighborhood of a test point and learns a suitable K for it with the help of artificial neural networks. This strategy for rightly classifying the test point is employed by Wettschereck and Dietterich in [11] in which, the value of K is determined for different portions of input space by applying cross-validation in its local neighborhood. The Ada-KNN2 is proposed as an extension to the Ada-KNN algorithm in which the neural network is replaced with a heuristic learning method based on local density indicator of a test point and information about its neighboring training points.

The large value of K would increase the computational cost and time in case of large data sets. To solve this problem, in [12] the variant value of K is proposed so that the early break of the algorithm can be possible, which ultimately saves computational time.

In [13] Adaptive KNN algorithm is developed by choosing optimal k for each item by maximizing its expected accuracy computed on similar points. The evaluation is done on three different datasets of Geo-Spatial Data.

In [14] the author employed a correlation Matrix, to reconstruct test data and assign different K values to the different test data points. The proposed algorithm achieved high accuracy and efficiency in applications of classification, regression, and missing data assertion.

The prediction of K value with the cross-validation method is usually time-consuming. In [15] authors introduced the training phase in the KNN classification algorithm and proposed a k\*Tree method to learn different optimal k values for different test samples. The proposed K\*Tree method reduced the running cost of the test phase. The efficient working of the proposed method is observed using 20 different real datasets.

In ICM the lots of work done in Raga recognition using KNN algorithm [5, 16, 17, 18, 19]. The researchers focused either on Features or compared using the different classifiers. The classifiers are used in their traditional form. In Data Mining as the application changes, the keen thinking about the parameters used in classifiers is required. The impact of these parameters on the performance also need to be observed.

The paper is organized as follows: Section II briefs about the proposed Modified Variant K Nearest Neighbor (MVKNN) algorithm. Section III gives details of experimental results and the analysis. Section IV Conclusion.

## II. PROPOSED ALGORITHM

The Ragas is the central notion of Indian Classical Music. Usually, researchers find Pitch Class Distribution (PCD) features and apply classifiers. In literature authors used traditional classifiers. The traditional KNN works as follows.

---

### Traditional KNN Algorithm

---

Procedure: - To find a class label for test input using KNN

Input: - D the set of Test samples, T the set of training samples,

Output: - P the class labels of test samples

---

#### Steps

1. SET 'K' Value
  2. Read training samples
  3. Read test samples
  4.  $P = \{ \}$
  5. **For each** d in D
    - 5.1 **For each** t in T
      - 5.1.1 Dis = distance(d,t)
    - Endfor**
    - Endfor**
    - 5.2 Sort Dis in ascending order
    - 5.3 Select first 'K' entries
    - 5.4 Find class labels of first 'K' entries
    - 5.5 Allocate class label of maximum in first 'K' entries
- 

In traditional KNN the K value is expected to provide in advanced which is very impractical. In this section, a Modified K Nearest Neighbor algorithm using variant K value for each test sample is proposed.

---

### Modified Variant K Nearest Neighbor (MVKNN) algorithm using Min\_Heap for Raga Identification

---

Procedure: - To find class label for test input

Input: - D the set of Test samples, T the set of training samples,

Output: - P the class labels of test samples

---

#### Steps

1. Read training samples
2. Read test samples
3.  $P = \{ \}$
4. **For each** c in C **do** // C the count of samples belong to each class in training set (T)
  - 4.1  $C\{c\} = \text{count}(t)$  where  $\text{class\_label}(t) = c$
- Endfor**
5. **For each** c in C **do**
  - 5.1  $K\{c\} = \text{round}(C\{c\} * 100 / \text{length}(T))$
  - 5.2  $M\_K = \max(K)$
- Endfor**
6. **For each** t in T **do**
  - 6.1 **For each**  $t_1 = t + 1$  in T **do**
    - 6.1.1 Dis = distance(d,t)
    - 6.1.2 Add Dis in min\_heap[t][t<sub>1</sub>] of size  $M\_K\{c\}$
    - 6.1.3 Add 't<sub>1</sub>' in neighbor\_heap[t] of size  $M\_K\{c\}$
    - 6.1.4 Add Dis in min\_heap[t<sub>1</sub>][t] of size  $M\_K\{c\}$
    - 6.1.5 Add 't' in neighbor\_heap[t<sub>1</sub>] of size  $M\_K\{c\}$
  - Endfor**
  - Endfor**
  7. **For each** k in K **do**
    - 7.1  $\text{Class\_neighbor}\{1..k\} = \text{findClass}(\text{neighbor\_heap})$
    - 7.2  $P\{d\} = \max(\text{count}(\text{Class\_neighbor}))$
    - 7.3  $\text{TP}[k,c] = \text{countif}(\text{class\_label}(t) == \text{class\_label}(P))$
  - Endfor**
  8. **For each** c in C **do**
    - 8.1  $K\_test\{c\} = \max(\text{TP}[c,k])$
  - Endfor**
  9. **For each** d in D **do**
    - 9.1 **For each** t in T **do**
      - 9.1.1  $T\_label = \text{class\_label}(t)$
      - 9.1.2 Dis = distance(d,t)
      - 9.1.3 Add Dis in min\_heap of size  $K\_test\{T\_label\}$
      - 9.1.4 Add 't' in neighbour\_heap of size  $K\{T\_label\}$
    - Endfor**
    - 9.2  $\text{Class\_neighbors}\{1..K\} = \text{findClass}(\text{neighbour\_heap}\{1..K\})$
    - 9.3  $P\{d\} = \max(\text{count}(\text{Class\_neighbour}))$
  - Endfor**

Note:  
\\ findClass(n) returns class label of samples in mean-heap  
\\ max() returns class label appearing in 'K' nearest neighbor  
\\ count() returns number of training samples class label is equal to predicted class label.

---

The traditional KNN does not have a training phase. It calculates the distance between every sample in test data with every sample in training data. The most nearest 'K' neighbors are identified for every sample based on distance. The class having maximum count belong to 'K' nearest Neighbor is assign to test sample.



In the proposed method algorithm is divided in two phases training and testing. In step 4.1 the samples per class are present in training data are calculated. The step 5.1 calculates K value for each class label considering its percentage contribution in training data. In steps 6 and 6.1 the Euclidean distance is calculated between every sample in training data and stored in Min-Heap of size  $2M_K$ . In this  $M_K$  is the maximum size of Heap.

Once the Min Heap is ready, in step 7.1 the class labels are identified for every test sample from first entries in Min-Heap. The class label with maximum count will be assigned to the test sample in step 7.2. Step 7.3 counts the correctly classified samples for every class and stored in the TP array. Where TP gives True Positive values for each class. The steps 7.1 to 7.3 are executed for every distinct value of K which was calculated in step 5.1. The value of K will vary from minimum to maximum value of K for classes calculated in step 5.1. After calculating TP for all different 'K' values. The optimal 'K' value for every class is calculated by finding maximum true positive count of every class. This completes the training phase. In the best case for all classes, the same 'K' may come. In the worst-case, every class will get different optimal 'K'.

In testing phase distance between every test sample and training sample is calculated and the Min-Heap is constructed for maximum optimal 'K' value which has got from the training phase. The nearest neighbors are identified from the first K entries in Min-Heap. The class label of maximum count of neighbors is assigned to the test sample.

The computational complexity of KNN is one of the limitations of KNN. In traditional KNN training phase is not available. The Time complexity of traditional KNN is  $O(T * D) + O(D * T \log_2 T) + O(D * K)$ . The complexity for calculating distance between every testing sample with training samples is  $O(T * D)$ . After calculating the distance between samples the sorting algorithm with average-case complexity  $N \log_2 N$  is required to sort the distance array. So to sort D tuples the sorting complexity will be  $O(D * T \log_2 T)$ . To get 'K' nearest neighbor from sorted data will be  $O(K)$  which will be finally  $O(D * K)$  for D test samples. Even if instead of sorting the Heap data structure is used to get 'K' nearest neighbor, complexity will reduced to  $O(D * T \log_2 T) + O(D * K \log_2 T)$ .

In MVKNN training and testing phases are introduced. The complexity of training phase is  $(O(T * (T+1)/2) + O(T * T \log_2 K) + O(K * K \log_2 K))$ . In the worst-case, number of distinct K values, will become equal to the distinct value of percentage of records belonging to the number of classes present in Dataset, and in the best case, only the same K value is for all classes. The complexity to calculate the distance between every training sample with other training sample is  $O(T * (T-1)/2)$ . To find the K nearest neighbor first it will create 'T' number of Min-Heap of  $2K$  size. So the complexity to create the T number of Min-Heap with T elements of size  $2K$  will be  $O(T * T \log_2 K)$ . To get K nearest neighbor Delete\_min operation will be performed K times so its complexity will be  $O(K \log_2 K)$ .

The testing phase complexity will be  $O(D * T) + O(D * T \log_2 K) + O(K \log_2 K)$ . The  $O(D * T)$  is complexity for calculating distance between every test sample with training

sample. The  $O(D * T \log_2 K)$  is complexity for creating Min-Heap of K size for T distance values. The Heap will be generated for every test sample.

The computation complexity of traditional KNN is higher than the computation complexity of the testing phase. If the complexity of both training and testing phase in MVKNN is considered then it is higher than traditional KNN but as we know the training of classifier is done only ones and are not required to perform whenever testing is executed. So based on this assumption the computational complexity of MVKNN testing phase is lower than traditional KNN.

The computational calculations can be understand more clearly by taking a small example.

Let us consider total samples 1000. Take a 70:30 ratio for training and testing. So  $T = 700$  and  $D = 300$ , the number of classes present in the dataset are 8.

The total computations in traditional KNN will be.

Distance calculations = 210000.

Finding K nearest neighbor = 20, 32,949.

Total computations = 22, 42, 949.

The total computations in the training phase of MVKNN for the worst case will be.

Distance calculations = 2, 45, 350.

Finding K nearest neighbor = 25, 14, 780.

Total computations = 27, 60, 130.

The total computations in the testing phase of MVKNN for the worst case will be.

Distance calculations = 210000.

Finding K nearest neighbor = 10, 75, 379.

Total computations = 12, 85, 379.

This case study shows that computation for the training phase in the worst-case nearly one and half times of computations in traditional KNN. The testing computations are almost half of the computations in traditional KNN. So this work may conclude that MVKNN is computationally efficient than traditional KNN provided training should be performed occasionally.

The space complexity is also reduced. In traditional KNN  $O(D * T)$  memory will be required to store the distance in sorted array or Heap form. Wherein MVKNN space complexity for the training phase is  $O(T * \log_2 K)$  and testing phase  $O(T * \log_2 K)$ .

### III. EXPERIMENTAL RESULTS

The proposed algorithm is presented as an extension of the traditional KNN algorithm. The performance of both algorithms is compared with our data set and CompMusic dataset.

In our dataset, 1450 samples of 8 different Ragas are present sung by different singers. The samples are stored in

.wav format with sampling frequency 44100Hz and 16bps. The frame size is considered as 20ms with 25% overlapping.

CompMusic dataset [16, 17] includes full-length audio recordings with the Raga label. It is a collection of several artists' vocal as well as instrumental performances. The clips were extracted from the live performances and CD recordings of 13 artists. Total 129 tunes for 08 ragas are considered. The dataset is downloaded as per instructions given in [20]. The duration of each tune averages 5-6 minutes. The tunes are converted to mono-channel, 44100 Hz sampling rate, 16 bit PCM.

The Pitch values are calculated as mentioned in [21]. The Pitch values are divided into 36 bins and constructed Pitch Class Distribution of every sample. Fig. 1 show the PCD for one sample of Raag Asavari. The PCD of the sample shows the frequency count of every bin. This sample is sung in the second octave so the Notes are present between bin numbers 13 to 25.

The PCD is calculated for all the samples and created a feature vector to give input to traditional KNN and MVKNN algorithm.

The experimentation for traditional KNN is done for varying K values from 1 to sqrt(T). The elbow method is applied and observed that after K=11, the accuracy is nearly constant up to K=20. Similarly with Decision Tree and SVM classifiers are also implemented with same datasets. Accuracy and F1 score is calculate as per following equations 1 and 2 respectively [22]. The results are documented in Table I.

$$Accuracy = \frac{(TP+TN)}{(TP+TN+FP+FN)} \tag{1}$$

$$F1 - Score = \frac{2*TP}{(2*TP+FP+FN)} \tag{2}$$

The PCD input is given to the MVKNN algorithm. For one instance the dataset is split into 30% testing and 70% training using train\_test\_split in Python. The training is performed for k=10, 11, 12, 13, 14 distinct 'K' values using Min-Heap. The confusion matrix containing True Positive, True Negative, False Positive and False Negative values is calculated for given dataset. The True Positive values are observed in every class for each 'K'. The 'K' having maximum True Positives is taken as an optimal K value for that class during the testing phase. In Table II the optimal K values are shown for every class for one instance.

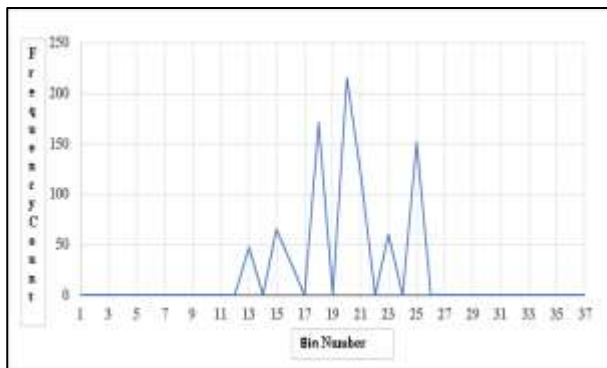


Fig. 1. PCD for One Sample.

TABLE I. RESULTS OF DECISION TREE, SVM CLASSIFIER

|                               | Self-Generated Data | CompMusic Data |
|-------------------------------|---------------------|----------------|
| <b>Decision Tree Accuracy</b> | 94.02%              | 86.33%         |
| <b>SVM Accuracy</b>           | 84.74%              | 82.72%         |
| <b>Decision Tree F1-Score</b> | 79.30%              | 49.13 %        |
| <b>SVM F1-Score</b>           | 38.99%              | 38.70%         |

TABLE II. OPTIMAL K VALUE FOR EACH CLASS

| Class No. | 1  | 2  | 3  | 4  | 5  | 6  | 7  | 8  |
|-----------|----|----|----|----|----|----|----|----|
| K value   | 14 | 12 | 14 | 13 | 13 | 13 | 11 | 12 |

Table III shows a comparison of Accuracy and F1-score of traditional KNN and MVKNN for self-Generated data and CompMusic data. It is observed that Accuracy and F1-Score are improved for both datasets.

TABLE III. RESULTS OF KNN AND MVKNN

|                       | Self-Generated Data | CompMusic Data |
|-----------------------|---------------------|----------------|
| <b>KNN Accuracy</b>   | 89.46%              | 86.02%         |
| <b>MVKNN Accuracy</b> | 95.82%              | 89.45%         |
| <b>KNN F1-Score</b>   | 57.90%              | 44.11 %        |
| <b>MVKNN F1-Score</b> | 83.28%              | 57.81%         |

The experimentation is done several times by taking an equal number of samples belonging to each class as well as by making imbalanced classes. It is observed that the variation in 'K' values always improved results than the same value of 'K'.

#### IV. CONCLUSION

In this paper, the survey of modified KNN algorithms is done. The KNN algorithm for variant K values for every test sample is proposed. The training phase is introduced to identify the optimal K value. The use of the Min-Heap data structure of 'K' size has reduced the space complexity. The algorithm was implemented using Indian Classical Music for classifying it based on the Raga. The PCD features of two different datasets are considered as an input vector. The Accuracy and F1-score measures are considered for comparing performance. The improvement in Accuracy and F1-score is observed using the proposed MVKNN algorithm in comparison with traditional KNN, Decision Tree and SVM. In Indian Classical Music, the repeating patterns play a very important role for Raga identification. In the future, the plan to apply the proposed algorithm on high dimensional feature vector of repeating patterns in a signal to improve the results of Raga identification.

#### REFERENCES

- [1] Alka Lamba and Dharmender Kumar, "Survey on KNN and its Variants," in International Journal of Advanced Research in Computer and Communication Engineering Vol. 5, Issue 5, pp.430- 435, May 2016.
- [2] Eui-Hong (Sam) Han, George Karypis and Vipin Kumar, "Text categorization using weight adjusted k-nearest neighbour classification," in Text categorization using weight adjusted k-nearest neighbour classification, Springer Berlin Heidelberg, 2001, pp. 53-65.
- [3] Guo-Feng Fan, Yan-Hui Guo, Jia-Mei Zheng, and Wei-Chiang Hong, "Application of the Weighted K-Nearest Neighbour Algorithm for

- Short-Term Load Forecasting,” *Energies* 2019, 12, 916; doi:10.3390/en12050916, pp.1-19.
- [4] Li-Yu Hu, Min-Wei Huang, Shih-Wen Ke, Chih-Fong Tsai, “The distance function effect on k-nearest neighbour Classification for medical datasets,” *Springer Plus*, Vol. 5, issue 1, Dec.2017, pp.1-9.
- [5] Parag Chordia and Senturk Sertan, “Joint recognition of Raag and Tonic in North Indian Music,” in *IEEE Computer Music Journal*, Vol. 37, No-3, Sept. 2013, pp.82-98.
- [6] Zhiwen Yu, Hantao Chen, Jiming Liu, Jane You, Hareton Leung, and Guoqiang Han, “Hybrid k-Nearest Neighbour Classifier,” in *IEEE Transactions on Cybernetics*, Vol. 46, No. 6, June2016, pp.1263-1275.
- [7] YANG Rui-jun, DING Dan-feng, YAN Feng, “Application of Improved KNN Algorithm in Air Quality Assessment,” in *HPCCT 2019*, June 22–24, 2019, Guangzhou, China, pp.108-112.
- [8] Hamid Saadatfar, Samiyeh Khosravi, Javad Hassannataj Joloudari, Amir Mosavi and Shahaboddin Shamsheirband, “A New K-Nearest Neighbors Classifier for Big Data Based on Efficient Data Pruning,” in *Mathematics* 2020, 8, 286.
- [9] Jianping Gou, Wenmo Qiu, Zhang Yi, Yong Xu, Qirong Mao, and Yongzhao Zhan, “A Local Mean Representation-based K-Nearest Neighbour Classifier,” *ACM Transaction Intelligent System and Technology*, Vol. 10, No. 3, May 2019, pp. 1-29.
- [10] Sankha Subhra Mullick, Shounak Datta, and Swagatam Das, “Adaptive Learning-Based k-Nearest Neighbour Classifiers With Resilience to Class Imbalance,” in *IEEE Transaction on Neural Networks and Learning systems*, Vol. 29, No. 11, Nov.2018, pp.5713-5725.
- [11] Dietrich Wetschereck and Thomas G. Dietterich, “Locally adaptive nearest neighbour algorithms,” *Adv. Neural Inf. Process. Systems (NIPS)*, vol. 6, 1994, San Mateo, pp. 184–184.
- [12] S. Ougiaroglou, A. Nanopoulos, A. N. Papadopoulos, Y. Manolopoulos, and T. Welzer-Druzovec, “Adaptive k-Nearest-Neighbour Classification Using a Dynamic Number of Nearest Neighbours,” in *Advances in Databases and Information Systems*, Y. Ioannidis, B. Novikov, and B. Rachev, Eds. Springer Berlin Heidelberg, 2007, pp. 66–82.
- [13] Mark Kibanov, Martin Becker, Juergen Mueller, Martin Atzmueller, Andreas Hotho, Gerd Stumme, “Adaptive kNN using Expected Accuracy for Classification of Geo-Spatial Data,” in *Proceedings of Symposium on Applied Computing (SAC)*, 2017, pp.1-9.
- [14] Shichao Zhang, Xuelong Li, Ming Zong, Xiaofeng Zhu, and Debo Cheng, “Learning k for KNN Classification,” in *ACM Transactions on Intelligent Systems and Technology*, Vol. 8, No. 3, Jan. 2017, pp.1-19.
- [15] Shichao Zhang, Xuelong Li, Ming Zong, Xiaofeng Zhu, and Ruili Wang, “Efficient KNN Classification With Different Numbers of Nearest Neighbours,” in *IEEE Transactions on Neural Networks and Learning Systems*, vol. 29, no. 5, May 2018, pp. 1774-1785.
- [16] Sankalp Gulati, J. Serra, V. Ishwar, S. Senturk, Xavier Serra, “Phrased based Raga Recognition using vector space modelling,” in *IEEE International Conference on Acoustics, Speech, and Signal Processing*, Shanghai, China 20<sup>th</sup> -25<sup>th</sup> Mar. 2016, pp.66-70.
- [17] Sankalp Gulati, J. Serra, K. Ganguli, S. Senturk, Xavier Serra, “Time-Delayed Melody Surfaces for Raga Recognition,” in *Proceedings of 17<sup>th</sup> International Society for Music Information Retrieval Conference*, New York, USA, 7<sup>th</sup> -11<sup>th</sup> Aug.2016, pp.751-757.
- [18] Parag Chordia and Alex Rae, “Raga recognition using Pitch Class and Pitch Class Dyad Distribution,” in *8<sup>th</sup> International Society of Music Information Retrieval Conference*, Vienna, Austria, 2007, pp. 431-436.
- [19] Gopala Koduri, Sankalp Gulati, Preeti Rao, “A survey of Raaga Recognition techniques and improvements to the state-of-the-art,” in *Conference of sound and Music*, Padova, Italy, 6<sup>th</sup> -9<sup>th</sup> July 2011, pp.1-4.
- [20] <https://compmusic.upf.edu/node/300>.
- [21] Kalyani C. Waghmare, Balwant A. Sonkamble, “Timbre with Note Based Features for Improving Performance of Music Classification,” in *International Journal of Advanced Science and Technology*, Vol. 29, No. 3, (2020), pp. 10328 – 10338.
- [22] Jiawei Han, Micheline Kamber and Jian Pei, “Data Mining: Concepts and Techniques 3<sup>rd</sup> ed.,” in the *Morgan Kaufmann Series in Data Management Systems*, Morgan Kaufmann Publishers, July 2011, ch-8, sec-8.5, pp.-364-370.

# Binary Operating Antenna Array Elements by using Hausdorff and Euclidean Metric Distance

Elson Agastra<sup>1</sup>, Julian Imami<sup>2</sup>, Olimpjon Shurdi<sup>3</sup>

Faculty of Information Technology, Polytechnic University of Tirana  
Sheshi Nene Tereza 1, 1004, Tirana, Albania

**Abstract**—In this paper, the linear antenna array is designed by the usage of Woodward–Lawson method. The design procedure fits antenna array radiation pattern to a predefined/required radiation mask. In this study will be investigated the possibility of powering off some antenna elements without modifying the behavior and power ratio of the elements which remains on. The aim of powering off antenna elements is to reduce power consumption of the designed array antenna and to reduce power dissipation problems on modern full digital beam forming architecture. The choice of binary operation of antenna element (on/off) reduces computational effort required for complex beam forming techniques. The results can be stored on look-up tables, in order to be recalled on demand by antenna operator. There are used two different metrics to identify how close, to the required design, is the modified antenna pattern. Euclidean and Hausdorff distances are both used as score of the modified array performance. The obtained solutions shows the applicability of binary operations on existing antenna array and the metric can be effectively used as ranking solutions.

**Keywords**—Antenna array; Hausdorff distance; Woodward–Lawson

## I. INTRODUCTION

Array antennas are a set of two or more elements (with element we mean individual antenna) spread in one, two or three direction in the space. Through modifying the feed in amplitude and/or in phase can be achieved different radiation models [1][2].

The array antennas are of a great usage in nowadays technology. Used in fields like wireless communication, satellite communications, military, radar communications, astronomical studies, naval usage, telecommunication technologies etc., they have changed the way these fields have improved over the years.

The telecommunication technologies, in particular, have benefitted from their usages in 2G and 3G/B3G by increasing the system capacity. In the latest system, 4G LTE and 5G ratio, they have given their impact through increasing of the spectral efficiency (SE), antenna diversity and multiplexing gain, interference suppression, etc.[3][4].

In this paper we will use a linear antenna array as one of the 4G antennas configuration, which have equal distance throughout the  $N$  elements (of the same type). We will get the array factor (AF) using the Woodward–Lawson method, and we will compare it with the defined pattern mask.

The proposed analysis is based on changing the feed status of some antenna elements (powering on or off). The modification of the array elements behavior will reflect also in the array pattern. The aim of this work is to demonstrate that the modified pattern is also a valid trade-off between number of elements powered off and the requirements from relative array pattern mask. To score the obtained pattern output, will be used two different metrics: Euclidean and Hausdorff distance. Both metrics permits to score how close to the desired radiation, is the modified array.

Powering off a part of array elements will reduce the relative power consumption and thus, due to electronic efficiency that is always lower than 1 (digital beam forming network), there will be a reduction in the power dissipation issues. From the antenna operator perspective, reducing power consumption will increase antenna life and will decrease its relative OPEX (Operating Expenses).

A preliminary linear array will be designed to demonstrate the possibility of powering off part of array elements, and the relative pattern feet to a predefined mask. The methodology used for the preliminary array design is based on Woodward–Lawson method. Our aim is to get this array factor by not feeding (powering off) some elements of the antenna and to compare the obtained pattern with the mask using both methods.

The possibility of powering off array elements and their influence to multiple beam array behavior will be investigated in future works [5][6][7].

This paper is organized as follows: Section 2 describes mathematical definitions for linear antenna array design based on W-L method, followed by definitions of both metrics (Euclidean and Hausdorff) which are used to score how close to required pattern is the designed and modified antenna pattern. Section 3 describes the antenna array design and setup; Section 4 describes test case analysis, different array alternatives analysis and numerical useful data extraction. Conclusions and recommendations for future work will be emphasized in Section 5.

## II. MATHEMATICAL DEFINITIONS

### A. Woodward – Lawson Method

The method that we are going to use for the preliminary antenna design is the Woodward- Lawson method. It is a popular antenna pattern synthesis method used for beam shaping. It was introduced by Woodward and Lawson from

which it took also its name (in year 1947). Even though in the late '80 it was a debate related to its use after those years [8], the time has shown that it is the base for a lot of nowadays researches.

The Woodward- Lawson method is linear and the most important thing is the fact that in defined directions, responsible for the radiation, the virtual feed has the maximum of beam (in that direction). So if we don't want radiation in a specified direction, we can easily turn off the corresponding virtual array [9]. Woodward-Lawson method is possible if there are maintained two assumptions related to the feed and the phase:

- The formula of array factor based on the elements feed is a linear function.
- Through operating only in the phase of a set of elements with uniform feed (when possible), it is possibly to change the direction of maximal radiation of the array factor.

If this set is chosen carefully it will be possibly to reaches, not only the maximum radiation in different directions, but also the nulls of radiation to be in the same directions where the other arrays have their maximums. By combining also the appropriate feed of virtual array, we can achieve (in that direction) a radiation amplitude like the one needed by the radiation mask. The overlay of all the virtual arrays can create the desired array factor (AF) which is an interpolation of the factor of the virtual arrays as in Fig. 1.

The complex antenna array can be analyzed as an overlay of different virtual, independent and superposed arrays. An example feeding function can be expressed like (1):

$$I_n = I_n^{(1)} + I_n^{(2)} + I_n^{(3)} + \dots + I_n^{(N)}; \quad n = 0, \dots, N-1 \quad (1)$$

The feed for each of them is expressed as  $I_n = a_n e^{j\beta_n}$ . We can chose a set of virtual array that have the maximum of radiation in different directions.

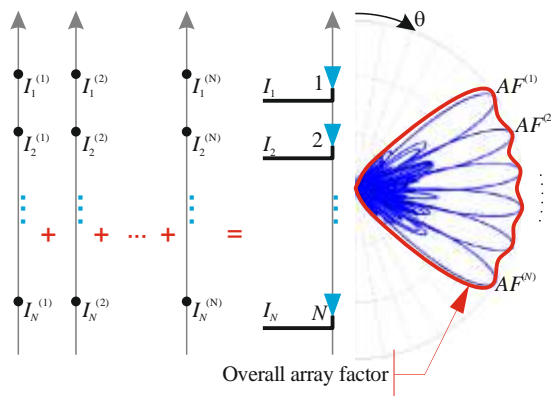


Fig. 1. Concept of Virtual Array Feeding and Beam Forming.

The realization of the pattern through the use of the chosen method follows the upcoming steps:

- The first function produced is a pattern in which the position of the beam is set on by the value of uniform progressive phase.
- The same concept is used also for the creation of second function but in this case a uniform progressive phase is adjusted in order that the maximum main lobe coordinates with the deepest null of the first step function. So an excitation in amplitude of this function determines the filling-in of the deepest null of the second function. The third function part of the main function is altered so the maximum of main lobe which occurs at the second deepest null of the first function and so on. In this way are created one after other all the functions part of the sum.

The array factor projected through the Woodward- Lawson method will be used as the original model in all the arrays. Based in this project, we will do the analysis of powering off some random elements to see the changes in the radiation model and how much it diverges from the desired model showed from the mask.

Based on this method, in this paper, we will focus on finding the distance in two different forms: Euclidean and Hausdorff distances as per below.

### B. Euclidean Distance

The Euclidean distance can be expressed as the straight line between two given points (of course that points can be vector or matrix). The length of the straight line represents the shortest distance between the two defined points. It is also used for higher dimensional problems [10].

Through this paper we will use the sum of all Euclidean distances (E) between array factor (AF) and the mask (M, the desired model) as given in equation (2) and shown in Fig. 2.

$$E = \sum_{\theta=0^\circ}^{180^\circ} \|AF(\theta) - M(\theta)\| \quad (2)$$

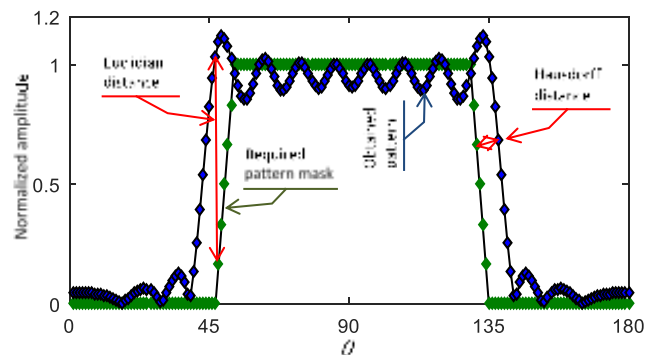


Fig. 2. Differences between Hausdorff and Euclidean Distances, Applied among the Antenna Pattern and Required Pattern Mask.

### C. Hausdorff Distance

This distance is named after Felix Hausdorff (first introduced in 1905). It is often referred as Pompeiu–Hausdorff distance. Hausdorff distance can be expressed as the maximum distance of a set to the nearest point in the other set [11]. Through this definition it is easy to understand that the distance expresses the longest distance that it might be forced to travel between two sets of points. Given 2 sets of points  $AF$  and  $M$ , the Hausdorff distance between them can be defined as in (3):

$$H(AF, M) = \max \{h(AF, M), h(M, AF)\} \quad (3)$$

Where  $h(AF, M)$  is called direct Hausdorff distance and defined as in (4):

$$h(AF, M) = \max_{AF(\theta_i) \in AF} \min_{M(\theta_j) \in M} \|AF(\theta_i) - M(\theta_j)\| \quad (4)$$

It identifies the point in  $AF$  that is the farthest from any point in  $M$  (*max* definition) and measures the Euclidean distance from that point to the nearest neighbor in  $M$  (*min* definition).

Likewise, the definition for  $h(M, AF)$  is in (5):

$$h(M, AF) = \max_{M(\theta_i) \in M} \min_{AF(\theta_j) \in AF} \|M(\theta_i) - AF(\theta_j)\| \quad (5)$$

Hausdorff and Euclidean distances applied to the actual antenna array design, are shown in Fig. 2.

### III. ANTENNA ARRAY SETUP

By using Woodward-Lawson method, we will build the standard linear antenna array which will have  $N = 21$  elements, an equidistance between elements of  $d = \lambda/2$  and will take in consideration a rectangular mask ( $M$ ) of unit amplitude (linear scale) from  $45^\circ$  to  $135^\circ$  and zero elsewhere (Fig. 3). For mobile operators the design of the array at a given center frequency of 2100MHz, gives an antenna with a high around 220 cm.

The Woodward-Lawson procedure does not specify how to generate the superposed sample beams or the required linear array complex element excitations. In 5G or in latest developments for 6G system the complex feed can be achieved through full digital beam forming network. In this case each antenna element of the array is directly connected to a dedicated RF chain (RF: Radio Frequency) comprising PA/LNA (Power Amplifier/Low Noise Amplifier) as in Fig. 4. One of the biggest drawbacks of this architecture, despite its cost, is the power consumption and high heat dissipation requirements [3][4].

To improve power consumption and extend antenna's life span, through decreasing its demand for power heat dissipation, in this paper we are investigating the possibility of intentionally turning off part of antenna elements (corresponding RF chain). Turning off some of antenna elements will inevitably also change the original radiation pattern. To understand how far from the desired radiation mask, the modified pattern is, it will be used a procedure of

measuring Euclidean and Hausdorff distances referring to the required mask.

Our intention is to compare both Euclidean and Hausdorff distances as an effective metric for antenna pattern deviation. But what is more important, to turn off part of RF chain network, which will bring more control to the mobile antenna operator, having so the possibility to decide whether to turn on or off part of antenna elements. This can be useful in case of low traffic or lower number of users connected for example by night or on low demand traffic hours. So the operator can reduce power consumption and heating dissipation, prolonging antenna life span without deteriorating the communication capabilities.

Instead of designing antenna array which focus in finding the best power feeding distribution network ratio for each element (which can be done with different methods) [12][13][14][15], in this paper, we will choose powering on or off (binary operation) selected antenna element and as well will be traced and scored modifications to the radiation pattern. In this case of all antenna elements powered on, its power ratio is defined by designing through W-L method. This choice of binary operation of antenna element (on/off) reduces computational effort required to complex beam forming techniques. The results can be stored on look-up tables to be recalled on demand. In this case, each RF chain operates as usual and can be on two states (on or off) based on mobile operator trade-offs.

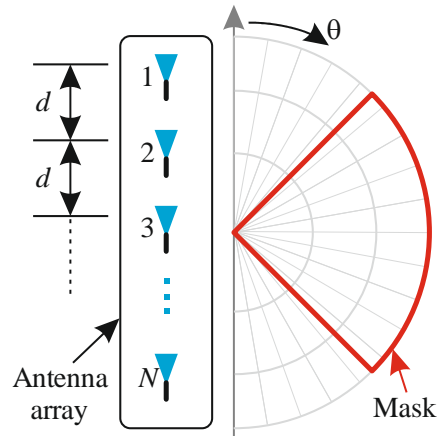


Fig. 3. Problem Defining Geometry.

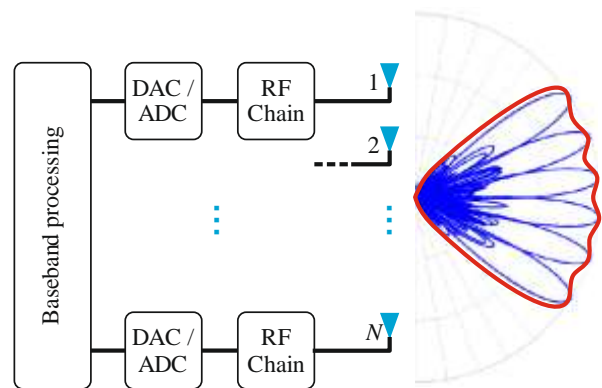


Fig. 4. Full Digital Beam Forming Architecture.

#### IV. ARRAY ANALYSIS AND SIMULATION

The original pattern designed as per W-L method (Fig. 5) is used to analyze the antenna array. The corresponding amplitude and phase of each element is presented in the second part of the same figure. This is a uniformly distributed antenna array, with non-uniform distribution feeding. By using the Linear Euclidean distance, can be easily noticed that: in case of all antennas up and running, Euclidean ( $E$ ) and Hausdorff ( $H$ ) distances are not null and are respectively  $E = 750.62$ ,  $H = 103.47$ .

In the analyzed scenario, since the possibilities for each antenna elements are only two (On or Off) there are a finite number of combinations to be tested ( $2^N = 2\ 097\ 152$ ). With the original antenna array power feeding ratio, designed as by W-L method, analyzing all the above combinations without modifying the feeding ratio between elements but only through changing their state, can be easily done through modern calculators.

Ranking the obtained solutions as for example by Euclidean distance (or the Hausdorff one) is inverse and not linear correlated to sorting solutions based on total number of powered off elements. As previously mentioned, the goal of mobile operators is to reach it without worsening the radiation pattern. These two goals are in contradiction with each other. In this case a more appropriate multiobjective optimization is required as in [16].

Turning off 6 antenna elements as in Fig. 6, the modified pattern shows a Euclidean distance  $E = 995.14$  and Hausdorff distance  $H = 117.18$ . Both distances are increased, but the obtained antenna pattern is still satisfactory in the main lobe.

Increasing the number of elements turned off from 6 to 10, especially those far from the array center, mainly modifies the side lobe level of the original W-L pattern. This can be evaluated by comparing Fig. 5 and Fig. 7 and theoretical analysis [14]. In this case, both metrics used show an increase in their respective values referred to the original W-L designed.

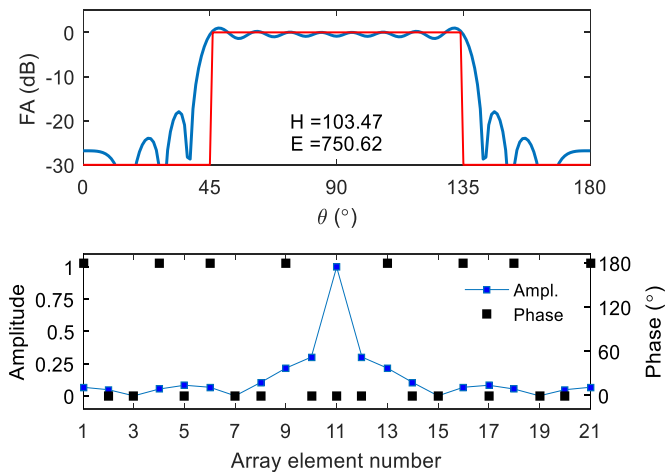


Fig. 5. Array Pattern and Relative Current at each Element as by W-L.

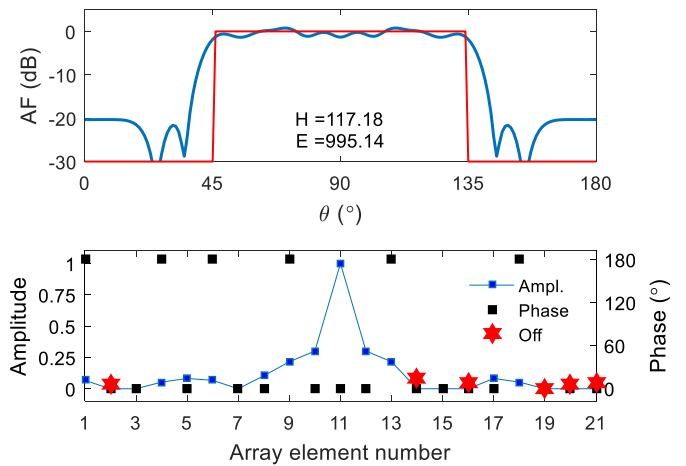


Fig. 6. Array Pattern and Relative Feed Ratio to all 21 Elements with 6 Antenna Elements turned off.

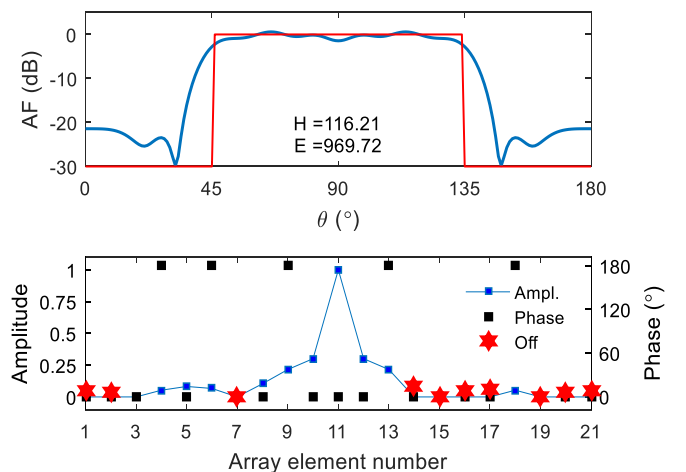


Fig. 7. Array Pattern and Relative Feed Ratio to all 21 Elements with 10 Antenna Elements turned off.

Increasing the number of elements turned off, not necessarily will bring worse results than the case with lower elements turned off. For this purpose, let us compare Fig. 8, Fig. 7 and Fig. 5 (original W-L, no elements turned off). In Fig. 8 there are 11 elements turned off (50% of all antenna elements) and both Euclidean and Hausdorff distances ( $E = 760.35$ ;  $H = 107.76$ ) are better than the case presented in Fig. 7 where both distances presents higher values ( $E = 969.72$ ;  $H = 116.21$ ). This means that we need to carefully choose which elements to turn off to have less distortion in the desired antenna pattern.

Comparing Fig. 9 and Fig. 10 brings a better insight to the above statement. Both configurations have nine antenna elements turned off, but visibly have very different radiation pattern. This can be confirmed also through comparing both metrics used. The solution presented in Fig. 9 has more uniformly distributed powered off elements which is similar to a spare antenna array [17][18].

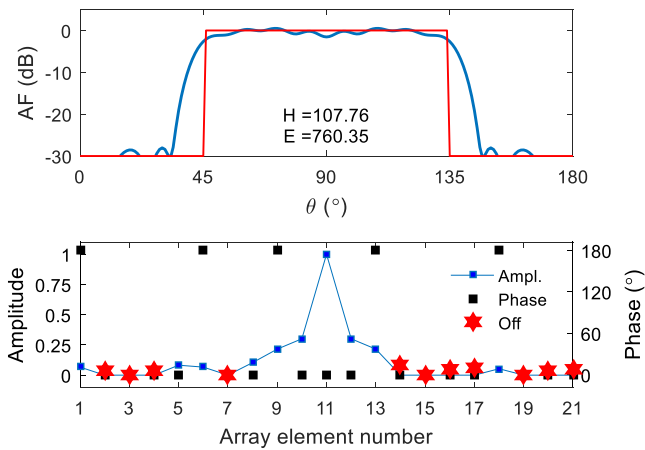


Fig. 8. Array Pattern and Relative Feed Ratio to all 21 Elements with 11 Antenna Elements turned off.

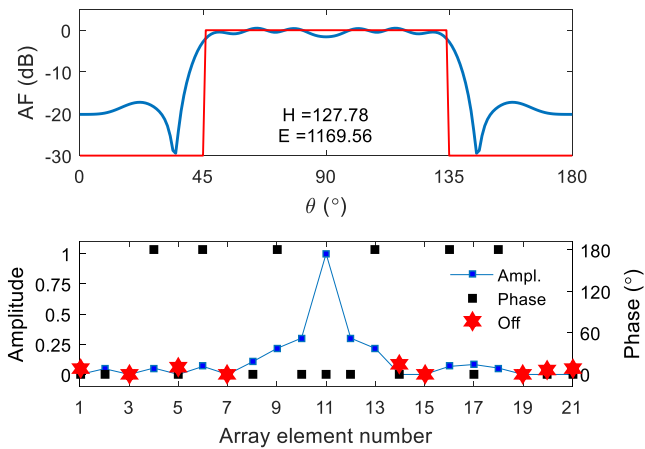


Fig. 9. Array Pattern and Relative Feed Ratio with 9 Antenna Elements turned off.

Referring Euclidean and Hausdorff distances in both figures (Fig. 9 and Fig. 10) compared to the result in Fig. 5 (original W-L configuration), we see an increase of 23% for  $H$  and 56% for  $E$  in Fig. 9, and 78% for  $H$  and 157% for  $E$  in Fig. 10.

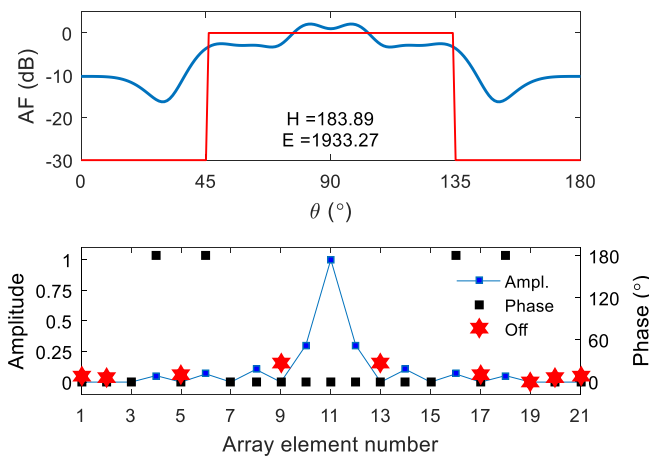


Fig. 10. Array Pattern and Relative Feed Ratio with 9 Antenna Elements turned off especially Element 9 and 13 have Higher Influence to the Pattern.

The last case, Fig. 11, presents the radiation pattern and relative elements powered for the same antenna array with 15 elements powered off. In this case there are around 71% of antenna elements powered off. It's observed an increase in side lobe level, but is maintained a contained variation to the main mask beam.

Both distance metrics can be efficiently used to evaluate how close is the modified antenna pattern to the required radiation mask. For this purpose, all presented structures, are compared in Table I. offering to interested readers all necessary information to recreate obtained results. In Table I is specified also which elements are turned on/off, the relative Euclidean and Hausdorff distances to the mask, and their variation to the original W-L ratio.

The ratio  $\Delta E/E_0$  and  $\Delta H/H_0$  are defined in (6) as relative  $E$  and  $H$  distances to the W-L respective distances to the desired mask.

$$\begin{cases} \frac{\Delta E}{E_0} = \frac{E - E_{WL}}{E_{WL}} \times 100\% \\ \frac{\Delta H}{H_0} = \frac{H - H_{WL}}{H_{WL}} \times 100\% \end{cases} \quad (6)$$

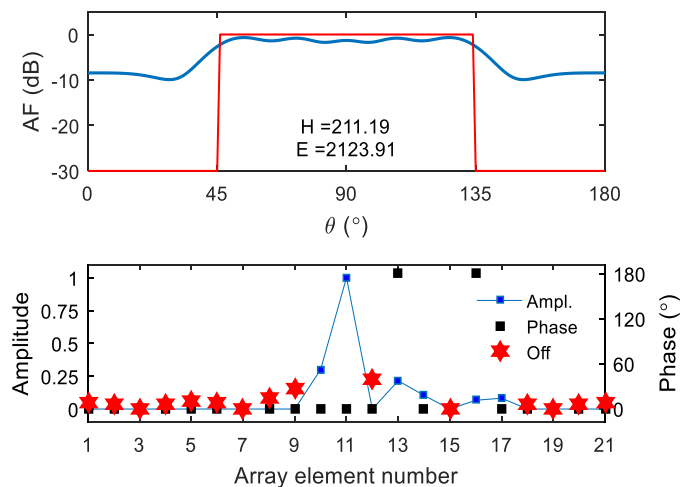


Fig. 11. Array Pattern and Relative Current at each Element with 15 Elements turned off.

TABLE I. EUCLIDEAN AND HAUSDORFF DISTANCES

| Fig. No. | Off No. | Off. Elements <sup>a</sup> | E    | H   | $\Delta E/E_0$ (%) | $\Delta H/H_0$ (%) |
|----------|---------|----------------------------|------|-----|--------------------|--------------------|
| 5        | 0       | 000000000000000000         | 750  | 103 | 0                  | 0                  |
| 6        | 6       | 01000000000010100111       | 995  | 117 | 32                 | 14                 |
| 7        | 10      | 1100001000000111101111     | 969  | 116 | 29                 | 13                 |
| 8        | 11      | 0111001000000111101111     | 760  | 107 | 1                  | 4                  |
| 9        | 9       | 1010101000000110001111     | 1169 | 127 | 56                 | 23                 |
| 10       | 9       | 1100100010001000101111     | 1933 | 183 | 157                | 78                 |
| 11       | 15      | 1111111110010010011111     | 2123 | 211 | 183                | 104                |

<sup>a</sup> Binary representation of powering on/off antenna array elements. 1: element off; 0: element on.



Referred to Table I, both metrics presents an increase in their distances due to the major modification of the radiation pattern. Hausdorff distances presents smaller variations respect to Euclidean distances as per the last row on Table I, where the modified pattern presents 183% variation on  $E$  metric and only 104% on  $H$  metric. In this way, Hausdorff distance brings a compressed scale for evaluating pattern variations.

## V. CONCLUSION AND FUTURE WORK

In this material is presented the analysis of an antenna array by turning off a part of antenna elements, in order to decrease power consumption without major modifications in radiation pattern.

The presented analysis is focused on binary format of turning on/off antenna elements which is easier and does not require higher processing capabilities for beam forming evaluating techniques. Modifying antenna array behavior is faster with just powering on/off elements on demand rather than changing power and phase distribution network or beam forming network.

In this case, the solution of the elements that can be turned off can be stored on look-up table, for faster reference similar to that presented in Table I.

Powering off up to 50% of array elements made possible to have less heat, to save energy without worsening the radiation pattern and increasing the lifecycle of antenna array.

Using Euclidean distance as a metric, brings to a spread of solutions, Hausdorff evaluates the same closer solutions. The other point is that the usage of Hausdorff distance against the traditional one the Euclidean, is more appropriate to choose the deterioration of the radiation models and/or the differences among them.

This work will be the base which will lead us in future works like how to choose in an intelligent way the elements to be powered on/off. Also, the procedure will be extended to a more complex antenna array design as planar and conformal array, and multi beam array systems.

### REFERENCES

[1] Robert J. Mailloux, "Phased Array Antenna Handbook", 3rd Edition; Artech House Publishers, 2017.

[2] Comisso, M.; Palese, G.; Babich, F.; Vatta, F.; Buttazzoni, G. "3D multi-beam and null synthesis by phase-only control for 5G antenna arrays", *Electronics* 2019, 8, 656.

[3] E. Björnson, L. Sanguinetti, H. Wymeersch, J. Hoydis, T.L. Marzetta, "Massive MIMO is a reality—What is next? Five promising research

directions for antenna arrays", Elsevier, *Digital Signal Processing*, Volume 94, November 2019, Pages 3-20.

[4] Rowell, C.; Han, S. "Practical large scale antenna systems for 5G cellular networks". In *Proceedings of the 2015 IEEE International Wireless Symposium (IWS 2015)*, Shenzhen, China, 30 March–1 April 2015.

[5] Molisch, A.F.; Ratnam, V.V.; Han, S.; Li, Z.; Nguyen, S.L.H.; Li, L.; Haneda, K. Hybrid Beamforming for Massive MIMO: A Survey. *IEEE Commun. Mag.* 2017, 55, 134–141.

[6] Roh, W.; Seol, J.Y.; Park, J.; Lee, B.; Lee, J.; Kim, Y.; Cho, J.; Cheun, K.; Aryanfar, F. Millimeter-Wave beamforming as an enabling technology for 5G cellular communications: Theoretical feasibility and prototype results. *IEEE Commun. Mag.* 2017, 52, 106–113.

[7] D. I. Lialios, N. Ntetsikas, K. D. Paschaloudis, C. L. Zekios, S. V. Georgakopoulos, G. A. Kyriacou, "Design of True Time Delay Millimeter Wave Beamformers for 5G Multibeam Phased Arrays," *Electronics* 2020, 9, 1331.

[8] G. A. Somers, "A proof of the Woodward-Lawson sampling method for a finite linear array," in *Radio Science*, vol. 28, no. 04, pp. 481-485, July-Aug. 1993.

[9] M. D. Migliore, "MIMO Antennas Explained Using the Woodward-Lawson Synthesis Method [Wireless Corner]," in *IEEE Antennas and Propagation Magazine*, vol. 49, no. 5, pp. 175-182, Oct. 2007.

[10] R. Rajashekar, K. V. S. Hari and L. Hanzo, "Quantifying the Transmit Diversity Order of Euclidean Distance Based Antenna Selection in Spatial Modulation," in *IEEE Signal Processing Letters*, vol. 22, no. 9, pp. 1434-1437, Sept. 2015.

[11] Gao Y. "Efficiently comparing face images using a modified Hausdorff distance," *Image and Signal Processing*, *IEEE Proceedings*, vol. 150, pp. 346-350, 2003.

[12] Deotale, N.; Kolekar, U.; Kondelwar, A. "Grey wolf optimization based transmit antenna selection for LTE system", In *Proceedings of the 2017 International Conference on Wireless Communications, Signal Processing and Networking (WiSPNET)*, Chennai, India, 22–24 March 2017.

[13] A. Magdy, O.M. EL-Ghandour and H. F. A. Hamed, "Improvement of Adaptive Smart Concentric Circular Antenna Array Based Hybrid PSO/GA Optimizer" *International Journal of Advanced Computer Science and Applications (IJACSA)*, 7(6), 2016.

[14] S. E. Nai, W. Ser, Z. L. Yu and H. Chen, "Beampattern Synthesis for Linear and Planar Arrays With Antenna Selection by Convex Optimization," in *IEEE Transactions on Antennas and Propagation*, vol. 58, no. 12, pp. 3923-3930, Dec. 2010.

[15] Z.K. Chen, F.G. Yan, X.L. Qiao, Y.N. Zhao, "Sparse Antenna Array Design for MIMO Radar Using Multiobjective Differential Evolution", *International Journal of Antennas and Propagation*, vol. 2016.

[16] E. Agastra, G. Pelosi, S. Selli, R. Taddei, "Multi-Objective Optimization Techniques", In *Wiley Encyclopedia of Electrical and Electronics Engineering*, Vol. 1-29, September 2014.

[17] R. Harrington, "Sidelobe reduction by nonuniform element spacing", *IRE Trans. Antennas Propag.* 1961,9, 187–192.

[18] P. Fan, J. Li, X. Wang and J. Gu, "A low sidelobe sparse array antenna," 2016 *CIE International Conference on Radar (RADAR)*, Guangzhou, 2016, pp. 1-4.

# Environmental Sustainability Coding Techniques for Cloud Computing

Shakeel Ahmed

College of Computer Sciences and Information Technology  
King Faisal University, Al-Ahsa, Saudi Arabia

**Abstract**—Cloud Computing (CC) has recently received substantial attention, as a promising approach for providing various information and communication technologies (ICT) services. Running enormously complicated and sophisticated software on the cloud requires more energy and most of the energy is wasted. It is required to explore opportunities to reduce emission of carbon in the CC environment that causes global warming. Global warming affects environment and it is required to lessen greenhouse gas emissions which can be achieved by adopting energy-efficient technologies that largely need to reduce the energy consumption caused during computations, for storing data and during communications to achieve Green computing. In literature, most of the energy-saving techniques focus on hardware aspects. Many improvements can be done in regard to energy efficiency from the software perspective by considering and paying attention to the energy consumption aspects of software for environmental sustainability. The aim of the research is to propose energy-aware profiling environmental sustainability techniques based on parameterized development technique to reduce the energy that has been spent and measure its efficiency inured to support software developers to enhance their code development process in terms of reducing energy. Experiments have been carried out and results prove that the suggested techniques have enabled in achieving energy consumption and achieve environmental sustainability.

**Keywords**—Environmental sustainability; cloud computing; energy-efficient; software development life cycle; parameterized development; green computing

## I. INTRODUCTION

Cloud Computing services comprised of large data centers, several virtualized server instances, networks with high band, and supporting systems for cooling and power supply. These equipment's can be classified into hardware and software and are accessed by remote users as shown in Fig. 1, and Cloud services are made accessible to the users through the usage of network equipment which connects the servers to the Internet which makes up the hardware equipment [1]. The user's applications/software managed by Cloud management system (CMS) are commonly referred as appliance and which runs on top of servers and is other supporting equipment includes power supply, cooling system, and data center building.

Green cloud computing became widely thought of issue in large organizations and they have targets to minimize the energy consumption and reduce unnecessary resources. Cloud computing is cost effective and highly scalable infrastructure for running High Performance Computing (HPC), enterprise and web applications. Moreover, there has been drastically

growing demand of cloud infrastructure by different organizations which have resulted in the increased consumption of energy to run these data centers, which has become a serious concern. Where High energy consumptions increase the operational cost and decrease the profit margin of cloud providers. Further, this also leads to high carbon emissions which is not eco-friendly [2].

### A. Energy Optimization in Cloud Computing

Energy efficiency can be well-defined as reduction of energy used for a given service or level of activity [4]. Nevertheless, owing to measure and convolution of data center equipment it is very difficult to describe service or bustle that could be observed for energy efficiency. Hence, [3] identified four scenarios within a system where energy is not used in well-organized way but it's lost or not used, as shown in Fig. 2.

Today, energy efficiency is the most vital constraints for cloud computing. It decides the operational costs and the benefits of capital investment. Since CC depend on data center industry deployed worldwide. Cloud applications optimization will not only reduces the data centers energy consumption, rather also will contribute in optimize overall cloud computing systems globally. In [5], issues are addressed in regards to reducing energy consumption of data centers, as well as in cloud computing. They include but not limited to virtual machines placement workload scheduling or load balancing as illustrated below:

1) *Virtual machines placement*: Virtualization is an efficient operation in cloud data centers. The physical equipment that is energy consumption can be replaced virtually in data center. VMs merging approaches try to accommodate lowermost conceivable number of physical machines to multitude a number of VMs. In virtualized environment, scheduling and load balancing are some techniques used effectively to manage operation in data centers. VM is ensuring efficient utilization of storage to serve hosted application workloads and then lead to minimize energy consumption in data center.

2) *Workload scheduling*: It contributes in improving the efficiency of data center in a way that specifies the resources that would be used to complete the work. The work could be data flow, processes or threads that are in turn waiting to being processed. The focus is to achieve efficient utilization of resources selected from the server with cost and energy

effective. Additionally, energy efficient workload scheduling tends to ponder all active workloads onto a few numbers of servers with least possible communication resources.

3) *Load balancing*: The aim of load balancing is to optimize the resource usage, maximize the throughput and minimize response time, as well as to avoid overload for particular resource(s). Load balancing can efficiently distribute the incoming traffic among available servers in fast and reliable manner. It ensures that no one server has overloaded more than other, that may cause it to be down. As the inactive server (in case of shutdown) require energy to turn it on, and then heat is generated more and cooling system will consume electrical energy to keep good temperature. Load balancing is the important enabler for saving energy by avoiding unnecessary power consumption. However, recoveries after the server turned ON will causes some delays.

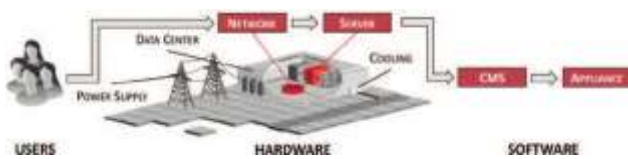


Fig. 1. Cloud Computing Data Center Domains [3].

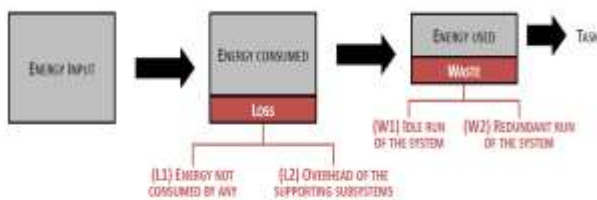


Fig. 2. Scenarios where Energy is Lost or Wasted within a System [3].

The structure of the article is as follows: Section 2 is related to the literature review and presents the discussion on the tools used by the developers for code development. Section 3 presents the framework of parameterized development phase. Section 4 presents the results, and Section 5 summarizes and concludes the paper.

## II. LITERATURE REVIEW

There are quite many platforms/tools used by the developers in code development and deployment of Cloud based services and applications which include Windows Azure [6], Hadoop [7], Twister [8], Google App Engine [9], Microsoft Daytona [10] and Manjrasoft Aneka [11] in all these platform there is a lack of consideration for energy efficiency techniques to be followed by the developer. Although a general-purpose programming environment to rationalize and support designers and developers in creating energy-aware and energy-efficient applications is proposed in [12]. Most of the consideration in the literature has thorough research on to enhance the Cloud Computing energy efficiency and considering improved resource management to circumvent specific concerns like excessive power consumption and service-level agreements (SLA) violation reliability [13].

Consequently, various progresses have been presented like, Dynamic voltage and frequency scaling (DVFS) and Dynamic Power Management (DPM) methodologies used in monitoring the power consumption of servers according to the workload [14]. To optimize hosts virtual machine consolidation policies are used by migrating virtual machines (VMs) from one host VM to another VM [13]. Few models are proposed for improved forecast of the task consolidation in order to maximize resource utilization [15] power consumption for the servers [16]. A general outline/framework known as Mistral for optimizing physical hosts' power consumption [17], a CPU re-allocation algorithm which combines live migration techniques and DVFS and to cut the energy consumption and raise the performances in Cloud datacenters [18]. Though, there is a deficiency of research that grabs the concern of appropriately confirming energy-awareness from the design stage. Therefore, it is still a need for establishing the energy efficiency of Cloud infrastructures to increase a better understanding of energy efficiency and to nourish the policymaking at the service design stage. So, the applications or software must be prepared with energy efficient techniques at the implementation phase. This means that the developers need to design the software with Green Software Development Life Cycle (G-SDLC). Where the source code is studied by identifying and analyzing the hotspots, which causes energy consumption with help of tools or methods. Cloud computing and software development are the backbone to design software which is most energy efficient for cloud based applications.

As results, the researchers focus on the side of implementation of cloud components that affect energy consumption. Thus, components decide the type of cloud computing service models that are being used in the environment of cloud. Our effort in this research project is on software implementation by elaborating in energy optimization at software or application level. Focusing on energy consumption of applications' profiling at runtime and narrow down hotspots iteratively; to achieve G-SDLC.

Developers need to understand the estimation of the program energy consumption to avoid the power waste in early stage of development. The current research focuses on elucidate of green software development life cycle, especially in software implementation and parameterized methodologies to contribute in reducing energy consumption when it is running on cloud. The fact is that when the developers improve the source code with the help of parameterized phase; energy optimization of software can be achieved by determining the part of code that consumes high energy during the runtime in alignment with regular SDLC phases. Our enhancement is adding parameterized development phase which focus on code generated in implementation phase. As stated, the source code plays a vital role in achieving energy efficient software. Therefore, all efforts focused on unnecessary use of controls, libraries and some unnecessary instructions by applying the parameters to reduce the energy consumption of software when running in cloud environment.

### III. PROPOSED SYSTEM

The aim of this work to propose and investigate the framework of software development life cycle that introduces a new phase called parameterized development phase to enhance the energy efficiency of the software as shown in Fig. 3, which helps the developers to optimize energy efficiency of software applications when it is being developed. Parameterized phase improves the software code by generating energy efficient code and to get efficient software which improves the source code for optimizing energy consumption and to determine the highest power consumption part in code. Therefore, the software application would be environment-friendly in cloud and same functionalities with other aspects of quality still maintained. This is of our interest in achieving and optimizing energy by implementing G-SDLC in cloud computing environment.

Parameterized phase provides guidelines and appropriate methodologies for developers that promote software's implementation phase. Set of parameters works as checklist that help in software code development. Such as data structure design, architectural design, abstract specification, and algorithm design. Applying the parameters should be based upon programming language used, application function and engineering hardware architecture. All these should be presented in earlier phase of software's specification and requirement. Thus, developers can modify those parts consuming the energy instead of re-writing the code from scratch. Energy optimization comes with best practice and experience; developers will be able to identify the part of the code demand a particular pattern to be modified.

Efficient code can be cost effective using different programming techniques that are used as parameters to adopt on source code. As result, developers can undertake code manually. Such as loop unrolling mechanism by executing the instructions within the loop in parallel. This will optimize compiler time as well as the energy required to compile the sequence loop instruction. For example, in a program that deletes 100 items a simple For loop can accomplish this task by calling the function delete( ). As a result of this adaptation, the enhancement with "loop unrolling" only 20 iterations of the jumps and conditional branches need to be run, instead of 100. Developers are responsible to choose loop control variables and number of operations inside the unrolled loop structure. So, the output is same as the original code produced.

#### A. Code Performance Measurement

The energy consumption depends on the application itself. If the code/application is extensively running with high usage of CPU and memory requirements then its execution will result in high energy consumption. Therefore, energy consumption here will be directly relational to the applications. Developer must put more efforts in regards to optimize the performance of code. Performance optimization is endless process. There is always an opportunity for the developer to improve and make the code run fast in efficient manner. Hence, software should be developed to be energy efficient either at earlier stage or during runtime.

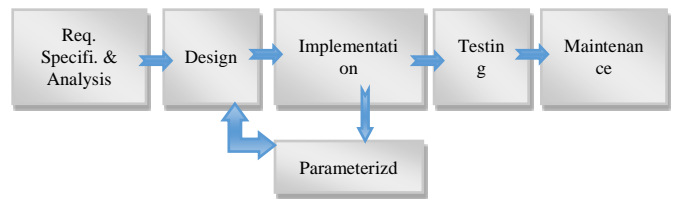


Fig. 3. Green Software Development Life Cycle.

The measurement of these parameters is the roadmap to know whether the software has good or low performance in terms of CPU utilization and memory it consumes. In other words, efficient application has good performance when its execution takes less time. However, inefficient application has low performance that leads to higher CPU and memory utilization, then higher energy consumption more time to execute Object-Oriented Programming Language most probably provides integrated garbage collection that helps the developer from dealing with memory de-allocation. However, garbage collection may consume resources in computation to take decision of which memory to free. Therefore, this could lead to decreased performance of the code [19]. Manual optimization remains mostly important at the source code level. Developer can use their experience and knowledge to perform optimization in creative manner to obtain good performance [20].

Optimizing the code will indicate good performance in regards to CPU and memory utilization. This can be measured by using performance profiler to identify code bottleneck. The code bottleneck can be found, for example, in loop that is executed hundreds/ thousands of times. Developer can redesign the body of loop in order to form in way that does not need to be executed hundreds/thousands of times [21].

#### B. Measure the Performance using Performance Profiler Tool in Microsoft Visual Studio 2017

Microsoft Visual Studio 2017 profiling tool, allows developer to analyze performance issues in their application code that is written with any programming languages of ASP.NET. It reports the performance from different perspective, including CPU usage, memory usage, performance wizard and others. It reports the performance of code by collecting information about the functions that performing work. Furthermore, provides timeline graph the developer can focus on precise sections of code [22]. Measuring the performance of code can be done using performance profiler in two steps: collect CPU/memory usage data and analyze CPU/memory usage data. To measure the time CPU is spending the CPU usage tool are used so that the developer can modify the code accordingly. Similarly, memory allocation shows the total memory allocated to execute the subject code [23] [24].

#### C. Performance Optimization Experiments using Proposed Parameter

One cannot really know about performance of code without measuring it. However, the function code of an application can be measured to see how long it takes and memory occupies. The good performance is defined by the function that taking less time to be executed with less memory

utilization. On other hand, the low performance is defined by function that taking more time to be executed and consuming the system resources. The various Code Optimization techniques/parameters introduced in the earlier section are performed on two experiments discussed below by applying these parameters to observe how memory and CPU usage is optimized to enhance the source code and makes it performs efficiently. ASP.NET was used framework to develop website with traditional software development life cycle, and another version with G-SDLC. The reasons behind selecting ASP.NET are that, it is language independent in which support more than one programming language. It reduced the long lines of code. ASP.NET framework has magnificent features, in which gives alert for infinite loops, memory leaks and other wrong behaviors. It handles this immediately by killing the wrong behaviors and restarts them over again. This will help in increasing the performance and achieving efficient website/application. Microsoft Visual Studio 2017 is used to create these versions of website.

#### IV. RESULTS

To demonstrate our proposed method, simple website with two versions which consists of four pages with similar design is developed. These websites run functions of reading around 400 records of data and inserts them into database in two different ways. Moreover, these records can be deleted from the database using two different methods. The database used is Microsoft Access 2010. Two different methodologies or functions on source code are used to deliver the same output. Performance measurements are made for the websites in regards to CPU usage and memory allocation using the performance profiler tool in Microsoft Visual Studio 2017. For simplicity, the website that needs to be enhanced is referred as website1. On other hand, the enhanced website is referred as website2. Both websites performed two functions insert and delete records from the database table. Performance assessment is performed on website1 regarding the insertion and deletion of records. Later, same assessment is performed on website2. In Website1, the insertion of records is done using for loop as follow:

```
For cnt = 0 To dt2.Rows.Count - 1
sql = "insert into ToEmployees (EmpName, EmpLog) values "
& _("'" & dt2.Rows(cnt).Item("SrcEmpName") & "' ,'" &
dt2.Rows(cnt).Item("SrcEmpLog") & "'")"
Try
conn.ConnectionString = ConStr
adapter.SelectCommand = New OleDbCommand(sql, conn)
adapter.Fill(dt)
Catch ex As System.Exception
Throw (ex)
Finally
conn.Close()
End Try
conn.Close()
```

Based on performance profiler tool, Fig. 4 indicates that the developer needs to implement some modification in order to improve the highlighted lines. These highlights can be accessed by investigating the peak point reported by CPU

usage or running time addressed in Fig. 5 which shows that website1 executed with total of 1,792 samples collected as CPU usage to insert 400 records. The sampling is recommended method for starting the investigation of code and it is useful for finding issue of processor utilization [25].

Based on the performance profiler tool, the insertion function in Website1 is executed with total of 5,759 KB allocated as illustrated in Fig. 6. In this version of website1, the inserted records in the database table can be deleted using for loop.

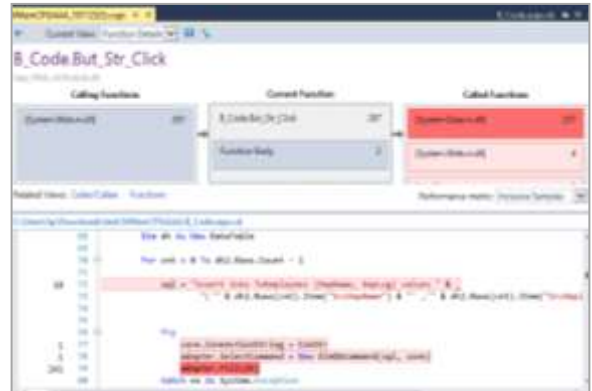


Fig. 4. Hot Spot Code of Inserting Records in Website1.



Fig. 5. Total CPU usage of Inserting Records in Website1.

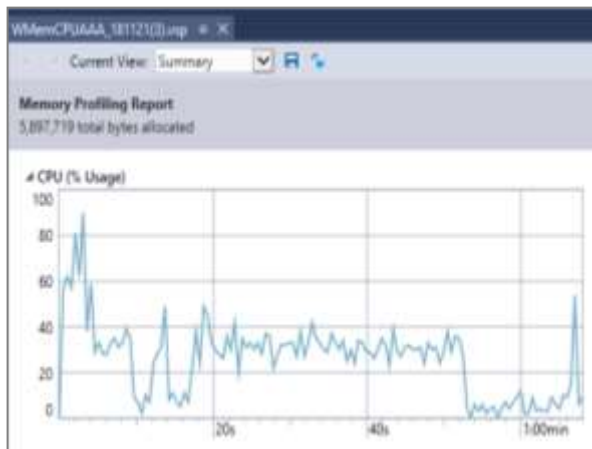


Fig. 6. Total Memory Allocation of Inserting Records in Website1.

```
For cnt = 0 To dt2.Rows.Count - 1
sql = "Delete from ToEmployees where EmpLog = '" &
dt2.Rows(cnt).Item("SrcEmpLog") & "'"
Dim adapter As New OleDbDataAdapter()
Dim conn As New OleDbConnection
Dim dt As New DataTable
Try conn.ConnectionString = ConStr
adapter.SelectCommand=NewOleDbCommand(sql, conn)
adapter.Fill(dt)
Catch ex As System.Exception
Throw (ex)
Finally
conn.Close()
```

This function is executed with total of 4,358 samples collected as CPU usage to delete 400 records. Fig 7, is snapshot reported from the performance profiler tool. As this deletion function causes to release memory space, there was no result to report memory usage for this function, i.e. no need to locate memory.

The Website1 underwent modification after getting the performance assessment of it. This modification reflected on Website2. It uses methodology of inserting and deleting the data into database using single SQL command instead of having a loop. The following code is the modified part to insert records into database table:

```
Dim sql As String = " INSERT INTO ToEmployees
(EmpName, EmpLog) SELECT SrcEmpName, SrcEmpLog
FROM(Employees) WHERE EmpChk= true"
adapter.SelectCommand = New OleDbCommand(sql, conn)
adapter.Fill(dt)
conn.Close()
```

Moreover, proper modification is applied in deletion function that causes deletion of the records that had been inserted into database table as follows:

```
Dim sql As String = "Delete * from ToEmployees "
Dim adapter As New OleDbDataAdapter()
Dim conn As New OleDbConnection
Dim dt As New DataTable
Tryconn.ConnectionString = ConStr
adapter.SelectCommand=NewOleDbCommand(sql, conn)
adapter.Fill(dt) Catch ex As System.Exception
Throw (ex)
Finally
conn.Close()
End Try
```

Same procedures is followed to assess the performance in website1's followed by website2.Starting with insertion method; Fig. 8 indicates that the code is executed with total of 713 samples collected as CPU usage. This show an improvement of 60% in CPU performance compared to website1. This reflected the enhancement of insertion function that insert around 400 records in database table. This led to have faster execution in short duration as illustrated.

Fig. 9 shows total of 1,098 samples collected as CPU usage of delete command. This is an improvement of 74% of delete function compared to website1.

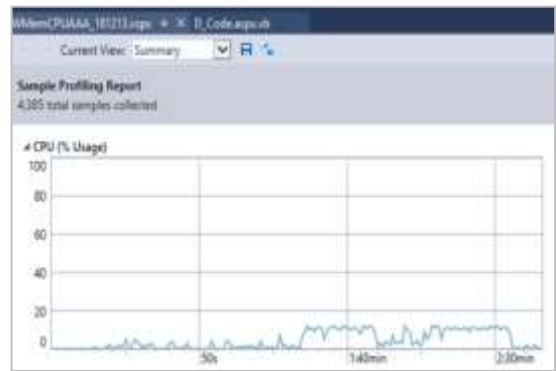


Fig. 7. Total CPU usage of Deleting Records in Website1.

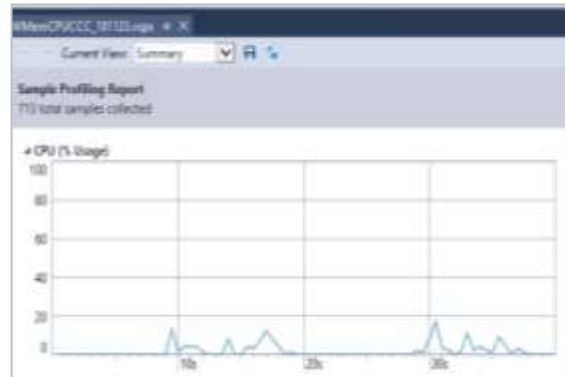


Fig. 8. Total CPU usage of Inserting Records in Website2.

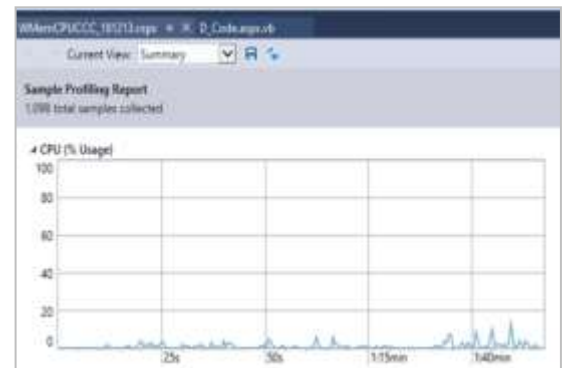


Fig. 9. Total CPU usage of Deleting Records in Website2.

Fig. 10 show that Website2 is executed with total of 3,033 KB allocated. This is an improvement of 47% in memory allocation compared to website1.

Fig. 11 summaries the result of performance assessment for the developed websites. This summary gives clear view of website2 improvement compared to website1 in regards to CPU usage and memory allocation. The insertion function of website1 is using for loop to populate database table with the selected records. On the other hand, website2 is using single SQL command to insert the records that meet the requirements with total improvement of 60% in regards to collected samples.

The reduction of total samples means less time of execution and response [26]. Fig. 12 illustrates the comparison

of CPU usage for delete function in website 1 and website2 with total improvement of 74% in regards to collected samples.

Fig. 13 illustrates the improvement of total memory allocation of website1 and website 2by using appropriate methodology to insert data in database table. Memory allocation reduced by 47% in website2 compared to website1. Overall, this initial energy reduction will help in deliver energy efficient website when in it deployed in server.

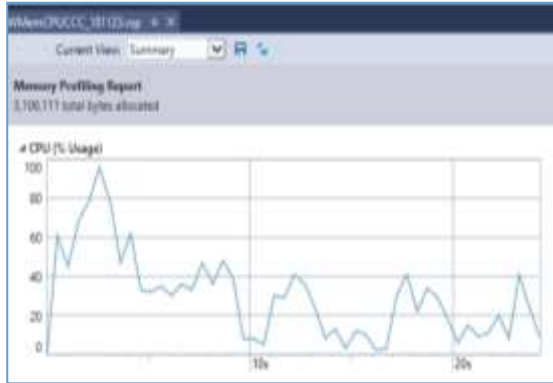


Fig. 10. Total Memory Allocation of Website2.



Fig. 11. CPU Collected Sample Improvement for Insert Function.



Fig. 12. CPU Collected Sample Improvement for Delete Function.



Fig. 13. CPU Collected Sample Improvement for Total Memory Allocation.

## V. CONCLUSION

Energy efficiency ought to be the first priority of software or website development. A main concept is that developer must use his/her experience for any chance to optimize the source code. SDLC with the additional phase of parameters, produced energy efficient website in regards to CPU and memory usage. This optimization had been measured using performance profiler built-in tool in Microsoft Visual Studio 2017. The initial energy optimization version of the website provides perception of the website's performance for the developer before deploying it in server. This perception gives an opportunity to re-assess the performance, if website does not comply with the required criteria of having green cloud computing. Hence, the cloud energy consumption is controlled from software side as well as hardware side.

Software development improvement leads to reduce power costs. Therefore, getting green cloud and saving money. The latest processors have improved energy efficiency in hardware side. In software side, developer needs to contribute and follow appropriate parameters in implementation phase, as small change to software engineering can make a large difference in regards to energy and for environmental sustainability.

## REFERENCES

- [1] AlNuaim, A. and Ahmed, S., 2018. Fog Computing: A Novel Approach to provide Security in Cloud Computing. Indian Journal of Science and Technology, 11(15), pp.1-6.
- [2] Rajkumar Buyya, and Sukhpal Singh Gill. 2018. Sustainable Cloud Computing: Foundations and Future Directions. Business Technology & Digital Transformation Strategies, Cutter Consortium, 21, 6, 1-10.
- [3] Mastelic, T., & Brandic, I. 2015. Recent Trends in Energy-Efficient Cloud Computing. IEEE Cloud Computing, 2, 40-47.
- [4] M.M. Islam, M. Hasanuzzaman, Introduction to energy and sustainable development ,Energy for Sustainable Development, Academic Press, 2020, Pages 1-18, ISBN 9780128146453.
- [5] Rengadevi, T.; Geetha, K.; Muthukumar, K.; Geem, Z.W. Optimized Energy Cost and Carbon Emission-Aware Virtual Machine Allocation in Sustainable Data Centers. Sustainability 2020, 12, 6383.
- [6] Windows Azure: Microsoft's Cloud Platform — Cloud Hosting — Cloud Services. Available at <http://www.windowsazure.com/en-us/>, 2020.
- [7] Welcome to Apache, Hadoop! Available at <http://hadoop.apache.org/>, 2020.
- [8] J. Ekanayake. Twister: Iterative MapReduce. Available at <http://www.iterativemapreduce.org/>, 2009.
- [9] Google App Engine - Google Developers. Available at <https://developers.google.com/>, 2020.
- [10] Daytona - Microsoft Research. Available at <http://research.microsoft.com/en-us/projects/daytona/>, 2013.
- [11] Manjrasoft Products Available at <http://www.manjrasoft.com/products.html>, 2020.
- [12] Xian, Y. Lu, and Z. Li. A programming environment with runtime energy characterization for energyaware applications. In Low Power Electronics and Design (ISLPED), 2007 ACM/IEEE International Symposium on, pages 141–146, 2007.
- [13] Beloglazov, J. Abawajy, and R. Buyya. Energy-aware resource allocation heuristics for efficient management of data centers for Cloud computing. Future Generation Computer Systems, 28(5):755– 768, May 2012.
- [14] Kliazovich, P. Bouvry, and S. Khan. DENS: Data Center Energy-Efficient Network-Aware Scheduling. In 2010 IEEE/ACM Int'l Conference on Green Computing and Communications & Int'l

- Conference on Cyber, Physical and Social Computing, pages 69–75. IEEE, December 2010.
- [15] R. Basmadjian, F. Niedermeier, and H. De Meer. Modelling and analysing the power consumption of idle servers. *Sustainable Internet and ICT for Sustainability (SustainIT)*, 2012, pages 1–9, 2012.
- [16] Y. Lee and A. Zomaya. Energy efficient utilization of resources in cloud computing systems. *The Journal of Supercomputing*, 60(2):268–280, March 2010.
- [17] G. Jung, M. Hiltunen, K. Joshi, R. Schlichting, and C. Pu. Mistral: Dynamically Managing Power, Performance, and Adaptation Cost in Cloud Infrastructures. 2010 IEEE 30th International Conference on Distributed Computing Systems, pages 62–73, 2010.
- [18] W. Chawarut and L. Woraphon. Energy-aware and real-time service management in cloud computing. In *Electrical Engineering/Electronics, Computer, Telecommunications and Information Technology (ECTI-CON)*, 2013 10th International Conference on, pages 1–5, 2013.
- [19] Matthew Hertz and Emery D. Berger, “Quantifying the Performance of Garbage Collection vs. Explicit Memory Management,” San Diego, California, USA, Rep. 1-59593-031-0/05/0010, October 2005.
- [20] Rudrik Upadhyay et al. (2017, September 7). A Practical Approach to Optimize Code Implementation [Online]. Available: <https://www.einfochips.com/wp-content/uploads/resources/a-practical-approach-to-optimize-code-implementation.pdf>.
- [21] Michael E. Lee, “Optimization of Computer Programs in C”, Ontek Corporation, Laguna Hills, USA, 1997.
- [22] Mike Jones et al. (2017, February 27). Profile application performance in Visual Studio [Online]. Available: <https://docs.microsoft.com/en-us/visualstudio/profiling/beginners-guide-to-performance-profiling?view=vs-2017>.
- [23] Theano Petersen et al. (2018, April 11). Analyze CPU usage [Online]. Available: <https://docs.microsoft.com/en-us/visualstudio/profiling/cpu-usage?view=vs-2017>.
- [24] Genevieve Warren et al. (2018, February 1). Analyze memory usage [Online]. Available: <https://docs.microsoft.com/en-us/visualstudio/profiling/analyze-memory-usage?view=vs-2017>.
- [25] Mark McGee et al. (2017, February 27). Beginners guide to CPU sampling [Online]. Available: <https://docs.microsoft.com/en-us/visualstudio/profiling/beginners-guide-to-cpu-sampling?view=vs-2017>.
- [26] Nikhil Joglekar (2016, April 28). How CPU Sampling Works [Online]. Available: <https://blogs.msdn.microsoft.com/devops/2016/04/28/how-cpu-sampling-works/>.



# High Priority Requests in Grid Environment

Tariq Alwada<sup>n1</sup>

School of Computing, Engineering  
and Digital Technologies  
Teesside University  
Middlesbrough, UK

Salah Alghyaline<sup>2</sup>

Department of Computer Science  
The World Islamic Sciences and  
Education University  
Amman, Jordan

Azmi Alazzam<sup>3</sup>

Computer Information System  
Department  
Higher Colleges of Technology  
Al Ain, UAE

**Abstract**—Grid computing is an enhanced technology consisting of a pool of connected machines that belong to multiple organizations in different sites to form a distributed system. This system can be used to deal with complex scientific or business problems. It is developed to help share distributed resources that may be diverted in nature and solve many computing problems. The typical decentralized grid computing model faces many challenges, such as; different systems and software architectures, quickly handling the enormous amount of grid requesters, and finding the appropriate resources for the grid users. Some of the grid requests might need to get significant attention and fast response to the other requests. Usually, the Grid Broker (GB) works as a third party or mediator between grid service providers and grid service requesters. This paper introduced a new automated system that can help exploit the grid power, improve its functionality, and enhance its performance. This research presents a new architecture for the Grid Broker that can assist with high priority requests and be processed first. This system is also used to monitor and provision the grid providers' work during the job running. It uses a multi-agent system to facilitate its work and accomplish its tasks. The proposed approach is evaluated using the Jade simulator. The results show that using the proposed approach can enhance the way of dealing with high priority requests coming to the grid.

**Keywords**—Grid computing; multi-agents system; grid broker; static priority mechanism; distributed resources

## I. INTRODUCTION

### A. Grid Computing

A grid is a system that has the capability to organize and manage resources and services that are distributed among different control domains, utilize protocols and interfaces, and provide a high quality of services [1, 2]. The primary goal of grid computing is to increase reliability, reduce computing costs, and increase flexibility by moving computers from an entity that we buy and run by ourselves to an entity run by a third party [3, 4].

Grid computing comes into sight due to combining multi-network computer systems to create a wide-scale and heterogeneous system used to resolve scientific or industrial problems [1]. Therefore, grid computing faces many challenges, such as reducing the number of rejected jobs, finding appropriate resources, and prioritizing some requests from grid users [5]. "Fig. 1" shows an example of a Grid Model.

Grid depends on improved software that ensures seamless communication between grid nodes [6]. The Grid architecture

comprises the following elements [7]: A- Grid Portal (GP): it is also called a grid interface, a virtual computing interface used by the grid users to reach the grid resources. A portal contains many characteristics, such as hiding the grid's complexity from users using a simple interface. In this way, it facilitates the classification of grid job requirements. B- The Grid Broker (GB): this element is considered the heart of grid computing. It performs significant functions in building an effective grid environment by organizing user jobs to suitable grid resources to accomplish specific targets, such as; raising resource utilization, reducing communication delays, and effectively delivering jobs among resources. It is also responsible for monitoring and provisioning jobs and sending back the outputs to the grid users.

To find appropriate resources for the grid users, the resource broker receives the GP's job requirements and searches for the right resources to meet these requirements. To do that, first, the Broker asks for all information about the free resources from the Information Service (IS) and the data information stored in the Replica Catalogue (RC) components. Then it selects the resources that can meet the job requirements. The (IS) Information is a critical element in grid computing. It is considered a directory service that keeps data about all the grid resources and their running jobs. This information can be static or dynamic. The static data can be used for specifying the hardware and the operating system requirements, while the dynamic information one is related to the job presently running, the resources available time, type of application software, policies, and disk space. All the grid resources have to register their information in the IS so that the GB can quickly locate them. The (RC) is another essential element for the GB. It offers information to help in accessing the stored data in the grid. It defines the places of data in the grid, maps logical file names to the real physical locations on grid resources, and updates data resources. The GB asks the RC for information about the data place and the access control mechanism required to use this data to utilize the grid data.

### B. Multi-Agent System (MAS)

An intelligent agent is a pre-programmed component intended to support other parts to accomplish a task or fulfill a pre-defined job. MAS is a group of agents that cooperate and work together with the outer system. It can work with a pre-defined level of self-government to do the requested jobs or complete particular tasks. MAS is incorporated to operate independently in a changing environment [8]. It has many features such as [9], the ability to cooperate, and connect with other agents to acquire commands, exchange data, and supply

responses. The MAS can also work dynamically on behalf of the programs or clients, enhance the performance regularly while working with the external environment, and negotiate where the MAS can run channels for communication between agents to achieve a specific level of cooperation.



Fig. 1. Grid Computing Model.

Several methods were introduced for the development of a system that includes many agents. For example, knowledge-based methodologies, such as CommonKADS [10] or Multi-agent System Engineering (MaSE) [11]. The proposed system in this research is based on MaSE, where the GB is employing the MAS to negotiate the job requirements and conditions with the grid users. The GB also uses the MAS to monitor and exchange information with the grid providers and provision the running jobs.

### C. Congestion Management Algorithms

Due to the rising requests on the grid services, applications, and grid service requesters request to reduce the running time for their tasks while minimizing the related cost. Also, both ask for the minimum QoS through the execution of their jobs. Most of the applications now are somewhat sensitive to the delays faced when transmitting and running their jobs to the grid. So, it is required to support different types of traffic with various QoS [12]. One crucial question to answer is distributing the users' jobs with a high priority value to the available resources on the grid.

This research introduces an advance redirecting policy that can be used to pick high priority requests from the grid users (as a paid service) and pass them by the GB to the appropriate grid resources. To do that, there is a demand for queuing the low priority requests and keep them in the GB memory until the high priority requests get processed by the Broker.

Our proposed technique is adopted from the cisco mechanism for queuing on router interfaces, where the queuing on cisco consists of hardware and software modules [13]. The proposed technique is used to facilitate the management of the congestion that might occur on the GB side. The chosen mechanism is the Static Priority Scheduler mechanism. This mechanism classifies packets automatically,

with every flow being situated into a separate queue according to its priority [13]. In the proposed system, if there are any jobs with high priority flags coming to the grid, the GB directly processes these jobs and put them at the beginning of the queue to forward them to the appropriate grid resources first. In this case, the GB guarantees high-speed processing time for this type of traffic.

This paper is organized as follows. Section 2 presents a literature review. Section 3 offers the proposed system model. The experimental results are discussed in Section 4. Finally, the conclusion of this paper is presented in Section 5.

## II. RELATED WORKS

G. Garimella, in [14], applies a reservation server that runs in cooperation with the Dynamic Soft Real-Time system [15]. The Garimella system aims to preserve the resource of the CPU in advance. In Advance Reservations Server, the client requires to state some QoS factors, such as that CPU percentage needed, the start time, and the duration. After the reservation request is initiated, the booked resources shall be accessible for the user following the beginning time for the time at the predetermined percentage. Yet, in practice, the majority of applications have QoS conditions that are negotiable. Since the reservation server does not keep up re-negotiations, this produces many reservation requests that have been rejected.

Another suggested model is the Resource Broker (RB) indicated in [16] combined with the reservation server introduced in [14]. The RB enhances the reservation server to give constant and fast reply time and several negotiation possibilities for the clients. The amount of re-negotiation inserts additional extensive overhead to the system in case of an unexpected shortage of resources. Thus, to preserve a resource to several contending applications, there is a need for a mechanism by the admission control to estimate and differentiate between different applications to refuse fewer priority applications first to assure the full set of clients obtain most of the benefit.

W. Smith and others in [17] introduced and evaluated many algorithms for maintaining enhanced reservations method in scheduling systems for supercomputers. These algorithms enhance regular organizing algorithms by uniting routine scheduling jobs from queues with the reservation demand. These enhanced reservations allow users to ask for multiple resources concurrently from scheduling systems at certain times. Nevertheless, [17] allocates the "time slots" entirely. In other words, the resources are not kept up in a shared way by many users for the same period. The applications are presumed to run on a best-effort basis, and the booking requests are then assumed to have diverse priority between the applications. These priorities are taken into account as the applications and the system schedules the reservations.

In [18], R. Min and M. Maheswaran suggested a Functions called (RSPB). The RSPB stands for Reservation Scheduler with Priorities and Benefit, which allows for algorithm program reservations while allowing for the relation priorities of the several reservation requests. In RSPB, every reservation

call has a related profit function that measures the client's profit by saving the resource at the needed stage. Once the user is prepared to negotiate for short service stages, it could specify this by offering a profit function that displays a cut but significant profit for short resource stages. This capability provided by the functions eliminates the necessity for negotiations as there is a resource shortage.

### III. SYSTEM MODEL

In this section, the details of our proposed system are presented. The system is a multi-agent system that considers several aspects when making the final decisions, such as the number and shortage of grid provider (resources), the hardware and software specifications, and the customers' priority.

"Fig. 2" shows the Architecture of our automated system, which can assist in exploiting the grid power, improving its functionality, and enhancing its performance. The system is designed to allow the GB to deal with high priority requests and be processed first. The system is divided into three parts; The Grid Portal part, the Grid Broker part, and the Grid Service Provider part.

#### A. The Grid Portal Part

A grid portal or grid interface is an interface for authorized grid users to reach the grid. A portal is essential as it is hiding the grid's complexity from users by a friendly interface, which can simplify the organization of grid job requirements. Our system has used the multi-agent system by creating a local agent attached to each grid user. The local agent is responsible for classifying the priority of the grid jobs. As a paid services, the grid users can flag their careers with a high priority in order to notify the GB about this job.

#### B. Grid Broker Part

This part is divided into three main elements. The main one is the monitor and the scheduler. This element is responsible for receiving the grid users' jobs and determining the appropriate free resources. The scheduler is responsible for checking the users' jobs for a priority flag. If there is no flag, that means the job is treated as a normal priority (low priority), and it will be served according to the First-In-First-Out mechanism. If the job flag is high, it will be moved to the next one in the queue. The scheduler asks for all information about the free resources from the Information Service (IS) element and the data information stored in the Replica Catalogue (RC) elements. The monitor is responsible for monitoring and provisioning the running jobs in the grid providers.

#### C. Grid Provider Part

After the Monitor and Scheduler sends the jobs to the appropriate resource(s) for operating, it gets messages periodically from the agents at the providers' side to check the status of the running jobs. The local agent at the providers is also responsible for informing the Broker when the job is done. The provider can contain many physical and virtual machines. The Hypervisor in each machine is responsible for creating and organizing the virtual machines on top of each physical machine.

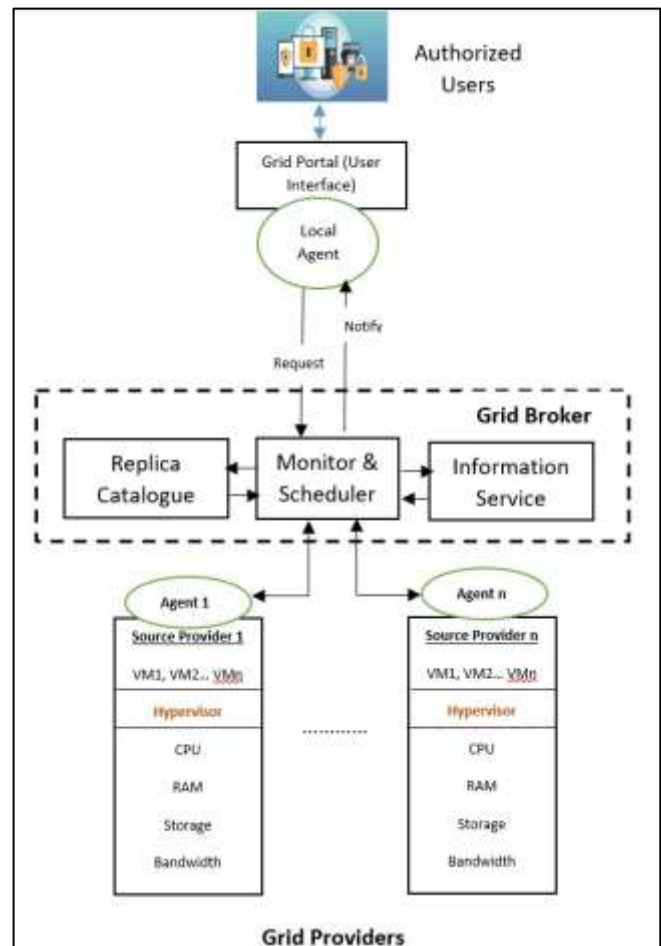


Fig. 2. System Architecture.

### IV. EXPERIMENTS AND RESULTS

In order to evaluate the performance of our proposed system, a Jade tool was employed. Jade is designed to support the agent software development as specified by the FIPA qualities for applied smart multi-agent systems.

In our experiment, two tests were created. Both tests have the same settings. These settings include 225 jobs from 3 grid users (75 each), with one physical machine and 4 virtual machines as grid providers. The Grid Broker is programmed to accept up to 125 jobs and reject all the jobs above that. The simulation time is 300 seconds. "Tables I, II and III" show the properties of the physical machine, the VMs, and the jobs, respectively.

Table I shows the number of virtual machines and their types. Also, it shows the Microprocessor without Interlocked Pipelined Stages (MIPS) for the CPU, Ram capacity, the network bandwidth for each VM, and the storage capacity.

Table II shows the characteristics of the physical machine used in the experiment. This includes the number of hosts and types of VMs and MIPS of the CPU, RAM, storage capacity, and network bandwidth.

Table III shows the characteristics of each job include job length and size.

TABLE I. VMS CHARACTERISTICS

|                  |            |
|------------------|------------|
| Number of VMs    | 4          |
| VMs types        | 4          |
| MIPS of CPU      | 1000       |
| Number of PEs    | 1          |
| RAM Capacity     | 1048       |
| Bandwidth        | 100 Mbit/s |
| Storage Capacity | 10 GB      |

TABLE II. PHYSICAL MACHINES CHARACTERISTICS

|                  |          |
|------------------|----------|
| Number of Hosts  | 1        |
| VMs types        | 4        |
| MIPS of CPU      | 1000     |
| Number of PEs    | 1        |
| RAM Capacity     | 2048     |
| Bandwidth        | 1 Gbit/s |
| Storage Capacity | 10 GB    |

TABLE III. JOBS CHARACTERISTICS

|                |      |
|----------------|------|
| Number of jobs | 225  |
| Job Length     | 1200 |
| File Size      | 300  |
| Output Size    | 300  |

In the first part of the experiment, no paid services for high priority jobs were done. In this case, the local agents for each of the three users will consider all the jobs as a low priority (priority is equal for the three users). In the second part of the experiment, the local agent for one of the users labeled the jobs as a high priority while the other two grid users with low priority.

Both tests planned to send all the jobs to the grid broker at the same time to check the time required to process all the jobs together. It is also intended to check the number of rejected jobs because of the large number of requests.

The experiment's two tests were compared and assessed on several facets, such as the time needed to complete the jobs and the number of jobs rejected for each user.

First Part: 225 jobs were sent to the grid broker from 3 users (75 jobs from each). No priority in this part. The Broker got the jobs and processed them as FIFO jobs. "Fig. 4" shows that the first 75 jobs were coming from the first user treated without any rejection. For the second user, only 50 jobs were accepted, and 25 rejected. But the Broker declined all jobs from the third user as the Broker reached the boundaries of the accepted jobs (as in its policy). The last user had to resend the jobs later for processing. "Fig. 5" shows the processing time for the first part of the experiment. The needed time to complete the first user's jobs is less than the second and third users. The processing time for the third user is the longest one, as the user has to resend the jobs again to the grid and wait until the services at the grid become available.

Second Part: 225 jobs were sent again to the Broker. This time the local agent labeled the jobs for user number 3 as high priority (paid service). The other users stay as a low priority (normal priority). "Fig. 4" and "Fig. 5" present the rejected jobs and the processing time correspondingly for the second part of the experiment. "Fig. 3" shows the part of the simulation for this experiment.

"Fig. 4" shows that user 3 has made use of the paid service priority service, as all of user 3's jobs were fulfilled. While "Fig. 5" shows that the time needed for the processing of user 3's jobs was minimal compare to the first part. Furthermore, there are no rejected jobs for user 3. The other results show that user 1 has 25 rejected jobs, while user 2 has 75 rejected jobs, and that was because the Broker processed their jobs according to the FIFO mechanism.

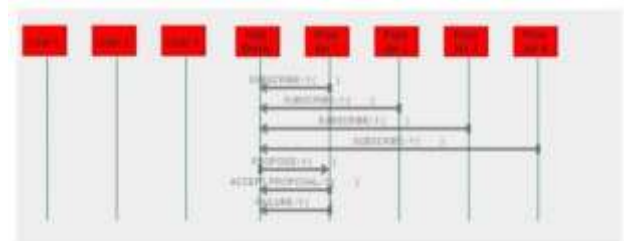


Fig. 3. Simulation for both Parts.

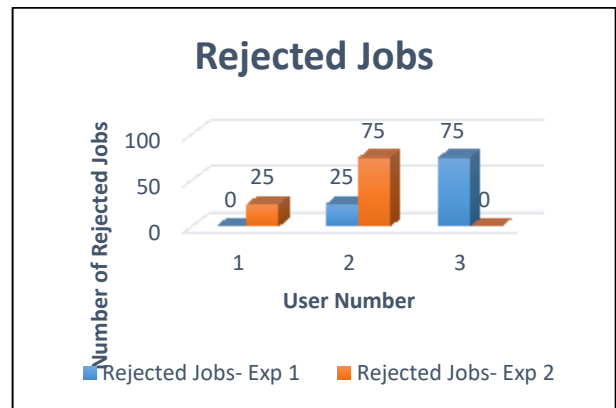


Fig. 4. Rejected Jobs for both Parts.

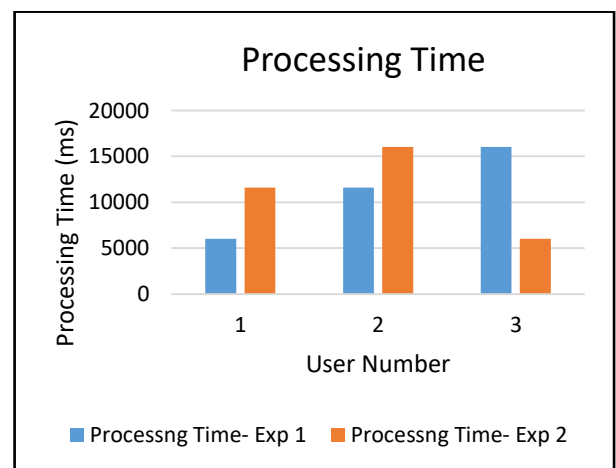


Fig. 5. Processing Time for both Parts.

## V. CONCLUSIONS AND FUTURE WORKS

Grid computing comes into sight due to combining multi-network computer systems to create a wide-scale and heterogeneous system used to resolve scientific or industrial problems. This paper presented a dynamic management system that can handle the high priority client requests as paid service to get a fast response for their jobs. Also, this system is used to provision and monitor the grid providers' work during the job running. The proposed system is evaluated using the Jade tool. The results show that using our system enhances the degree of customers' (QoS) requirements during the resource utilization, helps exploit the grid power, improves its functionality, and enhances its performance. Our future work includes improving our proposed system's functionality when dealing with multiple grid brokers instead of one Broker.

### REFERENCES

- [1] Ian Foster and Carl Kesselman, editors. *The Grid: Blueprint for a New Computing Infrastructure*. Morgan Kaufmann Publishers Inc., San Francisco, CA, USA, 1999.
- [2] T. Alwada'n, H. Aldabbas, H. Janicke, T. Khmour and O. Aldabba. Dynamic policy management in approach grid environments. *International Journal of Computer Networks & Caproachections (IJCNC)*, 4(2), 35–51. 2012.
- [3] I. Foster's. weblog. <http://ianfoster.typepad.com/blog/2008/01/theres-grid-in.html>. 2008.
- [4] H. Alhakami, H. Aldabbas, and T. Alwadan. Comparison between cloud and grid computing: Review paper. *International Journal on Cloud Computing: Services and Architecture (IJCCSA)*, 2, 08 2012.
- [5] T. Alwadan, H. Janicke, O. Aldabbas, and M. Alfawair. New framework for policy support for mobile grid services. *The 6th International Conference on Risks and Security of Internet and Systems (CRISIS2011)*, Romania 2011.
- [6] T. Alwadan, H. Janicke, O. Aldabbas, and H. Aldabbas. New framework for dynamic policy management in grid environments. In *Recent Trends in Wireless and Mobile Networks, Third International Conferences, WiMo 2011 and CoNeCo 2011*, volume 162, pages 297–304. Springer, 2011.
- [7] T. Alwadan, H. Janicke, A. Alarabeyyat, A. Alkharabsh, and T. Khmour. Policy-based support for mobile grid services. *International Journal of Computer Science Issues (IJCSI)*, 10, 01 2013.
- [8] T. Alwada'n, A. Alarabeyyat, T. Khmour and A. Rodan. "Utilizing Multi-Agent Systems in Grid Environments," 2019 Sixth HCT Information Technology Trends (ITT), Ras Al Khaimah, United Arab Emirates, pp. 138-143, doi: 10.1109/ITT48889.2019.9075099, 2019.
- [9] A. S. Grimshaw, M. A. Humphrey, and A. Natrajan. A philosophical and technical comparison of legion and globus. *IBM J. Res. Dev.*, 48:233–254, March 2004.
- [10] Rajkumar Buyya, David Abramson, and Jonathan Giddy. A case for economy grid architecture for service-oriented grid computing. In *Proceedings of the 15th International Parallel & Distributed Processing Symposium, IPDPS '01*, pages 83–, Washington, DC, USA. IEEE Computer Society. 2001.
- [11] Zsolt N. Ne'meth and Vaidy Sunderam. A formal framework for defining grid systems. In *Proceedings of the 2nd IEEE/ACM International Symposium on Cluster Computing and the Grid, CCGRID '02*, pages 202–, Washington, DC, USA. IEEE Computer Society. 2002.
- [12] Szilágyi, Szabolcs and Béla, Almási. (2012). A Review of Congestion Management Algorithms on Cisco Routers. *Journal of Computer Science and Control Systems*. 5. 103-107.
- [13] QOS, "Implementing Cisco Quality of Service", Student Guide, Volume 2, Version 2.2, © 2006 Cisco Systems Inc.
- [14] G. Garimella, "Advance CPU Reservations with the Dynamic Soft Real-Time Scheduler", Master's Thesis, University of Illinois at Urbana-Champaign, 1999.
- [15] H. Chu and K. Nahrstedt, "A Soft Real Time Scheduling Server in UNIX Operating System," *European Workshop on Interactive Distributed Multimedia Systems and Telecommunication Services (IDMS '97)*, Sep. 1997.
- [16] K. Kim and K. Nahrstedt, "A Resource Broker Model with Integrated Reservation Scheme," *IEEE International Conference on Multimedia and Expo 2000 (ICME '00)*, Aug. 2000.
- [17] W. Smith, I. Foster, and V. Taylor, "Scheduling with Advanced Reservations," *International Parallel and Distributed Processing Symposium (IPDPS '00)*, May 2000.
- [18] Rui Min and Muthucumara Maheswaran. *Scheduling Co-Reservations with Priorities in Grid Computing Systems*. 13th International Conference on Parallel and Distributed Systems, Anaheim, 2002. pages 266–268. 2002.

# A Hybrid Approach for Single Channel Speech Enhancement using Deep Neural Network and Harmonic Regeneration Noise Reduction

Norezmi Jamal<sup>1</sup>, N. Fuad<sup>2</sup>, MNAH. Sha'abani<sup>3</sup>  
Faculty of Electrical and Electronic Engineering  
Universiti Tun Hussein Onn Malaysia  
Johor, Malaysia

**Abstract**—This paper presents a hybrid approach for single channel speech enhancement using deep neural network (DNN) and harmonic regeneration noise reduction (HRNR). The DNN was used as a supervised algorithm to predict new target mask such as constrained Wiener Filter (cWF) target mask from noisy mixture signal that was transformed into gammatone filter bank features. Meanwhile, HRNR algorithm was applied in the post-filtering strategy to eliminate residual noise. The DNN algorithm is an emerging supervised speech enhancement to overcome heavy nonstationary noise and low signal-to-noise ratio (SNR) issues. To validate the proposed algorithm with new target mask, 600 Malay utterances combining male and female speakers were used in a training session while 120 Malay utterances were used in a prediction session. The short time objective intelligibility (STOI) and perceptual evaluation of speech quality (PESQ) scores were calculated as the performance metrics. In this work, the proposed target mask outperformed other baseline target masks. Thus, PESQ and STOI scores for the hybrid speech enhancement algorithm is 1.17 and 0.79, respectively, at - 5 dB babble noise SNR.

**Keywords**—Speech enhancement; single channel microphone; deep neural network; constrained Wiener Filter; post-filtering

## I. INTRODUCTION

Over the past few decades, automatic speech recognition (ASR) has gained a surge of interest among researchers in the speech processing research area. This is because ASR is widely used in mobile device applications, especially for navigation purposes. It allows human to talk to a computer, which responds to the given command. Basically, to capture human speech signals, a single microphone is practical enough to be used as an input device for speech data acquisition. Meanwhile, computer acts as a system to process the captured speech signal to realize human computer interaction (HCI) by applying mathematical algorithms and signal processing techniques. However, as the captured speech signals are in mobile remote condition [1], the speech signals could be easily contaminated by background noises, which may lead to complex computation and further processes. Thus, speech recognition may yield low speech recognition accuracy especially at low signal-to-noise ratio (SNR) and nonstationary noise, which the quality and intelligibility of speech are affected [2]. Thus, past studies proposed the Deep Neural Network (DNN)-based mask estimation approach to guarantee high intelligibility and quality of speech signal [3-9].

The first DNN-based mask estimation approach was pioneered by Wang, who demonstrated a DNN with promising results, owns good scalability and flexibility compared to other machine learning techniques [10], especially at high SNR. As mentioned in a study [4], DNN outperformed SVM algorithm during speech separation from noisy background as cited by [11]. The DNN algorithm became a great attention among researchers and most of them were interested to extend their work to improve in terms of features, target masks, and learning network [7, 12-15]. But when the mixture signal is at low SNR [10], the estimation between speech and noise signal is very challenging due to overlapping events. Excessive estimation of noise will cause speech distortion. Otherwise, when noise signal is underestimated, residual noise could be introduced after speech reconstruction [16]. For the first time, this study aims to propose a new target mask that could control speech distortion and noise distortion by using constrained Wiener Filter (cWF) in gammatone representation as the target mask for DNN algorithm with longer duration of speech utterance. The harmonic regeneration noise reduction (HRNR) was applied to reduce residual noise and generate new speech harmonic after the speech reconstruction.

This paper is organized as follows: Section II discusses the related works; Section III describes the methodology of research work; Section IV presents the experimental results and compares the results with the baseline approach and Section V summarizes the findings and proposes recommendations for improvement.

## II. RELATED WORKS

Features, target masks and learning network are the three important elements in the DNN-based mask estimation approach. Previously, several studies on the effect of different features in a supervised DNN-based mask estimation were done [14, 15]. The findings revealed that gammatone features is one of the outperform features. Various speech dataset such as IEEE [10, 14, 15, 17] and TIMIT [18] were used to analyze the performance, which normally in short duration of speech utterance. A study in [10] also compared the training targets in DNN algorithm. From the results, the combination of features such as mel-frequency cepstral coefficient (MFCC), relative spectral transform perceptual linear prediction coefficient (RASTA- PLP), amplitude modulation spectrogram (AMS) and gammatone filter bank power spectra (GF) outperformed

with ideal ratio mask (IRM), which produced the STOI and PESQ scores of 0.72 and 1.92, respectively, during -5dB SNR for duration length of 2 s using three hidden layers of DNN algorithm [10]. Otherwise, the authors studied the effect of different learning networks, which increasing the hidden layers by five [12].

A similar method of DNN-based mask estimation was done in past studies [19-23]. A study in [19] modified the feature and proposed adaptive masks in the DNN-based mask estimation with four hidden layers and 1024 hidden nodes. As a result, average PESQ and STOI scores of 2.12 and 0.78, respectively, were obtained at -5dB SNR [19]. Another study in [23] used the features fusion technique for the DNN input, while the phase-aware and magnitude mask were applied as the target mask. Five-layer structures, including one input layer, three hidden layers, and one output layer with 2048 rectified linear unit (ReLU) neurons were used for the network architecture. As a result, the STOI and PESQ scores of 0.74 and 2.01, respectively, were obtained. Some studies proposed a new target mask in the DNN such as less aggressive Wiener filtering, phase aware, and complex ratio mask [20-22]. Other studies also proposed an alternative approach using post-filtering techniques such as global variance equalization [17, 24] after the DNN-based mask estimation and speech reconstruction.

Another study also proposed a combination algorithm between the DNN-based approach and statistical-based approach to separate speech signals from background noise with TIMIT database [18]. The standard sparse non-negative matrix factorizations (SNMF) features were extracted from the noisy mixture. Five layers which consist of input layer, three hidden layers and one output layer were used. Then, 1024 number of neurons per layer and ReLU activation were applied in the network architecture. The SNMF-DNN with ideal ratio mask (IRM) target produced promising results compared to ideal binary mask (IBM) target. Even though the proposed approach outperformed, it suffered from features complexity. While another study in [5] investigated the generalization of DNN based mask estimation and contribution to modify a DNN model with permutation invariant training by [25]. This approach is time consuming and complex.

### III. RESEARCH METHODOLOGY

Fig. 1 shows the DNN-based mask estimation framework in this study. The framework was proposed to overcome background noise issue. Firstly, the clean speech and noise signal were resampled simultaneously at fixed sampling frequency of 16 kHz, amplified, normalized and scaled with the equal length of data to generate the mixture noisy speech signal in the data preparation stage. The clean and noise speech signals were converted into a time-frequency domain, to be used in the target mask stage. Prior to the mixture signal processing to be parameterized in the time-frequency domain or known as spectrogram, the mixture signal was transformed into gammatone filter bank power spectra (GF) in the feature engineering stage. The parameterized mixture signal was used as the input features of DNN algorithm. The target output was predicted from the input features using the DNN algorithm. Specifically, cWF was used as the target mask in the

gammatone time-frequency domain representation. Each frame of the proposed mask spectrogram corresponding to speech or noise for every audio samples was learnt by the DNN. The overall system involved similar process in the training and test sessions, excluding the post-filtering process. Lastly, a post-filtering strategy using HRNR was applied to overcome the residual noise issue after the speech synthesis process. The speech synthesis was done to reconstruct speech signals in time domain from the time-frequency domain using an inverse gammatone.

#### A. Data Preparation

MASS corpus dataset was used as the clean speech signal with sampling frequency of 22050 Hz [26]. Meanwhile, babble noise was used for background noise with the sampling frequency of 8000 Hz. The noise was artificially combined with the clean signal to produce mixture signal with different signal to noise ratio (SNR) of -10 and -5 dB. The mixture signal is as shown in Equation (1) below:

$$y(t) = x(t) + \alpha n(t) \tag{1}$$

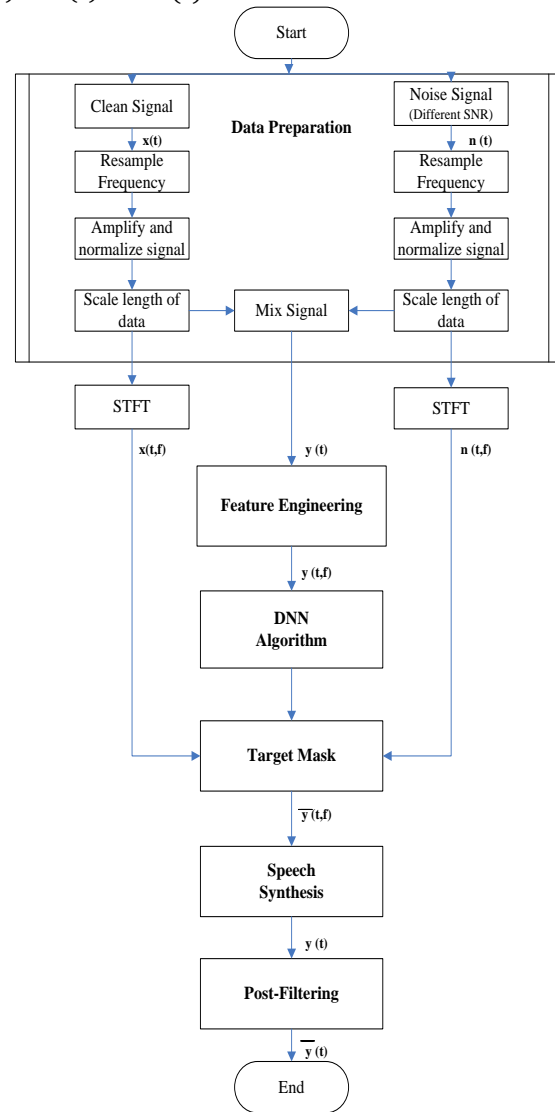


Fig. 1. Research Workflow.

where  $\alpha$  is assumed as the gain for scale noise energy signal at different required SNR value as in Equation (2):

$$\alpha = \sqrt{\frac{\sum P_x(t)}{\sum P_n(t) \cdot 10^{SNR/10}}} \quad (2)$$

Then, 600 utterance samples were used for data training, while the remaining 120 samples were used for evaluation performance.

### B. Feature Engineering

Gammatone filter bank power spectra (GF) was used because it can produce nonuniform time-frequency resolutions between the high and low frequency regions [27]. The 64-D GF vector was extracted by using 64 channels gammatone filter bank to produce an array of filtered responses with frequency range between 50 and 8000 Hz and loudness gain adjustment. A gammatone filter impulse response is simply defined in time-domain as the product of a gamma distribution and tone. Thus, the gammatone function can be defined as in Equation 3 [28].

$$g(t) = at^{n-1}e^{-2\pi bt} \cos(2\pi f_c t + \varphi), \quad (3)$$

where  $a$  is the gain value based on loudness theory,  $t^{n-1}$  is the time onset, exponent function in negative term defines bandwidth, decay rate,  $f_c$  is the characteristic frequency in equivalent rectangular bandwidth (ERB), and  $\varphi$  is the initial phase. Typically,  $b$  is 1.019 ERB. The ERB of the filter is given in the Equation (4) [28]:

$$ERB = 24.7 \left( \frac{4.37f_c}{1000} + 1 \right) \quad (4)$$

### C. Deep Neural Network (DNN)

The features were trained in a DNN architecture as shown in Fig. 2. The input and output nodes are represented by the blue colour with 640 input nodes and 64 output nodes. Meanwhile, the hidden nodes of four layers are represented by the orange colour. Next, the black arrow represents the forward network while the blue arrow represents the backpropagation network. 4 hidden layers DNN with ReLU hidden and output activation function were applied. Specifically, 430 hidden nodes in each hidden layer with adaptive gradient descent (AGD) and 64 output nodes were applied. Other hyper parameters of DNN to train the networks include 0.2 of dropout rate for backpropagation algorithm, 20 training epoch numbers, 0.5 of initial momentum rate, 0.9 of final momentum rate and loss function of mean squared error.

### D. Target Mask

The cWF was proposed as the training target in DNN algorithm to control individual noise and speech distortion. The cWF and IBM target output masks were obtained by using 64 channels of gammatone filter bank, with 20-ms analysis window and 10-ms overlap. The equation of cWF is as follows [29]:

$$y = \hat{W}(\omega) = \frac{1}{1 + \sqrt{\frac{P_n(\omega)}{P_x(\omega)}}} \quad (5)$$

Next, the proposed target was evaluated and compared with other two target outputs such as ideal binary mask (IBM) and

gammatone filter bank power spectrum of clean speech (GF-POW). The IBM is typically represented in the time-frequency domain. It is constructed from premixed signals between noise signal and speech signal based on the perceptual principles of auditory scene analysis [14]. The IBM is usually computed from a true signal-to-noise ratio (SNR) through thresholding with local SNR criterion (LC) as shown in Equation (6):

$$IBM(t, f) = \begin{cases} 1, & \text{if } SNR(t, f) > LC \\ 0, & \text{otherwise} \end{cases} \quad (6)$$

### E. Post-Filtering Strategy

The HRNR technique is used to preserve the harmonics and to avoid speech distortion [30]. By applying the algorithm, the distorted speech signal could be processed by creating a fully harmonic signal where all the missing harmonics are regenerated. Then, the synthesized speech signal was used to compute a spectral gain and preserve the speech harmonics as shown in Equation (7) [30]:

$$G_{HRNR}(p, k) = \frac{\hat{SNR}_{prio}^{HRNR}(p, k)}{1 + \hat{SNR}_{prio}^{HRNR}(p, k)} \quad (7)$$

Finally, the resulting speech spectrum was estimated using Equation (8) [30].

$$\hat{S}(p, k) = G_{HRNR}(p, k)X(p, k) \quad (8)$$

### F. Performance Measure

Two objective performance measures such as perceptual evaluation of speech quality (PESQ) and short-time objective intelligibility (STOI) were applied to evaluate the performance between enhanced and clean speech signals after the speech enhancement process. To measure the quality of enhanced speech signal, PESQ is widely used compared to other performance metrics which is more useful even though it is complicated [16]. The PESQ estimates the enhanced speech quality by measuring the distortion difference between the clean speech and the enhanced speech signals. The PESQ score between 0.5 and 4.5 represents bad quality and good quality, respectively [16]. Meanwhile, STOI is widely used to evaluate the performance of enhanced speech signal in terms of speech intelligibility. It computes the correlation in time-frequency domain between the enhanced and clean speech signals without speech perception theory by representing higher correlation when the value of STOI score is greater than 0.9 [13].

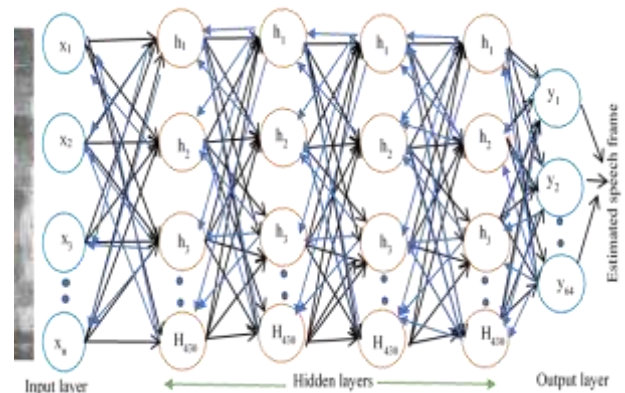


Fig. 2. DNN Architecture.



#### IV. RESULTS AND DISCUSSION

Fig. 3 shows the illustration of spectrograms for different target masks and reference of clean signal spectrogram. The speech utterance activity is represented by the yellow colour. The gammatone filter bank power (GF-PW) target mask suffered several speech components loss from the speech harmonics as shown in Fig. 3(a), which may lead to low intelligible compared to Fig. 3(d). Fig. 3(b) shows that Ideal binary mask (IBM) mask with GF-PW was better than the GF-PW, where the background noise that overlapped with speech event and some harmonics of speech components were removed. Moreover, higher residual noise was also introduced in Fig. 3(b).

Fig. 3(c) shows that the proposed target mask for DNN algorithm, cWF with GF-PW did not fully eradicate the background noise that overlapped with speech event at the band frequency of 0 to 4 kHz. As a result, loss of useful speech components from excessive noise elimination could be avoided. The STOI and PESQ scores for the three target masks in seen noise conditions at  $-5$  dB babble noise of SNR, are illustrated in Fig. 4. Target mask B (IBM + GF-PW) performed better with the STOI score of 0.2 higher than that of Target mask A (GF-PW) at  $-5$  dB of SNR for babble noise. This is because, Target mask B was constructed to retain time-frequency (T-F) units when the estimated speech is stronger than disturbing noise when SNR is greater than local criterion (LC) of  $-5$  dB and remove the T-F units when disturbing noise is dominant when SNR less than LC. Meanwhile, Target mask A applied gammatone filter bank power in clean speech signal without prior noise signal information. Next, the proposed Target mask C (cWF+GF-PW) also performed better than the other two target masks. However, only a small STOI score difference was recorded between the highest STOI score for  $-5$  dB babble noise by Target mask C compared to that of Target masks B and A.

Although Target mask A obtained worse STOI scores than either Target mask B or C, the PESQ scores were better than those of Target mask B. Hence, the proposed Target mask C provided a promising result in PESQ and STOI scores. For example, at babble noise condition, Target mask C obtained the highest PESQ scores of 1.17 for  $-5$  SNR. Therefore, it shows that Target mask B tends to improve speech intelligibility but not speech quality, while Target mask A tends to improve speech quality but not speech intelligibility. In short, Target mask C prediction in DNN-based mask estimation approach seems to be especially beneficial on improving speech quality and speech intelligibility. Furthermore, the difference in performance between the three training targets also reduced when the SNR reduced. This is because, noise signal is more dominant compared to speech signal that may lead to complexity to be predicted.

Fig. 5 shows the spectrogram of enhanced speech with different speech enhancement algorithms: DNN algorithm, HRNR algorithm, DNN+HRNR algorithm and log-MMSE algorithm. The speech utterance was corrupted by babble noise at  $-5$  dB SNR. Among the four spectrograms, the DNN+HRNR algorithm in Fig. 5(c) was outperformed, the residual noise was reduced considerably without distorting the

speech signal. Fig. 5(b) and Fig. 5(d) show that some harmonics in the enhanced speech signals were eliminated by HRNR and Log-MMSE algorithms. Therefore, both algorithms are not suitable for noisy speech signals at low SNR values. This happened when the fix threshold is applied, it may lead to excessive speech distortion and less noise distortion.

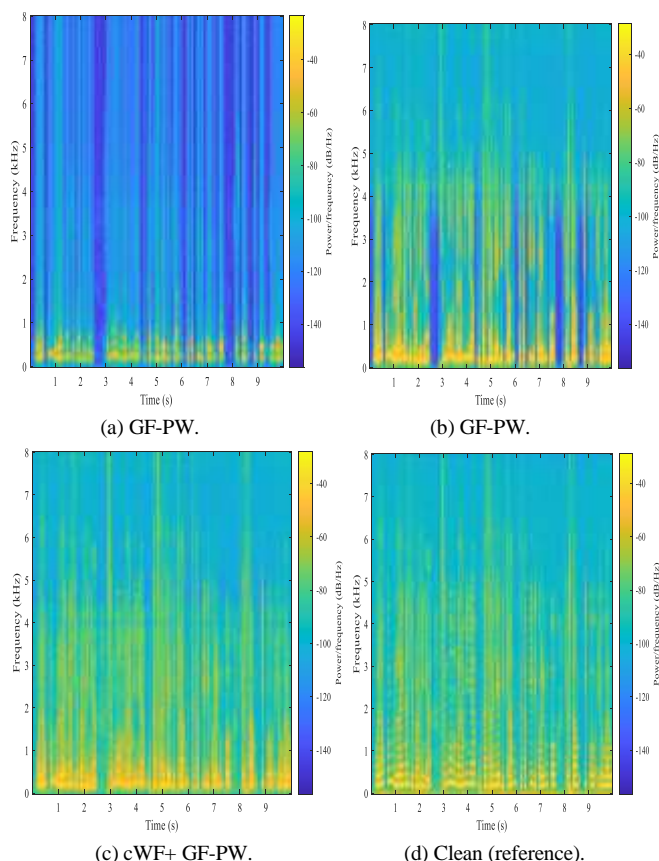


Fig. 3. Illustration of different Target Masks.

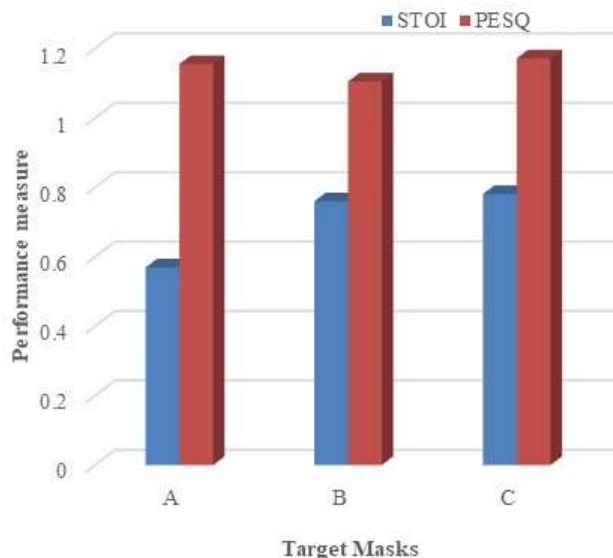


Fig. 4. STOI and PESQ Score for different Target Mask at  $-5$  dB Babble Noise SNR.

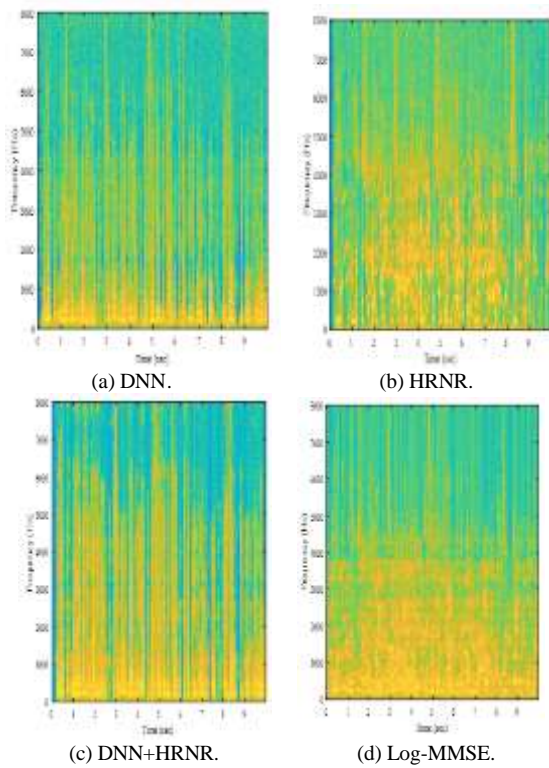


Fig. 5. Spectrogram of Enhanced Speech Signal with different Speech Enhancement Algorithms.

However, to achieve performance like the human speech perception after the DNN-based mask estimation remains a challenging task because the PESQ value was still below 2.0 during low SNR due to the introduction of residual noise after the speech reconstruction. It is supported by illustration of Fig. 6 when measuring the magnitude coherence between estimated and clean speech signal using Welch’s overlapped averaged periodogram method. The measured magnitude-squared coherence is a function of frequency with values between 0 and 1 by calculating the power spectral density correlation between estimated and clean speech signal. The values indicate the accuracy of speech signal estimation corresponds to clean speech signal at each frequency. It shows that higher correlation or cross power spectral density occurs after 4 kHz, while lower correlation or cross power spectral density occurs before 4 kHz due to the existence of residual noise.

The calculated STOI score of different algorithms at different SNR for long recorded speech signal length is shown in Fig. 7. The STOI score was slightly increased when the SNR value increased for different types of speech enhancement algorithms. DNN+HRNR improved the STOI score of DNN-based mask estimation approach by 0.01 at -10 and -5 dB SNR. The lowest STOI score was 0.2 at -10 dB SNR produced by the HRNR algorithm, followed by Log-MMSE algorithm, which is 0.35. Fig. 8 shows the calculated PESQ score of different algorithms at different SNR for long recorded speech signal length. The PESQ score at -10 and -5 SNR for DNN+HRNR and DNN did not improve significantly. PESQ is used to calculate distortion in speech signal. It is determined

that residual noise is remain issue in speech enhancement algorithm due to overlapping between noise and speech signal.

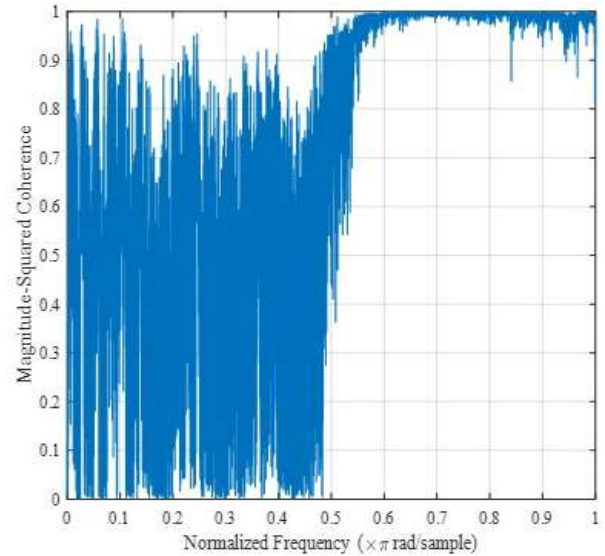


Fig. 6. Magnitude Coherence between Estimated and Clean Speech Signal.

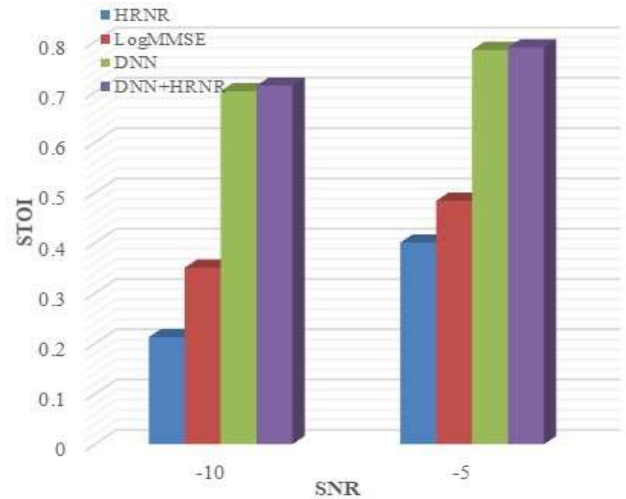


Fig. 7. Comparative STOI Score for different Speech Enhancement Algorithms and SNR Value.

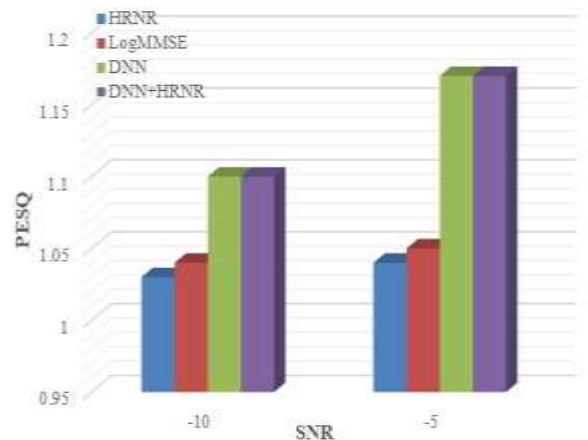


Fig. 8. PESQ Score for different Speech Enhancement Algorithms and SNR Value.

## V. CONCLUSION

In conclusion, a supervised speech enhancement algorithm using Deep Neural Network (DNN)-based mask estimation approach has developed and analysed accordingly. A hybrid algorithm between the DNN-based cWF mask estimation and HRNR algorithm has proposed to overcome the heavy non-stationary noise case and low signal to noise ratio (SNR), especially for babble noise at - 5 dB SNR. The proposed mask provided promising results in speech intelligibility due to high STOI score. Moreover, the proposed target mask outperformed other baseline target masks and the hybrid approach has compared to the conventional approach. To be more robust, network architectures such convolution neural network (CNN) and recurrent neural network (RNN) are recommended to be designed.

## ACKNOWLEDGMENT

Highly appreciation to Universiti Tun Hussein Onn Malaysia (UTHM) for funding this research work under GPPS (U712) and TIER1 (H268).

## REFERENCES

- [1] M. Wölfel and J. W. McDonough, Distant speech recognition. Wiley Online Library, 2009.
- [2] R. Yao, Z. Zeng, and P. Zhu, "A priori SNR estimation and noise estimation for speech enhancement," *EURASIP journal on advances in signal processing*, vol. 2016, no. 1, p. 101, 2016.
- [3] D. Wang and J. Chen, "Supervised speech separation based on deep learning: An overview," *IEEE/ACM Transactions on Audio, Speech, and Language Processing*, vol. 26, no. 10, pp. 1702-1726, 2018.
- [4] N. Saleem and M. I. Khattak, "A review of supervised learning algorithms for single channel speech enhancement," *International Journal of Speech Technology*, vol. 22, no. 4, pp. 1051-1075, 2019.
- [5] M. Kolbæk, Z.-H. Tan, and J. Jensen, "Speech intelligibility potential of general and specialized deep neural network based speech enhancement systems," *IEEE/ACM Transactions on Audio, Speech, and Language Processing*, vol. 25, no. 1, pp. 153-167, 2016.
- [6] H. Yu, W.-P. Zhu, Z. Ouyang, and B. Champagne, "A hybrid speech enhancement system with DNN based speech reconstruction and Kalman filtering," *Multimedia Tools and Applications*, pp. 1-21, 2020.
- [7] P. P. Ingale and S. L. Nalbalwar, "Deep neural network based speech enhancement using mono channel mask," *International Journal of Speech Technology*, vol. 22, no. 3, pp. 841-850, 2019.
- [8] X. Li, J. Li, and Y. Yan, "Ideal Ratio Mask Estimation Using Deep Neural Networks for Monaural Speech Segregation in Noisy Reverberant Conditions," in *Interspeech*, 2017, pp. 1203-1207.
- [9] A. Narayanan and D. Wang, "Ideal ratio mask estimation using deep neural networks for robust speech recognition," in *2013 IEEE International Conference on Acoustics, Speech and Signal Processing*, 2013, pp. 7092-7096: IEEE.
- [10] Y. Wang, A. Narayanan, and D. Wang, "On training targets for supervised speech separation," *IEEE/ACM transactions on audio, speech, and language processing*, vol. 22, no. 12, pp. 1849-1858, 2014.
- [11] Y. Wang and D. Wang, "Towards scaling up classification-based speech separation," *IEEE Transactions on Audio, Speech, and Language Processing*, vol. 21, no. 7, pp. 1381-1390, 2013.
- [12] J. Chen and D. Wang, "Dnn based mask estimation for supervised speech separation," in *Audio source separation*: Springer, 2018, pp. 207-235.
- [13] D. S. Williamson, Y. Wang, and D. Wang, "Complex ratio masking for monaural speech separation," *IEEE/ACM transactions on audio, speech, and language processing*, vol. 24, no. 3, pp. 483-492, 2015.
- [14] J. Chen, Y. Wang, and D. Wang, "A feature study for classification-based speech separation at low signal-to-noise ratios," *IEEE/ACM Transactions on Audio, Speech, and Language Processing*, vol. 22, no. 12, pp. 1993-2002, 2014.
- [15] Y. Wang, K. Han, and D. Wang, "Exploring monaural features for classification-based speech segregation," *IEEE Transactions on Audio, Speech, and Language Processing*, vol. 21, no. 2, pp. 270-279, 2012.
- [16] P. C. Loizou, *Speech enhancement: theory and practice*. CRC press, 2013.
- [17] N. Saleem, M. I. Khattak, and E. Perez, "Spectral Phase Estimation Based on Deep Neural Networks for Single Channel Speech Enhancement," *Journal of Communications Technology and Electronics*, vol. 64, no. 12, pp. 1372-1382, 2019.
- [18] H.-W. Tseng, M. Hong, and Z.-Q. Luo, "Combining sparse NMF with deep neural network: A new classification-based approach for speech enhancement," in *2015 IEEE International Conference on Acoustics, Speech and Signal Processing (ICASSP)*, 2015, pp. 2145-2149: IEEE.
- [19] R. Li, X. Sun, Y. Liu, D. Yang, and L. Dong, "Multi-resolution auditory cepstral coefficient and adaptive mask for speech enhancement with deep neural network," *EURASIP Journal on Advances in Signal Processing*, vol. 2019, no. 1, p. 22, 2019.
- [20] N. Saleem, M. Irfan Khattak, M. Y. Ali, and M. Shafi, "Deep neural network for supervised single-channel speech enhancement," *Archives of Acoustics*, vol. 44, 2019.
- [21] F. Bao and W. H. Abdulla, "Noise masking method based on an effective ratio mask estimation in Gammatone channels," *APSIPA Transactions on Signal and Information Processing*, vol. 7, 2018.
- [22] N. Zheng and X.-L. Zhang, "Phase-aware speech enhancement based on deep neural networks," *IEEE/ACM Transactions on Audio, Speech, and Language Processing*, vol. 27, no. 1, pp. 63-76, 2018.
- [23] H. Lang and J. Yang, "Speech Enhancement Based on Fusion of Both Magnitude/Phase-Aware Features and Targets," *Electronics*, vol. 9, no. 7, p. 1125, 2020.
- [24] Z. Huimin, J. Xupeng, and L. Dongmei, "An Iterative Post-processing Approach for Speech Enhancement," in *Proceedings of the 2019 4th International Conference on Multimedia Systems and Signal Processing*, 2019, pp. 130-134.
- [25] D. Yu, M. Kolbæk, Z.-H. Tan, and J. Jensen, "Permutation invariant training of deep models for speaker-independent multi-talker speech separation," in *2017 IEEE International Conference on Acoustics, Speech and Signal Processing (ICASSP)*, 2017, pp. 241-245: IEEE.
- [26] T.-P. Tan, X. Xiao, E. K. Tang, E. S. Chng, and H. Li, "MASS: A Malay language LVCSR corpus resource," in *2009 Oriental COCODA International Conference on Speech Database and Assessments*, 2009, pp. 25-30: IEEE.
- [27] B. Gao, W. L. Woo, and L. Khor, "Cochleagram-based audio pattern separation using two-dimensional non-negative matrix factorization with automatic sparsity adaptation," *The Journal of the Acoustical Society of America*, vol. 135, no. 3, pp. 1171-1185, 2014.
- [28] M. Russo, M. Stella, M. Sikora, and V. Pekić, "Robust cochlear-model-based speech recognition," *Computers*, vol. 8, no. 1, p. 5, 2019.
- [29] M. Parchami, W.-P. Zhu, B. Champagne, and E. Plourde, "Recent developments in speech enhancement in the short-time Fourier transform domain," *IEEE Circuits and Systems Magazine*, vol. 16, no. 3, pp. 45-77, 2016.
- [30] C. Plapous, C. Marro, and P. Scalart, "Improved signal-to-noise ratio estimation for speech enhancement," *IEEE Transactions on Audio, Speech, and Language Processing*, vol. 14, no. 6, pp. 2098-2108, 2006.

# Improving the Performance of Various Privacy Preserving Databases using Hybrid Geometric Data Perturbation Classification Model

Sk. Mohammed Gouse<sup>1</sup>, Dr.G.Krishna Mohan<sup>2</sup>  
Department of Computer Science and Engineering  
Koneru Lakshmaiah Education Foundation  
Vaddeswaram, 522502  
Andhra Pradesh, India

**Abstract**—As the size of the privacy preserving databases is increasing, it is difficult to improve the privacy and accuracy of these databases due to dimensionality and runtime. However, most of the traditional privacy preserving models are independent of privacy and runtime. Also, it is essential to preserve the privacy of the large sensitive attributes before publishing it to the third-party servers. As a result, a novel framework is required to improve the privacy as well as accuracy on the high dimensional privacy preserving data with less runtime. In order to improve the privacy, accuracy and runtime of the traditional privacy preserving models, a hybrid perturbation based privacy preserving classification model is proposed on the multiple databases. In this work, a new data transformation approach, hybrid geometrical perturbation approach and hybrid boosting classifier are proposed in order to enhance the overall efficiency of the model on the privacy preserving databases. In this work, a hybrid geometric perturbation approach is used to enhance the privacy preserving on the sensitive attributes. Initially, a pre-processing method is applied on the input dataset in order to remove the noise in the feature values. A hybrid machine learning classifier is proposed to predict the privacy preserving class label based on the training data. Experimental results represents the proposed hybrid geometric perturbation based boosting classifier has better statistical accuracy, recall, precision and runtime than the conventional models.

**Keywords**—Privacy preserving databases; machine learning; perturbation; high dimensionality; data filtering; data classification

## I. INTRODUCTION

Data mining focuses on the problem of discovering patterns that are unknown or hidden. It includes building data models, providing a human-comprehensible statistical summary of data, deciding strategies based on mined information [1]. Recently, researchers have drawn much attention to integrate utility constraints into data mining tasks. Utility mining is commonly used in many practical applications. A sensitive pattern is the repeated object with a sensitive information. The datasets used for data mining are represented in centralized or distributed way. In the centralized way, data are stored in the physical location, but that data accessibility / possession is involved. In the distributed manner, data are shared by two or more parties who do not really have trust in their personal information but

are interested in the extraction of their common data. The dataset can be heterogeneous, i.e. horizontally partitioned, if each group has the same set of records with various sub-sets of attributes. Centralized data is usually more complete than a portion of the distributed data, as it contains complete records and attributes for collecting and mining purposes. Many real-time applications, telecommunications networks, internet traffic flows, online banking and financial transactions, retail markets, manufacturing process data, sensor-based application data flows, satellite data, research laboratory data, electrical grids, engineering data, and other dynamic environments often use data mining tools and techniques. Data streams are enormous in volumes and possibly infinite. To recognize trends and patterns, these data streams need to be analysed, which benefit us in isolating anomalies and predicting future behaviour. However, due to some reasons, most notably privacy considerations, data proprietors or originators may not be willing to accurately discover the true values of their data. A certain amount of privacy preservation must therefore be done on the data before it can be made widely accessible. Data understanding is important and is combined with the need to use appropriate algorithms to preserve privacy. Various approaches such as data perturbation, k-anonymity, association rule mining, masking and encryption have been suggested for this purpose. It is not possible to apply existing techniques directly to data streams. In addition, robust assurances on the maximum permitted interval between incoming data and its anonymous output with minimum data losses and maximum privacy gain are required in data mining applications. Another approach to privacy preservation is to perform anonymization that ensures that the record of any individual in a dataset cannot be distinguished from a group of similar individuals. The availability of raw data is the most significant consideration in data mining privacy. For detailed statistical details about the data, the data miner should not be able to access all sensitive information into its original form. This calls for more rigorous data mining techniques, which will intentionally modify data in order to mask sensitive information and preserve the data statistics inherent in mining. The latest trend in corporate cooperation is that they want to exchange data and mining findings to help each other. Nevertheless, the disclosure of sensitive information also increased the potential threat. Sanitization of information is the process that covers the sensitive items in the source

database by appropriate modification and exposes the updated database [2]. In this work, they presented an efficient algorithm to maintain the privacy of high-value items from mining that extends our proposal to weighted utilities. The majority of data mining techniques that safeguard privacy turn original data into technologies or algorithms for data mining to decrease performance. There is also a common compromise between privacy and accuracy, but this compromise is endured by certain particular algorithms used for protecting privacy. Deep learning is a multi-layered data processing network that consists of multiple levels of abstraction to train the data for pattern analysis [3]. This network uses a non-linear transformation approach to transform and learn the data in each level. Recently, a large number of composite functions have been used in the deep learning framework for pattern analysis.

Data partitioning, there are two scenarios that require using of cluster analysis in a distributed way. In the first, the volume of data that is to be analysed is fairly great. Therefore, this requires a huge amount of computational effort—so much so, sometimes, it is not feasible to complete this computation. In such a case, a better alternative is to split the data and cluster it in a distributed manner and, finally, unify the distributed results. In centralized database, data will be located and maintained at single place where as in distributed database, data may be distributed vertically or horizontally to various sources. When the database is centralized, all the data is stored in one place. This type of database is completely different from the distributed database. One of the issues the centralized database faces is that as the entire data resides at one central location [4], there can be problems with bottlenecks occurring at key points where the data is released or assimilated.

Anonymity is "nameless." Anonymity is the identification of the information with their identity. Data anonymization is the process of removing personal information from the dataset to protect the privacy of individuals and allows data users and holders to safely reveal data for data analysis, decision making, testing and other purposes so that people whose information is in the dataset remain anonymous. Even if the specific identifiers are removed, the availability of individual's background information (e.g. in the public voter list) makes it easier for the adversary to re-identify individuals by linking the released data making it very hard to publish data without disclosing privacy [5]. Once the data is released to the third party, it is hard for the owners to control the way the data is manipulated.

K-anonymity protects privacy against the identification of records; however, it is not generally successful for protecting privacy against inference attacks of the sensitive attributes. k-anonymity is characterized as the degree of inference data protection. For example, a politician who intends to be elected to a post in the governance of a state utilizes the medical history of his opponent in demonstrating to the populace that his opponent cannot or is not ready to deal with the obligations as an agent of the state due to his medical problems. In the former scenario, l-diversity [6] fails to prevent attribute disclosure because the distribution for the real population is different from the dataset. K-anonymity is

designed for single data set where each row represents a different person. In case of relational database, k-anonymity might distort data too much or leak privacy. They proposed L-diversity to avoid attribute linkage attack. L-diversity demands that at least one responsive attribute value in each quasi identifier (QID) class [7]. This provision also satisfies the k-anonymity criterion where  $k= l$ . L-diversity varies from k-anonymity, while k-anonymity demands that a group contain at least k individuals with the same QID, l-diversity means that a group contain at least l of sensitive attributes.

L-diversity does not offer sufficient protection against probabilistic attack because some attributes appear more often than others [8]. In probabilistic, the sensitive attribute is inferred because it appears more frequently than other sensitive attributes and therefore attacker can infer that his victim must also have that value for the sensitive attribute. Isolating the sensitive attributes are considered as anonymous. The underlying principle here is isolation: if it cannot be isolated from its neighbours, a record is personal. In particular, when removed from the database, an opponent takes advantage of discovering the identity of the data. This is embedded in the breach of privacy that anonymizes a server. The attacker targets a server when entire data is accessed as a single large entity. If the selected data are removed from the server, the opponent cannot detect missing data and must change the attack strategy. Re-identification of individual records through quasi-identifiers is one of the major types of privacy outbreaks. Anonymization solves this type of attack. The idea behind k-anonymity is to suppress or generalize the publicly available selected data in order to make each record very similar from at least k-1 other records. Sensitive data can therefore be linked to collections of at least k size records. Quasi-identifier attribute values are a set of minimum values for the information attribute that can identify individuals in combination with other dataset. K-anonymity is intended to prevent the privacy of individuals without altering the attribute values. The traditional k-anonymity cannot be applied directly to the census data primarily for static dataset. The K-anonymity approach is the most widely used in PPDM while maintaining confidentiality.[9] proposed a K-anonymity approach by splitting the original dataset into data estimates, so that each one follows the K-anonymity. A classifier was trained on each projection and then an unknown instance was classified by combining all classifiers.

Perturbation is known for its long history, simplicity and effectiveness. It works by replacing original data with synthetic data which has similar statistical properties. Attacker cannot gain sensitive information from perturbed data because it does not correspond to original data. The downside of perturbation is that the data is meaningless for humans and it is only useful for computing statistical properties such as minimum, maximum, average, mean and so on. Additive noise is perturbation method that works by adding some random value to original value so that statistical properties of the original table would not differ too much from original ones. The downside of additive noise is that it does always offer sufficient protection to sensitive attribute. For example, when there is high correlation between QID and sensitive attribute and noise is low, the sensitive attribute's original value can be

covered from perturbed data [10]. The perturbation function requires a minor or major alteration of the problem-solving scenario to mathematically obtain the expected return. The perturbation functions were concerned with mathematical issues dealing with duality and primacy. The name of the function is appropriate for those which alter or trigger function changes at the start of the problem, and the function is twofold which is generally used to modify the limitations in order to obtain the desired solution. This contrasts with the previously proposed data mining strategies focused on additive random perturbation in order to show a significant breach of privacy. It also discusses the possibilities of proposed feature filtering techniques on various data types and interference approaches such as discrete and exclusive data or noise. Such data are widely available as statistical or categorical data. Numeric data are values that can be enumerated by categorical data. As the data of a database typically consists of ordered objects like tables and instances, the whole table or instance is not affected by the identity as a whole. The analyst or the miner is aware of the table or example but the information within the organizations are held privately. The sections or structural elements of the object are therefore chosen to cause randomization. In a database, each user typically comes up with a table consisting of multiple attributes where the user may pick the set of attributes for the query or where the attributes are appropriate for the query operations.

Increasing amounts of personal data collected and processed by companies also increases the complexity of information systems that protect information. Mainly, Privacy Preserving Data Mining (PPDM) problem focuses on two important aspects. Research's first facet: maintaining server confidentiality based on analysts' confidence rates and key attributes for their data mining queries. The second facet of analysis is to determine the level of sensitivity of the information disseminated from the database based on the queries of the analysts. In centralized database, data will be located and maintained at single place whereas in distributed database, data may be distributed vertically or horizontally to various sources. When the database is centralized, all the data is stored in one place. This type of database is completely different from the distributed database. One of the issues the centralized database faces is that as the entire data resides at one central location, there can be problems with bottle-necks occurring at key points where the data is released or assimilated. As a result, when looking for the availability of data, the efficiency with which it is retrieved is not as strong as in the distributed database system.

The rest of the paper is organized as follows. Section 2, describes the related works of the privacy preserving models and its limitations. Section 3, describes the proposed solution to the privacy preserving based machine learning framework on high dimensional data. Section 4, describes the experimental results and analysis. Finally, we conclude the paper in Section 5.

## II. RELATED WORKS

Privacy Preservation Data Mining (PPDM) is a data-protection research field focused on personally identifiable information that is considered for the creation of data-mining

information systems. Therefore, numerous efforts have been made to integrate data protection techniques with data mining algorithms. The current data storage technologies for data extraction are viewed in four dimensions: (i) data delivery (central or distributed); (ii) modification used (encryption, perturbation, generalization, etc.) to sanitize data; (iii) data mining algorithms optimized for the protection of privacy techniques; (iv) data mining techniques; This study incorporates techniques for noise generation that represent the sensitivity of the attributes and disturbance techniques. Data analysis, usually a realistic, multi-story business procedure, involves people using standardized methods to detect and analyse suitable problems, find approaches and techniques for implementation, and achieve measurable results. In general, information on privacy for data mining is taken as in tuples that contain several attributes. Each privacy data is scanned and transformed into normalized continuous data. The main issues of the privacy datasets are high dimensionality and imbalance nature. Traditional machine learning classifiers consider subset of features for classification and privacy prediction with high true negative rate and error rates. Attribute selection is used to compute the measure for each feature and rank them accordingly. These ranking methods select the top 'k' features based on highest rank and eliminate those having lower feature ranks.

The Privacy Preserving Data Mining (PPDM) problem in this traditional work concentrates on two important aspects. The first facet of the research: Assuring privacy of database based on the trust levels of the analysts and with respect to the key attributes for their data mining queries. The second facet of the research is to assess the sensitivity level of the information that is disseminated from the database based on the analysts' queries. The issue of utility-based privacy controlling data mining was reviewed in [11]. In [12], a technique for the suppression of anonymization of data. Disclosure top-down does not require a tree of taxonomy. The process begins with a set of deleted records and identifies the best specific candidate value that satisfies the privacy constraint for disclosure. The multidimensional k-anonymity is a multidimensional QID global recoding technique. In order to determine the optimum generalization, they consider Discernibility metric and Equivalence Class Size metric parameters. Multidimensional partitioning compared to single-dimensional partitioning to achieve the generalization error rate. The principle of t-closeness is that the distribution of sensitive values is as close to the distribution of sensitive values in the original data set in each equivalence class.

Support vector machine is an optimization technique for solving a variety of approaches such as classification, learning and outlier problems. The basic support vector machine (SVM) solves the two class problems, in which the data are partitioned by a hyper-plane using support vectors. If the support vector machine fails to separate two classes, then it solves this problem using a kernel function. Various kernel functions can be used in the SVM model such as linear, polynomial, Gaussian, regression, etc. to preserve the privacy on training dataset [13]. The author in [14] studied the utility-based problem of PPDM on large dataset. The idea was to extend the cursed dimensionality by distributing disjointed

matrices covering efficient attributes (Utility), but it is also challenging for privacy to be preserved. In Xu et al. proposed the use of local utility-based data mining method. The method is based on the fact that different attributes have varied utility from a software point of view. In local data partitioning, the data space is separated into many areas and the instance plotting to generalize value is local to that area. Another alternative way of using utility-based PPDM to anonymize data is that its residues beneficial to specific types of knowledge discovery process. This form of approach is frequently modelled with the k-anonymity framework and its derivatives: l-diversity, t-closeness, etc. Another popular model of privacy is that of  $\pi$ -differential privacy, which ensures that the addition or removal of data from a dataset results in a maximum change in any published information relative to  $\pi$  [15]. This ensures that a particular individual's presence or absence in the dataset has a limited impact on the information released, thus protecting the privacy of each individual. Data will be located and maintained at a single location in a centralized database, where data can be distributed vertically or horizontally to different sources, as in the distributed database. All data is stored in one place when the database is centralized. This database type is entirely different from the distributed database. One of the issues facing the centralized database is that since the entire data is located at one central location, bottle-neck problems can occur at key points where the data is released or published. As a result, the efficiency with which it is retrieved when searching for data availability is not as strong as in the distributed database system. Some of the traditional approaches, including k-anonymity, l-diversity, t-closeness and incognito, provide solutions to the problem of disclosure. They introduced a solution, namely, k-anonymity, which is considered a standard approach to dealing with the problem of linking attack. The anonymization-based study to protect individual privacy has become popular for the past decade. They conducted [16] a survey of U.S. census summary data to state the privacy risk of individuals.

### III. PROPOSED GEOMETRIC PERTURBATION BASED PRIVACY PRESERVING CLASSIFIER

In this proposed an advanced privacy preserving classification model is designed and implemented on the various datasets. Initially, each input data is pre-processing using the novel data filtering method. This transformation method is used to transform the numerical and nominal values and to fill the sparsity values on large datasets. After the data pre-processing step, a hybrid geometric perturbation method is developed to improve the classification rate on the filtered data. Finally, a novel boosting classification model is applied on the perturbation data for privacy preserving as shown in Fig. 1.

In this work, a hybrid data filtering method is designed and implemented on each PPDM input dataset. In the proposed data filtering method, each numerical attribute is normalized using the hybrid data transformation equation.

### Algorithm 1: Privacy preserving based data filter ( PPDF)

**Input:** PPDatasets PD={D1,D2...Dn}, Attributes List: AL  
 ,Max attribute value  $M_x$ , Minimum attribute value  $M_n$ .  
 Maximum attribute value:  $M_x(A)$ , Minimum Attribute value :  $M_n(A)$ ,  
 Mean of the attribute:  $\mu_A$ , Standard deviation of the attribute:  $\sigma_A$ .

1. Read input PPDM datasets D
2. To each dataset  $PD_i$
3. Do
4. To each attribute  $PD_{A[j]}$
5. Do
6. For each attribute value of  $PDV_{A[j][k]}$
7. Do
8. If ( $PD_{A[j]}$  is numerical attribute and NOTNULL)
9. Then
10. Transform  $PDA_{[j]}$  using the following eq .(1)
- 11.

$$PDV_{A[j][k]} = \frac{|PDV_{A[j][k]} - \max\{\mu_{PD_{A[j]}}, (M_x(PD_{A[j]}) - M_n(PD_{A[j]})) / \sigma_{PD_{A[j]}}\}|}{2 * (M_x(PD_{A[j]}) - M_n(PD_{A[j]}))} \quad \text{--(1)}$$

12. End if
13. If ( $PD_{A[j]}$  is nominal &&  $PD_{A[j]}$  is not null)
14. Then
15. Replace  $PDV_{A[j][k]}$  using the eq.(2)
- 16.

$$PDV_{A[j][k]} = \frac{\sum_{i=j, m=c} \Pr(PD_{A[j]} / c_m) \cdot \max\{\Pr(c_m)\}}{|c| \cdot \sigma_x \cdot \min\{\Pr(PD_{A[j]} / c_m)\}} \quad \text{-----(2)}$$

$i = 1..n; m = 1..c(\#classes)$

17. Done
18. Done
19. Done

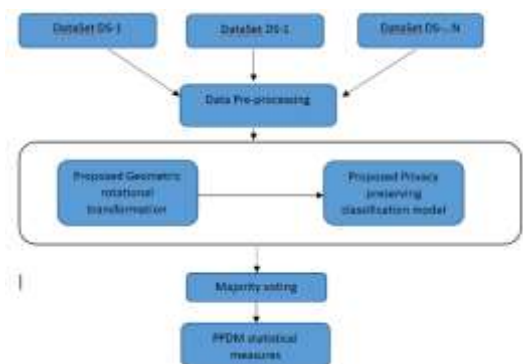


Fig. 1. Proposed Ensemble Deep Learning Framework for Privacy Preserving.

In the algorithm 1, each attribute of the input privacy preserving dataset is taken as input and transform the value using the equation 1 and 2. Initially, each attribute is tested for numerical data type or nominal type. If the attribute is numerical and it is not empty then each value in the attribute is transformed to new value by using eq.1. Similarly, if the attribute is nominal type then each value is estimated by using the maximization and minimization of its class probabilities.

**Algorithm 2: Geometric Homo Perturbation (Attribute A, Value V):**

- 1: Input: Transformed Sensitive attributes list S (AL).
- 2: Parameter initialization for homomorphic based attribute perturbation.

In the homomorphic based geometrical transformation, each attribute is perturbed using the additive and multiplicative transformation as given below.

$$: h \rightarrow h_0 = \begin{pmatrix} h_1 & h_2 \\ h_2 & h_1 \end{pmatrix}, \text{ where } h = h_1 + h_2$$

(1) The addition homomorphism holds since

$$h_0 + \bar{h}_0 = \begin{pmatrix} h_1 & h_2 \\ h_2 & h_1 \end{pmatrix} + \begin{pmatrix} \bar{h}_1 & \bar{h}_2 \\ \bar{h}_2 & \bar{h}_1 \end{pmatrix} = \begin{pmatrix} h_1 + \bar{h}_1 & h_2 + \bar{h}_2 \\ h_2 + \bar{h}_2 & h_1 + \bar{h}_1 \end{pmatrix}$$

(2) The subtraction homomorphism holds since

$$h_0 - \bar{h}_0 = \begin{pmatrix} h_1 & h_2 \\ h_2 & h_1 \end{pmatrix} - \begin{pmatrix} \bar{h}_1 & \bar{h}_2 \\ \bar{h}_2 & \bar{h}_1 \end{pmatrix} = \begin{pmatrix} h_1 - \bar{h}_1 & h_2 - \bar{h}_2 \\ h_2 - \bar{h}_2 & h_1 - \bar{h}_1 \end{pmatrix}$$

Then,  $h + \bar{h} = h_1$

(3) The multiplication  $+ h_2 - (\bar{h}_1 + \bar{h}_2) = (h_1 - \bar{h}_1) + (h_2 - \bar{h}_2) = (h_0 - \bar{h}_0)_{11} + (h_0 - \bar{h}_0)_{12}$ , Hence,  $\text{Dec}(C_0^*) = h - \bar{h}$ .

$$h_0 \cdot \bar{h}_0 = \begin{pmatrix} h_1 & h_2 \\ h_2 & h_1 \end{pmatrix} \cdot \begin{pmatrix} \bar{h}_1 & \bar{h}_2 \\ \bar{h}_2 & \bar{h}_1 \end{pmatrix}$$

Here,  $h_i, \bar{h}_j \in F$  are pairwise commutative. Furthermore,  $h = h_1 + h_2, \bar{h} = \bar{h}_1 + \bar{h}_2$  and  $m \cdot \bar{h} = (h_1 \bar{h}_1 + h_2 \bar{h}_2)$   
 $(h_1 \bar{h}_2 + h_2 \bar{h}_1) = (h_0 \cdot \bar{h}_0)_{11} + (h_0 \cdot \bar{h}_0)_{12}$ . Hence,  $\text{Dec}(C_0^*) = h\bar{h}$

The division homomorphism holds since

$$\bar{h}_0^{-1} = \begin{pmatrix} \bar{h}_1 & \bar{h}_2 \\ \bar{h}_2 & \bar{h}_1 \end{pmatrix}^{-1} = \frac{1}{(\bar{h}_1 - \bar{h}_2) \cdot (\bar{h}_1 + \bar{h}_2)} \cdot \begin{pmatrix} \bar{h}_1 & -\bar{h}_2 \\ -\bar{h}_2 & \bar{h}_1 \end{pmatrix}$$

and  $\bar{h}_1 + \bar{h}_2 = \bar{h}$  for  $\bar{h}_1 \neq \bar{h}_2$ . Therefore,

$$\begin{aligned} (\bar{h}_0^{-1})_{11} + (\bar{h}_0^{-1})_{12} &= \frac{1}{(\bar{h}_1 - \bar{h}_2) \cdot (\bar{h}_1 + \bar{h}_2)} \cdot \bar{h}_1 + \frac{1}{(\bar{h}_1 - \bar{h}_2) \cdot (\bar{h}_1 + \bar{h}_2)} \cdot (-\bar{h}_2) \\ &= \frac{\bar{h}_1 - \bar{h}_2}{(\bar{h}_1 - \bar{h}_2) \cdot (\bar{h}_1 + \bar{h}_2)} = \frac{1}{\bar{h}_1 + \bar{h}_2} = \frac{1}{\bar{h}} \end{aligned}$$

In the geometrical homomorphic perturbation, two keys are generated to each communication parties for data sharing and data re-construction process. The two keys public key and private keys are generated using the non-linear cyclic group elements.

Choose two cyclic group elements with prime orders  $k_1, k_2$ .

$\mu_A = \text{mean}$

$\eta_A = \text{VAR(AL)}; // \text{Variance}$

$$h_p = \text{gdf(AL)} = \frac{\eta_A^\alpha x^{\alpha-1} e^{-\eta_A x}}{\Gamma(\alpha)}, \text{ for } \eta_A, \alpha > 0$$

$$h_q = \log\left(\frac{\eta_A e^{-\eta_A (ALV[i]-\tau)}}{(1 + e^{-\eta_A (ALV[i]-\tau)})^2} * \text{gdf(AL).mean}\right)$$

$$n = h_p * h_q;$$

$$s = n * n;$$

Choose a random noise  $r_n \in (0, 1)$

$$\Psi = \frac{h_p \cdot h_q}{(n^{(h_p)} \text{mod}(r_n))^{(h_q)} \text{mod}(r_n)}$$

$$\theta = \Psi_A^{\text{gcd}(h_p, h_q, r_n)}$$

Step 3: Geometric attribute perturbation is given as

$$\text{GP}[] = \text{E(PB[]}]) =$$

$$r_n^{\text{ALV}[i]} \text{mod}(s) \cdot \theta^n \text{mod}(s) \cdot \text{mod}(s)$$

Step 4: Geometric data re-construction process is given as  $\text{D(CB[]}])$

$$h_1 = r_n^\theta \text{mod}(s) - \left(\frac{\theta}{n}\right)^{-1} \text{mod}(n)$$

$$\text{PB[]} = \text{GP}[i]^\theta \text{mod}(s) - \frac{\theta}{n} \cdot h_1 \text{mod}(n)$$

**Algorithm 3: Boosting Privacy Preserving Classification model**

In this algorithm, a hybrid privacy preserving based classification model is designed and implemented on the input datasets. This algorithm is used to check the performance of the privacy preserving model on the geometric perturbation data and the original data. Here, multiple boosting classifiers are integrated to improve the voting rate of the overall classification model. In this proposed classification model, a novel random tree and non-linear kernel function based multi-class SVM approach. In the boosting classification model KNN, random tree and non-linear kernel based SVM are used to improve the overall accuracy on the perturbation data.

**Algorithm: Boosting Privacy Preserving Classification model Random Tree**

1. To each input dataset PD
2. Do
3. Partition data into k number of classes and compute the best feature ranking measure using the following measure.



4. To each partition PFD
5. Do
6. For each attribute  $FD(A_i)$  in PFD
7. Do
8. 
$$\text{RandomTree Ranking Measure} = \text{RTRM}[FD(A_i), k] = \frac{-\text{Prob}(C_k) \cdot \sum \log(FD(A_i)) \cdot \text{Prob}(FD(A_i)/C_k)}{FD(A_i) \cdot \sqrt{\text{Entropy}(FD(A_i))}}$$
9. End for
10. Done
11. Done

### Non-linear SVM

Apply SVM multi-class optimization models as

$$\min_{W_k, a_k} \frac{1}{2} \|W_k\|_1^2 + \text{ker} \langle v, m \rangle \cdot \sum_{i=1}^n \exp(W_k) + \eta$$

s.t

$$W_k^T D_i + b_k \geq 1 - \eta, \text{ if } m_i = k$$

$$W_k^T D_i + b_k \leq -1 + \eta, \text{ if } m_i \neq k$$

$$\eta > 0; m = 1 \dots \text{classes}$$

In the above multi-objective function, a new kernel function is defined to improve the performance of the privacy preserving classification model. Here kernel function  $\text{ker}(x, y)$  defines the  $v$  input values that are mapped to  $m$  dimensional space as:

$$F_0(v) = 1$$

$$F_1(v) = v$$

$$F_{k+1}(v) = 2vT_k(v) - T_{k-1}(v)$$

$$\text{Ker}(v, m) = \min \left\{ \frac{\sum_{i=0}^n T_i(v) T_i^T(m)}{\sqrt{a - vm}}, \frac{\sum_{i=0}^n T_i(x) T_i(m_j)}{\sqrt{1 - v_j m_j}} \right\} \times \prod_{i=1}^m \left( \cos \left( 2 \cdot \frac{v_j - m_j}{a} \right) \exp \left( -\frac{\|v - m\|^2}{2a^2} \right) \right)$$

To each pattern in the decision tree construction, rule type is considered as either left side or right side of the pattern for privacy preserving.

### IV. EXPERIMENTAL RESULTS

Experimental results are carried out in java environment with multiple privacy preserving datasets. In this experimental results, proposed privacy preserving model is simulated on original datasets and transformed datasets. Different statistical measures such as accuracy, recall, precision and runtime are computed on the different datasets. These statistical metrics are used to check the performance of the privacy preserving based model on the perturbation dataset. Here, all the sensitive features are perturbed in order to preserve the privacy on machine learning decision patterns. Experimental results are compared on different privacy preserving models such as geometric perturbation, rotational perturbation and PABIDOT.

Our models is tested on different datasets such as FRDS, WQDS, ELDS, LRDS taken from [16].

The proposed algorithm is applied on Bank Marketing dataset from UCI repository. The dataset contains 17 attributes and 45211 rows along with other datasets. The attributes in bank dataset are age(numeric), job(categorical), marital status(categorical), education(categorical), credit default(categorical), housing loan(categorical), personal loan(categorical), contact communication type (categorical), last contact month(categorical), contact day of month(categorical), duration (numeric), campaign (numeric), pdays (numeric), previous(numeric), pout come (categorical), client subscribed to term deposit(yes or no)(categorical).

Among the attributes of bank marketing dataset, 'client subscribed to term deposit' attribute is sensitive attribute. There are no identifier attributes to be removed from given dataset. Attributes age, job, marital status and education are considered as quasi identifiers. Age is numerical quasi identifier and job, marital status, education are categorical quasi identifiers. Various utility measurements are used to measure the usefulness of generalized data. Some are loss metrics, ambiguity metrics, differentiation in discernibility, KL, entropy-based loss of information, and so on. In this work, traditional model PABIDOT and other perturbation models are used to compare the proposed model on the input training data. These traditional models have issues on high dimensionality and sparsity problems.

Metric Loss (LM): LM is calculated for each tuple attribute. The value  $t[A]$  is widespread tox where  $t$  is tuple and  $A$  is categorical. Suppose the domain size of  $A$  is  $M$  and the number of values generalized tox and the value of  $t[A]$   $(M-1)/(A-1)$  is lost. Loss of attributes is calculated for all tuple  $t$  as average loss  $t[A]$ . LM is the sum of losses for each attribute for the dataset.

Discernability metric (DM): Each tuple in the database has a penalty based on the number of other tuples that cannot be distinguished from it. For a size  $n$  database, DM assigns  $n$  to each deleted tuple as a penalty. Penalty shall be the total number of tuples with the same quasi-identifier values for unrestrained tuples. Thus, if tuples are grouped by a quasi-identifier, the DM shall be defined as the total number of squared groups plus  $n$  times the number of deletes.

Metric ambiguity: This metric is highly suitable for the k-anonymity framework. AM calculates the number of tuples for every tuple  $t$ , generalized to tuple  $t^*$ , in the sanitized data domain. This is the ambiguity of  $t^*$ . The AM for sanitized data is an average ambiguity of all tuples in the sanitized dataset.

KL-Divergence: The original table is treated as a distribution probability  $p1$  to use KL-divergence.  $P1(t)$  is the tuple fraction equal to  $t$ . The sanitized data will also be converted to  $p2$  (possible ways to do this will be discussed). The KL-divergence among the two is the same as for  $p1(t) \log(p1(t)/p2(t))$ .

Table I illustrates the performance of the present proposed hybrid perturbation-based privacy preserving model to the traditional models on different training datasets. Here, the average of F-measure is computed on the training datasets. As

shown in the table, it is noted that the proposed geometric perturbation based boosting classifier has better F-measure than the traditional models.

Fig. 2 illustrates the performance of the present proposed hybrid perturbation-based privacy preserving model to the traditional models on different training datasets. Here, the average of recall measure is computed on the training datasets. As shown in the figure, it is noted that the proposed geometric perturbation based boosting classifier has better recall measure than the traditional models.

Fig. 3 illustrates the performance of the present proposed hybrid perturbation-based privacy preserving model to the traditional models on different training datasets. Here, the average of precision measure is computed on the training datasets. As shown in the figure, it is noted that the proposed geometric perturbation based boosting classifier has better precision measure than the traditional models.

Fig. 4 illustrates the performance of the present proposed hybrid perturbation-based privacy preserving model to the traditional models on different training datasets. Here, the average of accuracy measure is computed on the training datasets. As shown in the figure, it is noted that the proposed geometric perturbation based boosting classifier has better accuracy measure than the traditional models.

TABLE I. PERFORMANCE ANALYSIS OF HYBRID PERTURBATION BASED PRIVACY PRESERVING MODEL TO THE CONVENTIONAL MODELS USING STATISTICAL F-MEASURE

| TestData  | GP    | RP    | PABIDOT | ProposedGPBC |
|-----------|-------|-------|---------|--------------|
| Test(#1)  | 68.31 | 69.96 | 79      | 85.11        |
| Test(#2)  | 69.77 | 69.2  | 79.41   | 87.11        |
| Test(#3)  | 70.05 | 69.03 | 81.87   | 90.9         |
| Test(#4)  | 69.25 | 69.17 | 79.79   | 91.03        |
| Test(#5)  | 69.54 | 70.99 | 80.07   | 91.81        |
| Test(#6)  | 68.56 | 75.18 | 79.03   | 88.47        |
| Test(#7)  | 69.47 | 70.67 | 78.16   | 91.96        |
| Test(#8)  | 67.57 | 75.9  | 80.52   | 89.43        |
| Test(#9)  | 70.61 | 75.96 | 81.24   | 88.22        |
| Test(#10) | 67.63 | 73.58 | 81.6    | 87.55        |

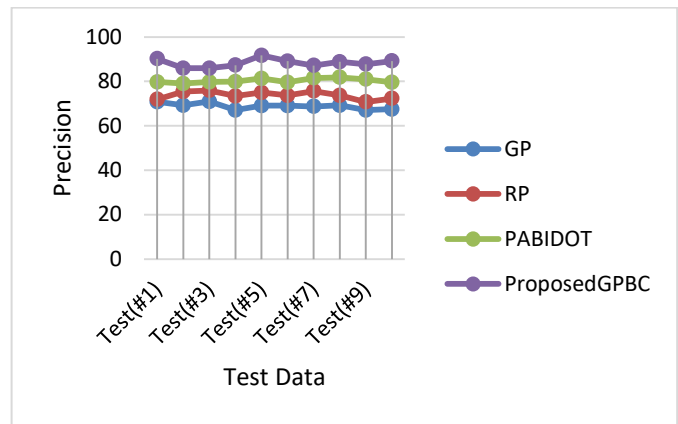


Fig. 3. Performance Analysis of Hybrid Perturbation based Privacy Preserving Model to the Conventional Models using Statistical Precision.

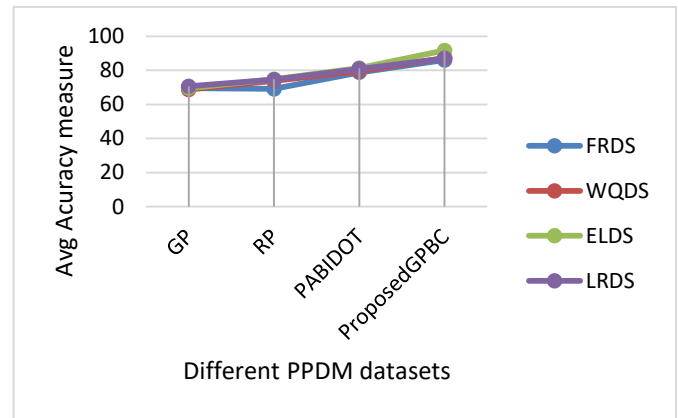


Fig. 4. Performance Analysis of Hybrid Perturbation based Privacy Preserving Model to the Conventional Models using Statistical Accuracy on different Datasets.

Fig. 5 illustrates the performance of the present proposed hybrid perturbation-based privacy preserving model to the traditional models on different training datasets. Here, the average of error rate measure is computed on the training datasets. As shown in the figure, it is noted that the proposed geometric perturbation based boosting classifier has better error rate than the traditional models.

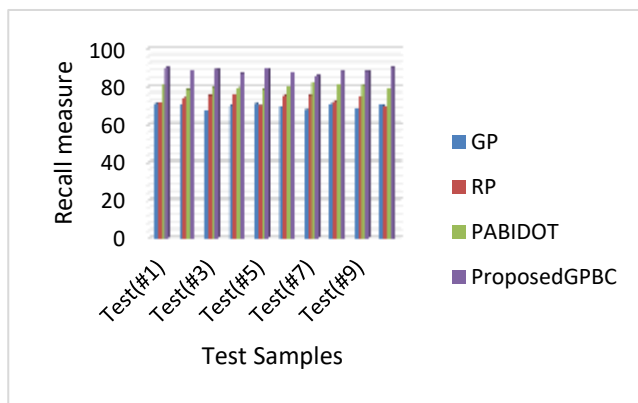


Fig. 2. Performance Analysis of Hybrid Perturbation based Privacy Preserving Model to the Conventional Models using Statistical Recall measure.

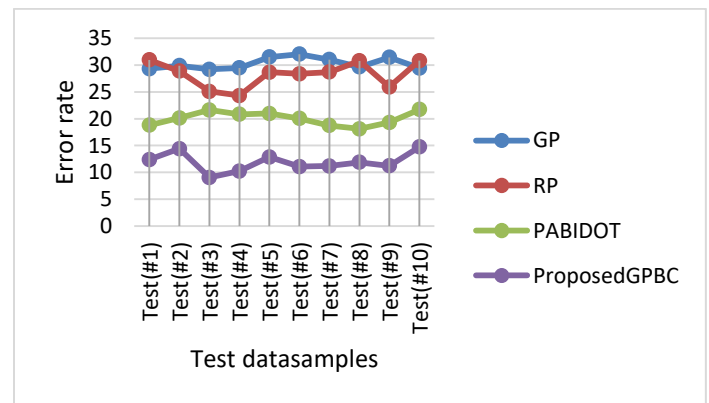


Fig. 5. Performance Analysis of Hybrid Perturbation based Privacy Preserving Model to the Conventional Models using Statistical Error Rate on different Datasets.

TABLE II. PERFORMANCE ANALYSIS OF HYBRID PERTURBATION BASED PRIVACY PRESERVING MODEL TO THE CONVENTIONAL MODELS USING STATISTICAL RUNTIME (MS) ON DIFFERENT DATASETS

| TestData  | GP   | RP   | PABIDOT | ProposedGPBC |
|-----------|------|------|---------|--------------|
| Test(#1)  | 4203 | 4853 | 3947    | 3138         |
| Test(#2)  | 4217 | 4376 | 3707    | 3052         |
| Test(#3)  | 4440 | 4183 | 4147    | 3106         |
| Test(#4)  | 4265 | 4792 | 4608    | 3247         |
| Test(#5)  | 3903 | 5164 | 4008    | 2894         |
| Test(#6)  | 3622 | 3826 | 5204    | 2910         |
| Test(#7)  | 4335 | 4257 | 4042    | 2921         |
| Test(#8)  | 4118 | 4633 | 5007    | 2880         |
| Test(#9)  | 4437 | 4906 | 3706    | 3092         |
| Test(#10) | 4000 | 4814 | 3691    | 2962         |

Table II illustrates the performance of the present proposed hybrid perturbation-based privacy preserving model to the traditional models on different training datasets. Here, the average of runtime (ms) measure is computed on the training datasets. As shown in the table, it is noted that the proposed geometric perturbation based boosting classifier has better runtime (ms) measure than the traditional models.

#### A. Results Analysis

A new privacy preserving data mining method is proposed. The proposed method is applied on various data sets and results were observed. The proposed method retains the classification accuracy while balancing data utility. Traditional approaches are limited to fixed sensitive attributes for privacy preserving. Also, these models are not appropriate on large data size. Also, the experimental results simulated on the perturbation anonymization bank data were improved by nearly 2% than the original data and nearly over 1% on the perturbation bank data. Experimental results suggested that the proposed geometric perturbation model achieves better efficiency in terms of high dimensionality and large data size than the conventional models.

### V. CONCLUSION

In this work, a novel filtered based privacy preserving model is designed and implemented on the different datasets. Since, most of the conventional privacy preserving models are depend on the data size and number of features, it is difficult to provide the privacy to a large number of attributes due to computational time and accuracy. Also, it is essential to preserve the privacy of the large sensitive attributes before publishing it to the third-party servers. As a result, a novel framework is required to improve the privacy as well as accuracy on the high dimensional privacy preserving data with less runtime. In this work, a filter-based hybrid privacy preserving model is designed and implemented on the different complex datasets in order to optimize the privacy preserving accuracy and the runtime. Experimental results proved that the proposed privacy preserving model has better efficiency on the different domain datasets compared to the conventional models. In the future work, this work can be extended to a cryptographic based perturbation method for big

datasets in order to minimize the error rate and to improve the privacy preserving policies.

#### REFERENCES

- [1] R. M. Alguliyev, R. M. Aliguliyev, and F. J. Abdullayeva, "Privacy-preserving deep learning algorithm for big personal data analysis," *Journal of Industrial Information Integration*, vol. 15, pp. 1–14, Sep. 2019, doi: 10.1016/j.jii.2019.07.002.
- [2] M. Amiri-Zarandi, R. A. Dara, and E. Fraser, "A survey of machine learning-based solutions to protect privacy in the Internet of Things," *Computers & Security*, vol. 96, p. 101921, Sep. 2020, doi: 10.1016/j.cose.2020.101921.
- [3] A. Boulemtafes, A. Derhab, and Y. Challal, "A review of privacy-preserving techniques for deep learning," *Neurocomputing*, vol. 384, pp. 21–45, Apr. 2020, doi: 10.1016/j.neucom.2019.11.041.
- [4] M. A. P. Chamikara, P. Bertok, I. Khalil, D. Liu, and S. Camtepe, "Privacy Preserving Face Recognition Utilizing Differential Privacy," *Computers & Security*, vol. 97, p. 101951, Oct. 2020, doi: 10.1016/j.cose.2020.101951.
- [5] Y. Chen, F. Luo, T. Li, T. Xiang, Z. Liu, and J. Li, "A training-integrity privacy-preserving federated learning scheme with trusted execution environment," *Information Sciences*, vol. 522, pp. 69–79, Jun. 2020, doi: 10.1016/j.ins.2020.02.037.
- [6] Y. Dong, X. Chen, L. Shen, and D. Wang, "EaSTFLy: Efficient and secure ternary federated learning," *Computers & Security*, vol. 94, p. 101824, Jul. 2020, doi: 10.1016/j.cose.2020.101824.
- [7] J. Duan, J. Zhou, and Y. Li, "Privacy-Preserving distributed deep learning based on secret sharing," *Information Sciences*, vol. 527, pp. 108–127, Jul. 2020, doi: 10.1016/j.ins.2020.03.074.
- [8] Y. Fan et al., "Privacy preserving based logistic regression on big data," *Journal of Network and Computer Applications*, p. 102769, Aug. 2020, doi: 10.1016/j.jnca.2020.102769.
- [9] C. Fang, Y. Guo, N. Wang, and A. Ju, "Highly efficient federated learning with strong privacy preservation in cloud computing," *Computers & Security*, vol. 96, p. 101889, Sep. 2020, doi: 10.1016/j.cose.2020.101889.
- [10] M. Gong, J. Feng, and Y. Xie, "Privacy-enhanced multi-party deep learning," *Neural Networks*, vol. 121, pp. 484–496, Jan. 2020, doi: 10.1016/j.neunet.2019.10.001.
- [11] M. Gong, K. Pan, Y. Xie, A. K. Qin, and Z. Tang, "Preserving differential privacy in deep neural networks with relevance-based adaptive noise imposition," *Neural Networks*, vol. 125, pp. 131–141, May 2020, doi: 10.1016/j.neunet.2020.02.001.
- [12] Z. Guan, Z. Lv, X. Du, L. Wu, and M. Guizani, "Achieving data utility-privacy tradeoff in Internet of Medical Things: A machine learning approach," *Future Generation Computer Systems*, vol. 98, pp. 60–68, Sep. 2019, doi: 10.1016/j.future.2019.01.058.
- [13] P. Li, T. Li, H. Ye, J. Li, X. Chen, and Y. Xiang, "Privacy-preserving machine learning with multiple data providers," *Future Generation Computer Systems*, vol. 87, pp. 341–350, Oct. 2018, doi: 10.1016/j.future.2018.04.076.
- [14] X. Li, Y. Gu, N. Dvornek, L. H. Staib, P. Ventola, and J. S. Duncan, "Multi-site fMRI analysis using privacy-preserving federated learning and domain adaptation: ABIDE results," *Medical Image Analysis*, vol. 65, p. 101765, Oct. 2020, doi: 10.1016/j.media.2020.101765.
- [15] Y. Liu, Z. Ma, Z. Yan, Z. Wang, X. Liu, and J. Ma, "Privacy-preserving federated k-means for proactive caching in next generation cellular networks," *Information Sciences*, vol. 521, pp. 14–31, Jun. 2020, doi: 10.1016/j.ins.2020.02.042.
- [16] M. A. P. Chamikara, P. Bertok, D. Liu, S. Camtepe, and I. Khalil, "Efficient privacy preservation of big data for accurate data mining," *Information Sciences*, vol. 527, pp. 420–443, Jul. 2020, doi: 10.1016/j.ins.2019.05.053.

AUTHORS' PROFILE



Shaik Mohammed Gouse research scholar. He obtained his Bachelors degree in Electronics From Acharya Nagarjuna University, M.C.A degree from Madurai Kamaraj U niversity, M.Tech ( CSE ) from Jawaharlal Nehru Technological University, Kakinada, He is currently pursuing Ph.D (CSE) degree with Department of Computer Science and Engineering Koneru Lakshmaiah Education Foundation, Vaddeswaram, 522502 Andhra Pradesh, India. His research interests lie in Bigdata Analytics, AI and Data science.



Dr. G. Krishna Mohan, working as Professor in the Department of Computer Science & Engineering, KL University. He obtained his M.C.A degree from Acharya Nagarjuna University, M.Tech(CSE) from Jawaharlal Nehru Technological University, Kakinada, Ph.D(CSE) from Acharya Nagarjuna University. Qualified, AP State Level Eligibility Test. His research interests lie in Data Mining and Software Engineering. He published 26 research papers in SCOPUS indexed, 45 research papers in various National and International journals. Editorial board member of SAS Publishers (Scholars Academic & Scientific Publishers) & SCIREA journal of computer. Reviewer of Australasian Journal of Information Systems & International Journal of Engineering &Technology. Authored three book chapters in Springer.

# High-Level Description of Robot Architecture

Sabah Al-Fedaghi<sup>1</sup>, Manar AlSaraf<sup>2</sup>  
Computer Engineering Department  
Kuwait University  
Kuwait

**Abstract**—Architectural Description (AD) is the backbone that facilitates the implementation and validation of robotic systems. In general, current high-level ADs reflect great variation and lead to various difficulties, including mixing ADs with implementation issues. They lack the qualities of being systematic and coherent, as well as lacking technical-related forms (e.g., icons of faces, computer screens). Additionally, a variety of languages exist for eliciting requirements, such as object-oriented analysis methods susceptible to inconsistency (e.g., those using multiple diagrams in UML and SysML). In this paper, we orient our research toward a more generic conceptualization of ADs in robotics. We apply a new modeling methodology, namely the Thing Machine (TM), to describe the architecture in robotic systems. The focus of such an application is on high-level specification, which is one important aspect for realizing the design and implementation in such systems. TM modeling can be utilized in documentation and communication and as the first step in the system’s design phase. Accordingly, sample robot architectures are re-expressed in terms of TM, thus developing (1) a static model that captures the robot’s atemporal aspects, (2) a dynamic model that identifies states, and (3) a behavioral model that specifies the chronology of events in the system. This result shows a viable approach in robot modeling that determines a robot system’s behavior through its static description.

**Keywords**—Conceptual model; robot architectural specification; robot behavior; static diagram; dynamism

## I. INTRODUCTION

Robotic systems are multifaceted and challenging. Thus, the robotic systems must interact with a dynamic environment to be reactive and flexible to unexpected changes. Such challenges require good frameworks and models that embody well-defined concepts to effectively manage this complexity. The use of a well-conceived architectural description (AD) can often help to manage that complexity [1]. An AD is a representation of a system, its structure, and associated behaviors, such as the AD languages UML and SysML [2].

An architectural model is the backbone that facilitates the description, implementation, and validation of robotic systems [3]. It is important for communication among stakeholders to provide a common language in which different concerns can be expressed, negotiated, and resolved at a level that is manageable even for complex systems [4]. Additionally, the architecture helps with recognizing constraints, dictating organizational structures, enabling a system’s quality attributes, managing changes, and providing the basis for training [4].

This paper applies a new modeling methodology, the thing machine (TM), for architecting robotic systems. The

focus of such an application is on a *high-level AD*, which is one important aspect of designing and implementing a robotic system [4]. The AD can be utilized in documentation and communication and as the first step in the system’s design.

## II. RELATED WORKS

Robot architecture is a subtopic of system architecture. Robot architecture is hardly recognized as an independent subject. For example, a search on “robot architecture” on Wikipedia produces the response, “The page ‘Robot architecture’ does not exist”; instead, several pages are given, such as “autonomous robot architecture” and “subsumption architecture.”

We outline here some of the many sources in the rich field of system architecture, starting with the types of structures in this field. England [2] lists 28 sample architectural domains, including conceptual architecture, computer (hardware) architecture, software architecture, communication architecture, technical architecture, and reference architecture. Architecture-related standards have been adopted to address lifecycle processes, activities, and tasks, such as the IEEE Standard Ontology for Robotics and Automation, IEEE/RS, INCOSE UK’s Practice of System Architecture (2014), and ISO/PAS 19450:2015 Automation Systems and Integration—Object-Process Methodology. A survey reported a list of 120+ AD languages, which are detailed in [2]. Because of space limitations, we focus on four representative samples of robot ADs.

An architecture comprises the high-level schema that show a system’s overall structure [4]. The term refers to “determining the needs of the user of a structure and then designing to meet those needs as effectively as possible within economic and technological constraints... The emphasis in architecture is upon the needs of the user, whereas in engineering the emphasis is upon the needs of the fabricator” [5]. The term architecture is used here to describe the conceptual structure and functional behavior, as distinct from the organization of the logical design and the physical implementation [6].

The Software Engineering Institute defines software architecture as a system’s structure, which includes system elements, their externally visible interfaces, and the relationships among them in the system [4]. Software architecture deals with an abstraction of a system, by defining how elements interact within this abstraction but not how individual elements are implemented [7]. According to Bass, Clements, and Kazman [4], there is “little difference” between software architecture and system architecture. The

architectural view is abstract, distilling implementation details and concentrating on the system elements' behavior and interactions [4]. Architecture prescribes a system's structure by accommodating combinations of both physical structure and functionality (utility) [2].

Coste-Maniere and Simmons [3] assert that the "architectural structure refers to how a system is divided into subsystems, and how those subsystems interact. This is often represented by the traditional 'boxes and arrows' diagrams." If there is no system architecture, the project should not proceed to full-scale system development [8]. According to Coste-Maniere and Simmons [3], a robot system often uses several architecture styles together, so it is sometimes difficult to determine exactly what architecture is used—to describe the robot's system—because the architecture and the implementation are often intimately tied together. Coste-Maniere and Simmons [3] continue, "This is unfortunate, as a well-conceived architecture can have many advantages in the specification, execution, and validation of robot systems."

To exemplify the types of robot AD, we show four representative cases. The purpose is not to give fair accounts of them, but to show the types of diagrams used for those cases for contrast with the TM diagrams developed later in the paper.

Loza-Matovelle, Verdugo, Zalama, and Gómez-García-Bermejo [9] developed a system that combines robots with a network of sensors and actuators, as illustrated in Fig. 1. Different devices are represented by heterogeneous icons such as a device, a face, a hand, and a telephone. Servers in the system are represented as circles or rounded rectangles. Snoswell et al. [10] presented a robot system architecture (Fig. 2) for a manipulator that grasps and completes tasks. The system is distributed across multiple computers. They tested this system architecture using the so-called MOVO mobile manipulation platform from Kinova Robotics.

As shown in Fig. 3, PatentSwarm [11] (in an invention) incorporates state machines into the robot AD. Note that these high-level ADs are static depictions that do not incorporate dynamic features or facilitate movement to the next level of development (i.e., design). This is an important point to consider when contrasting them with the proposed TM modeling.

The fourth type of AD lacks a holistic view of the robot system. According to Bass, Clements, and Kazman [4], architectural structures can be divided into three groups: module structures, component-and-connector structures, and allocation structures. Module-based structures include decomposition and use layers and classes or generalization. Component-and-connector structures include processes, concurrency, and the client-server structure. Finally, allocation structures include allocation and deployment. Bass, Clements, and Kazman [4] used many diagrams, such as UML diagrams, to describe different aspects of architecture. Fig. 4 shows a sample of these diagrams, called data flow architectural views.

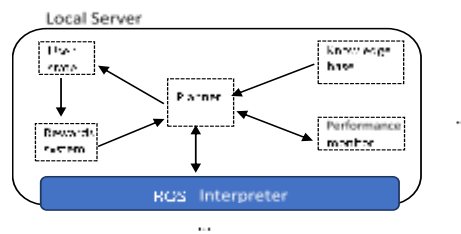


Fig. 1. Sample AD that Combines Robots with a Network of Sensors and Actuators (Adapted from [9]).

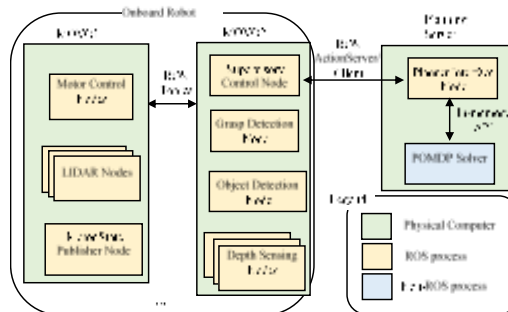


Fig. 2. Architecture for a Distributed Robot-Planning System (Adapted from [10]).

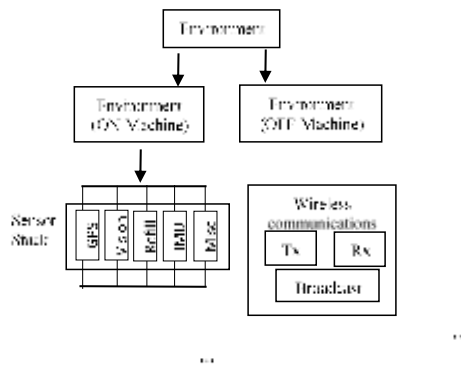


Fig. 3. A Schematic Illustration of an Embodiment of the Robot Control Architecture (Partially from [11]).

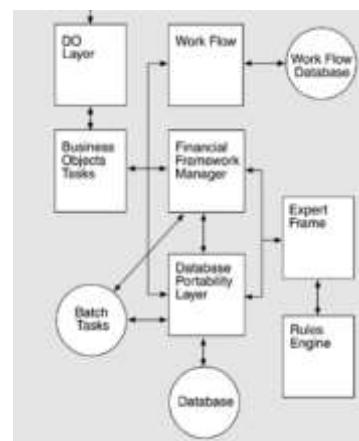


Fig. 4. Data Flow Architectural view (Partially from [4]).

### III. RESEARCH PROBLEM AND PROPOSED SOLUTION

The samples presented in the previous section demonstrate the need for an AD that reduces ambiguity and misunderstandings (e.g., via consistent model usage), manages complexity (e.g., via abstraction, with only the salient features presented), and affords assurance (i.e., correct interpretation) [2]. Bass, Clements, and Kazman's [4] representation of AD systems can be criticized as over-described when using a version of Occam's razor indicating that things should not be multiplied without necessity. In general, current architecture specifications might vary and lead to various difficulties, including mixing architectural specifications with implementation issues. Such descriptions lack the qualities of being systemic and coherent, as well as technical-related forms (vs. drawings of physical layouts and structural compositions in housing). Many system architectures use icons (e.g., faces, hands, computer screens) without a reasonable level of detail. Additionally, a variety of languages exist for eliciting requirements (e.g., object-oriented analyses use scenarios or "use cases" to embody requirements) and finite-state-machine models [4] that are susceptible to inconsistency (e.g., multiplicity of diagrams in UML and SysML). From the modeling point of view, such representations mix static modeling with dynamism that incorporates time. The difference between staticity and dynamism will become clearer when we discuss our method of modeling robot architecture.

On the other hand, for a robot architecture to be effective as the backbone of a project's design, the architecture's documentation should be informative, unambiguous, and readable by many people with various backgrounds [4]. We will show that our TM AD (called the static model, denoted by S) can be specified by a single ontological element called the thimac (things/machines). S is decomposed to produce sub-diagrams that can be converted to events by infusing a time element into the model. The events' chronology models the system's behavior.

Before applying TM to robot architecture specification, the next section provides a summary review of TMs. TM modeling is a promising modeling approach that has been applied in diverse areas such as designing unmanned aerial vehicles [12], documenting computer networks [13], modeling network architectures [14], modeling advanced persistent threats [15], modeling an IP phone communication system [16], and programming [17]. The TM model can also be used to model service-oriented systems [18], business systems [19], a tendering system [20], a robot's architectural structure [21], the VLSI engineering process [22], physical security [23], the privacy of the processing cycle for bank checks [24], a small company process [25], wastewater treatment controls [26], asset-management systems [27], IT processes using Microsoft Orchestrator [28], digital circuits [29], and automobile tracking systems [30].

### IV. THING MACHINE MODELING

According to the IEEE-RAS (Robotics and Autonomous Systems) working group on ontologies for robotics and automation, with the growing complexity of behaviors that robots are expected to perform, the need for well-defined

knowledge representation is becoming more evident [31]. In this context, ontologies are defined as "[consisting of] a formal conceptualization of the knowledge representation and [providing] the definitions of the concepts and relations capturing the knowledge of a domain in an interoperable way" [32]. Examples of such ontologies include those of Cheng et al. [33]: device (e.g., concepts such as that of a machine), process (e.g., operations performed by technical equipment), parametric (e.g., quality of service), and product ontologies (e.g., product information). Engel, Greiner, and Seifert [34] proposed ontologies for batch process plants that include operations, architectures, and general system characteristics and relations.

In this paper, we orient our research toward a more generic conceptualization of ontologies' role in robotics. An ontology is a crucial mechanism with which to model a robot system and its activities. A model refers to a conceptual description of a robot system and its processes. Developing such a model restrains and guides the robot system's design, development, and use. The issue, in this context, is a cross-area study between modeling and ontology in robotics. This paper provides a broad ontological foundation for conceptual modeling in the robotics domain by suggesting a practical ontology in terms of the notion of TMs. TM modeling uses a one-category ontology called a thimac in contrast to objects, attributes, and relations in the object-oriented paradigm. In philosophy, tropes are a well-known one-category ontology. According to Cheng et al. [32], "One-category ontologies are deeply appealing, because their ontological simplicity gives them an unmatched elegance and sparseness."

Let a thimac be denoted by  $\Delta$ ; then,  $\Delta = (M, T)$ , where  $\Delta$  has a dual mode of being: a machine denoted as M and a thing denoted by T. Fig. 5 shows a general form of TM modeling machines, and Fig. 6 is a simplification of Fig. 5. M includes generic actions described as follows. A sample of the two sides of a thimac will be given later.

The actions (also called stages) in M (Fig. 5) can be described as follows:

- Arrival: A thing reaches a new machine.
- Acceptance: A thing is allowed to enter the machine. If arriving things are always accepted, then arrival and acceptance can be combined into a "receiving" stage. For simplicity, we will assume that a receiving stage exists.
- Processing (alteration): A thing undergoes modifications without creating a new thing.
- Release: A thing is marked as ready to be transferred outside of the machine.
- Transference: A thing is input or output outside of or within the machine.
- Creation: A new thing is born (created) within a machine. Creation can designate bringing into existence (e.g.,  $\exists$  in logic) in the system because what exists is what is found. Creation in M indicates "there is" in the system, but not at any particular time.

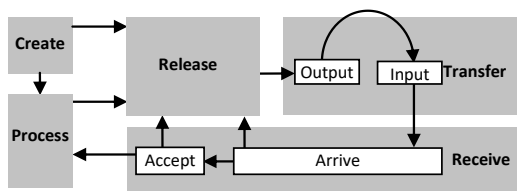


Fig. 5. The Thinging Machine, M.

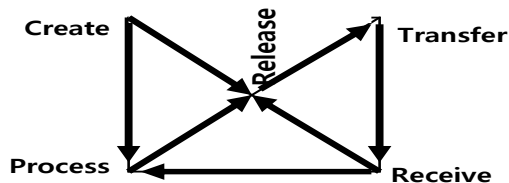


Fig. 6. Simplification of Machine, M.

The TM model also includes the notion of triggering, which connects two sub-diagrams between which there is no flow. Triggering is represented by dashed arrows in the TM diagram.

To informally justify the five TM actions, consider a robot's actions. The robot interacts with the environment either through inputting or outputting. Through its interface (transfer), it receives things (e.g., data or actions) and outputs (transfers) things (e.g., data or sound). Some of these output things might be "stocked" (released), waiting until the right time for output. Accordingly, the transfer, receive, and release actions are all types of interactions with the outside, which are usually referred to as sending data, receiving actions (e.g., physical hits), outputting movement (e.g., walking to a certain position), etc. Additionally, the robot might process incoming things such as converting a signal to data, analyzing a scene, inspecting a sound, and so on. It also could create (generate, produce) things such as a sound, movement, or plan. All activities can be specified in terms of the five actions—create, process, release, transfer, and receive—or a subset of these actions.

## V. EXAMPLE: A WINDOW-OPENING ROBOT

Cassinis [35] developed a robot that, when given the goal "open the window," could perform the following sequence of steps: (1) locate the window, (2) reach near the window, (3) locate the handle, (4) reach the handle, (5) turn the handle, and (6) pull the handle.

### A. The Static TM Model

Fig. 7 shows the TM model S of this window-opening task. We assume that the window's location is communicated by a sensor and that the handle position is recognized through a camera on the robot.

Upon being activated to open a window, the robot receives data about the window's location (circle 1 in the figure) and processes the data (2) to trigger (3) the window position's generation (4). The window position and robot's current position (5) both flow (6 and 7) to be processed (8), triggering (9) the creation of a description of the path to reach the window (10). This path flows (11) to the wheel control (12), where the path data are processed (13) to generate movement

(14) toward the window. Upon reaching the window (15), two triggering actions occur

- The robot's new location replaces its current location (16 and 17).
- The camera is turned on to search for the handle (18 and 19).

Upon collecting the data about the handle (20), the handle position is recognized and processed (21). Such a process triggers the creation (22) of the required trajectory to reach the handle (23), which flows (24) to the handle (25). There, the trajectory is processed (26) to trigger the handle's movement (27) to perform the following:

- Turning the handle (28) and
- Pulling it (29).

Note that TMs are applied uniformly for all types of things: data, processes, wheels, handles, camera, movement, pulling, and turning. Every machine is constructed from the create, process, release, transfer, and receive actions, or from a subset of these actions. Model S is richer than the so-called ADs; however, if we are interested in the system in terms of its components and their relations, then these can be extracted from S by eliminating the actions, as shown in Fig. 8. Every component in Fig. 8 is a thimac. To illustrate the notion of thimac, Fig. 9 shows the window-opening robot as a thimac. It is a machine and a thing simultaneously. For example, as a thing, it can include its physical attributes, manufacturer, etc., as in the case of a class's attributes in the object-oriented model. In addition, as a thing, it can be shipped, cleaned, etc.

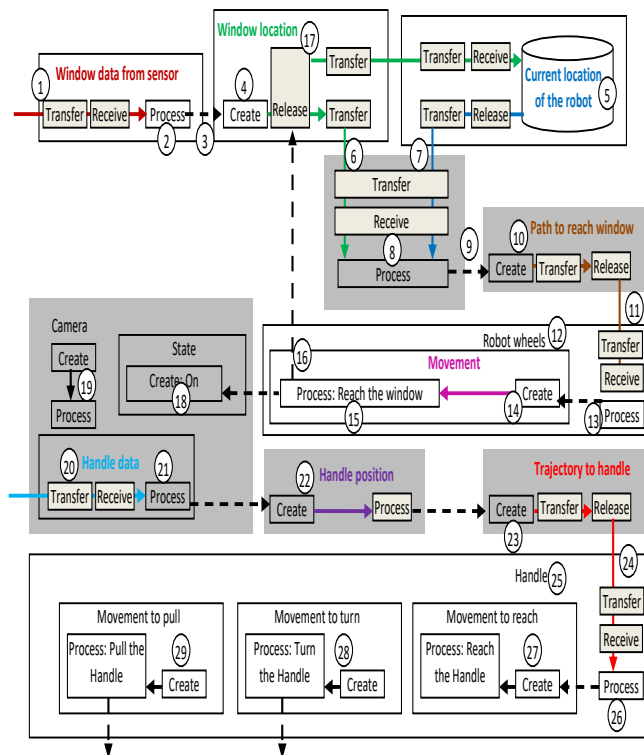


Fig. 7. Static TM Model, S.



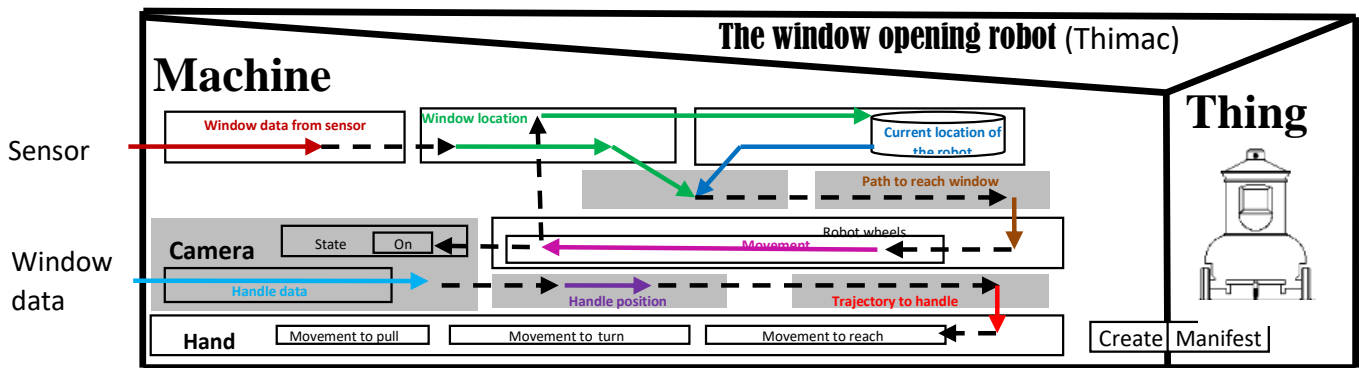


Fig. 8. The Window-Opening Robot as Components and their Relationships.

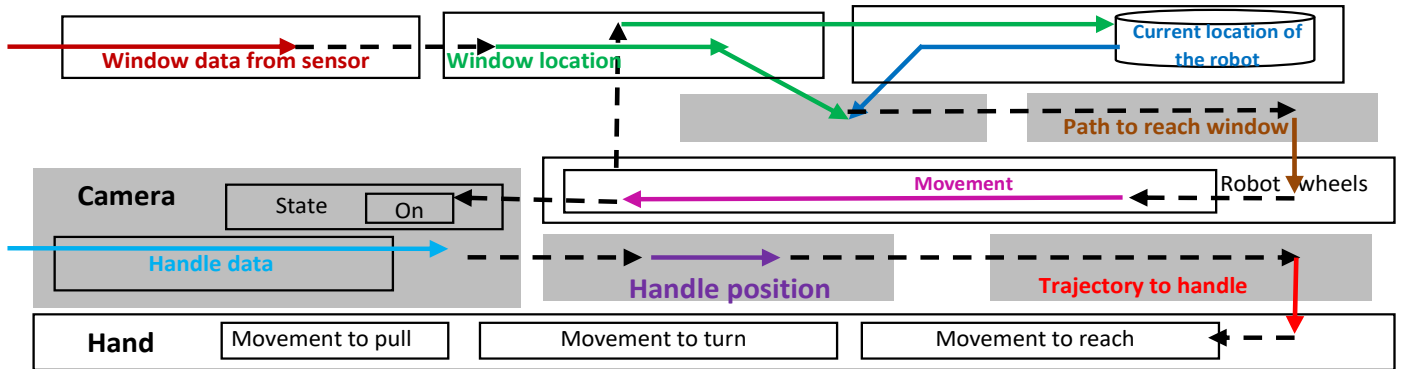


Fig. 9. The Window-Opening Robot as a Thimac.

Alternatively, if we want to go in the opposite direction into the model's fine details, we can apply the same TM machine to the subthimacs. Suppose that we add an obstacle in the path to the window. Fig. 10 shows the needed modifications to the original model S (Fig. 7).

The modification starts in the wheels machine, where the original path to the window (circle 1) reaches the wheels' controller to be processed (2), triggering a movement (3) to reach the window (4). Suppose the movement instead meets an obstacle (5), which triggers (6) a warning. The warning flows (7) to a control module, which processes it (8) to trigger, (a) activating a camera on the robot (9) and (b) saving the current path in storage (10 and 11) to continue later after overcoming the obstacle.

The camera data (12) are analyzed (13) to trigger the creation of a new path (14). The new path flows to the wheels system (15), where it is processed to create movement. After the obstacle is overcome (16), the path to the window is restored (17).

**B. The Dynamic Model**

S is a machine schema that can be decomposed to generate a new organizational level (multiplicity) from the "meaningful" parts of S. Model S (Fig. 7) is a static description that represents a still or resting (no time) condition. The meaningfulness of a part of S resides in the isomorphism between the part and the thing it is supposed to represent (in the modeler's conceptual framework).

Decomposition is necessary because the system described by S is clearly "activated" behaviorally, piece by piece (sub-diagrams). Fig. 11 shows a selected division of S for the robot system in 15 static changes. The robot's dynamism originates from conceptually dividing it as a whole and replacing it with its 15 sub-diagrams, which then become viewed as events by injecting a time sub-machine into each of them. For example, the event Replace the old robot location with the current location is modeled as shown in Fig. 12. The chronology of events is shown in Fig. 13.

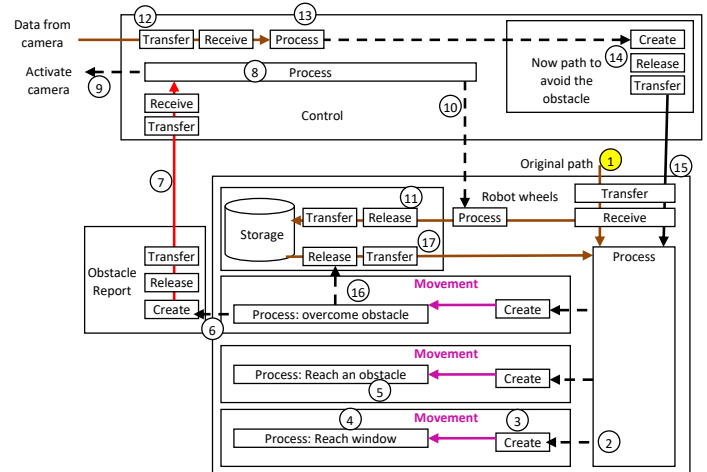


Fig. 10. Adding an Obstacle to the Window-Opening Robot.

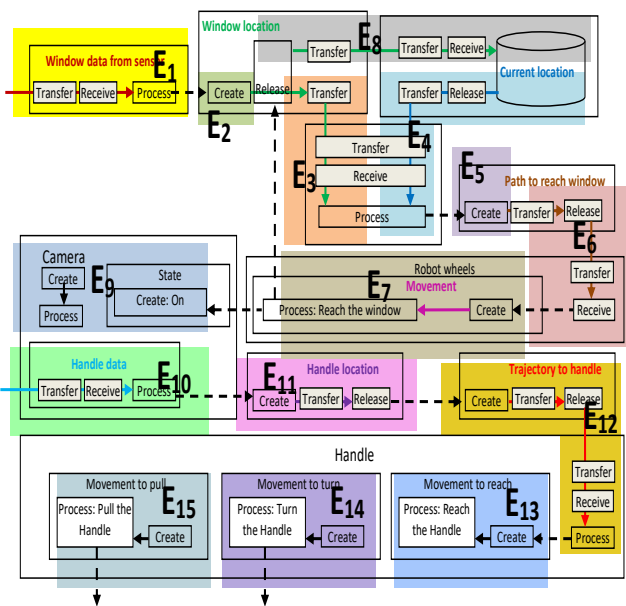


Fig. 11. Dividing the Static Model into Parts.

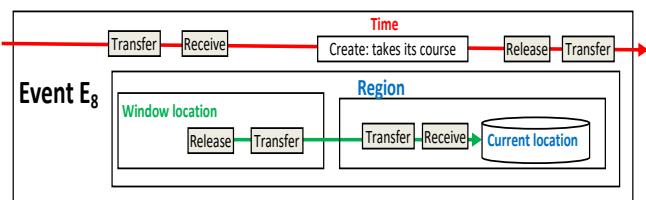


Fig. 12. Event E8.

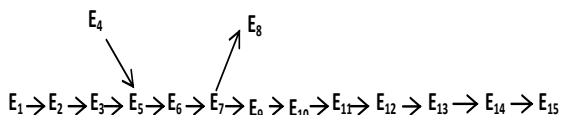


Fig. 13. The Window-Opening Robot's behavior in Terms of the Chronology of Events.

## VI. CASE STUDY

For our study, without loss of generality, we selected one architectural description for a robot called the NAO robot, the first autonomous, programmable humanoid robot created by SoftBank Group. It is an effective programming tool used in education and research. In addition, companies and health care centers might use it to welcome, inform, and entertain visitors [36]. NAO's documentation and user guide show how to start the robot and describe the result of turning the robot ON. In addition, they describe what happens when someone approaches the robot [37]. Furthermore, the robot's actions can be created and modified using the Choregraphe software. Choregraphe is a multiplatform desktop application that allows users to create animations and dialogues for robots. It also permits users to monitor and control the robot [36]. In addition, Fig. 14 and 15 show the general architecture of interacting with the robot using Choregraphe software and Microsoft Azure, respectively [38]. Microsoft Azure is a continuously expanding cloud-computing service that allows users to build, manage, and deploy applications on a global

network using their preferred tools and frameworks [39]. Our case study involves combining NAO's manual switching/approaching of the robot with the architecture in Fig. 14 and 15. The result is demonstrated using a TM model to obtain an A-to-Z architecture of the robot.

The basic description of a user interacting with the robot is described below [38]:

- 1) Check the Internet connection.
- 2) Notify the users if NAO is in online mode.
- 3) Start speech recognition; by default, NAO will record a sound file when speech is detected.
- 4) The file path of the recorded sound clip will be sent to the Bing Speech API to extract text.
- 5) The text will then be sent to Azure Function to process the response.
- 6) In Azure Function, first, we will analyze the sentiment of the input, which will trigger a negative response (e.g., "Please don't scold me") when it detects that the users are upset.
- 7) If not, it will call QnA Maker API to obtain a response.
- 8) If an answer is found, then Azure Function will output the response. Otherwise, it will be recorded in Table Storage for admin to update.
- 9) Both the input and output are archived in Table Storage for validation.
- 10) Keywords in the responses from Azure Function will trigger specific movements.
- 11) Repeat step 3.
- 12) At any point in time, if the head is tapped, it will stop the conversation [38].

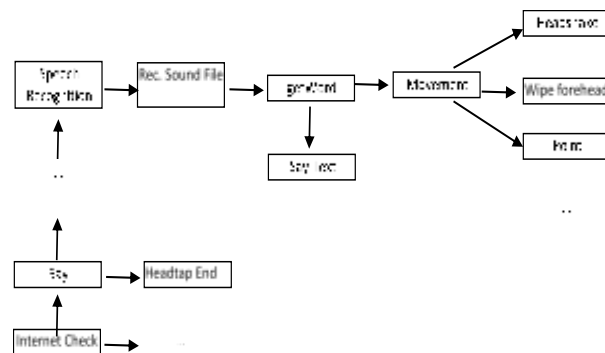


Fig. 14. An Overall Architecture of NAO Robot using Choregraphe (Partially from [38]).

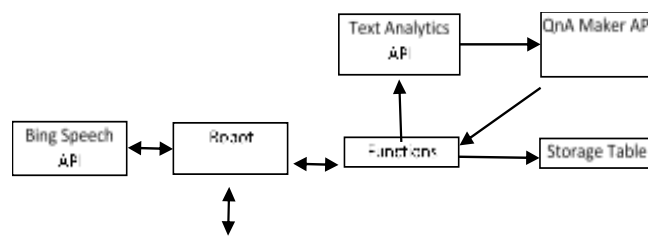


Fig. 15. An Overall Architecture using Azure (Partially from [38]).

### A. TM Static Model

The robot consists of four parts: the sensors, the controller, the microphone, and the physical parts of the robot (head and body).

- Through the sensors, the user generates a signal (circle 1) that flows (2) to the robot to trigger the robot's state to be ON (3). Switching the robot ON triggers two actions: The LEDs are switched ON (4), and sound is created (5).
- When the LEDs are switched ON, the black-and-white light module creates (6) blinking, and a process (7) takes its course, changing color from black to white.
- Continuing at circle (5), a greeting sound is generated (8).
- Approaching the robot: A talking distance (assuming a maximum of 1.5 meters) is assumed to be initialized for the first time using the robot (9). When the user walks within this distance (10), a current distance is created (11) by the sensor, and its value flows (12) to the controller, where it is processed (13) to trigger (14) creation of the navy color (15) on the LEDs.
- Interacting with the robot: Once the user speaks (16—bottom-left corner of the figure), this act is detected (17) by the sensors and processed (18) to create (19) digital data from the analog sound. The digital data flow to the controller, where the data are processed to be recorded (20) and stored (21). Later, the stored data are retrieved and extracted as text (22) to create (23) sound clips. The sound clip is processed (24) to create (identify) its function (as a question or order).
- If the function is a question (25), it flows to be processed (26) such that:
  - The question is compared with the questions stored in the database.
    - (i) If the question is found, the answer is retrieved (27) and flows to the microphone (28) to be processed (29). Accordingly, the corresponding speech is created (30).
    - (ii) Otherwise, the question is stored in a database for validation (31).
- If the function is an order (32), the order flows to the physical head and body (33) to be processed (34). Based on the type of order, a physical action is performed as follows:
  - I. Head shaking (35),
  - II. Wiping forehead (36), or
  - III. Pointing (37) in a certain direction.
- Interruption: At any moment, the user can tap the robot's head (38—bottom left), which generates a signal (39) from the tactile head sensors that flows (40) to the microphone. The signal is processed (41) to trigger stopping of the speech (42).

Fig. 16 shows the TM model of the NAO robot's architecture.

### B. The Dynamic Model

The decomposition of the S model forms the foundation upon which to understand events. The resulting parts of S should be sufficiently "meaningful." The meaningfulness of a part of S resides in the isomorphism between the part and the thing it is supposed to represent (in the modeler's conceptual framework). For example, "release" by itself as a sub-diagram does not seem to have this meaningfulness, but "release, transfer, transfer, and receive" is an ideal whole/part because it corresponds to the familiar notion of "moving from to" The resulting TM states (parts of S) are altered by inducing time (the time subthimac) to be transformed into events.

To construct the dynamic model, we identify the following events (see Fig. 17):

Event 1 ( $E_1$ ): The user presses the start button and creates a signal through the sensors.

Event 2 ( $E_2$ ): The signal triggers the robot to be switched ON, which causes (i) the LEDs to blink, (ii) a greeting sound, and (iii) initialization of the talking distance.

Event 3 ( $E_3$ ): The user approaches the robot within 1.5 m, which triggers creation of the current approaching distance.

Event 4 ( $E_4$ ): The current distance flows to the controller.

Event 5 ( $E_5$ ): The controller processes the current distance, and the LED light changes to navy.

Event 6 ( $E_6$ ): The user speaks, which is received by the sensor.

Event 7 ( $E_7$ ): The analog sound is processed and converted to digital data.

Event 8 ( $E_8$ ): The digital data are released to the controller, where the data are stored.

Event 9 ( $E_9$ ): The digital data are retrieved and extracted as text, then processed to create sound clips.

Event 10 ( $E_{10}$ ): The sound clips are processed to trigger creation (identification) of the function.

Event 11 ( $E_{11}$ ): The function is processed to distinguish a question from an order.

Event 12 ( $E_{12}$ ): The function is a question, which is sent to the Q&A module.

Event 13 ( $E_{13}$ ): The answer to the question is sent to the microphone.

Event 14 ( $E_{14}$ ): The answer cannot be found; hence, it is stored.

Event 15 ( $E_{15}$ ): The function is an order; hence, it is sent to the control of the physical body and head.

Event 16 ( $E_{16}$ ): The order is processed.

Event 17 ( $E_{17}$ ): The order is for the robot to shake its head.

Event 18 ( $E_{18}$ ): The order is for the robot to wipe its forehead.

Event 19 ( $E_{19}$ ): The order is for the robot to point.

Event 20 ( $E_{20}$ ): The user taps the robot's head, creating a signal that is received by the microphone, thus stopping the sound.

Lastly, the robot's behavior can be specified by the chronology of events shown in Fig. 18.

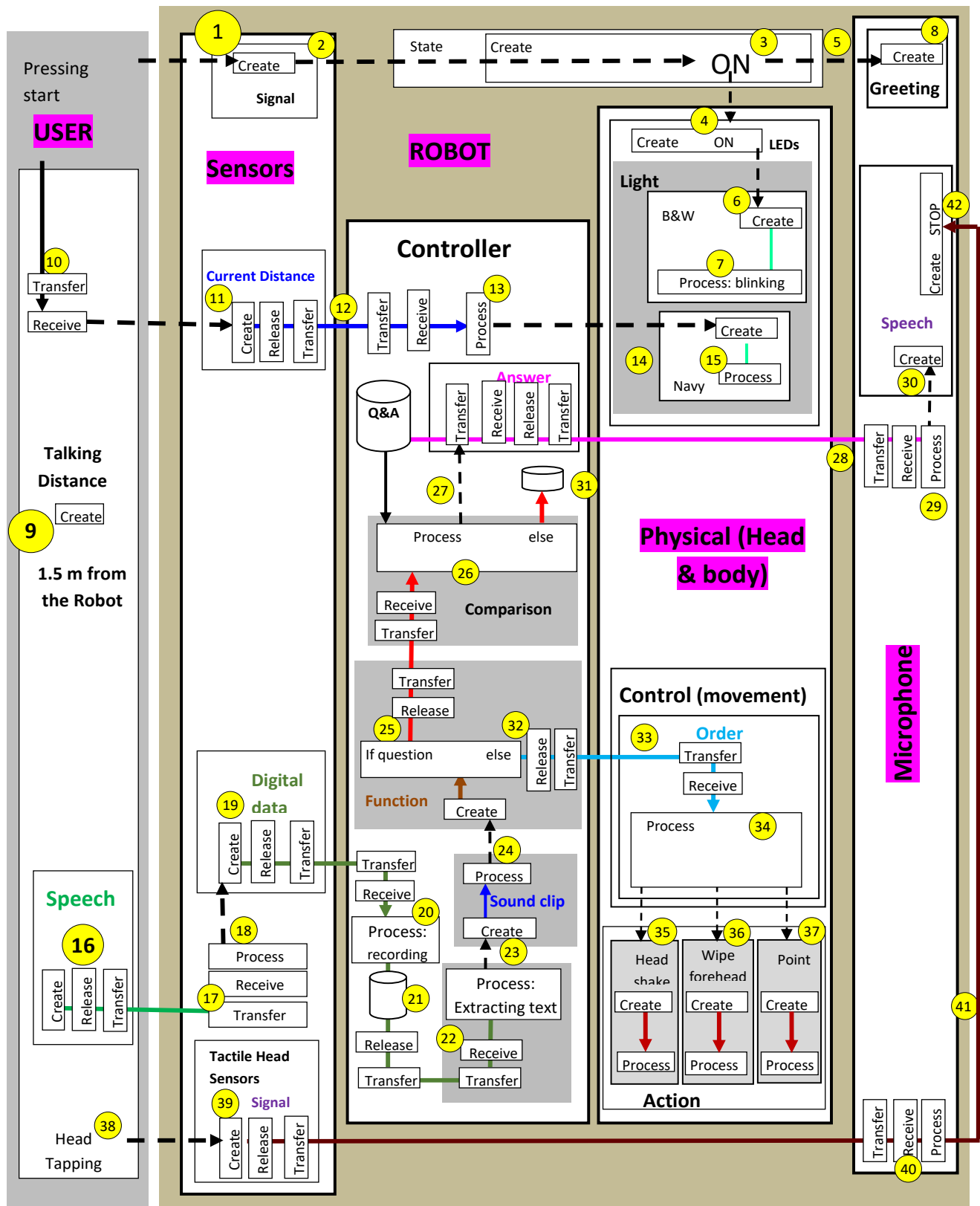


Fig. 16. TM Model of the NAO Robot's Architecture.

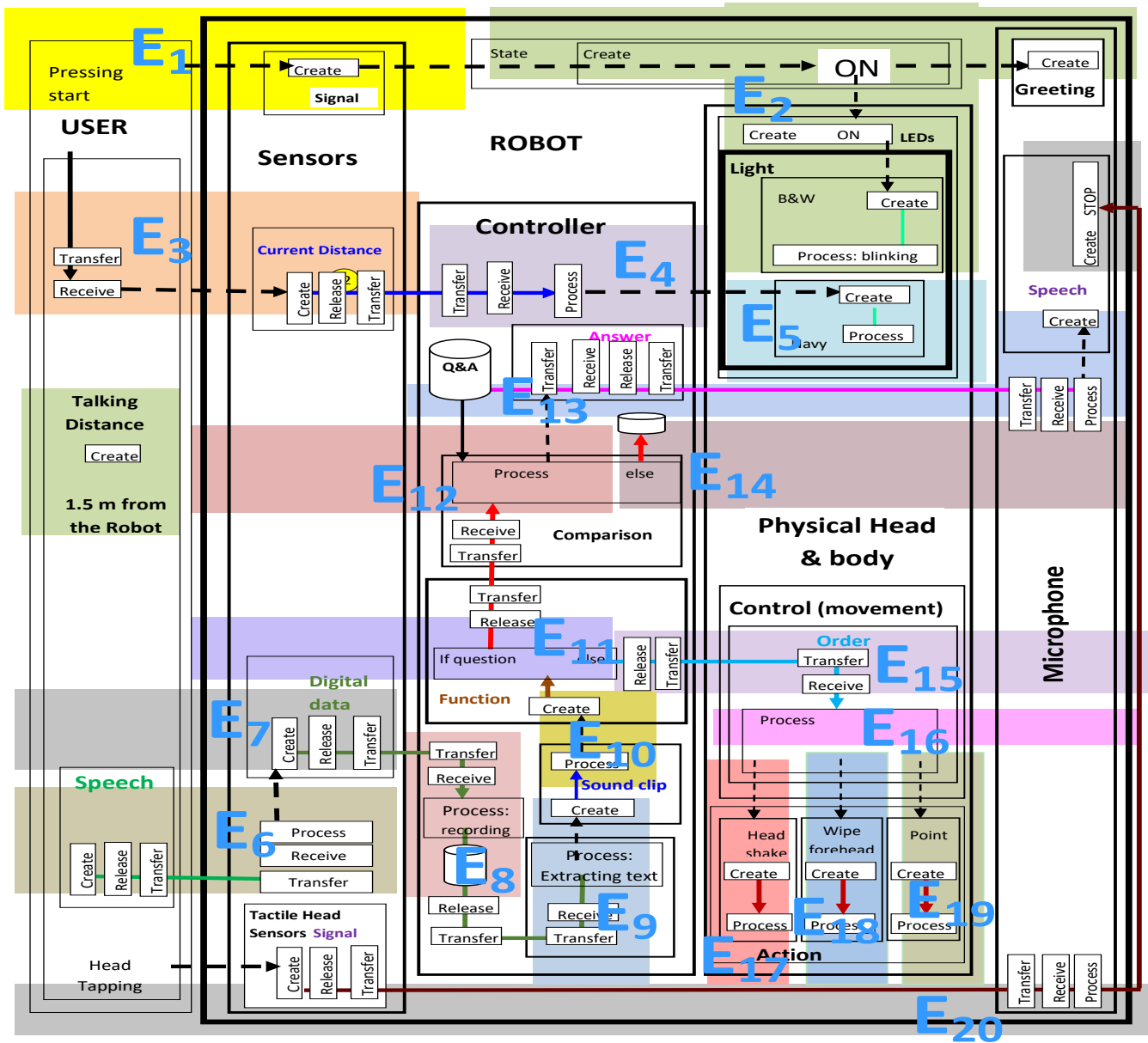


Fig. 17. The Selected Events.

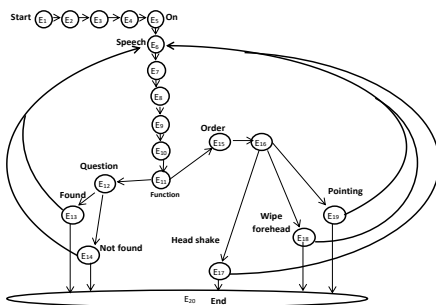


Fig. 18. The General Architecture of Interacting with the Robot (from [38]).

## VII. CONCLUSION

This paper contributes to establishing a broad foundation for describing a high-level specification of robot systems. This involved developing the system, from static modeling to identifying the system's behavior. Our approach to present the benefits of such an approach was to contrast current architectural descriptions (Fig. 1 to 4, 14 and 15) with static and dynamic TM modeling to obtain a more detailed structure of the robot's processes, which is important to complete the designing and implementing phases of any robot structure. Further research will apply TM modeling to different aspects in robotics.

REFERENCES

- [1] D. Kortenkamp and R. Simmons, "Robotic systems architectures and programming," in Springer Handbook of Robotics, B. Siciliano and O. Khatib, Eds. Berlin, Germany: Springer, 2008, pp. 187–206.
- [2] R. England, "Elements of (system) architecture—an introduction, v1.0," Project: Human Centric Systems Engineering, 2016. DOI: 10.13140/RG.2.2.31541.78566.
- [3] E. Coste-Maniere and R. Simmons, "Architecture, the backbone of robotic systems," Proceedings of the 2000 IEEE International Conf. on Robotics & Automation. San Francisco, CA, USA, April 2000, pp. 67–72.
- [4] L. Bass, P. Clements, and R. Kazman, Software Architecture in Practice, 2nd ed. Addison Wesley, 2003.
- [5] F. Brooks, "Architectural philosophy," in Planning a Computer System - Project Stretch, W. Buchholz, Ed. New York: McGraw-Hill, 1962, pp. 5–16.
- [6] G. Amdahl, G. Blaauw, and F. Brooks, "Architecture of the IBM System/360," IBM Journal of Research and Development, vol. 8, pp. 87–101, 1964.
- [7] M. T. Long, Creating a distributed field robot architecture for multiple robots. (2004). Ph.D. Thesis, University of San Francisco, San Francisco, CA, USA, 1 November 2004. <https://scholarcommons.usf.edu/etd/1137>.
- [8] Workshop on Architectures for Software Systems, School of Computer Science, Carnegie Mellon University, Pittsburgh, PA, USA, April 1995. CMU-CS-TR-95-151.
- [9] D. Loza-Matovelle, A. Verdugo, E. Zalama, and J. Gómez-García-Bermejo, "An architecture for the integration of robots and sensors for the care of the elderly in an ambient assisted living environment," Robotics, vol. 8, 2019.
- [10] A. J. Snoswell, V. Dewanto, M. Hoerger, J. Song, H. Kurniawati, and S. P. N. Singh, "A distributed, any-time robot architecture for robust manipulation," Australasian Conference on Robotics and Automation, Lincoln, New Zealand, December 4-6, 2018.
- [11] PatentSwarm, Control architecture for multi-robot system US 9 527 211B2, INVENTION Claim. Available online: <https://patentswarm.com/patents/US9527211B2> (accessed July 7, 2020).
- [12] S. Al-Fedaghi and J. Al-Fadhli, "Thing-oriented modeling of unmanned aerial vehicles," Int. J. Adv. Comput. Sci. Applic., vol. 11, pp. 610–619, 2020. DOI: 10.14569/IJACSA.2020.0110575.
- [13] S. Al-Fedaghi and B. Behbehani, "How to document computer networks," Journal of Computer Science, vol. 16, pp. 423–434, 2020.
- [14] S. Al-Fedaghi and D. Al-Qemlas, "Modeling network architecture: A cloud case study," IJCSNS, vol. 20, pp. 195–209, 2020.
- [15] S. Al-Fedaghi and M. Bayoumi, "Modeling advanced persistent threats: A case study of APT38," 14th International Conference for Internet Technology and Secured Transactions (ICITST-2019), London, UK, December 9-11, 2019.
- [16] S. Al-Fedaghi and G. Aldamkhi, "Conceptual modeling of an IP phone communication system: A case study," 18th Annual Wireless Telecommunications Symposium (WTS 2019), New York City, New York, USA, April 9-12, 2019.
- [17] S. Al-Fedaghi and E. Haidar, "Programming is diagramming is programming," J. Software, vol. 14, pp. 410–422, 2019.
- [18] S. Al-Fedaghi and M. Al-Otaibi, "Service-oriented systems as a thing machine: A case study of customer relationship management," IEEE Intern. Conf. on Information and Computer Technologies, University of Hawaii, Maui College, Hawaii, USA, March 14-17, 2019, pp. 243–254.
- [19] S. Al-Fedaghi and M. Makdessi, "Modeling business process and events," 9th Computer Science On-line Conference, Springer, Applied Informatics and Cybernetics in Intelligent Systems, April 23-26, 2020, pp. 83–97. doi.org/10.1007/978-3-030-30329-7\_8.
- [20] S. Al-Fedaghi and E. Haidar, "Thing-based conceptual modeling: Case study of a tendering system," Journal of Computer Science, vol. 16, pp. 452–466, 2020. DOI: 10.3844/jcssp.2020.452.466.
- [21] S. Al-Fedaghi and M. Al-Saraf, "Thinging the robotic architectural structure," The 3rd Intern. Conf. on Mechatronics, Control and Robotics, Tokyo, Japan, Feb. 22-24, 2020.
- [22] S. Al-Fedaghi and A. Hassouneh, "Modeling the engineering process as a thinging machine: A case study of chip manufacturing," The 8th Computer Science On-line Conference, April 24, 2019. L pp. 67–77.
- [23] S. Al-Fedaghi and O. Alsumait, "Toward a conceptual foundation for physical security: Case study of an IT department," International Journal of Safety and Security Engineering, vol. 9, pp. 137–156, 2019.
- [24] S. Al-Fedaghi and M. Alsulaimi, "Privacy thinging applied to the processing cycle of bank cheques," 3rd International Conference on System Reliability and Safety, Barcelona, Spain, Nov. 24-26, 2018.
- [25] S. Al-Fedaghi and H. Aljenfawi, "A small company as a thinging machine," 10th International Conference on Information Management and Engineering (ICIME 2018), University of Salford, Manchester, UK, September 22-24, 2018, pp. 27–34. doi.org/10.1145/3285957.3285988.
- [26] S. Al-Fedaghi and R. Al-Azmi, "Control of waste water treatment as a flow machine: A case study," The 24th IEEE International Conference on Automation and Computing (ICAC'18), Newcastle University, Newcastle upon Tyne, UK, September 6-7, 2018.
- [27] S. Al-Fedaghi and N. Al-Huwais, "Toward modeling information in asset management: Case study using Maximo, 2018," 4th International Conf. on Information Management, Oxford, UK, 2018, pp. 117–124.
- [28] S. Al-Fedaghi and M. Alsharah, "Modeling IT processes: A case study using Microsoft Orchestrator," 2018 International Conference on Advances in Computing and Communication Engineering (ICACCE), Paris, France, June 22-23, 2018, pp. 394–401.
- [29] S. Al-Fedaghi and A. Esmaeel, "Modeling digital circuits as machines of things that flow," 2018 International Conference on Mechatronics Systems and Control Engineering (ICMSCE 2018), Amsterdam, Netherlands, February 21-23, 2018.
- [30] S. Al-Fedaghi and Y. Atiyah, "Tracking systems as thinging machine: A case study of a service company," IJACSA, vol. 9, pp. 110–119, 2018.
- [31] C. Schlenoff, E. Prestes, R. Madhavan, P. Goncalves, H. Li, S. Balakirsky, T. Kramer, and E. Miguelanez, "An IEEE standard ontology for robotics and automation," IEEE/RSJ International Conference on Intelligent Robots and Systems, Vilamoura, Portugal, Oct. 7-12, 2012.
- [32] V. R. S. Kumar, A. Khamis, S. Fiorini, J. L. Carbonera, A. O. Alarcos, M. Habib, P. Goncalves, H. Li, and J. I. Olszewska, "Ontologies for industry 4.0.," The Knowledge Engineering Review, vol. 34, e17, 2019. DOI: 10.1017/S0269888919000109.
- [33] H. Cheng, P. Zeng, L. Xue, Z. Shi, P. Wang, and H. Yu, "Manufacturing ontology development based on industry 4.0 demonstration production line," IEEE International Conference on Trustworthy Systems and Their Applications, Wuhan, China, September 22-23, 2016, pp. 42–47.
- [34] G. Engel, T. Greiner, and S. Seifert, "Ontology-assisted engineering of cyber-physical production systems in the field of process technology," IEEE Trans. on Industrial Informatics, vol. 14, pp. 2792–2802, 2018.
- [35] R. Cassinis, BARCS: A new way of building robots. Laboratorio di Calcolatori, Dipartimento di Elettronica, Politecnico di Milano, Milan, Italy, September 1987. Available online: [http://www.cassinis.it/Siti%20ex%20Uni/ARL/docs/papers/05\\_002.pdf](http://www.cassinis.it/Siti%20ex%20Uni/ARL/docs/papers/05_002.pdf).
- [36] X. Lacherade, SoftBank Robotics Europe – SAS (Limited Company). 2020. Available online: <https://www.softbankrobotics.com/emea/index.php/en/nao> (accessed on July 10, 2020).
- [37] SoftBank Robotics Europe. Aldebaran documentation. 2017. Available online: [http://doc.aldebaran.com/2-1/home\\_nao.html](http://doc.aldebaran.com/2-1/home_nao.html) (accessed on July 10, 2020).
- [38] M. T. G. Ying, NaoRobot. November 2017. Available online: <https://github.com/guangying94/NaoRobot#start-of-content> (accessed on July 10, 2020).
- [39] Microsoft. Microsoft Azure. 2020. Available online: <https://azure.microsoft.com/en-us/overview/> (accessed on July 10, 2020).

# Enhancing Acceptance Test Driven Development Model with Combinatorial Logic

Subhash Tatal<sup>1</sup>

Research Scholar, Dept. of CSE  
Koneru Lakshmaiah Education Foundation  
Vaddeswaram Vijayawada, India

Dr. V. Chandra Prakash<sup>2</sup>

Professor, Dept. of CSE  
Koneru Lakshmaiah Education Foundation  
Vaddeswaram Vijayawada, India

**Abstract**—In the Software Development Life Cycle, modelling plays a most significant role in designing and developing software efficiently. Acceptance Test-Driven Development (ATDD) is a powerful agile software development model where a customer provides user acceptance test suits as a part of Software Requirements Specifications. A design has to develop a system so that User Acceptance Tests will be successful. In some systems, the Combinatorial Logic and Combinatorial Testing play a very crucial role. The authors have proposed a novel approach to enhance the existing Acceptance Test Driven Development model to Combinatorial Logic Oriented-ATDD model by incorporating combinatorial logic. Refinement with respect to combinatorial logic needs to be incorporated in all the stages of Software Development Life Cycle, i.e. starting from Software Requirement Specifications to User Acceptance Tests. This comprehensive approach derives the acceptance tests from user requirements effectively and efficiently. In this paper, the existing Indian Railway Reservation System is considered as a case study, and it was fully implemented as per proposed Combinatorial Logic Oriented-ATDD model.

**Keywords**—Software requirements specification; software development life cycle; acceptance test driven development; combinatorial logic; combinatorial testing; user acceptance tests; railway reservation system

## I. INTRODUCTION

This Nowadays, software systems are becoming increasingly complex. It is more challenging to verify the correctness of complex software requirements specification [1]. Formal verification approaches are highly sensitive to the software's complexity and might require costly resources, namely tools and human resources. During functional testing, many errors can be captured. It is not very easy to validate software requirements specification from a potentially huge set of parameters, values, or conditions of the system [2][3].

In the systems such as reservation system, college admission system, concession management system, etc. combinations of a set of parameters, values, or conditions are present. Combinatorial logic plays a considerable role in such type of systems. For example, in the current railway reservation system, a passenger avail only one type of concession at a time. A passenger can avail multiple concessions at a time by applying combinatorial logic on a set of concession categories and types. Suppose a passenger who wants to avail concession is a senior citizen and physically handicapped, then the passenger can get more percentage of

concession than percentage of concession offered in single concession using pairwise combinatorial logic. If a passenger is a senior citizen, cancer patient, and physically handicapped, then the passenger can get more percentage of concession than percentage of concession offered in pairwise concession using 3-way combinatorial logic. In addition to standard testing techniques, combinatorial testing is also very much essential to test this combinatorial logic to ensure the reliability of such systems.

The combinatorial logic is applied to various systems and performed combinatorial testing to ensure the reliability of those systems. The researchers claimed that 67% of the faults were triggered by only a single parameter value, 93% by 2-way combinations, and 98% by 3-way combinations of a complex application. For some applications, 100% faults were detected with 4 to 6- way interactions [4].

The authors made a survey to find out a model among the classical process models viz. waterfall, spiral, incremental, etc., and agile process models viz. extreme programming, scrum, etc., that is most suitable to represent combinatorial logic. The authors found that Test Driven Development (TDD) and Acceptance Test Driven Development (ATDD) are more suitable to represent combinatorial logic.

There are many systems where combinatorial logic is found as a must and hence there is need to put focus on how to incorporate combinatorial logic in all the stages of Software Development Life Cycle (SDLC) in a better way. Combinatorial logic can be incorporated into all the stages of SDLC. Out of earlier mentioned process models, the authors identified that the TDD and ATDD models are suitable to represent the combinatorial logic. In this section, concepts related to combinatorial testing and the ATDD model are discussed.

### A. Combinatorial Testing

Combinatorial Testing (CT) is a specification based technique. It provides a systematic way to select combinations of program inputs or parameters for testing. It is a useful testing technique to test hardware or software system which identifies failures based on input or output combinations of parameters. Over the years, this technique has been applied to test system configurations, web forms, protocols, graphical user interfaces, and software product lines [5]. The possible n-way (n=2, 3, 4, 5, 6, or more) combinatorial interactions

among the input variables can be detected by testers using the combinatorial testing technique [6].

1) *Pairwise testing*: Pairwise testing technique is the most commonly used combinatorial testing. It is a useful testing technique which involves all possible discrete combinations of each pair of input parameters of the system. Pairwise testing can be performed much faster than exhaustive testing that tests all combinations of all input parameters. The majority of software faults are triggered by a single input parameter or a combination of two input parameters. Pairwise testing requires that each pair of input parameter values should be represented at least by one test case. Let us consider software that takes three input parameters say  $x, y, z$ . If each parameter has four different values, then there will be 64 different pairs;  $\{(x_1, y_1) (x_1, y_2) \dots (y_4, z_4)\}$ . A test case  $(x_1, y_3, z_2)$ , for example, represents three of these 64 pairs:  $(x_1, y_3), (x_1, z_2), (y_3, z_2)$ . The pairwise testing method is highly useful for cases with a limited number of parameters with multiple possible values to reduce the test suite size and detect about 70% to more than 90% of software faults [7].

2) *n-way testing*: Some faults are triggered only by a combination of 3, 4, or more parameter values. These combinations cannot be detected by the pairwise testing. There is a need to test 3-way and 4-way combinations of parameter values for those cases. The study showed that across a variety of domains, all faults are detected by a maximum of 4-way to 6-way interactions. The fault detection rate increases rapidly with interaction strength (n-way combinations).

### B. Acceptance Test Driven Development

Acceptance Test-Driven Development (ATDD) [8] supports collaboration among the customers, developers, and testers to ensure that acceptance tests exist before writing any code. The acceptance tests are written from the perspective of the end-user. In the ATDD model, acceptance tests are written before developers start coding. The ATDD model has been used from time to time by considering the following goals [9].

1) ATDD is a specification and not validation. It is one way of thinking through the software requirements specifications followed by user acceptance tests before writing the functional code.

2) ATDD is simply a programming technique to write a clean code that works effectively.

3) ATDD is not testing software, but it stands as an aid to the programmer and customer during the development process to establish unambiguous requirements.

There is a scope for research to apply the ATDD model to the applications where requirements are specified using the combinatorial logic. This paper is organized as follows. Section 2 reviews the related work on combinatorial testing and the ATDD model. Section 3 discusses the classical and combinatorial logic oriented -ATDD model. In section 4, Railway Reservation System based on combinatorial logic oriented-ATDD model is presented. Section 5 reports

experimental results. Section 6 concludes this paper and provides the guidelines of the future work.

## II. RELATED WORK

Several researchers have attempted to pursue research in the field of combinatorial testing technique and ATDD model. In this section, related work on combinatorial testing and the ATDD model has been discussed.

### A. Combinatorial Testing

The combinatorial testing technique used to generate tests that cover pairwise or n-way combinations of parameters of the system by implementing the AETG system. The AETG system [10] is in a variety of applications for the unit, system, and interoperability testing. Automated Combinatorial Testing for Software Tool (ACTS) developed to apply high-strength combinatorial testing to detect intangible failures that occur when multiple components interact with each other. ACTS tool uses IPOG, IPOG-F, IPOG-F2, IPOG-D, and Base Choice algorithms for test case generation [11-13]. The fault localization approach [14] is used that can help programmers in locating faults with less manual interference. The available algorithms/tools of combinatorial testing are categorized based on different comparison criteria [15], including the test suite generation technique, combination criteria, mixed covering array, the strength of coverage, and the support for constraints between parameters.

The different search algorithms like the Genetic Algorithm, Particle Swarm Optimization, Ant Colony Algorithm, Bee Colony Optimization, and Simulate Annealing [16-17] are used to test embedded systems using test cases generated through combinatorial testing techniques. The combinatorial test cases are derived from the output domain in systems such as safety-critical embedded systems, which ensure maximum output combinations tested in detail. These test cases are derived using a genetic algorithm [18-19] and adjacent pairwise testing [20]. The various constraint handling, identification, and maintenance techniques [21] of combinatorial testing are analyzed. A Neural Network approach [22] is used to improve combinatorial coverage in the combinatorial testing approach [23]. A multi-objective crow search and fruit-fly optimization techniques [24] are used to optimize combinatorial test cases in constraints handling environment.

System requirements and corresponding models [25] are proposed for applying the combinatorial approach to those requirements. A structured modelling method [26] used to translate requirements expressed in a general format into an input parameter model suitable for combination strategies. A number of Articles [27-39] have been presented for testing embedded systems using combinatorial methods in the literature for testing distributed embedded systems.

### B. Acceptance Test Driven Development Model

ATDD is the developer-focused model where the entire team collaborates to define the acceptance criteria of a user scenario before the actual implementation starts. ATDD model is implemented using the Given-When-Then format [40] that uses unit tests to deliver small pieces of functionality



incrementally. A hybrid approach of combining user-centered agile methodology with ATDD model [41] is proposed in an efficient manner. It makes the possibility of software reusability based on the needs of end-users for decreasing development costs. The various case studies of a Real-Time Embedded system [42-43] and web applications [44] from industry are developed using Project-Based Learning [45], ATDD, and agile development. This helps to detect unauthorized access and fraud.

A combination of ATDD and Model-Based Testing (MBT) [46] is applied in several real-world projects. This approach increased test coverage and extended testing to user scenarios. It is exercised by the existing acceptance tests to minimize the risks and to reduce the effort involved in introducing MBT in the projects. The idea of collaborating Quality Function Deployment (QFD) and ATDD [47] is proposed. The principles of QFD are applied to capture the customer requirements and deploy them into functional and non-functional requirements. These requirements are mapped into user scenarios, which then became the acceptance tests. The development is performed based on those acceptance tests using the ATDD model. Production code is validated later against the customer requirements instead of the interpretation of the requirements by the developer team. An AnnoTest Web/Run tool [48] is used by expert customers to specify acceptance tests through the reuse of existing requirements specification.

The development teams have a better understanding of the software requirements as it mandates the exact behavior in terms of acceptance criteria using ATDD. The improved understanding of requirements results in reduced defect density and hence reduced Cost of Quality. This improvement also helps in simplifying the need for repetitive or breakthrough improvement as per changing business requirements. The ATDD model is an effective way of developing an application in a continuously evolving environment [49]. The open-source Quality Assurance of Complex Event Processing (CEP) Testing System [50] is introduced for realizing the executable acceptance test-driven development of complex event processing applications.

### III. COMBINATORIAL LOGIC ORIENTED-ATDD (CLO-ATDD) MODEL

Combinatorial logic plays an essential role in designing and developing systems like Reservation Systems, Concession Management System, College Admission System, etc.

As mentioned in section I, the authors found that TDD and ATDD models are suitable to represent combinatorial logic. In the TDD model, test cases are written in the same language in which the features are implemented. If the features are implemented in Java programming language, then test cases are written in Java (e.g., JUnit test cases which are written Java). The TDD model focuses on the implementation of the features. In the ATDD model, test cases are written in simple business language. The authors propose that combinatorial logic can be incorporated in acceptance tests of the ATDD model. User acceptance tests are written from the user's point of view. Developers implement the system using these user acceptance tests. Hence, ATDD is more suitable model than

TDD to incorporate combinatorial logic while framing the SRS document. The authors propose enhancement in the existing ATDD model by incorporating combinatorial logic in all the stages of SDLC. In the next section, classical SDLC and Combinatorial Logic Oriented-ATDD (CLO-ATDD) models are explained.

#### A. Classical SDLC

SDLC defines a methodology for the overall development process, which improves the quality of software. It consists of a detailed plan illustrating how to develop, maintain, replace, and enhance specific software.

The following are the various stages of a classical SDLC.

- 1) Communication.
- 2) Planning.
- 3) Modeling.
- 4) Construction.
- 5) Deployment.

Every software process has its limitations, and the SDLC stands as unexceptional to that. The selection of the appropriate SDLC model is a very challenging task. Each model has definite advantages and disadvantages; therefore, it is essential to assess each one to ensure fitness. Most SDLC models are designed around a business partner or customer requirements. It is difficult for business partners and customers to deliver the detailed requirements specification of the systems, which is to be developed as per their expectations within time, cost, and quality. A successful implementation requires dedicated user involvement to capture the true essence of the system requirements. If the business partners or customers are not satisfied with the working functionality/features, the development team has to modify the functionality/features. Multiple modifications in software development cause a potential delay in deliverable components. If changes are delayed to be implemented in the process, it increases the total cost of the system while extending the time to completion. In the next section, the authors proposed CLO-ATDD model.

#### B. Proposed CLO-ATDD Model

The proposed CLO-ATDD model is an enhancement of the existing ATDD model. In CLO-ATDD, user acceptance tests are prepared in a business language. These tests are prepared based on the combinatorial logic oriented rules, as discussed in section 3.2.1. Gherkin syntax [51] is used to prepare the test cases. It is easy to learn Gherkin syntax which is specified in a business language. The Gherkin syntax has a structured format to illustrate the business rules of real-world applications. The user acceptance tests are prepared using a well-defined Given-When-Then structure format and a few keywords. In Gherkin syntax, each feature contains multiple user scenarios. Each feature starts with a keyword, followed by a description of the feature. Each test starts with a sequence of these keywords: Given, When, Then. And and But is used whenever necessary. The description of these keywords is given below.

- Given – It describes the preconditions for the scenario.

- When – It describes the operation that we want to test.
- Then – It describes the expected result.
- And and But – They are optional. These keywords are used as conjunctions and semantically continue the meaning of previous sentences.
- Comment –It is optional. This can be used to provide explanation of the test case.

In this section, the CLO-ATDD model is discussed. The different stages of SDLC with respect to the CLO-ATDD model are described below.

1) *Communication*: In the classical SDLC, only requirements are prepared and finalized during this phase. In ATDD, communication among the business customers, the developers, and the testers happen to discuss the requirements specification. In ATDD, acceptance tests are written before the developer team starts coding. In CLO-ATDD model, the following activities are carried out.

a) Preparation & finalization of the SRS document of the system by different stakeholders such as developer, customer, etc.

b) This SRS document is prepared using combinatorial logic oriented rules. The rules are an essential part of the SRS document. The SRS consists of a set of scenarios, configurations, or conditions. The combinatorial logic is applied to these sets of scenarios, configurations, or conditions to prepare the combinatorial logic oriented rules. These combinatorial logic oriented rules are used by a business analyst to analyze the system, a designer to design the system, by a programmer during coding, and by a tester to test the system using combinatorial testing.

c) Preparation & finalization of the test suite for the user acceptance tests. Test cases are prepared from the requirements specification for the user acceptance test. These user acceptance tests are prepared by using the Given-When-Then format [51].

The SRS document is very much important in this phase of the CLO-ATDD model. It consists of combinatorial logic oriented rules and user acceptance tests.

2) *Planning*: The planning phase consists of project cost estimation, project scheduling, and resources like human resources, hardware, software, and network resources. The team members are allocated as per skill sets of the members for the project's active development. In the proposed approach, combinatorial testing is very much essential. The team members having skill-sets of combinatorial testing are preferred in this model. Regarding software resources, many combinatorial logic-oriented tools are available. Developing new tools require more time and cost. Existing available combinatorial testing tools like AETG and ACTS are used to complete the projects as per the schedule and to save the project's cost.

3) *Modeling*: In this section, the analysis and design of the proposed model are discussed. Combinatorial logic is applied while designing the system.

In the analysis stage, an in-depth analysis of the requirements is performed to obtain a detailed understanding of the system's business needs. System requirements are studied and structured. The result after this stage is a requirement document called the SRS document. The SRS document tries to capture the requirements from the customer's perspective. Combinatorial logic oriented UML diagrams are drawn to specify, analyze, and visualize the requirements specification.

It is an important stage in which the requirements specifications are designed by using combinatorial logic. This design is represented by a set of parameters, their respective values, and constraints on the value combinations. If a set of parameters and their respective values are high, then a huge number of parameter-value combinations are generated.

There is a need to give solutions for efficiently generating input combinations to represent software interaction and generation of test suites using efficient techniques. While generating test cases automatically for conducting combinatorial testing, sometimes, the size of test suite may be extremely large because of too many parameters and values in input. This is called as Combinatorial Explosion of test cases. To avoid the occurrence of the combinatorial explosion, we proposed CLO-ATDD design.

4) *Construction*: In this phase, the system is implemented and tested by using combinatorial logic. Many algorithms are available for generating combinatorial test suites.

After completion of the system designing phase, the coding phase begins. In this phase, developers start to develop the system by writing code based on the combinatorial logic oriented rules. It is the most extended phase of the SDLC process. The stakeholders should be involved regularly to ensure that their expectations are being fulfilled. The output of this phase is testable and functional software.

Exhaustive testing of any system may be impossible sometimes because the domain of input parameters to most software systems is huge. There is a need to design optimized test suites that are of reasonable size and are useful to detect as many defects present in the system as possible. If test cases are selected randomly, many of these randomly selected test cases do not contribute to the significance of the test suite. Thus, the number of random test cases in a test suite is not an indication of the effectiveness of the testing. User acceptance tests are prepared based on the combinatorial logic oriented rules. User acceptance testing is defined as testing the software by the user or client to verify whether it can be accepted or not.

5) *Deployment*: Once the software testing phase is completed, and defects are not present in the system, then the final deployment process starts. As per the proposed CLO-ATDD model, the final software is deployed after the user

accepts the user acceptance tests. The deployment manager does the deployment.

#### IV. RAILWAY RESERVATION SYSTEM: A CASE STUDY OF THE PROPOSED MODEL

In this section, a case study of Concession Management Subsystem (CMSS) of the proposed Railway Reservation System (RRS) is explained by using CLO-ATDD model.

##### A. Framing SRS using CLO-ATDD Model

Indian Railways is one of the most prominent organizations of the Government of India. Indian Railways offers concessions on ticket fares with respect to different concession categories such as Disabled Passengers, Patients, Senior Citizens, Awardees, War Widows, Students, and Youths etc. These concessions are available for various types of journey classes viz. Sleeper (SL) Class, Second Class (2ND), First Class (1ST), 1-2-3- Tier AC Class and Ac Chair. The list of different concession categories and concession types along with the journey class are shown in Table I.

1) Limitations of the existing reservation policy of Indian Railways:

a) All the concession types mentioned in Table I are not available on on-line ticketing platform of Indian Railways. The concession types like senior citizens, divyangjan, general, press person, press child, press spouse, and press companion are available on the on-line ticketing platform. The remaining concession types can be availed by the passenger at the Passenger Reservation System (PRS) counters at any reservation office of Indian Railways.

b) Only one type of concession is applicable at a time as per the choice of a passenger. The passenger is not allowed to avail more than one concession at a time.

There is a need to re-design, re-develop the railway reservation system to overcome the limitations of the existing railway reservation system. In the next section, the authors proposed a new reservation system by revising the software requirements specification of the existing Railway Reservation System by using the CLO-ATDD model.

2) *Proposal for revision of SRS using CLO-ATDD Model:* The following are subsystems of the present RRS of Indian Railways which provide on-line facility for reservation.

- Search Train.
- Plan Journey.
- Cancel Ticket.

The authors propose a new RRS by incorporating combinatorial logic in the system using CLO-ATDD model. In the new RRS, Concession Management Subsystem (CMSS) is enhanced to manage the concessions. CMSS is used to manage

multiple concessions at a time which can be availed by a passenger. Here, a novel approach is proposed to enhance the CMSS so that a passenger can be benefited by availing multiple concessions at a time. The existing SRS document is enhanced by incorporating combinatorial logic oriented rules and user acceptance tests. In the SRS document, two sections are added. These sections are very much important. First section consists of combinatorial logic oriented rules and second section consists of user acceptance tests. The proposed rules for availing multiple types of concession are shown in Table II. User acceptance tests are prepared using the Given-When-Then format as shown in Table III.

##### B. Design of Concession Management Subsystem

Software systems have five types of design such as Database Design, Program Architecture Design, File Design, Input Design and Output Design. Screen design can be used to represent both input and output design of a system wherever it is relevant. Now-a-days, Graphical User Interface (GUI) is used to design screens. In this section, the authors propose combinatorial logic oriented design of CMSS of RRS.

In the existing RRS, a passenger has to fill up a concession form at passenger reservation counter at any railway reservation office. There are some concessions viz. senior citizen, child, divyangjan etc. for which there is no need to fill up a separate concession claim form. The proof of these concession types is verified by a reservation clerk. For other concession types, the passenger has to fill up a concession claim form and submit it along with the necessary proofs to the reservation manager. The manager verifies the document proofs for the claim and sanctions concession for only one concession type as mentioned in Table I. The reservation manager issues a document termed as concession sanction order which consists of the maximum percentage of concession sanctioned along with signature and stamp of reservation manager. All this procedure is to be performed off-line and a lot of time may be required to complete this procedure. After this, the passenger will go to reservation counter to reserve his/her ticket. The reservation clerk verifies the concession sanction order, provides concession in the ticket fare, and reserves the seat/berth for the passenger.

The authors proposed a new CMSS of RRS using combinatorial logic so that a passenger can avail more than one concession type at a time. A passenger uses CMSS and fills up a concession claim form by selecting one or multiple concession types and submits it along with the necessary proofs to reservation manager. The manager will verify all the concessions claims and sanctions the total concession allowed to the passenger by using CMSS. The reservation manager uses CMSS and issues the concession sanction order consist of total percentage of concession offered along with signature and stamp. The passenger will reserve the ticket as per the total percentage of concession sanctioned.

TABLE I. LIST OF CONCESSION CATEGORIES AND CONCESSION TYPES ALONG WITH JOURNEY CLASS

| Category of Concession                                                                                                                                                                                                                                                                                      | Journey Class   |         |         |         |         |         |             |
|-------------------------------------------------------------------------------------------------------------------------------------------------------------------------------------------------------------------------------------------------------------------------------------------------------------|-----------------|---------|---------|---------|---------|---------|-------------|
|                                                                                                                                                                                                                                                                                                             | SL              | 2ND     | 1ST     | 1AC     | 2AC     | 3AC     | AC Chair    |
|                                                                                                                                                                                                                                                                                                             | % of Concession |         |         |         |         |         |             |
| <b>Disabled Passengers</b>                                                                                                                                                                                                                                                                                  |                 |         |         |         |         |         |             |
| Orthopedically Handicapped, Mentally retarded, Blind                                                                                                                                                                                                                                                        | 75              | 75      | 75      | 50      | 50      | 75      | 75          |
| Deaf & Dumb                                                                                                                                                                                                                                                                                                 | 50              | 50      | 50      | NA      | NA      | NA      | NA          |
| <b>Patients</b>                                                                                                                                                                                                                                                                                             |                 |         |         |         |         |         |             |
| Cancer                                                                                                                                                                                                                                                                                                      | 100             | 75      | 75      | 50      | 50      | 100     | 75          |
| Thalassemia, Heart, Kidney                                                                                                                                                                                                                                                                                  | 75              | 75      | 75      | 50      | 50      | 75      | 75          |
| Hemophilia                                                                                                                                                                                                                                                                                                  | 75              | 75      | 75      | NA      | NA      | 75      | 75          |
| T.B./Lupus Valgaris, Non-infectious Leprosy                                                                                                                                                                                                                                                                 | 75              | 75      | 75      | NA      | NA      | NA      | NA          |
| AIDS                                                                                                                                                                                                                                                                                                        | NA              | 50      | NA      | NA      | NA      | NA      | NA          |
| Sickle & Aplastic Anaemia                                                                                                                                                                                                                                                                                   | 50              | NA      | NA      | NA      | 50      | 50      | 50          |
| <b>Senior Citizens</b>                                                                                                                                                                                                                                                                                      |                 |         |         |         |         |         |             |
| Men- 60 years and above.                                                                                                                                                                                                                                                                                    | 40              | 40      | 40      | 40      | 40      | 40      | 40          |
| Women- 58 years and above                                                                                                                                                                                                                                                                                   | 50              | 50      | 50      | 50      | 50      | 50      | 50          |
| <b>Awardees</b>                                                                                                                                                                                                                                                                                             |                 |         |         |         |         |         |             |
| President's Police Medal, Indian Police Award (Age>=60)                                                                                                                                                                                                                                                     | 50M/<br>60F     | 50M/60F | 50M/60F | 50M/60F | 50M/60F | 50M/60F | 50M/<br>60F |
| Shram                                                                                                                                                                                                                                                                                                       | 75              | 75      | NA      | NA      | NA      | NA      | NA          |
| National Awardee Teachers /Bravery Award                                                                                                                                                                                                                                                                    | 50              | 50      | NA      | NA      | NA      | NA      | NA          |
| <b>War Widows</b>                                                                                                                                                                                                                                                                                           |                 |         |         |         |         |         |             |
| War Widows, Widows <sup>3</sup>                                                                                                                                                                                                                                                                             | 75              | 75      | NA      | NA      | NA      | NA      | NA          |
| <b>Students</b>                                                                                                                                                                                                                                                                                             |                 |         |         |         |         |         |             |
| SC/ST Category for hometown & educational tours                                                                                                                                                                                                                                                             | 75              | 75      | NA      | NA      | NA      | NA      | NA          |
| Students of Govt. schools for study tour, Entrance exam - Girls of Govt. schools in rural areas                                                                                                                                                                                                             | NA              | 75      | NA      | NA      | NA      | NA      | NA          |
| Main written examination conducted by UPSC & SSC                                                                                                                                                                                                                                                            | NA              | 50      | NA      | NA      | NA      | NA      | NA          |
| Foreign students, Research scholars' for journeys <sup>4</sup> , Cadets and Marine Engineers <sup>5</sup> , , Hometown & educational tours                                                                                                                                                                  | 50              | 50      | NA      | NA      | NA      | NA      | NA          |
| Students and non-students participating in Camps                                                                                                                                                                                                                                                            | 25              | 25      | NA      | NA      | NA      | NA      | NA          |
| <b>Youths</b>                                                                                                                                                                                                                                                                                               |                 |         |         |         |         |         |             |
| National Youth Project, To attend job interview in Statutory Bodies, Bharat Scouts &                                                                                                                                                                                                                        | 50              | 50      | NA      | NA      | NA      | NA      | NA          |
| ManavUththanSewaSamiti                                                                                                                                                                                                                                                                                      | 40              | 40      | NA      | NA      | NA      | NA      | NA          |
| To attend job interviews in Central & State Govt.                                                                                                                                                                                                                                                           | 50              | 100     | NA      | NA      | NA      | NA      | NA          |
| <b>Kisans</b>                                                                                                                                                                                                                                                                                               |                 |         |         |         |         |         |             |
| Kisans and Industrial Labourers                                                                                                                                                                                                                                                                             | 25              | 25      | NA      | NA      | NA      | NA      | NA          |
| Kisans travelling                                                                                                                                                                                                                                                                                           | 33              | 33      | NA      | NA      | NA      | NA      | NA          |
| Kisans& Milk Producers, Delegates for attending Annual Conferences <sup>6</sup>                                                                                                                                                                                                                             | 50              | 50      | NA      | NA      | NA      | NA      | NA          |
| <b>Artists &amp; Sportspersons</b>                                                                                                                                                                                                                                                                          |                 |         |         |         |         |         |             |
| Artistes & Film technicians                                                                                                                                                                                                                                                                                 | 75              | 75      | 50      | NA      | 50      | 50      | 50          |
| All India, State, National tournaments Sportsmen, Mountaineering Expeditions                                                                                                                                                                                                                                | 75              | 75      | 50      | NA      | NA      | NA      | NA          |
| Press Correspondents                                                                                                                                                                                                                                                                                        | 50              | 50      | 50      | 50      | 50      | 50      | 50          |
| <b>Medical Professionals</b>                                                                                                                                                                                                                                                                                |                 |         |         |         |         |         |             |
| Doctors – Allopathic - travelling for any purpose                                                                                                                                                                                                                                                           | 10              | 10      | 10      | 10      | 10      | 10      | 10          |
| Nurses & Midwives - for leave and duty                                                                                                                                                                                                                                                                      | 25              | 25      | NA      | NA      | NA      | NA      | NA          |
| (3 widow of I.P.K.F. Personnel, Policemen & Paramilitary personnel, defense personnel, Martyrs of Operation Vijay in Kargil, 4 journey in connection with research work. (age<=35), 5 apprentices for travel between home and training ship, 6 delegates of Bharat Krishak Samaj & Sarvodaya Samaj, Wardha) |                 |         |         |         |         |         |             |

TABLE II. RULES FOR AVAILING CONCESSION IN SRS DOCUMENT USING CLO-ATDD MODEL

| Rule No. | Criteria                                                 | % of total concession                                                                                  |
|----------|----------------------------------------------------------|--------------------------------------------------------------------------------------------------------|
| 1        | No. of concession types selected= 1                      | % of total concession is applicable as per Table I.                                                    |
| 2        | No. of concession types selected= 2                      | % of total concession = % of highest concession type + 5% of remaining concession type                 |
| 3        | No. of concession types selected= 3                      | % of total concession = % of highest concession type + 7% of remaining higher concession type          |
| 4        | No. of concession types selected > 3                     | % of total concession = % of highest concession type + 10% of highest of the remaining concession type |
| 5        | % of total concession exceeds maximum allowed concession | % of total concession = maximum allowed concession (=100%)                                             |

TABLE III. SAMPLE USER ACCEPTANCE TEST

| Test Case No. | Keyword | Description                                                                                                                                                 |
|---------------|---------|-------------------------------------------------------------------------------------------------------------------------------------------------------------|
| 1             | Given   | The passenger selects concession type as orthopedically handicapped for second class journey.                                                               |
|               | When    | Rule 1 is applied. (Refer Table II)                                                                                                                         |
|               | Then    | The passenger gets 75% concession in ticket fare. (Refer Table I)                                                                                           |
| 2             | Given   | The passenger selects concession types as an orthopedically handicapped and a cancer patient for second class journey.                                      |
|               | When    | Rule 2 is applied.                                                                                                                                          |
|               | Then    | The passenger gets 78.75% concession in ticket fare.                                                                                                        |
|               | Comment | % of total concession= 75% (orthopedically handicapped) + 5% of 75 (cancer patients) = 75 % + 3.75% = 78.75% (Refer Table I & Rule 2 of Table II)           |
| 3             | Given   | The passenger selects concession types as a female senior citizen, an orthopedically handicapped and a cancer patient for second class journey.             |
|               | When    | Rule 3 is applied.                                                                                                                                          |
|               | Then    | The passenger gets 80.25% concession in ticket fare.                                                                                                        |
|               | Comment | % of total concession= 75% (orthopedically handicapped) + 7% of 75 (cancer patients) = 75 % + 5.25% = 80.25% (Refer Table I & Rule 3 of Table II)           |
| 4             | Given   | The passenger selects concession types as a female senior citizen, war widow, an orthopedically handicapped and cancer patient for sleeper class journey.   |
|               | When    | Rule 4 & Rule 5 are applied.                                                                                                                                |
|               | Then    | The passenger gets 100% concession in ticket fare. (Refer Table I & Rule 4 of Table II)                                                                     |
|               | Comment | % of total concession= 100% (cancer patient) + 10% of 75 (war widow) = 100 % + 7.5% = 107.5% (As per rule 4)<br>As per rule 5, % of total concession = 100% |

For input and output design, GUI based screen is designed as shown in Fig. 1. The CMSS is role based viz. passenger and reservation manager. The GUI consists of all concession categories and types as mentioned in Table I. A passenger has to fill up his/her personal information, journey details, and has to select one or multiple concession types. For example, the passenger can select concession types as a female senior citizen, war widow, an orthopedically handicapped and cancer patient for sleeper class journey and submits the form. A passenger cannot select infeasible combination of concession types. For example, a male senior citizen passenger cannot select for concession type of war widow. The GUI is designed in such a way that a passenger cannot select infeasible combination of concessions types. When a passenger is filling the concession claim form, only Submit and Print buttons are enabled and Approve button is disabled.

In case of a reservation manager, Approve and Print buttons are enabled. The reservation manager verifies the document proofs of selected concessions claimed by the passenger. If any claim is not valid then the manager can unselects the concession claim. The manager can then approve the concession claim. The combinatorial logic oriented rules mentioned in Table II are used by CMSS to calculate total concession in ticket fare. Finally, the concession sanction

order is printed which consists of original ticket fare, total number of concessions submitted by the passenger, total number of concessions sanctioned by the reservation manager, and net ticket fare.

### C. Implementation

In this section, implementation strategy of proposed CMSS and technique of test case generation is discussed.

1) *Implementation strategy of proposed CMSS*: The inputs of the proposed system are parameters and values. In CMSS, the concession categories and concession types are considered as parameters and values, respectively. Each concession category includes multiple concession types. The CMSS system has some constraints and conditions; for example, a male passenger cannot avail concessions of widow concession type because of infeasible combinations of parameters and values.

Client-server architecture is used to implement the proposed CMSS, as shown in Fig. 2. Interactive web pages at the client-side are designed by using Vue JS open source JavaScript framework. Express Node.js framework is used to develop a robust set of features of the proposed system at the server-side.

Fig. 1. GUI of CMSS.

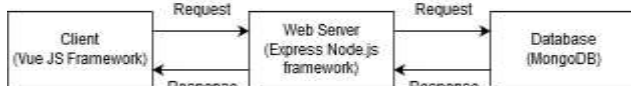


Fig. 2. Client-Server Architecture of the Proposed CMSS.

A request is sent by the user at the client-side and a request object is generated. It represents the HTTP request and has properties for the request query string, parameters, body, HTTP headers. Response to the request is generated at the server-side and it creates a response object. It represents the HTTP response that an Express app sends when it gets an HTTP request. MongoDB open-source document-based database is used in the proposed system to store the user and concession details. The system is implemented as per the specifications mentioned in Table I, CLO-ATDD rules for availing concessions mentioned in Table II and user acceptance tests mentioned in Table III.

2) *Test case generation technique:* Test case generation technique of the proposed system is explained in this section. The percentage of concession is dependent on journey class and concession categories which are mentioned in Table I. Only widow concession is gender-specific and so it applies to

the females only. The fare of the ticket is based on Child and Adult passenger types. Children above the age of 5 years and under 12 years of age are charged as 50% of adult ticket fare and considered as a child passenger. The fare of the ticket is exempted for the children under five years of age. Necessary information details for reservation class are shown in Table IV. The concession categories, types, selection mode of concession types and feasibility details of proposed CMSS are shown in Table V. The concession categories are infeasible to passenger types, gender and age. Some concessions are infeasible to child passenger type and some are infeasible to an adult passenger type. The passengers can select multiple concession types in the disabled passenger and patient concession category. For the remaining concession types, only one concession type is selected.

3) *Proposed algorithm to generate the test cases:* Step 1:- A dictionary in python for all types of journey class declared named class\_dict and a dictionary for the type of passenger names type\_dict.  
e.g. type\_dict={"1":"Child","2":"Adult"}

TABLE IV. BASIC INFORMATION DETAILS FOR RESERVATION CLASS

|                       |                         |                     |     |     |     |     |          |
|-----------------------|-------------------------|---------------------|-----|-----|-----|-----|----------|
| <b>Journey Class</b>  | SL                      | 2ND                 | 1ST | 1AC | 2AC | 3AC | AC Chair |
| <b>Gender</b>         | Male                    | Female              |     |     |     |     |          |
| <b>Passenger Type</b> | Child (5<=Age<= 12 yrs) | Adult (Age> 12 yrs) |     |     |     |     |          |

TABLE V. CONCESSION CATEGORIES AND TYPES ALONG WITH SELECTION MODE BASED ON PASSENGER TYPES

| <b>Concession categories</b>        | Disabled Passenger | Patient      | Senior Citizen       | Widow        | Student | Awardee | Artists & Sports-person | Youth  | Kisan  | Medical Professionals |
|-------------------------------------|--------------------|--------------|----------------------|--------------|---------|---------|-------------------------|--------|--------|-----------------------|
| <b>No. of concession types</b>      | 04                 | 10           | 2                    | 5            | 8       | 5       | 5                       | 4      | 3      | 2                     |
| <b>Selection Mode</b>               | Multiple           | Multiple     | Single               | Single       | Single  | Single  | Single                  | Single | Single | Single                |
| <b>Applicable to passenger type</b> | Adult, Child       | Adult, Child | Adult (based on age) | Adult female | Adult   | Adult   | Adult                   | Adult  | Adult  | Adult                 |

Step 2:- A dictionary of all the concession categories declared with keys against the values of the patient, disabled passenger etc. A dictionary named categories is defined with the keys being broad categories like Patient, Disability etc. and the keys a dictionary which contains the specifications of that category, e.g. categories = {'type':type\_dict}.

Step 3:- An empty dictionary concession\_class declared where the keys of each concession type against a list of values of concession in order of journey class. e.g. concession\_class["Cancer"] = [100, 75, 75, 50, 50, 100, 75].

Step 4:- A function concession defined to calculate the concession in case of multiple values for patients and disabled passenger category. This concession function takes in the list of disability, patients etc. as pairs for 2-way testing and as triplets for 3-way testing along with the journey class as resvClass. It then calculates the length of this list and sorts it in ascending order. This sorted list has concession values, the last element being the highest concession. Depending on the number of concession values, they are multiplied with a multiplier to calculate final concession and a final concession is returned through this function.

Step 5:- A function printCombination ( ) defined which takes in an array, n and r to calculate all combinations of size r in an array of size n (nCr).

Step 6:- A function combinationUtil ( ) defined which takes in the array, a temporary array named data, start which is the starting index of the array, end which is the end index of the array and r which is the size of combination. Both these functions are in the main function called getCombination ( ) which gives us a result of all combinations. All of these combinations are stored in the form of a dictionary where the keys are the broad categories i.e. Disability, Patient, Awardee etc. and the values are a list of all possible combinations of that category. e.g. {'Disability': [['Orthopedically Handicapped', 'Mentally retarded']]}

Step 7:- A final concession\_list dictionary is declared whose keys are as same as the final result, i.e. the broad category. Furthermore, the values will be all the information for that broad category, i.e., the journey class, the type of customer, the combination of that broad category and the concession given.

Step 8:- Iterating through a loop, in the dictionary final\_result, we go through the dictionary values to pick up each possible combination that we have calculated through getCombination ( ) function.

Step 9:- Another for loop iterates class\_dict to calculate journey class to display for a particular combination and to go through type\_dict to find out the type of customer for that combination.

Step 10:- Two lists are declared to append the list of all the combinations against the journey class and its respective concession.

Step 11:- The first list goes through the final\_result, makes a list of journey class, type of customer, concession value and the particular combination. The second loop is used to take this entire list having information about a particular combination to store it in a different list called final which has values as list, i.e., temp\_final.

Examples-

```
{'Disability': [['SL', 'Adult/Child', 78.75, ['Orthopedically Handicapped', 'Mentally retarded']], ['2nd', 'Adult/Child', 78.75, ['Orthopedically Handicapped', 'Mentally retarded']]}
```

Step 12:- This final list for a broad category is created and then stored in concession\_list against its key i.e., Disability, Patient etc.

Step 13:- Edit concession\_list according to particular conditions by using a loop, iterating through the final concession\_list to make changes wherever it is needed. All the test cases having the same concession for all seven journey classes have been combined into one test case.

Step 14:- Writing all of the results into a text file by taking the console output and creating a new text file which contains all the test cases. The unsuccessful cases for each broad category are written at the end of the file.

## V. RESULT ANALYSIS AND DISCUSSION

The authors proposed the technique of generation of combinatorial test cases to reduce the time and improve the effectiveness of the testing. Total of 665 test cases are generated using 2-way combinatorial strategy, and 1435 test cases are generated through 3-way combinatorial strategy. The authors claimed that proposed testing technique gives

reliability and efficiency completely. The user acceptance test is fully satisfied. The combinatorial explosion of test cases is avoided using CLO-ATDD model. The result of the proposed technique is shown in Table VI.

### A. Findings

There are some systems such as Reservation system, College admission system, Concession management system, etc. where combinatorial logic plays an extremely important role. The authors made a survey to find a suitable model among the classical process models viz. Waterfall, Spiral, Incremental, etc., and agile process models viz. Extreme Programming, Scrum, etc., to represent combinatorial logic. The authors found that TDD and ATDD models are more suitable to represent combinatorial logic. Compared to TDD model, ATDD is most suitable model. The authors proposed to enhance the existing ATDD model to CLO-ATDD model.

### B. Comparison with Existing Models

In the TDD model, test cases are written in the same language in which the features are implemented. The TDD model focuses on the implementation of the features. In the ATDD model, test cases are written in simple business language. User acceptance tests are written from the user's point of view. Developers implement the system using these user acceptance tests. In CLO-ATDD model, user acceptance tests are prepared in a business language using combinatorial logic oriented rules. Hence, CLO-ATDD is more suitable model than TDD and ATDD to incorporate combinatorial logic.

### C. Limitations of the Proposed Model

The first limitation is generating more than 6-way combinations of parameters for combinatorial testing. In case, if we have to go for higher values of interaction strength, we may have to find new algorithms and techniques. The second limitation is exhaustive testing. But, if the size of test suite is small and manageable, then we recommend exhaustive testing. The third limitation is combinatorial explosion problem as discussed in section (III (B(c))) which is a universal problem in software testing. Our proposed model attempts to avoid this combinatorial explosion problem to some extent.

TABLE VI. RESULTS OF PROPOSED TECHNIQUE

| No. test cases/test case generation | Combinatorial test case generation |       |
|-------------------------------------|------------------------------------|-------|
|                                     | 2-way                              | 3-way |
| Number of test cases generated      | 665                                | 1435  |

## VI. CONCLUSION AND FUTURE WORK

The present paper has explored an enhancement of the Acceptance Test Driven Development model to improve the software development life cycle by applying combinatorial logic. The proposed Combinatorial Logic Oriented-Acceptance Test Driven Development (CLO-ATDD) model has been illustrated with a case study of the Indian Railway Reservation System. This system was fully implemented and verified by using the combinatorial testing and combinatorial testing approach. This system typically considers multiple

concession types and calculates an appropriate percentage of concession in ticket fare to the passenger as per proposed CLO-ATDD model. The authors hope that this proposal would be valuable for end-user, i.e. the tourism community ultimately. In future, the aforementioned CLO-ATDD model can be applied to design various systems where combinatorial logic is essential. Also, this model will also helpful to generate combinatorial logic oriented test cases using UML diagrams.

### REFERENCES

- [1] Lei, Yu, and Kuo-Chung Tai. "In-parameter-order: A test generation strategy for pairwise testing." In Proceedings Third IEEE International High-Assurance Systems Engineering Symposium (Cat. No. 98EX231), pp. 254-261 (1998).
- [2] Grindal, Mats, Jeff Offutt, and Sten F. Andler. "Combination testing strategies: a survey." *Software Testing, Verification and Reliability* 15, no. 3 (2005): 167-199.
- [3] Nie, Changhai, and Hareton Leung. "A survey of combinatorial testing." *ACM Computing Surveys (CSUR)* 43, no. 2 (2011): 1-29.
- [4] Kuhn, D. Richard, Renee Bryce, Feng Duan, Laleh Sh Ghandehari, Yu Lei, and Raghu N. Kacker. "Combinatorial testing: Theory and practice." In *Advances in Computers*, vol. 99, pp. 1-66. Elsevier, 2015.
- [5] Lott, C., Ashish Jain, and S. Dalal. "Modeling requirements for combinatorial software testing." In *ACM SIGSOFT Software Engineering Notes*, vol. 30, no. 4 (2005), pp. 1-7.
- [6] Zamansky, Anna, and Eitan Farchi. "Helping the tester get it right: Towards supporting agile combinatorial test design." In *SEFM 2015 Collocated Workshops*, pp. 35-42. Springer, Berlin, Heidelberg, 2015.
- [7] Lei, Yu, and Kuo-Chung Tai. "In-parameter-order: A test generation strategy for pairwise testing." In *Proceedings Third IEEE International High-Assurance Systems Engineering*.
- [8] Mondal, Sayani, and Partha Pratim Das. "Effectiveness of Test-Driven Development as an SDLC Model: A case study of an elevator controller design." In *Emerging Trends in Computing and Communication*, pp. 225-233. Springer, New Delhi, 2014.
- [9] Dogša, Tomaž, and David Batič. "The effectiveness of test-driven development: an industrial case study." *Software Quality Journal* 19, no. 4 (2011): 643-661.
- [10] Cohen, David M., Siddhartha R. Dalal, Michael L. Fredman, and Gardner C. Patton. "The AETG system: An approach to testing based on combinatorial design." *IEEE Transactions on Software Engineering* Vol.23, No. 7 (1997), pp. 437-444.
- [11] R. Kuhn, Yu Lei and Raghu Kacker, "Practical Combinatorial Testing: beyond Pair wise", *IEEE Computer Society - IT Professional*, Vol. 10, No. 3 (2008).
- [12] D. Richard Kuhn, Raghu N. Kacker and Yu Lei, "Practical combinatorial testing", *NIST Special Publication*, (2010).
- [13] Bhuvana, S., and M. V. Srinath. "A survey on Automated Combinatorial Testing for Software Tool (ACTS) with experimental revise based on T-way test generation." (2016).
- [14] Jayaram, Rekha, and R. Krishnan. "Approaches to Fault Localization in Combinatorial Testing: A Survey." In *Smart Computing and Informatics*, pp. 533-540. Springer, Singapore, 2018.
- [15] Khalsa, Sunint Kaur, and Yvan Labiche. "An orchestrated survey of available algorithms and tools for combinatorial testing." In *2014 IEEE 25th International Symposium on Software Reliability Engineering*, pp. 323-334.
- [16] Mudarakola, Lakshmi Prasad, and M. Padmaja. "The survey on artificial life techniques for generating the test cases for combinatorial testing." *International Journal of Research Studies in Computer Science and Engineering (IJRSCSE)* 2, no. 6 (2015): 19-26.
- [17] Mudarakola, Lakshmi Prasad, J. K. R. Sastry, and V. Chandra Prakash. "Testing embedded systems using test cases generated through combinatorial techniques." *International Journal of Engineering & Technology* 7, no. 2.7 (2018): 146-158.
- [18] Vudatha, Chandra Prakash, Sateesh Nalliboena, Sastry Kr Jammalamadaka, Bala Krishna Kamesh Duvvuri, and L. S. S. Reddy.



- "Automated generation of test cases from output domain of an embedded system using Genetic algorithms." 3rd International In Electronics Computer Technology (ICECT), IEEE (2011), vol. 5, pp. 216-220.
- [19] Vudatha, Chandra Prakash, Sateesh Nalliboena, Sastry KR Jammalamadaka, Bala Krishna Kamesh Duvvuri, and L. S. S. Reddy. "Automated generation of test cases from output domain and critical regions of embedded systems using genetic algorithms." *2nd National Conference on Emerging Trends and Applications in Computer Science*, pp. 1-6. IEEE, 2011.
- [20] Vudatha Chandra Prakash, Sastry K R Jammalamadaka, and Bala Krishna Kamesh Duvvuri. "Automated generation of Test cases for testing critical regions of embedded systems through Adjacent Pair-wise Testing." *International Journal of Mathematics and Computational Methods in Science & Technology* Vol.2, No.2, (2012), pp. 10-15.
- [21] Wu, Huayao, Changhai Nie, Justyna Petke, Yue Jia, and Mark Harman. "A Survey of Constrained Combinatorial Testing." (2019).
- [22] Ramgouda Patil, V Chandra Prakash, "Neural Network Based Approach for Improving Combinatorial Coverage in Combinatorial Testing Approach", *Journal of Theoretical and Applied Information Technology*, Vol.96. No 20 (2018),pp.6677-6687
- [23] Gouda, Ram, and V. Chandraprakash. "Optimization Driven Constraints Handling in Combinatorial Interaction Testing." *International Journal of Open Source Software and Processes (IJOSSP)* 10, no. 3 (2019): 19-37.
- [24] Ramgouda, P., and V. Chandraprakash. "Constraints handling in combinatorial interaction testing using multi-objective crow search and fruitfly optimization." *Soft Computing* 23, no. 8 (2019): 2713-2726.
- [25] Lott, C., Ashish Jain, and S. Dalal. "Modeling requirements for combinatorial software testing." In *ACM SIGSOFT Software Engineering Notes*, vol. 30, no. 4 (2005), pp. 1-7.
- [26] Grindal, Mats, and Jeff Offutt. "Input parameter modeling for combination strategies." In *Proceedings of the 25th conference on IASTED International Multi-Conference: Software Engineering*, pp. 255-260. ACTA Press, 2007.
- [27] V.Chandra Prakash and Kadiyala Priyanka, 2016. "Test Case Generation for Pairwise + Testing." *Asian Journal of Information Technology*. Vol. 15 No.23 (2016), pp.4800-4805.
- [28] Vrushali Kondhalkar, V.Chandra Prakash. "Automated Generation of Test Cases for Conducting Pairwise plus Testing". *Journal of Advanced Research in Dynamical and Control Systems (ISSN 1943-023X)*, Issue 7 (2018), pp.1484-1492.
- [29] Dr.V.Chandra Prakash, Subhash Tatale, Vrushali Kondhalkar, Laxmi Bewoor. "A critical review on automated test case generation for conducting combinatorial testing using particle swarm optimization." *International Journal of Engineering & Technology (UAE)*, Vol.7, No.3.8, (2018), pp. 22-28.
- [30] Dhadyalla, Gunwant, Neelu Kumari, and Timothy Snell. "Combinatorial testing for an automotive hybrid electric vehicle control system: a case study." In *Software Testing, Verification and Validation Workshops (ICSTW)*, 2014 IEEE Seventh International Conference on, pp. 51-57.
- [31] Dr.ChandraPrakash V, Dr.Sastry JKR, Sravani G, Manasa USL, Khyathi A, Harini A, Testing Software Through Genetic Algorithms – A Survey, *Journal of Advanced Research in Dynamical and Control Systems* Vol. 9. Sp– 12. (2017).
- [32] M. Lakshmi Prasad,Dr.J.K.R. Sastry, A Graph Based Strategy (GBS) for Generating Test Cases Meant for Testing Embedded Systems Using Combinatorial Approaches, *Jour of Adv Research in Dynamical & Control Systems*, Vol. 10, 01-Special Issue, (2018).
- [33] J. Sasi Bhanu, M. Lakshmi Prasad, Dr. JKR Sastry, A Combinatorial Particle Swarm Optimization (PSO) Technique for Testing an Embedded System, *Jour of Adv Research in Dynamical & Control Systems*, Vol. 10, 07-Special Issue, 2018, pp. (321-336).
- [34] M. Lakshmi Prasad, Dr. JKR Sastry, Building Test Cases by Particle Swarm Optimization (PSO) For Multi Output Domain Embedded Systems Using Combinatorial Techniques, *Jour of Adv Research in Dynamical & Control Systems*, Vol. 10, 06-Special Issue, 2018.
- [35] Dr. J Sasi Bhanu, M. Lakshmi Prasad, Dr. J. K. R. Sastry, Combinatorial Neural Network Based a Testing of an Embedded System, *Jour of Adv Research in Dynamical & Control Systems*, Vol. 10, 07-Special Issue, 2018.
- [36] Dr. J Sasi Bhanu, M. Lakshmi Prasad, Dr. J. K. R. Sastry, Testing Embedded System through Optimal Combinatorial Mining Technique, *Jour of Adv Research in Dynamical & Control Systems*, Vol. 10, 07-Special Issue, 2018, pp. (337-354).
- [37] Dr. J Sasi Bhanu, M. Lakshmi Prasad, Dr. J. K. R. Sastry, Testing Embedded Systems Using - A Graph Based Combinatorial Method (GBCM), *Jour of Adv Research in Dynamical & Control Systems*, Vol. 10, 07-Special Issue, 2018, pp. (355-375).
- [38] M. Lakshmi Prasad, A. Raja Sekhar Reddy, J.K.R. Sastry, GAPSO: Optimal Test Set Generator for Pairwise Testing, *International Journal of Engineering and Advanced Technology (IJEAT)* ISSN: 2249 – 8958, Volume-8 Issue-6, August 2019.
- [39] Dr.Sasi BhanuJ, Dr.Baswaraj D, Sunitha Devi Bigul, Dr. JKR Sastry, Generating Test cases for Testing Embedded Systems using Combinatorial Techniques and Neural Networks based Learning Model, *International Journal of Emerging Trends in Engineering Research*, Volume 7, No. 11 November 2019, pp 417-429.
- [40] Moe, Myint Myint. "Comparative Study of Test-Driven Development (TDD), Behavior-Driven Development (BDD) and Acceptance Test-Driven Development (ATDD)." (2019).
- [41] Losada, Begoña, Juan-Miguel López-Gil, and Maite Urretavizcaya. "Improving Agile Software Development Methods by means of User Objectives: An End User Guided Acceptance Test-Driven Development Proposal." In *Proceedings of the International Conference on Human Computer Interaction*, pp. 1-4. 2019.
- [42] Hoffmann, Luiz Felipe Simoes, Luiz Eduardo Guarino de Vasconcelos, Etiene Lamas, Adilson Marques da Cunha, and Luiz Alberto Vieira Dias. "Applying acceptance test driven development to a problem based learning academic real-time system." In *2014 11th International Conference on Information Technology: New Generations*, pp. 3-8. IEEE.
- [43] Basit, Mujeeb A., Krystal L. Baldwin, Vaishnavi Kannan, Emily L. Flahaven, Cassandra J. Parks, Jason M. Ott, and Duwayne L. Willett. "Agile Acceptance Test-Driven Development of Clinical Decision Support Advisories: Feasibility of Using Open Source Software." *JMIR medical informatics* 6, no. 2 (2018).
- [44] Clerissi, Diego, Maurizio Leotta, Gianna Reggio, and Filippo Ricca. "A lightweight semi-automated acceptance test-driven development approach for web applications." In *International Conference on Web Engineering*, pp. 593-597. Springer, Cham, 2016.
- [45] Nilsson, Johan, and Xiaoqian Xiong. "Applicability of Acceptance Test Driven Development in Integration and Verification Process in a Large Scale Company." (2016).
- [46] Ramler, Rudolf, and Claus Klammer. "Enhancing Acceptance Test-Driven Development with Model-based Test Generation." In *2019 IEEE 19th International Conference on Software Quality, Reliability and Security Companion (QRS-C)*, pp. 503-504.
- [47] Anang, Yunarso, Masakazu Takahashi, and Yoshimichi Watanabe. "Collaborating Acceptance Test-Driven Development and QFD in Business System Software Development." (2017).
- [48] Connolly, David, Frank Keenan, and Fergal McCaffery. "Acceptance test-driven development by annotation of existing documentation." (2010).
- [49] Aggarwal, Vishal, and Manpreet Singh. "Acceptance Test Driven Development." *Journal of Advanced Computing and Communication Technologies (ISSN: 2347-2804)* (2014): 1-4.
- [50] Weiss, Johannes, Peter Mandl, and Alexander Schill. "Introducing the QCEP-testing system for executable acceptance test driven development of complex event processing applications." In *Proceedings of the 2013 International Workshop on Joining AcadeMiA and Industry Contributions to testing Automation*, pp. 13-18.
- [51] Axelrod, Arnon. "Acceptance Test Driven Development." In *Complete Guide to Test Automation*, pp. 371-394. Apress, Berkeley, CA, 2018

# A Comprehensive Study of Blockchain Services: Future of Cryptography

Sathya AR<sup>1</sup>, Barnali Gupta Banik<sup>2</sup>

Department of Computer Science and Engineering  
Koneru Lakshmaiah Education Foundation, Deemed to be University  
Hyderabad, Telangana-500075

**Abstract**—Cryptography is the process of protecting information from intruders and letting only the intended users' access and understand it. It is a technique originated in 2000 BC where simple methods were used in earlier times to keep the information in a way that is not understandable by everyone. Only the intended receiver knows how to decode the information. Later, as technology advances, many sophisticated techniques were used to protect the message so that no intrusion can invade the information. Many mathematically complex algorithms like AES, RSA are used to encrypt and decrypt the data. Due to the advancements in the computer science field, recently, cryptography is used in the development of cryptographic currencies of cryptocurrencies. Blockchain technology, a distributed ledger technology identified to be the foundation of Bitcoin cryptocurrency, implements a high-level cryptographic technique like public-key cryptography, Hash Functions, Merkle Trees, Digital signatures like Elliptic curve digital signatures, etc. These advanced cryptographic techniques are used to provide security to blockchain data and for the secure transmission of information, thereby making Blockchain more popular and demandable. Blockchain applies cryptography in various phases, and some of the techniques used in Blockchain are advanced in cryptographic sciences. This paper intends to provide a brief introduction to cryptography and Blockchain Technology and discusses how both technologies can be integrated to provide the best of the security to the data. This paper reviews the various cryptographic attacks in Blockchain and the various security services offered in Blockchain. The challenges of blockchain security are also analyzed and presented briefly in this paper.

**Keywords**—Cryptography; cryptocurrencies; blockchain; bitcoin

## I. INTRODUCTION

Blockchain is a distributed, P2P, decentralized network where data is secure and tamper-proof. The transaction over the networks are recorded transparently without any third party. Although Blockchain technology was developed to support cryptocurrencies, industries of various sectors show great interest in adapting them for their interest. Like financial transactions, supply chain, secure contracts, sharing sensitive information, governance, and many more. The critical issues of existing systems are information security and data storage. Blockchain technology resolves these issues by assuring transparency and maintaining the integrity of the stored data. Generally, it is believed that the data is authentic if there is a central server or a third party to maintain the data. It is very much essential to encrypt the data if there is no trusted central system. Therefore, cryptography plays a vital role in

Blockchain. In Blockchain, cryptography is adapted to ensure the consistency of the data, guard user privacy, and transaction information [1].

The organization of the paper is as follows. Section II elaborates the cryptography background of Blockchain Technology. Section III discusses the convergence of cryptography and Blockchain. The various security attacks and security services are presented in detail in Sections IV and V, respectively. Section VI summarizes the applications of blockchain technology and the different challenges are described in Section VII.

## II. BACKGROUND

### A. Related Knowledge on Blockchain Technology

Blockchain is a decentralized public ledger distributed over the network recording the transactions of the network [2]. The distributed ledger is open to the public, and every node in the network has a copy of the ledger. Transactions over the network are combined as blocks, and every block is connected to the previous block using hashing algorithms. The network nodes strictly protect the data into blocks and broadcast the information to the network. Hashing helps in ensuring the data integrity by linking each block with the other by the hash code. Thus, a chain of blocks linked via a hash is called Blockchain. The simple architecture of Blockchain has been demonstrated in Fig. 1. Blockchain is the underlying technology of the most popular cryptocurrency Bitcoin. Later many other cryptocurrencies, like altcoins, peercoins, litecoins added more popularity to this technology. At present, Blockchain is one of the fastest-growing technologies due to its unique features like immutability, integrity, security, and reliability. After bitcoin, Ethereum is the most successful Blockchain-based project. Ethereum is a platform used to develop decentralized applications (DApps) and Smart contracts. Over the last decade, there are several MNC's that backs up many start-up companies for Blockchain-based projects. At present, companies of various domains are researching to find the possible use-case to fit in Blockchain so that maximum benefits can be achieved. However, many Blockchain-based solutions are still in the pilot stage and need more research and regulations to standardize. FinTech, Supply-chain, Healthcare, IoT, Decentralized storage, smart contracts are some of the most researching areas of Blockchain.

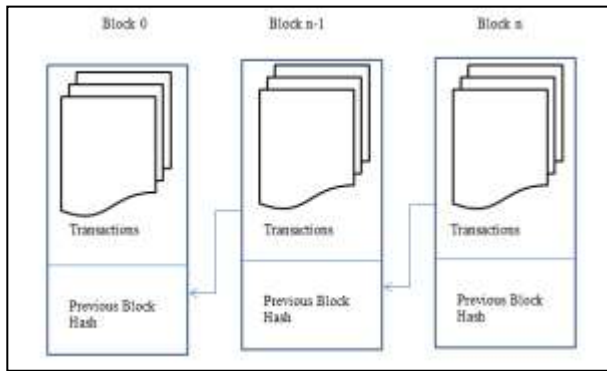


Fig. 1. A Simple Blockchain Architecture.

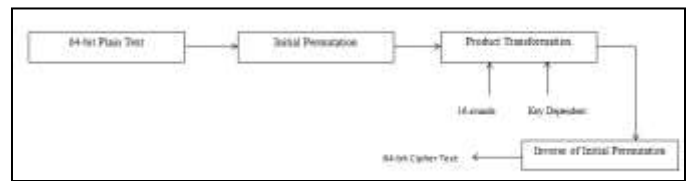
### B. Related Knowledge on Cryptography

Cryptography came into existence even before the age of computing. In ancient times, a simple cryptography algorithm called Caesar cipher is used to transmit messages. In Caesar cipher, each alphabet will be replaced by a letter three places after that. For example, A becomes D, B becomes E, and so on. The message remains private as long as the system used in creating the ciphertext remains secret. Therefore, the process of keeping information safe and protecting them from attack is termed cryptography. So, cryptographic algorithms are introduced with encryption keys to decrypt the secret messages. These methods can be easily broken by identifying the frequency of letters. Later, Enigma Machine, a system using multiple rotors, is used to generate ciphertext, which cannot be broken quickly based on letter frequency. The need for protecting business secrets gave rise to the development of the Data Encryption Standard (DES) by IBM. As the computing power increases, Advanced Encryption Standards (AES) are developed due to inadequacies of DES. Encryption has become an integral part of everyday life, which is also the backbone of cryptocurrencies. Although many of the cryptography algorithms become obsolete, Blockchain uses hashing, public-key cryptography, and Merkle Tree cryptographic methods [3].

1) *Symmetric encryption*: Two popular methods used to encrypt the data are Symmetric and Asymmetric encryption. Symmetric key algorithms are traditional encryption algorithms. It uses a single private key is used to encrypt and decrypt a message. Symmetric algorithms needed both the sender and the receiver to agree upon the private key before information exchange. Symmetric methods are faster compared to asymmetric methods. Nevertheless, the algorithm's security depends on keeping the key secret. If the key is lost, the encryption algorithm can be cracked easily. Also, by using a complex mathematical formula on an encrypted plaintext, it is possible to find the key used to decrypt the plain text. The symmetric key algorithms are of two types Sequence and packet encryption algorithm. In a sequence encryption algorithm at a time, a single bit of data is encrypted, whereas a set of bits is encrypted in packet encryption. DES algorithm, a popular symmetric encryption scheme, uses the conventional form of Encryption, block cipher. The general process of the DES encryption technique

is shown in Fig. 2.a, whereas the detailed internal process is shown in Fig. 2.b.

The plaintext has to be transformed, and the block containing the information will be divided into two parts and then is transformed by a function  $f$ . It will be repeated 16 times. The two parts of the information are combined after product transformation. An inverse transformation will be applied to the combined information. As an example, the original first reverse transformation, the left shifted message is 48 bits, and then the existing 32-bit value is replaced by the final result instead of the substitution result. The substitution operation is done as per the steps above. The method mentioned above is the execution cycle of the function  $f$ , and the output is XOR worked with the left part, replacing the current output with the actual part. The DES encryption method was finished after 16 run cycles. The same algorithm is used for decryption as well. The key must be in reverse, while decrypting is the only difference. A circular key is generated for every circle by DES, and transfers for relocation to the right in turn [5]. One of the significant drawbacks of symmetric algorithms is weak keys. The weak key is the one that contains all 0's, all 1's or half 0's, and half 1's after symmetry drop operation. The weak key allows the attacker to decipher the DES encryption at a reduced time.



(a) A High-Level view of a Symmetric Encryption Method.

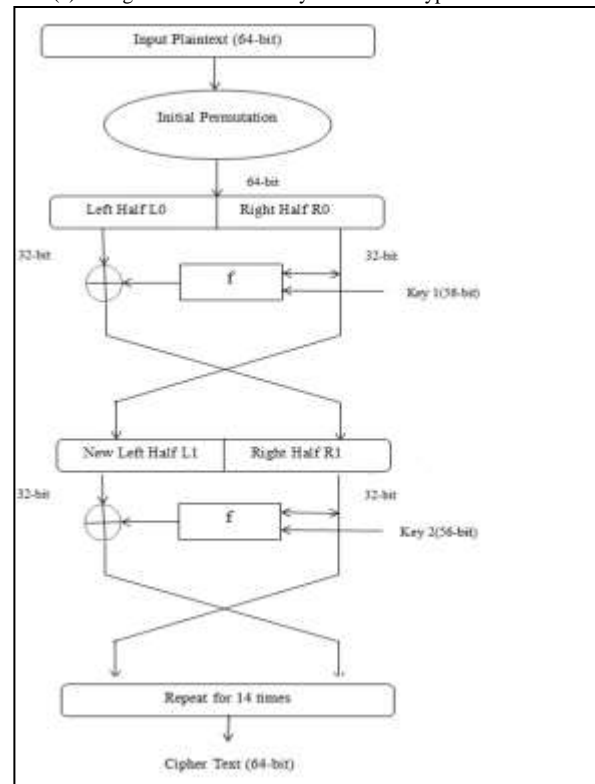


Fig. 2. (b). Internal Process of DES Encryption Algorithm [4].

2) *Asymmetric encryption*: The Asymmetric Encryption was developed to resolve the problems of symmetric key algorithms. It is otherwise called as public-key cryptography. In asymmetric Encryption, two different keys name public and private keys are used in encryption and decryption process. Both the keys are mathematically linked. The public key is used in the encryption process, and it can be decrypted using the private key. The security of the network is assured by two unrelated keys in public-key cryptography. The process of public key Encryption and decryption can be denoted by the equation below.

$$\text{EncryptKey1(Plaintext)} = \text{Cipher} \quad (1)$$

$$\text{DecryptKey2(Cipher)} = \text{Plaintext} \quad (2)$$

$$\text{DecryptKey2(EncryptKey1(Plaintext))} = \text{Plaintext} \quad (3)$$

3) *Comparison between symmetric and asymmetric key encryption*: Both symmetric and asymmetric key Encryption has its advantages and disadvantages. In a secure transmission, the symmetric key algorithm is highly efficient, whereas efficiency is relatively low in public key cryptography. Though the use of two different keys in the asymmetric method significantly improves the security process, there is a decline in the transaction speed when compared with symmetric methods [6]. Thus, the combination of the public key and symmetric key gave rise to digital envelopes for transmitting data safely. It allows the data to be encrypted as fast as symmetric key and as secure as the public key.

### III. THE CONVERGENCE OF CRYPTOGRAPHY AND BLOCKCHAIN NETWORK

Blockchain Technology is a combination of a peer-to-peer network, cryptography, and Game Theory. Blockchain uses cryptography in various ways, especially security and privacy mechanisms [7]. Enabling digital signatures, wallets creation, secure and transparent transactions are some of the areas where Blockchain uses cryptography. Some of the essential cryptographic techniques used in Blockchain are Hashing, Digital signatures, and Merkle Trees [8].

Fig. 3 summarizes the different cryptographic components included in Blockchain.

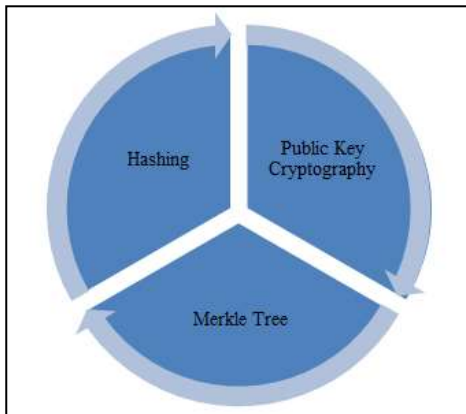


Fig. 3. Role of Cryptography in Blockchain.

#### A. Hashing Mechanism

Hashing is a cryptographic method in which any kind of data is converted to character strings. Hashing not only provides security, but it also provides efficient storage of data as the size of hashing output is fixed. Any hash algorithm, only if it confirms specific properties, it can be used for providing security services. These properties are not inherently provided by any general-purpose hash functions. This is the reason why algorithms like SHA-2 are considered as cryptographic hash functions. Some of the critical features of hashing are the one-way or pre-image resistance nature, which is why it always produces the same output for the same input. Also, by using hashing output, it is impossible to deduce the input. The second pre-image resistance property assures that no two different messages can have the same hash value. Any minor change in the input also creates an entirely different hashing output, and no two inputs can ever produce the same hash output. This is due to the collision resistance property of the hashing function [9]. The only concern of hashing is that generating hash values should be fast and should not use much computing power. The hashing algorithm used in bitcoin blockchain is SHA-256. SHA-256 is a part of the SHA-2 cluster and generates a 256 bits or 64 hexadecimal characters output. Refer Fig. 1 of blockchain architecture, which shows how the blocks are connected using the hash of the previous blocks.

SHA-256 algorithm follows a two-phased approach: pre-processing of the message and main loop. In the first phase, i.e., the message pre-processing phase, the process of filling the message length and binary bit on any message length is performed. Later, the messages are split into many 512 bit message blocks. In the second phase, a compression function processes the entire message blocks of phase-I. In other words, the input of a new compression function is the output of the previous compression function, and the output of the final compression function is the hash of the final message.

In Blockchain, each transaction is hashed and bundled together in blocks, and each block is connected to the predecessor block using a hash pointer, i.e., the hash of all information of every previous block is stored in the Header of every block. Hashing is responsible for Blockchain's distinct feature of immutability and is used for verifying any transaction's integrity. This can be achieved by comparing the calculated hash with the stored hash value in the block header. Once the public keys are generated using ECDSA, a set of hash functions are applied to the key to generating a unique hash address. The public-private key pairs can also be generated using a hash function [10].

The block view is given in Fig. 4. A block contains a block header and a block body. The Header includes many data like the hash value of the previous block, nonce- a random number, timestamp, target value, and Merkle root. The block body includes the set of all transactions in the block. Prev Hash: It is the hash value of all the information of the previous block. This also assures the integrity of the previous block data. Nonce: A random number whose initial value is 0. The bitcoin node always conducts an SHA-256 procedure on the block's total data. If the SHA-256 value determined by the current random number does not satisfy the criteria; instead,

one unit reduces the random number and the SHA-256 operation proceeds. A new data block is created and approved by the P2P network if the value of SHA-256 is smaller than the current block's SHA-256 value. This process of block generation is called Proof-of-Work (PoW). **Timestamp:** This is the time at which the data is written in the block. The data blocks are arranged in chronological order based on the timestamp on the header block. **Target:** A target hash is a value that a hashed block header needs to be below or equivalent to in order to create a new block. The SHA-256 value in the block determines the target value. **Merkle Root:** Merkle tree is a hash tree to verify the integrity of a large amount of data. **Transaction List:** All information about the transactions like Payer, Receiver, Timestamp, the amount transferred, transaction id, etc.

The usage of the hashing mechanism in Blockchain is categorized into the following. Address generation, Proof-of-Work (PoW), Block generation, Random number generator, Message Digest (MD) signatures, and bridge components [11].

Due to the advancements in the mining techniques, the possibility of having 51% attacks [12] is increasing, thereby giving rise to new hashing mechanisms. It is well known that SHA-256 is the hashing algorithm used in Blockchain. Some of the other popular hashing algorithms are SCrypt, a memory hard hash function used in Litecoin, Fairbrix and Tenebrix [13], X11, which is used in Darkcoin is a combination of 11 hash functions taken from SHA-3 [14], Equihash, another hard memory function proposed by [15] and Ethash an ASIC-resistant hash function widely adapted in Ethereum based cryptocurrencies [16].

### B. Digital Signatures

Digital Signature is an Asymmetric Cryptographic method, specifically public key Encryption. Unlike symmetric cryptography, where the same key is used by both the sender and receiver asymmetric method uses a pair of the key is connected by cryptography. If user A wants to prove certain information is authentic and wants to maintain data integrity, then he/she can digitally sign the information and can transmit over the network. In bitcoin, digital signatures are used to make cryptocurrency transactions. To create a digital signature, the information to be sent will be processed by a hashing algorithm to generate unique strings. Later, these strings can be digitally signed using user A's private key. In more straightforward ways, the digital signature is a combination of hash code and the private key of the user. Moreover, to verify, the user's public key can be used to check the authenticity of the user as well as the data. Fig. 5 shows the sending and verification of digital signatures. Elliptic Curve Digital Signature Algorithm (ECDSA) and RSA are some of the algorithms used in generating the public and private key pairs. DSA's elliptic curve version, ECDSA, is widely used in blockchain implementation as it provides many benefits, such as decreased key size and quicker calculation compared to other discrete algorithms based on logarithms and factoring algorithms based on modules [17]. Relevant domain parameters specify elliptic curves are ideal for cryptographic operations [18]. A variety of such curves are available, and few are standardized by NIST, IEEE, ANSI, and others.

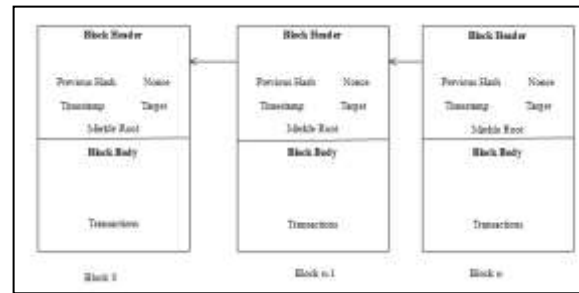


Fig. 4. Structure of a Block.

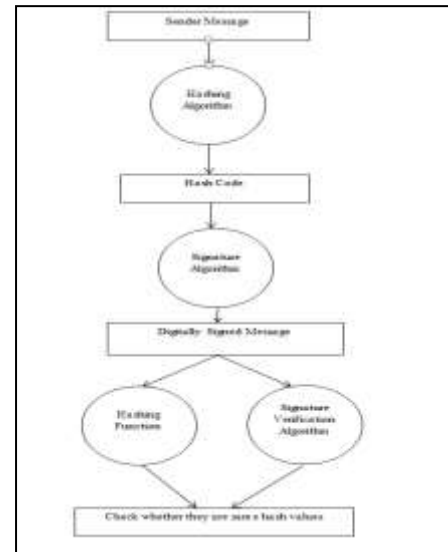


Fig. 5. Signing and Verification of Digital Signatures.

### C. ECDSA

The digital signature scheme used in bitcoin blockchain for signing the transaction is the Elliptic Curve Digital Signature Algorithm, i.e., ECDSA [19]. The standard "secp256k1" elliptic curve algorithm is used in Blockchain. Secp256k1 is built on a finite field with an elliptic curve. Its engineered design will produce an advantage of 30 percent over other curves due to its unique structure. The sep256k1 constant will effectively eliminate loophole possibilities. ECDSA is immune to 'chosen-message attack,' where a genuine entity E intends to fabricate a valid signature on an unknown message m, once the attacker acquired the signature of the entity E by posting a set of queries to a collection of messages (other than m).

It is known that Blockchain uses public/private key pair. The public key encryption method is used to generate key pairs. A private key is a random number, whereas the public key is generated by encrypting private keys using the elliptic curve multiplication technique. A public key generates the bitcoin address of a user through a single entry encrypted hash function. The private key is created by selecting a random number between 1 and  $2^{256}$ . The number should be selected in such a way that it should not repeat and predicted easily. In bitcoin to generate the 256-bit random number, the random number generator of the OS is used. This generated random number is the private key k. The private key k is multiplied with the defined generation point G of the curve to get another

point in the curve. That would be the corresponding public key K. The connection between K and K is static in a uni-directional way. In other words, it is possible to detect K from k but not the other way. Several algorithms are used in different cryptocurrency platforms to generate addresses. For instance, SHA-256 and RIPEMD160 are used in Bitcoin, whereas Keccak 256 is used in Ethereum [20].

#### D. Merkle Trees

Merkle tree is a method of hashing a considerable amount of data that is divided into small blocks, and each block is hashed and is combined and re-hashed again with another block to generate a combined hash. This is a repetitive process and will be continued until a single hash code is achieved from a group of blocks. Refer Fig. 6 below for a Merkle tree representation.

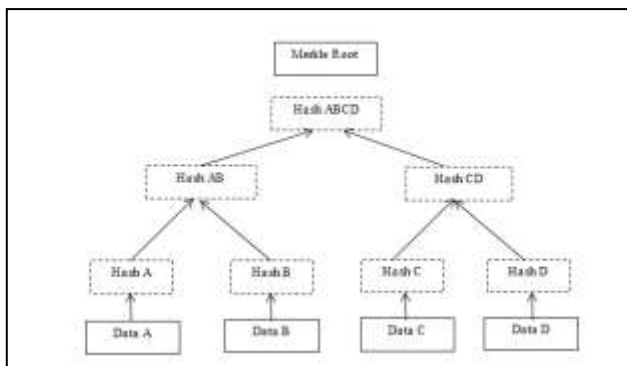


Fig. 6. Representation of a Merkle Tree.

Merkle tree uses a hashing mechanism and stores the hash output rather than storing the data itself. The Merkle root is the root node of a Merkle tree, which has the combined hashes of the left and right sub-trees. Since each block holds the hash value of the previous block, the data in Blockchain is unchangeable [21]. A double SHA-256 hash algorithm is used in the Bitcoin blockchain. In other words, the original data of any length is applied to two SHA256 hashing operations. For uniform identification and storage, a 256-binary digit is used. Various cryptographic algorithms are used by different Blockchain. SHA-256 is being used by Bitcoin blockchain. Ethereum uses Keccak256, whereas Litecoin and Dogecoin use a lighter and faster cryptographic algorithm Scrypt. Hashing helps in ensuring the integrity of the data in Blockchain.

#### IV. POSSIBLE SECURITY ATTACKS ON BLOCKCHAIN

Despite its nature to secure data, Blockchain is susceptible to different security-related attacks [22][23]. Fig. 7 shows the various security attacks on a blockchain network, and possible solutions for those attacks are listed in Table I.

##### A. Key Attacks

1) *Cryptographic algorithm attacks*: The elliptical curves used in Blockchain cryptographic operations are derived using parameters that may be compromised and can allow an attacker to know the secret numbers to break the encrypted messages of 32-bit size [24].

2) *Hashing attacks*: Most of the blockchain implementations use the SHA-256 algorithm as it is considered to be secured. However, SHA algorithms can be attacked by length extension attacks. Through this attack, one can add intruder-controlled data to digitally signed information and can change the hash of the message without revealing the shared information. Hashing algorithms are also prone to birthday attacks in which the collision resistance property of the hashing can be broken [26].

##### B. Identity Attacks

1) *Sybil attacks*: In Blockchain, few specific nodes will be identified as the target node, and the intruder will not relay any transactions to and from the target node and deploys double-spending attacks using the target nodes.

2) *Impersonation attacks*: Imitating like honest nodes to gain access.

3) *Replay attacks*: Communication between two genuine users is imitated by the intruder to gain access and steal the hash key. Reusing the hash key makes the intruder an authentic user.

##### C. Manipulation Attacks

1) *Eclipse attack*: A particular node will be identified and will be isolated from the network and will not get any transactions or blocks from the rest of the network. The intruder will waste the resources of the target node or use it for malicious activities [31].

2) *Transaction malleability*: It is a bitcoin design issue where the transactions can be changed after creation but before getting added to a block. Information like sender and receivers address, money transferred will not be changed, but data like transaction id can be modified. As the transaction id gets changed, it is not possible to validate the transactions, and attackers can withdraw money transferred.

3) *TimeJacking attacks*: Timejacking is an attack that aims to bias the timestamp of a target node by linking several peers to a target and transmitting an incorrect time to the target. This lets the node to reject transactions due to wrong timestamps. It is thereby letting the malicious user to do fraudulent transactions.

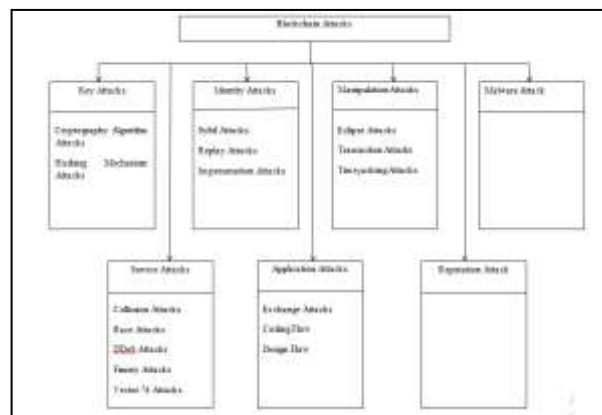


Fig. 7. Various Blockchain Security Attacks.

TABLE I. SUMMARY OF SECURITY ATTACKS IN BLOCKCHAIN

| Category             | Attacks                         | Solution                                                                                                              |
|----------------------|---------------------------------|-----------------------------------------------------------------------------------------------------------------------|
| Key Attacks          | Cryptographic Algorithm Attacks | Use cryptographically secure random number generator                                                                  |
|                      | Hashing Attacks                 | Use double SHA-256 [25]                                                                                               |
| Identity Attacks     | Sybil Attacks                   | Create unchangeable chains where interactions between users are assessed periodically [27].                           |
|                      | Impersonation Attacks           | Use Feature-based Signatures and distributed incentives approach [28][29].                                            |
|                      | Replay Attacks                  | Use elliptic curve based Encryption or have one-time private-public key pairs [30]                                    |
| Manipulation Attacks | Eclipse Attack                  |                                                                                                                       |
|                      | Transaction Malleability        |                                                                                                                       |
|                      | TimeJacking Attacks             | Several countermeasures suggested like time monitor, network encryption, checking the node connection diversity [32]. |
| Reputation Attack    |                                 | No proper approaches yet                                                                                              |
| Service Attacks      | Race Attacks                    | Hold till at least a minimum number of confirmations are received.                                                    |
|                      | DDoS Attacks                    | No standard solutions yet.                                                                                            |
|                      | Double Spending Attacks         |                                                                                                                       |
|                      | Finney Attacks                  | Wait for more confirmation.                                                                                           |
|                      | Vector 76 Attacks               |                                                                                                                       |
|                      | Collusion Attacks               |                                                                                                                       |
| Malware Attacks      |                                 |                                                                                                                       |
| Application Attacks  | Design Errors                   | It is fixed by dividing Ethereum Blockchain into Ethereum Classic and Ethereum. Better desi.gn                        |
|                      | Coding Errors                   | Better design and coding principles                                                                                   |

#### D. Reputation Attack

Act of changing the reputation of a user from bad to good. This can be done by having a new account or by hiding the fraudulent transactions.

#### E. Service Attacks

1) *Race attacks*: Malicious users create two transactions one genuine and one false. Any node which takes zero confirmations (a transaction yet to be included in the block) is then targeted, and the false transaction is directly sent to the target, whereas the genuine transaction is sent to the pool. The target may approve the transaction that is not genuine and may provide the service.

2) *DDoS attacks*: The network may be seized, and a vast amount of service requests may be sent that the network may not be able to handle [33].

3) *Double spending attacks*: By bribing the significant number of nodes, a user may be able to spend the assets more than once.

4) *Finney attacks*: These are the continuation of double-spending attacks, where the attacker adds all his internal transactions to his block and releases only when he finishes double-spending them by zero-confirmation methods.

5) *Vector 76 attacks*: A mixture of Finney and Race Attacks.

**Collusion Attacks**: Popularly it is the 51% attack where more than 51% of the network resources are compromised or controlled by a single source. This enables any malicious activity to take place within the network.

#### F. Malware Attacks

It is a standard attack in pocketing cryptocurrencies. This can get into Blockchain by mining software or storing some arbitrary data along with immutable data. Leads to several other attacks like DNS, Man-in-the-Middle Attacks [34].

#### G. Application Attacks

1) *Design errors*: The design of the Decentralized Autonomous Organization (DAO) allows the users to take their money out or put them in a separate DAO. This system was later hacked and led this feature to repeatedly put the funds in child DAO but before the actual fund transmission.

2) *Coding errors*: A bug in coding led to the attacks of wallets.

### V. SECURITY AND PRIVACY SERVICES OF BLOCKCHAIN

Every node in the blockchain network maintains a copy of the Blockchain, and a miner is the one who creates and validates the block. A Blockchain network is a peer-to-peer network that verifies itself and eliminates the third party for verification. It offers rewards to the network nodes that do the validation process honestly. This process of validating the transactional data is called mining. The Blockchain uses concepts like Proof-of-Work (PoW), Proof-of-Stake (PoS), Proof-of-Space (PoSpace), Practical Byzantine Fault Tolerance (PBFT), etc. based on a hashing scheme to validate the data. A cryptographic puzzle has to be solved by a network and then broadcasts the results to the network for verification to include a timestamp to the network. This proof-of-work concept keeps the network authentic. The SHA-256 algorithm is used in PoW as it is comparatively complex to solve but can be verified easily. The variety of security and privacy services offered by Blockchain are listed below [35].

#### A. Services of Encryption and Authentication

1) *Traditional systems*: The vital security services that any network can offer are Authentication and Encryption. This can be achieved by using public-key cryptography (PKI) framework. Of all the security services offered by PKI, user authentication, and message confidentiality are the most severe service in all network applications. User authentication can be done by having digital signatures and confidentiality by using simple encryption/decryption techniques [36]. It is well known that traditional PKI systems use a trusted third-party certificate

authority (CA) to manage the key distribution. Another approach is Web of Trust (WoT), which follows a decentralized approach by locally generating the key and verified by a trusted third-party. Some of the challenges of these traditional PKI systems are security, cost, and centralized system. Security of generating and distributing the key is at risk if the trusted third-party (CA) is negotiated. Since there is a central system involved the risk of a system failure leading to data loss and increased cost for maintenance by a single entity. On the other hand, in WoT systems to join a network, the users have to create trust with the existing users, who might be a difficult task for new users. Moreover, both the traditional systems lack in identity retention, i.e., it lets the users impersonate the identity of a user who already registered in the network.

- 2) Current Blockchain-based PKI
- 3) Authentication services through Encryption

The drawbacks of traditional PKI systems can be resolved by Blockchain-based PKI. Since Blockchain is distributed in nature, it does not need a centralized repository of data. Prior trusts among the users are not necessary as the trust is created based on the majority of votes by the nodes (miners) [37]. Blockchain has many open-source implementations leading to economical and efficient solutions. Several approaches are followed to attain Blockchain-based PKI solutions.

*a) Instant Karma PKI:* The traditional CA approach is extended in this approach, where the activity of CA is recorded in Blockchain. This helps to identify the compromised CA's, thus eliminating trust related issues of the traditional PKI system. However, including a CA still creates a dependency on the third party.

*b) Distributed PKI:* Distributed PKI uses a web-based domain registration system in which the user generates the private and public key pair, and as a transaction, the public key is registered in the Blockchain. This approach avoids the man in the middle attacks by connecting the identity of the user with the latest key of the user [38].

*c) Gan's Approach:* A key based verification system exclusively for IoT environments is proposed by Gan [39]. This aims to have a private blockchain to store the nodes' public keys and validating them. It includes a centralized CA which is connected to some validators who are responsible for generating the keys and maintaining the blockchain database. The IoT devices are connected to these validators. This is a cyclic process where a validator brings in the public key of an IoT node, gets it validated, and signed through the CCA and records the transaction on Blockchain. However, this approach as well suffers the central point of failure due to a centralized CA.

*d) Blockstack:* Namecoin [40], a division of bitcoin, is used here to develop a distributed PKI system. Namecoin enables data storage in blockchain transactions. This system uses a name-value pair to record the user names and will be stored in the Blockchain. Blockstack modifies the Namecoin system by including the public key as another name-value

pair. Similar to Namecoin, Certcoin [41], another decentralized network is used for identity retention services.

*e) Blockchain-based IBC:* Identity-based cryptography techniques need a centralized system to generate private keys. Hence, if this central system is compromised, the entire system can be compromised. This problem of centralization can be resolved by using a Blockchain-based approach as it adapts a decentralized approach. Since users can generate their keys in the blockchain network, there is no need for a central system to generate the key pairs.

## B. Services of Confidentiality

A privacy service lets the user set the control and accessibility of the data by the network. It enables complete ownership of the data. Data privacy is more important in the case of networking systems as the network is shared by many users.

*1) Traditional techniques:* In general, data privacy can be achieved by defining Access Control List (ACL) where the user lists who can access what information and when. An encryption technique, like homomorphic Encryption [33], can be used to prevent unauthorized access. Another traditional approach is Data anonymization, where the user's identity can be hidden and hence not possible to link them with the data. Some of the techniques to achieve data anonymization are K-anonymity, T-closeness, and L-diversity. Although several approaches are available to assure data privacy, there are few drawbacks like scalability, efficiency, lack of ownership, and methodical lifecycle approach, which cannot be overlooked.

*2) Blockchain-based privacy:* The decentralized data privacy based on Blockchain can resolve the drawbacks of traditional systems. It guarantees complete ownership of data by the users and enables a dynamic ACL as and when needed. Blockchain-based systems are highly dependent on cryptographic techniques; hence they are still challenging to implement. The objective of data privacy based on Blockchain is to construct a layer named the blockchain layer above the data storage layer [42]. This allows the users to define their ACL and publish them through smart contracts. This enables the data to be stored as blockchain transactions which are encrypted. Therefore, no central entity can own the data as in traditional systems. Nevertheless, the data can be accessed if they are part of the blockchain network and only if the ACL allows them. Some of the privacy preserving techniques based on Blockchain are listed below:

*a) Zyskind's Technique:* This is a decentralized approach in which data and ACL are stored in blocks of the Blockchain, and the user (owner) is provided complete access to it. The user can send ACL and data as a transaction over the blockchain network and will be verified by the nodes of the network. Whenever some other user needs to access the data, a request can be sent to the network and can receive an encrypted response only if he has given access to ACL.

*b) Fair Access and IoT:* Fair access is a decentralized, pseudonymous privacy preserving mechanism that enables the user to access and control their data. Through Fair-Access, a



user can grant, receive, request, and revoke access through smart contracts.

### C. Data Integrity Services

Integrity means that data is correct and valid. This property guarantees that data have not tampered when stored or during transmission. In Blockchain, the data can be the ones that are stored, produces, and accessed by the network. Integrity in Blockchain is assured by digital signatures and public-key encryption methods [43].

1) *Traditional techniques:* Currently, using data replication techniques and cryptographic tools, data integrity is maintained. Cryptographic tools can be public-key cryptography and digital signatures, which will not allow any unauthorized person to access the information. It is possible to identify whether the data has been modified by using any signature verifying technique. Keeping the keys secret is the main task in traditional methods, but if the key is identified once, it is not possible to foresee the attacks that can happen [44].

In traditional techniques, identifying an intruder in case of an attack is a severe problem. This is because intrusion could have happened anywhere, like transmission, processing, or storage. The need to identify the intruder can be various like to detect the kind of mischievous activities, to modify the access mechanism, or to punish the intruders. Dependency on a third party is another factor where trust can be an issue. Also, integrity is another added security that would need additional resources and adds complexity to the system.

2) *Blockchain based integrity:* Blockchain has built-in integrity checks where the sender signs the transactions, and a miner verifies it. It is known that data, once saved in Blockchain, is tamper-proof forever, thereby assuring integrity. For IoT devices, a specialized framework for data integrity has been proposed [45]. The objective of this framework is to store the encrypted hash values of user data on Blockchain. Later, the hash values can be used to verify integrity. Another approach is Storj, a P2P system used for storage. It stores the hash values of the blockchain database, which is immutable and ensures data integrity.

## VI. APPLICATIONS OF BLOCKCHAIN TECHNOLOGY

Decentralized nature, immutability and the security services feature of blockchain makes the technology to dive in various domains. Many industries currently focusing to identify an appropriate use case for Blockchain to fit in. Some of the major areas where Blockchain is applied other than Financial services are Education [46], Healthcare [47], Supplychain, IoT [48], Data Management and security services [49], Energy sector [50] and so on. The wide variety of applications where Blockchain can be adopted is shown in Fig. 8.

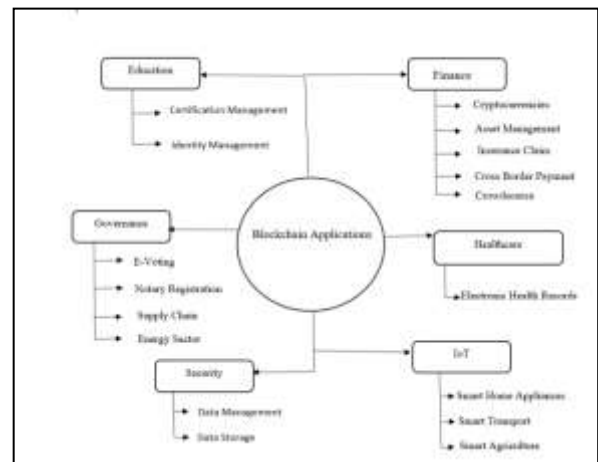


Fig. 8. Applications of Blockchain Technology.

## VII. CHALLENGES OF BLOCKCHAIN SECURITY

### A. Scalability

Many of the blockchain implementations have scalability issues due to the block size and the approximate time taken to publish the blocks. Few types of research suggest enhancing the scalability by increasing block size. More transactions can be accommodated if the block size is increased [51]. However, increasing block size delays the propagation speed. However, as per the discussion in [52], the current propagation techniques are not optimized and increase the risk of several attacks. So if the block size increment decreases the block propagation speed, it may increase the possibility of more attacks. Another countermeasure for this scalability problem is SegWit. SegWit, otherwise called Segregated Witness, creates a certain amount of space in a block by separating the data used for verifying the transactions. i.e., signature data and transaction data. However, this approach alone cannot suffice to handle Blockchain's scalability issue.

### B. Privacy

As discussed before, bitcoin and several other cryptocurrencies, though considered to be anonymous they genuinely are not [53]. It may not be easy but not impossible to find the real identity of the user using their transaction history. Thus, they can be termed as pseudonymous. There is some software available to de-anonymize the cryptocurrencies. The possible approach to solve this privacy issue has CoinJoin services. CoinJoin combines several accounts and then transfers the coin in a pseudo-random manner and makes the transaction anonymous. Ethereum blockchain, where smart contracts and DApps are used, are highly susceptible to privacy issues. To keep the smart contracts, secure and anonymous many methods are suggested by V Buterin in [54].

### C. Computations and Time Consumption

Majority of the applications that are currently used are simple and does not require high computational resources, whereas blockchain client needs very high computational abilities to handle the mining activity. Providing any security service needs quick processing capabilities, but in Blockchain, the consensus mechanism and mining process is time-

consuming [55]. However, this issue has been addressed in Ethereum and Hyperledger platforms but still needs many improvements to handle this issue.

### VIII. DISCUSSION

In this paper, a comprehensive study on the cryptographic techniques with a specific emphasis on blockchain technology and related security and privacy aspects of it. We have provided in the survey the cryptographic techniques that are included in blockchain and an in-depth study on various attacks on the blockchain network. We have also presented a detailed investigation of various security and privacy services of blockchain. The application areas and the challenges of the technology are also briefly discussed in this paper. The paper included referrals from peer-reviewed works aiming to provide a detailed insight of the blockchain technology from the security perspective.

### IX. CONCLUSION

In the past decade, Blockchain Technology is the interesting inventions of cryptography and information & communications. This paper presents the evolution of cryptographic mechanisms and the different cryptographic methods used in Blockchain. The various security attacks aimed at Blockchain are also discussed. The different security services offered for authentication and privacy and the challenges of Blockchain are discussed in brief. This study highlights that blockchain implementations are majorly based on the cryptographic concepts and provides a roadmap for future developments in blockchain technology. Thus, it can be concluded that cryptography plays a major role in the internal functioning of blockchain technology. The foundation for blockchain transactions and wallets are based on public-key Encryption, and the use of cryptographic hashing mechanism along with Merkle tree concepts enables the immutable nature of Blockchain and providing a high-end security.

### REFERENCES

- [1] W. Diffie and M. Hellman, "New directions in cryptography," in *IEEE Transactions on Information Theory*, vol. 22, no. 6, pp. 644-654, November 1976. DOI: 10.1109/TIT.1976.1055638.
- [2] S. Nakamoto. Bitcoin: A Peer-to-Peer Electronic Cash System. 2009. Accessed: February 13, 2018. [Online]. Available: <http://www.bitcoin.org/bitcoin.pdf>.
- [3] Xiaochun Yun • Weiping Wen Bo Lang • Hanbing Yan • Li Ding Jia Li Yu Zhou (Eds.), *Cyber Security, 15th International Annual Conference, CNCERT 2018, Beijing, China, August 14-16, 2018*, doi.org/10.1007/978-981-13-6621-5.
- [4] W. Stallings, *Cryptography and Network Security Principles and Practices*, 4th ed. Prentice-Hall, 2005.
- [5] J. Shivani and Ranjan Senapati. "Robust Image Embedded Watermarking Using DCT and Listless SPIHT." *Future Internet*, vol. 9, no. 3, July 2017, p. 33. DOI.org (Crossref), doi:10.3390/fi9030033.
- [6] Aparna, Puvvadi, and Polurie Venkata Vijay Kishore. "An Efficient Medical Image Watermarking Technique in E-Healthcare Application Using Hybridization of Compression and Cryptography Algorithm." *Journal of Intelligent Systems*, vol. 27, no. 1, Jan. 2018, pp. 115-33. DOI.org (Crossref), doi:10.1515/jisys-2017-0266.
- [7] Sheping Zhai, Yuanyuan Yang, Jing Li, Cheng Qiu, Jiangming Zhao. "Research on the Application of Cryptography on the Blockchain," *Journal of Physics: Conference Series*, 2019, DOI:10.1088/1742-6596/1168/3/032077.
- [8] S. G. Aruna Sri, P., and D. Lalitha Bhaskari. "A Study on Blockchain Technology." *International Journal of Engineering & Technology*, vol. 7, no. 2.7, Mar. 2018, p. 418. DOI.org (Crossref), doi:10.14419/ijet.v7i2.7.10757.
- [9] R. Martino and A. Cilardo, "SHA-2 Acceleration Meeting the Needs of Emerging Applications: A Comparative Survey," in *IEEE Access*, vol. 8, pp. 28415-28436, 2020. DOI: 10.1109/ACCESS.2020.2972265.
- [10] Sahu, Aditya Kumar, et al. "Digital Image Steganography Using Bit Flipping." *Cybernetics and Information Technologies*, vol. 18, no. 1, Mar. 2018, pp. 69-80. DOI.org (Crossref), doi:10.2478/cait-2018-0006.
- [11] Wang, Licheng, Xiaoying Shen, Jing Li, Jun Shao, and Yixian Yang. "Cryptographic primitives in blockchains." *J. Netw. Comput. Appl.* 127, (2019): 43-58. <https://doi.org/10.1016/j.jnca.2018.11.003>.
- [12] Tara Salman, Maede Zolanvari, Aiman Erbad, Raj Jain, Mohammed Samaka. "SecurityServices Using Blockchains: A State of the Art Survey," *IEEE Communications Surveys & Tutorials*, 2019, DOI: 10.1109/COMST.2018.2863956.
- [13] Krawczyk H. (2010) Cryptographic Extraction and Key Derivation: The HKDF Scheme. In: Rabin T. (eds) *Advances in Cryptology – CRYPTO 2010*. CRYPTO 2010. Lecture Notes in Computer Science, vol 6223. Springer, Berlin, Heidelberg. DOI: [https://doi.org/10.1007/978-3-642-14623-7\\_34](https://doi.org/10.1007/978-3-642-14623-7_34).
- [14] E. Duffield and K. Hagan, "Darkcoin: Peer-to-peer crypto-currency with anonymous blockchain transactions and an improved proof-of-work system," Mar. 2014 [Online]. Available: <http://www.darkcoin.io/downloads/DarkcoinWhitepaper.pdf>.
- [15] Biryukov, Alex, and Dmitry Khovratovich. "Equihash: Asymmetric Proof-of-Work Based on the Generalized Birthday Problem." *IACR Cryptology ePrint Archive* 2015 (2015): 946. DOI: <https://doi.org/10.5195/ledger.2017.48>.
- [16] Q. Zhou, "Irregular-Program-Based Hash Algorithms," 2019 IEEE International Conference on Decentralized Applications and Infrastructures (DAPPCON), Newark, CA, USA, 2019, pp. 125-128. DOI: 10.1109/DAPPCON.2019.00024.
- [17] Li, Xiaoqi et al. "A Survey on the Security of Blockchain Systems." *ArXiv abs/1802.06993* (2018): n. pag. <https://doi.org/10.1016/j.future.2017.08.020>.
- [18] Certicom-Research, 2000. Sec2: Recommended Elliptic Curve Domain Parameters. <http://www.secg.org/SEC2-Ver-1.0.pdf>.
- [19] Johnson, D., Menezes, A. & Vanstone, S. The Elliptic Curve Digital Signature Algorithm (ECDSA). *IJIS* 1, 36-63 (2001). <https://doi.org/10.1007/s102070100002>.
- [20] Z. Zheng, S. Xie, H. Dai, X. Chen and H. Wang, "An Overview of Blockchain Technology: Architecture, Consensus, and Future Trends," 2017 IEEE International Congress on Big Data (BigData Congress), Honolulu, HI, 2017, pp. 557-564. DOI: 10.1109/BigDataCongress.2017.85.
- [21] R.C. Merkle, "A Digital Signature Based on a Conventional Encryption Function," *Advances in Cryptology — CRYPTO '87*, Springer, 1987. DOI:10.5555/646752.704751.
- [22] Dasgupta, D., Shrein, J.M. & Gupta, K.D. A survey of Blockchain from the security perspective. *J BANK FINANC TECHNOL* 3, 1-17 (2019). <https://doi.org/10.1007/s42786-018-00002-6>.
- [23] A. Averin and O. Averina, "Review of Blockchain Technology Vulnerabilities and Blockchain-System Attacks," 2019 International Multi-Conference on Industrial Engineering and Modern Technologies (FarEastCon), Vladivostok, Russia, 2019, pp. 1-6. DOI: 10.1109/FarEastCon.2019.8934243.
- [24] Schneier on Security (2007) Retrieved November 1, 2018, from [https://www.schneier.com/essay/s/archi-ves/2007/11/did\\_nsa\\_put\\_a\\_secret.html](https://www.schneier.com/essay/s/archi-ves/2007/11/did_nsa_put_a_secret.html).
- [25] M. Raikwar, D. Gligoroski and K. Kravlevska, "SoK of Used Cryptography in Blockchain," in *IEEE Access*, vol. 7, pp. 148550-148575, 2019. DOI: 10.1109/ACCESS.2019.2946983.
- [26] N. Anita. and M. Vijayalakshmi., "Blockchain Security Attack: A Brief Survey," 2019 10th International Conference on Computing, Communication and Networking Technologies (ICCCNT), Kanpur, India, 2019, pp. 1-6. DOI: 10.1109/ICCCNT45670.2019.8944615.
- [27] Keutmann (2018) Keutmann/Trustchain. Retrieved November 1, 2018, from <https://github.com/keutmann/Trustchain>.

- [28] Wang Q, Qin B, Hu J, Xiao F (2017) Preserving transaction privacy in bitcoin. *Future Generation Comput Syst.* <https://doi.org/10.1016/j.future.2017.08.026>.
- [29] Choo R, He X, Lin C, He D, Vasilakos AV (2018) Bsein: a blockchain-based secure mutual authentication with fine-grained access control system for industry 4.0. *Netw Comput Appl* 116:42–52. <https://doi.org/10.1016/j.nca.2018.05.005>.
- [30] Huang X, Xu C, Wang P, Liu H (2018) LNSC: a security model for electric vehicle and charging pile management based on blockchain ecosystem. *IEEE Access* 6:13565–13574. DOI: 10.1109/ACCESS.2018.2812176.
- [31] L. Wan, D. Eysers and H. Zhang, "Evaluating the Impact of Network Latency on the Safety of Blockchain Transactions," 2019 IEEE International Conference on Blockchain (Blockchain), Atlanta, GA, USA, 2019, pp. 194-201. DOI: 10.1109/Blockchain.2019.00033.
- [32] Maria A, Zohar V (2017) Hijacking bitcoin: routing attacks on cryptocurrencies. In: IEEE symposium on security and privacy, pp 375–392. <https://arxiv.org/abs/1605.07524>.
- [33] A. A. Andryukhin, "Phishing Attacks and Preventions in Blockchain-Based Projects," 2019 International Conference on Engineering Technologies and Computer Science (EnT), Moscow, Russia, 2019, pp. 15-19. DOI: 10.1109/EnT.2019.00008.
- [34] Arunima Ghosh, Shashank Gupta, Amit Dua, Neeraj Kumar, Security of Cryptocurrencies in blockchain technology: State-of-art, challenges and future prospects, *Journal of Network and Computer Applications*, Volume 163, 2020, 102635, <https://doi.org/10.1016/j.jnca.2020.102635>.
- [35] Leiyong Guo, Hui Xie, Yu Li, Data Encryption based Blockchain and Privacy-Preserving Mechanisms towards Big Data, *Journal of Visual Communication and Image Representation*, 2019, 102741, <https://doi.org/10.1016/j.jvcir.2019.102741>.
- [36] R. Canetti, "Universally composable security: a new paradigm for cryptographic protocols," *Proceedings 42nd IEEE Symposium on Foundations of Computer Science*, Newport Beach, CA, USA, 2001, pp. 136-145. DOI: 10.1109/SFCS.2001.959888.
- [37] G. Karame and S. Capkun, "Blockchain Security and Privacy" in *IEEE Security & Privacy*, vol. 16, no. 04, pp. 11-12, 2018. DOI: 10.1109/MSP.2018.3111241.
- [38] S. Singh and N. Singh, "Blockchain: Future of financial and cybersecurity," 2016 2nd International Conference on Contemporary Computing and Informatics (IC3I), Noida, 2016, pp. 463-467. DOI: 10.1109/IC3I.2016.7918009.
- [39] S. Gan, "An IoT simulator in NS3 and a key-based authentication architecture for IoT devices using blockchain," M.S. thesis, Indian Inst. Technol. At Kanpur, Kanpur, India, 2017. Accessed: February 13, 2018. [Online]. Available: <https://security.cse.iitk.ac.in/node/240>.
- [40] T. Chang and D. Svetinovic, "Data Analysis of Digital Currency Networks: Namecoin Case Study," 2016 21st International Conference on Engineering of Complex Computer Systems (ICECCS), Dubai, 2016, pp. 122-125. DOI: 10.1109/ICECCS.2016.023.
- [41] C. Fromknecht, D. Velicanu, and S. Yakoubov, "A decentralized public key infrastructure with identity retention," *IACR Cryptol. ePrint Archive*, p. 803, 2014.
- [42] M. C. Kus Khalilov and A. Levi, "A Survey on Anonymity and Privacy in Bitcoin-Like Digital Cash Systems," in *IEEE Communications Surveys & Tutorials*, vol. 20, no. 3, pp. 2543-2585, third quarter 2018. DOI: 10.1109/COMST.2018.2818623.
- [43] X. Yi, R. Paulet, and E. Bertino, *Homomorphic Encryption and Applications* (Springer Briefs in Computer Science), vol. 2. Cham, Switzerland: Springer Int., 2014, pp. 27–46. <https://doi.org/10.1007/978-3-319-12229-8>.
- [44] J. Lou, Q. Zhang, Z. Qi and K. Lei, "A Blockchain-based key Management Scheme for Named Data Networking," 2018 1st IEEE International Conference on Hot Information-Centric Networking (HotICN), Shenzhen, 2018, pp. 141-146. DOI: 10.1109/HOTICN.2018.8605993.
- [45] B. Liu, X. L. Yu, S. Chen, X. Xu, and L. Zhu, "Blockchain based data integrity service framework for IoT data," in *Proc. IEEE Int. Conf. Web Services (ICWS)*, Honolulu, HI, USA, 2017, pp. 468–475. DOI:10.1109/ICWS.2017.54.
- [46] Kumar, S.M.K.V., et al. "Incorporation of Blockchain in Student Management System." *International Journal of Innovative Technology and Exploring*, vol. 8, no. 6, Apr. 2019, pp. 664–68.
- [47] KusumaLatha, K., et al. "Warehousing Of Medical Data Using Blockchain." *International Journal of Innovative Technology and Exploring Engineering*, vol. 8, no. 7, May 2019, pp. 604–07.
- [48] P, Tejaswi, et al. "An Efficient Blockchain Security for Distributed System." *International Journal of Innovative Technology and Exploring Engineering*, vol. 8, no. 6, Apr. 2019, pp. 1265–69.
- [49] Poluri, M., et al. "IOT Ecosystem with Blockchain and Smart Contracts." *International Journal of Recent Technology and Engineering*, vol. 7, no. 6, Mar. 2019, pp. 638–41.
- [50] Uppalapati Krishna, Tapasvi, et al. "A Framework Using Blockchain Application to Monitor & Control Logs." *Journal of Advanced Research in Dynamical and Control Systems*, no. Special Issue 2, 2018, pp. 459–65.
- [51] Ammbika, V. M., and D. S. Rao. "Limitations of Blockchain Technology with Its Applications." *International Journal of Recent Technology and Engineering*, vol. 8, no. 2S11, Nov. 2019, pp. 3646–52. DOI.org (Crossref), doi:10.35940/ijrte.B1459.0982S1119.
- [52] Decker C, Wattenhofer R (2013) Information propagation in the Bitcoin network. *IEEE P2P 2013 Proceedings*, pp. 1–10. DOI: 10.1109/P2P.2013.6688704.
- [53] Khalilov, Merve Can Kus and Albert Levi. "A Survey on Anonymity and Privacy in Bitcoin-Like Digital Cash Systems." *IEEE Communications Surveys & Tutorials* 20 (2018): 2543-2585. DOI: 10.1109/COMST.2018.2818623. DOI: 10.1109/Blockchain.2019.00033.
- [54] Foundation E (ed.) (n.d.) Privacy on the Blockchain. Retrieved November 01, 2018, from <https://blog.ethereum.org/2016/01/15/privacy-on-the-block-chain>.
- [55] Junfeng Xie, Helen Tang, Tao Huang, F. Richard Yu, Renchao Xie, Jiang Liu, Yunjie Liu. "A Survey of Blockchain Technology Applied to Smart Cities: Research Issues and Challenges," *IEEE Communications Surveys & Tutorials*, 2019. DOI: 10.1109/COMST.2019.2899617.

# Prototyping with Raspberry Pi in Healthcare Domain

## A Bibliometric Analysis

Hari Kishan Kondaveeti<sup>1</sup>, Sruti Raman<sup>2</sup>, Praveen Raj<sup>3</sup>  
Computer Science and Engineering, Vellore Institute of Technology  
AP, Amaravati, India

**Abstract**—The objective of this paper is to conduct a bibliometric study on the use of Raspberry Pi in the medical field. In the past several decades healthcare advancements have played a major role and Raspberry Pi being the charm with its extensive features and low cost, it is of interest to know whether the development in health care technologies with respect to Raspberry Pi has created an impact or not. A platform known as Biblioshiny has been used to collect statistical information and perform the analysis. A total of 154 journal articles have been collected from PubMed, a free full-text archive of biomedical and life sciences journal literature at the U.S. National Institutes of Health's National Library of Medicine (NIH/NLM) and analysis has been made on various parameters such as top authors, countries and affiliations etc. The conclusions drawn help us to understand the usage of Raspberry Pi in the healthcare domain. The Bibliometric Analysis done indicates that there has been an increase in the research over the years and the authors from various countries have been working elaborately indicating that there has been a good amount of usage of Raspberry Pi in the healthcare domain. Overall, our results demonstrate the trending topics the authors currently working on and collaborations amongst authors and countries. Finally, this paper identifies that there are no motor themes but displays the budding keywords (or the ideas where authors have worked on) in the health care domain emerging with the prototyping of Raspberry Pi.

**Keywords**—Information extraction; bibliometric study; prototype; Raspberry Pi; healthcare

### I. INTRODUCTION

Raspberry Pi is a mini-sized computer, often denoted as credit-card-sized board established by the “Raspberry Pi Foundation”. Originally, Raspberry Pi was developed for students so that they could learn programming which would help them implement innovative projects in various fields [1]. It is essentially a motherboard which has a provision for general purpose input/output pins and enables one to modulate myriad of electronic components. This mini-sized computer comes with its own set of fringe benefits and is known for its affordable price and high computing capability. It runs on various operating systems and is compatible with plenty of programming languages such as C, C++, Java, Perl and Ruby [2]. It supports various operating systems; it also requires power to boot. However, there are versions of the Raspberry Pi which can boot directly from the network for which file storage system is required [3] Raspberry Pi is an excellent platform for prototyping (preferably, small scale) [4]. Prototyping ideally deals with validating idea, hypotheses or hardware design. It helps understand vindicate electronic design in an operating system. Prototyping helps weigh the

positives and the negatives of the features being implemented in a model. Raspberry Pi also behaves as an enabler technology [3] The Pi is used to create and develop unconventional projects -widely used in home automation, robot controlling, bots making etc. Due to its high usability, the Pi is used in the evergreen “Healthcare Field” for health monitoring and MRI analysis by making use of the Internet of Things, Smart Devices etc. According to the British Standard Institution (1976), bibliometrics is coined as the ‘application of mathematical and statistical methods in the study of the use of documents and publication patterns.’ To put the above definition in Layman’s terms, bibliometrics can be considered as a procedure which counts the publications and citations relevant to a certain topic. The amalgamation of bibliometrics to science is known as ‘Scientometrics’. It is typically defined as the “quantitative study of science and technology” [5].

The most commonly used methods in the field of library and information science are – citation analysis and content analysis. The study of bibliometrics consists of three major bibliometric indicators which are quantity indicators, performance indicators and structural indicators [6]. To measure the productiveness of a researcher or research group, the quantity indicator is utilized for evaluating the standard of the journal or the research and the research journal. Structural indicators measure the linkage or the connection amongst various authors, publications etc. [7] Predominantly, the bibliometric study involves the elucidation of activities concerning the topic carried out by researchers, institutions and countries which will help establish trends in research [8] Since, Raspberry Pi is attracting attention in the medical field, this paper attempts to throw light on the popularity of Raspberry Pi over the years in healthcare domain and bring out the trends in various and distinct metrics by conducting the bibliometric analysis.

The rest of the paper is divided into four sections. Section I presents the research methodology to perform the bibliometric analysis. Section II presents the results obtained from the study. Section III shows the conclusions obtained from the study and an acknowledgment. Section IV shows the references which assisted in conducting the study.

### II. METHODOLOGY

The data for the analysis has been collected from the PubMed database, which collects the information from the Medline database compiled by the United States Library of Medicine [9]. The search strategy which was used to collect the information was – “Raspberry Pi”. The data was analyzed

using a web-based Bibliometrix tool in R called Biblioshiny [10]. The information thus collected has been filtered to obtain precise results. *Summary* of the findings are as below:

Initially, one hundred and ninety-one (191) articles have been extracted for the analysis. To remove the uncertainties, they are further filtered to document type, “Journal Articles”, which fetched one hundred and fifty-four (154) items. These Articles relate to the period between 2013 and 2020 with contributions from six hundred and ninety-seven (697) authors. Conceptual and Social Structure of these articles were analyzed to draw meaningful conclusions.

Table I gives a brief on the data extracted for the period between 2013 and 2020. There are 191 articles as mentioned above, which include those from journals and books numbering 61.249 ‘Keywords’ from these articles are captured for the analysis. ‘Keywords’ are index terms used by the authors to present the main content of their paper.

TABLE I. MAIN INFORMATION OF DATA COLLECTED

| Description                          | Results   |
|--------------------------------------|-----------|
| Timespan                             | 2013:2020 |
| Sources (Journals, Books, etc)       | 61        |
| Documents                            | 154       |
| Average years from publication       | 1.92      |
| References                           | 1         |
| Keywords Plus (ID)                   | 249       |
| Keywords Plus (ID)                   | 249       |
| Author's Keywords (DE)               | 249       |
| Authors                              | 697       |
| Author Appearances                   | 733       |
| Authors of single-authored documents | 7         |
| Authors of multi-authored documents  | 690       |
| Documents per Author                 | 0.221     |
| Authors per Document                 | 4.53      |
| Co-Authors per Documents             | 4.76      |
| Collaboration Index                  | 4.69      |

Out of contributions from 697 authors in all, 7 are single-authored documents and the balance 690 documents are multi-authored. Single authored documents are the documents which have been journaled by only one author whereas multi-authored documents are the ones in which there is a collaboration among two or more authors. To assess the overall contribution of an author, the data is further analysed based on ‘author appearances’. ‘Author appearances’ demonstrate whether an author has more than one journal article on his name. In our analysis, considering the count of articles and the frequency of the author’s name, seven hundred and thirty-three (733) records have been discovered. Authors per document come to 4.53, which is calculated by finding the ratio of the total number of authors and documents by them. Likewise, the documents per author come to 0.221 by evaluating the ratio of documents and authors. Co-author per document comes to 4.76, which is the ratio of the total number of author appearances and documents. The collaboration index

is established by correlating the data of authors of multi-authored articles divided by the number of multi-authored articles. [11]. The details are explicitly mentioned in Table I.

### III. RESULTS AND DISCUSSION

#### A. Trends in the Number of Articles

The first publication in the health care domain using Raspberry Pi appeared in the year 2013 with only one article in the entire year. Between 2014 and 2016, the number of articles published on the subject did not cross double-digit. Since 2017, a moderate increase is noticed as shown in Table II. The Annual Scientific Production of the topics is captured in the diagram depicted in Fig. 1, where Y-axis represents the number of articles and X-axis years establishing the relationship of the number of articles to the years. During the initial phase starting from 2013 to 2016, as depicted in Fig. 1, there have been less number of articles in this field but the year 2017 witnessed 23 articles and there has been an increase in the number of articles published since then. In the year 2020, 28 articles have been published. The annual growth is estimated at 60.97%. Annual growth rate establishes the geometric progression ratio that provides a return of constant rate over some time. [12].

TABLE II. NUMBER OF ARTICLES PUBLISHED IN THE CORRESPONDING YEAR

| Year | Articles |
|------|----------|
| 2013 | 1        |
| 2014 | 7        |
| 2015 | 7        |
| 2016 | 8        |
| 2017 | 23       |
| 2018 | 31       |
| 2019 | 49       |
| 2020 | 28       |

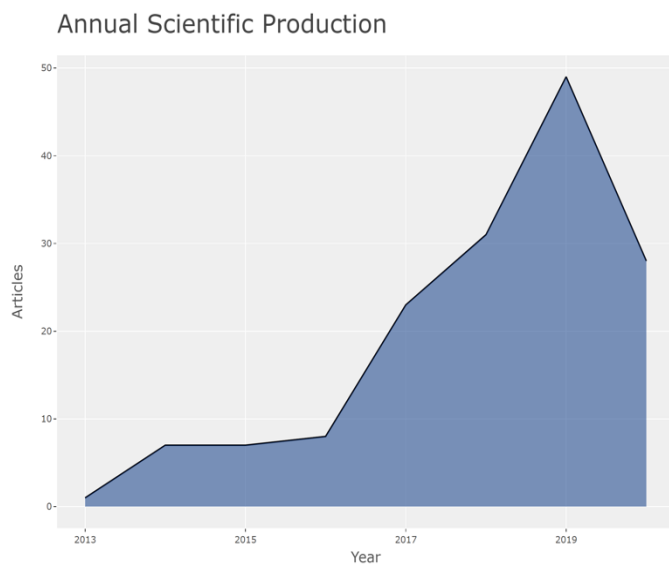


Fig. 1. Trends in the Number of Articles over the Years from 2013-2020.

**B. Top 10 Most Relevant Sources**

A source is essentially is a journal, a book etc. which has issued plenty of documents. This is denoted as sourcing the article/subject of the original author. Table III lists out top 10 sources of articles found on PubMed and the number of times these have been utilized. The observation which can be drawn is that “Sensors” (Basel Switzerland) has been sourced by many articles and “Application in Plant Sciences” has been least sourced.

**C. Documents of Top 3 Authors**

Table IV shows the list of documents journalled by the top three authors. Although ‘PLOS one’ has several articles under them, the documents written by top five authors are not sourced by “PLOS one”. However, multiple authors have worked on the same article.

**D. Top 10 Most Relevant Affiliations**

The affiliations on a research paper imply that the author worked at an institute that oversees the research integrity of the paper published. Affiliations give credibility to the research paper. A study conducted at a reputed University is more respected rather than by the authors affiliated with a university none ever heard of. This explains the reason why researchers from less-known institutions collaborate with researchers of well-known universities.

Table V and the Fig. 2 give an analysis of university affiliations of the authors who published articles on the subject under study. The largest number of affiliations are to the University of British Columbia with 25 articles which are represented by a dark shade of blue in the Fig. 2. In the Fig. 2, the X-axis denotes the number of articles and the Y-axis denotes the name of the affiliation. The intensity of the color decreases as we go down the graph indicating the decrease in the frequency of articles. Kinsmen Laboratory of Neurological research has the least number of articles affiliated. However, the other universities, to cite a few, Tucson, University of Alberta, etc. have a good number of papers that are affiliated.

TABLE III. A TABULAR REPRESENTATION OF THE SOURCES AND CORRESPONDING NUMBER OF ARTICLES

| Sources                                                                                                           | Articles |
|-------------------------------------------------------------------------------------------------------------------|----------|
| Sensors (Basel Switzerland)                                                                                       | 68       |
| PLOS one                                                                                                          | 68       |
| Conference proceedings – Annual International Conference of the IEEE, Engineering in Medicine and Biology Society | 7        |
| Review of scientific instruments                                                                                  | 6        |
| Journal of Neuroscience methods                                                                                   | 5        |
| Biosensors and Bioelectronics                                                                                     | 3        |
| Journal of medical systems                                                                                        | 3        |
| Plant methods                                                                                                     | 3        |
| PLOS Biology                                                                                                      | 3        |
| Applications in plant sciences                                                                                    | 2        |

TABLE IV. TOP AUTHORS AND THE CITATION OF THEIR CORRESPONDING ARTICLES

| Author    | Citation                     |
|-----------|------------------------------|
| Murphy Th | [18], [19], [20], [21], [22] |
| Barker D  | [23], [24], [25], [26]       |
| Boyd Jed  | [18], [19], [22]             |

TABLE V. TOP 10 AFFILIATIONS AND THE NUMBER OF DOCUMENTS AFFILIATED

| Affiliations                                  | Articles |
|-----------------------------------------------|----------|
| University of British Columbia                | 25       |
| Zhejiang University                           | 17       |
| Tucson                                        | 16       |
| University of Science and Technology of China | 16       |
| Universidad Carlos III De Madrid              | 15       |
| University of Alberta                         | 15       |
| University of Tubingen                        | 13       |
| The University of Sheffield                   | 12       |
| University of California                      | 12       |
| Kinsmen Laboratory of Neurological Research   | 11       |

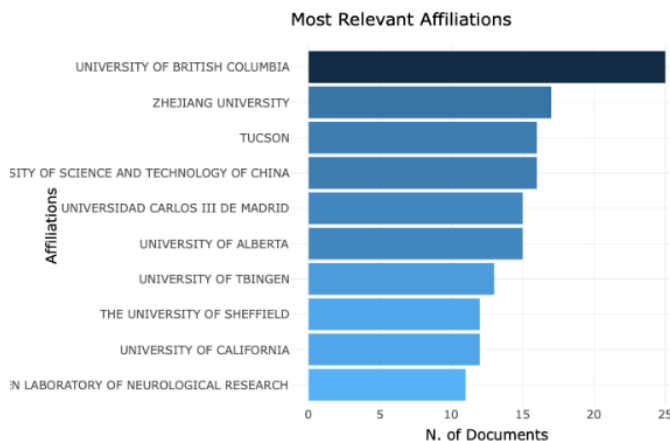


Fig. 2. A Graphical Representation of Top-10 Affiliations and the Number of Documents Affiliated.

**E. Top 10 Corresponding Author’s Countries**

The leading authors of the articles belong to China, USA, France and Korea; most of the authors are from China and the USA as shown in the graph (Fig. 3). The X-axis represents the number of documents and the Y-axis represents the countries. SCP is the abbreviation for Single Country Publication and MCP is an abbreviation for Multiple Countries Publication. It can be concluded that there are no documents where a co-author from a different country is working on in the dataset under analysis.

**F. Top-10 Country Specific Production**

Country specific production gives us an insight into the number of journal articles produced in a specific country. From the Table VI, it can be observed that the USA tops the list by producing 117 articles over the years and the UK appears at the bottom by producing the least with 26 articles.

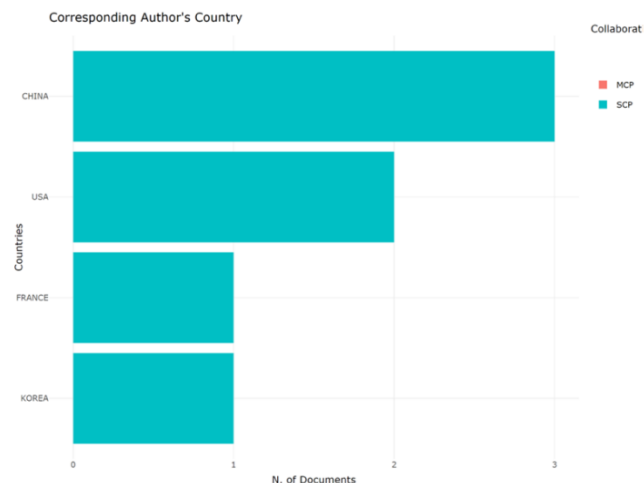


Fig. 3. A Graphical Diagram Representing the Top 10 Author's Countries.

TABLE VI. TOP 10 COUNTRIES WITH THE HIGHEST NUMBER OF PRODUCTIONS

| Terms      | Frequency |
|------------|-----------|
| system     | 29        |
| raspberry  | 22        |
| low-cost   | 21        |
| monitoring | 19        |
| based      | 18        |
| pi         | 18        |
| open       | 13        |
| platform   | 13        |
| data       | 12        |

G. Frequently used Words – Author's Keywords, Title, Abstract

A word cloud is a pictorial representation of the collection of words related to a specific parameter, be it author's keywords or title or abstract. The cloud is essentially designed such a way that the word with higher importance or most re-occurring is typically depicted in a bigger font and the words with less frequency gradually decrease in size. Various data transformations can be used to understand the occurrence of words. Since dataset under observation is not humongous, the analysis is confined to the measure of "frequency". Other options such as log, square root transformations are available which will give the preview of the word cloud, based on the scaled transformation applied to the data [13].

1) *Author's keywords:* Author's keywords, as mentioned earlier is a list of terms which relate to the main topic of the author's paper. Fig. 4 captures, the terms and Table VII gives the details about the word and their frequency. An interesting observation made in the analysis is that the most commonly used words by the authors are 'humans', 'software', 'animals', 'female' etc. The frequency of usage of the word 'humans' was 48 times, which gives a conclusion that the application of Raspberry Pi has been essentially used to the benefit of human beings.

2) *Most Commonly used words in titles:* It is also analyzed whether the term Raspberry Pi appears in the title and the abstract of the articles produced. From Table VIII and the Fig. 5, it is interpreted that the word "system" has the highest frequency which can be seen from the cloud of words such as.

- Prototyping of Raspberry pi is used.
- Integration of IoT.
- Open-source platform.
- Working on low cost, smart, robust systems.
- Applications of the raspberry pi for monitoring purposes.

3) *Most commonly used words in abstract:* "System" and "data" are the two terms with the highest frequencies. It is quite evident that most of the terms in the title and the abstract have been repetitive. An amusing observation here is that the usage of the term Raspberry Pi is more when compared to its usage to the title and author's keywords. The occurrence of the terms can be seen in Table IX and Fig. 6.



Fig. 4. Word cloud depicting the most Common Author's Keywords.

TABLE VII. MOST FREQUENT TERMS AND ITS OCCURRENCE IN AUTHOR'S KEYWORDS

| Region      | Freq |
|-------------|------|
| USA         | 151  |
| CHINA       | 82   |
| SPAIN       | 81   |
| CANADA      | 67   |
| GERMANY     | 39   |
| BRAZIL      | 38   |
| ITALY       | 37   |
| SOUTH KOREA | 31   |
| MEXICO      | 30   |
| UK          | 26   |

TABLE VIII. MOST FREQUENT TERMS AND ITS OCCURRENCE IN TITLES

| Terms                              | Frequency |
|------------------------------------|-----------|
| humans                             | 48        |
| software                           | 20        |
| animals                            | 17        |
| female                             | 13        |
| algorithms                         | 12        |
| equipment design                   | 12        |
| male                               | 12        |
| computers                          | 7         |
| image-processing computer-assisted | 7         |
| internet                           | 7         |



Fig. 5. Word cloud depicting the Most Common Words Found in titles.

TABLE IX. MOST FREQUENT TERMS AND ITS OCCURRENCE IN ABSTRACT

| Terms     | Frequency |
|-----------|-----------|
| system    | 209       |
| data      | 159       |
| pi        | 153       |
| raspberry | 153       |
| device    | 89        |
| based     | 86        |
| proposed  | 82        |
| low-cost  | 77        |
| devices   | 76        |
| sensor    | 71        |



Fig. 6. Word cloud Depicting the Most Common Words Found in the Abstract.

H. Graphical Analysis

Biblioshiny platform has a graphical analysis tool known as “Three-Field-Plot” which helps in determining the relationship between three metrics in a graph. It works on the principle of the Sankey diagram. Three field plot is divided into 3 fields namely-

- Middle field
- Leftfield
- Right field

Sankey diagram consists of boxes; the size and the dimensions of the box are directly proportional to the frequency or the count of the entered metrics.

For the first analysis three fields viz., Middle: Keyword, Left: Author, Right: Sources are considered confining to top 10 interactions amongst them.

Fig. 7 re-establishes that “Human” is the most commonly used keyword and has been frequently used by most of the sources such as “Sensors (Basel, Switzerland)”. The authors, to name a few, Sahoo n and Lin hw have been working on projects which use the keywords (topics) such as ‘humans’, ‘user computer interface’, ‘equipment design’ etc.

For the second analysis the three fields viz., Middle: Keyword, Left: Country, Right: Sources are considered restricting again to top 10 interactions amongst them.

The graph (Fig. 8) depicts that the highest production of articles is from the country – “China” and the authors have utilized the topics/keywords such as ‘keywords’, ‘algorithms’, ‘image processing’, ‘computer-assisted’, ‘equipment design’ and ‘user computer interface’. Interestingly, the most frequently used keyword - “Humans” has been used in the journal articles produced by all the countries present in the graph (Spain, China, France, Korea, Mexico, USA, Italy, Germany, Canada). It has been sourced by all except for journal of neuroscience methods. We can also see that that ‘Sensors’ (Basel, Switzerland) has been sourced by all the keywords. Table X lists out the country and the topics the countries have been working on. By analyzing the width between the country and the keyword, Table XI is prepared to give an insight into the topic(s) the respective countries are specifically working on.

The third graphical analysis involves the three fields, viz., Middle: Author, Left: Affiliations, Right: keywords; restricting to top 10 interactions. The graph (Fig. 9) represents the keywords used by the author and the university the author has been affiliated to.

The fourth graphical analysis (Fig. 10) gives us an insight into the author’s country. Considering the three fields viz., Middle: Author, Left: Countries, Right: Affiliations. The relationship between the three is established.

The fifth graphical analysis (Fig. 11) uses Middle: Affiliation, Left: Authors, Right: Countries, restricting the number of items to 24 to find out the affiliation of later items.



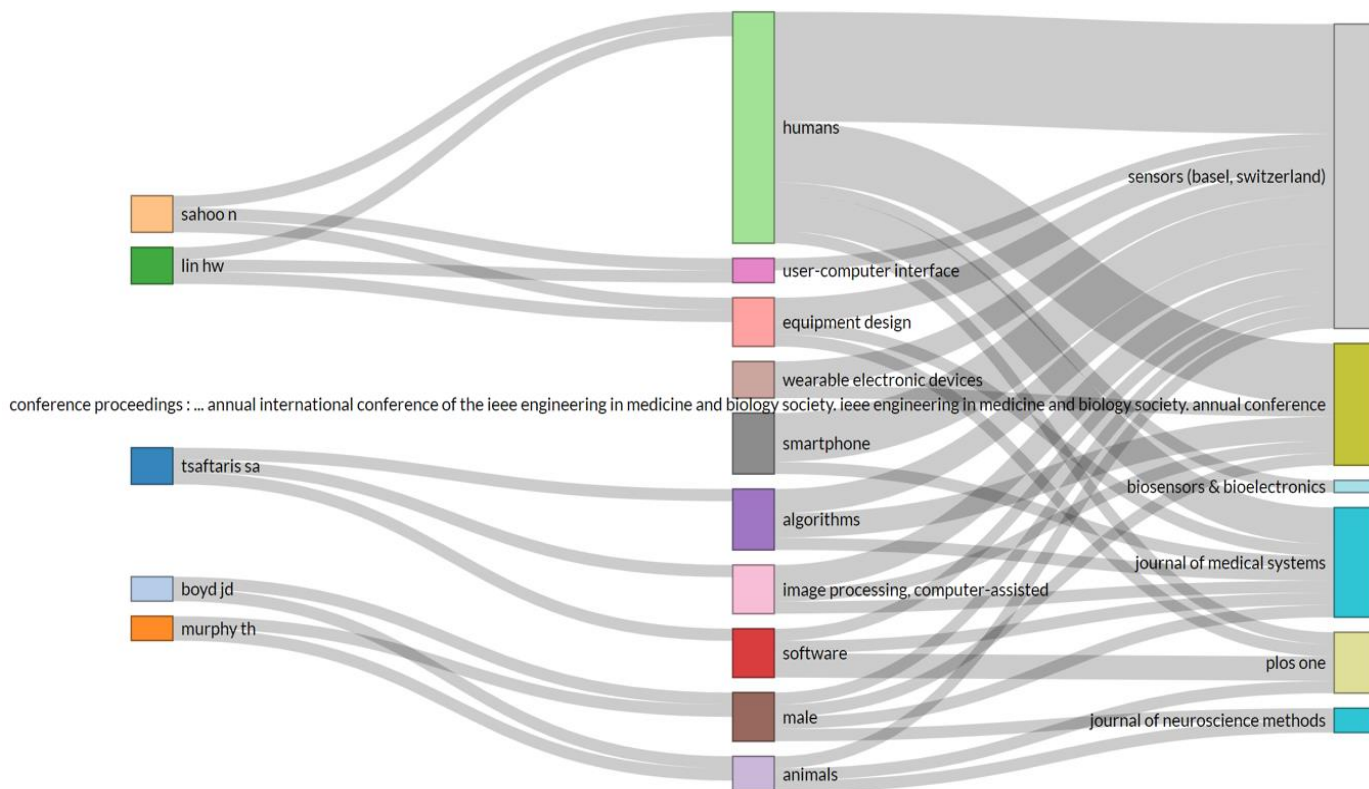


Fig. 7. Three Plot Diagram Representing the Relationship among Keywords, Authors and Sources.

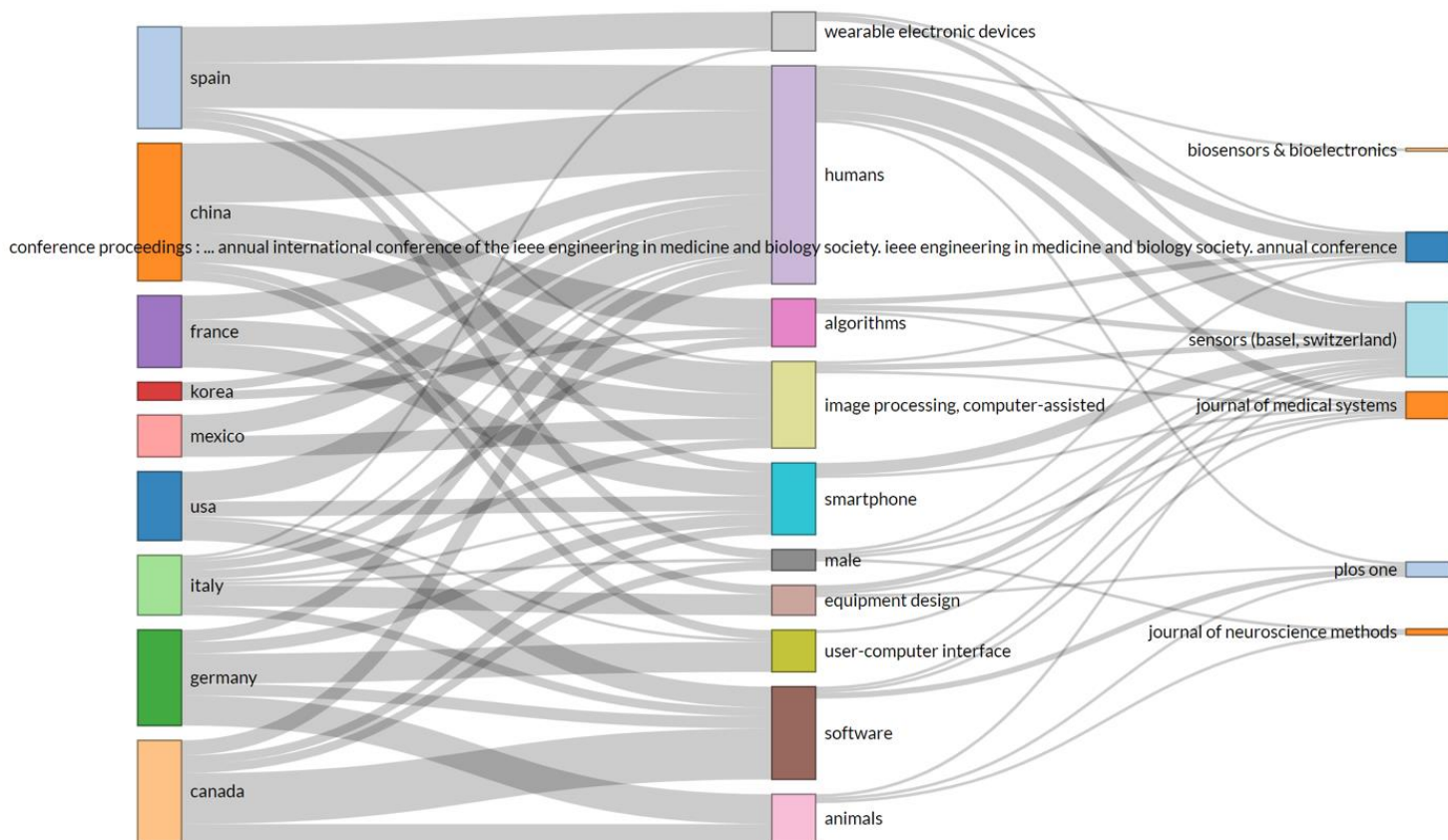


Fig. 8. Three Plot Diagram Representing the Relationship among Keywords, Country and Sources.

TABLE X. LIST OF COUNTRIES AND THE RELATED CORRESPONDING TOPICS

| Country | Topic(s)                                                                                                                  |
|---------|---------------------------------------------------------------------------------------------------------------------------|
| Spain   | The wearable electronic device, humans, image processing-computer assisted, smartphone, male                              |
| China   | Humans, algorithms, image processing- computer-assisted equipment design, user computer interface                         |
| France  | Humans, image, processing, computer-assisted, smartphone                                                                  |
| Korea   | Humans, algorithms                                                                                                        |
| Mexico  | Humans, image processing-computer assisted                                                                                |
| USA     | Humans, smartphone, user computer interface, software                                                                     |
| Italy   | The wearable electronic device, humans, algorithms, image processing, computer-assisted, male, equipment design, software |
| Germany | Humans, smartphones , user computer interface, software animals                                                           |
| Canada  | Humans, smartphones, male, software, animals                                                                              |

TABLE XI. LIST OF COUNTRIES AND THE CORRESPONDING MAJOR TOPICS

| Country | Topic(s)                                                                    |
|---------|-----------------------------------------------------------------------------|
| Spain   | Wearable electronic device, humans                                          |
| China   | Humans, algorithms<br>image processing, computer-assisted                   |
| France  | Humans, image processing, computer-assisted, smartphone                     |
| Korea   | Humans, algorithms                                                          |
| Mexico  | Humans, image processing, computer-assisted                                 |
| USA     | Humans, smartphone, software                                                |
| Italy   | Algorithms, image processing, computer-assisted, equipment design, software |
| Germany | User computer interface, animals                                            |
| Canada  | Software, animals                                                           |

By analyzing the three graphs (Fig. 9, Fig. 10, Fig. 11), the most common keywords used by the author, the paper's affiliation and the country in which the author has published the journal article can be identified. The keywords for authors whose papers were published in Korea are not available, however, it can be noticed as mentioned in the Table X that Korea has essentially worked on 'Humans' and 'algorithms'. So, for the current analysis, these keywords have been added against their names. The tabulated chart can be seen in Table XII. Table XII gives the impression that the most popular topics on which the top authors are working relate to humans and animals. To analyze whether the topic on which the authors are working on is a trending topic or a general topic with scope for further development, network analysis is conducted.

### I. Knowledge Synthesis

Knowledge synthesis is made up of three fragments which are.

- Conceptual structure
- Intellectual structure

- Social structure

The conceptual structure involves network analysis of the co-words' networks, which is ideally studying and analyzing of graphs depicting a collection of words appearing together.

To identify the evolution of themes and infer the topics, the thematic map is used. A graph has nodes also known as vertices which are linked by lines or edges.

The colors represent the clusters to which the words belong to as shown in Fig. 12. The parameter used for constructing the graph is the author's 'keywords'. Salton's cosine, Jaccard's Index and Association Strength [14] are used for measuring the co-occurrence and Louvain algorithm for clustering [15].

The map as shown in Fig. 12 gives a visual representation of the most co-occurring words and it is observed that the vertex representing "Humans" has highly reoccurred. The strength of the edges is proportional to the co-occurrences. The link between "Humans" and "image processing", "computer-based" is much stronger than the other edges inferring that the Raspberry Pi is being used or studied concerning applications which have the ability of image processing.

### J. Thematic Evolution – A Longitudinal Thematic Map Analysis

A thematic map is used for visualizing a certain topic and the concept used in the paper by choosing "author's keywords". The map is divided into four plots or quadrants viz., Upper left plot: highly developed and isolated themes, Upper right plot: Motor themes; Lower left plot: emerging or declining themes; Lower right plot: Basic and transversal themes. Each quadrant is depicted as a Thematic map [16] As shown in the map (Fig. 13) each bubble depicts a network cluster and the word which is being represented in the bubble has the highest occurrence value. The position of the bubbles is according to the Centrality and Density which are captured in X and Y axes, respectively [17].

Centrality helps to measure the degree of interaction amongst the myriad clusters present in the graph. It helps in estimating the importance of the theme in the entire research area. Density estimates the internal strength of the cluster, in other words, it is the measure of the theme's development in the entire research.

The purpose of using thematic evolution for the analysis is to discover if there are any topics which have emerged into any other quadrants and more so to understand the topic's evolution over some time. The span of years is divided into two parts, and the cutting point emerged as 1. (2013-2017, 2018-2020).

Time Slice-1: The conjecture made from the Fig. 13 is that "wireless technology/instrumentation" is a motor theme and was a Central Point for conducting research studies concerning Raspberry Pi.

The second observation of the analysis is that the bubbles referring to "humans" is in emerging or declining themes as the frequency of words in the cluster are in the declining zone.

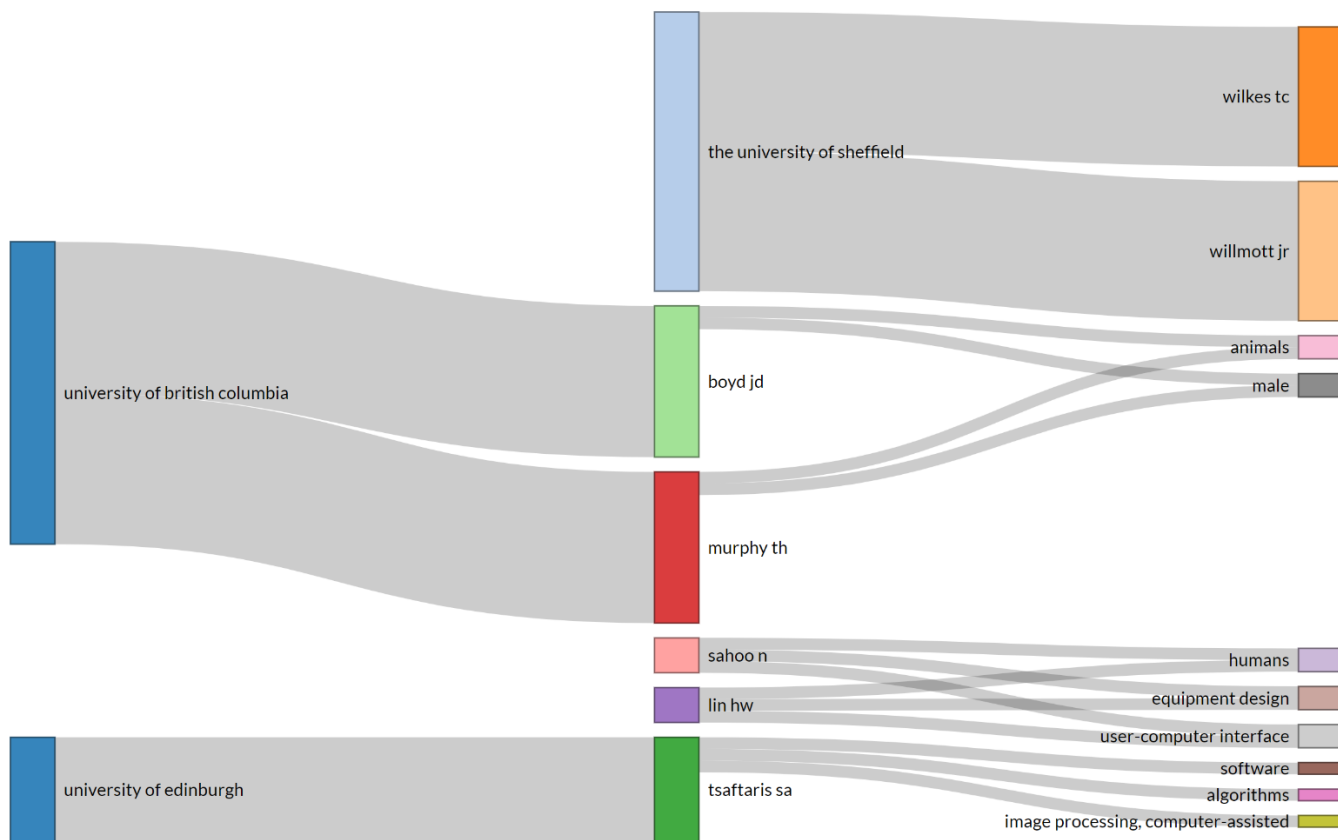


Fig. 9. Three Plot Diagram Representing the Relationship among Authors, Affiliations and Keywords.

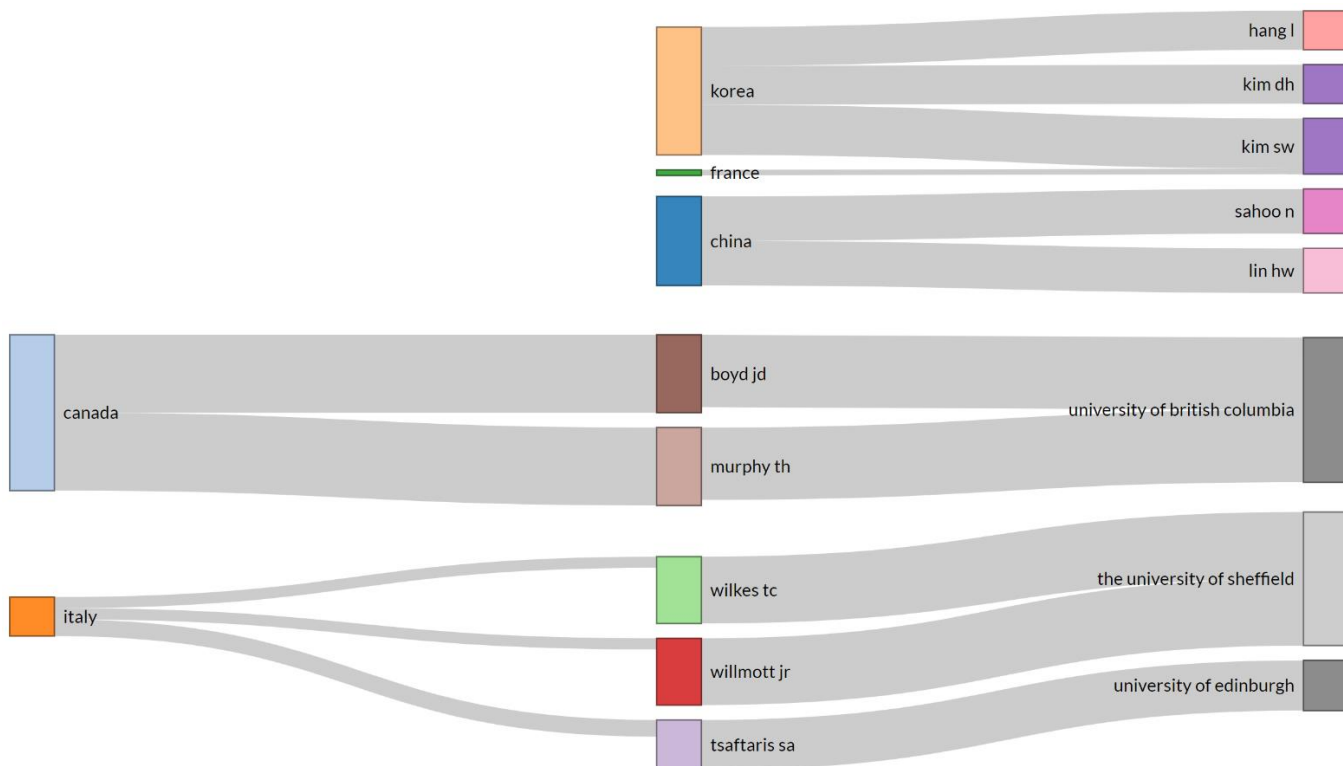


Fig. 10. Three Plot Diagram Representing the Relationship among Authors, Countries and Affiliation.

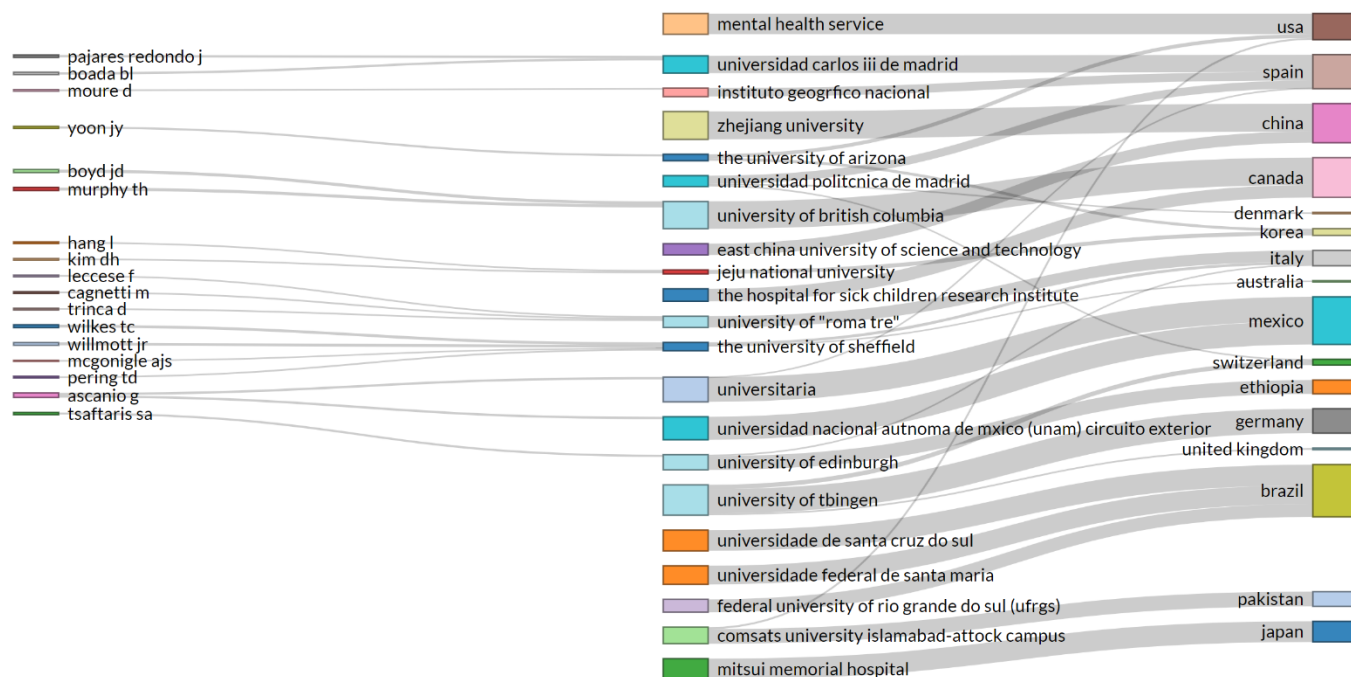


Fig. 11. Three Plot Diagram Representing the Relationship among Affiliations, Authors and Countries.

TABLE XII. LIST OF AUTHORS, MOST COMMON KEYWORDS USED BY AUTHORS, AFFILIATION, COUNTRY OF PRODUCTION OF ARTICLES AND SOURCES

| Author       | Keywords used by the author                               | Affiliation                    | Country       | Sources                         |
|--------------|-----------------------------------------------------------|--------------------------------|---------------|---------------------------------|
| Wilkes Tc    | unavailable                                               | The University of Sheffield    | Italy         | Sensors (Basel, Switzerland)    |
| Willmott Jr  | unavailable                                               | The University of Sheffield    | Italy         | Sensors (Basel, Switzerland)    |
| Boyd Jd      | Animals, male                                             | University of British Columbia | Canada        | Journal of Neuroscience Methods |
| Murphy Th    | Animals, male                                             | University of British Columbia | Canada        | Journal of Neuroscience Methods |
| Sahoo n      | Humans, equipment design, user computer interface         | Unavailable                    | China         | Sensors (Basel, Switzerland)    |
| Lin Hw       | Humans, equipment design, user computer interface         | Unavailable                    | China         | Sensors (Basel, Switzerland)    |
| Tsaftaris Sa | Software, algorithms, image processing, computer-assisted | University of Edinburgh        | Italy         | Plant methods.                  |
| Hang l       | Humans, algorithms                                        | Jeju National University       | Korea         | Sensors (Basel, Switzerland)    |
| Kim DH       | Humans, algorithms                                        | Jeju National University       | Korea         | Sensors (Basel, Switzerland)    |
| Kim SW       | Unavailable                                               | Unavailable                    | Korea, France | Sensors (Basel, Switzerland)    |

‘Software’, ‘behaviour,’ and ‘animal/physiology’ belong to the basic and transversal themes which establish that those were the general topics during the years 2013-2017. It is also observed that ‘equipment design’ is right in the middle of the map, covering a tiny portion from all the quadrants.

Time Slice-2: In the Fig. 14, plenty of new keywords can be noticed in the graph and ‘humans’ has its locomotion from emerging/declining topics to general and transversal themes whereas ‘wireless technology’ or ‘instrumentation’ is no more a “motor theme” which insinuates that there are new topics which have merged or have been split into individual topics.

The Fig. 15 gives distribution and diversity of topics (author’s keywords) over the years in the given time slice. In

the first slice, all the topics have started uniquely and topics such as ‘humans’, ‘wireless technology/instrumentation’ and ‘software’ have diverged into various fields. However, the whole of behavior, ‘animal/physiology’ has shifted to ‘female’ and ‘animals’ has shifted into; automation’, ‘laboratory/instrumentation’. The keywords popular in the time slice between 2018-2020 are ‘humans’, ‘automation’, ‘laboratory/instrumentation’, ‘female’, ‘software’, ‘anticoagulants’, ‘equipment design’, ‘wearable electronic devices’ and ‘algorithms’.

Fig. 16 captures the clusters from 2013-2020 by combining the occurrences of various topics and keywords in the thematic map.



Fig. 12. A Graphical Representation of a Network of the most co-Occurring Words in all the Articles.

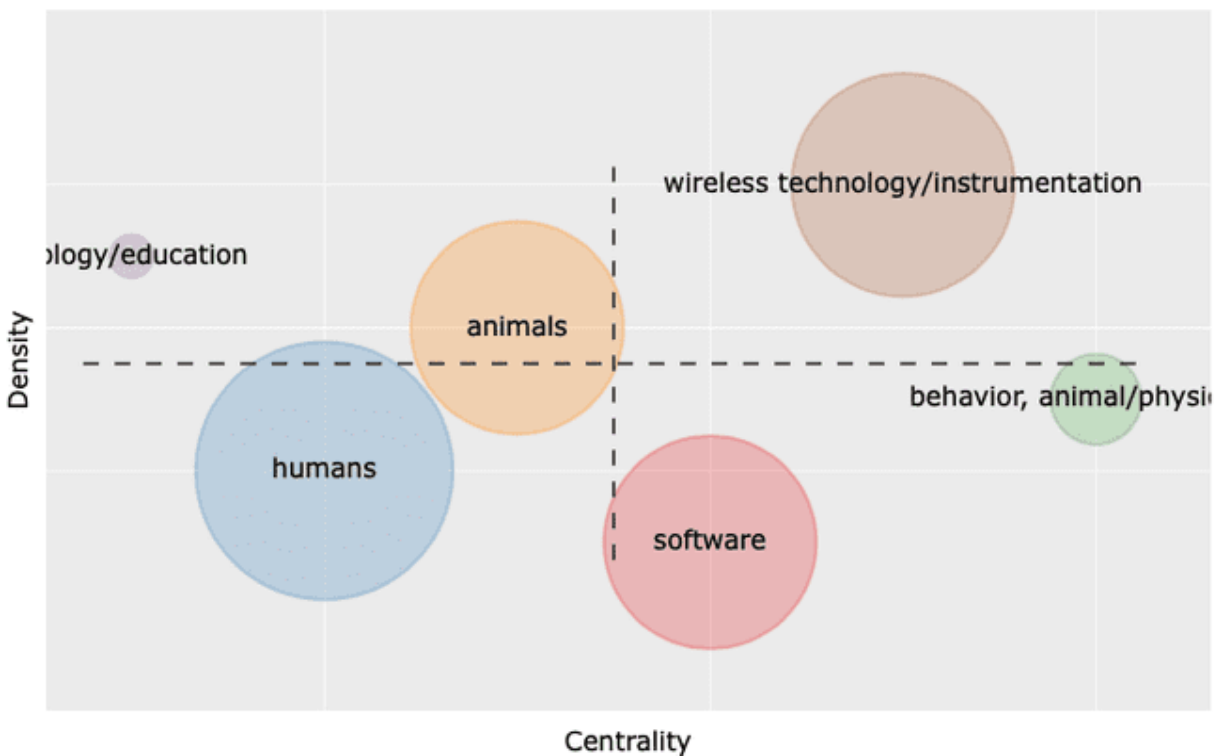


Fig. 13. Strategic Diagram Representing the Author's Keywords in Time Slice – 1.

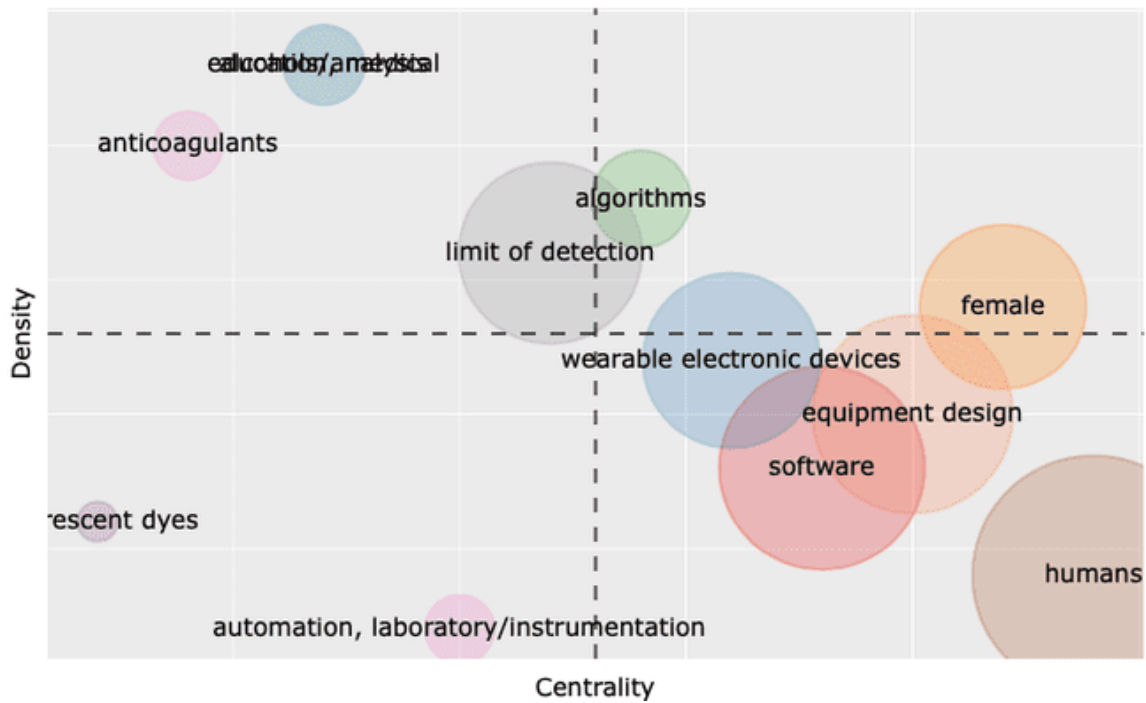


Fig. 14. Strategic Diagram Representing the Evolution of the Author's Keywords in Time Slice -2.

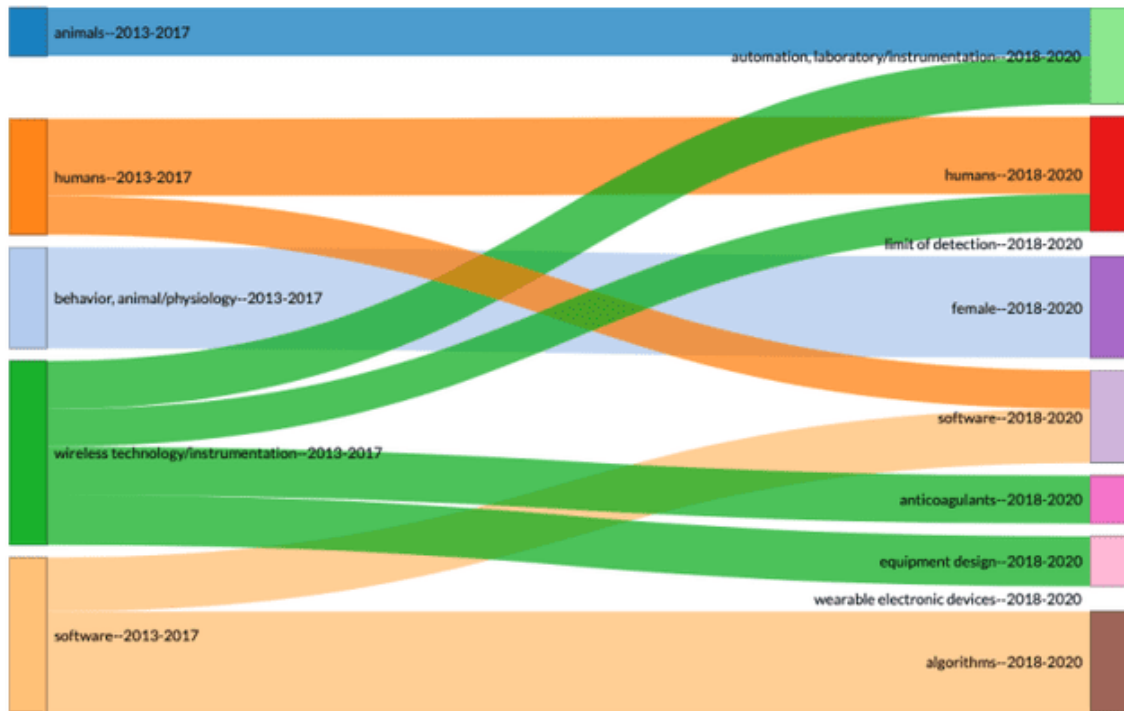


Fig. 15. 2-Plot Diagram for the Evolution of Author's Keywords over the Year.

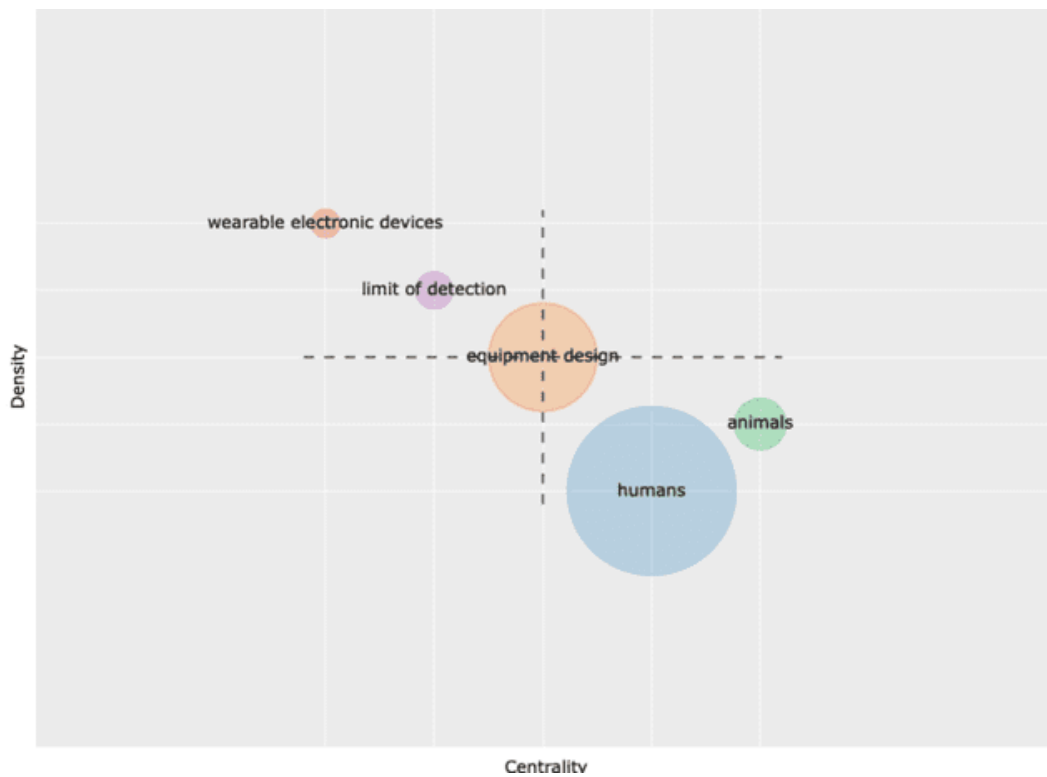


Fig. 16. Overall Strategic Diagram for Author's Keywords from 2013-2020.

It can be noticed that the bubble-“human”, belongs to the basic and transversal themes indicating that the bubble has shifted its position from one plot to the other, which can be seen in the evolution in the latter part. Two of the terms which are highly recurring in the ‘humans bubble’ are ‘software’ and ‘algorithm’ which reflects that dynamic problem solving requires the usage of algorithms. In the ‘animals bubble’, the recurring terms are ‘physiology’ and ‘three dimensional/printing’. The analogy here seems to be the development of a health monitoring system or something similar which requires 3D printing for various parts and physiological parameters for monitoring the health status of individuals. It is noticed that there is no particular bubble positioned in the ‘motor theme plot’ signaling that there are no mainstream fields in the research topic. ‘Wearable electronic devices’ and ‘limit of detection’ do not hold much of place in the research field since they lie in the upper left quadrant. However, ‘humans’ and ‘animals bubble’ are vital in the research study but it could be interpreted that they are not yet evolved fully or the researchers are still working on their development. They are the basic general topics with good scope for further development. Intellectual Structure involves citation analysis, which is not attempted in the paper due to the current restriction in accessing the citation details from PubMed.

#### K. Social Structure

Social structure deals with the relationship between countries and authors in the research area.

1) *Country collaboration*: Fig. 17 depicts a list of countries arranged randomly, with each color of the node representing a unique cluster. Countries which have collaborated or are collaborating are categorized in the clusters joined through links. It is noticed that Spain has collaborations with both Mexico and USA; Germany and Switzerland also appear in the collaborated list. The rest of the countries remain independent. The observations are recorded in Table XIII.

2) *Co-author collaboration*: Co-author collaboration helps us in perceiving a pictorial representation of collaboration amongst authors. The same understanding of the graph applies here which is each unique color represents a cluster and the authors which are working together are connected by links. From the Fig. 18, it is observed that there are 39 clusters in all, out of which there are 4 clusters which represent the collaboration of authors which has been recorded in Table XIV.





#### IV. CONCLUSION

The analysis leads to the following conclusion:

- A total of 154 articles have been published from 2013-2020 in the health-care field using Raspberry Pi, with the year 2019 having the highest number of journal articles published.
- The United States of America leads the table with the highest number of specific country production and most of the authors working on the topic belong to China with less representation from Korea.
- University of British Columbia, Canada has the greatest number of affiliations to the topic. Considering all the data and analyzing the graphs with various parameters, a table (Table XII) has been constructed which represents the most common keywords used by the top authors and the country from which the paper has been published and its corresponding source.
- The most trending keyword by the top authors is "Humans." On performing knowledge analysis (conceptual structure – discovering major themes and trends), the graphs insinuate that there is no "Motor Theme" as yet in the healthcare domain. On the contrary, a lot of research work is being done on 'Humans' and 'animals' in this field, for instance, 'Health monitoring system for animals and humans.
- By making use of Social Structure which per se helps us to identify the relationships between authors and countries who have collaborated, the results deduce that there are a couple of authors who are working in harmony towards this budding topic in the research field and the USA, Mexico, Spain; Switzerland and Germany are the countries which are working collaboratively in this research field.

Despite the limitations of not conducting intellectual structure analysis because of restriction of citation details from PubMed, the findings are valuable in light of a strong basic analysis for future research. Thematic analysis has been a game-changer in our trend analysis. Broadly translated, our findings indicate that there is no motor theme emerging in the present context but more research in the upcoming years may alter the position. However the present findings do confirm that there has been a progress in affairs which involve amalgamation of Raspberry Pi along with wearable electronic devices, various algorithms, image processing techniques, etc.

#### V. FUTURE WORK

Future studies could fruitfully explore more domains on the applicative trends of Raspberry Pi in healthcare. Few recommendations for future research are given.

- Enhancements in the current technologies with respect to the Pi in order to boost compatibility, connectivity and productivity.
- Security, privacy, legal issues which have to be tackled while using the same.

Looking forward, further attempts could prove quite beneficial to the literature.

#### ACKNOWLEDGMENT

We would like to express our special thanks of gratitude to our Prof. Hari Kishan Kondaveeti for his valuable and constructive suggestions during the planning and development of this research. He has been a constant support for us in bringing the best out of us and shaping the paper with his immense knowledge and patience.

#### REFERENCES

- [1] R. B. Kent, *Science and Computing with Raspberry Pi*, IOP Concise Physics, 2018.
- [2] P. Sachdeva and S. Katchi, "A Review Paper on Raspberry Pi," *International Journal of Current Engineering and Technology*, 2014.
- [3] J. ., S. Johnston and J. ., S. Cox, *Raspberry Pi Technology*, 2018.
- [4] M. Saari, b. M. ., A. Baharudin and S. Hyrynsalmi, *Survey of Prototyping Solutions Utilizing Raspberry Pi*, 2017.
- [5] V. Raan, "In matters of quantitative studies of science the fault of theorists is offering too little and asking too much," *Scientometrics*, vol. 43, p. 129–139, 1998.
- [6] J. Lundberg, "Bibliometrics as a research assessment tool : impact beyond the impact factor," 2006.
- [7] V. Durieux and P. Gevenois, " Bibliometric Indicators: Quality Measurements of Scientific Publication," *Radiology*, vol. 255, no. 2, pp. 342-51, 2010.
- [8] L. L. Li, G. Ding, N. Feng, M. H. Wang and Y. S. Ho, "Global stem cell research trend: Bibliometric analysis as a tool for mapping of trends from 1991 to 2006," *Scientometrics*, vol. 80, pp. 39-58, 2009.
- [9] F. Fatehi, G. Leonard and W. Richard, "How to improve your PubMed/MEDLINE searches: 1. background and basic searching," *Journal of telemedicine and telecare*, 2013.
- [10] M. Aria, "bibliometrix: An R-tool for comprehensive science mapping analysis," *Journal of Infometrics*, 2017.
- [11] B. Elango and P. Rajendran, "Authorship trends and collaboration pattern in the marine sciences literature : a scientometric study.," *International Journal of Information Dissemination and Technology*, 2, pp. 166-169, 2012.
- [12] W. contributors, "Compound annual growth rate," 28 March 2020. [Online]. Available: [https://en.wikipedia.org/w/index.php?title=Compound\\_annual\\_growth\\_rate&oldid=947842856](https://en.wikipedia.org/w/index.php?title=Compound_annual_growth_rate&oldid=947842856).
- [13] J. H. McDonald, *Handbook of Biological Statistics*, Sparkly house publishing, 2009.
- [14] L. W. Nees Jan van Eck, "How to Normalize Co-Occurrence Data? An Analysis of Some Well-Known Similarity Measure," *Journal of the American Society for Information science and Technology*, 2009.
- [15] A. L. a. S. Fortunato, "Community detection algorithms : a comparative analysis," *Physical review*, 2009.
- [16] M. J. Cobo, G. ., A. Lopez - Herrera, E. Herrera - Viedma and F. Herrera, "An approach for detecting, quantifying, and visualizing the evolution of a research field: A practical application to the Fuzzy Sets Theory field," *Journal of Infometrics*, pp. 146-166, 2010.
- [17] M. Callon, J. ., P. Courtial and F. Laville, "Co-word analysis as a tool for describing the network of interactions between basic and technological research: The case of polymer chemistry," *Scientometrics*, pp. 155-205, 1991.
- [18] M. Th, J. Boyd and O. Noorshams, "Automating Mouse Weighing In Group Homecages With Raspberry Pi Micro-Computers.," *Journal of Neuroscience Methods*, vol. 285, 2017.
- [19] Automated Task Training And Longitudinal Monitoring Of Mouse Mesoscale Cortical Circuits Using Home Cages..

- [20] F. Bolaños, J. LeDue and T. Murphy, "Cost effective raspberry pi-based radio frequency identification tagging of mice suitable for automated in vivo imaging," *Journal of Neuroscience Methods*, vol. 276, 2016.
- [21] D. J. Ardesch, M. Balbi and T. Murphy, "Automated Touch Sensing In The Mouse Tapered Beam Test Using Raspberry Pi.," *Journal of Neuroscience Methods*, vol. 291, 2017.
- [22] D. J. Boyd, H. Murphy, Timothy, H. . S. ., B. ., F. Scott and G. Silasi, "Individualized Tracking Of Self-Directed Motor Learning In Group-Housed Mice Performing A Skilled Lever Positioning Task In The Home Cage.," *Journal of Neurophysiology*, vol. 119, no. 1, pp. 337-346, 2018.
- [23] S. McGill and D. Barker, "Comparison Of The Protein-Coding Genomes Of Three Deep-Sea, Sulfur-Oxidising Bacteria: "Candidatus Ruthia Magnifica", "Candidatus Vesicomysocius Okutanii" And Thiomicrospira Crunogena.," *BMC Research Notes*, vol. 10, 2017.
- [24] F. R. James and B. Daniel, "Comparison of the protein-coding gene content of Chlamydia trachomatis and Protochlamydia amoebophila using a Raspberry Pi computer," *BMC Res Notes*, vol. 8, 2015.
- [25] D. Barker, D. Ferrier, P. Holland, J. Mitchell, H. Plaisier, M. Ritchie and S. Smart, "4273π: Bioinformatics education on low cost ARM hardware," *BMC bioinformatics*, vol. 14, 2013.
- [26] J. McDonagh, D. Barker and R. G. Alderson, "Bringing computational science to public," *SpringerPlus*, vol. 5, no. 259, 2016.

# Effect of Route Length and Signal Attenuation on Energy Consumption in V2V Communication

Mahmoud Zaki Iskandarani  
Faculty of Engineering  
Al-Ahliyya Amman University  
Amman, Jordan

**Abstract**—Simulation of Vehicle-to Vehicle (V2V) communication and connectivity is carried out. The main objective of the carried out V2V communication simulation is to study the effect of route length, number of hops per route, attenuation related parameter and message size on energy consumption of transmitted bits per sent message. Mathematical modeling (using the original radio energy model), and analysis, is carried out to quantify and approximate the effect of attenuation related parameter ( $\alpha$ ) and Route Length (LR) on energy consumption of transmitted Basic Safety Message (BSM) for both, 256 Bytes and 320 Bytes size. The original energy radio model is expanded to include not only message size, but also the effect of number of hops on energy consumption. The work successfully proved the critical effect of  $\alpha$  and number of hops on energy consumption for a fixed BSM size and the effect of  $\alpha$  on the transitional characteristics of routes as a function of number of hops. It is clear from the simulation that  $\alpha$  has an adverse effect on consumed energy for transmitted BSMs and also has a marked effect on routes, where any value of  $\alpha$  above 3 will lead to energy depletion among, other negative effects on communicating devices.

**Keywords**—Intelligent transportation systems; routing; connected vehicles; energy; V2V; multipath fading; BSM

## I. INTRODUCTION

Advances in information and communication technologies and their applications to infrastructure and traffic under intelligent transportation systems generated much work on vehicular networking. Objectives for such work is to provide vehicles and roads with safe and reliable travelling infrastructure. Additional benefits from securing increasing the efficiency of roads and vehicles interaction is to enable a more relaxed and comfortable journeys. To achieve such objectives, a secure, efficient, effective, and reliable information need to be conveyed to vehicles concerning road conditions, accidents, incidents, congestion, weather conditions, alternative routes, alternative services on different routes and roads. This is for all travelling vehicles on the roads network, and for vehicles sharing the same road over a period of time, speed, distance, and location information need to be exchanged between vehicles as well as all other information that is received by vehicles from traffic management centers and from traffic control centers [1-4].

The delivered information to vehicles and information exchanged between vehicles, contributes to better and safer journeys, improves economic conditions and business efficiency, reduce pollution, fuel consumption, running cost.

To achieve intelligent transportation systems objectives, vehicular ad-hoc network (VANET) is devised based on the existing mobile ad-hoc network (MANET), to form a wireless communication infrastructure for information exchange among vehicles. In VANETS, vehicles are equipped through on board units (OBUs) with wireless communication capabilities, which prepare them to form temporary networks while sharing same road within a transmittable distance, without the need for infrastructure connections or road side units (RSUs) [5-9].

The main task of a VANET is to enable data exchange through wireless communication through an effective Basic Safety Messages (BSMs), covering Vehicle-to-Vehicle communication (V2V) for speed, distance, location and general safety applications. Vehicle-to-Infrastructure communication (V2I) for safety and information collection applications, and in some scenarios, when the vehicles are at a long distance, V2V can occur through V2I, or when internet access is required for cloud computing applications and for temporary vehicular networks through cloud, V2I and V2V is employed a blended way for vehicular networking applications [10-16].

Vehicles travel in different areas and undergo different traffic environments due to the infrastructure mapping, such as urban, rural and large cities roads. Thus, communication within a vehicular ad-hoc network should operate satisfactory in all these areas which, have different communication impairments, which affects transmission energy of BSMs.

For communication to operate successfully, the default signal propagation model (free-space), needs to be modified according to the existing types of interference and blockage that might exist. The existence of such obstacles that can cause signal fading due to many factors, such as reflection, refraction and adsorption due surfaces such as building, high traffic density, trees, among others, which can also cause shadowing of signal propagation and end with multi-path fading., hence, free-space model cannot be assumed due to general signal attenuation [17-20].

Vehicular networks have to communicate with nearby vehicles, road side units (RSUs) with different requirements. Thus, and regardless of mechanism of communication, consideration of multipath fading and frequency displacements due to dynamic movements of vehicles (nodes) during travelling on different road environments is essential. Radio waves V2V communication using different frequencies

and wavelengths are very much developed with energy consumption as a measuring factor of efficient data exchanged between vehicles in a vehicular network [21-22].

In this paper, the extent of influence of the attenuation dependent parameter ( $\alpha$ ) and Route Length (RL) is analyzed and modeled using the basic radio energy model. The effect of fading and route length is also related to the number of hops per route and to energy consumption for 256 Bytes and 320 Bytes BSMs.

## II. METHODOLOGY

The purpose of this work is to use simulation of connected vehicles under different communication conditions, to assess V2V connectivity through energy consumption and its relationship with both route length and fading factors. The results of the simulation is used to develop the energy radio model to explicitly show effect of route length, hops, and fading factors (attenuation) in the consumed energy.

Modeling of energy consumption through data exchange between vehicles through routing using radio model is expressed by the general equation (1) and is derived as the energy per bit as a function of single hop.

$$E = E_{tx} + E_{rx}. \quad (1)$$

Where;

$E_{tx}$ : Energy consumption of transmitter electronics.

$E_{rx}$ : Energy consumption of receiver electronics.

The components of equation (1) are:

$$E_{tx} = E_{elect} + E_{tx(d)}(d)^\alpha. \quad (2)$$

$$E_{rx} = E_{elect}. \quad (3)$$

$E_{elect}$ : Energy consumption of radio dissipation.

$E_{tx(d)}$ : Energy consumption of the amplifier in the free space channel model used to transmit 1-bit over 1-meter distance, which can be substituted with the term  $E_{(initial)}$ .

$\alpha$ : Attenuation dependent parameter, function of communication environment usually between 2 and 5.

$d$ : Transmission range or distance.

To account for size of exchanged data in bits, equation (4) needs to be taken into consideration.

$$k = N * packetsize * 8. \quad (4)$$

Where;

$N$ : Number of transmitted packets.

Thus; equations (2) and (3) become:

$$E_{tx} = k * (E_{elect} + E_{(initial)}(d)^\alpha) \quad (5)$$

$$E_{rx} = k * E_{elect}. \quad (6)$$

It is assumed in this work that both  $E_{elec}$  and  $E_{(initial)}$  have fixed values of ( $E_{elec} = 50\text{nJ/bit}$ ,  $E_{(initial)} = 0.105\text{nJ/bit/m}^2$ ). Thus the variation in consumed energy is mainly due to the factors of distance and the attenuation factor  $\alpha$ .

Energy for transmitted bits is a function of distance, as more energy is needed for longer distances, due to fading and attenuating factors, and distance between transmitter and receiver (which is varying in real time). Energy is also related to the number of hops required to pass a message from vehicle A to vehicle B under consideration. The number of hops and consequently route length (RL) indicative of traffic condition and smoothness of traffic flow.

Thus, energy will be consumed more in relation to route length (RL), which is related to the number of hops. This means that, the distance ( $d$ ) can be replaced by Route Length (RL), which will enable measuring distances as a function of hops based on the following assumptions:

1) Each vehicle will transmit to a fixed range such that route length for each hop does not exceed that range.

2) The range of transmission for each vehicle is widened if no communication achieved with the current range within a period of time  $T$ .

3) Route length will increase as more hops are needed for V2V connection, which will require longer communication time and more energy consumption. Hence, equation (5) becomes:

$$E_{tx} = k * (E_{elect} + E_{(initial)}(Route\ Length)^\alpha) \quad (7)$$

As Route length (RL) is related to the number of hops, then, Route length can be approximated and represented as shown in equation (8), which presents the effect of average hop length (AVH) or in general shows the effect of hop length as hops constitute travelled message route.

$$Route\ Length(RL) = (M * Average\ Hop\ Length). \quad (8)$$

Where  $M$  represents number of hops per specific route. So, equation (7) can be fairly represented as shown in equation (9).

$$E_{tx} = k * (E_{elect} + E_{(initial)}(M * AHL)^\alpha) \quad (9)$$

As the number of hops increases, the average hop length decrease, indicative of more traffic and more consumed energy.

To obtain a good approximation for Average Hop Length (AHL), the average of all routes length with different number of hops should be computed.

Thus, number of hops and average hop length need to be reduced in order to preserve consumed energy, at the same time, such hop count can be used to indicate traffic conditions.

## III. RESULTS AND DISCUSSION

Tables I to IV present the initial simulated results for road traffic and V2V communication using BSMs.

TABLE II. BSM COMUNICATION FOR  $\alpha = 1$

| M | RL (m) | E <sub>tx</sub> (J) |               |
|---|--------|---------------------|---------------|
|   |        | BSM=256 Bytes       | BSM=320 Bytes |
| 2 | 50.62  | 0.0001128           | 0.0001410     |
| 2 | 55.00  | 0.0001137           | 0.0001421     |
| 2 | 55.64  | 0.0001138           | 0.0001422     |
| 2 | 55.81  | 0.0001138           | 0.0001423     |
| 2 | 55.88  | 0.0001138           | 0.0001423     |
| 2 | 56.21  | 0.0001139           | 0.0001424     |
| 2 | 56.34  | 0.0001139           | 0.0001424     |
| 2 | 56.82  | 0.0001140           | 0.0001425     |
| 2 | 56.99  | 0.0001141           | 0.0001426     |
| 2 | 57.63  | 0.0001142           | 0.0001428     |
| 2 | 57.84  | 0.0001142           | 0.0001428     |
| 2 | 58.87  | 0.0001145           | 0.0001431     |
| 2 | 59.82  | 0.0001147           | 0.0001433     |
| 3 | 61.17  | 0.0001149           | 0.0001437     |
| 3 | 61.86  | 0.0001151           | 0.0001438     |
| 3 | 62.43  | 0.0001152           | 0.0001440     |
| 3 | 62.66  | 0.0001152           | 0.0001440     |
| 3 | 63.33  | 0.0001154           | 0.0001442     |
| 3 | 64.30  | 0.0001156           | 0.0001445     |
| 3 | 64.47  | 0.0001156           | 0.0001445     |
| 3 | 65.81  | 0.0001159           | 0.0001448     |
| 3 | 66.05  | 0.0001159           | 0.0001449     |
| 3 | 67.28  | 0.0001162           | 0.0001452     |
| 3 | 67.91  | 0.0001163           | 0.0001454     |
| 3 | 68.87  | 0.0001165           | 0.0001456     |
| 3 | 69.87  | 0.0001167           | 0.0001459     |
| 3 | 70.53  | 0.0001168           | 0.0001461     |
| 3 | 71.91  | 0.0001171           | 0.0001464     |
| 3 | 72.26  | 0.0001172           | 0.0001465     |

TABLE III. BSM COMUNICATION FOR  $\alpha = 2$

| M | RL (m) | E <sub>tx</sub> (J) |               |
|---|--------|---------------------|---------------|
|   |        | BSM=256 Bytes       | BSM=320 Bytes |
| 2 | 50.62  | 0.00063             | 0.00078       |
| 2 | 56.91  | 0.00077             | 0.00096       |
| 2 | 56.99  | 0.00077             | 0.00096       |
| 2 | 57.30  | 0.00077             | 0.00097       |
| 2 | 58.04  | 0.00079             | 0.00099       |
| 2 | 58.05  | 0.00079             | 0.00099       |
| 2 | 58.21  | 0.00080             | 0.00100       |
| 2 | 59.07  | 0.00082             | 0.00102       |
| 2 | 59.17  | 0.00082             | 0.00102       |
| 3 | 63.27  | 0.00092             | 0.00115       |
| 3 | 64.60  | 0.00096             | 0.00120       |
| 3 | 64.89  | 0.00096             | 0.00121       |
| 3 | 64.93  | 0.00097             | 0.00121       |

|   |       |         |         |
|---|-------|---------|---------|
| 3 | 66.02 | 0.00099 | 0.00124 |
| 3 | 67.61 | 0.00104 | 0.00130 |
| 3 | 68.83 | 0.00107 | 0.00134 |
| 3 | 68.92 | 0.00108 | 0.00134 |
| 3 | 68.96 | 0.00108 | 0.00135 |
| 3 | 69.29 | 0.00109 | 0.00136 |
| 3 | 69.78 | 0.00110 | 0.00137 |
| 3 | 69.80 | 0.00110 | 0.00138 |
| 3 | 70.22 | 0.00111 | 0.00139 |
| 3 | 70.50 | 0.00112 | 0.00140 |
| 3 | 70.57 | 0.00112 | 0.00140 |
| 3 | 70.91 | 0.00113 | 0.00142 |
| 3 | 71.31 | 0.00114 | 0.00143 |
| 3 | 71.36 | 0.00115 | 0.00143 |
| 3 | 71.75 | 0.00116 | 0.00145 |
| 3 | 72.24 | 0.00117 | 0.00146 |

TABLE IV. BSM COMUNICATION FOR  $\alpha = 3$

| M | RL (m) | E <sub>tx</sub> (J) |               |
|---|--------|---------------------|---------------|
|   |        | BSM=256 Bytes       | BSM=320 Bytes |
| 2 | 51.93  | 0.02878             | 0.03597       |
| 2 | 51.96  | 0.02883             | 0.03604       |
| 2 | 52.01  | 0.02892             | 0.03614       |
| 2 | 52.11  | 0.02908             | 0.03635       |
| 2 | 52.21  | 0.02925             | 0.03657       |
| 2 | 52.37  | 0.02953             | 0.03691       |
| 2 | 52.53  | 0.02980             | 0.03724       |
| 2 | 52.76  | 0.03017             | 0.03772       |
| 2 | 53.26  | 0.03104             | 0.03879       |
| 2 | 53.26  | 0.03104             | 0.03879       |
| 2 | 53.57  | 0.03159             | 0.03949       |
| 2 | 53.93  | 0.03222             | 0.04027       |
| 2 | 54.32  | 0.03293             | 0.04116       |
| 2 | 54.76  | 0.03373             | 0.04217       |
| 3 | 66.55  | 0.06045             | 0.07557       |
| 3 | 71.39  | 0.07461             | 0.09326       |
| 3 | 72.65  | 0.07863             | 0.09828       |
| 3 | 72.99  | 0.07975             | 0.09968       |
| 3 | 73.42  | 0.08115             | 0.10144       |
| 3 | 74.20  | 0.08377             | 0.10471       |
| 3 | 74.35  | 0.08428             | 0.10536       |
| 3 | 74.55  | 0.08494             | 0.10618       |
| 3 | 74.60  | 0.08513             | 0.10642       |
| 3 | 74.89  | 0.08611             | 0.10764       |
| 3 | 75.06  | 0.08671             | 0.10839       |
| 3 | 75.19  | 0.08716             | 0.10895       |
| 3 | 75.52  | 0.08830             | 0.11037       |
| 3 | 75.54  | 0.08837             | 0.11046       |
| 3 | 75.93  | 0.08974             | 0.11218       |

TABLE V. BSM COMMUNICATION FOR  $\alpha = 4$

| M | RL (m) | $E_{tx}$ (J)  |               |
|---|--------|---------------|---------------|
|   |        | BSM=256 Bytes | BSM=320 Bytes |
| 2 | 53.54  | 1.68287       | 2.10359       |
| 2 | 54.18  | 1.76491       | 2.20614       |
| 2 | 54.88  | 1.85787       | 2.32234       |
| 2 | 55.46  | 1.93788       | 2.42235       |
| 2 | 55.47  | 1.93882       | 2.42352       |
| 2 | 55.49  | 1.94197       | 2.42747       |
| 2 | 55.53  | 1.94739       | 2.43423       |
| 2 | 55.64  | 1.96315       | 2.45394       |
| 2 | 56.04  | 2.01967       | 2.52459       |
| 2 | 56.18  | 2.03995       | 2.54994       |
| 2 | 56.34  | 2.06309       | 2.57886       |
| 2 | 56.47  | 2.08235       | 2.60294       |
| 3 | 63.08  | 3.24238       | 4.05298       |
| 3 | 64.76  | 3.60191       | 4.50239       |
| 3 | 66.56  | 4.02014       | 5.02518       |
| 3 | 67.52  | 4.25767       | 5.32208       |
| 3 | 67.63  | 4.28495       | 5.35618       |
| 3 | 67.91  | 4.35545       | 5.44432       |
| 3 | 68.03  | 4.38557       | 5.48197       |
| 3 | 68.49  | 4.50628       | 5.63284       |
| 3 | 69.60  | 4.80694       | 6.00867       |
| 3 | 70.54  | 5.07095       | 6.33869       |
| 3 | 71.35  | 5.30825       | 6.63531       |
| 3 | 72.72  | 5.72646       | 7.15807       |
| 3 | 73.14  | 5.86081       | 7.32602       |
| 3 | 74.03  | 6.15081       | 7.68851       |
| 3 | 74.96  | 6.46646       | 8.08307       |
| 3 | 75.02  | 6.48689       | 8.10862       |
| 3 | 76.58  | 7.04254       | 8.80317       |

Fig. 1 to 4 show effect of the attenuation related parameter ( $\alpha$ ), Route Length (RL), BSM size on energy consumption during transmission ( $E_{tx}$ ). From the figures, it is realized that:

- 1) The clear increase in the energy consumption of the transmitted messages as a function of Route Length (RL).
- 2) The expected increase in the energy consumption of the transmitted messages as a function of message size.
- 3) A marked increase in the energy consumption of the transmitted messages as a function of increasing the attenuation dependent parameter ( $\alpha$ ).
- 4) The increase in ( $\alpha$ ) caused a change in the energy consumption function behavior from linear to quadratic, which has an ability to increase in a dramatic manner causing communication failure due to energy depletion.

Tables V and VI present statistical data regarding average hops lengths (AHL), attenuation dependent parameter ( $\alpha$ ), and average consumed energy (ACE) during BSM transmission. From the tables, the following is noted:

- 1) As  $\alpha$  increases, AHL is also affected.
- 2) AHL (2 Hops) changes dynamically with AHL (3 Hops), so if one increases the other decreases.
- 3) For all  $\alpha$  values, AHL (2 Hops) is larger than AHL (3Hops).
- 4) The number of hops forming a route is independent of BSM size.
- 5) The average consumed energy per hop (ACE) is inversely related to the number of hops with overall average consumed energy directly proportional to route length (RL) and to the transmitted message size (BSM).
- 6) The average consumed energy per hop is directly proportional to the attenuation related parameter ( $\alpha$ ).

From the observations on data presented in Tables V and VI, equation (10) shows a reasonable representation of obtained data within the radio model context.

$$ACE = k * (E_{elect} + E_{(initial)}(M * AHL)^\alpha) \tag{10}$$

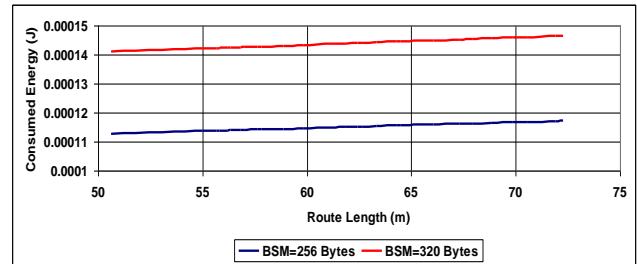


Fig. 1. Consumed Transmission Energy as a Function of Route Length ( $\alpha=1$ ).

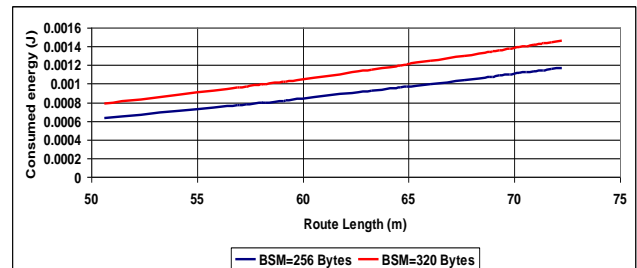


Fig. 2. Consumed Transmission Energy as a Function of Route Length ( $\alpha=2$ ).

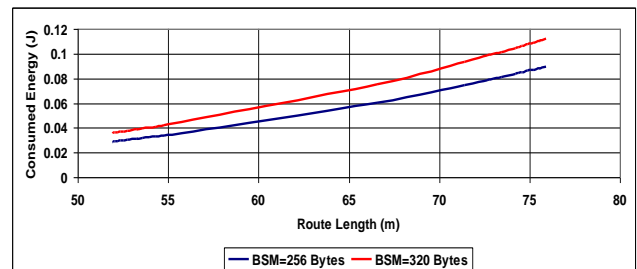


Fig. 3. Consumed Transmission Energy as a Function of Route Length ( $\alpha=3$ ).

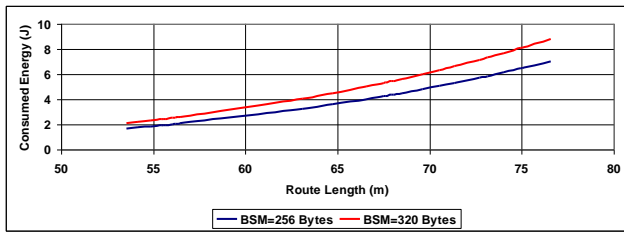


Fig. 4. Consumed Transmission Energy as a Function of Route Length ( $\alpha=4$ ).

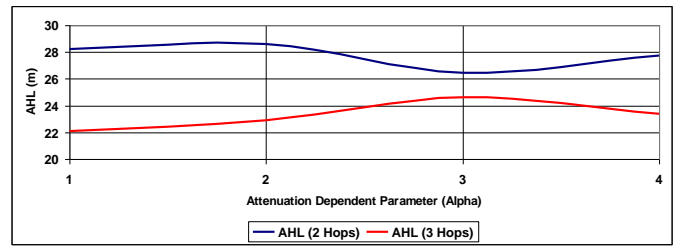


Fig. 5. Effect of  $\alpha$  on Route Characteristics.

TABLE VI. EFFECT OF  $\alpha$  AND AHL ON AVERAGE ENERGY CONSUMPTION (ACE) FOR BSM=256 BYTES

| $\alpha$ | AHL (m) |        | ACE (J) |         |
|----------|---------|--------|---------|---------|
|          | 2 Hops  | 3 Hops | 2 Hops  | 3 Hops  |
| 1        | 28.21   | 22.10  | 0.00006 | 0.00004 |
| 2        | 28.60   | 22.93  | 0.00039 | 0.00036 |
| 3        | 26.46   | 24.60  | 0.01525 | 0.02754 |
| 4        | 27.72   | 23.37  | 0.96830 | 1.67793 |

TABLE VII. EFFECT OF  $\alpha$  AND AHL ON AVERAGE ENERGY CONSUMPTION (ACE) FOR BSM=320 BYTES

| $\alpha$ | AHL (m) |        | ACE (J) |         |
|----------|---------|--------|---------|---------|
|          | 2 Hops  | 3 Hops | 2 Hops  | 3 Hops  |
| 1        | 28.21   | 22.10  | 0.00007 | 0.00005 |
| 2        | 28.60   | 22.93  | 0.00048 | 0.00045 |
| 3        | 26.46   | 24.60  | 0.01906 | 0.03442 |
| 4        | 27.72   | 23.37  | 1.21000 | 2.09741 |

For large values of  $\alpha$ ,  $E_{elec}$  can be ignored as most of the consumed energy is influenced and affected by route length (RL), which contains hops. Thus, equation (10) can be reduced and simplified to obtain equation (11).

$$ACE = k * (E_{(initial)} (M * AHL)^\alpha) \tag{11}$$

The differential change in ACE in response to AHL will also follow a power law representation affected by both BSM and  $\alpha$ .

Fig. 5 shows the behavior of 3 Hops routes versus 2 Hops routes as a function of the attenuation dependent parameter  $\alpha$ . The figure clearly shows an opposite dynamic behavior, which points towards a dependence relationship between  $\alpha$  and its effect on the differential characteristics of routes. Such effect of  $\alpha$  is critical in routing considerations for BSMs exchanged between vehicles and for vehicular ad-hoc networks under communication networks affected by transmitting frequency and processing speed within environmental parameters with associated multi path fading factors.

#### IV. CONCLUSIONS

This work presents a new approach to analyze energy consumption by transmitted BSMs during V2V communication. The analysis showed a marked and non-linear effect of the attenuation dependent parameter ( $\alpha$ ) on both route length and consumed energy. Route length also has an effect of increasing the energy consumed in a transmitted message as a function of number of hops. The conventional energy radio model is used to analyze such effects and successfully showed that the original distance term in the model can be replaced with route length and further with an expression relating number of hops and average hops length. Based on this work, traffic movements and congestion can be estimated as energy consumption is related to the number of BSMs exchanged and to number of hops per route. Energy harvesting in BSM exchanges with advanced information and communication technologies with smart cities traffic applications and internet of things IoT will much benefit from such approach, as routing algorithms always search for shortest route with minimum number of hops and energy dissipation and consumption.

#### REFERENCES

- [1] S. Mignardi, C. Buratti, A. Bazzi, R. Verdone "Trajectories and Resource Management of Flying Base Stations for C-V2X," Sensors, vol. 19, no. 811, pp. 1–15, 2019.
- [2] M. Baek, D. Jeong, D. Choi, S. Lee, "Vehicle Trajectory Prediction and CollisionWarning via Fusion of Multisensors and Wireless Vehicular Communications," Sensors, Vol. 20, No. 288, pp. 1-26, 2020.
- [3] J S. Hussain, D. Wu, W. Xin, S. Memon, N. Bux, A. Saleem, "Reliability and Connectivity Analysis of Vehicular Ad Hoc Networks for a Highway Tunnel , " International Journal of Advanced Computer Science and Applications, Vol. 10, No. 4, pp. 181-186, 2019.
- [4] T. Li, N. Ngoduy, F. Hui, X. Zhao, "A car-following model to assess the impact of V2V messages on traffic dynamics," Transportmetric B: Transport Dynamics, Vol. 8, No. 1, pp. 150-165, 2020.
- [5] Y. Bai, K. Zheng, Z. Wang, X. Wang, "MC-Safe: Multi-channel Real-time V2V Communication for Enhancing Driving Safety," ACM Transactions on Cyber-Physical Systems, Vol. 4, No. 4, pp. 1-27, 2020.
- [6] C. Jung, D. Lee, S. Lee, D. Shim, "V2X-Communication-Aided Autonomous Driving: System Design and Experimental Validation," Sensors, Vol. 20, No. 2903, pp. 1-21, 2020.
- [7] D. Xie, Y. Wen, X. Zhao, X. Li, Z. He, "Cooperative driving strategies of connected vehicles for stabilizing traffic flow," Transportmetric B: Transport Dynamics, Vol. 8, No. 1, pp.166-181, 2020.
- [8] Y. Chen, C. Lu, W. Chu, "A Cooperative Driving Strategy Based on Velocity Prediction for Connected Vehicles With Robust Path-Following Control," IEEE Internet of Things Journal, Vol. 7, No. 5, pp. 3822-3832, 2020.
- [9] J. Mertens, C. Knies, F. Diermeyer, S. Escherle, S. Kraus, "The Need for Cooperative Automated Driving," Electronics, Vol. 9, No. 754, pp. 1-20, 2020.

- [10] K. Yu, L. Peng, X. Ding, F. Zhang, M. Chen, "Prediction of instantaneous driving safety in emergency scenarios based on connected vehicle basic safety messages," *Journal of Intelligent and Connected Vehicles*, Vol. 2 · No. 2, pp. 78–90, 2019.
- [11] M. El Zorkany, A. Yasser, A. I. Galal, "Vehicle To Vehicle "V2V" Communication: Scope, Importance, Challenges, Research Directions and Future," *The Open Transportation Journal*, Vol. 14, pp. 86-98, 2020.
- [12] V. Nampally, R. Sharma, "A Novel Protocol for Safety Messaging and Secure Communication for VANET System: DSRC," *International Journal of Engineering Research & Technology*, Vol. 9, No. 01, pp. 391-397, 2020.
- [13] H. Kim, T. Kim, "Vehicle-to-Vehicle (V2V) Message Content Plausibility Check for Platoons through Low-Power Beaconing," *Sensors*, Vol. 19, No. 5493, pp. 1-20, 2019.
- [14] X. Liu, A. Jaekel, "Congestion Control in V2V Safety Communication: Problem, Analysis, Approaches," *Electronics*, Vol. 8, No. 540, pp. 1-243, 2019.
- [15] A. Seyd Ammar, H. Abolfazl, K. Hariharan, A. Farid, M. Ehsan, "V2V System Congestion Control Validation and Performance," *IEEE Transactions on Vehicular Technology*, Vol. 86, No. 3, pp. 2102-2110, 2019.
- [16] S. Son, K. Park, "BEAT: Beacon Inter-Reception Time Ensured Adaptive Transmission for Vehicle-to-Vehicle Safety Communication," *Sensors*, Vol. 19, No. 3061, pp. 1-11, 2019.
- [17] C. Del-Valle-Soto, C. Mex-Perera, J. Nolasco-Flores, R. Velázquez, A. Rossa-Sierra, "Wireless Sensor Network Energy Model and Its Use in the Optimization of Routing Protocols," *Energies*, Vol. 13, No. 728, pp. 1-33, 2020.
- [18] O. Eyobu, J. Joo, D. Han, "A broadcast scheme for vehicle-to-pedestrian safety message dissemination," *International Journal of Distributed Sensor Networks*, Vol. 13, No. 11, pp. 1-19, 2017.
- [19] Q. Yan, W. Peng, G. Zhang, "Optimal Energy Consumption Tasks Scheduling Strategy for Multi-Radio WSNs," *Sensors*, Vol. 20, No. 881, pp. 1-15, 2020.
- [20] R. Sinda, F. Begum, K. Njau, S. Kaijage, "Refining Network Lifetime of Wireless Sensor Network Using Energy-Efficient Clustering and DRL-Based Sleep Scheduling," *Sensors*, Vol. 20, No. 1540, pp. 1-26, 2020.
- [21] M. Al-Absi, A. Al-Absi, T. Kim, H. Lee, "An environmental channel throughput and radio propagation modeling for vehicle-to-vehicle communication," *International Journal of Distributed Sensor Networks*, Vol. 14, No. 4, pp. 1-10, 2018.
- [22] Y. Song, H. Choi, "Analysis of V2V Broadcast Performance Limit for WAVE Communication Systems Using Two-Ray Path Loss Model," *ETRI Journal*, Vol. 39, No. 2, pp. 213-221, 2017.



# Handwritten Numeric Image Classification with Quantum Neural Network using Quantum Computer Circuit Simulator

Achmad Benny Mutiara<sup>1</sup>, Muhammad Amir Slamet<sup>2</sup>, Rina Refianti<sup>3</sup>, Yusuf Sutanto<sup>4</sup>  
Faculty of Computer Science and Information Technology, Gunadarma University<sup>1,3,4</sup>  
Department of Informatic Engineering, Gunadarma University<sup>2</sup>  
Jl. Margonda Raya No. 100, Depok 16424, Jawa Barat<sup>1,2,3,4</sup>

**Abstract**—Quantum Computer is a computer machine using principles of quantum mechanics in doing its computation. The Quantum Computer Machine itself is still in the development stage and has not been deployed yet, however TensorFlow provides a library for hybrid quantum-classical machine learning called TensorFlow Quantum (TFQ). One of the quantum computing models is the Quantum Neural Network (QNN). QNN is adapted from classical neural networks capable of processing qubit data and passing quantum circuits. QNN is a machine learning model that allows quantum computers to classify image data. The image data used is classical data, but classical data cannot reach a superposition state. So in order to carry out this protocol, the data must be readable into a quantum device that provides superposition. QNN uses a supervised learning method to predict image data. Quantum Neural Network (QNN) with a supervised learning method for classifying handwritten numeric image data is implemented using a quantum computer circuit simulation using the Python 3.6 programming language. The quantum computer circuit simulation is designed using library Cirq and TFQ. The classification process is carried out on Google Colab. The results of training on the QNN model obtained a value of 0.337 for the loss value and 0.3427 for the validation loss value. Meanwhile, the hinge accuracy value from the training results is 0.8603 for the hinge accuracy value with training data and 0.8669 for the hinge accuracy validation value. Model testing is done by providing 100 handwritten number images that are tested, with 53 image data of number three and 47 image data of number six. The results obtained for the percentage of testing accuracy are 100% for the number three image and 100% for the number six image. Thus, the total percentage of testing is 100%.

**Keywords**—Image classification; quantum neural network; quantum computer; TensorFlow

## I. INTRODUCTION

Quantum Computer is a computer machine which uses quantum mechanics for doing its computation [10], [11]. The intensity of the most sophisticated computer now days, has not been satisfied human to possess a super speedy computer. It is not impossible; in the future the most sophisticated super computer will be left by many companies and replaced by quantum computer [10]. Quantum computer machine itself is still in developing phase and has not been spread, but TensorFlow supplies library to hybrid quantum-classical machine learning which is called TensorFlow Quantum

(TFQ). One model of quantum computing is quantum neural network (QNN). QNN is adapted from classical neural network which is able to proceed qubit data and surpass quantum circuit. Qubit is a measurement unit data in quantum computer [1], [2], [3], [4], [5], [6].

QNN is a machine learning model that allows quantum computers to classify image data. The image data used is classical data, but classical data cannot reach a superposition state. So in order to carry out this protocol, the data must be readable into a quantum device that provides superposition. QNN uses a supervised learning method to predict image data [7], [9]. Supervised learning is an approach where trained data is already available, and consists of variable which is targeted [8].

Based on the background above, the following problems are formulated: How to implement the supervised learning method to classify handwritten numeric image data in the Quantum Neural Network (QNN) model in order to achieve a superposition state?

The paper focuses on implementing the quantum neural network (QNN) by using supervised learning method in order to classify numeric handwritten data image. QNN is modelled by using computer quantum simulator circuit which is designed by making use of python-based library Cirq and TFQ. Furthermore, the implementation of the classification process is carried out on Google Colab.

The limitations of the problem in this paper are:

- 1) Handwritten image data obtained from MNIST (Modified National Institute Of Standards and Technology) [12].
- 2) Handwritten image data used are handwritten images of number 3 and handwritten images of number 6 with 11,520 training data and 1,968 testing data.
- 3) The size of the handwritten image data used is 28x28 pixels which are converted to 4x4 pixels.
- 4) The resulting output is a Boolean number where the value 1.0 or true represents the number 3 and the value -1.0 or false represents the number 6.
- 5) The programming language used is Python 3.6 and utilizes the Keras, TensorFlow 2.1, Sympy, Matplotlib, Numpy, and Collections libraries.

6) Quantum computation is performed using a quantum computer circuit simulator provided by TensorFlow Quantum (TFQ) and Cirq.

7) The learning method used is a supervised learning method.

In the rest of paper, we show the research methodology in Section II. In Section III, the implementation and testing of model is presented. The last section is conclusion of our research.

## II. RESEARCH METHODOLOGY

The research method in this research is shown in the following Fig. 1.

### A. Collecting and Processing of Classical Data Image

Data that is used to train model consist of classical image data. Those data are divided into 60.000 train data and 10.000 validity data. Classic image data is used constitute data which is obtained from MNIST database (Modified National Institute of Standards and Technology database).

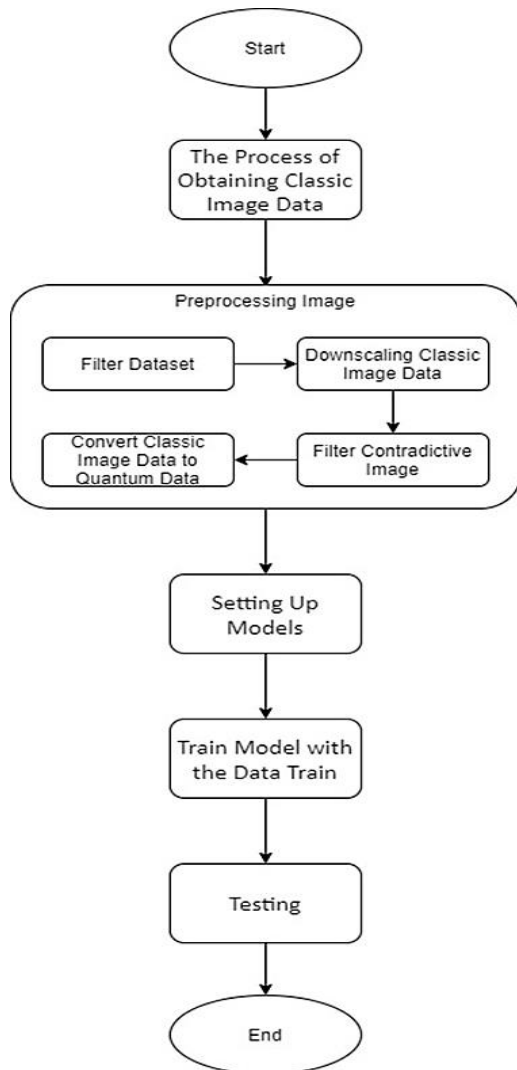


Fig. 1. Research Method.

### B. Preprocessing Data

Pre-processing data image is done by the following steps:

1) *Filtering datasets*: In MNIST datasets consist of ten labels in various images of handwritten number. At the time of writing, quantum computation could only identify Boolean values, so the dataset needed to be filtered so that it could be operated on quantum circuits. The data used comes from dataset 3 and dataset 6, where dataset 3 contains data handwritten image number three and dataset 6 contains data handwritten image number six.

The filter-function is as in the following Fig. 2:

```
def Filter_36(x, y):
 keep = (y == 3) | (y == 6)
 x, y = x[keep], y[keep]
 y = y == 3
 return x, y
```

Fig. 2. Filter-Function for Label 3 and Label 6.

Furthermore, the training data and test data are filtered, and at the same time labe y is converted into Boolean numbers, i.e. “true” value for number three and “false” value for number six. This process reduced the number of training data to 12,049 and test data to 1,968.

2) *Downscaling/Resizing classic image data*: The classic MNIST image data is 28x28 pixels. This size is too large for the quantum computations running on conventional computers at this time. The image will be resized to 4x4 pixels so that it can be fed into the quantum circuit.

Image training data used during training is image data that has gone through the downscaling stage. Below are the before and after downscaling images, as seen respectively in Fig. 3 and Fig. 4.

3) *Filtering contradictive image*: Contradictory images are images labeled 3 and 6. This is done to reduce data barriers which will reduce accuracy when conducting training data on the model to be created. Fig. 5 shows the steps of filtering the contradictive image.

Classical class 3 and class 6 image dataset will be filtered, contradictory images will be deleted and non-contradictory images will be saved. Unique handwritten image data will be saved while image data that is more than one and classified into two (contradictory) labels will be deleted. This process reduced the number of training data to 11,520.

4) *Convert classic image data to quantum data*: Image processing using quantum computers requires quantum data in qubits. An image is made up of pixels, each pixel in the classic image data representing one qubit of data, with a state that depends on its pixel value. The first step is to convert the classic image data to binary coding (see Fig. 6).

Classical image data that has gone through the binary coding process will be converted into quantum data using the Cirq library (see Fig. 7).

After the classical image data becomes quantum data using circuits from Cirq, the circuits are converted to tensors (see Fig. 8).

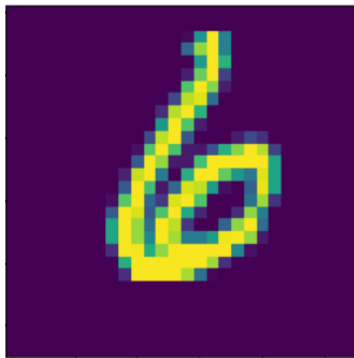


Fig. 3. Image before Downscaling.



Fig. 4. Image after Downscaling.

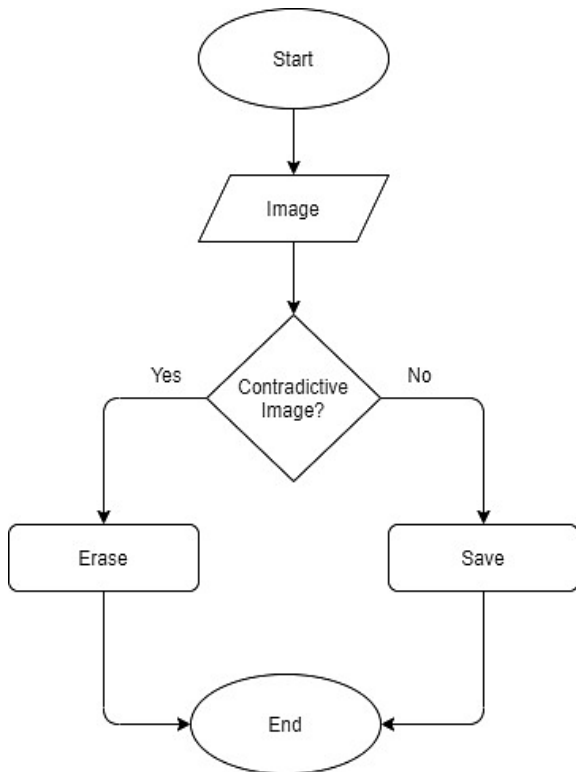


Fig. 5. Filter Contradictive Image Flowchart.

```

THRESHOLD = 0.5

x_train_bin = np.array(x_train_nocon > THRESHOLD, dtype=np.float32)
x_test_bin = np.array(x_test_small > THRESHOLD, dtype=np.float32)

```

Fig. 6. Binary Encoding.

```

def convert_to_circuit(image):
 values = np.ndarray.flatten(image)
 qubits = cirq.GridQubit.rect(4, 4)
 circuit = cirq.Circuit()
 for i, value in enumerate(values):
 if value:
 circuit.append(cirq.X(qubits[i]))
 return circuit

x_train_circ = [convert_to_circuit(x) for x in x_train_bin]
x_test_circ = [convert_to_circuit(x) for x in x_test_bin]

```

Fig. 7. Classic Data Convert to Quantum Data.

```

x_train_tfcirc = tfq.convert_to_tensor(x_train_circ)
x_test_tfcirc = tfq.convert_to_tensor(x_test_circ)

```

Fig. 8. Convert Cirq to Tensor.

### C. Setting up Model

The quantum neural network (QNN) model that is built will be used to recognize images. This model uses two qubit gates, with continuously readout qubit. Thus, this model use layered approach; each layer will pass through the same gate. Each qubit data plays a role in the qubit readout.

The script above in Fig. 9 is a readout preparation for creating a gate layer, then entering it into the circuit in Fig. 10, as well as preparing for building a quantum model.

```

class CircuitLayerBuilder():
 def __init__(self, data_qubits, readout):
 self.data_qubits = data_qubits
 self.readout = readout

 def add_layer(self, circuit, gate, prefix):
 for i, qubit in enumerate(self.data_qubits):
 symbol = sympy.Symbol(prefix + '-' + str(i))
 circuit.append(gate(qubit, self.readout)**symbol)

```

Fig. 9. Build Gate Layer.

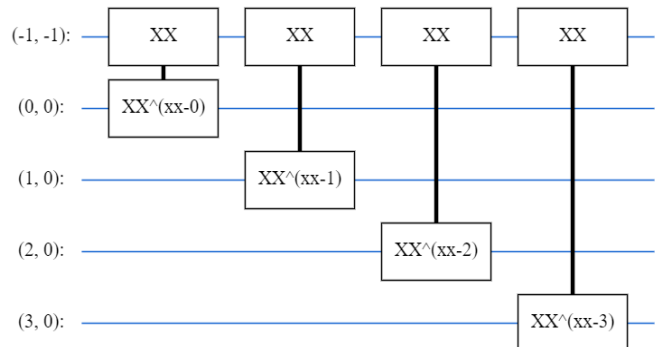


Fig. 10. Grid 4x4.

Data entered through gate XX, each qubit data will become one qubit that is read. The image used is 4x4 pixels in size. Each qubit in its pixel will be read to predict the image. After the XX gate circuit is built, next build a two layer model equal to the circuit size and enter the readout preparation that was made previously. The process of building the two layer model is shown in Fig. 11.

The model is wrapped into the tfq-keras Model. Here, the Keras model is built with quantum components. This model uses quantum data by using the Parameterized Quantum Circuits (PQC) layer for training circuit models on quantum data [7].

Range readout from layer PQC is [-1, 1], thus, optimum hinge loss is required. Re-adjust is required. The data type label y\_train\_nocon which is initially Boolean will be converted to a matrix [-1, 1], according to the hinge loss. Threshold 0.0 is used to change data type when the output emerges, data type will return to be Boolean. Thus the output which comes out there is -1.0 for false value and 1.0 for true value.

Describing training procedures to the model is carried out using the compile method. Image data originating from conventional computers will enter through the PQC layer, then the image data will be quantum processed and the processed data will be sent again to a conventional computer to display the output.

```
def create_quantum_model():
 data_qubits = cirq.GridQubit.rect(4, 4)
 readout = cirq.GridQubit(-1, -1)
 circuit = cirq.Circuit()

 circuit.append(cirq.X(readout))
 circuit.append(cirq.H(readout))

 builder = CircuitLayerBuilder(
 data_qubits = data_qubits,
 readout=readout)

 builder.add_layer(circuit, cirq.XX, "xx1")
 builder.add_layer(circuit, cirq.ZZ, "zz1")

 circuit.append(cirq.H(readout))

 return circuit, cirq.Z(readout)
```

Fig. 11. Quantum Model Function.

Fig.12 shows the summary of model that is built.

| Layer (type)            | Output Shape | Param # |
|-------------------------|--------------|---------|
| pqc (PQC)               | (None, 1)    | 32      |
| Total params: 32        |              |         |
| Trainable params: 32    |              |         |
| Non-trainable params: 0 |              |         |
| None                    |              |         |

Fig. 12. Model Summary.

#### D. Training Model with the Data Train

Model is trained by using trained image data and the output to be validated.

#### E. Testing

Classic image data handwritten which was trained will be tested by image. The output in the form of Boolean number where value of 1.0 or true represents number 3 and value of -1.0 or false represents number 6.

### III. IMPLEMENTATION AND TESTING

Testing of the model is performed using image test data. The testing is recorded by observing the results of the QNN testing process which is processed using the supervised learning method to predict classical handwritten image data.

#### A. Results of Model Training

Fig. 13 shows a graph of the loss value from the results of the training that has been performed. The level of learning in the model built is 0.3370 for the loss value with training data and 0.3427 for the validation loss value.

Meanwhile, the hinge accuracy value from the training results is 0.8603 for the accuracy value on the training data and 0.8669 for the validation hinge accuracy value. The graph of the training accuracy and validation accuracy values can be seen in Fig. 14.

#### B. Results of Model Testing

Testing is performed by providing several images; the model will predict the answer. Image number 3 will be represented as true with an answer output of 1.0 and image number six 6 will be represented as false with an answer output of -1.0. The model will be tested with 100 handwritten numeric images. The test results of the test data can be seen in the Table I.

Based on the data from the results of the tests that have been carried out, the accuracy percentage can be obtained with the following calculations:

$$\text{Accuracy Percentage} = \frac{\text{The Quantity of True Testing Data}}{\text{The Quantity of Testing Data}} \times 100\%$$

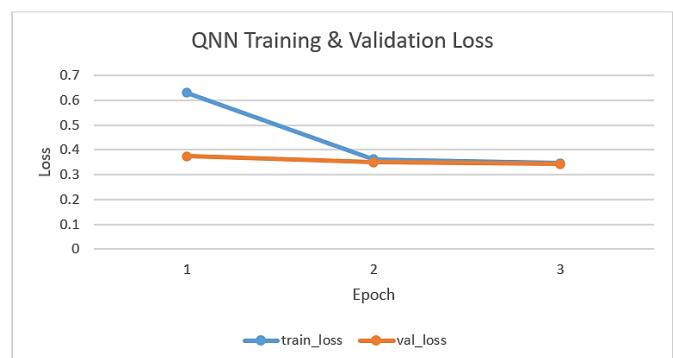


Fig. 13. Loss Value of the Training Process Diagram.

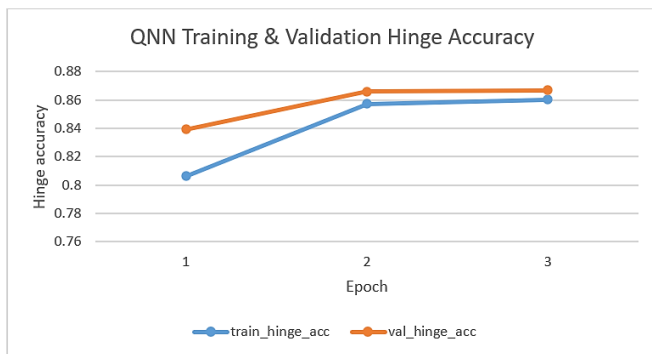


Fig. 14. Accuracy Value of the Training Process Diagram.


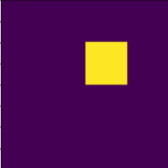
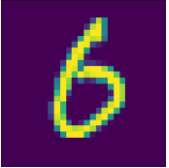


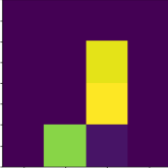
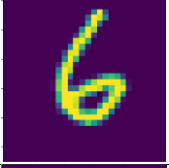
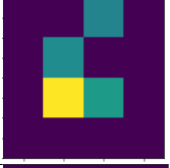


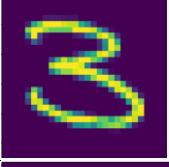
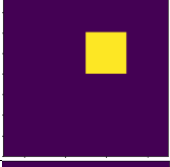
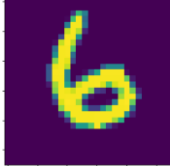


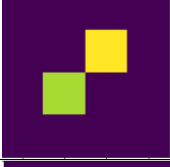
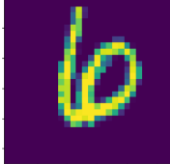



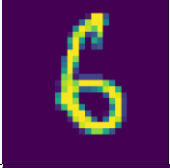

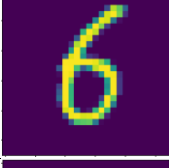


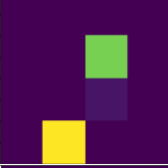
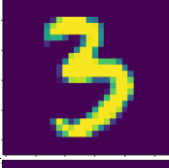

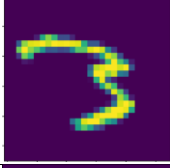

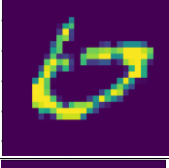


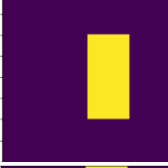
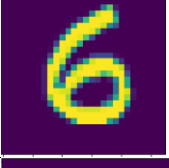
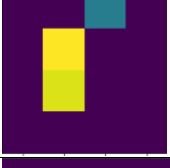
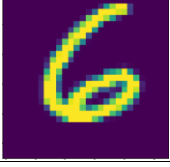
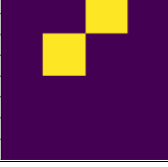
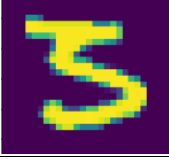

TABLE I. MODEL TEST RESULT

| No. | Original Test Image | Test Image That the Model Read | Answer |
|-----|---------------------|--------------------------------|--------|
| 1.  |                     |                                | -1.0   |
| 2.  |                     |                                | 1.0    |
| 3.  |                     |                                | -1.0   |
| 4.  |                     |                                | -1.0   |
| 5.  |                     |                                | 1.0    |
| 6.  |                     |                                | 1.0    |
| 7.  |                     |                                | 1.0    |

| No. | Original Test Image | Test Image That the Model Read | Answer |
|-----|---------------------|--------------------------------|--------|
| 8.  |                     |                                | -1.0   |
| 9.  |                     |                                | 1.0    |
| 10. |                     |                                | -1.0   |
| 11. |                     |                                | 1.0    |
| 12. |                     |                                | -1.0   |
| 13. |                     |                                | 1.0    |
| 14. |                     |                                | 1.0    |
| 15. |                     |                                | -1.0   |
| 16. |                     |                                | 1.0    |
| 17. |                     |                                | -1.0   |

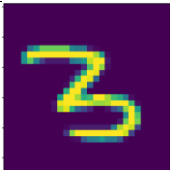



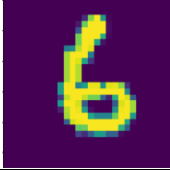

| No. | Original Test Image | Test Image That the Model Read | Answer | No. | Original Test Image | Test Image That the Model Read | Answer |
|-----|---------------------|--------------------------------|--------|-----|---------------------|--------------------------------|--------|
| 18. |                     |                                | 1.0    | 28. |                     |                                | -1.0   |
| 19. |                     |                                | -1.0   | 29. |                     |                                | 1.0    |
| 20. |                     |                                | 1.0    | 30. |                     |                                | -1.0   |
| 21. |                     |                                | -1.0   | 31. |                     |                                | 1.0    |
| 22. |                     |                                | -1.0   | 32. |                     |                                | -1.0   |
| 23. |                     |                                | 1.0    | 33. |                     |                                | -1.0   |
| 24. |                     |                                | -1.0   | 34. |                     |                                | 1.0    |
| 25. |                     |                                | -1.0   | 35. |                     |                                | 1.0    |
| 26. |                     |                                | -1.0   | 36. |                     |                                | -1.0   |
| 27. |                     |                                | -1.0   | 37. |                     |                                | 1.0    |

| No. | Original Test Image | Test Image That the Model Read | Answer | No. | Original Test Image | Test Image That the Model Read | Answer |
|-----|---------------------|--------------------------------|--------|-----|---------------------|--------------------------------|--------|
| 38. |                     |                                | -1.0   | 48. |                     |                                | -1.0   |
| 39. |                     |                                | 1.0    | 49. |                     |                                | 1.0    |
| 40. |                     |                                | 1.0    | 50. |                     |                                | 1.0    |
| 41. |                     |                                | 1.0    | 51. |                     |                                | 1.0    |
| 42. |                     |                                | -1.0   | 52. |                     |                                | -1.0   |
| 43. |                     |                                | 1.0    | 53. |                     |                                | 1.0    |
| 44. |                     |                                | 1.0    | 54. |                     |                                | 1.0    |
| 45. |                     |                                | 1.0    | 55. |                     |                                | 1.0    |
| 46. |                     |                                | -1.0   | 56. |                     |                                | -1.0   |
| 47. |                     |                                | 1.0    | 57. |                     |                                | -1.0   |

| No. | Original Test Image                                                                 | Test Image That the Model Read                                                      | Answer | No. | Original Test Image                                                                  | Test Image That the Model Read                                                        | Answer |
|-----|-------------------------------------------------------------------------------------|-------------------------------------------------------------------------------------|--------|-----|--------------------------------------------------------------------------------------|---------------------------------------------------------------------------------------|--------|
| 58. |    |    | 1.0    | 68. |    |    | -1.0   |
| 59. |    |    | 1.0    | 69. |    |    | -1.0   |
| 60. |    |    | -1.0   | 70. |    |    | 1.0    |
| 61. |    |    | -1.0   | 71. |    |    | 1.0    |
| 62. |   |   | -1.0   | 72. |   |   | 1.0    |
| 63. |  |  | -1.0   | 73. |  |  | -1.0   |
| 64. |  |  | 1.0    | 74. |  |  | 1.0    |
| 65. |  |  | 1.0    | 75. |  |  | -1.0   |
| 66. |  |  | 1.0    | 76. |  |  | -1.0   |
| 67. |  |  | -1.0   | 77. |  |  | 1.0    |



| No. | Original Test Image | Test Image That the Model Read | Answer | No. | Original Test Image | Test Image That the Model Read | Answer |
|-----|---------------------|--------------------------------|--------|-----|---------------------|--------------------------------|--------|
| 78. |                     |                                | 1.0    | 88. |                     |                                | -1.0   |
| 79. |                     |                                | 1.0    | 89. |                     |                                | 1.0    |
| 80. |                     |                                | 1.0    | 90. |                     |                                | 1.0    |
| 81. |                     |                                | -1.0   | 91. |                     |                                | 1.0    |
| 82. |                     |                                | -1.0   | 92. |                     |                                | -1.0   |
| 83. |                     |                                | -1.0   | 93. |                     |                                | -1.0   |
| 84. |                     |                                | -1.0   | 94. |                     |                                | 1.0    |
| 85. |                     |                                | 1.0    | 95. |                     |                                | -1.0   |
| 86. |                     |                                | -1.0   | 96. |                     |                                | 1.0    |
| 87. |                     |                                | 1.0    | 97. |                     |                                | 1.0    |

| No.  | Original Test Image                                                               | Test Image That the Model Read                                                    | Answer |
|------|-----------------------------------------------------------------------------------|-----------------------------------------------------------------------------------|--------|
| 98.  |  |  | 1.0    |
| 99.  |  |  | 1.0    |
| 100. |  |  | -1.0   |

The testing with 53 image data of number three represented by a value of 1.0 or true, the percentage of accuracy is obtained as follows:

$$\text{Accuracy Percentage} = \frac{53}{53} \times 100\%$$

$$\text{Accuracy Percentage} = 100\%$$

The testing with 47 image data of number six represented by a value -1.0 or false, the percentage of accuracy is obtained as follows:

$$\text{Accuracy Percentage} = \frac{47}{47} \times 100\%$$

$$\text{Accuracy Percentage} = 100\%$$

### C. Summary of Test Results

From the results of tests that have been carried out using 100 handwritten numeric image data with the Quantum Neural Network (QNN) model, it shows that the accuracy results for each image type and the overall accuracy results are in the following Table II:

TABLE II. SUMMARY OF TEST RESULT

| Type of Images        | Last Percentage |
|-----------------------|-----------------|
| Image of number three | 100%            |
| Image of number six   | 100%            |
| Total                 | 100%            |

## IV. CONCLUSION

The implementation of the supervised learning method to classify handwritten numeric image data on the Quantum Neural Network (QNN) model in order to achieve a superposition state has been successful and the data can be read on a quantum computer circuit simulator.

The results of training on the QNN model obtained a value of 0.337 for the loss value and 0.3427 for the validation loss value. Meanwhile, the hinge accuracy value from the training results is 0.8603 for the hinge accuracy value with training data and 0.8669 for the hinge accuracy validation value.

Model testing is done by providing 100 handwritten numeric images that are tested, with 53 image data of number three and 47 image data of number six. The results obtained for the percentage of testing accuracy are 100% for the number three image and 100% for the number six image. Thus, the total percentage of testing is 100%. Based on the results of the total accuracy, the overall performance of the model is maximized.

## ACKNOWLEDGMENT

This document is the results of the research project funded by the Ministry of Research and Technology / the national agency for Research and Innovation of Indonesia (Grant No. 079/SP2H/LT/DRPM/2020).

## REFERENCES

- [1] Abadi, M., Agarwal, A., Barham, P., Brevdo, E., Chen, Z., Citro, C., Corrado, G., Davis, A., Dean, J., Devin, M., Ghemawat, S., Goodfellow, I., Harp, A., Irving, G., Isard, M., Jia, Y., Jozefowicz, R., Kaiser, L., Kudlur, M., Levenberg, J., Mane, D., Monga, R., Moore, S., Murray, D., Olah, C., Schuster, M., Shlens, J., Steiner, B., Sutskever, I., Talwar, K., Tucker, P., Vanhoucke, V., Vasudevan, V., Viegas, F., Vinyals, O., Warden, P., Wattenberg, M., Wicke, M., Yu, Y., and Zheng, X. 2016. Tensorflow: Largescale Machine Learning on Heterogeneous Distributed Systems. <https://arxiv.org/abs/1603.04467>.
- [2] Anonim. 2020. About Keras, <https://keras.io/about/>.
- [3] Anonim. 2018. Apa Itu Colabotory?. <https://colab.research.google.com/notebooks/welcome.ipynb?hl=id>.
- [4] Anonim. 2020. Quantum Machine Learning Concept. <https://www.tensorflow.org/quantum/concepts>.
- [5] Anonim. 2020. Tensorflow Quantum. <https://www.tensorflow.org/quantum/overview>.
- [6] Anonim. 2020. Tensorflow Quantum Design. <https://www.tensorflow.org/quantum/design>.
- [7] Benedetti, M., Lloyd, E., Sack, S., and Fiorentini, M. 2019. Parameterized Quantum Circuit As Machine Learning Models. <https://arxiv.org/abs/1906.07682>.
- [8] Fahriz. 2019. Mengenal Jenis Pembelajaran Mesin Supervised Learning dan Unsupervised Learning. <https://medium.com/kelompok1/mengenal-jenis-pembelajaran-mesin-supervised-learning-dan-unsupervised-learning-c588881e8ef5>.
- [9] Farhi, E. and Neven, H. 2018. Classification with Quantum Neural Networks on Near Term Processors. California: Google.Inc. URL: <https://arxiv.org/pdf/1802.06002.pdf>.
- [10] Gotarane, V. and Gandhi, S. 2016. Quantum Computing: Future Computing. Mumbai: P.G. Scholar A.R.M.I.E.T. Vol. 3. [https://www.researchgate.net/publication/328133812\\_Quantum\\_Computing\\_Future\\_Computing](https://www.researchgate.net/publication/328133812_Quantum_Computing_Future_Computing).
- [11] Hidary, J. 2019. Quantum Computing: An Applied Approach. California: Springer Nature Switzerland AG.
- [12] LeCun, Y., Cortes, C., and Burges, C. 2016. The MNIST Database of Handwritten. <http://yann.lecun.com/exdb/mnist/>.

# A Novel Approach to Mammogram Classification using Spatio-Temporal and Texture Feature Extraction using Dictionary based Sparse Representation Classifier

Vaishali D. Shinde<sup>1</sup>

Department of Computer Science and Engineering  
Koneru Lakshmaiah Education Foundation  
Vaddeswaram, Andhra Pradesh, India

Dr. B. Thirumala Rao<sup>2</sup>

Department of Computer Science and Engineering  
Lakireddy Bali Reddy College of Engineering  
Mylavaram, Andhra Pradesh, India

**Abstract**—Cancer is a chronic disease and increasing rapidly worldwide. Breast cancer is one of the most crucial cancer which affects the women health and causes death of the women. In order to predict the breast cancer, mammogram is considered as a promising technique which helps to identify the early stages of cancer. However, several schemes have been developed during last decade to overcome the performance related issues but achieving the desired performance is still challenging task. To overcome this issue, we introduce a novel and robust approach of feature extraction and classification. According to the proposed approach, first of all, we apply pre-processing stage where image binarization is applied using Niblack's method and later Region of Interest (ROI) extraction and segmentation schemes are applied. In the next phase of work, we developed a mixed strategy of feature extraction where we consider Gray Level Co-occurrence Matrix (GLCM), Histogram of oriented Gradients (HoG) with Principal Component Analysis (PCA) for dimension reduction, Scale-invariant Feature Transform (SIFT), and non-parametric Discrete Wavelet Transform (DWT) features are extracted. Finally, we present K-Singular value decomposition (SVD) based dictionary learning scheme and applied the Sparse representation classifier (SRC) classification approach and performance is evaluated using MATLAB tool. An extensive experimental study is carried out which shows that the proposed approach achieves classification accuracy as 98.13%, Precision as 97.58%, Recall as 98.36%, and F-Score 97.95%. The performance of proposed approach is compared with the state-of-art techniques which shows that the proposed approach gives better performance.

**Keywords**—Mammogram; segmentation; classification; feature extraction

## I. INTRODUCTION

Cancer is a paramount root of death worldwide among men and woman. The burden of cancer is increasing worldwide due to different lifestyles. In complete worldwide population, 49.5% of population is covered by the females where larger portion is occupied by the population over 60 years [1]. Recently, American Cancer Society (ACS) presented a study where it was concluded that breast cancer is repeatedly diagnosed cancer and considered as a chronic disease which is second leading source of cancer death among

U.S. women [2]. Also, the facts and figures indicate that there is increase in deaths in female due to breast cancer [45]. Breast cancer is considered as a vital health issue and generally, it is found in the women around age of 40. ACS revealed new cases of cancer which shows that total 231,840 cancer patients are women and 2350 cases are men and this study also presented that 40,730 number of deaths are also estimated during 2015 [3]. Hence, early prediction and detection of breast cancer is highly recommended to reduce the death counts due to the breast cancer.

Breast cancer is a most familiar type of cancer which is generally found among women after the skin cancer. Lower region of breast tissue structure is analyzed for identification of abnormality. In general, several techniques are present for detection and identification of breast cancer in its early stage such as biopsy, thermography, ultra sound imaging and mammography. Mammography is considered as most promising way for detection and diagnosis of breast cancer and can reduce the breast cancer mortality [4]. It is a medical imaging process where less intensity and energy X-ray systems are used to visualize the inner region of breast and images are acquired which are known as mammograms [5]. However, performance of mammography screening is a challenging task and all radiologists cannot achieve the uniformly higher accuracy because of tedious and error-prone process of analysis. This screening-based analysis suffer from various issues such as higher false positive rates, variability among clinicians and over-diagnosis of insignificant lesions [6]. In general, higher false positive rates can cause unnecessary cost and stress on the patient. In order to deal with these issues, a fully automated mammogram image analysis tool need to be developed which can efficiently analyze the mammogram images resulting in improved performance for detection of breast cancer and reduction in false positive rates using machine vision-based solution.

In this field of medical imaging, computer-aided diagnosis (CAD) and detection-based techniques has demonstrated a significant impact on the early detection process of several diseases. These systems are developed for various medical applications such as lung cancer, brain tumour, CT image

processing, mammography and other pathology images. In this work, focus is on the CAD systems for mammogram image analysis because of its significant performance for breast cancer mammogram image analysis. The complete process of mammogram analysis requires multiple stages such as ROI extraction, pectoral muscle segmentation image binarization, feature extraction and classifier construction. A general process flow is depicted in Fig. 1 where input image, image segmentation, ROI extraction and pectoral muscle removal are presented.

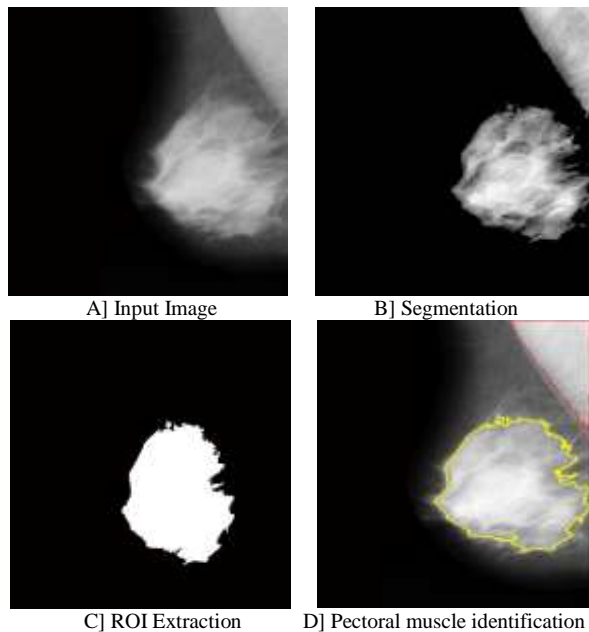


Fig. 1. General Process of Mammogram Analysis.

Conventional approaches of mammogram classification require several extra information such as bounding box or ground truth images to perform the segmentation. These techniques are based on the handcrafted features where manual screening process is applied which is a tedious and time-consuming task. Moreover, analysis becomes inappropriate which may cause inaccurate diagnosis.

Hence, CAD based automated systems are developed for detection and classification of breast cancer [7]. Several techniques have been presented in the field of mammogram classification where image pre-processing, feature extraction and classifier construction are considered the fundamental stages. During image pre-processing, image enhancement and image denoising plays important role. Maitra et al. [8] presented contrast enhancement strategy using contrast limited adaptive histogram equalization (CLAHE) scheme. Later, modified seeded region growing (SRG) algorithm is applied for pectoral muscle segmentation. For image enhancement spatial [9] and transform domain [10] techniques are adopted. As discussed before, image binarization also plays an important role in mammogram image analysis. Various schemes have been used such as Otsu's thresholding method [11], adaptive thresholding [12] and Kittler's Method [13]. P. S. Vikhe proposed an adaptive threshold-based contrast enhancement method for enhancement of suspicious regions in mammograms masses in mammograms [46]. Homomorphic

filtering and wavelet shrinkage methods are used for denoising and enhancement of mammograms in [47]. In the next stage, ROI extraction and segmentation is considered as main objective. Accurate image segmentation can help to obtain the desired information without mixing the unwanted sources. In order to perform the image segmentation, several techniques such as region growing [14] and watershed segmentation [15] are used. In order to obtain the robust performance of classification, feature extraction techniques are implemented for better leaning. In this field, GLCM (Gray-Level Concurrence) features [16-17], wavelet transform [17-18,22], LBP (Local Binary pattern) [19-20], HoG (Histogram of gradient) [21], SIFT (Scale-invariant feature extraction) [22], CNN [23-24] based features and texture features are widely applied to obtain the efficient accuracy. With the help of these techniques, classifiers are constructed for pattern learning and classification of the breast cancer. These classifiers are known as DNN (Deep Neural Network) [25], SVM (Support Vector Machines) [26] and Neural Network Classifier [27], etc.

Significant amount of work has been presented in this field of medical imaging for breast cancer detection and classification. Most of the schemes are focused on the feature extraction where multiple features are extracted and classified using different classifier modules. However, during image capturing, degraded image quality may cause poor performance. Moreover, image binarization, pectoral muscle segmentation and ROI (Region of interest) also need to be considered for better performance of classification. An optimum ROI can significantly improve the classification performance because of robust feature extraction region. Later, improved and hybrid feature extraction also can be helpful for image analysis and classification of breast cancer. According to the current classification studies, feature vectors are directly provided to the learning scheme where data range and its distribution becomes unpredictable which results in erroneous learning and poor classification performance. Hence, there is a need to develop a novel robust computer vision-based image mammogram image analysis tool for improved early prediction breast cancer.

In order to deal with these issues, an end-to-end image analysis tool is presented where novel methods are applied for image pre-processing, feature extraction and classification. According to image pre-processing phase, first of all, image binarization scheme is applied where Niblack image binarization is applied which helps to preserve the edges of image. This edge preserving can improve the segmentation process by accurate boundary identification. In the next phase of pre-processing, pectoral muscle segmentation is performed using convex hull modeling and ROI is extracted. Next, important phase considers feature extraction task where multiple scheme for feature extraction are applied. GLCM, improved HoG, improved SIFT and geometric non-parametric based features extraction schemes are implemented. For further process, these features are processed through the sparse representation to obtain the generalized features with a known distribution which helps to reduce the training error. Finally, heuristic SRC classification scheme is presented which is self-adaptive in nature and can perform efficiently for high dimension complex data. This article shows that

proposed non-parametric feature extraction in combination with SIFT, GLCM, and HoG feature is an important contribution. This combination provides detailed information about mammogram images. Moreover, this scheme of feature extraction can be helpful for other bio-medical imaging applications.

Rest of the article is arranged as follows: Section II presents recent trends and techniques in field of breast cancer detection and classification, proposed model and its description is presented in Section III, Section IV presents experimental and comparative study using proposed approach and finally, Sections V and VI gives concluding remarks and future direction of the work.

## II. LITERATURE SURVEY

In previous section, a brief discussion about the breast cancer is done, its effects and solutions using computer aided designs are presented. As discussed before, several techniques have been presented recently for breast cancer detection and classification using mammography mechanism. This section presents a brief discussion about recent trends and techniques in the field of mammogram classification using machine vision methodology. Many researches have been presented which are mainly focused on the robust feature extraction. Singh et al. [28] studied about the mammogram classification and introduced a center-symmetric based approach for texture feature extraction which is called as wavelet-based center-symmetric local binary pattern (WCS-LBP) and concluded that these features are adequate to achieve better performance. This approach extracts the features from non-overlapping region. In addition to this, relevant feature selection and reduction is also applied using SVM based recursive feature elimination process. Finally, decision tree based random forests classifier is constructed and performance is obtained. However, this approach is applied for the raw data where input image is divided into four frequency bands and LL band is considered for the LBP feature extraction. Due to this process, accurate ROI extraction becomes a tedious task hence complete image need to be considered for processing which may result in false positives. Shastri et al. [29] proposed a novel feature extraction process for mammogram classification. In this work, Histogram of oriented texture features are computed which are obtained using histogram of gradients and Gabor filter combination. For improved texture analysis, Pass Band - Discrete Cosine Transform (PB-DCT) scheme is also applied followed by a feature selection technique. This approach achieves better performance but fails to study about the mammogram density which becomes a crucial task during ROI extraction. In this approach, the images are divided into different patches but sometimes all patches do not play significant role in feature extraction hence authors introduced Discrimination Potentiality scheme for feature selection.

In medical imaging applications, texture feature extraction plays important role. Texture features can be categorized into four groups as: statistical texture feature, local pattern histogram, directional features and transform based texture features. Khan et al. [30] utilized the statistical texture feature analysis and presented optimized Gabor feature extraction for

mass classification in mammography and for improving the performance by reducing the false positives. In order to formulate an optimized filter bank, Particle Swarm Optimization and incremental clustering algorithm is applied. Moreover, Gaussian kernel SVM is applied as the fitness function for PSO. In [31] Abdel-Nasser et al. focused on the local patterns for image classification process and implemented for breast tissue classification. The classification works carried out in this study are as follows: classification of breast tissue within the region of interest and classification of breast density. The complete process is implemented into three main stages as ROI segmentation, feature extraction and classification. This study shows that detection of mass and breast density is a challenging and it has a serious impact on the breast tissue classification. Hence, presented feature extraction mode called as uniform local directional pattern. However, due to insignificant feature extraction and modelling, this study fails to obtain the promising estimation of breast density and mass identification. Recently, Gedik et al. The author in [32] presented transform based feature extraction method using fast finite shearlet transform where transform coefficients are used for feature vector construction. Later, thresholding process is implemented to distinguish between different classes and finally SVM based classification approach is implemented to measure the performance. This technique doesn't focus on the image segmentation and ROI extraction process which causes inaccurate feature extraction resulting in poor pattern learning.

In this field, machine learning based schemes are also widely adopted for various feature extraction and classification. In this field, CNN (Convolutional Neural Network) based feature extraction and classification scheme is used in many studies. Wu et al. [23] presented 2D mammogram classification study using CNN. According to this approach, loop interpretation method is applied for identifying the behavior of CNN model which helps to detect the breast tissue pattern. Later, these patterns can be analyzed by the experts to find the correlation with mass tissue and calcificated vessels. The developed system is not fully automated and it requires expert knowledge for analysis of brain tissues. Recently, Tusa et al. [33] presented a comparative study for mammogram classification based on the CNN models. These two different classifiers are different from each other in terms of connected layers, feature extraction techniques and bit per pixel. Further, CNN classifier uses Tensor-Flow library for classifying the mammograms. Total optimal number of layers and computational complexity is considered a challenging task in these processes. Gardezi et al. [34] introduced a classification approach for classifying the normal and abnormal mammograms using deep learning approach. In order to obtain this architecture, authors have used VGG-16 based CNN deep learning model. Moreover, ROI extraction is performed by applying 3x3 convolutional filter and 10-fold cross-validation is used for SVM, simple logistics classifier, binary tree, and KNN classifier with the varied values of K as 1,3, and 5. Lizzi et al. [35] discussed about the rules and regulations of the use of ionizing radiation and information about the radiation dose according to the European Directive 59/2013/EURATOM. Dose controlling during the cancer

screening process is a very crucial and important process because breast contains radio-sensitive tissues and during screening processed these are exposed to the radiation. Inaccurate dose of radiations may cause damage in tissues. In order to optimize the dose for each patient, we perform classification of mammograms using CNN in BIRADS standard. This process helps to personalize the doses according the severity of the breast cancer.

In this section, detailed study of recent techniques for breast cancer classification using mammogram image classification techniques is done. These techniques are based on the image pre-processing, feature extraction and classification. Some of the state-of-art techniques use feature extraction but ROI extraction and segmentation is not

considered which results in the poor feature extraction. On other hand, CNN and machine learning based strategies are also considered which are capable to achieve the improved performance but computational complexity remains a challenging issue. Hence, still there is a need to improve the mammogram image analysis for breast cancer detection and classification. Below given Table I shows a comparative analysis of these techniques.

The existing techniques suffer from poor accuracy performance which is the main disadvantage of these techniques. The classification accuracy depends on the robustness of features. Hence, we focus on the feature extraction process and introduce a new feature vector model to improve the classification accuracy.

TABLE I. COMPARATIVE ANALYSIS OF MAMMOGRAM CLASSIFICATION

| Authors                  | Work Contribution                                                                       | Features                                                                                    | Research Gap                                             | Performance Measurement                                                               |
|--------------------------|-----------------------------------------------------------------------------------------|---------------------------------------------------------------------------------------------|----------------------------------------------------------|---------------------------------------------------------------------------------------|
| Wu et al. [23]           | Mammogram classification using CNN                                                      | Low-level gradients                                                                         | Not fully automated, expert knowledge is required        | AUC                                                                                   |
| Singh et al. [28]        | Mammogram classification support vector machine-recursive feature elimination (SVM-RFE) | CS-LBP texture                                                                              | Pectoral muscle identification is not considered         | Sensitivity, Specificity, Classification accuracy & precision                         |
| Shastri et al. [29]      | Hitogram related features, Discrimination Potentiality (DP) for feature selection and   | Histogram of Oriented Texture and Pass Band - Discrete Cosine Transform (PB-DCT) descriptor | Scale based orientation features are not considered      | AUC (Area Under Curve), Sensitivity, Specificity, Classification accuracy & precision |
| Khan et al. [30]         | Mammogram mass classification using Gabor feature and SVM classifier                    | Gabor feature and PSO feature selection                                                     | Abnormality classification is not incorporated           | Sensitivity, Specificity, Classification accuracy & precision                         |
| Abdel-Nasser et al. [31] | Breast cancer classification SVM class                                                  | Uniform local directional pattern                                                           | Local directional pattern (LDP)                          | AUC, Classification                                                                   |
| Gedik et al. [32]        | 5-fold cross validation with support vector machine (SVM) classifier                    | fast finite shearlet transform                                                              | Segmentation, dimension reduction                        | Accuracy                                                                              |
| Tusa et al. [33]         | Tensor Floe with convolutional neural networks (CNN) for mammogram classification       | Texture                                                                                     | Segmentation, Pectoral muscle and computation complexity | Accuracy and MSE (Mean Squared Error)                                                 |
| Gardezi et al. [34]      | Mammogram classification using Deep learning                                            | Deep features using multiple layers                                                         | Pre-processing, and computation complexity               | Accuracy and AUC                                                                      |
| Lizzi et al. [35]        | CNN for mammogram Classification                                                        | Convolution Layer Features                                                                  | Accuracy                                                 | Accuracy                                                                              |

### III. PROPOSED MODEL AND METHODOLOGY

Previous section described about the current techniques in the field of medical imaging and presented a brief discussion about recent techniques for mammogram classification and their drawbacks. This section presents a novel and robust solution for the mammogram image classification using computer vision-based approaches. As discussed before, computer vision-based pattern learning and classification scheme requires three basic steps which are image pre-processing, feature extraction and classification. The proposed work is also divided into three main stages which is as follows:

- *Image pre-processing:* This is an important phase of any pattern learning and classification model. In this work, image binarization using Niblack algorithm is applied which helps to preserve the edges of image this edge preserving nature help to identify the object

boundaries and can improve the segmentation process. Later, pectoral muscle segmentation is applied to obtain the segmented breast region and finally ROI is extracted.

- *Feature extraction:* In next stage, feature extraction process is applied where conventional GLCM features are extracted for texture analysis, HoG (Histogram of gradient) features are extracted for improved histogram analysis and object localization. In addition to this, SIFT (Scale Invariant Feature Transforms) are also computed which helps to improve the feature extraction for varied scales and angles of image acquisition. Later, geometry based non-parametric features are also extracted which makes features more robust without taking any pre-defined parameters. Once the feature extraction is done, we apply sparse representation which performs feature normalization and reduces the feature redundancy.

- Finally, presented heuristic self-adaptive SRC classifier which can provide the robust performance for high dimension datasets.
- The complete process of proposed approach is depicted in Fig. 2.

### A. Image Pre-Processing

According to the proposed approach, first of all, image binarization scheme for boundary identification is applied. In computer vision-based applications, binarization is also known as thresholding where a basic function is applied to compare the gray levels with the computed threshold. In this process, it converts all pixels zero if the pixel values are less than the threshold and higher pixel values are converted to 1. Let us consider that the threshold outcome is  $t(x, y)$  and input image is expressed as  $f(x, y)$  and the threshold is given as  $Thr$ , then the image binarization or thresholding relation can be expressed as.

$$t(x, y) = \begin{cases} 0, & \text{if } f(x, y) < Thr \\ 1, & \text{if } f(x, y) \geq Thr \end{cases} \quad (1)$$

In this process, optimal threshold plays important role hence Niblack's technique for image binarization is considered. According to this process, a rectangular window is created and pixel-wise sliding is performed over the input gray image. However, the size of the window may vary. In this process, local mean ( $m$ ) and standard deviation ( $S$ ) is considered to compute the threshold which can be expressed as:

$$Thr = (K \times S) + m \\ = K \sqrt{\frac{1}{NP} \sum (p_i - m)^2} + m \quad (2)$$

Where  $NP$  denotes total number of pixels in the image,  $m$  denotes average pixel values,  $K$  denotes then noise constant and  $p$  the current pixel value.

After performing the binarization, pectoral muscle identification and ROI extraction is performed where segmentation and connected component labelling is applied.

Where  $NP$  denotes total number of pixels in the image,  $m$  denotes average pixel values,  $K$  denotes then noise constant and  $p$  the current pixel value. Below given Fig. 3 shows a comparative analysis of image binarization using different techniques.

After performing the binarization, pectoral muscle identification and ROI extraction is performed where segmentation and connected component labelling is applied.

### B. Segmentation and ROI

With the help of this process, the ROI and other components are extracted as given in Fig. 4 where input image, binarized image, pectoral muscle removal, etc. are obtained. In this, final outcome is obtained as pectoral muscle removed ROI. This ROI can be processed further for feature extraction.

For pectoral muscle extraction, the mammogram image is segmented and extract the ROI from the segmented region. First of all, apply multi-level Otsu's image thresholding approach for segmentation and extract the ROI. The multi-level Otsu's thresholding helps to classify the pixels in different classes based on their gray levels. In the next phase, focus is on the pectoral muscle extraction. It is considered that the pectoral muscle has high intensity pixels whereas other regions have low-intensity pixels. In this process, initialize the extraction process with two thresholds and increase it by one to analyse the region which is having higher pixel intensities. Further, pectoral muscle region and intermediate region is considered which is adjacent to the pectoral muscle and measure the transitional area between two regions. If this region has a greater number of black pixels, then it is considered that further region is not useful for calculations and multi-level Otsu's thresholding is reinitialized with higher values of threshold.

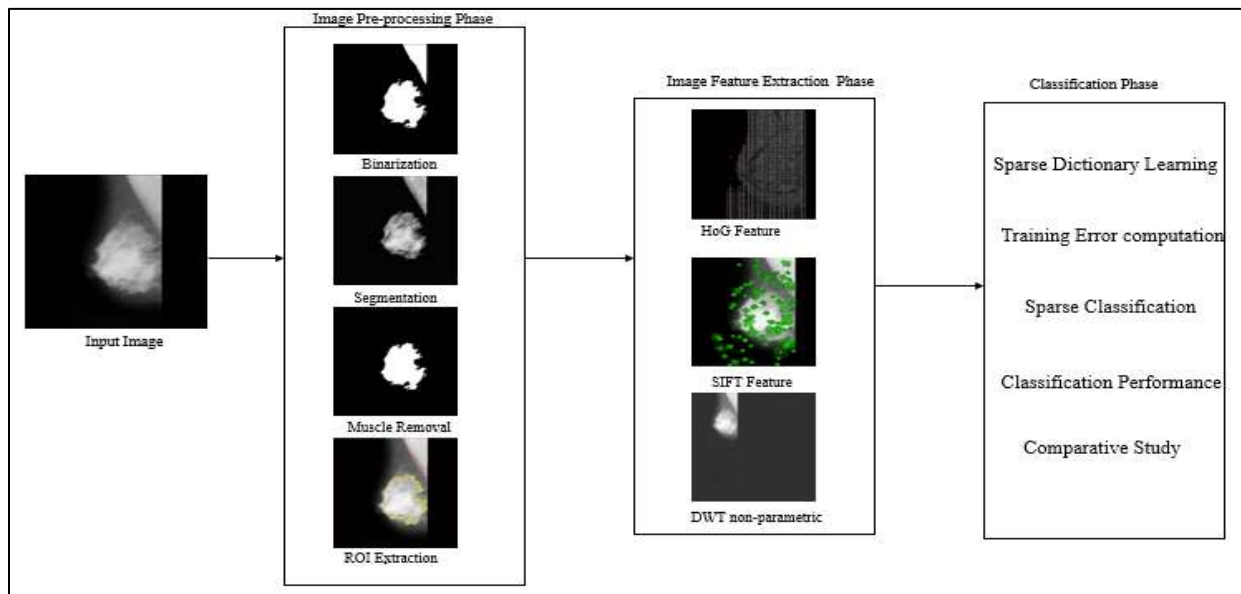


Fig. 2. Complete Process flow Chart.

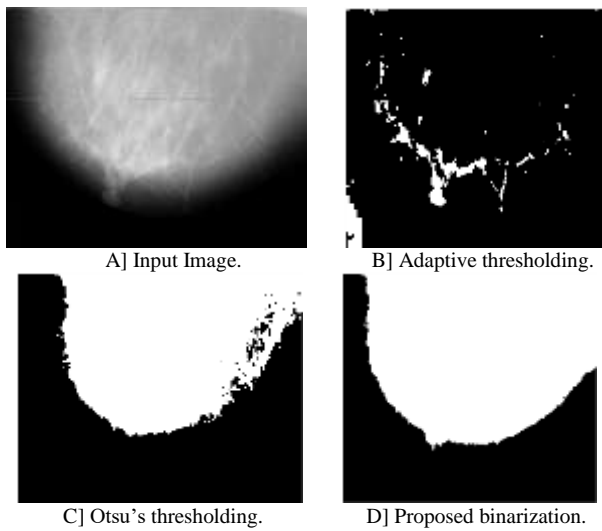


Fig. 3. Qualitative Comparison of Image Binarization.

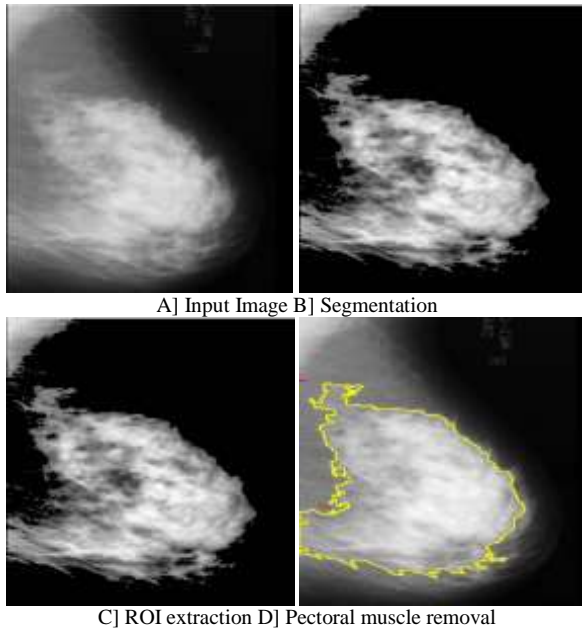


Fig. 4. Image Pre-Processing Phase.

1) *GLCM feature extraction:* In this sub-section, proposed feature extraction technique is presented where first of all GLCM features are computed for the given input image. In this phase, Haralick [24] based scheme for feature extraction is followed which have been adopted widely in various applications. General mathematical formulas for GLCM feature extraction are expressed in Table II.

GLCM features are considered as a matrix whose distribution is based on the angular and distance relation between pixels. The tabulated features provide degree of correlation between pixel pairs and texture information to analyze the image. Moreover, these are the statistics properties of GLCM which helps to construct the normalized GLCM. Generally, in image pixels vary at every position which can be used for identifying various texture information using GLCM. With the help of GLCM, several features can be computed

using this matrix which are classified as visual texture features, statistics feature, and information theory feature and information correlation measurement.

2) *Improved HoG feature extraction:* In this sub-section discussion is about the improved HoG feature extraction process for given input images. In order to improve the further performance, PCA (Principal Component Analysis) is applied for feature dimension reduction which is applied on every block. HoG features are known as gradient features and widely adopted for object recognition. These features are extracted by considering entire region of the input image. In other words, it can be expressed that the HoG features can represent the rough shape of the input as depicted in Fig. 5.

In order to efficiently extract the features, region or interest need to be extracted initially by using back ground subtraction or image binarization methods. Input image is normalized and the object in the form of breast is located on the image. In order to formulate the feature, first of all, image gradient need to be computed which is expressed as:

$$\begin{cases} f_x(u, v) = I(u + 1, v) - I(u - 1, v) \quad \forall_{u,v} \\ f_y(u, v) = I(u, v + 1) - I(u, v - 1), \quad \forall_{u,v} \end{cases} \quad (3)$$

TABLE II. GLCM FEATURE MATHEMATICAL FORMULA

| Feature     | Mathematical formula                        |
|-------------|---------------------------------------------|
| Entropy     | $\sum_i \sum_j P(i, j) \log P(i, j)$        |
| Contrast    | $\sum_i \sum_j (i - j)^2 P(i, j)$           |
| Energy      | $\sum_i \sum_j p^2(i, j)$                   |
| Homogeneity | $\sum_i \sum_j \frac{P(i, j)}{1 +  i - j }$ |

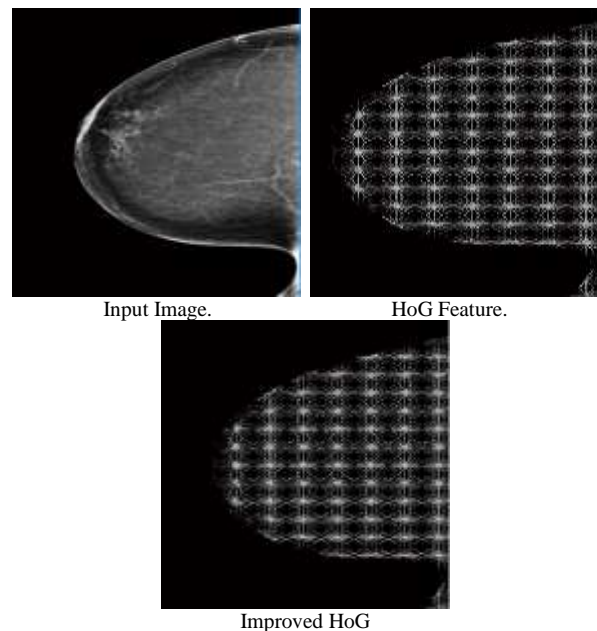


Fig. 5. HoG Feature Extraction Process.



Where gradient of  $x$  and  $y$  component are denoted by  $f_x$  and  $f_y$ , pixel value intensity is given by  $I(u, v)$  at the  $(u, v)$  coordinate locations. HoG feature contains magnitude  $m(u, v)$  and orientation variation  $\theta(u, v)$  which can be denoted as follows:

$$m(x, y) = \sqrt{f_x(x, y)^2 + f_y(x, y)^2}$$

$$\theta(x, y) = \tan^{-1}(f_y(x, y)/f_x(x, y)) \quad (4)$$

In order to make it more robust feature extraction model, we use unsigned orientation computation, given as follows:

$$\tilde{\theta}(u, v) = \begin{cases} \theta(u, v) + \pi & \text{if } \theta < (u, v) < 0 \\ \theta(u, v), & \text{otherwise} \end{cases} \quad (5)$$

The obtained gradient image is obtained and divided into cells as  $c_h \times c_w$  pixels where  $w$  is width of cell  $c$  and  $h$  is the height of cell  $v$ . In each cell, orientation bins ( $C_b$ ) are computed by quantizing the unsigned gradient orientations which are weighted by its magnitude for histogram computation. This process of histogram orientation and bin computation is presented in Fig. 6 where cell and blocks are presented. Any cell has orientation as  $C_b$ , hence the feature extraction block dimension can be given as  $d = C_b \times b_h \times b_w$  for each computing block. Let us consider that  $\mathcal{V}$  is a feature vector and  $\mathcal{H}_{ij}$  denotes the histogram of the current cell at the pixel position  $(i, j)$  and  $\{1 \leq i \leq b_w, 1 \leq j \leq b_h\}$ . Finally, a normalized feature vector of each block can be given as:

$$H'_{ij} = \frac{\mathcal{H}_{ij}}{\sqrt{\|\mathcal{V}\|^2 + \epsilon}} \quad (\epsilon = 1) \quad (6)$$

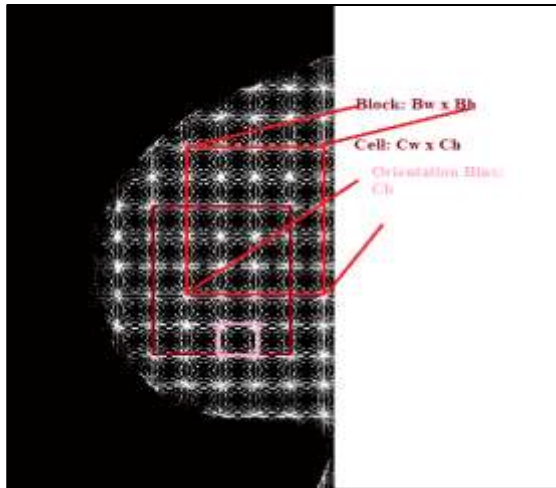


Fig. 6. Histogram Orientation Extraction.

In this process, the gradient over the entire image is computed hence the feature vector dimension is higher and for better classification, the features obtained from the object region only need to be considered and the background region features need to be eliminated to reduce the error. In order to perform this task, we present PCA based feature reduction strategy. In digital image processing, any input image can be represented in the form of pixel groups where pixels are arranged in the two-dimensional matrix form. Generally, these pixels are in the form of floating point for coloured image and

gray scale images contains discrete values which can be denoted in a matrix form as follows:

$$\mathcal{R}(u, v) = \begin{bmatrix} r(0,0) & \dots & r(0, m-1) \\ \vdots & \ddots & \vdots \\ r(n-1,0) & \dots & r(n-1, m-1) \end{bmatrix} \quad (7)$$

Where  $u$  and  $v$  denotes the pixel coordinates and  $d(u, v)$  denotes the corresponding pixel value from the image. Image feature dimension reduction can be categorized into four main steps such as: image normalization, covariance computation, eigen vector computation and data transformation.

First of all, apply image normalization process where mean value is subtracted from the original image which helps to improve the SNR quality. This process of data normalization can be obtained as:

$$\mathcal{R}_{norm}(x, y) = \begin{bmatrix} r(0,0) & \dots & r(0, m-1) \\ \vdots & \ddots & \vdots \\ r(n-1,0) & \dots & r(n-1, m-1) \end{bmatrix} - [\bar{r}(0,0), \dots, \bar{r}(0, m-1)] \quad (8)$$

Where  $[\bar{r}(0,0), \dots, \bar{r}(0, m-1)]$  denotes the mean value of the image. In next stage, we apply covariance computation which is used for identifying the lowest and highest variance points in the image. The covariance matrix of this normalized data ( $\mathcal{R}_{norm}$ ) can be obtained as follows:

$$C(U_1, V_1) = \frac{\mathcal{R}_{norm}(u,v) * \mathcal{R}_{norm}(u,v)^T}{m-1} \quad (9)$$

Where  $m$  denotes the total number of elements. In the next phase of PCA, eigen vectors and eigen values of covariance matrix is computed which can be obtained by the SVD equation and can be expressed as:

$$AA^T = Cov(U_1, V_1) = UU^T \mathcal{R}^2 \quad (10)$$

Where  $U$  denotes the eigen vectors of covariance and the square of singular values ( $\mathcal{R}^2$ ) denotes the eigen values of  $AA^T$ . Finally, transform the complete data into the new data with the reduced dimension, it can be expressed in the form of eigen vectors, as follows:

$$\mathcal{R}_{transform}(u, v) = U^T \mathcal{R}_{norm}(u, v) \quad (11)$$

Where  $\mathcal{R}_{norm}(u, v)$  is the adjusted, original image dataset and  $\mathcal{R}_{transform}(u, v)$  is the final reduced dimension dataset.

3) *SIFT feature extraction*: This section briefly describes the SIFT feature extraction process where key points of the image are extracted which are invariant to the image transform. The complete process is divided into four main stages: (a) Scale-space extrema detection: this is the first stage of SIFT, where Difference of Gaussian (DoG) is applied which is used for identifying the interest points, (b) key point localization: in this phase, location and scales are identified for each candidate point and later key points are selected based on the measurement of stability, (c) orientation assignment: each key point is assigned one or more number of orientation which are computed based on the image gradients, and (d) Key point descriptor: in this phase, image descriptors

are generated by considering the each key point computed from the local image gradient.

This approach generates huge number of features over multiple location and wide range of scales. However, the size of feature generation depends on the image size and input parameters. According to this process of SIFT, aim is to find the reliable locations in the given scale space where these locations can be extracted efficiently. First stage uses scale-space extrema computation in  $D(u, v, \theta)$  with the help of DoG function where two nearby images are considered which are separated by a multiplicative factor denoted as  $k$ , this computation can be given as:

$$\begin{aligned} DoG(u, v, \sigma) &= (G(u, v, k\sigma) - G(u, v, \sigma)) * I(u, v) \\ &= L(u, v, k\sigma) - L(u, v, \sigma) \end{aligned} \quad (12)$$

Where  $L(u, v, \sigma)$  is the scale space function which is obtained by performing the convolution between Gaussian kernel  $G(u, v, \sigma)$  and input image  $I(u, v)$ . Prior to the descriptor key point construction, the descriptors are transformed into the invariant to the rotation by assigning the key points. In order to compute the key point orientation, orientation histogram of local gradient is considered from the smoothed image as  $L(u, v, \sigma)$ . For any given input image sample  $L(u, v)$  scale, the gradient magnitude as  $m(u, v)$ , orientation  $\theta(u, v)$  can be by using pixel differences as:

$$\begin{aligned} m(u, v) &= \left( (L(u+1, v) - L(u-1, v))^2 \right. \\ &\quad \left. + (L(u, v+1) - L(u, v-1))^2 \right)^{\frac{1}{2}} \\ \theta(u, v) &= \tan^{-1} \frac{L(u, v+1) - L(u, v-1)}{L(u+1, v) - L(u-1, v)} \end{aligned} \quad (13)$$

4) *Non-parametric feature extraction*: In this section, non-parametric feature extraction process using wavelet transform for the input image  $I$  with the dimension as  $R \times C$  is presented. In this process, wavelet decomposition is applied with  $j$  decomposition levels and descriptors are computed in the patches form. These patches are characterized as feature vector for the decomposed sub-bands, first sub-band  $B_{j,1}$  is computed with the help of low-pass filtering computation in horizontal and vertical directions as LL band, next frequency sub-band are estimated with the help of low and high pass filtering computation which can be expressed as LH where low pass filtering is applied as horizontal manner and high pass filtering is applied as vertical, HH band where high pass filtering is applied in the both direction and HL band where high-pass filtering is applied in the horizontal and low-pass filtering is applied in the vertical direction.

A non-parametric feature vector is formed by computing the sub-band variance  $\gamma_{j,i}^2$ , mean value  $\mu_{j,i}$ , L1-norm  $\|B_{j,i}\|_1$ , L2-norm  $\|B_{j,i}\|_2$  and entropy for each sub-band. In addition to this, the variance of sub-band can be given as:

$$\gamma_{j,i}^2 = \frac{1}{R_j \cdot C_j} \sum_{r=0}^{R_j-1} \sum_{c=0}^{C_j-1} (B_{j,i}[r, c] - \mu_{j,i})^2 \quad (14)$$

Where  $B_{j,i}[r, c]$  denotes the wavelet coefficients and  $\mu$  is the mean of sub-band, which is expressed as:

$$\mu_{j,i} = \frac{1}{R_j \cdot C_j} \sum_{r=0}^{R_j-1} \sum_{c=0}^{C_j-1} (B_{j,i}[r, c]) \quad (15)$$

Similarly, the first order and second order norms are given as follows:

$$\|B_{j,i}\|_{\tau} = \frac{1}{R_j \cdot C_j} \sum_{r=0}^{R_j-1} \sum_{c=0}^{C_j-1} |B_{j,i}[m, n]|^{\tau} \quad (16)$$

where  $\tau$  denotes the norm-factor i.e. if  $\tau = 1$  then first order norm and  $\tau = 2$  denotes the second-order norm. In next phase of feature computation, entropy and coding gain are computed in each sub-band. In this work, we have considered Shannon's entropy which can be computed as:

$$E_{j,i} = \sum_k p_k \log_2 \left( \frac{1}{p_k} \right) \quad (17)$$

Where  $p_k$  denotes the pixel probability of occurring the sub-band.

In the next phase, the feature vector is constructed by combining all features in a row vector where GLCM, HoG, SIFT and non-parametric features are arranged in a sequence.

$$\min_{D,H} \|V - DH\|_F^2 \text{ s.t. } \|a_i\|_0 \leq T_{limit} \quad \forall_i \quad (18)$$

Where  $D$  denotes the dictionary to be learned as  $D \in R^{n \times m}$  where  $n > m$ ,  $H$  denotes the sparse coding vector as  $H = [h_1, h_2, \dots, h_M]$  and  $\|\cdot\|_F$  Frobenius norm and  $T$  denotes the sparsity limits which reduces non-zero coefficients in each sparse coding vector.

Let us consider that dictionary is given as  $D$  which need to be expressed in the linear combination as  $v = D\hat{a}$  where  $\hat{a}$  denotes the sparse. The solution for sparse can be given as:

$$\hat{a} = \operatorname{argmin}_a \|v - Da\|_2 \text{ subject to } \|a_i\|_0 \leq T_{limit} \quad (19)$$

After finishing the dictionary training for each class  $i \in \{1, \dots, N\}$ , classification of new incoming patch can be computed by the representation error, given as.

$$e_i(v_{new}) = \|v_{new} - D_i \hat{a}_i\|_2^2 \quad \forall_i \quad (20)$$

With the help of class error, pseudo probability ( $p$ ) measurement is computed for each class which is used for the class assignment rule:

$$i = \operatorname{argmin}_i p(C_i) \text{ where } p(C_i) = \frac{1}{N-1} \frac{\sum_{j=1, j \neq i}^N e_j}{\sum_{j=1}^N e_j} \quad (21)$$

In this approach, introduced a new model for significant feature extraction. This technique poses several advantages such as new hybrid approach for feature extraction, reducing the computational complexity, non-parametric feature extraction to achieve the transform domain information and designing a new scheme for learning to reduce the learning error.

### C. Classifier Construction

Previous section presents proposed feature extraction techniques and formulate a robust feature vector. In order to obtain the improved classification process, data pattern learning scheme need to be applied on the extracted features.

Here, dictionary learning based approach is considered for pattern learning where K-SVD approach is used. The main advantage of K-SVD is that prior to training it includes data sparsity followed by L2 normalization. Let us consider that input feature vector is given as  $V = [v_1, v_2, v_3 \dots, v_n]$  which is L2 normalized training samples as  $v_i \in \mathbb{R}^n$ . During this phase, K-SVD approach tries to solve the following problem.

#### IV. RESULTS AND DISCUSSION

This section presents complete experimental study using proposed approach for mammogram classification. The proposed approach is carried out using MATLAB 2013b simulation tool running on windows platform with Intel i3 processor. The proposed approach is carried out on open source database known as Mammographic image analysis society (MIAS) database [36]. Complete information about the dataset is given in the corresponding ids. In this database, total 322 images are present where 115 images are abnormal and 207 images are considered to be from normal class. Here we consider total 115 images for experimental study to classify the benign and malignant cases where 62 images are benign and 53 images are malignant.

##### A. Performance Measurement

In order to measure the performance of proposed approach the dataset is divided into multiple training and testing sets of images. The complete performance is evaluated by computing confusion matrix where true negative (TN), False Negative (FN), True positive (TP) and False Positive (FP) cases are present. With the help of confusion matrix, we compute various performance measurement parameters such as:

Precision: which is a measurement of the discrimination ability of the test images for other images and classes.

$$Precision = \frac{TP}{FP + TP}$$

Recall: It is a measurement of system's recognition performance for different type of mammograms. It is also known as sensitivity.

$$Recall = \frac{TP}{FN + TP}$$

False Positive Rate: it is a measurement of proportion of classification of images as particular class but actually it belongs to the different class.

$$FP\ Rate = \frac{FP}{TN + FP}$$

Later, F-measure is computed which is the combined measurement of precision and recall which is computed as:

$$F - Measure = \frac{2 * recall * precision}{Recall + Precision}$$

Finally, classification accuracy is measured which shows the overall classification performance, given as:

$$Accuracy = \frac{TN + TP}{TN + TP + FN + FP}$$

##### B. Experimental Results

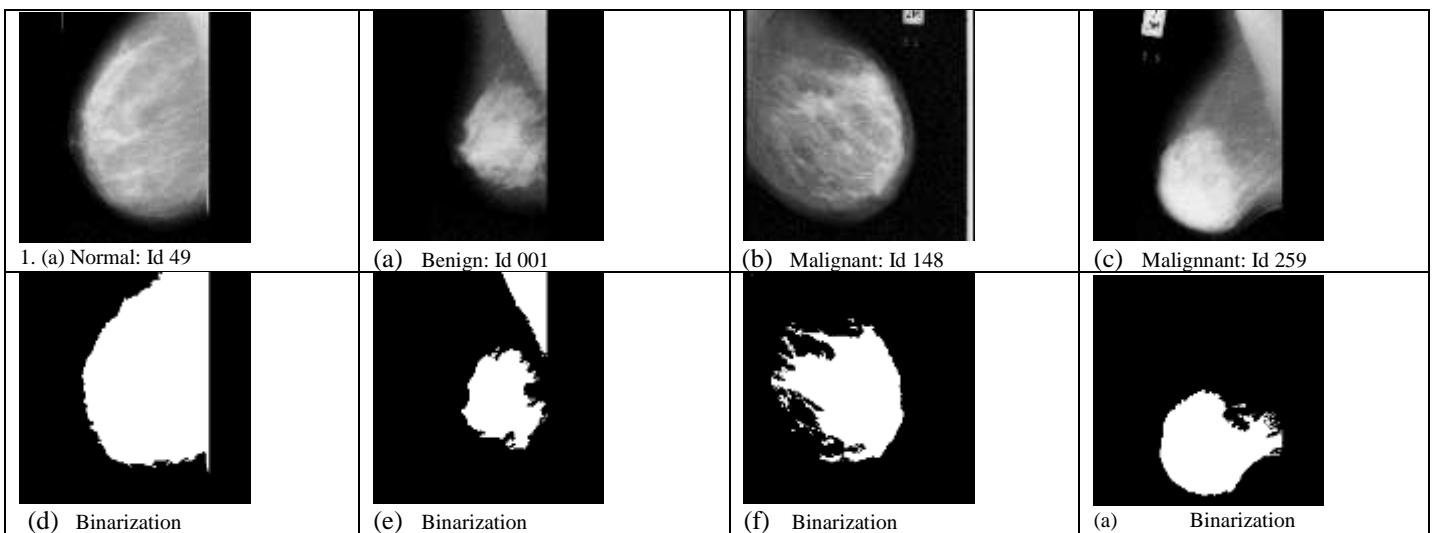
In this sub-section experimental result and their discussion for various test cases are presented. Moreover, the intermediate stages are also depicted for multiple test cases.

In the above given Fig. 7, different test cases such as normal, benign and malignant are considered. Each image is processed through different phases such as binarization, segmentation, muscle removal, ROI extraction, HoG features, SIFT features, and wavelet-based feature extraction.

##### C. Performance Measurements

In this section, presented are, comparative performance in terms of classification accuracy, confusion matrix and other statistical measurement parameters. With the help of proposed classifier, the obtained confuse matrix is given in Table III.

Based on the obtained confusion matrix, we compute other performance measurement parameters which are given in Table IV.



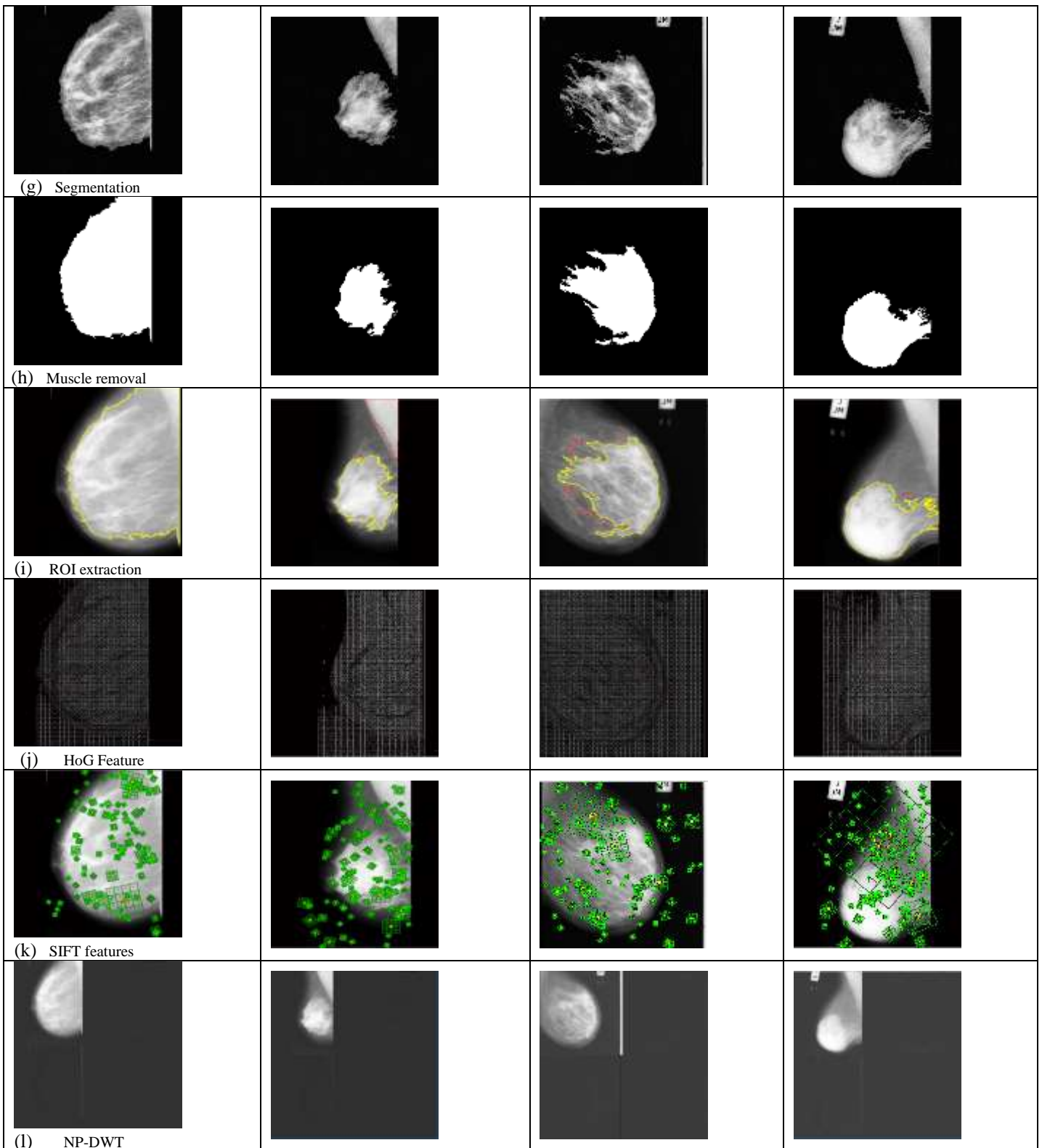


Fig. 7. Input Image and their Corresponding Intermediate Steps for Feature Extraction.

TABLE IV. CONFUSION MATRIX

| Class                | Abnormal (Actual) | Actual (Normal) |
|----------------------|-------------------|-----------------|
| Abnormal (Predicted) | 112               | 1               |
| Normal (Predicted)   | 1                 | 207             |

TABLE V. PERFORMANCE OF PROPOSED APPROACH

| Class                | Recall | Precision | Sensitivity | Specificity | F-Score | Accuracy |
|----------------------|--------|-----------|-------------|-------------|---------|----------|
| Abnormal (Predicted) | 0.990  | 0.956     | 0.990       | 0.976       | 0.973   | 98.13    |
| Normal (Predicted)   | 0.976  | 0.995     | 0.976       | 0.990       | 0.985   |          |

TABLE VI. COMPARATIVE PERFORMANCE ANALYSIS

| Authors/Article         | Techniques used                                                                                                 | Accuracy   | Precision | Recall | F-Score |
|-------------------------|-----------------------------------------------------------------------------------------------------------------|------------|-----------|--------|---------|
| Proposed                | Pre-processing+ GLCM + HoG + SIFT + wavelet based non-parametric                                                | 98.13%     | 97.58%    | 98.36% | 97.95%  |
| Singh et al. [28]       | Wavelet based LBP + feature selection+ random-forest classifier                                                 | 97.25%     | 97.30%    | 97.20% | 97.20%  |
| Srivastava et al. [37]  | CLAHE enhancement +Fuzzy C-Means segmentation+ Texture feature + Feature selection using GA +SVM-MLP classifier | 87%        | 75%       | 95%    | ×       |
| Beura et al. [17]       | GLCM feature + Back-propagation                                                                                 | 94.2%      | 97%       | ×      | ×       |
| Pratiwi et al. [38]     | GLCM feature + RBFNN                                                                                            | 93.98      | 93.62     | 94.44  |         |
| Tzikopoulos et al. [39] | Fractal texture features and Statistical features + SVM (Support vector machine) classifier                     | 84.47%     | ×         | ×      | ×       |
| Buciu et al. [40]       | Gabor wavelet + PCA+ SVM                                                                                        | ×          | 60.86%    | 97.56% | ×       |
| Liu et al. [41]         | Wavelet + Statistical feature + binary tree classifier                                                          | 84.20%     | ×         | ×      |         |
| Subashini et al. [42]   | Statistical features + SVM Classification                                                                       | 86.67%     | ×         | ×      | ×       |
| Dhabhi et al. [43]      | Discrete Curvelet transform + feature selection + k-NN classifier                                               | 91.27%     | ×         | ×      | ×       |
| Gedik [32]              | shearlet transform, t-test statistic and dynamic thresholding.                                                  | 97.84%     | ×         | ×      | ×       |
| Virmani et al. [44]     | Texture+ Statistical feature +PCA +SVM                                                                          | 92.5-94.4% | ×         | ×      | ×       |

The Table V shows a comparative performance analysis by considering various state-of-art techniques. In this analysis, we compared several parameters such as accuracy, precision, recall and F-score measurement. Experimental analysis shows that proposed approach achieves better performance in terms of Accuracy, Precision, Recall, and F-Score as 98.13%, 97.58%, 98.36% and 97.95%, respectively.

### V. CONCLUSION

In this article, focus is on the development of a novel framework for breast cancer classification using computer-vision based approach. In order to develop this model, first of all image pre-processing stage is presented where image binarization is performed using Niblack's method, later ROI segmentation and pectoral muscle removal techniques are presented. In the next phase, feature extraction process and developed a robust feature extraction model are considered where GLCM, HoG with PCA, SIFT and DWT based non-parametric features are calculated and represented in a sparse manner to reduce the data training error. Finally, pattern learning scheme is applied where K-SVD based dictionary learning approach is implemented and SRC classifier is applied and performance is evaluated. A comparative performance analysis is carried out which shows that the proposed approach achieves improved performance when compared with the state-of-art techniques. Moreover, this

approach reduces computational complexity which can be helpful for clinicians to achieve the faster and reliable outcome to provide the suitable diagnosis.

### VI. FUTURE WORK

Further, this work can be extended with the help of deep learning schemes such as convolutional neural networks to reduce the computational complexity related issues.

### REFERENCES

- [1] Torre, L.A., Islami, F., Siegel, R.L., Ward, E.M. and Jemal, A., Global cancer in women: burden and trends, 2017.
- [2] Zhu, Wentao, Qi Lou, Yeeleng Scott Vang, and Xiaohui Xie. "Deep multi-instance networks with sparse label assignment for whole mammogram classification." In International Conference on Medical Image Computing and Computer-Assisted Intervention, pp. 603-611. Springer, Cham, 2017.
- [3] American Cancer Society, Internet site address: <http://www.cancer.org/Research/CancerFactsFigures/index>, 2015.
- [4] Smith, Robert A., Kimberly S. Andrews, Durado Brooks, Stacey A. Fedewa, Deana Manassaram-Baptiste, Debbie Saslow, Otis W. Brawley, and Richard C. Wender. "Cancer screening in the United States, 2017: a review of current American Cancer Society guidelines and current issues in cancer screening." CA: a cancer journal for clinicians 67, no. 2 (2017): 100-121.
- [5] Svahn, T. M., N. Houssami, I. Sechopoulos, and Sören Mattsson. "Review of radiation dose estimates in digital breast tomosynthesis relative to those in two-view full-field digital mammography." The Breast 24, no. 2 (2015): 93-99.

- [6] Oeffinger, K.C., Fontham, E.T., Etzioni, R., Herzig, A., Michaelson, J.S., Shih, Y.C.T., Walter, L.C., Church, T.R., Flowers, C.R., LaMonte, S.J., et al.: Breast cancer screening for women at average risk: 2015 guideline update from the American Cancer Society. *Jama* 314(15), 1599–1614 (2015).
- [7] Dhungel, N., Carneiro, G. and Bradley, A.P.. Fully automated classification of mammograms using deep residual neural networks. In *Biomedical Imaging (ISBI 2017)*, 2017 IEEE 14th International Symposium on (pp. 310-314). IEEE, 2017, April.
- [8] Maitra, I.K., Nag, S. and Bandyopadhyay, S.K., 2012. Technique for preprocessing of digital mammogram. *Computer methods and programs in biomedicine*, 107(2), pp.175-188.
- [9] Panetta, K., Samani, A. and Aghaie, S., Choosing the optimal spatial domain measure of enhancement for mammogram images. *Journal of Biomedical Imaging*, 2014, p.3.
- [10] Padmavathy, T.V., Vimalkumar, M.N., Nagarajan, S., Babu, G.C. and Parthasarathy, P. Performance analysis of pre-cancerous mammographic image enhancement feature using non-sampled shearlet transform. *Multimedia Tools and Applications*, pp.1-16, 2018.
- [11] Jen, C.C. and Yu, S.S., Automatic detection of abnormal mammograms in mammographic images. *Expert Systems with Applications*, 42(6), pp.3048-3055, 2015.
- [12] Fooladivanda, Aida, Shahriar B. Shokouhi, Nasrin Ahmadijad, and Mohammad R. Mosavi. "Automatic segmentation of breast and fibroglandular tissue in breast MRI using local adaptive thresholding." In 2014 21th Iranian Conference on Biomedical Engineering (ICBME), pp. 195-200. IEEE, 2014.
- [13] Patil, H.T., Segmentation Method for ROI Detection in Mammographic Images using Wiener Filter and Kittler's Method, 2013.
- [14] Rouhi, Rahimeh, Mehdi Jafari, Shohreh Kasaei, and Peiman Keshavarzian. "Benign and malignant breast tumors classification based on region growing and CNN segmentation." *Expert Systems with Applications* 42, no. 3 (2015): 990-1002.
- [15] Sharma, Jaya, J. K. Rai, and R. P. Tewari. "A combined watershed segmentation approach using k-means clustering for mammograms." In 2015 2nd International Conference on Signal Processing and Integrated Networks (SPIN), pp. 109-113. IEEE, 2015.
- [16] Beura, Shradhananda, Banshidhar Majhi, Ratnakar Dash, and Susnata Roy. "Classification of mammogram using two-dimensional discrete orthonormal S-transform for breast cancer detection." *Healthcare technology letters* 2, no. 3 (2015): 46-51.
- [17] Beura, Shradhananda, Banshidhar Majhi, and Ratnakar Dash. "Mammogram classification using two dimensional discrete wavelet transform and gray-level co-occurrence matrix for detection of breast cancer." *Neurocomputing* 154 (2015): 1-14.
- [18] Pawar, Meenakshi M., and Sanjay N. Talbar. "Wavelet statistical feature selection using genetic algorithm with fuzzy classifier for breast cancer diagnosis." In *Progress in intelligent computing techniques: Theory, practice, and applications*, pp. 95-105. Springer, Singapore, 2018.
- [19] De Sampaio, Wener Borges, Aristófanés Corrêa Silva, Anselmo Cardoso de Paiva, and Marcelo Gattass. "Detection of masses in mammograms with adaptation to breast density using genetic algorithm, phylogenetic trees, LBP and SVM." *Expert Systems with Applications* 42, no. 22 (2015): 8911-8928.
- [20] Reyad, Yasser A., Mohamed A. Berbar, and Muhammad Hussain. "Comparison of statistical, LBP, and multi-resolution analysis features for breast mass classification." *Journal of medical systems* 38, no. 9 (2014): 100.
- [21] Arevalo, John, Fabio A. González, Raúl Ramos-Pollán, Jose L. Oliveira, and Miguel Angel Guevara Lopez. "Representation learning for mammography mass lesion classification with convolutional neural networks." *Computer methods and programs in biomedicine* 127 (2016): 248-257.
- [22] Ergin, Semih, and Onur Kilinc. "A new feature extraction framework based on wavelets for breast cancer diagnosis." *Computers in biology and medicine* 51 (2014): 171-182.
- [23] Wu, Jimmy, Diandra Peck, Scott Hsieh, Vandana Dialani, Constance D. Lehman, Bolei Zhou, Vasilis Syrgkanis, Lester Mackey, and Genevieve Patterson. "Expert identification of visual primitives used by CNNs during mammogram classification." In *Medical Imaging 2018: Computer-Aided Diagnosis*, vol. 10575, p. 105752T. International Society for Optics and Photonics, 2018.
- [24] Lotter, William, Greg Sorensen, and David Cox. "A multi-scale CNN and curriculum learning strategy for mammogram classification." In *Deep Learning in Medical Image Analysis and Multimodal Learning for Clinical Decision Support*, pp. 169-177. Springer, Cham, 2017.
- [25] Zhang, Xiaofei, Yi Zhang, Erik Y. Han, Nathan Jacobs, Qiong Han, Xiaoqin Wang, and Jinze Liu. "Classification of whole mammogram and tomosynthesis images using deep convolutional neural networks." *IEEE transactions on nanobioscience* 17, no. 3 (2018): 237-242.
- [26] Görgel, Pelin, Ahmet Sertbas, and Osman Nuri Uçan. "Computer-aided classification of breast masses in mammogram images based on spherical wavelet transform and support vector machines." *Expert Systems* 32, no. 1 (2015): 155-164.
- [27] Gautam, Aman, Vikrant Bhateja, Ananya Tiwari, and Suresh Chandra Satapathy. "An improved mammogram classification approach using back propagation neural network." In *Data Engineering and Intelligent Computing*, pp. 369-376. Springer, Singapore, 2018.
- [28] Singh, Vibhav Prakash, Subodh Srivastava, and Rajeev Srivastava. "Effective mammogram classification based on center symmetric-LBP features in wavelet domain using random forests." *Technology and Health Care* 25, no. 4 (2017): 709-727.
- [29] Shastri, Aditya A., Deepti Tamrakar, and Kapil Ahuja. "Density-wise two stage mammogram classification using texture exploiting descriptors." *Expert Systems with Applications* 99 (2018): 71-82.
- [30] Khan, Salabat, Muhammad Hussain, Hatim Aboalsamh, Hassan Mathkour, George Bebis, and Mohammed Zakariah. "Optimized Gabor features for mass classification in mammography." *Applied Soft Computing* 44 (2016): 267-280.
- [31] Abdel-Nasser, Mohamed, Hatem A. Rashwan, Domènec Puig, and Antonio Moreno. "Analysis of tissue abnormality and breast density in mammographic images using a uniform local directional pattern." *Expert Systems with Applications* 42, no. 24 (2015): 9499-9511.
- [32] Gedik, Nebi. "A new feature extraction method based on multi-resolution representations of mammograms." *Applied Soft Computing* 44 (2016): 128-133.
- [33] Soriano, Danny, Carlos Aguilar, Ivan Ramirez-Morales, Eduardo Tusa, Wilmer Rivas, and Maritza Pinta. "Mammogram classification schemes by using convolutional neural networks." In *International Conference on Technology Trends*, pp. 71-85. Springer, Cham, 2017.
- [34] Gardezi, Syed Jamal Safdar, Muhammad Awais, Ibrahim Faye, and Fabrice Meriaudeau. "Mammogram classification using deep learning features." In 2017 IEEE International Conference on Signal and Image Processing Applications (ICSIPA), pp. 485-488. IEEE, 2017.
- [35] Lizzi, Francesca, Paolo Bosco, Davide Caramella, Carolina Marini, Alessandra Retico, Antonio Traino, and Maria Evelina Fantacci. "Convolutional Neural Networks for mammogram classification in BIRADS standard: development and preliminary tests." (2018).
- [36] <http://peipa.essex.ac.uk/info/mias.html> last accessed on 13 July 2018.
- [37] Srivastava, Subodh, Neeraj Sharma, S. K. Singh, and Rajeev Srivastava. "Quantitative analysis of a general framework of a CAD tool for breast cancer detection from mammograms." *Journal of Medical Imaging and Health Informatics* 4, no. 5 (2014): 654-674.
- [38] Pratiwi, Mellisa, Jeklin Harefa, and Sakka Nanda. "Mammograms classification using gray-level co-occurrence matrix and radial basis function neural network." *Procedia Computer Science* 59 (2015): 83-91.
- [39] Tzikopoulos, Stylianos D., Michael E. Mavroforakis, Harris V. Georgiou, Nikos Dimitropoulos, and Sergios Theodoridis. "A fully automated scheme for mammographic segmentation and classification based on breast density and asymmetry." *Computer methods and programs in biomedicine* 102, no. 1 (2011): 47-63.
- [40] Buciu, Ioan, and Alexandru Gacsadi. "Directional features for automatic tumor classification of mammogram images." *Biomedical Signal Processing and Control* 6, no. 4 (2011): 370-378.
- [41] Liu, Sheng, Charles F. Babbs, and Edward J. Delp. "Multiresolution detection of spiculated lesions in digital mammograms." *IEEE transactions on Image Processing* 10, no. 6 (2001): 874-884.

- [42] Subashini, T. S., Vennila Ramalingam, and S. Palanivel. "Automated assessment of breast tissue density in digital mammograms." *Computer Vision and Image Understanding* 114, no. 1 (2010): 33-43.
- [43] Dhahbi, Sami, Walid Barhoumi, and Ezzeddine Zagrouba. "Breast cancer diagnosis in digitized mammograms using curvelet moments." *Computers in biology and medicine* 64 (2015): 79-90.
- [44] Virmani, Jitendra, Nilanjan Dey, and Vinod Kumar. "PCA-PNN and PCA-SVM based CAD systems for breast density classification." In *Applications of intelligent optimization in biology and medicine*, pp. 159-180. Springer, Cham, 2016.
- [45] Vikhe, P. S., and V. R. Thool. "Mass detection in mammographic images using wavelet processing and adaptive threshold technique." *Journal of medical systems* 40, no. 4 (2016): 82.
- [46] Vikhe, P. S., and V. R. Thool. "A wavelet and adaptive threshold-based contrast enhancement of masses in mammograms for visual screening." *International Journal of Biomedical Engineering and Technology* 30, no. 1 (2019): 31-53.
- [47] Vikhe, P. S., and V. R. Thool. "Contrast enhancement in mammograms using homomorphic filter technique." In *2016 International Conference on Signal and Information Processing (IconSIP)*, pp. 1-5. IEEE, 2016.

# A Hybrid POS Tagger for Khasi, an Under Resourced Language

Medari Janai Tham

Department of Computer Science and Engineering  
Assam Don Bosco University, Assam, India

**Abstract**—Khasi is an Austro-Asiatic language spoken mainly in the state of Meghalaya, India, and can be considered as an under resourced and under studied language from the natural language processing perspective. Part-of-speech (POS) tagging is one of the major initial requirements in any natural language processing tasks where part of speech is assigned automatically to each word in a sentence. Therefore, it is only natural to initiate the development of a POS tagger for Khasi and this paper presents the construction of a Hybrid POS tagger for Khasi. The tagger is developed to address the tagging errors of a Khasi Hidden Markov Model (HMM) POS tagger by integrating conditional random fields (CRF). This integration incorporates language features which are otherwise not feasible in an HMM POS tagger. The results of the Hybrid Khasi tagger have shown significant improvement in the tagger's accuracy as well as substantially reducing most of the tagging confusion of the HMM POS tagger.

**Keywords**—Khasi corpus; BIS tagset; Khasi POS tagger; Conditional Random Fields (CRF); Hidden Markov Model (HMM)

## I. INTRODUCTION

Part-of-speech (POS) tagging is the process of automatically assigning a part of speech to each word present in a sentence. It differs from a morphological analyzer, which gives a detailed analysis of a word such as root word, multiple parts of speech (if any), etc., by assigning a part of speech to the word depending on its context. These parts of speech are assigned from a specific list of POS tags called a tagset, applicable to the language at hand. The annotated corpus and tagset utilized in this work are described in [1]. The tagset was formulated according to the Bureau of Indian Standards (BIS) guidelines and referred to as the Khasi BIS tagset. In this paper, the Hidden Markov Model (HMM) approach has been incorporated in the development of a Khasi POS tagger and a ten-fold cross-validation has been carried out to rigorously test the performance of the tagger. To address the tagging errors of the Khasi HMM tagger, conditional random fields (CRF) have been integrated. The CRF approach has shown its capability in resolving issues in various natural language processing tasks [2], [3], [4], and integrating CRF allows the inclusion of features in a sentence such as capitalization, prefixes which are prevalent in Khasi, part of speech tag of the previous word, and context words. This leads to the development of a Hybrid POS tagger for Khasi with improved performance and the details of the tasks undertaken are given in the sections below. The background work is discussed in Section II, which briefly introduces Khasi and POS tagging approaches. Section III contains a description of the resources utilized in this work,

while the construction of the Khasi HMM POS tagger is described in Section IV. The integration of CRF in developing a Hybrid Khasi POS tagger is presented in Section V, and finally the conclusion of the paper is given in Section VI.

## II. BACKGROUND WORK

### A. A Brief Overview of the Khasi Language

Khasi belongs to the Austro-Asiatic language family and is categorized under the Mon-Khmer branch. It is a language spoken by the Khasi tribe who mainly inhabits the state of Meghalaya in India. As per the 2011 census of government of India, there are about 1.4 million speakers of the language in the state. Khasi is an analytic and isolating language, devoid of inflection, but typical of its Mon-Khmer features, it demonstrates simple derivational morphology contributing to the partial agglutination present in the language [5], [6]. Derivational morphology occurs when affixes attached themselves to a word base and they are easily distinguished from any given word. Another Mon-Khmer characteristic is that the word order is subject verb object (SVO). Khasi is written in the Latin script comprising of 23 letters with the exclusion of the letters c, f, q, v, x, z and the inclusion of the diacritic letters ĩ and ñ, and the diagraph ng [1].

### B. Part-of-Speech Tagging Approaches

India's rich language diversity can be understood by the presence of five language families namely Indo-Aryan, Dravidian, Austro-Asiatic, Tibeto-Burmese, and Semito-Hamitic. The reported accuracies for POS taggers for Hindi, a morphologically rich language and one of India's official languages, are 87.55% on a rule-based tagger [7], 93.45% accuracy using a small-sized training corpus of 15,562 words aided with an extensive morphological analyzer and a massive lexicon [8], and 93.12% using HMM on corpus size of 66,900 words [9]. A trend observed across POS taggers for Indian languages is that stochastic taggers have to deal with the availability of only small-sized training data. In the Khasi language scenario, two HMM POS taggers have been reported for Khasi but trained and tested on two independent data sets and tagsets. The first HMM POS tagger trained on a dataset of 86,087 tokens using the Khasi BIS tagset of 33 tags provided an accuracy of 95.68% [1]. The second HMM tagger was trained on 7,500 words with a custom-made tagset of 54 tags reporting an accuracy of 76.7% [10]. However, both taggers reported accuracy performing only in a single run on their respective test data.



### III. RESOURCES UTILIZED – KHASI CORPUS AND KHASI BIS TAGSET

The present available Khasi corpus comprises of Khasi literature containing 4,386 sentences and 94,651 tokens [1]. Excluding the punctuations, there are 83,312 tokens and 5,465 word types. Text segmentation has been performed on the corpus to visibly identify characters, words, and sentences. Written Khasi is very similar to written English because of the usage of the Latin script and the use of whitespace for marking word boundaries. Each sentence in the corpus is written in one line and marked with an end of sentence marker such as the period (.), the question mark (?), or the exclamation mark (!). Each token in a sentence is separated by a whitespace. Punctuations are also considered as tokens, except for two punctuations- the apostrophe (') which is part of a contracted word and the hyphen (-) which is part of a compound word. The data has been annotated with the Khasi BIS tagset containing 33 tags [1].

Corpus analysis revealed that 10.9% of the word types are multifunctional. The abbreviations used are in accordance with the Leipzig glossing rules except when clearly specified<sup>1</sup>. Table I shows the frequency of the most common words occurring more than five hundred times in the corpus. The statistics show that these 15 most frequent words account to 34.7% of the word tokens in the corpus. If the most frequent words occurring 100 times or more are taken into account, it amounts to 55.8% of the tokens in the corpus. However, from Table II we can see that approximately 47.7% of the word types occur only once in the corpus. These statistics are in line with what is reported by Manning and Shütze [11] about the difficulty in predicting the behavior of words even with the availability of a larger and bigger corpus.

Another phenomenon related to natural language data is the Zipfian distribution. When frequencies (f) of different word types is calculated and ranked in order of occurrences, then according to Zipf's law,  $f \propto \frac{1}{r}$  and we can also say that there is a constant k where  $f * r = k$ . Drawing this information from the training corpus, the extracted values and their respective calculations are shown in Table III. Based on this extraction, along with the usage of logarithmic scales, the graph of Fig. 1 shows the plot of the rank of word type on the X-axis versus the frequency of the respective word type on the Y-axis. The double line graph shows the ranks and frequencies of the words in the corpus, and the straight line shows Zipf's predicted value for  $k = 10000$ . The graph seems to approximately hold Zipf's law, except for very low rank and high rank words.

Table I also reveals other suspected language phenomena. For instance, pronouns such as *ka*, *u*, *i*, and *ki* can have other functions and various researchers [12], [13], [14], [15] have referred to them as articles, pronominal markers, noun gender markers, subject enclitic, and so on. The frequencies indicate that the third personal pronouns- *ka* 'singular feminine', *i* 'singular neutral' (183 occurrences as a pronominal marker versus 93 occurrences as a pronoun), and *ki* 'plural'- are more likely to have a sense of pronominal markers (tagged as PR\_PRP\_M) than of personal pronouns (tagged as PR\_PRP).

However, *u* "singular masculine" is more likely to be a personal pronoun than a pronominal marker. Since all animate and inanimate objects in Khasi have gender, and given that the Khasi tribe follows a matrilineal system, Khasi corpus analysis indicates that there are more objects tagged as feminine than masculine. The feminine pronominal marker *ka* is approximately 2 times more than the masculine pronominal marker *u* (Table I).

TABLE I. MOST COMMON WORD FREQUENCY

| Sl. No | Word          | Frequency | Frequency of Parts of Speech                                                                      |
|--------|---------------|-----------|---------------------------------------------------------------------------------------------------|
| 1.     | ka<br>3SF     | 7,212     | pronominal marker= 4,946;<br>pronoun= 2,263; others= 3                                            |
| 2.     | u<br>3SM      | 4,332     | pronominal marker= 2,040;<br>pronoun= 2,292                                                       |
| 3.     | ki<br>3PL     | 4,272     | pronominal marker= 2,515;<br>pronoun= 1,757                                                       |
| 4.     | la<br>AUX     | 3,214     | auxiliary verb= 2,590; possessive<br>particle= 506; subordinating<br>conjunction= 69 ; others= 49 |
| 5.     | ia<br>ACC     | 2,864     | preposition= 2,852; verb=12                                                                       |
| 6.     | bad<br>'and'  | 2,276     | coordinating conjunction= 2,166;<br>preposition=110                                               |
| 7.     | ha<br>DAT     | 1,540     | preposition= 1,534; others= 6                                                                     |
| 8.     | ba            | 1,452     | subordinating conjunction= 1,443;<br>coordinating conjunction = 6; others=3                       |
| 9.     | ban<br>INF    | 1,346     | infinitive= 1,311; preposition=19;<br>others=16                                                   |
| 10.    | jong<br>GEN   | 1,102     | preposition=1,096; others=6                                                                       |
| 11.    | nga<br>1SN    | 753       | pronoun = 752; noun = 1                                                                           |
| 12.    | da<br>INS     | 725       | preposition= 415; auxiliary verb= 308;<br>verb=2                                                  |
| 13.    | kaba<br>3SREL | 615       | relative pronoun                                                                                  |
| 14.    | na<br>'from'  | 576       | Preposition                                                                                       |
| 15.    | don<br>COP    | 545       | auxiliary verb = 527; proper noun=18                                                              |

TABLE II. FREQUENCY OF FREQUENCY

| Frequency | Frequency of Frequency |
|-----------|------------------------|
| 1         | 2608                   |
| 2         | 820                    |
| 3         | 397                    |
| 4         | 221                    |
| 5         | 188                    |
| 6         | 145                    |
| 7         | 108                    |
| 8         | 94                     |
| 9-10      | 111                    |
| 11-30     | 432                    |
| 31-100    | 240                    |
| >100      | 101                    |

<sup>1</sup> <http://www.eva.mpg.de/lingua/resources/glossing-rules.php>

TABLE III. EXPERIMENTAL CALCULATION OF ZIPF'S LAW ON THE CORPUS

| Word  | Frequency (f) | Rank | f*r   | Word      | Frequency (f) | Rank | f*r   |
|-------|---------------|------|-------|-----------|---------------|------|-------|
| ka    | 7212          | 1    | 7212  | phin      | 108           | 100  | 10800 |
| u     | 4332          | 2    | 8664  | yn        | 55            | 200  | 11000 |
| ki    | 4272          | 3    | 12816 | iarap     | 35            | 300  | 10500 |
| la    | 3214          | 4    | 12856 | jumai     | 25            | 400  | 10000 |
| ia    | 2864          | 5    | 14320 | phareng   | 19            | 500  | 9500  |
| jong  | 1102          | 10   | 11020 | pdeng     | 15            | 600  | 9000  |
| long  | 414           | 20   | 8280  | synshar   | 12            | 700  | 8400  |
| sa    | 321           | 30   | 9630  | nguh      | 10            | 800  | 8000  |
| haba  | 273           | 40   | 10920 | jingdum   | 8             | 900  | 7200  |
| iing  | 229           | 50   | 11450 | jingkylli | 7             | 1000 | 7000  |
| bha   | 180           | 60   | 10800 | syndakor  | 3             | 2000 | 6000  |
| ri    | 150           | 70   | 10500 | b.ed.     | 1             | 3000 | 3000  |
| shong | 138           | 80   | 11040 | keep      | 1             | 4000 | 4000  |
| ngam  | 126           | 90   | 11340 | satdam    | 1             | 5000 | 5000  |

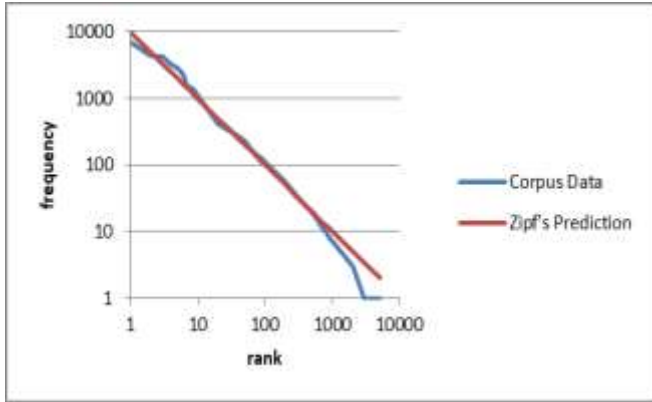


Fig. 1. Zipf's Law: The Red Line shows Relationship between Rank and Frequency Predicted by Zipf for  $k = 10000$ , that is  $f^*r = 10000$ . The Blue Line Corresponds to the Ranks and Frequencies of the Words in the Khasi Corpus. Logarithmic Scales are used for Both Rank and Frequency.

Finally, Table IV highlights the 10 most common tags in the training corpus excluding the punctuation tag. The most common tag is the common noun (N\_NN). Remarkably, the fact that Khasi is known to be rich in adverbs is also reflected by its usage in the corpus and its position in the table (RB is the fifth most common tag out of 33 tags).

TABLE IV. MOST FREQUENT TAGS

| Rank | Tags     | Frequency |
|------|----------|-----------|
| 1    | N_NN     | 13025     |
| 2    | V_VM     | 11193     |
| 3    | PR_PRP_M | 9708      |
| 4    | PR_PRP   | 8355      |
| 5    | RB       | 7490      |
| 6    | IN       | 7373      |
| 7    | V_VAUX   | 4970      |
| 8    | CC_CCD   | 3057      |
| 9    | JJ       | 2348      |
| 10   | CC_CCS   | 2225      |

#### IV. APPLYING THE HIDDEN MARKOV MODEL FOR POS TAGGING

Given a Khasi sentence of  $n$  words  $W = w_1 w_2 \dots w_n$ , we have to assign the best possible tag sequence  $T = t_1 t_2 \dots t_n$ , to the given sentence. Here,  $t_i$  is a tag from the BIS tagset for.

Khasi and assigned to word  $w_i$ , where  $1 \leq i \leq n$ . A Khasi sentence tagged using the Khasi BIS tagset is as follows:

Kane/DM\_DMD ka/PR\_PRP\_M shnong/N\_NN  
ka/PR\_PRP long/V\_VAUX halor/N\_NST u/PR\_PRP\_M  
lum/N\_NN u/PR\_PRP baitynnat/JJ shikatdei/RB eh/RP\_INTF  
./RD\_PUNC.

'This village is on a very beautiful hill.'

As proposed by Brants [16], a second-order Markov model along with additional tags  $t_{-1}$ ,  $t_0$ , and  $t_{n+1}$  for beginning and end of sentence indicators is incorporated in part of speech tagging for Khasi as follows:

$$\text{argmax}_T (\prod_{i=1}^n P(w_i|t_i)P(t_i|t_{i-1}, t_{i-2}))P(t_{n+1}|t_n) \quad (1)$$

To handle data sparsity in (1), he suggested linear interpolation of unigrams, bigrams, and trigrams. Hence, the probability is recalculated as in (2), where the  $\lambda$ s are evaluated using deleted interpolation and  $\lambda_1 + \lambda_2 + \lambda_3 = 1$ .

$$P(t_i|t_{i-2}, t_{i-1}) = \lambda_3 \hat{P}(t_i|t_{i-2}, t_{i-1}) + \lambda_2 \hat{P}(t_i|t_{i-1}) + \lambda_1 \hat{P}(t_i) \quad (2)$$

##### A. Integrating Khasi Morphology to Handle unknown Words

As mentioned in Tham [1], Khasi affixes are easily detectable, especially the prefixes which play a major role in Khasi derivational morphology. There is a consistent pattern of Khasi words with prefixes such as *jing-*, *nong-* and *maw-* mapping to common nouns (N\_NN), and prefixes such as *pyn-* and *ia-* (excluding the preposition *ia*) mapping to verbs (V\_VM). To estimate the probability of unknown words having these features, words in the Khasi corpus having prefixes *jing-*, *nong-*, *maw-*, *pyn-*, and *ia-* (excluding preposition) are mapped to pseudowords *\_JING\_*, *\_NONG\_*, *\_MAW\_*, *\_PYN\_* and *\_IA\_* respectively. To handle unknown

words which do not have the above-mentioned prefixes, low frequency words in the training data are mapped to pseudoword `_UNK_`. As suggested by Manning and Shütze [11], words occurring only once in the corpus are treated as rare words or out-of vocabulary items, and hence can be mapped to pseudoword `_UNK_`. They have stated that these words, correspondingly known as hapax legomena, tend to comprise half of the word types, but only a fraction of the tokens in the corpus. Hence, these words will not significantly affect the model. The same phenomenon is likewise observed in Khasi, where such words comprise 47.7% of the word types but only 0.03% of the tokens in the corpus. Therefore, low frequency is taken to be less than or equal to a selected value of  $\gamma$ , and in this tagger  $\gamma=1$ . After the mappings are done, the HMM parameters are evaluated as mentioned earlier where the pseudowords `_JING_`, `_PYN_`, `_NONG_`, `_IA_` and `_UNK_` are treated like regular words. This mapping is carried out to ensure that the probability of  $P(w_i|t_i)$  is never zero.

### B. Testing Results and Error Analysis of HMM POS Tagger

The corpus comprising of 94,651 tokens is used for training and testing a baseline tagger, a Natural Language Toolkit (NLTK) tagger [17], and an HMM POS tagger. The mappings mentioned in Section A are incorporated in the baseline tagger and HMM POS tagger. A baseline tagger employed here is a tagger that tags the most probable tag to each word in the test data as put forward by Jurafsky and Martin [18]. Unigram, bigram, trigram taggers, etc., are also provided in NLTK. In the case of the NLTK tagger, it integrates a trigram tagger which backs off to a bigram tagger, the bigram tagger which backs off to a unigram tagger, and the unigram tagger which backs off to a Khasi regular expression. The Khasi regular expression tagger incorporates Khasi morphology, tagging words with prefixes *jing-*, *nong-*, and *maw-* as common nouns (N<sub>NN</sub>), words with prefixes *pyn-* and *ia-* as verbs (V<sub>VM</sub>), and defaults to the most common tag which is the common noun (N<sub>NN</sub>). Hapax legomena words not containing the mentioned prefixes are preprocessed and mapped to pseudoword `_UNK_`. The results of all the three taggers using ten-fold cross-validation are given in Table V, with the HMM POS tagger giving a relatively good performance of 93.39% accuracy.

A confusion matrix of the HMM POS tagger, shown in Table VI, is used in analyzing the errors during the HMM POS tagging, with the values reflecting errors occurring at 0.5% and above (i.e., an average frequency of 3 and above). The rows in Table VI indicate the correct tags, the columns indicate the HMM tagger's predicted tags, and each cell indicates the percentage of the tagging error. The most common error which is difficult to disambiguate is when proper nouns are tagged as common nouns and vice versa, accounting to 12% of the errors. Here, the HMM tagger has not been able to take into consideration the capitalization feature of proper nouns. A brief discussion on some of the tagging errors is given as follows:

TABLE V. KHASI POS TAGGER RESULTS USING TEN-FOLD CROSS VALIDATION

| Tagger                | Accuracy      |
|-----------------------|---------------|
| Baseline Tagger       | 84.05%        |
| NLTK Tagger           | 87.58%        |
| <b>HMM POS Tagger</b> | <b>93.39%</b> |

Verb Noun / Noun Verb confusion.

An interesting phenomenon that mainly contributes to the collective occurrence of 20% of the errors is when pronouns are tagged as pronominal markers, the words following them are inadvertently tagged as nouns rather than verbs. When pronominal markers are tagged as pronouns, the words following them are likewise tagged as verbs rather than nouns. For example:

U/PR\_PRP lum/V\_VM ia/IN u/PR\_PRP\_M soh/N\_NN ka/PR\_PRP\_M jingtrei/N\_NN shitom/JJ jong/IN u/PR\_PRP /RD\_PUNC.

'He reaps the fruit of his hard work.'

In the sentence above, the verb *lum* 'reap' is incorrectly tagged as a noun *lum* 'hill/mountain' in the sentence given below. This is because the preceding word *u* was incorrectly tagged as a pronominal marker rather than a personal pronoun.

U/PR\_PRP\_M<sup>2</sup> lum/N\_NN<sup>\*</sup> ia/IN u/PR\_PRP\_M soh/N\_NN ka/PR\_PRP\_M jingtrei/N\_NN shitom/JJ jong/IN u/PR\_PRP /RD\_PUNC.

Another example where a noun is incorrectly tagged as a verb is shown in the sentences below:

Baroh/JJ ki/PR\_PRP\_M diengsohnamtra/N\_NN sawdong/RB ia/IN u/PR\_PRP ki/PR\_PRP don/V\_VAUX tang/RB kawei/QT\_QTC ban/V\_VAUX\_VINF iathuh/V\_VM /RD\_PUNC ka/PR\_PRP\_M jingjot/N\_NN bad/CC\_CCD ka/PR\_PRP\_M jinglehnohei/N\_NN /RD\_PUNC.

'All the orange trees have only one thing to tell, tales of destruction and lost.'

Baroh/JJ ki/PR\_PRP<sup>\*</sup> diengsohnamtra/V\_VM<sup>\*</sup> sawdong/RB ia/IN u/PR\_PRP ki/PR\_PRP don/V\_VAUX tang/RB kawei/QT\_QTC ban/V\_VAUX\_VINF iathuh/V\_VM /RD\_PUNC ka/PR\_PRP\_M jingjot/N\_NN bad/CC\_CCD ka/PR\_PRP\_M jinglehnohei/N\_NN /RD\_PUNC.

Apart from what is described above, other instances when a noun is erroneously tagged as a verb are when the tagger cannot distinguish a verb functioning as a noun.

Adjective Verb / Verb Adjective confusion

Various researchers have put forward their views on the existence of adjectives in Khasi due to their syntactic similarity with verbs [12], [19], [20]. The confusion matrix also indicates that the tagger has tagged some adjectives as verbs, especially when the words follow a subordinating conjunction *ba* or the auxiliary word *la*.

<sup>2</sup> \* Incorrect tag

TABLE VI. CONFUSION MATRIX IN % OF KHASI HMM POS TAGGER

|          | N_NN | PR_PRP | V_VM | PR_PRP_M | N_NNP | RB  | JJ  | RD_ECH | RD_RDF | CC_CCD | RP_RPD | QT_QTC | IN  | PR_PRF |
|----------|------|--------|------|----------|-------|-----|-----|--------|--------|--------|--------|--------|-----|--------|
| N_NNP    | 12.7 |        | 1.3  |          |       | 0.8 |     |        | 0.6    |        |        |        |     |        |
| V_VM     | 5.3  |        |      |          |       | 2.9 | 1.4 | 0.8    |        |        |        |        |     |        |
| PR_PRP   |      |        |      | 5.0      |       |     |     | 0.5    |        |        |        |        |     |        |
| N_NN     |      |        | 4.9  |          | 3.7   | 3.3 | 1.6 | 1.5    | 1.2    |        |        | 0.7    |     |        |
| PR_PRP_M |      | 4.8    |      |          |       |     |     | 1.0    |        |        |        |        |     |        |
| JJ       | 3.3  |        | 1.9  |          |       | 2.7 |     |        |        |        |        | 0.5    |     |        |
| RB       | 3.0  |        | 3.1  |          |       |     | 1.9 |        |        |        |        |        |     |        |
| IN       |      |        |      |          |       | 0.8 |     | 0.6    |        | 1.2    |        |        |     |        |
| QT_QTC   | 1.0  |        |      |          |       |     |     |        |        |        |        |        |     |        |
| PR_PRF   |      |        |      |          |       |     |     |        |        |        | 0.9    |        |     |        |
| RD_PUNC  |      |        |      |          |       |     |     | 0.6    |        |        |        |        |     |        |
| RP_INJ   |      |        |      |          |       | 0.6 |     |        |        |        |        |        |     |        |
| CC_CCD   |      |        |      |          |       |     |     | 0.5    |        |        |        |        | 0.5 |        |
| CC_CCS   |      |        |      |          |       | 0.5 |     |        |        |        |        |        |     |        |
| RP_RPD   |      |        |      |          |       |     |     |        |        |        |        |        |     | 0.5    |
| RD_RDF   | 0.5  |        |      |          |       |     |     |        |        |        |        |        |     |        |

Ka/PR\_PRP\_M khmat/N\_NN jong/IN ka/PR\_PRP  
ka/PR\_PRP la/V\_VAUX stem/JJ blaid/RB blaid/RB  
./RD\_PUNC

‘Her eyes have turned yellowish.’

Ka/PR\_PRP\_M khmat/N\_NN jong/IN ka/PR\_PRP  
ka/PR\_PRP la/V\_VAUX stem/V\_VM\* blaid/RB blaid/RB  
./RD\_PUNC

Likewise, there are some instances where a verb has also been tagged as an adjective. Here, *bah* ‘carry on the back/shoulders’ has been erroneously tagged as an adjective.

Nga/PR\_PRP la/V\_VAUX kit/V\_VM, /RD\_PUNC  
nga/PR\_PRP la/V\_VAUX bah/V\_VM, /RD\_PUNC  
bad/CC\_CCD nga/PR\_PRP la/V\_VAUX bysa/V\_VM  
la/V\_VAUX btiah/V\_VM ia/IN phi/PR\_PRP baroh/JJ  
./RD\_PUNC

‘I bore the burden and raised all of you.’

Nga/PR\_PRP la/V\_VAUX kit/V\_VM, /RD\_PUNC  
nga/PR\_PRP la/V\_VAUX bah/JJ\*, /RD\_PUNC bad/CC\_CCD  
nga/PR\_PRP la/V\_VAUX bysa/V\_VM la/V\_VAUX  
btiah/V\_VM ia/IN phi/PR\_PRP baroh/JJ ./RD\_PUNC

Noun Adverb confusion

When a noun is tagged as an adverb, it is because the noun follows the verb without a preceding pronominal marker. This is an example where the mandatory pronominal marker is dropped before the noun *Sein Iong* ‘black snake’.

U/PR\_PRP la/V\_VAUX kylla/V\_VM Sein/N\_NN  
Iong/N\_NN ./RD\_PUNC.

‘He turned into a black snake.’

U/PR\_PRP la/V\_VAUX kylla/V\_VM Sein/RB\* Iong/RB\*  
./RD\_PUNC.

Adjective Noun / Noun Adjective confusion

When an adjective is tagged as a noun, it is more likely that the tagger cannot differentiate a compound noun from a noun having a qualifying adjective. This is mainly because in most cases adjectives follow the nouns they qualify. Here the adjective *badon baem* ‘well-to-do’ is tagged as a compound noun.

Ka/PR\_PRP pher/JJ na/IN kiwei/JJ pat/RP\_RPD  
ki/PR\_PRP\_M khun/N\_NN badon/JJ baem/JJ kiba/PR\_PRL  
nga/PR\_PRP la/V\_VAUX iakynduh/V\_VM ./RD\_PUNC.

‘She is different from all the well-to-do kids that I have met.’

Ka/PR\_PRP pher/JJ na/IN kiwei/JJ pat/RP\_RPD  
ki/PR\_PRP\_M khun/N\_NN badon/N\_NN\* baem/N\_NN\*  
kiba/PR\_PRL nga/PR\_PRP la/V\_VAUX iakynduh/V\_VM  
./RD\_PUNC

Nouns are erroneously tagged as adjectives in compound nouns, or when an adjective or a verb semantically functions as a noun, as seen in the sentence below. Here *u rit u riat* ‘low-class people’ is confused as *rit* and *ria*, which means ‘small’ in another sense of the words. Additionally, the preceding word

being tagged as a pronoun rather than a pronominal marker adds to the confusion.

Mynta/RB ./RD\_PUNC u/PR\_PRP\_M rit/N\_NN  
u/PR\_PRP\_M ria/N\_NN u/PR\_PRP shu/RB pyrta/V\_VM  
shla/RB ./RD\_PUNC.

‘Now, the low-class people are just shouting angrily.’

Mynta/RB ./RD\_PUNC u/PR\_PRP\* rit/JJ\* u/PR\_PRP\*  
ria/JJ\* u/PR\_PRP shu/RB pyrta/V\_VM shla/RB ./RD\_PUNC.

The above discussion indicates that one way of addressing the existing confusion is to consider the properties or attributes of words such as capitalization, next occurring word, and others. These considerations are presented in the next section.

## V. A HYBRID KHASI POS TAGGER TO ADDRESS TAGGING ERRORS

To reduce the errors present in the HMM POS tagger output, the errors identified in Section IV B need to be addressed.

To do so, the *sklearn-crfsuite*<sup>3</sup> has been engaged as a means to achieve this purpose. *Sklearn-crfsuite* is a thin python-crfsuite wrapper which provides a fast implementation of conditional random fields (CRF). Unlike HMM, CRFs allow the inclusion of features that are non-independent and varied in depth even on the same observation [21]. Using CRF, given a sentence  $X = x_1 x_2 \dots x_T$ , the conditional probability of the tag sequence  $Y = y_1 y_2 \dots y_T$  is given by:

$$P(y|x) = \frac{1}{Z(x)} * \exp(\sum_{t=1}^T \sum_k \theta_k \cdot f_k(y_{t-1}, y_t, x)) \quad (3)$$

where  $Z(x) = \sum_T \exp(\sum_{t=1}^T \sum_k \theta_k \cdot f_k(y_{t-1}, y_t, x))$  is the normalization factor,  $\theta_k$  is the weight and  $f_k(y_{t-1}, y_t, x)$  is the feature function. Implementing POS tagging in *sklearn-crfsuite* permits the possibility to include as many word features as possible to aid the tagging process. The word features included for Khasi are capitalization, prefixes (prevalent in Khasi, unlike suffixation in English) of length  $\geq 2$  and length  $\leq 4$ , current word under consideration, previous word, next word, and whether a word begins or ends a sentence. An additional feature that can be included is the previous tag of a word. In the interface provided by *sklearn-crfsuite* the features are extracted from the training data and from the test data. It expects the training data to contain annotated data, i.e., the words and their respective POS tags. This will enable *sklearn-crfsuite* to extract all the specified features and learn the tagging process. However, when tagging the test data, the problem arises during feature extraction from the test data. In the provided interface, all the above-mentioned features are possible to extract from the test data except the previous word tag feature. This feature is not available in the test data because it contains only sentences where the respective words are yet to be tag. To overcome this problem, the output of the Khasi HMM POS tagger is used as input to the Khasi CRF POS tagger. This enables the previous tag feature to be easily extracted from the tagged output of the HMM tagger.

<sup>3</sup> <https://sklearn-crfsuite.readthedocs.io/en/latest/>

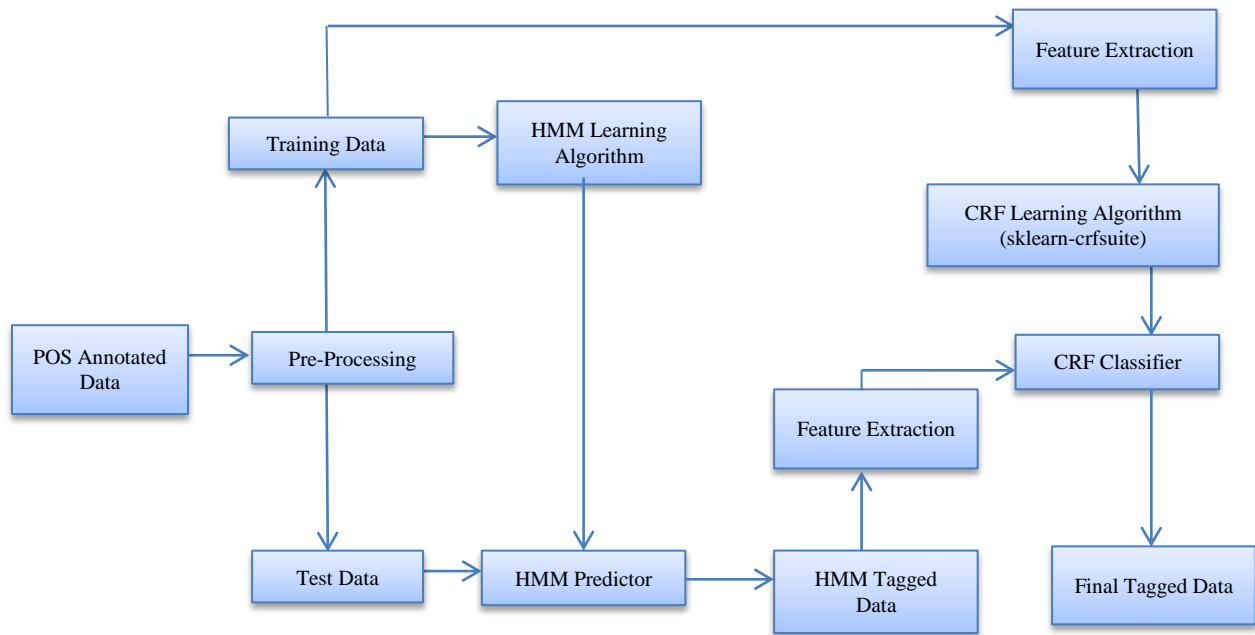


Fig. 2. Block Diagram of the Hybrid POS Tagger.

Fig. 2 shows the block diagram of the implementation. The features mentioned above are included in the CRF tagger. The CRF POS tagger is then trained on the same training data used by the HMM POS tagger. To ensure consistency, ten-fold cross-validation is undertaken for training and testing the CRF tagger. During tagging, the word features are extracted from the test data and the previous tag feature is provided by the output of the HMM tagger. In doing so, training on 4k sentences and tagging on 10% of the training sentences, an average tagging accuracy of **95.29%** is achieved with an average improvement of 1.9% over the performance of the HMM tagger shown earlier in Table V.

#### VI. EVALUATION OF HYBRID POS TAGGER

Table VII shows the average precision, recall, and F-measure of both the HMM POS Tagger and the Hybrid POS Tagger. The F-measure of the Hybrid POS Tagger shows a significant improvement over the F-measure of the HMM POS Tagger in 23 tags out of 32 tags, with one tag RD\_UNK (for unknown tags) giving 0 F-measure in both taggers. This may be attributed that RD\_UNK occurs exactly once in the corpus. Since the corpus captures only prose genre, it may be the factor where the frequency of symbols in the corpus is only 4. This may be the reason that the Hybrid POS Tagger has failed to predict the symbol tag by giving an F-measure of 0 for RD\_SYM symbol tag. Fig. 3 shows the graphical comparison of the average confusion frequency among the tags between the HMM tagger and the Hybrid tagger, arranged in descending order of the HMM tagger confusion percentage. Table VIII

shows the percentage of reduction or increase in confusion in the Hybrid POS tagger from the HMM POS tagger. The rows in Table VIII indicate the correct tags, the columns indicate the Hybrid tagger's predicted tags, and each cell indicates the percentage increase or reduction in tagging error from the HMM tagger. The biggest improvement of the Hybrid tagger is the 100% elimination of all the tags confused as echo tags (RD\_ECH) shown earlier in Table VI.

Another significant improvement is in its ability to disambiguate proper nouns (N\_NNP) from common nouns (N\_NN) with an 89% reduction of confusion; a trait where CRF classifiers are good at capturing word features such as capitalization. The same is observed in noun and foreign word confusion (N\_NN, RD\_RDF), noun and adverb confusion (N\_NN, RB), and the coordinating conjunction and preposition confusion (CC\_CCD, IN); all of them over the 80% confusion reduction. Overall, it is clear that the Hybrid tagger has reduced most of the confusion mentioned in Section IV-B. Interestingly, even the Hybrid tagger has a problem in disambiguating adjectives from verbs, a language phenomenon debated by researchers [11], [13], [19], [20]. In this category, the confusion has not reduced but increased by 65%. The other two tags that showed a relatively small increase in confusion are the adverb and noun (RB, N\_NN) -confusion by 10%- and the interjection and adverb (RP\_INJ, RB)- confusion by 8%. The remaining three confusing tags showed a 2% or less increase in confusion. All the most common confusion tags that have an average frequency of 3 or more are indicated in Table VIII.

TABLE VII. AVERAGE PRECISION, RECALL, AND F-MEASURE OF BOTH TAGGERS

| Sl. No | POS Tags    | HMM POS Tagger |        |           | Hybrid POS Tagger |        |           |
|--------|-------------|----------------|--------|-----------|-------------------|--------|-----------|
|        |             | Precision      | Recall | F-measure | Precision         | Recall | F-measure |
| 1      | CC_CCD      | 95.95          | 97     | 96.46     | 96.13             | 98.29  | 97.18     |
| 2      | CC_CCS      | 96.99          | 95.68  | 96.31     | 98.66             | 96.71  | 97.66     |
| 3      | DM_DMD      | 100            | 96.03  | 97.93     | 98.55             | 97.16  | 97.79     |
| 4      | IN          | 98.44          | 96.3   | 97.35     | 98.64             | 97.76  | 98.2      |
| 5      | JJ          | 82.6           | 75.16  | 78.54     | 89.03             | 78     | 83.01     |
| 6      | N_NN        | 87.38          | 91.69  | 89.45     | 92.75             | 93.57  | 93.15     |
| 7      | N_NNP       | 75.97          | 54.72  | 61.89     | 88.15             | 94.83  | 91.2      |
| 8      | N_NST       | 99.57          | 96.12  | 97.76     | 97.66             | 91.19  | 94.25     |
| 9      | PR_PRF      | 73.02          | 67.64  | 68.88     | 82.65             | 72.03  | 74.5      |
| 10     | PR_PRI      | 91.58          | 90.04  | 90.52     | 95.5              | 92.4   | 93.71     |
| 11     | PR_PRL      | 99.67          | 98.03  | 98.83     | 99.8              | 98.79  | 99.29     |
| 12     | PR_PRP      | 96.02          | 95.53  | 95.75     | 96.58             | 95.96  | 96.26     |
| 13     | PR_PRP_AUX  | 98.43          | 99.59  | 99        | 97.94             | 99.35  | 98.63     |
| 14     | PR_PRP_M    | 96.64          | 96.26  | 96.44     | 96.21             | 97.44  | 96.81     |
| 15     | PR_PRQ      | 92.56          | 75.23  | 82.01     | 96.24             | 77.69  | 85.06     |
| 16     | QT_QTC      | 85.37          | 83.43  | 83.93     | 96.25             | 88.46  | 92.02     |
| 17     | QT_QTF      | 97.79          | 97.15  | 97.43     | 96.86             | 96.82  | 96.76     |
| 18     | QT_QTO      | 83.17          | 78.22  | 78.64     | 97.15             | 64.71  | 74.01     |
| 19     | RB          | 88.29          | 91.06  | 89.64     | 91.53             | 93.41  | 92.46     |
| 20     | RD_ECH      | 21.28          | 22.5   | 13.88     | 30                | 13.34  | 17.53     |
| 21     | RD_PUNC     | 89.98          | 89.6   | 89.79     | 99.99             | 99.88  | 99.93     |
| 22     | RD_RDF      | 38.51          | 66.51  | 41.35     | 36.55             | 47.1   | 33.44     |
| 23     | RD_SYM      | 10             | 10     | 10        | 0                 | 0      | 0         |
| 24     | RD_UNK      | 0              | 0      | 0         | 0                 | 0      | 0         |
| 25     | RP_CL       | 98             | 98.23  | 97.96     | 100               | 98.75  | 99.34     |
| 26     | RP_INJ      | 71.04          | 71.95  | 70.87     | 76.71             | 73.46  | 74.36     |
| 27     | RP_INTF     | 95.05          | 95.67  | 95.18     | 94.82             | 99.51  | 96.95     |
| 28     | RP_NEG      | 99.73          | 98.88  | 99.3      | 100               | 98.84  | 99.42     |
| 29     | RP_POS      | 89.46          | 92.87  | 90.92     | 89.31             | 97.07  | 92.61     |
| 30     | RP_RPD      | 94.16          | 92.09  | 93.04     | 94.38             | 93.82  | 93.95     |
| 31     | V_VAUX      | 97.08          | 97.31  | 97.19     | 97.52             | 98.08  | 97.8      |
| 32     | V_VAUX_VINF | 98.25          | 98.24  | 98.24     | 97.91             | 99.45  | 98.67     |
| 33     | V_VM        | 92.71          | 92.86  | 92.76     | 93.22             | 94.38  | 93.78     |
|        |             |                |        |           |                   |        |           |

TABLE VIII. REDUCTION % IN CONFUSION OF HYBRID POS TAGGER

|          | N_NN              | PR_PRP | V_VM              | PR_PRP_M         | N_NNP | RB               | JJ   | RD_ECH | RD_RDF | CC_CCD           | RP_RPD           | QT_QTC | IN   | PR_PRF |
|----------|-------------------|--------|-------------------|------------------|-------|------------------|------|--------|--------|------------------|------------------|--------|------|--------|
| N_NNP    | 88.9              |        | 68.2              |                  |       | 84.9             |      |        | 85.4   |                  |                  |        |      |        |
| V_VM     | 1.7               |        |                   |                  |       | 42               | 23   | 100    |        |                  |                  |        |      |        |
| PR_PRP   |                   |        |                   | 2.2 <sup>#</sup> |       |                  |      | 100    |        |                  |                  |        |      |        |
| N_NN     |                   |        | 0.6               |                  | 15.7  | 13.6             | 37   | 100    | 86.1   |                  |                  | 87.5   |      |        |
| PR_PRP_M |                   | 18.6   |                   |                  |       |                  |      | 100    |        |                  |                  |        |      |        |
| JJ       | 21.8              |        | 65.3 <sup>#</sup> |                  |       | 31               |      |        |        |                  |                  | 76.5   |      |        |
| RB       | 10.3 <sup>#</sup> |        | 43.7              |                  |       |                  | 51.2 |        |        |                  |                  |        |      |        |
| IN       |                   |        |                   |                  |       | 47.1             |      | 100    |        | 1.3 <sup>#</sup> |                  |        |      |        |
| QT_QTC   | 48.2              |        |                   |                  |       |                  |      |        |        |                  |                  |        |      |        |
| PR_PRF   |                   |        |                   |                  |       |                  |      |        |        |                  | 1.8 <sup>#</sup> |        |      |        |
| RD_PUN_C |                   |        |                   |                  |       |                  |      | 100    |        |                  |                  |        |      |        |
| RP_INJ   |                   |        |                   |                  |       | 8.3 <sup>#</sup> |      |        |        |                  |                  |        |      |        |
| CC_CCD   |                   |        |                   |                  |       |                  |      | 100    |        |                  |                  |        | 82.9 |        |
| CC_CCS   |                   |        |                   |                  |       | 71               |      |        |        |                  |                  |        |      |        |
| RP_RPD   |                   |        |                   |                  |       |                  |      |        |        |                  |                  |        |      | 25.8   |
| RD_RDF   | 3.1               |        |                   |                  |       |                  |      |        |        |                  |                  |        |      |        |

<sup>#</sup>Increase % in confusion



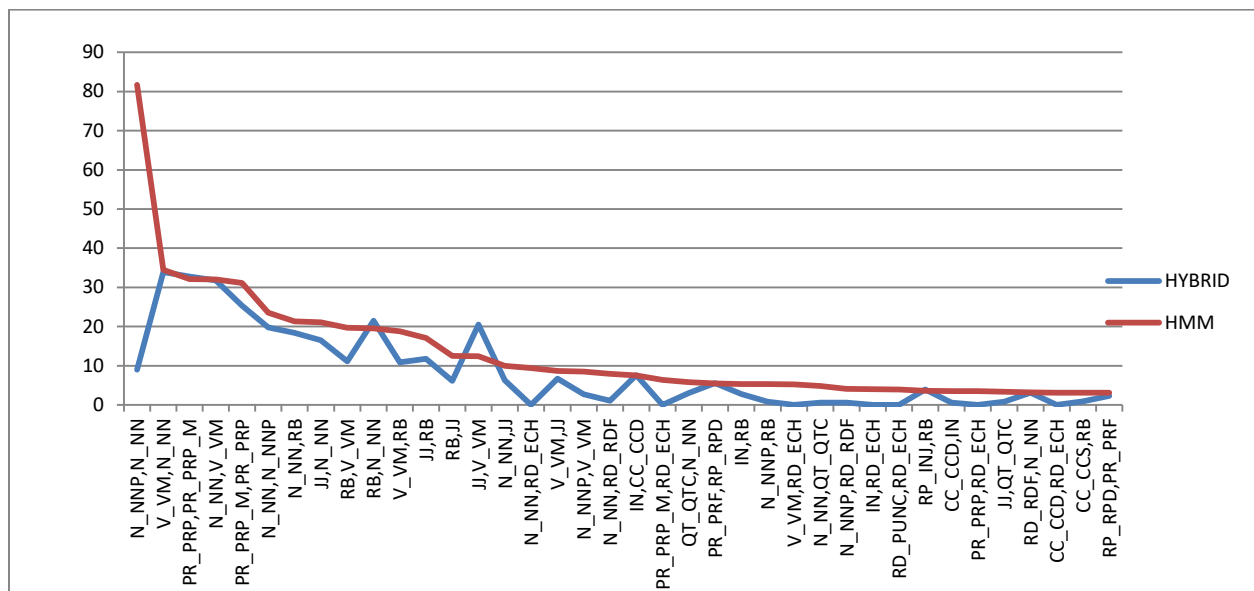


Fig. 3. The Graph Shows the Tag Confusion between the HMM POS Tagger and the Hybrid POS Tagger where Label x,y means Tag x is Confused as y.

### VII. CONCLUSION

Although the present annotated 90k corpus available for Khasi is relatively small, nevertheless experiments with automatic tagging using HMM along with the BIS tagset for Khasi have shown performance that does not lack behind reported performance in other languages. As shown in this paper, addressing the tagging errors of the HMM POS tagger by coupling it with the sklearn-crfsuite, a fast implementation of CRF has given a Hybrid POS tagger for Khasi with an improved accuracy of 95.29%.

The results are very promising for an under resourced language such as Khasi. Apart from the concerns regarding the performance of the tagger, Khasi POS tagger development has also highlighted issues that were often raised in the literature of Khasi language. Does the Hybrid tagger's confusion between verbs and adjectives imply that the confused adjectives are actually attributive verbs? However, to answer this question, further investigation in this direction is still needed. Finally, the next step is to include a wider range of genres for the corpus, which hopefully, with the current POS tagger in place, will ease the development towards a larger size annotated corpus.

#### REFERENCES

[1] M. J. Tham, "Challenges and issues in developing an annotated corpus and HMM POS tagger for Khasi", Proceedings of the 15th International Conference on Natural Language Processing (ICON 2018), Patiala, Punjab, India, pp. 15-18, December 2018.

[2] K. Darwish et al. "Multi-dialect Arabic POS tagging: a CRF approach", Proceedings of the Eleventh International Conference on Language Resources and Evaluation (LREC 2018), May 2018.

[3] W. Khan, et al. "Urdu part of speech tagging using conditional random fields", Language Resources and Evaluation, 53, pp. 331-362. 2018.

[4] S. Song, N. Zhang, and H. Huang, "Named entity recognition based on conditional random fields", Cluster Comput, 2017.

[5] K. S. Nagaraja, Word formation in Khasi, Bulletin of the Deccan College Research Institute 60/61:387-417, 2000.

[6] B. War, Ki sawa bad ki dur jong ka ktien Khasi, 2nd edn. Ri-Ia-dor, Shillong, Meghalaya, 2011.

[7] N. Garg, V. Goyal, and S.Preet, "Rule based Hindi part of speech tagger", Proceedings of COLING 2012, Mumbai, India, pp. 163-174, 2012.

[8] S. Singh, K. Gupta, M. Shrivastava, and P. Bhattacharyya. "Morphological richness offsets resource demand - experiences in constructing a POS Tagger for Hindi", Proceedings of the COLING/ACL 2006 Main Conference Poster Sessions. Sydney, Australia, pp. 779-786, 2006.

[9] M. Shrivastava, P. Bhattacharyya, "Hindi POS tagger using naive stemming: harnessing morphological information without extensive linguistic knowledge", Proceedings of the International Conference on NLP (ICON 08). Pune, India, 2008.

[10] S. Warjri, P. Pakray, S. Lyngdoh, and A. K. Maji, "Identification of POS tag for Khasi language based on Hidden Markov Model POS tagger". Computación y Sistemas, 23(3):795-802, 2019.

[11] C. D. Manning, and H. Schütze, Foundations of statistical natural language processing. MIT press, 1999.

[12] M. B. Jyrwa, A descriptive study of the noun phrase in Khasi. Dissertation, North Eastern Hill University, 1989.

[13] K. S. Nagaraja, Khasi a descriptive analysis, Deccan College Post-Graduate & Research Institute, Pune, India, 1985.

[14] L. Rabel, Gender in Khasi nouns, Mon Khmer Studies 6:247-272, 1977.

[15] H. Roberts, A grammar of the Khasi language, Mittal Publications, New Delhi, India , 2005.

[16] T. Brants, "TnT-A statistical part of speech tagger", Proceedings of the Sixth Conference on Applied Natural Language Processing, Seattle, Washington, USA, pp. 224-231, 2000.

[17] S. Bird, E. Klein, and E. Loper, Natural language processing with python. O'Reilly Media Inc, CA, 2009.

[18] D. Jurafsky, and J. H. Martin, Speech and language processing. An introduction to natural language processing, Computational Linguistics, and Speech Recognition, 2nd edn. Pearson India Education, Noida, 2009.

[19] L. Rabel, Khasi a language of Assam. Baton Rouge: Louisiana State University Press, 1961.

[20] I. M. Simon, "Some observations on the adjectives in Khasi", Khasi Studies 1(3), 1987.

[21] J. Lafferty, A. McCallum, and F. C Pereira, "Conditional random fields: Probabilistic models for segmenting and labeling sequence data", 2001.

# Robust Drowsiness Detection for Vehicle Driver using Deep Convolutional Neural Network

A F M Saifuddin Saif<sup>1</sup>

Faculty of Science and Technology  
American International University – Bangladesh  
Dhaka, Bangladesh

Zainal Rasyid Mahayuddin<sup>2</sup>

Faculty of Information Science and Technology  
Universiti Kebangsaan Malaysia  
43600 UKM, Bangi, Selangor, Malaysia

**Abstract**—Drowsiness detection during driving is still an unsolved research problem which needs to be addressed to reduce road accidents. Researchers have been trying to solve this problem using various methods where most of these solution lacks behind in accuracy, real-time performance, costly, complex to build, and has a higher computational cost with low frame rate. This research proposes robust method for drowsiness detection of vehicle drivers based on head pose estimation and pupil detection by extracting facial region initially. Proposed method used frame aggregation strategy in case of face region cannot be extracted in any frame due to shortcomings, i.e. light reflection, shadow. In order to improve identification under highly varying lighting conditions, proposed research used cascade of regressors cutting edge method where each regression refers estimation of facial landmarks. Proposed method used deep convolutional neural network (DCNN) for accurate pupil detection to learn non linear data pattern. In this context, challenges of varying illumination, blurring and reflections for robust pupil detection are overcome by using batch normalization for stabilizing distributions of internal activations during training phase which makes overall methodology less influenced by parameter initialization. Proposed research performed extensive experimentation where accuracy rate of 98.97% was achieved using frame rate of 35 fps which is higher comparing with previous research results. Experimental results reveal the effectiveness of the proposed methodology.

**Keywords**—Drowsiness detection; convolutional neural network; face region extraction; pupil detection

## I. INTRODUCTION

In this age of era, road accidents happens to be caused by lot of reasons where one of that reason happens to be driver feeling drowsy during driving known as fatigue driving. Previous research proposed two types of drowsiness detection system, i.e. subjective detection methods and objective detection methods. In subjective detection methods, drivers tend to determine their state of drowsiness by individual record data-sheet and own physiological response. Subjective methods are easy to build and simple in usage but lacks behind in accuracy and real-time performance. Objective detection methods use modern technologies to evaluate driver drowsiness state by extraction of driving characteristics, facial features analysis and come to a result base conclusion. However, simulation of objective detection methods are tends to be costly, complex to build, and has a higher computational cost. Objective detection methods can be divided into two categories based on detection parameters, i.e. driver

physiological parameters based detection method and driver facial features based detection method. In driver physiological parameters based detection method, normally driver response becomes slow due to drowsiness where EEG can be used to detect drowsiness state [1, 2, 3]. However, this approach tends to be costly and real time detection during driving is not robust. Driver facial features based detection methods are based on facial features using various methods, i.e. CNN based Deep Learning Model [4], Generative Adversarial Networks (GAN) [5], Principal Component Analysis [6], DriCare [7] where analysis was done on pupil, eyelids and head pose to detect drowsiness. This research proposes a robust method for vehicle driver drowsiness detection using facial features based head orientation and pupil detection where frame aggregation strategy is also used to ensure facial features processing under challenging circumstances, i.e. light reflection and shadow.

Research in [4] used neural network approach for face features based detection methods and utilized facial landmarks through Convolutional Neural Network (CNN) in order to categorize driver drowsiness. Deep learning model which is small in size with high accuracy was considered as their achievement. However, in case of wearing sunglasses in lieu with bad lighting conditions, their proposed approach could not provide expected performance. Research in [5] introduced a novel framework that remedies generalization failures under represented population groups in the training dataset. They improved Convolutional Neural Network (CNN) trained for prediction by using Generative Adversarial networks (GAN) for targeted data augmentation for population groups that face similar facial attributes and highlights where the model was failing. However, due to the lack of sufficient training data for various population groups, their research requires further investigation. Research in [6] showed that there are potential social challenges regarding the application of drowsiness detection by highlighting problems in detecting dark-skinned driver faces. They focused to use unrepresentative images to train driver drowsiness detection system using vision based approach. However, their accuracy obtained decreased substantially when their approach was evaluated using more representative test set. Research in [7] proposed a system called DriCare to detect the drivers' fatigue status, such as yawning, blinking, and using video images, duration of eye closure, without equipping their bodies with devices. However, they did not show any comparison of performance with the existing research methods. Proposed method for

drowsiness detection by this research extracts facial features initially followed by head orientation and pupil detection. In addition, to learn nonlinear data pattern proposed method used aggregation strategy and integral image construction in lieu with deep convolutional neural network (DCNN) to improve efficiency. Overall contributions by this research are stated below:

- Proposed method detects drowsiness for vehicle driver in the basis of visual analysis of eye and head orientation together followed by pupil detection.
- Proposed method uses deep convolutional neural network (DCNN) to learn non-linear data pattern.
- Proposed method handles highly varying lighting conditions by using cascade of regressors cutting edge method.
- Various challenges, i.e. unfixed illumination, blurring and reflections are overcome by the proposed method using batch normalization to stabilize distributions of internal activations during training phase.

Rest of this paper is organized as follows. Section 2 demonstrates comprehensive and critical reviews in the existing research, Section 3 illustrates proposed methodology for drowsiness detection, Section 4 depicts extensive experimental validation for the proposed method and finally Section 5 presents concluding remarks.

## II. BACKGROUND STUDY

Researchers used various methods for driver drowsiness detection mentioned in Fig. 1. Previously, researchers used artificial neural network (ANN) for drowsiness detection where information such as features are stored in the entire network and can learn from observing datasets and disappearances of few piece of information does not prevent network from functioning [8, 9, 14]. However, ANN requires higher computation due to parallel processing is needed which means that overall methodology will not always be robust and little suitable to use in a vehicle constantly [10, 11]. In this context, deep learning or a form of machine learning approach can be used to speed up analysis of datasets [12, 13, 15]. Research in [4] focused on the detection of drowsiness using neural network based methodology. Facial landmarks from frames captured by mobile device was detected using CNN-based machine learning approach by them and CNN-based trained deep learning model was used to detect drowsy driving behavior. However, in their research still better performance can be achieved using efficient facial features detection under bad lighting conditions. Research in [5] identified individuals with facial features by introducing a sampling strategy where the network was failing. They showed how a Generative Adversarial networks (GAN) can be used to produce training data or individuals where model is failing by generating realistic images. Their proposed approach did not rely on any meta-data or assumptions about the race or ethnicity of individuals in the datasets, which is a commonly used approach to determine algorithmic fairness or bias. However, their proposed methodology still requires that some training data be available for various population groups. A novel

visualization technique which can be assistance to identify groups of people was proposed by research in [6] where potential discrimination could arise due to the usage of Principal Component Analysis (PCA). They used PCA to produce a grid of faces sorted by similarity and combining these with a model accuracy overlay. They aimed to highlight the challenges of using unrepresentative images to train vision-based driver drowsiness detection systems. However, facial regions for the lighter skinned individuals were focused by them and failed to do so for darker skinned individuals pointed potential failure case. In addition, indication of some overfitting on more representative datasets was observed causes a decrease on more representative datasets. Research in [7], proposed a new face-tracking algorithm named Multiple Convolutional Neural Networks (CNN)-KCF (MC-KCF), which optimizes KCF algorithm. Their proposed DriCare provides three different criteria to evaluate the degree of the driver's drowsiness: blinking frequency, duration of the eyes closing, and yawning. They combined CNN with KCF algorithm to improve the performance under complex environment, such as low light. However, they did not compare effectiveness of their proposed DriCare with other existing methods.

Driving parameters in comparison with facial features and drivers physiological parameters is another widely used approach in detection of fatigue during driving. Karolinska sleepiness scale (KSS) is an ideal method for vehicle driving parameters which refers as questionnaire that depends on drivers to self-involvement and answers of drivers from the pre-set questionnaire [16, 17, 18]. Then, these answers tend to pass through KSS and results are generated from the KSS scale. Due to the simplicity of this approach to detect fatigue of vehicle driver is stated as simple approach which does not require complicated computation and processing [19, 20, 21]. However, core problem with the vehicle driving parameter in the detection of fatigue is that vehicle driving parameters often results in poor accuracy and sensitivity.

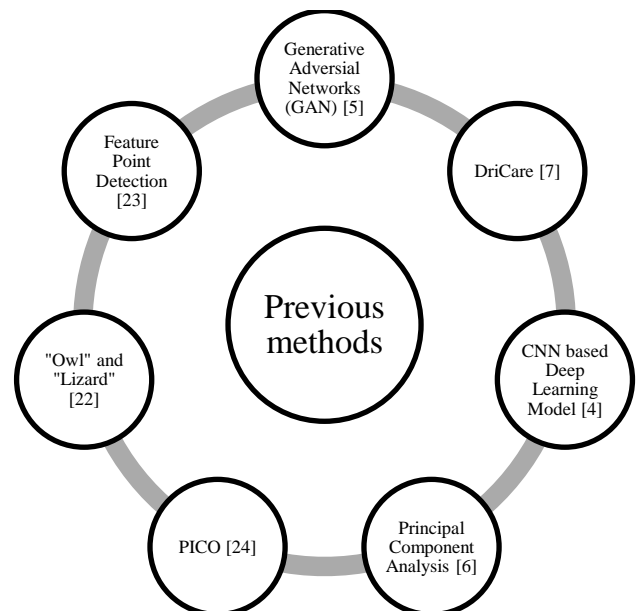


Fig. 1. Previous Research Methods for Driver Drowsiness Detection.

Research in [22] used random forest classifier for classification where they required a face and pupil under classification schemes and observed variation in accuracy among subjects before and after adding eye pose in the classification set. However, variation of performance in their proposed methodology was noticed results in unreliable validation. In this context, research in [23] experimented effects of facial sub regions to estimate accuracy where they combined eye and mouth areas. They used facial textures and landmarks extracted from image sequences and fused these features to enhance performance. However, due to lack of weak feature extraction mechanism used by their research caused higher error rate. Research in [24] used facial features as parameters for drowsiness detection. They used rigid face model which enables fast pose estimation, especially for on-board computers. Their 3D face model produced more robust recognition memory. However, rigid face model cannot update shape. Besides, research in [24] absolute deviations are mainly caused by rigid model which has geometry error for different subjects resulting in higher error rate.

This research proposes robust method for drowsiness detection using facial region extraction and head orientation estimation followed by pupil detection. To ensure the robustness of the proposed methodology, aggregation strategy is used during facial region extraction to overcome various shortcomings, i.e. light reflection, shadow. In addition, to overcome the challenges of varying illumination, blurring and reflections, this research used deep convolutional neural network (DCNN) to learn non-linear data pattern and high probability values are provided to the pixels enclosed by the generated circle instead of providing pupil's coordinates directly.

### III. PROPOSED METHODOLOGY

This research proposes an efficient method to reduce collisions associated with driver drowsiness. Difference between existing methods and proposed method is that proposed method detects drowsiness in the basis of visual analysis of eye state and head pose whereas in previous research methods, driver drowsiness or distraction level was determined by using eye closure or head-nodding angles. Various steps such as face detection, face alignment, pupil detection, classification and decision-making, Kalman filter are included in the proposed method mentioned in Fig. 2. All these steps for the proposed method are extensively explained.

#### A. Input Image

Proposed research used monocular video camera using 35 fps frame rate for input image collection. Proposed research used median filter [25, 26] to remove noise from the collected video frames. In this context, morphological processing such as resizing of the frame into 200x200 dimension, erosion and dilation were applied to ensure noise free frames to the next subsequent frames. In addition, this research also used two frame differential approaches to find the difference between frames to find the initial change between video frames.

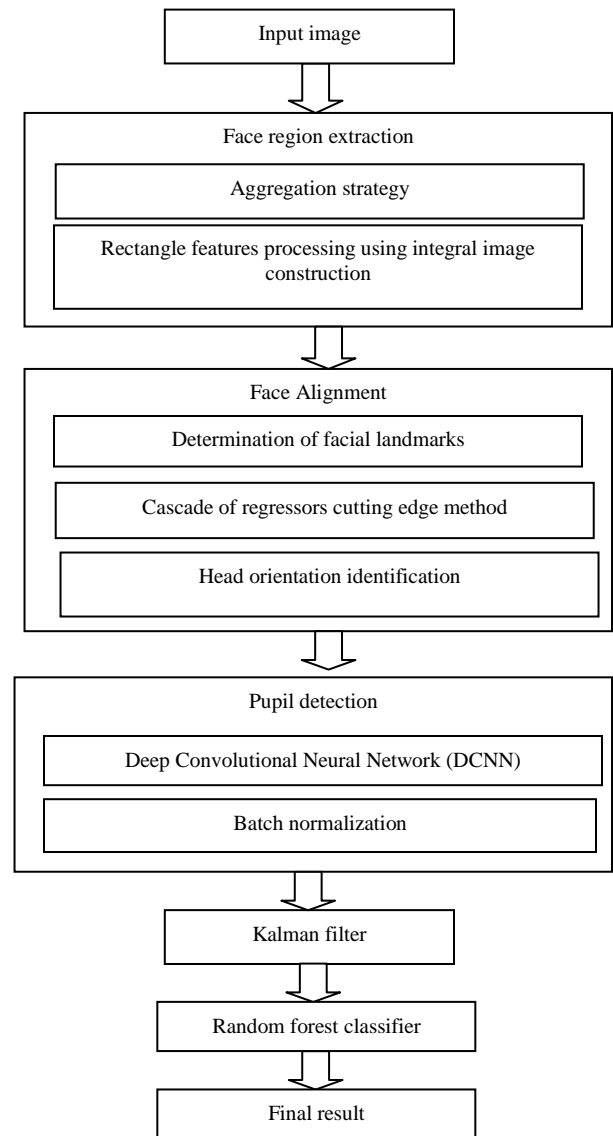


Fig. 2. Proposed Method for Drowsiness Detection.

#### B. Face Region Extraction

In this step, proposed research composed face detection into three more steps, i.e. implication of Viola-Jones algorithm for facial region extraction, aggregation strategy and integral image construction to process rectangle features. This research used Viola-Jones algorithm to extract facial region extraction due to maintain reliable frame rate for overall processing in every frame achieved in the previous step. In several frames, face region was not extracted due to some issues, i.e. light reflection, shadow. To overcome these shortcomings, frame aggregation strategy is used by this research. In frame aggregation strategy, frames without a detected face region are replaced by the previous frame. During face region extraction process, rectangle features are computed through intermediate representation in one pass over the original frames called as integral image. Thus, face region was extracted from the input frames achieved in the previous frames.

### C. Face Alignment

After face region extraction, various facial landmarks are determined from face region components, i.e. eyes, upper edge of eyebrows, upper edge of the eyebrows, inner and outer lips, jawline, and parts in and around the eye from the location and size of individual face region. In order to improve identification under highly varying lighting conditions for monocular video frames, proposed research used cascade of regressors cutting edge method. Cascade of regression was implemented as a sequence of regressors progressively refining the estimation of poses from individual frames where each regression refers an estimation of facial landmarks. In order to localize driver gaze localization as part of facial landmarks identification, two characteristics play significant role, i.e. robust to partial occlusion and self-occlusion, Running-time of cascade of regressors cutting edge method is significantly faster than 30 fps video frame rate. These two characteristics are mapped directly to gaze location using cascade of regression to compute head orientation. Extracted facial landmarks are also be mapped to a 3D model of the head. Orientation of the head is computed by the resulting 3D–2D point correspondence.

### D. Pupil Detection

Robust and accurate detection of pupil is a key for head mounted drowsiness detection after face alignment by the proposed research. Varying illumination, blurring and reflections are the main challenges for accurate pupil detection. Proposed method used deep convolutional neural network (DCNN) to obtain coordinates of the pupil center. DCNN consists of several layers which contain neurons that perform local convolutions and main variables of the model are the weights of local convolutions. Activation function such as rectified linear unit is used for DCNN network to introduce non linearity into the network in order to learn non-linear function. Proposed research used facial landmarks as the center of segmentation to be used through DCNN network. DCNN generates a mask in which pixels values provides the probability of being part of the circle centered in the pupil due to the usage of circular mask of size 25 pixels with value one was drawn in the position of pupil's center on a background of value zero. For this reason, high probability values are assigned by DCNN network to the pixels enclosed by the generated circle instead of providing pupil's coordinates directly. To overcome the challenges of varying illumination, blurring and reflections for robust pupil detection, this research used batch normalization for stabilizing distributions of internal activations during training of the model and makes model less impacted by parameter initialization. Batch normalization uses mean and variance of the mini-batch to normalize mean and variance before activation function and to estimate a moving average and variance that are used during inference.

### E. Kalman Filter

Kalman filter is used to provide the best estimation of states by using measurements from various sensors in the presence of noise. Proposed method used Kalman filters to optimally estimate variables for higher accuracy rate. After pupil detection, if there is any frame loss due to noise then

Kalman filter is used by the proposed method to process that frame by illuminating noise. Although, in the context of automotive drivers, face region does not change abruptly in consecutive frames, gaze point can be often still noise due to tiniest differences in the face location or endpoints of the fitted pupil ellipse cause deviation in the calculated gaze point. For this reason, estimation of the eye features and gaze point, fluctuate even when steadily fixating a single point which can even make the use of gaze information impractical. For this reason, gaze point is smoothed by Kalman filter to improve performance.

### F. Classification

Finally, decision for drowsiness from the extracted and filtered landmarks is performed using random forest classifier from single feature vector by generating a set of probabilities for each class. In this context, probabilities are estimated using mean predicted class probabilities of the trees in the forest where class probability of a single tree is the fraction of samples of the same class in the tree. Class with highest probability is the one that is assigned to the image as the "decision". In this context, ratio of the highest probability to the second highest probability is referred to as "confidence" of the decision. Proposed research fixed threshold of 10 based on various trials and depending on the facial landmark features with head pose movement and designated classes based on drowsiness behavior. Any decision with confidence more than threshold are accepted and others are ignored.

## IV. EXPERIMENTAL RESULTS AND DISCUSSION

### A. Hardware and Software Set up

Hardware and software set up are initial core part for validating proposed method before starting experimentation [27, 28]. Collection of datasets was done in real time during hardware set up followed by software set up. Usage the type of camera and CPU were fixed in the hardware set up stage where proposed method used monocular camera. Monocular camera has some advantages comparing with binocular and webcams. Monocular camera provides single eyepiece with good resolution during capturing frames from real time scene [29, 30]. In addition, this type of camera consists of night vision so low light issue or capturing frames during night time does not impact in the datasets used by this research. Besides, low cost and robustness of the monocular camera in lieu with reducing computational cost by using one camera instead of using multiple web cameras encourages proposed research to use monocular camera. Proposed research used Intel Core i7 8<sup>th</sup> generation to serve the purpose of processing training datasets faster. Python programming language was used during experimentation to validate the proposed method.

### B. Datasets

Proposed method was validated using iBUG 300 W dataset which consists of 300 indoor and 300 outdoor images [22]. iBUG 300 W dataset contains diverse pool of images in various perspectives, i.e. naturalistic, unconstrained face images, different variations such as pose, expression, background, occlusion, resolution, various expression such neutral, surprise, squint, smile, disgust, scream. In addition, various images related to various expressions were collected

from various sources, i.e. party, conference, protest, sport, celebrities. Besides, re-annotation was performed in iBUG 300 W datasets using semi-supervised approach to improve accuracy.

### C. Experimental Results

This research used various performance metrics, i.e. accuracy, error rate, frame rate as frame per second (fps) to validate proposed method [31, 32, 33]. Accuracy of the proposed method is calculated using (1) mentioned below:

$$K_a = \frac{k_{nt}}{k_{nt} + k_{rp}} \quad (1)$$

Here,  $k_{nt}$  denotes distance of nose tip and  $k_{rp}$  denotes distance of right pupil from their average position of the background model. Both distances are in the range of  $[0, \sqrt{2}]$  due to normalization of the features. Value of  $K_a$ , 0 indicates a shift in gaze involves only in eyes and value of  $K_a$ , 1 indicates a shift in gaze involves only head. Measurement of drowsiness for each subject is computed by averaging the result of  $K_a$ . This research categorized subjects into three groups, i.e. gaze in eye, gaze in head and mixed gaze based on the value of  $K_a$  using adaptive threshold mentioned in (2) [34, 35].

$$\theta = \psi - \frac{\psi \times (\log_2(K_a) + 1)}{100} \quad (2)$$

Here,  $K_a$  denotes total number of frames, mean value of pictorial intensities is denoted as  $\psi$  in a video frame. Threshold value is denoted as  $\theta$ .

Proposed method achieved accuracy rate of 98.97% which is higher than previous research methods. Proposed method received minimum error rate of 1.03% using frame rate of 35 fps shown in Table I.

### D. Comparison with Previous Research Results

Experimental results of the proposed method are compared with previous research results based on accuracy, error rate and frame rate shown in Table II, Table III and Table IV respectively. Research in [4] received accuracy rate of 83% using CNN-based trained Deep Learning model and used frame rate of 30 fps. In the presences of low light condition, their research could not provide satisfactory validation. Research in [5] received accuracy rate of 98.01% using Generative Adversarial Networks (GAN). However, lack of training data initiates the need of further investigation to validate their overall methodology. Research in [6] received accuracy rate of 98.7% using Principal Component Analysis (PCA) to deal with unrepresentative models. However, their research could not show expected accuracy rate when tested on more representative test dataset. Research in [7] received accuracy rate of 92% using their proposed DriCare. They used frame rate of 18 fps when environment was bright and 16 fps when environment was dark. However, they did not compare DriCare with existing research methods. Research in [24] received accuracy rate of 88.41% and 77.8% for day datasets and night datasets separately using PICO (Optimized).

However, PICO (Optimized) received error rate of 11.59%. Viola-Jones (OpenCV) based face detection methodology in the same research received accuracy rate of 78.43% for daytime dataset and 76.01% for night time datasets using 9 fps frame rate. However, higher error rate of 11.9% and 13.99% were received for day time and night time datasets respectively which are higher comparing with the proposed method by this research. Research in [36] received accuracy rate of 96.7% using 24fps frame rate by adopting face landmark. However, accuracy rate in the research fluctuates when temporal resolution was higher than 6 fps. Their research could not deal with interferences constraint which causes low performances comparing with the proposed method by this research. In addition, they used texture information which decreased average accuracy due to variations in illumination and skin colour. In this context, proposed method by this research used information, i.e. head and eye using 35 fps frame rate which causes higher accuracy than research in [36]. Research in [23] achieved accuracy rate of 95% using feature point extraction. They received error rate less than 5% by reducing computational complexity effectively. However, their method provided efficient result using 25 fps frame rate only whereas proposed method by this research has the ability to perform with 35 fps frame rate. In addition, proposed method received lower error rate of 1.03% comparing with research in [23]. Research in [22] received accuracy rate of 94.6% using 30 fps frame rate which also indicates low performance comparing with the proposed method by this research. In addition, variation in accuracy among subjects before and after adding eye pose to the classification set, research in [22] requires further investigation.

TABLE I. EXPERIMENTAL RESULTS USING PROPOSED METHOD

| Accuracy (%) | Error Rate (%) | Frame Rate (FPS) |
|--------------|----------------|------------------|
| 98.97        | 1.03           | 35               |

TABLE II. COMPARISON WITH PREVIOUS RESEARCH METHODS BASED ON ACCURACY

| Methods                                   | Accuracy   |        |
|-------------------------------------------|------------|--------|
| Proposed method                           | 98.97%     |        |
| CNN based Deep Learning model [4]         | 83%        |        |
| Generative Adversarial networks (GAN) [5] | 98.01%     |        |
| Principal Component Analysis (PCA) [6]    | 98.7%      |        |
| DriCare [7]                               | 92%        |        |
| Feature point detection [23]              | 95%        |        |
| Facial landmark location [36]             | 96.7%      |        |
| “owl” and “lizard” [22]                   | 94.6%      |        |
| PICO (Optimized) [24]                     | Day time   | 88.41% |
|                                           | Night time | 77.85% |
| Viola-Jones (OpenCV)[24]                  | Day time   | 78.43% |
|                                           | Night time | 76.01% |

TABLE III. COMPARISON WITH PREVIOUS RESEARCH METHODS BASED ON ERROR RATE

| Methods                      | Error Rate   |        |
|------------------------------|--------------|--------|
| Proposed method              | 1.03 %       |        |
| PICO (Optimized) [24]        | 11.59%       |        |
| Viola-Jones (OpenCV)[24]     | Day time     | 11.9%  |
|                              | Night time   | 13.99% |
| Feature point detection [23] | Less than 5% |        |

TABLE IV. COMPARISON WITH PREVIOUS RESEARCH METHODS BASED ON FRAME RATE

| Methods                           | Frame Rate |
|-----------------------------------|------------|
| Proposed method                   | 35 fps     |
| CNN based Deep Learning model [4] | 30 fps     |
| DriCare [7]                       | 18 fps     |
| Feature point detection [23]      | 25 fps     |
| Facial landmark location [36]     | 24 fps     |
| “owl” and “lizard” [21]           | 30 fps     |
| Viola-Jones (OpenCV)[24]          | 9 fps      |

### E. Analysis and Discussion

Although previous research attempted to achieve effective methodology for drowsiness detection, various concerns are still existed in terms with validating their methodology. Research in [4] used CNN based machine learning approach and achieved accuracy rate of 83% using 30 fps. They were able to detect facial landmarks to pass through CNN based deep learning model. However, in the presence of low light condition and obstructions due to wear glass by the subjects, their proposed methodology, could not provide expected validation results. Proposed method by this research used rich datasets where glasses or low light conditional scenario were overcome indicating by higher accuracy rate of 98.97% with higher frame rate of 35 fps than research in [4] shown in Fig. 3. Research in [5] used Generative Adversarial Networks (GAN) and introduced a sampling strategy to identify individuals with facial features where the network was failing. Although, they achieved accuracy rate of 98.01%, due to lack of population groups during validation, their methodology demands for further investigation to improve performance. In this context, research in [6] achieved accuracy rate of 98.7% by using Principal Component Analysis (PCA) where similarity based sorting was done by producing a grid of faces and combining these with a model accuracy overlay. However, Principal Component Analysis (PCA) method is mostly known as dimension reduction method which mainly depends of efficient extraction of features [13, 25]. In addition, in their research, accuracy decreased substantially when their proposed approach was validated using more representative test set. Accuracy of the proposed method by this research was not decreased during any stage of experimentation due to the usage of geometric structure identification of human face in lieu with that proposed method received lower error rate comparing with previous research results. Research in [7] proposed DriCare to estimate different

criteria about the degree of the driver’s drowsiness, i.e. blinking frequency, duration of eyes closure. They achieved accuracy rate of 92% using two different frame rates, i.e.18fps when the environment was bright, 16 fps when the environment was dark. In both context of accuracy rate and frame rate, proposed method achieved higher accuracy rate of 98.97% using higher frame rate of 35 fps. Research in [23] assessed effects of facial sub regions to estimate accuracy where they combined eye and mouth areas and caused accuracy rate of 95% in lieu with error rate of less than 5% using 25 fps shown in Fig. 4 and Fig. 5. They used facial texture and landmarks extracted from image sequences and fused these features to enhance the performance causes higher error rate than proposed method by this research. In this context, proposed method used pupil and head position to detect drowsiness causes better accuracy rate in lieu with frame rate of 35 fps using 1.03% error rate which are better than research in [23].

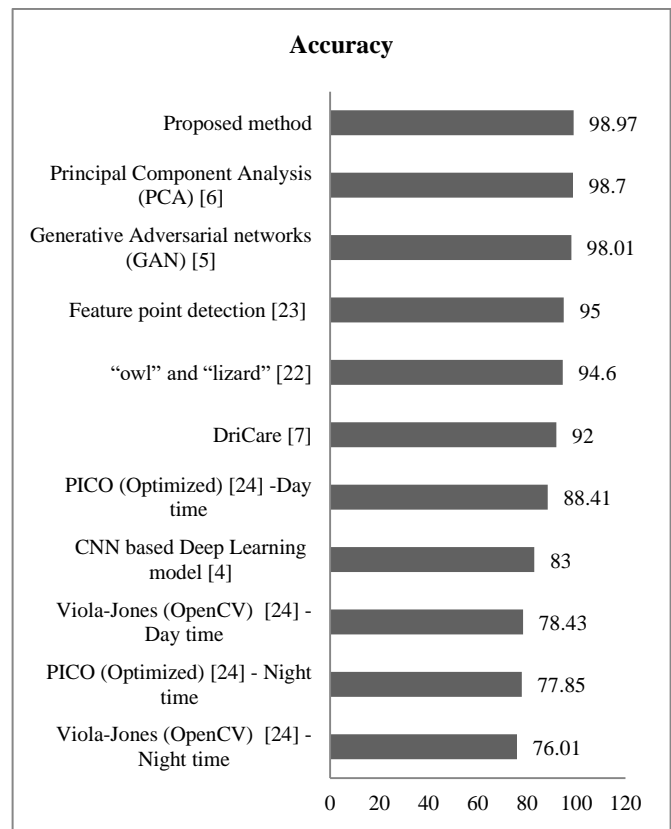


Fig. 3. Comparison among Proposed Method and Previous Research based on Accuracy.

Research in [22] required a face and pupil under classification schemes where they observed variation in accuracy among subjects before and after adding eye pose to the classification set. Although they received accuracy rate of 94.6% using 30 fps frame rate, their accuracy rate is not reliable enough due to the variation in accuracy which drops to below 80% and even to as low as 40%.In this context, proposed research used pupil and head position detection to detect drowsiness using 35 fps with higher accuracy rate of 98.97% than research in [22]. Research in [24], absolute deviations are mainly caused by the rigid face model, which

has geometry error for different subjects, and cannot update its shape like the flexible model or adaptive model. For this reason, research in [24] received higher error rate comparing with the proposed method by this research. In this context, proposed method detects facial regions of a driver when an image sequence is captured in lieu with applying Viola-Jones algorithm for facial region extraction. Proposed method used Viola-Jones algorithm for facial region extraction with higher frame rate processing perspectives which causes lower error rate at the same time.

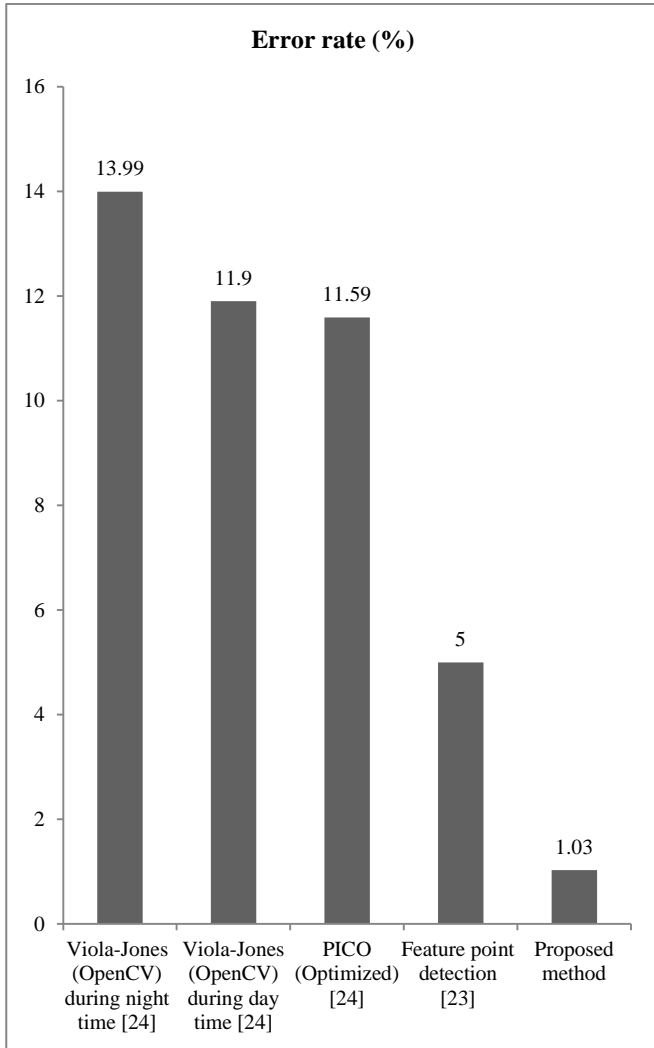


Fig. 4. Comparison among Proposed Method and Previous Research based on Error Rate.

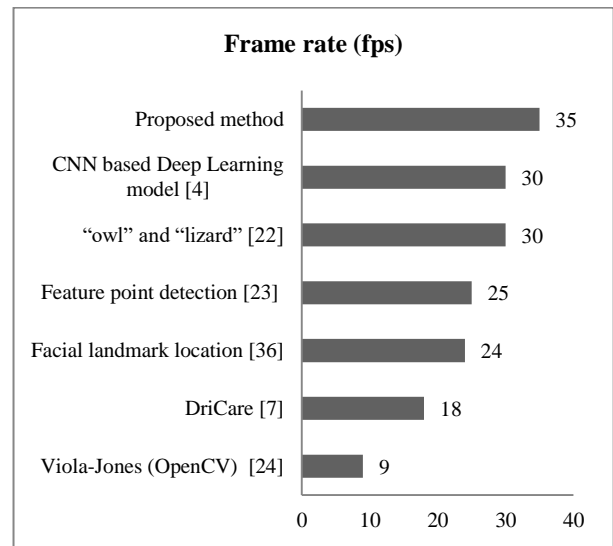


Fig. 5. Comparison among Proposed Method and Previous Research based on Frame Rate.

## V. CONCLUSION

Proposed method detects driver drowsiness by extracting facial features initially and then performs face alignment following by pupil detection and classification by random forest classifier. During facial features extractions proposed method used aggregation strategy and integral image construction to process rectangle features in case face region cannot be extracted due to some issues, i.e. light reflection, shadow in input frames. In face alignment phase, proposed method used cascade of regressors cutting edge method in order to improve identification of facial landmarks under highly varying lighting conditions for video frames. Later, in pupil detection step, proposed research used deep convolutional neural network (DCNN) for accurate pupil detection for nonlinear data pattern where proposed method used facial landmarks as the center of segmentation to be used through DCNN network. Although, in the context of automotive drivers, face region does not change abruptly in consecutive frames, gaze point is smoothed by Kalman filter to remove noise due to tiniest differences in the face location or endpoints of the fitted pupil ellipse cause deviation in the calculated gaze point and thus improve performance. In this context, appropriate features selection during facial features extraction in lieu with computational time measurement to compare with previous research is intended to investigate in future. Experimental results for the proposed method reveal higher efficiency comparing with previous research results in terms with accuracy rate, error rate and frame rate. Proposed method achieved accuracy rate of 98.97% with error rate of 1.03% using frame rate of 35 fps. Performance of the proposed method reveals the potentiality to impact significantly to reduce road accidents.



#### ACKNOWLEDGMENT

The authors would like to thank Universiti Kebangsaan Malaysia for providing financial support under the “Geran Universiti Penyelidikan” research grant, GUP-2020-064.

#### REFERENCES

- [1] Z. Guo, Y. Pan, G. Zhao, S. Cao, and J. Zhang, "Detection of driver vigilance level using EEG signals and driving contexts," *IEEE Transactions on Reliability*, vol. 67, pp. 370-380, 2017.
- [2] Z. Zhang, D. Luo, Y. Rasim, Y. Li, G. Meng, J. Xu, and C. Wang, "A vehicle active safety model: Vehicle speed control based on driver vigilance detection using wearable EEG and sparse representation," *Sensors*, vol. 16, p. 242, 2016.
- [3] Y. Liang, W. J. Horrey, M. E. Howard, M. L. Lee, C. Anderson, M. S. Shreeve, C. S. O'Brien, and C. A. Czeisler, "Prediction of drowsiness events in night shift workers during morning driving," *Accident Analysis & Prevention*, vol. 126, pp. 105-114, 2019.
- [4] R. Jabbar, M. Shinoy, M. Kharbeche, K. Al-Khalifa, M. Krichen, and K. Barkaoui, "Driver drowsiness detection model using convolutional neural networks techniques for android application," in *2020 IEEE International Conference on Informatics, IoT, and Enabling Technologies (ICIoT)*, 2020, pp. 237-242.
- [5] M. Ngxande, J.-R. Tapamo, and M. Burke, "Bias Remediation in Driver Drowsiness Detection Systems Using Generative Adversarial Networks," *IEEE Access*, vol. 8, pp. 55592-55601, 2020.
- [6] M. Ngxande, J.-R. Tapamo, and M. Burke, "Detecting inter-sectional accuracy differences in driver drowsiness detection algorithms," in *2020 International SAUPEC/RobMech/PRASA Conference*, 2020, pp. 1-6.
- [7] W. Deng and R. Wu, "Real-time driver-drowsiness detection system using facial features," *IEEE Access*, vol. 7, pp. 118727-118738, 2019.
- [8] C. J. de Naurois, C. Bourdin, A. Stratulat, E. Diaz, and J.-L. Vercher, "Detection and prediction of driver drowsiness using artificial neural network models," *Accident Analysis & Prevention*, vol. 126, pp. 95-104, 2019.
- [9] L. Chukoskie, S. Guo, E. Ho, Y. Zheng, Q. Chen, V. Meng, J. Cao, N. Devgan, S. Wu, and P. C. Cosman, "Quantifying gaze behavior during real-world interactions using automated object, face, and fixation detection," *IEEE Transactions on Cognitive and Developmental Systems*, vol. 10, pp. 1143-1152, 2018.
- [10] Z. R. Mahayuddin and A. F. M. S. Saif, "A Comprehensive Review Towards Segmentation and Detection of Cancer Cell and Tumor for Dynamic 3D Reconstruction," *Asia-Pacific Journal of Information Technology and Multimedia*, vol. 9, pp. 28-39, 2020.
- [11] Z. R. Mahayuddin and A. S. Saif, "A Comprehensive Review Towards Appropriate Feature Selection for Moving Object Detection Using Aerial Images," in *International Visual Informatics Conference*, 2019, pp. 227-236.
- [12] Z. R. Mahayuddin and A. S. Saif, "A Comparative Study of Three Corner Feature based Moving Object Detection Using Aerial Images," *Malaysian Journal of Computer Science*, pp. 25-33, 2019.
- [13] A. S. Saif, A. S. Prabuwo, and Z. R. Mahayuddin, "Moment feature based fast feature extraction algorithm for moving object detection using aerial images," *PloS one*, vol. 10, p. e0126212, 2015.
- [14] M. H. Alkinani, W. Z. Khan, and Q. Arshad, "Detecting Human Driver Inattentive and Aggressive Driving Behavior Using Deep Learning: Recent Advances, Requirements and Open Challenges," *IEEE Access*, vol. 8, pp. 105008-105030, 2020.
- [15] M. Dua, R. Singla, S. Raj, and A. Jangra, "Deep CNN models-based ensemble approach to driver drowsiness detection," *Neural Computing and Applications*, pp. 1-14, 2020.
- [16] T. Wilaiprasitporn and T. Yagi, "Feasibility study of drowsiness detection using hybrid brain-computer interface," in *Proceedings of the international Convention on Rehabilitation Engineering & Assistive Technology*, 2016, pp. 1-4.
- [17] B.-L. Lee, B.-G. Lee, and W.-Y. Chung, "Standalone wearable driver drowsiness detection system in a smartwatch," *IEEE Sensors Journal*, vol. 16, pp. 5444-5451, 2016.
- [18] C. B. S. Maior, M. J. das Chagas Moura, J. M. M. Santana, and I. D. Lins, "Real-time Classification for Autonomous Drowsiness Detection Using Eye Aspect Ratio," *Expert Systems with Applications*, p. 113505, 2020.
- [19] X. Zhang, X. Wang, X. Yang, C. Xu, X. Zhu, and J. Wei, "Driver drowsiness detection using mixed-effect ordered logit model considering time cumulative effect," *Analytic methods in accident research*, vol. 26, p. 100114, 2020.
- [20] T. Kundinger, A. Rieger, N. Sofra, and K. Weigl, "Driver drowsiness in automated and manual driving: insights from a test track study," in *Proceedings of the 25th International Conference on Intelligent User Interfaces*, 2020, pp. 369-379.
- [21] K. Mahajan and N. R. Velaga, "Effects of partial sleep deprivation on braking response of drivers in hazard scenarios," *Accident Analysis & Prevention*, vol. 142, p. 105545, 2020.
- [22] L. Fridman, J. Lee, B. Reimer, and T. Victor, "'Owl' and 'Lizard': Patterns of head pose and eye pose in driver gaze classification," *IET Computer Vision*, vol. 10, pp. 308-314, 2016.
- [23] C. Meng and X. Zhao, "Webcam-based eye movement analysis using CNN," *IEEE Access*, vol. 5, pp. 19581-19587, 2017.
- [24] C. Yin and X. Yang, "Real-time head pose estimation for driver assistance system using low-cost on-board computer," in *Proceedings of the 15th ACM SIGGRAPH Conference on Virtual-Reality Continuum and Its Applications in Industry-Volume 1*, 2016, pp. 43-46.
- [25] Z. R. Mahayuddin and A. F. M. S. Saif, "Efficient Hand Gesture Recognition Using Modified Extrusion Method based on Augmented Reality," *TEST Engineering and Management*, vol. 83, pp. 4020-4027, 2020.
- [26] Z. R. Mahayuddin and A. F. M. S. Saif, "Augmented Reality based Ar Alphabets Towards Improved Learning Process in Primary Education System," *Journal of Critical Reviews*, vol. 7, 2020.
- [27] Z. R. Mahayuddin, A. S. Saif, and A. S. Prabuwo, "Efficiency measurement of various denoise techniques for moving object detection using aerial images," in *2015 International Conference on Electrical Engineering and Informatics (ICEEI)*, 2015, pp. 161-165.
- [28] A. Saif and Z. R. Mahayuddin, "Moving Object Segmentation Using Various Features from Aerial Images: A Review," *Advanced Science Letters*, vol. 24, pp. 961-965, 2018.
- [29] A. Saif, A. Prabuwo, and Z. Mahayuddin, "Adaptive long term motion pattern analysis for moving object detection using UAV aerial images," *International Journal of Information System and Engineering*, vol. 1, pp. 50-59, 2013.
- [30] A. Saif, A. S. Prabuwo, and Z. R. Mahayuddin, "Moving object detection using dynamic motion modelling from UAV aerial images," *The Scientific World Journal*, vol. 2014, 2014.
- [31] A. S. Saif, A. S. Prabuwo, and Z. R. Mahayuddin, "Adaptive motion pattern analysis for machine vision based moving detection from UAV aerial images," in *International Visual Informatics Conference*, 2013, pp. 104-114.
- [32] A. S. Saif, A. S. Prabuwo, and Z. R. Mahayuddin, "Real time vision based object detection from UAV aerial images: a conceptual framework," in *FIRA RoboWorld Congress*, 2013, pp. 265-274.
- [33] A. S. Saif, A. S. Prabuwo, and Z. R. Mahayuddin, "Motion analysis for moving object detection from UAV aerial images: A review," in *2014 International Conference on Informatics, Electronics & Vision (ICIEV)*, 2014, pp. 1-6.
- [34] A. S. Saif, A. S. Prabuwo, Z. R. Mahayuddin, and T. Mantoro, "Vision-based human face recognition using extended principal component analysis," *International Journal of Mobile Computing and Multimedia Communications (IJMCMC)*, vol. 5, pp. 82-94, 2013.
- [35] A. S. Saif, A. S. Prabuwo, Z. R. Mahayuddin, and H. T. Himawan, "A review of machine vision based on moving objects: object detection from UAV aerial images," *International Journal of Advancements in Computing Technology*, vol. 5, p. 57, 2013.
- [36] L. Zhao, Z. Wang, X. Wang, and Q. Liu, "Driver drowsiness detection using facial dynamic fusion information and a DBN," *IET Intelligent Transport Systems*, vol. 12, pp. 127-133, 2017.

# Towards a Multi-Agent based Network Intrusion Detection System for a Fleet of Drones

Said OUIAZZANE<sup>1</sup>, Fatimazahra BARRAMOU<sup>2</sup>, Malika ADDOU<sup>3</sup>  
ASYR Team - LaGeS Laboratory, Hassania School of Public Works  
Casablanca, Morocco

**Abstract**—The objective of this research work is to propose a new model of intrusion detection system for a fleet of UAVs deployed with an ad hoc communication architecture. The security of a drone fleet is rarely addressed by the scientific community, and most research has focused on routing protocols and battery autonomy, while ignoring the security aspect. The multi-agent paradigm is considered the most adequate and appropriate solution to model an effective intrusion detection system capable of detecting intrusions targeting a drone fleet. Multi-agent systems can perfectly address the security problem of a drone fleet, given the mobility, autonomy, cooperation and distribution characteristics present in the network linking the different nodes of the fleet. The proposed model consists of a set of cooperative, autonomous, communicating, learning and intelligent agents that collaborate with each other to carry out intrusion and suspicious activity detection missions that can target the network of a fleet of drones. Our system is autonomous and can detect known and unknown cyber attacks in real time without the need for human experts, who generally design the signatures of known attacks for conventional intrusion detection systems.

**Keywords**—Fleet of drones; drone; intrusion detection; multi agent system; security; intrusion detection system; autonomy; distribution; UAV; unmanned aerial vehicle; unknown attacks; known attacks

## I. INTRODUCTION

Drones play a major role in the everyday life of individuals, given their extensive use in several areas of expertise, and will now be the trend worldwide. According to a study conducted on the prospects for European UAV (Unmanned Aerial Vehicle), the UAV market will be the trend in the coming years in various fields: agriculture, energy, public safety, e-commerce/delivery and mobility and transport [1]. The author in [2] highlights some applications of drones as illustrated by Fig. 1. As shown in the table (Fig. 1), UAVs are generally used respectively in the military sector, in the professional civilian sector and for leisure activities. In our work, we will focus mainly on the use of drones in the civilian professional field, given the important use of drones to solve human problems.

Drones have limited resources in terms of battery life and the geographical area they can cover. As a result, a single drone cannot perform all the missions it is assigned, especially when it has to cover a large geographic area. To overcome these limitations, a fleet of drones [3] is needed, which consists of connecting several drones via a network, so that

they can cooperate and collaborate with each other to accomplish more complex tasks.

In spite of the important research carried out in the scientific community on drones, the problem of security of UAV networks is still an issue, as these networks have not yet received much attention from researchers [4]. Moreover, the only security system implemented on UAVs is the Anti-collision system, which is insufficient to ensure the security of the drone against cybercrime [5]. Therefore, security issues need to be addressed and should be a major concern given the criticality of the information that transits in the network and which may be subject to various attacks.

The security issue is necessary for several reasons:

- Firstly, because the architecture of the Mobile Adhoc Network is generally vulnerable to various attacks due to the lack of a central entity monitoring the activities in the network.
- Secondly, this is due to the routing protocols used in an ad hoc network, which involve all nodes in the network in the routing operations without thinking about the presence of malicious nodes that can falsify the paths taken by the packets.
- Thirdly, because we can't distinguish between a malicious action undertaken by an attacker and another caused by the loss of linkage due to the mobility of the drones.

Fourthly and finally, we must take into consideration the problem of the drones's limited resources in terms of memory, bandwidth and energy.

| SECTOR                       | EXAMPLES OF APPLICATIONS                                        | ROLES                                                                                                            |
|------------------------------|-----------------------------------------------------------------|------------------------------------------------------------------------------------------------------------------|
| Law enforcement surveillance | Search and rescue                                               | Drone are equipped with cameras                                                                                  |
| Public safety communications | Voice communications in case of disaster                        | Aerial base stations                                                                                             |
| Environmental applications   | Climate change                                                  | Information gathering via sensors                                                                                |
| Logistics                    | Goods shipping and delivery in urban areas                      | Drones are used as a transportation medium                                                                       |
| Military                     | Searches for lost or injured soldiers                           | Drones use live streaming communications to send videos to ground troops, they can also be equipped with weapons |
| Medical field                | Delivering aid packages, medicines and vaccines to remote zones | Drones are used as a transportation medium                                                                       |
| Photography                  | Events such as social gatherings, sport games and competitions  | Drones are used to capture videos by using cameras                                                               |
| Agriculture                  | Crop monitoring and soil and field analysis                     | Sensors can be placed on drones to capture the information required by the agriculture field                     |

Fig. 1. Summary Table of the Fields of Application of UAVs [1] [2].

In light of these observations, it is necessary to ensure the security of a UAV network to detect intrusions that could affect the security principles summarized by the CIA triad (Confidentiality, Integrity and Authentication).

The flow of applications through the UAV network is of acritical importance not only for the mission requirement, but also for civilians (the critical risk would be, for example, the hijacking of a drone). The application flow is very sensitive and must be protected against illegitimate access that could corrupt the viability of the drone system [6].

A UAV network is a spontaneous environment that raises several security issues. First of all, the use of wireless links which are intrinsically vulnerable to eavesdropping attacks or denial of service. Secondly, because of the absence of message and node authentication services, knowing that it is possible to inject forged packets into the network to disrupt the proper functioning of the routing algorithm. This kind of attacks can corrupt the communication or decrease the network performance [7].

The rest of the document is organized as follows: Section 2 highlights the context of the study to define some concepts related to our work. Section 3 highlights the state of the art of the multi-agent paradigm and its use for handling complex problems. Section 4 discusses the proposed architecture of IDS, its components and its operating principle. Section 5 concludes the paper.

## II. RELATED WORK

In this section, we will highlight some of the concepts related to our research work. First, we're going to talk about drones, a fleet of drones, and the different communication architectures of a fleet of drones. Next, we'll look at the security aspects of a UAV network, while identifying the various vulnerabilities and attacks to which the UAVs in the fleet are exposed. Finally, we will close this part by defining the multi-agent paradigm, while citing the different types of agents that exist and that can deal with the security issue in a UAV network.

### A. Drone Definition

A drone is an unmanned aircraft with no pilot on board, remotely controlled by a ground station. It can fly autonomously according to a programmed flight plan or by controlling it via a smartphone or tablet connected to its network [8].

Examples of the use drones for different purposes are numerous in the literature. Notably, in [9] the author proposes to use a drone to capture multispectral images and to detect the difference in terrain in the field of agriculture. In [10], the authors propose to use drones to carry an X-ray camera, an IR camera and metal detectors. For e-commerce and delivery, applications are still in their early stages given the strong impact of weight on battery life and therefore on the distance to be travelled by the drone, knowing that the delivery of small objects is already a reality. In [11], a service for transporting small medicines and blood in Africa using a winged drone is proposed. For e-commerce, several proposals

have been made by large technology companies, namely Amazon's Prime Air service [12].

### B. Fleet of Drones

A UAV fleet consists of several drones that cooperate and collaborate with each other to accomplish more complex tasks [3]. In a UAV fleet, each drone executes its task to participate in achieving the mission objective for which the fleet is created. A UAV fleet can be designed according to three possible communication architectures: the centralized communication architecture, the cellular communication architecture, the satellite communication architecture and the adhoc communication architecture.

### C. Possible Communication Architectures of a UAV Fleet

1) *Centralized communication architecture*: A centralized UAV fleet communication architecture [13] is characterized by a direct wireless link between a centralized node (e.g. ground station) and the surrounding drones (Fig. 2). In this architecture, each drone is directly connected to the ground station to transmit payload data and to receive the command and control flow. UAVs are not directly connected to each other and the information can be sent between neighboring UAVs via the ground station. In this case, the ground station acts as a relay node.

2) *Cellular communication architecture*: This type of communication architecture is used in the field of telephony and is based on a base station infrastructure. Cells are deployed according to the density of the network sought and the geographical perimeter to be covered. Each cell includes a subset of UAVs and a ground station that manages the group [13] and communication between the members of a group must pass through the ground station (Fig. 3). Direct communication between UAVs belonging to the same cell can take place. This architecture is expensive and requires much more investment for its proper deployment.

3) *Satellite communication architecture*: Another communication architecture can be envisaged and it is based on the deployment of a satellite to make the different UAVs communicate with each other. In this architecture (Figure 4), the satellite plays the role of a communication relay [13]. The satellite's receiving antennas receive signals from the ground station; these signals undergo amplification and frequency conversion operations before they are retransmitted to the drones. However, this architecture requires the presence of a central entity which is the satellite to ensure routing between the control station and the drones. Given the real-time nature of the application traffic exchanged between the nodes of a fleet of UAVs, this could lead to significant latencies in exchanges between the nodes. In addition, in the presence of obstacles around the ground station (a building, for example), communication to the satellite can be partially attenuated or completely blocked.

4) *Adhoc communication architecture*: A wireless adhoc network consists of connecting several mobile drones equipped with one or more radio interfaces to weave a short-duration communication network to achieve the fleet's mission

objective [41]. The drones belonging to this network can enter or exit the network at any time. The adhoc communication architecture (Fig. 5) is decentralized and capable of self-organizing without the need for a fixed infrastructure. If a transmitting UAV, for example, is located outside the perimeter of coverage of the receiving UAV, the application flow is transmitted step by step to the destination point and the routing table is kept up to date by the network in case of a change in the network topology. The adhoc network enables two nodes that are out of direct reach of each other to communicate. [3].

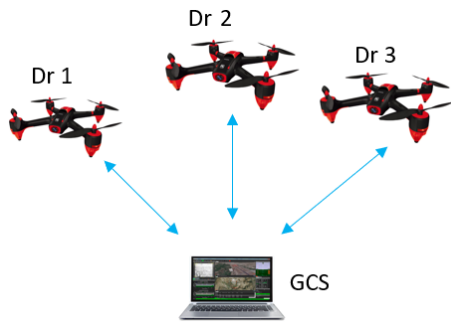


Fig. 2. Centralized Communication Architecture [13].

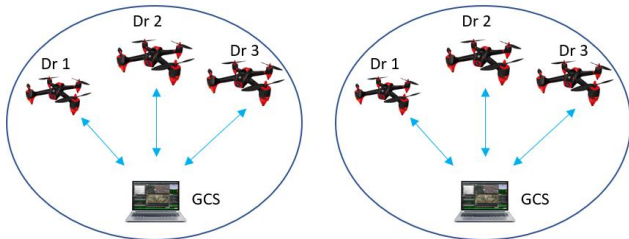


Fig. 3. Cellular Communication Architecture [13] [3].



Fig. 4. Satellite Communication Architecture [3].

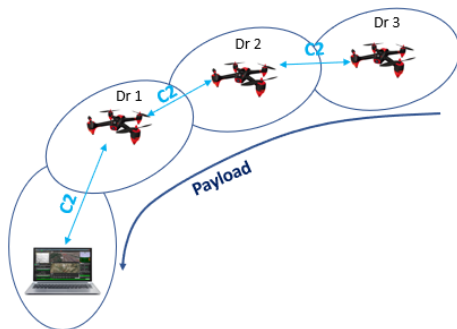


Fig. 5. Adhoc Communication Architecture [3].

#### D. Security in an Adhoc Network

The use of drones is becoming widespread, and that what is motivating Hackers to learn much more about drone vulnerabilities in order to exploit them and thus touch on the security principles summarized in the CIA triad (Confidentiality, Integrity and Availability). Consequently, it is imperative to ensure network security against cyber attacks to protect application flows and sensitive network data.

1) *Vulnerabilities in an adhoc network:* The adhoc mobile network architecture is generally vulnerable to various attacks due to the lack of a central entity monitoring the activities in the network. In addition, the routing protocols in an Adhoc network involve all nodes of the network in the routing operations and assume the absence of malicious nodes that can falsify the paths taken by packets [3].

UAV vulnerabilities can be related to the physical architecture of the nodes [14], to the different communication links, to the condition of the UAV fleet deployment (the need for cooperation between nodes) and to the possibility of malicious nodes presence in the network [15]. Radio links are often equipped with very low bandwidth and this is exactly what an attacker can exploit by saturating the network via packet broadcasting and thus succeeding in breaking the communication between the drones in the network [16].

The environment of an adhoc wireless network is uncontrolled due to its distribution and dynamic characteristics. That is, communication is shared and opportunistic between the nodes participating in the routing operations. As a result, it is very difficult to control the entry and exit of nodes into and out of the network. As a result, a malicious node could connect to the network and thus participate in the transfer of packets. It can also use the identity of a legitimate node (Identity Theft) to tamper with the routing mechanism while broadcasting incorrect information or replaying outdated information. This is notably the case of the rushing attack [17].

Drones can move at a very high speed (for example, DT18 type UAVs can reach a speed of 80 km/h), what leads to a continuous change of the network topology according to the commands issued by the ground station or those imposed by the UAV flight plan. The mobility of drones poses a security problem since a routing protocol cannot distinguish between a communication failure caused by UAV movements and an attacker trying to interrupt communications in the network [18].

An adhoc network works with the assumption that all nodes are cooperative and non-malicious in nature and the assumption that a malicious node can connect to the network is not taken into account. In this case, the authenticity of the identity of the nodes is not guaranteed since the possibility of the existence of malicious nodes is always present and they can publish routes with better metrics and thus participate in the routing operations.

Drones are very limited in terms of CPU and RAM capacities. In this case, the limited resources can be exhausted by the attackers while applying, for example, sleep deprivation

attacks [19] whose principle is the unlimited distribution of control messages to the network nodes. As a result, once these resources are exhausted, drones can be, for example, captured or hijacked by an attacker.

2) *Attacks in an adhoc network:* A fleet of drones relies on the wireless network to send and receive signals between nodes. The wireless network in turn relies on radio links that can be targeted by various attacks, namely eavesdropping and active interference [20].

The presence of an attacker using a high-gain antenna within range of a UAV can present a significant risk of eavesdropping on the entire network that supports the communication of the UAV fleet.

Ad hoc networks are generally targeted by different types of attacks, and drones are a new target for hackers given the importance of the application flows they carry. For example, the Eavesdropping on an adhoc network consists of placing a malicious node between two or more communicating nodes. Attackers can also explore the vulnerabilities of drone systems which can be the result of misconfiguration of UAV networks, a fault implementation, flawed designs and/ or protocols [21]. To listen to the whole network, the attacker can act on the routing protocols while trying to generate false packets or modify the routing packets.

The presence of an attacker using a high-gain antenna within range of a UAV can present a significant risk of illicit eavesdropping on the entire network constituting the communication medium of the UAV fleet.

Fig. 6 and 7 highlight possible attacks on an ad hoc network of UAVs. These intrusions can target both layers of the OSI model, the physical layer and the network layer. For example, attacks aimed at exploiting the physical layer can attack the wireless modem in use. Such attacks do not require any prior knowledge of the network topology. These attacks can take the form of eavesdropping on application flows, active interference to overlap transmission channels or jamming attacks.

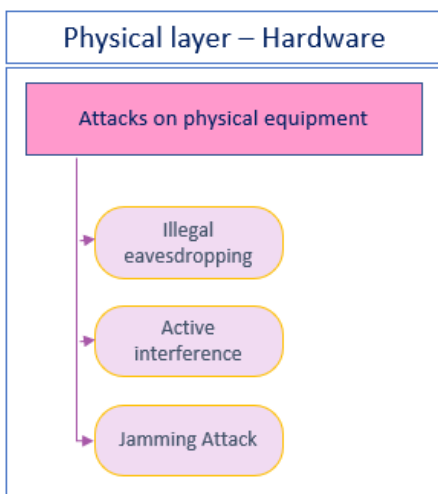


Fig. 6. Attacks Targeting the Physical Layer of a UAV [20].

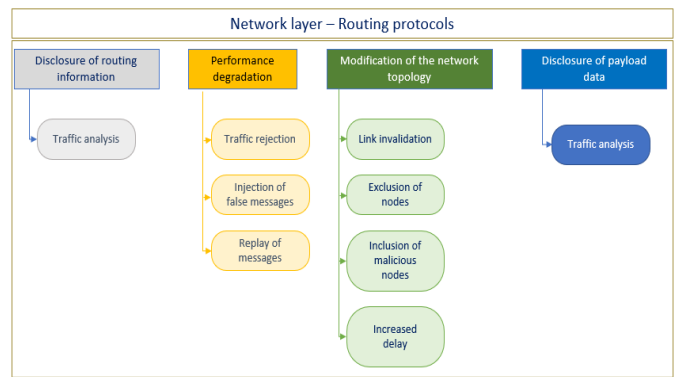


Fig. 7. Attacks that can Target the Network Layer [21][22].

Attacks aimed at attacking the network layer generally consist of disclosing routing information through traffic analysis, degrading network performance through traffic rejection, injecting false messages and replaying messages, and modifying the network topology while invalidating links, including or excluding malicious nodes, and increasing the delay of exchanges. And finally, these attacks can disclose payload data through sniffing and network traffic analysis.

### E. Multi-Agent Paradigm (MAS)

1) *Agent:* According to [23], an agent is a physical or virtual entity that has the following characteristics:

- It must be able to act in its environment,
- It can communicate and interact with other agents,
- It seeks to achieve and optimize its individual goals, satisfactions and survival,
- It has its own resources,
- It is able to perceive its environment in a limited way,
- It has only a partial representation of this environment (Or any),
- It has skills to offer services,
- It is capable of reproducing itself when needed,
- It behaves in such a way that it satisfies its objectives within the limits of its resources and skills and this, according to its perception, its representations and the communications it receives from other entities in the system.

In the field of computer science, an agent is any computer program that has some or all of these characteristics [24][25]:

- It is capable of perceiving the environment to which it belongs in order to act appropriately.
- An agent is independent, i.e. it can act alone without human intervention (or by other agents).
- An agent is flexible, i.e. it can react quickly to changes in its environment and always tries to take advantage of opportunities to achieve its goals.

According to the Multi-agent paradigm, There are four main types of agents [23] [24] [26] [25]:

- Reactive agent that responds to changes in its environment while acting appropriately to accomplish its missions.
- Deliberative agent which can conduct deliberations to accomplish its missions and thus achieve its objectives.
- Hybrid agent that performs both the tasks of a reactive agent and those of a deliberative agent.
- A learning agent which is able to learn through the perception of its environment in order to improve its ability to act in the future without any human intervention or by other agents.

2) *Multi-Agent system*: A Multi-Agent system can be defined as a set of autonomous entities that interact in a given environment to achieve objectives and deal with very different problems [27]. Multiagent Systems mainly aim to achieve the following objectives:

- Multi-agent systems aim to carry out their missions according to the phenomena and problems to be dealt with. There are different types of MAS that are:
  - Cooperative SMA (MAS) where each agent sets its own objective. The agents in this SMA trust each other and can make decisions together to achieve their common goal.
  - Competitive SMA: Each agent in this type of system sets its own objective relying on simulation by agents to reproduce a phenomenon external to the system.

### III. STATE OF THE ART

#### A. UAV Security and Multiagent Paradigm

1) *UAV security*: The security of UAV networks has not yet received much attention from researchers. Most of the research conducted by the scientific community has focused on routing protocols and optimizing UAV autonomy, while ignoring the security aspect, which has been of major importance lately and is now attracting the attention of manufacturers.

Several research projects have dealt with the safety aspect of UAV systems. Notably, in [28], the author carried out an audit of the behavior and vulnerability of UAVs used in the IoT as an intermediate communication medium. In [29], the authors proposed to use the Blockchain technology to transmit signals between the controller and the UAV. The author of [30] gave a secure routing protocol for UAV Ad hoc NETWORKS (UAANETS). In [4], a rule-based IDS is proposed to detect GPS Spoofing, Jamming and False information attacks. In [31], the focus was on the security of the physical layer to counter jamming, eavesdropping and spoofing attacks that can target UAV systems. The author in [32] proposed an IDS for the UAV using behavior rule specifications knowing

that most existing IDS for UAV use behavior based detection mechanisms [33].

From the above literature survey, we can identify that a simple framework based IDS is only designed for UAV against different types of attacks with major limitations.

2) *Multiagent paradigm for computer security*: The MAS (Multi-Agent System) paradigm is widely used by researchers to address complex problems that are difficult or impossible to address with traditional methods. Agent technology is already used to address the security aspect in traditional information systems. For example, in [34], the author considers the network as a set of nodes and opts for a multi-agent system as a solution to detect suspicious activities at the level of all nodes. The author in [35] highlights a hybrid intrusion detection system called MOVICAB IDS which is based on artificial neural networks and multi-agent architecture. In [36], a distributed intrusion detection system architecture is proposed and it is based on mobile agents allowing decision making and agent replication. The author of [37] gave a model of a PAID intrusion detection system using multi-agent technology. The proposed model is based on several agents capable of sharing their beliefs (Soft findings) and measuring values (Hard findings). This model allows to analyze the information contained in the system and to estimate the probability of intrusion according to its agents.

In [38], a framework named SPIDER is proposed, based on a set of autonomous agents with heterogeneous processing models. The author of [39] proposed the IA-NSM (Intelligent Agents for Network Security Management) system to detect intrusions by relying on intelligent agent technology. This architecture is hierarchical and is based on a set of agents that communicate and cooperate with each other in order to perform intrusion detection missions efficiently and with optimal processing performance. The author in [40] develops an approach for network intrusion detection based on multi-agent systems and the artificial immune system (AIS). The AIS system is based on autonomous, mobile, collaborative, adaptive and learning agents. The MAIS-IDS (Multi-agent Artificial Immune System - Intrusion Detection System) is a hybrid IDS by anomaly detection that is capable of analyzing system configurations to detect activities that may be real intrusions that threaten the security of the system.

#### B. Discussion

Based on the study of the state of the art conducted to better understand what is done in the literature regarding the security of drones. The security of a UAV fleet is rarely addressed, despite the fact that these fleets represent the future trend in the use of UAVs for civilian missions. Most of the work cited in the state of the art has focused on routing protocols, autonomy optimization, communication architectures... while ignoring the security aspect, which is receiving much more attention given the disastrous damage that can occur if the security principles of a UAV fleet are circumvented.

Research work in the field of the adhoc UAV network generally focuses on improving on-board ground communication between a drone and a ground station and optimizing inter-drone communication, and does not address the safety aspect of UAVs. The scientific community is opting for multi-agent systems to deal with complex problems affecting different fields. This technology is very effective in simplifying the most complex problems. The network of a fleet of UAVs is in turn very complicated due to the continuous modification of the network topology and the increased speed of the UAVs. As a result, dealing with the safety of an UAV fleet is a very difficult mission to accomplish.

The computer security of a UAV fleet based on an adhoc communication architecture is very complex to address due to the continuous change in the network topology and the rapid mobility of the nodes. In this case, opting for the multi-agent paradigm proves to be the most appropriate solution to address the security gaps in an adhoc UAV network.

In our work, we will propose a more efficient intrusion detection architecture allowing to detect intrusions in an adhoc UAV network in real time without any network latency or depletion of limited UAV resources (CPU, RAM, Storage...).

#### IV. PROPOSED APPROACH

##### A. General View

In a fleet of UAVs, all the nodes communicate with each other and generate very sensitive application flows. These flows include very critical information, which can be routing information, payload traffic (images, videos, sounds, etc.), control and command traffic (C2), GPS coordinates, etc. It is therefore necessary to secure these application flows against malicious persons who can exploit the vulnerabilities of the wireless ad hoc networks to impact the smooth operation of the UAV fleet.

Fig. 8 gives a brief description of the ad hoc communication most used in the deployment of UAV fleets. Indeed, the ad hoc network is a sub-category of the Manet mobile networks. This mode of communication consists of connecting a set of cooperative mini drones that have an enormous mobility speed. In an ad hoc UAV fleet network, we find exchanges of routing data and payloads. Therefore, we need to think about security to secure the data flow that passes through it.

##### B. Proposed Model

To fill the security gaps in adhoc UAV networks, we thought of designing and developing an intrusion detection system to detect intrusions targeting UAV fleets based on ad hoc networks. The IDS will be placed at the level of the adhoc network so that it captures all traffic circulating at the level of the UAV network including the control station. It will then proceed by comparing the captured traffic with the normal reference profile to determine whether it is an attack or not. Our system is designed to fully comply with the security principles of data confidentiality, integrity, availability and authenticity (Fig. 9).

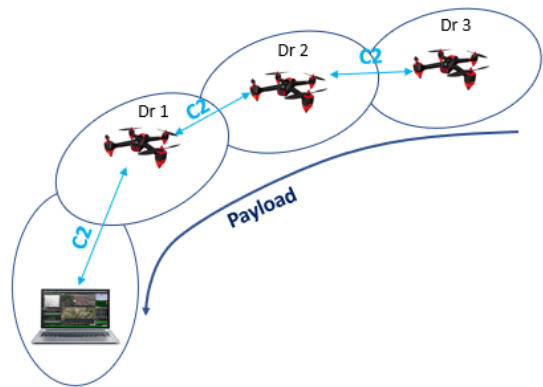


Fig. 8. Adhoc Architecture of a UAV Fleet [3].

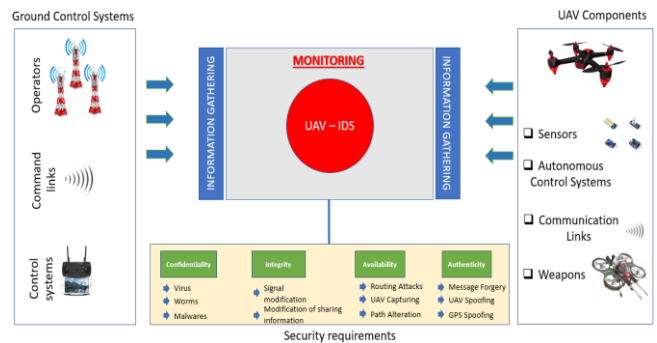


Fig. 9. General Overview of the Intrusion Detection System in an adhoc UAV Network.

Our approach, to detect intrusions and attacks targeting a fleet of drones based on an adhoc network, is to propose an intrusion detection system model based on the multi-agent paradigm. Indeed, the proposed system is distributed and includes a set of autonomous, learning, cooperative and communicating agents to undertake actions to detect attacks in an adhoc network of drones.

The proposed IDS model will be deployed in such a way that it receives all traffic from the UAV fleet's, including the ground station. Our IDS will be based on machine learning techniques while learning the normal operation of the UAV ad hoc network to model the normal reference profile, and from there any deviation from this profile is considered as an intrusion while notifying the fleet owner. Fig. 10 gives an overview of the location of our system in an UAV fleet ad hoc network.

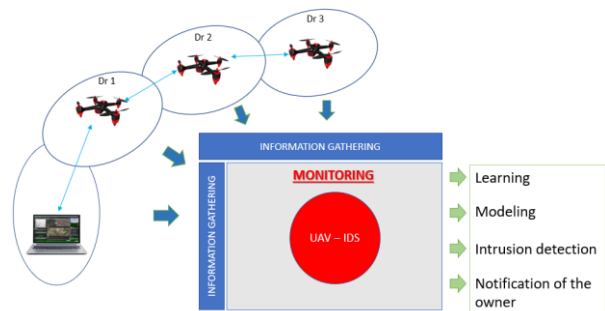


Fig. 10. General Overview of the Proposed IDS to Capture Attacks Targeting adhoc Networks.

The diagram (Fig. 11) illustrates our proposed IDS model. This system is composed of a set of cooperative and communicating agents that collaborate with each other to carry out intrusion detection missions.

Our model consists mainly of a total of seven agents which are: Sniffer Agent (SA), Filtering Agent (FA), Feature Selection Agent (FSA), Decision Maker Agent (DMA), Reporting Agent (RA), Alert Manager Agent (AMA) and Taking Action Agent (TAA). Each agent in the system is responsible for carrying out specific tasks to help achieve the system's strategic objectives, which are to detect intrusions in an efficient manner without impacting the resources of the drones belonging to the fleet.

### C. Components of the Proposed System

Our approach is based on the multi-agent paradigm given the complexity of adhoc UAV networks in terms of node mobility and the continuous change in the network topology of the fleet. To simplify the system, multi-agent technology proves to be the most appropriate solution to address the problem of intrusion detection in this type of network. The proposed intrusion detection system consists of the following components:

- Sniffer Agent (SA): This agent represents the entrance of our system; it takes care of capturing all the network traffic that transits in the adhoc network. To do so, this agent will be equipped with a high gain antenna that will be placed in a location so as to cover the entire perimeter of the fleet.
- Filtering Agent (FA): This is a reactive agent that checks the packet match against a knowledge base of all signatures of all known attacks and intrusions. If it finds a match, a notification will be generated to alert the user and if the packet is not recognized by the signature database, it will be sent to the Storage Cluster for processing.
- Feature Selection Agent (FSA): This agent is intelligent and relies on machine learning techniques to extract the features that best describe network packets. In addition, it uses size-reduction techniques to select only the relevant parameters that can characterize and distinguish network packets.
- Decision Maker Agent (DMA): This is a learning agent that uses machine learning techniques to model different types of attacks and normal traffic. It is based on the calculated values of the attributes extracted by the FSA.
- Alert Manager Agent (AMA): This agent is responsible for correlating the various alerts and alarms generated by the system in order to reduce their number and to keep only those that are true alerts and not false positives. It also allows the user, via the GUI interface, to intervene to mark alerts as true or false alarms. This allows the administrator's expertise to be exploited and leveraged to improve the accuracy of the IDS and reduce the false positive rate.

- Reporting Agent (RA): It allows reports to be developed according to the needs of administrators. The user can generate dashboards and reports so that he has more visibility on the security KPIs that need to be more meaningful through the use of graphs.
- Taking Action Agent (TAA): This agent allows to take actions in case of attack or intrusion. The user via its graphical interface can neutralize an attack by isolating the UAV concerned, for example, it can also ensure the RTH (Return To Home) of the drone before it is lost or captured by hackers and malveillant persons. The TAA communicates with the AMA and can be programmed according to the alerts generated. For example, it can trigger the landing of a legitimate drone as soon as a malicious UAV is detected trying to enter its adhoc network.
- Knowledge Base Module: This is a knowledge base that includes all known attack signatures. This base will be enriched by new signatures of attacks detected by the IDS.
- Storage Cluster: The traffic coming from the adhoc networks is very voluminous and transits with an increased speed. Therefore, choosing HDFS storage is more appropriate and allows for very fast processing without any latency or performance degradation.

### D. Principle of Operation of the Proposed System

The operating principle of the proposed model is illustrated in Fig. 12.

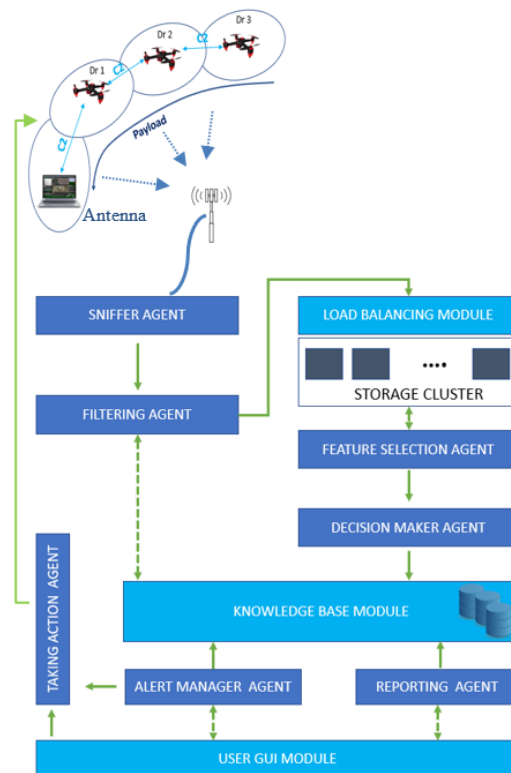


Fig. 11. The Proposed Model of IDS.



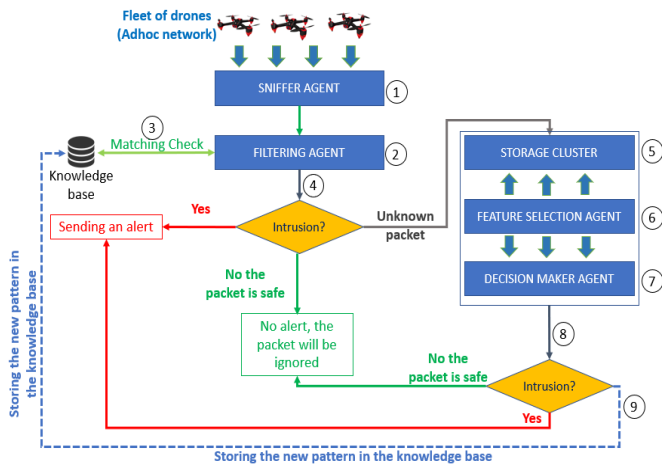


Fig. 12. Operating Principle of the Proposed Model.

As we can see in the diagram above, the intrusion detection mechanism at the level of an adhoc network of a UAV fleet is done according to nine steps which are:

- Step 1: In this step, the system, via its SA agent, captures all network traffic circulating in the UAV fleet, based on a high-gain antenna that can cover the entire perimeter of the fleet.
- Step 2: The captured traffic is sent to the next agent, which is the FA.
- Step 3: The FA opts for a matching check against a knowledge base containing all known attack and intrusion signatures.
- Step 4: Depending on the result of the matching verification, there are three possible scenarios:
  - Either the packet matches an attack signature already known by the knowledge base, in which case the FA alerts the system administrator to see the intrusion details,
  - Either the network packet is normal and does not represent any risk for the fleet network and in this case the packet will be ignored and will not undergo any further processing,
  - And finally, if the package is not recognized by the signature database, then in this case it will be sent to the following agents to undergo the necessary treatments to identify its nature.
- Step 5: Then, as we said in the previous step, if the packet is not recognized, it will automatically be stored in a HDFS (Hadoop Distributed File System) storage cluster to undergo the necessary treatments.
- Step 6: In this step, the FSA chooses to extract the characteristics and attributes that best describe the behavior of the packet. It also ensures dimension reduction through the use of machine learning algorithms in order to obtain good detection accuracy.

- Step 7: The DMA agent uses the attribute values calculated by the FSA and a model of normal traffic to detect deviations from normal traffic. The DMA uses machine learning techniques and must be trained beforehand on a training dataset so that it can recognize the nature of network packets.
- Step 8: Depending on the result of the processing, there are two scenarios:
  - The packet is normal, in this case no notification will be sent to the system administrator,
  - The packet is intrusive: An alert will be sent to the administrator to prompt him to see the details of the intrusion.
- Step 9: Whatever the result of the detection (Intrusion or not), the new pattern will be stored in the knowledge base to be used in step 3.

## V. EXPERIMENTATION

In this section, we will discuss the micro level of our system's operation. This section deals with the experimentation part related to the use of machine learning techniques to make the system learn the different known attacks and to make it possible for it to detect zero-day attacks by opting for semi-supervised machine learning techniques. In this part, we will be focusing on the two used techniques to detect known and unknown attacks.

### A. Dataset

To test our model, we used the CICIDS2017 dataset which is an up-to-date dataset encompassing all normal events as well as those of the various most recent known attacks. This dataset includes data annotated using the network analysis tool CICFlowMeter, which allows us to label the flow based on the timestamp, source and destination IP addresses, source and destination network ports, protocols used and the name of the attack [42].

The CICIDS2017 dataset contains all kinds of network traffic that can pass through a network. On the one hand, it includes normal network events that do not present any risk of compromising the security principles (CIA) and on the other hand, it gathers all events that may be generated by cyber attacks. CICIDS2017 recognizes the following attacks [42] [43]:

- Brute force attacks: This technique attempts to guess passwords or encryption keys by trying a large number of possible combinations. This technique requires much more effort depending on the complexity of passwords and encryption keys.
- Denial of Service (DoS) attacks: This type of attack prevents authorized users from using a service, network or computer system. During this attack, the attacker can act in several ways to make the target inaccessible and out of service: Notably, overloading a network with packets to cause network congestion and thus degrade its performance, or targeting a specific host computer to

make it out of service and thus prevent users from accessing it.

- Botnet attacks: This attack is very widespread and is based on the use of a network of Bots (zombies), these are usually computers infected with malware to become part of the Botnet network and therefore obey the commands of the C&C attacker against a specific target.
- Port scanning: This attack allows an attacker to send probe packets to a network or a system to extract information from the received responses. In particular, the attacker can detect ports that are open, closed and filtered by a firewall. Without forgetting that the hacker, via this technique, can identify the version of the used OS (Fingerprinting) and thus better understand the victim's vulnerabilities.
- SQL injections: This is the most dangerous attack since it allows inserting, reading and modifying information contained in a database. This attack takes advantage of coding vulnerabilities (No input validation, XSS vulnerability...) and web server vulnerabilities to inject SQL commands into text and search boxes.
- XSS (Cross-Site-Scripting) attacks: This attack can be undertaken if the attacker has the ability to place scripts in the HTML content of a web page. This attack occurs when the developer has not reinforced the input validation in his application during the development phase. Through this attack, the hacker can steal a user's cookies in order to impersonate him without any authentication or authorization.
- Heartbleed: This is a bug in the Open-SSL library used in asymmetric PKI (Public Key Infrastructure) cryptography. This attack was discovered in 2014 and allows an attacker to execute arbitrary code in the compromised target.

### B. Tools for Simulation

In order to test the proper functioning of our system we have used the data analysis tool called Knime. It is widely used in the field of data science to test machine learning techniques.

Knime is a software designed to create and produce scientific data using a simple and intuitive environment that allows each stakeholder in data science to focus on what they do best.

### C. Supervised Machine Learning

As we have seen in the "Proposed model" section, our IDS is based on two machine learning techniques which are: Supervised and unsupervised machine learning techniques. The supervised machine learning is performed using the Decision Tree algorithm, which has given conclusive results with 100% of accuracy and a zero false positive rate.

1) *Decision Tree workflow*: To train and test our model, we have opted for the following workflow (Fig. 13).

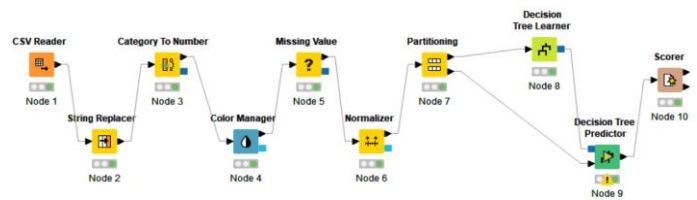


Fig. 13. Decision Tree Workflow.

As we see in the figure above, the data undergoes some pre-processing operations before being consumed by the machine learning decision tree algorithm. These operations generally consist of:

- String Replacer: The objective of this phase is to make data readable while replacing erroneous characters with readable and more meaningful ones.
- Data transformation: Data must be transformed into quantitative data to be consumed by the Decision Tree algorithm. As a result, all categorical values have been transformed into quantitative values that can be used by the mathematical equations of the Decision Tree algorithm.
- Missing data: This process allows missing data to be replaced by their average for example. This helps to have satisfactory results during the learning phase. The action of replacing null and missing values took place to make the CICIDS data more reliable and more readable by the Decision Tree algorithm.
- Data normalization: This technique allows to modify the values of the numerical columns of the dataset in order to use a common scale without markup or loss of information. The Decision Tree algorithm needs this normalization operation in order to model the data correctly.
- Data partitioning: During this phase, we segmented the data into two categories:
  - Training dataset: This is the data for training and represents 80% of the total dataset. The training dataset contains all possible categories of network events (normal traffic and malicious traffic), which allows the model to be trained on any possible type of event.
  - Test dataset: This dataset represents 20% of the dataset and allows to evaluate the implemented model.

2) *Results and metrics*: After preparing the training dataset, the Decision Tree algorithm uses this data to come up with a model capable of distinguishing normal traffic from other suspicious activities. The ML algorithm used has proven very good results in detecting known attacks, it was able to achieve 100% detection accuracy with zero false positives (FP) and false negatives (FN). Fig. 14 illustrates the obtained results using the Decision Tree algorithm. The results are conclusive and are represented by the following rates:

- True Positives: TP
- False Positives: FP
- True Negatives: TN
- False Negatives: FN

Fig. 15 below shows the confusion matrix of the used algorithm. This table illustrates the effectiveness of the Decision Tree against the modeling of known attacks contained in the CICIDS2017 dataset.

#### D. Semi-Supervised Machine Learning

In this part, we will clarify the mechanism for detecting unknown attacks that are not recognized by the first phase of filtering based on supervised machine learning. The figure 16 highlights the workflow adopted by network traffic before the nature of network events is identified. Network traffic that is not recognized by the FA (Supervised Machine Learning) moves on to the next steps to undergo semi-supervised machine learning operations.

| TRAFFIC                  | TP     | FP | TN     | FN |
|--------------------------|--------|----|--------|----|
| BENIGN                   | 454861 | 0  | 111288 | 0  |
| DDoS                     | 25671  | 0  | 540478 | 0  |
| PORT SCAN                | 31695  | 0  | 534454 | 0  |
| BOT                      | 384    | 0  | 565765 | 0  |
| INFILTRATION             | 7      | 0  | 566142 | 0  |
| WEB ATTACK BRUTE FORCE   | 307    | 0  | 565842 | 0  |
| WEB ATTACK XSS           | 130    | 0  | 566019 | 0  |
| WEB ATTACK SQL INJECTION | 4      | 0  | 566145 | 0  |
| FTP-PATATOR              | 1622   | 0  | 564527 | 0  |
| SSH-PATATOR              | 1192   | 0  | 564957 | 0  |
| DoS SLOWLORIS            | 1161   | 0  | 564988 | 0  |
| DoS SLOWHTTPTEST         | 1119   | 0  | 565030 | 0  |
| DoS HULK                 | 45933  | 0  | 520216 | 0  |
| DoS GOLDENEYE            | 2061   | 0  | 564088 | 0  |
| HEARTBLEED               | 2      | 0  | 566147 | 0  |

Fig. 14. Accuracy Statistics.

|                          | BENIGN | DDoS  | PORT SCAN | BOT | INFILTRATION | WEB ATTACK BRUTE FORCE | WEB ATTACK XSS | WEB ATTACK SQL INJECTION | FTP-PATATOR | SSH-PATATOR | DoS SLOWLORIS | DoS SLOWHTTPTEST | DoS HULK | DoS GOLDENEYE | HEARTBLEED |
|--------------------------|--------|-------|-----------|-----|--------------|------------------------|----------------|--------------------------|-------------|-------------|---------------|------------------|----------|---------------|------------|
| BENIGN                   | 454861 | 0     | 0         | 0   | 0            | 0                      | 0              | 0                        | 0           | 0           | 0             | 0                | 0        | 0             | 0          |
| DDoS                     | 0      | 25671 | 0         | 0   | 0            | 0                      | 0              | 0                        | 0           | 0           | 0             | 0                | 0        | 0             | 0          |
| PORT SCAN                | 0      | 0     | 31695     | 0   | 0            | 0                      | 0              | 0                        | 0           | 0           | 0             | 0                | 0        | 0             | 0          |
| BOT                      | 0      | 0     | 0         | 384 | 0            | 0                      | 0              | 0                        | 0           | 0           | 0             | 0                | 0        | 0             | 0          |
| INFILTRATION             | 0      | 0     | 0         | 0   | 7            | 0                      | 0              | 0                        | 0           | 0           | 0             | 0                | 0        | 0             | 0          |
| WEB ATTACK BRUTE FORCE   | 0      | 0     | 0         | 0   | 0            | 307                    | 0              | 0                        | 0           | 0           | 0             | 0                | 0        | 0             | 0          |
| WEB ATTACK XSS           | 0      | 0     | 0         | 0   | 0            | 0                      | 130            | 0                        | 0           | 0           | 0             | 0                | 0        | 0             | 0          |
| WEB ATTACK SQL INJECTION | 0      | 0     | 0         | 0   | 0            | 0                      | 0              | 4                        | 0           | 0           | 0             | 0                | 0        | 0             | 0          |
| FTP-PATATOR              | 0      | 0     | 0         | 0   | 0            | 0                      | 0              | 0                        | 1622        | 0           | 0             | 0                | 0        | 0             | 0          |
| SSH-PATATOR              | 0      | 0     | 0         | 0   | 0            | 0                      | 0              | 0                        | 0           | 1192        | 0             | 0                | 0        | 0             | 0          |
| DoS SLOWLORIS            | 0      | 0     | 0         | 0   | 0            | 0                      | 0              | 0                        | 0           | 0           | 1161          | 0                | 0        | 0             | 0          |
| DoS SLOWHTTPTEST         | 0      | 0     | 0         | 0   | 0            | 0                      | 0              | 0                        | 0           | 0           | 0             | 1119             | 0        | 0             | 0          |
| DoS HULK                 | 0      | 0     | 0         | 0   | 0            | 0                      | 0              | 0                        | 0           | 0           | 0             | 0                | 45933    | 0             | 0          |
| DoS GOLDENEYE            | 0      | 0     | 0         | 0   | 0            | 0                      | 0              | 0                        | 0           | 0           | 0             | 0                | 0        | 2061          | 0          |
| HEARTBLEED               | 0      | 0     | 0         | 0   | 0            | 0                      | 0              | 0                        | 0           | 0           | 0             | 0                | 0        | 0             | 2          |

Fig. 15. Confusion Matrix.

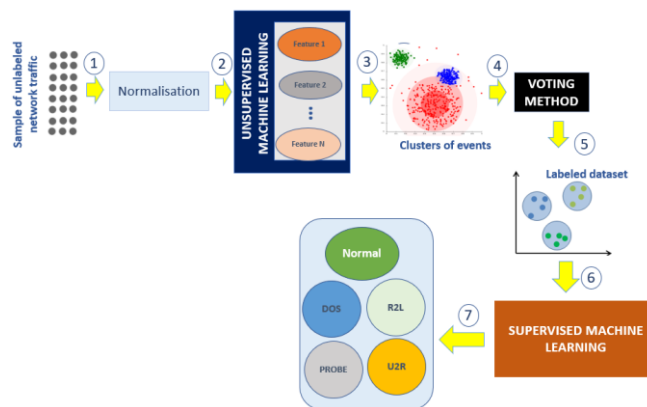


Fig. 16. Semi-Supervised Machine Learning Workflow.

Semi-supervised machine learning techniques consist in passing network traffic through the following phases:

- Phase 1 (Non-supervised machine learning): In this step, the unannotated network traffic is learned by an unannotated machine learning technique. At the end of this phase, the algorithm groups the network events into a set of Clusters (Each Cluster includes events that have certain similarities).
- Phase 2 (Voting Method): Arriving at this stage, the unannotated data are not yet annotated with labels. To do this, the voting method is used to be able to name the different Clusters with significant attack names [44]. The output of this operation gives us annotated data that can be learned using supervised machine learning techniques.
- Phase 3 (Supervised machine learning): After having produced the annotated data, the latter undergoes learning actions by the supervised machine learning algorithms so that the different events can be recognized later during the next filtering by the FA.

For the semi-supervised machine learning techniques, we have unfortunately not yet experimented with this part and it will be dealt with in another work in the near future.

#### VI. CONCLUSION AND PERSPECTIVES

In this paper, we put forward a model of an Intrusion Detection System (IDS) to detect intrusions in a UAV fleet using an adhoc communication architecture. The proposed IDS is distributed and based on the multi-agent paradigm and an HDFS storage cluster. Our system can detect any type of attacks and intrusions that can target a network of drones. It ensures the detection of known and unknown attacks in real time based on machine learning techniques that allow the modeling of the network traffic of the UAV fleet. This application demonstrates the usefulness of the methodologies proposed by the multi-agent community that can be used to ensure the security of a network of drones linked by adhoc. Our IDS model perfectly meets the security requirements of an UAV network based on adhoc networks in terms of:

- Distribution: Given the distributed nature of the network linking drones with small adhoc networks.

- **Dynamism:** The rapid and continuous change of the network topology due to the mobility of nodes and the possibility of losing a node at any time.
- **Volumetry:** The data generated by a network of a fleet of UAVs is voluminous and requires appropriate means to process it.
- **Cooperation:** UAVs in an adhoc communication architecture are communicative and cooperative; security systems must take this aspect into account.
- **Autonomy:** UAVs are autonomous, so the security system must be autonomous in order to effectively detect intrusions.
- **Learning:** The detection of unknown intrusions must be based on machine learning techniques, so our system is built using intelligent learning agents.
- **Performance:** The security system must be efficient to take into account the limited resources of the UAVs in the fleet in terms of CPU, RAM and storage.

The work is not finished yet, there are still several tasks to be done to make our system more efficient and able to detect known and unknown attacks in real time, we quote in particular:

- **Testing the semi-supervised machine learning with Knime:** This allows us to choose the right algorithms with increased detection accuracy and a much reduced false positive rate.
- **Setting up an HDFS (Hadoop Distributed File System) environment:** This allows us to evaluate the real-time character of our system. Bearing in mind that machine learning algorithms generally require CPU, RAM and storage resources.
- **Retrieving a real dataset gathering the set of network events generated by the nodes of a fleet of UAVs communicating by adhoc.**
- **Testing the entire system within a real fleet's network.**

#### REFERENCES

- [1] Undertaking, S.J. European Drones Outlook Study. Unlocking the Value for Europe; Technical Report; SESAR Joint Undertaking: Brussels, 2016.
- [2] Intrusion Detection Systems for Networked Unmanned Aerial Vehicles: A survey Gaurav Choudhary, Vishal Sharma, Ilsun You, Kangbin Yim, Ing-Ray Chen, Jin-Hee Cho
- [3] Architecture de communication sécurisée d'une flotte de drones Jean-Aimé Maxa.
- [4] A Hierarchical Detection and Response System to Enhance Security Against Lethal Cyber-Attacks in UAV Networks Hichem Sedjelmaci, Sidi Mohammed Senouci, Nirwan Ansari.
- [5] Detecting signal spoofing and Jamming Attacks in UAV networks using a light weight IDS Menaka Pushpa Arthur Menaka Pushpa Arthur.
- [6] Raja Naeem Akram, Pierre-François Bonnefoi, Serge Chaumette, Konstantinos Markantonakis, and Damien Sauveron. Improving security of autonomous uavs fleets by using new specific embedded secure elements a position paper.
- [7] Sonja Buchegger and J-Y Le Boudec. Nodes bearing grudges : Towards routing security, fairness, and robustness in mobile ad hoc networks. In Parallel, Distributed and Network-based Processing, 2002. Proceedings. 10th Euromicro Workshop on, pages 403–410. IEEE, 2002.
- [8] <https://www.drone-malin.com/pages/en-savoir-plus/les-drones/c-est-quoi-un-drone.html>.
- [9] Lum, C.; Mackenzie, M.; Shaw-Feather, C.; Luker, E.; Dunbabin, M. Multispectral Imaging and Elevation Mapping from an Unmanned Aerial System for Precision Agriculture Applications. In Proceedings of the 13th International Conference on Precision Agriculture, St. Louis, MO, USA, 31 July–4 August 2016.
- [10] Hamza, M.; Jehangir, A.; Ahmad, T.; Sohail, A.; Naeem, M. Design of surveillance drone with X-ray camera, IR camera and metal detector. In Proceedings of the 2017 Ninth International Conference on Ubiquitous and Future Networks (ICUFN), Milan, Italy, 4–7 July 2017; pp. 111–114.
- [11] Zipline. Zipline, 2017. Available online: <http://www.flyzipline.com> (accessed on 11 April 2018).
- [12] Amazon. Amazon Prime Air, 2016. Available online: <https://www.amazon.com/Amazon-Prime-Air/b?node=8037720011> (accessed on 11 April 2018).
- [13] Eric W Frew and Timothy X Brown. Networking issues for small unmanned aircraft systems. Journal of Intelligent and Robotic Systems, 54(1-3) :21–37, 2009.
- [14] Alan Kim, Brandon Wampler, James Goppert, Inseok Hwang, and Hal Aldridge. Cyber attack vulnerabilities analysis for unmanned aerial vehicles. Infotech@ Aerospace, 2012.
- [15] Ahmad Y Javaid, Weiqing Sun, Vijay K Devabhaktuni, and Mansoor Alam. Cyber security threat analysis and modeling of an unmanned aerial vehicle system. In Homeland Security (HST), 2012 IEEE Conference on Technologies for, pages 585–590. IEEE, 2012.
- [16] Ping Yi, Zhoulun Dai, Shiyong Zhang, and Yiping Zhong. A new routing attack in mobile ad hoc networks. International Journal of Information Technology, 11(2) :83–94, 2005.
- [17] Yih-Chun Hu, Adrian Perrig, and David B Johnson. Rushing attacks and defense in wireless ad hoc network routing protocols. In Proceedings of the 2nd ACM workshop on Wireless security, pages 30–40. ACM, 2003.
- [18] Jack Elston, Eric W Frew, Dale Lawrence, Peter Gray, and Brian Argrow. Net-centric communication and control for a heterogeneous unmanned aircraft system. Journal of Intelligent and Robotic Systems, 56(1-2) :199–232, 2009.
- [19] Matthew Pirretti, Sencun Zhu, Narayanan Vijaykrishnan, Patrick McDaniel, Mahmut Kandemir, and Richard Brooks. The sleep deprivation attack in sensor networks : Analysis and methods of defense. International Journal of Distributed Sensor Networks, 2(3) :267–287, 2006.
- [20] Bounpadith Kannhavong, Hidehisa Nakayama, Yoshiaki Nemoto, Nei Kato, and Abbas Jamalipour. A survey of routing attacks in mobile ad hoc networks. IEEE Wireless Communications, 14(5) :85–91, 2007.
- [21] H. Debar, M. Dacier, and A. Wespi, “Towards a taxonomy of intrusion-detection systems,” Computer Networks, vol. 31, no. 8, pp. 805–822, 1999.
- [22] Hao Yang, Haiyun Luo, Fan Ye, Songwu Lu, and Lixia Zhang. Security in mobile ad hoc networks: challenges and solutions. IEEE wireless communications, 11(1) :38–47, 2004.
- [23] J. Ferber – 1995 – “Les systèmes multi-agents, vers une intelligence collective”, Inter Editions (1995).
- [24] Said OUIAZZANE et all Toward Network Intrusion Detection System for Geographic Data.
- [25] Barramou F., Addou M. – 2012- An agent based approach for simulating complex systems with spatial dynamics application in the land use planning.
- [26] Said OUIAZZANE et al. A Multi-Agent Model for Network Intrusion Detection.
- [27] Philippe Caillou Présentation Des Systèmes Multi-Agents - Master IAC 2014 – 2014.
- [28] Behavior and Vulnerability Assessment of Drones-Enabled Industrial Internet of Things (IIoT) Vishal Sharma ; Gaurav Choudhary ; Yongho Ko ; Ilsun You.

- [29] An intelligent approach for UAV and drone privacy security Tarun Rana, Achyut Shanker, Mohd Karman Sultan, Rizwan.
- [30] J. Maxa, M. S. Ben Mahmoud and N. Larrieu, Secure routing protocol design for UAV Ad hoc NETWORKS. IEEE/AIAA 34th Digital Avionics Systems Conference (DASC), Prague, 2015, pp. 4A5-1-4A5-15.
- [31] User-Centric View of Unmanned Aerial Vehicle Transmission Against Smart Attacks Liang Xiao, Senior Member, IEEE, Caixia Xie, Minghui Min, Student Member, IEEE and Weihua Zhuang, Fellow, IEEE.
- [32] R. Mitchell and I. Chen. Adaptive Intrusion Detection of Malicious Unmanned Air Vehicles Using Behavior Rule Specifications. in IEEE Transactions on Systems, Man, and Cybernetics: Systems, vol. 44, no. 5, pp. 593-604, May 2014.
- [33] D. Shen, G. Chen, E. Blasch, and G. Tadda, "Adaptive markov game theoretic data fusion approach for cyber network defense," in IEEE Military Communications Conference (MILCOM 2007), 2007, pp. 1-7.
- [34] Lasheng et Chantal - Agent Based Distributed Intrusion Detection System.
- [35] Navarro et al. - 2010 - Approaching Real-Time Intrusion Detection through.
- [36] Manjula, D College, R M D Engineering Nadu, Tamil – 2012 – Dynamic Distributed Intrusion Detection System Based on Mobile Agents with Fault Tolerance Department of Computer Science and Engineering , Department of Computer Science and Engineering.
- [37] Gowadia, Vaibhav Farkas, Csilla Valtorta, Marco – 2005 – PAID: A probabilistic agent-based intrusion detection system.
- [38] Miller, P. Inoue, A. – 2003 – Collaborative intrusion detection system – Annual Conference of the North American Fuzzy Information Processing Society – NAFIPS.
- [39] Boudaoud, K. Labiod, H. Boutaba, R. Guessoum, Z. – 2000 – Network security management with intelligent agents – IEEE Symposium Record on Network Operations and Management Symposium.
- [40] Afzali, Neda Azmi, Reza – 2014 – Engineering Applications of Artificial Intelligence MAIS-IDS: A distributed intrusion detection system using multi-agent AIS approach.
- [41] Abdelilah Alshbatat, Liang Dong Performance Analysis of Mobile Ad Hoc Unmanned Aerial Vehicle Communication Networks with Directional Antennas.
- [42] A detailed analysis of CICIDS2017 dataset for designing Intrusion Detection Systems.
- [43] Vilhelm Gustavsson Machine Learning for a Networkbased Intrusion Detection System 2019.
- [44] Muhammad Aamir, Syed Mustafa Ali Zaidi - Clustering based semi-supervised machine learning for DDoS attack classification.

# MSTD: Moroccan Sentiment Twitter Dataset

Soukaina MIHI<sup>1</sup>, Brahim AIT BEN ALI<sup>2</sup>, Ismail EL BAZI<sup>3</sup>, Sara AREZKI<sup>4</sup>, Nabil LAACHFOUBI<sup>5</sup>

University Hassan first of Settat Morocco<sup>1, 2, 4, 5</sup>  
University Moulay Slimane of Beni Mellal<sup>3</sup>

**Abstract**—With the proliferation of social media and Internet accessibility, a massive amount of data has been produced. In most cases, the textual data available through the web comes mainly from people expressing their views in informal words. The Arabic language is one of the hardest Semitic languages to deal with because of its complex morphology. In this paper, a new contribution to the Arabic resources is presented as a large Moroccan dataset retrieved from Twitter and carefully annotated by native speakers. For the best of our knowledge, this dataset is the largest Moroccan dataset for sentiment analysis. It is distinguished by its size, its quality given by the commitment of annotators, and its accessibility for the research community. Furthermore, the MSTD (Moroccan Sentiment Twitter Dataset) is benchmarked through experiments carried out for 4-way classification as well as polarity classification (positive, negative). Various machine-learning algorithms are combined to feature extraction techniques to reach optimal settings. This work also presents the effect of stemming and lemmatization on the improvement of the obtained accuracies.

**Keywords**—Sentiment analysis; Moroccan dialect; machine-learning; stemming; lemmatization; feature extraction

## I. INTRODUCTION

Natural language processing (NLP) is a very active area of research that exploits the most advanced algorithms and techniques to give machines the ability to understand human language. This branch of Artificial Intelligence has several applications, including translation applications such as Google translate, personal assistance applications such as Cortana, topic detection, sentiment analysis, and others.

Sentiment analysis, also known as opinion mining, is a subfield of NLP that has experienced a strong interest during the last few years. Its study has become inevitable for many businesses wanting to analyze public opinions on the internet. It would be almost impossible for businesses to grow without being able to monitor their presence and brand image through customer interactions.

The applications of sentiment analysis are diverse and closely affecting our daily lives and decisions. In the healthcare field [1][2][3], the opinions published on health communities significantly help patients to find the right doctor for their cases, make the correspondence with their symptoms and take preventive measures. Also, doctors could adapt their prescriptions, schedules, and practices, even pharmaceutical companies benefit by analyzing the public effect of medications and planning studies based on patient attitudes. Moreover, politicians use posts and comments on social media

and news articles to determine people's political orientation [4], predict election results [5], and gauge public opinion about changes in legislation or policy projects. In conjunction with the expansion of digital marketing [6], business entities invest in the study of customer perceptions and preferences [7], by analyzing shared opinions about their products and services. Thus, marketers can monitor their brand image and e-reputation. Also, sentiment analysis allows corporations to meet customer expectations and increase their competitiveness.

The expansion of sentiment analysis is made possible, owing to the abundance of data available on social networks. Indeed, several techniques [8] have been proposed to analyze these unstructured data in different languages.

Arab data on social media has enormously increased in recent years. Arab internet users have more access to the internet, which they use every day to get news, share their ideas, buy products online, etc. There are different formats of the Arabic language, including Modern Standard Arabic and Dialectal Arabic. However, when talking about social media, it often implies colloquial forms of expression, users of these platforms create a virtual network of friends with whom they communicate in Dialectal Arabic. This generates more impact and reaches more people.

According to the digital report 2020 for Morocco<sup>1</sup>, Internet users represent a percentage of 69% of the Moroccan population with an annual growth of 13%. Today, there are 18 million active users of social networks, with a growth rate of 11% compared to 2019. However, there is very little research that focuses on Moroccan dialectal Arabic, let alone resources available to researchers in sentiment analysis. To the best of our knowledge, there is no publicly available Moroccan dataset for sentiment analysis task. Moreover, it is the need for such a resource to carry out experimentations that led us to develop a large-scale, multi-domain sentiment dataset in Moroccan dialectal Arabic.

The remainder of this paper is organized as follow: Section II details the challenges of analyzing Moroccan dialect as well as twitter posts. Section III presents a survey of works related to the dataset constitution for different dialects, and points out their availability for research community. The next section explains the process of collection and annotation of the MSTD (Moroccan Sentiment Twitter Dataset) to report afterward in Section V the experimentations and results. Finally, we conclude in Section VI.

<sup>1</sup> <https://datareportal.com/reports/digital-2020-morocco>

## II. CHALLENGES

### A. Moroccan Dialect Challenges

The Moroccan dialect, widely known as Darija is a variety of Arabic language; it is used in daily communication by Moroccan citizens, Media programs, brand pages on social media, commercial or government advertising to reach out to the general public. Darija is a part of the group of Maghrebi dialects spoken in North African countries and differs itself from one region to another [9]. For example, a distinction is made between the northern dialect, southeast dialect, southwest dialect, and the central dialect, which is the most widespread form.

Moroccan dialect (MD) shares some vocabulary and morphological properties with Modern Standard Arabic (MSA), and is characterized by its own spelling, syntax, lexicon, and phonology. Recently, it has become common to use Darija in writing thanks to the advent of the World Wide Web, blogs, and social media. The following are some of the difficulties in processing Darija in its textual format:

- Code-Switching: The history of Morocco is marked by the French-Spanish colonization, which fed Darija with French and Spanish terms along with the Berber language that is spoken by nearly 40% of the Moroccan population [10]. Consequently, when writing Darija, one can find a mix of MSA, Berber, French, Spanish, and English. An example of this: *عندنا الزلزل والشوماج وعسر من وبياء كورونا بزاف الشوماج* (*poverty and unemployment are more dangerous than the pandemic COVID-19*), here *الشوماج* is a French word (**chômage**/Unemployment) and (*وبياء*) is a word of MSA.
- Morphological Characteristics: Arabic is a Semitic language characterized by its morphological complexity [11]. It is written from right to left and does not contain capital letters, unlike English. Typically, Darija is very inflectional and derivational. By adding affixes to a word, you get several different words in categories and meanings. Thus, as an example from *عجب*/Ajaba we can get other words *عجيب*/Fabulous or *عجيني*/I like it.
- Orthography: Darija has no orthographic standard [12]. It can be written in the Arabic alphabet (28 letters), Latin (Arabizi). Commonly, on social media, we often find a mix of the two with the use of numbers to write letters that do not exist in the Roman alphabet, such as 3 for ع. (Darija) *عجيني*/3jebni (Arabizi)/I like it.
- Lack of resources: Research dedicated to Arabic Sentiment Analysis is recent and still scarce compared to other languages. Thus, lexicons and resources for Arabic and particularly dialectal Arabic, are very limited [13].

### B. Twitter Challenges

Twitter is a microblogging site that allows users to create personal accounts to share their ideas and activities with followers [14]. Tweets are limited to 140 characters and are usually written in a non-standard format. In Morocco, 17% of Internet users have active accounts on Twitter; they

continuously generate massive data which is challenging to process due to:

- Spelling errors: In order to overcome the restrictive length of 140 characters, users may concatenate two or more successive words, delete some letters from long words, and use Acronyms or Slang. Also, a common error is to repeat letters to emphasize a sentiment: *عجيبيب هادشي*/This is fabulous.
- Emoticons: used within a tweet to express a feeling, it is usually the combination of special characters and punctuation. For example, the combination of ":" and ")" usually implies a positive attitude.
- Twitter's features: Twitter is a powerful tool to disseminate information. It offers certain functions for users allowing them to mention other users by adding the "@" character. They can share interesting tweets by using the retweet function "RT". Further, tweets related to the same topic contain the hashtag "#". These special characters create noise in tweets and make the task of processing text from Twitter more difficult than other texts.

### C. Annotation Challenges

Annotating textual data for sentiment analysis is not a straightforward process, especially short tweets written in informal language. In the granular level of words, the task of labeling a word is often reduced to the emotion it conveys, is it a positive emotion (love, peace, excitement, etc.) or a negative one (hate, anger, fear, etc.) otherwise, the word is neutral. But as soon as we scale up to the sentence, it becomes complicated depending on the form of the sentence, and the combination of employed tokens [15].

Researchers distinguish three methods of annotation, manual annotation [16], which is based on the intuition of native speakers guided by an instruction scheme and possibly a word lexicon for each target category, automatic labeling [17] that considers the emojis in tweets with reference to an emoticon dictionary for correspondence with the equivalent sentiment and a semantic scoring of the text, and the hybrid method combining both human annotation and automatic techniques [18].

The automatic method can be efficient when managing simple annotation scenarios. It is the categorization of the text [19] in two dimensions of sentiments (positive/negative). However, once we move to a larger scale that concerns several multi-class objectives, with cases of sarcasm sentences, rhetorical questions, mixed sentiments, it is more appropriate to choose manual annotation framed by an annotation scheme and clear instructions.

## III. RELATED WORK

Until recently, building resources for sentiment analysis and subjectivity detection was more prevalent for English. These last five years have witnessed a considerable increase of researches devoted to the Arabic language, more specifically, one can find in the literature some recent works regarding the elaboration of materials for the analysis and evaluation of sentiments.

Following sections present various datasets and corpora produced by different research communities within the scope of work on sentiment analysis, with a distinction between three kinds of works, specifically ones related to the MSA, the datasets produced in Vernacular Arabic, and finally resources built on the Maghreb dialects, with an emphasis on research conducted on Tunisian, Algerian, as well as on the Moroccan colloquial languages.

#### A. MSA Datasets

The most popular datasets in Modern Standard Arabic (MSA) are OCA[20] and AWATIF[21]. The first one was published in 2011. Reviews have been manually extracted directly from various movie websites. Overall, there are 500 reviews from OCA, out of which 250 are positive and 250 negative. Manual processing for cleaning up the text has been performed while the Rapidminer software was used for assessing both Khoja and light stemming.

On the other side, AWATIF is a multi-genre corpus retrieved from three different sources, including Penn Arabic Treebank (PATB) with 2855 sentences, as well as Wikipedia Talk Pages containing 1508 sentences and Web Forums with 1019 sentences. Researchers have cleaned up the noise and text written in dialects to keep only the MSA, and have adopted a manual annotation process in order to compare labeling derived through native speakers with labeling obtained from the Amazon Mechanical Turk crowd-sourcing system. Annotators employed both linguistically motivated and nuance-genre guidelines.

#### B. Vernacular Arabic Datasets

A considerable effort has been made to build datasets for several Arabic dialects, in particular, the literature is marked by important works concerning the Egyptian dialect. In 2012, Abdul-Mageed and al. reported a corpus consisting of four datasets (DAR-TGRD-THR-MONT) [22] respectively gathered on Maktoob, Twitter, Wikipedia Talk Pages, and Web Forums. In 2013, Mohamed Aly and al. introduced the LABR dataset [23] containing a set of 63K auto-labeled book reviews, employing ratings (1,2) for negative, (4,5) for positive, and 3 for neutral. They eliminated the neutral category and made public the rest of the dataset. Following the same paradigm, Elnagar and al. presented two large scale datasets BRAD [24] for book reviews and HARD[25] for hotel reviews. The ASTD [26] is a popular dataset used extensively for benchmarking sentiment analysis methodologies. 10006 Tweets are covering the following four categories (799 positive tweets, 1684 negative tweets, 6691 objective tweets, 832 mixed tweets) while a manual annotation process was used for labeling all data.

In the same context and sharing the same objective, that of enriching the resources available for sentiment analysis applications in dialectal Arabic, other works have presented datasets in different dialects, including, but not limited to, the following: In Saudi dialect, the Arasenti-tweet [27], a dataset

retrieved on Twitter and manually annotated in four classes (positive, negative, neutral and mixed), other datasets have been reported in [28][29]. With regard to the Jordanian dialect, different datasets gathered on Facebook as well as Twitter, were introduced in [30][31][32]. Regarding the Levantine dialect, the works [33][34] yields valuable datasets. Last but not least, a strong focus has been placed on the Sudanese dialect, from which the followings resources can be cited [35][36].

#### C. Maghrebian Datasets

Maghrebian Arabic is a variety of the vernacular Arabic that is spoken in the North of Africa, including Morocco, Algeria, Libya, Tunisia, and Mauritania. Increasing efforts have been put in processing Maghrebian dialects. In 2018, Rehab and al. presented two Algerian datasets SIAAC[37] & SANA [38], for sentiment polarity identification on newspaper comments. The final corpus consists of 513 manually annotated comments in positive, negative, and neutral classes. They conducted some experiments in which they conclude that KNN outperforms SVM. The work in [39] describes an automated technique used to annotate 8000 Algerian messages into positive and negative, whilst [40] presented a corpus of 10K Facebook comments manually annotated into the two categories positive and negative.

Mdhafar et al. Introduced TSAC [41], a Tunisian corpus collected from Facebook comments and manually annotated, it contains 17K positive and negative comments. Another automated process is presented in [42], which used the Twitter API to collect about 6 million tweets, of which more than 170K written in Maghrebian. For the purpose of validating their approach, the authors have manually tagged 1000 tweets and reported the error rate. The resultant TEAD dataset is the largest Arabic corpus that we know so far. Concerning Libyan Arabic, [43] has recently set up a manual dataset of 2938 tweets annotated in three categories: positive, negative and neutral.

Furthermore, [44] presented a method for automated retrieval from Moroccan tweets according to the geographical localization and trained a Naives Bayes classifier for the multilingual collected dataset. Elouardighi et al. [45] produced a Facebook dataset containing approximately 10K positive and negative comments written in Moroccan and Modern Standard Arabic. Not long ago, [46] investigated deep learning models in processing Moroccan tweets, the authors introduced MSAC, a multi-domain balanced dataset of 2000 positive and negative tweets.

Above, Table I is summarizing the cited datasets that are also a compilation from the most commonly known datasets within the research community, covering the various dialects of Arabic along with their availability to the wider public. The table shows that despite recent efforts to build up resources in Arabic, especially the Moroccan dialect, datasets are not available to carry out studies and benchmark new approaches.



TABLE I. ARABIC DIALECTAL DATASETS FOR SENTIMENT ANALYSIS

| Dataset                  | Size   | Type      | Classes                      | Source          | Year | Publicly Available |
|--------------------------|--------|-----------|------------------------------|-----------------|------|--------------------|
| AWATIF[21]               | 4932   | MSA       | POS/NEG/NEU/OBJ              | WTP/WF/ATB1V3   | 2012 | No                 |
| OCA[20]                  | 500    | MSA       | POS/NEG                      | Movies Websites | 2011 | Yes                |
| LABR[23]                 | 63000  | Egyptian  | POS/NEG/NEU                  | Goodreads       | 2013 | Yes                |
| BRAD[24]                 | 510600 | Egyptian  | POS/NEG/NEU                  | Goodreads       | 2016 | Yes                |
| HARD[25]                 | 93700  | Egyptian  | POS/NEG/NEU                  | Booking.com     | 2016 | Yes                |
| ASTD[26]                 | 10006  | Egyptian  | POS/NEG/OBJ/MIX              | Twitter         | 2015 | Yes                |
| AraSenti-Tweet[27]       | 17573  | Saudi     | POS/NEG/NEU                  | Twitter         | 2017 | No                 |
| SDTC[28]                 | 5400   | Saudi     | POS/NEG/NEU/OBJ/SPAM/NOTSURE | Twitter         | 2018 | No                 |
| Saudi Twitter Corpus[29] | 4700   | Saudi     | POS/NEG/NEU                  | Twitter         | 2016 | No                 |
| Atoum &al.[30]           | 3550   | Jordanian | POS/NEG/NEU                  | Twitter         | 2019 | No                 |
| Al-harbi &al.[31]        | 2500   | Jordanian | POS/NEG                      | JEERAN/Jordan   | 2019 | No                 |
| Duwairi &al.[32]         | 22550  | Jordanian | POS/NEG/NEU                  | Twitter         | 2015 | No                 |
| ArSenTD-LEV[33]          | 4000   | Levantine | VPOS/POS/VNEG/NEG/NEU        | Twitter         | 2019 | Yes                |
| BBN Syrian dataset[34]   | 2000   | Levantine | POS/NEG/NEU                  | BBN             | 2015 | Yes                |
| SSA-SDA[35]              | 5456   | Sudanese  | POS/NEG/NEU                  | Twitter         | 2019 | No                 |
| Abdelhameed &al.[36]     | 4625   | Sudanese  | POS/NEG/NEU                  | Twitter         | 2019 | No                 |
| SANA[37]                 | 178    | Algerian  | POS/NEG/NEU                  | Newspapers      | 2019 | No                 |
| SentiALG[39]             | 4000   | Algerian  | POS/NEG                      | Facebook        | 2018 | No                 |
| DzSentiA[40]             | 49864  | Algerian  | POS/NEG                      | Facebook        | 2019 | Yes                |
| TSAC[41]                 | 17000  | Tunisian  | POS/NEG                      | Facebook        | 2017 | Yes                |
| TEAD[42]                 | 6m     | Tunisian  | POS/NEG                      | Twitter         | 2017 | Yes                |
| Ramadan &al.[43]         | 2938   | Lybian    | POS/NEU/NEG                  | Twitter         | 2019 | No                 |
| El Abdouli &al.[44]      | 930    | Moroccan  | POS/NEG                      | Twitter         | 2017 | No                 |
| Elouardighi &al.[45]     | 10254  | Moroccan  | POS/NEG                      | Facebook        | 2017 | No                 |
| Oussouss &al.[46]        | 2000   | Moroccan  | POS/NEG                      | Twitter         | 2019 | No                 |

#### IV. DATASET

The proposed model provides a large-scale dataset spanning several domains, including sports, arts, politics, education, and society. The adopted approach is depicted in Fig. 1. First, starting by collecting the data written in Moroccan dialect, then annotating the material into four different classes, after which data is prepared for experimentation; furthermore, the effect of stemming on classification outcomes is benchmarked, and an extended list of stop words is presented, this list is enriched with words from Moroccan dialect to closely observe the influence of using stop-words on determining the correct and incorrect predictions of sentiment categories.

##### A. Data Collection and Annotation

The collected data is provided from Twitter of users located geographically in Morocco and written only in Arabic. As a result, we have obtained approximately 35K tweets related to the domains of sports, arts, politics, education, and other social issues. While analyzing this data, we have noticed that it contained a high noise content, which makes it very difficult to process it automatically. We stored this data in textual formats, ready to be further analyzed.

A preliminary review of the tweets was performed. Many were cut out because of Twitter's limitation on the number of characters, and some only contained a word or two making reference to an URL and/or a picture. Some were containing nothing other than Hashtags. This initial scan was made to identify the most relevant categories from the collected data. We have noted that we cannot trust emoticons since they convey a fuzzy impression, e.g., Emojis that express a good sentiment were often employed for expressing jokes such as sarcasm and irony. Therefore, the agreement was made for manually labeling these tweets according to the same instructions and some sample annotations Table II.

For annotating tweets, the choice was made for the manual annotation method since it is more performant at giving good quality scores. A team of three native speakers was hired for the task. Total number of tweets was split over three so for each annotator to do one part based upon sample file as well as directions, at the end, an author revises all the annotations so that only those compliant with the initial instructions are kept, thus ensuring consistency with the guidelines established at the outset. We suggest a 4-way annotation that consists of the following four classes (positive, negative, sarcasm, objective).

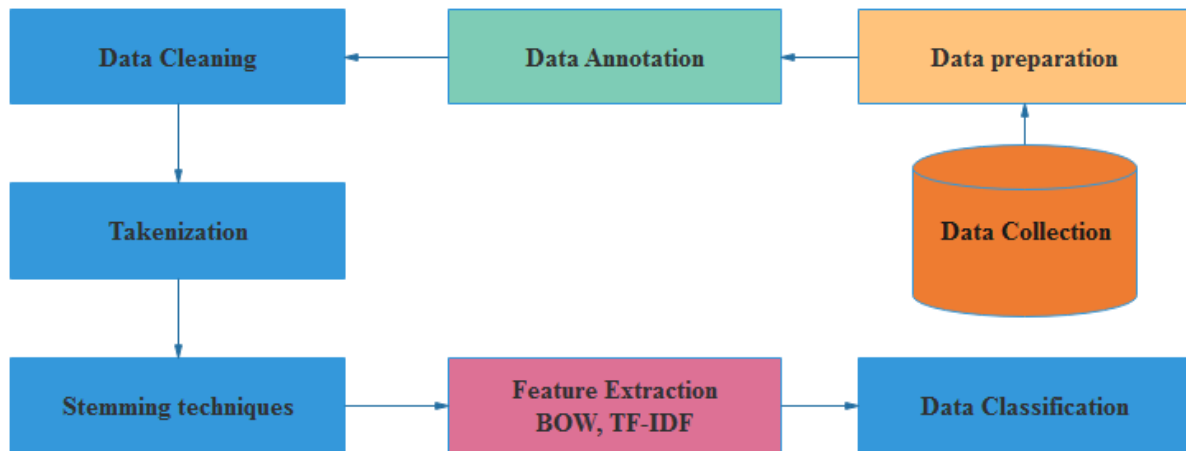


Fig. 1. Proposed System.

Below the guidelines to strive towards identical labeling:

1) *Objective*: is objectively marked, each sentence reporting a new, although this latter may be written with a negative or positive focus, each fact and description about reality without using expressions and/or qualifiers to convey a sentiment.

2) *Positive*: we assign a positive category to every statement representing a pleasant emotion from the perspective of the user regarding their own experience, about a public personality, a product or an event, and so forth. Such polarity is characterized by clear terms and the presence of a target of the sentiment.

3) *Negative*: On the contrary to the positive polarity, we give negative class for tweets that clearly employ some negative words and/or adjectives that express personal beliefs, including colloquial expressions revealing bad perceptions.

4) *Sarcasm*: A sarcastic text can be characterized either by a contradiction in the statement with the words being used to describe it or by a negative connotation being spoken in a positive way. In addition, there are also some popular sayings or idioms known to Moroccans, which convey sarcasm.

### B. Dataset Properties

The overall collected size of the dataset is approximately 35K. All three annotators were given a respective file containing one-third from the tweets, along with instructions and a labeled sampling. It was consented by the guidelines to remove the following tweets:

- Those marked as RT (retweet).
- Tweets in duplicates.
- Tweets that only contain hashtags.
- Tweets that are written entirely in non-Arabic letters.
- Texts representing Spam or insults.
- Tweets with a single word.

The annotators were able to annotate over 12K tweets with four separate classes: 6378 objective, 2769 negative, 866 positives, and 2188 sarcasm, as shown in Fig. 2.

In order to illustrate the frequency of tokens in the MSTD dataset corresponding to a given class, the following word cloud schemes in Fig. 3, Fig. 4, Fig. 5 and Fig. 6 show the word occurrences for the four labeled classes.

TABLE II. ANNOTATED SAMPLE

| Text                                                                            | Translation                                                                 | Class     | Label |
|---------------------------------------------------------------------------------|-----------------------------------------------------------------------------|-----------|-------|
| البوليس ديالنا احسن بوليس ماتفلت معاه حتى حاجة،واش غلبوكم الشفارة ولاخايين منهم | "Our police are the best in the world, did the thieves beat you or what ?!" | Sarcasm   | 3     |
| اجمل مدينة كانت مفخرة جهة سوس العالمية الجميلة                                  | "The most beautiful city, it's our proud, beautiful international Souss."   | Positive  | 2     |
| لحظة اعتقال تلميذ غش في امتحانات البكالوريا                                     | "The moment when a student stops for the baccalaureate exam."               | Objective | 0     |
| العلاقة بيناتنا متوترة بسبب الاختلاف في وجهات النظر                             | "Our relationship is upset because of the difference of opinion."           | Negative  | 1     |

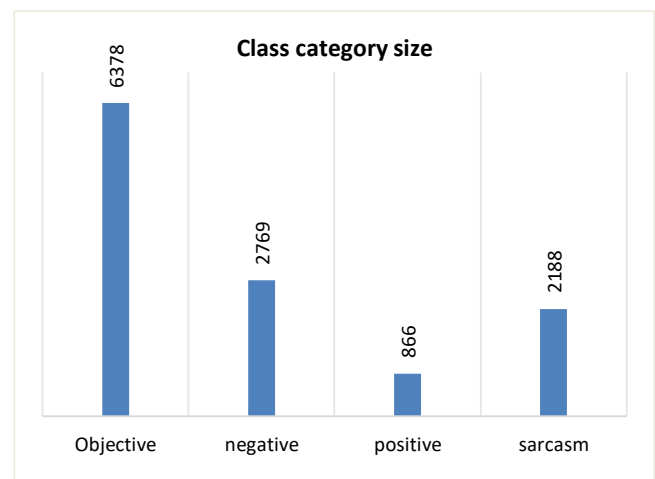


Fig. 2. Class Category Size.



Fig. 3. Word Occurrence for Objective Class.



Fig. 4. Word Occurrence for Negative Class.



Fig. 5. Word Occurrence for Positive Class.



Fig. 6. Word Occurrence for Sarcasm Class.

### C. Data Preprocessing

Data cleaning constitutes an extremely essential phase for NLP tasks, most notably for Arabic sentiment analysis, as proven through several studies [47][48]. Processing text in its plain format substantially enhances accuracy measures as well as reduces redundancy and irrelevant tokens to detect corresponding classifications. A cleaning phase of collected tweets was processed after annotating them.

The first step is to remove all special characters, emoticons, Hashtags, URLs, Html code, usernames, punctuation, and non-Arabic letters. This stage enables to reduce noise in text extensively. Then, we normalized the data by removing the diacritics (tashdid, Fatha, Tanwin Fath, Damma, Tanwin Damm, Kasra, Tanwin Kasr, Sukun, Tatwil). These signs that are placed above or under the Arabic letters can alter the meaning of a single word, for instance (مدرسة means school while مُدرسة means teacher). The last phase of normalization consisted of normalizing the various letters shapes (ة, ء) based on the Pyarabic library<sup>2</sup>.

Besides, stop words are words that do not add any sentiment to text; we have built up a list that contains Arabic and specific Moroccan stop words, which we removed from cleaned tweets to minimize the size of the features. The final step involved retrieving tokens from the text by performing the tokenization. Pyarabic library and NLTK provide tools for doing this tokenization.

### D. Data Stemming and Lemmatization

Arabic has a high inflectional degree since several words may be derived out of the same letters, although these words are necessarily synonyms in a sense. Stemming is a process consisting of the reduction of forms from each word into its root by cutting up prefixes and suffixes found in the beginning and the end of words. In contrast, lemmatization is a method with the same purpose to find the basis of the words but takes into account the morphological nature of words to extract a lemma that conserves meaning. Stemming can be classified into two types: root based stemming or heavy stemming and light stemming:

1) *Root-based stemming*: these methods attempt to use linguistic and heuristic analysis to extract the basic root of a word by removing its longest prefixes and suffixes. Despite its wide use, root-based methods may lead to different semantic meanings for the same extracted root. Example of use: considering the word "ينتصرون/they win", a root-based algorithm will remove "ي" and "ون" resulting in "نتصر" which has no semantic meaning.

2) *Light-stemming*: on its side, light stemming doesn't use deep linguistic analysis. Instead, it performs some heuristic analysis to strip off most frequent prefixes and suffixes attached to the beginning and the end of words, and it results in fewer errors in semantic meaning. Example of a light-stemming method: from the word "الخدمات/services", "ال" will be removed from the beginning and "ات" from the end. As a result, the root will be "خدم".

3) *Lemmatization*: uses morphological analysis and relies on vocabulary usage to derive lemma from words. Some studies show that lemmatizers lead to better results than stemmers. Example of a lemmatization method: considering the word "ينتصرون/they win", a lemmatizer algorithm will remove "ي" and "ون" resulting in "انتصر", a word that means "won".

<sup>2</sup> T. Zerrouki, Pyarabic, An Arabic language library for Python, <https://pypi.python.org/pypi/pyarabic/>, 2010.

## V. EXPERIMENTATION AND RESULTS

Within the scope of this research, we have investigated the multi-class classification issue through benchmarking the most popular classifiers for the NLP tasks to conduct the 4-way classification on unbalanced dataset firstly as well as to detect polarity for a balanced configuration. The results are compared for each method by combining the feature extraction methods with the machine learning algorithms. Then we try also to address how stemming impacts the classification of text that is written only in informal Moroccan Arabic with different local dialects.

### A. Feature Extraction

Feature extraction represents an essential process for optimizing machine learning models. It allows to avoid the over-fitting problem reducing the dimensionality of data. Thus, a selection is made of the most relevant features, which significantly enhances accuracy as well as decreases the time required in training models.

Two different feature extraction algorithms were used: the bag of words, this model provides a number vector that represents the occurrence frequencies associated with words, and TF-IDF (Term Frequency-Inverse Document Frequency), which does not just simply calculate the word occurrence, but assigns an individual TF-IDF score for each word as a ratio of two measurements: The TF representing a word's frequency within a document and the IDF computing its importance within a dataset, whereby the words appearing least often in documents are those that are most prominent for classification purposes. For both feature extraction models, we experiment the N-gram features.

### B. Classification Algorithms

The classification phase is handled through different machine learning algorithms benefiting from the implementation of the python sklearn library. Default settings were adopted to compare the following algorithms: SVC, Bernouli Naïve Bays, Multinomial Naives Bayes, LinearSVC, LogisticRegression, RandomForest, XGBoost, K-Nearest Neighbors, and the DecisionTree.

### C. Stemming Techniques

Different experiments were conducted on two stemmers as well as a lemmatizer. For this, the ISRI-Stemmer [49] algorithm is tested for root-based methods, the Tashafyn<sup>3</sup> algorithm for light stemming, and the Farasa [50] framework for lemmatization.

### D. Discussion

Table III presents the accuracy obtained by the selected algorithms for both vectorization methods (BOW, TF-IDF) combined with the stemming algorithms (ISRI Stemmer, Tashafyn light Stemmer). In order to evaluate the effect of stemming, also experiments were conducted on the preprocessed dataset without the stemming phase.

From the results achieved for the 4-way classification, it is obvious that the Logistic Regression algorithm outperforms the SVC algorithm. Indeed, the highest accuracy, 0.563, was given from experimentation Logistic Regression + ISRI Stemmer + TF-IDF tri-gram. Whilst using the Tashafyn light stemmer system, it was found out that the most accurate settings are SVC+Tashafyn+ BOW tri-gram with 0.556. We notice that for any algorithm of classification and whatever is the vectorization process, the stemming phase represents an essential and reliable way of improving both performance and accuracy rate.

Table IV shows obtained results using the balanced setup for polarity classification (positive, negative), and we consider the details of accuracy measurements concerning on one side, the ISRI Stemmer algorithm as well as those regarding the Lemmatizer Farasa with Ngram of both BOW Ngram and TF-IDF schemes.

The recorded findings demonstrate similarity in accuracy provided by each of the classification algorithms. With the TF-IDF model, the highest scoring is achieved by using the 1-gram scheme, in contrast with the BOW model, which has higher scores given using the 3-gram scheme. While comparing both methods Farasa and ISRI Stemmer, we can observe that with Farasa lemmatizer, a better overall accuracy is achieved when using SVM (SVC and LinearSVC) and Logistic Regression algorithms. At this point, it is worth mentioning the very fast processing time of the Logistic Regression algorithm with regard to SVC.

---

<sup>3</sup> <https://pypi.org/project/Tashaphyne/>

TABLE III. 4-WAY CLASSIFICATION EXPERIMENTATION RESULTS

| Stemming Mechanism     | Classifier         | TF-IDF       |              |              | Bag of Words |       |              |
|------------------------|--------------------|--------------|--------------|--------------|--------------|-------|--------------|
|                        |                    | 1g           | 1g+2g        | 1g+2g+3g     | 1g           | 1g+2g | 1g+2g+3g     |
| ISRI Stemmer           | SVC                | 0.561        | <b>0.562</b> | 0.550        | <b>0.559</b> | 0.555 | 0.556        |
|                        | XGB                | 0.552        | 0.551        | 0.544        | 0.547        | 0.547 | 0.547        |
|                        | BNB                | 0.555        | 0.555        | 0.558        | 0.558        | 0.556 | 0.555        |
|                        | LogisticRegression | 0.557        | 0.557        | <b>0.563</b> | 0.554        | 0.552 | 0.548        |
|                        | KNN                | 0.519        | 0.514        | 0.517        | 0.502        | 0.503 | 0.502        |
|                        | DecisionTree       | 0.476        | 0.481        | 0.489        | 0.476        | 0.481 | 0.484        |
|                        | RandomForest       | 0.555        | 0.548        | 0.544        | 0.548        | 0.551 | 0.548        |
| Tashafyn Light Stemmer | SVC                | 0.554        | 0.551        | 0.550        | 0.550        | 0.555 | <b>0.556</b> |
|                        | XGB                | 0.545        | 0.545        | 0.540        | 0.544        | 0.548 | 0.547        |
|                        | BNB                | <b>0.555</b> | 0.547        | 0.549        | 0.553        | 0.557 | 0.555        |
|                        | LogisticRegression | 0.548        | 0.548        | 0.546        | 0.539        | 0.552 | 0.548        |
|                        | KNN                | 0.513        | 0.519        | 0.520        | 0.525        | 0.503 | 0.502        |
|                        | DecisionTree       | 0.476        | 0.469        | 0.486        | 0.484        | 0.479 | 0.482        |
|                        | RandomForest       | 0.551        | 0.542        | 0.539        | 0.546        | 0.553 | 0.547        |
| No-Stemming            | SVC                | 0.549        | 0.547        | 0.547        | 0.548        | 0.546 | 0.546        |
|                        | XGB                | 0.541        | 0.540        | 0.539        | 0.539        | 0.540 | 0.541        |
|                        | BNB                | 0.555        | 0.546        | 0.546        | 0.549        | 0.549 | 0.549        |
|                        | LogisticRegression | 0.548        | 0.554        | 0.554        | 0.545        | 0.549 | 0.550        |
|                        | KNN                | 0.499        | 0.503        | 0.503        | 0.510        | 0.517 | 0.519        |
|                        | DecisionTree       | 0.479        | 0.488        | 0.488        | 0.479        | 0.485 | 0.473        |
|                        | RandomForest       | 0.548        | 0.546        | 0.548        | 0.549        | 0.540 | 0.538        |

TABLE IV. POLARITY CLASSIFICATION EXPERIMENTATION RESULTS

|              |           | TF-IDF       |              |              | BOW          |       |              |
|--------------|-----------|--------------|--------------|--------------|--------------|-------|--------------|
|              |           | 1g           | 1g+2g        | 1g+2g+3g     | 1g           | 1g+2g | 1g+2g+3g     |
| ISRI Stemmer | SVC       | 0.756        | <b>0.761</b> | 0.747        | <b>0.716</b> | 0.713 | 0.713        |
|              | BNB       | <b>0.670</b> | 0.606        | 0.552        | 0.718        | 0.739 | <b>0.744</b> |
|              | LR        | 0.741        | 0.744        | <b>0.750</b> | 0.739        | 0.741 | <b>0.744</b> |
|              | MNB       | 0.750        | <b>0.759</b> | 0.750        | 0.756        | 0.773 | <b>0.773</b> |
|              | LinearSVC | <b>0.747</b> | 0.747        | 0.736        | 0.730        | 0.713 | <b>0.716</b> |
| FARASA       | SVC       | 0.767        | <b>0.772</b> | 0.764        | 0.707        | 0.710 | <b>0.710</b> |
|              | BNB       | <b>0.695</b> | 0.606        | 0.537        | 0.730        | 0.747 | <b>0.747</b> |
|              | LR        | <b>0.772</b> | 0.761        | 0.753        | 0.733        | 0.747 | <b>0.747</b> |
|              | MNB       | <b>0.756</b> | 0.741        | 0.736        | 0.748        | 0.750 | <b>0.750</b> |
|              | LinearSVC | 0.773        | 0.767        | <b>0.776</b> | <b>0.698</b> | 0.672 | 0.672        |

## VI. CONCLUSION AND FUTURE WORK

Within this work's scope, a major contribution is presented aiming constitution of resources for sentiment analysis in Arabic language, especially the Moroccan dialect spoken by over 35 million people and widely spread through social media and awareness-raising programs, such as during the Covid-19 pandemic. We have collected and labeled on a large scale-dataset containing over 12k tweets, which is publicly

available<sup>4</sup> for the research community. A particularity with this dataset resides in its handling of various classes: positive, negative, sarcasm, and objective. This assumption comes from the fact that most of the posts on twitter emanate from the younger generation who in most cases, express themselves implicitly through expressions of sarcasm. In another part, substantial experiments were performed for the validation of

<sup>4</sup> <https://github.com/moroccanSA-NER/SA-Moroccan>

the MSTD dataset in both unbalanced and balanced configurations, also in order to compare the accuracy for 4-way classification and the classification of two classes. In addition, the effect of stemming on the improvement of the results was investigated, this leads to the conclusion that for the case of Arabic language, lemmatization remains a reliable choice. The annotation and processing of the dataset is really tedious and time-consuming work. However, we hope through manual annotation to contribute with a precise and accurate dataset.

Among the limitations encountered in developing this work is the computational capacity of the machines available for the experiments. However, the obtained outcomes of this study motivate us further to pursue this work at several levels, including an investigation into deep learning models as well as additional feature extraction methods in order to improve multi-class classification scoring. Furthermore, this dataset could be extended to include more valuable texts coming out of Facebook and/or YouTube.

#### REFERENCES

- [1] S. Gohil, S. Vuik, and A. Darzi, "Sentiment analysis of health care tweets: Review of the methods used," *J. Med. Internet Res.*, vol. 20, no. 4, 2018.
- [2] V. L. Mane, S. S. Panicker, and V. B. Patil, "Summarization and sentiment analysis from user health posts," 2015 Int. Conf. Pervasive Comput. Adv. Commun. Technol. Appl. Soc. ICPC 2015, vol. 00, no. c, 2015.
- [3] F. C. Yang, A. J. T. Lee, and S. C. Kuo, "Mining Health Social Media with Sentiment Analysis," *J. Med. Syst.*, vol. 40, no. 11, 2016.
- [4] A. P. Patil, D. Doshi, and D. Dalsaniya, "Applying Machine Learning Techniques for Sentiment Analysis in the Case Study of Indian Politics." eds) *Advances in Signal Processing and Intelligent Recognition Systems. SIRS 2017. Advances in Intelligent Systems and Computing*, vol. 678. Springer, Cham. [https://doi.org/10.1007/978-3-319-67934-1\\_31](https://doi.org/10.1007/978-3-319-67934-1_31).
- [5] T. Elghazaly and A. Mahmoud, "Political Sentiment Analysis Using Twitter Data," ICC '16: Proceedings of the International Conference on Internet of things and Cloud Computing. March 2016.
- [6] D. Al-Hajjar and A. Z. Syed, "Applying sentiment and emotion analysis on brand tweets for digital marketing," 2015 IEEE Jordan Conf. Appl. Electr. Eng. Comput. Technol. AEECT 2015, 2015.
- [7] A. Alamsyah, W. Rahmah, and H. Irawan, "Sentiment analysis based on appraisal theory for marketing intelligence in Indonesia's mobile phone market," *J. Theor. Appl. Inf. Technol.*, vol. 82, no. 2, pp. 335–340, 2015.
- [8] W. Medhat, A. Hassan, and H. Korashy, "Sentiment analysis algorithms and applications: A survey," *Ain Shams Eng. J.*, vol. 5, no. 4, pp. 1093–1113, 2014.
- [9] J. Heath, *Jewish and muslim dialects of moroccan arabic*. 2013.
- [10] Y. Samih and W. Maier, "An Arabic-moroccan Darija code-switched corpus," *Proc. 10th Int. Conf. Lang. Resour. Eval. Lr.* 2016, pp. 4170–4175, 2016.
- [11] S. Al-Osaimi and M. Badruddin, "Sentiment Analysis Challenges of Informal Arabic Language," *Int. J. Adv. Comput. Sci. Appl.*, vol. 8, no. 2, pp. 278–284, 2017.
- [12] R. Tachicart, K. Bouzoubaa, and H. Jaafar, "Lexical differences and similarities between Moroccan dialect and Arabic," *Colloq. Inf. Sci. Technol. Cist*, pp. 331–337, 2017.
- [13] L. Albraheem, "Exploring the problems of Sentiment Analysis in Informal Arabic," *IHWAS '12: Proceedings of the 14th International Conference on Information Integration and Web-based Applications & Services* December 2012 Pages 415–418.
- [14] E. Martínez-Cámara, M. T. Martín-Valdivia, L. A. Ureña-López, and A. R. Montejó-Ráez, "Sentiment analysis in Twitter," *Nat. Lang. Eng.*, vol. 20, no. 1, pp. 1–28, 2014.
- [15] S. Mohammad, "A Practical Guide to Sentiment Annotation: Challenges and Solutions," no. January, pp. 174–179, 2016.
- [16] R. F. de Azevedo, J. P. Santos Rodrigues, M. R. da Silva Reis, C. M. C. Moro, and E. C. Paraiso, "Temporal Tagging of Noisy Clinical Texts in Brazilian Portuguese. International Conference on Computational Processing of the Portuguese Language (PROPOR)," *Lncs*, vol. 11122, pp. 231–241, 2018.
- [17] A. Baccouche, B. Garcia-Zapirain, and A. Elmaghraby, "Annotation Technique for Health-Related Tweets Sentiment Analysis," 2018 IEEE Int. Symp. Signal Process. Inf. Technol. ISSPIT 2018, no. December, pp. 382–387, 2019.
- [18] L. Y. F. Su, M. A. Cacciatore, X. Liang, D. Brossard, D. A. Scheufele, and M. A. Xenos, "Analyzing public sentiments online: combining human- and computer-based content analysis," *Inf. Commun. Soc.*, vol. 20, no. 3, pp. 406–427, 2017.
- [19] C. Bosco, V. Patti, and A. Bolioli, "Developing corpora for sentiment analysis: The case of irony and senti-TUT," *IJCAI Int. Jt. Conf. Artif. Intell.*, vol. 2015-Janua, no. Ijcai, pp. 4158–4162, 2015.
- [20] X. Liu, "Full-Text Citation Analysis: A New Method to Enhance," *J. Am. Soc. Inf. Sci. Technol.*, vol. 64, no. July, pp. 1852–1863, 2013.
- [21] M. Abdul-Mageed and M. Diab, "AWATIF: A multi-genre corpus for modern standard Arabic subjectivity and sentiment analysis," *Proc. 8th Int. Conf. Lang. Resour. Eval. Lr.* 2012, no. April 2015, pp. 3907–3914, 2012.
- [22] M. Abdul-Mageed, M. Diab, and S. Kübler, "SAMAR: Subjectivity and sentiment analysis for Arabic social media," *Comput. Speech Lang.*, vol. 28, no. 1, pp. 20–37, 2014.
- [23] M. Aly and A. Atiya, "LABR: A large scale arabic book reviews dataset," *ACL 2013 - 51st Annu. Meet. Assoc. Comput. Linguist. Proc. Conf.*, vol. 2, no. October 2014, pp. 494–498, 2013.
- [24] A. Elnagar and O. Einea, "BRAD 1.0: Book Reviews in Arabic Dataset," 2016 IEEE/ACS 13th International Conference of Computer Systems and Applications (AICCSA).
- [25] A. Elnagar, Y. S. Khalifa, and A. Einea, "Hotel arabic-reviews dataset construction for sentiment analysis applications," *Stud. Comput. Intell.*, vol. 740, pp. 35–52, 2018.
- [26] M. Nabil, M. Aly, and A. Atiya, "ASTD: Arabic Sentiment Tweets Dataset," *Proceedings of the 2015 Conference on Empirical Methods in Natural Language Processing*, no. September, pp. 2515–2519, 2015.
- [27] N. Al-Twairesh, H. Al-Khalifa, A. Al-Salman, and Y. Al-Ohali, "AraSenTi-Tweet: A Corpus for Arabic Sentiment Analysis of Saudi Tweets," *Procedia Comput. Sci.*, vol. 117, pp. 63–72, 2017.
- [28] A. Al-thubaity and M. Alharbi, "A Saudi Dialect Twitter Corpus for Sentiment and Emotion Analysis," 2018 21st Saudi Comput. Soc. Natl. Comput. Conf., pp. 1–6, 2018.
- [29] A. Assiri, A. Emam, and H. Al-dossari, "Saudi Twitter Corpus for Sentiment Analysis," *International Journal of Computer and Information Engineering Vol:10, No:2*, 2016.
- [30] J. O. Atoum and M. Nouman, "Sentiment Analysis of Arabic Jordanian Dialect Tweets," (IJACSA) International Journal of Advanced Computer Science and Applications, Vol. 10, No. 2, 2019.
- [31] O. Al-harbi, "Classifying Sentiment of Dialectal Arabic Reviews: A Semi-Supervised Approach," *International Arab Journal Of Information Technology*, 16(6):995:1002.
- [32] R. M. Duwairi, "Sentiment Analysis for Dialectical Arabic," 2015 6th International Conference on Information and Communication Systems (ICICS) pp. 166–170, 2015.
- [33] R. Baly, A. Khaddaj, H. Hajj, W. El-hajj, and K. B. Shaban, "ArSentD-LEV: A Multi-Topic Corpus for Target-based Sentiment Analysis in," *Proceedings of the Eleventh International Conference on Language Resources and Evaluation (LREC 2018)*.
- [34] M. Salameh, "Sentiment after Translation: A Case-Study on Arabic Social Media Posts Sentiment after Translation: A Case-Study on Arabic Social Media Posts," *Proceedings of the 2015 Conference of the North American Chapter of the Association for Computational Linguistics: Human Language Technologies* no. June 2016, 2015.
- [35] M. E. M. Abo, N. A. K. Shah, V. Balakrishnan, M. Kamal, A. Abdelaziz, and K. Haruna, "SSA-SDA: Subjectivity and sentiment

- analysis of sudanese dialect Arabic," 2019 Int. Conf. Comput. Inf. Sci. ICCIS 2019, pp. 1–5, 2019.
- [36] H. Al-Rubaiee, R. Qiu, K. Alomar, and D. Li, "Sentiment Analysis of Arabic Tweets in e-Learning," *J. Comput. Sci.*, vol. 12, no. 11, pp. 553–563, 2016.
- [37] P. Silhavy, "Applied Computational Intelligence and Mathematical Methods," vol. 662, 2018.
- [38] H. Rahab, A. Zitouni, M. Djoudi, and S. Sentiment, "SANA : Sentiment analysis on newspapers comments in Algeria To cite this version : HAL Id: hal-02444686 SANA : Sentiment Analysis on Newspapers comments in Algeria," *J. King Saud Univ. - Comput. Inf. Sci.*, 2020.
- [39] I. Guellil, A. Adeel, F. Azouaou, and A. Hussain, SentiALG: Automated Corpus Annotation for Algerian Sentiment Analysis, vol. 10989 LNAI, no. Ml. Springer International Publishing, 2018.
- [40] A. Abdelli, F. Guerrouf, O. Tibermacine, and B. Abdelli, "Sentiment Analysis of Arabic Algerian Dialect Using a Supervised Method," *Proc. - 2019 Int. Conf. Intell. Syst. Adv. Comput. Sci. ISACS 2019*, 2019.
- [41] S. Medhaffar, F. Bougares, Y. Estève, and L. Hadrich-Belguith, "Sentiment Analysis of Tunisian Dialects: Linguistic Ressources and Experiments," no. January, pp. 55–61, 2017.
- [42] H. Abdellaoui and M. Zrigui, "Using tweets and emojis to build TEAD: An arabic dataset for sentiment analysis," *Comput. y Sist.*, vol. 22, no. 3, pp. 777–786, 2018.
- [43] R. Alfared, "A Topic-based Twitter Sentiment Analysis Training Dataset for Libyan Dialect," (IJACSA) International Journal of Advanced Computer Science and Applications, no. March, pp. 4–6, 2019.
- [44] A. El Abdouli, L. Hassouni, and H. Anoun, "Sentiment Analysis of Moroccan Tweets using Naive Bayes Algorithm," *International Journal of Computer Science and Information Security*, vol. 15, no. 12, 2017.
- [45] Maghfour M., Elouardighi A. (2018) Standard and "Dialectal Arabic Text Classification for Sentiment Analysis". In: Abdelwahed E., Bellatreche L., Golfarelli M., Méry D., Ordonez C. (eds) Model and Data Engineering. MEDI 2018. Lecture Notes in Computer Science, vol 11163. Springer, Cham. [https://doi.org/10.1007/978-3-030-00856-7\\_18](https://doi.org/10.1007/978-3-030-00856-7_18).
- [46] A. Oussous, F. Z. Benjelloun, A. A. Lahcen, and S. Belfkih, "ASA: A framework for Arabic sentiment analysis," *J. Inf. Sci.*, 2019.
- [47] R. Duwairi and M. El-Orfali, "A study of the effects of preprocessing strategies on sentiment analysis for Arabic text," *J. Inf. Sci.*, vol. 40, no. 4, pp. 501–513, 2014.
- [48] M. Sawalha et al., "Enhancing the Arabic sentiment analysis using different preprocessing operators.," *New Trends Inf. Technol.*, no. April, pp. 113–117, 2017.
- [49] M. G. Syarief, O. T. Kurahman, A. F. Huda, and W. Darmalaksana, "Improving Arabic Stemmer: ISRI Stemmer," *Proceeding 2019 5th Int. Conf. Wirel. Telemat. ICWT 2019*, 2019.
- [50] H. Mubarak, "Build fast and accurate lemmatization for Arabic," *Lr. 2018 - 11th Int. Conf. Lang. Resour. Eval.*, pp. 1128–1132, 2019.

# Load Balancing Problem on Hyper Hexa Cell Interconnection Network

Aryaf Al-Adwan<sup>1</sup>

Department of Computer and  
Networks Engineering  
Faculty of Engineering Technology  
Al-Balqa Applied University  
Amman, Jordan

Basel A. Mahafzah<sup>2</sup>

Computer Science Department  
King Abdullah II School for  
Information Technology  
The University of Jordan  
Amman, Jordan

An'am Aladwan<sup>3</sup>

Department of Management  
Information Systems  
Al-Ahliyya Amman University  
Amman, Jordan

**Abstract**—Dynamic load balancing techniques prevents computer nodes from overloading unevenly while leaving other idle. It is considered as one of the most challenging topics in parallel computing. Moreover, it is essential for increasing the efficiency of highly parallel systems especially in solving multitask problems with unpredictable load estimates. Particularly, over each processor in the parallel systems and interconnection networks. This paper focuses on developing an efficient algorithm for load balancing on Hyper Hexa Cell (HHC) interconnection network, namely, HHCLB algorithm. Basically, the Dimension Exchange Method (DEM) approach is used in this paper to construct a new load balancing approach on the network of HHC interconnections. Thus, an algorithm was introduced and simulated using java threads, where the performance of the algorithm is evaluated both analytically and experimentally. The evaluation was in terms of various performance metrics, including, execution time, load balancing accuracy, communication cost. By implementing the proposed load balancing algorithm to the HHC network, a high degree of accuracy and minimal execution time was achieved. It is important to highlight that the algorithm recorded small gap between the execution time for small number of processors and large number of processors. For instance, the algorithm achieved 0.14 seconds for balancing the load of 6 processors while 0.59 seconds for balancing the load of 3072 processors. This proves how effective the algorithm is in balancing the load for different network sizes from small to large number of processors, with a slight difference in execution time.

**Keywords**—Parallel computing; load balancing; Hyper Hexa-Cell; interconnection network; Dimension Exchange Method (DEM)

## I. INTRODUCTION

In parallel systems, during the processing of tasks, the load is dynamically modified. So, during the processing of each task, there is a need to consider the current node of each processor. The literature has suggested many techniques and methodologies for scheduling processes in a distributed or parallel environment. Load balancing is primarily aimed at equalizing the load between the nodes by minimizing execution time and communication delays, optimizing resource efficiency and maximizing throughput [1][2].

To prevent some processors from becoming idle when others have a significant amount of workload, load balancing is concerned with distributing the workload among the processors in a parallel system. Thus, either heavily loaded processors sending loads to other processors or idle processors demanding work from others will perform it. It is critical that a large number of communication steps do not significantly contribute to the overhead of executing the load balancing algorithm.

In any parallel machine, the interconnection network transfers information from the source processor to the destination processor. This task can be achieved with as little latency as possible, enabling a large number of such transfers to occur at the same time. Therefore, in reducing this latency, the topology of the interconnection network plays a significant role. Correspondingly, researchers in this field have proposed many interconnection networks and various parallel algorithms have been used to verify the topological properties of such architectures. One of these interconnection networks is Hyper Hexa Cell, which was built on the advantageous features of the hypercube interconnection network and had attractive topological properties such as diameter, minimum node degree, width of bisection and optical cost [3]. This encouraged the researchers to use this new architecture in solving many parallel algorithms in different fields, such as broadcast communication [4], unicast routing [5] and parallel prefix sum [6]. Moreover the optical links version of this interconnection network namely OTIS-HHC, was exploited by the researchers in order to solve various problems, such as communication algorithms[7], shortest path routing on OTIS-HHC[8], parallel heuristic local search algorithms [9], routing and sorting algorithms[10], parallel quick sort algorithm [11], and traveling salesman problem[12]. Due to the importance of load balancing in parallel architectures, different researches were addressed this problem [13-22]. Among these researches, HHC obtained high speedup as well as efficiency, this is due to the iterative structure that is provided by this interconnection network as well as the high computing capabilities and the minimum communication time that can be achieved by HHC. Therefore, it is worth to solve the load balancing problem on such interconnection network. Based on these observations this paper chose the HHC interconnection network.



This paper focuses on developing an efficient algorithm for load balancing on hyper Hexa Cell interconnection network where a new algorithm is introduced and its performance is evaluated analytically and experimentally, in terms of various performance metrics. To the best of our knowledge, there is no work that has been addressed in the literature to solve the load balancing problem on Hyper Hexa Cell interconnection network, since it is relatively a new optoelectronic architecture.

The structure of this study is as follows: Section 2 shows a brief background about the main concepts that are used throughout this study, Section 3 describes the proposed algorithms, Section 4 describes the analytical evaluation for the two algorithms, Section 5 shows the experimental results and the comparison analysis of our algorithms, and finally the conclusions and future work are presented in Section 6.

## II. BACKGROUND

Hyper Hexa-cell (HHC) which has a  $d$ h dimension, can be considered as an undirected graph that can be generated by substituting  $2^d$  nodes of a hypercube by HHC graph with one dimension [3]. A fusion of an HHC of dimension one and a hypercube of dimension  $d$  is each dimension of the HHC. One is the smallest dimension of an HHC and it is the basis for the other HHC dimensions. For more clarity, HHC of six processors and their labels is as shown in Fig. 1.

A summary of the topological characteristics of the HHC interconnection network in terms of diameter, maximum and minimum node degree, size, total cost and bisection width is provided in this section, as defined in [3]. These topological properties include the diameter, maximum node degree, size, number of links and bisection width. The diameter is the most important property that distinguish each interconnection from the other, it can be defined by the maximal distance between any two processors in the network is the diameter. The diameter of the HHC interconnection network is  $d+1$ , where the maximum distance between one of the top triangle's processors and one of the processors at the bottom of the opposite triangle will always be two steps in each sub-group. For instance, the diameter would be  $1 + 1 = 2$  in the first dimension, and  $2 + 1 = 3$  in the second dimension.

The maximum node degree of interconnection network can be defined by the maximum number of links to which it is connected. Consequently, the maximum node degree of the HHC interconnection network is  $d + 2$ , where each node within each HHC subgroup is connected to three nodes. Also, each node is connected to an equivalent node in an additional dimension by a single link. The maximum node degree, for example, is  $2 + 2 = 4$  in the second dimension.

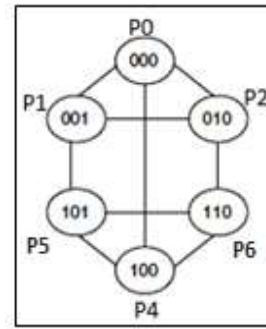


Fig. 1. One Dimensional HHC [3].

Basically, the size of an interconnection network can be considered as the number of processors or nodes in any interconnection network. The size of the HHC interconnection network is  $6 \times 2^{(d-1)}$ , because in HHC interconnection network, the minimum number of nodes is six. For example, the number of processors in the first dimension will be  $6 \times (2^0) = 6$  processors and in the second dimension will be  $6 \times (2^1) = 12$  processors.

The total cost is the total number of communication links that bind the processors within each network group, which can be calculated easily using the following equation:

$$\text{Number of links} = ((6 \times 2^{d-1}) \times (d + 2)) / 2 \quad (1)$$

Precisely, the bisection width is the minimum number of communication links to be eliminated in order to break the network into two equal halves, as defined in equation 2. For example, in the second dimension the cost of HHC will be  $(6 \times 2^1) / 2 = 6$ .

$$\text{Bisection width} = ((6 \times 2^{d-1}) / 2) \quad (2)$$

## III. DIMENSION EXCHANGE METHOD

Balancing is carried out between two processors in the DEM system in such a way that the processor with a greater load sends part of its load to the other processor, so that it has the same load as possible. If the load is indefinitely divisible, exactly the same amount of load will always be taken from each processor. But this is not a realistic assumption of fact in the distribution of tasks [15-16]. By redistributing the tasks through the links of each dimension, this approach goes across all dimensions, from  $d=1$  to  $d = n$ , and balances loads. The processors swap their load sizes in the first dimension, where the higher load processor transfers the excess load to the lower loaded processor; in the second, third and fourth dimensions, the same steps are performed between the processors related. Basically, the DEM approach is used in this paper to construct a new load balancing approach on the network of HHC interconnections.

#### IV. HYPER HEXA CELL LOAD BALANCING ALGORITHM

In this section , the Hyper Hexa Cell Load Balancing (HHCLB) algorithm is introduced, where the pseudo code for balancing the one-dimensional HHC interconnection network is provided, followed by the application of the DEM algorithm to balance the multidimensional HHC, and the best and worst cases of the algorithm are finally defined.

##### A. HHCLB Pseudo Code

The pseudo code of HHCLB basically contains two phases as follows:

Input: Unbalanced P-processors Hyper Hexa Cell

Output: Balanced HHC with equal or approximate load on each processor

##### Phase 1: Processors Load balancing

1. For ( $j=1; j \leq p-1; j++$ )
2. for all pairs of processors  $p_i, p_j$  such that the binary representation of  $i$  and  $j$  differ only in the  $d$ th bit position
3. do in parallel
4.  $avgload = floor( load(p_i) + load(p_j) ) / 2$
5. if  $(load(p_i) > avgload)$
6. send excess load  $(load(p_i) - avgload)$  to neighbor processor along dimension  $d$
7.  $load(p_i) = avgload$
8. else
9. receive excess load  $(load(p_j) - avgload)$  from neighbor processor
10.  $load(p_j) += ( load(p_i) - avgload )$

##### Phase 2: Triangle Load Balancing

11. Consider the HHC as two triangles and balance each one on parallel
12. Exchange  $p_i, p_j, p_k$  loads sizes
13.  $avgload = floor( load(p_i) + load(p_j) + load(p_k) ) / 3$
14. if  $(load(p_j) > avgload)$
15.  $p_j$  send excess load  $(load(p_j) - avgload)$  to  $p_i$  and  $p_k$  processors
16.  $load(p_j) = avgload$
17. else
18.  $p_j$  receive excess load  $(load(p_i) - avgload)$  and  $(load(p_k) - avgload)$  from  $p_i$  and  $p_k$  processors
19.  $load(p_i) = avgload$
20.  $load(p_k) = avgload$

The main phases of this algorithm are as follows:

**Phase1:** Perform load balancing on all HHC processors that differs only in the location of the  $d$ th bit. It includes the steps that follow:

Step 1: the load will be exchanged between the processors that will communicate to balance their loads. So, load balancing will be applied between the processors who differ in the Least Significant Bit (LSB) as depicted in Fig. 2(a) and (b). Then, the Second Significant Bit (SSB) as shown in Fig. 2(c) and (d). Finally, the Most Significant Bit (MSB) as shown in Fig. 2(e) and (f) (Line 2).

Step2: For each pair of processors directly linked along the  $d$ th dimension, the average load is computed. This can be accomplished by considering the floor of the sum of processor's load and dividing it by two (line 4). For example, adding and dividing the load of processors P0 and P1 in LSB step by two and calculate the average load of them as:  $[L_{P0} + L_{P1}] / 2$ . Also, the load of processor P5 and P4 in LSB step will be added and divided by two to calculate the average load of them  $[L_{P5} + L_{P4}] / 2$ . Notice that, we assume that if the average load contains fractions, the remainder, which equals to one, will be added to the AvgLoad of the processors as follows: between P0, P1  $\rightarrow$  P1, between P5, P4  $\rightarrow$  P5, between P1, P2  $\rightarrow$  P1, between P5, P6  $\rightarrow$  P5 in the LSB Step.

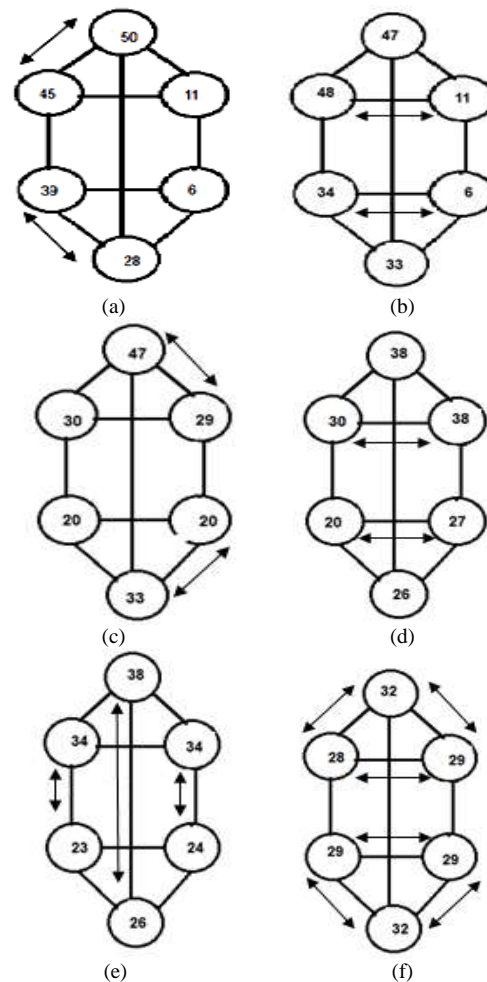


Fig. 2. HHC One Dimensional Load Balancing Example.

Step3: Processors' load redistribution. First, each processor compares its load to the average load (average of the processor's load and its neighbor processor's load). If the processor's load is greater than the average load (line 5), the processor sends the amount of excess load (processor's load minus average load) along the  $d^{\text{th}}$  dimension (line 6), and the processor's load is adjusted to be equal to the average load (line 7). Otherwise, the processor receives the amount of its neighbor's excess load along the  $d^{\text{th}}$  dimension (lines 9-10), and its load is incremented by the amount of its neighbor's excess load.

When the algorithm balances the loads for the processors based on the difference in the least significant bit the remainder will be added to the processors with labels (P1 and P5). When the algorithm balances the processors based on the difference in the second significant bit the remainder will be added to the processors with labels (P2 and P6). In the most significant bit balancing the remainder will be added to the processor with the lower load. After this phase you will have a balanced rectangle of processors P1, P2, P5, and P6 with maximum difference in weight = 2). And the loads of processors P0 and P4 will be either less than or greater than the loads of the processors in this rectangle.

**Phase 2: Triangle Load Balancing**

In this phase, the HHC will be considered as two triangles and the average processor's load in each triangle is calculated (lines 11-14). There will be two cases here: *Case 1* (in lines 15-16), in which the load of processor P0 is greater than the load of processors P1 and P2, in this case, processor P0 will send the excess load to both processor P1 and P2, as depicted in Fig. 2(f).

*Case 2* (in lines 17-20), the load of processor P0 are less than the load of processors with labels P1 and P2, in this case processor P0 will receive the excess load from both P1 processor and P2 processor. This will be applied in parallel with processors P4, P5, and P6. Finally, after applying the two phases a balanced one-dimensional HHC will be obtained, as depicted in Fig. 3.

Regarding the balancing of the other dimensions, where  $d > 1$ , the balancing will be started by applying the DEM algorithm [17-18] on the connected HHC cells. In the two-dimensional HHC, two steps are only needed for load balancing. The first, is to balance the HHC cells in the first dimension while in the second step each processor will be balanced with its directly connected neighbor in the second dimension.

**B. Best and Worst Cases of HHCLB Algorithm**

The best case occurred when the HHC interconnection is almost balanced; in this case, the algorithm will perform only global information collection and average calculation without load balancing steps, because each processor will find out that its load is equal or almost equal to the average load between them. On the other hand, the worst case occurred when all the workload is on one processor P1 while other processors are idle or have very minimum load as shown in Fig. 4.

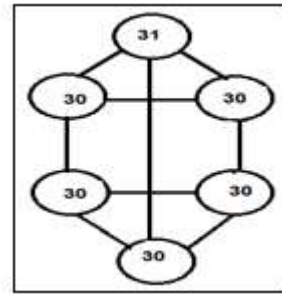


Fig. 3. Balanced HHC.

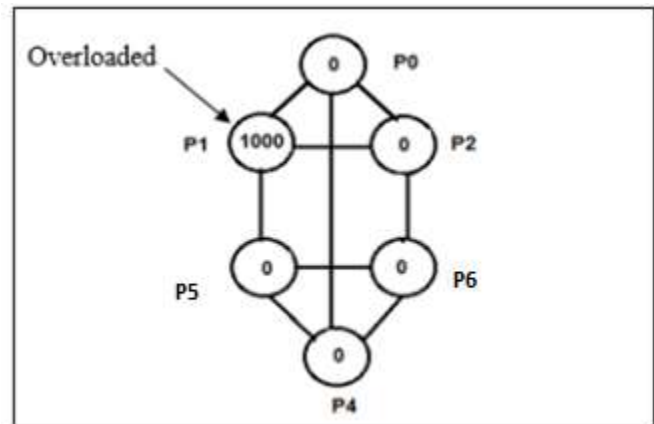


Fig. 4. Worst case of HHCLB Algorithm.

If each processor is assigned at most  $M$  tasks before the load balancing algorithm is performed, then at each step there are at most  $M/2$  tasks to be moved across the edges of dimension.

Assuming the maximum workload is  $M$ . In phase 1, the first step of the algorithm is required to transfer  $M/2$  excess load from  $P1$  to  $P0$ . In step 2,  $M/4$  load will be transferred from  $P1$  to  $P2$ . While in step 3,  $M/8$  load will be transferred from  $P0$  to  $P2$ . In step 4,  $M/16$  load will be transferred from  $P1$  to  $P2$ . In step 5,  $3M/16$  load will be transferred from  $P0$  to  $P4$ . Subsequently, in phase2,  $M/48$  excess load will be transferred by the algorithm. Adding all these loads would result in a first dimension execution time of  $1.2M$ . This will end with every load of  $M/6$  on each processor. On the second dimensions,  $M/6$  will be divided by 2 on the second dimension, resulting in an excess load of  $M/12$  that will be transferred between the two HHC cells. And so forth. Thus, in all dimensions, the total execution time will be as shown in equation (3).

Solving equation (3) results in  $O(M + \ln(d))$  execution time.

$$\text{Total execution time} = 1.2 M + \sum_{i=2}^d \frac{M}{6 \cdot i} \tag{3}$$

**V. ANALYTICAL EVALUATION**

HHCLB algorithm is evaluated in this section in terms of the following metrics: execution time, accuracy of load balancing, and number of communication steps.

### A. Execution Time for HHCLB

The execution time metric calculates the time required to achieve load balancing steps. The worst-case time complexity of the proposed load balancing algorithm on HHC, is the time taken to move the excess load  $M$  from one processor to another, which can be defined as the difference between the maximum load of one processor and the average load of the processor. When all processor loads are zero and processor  $P_1$  has the maximum load, the worst case of HHCLB occurred, this will generate  $O(M + \ln d)$ , as discussed in section IV.

### B. Load Balancing Accuracy

The accuracy in load balancing represents the difference between the maximum and the minimum number of tasks assigned to any processor in the whole interconnection which also defined as the error rate in the algorithm [14].

In the first dimension, HHCLB algorithm generates a maximum error equal to 2, and in the above dimensions it will achieve error with maximum  $e \leq d+1$ .

### C. Number of Communication Steps

Communication cost in load balancing is the number of communication steps that are needed for load balancing [14].

The number of communication steps in phase1 is five steps. But in each step, there are two more additional steps for load exchanging and average load calculation. Therefore, this will produce  $5*3 = 15$  steps. Additionally, in phase2, the number of communication steps will be  $2*3 = 6$  steps. So, in the first dimension, the total number of steps is 21. On the other hand, the maximum number of steps in all dimensions will be increased by three in each dimension, this will result in  $21+3*(d-1) = 3d+18$ . In the worst case, we may have additional three steps over each dimension, Thus the total number of communication steps will be  $6*(d-1) + 21 = 6d+15$ . The summary of the performance metrics is shown in Table I.

TABLE I. SUMMARY OF PERFORMANCE METRICS FOR EVALUATING HHCLB ALGORITHM

| Analysis Metric                           | Equation                                    |
|-------------------------------------------|---------------------------------------------|
| Execution Time in the First Dimension     | $1.2M \rightarrow O(M)$                     |
| Total Execution Time                      | $O(M + \ln(d))$                             |
| Maximum Number of Steps in all dimensions | In average $3d+18$<br>In worst case $6d+15$ |
| Accuracy                                  | $e \leq d+1$                                |
| Links utilized                            | All                                         |

## VI. EXPERIMENTAL RESULTS AND COMPARATIVE ANALYSIS

The experimental results obtained to validate the performance of the proposed algorithms for load balancing in HHC interconnection networks are shown in this section. To implement the algorithm, the simulation environment was set up using the Java Jdk7.2 and Eclipse Java EE IDE environments. All tests were performed on a 16 GB RAM Intel Processor (CPU 3.2 GHz) with 8 MB Cache memory and Windows10 as an operating system.

The implementation was based on the following classes:

- **Topology** class, which connects the multidimensional interconnection of the HHC cells.
- **HHC** class, which according to the HHC interconnection, connects the processors.
- **Node** class, which sets each processor's properties.

The simulation begins by constructing the desired network of interconnections according to the user-determined dimension. To allow parallel execution of the implemented load balancing algorithms, the load balancing mechanism is implemented using multithreading. The library of Java threads is used to build and manage a complex number of threads used to simultaneously perform load balancing steps. Our implementation was done by: load computation, calculation of average load, and transfer of excess load.

### A. Execution Time

Several experiments have been conducted to compute the time required to execute the proposed load balancing method, on 6, 12, 24, 48, 96, 192, 384, 768, 1536 and 3072-processor HHC. That indicates that the experiments were performed for several dimensions starting from dimension one up to dimension ten. The execution of the algorithm was done using the same random number sequences that represents the load of the processors using specific seeds for our random number generator. For this purpose, four seeds were selected: {1, 2, 8, and 12} to run the experiment. Finally, the results were recorded according to the execution time as shown in Table II.

Table II depicts the average execution time in seconds taken by HHCLB to balance the HHC interconnection in different dimensions, in this experiment, the maximum load which assigned to each processor was at most 200 workload units. A careful examination of this table shows that the execution time is increased as the number of processors increases too. For instance, the average execution time for balancing 24 processors is equal to 0.23 seconds, while it takes 0.56 seconds to balance 1536 processors. This shows the efficiency of the HHCLB algorithm, where a large number of processors only need a very limited amount of time to balance their loads.

The preceding discussion concerned with the effect of the size of the network on the execution time. Currently, it is the time to examine the contribution made by the number of workload units allocated to each processor. So, another experiment had been performed with variable average loads sizes assigned to each processor. The load sizes used are at most {10, 50, 100, 500} workload units assigned to each processor as shown in Table III.

Experiments have shown that the number of workloads units allocated to processors have a huge effect on the execution time for a large number of processors. This is more apparent with a greater number of processors. For example, the execution time for HHCLB algorithm with 200 workload units and 24 processors is 0.26 seconds while it is 1.31 seconds for 1000 workload units and 24 processors. As shown in Table III these findings were revealed.

TABLE II. AVERAGE EXECUTION TIME USING HHCLB ON SEVERAL DIMENSIONS OF HHC INTERCONNECTION NETWORK (MAXIMUM LOAD SIZE IS 200 WORKLOAD UNITS PER PROCESSOR)

| No of Processors | HCCLB Algorithm Execution time (Sec) |
|------------------|--------------------------------------|
| 6                | 0.14                                 |
| 12               | 0.19                                 |
| 24               | 0.25                                 |
| 48               | 0.29                                 |
| 96               | 0.35                                 |
| 192              | 0.39                                 |
| 384              | 0.46                                 |
| 768              | 0.53                                 |
| 1536             | 0.56                                 |
| 3072             | 0.59                                 |

TABLE III. AVERAGE EXECUTION TIME IN SECONDS USING HHCLB ALGORITHM ON SEVERAL DIMENSIONS OF HHC (WITH 10,200,400 AND 1000 WORKLOAD UNITS)

| Workload Units | HHC Dimension | No of Processors | HCCLB Algorithm Execution time (Sec) |
|----------------|---------------|------------------|--------------------------------------|
| 10             | 1D            | 6                | 0.01                                 |
|                | 2D            | 12               | 0.015                                |
|                | 3D            | 24               | 0.019                                |
|                | 4D            | 48               | 0.023                                |
|                | 5D            | 96               | 0.026                                |
| 200            | 1D            | 6                | 0.19                                 |
|                | 2D            | 12               | 0.24                                 |
|                | 3D            | 24               | 0.26                                 |
|                | 4D            | 48               | 0.29                                 |
|                | 5D            | 96               | 0.36                                 |
| 400            | 1D            | 6                | 0.29                                 |
|                | 2D            | 12               | 0.41                                 |
|                | 3D            | 24               | 0.54                                 |
|                | 4D            | 48               | 0.59                                 |
|                | 5D            | 96               | 0.63                                 |
| 1000           | 1D            | 6                | 0.77                                 |
|                | 2D            | 12               | 0.93                                 |
|                | 3D            | 24               | 1.31                                 |
|                | 4D            | 48               | 1.46                                 |
|                | 5D            | 96               | 1.72                                 |

### B. Communication Cost

The average number of communication steps was computed among several runs of HCCLB algorithm on different HHC cells in several dimensions from dimension one to dimension ten.

Table IV shows the average number of communication steps required by the algorithm to balance the loads on HHC interconnection network. It is clearly shown that HHCLB algorithm requires small number of communication steps.

TABLE IV. MAXIMUM NUMBER OF STEPS USING HCCLB ALGORITHM ON SEVERAL DIMENSIONS OF HHC INTERCONNECTION NETWORK (MAXIMUM LOAD SIZE IS 200 WORKLOAD UNITS PER PROCESSOR)

| No of Processors | HCCLB Algorithm Communication Steps |
|------------------|-------------------------------------|
| 6                | 18                                  |
| 12               | 24                                  |
| 24               | 30                                  |
| 48               | 33                                  |
| 96               | 39                                  |
| 192              | 45                                  |
| 384              | 48                                  |
| 768              | 51                                  |
| 1536             | 54                                  |
| 3072             | 60                                  |

### C. Load Balancing Accuracy

The variation between the maximum amount of workload units in each processor and the minimum amount of workload units in each other is known as the error which is responsible for determining the accuracy of the load balancing. The accuracy of HHCLB algorithm on different HHC cells in several dimensions from dimension one to dimension ten was computed. The experiments show that the error in the algorithm does not exceed  $d+1$ . For instance, the accuracy for 96 processors is equal to four which is less than the fifth dimension. In addition, Table V showed a very excellent performance, where the accuracy for a very large number of processors such as 3072 processors is only seven. Thus, when the network size becomes very large the error is very small for HHCLB algorithm.

Fig. 5 illustrates a slight increase in accuracy as the number of processors increases.

TABLE V. THE NUMBER OF ERRORS RESULTED AFTER EXECUTING HHCLB OVER DIFFERENT HHC DIMENSIONS

| No of Processors | Dimension of HHC | HHCLB Algorithm Load Balancing Accuracy |
|------------------|------------------|-----------------------------------------|
| 6                | 1D               | 2                                       |
| 12               | 2D               | 3                                       |
| 24               | 3D               | 3                                       |
| 48               | 4D               | 3                                       |
| 96               | 5D               | 4                                       |
| 192              | 6D               | 5                                       |
| 384              | 7D               | 5                                       |
| 768              | 8D               | 5                                       |
| 1536             | 9D               | 6                                       |
| 3072             | 10D              | 7                                       |

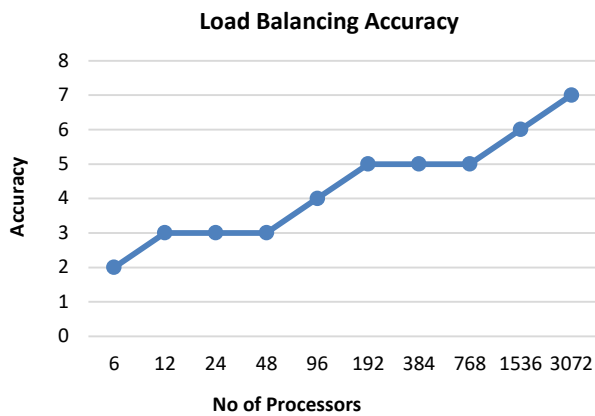


Fig. 5. Accuracy of HHCLB Algorithm.

## VII. CONCLUSIONS AND FUTURE WORK

We presented a new algorithm for balancing the load across the network of HHC interconnections in this paper. Moreover, it was evaluated and implemented. The efficacy of the HHCLB algorithm is proved not only by the parameters of the analytical evaluation, but also by the experimental findings. The results show the effectiveness of the HHCLB algorithm as regards to several performance metrics. Limited execution time was achieved, with a high degree of accuracy by applying the proposed load balancing approach to the HHC network. Consequently, with the time needed to perform load balancing on HHC, it was clear from the empirical and analytical results that the algorithm requires limited number of communication steps. So, the main goal of load balancing for equalizing the load among the processors with a minimization of the execution time and the communication delays is satisfied. Future work includes the extension of the proposed scheme for load balancing to be applied in optoelectronic architecture of the HHC interconnections.

### REFERENCES

- [1] Willebeek-LeMair, H. Marc, and A. P. Reeves, "Strategies for dynamic load balancing on highly parallel computers". *Parallel and Distributed Systems*, IEEE Trans, vol. 4, pp. 979-993, 1993.
- [2] P. Shah and SM. Shah, "Load Balancing in Distributed System Using Genetic Algorithm". *Special issues on IP Multimedia Communications*, vol. 1, pp. 139-142, October 2011.
- [3] B. Mahafzah, A. Sleit, N. Hamad, E. Ahmad, T. and Abu-Kabeer. "The OTIS hyper hexa-cell optoelectronic architecture". *Computing*, vol. 94, pp. 411-432, 2012.
- [4] B. Mahafzah, and I. Al-Zoubi. "Broadcast communication operations for hyper hexa-cell interconnection network." *Telecommunication Systems*, vol. 67, pp. 73-93, 2018.
- [5] J. Al-Sadi. "A New Unicast Routing Algorithm for Hyper Hexa-Cell Interconnection Networks." *International Journal of Information Systems and Social Change (IJSSC)*, vol. 8, pp. 45-57, 2017.
- [6] A. Gupta, and B. Sarkar. "Parallel Prefix Sum Algorithm on Optoelectronic Biswapped Network Hyper Hexa-cell." *International Journal of Computer Network & Information Security*, vol. 10, pp. 27-35, 2018.

- [7] A. Akhtar, K. Lucas, "Comparison of communication algorithms on OTIS-HHC and OTIS-ring parallel architectures". *International Journal of Engineering and Computer Science* vol. 3, pp. 8741-8745, 2014.
- [8] A. Gupta, and B. Sarkar. "Shortest path routing on OTIS hyper hexa-cell." In *Computing, Communication and Networking Technologies (ICCCNT)*, 8th International Conference on, pp. 1-6. IEEE, 2017.
- [9] A. Al-Adwan, B. Mahafzah, and A. Sharieh, "Parallel Heuristic Local Search Algorithm on OTIS Hyper Hexa-Cell and OTIS Mesh of Trees Optoelectronic Architectures", *Applied Intelligence*, vol. 49, pp. 661-688, 2019.
- [10] A. Akhtar, K. Lucas, "Routing and sorting on OTIS-hyper hexa-cell", *International Journal of Engineering & Computer Science* vol. 7, pp. 7388-7393, 2014.
- [11] A. Al-Adwan, R. Zaghoul, B. Mahafzah, and A. Sharieh, "Parallel quicksort algorithm on OTIS hyper hexa-cell optoelectronic architecture", *Journal of Parallel and Distributed Computing*, vol.141, pp. 61-73, 2020.
- [12] A. Al-Adwan, R. Zaghoul, B. Mahafzah, and A. Sharieh, "Solving traveling salesman problem using parallel repetitive nearest neighbor algorithm on OTIS-hypercube and OTIS-mesh optoelectronic architectures". *The Journal of Supercomputing* vol. 74, pp. 1-36, 2018.
- [13] A. Awwad, and J. Al-Sadi. "Efficient Load Balancing Algorithm for the Arrangement-Star Network." *Proceedings of the International Conference on Parallel and Distributed Processing Techniques and Applications (PDPTA)*. The Steering Committee of The World Congress in Computer Science, Computer Engineering and Applied Computing (WorldComp), 2016.
- [14] B. Mahafzah, B. and B. Jaradat, "The hybrid dynamic parallel scheduling algorithm for load balancing on Chained-Cubic Tree interconnection networks". *The Journal of Supercomputing*, vol. 52, pp. 224-252, 2010.
- [15] H. Rim, J. Jang and S. Kim, "An efficient dynamic load balancing using the dimension exchange method for balancing of quantized loads on hypercube multiprocessors". In *Parallel Processing, 1999. 13th International and 10th Symposium on Parallel and Distributed Processing, 1999. IPPS/SPDP. Proceedings IEEE*, pp. 708-712, April 1999.
- [16] G. Jan and Y. Hwang, "An efficient algorithm for perfect load balancing on hypercube multiprocessors". *The Journal of Supercomputing*, vol. 25, pp. 5-15, 2003.
- [17] H. Yuan-Shin H and E. Gene. "A Simple Algorithm for Optimal Load Balancing on Hypercube Multiprocessors", *The journal of supercomputing*, vol. 25, pp. 5-15, 2001.
- [18] B. Mahafzah and B. Jaradat, "The load balancing problem in OTIS-Hypercube interconnection networks". *The Journal of Supercomputing*, vol. 46, pp. 276-297, 2008.
- [19] B. Mahafzah, M. Alshraideh, L. Tahat, and N. Almasri, "Topological Properties Assessment for Hyper Hexa-Cell Interconnection Network", *International journal of computers*, vol. 13, pp 115-121, 2019.
- [20] J. Sadi, "Factor-Optical-Factor Factor Exchanges Method: a new load balancing method for Extended Optical Transpose Interconnection System-n-Cube networks", *Concurrency and Computation: Practice and Experience*, vol. 13, pp.3415-3428,(2015).
- [21] AM. Awwad, J. Al-Sadi, "Investigating the Distributed Load Balancing Approach for OTIS-Star Topology", *International Journal of Computer Science and Information Security*, vol. 14, pp.163-171, 2016.
- [22] AM. Awwad and J. Al-Sadi, J, "The Load Balancing Algorithm for the Star Interconnection Network", *International Journal of Computer, Information, Systems and Control Engineering*, vol. 8, pp.1598-1602. 2015.

# Attribute-Based Encryption for Fine-Grained Access Control on Secure Hybrid Clouds

Sridhar Reddy Vulapula<sup>1</sup>

Research Scholar- KLEF, Vijayawada, A.P. India

Srinivas Malladi<sup>2</sup>

Professor-KLEF, Vijayawada, A.P. India

**Abstract**—In the present scenario, the proliferation of cloud computing services allows hospitals and institutions to move their healthcare data to the cloud, enabling global access to data and on-demand high-quality services at a lower cost. Healthcare data has sensitive attributes to be shielded from leakage due to inference attacks by a curious intruder, either directly or indirectly. A hybrid cloud is a mix of both private and public clouds proposed for the storage of health data. Carefully distributing data between private and public clouds to provide protection. While there has been ample work for the delivery of health data for some time now, it does not appear to be more effective in terms of both data retrieval and consideration for fine-grained access control of the data. This work suggests a cordial approach for a more reliable delivery of data using geometric data disruption of health data over hybrid clouds. It is focused on an in-depth review of the results. The distribution enforces fine-grained data access control using attribute-based encryption. In addition, the approach also addresses a method to effectively extract relevant information from hybrid clouds.

**Keywords**—Secure hybrid cloud; geometric data perturbation; efficiency; fine-grained access control; attribute-based encryption

## I. INTRODUCTION

Recently, many organizations have been in the process of converting data management to cloud storage in the light of factors such as cost-effectiveness, affordability, redundancy, etc. [4]. The use of cloud computing in healthcare companies enables the exchange of inter-organizational medical data. Data protection and privacy are the two most critical things to remember when it comes to cloud data storage. Possible leakage of confidential medical data could compromise the privacy of the person [1]. While encryption methods are used, leakage of sensitive data can still occur by inference, likely contributing to anti-social activities such as extortion, defamation, etc. It is therefore of utmost importance to ascertain the protection and privacy of data stored in the cloud. All approaches currently used for the defense of privacy can be classified as follows:

- Anonymization.
- Randomization.
- Cryptographic techniques.
- Diversification.
- Aggregation.

However, these approaches have some deficiencies related to the size of operations. Lately, hybrid clouds have been

brought forth by many to improve security and privacy [3]. The data is obfuscated or transformed by using specific parameters. The obfuscated data is stored in the untrusted public cloud while the completely trusted private cloud is used to store the parameters used for obfuscation. Through transmitting obfuscated information and parameters used for various data stores, the confidentiality of the obfuscated data is guaranteed even when it is leaked. Certain open issues related to cloud-based hybrid storage solutions are listed here:

- Efficiency in storage and retrieval process.
- Fine-grained access control on the data.

The differential handling of the protection of attributes must be based on the degree of sensitivity. Besides, the fine-grained access control must be carried out for various classes of users. The disrupted data must be indexed for efficient retrieval. The retrieval method must also be secured from inference attacks. In addition to data security, the index must also be protected as private information may be accessed by inference. With these criteria, a stable geometric data disruption approach for health data using hybrid clouds is proposed in this work. The perturbation is controlled through attribute-based encryption [2]. The method also proposes a fine-grained access control on perturbed data with efficient secure indexing and retrieval of information.

## II. RELATED WORK

Authors in [1] suggested a novel means of inter-organizational data exchange for health data. The solution is designed to address the protection and privacy needs of patient data for semi-trusted clouds. Encryption dependent attributes were proposed for limited access in this work. Data distribution through several clouds is achieved by cryptographic hidden sharing [26]. Retrieval of the required data is becoming slightly inefficient in this approach due to the presence of more cloud service providers. A scalable data anonymization technique is proposed in [2]. A proximity privacy model dealing with the semantic proximity of sensitive values and multiple sensitive attributes is proposed to resolve privacy breaches. Proximity-aware agglomerative clustering algorithm groups similar records into hierarchical groups and differential privacy is proposed for these groups. Encryption based attributes (ABE) is used to enhance the security of electronic health records in [3][28]. With the use of ABE, the two-fold benefit of reducing connectivity costs and fine-grained access control is achieved. The authors evaluated the performance of four different ABE systems – CP-ABE, KP-ABE, HBE, DABE. Authors in [4] suggested a solution

to ABE's main distribution problems when used to protect electronic health records in the cloud. Besides, the key distribution method is often streamlined by using attributes and implicit authentication. The scheme is based on the premise that a centralized main issue of authority becomes an obstacle to failure. Encryption based attributes and searchable encryption are suggested for retrieval of fine-grained information-based keywords in [5]. It is a multi-authority scheme and the user hidden key distribution is proposed to solve the problem of key leakage. This scheme is successful for resource-restricted devices and most appropriate for fog computing nodes. A hybrid approach to protecting data sharing in the cloud for privacy is proposed in [6]. Authors in [7] used a reversible Privacy Contrast Mapping (RPCM) algorithm to disrupt info. The algorithm involves two phases of data destruction and data recovery. Perturbation is accomplished by grouping together two adjacent data values. In addition to embedding a watermark, this is accomplished. The troubling data is being restored at the recovery stage. An embedded watermark is used to verify the quality of the data being disturbed. A fast-disrupting tree structure algorithm is proposed in [8]. Disruption time is reduced by using a particular tree-crossing technique using specified tree and table structures [9]. Fuzzy keyword search is suggested along with fine-grained access control of encrypted data. The author also recommended that ABE be moved to the private cloud to reduce the cost of computation at the end of the customer. The Privacy Protection Data Publishing System, called the Hybrid Clouds Cocktail, is proposed in [10]. An Expanded Quasi-Identification-Partitioning (EQI) technique is proposed for the partitioning of data during the data publishing process. The differential privacy technique is used at the level of the data question to protect against infringements of privacy. In addition to reducing the loss of information, this strategy also requires data security. The implementation of an independent data partition strategy is suggested in [11]. Relevant data is stored in a private cloud while the public cloud includes disrespectful data in this scheme. Authors in [12] proposed a two-stage data interruption scheme called RG+RP. The user disrupts data using a non-linear Repeated Gompertz (RG) and then projects data to a lower dimension in a distance-preserving manner using a random project matrix (RP). The use of this two-stage scheme avoids the loss of data due to estimation attacks and independent component analysis attacks. Due to distance preservation, fuzzy c mean clustering can be performed on disrupted data with the same result as that applied to raw data. An assault of resilient geometric data disturbance is proposed in [13] [14]. In this thesis, a multidimensional geometric perturbation method called random disturbance projection is proposed. Authors in [15] suggested rapid indexing for data retrieval in a stable cloud. Compression sensing is used for sampling, compression, and recovery of data. To retrieve data, an encrypted high-performance index is created. A new method of anonymization, which is protected against an attack on identity disclosure, is proposed in [16]. The scheme translates data into fixed intervals and then replaces the original values with the averages. The transformation of data is one way and cannot be restored to the original state. An anonymization scheme based on the data classification capability is proposed

in [17]. The data classification capacity is calculated using shared knowledge. Two K-anonymity algorithms are proposed to transform the data without losing the ability to distinguish. A privacy protection system for association rules data is proposed in [18] [19]. Combined clustering and geometric data disturbance approach to enhancing the privacy of health data in hybrid clouds [20] [21] using the GDP algorithm, which separates data using K-means, making it difficult to identify. Higher entropy attributes are viewed as sensitive and transformed. Authors in [22] [23] proposed a system by which Cloud Service providers could deal with the protection of information provided by remote clients in the cloud. Furthermore, protection can be given to the general public in this application without understanding it personally. The client's confidentiality is done in this way. In this document, Hash Counter Hash (HCH) is the latest protection offered by the suppliers of the administration, and the information is accepted by the information owners, who have finally scrambled the information demanded by the clients and unscrambled the information for use. A modern decentralized approach to access control in [24] is implemented, i.e. Scalable Attribute-Based Encryption (SABE) to achieve versatile and scalable access control in cloud computing for safe cloud storage. SABE not only performs scalable due to its pyramid structure, but also shares powerful and versatile access control support for ABE, it also assigns user expiry and revocation time efficiently to existing schemes. Thus, in this paper, we propose and build Transmitted Team Key Management (TTKM) where each client (user) in the community shares a hidden trust key owner with subsequent re-keying for data sharing through entering or leaving users' needs only broadcast messages between data sharing in the cloud. We evaluate the privacy of the proposed TTKM scheme and compare it to the current SABE protection scheme for distributed data sharing. Experimental findings showed successful regulation of data access with security considerations. Writers of [25] projected how to provide protections for data stored in the cloud. Data stored in the cloud can be either public data requiring minimal protection or extremely sensitive data requiring high protection. We evaluate the privacy of the proposed TTKM scheme and compare it to the current SABE protection scheme for distributed data sharing. Writers of [25] projected how to provide protections for data stored in the cloud. Data stored in the cloud can be either public data requiring minimal protection or extremely sensitive data requiring high protection. This can be achieved by authenticating the client. In addition, there are a range of similar security and privacy concerns that fall under two broad categories: security and privacy concerns faced by cloud providers and their customers. With the available algorithms that are used to convert plain text to cypher text, apply the principle of steganography to the cypher text and make protection more effective and protect data from unauthorized access. We need a reliable framework to resolve security concerns at the time of data processing in the cloud. As a result, authors in [26] trying to find the best method for accessing cloud data by comparing all attribute-based encryption, such as KP-ABE, CP-ABE and HASBE, addressed the different features of these ABE systems by discussing all features of these schemes



in a tabular manner. Features such as Access Policy, Attributes Fine graininess Access Control, Overhead Computation, Performance, User Revocation, Scalability, and Collision-Resistance were addressed in depth, including Advantages and Limitations. It is suggested in the [27] Biometric Access Scheme that specifies that the biometric data is encrypted and submitted to the cloud server. In which biometric access is encrypted, database providers can then send data to the cloud. Cloud performs some encrypted database operations to send to it and returns the output to the database owner. Security analysis shows that the scheme is protected even though attackers try to target the database and want to access the data of users present in the cloud. Compared to the other protocols, the results inform us that the scheme has achieved better efficiency. Authors in [28] proposed a CSHQS (Cloud Protection Hybrid Querying System) algorithm that efficiently processes data security in a hybrid cloud, and that sub-query framework handles different components.

### III. SEARCHABLE FINE ACCESS CONTROL ON SECURE HYBRID CLOUDS (SFAC-SHC)

The architecture of the new Secure Hybrid Cloud Fine Access Control (SFAC-SHC) is shown in Fig. 1. The suggested solution includes the following steps:

- CP-ABE based key generation.
- Fine-grained access control.
- Geometric perturbation.
- Secure Retrieval.

#### A. CP-ABE based Key Generation

Of the four-basic setup, key generation, encryption, and decryption algorithms, only two stages of setup and key generation are used in this work. The key authority or generation center produces both public and private keys. When the data owner uploads the file, the key authority needs a policy of access for each user in terms of attributes to the key authority. The qualified key authority shall produce a single public and private key for each access policy. The public key / private keys corresponding to the policy are sent to the data owner and the private key is given to the corresponding data users when the information is requested.

The access policy used in this work consists of two sets of information:

- 1) Attribute – value pairs of the user
- 2) Fields or Column names in the dataset allowed for view for the user.

The key generation is based on the policy attribute-value pairs. The file or column name for access is managed by the fine-grained access control point.

#### B. Fine-Grained Access Control

The health care dataset uploaded by the data owner is a table format for each patient row and each column is a field. The dataset (Table I) has three classes of information: Class 1, Class 2 and Class 3.

The data owner encrypts Class 1 information with the public key obtained by the key authority using any symmetric key algorithm and generates a processed data set. Each row has an identifier that can be either a unique string or a number.

An association map is created between the policy private key and the field or column names permitted to be accessed by users who comply with this policy. The processed dataset and the association map are sent to a private cloud for geometric perturbation (Fig. 1).

#### C. Geometric Perturbation

The field or column names to be managed are collected for each mapping in the association map. A random geometric disturbance key is generated, which is a multiplication transformation sequence (TP), a translation (Vs) and a distance disturbance (D).

$$GDP(P) = TP + V_s + D$$

Where D is given as

$$D = \frac{1}{\sigma\sqrt{2\pi}} e^{-\frac{(x-\mu)^2}{2\sigma^2}}$$

TABLE I. DATASET AND ITS CLASSES

|         |                                                                                             |
|---------|---------------------------------------------------------------------------------------------|
| Class 1 | Overly sensitive information that cannot be shared by the data owner                        |
| Class 2 | Sensitive information that can be shared and fine grain controlled for the accessing users. |
| Class 3 | Insensitive information that can be shared without any security concerns                    |

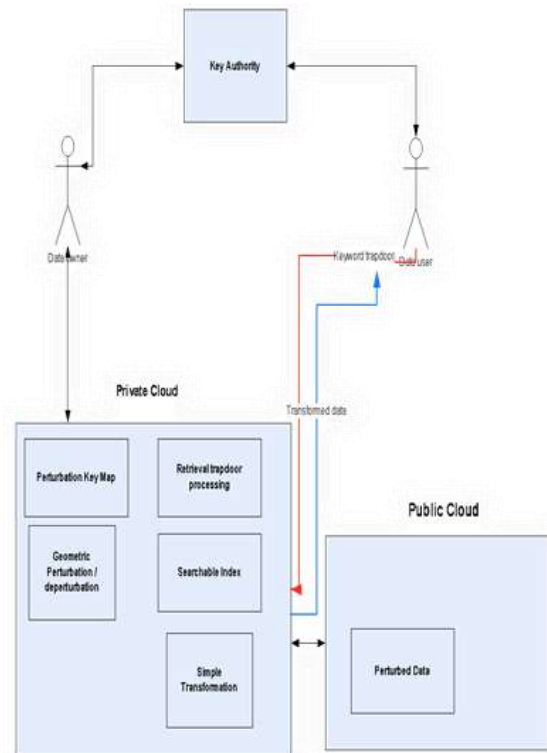


Fig. 1. Architecture of SFAC-SHC.

Where T is a random projection matrix, P is a matrix to be transformed, Vs is a translation matrix, D is a random Gaussian noise. The advantage in this disturbance is that even after the perturbation has been applied, geometric properties such as distance are preserved in the transformed dataset. The fields in the data to be tested are copied to a separate table along with the corresponding identifier. Leaving the identifier, the rest of the columns in the separate table are disturbed by using the generated geometric disturbance key. For this disturbed data, a random file name is created, and this file is transferred to the public cloud for storage. An entry is added to the perturbation key map mapping between the hash of the private key and the following information:

|                       |                                                                                                          |
|-----------------------|----------------------------------------------------------------------------------------------------------|
| Hash<br>(Private key) | Field name perturbed<br>Perturbation key<br>Perturbed file name (saved in a public cloud)<br>Private key |
|-----------------------|----------------------------------------------------------------------------------------------------------|

The hashing function to be used is transmitted to the private cloud by the data owner. The data owner also sends this hashing function to the main authority to distribute it to the data users. Data Perturbation algorithm is used for geometric disturbance.

#### D. Data Perturbation Algorithm

Input: Original data D, its size n and delicate characteristic [S]

output: Perturbed data set D<sup>I</sup>

Steps:

- The sensitive attributes are rotated 180° clockwise and the result is a rotation matrix  $[RT]_{n \times 1}$
- The result of  $[RT]_{n \times 1}$  and the  $[S]_{n \times 1}$  is obtained in step 3. The duplicated esteems will be,  $[X]_{n \times 1} = [RT]_{n \times 1} \times [S]_{n \times 1}$
- The translation transformation matrix is computed  $[T]$  as a mean of sensitive attribute  $[S]_{n \times 1}$
- Generate transformation  $[TS]_{n \times 1}$  by applying the transformation matrices to  $[S]_{n \times 1}$ .
- Compute Gaussian distribution as a probability density function for Gaussian noise

$$\Omega = \frac{1}{\sigma\sqrt{2\pi}} e^{-\frac{(x-\mu)^2}{2\sigma^2}}$$

where  $\mu$  = mean and  $\sigma$  = variance

- Now the perturbation data is  $D^I = [X]_{n \times 1} + [VS]_{n \times 1} + \Omega$

It is detailed in our earlier work [20].

In addition to perturbation, a searchable index is constructed between the field values to the row index of the dataset.

#### E. Secure Retrieval

The data user can retrieve data in two modes-all data or fit a specific field value pair.

For retrieval in all data mode, the data user first retrieves the private key from the key authority for its corresponding attributes. The private key and the hashing function are returned to the key authority. The secret key is hacked and then sent to the private cloud. At the private cloud, a lookup is performed on a disturbance key mapping to find a match for a hashed private key. If a match could not be identified, the retrieval would fail. If a match is found, the following information is retrieved from the mapping:

- 1) Field name perturbed
- 2) Perturbation key
- 3) Perturbed file name (saved in a public cloud)
- 4) Private key.

The disrupted file is retrieved from the public cloud, and the de-disruption key is retrieved from the files. We use the Data De-disruption algorithm given below for geometric de-disruption.

#### F. Data De - Perturbation Algorithm

Input: Perturbed data D<sup>I</sup>, sensitive attribute [S]

Output: Original data D of the perturbed data D<sup>I</sup>

Steps:

- Given the perturbed dataset D<sup>I</sup>, its tuple estimate n and the relating sensitive attribute  $[S]_{n \times 1}$
- Sensitive attribute  $[S]_{n \times 1}$  is rotated in 180° counter clock-wise direction, so the random rotation matrix  $[RT]_{n \times 1}$  is generated.
- The result of  $[RT]_{n \times 1}$  is and  $[S]_{n \times 1}$  is obtained in step 3. The duplicated esteems will be,  $[X^I]_{n \times 1} = [RT]_{n \times 1} \times [S]_{n \times 1}$
- Compute the translation transformation matrix  $[TS]_{n \times 1}$  as mean of sensitive attribute  $[S]_{n \times 1}$
- Generate transformation  $[VS^I]_{n \times 1}$  by applying the transformation matrices to  $[S]_{n \times 1}$
- Compute Gaussian distribution  $\Omega^I$
- Now the result data is  $P = [X^I]_{n \times 1} + [VS^I]_{n \times 1} + \Omega$

The data after de-disruption must not be submitted directly to the customer. The private key, along with the current hour, is hashed to a numeric code and a simple transformation operation is performed on the values of the field with a numeric code (like a progressive addition). This transition helps prevent attacks from being captured by the network. At the end of the data user, the opposite of simple transformation (like progressive subtraction) is performed using the private key and the current time to get the original data.

The retrieval method is secure against network capture attacks due to the exchange of only transformed data between the private cloud and the user. The data retrieval from cloud to user end is masked with a quick transformation. Without the details on the private key and the parameter used for hashing (here is the current time), the removal of the mask is not possible. Even if a network capture attack is performed, the recovered data is still masked and stable.

The proposed scheme also supports the importance of the field retrieval. The field and the corresponding value to be searched are encrypted by a private key using an asymmetric cryptographic algorithm and sent to a private cloud. This encrypted value is called a search door. Because the field name and corresponding value are encrypted, it is difficult for the network to catch attacks to compare between the search information and the outcome. The filed name and the corresponding meaning are decrypted in the private cloud. Lookup is performed on a disturbance key mapping to find the match. If a match could not be identified, the retrieval would fail. If a match is made, the following information is recovered from the mapping table:

- 1) Field name perturbed
- 2) Perturbation key
- 3) Perturbed file name (saved in the public cloud)
- 4) Private key.

If the field name given for the search in the field name list has been interrupted, the search will continue, otherwise the error will be returned. The fine-grained access control is then applied even while searching. The value of the search field is searched in the searchable index of the match field. If no matching row index is found, an error is returned. If indexes of the matching row are found, those specific row indexes will be retrieved from the public cloud. De-disruption occurs in the obtained row indexes. If the field name given for the search in the field name list has been interrupted, the search will continue, otherwise the error will be returned. The fine-grained access control is then applied even while searching. The value of the search field is searched in the searchable index of the match field. If no matching row index is found, an error is returned. If indexes of the matching row are found, those specific row indexes will be retrieved from the public cloud. De-disruption occurs in the obtained row indexes. The data after de-disruption must not be submitted directly to the customer. The private key, along with the current hour, is hashed to a numeric code and a simple transformation operation is performed on the values of the field with a numeric code (like a progressive addition). At the end of the data user, the opposite of simple transformation (like

progressive subtraction) is performed using the private key and the current time to get the original data.

#### IV. PROPOSED SOLUTION

The proposed solution has the following novel aspects:

1) The data owner has more control over highly confidential information and though the data is uploaded to the cloud. This is activated by transferring unnecessarily confidential information to Class 1 and encrypting the data owner's public key. This information cannot be accessed without the owner sharing this key.

2) The data transmitted from the cloud to the user is simply translated to the private key and the current time. It is also difficult for network attackers to collect and decode information from it.

3) Users accept two types of retrieval. Retrieval may be either a whole file or several records that meet a criterion.

4) Fine-grained field-level access control is implemented for users in both retrieval modes.

5) The data owner has more control about which users he wants to share data based on the user's attributes.

#### V. RESULTS

The performance of the proposed searchable fine access control on secure hybrid clouds (SFAC-SHC) is compared in different aspects of

- Perturbation efficiency.
- Data storage and retrieval efficiency.
- Security against attacks.

The arrhythmia dataset from the UCI machine learning repository is used for evaluation [21].

##### A. Perturbation Efficiency

The disturbance efficiency of the proposed solution is compared to the RG+RP algorithm proposed in [12]. K-Means clustering is done on the original data as well as on the disrupted data produced by the proposed RG+RP. The accuracy of the clustering is determined between.

1) The clusters used the proposed cluster and the initial data set cluster.

2) Clusters used RG+RP and the cluster of the original data set.

The clustering accuracy is calculated as

$$ACC = \frac{1}{N} \sum_{i=1}^k (|Cluster_i(P)| - |Cluster_i(P')|)$$

Where P is the original data, P' is the transformed data, k is the number of clusters and N is the number of items in the dataset. The result of clustering accuracy (Table II) is measured for different k values and the result.

The clustering accuracy (Fig. 2) lies more in the proposed solution as the transformation method adopted retains the geometrical properties even after transformation.

TABLE II. RESULT OF CLUSTERING ACCURACY FOR DIFFERENT VALUES OF K

| K | Clustering accuracy in RG+RP [12] | Clustering accuracy in Proposed |
|---|-----------------------------------|---------------------------------|
| 2 | 66.23                             | 65.89                           |
| 3 | 66.56                             | 71.25                           |
| 4 | 73.33                             | 74.59                           |
| 5 | 67.22                             | 79.58                           |

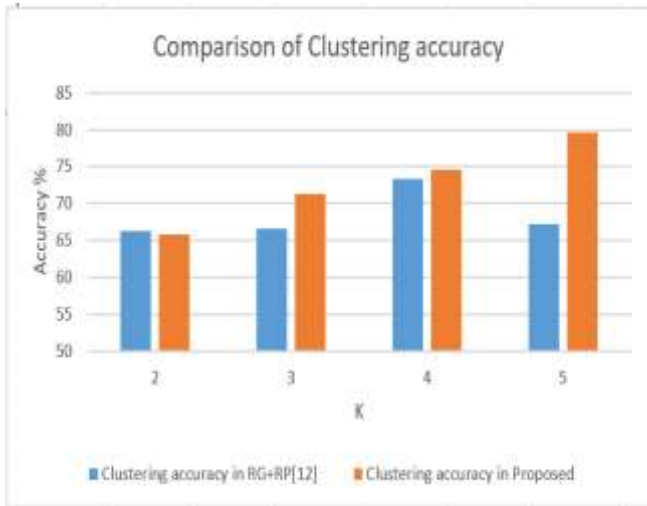


Fig. 2. Comparison of Clustering Accuracy.

### B. Data Storage and Retrieval Efficiency

Performance of the proposed method is compared with a similar approach to the fine-grained searchable retrieval system proposed in [5]. Output is contrasted with the following parameters by changing the number of attributes:

- 1) Key generation time.
- 2) Index generation time.
- 3) Trapdoor generation time.
- 4) Search time.

The key generation time (Fig. 3) is comparatively shorter in the proposed solution as the key size (16 bytes) is shorter in the proposed solution compared to [5].

The index generation time (Fig. 4) is shorter in the proposed solution compared to [5] as the index is computed only in certain fields as needed by users. But the index [5] is optimized for all fields, and this increases the generation time of the index.

The time of generation of trapdoor (Fig. 5) or encrypted search keywords in the proposed solution is lower than [5]. This reduction is due to the reduced key size and the less rounded AES for trapdoor generation in the proposed solution.

Retrieval time (Fig. 6) is also shorter in the proposed solution compared to [5]. Reasons for shorter recovery time are attributed to lower rate of trapdoor decryption, index scanning, and lower time for de-disruption and easy transformation.

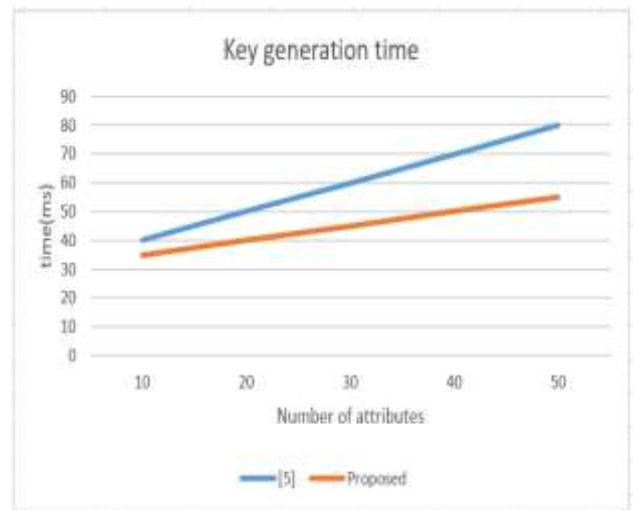


Fig. 3. Key Generation Time.

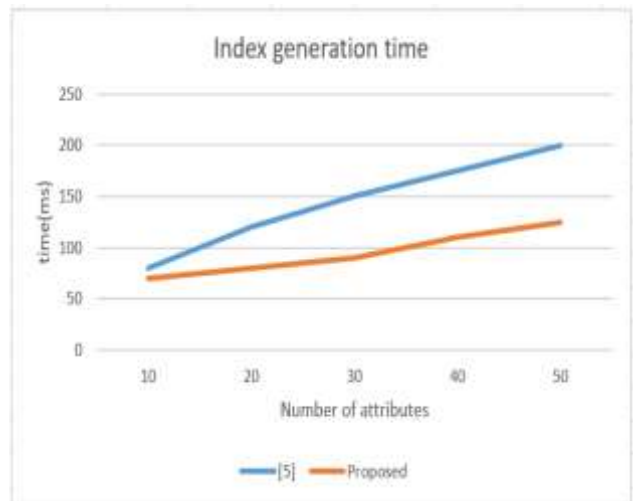


Fig. 4. Index Generation Time.

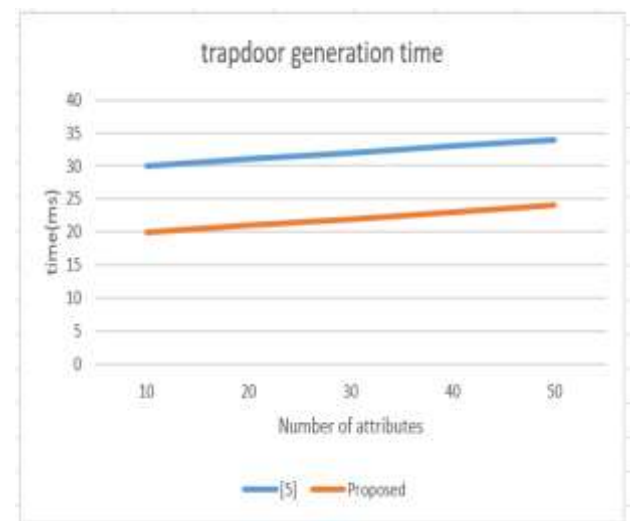


Fig. 5. Trapdoor Generation Time.

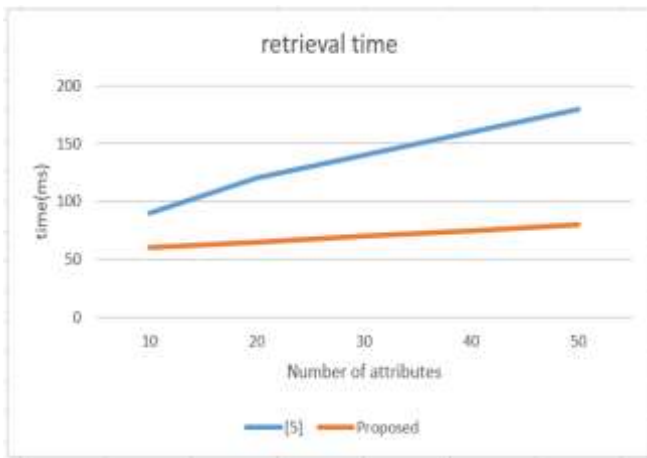


Fig. 6. Retrieval Time.

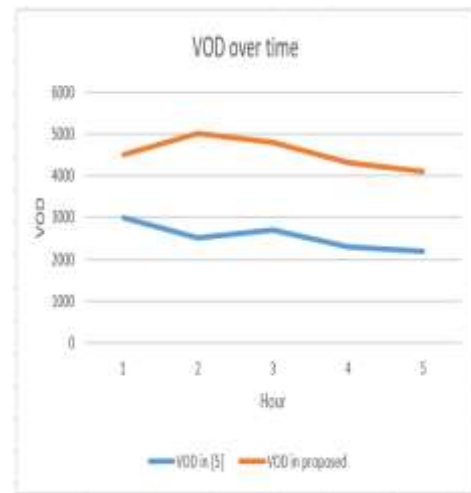


Fig. 7. VOD Overtime.

### C. Security against Attacks

The security of the proposed solution is measured in terms of the complexity of estimating the original data from the disrupted data by an intruder who extracts the disrupted data from the cloud. There are two types of fields to protect privacy in the dataset:

- 1) Class 1
- 2) Class 2

Class 1 data is overly sensitive. Class 2 is confidential information that can be shared, and fine grain regulated for users who have access to it. In the proposed scheme, the Class 1 fields are encrypted with AES and geometric disturbances are added if they need to be exchanged. Class 2 fields are subject only to geometric disturbance. The variance of the difference-based method is used to measure the degree of difficulty. Let the difference between the data in the original column and the projected data be the random variable  $D_i$ . Without any knowledge of the original results, there is a mean and variance of the difference in the accuracy of the calculation. Since the mean difference can be easily omitted if the attacker can approximate the original column distribution, only the difference variance (VoD) is used as the primary metric to evaluate the degree of difficulty in estimating the original results.

Let  $X_i$  be a random variable representing the column  $i$ ,  $X_i^I$  be the estimated result of  $X_i$  and difference  $D_i = X_i^I - X_i$ . Let mean of  $D$  be  $E(D_i)$  and variance is  $Var(D_i)$ . VOD for column  $i$  is  $Var(D_i)$ . VOD is measured for each column and average VOD is given as a privacy measure(pm)

$$pm = \frac{\sum_{i=1}^N VOD_i}{N}$$

A guess is launched for 5 hours on the perturbed data and the privacy measure (pm) is measured for every 1-hour interval and plotted below.

It can be seen from the results that VOD (Fig. 7) in the proposed solution is extremely high compared to VOD in [5]. Higher VOD means that it is difficult to locate the closest approximation of the original data from the disturbed data. VOD increased in the proposed solution due to geometric disruption combined with encryption for data fields of class 1.

### VI. CONCLUSION

In this work, a searchable fine access control for stable hybrid clouds (SFAC-SHC) is proposed. The scheme uses multiple concepts of CP-ABE, fine-grained access control, geometric disruption, and searchable indexing of disrupted data. Stable Perturbed data is maintained in an untrusted public cloud with no chance of leakage. The information needed to interrupt data on the public cloud is stored in the private cloud. The proposed scheme is safe against network capture attacks and unauthorized access attacks. Fine-grained access control is a field-wise exercise, so that knowledge is strictly regulated. The work is focused on the premise that there is full confidence in the private cloud. As future work, the work needs to be optimized for a semi-trusted private cloud by unloading some of the operations to the respective data owner or data consumers.

### REFERENCES

- [1] X. Liu, R.H. Deng, Y. Yang, H.N. Tran, and S.Zhong, Hybrid privacy-preserving clinical decision support system in fog-cloud computing, Future Generation Computer Systems.2018; vol.78,pp.825-837.
- [2] Zhang, Xuyun, et al. "Proximity-aware local-recoding anonymization with mapreduce for scalable big data privacy preservation in cloud." IEEE transactions on computers 64.8 (2014): 2293-2307.
- [3] Li, Jin, et al. "Secure attribute-based data sharing for resource-limited users in cloud computing." Computers & Security 72 (2018): 1-12.
- [4] Achampong, Emmanuel & Dzidonu, Clement. (2016). Optimising Attribute-based Encryption to Secure Electronic Health Records System within a Cloud Computing Environment. 27-34. 10.21742/ijcs.2016.3.2.04.
- [5] Jin Sun, Xiaoqing Wang, "A searchable personal health records framework with fine-grained access control in cloud-fog computing", PLOS ONE, 2018.
- [6] J. Yang, J. Li, and Y. Niu, "A hybrid solution for privacy preserving medical data sharing in the cloud environment", Future Generation Computer Systems, Vol. 43-44, No. 2, pp. 7486, 2015.

- [7] Kao, Yuan-Hung & Lee, Wei-Bin & Hsu, Tien-Yu & Lin, Chen-Yi & Tsai, Hui-Fang & Chen, Tung-Shou. (2015). Data Perturbation Method Based on Contrast Mapping for Reversible Privacy-preserving Data Mining. *Journal of Medical and Biological Engineering*. 35. 10.1007/s40846-015-0088-6.
- [8] Yun, Unil & Kim, Jiwon. (2015). A fast perturbation algorithm using tree structure for privacy preserving utility mining. *Expert Systems with Applications*. 42. 1149–1165. 10.1016/j.eswa.2014.08.037.
- [9] J.Li, J.Li, X.Chen, Z.Liu, and C.Jia, Privacy preserving data utilization in hybrid clouds, *Future Generation Computer Systems*.2014;vol.30, pp.98-106.
- [10] H. Zhang, Z. Zhou, L. Ye and X. Du, "Towards Privacy Preserving Publishing of Set-Valued Data on Hybrid Cloud," in *IEEE Transactions on Cloud Computing*, vol. 6, no. 2, pp. 316-329, 1 April-June 2018.
- [11] Z. Zhou, H. Zhang, X. Du, P. Li and X. Yu. Prometheus: Privacy-Aware Data Retrieval on Hybrid Clouds. In *Proc. of INFOCOM*, 2013.
- [12] Lyu, Lingjuan & Bezdek, James & Law, Yee Wei & He, Xuanli & Palaniswami, Marimuthu. (2018). Privacy-preserving collaborative fuzzy clustering. *Data & Knowledge Engineering*. 10.1016/j.datak.2018.05.002.
- [13] Chen, Keke & Sun, Gordon & Liu, Ling. (2007). Towards Attack-Resilient Geometric Data Perturbation. 10.1137/1.9781611972771.8.
- [14] Chen, K., Liu, L. Geometric data perturbation for privacy preserving outsourced data mining. *Knowl Inf Syst* 29, 657–695 (2011).
- [15] X. Yuan, X. Wang, C. Wang, J. Weng and K. Ren, "Enabling Secure and Fast Indexing for Privacy-Assured Healthcare Monitoring via Compressive Sensing," in *IEEE Transactions on Multimedia*, vol. 18, no. 10, pp. 2002-2014, Oct. 2016.
- [16] A. Majeed, "Attribute-centric anonymization scheme for improving user privacy and utility of publishing e-health data," *Journal of King Saud University - Computer and Information Sciences*, 2018.
- [17] Li, Jiuyong & Liu, Jixue & Baig, Muzammil & Wong, Raymond. (2011). Information based data anonymization for classification utility. *Data Knowledge. Eng.* 70. 1030-1045. 10.1016/j.datak.2011.07.001.
- [18] P. Cheng, J. Roddick, S. Chu, and C. Lin, "Privacy preservation through a greedy, distortion-based rule-hiding method," *Applied Intelligence*, vol. 44, no. 2, 2015, pp. 295-306.
- [19] Sabin Begum, R., Sugumar, R. Novel entropy-based approach for cost-effective privacy preservation of intermediate datasets in cloud. *Cluster Comput* 22, 9581–9588 (2019).
- [20] Vulapula Sridhar Reddy, Barige Thirumala Rao, "A Combined Clustering and Geometric Data Perturbation Approach for Enriching Privacy Preservation of Healthcare Data in Hybrid Clouds", *International journal of engineering and systems*, Oct 2017.
- [21] <https://archive.ics.uci.edu/ml/datasets/Arrhythmia>.
- [22] Ruth Ramya K., Saikrishna D.N.V., Sravya Nandini T., Tanmai Gayatri R., "A survey on using biometrics for cloud security". *International Journal of Engineering and Technology(UAE)*, 2018.
- [23] Vurukonda N., Thirumala Rao B., "Hash counter hash method for privacy and security in cloud computing with attribute-based encryption", *Journal of Advanced Research in Dynamical and Control Systems*, 2017.
- [24] Ranjeeth Kumar M., Srinivasu N., Reddy L.C., "Fine grained multi access control via group sharing in distributed cloud data", *Journal of Theoretical and Applied Information Technology*, 2017.
- [25] Wadhya R., Divya Harika B., Sandeep Reddy C., Krishna Reddy V., "Security for data storage in cloud", *Journal of Advanced Research in Dynamical and Control Systems*, 2017.
- [26] Vurukonda N., Thirumala Rao B., "Secure sharing of outsourced data in cloud computing with comparison of different attribute based encryption", *Journal of Advanced Research in Dynamical and Control Systems*, 2017.
- [27] Dr.V.Naresh, T.Gopi Venkata Ajay, T.Naga Sai Reddy, M.Srinivas, "An Efficient And Privacy Preserving Biometric Authentication Scheme In Cloud Computing", *International Journal Of Scientific & Technology Research* Volume 9, Issue 01, January 2020 Issn 2277-8616.
- [28] Vulapula Sridhar Reddy, Malladi Srinivas, "Secure Data Accessing Over Cloud Computing Environment Using Hybrid Query", *Jour of Adv Research in Dynamical & Control Systems*, Vol. 10, 14-Special Issue, 2018.

# Gabor Capsule Network for Plant Disease Detection

Patrick Mensah Kwabena<sup>1</sup>, Benjamin Asubam Weyori<sup>2</sup>

Department of Computer Science and Informatics  
University of Energy and Natural Resources  
Sunyani, Ghana

Ayidzoe Abra Mighty<sup>3</sup>

School of Information and Software Engineering  
University of Electronic Science and Technology of China  
Chengdu, China

**Abstract**—Crop diseases contribute significantly to food insecurity, malnutrition, and poverty in Africa where the majority of the population is into Agriculture. Manual plant disease recognition methods are widespread but limited, ineffective, costly, and time-consuming making the need to search for automatic and efficient methods of recognition more crucial. Machine learning and Convolutional Neural Networks have been applied in other jurisdictions in an attempt to solve these problems. They have achieved impressive results in this domain but tend to be ‘data-hungry’, invariant, and vulnerable to attacks that can easily lead to misclassifications. Capsule Networks, on the other hand, avoids the weaknesses of CNNs and has not been widely used in this area. This article, therefore, proposes the use of Gabor and Capsule network to recognize blurred, deformed, and unseen tomato and citrus disease images. Experimental results show that the proposed model can achieve a 98.13% test accuracy which is comparable to the performance of state-of-the-art CNN models in the literature. Also, the proposed model outperformed two state-of-the-art deep learning models (which were implemented as baseline models) in terms of robustness, flexibility, fast converges, and having fewer parameters. This work can be extended to other crops and may well serve as a useful tool for the recognition of unseen plant diseases under bad weather and bad illumination conditions.

**Keywords**—Convolutional neural networks; capsule network; gabor filters; crop diseases; machine learning

## I. INTRODUCTION

Tomatoes and Citrus are major economic crops that are widely cultivated in developing countries where the majority of the farmers have little or no knowledge about the diseases that can affect these crops and how they can be controlled. These crops also form part of the daily nutritional requirements of many people necessary to maintain good health. However, both crops are plagued with several types of diseases that require timely and accurate identification to prevent crop losses. Current identification methods are manual which is laborious, time-consuming, and error-prone especially during the early stages. Newer automatic recognition methods [1] are therefore needed. Convolutional Neural Networks (CNNs) including state-of-the-art deep transfer learning models such as AlexNet [2], ResNet [3], VGG [4] and GoogleNet [5] have been used to identify crop diseases [6][7][8][9]. However, the problem is that they use max-pooling and are deeper (the deeper the CNN, the better the performance [10]). Max-pooling makes the network invariant requiring a lot of data to avoid overfitting. Depth, on the other hand, comes with some drawbacks such as a large

number of parameters, high complexity, high memory requirements, and high computational demands.

Hasan et al. [11] collected a tomato disease dataset and used the pre-trained weights of GoogleNet and InceptionV3 for classification. A 90% and 10% division for training and test respectively resulted in 99% overall classification accuracy. A further division of 80%, 20% for training and testing respectively resulted in 92% accuracy. Fuentes et al. [12] combined Faster Region-based CNNs and Single Short Multibox Detector (SSD) algorithms with deep feature extractor pre-trained models such as VGG and ResNet for tomato disease/pest recognition to obtain 85.98% accuracy. Zhange et al. [13] trained AlexNet, ResNet, and GoogLeNet on the Plant Village (PV) [14] dataset obtaining 97.28% accuracy. This same dataset was used by Iandola et al. [15], Durmus et al. [16], and Krishnaswamy et al. [17], to evaluate the performance of AlexNet and SqueezeNet, AlexNet (95.65%), AlexNet and VGG16 (99.24% for 6 classes) respectively. In [18], a modified LeNet [19] was used to obtain 94.85% accuracy on the PV dataset. Nine out of ten classes of the PV dataset were used by Brahimi et al. [20] to fine-tune GoogleNet and AlexNet resulting in 99.18% accuracy. In [21], VGGnet was trained and evaluated on the PV dataset achieving a classification accuracy of 95.24% while AlexNet and GoogleNet obtained 84.58% test accuracy on the same dataset.

Wang et al. [22] collected sick tomato leaf images from the internet and trained a region-based CNN (R-CNN) to detect disease types and areas of infection. Their networks were so deep that ResNet-101 obtained 23.25 hours of training time.

Other plant disease detection models in the literature [23][1][24][25][26] achieved good results, however, most of them are deep, complex, invariant, not robust, low performing, and lack flexibility. Additionally, they are invariant, cannot encode hue, texture, spatial orientation, and deformation. These weaknesses led to the introduction of Capsule Networks (CapsNets) [27] which are capable of encoding spatial information, texture, hue, and deformation. Capsules perform well on smaller datasets and are well suited for crop disease recognition since texture and orientation play key roles in the recognition of leaf parts that do not conform to the other parts of the leaf. However, capsules have a problem in recognizing real images with complex backgrounds [28].

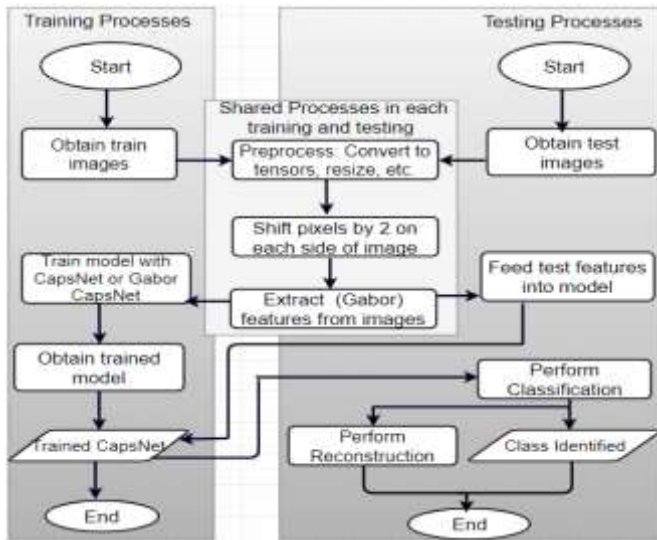


Fig. 1. Workflow Diagram Adopted in this Study.

This paper adopts Capsule’s dynamic routing algorithm by adding a Gabor layer [29] to further enhance its textural and spatial recognition capabilities. The workflow adopted for the proposed work is shown in Fig. 1.

Experimental results on two datasets show that the Gabor CapsNet outperformed both the state-of-the-art CNN baseline models and a CapsNet model on deformed images and unseen images. The proposed model also proved to be more flexible and converges faster than the baseline models. A model’s flexibility and ability to generalize on unseen/deformed data is crucial for the control of plant diseases such as the *early blight* tomato disease which is spread by wind and splashing rain.

The main contributions of this paper are: 1) reusing existing methods to improve the robustness and flexibility of CapsNets on deformed, blurred, and spatially rotated images. The results demonstrate the feasibility of using Gabor Capsules for plant disease recognition under subnormal conditions, 2) the proposed model outperforms existing state-of-the-art CNN models in terms of accuracy and also has fewer parameters compared to deep CNN models in the literature except for GoogleNet, 3) the Gabor-CapsNet architecture has superior texture extraction capabilities capable of identifying sick parts.

This paper is divided into the following sections: Section II presents an introduction to Gabor CapsNets followed by Section III which outlines the Materials and Methods used for this work leading to Sections IV where the experimental setup, the proposed model, and baseline models are presented. Results are presented and discussed in Section V followed by Section VI where the work is concluded and future works provided.

## II. GABOR CAPSULE NETWORK

A Capsule [27] is a group of neurons whose activity vector represents the instantiation parameters with the length of the vector representing the likelihood that an entity exists. The first layer of a Capsule network is a CNN layer followed by a Primary Capsule (PC) layer. The Class Capsule (CC) layer

performs the classification while the decoder network performs reconstruction. The CNN layer performs feature extraction to serve as input to the PC layer which in turn produces  $\hat{u}_{j|i} = W_{ij}u_i$  as output. A coupling coefficient  $c_{ij} = \frac{\exp(b_{ij})}{\sum_k \exp(b_{ik})}$  allows a lower-level capsule to choose a higher-level capsule as a cluster centre. The coupling coefficient is the SoftMax of the logits  $b_{ij} = b_{ij} + v_j \cdot \hat{u}_{j|i}$ . During the routing process, the  $c_{ij}$ s are updated based on the agreement  $a_{ij} = v_j \cdot \hat{u}_{j|i}$  between the prediction of a lower level capsule and a higher-level capsule. The total input to a higher-level capsule  $j$  takes as input the weighted sum of all prediction vectors  $\hat{u}_{j|i}$  of a given PC  $i$  for a given CC  $j$ . This is given by  $s_j = \sum_{i=1}^{N_1} c_{ij} \hat{u}_{j|i}$ . To constrain the value of the CC’s output between the range [0,1], the squashing function  $v_j = \frac{\|s_j\|^2}{1 + \|s_j\|^2} \frac{s_j}{\|s_j\|}$  is applied. CapsNets have performed well on a wide range of problems [30].

Gabor Filters [29] on the other hand are linear filters popularly used for texture [31] analysis, edge detection, and feature extraction. They can be used to approximate the characteristics of the visual cortex of some animals. A Gabor filter is composed of real and imaginary parts. The real part is described by equation (1), where  $\lambda$  = sinusoidal factor wavelength,  $\theta$  = orientation of the normal to the Gabor function parallel stripes,  $\sigma$  = standard deviation of the Gaussian envelope, and  $\gamma$  = spatial aspect ratio specifying the specificity.

$$g\lambda, \theta, \sigma, \gamma(x, y) = \exp\left(-\frac{x'^2 + \gamma y'^2}{2\sigma^2}\right) \cos\left(2\pi \frac{x'}{\lambda} + \phi\right) \quad (1)$$

where  $x' = x \cos \theta + y \sin \theta$ ,  $y' = -x \sin \theta + y \cos \theta$ .

Practically,  $\lambda$  regulates the width of the Gabor function strips; increasing  $\lambda$  will increase the width and vice versa.  $\theta$ , on the other hand, governs the orientation of the strips. A  $0^\circ \theta$  represents a vertical strip.  $\gamma$  and  $\sigma$  respectfully control the height and overall size of the strips.

Gabor filters recognize orientation and texture. During convolution, global Gabor Filter banks are used to extract the features. Given an input image  $I(x, y)$ , convolution (\*) of the image with a global Gabor filter bank  $G(x, y; w, \theta)$ , produces  $(O_{m,n}(x, y))$  features that can be approximated by equation (2).

$$O_{m,n}(x, y) = I(x, y) * G(x, y; w, \theta) \quad (2)$$

Gabor Capsules [32] (applied to Expectation maximization Capsules) and Gabor CNNs [33][31][34] have performed well on images through texture recognition.

## III. MATERIALS AND METHODS

### A. Image Acquisition and Preprocessing

*Tomato dataset:* It is a subset of the Plant Village dataset and consists of 18,159 images; nine categories of infected leaves and one healthy leaves class. Data imbalance, the similarity of images from different classes, and varied image backgrounds make the dataset challenging for classification models.



*Citrus dataset* [35]: This dataset is made up of sick and healthy leaves and fruits with the following categories: Blackspot, Canker, Scab, Greening, and Melanose. The dataset is made up of 759, 256 x 256x3 images acquired from crop-fields making it complex as well as having the data imbalance problem that plagues most data sets. It was used for the classification of citrus diseases in [36]. Fig. 2 depicts sample raw images from the two datasets.



Fig. 2. Sample Images from the Two Datasets. Top Row: Tomato Dataset. Bottom Row: Citrus Dataset.

The images were resized from the original 256x256 to 48x48, 68x68, and 224x224 depending on which model was being trained. Standard data augmentation techniques such as vertical and horizontal mirroring, blurring, deformation, and rotation were applied to 50% of the images in each class of the test sets. The deformation was achieved using Moving Least Squares’ affine transformation [37] and the blurring by the use of Gaussian function in what is known as Gaussian Blur [38] with a kernel size of 15x15. These steps were necessary to test the ability of the models to generalize on unseen data and also under bad illumination conditions. Some of the preprocessed images are shown in Fig. 3.

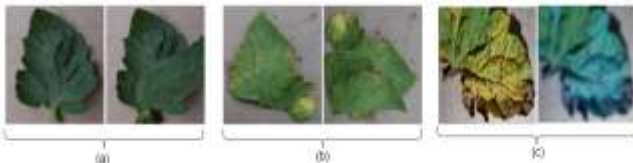


Fig. 3. Sample Preprocessed Images: (a) *Bacterial\_Spot* Infected Original Image on the Left and its Deformed Counterpart on the Right, (b) *Bacterial\_Spot* Infected Original Image on the Left and its Deformed-Rotated Counterpart on the Right, (c) *Early\_Blight* Infected Original Image on the Left and its Gaussian Blurred Counterpart on the Right.

#### IV. EXPERIMENTS

This work was carried out in Python 3.7. PyTorch 1.3 was used to design all the models with visualizations produced in Visdom server. The computing hardware was a 64bit Windows machine with NVIDIA GeForce GTX 1060 Graphic Processing Unit (GPU) running on CUDA 10.1 with a dedicated memory of 8GB. The CPU is an Intel Core i7, 8th generation.

In this work, a Gabor Capsule network is proposed and trained from scratch. Three baseline models were used to evaluate the performance of the proposed model. The baseline models are 1) Capsule network based on dynamic routing, 2) AlexNet, and 3) GoogleNet. The last two were fine-tuned

based on the implementation in [20]. The models were each trained for 400 epochs with a batch size of 60. Other hyperparameters for implementing the CapsNets include three routing iterations, rectified linear unit (ReLU) for non-linearity, use of the sigmoid function in the last FC layer, SoftMax function, and the Adam optimizer.

#### A. Proposed Gabor Capsule Model

This paper uses the properties of Gabor filters in Capsule networks to develop a plant disease detection model. Fig. 4 shows the proposed architecture which is made up of one Gabor layer, one CNN layer, a PC layer, and the class capsule (*DiseaseRecognition*) layer. The Gabor layer is implemented as a convolutional layer with its filters constrained to fit a Gabor function [33]. The Gabor layer uses 96, 7x7 kernels to produce 96, 42x42 feature maps for the subsequent convolutional layer at a stride of 1. The first convolutional layer (*Conv1*) uses ReLU non-linear activation and has 96, 9x9 kernels producing 96, 34x34 feature maps. *Conv1* runs at a stride of 1.

The primary capsule layer is a convolutional capsule layer with 12 channels of convolutional 8D capsules. Each component capsule in the primary capsule layer has 13x13 capsules. The PC layer outputs 13\*13\*12, 8D capsules. The decoder network is a fully connected layer with 512 neurons followed by 1024 and 6912 neurons for the first, second, and third FC layers respectively. It is the responsibility of the decoder network to perform reconstruction of the original images. The frequency  $f_n$  and orientation  $\theta_m$  of the Gabor filters in the Gabor layer is set using the expressions in equations 3 and 4 [33].

$$f_n = \frac{\pi}{2} \sqrt{2}^{-(n-1)} \tag{3}$$

$$\theta_m = \frac{\pi}{8} (m - 1) \tag{4}$$

where  $n=1,2, \dots, 5$  and  $m=1, 2, \dots, 8$ .

#### B. Baseline Models

In this section, the three baseline models are discussed in detail.

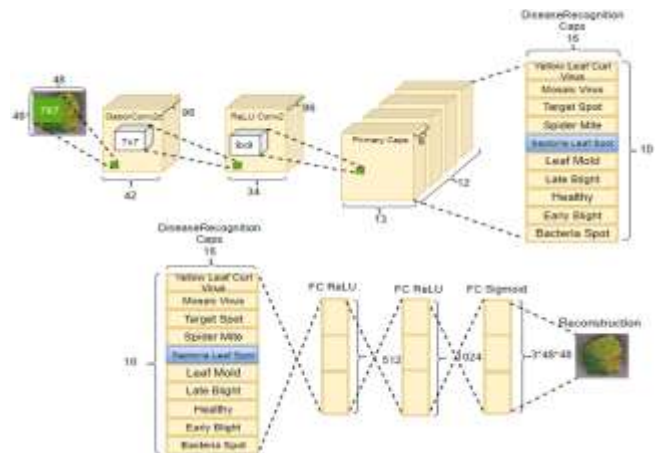


Fig. 4. Gabor CapsNet Architecture for Plant Disease Recognition.

### C. CNN Baseline Models

The two CNN models in [20] were implemented in this paper as baseline models to provide a common implementation platform for a fair comparison of results between the proposed and baseline models.

1) *GoogLeNet*: In 2014, GoogLeNet [5] achieved an impressive top-5 error rate of 6.67% in the ImageNet Large Scale Visual Recognition Challenge (ILSVRC). The network was built on LeNet [19] with an Inception module and global average pooling. Its architecture is a 22-layer deep CNN. 1x1 convolutions were used for reduction in dimensionality and computations. Its pre-trained weights have since been reused and transferred to solve other image recognition tasks. In this work, GoogLeNet was implemented as one of the baseline models occupying 25.91MB disk space with approximately 6.55 Million parameters. The following changes were made to the pre-trained model to solve the problem at hand: 1) the output layer was changed from 1000 to 10 since there are ten classes in the tomato dataset, 2) the top three layers were fine-tuned since the initial layers usually extract generic features (e.g. edge detectors or color blob detectors) while the upper layers are dataset-specific.

2) *AlexNet*: AlexNet [2] won the 2012 ILSVR Challenge with a top-5 error of 26% to 15.3%. The network comprises stacked convolutional layers of 11x11, 5x5, 3x3 convolutions. It utilized dropout, stochastic gradient descent (SGD), does max pooling, and uses a rectified linear unit (ReLU) for non-linearity. The architecture of AlexNet is such that it occupied 242.03 MB disk space with approximately 61 million parameters. The pre-trained model was loaded and the last three layers fine-tuned to adapt to the new classification problems with 10 and 6 classes respectively for the tomato and citrus datasets as well as reducing the image sizes from 227x227, 3 to 224x224, 3 channels.

### D. Capsule Baseline Model

Fig. 5 is the architecture of the baseline Capsule network model. The input images are resized from (256x256x3) to (48x48x3). They are then fed into the first convolutional layer (Conv1) with 7x7, 96 kernels with ReLU non-linear activation. The convolutions in the Conv1 layer are performed with a stride of 1. Conv1 then produces 256, 42x42 feature maps which are fed into the second convolutional layer (Conv2) also with ReLU non-linear activation. Conv2 is made up of 96, 9x9 kernels performing convolution over the image at a stride of 1. Conv2 then produces 96, 34x34 feature maps as input to the primary capsule (PC) layer. The primary capsule layer is a convolutional capsule layer with a kernel size of 9x9 and a stride of 2. In the PC layer, the output of the standard convolution layer comes in the form of 96 channels of scalars in 13x13 arrays. These are seen as 12 channels of 8-dimensional vectors organized in 13x13 arrays. The resulting value for the PC output is a 13\*13\*12, 8-dimensional vectors (also called the routing nodes) which are changed into a 16-dimensional vector in the DiseaseRecognitionCaps layer. These dimensions may hold features such as size, texture, deformation, orientation, hue, and position. A tensor product

between  $u$  and the weights ( $W$ ) produces  $\hat{u}_{ij}$  which is made up of 2028, 16-dimensional vectors for each DiseaseRecognitionCaps output. Since there are 10 classes in all, the total number of outputs for the DiseaseRecognitionCaps is 2028\*10, 16D vectors. These are fed into a Fully connected (FC) layer consisting of three layers. This part is usually referred to as the decoder and is made up of 512 neurons in the first FC layer followed by 1024 neurons. The last layer of the decoder network is made up of 6912 neurons necessary for reconstructing the input image.

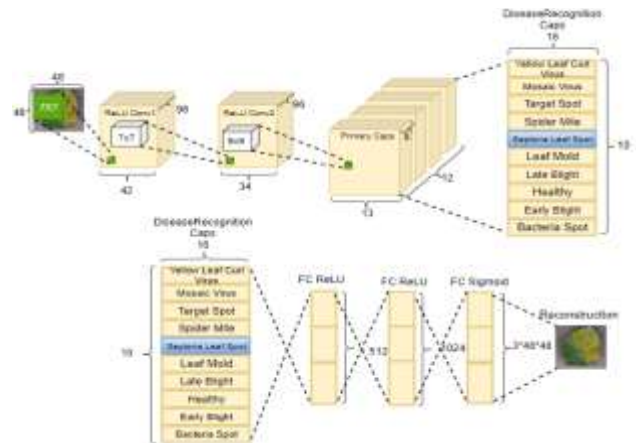


Fig. 5. The Baseline CapsNet Architecture for Plant Disease Recognition.

## V. RESULTS AND DISCUSSION

The datasets were divided with a ratio of 8:2 for training and testing respectively for all the models. The loss function used to train the model is made up of the margin and reconstruction losses as depicted in Fig. 6(a) and (c) and Appendix A (Fig. 11). The default values for  $m+$ ,  $m-$ , and  $\lambda$  of the loss function in [27] were maintained in this implementation. Three routing iterations were used during training for the Capsule models. The proposed model obtained 98.13% and 93.33% accuracies for the tomato and citrus datasets respectively. The proposed model outperformed all the other models on both datasets. Fig. 7 and 8 depict the confusion matrices obtained by training the proposed model with the datasets. It can be seen from Table I that GoogLeNet achieved 97.60% accuracy outperforming the CapsNet (95.29%) and AlexNet (94.40%) baseline models on the tomato dataset.

### A. Model Flexibility and Robustness

Random changes to parameter values and/or intermediate layers in all the models were carried out to determine how sensitive each model is to these changes. The effect of these changes adversely affected the performance of the CNN models as compared to the proposed Capsule models.

Varying the momentum, batch size, learning rate, dropout, and learning rate decay did not significantly affect the performance of the CapsNets models as observed in [30]. The single most important hyperparameter that significantly affected the performance of the CapsNet models was the number of routing iterations with three producing the best performance values. To illustrate the flexibility and robustness of the CapsNets, the input images were resized from 256x256

to 48x48, 68x68, and 224x224, and the models trained. The results in Table I show that the performance of the baseline CNN models was affected by simple resizing. The default settings in AlexNet could not train with the 48x48 images.

On the other hand, as the image size was increased, the CapsNet models produced almost consistent results. However, increasing the image size to 224x224 required more computational resources and training time and could not be implemented for this study.

It is noted here that Pytorch can accumulate gradients over multiple smaller batches as long as enough memory exists for a batch, however, 400 epochs were excessive, slow to train, and was taking too long a time.

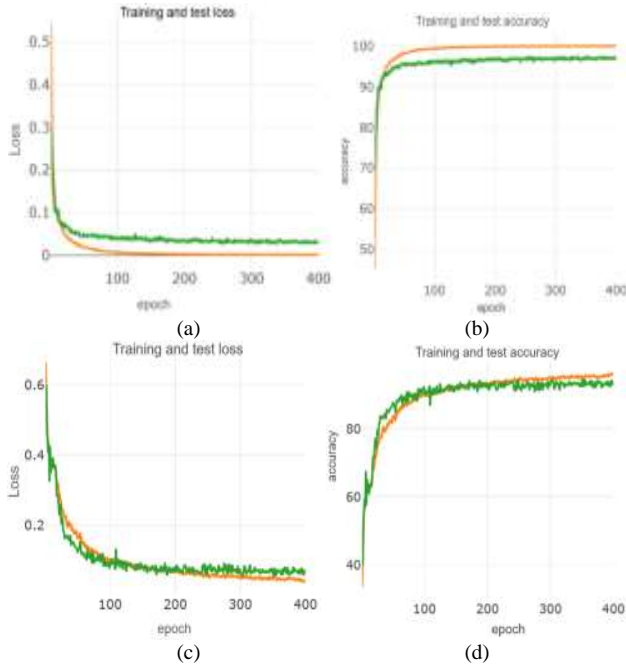


Fig. 6. Loss and Accuracy of the Proposed Gabor CapsNet Model Trained on (a) and (b) Tomato Dataset, (c), and (d) Citrus Dataset. The Training Curves are shown in Orange with the Test Result Curves shown in Green.

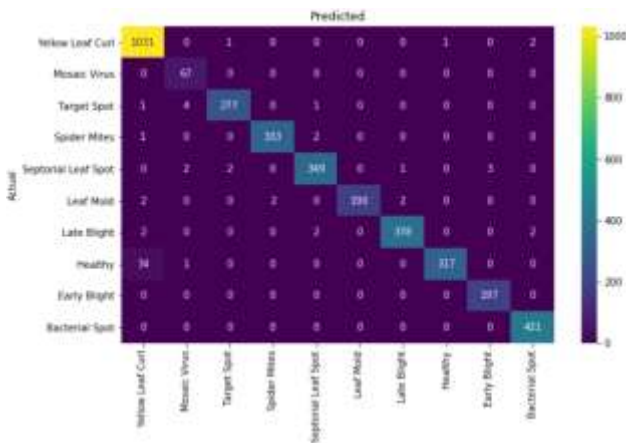


Fig. 7. Confusion Matrix for Tomato Dataset.

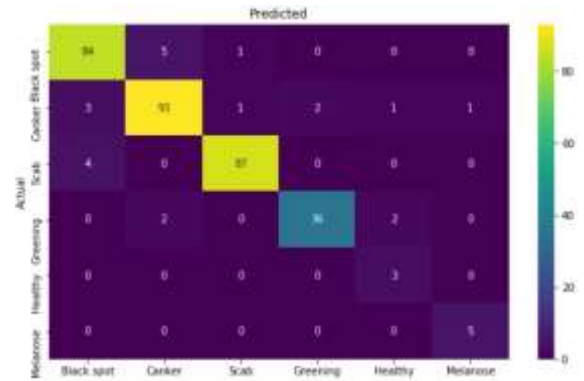


Fig. 8. Confusion Matrix for Citrus Dataset.

B. Model Convergence

The resulting plots in Fig. 9 and 10 show that the proposed Gabor CapsNet learns and converges faster than the other models. For instance, between epochs 0 to 100, the Gabor CapsNet attains accuracies higher than all the other models. The final accuracies are approximately equal to the accuracies they assume in the initial stages. As a result, the final accuracy of the proposed Capsule network can be approximated during the first few epochs.

On the contrary, the baseline models rise gradually through each epoch up to the last epoch. The final accuracy of the baseline models can therefore not be approximated at the initial stages. One has to wait for the entire duration of the training before a determination of the final accuracy can be made. This convergence is attributed to the ability of the Gabor filters to encode the texture of the diseased parts of leaves. The ensuing capsule layer after the Gabor layer also can encode texture, pose, and deformation. Fast learning and convergence are the results of the working together of these layers. These are particularly useful during a preliminary investigation into crop diseases and for prototyping.

TABLE I. ACCURACY DECREASES AS IMAGE SIZE IS REDUCED FOR THE BASELINE CNN MODELS. CAPSNET MODELS DID NOT SHOW ANY SIGNIFICANT CHANGE IN ACCURACY

| Model (dataset)        | Accuracy     |              |                |
|------------------------|--------------|--------------|----------------|
|                        | 48x48 images | 68x68 images | 224x224 images |
| Gabor CapsNet (tomato) | 98.12%       | 98.93%       | -----          |
| CapsNet (tomato)       | 95.29%       | 95.11%       | -----          |
| AlexNet (tomato)       | -----        | 81.85%       | 94.40%         |
| GoogleNet (tomato)     | 90.20%       | 95.98%       | 97.60%         |
| Gabor CapsNet (Citrus) | 93.33%       | 92.85%       | -----          |
| CapsNet (Citrus)       | 90.69%       | 90.26%       | -----          |
| AlexNet (Citrus)       | -----        | 81.85%       | 90.90%         |
| GoogleNet (Citrus)     | 88.81%       | 90.17%       | 91.04%         |

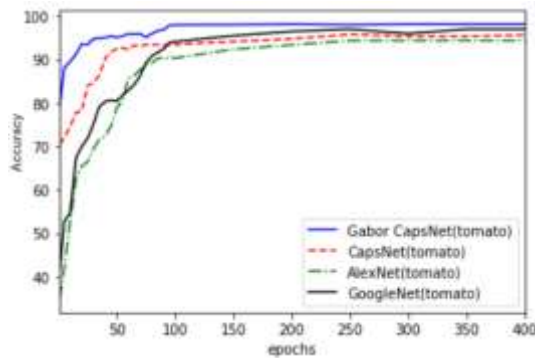


Fig. 9. Model Convergence on Tomato Dataset.

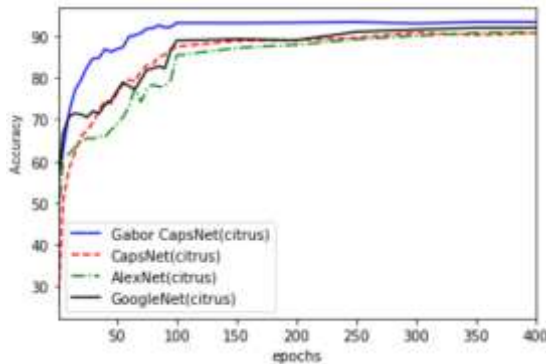


Fig. 10. Model Convergence on the Citrus Dataset.

C. Reduced Parameters

The models were evaluated on the number of trainable parameters using the 68x68 images and the results shown in Table II. The complexity of a model can be inferred from the number of trainable parameters it generates. As shown in Table II, the proposed model had fewer parameters than the AlexNet baseline model. This is a contribution to the state-of-the-art since fewer parameters are needed to reduce model complexity and its ability to over-fit smaller datasets.

D. Comparison to Related Works in Literature

The tomato dataset has been used in the literature to fit several CNN and deep learning models. In Table III, a comparison between these models and the proposed model based on average test accuracies is provided for the tomato dataset. For a fair comparison, other implementations in the literature using custom tomato datasets [12][11][22] were not adopted for this exercise. It can be seen from Table III that the proposed model produced results that are comparable to the state-of-the-art models irrespective of the complexity of the input images.

TABLE II. COMPARISON OF PARAMETERS BETWEEN THE PROPOSED MODEL AND THE BASELINE MODELS

| Model              | Number of Parameters    |
|--------------------|-------------------------|
| Gabor CapsNet      | 12,397,216 ~ 12 Million |
| CapsNet            | 9,583,936 ~ 10 Million  |
| Baseline AlexNet   | 61 Million              |
| Baseline GoogleNet | 6.55 Million            |

TABLE III. COMPARISON OF RESULTS OF THE PROPOSED MODEL TO THOSE IN THE LITERATURE. NOTICE THAT SOME OF THE MODELS USED 6 OR 9 CLASSES OUT OF THE TOTAL 10 CLASSES

| Reference       | Model Algorithm                  | Number of Classes | Accuracy      |
|-----------------|----------------------------------|-------------------|---------------|
| [16]            | AlexNet (pre-trained weights)    | 10                | 95.65%        |
| [16]            | SqueezeNet (pre-trained weights) | 10                | 94.30%        |
| [18]            | Variation of LeNet [19]          | 10                | 94.85%        |
| [21]            | VGG                              | 10                | 95.24%        |
| [20]            | AlexNet                          | 9                 | 98.66%        |
| [20]            | GoogleNet                        | 9                 | 99.18%        |
| [13]            | ResNet [3]                       | 10                | 97.28%        |
| [17]            | VGG16                            | 6                 | 99.24%        |
| <b>Proposed</b> | <b>Gabor CapsNet</b>             | <b>10</b>         | <b>98.12%</b> |
| <b>Baseline</b> | <b>CapsNet</b>                   | <b>10</b>         | <b>95.29%</b> |

VI. CONCLUSION

In this work, Gabor Capsule Network for the recognition of tomato and citrus diseases has been proposed. Two state-of-the-art CNN and one capsule baseline models were also implemented for comparison. To determine the robustness of the proposed models, extensive preprocessing such as rotation, deformation, and Gaussian blur was applied to a proportion of the test set and used to test each of the models. The Gabor CapsNet outperformed the other models on the two datasets in terms of accuracy, convergence, robustness, complexity, and flexibility. The results suggest that Capsule Networks can outperform other deep learning methods on complex real-world datasets. Furthermore, they can recognize unhealthy plants even in challenging weather and illumination conditions as well as from diverse angles. The results in this paper show that Capsules have a huge potential to improve agriculture especially as the algorithm is being improved by researchers to enable it mature for practical adoption.

In the future, a further reduction in the number of parameters for possible implementation on mobile devices like smartphones will be pursued since a high percentage of farmers have mobile phones. The possibility of using a custom routing algorithm will also be considered.

REFERENCES

- [1] M. Dong, S. Mu, T. Su, and W. Sun, "Image Recognition of Peanut Leaf Diseases Based on Capsule Networks," in ICAI 2019, 2019, pp. 43–52, doi: 10.1007/978-981-32-9298-7\_4.
- [2] A. Krizhevsky, I. Sutskever, and G. E. Hinton, "ImageNet Classification with Deep Convolutional Neural Networks," Commun. ACM, vol. 60, no. 6, pp. 84–90, 2017, doi: 10.1145/3065386.
- [3] K. He, X. Zhang, S. Ren, and J. Sun, "Deep residual learning for image recognition," in Proceedings of the IEEE Computer Society Conference on Computer Vision and Pattern Recognition, 2016, vol. 2016-December, pp. 770–778, doi: 10.1109/CVPR.2016.90.
- [4] K. Simonyan and A. Zisserman, "Very Deep Convolutional Networks for Large-Scale Image Recognition," in ICLR 2015 Conference proceedings, arXiv:1409.1556v6 [cs.CV], 2015, pp. 1–14.
- [5] C. Szegedy et al., "Going deeper with convolutions," in Proceedings of the IEEE Conference on Computer Vision and Pattern Recognition (CVPR '15), 2015, pp. 95–111, doi: 10.1109/CVPR.2015.7298594.

- [6] A. F. Fuentes, S. Yoon, J. Lee, and D. S. Park, "High-performance deep neural network-based tomato plant diseases and pests diagnosis system with refinement filter bank," *Front. Plant Sci.*, vol. 9, no. August, pp. 1–15, 2018, doi: 10.3389/fpls.2018.01162.
- [7] J. G. M. Esgario, R. A. Krohling, and J. A. Ventura, "Deep learning for classification and severity estimation of coffee leaf biotic stress," *Comput. Electron. Agric.*, vol. 169, no. July 2019, 2020, doi: 10.1016/j.compag.2019.105162.
- [8] S. Zhang, W. Huang, and C. Zhang, "Three-channel convolutional neural networks for vegetable leaf disease recognition," *Cogn. Syst. Res.*, pp. 1–11, 2018, doi: 10.1016/j.cogsys.2018.04.006.
- [9] M. Brahimi, S. Mahmoudi, K. Boukhalfa, and A. Moussaoui, "Deep interpretable architecture for plant diseases classification," *Signal Process. - Algorithms, Archit. Arrange. Appl. Conf. Proceedings, SPA*, vol. 2019-Septe, pp. 111–116, 2019, doi: 10.23919/SPA.2019.8936759.
- [10] R. Cadène, "Deep Learning for Visual Recognition," 2016.
- [11] M. Hasan, B. Tanawala, and K. J. Patel, "Deep Learning Precision Farming: Tomato Leaf Disease Detection by Transfer Learning," in *2nd International Conference on Advanced Computing and Software Engineering (ICACSE-2019)*, 2019, pp. 1–5, doi: 10.2139/ssrn.3349597.
- [12] A. Fuentes, S. Yoon, S. C. Kim, and D. S. Park, "A robust deep-learning-based detector for real-time tomato plant diseases and pests recognition," *Sensors (Switzerland)*, vol. 17, no. 9, 2017, doi: 10.3390/s17092022.
- [13] K. Zhang, Q. Wu, A. Liu, and X. Meng, "Can deep learning identify tomato leaf disease?," *Adv. Multimed.*, vol. 2018, 2018, doi: 10.1155/2018/6710865.
- [14] D. P. Hughes and M. Salathe, "An open access repository of images on plant health to enable the development of mobile disease diagnostics," <https://arxiv.org/abs/1511.08060>, 2015.
- [15] F. N. Iandola, S. Han, M. W. Moskewicz, K. Ashraf, W. J. Dally, and K. Keutzer, "Squeezenet: Alexnet-Level Accuracy with 50 X Fewer Parameters and < 0.5mb Model Size," *arXiv1602.07360v4 [cs.CV]*, pp. 1–13, 2017.
- [16] H. Durmus, E. O. Gunes, and M. Kirci, "Disease detection on the leaves of the tomato plants by using deep learning," in *2017 6th International Conference on Agro-Geoinformatics, Agro-Geoinformatics 2017*, 2017, doi: 10.1109/Agro-Geoinformatics.2017.8047016.
- [17] A. K. Rangarajan, R. Purushothaman, and A. Ramesh, "Tomato crop disease classification using pre-trained deep learning algorithm," *Procedia Comput. Sci.*, vol. 133, pp. 1040–1047, 2018, doi: 10.1016/j.procs.2018.07.070.
- [18] P. T. A. Pranathi, K. S. Ashritha, N. B. Chittaragi, and S. G. Koolagudi, "Tomato Leaf Disease Detection Using Convolutional Neural Networks," in *2018 11th International Conference on Contemporary Computing, IC3 2018*, 2018, pp. 2–4, doi: 10.1109/IC3.2018.8530532.
- [19] Y. LeCun et al., "Backpropagation Applied to Handwritten Zip Code Recognition," *Sci. Signal.*, vol. 7, no. 329, pp. 541–551, 2014, doi: 10.1126/scisignal.2005580.
- [20] M. Brahimi, K. Boukhalfa, and A. Moussaoui, "Deep Learning for Tomato Diseases: Classification and Symptoms Visualization," *Appl. Artif. Intell.*, vol. 31, no. 4, pp. 299–315, 2017, doi: 10.1080/08839514.2017.1315516.
- [21] E. Suryawati, R. Sustika, R. S. Yuwana, A. Subekti, and H. F. Pardede, "Deep structured convolutional neural network for tomato diseases detection," in *2018 International Conference on Advanced Computer Science and Information Systems, ICACSIS 2018*, 2019, no. October 2019, pp. 385–390, doi: 10.1109/ICACSIS.2018.8618169.
- [22] Q. Wang, F. Qi, M. Sun, J. Qu, and J. Xue, "Identification of Tomato Disease Types and Detection of Infected Areas Based on Deep Convolutional Neural Networks and Object Detection Techniques," *Comput. Intell. Neurosci.*, vol. 2019, 2019, doi: 10.1155/2019/9142753.
- [23] R. V. Kurup, M. A. Anupama, R. Vinayakumar, V. Sowmya, and S. K. P., "Capsule Network for Plant Disease and Plant Species Classification," in *ICCVBIC -Advances in Intelligent Systems and Computing*, 2019, vol. 186 AISC, pp. 413–421, doi: 10.1007/978-3-030-37218-7.
- [24] S. Sladojevic, M. Arsenovic, A. Anderla, D. Culibrk, and D. Stefanovic, "Deep Neural Networks Based Recognition of Plant Diseases by Leaf Image Classification," *Comput. Intell. Neurosci.*, vol. 2016, 2016, doi: 10.1155/2016/3289801.
- [25] Y. Toda and F. Okura, "How Convolutional Neural Networks Diagnose Plant Disease," *Plant Phenomics*, vol. 2019, pp. 1–14, 2019, doi: 10.34133/2019/9237136.
- [26] S. Verma, A. Chug, and A. P. Singh, "Exploring capsule networks for disease classification in plants," *J. Stat. Manag. Syst.*, vol. 23, no. 2, pp. 307–315, 2020, doi: 10.1080/09720510.2020.1724628.
- [27] S. Sabour, N. Frosst, and G. E. Hinton, "Dynamic routing between capsules," in *31st Conference on Neural Information Processing Systems (NIPS 2017)*, 2017, vol. 2017-Decem, no. NIPS 2017, pp. 3857–3867.
- [28] R. Mukhometzianov and J. Carrillo, "CapsNet comparative performance evaluation for image classification," <https://arxiv.org/abs/1805.11195>, pp. 1–14, 2018.
- [29] D. Gabor, "Theory of communication. Part 1: The analysis of information," *J. Inst. Electr. Eng. - Part III Radio Commun. Eng.*, vol. 93, no. 26, pp. 429–441, 1946, doi: 10.1049/ji-3-2.1946.0074.
- [30] M. Kwabena Patrick, A. Felix Adekoya, A. Abra Mighty, and B. Y. Edward, "Capsule Networks – A survey," *J. King Saud Univ. - Comput. Inf. Sci.*, 2019, doi: 10.1016/j.jksuci.2019.09.014.
- [31] I. Fogel and D. Sagi, "Gabor filters as texture discriminator," *Biol. Cybern.*, vol. 61, no. 2, pp. 103–113, 1989, doi: 10.1007/BF00204594.
- [32] S. Hosseini and N. I. Cho, "GF-CapsNet: Using Gabor Jet and Capsule Networks for Facial Age, Gender, and Expression Recognition," in *2019 14th IEEE International Conference on Automatic Face & Gesture Recognition (FG 2019)*, 2019, pp. 1–8, doi: 10.1109/fg.2019.8756552.
- [33] A. Alekseev, "GaborNet: Gabor filters with learnable parameters in deep convolutional neural networks Gabor function," *AXRIV Arch.*, 2019.
- [34] S. Luan, C. Chen, B. Zhang, J. Han, and J. Liu, "Gabor Convolutional Networks," *IEEE Trans. Image Process.*, vol. 27, no. 9, pp. 4357–4366, 2018, doi: 10.1109/TIP.2018.2835143.
- [35] H. T. Rauf, B. A. Saleem, M. I. U. Lali, M. A. Khan, M. Sharif, and S. A. C. Bukhari, "A citrus fruits and leaves dataset for detection and classification of citrus diseases through machine learning," *Data Br.*, vol. 26, pp. 1–7, 2019, doi: 10.1016/j.dib.2019.104340.
- [36] M. Sharif, M. A. Khan, Z. Iqbal, M. F. Azam, M. I. U. Lali, and M. Y. Javed, "Detection and classification of citrus diseases in agriculture based on optimized weighted segmentation and feature selection," *Comput. Electron. Agric.*, vol. 150, no. April, pp. 220–234, 2018, doi: 10.1016/j.compag.2018.04.023.
- [37] S. Schaefer, T. Mcphail, and J. Warren, "Image Deformation Using Moving Least Squares," *ACM SIGGRAPH 2006*, vol. 1, no. 212, pp. 533–540, 2006.
- [38] J. Flusser, S. Member, S. Farokhi, C. H. Iv, and M. Pedone, "Recognition of Images Degraded by Gaussian Blur," *IEEE Trans. IMAGE Process.*, vol. 25, no. 2, pp. 790–806, 2016.

APPENDIX A

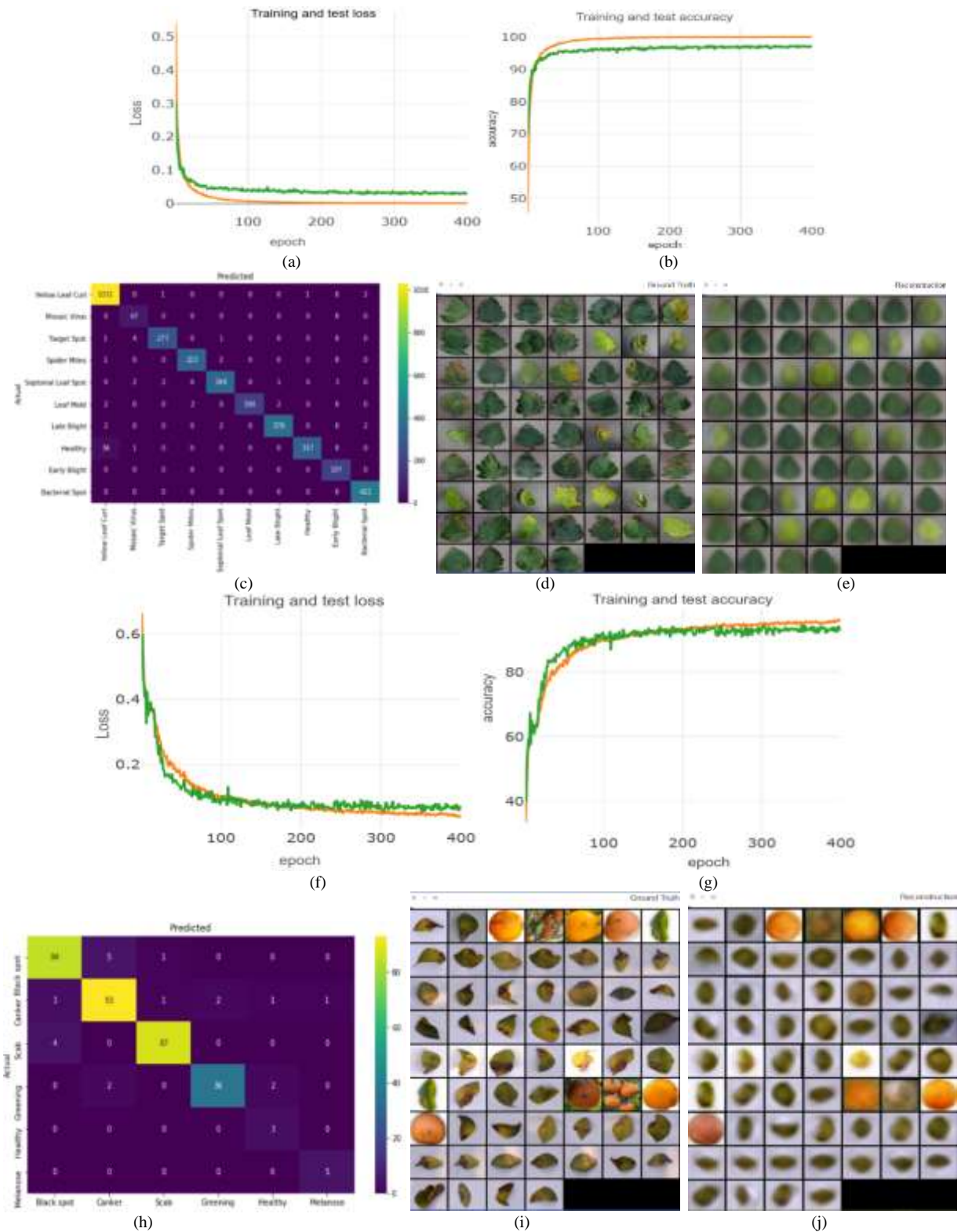


Fig. 11. Sample Results from the Proposed Gabor Capsule Network: (a)-(e) Tomato Dataset, (f)-(j) Citrus Dataset. (a), (b), (f), and (g) are Loss and Accuracy for Training and Test. (c) and (h) are the Confusion Matrices. (d), (e), (i), and (j) are the Ground Truth and Reconstructed Images.

# Comparison Performance of Lymphocyte Classification for Various Datasets using Deep Learning

Syadia Nabilah Mohd Safuan<sup>1</sup>, Mohd Razali Md Tomari<sup>2</sup>, Wan Nurshazwani Wan Zakaria<sup>3</sup>, Nor Surayahani Suriani<sup>4</sup>  
Faculty of Electronic and Electrical Engineering, Universiti Tun Hussein Onn Malaysia, Johor, Malaysia<sup>1,3,4</sup>  
Principle Researcher in Research Centre for Applied Electromagnetics, Universiti Tun Hussein Onn Malaysia, Johor, Malaysia<sup>2</sup>

**Abstract**—Analyzing and classifying five types of Lymphocyte White Blood Cell (WBC) is important to monitor the lack or excessive amount of cell in human body. These harmful amount of cell must be detected early for the early treatment can be run to the patient. However, the process may be tedious and time consuming as it is done manually by the experts. Other than that, it may yield inaccurate result as it depends on the pathologist skill and experience. This work presents a way that can be the second opinion to the experts using computer aided system as a solution. Convolutional Neural Network (CNN) is applied to the system to avoid complex structure and to eliminate the features extraction process. Three CNN models of mobilenet, resnet and VGG-16 is experimented on three different datasets which are kaggle, LISC and IDB-2. Kaggle, LISC and IDB-2 dataset consist of 6000, 242 and 260 images respectively. The result is divided into two parts which are dataset and model. As for IDB-2 dataset, the best model is VGG with training and validation accuracy of 0.9721 and 0.7913 respectively. While for kaggle and LISC dataset, the best model is resnet as it achieved training accuracy of 0.9713 and 0.9771 respectively. The highest validation accuracy for kaggle is 0.5955 and 0.5781 for LISC. Lastly, the best database that is most suitable for all model is IDB-2 database. It obtained highest training and validation accuracy for all model of mobilenet, resnet and VGG-16.

**Keywords**—Convolutional neural network; Google colab; training accuracy; validation accuracy; white blood cell

## I. INTRODUCTION

White Blood Cell (WBC) is one of other particles in human blood. This cells help to fight disease and virus as its presence help to boost the immune system [1]. However, having extra and unnecessary WBC in the blood could be harmful. This is where the WBC analysis is needed. WBC analysis is undeniably important as it helps to prevent disease's complications and an early prevention can be made [2]. Other than that, it is very helpful for diagnosing the patient's health condition [3].

WBC has five types which are Eosinophil, Basophil, Neutrophil, Lymphocyte and Monocyte [4]. They vary in terms of its shape, number or lobes and sizes of its nucleus and cytoplasm as showed in Fig. 1 [5, 6]. It is also differentiated by the nucleus' stain [7]. The number of each cells must be maintained as excessive number of cell will create problem to the patient's health.

Conventionally, WBC analysis is done manually where the images were placed under the microscope and pathologist analyze it manually [8]. This process takes time and creates confusion as the result is highly dependent on the pathologist's skills which will yield inaccurate result [9]. Moreover, it will be more challenging as the number of sample increases [10]. However, there is hematology counter in the market which is automated, fast and accurate but it is expensive [11]. In this work, the same objective is made but with a low cost approach.

The approach that this work offers is by using Convolutional Neural Network (CNN) which apply deep learning technique. It is less complex than the conventional method which the image has to go through many process and steps before being classified [12]. Preprocessing and feature extraction has to be done for conventional method [13]. It is important to extract the suitable features as it gives a huge impact to the classification accuracy. While in CNN, the structure is specially built to tackle the image variation and feature extraction problem. The image need to fed for the model to study and learn the pattern of each classes [14].

Deep CNN also known to solve computer vision issues successfully such as object recognition, semantic segmentation, object detection and video analysis [15]. It is widely used and applied on such as heartbeats classification [16], road crack detection [17], segmentation of blood vessels in retina image, skin cancer and lung lesion [18]. Other than that, some researchers use CNN for dynamic scene deblurring [19]. Google Colaboratory or Google colab is used along with CNN as it provides server less Jupyter notebook and it is free to use [20]. Some of works use Google colab for video- based emotion recognition [21] and breast cancer identification [22]. While this paper focuses on WBC classification using CNN. However, many works related to CNN WBC classification done but limited to one dataset which no comparison in terms of its performance has been made.

In conclusion, this paper emphasizes on the study of WBC classification performance for various datasets as WBC analysis is undeniably important to monitor a patient's health condition. It is done by using CNN of deep learning and it is applied through Google Colab medium as it is fast and requires less time for data training process. Three datasets were used with three CNN pre-trained models and the result of training and validation accuracy is compared. Result will show the best model for each dataset and which dataset suits a certain model

best. The datasets used are Kaggle, IDB-2 and LISC. While pretrained models involved are VGG-16, Mobilenet and Resnet.

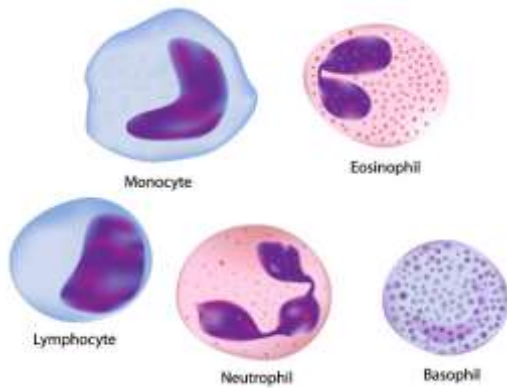


Fig. 1. Five types of WBC

This paper is organized as follows: Section II explains the flow of the method used. Section III shows the result and analysis. Lastly, Section IV concludes the result obtained and recommendations of future works.

## II. SYSTEM OVERVIEW

### A. Google Colab

In this paper, Google Colab is used as a platform to execute machine learning models in the cloud. It is a free Jupyter notebook and in Python. One of its advantages is it can be edited by the team members and easy to access without requiring any setup. It supported many types of machine learning libraries and can be easily loaded. As for this project, the flowchart of starting Google Colab is as depicted in Fig. 2.

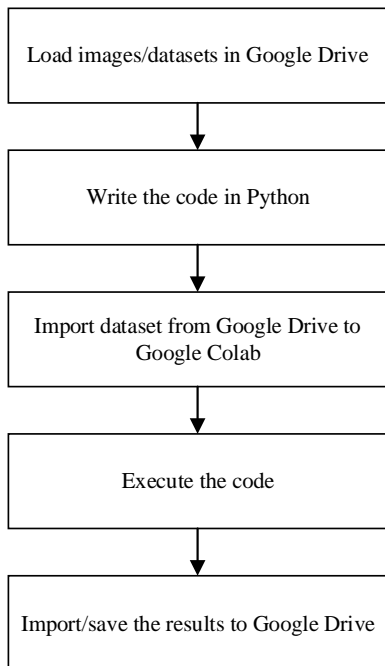


Fig. 2. Flowchart of Google Colab Settings.

Referring to the flowchart, setting up Google Colab is easy and does not require complicated steps to follow. Firstly, external dataset is uploaded to Google Drive. There are mainly two files for each dataset which are training and validation files. Before executing code in Google Colab, the dataset must be imported from Google Drive. Next, training and validation data directory is created. Pretrained model is constructed by integrating TensorFlow and Keras. After that, the training process is done and the outcome is plotted. The result is then saved in Google Drive file.

### B. Convolutional Neural Network (CNN)

Varies of pretrained models from CNN is used in this project which are VGG-16, mobilenet and resnet. These models are different from one another but the main elements are the same which are convolution layer, non-linearity and fully connected layer [23]. Basically, images will be fed to convolution layer that act as a filter of different sizes for every model. The image size will be different after the convolution layer. The number of layer also differ depending on the model itself. Next, the features vector is minimized by applying non-linearity layer. Lastly, fully connected layer is assigned to classify the categories of the images.

- VGG-16: Structure of VGG-16 is considered simple as it consists only three main elements of convolution, max pooling and fully connected as shown in Fig. 3. Max pooling in VGG-16 is used to help with overfitting. Other than that, it reduces the number of parameters to learn which will reduce the computational cost. Overall, it has 13 convolution layers and 3 fully connected layers. Input image size for VGG-16 is fixed 224x224 RGB image.
- Mobilenet: Mobilenet is known as a small, low latency and low power model. It consists of 27 convolutional layers which includes depthwise convolution as depicted in Fig. 4. In mobilenet structure, initially, 3x3 convolutional layer is applied. Then followed by depthwise convolution layer and 1x1 convolution layer. These process is applied for 13 times as it has 13 depthwise convolution layers and 13 1x1 convolution layers. Next, average pool layer, fully connected and softmax layer is added to classify the classes of the image.

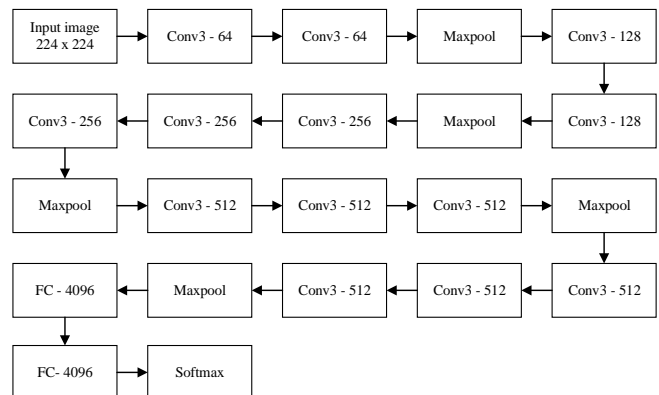


Fig. 3. VGG-16 Architecture.



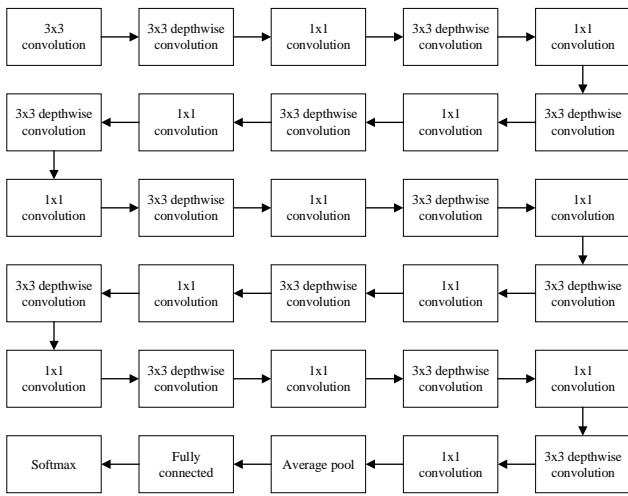


Fig. 4. Mobilenet Architecture.

- Resnet: Resnet architecture is acquired based on the Residual Network. It has 34-layer residual and this network implemented the skip connected as depicted in Fig. 5. Basically, it trains few layers and the output is connected directly. One of its advantages is any layer that can affect the performance of the network will be ignored and skipped by regularization. Hence, problems caused by vanishing or exploding gradient can be tackled by using this network.

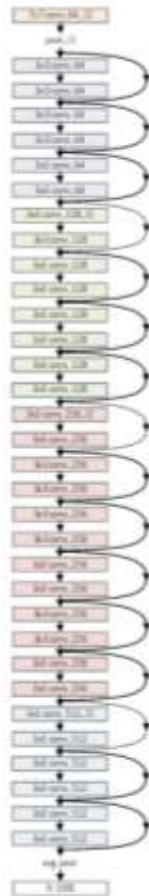


Fig. 5. Resnet Architecture.

### C. Dataset

There are three datasets used in this paper which are Kaggle, IDB-2 and LISC.

1) *Kaggle*: In this database, there are four classes of white blood cell image which are Eosinophil, Neutrophil, Lymphocyte and Monocyte. The samples of images in this database is as shown in Fig. 6. There are 1500 images for each class and total image in the database is 6000 images for training. The images are in RGB and it has variation of image rotation.

2) *IDB-2*: There are only two classes which are Lymphoblast and Non-lymphoblast and the sample images are as depicted in Fig. 7. In this database, there are 130 images of lymphoblast and 130 of non-lymphoblast which makes the total image is 260. In this case, lymphoblast is an abnormal lymphocyte cells. The motive of using this dataset is to classify the lymphoblast and non-lymphoblast cell.

3) *LISC*: Images from this dataset is a healthy subject images that consists of five types of WBC which are Eosinophil, Neutrophil, Basophil, Lymphocyte and Monocyte. The sample image in LISC dataset is as shown in Fig. 8. The number of images in this dataset for Eosinophil, Neutrophil, Basophil, Lymphocyte and Monocyte is 39, 50, 53, 52 and 48 respectively. This dataset is different from the other two datasets by its image magnification which make the image contains all cell types and particles such as white blood cell, red blood cell and platelet. While the Kaggle and IDB focus more on the WBC region.

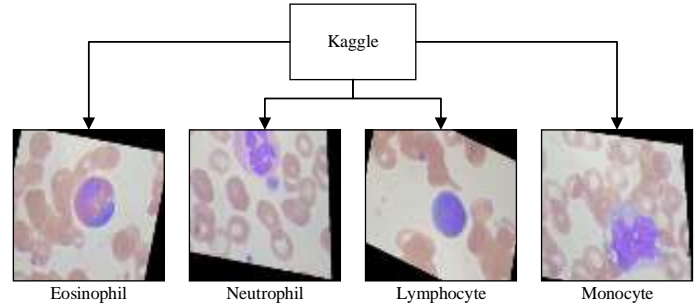


Fig. 6. Sample Images in Kaggle.

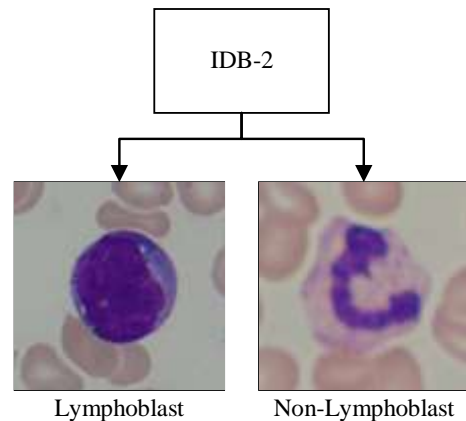


Fig. 7. Sample Images in IDB-2.

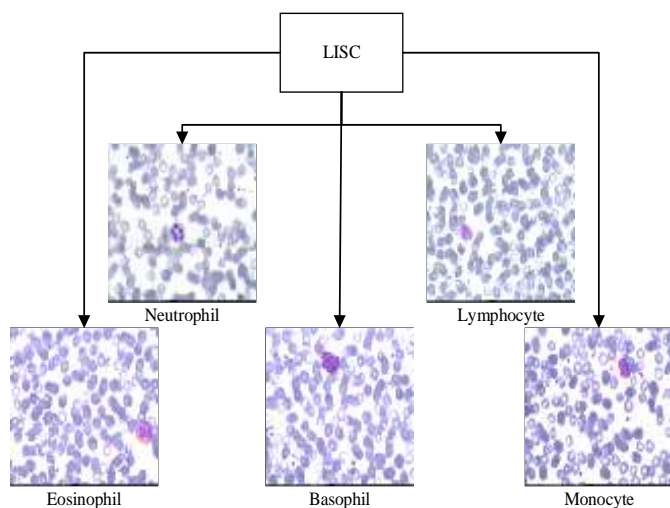


Fig. 8. Sample Images in LISC.

### III. RESULT AND ANALYSIS

In this paper, three CNN models were tested using three different datasets to prove which model suits which dataset the best. Each dataset of Kaggle, IDB2 and LISC is trained using three models which are mobilenet, resnet and VGG-16. 70% of the images in each dataset were used for training and remaining 30% used for validation. Total number of image in IDB2 is 260 images and 182 images were used for training and 78 images were used for validation. While for LISC dataset, 168 images were used for training and 74 images were used for validation purpose. Epoch is fixed to 50 and the batch size is 64 in training process.

#### A. Dataset

Each dataset is tested using three different models of mobilenet, resnet and VGG-16. The results obtained is compared.

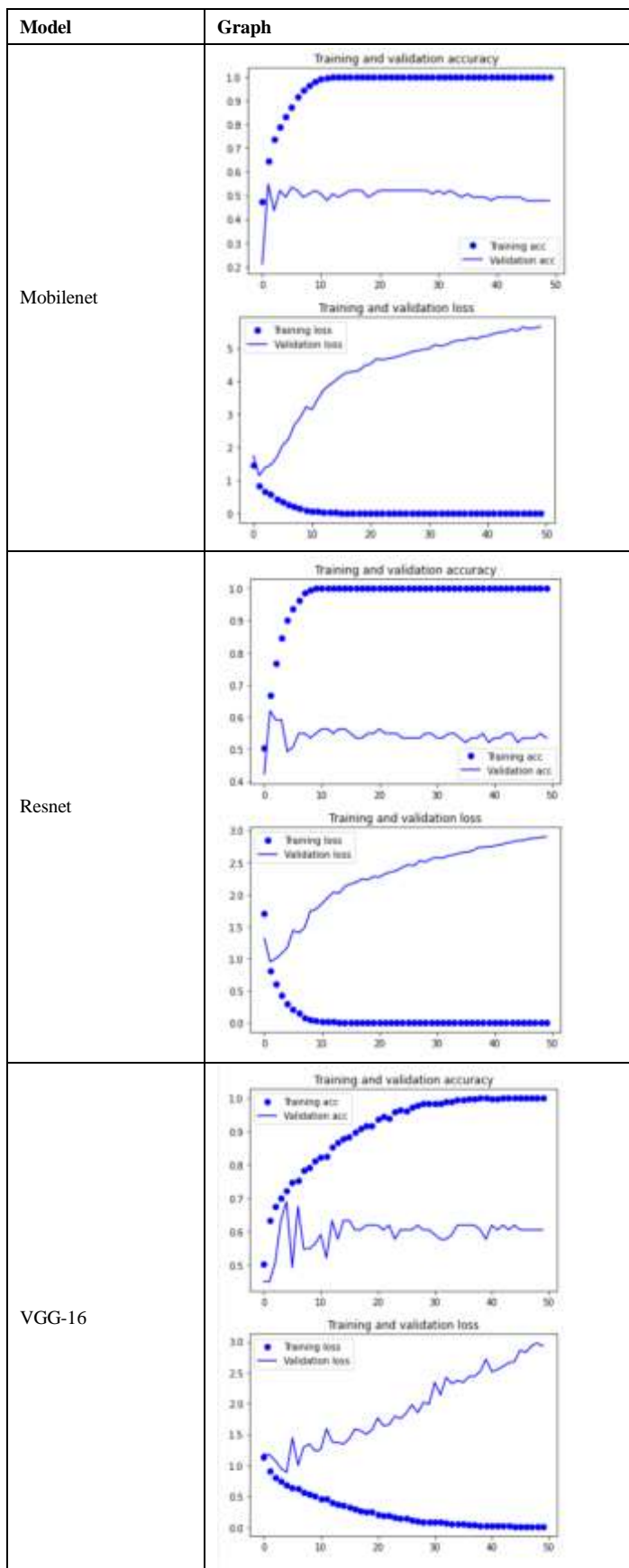
- Kaggle: As mentioned before, there are total of 6000 images in this dataset. It is trained using three models and the result is as tabulated in Table I.

Based on the table above, it can be seen that for training, the highest accuracy can be obtained by Resnet with lowest training loss. While for validation, highest accuracy is VGG-16 with lowest validation loss of 1.9219. Table II visualizes the graph plotting for both training and validation accuracy and loss. It can be seen that Resnet training accuracy pattern is more stable than the other two models. While for validation, the highest accuracy obtained is 0.6901 by VGG-16 model compared to the other two models, which barely obtained 0.6500 accuracy.

TABLE I. KAGGLE RESULT

| Model \ Result | Training |          | Validation |          |
|----------------|----------|----------|------------|----------|
|                | Loss     | Accuracy | Loss       | Accuracy |
| Mobilenet      | 0.1049   | 0.9629   | 4.3103     | 0.4983   |
| Resnet         | 0.0884   | 0.9713   | 2.2724     | 0.5425   |
| VGG-16         | 0.2547   | 0.9091   | 1.9219     | 0.5955   |

TABLE II. GRAPH OF TRAINING AND VALIDATION FOR KAGGLE



- IDB-2: In IDB-2, there are two classes of image which are Lymphoblast and Non-Lymphoblast cell. Both contains equal number of 130 images and the total for both classes is 260 images. All the images undergo all three models to get the result for comparison.

Based on the Table III, highest training accuracy of 0.9721 is obtained by VGG-16 model. It is the same for validation which achieved 0.7913 validation accuracy. The lowest accuracy for training is mobilenet by 0.0025 and for validation, the lowest is 0.6999 which obtained by resnet model. Next, Table IV compares the graph plotting for training and validation.

It can be seen that for training accuracy, VGG-16 is not the most stable but it increases gradually and its average accuracy is the highest. While for validation, it is clearly can be seen that VGG-16 can achieve more than 0.8 accuracy compared to mobilenet and resnet. VGG-16 is the most suitable model for IDB-2 database.

- LISC: LISC has the most classes consists of Basophil, Eosinophil, Neutrophil, Lymphocyte and Monocyte. The result for model comparison is as tabulated in Table V.

Resnet achieved the highest training accuracy of 0.9771 and lowest loss which is 0.0819. However, for validation, the highest accuracy is 0.5781 achieved by VGG-16. The validation accuracy for LISC database is not high and satisfactory. Table VI compares the graph for training and validation for each model of mobilenet, resnet and VGG-16. It can be seen that the consistency of training accuracy for resnet is better compared to mobilenet and VGG-16. However, it is different for validation accuracy where it fluctuated and not stable.

**B. Model**

This section explains the performance comparison of each dataset by model. Results showed the best dataset for which model.

- Mobilenet: In mobilenet, there are 27 convolutional layers which consist of 13 depthwise layers, 1 3x3 convolution layer and 13 1x1 convolution layers. This model is small, low latency and low power models.

Three datasets have been tested using this model for classification purposes and the result is as tabulated in Table VII.

Based on this result, it can clearly be seen that highest training accuracy is achieved on IDB-2 dataset by 96.96% and same applied to validation accuracy which 0.7210 is achieved for IDB-2. It can be said that IDB dataset is the most suitable dataset for mobilenet.

TABLE III. IDB-2 RESULT

| Model \ Result | Training |          | Validation |          |
|----------------|----------|----------|------------|----------|
|                | Loss     | Accuracy | Loss       | Accuracy |
| Mobilenet      | 0.1779   | 0.9696   | 1.0633     | 0.7210   |
| Resnet         | 0.2286   | 0.9718   | 1.3799     | 0.6999   |
| VGG-16         | 0.1279   | 0.9721   | 0.6396     | 0.7913   |

TABLE IV. GRAPH OF TRAINING AND VALIDATION FOR IDB-2

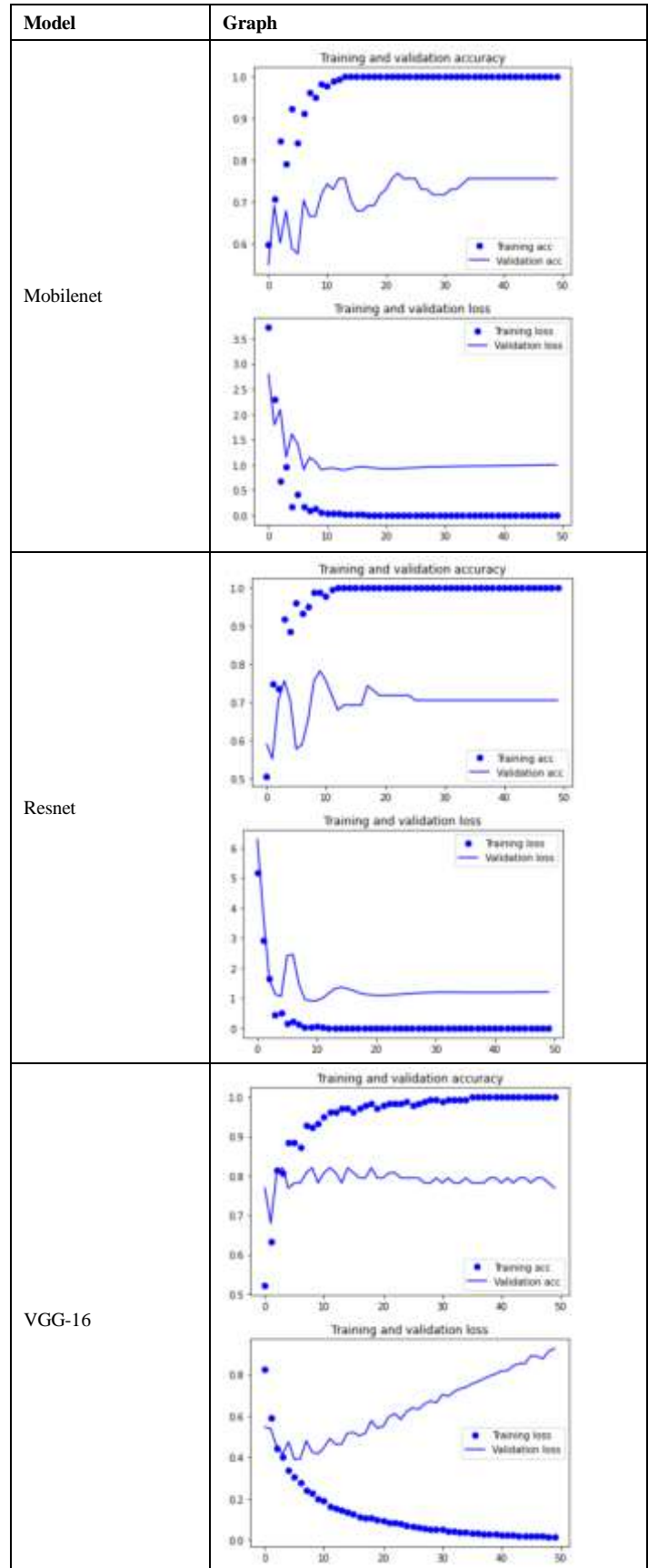


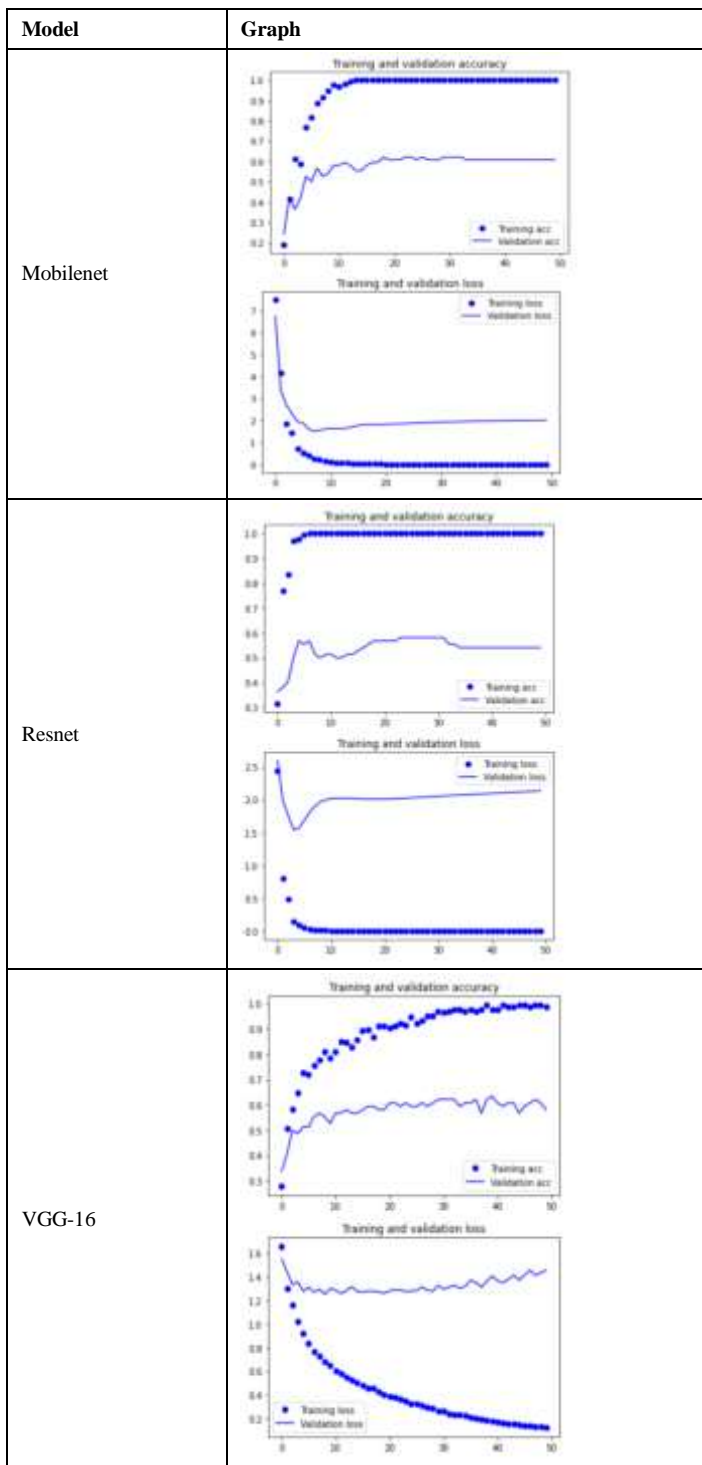
TABLE V. LISC RESULT

| Result / Model | Training |          | Validation |          |
|----------------|----------|----------|------------|----------|
|                | Loss     | Accuracy | Loss       | Accuracy |
| Mobilenet      | 0.3595   | 0.9413   | 2.0149     | 0.5778   |
| Resnet         | 0.0819   | 0.9771   | 2.0235     | 0.5370   |
| VGG-16         | 0.4332   | 0.8849   | 1.3299     | 0.5781   |

TABLE VII. DATASET COMPARISON FOR MOBILENET

| Result / Model | Training |          | Validation |          |
|----------------|----------|----------|------------|----------|
|                | Loss     | Accuracy | Loss       | Accuracy |
| Kaggle         | 0.1049   | 0.9629   | 4.3103     | 0.4983   |
| IDB-2          | 0.1779   | 0.9696   | 1.0633     | 0.7210   |
| LISC           | 0.3595   | 0.9413   | 2.0149     | 0.5778   |

TABLE VI. GRAPH OF TRAINING AND VALIDATION FOR IDB-2



- Resnet: Resnet is taken from Residual Network which means it contains residual layers. It has 34 residual layers and it also implement skip connection. The advantage of skip connection is to train without problems caused by vanishing and exploding gradient. The best dataset for resnet model is as shown in Table VIII.

TABLE VIII. DATASET COMPARISON FOR RESNET

| Result / Model | Training |          | Validation |          |
|----------------|----------|----------|------------|----------|
|                | Loss     | Accuracy | Loss       | Accuracy |
| Kaggle         | 0.0884   | 0.9713   | 2.2724     | 0.5425   |
| IDB-2          | 0.2286   | 0.9718   | 1.3799     | 0.6999   |
| LISC           | 0.0819   | 0.9771   | 2.0235     | 0.5370   |

As for training accuracy, the highest is obtained by LISC database. However, the differences between all the three datasets are not huge. While highest validation accuracy is achieved on IDB-2 dataset which is 0.6999.

- VGG-16: This model contains 16 layers which consist of 13 convolution layers and 3 fully connected layers. It is the simplest model compared to the other two models. The comparison for each dataset using VGG-16 is as tabulated in Table IX.

TABLE IX. DATASET COMPARISON FOR VGG-16

| Result / Model | Training |          | Validation |          |
|----------------|----------|----------|------------|----------|
|                | Loss     | Accuracy | Loss       | Accuracy |
| Kaggle         | 0.2547   | 0.9091   | 1.9219     | 0.5955   |
| IDB-2          | 0.1279   | 0.9721   | 0.6396     | 0.7913   |
| LISC           | 0.4332   | 0.8849   | 1.3299     | 0.5781   |

It can be seen that IDB-2 dataset able to obtain highest training and validation accuracy of 0.9721 and 0.7913 respectively. Lowest accuracy for training and validation for VGG-16 is by LISC dataset.

#### IV. CONCLUSION AND FUTURE WORKS

This paper concludes the comparison of three models using three different databases to classify different classes. Google Colab was used for this project as it is fast, and can be edited by the team members. Other than that, it is free and supports many machine learning such as CNN. The CNN models involved in this paper are Mobilenet, Resnet and VGG-16. All the models tested using three different datasets of Kaggle, IDB-2 and LISC which contains 6000, 260 and 242 images respectively. Kaggle consists of four classes, IDB-2 consists of two classes and LISC consists of five classes of WBC types.

Firstly, Kaggle dataset is trained and validated using mobilenet, resnet and VGG-16 to know which model suits kaggle the best. It has four classes of data which are

Eosinophil, Neutrophil, Lymphocyte and Monocyte. Based on the experiment, resnet able to achieve highest training accuracy by 0.9713. However, VGG-16 is the highest for validation accuracy. But the differences between resnet and VGG-16 is 0.053. It can be said that resnet is the best model to classification of kaggle dataset. Next, IDB-2 database consists of two classes which are Lymphoblast and Non-Lymphoblast. The models are expected to detect and classify these two type of cells. Both training and validation accuracy is highest with VGG-16 model for IDB-2. Training accuracy achieved is 0.9721 and validation accuracy is 0.7913. It is clearly seen that VGG-16 is the best model to classify IDB-2 database. Last database tested is LISC database. It has five classes of data which are Basophil, Eosinophil, Neutrophil, Lymphocyte and Monocyte. In this case, highest training accuracy is obtained by resnet while highest validation accuracy is achieved by VGG-16 which is 0.9771 and 0.5781 respectively. The difference of validation accuracy between resnet and VGG-16 is 0.0411 which is not huge. As for LISC database, resnet is the best model to classify five classes of LISC database.

Next, the result is also manipulated by comparing the dataset result for each model. Firstly, for mobilenet, highest training and validation accuracy is from IDB-2 database which is 0.9696 and 0.7210 respectively. While for resnet, highest training accuracy is from LISC dataset. However, the differences between LISC and IDB-2 is only 0.0053. But for validation accuracy, IDB-2 is the highest which is 0.6999. Lastly, both training and validation accuracy is highest with IDB-2 database for VGG-16 model. The training accuracy is 0.9721 and the validation accuracy is 0.7913.

As a conclusion, resnet works best for kaggle and LISC dataset but VGG-16 works best for IDB-2 dataset. Other than that, the best dataset that can work with each model of mobilenet, resnet and VGG-16 is IDB-2 as it is less complex and it only has two classes of data. The images are also focused on the region of interest compared to the other two datasets which have more elements in the blood image.

In future, the own model is expected to be built which is better than the existing model to improve the training and validation accuracy. Next, other than classification, the system is also expected to localize the referred cell to make sure it is classifying the correct region. Experts' validation need to be obtained to strengthen the result's justification. Lastly, the number of dataset should be increased and undergo the same pretrained model.

#### ACKNOWLEDGMENT

This research is supported by a Fundamental Research Grant Scheme (FRGS) FRGS/1/2019/TK04/UTHM/02/6 (Vot. no K191) sponsored by the Ministry of Higher Education (MOHE). The research also received funding from the Office for Research, Innovation, Commercialization and Consultancy Management (ORICC), UTHM under Postgraduate Research Grant GPPS (Vot. No. H400).

#### REFERENCES

[1] Wang, X., et al., White blood cell counting on smartphone paper electrochemical sensor. *Biosensors and Bioelectronics*, 2017. 90: p. 549-557.

[2] Wang, Q., et al., A spectral and morphologic method for white blood cell classification. *Optics & Laser Technology*, 2016. 84: p. 144-148.

[3] Manik, S., L.M. Saini, and N. Vadera. Counting and classification of white blood cell using artificial neural network (ANN). in 2016 IEEE 1st International Conference on Power Electronics, Intelligent Control and Energy Systems (ICPEICES). 2016. IEEE.

[4] Macawile, M.J., et al. White blood cell classification and counting using convolutional neural network. in 2018 3rd International Conference on Control and Robotics Engineering (ICCRE). 2018. IEEE.

[5] Othman, M.Z., T.S. Mohammed, and A.B. Ali, Neural network classification of white blood cell using microscopic images. *Int. J. Adv. Comput. Sci. Appl.*, 2017. 8(5): p. 99-104.

[6] Throngnumchai, K., et al. Classification of White blood cell using Deep Convolutional Neural Network. in 2019 12th Biomedical Engineering International Conference (BMEiCON). 2019. IEEE.

[7] Zheng, X., et al., Fast and robust segmentation of white blood cell images by self-supervised learning. *Micron*, 2018. 107: p. 55-71.

[8] Sona, K., C. Sriragavi, And A.V.B. Varshini, Detection Of White Blood Sample Cells Using Cnn. 2019.

[9] Habibzadeh, M., et al. Automatic white blood cell classification using pre-trained deep learning models: Resnet and inception. in Tenth International Conference on Machine Vision (ICMV 2017). 2018. International Society for Optics and Photonics.

[10] Safuan, S.N.M., M.R.M. Tomari, and W.N.W. Zakaria, White blood cell (WBC) counting analysis in blood smear images using various color segmentation methods. *Measurement*, 2018. 116: p. 543-555.

[11] Safuan, S.N.M., et al. Lymphoblast cell morphology identification to detect Acute Lymphoblastic Leukemia (ALL) using various color segmentation. in *Journal of Physics: Conference Series*. 2020. IOP Publishing.

[12] Dong, N., et al., White blood cell classification. *arXiv preprint arXiv:2008.07181*, 2020.

[13] Andrade, A.R., et al., Recent computational methods for white blood cell nuclei segmentation: A comparative study. *Computer Methods and Programs in Biomedicine*, 2019. 173: p. 1-14.

[14] Wang, R., et al. Convolutional recurrent neural networks for text classification. in 2019 International Joint Conference on Neural Networks (IJCNN). 2019. IEEE.

[15] Zhao, C., et al. Variational convolutional neural network pruning. in *Proceedings of the IEEE Conference on Computer Vision and Pattern Recognition*. 2019.

[16] Acharya, U.R., et al., A deep convolutional neural network model to classify heartbeats. *Computers in biology and medicine*, 2017. 89: p. 389-396.

[17] Zhang, L., et al. Road crack detection using deep convolutional neural network. in 2016 IEEE international conference on image processing (ICIP). 2016. IEEE.

[18] Alom, M.Z., et al., Recurrent residual convolutional neural network based on u-net (r2u-net) for medical image segmentation. *arXiv preprint arXiv:1802.06955*, 2018.

[19] Nah, S., T. Hyun Kim, and K. Mu Lee. Deep multi-scale convolutional neural network for dynamic scene deblurring. in *Proceedings of the IEEE Conference on Computer Vision and Pattern Recognition*. 2017.

[20] Bisong, E., Google Colaboratory, in *Building Machine Learning and Deep Learning Models on Google Cloud Platform*. 2019, Springer. p. 59-64.

[21] Gunawan, T.S., et al., Development of video-based emotion recognition using deep learning with Google Colab. *TELKOMNIKA*, 2020. 18(5): p. 2463-2471.

[22] Balaraman, S., Comparison of Classification Models for Breast Cancer Identification using Google Colab. *Preprints*, 2020.

[23] Albawi, S., T.A. Mohammed, and S. Al-Zawi. Understanding of a convolutional neural network. in 2017 International Conference on Engineering and Technology (ICET). 2017. IEEE.

# Supervised Hyperspectral Image Classification using SVM and Linear Discriminant Analysis

Shambulinga M<sup>1</sup>, G. Sadashivappa<sup>2</sup>

Dept. of Electronics and Telecommunication Engineering  
RV College of Engineering, Bengaluru

**Abstract**—Hyperspectral images are used to recognize and determine the objects on the earth's surface. This image contains more number of spectral bands and classifying the image becoming a difficult task. Problems of higher number of spectral dimensions are addressed through feature extraction and reduction. However, accuracy and computational time are the important challenges involved in the classification of hyperspectral images. Hence in this paper, a supervised method has been developed to classify the hyperspectral image using support vector machine (SVM) and Linear Discriminant Analysis (LDA). In this work, spectral features of the images are extracted and reduced using LDA. Spectral features of hyperspectral images are classified using SVM with RBF kernel like buildings, vegetation fields, etc. The simulation results show that the SVM algorithm combined with LDA has good accuracy and less computational time. Furthermore, the accuracy of classification is enhanced by incorporating the spatial features using edge-preserving filters.

**Keywords**—Linear discriminant analysis; support vector machine; guided image filtering; bilateral filter

## I. INTRODUCTION

Hyperspectral image classification helps in identifying the various objects present on the earth's surface. The important application of this classification involves urban planning and development, flood monitoring, forest management, resource monitoring, vegetation fields, etc. A Hyperspectral image is captured with different wavelengths and contains a number of spectral bands. Classification of hyperspectral image is based on the spectral signature of the various materials. Spectral signature contains the reflected and absorbed light of the material with respect to different wavelength of electromagnetic spectrum. Various materials on the earth surface such as vegetation land, buildings, roads, etc. has different reflection and absorption at various channel wavelength. These spectral signatures of various materials on the earth are measured using spectrometer. The number of spectral signature values of various spectral wavelength bands, increases the spectral dimensions of the hyperspectral image. The problem with higher spectral dimensions in classification results in Hughes phenomenon [1], which means, the accuracy of the classification reduces as the spectral band dimension increases. To overcome the problem with higher dimensions of image, researchers have developed various band reduction techniques to reduce the number of spectral bands in hyperspectral images.

Principal component analysis (PCA) [2] is one of the unsupervised band reduction techniques in various data

analysis for pattern classification. It is designed to decrease the mean square error between the original dimensions and reduced dimensions. PCA will not maximize or minimize any metric related to automatic target recognition. The first problem in pattern classification is encountered when there is large size of training data samples compared with dimensions of the features space considered for classification. These features space contains very less redundancy information. Second, it is difficult to model the patterns by considering very less training data features and it results in rank-deficient covariance matrix if a feature has very high redundancy. The experimental evidence has been provided for the hyperspectral image that dimensionality reduction technique using PCA is not much effective for solving small sample size problems, with the number of training pixels are less than the dimensionality of feature space. On the other hand, few techniques have been developed in order to resolve the small sample size problems are Linear discriminant (LDA) transformation. LDA is developed to maximize the separation between the class scatters and minimize the separation within class scatters.

Hyperspectral image classification is divided into supervised and unsupervised classification. Supervised classification can achieve the higher classification accuracy compared with unsupervised classification due to the learning phase using training samples. In literature, Various supervised classifier has been developed for the classification of hyperspectral image based on some statistical parameters such as artificial neural networks [3], minimum distance [4], k-nearest neighbor [5], parallelepiped, Adaboost [6], Mahalanobis distance [7], Gaussian maximum likelihood [8], decision trees [9], Logistic Regression [10] and Convolutional neural network [11].

The mentioned methods are the pixel wise classifier and will not provide the very good classification results due to the complexity involved in the hyperspectral images. The numbers of training samples present in the dataset are very limited compare to the spectral bands present in the image which results in decreased classification accuracy. Moreover, hyperspectral bands are highly correlated which results in certain kind of noise that exists between the bands. However, certain techniques have been adopted to overcome the difficulties present in classifying the hyperspectral data. The one approach is developing the spectral and spatial classifier which results in accurate classification and combines the pixels wise classifier with spatial information of the image.

SVM [12] is one of the power full classifier for the hyperspectral image as it has good accuracy compared to the other classifiers that are mentioned above. To achieve more accuracy in SVM classification, several variations have been made to SVM which includes transductive SVM and SVM with composite kernels. Labeled and unlabeled samples are exploited in the transductive SVM. The Spectral features are directly incorporated into the SVM kernels. SVM is the pixel based classifier and includes only the spectral features for the classification and it does not include the spatial information of the image. To overcome problem related to including spatial features to the SVM, many researchers have explored and made an effort to enhance the reliability of classification by incorporating the spatial and spectral features [13] using image fusion techniques [14] and edge-preserving filter.

Guided image filter [15] and bilateral filter are the edge-preserving filter that incorporates the spatial features to the SVM algorithm. These edge-preserving filters improve the accuracy of the SVM algorithm by correcting the misclassified samples in the hyperspectral image.

In this paper, the hyperspectral image is classified by using SVM and LDA. The LDA is used as a band reduction technique and to extract spectral features of image. These spectral features contain the reflected and absorbed light information of the earth surface. Furthermore, to improve the performance of SVM classification, the two edge-preserving filters such as guided image filter and bilateral filter is used as post processing. Both filters use the first component of linear discriminant analysis as a guidance image.

This paper is organized as follows: Section II presents the feature extraction and reduction of the image based on LDA. Section III presents the classification of images with the help of SVM and RBF kernel using spectral features. Section IV presents the edge-preserving filter such as guided image filter and bilateral filter to enhance the classification accuracy by incorporating spatial features. Section V discusses the flowcharts and implementation of hyperspectral classification. The results and analysis of Indian pines image is discussed in section VI and conclusion derived in section VII.

## II. LINEAR DISCRIMINANT ANALYSIS

LDA is the supervised dimensionality reduction method used in the hyperspectral image. It reduces the number of spectral bands in the image and extract spectral features for classification. The technique is used to convert the high dimensional spectral feature space to the low dimensional spectral feature space using known class labels in the image. This will lead to enhance the class separation to eliminate the overfitting problem by reducing the error while estimating the parameter and reduces the computation time of the classification. However, even though spectral bands are reduced, the information required for the classification is maintained in very few numbers of linear discriminant components.

Steps to be followed in determining the LDA for feature reduction.

- 1) Calculate the mean of spectral signature for the various classes in the hyperspectral image.
- 2) Obtain the scatter matrices between and within the classes of the data.

Scatter matrix for within class is calculated by using equation (1).

$$S_w = \sum_{i=1}^c S_i \quad (1)$$

Where, c is total classes in the hyperspectral dataset

$$S_i = \sum_{x \in D_i}^n (x - m_i)(x - m_i)^T \quad (2)$$

$$m_i = \frac{1}{n_i} \sum_{x \in D_i}^n x_k$$

Where, x is a spectral value and n is the number of spectral values for each class.

Scatter matrix for between classes matrix is calculated using equation (3)

$$S_B = \sum_{i=1}^c N_i(m_i - m)(m_i - m)^T \quad (3)$$

Where,

$$m_i = \frac{1}{n_i} \sum_{x \in D_i}^n x_k$$

3) The eigenvectors and eigenvalues of the above scatter matrix are calculated.

4) Arrange the eigenvalues and vector in decreasing values. Furthermore, form the matrix W, of dimension  $d \times k$ , by selecting k eigenvectors with the highest eigenvalues.

5) The new sample subspace is created by using the  $d \times k$  eigenvector matrix. This can be transformed by matrix multiplication:  $Y=X \times W$ . where X contains the n samples and Y contains the newly transformed subspace.

The new sample subspace which contains the linear discriminant component values, which are used for the classification of hyperspectral images.

## III. SUPPORT VECTOR MACHINE

SVM is the supervised classification algorithm developed by Vapnik in 1998, which can be used for the classification of hyperspectral images. SVM classification depends on the optimal hyperplane that has been generated from support vectors. SVM is basically designed for binary classification, however multiclass SVM is developed by using original binary SVM. SVM model requires training spectral signature and testing spectral signature with corresponding class labels. Training spectral signature with labels are used to train the model and a trained model is tested using the testing spectral signature.

Now let X is the input spectral signature data and Y is the corresponding class label for each spectral signature. The training samples for the model is  $\{(x_1, y_1), (x_2, y_2), \dots, (x_m, y_m)\}$ . Now train the model and identify the acceptable value of  $y \in Y$  from the earlier seen value  $x \in X$ .

SVM model using training samples can be created by the equation.

$$Y = f(x, \alpha) \quad (4)$$

where,  $\alpha$  is kernel function parameters. These parameters are identified properly for exact classification. SVM is modeled with different kinds of kernel functions such as linear, polynomial functions, and radial basis functions. From the literature, it is proven that RBF kernel had achieved the highest classification accuracy for hyper spectral image.

The SVM decision function is given by equation (5).

$$f(x) = \sum_{i \in S} \alpha_i y_i K(x_i, x_j) + b \quad (5)$$

$K(x_i, x_j)$  is the kernel function, S is training features and labels.

Radial basis function:

$$K(x_i, x_j) = \exp\left\{-\frac{\|x_i - x_j\|^2}{2\sigma^2}\right\} \quad (6)$$

#### IV. EDGE PRESERVING FILTER

There are two types of edge-preserving filters, namely, bilateral filter and guided image filter. These filters are used to separate the noise present in the classified image. Noise in the classified image is mainly because of the wrong classification of each pixel. These misclassified pixels are corrected using bilateral and guided image filters. These two filters use the smoothing concept to correct the misclassified pixel by comparing the neighboring correctly classified pixels. Guided image filter is better than a bilateral filter at the edges of the image during the smoothing process due to gradient reversal artifacts present in the detailed composition.

##### A. Guided Image Filter

Guided image filter includes the spatial feature to the classified image and acts as an edge-preserving filter. The output of the filter is computed for each pixel by considering the input image p and guidance image I. The guidance image for the filter is as same as input image or any other type of image and it depends on the application. The output of the filter is calculated for each pixel by considering the window of size  $\omega_k$  as shown in equation (7). It is basically the linear transformation of guidance image and calculated for each pixel of an input image.

$$q_i = a_k I_i + b_k, \forall i \in \omega_k \quad (7)$$

$a_k$  and  $b_k$  are the linear coefficients that are calculated by reducing cost function between the filter input p and filter output q

$$E(a_k, b_k) = \sum_{i \in \omega_k} ((a_k I_i + b_k - p_i)^2 + \epsilon a_k^2) \quad (8)$$

$\epsilon$  is the regularization parameter and linear regression is used to calculate the solution to equation (8).

$$a_k = \frac{\frac{1}{|\omega|} \sum_{i \in \omega_k} I_i p_i - \mu_k \bar{p}_k}{\sigma_k^2 + \epsilon} \quad (9)$$

$$b_k = \bar{p}_k - a_k \mu_k \quad (10)$$

Here,  $\mu_k$  and  $\sigma_k^2$  are the mean and variance value of guidance image I in  $\omega_k$ ,  $|\omega|$  is the total number of pixel values in  $\omega_k$ .

Linear modeled for every local window is applied and compute the filter output by equation (11).

$$q_i = \frac{1}{|\omega|} \sum_{k: i \in \omega_k} (a_k I_k + b_k) = \bar{a}_i I_i + \bar{b}_i \quad (11)$$

where  $\bar{a}_i = \frac{1}{|\omega|} \sum_{k \in \omega_i} a_k$  and  $\bar{b}_i = \frac{1}{|\omega|} \sum_{k \in \omega_i} b_k$

##### B. Bilateral Filter

The bilateral filter output of each pixel is computed by the weighted average of the nearby pixels. The bilateral filter preserves the edges while smoothing by considering the difference in values of the neighboring pixels. The bilateral filter is defined by.

$$BF[I]_p = \frac{1}{W_p} \sum_{q \in S} G_{\sigma_s}(\|p - q\|) G_{\sigma_r}(|I_p - I_q|) I_q \quad (12)$$

where,  $W_p$  is the normalization factor, the sum of its weight is equal to 1.

$$W_p = \sum_{q \in S} G_{\sigma_s}(\|p - q\|) G_{\sigma_r}(|I_p - I_q|) \quad (13)$$

Here, parameter  $\sigma_s$  and  $\sigma_r$  define the filtering amount for the image I.

$G_{\sigma_s}$  is the spatial Gaussian weight that minimizes the effect of distant pixels.

$G_{\sigma_r}$  is a range Gaussian minimize the effect of pixel q when their intensity values vary from  $I_p$ .

#### V. METHODOLOGY

The methodology followed in the classification of hyperspectral image classification consists of the implementation of SVM algorithm, LDA algorithm, and Edge preserving filters such as guided image filter and bilateral filter. Matlab with various toolbox are used in the implementing the algorithm. The implementation of the hyperspectral image classification is shown in Fig. 1. Here hyperspectral image with 224 spectral bands have been considered for the classification. LDA extracts and reduces the spectral features of the hyperspectral image. These spectral features contain the reflected and absorbed light information at different wavelengths. These high dimensionality spectral bands at different wavelength of the image are converted to the low dimensionality spectral bands for reducing the computational complexity in classification. The implementation of the LDA algorithm is shown in Fig. 2. The LDA is the supervised dimensionality reduction algorithm and uses the spectral signature of the image and known labels of the dataset as input data. LDA calculates the mean, scatter matrix, and eigen values and eigen vectors of the spectral signature of the materials present in the hyperspectral image and also uses known labels present in the dataset for the calculation. Finally, the k eigenvector is selected as a feature vector and this feature vector is used to derive the new set of data by multiplying the feature vector with spectral signature. The obtained new data vectors are the linear discriminant components of the spectral signature. The maximum linear



discriminant components obtained here is the number of classes present in the image. The number of linear discriminant components depends on the selection of eigenvector. Linear components contain the spectral features values and these values are used for SVM classification. These spectral features along with labels of each class are divided into the training and testing samples for SVM classification. SVM model is trained using the RBF kernel by computing the cost function and gamma parameter using a five-fold cross-validation method.

The implementation of the five-fold cross-validation method is shown in Fig. 3. This method calculates the cost function and gamma parameter required for RBF kernel using training samples and labels based on maximum classification accuracy achieved at each iteration of C and g value. Now predict the test samples using a trained SVM model and calculate the overall accuracy of classification by plotting the confusion matrix. Few pixels of the hyperspectral image are correctly classified and few pixels are wrongly classified into different classes. The misclassified pixels in the image are corrected using edge preserving filter such as guided image filter and bilateral filter.

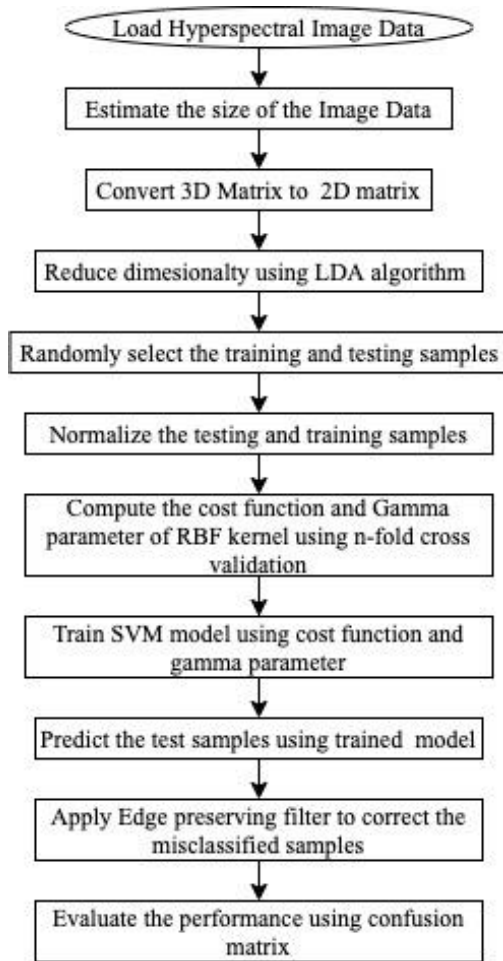


Fig. 1. Implementation of Hyperspectral Image Classification.

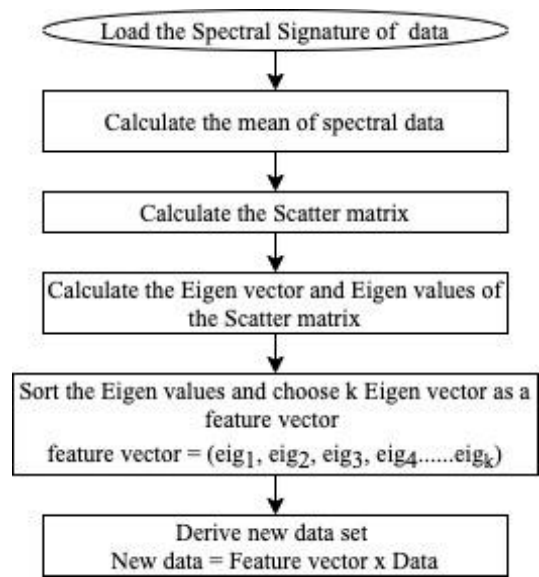


Fig. 2. LDA Implementation flow Chart.

The implementation of this filter is shown in Fig. 4 and Fig. 5. This edge-preserving filters includes the spatial features for the classification of images. Misclassified pixels in the SVM classification are considered as noise and filter removes the noise by comparing the neighbor pixels. The filter uses the SVM classified image as an input image and first component of linear discriminant analysis image as a guidance image for both filters. Filter coefficients required for both edge-preserving filter is determined based on (9) and (10) for the selected window of 3x3. The output of the filter is derived based on (11) and (12). The output of the filter contains the pixels with correctly classified classes. Finally, the overall classification accuracy of SVM with both edge-preserving filter is measured by plotting the confusion matrix and simulation results are compared with previous SVM outputs.

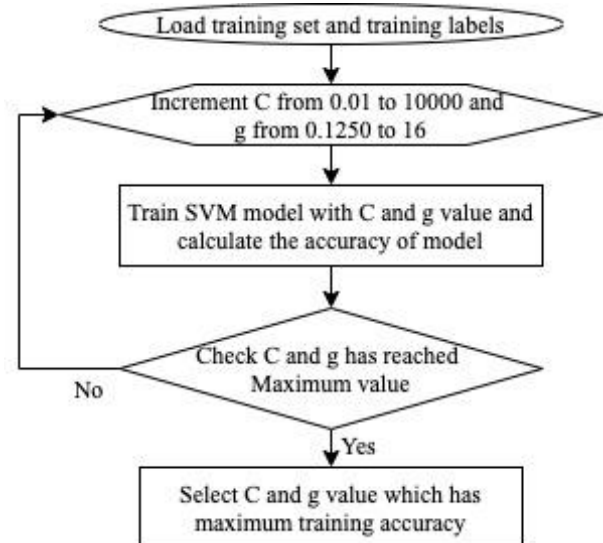


Fig. 3. Flow Chart for Five-fold Cross Validation Method.

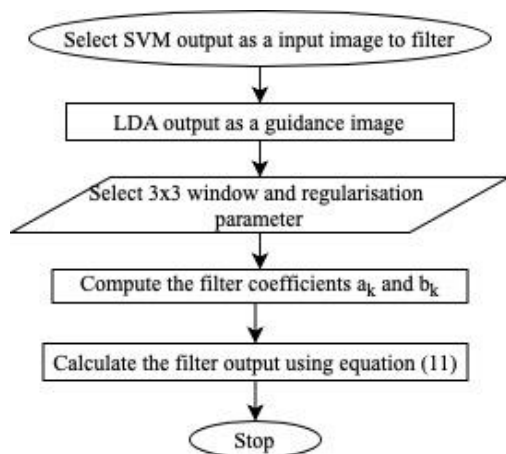


Fig. 4. Flow Chart for Guided Image Filter.

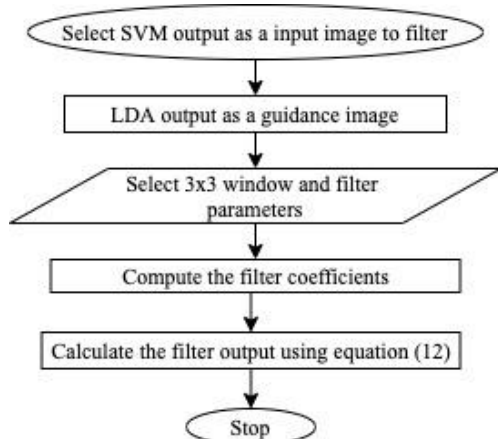


Fig. 5. Flow Chart for Bilateral Filter.

## VI. RESULTS AND ANALYSIS

### A. Hyperspectral Image

The Indian pines image as shown in Fig. 6(a) is captured through the AVIRIS sensor (Airborne Visible / Infrared Imaging spectrometer). These image are captured at the North-Western Indiana test place. Recorded image comprises of 220 bands spectral information. The spectral wavelength of the AVIRIS sensor is 0.4 to 2.5 $\mu$ m. The total size and spatial resolution of the image is 145x145 pixels and 20m per pixel, respectively. The image consists of forest land, agriculture land, and various vegetation fields, and totally it has 16 classes of information. Spectral bands covered with water absorption region are removed and total bands of the image are reduced to 200 bands. Color image and ground truth data indicating all the classes are shown in Fig. 6. The parameters considered to evaluate the performance of the developed methods are Kappa coefficient, Average accuracy (AA), and overall accuracy (OA).

### B. Classification Results

The Indian pines image as shown in Fig. 6(a) is classified using a SVM with RBF kernel and simulation results of different proposed approaches are shown in Table I. The training data used in the generation of the SVM model is 10%

of the total samples. Fig. 7 shows the classified image of different vegetation fields using the trained SVM model with RBF kernel using spectral features. The resultant overall classification accuracy obtained for the classified image is 81.15% and the computation time required to simulate the algorithm is 155 seconds. This computation time of SVM classification is reduced by removing the unnecessary spectral information by using LDA. The computation time is reduced to 25 seconds with the same classification accuracy, if only 15 linear components are used to train and test the SVM model. It can be infer from Fig. 7 that there are few pixels in the resultant image are wrongly classified to the different classes. These pixels appear like a noise in the resultant image which degrades the overall classification accuracy. These noises in the resultant image is removed by considering the edge preserving filter such as guided image filter and bilateral filter.

The overall classification accuracy of the SVM model is improved by adding spatial features to the SVM classified image. These features are added by using a guided image filter and bilateral filter with the first linear component of LDA as a guided image. Fig. 8 and 9 shows the SVM classified image using a guided image filter and bilateral filter, respectively. From the figure, it can be infer that noise in the resultant image are removed when compared to the previous SVM resultant image. The removal of noise increases the overall classification accuracy. Guided image filter improves the overall classification accuracy of SVM from 81.15% to 93.41%. Bilateral filter improves the overall classification accuracy of SVM from 81.15% to 92.41%. Guided image filter performs better compare to bilateral filter and it has better behavior near edges.

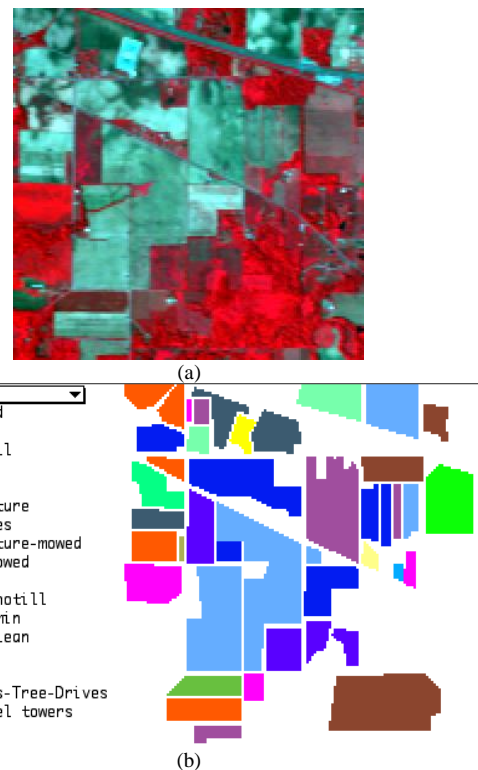


Fig. 6. (a) Three Band Color Image (b) Ground Truth Data, of Indian Pines Image.

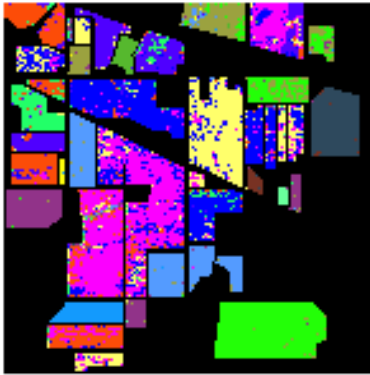


Fig. 7. Classified Hyperspectral Image using SVM with RBF Kernel.



Fig. 8. Classified Hyperspectral Image using SVM and Guided Image Filter.



Fig. 9. Classified Hyperspectral Image using SVM and Bilateral Filter.

The linear components are used to reduce the computational time by maintaining the same accuracy level of the SVM model. Fig. 10 shows the variation of overall classification accuracy of SVM with a number of linear components used to train the SVM model.

A few numbers of linear components are more enough to get the same accuracy when compared to the classification accuracy of SVM with all features are considered. From the simulation experiments it can be infer that liner components with more than 7 are giving almost same classification accuracy. By considering very few linear components the computation time for classification is reduced and Fig. 11 shows the computation time with a number of linear

components considered for SVM classification. From figure it can be infer that first few liner components require more computation time for classification. The computation time is minimum for the liner components from 6 to 8 and later for higher linear components the computation time increases. This computation time for classification includes reading of the image data, extracting the spectral features using LDA, training and testing the SVM model.

TABLE I. SIMULATION RESULTS OF HYPERSPECTRAL IMAGE CLASSIFICATION

| Methods                      | SVM    | SVM LDA | SVM LDA_GF | SVM LDA_BF |
|------------------------------|--------|---------|------------|------------|
| OA                           | 81.15  | 82.75   | 93.41      | 92.41      |
| AA                           | 79.77  | 84.32   | 93.82      | 93.45      |
| Kappa                        | 78.43  | 80.20   | 92.41      | 91.28      |
| Alfalfa                      | 70.00  | 86.96   | 100.00     | 100.00     |
| Corn-notill                  | 75.95  | 79.30   | 98.02      | 98.36      |
| Corn-mintill                 | 64.71  | 72.48   | 89.00      | 95.81      |
| Corn                         | 63.43  | 64.22   | 69.67      | 69.49      |
| Grass-pasture                | 88.71  | 88.19   | 91.17      | 95.02      |
| Grass-trees                  | 92.40  | 94.97   | 99.85      | 100.00     |
| Grass-pasture-mowed          | 86.67  | 100.00  | 100.00     | 100.00     |
| Hay-windrowed                | 100.00 | 99.51   | 100.00     | 100.00     |
| Oats                         | 52.63  | 62.50   | 100.00     | 100.00     |
| Soybean-notill               | 73.15  | 69.08   | 88.33      | 80.49      |
| Soybean-mintill              | 82.18  | 81.16   | 92.08      | 91.48      |
| Soybean-clean                | 78.37  | 83.94   | 99.53      | 85.79      |
| Wheat                        | 97.16  | 100.00  | 100.00     | 100.00     |
| Woods                        | 95.28  | 98.88   | 99.91      | 99.82      |
| Buildings-Grass-Trees-Drives | 68.90  | 70.02   | 77.64      | 81.19      |
| Stone-Steel-Towers           | 86.79  | 97.92   | 95.92      | 97.67      |

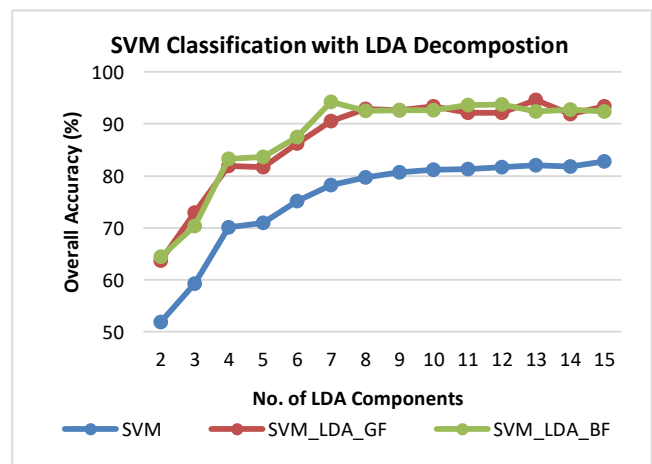


Fig. 10. Graph of Overall Accuracy vs No. of LDA Components.

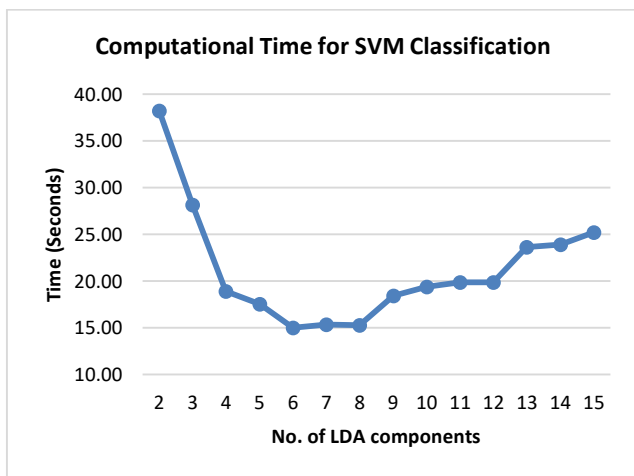


Fig. 11. Graph of Computation Time vs. No. of LDA Components.

## VII. CONCLUSION

In this paper, hyperspectral image classification was developed based on spectral and spatial features. SVM with RBF kernel was used in the proposed approach for classification. More computation time required for SVM to compute its kernel parameter and classify, if all the spectral features of the images are considered. These spectral features of the hyperspectral image are reduced by linear discriminant analysis and only a few linear components are considered for the SVM classification in order to reduce the computational time. Furthermore, the classification accuracy was increased by incorporating the spatial features to the classification. These spatial features are included in classification by using edge-preserving filters such as guided image filter and bilateral filter. Simulation results shows that the guided image filter improves the classification accuracy from 81.15% to 93.41% and bilateral filter improves the classification accuracy to 92.41%. In future, computation time and accuracy of SVM can be improved by using various dimensionality reduction algorithms.

## REFERENCES

- [1] G. Hughes, "On the mean accuracy of statistical pattern recognizers," *IEEE Transactions Information Theory*, vol. IT-14(1), pp. 55–63, 1968.
- [2] Saurabh Prasad and Lori Mann Bruce, "Limitations of principal components analysis for hyperspectral target recognition," *IEEE Geoscience Remote Sensing Letter*, vol. 5(4), pp. 625–629, 2008.
- [3] Y. Zhong and L. Zhang, "An adaptive artificial immune network for supervised classification of multi-/hyperspectral remote sensing imagery," *IEEE Transactions Geoscience Remote Sensing*, vol. 50(3), pp. 894–909, 2012.
- [4] W. Li, S. Prasad, E. W. Tramel, J. E. Fowler and Q. Du, "Decision fusion for hyperspectral image classification based on minimum-distance classifiers in the wavelet domain," *IEEE China Summit & International Conference on Signal and Information Processing*, Xi'an, 2014, pp. 162-165.
- [5] B. Tu, J. Wang, X. Kang, G. Zhang, X. Ou and L. Guo, "KNN-Based Representation of Superpixels for Hyperspectral Image Classification," in *IEEE Journal of Selected Topics in Applied Earth Observations and Remote Sensing*, vol. 11, no. 11, pp. 4032-4047, Nov. 2018.
- [6] B. Kuo, S. Lin, H. Wu and C. Chuang, "A novel classification processing based on the spatial information and the concept of Adaboost for hyperspectral image classification," *2010 IEEE International Geoscience and Remote Sensing Symposium*, Honolulu, HI, 2010, pp. 2816-2819.
- [7] V. Natarajan, L. Anush Bharadwaj, K. Hari Krishna and J. Aravindh, "Urban Objects Classification from HSR-HTIR Data Using Gaussian and Mahalanobis Distance Classifiers," *2018 International Conference on Communication and Signal Processing (ICCS)*, Chennai, 2018, pp. 1041-1045.
- [8] D. Saqui, J. H. Saito, L. A. D. C. Jorge, E. J. Ferreira, D. C. Lima and J. P. Herrera, "Methodology for Band Selection of Hyperspectral Images Using Genetic Algorithms and Gaussian Maximum Likelihood Classifier," *International Conference on Computational Science and Computational Intelligence (CSCI)*, Las Vegas, NV, 2016, pp. 733-738.
- [9] P. P. Shingare, P. M. Hemane and D. S. Dandekar, "Fusion classification of multispectral and panchromatic image using improved decision tree algorithm," *International Conference on Signal Propagation and Computer Technology*, Ajmer, 2014, pp. 598-603.
- [10] S. Bajpai, H. V. Singh and N. R. Kidwai, "Feature extraction & classification of hyperspectral images using singular spectrum analysis & multinomial logistic regression classifiers," *2017 International Conference on Multimedia, Signal Processing and Communication Technologies (IMPACT)*, Aligarh, 2017, pp. 97-100.
- [11] L. Fang, G. Liu, S. Li, P. Ghamisi and J. A. Benediktsson, "Hyperspectral Image Classification With Squeeze Multibias Network," *IEEE Transactions on Geoscience and Remote Sensing*, vol. 57(3), pp. 1291-1301, 2019.
- [12] Y. Chen, N. M. Nasrabadi, and T. Tran, "Hyperspectral image classification via kernel sparse representation," *IEEE Transactions Geoscience Remote Sensing*, vol. 51(1), pp. 217–231, 2013.
- [13] Z. He, Y. Shen, M. Zhang, Q. Wang, Y. Wang and R. Yu, "Spectral-spatial hyperspectral image classification via SVM and superpixel segmentation," in the proceedings of *IEEE International Instrumentation and Measurement Technology*, 2014, pp. 422-427.
- [14] Suchitha K., Premananda B.S. and A.K. Singh, "High spatial resolution hyperspectral image using fusion technique," in the Proceedings of *International Conference on Trends in Electronics and Informatics*, pp. 348-353, 2017.
- [15] Shambulinga M and Sadashivappa G., "Hyperspectral Image Classification using Support Vector Machine with Guided Image Filter" *International Journal of Advanced Computer Science and Applications*, vol. 10(10), 2019.

# Manar: An Arabic Game-Based Application Aimed for Teaching Cybersecurity using Image Processing

Afnan Alsadhan<sup>1</sup>, Asma Alotaibi<sup>2</sup>, Lulu Altamran<sup>3</sup>, Majd Almalki<sup>4</sup>, Moneera Alfulaij<sup>5</sup>, Tarfa Almoneef<sup>6</sup>

Information Systems Department  
King Saud University, Riyadh, Saudi Arabia

**Abstract**—People use the Internet for various activities, including exchanging money, playing games, and shopping. However, this powerful network came at a cost: the features that provide the Internet with these capabilities are also what make it vulnerable. The need for cybersecurity tools and practices was recognized, especially for children, since they tend to be naive and can be easily tricked. Aimed at children from 6 to 12 years old, Manar is an Arabic smartphone game that seeks to build a generation who are well-informed about cybersecurity issues. It teaches them about notable cybersecurity topics such as social engineering and cryptography, it also has a very appealing theme to attract children to play the game. The theme being “pirates and islands”, each level will be represented as an island and a moving pirate ship will navigate between the levels. The application introduces the technology of image processing in a unique way, allowing children to move around and look for objects, which makes the game as interactive as possible to attract children’s attention.

**Keywords**—Cybersecurity; image processing; social engineering; cryptography

## I. INTRODUCTION

As the Internet is increasingly becoming part of people’s lives, users must be wary of the risks. Cybersecurity awareness is essential. Internet users are at constant risk of hacking, phishing, sniffing and many other threats. Many children spend an unhealthy amount of time on the Internet, using it to study and complete homework or to play online games and browse social media. Such activities may lead to unwanted exposure to risk and potential harm.

This project proposes a smartphone game directed at children which is intended to help them become more informed about cybersecurity. The application consists of various levels that focus on different cybersecurity concepts. In each level, the player learns a new concept of cybersecurity that helps them to be more careful and safer. It is hoped that they will develop a responsible attitude towards communicating in cyberspace.

Furthermore, cybersecurity and the information technology field in general became a primary interest and concern in Saudi Arabia’s Vision 2030 plan, as evidenced, for example, by the establishment of a national cybersecurity authority. Hence, the game will contribute to the goals and objectives of the Vision 2030 plan through raising awareness among young people who are not currently interested in or aware of these topics. It is hoped that through the game, awareness can be raised in a way that intrigues the children. The number of

Internet users has increased significantly, which increases the risk of hacking and other harmful activities. This increased risk raises the need for cybersecurity to protect users, especially children because they lack enough knowledge to be safe online.

This paper is structured as follows. Section II illustrates the literature review that discusses related studies and applications. The definition of the problem, the proposed solution, and the project objectives are outlined in Section III. Section IV presents the application development process used in the project. Section V discusses the limitations and future work, and Section VI concludes the paper.

## II. LITERATURE REVIEW

This section describes the differences between Manar application and similar systems. First, the features of existing systems are described. Manar application is then compared with those systems. Next, how the application’s features overcome the limitations of similar systems will be explained in more details.

### A. Related Studies

The number of Internet users has increased significantly, which increases the risk of hacking and other harmful activities. This increased risk raises the need for cybersecurity to protect users, especially children because they lack enough knowledge to be safe online.

**Cyber security** is defined as "technologies and processes constructed to protect computers, computer hardware, software, networks and data from unauthorized access, vulnerabilities supplied through the Internet by cybercriminals, terrorist groups and hackers" [1].

**Image processing** is "a method to convert an image into digital form and perform some operations on it, in order to get an enhanced image or to extract some useful information from it" [2].

Risks and concerns about Internet use range from situations where innocent children are victimized by others, to situations where children have engaged in actions that are risky, irresponsible, harmful, or even illegal. The following are some key risks and concerns [3]:

1) *Cyberbullying* is bullying that takes place over digital devices like cell phones, computers, and tablets. Cyberbullying can occur through SMS, Text, and apps, or online in social media, forums, or gaming where people can

view, participate in, or share content. Cyberbullying includes sending, posting, or sharing negative, harmful, false, or mean content about someone else. It can include sharing personal or private information about someone else causing embarrassment or humiliation. Some cyberbullying crosses the line into unlawful or criminal behavior [4].

2) *Hacking* is the process of attempting to gain or successfully gaining, unauthorized access to computer resources. Computer hacking is the practice of modifying computer hardware and software to accomplish a goal outside of the creator's original purpose [5].

3) *Online gaming* describes any video game that offers online interactions with other players [6].

These risks and concerns can be effectively addressed through education and parental supervision.

The most common issues children face online [7]:

1) *Cyberbullying*: 1 in 5 repeatedly cyberbullied teens contemplate suicide.

2) *Sexual Solicitation and Exposure to Sexual Content*: A recent study found that one in five youth experienced unwanted sexual solicitation online.

3) *Maintaining Privacy*: The report estimates that by the age of 13, parents have posted roughly 1300 photos and videos of their children online. According to the UK report, Barclays has forecast that by 2030 "sharenting" will account for 2/3 of identity fraud, costing hundreds of millions of dollars a year. With just a name, date of birth, and address (easy enough to find in a geotagged birthday party photo on Facebook, for example), bad actors can store this information until a person turns 18 and then begin opening accounts [8].

4) *The Generational (or Communication) Gap*: Children tend to view their lives online and offline as one and the same, whereas adults tend to view them as separate spheres. Having spent the majority of their life interacting with technology, children have an inherent advantage when it comes to navigating the Internet. The only way parents and educators can close this generational disparity is to open clear communication channels with students.

"On 15 November 2013 the online video-sharing website YouTube was searched for various cyber-safety related videos. On searching the word 'e-Safety', 141 million possibilities were identified. A search for the phrase 'e-Safety for children' produced 11 million videos and the phrase 'e-Safety for children cartoon' indicated that more than 1.8 million possible cartoon videos exist" [3]. See Table I. This shows that the best way to teach children about cybersecurity is by using cartoons as much as possible.

TABLE I. YOUTUBE SEARCHES (15 NOVEMBER 2013)

|          | Safety | For children | Cartoons |
|----------|--------|--------------|----------|
| e-       | 141 m  | 11 m         | 1.8 m    |
| Cyber    | 2.1 m  | 305 k        | 285 k    |
| Internet | 19 m   | 2 m          | 244 k    |

Recently there have been some initiatives and campaigns concerning cybersecurity in Saudi Arabia for children [9]. One example is the campaign Safe Online, it was published in 2016 by the Communications and Information Technology Commission in cooperation with the Ministry of Education. The campaign's goal was to raise children's awareness of the proper use of the Internet in a fun and educational way. They targeted children and their guardians in the cities of Riyadh, Jeddah, and Dammam to teach them about cybersecurity courses.

NEW YORK, 15 April 2020 [10] – Millions of children are at increased risk of harm as their lives move increasingly online during lockdown in the COVID-19 pandemic, UNICEF and partners said today.

"The coronavirus pandemic has led to an unprecedented rise in screen time," said Global Partnership to End Violence Executive Director Dr. Howard Taylor. "School closures and strict containment measures mean more and more families are relying on technology and digital solutions to keep children learning, entertained and connected to the outside world, but not all children have the necessary knowledge, skills and resources to keep themselves safe online."

#### B. Related Applications

- *CYBER-FIVE*: CYBER-FIVE [11] is a web-based game provided by ABCya.com that aims to teach children five rules of cybersecurity by showing them a short animation of a dialogue between two friends, Hippo and Hedgehog. Hedgehog breaks the five security rules one by one, and Hippo advises him to avoid each mistake. The game provides animation with audio for the two friends, quizzes and tests.
- *Talented & Gifted Games*: Talented & Gifted Games [12] is an Android and iOS application developed by Kids Academy that teaches that teaches children many courses like math and English. Each course consists of an educational video, game and quiz. All the courses are divided into grades: preschool (ages 2–4), kindergarten (ages 4–5), 1st grade (ages 5–7), 2nd grade (Ages 6–8), and 3rd grade (ages 9–10). The application features include augmented reality and educational videos provided by specialists.
- *Play safe! Be safe Fire safety game*: Fire safety game [13] Created in 1994, play safe! be safe! is a web-based game by the BIC corporation aimed at teaching children fire safety. It supports only the English language. The game teaches the children different things in safety like fire safety and n safe and unsafe objects to play with and so on.
- *MentalUP game*: MentalUPgame [14] measures children's performance and development with a regular report so they can discover their strengths and weaknesses and they can track their improvement over time. It provides advice after each set is terminated by the games. Also, it improves child skills like creative thinking and problem-solving.

- *Khan Academy Kids*: Khan Academy Kids [15] is an educational app dedicated to children from the ages of 2 to 6. It supports only the English language, and it operates on Apple's iOS and Google's Android. The app's main goal is to teach children about science, reading, writing, problem-solving skills and social-emotional learning in a fun and interactive way with original content. It provides multiple levels of different activities, such as drawing, matching and storytelling.
- *TripLens*: TripLens [16] is an Android and iOS application developed by Kita Bilgi to improve the user's travel experience even if they speak the local language very well. For instance, the user may not remember translating an object in that foreign language, and it is a wonderful assistant for text translations.
- *Make it*: Make it [17] is an Android and iOS application developed by Learn Land that allows teachers to make fun and interactive quizzes or games with a wide assortment of templates available. Teachers can customize the games or quizzes to suit their students' needs. The application makes it easy to add images, sounds and other educational resources to the game or quiz. Finally, students learn by doing they can make their own game at home or at school.

### C. Discussion

Early childhood education about cybersecurity results in increased social awareness. Children become more aware of how to protect themselves and their information on the Internet. The Manar application will raise awareness about cybersecurity in a way that is superior to traditional methods of education. Additionally, as the game uses the Arabic language, it will contribute to Arabic content in the IT field and promote the value of the Arabic language among children. Moreover, Manar will contribute to the goals and objectives of the country's Vision 2030 [18].

The systems introduced above helped us understand the available features in children games to consider missing features and improve existing features to provide an interactive and interesting game. As mentioned in Table II games have many features, but they also have many limitations. Some of the most common limitations are that they do not support mobile devices, they do not support Arabic language, they do not use a reward system, they do not support image processing, and they do not teach cybersecurity. In contrast, Manar application provides all these features, among others.

### III. PROBLEM DEFINITION

Smart devices and technology in general have become a significant part of people's lives, and they are easily accessible to all generations. However, it is well-known that the cyber world is in many ways potentially harmful to adults and even more so for children, who may be incautious in regard to online activity.

This raises concerns about children's use of the Internet, as they are exposed to computers, smartphones, and tablets at an

early age, often using them without supervision and with direct connection to complete strangers. This situation may lead to various threats, such as exposure to inappropriate content, cyberbullying, and online scams.

Manar is our proposed solution. It's an application, a smartphone game that teaches children about cybersecurity in a fun and interactive way. The theme will be "pirates and islands", which will add flamboyance to the application.

The game will be divided into different levels, each level representing a new island. The game will also include a reward system, and the child must pass each level to collect rewards. These rewards will add an element of excitement and motivation to the game.

To add an interactive element, the game will include image-processing technology, specifically image recognition. At the beginning of each level, a hint will be given of what the level is going to be about, and the child will be asked a question which they must respond to with a photograph of an object.

The application will be developed for Android OS through Android Studio using the Java programming language.

The main goals of the project are to raise awareness of cybersecurity among children, using a fun, interactive game that lets children move around and protects them from potential threats of the cyber world. From these goals are derived the following objectives:

- Teaching children about various cybersecurity concepts, such as hacking, protection, and social engineering.
- Designing a vivid interface with fun characters and themes.
- Applying the concepts illustrated and taught in the game by asking different types of questions.
- Using the reward system to motivate the players.
- Increasing children's physical activity by adding image-processing (image recognition) technology, which allows them to move around their environment looking for certain objects.

### IV. APPLICATION DEVELOPMENT

This section outlines the process by which we developed the application, beginning with the information gathering strategies used in the analysis phase then continuing with an overview of the system design, user interfaces, system implementation and lastly system Implementation and testing.

#### A. Information Gathering

The first method of information gathering in conducting interviews. A meeting was held with Hanan AlShehri, a coordinator at the Cybersecurity for Kids initiative. The meeting was held on the 25th of September 2020, with all team members present. The purpose of the meeting was to learn how to provide interactive games dedicated to children, since this initiative is already providing activities to children in the cybersecurity field. Also, the project team interviewed

three children from ages 11 to 12, it was conducted on the 30th of September. The interviews were useful, as these children were in the target demographic of the application.

The second method was conducting an online questionnaire, it received 624 responses and targeted parents in Saudi Arabia. The results of the survey indicated that 55.9% of children spend more than four hours on their devices and 9.1% of them spend one hour. Another observation was that 44.6% of children sometimes talk to unknown people on social media or online games and 39.9% of them never talk to unknown people. Some children are aware, but the majority still lack perception. The respondents were also asked “Are you keen to add anti-virus programs to your child’s device?”, to which 67.3% answered “I do not care about downloading antivirus software” and 32.7% answered “I download antivirus software for my child’s devices”. Another question was “Does your child connect to public Wi-Fi networks (such as restaurants and hotels)?”, to which 46% answered “Sometimes” and 30.1% answered “Never”. Also, it showed that 47.4% of children do not have different passwords chosen for each account, and only 16% do. Another question was “Do you think your children need to significantly increase their level of awareness about cybersecurity?” to which 87.7% agreed and 2.7% disagreed. Another question was “Do you support an educational application. Finally, the respondents were asked for suggestions and features to include in the Manar application. They responded that they wanted the application to avoid difficult terms, to use other non-educational characteristics to attract children, and to not advertise it as a purely educational program because most children are averse to anything that benefits them. The respondents commented that the attractive appearance of the application attracts children, and they hoped that the

application would reach the widest range of children through dissemination by the Ministry of Education. Designed to teach children the principles of cybersecurity in fun ways?”, to which 92.3% answered “Yes” and 2.9% answered “No”.

The conclusion is that all information gathered from this section will be taken into consideration when developing Manar. Manar will help parents to protect their children from threats that they may face on the Internet. It will teach children about various cybersecurity concepts using a vivid interface to make learning fun. All the information gathered and presented in this section will be helpful for system analysis.

### B. System Design

Manar application is designed as a smartphone game that teaches children about cybersecurity in a fun and interactive way. The application targets Saudi children, both boys and girls, in the age range 6–12 years. It will support only the Arabic language, and it will be directed to schools and children’s institutes.

As the game targets children, the design and look of it is very important. The theme is “pirates and islands”, which will add flamboyance to the application and a parrot character designed to guide the child throughout the application. The game will be divided into different levels, each level representing a new island. The game will also include a reward system, and the child must pass each level to collect rewards. These rewards will add an element of excitement and motivation to the game. To add an interactive element, the game will include image-processing technology, specifically image recognition. At the beginning of each level, a hint will be given of what the level is going to be about, and the child will be asked a question which they must respond to with a photograph of an object.

TABLE II. COMPARISON BETWEEN SIMILAR SYSTEMS AND MANAR

| Application features                                         | Make it   | CYBER-FIVE | TripLens | Talented & gifted | Fire safety game | MentalUP | Khan Academy Kids | Manar |
|--------------------------------------------------------------|-----------|------------|----------|-------------------|------------------|----------|-------------------|-------|
| Mobile Application                                           | ✓         | ✗          | ✓        | ✓                 | ✗                | ✓        | ✓                 | ✓     |
| Support Arabic language                                      | partially | ✗          | ✗        | ✗                 | ✗                | ✗        | ✗                 | ✓     |
| Support image processing                                     | ✗         | ✗          | ✓        | ✓                 | ✗                | ✗        | ✗                 | ✓     |
| Teach cybersecurity                                          | ✗         | ✓          | ✗        | ✗                 | ✗                | ✗        | ✗                 | ✓     |
| Provide certification at the end / Applied the reward system | ✗         | ✗          | ✗        | ✓                 | ✗                | ✗        | ✓                 | ✓     |
| User has more than one Account                               | ✗         | ✗          | ✗        | ✗                 | ✗                | ✓        | ✓                 | ✓     |
| Provide quiz                                                 | ✓         | ✓          | ✗        | ✓                 | ✓                | ✓        | ✓                 | ✓     |
| Has multiple levels                                          | ✓         | ✗          | ✗        | ✗                 | ✓                | ✓        | ✓                 | ✓     |



Manar application uses a hybrid architecture [19] that consists of an MVP (model–view–presenter) pattern for the client side and a client–server model for the whole system. The MVP pattern was chosen because of its ability to facilitate automated unit testing and improve the separation of concerns in presentation logic. The Presenter contains the user-interface business logic for the View. All invocations from the View are delegated directly to the Presenter. The Presenter is also decoupled directly from the View and communicates with it through an interface, as shown in Fig. 1.

The client–server architecture was chosen because of the system’s requirement to acquire information from an external source acting as a server, namely, the IBM image-recognition API. In the client–server model, any process can act as server or client. It is not the type, size, or computing power of the machine that makes it a server; it is its ability to serve requests that makes a machine a server. For the Manar application, a repository architecture was not chosen because the application does not have large volumes of data. A peer-to-peer architecture was not chosen because the application does not have multiple clients with equal capabilities and responsibilities.

### C. User Interfaces

This part presents a sample of screen shots in Manar application to illustrate the user interface design (Fig. 2 to 9).

### D. System Implementation

Manar used the Android Studio environment to program the application by using the Java programming language. Furthermore, to execute and test Manar application, the team used Android mobile and virtual devices provided by Android Studio. Moreover, Adobe illustrator and Photoshop applications were used to design the pictures and instructions included in the application. For Manar’s database, we chose Firebase because it is the most suitable since it is a real-time and cloud database dealing with cloud and real-time data. We used the database to save the user’s information, lessons and quizzes questions. Finally, we used the IBM Watson API to Recognition image by extract images and detect for specific content.

In the beginning, the application starts to run with the start window then a registration window that contains the user registration with the name and characters (boy and girl). Next, a map window showing a series of locked islands that the child must unlock to reach the last island is displayed. Each island represents a level in the application and introduces one of the cybersecurity concepts, to unlock the island the child must solve a puzzle by photographing a specific object and the IBM Watson API recognize and detect the image. The island (level) contains lessons, then interactive quiz after the lessons that measures the child’s understanding. A “Hint” option will be provided with each question to assist the child if needed after three wrong attempts. The application is applying a reward strategy to motivate children. Once the child finishes the quiz, the total score will be given that represented by coins which will be added to his/her treasure. After that the child will be able to move to the next island. The child’s progress will be shown throughout each level. The child will visit five islands that provide five cybersecurity concepts: Password

level, Social engineering level, Viruses level, Cyber Bully level and Encryption level. Finally, when the child finishes all the levels successfully if the child collects 100 coins, he/she will encrypt his/her name as a prize for him. Regardless of the number of coins, the child will receive a certificate, the certificate will contain the child’s name and total score and can be saved or shared through different social applications.

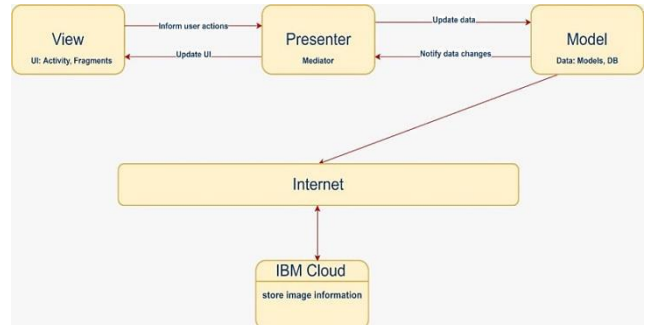


Fig. 1. Manar’s Hybrid Architecture (Combines MVP and Client–Server Architectures).

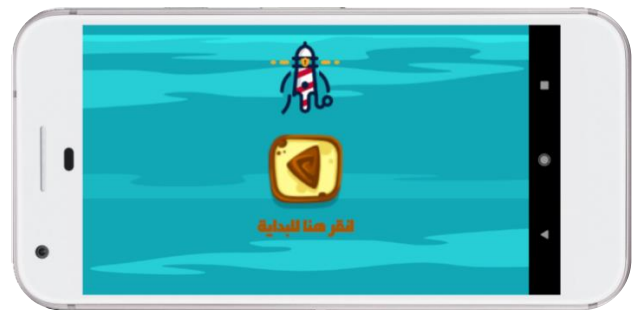


Fig. 2. Beginning Page, the First UI Seen by the user.



Fig. 3. Registration Page, the user has to Choose a Name and a Profile Picture.



Fig. 4. Welcome Page, a Nice Welcoming to the user.



Fig. 5. Choose Account Page, Appears when the user wants to Switch Accounts.



Fig. 9. Child's Certificate, the end Reward of completing all the Levels.



Fig. 6. Map Page, Appears when the user completes a Level and uses it to go to the Next.



Fig. 7. Level Unlock Question, the user is presented with a Puzzle that is solved by taking a Picture of the Answer.



Fig. 8. Match Question, an Example of a Type of Question that the user could Face.

### E. System Evaluation and Testing

To assure that the system performs all requirements, meet the objective and to uncover errors there must a testing method preformed. Manar application applied several test strategies such as unit testing, integration testing, user acceptance testing, and performance testing.

User Acceptance Testing (UAT) [20] is a type of testing performed by the end user or the client to verify/accept the software system before moving the software application to the production environment. The Test has been conducted on five Arab children, their ages, ranges from 6 to 12 years old. The users' feedback, sectioned according to task, are illustrated in Table III.

TABLE III. USER ACCEPTANCE TESTING

| Username             | Tamim Almalki    |                            |                                    |                   |
|----------------------|------------------|----------------------------|------------------------------------|-------------------|
| Task                 | Number of Errors | Time Needed min: sec: msec | User Feedback                      | Completion status |
| Enter Name           | 0                | 00:15:25                   | I want to enter my name in English | Pass              |
| Take Picture         | 0                | 00:13:02                   | Wow                                | Pass              |
| View Level           | 0                | 59:05:10                   | -                                  | Pass              |
| View Lessons         | 0                | 34:07:39                   | New information                    | Pass              |
| Solve Quiz           | 0                | 20:00:05                   | This is funny                      | Pass              |
| View Hint            | 0                | 00:05:75                   | Oh, I understand                   | Pass              |
| Display Result sheet | 0                | 00:07:22                   |                                    | Pass              |
| View Certificate     | 0                | 00:09:22                   | Its colors are beautiful           | Pass              |
| Save Certificate     | 0                | 00:10:59                   |                                    | Pass              |
| Share Certificate    | 0                | 00:13:55                   | Great                              | Pass              |

## V. LIMITATIONS AND FUTURE WORK

One of the limitations of Manar application is that it will only be available for Android devices. Also, Manar is only available in Arabic, which limits the number of users that it can reach.

## VI. CONCLUSION

In this project, the Manar smartphone game was developed to teach children about cybersecurity in a fun and interactive way.

The theme is “pirates and islands”, which are added to the application. The game divides into different levels, each level representing a new island. The game also includes a reward system, and the child must pass each level to collect rewards. These rewards will add an element of excitement and motivation to the game. To add an interactive element, the game includes image-processing technology, specifically image recognition. At the beginning of each level, a hint will be given of what the level is going to be about, and the child will be asked a question which they must respond to with a photograph of an object. Finally, the number of Internet users has increased significantly, which increases the risk of hacking and other harmful activities. This increased risk raises the need for cybersecurity to protect users, especially children because they lack enough knowledge to be safe online. We hope that the Manar application reaches all children to spread awareness of cybersecurity among them

## VII. FUTURE WORK

Support iOS device is one of the planned features for the application and to extend the scope of the application and reach more users the intention is to support more languages. Also, because the field of cybersecurity is wide-ranging, more lessons, levels and quizzes will be added to introduce more information and concepts. Moreover, another planned addition to the application is a live scoreboard, which would keep the scores for each player and motivate players to compete against one another.

## REFERENCES

- [1] R. Kumargoutam, “Importance of Cyber Security,” International Journal of Computer Applications, vol. 111, no. 7, pp. 14–17, 2015.
- [2] F. Jalled, Object Detection Using Image Processing. Moscow: Moscow Institute of Physics & Technology, 2016, pp. 1-6.
- [3] D. L. Espelage, J. S. Hong, and A. Valido, “Cyberbullying in the United States,” International Perspectives on Cyberbullying, pp. 65–99, 2018.
- [4] StopBullying.gov. 2020. What Is Cyberbullying. [online] Available at: <<https://www.stopbullying.gov/cyberbullying/what-is-it>> [Accessed 25 October 2020].
- [5] Mahavidyalaya, P. and Medinipur, P., 2016. Overview of Hacking. Overview of Hacking, [online] 18(4), p.90. Available at: <<http://www.iosrjournals.org/iosr-jce/papers/Vol18-issue4/Version-4/N1804049092.pdf>> [Accessed 25 October 2020].
- [6] Hub, G. and basics, O., 2020. Online Gaming | The Basics - Internet Matters. [online] Internet Matters. Available at: <<https://www.internetmatters.org/resources/online-gaming-advice/the-basics/>> [Accessed 25 October 2020].
- [7] Goguardian.com. 2020. [online] Available at: <<https://www.goguardian.com/blog/safety/the-4-biggest-risks-kids-face-online/>> [Accessed 25 October 2020].
- [8] Baron, J., 2020. Posting About Your Kids Online Could Damage Their Futures. [online] Forbes. Available at: <<https://www.forbes.com/sites/jessicabaron/2018/12/16/parents-who-post-about-their-kids-online-could-be-damaging-their-futures/#f4709cf27b71>> [Accessed 25 October 2020].
- [9] Communications and Information Technology Commission. [Online]. Available: <https://www.citc.gov.sa/ar/Pages/default.aspx>. [Accessed: 23-Sep-2019].
- [10] Unicef.org. 2020. Children At Increased Risk Of Harm Online During Global COVID-19 Pandemic. [online] Available at: <<https://www.unicef.org/press-releases/children-increased-risk-harm-online-during-global-covid-19-pandemic>> [Accessed 25 October 2020].
- [11] ABCya! Educational Computer Games and Apps for Kids. [Online]. Available: [https://www.abcya.com/games/cyber\\_five\\_internet\\_safety](https://www.abcya.com/games/cyber_five_internet_safety). [Accessed: 08-Oct-2019].
- [12] Games, K. (2019). Educational Games for Preschoolers | Kids Academy. [online] Kidsacademy.mobi. Available at: <https://www.kidsacademy.mobi/playground/interactive-preschool-educational-games/> [Accessed 8 Oct. 2019].
- [13] “Hero’s World,” BIC Play Safe! Be Safe! - Fire Safety Education for Children. [Online]. Available: <http://playsafebesafe.com/games-activities/>. [Accessed: 08-Oct-2019].
- [14] Games, M. (2019). Brain Games For Children | MentalUP. [online] MentalUP. Available at: <https://www.mentalup.co/> [Accessed 8 Oct. 2019].
- [15] Khan Academy. (2019). Khan Academy. [online] Available at: <https://www.khanacademy.org/kids> [Accessed 8 Oct. 2019].
- [16] Triplens.kitabligiapps.com. (2019). TRIPLENS. [online] Available at: <https://triplens.kitabligiapps.com/> [Accessed 8 Oct. 2019].
- [17] Ltd, E. (2019). Make It for Teachers Review | Educational App Store. [online] Educational App Store. Available at: <https://www.educationalappstore.com/app/make-it-for-teachers> [Accessed 8 Oct. 2019].
- [18] Vision2030.gov.sa. 2020. Saudi Vision 2030. [online] Available at: <<https://www.vision2030.gov.sa/en>> [Accessed 25 October 2020].
- [19] “Model–view–presenter”, En.wikipedia.org, 2019. [Online]. Available: <https://en.wikipedia.org/wiki/Model–view–presenter>. [Accessed: 13-Nov- 2019].
- [20] “What is User Acceptance Testing (UAT)? with Examples,” Guru99. [Online]. Available: <https://www.guru99.com/user-acceptance-testing.html>. [Accessed: 23-Apr-2020].

# A Machine Learning Approach to Identifying Students at Risk of Dropout: A Case Study

Roderick Lottering<sup>1</sup>, Robert Hans<sup>2</sup>, Manoj Lall<sup>3</sup>

Department of Computer Science  
Tshwane University of Technology  
Gauteng, South Africa

**Abstract**—The increase in students' dropout rate is a huge concern for institutions of higher learning. In this article, classification techniques are applied to determine students "at-risk" of dropping out of their registered qualifications. Being able to identify such students timeously will be beneficial to both the students and the institutions with which they are registered. This study makes use of Random Forest, Support Vector Machines, Decision Trees, Naïve Bayes, K-Nearest Neighbor, and Logistic Regression for classification purposes. The selected algorithms were applied on a dataset of 4419 student records obtained from the institutional database related to Diploma students enrolled in the Faculty of Information, Communication and Technology. The results reveal that the overall accuracy rate of Random Forest (94.14%) was better than the other algorithms in identifying students at risk of dropout.

**Keywords**—EDM; student dropout; binary classification; ensemble method; KDD

## I. INTRODUCTION

Globally, institutions of higher learning have to deal with an increasingly serious problem of student's dropping out of their registered qualifications. Many reasons including absenteeism and financial conditions have been cited for their dropout. The impact of dropout on institutes of higher learning, whether government or privately funded, can be dire as they are often "tuition-dependent". In some countries, including South Africa, the government funding to the institutions is tied to students who graduate. Being able to identify such students, educational institutes can provide a targeted support mechanism to the needy students [1]. Additionally, a high dropout rate is perceived by some as a measure of the quality of educational institutions [2]. To address the problem of student dropout, institutions apply various strategies depending on the perceived student needs and available resources. Examples of strategies put in place to reduce the dropout rate are - assign tutors to needy students, set up learning communities, and provide extended labs access (for practical subjects) [3]. From the discussion presented here, it is apparent that the identification of students at risk of dropout is of significant importance; hence this article aims to formulate a model to address this problem.

Amongst the various approaches adopted to address this problem of identifying students at risk of dropout, educational data mining (EDM) techniques continue to receive great attention. EDM is an area of study to find patterns in educational data through statistics, machine learning (ML),

and data mining (DM) algorithms. EDM's aim is to evaluate educational data in order to address the problems of educational research [4]. EDM is interested in the development of methods to evaluate data from educational settings in order to better understand the learners, the learning process and the environment [5] [6].

Data mining and ML continue to receive attention from researchers in diverse fields including education, business and health care. Accordingly, this paper focuses on a comparative analysis of various machine learning techniques including Decision Trees (DT), K-Nearest Neighbor (KNN), Logistic Regression (LR), Naïve Bayes (NB) and Support Vector Machines (SVM) classification algorithms to determine students at risk of dropout. Random Forest as an ensemble method is used to enhance the prediction output of these machine learning techniques.

The institutional guideline in this case study allows a student a maximum of six years to complete the Diploma studies, failing which the student is excluded (forced dropout). Depending on the credits obtained at a certain period during the studies, a student is provided with an opportunity to comply with the academic performance requirements, in order to avoid final exclusion. This study is aimed to determine the students at risk of dropout due to exclusion.

The rest of this article is structured as follows: a literature review is presented in Section II. Section III presents the methodology followed in achieving the research objective. Section IV discusses the results and the conclusion is presented in Section V.

## II. LITERATURE REVIEW

According to Yukselturk, Ozekes & Türel [7], data mining has been applied to retrieve data from the various implementations of instructional modes including computer-based, web-based and traditional (face-to-face) education. As indicated by [8], data mining may be used to discover unexpected relationships between student characteristics, teaching strategies and assessments. In the context of online courses, they used Association Rules (AR) to evaluate and produce useful information about dropouts. This model was applied to a Moodle-based Learner Management System (LMS) at the Institute of Computing of a federal university in Brazil with a mix of in-classroom and distant learning students. A total of 27 courses with a student population of 1421 were selected. This population included 242 dropouts.

These study findings showed that reducing the number of dropouts from online courses mediated through the LMS was a relative goal to boost resource utilization where classes for students are small.

Liang, Li & Zheng [2] focused on the student performance in Massive Open Online Courses (MOOCs) using users' behaviour logs. Metadata on classes, course registration records for students and most importantly, user activity logs were collected from their online analytics platform. Their sample of data included thirty-nine (39) courses, with each course containing user activity logs of over 20 000 students over 40 days. Commonly used supervised machine learning algorithms such as LR, NB, SVM, and DT have been used to address this problem. The best performance was the Gradient Boosting Decision Tree (GBDT) with an 88% accuracy.

Adhatrao et al. [9] include merit for examination marks, gender, and marks scored in Science, Technology and Mathematics in the examination of Grade 12 in their dataset to predict student performance. A class label was retained with the expected result, either "Pass" or "Fail". As such, attributes will include distinct values where there was a description of different groups to predict better outcomes. If the merit scored was 120 and above, the merit rating had a "good" value and merit was graded as "bad" if less than 120. This dataset was derived from a university database containing 123 documents.

Aulck et al. [10] analyzed a large, heterogeneous dataset from the University of Washington's Information school. The data included demographic information, school exit information and records from the university. They focused on cohorts over a defined period in a population of 69 116 students. Those who did not complete their studies were marked as dropouts. Three machine learning algorithms (regularized LR, KNN and RF) were applied to the datasets to predict a dropout. The strongest individual predictors of student retention were the Grade Point Average (GPA) in Mathematics, English, Chemistry and Psychology classes. Regularized LR provided the strongest predictions for the dataset.

Bergin et al. [11] reported: "Identifying struggling students at an early stage was not easy as introductory programming modules often have a high student to lecture ratio (100:1 or greater) and early assessment may not be a reliable indicator of overall performance". The factors include: (i) background information, (ii) perceived comfort level factors at the start of the module and (iii) motivation and use of learning strategies. Some of the background factors include among others previous academic experience for example mathematics, science and language. Six different types of algorithms under evaluation included: (i) Logistic Regression, (ii) K-Nearest Neighbor, (iii) Backpropagation, (iv) C4.5, (v) Naïve Bayes and (vi) SVM using Sequential Minimal Optimization (SMO). Three measurement techniques such as overall classifier accuracy, precision and recall were employed in this study. Naïve Bayes produced the highest result among these algorithms in the study.

Whiting et al. [12] included Stochastic Gradient Boosting, RF and rule ensembles (RuleFit) in their approach to implement ensemble methods. Compared to partially adaptive

models, the ensemble models provided a better classification and did particularly well. The rule ensemble was appealing in that while providing interpretability, it achieved competitive levels of precision. The dataset was made up of 228 firms, 114 real fraud firms and 114 model companies in the industry.

### III. METHODOLOGY

In this study, the KDD (see Fig. 1) approach is applied to the dataset in determining the students at risk of dropout. In KDD approach [13], the selected data is subjected to certain preprocessing steps such as removal of outliers and imputation of missing values. Thereafter, dimensionality reduction or transformation techniques to reduce the effective number of variables are performed on the dataset. Subsequently, selected algorithms are applied to the dataset in search of a pattern. The mined pattern is then interpreted to gain knowledge.

#### A. Dataset

The dataset consisting of 4419 full-time students who enrolled in the Diploma qualifications offered in the Faculty of Information, Communication and Technology (ICT) between 2013 and 2017 academic year was harvested from the institutional database. The normal duration of these Diploma qualifications is three years and requires a student to pass 24 subjects. The total credit value of these 24 subjects is three (3). The dataset consisted of student biographical information and student academic information. Student biographical data includes accommodation indicator, age, disability indicator, financial aid indicator, gender, home language and previous year activity indicator. Student academic record data included qualification, modules and the final mark obtained.

The dataset was enriched with derived values for credits obtained (total number of credits for subjects passed), Number of modules completed, Number of modules repeated (passed on subsequent attempts), Number of modules passed in the first attempt, persistence (a count of modules attempted), years in the system (nr of years in the system from registration) and a final decision class attribute. Accommodation indicates if a student is staying in the university provided residence or not. Persistence is the number of times a student takes a particular subject and therefore measures extra effort a student put into the enrolled studies. An overview of the variables and possible values of the dataset is provided in Table I.

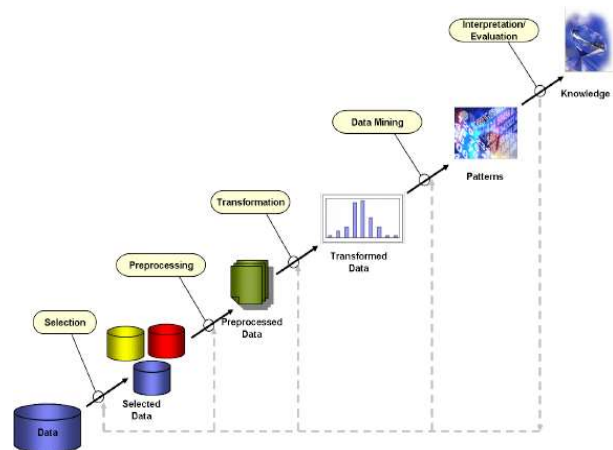


Fig. 1. Knowledge Discovery in Database [14].

TABLE I. OVERVIEW OF DATASET

| VARIABLE / FEATURE               | VALUES                                                                                                                                       |
|----------------------------------|----------------------------------------------------------------------------------------------------------------------------------------------|
| ACCOMODATION                     | Y or N                                                                                                                                       |
| AGE                              | 17 to 48                                                                                                                                     |
| CALENDER_YEAR                    | 2013 to 2017                                                                                                                                 |
| CREDITS_COLLECTED                | 0 to 3480                                                                                                                                    |
| DISABILITY                       | Y or N                                                                                                                                       |
| FINANCIAL_AID                    | Y or N                                                                                                                                       |
| GENDER                           | M or F                                                                                                                                       |
| HOME_LANGAUGE                    | AFRI, ENGL, ISIN, ISIX, ISIZ, OTHR, SESO, SESS, SETS, SISW, TSHI, XITS                                                                       |
| MODULES_COMPLETED                | 0 to 55                                                                                                                                      |
| MODULES_REPEATED                 | 0 to 22                                                                                                                                      |
| MODULES_FIRST_TIME               | 0 to24                                                                                                                                       |
| PERSISTENCE                      | 0 to 70                                                                                                                                      |
| PREVIOUS_YEAR_ACTIVITY           | S or NS                                                                                                                                      |
| QUALIFICATION CODE               | NDIB12, NDIBF1, NDII12, NDIIF1, NDIK12, NDIKF1, NDIL12, NDILF1, NDIP12, DIPF1, NDIS12, NDISF1, NDT12, NDITF1, NDUI12, NDUIF1, NDIW12, NDIWF1 |
| YEARS_IN_SYSTEM                  | 1 to 7                                                                                                                                       |
| FINAL_DECISION (CLASS ATTRIBUTE) | PROBATION /EXCLUDED                                                                                                                          |

As per the instructional guideline, a student is allowed a maximum of six years to complete the Diploma or else the student is excluded (forced dropout) from the qualification. The exclusion of poor-performing students is necessary as they impact on the success rate, throughput rate, earnings and reputation of the institution. In order to identify students at risk of exclusion, constant monitoring of the progress of students is essential. Depending on the credits accumulated in a certain time period, a student may continue without any restrictions placed on him or be placed on probation. Probation is essentially a conditional grace period in the exclusion process which provides the student with the opportunity, through specific conditions and interventions, to comply with the academic performance requirements, in order to avoid final exclusion. Table II shows the minimum credit requirements by the students to avoid being excluded or placed on probation. A student that obtains 0.5 credits or more per year is considered to be on the safe side and therefore "NOT AT RISK". A student who obtains less than 0.5 credits is considered "AT RISK" [15].

To derive the values of the class attribute (FINAL\_DECISION), Equation 1 was applied to obtain the RISK RATIO.

$$RISK\_RATIO = 1 - (ACCUMULATED\_CREDITS / YEARS\_REGISTERED) \tag{1}$$

If the RISK RATIO is greater than 0.469 and less than 0.55, the value of the class attribute (FINAL-DECISION) is "probation". If the RISK RATIO is greater than 0.55 then

FINAL-DECISION is "exclusion". Otherwise, the student is performing satisfactorily and is considered "not at risk" as proposed by Lottering, Hans and Lall [15]. The dataset had instances with the following class categories: "At risk" had 1654 students and the "Not At Risk" category had 2765 records.

*B. Preprocessing*

All the records with the "Not At Risk" class label was removed before any analysis on the dataset was performed. Preprocessed catered for missing values, outliers and type conversion. The dataset was then subjected to a feature selection process using Regularized Random Forest to reduce the dimensionality of the dataset and consider only the attributes that have some predictive power. Fig. 2 highlights that 9 attributes and their relative importance in the classification process.

TABLE II. CREDIT REQUIREMENTS PER STUDY YEAR

| Number of Years registered for a qualification | Maximum Credits obtainable/year | Minimum credits required / year to avoid exclusion. | Accumulated Credits | Risk ratio |
|------------------------------------------------|---------------------------------|-----------------------------------------------------|---------------------|------------|
| 1                                              | 1.0                             | 0.45                                                | 0.45                | 0.55       |
| 2                                              | 1.0                             | 0.45                                                | 0.90                | 0.55       |
| 3                                              | 1.0                             | 0.495                                               | 1.395               | 0.535      |
| 4                                              |                                 | 0.6                                                 | 1.995               | 0.50       |
| 5                                              |                                 | 0.66                                                | 2.655               | 0.469      |
| 6                                              |                                 | 0.345                                               | 3.00                | 0.5        |
| Total credits                                  | 3.0                             | 3.0                                                 |                     |            |

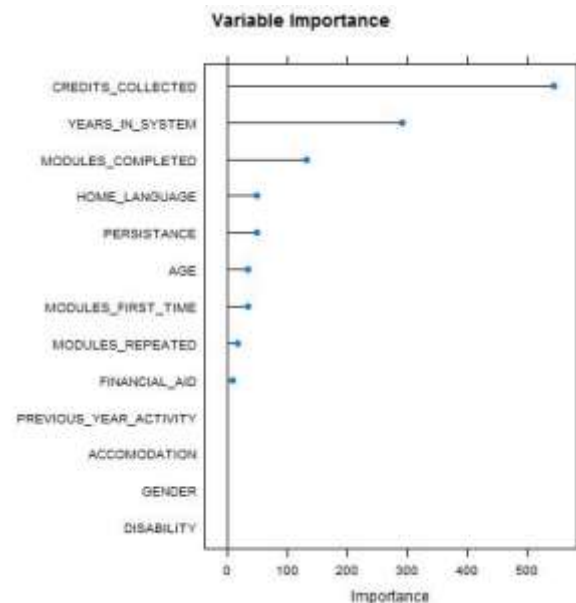


Fig. 2. Feature Selection.

The mean values and standard deviation presented in Fig. 3, contains the range of values reported in Table I. Trends that emerge include a big spread in PERSISTANCE, MODULES\_FIRST\_TIME and MODULES\_COMPLETED due to the standard deviation that is more than 3. The other variables are within the standard deviation of less than 2, indicating a higher concentration around the mean of these features. From the descriptive analysis performed and reported (Table III), it was observed that forty-seven per cent (n=780) had received some form of scholarship. The dominant home language was Sesotho (SESO) which represented 27%. Off these instances, 1074 belonged to the “EXCLUSION” class label compared to the 580 instances that were of the “PROBATION” class label.

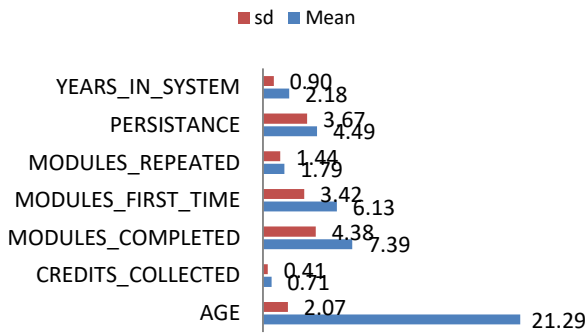


Fig. 3. Mean and Standard Deviation for the Dataset.

TABLE III. DESCRIPTIVE STATISTICS OF THE DATASET

|                | Frequency | Percentage |
|----------------|-----------|------------|
| FINANCIAL_AID  |           |            |
| Yes            | 780       | 47%        |
| No             | 874       | 53%        |
| HOME_LANGUAGE  |           |            |
| AFRI           | 3         | 0%         |
| ENGL           | 31        | 2%         |
| ISIN           | 73        | 4%         |
| ISIX           | 72        | 4%         |
| ISIZ           | 300       | 18%        |
| OTHR           | 96        | 6%         |
| SESO           | 440       | 27%        |
| SESS           | 126       | 8%         |
| SETS           | 148       | 9%         |
| SISW           | 120       | 7%         |
| TSHI           | 106       | 6%         |
| XITS           | 139       | 8%         |
| FINAL_DECISION |           |            |
| Probation      | 580       | 35%        |
| Exclusion      | 1074      | 65%        |

### C. Data Transformation

To classify the students as being at risk of "PROBATION" or "EXCLUSION", the values of attributes listed in Table I, was converted into normalized numerical values. Thereafter, imbalances in the dataset were removed by undersampling the exclusion class label to equal size of the probation class label. Seventy-five per cent (75%) of the dataset was used as a training and validation set while 25% was used for testing purposes. A ten (10) fold cross-validation was used on the training set. Table IV provides an overview of the training and testing balanced datasets for classification purposes.

TABLE IV. TRAINING AND TESTING DATASET

| Dataset                                 | Probation | Exclusion |
|-----------------------------------------|-----------|-----------|
| Original balanced dataset (N=1160)      | 580       | 580       |
| Training and validation dataset (N=870) | 435 (50%) | 435 (50%) |
| Testing dataset (N=290)                 | 145 (50%) | 145 (50%) |

### D. Data Mining

Parmar *et al.* [6] defined machine learning as “computational methods/models using experience (data) to enhance performance”. Such programmable computational methods are capable of ‘learning’ from data and can thus simplify and improve the process of prediction. For the purpose of classification, the following algorithms were used - DT [11], KNN [13], LR [16], NB [11], SVM[11] and RF [8] as ensemble method. These six classifiers are the most suitable classifiers to be used in the identification of students at risk of dropout. A brief explanation of each of these classifiers mentioned above is presented below.

DT are non-parametric classifiers that partitions one feature of a feature vector at a time when the tree’s interior nodes correspond to partitioning laws and the class attribute corresponds to the leaf nodes. A vector x function is defined by following the tree starting from the root and applying each node’s partitioning rules to decide which branch to follow until a leaf node is reached. The value at the leaf node is classification results [17].

Rovira, Puertas and Igual [18], define SVM is classification models based on the idea of using hyperplanes to separate data. It considers feature vectors as references in the real Euclidean space. It presupposes that each dot has a single class (0 or 1) and addresses the problem of separating points from any class by constructing the hyperplane from the points of class 0 and class 1 at the greatest distance.

NB is a probability model based on the theorem of Bayes [19]. The algorithm uses Bayes theorem to measure  $p(C/x_1, \dots, x_n)$  given the n-dimensional function vector of classification class C. In practice, it is assumed that variables are independent.

KNN indicates how many nearby neighbors are supposed to represent the data-point sample class based on the nearest neighbor on k estimates. This kind of learning is ‘lazy’ as it prevents generalization into the classification stage. The NN algorithm is based on the concept of the probability of the properties of a particular instance in its neighborhood. Each

new instance is compared to existing instances using a distance metric and the new instance is classed according to the majority class of the nearest  $K$  neighbors [19].

LR uses a logistic function to model a binary dependent variable, although several extensions that are more complex exist. Brownlee [16] explains this as a way to deal with binary classification problems (two-class problems).

RF classifiers are an ensemble learning technique, which creates a set of decision trees, and the performance is the way individual trees are studied. This model is trained with Feature Bagging [17].

E. Evaluation

Accuracy, Kappa, Precision and Recall are the measures that were used to assess classifier performance. Equations 2 to 4 provide definitions of these performance measures.

$$Accuracy = \frac{tp+tn}{tp+tn+fp+fn} \tag{2}$$

$$Precision = \frac{tp}{tp+fp} \tag{3}$$

$$Recall = \frac{tp}{tp+fn} \tag{4}$$

Where  $tn$  is a true negative,  $tp$  is true positive,  $fn$  false negative and  $fp$  false positive. Dropout is considered the positive class and non-dropout as the negative class. Since we want to eliminate false negatives (students who drop out are expected to be students who do not drop out) we will pick models with the higher specificity over those with better recall.

For interrater or intra-rater reliability testing, Kappa is a solid statistics. Its range varies from -1 to +1, where 0 represent a random change and 1 stand for perfect agreement among raters. The result is interpreted as follows: values  $\leq 0$  as indicating no agreement and 0.01–0.20 as none to poor, 0.21–0.40 as fair, 0.41– 0.60 as moderate, 0.61–0.80 as good, and 0.81–1.00 as very good [14].

IV. RESULTS AND DISCUSSIONS

It was observed that NB is the worst performing classifier of the five classifiers under consideration. Fig. 4 presents an overview of the performance of the classifiers. SVM was the best performing classifier among these models. With an accuracy rate of 89.31% and a specificity rate of 91.25%, this classifier is categorised a “substantial” among the raters from a kappa statistic perspective. Recall measured at 86.92%. The best predictor from a precision perspective is Decision Tree, which measured 88.46%. This is the most important measure to select classifiers since the researcher intends to minimise false negatives. KNN was the worst-performing classifier among the supervised machine learning algorithms although it outperformed NB from a precision perspective. The kappa statistic performance of the classifiers is “substantial” among the raters.

The performance indicators of ensemble methods are presented in Fig. 5. Random Forest (RF) had an accuracy of 94.14%, outperforming the initial five classifiers. The RF

measured 88.12% from a kappa statistic perspective and attracted an “almost perfect” agreement among the raters.

Fig. 6 presents the performance of the binary classifiers in this study. In general, an AUC of 50% suggests no discrimination (ability to predict students at risk of probation or exclusion based on the test). All the classifiers are therefore categories as “outstanding” since all of them have a measure of more than 90%. The AUC score presents an aggregate measure of performance across all classification thresholds. Random Forest is the best performing classifier with a 99% measure and DT and KNN measured 91% as the least favourable classifier.

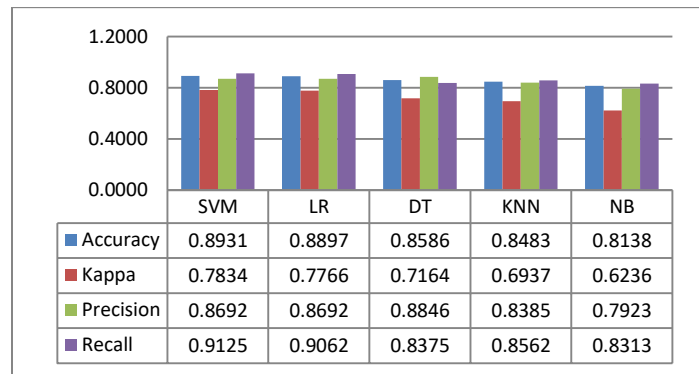


Fig. 4. Overall Classifier Performance.

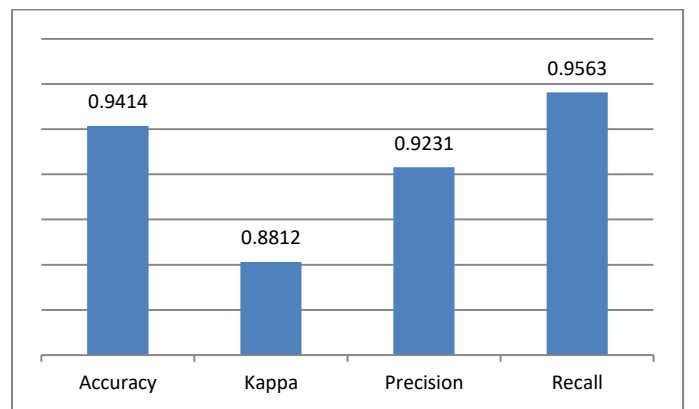


Fig. 5. Performance of Random Forest.

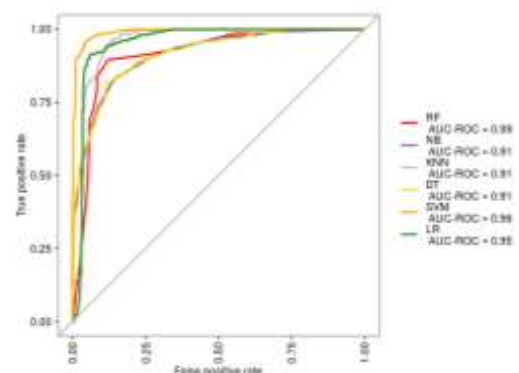


Fig. 6. ROC Curves for Classifiers with a Reduced Dataset.



## V. CONCLUSION

In this paper, we examined the factors that could be used to identify a student at risk of dropout at a university of technology. The Tshwane University of Technology was used at a case study. Data of fulltime students for the academic years 2013 to 2017 in various course offerings in the Faculty of Information and Communication Technology was harvested from the institutional database. The data mining process was accomplished by applying the KDD approach. We applied Decision Trees, K-Nearest Neighbor, Logistic Regression, Naïve Bayes, Support Vector Machines and Random Forest for classification purposes. It was observed that Random Forest outperformed the other classifiers for the given dataset. The accuracy achieved by the Random Forest model was 94.14%.

For future work, these models will be tested with new students' data over a longer period. In parallel, the number of students and a variety of degrees will be increased to evaluate these models in other scenarios. Although this research can predict students at risk of dropout, the conclusion cannot be generalized as the data is from a specific University of Technology.

## ACKNOWLEDGMENTS

The researchers acknowledge the National Research Foundation (NRF, grant number: 105218) for their enabling support of this research paper.

## REFERENCE

- [1] F. MAKOMBE AND M. LALL. A predictive model for the determination of academic performance in private higher education institutions. *International Journal of Advanced Computer Science and Applications (IJACSA)*, 11(9), 2020.
- [2] LIANG, C. LI, and L. ZHENG, Machine learning application in MOOCs: Dropout prediction, Paper presented at the 2016 11th International Conference on Computer Science & Education (ICCSE) 23-25 Aug 2016.
- [3] B.O. BAREFOOT, Higher education's revolving door: confronting the problem of student drop-out in US colleges and universities, *Open Learning: The Journal of Open, Distance and e-Learning*, 19:1, 9-18, DOI: 10.1080/0268051042000177818, 2004.
- [4] T. BARNES, M. DESMARAIS, C. ROMERO and S. VENTURA, Presented at the 2nd Int. Conf. Educ. Data Mining, Cordoba, Spain. 2009.
- [5] R. BAKER, "Data mining for education," in *International Encyclopedia of Education*, B. McGaw, P. Peterson, and E. Baker, Eds., 3rd ed. Oxford, U.K.: Elsevier, 2010.
- [6] C. PARMAR, P. GROSSMANN, J. BUSSINK, P. LAMBIN and H.J.W.L. AERTS, Machine Learning methods for Quantitative Radiomic Biomarkers, *Scientific Reports*, 5:13087, 2015.
- [7] E. YUKSELTURK, S. OZEKES and Y TÜREL, Predicting Dropout Student: An Application of Data Mining Methods in an Online Education Program, *European Journal of Open, Distance and E-Learning*, 17(1):118-133, 2014.
- [8] M.R. BEIKZADEH, S. PHON-AMNUAISUK and N. DELAVARI, Data mining application in higher learning institutions, *International Journal of Informatics in Education*, 7(1):31-54, 2008.
- [9] K. ADHATRAO, A. GAYKAR, A. DHAWAN, R. JHA and V. HONRAO, Predicting students' performance using id3 and c4.5 classification algorithms. *International Journal of Data Mining & Knowledge Management Process*, 3(5):39-52. 2013.
- [10] L. AULCK, N. VELAGAPUDI, J. BLUMENSTOCK and J. WEST, Predicting Student Dropout in Higher Education, 16-20. 2017.
- [11] S. BERGIN, A. MOONEY, J. GHENT, and K. QUILLE, Using Machine Learning Techniques to Predict Introductory Programming Performance, *International Journal of Computer Science and Software Engineering (IJCSSE)*, 4(12):323-328, 2015.
- [12] D.G. WHITING, J.V. HANSEN, J.B., MCDONALD, C. ALBRECHT and W.S. ALBRECHT, Machine learning methods for detecting patterns of management fraud. *Computational Intelligence*, 28(4):24, 2012.
- [13] S.A. ALASADI and W.S. BHAYA, Review of Data Processing Techniques in Data Mining. *Journal of Engineering and Applied Sciences*, 12(16): 4192 – 4107, 2017.
- [14] A. GUERRA-HERNÁNDEZ, R. MONDRAGÓN-BECERRA and N. CRUZ-RAMIREZ, Explorations of the BDI multi-agent support for the knowledge discovery in databases process. *Research in Computing Science* 39, 221-238, 2008.
- [15] R. LOTTERING, R. HANS AND M LALL. A model for the identification of students at risk of dropout at a university of technology. 2020 International Conference on Artificial Intelligence, Big Data, Computing and Data Communication Systems (icABCD). IEEE, 2020.
- [16] J. BROWNLEE, Logistic regression for Machine learning. *Machine Learning Algorithms*, <https://machinelearningmastery.com/logistic-regression-for-machine-learning>, 2016, Accessed 19/06/2020.
- [17] R. BOST, A. RALUCA, T. STEPHEN and G. SHAFI, Machine Learning Classification over Encrypted Data [Electronic Version], 2015.
- [18] S. ROVIRA, E. PUERTAS and L. IGUAL, Data-driven system to predict academic grades and dropout, *PLoS ONE* 12(2): e0171207. DOI:10.1371/journal.pone.0171207, 2017.
- [19] C. ROMERO, S. VENTURA, and E. GARCÍA, Data mining in course management systems: Moodle case study and tutorial, *Computers & Education*, 51(1):368-384. 2008.

# Customized BERT with Convolution Model: A New Heuristic Enabled Encoder for Twitter Sentiment Analysis

Fatima-ezzahra LAGRARI<sup>1</sup>, Youssfi ELKETTANI<sup>2</sup>

Department of Mathematics, Ibn Tofail University of Science  
Kenitra, Morocco

**Abstract**—The Twitter messaging service has turned out to be a domain for news consumers and patrons to convey their sentiments. Capturing these emotions or sentiments in an accurate manner remains a major challenge for analysts. Moreover, the Twitter data include both spam and authentic contents that often affects accurate sentiment categorization. This paper introduces a new customized BERT (Bidirectional Encoder Representations from Transformers) based sentiment classification. The proposed work consists on pre-processing and tokenization step followed by a customized BERT based classification via optimization concept. Initially, the collected raw tweets are pre-processed via "stop word removal, stemming and blank space removal". Prevailing semantic words are acquired, from which the tokens (meaningful words) are extracted in the tokenization phase. Subsequently, these extracted tokens will be subjected to classification via optimized BERT, which weights and biases are optimally tuned by Standard Lion Algorithm (LA). In addition, the maximum sequence length of BERT encoder is updated with standard LA. Finally, the performance of the proposed work is compared over other state-of-the-art models with respect to different performance measures.

**Keywords**—Twitter data; sentiment analysis; tokenization; optimized BERT; Lion Algorithm

## I. INTRODUCTION

The Internet has become a platform for online learning, exchanging ideas and sharing opinions. Social media like Twitter, Facebook, Google+ can be referred to the group of internet-based applications that build on the ideological and technological foundations of Web 2.0, and that allow the creation and exchange of user-generated content”, as defined by Kaplan and Haenlein [9,8].

After the introduction of social media, the globe is entirely connected and hence aids users to exchange their information at any instance of time with lower cost and lower delivery time. In real-time, Twitter is a renowned “social micro-blogging service” that permits the users to post their opinions in the form of shorter messages within 140 characters or less and these short messages are referred as tweets [10-14]. In Twitter, training data are typically obtained by either assuming that tweets’ polarities (positive, negative, neutral) can be inferred using emotions or by taking consensus from the results returned by the sentiment detection websites. Sentimental Analysis deals with getting know the real

opinion/voice of people on specific product, services, organization, movies, news, events, issues and their attributes.

Twitter sentiment analysis has attracted much attention due to the rapid growth in Twitter’s popularity as a platform for people to express their opinions towards a great variety of topics [15-17]. Approaches to Twitter sentiment analysis tend to focus on the identification of sentiment of individual tweets (tweet-level sentiment detection). Broadly speaking, existing work on tweet-level sentiment detection follows two main approaches, namely machine learning and lexicon-based approach. The supervised learning and unsupervised learning are the two categories of the machine learning approach. Sentiment classification using machine learning approach consists of two steps: feature extraction and classification with algorithms. Supervised learning approaches require training data for sentiment classifier learning, which is more computationally complex [18-21]. The conventional techniques on the Twitter sentiment analysis comprise of supervised learning schemes and dictionary-oriented techniques for sentiment classification. However, a most important challenge regarding the machine learning scheme is the selection of features that lead to minimal sparsity. The two main challenges of sentiment analysis are: (1) tweets are generally written in informal language (2) short messages show limited cues about sentiment and (3) acronyms and abbreviations are extensively used on Twitter [25,23].

Moreover, ANN (Artificial Neural Network) model performs better in most of the experiments while comparing to Fuzzy logic. ANN for the purpose of classification of sentiments helps to gain the accuracy in terms of correlations and dependencies [22,24]. The optimization algorithms have undergone various improvements in terms of many factors. One among them is by introducing adaptive operators or adaptive functions [26-29].

The major contribution of this research work consists of:

- An optimized BERT (framework, whose maximum sequence length of encoder is updated by the renowned standard LA.
- Further, the weight and bias of BERT framework are fine-tuned by the LA that ensures the prediction accuracy.

The rest of the paper is organized as follows: the recent works in sentiment analysis are discussed in Section 2. The pre-processing and tokenization steps are depicted in Section 3. Further, in Section 4 the optimized BERT for sentiment classification with Lion Algorithm: objective function and solution encoding are presented. The resultant acquired with the presented work is discussed in Section 5. A strong conclusion of this research work is provided in Section 6.

## II. LITERATURE REVIEW

### A. Related Works

In 2018, Jianqiang *et al.* [1] have introduced word embedding using unsupervised learning on large Twitter corpora. Further, in between the tweet and the word there is a co-occurrence statistical character and in supplement the latent contextual semantic relationships are also present. The sentiment feature set was formed by word sentiment polarity score features as well as the n-grams features with the aid of the word embedding. Finally, the sentiment classification labels were trained and determined in the deep convolution neural network, which intakes the sentiment feature set of tweets as input.

In 2020, Phan *et al.* [2] have introduced a novel approach for sentiment analysis from the Twitter data. This approach was developed on the basis of a “feature ensemble model” that had encapsulated the fuzzy sentiment, which had considered the elements like the “lexical, word-type, semantic, position, and sentiment polarity of the words”.

In 2019, Iqbal *et al.* [3] have constructed a novel integrated framework for Twitter sentiment analysis. The authors have introduced a novel GA (Genetic algorithm) with the intention of enhancing the scalability of the classifier by means of reducing the feature dimensions. The evaluation of the proposed model was made over the existing feature reduction approaches like the PCA (Principal component analysis) and LSA (Latent Semantic Analysis).

In 2020, Ruz *et al.* [4] have developed a new Sentiment analysis approach based on Bayesian network classifiers. The authors used the Bayes factor approach in order to curtail the edges automatically during the training mechanism. The evaluation of the proposed approach was made on two Spanish datasets: The 2010 Chilean earthquake and the 2017 Catalan independence referendum. The resultant of the evaluation had exhibited the effectiveness of the presented work over the existing works.

In 2020, Nagamanjula and Pethalakshmi [5] have developed LAN<sup>2</sup>FIS for opinion mining and sentiment analysis. Here, the features were selected from the data (public tweets) using a bi-objective optimization (minimum redundancy and maximum relevancy). Further, with the intention of solving the issues regarding the computation time, they have implemented the proposed framework in a “parallel and distributed way” with the aid of the “Hadoop framework with the MongoDB database”.

In 2020, Ombabi *et al.* [6] have introduced a novel deep learning model on the basis of the one-layer CNN architecture for more efficient Arabic language sentiment analysis. The authors have extracted the local feature using the one-layer CNN architecture and the long-term dependencies were maintained with two layers LSTM (Long Short-Term Memory). The final classification resultant was acquired from SVM (Support Vector Machine), which intakes the resultant from LSTM and CNN.

In 2017, Pandey *et al.* [7] have developed a novel met heuristic method (CSK) for efficient Sentiment analysis and this approach was based on the “K-means” and Cuckoo Search. From the Twitter dataset, the sentimental contents having the optimum cluster-heads were explored with the proposed method. They have compared the proposed work over the existing models and the resultant had exhibited the efficiency of the proposed model.

In 2019, Abid *et al.* [8] have constructed joint architecture by means of combing the CNN and the RNN (Recurrent Neural Network) for Sentiment analysis. Initially, the “long-term dependencies” were captured with the RNN, they were captured with the help of the CNN global average pooling layer, the syntax and vocabulary. Based sentiments issues were solved with the GloVe (Global Vectors) based word embedding method. The resultant of the model had exhibited a higher performance with this slight hyper parameter tuning.

### B. Review

Table I gives a summary of the related works presented in the literature section in terms of features and challenges.

At first, DCNN was introduced in [1], which offers a better product model and it also includes improved purchase decisions. However, there was no consideration of positive and negative opinion words. Fuzzy approach was exploited in [2] that fuses more online reviews and it also offers better ranking on products, but it needs more convenient purchase decisions. In addition, GA was deployed in [3,33] that avoid the redundant outcomes and it offers improved accuracy. Anyhow, it requires automatic syntactic rule extraction. Likewise, Bayesian network was suggested in [4] that offers improved analysis of service and products and it also concerns on better prediction on sentiments, however, it needs implementation of feedback loop during the training process. Likewise, LAN<sup>2</sup>FIS was exploited in [5], which deals rapidly with consumer reviews and it is more effective but requires more application studies. Further, CNN was exploited in [6] that eliminates noise and it offers a better classification of sentiments, anyhow it was not much adaptable to all languages. CSK was implemented in [7], it offers better sensitivity and it also offers improved accuracy, but it will be interesting to include more attributes. At last, CNN and RNN was suggested in [8] that provides timely responses and it also recognizes negative reviews. However, it necessitates additional contextual factors. These limitations have to be considered for improving the sentiment analysis currently, and in future as well.

TABLE I. FEATURES AND CHALLENGES OF EXISTING SENTIMENT ANALYSIS APPROACH

| Author                 | Approach                 | Features                                                                      | Challenges                                                              |
|------------------------|--------------------------|-------------------------------------------------------------------------------|-------------------------------------------------------------------------|
| Jianqiang et al. [1]   | DCNN                     | Improved purchase decisions<br>Better product model                           | No consideration on positive and negative opinion words                 |
| Phan et al. [2]        | Fuzzy                    | Fuses more online reviews.<br>Better ranking on products                      | Needs more convenient purchase decisions                                |
| Iqbal et al. [3]       | GA                       | Avoids the redundant outcomes<br>Better accuracy                              | Requires automatic syntactic rule extraction                            |
| Ruz et al. [4]         | Bayesian network         | Improved analysis on service and products.<br>Better prediction on sentiments | Needs implementation of feedback loop during training process           |
| Nagamanjula et al. [5] | LAN2FIS                  | Deals rapidly with consumer reviews.<br>More effective.                       | Requires more application studies                                       |
| Ombabi et al. [6]      | CNN                      | Eliminates noise.<br>Better classification of sentiments                      | It was not much adaptable to all languages                              |
| Pandey et al. [7]      | CSK                      | Better sensitivity<br>Improved prediction accuracy                            | Need to concern on more attributes                                      |
| Abid et al. [8]        | CNN and RNN              | Enhanced timely responses. Recognizes negative reviews                        | Necessitates additional contextual factors                              |
| Lagrari et al. [33]    | GA and random forests    | Avoids the redundant outcomes.<br>Better accuracy                             | Computationally expensive<br>Difficulty of designing objective function |
| Elkhechafi et al. [35] | GA and Firefly algorithm | Best Success rate<br>Good ability to deal with multimodality                  | efficient in solving optimization problem<br>Better in terms of time    |

### III. PROPOSED TWITTER SENTIMENT ANALYSIS MODEL

A novel sentiment classification approach is developed for accurate detection of the sentiments from the Twitter data  $D$ . The proposed model encapsulates two major steps: “(a) Pre-processing and tokenization, (b) classification”. The diagrammatic representation of the presented work is illustrated in Fig. 1. Initially, the raw data are subjected to pre-processing that includes three different steps like “stop word removal, stemming, blank space removal”. The pre-processed words  $D_{pre-process}$  are subjected to tokenization, in which the stream of words is broken into symbols, words and other meaningful elements referred as “tokens”. At the end of tokenization, only specific meaningful words are selected. These tokenized words are denoted as  $D_{Token}$ , which is classified via optimized BERT framework [32]. As a major contribution, the weight and bias of the BERT framework is optimized using the standard LA (Lion Algorithm) [31]. In addition, to make the proposed work applicable for huge datasets, the proposed optimized BERT is customized by updating the maximum sequence length of BERT encoder by standard LA. Finally, the optimized BERT framework generates the classified results such as positive, negative or neutral sentiment.

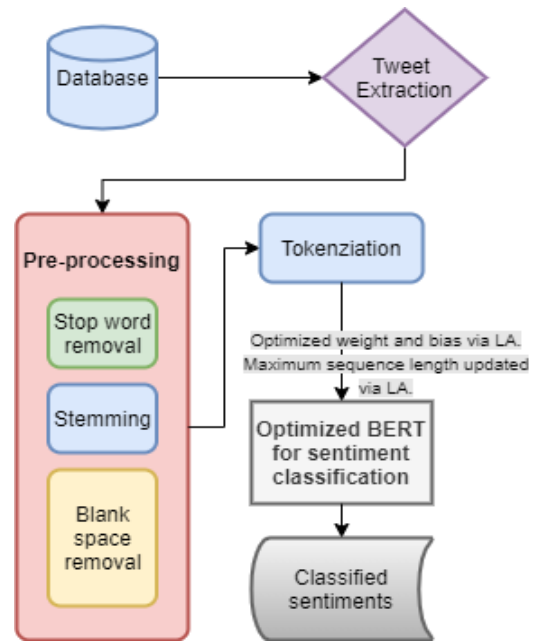


Fig. 1. Proposed Sentiment Analysis Framework.

### IV. PRE-PROCESSING AND TOKENIZATION

#### A. Pre-Processing

Initially, the raw tweets  $D$  are collected from three standard databases (see the experimental section).

The data-processing is a crucial step that is applied to any of the collected data before embedding it with sentiment extraction approach. In general, the data pre-processing permits generating text classification via higher quality as well as to diminish the computational complexity. In this research work, the pre-processing step consists of stemming, stop words removal and blank space removal.

1) *Stemming*: It is the mechanism of supplanting words with their stems, or roots. For the BOW (bag of words), the dimensions are lessened during the mapping of the root-related words into a unit word. For illustration, the words “reading, read and reader” are the root-related words and they get mapped into a single word “read”. Apart from this, during the application of the stemming, the bias might get increased. As a resultant, the over-stemming (i.e. “experiment” and “experience” gets mapped into “exper”) and under-stemming (“adhere” and “adhesion” gets merged) errors might occur. Over stemming brings down accuracy and under-stemming brings down recall.

2) *Stop-words removal*: In a sentence, the connecting function between the words is given by the stop words. These stop words add meaning to the document during the construction of the Natural Language Processing model or text data assessment. The most commonly utilized stop-words are “the”, “is”, “at”, “which” and “on”. Further, before performing the classification, the removal of the stop-words takes place as they are more frequent and do not influence the sentence’s final sentiment.

3) *Blank space removal*: Since the blank space increases the dimensionality between the words, they are to be rejected. Once the blank space or extra whitespace or tab spaces are identified in the sentence, they are removed and replaced by a whitespace. In addition, the “Twitter hashtags, retweets, word capitalization, word lengthening, question marks, presence of web addresses in tweets, exclamation marks, internet emoticons and internet shorthand/slangs” are also removed. At the end of pre-processing, extraction of certain keywords takes place. The extracted keywords are subjected to further processing. The pre-processed words  $D_{pre-process}$  are subjected to tokenization.

**B. Tokenization**

In general, the tokenization is the mechanism of creating a BOW from  $D_{pre-process}$ . The breaking of the approaching string into comprising words and different components. The singular words can be distinguished with normal separator like whitespace; anyway, different symbols can likewise be utilized. Tokenization of web-based social networking information is significantly more troublesome than tokenization of the overall content since it contains various emojis, URL links, contractions that can't be effectively isolated as entirety substances. The consolidation of the accompanying words into “phrases or n-grams” is the overall practice and it can be “unigrams, bigrams, trigrams, and so on”. In general, a single word is said to be a Unigrams, while assortments of two neighbouring words in a text is said to be bi-grams and trigrams are assortments of three neighbouring words. N-grams based tokenization technique can diminish predisposition, yet may increment factual inadequacy. It has been demonstrated that the utilization of n-grams can improve the quality of text characterization. At the end of tokenization, only specific meaningful words are selected. These tokenized words are denoted as  $D_{Token}$ , which is classified via optimized BERT framework.

**V. OPTIMIZED BERT FOR SENTIMENT CLASSIFICATION WITH LION ALGORITHM THE TEMPLATE**

**A. Optimized BERT Framework**

BERT is referred as “Bidirectional Encoder Representations from Transformers”. This approach was developed in [32] with the objective of pre-training the deep bidirectional representations that was utilized to create the NLP from unlabelled texts. This was done in all layers by means of conditioning both the left and right context. Typically, the BERT framework encloses three major parts: Input layer, BERT encoder and output layer. The BERT framework is illustrated in Fig. 2.

1) *Input Layer*: The input layer is fed with  $D_{Token}$  that has  $K$  count of words. This is denoted as  $D_{Token(1:K)} = D_{Token(1)}, D_{Token(2)}, \dots, D_{Token(i)}, \dots, D_{Token(K)}$ , in which  $D_{Token(i)}$  is the  $i^{th}$  word of the tokenized input sequence and it is  $1 \leq D_{Token(i)} \leq K$ . In one token sequence, the input sequence can be represented either be a couple of text sequence or a unit text sequence. The first token is always the “CLS”

which encapsulates the classification embedding. In addition, the segments are separated with special token “SEP”.

2) *Proposed BERT encoder*: It is a “multi-layer bidirectional Transformer encoder” with 12 transfer blocks and the maximum sequence length of 512 tokens (pre-trained). The output from the encoder is the representations of the sequence and it can be a hidden state vector or the “hidden state vector’s time-step sequence”. Here, the final “hidden state vector” is utilized in this research work and the standard LA is deployed here to predict the best sequence token among the maximum sequence count. Moreover, the maximum sequence count is pre-trained and it couldn’t be utilized for huge datasets. Thus, to make the sentiment classification applicable for huge datasets, the maximum sequence count of the BERT encoder is updated with standard LA.

3) *Output layer*: It is a simple “softmax classifier” that is embedded at the top of the Proposed BERT encoder. This helps in predicting the probability of the labels  $C$  in the  $D_{Token}$ . This is mathematically expressed in Eq. (1), in which  $H$  is the final hidden state and  $T$  is the task-specific parameter matrix.

$$P(C|H) = \text{Soft max}(T \cdot H) \tag{1}$$

On the other hand, during the training stage, the weight as well as bias is fixed and pre-trained, since BERT is a “pre-trained model”. But a natural question has arisen, whether the pre-trained bias could be proficient in processing natural languages of any data scale. This is bit complex with the pre-trained bias as well as pre-trained weights, since the datasets of Twitter is bulky. Thus, in this research work, the bias ( $B$ ) and the weight ( $W$ ) of BERT will be trained with the standard LA.

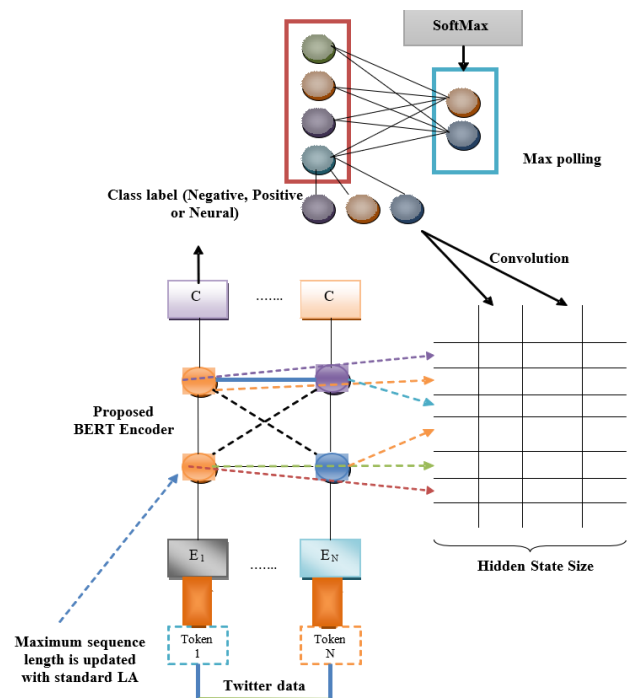


Fig. 2. Proposed Bert Framework.

### B. Objective Function and Solution Encoding

As mentioned above, the weight ( $W$ ) and the bias ( $B$ ) of the BERT model is fine-tuned by LA model. The input solution to the algorithm is shown in Fig. 3. Moreover, the objective function defined in the work is enhancing accuracy ( $Acc$ ), which is expressed in Eq. (2).

$$Ob = \max(Acc) \quad (2)$$

### C. Standard LA

LA is a natural inspired optimization algorithm that was developed on the basis of the unique social behaviour of the lions, particularly, terrestrial defence and territorial takeover. In between the nomadic as well as residual males occurs the terrestrial defence, while the terrestrial take over exists between the old territorial and the new territorial males. The steps followed in the standard LA are described below [31].

1) *Step 1 - Pride Generation and fitness evaluation:* In this step, the initialization of the pride's male territorial lion  $X^{male}$  and female territorial lion  $X^{female}$  and nomad lion  $X^{nomad}$  take place. The arbitrary solutions for  $X^{male}$ ,  $X^{female}$  and  $X_1^{nomad}$  are termed as  $P$ . In addition  $fn(X^{male})$ ,  $fn(X^{female})$  and  $fn(X_1^{nomad})$  refers to the fitness of  $X^{male}$ ,  $X^{female}$  and  $X_1^{nomad}$ . During the initialization, the reference fitness is set as  $fn^{ref} = fn(X^{male})$  and the generation count is fixed as  $N_g = 0$ , which is described at the termination step.

2) *Step 2 - Fertility Evaluation:*  $X^{male}$  and  $X^{female}$  are used for fertility and this fertility evaluation benefits the solutions to get away from local optima as well as convergence issues. The updated female lion is denoted by  $X^{female+}$ , which is ensured by the "sterility rate"  $S_r$  that increases by 1 at the end of the crossover. The updated female lion is achieved with  $X^{female}$  and the random integer  $p$  that is within the interval  $[1, P]$ . This is expressed in Eq. (3).

$$\{X^{female+} = \min[X_p^{max}, \max(X_p^{min}, \lambda_p)]\} \quad (3)$$

Moreover, the female renewal function  $\lambda$  and the random integers  $ra_1$  and  $ra_2$  are generated within the interval  $[0, 1]$ .

$$\lambda_p = \{X_p^{female} + [0.1ra_2 - 0.05(X_p^{male} - ra_1X_p^{female})]\} \quad (4)$$

3) *Step 3 - Mating and Cub growth:*  $X^{male}$  and  $X^{female}$  goes through crossover and mutation operation. Among them, the crossover is performed initially and it is based on the littering rate of the lion. At the end of crossover and mutation,  $X^{cubs}$  with  $X^{m\_cub}$  male cub and  $X^{f\_cub}$  female cub are produced. On the basis of the fitness,  $X^{cubs}$  are formed. Further, "Cub growth function is a local solution search function" for the male and female cubs. The random mutation rate  $G_r$  approves this mechanism. The previous  $X^{m\_cub}$  and  $X^{f\_cub}$  is replaced by the mutated  $X^{m\_cub}$  and  $X^{f\_cub}$ , only if  $X^{m\_cub}$  and  $X^{f\_cub}$  is better when compared to the existed mutation.

4) *Step 4 - Territorial Defence and takeover:* With the aid of search space, the identification of the territorial defence takes place. This can be given as "nomad coalition, pride and survival fight". In general, the territorial takeover is said to be

the mechanism of providing territory to the male as well as female cubs as they become matured and stronger. More particularly, terrestrial take over occurs only, when the age of the cub ( $A^{cub}$ ) is greater than or equal to the maturity age. The mathematical equation corresponding to the selection of  $X^{e\_nomad}$  are depicted in Eq. (5), Eq. (6) and (7), respectively.

$$fn(X^{e\_nomad}) < fn(X^{male}) \quad (5)$$

$$fn(X^{e\_nomad}) < fn(X^{m\_cub}) \quad (6)$$

$$fn(X^{e\_nomad}) < fn(X^{f\_cub}) \quad (7)$$

5) *Step 5 - Termination:* The algorithm terminates when the count of fitness goes beyond the limit. This is expressed via two conditions as per Eq. (8) and Eq. (9), respectively.

$$N_g > N_{g(max)} \quad (8)$$

$$|fn(X^{male}) - fn(X^{optimal})| \leq T_e \quad (9)$$

The error threshold is specified as  $T_e$ , and "maximum count of the generations" is represented and the target minimum is depicted as  $N_{g(max)}$  and  $f(X^{optimal})$ . The flow chart of standard LA is shown in Fig. 4.

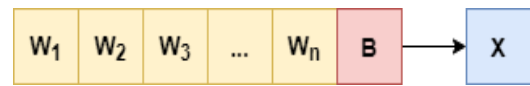


Fig. 3. Solution Encoding.

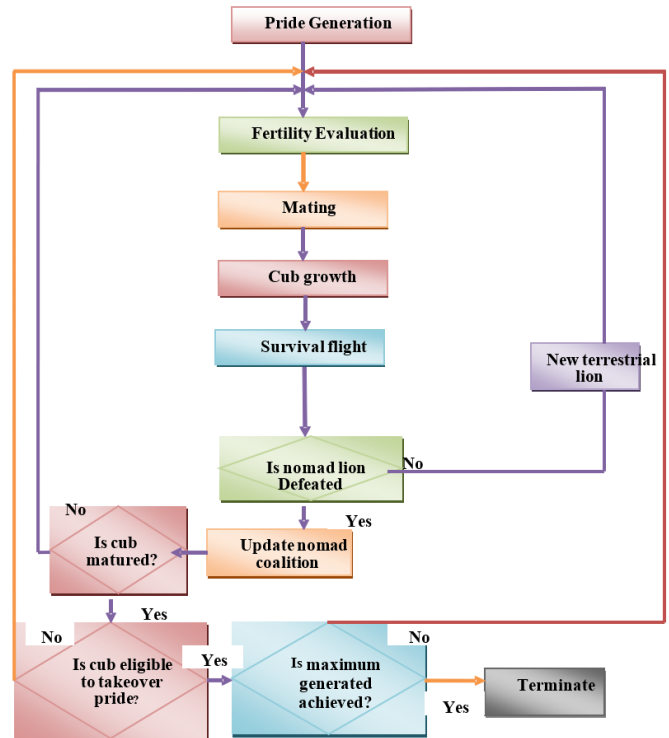


Fig. 4. Flowchart of Standard LA.

## VI. RESULTS AND DISCUSSIONS

### A. Experiments

The proposed sentiment classification with optimized BERT was implemented in Python and the corresponding outcomes acquired are noted. The experimentation was carried out using three Datasets:

Dataset 1 (Brands and Product Emotions<sup>1</sup>) contains 9094 rows with 3 variables where contributors evaluated tweets about multiple brands and products. The crowd was asked if the tweet expressed positive, negative, or no emotion towards a brand and/or product. If some emotion was expressed, they were also asked to say which brand or product was the target of that emotion.

Dataset 2 (TWCS for Customer Support on Twitter<sup>2</sup>) is a large (3 million tweets), modern corpus of tweets and replies to aid innovation in natural language understanding and conversational models, and for study of modern customer support practices and impact.

Dataset 3 is called sentiment 120 Dataset, which contains 1,600,000 tweets extracted using the Twitter API. The tweets have been annotated (0 = negative, 4 = positive) and they can be used to detect sentiments [34].

Further, the proposed optimized BERT model was compared over the existing models like IB-K[3], NB [9], SMO [3], Bayesian Net [4], jRip [3], j48 [3], PART [3], CNN[1] and BERT [30] in terms of specificity (true negative rate), sensitivity (True positive rate), accuracy, precision (Positive Predictive Value), FPR (False positive rate), FNR (False negative rate), FOR (False omission rate), NPV (Negative predictive value), FDR (False discovery rate), F1-Score and MCC (Matthews correlation coefficient), respectively. This evaluation is done by varying the Training Percentage (TP).

### B. Analysis on Dataset 1 (Brands and Product Emotions): Performance and Error

The Dataset is evaluated in terms of positive measures, negative and other measures. The resultants are graphically exhibited in Fig. 5, Fig. 6 and Fig. 7, respectively. The positive measures like “Accuracy, sensitivity, balancing accuracy” and precision are shown in Fig. 5. It is observed that the proposed work attains accurate results when compared over other conventional models, which ensures the fulfilment of the objective defined in this work. On observing the accuracy of the presented work at TP = 90 is 92.2, which is 15.9%, 14.4%, 11%, 10.3%, 9.46%, 5.85%, 3.15%, 1.67% and 0.75% better than the existing approaches like IB-K, NB, SMO, Bayesian Net, jRip, j48, PART, CNN and BERT, respectively.

In case of sensitivity, the maximum sensitivity is recorded by the presented work for every variation in TP Fig. 5(b). Among the sensitivity of the presented work, the maximal sensitivity of 91.2 is recorded at TP=90. Moreover, the balancing accuracy of the presented work is higher at TP=90

and it is 22%, 17.8%, 14.2%, 13%, 8.87%, 7.47%, 4.4%, 2.2% and 0.757% better than the existing models like IB-K, NB, SMO, Bayesian Net, jRip, j48, PART, CNN and BERT, respectively. In addition, the precision of the presented work is higher than all the existing works as per Fig. 5(d). The highest values recorded by the presented work at TP= 40, TP=50, TP=60, TP=70, TP=80 and TP=90 are 74.4, 81.6, 81.8, 86.8, 93.2 and 94, respectively.

On the other hand, the negative measures like FNR, FPR, and FDR and FOR also help in exhibiting the enhancement level of the presented work. The lower the error measures, higher the accuracy of the classification. The FNR (in Fig. 6(a)) of the presented work is lower at every variation in TP. At TP=90, the FNR of the presented work is 78.5 and it is 65.1%, 62.97%, 56.3%, 53.82%, 50.93%, 40.53%, 21.5%, 16.4% and 8.18% better than IB-K, NB, SMO, Bayesian Net, jRip, j48, PART, CNN and BERT, respectively. Then, in case of FPR, the lowest value is recorded by the presented work as 76.2 at TP=40% and in all other variation in TP's also the presented work records the lowest value. In addition, the FDR and FOR of the presented work is lower for every variation in TP. The lowest FDR is recorded by the presented work at TP=60 (10.9).

In addition, the other measures like NPV, PPV, MCC and F1-Score of the concern database is shown in Fig. 7. All these measures exhibit higher performance with the presented work, while compared with the existing one. The NPV of the presented work is higher at TP=90 and it is 22%, 17.8%, 14.2%, 13%, 8.87%, 7.47%, 4.4%, 2.22% and 7.57% better than IB-K, NB, SMO, Bayesian Net, jRip, j48, PART, CNN and BERT, respectively. Thus, as a whole the presented work shows the highest positive performance and lowest negative performance, which makes it much suitable for sentiment classification.

The overall training error performance of the presented work over the existing work is shown in Table II. The overall error performance of the presented work is lower at TP=90 and it is 75.1%, 73.5%, 67.7%, 66%, 64.3%, 52.8%, 37.4%, 24.1% and 12.6% better than existing IB-K, NB, SMO, Bayesian Net, jRip, j48, PART, CNN and BERT, respectively.

### C. Analysis on Customer Support on Twitter Dataset (TWCS)

For a matter of clarity, we present here only the overall training error performance of the proposed work over the existing work is shown in Table III. Here, the presented work shows the lowest performance, while compared to the existing works. The lowest performance is revealed by the presented work at TP=90.

### D. Analysis on Sentiment 120 Dataset

The overall training performance of the presented work over the existing work is tabulated in Table IV. The lowest error performance is recorded by the presented work, while compared to the existent works. At TP= 90, the presented work shows the lowest error value is 5.72, which is 68.75, 64.4%, 60.2%, 51.95, 43.8%, 40%, 39.4%, 25.7% and 12.75 better than the existing models like IB-K, NB, SMO, Bayesian Net, jRip, j48, PART, CNN and BERT, respectively.

<sup>1</sup> <https://data.world/crowdfunder/brands-and-product-emotions>

<sup>2</sup> <https://www.kaggle.com/thoughtvector/customer-support-on-twitter>

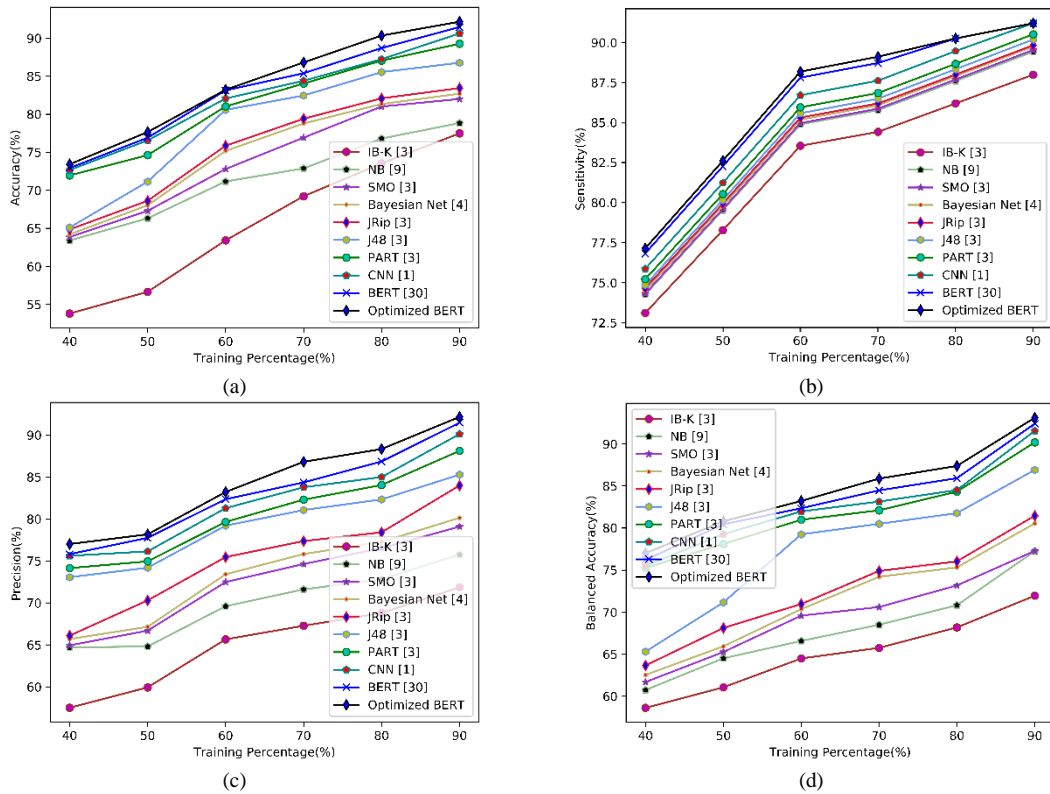


Fig. 5. Performance Analysis of Presented Work over Existing Approaches in Terms of Positive Measures for Brands and Product Emotions Dataset Showing (a) Accuracy, (b) Sensitivity, (c) Precision and (d) Balanced Accuracy.

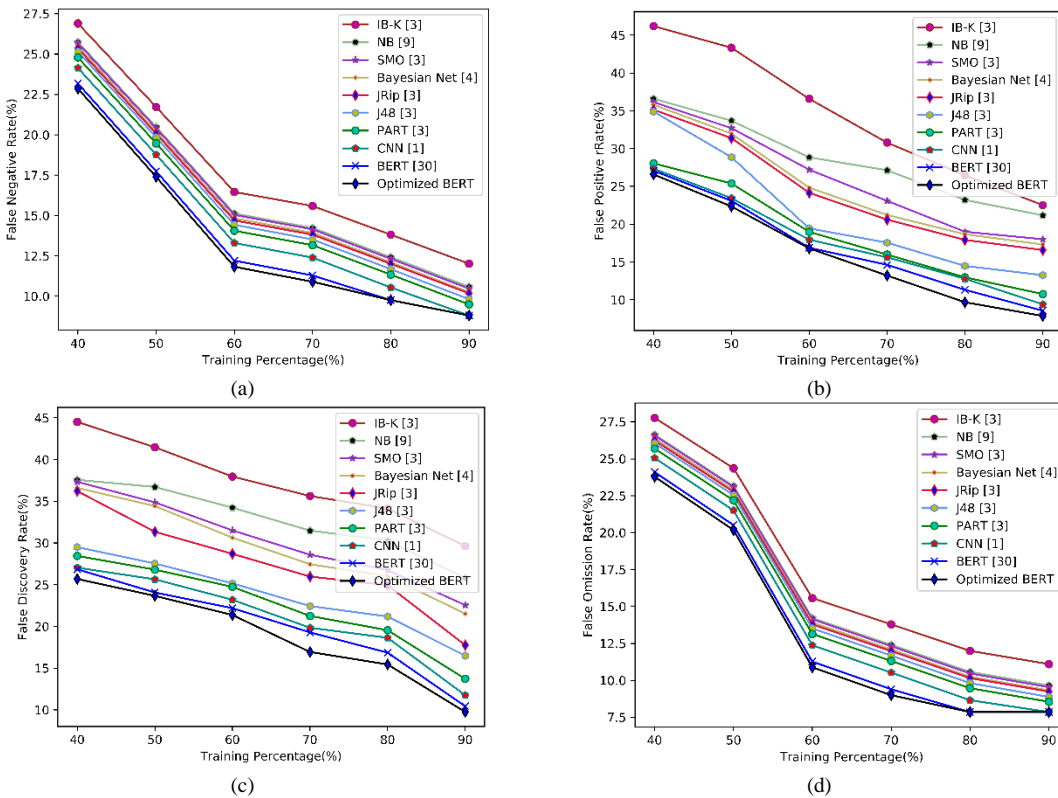


Fig. 6. Performance Analysis of Presented Work over Existing Approaches in Terms of Negative Measures for Brands and Product Emotions Dataset Showing (a) FNR, (b) FPR, (c) FDR and (d) FOR.



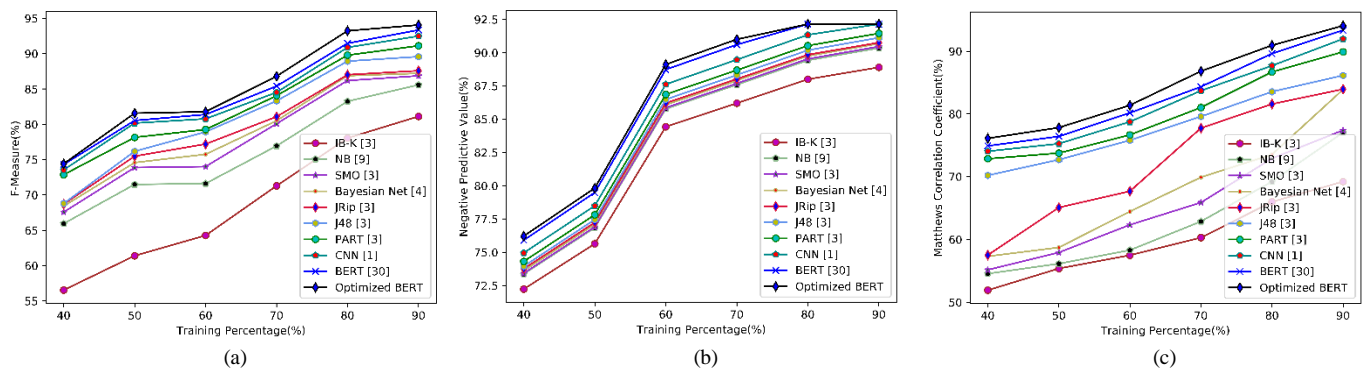


Fig. 7. Performance Analysis of Presented Work over Existing Approaches in Terms of other Measures for Brands and Product Emotions Dataset (a) F1-Score, (b) NPV, (c) MCC.

TABLE II. OVERALL TRAINING ERROR PERFORMANCE EVALUATION OF BRANDS AND PRODUCT EMOTIONS DATASET (%)

| Methods               | TP=40       | TP=50       | TP=60       | TP=70       | TP=80       | TP=90       |
|-----------------------|-------------|-------------|-------------|-------------|-------------|-------------|
| IB-K [3]              | 34.4        | 33.3        | 30.3        | 25.6        | 23.4        | 20.1        |
| NB [9]                | 22.7        | 22          | 21.8        | 21.6        | 20          | 18.7        |
| SMO [3]               | 22.1        | 20.8        | 20          | 17.3        | 15.6        | 1.55        |
| Bayesian Net [4]      | 21.7        | 20          | 17.4        | 15.3        | 15.3        | 14.7        |
| jRip [3]              | 20.9        | 19.3        | 16.6        | 14.6        | 14.5        | 14          |
| j48 [3]               | 20.6        | 16.3        | 11.5        | 11.3        | 10.9        | 10.6        |
| PART [3]              | 12.2        | 12.2        | 11          | 9.65        | 9.34        | 7.99        |
| CNN [1]               | 11.4        | 9.93        | 9.82        | 9.26        | 9.13        | 6.59        |
| BERT [30]             | 11.1        | 9.51        | 8.65        | 8.19        | 7.62        | 5.72        |
| <b>Optimized BERT</b> | <b>10.5</b> | <b>8.64</b> | <b>8.56</b> | <b>6.67</b> | <b>5.91</b> | <b>5.00</b> |

TABLE IV. OVERALL TRAINING ERROR ANALYSIS OF SENTIMENT 120 DATASET (%)

| Methods               | TP=40       | TP=50       | TP=60       | TP=70       | TP=80       | TP=90       |
|-----------------------|-------------|-------------|-------------|-------------|-------------|-------------|
| IB-K [3]              | 27.7        | 25.8        | 24.3        | 23.8        | 22.9        | 18.3        |
| NB [9]                | 21.3        | 20.1        | 19.5        | 19.4        | 16.7        | 16.1        |
| SMO [3]               | 19.7        | 18.6        | 17.4        | 16.7        | 15          | 14.4        |
| Bayesian Net [4]      | 16.2        | 16          | 13.6        | 12.9        | 12.4        | 11.9        |
| jRip [3]              | 16          | 15          | 12.7        | 12.4        | 10.2        | 10.2        |
| j48 [3]               | 15.9        | 14.9        | 12.3        | 11.7        | 9.90        | 9.57        |
| PART [3]              | 15.5        | 12          | 11.6        | 11.3        | 9.49        | 9.44        |
| CNN [1]               | 14.3        | 11.9        | 10.5        | 10.1        | 8.64        | 7.71        |
| <b>Optimized BERT</b> | <b>12.9</b> | <b>11.5</b> | <b>9.99</b> | <b>9.56</b> | <b>8.34</b> | <b>6.55</b> |

TABLE III. OVERALL TRAINING ERROR PERFORMANCE OF TWCS DATASET (%)

| Methods               | TP=40       | TP=50       | TP=60       | TP=70       | TP=80       | TP=90       |
|-----------------------|-------------|-------------|-------------|-------------|-------------|-------------|
| IB-K [3]              | 33.8        | 31.2        | 29.8        | 25.2        | 21.1        | 18.9        |
| NB [9]                | 21.6        | 20.6        | 19.9        | 19.5        | 17.6        | 11.8        |
| SMO [3]               | 21.3        | 19.1        | 18.6        | 18.2        | 12.2        | 11.5        |
| Bayesian Net [4]      | 20.8        | 18.1        | 18          | 15.5        | 12          | 10.9        |
| jRip [3]              | 20.6        | 16.7        | 15.6        | 14.6        | 11.6        | 10.8        |
| j48 [3]               | 16.3        | 14.8        | 13.9        | 13.6        | 11.4        | 9.92        |
| PART [3]              | 16.2        | 14.2        | 12.5        | 12.3        | 10          | 9.87        |
| CNN [1]               | 15.6        | 13.9        | 12.2        | 12.1        | 9.77        | 9.01        |
| BERT [30]             | 14.3        | 13.4        | 11.9        | 10.7        | 9.63        | 8.07        |
| <b>Optimized BERT</b> | <b>12.6</b> | <b>12.1</b> | <b>10.9</b> | <b>10.4</b> | <b>9.18</b> | <b>7.68</b> |

Both positive and negative measurements of optimized BERT on the three datasets gives a better result over the existing approaches.

For future work, we plan to take into consideration an important aspect in sentiment analysis which is emoticons that can reflect the mood of the writer. Another aspect could be the comparison of the training and execution time over the existing approaches.

VII. CONCLUSION

A new customized BERT based sentiment classification was introduced in this research work. The proposed work includes two major phases: pre-processing and tokenization, and Customized BERT based classification via optimization concept. The data collected was pre-processed with “based classification via optimization concept”, which was then tokenized. Prevailing semantic words were acquired, from which the tokens (meaningful words) were extracted in the tokenization phase. The optimized BERT was introduced for classifying the tokens. In the optimized BERT, the weight and biases are optimally tuned by Standard LA. In addition, the maximum sequence length of BERT encoder was updated with standard LA. It is observed that the proposed work attains accurate results when compared over other conventional models, which ensures the fulfilment of objective defined in this work. On observing the accuracy of the presented work for Brands and Product Emotions dataset at TP =90 is 92.2, which is 15.9%, 14.4%, 11%, 10.3%, 9.46%, 5.85%, 3.15%, 1.67% and 0.75% better than the existing approaches like IB-K, NB, SMO, Bayesian Net, jRip, j48, PART, CNN and BERT, respectively.

REFERENCES

[1] Jianqiang, Z., Xiaolin, G., & Xuejun, Z. (2018). Deep convolution neural networks for twitter sentiment analysis. *IEEE Access*, 6, 23253-23260.

[2] Phan, H. T., Tran, V. C., Nguyen, N. T., & Hwang, D. (2020). Improving the performance of sentiment analysis of tweets containing

- fuzzy sentiment using the feature ensemble model. *IEEE Access*, 8, 14630-14641.
- [3] Iqbal, F., Hashmi, J. M., Fung, B. C., Batool, R., Khattak, A. M., Aleem, S., & Hung, P. C. (2019). A hybrid framework for sentiment analysis using genetic algorithm based feature reduction. *IEEE Access*, 7, 14637-14652.
- [4] Ruz, G. A., Henríquez, P. A., & Mascareño, A. (2020). Sentiment analysis of Twitter data during critical events through Bayesian networks classifiers. *Future Generation Computer Systems*, 106, 92-104.
- [5] Nagamanjula, R., & Pethalakshmi, A. (2020). A novel framework based on bi-objective optimization and LAN2FIS for Twitter sentiment analysis. *Social Netw. Analys. Mining*, 10(1), 34.
- [6] Ombabi, A. H., Ouarda, W., & Alimi, A. M. (2020). Deep learning CNN-LSTM framework for Arabic sentiment analysis using textual information shared in social networks. *Social Network Analysis and Mining*, 10(1), 1-13.
- [7] Pandey, A. C., Rajpoot, D. S., & Saraswat, M. (2017). Twitter sentiment analysis using hybrid cuckoo search method. *Information Processing & Management*, 53(4), 764-779.
- [8] Abid, F., Alam, M., Yasir, M., & Li, C. (2019). Sentiment analysis through recurrent variants latterly on convolutional neural network of Twitter. *Future Generation Computer Systems*, 95, 292-308.
- [9] Sailunaz, K., & Alhajj, R. (2019). Emotion and sentiment analysis from Twitter text. *Journal of Computational Science*, 36, 101003.
- [10] Fang, Y., Tan, H., & Zhang, J. (2018). Multi-strategy sentiment analysis of consumer reviews based on semantic fuzziness. *Ieee Access*, 6, 20625-20631.
- [11] Ahmad, S., Asghar, M. Z., Alotaibi, F. M., & Awan, I. (2019). Detection and classification of social media-based extremist affiliations using sentiment analysis techniques. *Human-centric Computing and Information Sciences*, 9(1), 24.
- [12] Gutiérrez-Batista, K., Campaña, J. R., Vila, M. A., & Martin-Bautista, M. J. (2018, June). Fuzzy Analysis of Sentiment Terms for Topic Detection Process in Social Networks. In *International Conference on Information Processing and Management of Uncertainty in Knowledge-Based Systems* (pp. 3-14). Springer, Cham.
- [13] Wang, D., Li, J., Xu, K., & Wu, Y. (2017). Sentiment community detection: exploring sentiments and relationships in social networks. *Electronic Commerce Research*, 17(1), 103-132.
- [14] del Pilar Salas-Zárate, M., Medina-Moreira, J., Álvarez-Sagubay, P. J., Lagos-Ortiz, K., Paredes-Valverde, M. A., & Valencia-García, R. (2016, November). Sentiment analysis and trend detection in Twitter. In *International Conference on Technologies and Innovation* (pp. 63-76). Springer, Cham.
- [15] Sánchez-Rada, J. F., & Iglesias, C. A. (2019). Social context in sentiment analysis: Formal definition, overview of current trends and framework for comparison. *Information Fusion*, 52, 344-356.
- [16] Liu, N., & Shen, B. (2020). Aspect-based sentiment analysis with gated alternate neural network. *Knowledge-Based Systems*, 188, 105010.
- [17] Ahuja, R., Chug, A., Kohli, S., Gupta, S., & Ahuja, P. (2019). The impact of features extraction on the sentiment analysis. *Procedia Computer Science*, 152, 341-348.
- [18] Ren, R., Wu, D. D., & Liu, T. (2018). Forecasting stock market movement direction using sentiment analysis and support vector machine. *IEEE Systems Journal*, 13(1), 760-770
- [19] Tang, F., Fu, L., Yao, B., & Xu, W. (2019). Aspect based fine-grained sentiment analysis for online reviews. *Information Sciences*, 488, 190-204.
- [20] Geetha, M., Singha, P., & Sinha, S. (2017). Relationship between customer sentiment and online customer ratings for hotels-An empirical analysis. *Tourism Management*, 61, 43-54.
- [21] Qiu, J., Liu, C., Li, Y., & Lin, Z. (2018). Leveraging sentiment analysis at the aspects level to predict ratings of reviews. *Information Sciences*, 451, 295-309.
- [22] López, M., Valdivia, A., Martínez-Cámara, E., Luzón, M. V., & Herrera, F. (2019). E2SAM: evolutionary ensemble of sentiment analysis methods for domain adaptation. *Information Sciences*, 480, 273-286.
- [23] Ibrahim, N. F., & Wang, X. (2019). Decoding the sentiment dynamics of online retailing customers: Time series analysis of social media. *Computers in Human Behavior*, 96, 32-45.
- [24] Xiong, S., Wang, K., Ji, D., & Wang, B. (2018). A short text sentiment-topic model for product reviews. *Neurocomputing*, 297, 94-102.
- [25] Chen, M. H., Chen, W. F., & Ku, L. W. (2018). Application of Sentiment Analysis to Language Learning. *IEEE Access*, 6, 24433-24442.
- [26] Rajakumar, B. R. (2013). Impact of static and adaptive mutation techniques on the performance of Genetic Algorithm. *International Journal of Hybrid Intelligent Systems*, 10(1), 11-22.
- [27] Rajakumar, B. R. (2013). Static and adaptive mutation techniques for genetic algorithm: a systematic comparative analysis. *International Journal of Computational Science and Engineering*, 8(2), 180-193.
- [28] Swamy, S. M., Rajakumar, B. R., & Valarmathi, I. R. (2013). Design of hybrid wind and photovoltaic power system using opposition-based genetic algorithm with Cauchy mutation.
- [29] Rajakumar, B. R., & George, A. (2013). APOGA: An adaptive population pool size based genetic algorithm. *AASRI Procedia*, 4, 288-296.
- [30] Sun, C., Qiu, X., Xu, Y., & Huang, X. (2019, October). How to fine-tune bert for text classification?. In *China National Conference on Chinese Computational Linguistics* (pp. 194-206). Springer, Cham.
- [31] Boothalingam, R. (2018). Optimization using lion algorithm: a biological inspiration from lion's social behavior. *Evolutionary Intelligence*, 11(1-2), 31-52.
- [32] Devlin, J., Chang, M. W., Lee, K., & Toutanova, K. (2018). Bert: Pre-training of deep bidirectional transformers for language understanding. *arXiv preprint arXiv:1810.04805*.
- [33] Lagrari, F. E., Ziyati, H., & El Kettani, Y. (2018, July). An Efficient Model of Text Categorization Based on Feature Selection and Random Forests: Case for Business Documents. In *International Conference on Advanced Intelligent Systems for Sustainable Development* (pp. 465-476). Springer, Cham.
- [34] Go, A., Bhayani, R., & Huang, L. (2009). Twitter sentiment classification using distant supervision. *CS224N project report*, Stanford, 1(12), 2009.
- [35] Elkhechafi, M., Hachimi, H., & Elkettani, Y. (2017). A new hybrid firefly with genetic algorithm for global optimization. *Int. J. Manag. Appl. Sci*, 3, 47-51.

# Empirical Oversampling Threshold Strategy for Machine Learning Performance Optimisation in Insurance Fraud Detection

Bouzgarne Itri<sup>1</sup>, Youssfi Mohamed<sup>2</sup>, Bouattane Omar<sup>3</sup>, Qbadou Mohamed<sup>4</sup>  
SSDIA Laboratory  
ENSET Mohammedia University Hassan 2  
Casablanca, Morocco

**Abstract**—Insurance fraud is one of the most practiced frauds in the sectors of the economy. Faced with increasingly imaginative underwriters to create fraud scenarios and the emergence of organized crime groups, the fraud detection process based on artificial intelligence remains one of the most effective approaches. Real world datasets are usually unbalanced and are mainly composed of "no-fraudulent" class with a very small percentage of "fraudulent" examples to train our model, thus prediction models see their performance severely degraded when the target class appears so poorly represented. Therefore, the present work aims to propose an approach that improves the relevance of the results of the best-known machine learning algorithms and deals with imbalanced classes in classification problems for prediction against insurance fraud. We use one of the most efficient approaches to re-balance training data: SMOTE. We adopted the supervised method applied to automobile claims dataset "carclaims.txt". We compare the results of the different measurements and question the results and relevance of the measurements in the field of study of unbalanced and labeled datasets. This work shows that the SMOTE Method with the KNN Algorithm can achieve better classifier performance in a True Positive Rate than the previous research. The goal of this work is to lead a study of algorithm selections and performance evaluation among different ML classification algorithms, as well as to propose a new approach TH-SMOTE for performance improvement using the SMOTE method by defining the optimum oversampling threshold according to the G-mean measure.

**Keywords**—Machine learning; oversampling; SMOTE; insurance fraud

## I. INTRODUCTION

Insurance fraud costs several million dollars each year. In 2017, the Insurance Fraud Bureau of Australia (IFBA) detected \$280 million in fraudulent claims [1]. In Morocco, according to the Economist newspaper [2], the FMSAR claims that traffic accident compensation fraud accounts for more than 21% of insurers' compensation. In France, according to the Agency for the Fight against Insurance Fraud (ALFA) 44814 acts were detected in 2013, for a recovered amount of 214 million Euros; In 2018, the amount is increased to 500 million Euro [3].

Fraudulent cases often have relatively similar characteristics to non-fraudulent cases, which also depends on the information entered by claim handlers on the system and its relevance. What makes fraud detection very difficult is that

there is no particular variable or rule to characterize fraud cases in a simple and robust way. Thus, the use of automatic detection models based on machine learning algorithms becomes an operational necessity to fight fraud effectively. In our case study, we focus on the type of fraud in automobile claims. Our model is based on the supervised method to solve a classification problem. We build a statistical learning model to predict the affiliation of claims reported to one of the following classes (fraudulent claims, non-fraudulent claims). We try also to find the best classification model to estimate a high probability of belonging to the "fraudulent claim" class. A comparative analysis of ten best-known machine-learning algorithms are presented in this work. However, one of the main problems of these machine learning models, as in our case, is that they suffer from the problem of imbalanced classes in the data set. The class of fraudulent claims represents only 6% in our dataset. Indeed, when a binary classification problem has a lot less data in a "fraudulent" class than in a "non fraudulent" class, some machine learning algorithms will simply learn to ignore the minority class and classify all cases into the majority class, because this will trivially yield high classification accuracy, but the performance of the prediction models will be strongly degraded. Common methods to address this problem are called sampling techniques. Furthermore, the Synthetic Minority Oversampling Technique (SMOTE) [4] method is known as the pioneer in the development of oversampling techniques based on synthetic data. Based on the SMOTE method, we are inspired to develop and process our unbalanced dataset, notably to oversample the minority class in order to improve the performance, compare algorithms and present a new approach Threshold Synthetic Minority Oversampling Technique (TH-SMOTE) to determine an optimal oversampling threshold with a G-mean Score.

Our paper is organized as follows. Section 2 provides a brief overview of the research conducted in this study and the problem of data imbalance. In Section 3, we detail the methodology of our approach, including the different steps of data preparation, the oversampling method, and the different evaluation measures. Section 4 presents the result of our experience. We discuss the performance results between the different algorithms through the iterations of oversampling, comparing our result with previous study. Finally, we present our conclusions in Section 5.

## II. RELATED WORK

Several authors find a modeling approach that sheds some light on the empirical investigation of fraud. They worked on data analytics and data mining approaches to improve model performance in the prediction, but some authors have addressed the same problem of our study, by dealing with the same dataset known as "carclaims.txt". Xu et al. [5] in 2011, proposed a neural network combined with a random rough subspace method to improve the consistency in the datasets. Sundarkumar et al. in 2015 [6], proposed an hybrid approach for rectifying the imbalance dataset problem by employing k Reverse Nearest Neighborhood and one class support vector machine (OCSVM). Nian et al. in 2016 [7], proposed an unsupervised spectral ranking method for detection anomaly (SRA) of forged instances in fraud detection problems, using auto insurance claim dataset. S. Subudhi and S. Panigrahi [8] in 2017, proposed a hybrid approach for detecting frauds in automobile insurance claims by applying Genetic Algorithm (GA) based Fuzzy C-Means (FCM) clustering and various supervised classifier models. Itri and Youssefi [9] in 2019, presented a new approach to improving the probability of fraud predictions by resampling methods with imbalanced dataset, as well as the methodology for evaluating performance of the ten best-known machine learning algorithms.

Furthermore, the problem of learning performance related to unbalanced datasets has received attention in different areas of research. Tora et al. (2019) [10] subdivided the resolution into three groups: Solution at data level, Solution at algorithm level and Hybrid solution. We focus like most of the articles on the techniques in the solution at the data level. Kubat and Matwin (1997) [10] applied the under sampling technique selectively on the majority class, while retaining the original population of the minority class. They applied the selection technique by subdividing the minority examples into four groups to eliminate overlapping noise data in the borderline region, as well as redundant samples. Chawla et al. (2002) [4] proposed the Synthetic Minority Oversampling Technique (SMOTE) method as a new approach to over-sampling the minority class, they are the founders of the SMOTE method, which has proven its worth in the problems of unbalanced datasets and oversampling techniques, in their approach. They have revolutionized the classical oversampling method, which inspired several authors [9][12][13][14] by proposing new methods derived from SMOTE to improve or remedy these weaknesses, such as neighbors, noise and wrong sample generation.

## III. PROPOSED METHODOLOGY

In order to have a good choice between the classification algorithms, we have chosen to compare the performance of the ten best-known algorithms: KNN, C4.5, Naive Bayes, Random Forest, Multilayer Perceptron, Machine Vector Support, Logistic, Partial Decision Trees (PART), Decision Table, and Adaptive. Before training our model, we processed the data and subsequently applied the SMOTE oversampling method by increasing the percentage of the minority class, iteration by

iteration, until the threshold where the performance becomes optimal. We chose a tenfold cross-validation method to train the model [15]. In the end, several classification measures are defined and discussed to evaluate these classifiers for each iteration. These steps are detailed in the following sections.

### A. Data Collection and Data Pre-Processing

The data set for our study is represented by real data from an anonymous insurance company on automobile claims provided by Angoss Knowledge Seeker Software, known in the literature as "carclaims.txt". The dataset comprises 15420 claims reported between January 1994 and December 1996, with 32 predictor variables and one target variable representing the values 1 "Fraud" and 0 "No Fraud". Fraudulent claims constitute 6% of the data set, i.e. 923 samples. The data set is in CSV format. We have converted the attributes to nominal because, on the one hand, several classifiers only support nominal attribute types, on the other hand, when importing data, heuristics cannot always predict the exact type of the attribute.

### B. Data Sampling

When working with real-world data such as the case of our study, in general cases, the datasets are highly composed of "normal" instances and only a small percentage represent target and abnormal instances. "Sampling" is a pre-processing procedure whose objective is to address the imbalance of a given data set by increasing or decreasing the training data before building a model, either by increasing examples from the minority class (over-sampling) or removing examples from the majority class (under-sampling). This one is only relevant if we have a large amount of data, which is not the case for our dataset. Therefore, we propose an over-sampling method SMOTE [4], whose approach generates new examples of the minority class by combining the data with those of their nearest neighbors, judged by the Euclidean Distance. But our new approach aims to define an optimal threshold of oversampling based on the evolution of the G-mean indicator and SMOTE method.

### C. Classification Evaluation

This section presents the application of the methods to train our model and the evaluation and selection criteria to decide on the best performing classification algorithms given a case study.

Through the confusion matrix a whole bunch of performance criteria can be derived. The following Table I presents the confusion matrix for a binary classifier with four different combinations of predicted and actual values.

TABLE I. CONFUSION MATRIX

| Actual \ Prediction | Fraud               | No Fraud           |
|---------------------|---------------------|--------------------|
|                     | Fraud               | TP - true positive |
| No Fraud            | FP - false positive | TN - true negative |

The following are the various measures derived from the indicators obtained through the fusion matrix:

1) *Accuracy*: is the number of correct predictions (TP and TN) made by the model over all kinds predictions made. Accuracy is a great measure but only when the given dataset is symmetric and balanced. However, when the data is imbalanced as in the case of our study, accuracy doesn't really capture the effectiveness of a classifier, because our models look at the data and cleverly decide that the best thing to do is to always predict "NoFraud Class" and achieve high accuracy (accuracy paradox). The formula is given by

$$Accuracy = \frac{TP + TN}{TP + FP + TN + FN}$$

2) *F-Measure*: Several evaluation criteria can be used, indicating the better or worse performance of a prediction function. But it is difficult to compare two models with low precision and high recall or vice versa. To facilitate the interpretation of the algorithm performance, Van Rijsbergen, 1979 [16] created a synthetic measure F1-Measure or F-score, defined as the harmonic mean of the precision and recall of a binary decision rule. It is given by.

$$F - Measure = \frac{((1 + \beta^2) \times Precision \times Recall)}{(\beta^2 \times Precision) + Recall}$$

Precision is a measure that tells us what proportion of claims that we predict as fraudulent (TP and FP), actually are fraudulent (TP). It is given by.

$$Precision = \frac{TP}{TP + FP}$$

Recall or Sensitivity is a measure that tells us what proportion of claims that actually fraudulent (TP and FP), was predicted by the algorithm as fraudulent (TP). It is given by.

$$Recall = \frac{TP}{TP + FN}$$

The  $\beta$  parameter determines the weight of precision in the combined score. If we set parameter  $\beta$  to 1, it means that precision and recall have equal importance.  $\beta < 1$  lends more weight to precision, while  $\beta > 1$  favors recall.

3) *AUC-ROC*: To support and compare the results of our study, we introduced another measure, Area Under Receiver Operating Characteristic (AUC-ROC) curve. The ROC curve is the plot between Recall and (1- specificity), the greater its value, the more predictive the model is able to distinguish between fraudulent and non-fraudulent groups.

4) *G-mean*: Called Geometric Mean, was proposed by Kubat et al. (1997) [11]. This evaluation parameter shows the balance between sensitivity and specificity, calculated as:

$$G - mean = \sqrt{Recall \times Specificity}$$

Specificity is a measure that tells us what proportion of claims that actually not fraudulent, was predicted by the model as not fraudulent. It's the opposite of Recall, that's why we're going to settle for this one instead. It is given by.

$$Specificity = \frac{TN}{TN + FP}$$

We used G-mean measure to decide on the oversampling threshold, by studying the evolution of the two indicators recall and specificity through the increase of the minority class percentage. Thus, the oversampling threshold will be calculated when the evolution curve becomes stagnant as the percentage of the minority class increases. In other words, the threshold is equal to the percentage of the minority class where the values of G-mean begins to converge towards a constant and its derivative is around zero.

#### IV. EXPERIMENTAL ANALYSIS

##### A. Experimental Results Discussion

To improve the model's performance, we will study the evolution of the measures according to the minority class percentage after each SMOTE oversampling iteration. As a first step, we start with an overview of the performance for all contending algorithms. We calculate the overall average of each measure in each iteration for all algorithms whose results and evolution are shown in Fig. 1.

Before applying oversampling, we have a high value of Accuracy and specificity measurement, due to the low percentage of the minority class. Our model tends to predict that almost all claims are non-fraudulent, so we confront the accuracy paradox. Therefore, the accuracy measurement is not a relevant measure for evaluating the performance of an unbalanced dataset. On the other hand, the Specificity has an average of 99% while the average recall is less than 1%, but the Recall remains a more important metric to consider in the process of detecting fraudulent claims, because it is important to detect all possible frauds, even if it means that the insurer may have to tolerate some false positives. This involves that we will have to give more weight to the recall in the  $\beta$  parameter of the F-measure formula.

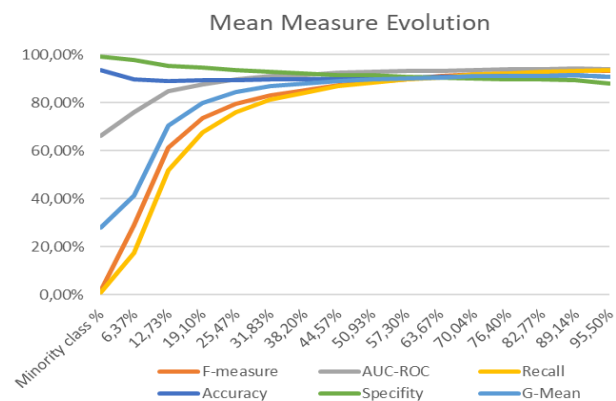


Fig. 1. Average Evolution of the Overall Algorithm Measures per Oversampling Iteration.

However, to compare and illustrate the importance of the parameter  $\beta$  for the evaluation according to the F-measure, we will keep the parameter  $\beta=1$  in a first step as shown in Fig. 1. Then we scale this parameter in a second step when the results of the algorithms evolve and become closer. We applied fifteen iterations to oversample – with the SMOTE method - the minority class, increasing its percentage in the dataset to 12.73%, 19.10%, 25.47% ... up to 100% where both fraudulent and non-fraudulent classes will have the same proportion. After the first iteration (12.73%) as shown in Fig. 1, we see that the average measures results increase significantly after the first oversampling operations, even exponentially for the F-Measure and Recall, except for the Accuracy (accuracy paradox), which decreases in the first iterations. After the second iteration (25.47%), the average of the measurements, including accuracy, increases linearly to reach higher values close to 100%.

If we have a closer look at the measures by the five algorithms that inflate as presented in Table II, focusing on the top five algorithms with the highest F-measure and AUC-ROC values, the recall of KNN algorithm makes a considerable leap from a score of 8% to 79.60% after the first iteration (12.7%), far surpassing the other algorithms. As for the Area Under ROC values, KNN is ranked second with a value of 91.86% not far from the first place attributed to the Random Forest with 93.26%, but has a low Recall value with 22.48%. While the value of F-measure is increased by KNN with the highest value 70.82%, against Random Forest which holds the value 36.63% well far from the first place held by KNN.

Up to now, in this first iteration we can conclude that KNN takes the lead in the ranking of the algorithms, reacts faster on the Recall indicator. On the other hand, considering the importance of the recall measure, the Area Under Roc measure remains irrelevant at this stage in comparison with F-measure to evaluate and rank the algorithms' performances.

In the last iteration (100% SMOTE), as presented in Table III when the minority class reaches the same proportion as the majority class, Random Forest increases all measures including F-measure except the recall measure which is held by KNN with a value of 98.94%, followed by C4.5.

On the other hand, for the performance ranking according to the F-measure, we have considered until now that the recall and the precision have the same importance when we assigned the  $\beta$  parameter value to 1. However, we should give more attention to the Recall measure compared to the precision. In this case we need to give more weight to the recall ( $\beta>1$ ). Thus, we assign the value 2 to  $\beta$ , meaning that recall is twice as important for us. According to the F-Measure results in Table III, we observe that the weight of the Recall indicator is taken into account, with an increase in the KNN algorithm not far from Random Forest. We conclude that KNN remains the most efficient algorithm to improve the model from the first iteration to the last. It is the most effective algorithm to increase the percentage of fraudulent instance we recalled from all fraudulent instance.

As some regions of minority and majority class groups are closely neighbored, SMOTE may overgeneralize the region of minority classes that is in the proximity of majority classes. Thus, new noisy instances may be generated [17], and may reduce the reliability of predictions for both minority and majority classes. If we repeat this generation several times, our model may deviate from reality because of the noisy instances, despite the improvement of the indicators over iterations. Therefore, according to the evolution of the performance of the KNN algorithm through the iterations of oversampling (see Fig. 2), if we look at the curve of the G-means indicator, the optimal is reached at the third iteration (25.47%), at this level the values of the measurements are very optimal to constitute our prediction model (Recall = 95.10%; Specificity = 90.62%; AUC-ROC = 95.37%).

TABLE II. PERFORMANCE ANALYSIS AFTER FIRST OVERSAMPLING ITERATION

| Model        | Precision | Recall        | Accuracy | Specificity | AUC-ROC       | F-measure     |
|--------------|-----------|---------------|----------|-------------|---------------|---------------|
| KNN          | 63,73%    | <b>79,69%</b> | 92,58%   | 94,23%      | <b>91,86%</b> | <b>70,82%</b> |
| PART         | 55,33%    | 39,06%        | 89,56%   | 95,99%      | 83,09%        | 45,79%        |
| Naive Bayes  | 42,60%    | 45,83%        | 86,91%   | 92,14%      | 83,83%        | 44,15%        |
| M.Perceptron | 56,92%    | 29,20%        | 89,51%   | 97,19%      | 81,33%        | 38,60%        |
| RandomForest | 98,81%    | 22,48%        | 91,21%   | 99,97%      | <b>93,26%</b> | <b>36,63%</b> |

TABLE III. PERFORMANCE ANALYSIS IN THE LAST OVERSAMPLING ITERATION (100% SMOTE)

| Model        | Precision | Recall        | Accuracy | Specificity | F-measure     |               |
|--------------|-----------|---------------|----------|-------------|---------------|---------------|
|              |           |               |          |             | $\beta = 1$   | $\beta = 2$   |
| KNN          | 88,47%    | <b>98,94%</b> | 93,02%   | 87,10%      | 93,41%        | <b>57,99%</b> |
| RandomForest | 99,42%    | 95,29%        | 97,37%   | 99,45%      | <b>97,31%</b> | 57,65%        |
| M.Perceptron | 90,07%    | 94,49%        | 92,03%   | 89,58%      | 92,22%        | 56,14%        |
| C4.5         | 92,14%    | <b>96,26%</b> | 94,03%   | 91,79%      | 94,16%        | 57,24%        |
| PART         | 94,60%    | 95,56%        | 95,05%   | 94,55%      | 95,08%        | 57,22%        |

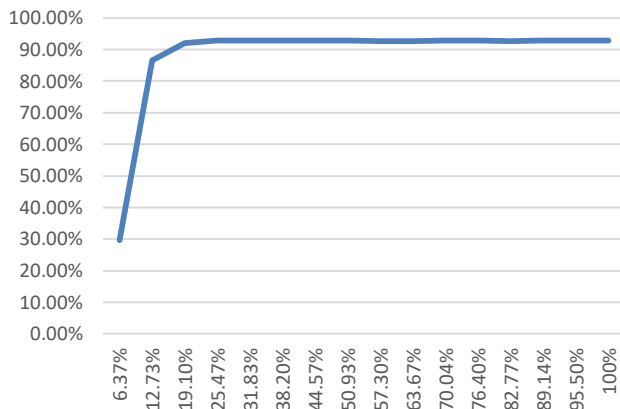


Fig. 2. G-Mean Evolution for KNN Algorithm through Iterations of SMOTE Percentage.

### B. Comparison with Previous Literature in the Same Scope

Several research works have addressed the same dataset. We present in Table IV, a comparison of the expected results by referring to the same measures (accuracy, recall, Specificity) used in the same literature.

TABLE IV. COMPARATIVE PERFORMANCE ANALYSIS USING CARCLAIMS.TXT

| Research Articles              | Accuracy | Recall | Specificity |
|--------------------------------|----------|--------|-------------|
| Xu et al. (2010)               | 88,7     | -      | -           |
| Sundarkumar et al. (2015)      | 58,92    | 95,52  | 56,58       |
| Sundarkumar and Ravi (2015)    | 60,31    | 90,79  | 58,69       |
| Nian et al. (2016)             | -        | 91     | 52,00       |
| Sharmila and Panigrahi. (2017) | 87,02    | 83,21  | 88,45       |
| Bouzarne and Youssefi (2020)   | 91,52    | 95,1   | 90,62       |

We obtained the best performance compared to previous studies. We can still improve the results by pushing the oversampling percentage to 100% when the dataset becomes balanced and symmetrical, however this will generate a large amount of non-real data that will penalize the quality of the training data, impacting the model veracity with the risks of oversampling. This is why in our approach, we oversampled the minority class only up to the threshold (25%), determined by the mean G curve, thus achieving a better result.

### V. CONCLUSION

In this article, an approach TH-SMOTE to improving the performance of the prediction model in auto insurance fraud was proposed. A comparative study of machine learning classification algorithms applied on a labeled and unbalanced dataset was carried out. Over-sampling based on the SMOTE method was applied, by increasing the minority class by iteration to the threshold where the measurements became more significant for the model. Particular attention was given to the performance evaluation methods of the classification model. The relevance of the results of the most known measure to classify the algorithms were discussed, by giving more weight to the Recall indicator, one of the most important indicators in detecting fraud.

The results show that the TH-SMOTE approach can significantly improve the performance of the classifiers for the whole set of classification algorithms. In particular, the KNN algorithm reacts faster to the first over-sampling percentages to offer better model performance, notably through the Recall indicator.

Furthermore, we have shown that the F-Measure allows a better comparison of the performance of the classification algorithms for unbalanced datasets cases in comparison with the AUC-ROC measurement, provided that more weight is given to the True Positive Rate (recall) via its  $\beta$  parameter. In contrast, the G-mean measure allowed us to measure and define the threshold of the percentage of oversampling, along with the minority class to avoid too much over-sampling at the expense of the model quality. Specifically, it is to prevent overfitting and to reduce generating noisy examples into the dataset without skewing the performance results.

Finally, this study's results were compared with previous research on the same scope, our approach found a higher result.

Although the experimental results of this study have proven that this approach allows a comparison and choose the best algorithm for the case of an unbalanced dataset using the TH-SMOTE method combined with G-mean, there are also other research works in the same area of study which offer variants of the SMOTE method. Hence, the extension of our approach to these variants may be possible in future work.

### REFERENCES

- [1] Insurance Fraud Bureau of Australia Homepage, <https://ifba.org.au>, last accessed 30/05/2020.
- [2] Assurance auto: La fraude explose. Edition N°:5302, 27/06/2018. <https://www.leconomiste.com/article/1030288-assurance-auto-la-fraude-explose>, last accessed 30/05/2020.
- [3] French Agency for the Fight against Insurance Fraud – ALFA. <https://www.alfa.asso.fr/>.
- [4] Chawla et al. 2002. "SMOTE: synthetic minority over-sampling technique." Journal of artificial intelligence research 16 : 321–357.
- [5] Xu, W., Wang, S., Zhang, D., Yang, B., 2011. Random rough subspace based neural network ensemble for insurance fraud detection. In: Computational Sciences and Optimization (CSO), 2011 Fourth International Joint Conference on. IEEE, pp. 1276–1280.
- [6] Sundarkumar, G.G., Ravi, V., 2015. A novel hybrid undersampling method for mining unbalanced datasets in banking and insurance. Eng. Appl. Artif. Intell. 37, 368–377.
- [7] Nian, K., Zhang, H., Tayal, A., Coleman, T., Li, Y., 2016. Auto insurance fraud detection using unsupervised spectral ranking for anomaly. J. Finance Data Sci. 2 (1), 58–75.
- [8] Sharmila Subudhi, Suvasini Panigrahi, 2017. Use of optimized Fuzzy C-Means clustering and supervised classifiers for automobile insurance fraud detection; Department of Computer Science and Engineering & IT, Veer Surendra Sai University of Technology, Burla, Odisha 768018, India.
- [9] Bouzarne Itri and Youssefi Mohammed, et al.2019:"Performance comparative study of machine learning algorithms for automobile insurance fraud detection".2019 Third International Conference on Intelligent Computing in Data Sciences (ICDS), 28-30 Oct. 2019.
- [10] Tora Fahrudin, et al. 2019. Enhancing the performance of smote algorithm by using attribute weighting scheme and new selective sampling method for imbalanced data set. ICIC International, 2019 ISSN 1349-4198, pp. 423-444.
- [11] Miroslav Kubat and Stan Matwin: "Addressing the Curse of Imbalanced Training Sets: One-Sided Selection". Proceedings of the 14th International Conference on Machine Learning, (1997)179-186.

- [12] E.Ramentol, Y.Caballero, R.Bello, F.Herrera, 2012. Smote-rsb: a hybrid preprocessing approach based on oversampling and undersampling for high imbalanced data-sets using smote and rough sets theory. *Knowl. inf. Syst.* 33 (2012), 245–265.
- [13] S. Barua et al., Mwmote–majority weighted minority oversampling technique for imbalanced data set learning, *IEEE Trans. Knowl. Data Eng.* 26 (2014), 405–425.
- [14] Z. Zheng et al., Oversampling method for imbalanced classification, *Comput. Informat.* 34 (2016), 1017–1037.
- [15] Refaeilzadeh et al. 2009. Cross-validation. In: *Encyclopedia of Database Systems*. Springer, pp. 532–538.
- [16] C. J. V. Rijsbergen, 1979. *Information Retrieval*. Butterworth-Heinemann, Newton, MA, USA, 2nd edition.
- [17] Haibo He and Edwardo A Garcia. 2009. Learning from imbalanced data. *Knowledge and Data Engineering, IEEE Transactions on*, 21(9):1263-1284.



# Design of an Electro-Stimulator Controlled by Bluetooth for the Improvement of Muscular Atrophy

Paul Portilla Achata<sup>1</sup>, Raúl Sulla Torres<sup>2</sup>, Juan Carlos Copa Pineda<sup>3</sup>  
Agueda Muñoz del Carpio Toia<sup>4</sup>, Jose Sulla-Torres<sup>5</sup>

Electronic Engineering, Universidad Católica de Santa María, Arequipa, Perú<sup>1, 2, 3</sup>  
Medicine, Universidad Católica de Santa María, Arequipa, Perú<sup>4</sup>  
Systems Engineering, Universidad Católica de Santa María, Arequipa, Perú<sup>5</sup>

**Abstract**—Muscle stimulation consists of a muscle's work when it is in constant exercise or contraction. This article presents an electro-stimulator design that generates electrical pulses in muscle cells through two electrodes positioned in an area of the body, causing the response of said cells to improve muscle atrophy. The steps that were followed were the construction of the block diagram, the design, and development of the circuit, the design and development of the control based on the pic12F683 and pic 16F690 microcontrollers, finally, the development of the software of the mobile application that controls the equipment using Bluetooth signals, based on the standard of IEC 60601-1 for basic safety and essential equipment performance. It was possible to obtain control of the frequency, application time, and amplitude of the duty cycle to have better results when applying therapy in specific areas of the body through the mobile application. Finally, the design is developed to respond to the user's parameters, using the Bluetooth of a mobile device and allowing the generation of electrical pulses in the muscle cells to improve muscle atrophy. The team can be part of therapeutic sessions for people with quadriplegia, improving the physiotherapy sessions performed on patients.

**Keywords**—Design; electro-stimulator; microcontroller; electric pulses; muscular atrophy

## I. INTRODUCTION

The World Health Organization (WHO) defines disability as "a generic term that encompasses deficiencies, activity limitations, and participation restrictions," all this in terms of the environment in which the person develops [1].

Within the context of disability, there are different types, of which we can mention cerebral palsy, Down syndrome, depression, so on. In the article "Disability in Peru: An analysis of reality from statistical data" [2], it is mentioned that in Peru, the reality of disability is not indifferent, thus having 10.4% of the general population has some disability, and in this subset, it has that 57% occurs in women and 43% occurs in men, within this population, we take into account those who have a motor or physical disability such as paraplegia, quadriplegia, amputations limbs, so on.

Muscular atrophy and motor or physical disability refer to the consequence of having a disability, that is, muscular atrophy is the loss of muscle mass due to the lack of exercise or movement of muscles that are in the affected area [3]. In the field of medicine, specifically in the area of therapeutic treatments, It can find electronic equipment that gives us a

facility for the implementation of these treatments, known as electro-stimulators [4], which seeks to replace the natural physiological stimuli of the body with electrical ones, caused from the outside by equipment with a specific potential and a given current form.

In Peru, one of the main problems with electrostimulation is the lack of application in the various forms of disability, being more specific about its use in the development of people's muscles. However, of the articles that have been reviewed to date, there are very few studies related to the design of a muscle electro-stimulator to muscular atrophy, especially in Latin America. That is why this work aims to design an electro-stimulator controlled by Bluetooth to improve muscle atrophy that will develop using electrical pulses in muscle cells through two electrodes positioned in an area of the body.

The rest of this paper is organized as follows: The second section is the background and related work. The third section describes the methodology. The fourth section presents the results and discussion of this research. Finally, this paper is concluded with the future works of this study.

## II. THEORETICAL FRAMEWORK

The application of engineering in the different fields of society seeks to generate a new way in which well-being and what is offered is in the best way. This research aims to develop a team that achieves favorable results in patients suffering from muscle atrophy by improving muscle function to improve their motor disability.

In this sense, the theoretical framework on the main concepts and related works of the research developed is presented.

### A. Disability

Disability is a human condition, which every person can suffer, either temporarily or permanently. In turn, the WHO mentions disability as a generic term that can encompass deficiencies, limitations, and restrictions to perform motor activities.

It must be clear when talking about disability since there are different types, and in turn, within each one, we have the form and the degree with which it occurs. In the article by Jalayondeja et al. [5], it is mentioned that disability, from the medical point of view, can be classified into five categories,

and mentions motor or physical disability such as hemiplegia, paraplegia, and quadriplegia, limb amputations, poliomyelitis, arthritis; there is also intellectual disability [6], which are limitations in intellectual functioning and the development of adaptive skills; there is mental disability [7], which refers to biochemical alterations that limit thinking, humor, feelings, as well as behavior with others; when talking about sensory disability [8], it refers to the limitations in the function of perception of external sounds - hearing, objects - sight and finally there is multiple disability [9], as the presence of two or more disabilities.

### B. Muscle Atrophies

To refer to muscular atrophies, we will first define what atrophy is; in [10] explains that atrophy refers to the decrease in the size of an organ due to loss of protoplasmic mass, it is necessary to specify that, unlike hypoplasia, where the organ does not develop or there is arrested development, atrophy is the reduction of the organ that reached its normal development.

In [11], they speak of muscle atrophy, referring to the wasting, thinning, or loss of muscle tissue due to lack of activity since it is found in long periods of rest.

Some diseases and disorders cause a decrease in muscle mass, including inactivity, cachexia present in cancer patients or heart failure, chronic obstructive pulmonary disease, extensive burns, liver failure, electrolyte disorders, anemia, so on. Other syndromes can cause muscle atrophy such as malnutrition, denervation of motor neurons, childhood spinal muscular atrophy, and inflammatory myopathies and dystrophies, among others.

There are different types of muscle atrophies [12]: physiological, which is caused by not using your muscles enough, can be reversed with exercise and good nutrition; pathological, which is caused by aging, starvation, and diseases, such as Cushing's syndrome, and the neurogenic that is due to an injury, or a disease, in the nerves that connect to the muscles. This type of muscle atrophy tends to happen more suddenly than disuse atrophy.

However, when it comes to diagnosis, the process comes in carefully reviewing the patient's medical history in search of family history or a disease that affects tissues or organs.

### C. Electro Stimulating Equipment

An electro-stimulator is electronic equipment used in the development of protocols for performance evaluation and physical rehabilitation through electrical pulses. There are different electrostimulation equipment oriented to the sports field, health, among others [13].

The basis of electro-stimulators' action is based on the reproduction of the body's impulses, which are transmitted through the skin utilizing electrodes to the nerve fibers, respectively muscle fibers [14] [15]. For these purposes, it is essential to place the electrodes in various parts of the body; electrical stimuli are harmless and dynamic and do not produce pain. During the applications, It only feels a slight tingling or a slight vibration. The electrical impulses that penetrate the box influence the emanation of the nerve

pathways and the nerve ganglia and muscle groups in application areas.

Neuromuscular electrical stimulation (NMES) has emerged as a new therapeutic alternative to improve patients' physical condition with muscle loss problems [16]. There has also been some rehabilitation research aimed at the particularities of women [17], and rehabilitations may even be carried out at a robotic level [18], where the development of a novel functional electrical stimulation system (FES) is presented. New approaches to emergent rehabilitation robotics propose residual muscle activity or limb movements during the neuromotor rehabilitation process.

Electrostimulating equipment contains different parameters that vary; one of these is the operating frequencies; Table I shows the frequencies at which it operates in a general way:

TABLE I. FREQUENCIES OF ELECTRO-STIMULATOR WORK

| Frequency   | Operation                            |
|-------------|--------------------------------------|
| 1 – 3 Hz    | Decontracting                        |
| 4 – 7 Hz    | Relaxation                           |
| 8 – 10 Hz   | Increased blood flow Capillarization |
| 10 – 33 Hz  | Aerobic resistance                   |
| 33 – 50 Hz  | Muscle firmness                      |
| 50 – 75 Hz  | Force and resistance                 |
| 75 – 120 Hz | Explosive force                      |

Regarding the wirelessly controlled electro-stimulator, Araujo et al. [19] present an approach to hardware and software-controlled solutions in the field of electrical stimulation. A miniaturized, portable, and wireless electro-stimulator was designed controlling the stimulation parameters in real-time for stimulation sessions with high flexibility and ease, using a friendly interface for a computer or Android platform that communicates with the portable and wireless device.

### III. METHODOLOGY

As mentioned in the previous section, electrostimulating equipment is based on the generation of an impulse that generates the contraction of the cells, which causes a depolarization of the electrical changes.

Since the research is focused on the design of an electro-stimulator, its design is based on the use of different parameters of the electrical signal that allows the prevention and treatment of muscle atrophy in patients, which must have a user interface- friendly machine for the application and control of said signals.

To start with the design of the equipment, some characteristics that must be met in order to make it safe and reliable for the user:

- Have control of the parameters of the stimulation signal at all times.
- Maintain accuracy against input values such as supplied voltage and current.

- Comply with safety for both patient and user.
- Have a user-machine interface that is easy to use and implement.

The Block Diagram used in the electro-stimulator design is presented below.

#### A. Blocks Diagram

The user defines the parameters and time of application of the signal through the mobile equipment. With this information already determined, the microcontroller receives said instructions to generate the necessary routines and fulfill what the user is looking for. The signal generator with the signal already adapted goes through an amplification circuit, ending all this in the signal's adapter circuit to be transmitted through the electrodes positioned on the body.

In Fig. 1, the block diagram of the equipment is shown.

#### B. Design and Development of the Circuit

Having control of the parameters, such as the frequency and the operating time of the device, is a great advantage in terms of the application of therapy; all this is controlled from a graphical interface (computer with Android operating system), which communicates wirelessly with the computer through the Bluetooth protocol; the equipment has the PIC 16F690 as its receiver and the PIC 12F683 as the pulse generator.

The PIC 12F683 microcontroller produces two signals; the first is a square wave pulse train; this is going to be connected to a non-inverting Buffer (CD4050) that helps to adjust the signal of the electrical pulses to the base of the transistor to pass to the two-phase isolation coil. The second signal to generate is a pulse width modulation (PWM) signal, connected to a resistor-capacitive (RC) circuit, passed to an operational amplifier in non-inverting mode, with positive gain to amplify the signal. The LM 358 integrated circuit provides us with two operational amplifiers, one is used in non-inverting mode, at the + input of the amplifier with an RC circuit; this circuit is configured as a low pass filter, thus obtaining the pass of the frequencies low and reject high frequencies. For the calculation of the filter cutoff frequency, the following Eq. 1:

$$f_c = \frac{1}{2\pi RC} \quad (1)$$

Suppose the amount of ohms used is not adequate; for example, 1500 ohms, the work's intensity decreases. Consequently, the induction of muscle contractions is reduced; therefore, to achieve the desired effect, the current must remain constant despite variations in our body's resistance. In this case, 1000 ohms was used as resistance (R) and 1 $\mu$ F as a capacitor (C). Replacing is shown in Eq. 2:

$$f_c = \frac{1}{2\pi * 1000 * 1 * 10^{-6}} = 159.24 \text{ Hz} = 159 \text{ Hz} \quad (2)$$

The PIC 12F683 generates two PWM frequencies, the first of 490 Hz and the other of 980 Hz, all this in order to obtain an average voltage in the charge and discharge of the capacitor. This signal enters the pin + of the operational amplifier, which is in a non-inverting configuration with a positive gain.

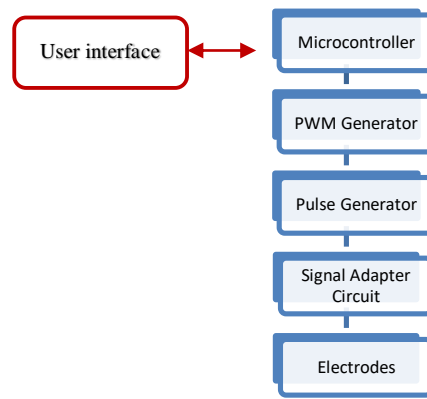


Fig. 1. Blocks Diagram.

At the same time, the signal for the output must be conditioned; in this case, a train of pulses is generated which passes through the non-inverting buffer CD4050; A Darlington configuration is used for the amplification of the current using the NPN 2N2222 transistors, with that the signal already conditioned passes through the isolation transformer and is applied to the patient. For protection in this stage, a fast-acting diode 1N4148 is used.

#### C. Control Design and Development

About the control stage, two fundamental components are used for this equipment: the PIC 12F683 and the PIC 16F690, from the Microchip brand, they are high-end devices accessible to the market. Regarding the PIC 12F683 to implement the pulse width modulation (PWM), we use the CCP module; in this module, we have three types of operation: capture, comparison, and PWM. When the PWM module is activated using the CCP1CON register, different working frequencies can be generated, and there is even the option of varying the duty cycle while maintaining one frequency.

In this operating mode, the Prescaler is used, and TIMER2; the PR2 register varies from 0 to 255 (this being 8 bits but with the availability of being able to extend to 10 bits and work from 0 to 1024 as necessary), for its calculation Eq. 3:

$$PR2 = \frac{\frac{1}{F}}{\left(\frac{4}{F_{osc}} * Prescale\right) - 1} \quad (3)$$

To calculate the Duty Cycle, we have Eq. 4:

$$PWM \text{ Duty Cycle} = \frac{\frac{1}{F}}{\frac{1}{F_{osc}} * Prescale} \quad (4)$$

Regarding communication with the mobile device, the PIC 16F690 was used, which has various functions that facilitate its programming; this microcontroller processes the data it receives from the mobile device through the Bluetooth module. For this communication, the EUSART module (Enhanced Universal Synchronous Asynchronous Receiver Transmitter) was used, which works in asynchronous mode, since the Bluetooth module has an internal clock signal, the TXSTA, RCSTA, and BAUDCTL work registers are used.

Fig. 2 shows the signal conditioning circuit together with the microcontroller:

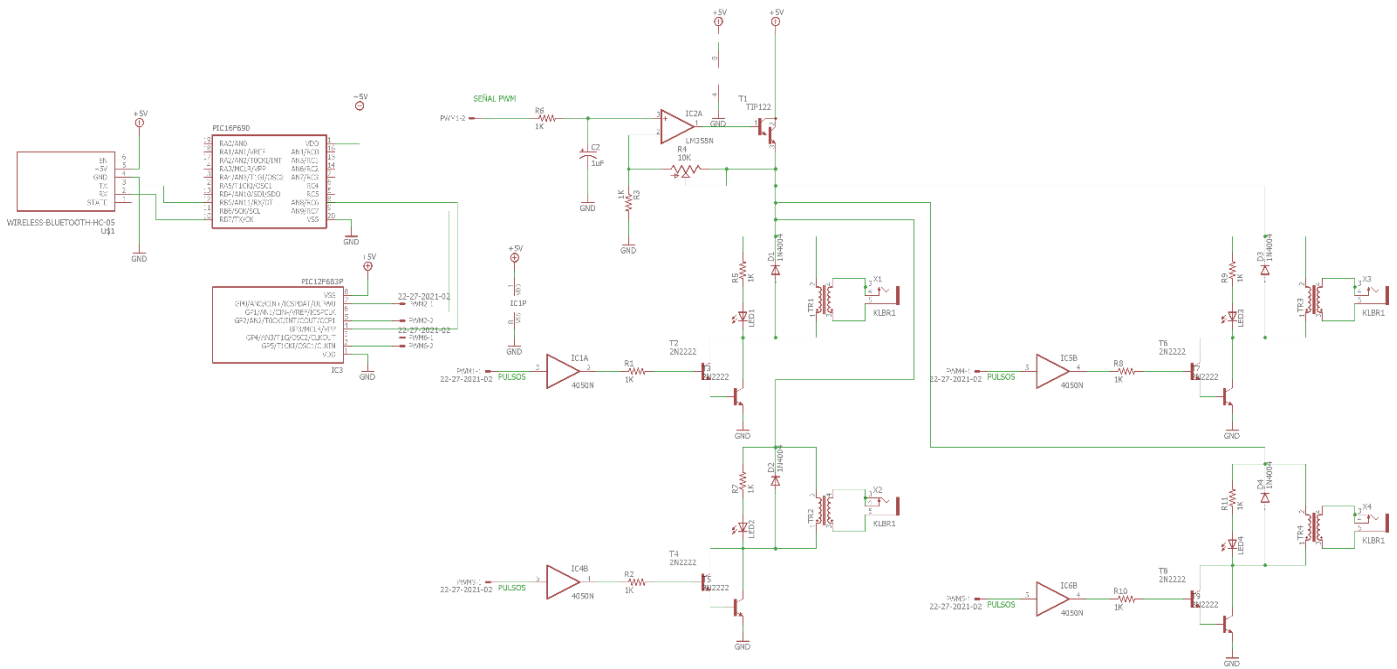


Fig. 2. Schematic Circuit of the Electro Stimulator.

Once the data transmission speed with which the microcontroller is working has been configured, the reception and transmission of this data are configured; through the Android application, the electrode site's configuration is configured, along with with the intensity and the time of the application of the electrical impulses. These signals are transmitted from the mobile to the microcontroller by the HC-05 Bluetooth module. Bluetooth is an open system communications protocol of IEEE 802.15, enabling data passage between devices through short-distance wireless communication around the 2.4 GHz free band [20].

It can be established that the design of the electrostimulation equipment controlled remotely by the user can contribute to the science regarding the use of the Myostimulation vest.

Fig. 3 shows the electrodes' positioning in the Myostimulation vest developed suggested by Beurer [13]; this vest has the connection points in the lower part, where the equipment connects and generates the signal of the electrical pulses in patients.

Fig. 4 shows the prototype of the Myostimulation vest developed for the study.

Likewise, the IEC 60601-1 standard recommendations were followed, which is a series of technical standards for the safety and essential performance of medical electrical equipment [21]. The standard's main requirement is the creation of an excellent and complete structure that must contain the complete documentation of the project development.

#### D. Mobile Application for Equipment Control

Our equipment parameters will be entered through a mobile device with an Android operating system [22]. In the current market, we have several programs for the development

of these applications; the MIT App Inventor 2 software [23] contains two parts of programming: the first dedicated specifically to the graphic design of the user interface, and the second refers clearly to programming, this programming is by blocks of essential functions that are based on the C ++ language.

When starting the application, there is a screen with two buttons: "Bluetooth connection" and "EMS" the first button allows establishing a connection with the electro-stimulator equipment, and the second access the configuration of the equipment parameters. When you click on the "Bluetooth connection," it generates the second screen of the application to link the mobile device's equipment.

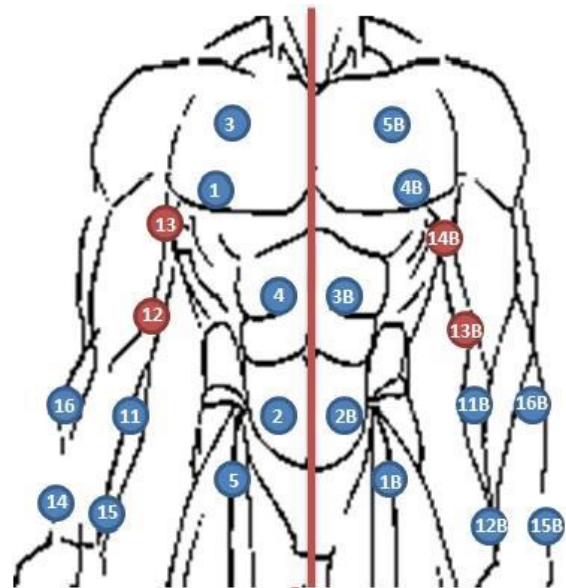


Fig. 3. Electrode Positioning on the Vest [13].



Fig. 4. Vest Prototype Proposed in the Study.

The "EMS" button generates the second screen of the application in which several parts are shown: in the first, the application channel is selected, the equipment has four output channels, where you can select the four output channels or on the contrary, only the working channel; In a second part, you can select the team's work area, where you have four options, similarly when one is selected, it will turn green, while the others will turn lead, showing that they cannot be activated.

When selecting a part of the work, there are two images on the display screen. These images provide us with the positions in which we will connect the electrodes; As a third party, you have the program to select; this refers to the frequency of work that the equipment will have; as mentioned, there are seven work modes, and finally, two fields are presented to fill, the first one referring to the time of application of the equipment (in seconds) and the second field focused on the intensity, for this case there are intensities from 1 to 10. There is also a button called "Load" for the data established in applying to the electro stimulator equipment.

In Fig. 5, the interface of the mobile application with which the user interacts is shown.



Fig. 5. Mobile App Interface.

#### IV. RESULTS

Having the PIC 12F683 generating the pulse trains and the PWM helps us better control the user's stimulation parameters.

In Fig. 6, the pulses at the output of the transformer are observed, which through the electrodes will be transmitted to the patient; in the image on the left side, we have a frequency of 50 Hz, thus obtaining the muscle firmness that the patient needs for the depolarization of muscle cells, while in the image on the right we have a frequency of 100 Hz, generating an explosive force in the muscle with which we will progressively contract the muscle obtaining a response in each muscle cell.

At the moment of stimulating a cell, a positive net internal charge effect is produced; this is given by a change in the ionic fluxes of Na and K, the K ions are directed towards the outside of the cell while the Na ions go inside; this movement produces the effect of positive net internal charge. Once the cells present a resting voltage, the stimulation that generates is that that voltage is exceeded, which will cause the membrane to depolarize.

According to the results obtained, you can control and select the different working frequencies and signal parameters.

Likewise, Table II shows the comparison between four implemented equipment, a commercial product that is sold in the market (BEURER EM80) [13], the other is a revised research work by Tame [24], the third equipment is the Muscular Strain of Different Whole-Body Electromyostimulation [25], and the fourth equipment is the one proposed in this study.

Within this table, it can notice the different characteristics regarding the proposed equipment, among which the following stand out:

- The proposed equipment has an output signal based on biphasic pulse trains, compared to the other two devices

with a biphasic pulse signal or only non-biphasic pulse trains.

- By having a lower current than the BEURER EM80 equipment, the equipment's size is reduced.
- The proposed equipment has four application channels (8 electrodes) to better apply for the treatment programs.
- The four computers have a user interface, but it can be highlighted that the proposed equipment does not

depend on the use of a screen on the equipment, that if the equipment fails, it will be inoperative.

- Compared to the three teams, an application for mobile devices was developed for the team, in which different actions will be generated for the team; on the contrary, the other two teams do not have this benefit.
- The mobile application presented has a registry of patients in which the equipment will be used.
- Besides, it also has a record of the results obtained in the sessions and displays different results.

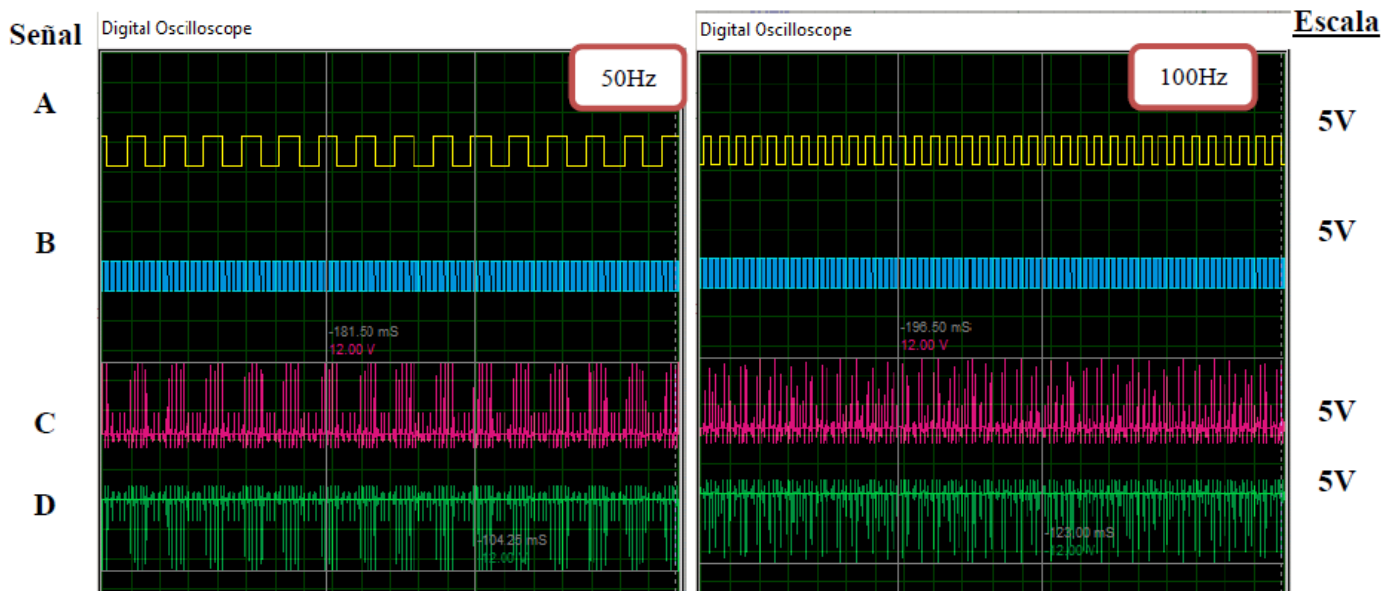
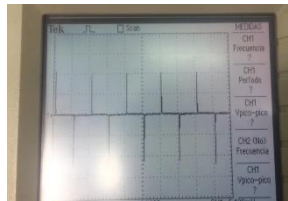
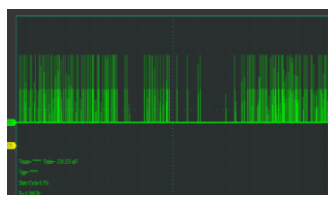
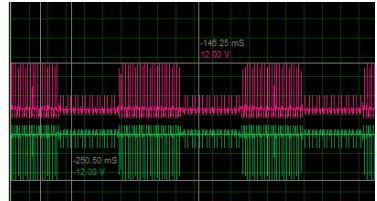


Fig. 6. Simulation of Electrical Pulses at 50 and 100 Hz, respectively.

TABLE II. COMPARISON BETWEEN EQUIPMENT ON THE MARKET

|                    | Beurer 80                   | Electro-stimulator -Talme | Muscular Strain of Different Whole-Body Electromyostimulation (WB-EMS) Protocols<br>Used equipment: miha bodytec (Gersthofen, Germany) | Proposed electro-stimulator v. 1.0         |
|--------------------|-----------------------------|---------------------------|----------------------------------------------------------------------------------------------------------------------------------------|--------------------------------------------|
| Output curve shape | Biphasic rectangular pulses | Rectangular pulses        | Symmetric biphasic                                                                                                                     | Biphasic rectangular pulses (pulse trains) |
| Pulse frequency    | 1 – 120 Hz                  | 1 – 150 Hz                | 2 – 150 Hz                                                                                                                             | 1 – 120 Hz                                 |
| Output voltage     | Máx 90 Vpp                  | Does not specify          | <= 74Vp @ 500Ω (54-74 Vp)<br><= 152Vp @ 2kΩ (110...152 Vp)<br><= 152Vp @ 10kΩ (130 ... 152 Vp)                                         | Máx 24 Vpp                                 |
| Output current     | 180 mA                      | 100 mA                    | < 148mA @ 500Ω (108-148mA)<br>< 76mA @ 2kΩ (55-76mA)<br>< 15 mA @ 10kΩ (13-15mA)                                                       | 100 mA                                     |

|                                  |                                                                                   |                                                                                   |                                                                                                                                                                                |                                                                                     |
|----------------------------------|-----------------------------------------------------------------------------------|-----------------------------------------------------------------------------------|--------------------------------------------------------------------------------------------------------------------------------------------------------------------------------|-------------------------------------------------------------------------------------|
| <i>Voltage supply</i>            | 3x batteries type AA                                                              | Battery 9V                                                                        | Control unit: 15 V – 19 V; External power supply (100– 240 V ~ 50 – 60 Hz)                                                                                                     | Battery 9V                                                                          |
| <i>Treatment duration</i>        | Adjustable from 5 to 90 minutes                                                   | Does not specify                                                                  | Training should not exceed 20 minutes; Screen shows remaining time in minutes and displays image showing time remaining                                                        | Dimmable in seconds                                                                 |
| <i>Intensity</i>                 | Adjustable from 0 to 15                                                           | Does not specify                                                                  | Does not specify                                                                                                                                                               | Adjustable 0 to 10                                                                  |
| <i>Operating conditions</i>      | 0°C – 40°C                                                                        | Does not specify                                                                  | Does not specify                                                                                                                                                               | 10°C-50°C (ideal 20°C-30°C)                                                         |
| <i>Stimulation channels</i>      | 4 channels (8 electrodes)                                                         | 2 channels (4 electrodes)                                                         | 10, channel selective stimulation. Maximum one channel is active at any time.                                                                                                  | 4 channels (8 electrodes)                                                           |
| <i>Signs</i>                     |  |  | Does not specify                                                                                                                                                               |  |
| <i>User interface - computer</i> | Black white screen on the computer                                                | Nextion screen in equipment                                                       | 10.1 inch non-touch LC color display for program / training plan selection via menu, settings, device status, training mode display (animated avatar, timer, selected program) | Electro-stimulator application for mobile equipment                                 |
| <i>Equipment setup</i>           | By buttons on the computer                                                        | By screen on the computer                                                         | The device must only be operated by a trainer, who received full training                                                                                                      | By application from a mobile device                                                 |
| <i>Patient registration</i>      | Does not count                                                                    | Does not count                                                                    | Yes, while a program is active the patient is supervised by a trainer and able to manipulate intensity                                                                         | In application, the patient registration window                                     |
| <i>Session log</i>               | Does not count                                                                    | Does not count                                                                    | Does not specify                                                                                                                                                               | In application, measurement window                                                  |

## V. CONCLUSIONS

A Bluetooth-controlled Electro Stimulator was designed to improve muscle atrophy. The equipment responds to the user's parameters through wireless communication from a mobile device, always considering the standards that govern its design. We have an EMS electro stimulator with components and materials to obtain muscle activation in the local market.

It was possible to build an interface for mobile devices with Android operating system, easy to use for the user or therapist, which allows us to connect with the equipment wirelessly through the Bluetooth protocol, having as possible future designs the incorporation of a web server such as use and storage of data where the therapist can easily access the patient's medical history.

It was possible to obtain control of the frequency, application time, and amplitude of the duty cycle to have better results when applying therapy in specific areas of the body, all this through the mobile device.

The team can be part of therapeutic sessions for people with quadriplegia, improving the muscular atrophies that these patients present. This equipment is exposed to improvements in its design and programming, the change in technology, and the initial algorithm's different parameters.

As future work, the design of the programming can be changed for use through web servers, with which the patient's medical history can be saved so that doctors can access it more easily. Likewise, you can double the pulse stage for conditioning and thus obtain more outputs for the application.

## ACKNOWLEDGMENTS

To the Universidad Católica de Santa María, Arequipa-Perú which has financed the approved project with 25789-R-2018-UCSM granted for the development of the article.

## REFERENCES

- [1] WHO, "WHO Global Disability Action Plan 2014-2021: Better Health for All People With Disability," Who, 2015.

- [2] J. R. Diaz Dumont, "Disability and analysis of case statistics in Perú abstract," *Rev. Venez. Gerenc.*, vol. 24, no. 85, 2019.
- [3] R. Y. Cao, J. Li, Q. Dai, Q. Li, and J. Yang, "Muscle atrophy: Present and future," in *Advances in Experimental Medicine and Biology*, 2018.
- [4] A. L. Aragón, C. Bao-Varela, E. Pérez, A. Pazos, and D. Nieto, "Fabrication and characterization of a cell electrostimulator device combining physical vapor deposition and laser ablation," 2017.
- [5] C. Jalayondeja, W. Jalayondeja, J. Suttiwong, P. E. Sullivan, and D. L. H. K. Nilanthi, "Physical activity, self-esteem, and quality of life among people with physical disability," *Southeast Asian J. Trop. Med. Public Health*, 2016.
- [6] F. Gaese, F. Häßler, and M. Menzel, "Intellectual Disability," *Fortschritte der Neurologie Psychiatrie*. 2019.
- [7] World Health Organisation, "Depression and other common mental disorders: global health estimates," *World Heal. Organ.*, 2017.
- [8] M. Piquart and J. P. Pfeiffer, "Solving Developmental Tasks in Adolescents with a Chronic Physical Illness or Physical/Sensory Disability: A Meta-analysis," *Int. J. Disabil. Dev. Educ.*, 2015.
- [9] G. A. and S. S., "Inclusive research and people with profound and multiple disability," *J. Intellect. Disabil. Res.*, 2019.
- [10] S. Ramdas and L. Servais, "New treatments in spinal muscular atrophy: an overview of currently available data," *Expert Opinion on Pharmacotherapy*. 2020.
- [11] S. Messina and M. Sframeli, "New Treatments in Spinal Muscular Atrophy: Positive Results and New Challenges," *J. Clin. Med.*, vol. 9, no. 7, p. 2222, 2020.
- [12] J. Li et al., "MiR-29b contributes to multiple types of muscle atrophy," *Nat. Commun.*, 2017.
- [13] Beurer TENS/EMS electrostimulation, "TENS/EMS | beurer," beurer, 2020. [Online]. Available: <https://www.beurer.com/web/gb/products/medical/electrostimulation/tens-ems/>. [Accessed: 01-Sep-2020].
- [14] J. Day and J. Newman, "The effect of neuromuscular electrical stimulation on function outcome measures following muscle fatigue: A systematic review," *Current Orthopaedic Practice*. Lippincott Williams and Wilkins, 2020.
- [15] J. Bílý, J. Cacek, and T. Kalina, "Electroestimulation: Part of the warm-up before the performance in counter movement jump," in *10th International Conference on Kinanthropology*, 2016, p. 131.
- [16] V. Esteve et al., "The effect of neuromuscular electrical stimulation on muscle strength, functional capacity and body composition in haemodialysis patients," *Nefrologia*, 2017.
- [17] P. Lopès, F. Rimbault, M. Scheffler, C. André, M. C. Cappelletti, and P. Marès, "Étude prospective multicentrique randomisée évaluant l'intérêt de l'électrostimulation intravaginale à domicile après rééducation périméale pour incontinence urinaire," *Gynecol. Obstet. Fertil.*, 2014.
- [18] F. Brunetti, Á. Garay, J. C. Moreno, and J. L. Pons, "Enhancing functional electrical stimulation for emerging rehabilitation robotics in the framework of hyper project," in *IEEE International Conference on Rehabilitation Robotics*, 2011.
- [19] T. Araújo, N. Nunes, and H. Gamboa, "Miniaturized wireless controlled electrostimulator," in *BIODEVICES 2012 - Proceedings of the International Conference on Biomedical Electronics and Devices*, 2012.
- [20] B. M. Vladimirovich, S. D. Andreyevich, B. L. Vladimirovna, and S. A. Leonidovich, "Development of the mobile application for control of the neuro-electrostimulator of type 'SYMPATHOCOR-01' using apache cordova," in *Proceedings - 2018 Ural Symposium on Biomedical Engineering, Radioelectronics and Information Technology, USBEREIT 2018*, 2018.
- [21] H. Buchwald, "Lab Experiences with IEC 60601-1-2 4th Edition," in *2018 IEEE Symposium on Electromagnetic Compatibility, Signal Integrity and Power Integrity, EMC, SI and PI 2018*, 2018.
- [22] V. H. Goh and Y. W. Hau, "Android-based mobile application for home-based electrocardiogram monitoring device with google technology and bluetooth wireless communication," in *2018 IEEE EMBS Conference on Biomedical Engineering and Sciences, IECBES 2018 - Proceedings*, 2019.
- [23] T. Adiono, S. F. Anindya, S. Fuada, K. Afifah, and I. G. Purwanda, "Efficient Android Software Development Using MIT App Inventor 2 for Bluetooth-Based Smart Home," *Wirel. Pers. Commun.*, 2019.
- [24] C. Tame Cuba, "Diseño e implementación de un dispositivo electroestimulador portátil utilizando un microcontrolador e interfaz gráfica para reducir el estrés laboral de los trabajadores administrativos de la empresa Medinet SAC," 2019.
- [25] W. Kemmler, "Muscular Strain of Different Whole-Body Electromyostimulation (WB-EMS) Protocols - A Crossover Study with Athletes without Experience in WB-EMS," *Phys. Medizin Rehabil. Kurortmedizin*, 2020.



# Dual Annular Ring Coupled Stacked Psi Shape Patch Antenna for Wireless Applications

K. Mahesh Babu<sup>1</sup>

Research Scholar, Dept. of ECE  
KL Deemed to be university  
KLEF, Green Fields, Vaddeswaram  
Guntur, Andhra Pradesh, India

T.V. Rama Krishna<sup>2</sup>

Professor, Dept. of ECE  
KL Deemed to be university  
KLEF, Green Fields, Vaddeswaram  
Guntur, Andhra Pradesh, India

**Abstract**—The paper aims to design and analyze an annular ring coupled stacked Psi shaped patch antenna with coplanar waveguide (CPW) feed technique operating for dual band frequency applications. The proposed model comprises of stacked Psi shapes resonating for lower order frequency. The second order resonating band was obtained through capacitively coupled overlapped annular rings. The geometrical dimensions of the proposed model are  $3.5 \times 2$  (L\*W) based on lower order resonating band. The design and simulations were performed using DS CST Microwave Studio suite. The model achieves dual resonant bands, (2.19- 2.68) GHz with impedance bandwidth 490 MHz and (5.569 – 6.09) GHz with 530 MHz impedance bandwidth. The center frequencies are 2.42 GHz and 5.815 GHz with return loss -28.97 dB and -28.99 dB respectively. The design exhibited a maximum gain of 5 dB with bidirectional and omni directional patterns in E and H- planes. The axial ratio at the two resonating bands was less than 3 dB. Parametric analysis was performed for reflection co-efficient on geometric variables like ground width, ground length and permittivity. From (3-5) GHz frequency range, a perfect notch band was also exhibited. Simulated and measured results have shown a good concurrence. The model was suitable for WLAN (Wireless Local Area Network) and ISM (Industrial, Scientific and Medical) Band applications.

**Keywords**—Annular ring; stacked psi shape; WLAN; ISM band

## I. INTRODUCTION

Modern era of wireless communications has begun with the implementation of Micro Strip Patch Antennas (MSPAs) for transmission or reception of EM waves replacing the conventional antennas. Despite of their advantages, MSPAs have numerous disadvantages like narrow bandwidth, low gain, radiation loss, etc. To overcome these drawbacks, various techniques have been implemented in the design of MSPAs [1, 2, 3, 4] for performance improvement. Out of these techniques, coupling mechanism [5] have shown good results in enhancing the features like multi-band, reduction in Radiation Loss, high gain as well as directivity. The coupled structures have to be chosen based on the driven elements so that performance of the MSPA improves. Annular Ring structures [6, 7, 8, 9, 10] as coupling elements have provided striking progress in the operation of MSPAs. Out of numerous wireless applications, commercial frequency bands like WLAN (2.4/ 5.8 GHz), ISM band (2.45/ 5.8 GHz) and WiMAX (2.5 GHz) have a significant prominence in today's communication systems. A heart shape antenna with planar

AMC on Frequency selective surface (FSS) was designed in [11] for WiMAX and WLAN Applications. Annular Ring coupled by monopolar broadband circular patch antenna with short vias was presented in [12] to generate multi resonant modes for WLAN applications. Annular ring structure with slot coupled square patch was implemented in [13] for GPS and SDARS applications. A compact asymmetric Coplanar waveguide fed SRR patch antenna [14] was proposed for WLAN/WiMAX Applications. A detail mathematical analysis and experimental verification on annular ring patch antennas with shorted wires modelled in [15]. For the proposed applications numerous various shapes and structures of patch antennas have been studied and surveyed [16, 17, 18, 19, 20, 21]. A compact stacked psi shaped patch antenna with a coplanar waveguide feed is proposed in this paper operating for WLAN/WiMAX/ISM band applications. The desired bands were obtained through dual annular ring coupling, improving the antenna performance. In the further description of the paper, the design geometry as well as design development was depicted followed by mathematical analysis, parametric analysis, comparison of measured and simulated parameters like reflection co-efficient, radiation patterns and 3D gain plots were also studied. The simulation results of the proposed model were obtained using Dassault Systems CST studio suite and measurements using combinational analyzer in an anechoic chamber.

## II. ANTENNA DESIGN AND ANALYSIS

### A. Antenna Design and Geometry

The design development of the proposed antenna is shown in Fig. 1. A stacked psi shaped structure coupled with dual annular rings and coplanar waveguide feed is fabricated on a substrate with permittivity  $\epsilon_r$  of 2.0, loss tangent 0.009 and thickness  $h$  of 0.127 cm. In addition to this, the proposed model was also analyzed for FR-4 substrate with permittivity  $\epsilon_r$  of 4.3, loss tangent 0.009 and thickness of  $h$  of 0.156 cm.

The arms of the stacked psi shapes have different dimensions with  $X_p$  as the widths of the side arms and  $X_{p1}$  is the width of middle arm. All the arms of the psi shape have a length of  $Y_p$ . The separation between the two psi shapes is equal to length of the arm ( $Y_{p1}=Y_p$ ). To enhance proper impedance matching, two overlapped annular rings are coupled the stacked psi shaped with outer radii of  $R_o$  and Inner radii or  $R_i$ . The separation between the two centers of

the coupled rings is maintained as  $3 \cdot R_i$  so the two rings will coincide to their widths which can be etched in further design process. A circular ring slot was introduced in each coupled ring to increase the capacitive effect which further improves the coupling phenomena. The geometry of the proposed antenna is shown in Fig. 2(a). The geometry variables are represented in Fig. 2(b) and their optimized values are tabulated in Table I.

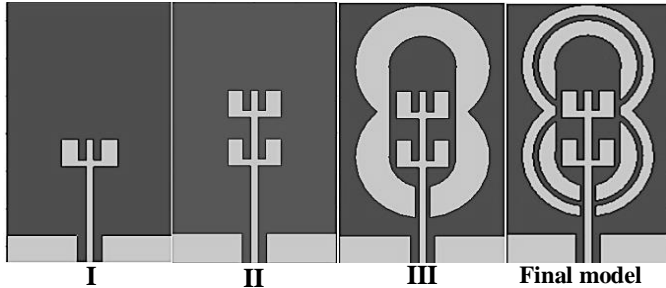


Fig. 1. Design Development of the Proposed Antenna.

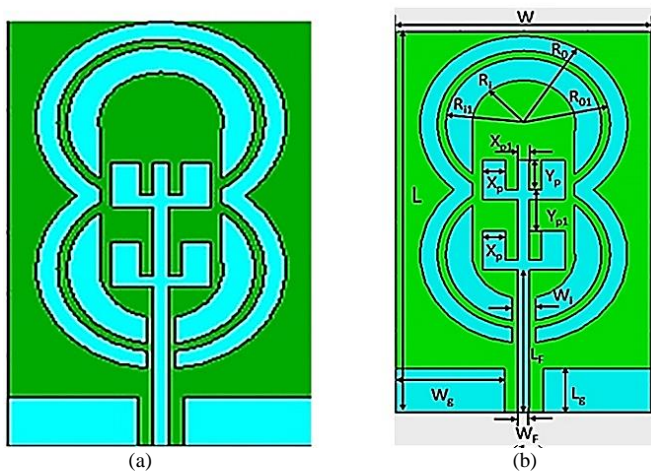


Fig. 2. (a) Geometry of the Proposed Model. (b) Geometry Parameters of the Proposed Antenna.

TABLE I. GEOMETRY PARAMETER VALUES OF THE PROPOSED MODEL

| Parameter    | Value(cm) | Parameter | Value(cm) |
|--------------|-----------|-----------|-----------|
| L            | 3.5       | $W_f$     | 0.09      |
| W            | 2         | $W_1$     | 0.18      |
| $\epsilon_r$ | 2         | $L_g$     | 0.4       |
| h            | 0.127     | $W_g$     | 0.85      |
| $R_0$        | 0.812     | $X_p$     | 0.18      |
| $R_i$        | 0.406     | $X_{p1}$  | 0.09      |
| $R_{01}$     | 0.67      | $X_{p2}$  | 0.1       |
| $R_{11}$     | 0.6       | $Y_p$     | 0.27      |
| $L_f$        | 1.31      | $Y_{p1}$  | 0.27      |

### B. Electrical Equivalent Circuit

The equivalent circuit of the proposed model was determined based on the transmission line model technique. The total structure of the patch antenna is represented in its equivalent electrical lumped parameters. The Electro Magnetic force (EMF) induced in the patch is considered as Inductance (L) and the electrostatic force between the copper material and dielectric mediums (air and duroid) is considered as capacitive effect (C). The resistive nature of the patch (R) is neglected as the calculated resistance is very small compared with other two passive effects. The equivalent circuit of the proposed model is shown in Fig. 3.

The stacked psi shape provides the impedance ( $Z_1$ ) with series LC Circuit resonating for Zeroth Order Resonance (ZOR) and the addition of coupled annular ring shape makes the structure to resonate for First Order Resonance (FOR) with an impedance ( $Z_2$ ) forming parallel resonant circuit. The electrical equivalent block diagram for stacked psi shape using passive components is represented in Fig. 4. The arms of psi shape provide inductive effect. The capacitive effect is obtained through the separation between the two arms of psi shape as shown in Fig. 4(b). Two psi shapes are connected by using a microstrip line which provides inductance ( $Z_l$ ) as shown in Fig. 4(a).

The total impedance of the stacked psi shaped arm is given by

$$Z_1 = 2 \cdot Z_{p1} + Z_l \quad (1)$$

The impedance of the psi shape ( $Z_{p1}$ ) in (1) is given by

$$Z_{p1} = \frac{j\omega [L_3 - \omega^2 (L_1 + L_2) \cdot CL_3]}{1 - \omega^2 (L_1 + L_2)C + 2L_3C} \quad (2)$$

$$Z_l = j\omega L_4 \quad (3)$$

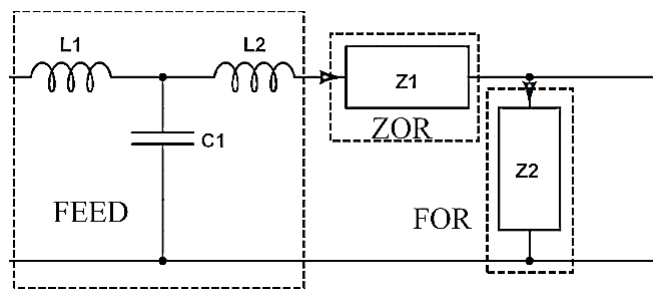


Fig. 3. Electrical Equivalent Circuit of the Proposed Model.

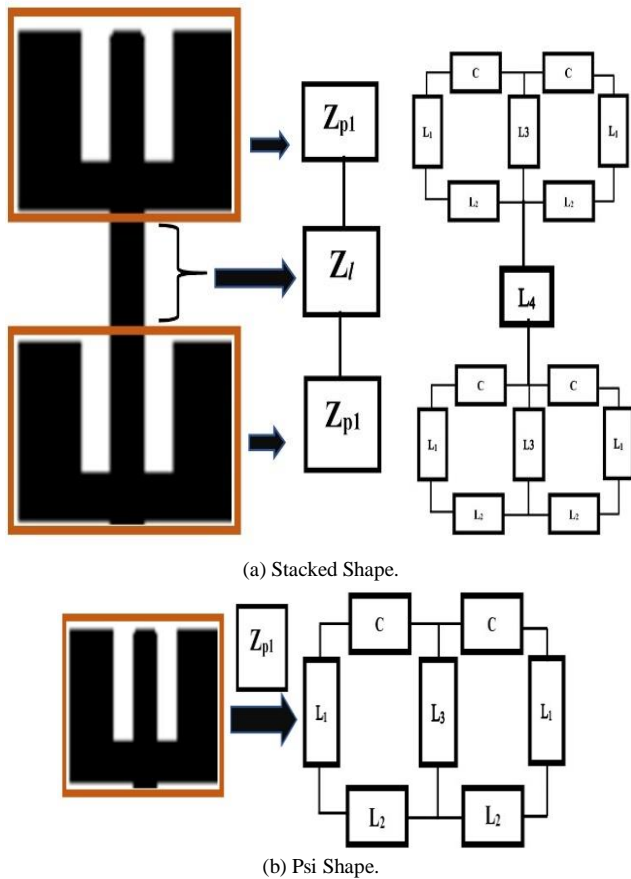


Fig. 4. Electrical Equivalent Block Diagram.

The inductance and capacitance values [22, 23] of (3) can be calculated using the following formulae:

$$L = \begin{cases} \frac{377\pi l}{C_0 \ln \left[ 2 * \frac{1 + \sqrt{1 - \frac{d^2}{(2w_1 + d)^2}}}{1 - \sqrt{1 - \frac{d^2}{(2w_1 + d)^2}}} \right]} & 0 < \frac{d}{2w_1 + d} \leq \frac{1}{\sqrt{2}} \\ \frac{120l}{C_0} \ln \left[ 2 * \frac{1 + \sqrt{\frac{d}{2w_1 + d}}}{1 - \sqrt{\frac{d}{2w_1 + d}}} \right] & \frac{1}{\sqrt{2}} < \frac{d}{2w_1 + d} \leq 1 \end{cases} \quad (4)$$

$$C = \begin{cases} \frac{\epsilon_r l * \ln \left[ \frac{2}{\sqrt{1 - \frac{d^2}{(2w_1 + d)^2}} - 1} \left( \sqrt{1 - \frac{d^2}{(2w_1 + d)^2}} + 1 \right) \right]}{377\pi C_0} & 0 < \frac{d}{2w_1 + d} \leq \frac{1}{\sqrt{2}} \\ \frac{\epsilon_r l}{120C_0 \ln \left[ \frac{2}{\sqrt{\frac{d}{2w_1 + d}} - 1} \left( \sqrt{\frac{d}{2w_1 + d}} + 1 \right) \right]} & \frac{1}{\sqrt{2}} < \frac{d}{2w_1 + d} \leq 1 \end{cases} \quad (5)$$

Where  $d$  is separation between the arms of the psi shape arm,  $w_1$  is width of the psi shape arm,  $l$  is the length of the arm in psi shape,  $C_0$  is the velocity of light and  $\epsilon_{re}$  is the effective permittivity of the patch antenna in (4) and (5).

$$Z_1 = \frac{j\omega [2 * L_3 + L_4 + L_3 L_4 C - \omega^2 [(L_1 + L_2)(L_4 + 2L_3 C)]]}{1 - \omega^2 (L_1 + L_2) C + 2L_3 C} \quad (6)$$

Making the impedance part to zero (6) for resonance condition, we get.

$$f_0 = \frac{1}{2\pi} \sqrt{\frac{2L_3 + L_4 + L_3 L_4 C}{(L_1 + L_2)(L_4 + 2L_3 C)}} \quad (7)$$

Equation (7) represents resonant equation for the proposed patch structure providing 2.4 GHz at ZOR which will be considered as the fundamental resonant frequency.

### III. RESULTS AND DISCUSSION

#### A. Return Loss

Various parameters of the proposed mode were studied and analyzed through simulation and practical measurements. The reflection co-efficient parameter analysis with respect to frequency variation was considered for the study for the design development is shown in Fig. 5. Apart from single psi shape, all the iterations up to the final model have shown dual band response. All the iterations have resonated for ZOR band as it solely depends on the stacked psi shape. Although iteration III has shown least return loss ( $S_{11}$ ) value, the center frequency is not desirable.

The fabricated prototype of the proposed model is shown in Fig. 6 and the measurement setup for the prototype antenna is shown in Fig. 7. The simulated and measured reflection co-efficient results of the annular ring coupled stacked psi shape is presented in Fig. 8. The patch antenna was designed and simulated in CST studio suite. The antenna has resonated for dual frequency bands with -10 dB impedance bands (2.19 – 2.68) GHz and (5.569 – 6.09) GHz with 490 MHz and 530 MHz bandwidths, respectively. The center frequencies have a reflection co-efficient of -28.97dB at 2.42 GHz and -28.99 dB at 5.815 GHz. The measured results have shown minimal variation with simulated values exhibiting the same dual resonant bands with (2.09 to 2.66) GHz and (5.49 – 6.12) GHz frequency bands with bandwidths 570 MHz and 630 MHz respectively. The return loss at center frequencies are -25.21 dB at 2.4 GHz and -23.21 dB at 5.815 GHz. Apart from these, the antenna was also fabricated on Fr-4 substrate and comparison was made between simulated and measured values. The main reason for choosing Fr-4 substrate is due to its economical factor and most of the commercial applications use patches with this substrate for wireless communication media. The comparison of different parameters of patch antenna on these substrates was presented in Table II.

#### B. Ground Analysis

To analyze the behavior of the proposed model, parametric analysis was carried out ground dimensions of the patch antenna. The ground length ( $L_g$ ) and ground width ( $W_g$ ) of the

patch antenna were varied and the reflection co-efficient ( $S_{11}$ ) was observed for the variations as shown in Fig. 9.

When the length of ground varies, there is no much deviation on the ZOR center frequency (2.4 GHz) as it mainly depends on the stacked psi shape. The center frequency of FOR deviates towards the higher frequency as the ground length ( $L_g$ ) decreases. This is due to decrease in the cross-sectional area of the feed capacitance. In the case of ground width ( $W_g$ ) variation, the FOR-frequency band deviates to the higher frequencies as the coupling existing between the feed and ground weakens. The parametric analysis was carried out on ring slot width  $d$ . The reflection co-efficient curve for slot width variation is presented in Fig. 10.

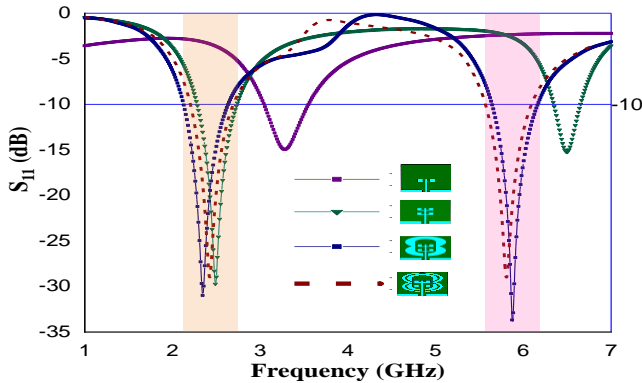


Fig. 5. Reflection Co-efficient Vs Frequency Characteristics for Design Development.

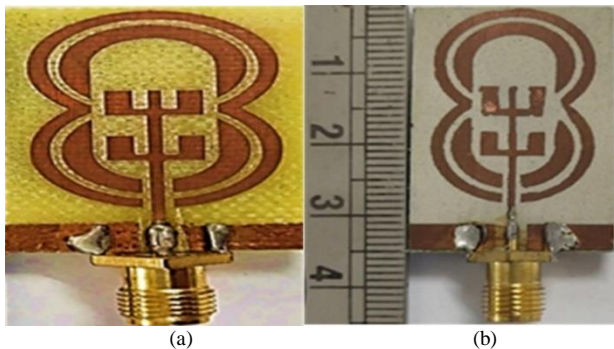


Fig. 6. Fabricated Prototype of the Proposed Patch Antenna (a) on FR-4 Substrate  $\epsilon_r = 4.3$  (b) on Rogers RT Duroid  $\epsilon_r = 2.0$ .

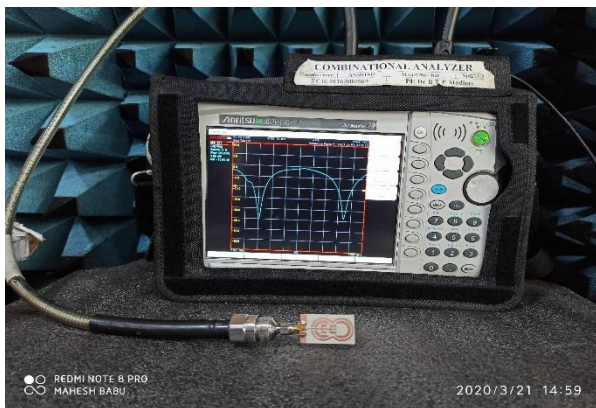


Fig. 7. Photograph of Measurement Setup for the Fabricated Prototype with Measured Reflection Co-efficient Curve.

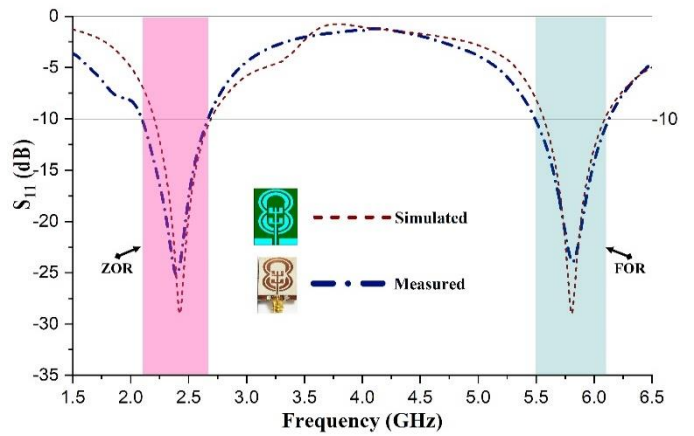
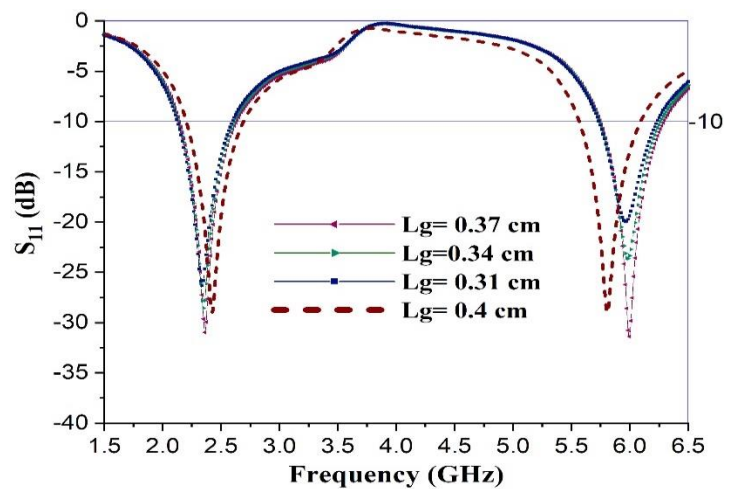
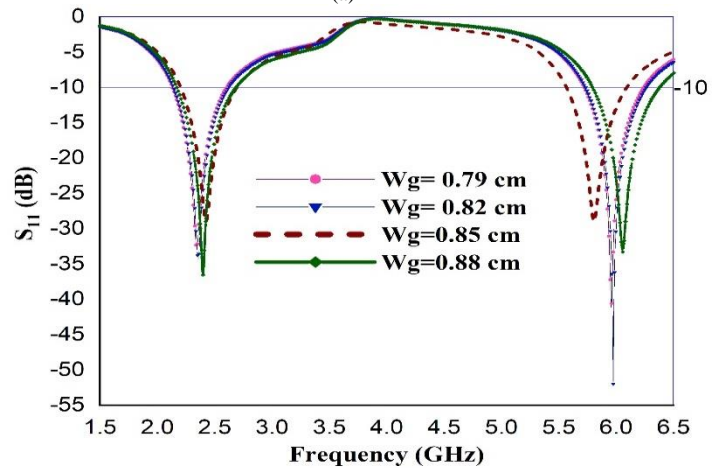


Fig. 8. Simulated and Measured Reflection Co-efficient ( $S_{11}$ ) Curves of the Proposed Model



(a)



(b)

Fig. 9. Reflection Co-efficient ( $S_{11}$ ) Curve for Ground Analysis (a) Length ( $L_g$ ) Variation (b) Width ( $W_g$ ) Variation.

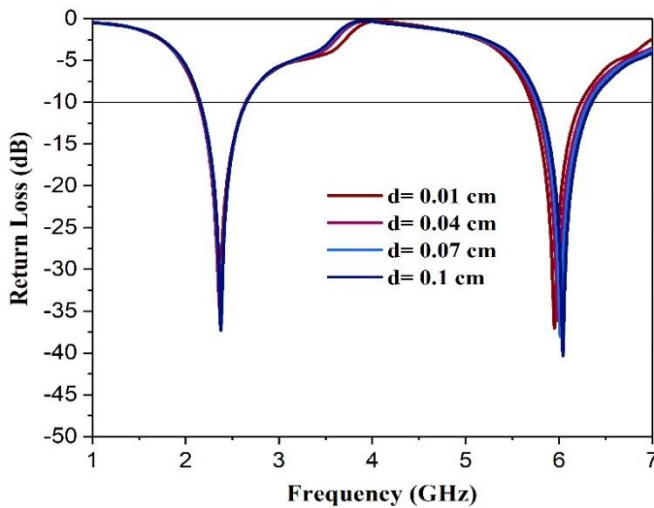


Fig. 10. Reflection Co-efficient Curve for Ring Slot width Variation.

### C. Substrate Analysis

The substrate analysis was carried out on the patch antenna for other substrates like FR-4 and polyimide. The reflection co-efficient ( $S_{11}$ ) characteristics for various substrates is presented in Fig. 11. All these substrates have commonly resonated at ZOR band. The patch antenna has commonly resonated for dual bands for the considered substrates. The polyimide substrate has resonated for two bands namely 2.1 GHz and 5.2 GHz while the FR-4 substrate has 2.0 GHz and 5.1 GHz resonating bands. The response curve shifted towards the lower frequencies as the permittivity increases as the capacitance effect increases. The comparison between the various parameters for the three substrates is presented in Table II. The rogers RT duroid material has shown reliable and precise results than the other two substrates.

### D. Axial Ratio

The axial ratio defines the capability of a patch antenna to exhibit circular polarization. If the resonating frequency of a patch antenna has axial ratio less than 3 dB, the patch is said to have circular polarization which is mostly desirable for wireless applications. The simulated axial ratio response curve with respect to frequency was plotted in Fig. 12. The center frequencies of ZOR and FOR bands have axial ratios less than 3dB i.e., 1.5 dBi at 2.4 GHz and 1.58 dBi at 5.815 GHz.

### E. Radiation Patterns

The radiation patterns are simulated and measured for the proposed patch antenna at both operating frequencies. The patterns are observed in all the corresponding XZ, YZ and XY planes as shown in Fig. 13. At 2.4 GHz frequency, the XZ-plane has omnidirectional radiation whereas bi-directional radiation pattern can be observed for both YZ and XY planes with a gain difference between them. The main lobe direction of the YZ-plane radiation is at  $2^\circ$  with a -3dB angular width of  $87.4^\circ$ . XY-plane radiation has  $87.8^\circ$  angular bandwidth radiating main lobe at  $178^\circ$ . In the case of higher order frequency 5.815 GHz, the XZ- plane has semi omnidirectional radiation pattern with -3dB angular of  $131^\circ$ . The radiation patterns in YZ and XY planes are in butterfly shape

with angular widths of  $59.2^\circ$  and  $56.6^\circ$  respectively where as the main lobe directions are  $28^\circ$  and  $34^\circ$ .

### F. 3D Gain Plots

Fig. 14 represents the 3-Dimensional gain plot of the proposed model for the center frequencies of ZOR and FOR. At ZOR frequency band, the radiation is almost omnidirectional for all the frequencies with a peak gain of 5 dBi. While the FOR-frequency band exhibits bi-directional with butterfly like shape having peak gain of 4.45 dBi.

### G. Surface Currents

The gain of the patch antenna depends on the surface currents. The propose model has major current distribution on the edges of the shape with minimum surface currents on the surface there by improving the gain of the antenna. At 2.4 GHz, the maximum surface current is 72 A/m having current distributions on the feed, outer edges and ground. Similarly, for 5.815 GHz frequency, the maximum current is 110 A/m with surface currents propagating on the surface between two psi shapes and outer edges of coupled annular ring. The surface current distributions of the model are presented in Fig. 15.

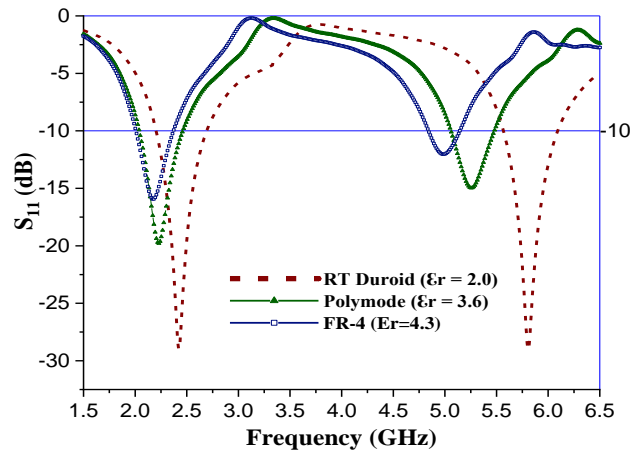


Fig. 11. Reflection Co-efficient Curve for Various Substrates.

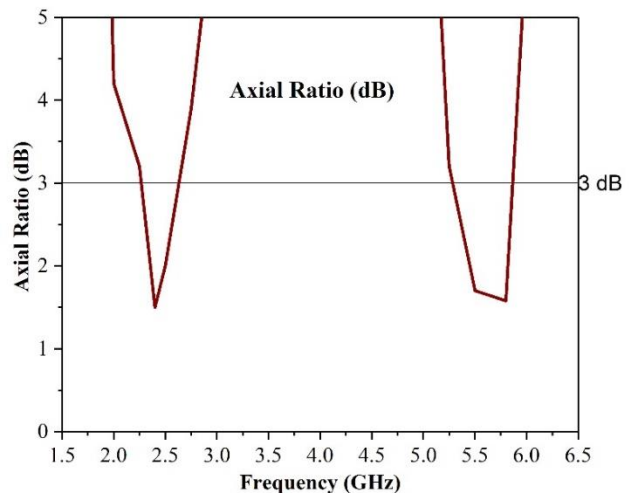


Fig. 12. Axial Ratio Response Curve for the Proposed Model.

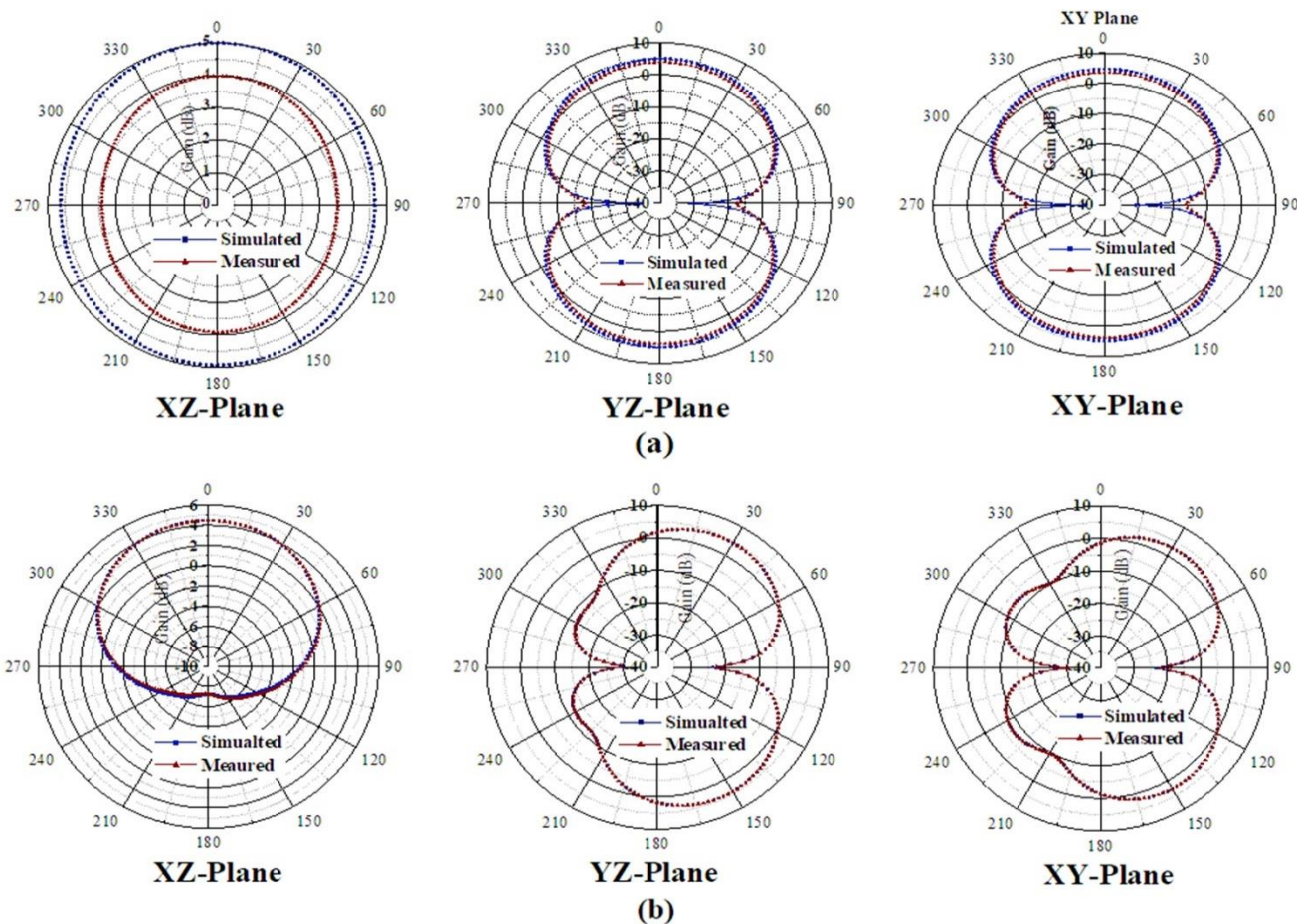


Fig. 13. Radiation Patterns of Proposed Model in XZ, YZ and XY Planes at (a) 2.4 GHz (b) 5.815 GHz.

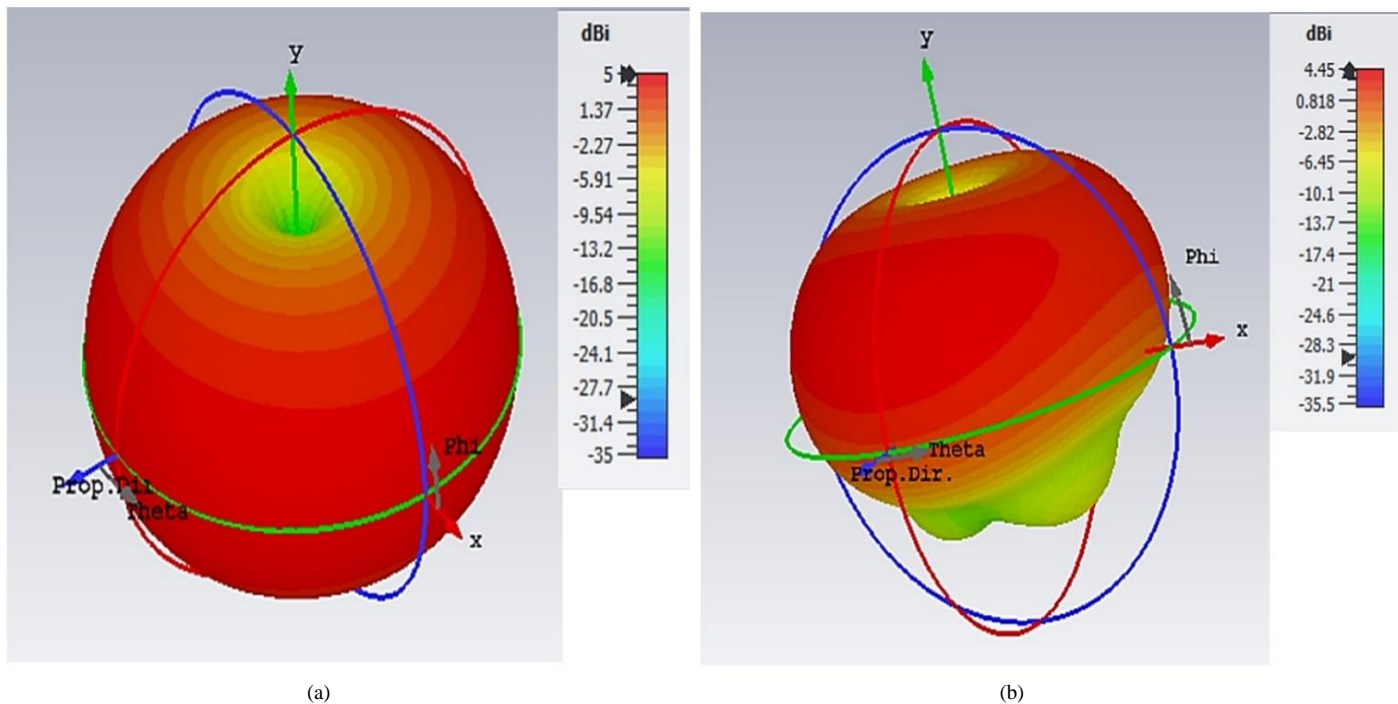


Fig. 14. 3D Gain Plots of Proposed Model (a) 2.4 GHz (b) 5.815 GHz.

TABLE II. GEOMETRY PARAMETER VALUES OF THE PROPOSED MODEL

| Substrate                                               | Center Frequency (GHz) | Reflection coefficient (dB) | Bandwidth (MHz)    | Bandwidth (%) | Gain (dBi)   |
|---------------------------------------------------------|------------------------|-----------------------------|--------------------|---------------|--------------|
| Rogers RT Duroid<br>( $\epsilon_r = 2.0$ )<br>simulated | 2.42<br>5.815          | -28.9<br>-28.9              | 490 MHz<br>530 MHz | 20.24<br>9.12 | 5.00<br>4.45 |
| RT Duroid<br>( $\epsilon_r = 2.0$ )<br>measured         | 2.4<br>5.815           | -25.2<br>-23.2              | 570 MHz<br>630 MHz | 23.5<br>10.8  | 4.95<br>4.2  |
| FR-4 ( $\epsilon_r = 4.3$ )<br>simulated                | 2.17<br>4.99           | -15.94<br>-12.02            | 370 MHz<br>300 MHz | 17.05<br>6.01 | 2 dB<br>2.28 |
| FR-4 ( $\epsilon_r = 4.3$ )<br>measured                 | 2.32<br>5.24           | -13.35<br>-16.81            | 620<br>460         | 26.72<br>8.77 | 1.8<br>1.72  |
| Polymide<br>( $\epsilon_r = 3.5$ )<br>simulated         | 2.23<br>5.26           | -19.78<br>-14.95            | 420<br>420         | 18<br>7.98    | 2.04<br>2.79 |

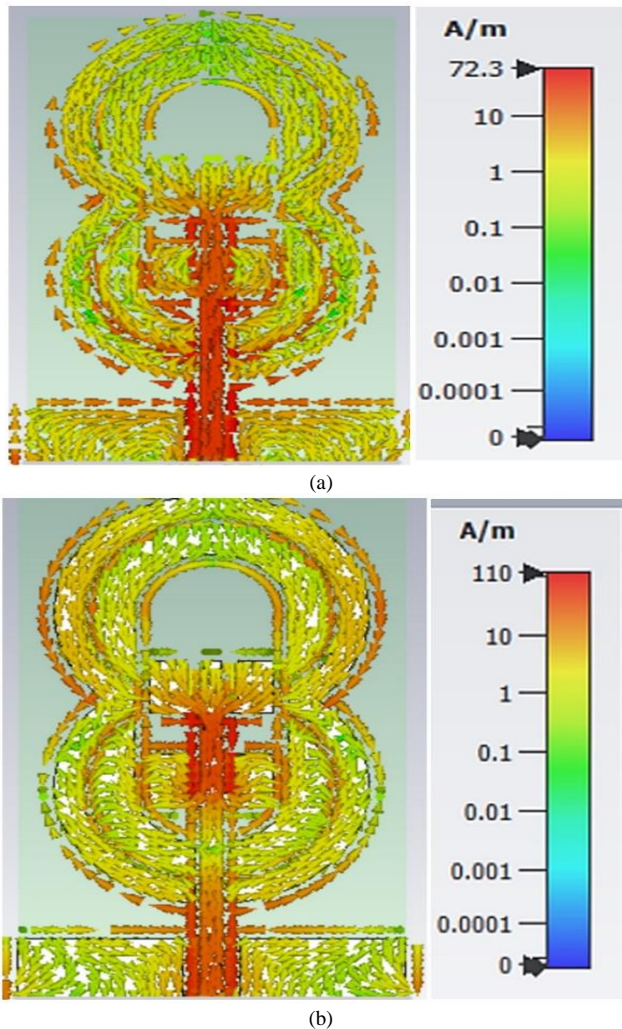


Fig. 15. Surface Current Distribution at (a) 2.4 GHz (b) 5.815 GHz.

#### IV. CONCLUSION

In this paper, a dual annular ring coupled stacked psi shape patch antenna was proposed with dual resonating bands and high gain for wireless applications. The dual annular ring and the ring slot enhance the impedance bandwidth of the patch. The prototype antenna resonates at 2.4 GHz and 5.815 GHz

having reflection co-efficient of -28.9 dB at both frequencies. The impedance bandwidths are 23.5% and 10.85% with respect to center frequencies having measured gains of 5 dBi at 2.4 GHz and 4.45 dBi at 5.815 GHz. Mathematical analysis was carried out to prove ZOR center frequency. A good consistency was observed between the measured and simulated values. The proposed antenna operates for WLAN, ISM band and WiMAX applications.

#### REFERENCES

- [1] Frank Zavosh and James T. Aberle, "Improving the Performance of Microstrip-Patch Antennas," IEEE Antennas and Propagation Magazine, vol. 38, no. 4, pp. 7-12, 1996.
- [2] Hsi-Tseng Chou, Chung-Yi Chung and Yu-Ting Hsiao, "Radiation Performance Improvement of Microstrip Antennas by a Mounted Horn and R-card for the Car Communication Applications," Electromagnetics, vol. 27, no. 1, pp. 9-22, 2007.
- [3] M.K.Abdulhameed, M. Isa, M. Ibrahim, Mowafak. K.Mohsen, S.R.Hashim and Mothana L. Attiah, "Improvement of Microstrip Antenna Performance on Thick and High Permittivity Substrate with Electromagnetic Band Gap," Journal of Advanced Research in Dynamical & Control Systems, vol. 10, no. 4, pp. 661-669, 2018.
- [4] A. K. M. Baki, Md. Nurur Rahman and Shawon Kumar Mondal, "Analysis of Performance-Improvement of Microstrip Antenna at 2.45 GHz Through Inset Feed Method," in International Conference on Advances in Science, Engineering and Robotics Technology 2019 (ICASERT 2019), 2019.
- [5] Yi-Fang Lin, Hua-Ming Chen and Shih-Chieh Lin, "A New Coupling Mechanism for Circularly Polarized Annular-Ring Patch Antenna," IEEE Transactions on Antennas and Propagation, vol. 56, no. 1, pp. 11-16, 2008.
- [6] G. B. G Tilak, Sarat K. Kotamraju, Boddapati T. P. Madhav, K. CH. Sri Kavya and M. Venkateswara Rao, "Dual Sensed High Gain Heart Shaped Monopole Antenna with Planar Artificial Magnetic Conductor," Journal of Engineering Science and Technology, vol. 15, no. 3, pp. 1952-1971, 2020.
- [7] Juhua Liu, Shaoyong Zheng, Yuanxin Li and Yunliang Long, "Broadband Monopolar Microstrip Patch Antenna With Shorting Vias and Coupled Ring," IEEE Antennas and Wireless Propagation Letters, vol. 13, pp. 39-42, 2014.
- [8] M. M. Bilgic and K. Yegin, "Modified Annular Ring Antenna for GPS and SDARS Automotive Applications," IEEE Antennas And Wireless Propagation Letters, vol. 15, pp. 1442-1445, 2016.
- [9] Binod K. Kanaujia and Babau R. Vishvakarma, "Analysis of Two-Concentric Annular Ring Microstrip Antenna," Microwave and Optical Technology Letters, vol. 36, no. 2, pp. 104-108, 2003.
- [10] Mahesh Babu Kota and T.V. Rama Krishna, "Design Analysis and Performance Evaluation of Annulus Patch Antennas," International Journal of Recent Technology and Engineering (IJRTE), vol. 8, no. 3, pp. 3116-3122, 2019.

- [11] D.M. Kokotoff, R.B. Waterhouse, C.R. Birtcher and J.T. Aberle, "Annular Ring Coupled Circular Patch with enhanced performance," IEEE Electronic Letters, vol. 33, no. 24, pp. 2000-2001, 1997.
- [12] S.H. Al-Charchafchi, W.K. Wan Ali and S. Sinkere, "A Stacked Annular-ring Microstrip Patch Antenna," in IEEE Antennas and Propagation Society International Symposium 1997, 1997.
- [13] Binod Kumar Kanaujia and Anil Kumar Singh, "Analysis and Design of Gap-Coupled Annular Ring Microstrip Antenna," International Journal of Antennas and Propagation, vol. 2008, no. 1, pp. 1-5, 2008.
- [14] K. K. Naik, "Asymmetric CPW-fed SRR Patch Antenna for WLAN/WiMAX Applications," International Journal of Electronics and Communications, 2018.
- [15] Stanislav B. Glybovski, Valeri P. Akimov and Alexander E. Popugaev, "Analytical Study of Annular-Ring Microstrip Antennas," IEEE Transactions on Antennas and Propagation, vol. 62, no. 6, pp. 3348-3353, 2014.
- [16] "A Quad-Band Dual-Sense Circularly-Polarized Square-Ring Antenna for Multi-Functional Wireless Applications," IEEE Access, vol. 7, pp. 149634-149640, 2019.
- [17] Q. Gong, Meizhen Xiao, Peng Luo and Yuehui Cui, "Dual-band horizontally/dual polarized antennas for WLAN/ISM applications," Microwave and Optical Technology Letters, vol. 62, no. 3, pp. 1-11, 2019.
- [18] D. K. Naji, "Miniature Slotted Semi-Circular Dual-Band Antenna for WiMAX and WLAN Applications," Journal of Electromagnetic Engineering and Science, vol. 20, no. 2, pp. 115-124, 2020.
- [19] Karteek Viswanadha and Nallanthighal Srinivasa Raghava, "Design and Analysis of a Multi-band Flower Shaped Patch Antenna for WLAN/WiMAX/ISM Band Applications," Wireless Personal Communications, pp. 863-887, 2020.
- [20] Z. DING, Z. DAN and M. CHUNYU, "Broadband Antenna Design With Integrated CB-CPW and Parasitic Patch Structure for WLAN, RFID, WiMAX, and 5G Applications," IEEE Access, vol. 8, pp. 42877-42883, 2020.
- [21] K. Kumar Naik, S. Sandhya Rani, G. Dattatreya and P. Ravi Kumar, "Design of Inverted U-shaped Radiating Patch Antenna for LTE/WiMAX Applications," in IEEE Indian Conference on Antennas and Propagation (InCAP), Hyderabad, 2018.
- [22] C. R. Paul, Analysis of Multiconductor Transmission Lines, 2nd Edition, Wiley-IEEE Press, 2007.
- [23] C. R. Paul, Inductance: Loop and Partial, Wiley-IEEE Press, 2010.

#### AUTHORS' PROFILE



Mr. K. Mahesh Babu received his bachelor's degree from JNTUA, Anantapur in 2011, Master's Degree in VLSI System Design from JNTUA, Anantapur in 2015. He worked as an Assistant Professor from Aug, 2011 to Nov 2012 and July, 2015 to Jan 2018 with total experience of 3 years and 10 months. He published 6 articles in National/International Journals/ Conferences. He is currently pursuing fulltime PHD in KLEF Deemed to be University, Vaddeswaram since Jan 2018.



Dr. T. Venkata Rama Krishna received his Bachelor's Degree from Acharya Nagarjun a University in 1997, Master Degree (ME) from Bharatiar University in 2000. ME(ECE) with specialization in Communication Systems and PHD Degree in Antenna Measurements, College of Engineering, JNT University, Kakinada in 2011, collaboration with DLRL Hyderabad and had work experience in design, development of Satellite Antennas, Receivers, Jamming Decoys etc. He completed sponsored projects successfully from agencies like UGC, ACITE, as an Investigator. He is a life member of IETE, IE, ISTE, ISI, CRSI, SEMCEI and published 51 articles in National/International Journals/ Conferences. He is currently working as Professor in ECE Department and Director(E-Resources) in KLEF Deemed to be University, Vaddeswaram from 2014 to till date.



# Secure Communication across the Internet by Encrypting the Data using Cryptography and Image Steganography

Dr P Rajesh<sup>1</sup>, Dr Mansoor Alam<sup>2</sup>, Dr Mansour Tahernezehadi<sup>3</sup>, T Ravi Kumar<sup>4</sup>, Vikram Phaneendra Rajesh<sup>5</sup>

Associate Professor, KLEF University, India<sup>1,4</sup>  
Professor, Northern Illinois University, USA<sup>2,3</sup>  
Researcher, KLEF University, India<sup>5</sup>

**Abstract**—Sharing the information has become a facile task nowadays just like one-tap which can take the information to any component of the world. This whole thing transpired over the evolution of the cyber world, which avails to stay connected with the entire world. Due to the wide-spread utilization of the cyber world, it leads a peril of data breaching by some incognito or unauthorized people while it is being sent from one utilizer to another. Unauthorized people can get access to the data and extract utilizable information from it. The confidential data being sent through the web which may get tampered while reaching the other end-utilizer. So, to dispense this data breaching, we can encrypt the data being sent and the receiver can only decrypt the message so that we can conceal the data. It routes a tremendous way to do this, the most popular one is cryptography, and another is steganography. Anteriorly there subsist many ways in these techniques like Image Steganography, Secret key Cryptography, LSB method, and so on which are being used to encrypt data and secure communication. One of the algorithms of cryptography is utilized along with Image Steganography to encrypt the data to ascertain more security which resembles the two-step verification process. In proposed paper we utilized new Huffman coding algorithm in step of the Image Steganography to ascertain that even an astronomically immense data can fit into a minute image. The ciphertext is compressed utilizing Huffman Coding and then it gets embedded into an image utilizing LSB method of Image Steganography in which the least paramount bits of the image are superseded with the data from the antecedent step. We implemented the analytical using python and it shows better compression results with large volumes of data to transfer easily through network.

**Keywords**—Cryptography; image steganography; least significant bits; secure communication; Huffman coding; data encryption; data compression

## I. INTRODUCTION

### A. Encryption

Encryption is a process that a message to be encoded to be private so then it will read by a Specific Person or Specific people [1]. The message in encrypted data is referred to as a secret message that uses an algorithm to enhance more security [2]. A plaintext or a message is converted to ciphertext by using an algorithm that encrypts data and uses a symmetric key that will receive by the destined party to unencrypt or decrypt the encrypted data to grab the message or

information from the ciphertext [3]. There are three types of Encryption, they are:

#### 1) Symmetric Encryption (Fig. 1)

In this encryption, a single key is used for both encryption and decryption, also called secret-key cryptography [4].

In the process of encrypting the message, a Symmetric key is injected into the Encryption.

In the process of decrypting the message, the same key is injected to decrypt the information from the ciphertext [5].

It is mainly used for confidentiality and privacy.

#### 2) Asymmetric Encryption (Fig. 2)

In this encryption, one key is for encryption and another key is for decryption, also called public key cryptography [6].

In the process of encrypting the message, a public key is injected into the Encryption.

In the process of decrypting the message, a private key is injected to decrypt the information from the ciphertext [7][8].

It is mainly used for non-repudiation, authentication, and key exchange.

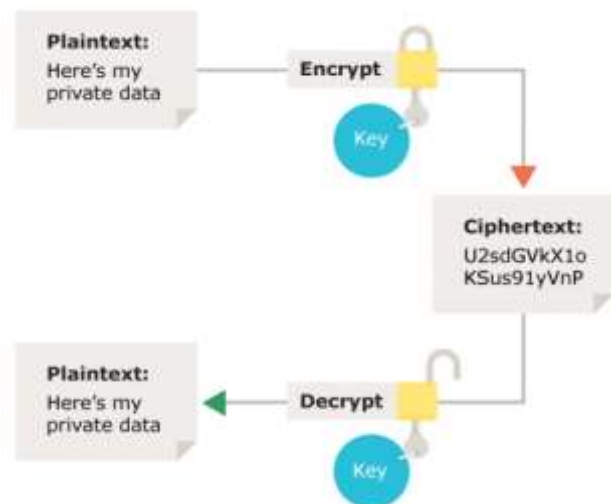


Fig. 1. Symmetric Encryption of Data.

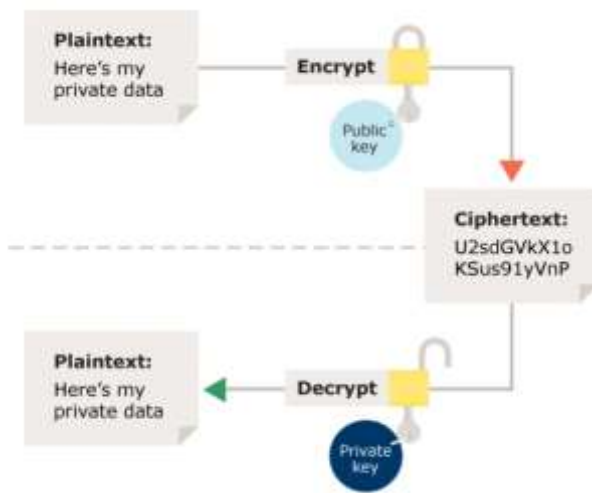


Fig. 2. Asymmetric Encryption of Data.

### 3) Hash Functions

- In the process of encrypting, a mathematical transformation is used to encrypt the information irreversibly by providing a digital fingerprint.
- It is mainly used for message integrity.

### B. Decryption

The process of converting the encoded data to the useful information by following the needs of transformation like algorithm and a shared key or a private key depending on the type of encryption that the information is molded with a ciphertext [9][10] (see Fig. 3). And it is a reverse process of Encryption. To grab the information through a ciphertext an authorized user can only be the person to unscramble the encoded data through a password or a key [11].

### C. Steganography

Steganography is a technique used to hide the top-secret data with an ordinary image or audio or video to avoid the cyberattacks and the hided data is unscrambled at the end receiver [12][13]. The use of steganography is to encrypt the secret message with a Symmetric key using one of the algorithms and this encryption is embedded into an ordinary resource as mentioned above. For computer applications like text, sound, etc. it replaces the unwanted bits at the time of encryption so that the resource that we use will remain same.

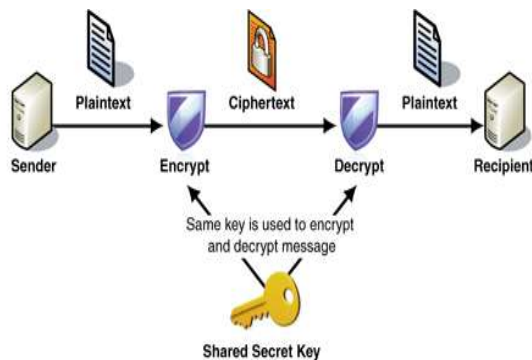


Fig. 3. Process of Encryption and Decryption of Data.

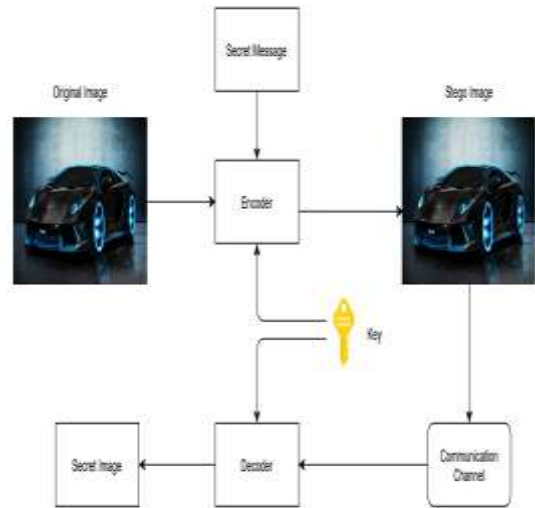


Fig. 4. Formation of Normal Image to a Stego-Image.

If we differentiate the cryptography with steganography the main part that the steganography concentrates on the advancement of security to the secret message that to embedding the bits into any type of digital object will be ordinary to all over the world as the cryptography is masking only on the content of the message and sending to the end receiver it may have some more reveal factor to the world while it is in World Wide Web (WWW) [14][15] (Fig. 4). Steganography can use the combination with encryption, the encrypted data can be inserted into an image or the other normal things and if the case occurs of decrypting the ciphertext the hidden message will remain secure [16].

#### 1) Types of steganography

a) *Direct embedding*: This type of Steganography approach will lead to an increase in the size of the normal file or an ordinary image depending upon the secret message by embedding the secret message into the resource [17].

b) *LSB embedding*: This type has a different approach to solve the above type of embedding, to reduce the size by fitting the bits of a secret message into the unwanted bits or fewer priority bits of available normal objects [18].

There are four types of objects where we can insert the bits:

- Image
- Audio
- Video
- Document

#### 2) Image steganography

Images are the most used resource in steganography. An image is an ordinary object that we use in real life but in computer applications, it is a group of bytes or matrices or pixels also called Digital Images [19][20]. Using these Bytes of an image, a secret message is passed through the network where we can achieve more security. By looking intensely, every byte will contain 8 bits in the image and changing the

least significant bits in every byte will attain to hide the data [21][22]. It may lead to exists a drawback in this technique, if message size in bits exceeds the size of the image then the algorithm will not work for this type of case.

In cryptography, the encrypted data that is the coded data will be visible to the unapproved users, but can't use them unless they decrypt it using appropriate technique whereas, in the steganography, the encrypted data cannot be seen directly, can be seen in digital format, makes unapproved users difficult to tamper the data [23].

The most popular usage of these techniques is encrypting the data with both the flavors like using steganography along with cryptography [24][25]. In this research, an encrypted key is generated with the data at the sender's side using cryptography, and then the data is encrypted into multimedia tools such as image, video, or audio using steganography.

3) Steps involved in this process:

- Encryption key generation with the input data using Cryptography.
- Data encryption using LSB method of Image steganography.
- Data compression using Huffman coding.
- Sending the stego image along with the generated encryption key at the receiver side, retrieve the hidden data in the stego image and then decrypt it using the encryption key.

II. BLOCK DIAGRAM FOR PROPOSED SYSTEM

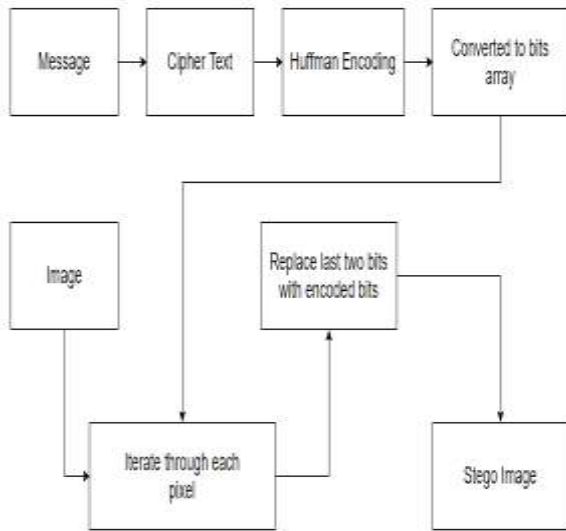


Fig. 5. Block Diagram for Proposed Methodology.

III. IMPLEMENTATION

The main theme is that the message should be seen only by the receiver. So, in this paper, the encryption key is merged to the message and converted to ciphertext so that the one person knows and reads the encryption key and then the ciphertext is hidden inside the image.

A. Encryption Key Generation using Cryptography

Cryptography is a standard method used to encrypt the data, the data say a text is converted some other text in an illegible format called as ciphertext using encrypting algorithms and send the original data along with encryption key, then the receiver should know the decryption key so that the data can be retrieved using that key when it has arrived. Most of the time, those encryption keys are private since the receiver of the data can only use the data.

B. Data Encryption using LSB Method of Image Steganography

Mainly the steganography is used to hide messages inside the image. So many ways are making their way to existing methodology to store the message inside the image. Here, the LSB method means the least significant bits method is used. Every image has so many pixels, each pixel is the smallest individual element of the image. In the color imaging system, color is represented by three or four components such as RGB (Red, Green, Blue), CMYB (Cyan, Magenta, Yellow, and Black). The CMYB is mainly used in printers.

Each pixel is composed of three value RGB having 8-bit values. The rightmost bits have less impact on the image. So, the last two bits are changed, and the result is an altered image also called stego image.

Here, Fig. 6 is an RGB pixel representation. In each 8-bit representation, the last two bits are changed because of having less impact on the resultant image that can be difficult to identify the difference with the naked eye.

Each Image can store only a certain number of bits it can be calculated by the  $(\text{height} \times \text{width} \times (\text{color component})^2) / 8000$  (KB of data).

C. Data Compression using Huffman Coding

Huffman coding is a data compression algorithm. In this algorithm, all the characters are replaced with numbers because the character's bit length is more than the number's bit length. While transmitting the message, a table that maps the character and the number bits of the message will be sent. So after ciphertext is generated, a number will be mapped to each unique character in the message and a mapping function is generated so that all the characters in the message are replaced by that corresponding number, the bit representation of a number is less than the bit representation of character so it can reduce the size of the message to a great extent.

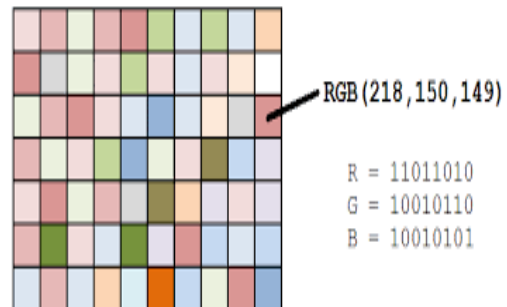


Fig. 6. RGB Pixel Representation.

**Example:**

"Hi, this is the secret message" is the message to be encoded in the image and send it to the receiver, Steganography is the practice of concealing a file, message, image, or video within another file, message, image, or video hence the message remains confidential.

Length of the binary representation of cipher text is:1816 (0.227KB).

Length of the binary representation of cipher text Applying Huffman approach is:1429 (0.1786KB).

**Huffman table for the above message:**

So, the message size is reduced. In this way, a long message can be stored in small images.

**D. Sending the Stego Image along with Generated Encryption Key**

The image generated after the data compression using Huffman coding that is from the step-3 is sent to the receiver along with the encryption key, generated from the step-1.

At the receiver end, this image is then converted to binary bits, and then by the reverse of the Huffman approach, it is decoded as strings then decoded as the original message by using the encryption key.

**E. Results**

Fig. 7 is the image where the message to be stored. Image shape: 1024\*1820\*3 and can store 1397.76 KB of information. Then this image is converted to binary and the last two bits are replaced with message bits using LSB method of image steganography.

Fig. 8 is the final image generated after data compression using Huffman coding that helps to store large information.



Fig. 7. Original Image.



Fig. 8. Stego Image.

|               |          |          |          |          |          |          |
|---------------|----------|----------|----------|----------|----------|----------|
| 1 --> (space) | 2 --> (, | 3 --> A  | 4 --> B  | 5 --> C  | 6 --> D  | 7 --> E  |
| 8 --> F       | 9 --> G  | 10 --> H | 11 --> I | 12 --> L | 13 --> M | 14 --> N |
| 15 --> O      | 16 --> P | 17 --> R | 18 --> S | 19 --> T | 20 --> V | 21 --> W |
| 22 --> Y      |          |          |          |          |          |          |

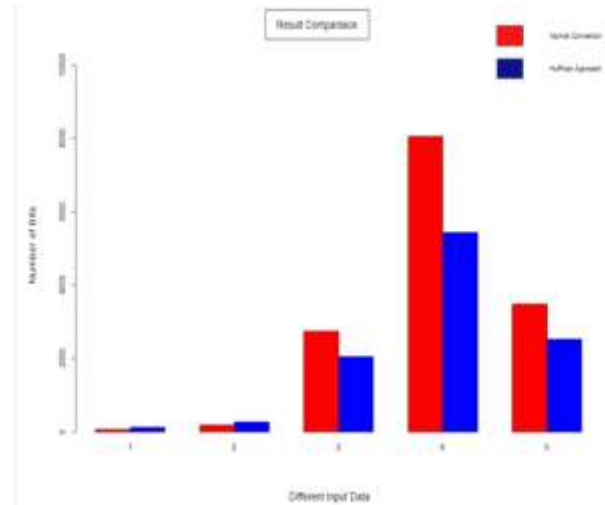


Fig. 9. Histogram Analysis for Steganography.

So, it means this image contains the information, but it seems to look the same as the original image. This is the main advantage of encrypting the data and then send it to the receiver.

Fig. 9 clearly states information about the bits of a Normal Conversion and Huffman Approach Conversion, taking the different sets of data with differences in their sizes by the above graph we can say that the algorithm will reduce the bits by approaching Huffman encoding and decoding method. Conclusion and Future Scope

Encryption of data and Decrypting back is to protect the crucial data that will use mainly by companies to safeguard their data like formulas or particulars of their clients etc., by using this steganography method with the conjunction of cryptography we can accomplish more security to provide for the user. This research came into the action to provide an algorithm to send the message over the expectation through an average resolution image and for a situation where we cannot send a message through image due to the size or the resolution or low pixels quality of the image then our research made the situation easier to handle.

- Multilevel Steganography by fitting the Image steganography into another ordinary image.
- In the future, by using this Huffman optimization method we can reduce the duplicate bytes and assigning every unique byte with a unique symbol and replacing all the duplicate bytes with the unique symbol gives a solution for fitting the heavier Steganography image into an average resolution image.

REFERENCES

- [1] MehtapUlker, Bilgehan Arslan(2018). "A Novel Secure Model: Image Steganography with Logistic Map and Secret Key", IEEE.
- [2] Pooja Chandarana, Prof. Purnima Ahirao. "ADVANCED IMAGE STEGANOGRAPHY", International Journal of Innovative Research in Information Security, Issue 07, Volume 5, (September 2018).
- [3] Huma Jabeen, Professor Abdul Wahid. "Image Steganography using Pseudo-Random Number Generator", International Journal of Advanced Research in Computer Engineering & Technology (IJARCET) Volume 8, Issue 3, March 2019.
- [4] K. Surekha, J. S. S. Sekhar, V. Devi Prasanna, P. Srividya, S. S. S. Anusha, V. Manogna. "Hidden Secrets Behind the Images", International Journal for Research in Applied Science & Engineering Technology (IJRASET), Volume 8 Issue V May 2020.
- [5] Dong Wu. "minimizing distortion in steganography based on image feature", International Journal of Computer Science & Information Technology (IJCSIT) Vol 11, No 1, February 2019.
- [6] Aung Myint Aye. "LSB Based Image Steganography for Information Security System", International Journal of Trend in Scientific Research and Development (IJTSRD) International Open Access Journal, ISSN No. 2456 – 6470, Volume-3, Issue-1, Nov-Dec 2018.
- [7] Urvashi Kodwani, Sakshi Agrawal, JuiDiwale, Samiksha Thakur, Devishree Naidu. "Secure and transparent file encryption system", International Journal of Advance Research, Ideas and Innovations in Technology, Volume 5, Issue 1, 2019.
- [8] Giridhar Maji, Sharmistha Mandal. "Secure and Robust Image Steganography Using a Reference Image as Key", International Journal of Innovative Technology and Exploring Engineering (IJITEE) ISSN: 2278-3075, Volume-8, Issue-7, May,2019.
- [9] Ernest Andreigh C. Centina. "Image Steganography of Multiple File Types with Encryption and Compression Algorithms", Asia Pacific Journal of Multidisciplinary Research, Vol. 5, No. 3, August 2017.
- [10] srishti Rajvanshi, Shrikrishna Sawant, Vedant Tiwari, Anurag Waghmare, ManjiriGogate. "Image Steganography", International Journal for Research in Applied Science & Engineering Technology (IJRASET) ISSN: 2321-9653; IC Value: 45.98; SJ Impact Factor: 7.177 Volume 7 Issue XI, Nov 2019.
- [11] Walaa Ali H. Jumiawi, Haider A. Abbas Mohammed. "Chained QR Keys Generation Based on Chaotic Hybrid Encoding and Fourier Transform Shifting for Image Encryption", DOI 10.5013/IJSSST.a.21.02.09.
- [12] Salah Harb, M. Omair Ahmad, M.N.S Swamy. "Design and hardware implementation of a separable image steganographic scheme using public-key cryptosystem", Electrical and Computer Engineering Department, Concordia University, 1440 De Maisonneuve, Montreal, Canada.
- [13] Abhijeet Bhaskar, Mr. Upendra Kumar Acharya. "Image Steganography Using Modified LSB".
- [14] J. K. Mandal, Debashis Das. "Colour Image Steganography Based on Pixel Value Differencing in Spatial Domain", International Journal of Information Sciences and Techniques (IJIST) Vol.2, No.4, July 2012.
- [15] Anusha T and Venkatesan R, PSG College of Technology, India. "Steganography Based Asymmetric Key Cryptosystem Using Trellis Coded Genetic Algorithm Random Key Generator", International Journal of Embedded Systems and Applications (IJESA), March 2019, Volume 9, Number 1.
- [16] Dr P Rajesh, Dr M Alam, " A Data Science Approach to Football Team Player Selection" at 20th Annual IEEE International Conference On Electro Information Technology (eit2020). July 31 - August 1, 2020, USA. <https://ieeexplore.ieee.org/document/9208331>.
- [17] Dr Dr P Rajesh, Dr M Alam, " Machine Learning and Statistical Analysis Techniques on Terrorism" at The 6th International Conference onFuzzy Systems and Data Mining (FSDM 2020)November 13-16, 2020, Xiamen, China.
- [18] Dr.P.Rajesh, Sai Prasanna " A Forensic Approach To Perform Android Device Analysis " at National Women Conference on Technological Innovations", 2019, Scopus, with Best paper award of conference.
- [19] SK.Wasim Akram, P.Rajesh "Avoiding Cross Site Request Forgery (CSRF) Attack Using TwoFish Security Approach" in International Journal of Computer Trends and Technology.2015.
- [20] P.Rajesh, Dr.G.Narsimha, " Cerebration Of Privacy Preserving Data Mining Algorithms" in International conference on machine learning and data analysis ICMLDA\_ 2014, USA in association with springer, IEEE Explore, DBLP.
- [21] P.Rajesh, Dr.G.Narsimha, "Fuzzy based privacy preserving classification of data streams." in ACM conference (CUBE), Pune, PP: 784-788, 2012, DBLP, ISBN: 978-1-4503-1185-4.
- [22] Sahu, Aditya Kumar; Swain, Gandharba , Data hiding using adaptive LSB and PVD technique resisting PDH and RS analysis, International Journal Of Electronic Security And Digital Forensics,2019, 10.1504/IJESDF.2019.102567.
- [23] Ranjeeth Kumar M , Srinivasu N, Reddy, Advanced hybrid approach to provide privacy for cross-site and XSS attacks in cloud computing, Journal of Advanced Research in Dynamical and Control Systems (2018).
- [24] Srinivasu N, Sahil M, Francis J, Security enhanced using honey encryption for private data sharing in cloud, International Journal of Engineering and Technology(UAE) (2018).
- [25] Balakrishna A, Srinivasu N, Security analysis for control policy in OSNs, ARPN Journal of Engineering and Applied Sciences (2016).

# White Blood Cells Detection using YOLOv3 with CNN Feature Extraction Models

Nurasyeera Rohaziat<sup>1</sup>, Mohd Razali Md Tomari<sup>2</sup>, Wan Nurshazwani Wan Zakaria<sup>3</sup>, Nurmiza Othman<sup>4</sup>

Faculty of Electrical and Electronic Engineering  
Universiti Tun Hussein Onn Malaysia  
Malaysia

**Abstract**—There are several types of blood cancer. One of them is Leukaemia. This is due to leukocyte or white blood cell (WBCs) production problem in the bone marrow. Detection at earlier stage is important so that the patient is able to get a proper treatment. The conventional detection and blood count method is less efficient and it is done manually by pathologist. Thus, there will be a long line to wait for the results and also delay the treatment. A faster detection procedure and technique will have high impact on the real time diagnostic. Fortunately, these problems are able to overcome by making the blood test procedures automatic. One of the effort is the development of deep learning for WBCs detection and classification. In computer aided WBCs detection, the You Only Look Once (YOLO) based platform present a promising outcome. However, the investigation of optimal YOLO structure remains vague. This paper investigate the effect of the deep learning based WBCs detection using You Only Look Once version 3 (YOLOv3) with different pretrained Convolutional Neural Network (CNN) model. The models that been tested are the Alexnet, Visual Geometry Group 16 (VGG16), Darknet19 and the existing YOLOv3 feature extraction model, the Darknet53. The architecture consist of the bounding box for class prediction, feature extraction, and additional convolutional layers. It was trained with 242 WBCs images from Local Initiatives Support Corporation (LISC) dataset. The final outcome shows that the YOLOv3 architecture with Alexnet as its feature extractor produced the highest mean average precision of 98% and have better performance than the other models.

**Keywords**—Alexnet; darknet19; darknet53; detection; VGG16; white blood cells; YOLO

## I. INTRODUCTION

The human body immunization system depends on the white blood cells condition. Normal WBCs consist of Basophil, Eosinophil, Lymphocyte, Monocyte and Neutrophil. Immune system will be affected if there are any abnormality detected in the WBCs. Blood cancer such as leukemia is most common WBCs abnormality. Patient with this type of cancerous cell will have problem to fight virus and bacteria in the body system and weaken the immune system [1] [2]. It also affect the production of red blood cells and platelets in the bone marrow. There are several type of leukemia. An Acute Lymphoblastic Leukemia (ALL) is the one of it, which have abnormal lymphocyte which called leukocytes. This condition is crucial for early detection in order to establish a proper treatment for the patient. A typical diagnose method is the WBCs blood count which provide the data for the immune system and any blood related disease [3]. The conventional

method for leukemia diagnose are by bone marrow biopsy, lymph node biopsy, flow cytometry, lumbar puncture, lab test and also image tests, which is very challenging. However, the current automated system is depending on the application image processing, segmentation, feature extraction and finally the classification steps. Unfortunately, this method have an optimization issue [4]. A simple automated blood count method have been developed by using Convolutional Neural Network (CNN) architecture. The microscopic images are fed directly into the architecture for the classification and produce an output result [5]. On top of that, the neural network (NN) method have been evolve over the years and become the basic of a faster detection method.

The YOLOv3 detection method which been implemented in this project utilized the fundamental of neural network. This detection method practice a deep learning method for localization step which by using bounding box prediction, instead of the common sliding window search method [6]. The training process uses the sum of squared error loss and the logistic regression analysis for the objects' score prediction. The score will become 1 if the bounding box is overlap with the ground truth prior than another bounding box. Next, for the prediction of the classes, the independent logistic classifier and the cross-entropy loss are implemented. Then, as for the step prediction, three scale sizes are used. Meanwhile, for the feature extraction, Darknet-53 is used and followed by a few layers of convolutional layers. Lastly it produced a labeled output image.

This project investigated the implementation of different pretrained models (Alexnet, VGG16, Darknet-19) as the YOLOv3 feature extractor. LISC dataset images were used during the training and testing of the system. The finding of this research is the effect of different feature extractor on the detection rate and the detection average precision. The Alexnet as the feature extractor showed the highest detection mean average precision. Thus, this model can improve the existing blood smear detection method.

## II. YOU ONLY LOOK ONCE (YOLO)

Initially, the You Only Look Once (YOLO) was first introduced by J. Redmond et al. [7]. The YOLO detection system is illustrated in Fig. 1. In essence, the system will first resize the image, then undergo the convolutional network, and lastly the non-max suppression layer. The outcome is the detected labeled image. In the paper, the object detection is shown as a regression problem as the spatially separated the

bounding boxes and the associated class probabilities. From a full image, a single neural network is able to predict both the bounding boxes and the class probabilities with one evaluation. The speed of the model is at 45 frames per second. On the other hand, the Fast YOLO (smaller version) has higher process speed which is at 155 frames per second and had attained higher mean average precision in comparison with the other real time detectors.

The convolutional layers network of the YOLO detection is shown in the Fig. 2. It consist of 24 convolutional layers, two fully connected layers and interchanging 1x1 convolutional layers for feature space reduction from the preceding layers.

The convolutional layers of the YOLO detection network are illustrated in Fig. 2. It consist of 24 convolutional layers, two fully connected layers with 1x1 convolutional layers

alternately. This is to reduce the feature space from preceding layers. The overall YOLO model is trained together with the loss function that directly resembled the performance of the detection.

The authors presented another paper in the same year with YOLOv2 which is the upgraded from the previous YOLO model [8]. It is also named YOLO9000 due to its ability to detect 9000 or more objects' categories in real-time. The Darknet-19 was implemented in the architecture as the classifier. It consist of 19 convolutional layers and five maximum pooling layers. The model is able to process different image sizes while performing a balance of speed and accuracy. After that, the author updated the YOLOv2 to YOLOv3 [9]. In this new version, the Darknet19 had been upgrade to Darknet53 as the feature extractor. Its improvement include the extractor shortcut connection, feature map upsampling and concatenation.

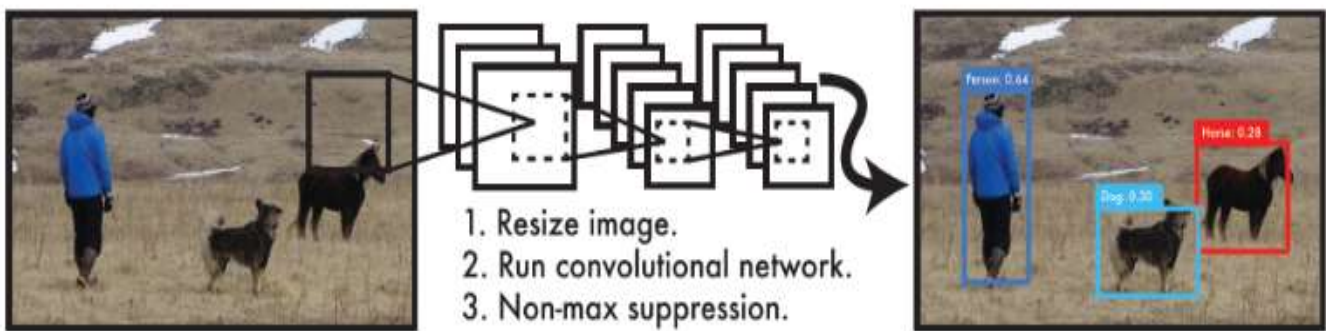


Fig. 1. YOLO Detection System [7].

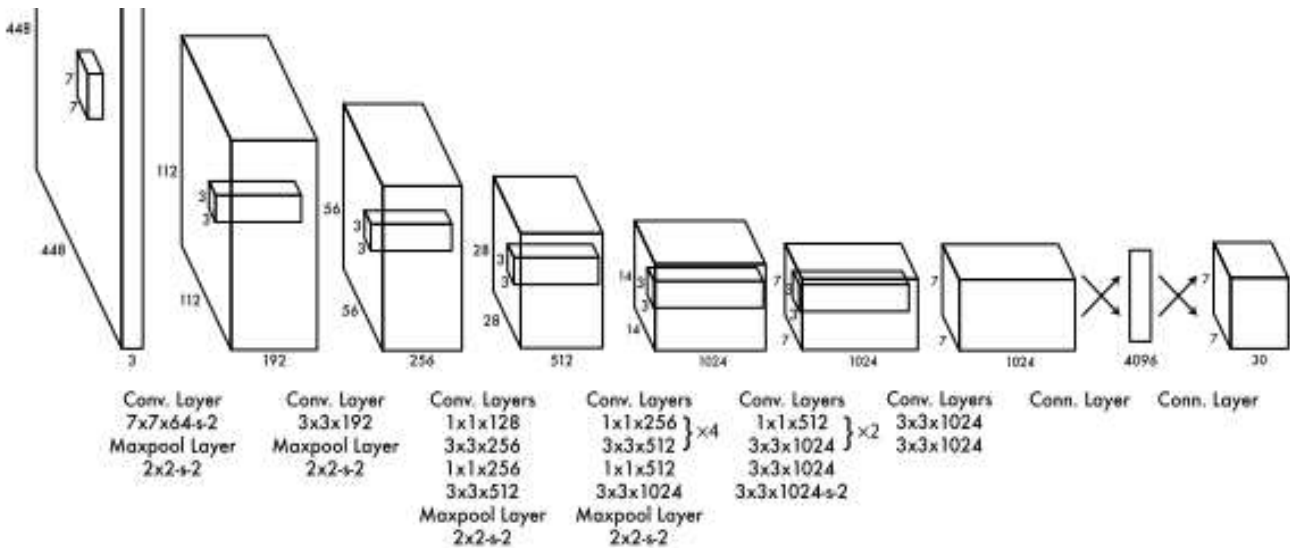


Fig. 2. YOLO Architecture [7].

#### IV. PRE-TRAINED MODELS

There are many types of pretrained model that been implemented in any machine learning architecture. Models like Alexnet, VGG16, and Darknet that had been trained with Imagenet and the weight is kept and ready to use for future implementation. Most of these models are CNN based.

Alexnet consist of five convolutional layers (only layer 1, 2 and 5 are followed by the max pooling) and three full connected layers [10]. All the inner layers applied Rectified Linear Units (ReLu) function as it activation function and softmax activation function in the final output layer. The application of the ReLu activation function speed up the training time up to six times on the Canadian Institute for Advanced Research 10 (CIFAR-10) dataset, instead of using the tanh activation function. Other than that, Alexnet allowed a multi graphics processing unit (GPU) training. Thus, it able to train bigger model and also shorten the training time. The conventional CNN pooling process will pool output from its neighbor groups of neurons without overlapping. Nevertheless, overlapping pooling was introduced in Alexnet which shows 0.5% loss reduction and the model less likely to overfit. The summary of the Alexnet architecture is tabulated as in Table I and the architecture diagram is as in Fig. 3.

The VGG16 model has more layers compare to the Alexnet structure. VGG16 architecture is illustrated in the Fig. 4. It was introduced in 2014 and to be an improvement of the Alexnet [11]. The large kernel-sized filters in Alexnet is

replace with a multiple 3x3 kernel-sized filters. The model had achieved 92.7% test accuracy in ImageNet. The structure has 16 layers depth and the VGG16 model is summarized in Table II. The input of the first convolutional layers is 224x224 RGB image and passed through the layers of convolutional layers then it applied maximum maximum pooling layer together with the 3x3 sized kernel filter. This produced a smaller image with dimension of 112x112x64. Then, it followed by two more convolutional layer, 3x3 sized 128 feature maps. Next, the maximum pooling with same size. Convolutional layers with 3x3 sized filter with 256 feature maps followed by maximum pooling are in the fifth and sixth layers. In the seventh to twelfth layer, there are two groups of three 3x3 sized 512 filters convolutional layers and maximum pooling layer. The last reduced size output is 7x7x512. Then, the output from the convolutional layer is flatten through the fully connected layers. Lastly, the layer of softmax function. All the hidden layers consist of the ReLu activation function.

Another CNN base model is the Darknet-19. It is initially used in YOLOv2 [8]. The model used filters and after each pooling step, there will be a couple of channel. The global average pooling is used for making the prediction and the filters for feature representation compression between convolutions. In order to stabilize the training, increase the convergence timing, and to make the model batch regulated, the paper used Batch Normalization technique. The Darknet19 consist of 19 convolutional layers and five maximum pooling layers. The summary of the model is tabulated in Table III.

TABLE I. SUMMARY OF ALEXNET ARCHITECTURE

| Layer  |             | Feature Map | Size      | Kernel Size | Stride | Activation |
|--------|-------------|-------------|-----------|-------------|--------|------------|
| Input  | Image       | 1           | 227x227x3 | -           | -      | -          |
| 1      | Convolution | 96          | 55x55x96  | 11x11       | 4      | Relu       |
|        | Max Pooling | 96          | 27x27x96  | 3x3         | 2      | Relu       |
| 2      | Convolution | 256         | 27x27x96  | 5x5         | 1      | Relu       |
|        | Max Pooling | 256         | 13x13x256 | 3x3         | 2      | Relu       |
| 3      | Convolution | 384         | 13x13x384 | 3x3         | 1      | Relu       |
| 4      | Convolution | 384         | 13x13x384 | 3x3         | 1      | Relu       |
| 5      | Convolution | 256         | 13x13x256 | 3x3         | 1      | Relu       |
|        | Max Pooling | 256         | 6x6x256   | 3x3         | 2      | Relu       |
| 6      | FC          | -           | 9216      | -           | -      | Relu       |
| 7      | FC          | -           | 4096      | -           | -      | Relu       |
| 8      | FC          | -           | 4096      | -           | -      | Relu       |
| Output | FC          | -           | 1000      | -           | -      | Softmax    |

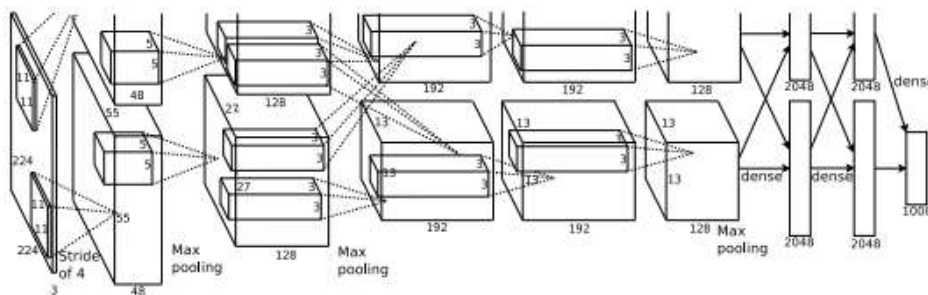


Fig. 3. Alexnet Architecture.



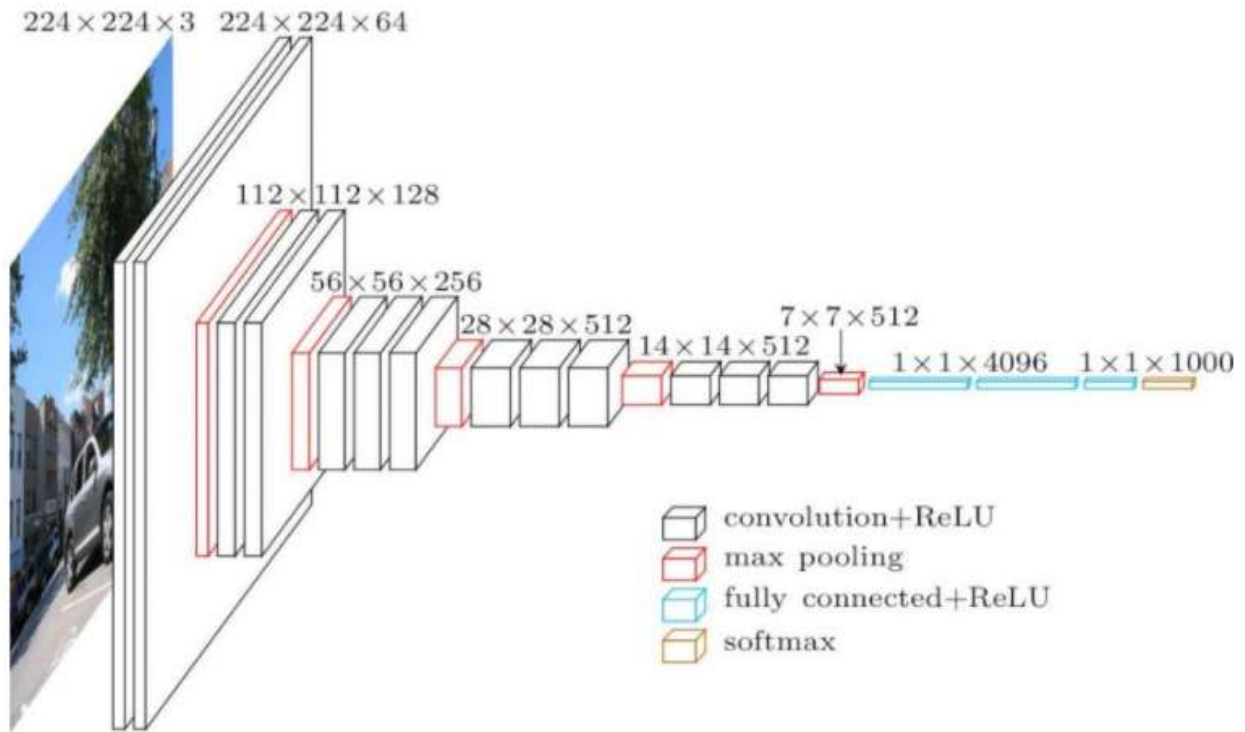


Fig. 4. VGG16 Architecture.

TABLE II. SUMMARY OF VGG16 ARCHITECTURE

| Layer  | Feature Map     | Size | Kernel Size | Stride | Activation |         |
|--------|-----------------|------|-------------|--------|------------|---------|
| Input  | Image           | 1    | 224x224x3   | -      | -          |         |
| 1      | 2 x Convolution | 64   | 224x224x64  | 3x3    | 1          | Relu    |
|        | Max Pooling     | 64   | 112x112x64  | 3x3    | 2          | Relu    |
| 3      | 2 x Convolution | 128  | 112x112x128 | 3x3    | 1          | Relu    |
|        | Max Pooling     | 128  | 56x56x128   | 3x3    | 2          | Relu    |
| 5      | 2 x Convolution | 256  | 56x56x256   | 3x3    | 1          | Relu    |
|        | Max Pooling     | 256  | 28x28x256   | 3x3    | 2          | Relu    |
| 7      | 3 x Convolution | 512  | 28x28x512   | 3x3    | 1          | Relu    |
|        | Max Pooling     | 512  | 14x14x512   | 3x3    | 2          | Relu    |
| 10     | 3 x Convolution | 512  | 14x14x512   | 3x3    | 1          | Relu    |
|        | Max Pooling     | 512  | 7x7x512     | 3x3    | 2          | Relu    |
| 13     | FC              | -    | 25088       | -      | -          | Relu    |
| 14     | FC              | -    | 4096        | -      | -          | Relu    |
| 15     | FC              | -    | 4096        | -      | -          | Relu    |
| Output | FC              | -    | 1000        | -      | -          | Softmax |

TABLE III. SUMMARY OF DARKNET19 ARCHITECTURE

| Type          | Filter | Size / Stride | Output  |
|---------------|--------|---------------|---------|
| Convolutional | 32     | 3x3           | 224x224 |
| Max Pooling   |        | 2x2/2         | 112x112 |
| Convolutional | 64     | 3x3           | 112x112 |
| Max Pooling   |        | 2x2/2         | 56x56   |
| Convolutional | 128    | 3x3           | 56x56   |
| Convolutional | 64     | 1x1           | 56x56   |
| Convolutional | 128    | 3x3           | 56x56   |
| Max Pooling   |        | 2x2/2         | 28x28   |
| Convolutional | 256    | 3x3           | 28x28   |
| Convolutional | 128    | 1x1           | 28x28   |
| Convolutional | 256    | 3x3           | 28x28   |
| Max Pooling   |        | 2x2/2         | 14x14   |
| Convolutional | 512    | 3x3           | 14x14   |
| Convolutional | 256    | 1x1           | 14x14   |
| Convolutional | 512    | 3x3           | 14x14   |
| Convolutional | 256    | 1x1           | 14x14   |
| Convolutional | 512    | 3x3           | 14x14   |
| Max Pooling   |        | 2x2/2         | 7x7     |
| Convolutional | 1024   | 3x3           | 7x7     |
| Convolutional | 512    | 1x1           | 7x7     |
| Convolutional | 1024   | 3x3           | 7x7     |
| Convolutional | 512    | 1x1           | 7x7     |
| Convolutional | 1024   | 3x3           | 7x7     |
| Convolutional | 1000   | 1x1           | 7x7     |
| Average pool  | -      | Global        | 1000    |
| Softmax       | -      | -             | -       |

## V. RELATED WORKS

The detection and classification method of the WBCs has been studied widely in medical and also engineering field. One of the study presented a Regional Convolutional Neural Network (RCNN) which was trained by transfer learning using Alexnet, VGG16, Googlenet and Resnet50 [12]. The Resnet50 transfer learning shows the highest performance.

The author also have tested another CNN based architecture that tested on different pretrained models as its feature extractor with the Extreme Learning Machine (ELM) classifier [13]. The output from these feature extractors were then combined and the minimum redundancy maximum relevance method was used to select the efficient features. Finally, the ELM was enabled. The results shows accuracy rate of 96.03%. There are three studies that had been done. The Alexnet-ELM method which used ELM as classifier for the features at the fully connected layers of each CNN models. It obtained an accuracy rate of 95.29%. Then, the performance of classifier were tested and the Resnet model achieved 95.2% accuracy rate. Lastly, the paper studied the CNN - Minimum Redundancy Maximum Relevance (MRMR) - ELM method

on the WBCs data. MRMR feature selection algorithm was used for features combination at the last layers of the tested models. This method achieved the accuracy rate of 96.03%.

A project also had demonstrated that Alexnet has the best performance as feature extraction for WBCs type classification in comparison with Lenet, and VGG16 architectures [14]. The Discrete Transform (DT), quadratic discriminant analysis (QDA), linear discriminant analysis (LDA), Support vector machine (SVM), k- nearest neighbors (kNN) with Alexnet also been compared to a softmax classifiers and the highest accuracy is the combination of QDA-Alexnet which is 97.78%.

Additional application other than WBCs detection, Alexnet also been implemented in the detection and classification of the red blood cell (RBCs) [15]. The designed framework was able to classify 15 types of RBCs. The results obtained were: 95.92% accuracy, 77% sensitivity, 98.82% specificity, and 90% precision.

A different comparison had been made between the VGG16 and Resnet50 for WBCs classification [16] and the Resnet50 achieved 88.29% of accuracy. One of the project that utilized VGG16 is by M. Shahzad [17]. The framework starts with feeding the original images and ground truth images to the preprocessing stage. This include labeling of the pixel-level and conversion of RGB-Grayscale. The VGG16 later fed into the system as a feature extractor. Then the training process begin. The system accuracies are 97.45% for RBCs, 93.34% for WBCs, and 85.11% for platelets. Meanwhile, another paper also had compared the utilization of CNN models and Alexnet had perform better than GoogleNet and Resnet-101 [18]. A paper had implement image processing algorithm based for preprocessing and together with VGG16 as its classifier [19]. The experiment achieved 95.89% accuracy. In addition, a paper had use the concept of capsule for the classification model of WBCs [20]. The developed model proved that it had higher precision value than using the Resnet and VGG model.

A paper by K. Almezghwi also apply the VGG16, Resnet and Densenet in the project. The paper studied the generative adversarial networks (GAN) and image transformation operation for data augmentaion together with the deep neural networks for feature extraction [21]. The outcome of the experiments is that the highest accuracy was achieved by using the Densenet-169 as the feature extractor which is 98.8%.

## VI. METHODOLOGY

The project starts with preparing the hardware, software and datasets. The hardware used for this experiment is the Intel® Core™ i5-5200U CPU @ 2.20GHz processor. Whereas the Spyder by Anaconda software is used for all the programming activity include training, detecting and result analysis.

### A. Datasets

This project worked with the dataset from LISC which is a public dataset. There are five image categories which are Basophil, Eosinophil, Lymphocytes, Monocytes and the

Neutrophil. Images are parted into training and testing as in Table IV. The number of training images is as 53, 39, 52, 48, and 50, respectively. Whilst the number of testing images is five for each category and eight images containing multiple WBCs type. The preparation of the datasets starts with annotating the images. The labelling process is done in the Microsoft’s Visual Object Tagging Tool (VoTT) software. After completing the preparation of datasets, the experiment continue with the training and detecting process.

**B. YOLOv3**

The main structure of this project is the YOLOv3 image detection. It starts with the forming of bounding box. Next, followed by the class prediction, prediction across scales, feature extraction, and the convolutional layer. Based on the YOLOv3 architecture in Fig. 5, it used a multi-scale method for the multiple target detection. The finer grid cell enable for smaller target detection. In every grid, three bounding boxes are predicted. Then, it will predict the three categories and five basic parameters which are x, y, w, h, and c.

Then, the multilabel classification will predict the classes in each bounding box. The classes will be predicted by using the binary cross-entropy loss during the training. Three sizes scales will then go through feature extraction. In addition, the Darknet-53 model will supported by additional convolutional layers. The feature map from the previous two layers were upsampled by double and concatenation the feature map from the prior layer in the network which produced a semantic and finer grained data.

Fig. 6 shows the flow process of the YOLOv3. The dataset was split into training set and testing set. The training set was

then undergo a bounding box step, class prediction and the prediction across scales. Later, the features were extracted by the Darknet53 model before it pass through convolutional layer and produced output. The steps were repeated by replacing the extractor with different CNN models. This project tested on the Alexnet, VGG16 and Darknet19 model which shows in Fig. 7.

**C. Evaluation of the Classifier Test Data**

The performance of the architectures was determined based on its accuracy, precision and sensitivity ratios as in equation (1), (2), and (3), respectively.

$$Accuracy (Acc.) = \frac{TP+TN}{TP+TN+FP+FN} \tag{1}$$

$$Precision (Pre.) = \frac{TP}{TP+FP} \tag{2}$$

$$Sensitivity \text{ or } Recall (Rec.) = \frac{TP}{TP+FN} \tag{3}$$

TABLE IV. NUMBER OF IMAGE DATASET IN EACH WBCS CATEGORY

| Images      | Training | Testing |
|-------------|----------|---------|
| Basophil    | 53       | 5       |
| Eosinophil  | 39       | 5       |
| Lymphocytes | 52       | 5       |
| Monocytes   | 48       | 5       |
| Neutrophil  | 50       | 5       |
| Mixed       | -        | 8       |
| Total       | 242      | 33      |

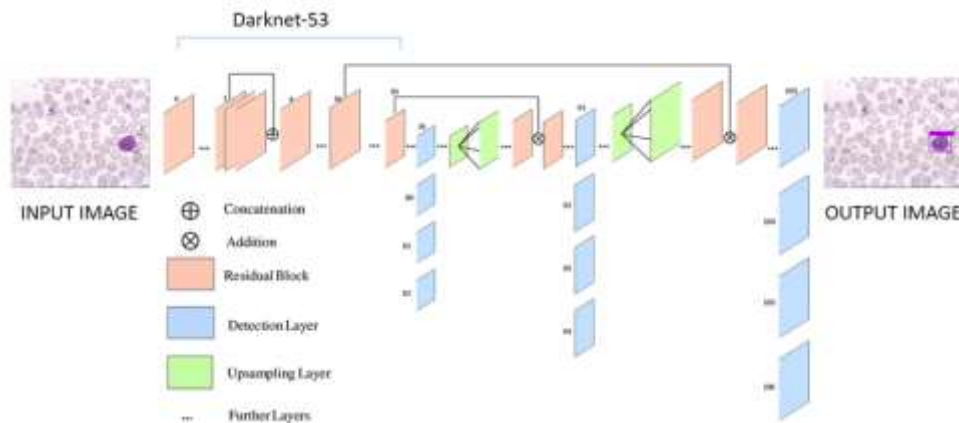


Fig. 5. YOLOv3 Architecture for WBCs Detection.

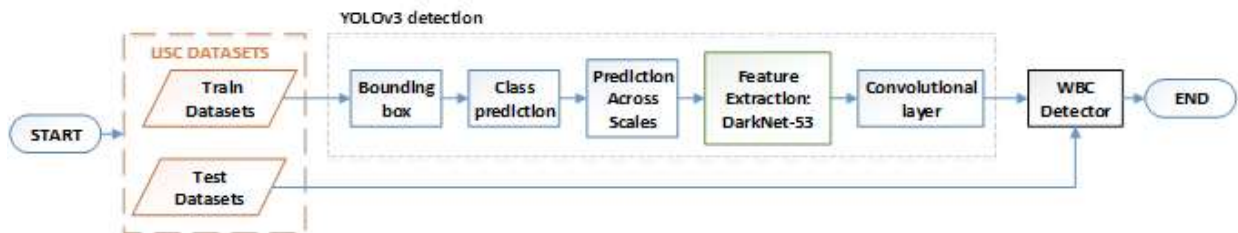


Fig. 6. YOLOv3 Process Flow.

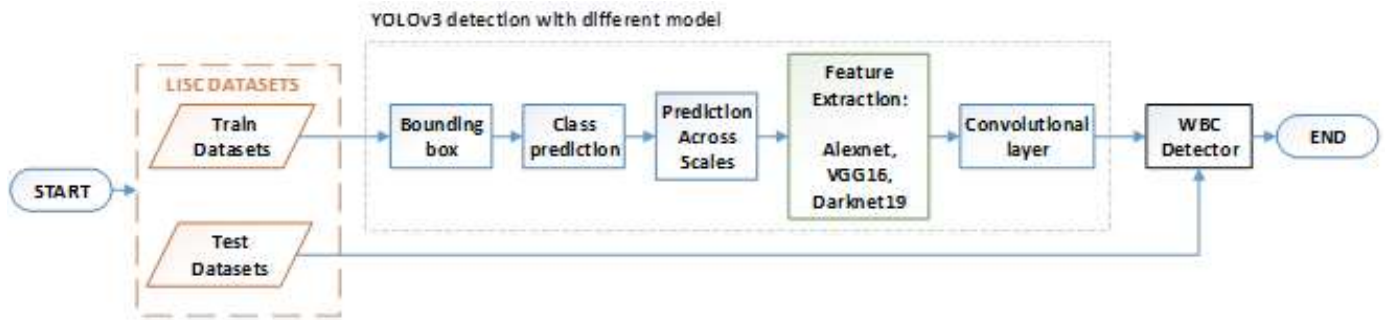


Fig. 7. YOLOv3 with different Model Process Flow.

The abbreviations are define as: TP = true positive, TN = true negative, FP = false positive, FN = false negative.

Then, the mean average precision (mAP) value is obtained by using (4).

$$AP = \int_0^1 Pre.(Rec.) dRec. \quad (4)$$

### VII. RESULTS AND DISCUSSION

The Table V presented the results of the training loss, validation loss, testing time, detection rate, and the detection mean average precision for each model used. The training loss and validation loss for all for models were between 13.8492 to 14.9078 and 13.4578 to 14.3617 respectively. Alexnet reached the lowest number of training loss, validation loss and also the

testing time. Based on the tabulated data, Alexnet has the highest detection mean average precision, 98%. However, the VGG-16 achieved the lowest, 96.61%.

The summary of mean average precision of each WBCs type is presented in Table VI. All four model had detected Basophil and Neutrophil with highest mAP. Meanwhile, only Darknet-19 achieved 100% of mAP. The lowest value of mAP, was the detection Monocyte cell by VGG16, which only 75%. The visual characteristic of the basophil and neutrophil are clearly able to differentiate compared to the visual characteristic of the monocyte. The output images were presented in the Table VII. The images were labelled with predicted class.


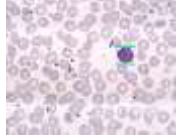

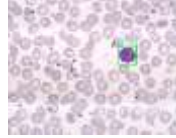
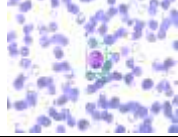
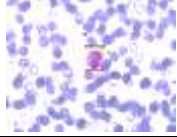
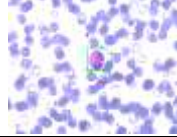
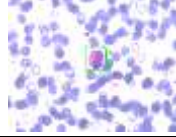
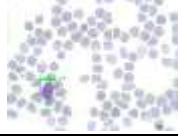



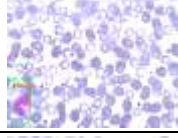



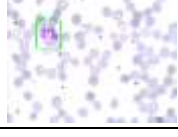

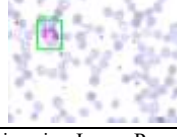
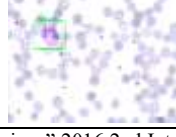
TABLE V. TRAINING AND DETECTION RESULTS

| Model      | Training Loss | Validation Loss | Testing time | Detection rate | Detection Mean Average Precision (mAP / %) |
|------------|---------------|-----------------|--------------|----------------|--------------------------------------------|
| AlexNet    | 13.8492       | 13.4578         | 74.4sec      | 0.4FPS         | 98%                                        |
| VGG-16     | 14.9078       | 13.9120         | 103.1sec     | 0.3FPS         | 93.06%                                     |
| Darknet-19 | 14.5619       | 14.2912         | 105.9sec     | 0.3FPS         | 96.61%                                     |
| Darknet-53 | 14.0242       | 14.3617         | 78.5sec      | 0.4FPS         | 96.19%                                     |

TABLE VI. THE MEAN AVERAGE PRECISION VALUE OF EACH CELL TYPE IN EVERY TEST

| Cell Type                               | Model   |        |            |            |
|-----------------------------------------|---------|--------|------------|------------|
|                                         | AlexNet | VGG-16 | Darknet-19 | Darknet-53 |
| Basophil                                | 1       | 1      | 1          | 1          |
| Eosinophil                              | 1       | 0.9    | 1          | 0.94       |
| Lymphocyte                              | 1       | 1      | 0.83       | 1          |
| Monocyte                                | 0.9     | 0.75   | 1          | 0.87       |
| Neutrophil                              | 1       | 1      | 1          | 1          |
| <b>Mean Average Precision (mAP / %)</b> | 98%     | 93.06% | 96.61%     | 96.19%     |

TABLE VII. IMAGES OUTCOME

| Images       | Model                                                                              |                                                                                    |                                                                                     |                                                                                      |
|--------------|------------------------------------------------------------------------------------|------------------------------------------------------------------------------------|-------------------------------------------------------------------------------------|--------------------------------------------------------------------------------------|
|              | AlexNet                                                                            | VGG-16                                                                             | Darknet-19                                                                          | Darknet-53                                                                           |
| Basophil12   |   |   |   |   |
| Eosinophil22 |   |   |   |   |
| Lymphocyte12 |   |   |   |   |
| Monocyte38   |   |   |   |   |
| Neutrophil35 |  |  |  |  |

### VIII. CONCLUSION

The YOLOv3 architecture originally implement the Darknet53 as its feature extractor. This paper investigated the effect of using different feature extractor (Alexnet, VGG16, and Darknet19). The outcome of the experiment shows that the YOLOv3 with Alexnet as feature extractor obtained the highest mean average precision which was 98%. It also have the lowest losses and shortest testing time. As a result, it demonstrated to have higher performance compared to other models. On the other hand, more improvement is able to apply as a continuous project, such as to train on greater number of dataset, testing on several different source of datasets and also to use GPU to increase the training speed.

### ACKNOWLEDGMENT

This research is supported by a Fundamental Research Grant Scheme (FRGS) FRGS/1/2019/TK04/UTHM/02/6 (Vot. No. K191) sponsored by the Ministry of Higher Education (MOHE) Malaysia.

### REFERENCES

- [1] B. J. Bain, "The Nature of Leukaemia, Cytology, Cytochemistry and the FAB Classification of Acute Leukaemia," in *Leukaemia Diagnosis*, Fifth., B. J. Bain, Ed. John Wiley & Sons Ltd, 2011, pp. 1–63.
- [2] A. Vora, *Childhood Acute Lymphoblastic Leukemia*. Springer, 2017.
- [3] B. Martin, "Leukemia," in *Harmful Interaction between the Living and the Dead in Greek Tragedy*, U. Popat and J. Abraham, Eds. Demos Medical Publishing, 2011, pp. 191–194.
- [4] R. G. Bagasjvara, I. Candradewi, S. Hartati, and A. Harjoko, "Automated Detection and Classification Techniques of Acute

Leukemia using Image Processing : A Review," 2016 2nd Int. Conf. Sci. Technol., pp. 35–43, 2016.

- [5] F. Novoselnic, R. Grbic, I. Galic, and F. Doric, "Automatic White Blood Cell Detection and Identification Using Convolutional Neural Network," *Proc. Int. Conf. Smart Syst. Technol.* 2018, SST 2018, pp. 163–167, 2018.
- [6] A. Gautam, "Automatic Classification of Leukocytes using Morphological Features and Naïve Bayes Classifier," 2016 IEEE Reg. 10 Conf., pp. 1023–1027, 2016.
- [7] J. Redmon, S. Divvala, R. Girshick, and A. Farhadi, "You only look once: Unified, real-time object detection," *Proc. IEEE Comput. Soc. Conf. Comput. Vis. Pattern Recognit.*, vol. 2016-Decem, pp. 779–788, 2016.
- [8] J. Redmon and A. Farhadi, "YOLO9000: Better, faster, stronger," *Proc. - 30th IEEE Conf. Comput. Vis. Pattern Recognition, CVPR 2017*, vol. 2017-Janua, pp. 6517–6525, 2017.
- [9] J. Redmon and A. Farhadi, "YOLOv3: An Incremental Improvement," 2018.
- [10] A. Krizhevsky, I. Sutskever, and Geoffrey E. Hinton, "ImageNet Classification with Deep Convolutional Neural Networks," *Handb. Approx. Algorithms Metaheuristics*, pp. 1–1432, 2007.
- [11] K. Simonyan and A. Zisserman, "Very deep convolutional networks for large-scale image recognition," 3rd Int. Conf. Learn. Represent. ICLR 2015 - Conf. Track Proc., pp. 1–14, 2015.
- [12] H. Kutlu, E. Avci, and F. Özyurt, "White blood cells detection and classification based on regional convolutional neural networks," *Med. Hypotheses*, vol. 135, no. October 2019, p. 109472, 2020.
- [13] F. Özyurt, "A fused CNN model for WBC detection with MRMR feature selection and extreme learning machine," *Soft Comput.*, vol. 24, no. 11, pp. 8163–8172, 2020.
- [14] M. Togacar, B. Ergen, and M. E. Sertkaya, "Subclass separation of white blood cell images using convolutional neural network models," *Elektron. ir Elektrotehnika*, vol. 25, no. 5, pp. 63–68, 2019.

- [15] H. A. Aliyu, M. A. A. Razak, R. Sudirman, and N. Ramli, "A deep learning alexnet model for classification of red blood cells in sickle cell anemia," *IAES Int. J. Artif. Intell.*, vol. 9, no. 2, pp. 221–228, 2020.
- [16] S. Vathavanarao, S. Tungjitnob, and K. Pasupa, "White Blood Cell Classification: A Comparison between VGG-16 and ResNet-50 Models," p. 2.
- [17] M. Shahzad, A. I. Umar, M. A. Khan, S. H. Shirazi, Z. Khan, and W. Yousaf, "Robust Method for Semantic Segmentation of Whole-Slide Blood Cell Microscopic Images," *Comput. Math. Methods Med.*, vol. 2020, 2020.
- [18] M. Sharma, A. Bhave, and R. R. Janghel, "White Blood Cell Classification and Counting Using Convolutional Neural Network," *Adv. Intell. Syst. Comput.*, vol. 900, pp. 135–143, 2019.
- [19] C. B. Wijesinghe, D. N. Wickramarachchi, I. N. Kalupahana, L. R. De Seram, I. D. Silva, and N. D. Nanayakkara, "Fully Automated Detection and Classification of White Blood Cells," *Proc. Annu. Int. Conf. IEEE Eng. Med. Biol. Soc. EMBS*, vol. 2020-July, pp. 1816–1819, 2020.
- [20] Y. Liu, Y. Fu, and P. Chen, "WBCaps: A Capsule Architecture-based Classification Model Designed for White Blood Cells Identification," *Proc. Annu. Int. Conf. IEEE Eng. Med. Biol. Soc. EMBS*, pp. 7027–7030, 2019.
- [21] K. Almezghwi and S. Serte, "Improved Classification of White Blood Cells with the Generative Adversarial Network and Deep Convolutional Neural Network," *Comput. Intell. Neurosci.*, vol. 2020, 2020.

# A Novel Solution for Distributed Database Problems

Bishoy Sameeh Matta Sawiris<sup>1</sup>

Business Information System Department  
Faculty of Commerce and Business Administration  
Helwan University  
Cairo, Egypt

Manal A. Abdel-Fattah<sup>2</sup>, Assoc.Prof.

Faculty of Computers and Information  
Information Systems Department  
Helwan University  
Cairo, Egypt

**Abstract**—Distributed Databases Systems (DDBS) are a set of logically networked computer databases, managed by different sites, locations and accessible to the user as a single database. DDBS is an emerging technology that is useful in data storage and retrieval purposes. Still, there are some problems and issues that degrade the performance of distributed databases. The Aim of this paper is to provide a novel solution to distributed database problems that is based on distributed database challenges collected in one diagram and on the relationship among DDB challenges in another diagram. This solution presents two methodologies for Distributed Databases management Systems: deep learning-based fragmentation and allocation, and blockchain technology-based security provisioning. The contribution of this paper is twofold. First, it summarizes major issues and challenges in the distributed database. Additionally, it reviews the research efforts presented to resolve the issues. Secondly, this paper presents a distributed database solution that resolves the major issue of distributed database technology. This paper also highlights the future research directions that are appropriate for distributed database technology after the implementation in a large-scale environment and recommended the technologies that can be used to ensure the best implementation of the proposed solution.

**Keywords**—Distributed database; database challenges; deep learning; fragmentation; blockchain; security

## I. INTRODUCTION

Distributed Database (DDB) is the storage paradigm where the users are allowed to store and preserve their data anywhere and are also allowed to access data from any locations [1]. In other words, DDB is constructed with logically distributed multiple databases that are interrelated with. DDB is illustrated in Fig. 1.

As shown in Fig. 1, DDB has multiple databases that are run over different physical or virtual machines at various locations. For an end user, it looks like a single centralized database (i.e.) the user accesses data or uploads data through a centralized server. The centralized server is responsible for managing multiple databases over the system. The main objective of DDB is to prevent overloading at a single point [2]. In conventional centralized databases, all data is stored and accessed in a single server, which increases load on the central server. To overcome this, DDB distributes the load among multiple servers to prevent single point overloading. In DDB, the distributed servers are connected through wire or wirelessly but do not share the memory or clock. In recent times, several advantages have been addressed in DDB systems and those are provided in Table I [3].

Recently, DDB has been adapted in cloud computing technology [4].

Integration of DDB in cloud computing improves usability, scalability and system monitoring. Although DDB has many advantages, it also has some issues that can be listed as follows:

- High Complexity.
- Lack of Security.
- High Cost.
- Lack of Integrity.
- Lack of Standards.
- Complex Design.
- Difficulty in Operating System.

Current research efforts have aimed at optimizing the above issues in DDB system.

## A. PROCESS IN DB

In DDB and distributed database management systems (DBMS), two major processes are included. The main processes are:

1) *Replication* – This process looks for changes in DDB. If any change occurs, then a replication process is initiated to make all servers look exactly the same.

2) *Duplication* – To ensure the data is available in all distributed databases, a duplication process is performed. In duplication, a server is considered as master then the database is duplicated as required. Through this process the user is allowed to change the master database without overwriting other distributed databases [5].

## B. DB Architecture Model

These processes are important in both homogeneous and heterogeneous databases. In a homogeneous database, all servers have identical software while a heterogeneous database has different software for different servers [6]. In general, there are three common architecture models for DDB. Those are,

- Client-server Architecture.
- Peer-to-Peer Architecture.
- Multi-DBMS Architecture.

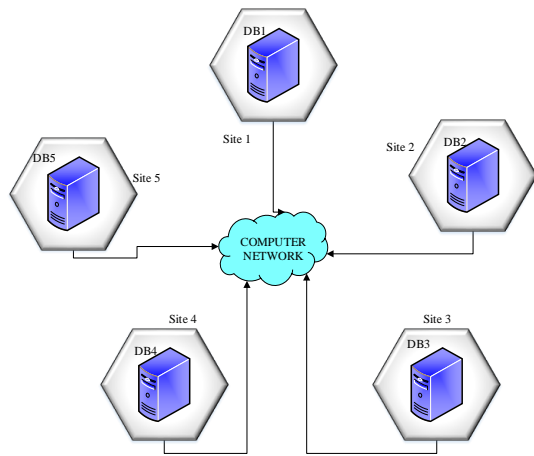


Fig. 1. Distributed Database System.

TABLE I. ADVANTAGES OF DDB

| Advantage        | Description                                                                                                                                                                              |
|------------------|------------------------------------------------------------------------------------------------------------------------------------------------------------------------------------------|
| Availability     | As the data is replicated in multiple sites, DDB generally assures availability of data at all times. If any one of the servers failed to provide data, then the other servers can help. |
| Data Sharing     | Users from anywhere are allowed to share and transmit data in any distributed server.                                                                                                    |
| Robustness       | Failures in any one of the servers will not affect the entire DDB system since multiple servers are connected and work together.                                                         |
| High Performance | DDB, in general, enables concurrent data transmissions, which assures a high level of performance. It also shows better delay performance as the local queries are at local servers.     |
| Scalability      | In DDB, overloading is not an issue such that it is easy to add more users in the system.                                                                                                |

In the client-server architecture model, the functionality is divided into servers and clients. Here, a client server function manages user interface, while a server function covers data

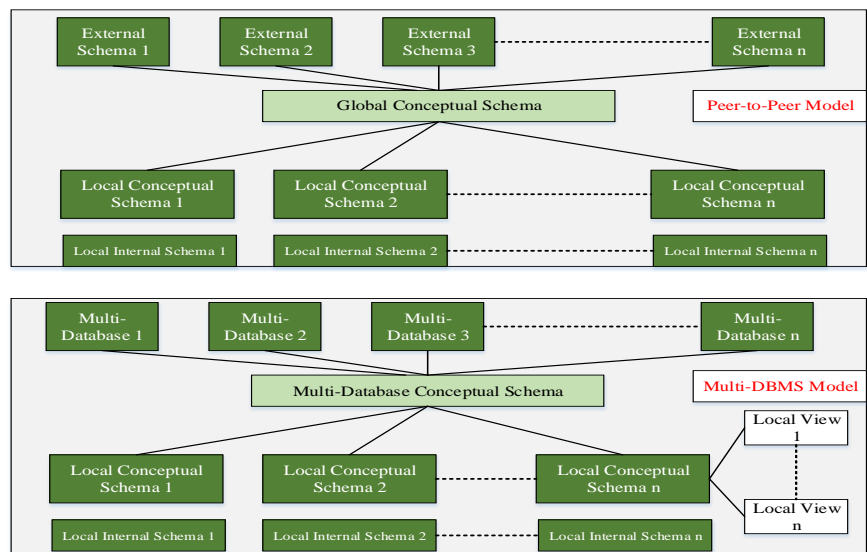
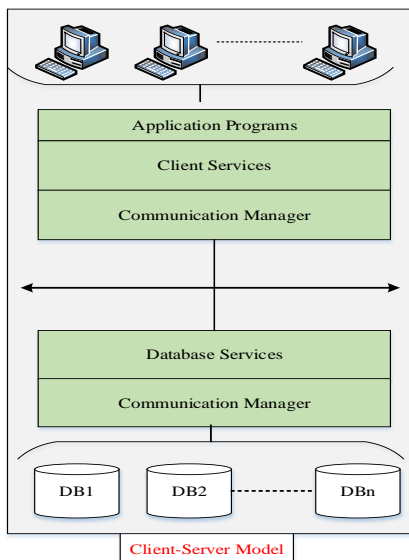


Fig. 2. DDB Architecture Models.

management, query processing, optimization and transaction management. Further, the client-server model involves two different models: single server multiple clients and multiple server multiple clients. In a peer-to-peer model, all servers and clients are connected as peers. For co-ordination, it uses global conceptual schema, local conceptual schema, local interface schema and external schema. The multi-DBMS is formulated by collection of more databases. It uses six level schemas for functioning. Those are multi-database view level, multi-database conceptual level, multi-database internal level, local database view level, local database conceptual level and local database internal level [7]. All three kinds of architectures are illustrated in Fig. 2.

C. Contributions

The major contribution of this paper relies on summarization of research issues in DDB and DBMS. Further contributions are provided as follows:

- The research issues of DDB and DBMS are clearly analyzed and summarized. Background of all issues has been analyzed.
- A novel DDB system is designed as the solution to resolve the research issues. The proposed system relies upon optimizing overall DDB and DBMS through an optimal architectural design.
- Future research directions for improving DDB performance is provided in the conclusion of this paper.

D. Paper Organization

The rest of this paper is organized as follows: Section 2 clearly explains the issues of DDB in architectural and performance aspects. Section 3 reviews the existing research works held on DDB and DBMS. In Section 3, the main research gap is identified and summarized. In Section 4, the researcher’s proposed solution for DDB system is presented. Section 5 concludes the researcher’s contributions and highlights the future research directions.



## II. OVERVIEW ON DDB PROBLEMS

This section provides a detailed summary of the research problems in DDB systems. The major problems are depicted in Fig. 3.

### A. Distributed Query Processing

The first and foremost problem in DDB is the development of distributed design. The problem is related to placing data and applications in the optimal place across the distributed sites. In DDB, non-replicated (portioned) and replicated alternatives are utilized for placing data optimally. Here, the major issue relies on fragmentation which separates the database into partitions. The other issue is the optimum distribution of those fragments [8].

### B. Directory Management

In DDB, the data can be stored in any server across the system. Database directory generally contains the information about the all data items in the DDB system. The directory

maintains descriptions and locations of all data items stored across the distributed system. The main issue is related to the management of directory (i.e.) updating and deletion of data item description and location (i.e. in the system) [9].

### C. Distributed Query Processing

Query processing involves acquisition of user query and processing it to retrieve the required data. For that designing optimum algorithms is still an issue since the process of analyzing queries and converting queries into data manipulation operations are complex issues. Thus, designing and optimizing algorithms for query processing is still an issue [8].

### D. Concurrent Processing Control

The main aim of DDB system is to serve multiple users concurrently by distributing workload to multiple servers. However, synchronization of these processes is the foremost issue in DDB.



Fig. 3. DDB System Problems.

### E. Deadlock Management

Deadlock is an important issue in DDB system that occurs due to the competition between users for accessing the same set of resources, for instance, if many users are requesting for the same data at the same time. Here, the synchronization works upon the locking [10].

### F. Reliability

Maintaining consistency of the database affects the reliability of the DDB system. In addition, occurrence of failures is also the main issue for reliability degradation. To ensure reliability, prevention, detection and mitigation of faults improve reliability.

### G. Replication Problem

Though replication is one of the key processes of DDB, the algorithm design must ensure the consistency of the copies of data items stored in distributed system.

### H. Heterogeneity

Middleware design of DDB system for managing a heterogeneous environment is still a major problem. Middleware is the set of services that acts as interface between end users and DDB system. However, designing such middleware to support heterogeneous users is the main issue.

### I. Security and Trust

Security and trust management of the stored data remains an unsolved issue since involvement of attackers crack the security of the system. Unauthorized user access and insecure data storage degrades the security level of overall system [11].

### J. Transparency

The main goal of DDB system is that it looks like a single system for the end users. The transparency quality also ensures that the DDB is perceived by the users as a single entity rather than a collection of autonomous systems [12].

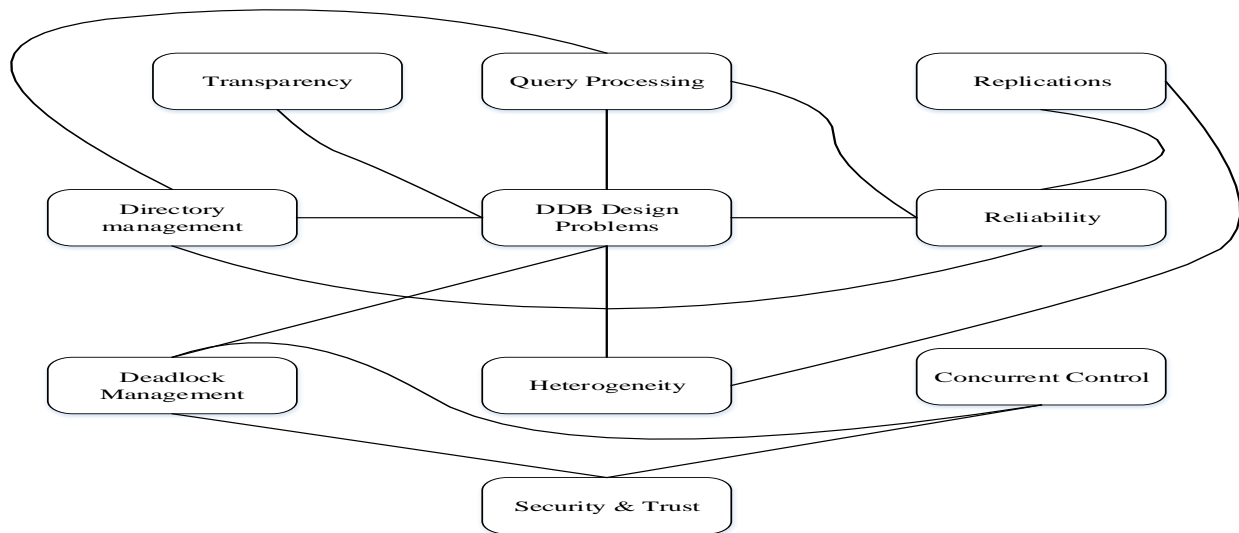


Fig. 4. Relationship among DDB Problems.

All these problems are unsolved in the DDB systems. Although all problems seem to be individual, there is a relationship among them. In Fig. 4, the relationship among DDB problems is summarized.

## III. LITERATURE REVIEW

In recent years, many research works have been focused on optimizing the performance of DDB systems. The significant works are analyzed in this section.

Many research works have concentrated on replication and fragmentation management. A new approach was presented in DDB for managing fragmentation and data allocation [13]. This approach splits the data into pair-wise disjoint fragments. Then, it determines whether the fragments were already allocated to any system. Further, high speed clustering technique was presented. First, data was allocated to a single cluster. Then, it was replicated to other clusters. However, this work increases complexity since replication is performed in a non-optimal manner. A cluster-based fragmentation and data replication methodology was presented for flexible query answering in DDB systems [14]. This work uses a standard

clustering algorithm to determine the semantic fragmentation of data in the database. Further, an intelligent query processing methodology was introduced for managing queries in distributed databases. This work also supports load balancing in distributed systems. A combined approach was presented for DDB systems [15]. An optimized heuristic algorithm was designed for horizontal fragmentation and data allocation. The heuristic approach was made up of data fragmentation strategy, data allocation and replication, and clustering strategies. In general, heuristic approaches consume a large amount of time and addition of multiple strategies in the heuristic approach increases time consumption rapidly. A distance-based site clustering approach was presented to support effectual fragmentation [16]. The method of cluster relies on the distance between sites i.e. nearer sites form clusters. For fragmentation, dynamic methods were utilized since static allocation of fragments degrades the response system.

Although this system works better than static methods, this work is unsuitable for large-scale database systems. However, the DDB system is generally large-scale that has to support a

large number of users and data. A query processing methodology was presented to optimize DDB system [17]. Here, the query execution plan was executed then it was used in the search space. The input SQL query was parsed and translated at first. An optimal query search strategy was introduced upon a new tree structure. This work has a higher computational cost in terms of time consumption and computations.

Another main aspect focused upon by many researches works and emerging in DDB is security. A key agreement protocol was used to secure the DDB environment [18]. The proposed scheme was named as key agreement based secure Kerberos authentication protocol (KASKAP). The KASKAP authenticates the distributed servers in order to ensure that only trusted nodes process the user queries.

Further, the trusted nodes were allowed to adjust the process of the DDB system. The conventional Kerberos protocol, which has a lower security level, is used in this work. Thus, this work is not able to achieve the required level of security. In addition to key agreement, cryptography algorithms are also useful in providing security for DDB systems [19]. Symmetrical encryption algorithms were utilized to secure the system. Considered algorithms were: Rijndael algorithm, Reverts Cipher (RC2), advanced

encryption standard (AES), data encryption standard (DES) and triple data encryption standard (TDES). All these conventional algorithms are lower in security level but higher in complexity. However, lightweight and fast algorithms are more suitable for DDB security. An access control mechanism was introduced to ensure security level in DDB systems [20]. Here, the access control policy was applied for the users validating the user's identity. Security dimension was applied for the users to calculate the permission level. The access control policy is applied based on a single metric which is ineffectual, and the policies are static, which increases malicious user access.

Table II summarizes the research works held in DDB systems and their contributions towards solving the DDB problems. It can be seen that still there are major gaps to be addressed in DDB systems. It can be formulated as follows:

- The fragmentation and query processing must have lower delay and complexity while providing better performance.
- Security mechanisms must ensure high level security without increasing time complexity. The solution must be lightweight and capable of handling large numbers of users.

TABLE II. SUMMARIZATION OF EXISTING WORKS

| Work | Problem Focused |                      |                  |                    |                     |             |             |               |          | Research Issue                                   |
|------|-----------------|----------------------|------------------|--------------------|---------------------|-------------|-------------|---------------|----------|--------------------------------------------------|
|      | Design Issue    | Directory Management | Query Processing | Concurrent Control | Deadlock Management | Reliability | Replication | Heterogeneity | Security |                                                  |
| [8]  | ✓               | ✗                    | ✓                | ✓                  | ✗                   | ✓           | ✓           | ✗             | ✗        | High Complexity<br>Non-optimal<br>Replication    |
| [9]  | ✓               | ✗                    | ✓                | ✓                  | ✗                   | ✓           | ✗           | ✗             | ✗        | Ineffective<br>concurrent<br>processing          |
| [10] | ✓               | ✗                    | ✗                | ✗                  | ✗                   | ✗           | ✗           | ✗             | ✗        | Higher time<br>consumption                       |
| [11] | ✓               | ✓                    | ✗                | ✗                  | ✗                   | ✓           | ✓           | ✗             | ✗        | Not suitable<br>for large-<br>scale system       |
| [12] | ✓               | ✗                    | ✗                | ✓                  | ✗                   | ✓           | ✗           | ✗             | ✗        | Higher<br>computational<br>cost                  |
| [13] | ✗               | ✗                    | ✗                | ✗                  | ✗                   | ✗           | ✗           | ✗             | ✓        | Security level<br>is marginal                    |
| [14] | ✗               | ✗                    | ✗                | ✗                  | ✗                   | ✗           | ✗           | ✗             | ✓        | Slow<br>processing<br>and security<br>level      |
| [15] | ✗               | ✗                    | ✗                | ✗                  | ✗                   | ✗           | ✗           | ✗             | ✓        | Unable to<br>prevent<br>malicious<br>user access |

✓-Focused; ✗-Not Focused;

#### IV. PROPOSED SOLUTIONS

In this section, the researcher introduces an overview of the proposed solution for DDB problems. Two methodologies for DDB management are presented. The first one is deep learning-based fragmentation and allocation. The second one is blockchain technology-based security provisioning. Deep learning is the evolving Artificial Intelligence (AI) technique that resembles the artificial neurons in a deep manner. General Deep Neural network (DNN) involves three kinds of layers. Those are the input layer, the hidden layer and the output layer. Input layer is responsible to get input from the users (in this work, the input is the user query or data). In the hidden layer, the weight value is tuned for each input upon a set of criteria. In the output layer, the output of the given input is obtained. The logical structure of DNN is illustrated in Fig. 5.

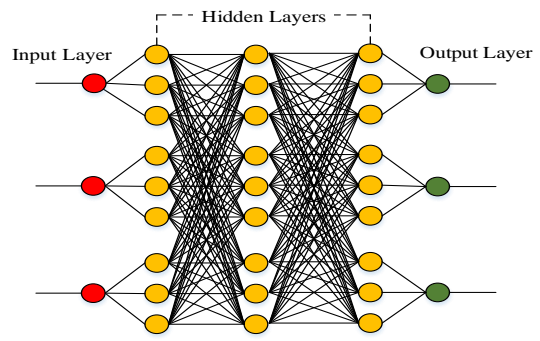


Fig. 5. DNN Architecture.

Deep learning has many advantages over DDB systems. The important benefit is that it assures a high-level performance by providing an optimal solution in fragmentation and query optimization. In the following pseudocode, the process of DNN is explained in detail. This procedure is adapted in processing of data in the DDB system. Here, the hidden layer is responsible to compute weight value upon objective function. For example, if DNN is sued for clustering sites then the weight value is computed in terms of distance between the sites.

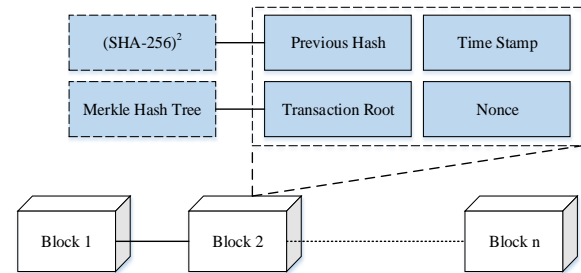


Fig. 6. Blockchain Model for DDB.

---

#### Pseudocode for DNN

---

Input: Data Points  $\{ X = X_1, X_2, X_3, \dots, X_n \}$

Output: Processing outcome as  $\{ Y = Y_1, Y_2, Y_3, \dots, Y_n \}$

---

Begin

    Initialize {bias}

    Assign weight  $w = 0$

    While {Iteration < Maximum Iteration} do

        Update weight as  $w_i$  //Hidden Layer

        Obtain average weight //Output Layer

        Update Learning rates

        Return (Y)

    End While

End

---

When it comes to blockchain technology, it is a distributed ledger technology that supports effectual security management over the DDB systems. In blockchain, all transactions (like user credentials, queries, retrievals, server credentials, transaction logs) are stored in the distributed blocks. For each transaction, corresponding hash value is generated and stored in the blockchain structure. For hashing, secure hashing algorithm-256 is applied twice as  $(SHA-256)^2$  and signature is verified based on elliptic curve signature generation. The model of blockchain is illustrated in Fig. 6.

With the aid of blockchain ledger, it is possible to perform secure operations in the system. It assures security, integrity, authenticity, access control and non-repudiation, which are important security requirements. The following pseudocode explains the procedure of secure hashing performed in the blockchain. Here, each data accessed or stored in the DDB system is provided with the secure hash function.

---

#### Pseudocode for Hash Generation

---

Input: Data  $\{ X = X_1, X_2, X_3, \dots, X_n \}$

Output: Hash of Data  $(H\{X = X_1, X_2, X_3, \dots, X_n\})$

---

Begin

    Initialize hash values

    From  $\{h_0$  to  $h_7\}$  as primes

    Initialize Round Constants

    Perform padding on X

    Make X into 512 bits Chunks

    For each chunk Do

        Create Schedule Array

        Extend Schedule Array

        Initialize working variables

        Compress schedule array

        Add compressed Chunk to  $H\{Y\}$

    End for

End

---

In Fig. 7, overall proposed architecture is illustrated. In the proposed solution, all users and DDB system are connected through distributed blockchain to ensure high-level security. In general, blockchain stores the current hash value and previous block hash value which ensures non-repudiation and integrity for the data stored in DDB.

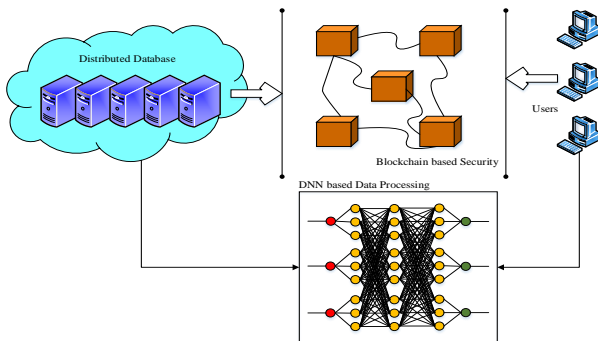


Fig. 7. Proposed DDB Architecture.

Further, user authentication credentials can be stored in the blockchain as an alternate for traditional centralized server. As a result, the single point failure issue of centralized server is overwhelmed. For fragmentation and data allocation problem, DNN based data processing procedure is proposed. Thus, solutions are presented for major problems of DDB systems. Both solutions can work together to ensure efficiency and security.

## V. CONCLUSION AND FUTURE DIRECTION

This paper presents an overview on distributed database (DDB) system. First, it summarizes major research problems of DDB and the relationship among the problems. Then, it reviews significant works focus on resolving the problems of DDB. The analysis shows that still there are several issues that are unsolved in DDB systems. After critical analysis, the researcher proposes a novel solution that combines Blockchain and Deep Learning for DDB security and data processing respectively. Overview on the proposed solution is given in detail. Further research can be carried over the following directions:

- The system needs to be tested and evaluated in a large-scale environment.
- Proposed DDB system can be combined with Hadoop file systems to make the processes faster and more efficient.
- Lightweight and scalable blockchain technology will be useful to cope with the DDB environment.
- Lightweight cryptography techniques can be employed to improve security level.
- Unsupervised clustering methods can be tested for fragmentation process.

## REFERENCES

- [1] D.S.Hiremath, Dr.S.B.Kishor, (2016). "Distributed Database Problem areas and Approaches", IOSR Journal of Computer Engineering, 15-18.
- [2] Raouf, A.A., Badr, N., & Tolba, M. (2017). Distributed Database System (DSS) Design Over a Cloud Environment.
- [3] Sharma, M., Singh, G., & Singh, R. (2016). Design and analysis of stochastic DSS query optimizers in a distributed database system. Egyptian Informatics Journal, 17, 161-173.
- [4] Seybold, D., & Domaschka, J. (2017). Is Distributed Database Evaluation Cloud-Ready? ADBIS.
- [5] Xiong, X., Shen, Y., Feng, G., Guo, M., & Wang, B. (2019). Research on Multi-level Distributed Storage Method of Economic and Financial Management Database. 2019 International Conference on Virtual Reality and Intelligent Systems (ICVRIS), 411-414.
- [6] Zhou, Y., Chen, Q., Shan, B., Jiang, F., & Pang, Y. (2019). A Distributed Storage Strategy For Trajectory Data Based On Nosql Database. IGARSS 2019 - 2019 IEEE International Geoscience and Remote Sensing Symposium, 3487-3490.
- [7] Gupta, Swati & Saroha, Kuntal & Bhawna, & Tech, M & Scholar, Pdmce & Bahadurgarh., (2011). Fundamental Research of Distributed Database. International Journal of Computer Science and Management Studies. 11.
- [8] Katembo Kituta Ezéchiél, Shri Kant, Ruchi Agarwal, (2019). A Systematic Review On Distributed Databases Systems And Their Techniques. 15th January 2019. Vol.96. No 1, 1992-8645.
- [9] M.T. O' zsu, U. Dayal and P. Valduriez (eds.), Morgan-Kaufmann An Introduction to Distributed Object Management, 1994, pages 1-24.
- [10] Swati Gupta, 21, July 2013, Deadlock Detection Techniques in Distributed Database System, International Journal of Computer Applications (0975 - 8887).
- [11] Abubakar Mohammed, Bashir Maina Saleh, January 2017, Centralized Database: A Prerequisite for Security and Sustainable Development in Nigeria, International Journal of Innovative Research in Computer Science & Technology (IJIRCST).
- [12] Shital Jadhav, Ashwini Gawande, February 2017, An Overview of Distributed Database System's Advantages and its Problem Areas, International Journal of Innovative Research in Computer and Communication Engineering, (3297: 2007).
- [13] Al-Sayyed, R.M., Zaghoul, F.A., Suleiman, D., Itriq, M., & Hababeh, I. (2014). A New Approach for Database Fragmentation and Allocation to Improve the Distributed Database Management System Performance. Journal of Software Engineering and Applications, 07, 891-905.
- [14] Wiese, L. (2014). Clustering-based fragmentation and data replication for flexible query answering in distributed databases. Journal of Cloud Computing, 3, 1-15.
- [15] AliA.Amer, Adela.Sewisy, TahaM.A.Elghendy. (2017). An optimized approach for simultaneous horizontal data fragmentation and allocation in Distributed Database Systems (DDBSs). Heliyon3.
- [16] Suganya, A., & Kalaiselvi, R. (2013). Efficient Fragmentation and Allocation in Distributed Databases. International journal of engineering research and technology, 2.
- [17] Alom, B., Henskens, F., & Hannaford, M. (2009). Query processing and optimization in distributed database systems.
- [18] Natarajan, M., & Manimegalai, R. (2018). Key agreement based secure Kerberos authentication protocol (KASKAP) for distributed database access in secured manner. International journal of engineering and technology, 7, 24.
- [19] Khamis, A.D., & Subair, S.O. (2019). Security Framework for Distributed Database System.
- [20] Guclu, A., Bakir, C., & Hakkoymaz, V. (2020). A New Scalable and Expandable Access Control Model for Distributed Database Systems in Data Security. Hindawi.

# Secure Software Defined Networks Controller Storage using Intel Software Guard Extensions

Qasmaoui Youssef<sup>1</sup>

Hassan First University, Faculty of  
Sciences and Techniques, Computer  
Networks, Mobility and Modeling  
laboratory: IR2M, Settat, Morocco

Maleh Yassine<sup>2</sup>

IEEE Senior Member  
Sultan Moulay Slimane University  
LaSTI Laboratory, Beni Mellal  
Morocco, Settat, Morocco

Abdelkrim Haqiq<sup>3</sup>

IEEE Senior Member  
Hassan First University, Faculty of  
Sciences and Techniques, Computer  
Networks, Mobility and Modeling  
laboratory: IR2M, Settat, Morocco

**Abstract**—The SDN controller is the core of the software-defined network (SDN), which provides important network operations that needs to be protected from all type of threats. Many researches have been focusing on different layers of security regarding the SDN controller such as Anti-DDOS system or enforcement of TLS connection between the controller and the Open-vswitches. One of the major security threats targeting any program is the environment execution itself (e.g. Operating system and the hardware itself). Intel's Software Guard Extension (SGX) offers a solid layer of security applied to applications by creating a Trusted execution environment. SDN controller relay on a storage module to keep sensitive data such as Flow Rules, users' credentials and configuration files. Protecting this side of the SDN controller is a must in term of security. To date, no work has been conducted considering SDN controller storage security using Intel SGX. This paper introduces an SGX enabled SDN controller. The new controller ensures the integrity and the confidentiality in a trusted execution environment by leveraging a recent hardware technology called intel SGX. This technology provides a trusted and secure enclave. Enclaves are sealed and unsealed by intel SGX attestation mechanisms to protect the executed code and data inside live memory and disk from being altered by any unauthorized access. High privileged codes such as the OS itself is kept from altering data inside enclaves. We implemented the Intel SGX using the Floodlight SDN controller running a real enabled Intel SGX hardware. Our evaluation shows that the SGX enabled SDN controller introduces a slightly observable performance overhead to the floodlight controller compared to advantages in term of security.

**Keywords**—Software defined networks; software guard extensions; storage; integrity; confidentiality

## I. INTRODUCTION

In recent years, the network research community has experienced a period of intense activity that has led to the emergence of different architectures or paradigms such as the SDN. The centralization (logical or physical) of the control plan, had to bring the expected flexibility to the network applications and allow to respond to many concrete use cases.

Software-Defined Network is a new paradigm of network architecture that aims to design a data plane that is fully programmable and separated from the control plane [1]. The Control Plane manages decisions about how and where to transmit network traffic through system configuration,

management and exchange of routing table information. The Data/Forwarding Plane manages the actual transmission of packets to the destination network according to the logic of the control plan. Behind this separation, there are three main objectives:

- The separation of network intelligence (control plan) from equipment (data plan).
- The provision of a logically centralized view of the global physical network.
- Providing an abstraction of programmable network equipment using Interfaces of application programming (API).

Among the innovations of this new paradigm is the programmability of network equipment and applications. New network applications can be transparently programmed and deployed using standard APIs. However, its implementation in the data plane remains one of the greatest challenges for research.

Protecting sensitive data from been altered or access gained by any authorized manner is present since the beginning of the programming time, a challenge that many have taken the race to solve it [2]. SDN technology has been introduced to solve the complexity of configuring network hardware. SDN enabled networks relay on a central decision making called the SDN controller to handle request coming from network devices such as switches and routers [3], [4]. Those requests are transported via API's using open flow protocol [5] and optionally secured using TLS.

The SDN controllers represent the most delicate part of the SDN architecture as it consists of the brain of the network, making it vulnerable to all sort of attacks [6], [7]. Security issues may vary depending on the level of interest targeted by a malicious person; it goes from Denial of service to traffic redirection and flow rules modification [8]. The SDN controller software is run on vast untrusted platforms, including operating systems, hypervisors, firmware, and hardware. This large machine base is growing complex and difficult to verify. For e.g., an OS such as Linux has 17 million line of code, however 662 vulnerabilities related to CVE have been recorded in 2019, such as memory corruption, transverse directory, unauthorized code execution. Execution

of normal and security-critical applications running on shared resources controlled by untrusted computing machines raises security threats. Running the SDN programs in such environments represent a considerable threat to its normal operations.

To solve the issue, one of the solutions is Trusted execution environments (TEE). TEE guarantee security by relying on less hardware and software computing base. Hardware is commonly considered to be a stable base since the cost and sophistication of hardware attacks usually are high. This has lead to the development of a secure running environment by industrial hardware companies for a safety-critical application that maintains little reliance or less dependency upon the operating system and hypervisor. Up to today, we found two main technology which are ARM Trust Zone Technology, Intel Software Guard Extensions (SGX) [9][10].

The objective of this work is to propose a secure architecture by programming new modules and adding security functions at the control plan storage based on Intel SGX. Then, evaluate the impact of SDN architectures at the performance level.

The rest of the paper is organized as follow. The next section will include a background and related works followed by the proposed model to secure SDN controller storage using Intel SGX, then we present the results of the implementation with discussion. Finally, we conclude this work with a conclusion and perspectives for future work.

## II. BACKGROUND

Trusted Execution Environment (TEE) is a tamper-resistant computing ecosystem that works on a separate kernel. It guarantees the validity of the executed programs, the security of the runtime components (e.g. memory, CPU registers, and critical Input / Outputs) and the secrecy of the executed code, data and runtime states are maintained in non-volatile memory [11]. In addition, the remote certificate shall be given to show its trustworthiness to third parties. The contents of TEE are not static; they can be changed safely. TEE condemns all software-related threats as well as hardware threats against the main memory of the operating system. Attacks leveraging backdoor authentication bugs are futile.

Fig. 1 illustrates the difference between a Trusted execution environment and an ordinary OS.

The most common TEE environments are Intel SGX and ARM TrustZone [12]. Both Intel SGX and ARM TrustZone are hardware TEE environments, but the process behind building a trusted environment with trusted code is distinct. Intel SGX provides a trusted environment for trusted programs that run on top of current untrusted device software. Whereas, ARM TrustZone is building a new, trusted ecosystem for trustworthy applications that operate on trustworthy device software and hardware that are only accessible to the trusted Configuration.

In this paper we focused on intel SGX technology to deploy our secure SDN controller. The Choice of using Intel SGX was taken depending on the much benefit that supersede ARM TrustZone, benefits such as documentation, maturity

and the availability of hardware enabled machines. The majority of researchers uses Intel SGX to deploy a trusted execution environment.

Intel Software Guard Extensions (Intel SGX) provides hardware-based memory encryption to isolate portions of code and application-specific data in memory. Intel® SGX allows user-level code to assign private memory regions (called enclaves) designed to be protected against processes running at higher privilege levels. Only the Intel® SGX solution provides such a granular level of control and protection.

Intel SGX has been used to secure flow tables inside OpenVswitches as mentioned in related works.

Fig. 2 shows the architecture of a typical intel SGX enabled environment.

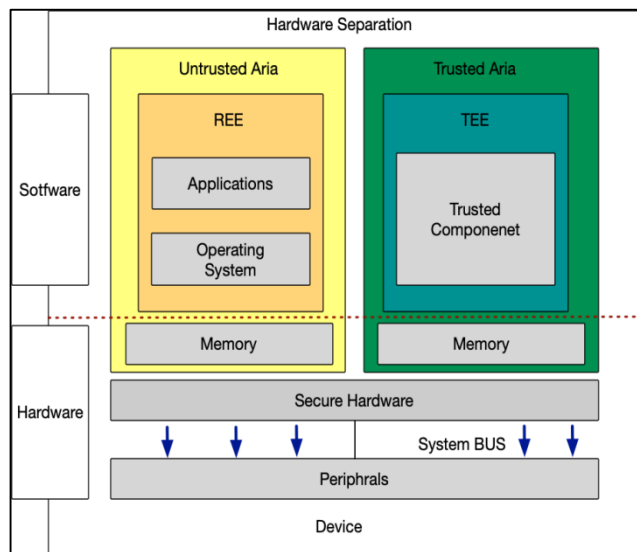


Fig. 1. Trusted Execution Environment.

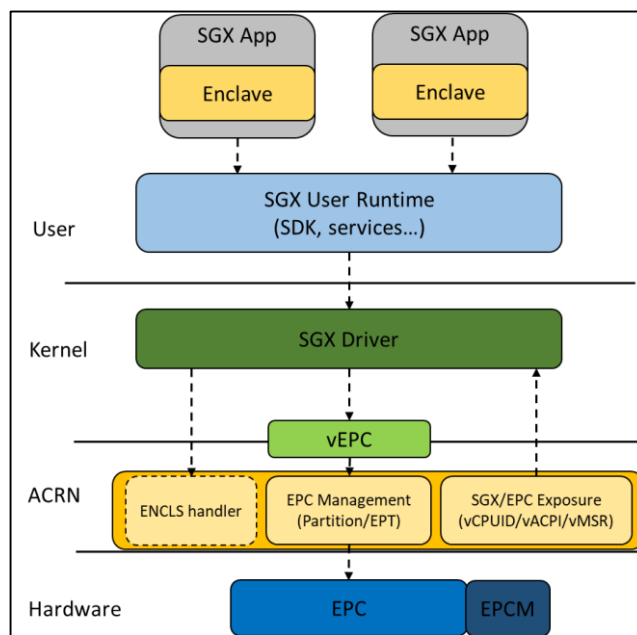


Fig. 2. Intel SGX Architecture.

SGX is built to be reliable; this is done in a variety of ways, including robust enclave delivery, sealing and attestation. Intel summarizes SGX's protections [13], [14] as follows;

- Memory is secured against observation and modification from outside the enclave, using an in-die Memory Encryption Engine (MEE) [15], with a secret that rotates on every boot. This protection notably works against host hypervisors, other enclaves, and anything running in supervisor mode.
- Enclaves will attest or confirm their identities to a competitor with the aid of a permanent hardware identification key for asymmetric encryption.
- Computer calls are designed to schedule and pass power in and out of the enclave. Arguments are safely mapped according to the concept of a static enclave.
- SGX does not protect itself against reverse engineering or side-channel attacks: to counteract this is the responsibility of the client.

### III. RELATED WORKS

There are only a few works in the literature that discuss SDN security using SGX. Intel Software Guard Extensions (SGX) has provided the general purpose of the hardware-assisted TEE referred to as Intel SGX. Intel SGX is an expansion of the x86 architecture with a new range of security-related instructions [16]. These instructions are used by security-critical programs to create a hardware-assisted trust environment referred to as an enclave [17]. Intel SGX enclave maintains secrecy through hardware-maintained data layout and honesty tests by encrypting data and code when it is outside the CPU package [18]. Intel SGX is a centralized security architecture, and the trustworthy TCB computing foundation is known to be a CPU package.

TruSDN is a mechanism for bootstrapping confidence in the technology of SDN [19]. Supports the safe supply of switches in SGX enclaves, a protected communication channel between switches and SDN controllers, and secure communication between endpoints.

Trusted Click [20] investigates the viability of network processing in SGX enclaves. Although none of the above methods discusses the credibility and anonymity of OpenFlow flow tables, they can be complemented by OFTinSGX to accomplish this. SCONE allows operators to protect the secrecy and integrity of computing in containers against host root access adversaries [21]. An alternative approach to securing virtual network functions running in containers, which prevents the unnecessary expansion of the trusted computing foundation, is proposed in [22]. Event Controller Eviction mitigates DoS attacks and OpenFlow Application overflow [23]. This framework uses two different frameworks – the learning module and the flow control module – while the case handler system prevents overload and DoS attacks, the OpenFlow flow tables have no security guarantees. OFTinSGX maintains the integrity and confidentiality of

OpenFlow tables and the reasoning for forwarding and disposal procedures.

TLSonSGX guarantees that OvS authorities retain communication with SDN controllers and the cryptographic material they use [24]. This methodology can be paired with OFTinSGX to provide broader security assurances for OpenFlow switches. Fig. 3 shows the TLSonSGX system design.

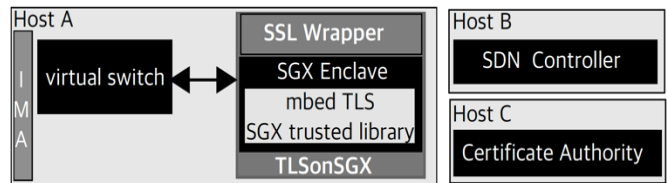


Fig. 3. TLSonSGX System Design.

In recent works OFTinSGX has been proposed by [9], which has four components: SGX OpenFlow table, SGX rule structure, SGX Eviction component, and SGX tables dpif, which helps OvS to delegate its OpenFlow tables and forward logic to enclave memory.

The important limitation of this work is that the abstraction of only the contents of the OpenFlow flow tables does not address all security concerns, as the classifier only includes references to the classification rules. The procedure used to control the OpenFlow flow tables can cover both the contents of the tables and the full description of the rules assigned to the untrusted memory.

Fig. 4 illustrates the OFTinSGX Architecture.

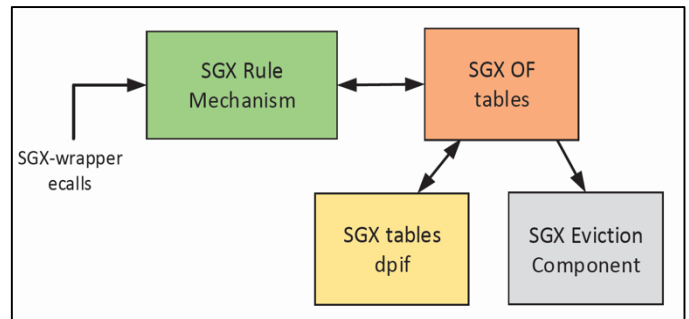


Fig. 4. OFTinSGX Architecture.

## IV. THE PROPOSED SGX SDN CONTROLLER

### A. SDN Storage Module Overview

This section presents the design and the architecture of the proposed model to secure SDN controller storage using Intel SGX.

Generally, the SDN controller is relying on a storage module that handles all sensitive data; controller data are mostly configuration files such as flow rules. In our case, we use the floodlight SDN controller to implement our approach. Fig. 5 illustrates the Floodlight architecture. The proposed model consists of rewriting the storage module code taking into consideration the Intel SGX technology.



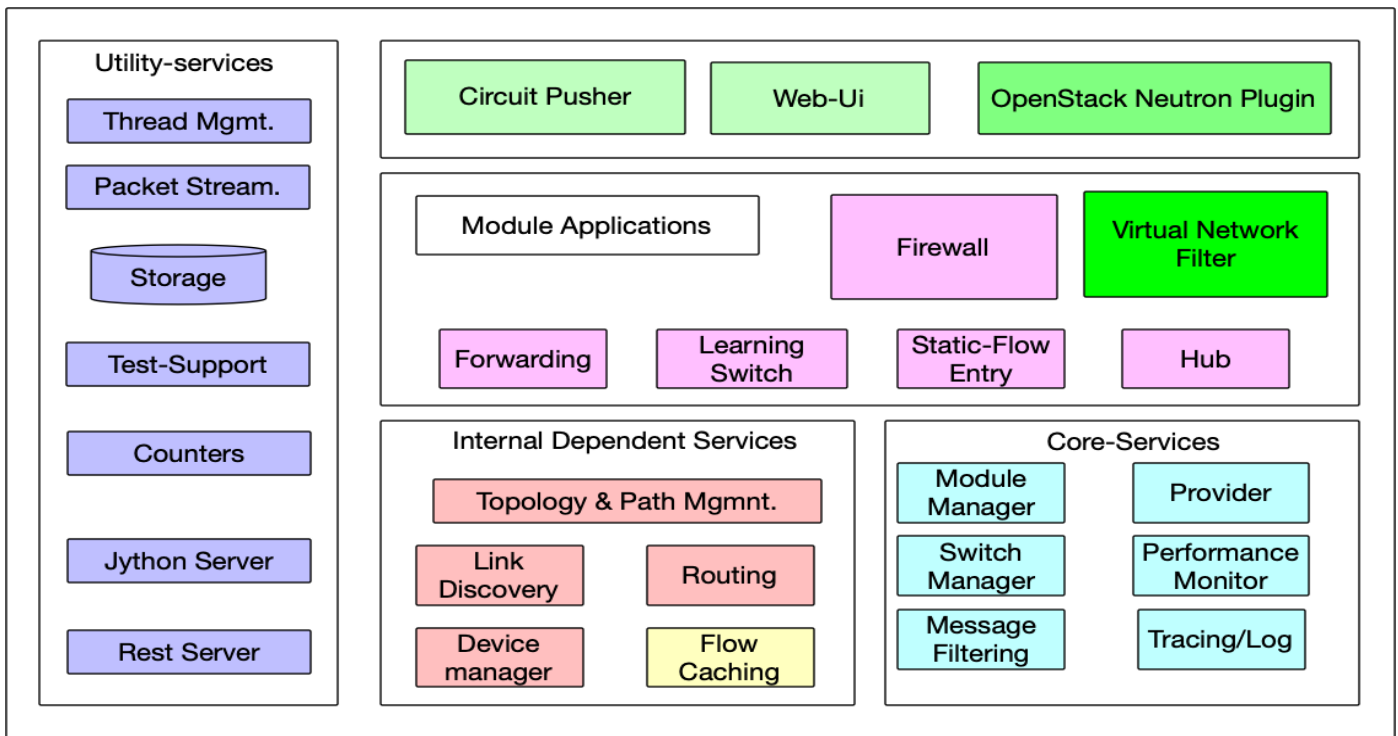


Fig. 5. Floodlight Architecture.

The storage module consists of four main modules: link discovery module (responsible for discovering and maintaining the status of links in the OpenFlow network), Device manager module (tracks devices as they move around a network and defines the destination device for a new flow), Static flow entry pusher (allows a user to manually insert flows and groups into an OpenFlow network) module and QoS module (give a user a way to simply push QoS state to switches that support these features) interacting with the primary storage module which is mainly a NoSQL database residing in the random-access memory. Fig. 6 shows the interaction between the four-module and the storage module.

A compromised host can present a huge issue to the NoSQL database making it vulnerable to several attacks such memory dump or memory exhaustion attacks. Our method consists of hardening all the space used by the NoSQL database by implementing the Intel SGX technology to prevent any damage to the RAM area used by the SDN controller.

**B. SDN Enabled SGX Architecture**

SDN enabled SGX model operates as an intermediate system. Specifically, it executes a process daemon that intercepts all the call made to the ordinary storage module by the controller application. These calls are translated into corresponding functions of the SDN enabled SGX model enclave. For instance, when a new open flow rules need to be inserted, the call is made via our interface and call the corresponding function inside the enclave via a JNI (Java Native Interface). The code residing in the enclave return the right value depending on the result of the function via the interface. In this design, all the data structures related to the file system are continuously kept in the Enclave Page

Cache(EPC), which is a subset of DRAM that cannot be directly accessed by other software, including system software and SMM code. The CPU's included memory controllers also reject DMA transmissions targeting the EPC, thus protecting it from access by other peripherals.

The NoSQL database files are maintained by the enclave and protected by the encryption mechanisms of the SGX technology, making a dump of the memory useless as its encrypted and cannot be read.

Data is decrypted by the SGX unsealing mechanism: this process occurs while entering the enclave and is thus secured by the CPU borders. Consequently, a dump of the EPC (enclave page cache) would be captured and blocked by the SGX protection mechanisms.

Fig. 7 shows the proposed SDN enabled SGX model.

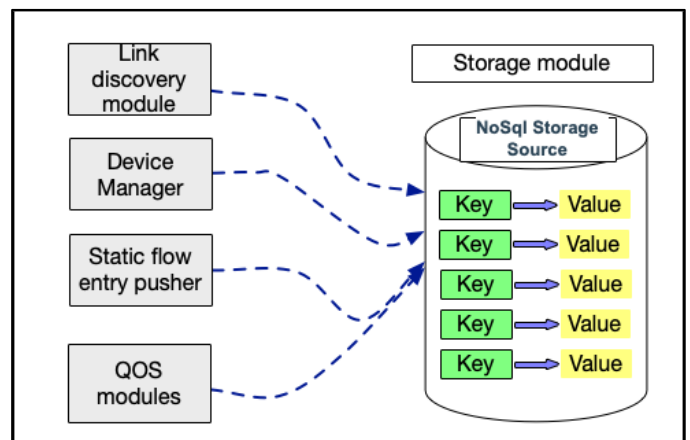


Fig. 6. The Proposed Storage Module.

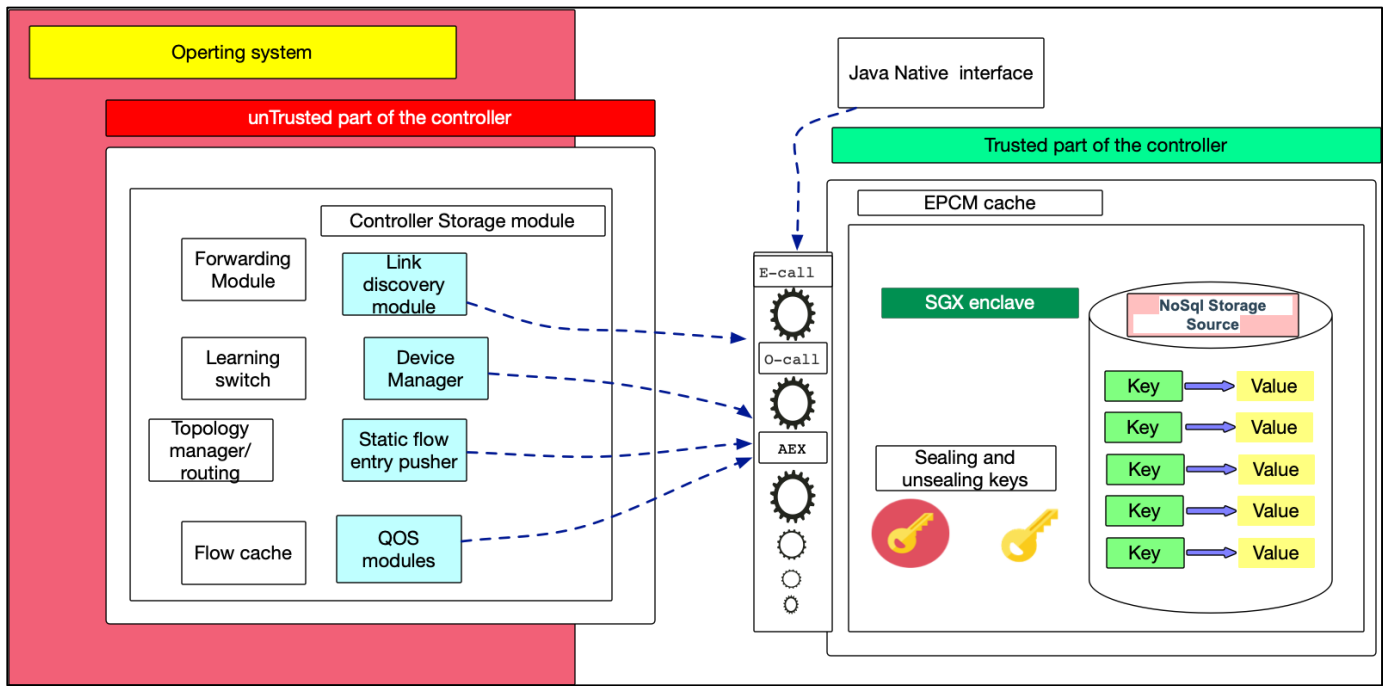


Fig. 7. The Proposed SDN Enabled SGX Model.

## V. IMPLEMENTATION AND EVALUATION

### A. Implementation Setup

We implemented the SDN controller enabled SGX on a Linux platform holding an SDN controller named floodlight developed using JAVA programming language. Since intel SGX SDK support only C/C++ language, we used the Java Native Interface (JNI) to make the right call to C functions to handle intel SGX operations. The next scenario demonstrates the different phases of the implementation, this scenario is almost generic to any Intel SGX enabled case:

- Step 1: An enclave is created by the untrusted part of the application.
- Step 2: The enclave must be initialized via a launch token, fetched and provided by Intel's launch enclave.
- Step 3: Access to the LE and other architectural enclaves, e.g., the quoting enclave (QE) and the provisioning enclave (PE), is provided by the Intel application enclave service manager (AESM). SGX libraries provide an abstraction layer for communicating with the AESM.
- Step 4: Execution of a trusted function which executes an ECALL.
- Step 5: The ECALL goes through the SGX call interface to bring the executing thread inside the enclave.
- Step 6: An OCALL is executed once the execution in the trusted environment completes.
- Step 7: Finally giving the control back to the caller.

The program run on HP Proliant gen10 server with the following Configuration:

- Intel XEON E-2174G with intel SGX support.
- 32GB of RAM.

To generate traffic we use mininet simulator [25], mininet was setup and configured on five different computers to be able to generate 2000 request by each one.

The written code mainly focuses on the Storage Source Service, which is the main interface of the storage module of floodlight controller, also some of the dependencies were taken into accounts such as IDebugCounterService and IRestApiService.

Table I shows a summary of the code changes made to the storage module inside the floodlight controller. The most significant part of the added code consists of new (JAVA NATIVE INTERFACE) JNI interface and make files, floodlight storage also has been modified to accept the call from OCALL I/O peripherals.

### B. Performance Analysis

Our evaluation is based on the scenario that involves a number of nodes making calls to the SDN controller. In this case, the network devices receive various request to dispatch packets from a script that run on several separated machines. Decision making is sent from the data layer represented by the network devices. Next, the controller responds with the corresponding flow rule. Rules present inside the Open-switches are deleted, so the network devices are forced to make calls to the controller. The script sends over 10000 requests to several separated switches. The generated traffic sent to the controller allows us to take statistics and compare them to the normal scenario.

TABLE I. SUMMARY OF THE CODE CHANGES

| Lines of code of SGX enabled SDN controller |                        |                   |
|---------------------------------------------|------------------------|-------------------|
| component                                   | Lines of original code | % changed         |
| Floodlight storage module                   | 3688                   | 9.05% (350 lines) |
| JNI interface                               | 1203                   | 100% (1203 line)  |
| Other(e.g. make files )                     | 200                    | 100% (200 lines)  |

A normal scenario consists of the same use case but with non-modified controller. Table II, shows the collected measures and a relative Overhead. Overhead is between 7 and 10% in the first run. The overhead is calculated as shown in the following equation:

$$OH = (E[SGX] - E[normal])/E[normal]*100$$

The increase of the overhead is caused by the use of SGX enclaves. For each ECALL to the storage module to gather flow rules, the CPU switch to the enclave mode, resulting to an increase of execution time. Overhead increases linearly with the number of e-call invocations. The state of the controller gets stabilized after a while since the flow rules are cached inside the open flow tables within the open vswitches.

TABLE II. COLLECTED MEASURES AND OVERHEAD

| Controller response time                 |                 |                                  |          |
|------------------------------------------|-----------------|----------------------------------|----------|
| Number of requests to the SDN controller | Normal scenario | Intel SGX enabled SDN controller | Overhead |
| 10000 (first run)                        | 3300 us         | 3630                             | 10 %     |
| 10000 (second run)                       | 2170 us         | 2320                             | 7 %      |
| 10000 (third run no flow flashing)       | 300 us          | 313 us                           | 4.33 %   |

Table II shows the Overhead interval between two test cases. The same parameters are kept during the two tests. The deference between the overhead in both runs is due to CPU consumption by the OS itself and other floodlight operations.

The third run on the scenario was conducted in a special case where the open-vswitches are not flushed so flow rules are kept inside the switches flow tables, open flow switches call the SDN controller only if there is no entry matching the upcoming packets. There was a slit increase in time execution in this case and that was because of normal operations executed by the controller itself.

## VI. CONCLUSION

The concept of SDNs or Software Defined Networks is an architecture that facilitates network management and control, and allows rapid introduction of network services through programming and separation of the control plane from the data plane. With this new architecture, administrators can manage the network in a unified way from the control plane, and can introduce or eliminate any service through the application plane without changing the physical infrastructure. New network applications can be transparently programmed and deployed using standard APIs. Most modern SDN controllers can run on any OS However, its implementation in the data domain remains one of the biggest challenges for storage security at the control plane level.

In this work, we proposed using Intel SGX to provide additional security to the general intent of the Execution Environment of applications.

In order to evaluate the performance impact of our SDN enabled Intel SGX architecture we implemented our SDN controller model enabled SGX on a Linux platform holing an SDN controller named floodlight. The results of our model implementation show the efficiency of our model without any major cost in term of performance.

## VII. FUTURE WORKS

As a perspective, we would like to test our model in large test platforms to estimate its capacity and limitations and compare it to the TEE provided by ARM named ARM Trustzone.

Other evolution will be conducted on other point of views such as using intel SGX to build the entire application instead of the storage module alone.

## REFERENCES

- [1] M. F. H. and M. A. Ismail, "Distributed Shadow Controllers based Moving Target Defense Framework for Control Plane Security," Int. J. Adv. Comput. Sci. Appl., vol. 10, no. 12, pp. 150–156, 2019, doi: 10.14569/IJACSA.2019.0101221.
- [2] Safaa MAHRACH and Abdelkrim HAQIQ, "DDoS Flooding Attack Mitigation in Software Defined Networks," Int. J. Adv. Comput. Sci. Appl., vol. 11, no. 1, pp. 693–700, 2020, doi: 10.14569/IJACSA.2020.0110185.
- [3] T. Dargahi, A. Caponi, M. Ambrosin, G. Bianchi, and M. Conti, "A Survey on the Security of Stateful SDN Data Planes," IEEE Commun. Surv. Tutorials, 2017.
- [4] J. Son and R. Buyya, "A Taxonomy of Software-Defined Networking (SDN)-Enabled Cloud Computing," ACM Comput. Surv., vol. 51, no. 3, p. 59, 2018.
- [5] N. McKeown et al., "OpenFlow: enabling innovation in campus networks," ACM SIGCOMM Comput. Commun. Rev., vol. 38, no. 2, pp. 69–74, 2008.
- [6] K. Bhushan and B. B. Gupta, "Distributed denial of service (DDoS) attack mitigation in software defined network (SDN)-based cloud computing environment," J. Ambient Intell. Humaniz. Comput., pp. 1–13, 2018.
- [7] H. D’Cruze, P. Wang, R. O. Sbeit, and A. Ray, "A Software-Defined Networking (SDN) Approach to Mitigating DDoS Attacks," in Information Technology-New Generations, Springer, 2018, pp. 141–145.
- [8] A. QASMAOUI, Y., & HAQIQ, "Enhanced Solid-Flow: An Enhanced Flow Rules Security Mechanism for SDN," IAENG Int. J. Comput. Sci., vol. 47, no. 3, 2020.
- [9] J. Medina, N. Paladiy, and P. Arlosz, "Protecting OpenFlow using Intel SGX," in 2019 IEEE Conference on Network Function Virtualization and Software Defined Networks (NFV-SDN), Nov. 2019, pp. 1–6, doi: 10.1109/NFV-SDN47374.2019.9039980.
- [10] S. Costan, V., & Devadas, "Intel SGX Explained," IACR Cryptol. ePrint Arch., vol. 86, pp. 1–118, 2016.
- [11] V. Lefebvre, G. Santinelli, T. Müller, and J. Götzfried, "Universal Trusted Execution Environments for Securing SDN/NFV Operations," 2018, doi: 10.1145/3230833.3233256.
- [12] J. Winter, "Trusted Computing Building Blocks for Embedded Linux-Based ARM Trustzone Platforms," in Proceedings of the 3rd ACM Workshop on Scalable Trusted Computing, 2008, pp. 21–30, doi: 10.1145/1456455.1456460.
- [13] S. Kim, Y. Shin, J. Ha, T. Kim, and D. Han, "A First Step Towards Leveraging Commodity Trusted Execution Environments for Network Applications," 2015, doi: 10.1145/2834050.2834100.

- [14] A. Baumann, M. Peinado, and G. Hunt, "Shielding Applications from an Untrusted Cloud with Haven," *ACM Trans. Comput. Syst.*, vol. 33, no. 3, Aug. 2015, doi: 10.1145/2799647.
- [15] S. Gueron, "A Memory Encryption Engine Suitable for General Purpose Processors," *Cryptol. ePrint Arch. Rep.* 2016/204, 2016.
- [16] Intel®, "Intel® Software Guard Extensions Programming Reference," (Cited pages 13 14.), 2014.
- [17] I. Graydon, E. Beatty, S. Paul, M. N. Us, and J. A. Hauck, "Method and apparatus to provide secure application execution," 2006.
- [18] F. X. Simon P Johnson, Uday R Savagaonkar, Vincent R Scarlata and C. V. R. McKeen, "Technique for supporting multiple secure enclaves," *US Patent 8,972,746.*, 2015.
- [19] N. Paladi and C. Gehrman, "TruSDN: Bootstrapping Trust in Cloud Network Infrastructure," in *International Conference on Security and Privacy in Communication Systems* (pp. 104-124), 2017, pp. 104–124.
- [20] M. Coughlin, E. Keller, and E. Wustrow, "Trusted Click: Overcoming Security Issues of NFV in the Cloud," in *Proceedings of the ACM International Workshop on Security in Software Defined Networks & Network Function Virtualization*, 2017, pp. 31–36, doi: 10.1145/3040992.3040994.
- [21] S. Arnautov et al., "{SCONE}: Secure Linux Containers with Intel {SGX}," in *12th {USENIX} Symposium on Operating Systems Design and Implementation ({OSDI} 16)*, Nov. 2016, pp. 689–703, [Online]. Available: <https://www.usenix.org/conference/osdi16/technical-sessions/presentation/arnautov>.
- [22] D. Girtler and N. Paladi, "Component integrity guarantees in software-defined networking infrastructure," in *2017 IEEE Conference on Network Function Virtualization and Software Defined Networks (NFV-SDN)*, Nov. 2017, pp. 292–296, doi: 10.1109/NFV-SDN.2017.8169858.
- [23] Ying Qian, Wanqing You, and Kai Qian, "OpenFlow flow table overflow attacks and countermeasures," in *2016 European Conference on Networks and Communications (EuCNC)*, Jun. 2016, pp. 205–209, doi: 10.1109/EuCNC.2016.7561033.
- [24] N. Paladi, L. Karlsson, and K. Elbashir, "Trust Anchors in Software Defined Networks," in *Computer Security*, 2018, pp. 485–504.
- [25] R. L. S. de Oliveira, C. M. Schweitzer, A. A. Shinoda, and L. R. Prete, "Using Mininet for emulation and prototyping Software-Defined Networks," in *2014 IEEE Colombian Conference on Communications and Computing (COLCOM)*, 2014, pp. 1–6, doi: 10.1109/ColCom.Con.2014.6860404.

#### AUTHORS' PROFILE

**Youssef Qasmaoui** received his Master degree in Networks and IT Security and his Bachelor degree in Networks and IT Systems, respectively in 2012 and 2010 from the Faculty of Sciences and Techniques (FST), Serrat – Morocco. He also received a second Master degree in Information System Engineering at the University of Western Brittany at Brest – France. He is also doing his Ph.D. thesis at the FST, Serrat - Morocco. His research interests include Software Defined Networks, Virtual Laboratory and Networks Security.

**Yassine MALEH** is a cybersecurity professor and practitioner with industry and academic experience. He is a Ph.D. degree in Computer Sciences. Since 2019, He working as a professor of cybersecurity at Sultan Moulay Slimane University, Morocco. He was working for the National Port

agency (ANP) in Morocco as an IT Security Manager from 2012 to 2019. He has published more than 60 research papers. This includes 7 books, 20 book chapters, 14 peer-reviewed journal articles, and 20 peer-reviewed conference manuscripts.

He has served on Program Committees of more than 20 conferences and events and has organized many Symposia/Workshops as a General Chair. He is an editor of a number of journals including Editor in Chief: *International Journal of Smart Security Technologies (IJSST)*. Associate Editor: *IEEE Access* (Impact Factor: 4.09), *International Journal of Digital Crime and Forensics (IJDCF)* and *International Journal of Information Security and Privacy (IJISP)*. He was also a Guest Editor of a special issue on *Recent Advances on Cyber Security and Privacy for Cloud-of-Things of the International Journal of Digital Crime and Forensics (IJDCF)*, Volume 10, Issue 3, July-September 2019. He served and continues to serve as a reviewer of numerous prestigious journals such as *Elsevier Ad Hoc Networks*, *IEEE Network Magazine*, *IEEE Sensor Journal*, *ICT Express*, and *Springer Cluster Computing*, etc...

**Prof. Abdelkrim HAQIQ** has a High Study Degree (Diplôme des Etudes Supérieures de troisième cycle) and a PhD (Doctorat d'Etat), both in the field of modeling and performance evaluation of computer communication networks, from Mohammed V University, Faculty of Sciences, Rabat, Morocco. Since September 1995 he has been working as a Professor at the department of Applied Mathematics and Computer at the Faculty of Sciences and Techniques, Serrat, Morocco. He is the Director of Computer, Networks, Mobility and Modeling laboratory: IR2M. He is an IEEE senior member and an IEEE Communications Society member. He is also a member of Machine Intelligence Research Labs (MIR Labs), Washington, USA. He was a co-director of a NATO Multi-Year project entitled "Cyber Security Analysis and Assurance using Cloud-Based Security Measurement system", having the code: SPS-984425. Prof. Abdelkrim HAQIQ's interests lie in the areas of modeling and performance evaluation of communication networks, mobile communications networks, cloud computing and security, emergent technologies, Markov chains and queueing theory, Markov decision processes theory, and game theory. He is the author and co-author of more than 170 papers (international journals and conferences/workshops). He supervised 15 PhD thesis and co-supervised 3 PhD thesis. Actually, he is supervising and co-supervising other PhD thesis. He is an associate editor of the *International Journal of Computer International Systems and Industrial Management Applications (IJCISM)*, an editorial board member of the *International Journal of Intelligent Engineering Informatics (IJIEI)* and of the *International Journal of Blockchains and Cryptocurrencies (IJBC)*, an international advisory board member of the *International Journal of Smart Security Technologies (IJSST)* and of the *International Journal of Applied Research on Smart Surveillance Technologies and Society (IJARSSTS)*. He is also an editorial review board of the *International Journal of Fog Computing (IJFC)* and of the *International Journal of Digital Crime and Forensics (IJDCF)*. Prof. Abdelkrim HAQIQ was a chair and a technical program committee chair/member of many international conferences and scientific events. He was also a Guest Editor and Co-Editor of special issues of some journals, books and international conference proceedings. From January 1999 to December 1999 he had a Post-Doctoral Research appointment at the department of Systems and Computers Engineering at Carleton University in Canada. He also has held visiting positions at the High National School of Telecommunications of Paris, the Universities of Dijon, Versailles St-Quentin-en-Yvelines and LAAS CNRS, Toulouse in France, the University of Ottawa in Canada, the FUCAM in Belgium, the National Engineering School of Sfax, Tunisia, the University of Naples Federico II, Italy and the University of Algarve, Portugal.

# Dynamics of Organizational Change

Maximo Flores-Cabezas<sup>1</sup>

Faculty of Accounting, Economic  
and Financial Sciences  
Universidad de Ciencias y  
Humanidades, Lima, Perú

Desiree Flores-Moya<sup>2</sup>

Faculty of Engineering  
Universidad de Ciencias y  
Humanidades  
Lima, Perú

Brian Meneses-Claudio<sup>3</sup>

Image Processing Research  
Laboratory (INTI-Lab)  
Universidad de Ciencias y  
Humanidades, Lima, Perú

**Abstract**—In this research, the evolution of change in an organization, due to continuous changes in the market, is disclosed in a qualitative and quantitative way. The changes developed in the organizational structure were aimed at the search for a flexible, dynamic and agile organization, which would allow adapting to the demands of increasingly informed customers, this engine of change called customer required the company to develop a flexible organizational structure. For this, the key concepts were reviewed, such as: systems, processes, activities, modeling and the use of the Systems Dynamics tool for the elaboration of the causal diagram and flow diagram, which allowed to identify, analyze and evaluate the variables that affected each stage of organizational change. The evolution of the change that the organization developed was carried out in an unplanned sequential manner, in the following stages: first a vertical organization, second an organization by processes, third a focused organization, fourth a modular organization and later a flexible organization, which allowed adapt to changes in customer orders, orders that each time increased in the characteristics of the product model, but decreased in quantities. The changes developed by the organization allowed to increase the response speed in order delivery by 43%.

**Keywords**—System dynamics; diagram; vertical organization; process organization; focused organization; modular organization; flexible organization

## I. INTRODUCTION

The present research work explains the evolution of the organization of an XXX textile-clothing company, in which the level of change in the behavior of its organizational structure was analyzed [1,2], as a result of the level of change in demand in the market. Initially, the company was developed through a vertical structure in a traditional hierarchical and highly bureaucratic way, it was formed by the administrative areas considered as support, and the operational areas that carried out from the storage of raw materials and supplies, transformation to packaging for the obtaining the final product, which are clothing. The company was considered as a system that consisted of a set of productive resources, led by management, decision-making was centralized, as well as the administrative area, the control of this area was done by management, this type of organization [3,4] gave results when the company was in its infancy, but due to the increase in demand for orders, the company began to expand its production capacity by increasing its infrastructure, machines, equipment and personnel for the different operational and administrative areas, it was

becoming increasingly clear that the company required new organizational models.

The company exports garments to the US, Canada among other countries, in a greater proportion to the US. These clients requested garments through a contract, their orders were greater than 5,000 garments per model with little variability in color, and type of fabric, it could have one type of application: print or embroidery, or both. The organization was forced to make the change where the type of order was suitable for a mass production line, the higher the production, the utility tends to increase and the unit costs to decrease, and this is due to the variable costs they increase according to the units produced and fixed costs remain constant over time, as can be seen in Fig. 1. Market changes began to appear when customers requested smaller and smaller quantities of garments through their orders to 5,000 garments, with varieties of colors, type of fabric and applications, that is, it became unstable, but this instability brought benefits to the company because it seeks a change from a company with a traditional structure to a dynamic, agile company. Organizations are defined as “open systems whose parts are related to each other and to their environment. The nature of this relationship is one of interdependence because all parts of the system affect and are mutually affected” [5].

In Section II, the methods applied in the collection, analysis and evaluation of information and System Dynamics as a tool for the design of scenario models using the Vensim software. And as an understanding of the development of these models, the concepts of systems, processes and activity are provided. In this section, the evolution of organizational change is rigorously detailed in four stages. In Section III, the results of the organizational change are presented in a quantitative way and graphically presenting its various behaviors from a modular structure to a flexible structure and the incidence of the configuration of production batches in process. In Section IV, the results obtained and the consequences that generated the changes are explained, such as the reduction of personnel, lack of commitment of the personnel and the decisions that the organization makes to reverse the lack of skilled workforce, the prevalence of the organization to maintain control through its authority. In Section V, the conclusions of the obtained results are explained and the future research to be carried out on organizational change through the concepts of chaos and complex systems in a qualitative and quantitative way is presented.

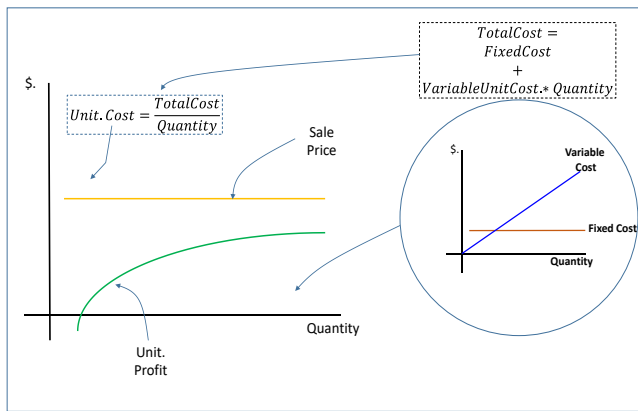


Fig. 1. Fluctuation of Prices, Costs and Profit.

### A. Statement of the Problem

Due to the rigidity with which the organization was developed through a vertical and centralized structure and with operational areas configured as mass production lines, it was not going to meet the changes in customer demand, in such a situation the management needed to respond to the following questions:

- Is the company prepared for a transition and know how to transform this implicit threat into growth?
- If the company with the type of structure could not adapt to changes in demand, what should be the type of agile and flexible organizational structure to demand?
- What positive effects will decentralization of administrative areas generate within operational areas?
- Reconfigure the operational areas from a type of organization by processes to a flexible organization with a pull system, would it adapt to changes in demand?

### B. Objective

It is to make known the stages of dynamic changes and the results of adaptability of the organization, based on the change in customer demand. From a rigid organization to a flexible, dynamic, results-oriented organization, allowing its members to think, innovate, collaborate, improve their capacities and assume a personal commitment to the collective future and to the objectives of the company.

### C. Hypothesis

A flexible organization is a dynamic and agile organization that adapts to changes in market demand, with personnel specialized in carrying out different types of activities that add value, in handling different types of machine, in the shortest possible time, reducing lead time, the costs of its resources and producing only the quantity requested by the client, efficiently and effectively fulfilling delivery times and with superior quality for the client.

## II. METHODOLOGY

The method used in the present study is empirical-analytical because through the stages of implementation of the change in the organizational structure, direct experience was

acquired and the evidence of the assimilation of the change was collected in each stage, making itself known in the present research work.

Also, a quantitative method because through the change that was made, the Systems Dynamics tool was used for modeling scenarios, identifying the relationship and interaction of the variables involved, assigning numerical values and algorithms, to apply formal techniques to the study.

### A. Systems Dynamics

Systems Dynamics is a tool that allows to analyze the level of behavior of a certain system, the interaction, the cause and effect of the variables that intervene [6, 7, 8], it also allows simulations through the construction of scenario models which we will do through of the Vensim software, defining the types of variables that act and interact. Through it, the level of incidence between the areas was evaluated: administrative with the operational part through the development of causal diagrams and flow diagrams.

Causal diagrams analyze the cause and effect that occur between two variables:

- $\uparrow A \rightarrow \uparrow B$ , if variable A increases or decreases variable B will also present the same behavior.
- $\uparrow A \rightarrow \downarrow B$ , if variable A increases or decreases variable B will present the opposite behavior.

This tool allowed to carry out experiments, gathering knowledge of the system, initially in a non-structured way, but as the cause-effect relationships of the variables were understood, this knowledge was organized in a more structured way [9].

### B. System

A system is a unit that is formed by a set of elements that interact with each other, to achieve a common goal [10, 11, 12]. The company as a system is visualized through an organization chart, where the set of areas that is organized is observed. Each area has a function and resources for the fulfillment of its objectives, as well as the level of responsibility. It can also consider that each area is a subsystem and is also made up of resources that interact towards a specific objective.

### C. Process

A process (P) is formed by a set of sub-processes (Sp) and each sub-process by a set of activities (a), it can also be considered that a process is made up of a set of activities, this will depend on the type of development of the organization [13, 14, 15].

$$P = \sum_{j=1}^n Sp_j, Sp = \sum_{i=1}^n a_i, P = \sum_{i=1}^n a_i \quad (1)$$

In operational processes, there are two types of push and pull systems. The push system adjusts to the capacity of the activity carried out by pushing the raw material, products in process or finished products from one activity to another, in this type of system inventories are presented, this is due to the difference in capabilities between activities.

The pull system [16] adjusts to market demand, when demand is present, production becomes effective. In this type of system, it does not present inventories since production is carried out according to the order between activities, that is, the activity that precedes pulls the raw material or product in process to the activity that precedes it. As will be seen later in the development, the change and their implementation of these systems in the operational areas had an impact on their adaptability to customer demand.

#### D. Activity

An activity (a) is made up of a set of tasks [17, 18], executed by the person or machine and person-machine. For each process, the following resources used were identified:

Cut  $\rightarrow a=f(T, RM, Inp, Mac., Pers., T.)$

Sewing  $\rightarrow a=f(Mac., Pp, Pers., T.)$

Cleanliness  $\rightarrow a=f(T, Pp., Pers., T.)$

Review  $\rightarrow a=f(Pp, Pers., T.)$

Packing  $\rightarrow a=f(Mac., T, Inp, Pp, Pers., T.)$

Where:

T = Table, RM = Raw Material, Inp. = Input, Mac = Machine, Pers. = Personnel, Pp = Product in process, T. = Tool.

#### E. Model

A model is an object that represents another object. As defined by Marvin Minsky [19], "For an observer O an object M is a model of an object S and an experiment E, if O can use M to apply E and solve important questions in relation to S".

#### F. Dynamics of Organizational Change

The management began to develop changes in the administrative areas and in the operational areas, the objective is for the company to be flexible to changes in demand. The administrative and operational organization must be able to adapt to rapid changes in demand efficiently and effectively. The type of organization that was developed was a vertical and rigid structure, the level of information from the operational and administrative areas reached the management for control, evaluation and decision-making, time was very limited for the review of all the reports. Faced with such complexity, management chose to make changes in the administrative areas as well as in the operational areas. Although, the changes developed by management were not planned but guided by instinct.

The change process in a given organization goes from top to bottom, management leadership for change determines the level of strength, flexibility and agility of the organization's response to the client. As the following researchers point out:

Gonzales [20] "in order to have adaptable organizations, it is necessary to create heterarchical structures, with flexible and flat models".

Ponce [21] "the company's ability to integrate, build and reconfigure internal and external competencies to address rapid changes in the environment."

The fundamental thing about change in an organization is that it remains constant, for this the design of the organization must be supported by a decentralized and flexible hierarchical structure: encourage teamwork, exchange and delegation of power: and put in motion systems that recognize and celebrate personal achievements.

The unplanned changes began in the operational part and later in the administrative part, as follows:

1) *1st Change from a vertical structure to a process structure:* In this type of vertical organization, the administrative part was separated from the operative part, as shown in Fig. 2. In the administrative part are the areas of Planning, Purchasing, Quality, Accounting, Modeling, Systems, Maintenance and Commercial. The Maintenance and Quality areas were centralized within the administrative part, not as part of the transformation of the product but as support areas for the operational part. The objective of the management was to maintain control of the administrative part, and the decisions of the management of the operative part were entrusted to the production manager, which only reported to the management the progress for each production order. The characteristic in this type of organization was that the communication flows are vertical from top to bottom and spread through the hierarchical structure, the leadership of the organization was in charge of an insider that is, the management controlled every activity that was executed in the administrative part. This organization provided a stable and predictable environment, it was conceived as a machine, the objective of the administrative and operational staff was its self-preservation, and physically the administrative part was separated from the production part.

As this type of structure did not help the strategic objectives of the company, changes in the organizational structure began, especially in those operational processes that used more labor, machine and production time and it's began from the receipt of the raw material, transformation, to turn into a final product such as the warehouse, cutting, sewing, cleaning-review and packaging areas.

In this type of organization, as can be seen in Fig. 3, the company developed it with the aim of maintaining control of the capacity and ability of each operating process separately, when it enters a certain garment model for its manufacture.

The type of demand requested by the client through a contract, the company converted it into a production order for internal administrative management in all operational processes, and the production orders were higher than 5,000 garments, the degree of complexity in their Manufacturing was minimal since it presented a single type of fabric, fewer than four colors, each color on average was 1,250 garments.

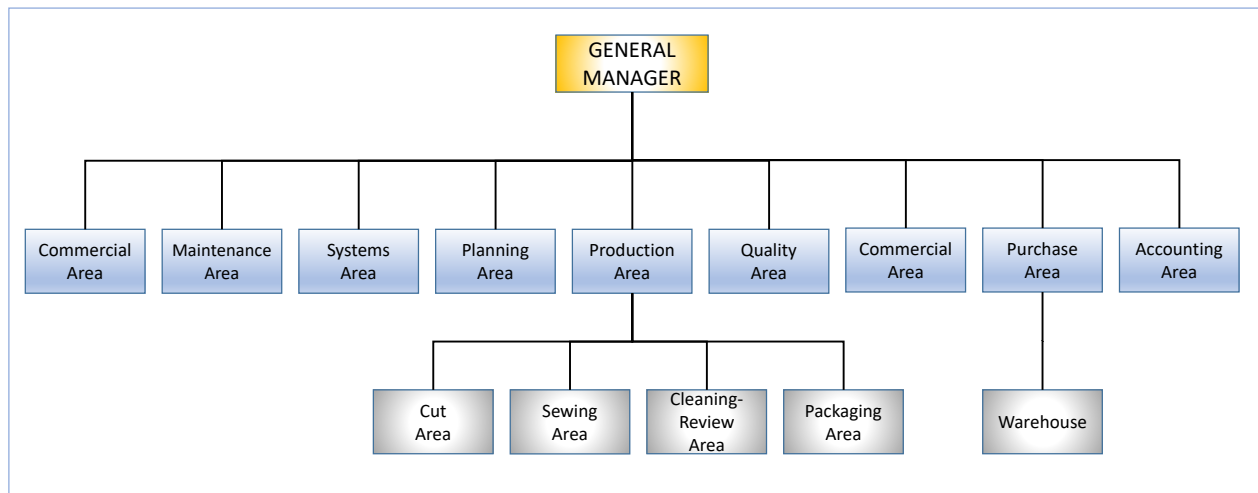


Fig. 2. Vertical Organization Chart.

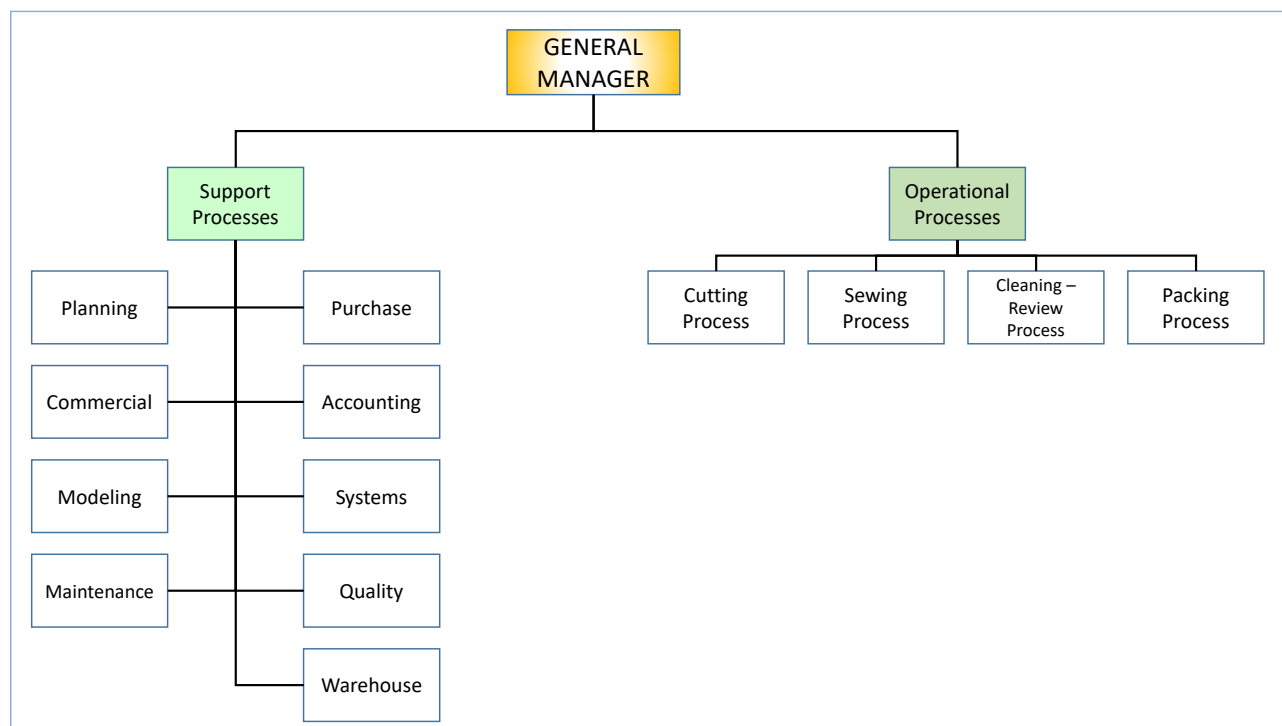


Fig. 3. Organization Chart by Processes.

The cutting area received the information of the production orders, coming from the planning area and the fabric from the dyeing area, later it made the cut according to the FIFO method (first in, first out), that is, the first to arrive is the first cut and then sent to the sewing area or according to the programmed date of entry to sewing. It was commonly carried out according to the FIFO method, since removing the laying of the fabric that was on the table was unproductive for the cutting area, the area manager avoided that in the monthly report that he presented to management, efficiency and productivity were low.

This decision of the cutting area affected the availability of time in the areas that preceded it, such as: sewing, cleaning-review and packaging. Progressively, the time available was

reduced for its delivery, that is, the cutting area did not consider the needs of its internal client.

In order that these areas are not affected by non-compliance on the delivery date to the customer, the sewing, cleaning-review and packaging supervisors increased with productive hours, carrying out the overtime programming, especially the packaging area which was the area with the least available hours at the end of the entire process, this type of decision affected manufacturing costs.

The clothing area, maintained a planned production according to its capacity applying the push system as can be seen in the Fig. 12, it was configured as a mass production line, that is, the sewing operations that preceded the previous operation should wait, until the assembly of the garments of



the batch production was completed, not presenting a continuous production flow but unproductive times between activities, although its flow presented a consecutive sequence according to the sewing activities of the garment model. Its speed and its skill level of the seamstresses at the beginning of production of the model was low, but as time passed, it increased its production of the same model, the staff increased their degree of skill and speed since the activity was monotonous, performing the same operation on the same machine and its level of defects was minimal. The operational ability of the sewing personnel only had dexterity in the handling of a single type of machine, performing different types of complex and non-complex operations, their salary was piecework, that is, according to what they produced, they did not assume the challenges in handling other types of machines, in addition to the fact that the applied production system did not allow it. For the present cause and effect model, the relationships of each of the variables are exposed as shown in Fig. 4.

**Client:** This variable, made up of other variables, has a positive influence relationship with the orders it places, and presents a positive feedback with the receipt of the shipments made by the company.

**Production:** The quantity produced is positively influenced by the number of orders placed by the client, and is also negatively influenced by the number of work centers, production time, and the number of defects.

**Ability:** It is a variable that is related to the activity carried out by the person, and has negative influences: with the number of personnel required, with the production time and the defects due to the execution of their activity.

**Dispatch:** It is a compound variable that is positively influenced by the quantity produced and that has a positive influence on clients.

Continuously in the sewing process, the supervisor controlled the Lead Time or processing time as seen in Fig. 5, when a garment model change occurred, before entering the production unit or batch to the line, the supervisor carried out the distribution of personnel and machine, executed in any of the following ways:

a) When personnel were placed in the machines in a single time. Here, waiting or unproductive times were presented from the second operation and accumulated until the last sewing operation. The waiting time between activities is directly related to the size of the production batch, as observed in equation 1 and 2.

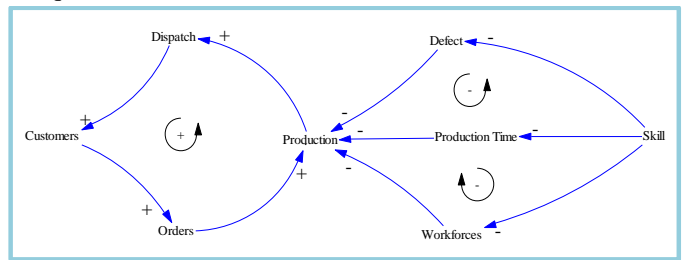


Fig. 4. Cause and Effect Diagram.

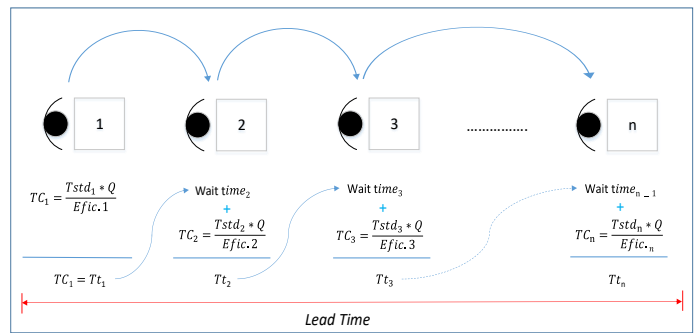


Fig. 5. Lead time with Waiting Times.

$$LeadTime = WaitingTimes + \frac{Tstd_n * Q}{Efic.n} \quad (2)$$

$$WaitingTimes_n = \frac{Tstd_{n-1} * Q}{Efic.n-1} \quad (3)$$

$TC_n$ = Sewing time of activity “n”.

$Tstd_n$ = Standard time of activity “n”

$Tt_n$ = Total time in sewing activity “n”

$Q$ = Number of pieces per package

b) When personnel are located as the batch of 20 units progresses for each operation, the waiting time does not appear, for this the supervisor must previously schedule activities for the personnel before being placed on the line, as observed in Fig. 6 and equation 1.

In Fig. 7, the causal diagram is shown where the cause-effect relationship between the administrative part and the operational part is revealed, the greater the physical separation distance between these areas, the less their interaction and communication. The administrative part presented ignorance of the programmed orders in the processes, control and ignorance of the operational decisions. The reports presented by the administrative areas to the operative part were inadequate, since in the operative part it generated limitations in the management of their productive resources which implied problems of quality, productivity, efficiency and effectiveness, due to lack of coordination and adequate information and timely, which presented organizational confusion and delays in the delivery of production orders to the client in the requested time.

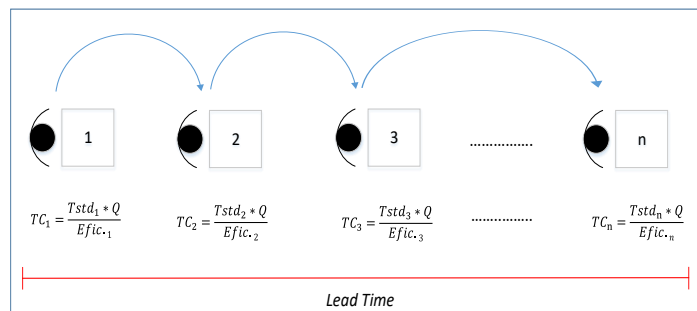


Fig. 6. Lead Time without Waiting Times.

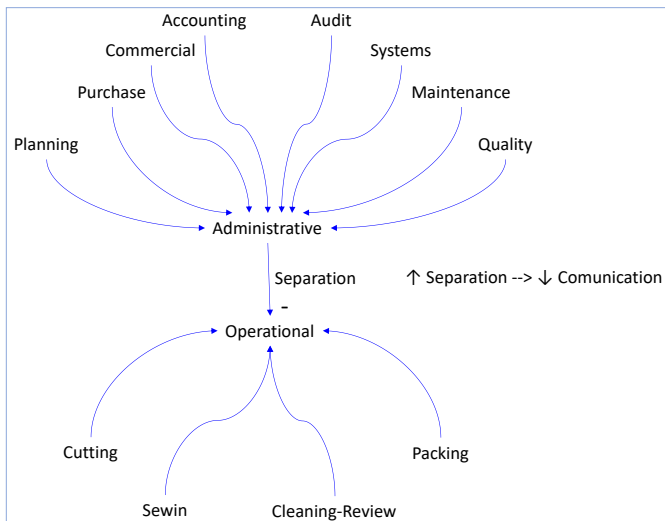


Fig. 7. Causal Diagram: Greater Administrative-Operational Separation.

Each operational area was physically separated and was responsible for its own process and sought in any case to increase its productivity, quality and efficiency, but it did not observe its internal client, that is, the other processes that carried out the transformation of the raw material or product in process. The cutting area carried out its activities in the shortest possible time and sent the fabrics cut into pieces by transport to the sewing area for their preparation, in this area as it was observed that some pieces cut within the packages did not comply with the measurements according to the specification sheet, which was returned to the cutting area for rectification or replacement, in the same way it was presented in the cleaning-review and packaging process, the accumulation of unproductive times due to return each time it increased for each operating area, presenting a bottleneck, limiting its advance for each production order.

2) *2nd change from a process structure to a focused organizational structure:* In this type of organization, although the operational processes were still physically separated, as shown in Fig. 8, internal changes were made in each process. The cutting process that consisted of a set of tables was organized so that each of them worked taking into account the garment model, in the same way it was carried out in the sewing, cleaning-review and packaging processes, with the aim of maintaining a linear orientation at the flow level, which allowed better coordination between processes and better control for those in charge.

In this type of organization, it was considered more orderly since it was identified which are the sub-processes and activities for each process as shown in Fig. 9, which allowed better control of production and quality control. In the cutting process, a single type of model was assigned for a certain table, its degree of complexity decreases and its efficiency increases, its production time is less and less, as well as the machine configuration time (set up), which allowed to reduce operating costs, in the same way it was organized for the sewing, cleaning-review and packaging processes. But the administrative part was still detached from the operational part

and under management control, which continued to affect the level of communication.

3) *3rd change from a focused structure to a modular structure:* As can be seen in Fig. 10, the change developed in the operational part is the implementation of modules, which is constituted by a set of processes and organized sequentially according to the construction of the garment model and that combine different types of machines and multi-functional people to execute different types of activities within each sub-process or process, with the objective of transforming a complete production unit. Within its characteristic, it can be noted that there is a high level of operational communication, the production flow is aligned and continuous. It presents higher quality in the activities, increases the production speed, that is, reducing manufacturing times and reducing operating costs.

This type of organization implemented by the company, each module consisted of the areas of cutting, sewing, review-cleaning and packaging, as seen in the organization chart, and was carried out as a result of the client's demand increasing in orders, no longer in quantity per model but in variety, from a production order of 5,000 garments it was now the equivalent of 10 order orders with different types of models, different types of fabric, different colors and with stamping or embroidery applications, with minimum quantities for each color.

With the type of focused structure on which the sewing process was configured as a mass production line for orders greater than 5,000 garments, it could not be adapted to orders of less than 400 garments, what was to redesign the production lines for minimum quantities.

With this type of organizational change, the company only focused on operational processes, which consumed more activity, personnel, machine and production time, such as: cutting, sewing, cleaning-review and packaging. The area was redesigned in a modular way, so that these activities are within them led by a boss. The distribution of the process, sub-processes and activities within the module, must have a sequential form maintaining a constant flow of production, with the same configuration of the batch or production unit from the beginning of the cutting activity, passing through all the activities of sewing, cleaning-inspection and packaging as seen in Fig. 11.

The distribution of the production batch between activities continued to be maintained with the push system, as shown in Fig. 12. In this type of modular organization, a higher level of interaction between processes, sub-processes and activities was observed since it was within one module, it was more dynamic, the control and exchange of information was more fluid and effective, and the degree of response and communication was greater. But the interaction with the administrative areas was still inefficient, since it was physically separated from the operative part and inadequate or delayed information continued to be presented for the operative part.

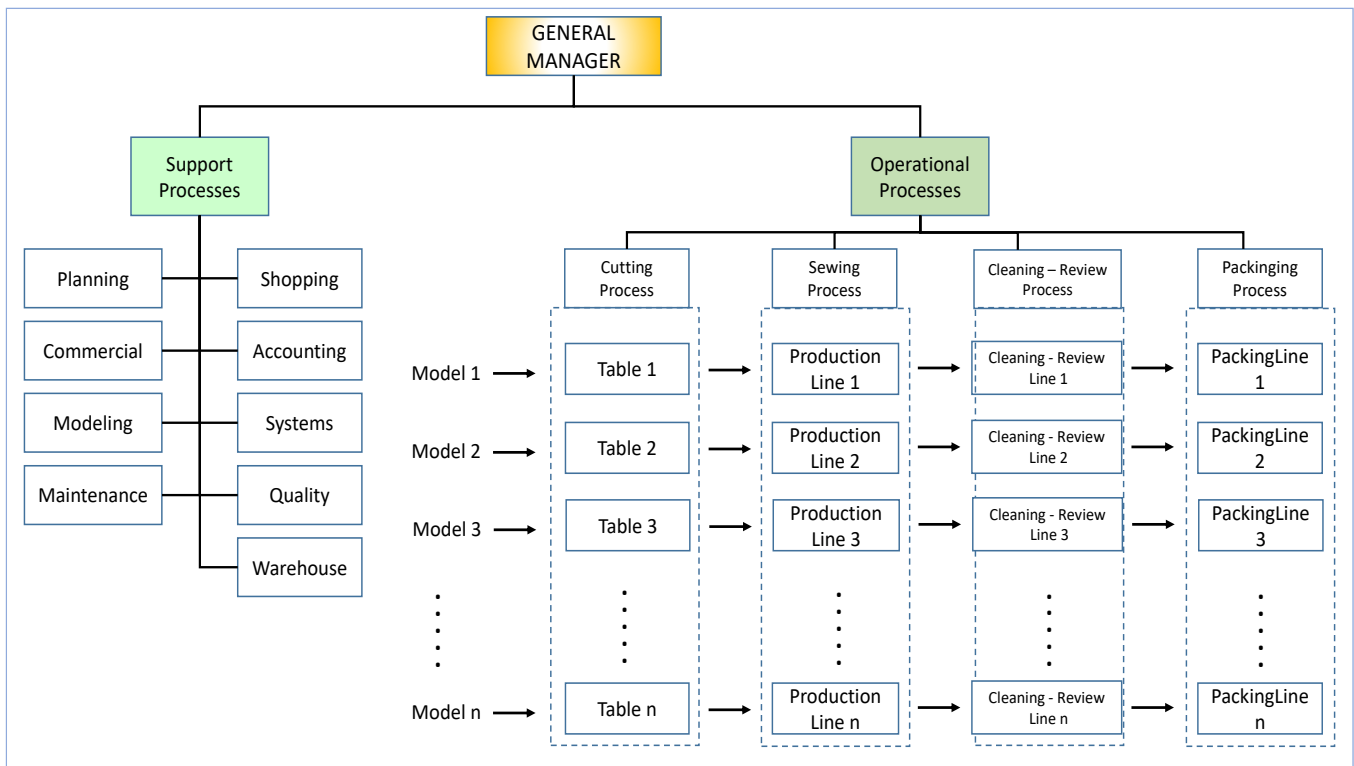


Fig. 8. Model Focused Organization Chart.

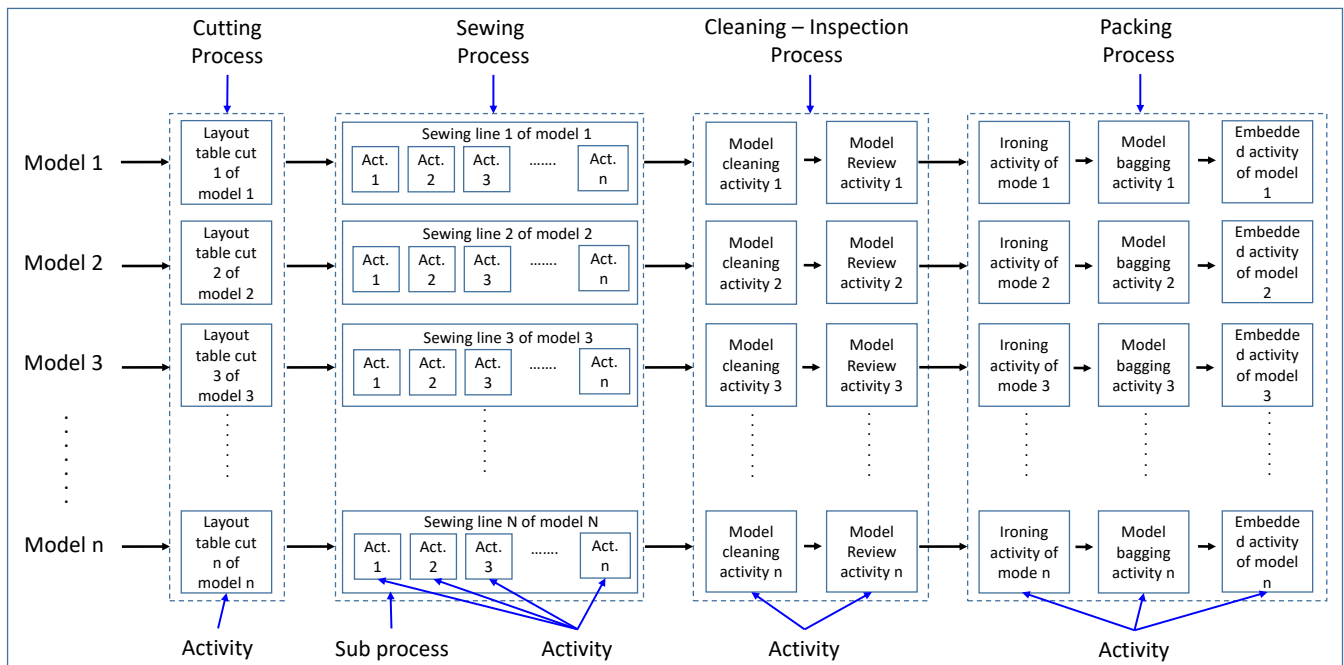


Fig. 9. Organization by Processes, Sub-processes and Activities.

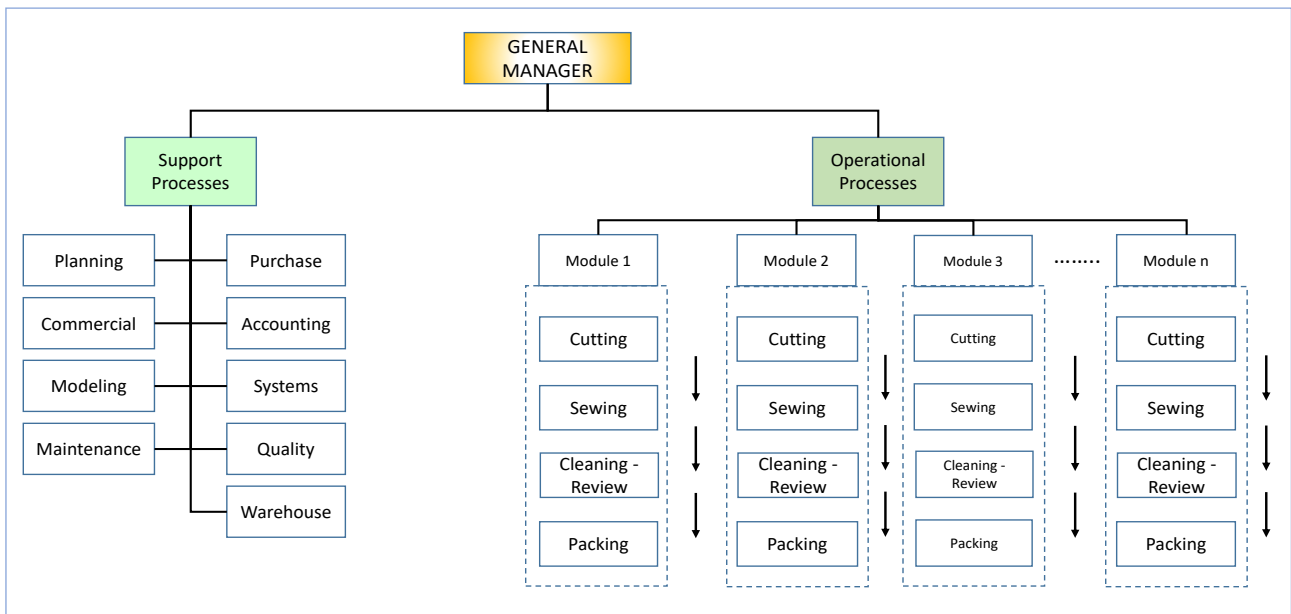


Fig. 10. Modular Organization Chart.

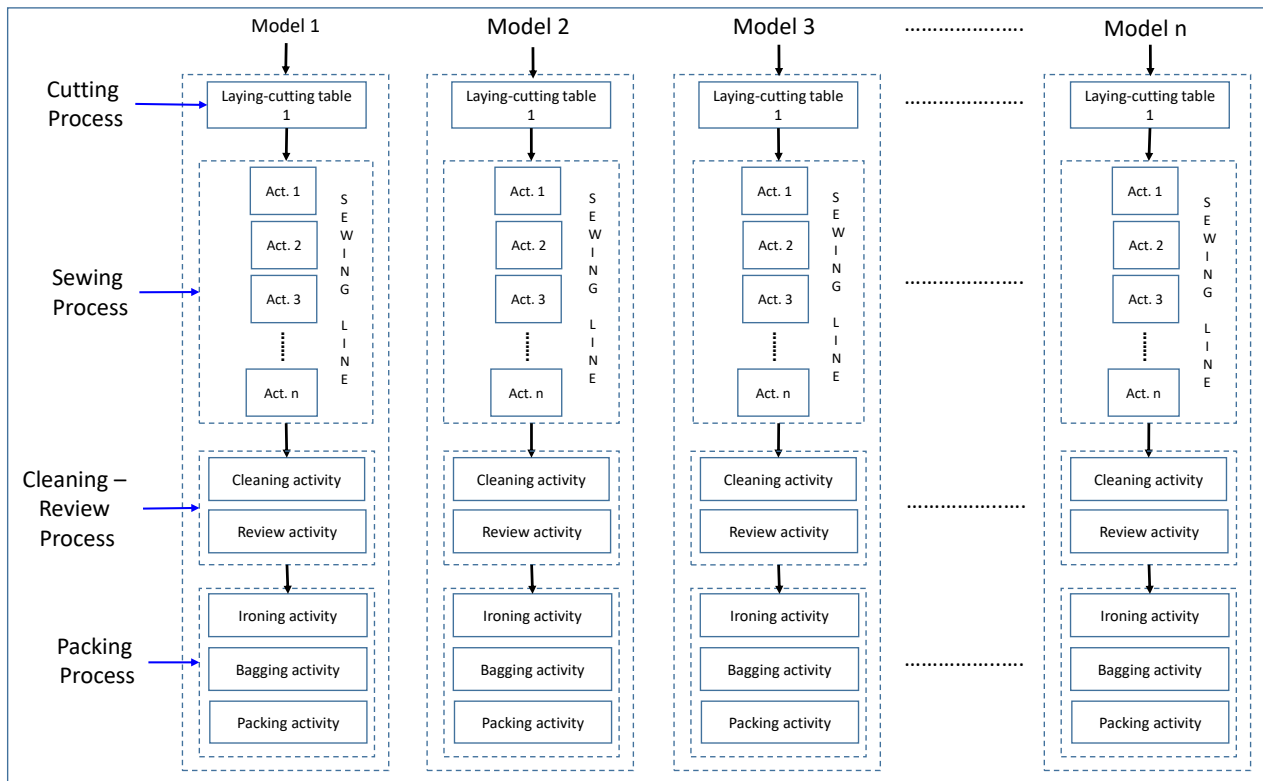


Fig. 11. Organizacion por Modulo de los Procesos Subprocesos y Actividades.

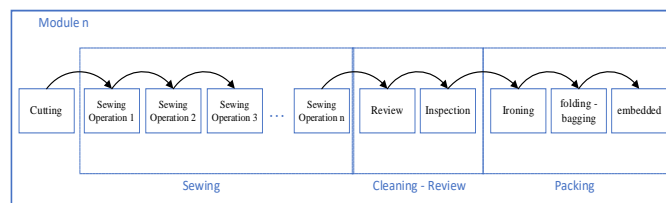


Fig. 12. Push System.

a) *Flowchart*: The development of this diagram was carried out to understand the variables that influence the production system, in order to quantitatively determine the level of incidence of the variables and how changes affect the system, as a previous step to the simulation. It should be remembered that, in the hypothesis to be solved, is that the organization identifies and executes activities that add value, through the variables requested, days required, efficiency, defect levels and lead time, which affect each process, it can identify quantitatively the limiting effect on the system. Fig. 13 shows the flow diagram that is made up of 23 constants, 15 auxiliary variables, 10 flow variables and 5 level variables.

b) *Dynamic Formulation of a Modular Structure*

TTU: Total Time Used by the area (cutting, sewing, cleaning, Review and finishing).

$$TTU_{area} = TC_{area} + TP_{area} + TT_{area} \quad (4)$$

TC\_area = Loading time of the area (cutting, sewing, cleaning, Review and finishing).

$$TC_{area} = \frac{Q_{area} * Tstd_{area} * \#package}{Efc_{area}} \quad (5)$$

Where:

Q\_area= Number of units per package or batch.

Tstd\_area= Standard time of the model that is carried out in the area.

#package= It is the first package or batch that enters the area.

Efc\_area= Load efficiency of the first package of the model that enters the area. The speed in the use of resources to

perform the configuration of machines and the degree of skill of the personnel to carry out the assigned operation are considered.

TP\_area: Production time of the area (cutting, sewing, cleaning, Review and finishing).

$$TP_{area} = \frac{Ped * Tstd_{area}}{Op_{area} * Efp_{area}} \quad (6)$$

Where;

Ped. = The quantity ordered by the client.

Tstd\_area= Standard time of the model that is carried out in the area.

Op\_area= Number of operators assigned to the area for a specific model.

Efp\_area= Production efficiency of the area regarding to the model.

TT\_area = Time for transfer of production to the next area.

$$TT_{area} = \frac{TP_{area} * Tt_{area}}{T_{dispon}} \quad (7)$$

Where:

TP\_area = Production time of the area (cutting, sewing, cleaning, Review and finishing).

TT\_area = Transportation time performed by the preceding area.

T. dispon= Time available for the area.

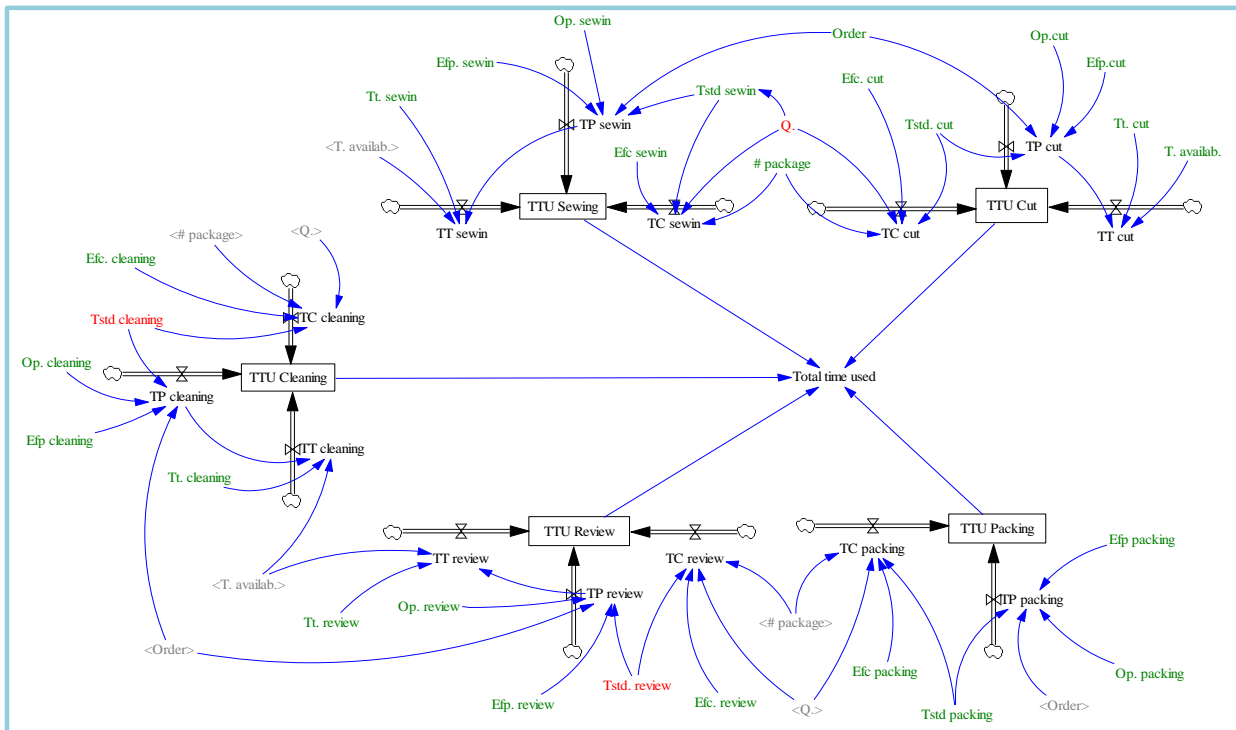


Fig. 13. Manufacturing Flow Diagram.

4) 4th change from a modular structure to a flexible manufacturing: As the administrative areas were not effective in communicating and transferring information with the operational part due to the physical separation distance, the management made the decision to distribute the personnel in charge of planning, purchasing, commercial, maintenance, quality and payroll, (Regarding to the last one, this function was considered in replacement of accounting), within each module, as observed in the causal diagram of Fig. 14, the smaller the separation distance between the administrative and operational areas, the greater the level of communication and under the direction of the head of module.

The responsibility of the dispatches of the production orders fell to the head of the module, as can be seen in the new organization chart in Fig. 15. This type of decentralized organization [22] presented autonomy in the module to make its own decisions, which generated effects positive, there was already more interaction between the administrative and operational part within the module, as Vásquez points out [23] "Reinforcing communication processes and strengthening social and human capital through teamwork and communications".

In addition, changes were made in the operational part, the cleaning and Review processes as it did not generate added value to the product only inventories, waiting times, occupation of spaces and consumption of resources, their permanence generated a negative effect, since when the operating personnel of the sewing department observed this activity carried out by manual personnel, it did not give the importance of quality in its activity, generating even more re-inspections and reprocesses, which shortened the delivery time to the client, in addition to considering that the sewing lines were configured as a mass production with push system, the personnel at least knew how to operate one type of sewing machine. For this, the management made the decision to implement a training area, with the aim of training personnel in the handling of three types of machines (serger, coating machine and straight) at least, to perform different types of

complex and non-complex activities, in other words, those activities that take longer, in addition, the same sewing staff must clean the garment, trimming the threads by using a picket and reviewing its activity avoiding the occurrence: skipped stitch, thread tension, thread breakage, etc., before to move on to the next activity.

Given the increase in time for carrying out these activities, the payment method was modified, from piecework (individual) to group, according to the amount of garments made by the sewing line. The type of training developed by the company to the operational personnel, facilitated the module supervisor in making decisions to assign activities in the event of any absence, since the personnel had the training and ability to handle any type of machine, which allowed avoid bottlenecks or extend overtime for any need with the available staff. It was also considered to modify the production system from the push system to the pull system [24], such as in Fig. 16. For the implementation of the system, the batch or production unit of 20 garments was modified to one garment, that is, the Inventory in process and the sewing activities that preceded should pull the progress of the previous activity, the objective of reducing downtime between activities and meeting the delivery to the customer in the requested time.

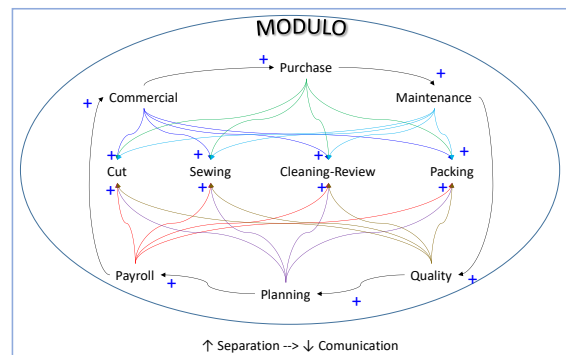


Fig. 14. Causal Diagram: Minor Administrative-Operational Separation.

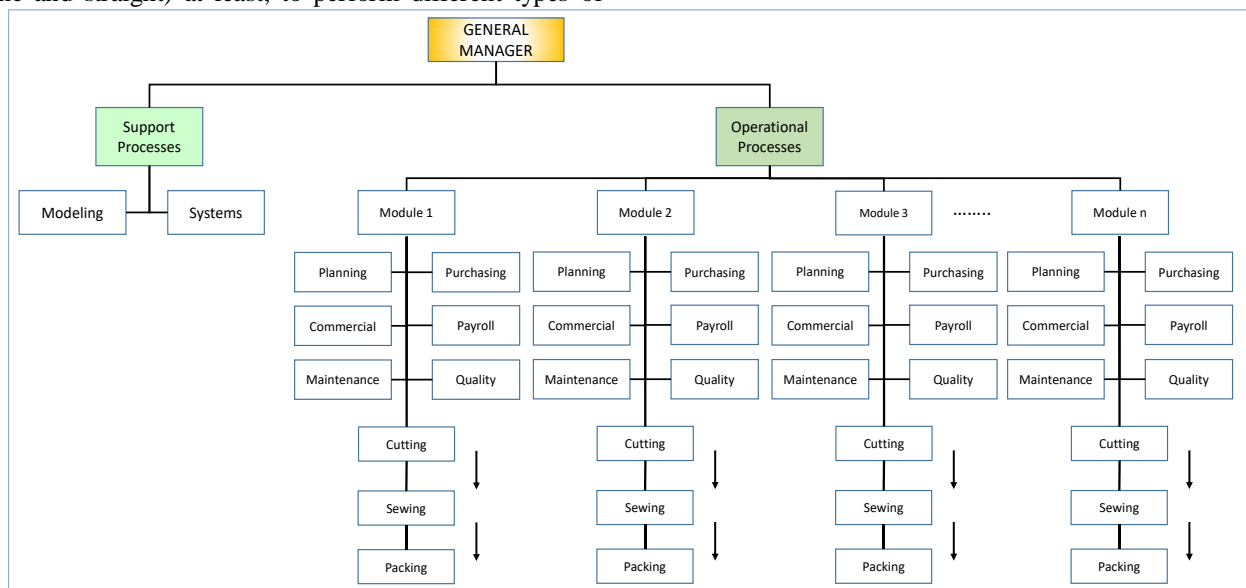


Fig. 15. Flexible Organization Chart.

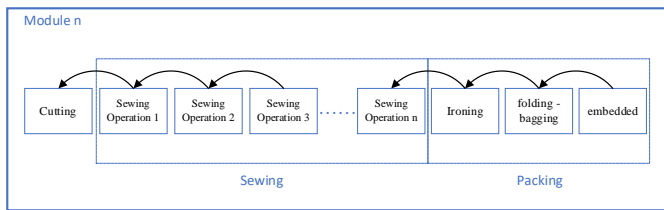


Fig. 16. Pull System.

Considering the changes made in the modules and the available times, standard times and assigned personnel, each person in charge of the area began to carry out their planning, programming and control of their production processes according to their new flexible structure, determining the required loading times, production time and delivery time to the client.

### III. RESULTS

The management maintained a high level of leadership that allowed the organization to seek to adapt to changes in the external environment, its leadership project perseverance, creativity and innovation to change. To compare the results obtained by the application of a Modular structure with a flexible structure, the following Table presents 1, 2, 3, 4 and 5 the parameters or constants used in the flow diagram in Fig. 13.

Tables I, II, III, IV and V detail the entry of the initial information for each area: the order, available time, loading time of the batch in the process, the production batch or package as a work unit within of the processes, quantity that is constituted in a batch, efficiency of the area, standard production time of the garment model, number of operators used by each area, average efficiency of the personnel and their total time.

Comparing these results with the application of a flexible structure, where the cleaning and review areas are no longer considered within the operational organization and the application of the pull system, configuring as a production batch of one unit, the following variables were modified of the same scenario flow, entering the following data:

$$Q=1 \text{ garment} / (\text{package} * \text{operators}).$$

$$\text{Tstd. Cleaning} = 0 \text{ minutes} * \text{operators} / \text{garment}.$$

$$\text{Tstd. Review} = 0 \text{ minutes} * \text{operators} / \text{garment}.$$

As can be seen in Fig. 17, the behavior of the loading time in the production line of a batch of 20 garments is greater than the loading time of a unit. The reduction times were:

- Cut load time reduced from 13.11 to 0.655 minutes.
- Sewing load time reduced from 133.52 to 8,664 minutes.
- The loading times of the cleaning and review areas were reduced to zero, since these were eliminated from the process since they did not add value to the product.
- Finishing area loading time reduced from 27.55 to 1.3755 minutes.

As the cleaning and review areas are no longer presented in the flexible structure, the personnel were reduced by 19%. As a result of the changes made, the organization presented a faster response speed reducing its loading time by 43%, in Fig. 18, it is observed quantitatively without considering and considering the changes made by the organization.

TABLE I. PARAMETERS OR CONSTANTS USED FOR THE CUTTING AREA, AS INPUT IN THE FLOW DIAGRAM OF FIG. 13

|            | Unity         | Modular Structure              |
|------------|---------------|--------------------------------|
| Order      | Garment/Order | 5,000                          |
| T. dispon. | Minutes/Day   | 480                            |
| TC Corte   | # package     | Package/Order                  |
|            | Q.            | garment/ (package * operators) |
|            | Efc. Cut      | Dmnl                           |
|            | Tstd. Cut     | minutes * operators / garment  |
| TP Cut     | Op. Cut       | Operators                      |
|            | Efp. Cut      | Dmnl                           |
| TT Cut     | Tt. Cut       | Minutes/Day                    |

TABLE II. PARAMETERS OR CONSTANTS USED FOR THE SEWING AREA, AS INPUT IN THE FLOW DIAGRAM OF FIG. 13

|            | Unity         | Modular Structure             |
|------------|---------------|-------------------------------|
| Order      | Garment/Order | 5,000                         |
| T. dispon. | Minutes/Day   | 480                           |
| TC Sewing  | # package     | Package/Order                 |
|            | Q.            | garment/(package * operators) |
|            | Efc. Sewing   | Dmnl                          |
|            | Tstd. Sewing  | minutes*operators / garment   |
| TP Sewing  | Op. Sewing    | Operators                     |
|            | Efp. Sewing   | Dmnl                          |
| TT Sewing  | Tt. Sewing    | Minutes/Day                   |

TABLE III. PARAMETERS OR CONSTANTS USED FOR THE CLEANING AREA, AS INPUT IN THE FLOW DIAGRAM OF FIG. 13

|             | Unity          | Modular Structure              |
|-------------|----------------|--------------------------------|
| Order       | Garment/Order  | 5,000                          |
| T. dispon.  | Minutes/Day    | 480                            |
| TC Cleaning | # package      | Package/Order                  |
|             | Q.             | garment/ (package * operators) |
|             | Efc. Cleaning  | Dmnl                           |
|             | Tstd. Cleaning | minutes*operators / garment    |
| TP Cleaning | Op. Cleaning   | Operators                      |
|             | Efp. Cleaning  | Dmnl                           |
| TT Cleaning | Tt. Cleaning   | Minutes/Day                    |

TABLE IV. PARAMETERS OR CONSTANTS USED FOR THE REVIEW AREA, AS AN ENTRY IN THE FLOW DIAGRAM OF FIG. 13

|            | Unity         | Modular Structure             |
|------------|---------------|-------------------------------|
| Order      | Garment/Order | 5,000                         |
| T. dispon. | Minutes/Day   | 480                           |
| TC Review  | # package     | Package/Order                 |
|            | Q.            | garment/(package * operators) |
|            | Efc. Review   | Dmnl                          |
|            | Tstd. Review  | minutes*operators / garment   |
| TP Review  | Op. Review    | Operators                     |
|            | Efp. Review   | Dmnl                          |
| TT Review  | Tt. Review    | Minutes/Day                   |

TABLE V. PARAMETERS OR CONSTANTS USED FOR THE FINISHES AREA, AS INPUT IN THE FLOW DIAGRAM OF FIG. 13

|             | Unity         | Modular Structure              |
|-------------|---------------|--------------------------------|
| Order       | Garment/Order | 5,000                          |
| T. dispon.  | Minutes/Day   | 480                            |
| TC Finishes | # package     | Package/Order                  |
|             | Q.            | garment/ (package * operators) |
|             | Efc Finishes  | Dmnl                           |
|             | Tstd Finishes | minutes*operators / garment    |
| TP Finishes | Op. Finishes  | Operators                      |
|             | Efp Finishes  | Dmnl                           |

#### IV. DISCUSSION

The development of organizational change was carried out reactively according to the evolution of the international market.

The changes made by the organization to arrive at a flexible structure caused the sewing operating personnel to be reduced by 20% by own decision.

The personnel only wanted to work piecework with a sewing time without considering the cleaning time and review of their activity, this allowed them to have greater income but affected the changes and the productivity of the company, in such a situation the company had to compensate for this loss of seamstresses with personnel who carried out manual tasks (cleaning and Review) through training in the handling of different types of machines, being considered by the personnel as an added value to their professional career as a technician, increasing their value in the company and their salary.

Alonso [3] points out that organizations exercise subtle mechanisms of domination and control, it is correct, but it was necessary to prevail the sense of authority in a group of people of different types of education, cultures and values in organizational change.

The company developed a training center called "Little School" which allowed to prepare the personnel who performed manual labor in sewing. The trained personnel generated greater involvement in the changes of the organization, which translated into greater productivity and fewer limitations in their performance in the production areas.

What the company did need was a management that would lead the change involving not only administrative but also operational personnel, through successive meetings pointing out the short, medium- and long-term objectives and the positive effects that changes would bring for employers.

The research work carried out by Galvan [1-3] are oriented to the internal analysis of the organization, revealing the level of intrapreneurship, Delgado's study analyzes the organizational structure, human capital and collaboration networks to increase the development of the capacity for innovation and the research carried out by Gonzales statistically concludes that the problems generated by change within an organization are solved through communication. But none of these researchers reveals how the evolution of change in an organization is presented in its organic structure both in the administrative and operational part and how this affects the redesign of the processes in each stage of change, as presented in this research work.

#### V. CONCLUSIONS

The company dealt with the problems of change holistically and responding in a systematic, but unplanned way, forming a type of flexible organization for change.

The changes made by the company produced results that allowed it to adapt to the changes in demand requested by clients. Going through five types of transitions or changes, allowed to know the level of commitment and adaptability on the part of the organization, which generated positive results.

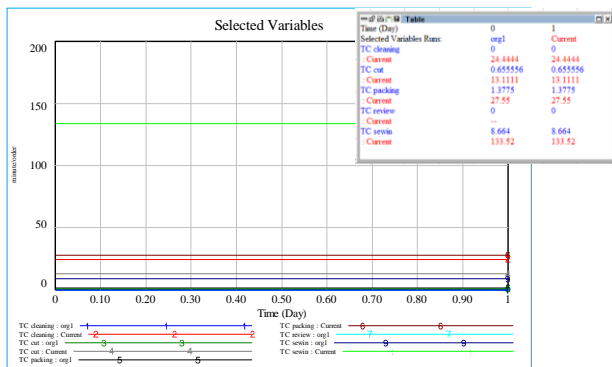


Fig. 17. Behavior of Loading Times with Q = 20 Garments / Order and Q = 1 Garment / Order.

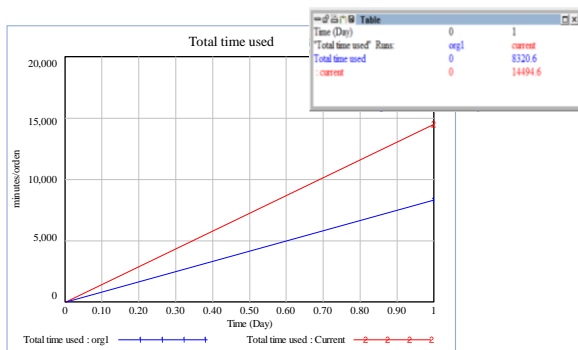


Fig. 18. Behavior of the Total Time used between a Modular Structure vs a Flexible structure.



Employee involvement in each stage of change was developed through interactions, training, and knowledge sharing. The management understood that, to make the changes, they should first change their type of leadership from centralist to decentralist, less hierarchical, giving the power of decision (empowerment) to administrative and operational personnel, while still controlling the progress of requests for clients in every operational process.

Each module was considered an agile, dynamic, flexible organization that evolves and generates change through interaction with the client, creating economic and social value in a sustainable way, each order is analyzed, evaluated in quantity, degree of difficulty of the model and availability of resources, establishing processing times and delivery dates.

The result obtained as a result of the research allowed to know the degree of evolution of each stage of change within a manufacturing organization, developing and analyzing the levels of behavior in a quantitative and graphical way at each stage of the change through scenario models and algorithms and their interrelation in the use of productive resources as dependent variables of the system.

For future work, the incidence of dynamic organizational change will be expanded with the concepts of chaos, as Pacheco [25] points out, learning is connected and weaves growing interactive networks of progressive complexity. And complex systems or sciences of complexities [26] where adaptive, non-linear systems will be analyzed taking as references Edward Lorenz and Benoit Mandelbrot. The main asset of an organization is the person and as such their degree of knowledge differ, this knowledge is found in their brain which is a non-linear product of a non-linear evolution.

#### REFERENCES

- [1] M. Chudnovsky, M. Cafarelli, Changes in the Organizational Structures of the State And their Link to the Composition of Public Employment. Argentina 2003-2016, Foro Internacional (FI) 232, LVIII, 2018 (2), p. 281.
- [2] G. Millan, R. Diaz, M. Gonzales, Oscar U., Cambio Organizacional en las Medianas y Grandes Empresas del Valle de SugamuxI, Dimension Empresarial 15(1) 2016, p. 210.
- [3] E. Galvan y M. Sanchez, Factores organizacionales relacionados con el comportamiento intraemprendedor, Innovar vol. 29, No 71 2019, p. 61.
- [4] A. Delgado, E. Vargas, F. Rodriguez y J. Monets, Organizational Structure, Human Capital and Collaboration Networks: Determinants of Innovation Capability in Restaurants, Ad-Minister No 32, 2018, p. 12.
- [5] A. Segredo, Theoretical approach to the evolution, theories, criteria and characteristics supporting the development of organizations, Revista Cubana de Salud Pública 2016, p. 588.
- [6] C. Reis, L. Benvenuti, L. Campos, M. Uriona, The Influence of Company Size on Energy Management Systems Adoption: A System Dynamics Model, Brazilian Business Review 2020, p. 584.
- [7] J. Calpa, Validation of a Model of Reverse Logistics for the recovery of WEEE from the city of Cali, based on the Systemic Thinking using a simulation of System Dynamics, Tecnologicas vol. 23, N° 48, 2020, p. 66.
- [8] L. Rodriguez, J. Loyo, M. Lopez, J. Gonzales, Dynamic simulation of a back-fedged production system, II Ingenieria Industrial vol. XL, N° 2, 2019, p. 172.
- [9] D. Zapata y J. Oviedo, Modelo de Simulación de Alternativas de Productividad para Apoyar los Procesos de Toma de Decisiones en Empresas del Sector Floricultor Antioqueño, Información Tecnológica 2019, p. 58.
- [10] Y. Palmas, A. Franco, L. Lopez, C. Giraldo, Sistemas complejos y turismo: aplicación del modelo de turismo armónico en dos localidades de países latinoamericanos, Cuadernos de Geografía vol. 29, N° 2, 2020, p. 356.
- [11] G. Becerra, Complex Systems Theory and Social Systems Theory in the controversies of complexity, Convergencia e-ISSN 2448-5799, vol. 27, 2020, p. 5.
- [12] L. Rodriguez, Contribución a la crítica de la teoría de los sistemas complejos: bases para un programa de investigación. Estudios Sociologicos, DOI: 10.24201, vol. 36 N° 106, 2018, p. 76.
- [13] Z. Yang, Z. Ge, Monitoring and prediction of big process data with deep latent variable models and parallel computing, Journal of Process Control, 2020, p. 19.
- [14] D. Van, M. Mandegari, S. Farzad, J. Gorgens, Techno-economic and environmental analysis of bio-oil production from forest residues via non-catalytic and catalytic pyrolysis processes, Energy Conversion and Management 213 (2020) 112815, p. 3.
- [15] W. Tupia, L. Brañez, A. Arribasplata, J. Acosta, An experimental methodology to determine the parameters of the compression molding process of composite materials made of recycled thermoplastic and recovered wood, Revista Materia vol. 23, N° 3, 2020, p. 2.
- [16] J. Vargas, F. Jimenez, J. Toro, Y. Rodriguez, Comparing Push and Pull Manufacturing Systems via Simulation, Ciencia e Ingenieria Neogranadina 2019, p. 84.
- [17] F. Ferreiro, M. Del Campo. M. Santos, Training and talent management of the most valued human resources companies in Spain, Contaduría y Administración 64 (3), 2019, p. 5.
- [18] E. Arvizu, L. Velasquez, Corporate social responsibility: Distinctive, practices and processes of the mining sector in Sonora, Mexico, Revista de Alimentación Contemporánea y Desarrollo Regional Volumen 29, Número 54, 2019, p. 5.
- [19] J. Gray, M. Minsky, Models in Simulation, Softw Syst. Model 2016, p. 605.
- [20] J. Gonzales, M. Rodriguez y O. Gonzales, Organizational Change In Medium And Large Companies Of Sugamuxi Valley, Dimension Empresarial vol. 15, No 1, 2017, p. 210.
- [21] G. Ponce, D. Espinoza, J. Zamura y K. Tapia, Organizational capacities to generate value: analysis of industrial sector, Retos vol. 7 No 13, 2017, p. 144.
- [22] H. Aray, Effects of decentralization on public infrastructure accumulation: The case of Spain, El trimestre económico vol. 85, No 340, 2018, p. 862.
- [23] S. Vasquez, C. Lujan, J. Olivas, H. Gonzales y H. Lujas, Prospective of forest sector's organizational system in Chihuahua, Mexico, Madera y Bosquez vol. 23, No 2, 2017, p. 220.
- [24] L. Rodriguez, J. Loyo, M. Lopez, J. Gonzales, Simulación dinámica de un sistema de producción retroalimentado, Ingeniería Industrial 2019, p. 173.
- [25] P. Pacheco, Study of a learning process in experimental sciences by the Chaos Theory, Formación Universitaria vol. 13 N° 3, 2020, p. 78.
- [26] G. Becerra, Complex Systems Theory and Social Systems Theory in the controversies of complexity, Convergencia vol.27, 2020, p. 2.

# Impact of Change in Business IT Alignment: Evaluation with CBITA Tool

Imgharene Kawtar<sup>1</sup>, Baina Salah<sup>3</sup>  
Mohammed V University  
ENSIAS, Rabat  
Morocco

Doumi Karim<sup>2</sup>  
Mohammed V University  
FSJES, Rabat  
Morocco

**Abstract**—Organizations introduce changes to adapt to an agile context in a turbulent environment. These change often have an impact on business and information technology. In most cases, the change impacts organizational elements that make the adaptation not well defined, leaving out elements that can lead to misalignment. The change is realized in this article as a project, which will impact all the Business-IT alignment elements. It is important to know the scope of the impact in order to make a complete adaptation. By reviewing the literature, we found that there is no work dealing with this aspect. To fill this gap, we determine the impact of the project on the organization by considering of Business-IT alignment and we proceed with a comparison of the AS IS model of the organization with the TO BE model which is the target to be implemented keeping the system aligned. Accordingly, we propose a metamodel for change by the impact of the project on the Business-IT alignment and a set of rules and algorithms to predict the impact and adaptation. To make these contributions operational, the implementation of Change Business-IT Alignment Tool and demonstrate its applicability through a case study of an urban agency.

**Keywords**—Agility; business IT alignment; change; project

## I. INTRODUCTION

Today's businesses are facing rapid and dynamic changes in the business environment, making agility a critical step in achieving competitive advantage over competitors. At that time, when the importance of alignment for effective organizational performance was emerging is now well recognized and must be invoked: it is "Business IT Alignment" which is dedicated to providing an aligned system where the elements of a business are not communicated with each other. The world is spinning, not necessarily very round, but certainly faster and faster, and the man in the middle of it all, if he creates the conditions for this acceleration, must also face it. Change is the scale of any organization, when it's needed it affects all the elements of business IT alignment. The last one is defined and modeled on good theoretical [1], presented [2] and empirical [3] standards, but rarely who talks about agility or change with the alignment Business IT [4]–[6].

As cited during our previous research as there is little research into the dynamics of alignment, the old research before technology, digital transformation appears, R. Greenwood and C. R. Hinings [7] views alignment as a dying target on which organizations are heading, while S. L. Jarvenpaa and B. Ives [1] suggest that it should be examined

as an emerging process. But today's environment is constantly changing, it continues to change, slowly or rapidly, but it is changing all the time. Even after an organization has achieved alignment, its environment would continue to change.

However, organizations may not be able to adapt their alignment models to changes in the external environment for one main reason: Too much emphasis on alignment may restrict the organization's perspective, impede the recognition of other perspectives, and reduce the ability to "recognize and respond to the need for change" [8]. Alignment facilitates short-term success, which leads to structural and cultural inertia, and inertia, in turn, leads to failure when market conditions suddenly change [9].

As a result, when organizations with a high level of alignment are faced with unexpected changes in industry conditions, they may find it difficult to respond with evolutionary changes. Revolutionary change would be more likely [10]. If the strategy or structure of the company is changed accordingly:

- Will the other elements be modified in a synchronized way to maintain alignment?
- Or would there be periods of poor alignment until the other elements are realigned?

During previous research, it was found that there is no study regarding the impact of change on business IT alignment, the comparative study of [11] concluded that few strategic alignment approaches address the impact of change, therefore this paper will demonstrate the impact of the project as a change to an aligned system.

The main objective of this article is to define and maintain over time, the model that will allow analysing the impact of the change and the change itself to maintain adaptability between elements and maintain Business IT alignment. In our previous research [12], agility was seen as a change with concrete and valid definitions. This paper will define change as a project, the impact of the project in an enterprise will involve the change in the elements of the Business IT alignment, and the goal is to define its changes by analyzing the study of the existing with the project to define the goal to be implemented without a misalignment. The analysis will be done through a project that will be modeled by rules involved with the Business IT alignment, a description of the study of the existing will be modeled by the Archimate language and a

homogeneity will be done with the project to have a future model also modeled by the Archimate language which will be the future target to implement.

The objective is to integrate a new project in the company by analyzing the change that will impact the elements by comparing the study of the existing (AS IS) with the target to be maintained (TO BE) taking into consideration the modeling of the project and integrating the French state urbanization model as a repository of Business IT alignment. A 3-step process will be explained in the following sections. A process that will define that the project will be quantifiable for the company without damaging the Business IT alignment too much and by analyzing the change and the Business IT alignment elements impacting, then we have a prototype that will concretize this contribution and will be simulated by a case study of a Moroccan urban agency. Section 1 defines the work related between the Business IT alignment and an aligned project, Section 2 will define the approach that will be concretized by an AS IS model and a TO BE model using Archimate language, Section 3 elaborates the impact analysis of the change on an aligned system and finally a Section 4 that elaborates the CBITA prototype that will be validated by a case study of a Moroccan urban agency.

## II. RELATED WORK

### A. Impact Change in Alignment Business IT

The research [13] has mentioned that the relationship between agile changes largely affects all elements of business IT alignment; they have described that when there is a change in an entity that contributes to strategic alignment automatically it is all the entities that touch each other. Over the course of the literature, we find that the majority of the work concerning the changes that impact the system and not precisely the harmonization between the elements of the strategic alignment, these works are essentially in different domains including the modeling of company or the software architecture. For the latter, we examined the work of [14] Williams et al. provided a framework for assessing change characteristics (e.g., sources, types of change, granular effect, etc.) and their impact on architecture, [15] they also determine the different characteristics of agile change, they develop the sources of change and integrate them into the system. This paper concludes with a focus on the impact of agile change on business IT alignment, primarily: (i) change is triggered by sources as well as type of change, (ii) impact touches all the components and entities of a business IT alignment whether it is Bottom Up or Top Down.

### B. Alignment Business IT with an Aligned Project

The selection of projects and initiatives is an area where Business IT alignment can be easily and quickly improved and where this work has a massive impact on organizational performance. Selection is often done by an executive committee and, because of this level of visibility, people tend to assume that the resulting project portfolio is aligned with strategy. It is not easy to lead a change in a company, especially when you know that a % of projects are not supported, i.e. do not achieve their objectives. There are many indicators to be taken into account to start a transformation.

By focusing on the resources of the most strategically important projects, value is created with less risk. Therefore, projects that are aligned with strategy have a better chance of achieving their objectives. In other words, by measuring the Business IT alignment of projects and eliminating projects that are not aligned, these resources can be redirected to important projects that are in difficulty and turned into successful projects. Project prioritization is the basis for successful project implementation. This is where the alignment of projects to strategy requires.

Incorrect prioritization leads to the failure of projects and, ultimately, to the non-attainment of objectives. Properly conducted, a good project process will strategically align resource allocation decisions while achieving more successful projects. This seems to be reason enough to invest in improving the project prioritization process, but many organizations do not even realize that their current process is flawed; it has evolved over time, it worked last year and it will work next year.

The environment is constantly changing around us, and if we do not have a well-structured process to recognize and respond to change in a way that has broad management support, then the organization will fail to achieve its goals.

This is where we need to prioritize projects:

- Align projects with strategy;
- Compare the study of the existing (existing project) with the study to be implemented (future project) and;
- Analyse the impact of the project on the aligned system to quantify the projects that add value and the ones that do not.

To achieve this, an approach consisting of three important phases will be followed in the following section.

## III. PROCESS FOR IMPACT A PROJECT ON AN ALIGNED SYSTEM

The contribution will begin with an approach that consists of 3 important phases as shown in Fig. 1. It includes (1) a model of the study of the existing of the enterprise (AS IS) defined by the Archimate language that will be the first step, then (2) the project that is the source of change and after (3) the impact of this project on the study of the existing to have the model defined by the Archimate language that we want to put in place taking into consideration the Business IT alignment (TO BE) [16].

- Pre-requisites: Study of the existing 'AS-IS' using the of Urbanisation reference of the information system frame of the French government's;
- IT project modeling: Modeling of the project with different missions and processes of different levels of abstraction (same repository as AS-IS but with the project objectives);
- Change analysis: To determine if the project will be suitable for adoption by the AS-IS, a comparison is needed to determine the changes that will be supported.

A. Phase 1: AS-IS

In this step, an "AS IS" is carried out on four levels, (1) the processes with high added value of the company, (2) the organization of the application architecture, (3) functional and flows, (4) the organization of the technical architecture.

The inventory identifies the points of difficulty and possible risks associated with the information system and/or the IT system. These risk points may be the subject of projects to be implemented as part of the improvement of the information system using the 'French State Urbanization reference system' [17].

Previous research on business IT alignment [18]–[20] ... has approached strategic alignment from a modelling and evaluation point of view with an appropriate result, but little research has been carried out on the evolution of this Business IT alignment with unforeseen events and changes.

This model [17] will be our referential on the existing as shown in Fig. 2, it is a French state urbanization model which in order to facilitate mutual understanding both of patrimony but also of initiatives and projects of transformation. It will allow us to list and classify the subjects concerned: data, applications, processes, but also software components or technical equipment, as the initiatives and transformation projects. The objective is to define and maintain for each viewpoint on the IS (strategy view, business view, functional view, application view, infrastructure view) a reference nomenclature that allows:

- Structure the assets and their transformation;
- Facilitate communication and understanding of heritage and projects;
- Definition of the existing technical architecture.

B. Phase 2: Modelling Project

The project will have its own modelling is presented in Fig. 3 independent of the AS IS model where we will define its strategy, its declination on the business processes and its declination on the functions of the information system and we will see further on if this project will have an added value by keeping the alignment between the strategy and the information system.

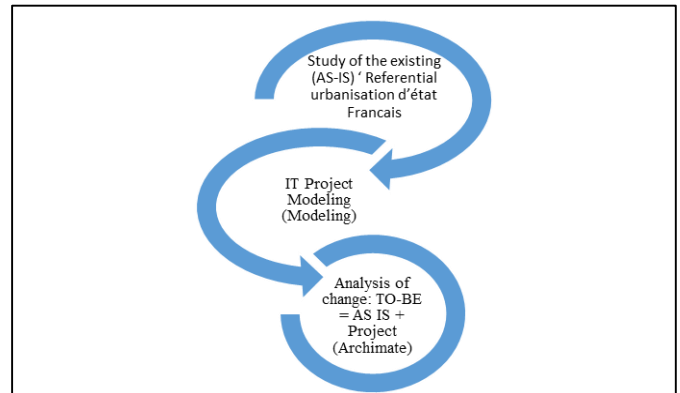


Fig. 1. Process of Impact of a Project on Business IT Alignment.

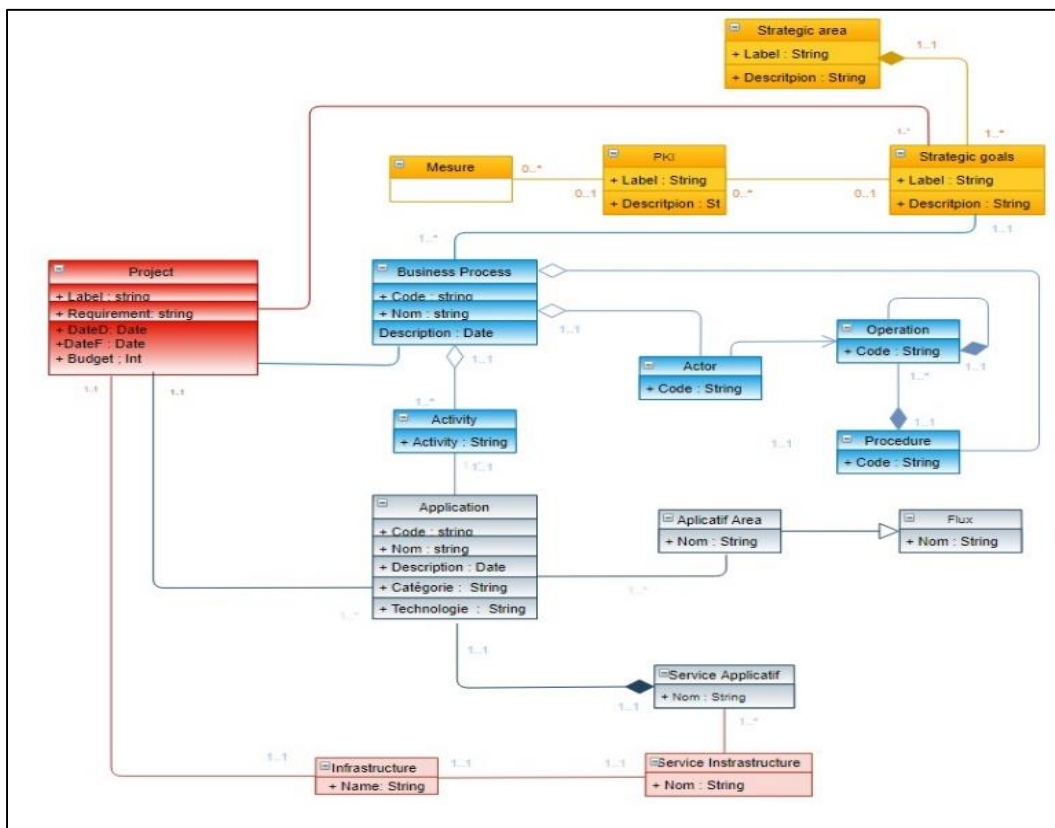


Fig. 2. French State Urbanization Reference Information System.

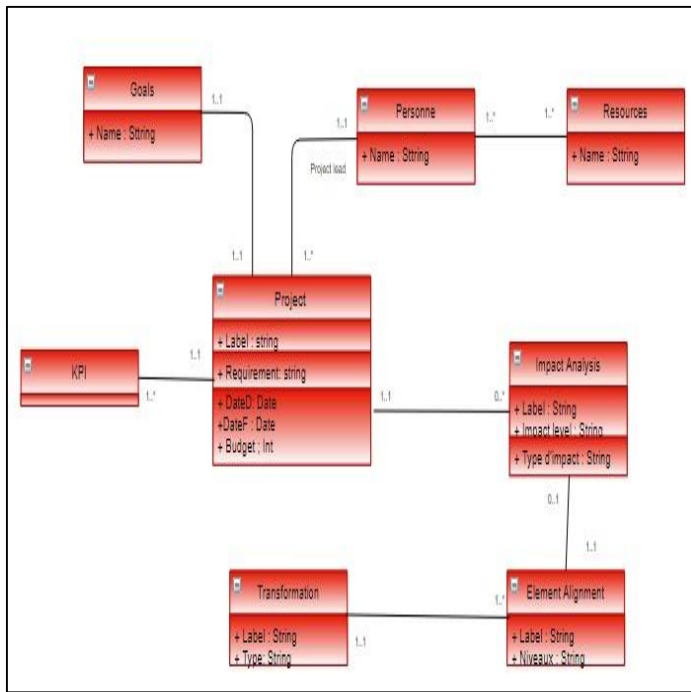


Fig. 3. Project Modeling.

The model will be characterized by a modeling process is presented in Fig. 4 aimed at obtaining an acceptable solution from the computer system. The solution finally selected is not obtained in a single iteration. Several steps are necessary; these successive steps allow the level of detail of the system to be refined. The first steps give a very large vision and allow to progress in the understanding of the problem.

C. Phase 3: To be - Change Analysis

Before starting a project, an impact analysis should be conducted in order to identify all the consequences of a change on employees, processes, business functions, other ongoing projects, etc. as mentioned in Fig. 5.

Fig. 5 shows the following steps:

- Expression of needs: The need expression phase involves identifying the request, clarifying and specifying the need;
- Feasibility study: The feasibility study concerns the technical, financial and availability of means for the project;
- Action plan: Defining, organizing, planning and implementing all the means to achieve the set objectives.

A mechanism must therefore make it possible to define "what should be done" (i.e. in compliance with the rules of business IT alignment) and compare it as soon as possible with "what can be done" (i.e. in compliance with cost and time constraints).

Phase 3 will be formalized by the ArchiMate language [13] which is relatively a new standard for high-level enterprise architecture modeling. It provides a comprehensive modeling language that has been formally developed to describe and analyse the architecture of an enterprise. It provides a meta-model and graphical notations to visually describe and analyse the three layers of EA (Business, Application and Infrastructure), their relationships and dependencies. The main advantage of ArchiMate is its ability to cover all layers of the enterprise, a single language for all layers and viewpoints of the business, from the business to the technical foundation.

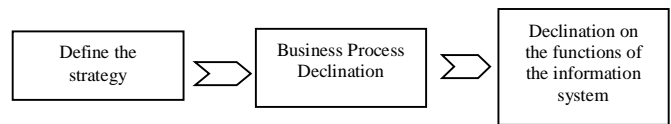


Fig. 4. Strategy of a Project Modeling.

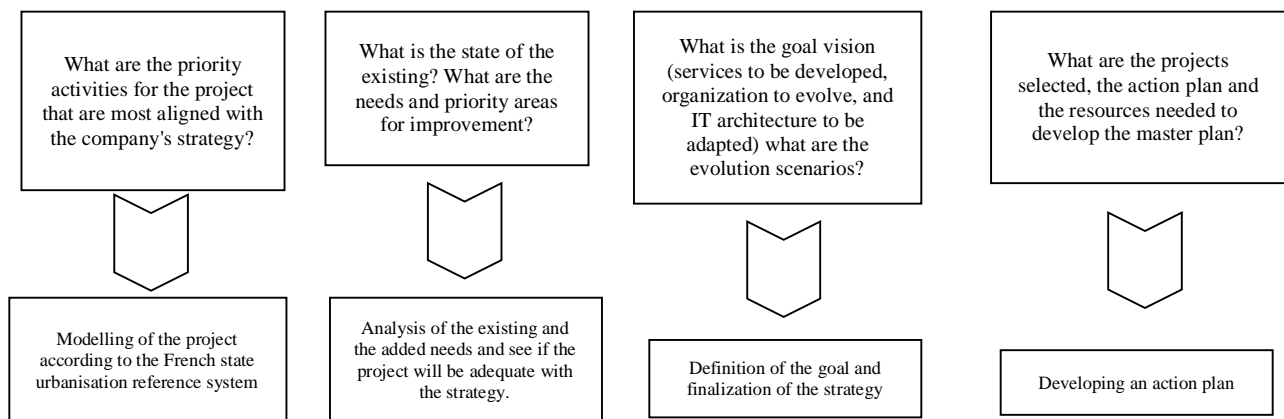


Fig. 5. Change Analysis.

#### IV. THE IMPACT OF THE ALIGNED PROJECT ON AN ALIGNED SYSTEM

Alignment takes place at the business and functional levels, from a technological and organizational point of view presented in Fig. 6. Through projects, the information system tries to structure itself in an organized way [21]. From an economic point of view, the application of an investment typology at the project portfolio level makes it possible to respond to two complementary management challenges:

- A gradual realignment of the value provided: a strategic opportunity approach may emerge for the business and IT.
- Taking into consideration the nature of the projects and their specificities in order to compare them in a common framework: response to the prioritization difficulties frequently encountered (between strategic projects and infrastructure projects, for example).

The impact of a project includes all related information in terms of resources, schedules, budgets, benefits and risks. It can also include other information related to the nature of the company's activity or principles related to the Business IT alignment of all levels of abstraction. The project manager will define the cost and quality of the project and the duration. The business IT Alignment Architect will define the limit and weight of the Business IT alignment entity elements and will make a comparison between AS-IS and TO-BE model from Archi tool to distinguish between projects that are supported and projects that are not supported by the project management system presented in Fig. 7.

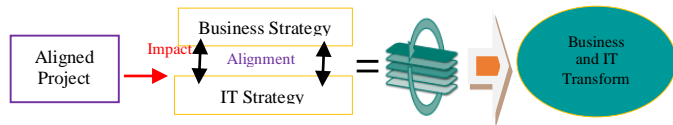


Fig. 6. Impact of an Aligned Project.

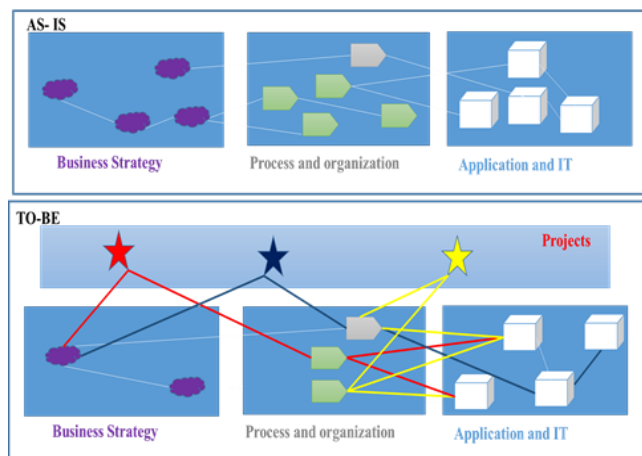


Fig. 7. Impact of an Aligned Project on an Aligned System.

#### V. CASE STUDY: URBAN AGENCY IMPLEMENTING A GEOGRAPHIC INFORMATION SYSTEM

The process explained in the previous sections will be validated by the case study of an Urban Agency implementing a Geographic Information System.

##### A. Study of the Existing

Several interviews were held with the various stakeholders of the basic departments of the Laayoune-Sakia el Hamra Urban Agency with a view, on the one hand, to detail the areas to be computerized and, on the other hand, to collect the expected needs of the GIS to be set up.

These interviews focused on the following points:

- Existing organization and procedures,
- Data produced by the Agency: nature and media of the data;
- Existing alphanumeric and cartographic data;
- Existing in terms of available databases and applications;
- Existing in terms of IT platform;
- Needs in terms of data and processing;
- Existing in terms of completed project.

The analysis of the existing is part of the detailed analysis phase of the project. This step, which is essential to any project start-up, helps to define and encourage the creativity of the team in charge of developing the new GIS.

Fig. 9 illustrates the study of the existing which is modelled by the Archi tool, which is a visual design and modelling tool for creating ArchiMate models and modelling designs. The AS IS will be formalized to understand the concept of the study of the existing.

The export of the AS IS model in CSV is presented in Fig. 8 by the Archi tool will help us to make a comparison with the CSV of the TO BE model to feed the change impacted by the project, a prototype will be created to compare the 2 CSV files and determine the change that was achieved.

| ID                          | Type             | Name                                                           | Documentation |
|-----------------------------|------------------|----------------------------------------------------------------|---------------|
| 0d7f4b0d-f1d1-4f5a-b578-a6  | ArchimateModel   | AS IS F                                                        |               |
| 9b72f94a-2db4-4024-8bd0-3   | BusinessActor    | Agent                                                          |               |
| 5437a090-b03a-44a4-9426-fc  | BusinessActor    | DAJF                                                           |               |
| da1b3d65-c0e2-4478-99b4-b   | BusinessFunction | Accessibilit s aux donn es                                     |               |
| 000a9c3f-6c53-404c-a276-bb  | BusinessFunction | Gestion des dossiers                                           |               |
| f30198ae-0393-4c7c-86ee-15  | BusinessFunction | Gestion des infractions                                        |               |
| e56ec39f-d7a1-49e1-9586-b   | BusinessProcess  | Accessibilit s aux donn es                                     |               |
| ae385912-561e-4eb3-a5a1-f   | BusinessProcess  | Commission                                                     |               |
| 3ae0b003-e33f-4066-ae88-7   | BusinessProcess  | Convocation                                                    |               |
| e4ad49f-054a-4826-80cd-49   | BusinessProcess  | Dispatching                                                    |               |
| fa16a719-cfca-422d-8367-e2  | BusinessProcess  | Documenter les donn es                                         |               |
| 8c48d354-f1b2-4ddf-8ee2-2f  | BusinessProcess  | Elaborer les demandes                                          |               |
| 22952cd4-3749-4f64-a5e0-bc  | BusinessProcess  | Enregistrement                                                 |               |
| fc0ea7c5-bf2c-466f-9a1f-3ac | BusinessProcess  | Envoi de la lettre et copie des PV pour la signature par le DG |               |

Fig. 8. AS IS Model Export in CSV.

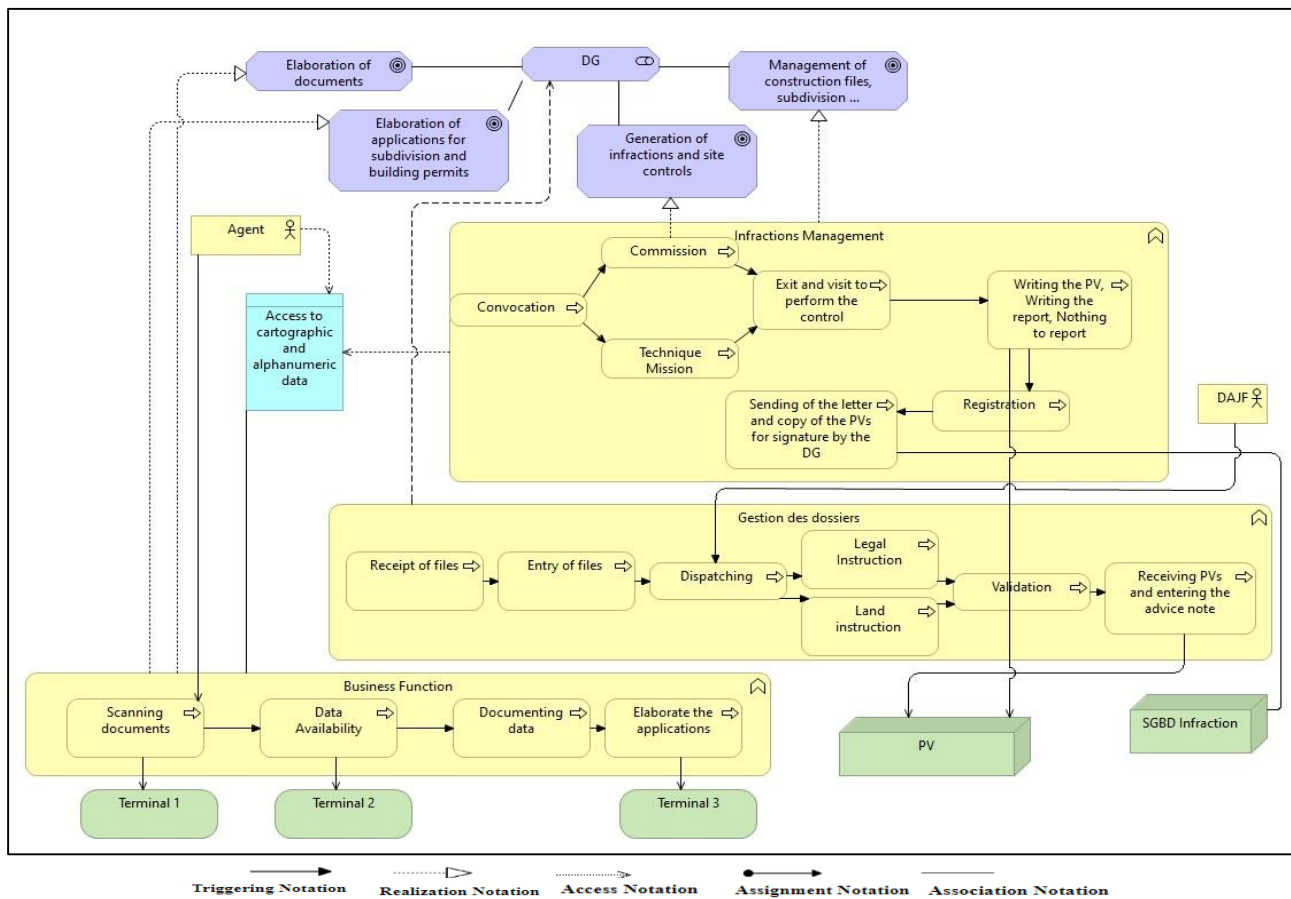


Fig. 9. Modeling of the GIS Project with AS IS Model.

### B. Modeling of the GIS Project

The Urban Agency, as a public agency in charge of Urban Planning and technical assistance to its partners in its territorial area, is required to manage on a regular basis a large amount of information from different sources, natures and media.

The implementation of a WEB GIS (Geographical Information System) platform and online services, on behalf of the Urban Agency, with the aim of controlling the information possessed and acquired, rationalizing the archiving and updating of information and accessing various statistics and carrying out spatial analyses.

The GIS tool presented in Fig. 10 must ensure the following functionalities: information, production and decision, it must cover all the basic procedures relating to the operation of the Urban Agency of Laayoune. This system must allow the automation of its procedures, support processes and business processes. The technical specifications relating to the implementation of this system must meet the overall constraints indicated below:

- Consultation and quick reading of urban planning documents and regulatory databases;
- The delivery of the information note;

- The automatic generation of monitoring and historical records of activities at the level of plots and specific study areas;
- The facility of exchanges with the various partners and customers by the GIS-WEB; (results of the files, information notes...);
- The electronic management of documents;
- Management of claims.

The proposed solution presented in Fig. 10 must respond precisely to the specific needs of the Administration in terms of data exploitation and functional organization. In particular, it must be based on an internationally recognized GIS & DBMS solution that can guarantee interoperability, data sharing and ensure the durability and evolution of the solution. The final objective being: the achievement of the following missions:

- Electronic document management;
- E-note;
- E-reclamation;
- E- infraction;
- Geoportail for urban planning.

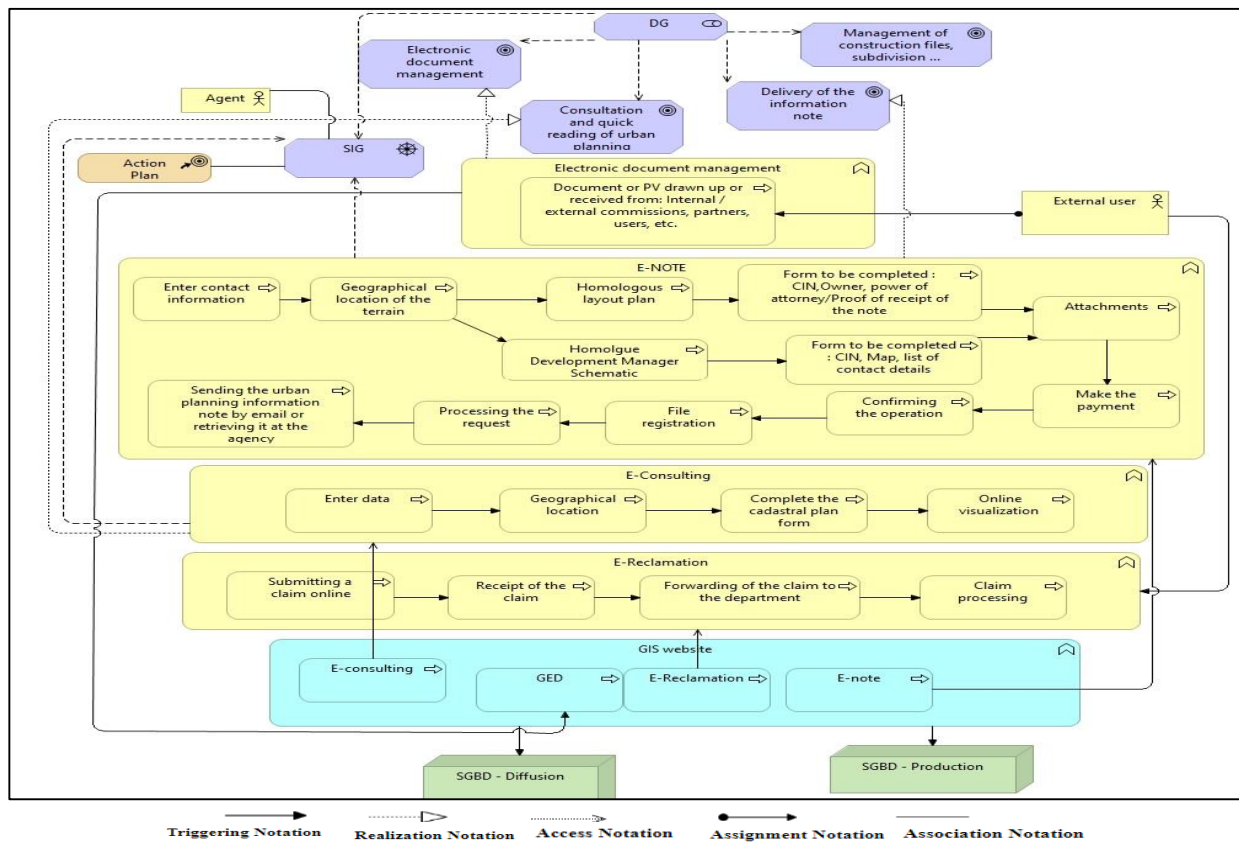


Fig. 10. Modeling of the GIS Project.

### C. Analysis of Change: TO BE

After the analysis on the basis of the 'Special Conditions' which was transmitted by the agency, the impact of the project on the study of the existing will transform all the objectives of the agency to different modules developed in the GIS:

The TO BE model is presented in Fig. 12 will be determined as follows:

- The proposed GIS platform must be based on a secure Intra/Internet solution for its deployment and operation;
- The solution must make use of the digital mapping tools available, which the contractor undertakes to acquire on behalf of the management, and must take into consideration all the applications and databases already deployed within the management and at the supervisory Ministry (possibility of integrating the ministerial frameworks to save time and guarantee the reliability of the data provided).
- The solution must ensure the integration, management, centralization, in databases and the updating, if necessary, of all the data involved in the business, such as cartographic, photogrammetric, remote sensing and socio-economic data;

The system will have to take into account all the information essential for its implementation by integrating

georeferenced or non-geo-referenced information (documentation, authorization file, Image...) with their metadata to define all the technical and descriptive information (digitization scale, accuracy...);

Objectives are added to complete the overall goal of the agency, these objectives are aligned with business processes that will be modulated by activities, using the WEB GIS platform to disseminate all the services that will be handled by the agency's agents. After the modelling of the impact of the project on the study of the existing, the 'TO BE' model will be imported in CSV presented in Fig. 11 format in order to execute the comparison with the CSV file of the study of the existing 'AS IS' mentioned above to determine the acquired transformations and to analyse the change. The following section will demonstrate the prototype that supports this comparison.

| ID                      | Type             | Name                                           | Documentation |
|-------------------------|------------------|------------------------------------------------|---------------|
| 0d7f4b0d-f1d1-4f5a-b57  | ArchimateModel   | TO BE F                                        |               |
| 9b72f94a-2db4-4024-8bc  | BusinessActor    | Agent                                          |               |
| 5437a090-b03a-44a4-942  | BusinessActor    | DAF                                            |               |
| daf5d87-84e3-4d39-abi   | BusinessActor    | Responsable du dÃ©partement de Gestion urbaine |               |
| 8635cd2-57e3-468e-94f   | BusinessActor    | Utilisateur externe                            |               |
| 347bca8b-cfe0-44a1-8b3  | BusinessFunction | E-Consultation                                 |               |
| a7f1653f-2081-47c8-8bbi | BusinessFunction | E-NOTE                                         |               |
| 1549a78a-83e9-44a1-bf7  | BusinessFunction | E-RÃ©clamation                                 |               |
| f30198ae-0393-4c7c-86e  | BusinessFunction | Gestion des Infractions et Controles           |               |
| 358d741c-9699-4c3e-845  | BusinessFunction | Gestion Ã©lectronique des documents            |               |
| 00a9c3f-6c53-404c-a27f  | BusinessFunction | IntÃ©gration Gestion de dossier dans LE SIG    |               |
| 0c65d51-9606-4fa2-a93   | BusinessFunction | Sauvegarde Des documents                       |               |
| afaa5f9-5b93-4d7e-bc1   | BusinessProcess  | Archivage dans une base de donnÃ©es            |               |
| 08a03972-c884-4fa2-bfc  | BusinessProcess  | Confirmation de l'opÃ©ration                   |               |
| 2340be5e-5852-4ecc-90   | BusinessProcess  | Diffusion de la rÃ©clamation au dÃ©partement   |               |

Fig. 11. To be Model Export in CSV.



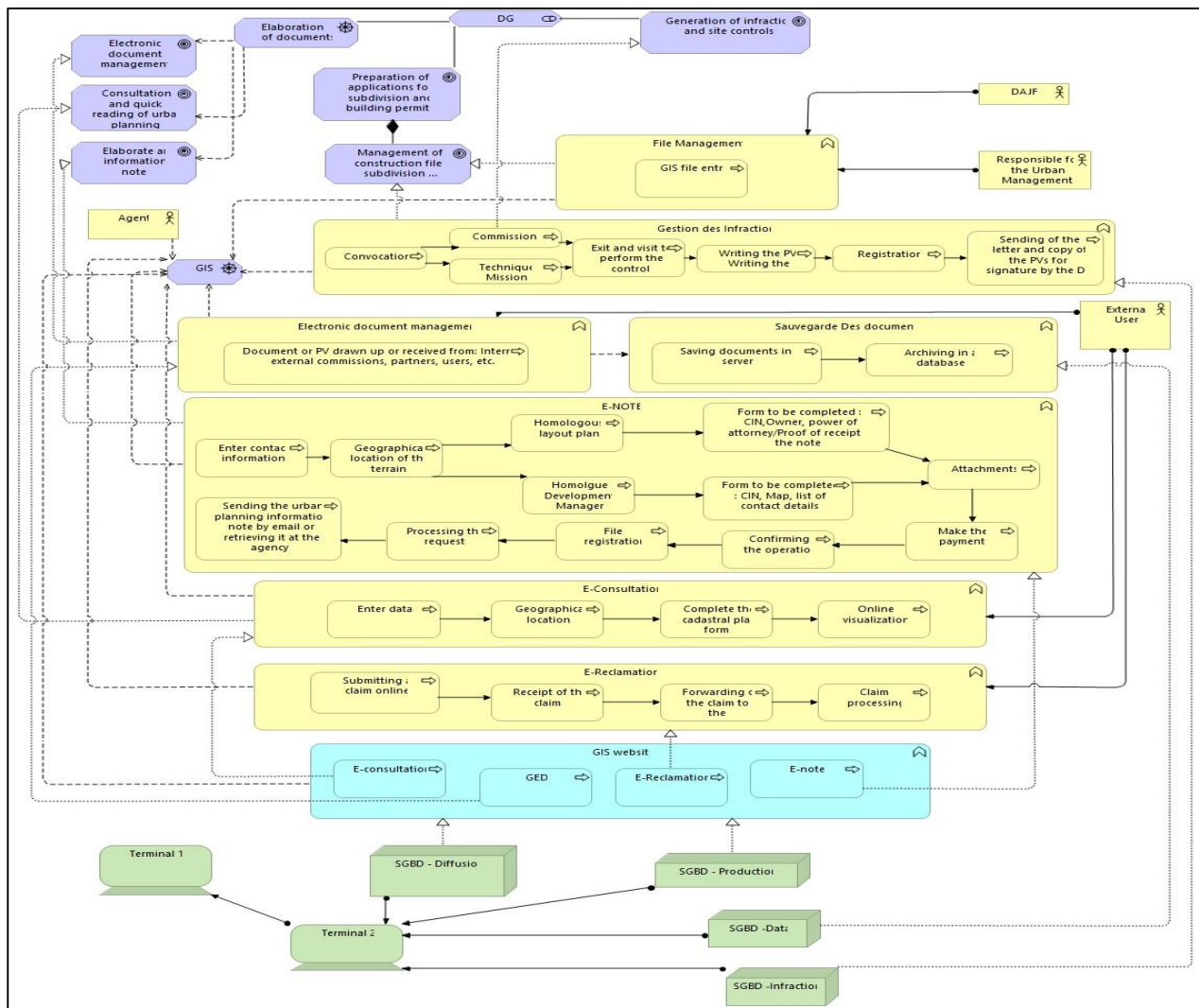


Fig. 12. Modeling of the GIS Project with AS IS Model = TO BE.

## VI. CHANGE IN BUSINESS IT ALIGNMENT (CBITA) TOOL

The CBITA (Change in Business IT Alignment) Tool developed to support change evaluation by comparing CSV files exported from the AS IS and TO BE modeling by the Archi tool proposed in the previous section.

The goal of this prototype is to provide a comparator by general algorithms that gives us the result of the evaluation of the impact of Project (Strategic Project Objectives and IT Project Objectives) on the study of the existing (an aligned system = strategic objectives aligned with the IT objectives) by presenting the changes by entity of alignment, the modifications made, the redundancy, the deletion or addition of entities and to clarify the good project that will be eligible

for the study of the existing. This Tool will allow the users (it can be the project manager, the strategic alignment architect ...) to know the appropriate alignment model for the study of the existing in relation to the project and to define the set of analysis of changes that the project can establish to the whole existing aligned system. This tool therefore allows: Fig. 13 show the comparison between 2 CSV files (AS IS and TO BE) to analysis the change, the Fig. 14 the evaluation of the alignment through algorithms to determine the number of changes between the different entities of Business IT alignment as also the exact change between the entities, and finally the Fig. 15 defines a graph which qualifies the best project by change (modification, deletion, addition).

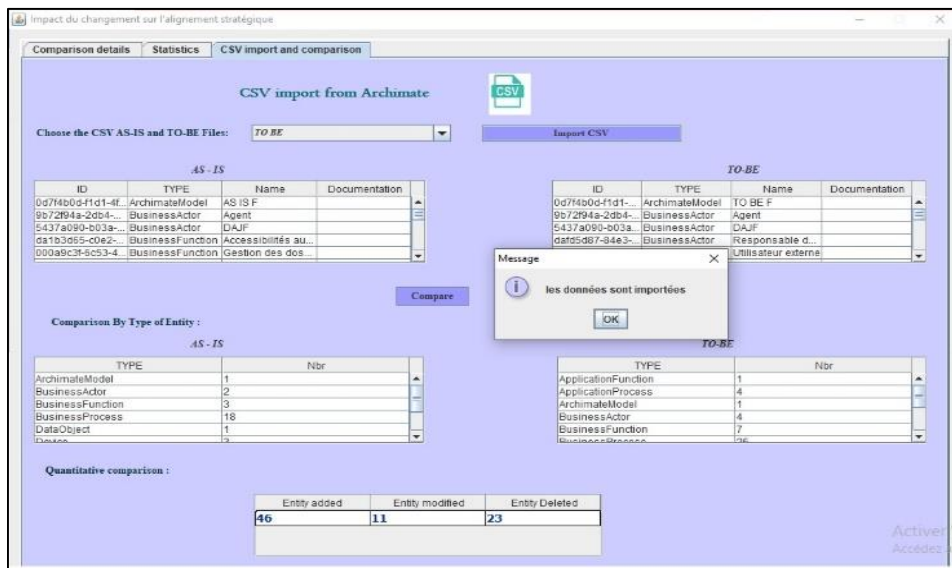


Fig. 13. Comparison between CSV Files = AS IS and TO BE.

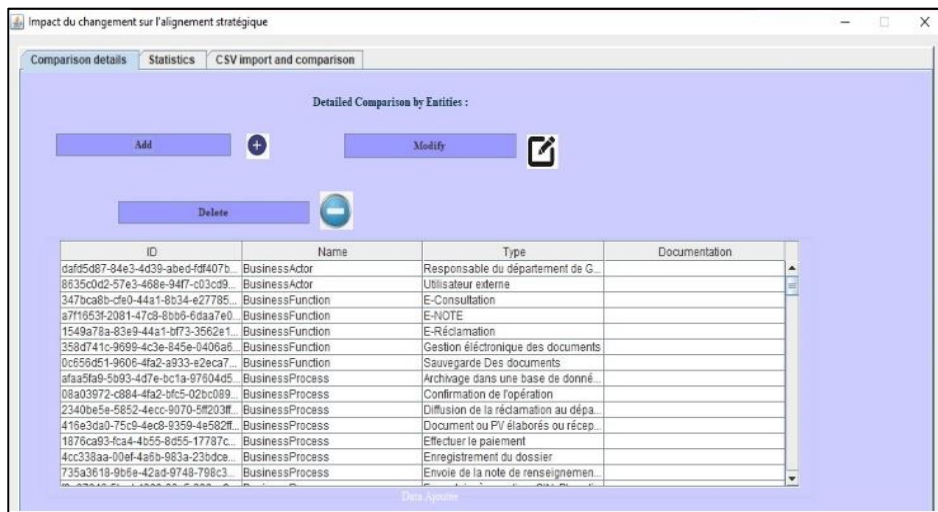


Fig. 14. Analyses of Change between the CSV Files.

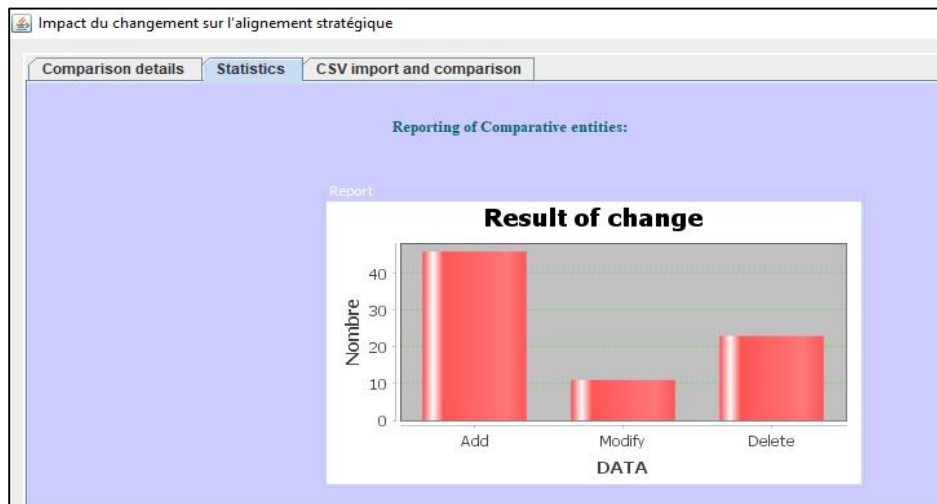


Fig. 15. Graph Illustrating the Impact of Change.

## VII. CONCLUSION AND FUTURE DIRECTION

To conclude, this was possible to determine the impact of a project on an aligned system. A process was to be carried out to analyse the change in the impact of a project on an aligned system. The conclusion is that when a change affects the aligned system, it is all the system which changes: objectives change, business processes, activities, information system, technical infrastructure all change, so when a change affects the system automatically the whole system changes. The main objective of the contribution despite the change we must keep the strategic alignment. Future work will focus firstly on comparing the approach detailed previously with the other approaches in order to benefit from the comparative criteria. Secondly, we will try to add to the CBITA approach the option of choosing between several projects to demonstrate the most quantifiable project for an aligned system.

### REFERENCES

- [1] S. L. Jarvenpaa and B. Ives, "Organizing for Global Competition," *Decis. Sci.*, vol. 24, no 3, p. 547-580, mai 1993.
- [2] Andrew H. Van de Ven and Robert Drazin, "The Concept of Fit in Contingency Theory," p. 71, 1985.
- [3] D. Miller, "Environmental Fit versus Internal Fit," *Organ. Sci.*, vol. 3, no 2, p. 159-178, mai 1992.
- [4] Tallon and A. Pinsonneault, "Competing perspectives on the link between strategic information technology alignment and organizational agility: insights from a mediation model," *Mis Q.*, vol. 35, no 2, p. 463-486, 2011.
- [5] O. Avila and K. Garcés, "Change management support to preserve Business-Information technology alignment," *J. Comput. Inf. Syst.*, vol. 57, no 3, p. 218-228, 2017.
- [6] O. Avila and K. Garcés, "Change management contributions for business-IT alignment," in *International Conference on Business Information Systems*, 2014, p. 156-167.
- [7] R. L. Thompson and C. L. Iacovou, "Information technology, critical success factors and organizational performance of small firms: a causal modelling approach," School of Business Administration, University of Vermont, Burlington, VT, Working Paper WP-MIS-93-006-1., 1993.
- [8] D. Miller, "Configurations Revisited," *Strateg. Manag. J.*, vol. 17, no 7, p. 505-512, 1996.
- [9] M. L. Tushman and C. A. O'Reilly, "Ambidextrous Organizations: Managing Evolutionary and Revolutionary Change," *Calif. Manage. Rev.*, vol. 38, no 4, p. 8-29, juill. 1996.
- [10] R. Greenwood and C. R. Hinings, "Understanding Radical Organizational Change: Bringing Together the Old and the New Institutionalism," *Acad. Manage. Rev.*, vol. 21, no 4, p. 1022-1054, oct. 1996.
- [11] K. Imgharene, K.doumi, and S.Baina, "Impact of Agility on the Business IT Alignment Conference the International Symposium on Business Modeling and Software Design," BMSD, 2017.
- [12] K. Imgharene, K. Doumi, and S. Baina, "Proposal model of change for Business IT Alignment," *Procedia Comput. Sci.*, 2019.
- [13] K. Imgharene, K. Doumi, and S. Baina, "Toward a model for agility and Business IT Alignment," *BDCA*, avr. 2018.
- [14] B. J. Williams and J. C. Carver, MSU-081216 "Characterizing Software Architecture Changes: A Systematic Review,"
- [15] R. Sartori, A. Costantini, A. Ceschi, and F. Tommasi, "How Do You Manage Change in Organizations? Training, Development, Innovation, and Their Relationships," *Front. Psychol.*, vol. 9, mars 2018.
- [16] The Open Group "ArchiMate 3.1 Specification," p. 206, 2019.
- [17] Etat Francais "Cadre commun d'urbanisation du SI de l'Etat Francais," 2016.
- [18] K. Doumi, S. Baïna, and K. Baïna, "Modeling Approach Using Goal Modeling and Enterprise Architecture for Business IT Alignment," in *Model and Data Engineering*, sept. 2011, p. 249-261.
- [19] A. Etien, "Ingénierie de l'alignement: concepts, modèles et processus: la méthode ACEM pour l'alignement d'un système d'information aux processus d'entreprise," Paris 1, 2006.
- [20] L.-H. Thevenet, "Proposition d'une modélisation conceptuelle d'alignement stratégique: La méthode INSTAL," Université Panthéon-Sorbonne-Paris I, 2009.
- [21] A. Asil, "Design and Implementation of Strategic Agility Evaluation Model with Structural Equation Modelling Approach," *Acad. Strateg. Manag. J.*, févr. 2019, Consulté le: juill. 26, 2019.

# Enhancing VoIP BW Utilization over ITTP Protocol

AbdelRahman H. Hussein<sup>1\*</sup>, Mahran Al-Zyouid<sup>2</sup>

Dept. of Computer Science  
Al-Ahliyya Amman University (AAU)  
Amman, Jordan

Kholoud Nairoukh<sup>3</sup>, Sumaya N. Al-Khatib<sup>4</sup>

Dept. of Networks and Information Security  
Al-Ahliyya Amman University  
Amman, Jordan

**Abstract**—The revolution of Voice over Internet Protocol (VoIP) technology has propagated everywhere and replaced the conventional telecommunication technology (e.g. landline). Nevertheless, several enhancements need to be done on VoIP technology to improve its performance. One of the main issues is to improve the VoIP network bandwidth (BW) utilization. VoIP packet payload compression is one of the key approaches to do that. This paper proposes a new method to compress VoIP packet payload. The suggested method works over internet telephony transport protocol (ITTP) and named Delta-ITTP method. The core idea of the Delta-ITTP method is to find and transmit the delta between the successive VoIP packet payloads, which is typically smaller than the original VoIP packet payload. The suggested Delta-ITTP method implements VoIP packet payload compression at the sender side and decompression at the receiver side. During the compression process, the Delta-ITTP method needs to keep some values to restore the original VoIP packet payload at the receiver side. For this, the Delta-ITTP method utilizes some of the IP protocol fields and no additional header is needed. The Delta-ITTP method has been deployed and compared with the traditional ITTP protocol without compression. The result showed that up to 19% BW saving was achieved in the tested cases leading to the desired enhancement in the VoIP network BW utilization.

**Keywords**—Voice over IP (VoIP); VoIP protocols; Internet Telephony Transport Protocol (ITTP); payload compression; bandwidth utilization

## I. INTRODUCTION

Voice over Internet Protocol (VoIP) is everywhere. There is a very high growing demand for VoIP in just about all companies and even by the normal people [1][2]. However, two main dilemmas need to be addressed for VoIP to replace the traditional telecommunication systems. The first one is the faint quality of the VoIP calls when compared with the traditional telecommunication system calls. This is because VoIP works over IP networks which, as opposite to the traditional telecommunication systems, do not provide a dedicated channel for the VoIP call [3][4]. The second dilemma is the failure to make the best use of VoIP network bandwidth (BW) [4][5]. This is mainly because the VoIP codecs produce a very small voice frame (VoIP packet payload) in order to avoid exceeding the acceptable 150ms delay of VoIP calls. The codec voice frame is usually 10 to 30 bytes in length while the size of the protocols (VoIP packet header) that used to carry the voice data can reach up to 40 bytes. Therefore, only 20% to 43% of the VoIP network BW is used to carry the VoIP data while the remaining share of the BW is wasted to carry the VoIP packet header. Clearly, this is a very high ratio of waste of the VoIP network BW [6][7].

There are several protocols used by VoIP technology to carry the VoIP data. They are typically classified into signaling protocols and media transfer protocols. The signaling protocols are used to establish and negotiate the parameters to be used in a call. The two main examples of VoIP signaling protocols are SIP and H.323 protocol [8][9]. The media transfer protocol is used to convey the voice data, after establishing the call, from point to point over the VoIP network. The 12-byte Real-time Transport Protocol (RTP), 6-byte Internet Telephony Transport Protocol (ITTP), and 4-byte Inter-Asterisk eXchange (IAX) are the main examples of media transfer protocols. Both RTP and IAX take the help of the 8-byte User Datagram Protocol (UDP) to be able to convey the voice data, while ITTP is able to carry the voice data by itself [10][11][12]. As mentioned earlier, adding these protocols along with the 20-byte IP protocol to the small VoIP packet payload leads to a considerable amount of BW waste. Table I shows the wasted BW, caused by media transfer protocols along with the IP protocol. The wasted BW is calculated by dividing the protocol size over packet size (payload and protocol).

The VoIP researchers have followed several ways to deal with the wasted BW resulting from the VoIP applications. These approaches include VoIP packet grouping, VoIP packet payload compression, and VoIP packet header compression [13][14][15]. In this research paper, we propose a new method to save the VoIP network BW by compressing the VoIP packet payload. The suggested method computes the delta of the consecutive VoIP packets payload with a specific mechanism to compress VoIP packet payload. Additionally, the suggested method utilizes some of the IP protocol fields to serve and save the values needed by the compression algorithm. Thus, no extra header needs to be added to the VoIP packet.

TABLE I. CONSUMED BW BY MEDIA TRANSFER PROTOCOLS AND IP PROTOCOL

| Protocol Name | Protocol Size | Wasted BW(%)     |                  |                  |
|---------------|---------------|------------------|------------------|------------------|
|               |               | 10-bytes payload | 20-bytes payload | 30-bytes payload |
| IAX/UDP/IP    | 32            | 76.1%            | 61.5%            | 51.6%            |
| RTP/UDP/IP    | 40            | 80%              | 66.6%            | 57.1%            |
| ITTP/IP       | 26            | 72.2%            | 56.5%            | 46.5%            |

\*Corresponding Author

The hierarchy of the paper is as follows: Section 2 spotlights one of the grouping methods that addresses the BW utilization problem. Section 3 discusses the internal operations and procedures of the suggested method. Section 4 shows the evaluation parameters of the suggested method and investigates its robustness against the traditional ITTP method. In the end, Section 5 summarizes the findings.

## II. RELATED WORKS

The issue of VoIP BW utilization has been investigated by many researchers. This section discusses some of the methods that were suggested to improve VoIP network BW utilization.

Teymoori, Peyman, et al. suggested a packet grouping method to improve the VoIP network BW in wireless LAN (WLAN). To achieve this, the suggested method grouped the incoming VoIP frames in one layer 2 header. Besides packet grouping, the suggested method focused on the ideal size of the resulted grouped packet, particularly for the delay-sensitive applications in the high speed WLAN. Thinking about the impact of packet grouping on delay, Teymoori, Peyman, et al. suggested an investigative model to get the ideal grouped packet size with respect to delay limitations forced by real-time applications. Specifically, the authors defined a packet grouping scheme as a constrained convex optimization issue to expand the overall WLAN throughput. First, Teymoori, Peyman, et al. displayed the channel access delay of nodes using the IEEE 802.11n packet grouping scheme. Second, through a general strictly concave network utility function, the optimization problem is constructed and the distributed solution is suggested to reach at its ideal point. The result proved that the suggested model reached the ideal point within little iterations in long term with no extra overhead. Moreover, delay requirements of nodes are actually fulfilled showing the precision of the suggested investigative model [16].

Sze et al. suggested a method that performs both header compression and packet grouping. The suggested method involved a module located at the sender device and another one located at the receiver device. The first module stripes the header from the data, compresses the RTP header based on certain mechanism, attaches the compressed RTP to the data, groups the resulted frames in one UDP/IP header, and transmits the resulted large packet to the receiver. The frames are grouped in one large packet until reaching a specific delay limit. The receiver side module de-groups the received large packet, separates the compressed RTP from the data, restores the original RTP header, attaches the RTP header along with UDP/IP header to the data, and sends the resulted original packet to its final destination. Besides header compression and packet grouping, the suggested method modifies the initial process of establishing the VoIP call. This modification is necessary for the sender to inform the receiver that the transmitted packets are grouped together and not the normal VoIP packet. The suggested method was tested and evaluated against the traditional method without grouping. The results showed an improvement in the BW utilization that reached up to 300% in the tested scenarios [17].

All of the previously mentioned methods were deployed over RTP/UDP/IP protocols header. In contrary to those

methods, Abualhaj, M. et al suggested a grouping method, called ITTP-Mux that works over the ITTP protocol header. The method, involved two modules located at the sender side gateway (named S-Mux) and the receiver side gateway (named S-DMux). The main purpose of the S-Mux is to group the packets that share the same path to the same gateway together in one IP header rather than a separate IP header to each packet. Before being grouped in one large packet with one IP header, a small header is attached to each of the mini-packets to be grouped in the large packet. The main purpose of the S-DMux is to segregate the large packet to the mini-packets, by inspecting the small header, and restore the original VoIP packet. The restored VoIP packets are then transmitted to their final destinations. The suggested method was tested and evaluated against the traditional ITTP method without grouping. The result showed an improvement in the BW utilization by up to 29.1% in the tested scenarios [18]. Another grouping method that works over ITTP protocol was in 2019. However, the suggested method, named CA-ITTP, combines between VoIP packets grouping and VoIP packets payload compression. Similar to the ITTP-Mux method, CA-ITTP method involved two modules located at the sender side gateway (named SCA) and the receiver side gateway (named RCD). The SCA module performs the same functions of the S-Mux in addition to payload compression based on a certain algorithm. The RCD module performs the same functions of the S-DMux in addition to payload decompression. The compression algorithm reduces the size of the VoIP packet payload based on a specific mathematical mechanism, which produces a smaller payload than the original payload. The decompression algorithm reinstates the size of the VoIP packet payload at the receiver side gateway. The suggested CA-ITTP method was tested and evaluated against the traditional ITTP method without grouping or compression. The result showed that the BW waste was reduced by half in the tested scenarios [19]. In this paper, we propose a new method to compress the VoIP packet payload, called Delta-ITTP. The suggested Delta-ITTP method computes and sends the variation of the consecutive VoIP packets payload, which is usually smaller than the original VoIP packet payload, using a specific delta algorithm. In addition, unlike the afore-discussed method, no additional header is needed since the suggested method utilizes some of the IP protocol fields to serve the purpose of the compression algorithm. The following section discusses the details of the Delta-ITTP method.

## III. THE SUGGESTED DELTA-ITTP METHOD

This section discusses the internal algorithm of the suggested Delta-ITTP method. The main purpose of the Delta-ITTP method is to enhance the VoIP network BW utilization. The desired utilization is achieved by shrinking the VoIP packet payload. The core shrinking idea used by the Delta-ITTP method is to consider the VoIP packet payload a digital number. By doing so, the VoIP packet payload of the consecutive packets can be subtracted from each other. The result of the subtraction is usually less in size than the VoIP packet payload. Then, the subtraction result replaces the VoIP packet payload and is sent to the receiver, saving the BW due to its smaller size. For demonstration, assume that the payload

of the first VoIP packet is X and the payload of the second VoIP packet is Y. The size of payload X is fifteen bits “111001100110101” and the size of payload Y is fifteen bits “110011101001001”. Then the result of subtracting the payload Y from the payload X is thirteen bits 10111101100, which is smaller than the normal payload size (110011101001001), thus lessens the consumed BW. There is a set of operations that are performed at the sender side to shrink the VoIP packet payload, as discussed in section (III.A). At the receiver side, the VoIP packet payload needs to be filled in order to recover its initial shape and size as produced by the codec at the sender side. Section 3.2 discusses the operations to recover the VoIP packet payload initial shape and size.

A. Delta-ITTP Operations at Sender Side

The main aim of the suggested Delta-ITTP method is to shrink the VoIP packet payload and, thus, save the VoIP network BW. Several operations must occur to achieve this. First, dissociation of the VoIP packets payload from the VoIP packets header. Second, subtraction of the VoIP packets payload that follow each other. For example, assume there are two payloads x and y, where x is the payload of packet n and y is the payload of packet n+1. If the value, as a digital number, of x is greater than y, then subtract y from x. Otherwise, subtract x from y. If the subtraction result is less than y, then replace y by the subtraction result, otherwise, keep y value as it is. Clearly, the first packet’s payload remains unchanged because no packets had arrived before it. Third, update the flag fields of the IP protocol in the VoIP packet header. The value of these fields is used to recover the VoIP packet payload initial shape and size as produced by the codec at the sender side. The process of updating these fields will be discussed below. Fourth, reconstruct the VoIP packet by associating the y packet payload to its header. Fifth, send the resulted VoIP packet to its destination. Fig. 1 illustrates the set of operations performed by the suggested Delta-ITTP at the sender side.

As mentioned above (Third operation), the flag fields of the IP protocol in the VoIP packet header need to be updated. There are three 1-bit flag fields within the IP protocol header. These fields are typically used to control the fragmentation process and identify the fragments of the large IP packets. However, the VoIP packets size is typically between 36 bytes to 56 bytes when ITTP protocol is used; thus, no fragmentation of the ITTP VoIP packets occur. Therefore, the three 1-bit flag fields within the IP protocol header are unused in case of VoIP over ITTP and remain zeros. Accordingly, the suggested Delta-ITTP method will use them to denote i) whether x is greater than y or the opposite and ii) whether y value is replaced by the subtraction result or kept as it is. Only two bits are needed to denote these two cases; therefore, the leftmost two bits of the three will be used. The first leftmost bit is used to denote whether x is greater than y or the opposite. Setting it to one denotes that x is greater than y and setting it to zero denotes the opposite. The second leftmost bit is used to denote whether y value is replaced by the subtraction result or kept as it is. Setting it to one denotes that y value kept as it is and setting it to 0 denotes that y value is replaced by the subtraction result. These values are used to

recover the VoIP packet payload initial shape and size as produced by the codec at the sender side. Fig. 2 shows the pseudocode of the subtraction process (Second operation) and updating of the IP protocol header flag fields (Third operation).

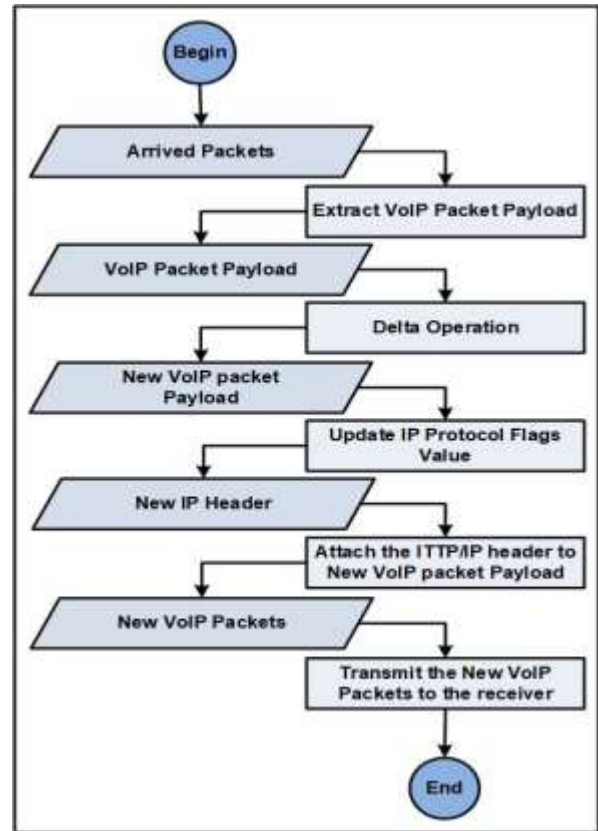


Fig. 1. Delta-ITTP Operations (Sender Side).

```

Delta Algorithm @ Sender Side
1 // X is packet n payload
2 // Y is packet n+1 payload
3 // FF First leftmost flag bit
4 // SF Second leftmost flag bit

5 if (X > Y) {
6 result= X - Y
7 FF = 1
8 } else
9 result= Y - X
10 FF = 0
11 }
12 if (result < Y) {
13 Y= result
14 SF = 0
15 } else
16 Y= Y
17 SF = 1
18 }

```

Fig. 2. Delta Algorithm (Sender Side).

### B. Delta-ITTP Operations at Receiver

The VoIP packet payload must be recovered to its initial shape and size as produced by the codec at the sender side. The receiver side performs a set of operations to do so. First, dissociation of the VoIP packets payload from the VoIP packets header. Second, recovering the VoIP packet payload initial shape and size as produced by the codec at the sender side. This is achieved by performing the addition or subtraction operation with the previous VoIP packet payload, based on the IP protocol header flag field's value. For example, assume that there are two payloads  $x$  and  $y$ , where  $x$  is the payload of packet  $n$  and  $y$  is the payload of packet  $n+1$ . If the second leftmost bit of the IP protocol header flag fields is equal to one, then the VoIP packet payload equals  $y$ . However, if the second leftmost bit of the IP protocol header flag fields is equal to zero and the first leftmost bit of the IP protocol header flag fields is equal to zero, then add  $y$  to  $x$  to produce the VoIP packet payload initial shape and size. Otherwise, subtract  $y$  from  $x$  to produce the VoIP packet payload initial shape and size. Clearly, no operations are performed on the first packet's payload because it did not change at the sender side. Third, set the IP protocol header flag field's value to zero to avoid any misinterpretation by the receiver. Fig. 3 shows the pseudocode of recovering the VoIP packet payload initial shape and size (Second operation) and updating of the IP protocol header flag fields (Third operation). Fourth, reconstruct the VoIP packet by associating the  $y$  packet payload to its header. Fig. 4 illustrates the set of operations performed by the suggested Delta-ITTP at receiver side.

#### Delta Algorithm @ Receiver Side

```

1 // X is packet n payload
2 // Y is packet n+1 payload
3 // FF First leftmost flag bit
4 // SF Second leftmost flag bit

5 if (SF is equal to 1) {
6 Payload-Size= Y
7 else if (SF is equal to 0) {
8 if (FF is equal to 0) {
9 Payload-Size= Y + X
10 else if (FF is equal to 1)
11 Payload-Size= X - Y
12 }

```

Fig. 3. Delta Algorithm (Receiver Side).

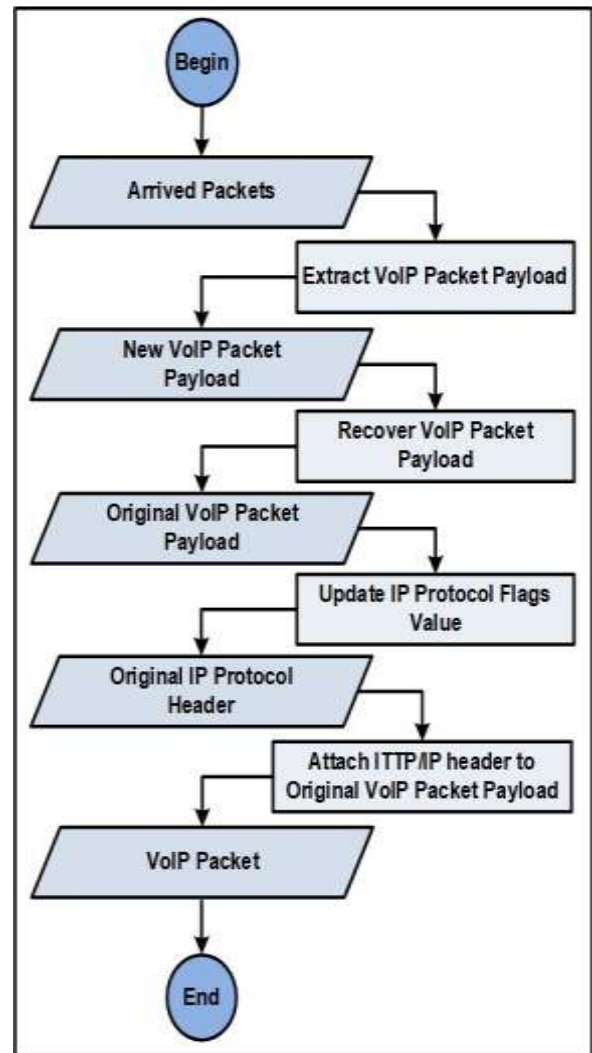


Fig. 4. Delta-ITTP Operations (Receiver Side).

## IV. DELTA-ITTP RESULTS AND PERFORMANCE EVALUATION

This section discusses the suggested Delta-ITTP performance evaluation. The main aim of the suggested Delta-ITTP method is to shrink the VoIP packet payload; thus, saving the VoIP network BW. The VoIP network BW of the suggested Delta-ITTP method was investigated on the basis of three different metrics, namely, shrunk bits per VoIP packet payload, saved BW, and capacity improvement.

### A. Shrunk Bits Per VoIP Packet Payload

This section discusses the payload shrunk bits when using the suggested Delta-ITTP method. The payload shrunk bits were investigated for five different streams, with a sample of seven packets for each, in comparison to the original VoIP packet payload size ( $O\_Size$ ). The size of the first VoIP packet payload of each stream is equal to the  $O\_Size$  because no packets had arrived before it and, thus, no shrinking occurred. The rest of the VoIP packets' payloads, starting from the second packet, were shrunk with different values. The difference of the shrunk bits' value is due to the different distribution style of each VoIP packet payload. The more the

number of shrunk bits, the better the BW utilization [20]. Fig. 5 shows the payload shrunk bits of the suggested Delta-ITTP method.

### B. Saved BW

This section discusses the saved BW ratio when using the suggested Delta-ITTP method. The saved BW ratio was investigated for 10 different streams. The BW saving was improved by approximately 12% to 19%; thus, enhancing the BW utilization [21]. The difference of the saved BW ratio between the 10 streams is due to the different distribution style of each VoIP packet payload. Fig. 6 shows the saved BW ratio of the suggested Delta-ITTP method.

### C. Capacity Improvement

This section discusses the capacity improvement ratio when using the suggested Delta-ITTP method. Capacity is the number of calls running concurrently at a specific period. The capacity improvement ratio was investigated for 10 different streams. The capacity improvement was approximately between 3% and 7%; thus, enhancing the BW utilization. Again, the difference of the capacity improvement ratio between the 10 streams is due to the different distribution style of each VoIP packet payload. Fig. 7 shows the capacity improvement ratio of the suggested Delta-ITTP method.

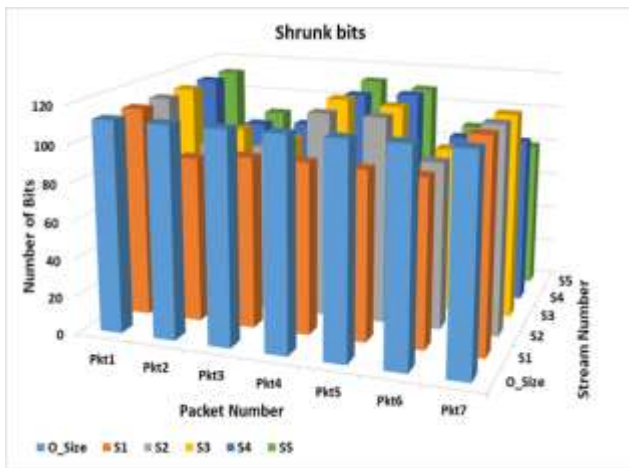


Fig. 5. VoIP Packet Payload Shrunk Bits.

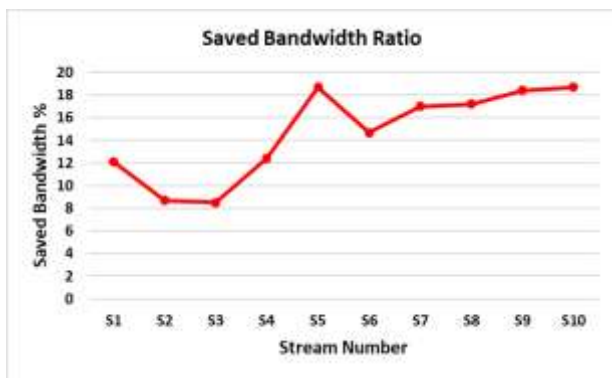


Fig. 6. Saved Bandwidth Ratio.

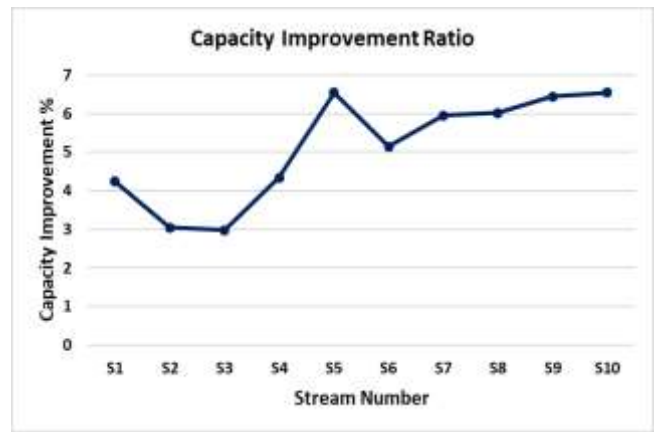


Fig. 7. Capacity Improvement Ratio.

## V. CONCLUSION

VoIP technology has evolved rapidly to serve most of the big companies in private and public sectors. However, the BW utilization of VoIP networks needs to be improved. This paper suggests a new method, called Delta-ITTP, to improve VoIP networks BW utilization. The Delta-ITTP method achieves this by shrinking the VoIP packet payload using the suggested delta algorithm. The core idea of the delta algorithm is to find the delta of the VoIP packets payload that follow each other and send this delta, instead of the full VoIP packet payload. The Delta-ITTP method utilizes the IP protocol flag fields to keep the needed information by the delta algorithm; thus, no additional header is needed. The Delta-ITTP method was deployed and compared with the traditional ITTP protocol without compression. The results show that the number of shrunk bits varies, between the VoIP packets payload, based on the bits' pattern. The improvement in BW saving and capacity reached up to 19% and 7%, respectively. Therefore, the suggested Delta-ITTP method enhances the VoIP network BW utilization and achieves its design goal. In the future, we will deploy the suggested Delta-ITTP method with other VoIP network BW utilization methods, such as VoIP packets aggregation methods.

## REFERENCES

- [1] Y. Zhang, K. Xie, and O. Ruan, "An improved and efficient mutual authentication scheme for session initiation protocol," *PloS one*, vol. 14(3), pp. e0213688, 2019.
- [2] M. M. Abualhaj, M. M. Al-Tahrawi, and S. N. Al-Khatib, "Performance Evaluation of VOIP Systems in Cloud Computing," *Journal of Engineering Science and Technology*, vol. 14(3), pp. 1398-1405, 2019.
- [3] H.M. Mahdi, A.M. Suhail, A. Maaruf, H. H. AbdelRahman, and A.G. Muzafar, "Simulation and Analysis of Quality of Service (QoS) Parameters of Voice over IP (VoIP) Traffic through Heterogeneous Networks", *International Journal of Advanced Computer Science and Applications (IJACSA)*, vol. 8, no. 7, 2017.
- [4] T. T. Nguyen, and G. Armitage, "A survey of techniques for internet traffic classification using machine learning," *IEEE communications surveys & tutorials*, vol. 10(4), pp. 56-76, 2008.
- [5] M. M. Abualhaj, S. N. Al-Khatib, M. Kolhar, A. Munther, and Y. Alraba'nah, "Effective Voice Frame Pruning Method to Increase VoIP Call Capacity," *TEM Journal*, vol. 9(1), pp. 48-54, 2020.



- [6] M. O. Ortega, G. C. Altamirano, C. L. Barros, and M. F. Abad, "Comparison between the real and theoretical values of the technical parameters of the VoIP codecs," 2019 IEEE Colombian Conference on Communications and Computing (COLCOM), pp. 1-6, 2019.
- [7] J. M. Valin, T. B. Terriberry, C. Montgomery, and G. T. Maxwell, "A high-quality speech and audio codec with less than 10-ms delay," IEEE transactions on audio, speech, and language processing, vol. 18(1), pp. 58-67, 2009.
- [8] A. Irshad, M. Sher, E. Rehman, S. A. Ch, M. U. Hassan, and A. Ghani, "A single round-trip sip authentication scheme for voice over internet protocol using smart card," Multimedia Tools and Applications, vol. 74(11), pp. 3967-3984, 2015.
- [9] S. Stelios Antoniou, Introducing VoIP Signaling - <https://www.pluralsight.com/blog/it-ops/voip-signaling-protocols>, July 2020.
- [10] M. M. Abualhaj, M. M. Al-Tahrawi, and S. N. Al-Khatib, "A New Method to Improve Voice over IP (VoIP) Bandwidth Utilization over Internet Telephony Transport Protocol (ITTP)," Proceedings of the 2019 8th International Conference on Software and Information Engineering, pp. 192-195, 2019.
- [11] G. Kaur, J. Kaur, S. Aggarwal, C. Singla, N. Mahajan, S. Kaushal, and Sangaiah, A.K, "An optimized hardware calibration technique for transmission of real-time applications in VoIP network," Multimedia Tools and Applications, vol. 78(5), pp. 5537-5570, 2019.
- [12] M. Spencer, B. Capouch, E. Guy, F. Miller, and K. Shumard, "Iax: Inter-asterisk exchange version 2," Internet Request for Comments, 2010.
- [13] P. Fortuna, and M. Ricardo, "Header compressed VoIP in IEEE 802.11," IEEE Wireless communications, vol. 16(3), pp. 69-75, 2009.
- [14] R. F. Aji, S. Yazidb, H. Suhartantoc, and I. Budid, "Throughput Fairness Using Packet Aggregation on 802.11 g Networks," 2016.
- [15] Shambour, Qusai, et al. " Effective Voice Frame Shrinking Method to Enhance VoIP bandwidth Exploitation." International Journal of Advanced Computer Science and Applications (IJACSA), IEEE, vol. 11(7), pp. 313-319, 2020.
- [16] Teymoori, Peyman, et al. "An optimal packet aggregation scheme in delay-constrained IEEE 802.11 n WLANs." 2012 8th International Conference on Wireless Communications, Networking and Mobile Computing. IEEE, 2012.
- [17] H. P. Sze, S. C. Liew, J. Y. Lee, and D. C. Yip, "A multiplexing scheme for H. 323 voice-over-IP applications," IEEE Journal on Selected Areas in Communications, vol. 20(7), pp. 1360-1368, 2002.
- [18] M. M. Abualhaj, "ITTP-MUX: An efficient multiplexing mechanism to improve voip applications bandwidth utilization," International Journal of Innovative Computing Information and Control, vol. 11(6), pp. 2063-2073, 2015.
- [19] M. M. Abualhaj, "CA-ITTP: An efficient method to aggregate voip packets over ittp protocol," International Journal of Innovative Computing Information and Control, vol. 15(3), pp. 1067-1077, 2019.
- [20] M. M. Abualhaj, et al. "PS-PC: An effective method to improve voip technology bandwidth utilization over ittp protocol." Cybernetics and Information Technologies (CIT) 20(3), pp. 147-158, 2020.
- [21] M. M. Abualhaj, et al. "Multiplexing voip packets over wireless mesh networks: A survey," KSII Transactions on Internet & Information Systems 10(8), pp. 3728-3752, 2016.

# High-Security Image Steganography Technique using XNOR Operation and Fibonacci Algorithm

Ali Abdulzahra Almayyahi<sup>1</sup>, Rossilawati Sulaiman<sup>2</sup>, Faizan Qamar<sup>3</sup>, Abdulwahhab Essa Hamzah<sup>4</sup>

Faculty of Information Science and Technology, Universiti Kebangsaan Malaysia UKM Bangi 43600, Selangor, Malaysia<sup>1, 2, 3</sup>  
Photonics Technology Laboratory, Department of Electrical, Electronic and Systems Engineering, Faculty of Engineering and Built Environment, Universiti Kebangsaan Malaysia, UKM Bangi 43600, Selangor, Malaysia<sup>4</sup>

**Abstract**—Since the number of internet users is increasing and sensitive information is exchanging continuously, data security has become a problem. Image steganography is one of the ways to exchange secret data securely using images. However, several issues need to be mitigated, especially in the imperceptibility (security) aspect, which is the process of embedding secret data in the images that can be vulnerable to attacks. This paper focuses on developing a secure method for hiding secret messages in an image, based on the standard Least Significant Bit (LSB). Before proceeding with the embedding stage, the secret message's size is reduced by compression using the Huffman algorithm, followed by two operations, which are the Boolean operation Exclusive-NOR (XNOR) operation and the Fibonacci algorithm when selecting pixels to embed the secret message. As a result of these processes, a stego-image is created with two secret keys. We obtained promising results against standard images with higher Peak Signal-to-Noise Ratio (PSNR) values of 66.6170, 65.8928, and 65.9386 dB for Lena.bmp, Baboon.bmp, and Pepper.bmp, respectively, as compared to other state-of-the-art schemes. The evaluation stage proves the increasing level of security as well as imperceptibility.

**Keywords**—Image steganography; Huffman algorithm; XNOR operation; Fibonacci algorithm; LSB; PSNR

## I. INTRODUCTION

Steganography is the technique used to hide secret data in a cover-media. It consists of two parts, "stego" which means "cover" in Greek and "grafia" which means "writing" and both can be defined as "covered writing" [1]. Various types of multimedia files can be used to conceal secret data such as text [2], image [3], video [4]-[5], audio [6][39] protocols, and Deoxyribonucleic acid (DNA), with the most commonly used, are images as a cover-media [7]-[9]. The cover-media can also be referred to as stego-media. There are two types of embedding methods in a steganography system, which are spatial domain and frequency domain. In the spatial domain, pixels intensity is used to insert or embed the secret message directly into the Least Significant Bit (LSB) of a pixel. The LSB substitution is the most common technique of embedding in the spatial domain, whereas, in the frequency domain, the image is converted into various frequency classes, and the embedding process has been performed by using the coefficient factors [10]-[12].

Several issues and challenges are associated with steganography, which includes (1) lack of security of the secret message hidden in the image, (2) lack of payload capacity, which reflects the amount of data that can be embedded into

the image, and (3) maintain high imperceptibility or quality of the stego-image as similar as the cover image (original image), which is the desired property that supports security [13]-[15]. Several literature attempts to find a balance between the quantity of data embedded and the protection of the secret message while maintaining the quality of the image [16], [17]. Some algorithms have succeeded in increasing the data hiding while keeping the image's quality, but the majority have not [18], [19]. These existing methods have made more efforts in hiding information to get high security so that the concealing method makes the hidden secret message not to be seen by a hacker (or not seen by human eyes). However, more research in steganography techniques need to do to achieve high security and high capacity [20].

This paper proposes a new technique for enhancing the security and capacity of the standard LSB method. A balance between high security and high capacity is important to maintain the cover-image quality similar to stego-image after embedding stage. We exploit the Most Significant Bit (MSB) and LSB in the cover-images to add a security level of the standard LSB steganography methods. Also, capacity can be increased by applying compression to the secret message.

The rest of the paper is organized as follows: Section II defined related works on secret data hiding techniques. Then, Section III illustrates the proposed method in details, followed by Section IV, which presents the experimental results. Section V states the conclusion of the work, and lastly, Section VI shows recommendations for future research work.

## II. RELATED WORK

This section discusses the existing solutions to counter the issues in image steganography. Various versions of bit inversion techniques are proposed to enhance the LSB embedding process. In [3], the authors proposed an improved LSB technique where the LSB's of some pixels of the cover-image is inverted when inputs of specific bit patterns are found. Their result shows that a high quality of invisibility and imperceptibility in the stego-image. Another bit inversion technique is suggested in [21], which uses a bit inversion based on specific patterns to improve the quality of the stego-image. The idea is to conceal the secret message after a lossless compression of smoother areas of the image, resulting in fewer pixels being modified in the stego-image.

The authors in [22] proposed a novel steganographic algorithm in the spatial domain using the concept of pixel

modulation, which diminishes the changes that occur in the stego-image generated from the cover-image. In this method, the LSB of the image's intensity values is modified according to the secret data. The secret data is converted into a binary string based on each character's ASCII value that is represented in the 8-bit notation. Then, all bits are embedded in a matrix containing the adjacent pixel values. Their result shows a lower average embedding capacity, but the PSNR values of the stego-images produced are high. In order to improve the security of the hidden secret message, the XOR transposition encryption based on the LSB approach is proposed in [23]. The embedded secret message is encrypted by transposing the message based on the order of the key. The result of this process is converted into binary and embedded into the cover-image using the XOR operation.

An LSB method is developed by [24] for embedded secret message into a 24-bit colour image, where the last two bit of LSB of each channel (red, green and blue) of the cover-image, are substituted by two bits of the secret message. This means that the last two bits of LSB of the red channel are substituted by the first two bits of the secret message; the last two bits of LSB of the green channel are substituted by the second two bits of the secret message, and the last two bits of LSB of the blue channel are substituted by the third two bits of the secret message. Therefore, a total of six bits of the secret image can be concealed in a 24-bit colour image. Another approach in [25] proposed a new technique intending to keep secure communication intact. The proposed method merged the advantage of the two bits of LSB and the XOR operation. the 8th bit of the cover-image is XORed with the 1st bit of the secret data, and the 7<sup>th</sup> bit is XORed with the 2nd bit of the secret data. The bits from the final result are inserted into the last two LSBs of the image pixel. The results proved that this approach achieved high capacity and high security. An efficient LSB steganography method is proposed in [26] for transferring secret data in the digital format using the number theory. This research focuses on the spatial domain using the Fibonacci sequence and Zeckendorf theorem, which increase the embedding rate from 8-bit to 12-bit, on a grayscale image. This method achieves a high embedding capacity.

An adaptive LSB replacement was suggested by [27] for several colour images. In this method, the RGB colour channels are converted into the YCbCr form [28], where the Cr channel is selected and divided into an 8\*8 size block. Each block is then transformed into discrete cosine, and a coefficient is selected where the bit sequence of the secret message is embedded to this coefficient. The image quality is preserved and robust against stego-attacks. An image steganography method was developed by [29], which is based on the use of two secret keys to randomize the embedding process of secret messages. Randomization increases the security of the secret message. The proposed method used some colour such as Red, Green, and Blue to enhance the pixel's values and calculate the location of the pixels' random position to embed the secret message. This approach provides high data hiding capacity and a high-security level compared with the standard LSB substitution technique.

A method of using a modified LSB algorithm is proposed in [30], based on the three RGB channels to increase the

security level of the hidden message. This method relied on encryption of secret text message using the encryption key and the XNOR operation before embedding it in a colour image using LSB. The idea of concealing the message depends on the extraction of chromatic channels of the three RGB channels for each pixel and specifying the channel in which the bit of the encryption message is hidden.

A highly secure chaos-based image steganography method is proposed in [31]. Encryption to the secret message is performed using Caesar cipher and Chaos theory. The ciphertext obtained after the encryption process is embedded in a cover image using a 3, 3, 2 LSB replacement algorithm, which gave better security and performance than the traditional LSB technique. Another approach that combines the cryptography and steganography methods was presented in [32]. The Vigenere Cipher and Huffman Coding techniques are used to encrypt and compress the secret message. This method improved the security level and ensured the message content could not be recovered without knowledge of the decrypting key and the Huffman Dictionary table.

An approach for data hiding in RGB images based on the grey level modification (GLM) and multi-level encryption (MLE) is proposed in [33]. The secret key and secret messages are encrypted using the MLE algorithm before mapping it to the grayscale cover-image. A transposition function is applied to the cover-image before data embedding. The use of a secret key, MLE, and GLM adds various security levels to the algorithm, making it very complicated for a malicious user to recover the original secret data.

Based on the literature, many solutions have been proposed to solve standard LSB's main problems, which are related to security, capacity, and imperceptibility. Security focuses on the embedding methods, which is considered secure if an attacker finds it challenging to extract secret data from the cover medium. On the other hand, high capacity means that there are larger spaces to store secret messages in the cover-image. Lastly, imperceptibility is related to the high quality of the stego-image generated by the algorithm that is close to the original cover-image. In this study, the focus is on increasing the security level of a stego-image (maintaining imperceptibility) while improving the embedding capacity by utilizing the standard LSB image technique.

### III. PROPOSED METHODOLOGY

The proposed methodology is explained in Fig. 1. It consists of four different stages as following:

- Data Preparation stage.
- Data Embedding stage.
- Evaluating stag.
- Extracting stage.

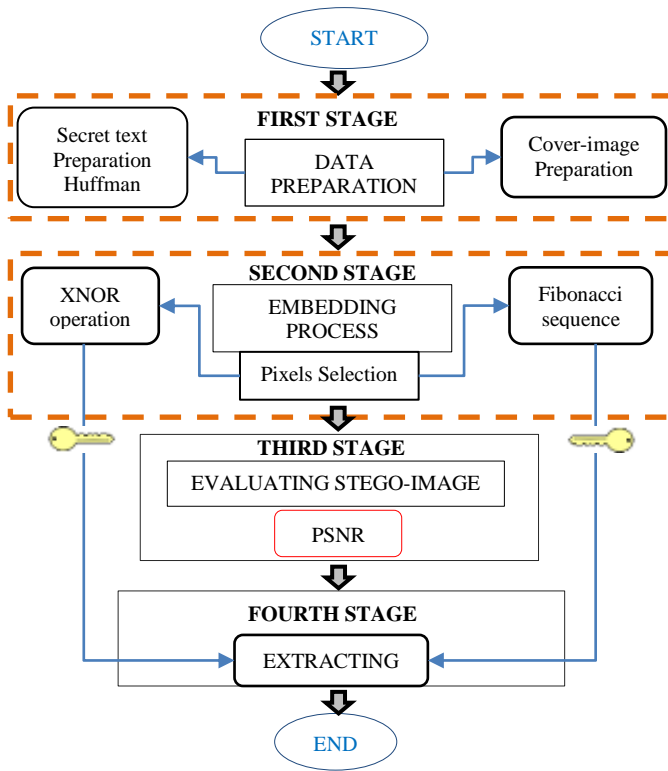


Fig. 1. Proposed Method.

A. First Stage: Data Preparation

1) *Huffman coding*: Before proceeding with the embedding stage, the Huffman algorithm is applied to the secret message to compress the message and then transform it into streams of bits. Later, each stream is converted into a secret code using the Huffman table. The result after the compression process is the vector of secret codes. The advantages of Huffman encoding are 1) lossless compression that improves the embedding capacity and 2) security because the encoded bitstream does not really disclose any information and only can be decoded using the Huffman table [34]. However, if the Huffman coded bitstream changes with just one bit, the Huffman table could not decode it. Huffman coding also satisfies the desired condition of high embedding capacity [21].

Next, a numerical example is provided to explain how Huffman will work within the proposed system. This example used five different symbols as B, E, A, D, and C with their frequencies of 14, 8, 56, 10, 12, respectively, as shown in Table I. The following seven steps are performed:

- **Step 1:** Construct a table that contains the source symbols and their respective frequency numbers.
- **Step 2:** Arrange the source symbols in ascending order according to their frequency numbers.
- **Step 3:** Merge the first two frequency numbers and then rearrange the table.

- **Step 4:** Repeat Step 3 until a single frequency number is obtained.
- **Step 5:** Construct a Huffman tree by assigning the value of 0 or 1 to each pair of branches in the tree.
- **Step 6:** Construct the final table (Huffman coding) that contains the leaf nodes and their respective codes according to the Huffman tree.
- **Step 7:** Create the compressed secret text by rewriting the output codes using the table of Huffman coding [1, 011, 010, 001, 000], as mentioned in Table II (in the 'Code' column).

As illustrated in the Huffman tree (Fig. 2), the two-parent nodes have the frequencies of 18 and 26, from accumulating the frequency of their children (8,10) and (12, 14), respectively. The high-frequency letter 'A' will be created at a high level to construct the final tree will connect both children in one parent with a frequency of 100.

For the output code in Step 7, each leaf has a path to reach the main node (100), so the paths' numbers and direction refer to these values. For example, the code for 'C' is 010, from following the path from 'C' to 100. For 'A', the code is 1, as it has only one path to the main node. After completing the Huffman tree to the text, we obtain (188 bits) while the text in ASCII code is represented by 800 bits (100 characters × 8 bits), as shown in Table II.

Huffman:  $56*1+14*3+12*3+10*3+8*3=188$  bits

ASCII:  $(56+14+12+10+8)*8=800$  bits

TABLE I. CONSTRUCTION OF THE HUFFMAN TREE

| Step | Symbol    | B     | E  | A  | D  | C  |
|------|-----------|-------|----|----|----|----|
| 1    | Frequency | 14    | 8  | 56 | 10 | 12 |
|      | Symbol    | E     | D  | C  | B  | A  |
| 2    | Frequency | 8     | 10 | 12 | 14 | 56 |
|      | Symbol    | ED    | C  | B  | A  |    |
| 3.1  | Frequency | 18    | 12 | 14 | 56 |    |
|      | Symbol    | ED    | CB | A  |    |    |
| 3.2  | Frequency | 18    | 26 | 56 |    |    |
|      | Symbol    | EDCB  | A  |    |    |    |
| 3.3  | Frequency | 44    | 56 |    |    |    |
|      | Symbol    | EDCBA |    |    |    |    |
| 3.4  | Frequency | 100   |    |    |    |    |

TABLE II. THE SEQUENCE OF SYMBOLS AND CODES USING THE HUFFMAN TREE

| Symbols | Code | Length | Frequency |
|---------|------|--------|-----------|
| A       | 1    | 1      | 56        |
| B       | 011  | 3      | 14        |
| C       | 010  | 3      | 12        |
| D       | 001  | 3      | 10        |
| E       | 000  | 3      | 8         |

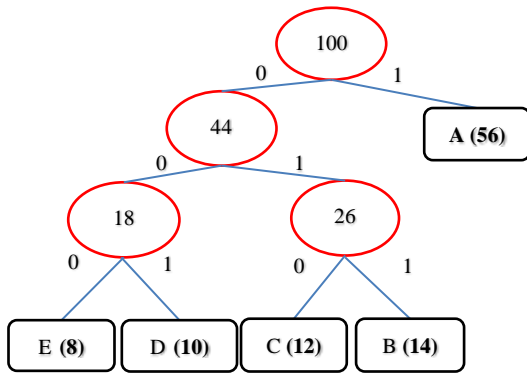


Fig. 2. Huffman Tree.

Therefore, 76.5% of space can be saved using Huffman coding.

2) *Image preparation:* The cover-image is the original image that is selected to host the secret messages before embedding. RGB colour images or grayscale images are used as a cover-medium in this research. The images can be downloaded from <http://sipi.usc.edu/database/database.php?volume=misc> (USC-SIPI) [32] with different sizes as a data set. The size of the cover-images is 512\*512 pixels to hide the secret messages. Lena.bmp, Baboon.bmp, Pepper.bmp, Airplane.bmp, Camera.bmp, Barbara.bmp, Tiffany.bmp, and Tree.bmp are used to cover-images.

**B. Second Stage: Proposed Embedding Process**

1) *Pixel selections:* The embedding method deals with the process of selecting and preparing pixels for embedding. Fig. 3 shows an example of pixel selections. The text message represents the secret message, and it will be encoded with the Huffman algorithm. The encoded message will be embedded into a cover-image. In this example, Lena.bmp is chosen as a cover-image. The embedding process starts at the top left of the row and column (the x and y) position of Lena.bmp. The pixel position of x and y is compared to determine whether to embed using the XNOR operation or using the Fibonacci sequence. If the x value is higher than the y value, the Fibonacci sequence is used to embed it; otherwise, the XNOR operation is applied. Whereas, in the case where the value of x is equal to y, the embedding is skipped. Therefore, half of the pixels use the XNOR operation while the other half use the Fibonacci algorithm. After all secret messages are embedded, the output will be a stego-image.

2) *XNOR operation:* In embedding with XNOR, the idea is to use the last bit of MSB of the red channel as a secret key, which is agreed by the sender and recipient. The red channel will specify which channel (either green or blue) that the bit of the secret text message will be hidden inside it. The red channel is chosen as the secret key, while the embedding process happens in either green and blue. The reason is that human eyes are most sensitive to red, followed by green and blue [40-41], and therefore we avoid embedding secret data in the red channel.

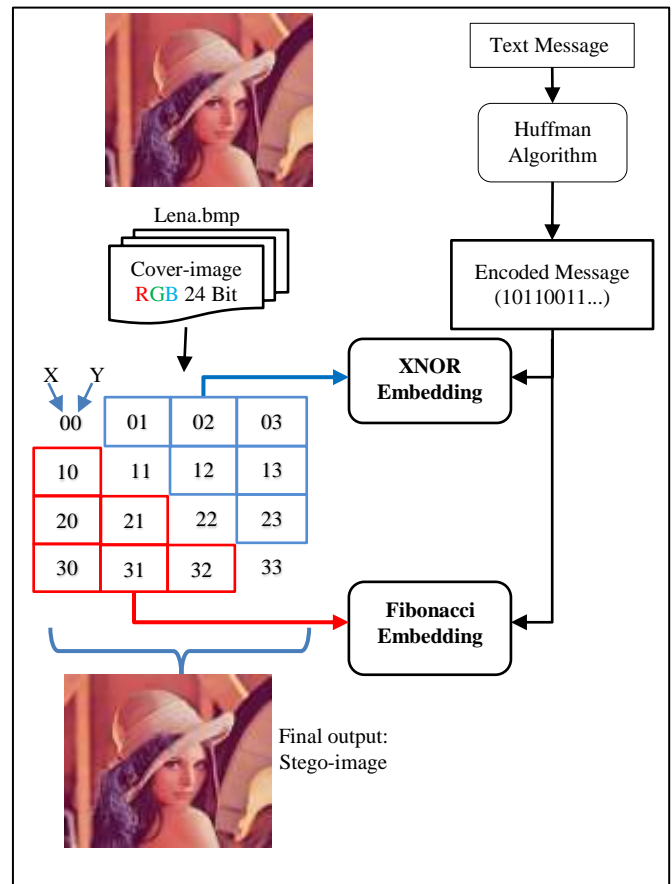


Fig. 3. Pixel Selections Flowchart.

The algorithm for pixel selections is shown in Fig. 4.

**Algorithm 1:** Pixel selections for embedding

**Input:**

Image Pixel points (x, y)

**Output:**

Selected Points for embedding

**Steps:**

1. Image size = 512\*512
2. For x, y in a range of (image\_size)
3. Select the points of x as a key
4. If (x > y) then  
Apply Fibonacci Embedding
5. If (x < y) then  
Apply XNOR Embedding

Fig. 4. Pixel Selections based on Values of x and y.

There are two processes inside the embedding stage, which are channel selections and data insertion. Firstly, in the channel selections for embedding, the last bit of the red channel's LSB is specified, either '0' (to select BLUE channel) or '1' (to select GREEN channel). Secondly, in the data insertion, it performs the XNOR operation of the last MSB red channel with one bit of the secret text. Finally, the result (0 or 1) will be carried to the selected channel and replace it with LSB's first bit in the cover-image (as shown in Table III). Fig. 5 and Fig. 6 provides an example of embedding using the XNOR operation.

TABLE III. INPUT, OUTPUT AND CHANNEL SELECTIONS

| XNOR operation                                 |            |        | First bit LSB for channel selection |
|------------------------------------------------|------------|--------|-------------------------------------|
| Last bit of MSB red channel of the cover-image | Secret bit | Result |                                     |
| 0                                              | 0          | 1      | BLUE                                |
| 0                                              | 1          | 0      | BLUE                                |
| 1                                              | 0          | 0      | GREEN                               |
| 1                                              | 1          | 1      | GREEN                               |

Fig. 5 explains an example of embedding one bit of secret data using the XNOR operation inside the Green channel.

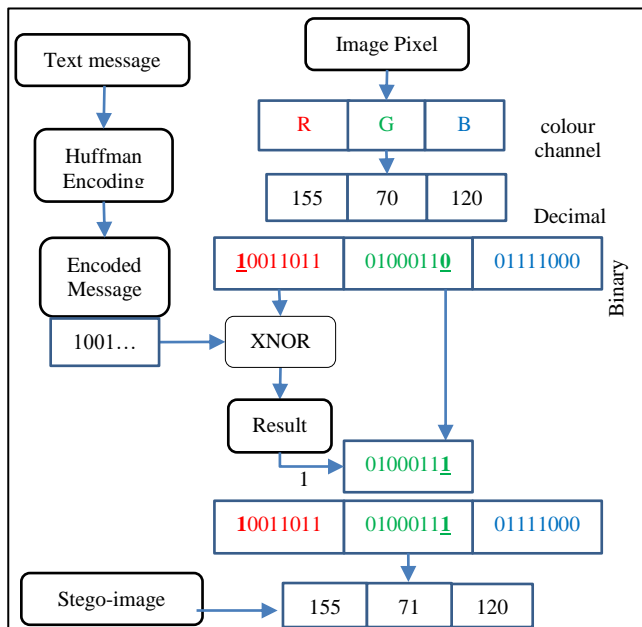


Fig. 5. Embedding One Bit with XNOR Operation Inside Green Channel.

The text message in Fig. 5 represents the secret message, which is encoded with the Huffman algorithm. Consider an image pixel with Red, Green, and Blue colour channels, which has decimal values of 155, 70, and 120, respectively. These decimal values are converted to binary values. Consider also that the encoded message starts with 1001 and so on.

The MSB of the red channel, which is '1', will be XNORed with the secret message bit '1', and the results, in this case, is also '1'. Therefore, this result will be embedded in the green channel, according to Table III. As a result, the final decimal values has been changed to 155, 71, and 120, respectively.

On the other hand, Fig. 6 has '0' for the MSB red channel, XNORed with '0' of the secret bit, and the result is '1'. Therefore, it will be embedded in the blue channel. The decimal values have changed to 27, 70, and 121, respectively.

The embedding process using the XNOR operation is summarized in Fig. 7.

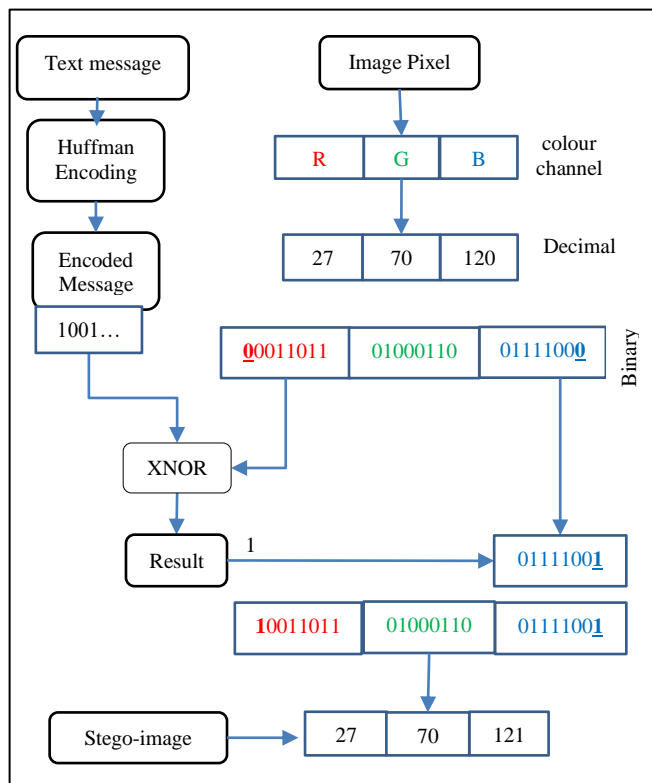


Fig. 6. Embedding One Bit with XNOR Operation Inside Blue Channel.

**Algorithm 2:** XNOR Image Embedding

**Input:**

Image Pixels of RGB:

$$R = \{P_{r1}, P_{r2}, \dots, P_{rm}\},$$

$$G = \{P_{g1}, P_{g2}, \dots, P_{gm}\}$$

$$B = \{P_{b1}, P_{b2}, \dots, P_{bm}\}$$

Message ( $M_x$ )

**Output:** Stego-image

**Steps:**

1. Apply Huffman encoding on the message  $H(M_x)$
2. Get the binary representation of the encoded message  $H(M_x) = \{b_{m1}, b_{m2}, \dots, b_{mh}\}$
3. Get Binary values of each Red, Green and Blue pixels  $P_{ri} = \{b_{r1}, b_{r2}, \dots, b_{r8}\},$   
 $P_{gi} = \{b_{g1}, b_{g2}, \dots, b_{g8}\},$   
 $P_{bi} = \{b_{b1}, b_{b2}, \dots, b_{b8}\}$
4. Get last bit **MSB** of Red array ( $br_8$ )
5. Get first bit **LSB** of Green and Blue arrays ( $bg_1, bb_1$ )
6. Get first bit of the message binary array ( $bm_1$ )
7. **If** ( $br_8$ ) == 1 **then**  
 $(br_8) \text{ XNOR } (bm_1) == (bg_1)$
8. **If** ( $br_8$ ) == 0 **then**  
 $(br_8) \text{ XNOR } (bm_1) == (bb_1)$
9. Initiate stego-image with the new values of RGB pixels

Fig. 7. Embedding Algorithm of the XNOR.

3) *Fibonacci decomposition*: Fibonacci numbers are a sequence of numbers that begin with zero or one, and then the next value is the summation of the two previous numbers [35]. In this research, we convert pixel values from binary into Fibonacci representation for the image. Binary consists of 8-bit planes, and the pixel values will occupy these bit. However, the bit planes with Fibonacci decomposition consists of 12-bit planes, therefore manipulating the LSB of Fibonacci is more flexible and efficient [26], as shown in Fig. 8.

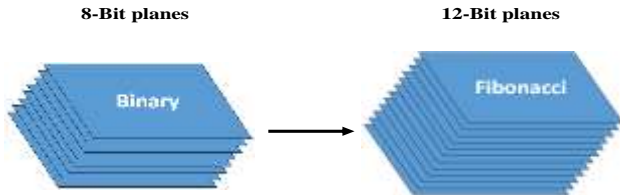


Fig. 8. Bit Plane Distribution in Binary and Fibonacci Representation.

In the 13<sup>th</sup> century, Leonardo of Pisa introduced the classical Fibonacci number [36]. The general definition of the Fibonacci sequence can be explained by using equation (1).

$$F_{(N)} = F_{(N-1)} + F_{(N-2)} \quad (1)$$

Where  $F_0 = 0$ ,  $F_1 = 1$ , and  $F_2 = 1$ ,  $N$  Fibonacci number. The sequence of Fibonacci is as follows:

1, 1, 2, 3, 5, 8, 13, 21, 34, 55, 89, 144,... and so on; such that any numeric value can be represented as binary representation [35]–[37]. Table IV distinguishes between two representations, Binary and Fibonacci for 8-bit and 12-bit planes. In the binary representation, a large range of numbers is available for 8 bits that are [0-255], whereas Fibonacci representation provides the same range [0-255] to represent 12 bits, like the following:

- Binary representation for  $255=128 +127 = 11111111$
- Fibonacci binary representation for  $255 = 233+21+1 = 100001000001$ .

It is important to note that the binary representation does not introduce redundancy. On the other hand, the Fibonacci representation is redundant, which means that different sequences may represent a single number. For instance, using the Fibonacci representation, a number 70 can have different representations such as the following:

- 1)  $55+13+2$
- 2)  $34+21+13+2$
- 3)  $55+8+5+2$
- 4)  $34+21+8+5+2$

Thus, it could be represented as follows (shown in Table V):

In order to obtain the unique representation of the given number, the Zeckendorf theorem can be applied, which states that "each positive integer  $m$  can be represented as the sum of distinct numbers in the sequence of Fibonacci numbers, using no two consecutive Fibonacci numbers" [38]. Consequently,

any positive number can be represented using equation (2) [25].

$$\alpha_F = \alpha_0 + \alpha_1 F^1 + \alpha_2 F^2 + \dots = \sum_{i=0}^N b_i F^i \quad (2)$$

As can be seen in Table V, there are four representations for number 70. However, only one representation should be selected. Thus, to choose only one of them, the one with the lexicographically lowest value of 1 will always be selected. In the case of number 70, the one which has a minimum number of '1' will be selected as the Fibonacci representation, which is the first rows of Table V (which has three '1'). Thus, a sequence produced using Fibonacci numbers would be valid if there are *no two repeating '1'* in a sequence. Therefore, the probabilities for the first two bits LSBs of a cover-image pixel in Fibonacci representation are '00', '01', or '10' with no repeating of '1'. For embedding purposes, one bit from the secret message (either 0 or 1) can be hidden in the first bit of Fibonacci LSB in the cover-image. Depending on these probabilities, our mapping is proposed, as illustrated in Table VI.

TABLE IV. BIT PLANE REPRESENTATION IN BINARY AND FIBONACCI

| Bit plane | Binary | Fibonacci |
|-----------|--------|-----------|
| 1         | 1      | 1         |
| 2         | 2      | 2         |
| 3         | 4      | 3         |
| 4         | 8      | 5         |
| 5         | 16     | 8         |
| 6         | 32     | 13        |
| 7         | 64     | 21        |
| 8         | 128    | 34        |
| 9         | -      | 55        |
| 10        | -      | 89        |
| 11        | -      | 144       |
| 12        | -      | 233       |

TABLE V. REPRESENTATION NUMBER 70 IN FIBONACCI

| Number | Fibonacci                                                  | Binary       |
|--------|------------------------------------------------------------|--------------|
| 70     | $0*1+1*2+0*3+0*5+0*8+1*13+0*21+0*34+1*55+0*89+0*144+0*233$ | 010001001000 |
|        | $0*1+1*2+0*3+1*5+1*8+0*13+0*21+0*34+1*55+0*89+0*144+0*233$ | 010110001000 |
|        | $0*1+1*2+0*3+1*5+1*8+0*13+1*21+1*34+0*55+0*89+0*144+0*233$ | 010110110000 |
|        | $0*1+1*2+0*3+0*5+0*8+1*13+1*21+1*34+0*55+0*89+0*144+0*233$ | 010001110000 |

TABLE VI. MAPPING ALGORITHM FOR FIBONACCI

| Cover bits \ Secret bits | 0  | 1  |
|--------------------------|----|----|
|                          | 00 | 00 |
| 01                       | 00 | 01 |
| 10                       | 10 | 01 |

In the proposed method, the idea of embedding using Fibonacci is by using the green channel of each pixel for the cover-image as a secret key. The secret bit will be inserted to the first bit of the LSB of the green channel, according to Table VI. For example, if the first two bits from the cover-image is '00', and the secret bit is '0', then the stego-image bit is not changed, which is '00'. Otherwise, the stego-image is changed to '01'. Only the green channel is selected to make it harder for the attacker to guess the embedding channel.

Another example is shown in Fig. 9, with the cover-image in the Fibonacci code is represented as 000100100010 in the Green channel. The secret bit can be either '0' or '1'. According to the mapping in Table VI, if the secret bit is '1', and the first two bits is '10', the result after embedding will become '01', which means that the Fibonacci code now becomes 000100100011.

However, this Fibonacci code is not valid according to the Zeckendorf theorem because it has two consecutive '1'. Therefore, a condition is given where the second bit is changed to 0, to avoid the consecutive ones. The final result will be 000100100001. Meanwhile, if the secret bit is '0', and the first two bits is '10', the green bits on the cover-image is not changed. If there is no change to the cover-image, it means less distortion on the stego-image after the embedding process, which results in a high level of security for the hidden message.

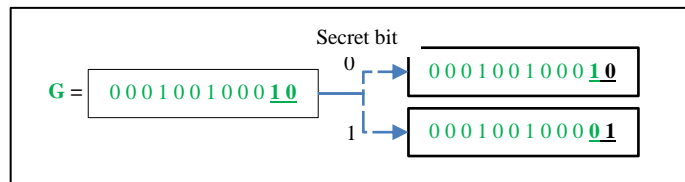


Fig. 9. An Example of Fibonacci Pixel Embedding in the Proposed Method.

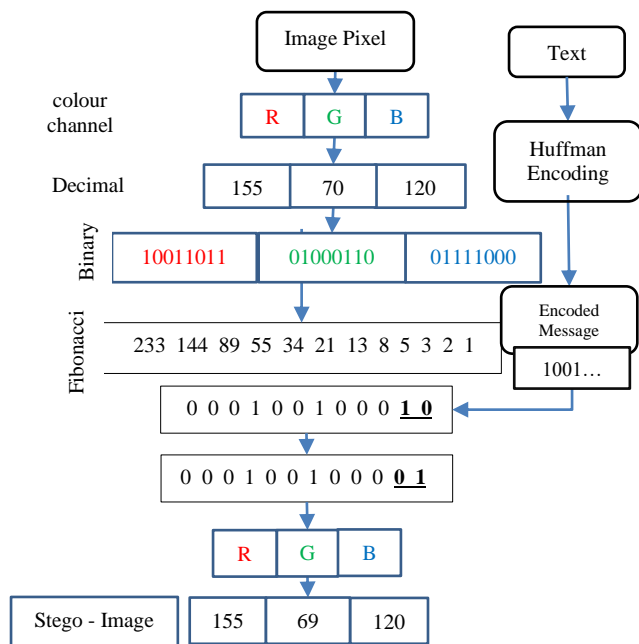


Fig. 10. Embedding One bit in the Fibonacci Algorithm.

Fig. 10 explains another example of the Fibonacci embedding process. Similar to the previous example, we choose 155, 70, and 120 as the values for Red, Green, and Blue channels. The Fibonacci value for 70 is given as a sequence, as well as its binary representation, which is 000100100010. The first two bits of the Fibonacci representation is '10' (Bold and underlined), and the secret message is '1'. Therefore, the embedding results, according to Table VI, is 000100100011, but this representation is not valid according to the Zeckendorf theorem. So, we change the second bit to '0': 000100100001, which is also representing 69 in decimal value.

The algorithm for the embedding process is summarized in Fig. 11.

**Algorithm 3:** Image Embedding using Fibonacci

**Input:**

Image Pixels of RGB where:

$$R = \{P_{r1}, P_{r2}, \dots, P_{rm}\}$$

$$G = \{P_{g1}, P_{g2}, \dots, P_{gm}\}$$

$$B = \{P_{b1}, P_{b2}, \dots, P_{bm}\}$$

Message( $Mx$ )

**Output:**Stego-image

**Steps:**

1. Apply Huffman encoding on the message  $H(Mx)$
2. Get the binary representation of the encoded message  $H(Mx) = \{b_{m1}, b_{m2}, \dots, b_{mh}\}$
3. Select the Green pixels  $G = \{P_{g1}, P_{g2}, \dots, P_{g3}\}$
4. Get the Binary values of each Green pixel  $P_{gi} = \{b_1, b_2, \dots, b_8\}$
5. Transform the binary array of Green pixel into Fibonacci representation  $Fib(P_{gi}) = \{b_{f1}, b_{f2}, \dots, b_{f11}, b_{f12}\}$
6. Get the first two bits LSB of green pixel Fibonacci ( $b_{f1}, b_{f2}$ )
7. Get the first bit of the encoded message ( $b_{m1}$ )
  - 7.1 **If**  $b_{f1}=0 \ \&\& \ b_{f2}=0 \ \&\& \ b_{m1}=0$   
 $b_{f1}=0, b_{f2}=0$
  - 7.2 **Else If**  $b_{f1}=0 \ \&\& \ b_{f2}=0 \ \&\& \ b_{m1}=1$   
 $b_{f1}=1, b_{f2}=0$
  - 7.3 **Else If**  $b_{f1}=1 \ \&\& \ b_{f2}=0 \ \&\& \ b_{m1}=0$   
 $b_{f1}=0, b_{f2}=0$
  - 7.4 **Else If**  $b_{f1}=1 \ \&\& \ b_{f2}=0 \ \&\& \ b_{m1}=1$   
 $b_{f1}=1, b_{f2}=0$
  - 7.5 **Else If**  $b_{f1}=0 \ \&\& \ b_{f2}=1 \ \&\& \ b_{m1}=0$   
 $b_{f1}=0, b_{f2}=1$
  - 7.6 **Else**  
 $b_{f1}=1, b_{f2}=0$
8. Get the decimal value of the new green pixel Fibonacci array  $Fib(P_{gi}) = \{\text{NEW}b_{f1}, \text{NEW}b_{f2}, \dots, b_{f11}, b_{f12}\} \rightarrow D$
9. Initiate the stego-image with the new values of RGB pixels

Fig. 11. Embedding Process using Fibonacci.

**C. Third Stage: Performance Evaluation**

Any steganography system aims to build a secure communication system that cannot be detected by a third party. The attacker can use statistical methods to identify the stego-image such as histogram analysis and chi-square attack, even if the cover-image is unknown [26],[32]. As mentioned before,



after the embedding stage, the image produced is called stego-image. The PSNR values are used to evaluate the quality of this stego-image, and the desired value for PSNR is as similar as possible with the cover-image. When the value of PSNR is high, that indicates the proposed method does not damage or distort the cover-image. The PSNR value is calculated like the following equation (3).

$$PSNR = 10 \log_{10} \frac{(255)^2}{MSE} \quad (3)$$

Equation (4) is used to calculate the mean squared error. MSE is calculated by obtaining the average square error. Then its result will be used to calculate PSNR to evaluate the resolution and quality of the stego-image.

$$MSE = \frac{1}{mn} \sum_{i=1}^m \sum_{j=1}^n (x_{ij} - y_{ij})^2 \quad (4)$$

Here,  $m$  and  $n$  are the images sizes while  $x$  and  $y$  are the cover and stego-images, respectively.

#### D. Fourth Stage: Extracting Stage

The information hiding process always follows specific procedures, which are an embedding method, and the main steps in this method with information of the embedding process should also be known to the receiver. The receiver uses the secret keys, which contain the embedding information. In order to extract from the secret message embedded in a stego-image, the same procedure for embedding is used but in a reverse manner. The pixel selection process summarized in Fig. 12.

---

#### Algorithm 4: Pixel Selections for Extracting Process

---

**Input:**

Stego-Image Pixel points (x, y)

**Output:**

Selected Points for extracting

---

**Steps:**

- 1 Image size = 512\*512
  - 2 For x,y in a range of (image\_size)
  - 3 Select the points of x as a key
  - 4 If (x > y) **then**  
    Apply Fibonacci Extracting
  - 5 If (x < y) **then**  
    Apply XNOR Extracting
- 

Fig. 12. Pixel Selection for the Extracting Process.

Fig. 13 and Fig. 14 explains the extracting processes for XNOR and Fibonacci, respectively.

---

#### Algorithm 5: Image Extracting using XNOR

---

**Input:** Stego-image Pixels of RGB

$R = \{P_{r1}, P_{r2}, \dots, P_{rm}\}$

$G = \{P_{g1}, P_{g2}, \dots, P_{gn}\}$

$B = \{P_{b1}, P_{b2}, \dots, P_{bn}\}$

**Output:**Message (Mx)**Steps:**

1. Initialize an empty array of bits  $Ex$
  2. Get Binary values of each Red, Green and Blue pixels  
 $P_{ri} = \{b_{r1}, b_{r2}, \dots, b_{r8}\}$ ,  $P_{gi} = \{b_{g1}, b_{g2}, \dots, b_{g8}\}$ ,  $P_{bi} = \{b_{b1}, b_{b2}, \dots, b_{b8}\}$
  3. Get last bit MSB of Red array (br8)
  4. Get first bit LSB of Green and Blue arrays (bg1,bb1)
  5. **If** (br8) == 1  
    (br8) XNOR (bg1) == (bm1) **then**  
    Add (bg1) to H(Mx)
  6. **If** (br8) == 0 && (bb1) == 0  
    (br8) XNOR (bb1) == (bm1) **then**  
    Add (1) to H(Mx)
  7. **If** (br8) == 0 && (bb1) == 1  
    (br8) XNOR (bb1) == (bm1) **then**  
    Add (br8) to H(Mx)
  8. Get binary representation of the encode message  
 $H(Mx) = \{bm1, bm2, \dots, bmh\}$
  9. Apply Huffman to decode H(Mx)
- 

Fig. 13. Extracting Process with XNOR Operation.

---

#### Algorithm 6: Image Extracting using Fibonacci

---

**Input:**

Image Pixels of RGB where:

$R = \{P_{r1}, P_{r2}, \dots, P_{rm}\}$

$G = \{P_{g1}, P_{g2}, \dots, P_{gn}\}$

$B = \{P_{b1}, P_{b2}, \dots, P_{bn}\}$

**Output:**Message Mx**Steps:**

1. Initialize an empty array of bits  $Ex$
  2. Select the Green pixels,  $G = \{Pg1, Pg2, \dots, Pgn\}$
  3. Get the Binary values of each Green pixel  $Pgi = \{b1, b2, \dots, b8\}$
  4. Transform the binary array of Green pixel into Fibonacci representation  $Fib(Pgi) = \{bf1, bf2, \dots, bf11, bf12\}$
  5. Get the first two LSB bits of green pixel Fibonacci (bf1, bf2)
  6. **If** (bf1 = 1 | bf2 = 0)  
    add 1 to H(Mx)
  7. **Else:**  
    add 0 to H(Mx)
  8. Get the binary representation of the encoded message  
 $H(Mx) = \{bm1, bm2, \dots, bmh\}$
  9. Apply Huffman to decode H(Mx)
- 

Fig. 14. Extracting Process with the Fibonacci Algorithm.

#### IV. EXPERIMENTAL RESULTS

##### A. Dataset

A dataset is defined as a group of images that is used to benchmark the observation of this research with the existing literature. The study follows the same strategy to evaluate and benchmark the experimental results obtained using the proposed method. RGB colour images with size 512\*512 have been used as benchmarks in the evaluation stage. The following images are selected as cover-images, as shown in Fig. 15.

##### B. PSNR Comparison and Analysis

The PSNR is an expression for the ratio between the maximum possible value of a signal and the distorting noise that affects its representation quality. If the PSNR values are greater than 50 dB when tested on several images, the images are high in quality [37]. This type of evaluation is used to measure the quality of the image after embedding. PSNR is most commonly used to measure the quality of reconstruction of lossy presentation codecs (e.g., for image hiding). In this case, the signal is the original data, and the noise is the error introduced by the embedding process. When comparing image representation codecs, PSNR approximates the human perception of reconstruction quality. Although a higher PSNR generally indicates that the reconstruction is of higher quality, in some cases, it may not [38]. PSNR is most easily defined via the mean squared error (MSE), as mentioned before, which is based on the dimensions of the image.

The MSE is calculated by obtaining the average square error. Then its result will be used to calculate PSNR to evaluate the resolution and quality of the stego-image, as shown in Table VII.

Table VIII shows the comparison stages of the results with four other methods in [30], [32], [26], and [33], with 8Kb, 10Kb, 13Kb, and 16Kb of secret messages, and 512\*512 size of cover images. We note that the bigger the secret messages' size, the lower the PSNR value as more significant data will cause more distortion to the stego-image. From the results, high values of PSNR are obtained compared with previous findings. This indicates that the proposed method is very efficient in hiding data, which means that this technique can keep changes to the stego-image to a minimum. Therefore, we can conclude that this technique has a good quality of imperceptibility.



Fig. 15. Dataset used as Cover-Images.

TABLE VII. PSNR AND MSE VALUES FOR STEGO-IMAGES

| Cover- image | Secret Message 8 KB |           | Secret Message 16 KB |         |
|--------------|---------------------|-----------|----------------------|---------|
|              | MSE                 | PSNR      | MSE                  | PSNR    |
| Lena.bmp     | 0.002477            | 74.191525 | 0.014170             | 66.6170 |
| Camera.bmp   | 0.006153            | 70.239859 | 0.019850             | 65.1531 |
| Babbon.bmp   | 0.004360            | 71.735740 | 0.016741             | 65.8928 |
| Airplane.bmp | 0.004323            | 71.772626 | 0.016536             | 65.9463 |
| Tiffany.bmp  | 0.004240            | 71.856456 | 0.016924             | 65.8456 |
| Peppers.bmp  | 0.004189            | 71.908861 | 0.016565             | 65.9386 |
| Tree.bmp     | 0.004057            | 72.048147 | 0.017345             | 65.7389 |
| Barbara.bmp  | 0.003378            | 72.843499 | 0.016370             | 65.9902 |

TABLE VIII. COMPARISON OF PSNR AND MSE VALUES IN (DB) WITH THE LITERATURE

| Methods         | Size of Secret Message (Kb) | PSNR   |          |        |
|-----------------|-----------------------------|--------|----------|--------|
|                 |                             | Lena   | Baboon   | Pepper |
| [26]            | 12.79                       | 51.045 | 51.997   | 49.442 |
| [32]            | 10                          | 62.32  | 62.29    | 62.22  |
| [33]            | 8                           | 57.411 | -        | 57.442 |
| [30]            | 2.96                        | 53.65  | 40.89    | 39.99  |
| Proposed Method | 8                           | 74.192 | 71.736   | 71.909 |
|                 | 10                          | 72.750 | 69.927   | 69.971 |
|                 | 13                          | 70.301 | 67.64012 | 67.681 |
|                 | 16                          | 66.617 | 65.893   | 65.939 |

##### C. Histogram Analysis

One way to discover a good steganography method is to analyze the histogram of all stego-images and then compare them with the original. It represents the number of pixels that have colours in the image's colour space. The histogram for the original cover-image and stego-image for Lena and baboon, with 16KB size of secret messages embedded, are shown in Fig. 16 to Fig. 19, respectively.

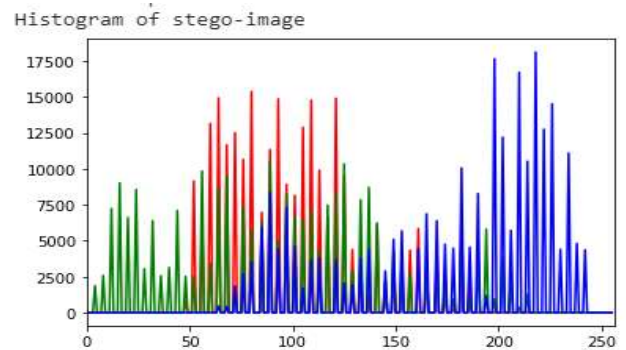


Fig. 16. Histogram of Cover-Image Lena.bmp.

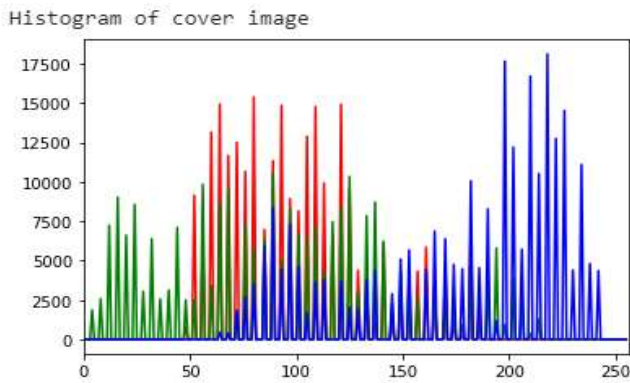


Fig. 17. Histogram of Lena.bmp Stego-Image.

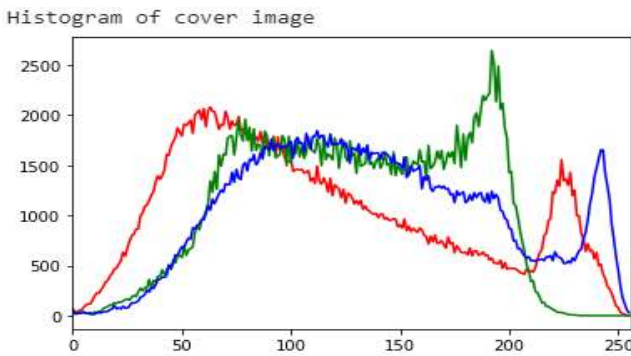


Fig. 18. Histogram of Cover-Image Baboon.bmp.

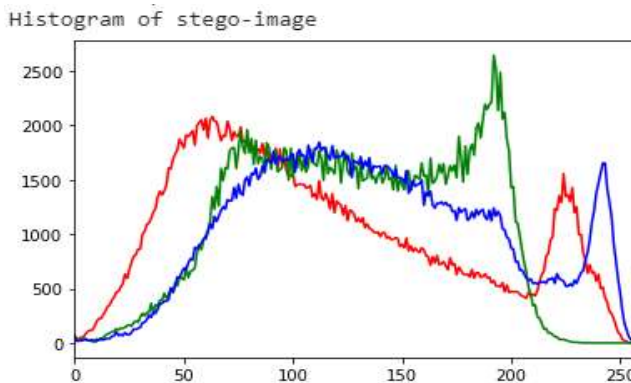


Fig. 19. Histogram of Baboon.bmp Stego-Image.

From the figures of Lena's and Baboon's stego-images, the histogram of the stego-images was similar to that of the cover images, resulting from alternately choosing either green or blue channels to embed the secret data, which does not give any significant difference between the two images. This means that the proposed technique can embed secret messages with minimum changes in the stego-image.

#### D. Embedding Capacity

The embedding capacity or ratio capacity depends on how much secret data bits can be hidden in the cover-image. It is calculated using equation (5).

$$EC = \frac{\text{number of secret message bits}}{\text{number of cover image pixels}} \text{ (bpp)} \quad (5)$$

Table IX shows the comparison of the hiding capacity between our proposed method and four other methods. The results show that the proposed method yields similar results to the other methods in terms of capacity.

TABLE IX. COMPARISON OF HIDING CAPACITY

| Methods                | Capacity (Kb) | Ratio capacity |
|------------------------|---------------|----------------|
| [30]                   | 2.9           | 0.093          |
| [33]                   | 8             | 0.25           |
| [32]                   | 10            | 0.313          |
| [26]                   | 12.79         | 0.399          |
| <b>Proposed Method</b> | <b>8</b>      | <b>0.250</b>   |
|                        | <b>10</b>     | <b>0.313</b>   |
|                        | <b>13</b>     | <b>0.406</b>   |
|                        | <b>16</b>     | <b>0.501</b>   |

#### V. CONCLUSION

The standard LSB method is the most popular steganography technique, as it is more efficient to use. However, this method's main weakness is that it is easy to recover the secret text message from the image, which is always hidden in the LSB of each pixel in an image. The developed XNOR operation with the Fibonacci sequence presents several characteristics that have enhanced the LSB standard technique's limitation. In terms of security level, there are three criteria integrated for higher security. Firstly, the Fibonacci algorithm uses only the green channel for embedding instead of the three channels red, green, and blue. The advantage of this is that the red and blue channels will act as noise data, which makes the extraction process harder for any intruder. Secondly, similar to the Fibonacci embedding operation, the XNOR operation also uses only one channel (the green or blue channels), while the other two channels act as noise data. Lastly, this method exploits the pixel selection to conceal the secret message, either use the Fibonacci algorithm or XNOR operation, to make the extraction process more secure. In this paper, we exploited the characteristics of both the XNOR operation and the Fibonacci algorithm to obtain high security and capacity to embed the secret message. Another important thing is that using the green or blue channel for each pixel on the cover-image gives an advantage as almost all of the pixels will be exploited to conceal secret data, and thus, capacity will be increased.

#### VI. FUTURE WORK

For future work, the three channels of RGB can be exploited to use as an indicator for embedding with the XNOR operation. The proposed method used the red channel as the key or supplier for embedding to green or blue channels (that means the red channel that will select which channel for embedding) as well as exploit one channel of RGB with the Fibonacci algorithm. In the proposed method, the green channel is used only for embedding, and that will let the proposed method be applied on three-channel RGB for embedding instead of using only the green channel. Another recommendation is to apply the proposed method with other cover-media types, such as text or audio.

#### ACKNOWLEDGMENT

This work was supported by Universiti Kebangsaan Malaysia under research grant PP-FTSM-2020.

#### REFERENCES

- [1] Ghosh, A. K. Chattopadhyay, and A. Nag, "A novel approach of image steganography with encoding and location selection," in *Advances in Intelligent Systems and Computing*, 2019, doi: 10.1007/978-981-13-1544-2\_10.
- [2] S. S. Baawi, M. R. Mokhtar, and R. Sulaiman, "New text steganography technique based on a set of two-letter words," *Journal of Theoretical and Applied Information Technology*, vol. 95, no. 22, pp. 6247–6255, 2017.
- [3] M. A. Majeed and R. Sulaiman, "An improved LSB image steganography technique using bit-inverse in 24 bit colour image," *Journal of Theoretical and Applied Information Technology*, vol. 80, no. 2, pp. 342–348, 2015.
- [4] S. Kamil, M. A. Authors, S. N. H. S. Abdullah, and Z. Ahmad, "Lightweight and optimized multi-layer data hiding using video steganography paper," *International Journal of Advanced Computer Science and Applications*, vol. 9, no. 12, pp. 256–262, 2018, doi: 10.14569/IJACSA.2018.091237.
- [5] S. Kamil, M. Ayob, S. N. H. Sheikh Abdullah, and Z. Ahmad, "Optimized Data Hiding in Complemented or Non-Complemented Form in Video Steganography," *Proceedings of the 2018 Cyber Resilience Conference, CRC 2018*, pp. 1–4, 2019, doi: 10.1109/CR.2018.8626871.
- [6] A. H. Ali, L. E. George, A. A. Zaidan, and M. R. Mokhtar, "High capacity, transparent and secure audio steganography model based on fractal coding and chaotic map in temporal domain," *Multimedia Tools and Applications*, vol. 77, no. 23, pp. 31487–31516, 2018, doi: 10.1007/s11042-018-6213-0.
- [7] F. Akhter and M. Selim, "A New Approach of Graph Realization for Data Hiding using Human Encoding," *International Journal of Advanced Computer Science and Applications*, vol. 7, no. 12, pp. 436–442, 2016, doi: 10.14569/ijacsa.2016.071256.
- [8] S. Mavanai, A. Pal, R. Pandey, A. Prof, and D. Nadar, "Message transmission using DNA crypto-system," *International Journal of Computer Science and Mobile Computing*, vol. 8, no. 4, pp. 108–114, 2019.
- [9] M. Cui and Y. Zhang, "Incorporating randomness into DNA steganography to realize secondary secret key, self-destruction, and quantum key distribution-like function," pp. 1–19, 2019, doi: <https://doi.org/10.1101/725499>.
- [10] R. A. Watheq, F. Almasalha, and M. H. Qutqut, "A new steganography technique using JPEG images," *International Journal of Advanced Computer Science and Applications*, vol. 9, no. 11, pp. 751–760, 2018, doi: 10.14569/ijacsa.2018.0911107.
- [11] A. Pradhan, K. R. Sekhar, and G. Swain, "Digital image steganography using LSB substitution, PVD, and EMD," *Mathematical Problems in Engineering*, vol. 2018, 2018, doi: 10.1155/2018/1804953.
- [12] S. Jeevitha and N. Amutha Prabha, "A comprehensive review on steganographic techniques and implementation," *ARPJ Journal of Engineering and Applied Sciences*, vol. 13, no. 17, pp. 4780–4791, 2018.
- [13] R. Gupta, S. Gupta, and A. Singhal, "Importance and techniques of information hiding: A review," *International Journal of Computer Trends and Technology*, vol. 9, no. 5, pp. 260–265, 2014, doi: 10.14445/22312803/ijctt-v9p149.
- [14] M. S. Subhedar and V. H. Mankar, "Current status and key issues in image steganography: A survey," *Computer Science Review*, vol. 13–14, pp. 95–113, 2014, doi: 10.1016/j.cosrev.2014.09.001.
- [15] E. Satir and H. Isik, "A Huffman compression based text steganography method," *Multimedia Tools and Applications*, vol. 70, no. 3, pp. 2085–2110, 2014, doi: 10.1007/s11042-012-1223-9.
- [16] A. Gutub and N. Al-juaid, "Multi-bits stego-system for hiding text in multimedia images based on user security priority," *Journal of Computer Hardware Engineering*, vol. 1, no. April, pp. 1–9, 2018, doi: 10.63019/jche.v1i2.513.
- [17] G. V. K. Murugan and R. Uthandipalayam Subramaniyam, "Performance analysis of image steganography using wavelet transform for safe and secured transaction," *Multimedia Tools and Applications*, vol. 79, no. 13–14, pp. 9101–9115, 2019, doi: 10.1007/s11042-019-7507-6.
- [18] T. Rabie, M. Baziyad, and I. Kamel, "Enhanced high capacity image steganography using discrete wavelet transform and the Laplacian pyramid," *Multimedia Tools and Applications*, vol. 77, no. 18, pp. 23673–23698, 2018, doi: 10.1007/s11042-018-5713-2.
- [19] Y. Yeung, W. Lu, Y. Xue, J. Huang, and Y.-Q. Shi, "Secure binary image steganography with distortion measurement based on prediction," *IEEE Transactions on Circuits and Systems for Video Technology*, vol. 30, no. 5, pp. 1423–1434, 2019, doi: 10.1109/tcsvt.2019.2903432.
- [20] D. Laishram and T. Tuithung, "A survey on digital image steganography: current trends and challenges," *Proceedings of 3rd International Conference on Internet of Things and Connected Technologies (ICIOTCT)*, 2018, Malaviya National Institute of Technology, Jaipur (India), March 26–27, 2018.
- [21] N. Akhtar, "An LSB substitution with bit inversion steganography method," *Springer India 2016. Proceedings of 3rd International Conference on Advanced Computing, Networking and Informatics, Smart Innovation, Systems and Technologies*, vol. 43, pp. 515–521, 2016, doi: DOI 10.1007/978-81-322-2538-6\_53.
- [22] S. Das, S. Sharma, S. Bakshi, and I. Mukherjee, "A framework for pixel intensity modulation based image steganography," *Advances in Intelligent Systems and Computing*, vol. 563, pp. 3–14, 2018, doi: 10.1007/978-981-10-6872-0\_1.
- [23] A. Setyono and D. R. I. M. Setiadi, "Securing and hiding secret message in image using XOR transposition encryption and lsb method," *Journal of Physics: Conference Series*, vol. 1196, no. 1, 2019, doi: 10.1088/1742-6596/1196/1/012039.
- [24] D. Rawat and V. Bhandari, "A steganography technique for hiding image in an image using LSB method for 24 bit colour image," *International Journal of Computer Applications*, vol. 64, no. 20, pp. 15–19, 2013, doi: 10.5120/10749-5625.
- [25] K. Joshi, R. Yadav, and G. Chawla, "an enhanced method for data hiding using 2-bit XOR in image steganography," *International Journal of Engineering and Technology*, vol. 8, no. 6, pp. 3043–3055, 2017, doi: 10.21817/ijet/2016/v8i6/160806266.
- [26] A. Rehman, T. Saba, T. Mahmood, Z. Mehmood, M. Shah, and A. Anjum, "Data hiding technique in steganography for information security using number theory," *Journal of Information Science*, vol. 45, no. 6, pp. 767–778, 2019, doi: 10.1177/0165551518816303.
- [27] S. Maurya and V. Shrivastava, "An improved novel steganographic technique for RGB and YCbCr colour space," *IOSR Journal of Computer Engineering*, vol. 16, no. 2, pp. 155–157, 2014.
- [28] Y. G. Yang, L. Zou, Y. H. Zhou, and W. M. Shi, "Visually meaningful encryption for colour images by using Qi hyper-chaotic system and singular value decomposition in YCbCr colour space," *Optik*, vol. 213, p. 164422, 2020, doi: 10.1016/j.jlileo.2020.164422.
- [29] S. Dagar, "Highly randomized image steganography using secret keys," *International Conference on Recent Advances and Innovations in Engineering, ICRAIE 2014*, 2014, doi: 10.1109/ICRAIE.2014.6909116.
- [30] R. M. Neamah, J. A. Abed, and E. A. Abboud, "Hide text depending on the three channels of pixels in colour images using the modified LSB algorithm," *International Journal of Electrical and Computer Engineering*, vol. 10, no. 1, pp. 809–815, 2020, doi: 10.11591/ijece.v10i1.pp809-815.
- [31] G. S. Charan, S. S. V. Nithin Kumar, B. Karthikeyan, V. Vaithyanathan, and K. Divya Lakshmi, "A novel LSB based image steganography with multi-level encryption," *ICIIIECS 2015 - 2015 IEEE International Conference on Innovations in Information, Embedded and Communication Systems*, pp. 1–5, 2015, doi: 10.1109/ICIIIECS.2015.7192867.
- [32] Z. S. Younus and M. K. Hussain, "Image steganography using exploiting modification direction for compressed encrypted data," *Journal of King Saud University - Computer and Information Sciences*, 2019, doi: 10.1016/j.jksuci.2019.04.008.

- [33] K. Muhammad, J. Ahmad, H. Farman, Z. Jan, M. Sajjad, and S. W. Baik, "A secure method for colour image steganography using gray-level modification and multi-level encryption," *KSIIT Transactions on Internet and Information Systems*, vol. 9, no. 5, pp. 1938–1962, 2015, doi: 10.3837/tiis.2015.05.022.
- [34] A. Nag, S. Biswas, D. Sarkar, and P. P. Sarkar, "A novel technique for image steganography based on DWT and Huffman," *International Journal of Computer Science and Security (IJCSS)*, vol. 4, no. 6, pp. 73–82, 2013, doi: 10.1017/CBO9781107415324.004.
- [35] M. N. Abdulwahed, "An effective and secure digital image steganography scheme using two random function and chaotic map," *Journal of Theoretical and Applied Information Technology*, vol. 98, no. 1, pp. 78–91, 2020.
- [36] A. A. Abdulla, S. A. Jassim, and H. Sellahewa, "Efficient high-capacity steganography technique," *Mobile Multimedia/Image Processing, Security, and Applications 2013*, vol. 8755, no. February 2019, p. 875508, 2013, doi: 10.1117/12.2018994.
- [37] M. Sherif, "StegoCrypt : Geometric and Rudin – Shapiro Sequence – Based Bit – Cycling and 3DES", Bachelor Thesis, 2019.
- [38] Aroukatos N.G., Manes K., Zimeras S., "Social networks medical image steganography using sub-Fibonacci sequences," *Springer International Publishing Switzerland 2016* A.A. Lazakidou et al. (eds.), *mHealth Ecosystems and Social Networks in Healthcare, Annals of Information Systems 20*, pp. 171–185, 2016, doi: 10.1007/978-3-319-23341-3.
- [39] S. Kamil, M. Ayob, S. N. H. S. Abdullah, and Z. Ahmad, Challenges in multi-layer data security for video steganography revisited, *Asia-Pacific Journal of Information Technology and Multimedia (APJITM)*, pp. 53-62, 2018, doi: dx.doi.org/10.17576/apjitm-2018-0702(02)-05
- [40] S. Roy and A. K. Pal, "A blind DCT based color watermarking algorithm for embedding multiple watermarks," *AEU - International Journal of Electronics and Communications*, vol. 72, pp. 149–161, 2017, doi: 10.1016/j.aeue.2016.12.003.
- [41] S. Rajagopala et al., "MSB Based Embedding with Integrity: An Adaptive RGB Stego on FPGA Platform," *Information Technology Journal*, vol. 13, no. 12, pp. 1945–1952, 2014, doi: 10.3923/itj.2014.1945.1952.

# Very Deep Neural Networks for Extracting MITE Families Features and Classifying them based on DNA Scalograms

Mael SALAH JRAD<sup>1</sup>, Afef ELLOUMI OUESLATI<sup>2</sup>, Zied LACHIRI<sup>3</sup>

University of Tunis El Manar, SITI Laboratory, National School of Engineers of Tunis (ENIT)  
BP 37, le Belvédère, 1002, Tunis Tunisia<sup>1,2,3</sup>

University of Carthage, National School of Engineers of Carthage (ENICarthage)  
Electrical Engineering Department, Tunisia<sup>2</sup>

**Abstract**—DNA sequencing has recently generated a very large volume of data in digital format. These data can be compressed, processed and classified only by using automatic tools which have been employed in biological experiments. In this work, we are interested in the classification of particular regions in *C. Elegans* Genome, a recently described group of transposable elements (TE) called Miniature Inverted-repeat Transposable Elements (MITEs). We particularly focus on the four MITE families (Cele1, Cele2, Cele14, and Cele42). These elements have distinct chromosomal distribution patterns and specific number conserved on the six autosomes of *C. Elegans*. Thus, it is necessary to define specific chromosomal domains and the potential relationship between MITEs and Tc / mariner elements, which makes it difficult to determine the similarities between MITEs and TC classes. To solve this problem and more precisely to identify these TEs, these data are classified and compressed, in this study, using an efficient classifier model. The application of this model consists of four steps. First, the DNA sequence are mapped in a scalogram's form. Second, the characteristic motifs are extracted in order to obtain a genomic signature. Third, MITE database is randomly divided into two data sets: 70% for training and 30% for tests. Finally, these scalograms are classified using Transfer Learning Approach based on pre-trained models like VGGNet. The introduced model is efficient as it achieved the highest accuracy rates thanks to the recognition of the correct characteristic patterns and the overall accuracy rate reached 97.11% for these TEs samples classification. Our approach allowed also classifying and identifying the MITEs Classes compared to the TC class despite their strong similarity. By extracting the features and the characteristic patterns, the volume of massive data was considerably reduced.

**Keywords**—DNA scalograms; genomic signature; classification; deep learning; transfer learning; VGGNET; accuracy

## I. INTRODUCTION

DNA is a molecule composed of a long chain of four nucleotides: Adenine (A), Thymine (T), Cytosine (C) and Guanine (G) [1, 2]. It comprises a multitude of periodic structures; the majority of which have an unknown biological function. This molecule adopts a three-dimensional double-helix having a curve shape [3]. In our work, the character's string was mapped into a scalogram form, based on wavelet

transform applied on a signal extracted from experimental measurements of the DNA curve. From these scalograms, we extracted patterns to classify some DNA regions. We chose, as model, the *Caenorhabditis Elegans* organism, which is an invertebrate combining simplicity and complexity. This duality makes it the most widely used versatile model for nearly all aspects of biological and genomic research. We also investigated a recently-described ET group, called Miniature Inverted-repeat Transposable Elements (MITEs). The latter were first discovered when studying the genes of several grass species including maize [4,5], rice [6] and barley [7]. They are genomic components abundant in many species, such as green pepper [8] and *Arabidopsis* [9, 10], as well as in several animal genomes including *Caenorhabditis elegans* [11], insects [12], humans [13] and zebrafish [14]. These species represent 1 % to 2% of the total sequence of the genomes. In these MITEs, we focused on four families, which are Cele1, Cele2, Cele14 and Cele42, because they have distinct chromosomal distribution patterns. In fact, Cele14 MITEs show clustering near the autosomes' ends. In contrast, the Cele2 MITEs display an even distribution through the central autosome domains, with no evidence for clustering at the ends. These patterns complicate the classification tasks. So far, there is no model for the systematic classification of 4 MITEs family.

However, more extensive sequence relationships between the MITEs and the Tc / mariner elements were established for the first time in *C. Elegans*. Most MITE families of this genome share their endings (~ 20 bp to 150 bp) and their TSD sequence with, at least, one of the described Tc1 / mariner transposons in this species. The comparison of the Tc elements coding of transposase and the numerous MITE families suggests possible scenarios for the origin of MITE in the *C. Elegans* genome.

As the distinction between the MITE families and the "transposable elements" (TC1, TC2, TC5) [15, 16, 17, 18] is a very difficult task, we thought about creating an efficient automatic model to classify them. In this paper, we introduce a new approach to classify DNA scalograms employing VGGNET while considering these scalograms as characteristic motifs of DNA. Our proposed method started first by converting the DNA string into DNA scalograms.

Afterward, a deep learning approach, that formed a Deep Neural Network (VGGNET) [19] for the prediction of database-derived tags from the original scalogram, was used. It allowed extracting high-level abstraction of characteristics from minimal preprocessing data. An evaluation of different CNN architectures namely, ResNet [37,38,39], inceptionv3 [40,41], Mobilnet [35,36] and Xception [42] was performed. This assessment shows that transfer learning achieved top-scoring performance.

The paper is organized as follows. Section II describes the utilized materials (the MITE and Transposons families, etc.) and the applied methods (DNA coding, continuous wavelet transform and the VGGNET classification methodology). It also details the criteria considered to evaluate the model performance (Accuracy and Confusion Matrix). Section III presents the different proposed approaches applied to classify and identify the four MITEs families applying these classification techniques. Section IV presents the experiments carried out to classify the MITE classes of *C. Elegans* and discusses the obtained results. Finally, Section V presents some concluding remarks.

## II. MATERIALS AND METHOD

### A. Materials

In this study, we focus on *Caenorhabditis Elegans* as an invertebrate combining simplicity and complexity, which makes it efficiently used to examine the important biological processes relevant to all eukaryotes. *C. Elegans* sequences were extracted from the National Center for Biotechnology Information (NCBI) public database [20]. Two sets of genomic data (the MITE dataset, composed of Cele1, Cele2, Cele14, and Cele42 [12], and non-ITE sequences which are the TEs TC1, TC2 and TC5 [15, 16, 17, 18]) are considered.

The MITEs are small non-autonomous elements derived from transposons. Their identification is usually based on the presence of target site duplications and terminal inverted repeats [10,11,12]. These elements are structurally comparable to defective class II. They are characterized by their small size (usually varying between 100bp and 458 bp in length) and their lack of coding capacity for transposase. They carry Terminal Inverted Repeats (TIR) and two adjacent short direct repeats called Target Site Duplications (TSD). MITEs are often located near or within genes, where they can affect gene expression [13,14]. They are preferentially located in single or weak copy regions. Thus, they can be used as genetic markers, especially for large genomes with low gene content [21]. MITEs can be grouped into super-families based on their association with TEs because they have almost the same TIRs. A relation between a given MITE family and its potential source of transposase is often based on limited sequence similarity in TIRs. The choice of a given family of TC as a non-MITE is justified by the fact that MITEs themselves contain TC sequences; which increases considerably MITE recognition rates in most bioinformatics tools. The studied MITE families are: CELE 1, CELE 2, CELE 14 and CELE 42. They have complex and variable structures and sizes.

Our database is composed of 7862 MITEs elements whose frequency occurrence in the *C. Elegans* genome of varies from

20 to 458, according to the class of family they belong to (Table I). The variability of length, composition and structure of these regions complicate their identification. Table I shows that MITEs have also a non-uniform distribution in the chromosomes. In fact, chromosome I (Chr I) contains the largest number of MITEs which is equal to 1799 with a size varying between 29 base pair(pb) and 380pb. Table I also demonstrate a high variability characterizing the sequences of MITE family; hence it is challenging to introduce an automated algorithm to predict them. Table II reveals that the sequences of Transposon family (TC1, TC2, TC5) are completely different. Although TC1, TC2 and TC5 are structurally characterized by more reduced numbers, they have big sizes (usually varying between 12 and 2088 bp in length).

$N_{Occ}$  is the number of occurrences of a class in 6 chromosomes of *C. Elegans*, and  $S_{min-max}$  represents the range of the minimum and maximum sizes and occurrences of a class in 6 chromosomes of *C. Elegans*.

In this research work, DNA scalograms are used to characterize these regions and transfer learning is applied to classify them.

TABLE I. NUMBER OF OCCURRENCES OF THE FOUR MITEs FAMILIES IN 6 CHROMOSOMES OF *C. ELEGANS* AND SIZE OF THE SCALOGRAMS OF EACH CLASS OF THESE FAMILIES

|                  |               | CELE1    | CELE2    | CELE14   | CELE42   |
|------------------|---------------|----------|----------|----------|----------|
| Chr I            | $N_{Occ}$     | 509      | 643      | 761      | 336      |
|                  | $S_{min-max}$ | [32-371] | [36-380] | [29-201] | [33-251] |
| Chr II           | $N_{Occ}$     | 148      | 578      | 438      | 101      |
|                  | $S_{min-max}$ | [45-372] | [34-367] | [30-202] | [34-247] |
| Chr III          | $N_{Occ}$     | 362      | 714      | 429      | 179      |
|                  | $S_{min-max}$ | [22-382] | [37-363] | [30-207] | [30-245] |
| Chr IV           | $N_{Occ}$     | 179      | 430      | 360      | 129      |
|                  | $S_{min-max}$ | [49-373] | [38-379] | [43-445] | [37-251] |
| Chr V            | $N_{Occ}$     | 366      | 394      | 677      | 178      |
|                  | $S_{min-max}$ | [20-458] | [36-363] | [34-225] | [47-273] |
| ChrX             | $N_{Occ}$     | 16       | 56       | 268      | 11       |
|                  | $S_{min-max}$ | [74-301] | [40-317] | [40-191] | [54-237] |
| Total occurrence |               | 1180     | 2815     | 2933     | 934      |
| Total            |               | 7862     |          |          |          |

TABLE II. NUMBER OF OCCURRENCES OF TRANSPOSON FAMILIES IN 6 CHROMOSOMES OF *C. ELEGANS* AND SIZE OF THE SCALOGRAMS OF EACH CLASS OF THESE FAMILIES

|                  |               | TC1        | TC2       | TC5       |
|------------------|---------------|------------|-----------|-----------|
| Chr I            | $N_{Occ}$     | 36         | 24        | 29        |
|                  | $S_{min-max}$ | [50-1610]  | [53-230]  | [54-1606] |
| Chr II           | $N_{Occ}$     | 42         | 19        | 26        |
|                  | $S_{min-max}$ | [62-1611]  | [47-2074] | [24-1611] |
| Chr III          | $N_{Occ}$     | 21         | 15        | 22        |
|                  | $S_{min-max}$ | [111-1610] | [61-157]  | [12-1608] |
| Chr IV           | $N_{Occ}$     | 23         | 31        | 34        |
|                  | $S_{min-max}$ | [15-1610]  | [12-154]  | [35-844]  |
| Chr V            | $N_{Occ}$     | 91         | 33        | 62        |
|                  | $S_{min-max}$ | [64-1611]  | [39-2088] | [28-1611] |
| ChrX             | $N_{Occ}$     | 83         | 52        | 28        |
|                  | $S_{min-max}$ | [33-1610]  | [12-155]  | [64-1631] |
| Total occurrence |               | 296        | 174       | 201       |
| Total            |               | 671        |           |           |

In bio-informatics field, two sequences are considered homologous if they come from a common ancestor. Multiple sequence alignment techniques allow specifying the homologous regions of each sequence. Fig. 1, shows that the DNA scalograms highlight DNA homology, a degree of identity or similarity, between scalograms of different regions of CELE2 and similar homology for different elements of TC2. It also reveals a slight difference between the CELE2 and TC2 images [12,21].

**B. Methods**

To classify the MITE families, it is necessary to parameterize the DNA sequences regardless to their heterogeneity. Thus, we choose the DNA mapping into image based on scalograms. For this reason, we use PNUC coding technique [22, 23] and Continuous Wavelet Transform (CWT) [24, 25, 26] to highlight features. Then, we extract these features from DNA images using VGGNet, a powerful CNN architecture, pre-trained on ImageNet. Finally, a classification is performed based on deep learning model (VGG19 and VGG16) [19, 27].

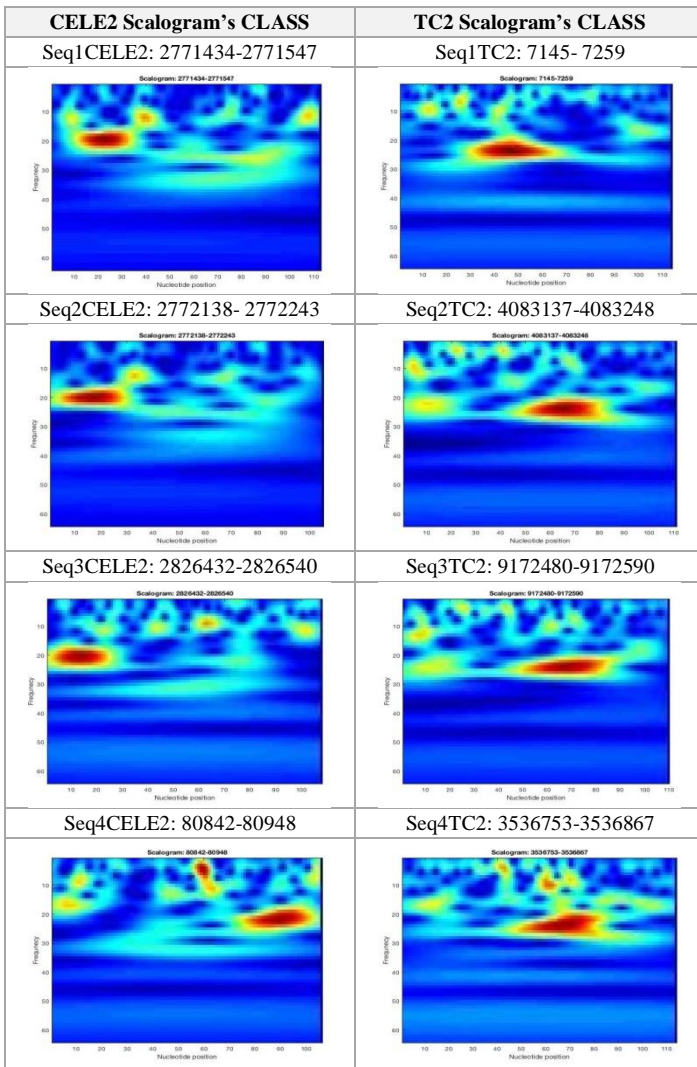


Fig. 1. Samples taken from the CELE2 Scalogram Class and TC2 Scalogram Class.

Transfer Learning consists first in training a base network on a dataset and then transferring the learned features to a second target network to train them to a target dataset.

1) *PNUC coding technique and Wavelet Transform:* For our classification technique, we consider DNA images. These images represent scalograms which are energy distributions obtained by taking the square module of the continuous wavelet transform applied to sequences encoded in PNUC [22, 23]. Considering the square module, time-frequency localization is enhanced, and a new database of DNA scalograms is generated.

PNUC coding is based on curvature measurements. This curvature is directly related to the nucleosome structures presence. Applying this technique, the pairing of the two DNA helix (A-T and CG) along the helix is taken into account. PNUC coding consists in assigning, to each codon or trinucleotide, the numerical value given by the experimental values associated with each codon [23].

For example, the  $S_{DNA}$  is replaced by the numerical sequence.

$$S_{DNA} = \text{'AAG TTT CTT GTG AAA ACG TGC AGC'}$$

The Pnuc coding of  $S_{DNA}$  is :

$$CS_{DNA} = \text{'7.3 0 7.3 9.2 0 7.6 8.5 1'}$$

DNA has a multitude of periodic structures and the wavelet analysis was proposed to reveal the local and frequential properties of the DNA periodic motifs. The analysis based on the Morlet Complex wavelet allows detecting the different periodicities in various types of C. Elegans chromosomal DNA [24, 25, 26].

Wavelet analysis relies essentially on the signal's decomposition into a sum of time-frequency atoms. The latter, called "wavelets", are obtained by dilating or contracting a Mother Wavelet  $\psi(t)$  [28, 29] and translating it along the time axis. The versions obtained after these transformations are noted  $\psi[(t-b)/a]$ .

The dilation and compression of a mother wavelet depend on a scaling factor (a), while the translation is ensured using a translation parameter (b). The wavelet family of scales and positions is then generated by the following expression:

$$\psi_{a,b}(t) = \frac{1}{\sqrt{a}} \psi^* \left( \frac{t-b}{a} \right), a > 0, b \in \mathbb{R} \tag{1}$$

In general, the wavelet transform of a signal f(t) is given by Equation (2):

$$T_{\psi}(f)(a, b) = \frac{1}{\sqrt{a}} \int_{-\infty}^{\infty} f(t) \psi^* \left( \frac{t-b}{a} \right) dt \tag{2}$$

where the symbol \* indicates the complex conjugate. The obtained  $T_{\psi}(a, b)$  numbers are called coefficients of wavelets. The Morlet Complex wavelet is the most efficient technique applied to analyze and characterize DNA structures [24] and presented as an exponential-modulated Gaussian envelope. It is defined by the following equation:

$$\psi(t) = \pi^{-\frac{1}{4}} \left( e^{i\omega_0 t} - e^{-\frac{1}{2}\omega_0^2} \right) e^{-\frac{1}{2}t^2} \tag{3}$$



where the parameter  $\omega_0$  designates the number of oscillations of the mother wavelet. It must be greater than 5 to satisfy the eligibility requirement. Using  $M$  scales, we obtain a matrix of  $N \times M$  coefficients representing the time-frequency plane where  $N$  is the length of the analyzed signal. The modulus of wavelet coefficients  $|\text{Tr}\psi(a, b)|$  is called "scalogram".

In our study, the performed analysis consists in applying a continuous wavelet transform based on the complex Morlet wavelet [24, 25, 26]. This analysis highlights the periodicities that reside in the DNA (represented by its inverse the frequency on the  $y$  axis) with precision on location in the nucleotides position (equivalent to time in the  $x$  axes). The result of analysis generates scalograms which are the images used in the classification.

2) VGGNET model for classification of DNA scalograms:

We are interested in studying the VGGNET which is a convolutional neural network trained on more than one million images from the ImageNet database [30].

We use transfer learning to classify the DNA scalograms. The main idea of transfer learning based on very deep neural networks is to apply a pre-trained deep learning model, previously trained on a large-scale dataset such as ImageNet. Containing 1.2 million images with another 50,000 images for validation and 100,000 images for testing, on 1000 different categories, and re-purpose, to handle an entirely different problem [31].

The used model treats the input image. Then, it outputs the vector containing 1000 values. This vector represents the corresponding class classification probability. If a model is utilized to predict that an image belongs to class 0, class 1, class 2, class 3, class 780, class 999 with probability 1, 0.05, 0.05, 0.03, 0.72, 0.05, respectively and the remaining classes with probability 0, the classification vector of this model will be:

$$\hat{y} = \begin{bmatrix} \hat{y}_0 = 0.1 \\ 0.05 \\ 0.05 \\ 0.03 \\ \vdots \\ \vdots \\ \hat{y}_{780} = 0.72 \\ \vdots \\ \vdots \\ \hat{y}_{999} = 0.05 \end{bmatrix}$$

Softmax function, defined below, is used to ensure that these probabilities add to 1:

$$P(y = j | \theta^{(i)}) = \frac{e^{\theta_j^{(i)}}}{\sum_{k=0}^K e^{\theta_k^{(i)}}} \quad (4)$$

where:

$$\theta = w_0 x_0 + w_1 x_1 + \dots + w_k x_k = \sum_{i=0}^k w_i x_i = W^T x$$

After learning certain features from a large dataset (ImageNET), they are used by VGGNet model as a base to learn the presented classification problem. As demonstrated in Fig. 2, we employ a popular and reliable CNN architecture called VGGNet with 16 convolutional and 3 fully-connected layers [27]. The width of convolutional layers (the number of channels) is rather small, starting from 64, in the first layer, and increasing by a factor of 2, after each max-pooling layer, up to 512. The input of the CNN is a fixed-size 224 x 224 RGB image. Each image passes through a stack of convolutional (conv.) layers. Subsequently, the convolution stride is added such that the spatial resolution will be preserved after convolution, i.e. the padding is considered also in Conv. layers. Spatial pooling is carried out by five max-pooling layers, which follow some but not all of the Conv. Layers. Max-pooling is performed over a specific pixel window; with stride. A stack of Conv. Layers, having different depths in various architectures, are followed by three fully-connected (FC) layers: each of the two first layers has 4096 channels, while the third one performs the classification of 2 after each max-pooling layer, up to 512 [32,33].

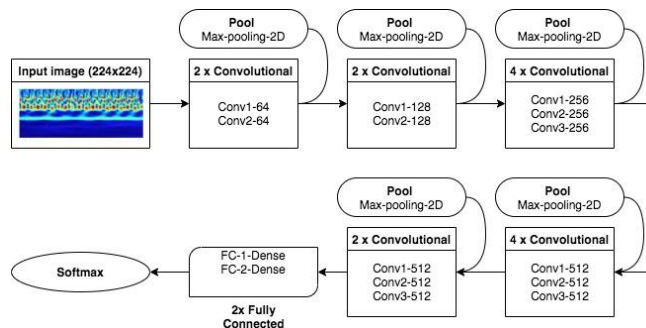


Fig. 2. Overview of the VGG16 Layer Structure (Left) and Corresponding Parameters (Right).

III. PROPOSED APPROACH

The adopted methodology includes three steps. Fig. 3 represents the flowchart describing our proposed approach whose application consists in:

- Extracting the MITEs sequences (CELE1, CELE2) and the TEs (TC1, TC2 and TC5) of all the chromosomes of *C. Elegans* from the NCBI database. The extraction phase can be divide into the following two sub-steps:
  - Generating the corresponding PNUC sequences to convert the DNA string into a 1D signal.
  - Applying Continuous Wavelet analysis to transform the signal to scalogram images.
- Extracting features using convolutional neural networks
- Using the VGGNET model to classify the studied sequences.

A. Creating MITE Signal Database

In the first step of our methodology, we extract the entire DNA sequences corresponding to the *C. Elegans* genome from the NCBI database [20]. Then, we apply PNUC coding on all chromosomes (6 chromosomes). Thereby, a chromosomal

signal database (1D signal) is created after applying the module on the square of the continuous wavelet transform [24, 25, 26], which enhances time-frequency localization and generates a new DNA database of DNA containing images (or scalograms) which represent energy distributions).

**B. Extraction of Features using Convolutional Neural Networks**

Several models were used to extract the characteristics of AND scalograms in the field of deep learning. In this work, we use a model adapted for their extraction (Fig. 4). These Different values of independent variables are also considered as the input of the classifier to predict the corresponding class to which the independent variable belongs. The architecture of introduced model is presented in Table III.

As shown in Fig. 4, the shape of the input image is (224, 224, 3) and the last layer produced from VGGNet has the shape (7, 7, 512). This means that VGGNet returns a feature vector of  $7 \times 7 \times 512 = 25088$  features. In order to perform transfer learning with VGGNet, we first save the extracted features (bottleneck features) from the pre-trained model. Then, top model is trained to classify our data using the saved bottleneck features. Finally, we combine our training data and the VGGNet model with the top model to predict DNA Pattern of scalograms [34].

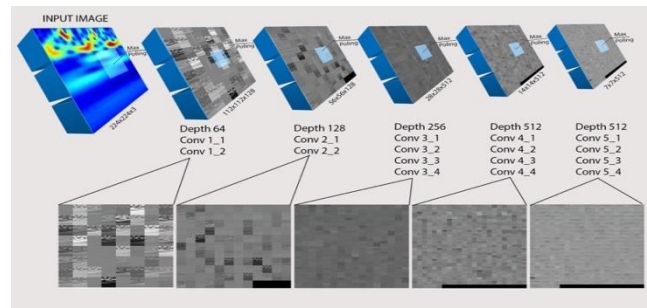


Fig. 4. Feature Extraction by VGG19 Model and Corresponding Parameters.

**C. Classification Algorithm**

For our classification algorithm, we use the third convolutional layer containing only two channels (one for each class). The final layer is the soft-max layer. All hidden layers are equipped with the non-linearity rectification [19,27]. For each image X of study type T in the training set, the weighted binary cross-entropy loss is optimized. The VGGNet specifications are described in Fig. 3.

The major limitation of VGGNet lays in the fact that this architecture necessitates huge memory requirements. Because of the number of fully-linked nodes and its depth, the size of VGGNet is equal to 574 MB, which complicates its use as features extractor.

We also employ the VGG16 and compare its results with those provided by the VGG19. The VGG-16 is a 16-layer CNN developed by Simon et al. for image recognition in the 2014 ImageNet large scale visual recognition challenge (ILSVRC) [19]. The filters  $3 \times 3$  are employed for all convolutional layers. This network accepts the input image with a dimension of  $224 \times 224$ . The image passes through a sequence of 16 convolutional layers. A multilayer perceptron (MLP) classifier, including three fully connected (FC) layers and the convolutional layers, is utilized in the classification step. The Rectified linear unit (ReLU) layers and max-pooling layers are also used in the whole network to prevent overfitting.

To evaluate our classification model, we apply the classification rate calculation and the confusion matrix as classification criteria. The performance of the proposed approach is tested in terms of accuracy, precision, sensitivity, specificity, F-measure (F1), Confusion matrix illustrated in Fig. 5 and loss functions value to select features of DNA scalograms. These measures are described below:

$$Accuracy = \frac{TP+TN}{TP+TN+FP+FN} \tag{5}$$

$$Recall = \frac{TP}{TP+FN} \tag{6}$$

$$Precision = \frac{TP}{TP+FP} \tag{7}$$

$$Sensitivity = \frac{TP}{TP+FN} \tag{8}$$

$$Specificity = \frac{TN}{TN+FP} \tag{9}$$

$$F1 = 2 \times \frac{Specificity \times Sensitivity}{Specificity+Sensitivity} \tag{10}$$

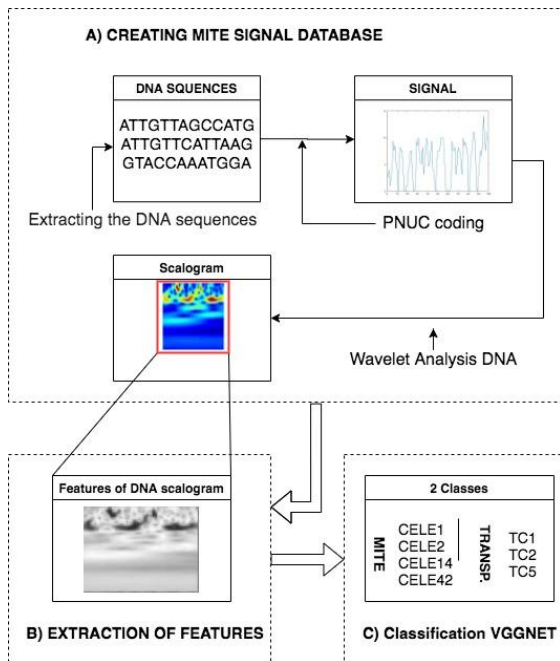


Fig. 3. Flow Chart of the Proposed Approach.

TABLE III. CONVOLUTIONAL NEURAL NETWORK ARCHITECTURE

| Feature            | value     |
|--------------------|-----------|
| Convolution layer  | 3x3       |
| Max pooling layer  | 2x2       |
| Convolution stride | 1 pixel   |
| Padding            | 2 pixel   |
| Rectification      | ReLU      |
| Fac layer          | softmax   |
| Fac layer nodes    | 4096      |
| Total layers       | 19 Layers |

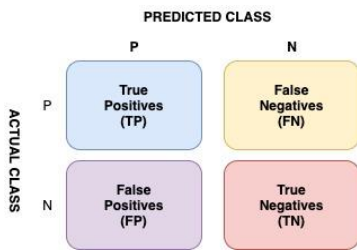


Fig. 5. Confusion Matrix.

where "TP" (True Positives) refers to the CELE samples correctly labeled by the classifier, "TNs" (True Negatives) are the Transposon samples correctly labeled by the classifier, "FPs" (False Positives) denotes the CELE scalograms incorrectly labeled as Transposons TC and "FNs" (False Negatives) are the transposon samples mislabeled as CELE.

The two most crucial and most intensively-employed loss functions are: the cross entropy function and the MSE function. Both of them are applied in regression and classification problems, respectively. The can be formulated as follows:

$$\mathcal{L}_{MSE}(\mathbf{W}) = \frac{1}{n-1} \sum_{i=0}^{n-1} (y_i - \hat{y}_i)^2 \quad (11)$$

$$\mathcal{L}_{\text{cross-entropy}}(\mathbf{W}) = - \sum_{i=0}^{n-1} \sum_{c=0}^M y_{i,c} \log \hat{y}_{i,c} \quad (12)$$

where n is the total number of samples in the dataset, M denotes the number of classes with in the dataset,  $y_{i,c}$  designates a binary indicator indicating if class c represents the correct classification for sample i and  $\hat{y}_{i,c}$  refers to the predicted probability of sample i which belongs to class c. The first previously-mentioned loss produces high loss when the predicted value is close to the true value; whereas the cross-entropy loss punishes uncertain prediction probabilities.

#### IV. RESULTS

The main objectives of this study are to characterize MITE families and distinguish them from other regions. For this purpose, genomic sequences used in this work are composed of two parts: a part containing MITE family sequences (CELE1, CELE2, CELE14 and CELE42) and another one including TC1, TC2, TC5.

The examination of the structure and distribution of MITEs reveals that the number of appearances of these elements are variable and that the TC family number of scalograms is reduced compared to them, which complicates the MITE classification process. To solve this problem of unbalanced data, we enlarge the database of TC and MITEs signals by grouping all the elements of the TC family in the same class and applying a binary classification. Here, the idea is based on the identification of the MITE family of elements (CELE1 CELE2 CELE14 and CELE42) with respect to other non-MITE families (Tc1, Tc2, Tc5). Thereafter, this dataset is split into two parts 70% for training and 30% for test). Then, VGGNET is applied with softmax activation mode. The Recognition process consists of two stages: features extraction and features recognition. The performance of the proposed system strongly depends on the choice of the extraction method.

The experimental results demonstrate that most of the CELE elements are correctly recognized with the Tc elements. Obviously, the VGG16 trained model achieves an accuracy rate of 97.11% for CELE14 identification, 93.38% for CELE1 identification, 91.79% for CELE42 identification and 89.66% for CELE2 identification. Fig. 6 illustrates the accuracy of the VGG-16 model over the Test images.

Similarly, Fig. 8 illustrates the accuracy rate obtained by applying the VGG-19 model on the validation dataset. The trained model reaches an accuracy rate equal to 96.44%, 94.52 %, 91.05 and 90.17 for the identification of CELE14, CELE42, CELE1 and CELE2, respectively.

Fig. 6, 7, 8 and 9 demonstrate that the learning and validation curves are remarkably enhanced for VGG16 and VGG19 Models. It is also clear that the network converges from the second epoch and, with the rise in the epochs, and the cross entropy loss tends to zero.

These figures represent the accuracy curves of train set and those of validation set. Each point of the precision curve corresponds to the accurate prediction rate for train or validation images. The accuracy curve follows similar smooth processing as that adopted by the loss curve. It is obvious that the train set accuracy and the validation set accuracy approach 100% after 2 epochs.

Fig. 6 and 7 show that the VGG16 model accuracy value is higher, compare to that of VGG19 model. However, this is not true depending on the element to be identified. Thus, the accuracy average is computed to classify the 4 MITE families. The accuracy rate attains 92.98, for VGG16, and 93.045, for VGG19, revealing that VGG16 is more effective in the classification of MITEs scalograms, compared to VGG19 model.

Additionally, testing results are given in Fig. 10 and 11 representing the Confusion Matrix for the validation data.

The performance measurement is with four different combinations of predicted and target classes which are the true positive, false positive, false negative, and the true negative. In this format, the number and percentage of the correct classifications performed by the trained network are indicated in the diagonal.

The confusion matrix shows that the used models clearly differentiate the families of MITE, compared to TC1, TC2, TC5, despite the similarities between the CELE and TC1, TC2, TC5, as cited in the first part (Section 3) of this paper [21].

As seen in Fig. 10, all the classes of MITEs are correctly classified. Our model, using VGG16, recognizes CELE2 with a very promising rate of 99.52%, and 99.19%, for CELE14 identification, 96.48%, for CELE1 identification, and 86.19% for identification of CELE42.

Comparison of our models with other CNN architectures

Similarly, a comparative analysis of the results obtained by the VGGNET framework, employing four well-known methods, was carried out to shed light on the efficiency of VGGNET in identifying the four MITE families, as given in

this table (Table IV). We show that Mobilenet [35,36], Resnet [37,38,39], InceptionV3 [40,41] and Xception [42] give average accuracy rates (Acc.) of 88.85%, 86.92%, 86.23% and 88.06%, respectively, to classify the four MITE families.

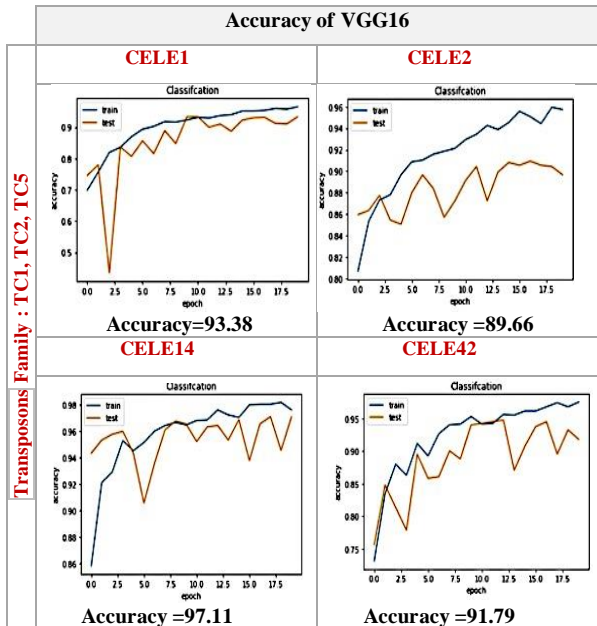


Fig. 6. Accuracy Rate Obtained for the Identification of Mites Families to Transposon Families DNA Scalograms VGG16.

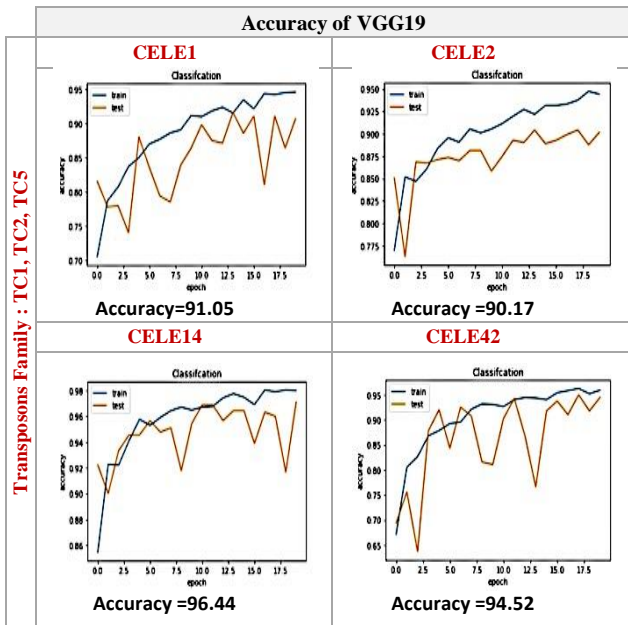


Fig. 7. Accuracy Rate Obtained for the Identification of Mite Family to Transposon Family DNA Scalograms VGG19.

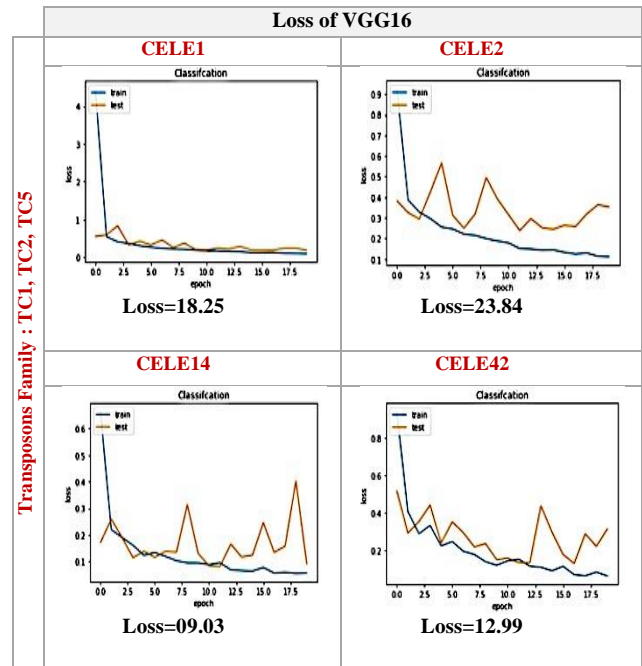


Fig. 8. Loss for the Identification of Mite Family to Transposon Family DNA Scalograms VGG16.

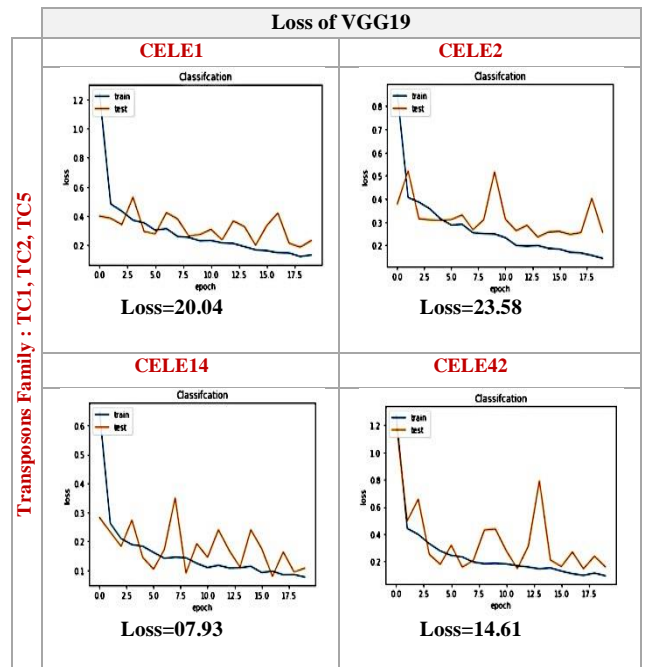


Fig. 9. Loss for the Identification of Mite Family to Transposon Family DNA Scalograms VGG19.

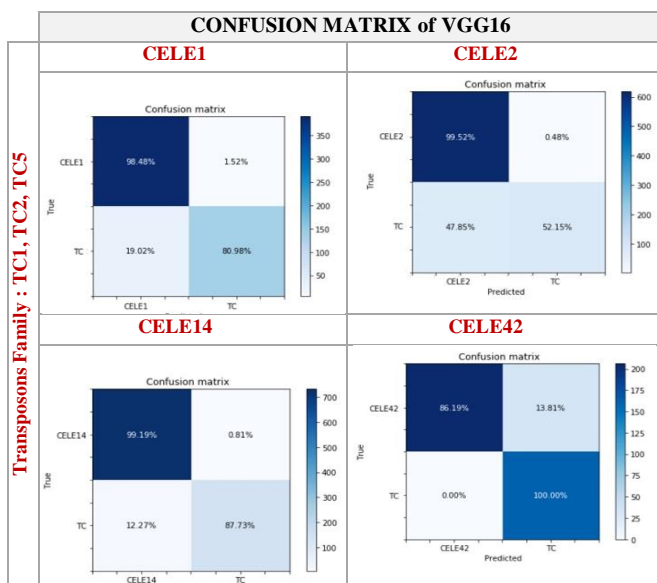


Fig. 10. Confusion Matrix for the Identification of MITE Families to Transposon Family of DNA Scalograms VGG16.

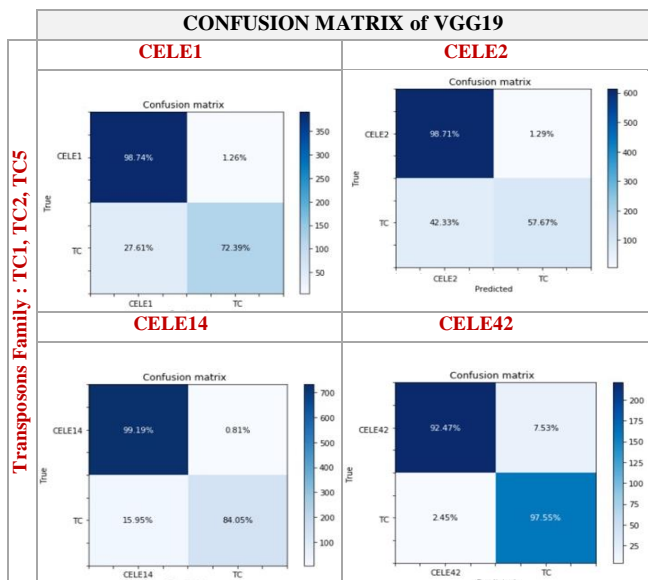


Fig. 11. Confusion Matrix for the Identification of MITE Families to Transposon Family of DNA Scalograms VGG19.

However, findings obtained using the VGGNET provide the highest accuracy of 97.11% for the identification of the CELE1 element. These results reveal that our architectures more powerful and promising than other deep models

Table IV demonstrates also the performance achieved by other CNN architectures [43,44] using Loss, Recall (Rec.), Precision (Pre.), sensitivity (Sens.), specificity (Spec.) and F1 metrics.

The proposed approach shows high performance by achieving accuracy, loss, recall, precision and f1-score of 97.11, 09.03, 99.18, 97.34, and 85.64, respectively.

TABLE IV. SPLATTING BASED COMPARATIVE WITH OTHER CNN ARCHITECTURE TO IDENTIFY CELE 1, CELE2, CELE14 AND CELE42

| CELE1       | AcC.         | LosS         | REc          | Pre.         | Sen.         | Spec.        | F1           |
|-------------|--------------|--------------|--------------|--------------|--------------|--------------|--------------|
| VGG16       | <b>93.38</b> | <b>18.25</b> | 98.48        | <b>92.63</b> | 74.71        | 80.98        | <b>77.71</b> |
| VGG19       | 91.05        | 20.04        | 98.73        | 89.67        | 76.81        | 72.39        | 74.53        |
| Resnet 152  | 83.89        | 35.92        | 97.97        | 82.55        | 82.72        | 49.69        | 62.08        |
| Mobilnet    | 84.97        | 33.67        | 85.60        | 92.62        | 71.36        | <b>83.43</b> | 76.92        |
| InCEPtionV3 | 85.86        | 34.26        | <b>99.24</b> | 83.80        | <b>83.79</b> | 53.37        | 65.2         |
| Xception    | 88.01        | 29.28        | 95.20        | 88.70        | 76.62        | 70.55        | 73.45        |

CELE2

| CELE2       | AcC.         | LosS         | REc        | Pre.         | Sen.         | Spec.        | F1           |
|-------------|--------------|--------------|------------|--------------|--------------|--------------|--------------|
| VGG16       | 89.66        | 23.84        | 99.51      | 88.79        | 87.90        | 52.14        | 65.45        |
| VGG19       | <b>90.17</b> | <b>23.58</b> | 98.71      | 89.88        | 86.88        | 57.66        | 69.25        |
| Resnet 152  | 84.69        | 34.32        | 100        | 83.80        | <b>93.52</b> | 26.38        | 41.15        |
| Mobilnet    | 86.47        | 20.578       | <b>100</b> | 85.41        | 91.59        | 34.96        | 50.60        |
| InCEPtionV3 | 86.66        | 34.66        | 93.23      | <b>90.04</b> | 85.65        | <b>59.50</b> | <b>70.21</b> |
| Xception    | 87.11        | 33.97        | 98.71      | 86.82        | 89.75        | 42.94        | 58.08        |

CELE14

| CELE14      | AcC.         | LosS         | REc        | Pre.         | Sen.         | Spec.        | F1           |
|-------------|--------------|--------------|------------|--------------|--------------|--------------|--------------|
| VGG16       | <b>97.11</b> | 09.03        | 99.18      | 97.34        | 83.65        | <b>87.73</b> | <b>85.64</b> |
| VGG19       | 96.44        | <b>07.93</b> | 99.18      | 96.56        | 84.23        | 84.04        | 84.13        |
| Resnet 152  | 93.56        | 14.27        | 99.72      | 92.92        | 87.30        | 65.64        | 74.93        |
| Mobilnet    | 90.45        | 12.536       | <b>100</b> | 89.56        | <b>90.55</b> | 47.23        | 62.07        |
| InCEPtionV3 | 91.56        | 21.28        | 99.45      | 91.06        | 88.96        | 55.82        | 68.59        |
| Xception    | 94.56        | 15.30        | 99.18      | <b>99.45</b> | 85.91        | 73.61        | 79.28        |

CELE42

| CELE42      | AcC.         | LosS         | REc          | Pre.       | Sen.         | Spec.      | F1           |
|-------------|--------------|--------------|--------------|------------|--------------|------------|--------------|
| VGG16       | 91.79        | <b>12.99</b> | 86.19        | <b>100</b> | 55.82        | <b>100</b> | 71.64        |
| VGG19       | <b>94.52</b> | 14.61        | 92.46        | 98.22      | 58.15        | 97.54      | <b>72.86</b> |
| Resnet 152  | 85.57        | 26.66        | 98.32        | 81.13      | 68.31        | 66.87      | 67.58        |
| Mobilnet    | 93.53        | 33.62        | 98.32        | 91.43      | 62.50        | 86.50      | 72.56        |
| InCEPtionV3 | 80.84        | 26.93        | <b>99.58</b> | 75.79      | <b>73.23</b> | 53.37      | 57.83        |
| Xception    | 82.58        | 28.48        | 71.54        | 98.84      | 51.50        | 98.77      | 67.70        |

Table V presents the existing works based on supervised machine learning algorithms used in the classification step and compares the results obtained employing DNA sequences database. As shown in this table, several studies utilized CNN (Convolutional neural networks) [47], C-KNN [45] and support vector machines utilized [46].

Nevertheless, successful categorization rate ranges between 70% and 90%. Obviously, a successful categorization relies mainly on the entry variability. The majority of the studies listed in Table V and those based on the machine learning dealt with correctly detecting and classifying the highest number of defects applying features extractions and classifiers. Measures reported in the literature (classification,

accuracy, number of features and computation time) are also compared. They demonstrate that transferred VGGNET models attain the highest accuracy rate. The major benefit of pre-trained VGGNET models, compared to those applied in the existing studies, lays in the fact that they do not necessitate a feature extraction mechanism or an intermediate feature selection phase.

TABLE V. COMPARISON OF THE TRANSFER LEARNING-BASED VGGNET MODELS WITH THE EXISTING WORKS

| Study                                   | Method                                   | Accuracy        |
|-----------------------------------------|------------------------------------------|-----------------|
| [43] Nguyen, N.G.<br>[44] Amerah Kassim | DNA Sequence<br>Classification by<br>CNN | 82 %            |
| [45] Mochammad Anshori                  | LDA-SVM                                  | 92.7%           |
| [46] Alhersh                            | C-KNN                                    | 73.72 % -91.82% |
| Proposed Approach                       |                                          | 97.11%          |

## V. CONCLUSION

In this paper, we focused on DNA images. Our main purpose is to identify the MITES Families from Transposon families and classify them. The DNA images represent the scalograms. In fact, the ATCG chain was first converted, using a PNUC coding technique, into a signal based on the experimental DNA curve measures. Then, the Continuous Wavelet Transform by Morlet Complex wavelet allowed converting this signal into particular images. Thirdly, a selection of features was performed applying Transfer learning approach. Finally, each produced feature set was tested by several classifiers to validate the proposed model.

This approach showed high performance by achieving accuracy, loss, recall, precision and f1-score of 97.11%, 09.03, 99.18, 97.34, and 85.64, respectively. The obtained results are the highest among all known published works on the same dataset, even if compared to other convolutional network models. In fact, the classification rate obtained in previous works did not exceed 90%.

## REFERENCES

[1] R. B. Macgregor, and G. M. Poon, "The DNA double helix fifty years on. Computational biology and chemistry", 27(4), pp.461-467, 2003.

[2] F. Rechenmann, and C. Gautier, "Interpreting the genome. La recherche", (332), pp.39-45, 2000.

[3] Craig NL, Craigie R, Gellert M, Lambowitz AM. Mobile DNA II. Washington, DC: Am. Soc. Microbiol. Press, 2002.

[4] Bureau, T. E. & Wessler, S. R. Plant Cell 4, pp.1283-1294, 1992.

[5] Bureau, T. E. & Wessler, S. R. Proc. Natl. Acad. Sci. USA 91, pp.1411-1415, 1994.

[6] Bureau, T. E., Ronald, P. C. & Wessler, S. R. Proc. Natl. Acad. Sci. USA, 93, pp.8524-8529, 1996.

[7] Shirasu, K., Schulman, A. H., Lahaye, T. & Schulze-Lefert, P. Genome Res. 10, pp.908-915, 2000.

[8] Pozueta-Romero, J., Houlne, G. & Schantz, R. Gene 171, pp. 147-153, 1996.

[9] Casacuberta, E., Casacuberta, J. M., Puigdomenech, P. & Monfort, A., Plant J. 16, pp.79-85, 1998.

[10] Surzycki, S. A. & Belknap, W. R. J. Mol. Evol. 48, pp. 684-691, 1991.

[11] Oosumi, T., Belknap, W. R. & Garlick, B. Nature (London) 378, 672, 1995.

[12] Surzycki, S. A., and W. R. Belknap, Repetitive-DNA elements are similarly distributed on Caenorhabditis elegans autosomes. Proc. Natl. Acad. Sci. USA 97: pp.245-249, 2000.

[13] Tu, Z. Proc. Natl. Acad. Sci. USA 94, pp.7475-7480, 1997.

[14] Izsvak, Z., Ivics, Z., Shimoda, N., Mohn, D., Okamoto, H. & Hackett, P. B. J. Mol. Evol. 48, pp.13-21, 1999.

[15] Mello CC, Kramer JM, Stinchcomb D, Ambros V. Efficient genetransfer in C. elegans: extrachromosomal maintenance and integration of transforming sequences. Embo J; 10 : 959-70, 1991.

[16] Duret, L., G. Marais & C. Biemont. Transposons but not retrotransposons are located preferentially in regions of high recombination rate in Caenorhabditis elegans. Genetics 156: pp. 1661-1669, 2000.

[17] Kidwell MG. Transposable elements and the evolution of genome size in eukaryotes. Genetica 115: pp. 49-63, 2002.

[18] Feschotte C, Pritham EJ. DNA transposons and the evolution of eukaryotic genomes. Annu Rev Genet 41: pp.331-368, 2007.

[19] K. Simonyan and A. Zisserman. Very deep convolutional networks for large-scale image recognition. In ICLR, 2015.

[20] The NCBI GenBank database. [Online]. Available: <http://www.ncbi.nlm.nih.gov/Genbank/>. Accessed 15 Sept 2005.

[21] Casa, Alexandra M., et al. "The MITE family Heartbreaker (Hbr): molecular markers in maize." Proceedings of the National Academy of Sciences 97.18: pp.10083-10089, 2000.

[22] AE Oueslati, Messaoudi I, Z Lachiri, N Ellouze, ed. by Salih Salih Dr, Spectral analysis of global behaviour of C. elegans chromosomes, in Fourier Transform Applications, pp. 205-228, 2012.

[23] Oueslati, A. E., Messaoudi, I., Lachiri, Z., & Ellouze, N. A new way to visualize DNA's base succession: the Caenorhabditis elegans chromosome landscapes. Medical & biological engineering & computing, 53(11), pp.1165-1176, 2015.

[24] I Messaoudi, A Elloumi, Z Lachiri, in C. elegans, International Conference on Control, Engineering & Information Technology (CEIT2013), vol. 3., Complex Morlet wavelet analysis of the DNA frequency chaos game signal and revealing specific motifs of introns (Sousse, Tunisia, 4-7 June), pp. 27-32, 2013.

[25] Messaoudi, I., Oueslati, A. E., & Lachiri, Z. Revealing Helitron signatures in Caenorhabditis elegans by the Complex Morlet Analysis based on the Frequency Chaos Game Signals. In IWBBIO (pp. 1434-1444), 2014.

[26] Messaoudi, I., Oueslati, A. E., & Lachiri, Z. Wavelet analysis of frequency chaos game signal: a time frequency signature of the C. elegans DNA. EURASIP Journal on Bioinformatics and Systems Biology, 2014(1), 16.

[27] B. Liu, X. Zhang, Z. Gao, and L. Chen, "Weld defect images classification with vgg16-based neural network," in Proceedings of the International Forum on Digital TV and Wireless Multimedia Communications, pp. pp.215-223, 2017.

[28] NAJMI AH, SADOWSKY J, The continuous wavelet transform and variable resolution timefrequency analysis. Johns Hopkins APL Tech Dig 18:1pp. 34-140,1997.

[29] Ngui, Wai Keng, et al. "Wavelet analysis: mother wavelet selection methods." Applied mechanics and materials. Vol. 393. Trans Tech Publications, 2013.

[30] Russakovsky, Olga, et al. "Imagenet large scale visual recognition challenge." International journal of computer vision 115.3 : pp.211-252, 2015.

[31] Chen, L.-C., Papandreou, G., Kokkinos, I., Murphy, K. & Yuille, A. L. Deep lab: Semantic image segmentation with 290 deep convolutional nets, a trous convolution, and fullyconnectedcrfs. IEEE Transactions on pattern analysis machine 291 intelligence 40, pp.834-848, 2017.

[32] Sahlol, Ahmed T., Philip Kollmannsberger, and Ahmed A. Ewees. "Efficient classification of white blood cell leukemia with improved Swarm optimization of deep features." Scientific Reports 10.1 (2020): 1-11.

[33] Busia, Akosua, et al. "A deep learning approach to pattern recognition for short DNA sequences." BioRxiv : pp.353474, 2019.

- [34] Bengio, Y., Courville, A. & Vincent, P. Representation learning: A review and new perspectives. *IEEE Transactions on pattern analysis and machine intelligence* 35, pp.1798–1828, 2013.
- [35] A. G. Howard, M. Zhu, B. Chen, D. Kalenichenko, W. Wang, T. Weyand, M. Andreetto, and H. Adam. Mobilenets: Efficient convolutional neural networks for mobile vision applications, 2017.
- [36] Z. Qin, Z. Zhang, X. Chen, and Y. Peng. "FD-MobileNet: Improved MobileNet with a Fast Downsampling Strategy," 2018.
- [37] C. Szegedy, S. Ioffe, V. Vanhoucke, and A. A. Alemi, "Inceptionv4, inception-ResNet and the impact of residual connections on learning," in *Proceedings of the AAAI Conference on Artificial Intelligence*, San Francisco, CA, USA, 2017.
- [38] K. He, X. Zhang, S. Ren, and J. Sun. Deep residual learning for image recognition. In *Proceedings of CVPR*, pp. 770–778, 2016.
- [39] S. Xie, R. Girshick, P. Dollár, Z. Tu, and K. He, "Aggregated Residual Transformations for Deep Neural Networks," in *Proc. of CVPR*, 2017.
- [40] C. Szegedy, W. Liu, Y. Jia, P. Sermanet, S. Reed, D. Anguelov, D. Erhan, V. Vanhoucke, and A. Rabinovich. Going deeper with convolutions. In *Proceedings of the IEEE Conference on Computer Vision and Pattern Recognition*, pp.1–9, 2015.
- [41] Szegedy, Christian, et al. "Rethinking the inception architecture for computer vision." *Proceedings of the IEEE conference on computer vision and pattern recognition*, 2016.
- [42] Chollet, "Xception: Deep Learning with Depthwise Separable Convolutions," in *Proc. of CVPR*, 2017.
- [43] Nguyen, N.; Tran, V.; Ngo, D.; Phan, D.; Lumbanraja, F.; Faisal, M.; Abapihi, B.; Kubo, M.; Satou, K. DNA sequence classification by convolutional neural network. *J. Biomed. Sci. Eng*, 9, pp.280–286, 2016.
- [44] Nurul Amerah Kassim1, and Dr Afnizanfaizal Abdullah2. Classification of DNA Sequences Using Convolutional Neural Network Approach. *Innovations in Computing Technology and Ap*.
- [45] Alhersh, Taha, et al. "Species identification using part of DNA sequence: evidence from machine learning algorithms." *Proceedings of the 9th EAI International Conference on Bio-inspired Information and Communications Technologies (formerly BIONETICS)*, 2016.
- [46] Anshori, Mochammad, Wayan Firdaus Mahmudy, and Ahmad Afif Supianto. "Classification Tuberculosis DNA using LDA-SVM." *Journal of Information Technology and Computer Science* 4.3:pp. 233-240, 2019.
- [47] Vu, Duong, Marizeth Groenewald, and Gerard Verkley. "Convolutional neural networks improve fungal classification." *Scientific reports* 10.1 : pp.1-12, 2020.

# The Prediction of Outpatient No-Show Visits by using Deep Neural Network from Large Data

Riyad Alshammari<sup>1</sup>, Tahani Daghistani<sup>2</sup>, Abdulwahhab Alshammari<sup>3</sup>  
Health Informatics Department, College of Public Health and Health Informatics  
King Saud Bin Abdulaziz University of Health Sciences  
King Abdullah International Medical Research Center (KAIMRC)  
Ministry of National Guard Health Affairs, Riyadh, KSA

**Abstract**—Patients' no-show is one of the leading causes of increasing financial burden for healthcare organizations and is an indicator of healthcare systems' quality and performance. Patients' no-show affects healthcare delivery, workflow, and resource planning. The study aims to develop a prediction model predict no-show visits using a machine learning approach. A large volume of data was extracted from electronic health records of patient visits in outpatient clinics under the umbrella of large medical cities in Saudi Arabia. The data consists of more than 33 million visits, with an 85% no-show rate. A total of 29 features were utilized based on demographic, clinical, and appointment characteristics. Nine features were an original data element, while data elements derived 20 features. This study used and compared three machine learning algorithms; Deep Neural Network (DNN), AdaBoost, and Naive Bayes (NB). Results revealed that the DNN performed better in comparison to NB and AdaBoost. DNN achieved a weighted average of 98.2% and 94.3% of precision and recall, respectively. This study shows that machine learning has the potential to improve the efficiency and effectiveness of healthcare. The results are considered promising, and the model can be an excellent candidate for implementation.

**Keywords**—No-show; outpatients; machine learning; prediction model introduction

## I. INTRODUCTION

Reducing outpatient appointment no-show is essential to health care organizations to utilize resources, decrease the financial burden, and treat the patients who need care. Hence, accurately predicting outpatient appointment no-show can efficiently use the hospital resources, reduce the waiting list considerably, and improve patient satisfaction significantly. Thus, "improve the quality of healthcare" [1] [2] [3] [4]. The request for outpatient services in Saudi Arabia is increasing sharply, and the appointment booking system is suffering from the high outpatient's appointment no-show [5]. There is currently no useful tool in the electric health care system to identify patients of a high risk of a no-show [5] [6] [7]. The current practice is to allow overbooking and walk-in. Therefore, healthcare systems in Saudi Arabia require a useful tool to predict outpatient no-show accurately.

Existing research on clinic no-show focuses on finding factors and developing models in specific patient groups such as diabetes or particular departments such as radiology. Moreover, rely on quantitative or traditional methods to serve the prediction of no-show risk. Few kinds of research are studying high-dimensional and high-volume

big data incorporating behavioral factors for no-show prediction. Many institutions are investing heavily in technology and digitalizing the work task, especially in the healthcare sector. A massive amount of data is collected over the years by the healthcare sector. Healthcare data is forecast by the International Data Corporation (ICD) to grow to more than 163 zettabytes by 2025 [8]. Hence, Big data solution becomes an essential part of the healthcare sector to extract knowledge and insights from the vast collected digital data records. One exciting area of data science, gaining massive attention from data science and big data analytics communities is Deep learning [9] [10]. Deep learning algorithms succeed in other domains [10] [11] and becoming more popular in the medical field [12] [13]. Deep learning algorithms become a promising type of machine learning algorithm that can model complex data characteristics at a high generalization level. One of the assuring platforms that can effectively handle big data and discover insights using machine learning algorithms is Google TensorFlow [14]. Google Tensorflow is a deep learning platform that can run a complex computation on different data types. It has been created to work efficiently and quickly to find knowledge/insights from a considerable amount of data.

This paper aims to construct a data-driven approach based on a deep machine algorithm to learn from over 30 million records to predict no-show in Outpatient clinics. The goal is to seek a patient's behavioral patterns by considering the patient's history of appointments that predict no-shows' probability. The main research contributions of this paper are:

Demonstrating the ability to predict no-show using only a minimalist feature set;

Exploring the performance of training machine learning algorithm with different machine learning tools;

Exploring the power of using Big Data Machine Learning platforms to build a model from large data size.

The rest of this paper is organized as follows. Section II presents the related work, and Section III provides the methods. The results are shown in Section IV. The analysis and discussion are given in Section V. Conclusions, and future work are drawn in Section VI.



## II. RELATED WORK

### A. Discovering Factors Related to No-Show

There are existing research mainly focuses on discovering the factors that contribute to predicting the probability of no-show patients. Harvey et al. [15] applied statistics and logistic regression models to assess the effectiveness of using factors available in the Electronic Medical Record (EMR) such as Demographic, clinical, and health services utilization factors in predicting the absence of patients from scheduled radiology examinations. Factors that successfully predict radiology no-shows included days between scheduling and appointments, modality type (mammography, CT, PET, and MRI), and insurance type. The predictive ability was determined using the area under the receiver operator curve was 0.753.

Chua and Chow [16] applied Multiple Logistic Regression (MLR) on routinely collected administrative data to define factors associated with no-shows. Using parameter estimates from MLR, a risk-scoring model was developed to classify patients according to their risk of a no-show. The model's predictive ability was 72%, evaluated using the area under the curve (AUC). A study conducted by Dantas et al. [17] investigated each patient-related factor's influence on appointment no-show behavior in the bariatric surgery clinic. A data set of 13,230 records was used to run Logistic Regression to examine specific factors on no-show rates. As a result, predictive models were developed and perform effectively (Accuracy: 71%) with eight variables. They are later hours appointment, summer months or not, pre/post-surgery appointment, high/low lead time, higher/little no-show history, numbers of previous appointments, home distance (20 to 50 km) from the clinic, or another scheduled medical specialty than a bariatric surgeon. In contrast, gender, age, weekday, and payment were not significant factors to predict patients' no-show.

### B. Using Traditional Machine Learning Algorithms to Predict No-Show

Few research studies had focused on predicting no-show of patients using different machine learning techniques, mainly logistic regression. Kurasawa et al. [18] build a logistic regression model to predict missed appointments by diabetes patients. Data were classified into two groups: the first group for clinical condition and the other for previous findings. The best predictor model was achieved in an area under the curve (AUC) = 0.958 using both groups. Precision and recall were, respectively, 0.757 and 0.659. Among all data, the appointment's day was the strongest predictor of missing the appointments (weight = 2.22).

Mohammadi et al. [19] used statistical and machine learning models to predict the next medical appointment show's chance. They applied logistic regression, artificial neural network, and Naive Bayes classifier applied on 73,811 unique appointments to identify critical features. As for finding, predictors were created, in addition to the EHR variable, as significant predictors to consider no-show

appointments. The new predictors included lead-time, prior no-show, tobacco use, cell phone ownership, and the number of days since the last appointment. Naive Bayes models had a relatively high area under the curve among three models; the model achieved 0.86.

On the other hand, Nelson et al. [20] suggested complex, high-dimensional, and non-linear predictive models based on training and evaluating a set of 22,318 sequential scheduled magnetic resonance imaging appointments. They used logistic regression, support vector machines, random forests, and AdaBoost to predict two hospitals' attendance. The results showed that Gradient Boosting models achieved the best performance with an area under the receiver operating characteristic curve of 0.852 and an average precision of 0.511.

Lenzi et al. [21] developed and validated a no-show's predictive model based on empirical data. The models were developed using Naïve and logistic regression and the Akaike Information Criteria to select the highest performance model. Fifty percent of scheduled appointments collected from a public primary care setting were used to train the model, and fifty percent were used to validate the model. Experimental results showed that an AUC of 80.9% (95% CI 80.181.7) was achieved using the two most important predictors: previous attendance and same-day appointments. Lee et al. [22] collected two years of follow up data with 25% of a no-show rate. They deployed three machine learning algorithms, namely RandomForest, Logistic regression, and decision tree. They achieved the best performance using Random Forest with an accuracy of 72.9. However, the collected dataset was for a small group of 400 patients.

### C. Using Deep Learning Algorithms

On the other hand, deep learning methods have attracted many researchers and organizations in the health care field. Deep learning methods are useful with Problems, which are difficult to solve with traditional methods. They provide the optimal way to deal with high dimensional and volume data. Furthermore, present a whole picture embedded in large-scale data and disclose unknown structure. It has proven to be a superior prediction of no-show. Thus, effective optimizing of health resource usage. There is a minimal effort in using deep learning in the prediction of the patient's no-show. Only one study using deep learning had been found to predict no-show patients in outpatient clinics. Dashtban and Li [23] represented a novel prediction method for outpatients' non-attendance based on a wide range of health, environmental, and socioeconomic factors. The model was based on deep neural networks, which have integrated data reconstruction and prediction steps from in-hospital data. This integration was aiming to have higher performance than the separated classification model in predicting tasks. Comparing the proposed model with other machine learning classifiers showed that deep learning models outperform other practice methods. The model achieved (AUC (0.71), recall (0.78), accuracy (0.69). Finally, the constructed model was deployed and connected to a reminder system. To the best of our knowledge, all the previous studies were applied in small data sizes. One of this study's objectives is to

use a larger data size to predict the no-show at high accuracy. For a summary of the related work, see Table I.

TABLE I. THE SUMMARY OF RELATED WORK

| The Summary of Related Work |                                                                              |                      |                                                    |
|-----------------------------|------------------------------------------------------------------------------|----------------------|----------------------------------------------------|
| Authors                     | Algorithms                                                                   | Best Algorithm       | Result                                             |
| Kurasawa et al. (2016)      | Logistic Regression                                                          | Logistic Regression  | AUC = 0.958<br>Precision = 0.757<br>Recall = 0.659 |
| Mohammadi et al. (2018)     | logistic regression<br>artificial neural network<br>NaïveBayes               | NaïveBayes           | AUC = 0.86                                         |
| Nelson et al. (2019)        | logistic regression<br>support vector machines<br>random forests<br>AdaBoost | Gradient Boosting    | AUC = 0.852<br>Precision = 0.511                   |
| Lenzi et al. (2019)         | Naïve Bayes<br>Logistic Regression                                           | Naïve Bayes          | AUC = 80.9                                         |
| Lee et al. (2017)           | RandomForest<br>Logistic regression<br>decision tree                         | Random Forest        | accuracy = 72.9                                    |
| Dashtban and Li (2019)      | deep neural networks                                                         | deep neural networks | AUC = 0.71<br>Recall = 0.78<br>Accuracy = 0.69     |

### III. EVALUATION METHODOLOGY

This section details the research methodology describing the datasets, features, preprocessing, machine learning algorithms, and evaluation criteria.

#### A. Dataset Description

Three-year datasets (Jan 2016-July, 2019) were extracted from the Medical Record Number (MRN) system at all the facilities at the central region (Riyadh) at the Ministry of National Guard Health Affairs (MNGHA) to reflect on the outpatient visits. King Abdullah International Medical Research Center (KAIMRC) review boards approved the study, and a waiver of individual consent was authorized. MNGHA has many hospitals and primary health care clinics that provide quality services for MNGHA staff and their eligible dependents. The three regions are Central (Riyadh city), Eastern (Dammam and Al-Hasa cities), and Western (Jeddah and Al-Madaina cities) and many primary health care centers all over Saudi Arabia. Approximately 77000 scheduled appointments are booked monthly on the Riyadh hospital. The central region has an on average of 77k booked appointments every month, Fig. 1.

Most outpatients live in major cities of Saudi Arabia, but many outpatients travel from across the country to Riyadh. A text reminder is sent to all outpatient three days before the appointment. The dataset includes more than 33 million (33,050,363) outpatient appointments. Table II shows a statistic description of the MNGHA

dataset according to age groups, gender, appointment type, and nationalities used in this research.

More than 33 million patients' appointments were booked in outpatients' clinics of MNGHA between January 2016 and July 2019. Of these, label classes included (85%) and (15%) for no-show class and show class, respectively. A huge no-show for the follow-up appointments (98.96%) was noticed. The noticed no-show for follow-up appointments are mainly for two reasons: I) patient need to travel a long distance to come to the hospital, and II) most of the missed appointments were related to diabetic follow up, and there is no overbook for them.

The largest group of the patients' age were between 5 and 69 years old, and the no-show rate was higher for patients over 45 years old. Most of the no-show was among national citizens (85%). The show rate for the first appointment was 76%, and more than half the patient showed up for the first visit. Of the total, (26,625,488) of the appointments were follow-up with (98.96%) no-show rate. There was a high no-show among adult patients in terms of age group, and there were no significant differences in the no-show rate among gender. Fig. 2 shows the machine learning process of the no-show prediction model.

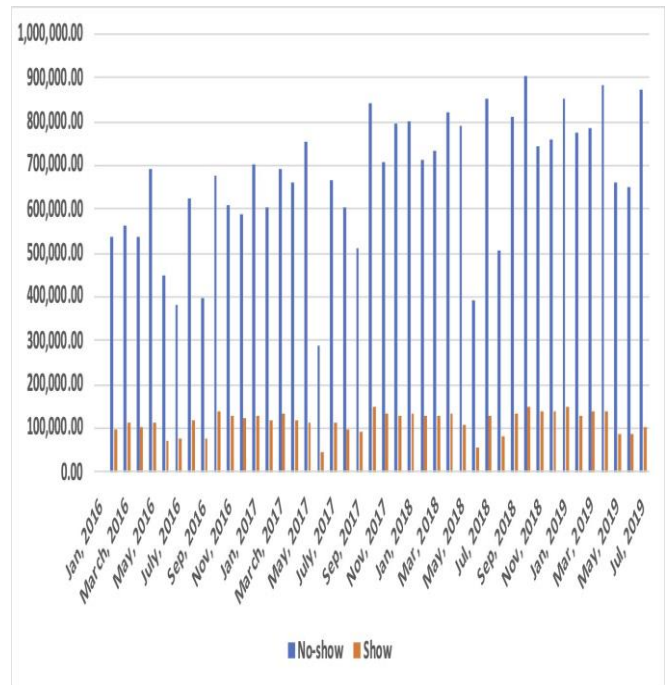


Fig. 1. Distribution of show and No-Show of Patients' Appointments from 2016 to 2019 in the Central Region.

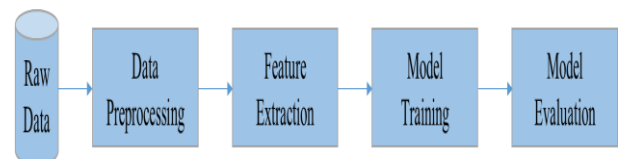


Fig. 2. Machine-Learning Process of the No-Show Prediction Model.

TABLE II. DESCRIPTIVE CHARACTERISTICS OF THE DATASET  
(N=33,050,363)

| Features                   | No-Show (N%)        | Show (N%)      | Total (N)  |
|----------------------------|---------------------|----------------|------------|
| <b>Age Group</b>           |                     |                |            |
| 1-4                        | 250,537 (65%)       | 134,715 (35%)  | 385,252    |
| 5-9                        | 728,676 (66.9%)     | 360,698        | 1,089,374  |
| 10-14                      | 1,004,354 (76%)     | (33.1%)        | 1,321,454  |
| 15-19                      | 804,462 (72%)       | 317,100 (30%)  | 1,114,550  |
| 20-24                      | 695,384 (68.6%)     | 310,088 (28%)  | 1,014,202  |
| 25-29                      | 729,945 (67.1%)     | 318,818        | 1,087,043  |
| 30-34                      | 920,858 (69.2%)     | (31.4%)        | 1,329,993  |
| 35-39                      | 1,114,211 (73%)     | 357,098        | 1,525,420  |
| 40-44                      | 1,274,528 (78.4%)   | (32.9%)        | 1,626,470  |
| 45-49                      | 1,886,169 (85.1%)   | 409,135        | 2,216,686  |
| 50-54                      | 2,626,922 (89.9%)   | (30.8%)        | 2,923,219  |
| 55-59                      | 3,373,995 (92.8%)   | 411,209 (27%)  | 3,637,547  |
| 60-64                      | 3,512,907 (94.1%)   | 351,942        | 3,732,703  |
| 65-69                      | 3,005,732 (94.9%)   | (21.6%)        | 3,168,725  |
| 70-74                      | 238,1034 (94.9%)    | 330,517        | 2,509,008  |
| 75-79                      | 1,820,760 (95.3%)   | (14.9%)        | 1,910,993  |
| 80-84                      | 912,299 (95%)       | 296,297        | 960,419    |
| ≥                          | 583,117 (94.7%)     | (10.1%)        | 615,913    |
|                            |                     | 263,552 (7.2%) |            |
|                            |                     | 219,796 (5.9%) |            |
|                            |                     | 162,993 (5.1%) |            |
|                            |                     | 127,974 (5.1%) |            |
|                            |                     | 90,233 (4.7%)  |            |
|                            |                     | 48,120 (5%)    |            |
|                            |                     | 32,796 (5.3%)  |            |
| <b>Gender</b>              |                     |                |            |
| Male                       | 15,989,649 (84.2%)  | 3,005,006      | 18,994,655 |
| Female                     | 12,189,970 (86.8%)  | (15.8%)        | 14,051,241 |
|                            |                     | 186,1271       |            |
|                            |                     | (13.2%)        |            |
| <b>Appointment type</b>    |                     |                |            |
| New Patient (NP)           | 936,387 (23.4%)     | 3,060,598      | 3,996,985  |
| First visit (FV)           | 899,145 (37%)       | (76.6%)        | 2,427,890  |
| Follow up (FU)             | 26,347,841 (98.96%) | 1,528,745      | 26,625,488 |
|                            |                     | (63%)          |            |
|                            |                     | 277,647        |            |
|                            |                     | (1.04%)        |            |
| <b>Nationalities</b>       |                     |                |            |
| Saudi                      | 27,891,825 (85%)    | 4,799,871      | 32,691,696 |
| Egypt Sudan                | 63,562(88%)         | (15%)          | 72,200     |
| Philippines Pakistan Syria | 43,753 (85%)        | 8,638 (12%)    | 51,627     |
| Other Countries            | 30,696 (65%)        | 7,874 (15%)    | 46,967     |
|                            | 20,261 (84%)        | 16,271 (35%)   | 24,087     |
|                            | 7,059(67%)          | 3,826 (16%)    | 10,592     |
|                            | 107,617 (82%)       | 3,533 (33%)    | 131,089    |
|                            |                     | 23,477 (18%)   |            |

### B. Data Preprocessing

Processing raw data needs computational powers. The data warehouse provided by the database management team was used to filter unnecessary data that is not needed in the prediction model. Data cleanings were applied to reduce noise. Categorical variables were converted into numbers, such as age and gender. For example, the age calculated based on the year and categorize by grouping every four years together.

Data cleanings methods were applied to reduce noise and remove outliers. Categorical data were transferred to numeric types such as sex and age. Data were normalized to make the data suitable for building machine learning models [24] [25].

### C. Feature Extraction

New features were derived from the data. For instance, the lead-time feature was calculated, representing a

difference in days between the appointments' booking and the day of the appointments. Also, calculate the percentage of show and no-show on all the previous visits. The past behavior of patients could be a potential feature for predicting future patient's behavior. From the "Medical Treatment Reservation Type Code" feature, two categorical predictors were added to calculate the count number of walk-in and scheduled appointments. In addition to calculating the count of on foot and emergency appointments. For the "Cancellation Flag" predictor, where the patient cancelled the appointment, new predictors were added to calculate the count of Cancellation Flag Yes and No. In addition to the extracted data from the electronic medical records, the features derived were candidates for the predictive model.

The list of generated features is shown in Table III. A total of (29) categorical or numerical data elements considered: (9) original data elements and (20) derived data elements. The dataset contained three categories: demographic attributes, clinical attributes, and appointment characteristics considered relevant to patient appointment history. The dataset contained imbalanced classes with 83.89% of the records for no-show class and 16.12% of the show class records. Finally, data transformation applied where all nominal values were converted to binary attributes.

### D. Machine Learning Algorithms

Three machine learning algorithms were applied in this work: Deep Neural Network, AdaBoost, and Naive Bayes. Multilayer Perceptron (MLP) algorithm is a type of machine learning algorithm developed by researchers to simulate how humans function and learn. Backpropagation was added to MLP as an improvement [26]. The MLP becomes one of the golden standard algorithms in the machine learning domain because it can learn despite the lack of prior information. Deep Neural Network (DNN) Learning algorithm is an extension of the MLP algorithm with many hidden layers [27] [28]. DNN applies various activation functions, such as Rectified Linear Unit (ReLU). DNN used gradient descent optimizers and various activation functions, such as Rectified Linear Unit (ReLU). These optimizers' main task is to find the local minimum solution with the assistant of hyperparameters like the learning rate. To model the deep neural network model, the values of the hyperparameters, such as the number of hidden layers, neurons, and type of activation function, need to be chosen wisely. The hyperparameter's values have a huge effect on the training time and the model's learning capability. Having large values is going to increase the training time, while having small values will minimize the learning abilities of the model. The model was trained by choosing smaller hyperparameters and increasing the hyperparameters' values/dimensionalities depending on the model's accuracy. The final DNN model builds by using Tensorflow [14] implementing DNN. The DNN model consists of four layers: input layers (28 nodes), two hidden layers (14 nodes and 7 nodes), and one output layer with ReLU as activation function, Fig. 3.

TABLE III. DATA CATEGORIES AND PREPROCOESSING FOR PATIENT HISTORICAL DATA

| Data Features and Description                                                    |                                                                                                                                                                                                                                  |
|----------------------------------------------------------------------------------|----------------------------------------------------------------------------------------------------------------------------------------------------------------------------------------------------------------------------------|
| Feature                                                                          | Description                                                                                                                                                                                                                      |
| 1) Gender                                                                        | Male, Female and Unknown                                                                                                                                                                                                         |
| 2) Age Category                                                                  | 18 age categories                                                                                                                                                                                                                |
| 3) Nationality                                                                   | The nationality of the patient                                                                                                                                                                                                   |
| 4) Address code                                                                  | The primary health care clinic location (used for the patient address)                                                                                                                                                           |
| 5)Medical Treatment Service Code                                                 | The code of the medical service                                                                                                                                                                                                  |
| 6)Appointment type code<br>New Patient(NP)<br>First visit (FV)<br>Follow up (FU) | Type of Appointment<br>New Patient<br>First visit<br>Follow up visit                                                                                                                                                             |
| 7) Patient Services<br>Department Type Cod<br>First visit (FV) Follow up (FU)    | Type of patient insurance<br>First visit<br>Follow up visit                                                                                                                                                                      |
| 8) Hospital code                                                                 | The code of referral hospital /clinic                                                                                                                                                                                            |
| 9)Medical Department code                                                        | The code of medical/clinic                                                                                                                                                                                                       |
| 10) Visit Number Count                                                           | Derived: count how many Visit Number                                                                                                                                                                                             |
| 11) Percentage of Show visits                                                    | Derived: Calculate the percentage of a show on all the previous visits                                                                                                                                                           |
| 12) Percentage of No-Show visits                                                 | Derived: Calculate the percentage of no show on all the previous visits                                                                                                                                                          |
| 13) Lead Time                                                                    | Derived: the time difference in days between the booking of the appointments and the day of the appointments                                                                                                                     |
| Cancellation Flag<br>14) Yes= appointment cancelled<br>15) No = not cancelled    | Derived: count how many Check-in Cancellation was Yes as total<br>Derived: count how many Check-in Cancellation was No as total                                                                                                  |
| Medical Treatment Reservation Type Code<br>16) 1= Schedule<br>17) 2= Walk-in     | Derived: count how many Scheduled reservation as total<br>Derived: count how many Walk-in reservations as total                                                                                                                  |
| Medical Treatment<br>18) Yes= patient treated<br>19)N= not treated               | Derived: count how many patients treated as total<br>Derived: count how many patients not treated as total                                                                                                                       |
| On Foot visit<br>20) 1= Yes<br>21)0 = No                                         | Derived: count how many On Foot visit was Yes as total<br>Derived: count how many On Foot visit was No as total                                                                                                                  |
| Emergency visit<br>22) 1= Yes<br>23)0 = No                                       | Derived: count how many Emergency visits was Yes as total<br>Derived: count how many Emergency visits was No as total                                                                                                            |
| 24)Count of Medical Reservation Date & Time                                      | Derived: count how much medical reservation date and time as total                                                                                                                                                               |
| 25) Count of Medical Arrival Date & Time                                         | Derived: count how many medical arrival dates and time as total                                                                                                                                                                  |
| Medical Treatment Room Arrival Date & Time<br>26) Show<br>27) No-Show            | Derived: count how much medical treatment room arrival date and time as total<br>Derived: count how many times the patient came for his/her appointment<br>Derived: count how many patients did not show for his/her appointment |
| Patient arrival confirmation<br>28) 1= Yes<br>29)0 = No                          | Derived: count how many patient arrival confirmations was Yes as total<br>Derived: count how many patient arrival confirmations was No as total                                                                                  |
| Class No-Show                                                                    | class show=0 or No-show=1                                                                                                                                                                                                        |

AdaBoost is a meta-learning algorithm that is used to reduce the error of weak learning algorithms significantly. Boosting works by repeatedly running input a training set in series rounds and then combing the classifiers into a single ensemble model. The model's prediction is taken as a sum of the weighted predictions [25]. On the other hand, Naive Bayes (NB) classifiers are derived from the Bayes' theorem, which assumes each attribute is independent. Each attribute has the probability to determine the classification outcomes independently [29].

E. Evaluation Criteria

The dataset was divided into two sets: the training set was used to develop the model while the testing set was used for validation. The training set included 23,135,254 records (70%) outpatient records, while the remaining 30% is used for testing the trained models. The evaluation metrics used to choose the best model are Precision and Recall that are defined as follows:

- Precision: shows how many of the predictions were correctly identified. Eq. 1 shows the calculation of it.
- Recall: presents how many of the correct outcomes were identified. Eq. 2 shows the calculation of it.

Precision = (TruePositive)/ (TruePositive + FalsePositive) (1)

Recall = (TruePositive)/ (TruePositive + FalseNegative) (2)

The precision and recall were used since they are influenced by the false positive and false negative. The administration is trying to minimize the costs of a no-show by reducing the false positive while physicians were interested in minimizing the overbooking by reducing the false negative. However, the trained model might be sufficient by deficit prediction using recall and precision [30].

IV. EXPERIMENTAL SETUP AND RESULTS

To show the DNN model's performance using real data, the DNN is compared with AdaBoost and NB. Weka version 3.8 is used to run AdaBoost and NB. Weka is a data mining tool developed by the University of Waikato, Hamilton, New Zealand, in 1992 [31]. On the other hand, TensorFlow [14] developed by Google is applied to build the DNN model. All the models were trained on a standalone server running Linux Centos version 6.9 with 12 CPU cores and 48GB of RAM.

Table IV shows the performance of the machine learning models per class on an unseen testing dataset. The best performing model was the Deep Neural Network (DNN). It achieved better precision and recall per class compared to AdaBoost and NB. The AdaBoost model was the second-best model, while NB was the lowest one.

Table V shows the weighted average performance of the machine learning models. DNN was the best model too. It achieved a precision and recall of 98.2% and 94.3%, respectively. The result showed that DNN performed excellently in the prediction of no-show and show based on evaluation criteria. Overall, the best machine learning models were chosen based on the highest performance using the evaluation metrics discussed.

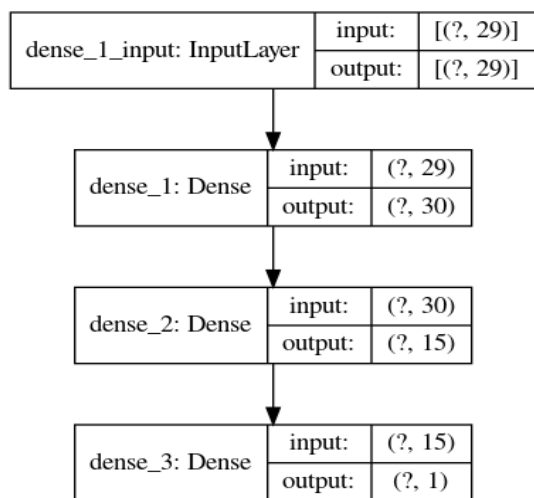


Fig. 3. The Deep Neural Network (DNN) Model Graphed by Tensorflow.

TABLE IV. THE PERFORMANCE PER CLASS FOR THE MACHINE LEARNING MODELS ON THE TEST DATASET

|                  | DNN    |        | AdaBoost |       | NB    |       |
|------------------|--------|--------|----------|-------|-------|-------|
|                  | S      | NS     | S        | NS    | S     | NS    |
| <b>Precision</b> | 0.7533 | 0.9815 | 0.732    | 0.977 | 0.416 | 0.987 |
| <b>Recall</b>    | 0.9068 | 0.9433 | 0.886    | 0.938 | 0.947 | 0.747 |

S=Show, NS= No-show

TABLE V. THE WEIGHTED AVERAGE PERFORMANCE OF THE MACHINE LEARNING MODELS ON THE TEST DATASET

|                  | DNN   | AdaBoost | NB    |
|------------------|-------|----------|-------|
| <b>Precision</b> | 0.982 | 0.938    | 0.895 |
| <b>Recall</b>    | 0.943 | 0.930    | 0.779 |

### V. DISCUSSION

The accurate prediction of a patient's show is one of the most interesting and challenging healthcare providers' tasks. With the advent of new technologies in health learning, large amounts of outpatients' data have been collected and available to the health research community. Accordingly, machine-learning methods have become a popular tool for health researchers. These techniques can discover and recognize patterns and relationships using big datasets while they can effectively predict future outcomes.

In this proof-of-concept study, a vast amount of data were collected from electronic health records. With the potential to improve healthcare quality while reducing the waiting list time, these massive amounts of data, so-called 'big data' support a variety of healthcare functions, including outcome prediction, decision support, and health management. Random forests have been applied successfully using high-dimensional data (33,050,363) visits to investigate machine learning performance for the early predicting no-show in the outpatient clinic and discover potential predictors of no show.

This is the first study that identified big data-derived to the best of our knowledge and included complex relations

between predictors using advanced machine learning. Three key differences in the current study compared to the other studies that need to be recognized. Our work for the prediction of a no-show demonstrates several feasible advantages for outpatient clinics and provides valid prognostic information from simple features. The result was superior to traditional models (e.g., AdaBoost and NB) in predicting patients with no-show that were adopted in previous studies. The approach here classifies the clinical features and extracts rules for identifying patients at high risk of no-show for individual records. The question is how to intervene when a patient is predicted as a no-show. The management could utilize different methods, such as SMS or phone call, to remind high-risk patients of no-show about their appointment, especially in the case of a long time since the last appointment.

Thus, appointments will be managed effectively, and the negative impact they have on the operational efficiency of systems in healthcare organizations will be decreased. A patient can benefit from additional engagement through SMS reminders or investigate associated factors to avoid no-show to avoid no-shows. According to Stubbs et al. [32], SMS is the most effective way to remind patients and decrease the no-show rate. Lastly, our framework is generic and can be adopted by other outpatient clinics characterized by rates of no-shows and appointment-based patient history. Our study has two limitations. First, given that the study was limited to the central region facilities, generalizing the results across other regions is unclear. Second, our study did not account for many of the personal or environmental factors that were not available in the EMR, such as transportation and weather.

The developed model will be adopted in practice leading by the Information System and Informatics Division (ISID) under the umbrella of the MNGHA. With the model's ability to provide no-show prediction back in a meaningful way, the expectation is that the deployment will reflect the test data's results. The research team's intent and the ISID to deploy this model in the central region into production as a pilot phase, then a full roll-out to the entire organization in all regions, would follow. In addition to providing the classifications, the research team will design studies to determine the current model's effectiveness and several interventions to reduce no-shows. Additionally, the model can be improved by adding more features, e.g., medication refills, lab appointments, or special clinic orders. Besides, the model will be retrained every 6-12 months in order to maintain the model accuracy.

The deep learning model showed a high performance in predicting no-show. However, deep learning has some disadvantages, such it will not be able to provide specific recommendations to manage the risk factors that influence no-show. The DNN cannot rank the importance of the features due to the neural network's hidden layers. Furthermore, the research study has other limitations. The knowledge extracted by the machine learning algorithms were based on medical record databases. Other data based on weather conditions, cultural factors, patient education, etc. might improve model accuracy and explain the no-show rate.

## VI. CONCLUSION

This work shows how machine learning can be effectively adopted in the health field to derive models that use patient data to predict an outcome of interest. Machine learning may be applied to the construction of models to predict patients at high risk of no-show for appointments using a data-driven approach, which – once evaluated and tested – may be embedded within health care systems. DNN, AdaBoost, and NB algorithms used to utilize EMR data in predicting no-show. The results show that the built model is effective and provides insightful implications for decision-making by management. The best predictive model was DNN with Precision and Recall of 0.982 and 0.943, respectively. More improvement can be achieved by adding more features, e.g., medication refills, lab appointments, or special clinic orders.

## VII. FUTURE WORK

Future research should evaluate the ability of such approaches to predict no-show patients and missed by traditional algorithms then translate into better-quality clinic outcomes. Furthermore, a multistage machine learning platform is considered a future improvement where the follow-up appointments have its prediction model.

## VIII. CONFLICT OF INTEREST

None of the authors has any competing interests.

## IX. HUMAN SUBJECTS PROTECTIONS

No human subjects were involved in the project.

### REFERENCES

- [1] Chariatte V, Berchtold A, Akre C, Pierre-André M (2008) Missed Appointments in an Outpatient Clinic for Adolescents, an Approach to Predict the Risk of Missing. *J Adolesc Heal* 43:38–45.
- [2] Carlsen KH, Carlsen KM, Serup J (2016) Non-attendance, predictors and interventions. *Adherence in Dermatology* 29–35.
- [3] Davies M, Goffman R, May J, Monte R, Rodriguez K, Tjader Y, Vargas D (2016) Large-Scale No-Show Patterns and Distributions for Clinic Operational Research. *Healthcare* 4:15.
- [4] O. AlRowaili M, Ahmed AE, Areabi HA (2016) Factors associated with No-Shows and rescheduling MRI appointments. *BMC Health Serv Res* 16:1–7.
- [5] Almomani I, AlSarheed A (2016) Enhancing outpatient clinics management software by reducing patients waiting time. *Journal of Infection and Public Health. J Infect Public Health* 9:734–743.
- [6] Samorani M, Laganga LR (2015) Outpatient appointment scheduling given individual day-dependent no-show predictions. *Eur J Oper Res* 240:245–257.
- [7] Srinivas S, Ravindran AR (2018) Optimizing outpatient appointment system using machine learning algorithms and scheduling rules: A prescriptive analytics framework. *Expert Syst Appl* 102:245–261.
- [8] Reinsel D, Gantz J, Rydning J (2017) *Data Age 2025 : Don't Focus on Big Data; Focus on the Data That's Big*. IDC White Pap 1–25.
- [9] El Fouki M, Aknin N, El Kadiri KE (2017) Intelligent adapted e-learning system based on deep reinforcement learning. *ACM Int Conf Proceeding Ser* 2–5.
- [10] Zuech R, Khoshgoftaar TM, Wald R (2015) Intrusion detection and Big Heterogeneous Data: a Survey. *J Big Data*. doi: 10.1186/s40537-015-0013-4.
- [11] Hossain M, Rahman SN, Bhattacharya P, Jacks G, Saha R, Rahman M (2015) Sustainability of arsenic mitigation interventions-an evaluation of different alternative safe drinking water options provided in Matlab, an arsenic hot spot in Bangladesh. *Front Environ Sci*. doi: 10.3389/fenvs.2015.00030.
- [12] Lipton ZC, Kale DC, Elkan C, Wetzel R (2016) Learning to diagnose with LSTM recurrent neural networks. 4th Int Conf Learn Represent ICLR 2016 - Conf Track Proc 1–18.
- [13] Esteva A, Kuprel B, Novoa RA, Ko J, Swetter SM, Blau HM, Thrun S (2017) Dermatologist-level classification of skin cancer with deep neural networks. *Nature* 542:115–118.
- [14] Abadi M, Barham P, Chen J, et al (2016) TensorFlow : A System for Large-Scale Machine Learning This paper is included in the Proceedings of the TensorFlow : A system for large-scale machine learning. 12th USENIX Symp Oper Syst Des Implement (OSDI '16) 265–283.
- [15] Harvey HB, Liu C, Ai J, Jaworsky C, Guerrier CE, Flores E, Pianykh O (2017) Predicting No-Shows in Radiology Using Regression Modeling of Data Available in the Electronic Medical Record. *J Am Coll Radiol* 14:1303–1309.
- [16] Chua SL, Chow WL (2019) Development of predictive scoring model for risk stratification of no-show at a public hospital specialist outpatient clinic. *Proc Singapore Healthc* 28:96–104.
- [17] Dantas LF, Hamacher S, Cyrino Oliveira FL, Barbosa SDJ, Viegas F (2019) Predicting Patient No-show Behavior: a Study in a Bariatric Clinic. *Obes Surg* 29:40–47.
- [18] Kurasawa H, Hayashi K, Fujino A, Takasugi K, Haga T, Waki K, Noguchi T, Ohe K (2016) Machine-Learning-Based Prediction of a Missed Scheduled Clinical Appointment by Patients with Diabetes. *J Diabetes Sci Technol* 10:730–736.
- [19] Mohammadi I, Wu H, Turkcan A, Toscos T, Doebbeling BN (2018) Data Analytics and Modeling for Appointment No-show in Community Health Centers. *J Prim Care Community Heal* 9:1–11.
- [20] Nelson A, Herron D, Rees G, Nachev P (2019) Predicting scheduled hospital attendance with artificial intelligence. *npj Digit Med* 2:1–7.
- [21] Lenzi H, Ben ÂJ, Stein AT (2019) Development and validation of a patient no-show predictive model at a primary care setting in Southern Brazil. *PLoS One* 14:1–14.
- [22] Lee G, Wang S, Dipuro F, Hou J, Grover P, Low LL, Liu N, Loke CY (2017) Leveraging on predictive analytics to manage clinic No-Show and improve accessibility of care. In: *Proc. - 2017 Int. Conf. Data Sci. Adv. Anal. DSAA 2017*. pp 429–438.
- [23] Dashtban M, Li W (2019) Deep Learning for Predicting Non-attendance in Hospital Outpatient Appointments. In: *Proc. 52nd Hawaii Int. Conf. Syst. Sci*. pp 3731–3740.
- [24] Biau G, Scornet E (2016) A random forest guided tour. *Test* 25:197–227.
- [25] Freund Y, Schapire RE (1996) Experiments with a New Boosting Algorithm. In: *Proc. 13th Int. Conf. Mach. Learn*. pp 148–156.
- [26] Rumelhart DE, Hinton GE, Williams RJ (1986) Learning representations by back-propagating errors. *Nature* 323:533–536.
- [27] Bengio Y (2009) Learning deep architectures for AI. doi: 10.1561/2200000006.
- [28] Bengio Y, Courville A, Vincent P (2013) Representation learning: A review and new perspectives. *IEEE Trans Pattern Anal Mach Intell* 35:1798–1828.
- [29] Bricher D, Müller A (2020) A supervised machine learning approach for intelligent process automation in container logistics. *J Comput Inf Sci Eng* 20:1–9.
- [30] Ghosh S, Rana A, Kansal V (2020) A benchmarking framework using non-linear manifold detection techniques for software defect prediction. *Int J Comput Sci Eng* 21:593–614.
- [31] Hall M, Frank E, Holmes G, Pfahringer B, Reutemann P, Witten IH (2009) The WEKA data mining software. *ACM SIGKDD Explor Newsl* 11:10–18.
- [32] Stubbs ND, Geraci SA, Stephenson PL, Jones DB, Sanders S (2012) Methods to reduce outpatient non-attendance. *Am J Med Sci* 344:211–219.

# Virtual Simulation for Entertainment using Genetic Information

Jin Woo Kim<sup>1</sup>, Hun Lim<sup>2</sup>, Taeho You<sup>3</sup>, Mee Young Sung<sup>4\*</sup>

Department of Computer Science, Kent State University, Ohio, USA<sup>1</sup>

Department of Computer Science and Engineering, Incheon National University, South Korea<sup>2,3,4</sup>

**Abstract**—The genetic information has been researched to predict the disease and to discover the clue of biological causes, especially in the medical field. However, based on the reliability of genetic information, it also gives a powerful realistic experience with VR devices. In this paper, we developed a dating simulation game that users can meet celebrities. The human personality of the celebrity, the favorability feedback depends on each choice of the conversation and a proper choice creation is based on the genetic information of the user and a celebrity. Besides, a method for utilizing genetic DNA information for virtual simulations is proposed. In this study, we have established that DNA information is related to human relationships both in the real and virtual worlds. Also, we concluded that the DNA information contributes to the development of interpersonal and mental health. However, a person's personality or preference for a specific situation or object, etc. are not determined only through genes. Therefore, more quantitative and multifaceted studies will need to be conducted on the effect of genes on personal preferences. We only experimented with virtual characters in virtual reality. It would be meaningful to proceed with the human experiment not only with a virtual character in the virtual environment, but also another human in the virtual environment. Eventually, the result of the experiment between virtual characters and humans should be compared.

**Keywords**—Virtual simulation; entertainment; genetic information; DeoxyriboNucleic Acid (DNA) matching; celebrity; favorability

## I. INTRODUCTION

The research goal of this study is to validate how the similarity between the genetic information of a celebrity and that of a user influences the user's preference in virtual simulations for entertainment. To achieve this objective, we developed a dating simulation with celebrities utilizing DeoxyriboNucleic Acid (DNA) data. It also proposes a method to measure the similarity between the celebrity and the user's genetic DNA information so that the user experiences a strong intimacy with the celebrity.

By analyzing the DNA information, the constitution and personality of a celebrity can be grasped [1]. The genetic characteristics of a celebrity chosen by a user can allow the user to feel close to the celebrity and feel lively in Virtual Reality (VR) simulations.

Genetic information analysis companies, such as 23andMe [2], Illumina [3], etc. try to collect genetic information and have focused on medical research and applications. To increase

the speed of collecting genetic information, researches on entertainment using genetic information are needed to be accelerated.

It is also necessary to build a database by understanding the meaning of domestic genetic information and organizing the data to be extracted. Besides, the interaction between genetic data and new functionalities that may arise due to it should be studied. It also demands the analysis of the applications and related technologies concerning VR. To maximize the visual effects of VR, researches on 360-degree image rendering and shooting techniques are also needed.

Besides, researches on how to form an intimacy with celebrities are required. We research the psychological effects of users who are not intimate with celebrities through the relationship between the visual effects of VR and genetic information.

The rest of this paper proceeds with a presentation of the background including genetic information analysis and artificial reality/virtual reality/mixed reality (AR/VR/MR) simulations. Then, our system model's conceptual structure and DNA matching methods are described. Next, the details of the implementation of our prototype for experiments and the methods of experiments are explained. Lastly, our conclusion and future work are followed.

## II. BACKGROUND

### A. Genetic Information Analysis

Humans have 23 pairs of chromosomes including 22 pairs of autosomes and 1 pair of sex chromosomes. The 23andMe, an American personal genetic information analysis company, provides various benefits with consumer's genetic information by using a Direct-to-Consumer (DTC) method that sells directly to consumers without going through a doctor. With this genetic information, more than 250 types of analysis, including risk analysis for various diseases, sensitivity to drugs, genetic characteristics, and ancestor analysis, are becoming a boom by improving the quality of life of users [4]. Such attempts have also begun in Korea. Ewon Diagnostics Genome Center (EDGC) [5], a genome-specialized analysis company, started the DTC genetic test service under the official brand name Gene2Me [6] for the first time.

However, Korean genetic testing regulations are much stricter than in the US, so there is a limit to the market formation. This is because commercial genetic testing is considered ethical. As a result, it is not getting more users.

\*Corresponding Author

This work was supported by Incheon National University Research Grant in 2017 (No. 2017-0320).

Nevertheless, since June 2016, regulations have been easing, and as the number of users of genetic information increases, the importance of genetic information will emerge and the easing will accelerate.

It is difficult to attract the attention of young adolescents that the main service using this data is medical. This is because the health issues do not immediately urgent and their interests are relatively low. Conversely, for the youth who enjoy numerous cultural activities, there is merit in the entertainment field. Gene2Me focuses on these popular cultural functions, however, it is still insufficient for entertainment. The more pioneering this field, the more we will use genetic information to make a ripple effect to our users.

The mediators that connect genes and entertainment are diverse. Representatively, there are games, movies, music, and simulations. In particular, VR is a field with potential, interest, and various challenges. VR amplifies the sense of reality and has the advantage that it can be used by fusion with various devices and technologies, so it is suitable for the entertainment field [7].

Celebrity is the most influential factor that can have a ripple effect. An American actress underwent a mastectomy after genetic testing revealed she had an 87% chance of getting breast cancer. As this incident became a big issue, 23andMe received the public's attention. Celebrities have recently become more influential due to increased accessibility through SNS. The Ice Bucket Challenge started with the purpose of indirectly experiencing the pain of amyotrophic lateral sclerosis (ALS), also known as Lou Gehrig's disease patients suffering from muscle contraction by flipping ice water. The propagation power of this movement was minimal at first, but when celebrities announced their participation in the movement on social media, it spread exponentially around the world [8]. If entertainment using VR is connected with celebrities, the purpose of this study would be maximized.

The main study is a simulation that combines these factors generated by the genetic information of the celebrity and the users to feel the realistic familiarity with the celebrity. The user can recognize the gap between personalities, what kind of effort is needed to get close to the celebrity, and the real interest of the celebrity through the genetic information of the celebrity.

Besides, by maximizing the intimacy with celebrities with VR, it can induce curiosity and interest in youths who are interested in celebrities, and the fact that celebrities have received genetic information service can have ripple effects. Also, it can be extended to express relationships with interested users through genetic information between users as well as celebrities. A system that checks intimacy by comparing his or her data with a person who has genetic data through AR or MR could also be configured.

### B. AR/VR/MR Simulations

VR has been a hot topic for a few years and the VR industry is developing rapidly. New terms and abbreviations can feel difficult in these situations.

In virtual reality, the user's view is completely blocked and only the virtual world is visible. The "virtual reality" includes the word "reality", but is called "virtual reality" to indicate the meaning of "another reality" that is completely separate from the "reality" we live in. In other words, "reality" and "virtual reality" can be said to be opposite concepts.

In the term "augmented reality", "reality" means the real world we live in. Thus, "augmented reality" means augmenting the real world. It is to use a glass headset that can be seen outside or to project a reality with a mobile phone camera and display additional information on it. Among vehicle navigation, some products display the direction of the vehicle or surrounding buildings on the image received from the camera during operation, which is a representative example of augmented reality.

MR stands for "mixed reality" and "reality" means both real and virtual reality. The mixture of these two realities is called mixed reality. While the concept of AR is to show additional information, in reality, MR can be said to place a virtual object in real space or to recognize a real object and construct a virtual space around it. An example of MR is an application that allows real cars, which are real objects, to be virtually changed.

Fig. 1 depicts the reality-virtuality continuum.

Popular AR/VR/MR devices are illustrated in Fig. 2.

HTC VIVE™ is a device for virtual reality games created jointly by SteamVR™ Tracking [10], [11] and head mounted display (HMD) with a 2\*1080\*1200 90Hz display. It uses a laser sensor, not a general HMD with a conventional gyro sensor or an infrared camera, and boasts higher freedom and faster tracking speed than the existing HMD. The laser sensor tracks the controller and the HMD in real-time and projects a 360-degree image to the user's eyes. HMD is a device that makes 3D images using binocular parallax. This provides a wide viewing angle, so you can see the virtual reality display even if you move your eyes.

SteamVR™ Tracking library provides libraries for user experience/user interface (UX/UI) using HTC VIVE™. Through this, it contains the basic information and technology necessary for VR development, such as performing various actions using the camera viewpoint or controller of the protagonist, which should be displayed in VR, which greatly helps to develop with VIVE equipment.

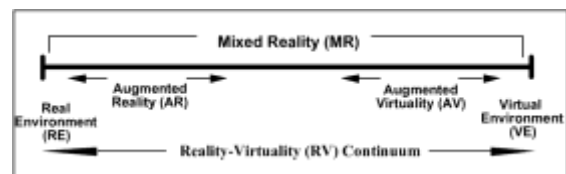


Fig. 1. Reality-virtuality continuum [9]



Fig. 2. AR/VR/MR Devices (from Left to Right and Top to Bottom: Google Glasses, Oculus Rift VR Headset, VIVE VR Headset, Microsoft Holo Lens).



In the case of VR types of equipment, it is easy to overload because it tracks in real-time and runs software. In particular, since the image is made up of 360 degrees, appropriate graphic efficiency is required.

It is a VR Anti-aliasing that helps in this part. Existing anti-aliasing uses a method of reducing frames of distant elements, but VR is applying this method by changing it for VR.

### III. SYSTEM MODEL

#### A. Conceptual Structure of the Simulation System

For those who want to get acquainted with celebrities and know more, we use HTC VIVE™ to create simulations with celebrities. This simulation makes it possible to interact with users based on facts through genetic information of real celebrities rather than virtual celebrities. Through this genetic information, the relationship between the user and the celebrity can be expressed and the constitution and personality can be understood. The basic interaction structure of our simulation system is described in Fig. 3.

After developing the simulation in both AR/VR/MR environments, not only the user dating celebrities but also meeting other users to communicate by interacting between AR/VR/MR environments. It is an extension of the original simulation to influence the genetic information between users.

- 1) Realization of three-dimensionalization with celebrities in virtual through VR.
- 2) Realization of visualization through the 3D engine.
- 3) Linkage of genetic information to 3D engine and visualization of data.

Table I summarizes the scopes and their methods to achieve the above three topics of this study.

#### B. DNA Matching

Thanks to much researches undergone on DNA sequences pattern matching have been actively undergone [12], [13], it is revealed that particular genes are related to a feature of human personality. C15orf17, message passing interface (MPI), secretory carrier membrane protein 2 (SCAMP2), protein kinase (ULK3), Cytochrome c oxidase subunit 5a (COX5A) are associated with neuroticism [14], Fyn interacts with N-methyl-D-aspartate (NDMA) receptors and inositol-1,4,5-trisphosphate (IP3)-gated channels to regulate calcium influx and intracellular release in the post-synaptic density. It causes an angry temperament [15]. Similarly, a single nucleotide polymorphism, rs322931, is significantly associated with a positive effect [16]. Based on genes that affect human personality, match the conversation choice with the user's genetic information, and match the favorability points of each conversation choice with the celebrity's genetic information.

To match the DNA comparison between the user and the virtual character, a compression algorithm [17] is used. The first step of the compression is encoding edit operation which is replaced, insert and delete. Lempel and Ziv [18], [19] proposed two algorithms to compress data sequences. These algorithms are based on a dictionary that relies on exact repeat. Similarly, a one-pass algorithm based on approximate matching called "Genome Compression" is implemented. The

compression gain function based on the optimal prefix is used to evaluate if a particular approximate repeat provides a profit in the encoding.

$$G(s, t, \lambda) = \max\{2|s| - |(|s|, i)| - w_\lambda * |\lambda(s, t)| - c, 0\}$$

In the formula above, s is a prefix of u, t is a substring appear at position i in v,  $2|s|$  is the number of bits we use: 2bits per base  $|(|s|, i)|$  is the encoding size of  $(|s|, i)$ ,  $|\lambda(s, t)|$  is the number of edit operations in  $\lambda(s, t)$  and c is the overhead proportional to the size of control bits. The optimal prefix is a prefix s of u when  $G(s, t, \lambda)$  is maximized over all  $\lambda$  and t while the input is  $w = vu$ . After the parsing and encoding procedure, the optimal prefix search is implemented. The compression is used to find the relatedness between two DNA sequences [17].

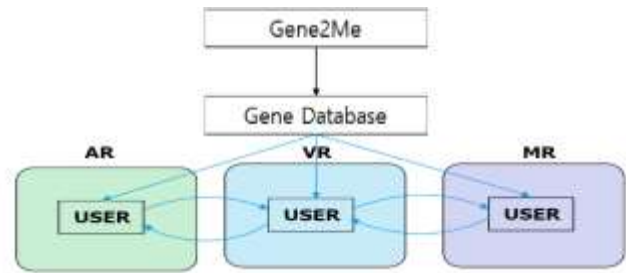


Fig. 3. Interactions between Simulation Environments of the Simulation.

TABLE I. RESEARCH SCOPES AND METHODS

| Scope                                                                                  | Method                                                                                                                                                                                                                                                                                                                                                                                                                                                                                                           |
|----------------------------------------------------------------------------------------|------------------------------------------------------------------------------------------------------------------------------------------------------------------------------------------------------------------------------------------------------------------------------------------------------------------------------------------------------------------------------------------------------------------------------------------------------------------------------------------------------------------|
| Research on 12 genes provided by Gene2me                                               | Collect and analyze research data of EDGC along with existing genetic data. In addition, the upper limit of the research range should be found by comparing it with the limited genes.                                                                                                                                                                                                                                                                                                                           |
| Psychological interaction study according to personality difference between one-to-one | Study how the other person feels generally according to the psychology of each individual, which can be known by genetic information. Through this, we create a manual that can organize the relationship by setting the standard of interaction.                                                                                                                                                                                                                                                                |
| Research on genetic information databaseization                                        | Organize and use various secondary information known as genetic information into data. Besides, the database is made in consideration of the case of interaction between secondary information.                                                                                                                                                                                                                                                                                                                  |
| Research on AR, VR, and 360-degree rendering of 3D images                              | Study the function of reading the genetic information of users through AR, confirming their genetic relationship, and viewing individual genetic information. Also, study how to express the relationship with celebrities through the AR effect in VR. We study what effect can be achieved by linking a 360-degree camera and VR. The reason for using VR in this study is to maximize the sense of reality and experience. This is not simply seen as an image, but visually makes you feel the most vibrant. |
| Maximizing intimacy with celebrities                                                   | Research how users feel intimacy through the relationship of genetic information and visual experiences, despite users do not have acquaintances with celebrities. Besides, maximize intimacy are studied by analyzing the field of celebrity marketing.                                                                                                                                                                                                                                                         |

IV. EXPERIMENTS

Most of the existing studies using genetic information are for medical purposes. The value of genetic information not only for medical purposes but also for entertainment is created through VR. The data of genetic information are specified in detail in a web genetic information database called gene cards. Among the genetic information listed in this GeneCards, the database was reconstructed with the focus on genetic information related to constitution and personality.

When reorganizing the gene database such as Fig. 4, the user, geneInfo, and relation tables were created using MySQL. The user saved the user's genetic information, the geneInfo saved the information of each gene, and the relation saved the correlation of each gene relationship. In this way, the data of gene cards was rearranged and used, and the data was visualized through the GUI of PHPMyAdmin.

It is linked with Unity through SteamVR so that you can see celebrities in a virtual space through HMD VIVE. The viewing angle of the existing VR is about 120 degrees, which is slightly wider than the viewing angle that humans can see, but it has been adjusted to 110 degrees to prevent dizziness. Using 3DMax, a frame was created to visualize and display the data values, and videos taken with a 360-degree camera [21] can be viewed in VR using Unity. Fig. 5 demonstrates a screenshot of our implementation of 360-degree linkage streaming.

When you run the program, a window to select your information appears. Jinwoo Kim, Hun Lim, or Taeho You and will be examples. When you select the name, a window appears where you can choose which celebrity you want to know about. Jinkiskan, Angelina Jolie, etc. are examples. When you select Jinkisukan, Jinkisukan appears in front of you on the VR screen, and the video taken with a 360-degree camera starts. After that, the simulation begins. The correlation with the user through the genetic information required for the simulation is visualized in the background near the celebrity. The following is an example of the simulation process.

If you select Jinkisu Khan, the valiant appearance of Jinkisukhan appears. It gives the feeling of actually talking to the user through VR. After that, a window pops up where you can find out the genetic information about Jinkis Khan's body parts. If you choose an eye, you can get information about the eye and know the protein or food that suits your constitution. And if you click the personality window, you can see the personality created based on the genetic information of Jinkisu Khan. If you click on the relationship, you can compare your personality and see which part is right and which part is not. And a solution comes up as to what kind of effort to make to become close or similar to the celebrity. If you press the home button of the VIVE controller, you will be taken to the screen where you can see your information.

Visual processing is performed so that images taken with a 360 degrees camera can be viewed in VR through the 3D engine Unity, and additional 3D objects are created using 3D editors, such as 3D-DOCTOR, 3D MAX, etc. It can be seen in Fig. 5. Also, the object appearance The texture of the image

can be viewed more realistically using the image editors, such as Photoshop, etc.

Using many VR engines, such as Unity, Unreal, etc., compatible with SteamVR, you can easily develop UX/UI for using HTC VIVE™, and you can easily design the background through the terrain engine, and asset various anti-aliasing techniques that can prevent overload as much as possible when using VR. Provided as.

Table II shows the development environment that we chose. We use the Unity Engine, an engine that has an advantage in multi-platform interconnection, to interact among different platforms. Also, we decided to use the SteamVR library and HTC VIVE™ which have a laser tracking method that has the advantage of less delay time of tracking while moving in a wide space compare to infrared tracking.



Fig. 4. ADAM10 Genetic Information through GeneCards Database [20].



Fig. 5. Screenshot of the Implementation of 360-Degree Linkage Streaming.

TABLE II. SOFTWARE DEVELOPMENT ENVIRONMENTS

| 3D Engines   |               | VR Frameworks |        |
|--------------|---------------|---------------|--------|
| Unity Engine | Unreal Engine | SteamVR       | Oculus |
| ✓            |               | ✓             |        |



Fig. 6. Examples of an Answer Choice Selection in our Dating Simulation Prototype.

Based on the genetic information, one selection of the answer choices is created depends on the user's personality. In Fig. 6, due to the user's main personality is anger, the second choice "Go away. I'm busy!" shows the appropriate answer that the user might want to choose. The goal of the game is to gain the most favorable points. The favorability points exist per each choice. Based on the genetic information, the algorithm of determining favorability points is built depending on the celebrity's personality. The system does not tell the user the number of favorability points, instead, the character shows different reactions depends on the result.

In our experiments, participants survey self-personality. The survey determines the genetic information of each participant. play the simulation with two different settings, simulation with random conversation choices and simulation with conversation choices based on the survey. After playing each simulation, record the heart beating, eye tracking position, the favorability point the participants gained, and survey on the satisfaction.

Experiments are performed with the environment of Intel(R) Core(TM) i7-9700 CPU @ 3.00GHz 3.00 GHz, RAM: 16.0GB, GPU RTX 2070 Super, and HTC VIVE™ with Dual AMOLED 3.6" diagonal screen, 1080\*1200 pixels per eye (2160 x 1200 pixels combined), 90 Hz refresh rate and 110 degrees of field of view.

## V. DISCUSSION

We discovered the improvement of human relationships by providing guidelines in the answer choice created based on the genetic information, however, the variety of the human personality is needed to evaluate in detail. To solve this problem, we need to discover more genetic information that influences the human personality. It will solve the limit of selecting the answer in a few options. We only experimented with the virtual characters in virtual reality. It would be meaningful to proceed with the human experiment not only with a virtual character in the virtual environment, but also another human in the virtual environment. Eventually, the result of the experiment between virtual characters and humans should be compared.

To give users more enjoyment, the influence of genes on personality or preference should be more clearly revealed through additional researches. If further researches can provide information that is likely to be preferred according to each individual's genetic information, users can be more interested in and pleased in entertainment based on DNA information.

Besides, it is expected to attract more people's attention through the function of entertainment, not the medical function of the original genetic information. This effect is expected to accelerate the domestic collection of personal genetic information.

## VI. CONCLUSIONS

This paper explains a virtual simulation for entertainment utilizing genetic DNA matching. It also demonstrates that the relationship between celebrities and the user's genetic DNA information, allowing the user to experience a strong affinity with it.

The realistic favorability system based on DNA information can influence the development of human relationships and sociality as well as used as a therapy for people with mental illness. This study contributes that DNA information is related to the formation of human relationships in virtual or real, and it contributed to the discovery that DNA information can contribute to the improvement of interpersonal relationships and mental health. This study also demonstrates the possibility of a new field by utilizing DNA genetic information in the entertainment field using AR/VR/MR technologies.

In future work, we will concentrate on the development of AI agents for helping users to augment the intimacy with a celebrity in the virtual and real world.

## ACKNOWLEDGMENT

This work was supported by Incheon National University Research Grant in 2017 (No. 2017-0320).

## REFERENCES

- [1] P. T. Williams, "Quantile-Specific Heritability may Account for Gene-Environment Interactions Involving Coffee Consumption," *Behavior Genetics*, Cite this article 50, pp. 119–126, 2020. <https://doi.org/10.1007/s10519-019-09989-0>.
- [2] <http://www.23andMe.com> (Retrieved September 25, 2020).
- [3] <https://steamcommunity.com/steamvr> (Retrieved September 25, 2020).
- [4] R. Plomin, H. M. Chipuer, J. C. Loehlin, "Behavioral genetics and personality," In L. A. Pervin (Ed.), *Handbook of personality: Theory and research*, pp. 225–243, The Guilford Press, 1990.
- [5] <http://www.edgc.com> (Retrieved September 25, 2020).
- [6] <http://www.gene2.me> (Retrieved September 25, 2020).
- [7] M.-L. Champel and S. Lasserre, "The special challenges of offering high quality experience for VR video," *Annual Technical Conference and Exhibition, SMPTE 2016*, pp. 1–10, 2016. <https://doi.org/10.5594/M001729>.
- [8] C. W. Chang, P. A. Yang, M. H. Lyu, and K. T. Chuang, "Influential Sustainability on Social Networks," *Data Mining (ICDM), 2015 IEEE International Conference on*. IEEE, pp. 31–40, 2015. <http://dx.doi.org/10.1109/ICDM.2015.129>.
- [9] P. Milgram, "Milgram, Paul. Some human factors considerations for designing mixed reality interfaces," *Toronto University (Ontario) Dept of Mechanical Engineering*, 2006.
- [10] J. W. Murray, "Building virtual reality with Unity and Steam VR," CRC Press, 2017.
- [11] S. M. LaValle, A. Yershova, M. Katsev, and M. Antonov, "Head tracking for the Oculus Rift," *2014 IEEE International Conference on Robotics and Automation (ICRA)*. IEEE, pp. 187–194, 2014. <https://doi.org/10.1109/ICRA.2014.6906608>.
- [12] H. T. Chang, C. J. Kuo, N. W. Lo, and W. Z. Lv, "DNA sequence representation and comparison based on quaternion number system," *International Journal of Advanced Computer Science and Applications (IJACSA)*, vol. 3, no. 11, 2012. <https://doi.org/10.14569/IJACSA.2012.031107>.
- [13] Y. Kim, "GenieHD: Efficient DNA pattern matching accelerator using hyperdimensional computing," In: *2020 Design, Automation & Test in Europe Conference & Exhibition (DATE)*, IEEE, pp. 115–120, 2020. <https://doi.org/10.23919/DATE48585.2020.9116397>.
- [14] M. Luciano, J. E. Huffman, A. Arias-Vásquez, A. A. Vinkhuyzen, C. M. Middeldorp, I. Giegling, A. Payton, G. Davies, L. Zgaga, J. Janzing, and X. Ke, "Genome-wide association uncovers shared genetic effects among personality traits and mood states," *American Journal of Medical Genetics Part B: Neuropsychiatric Genetics*, vol. 159, no. 6, pp. 684–695, 2012. <https://doi.org/10.1002/ajmg.b.32072>.
- [15] E. Mick, J. McGough, C. K. Deutsch, J. A. Frazier, D. Kennedy, and R. J. Goldberg, "Genome-wide association study of proneness to anger,"

- PloS one, vol.9, no. 1, e87257, 2014. <https://doi.org/10.1371/journal.pone.0087257>.
- [16] X. Chen, S. Kwong, & M. Li, "A compression algorithm for DNA sequences and its applications in genome comparison," *Genome informatics*, 10, pp. 51–61, 1999. <https://doi.org/10.1145/332306.332352>.
- [17] J. Ziv, & A. Lempel, "A universal algorithm for sequential data compression," *IEEE Transactions on information theory*, vol. 23, no. 33, pp. 337–343, 1977. <https://doi.org/10.1109/TIT.1977.1055714>.
- [18] Ziv, & A. Lempel, "Compression of individual sequences via variable-rate coding," *IEEE transactions on Information Theory*, vol. 24, no. 5, pp. 530–536, 1978. <https://doi.org/10.1109/TIT.1978.1055934>.
- [19] M. Safran, I. Bahir, T. Doniger, H. Krug, and A. Sirota-Madi, "GeneCards Version 3: the human gene integrator," *Database*, 2010. <https://doi.org/10.1093/database/baq020>.
- [20] A. P. Wingo, L. M. Almlı, J. S. Stevens, T. Jovanovic, T. S. Wingo, G. Tharp, Y. Li, A. Lori, M. Briscione, P. Jin, and E. B. Binder, "Genome-wide association study of positive emotion identifies a genetic variant and a role for microRNAs," *Molecular Psychiatry*, vol. 22, no. 5, pp. 774–783, 2017.
- [21] X. Corbillon, F. De Simone, & G. Simon, "360-degree video head movement dataset," In *Proceedings of the 8<sup>th</sup> ACM on Multimedia Systems Conference*, pp. 199–204, June 2017.

# Level of Depression in Positive Patients for COVID-19 in the Puente Piedra District of North Lima, 2020

Rosa Perez-Siguas<sup>1</sup>, Eduardo Matta-Solis<sup>2</sup>, Hernan Matta-Solis<sup>3</sup>  
Anika Remuzgo-Artezano<sup>4</sup>, Lourdes Matta-Zamudio<sup>5</sup>, Melissa Yauri-Machaca<sup>6</sup>  
Research and Intellectual Creativity Direction, Universidad María Auxiliadora, Lima, Perú<sup>1, 2, 3, 4</sup>  
Health Sciences, Instituto Peruano de Salud Familiar, Lima, Perú<sup>5</sup>  
Research and Technology Direction, Business on Making Technologies, Lima, Perú<sup>6</sup>

**Abstract**—Depression in the positive patient for COVID-19 is one of the emotional confrontations that must endure during isolation and quarantine, therefore, the objective of the research study is to determine the Level of Depression in positive patients for COVID-19 in the district of Puente Piedra in North Lima, 2020. This is a quantitative, non-experimental, descriptive and cross-sectional study, making a flow chart in relation to home care by the nursing professional in a population of 23 Positive patient for COVID-19 from the Puente Piedra district of North Lima, who answered a questionnaire with Sociodemographic data and the self-assessment scale for Zung's depression. In the results where we can observe, with respect to the level of depression in patients positive for COVID-19, where 14 patients represent 60.9% of the total are with a normal level of depression, 9 patients represent 39.1% of the total are slightly depressed. In conclusion, it is necessary to intervene in the psychological aspect according to the characteristics of each patient such as gender and age, in the future, it is recommended to carry out more research at the national level, as it will allow researchers to go into more detail about the mental health of the patient during and after the COVID-19 pandemic.

**Keywords**—Depression; coronavirus; patients; home care

## I. INTRODUCTION

The coronavirus disease (COVID - 19) has had a great impact on the world population both in their mental and physical health, therefore, it is expected that COVID - 19 since it appeared in December 2019, was widely recognized as a traumatic event for patients who tested positive for this disease, because it imposes a threat not only due to concerns at the physical level [1], but also at the mental level of infected patients, since they experience fear, sadness, melancholy, insomnia, and helplessness, where all this affects the patient exposing them to serious health problems related to the disease [2].

In the positive patients for COVID-19, they have been considered vulnerable in the mental aspect, because this disease presents depressive symptoms that prevent them from advancing in their life, it has been expected that positive patients with depressive symptoms do not tend to communicate with others and do not seek support from their relatives, because their perception of dignity and shame have been barriers that prevent them from seeking help [3], also, in

positive patients for COVID-19 who are at risk or who suffer depression during and after the disease outbreak as a result of isolation and quarantine, an increase in suicidal thinking and behavior could be considered in the short or long term [4].

Therefore, the mental health of the patient plays an important role during this crisis due to the COVID-19 pandemic [5] since they are predisposed to be vulnerable and lead to serious psychological consequences in the patient in relation to their person, environment and family.

In Hong Kong [6], it could be observed in 500 participants surveyed in the research work on depression during the COVID-19 pandemic, indicating that the prevalence rate for depression is considerable in the population, where 29% of people presented mild depression, 12.8% moderate depression, 6.2% moderately severe depression and 0.8% severe depression allowing to observe that depressive conditions affect the population during the COVID-19 pandemic.

In China [7], a study was conducted in 1593 participants in relation to the comparison between prevalence and factors associated with depression during the quarantine due to the COVID-19 pandemic in Southwest China in a population infected and not infected by the coronavirus, where the prevalence of depression in the infected population was 14.6%, stating that 8.3% had mild depression, 5.2% had moderate depression and 1.1% had severe depression, due to this they showed a high prevalence of depression in the infected population than in the uninfected population.

In Spain [8], a virtual survey was conducted with 976 participants during the first phase of the COVID - 19 outbreak in northern Spain, mentioning depression during the first phase of the COVID - 19 outbreak in Basque men and women, where 78 (8.6%) of the women presented mild depression, 16 (7.1%) moderate depression, 20 (2.3%) severe depression and 34 (3.0%) extremely severe depression, in men 19 (8.7%) had mild depression, 9 (4.0%) moderate depression, 5 (2.9%) severe depression and 3 (1.7%) extremely severe depression, concluding that Basque men and women present evidence of depressive symptoms from the COVID-19 pandemic.

The objective of the research work is to determine the level of depression in positive patients for COVID-19 in the

Puente Piedra district of North Lima, 2020. This study is important since it provides relevant and real data on mental vulnerability with respect to depression in COVID-19 positive patients treated at home by nursing professionals. In this research work, the survey will be used as a data collection instrument, the data to be entered will be given in a data matrix that will be designed in the statistical program IBM SPSS Statistics Base 25.0, its corresponding analysis was carried out, in which it will allow a better data processing for the realization of statistical tables and graphs so that they are later described and interpreted in results and discussions, respectively.

The following research work is structured as follows: In Section II, the development of the data collection processing of hospitalized patients will be presented and also the guidelines to be considered so that they are within the research work. In Section III, the results will show the level of depression in coronavirus positive patients according to the specified dimensions of the instrument in the measurement of the variable. In Section IV, we present the discussions of the research work and in Section V the conclusions.

## II. METHODOLOGY

In this part, a flow chart will be developed based on protocols to be followed by the nurse's care towards the coronavirus positive patient at home, the type and design of the research work, also the population and sample that it will be carried out in the research work, the inclusion criteria in detail and finally the data collection technique and instrument that is the survey, where it was taken by the nurse in charge of caring for the patient with COVID – 19, see Fig. 1. In this flow chart the protocols to be followed in patient care will be described, it starts in two partitions:

First, the nursing protocols will be given on the care of the patient at home, this refers to the care performed by the nursing professional towards the patient, the care to be carried out will manifest itself in five processes:

- First, it is the use of biosafety equipment such as N95 mask, face shield, protective glasses, gloves, and overalls, this allows the safety of both the nursing professional to come into contact with the patient and the family and thus be able to carry out the corresponding care.
- Second, it is the disinfection process, such as hand hygiene with soap, water and alcohol gel.
- Third, it is the monitoring of the COVID-19 disease, this process the nursing professional will monitor the patient their vital functions such as oxygen saturation, respiratory rate, temperature, blood pressure and heart rate allowing to observe if there is any alteration that predisposes that the disease is still active.
- Fourth, it is the treatment of the COVID-19 disease, in this process the procedures will be carried out according to the severity of the disease in the patient, if the disease is mild or moderate in which it will be verified if the patient is in oral treatment or it is on oral treatment and injection therapy [20].

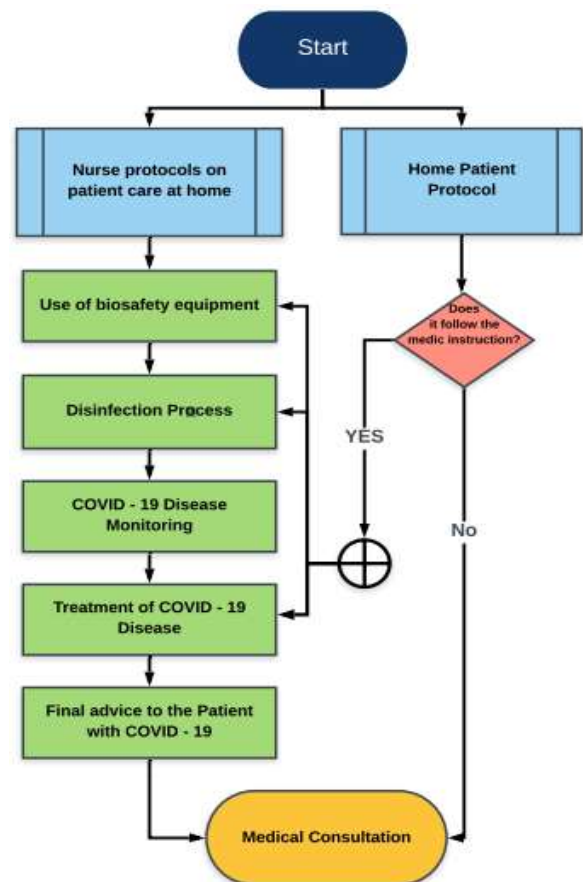


Fig. 1. Flowchart of the Nursing Professional on the Home Care Performed for the Patient with COVID-19.

- In fifth place, it is the final counseling to the patient with COVID-19, in this process the nursing professional will provide information to the patient about hand hygiene (the steps to follow and how to do them), healthy eating (foods rich in vitamins and minerals; and what foods are not).

Once all this is done, the patient will have their routine medical consultation, in which the physical examination will be performed, and also the laboratory examination to rule out if the disease is still active in the patient.

Second, the protocols to be followed by the patient at home will be given, but it will depend on a question with two answers, the question is, does patient follow all the steps? referring to the care that the doctor referred them, and the answers are, if they meet them or do not comply with them [21], the first response if it does, the patient will follow three processes:

- The first process is the use of biosafety equipment, where the patient must have the mask available, either simple or the N95, this will allow the patient through sneezing and the presence of cough, do not infect family members who live with them.
- Second process is the disinfection process, this process the patient should perform hand hygiene with soap and water, this will eliminate the bacteria present on the

hand and not spread through the skin to family members.

- Third process is the treatment of the COVID-19 disease, in this process the patient must follow the indications prescribed by the doctor, but depending on the degree to which the mild or moderate disease is found, in which oral treatment or oral treatment and injection therapy.

After all these processes, they should go to routine medical consultations for controls, the second answer if they do not comply with the instruction of the doctor, the patient should go to a medical consultation to verify the degree of the disease, it is very important to take into account that when at the time of the general examination of the patient, if a decrease in oxygen saturation is observed, the doctor will indicate if they will transfer to the hospital where they are subscribed to a life security because they will need support oxygen and also will continue the treatment indicated.

#### A. Research Type and Design

The present study, due to its characteristics, way of collecting data and measuring the variables involved, has a quantitative approach. Regarding the methodological design, it is a non-experimental, descriptive, cross-sectional study [9].

#### B. Population and Sample

In the present study, the population is made up of 23 COVID-19 positive patients who are undergoing treatment at their home in North Lima in the Puente Piedra district of the Micaela Bastidas Association.

#### C. Inclusion Criteria

- COVID-19 positive patients in the Puente Piedra district, Micaela Bastidas Association - Zapallal.
- Patients who are undergoing COVID-19 treatment at home.

#### D. Technique and Instrument

The technique used is the survey, through the questionnaire or data collection instrument of the Zung Depression Self-Assessment Scale (SDS), which aims to measure depression in coronavirus-positive patients.

The Zung Depression Self-Assessment Scale (SDS) is self-administered to assess how depressed a patient is, the scale consists of 20 items that indicate 4 most common characteristics of depression: the dominant effect, the physiological equivalents, other disturbances and psychomotor activities. There are 10 items elaborated in a positive way and 10 items in a negative way that are evaluated on a Likert-type scale where 1 "little time", 2 "some of the time", 3 "a good part of the time" and 4 "most of the time". The range of the scale goes from 20 to 80 [10], the higher the score, the more depression the patient presents.

#### E. Place and Application of the Instrument

The questionnaire carried out to measure the level of depression in positive patients for coronavirus, was carried out in North Lima, in the Puente Piedra district, of the Micaela Bastidas - Zapallal Association.

First, the necessary permits were made for this research work, coordinated with the family in charge of the patient to carry out the questionnaire, then the permission to the patient explaining about the questionnaire and why the research work is being carried out so that they have knowledge about of what is going to be done.

The questionnaire was carried out in the mornings with an approximate time of 15 minutes in each patient surveyed in the research work [19], reaching a conclusion with good satisfaction at the time of collecting the questionnaires that the patients supported for the research work.

It is important to emphasize the presence of the family in charge of the patient at the time of filling he questionnaire, because there is a possible adverse event from the disease in the patient and that the family member provides the treatment that it is receiving and thus avoid damages that can be considerable in the health of the patient. At the same time, the presence of the nursing professional is also important, since they will perform the care of the patient and also have knowledge about the necessary care of COVID-19 patients who are cared for at home.

### III. RESULTS

There are figures of the surveys carried out following the guidelines corresponding to the research work will be shown.

In Fig. 2, it has the data of the study patients, where it can observe with respect to the level of depression in patients positive for coronavirus in North Lima, where 14 patients represent 60.9% of the total with a normal level of depression, 9 patients represent 39.1% of the total are slightly depressed.

Fig. 3 shows the data of the study patients in relation to gender, where it can see that 13 represents 65% of the total male sex who are with a normal level of depression, 7 represents 35% of the total sex males who are slightly depressed, 1 represents 33.3% of the total female sex who are with a normal level of depression and 2 represents 66.7% of the total female sex who are slightly depressed.

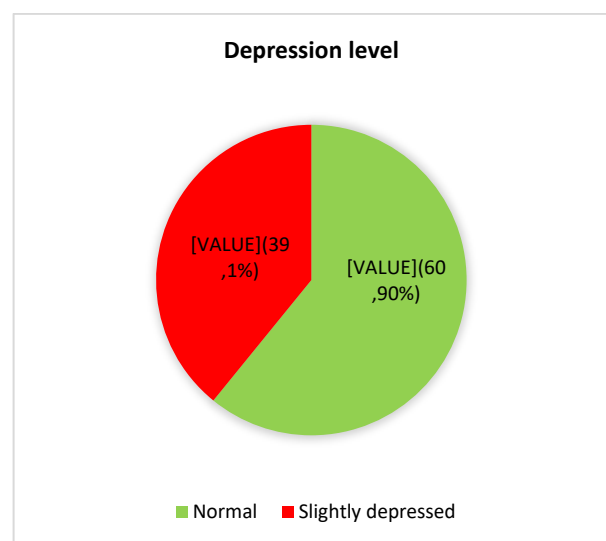


Fig. 2. Level of Depression in COVID-19 Positive Patients in the Puente Piedra District of North Lima, 2020.

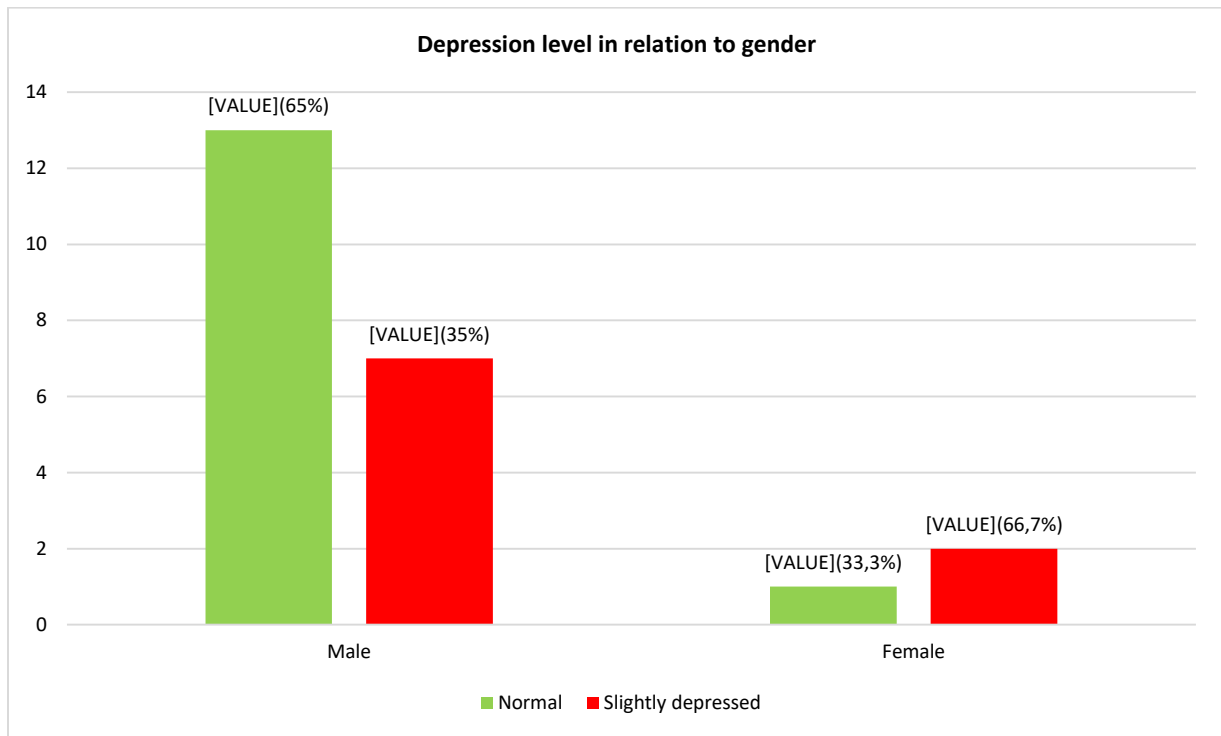


Fig. 3. Level of Depression in Relation to Gender in COVID-19 Positive Patients in the Puente Piedra District in North Lima, 2020.

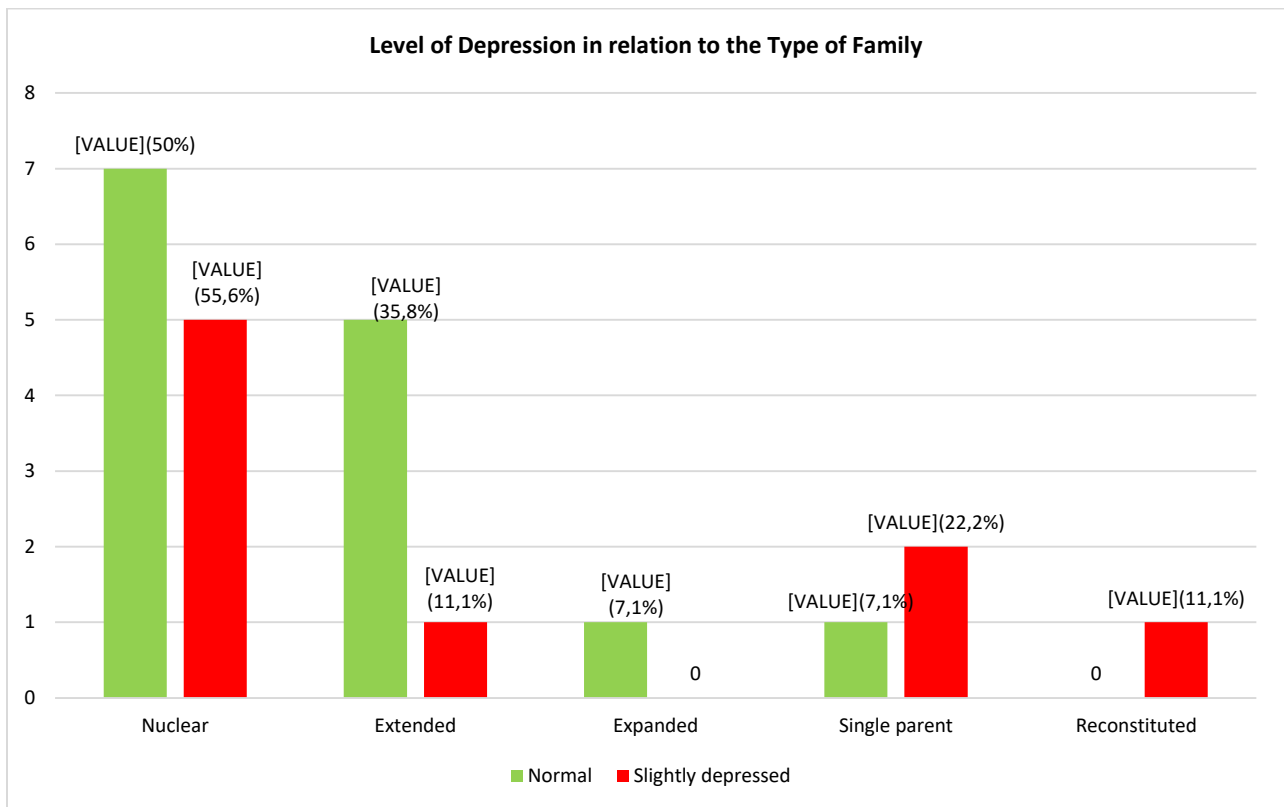


Fig. 4. Level of Depression in Relation to the Type of Family in Positive Patients for COVID-19 in the Puente Piedra District in North Lima, 2020.



Fig. 4 shows the data of the study patients in relation to the type of family, where it can be seen that 7 (50%) of the nuclear family type have a normal level of depression, 5 (55.6%) of the type nuclear family are slightly depressed, 5 (35.8%) of the extended family type have a normal level of depression, 1 (11.1%) of the extended family type are slightly depressed, 1 (7.1%) of the type expanded family have a normal level of depression, 1 (7.1%) of the type of single parent have a normal level of depression, 2 (22.2%) of the type of single parent are slightly depressed and 1 (11.1%) of the reconstituted family type are slightly depressed.

These results are important since they will give data to know if the COVID-19 positive patient is depressed because of the disease.

#### IV. DISCUSSION

In this research work, an approach is given to the mental health of the COVID-19 positive patient who is treated at home, although it is true because of the isolation due to the disease, the patient suffers a depressive state that affects themselves daily life and at the same time generates an impact on the family, causing a degree of psycho-emotional decline because of it.

In the results on the level of depression, it can be seen that the patients present a degree of depression due to COVID-19, this is because the disease has generated a substantial impact on the mental health of patients who tested positive for COVID-19 [18], although it is true some patients tend to show depressive symptoms because they feel distressed and worried about thinking that they can infect their families, therefore their psycho-emotional state tends to decrease and they do not face the situation properly. In the study by Choi E. et al. [6], they argue that patients who tested positive for COVID-19 had a deterioration in mental health and therefore had depression, this is because the patients felt overwhelmed by receiving information about COVID - 19 generating more anguish and concern in them, affecting them and altering the mental health of patients. Likewise Vindegaard N. and collaborator [15], argue that COVID-19 positive patients present a high index of depressive symptoms due to low psychological well-being and poor quality of sleep and being worried about their families increased symptoms regarding depression.

In the results on the level of depression in relation to sex, it was observed that in men there is evidence of a degree of depression due to COVID-19, this is due to the fact that men as head of the family, by testing positive for the disease, they have to think that they will not be able to work, in how to support their family, and also how to handle the situation due to isolation and quarantine, all this has generated in their mental health concern not only for themselves but for the rest of their family. Likewise, in the study by Ozamiz N. and collaborators [8], it was evidenced that women tended to manifest higher levels of depression than men, this is due to the fact that women have a high vulnerability with respect to health mentally, this is because stressors from COVID-19 make them more susceptible to depression [17], as their role as mother, wife, and caregiver coupled with pressure at home from isolation and quarantine has increased its stress therefore

leads to depression. Similarly, Newby J. and collaborators [12], highlight that the mental health of the caregiver or parent who stays at home was associated with loneliness, the future and financial worries that were indications of having high levels of depression more frequently in women. Jia R. and collaborators [13], stated in their study that women were more associated with high levels of depression due to their mood, loneliness and concern about the COVID-19 pandemic. In the same way, Dai L. and collaborators [14], reported that women with relatives with COVID-19 had a high probability of presenting symptoms of depression due to family burden and psychological distress to care for their relatives.

In the results on the level of depression in relation to the type of family, it can be seen that the type of nuclear family has a degree of depression due to COVID-19, this is because the families had a negative impact at the time of knowing that a relative tested positive for COVID-19, although it is true that the family must emotionally support the patient but at the same time they must also seek emotional support with their other relatives because the effect on mental health exerted by COVID-19 towards families is alarming because they show signs of concern, anguish and despair when they know that a relative suffers from the disease [16], therefore, the union in the family is very important to be able to cope with these moments of isolation and quarantine due to COVID-19. Likewise, Orte C. and collaborators [11] refer that they maintain that family support during isolation due to COVID-19 is very important in the family since this allows for a good life bond with other relatives and that the impact on mental health exerted by COVID-19 does not affect another member of the family.

#### V. CONCLUSION

In conclusion, brief psychological support should be given at home to patients who tested positive for COVID - 19 in which it will allow them to maintain their balanced health and be able to handle the situation properly.

In conclusion, intervention should be made on the psychological aspect according to the characteristics of each patient such as gender and age.

In conclusion, it is necessary to intervene in the psychological aspect to prevent and treat the decrease in depression in COVID-19 positive patients that it may create during and after the pandemic.

In conclusion, it is recommended to carry out continuous follow-ups by the nursing professional through home visits to observe the psychological aspect of the patient and provide emotional support in each visit that is made.

In a future research work, it is recommended to carry out more research at the national level, since it will allow researchers to go into more detail about the mental health of the patient during and after the COVID-19 pandemic.

The limitation in this research work is access to the homes of each patient, due to the fact that the relatives expressed mistrust at the time of conducting the surveys.

REFERENCES

- [1] Jakovljevic M, Bjedov S, Jaksic N, and Jakovljevic I, "Covid-19 pandemia and public and global mental health from the perspective of global health security. *Psychiatria Danubina*[revista en internet] 2020 [acceso 25 de agosto del 2020]; 31(1): 6-14."
- [2] Wei N et al., "Efficacy of internet-based integrated intervention on depression and anxiety symptoms in patients with COVID-19. *Journal of Zhejiang University: Science B*[revista en internet] 2020 [acceso 25 de agosto del 2020]; 21(5): 400-404."
- [3] Liu X et al., "Psychological status and behavior changes of the public during the COVID-19 epidemic in China. *Infectious Diseases of Poverty*[revista en internet] 2020 [acceso 25 de agosto del 2020]; 9(1): 1-11."
- [4] Klomek A, "Suicide prevention during the COVID-19 outbreak. *The Lancet Psychiatry*[revista en internet] 2020 [acceso 25 de agosto del 2020]; 7(5): 390."
- [5] Cullen W, Gulati G, and Kelly B, "Mental health in the COVID-19 pandemic. *QJM: monthly journal of the Association of Physicians*[revista en internet] 2020 [acceso 26 de agosto del 2020]; 113(5): 311-312."
- [6] Choi E, Hui B, and Wan E, "Depression and anxiety in Hong Kong during covid-19. *International Journal of Environmental Research and Public Health*[revista en internet] 2020 [acceso 25 de agosto del 2020]; 17(10): 10."
- [7] Lei L, Huang X, Zhang S, Yang J, Yang L, and Xu M, "Comparison of Prevalence and Associated Factors of Anxiety and Depression among People Affected by versus People Unaffected by Quarantine during the COVID-19 Epidemic in Southwestern China. *Medical Science Monitor*[revista en internet] 2020 [acceso 25 de agosto del 2020]."
- [8] Ozamiz N, Dosil M, Picaza M, and Idoiaga N, "Niveles de estrés, ansiedad y depresión en la primera fase del brote del COVID-19 en una muestra recogida en el norte de España. *Cadernos de Saude Publica*[revista en internet] 2020 [acceso 25 de agosto del 2020]; 36(4): 1-10."
- [9] Fernández C and Baptista P, *Metodología de la Investigación*. 6ta ed. México: Mc Graw-Hill/Interamericana; 2015.
- [10] Zung W, "Escala de Autoevaluación para la Depresión de Zung." pp. 1–2, 1965.
- [11] Orte C, Ballester B, and Nevot L, "Apoyo Familiar ante el COVID - 19 en España. *Universitat de les Illes Balears*[revista en internet] 2020 [acceso 16 de setiembre del 2020]; 1-12."
- [12] Newby J, O'Moore K, Tang S, Christensen H, and Faasse K, "Acute mental health responses during the COVID-19 pandemic in Australia. *PLoS ONE*[revista en internet] 2020 [acceso 28 de octubre del 2020]; 15(7):1-21.," doi: 10.1371/journal.pone.0236562.
- [13] Jia R et al., "Mental health in the UK during the COVID-19 pandemic: cross-sectional analyses from a community cohort study. *BMJ open*[revista en internet] 2020 [acceso 28 de octubre del 2020]; 9(10): 40620.," doi: 10.1136/bmjopen-2020-040620.
- [14] Dai L et al., "Anxiety and depressive symptoms among COVID-19 patients in Jiangnan Fangcang Shelter Hospital in Wuhan, China. *PLoS ONE*[revista en internet] 2020 [acceso 28 de octubre del 2020]; 15(8):1-11.," doi: 10.1371/journal.pone.0238416.
- [15] Vindegaard N and Benros M, "COVID-19 pandemic and mental health consequences: Systematic review of the current evidence. *Brain, Behavior, and Immunity* 2020; 89: 531-542.," Available: <https://www.ncbi.nlm.nih.gov/pmc/articles/PMC7260522/pdf/main.pdf>.
- [16] P. Herrera-Añazco and C. Toro-Huamanchumo, "Medical education during the COVID -19 pandemic: global initiatives for undergraduate, internship, and medical residency," *Acta Med Peru*, vol. 37, no. 2, p. 175, Apr. 2020, doi: 10.35663/amp.2020.372.999.
- [17] M. Walton, E. Murray, and M. D. Christian, "Mental health care for medical staff and affiliated healthcare workers during the COVID-19 pandemic," *Eur. Hear. J. Acute Cardiovasc. Care*, vol. 9, no. 3, pp. 241–247, Apr. 2020, doi: 10.1177/2048872620922795.
- [18] WHO, "Mental health and COVID-19," World Health Organization, 2019. <https://www.euro.who.int/en/health-topics/health-emergencies/coronavirus-covid-19/technical-guidance/mental-health-and-covid-19> (accessed Aug. 03, 2020).
- [19] N. W. S. Chew et al., "A multinational, multicentre study on the psychological outcomes and associated physical symptoms amongst healthcare workers during COVID-19 outbreak," *Brain. Behav. Immun.*, vol. 88, p. 565, Apr. 2020, doi: 10.1016/j.bbi.2020.04.049.
- [20] OPS/OMS, "Enfermedad por el Coronavirus (COVID-19)," Organización Panamericana de la Salud, Mar. 15, 2020. <https://www.paho.org/es/tag/enfermedad-por-coronavirus-covid-19> (accessed Aug. 17, 2020).
- [21] X. Xiao, X. Zhu, S. Fu, Y. Hu, X. Li, and J. Xiao, "Psychological impact of healthcare workers in China during COVID-19 pneumonia epidemic: A multi-center cross-sectional survey investigation," *J. Affect. Disord.*, vol. 274, pp. 405–410, May 2020, doi: 10.1016/j.jad.2020.05.081.

# Blockchain and Internet of Things for Business Process Management: Theory, Challenges, and Key Success Factors

Mabrook S. Al-Rakhami<sup>1</sup>, Majed Al-Mashari<sup>2</sup>

Information Systems Department  
College of Computer and Information Sciences  
King Saud University, Riyadh, Saudi Arabia

**Abstract**—The combination of business process management (BPM) and emerging technologies is a logical step. The evolving number of advanced technologies shows that contributions are with a high value for business processes. From a BPM point of view, value creation from the modern technologies such as Internet of things and Blockchain technology is pivotal on a progressively higher scale and affect the business process in different aspects. However, current research in this area still at the beginning. In order to close this research gap and the lack of experience in this area, the topic of integrating Blockchain and IoT technologies with BPM will play an essential role in a corporate context, particularly in the context of inter/intra-organizational information systems and their diverse design options. This review paper aims to survey the impact of two emerging technologies: Internet of Things and Blockchain technology on BPM and illustrates the current state of the art in this research domain. Each technology was investigated through a design science research approach to provide as a descriptive theoretical overview, characterize its theoretical background, challenges, and key success factors.

**Keywords**—Business process management; BPM; Internet of things; IoT; blockchain technology

## I. INTRODUCTION

The development of business at the national and international levels requires processes that dominate market instruments. Imagination, creativity, and technical instruments should be at the highest level to meet the market needs and high international competition. Today, selling alone is not enough. The client is given what he wants and needs at the right moment. Hence, thinking strategically is also necessary for relational marketing with advertising support to obtain a perfect mix in the competitiveness of companies [1].

In these times of global and ongoing progression of digital transformation, the evaluation of emerging technologies and the study of their potential research and application domains are of significance. Organizations have to develop their core process to remain competitive, transform their businesses, and stay more effective. Sometimes, they even need to change the entire business models.

By reviewing relevant publications [1-12], this study develops a clear articulation of the concept, nature, components, and elements of business process management (BPM), which is significant in understanding the BPM research

better. With the rapid growth of the volume of research output on the BPM topic [7], this study considers two recent technologies to draw conclusions on the current status and possible future directions.

Over the last decade, many technologies have emerged as promising paradigms for integrating and extending business processes at both intra- and inter-organizational levels, which are well known as industry 4.0. These emerging technologies have been fueled by the recent development of information and communications technology. The developments and technological advances will provide a viable array of solutions to the growing needs of information in different units of organizations. This viability has been evidenced by the fact that a growing number of enterprises worldwide have explored the benefits of digitizing enterprises' horizontal and vertical chains and adopted recent and advanced technologies in the process of becoming leading digital enterprises in tomorrow's complex industrial ecosystems.

Various technologies can be used for implementing the fourth industrial revolution (Industry 4.0) which affect strongly how BPM works. These technologies include the Internet-of-Things (IoT), blockchain, embedded systems, wireless sensor network, industrial robots and artificial intelligence among other technologies. In this article, two selected technologies are selected which are particularly significant for BPM. These technologies are the IoT and Blockchain technology. However, the coverage of all enabling technologies is by no means meant to be exhaustive. In this regard, this review article is designed to answer the following questions, which are as follows: How the selected technologies affect the IT aspect of BPM?, and what are the challenges for the application of these technologies? Moreover, what are the key factors to ensure the successful application of these technologies for BPM?

The contribution of this article is threefold: First, this work presents a survey on how BPM could be integrated with two of the recent technologies which are IoT and Blockchain. Second, it highlights the challenges that face the integration process. Third, it describes and discuss the key success factors of the integration between the technologies under investigation.

The remainder of this paper is structured as follows: Section II describes research methodology. Section III provides a theoretical background of the BPM by considering the BPM

six-core element model. Section IV elaborates on the fundamental concepts of the selected technologies, namely IoT and Blockchain technology, where each sub-section presents the overview, challenges, and key success factors for the abovementioned technologies. Section V provides a discussion on final thoughts and key point summary. Finally, section VI concludes the paper and presents the future work.

II. MATERIALS AND METHODS

The objective of this article is to investigate the impact of two emerging technologies on BPM, precisely, to study their challenges and key success factors. In order to achieve this objective, and to formulate the scope for the reviewed papers, this work adapted the steps shown in Fig. 1.

As a first step, the search for selected keywords related to recent technologies associated with BPM has been conducted on the indexed Web of Sciences (WoS) dataset. WoS is a recognized multidisciplinary proprietary database for peer-reviewed journal content. In addition, it has a powerful feature of tracking citing items. WoS is mainly used because it searches over 33,000 journals and over 21,000 books and conference proceedings, which was sufficient for this study.

The next step was to analyze the highly cited articles and investigate the mentioned challenges and key success factors for the application of selected topics with BPM direction. Although challenges and key success factors weren't necessarily mentioned directly, so it was necessary to figure it out based on our understanding of the discussions and conclusion of these articles. Table 1 illustrates the used queries for each topic and the statistics of retrieved articles. The query was carried out from All Databases.

For each topic, the number of related publications, average citations per item, the sum of times cited and the number of citing articles are calculated as shown in Table 1. Figs. 2 and 3 show the number of publications per topic. Figures demonstrate the importance of the selected technologies over the years, where the increase in the number of publications over the years is clear.

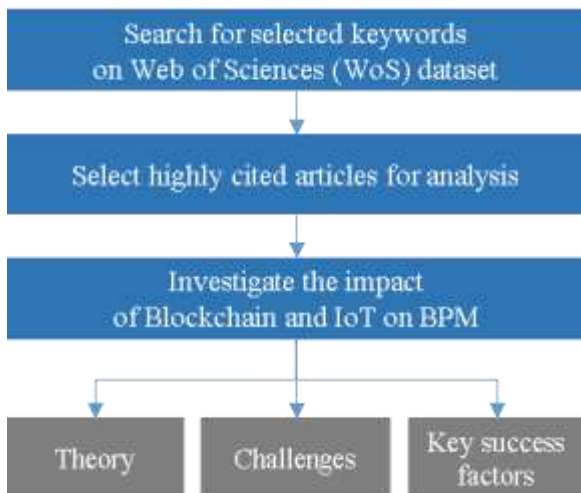


Fig. 1. Research Methodology.

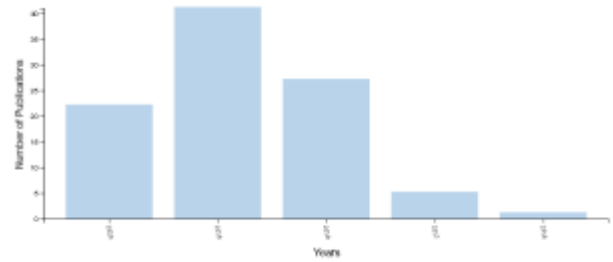


Fig. 2. Blockchain Technology for Business Process Management Publications Count per Year.

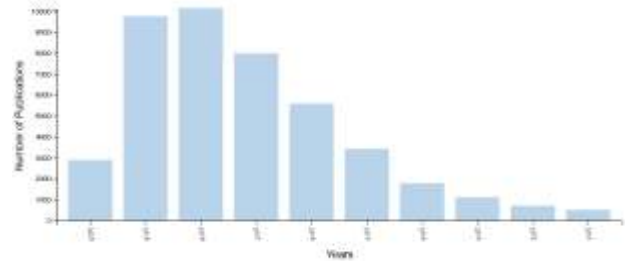


Fig. 3. IoT-based Business Process Management Publications Count per Year.

TABLE I. WoS QUERY KEYWORDS AND STATISTICS OF THE SELECTED TECHNOLOGIES RELATED TO BPM

| Topic                                                                                                              | Total publications | Average citations per item | Sum of times cited | Citing articles |
|--------------------------------------------------------------------------------------------------------------------|--------------------|----------------------------|--------------------|-----------------|
| TOPIC: ('business process management' OR 'BPM') AND inTITLE: ('Blockchain')                                        | 176                | 1.75                       | 308                | 244             |
| TOPIC: ('business process management' OR 'BPM') AND inTITLE: (IoT OR 'Internet-of-Things' OR 'Internet of Things') | 298                | 4.05                       | 1,208              | 1,105           |

III. BPM: THE ORETICAL BACKGROUND

A. Motivation and Definition

The competitiveness of companies depends on improving their efficiency, increasing productivity, reducing costs, matching products/services to customer expectations, the global vision between different processes, and the strategic alignment of their information system [14]. This requires an organization of the company around strategic and transversal processes.

BPM has recently received considerable attention from both business administration and computer science communities [10]. BPM is a discipline that combines methods, technologies, and tools to handle the entire life cycle of business processes in a single approach, collaborating systems, software, and people. BPM can be defined as "supporting business processes using methods, techniques and software to design, enact, control and analyze operational processes involving humans, organizations, applications, documents and other sources of information" [15].

**B. BPM Six-Core Elements Model**

Several theorists wrote about the key elements of business processes. They generally agree on identifying six basic elements that must be evaluated for business process management: strategic alignment, government, methods, information technologies, people, and culture. Fig. 4 illustrates a further level of detail for the six core elements associated with their capability areas.

1) *Strategic alignment*: Strategic alignment is defined as the close link of the priorities of the organization and processes of the company that allows a continuous and effective action to improve the business performance. Five different capacity areas are identified as part of an assessment of the strategic alignment of business processes.

2) *Government*: The government of BPM is dedicated to accountability in an orderly and transparent manner in terms of the roles and responsibilities of the different BPM levels (portfolio of programs, projects, and operations).

3) *Methods*: In the context of BPM, methods are defined as the tools and techniques that support and allow consistent activities at all BPM levels (portfolio of programs, projects, and operations). Different methods can be performed in the most important stages in the different stages of their life cycle.

4) *Information technology*: Information technology (IT) refers to software, hardware, and information systems that enable processes. The decomposition of IT as one of the basic elements of BPM is similar to that of BPM methods and also refers to the stages of the life cycle process. Like the dimension of methods, IT components focus on the specific needs of each stage of the process cycle and are evaluated from certain points of view.

5) *People*: People are defined as individuals and groups that continuously improve and use their expertise, ability to manage processes, and knowledge to improve business performance.

6) *Culture*: Culture refers to the collective values and beliefs that shape the processes related to attitudes and behavior to improve business performance.

| Strategic Alignment                   | Government                            | Methods                              | Information Technology               | People                       | Culture                            | Factors          |
|---------------------------------------|---------------------------------------|--------------------------------------|--------------------------------------|------------------------------|------------------------------------|------------------|
| Process Improvement Planning          | Process Management Decision Making    | Process Design &Modelling            | Process Design &Modelling            | Process Skills &Expertise    | Responsiveness to Process Change   | Capability Areas |
| Strategy & Process Capability Linkage | Process Roles and Responsibilities    | Process Implementation &Execution    | Process Implementation &Execution    | Process Management Knowledge | Process Values & Beliefs           |                  |
| Enterprise Process Architecture       | Process Metrics & Performance Linkage | Process Monitoring &Control          | Process Monitoring &Control          | Process Education            | Process Attitudes & Behaviors      |                  |
| Process Measures                      | Process Related Standards             | Process Improvement &Innovation      | Process Improvement &Innovation      | Process Collaboration        | Leadership Attention to Process    |                  |
| Process Customers &Stakeholders       | Process Management Compliance         | Process Program & Project Management | Process Program & Project Management | Process Management Leaders   | Process Management Social Networks |                  |

Fig. 4. Six Core Elements of BPM. Adapted from [2].

**IV. EMERGING TECHNOLOGIES**

BPM continues to advance throughout the world and evolves because of the great advancement of new technologies, such as IoT, cloud computing, Big Data, social BPM, etc. the growing importance is given to the management of processes. However, it is not only about technologies, but also about managing business processes and resources, which should be aligned with the business strategy and achieving a true and complete business process management [16]. These same technologies are also achieving digital transformation, which cannot be separated from business processes, because everything is related to processes. These must be managed and aligned with the business strategy [17].

This section introduces an overview of the two technologies that have a focus of the emergent body of research in BPM: IoT and Blockchain technology. In

accordance with the advances that continuously occur in both information systems and global business strategies, these technologies have emerged to improve the productivity and quality of business and its process in organizations of different sizes and operations. Fig. 5 presents the structure of this work.

**A. Internet of Things**

1) *Theoretical overview*: The vision of IoT will become the center of privacy and business in the future because billions of networked objects can communicate with each other [18]. The use of state-of-the-art technologies enables the emergence of new applications. Having instant access to information on the physical world and objects increases efficiency and productivity, creating great opportunities for business and personal life. The resulting new requirements also require existing business processes to be adapted to realize the full potential of IoT [19].

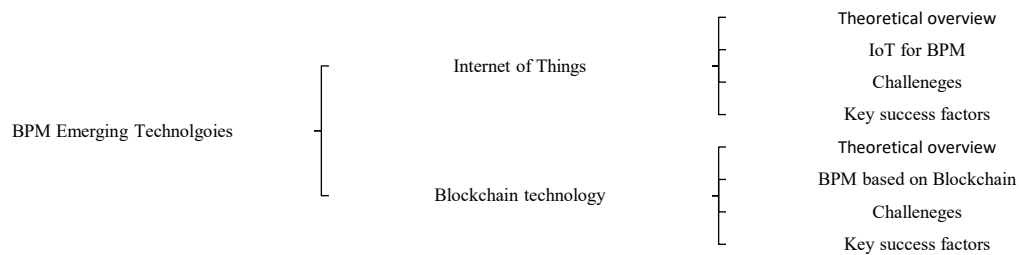


Fig. 5. Paper Structure.

This section deals with the concept of IoT and creates a holistic understanding of the topic. Therefore, both technologies and application scenarios, as well as the processes related to this topic, are presented and explained. The goal is to derive requirements for process support and technology compared to other works in the field and illustrate the impact of the IoT on processes. The use of IoT makes it possible to consider extensive real-time information in business processes. The result is more transparent processes and monitoring of business processes [20].

IoT is still at the beginning of its development. Every day, more machines, containers, houses, vehicles, and people are equipped with sensors to report their status, receive instructions, or even take action based on the information they receive. IoT has the potential to fundamentally change the way people interact with their environment. The ability to electronically monitor and control objects in the physical world enables automated, data-driven decision-making to optimize system and process performance, increase enterprise efficiency, and improve the quality of life. From monitoring machinery in production halls to tracking products on the high seas, sensors can help companies make better, more efficient use of their assets [21]. IoT also has the potential to significantly change or improve processes and procedures in private households or in the healthcare industry, especially in the treatment of chronically ill patients, such as those with diabetes. IoT can dramatically change the reach of information technology by blurring the physical real world with the digital world. To achieve this, technical and organizational hurdles must be overcome, and all the existing business processes have to be changed. In particular, companies that want to use the technologies of IoT in the future need better tools and methods to analyze the existing processes and adapt them to IoT [9].

In an environment of constant competition and ever-faster innovation, many companies are in a permanent process of change. Even in a company with a degree of stability, operational and technical processes need to be continuously improved and adjusted. Therefore, processes in a company have a high priority. However, the processes have to be adapted to the new possibilities of IoT to realize their full potential. The right people must use the right objects in the right situation at the right time. Hence, all parties involved, particularly people, systems, machines, and smart objects, must be coordinated. Countless sensors on devices in the industry, in cities, homes, and cars create a huge amount of real-time data

that needs to be analyzed. Networks can exchange these data and make decisions based on the processing logic. However, this logic only works according to previously planned rules of conduct. Unforeseen exceptions based on real events require a dynamic process adaptation.

Therefore, the use of IoT requires flexible business processes that are capable of dynamically adapting to the changes that can occur through process execution or the properties of the smart objects [22]. While some call IoT a short-term hype, there is no question about its spread. Gartner estimated that today, more than 8 billion devices, including smartphones and computers, are connected around the world. This number is expected to dramatically increase to as much as 25 billion over the next ten years. IoT attempts to coordinate this enormous number of different devices with people and applications through business processes. The goal is to close the gap that exists between business processes in the real world and the information systems in the digital world. Fig. 6 represents the BPMS framework that encompasses IoT entities and the middleware-based information system. Most IoT-based BPM frameworks are similar to the design in this figure [1].

2) *Challenges:* Processes: The deployments of IoT technologies would considerably affect and modify how businesses do business amid diverse segments of the social order, affecting several processes [13]. For being capable of gaining numerous latent profits that are proposed for the IoT, numerous challenges concerning the modeling and implementation of these kinds of processes must be resolved to comprehend the broader and profitable deployments of IoT [20,23]. The exceptional features of IoT services and processes must be considered. In addition, current business process modeling and execution and service description languages such as Unified Service Description Language (USDL) will probably be required to be protracted [24].

Adaptive and Event-driven Processes: Note that the processes get more accustomed to what is taking place in the actual world—chief benefits of IoT integration. Characteristically, it is founded on happenings identified either unswervingly or through a real-time study of sensor data. These kinds of events can occur in the process at any time [25, 26]. The probability of occurrence for certain events is extremely low, indicating their possibility to take place, but not when or if they will take place [27].

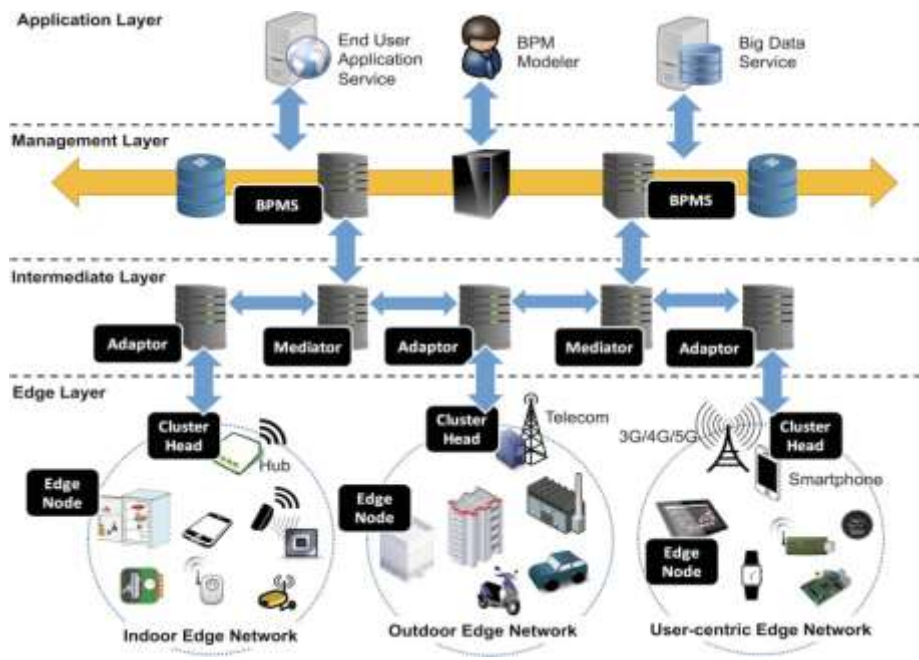


Fig. 6. BPM for the IoT Framework, Adapted from [1].

Modeling these kinds of events in a process is burdensome because these events must be encompassed in all probable activities, resulting in added difficulty as well as making it hard to comprehend the modeled process, specifically the chief process flow. Furthermore, the context will be considered to decide on how to respond to a lone event, the events that have been formerly perceived [28]. The study on event-driven and adaptive processes in IoT systems can reflect the extension and use of event-driven architectures (EDA) for activity checking and complex event processing (CEP). To start particular parts or steps of a business process, EDA can be joined with business process execution languages [29].

**Processes Dealing with Unreliable Data:** While working with events that are approaching from the physical world (like from signal-processing algorithms or sensors), some amount of undependability and doubt is put in the processes. In case the events with a certain doubt in them are used as a basis to take the conclusions in a business process, it is sensible to link all these events with a certain value for Quality of Information (QoI) [30].

In easy cases, this lets the process modeler describe thresholds. For instance, the event is presumed to have actually taken place if the degree of certainty is above 95%. In case it is amid 60–95%, we start to find out if certain other activities took place or not. The event is disregarded in case it is under 60%. Things become more difficult in cases when numerous events are involved. For instance, the degree of certainty of one event is 65%; one has 98%; and another has 83%. The principal services that fire the actual events need to be programmed to link these kinds of QoI values with the events [31]. From the viewpoint of a BPM, this kind of information must be taken, treated as well as articulated in a language like BPMN, which is a modeling notation language. Furthermore, the semantics and syntax of these kinds of QoI values must be standardized. As for the examples given earlier, is it merely a

certainty percentage, or must it be more expressive (like a range in which true value is there)? Applicable methods must not only merely look in the uncertainty flow of a business process based on IoT, but also in the total modeling and structuring of (perhaps unstructured or unknown) process flows. Practices for uncertain modeling of processes and data can be considered [32,33].

**Processes Dealing with Unreliable Resources:** The data from resources is characteristically undependable. The resources offering the data are also undependable because of the hosting device's failure [34]. Processes depending on these kinds of resources are required to be capable of adapting to these kinds of conditions. The major subject is to identify this kind of a failure. The detection, in which a process is calling a resource openly, is unimportant. It is tougher in the case of resources that may produce an event at one point in time (for instance, the resource that observes the temperature in the truck gives an alert in case it gets extremely hot) [35]. Resource failure can be a reason for not getting any event; however, one other reason can be that nothing was there to report. Similarly, the generated reports' quality must be frequently examined for accuracy. Certain monitoring software is required to sense these kinds of problems; however, if this kind of software must be a separate component or a segment of the BPM execution environment is unclear. Amid the challenges of the research is the management of monitoring processes with run-time actuating processes, provided that management planes have a tendency to function at diverse time scales from IoT processes [33].

**Highly Distributed Processes:** Performing a process in a decentralized manner is important; at the time, the interaction with real-world devices and objects is needed. The decentralization and the decomposition of current business processes upsurge performance and scalability and result in better decision making. It can even result in novel business

models. For instance, no messages are required to be sent to the central system in supply chain tracking or environmental monitoring applications if everything is in the limits. In case of a deviance, an alert (event) that can result in the adaptation of the whole process must be produced [34].

From the viewpoint of business process modeling, the process can probably explained centrally, providing that certain activities would be remotely performed. When the whole process is exhibited, linked services can probably be installed, which are to be implemented after this run and monitor the whole process. Appropriate issues of research comprise techniques and tools for the synthesis, authentication, and alteration of distributed processes in a volatile environment (e.g., altering settings, movement, and devices/objects connected to internet that leave or join) [36].

3) *Key success factors: Build IoT-BPM Ecosystems:* To control all aspects of the challenges that the BPM based on IoT, business ecosystems that are comparable to a coral reef, where a diversity of species can be found living in symbiosis with a shared development, must be built. This ecosystem must be friendly to all those who integrate it based on collaboration. The ecosystem allows every organization to stay alive and adapt to changes. Decisions are made as a team, and competitors are often partners too, sharing market and values [36].

Innovation as a business model: One of the main objectives of companies is to maintain and expand business relationships with their customers. Value-added services and new business models are a fundamental tool to achieve this and represent new opportunities. IoT technologies allow offering proposals to old customers and attracting new ones, enriching their services, obtaining more information, improving efficiency, and differentiating from competitors [20].

Entrepreneurial spirit: The connected world is highly volatile and dynamic, and the task of entrepreneurs and managers is to shape it by constantly taking advantage of the changes that are presented. This includes being prepared to deal with new environments that are presented at high speed in much the same way as when a new company is launched. Thus, IoT makes recommendable business structures divided into small, independent, agile business units that continually explore their environments and learn to prevent and minimize risks, but at the same time from a global perspective.

The use of Open source tools and cheap devices: One possible approach is to use open source software tools and non-expensive devices (such raspberry Pi) to deploy IoT solutions and integrate them with existing machines and systems in industries, in order to achieve full coverage of the organization's activity. It is necessary to adapt the elements that the industry already has to new technologies; this allows a reuse that not only economically favors companies, but also reduces the impact of discarding them.

### B. Blockchain Technology

1) *Theoretical overview:* Blockchain is commonly acknowledged as the technology behind Bitcoin [37]. However, the possible applications of Blockchain are much

more than merely facilitating digital currencies [38]. Blockchain allows a growing set of parties to keep a tamperproof, safe, and permanent transactions' ledger without a chief authority. Moreover, the transactions are not noted centrally, which is a vital aspect of this technology [39].

The technology of Blockchain unlocks various prospects to reform collaborative business processes, such as logistics and supply chain processes. These kinds of processes are usually performed by depending on reliable third-party providers, such as electronic data interchange escrows or hubs. The central design forms barriers to entry and deters process innovation. With the help of Blockchain, these processes can be performed in a peer-to-peer style without entrusting trust to central authorities nor needing mutual trust amid all groups of parties [40].

Prior works [41-43] show the viability of conducting collaborative business processes on a Blockchain platform. This is done by altering a collaborative process model into a smart contract serving like a template. After this, instance-specific smart contracts are produced from this template, which is done to observe or perform all instances of the process. This primary proof-of-concept design has bought out the requirement to enhance the usage of resource. Certainly, the Blockchain technology's cost is extremely subtle to the size of data registered on the ledger as well as the rate with which the smart contracts update the data [44,39]. Reducing the code size, rate of data writes, and data retained in the smart contracts is essential in making the Blockchain technology a feasible substitute for performing collaborative business processes.

2) *Blockchain technology improvement opportunities for BPM:* What kind of business process enhancement prospects does the Blockchain technology allow? To answer this, the value-driven BPM (VBPM) structure is used[45]. The VBPM structure (Fig. 7) categorizes the value, which the BPM can obtain for a business in seven groups. The "transparency" value is the main value in this framework, and states the capability for BPM to assist the shareholders of a business to monitor as well as comprehend their business processes in a better way.

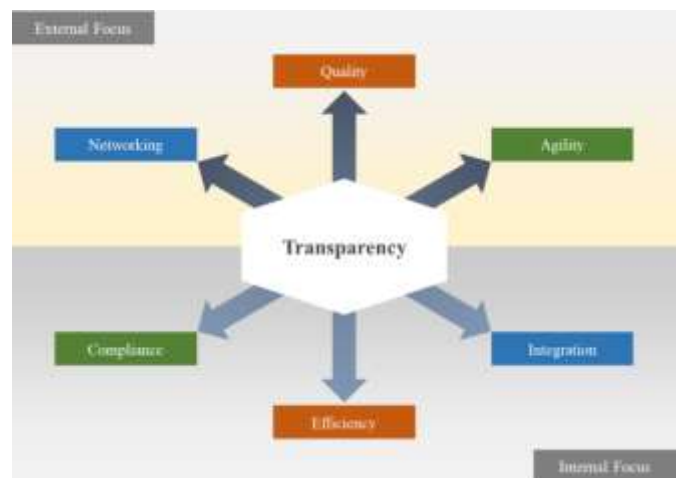


Fig. 7. Value-Driven BPM, Adapted from [45].



After the transparency is attained, BPM can bring value in three axes, with every axis equating to a pair of values. The efficiency–quality pair is the first axis, which shows a regularly recognized dichotomy amid efficiently satisfying the customer’s needs (quality) and restructuring the processes to proficiently satisfy these needs (like, at minimum cost). The agility–compliance pair is the second axis, which takes the contrast amid being capable to quickly adjust to a varying business environment (flexibility) vs. protecting the processes to make sure that they obey the applicable standards and rules. The third axis (integration–networking pair) takes the double imperative for businesses to keep their inner systems combined to avert siloes and depict the systems to external business partners to make use of collaborative business prospects [46].

**Efficiency vs. quality:** Several cases are suggested for Blockchain emphasis on augmenting competence by decreasing costs and time. The business of banking has profoundly invested in start-ups based on Blockchain, which functions with forming new arrangements for clearing of fiscal products. In partnership with more than 40 banks, the Corda platform has been presented by R3. The platform can re-design the present settlement processes by allowing the registration of financial agreements once, thus, removing the repetition of data to save costs and time from redundant reconciliation processes. Similarly, the Australian Stock Exchange is keenly looking to substitute its established CHES payment system with a distributed ledger based on Blockchain to decrease costs and settlement times [39].

Blockchain can also improve the quality of the consequence of business processes. When it comes to supply chains, tracking of materials and goods based on Blockchain could let a thorough tracking as well as avert fake products getting into the chain and avert replacement of good quality with inferior quality materials. One more instance is from the insurance sector, in which the eminence of the claim-handling course could be enhanced with the usage of the Blockchain technology. Blockchain would offer means to avert the usage of outdated or flawed data in the procedure.

**Agility versus compliance:** Agility is the ease and speed with which a business can retort to diverse modifications. The technology of Blockchain lets “smart contracts,” which automatically perform particular actions as mentioned in its conditions. These kinds of constructs could advance the agility of a course by shifting run-time implementations to smart contracts, thus describing the procedure per contract instead of the entire system. For example, with the goal of attaining safer, tailored, and auditable pay-outs, the UK government wants to put their welfare payment procedure on Blockchain.

The Blockchain technology can also make the compliance simpler by letting the dispensing of private data safely. Financial businesses, which are frequently put through new compliance guidelines, could dispense the data on Blockchain and give admission to financial regulatory agencies. It would eliminate the requirement of recording by giving the work of collecting data to the regulatory activities. This principal solution can be put on the accounting data of companies and their auditors.

**Integration vs. networking:** Blockchain could also be made use of to allow an enhanced incorporation of the processes in a firm. Blockchain has also been suggested for linking software, which will allow an inner network, in which the information systems are internally connected for data sharing. Although this practice is not much endorsed, the Blockchain’s networking feature is widespread [46].

The use of Blockchain as a registry of products is one of the most indorsed use. The notion is to record, register, and look into the transference of the possession of any product on distributed ledgers. Some of the benefits are being tamper-proof, avoiding third-party central ledgers, security, and clean records [47]. Nevertheless, this kind of solution allows collaborative processes. A research is taking place in Sweden to list and record land titles on a Blockchain solution. This will allow multi-party partnership, in which government agencies, banks, sellers, and buyers can cooperate and look at the development of the procedure.

The ability to considerably alter an extensive spectrum of business processes lies with the Blockchain technology [47]. With Blockchain making its presence known, it will possibly be the job of process experts to make sure that the value formed originates from discovering the prospects that Blockchain can support in business processes in place of merely substituting present technologies with others.

*3) Blockchain and BPM capabilities and challenges:* When new technologies show up, which are still in the first stages and far from reaching completeness, there is always a lot of debate [48,11]. In this section, the challenges and the opportunities that come from the Blockchain technology regarding the six BPM core competence areas are discussed. These core competencies are presented in Fig. 4, namely culture, methods, strategic alignment, information technology, governance, and people.

**Strategic alignment:** The Blockchain technology needs a study on how systematic analyses of the strategic effects of its usage on particular processes could be directed. As an unruly technology, Blockchain puts queries if the traditional process following a strategy model could be flipped with new processes based on Blockchain, challenging whole businesses like accounting. For numerous businesses, a possible disintermediation that could be allowed by the usage of Blockchain-based systems may result in a threat, and not an opportunity [11].

**Governance:** The Blockchain technology alters governance for the reason that it allows coooperation as a novel management style for processes [49]. This needs research on the description of devoted roles that communicate with external and internal partners for putting Blockchain provision for processes. Moreover, policies that describe when and where the Blockchain technology could be made use of or should not be made use of are needed for backing processes. For example, cryptocurrencies take exchange rates that are extremely volatile to old-style currencies, gains, and losses of 10–50% in a day are not rare. This instability would likely reduce with a wider uptake. At this time, it is a barricade for numerous applications.

Novel attack circumstances on Blockchain networks are hard to predict. As a result, strategies for making use of consortium, public-, or private-based Blockchains are needed. Lastly, smart contracts assure to ease self-governance of not merely processes, but of whole groups, like those presently role-modeled by the Decentralized Autonomous Organization. Making a decision on which applicants must have the discernibility of the parts of the transaction history also postures tests in trade-offs. On the one hand, advanced confidentiality and privacy will upsurge the receipt of the technology. On the other hand, more clearness in results in honesty, agreement checking, and optimization are founded on consistent data [50].

**Methods:** The Blockchain technology would need novel analysis approaches precisely with a focus on cost/benefit study and risk assessment and collaborative engineering approaches [44]. These need official reasoning competences regarding the precision and privacy protection of smart contracts. In addition, Blockchain would transmit attention from examining pain points back to looking for uncharted new prospects that may recover the certainty of the process re-engineering ideas argued in the early 1990s.

**Information technology:** The Blockchain technology needs novel answers, software components, and integrated development environments to apply business processes with Blockchains. Moreover, novel challenges have come out with issues of privacy and security, such as how to avert private business data leak. Though the discernibility of encoded data on a Blockchain is limited, it is in the hands of the contestants in the process to make sure that these devices are made use of in accordance to their confidentiality necessities. The certainty of these necessities is presently examined in the fiscal sector. Lastly, the characteristic boundaries of Blockchains are to be deliberated comprising throughput, computational power, processing costs, and data storage. Instead of making use of a present Blockchain, a substitute can be used to simply accept equivalent design philosophies, such as virtual transaction history [47].

**People:** The acceptance of Blockchains and the scheme of smart contracts would need novel means of thinking regarding individuals as the emphasis moves from processes in a sphere of control to alliance amid groups. Furthermore, individuals should be keen to make business partnerships in the frame of present rules to assist acceptance. This suggests that investigation of the Blockchain technology acceptance is required. Lastly, with inferences for work associations, giving incentives to third parties to add to current processes becomes simple because of the sincerity of Blockchains.

**Culture:** Blockchains need research in the organizational aspects, which ease initial and fruitful adoption. The organizational culture can probably be one of the aspects because the Blockchain model defies classical organizational structures [49].

Current research in the field of integrating a Blockchain into BPM is just beginning. At the moment there are still gaps in research and a lack of experience in this area. For the productive use of the Blockchain technology, the abovementioned challenges will have to be mastered in the

future. For example, there is currently a great need for specific requirements, conceptual models, procedures, case studies and technical solutions for successful integration into the system landscape of large companies and into the supplier network. A key aspect here is the integration of the Blockchain into the existing system landscapes.

Another practical example is connecting the Blockchain to the existing ERP systems; there are synergy effects for the improvement and efficient handling of the current process steps. When integrating both approaches, high care should be taken to ensure that the different concepts of the two systems harmonize with one another and are coordinated with one another. This is the only way to utilize the advantages and potential of both of them in an optimal way.

4) *Key success factors:* The biggest key success factor to turning Blockchain's potential into reality in BPM is the collaborative effort between organizations. Although business networks are a critical success factor for the adoption of the Blockchain technology, many other factors should also be considered [48]. One of these factors is the generation of an internal drive for the integration and application of Blockchain among enterprises, a factor that many organizations are struggling to achieve today [11]. Additional success factor that should be discussed is whether Blockchain capabilities contradiction with security challenges. Security is another reason why organizations might hesitate to adopt Blockchain, which is also reasonable. Ensuring process both secure and efficient is a challenge in itself, and it is a success factor for Blockchain generally. Although is not easy, however, it is not impossible as we have been a witness for many invocations in the usability of more secure solutions in the past years and the Blockchain will not be an exception. Beyond these factors, something is more fundamental: the need to make stakeholders within the organization be aware of the potential benefits of Blockchain and its positive effects. Finally, in order to apply Blockchain successfully, a common coordination among organizations must be fostered, which is vital in generating the positive network effects that make Blockchain very compelling [39].

## V. DISCUSSION

BPM is one of the most pronounced topics when dealing with information technology applied to the business environment. This paradigm encompasses the concepts, methods, techniques and software tools that support the life cycle of an organization's business processes. BPM is considered a multidisciplinary approach since it presents connectors with highly related business and technological elements. Along with the technological connectors as a type of application integration technologies incorporated into BPM, many merging technologies such Blockchain and IoT have evolved to change the way BPM is operated and managed, constitute a means to lead organizations to be more agile and innovative. This article conducted a review on how BPM could be integrated with the Blockchain and IoT technologies. It highlights the challenges that face the integration process,

describes and discuss the key success factors of the integration between the technologies under investigation.

Few reviews analyze the factors that influence the adoption of BPM technologies and emerging systems in the literature consulted. Reviews in this domain of knowledge focus on: assessing the characteristics of BPM technologies based on their proprietary or free nature [51, 52], analyzing their architecture and standards [53], and evaluating business process maturity models as evidence of its utilitarian nature and in relating BPM to software engineering in topics such as requirements engineering or the approach to software product lines.

In this section, a summary for our review on integrating Blockchain and IoT with BPM are listed:

- The first technology is the Internet-of-Things, which has the potential to fundamentally change the way people interact with their environment. IoT makes it possible to consider extensive real-time information in business processes. The result is processes that are more transparent and monitoring of business processes. The processes have to be adapted to the new possibilities of IoT to realize their full potential. The right people must use the right objects in the right situation at the right time. Therefore, the use of IoT requires flexible business processes that are capable of dynamically adapting to the changes that can occur through process execution or the properties of the smart objects. Numerous difficulties and challenges need to be investigated during the adoption of IoT for BPM, such as: extending and enhancing the current business process modeling and execution and service description languages, dealing with unreliable data, dealing with unreliable resources, and performing highly distributed processes.
- The second technology is the Blockchain which unlocks various prospects to reform collaborative business processes, such as logistics and supply chain processes. Moreover, Blockchain allows a growing set of parties to keep a tamperproof, safe, and permanent transactions' ledger without a chief authority. Moreover, the transactions are not noted centrally, which is a vital aspect of this technology. Some related challenges are as follow: Blockchain technology needs a study on how systematic analyses of the strategic effects of its usage on particular processes could be directed. Also consider the needs to a description of devoted roles that communicate with external and internal partners for putting Blockchain provision for processes. Finally, the policies that describe when and where the Blockchain technology could be made use of or should not be made use of are needed for backing processes and the needs for novel analysis approaches precisely with a focus on cost/benefit study and risk assessment and collaborative engineering approaches.

The research results should be interpreted taking into account some limitations, mainly with respect to the underlying research method. Specifically, the application of content analysis does not allow the study to be exempted from a certain

subjectivity. In order to avoid or minimize it, the authors have carried out this analysis, with an additional volunteer researcher intervening to coordinate the solution to discrepancies or different interpretations when quantifying the information. Similarly, another limitation is the number of databases consulted and that only academic articles published in journals and peer-reviewed have been searched. Perhaps, if the search is extended to a greater number of repositories and other types of publications (books, book chapters, contributions to congresses, doctoral theses or even informative works), more works could be found that confirm the findings and results of different research aspects. On the contrary, they suppose a new perspective for the literature in the field. In any case, it was decided to include only academic articles published in journals to guarantee their quality.

## VI. CONCLUSION

The digital transformation is revolutionizing every industry. The change is occurring at an exponential pace. Enterprises embarking on this new world have unlimited possibilities. New ways to connect with customers, more innovation for the workforce, the chance to engage and retain the most talented people, and the use of data analytics are just some of the possibilities of digitization. The benefits are clear: customers benefit from a successful delivery of higher sales, and can differentiate themselves from the competition in the market. The objective of this work was to investigate two emerging technologies and explain how they can be applied to improve business process management by studying their opportunities, challenges, and key success factors.

As a future work, more investigations on the impact of Blockchain and IoT on BPM can be applied through a qualitative and quantitative study on organizations of different sizes. Additional emerging technologies such as Cloud computing can be investigated also. Finally, reviewing more surveys that are recent and relevant could add a higher value to the overall work.

## REFERENCES

- [1] C. Chang, S. N. Srirama, and R. Buyya, Mobile Cloud business process management system for the internet of things: a survey, *ACM Computing Surveys*, vol. 49, no. 4, pp. 70, 2017.
- [2] M. Rosemann, and J. vom Brocke, The six core elements of business process management, *Handbook on business process management*, In *Handbook on business process management 1*, Springer, pp. 105-122, 2015.
- [3] J. vom Brocke, and J. Mendling, Frameworks for business process management: a taxonomy for business process management cases, *Business Process Management Cases*, Springer, , pp. 1-17, August, 2017.
- [4] L. Da Xu, Enterprise systems: state-of-the-art and future trends, *IEEE Transactions on Industrial Informatics*, vol. 7, no. 4, pp. 630-640, 2011.
- [5] M. Yang, and P. Gabrielsson, Entrepreneurial marketing of international high-tech business-to-business new ventures: A decision-making process perspective, *Industrial Marketing Management*, vol. 64, pp.147-160, July, 2017.
- [6] K. Korpela, J. Hallikas, and T. Dahlberg, Digital supply chain transformation toward blockchain integration., In *proceedings of the 50th Hawaii international conference on system sciences*, Village, Hawaii, , January, 2017.
- [7] J. F. Chang, *Business process management systems: strategy and implementation.*, CRC Press, , April, 2016.

- [8] N. J. A. S. Kratzke, A brief history of cloud application architectures, *Applied Sciences*, vol. 8, no. 8, pp. 1368, 2018.
- [9] L. Da Xu, W. He, and S. Li, Internet of things in industries: A survey, *IEEE Transactions on industrial informatics*, vol. 10, no. 4, pp. 2233-2243, 2014.
- [10] W. M. Van der Aalst, Business process management: a comprehensive survey, *ISRN Software Engineering*, vol. 2013, , 2013.
- [11] W. Viriyasitavat, L. Da Xu, Z. Bi, and A. Sapsomboon, Blockchain-based business process management (BPM) framework for service composition in industry 4.0, *Journal of Intelligent Manufacturing*, vol. 2018, No.1, pp. 1-12, May, 2018.
- [12] M. Klun, and P. Trkman, Business process management—at the crossroads, *Business Process Management Journal*, vol. 24, no. 3, pp. 786-813, 2018.
- [13] C. Chang, S. N. Srirama, and R. Buyya, Mobile Cloud Business Process Management System for the Internet of Things: A Survey, *ACM Computing Surveys*, vol. 49, no. 4, pp. 1-42, 2016.
- [14] J. Luftman, K. Lyytinen, and T. ben Zvi, Enhancing the measurement of information technology (IT) business alignment and its influence on company performance, *Journal of Information Technology*, vol. 32, no. 1, pp. 26-46, 2017.
- [15] W. van der Aalst, A. Ter Hofstede, and M. Weske, Business Process Management, *International Conference, BPM 2003, Proceedings: Springer Science & Business Media*, , Eindhoven, The Netherlands, June 26-27, 2003.
- [16] W. Viriyasitavat, L. Da Xu, Z. Bi, and V. Pungpapong, Blockchain and Internet of Things for Modern Business Process in Digital Economy--the State of the Art, *IEEE Transactions on Computational Social Systems*, vol. 6, No. 6, pp. 1420-1432, 2019.
- [17] H. Pervez, and I. U. Haq, Blockchain and IoT Based Disruption in Logistics., In *2019 2nd International Conference on Communication, Computing and Digital systems (C-CODE)*, Pakistan, Islamabad, pp. 276-281, March, 2019.
- [18] J. Gubbi, R. Buyya, S. Marusic, and M. Palaniswami, Internet of Things (IoT): A vision, architectural elements, and future directions, *Future generation computer systems*, vol. 29, no. 7, pp. 1645-1660, 2013.
- [19] L. Atzori, A. Iera, and G. Morabito, The internet of things: A survey, *Computer networks*, vol. 54, no. 15, pp. 2787-2805, 2010.
- [20] S. Meyer, A. Ruppen, and C. Magerkurth, Internet of things-aware process modeling: integrating IoT devices as business process resources., In *International conference on advanced information systems engineering*, pp. 84-98, Springer, Berlin, Heidelberg, 2013.
- [21] Y.-T. Chen, and M.-S. Wang, A study of extending BPMN to integrate IoT applications., In *2017 International Conference on Applied System Innovation (ICASI)*, Sapporo, Japan, pp. 1797-1800, May 13-17, 2017.
- [22] C. Janiesch, A. Koschmider, M. Mecella, B. Weber, A. Burattin, C. Di Ciccio, A. Gal, U. Kannengiesser, F. Mannhardt, and J. Mendling, The internet-of-things meets business process management: mutual benefits and challenges, *arXiv preprint, arXiv:1709.03628*, , 2017.
- [23] E. d. S. Zancul, S. M. Takey, A. P. B. Barquet, L. H. Kuwabara, P. A. Cauchick Miguel, and H. Rozenfeld, Business process support for IoT based product-service systems (PSS), *Business Process Management Journal*, vol. 22, no. 2, pp. 305-323, 2016.
- [24] S. Haller, and C. Magerkurth, The real-time enterprise: Iot-enabled business processes., In *IETF IAB Workshop on Interconnecting Smart Objects with the Internet*, Prague, pp. 1-3, 25th March 2011.
- [25] H.-H. Chiu, and M.-S. Wang, A study of iot-aware business process modeling, *International Journal of Modeling and Optimization*, vol. 3, no. 3, pp. 238, 2013.
- [26] M. Del Giudice, Discovering the Internet of Things (IoT): technology and business process management, inside and outside the innovative firms, *Business Process Management Journal*, vol. 22, no. 2, 2016.
- [27] M. Schief, C. Kuhn, P. Rösch, and T. Stoitsev, Enabling Business Process Integration of IoT-events to the Benefit of Sustainable Logistics., In *the International Conference on Logistics, Informatics and Service Science (LISS 2015)*, Beijing, China, pp. 40-49, February, 2011.
- [28] S. Appel, P. Kleber, S. Frischbier, T. Freudenreich, and A. Buchmann, Modeling and execution of event stream processing in business processes, *Information Systems*, vol. 46, pp. 140-156, 2014.
- [29] A.-M. Barthe-Delanoë, S. Truptil, F. Bénaben, and H. Pingaud, Event-driven agility of interoperability during the Run-time of collaborative processes, *Decision Support Systems*, vol. 59, pp. 171-179, 2014.
- [30] R. G. Lee, and B. G. Dale, Business process management: a review and evaluation, *Business process management journal*, vol. 4, no. 3, pp. 214-225, 1998.
- [31] G. Goldkuhl, and P. J. Ågerfalk, Action within information systems: outline of a requirements engineering method., In *the Fourth International Workshop on Requirements Engineering: Foundation for Software Quality*, Pisa, Italy, pp. 133-153, June 8-9 1998.
- [32] Y. Cheng, S. Zhao, B. Cheng, S. Hou, Y. Shi, and J. Chen, Modeling and Optimization for Collaborative Business Process Towards IoT Applications, *Mobile Information Systems*, vol. 2018, , 2018.
- [33] M. Papert, A. Pflaum, and A. Leischnig, A business process perspective on IoT implementation: findings from a comparative case analysis, *International Conference on Information Systems (ICIS)*, Seoul, , December 10th- 13th, 2017.
- [34] S. Haller, S. Karnouskos, and C. Schroth, The internet of things in an enterprise context., In *Future Internet Symposium*, Springer, Berlin, Heidelberg, pp. 14-28, 29 September, 2008.
- [35] S. Schönig, L. Ackermann, S. Jablonski, and A. Ermer, An integrated architecture for IoT-aware business process execution, In *Enterprise, Business-Process and Information Systems Modeling*, , pp. 19-34, Springer, Cham, 2018.
- [36] H.-G. Hong, Business Process Support Based on IoT Technology, *Journal of Convergence for Information Technology*, vol. 7, no. 1, pp. 75-79, 2017.
- [37] Eyal, A. E. Gencer, E. G. Sirer, and R. Van Renesse, Bitcoin-NG: A Scalable Blockchain Protocol., In *13th {USENIX} symposium on networked systems design and implementation ({NSDI} 16)*, Santa Clara, CA, USA, pp. 45-59, March 16–18, 2016.
- [38] D. Tapscott, and A. Tapscott, Blockchain Revolution: How the technology behind Bitcoin is changing money, business, and the world: aPenguin, *The Quality Management Journal*, Vol. 25, no. 1, pp.64-65, 2016.
- [39] Weber, X. Xu, R. Riveret, G. Governatori, A. Ponomarev, and J. Mendling, Untrusted business process monitoring and execution using blockchain., In *International Conference on Business Process Management*, Springer, Cham, pp. 329-347, 2016, September.
- [40] R. Hull, Blockchain: Distributed Event-based Processing in a Data-Centric World., In *Proceedings of the 11th ACM International Conference on Distributed and Event-based Systems*, Barcelona, Spain, pp. 2-4, June, 2017.
- [41] L. García-Bañuelos, A. Ponomarev, M. Dumas, and I. Weber, Optimized execution of business processes on blockchain., In *The International Conference on Business Process Management*, Barcelona, Spain, pp. 130-146, September 10-11, 2017.
- [42] C. Prybila, S. Schulte, C. Hocheiner, and I. Weber, Runtime Verification for Business Processes Utilizing the Bitcoin Blockchain, *arXiv preprint, rXiv:1706.04404*, 2017.
- [43] D. Verma, N. Desai, A. Preece, and I. Taylor, A blockchain based architecture for asset management in coalition operations., In *Ground/Air Multisensor Interoperability, Integration, and Networking for Persistent ISR VIII*, International Society for Optics and Photonics, vol. 10190, pp. 101900Y-101900Y-9, May, 2017.
- [44] J. Mendling, I. Weber, W. V. D. Aalst, J. V. Brocke, C. Cabanillas, F. Daniel, S. Debois, C. D. Ciccio, M. Dumas, and S. Dustdar, Blockchains for business process management-challenges and opportunities, *ACM Transactions on Management Information Systems (TMIS)*, vol. 9, no. 1, pp. 4, 2018.
- [45] F. Milani, L. García-Bañuelos, and M. Dumas, Blockchain and business process improvement, *BPTrends newsletter*, , October, 2016.
- [46] López - Pintado, L. García - Bañuelos, M. Dumas, I. Weber, and A. Ponomarev, CATERPILLAR: A business process execution engine on the Ethereum blockchain, *Software: Practice and Experience*, vol. 49, no. 7, pp. 1162-1193, 2019.

- [47] B. Tran, Q. Lu, and I. Weber, Lorikeet: A Model-Driven Engineering Tool for Blockchain-Based Business Process Execution and Asset Management., In BPM (Dissertation/Demos/Industry), , pp. 56-60, 2018.
- [48] S. Saberi, M. Kouhizadeh, J. Sarkis, and L. Shen, Blockchain technology and its relationships to sustainable supply chain management, International Journal of Production Research, vol. 57, no. 7, pp. 2117-2135, 2019.
- [49] J. Mendling, I. Weber, W. van der Aalst, J. v. Brocke, C. Cabanillas, F. Daniel, S. Debois, C. Di Ciccio, M. Dumas, and S. Dustdar, Blockchains for Business Process Management-Challenges and Opportunities, arXiv preprint, arXiv:1704.03610, , 2017.
- [50] Norta, Establishing Distributed Governance Infrastructures for Enacting Cross-Organization Collaborations., In International Conference on Service-Oriented Computing, Springer, Berlin, Heidelberg, pp. 24-35, November, 2015.
- [51] Sousa, Marco, et al. "Evaluation of BPM tools open source/freeware." 2018 13th Iberian Conference on Information Systems and Technologies (CISTI). IEEE, 2018.
- [52] Pourmirza, S., Peters, S., Dijkman, R., & Grefen, P. (2017). A systematic literature review on the architecture of business process management systems. Information Systems, 66, 43-58.
- [53] Correia, E., Carvalho, H., Azevedo, S. G., & Govindan, K. (2017). Maturity models in supply chain sustainability: A systematic literature review. Sustainability, 9(1), 64.

# A Trust-Based Collaborative Filtering Approach to Design Recommender Systems

Vineet K. Sejwal<sup>1</sup>

Department of Computer Science  
Jamia Millia Islamia, New Delhi, India

Muhammad Abulaish<sup>2</sup>, SMIEEE

Department of Computer Science  
South Asian University, New Delhi, India

**Abstract**—Collaborative Filtering (CF) is one of the most frequently used recommendation techniques to design recommender systems that improve accuracy in terms of recommendation, coverage, and rating prediction. Although CF is a well-established and popular algorithm, it suffers with issues like black-box recommendation, data sparsity, cold-start, and limited content problems that hamper its performance. Moreover, CF is fragile and it is not suitable to find similar users. The existing literatures on CF show that integrating users' social information with a recommender system can handle the above-mentioned issues effectively. Recently, *trustworthiness* among users is considered as one such social information that has been successfully combined with CF to predict ratings of the unrated items. In this paper, we propose a trust-based recommender system, **TrustRER**, which integrates users' trusts into an existing user-based CF algorithm for rating prediction. It uses both ratings and textual information of the items to generate a trust network for users and derives the trust scores. For trust score, we have defined three novel trust statements based on user rating values, emotion values, and review helpfulness votes. To generate a trust network, we have used trust propagation metrics to compute trust scores between those users who are not directly connected. The proposed **TrustRER** is experimentally evaluated over three datasets related to movie, music, and hotel and restaurant domains, and it performs significantly better in comparison to nine standard baselines and one state-of-the-art recommendation method. **TrustRER** is also able to effectively deal with the *cold-start* problem because it improves the rating prediction accuracy for *cold-start* users in comparison to baselines and state-of-the-art method.

**Keywords**—Recommender system; collaborative filtering; cold-start; trust; rating prediction

## I. INTRODUCTION

Personalized recommender systems recommend items based on the users' past experiences, previous ratings, and their preferences. Recommender systems handle *information overload* problem effectively where users find difficult to get right information at right time [1] [3]. Incorporating concepts like machine learning and information filtering with user profiling makes the recommender systems more effective towards product recommendation. Algorithms like content-based, collaborative filtering (CF), and hybrid methods are some well-known approaches for recommender systems [4]. Out of these CF is a frequently used algorithm to design recommender systems. It is very effective and simple to use in comparison to other approaches. CF can be categorized into memory-based (neighborhood) and model-based (latent factor) methods. In memory-based methods, similarities between users or items are used for rating prediction, whereas, model-based methods use machine learning approaches for creating rating prediction and

recommendation models. In recent years, matrix factorization (MF) based CF models have gained huge popularity due to their scalability and high accuracy [14]. However, one of the major issues with CF is to find similar users or items that are used to compute user- or item-based similarity in the recommending process. Moreover, CF algorithm alone is not capable to handle issues like *cold-start* and *data sparsity*.

Recently, researchers have shown that integrating users' social information with CF can handle the *cold-start* and *data sparsity* issues effectively with improved recommendations. Social networks play an important role in filtering user information because most of the information is obtained and diffused by the users' acquaintances, such as friends and colleagues [15] [26]. The social network-based recommendation approaches assume the existence of social ties between users, where users in the network are directly or indirectly connected to each other. One such promising social information is *trust* because users like to accept different viewpoints of other users in a trust-based social network. Abbasi et al. [5] defined trust as follows: "trust between two entities refers a situation where the first entity (trustor) rely on the activities of another entity (trustee)". Mayer et al. [2] defined trust as "the willingness of a party to be vulnerable to the actions of another party based on the expectation that the other will perform a particular action important to the trustor, irrespective of the ability to monitor or control that other party".

Since the incorporation of trust information into the recommender systems helps to improve rating prediction accuracy and handles *cold-start* and *data sparsity* problems, in this paper, we propose a trust-based recommender system, **TrustRER**, which predicts the ratings of the unrated items for the users based on their trust scores. We believe that only similar ratings between a user-pair are not ideal and sufficient for the recommendation, instead, they should have similar preferences, tastes, and trustworthiness. The proposed **TrustRER** computes the trust score between users using different trust statements. Unlike other trust-based models, where only user ratings are considered as a trust statement, we introduced three novel trust statements based on ratings, emotions, and review helpfulness votes. The users' trust scores are incorporated with the user-based CF model to enhance its rating prediction and recommendation capability. We generate a *trust-based* network for the users using the trust statements. It might be possible that users in a trust network are not directly connected because they do not rate the same items. To handle this issue, we incorporate one-hop trust propagation for those users who are not directly connected.

For experimental evaluation of TrustRER, we have used publicly available datasets – Amazon dataset (music domain) and Yelp (hotels and restaurants domain), and a movie dataset containing users’ reviews and movie-related information and used in one of our previous work [28]. TrustRER is compared with nine standard baselines and one state-of-the-art method using error-based and decision support-based metrics and outperforms these methods. TrustRER also improves rating prediction accuracy in comparison to comparative methods for *cold-start* users.

In short, the contributions of this work can be summarized as follows:

- Developing a recommendation method, TrustRER, combining trust and user-based collaborative filtering (UBCF) to predict the ratings of the unrated items.
- Defining three new trust statements to compute trust scores using both user ratings and reviews.
- Validating the proposed recommendation method using standard error-based and decision support-based metrics and comparing it with nine standard baselines and one state-of-the-art method over three datasets.
- Empirically evaluating the effectiveness of TrustRER to handle *cold-start* users in comparison to standard baselines and state-of-the-art methods.

The rest of the paper is organized as follows. Section II presents a brief discussion on the existing works to design recommender systems using trust statements and collaborative filtering. Section III presents a detailed description of the trust-related concepts, such as trust metrics, trust propagation, and trust aggregation. The work-flow of our proposed TrustRER method is discussed in Section IV. It also presents the computation of trust scores between users using three trust statements and trust models to predict ratings using the trust values and UBCF. Section V discusses the experimental and evaluation results. Finally, Section VI concludes the paper with future directions of research.

## II. LITERATURE REVIEW

In this section, we present a brief review of the existing literatures on trust-based recommender systems. We also review the approaches that have utilized both memory-based and model-based CF in trust-based recommender systems.

### A. Memory-based Trust-Aware Recommender Systems

In online social networks, *trust* represents the social relationships between users. Recently, trust has been used in many applications, such as multi-agents recommender systems, semantic web, and cloud computing. Rahman and Hailes presented a trust contextualization model in [6] that computes an explicit trust between a user-pair using *local trust* metric. This work was further extended by Massa and Bhattacharjee in [8], which proposed a model to compute local and explicit trust between a user-pair using the path (distance) that connects the respective users. The authors believed that only ratings of users are not sufficient for a recommender system to predict items because many users rate a few items. They introduced

the concept of *webs of trust* for users where trust propagation algorithms compute trust scores for indirectly connected users. The resultant trust value is binary. Further, Golbeck introduced a trust-based recommender system, *FilmTrust*, in [9] which recommends movies to users based on *Tidal* trust. *FilmTrust* computes an explicit *local trust* between users where trust values are gradual. To compute trust between directly and indirectly connected users, *FilmTrust* uses both trust propagation and trust aggregation techniques, respectively. In contrast to [9], O’Donovan and Smyth presented a *trust-based* recommendation technique [4] which computes an implicit local and global trust values. The trust value in the proposed work is gradual and uses trust metrics to compute the trust for user-pairs. The technique used in this work is based on the similarity between users. Hwang and Chen [27] incorporated both local and global trusts, respectively in a trust network that improves the rating prediction accuracy and coverage for recommendations. Massa and Avesani [10] introduced the *mole* trust algorithm, which computes the trust score for user-pairs using backward exploration. The path used for a user-pair in *mole* trust is based on the *maximum-depth*. Jamali and Ester [13] proposed *TrustWalker*, a coherent framework based on a random walk that combines both user-oriented approaches and user trust. The proposed model uses the ratings of the users that are directly/indirectly connected to the target user for the target item by performing a random walk. The methods discussed so far used rating-based trust statements for recommendations.

### B. Model-based Trust-Aware Recommender Systems

To improve the efficacy of recommender systems, there are various approaches where both trust and matrix factorization (MF) are incorporated in existing 2-dimensional recommender systems. Guo et al. [12] proposed *TrustSVD*, a SVD++-based MF method incorporated with users trust for rating prediction and recommendation. The idea behind the design of the *TrustSVD* model was to consider both users’ implicit and explicit ratings and trust for item recommendation. Yang et al. [17] proposed a variant of CF by incorporating users with social information and trust. The proposed model used MF technique, users sparse social trust network, and sparse rating data for rating prediction. Further, Jamali and Ester [7] proposed *SocialMF* model, a variant of MF which incorporates a trust propagation algorithm in an MF-based recommender system. The work proposed in [14] and [15] were based on co-factorization methods where the target user shares the same user and trust relation space. The co-factorization method factorizes the user-user trust relation matrix and user-item matrix using latent factors shared by the same user. Ma et al. [15] proposed *SoRec*, a social regularization model, which includes various social constraints of users. The proposed *SoRec* improves the rating prediction accuracy of recommender systems using social network information and also handles *cold-start* issue. Similarly, the works proposed in [16] and [19] were based on regularization methods which consider user preferences and assume that all user preferences should be available in their trust network. In another work, Jamali and Ester proposed a *SocialMF* model [16] that considered user preferences to generate a trust network.

Although, the approaches using either memory-based or model-based trust-aware recommendations have improved accuracy and coverage of the recommender systems, they

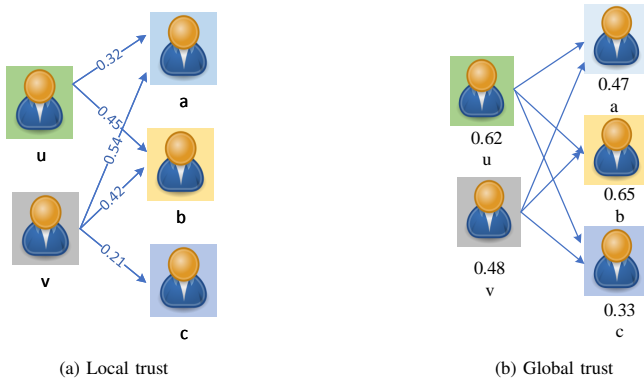


Fig. 1. Trust Metrics for Directly Connected users in a Trust Network.

still have certain limitations. First, the datasets used in these methods are either synthetic datasets or generated using questionnaire-based methods, such as Epinions and FilmTrust in which trust scores between users are provided. Second, the trust score between users is computed only using their ratings. In this paper, we overcome these limitations and compute the trust score automatically from the underlying datasets.

### III. PRELIMINARIES

In this section, we present a brief description of some trust-related concepts that are used to design trust-based recommender systems. We mainly describe trust metrics, which includes local and global trusts, trust propagation, and trust aggregation in the following sub-sections.

#### A. Trust

In a social network, the computation of a trust value between a user-pair is generally difficult because it is very tough to interpret users’ imagination, social behavior, and actual activities. To handle such issues, trust statements are defined and used to compute trust scores using users’ attributes and behavior. As discussed in section I, trust between a user-pair  $(u, v)$  determines the faith that a user (say  $u$ ) can keep on other user (say  $v$ ) based on their action and activities. Further, trust keeps various properties, such as *generic*, *asymmetric*, *distributive*, and *transitive* which are used to generate a trust network between users [18]. The trust metrics like *local trust* and *global trust* along with trust propagation and aggregation are useful to construct trust networks and discussed in the following sub-sections.

1) *Local Trust*: Local trust is always defined between a user-pair, and it is computed independently from every other users present in the trust network. Mathematically, local trust between a user-pair can be defined as  $LT : U \times U \rightarrow [0, 1]$ , where  $U$  is the set of users and  $[0, 1]$  is the range of trust score values. The local trust is said to be “local” because it is defined between a user-pair irrespective of the other users in the trust network, and computed using the trust statements. This implies that in a trust network comprising of  $n$  users, each user has maximum  $n - 1$  local trust scores. An example of local trust is given in figure 1a, where every connected user-pair shares a local trust value.

2) *Global Trust*: Global trust in a trust network represents a unique trust value for each user of the network. In general, global trust for a user is an aggregate single trust score computed using the trust statements. Mathematically, global trust can be defined as  $GT : U \rightarrow [0, 1]$ , where  $U$  is the set of users. This implies that in a trust network with  $n$  users there are  $n$  global trust scores, one for each user. An example of global trust is given in Fig. 1b, where every user has a global trust score value.

In comparison to *global trust*, *local trust* can handle various issues like *controversial topics* and *fake profiling* attack effectively. However, the time complexity of computing local trust is high in comparison to the global trust, because each user-pair is evaluated using the trust statements to compute the trust score values. There are various factors like topics, domains, and trust networks that can be taken into account while deciding to generate either local or global trust scores for a network.

#### B. Trust Propagation and Aggregation

In trust networks, there is a high chance that many users may not directly interact with other users. Therefore, trust propagation and aggregation algorithms are used for such users. A trust propagation algorithm computes both implicit and explicit trust values of the users in a trust network. Trust networks exhibit an atomic direct propagation relation which is also known as transitive relation. For example, if “Bob” trusts on “Alice”, and “Alice” trusts on another user “Eve” in a trust network, then using atomic direct propagation property, trust score between “Bob” and “Eve” can be calculated. However, trust networks not always hold the transitive relation property, which proves the subjectivity of trust [11]. In large trust networks where users are not directly connected, there is a chance that more than one path is available to set up connectivity between them. In such situations, propagating trust scores are not capable to compute trust between a user-pair. To handle this issue effectively, the aggregation of trust propagation scores are helpful to calculate trust values. Therefore, the structure of a trust network determines the requirement of both trust propagation and aggregation, as shown in Fig. 2a and 2b. To calculate the trust between a user pair  $E$  and  $J$  in Fig. 2a, the trust aggregation algorithm is required, because there are multiple paths between users  $E$  and  $J$ . On the other hand, trust propagation is sufficient in Fig. 2b for user pair  $(A, C)$  to estimate the trust score. Popular algorithms that are generally applied in a trust network to compute trust propagation and aggregation are briefly described in the following sub-sections.

1) *Mole Trust*: In a trust network, *mole* trust between a user-pair can be computed using both local trust and trust propagation metrics [22]. The working of *mole* trust is based on backward exploration, where a walk between a user-pair is initiated using the trust edges, as given in equation (1). In this equation,  $\mathcal{T}(v)$  represents trust value for user  $v$  for the previous walk, and  $\mathcal{T}_{edge}(v, u)$  represents trust edge score which connects the users  $v$  and  $u$ .

$$t_u = \frac{\sum_{v \in \text{precursors}} (\mathcal{T}(v) * \mathcal{T}_{edge}(v, u))}{\sum_{v \in \text{precursors}} (\mathcal{T}(v))} \quad (1)$$





Fig. 2. Trust Metrics for Indirectly Connected users in a Network.

2) *Tidal Trust*: *Tidal* trust was first proposed to recommend movies in a movie-based recommender system [20]. For a user-pair, *tidal* trust computes moderate trust in comparison to the *mole* trust which assigns a binary trust value. To compute *tidal* trust, first, all paths that connect a user-pair are identified, then the path having shortest distance is selected. Equation (2) presents a formal way to calculate *tidal* trust.

$$t_{m,n} = \frac{\sum_{p \in \text{adjacent}(m) | \mathcal{T}_{m,p} \geq \text{maximum}} \mathcal{T}_{m,p} \mathcal{T}_{p,n}}{\sum_{p \in \text{adj}(m) | \mathcal{T}_{m,p} \geq \text{maximum}} \mathcal{T}_{m,p}} \quad (2)$$

#### IV. PROPOSED APPROACH

In this section, we present a detailed description of the proposed TrustRER architecture, which is shown in Fig. 3. TrustRER predicts and recommends items to users using their trust values incorporated to the UBCF. First, a trust network is constructed using three novel trust statements based on users' ratings, emotions, and helpfulness votes. Thereafter, the trust score between users is incorporated into the UBCF model to find the top- $k$  users. Finally, ratings are predicted using users' trust scores with other users. A brief detail of different functioning modules of our proposed TrustRER architecture is presented in the following sub-sections.

##### A. Rating-based Deviation

In rating-based deviation, trust for a user-pair ( $a, u$ ) is computed using the rating values that represent their rating behavior. To calculate the trust score, we define a global trust function for both users  $a$  and  $u$ , as given in equations (3) and (4), where global trust shows the overall trust score for users  $a$  and  $u$ . In these equations,  $N$  represents the rating range for an item  $i$ ,  $\mathcal{R}$  represents the average rating value, and  $r_{ai}$  represents the rating value  $r$  given by user  $a$  on item  $i$ .

$$\mathcal{T}_{ai}^\delta = \begin{cases} \frac{-1}{N} |\mathcal{R} - r_{ai}| + 1, & \text{if } r_{ai} \neq 0 \\ 0, & \text{otherwise} \end{cases} \quad (3)$$

$$\mathcal{T}_{ui}^\delta = \begin{cases} \frac{-1}{N} |\mathcal{R} - r_{ui}| + 1, & \text{if } r_{ui} \neq 0 \\ 0, & \text{otherwise} \end{cases} \quad (4)$$

The deviation between the average rating  $\mathcal{R}$  and the ratings provided by users  $a$  and  $u$  on item  $i$  as  $r_{ai}$  and  $r_{ui}$  show the trust values of user  $a$  and  $u$ , respectively. Equation (5) computes the trust score for a user-pair ( $a, u$ ) using rating-based deviations. It can be observed from equation (5) that the trust value for a user pair ( $a, u$ ) is maximum only when both users rate nearly similar on identical items.

$$\mathcal{T}_{a,u,n}^\delta = \frac{\sum_{j=1}^n (1 - |\mathcal{T}_{aj}^\delta - \mathcal{T}_{uj}^\delta|)}{n} \quad (5)$$

##### B. Emotions-based Information

Emotions like *sadness*, *happiness*, *joy*, and *anger* between a user-pair ( $a, u$ ) can help to identify the trust/distrust relations between them. In [24] and [25], it has been proven by sociologists and psychologists that emotions are important parameters to compute trust/distrust values between users. Further, it has also been analyzed and observed that incorporation of emotions can reduce the data sparsity issue [23] [24]. Emotion values like *satisfaction*, *happiness*, and *joy* represent the positive emotions of users, whereas *sadness*, *anger*, and *fear* emotion values represent negative emotions [23]. The ratings and reviews provided by users on various e-commerce sites and platforms are highly correlated to their emotion values extracted from the reviews. The high ratings from users signify their positive emotions, whereas low ratings from users represent their negative emotions towards the consumption of the items. To calculate trust score for a user pair ( $a, u$ ), we define an emotion vector,  $\varepsilon = [\varepsilon_1, \varepsilon_2, \varepsilon_3, \varepsilon_4, \varepsilon_5]$  where,  $\varepsilon_1, \varepsilon_2, \varepsilon_3, \varepsilon_4$ , and  $\varepsilon_5$  represent *disgust*, *fear*, *sadness*, *joy*, and *anger*, respectively. Formally, (6) is used to compute the trust score using emotion vectors, where  $\mathcal{D}(a_j(\varepsilon), u_j(\varepsilon))$  is the Euclidean distance between the emotion vectors  $a_j(\varepsilon)$  and  $u_j(\varepsilon)$  for the user-pair ( $a, u$ ),  $\mathcal{T}_{a,u,n}$  is the aggregate trust score, and  $n$  represents the total number of similar items. The Euclidean

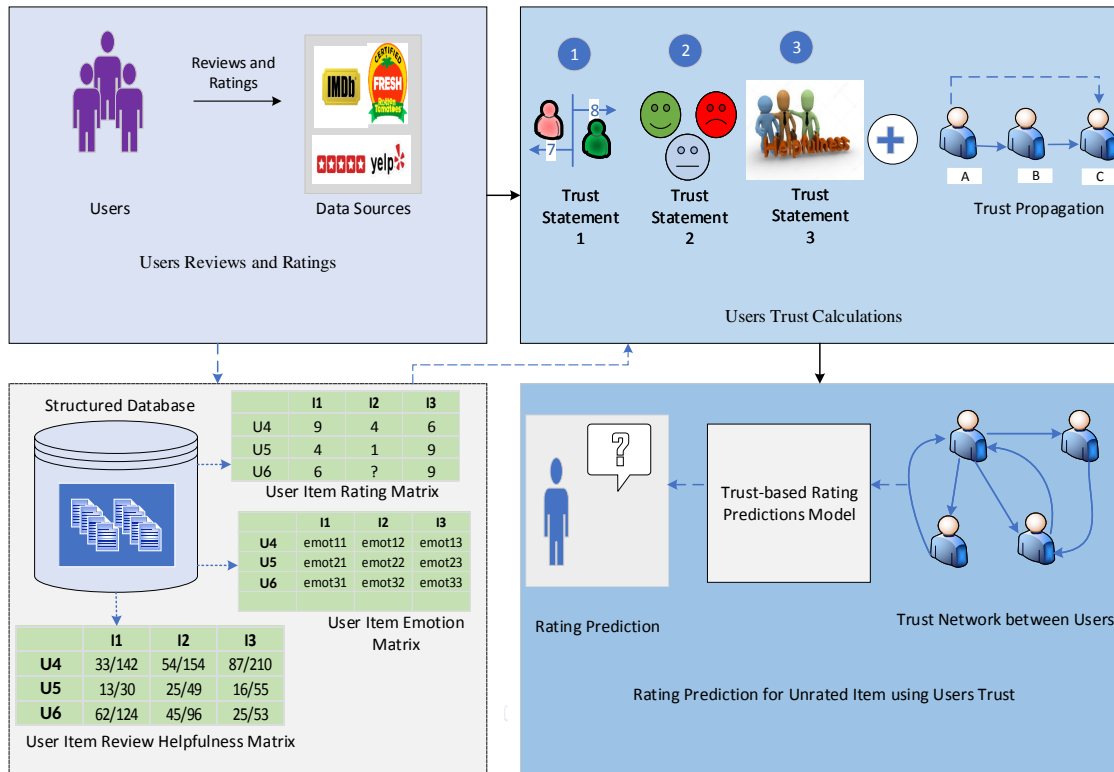


Fig. 3. Architecture of the Proposed TrustRER for Trust-based Recommendation.

distance between a user-pair  $(a, u)$  determines the correlation between them.

$$\mathcal{T}_{a,u,n}^\varepsilon = \frac{\sum_{j=1}^n (1 - \mathcal{D}(a_j(\varepsilon), u_j(\varepsilon)))}{n} \quad (6)$$

### C. Review Helpfulness

A user can rate and write reviews on various e-commerce sites and platforms. With ratings and reviews, users try to share their experiences and opinions on different aspects of the items. The e-commerce sites and platforms also provide voting facilities, where other users can cast votes to show whether they liked or disliked a particular review. The experiences and opinions are evaluated by users with a score of 0 or 1, in the form of *helpful* or *not helpful*. Review helpfulness can determine and infer trust score for users representing the reputation, reliability, and honesty score using their reviewed items. A number of websites, such as Yelp, Flipkart, and Amazon provide users' vote summary on reviews in the form, "17 out of 23 people find this review helpful". Ghose and Ipeirotis [29] described that the correlation between *review helpfulness* and reviewer reputation can be used to compute *trust*, *honesty*, and *reliability* values. In this study, we have used a variant of the trust statements given in [30] to compute trust score using review helpfulness. Equation (7) formally presents the way to compute trust score using review helpfulness votes. In equation (7),  $K$  shows the upper bound on trust value, and  $V$  is the *voting skewness*, which represents the number of positive and negative votes a reviewer has received on her reviews from different users. Voting skewness is formally defined in

equation (8), where  $f_{ip}$  and  $f_{in}$  represent the frequency of positive and negative votes, respectively, and  $N$  is the total number of reviews. Finally, the trust score using the *review helpfulness* trust statement can be computed using equation (9), where  $\mathcal{T}_a^{\mathcal{H}}$  and  $\mathcal{T}_u^{\mathcal{H}}$  are the trust score for users  $a$  and  $u$ , respectively calculated using the *review helpfulness* votes, and  $n$  is the number of common-rated items.

$$\mathcal{T}_u^{\mathcal{H}} = \frac{K}{1 + e^{-KV_u}} \quad (7)$$

$$V_u = \frac{\sum_{i=1}^m f_{ip} - \sum_{i=1}^m f_{in}}{N} \quad (8)$$

$$\mathcal{T}_{a,u,n}^{\mathcal{H}} = \frac{1 - |\mathcal{T}_a^{\mathcal{H}} - \mathcal{T}_u^{\mathcal{H}}|}{n} \quad (9)$$

Once the individual trust scores based on different trust statements are calculated for a user-pair  $(a, u)$ , the final trust score of  $(a, u)$  is calculated as their mean value, as given in equation (10).

$$\mathcal{T}_{a,u,n} = \frac{\mathcal{T}_{a,u,n}^\delta + \mathcal{T}_{a,u,n}^\varepsilon + \mathcal{T}_{a,u,n}^{\mathcal{H}}}{3} \quad (10)$$

### D. Trust Model for Rating Prediction

In this section, we discuss the rating prediction of the unrated items jointly using UBCF and trust scores in line to the proposed approach in [37]. Equation (11) formally describes

TABLE I. STATISTICS OF THE DATASETS

| Category          | Movie  | Yelp   | Amazon Music |
|-------------------|--------|--------|--------------|
| #Users            | 49080  | 45981  | 5542         |
| #Items            | 1300   | 11537  | 3569         |
| #Reviews          | 250882 | 229907 | 64719        |
| Data Sparsity     | 99.60% | 99.95% | 99.67%       |
| #Reviews per User | 5.11   | 5.00   | 11.67        |
| #Reviews per Item | 192.98 | 19.92  | 18.13        |

the computation of rating prediction on item  $i$  by user  $u$ , where  $sim\mathcal{T}(u, m)$  represents the trust score between users  $u$  and  $m$ ,  $r_{um}$  represents the rating score for user  $m$  on overlapping items, and  $U_u^n$  represents the top- $k$  users, similar to users  $u$  that have rated the same items.

$$\hat{r}_{ui} = \frac{\sum_{m \in U_u^n} sim\mathcal{T}(u, m)r_{um}}{\sum_{m \in U_u^n} |sim\mathcal{T}(u, m)|} \quad (11)$$

However, in a user-item interaction matrix, various users knowingly provide low or high ratings to certain items. They are bias users and their biasness or critical nature affects the rating prediction. In line to [37], we have used first-order approximation to handle users' biasness to improve rating predictions, as given in equation (12). In this equation,  $b_{ui} = b_u + \mu + b_i$ , where  $b_u$  and  $b_i$  are user and item deviations with respect to ratings, and  $\mu$  is the mean rating of the items.

$$\hat{r}_{ui} = b_{ui} + \frac{\sum_{m \in U_u^n} sim\mathcal{T}(u, m)(r_{um} - b_{um})}{\sum_{m \in U_u^n} |sim\mathcal{T}(u, m)|} \quad (12)$$

Similarly, to avoid the overfitting issue, we have used a regularized model used in [31] [32], which is formally described in equation (13). In this equation, the first term represents the mean square error (MSE), which helps to learn the best fit rating values for the user ( $b_u$ ) and item deviation ( $b_i$ ). The second term in equation (13) includes the regularization terms to avoid overfitting by controlling the size of parameters,  $\mathcal{K}$  is the set of ratings given by user  $u$  on item  $i$ , and  $\|\cdot\|$  denotes the Frobenius norm.

$$\min_{\mathcal{K}} \sum (r_{ui} - \hat{r}_{ui})^2 + \lambda(\|b_u^2\| + \|b_i^2\|) \quad (13)$$

Korean in [31] and Hu et al. in [32] proposed an approach to compute the values of bias terms  $b_u$  and  $b_i$  using rating deviation. However, the major issue with their proposed solution is that they are not accurate methods to predict the ratings. In order to handle this issue and to compute regularizing parameters, *Alternating Least Squares* (ALS) or *Stochastic Gradient Descent* (SGD) [33] methods can be applied on equation (13). In this work, we have used ALS to compute the regularizing parameters because it performs better on sparse data, it is scalable over large datasets, and it can perform parallel execution in comparison to other approaches.

## V. EXPERIMENT SETUP AND RESULTS

In this section, we present the experimental evaluation of TrustRER over three real-world datasets. It starts with a detailed description of the datasets used to perform experiments. Thereafter, it explains the evaluation metrics, baseline methods, and performance estimation results of TrustRER with baselines and state-of-the-art method. Finally, this section presents an empirical evaluation for *cold-start* users using TrustRER, baselines, and state-of-the-art method.

### A. Dataset Description

To demonstrate the effectiveness of TrustRER, we performed experiments on two real-world datasets – Yelp and Amazon, and one Movie dataset. The first dataset is associated to Yelp, a crowd-sourced review forum, which allows users to write reviews on hotels and restaurants. It contains review information related to *restaurants, shopping, nightlife, automotive, home services, beauty and spa, and active life*. In this paper, we have used restaurant datasets for experiments and evaluations. The *restaurants* review dataset contain information related to *user check ins, business, user information, tip, and user reviews*. The second dataset, Amazon, is used in [21], and contains user and item meta-data on various items like books, automotive, digital music, movies, sports and outdoors, video games, etc. In this paper, we have used Amazon digital music dataset that includes users' ratings, reviews, and helpfulness votes on the reviews provided by different users on different items. The third dataset is based on the movie domain and used in one of our previous works [28]. It contains meta-data, ratings, and reviews information for the movies. The statistics of these datasets are presented in table I.

### B. Evaluation Metrics

In this section, we briefly describe various metrics used to evaluate TrustRER and its comparison with the baselines and state-of-the-art method. We have used two types of standard evaluation metrics viz. error-based and decision support-based which are explained in the following paragraphs.

- *Error-based metrics*: In these metrics, the accuracy of filtering algorithms are evaluated by measuring the deviation between the real and estimated ratings. The absolute difference between the real and estimated ratings is used to compute the rating prediction accuracy. We have used two error-based metrics viz. MAE and RMSE for evaluations. MAE represents the average of absolute errors over a set of items, where absolute error is the deviation of the real and estimated ratings [34], as given in equation (14). RMSE computes the standard deviation of the predicted errors as given in equation (15). RMSE penalizes large errors because it gives a comparatively high weight to large errors. In equations (14) and (15),  $r_{ui}$  and  $\hat{r}_{ui}$  represent the real and estimated ratings for user  $u$  and item  $i$ , and  $\mathcal{T}$  is the test dataset.

$$MAE = \frac{\sum_{(ui) \in \mathcal{T}} |\hat{r}_{ui} - r_{ui}|}{|\mathcal{T}|} \quad (14)$$

$$RMSE = \sqrt{\frac{\sum_{(ui) \in \mathcal{T}} (\hat{r}_{ui} - r_{ui})^2}{|\mathcal{T}|}} \quad (15)$$

- **Decision support-based metrics:** In these metrics, accuracy of a recommender system is evaluated in terms of how well a recommender system facilitates its users to make good decisions. The term “good decisions” means recommending relevant items and filtering irrelevant items. In this work, we have used Precision, Recall, and F-score decision support-based metrics for evaluations. In recommender systems, relevant and recommended items are used to compute the values of Precision and Recall. Relevant items contain the real ratings on items provided by the users in past. On the other hand, recommended items contain the predicted ratings on the predicted items. Precision is defined as the fraction of the number of items that are both relevant and recommended to the number of items that are recommended, as given in equation (16). Recall is defined as the fraction of the number of items that are both relevant and recommended to the number of items that are relevant, as given in equation (17). In equations (16) and (17),  $\mathcal{R}_{rel}$  is the relevant items and  $\mathcal{R}_{rel,rec}$  is the relevant recommend items. The harmonic mean of Precision and Recall computes the F-score value.

$$Precision(P) = \frac{|\mathcal{R}_{rel,rec}|}{|\mathcal{R}_{rec}|} \quad (16)$$

$$Recall(R) = \frac{|\mathcal{R}_{rel,rec}|}{|\mathcal{R}_{rel}|} \quad (17)$$

$$F - score(F) = \frac{2 \times \frac{|\mathcal{R}_{rel,rec}|}{|\mathcal{R}_{rec}|} \times \frac{|\mathcal{R}_{rel,rec}|}{|\mathcal{R}_{rel}|}}{\frac{|\mathcal{R}_{rel,rec}|}{|\mathcal{R}_{rec}|} + \frac{|\mathcal{R}_{rel,rec}|}{|\mathcal{R}_{rel}|}} \quad (18)$$

### C. Baseline Methods

In order to show the effectiveness of TrustRER, we compare it with 9 standard baseline methods viz. normal predictor, k-nearest neighbors (KNN), baselines, co-clustering, non-negative matrix factorization (NMF), Singular Value Decomposition (SVD), slope one, and SVD++. The baseline methods are briefly described in the following paragraphs.

- Normal Predictor method is based on the concept of maximum likelihood estimation. The formulation of this method requires the values of mean ( $\mu$ ) and variance ( $\sigma$ ) to compute normal distribution as presented in equations (19) and (20), where  $R_{train}$  is the training dataset and  $r_{ab}$  shows user  $a$  rating on item  $b$ .

$$\mu = \frac{1}{|R_{train}|} \sum_{r_{ab} \in R_{train}} r_{ab} \quad (19)$$

$$\sigma = \sum_{r_{ab} \in R_{train}} \frac{(r_{ab} - \mu)}{|R_{train}|} \quad (20)$$

- K-nearest neighbors (KNN) is a machine learning approach that uses either users or items as nearest

neighbors for rating prediction. It needs a user-item interaction matrix and a similarity method to formulate a user or an item neighbors. Equation (21) shows the rating estimation of unrated items using KNN, where  $k$  is top- $k$  similar users and  $r_{vj}$  represents user  $v$  rating on item  $j$ .

$$\hat{r}_{vj} = \frac{\sum_{i \in N_{vj}^k} sim(j, i) \cdot r_{vi}}{\sum_{i \in N_{vj}^k} sim(j, i)} \quad (21)$$

- Co-clustering method uses the concept of pair-wise interactions of 2 types of concurrent entities. Equation (22) presents the rating estimation for co-clustering method, where  $\overline{Clust}_{vj}$  is the mean rating of the co-cluster  $\overline{Clust}_{vj}$ , and  $\overline{Clust}_v$  and  $\overline{Clust}_j$  represent the mean ratings of users' and items' clusters [35].

$$\hat{r}_{vj} = \overline{Clust}_{vj} + (\mu_v - \overline{Clust}_v) + (\mu_j - \overline{Clust}_j) \quad (22)$$

- Baseline method uses the biases of users and items to predict the ratings, as shown in equation (23), where  $\mu$  represents the mean ratings of all items in the dataset and  $bias_i$  and  $bias_u$  are the item and user rating deviations.

$$\hat{r}_{ui} = \mu + bias_i + bias_u \quad (23)$$

- SVD++, SVD, and NMF methods are used in collaborative filtering based recommendation techniques where a user-item rating matrix is decomposed into two low dimensional matrices viz. *user interest* and *item features*. The decomposed matrices help to compute the rating prediction for unrated items.
- Slope One method is designed for CF-based recommendation techniques, especially for item-based CF. It uses users' and items' mean ratings to predict the ratings of unrated items. Equation (24) presents the computation of slope one, where  $|R_j|$  represents a set of pertinent items,  $\bar{\mu}_v$  is mean rating of user  $v$ , and  $dev_{j,i}$  represents the difference in the ratings of items  $j$  and  $i$  [36].

$$\hat{r}_{vj} = \bar{\mu}_v + \frac{1}{|R_j|} \sum_{i \in R_j} dev_{j,i} \quad (24)$$

### D. Comparative Evaluation-1: TrustRER vs. Baseline Methods

This section presents a comparative analysis of TrustRER with nine baseline methods using error-based and decision support-based metrics. We have used SurPRISE (Simple Python Recommendation System Engine) [39] and RecQ Python libraries to implement the baseline methods. It can be observed from Fig. 4 that Yelp dataset has high error values in comparison to Movie and Amazon Music datasets because Yelp dataset contains minimum reviews for both users and items in comparison to the Movie and Amazon music datasets. This shows that Yelp dataset contains more *cold-start* users in comparison to the other two datasets. It can also be observed from Fig. 4 that SVD++ has minimum MAE and RMSE values in comparison to other baseline methods.

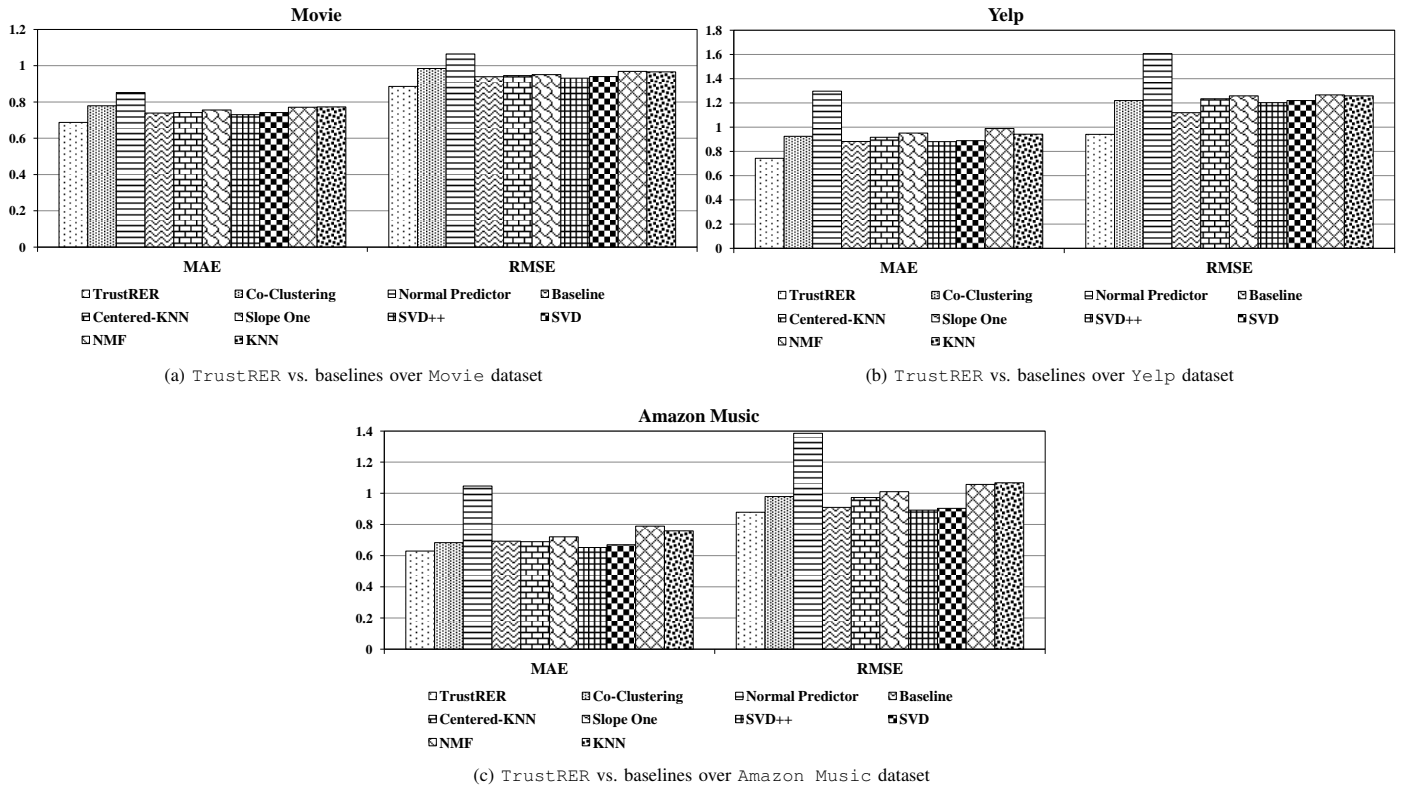


Fig. 4. Performance Comparison between TrustRER and Baselines in Terms of MAE and RMSE over different Datasets.

TABLE II. PERFORMANCE COMPARISON BETWEEN TRUSTRER AND SLOPE-ONE<sub>Trust</sub> IN TERMS OF MAE AND RMSE OVER DIFFERENT DATASETS

| Dataset      |                                 | k=20   |        | k=40   |        | k=60   |        | k=80   |        |
|--------------|---------------------------------|--------|--------|--------|--------|--------|--------|--------|--------|
|              |                                 | MAE    | RMSE   | MAE    | RMSE   | MAE    | RMSE   | MAE    | RMSE   |
| Movie        | TrustRER                        | 0.7198 | 0.9215 | 0.6738 | 0.8591 | 0.6625 | 0.8421 | 0.6799 | 0.8608 |
|              | Slope-One <sub>Trust</sub> [38] | 0.7616 | 0.9753 | 0.7329 | 0.9492 | 0.7017 | 0.8982 | 0.7293 | 0.9283 |
| Yelp         | CRecSys                         | 0.7916 | 0.9811 | 0.7537 | 0.9602 | 0.7233 | 0.9209 | 0.7319 | 0.9322 |
|              | Slope-One <sub>Trust</sub> [38] | 0.8428 | 1.0572 | 0.8028 | 1.0168 | 0.7759 | 0.9682 | 0.7822 | 0.9806 |
| Amazon Music | CRecSys                         | 0.6692 | 0.8624 | 0.6420 | 0.8382 | 0.6173 | 0.8082 | 0.6209 | 0.8120 |
|              | Slope-One <sub>Trust</sub> [38] | 0.6972 | 0.9023 | 0.6749 | 0.8825 | 0.6527 | 0.8528 | 0.6673 | 0.8603 |

TABLE III. PERFORMANCE COMPARISON BETWEEN TRUSTRER AND SLOPE-ONE<sub>Trust</sub> FOR DIFFERENT VALUES OF  $k$  IN TERMS OF PRECISION (P), RECALL (R), AND F-SCORE (F) OVER DIFFERENT DATASETS

| Dataset      |                                 | k=20   |        |        | k=40   |        |        | k=60   |        |        | k=80   |        |        |
|--------------|---------------------------------|--------|--------|--------|--------|--------|--------|--------|--------|--------|--------|--------|--------|
|              |                                 | P      | R      | F      | P      | R      | F      | P      | R      | F      | P      | R      | F      |
| Movie        | TrustRER                        | 0.7863 | 0.7171 | 0.7501 | 0.8001 | 0.7315 | 0.7642 | 0.8267 | 0.7527 | 0.7879 | 0.8191 | 0.7459 | 0.7807 |
|              | Slope-One <sub>Trust</sub> [38] | 0.7336 | 0.6717 | 0.7012 | 0.7510 | 0.6805 | 0.7140 | 0.7718 | 0.6981 | 0.7331 | 0.7657 | 0.7015 | 0.7321 |
| Yelp         | TrustRER                        | 0.7351 | 0.6524 | 0.6912 | 0.7410 | 0.6631 | 0.6998 | 0.7599 | 0.6994 | 0.7283 | 0.7514 | 0.6873 | 0.7179 |
|              | Slope-One <sub>Trust</sub> [38] | 0.6715 | 0.6027 | 0.6353 | 0.6855 | 0.6135 | 0.6475 | 0.7019 | 0.6250 | 0.6612 | 0.6950 | 0.6212 | 0.6560 |
| Amazon Music | TrustRER                        | 0.8011 | 0.7063 | 0.7507 | 0.8457 | 0.7367 | 0.7874 | 0.8632 | 0.7691 | 0.8134 | 0.8492 | 0.7552 | 0.7994 |
|              | Slope-One <sub>Trust</sub> [38] | 0.7764 | 0.6782 | 0.7239 | 0.8105 | 0.7019 | 0.7523 | 0.8327 | 0.7339 | 0.7801 | 0.8193 | 0.7250 | 0.7633 |

TABLE IV. PERFORMANCE COMPARISON BETWEEN TRUSTRER AND SLOPE-ONE<sub>Trust</sub> IN TERMS OF MAE AND RMSE FOR cold-start users OVER DIFFERENT DATASETS

| Dataset      |                                 | MAE (k@80) | RMSE (k@80) |
|--------------|---------------------------------|------------|-------------|
| Movie        | TrustRER                        | 0.8012     | 1.014       |
|              | Slope-One <sub>Trust</sub> [38] | 0.9182     | 1.1125      |
| Yelp         | TrustRER                        | 0.9214     | 1.1253      |
|              | Slope-One <sub>Trust</sub> [38] | 1.0421     | 1.2874      |
| Amazon Music | TrustRER                        | 0.7742     | 0.9861      |
|              | Slope-One <sub>Trust</sub> [38] | 0.8281     | 1.0375      |

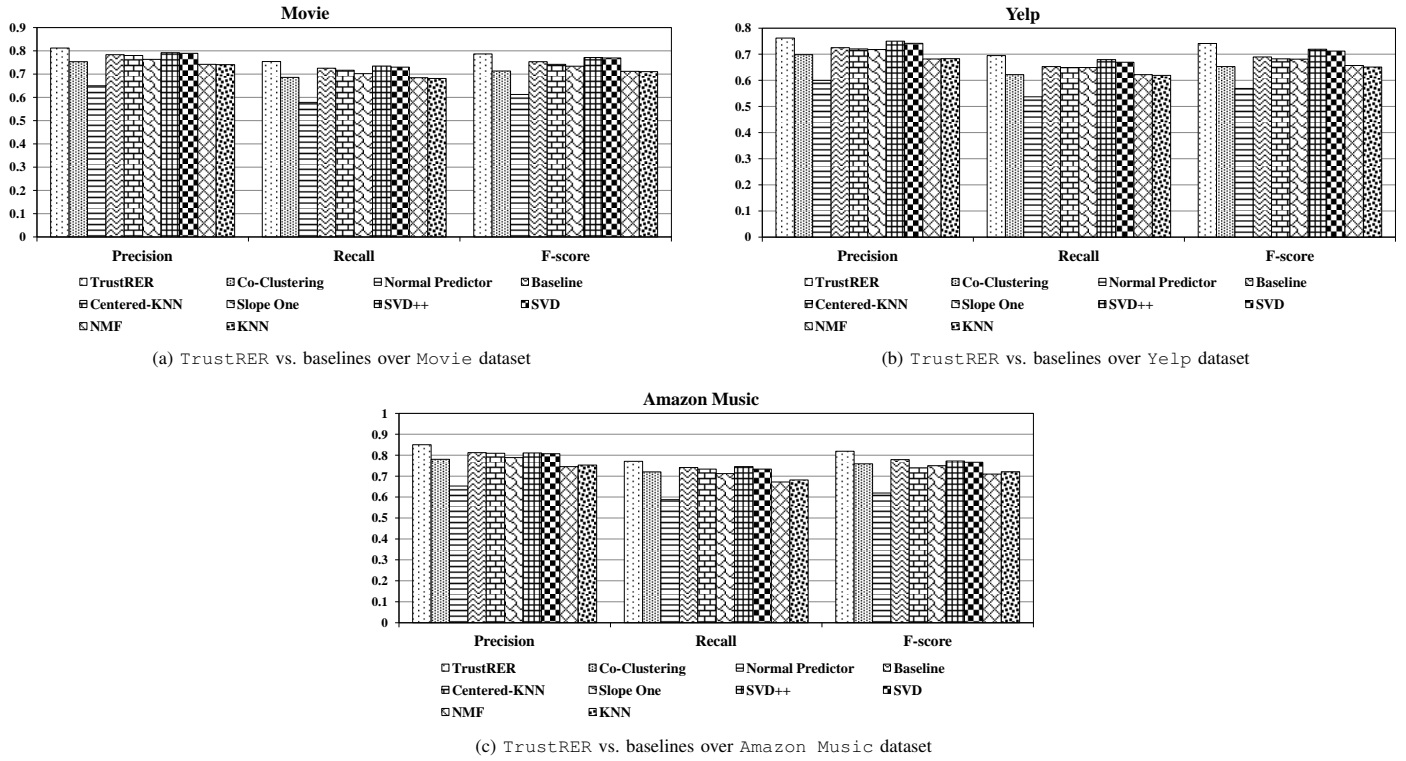


Fig. 5. Performance Comparison between TrustRER and Baselines in Terms of Precision, Recall and F-score over different Datasets.

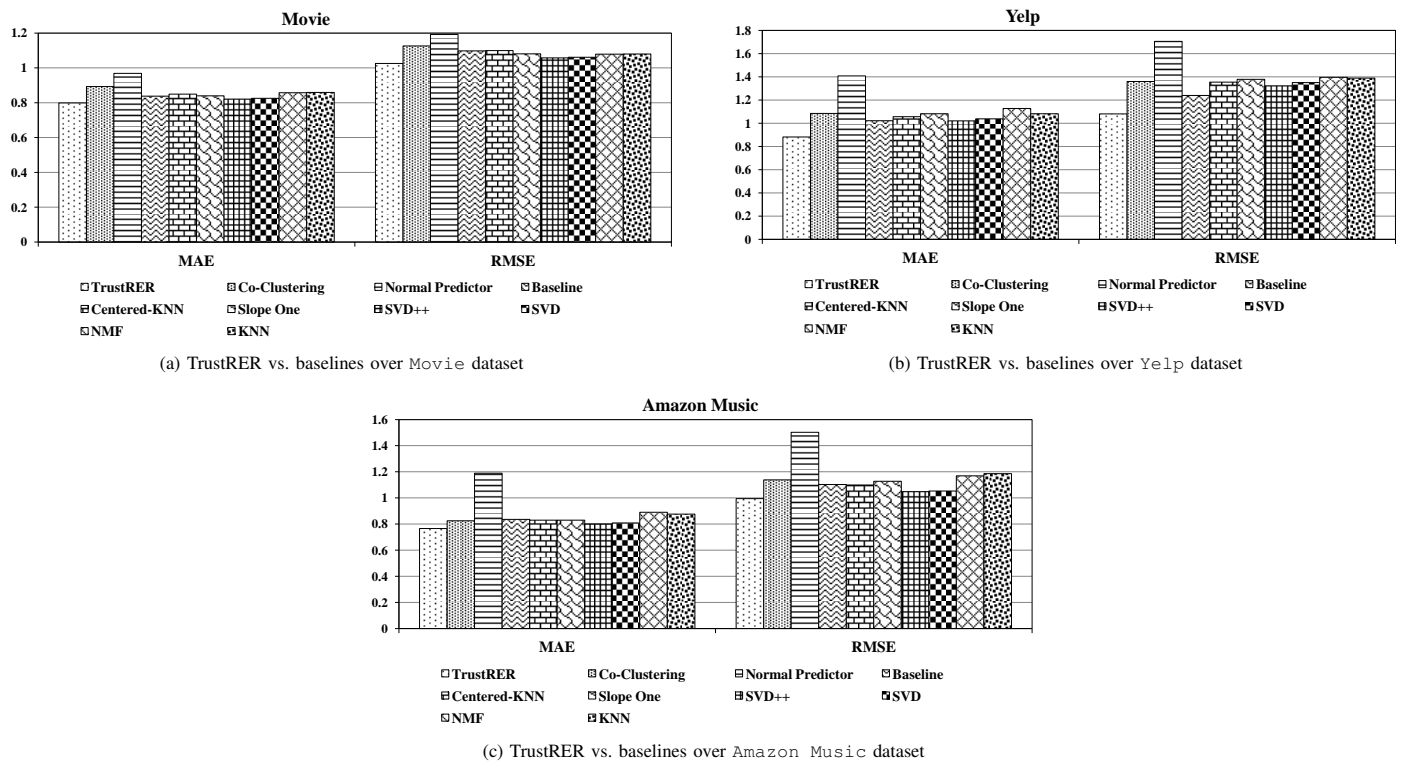


Fig. 6. Performance Comparison between TrustRER and Baselines in Terms of MAE and RMSE for the cold-start users on different Datasets.

SVD++ is a variant of MF and uses model-based collaborative filtering for rating predictions. SVD++ includes implicit ratings (implicit feedback information) which help to improve the predictions and recommendations. TrustRER outperforms SVD++ methods by 6.86% and 6.88% over Movie dataset, 15.70% and 21.68% over Yelp dataset, and 3.52% and 2.54% over Amazon music dataset for MAE and RMSE values. Similarly, Fig. 5 presents a comparative analysis of TrustRER with baseline methods using decision support metrics. It can be observed from Fig. 5 that TrustRER beats SVD++ with respect to Precision, Recall, and F-score by 5.07%, 6.44%, and 5.79% over Movie dataset, 7.27%, 9.76%, and 8.82% over Yelp dataset, and 5.55%, 4.76%, and 4.94% over Amazon Music dataset, respectively.

#### E. Comparative Evaluation-2: TrustRER vs. Slope-One<sub>Trust</sub> [38]

In this evaluation, TrustRER is compared with the state-of-the-art method, Slope-One<sub>Trust</sub> [38], which has used *slope one* algorithm to compute trust score between the users. Slope-One<sub>Trust</sub> approach proposed a *slope one* based trust algorithm that comprises the fusion of users' trust scores and their similarities for rating prediction and recommendation. The proposed approach first selects the trusted data of users and then computes similarities between them. The computed similarity scores are then added to the weight factor of the *slope one* algorithm to determine the ratings for the unrated items. Slope-One<sub>Trust</sub> method only uses rating deviations of users to generate the trust score, whereas TrustRER uses three novel trust statements, which seem very important to compute trust scores for the users.

Table II presents a comparative analysis of TrustRER and Slope-One<sub>Trust</sub> in terms of error-based metrics for  $k=20, 40, 60,$  and  $80$ . The different  $k$  values are the top- $k$  similar users for a target user. Similarly, Table III presents a comparative analysis of TrustRER and Slope-One<sub>Trust</sub> in terms of decision support-based metrics for different  $k$  values. It can be observed from table II that both TrustRER and Slope-One<sub>Trust</sub> received minimum MAE and RMSE values at  $k=60$ . On analysis, we found that TrustRER beats Slope-One<sub>Trust</sub> by 6.77% and 4.88% over Yelp dataset, 5.42% and 5.22% over Amazon Music dataset, and 5.58% and 6.24% over Movie dataset in terms of MAE and RMSE values, respectively. It can also be analyzed from table III that TrustRER beats Slope-One<sub>Trust</sub> and improved Precision, Recall, and F-score by 4.64%, 5.25%, and 4.95% over Movie dataset, 6.63%, 9.63%, and 8.21% over Yelp dataset, and 3.53%, 4.57%, and 4.09% over Amazon Music dataset.

#### F. Dealing with Cold-Start Users

In a user-item interaction matrix, some users provide very few ratings to items, and they are termed as *cold-start* users. With the availability of few ratings, it is very difficult to generate profiles for *cold-start* users and rating prediction for such users is a challenging task. Similarly, in the user-item interaction matrix, some items receive very few ratings from users, and such items are termed as *cold-start* items. However, in this work, we are predicting ratings for only *cold-start* users because we have used the UBCF model for rating prediction.

1) *TrustRER vs. Baseline Methods for Cold-Start Users:* To perform an empirical evaluation of TrustRER in comparison to the baseline methods for *cold-start* users, we conducted the same experiments as performed in Section V-D on Movie, Yelp, and Amazon Music datasets. In these experiments, the users who have estimated at most 5 items are considered as *cold-start* users, as used in [22]. The evaluated results are presented in Fig. 6a, 6b, and 6c. It can be observed from these figures that SVD++ outperformed all baseline methods on all datasets because of the availability of implicit feedback information. However, TrustRER beats the SVD++ method on all datasets because the user-based collaborative network in our approach considers both user ratings and reviews to generate the trust network and compute trust scores accordingly. Therefore, TrustRER computes trust for the users who consumed items but not directly interacted with other users using trust propagation metrics. In comparison to SVD++, TrustRER shows an improvement of MAE and RMSE values by 6.29% and 4.22% over Movie dataset, 15.02% and 19.9% over Yelp dataset, and 7.15% and 6.40% over Amazon Music dataset.

2) *TrustRER vs. Slope-One<sub>Trust</sub> [38] for Cold-Start Users:* TrustRER is compared with Slope-One<sub>Trust</sub> [38] for *cold-start* users on Movie, Yelp, and Amazon Music datasets. As discussed in Section V-F1, users who have estimated at most 5 items are considered as *cold-start* users. Table IV presents the comparative performance evaluation of TrustRER and Slope-One<sub>Trust</sub> with respect to MAE and RMSE values. It can be observed from Table IV that both TrustRER and Slope-One<sub>Trust</sub> have minimum MAE and RMSE values at  $k=80$ . Similarly, it can also be observed from Table IV that TrustRER beats Slope-One<sub>Trust</sub> by 12.74% and 8.85% over Movie dataset, 11.58% and 12.59% over Yelp dataset, and 6.62% and 5.01% over Amazon Music dataset in terms of MAE and RMSE values. This is because TrustRER considers both users' ratings and reviews to define trust statements. As a result, the *cold-start* users who have provided either ratings or reviews are able to find similar users. On the other hand, Slope-One<sub>Trust</sub> only considers rating deviations as trust statement, and accordingly *cold-start* users who provide only reviews are not considered.

## VI. CONCLUSION AND FUTURE WORK

In this paper, we have proposed TrustRER, a trust-based recommender system, which uses trust statements to calculate trust scores between the users based on their ratings and reviews for rating prediction and recommendation. We have incorporated trust scores of the users into a UBCF model for rating prediction and recommendation. The novelty of the proposed method lies in generating a trust network for users using their trust scores that are computed using both ratings and reviews of the users. To this end, we have proposed three trust statements based on users' *ratings*, *emotions*, and *helpfulness votes*. TrustRER is compared with nine standard baselines and one state-of-the-art recommendation method, Slope-One<sub>Trust</sub> [38] using both error-based and decision support metrics over three different datasets. TrustRER is able to resolve the *cold-start* user problem and the comparative performance results show that TrustRER beats both baselines methods and Slope-One<sub>Trust</sub> and provides better ratings. In the future, trust statements can be used to generate *trust-based*

embeddings for the users in the form of graph embeddings to construct trust networks, and they can be incorporated into a model-based CF to improve rating prediction and recommendation.

## REFERENCES

- [1] J. S. Breese, D. Heckerman and C. Kadie, "Empirical Analysis of Predictive Algorithms for Collaborative Filtering" Gregory F. Cooper and Serafin Moral, editors, in *Proc. UAI*, San Francisco, USA, 1998, pp. 43–52.
- [2] R. C. Mayer, J. H. Davis and F D. Schoorman, "An Integrative Model of Organizational Trust", in *Academy of Management Review*, vol. 20, no. 3, 1995, pp. 709–734.
- [3] D. O Sullivan, D. C. Wilson and B. Smyth, "Improving case-based Recommendation: A Collaborative Filtering Approach" in *Proc. ECCBR*, Aberdeen, Scotland, 2002, pp. 278–291.
- [4] J. O Donovan and J. Dunnion, "A Framework for Evaluation of Collaborative Recommendation Algorithms in An Adaptive Recommender System" in *Proc. CICLING*, Seoul, Korea, 2004, pp. 502–506.
- [5] M. A. Abbasi, J. Tang and H. Liu, "Trust-aware recommender systems," in *Machine Learning Book on Computational Trust*, Chapman and Hall/CRC Press, Boca Raton, FL, USA, 2014.
- [6] A. Abdul-Rahman and S. Hailes, "Supporting Trust in Virtual Communities", in *Proc. ICSS*, Maui, USA, 2000, pp. 1–9.
- [7] M. Jamali and M. Ester, "A Matrix Factorization Technique with Trust Propagation for Recommendation in Social Networks", in *Proc. RecSys*, Barcelona, Spain, 2010, pp. 135–142.
- [8] P. Massa and B. Bhattacharjee, "Using Trust in Recommender Systems: An Experimental Analysis", in *Proc. iTrust*, Oxford, United Kingdom, 2004, pp. 221–235.
- [9] J. A. Golbeck, "Computing and Applying Trust in Web-based Social Networks", in *Ph.D. dissertation, Dept. of Computer Science, Univ. of Maryland*, Maryland, USA, 2005.
- [10] P. Massa and P. Avesani, "Trust metrics on controversial users: Balancing between tyranny of the majority", in *IJSWIS*, vol. 3 no. 1, 2007, pp. 39–64.
- [11] A. Jøsang, R. Hayward and S. Pope, "Trust Network Analysis with Subjective Logic", in *Proc. ASCS*, Hobart, Australia, 2006, pp. 85–94.
- [12] G. Guo, J. Zhang and N. Yorke-Smith, "TrustSVD: Collaborative Filtering with Both the Explicit and Implicit Influence of User Trust and of Item Ratings", in *Proc. AAAI*, Austin Texas, USA, 2013, pp. 123–129.
- [13] M. Jamali and M. Ester, "Trustwalker: A Random Walk Model for Combining Trust-based and Item-based Recommendation", in *Proc. KDD*, San Diego, USA, 2009, pp. 397–406.
- [14] J. Tang, H. Gao, X. Hu and H. Liu, "Exploiting Homophily Effect for Trust Prediction", in *Proc. WSDM*, Rome, Italy, 2013, pages 53–62.
- [15] H. Ma, H. Yang, M. R. Lyu and I. King, "Sorec: Social Recommendation using Probabilistic Matrix Factorization", in *Proc. CIKM*, Galway, Ireland, 2008, pages 931–940.
- [16] M. Jamali and M. Ester, "A Matrix Factorization Technique with Trust Propagation for Recommendation in Social Networks", in *Proc. RecSys*, Barcelona, Spain, 2010, pp. 135–142.
- [17] B. Yang, Y. Lei, J. Liu and W. Li, "Social Collaborative Filtering by Trust", in *IEEE Transactions on Pattern Analysis and Machine Intelligence*, vol. 39, no. 8, 2017, pp. 1633–1647.
- [18] T. Bhuiyan, A. Josang and Y. Xu, "Managing Trust in online Social Networks", in *Handbook of Social Network Technologies and Applications*, 2010, pp. 471–496.
- [19] H. Ma, D. Zhou, C. Liu, M. R Lyu and I. King, "Recommender Systems with Social Regularization", in *Proc. WSDM*, Hong Kong, China, 2011, pp. 287–296.
- [20] J. Golbeck, "Generating Predictive Movie Recommendations from Trust in Social Networks", in *Proc. iTrust*, Pisa, Italy, 2006, pp. 93–104.
- [21] J. Ni, J. Li and J. McAuley, "Justifying Recommendations Using Distantly-labeled Reviews and Fined-grained Aspects" in *Proc. EMNLP*, Hong Kong, China, 2019, pp. 188–197.
- [22] P. Massa and P. Avesani, "Trust Metrics on Controversial Users: Balancing Between Tyranny of the Majority", in *IJSWIS*, vol. 3, no. 1, 2007, pp. 39–64.
- [23] G. Beigi, J. Tang, S. Wang and H. Liu, "Exploiting Emotional Information for Trust/Distrust Prediction", in *Proc. SDM*, Miami, USA, 2016, pp. 81–89.
- [24] G. R. Bewsell, "Distrust, Fear and Emotional Learning: An Online Auction Perspective", in *Journal of Theoretical and Applied Electronic Commerce Research*, vol. 7, no. 2, 2012, pp. 1–12.
- [25] J. R. Dunn and M. E. Schweitzer, "Feeling and Believing: The Influence of Emotion on Trust", in *Journal of Personality and Social Psychology*, vol. 88, no. 1, 2005, pp. 736–748.
- [26] C. Chen, J. Zeng, X. Zheng and D. Chen, "Recommender System based on Social Trust Relationships", in *Proc. ICEBE*, Coventry, UK, 2013, pp. 32–37.
- [27] C. Hwang and Y. Chen, "Using Trust in Collaborative Filtering Recommendation", in *Proc. IEA/AIE*, Kyoto, Japan, 2007, pp. 1052–1060.
- [28] V. K. Sejwal and M. Abulaish, "Context-Based Rating Prediction using Collaborative Filtering and Linked Open Data", in *Proc. WIMS*, Seoul, Korea, 2019, pp. 1–9.
- [29] A. Ghose and P. G. Ipeirotis, "Estimating the Helpfulness and Economic Impact of Product Reviews: Mining Text and Reviewer Characteristics", in *IEEE Transactions on Knowledge and Data Engineering*, vol. 23, no. 10, 2011, pp. 1498–1512.
- [30] G. Wang, S. Xie, B. Liu and S. Yu-Philip, "Review Graph Based Online Store Review Spammer Detection", in *Proc. ICDM*, Vancouver, Canada, 2011, pp. 1242–1247.
- [31] Y. Koren, "Factor in the neighbors: Scalable and accurate collaborative filtering", in *ACM Transactions on Knowledge Discovery from Data*, vol. 4, no. 1, 2010, pp. 1–24.
- [32] Y. Hu, Y. Koren and C. Volinsky, "Collaborative Filtering for Implicit Feedback Datasets", in *Proc. ICDM*, Pisa, Italy, 2008, pp. 263–272.
- [33] Y. Zhou, D. Wilkinson, R. Schreiber and R. Pan, "Large-Scale Parallel Collaborative Filtering for the Netflix Prize", in *Proc. AAIM*, Shanghai, China, 2008, pp. 337–348.
- [34] J. L. Herlocker, J. A. Konstan, L. G. Terveen and J. T. Riedl, "Evaluating Collaborative Filtering Recommender Systems", in *ACM Transactions on Information Systems (TOIS)*, vol. 22, no. 1, 2004, pp. 5–53.
- [35] T. George and S. Merugu "A Scalable Collaborative Filtering Framework Based on Co-Clustering", in *Proc. ICDM*, Houston, USA, 2005, pp. 625–628.
- [36] D. Lemire and A. Maclachlan "Slope One Predictors for Online Rating-Based Collaborative Filtering", in *Proc. SDM*, California, USA, 2005, pp. 1–5.
- [37] B. J. Schafer, D. Frankowski, J. L. Herlocker, and S. Sen, "Collaborative Filtering Recommender Systems", in *The Adaptive Web*, vol. 4321, 2007, pp. 291–324.
- [38] J. Liaoliang, C. Yuting, Y. Li, Li. Jing, Yan. Hongyang and W. Xiaojin, "A Trust-based Collaborative Filtering Algorithm for E-commerce Recommendation System", in *Journal of Ambient Intelligence and Humanized Computing*, vol. 10, no. 8, 2019, pp. 3023–3034.
- [39] N. Hug, "Surprise, a Python Library for Recommender Systems", 2017.



# A Game-Based Learning Approach to Improve Students' Spelling in Thai

Krittiya Saksrisathaporn

College of Arts, Media and Technology  
Chiang Mai University, Chiang Mai, Thailand 50200

**Abstract**—The problem of misspelled Thai words written in social media is increasing rapidly by youth in Thailand. To decrease the number of misspelled Thai words and improve the learning achievement for Thai youth, a first-person 3D mobile game was developed. The game is run on an Android smartphone applying a gyroscope sensor. This game has 3 levels in 5 stages. The learning achievement is evaluated from 37 players' pre- and post-test scores, who are bachelor's degree students of Animation and Game, College of Arts, Media and Technology, Chiang Mai University, Thailand. The data were statistically analysed by a paired sample t-test. Pre- and post-test scores were weakly and positively correlated ( $r = 0.666, p < 0.001$ ). There was a significant average difference between pre- and post-test scores ( $t_{36} = -11.776, p < 0.001$ ). On average, post-test scores were 15.027 points higher than pre-test scores (95% CI [-17.615, -12.439]). The results of the research show that the game-based learning approach significantly improved players' learning achievement in misspelled written Thai words.

**Keywords**—Game for learning; game-based learning; mobile game; paired sample t-test; Thai; misspelled words

## I. INTRODUCTION

Thai is the national language of Thailand, and it is intrinsically connected and interrelated to the culture of the Thai people, their identity, and Thai society. Thai people should understand the meaning of words and be able to use them correctly according to the principles of the Thai language, whether or not this is in the form of listening, speaking, reading, or writing. Although nowadays, many Thai youths have problems with spelling in writing, and misspelled words in writing are often seen on social media platforms, such as Facebook, Twitter, and LINE. This problem is increasing rapidly, and more so among the Thai youth.

Presently, using tools of communication in the digital era is inevitable. Mobile computing devices such as mobile phones have now evolved into the era of smartphones. Today, we possibly spent for 135 minutes per day on social media. People aged 16 to 24 spend the most time on social media – 3 hours and 1 minute daily [1]. Many people also spend time talking, communicating, studying online, or playing computer games on smartphones, which makes these devices extremely popular among mobile phone users today. Games for serious games or games for learning are tools that are easily accessible by people in the smartphone era, especially young people. Games for learning (G4L) and Game-based learning (GBL) have similar meanings and goals. In this paper, GBL was tested in a classroom while G4L may be implemented in the future for not only the purpose of the target group but for all Thai people.

The objective of the research, was to promote spelling and word recognition learning, and a first-person 3D mobile shooting game named “The Herd of Calf teach Thai” was developed. The game is run on a smartphone with an Android operating system by applying a gyroscope sensor [2]. The proposed game was designed to help motivate students to learn Thai and practice writing Thai by themselves by playing the game rather than memorizing words because language is a subject of frequent practice; and it will be more effective in the long-term. This mobile game aims to support students and players to learn and remember the often-misspelled Thai words with more interest and enthusiasm and to increase the resources that may help aid students in self-study. To further enhance this process the game was designed with vivid graphics.

The player must find the Thai consonants or vowels (letters) by turning the device, also known as a gyroscope control, then hit a shot to shoot a letter to the word until the correct word is formed. This game has 5 stages with 3 levels of difficulty. The player must find the Thai consonants or vowels (letters) by turning the device, also known as a gyroscope control, then hit a shot to shoot a letter to the word until the correct word is formed. This game has 5 stages with 13 words at each stage, including 3 levels of difficulty at each stage. To win the game, the player must pass 5 stages with at least 7 points in each stage. Many students spend time on YouTube video tutorials and other online materials hence find useful information on their own rather than in the classroom [3].

The prototype game was tested and evaluated with a student population, who are at the pre-working age, have a lot of energy, like playing games, like social communication, and mobile games. The evaluation used a paired sample t-test, which is suitable for the population sample data to compare scores before and after learning. Based on the pre- and post-test results, of the population, which were carried out under identical testing conditions, it was found that pre- and post-test scores were weakly and positively correlated ( $r = 0.666, p < 0.001$ ). There was also a significant average difference between pre- and post-test scores ( $t_{36} = -11.776, p < 0.001$ ). On average, post-test scores were 15.027 points higher than pre-test scores (95% CI [-17.615, -12.439]).

The game has several detailed steps in the game-making process that involved and needed integrated knowledge to produce the game. However, there are still opportunities to develop further the game, including some game techniques and art elements that can even be improved. System development can also be enhanced to collect playing statistics such as

identifying wrong and correct words to do further research in the future. To continue developing the game in other word categories or other Thai languages such as the Lanna language, including digital game development, which can work on a commercial.

The remainder of this study is structured as follows: Section II describes the background and related work. Section III presents a flow of the research methodology. Section IV presents the game design and development. Game testing and evaluation are discussed in Section V. Lastly, conclusions and future perspectives are discussed in Section VI.

## II. BACKGROUND AND RELATED WORK

### A. Thai Commonly Misspelled Words

According to Sanom Krutmueng, 2014 [4], it was stated that “Currently, writing wrong Thai words is considered a very important problem for Thai youth”, which is partly due to the creation of non-words and commonly misspelled words in everyday communication and writing by teenagers. This problem is becoming even more apparent in communication on social media, including listening, speaking, reading, and writing. There are also problems arising from the use of transliterated words that are commonly written incorrectly because the Thai language is a tonal language and is different from other foreign languages. Many spelling errors are related to pronunciation [5]. When incorrect writing is used continuously it results in new words being created that do not comply with Thai grammar, which creates ongoing problems in communication.

Misspelled words can be divided into two types [6]; [7]; [8]; [9] and include non-word misspelling errors and real-word misspellings. Real-word misspellings are the combination of characters of consonants, vowels, and tones, and create other words with meaning and appear in the dictionary. However, that word is not the word that the author intended to write [10] and is considered another type of misspelling that may cause the structure or meaning of the sentence to be distorted [7]. Misspelling can cause either a non-word error or an error, which is a real word but not the intended one. A non-word misspelling error is easier to detect by comparing it with a word list in a dictionary, while a real-word misspelling error cannot be detected with this method [11]. For example, “กษิฬพรท” (basil) is a real-word misspelling error in Thai while “กษิฬพรท” is a corrected word.

In 2019, Ronnayut found eight common mistakes in Thai misspelling from a random experiment with 1000 first-year students [12]. Moreover, in the same year, Rungnapha analyzed the misspellings in Thai and suggested that various teaching and learning innovations should be used to solve the problems of misspellings in order to improve academic achievement and performance [13].

### B. Game for Learning and Game-based Learning

Currently, there are many types of games, such as board games, card games, video games, and digital games [14]. These games can be type constructed as an entertainment game, educational game, game-based learning, game-based pedagogy simulation-based games, serious games, etc. [15].

An action game is a game that offers high-intensity action as the primary attraction. The reflex response is the primary skill needed to play these games well. The most common action games are shooters (Doom) and stealth (Metal Gear). The puzzle games are games that offer puzzles as the primary attraction. These games are mostly released on low budgets via the web. One of the most successful puzzle games is the famed Tetris, Lemmings, and Minesweeper [16]. Another example, Hangman, is a word guessing game, played by at least 2 or more players. One player sets 1 word, phrase, or sentence, and the other players try to guess that word by selecting letters or numbers within a limited time.

Presently, modern games are Multiple Game Types and Game Genres Combined. First-person shooter (FPS) is a video game genre centered on gun and other weapon-based combat in a first-person perspective, that is, the player experiences the action through the eyes of the protagonist. The genre shares common traits with other shooter games, which in turn makes it fall under the heading action game. Recently, Nintendo’s beloved Mario of Super Mario Bros went from humble beginnings as a simple side-scroller platform to now, where the Super Mario has mostly deviated from puzzle and adventure genres to a first-person Super Mario Bros shooter [17]. For example, the action game named Eliminate Gun Range, which is a target shooting game, there is a way to play in which players aim and shoot all targets in the allotted time.

According to Lorenz, 2015 [18] people who play video games have better memory and strategic planning capabilities compared to those who do not play video games. Additionally, in Jotham Msane, 2020, it was stated that students who like to play computer games are likely to succeed in programming [3]. In 2014, Andre proposed a method of a serious game to test the “Clean world” game. The learning of games occurs within multiple mechanisms, such as mini-games, puzzles, and quizzes played in parallel to the main game environment [19]. According to Becker, in 2014, she proposed a comparison table between the Game for Learning (G4L) and GBL. G4L is a game designed specifically with some learning goals in mind while GBL is the process and practice of learning using games. G4L is used for learning something while GBL is used to improve learning and to increase learning effectiveness, while both focus on content that what we are learning. However, GBL focuses more on learning objectives with the question of how to learn [15].

Educational games or edutainment games have been used as a tool for centuries and is much more attractive and interesting, and results in active learning rather than passive learning through textbooks and theory [20]. Game-based learning has been identified as an effective approach to making learning activities engaging and playful [21] serious game, and a serious game has become a hot topic in training and education as shown in the abundant academic research since 2012 [22]. Although, most digital game-based learning available in the market does not focus on graphics or level design.

Mobile devices have also become widely popular because they are easy to use, portable, and can support various applications. Many principles are considered in designing and developing these digital educational games, and many researchers focus on mobile game-based learning to enhance

the learning skills of students as interactive games enable intuitive content to be delivered directly to students through their devices. However, most education game-based learning is simple in both graphic and level design [14].

Up until now, there has quite a lot of research carried out on the Thai language while empirical research on digital game types for the Thai language is still scarce, should create innovative teaching and learning to solve a wide variety of problems of often written errors in Thai [13]. In addition, there are only a few other resources that can help students or young people learn Thai by themselves.

### III. RESEARCH METHODOLOGY

As shown in Fig. 1, the research started with a literature review and discussion with the teachers who teach Thai at Montfort College, a high school in Chiang Mai, Thailand. As mentioned in the introduction section, some problems were highlighted with incorrect writing and misspelled words. Game for Learning or Game-based learning were some of the approaches suggested. Moreover, commonly misspelled words in Thai writing was one of the topics that were selected for content to create a prototype game. To achieve the goal of improving knowledge in Thai writing, it was ascertained that the game needs to have a range of different levels to practice effectively. In this study, Unity software was a selected tool to develop the game. The game is divided into five stages with three levels at each stage. The game was tested and evaluated by 37 players. All game development process is detailed in the next section.



Fig. 1. Research Methodology.

### IV. GAME DESIGN AND DEVELOPMENT

A 3D mobile game was designed and developed that has an enhanced graphic design and provides an interactive playable game design for the player’s experience. Player experience as an individual experience goes beyond playability and game usability [23]. In this case, the 3D game was designed and developed by using Adobe Photoshop and Unity software. The Unity software is a game engine for developing 2-dimensional (2D) and 3-dimensional (3D) games, which can work on two platforms, Windows and OSX [14]. The popular 2D game name “Gardenarium” by Paloma and Kyler (2017) [24] with the support of KO-OP [25] was also made by Unity software. The game is designed from action games combined with puzzle games. Most people, even those who are not gamers, know how to play both games. The action game “Eliminate: Gun Range”, is a first-person shooter game, with the aim to shoot all targets in the allotted time, and uses Gyroscope control as the controller. Moreover, this game is combined with the classic letter guessing game “Hangman”.

In this study, 65 often misspelled Thai words were selected for the game, most of them are real-word spelling errors. By dividing all the words into three groups: 1 syllable, 2 syllables,

and 3 syllables, the criteria for selection of the 65 words was that the word is often seen or used in daily life and a hint was able to be set.

Game level design is divided into 5 stages, and each stage has three levels, with hints assigned to players. The first level of each stage is easy to give the players familiarity with how to play and control fire first. This creates incentives for playing and encourages them to not give up as they work up to the next level which will get harder and harder with new random words with more syllables added until the last level. Level 3 is the hardest level of each stage, and then players start the next stage on the first level again. This makes the gameplay dynamic between hard and easy. In each level, the player needs to remember the words before they can pass from one level to the next. The player needs to pass the first stage until the last stage by unlocking each level. To pass each level, players must complete the missing word within the time limit. The structure of the game levels at all stages is detailed in Table I.

The difficulty of the game depends on three factors: first, the number of syllables. Second, the time is limited, and finally, the ability of the enemy (monster), which is the calf herd. Additionally, in each level of the stage, the word appears randomly in a group so that the players are not bored and can not memorize the sequence of words to be played to increase the challenge for players. In the word manipulation, an algorithm was written to randomize the words by dividing them into 3 groups randomly at each level (see Fig.2).

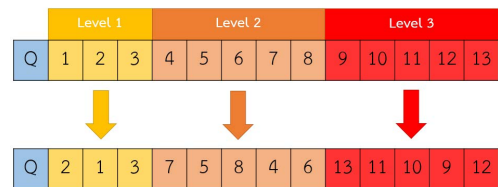


Fig. 2. Example of words Random in 3 Levels.

As shown in Fig. 3, the game flow or flowchart of the game starts with a menu selected which consists of how to play, stage selection, gameplay, and game result display. The gameplay starts playing from stage 1 level 1 to stage 5 level 3. The score will be given as follows: if correct > 3 words – the player gets 1 star (☆), > 8 words the player gets 2 stars (☆☆), and if the player can correct all words (13 words) he/she will get 3 stars (☆☆☆). The player must pass each stage and level to unlock the next stage until the game is won, players must also correct more than or equal to 7 words (>= 7 Word) within the time or life limits. The game will end when the player or score does not pass at each level 3 times.

As shown in Fig. 4, 5 and 6, to play the game, the player needs to fill in the incomplete letters by turning their mobile device around to find and shoot the monster with the correct letter attached to it. The player can remove letters from the latest one added and continue backward in case of shooting the wrong one. The player will need to complete each word within the set time. As aforementioned, the stage will end when the player completes all 13 words or is unable to complete one of the words in time.

TABLE I. GAME LEVEL DESIGN

|         | Level 1<br>1 syllable     |                           | Level 2<br>2 syllables    |                                                            | Level 3<br>3 syllables    |
|---------|---------------------------|---------------------------|---------------------------|------------------------------------------------------------|---------------------------|
| Stage 1 | Word count: 3             | จัน,<br>โย,<br>โล         | Word count: 5             | กะเพรา,<br>กันแสง, ศิระชะ,<br>กระทอง, มงกุฏ                | Word count: 5             |
|         | Alphabet time: 20s        |                           | Alphabet time: 15s        |                                                            | Alphabet time: 10s        |
|         | Word time: 40s            |                           | Word time: 45s            |                                                            | Word time: 50s            |
|         | Monster: idle             |                           | Monster: idle             |                                                            | Monster: idle             |
| Stage 2 | Word count: 3             | โน้ด,<br>ผลัด,<br>หงส์    | Word count: 5             | กุดผี, นิมนต์,<br>ทรวดทรง,<br>ทรุดโทรม, ดอกจัน             | Word count: 5             |
|         | Alphabet time: 20s        |                           | Alphabet time: 15s        |                                                            | Alphabet time: 10s        |
|         | Word time: 35s            |                           | Word time: 40s            |                                                            | Word time: 45s            |
|         | Monster: idle, walk       |                           | Monster: idle, walk       |                                                            | Monster: walk             |
| Stage 3 | Word count: 3             | แก๊ส,<br>ไซร์,<br>เกร็ด   | Word count: 5             | พิสูจน์, รื่นรมย์,<br>เกษียณ, เดียดจันท์,<br>เคร่าโตก      | Word count: 5             |
|         | Alphabet time: 15s        |                           | Alphabet time: 15s        |                                                            | Alphabet time: 10s        |
|         | Word time: 30s            |                           | Word time: 35s            |                                                            | Word time: 40s            |
|         | Monster: idle, walk, jump |                           | Monster: idle, walk, jump |                                                            | Monster: idle, walk, jump |
| Stage 4 | Word count: 3             | โจทย๋,<br>ขอสัก,<br>ฟิล์ม | Word count: 5             | ขาดแคล, บาดใหญ่,<br>ปราศรัย, ผลัดเวร,<br>ลายเซ็น           | Word count: 5             |
|         | Alphabet time: 15s        |                           | Alphabet time: 12s        |                                                            | Alphabet time: 8s         |
|         | Word time: 25s            |                           | Word time: 30s            |                                                            | Word time: 35s            |
|         | Monster: idle, walk       |                           | Monster: walk, jump       |                                                            | Monster: idle, walk, jump |
| Stage 5 | Word count: 3             | เด็นท์,<br>กะที้,<br>ขมา  | Word count: 5             | เวทมนตร์, สร้างสรรค์,<br>สายสัญญาณ, เหตุการณ์,<br>เลือกสรร | Word count: 5             |
|         | Alphabet time: 12s        |                           | Alphabet time: 10s        |                                                            | Alphabet time: 10s        |
|         | Word time: 20s            |                           | Word time: 25s            |                                                            | Word time: 30s            |
|         | Monster: walk, fly        |                           | Monster: walk, jump, fly  |                                                            | Monster: jump, fly        |

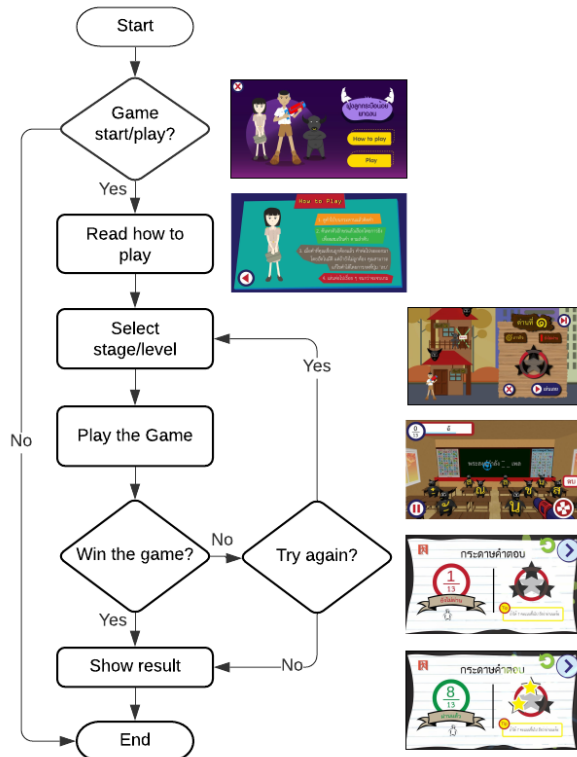


Fig. 3. Game Flow (Flowchart).

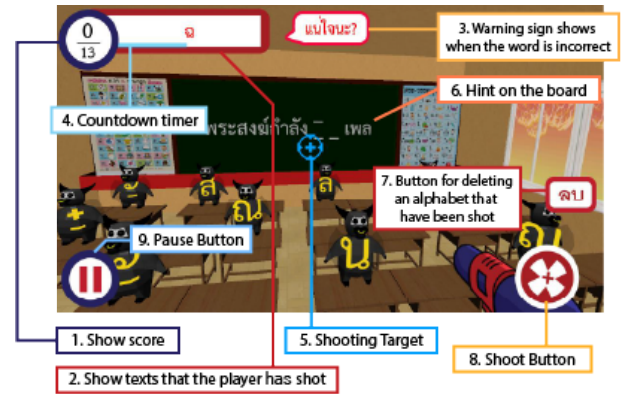


Fig. 4. Screenshot of Gameplay 1.

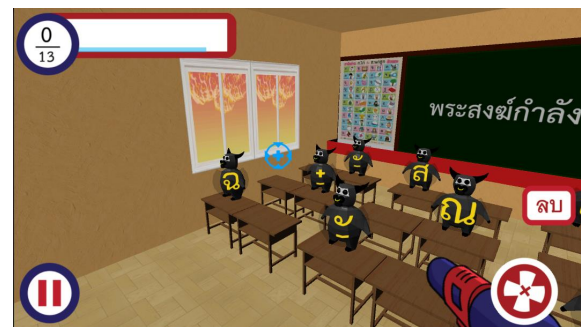


Fig. 5. Screenshot of Gameplay 2.

As shown in Table II, there are four types of monsters in the game. A standing still (idle) monster will exist since the first stage, a walking monster will start appearing from the second stage onwards, a jumping monster will start appearing from the third stage onwards and a flying monster will start appearing from the fifth stage onwards. The variation of position and movement causes it to be more difficult to aim and shoot accurately. Sometimes the correct letters will be blocked by another monster for some time. These difficulties make the

game more challenging. During the stages, help items will randomly fly into the scene in which players can then choose to shoot and use them. There are two types of help items, first is an item to help increase the time for 15 seconds to complete a word and the other is to stop monsters from moving for a limited time.

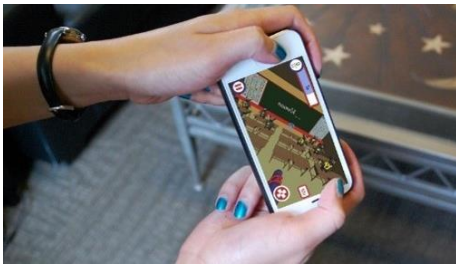


Fig. 6. “The Herd of Calf Teach Thai”, 3D Game using a Gyroscope Sensor.

TABLE II. MONSTER

| Idle | Walk | Jump | Fly |
|------|------|------|-----|
|      |      |      |     |

### V. EVALUATION

The paired sample t-test compares two means that are from the same individual, object, or related units. The two means can represent things like: A measurement is taken at two different times (e.g. pre- and post-test with an intervention administered between the two-time points) [26].

As shown in Table III, the paired sample t-test shows the actual test results. The sample dataset has placement test scores (out of 65 points) for pre- and post-tests (before and after playing the game). In this case, particular interest was paid to the learning outcome after playing the game to determine whether the pre-test or post-test had higher test scores on average. In this case, a paired t-test was used to test if there was a significant difference in the average of the two tests. The post-test scores of the students ( $x = 54.27$ , S.D. = 6.423) were significantly higher than the pre-test scores ( $x = 39.24$ , S.D. = 10.380). On average, post-test scores were 15.027 points higher than pre-test scores (95% CI [-17.615,-12.439]) (see Table V).

TABLE III. PRE- AND POST-TEST DATA (MEAN AND STD)

| Paired Samples Statistics |      |       |    |                |                 |
|---------------------------|------|-------|----|----------------|-----------------|
|                           |      | Mean  | N  | Std. Deviation | Std. Error Mean |
| Pair 1                    | pre  | 39.24 | 37 | 10.380         | 1.706           |
|                           | post | 54.27 | 37 | 6.423          | 1.056           |

Table IV indicates that the mean of the pre- and post-test scores of the students were weakly and positively correlated ( $r = 0.666, p < 0.001$ ). As shown in Table V, there was a significant average difference between pre- and post-test scores ( $t_{36} = -11.776, p < 0.001$ ). The result shows that the game enhanced learning outcomes for the population.

TABLE IV. PRE-AND POST-TEST SCORES CORRELATIONS

| Paired Samples Correlations |            |    |             |      |
|-----------------------------|------------|----|-------------|------|
|                             |            | N  | Correlation | Sig. |
| Pair 1                      | pre & post | 37 | .666        | .000 |

### VI. CONCLUSIONS AND FUTURE PERSPECTIVE

The development of the puzzle game, “The Herd of Calf teach Thai” to improve students’ spelling in Thai was created as a new alternative way of learning about Thai words that are often misspelled or written incorrectly. The game is a first-person shooter game that plays on mobile devices with the Android operating system. Most players have already played the game “Hangman” which means it does not take much time to learn how to play the game. They can play when gameplay appears with hints also assigned to help players. Then, players search for the missing letters which are shown in the scene. They then shoot the letters sequentially to mix into the correct words. The player can also replay until the condition is met or until the game is over which leads to learning the correct form of words from misspelled words.

The game level design is divided into five stages, and each stage has three levels. The difficulty of the game will change according to the level and stage. The evaluation was undertaken by a class of 37 students under 20 years old in the Department of Animation and Game within the College of Arts, Media, and Technology at Chiang Mai University, Thailand. In this case, a pre-game knowledge test was conducted. The data were then used for statistical testing using a pair sample t-test, and the results show that the game enhanced learning outcomes. Game design is both a science and an art, which has many steps and several approaches. This game has several detailed steps in the game-making process that involved and needed integrated knowledge to produce the game. It is often a challenge for developers to build on knowledge or content in the development of games. The uniqueness of this game is that it is not only entertaining for players, but it also offers players the ability to gain knowledge. Although players may not be able to achieve their goals all at once, they will be able to achieve them through repeated play and recognition. This is considered an important option as it creates creative learning and has the ability to attract a wide range of people.

However, there are still opportunities to develop the game further, including a Gyroscope game controller although this development requires the application of the Google Cardboard Software Development Kit, which is not fully customizable. Causing an error in the section of some impressions, including some art elements of the game can still be developed. Continued development in other word categories such as homonyms, words derived from foreign languages, couplets, etc. or the development in other Thai languages such as the Lanna language, etc. Development of a system to collect playing statistics such as identifying wrong and correct words to do further research in the future. As most game development works on a commercial basis, it is a mobile game on the Android operating system, and an In-App purchase system could be set up so that players can choose to purchase various levels or add-ons in the game through the Google Play Store.

### ACKNOWLEDGMENT

The authors are grateful to teachers in Montfort College, Chiang Mai, Thailand for who provided data that assisted the research, Mr. Panupong Maomoon, and the College of Arts, Media, and Technology, Chiang Mai University for support.

TABLE V. PRE-AND POST-TEST DATA OF THE STUDENT

|        |                | Paired Samples Test |                                           |       |         |         | t       | df | Sig. (2-tailed) |
|--------|----------------|---------------------|-------------------------------------------|-------|---------|---------|---------|----|-----------------|
|        |                | Paired Differences  |                                           |       |         |         |         |    |                 |
| Mean   | Std. Deviation | Std. Error Mean     | 95% Confidence Interval of the Difference |       |         |         |         |    |                 |
|        |                |                     | Lower                                     | Upper |         |         |         |    |                 |
| Pair 1 | pre-post       | -15.027             | 7.762                                     | 1.276 | -17.615 | -12.439 | -11.776 | 36 | 0.000           |

REFERENCES

[1] D. Metev, "How Much Time Do People Spend on Social Media", Retrieved Sep 2, 2020 from <https://review42.com/how-much-time-do-people-spend-on-social-media/>,2020.

[2] D. Patel, "Use of Accelerometers and Gyroscopes in Position Sensing," Retrieved Sep,29, 2015 from [http://www2.ece.gatech.edu/academic/courses/ece4007/08fall/ece4007101/al6/Dhaval\\_Patel\\_TRP.pdf](http://www2.ece.gatech.edu/academic/courses/ece4007/08fall/ece4007101/al6/Dhaval_Patel_TRP.pdf), 2009.

[3] M. Jotham, M. Bethel, and C. Tarirai, "Students Perception of the Effect of Cognitive Factors in Determining Success in Computer Programming: A Case Study," International Journal of Advanced Computer Science and Applications(IJACSA), 11(7), 2020.

[4] S. Krutmueng,"Often Written Words in Thai: An Analysis of Teaching Results," Journal of Management, Faculty of Management, Lampang Rajabhat University, 7(1), 42-55, 2014.

[5] P. Hui, "Spelling Errors in Thai Made by Chinese Students Learning Thai as a Foreign Language," The Social and Cultural Context of Language Situation in Southeast Asia Vol 22 No 3, 2019.

[6] R. Mishra and N. Kaur, "A survey of spelling error detection and correction techniques," International Journal of Computer Trends and Technology, 4(3), 372-374, 2013.

[7] R. Mitton, "Spelling checkers, spelling correctors and the misspellings of poor spellers," Information Processing and Management, 23(5), 495-505, 1987.

[8] S. Murthy, R. Madi and P. Kumar. "A non-word Kannada spell checker using morphological analyzer and dictionary lookup method," International Journal of Engineering Sciences and Emerging Technologies, 2(2), 43-52, 2012.

[9] S. Verberne, "Context-sensitive spell checking based on word trigram probabilities," (Master's thesis). University of Nijmegen, Netherlands, 2002.

[10] A. Wilcox-O'Hearn, G. Hirst and A. Budanitsky, "Real-word spelling errection with trigrams: A reconsideration of the Mays, Damerau, and Mercer model," Paper presented at the CICLing-2008, Haifa, 2008.

[11] P. Laimanu and W. Arunmanakul, "Analysis of Thai words that are often written incorrectly," Humanities Journal Vol.24 No.2 (July-December 2017) 318-342, 2017.

[12] R. Ueatrirat and N. Sornjitti, "The Analysis of Srinakharinwirot university students' errors in writing the thai language," Pimkanet Journal 15(1) Jan-June 2019 (87-100), 2019.

[13] R. Boonyim, "The Analysis of Causes of Misspelled Words in Thai," The fifth International and national conferences, Rajabhat Research Dec 2-5, 2018 ,Phetchaburi Rajabhat University, Thailand, 2018.

[14] K. Saksrisathaporn and P. Sribunthankul, "A Smartphone game to promote self-learning in chemistry," International Conference Cognition and Exploratory Learning in Digital Age 2019, Cagliari, Italy, pp. 347-354, 2019.

[15] K. Becker, "What is the difference between serious games, educational games, and game-based learning," Retrieved Feb 3, 2018 from <https://wp.me/p4Hsb6-1KS>, 2016.

[16] L. Grace, "Game Type and Game Genre. Chicago, IL: Illinois Institute of Art," Retrieved August 26, 2020 from [http://aai.lgrace.com/documents/Game\\_types\\_and\\_genres.pdf](http://aai.lgrace.com/documents/Game_types_and_genres.pdf), 2005.

[17] L. Bautista, "New Video Reimagines Super Mario Bros as a First-Person Shooter Game in Video Games," Retrieve Mar 12, 2020 from <https://www.highsnobiety.com/p/super-mario-bros-first-person-shooter>, 2020.

[18] R. C. Lorenz, T. Gleich, J. Gallinat and S. Kühn, "Video game training and the reward system," Frontiers in human neuroscience, No.9, pp 40, 2015.

[19] F. S. B. Andre, N. M. P. Pedro, A. F. F. D. Joo and G. M. S. Frutuoso, "A New Methodology of Design and Development of Serious Games," International Journal of Computer Games Technology, Article ID 817167, 8 pages, 2014.

[20] K. Saksrisathaporn and T. Maneevan, "A Web-based Traveling Game for the Preservation of Lanna Culture," 2012 IEEE Fourth International Conference on Digital Game and Intelligent Toy Enhanced Learning, Takamatsu, Japan, pp. 52-56, 2012.

[21] E. Klopfer, S. Osterweil and K. Salen, "Moving Learning Games Forward: Obstacles, Opportunities and Openness," MIT The Education Arcade. Cambridge, MA , 2009.

[22] V. Guillén-Nieto and M. Aleson-Carbonell, "Serious games and learning effectiveness: The case of It's a Deal!," Computers and Education, Vol 58, No. 1, pp 435-448, 2012.

[23] R. Dorner, S. Gobel, W. Effelsberg and J. Wiemeyer,"Serious Games Foundations, Concepts and Practice,". Springer International Publishing, 2016.

[24] Paloma. "Trippy, Dreamy Exploration: Gardenarium Released," Retrieved April 3, 2015 from <https://www.rockpapershotgun.com/2015/04/03/gardenarium-exploration-game-released>, 2017.

[25] K. Kiili, "Digital game-based learning: Towards an experiential gaming model," The Internet and higher education, Vol 8, No. 1, 13-24, 2005.

[26] Kent State University Libraries. "SPSS tutorials: Paired Samples t-Test," Retrieved Aug 26, 2020, from <https://libguides.library.kent.edu/SPSS/PairSamplestest>, 2017.

# Physical Parameter Estimation of Linear Voltage Regulators using Model-based Approach

Ng Len Luet<sup>1</sup>, Mohd Hairi Mohd Zaman<sup>2</sup>, Asraf Mohamed Moubark<sup>3</sup>, M Marzuki Mustafa<sup>4</sup>

Department of Electrical, Electronic and Systems Engineering  
Faculty of Engineering and Built Environment, Universiti Kebangsaan Malaysia  
43600 Bangi, Selangor, Malaysia

**Abstract**—Electronic systems are becoming increasingly sophisticated due to the emergence of advanced technology, which can produce robust integrated circuits by reducing the dimensions of transistors to just a few nanometers. Furthermore, most electronic systems nowadays are in the form of system-on-chip and thus require stable voltage specifications. One of the critical electronic components is the linear voltage regulator (LVR). LVRs are types of power converter used to maintain a stable and constant DC voltage to the load. Therefore, LVR stability is an essential aspect of voltage regulator design. The main factor influencing the stability of LVRs is the load disturbance. In general, disturbances such as a sudden change in load current can be compensated for by an output capacitor, which, contains a parasitic element known as equivalent series resistance (ESR). Therefore, the ESR and output capacitor specified in the datasheet is essential to compensate for load disturbance. However, LVR manufacturers typically do not provide detailed information, such as the internal physical parameters associated with the LVR in the datasheet. This situation leads to difficulties in identifying the behavior and stability of LVR. Therefore, this study aims to develop a method for estimating the internal physical parameters of LVR circuits that are difficult to measure directly by using a model-based approach (MBA). In this study, the MBA estimates the LVR model transfer function by analyzing the input and output signals via a linear regression method. Simulations through MATLAB and OrCAD Capture CIS software verify the estimated LVR model transfer function. Results show that the MBA has an excellent performance in estimating the physical parameters of LVRs and determining their stability.

**Keywords**—Linear voltage regulator; stability; capacitor; equivalent series resistance; physical parameter; model-based approach

## I. INTRODUCTION

Smart electronic devices or system-on-chip (SoC) applications have become an integral part of our daily necessities. This situation is due to the rapid development of technology that affects the way of life of individuals in the aspects of communication, learning, and thinking [1]. This development follows Moore's Law, which states that the number of transistors doubles every two years by reducing the dimensions of its transistors. With millions of transistors, stable voltage specifications are crucial in such SoC applications. Therefore, linear voltage regulators (LVRs) play an essential role in the field.

LVRs are a power converters that stabilize the output voltage within an acceptable range. Generally, an unstable output voltage for electronic devices causes oscillatory transients,

harmonics distortion and noise. All of these effects degrade the performance of electronic devices. Therefore, LVRs must be able to maintain a steady output voltage and be unaffected by changes in conditions [2].

In general, the main factor influencing the stability of LVRs is the disturbance, including a sudden change in load current. This disturbance can usually be compensated for by an output capacitor, which acts as an energy storage element. However, the output capacitor consists of a parasitic element called equivalent series resistance (ESR), which plays a critical role in the compensation of disturbance [3], [4]. Generally, a high ESR leads to large undershoot in transient response, and thus generates an unstable output voltage. Although a low ESR is always encouraged, it is not always the best option. When the ESR is too low, oscillation occurs and finally destroys the stability of the LVR. Hence, an optimum low ESR is encouraged in LVR design [5], [6], [7], [8].

Although LVR manufacturers provide the ESR and output capacitance information, they do not specify in the datasheet the required stability information, such as the internal physical parameters of the circuit. Hence, engineers face problems in analyzing and achieving stability for the LVRs they use. The available method for analyzing the stability of LVRs involves measuring the transient response manually via a real LVR circuit [9], [10], [11]. However, the process is time-consuming and limits the manufacturing productivity rate. Data-driven methods have been developed to analyze the failure regions of LVRs [12], [13], but they do not involve any circuit modeling.

Besides, some researches have been conducted to analyze the electronic device failure based on circuit models. For instance, the impact on the variation of the circuit transfer function coefficients has been investigated in detail to measure its performance [14], [15], [16], [17]. Furthermore, much research has been conducted to model the power management components, especially for the switching type power converters [18], [19], [20], [21], [22], [23]. However, most works, either model-based or data-driven method, assume the circuit under test as a black box system and did not consider the partially known physical parameters that exist in the circuit. For instance, in the LVR circuit, the output capacitor and feedback resistors can be regarded as the partially known parameters. Therefore, the current work aims to develop a model-based approach (MBA) to estimate the physical parameters of LVRs adequately via the linear regression (LR) method and subsequently determine the LVR stability by analyzing the transient response.

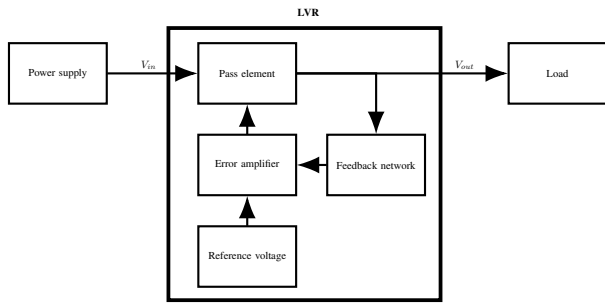


Fig. 1. Block Diagram of LVR.

### A. Linear Voltage Regulator

LVR consists of four main components, namely, reference voltage, error amplifier, feedback circuit, and pass element. Fig. 1 depicts the basic block diagram of an LVR. The error amplifier detects the output voltage through the feedback network and compares it with the reference voltage, thereby responding to the pass element. The pass element can be a BJT or MOSFET, and it maintains the voltage level such that the output voltage has the same value as the reference voltage by controlling the flow of current. For example, when the output voltage decreases due to a sudden change in load, the error amplifier triggers the pass element to control the current flow from the power supply to the load to ensure that the output voltage is at the same level as the reference voltage. The output voltage rises again to the initially controlled voltage [24].

### B. Output Capacitor

A capacitor is a type of passive component that contains two terminals to store electrostatic energy in the electric field. Typically, a capacitor connected in parallel to a circuit output is known as the output capacitor. The output capacitor acts as energy storage. The electrical energy stored is utilized during a sudden change in load. This component minimizes the effect of the disturbance by decreasing the ripple on the output voltage. Therefore, the output capacitor is a critical element in the stability aspect of LVRs.

In general, the value of the output capacitor exerts a significant impact on the stability of LVRs because the output capacitor influences the damping of the output voltage during the transient response. Low capacitor values are generally preferred. However, if the overall impedance of the output capacitor is too low, then oscillation or ring effect occurs and eventually reduces the stability of the output voltage.

### C. Equivalent Series Resistance

Ideally, capacitors are considered as pure elements and contain only capacitance. However, practically, capacitors used in reality are not pure elements and contain impurity. This impurity contributes to the existence of ESR. Typically, a resistor connected in series with the output capacitor simulates the ESR, as depicted in Fig. 2.

ESR values are essential in achieving LVR stability as they reflect characteristics that are essential to the output voltage, such as oscillation and undershoot during the transient response. For example, when the ESR is too high, it causes the

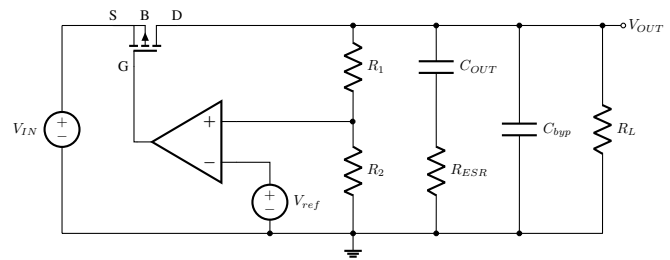


Fig. 2. ESR Connected in Series with the Output Capacitor.

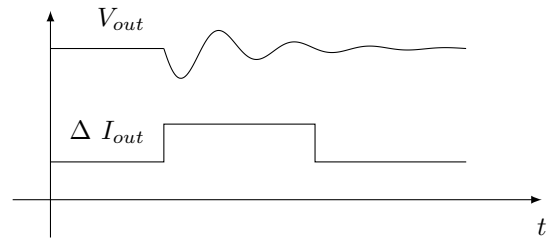


Fig. 3. Unstable Transient Response with Low ESR.

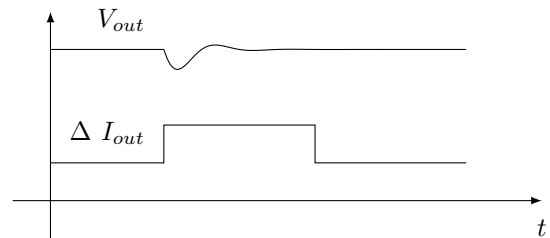


Fig. 4. Stable Transient Response with Optimum ESR.

output voltage to be less than the minimum operating voltage. Finally, this condition contributes to the unstable operation of the LVR. The difference between the output voltage and the minimum operating voltage is known as the undershoot. In sum, the higher the ESR is, the more significant the undershoot will be. This condition contributes to the instability of LVRs.

### D. Linear Voltage Regulator Stability

The main factor influencing the stability of LVRs is the load disturbance. For example, disturbances, such as sudden changes in load current due to short circuits, have a significant impact on LVR stability. Therefore, the designed LVR must be able to maintain a stable output voltage even if the current change occurs in a short period [12]. Fig. 3 and 4 show two examples of the relationship between ESR and transient response.

Fig. 3 shows that oscillations occur after the first peak, which indicates that the output voltage is unstable. Meanwhile, Fig. 4 depicts a stable output voltage. On the basis of both figures that illustrate the relationship between ESR and output voltage, we conclude that an extremely low ESR can cause oscillations and finally generate an unstable output voltage. Furthermore, LVR stability can be determined by the number of oscillations. For a stable LVR, in practice, the number of oscillations should be less than four.





Fig. 5. Block Diagram of MBA Process.

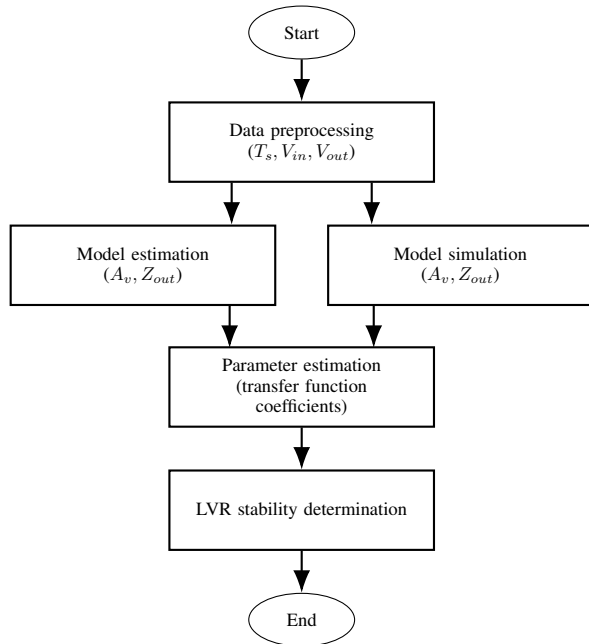


Fig. 6. Overall Flowchart of MBA Process.

## II. METHODS

### A. Model-based Approach

An MBA is a method for describing system behavior in the forms of transfer functions by analyzing the circuit. The transfer function of a system provides useful information regarding the input and output, such as stability, steady-state response, and dynamic response [25], [26]. In this study, the MBA is aimed at identifying all the coefficients or unknown parameters presented in a transfer function through the analysis of input and output signals. Fig. 5 depicts a simplified block diagram of the MBA process.

The MBA in this study utilizes the LR method to estimate the transfer function. LR is a method for modeling the relationship between two or more variables in a linear equation until they reach the desired level. This study aims to develop an efficient method for estimating the internal physical parameters of the LVR circuit on the basis of the LR method before determining the LVR stability. The study involves five main steps: preprocessing of data, model estimation, model simulation, parameter estimation, and determination of LVR stability. Fig. 6 displays the flowchart of this study.

This process starts with the preprocessing of data, which is aimed at determining the type of input signal. The model estimation process aims to obtain the transfer functions of output impedance,  $Z_{out}$  and the voltage gain,  $A_v$  via circuit analysis. At the same time, model simulations in the form of  $Z_{out}$  and  $A_v$  are carried out using OrCAD Capture CIS software. By

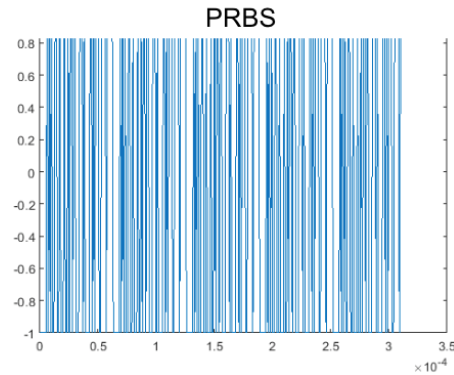


Fig. 7. PRBS Signal.

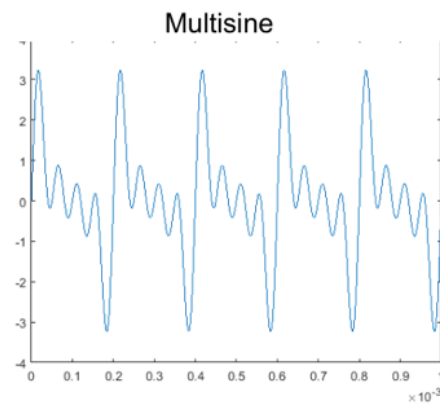


Fig. 8. Multisine Signal.

comparing  $A_v$  from model estimation and that from model simulation, we obtain the estimated physical parameters in this process. Finally, LVR stability is determined by using the estimated  $Z_{out}$  with estimated physical parameters.

### B. Preprocessing Data

The preprocessing of the data is intended to determine the type of excitation signal or input signal to excite the tested LVR circuit before the model estimation process is carried out. Two input signals are investigated: (a) PRBS signal and (b) multisine signal. The purpose of studying both signals is to select the input signal that is most appropriate for this study to increase the accuracy of the estimation of physical parameters.

The PRBS signal is known as a pseudorandom binary sequence. It is a succession of rectangular pulses that display statistical behavior similar to a random sequence. The PRBS signal is also a perfect white noise that is often used as a test signal. Fig. 7 shows an example of the PRBS signal.

The multisine signal is known as a multifrequency sinusoidal signal. It is an addition of at least two sinusoidal signals with different frequencies. Multisine is usually used to excite the tested circuit by manipulating the frequency of each sinusoidal signal. Fig. 8 shows an example of a multisine signal.

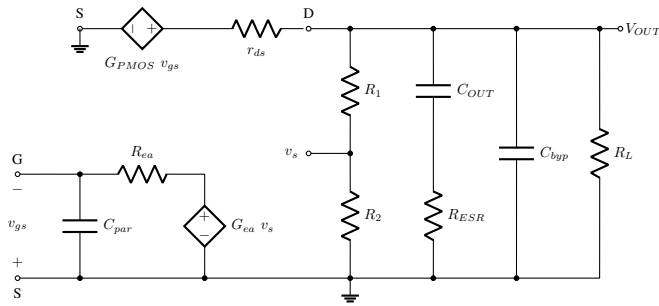


Fig. 9. LVR Circuit for  $Z_{out}$  Model.

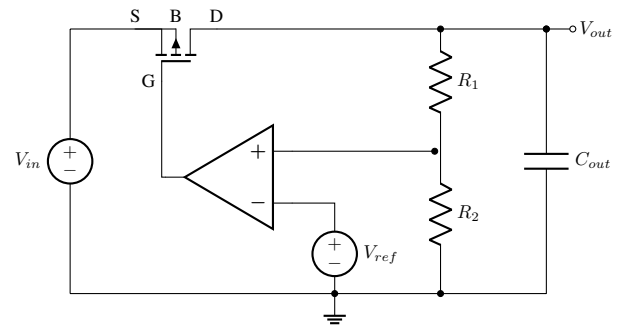


Fig. 10. LVR Circuit for  $A_v$  Model.

Theoretically, both signals are appropriate for this study. However, practically, PRBS is challenging to generate in the OrCAD Capture CIS software because this software does not supply PRBS generator components. Hence, the signal should be built from scratch by using discrete components. Thus, the multisine signal is selected as the input signal of the LVR circuit.

### C. Model Estimation

Once the input signal is specified, the subsequent model estimation can proceed. Generally, the LVR model estimation aims to obtain the model or transfer function of output impedance,  $Z_{out}$  and voltage gain,  $A_v$  through circuit analysis. Output impedance,  $Z_{out}$  describes the relationship between the output voltage and the output current during the transient response; it is defined as

$$Z_{out}(s) = \frac{v_{out}(s)}{i_{out}(s)} \quad (1)$$

$Z_{out}$  model is derived on the basis of (1) and the circuit analysis of the output impedance model, as shown in Fig. 9. Small-signal analysis on the LVR circuit, as shown in Fig. 9, is carried out to detect the effect of a sudden change in load current to an output voltage.

$Z_{out}$  in the discrete time domain can then be defined as

$$Z_{out_{CL}}(z) = \frac{1}{Z_1(z) Z_2(z)} \quad (2)$$

where

$$Z_1(z) = \frac{2}{T_s} \left( \frac{1-z^{-1}}{1+z^{-1}} \right) C_b + \frac{1}{R_1+R_2} + \frac{1}{R_L} + \frac{1}{r_{ds}} + \frac{1}{\left( \frac{2}{T_s} \left( \frac{1-z^{-1}}{1+z^{-1}} \right) C_{out} + R_{esr} \right)} \quad (3)$$

$$Z_2(z) = 1 + G_{fb} G_{ea} g_m r_{ds} \left( \frac{Z_3(z)}{r_{ds} + Z_3(z)} \right) \times \left( \frac{1}{1 + \frac{2}{T_s} \left( \frac{1-z^{-1}}{1+z^{-1}} \right) C_{gs} R_{oa}} \right) \quad (4)$$

$$Z_3(z) = \left( \frac{2}{T_s} \left( \frac{1-z^{-1}}{1+z^{-1}} \right) C_b + \frac{1}{R_L} \right) + \left( \frac{1}{R_{esr} + \frac{1}{\frac{2}{T_s} \left( \frac{1-z^{-1}}{1+z^{-1}} \right) C_{out}}} \right) \quad (5)$$

and

$$G_{fb} = \frac{R_2}{R_2 + R_1} \quad (6)$$

Next, the same method is used to obtain the transfer function of the  $A_v$  model but with different equations and circuit.  $A_v$  is derived as

$$A_v(s) = \frac{v_{out}(s)}{v_{in}(s)} \quad (7)$$

and the circuit analysis is conducted on the basis of the voltage gain model, as shown in Fig. 10.

Finally, the transfer function of  $A_v(z)$  in the discrete-time domain is obtained on the basis of (8).

$$A_v(z) = \frac{1 + g_m r_{ds}}{1 + Z_4(z) + Z_5(z)} \quad (8)$$

where

$$Z_4(z) = \frac{2}{T_s} \left( \frac{1-z^{-1}}{1+z^{-1}} \right) C_{out} r_{ds} + \frac{r_{ds}}{R_1 + R_2} \quad (9)$$

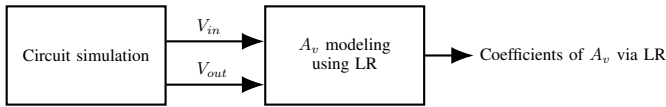


Fig. 11. Block Diagram of the MBA Process.

$$Z_5(z) = \frac{g_m r_{ds}}{(R_1 + R_2) \left( 1 + \frac{2}{T_s} \left( \frac{1 - z^{-1}}{1 + z^{-1}} \right) C_{gs} R_{oa} \right)} \quad (10)$$

In general, (8) can be simplified and expressed as

$$A_v(z) = \frac{b_0 + b_1 z^{-1} + b_2 z^{-2}}{a_0 + a_1 z^{-1} + a_2 z^{-2}} \quad (11)$$

where  $b_0$  to  $a_2$  are given as

$$b_0 = N_1 C_{gs} R_{oa} + N_2 C_{gs} R_{oa} g_m + N_3 g_m + N_4 \quad (12)$$

$$b_1 = N_5 g_m + N_6 \quad (13)$$

$$b_2 = N_7 C_{gs} R_{oa} + N_8 C_{gs} R_{oa} g_m + N_9 g_m + N_{10} \quad (14)$$

$$a_0 = D_1 C_{gs} R_{oa} + D_2 G_{ea} g_m + D_3 \quad (15)$$

$$a_1 = D_4 C_{gs} R_{oa} + D_5 G_{ea} g_m + D_6 \quad (16)$$

$$a_2 = D_7 C_{gs} R_{oa} + D_8 G_{ea} g_m + D_9 \quad (17)$$

where  $N_1$  to  $N_{10}$  represents the known constant values of the numerator while  $D_1$  to  $D_9$  represent the known constant values of the denominator that is made up of known and measurable physical parameters, such as  $R_1$ ,  $R_2$ ,  $C_{out}$ , and  $r_{ds}$ . Equations (12) to (17) show that the following physical parameters need to be estimated:  $C_{gs} R_{oa}$ ,  $C_{gs} R_{oa} g_m$ ,  $g_m$ , and  $G_{ea} g_m$ . To decrease the number of coefficients in the transfer function of  $A_v(z)$ , we can divide the result of (11) by  $a_0$ . Finally, the simplified transfer function can be written as (18).

$$A_{vMAL}(z) = \frac{b_{0MAL} + b_{1MAL} z^{-1} + b_{2MAL} z^{-2}}{1 + a_{1MAL} z^{-1} + a_{2MAL} z^{-2}} \quad (18)$$

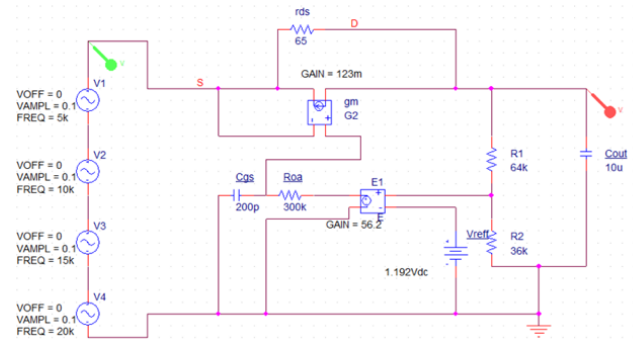


Fig. 12. Circuit Simulation of  $A_v$  Model.

#### D. Model Simulation

The next process in the MBA is the model simulation of the LVR circuit. This process aims to obtain the coefficients of the  $A_v$  model through the LR method by analyzing the input and output signals. Fig. 11 depicts the block diagram of the model simulation process.

Circuit simulation is conducted in OrCAD Capture CIS software. This process is aimed at obtaining the input signal,  $v_{in}$  and output signal,  $v_{out}$  of the  $A_v$  model. The circuit simulation for the  $A_v$  model, in the small-signal analysis circuit form, is constructed and shown in Fig. 12.

In this study, the selected input signal is a multisine signal with four different frequencies, namely, 5, 10, 15, and 20 kHz. Generally, each sinusoidal signal is capable of testing two frequency components at a time. Therefore, at least three different types of sinusoidal signals are needed for six frequency components or coefficients, as in (11). However, four sinusoidal signals are used to improve the accuracy of the estimated model.

Next, the input and output signals obtained from the LVR circuit simulation are used for the  $A_v$  modeling of the LVR circuit based on the LR method with the aid of MATLAB software. As the  $A_v$  model with the LR method generated by MATLAB is derived as

$$A_{vLR}(z) = \frac{y(k)}{x(k)} = \frac{b_{0LR} + b_{1LR} z^{-1} + b_{2LR} z^{-2}}{1 + a_{1LR} z^{-1} + a_{2LR} z^{-2}} \quad (19)$$

then (19) needs to be converted into

$$y(k) = -a_{1LR} y(k-1) - a_{2LR} y(k-2) + b_{0LR} x(k) + b_{1LR} x(k-1) + b_{2LR} x(k-2) \quad (20)$$

Then,  $\beta$  is defined as

$$\beta = [\beta_0, \beta_1, \beta_2, \beta_3, \beta_4, \beta_5]^T = [-a_{1LR}, -a_{2LR}, b_{0LR}, b_{1LR}, b_{2LR}]^T \quad (21)$$

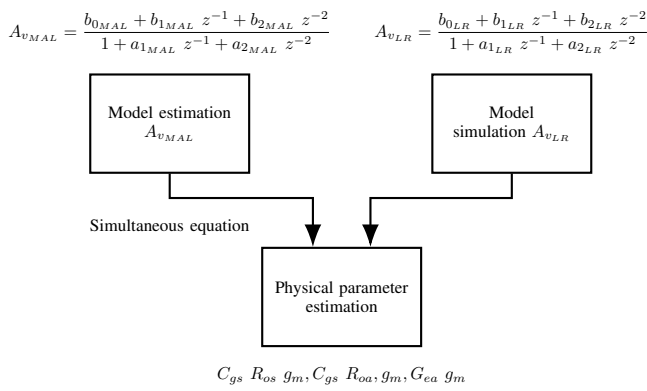


Fig. 13. Block Diagram of the Process of Parameter Estimation.

Equation (21) is used to determine the polarity of the estimated parameters. Furthermore, the derivation of vector  $\beta$  is started by the general equation of the LR method and is defined as

$$y = x^T \beta \quad (22)$$

$$\beta = (x^T x)^{-1} x^T y \quad (23)$$

where  $y$  is the output signal and  $x$  is the input signal. Finally, (21) is used to determine the polarity of the estimated parameters while (23) is used to estimate the coefficients such as  $b_{0_{LR}}, b_{1_{LR}}, b_{2_{LR}}, a_{1_{LR}},$  and  $a_{2_{LR}}$  in the  $A_{v_{LR}}$  model. The estimated coefficients are used to estimate the physical parameters of the LVR circuit in the next process.

#### E. Physical Parameter Estimation

This section explains the process of physical parameter estimation by comparing the two voltage gain transfer functions obtained from the model simulation,  $A_{v_{LR}}$ , and the model estimation,  $A_{v_{MAL}}$ . This process aims to estimate the physical parameters that are difficult to measure, i.e.,  $C_{gs}, R_{oa}, C_{gs}, R_{oa}, g_m,$  and  $G_{ea}, g_m,$  by using the simultaneous equation solution approach. Fig. 13 depicts the block diagram of the process of parameter estimation.

The coefficients of  $A_{v_{LR}}$  and  $A_{v_{MAL}}$  are equated to solve the following equations simultaneously:

$$b_{0_{MAL}} = b_{0_{LR}} \quad (24)$$

$$b_{1_{MAL}} = b_{1_{LR}} \quad (25)$$

$$b_{2_{MAL}} = b_{2_{LR}} \quad (26)$$

$$a_{1_{MAL}} = a_{1_{LR}} \quad (27)$$

$$a_{2_{MAL}} = a_{2_{LR}} \quad (28)$$

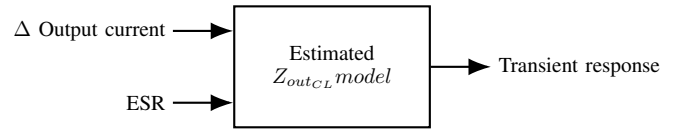


Fig. 14. Block Diagram of the Process of Obtaining a Transient Response via the Estimated Model.

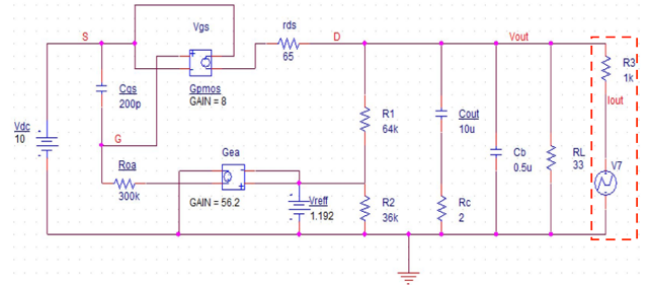


Fig. 15. LVR Circuit Simulation of  $Z_{out}(z)$  Model.

Then, the physical parameters, i.e.,  $C_{gs}, R_{oa}, C_{gs}, R_{oa}, g_m,$  and  $G_{ea}, g_m,$  are estimated. Thereafter, these estimated physical parameters are substituted into the  $Z_{out_{CL}}(z)$  model, as shown in (2). Moreover, parameters that are easy to measure and obtain, such as  $R_1, R_2, C_{out},$  and  $r_{ds},$  are also substituted by their measured values in (2). Finally, a complete estimated  $Z_{out_{CL}}(z)$  is obtained.

#### F. Determination of LVR Stability

This section explains the process of determination of LVR stability by analyzing the transient response of the LVR. The transient response is obtained when the input, such as a sudden change in the output current and ESR values, is applied to the estimated  $Z_{out_{CL}}(z)$  model. Fig. 14 depicts the process of obtaining a transient response.

The circuit simulation, as shown in Fig. 15, is used to generate the output voltage during the transient response. This result is known as the  $Z_{out_{CL}}(z)$  simulation result. Furthermore, instead of directly analyzing the output voltage from the simulation, we can generate the output voltage via the estimated model, the process of which is shown in Fig. 14. A disturbance signal, such as a sudden change in the output current at the tested ESR value, is applied to the circuit. Sudden change conditions can be simulated using a resistor,  $R_3$  and voltage generator,  $V_7$ , as shown in the right part of Fig. 15. Thereafter, the acquired disturbance signal is applied to the estimated  $Z_{out_{CL}}(z)$  model. Then, an output voltage during the transient response is acquired. This result is known as the  $Z_{out_{CL}}(z)$  estimation result. The simulation and estimated results are compared.

Two conditions must be met to ensure that the transient response is stable, that is, (a) the number of oscillations at the transient response does not exceed three and (b) the undershoot does not exceed the tolerance value given in the datasheet.

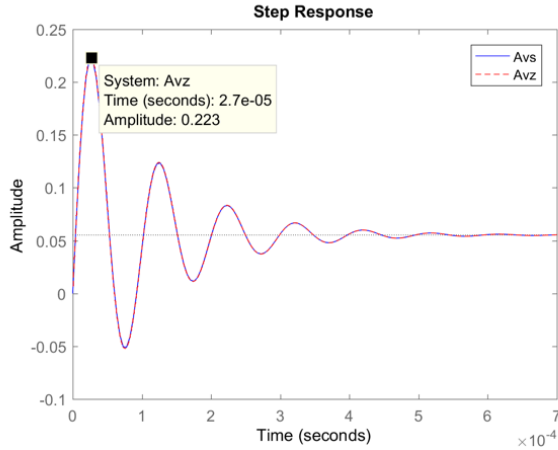


Fig. 16. Step Response with Rising Time of 27  $\mu$ s.

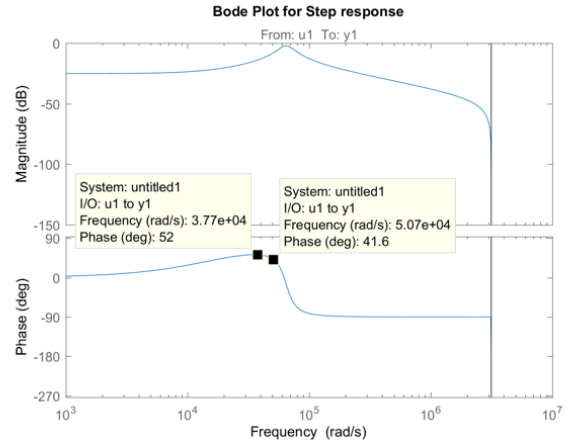


Fig. 17. Bode Plot with Frequencies of 37 dan 50 kHz.

### III. RESULTS AND DISCUSSION

#### A. Validation of Input Signal

As a multisine signal is selected as the input signal for the LR method, two important factors need to be considered: (a) the number of sinusoidal signals and (b) the values of the sinusoidal frequency. These two factors play an essential role in the accuracy of the estimated physical parameters. In sum, the more suitable the number of sinusoidal signals and the value of the sinusoidal frequency signal used are the more accurate the estimated physical parameters will be.

Firstly, the number of sinusoidal signals depends on the number of frequency components or the number of coefficients in the  $A_v$  model. In this study, we have six frequency components, as shown in (11); thus, at least three sinusoidal signals are required. However, four sinusoidal signals are used to increase the level of accuracy.

Secondly, the value of the sinusoidal frequency signal depends on the step response rising time of the  $A_v$  model. Hence, the selected sinusoidal frequencies must reach a maximum of 37 kHz. Fig. 16 depicts the step response of the  $A_v$  model. Selecting a frequency beyond 100 kHz is not recommended because when the frequency exceeds 100 kHz, the magnitude decreases and undergoes phase changes, as shown in Fig. 17. Thus, the stability of the LVR is affected.

#### B. Voltage Gain Model Estimation Results

This section discusses the voltage gain estimation results,  $A_{vLR}$  obtained via the LR method. In this study, the parameters that are easy to measure and obtain, such as  $R_1$ ,  $R_2$ ,  $C_{out}$ , and  $r_{ds}$ , are replaced by 64 k $\Omega$ , 36 k $\Omega$ , 10  $\mu$ F, and 65  $\Omega$ , respectively. The results of this estimation are shown in (29). The coefficients of the  $A_{vLR}$  model are listed in Table I.

$$A_{vLR}(z) = \frac{0.006905 + 0.000117 z^{-1} - 0.006794 z^{-2}}{1 - 1.978 z^{-1} + 0.982 z^{-2}} \quad (29)$$

Before the simultaneous equations are solved, the polarity for the coefficient must be noted. For example, the coefficient

TABLE I. ESTIMATION OF THE COEFFICIENTS OF VOLTAGE GAIN MODEL

| Coefficient | Coefficient values |
|-------------|--------------------|
| $a_{1LR}$   | 1.978000           |
| $a_{2LR}$   | -0.982000          |
| $b_{0LR}$   | 0.006905           |
| $b_{1LR}$   | 0.000117           |
| $b_{2LR}$   | -0.006794          |

for  $a_{1LR}$  is -1.978 based on (29), but it is incorrect because the polarity for the coefficient must be based on the equation of the LR method derived in (21). On the basis of (21),  $a_{1LR}$  and  $a_{2LR}$  have negative values. Therefore, the polarity for both coefficients must be inverted.

#### C. Physical Parameter Estimation Results

This section describes the results of the estimated internal physical parameters, i.e.,  $C_{gs}$ ,  $R_{oa}$ ,  $g_m$ ,  $C_{gs}$ ,  $R_{oa}$ ,  $g_m$ , and  $G_{ea}$ ,  $g_m$ . Before the physical parameter estimation process can be performed, the values of the physical parameters must be set randomly. Four examples of parameter sets are provided for the parameter estimation process, as shown in Table II, and the following equation is used to find the accuracy of the estimated physical parameters:

$$Accuracy = \left| \frac{TPP - EPP}{TPP} \right| \times 100\% \quad (30)$$

where TPP and EPP are target physical parameter and estimated physical parameter, respectively.

As shown in Table II, the results of the estimated physical parameters indicate that the MBA is capable of estimating the physical parameters of the LVR circuit with a high level of accuracy of approximately 90 %. However, the estimation results of these parameters are obtained on the basis of 1  $\mu$ s sampling time and multisine input signal with 5, 10, 15, and 20 kHz frequencies.

TABLE II. FOUR EXAMPLES OF PHYSICAL PARAMETERS OF THE LVR CIRCUIT

| Set | Parameters        | EPP                     | TPP                     | Accuracy (%) |
|-----|-------------------|-------------------------|-------------------------|--------------|
| A   | $C_{gs}R_{oa}g_m$ | $7.3865 \times 10^{-6}$ | $7.3800 \times 10^{-6}$ | 99.91        |
|     | $C_{gs}R_{oa}$    | $6.0088 \times 10^{-5}$ | $6.0000 \times 10^{-5}$ | 99.85        |
|     | $G_{ea}g_m$       | 6.7011                  | 6.9126                  | 96.94        |
|     | $g_m$             | $127.00 \times 10^{-3}$ | $123.00 \times 10^{-3}$ | 96.75        |
| B   | $C_{gs}R_{oa}g_m$ | $7.3900 \times 10^{-6}$ | $7.5000 \times 10^{-6}$ | 98.53        |
|     | $C_{gs}R_{oa}$    | $6.0456 \times 10^{-5}$ | $6.0500 \times 10^{-5}$ | 99.93        |
|     | $G_{ea}g_m$       | 6.9119                  | 6.9595                  | 99.32        |
|     | $g_m$             | $128.90 \times 10^{-3}$ | $123.50 \times 10^{-3}$ | 95.63        |
| C   | $C_{gs}R_{oa}g_m$ | $7.4410 \times 10^{-6}$ | $7.6200 \times 10^{-6}$ | 97.65        |
|     | $C_{gs}R_{oa}$    | $6.0829 \times 10^{-5}$ | $6.1000 \times 10^{-5}$ | 99.72        |
|     | $G_{ea}g_m$       | 7.1253                  | 6.8282                  | 95.64        |
|     | $g_m$             | $133.90 \times 10^{-3}$ | $122.50 \times 10^{-3}$ | 90.69        |
| D   | $C_{gs}R_{oa}g_m$ | $7.2637 \times 10^{-6}$ | $7.2699 \times 10^{-6}$ | 99.91        |
|     | $C_{gs}R_{oa}$    | $5.9304 \times 10^{-5}$ | $5.9400 \times 10^{-5}$ | 99.83        |
|     | $G_{ea}g_m$       | 6.2870                  | 6.8436                  | 91.87        |
|     | $g_m$             | $114.20 \times 10^{-3}$ | $122.38 \times 10^{-3}$ | 93.32        |

#### D. Output Impedance Model Estimation Results

This section explains the estimated output impedance model,  $Z_{out_{CL}}(z)$ , a comparison between the  $Z_{out_{CL}}(z)$  simulation results and the  $Z_{out_{CL}}(z)$  estimated results, and the transient response for different ESR values. Firstly, the estimated output impedance model is discussed. After the physical parameters are estimated, the values of the set A parameters shown in Table II are substituted into the estimated  $Z_{out_{CL}}(z)$  model. Finally, the transfer function of the  $Z_{out_{CL}}(z)$  model is generated, as shown in (31).

$$Z_{out_{CL}}(z) = \frac{(0.6521 z^7 - 2.276 z^6 + 2.336 z^5 + 0.474 z^4 - 2.5 z^3 + 1.756 z^2 - 0.4876 z + 0.0478)}{(1.013 z^7 - 4.84 z^6 + 9.458 z^5 - 9.782 z^4 + 5.718 z^3 - 1.876 z^2 + 0.3204 z - 0.0221)} \quad (31)$$

Secondly, a comparison of the simulation and estimation results of the  $Z_{out_{CL}}(z)$  model is displayed in Fig. 18, where the output current and ESR are set to 115 mA and 2  $\Omega$ , respectively.

Fig. 18 shows that the two results are nearly the same. This similarity is due to the accurate estimated physical parameters, as shown in Table II. In sum, the result of the estimated  $Z_{out_{CL}}(z)$  model is validated by the simulation of the LVR circuit with OrCAD Capture CIS software. Fig. 19 shows the input voltage of the input signal, while Fig. 20 shows the output voltage as the output signal.

Finally, the analysis of LVR stability is conducted on the basis of the estimated  $Z_{out_{CL}}(z)$  model, as shown in (31). In this study, the following conditions should be met to ensure the stable level of the LVR circuit: (a) the number of oscillations does not exceed three oscillations, and (b) the undershoot does not exceed the tolerance value as provided in the datasheet,

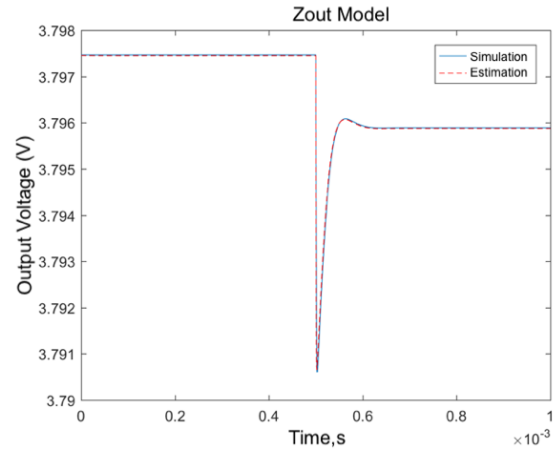


Fig. 18. Comparison of Simulation and Estimation of  $Z_{out_{CL}}(z)$  Model.

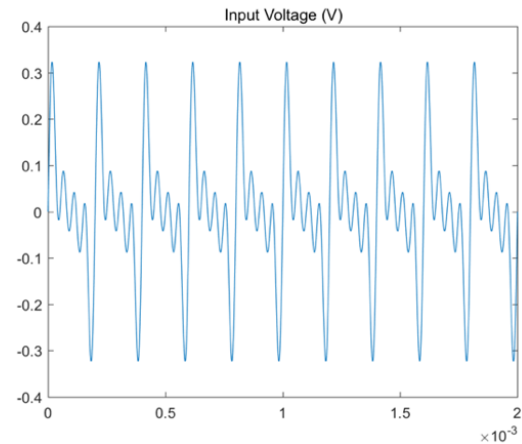


Fig. 19. Multisine as the Input Signal for the  $A_{v_{LR}}$  Model of LVR Circuit.

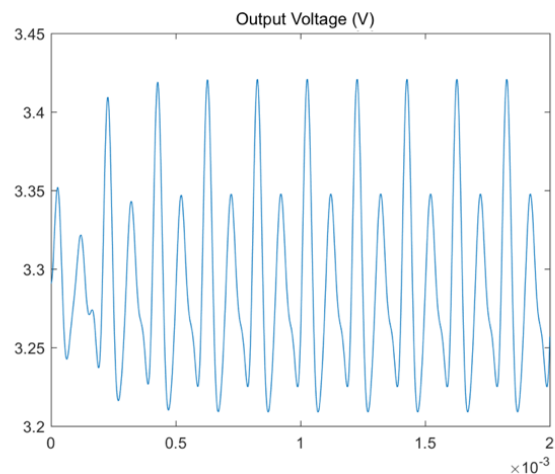


Fig. 20. Output Signal for the  $A_{v_{LR}}$  Model LVR Circuit.

which is 20 mV. Fig. 21 to 23 illustrate the transient response results along with the different ESR values given an output current is set at 115 mA.

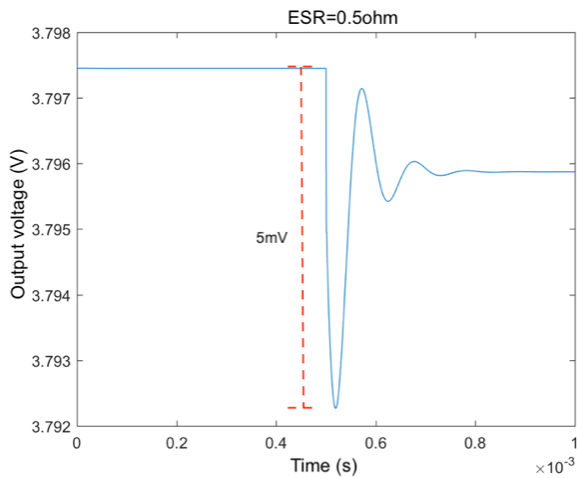


Fig. 21. Transient Response of Estimated  $Z_{outCL}(z)$  with ESR = 0.5  $\Omega$ .

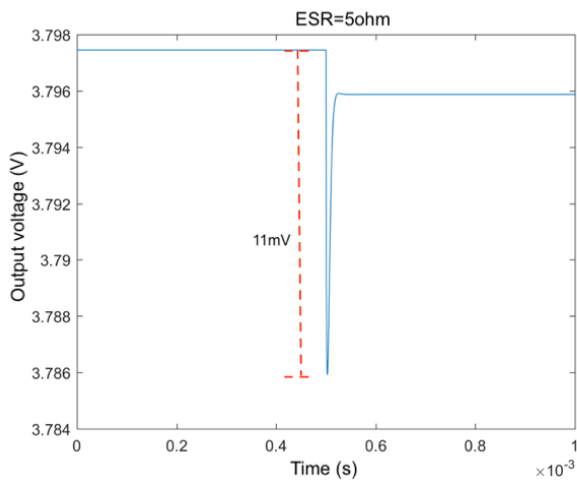


Fig. 22. Transient Response of Estimated  $Z_{outCL}(z)$  with ESR = 5  $\Omega$ .

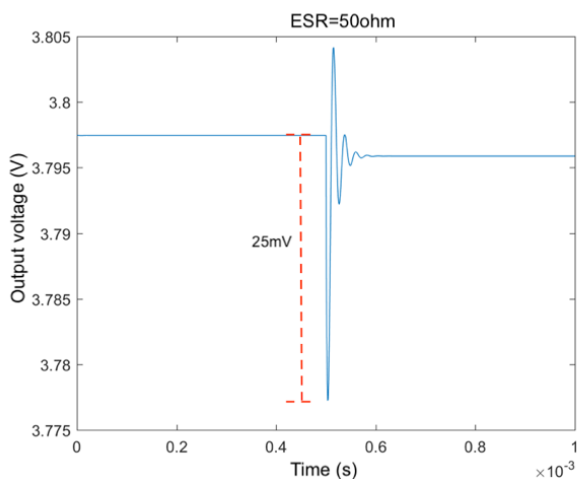


Fig. 23. Transient Response of Estimated  $Z_{outCL}(z)$  with ESR = 50  $\Omega$ .

Fig. 21 illustrates the results of a transient response with an ESR of 0.5  $\Omega$ . Although the results reflect a small undershoot,

the relatively high number of oscillations causes the LVR to operate in unstable conditions. Figure 22 shows a stable LVR with ESR of 5  $\Omega$ . This result is explained as follows: the transient response contains less than three oscillations, and the undershoot is in the appropriate range. Fig. 23 illustrates the results of a transient response with an ESR of 50  $\Omega$ . Although the number of oscillations does not exceed three oscillations, and the undershoot exceeds its tolerance value, the LVR fails to function correctly. In sum, an excessively low ESR causes oscillation to occur, whereas a high ESR produces a large undershoot. These two conditions result in an unstable output voltage.

#### IV. CONCLUSION

In conclusion, this study was successfully conducted, and the results obtained prove that the objectives were achieved. Firstly, this study successfully developed a method for estimating the physical parameters of LVR circuits through the MBA. Secondly, the results of the physical parameter estimation were successfully obtained with a high level of accuracy. Finally, LVR stability was successfully studied and analyzed through a transient response. Although the objectives of this study were achieved, the proposed MBA method may still be improved further. For example, study can be implemented using real LVR circuits to strengthen the concept of the MBA practically and validate the results obtained.

Herein, the MBA method is highly dependent on the LVR circuit supplied by the manufacturer, and this study can only be conducted when the LVR circuit is given in the datasheet. Therefore, this study can be improved in the future to solve the problem with the use of machine learning. For example, machine learning can analyze and provide some examples of possible LVR circuit sets through algorithmic learning and computing models.

#### ACKNOWLEDGMENT

The authors would like to thank Ministry of Higher Education Malaysia for the financial support under grant number FRGS/1/2019/TK04/UKM/03/1.

#### REFERENCES

- [1] C. Wilson, T. Hargreaves, and R. Hauxwell-Baldwin, "Benefits and risks of smart home technologies," *Energy Policy*, vol. 103, pp. 72–83, 2017.
- [2] Y. Shi, A. Wang, J. Cao, and Z. Zhou, "A transient-enhanced voltage regulator with stability and power-supply-rejection boosting," *Nanoscale Research Letters*, vol. 14, no. 368, pp. 1–11, 2019.
- [3] J. Wang, B. Bao, J. Xu, G. Zhou, and W. Hu, "Dynamical effects of equivalent series resistance of output capacitor in constant on-time controlled buck converter," *IEEE Transactions on Industrial Electronics*, vol. 60, no. 5, pp. 1759–1768, 2013.
- [4] C. K. Chava, and J. Silva-Martínez, "A frequency compensation scheme for LDO voltage regulators," *IEEE Transactions on Circuits and Systems I: Regular Papers*, vol. 51, no. 6, pp. 1041–1050, 2004.
- [5] M. Day, "Understanding low drop out (LDO) regulators," in *2006 Texas Instruments Portable Power Design Seminar*, pp. 1–7, 2006.
- [6] J. Falin, and J. Cummings, "ESR, stability, and the LDO regulator," *Texas Instruments Application Report*, pp. 1–6, 2020.
- [7] B. S. Lee, "Technical review of low dropout voltage regulator operation and performance," *Texas Instruments Application Report*, pp. 1–25, 1999.
- [8] E. Rogers, "Stability analysis of low-dropout linear regulators with a PMOS pass element," *Power Management*, pp. 10–13, 1999.

- [9] Rohm Semiconductor, "Simple test method for estimating the stability of linear regulators," Application Note, pp. 1–4, 2016.
- [10] A. H. Musa, M. H. M. Zaman, R. Mohamed, and M. M. Mustafa, "Characterization of voltage regulators by automated equivalent series resistance," in Proceedings of the 2014 IEEE Conference on System, Process and Control (ICSPC 2014), pp. 68–72, 2014.
- [11] S. Zamri, M. H. M. Zaman, M. F. Ibrahim, A. A. Ibrahim, and M. M. Mustafa, "Noninvasive stability measurement of linear voltage regulator in the closed-loop condition," International Journal of Advanced Trends in Computer Science and Engineering, vol. 10, no. 1.6, pp. 167–172, 2019.
- [12] M. H. M. Zaman, M. M. Mustafa, and A. Hussain, "Estimation of voltage regulator stable region using radial basis function neural network," Journal of Telecommunication, Electronic and Computer Engineering, vol. 10, no. 2–8, pp. 63–66, 2018.
- [13] M. H. M. Zaman, M. M. Mustafa, M. A. Hannan, and A. Hussain, "Neural network based prediction of stable equivalent series resistance in voltage regulator characterization," Bulletin of Electrical Engineering and Informatics, vol. 7, no. 1, pp. 134–142, 2018.
- [14] Z. Guo, and J. Savir, "Analog circuit test using transfer function coefficient estimates," in Proceedings of the International Test Conference, pp. 1155–1163, 2003.
- [15] Z. Guo, and J. Savir, "Coefficient-based test of parametric faults in analog circuits," IEEE Transactions on Instrumentation and Measurement, vol. 55, no. 1, pp. 150–157, 2006.
- [16] A. Kavithamani, V. Manikandan, and N. Devarajan, "Soft fault diagnosis of analog circuit using transfer function coefficients," in Proceedings of the International Conference on Process Automation, Control and Computing, pp. 1–6, 2011.
- [17] S. Sindhia, V. D. Agrawal, and V. Singh, "Non-linear analog circuit test and diagnosis under process variation using V-Transform coefficients," in Proceedings of the IEEE VLSI Test Symposium, pp. 64–69, 2011.
- [18] V. Valdivia, A. Barrado, A. Lazaro, P. Zumel, and C. Raga, "Easy modeling and identification procedure for "black box" behavioral models of power electronics converters with reduced order based on transient response analysis," in Proceedings of the IEEE Applied Power Electronics Conference and Exposition, pp. 318–324, 2009.
- [19] V. Valdivia, A. Barrado, A. M. Roldan, C. Fernandez, and P. Zumel, "Black box modeling of DC-DC converters based on transient response analysis and parametric identification methods," in Proceedings of the 25th Annual IEEE Applied Power Electronics Conference and Exposition, pp. 1131–1138, 2010.
- [20] V. Valdivia, A. Lazaro, A. Barrado, P. Zumel, C. Fernandez, and M. Sanz, "Black box modeling of three-phase voltage source inverters for system-level analysis," IEEE Transactions on Industrial Electronics, vol. 59, no. 9, pp. 3648–3662, 2012.
- [21] C. C. Bilberry, M. S. Mazzola, and J. Gafford, "Power supply on chip (PwrSoC) model identification using black-box modeling techniques," in Proceedings of the 27th Annual IEEE Applied Power Electronics Conference and Exposition, pp. 1821–1825, 2012.
- [22] H. Luo, Y. Wang, H. Lin, and Y. Jiang, "Module level fault diagnosis for analog circuits based on system identification and genetic algorithm," Measurement, vol. 45, no. 4, pp. 769–777, 2012.
- [23] Y. Yusof, N. Abd. Rahim, "Functional simulation model for single phase pulse width modulation-voltage source inverter (PWM-VSI) using switching function concept," Jurnal Kejuruteraan, vol. 23, pp. 49–56, 2011.
- [24] C. Simpson, "Linear and switching voltage regulator fundamental part 1," Texas Instruments, pp. 1–30, 2011.
- [25] S. Okiy, C. Chukwuemeka Nwobi-Okoye, and A. Clement Igboanugo, "Transfer function modelling: A literature survey," Research Journal of Applied Sciences, Engineering and Technology, vol. 11, no. 11, pp. 1265–1279, 2015.
- [26] M. H. M. Zaman, M. M. Mustafa, and A. Hussain, "Black-box modeling of low dropout voltage regulator based on two-port network parameter identification," in Proceedings of the 2015 IEEE 11th International Colloquium on Signal Processing and Its Applications, pp. 78–83, 2015.



# Artificial Bee Colony Algorithm Optimization for Video Summarization on VSUMM Dataset

Vinsent Paramanantham<sup>1</sup>

Research Scholar

Faculty of Computer Science and Engineering,  
Sathyabama Institute of Science and Technology  
(Deemed to be University)

Dr. S. SureshKumar<sup>2</sup>

Principal, Swarnandhra College of

Engineering and Technology, Narasapur, AP, India.

**Abstract**—This paper attempts to prove that the Artificial Bee Colony algorithm can be used as an optimization algorithm in sparse-land setup to solve Video Summarization. The critical challenge in doing quasi(real-time) video summarization is still time-consuming with ANN-based methods, as these methods require training time. By doing video summarization in a quasi (real-time), we can solve other challenges like anomaly detection and Online Video Highlighting. A simple threshold function is tested to see the reconstruction error of the current frame given the previous 50 frames from the dictionary. The frames with higher threshold errors form the video summarization. In this work, we have used Image histogram, HOG, HOOE, and Canny edge features as features to the ABC algorithm. We have used Matlab 2014a for doing the feature extraction and ABC algorithm for VS. The results are compared to the existing methods. The evaluation scores are calculated on the VSUMM dataset for all the 50 videos against the two user summaries. This research answers how the ABC algorithm can be used in a sparse-land setup to solve video summarization. Further studies are required to understand the performance evaluation scores as we change the threshold function.

**Keywords**—Artificial Bee Colony optimization; video summarization; online video highlighting; sparse-land; anomaly detection; image histogram; HOG; HOOE; canny edge

## I. INTRODUCTION

Since campuses, roads, and public places are monitored constantly by video surveillance, the adaptation of VS will be imperative. Skimming through a huge corpus of video data to derive meaningful summarization requires efficient VS techniques. The need of the hour is to come up with techniques that can be easily deployed and require less training of the algorithms as in ANN methods. Some of the frameworks work well in the object tracking environment or any others. In this framework, we have come up with a common approach to do VS, as seen in the result section evaluated across multiple genres of videos table reference. The main motivation behind this work is three-fold. Firstly, to prove the use of the ABC optimization algorithm in a sparse-land setup. Secondly, to apply this approach to a real-time (quasi) framework similar to [1]. Thirdly, to adapt any domains online video content so that it can be used to solve other challenges in real-time like anomaly detection [2].

The challenge to any video summarization is to adapt to any domain, some of the frameworks work well on a certain domain as the methods are restricted or concentrated

for a particular purpose like choosing humans and vehicle [3]. Methods like the sparse-land approach give the liberty to adapt to any domain videos, which is also proven in this work by the evaluation scores across multiple genre videos in VSUMM dataset in Table I, II. There has been a keen interest in the sparse-land based approach in the literature [4, 1, 5, 6, 7, 8], hence taking this approach in this paper is proven.

The rest of the paper is organized as follows: Section II briefs about the related works in VS. Section III describes the proposed ABC method for the VS framework, Section IV deals with the proposed methodology, Section V discusses the experimental results. Finally, Section VI concludes the paper.

## II. RELATED WORKS

The optimization algorithms play a vital role in selecting the right frames for video summarization and updating the dictionary  $D$ . Various studies on optimization algorithm and its performance metrics are based on storage reduction and computation time, as discussed in [9]. In this paper, we have evaluated the ABC algorithm against a well know dataset VSUMM [10], and the results benchmarked against a known dataset. In this section, we will go through optimization algorithm selection and different strategies to do VS. In the literature, we find lots of methods and techniques to do VS, based on clustering [11], saliency-based methods calculating the frame importance score on egocentric VS[lee2012discovering], traditional approaches with SVD [12]. In recent years there is an enormous amount of papers based on ANN [13, 14, 15, 16, 17, 18, 19]. ANN methods involve training in supervised, unsupervised approaches which may not be suitable for a near real-time VS. Graph-based methods [20, 21, 22, 23] also requires the data porting into a graph database before computation which specializes in keyframe retrievals and browsing system. Among all of the methods, the sparse-land based approach to solve VS still stands out of other techniques due to its simplicity in solving VS as an optimization problem. The other features can be easily plugged and played with any optimization algorithm, as demonstrated in [9], flexibility in selecting the right dictionary shapes and elements and support quasi (real-time) in solving the VS [1], followed by anomaly detection [2]. We also see recent advancement in the sparse-land approach using CSC(Convolutional Sparse Coding Model) as on par with the current ANN methods [24].

Optimization algorithm from Evolutionary methods like ABC [25], PSO [26], GA [27], ADMM [28] and *rmsprop*

[29] are quite common methods for optimization algorithm, In this paper, we have used the ABC method for optimization. In the recent literature, we can see ABC usage [30] for VS, where the authors have worked on another well-known dataset Summe [31] using segment level data on the Video for VS. The global effects of the entire video may not be captured well in such approaches [30].

[30] has used the ABC algorithm to identify key video segments and used clustering techniques to arrive at keyframes. The keyframes come from the center of the cluster. A region of interest approach is used to identify important frames, similar to the camshift algorithm proposed in our work to reduce the unwanted frames. The final reduction of keyframes is done via the hue histogram comparison. Also, the ABC algorithm has shown better convergence than other algorithms like PSO.

[9], in our previous approach, we have proposed four algorithms to test video summarization optimization time and storage reduction. The test was performed on random videos on youtube, whereas this paper accomplishes the performance of the ABC optimization algorithm against known VSUMM dataset in VS, also we have calculated the performance evaluation scores as indicated in the experiments and results section.

[1] has used ADMM optimization techniques in a sparse-land setup to solve VS challenge, these ideas are some of the key foundations in solving the VS framework along with dictionary initialization and sparse modeling. References for image restoration can be found in [32]. Image reconstruction is done with the current frame and frames from the dictionary. A high reconstruction error of  $\alpha$  denotes more changes between frames. When the reconstruction error  $\alpha$  is high the frame is included for summarization [33, 5, 34, 35].

#### A. Summary of the Contribution

Our contribution in this work is the usage of the ABC optimization algorithm in a sparse-land setup to do VS. The evaluation metrics *precision, recall, F1 – Score* are obtained for the individual video to showcase the working of the ABC algorithm on par with other methods as compared in Table III with earlier reference works [10]. The other two Tables I, II gives the *precision, recall, F1 – Score* for all the 50 individual videos in VSUMM dataset. This framework works as a near real-time(quasi-real-time) summarization and anomaly detection framework. The framework can also be easily extended to other advanced sparse-land setups such as CSC [24].

### III. THE ABC OPTIMIZATION FOR VS FRAMEWORK

The artificial bee colony (ABC) algorithm comes from the swarm intelligence branch. The ABC algorithm is modeled around the intelligent behavior of honey bee in performing their task efficiently to identify the target food locations [25, 36]. There are mainly three types of phase, Employed, onlooker, and scout bee phases. The employed bees are responsible for visiting the existing food sources, onlooker bees wait for the dance ceremony to select the next food source depending upon the performance of the bees, the scout bees do a random pickup of food sources. The main function of Employed phase is to update the  $X_{new}$  position variable and to find a suitable partner solution  $X_p$ , the update equation to

calculate the new position is as shown in the below equation 1.  $X$  is the current solution and  $X_p$  is the partner solution.  $\phi$  is a random value in the range [-1,1].

$$X_{new} = X + \phi(X - X_p), \phi \in [-1, 1] \quad (1)$$

The Onlooker bees are responsible for selecting the food sources with a highest nectar value  $F(\theta_i)$ ,  $\theta_i$  is the  $i^{th}$  food source, the probability of a cycle is given as  $P(c) = \{\theta_i(c) | i = 1, 2, \dots, S\}$ , (C: cycle, S:no. of food sources), probability function  $p(X_i)$  for choosing the food sources as given below.

$$p(x_i) = \frac{F(\theta_i)}{\sum_{i=1}^S F(\theta_k)} \quad (2)$$

The scout bees do a random discovery of the food sources with the predefined limits specified by the search space limits  $[X^{Min}, X^{Max}]$ , the randomness of the food sources are determined by the below equation 3.

$$X_{i,j} = X_j^{min} + rand_{i,j} \times (X_j^{max} - X_j^{min}) \quad (3)$$

Where  $i = 1, 2, \dots, S$ ,  $S$  is the number of food sources,  $j = 1, 2, \dots, d$ ,  $d$  dimensional vector solution,  $X^{min} = x_1^{min}, x_2^{min}, \dots, x_d^{min}$  and  $X^{max} = x_1^{max}, x_2^{max}, \dots, x_d^{max}$ ,  $rand_{i,j}$  is a value from a uniform distribution (0,1).

### IV. PROPOSED METHODOLOGY

The architectural flow for VS is similar to our previous work [9]. The features used are *HOG*(histogram of oriented gradients) with nine bins with a range of 20 degrees per bin, *HOF*(Histogram of Optical Flow), *HOOF*(Histogram of Optical Flow), Canny edge detection, the sample feature output of a frame can be seen in the below Fig. 1.

#### A. Preprocessing of Video Using

The camshift algorithm is used to preprocess the frames, a wide variety of applications can found for the camshift algorithm [37, 38, 39] including object tracking and frame rate and size reduction by only capturing the ROI areas. In our approach, we have used the camshift algorithm to reduce the number of frames. This is an important step to filter keyframes. The camshift algorithm usage and depiction can be seen in Fig. 2, similar methods can be seen in the literature [40].

| CA{1,1} | 1      | 2   | 3      | 4    |
|---------|--------|-----|--------|------|
| 1       | 0.2662 | 0   | 0.0125 | 3600 |
| 2       | 0.187  | 0   | 0      | 0    |
| 3       | 0.3927 | 0.5 | 0      | 0    |
| 4       | 0.2276 | 0   | 0      | 0    |
| 5       | 0.6122 | 0   | 0      | 0    |
| 6       | 0.1907 | 0   | 0      | 0    |
| 7       | 0.3722 | 0.5 | 0      | 0    |

Fig. 1. The Feature Matrix for HOG, HOF, Image Histogram, Canny Edge

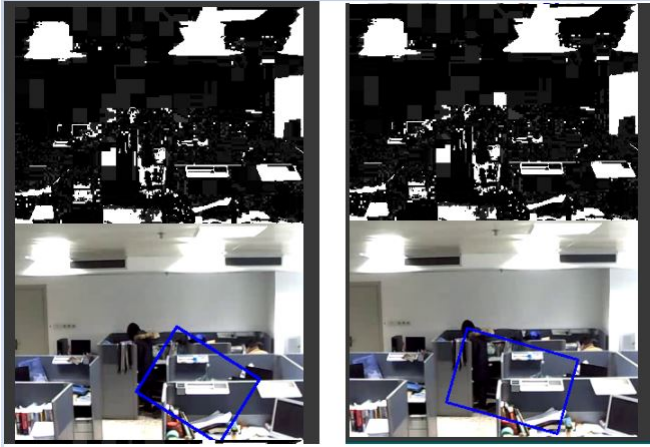


Fig. 2. The Camshift Algorithm usage for Frame Reduction

### B. Features Used

The features used can be seen in the code listing Matlab code below and the values as depicted in Fig. 1. *currF* is the current frame read, *Canny-edge* variable Contain the Canny edges, *HI* is the histogram image, *HOG* is the histogram of oriented gradients [41], *HOOF* is the Histograms of oriented flow.

```
% Matlab Code Listings of features
currF=rgb2gray(currFrame);
Canny-edge=mean2(edge(currF,'canny'));

HI1=mean(imhist(currF));

HOG = gradientHistogram(hx,hy',bin);

HOOF(1:size(ohog,1))=HOG;

CA{t}=[HOG HOOF Canny-edge HI1];
```

### C. Dictionary of Key Frames

The atom selection for the dictionary is done using a similar approach as followed in [2, 1]. We have selected 50 frames for dictionary comparison, the 50 frame is a selected as a computational limit, The current frame feature values are compared against and previous frames value as indicted in equation 4, where *pre* is the previous frames feature value, *cu* is the current frames feature value, the  $\alpha$  is calculated by the ABC algorithm as indicated in the algorithm section,  $\lambda$  is initialized to a small value of 0.01, 50 *k* atoms. Dictionary selection is again a great way to start the summarization with good representation from the video data, the dictionary initialization is discussed in [42, 43, 44].

$$\min_x f(x) = \sum_{i=1}^k (((pre - cu) \times \alpha)) + (\lambda \times \sum_{i=1}^k (\alpha)); \quad (4)$$

### D. Threshold as the Reconstruction Error

The threshold  $\alpha$  is calculated as a mean of the 50 frames in the current cycle comparison from the dictionary, as we increment by 50 frames for the next comparison. The threshold  $\alpha$  as compared with the value from equation 4 when there is a higher reconstruction error (higher value of  $\alpha$ ), we include the frame for summarization.

---

#### Algorithm 1 ABC Algorithm

---

```
1: CostFunction ← @(x)Sphere(x);
2: nVar ← 5; VarMin ← -10; VarMax ← 10;
3: MaxIt ← 10; nPop ← 10;
4: L = round(0.6 * nVar * nPop); (TrialLimit)
5: InitializationPopulationArray
6: pop ← repmat(emptybee, nPop, 1);
7: #InitBestSolutionEverFound BestSol.Cost ← inf;
8: #CreateInitialPopulationbyrandomsample
9: for i ← 1 : nPop do
10: updatethebestcost
11: BestSol = pop(i);
12: end for
13: #ABCMainLoop
14: #Choosepartner K randomly, != i
15: for it ← 1 : MaxIt do
16: for i ← 1 : nPop#RecruitedBees do
17: #NewBeePosition by eqn 1
18: newbee.Position ← pop(i).Position + φ ×
 (pop(i).Position - pop(k).Position);
19: end for
20: #Calculate Fitness Values and Selection Prob
21: for i ← 1 : nPop do
22: F(i) ← exp(-pop(i).Cost%MeanCost);
23: end for
24: Onlooker Bees
25: for m ← 1 : nOnlooker do
26: newbee.Cost ←
 CostFunction(newbee.Position);
27: end for
28: #Scout Bees
29: for i ← 1 : nPop do
30: pop(i).Cost ← C - Function(pop(i).Position);
31: end for
32: for i ← 1 : nPop do pop(i).Cost <
 BestSol.CostBestSol ← pop(i);
33: end for
34: return alpha ← min(BestCost);
```

---

## V. EXPERIMENTAL RESULT

In this section, we discuss the results obtained using the ABC optimization algorithm on a well-known dataset VSUMM [10]. The dataset consists of 50 videos from different genres and user summary keyframes for each video. In this experiment, we have compared the results for two user summaries and given the evaluation for each user summary against the automated summary generation as available in VSUMM dataset [10].

The average evaluation scores obtained in Table III indicate the approach using the ABC algorithm in a sparse-land approach is close to other results as compared to [10].

Fig. 3 depicts the results of one of the video # 30 from the VSUMM dataset giving a clear indication of the frame number matches and  $\pm 1$  frame matches, hence the results obtained demonstrate the approach for sparse-land based VS, a full framework for VS, anomaly detection, and online-highlighting. This approach is open to include any other Text/NLP [45, 46, 47, 48, 49, 50] based feature inputs. Frame importance rankings [45] with NLP caption generation methods [51, 52] combined with other video features are recent advancements in video summarization features [53, 50].

### A. Evaluation of Video Summary

The evaluation is based on the proposed approach as discussed in [54, 10] called Comparison of User Summaries (CUS). The user summary is composed of many user summaries and taken a common score approach in the VSUMM dataset. The results in our approach called the automatic summary are compared with two user summaries as depicted in Fig. 3.

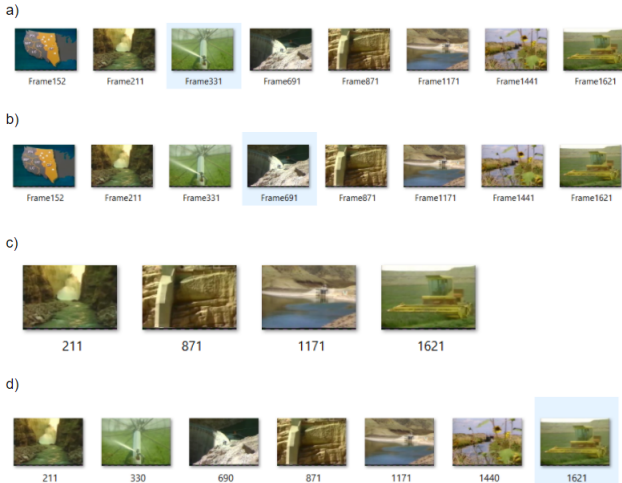


Fig. 3. CUS Evaluation Method for Video #30 in VSUMM Dataset, (a) User1 Summary (b) User2 Summary (c) Automatic Summary from ABC Method (d) Automatic Summary from ABC Method with  $\pm 1$  Frame Number. Frame Numbers for Each Group is Listed Below

- a) 152, 211, 331, 691, 871, 1171, 1441, 1621
- b) 152, 211, 331, 691, 871, 1171, 1441, 1621
- c) 211, 871, 1171, 1621
- d) 211, 330, 690, 871, 1171, 1440, 1621

Precision, recall, and F1-score are the common metrics to measure the performance of the VS framework, the formulas are followed from [54, 10]. The evaluation metrics for precision, recall, F1-score is depicted in Tables I and II against both the user summary in VSUMM dataset. The equation depicted below 5, 6, 7 are used for the evaluation metrics with the automated summary generated by our approach, the comparison scores are mean accuracy rate CUSA(precision) Error rate CUSE(Recall), and F1-Score. The F1-score obtained by our approach is close enough to other methods [10], by balancing the threshold parameters in ABC algorithm we can improve the F1-Score, also we need to take care of other scores that get affected like precision and recall. Finding the right balance with all the parameters of our ABC approach for

video summarization and evaluation by F1-Score is another open challenge.

$$Precision = \frac{N_{matched}}{N_{AS}} \quad (5)$$

$$Recall = \frac{N_{matched}}{N_{US}} \quad (6)$$

$$F1 - Score = \frac{2 \times P \times R}{P + R} \quad (7)$$

## VI. CONCLUSION

In this work, we propose the ABC optimization algorithm for Video summarization to reduce long video to short video, removing redundant frames. We have compared the performance metrics for evaluations with the known dataset VSUMM. The comparison metrics have given a better score with other methods with reasonable performance. This method can be easily used for (quasi) real-time VS and anomaly detection, also extendable with other advanced sparse-land approaches as CSC (Convolutional Sparse Coding Model) [24], and K-SVD approaches [55, 56]. Finding an optimal threshold function or value for summarization is still open as the performance measure gets affected as we decrease or increase the threshold function.

## REFERENCES

- [1] B. Zhao and E. P. Xing, "Quasi real-time summarization for consumer videos," in *Proceedings of the IEEE conference on computer vision and pattern recognition*, 2014, pp. 2513–2520.
- [2] B. Zhao, L. Fei-Fei, and E. P. Xing, "Online detection of unusual events in videos via dynamic sparse coding," in *CVPR 2011*. IEEE, 2011, pp. 3313–3320.
- [3] T. Hussain, K. Muhammad, A. Ullah, Z. Cao, S. W. Baik, and V. H. C. de Albuquerque, "Cloud-assisted multiview video summarization using cnn and bidirectional lstm," *IEEE Transactions on Industrial Informatics*, vol. 16, no. 1, pp. 77–86, 2019.
- [4] R. Panda and A. K. Roy-Chowdhury, "Multi-view surveillance video summarization via joint embedding and sparse optimization," *IEEE Transactions on Multimedia*, vol. 19, no. 9, pp. 2010–2021, 2017.
- [5] E. Elhamifar, G. Sapiro, and R. Vidal, "See all by looking at a few: Sparse modeling for finding representative objects," in *2012 IEEE conference on computer vision and pattern recognition*. IEEE, 2012, pp. 1600–1607.
- [6] J. Meng, H. Wang, J. Yuan, and Y.-P. Tan, "From keyframes to key objects: Video summarization by representative object proposal selection," in *Proceedings of the IEEE conference on computer vision and pattern recognition*, 2016, pp. 1039–1048.
- [7] S. Mei, G. Guan, Z. Wang, S. Wan, M. He, and D. D. Feng, "Video summarization via minimum sparse reconstruction," *Pattern Recognition*, vol. 48, no. 2, pp. 522–533, 2015.
- [8] F. Dornaika and I. K. Aldine, "Decremental sparse modeling representative selection for prototype selection," *Pattern Recognition*, vol. 48, no. 11, pp. 3714–3727, 2015.
- [9] D. S. K. Vinsent Paramanatham, "A real time video summarization for youtube videos and evaluation of computational algorithms for their time and storage reduction," *International Journal on Recent and Innovation Trends in Computing and Communication*, vol. 6, no. 4, pp. 176–186, 2018.
- [10] S. E. F. De Avila, A. P. B. Lopes, A. da Luz Jr, and A. de Albuquerque Araújo, "Vsumm: A mechanism designed to produce static video summaries and a novel evaluation method," *Pattern Recognition Letters*, vol. 32, no. 1, pp. 56–68, 2011.

- [11] A. Hanjalic and H. Zhang, "An integrated scheme for automated video abstraction based on unsupervised cluster-validity analysis," *IEEE Transactions on circuits and systems for video technology*, vol. 9, no. 8, pp. 1280–1289, 1999.
- [12] A. Packialatha and A. Chandrasekar, "Effective video summarization using eigen based classification," *Transylvanian Review*, no. 2, 2016.
- [13] K. Zhang, W.-L. Chao, F. Sha, and K. Grauman, "Video summarization with long short-term memory," in *ECCV*. Springer, 2016.
- [14] K. Zhou, Y. Qiao, and T. Xiang, "Deep reinforcement learning for unsupervised video summarization with diversity-representativeness reward," *arXiv preprint arXiv:1801.00054*, 2017.
- [15] J. Fajtl, H. S. Sokeh, V. Argyriou, D. Monekosso, and P. Remagnino, "Summarizing videos with attention," in *Asian Conference on Computer Vision*. Springer, 2018, pp. 39–54.
- [16] P. Koutras and P. Maragos, "Susinet: See, understand and summarize it," in *Proceedings of the IEEE Conference on Computer Vision and Pattern Recognition Workshops*, 2019, pp. 0–0.
- [17] N. Srivastava, E. Mansimov, and R. Salakhudinov, "Unsupervised learning of video representations using lstms," in *International conference on machine learning*, 2015, pp. 843–852.
- [18] H. Yang, B. Wang, S. Lin, D. Wipf, M. Guo, and B. Guo, "Unsupervised extraction of video highlights via robust recurrent auto-encoders," in *Proceedings of the IEEE international conference on computer vision*, 2015, pp. 4633–4641.
- [19] B. Mahasseni, M. Lam, and S. Todorovic, "Unsupervised video summarization with adversarial lstm networks," in *Proceedings of the IEEE conference on Computer Vision and Pattern Recognition*, 2017, pp. 202–211.
- [20] Y. He, C. Gao, N. Sang, Z. Qu, and J. Han, "Graph coloring based surveillance video synopsis," *Neurocomputing*, vol. 225, pp. 64–79, 2017.
- [21] Z. Ji, Y. Zhang, Y. Pang, and X. Li, "Hypergraph dominant set based multi-video summarization," *Signal Processing*, vol. 148, pp. 114–123, 2018.
- [22] M. Paul and M. M. Salehin, "Spatial and motion saliency prediction method using eye tracker data for video summarization," *IEEE Transactions on Circuits and Systems for Video Technology*, 2018.
- [23] A. Gupta, P. Srinivasan, J. Shi, and L. S. Davis, "Understanding videos, constructing plots learning a visually grounded storyline model from annotated videos," in *Computer vision and pattern recognition, 2009. CVPR 2009. IEEE conference on*. IEEE, 2009, pp. 2012–2019.
- [24] I. Rey-Otero, J. Sulam, and M. Elad, "Variations on the convolutional sparse coding model," *IEEE Transactions on Signal Processing*, vol. 68, pp. 519–528, 2020.
- [25] D. Karaboga and B. Basturk, "A powerful and efficient algorithm for numerical function optimization: artificial bee colony (abc) algorithm," *Journal of global optimization*, vol. 39, no. 3, pp. 459–471, 2007.
- [26] J. Kennedy and R. Eberhart, "Particle swarm optimization," in *Proceedings of ICNN'95-International Conference on Neural Networks*, vol. 4. IEEE, 1995, pp. 1942–1948.
- [27] J. H. Holland, "Genetic algorithms and the optimal allocation of trials," *SIAM Journal on Computing*, vol. 2, no. 2, pp. 88–105, 1973.
- [28] S. Boyd, N. Parikh, and E. Chu, *Distributed optimization and statistical learning via the alternating direction method of multipliers*. Now Publishers Inc, 2011.
- [29] T. Tieleman and G. Hinton, "Lecture 6.5-rmsprop: Divide the gradient by a running average of its recent magnitude," *COURSERA: Neural networks for machine learning*, vol. 4, no. 2, pp. 26–31, 2012.
- [30] T. Bhattacharjee, S. Saha, A. Konar, and A. K. Nagar, "Static video summarization using artificial bee colony optimization," in *2018 IEEE Symposium Series on Computational Intelligence (SSCI)*. IEEE, 2018, pp. 777–784.
- [31] M. Otani, Y. Nakashima, E. Rahtu, J. Heikkilä, and N. Yokoya, "Video summarization using deep semantic features," in *Asian Conference on Computer Vision*. Springer, 2016, pp. 361–377.
- [32] F. Bach, J. Mairal, J. Ponce, and G. Sapiro, "Sparse coding and dictionary learning for image analysis," in *Proceedings of IEEE International Conference on Computer Vision and Pattern Recognition*, 2010.
- [33] J. Mairal, F. Bach, J. Ponce, G. Sapiro, and A. Zisserman, "Non-local sparse models for image restoration," in *2009 IEEE 12th international conference on computer vision*. IEEE, 2009, pp. 2272–2279.
- [34] E. Elhamifar, G. Sapiro, and R. Vidal, "Sparse modeling for finding representative objects," *preparation*, vol. 4, no. 6, p. 8.
- [35] Y. Cong, J. Yuan, and J. Luo, "Towards scalable summarization of consumer videos via sparse dictionary selection," *IEEE Transactions on Multimedia*, vol. 14, no. 1, pp. 66–75, 2011.
- [36] D. Karaboga and B. Basturk, "On the performance of artificial bee colony (abc) algorithm," *Applied soft computing*, vol. 8, no. 1, pp. 687–697, 2008.
- [37] J. G. Allen, R. Y. Xu, J. S. Jin *et al.*, "Object tracking using camshift algorithm and multiple quantized feature spaces," in *ACM International Conference Proceeding Series*, vol. 100. Citeseer, 2004, pp. 3–7.
- [38] A. D. Mohammed and T. Morris, "A robust visual object tracking approach on a mobile device," in *Information and Communication Technology-EurAsia Conference*. Springer, 2014, pp. 190–198.
- [39] C. Zhang, Y. Qiao, E. Fallon, and C. Xu, "An improved camshift algorithm for target tracking in video surveillance," in *Conf. of 9th. Information Technology & Telecommunication*, 2009, pp. 19–26.
- [40] P. Korshunov and W. T. Ooi, "Reducing frame rate for object tracking," in *International Conference on Multimedia Modeling*. Springer, 2010, pp. 454–464.
- [41] N. Dalal and B. Triggs, "Histograms of oriented gradients for human detection," in *2005 IEEE computer society conference on computer vision and pattern recognition (CVPR'05)*, vol. 1. IEEE, 2005, pp. 886–893.
- [42] R. Rubinstein, M. Zibulevsky, and M. Elad, "Learning sparse dictionaries for sparse signal approximation?" Computer Science Department, Technion, Tech. Rep., 2009.
- [43] —, "Double sparsity: Learning sparse dictionaries for sparse signal approximation," *IEEE Transactions on signal processing*, vol. 58, no. 3, pp. 1553–1564, 2009.
- [44] S. Ibrahim, Y. M. Abd El-Latif, and N. M. Reda, "Anovel data dictionary learning for leaf recognition."
- [45] B. A. Plummer, M. Brown, and S. Lazebnik, "Enhancing video summarization via vision-language embedding," in *Proceedings of the IEEE conference on computer vision and pattern recognition*, 2017, pp. 5781–5789.
- [46] S. Yeung, A. Fathi, and L. Fei-Fei, "Videoset: Video summary evaluation through text," *arXiv preprint arXiv:1406.5824*, 2014.
- [47] S. Sah, S. Kulhare, A. Gray, S. Venugopalan, E. Prud'Hommeaux, and R. Ptucha, "Semantic text summarization of long videos," in *2017 IEEE Winter Conference on Applications of Computer Vision (WACV)*. IEEE, 2017, pp. 989–997.
- [48] D. Potapov, M. Douze, Z. Harchaoui, and C. Schmid, "Category-specific video summarization," in *European conference on computer vision*. Springer, 2014, pp. 540–555.
- [49] A. Sharghi, B. Gong, and M. Shah, "Query-focused extractive video summarization," in *European Conference on Computer Vision*. Springer, 2016, pp. 3–19.
- [50] A. Sharghi, N. d. v. Lobo, and M. Shah, "Text synopsis generation for egocentric videos," *arXiv preprint arXiv:2005.03804*, 2020.
- [51] L. Zhou, Y. Zhou, J. J. Corso, R. Socher, and C. Xiong, "End-to-end dense video captioning with masked transformer," in *Proceedings of the IEEE Conference on Computer Vision and Pattern Recognition*, 2018, pp. 8739–8748.
- [52] J. Wang, W. Jiang, L. Ma, W. Liu, and Y. Xu, "Bidirectional attentive fusion with context gating for dense video captioning," in *Proceedings of the IEEE Conference on Computer Vision and Pattern Recognition*, 2018, pp. 7190–7198.
- [53] Y. Song, J. Vallmitjana, A. Stent, and A. Jaimes, "Tvsum: Summarizing web videos using titles," in *Proceedings of the IEEE conference on computer vision and pattern recognition*, 2015, pp. 5179–5187.
- [54] M. Guironnet, D. Pellerin, N. Guyader, and P. Ladret, "Video summarization based on camera motion and a subjective evaluation method," *EURASIP Journal on Image and Video Processing*, vol. 2007, no. 1, p. 060245, 2007.
- [55] A. Mohammed, S. Yildirim, M. Pedersen, Ø. Hovde, and F. Cheikh, "Sparse coded handcrafted and deep features for colon capsule video summarization," in *2017 IEEE 30th International Symposium on Computer-Based Medical Systems (CBMS)*. IEEE, 2017, pp. 728–733.
- [56] M. Aharon, M. Elad, and A. Bruckstein, "K-svd: An algorithm for designing overcomplete dictionaries for sparse representation," *IEEE Transactions on signal processing*, vol. 54, no. 11, pp. 4311–4322, 2006.

## APPENDIX

Results of the ABC algorithm can be found in the following links and a short Video Description for the VS processing: <https://github.com/VinACE/ABC-VSUMM>

TABLE I. EVALUATION METRICS AGAINST USERSUMMARY 1 (VSUMM1 SUMMARY).

| Video #           | Automatic summary |               |               | Automatic Summary with +/- 1 Frame |               |               |
|-------------------|-------------------|---------------|---------------|------------------------------------|---------------|---------------|
|                   | Precision         | Recall        | F1-Score      | Precision                          | Recall        | F1-Score      |
| v21               | 1                 | 0.53          | 0.69          | 1                                  | 0.6           | 0.75          |
| v22               | 0.25              | 0.25          | 0.25          | 0.75                               | 0.75          | 0.75          |
| v21               | 1                 | 0.53          | 0.69          | 1                                  | 0.6           | 0.75          |
| v22               | 0.25              | 0.25          | 0.25          | 0.75                               | 0.75          | 0.75          |
| v23               | 0.33              | 0.33          | 0.33          | 0.46                               | 0.46          | 0.46          |
| v24               | 0.72              | 0.72          | 0.72          | 0.72                               | 0.72          | 0.72          |
| v25               | 1                 | 0.5           | 0.67          | 1                                  | 0.6           | 0.75          |
| v26               | 0.41              | 0.41          | 0.41          | 0.76                               | 0.76          | 0.76          |
| v27               | 0.54              | 0.54          | 0.54          | 0.7                                | 0.69          | 0.69          |
| v28               | 1                 | 0.95          | 0.97          | 1                                  | 1             | 1             |
| v29               | 0.44              | 0.44          | 0.44          | 0.55                               | 0.55          | 0.55          |
| v30               | 0.5               | 0.5           | 0.5           | 0.88                               | 0.88          | 0.88          |
| v31               | 0.27              | 0.27          | 0.27          | 0.36                               | 0.36          | 0.36          |
| v32               | 0.73              | 0.73          | 0.73          | 0.82                               | 0.82          | 0.82          |
| v33               | 0.14              | 0.14          | 0.14          | 0.47                               | 0.47          | 0.47          |
| v34               | 0.78              | 0.78          | 0.78          | 1                                  | 1             | 1             |
| v35               | 0.73              | 0.73          | 0.73          | 0.73                               | 0.73          | 0.73          |
| v36               | 0.63              | 0.63          | 0.63          | 0.63                               | 0.63          | 0.63          |
| v37               | 0.2               | 0.2           | 0.2           | 0.2                                | 0.2           | 0.2           |
| v38               | 0.64              | 0.64          | 0.64          | 0.71                               | 0.71          | 0.71          |
| v39               | 0.36              | 0.36          | 0.36          | 0.36                               | 0.36          | 0.36          |
| v40               | 0.54              | 0.54          | 0.54          | 0.92                               | 0.92          | 0.92          |
| v41               | 0.8               | 0.8           | 0.8           | 1                                  | 1             | 1             |
| v42               | 1                 | 1             | 1             | 1                                  | 1             | 1             |
| v43               | 0.68              | 0.68          | 0.68          | 0.81                               | 0.81          | 0.81          |
| v44               | 0.54              | 0.54          | 0.54          | 0.73                               | 0.73          | 0.73          |
| v45               | 0.14              | 0.14          | 0.14          | 0.29                               | 0.29          | 0.29          |
| v46               | 1                 | 1             | 1             | 1                                  | 1             | 1             |
| v47               | 0.8               | 0.8           | 0.8           | 0.8                                | 0.8           | 0.8           |
| v48               | 0.86              | 0.86          | 0.86          | 1                                  | 1             | 1             |
| v49               | 0.46              | 0.46          | 0.46          | 0.54                               | 0.54          | 0.54          |
| v50               | 0.75              | 0.75          | 0.75          | 0.86                               | 0.86          | 0.86          |
| v51               | 0                 | 0             | 0             | 0.14                               | 0.14          | 0.14          |
| v52               | 0.625             | 0.625         | 0.625         | 0.875                              | 0.875         | 0.875         |
| v53               | 0.4               | 0.4           | 0.4           | 1                                  | 1             | 1             |
| v54               | 0.86              | 0.86          | 0.86          | 1                                  | 1             | 1             |
| v55               | 0.5               | 0.5           | 0.5           | 0.5                                | 0.5           | 0.5           |
| v56               | 0.5               | 0.5           | 0.5           | 0.75                               | 0.75          | 0.75          |
| v57               | 0                 | 0             | 0             | 0.1                                | 0.1           | 0.1           |
| v58               | 0.78              | 0.78          | 0.78          | 1                                  | 1             | 1             |
| v59               | 0.5               | 0.5           | 0.5           | 1                                  | 1             | 1             |
| v60               | 0.56              | 0.56          | 0.56          | 0.91                               | 0.91          | 0.91          |
| v61               | 0.71              | 0.71          | 0.71          | 1                                  | 1             | 1             |
| v62               | 0.75              | 0.75          | 0.75          | 1                                  | 1             | 1             |
| v63               | 0                 | 0             | 0             | 0.22                               | 0.22          | 0.22          |
| v64               | 0.93              | 0.93          | 0.93          | 1                                  | 1             | 1             |
| v65               | 1                 | 1             | 1             | 1                                  | 1             | 1             |
| v66               | 0.78              | 0.78          | 0.78          | 1                                  | 1             | 1             |
| v67               | 0.86              | 0.86          | 0.86          | 1                                  | 1             | 1             |
| v68               | 1                 | 1             | 1             | 1                                  | 1             | 1             |
| v69               | 1                 | 1             | 1             | 1                                  | 1             | 1             |
| v70               | 0.6               | 0.6           | 0.6           | 1                                  | 1             | 1             |
| <b>Mean Score</b> | <b>0.6119</b>     | <b>0.5915</b> | <b>0.5985</b> | <b>0.7709</b>                      | <b>0.7547</b> | <b>0.7607</b> |

TABLE II. EVALUATION METRICS AGAINST USERSUMMARY 2 (VSUMM2 SUMMARY).

| Video #           | Automatic summary |               |               | Automatic Summary with +/- 1 Frame |               |               |
|-------------------|-------------------|---------------|---------------|------------------------------------|---------------|---------------|
|                   | Precision         | Recall        | F1-Score      | Precision                          | Recall        | F1-Score      |
| v21               | 1                 | 0.5           | 0.67          | 1                                  | 0.75          | 0.86          |
| v22               | 0.25              | 0.25          | 0.25          | 0.75                               | 0.75          | 0.75          |
| v23               | 0.31              | 0.31          | 0.31          | 0.46                               | 0.46          | 0.46          |
| v24               | 0.67              | 0.67          | 0.67          | 0.67                               | 0.67          | 0.67          |
| v25               | 1                 | 0.56          | 0.71          | 1                                  | 0.67          | 0.8           |
| v26               | 0.5               | 0.5           | 0.5           | 0.83                               | 0.83          | 0.83          |
| v27               | 0.33              | 0.33          | 0.33          | 0.44                               | 0.44          | 0.44          |
| v28               | 1                 | 0.94          | 0.97          | 1                                  | 1             | 1             |
| v29               | 1                 | 0.94          | 0.98          | 1                                  | 1             | 1             |
| v30               | 0.27              | 0.27          | 0.27          | 0.45                               | 0.45          | 0.45          |
| v31               | 0.25              | 0.25          | 0.25          | 0.5                                | 0.5           | 0.5           |
| v32               | 0.64              | 0.64          | 0.64          | 0.73                               | 0.73          | 0.73          |
| v33               | 0.23              | 0.23          | 0.23          | 0.69                               | 0.69          | 0.69          |
| v34               | 0.86              | 0.86          | 0.86          | 1                                  | 1             | 1             |
| v35               | 0.67              | 0.67          | 0.67          | 0.67                               | 0.67          | 0.67          |
| v36               | 0.38              | 0.38          | 0.38          | 0.63                               | 0.63          | 0.63          |
| v37               | 0.33              | 0.33          | 0.33          | 0.33                               | 0.33          | 0.33          |
| v38               | 0.68              | 0.68          | 0.68          | 0.79                               | 0.79          | 0.79          |
| v39               | 0.33              | 0.33          | 0.33          | 0.33                               | 0.33          | 0.33          |
| v40               | 0.4               | 0.4           | 0.4           | 0.9                                | 0.9           | 0.9           |
| v41               | 0.78              | 0.78          | 0.78          | 1                                  | 1             | 1             |
| v42               | 1                 | 1             | 1             | 1                                  | 1             | 1             |
| v43               | 0.7               | 0.7           | 0.7           | 0.8                                | 0.8           | 0.8           |
| v44               | 0.63              | 0.63          | 0.63          | 0.88                               | 0.88          | 0.88          |
| v45               | 0.16              | 0.16          | 0.16          | 0.33                               | 0.33          | 0.33          |
| v46               | 1                 | 1             | 1             | 1                                  | 1             | 1             |
| v47               | 0.75              | 0.75          | 0.75          | 0.75                               | 0.75          | 0.75          |
| v48               | 0.86              | 0.86          | 0.86          | 1                                  | 1             | 1             |
| v49               | 0.55              | 0.55          | 0.55          | 0.67                               | 0.67          | 0.67          |
| v50               | 0                 | 0             | 0             | 0                                  | 0             | 0             |
| v51               | 0.25              | 0.25          | 0.25          | 0.5                                | 0.5           | 0.5           |
| v52               | 0.5               | 0.5           | 0.5           | 0.83                               | 0.83          | 0.83          |
| v53               | 0.25              | 0.25          | 0.25          | 1                                  | 1             | 1             |
| v54               | 0.86              | 0.86          | 0.86          | 1                                  | 1             | 1             |
| v55               | 0.5               | 0.5           | 0.5           | 0.5                                | 0.5           | 0.5           |
| v56               | 0.4               | 0.4           | 0.4           | 0.6                                | 0.6           | 0.6           |
| v57               | 0                 | 0             | 0             | 0.12                               | 0.12          | 0.12          |
| v58               | 0.89              | 0.89          | 0.89          | 1                                  | 1             | 1             |
| v59               | 0.375             | 0.375         | 0.375         | 1                                  | 1             | 1             |
| v60               | 0.56              | 0.56          | 0.56          | 1                                  | 1             | 1             |
| v61               | 0.75              | 0.75          | 0.75          | 1                                  | 1             | 1             |
| v62               | 1                 | 1             | 1             | 1                                  | 1             | 1             |
| v63               | 0                 | 0             | 0             | 0.17                               | 0.17          | 0.17          |
| v64               | 0.92              | 0.92          | 0.92          | 1                                  | 1             | 1             |
| v65               | 1                 | 1             | 1             | 1                                  | 1             | 1             |
| v66               | 0.78              | 0.78          | 0.78          | 1                                  | 1             | 1             |
| v67               | 0.83              | 0.83          | 0.83          | 1                                  | 1             | 1             |
| v68               | 1                 | 1             | 1             | 1                                  | 1             | 1             |
| v69               | 1                 | 1             | 1             | 1                                  | 1             | 1             |
| v70               | 0.6               | 0.6           | 0.6           | 1                                  | 1             | 1             |
| <b>Mean Score</b> | <b>0.5999</b>     | <b>0.5787</b> | <b>0.5865</b> | <b>0.7664</b>                      | <b>0.7348</b> | <b>0.7596</b> |

TABLE III. MEAN ACCURACY RATE CUSA (PRECISION) AND MEAN ERROR RATE CUSE (RECALL) COMPARED AGAINST OTHER METHODS [10] AND OURS.

|                                  | OV  | DT   | STIMO | VSUMM1 | VSUMM2 | Our-Summ1   | Our-Summ2   |
|----------------------------------|-----|------|-------|--------|--------|-------------|-------------|
| <i>Precision/CUS<sub>A</sub></i> | 0.7 | 0.53 | 0.72  | 0.85   | 0.7    | <b>0.61</b> | <b>0.59</b> |
| <i>Recall/CUS<sub>E</sub></i>    | 0.7 | 0.53 | 0.72  | 0.85   | 0.7    | <b>0.61</b> | <b>0.59</b> |

# Continuous Human Activity Recognition in Logistics from Inertial Sensor Data using Temporal Convolutions in CNN

Abbas Shah Syed<sup>1</sup>  
University of Louisville, USA

Zafi Sherhan Syed<sup>2</sup>  
Mehran University, Pakistan

Arez Khalil Memon<sup>3</sup>  
University of Electronic Science and  
Technology of China (UESTC), P. R. China

**Abstract**—Human activity recognition has been an important task for the research community. With the introduction of deep learning architectures, the performance of activity recognition algorithms has improved significantly. However, most of the research in this area has focused on activity recognition for health/assisted living with other applications being given less attention. This paper considers continuous activity recognition in logistics (order picking and packing operations) using a convolutional neural network with temporal convolutions on inertial measurement sensor data from the recently released LARA dataset. Four variants of the popular CNN-IMU are experimented upon and a discussion of the results is provided. The results indicate that temporal convolutions are able to achieve satisfactory performance for some activities (hand center and cart) whereas they perform poorly for the activities of stand and hand up.

**Keywords**—Convolutional Neural Networks; deep learning; Human Activity Recognition (HAR); inertial sensors; LARA dataset

## I. INTRODUCTION

Activity recognition has been an important task for researchers in the field of gaming [1], assisted living [2], sports analysis [3], logistics and other industrial operations [4] and for monitoring of patients diseases, such as Parkinsons to build activity profiles for therapeutic purposes [5]. Eventhough activity recognition, generally speaking, can be performed in a variety of ways [6], [7], [8], inertial sensors have been far by the most popular modality to use for this purpose. This is due to the fact that they are mobile, less cumbersome to wear and cost less than sensing devices for other modalities. Moreover, with their incorporation in phones and smart watches etc, these sensors are usually easily available to the subject for use in activity recognition tasks. This ubiquitous presence combined with ease of data collection has resulted in large datasets being produced which has led to the use of deep learning for various aspects of activity recognition tasks as shown in [9], [10].

As mentioned, the field of activity recognition has been of attention to researchers in various domains, a domain that has not received as much interest is activity recognition in industrial settings. In this paper, data from the LARA dataset [11] is utilized to perform continuous recognition of activities in a logistics scenario using two different convolutional neural network (CNN) architectures, one is a typical convolutional network and the other is a modified version of the parallel CNN architecture called CNN-IMU suggested in [12] which performs convolutions in the temporal domain. The experiments

indicated that the parallel CNN architecture performed better than the considered typical CNN. The rest of the paper is organized as follows: section II discusses previous work carried out for activity recognition, section III presents an overview of the dataset used, section IV presents the methodology of the paper; the pre-processing steps and the discussion of the networks used in the experiments, section V discusses the results for the current work with a conclusion being provided in section VI and future directions in section VII.

## II. LITERATURE REVIEW

Activity recognition has been at the forefront of pervasive computing research and the development of cyber physical systems as this has enormous societal and economical impact potential [13]. This section covers previous work in the direction of activity recognition using utilizing inertial measurement sensors (IMUs).

Industrial activity recognition using IMUs has been targeted by multiple research works for varying applications, these include, wood shops [14], construction [15], assembly line [16], process optimization [17]. An early work using deep learning methods for activity recognition for industry was suggested by [18] on the Skoda dataset [19]. Their network consists of one convolutional layer, one pooling layer, two hidden layers and one softmax layer for classification. Moreover, the convolutional layer contains several convolutional blocks in parallel with partial weight sharing for the three axes of accelerometer sensor values. The pooling layer also pools convolutional blocks sharing their weights separately before the outputs are passed on to the later layers.

An interesting approach for segmenting different types of activities for health risk assessment in an order picking process is presented in [20] who utilize angles of human body joints from 17 IMUs placed on a workers body performing the order picking activity. Joint angles between body limbs are computed using an extended Kalman filter [21] and these are used to segment the sub-activities within the picking process. Risk assessment is performed using the rapid entire body assessment (REBA) standard [22]. The authors in [23] propose using accelerometer and gyroscope signal data to perform activity recognition for worker performance assessment in the meat industry. After extracting segments, they compute several features from both sensors and test the performance of multiple classifiers for determining output activity. Following from their



work in [24], the authors in [25] combine video and inertial measurement sensor data to determine grabbing actions in a picking process. They do this by extracting various time and frequency domain features from the IMU data as well as colour and descriptor features from the video data and then passing them on to three machine learning classifiers for prediction purposes.

The approach suggested in [12] makes use of CNNs on the data provided in [17]. They propose a CNN architecture called CNN-IMU based on the CNN proposed in [26]. Their network uses four CNN layers with parallel CNN blocks sharing their weights for each IMU, two pooling operations, fully connected layer before they are combined using a fully connected layer followed by a softmax for classification. The motivation to spread the network instead of making it deeper is that it becomes more descriptive. The authors in [27] make use of accelerometer sensor data in the dataset in [28] and CNNs to differentiate between activities in the industry. They achieve their best results when using raw signal data and sending it to the CNN for classification. The authors in [29] use the CNN-IMU on three different datasets of activity recognition, two consisting of various different activities in daily life and one of activities from a logistic scenario of order picking. Their experiments involved comparing two different CNN architectures, one a CNN-IMU and the other a baseline CNN with the same layerwise make up as the CNN-IMU. For the logistics scenario, their result indicates that the CNN-IMU outperforms the typical CNN in nearly all experiments. Their results indicate to the effectiveness of using wider networks consisting of parallel layers instead of using deeper ones. CNNs have also been used with other modalities for industrial processes, in [30] semantic representations have been used for activity recognition in a picking setup. Motion capture data from the MoCAP dataset is used with the CNN architecture described in [31]. The authors in [11] use the Logistics Activity Recognition Challenge (LARA) dataset provided by them to determine activities in a logistics scenario. They carry this out by using a modified version of the t-CNN in [26] which consists of four convolutional layers, two fully connected layers followed by two separate softmax and sigmoid layers to determine the sub-activity being performed and the attribute from an activity attribute list on motion capture data from the dataset.

It can be observed from the literature review that convolutional neural networks have proved to be very useful for performing activity recognition in industrial scenarios. This paper utilizes a convolutional neural network for performing continuous activity recognition for logistics using inertial sensor data from the LARA dataset. This paper compares the performance of a modified version of the CNN-IMU network presented in [26] and used in [11] to a typical CNN. The CNN utilizes convolutions in the temporal axis to extract important features from time series sensor data and is well suited for use with inertial measurement sensor signals.

### III. DATASET

The LARA dataset provides data of multiple modalities from recordings in a logistics scenario. Video recordings, Motion Capture data and data from inertial measurement units is recorded from 14 people in the dataset. Each of

the participants is asked to perform three tasks which are common in logistics operations, two of these are picking tasks and the third is packing. Motion capture data was captured using a Optical Marker-based Motion Capture (OMoCap) system which resulted in markers for the movements of the participants, moreover, several IMUs were used to record the movement patterns too along with RGB videos of the activities being performed. The total duration of the recorded data is 758 minutes which has been annotated in two ways, first, an annotation is provided for each intra-activity that comprises the picking and packing tasks and second, binary semantic representations of a different type of representation for the picking and packing tasks. The first representation represents the activities in terms of eight intra-activities and is used in this work and the second type of representation as attributes to describe the task recordings. The eight annotations are standing, walking, cart (participant is walking with the cart), handling upwards (participant has atleast one hand raised upward to shoulder height), handling centered (participant can handle things without bending, lifting their arms or needing to kneel), handling downwards (participant has hands below his knees while kneeling or otherwise), synchronization (waving motion before each recording) and a set of samples which were unrecognizable by the annotators and have been marked as *None*.

This dataset provides the opportunity to develop algorithms for both the picking and packing operations in logistics by containing recordings of multiple modalities to researchers. From these modalities, this paper focuses on the data from the IMUs collected in these experiments. Three types of IMUs were used in the trials with 14 people in total performing the said tasks with data being collected from five points on the body, both the arms, legs and the chest/mid-body. The sampling frequency for the IMUs is 100 Hz. A summary of the recordings present in the dataset are given in Table I. Readers interested in more detail are referred to [11].

TABLE I. SUMMARY OF IMU MEASUREMENTS IN THE LARA DATASET

| Subject ID | Gender | Age | Scenario 1 | Scenario 2 | Scenario 3 |
|------------|--------|-----|------------|------------|------------|
| S07        | M      | 23  | 2          | 13         | 14         |
| S08        | F      | 51  | 2          | 13         | 14         |
| S09        | M      | 35  | 2          | 14         | 13         |
| S10        | M      | 49  | 2          | 13         | 12         |
| S11        | F      | 47  | 2          | 12         | 0          |
| S12        | F      | 23  | 0          | 6          | 14         |
| S13        | F      | 25  | 2          | 14         | 14         |
| S14        | M      | 54  | 2          | 14         | 14         |
| Total      |        |     | 14         | 99         | 95         |

### IV. METHODOLOGY

To perform continuous monitoring of activities in logistics, we use a two step process. Segments are first extracted from the IMU sensor data for each trial which are then passed to the CNNs to test their performance. For the first two experiments, segmentation is performed for all IMUs together whereas for the last two experiments data segmentation takes place for each of the five IMUs individually. These are then fed to the CNN networks as inputs.

#### A. Preprocessing Stage

Windows of 100 samples are extracted from the recording for each sensor and position with a step size of 25 samples

(75% overlap) for successive windowed segments. An overlap is used to ensure that enough samples are generated to develop a large enough dataset for training of deep learning networks. Furthermore, since the annotations in the dataset are present on a sample by sample basis for each value of each sensor, an extracted segment is assigned a *segment annotation* by majority voting of the annotations of its samples. We then use the segment annotations as the appropriate annotation labels, a similar approach has been used in [29]. Once segments have been extracted from all the trials for all subjects, the segments belonging to the *synchronization* and *None* class are removed. The rest of the segments are used for classification with the convolutional neural network.

### B. Classification

For classification, we make use of a modified version of the convolutional neural network described in [12] named CNN-IMU. They propose a network which utilizes four convolutional layers, two max pooling layers, fully connected layer and a softmax layer for determining the output class. Each of the convolutional layers have multiple parallel convolutional blocks sharing their weights which perform convolution operations along the time axis. The number of convolutional blocks in each layer depends on the number of IMUs present in the data, one block for each IMU. Input to the network is provided as windowed segments of IMU sensor signal recordings over the temporal domain. The output of each of these parallel blocks and pooling layers is passed to a fully connected layer individually for computing an intermediate feature representation. These representations are then combined using a fully connected layer before being passed to the softmax layer for classification. Dropout was applied to the fully connected layers apart from the softmax layer.

This CNN-IMU network is used in two different variants in this work based on the results of [29] and [11]. The first network follows the network construction as described in [12] which includes the max pooling operations of the network. The second variant of the network skips the pooling operations as was used in [11] which were found to affect network performance negatively in [31]. Both these variants require that data from the IMUs be segmented individually as separate parallel inputs. Furthermore, to compare the performance of the two CNN-IMU architectures to typical CNNs utilizing temporal convolutions, typical CNNs that do not make use of parallel convolutional blocks for different IMUs but consist of the same layer-wise structure are used to perform classification as well. These networks require that the segments be extracted for all five IMUs as one frame/segment. The details of the networks are provided in Table II and the architectures are illustrated in Fig. 1. The pooling layers have been shown with a dotted border to indicate the absence of these operations in the network variations considered in this research work.

The data from the sensors was split in to train, validation and test sets and the network was trained using an Adam Optimizer with cross entropy as the loss function. A learning rate of  $1 \times 10^{-6}$  was used along with a batch size of 400. Moreover, training was performed for 12 epochs with early stopping utilized to retain the best model.

TABLE II. DETAILS OF CNN ARCHITECTURES

| CNN Architecture | Number of Layers        |         |              |
|------------------|-------------------------|---------|--------------|
|                  | Convolutional           | Pooling | FC + Softmax |
| Typical CNN-1    | 4                       | 2       | 3            |
| Typical CNN-2    | 4                       | 0       | 3            |
| CNN-IMU-1        | 4 (Five blocks/ layer)  | 2       | 3            |
| CNN-IMU-2        | 4 (Five blocks / layer) | 0       | 3            |

## V. EXPERIMENTATION, RESULTS AND DISCUSSION

In order to test the efficacy of the four CNNs considered in this work, we perform experiments for each of the four networks individually and report on the results obtained. The results for each experiment are reported in terms of the Precision, Recall and F1 score for each activity class.

### A. Experiment with Typical CNN-1

In this experiment we used the typical CNN-1 architecture that consists of 4 convolution layers, 2 max pooling layers, 2 fully connected layers and one softmax layer. The input to this network were segments/ frames consisting of the combined information from all the IMUs together. The results for the classification are provided in Table III. It can be observed from the table that the CNN has performed poorly for the activities *Hand up* and *Stand*. Moreover, as can be observed, the best performing activities were *Cart* and *Hand Center*.

TABLE III. SUMMARY OF RESULTS: TYPICAL CNN-1 (WITH MAX-POOLING)

| Activity    | Precision (%) | Recall (%) | F1 (%) |
|-------------|---------------|------------|--------|
| Stand       | 38.73         | 61.96      | 47.66  |
| Walk        | 71.27         | 70.76      | 71.01  |
| Cart        | 82.44         | 86.31      | 84.33  |
| Hand up     | 45.61         | 79.48      | 57.96  |
| Hand Center | 91.87         | 80.75      | 85.95  |
| Hand Down   | 71.93         | 76.44      | 74.12  |

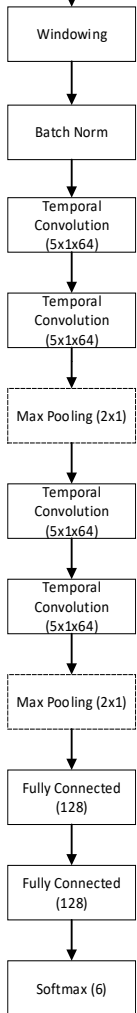
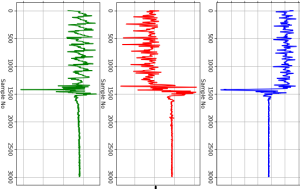
### B. Experiment with Typical CNN-2

For the second experiment, we use the typical CNN-2 architecture consisting of 4 convolution layers, 2 fully connected layers and one softmax layer. The input to this network too were segments/ frames consisting of the combined information from all the IMUs together. The results of the classification are presented in Table IV. It can be observed that the performance for this network is very similar to the *Typical CNN-1 network* of experiment 1 which used maxpooling layers, there has been some degradation in performance for some activities. In this experiment too, the network was able to best recognize the activities of *Cart* and *Hand Center* while poor performance was observed for the activities of *Stand* and *Hand up*.

TABLE IV. SUMMARY OF RESULTS: TYPICAL CNN-2 (WITHOUT MAX-POOLING)

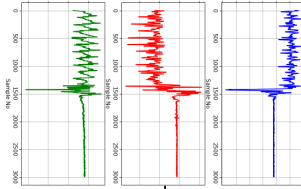
| Activity    | Precision (%) | Recall (%) | F1 (%) |
|-------------|---------------|------------|--------|
| Stand       | 39.06         | 47.95      | 43.05  |
| Walk        | 57.04         | 81.01      | 66.94  |
| Cart        | 80.38         | 85.42      | 82.83  |
| Hand up     | 34.99         | 79.03      | 48.51  |
| Hand Center | 92.21         | 78.99      | 85.09  |
| Hand Down   | 71.23         | 77.04      | 74.02  |

All IMU data segmented together

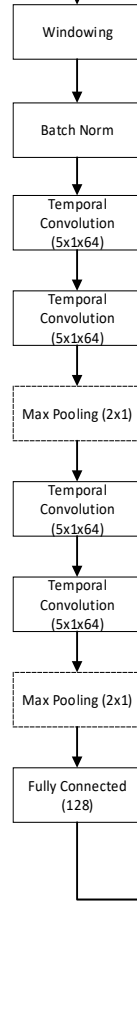
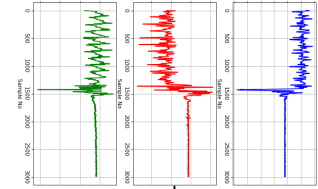


(a)

Data from IMUs segmented individually



• • •



• • •

(b)

Fig. 1. CNN Architectures used in this Work (a) Typical CNN (b) CNN-IMU.

### C. Experiment with CNN-IMU-1

This experiment involved the usage of the CNN-IMU-1 network to determine activity classes. This architecture consists of four convolutional layers with five convolutional blocks, one for each IMU data and these blocks share their weights. The IMU segments are individually fed to the blocks resulting in the classification scores shown in Table V. This network has also been able to recognize the activities of *Hand Center* and *Cart* well but the activity *Stand* is still the worst performing activity among the six activity classes being considered.

TABLE V. SUMMARY OF RESULTS: CNN-IMU-1 (WITH MAX-POOLING)

| Activity    | Precision (%) | Recall (%) | F1 (%) |
|-------------|---------------|------------|--------|
| Stand       | 27.68         | 66.85      | 39.15  |
| Walk        | 69.42         | 67.03      | 68.20  |
| Cart        | 87.95         | 79.67      | 83.61  |
| Hand up     | 43.62         | 60.18      | 50.58  |
| Hand Center | 90.34         | 80.04      | 84.88  |
| Hand Down   | 71.93         | 75.68      | 73.76  |

### D. Experiment with CNN-IMU-2

In this experiment we used the CNN-IMU-2 architecture which consists of four convolution layers, two fully connected layers and one softmax layer. The input to this network were segments/ frames consisting of the individual IMUs. The classification results are presented in Table VI. The omission of the pooling layer has impacted network performance positively as was observed in other works. Similar to the previous cases, this network produces the best results for the activities *Cart* and *Hand Center*.

TABLE VI. SUMMARY OF RESULTS: CNN-IMU-2 (WITHOUT MAX-POOLING)

| Activity    | Precision (%) | Recall (%) | F1 (%) |
|-------------|---------------|------------|--------|
| Stand       | 40.07         | 47.11      | 43.31  |
| Walk        | 49.08         | 82.73      | 61.61  |
| Cart        | 81.79         | 83.40      | 82.59  |
| Hand up     | 26.04         | 73.36      | 38.43  |
| Hand Center | 91.87         | 77.88      | 84.29  |
| Hand Down   | 71.46         | 75.37      | 73.37  |

Following from the experiments conducted in this work with the considered CNN architectures, the most suitable network for continuous activity recognition from inertial sensor data was found to be the Typical CNN-1 architecture which involves pooling operations. The best scores are achieved for the activities *Cart* and *Hand Cent* whereas the worst scores have been produced for the activities *Hand Up* and *Stand*, this was the case for all the networks considered in this research work. The F1 scores for each of the networks for the six activities are listed in Table VII.

## VI. CONCLUSION

This paper explores the usage of temporal convolutions in a CNN for the problem of continuous activity recognition in a logistics scenario using inertial measurement sensor data. Data from the LARA dataset which consists of video, OMOCap and IMU signal recordings from seven different people performing three different tasks concerning picking and packing has been used in this work. To accomplish the aims of this work, four

TABLE VII. SUMMARY OF RESULTS (F1 SCORE [%] FOR EACH CONSIDERED NETWORK)

| Activity    | F1 (%)        |               |           |           |
|-------------|---------------|---------------|-----------|-----------|
|             | Typical CNN-1 | Typical CNN-2 | CNN-IMU-1 | CNN-IMU-2 |
| Stand       | 47.66484      | 43.05043      | 39.14759  | 43.30519  |
| Walk        | 71.01347      | 66.94491      | 68.20405  | 61.60714  |
| Cart        | 84.32787      | 82.82695      | 83.60756  | 82.589    |
| Hand up     | 57.95574      | 48.50575      | 50.57692  | 38.43329  |
| Hand Center | 85.95271      | 85.0872       | 84.8763   | 84.29462  |
| Hand Down   | 74.11908      | 74.01961      | 73.76058  | 73.36562  |

CNN architectures, have been tested which take windowed segments of IMU recordings. From the experiments conducted, the typical CNN-1 architecture involving pooling operations was found to be the best performing model. High scores were achieved for the activities *Hand Center* and *Cart*; however, scores for the activity *Stand* and *Hand Up* weren't satisfactory. While satisfactory performance was achieved for the former activities, the performance of the considered networks for the latter activities was poor. Therefore, modifications need to be made for improvement of the network for such activities.

## VII. FUTURE WORK

This work presents experimental work for the continuous recognition of activities for logistics using the LARA dataset. In this paper, only CNN architectures have been considered, for future attempts at this task, other deep learning architectures could be considered to improve activity recognition such as Recurrent Neural Networks with attention, etc. Moreover, sensor fusion could also be used, especially OMOCap data from LARA dataset could be fused with IMU data and used with various deep learning networks to check for performance. Video data could also be combined to create a multimodal solution for activity recognition as suggested in [25]. Dependable activity recognition systems will help in the optimization of industrial processes as well as be used for health assessment purposes.

## REFERENCES

- [1] N. Jablonsky, S. McKenzie, S. Bangay, and T. Wilkin, "Evaluating sensor placement and modality for activity recognition in active games," in *Proceedings of the Australasian Computer Science Week Multiconference*, 2017, pp. 1–8.
- [2] J. Rafferty, C. D. Nugent, J. Liu, and L. Chen, "From activity recognition to intention recognition for assisted living within smart homes," *IEEE Transactions on Human-Machine Systems*, vol. 47, no. 3, pp. 368–379, 2017.
- [3] Y.-L. Hsu, S.-C. Yang, H.-C. Chang, and H.-C. Lai, "Human daily and sport activity recognition using a wearable inertial sensor network," *IEEE Access*, vol. 6, pp. 31 715–31 728, 2018.
- [4] C. Reining, F. Niemann, F. Moya Rueda, G. A. Fink, and M. ten Hompel, "Human activity recognition for production and logistics—a systematic literature review," *Information*, vol. 10, no. 8, p. 245, 2019.
- [5] W.-Y. Cheng, A. Scotland, F. Lipsmeier, T. Kilchenmann, L. Jin, J. Schjodt-Eriksen, D. Wolf, Y.-P. Zhang-Schaerer, I. F. Garcia, J. Siebourg-Polster *et al.*, "Human activity recognition from sensor-based large-scale continuous monitoring of parkinson's disease patients," in *2017 IEEE/ACM International Conference on Connected Health: Applications, Systems and Engineering Technologies (CHASE)*. IEEE, 2017, pp. 249–250.
- [6] S.-R. Ke, H. L. U. Thuc, Y.-J. Lee, J.-N. Hwang, J.-H. Yoo, and K.-H. Choi, "A review on video-based human activity recognition," *Computers*, vol. 2, no. 2, pp. 88–131, 2013.

- [7] A. Bulling, U. Blanke, and B. Schiele, "A tutorial on human activity recognition using body-worn inertial sensors," *ACM Computing Surveys (CSUR)*, vol. 46, no. 3, pp. 1–33, 2014.
- [8] X. Luo, Q. Guan, H. Tan, L. Gao, Z. Wang, and X. Luo, "Simultaneous indoor tracking and activity recognition using pyroelectric infrared sensors," *Sensors*, vol. 17, no. 8, p. 1738, 2017.
- [9] C. Xu, D. Chai, J. He, X. Zhang, and S. Duan, "Innohar: a deep neural network for complex human activity recognition," *Ieee Access*, vol. 7, pp. 9893–9902, 2019.
- [10] G. L. Santos, P. T. Endo, K. H. d. C. Monteiro, E. d. S. Rocha, I. Silva, and T. Lynn, "Accelerometer-based human fall detection using convolutional neural networks," *Sensors*, vol. 19, no. 7, p. 1644, 2019.
- [11] F. Niemann, C. Reining, F. M. Rueda, N. R. Nair, J. A. Steffens, G. A. Fink, and M. t. Hompel, "Lara: Creating a dataset for human activity recognition in logistics using semantic attributes," *Sensors*, vol. 20, no. 15, p. 4083, 2020.
- [12] R. Grzeszick, J. M. Lenk, F. M. Rueda, G. A. Fink, S. Feldhorst, and M. ten Hompel, "Deep neural network based human activity recognition for the order picking process," in *Proceedings of the 4th international Workshop on Sensor-based Activity Recognition and Interaction*, 2017, pp. 1–6.
- [13] P. Nikolov, O. Boumbarov, A. Manolova, K. Tonchev, and V. Poulkov, "Skeleton-based human activity recognition by spatio-temporal representation and convolutional neural networks with application to cyber physical systems with human in the loop," in *2018 41st International Conference on Telecommunications and Signal Processing (TSP)*, 2018, pp. 1–5.
- [14] J. A. Ward, P. Lukowicz, G. Troster, and T. E. Starner, "Activity recognition of assembly tasks using body-worn microphones and accelerometers," *IEEE transactions on pattern analysis and machine intelligence*, vol. 28, no. 10, pp. 1553–1567, 2006.
- [15] J. Zhao and E. Obonyo, "Towards a data-driven approach to injury prevention in construction," in *Workshop of the European Group for Intelligent Computing in Engineering*. Springer, 2018, pp. 385–411.
- [16] H. Koskimäki, V. Huikari, P. Siirtola, and J. Rönning, "Behavior modeling in industrial assembly lines using a wrist-worn inertial measurement unit," *Journal of Ambient Intelligence and Humanized Computing*, vol. 4, no. 2, pp. 187–194, 2013.
- [17] S. Feldhorst, M. Masoudenijad, M. ten Hompel, and G. A. Fink, "Motion classification for analyzing the order picking process using mobile sensors," in *Proc. Int. Conf. Pattern Recognition Applications and Methods*, 2016, pp. 706–713.
- [18] M. Zeng, L. T. Nguyen, B. Yu, O. J. Mengshoel, J. Zhu, P. Wu, and J. Zhang, "Convolutional neural networks for human activity recognition using mobile sensors," in *6th International Conference on Mobile Computing, Applications and Services*. IEEE, 2014, pp. 197–205.
- [19] P. Zappi, C. Lombriser, T. Stiefmeier, E. Farella, D. Roggen, L. Benini, and G. Tröster, "Activity recognition from on-body sensors: accuracy-power trade-off by dynamic sensor selection," in *European Conference on Wireless Sensor Networks*. Springer, 2008, pp. 17–33.
- [20] T. Hara, Y. Li, J. Ota, and T. Arai, "Automatic risk assessment integrated with activity segmentation in the order picking process to support health management," *CIRP Annals*, 2020.
- [21] C. Jakob, P. Kugler, F. Hebenstreit, S. Reinfelder, U. Jensen, D. Schuldhau, M. Lochmann, and B. M. Eskofier, "Estimation of the knee flexion-extension angle during dynamic sport motions using body-worn inertial sensors," in *Proceedings of the 8th International Conference on Body Area Networks*, 2013, pp. 289–295.
- [22] S. Hignett and L. McAtamney, "Rapid entire body assessment (reba)," *Applied ergonomics*, vol. 31, no. 2, pp. 201–205, 2000.
- [23] A. R. M. Forkan, F. Montori, D. Georgakopoulos, P. P. Jayaraman, A. Yavari, and A. Morshed, "An industrial iot solution for evaluating workers' performance via activity recognition," in *2019 IEEE 39th International Conference on Distributed Computing Systems (ICDCS)*. IEEE, 2019, pp. 1393–1403.
- [24] A. Diete, L. Weiland, T. Szytler, and H. Stuckenschmidt, "Exploring a multi-sensor picking process in the future warehouse," in *Proceedings of the 2016 ACM International Joint Conference on Pervasive and Ubiquitous Computing: Adjunct*, 2016, pp. 1755–1758.
- [25] A. Diete, T. Szytler, L. Weiland, and H. Stuckenschmidt, "Recognizing grabbing actions from inertial and video sensor data in a warehouse scenario," in *FNC/MobiSPC*, 2017, pp. 16–23.
- [26] J. Yang, M. N. Nguyen, P. P. San, X. Li, and S. Krishnaswamy, "Deep convolutional neural networks on multichannel time series for human activity recognition," in *Ijcai*, vol. 15. Citeseer, 2015, pp. 3995–4001.
- [27] X. Zheng, M. Wang, and J. Ordieres-Meré, "Comparison of data preprocessing approaches for applying deep learning to human activity recognition in the context of industry 4.0," *Sensors*, vol. 18, no. 7, p. 2146, 2018.
- [28] T. Szytler and H. Stuckenschmidt, "On-body localization of wearable devices: An investigation of position-aware activity recognition," in *2016 IEEE International Conference on Pervasive Computing and Communications (PerCom)*. IEEE, 2016, pp. 1–9.
- [29] F. Moya Rueda, R. Grzeszick, G. A. Fink, S. Feldhorst, and M. Ten Hompel, "Convolutional neural networks for human activity recognition using body-worn sensors," in *Informatics*, vol. 5, no. 2. Multidisciplinary Digital Publishing Institute, 2018, p. 26.
- [30] C. Reining, M. Schlangen, L. Hissmann, M. ten Hompel, F. Moya, and G. A. Fink, "Attribute representation for human activity recognition of manual order picking activities," in *Proceedings of the 5th international Workshop on Sensor-based Activity Recognition and Interaction*, 2018, pp. 1–10.
- [31] F. M. Rueda and G. A. Fink, "Learning attribute representation for human activity recognition," in *2018 24th International Conference on Pattern Recognition (ICPR)*. IEEE, 2018, pp. 523–528.

# Design of Multi-View Graph Embedding for Features Selection and Remotely Sensing Signal Classification

Abdullah Alhumaidi Alotaibi<sup>1</sup>

Department of Science and Technology,  
Taif University  
Taif, Saudi Arabia

Sattam Alotaibi<sup>2</sup>

Department of Electrical Engineering,  
Taif University  
Taif, Saudi Arabia

**Abstract**—Now-a-days, signal processing remains an intensive challenging area of research. In fact, various strategies have been suggested to address semi-supervised, feature selection and unlabeled samples challenges. The most frequent achievement was dedicated to exploit a single kind of feature/view from the original data. Recently, advanced techniques aimed to explore signals from different views and to, properly, integrate divergent kinds of interdependent features. In this paper, we propose a novel design of a multi-View Graph Embedding for features selection allowing a convenient integration of complementary weighted features. The proposed framework combines the singular properties of each feature space to accomplish a physically meaningful cooperative low-dimensional selection of input data. This allows us not only to perform a semi-supervised classification, but also to propagate narrow class information to unlabeled sample when only partial labeling knowledge is available. This paper makes the following contributions: (i) a feature selection schema for data refinement; and (ii) the adaptation of a multi-view graph-based approach by a better tackling of semi-supervised and dimensionality issues. Our experimental results, conducted by using a mixture of complementary features and aerial images datasets, demonstrate the effectiveness of the proposed framework without significantly increasing computational complexity.

**Keywords**—Signal processing; remote sensing images; features selection; graph embedding; unlabeled samples

## I. INTRODUCTION

In both signal processing/remotely sensing community, a considerable growth has been shown in the plenty and the capacity of images which deliver a noticeable defiance to the traditional signal processing techniques [1]. Dealing with remotely sensed images, multifarious types of features (e.g., spectral, texture, or spatial features) can be used to characterize pixels from different kind of views [2]. In fact, due to the progressively intense computational capabilities and the diligent advancement of feature extraction methods, signals are consequently outlined by disparate aspects [3]. Hence, a single pixel can be uniformly seen from different “views”, where each of them is composed of a particular subspace of descriptors.

With the availability of this infinitude set of features, multiple feature views are going to have, generally, a multitude of statistical dispositions. Hence, the concatenation of these views allows to take advantage of the complementary aspect between these spaces and consequently to increase the classification accuracy. Thus, it will be very interesting to handle all the input space, including all available descriptors. Nevertheless, the simple concatenation, without a proper modeling, will lead to some problems such as feature biasing [4]. In other terms, this

investigation confronts two major challenges. The first problem is the computational complexity which will be increased by the size of the input space. Moreover, the model sensitivity of classification schema will be affected by the insignificant features which should be ignored [5].

Now-a-days, multi-view learning has received noticeable immersion for signal processing applications [6]. While there have been progress in multi-view classification, most existent techniques are based only on the classical vector representation of features for each view and their fusion in the classification step. Nonetheless, the complex structure of most signal common forms and the inadequacy of vector modeling design induct significant challenges [7]. Then, a more adapted modelling of extracted features allows a finest capture and modeling of the inherent structural information. To address this issue, we propose, in this work, a novel approach involving a graph based classification enhanced by a feature selection schema. The major intention of this investigation is to find low-dimensional representations as a gateway for graph embedding while preserving the inherent structure of original data.

To outline, our principle contributions are threefold:

- A novel graph embedding schema is introduced for multi-view classification and an alternating model based on SSMF algorithm [8] is presented to efficiently optimize remote sensing signal classification.
- The feature selection step, considered in previous works as a pre-processing step, has been incorporated to the proposed algorithm, thus enabling us to eliminate superfluous features while controlling the dimensionality issue.
- Expanded experiments conducted on two different datasets reflect the capability of the proposed technique.

The remainder of the paper is organized as follows. Section II is dedicated to problem formulation and literature review, Section III presents in greater details the proposed approach. Section IV shows the experiment on a synthetic/real data set and highlights the obtained outcomes. Section V presents the discussion. Section VI finally establish the conclusions and the future directions of our work.

## II. RELATED WORKS

The classification approaches dedicated to image processing can be decomposed into three main families : super-

vised, semi-supervised and unsupervised techniques. These approaches can be also decomposed into hard and soft techniques. The so-called full pixel techniques, adopting the assumption that each pixel is associated with a pure land cover type, have been evaluated as no appropriate for the processing of mixed pixels. A widely alternative way is the use of soft classification approaches [9]. These methods do not appoint a pixel to exactly one class, although they generate a set of fractions that reflects, for each pixel, the membership amplitude for a given class. This fact imposes to include different types of features/view in order to better classify this kind of pixels.

When tackling image processing from a multi-view perspective, various refinements can be envisaged by considering remotely sensed images as a valuable source of information. In fact, combining information from various data sources has become a prominent research topic in machine learning. Nevertheless, representing images is not an unequivocal exercise in the domain of signal processing, as the amount of candidate image features is practically unlimited [10]. The election of features/model is generally related to the target appliance. Features examples can be divided into spectral, textural, structural groups. The textural group such as SIFT and Gabor texture features. The spectral group includes radiometric features, Gray Level Co-Occurrence Matrix (GLCM). The third group includes Gaussian wavelet features, shape features, etc. [11]. Major works adopt the instinctive idea stipulating that if we increase the number of features, the accuracy will increase unquestionably.

The associated literature was faintly focused on a same linear fusion schema from different views for all objects. Zhand et al. [12] propose an object-oriented segmentation combined with Support vector machines. Nweke et al. propose a multiple classifiers system based on k-Nearest Neighbors [13]. Wu et al. introduce a deep learning algorithm for multi-view medical images processing [14]. Alhumaidi et al. use a serious gaming approach to manage interferences in ad hoc femtocell, Stackelberg competition is used to elect the best FAPs without making a random choice [15]. Unfortunately, the proper integration of the features with different input space is missing. Conceivably, the classifier performance was not automatically improved (reduced in some cases) by the profusion of multi-bands images [16]. Concurrently, this phenomenon is the after effect of the increase of spectral class variability. Hughes showed that classification performance decreased, as further features were involved. This phenomena is designed by “the curse of dimensionality” [17].

As an extension to the discussed works, an emerging family related to multi-view approaches are becoming an interesting area of research. The existing approaches adopt a “one-combo-fits-all” schema. Therefore, the final model based on features concatenation and manifold ranking is done linearly by combining multi-views spaces. This will lead to a single similarity graph [18]. More readily, the propagation fusion approach investigates the label propagation or for each features space, then a federation step allows to combine the obtained outcomes. Furthermore, the feature selection step is not included in the manifold ranking, which induce some errors in the final result. In order to boost the classification accuracy, a balance should be raised between the dimensionality of the

input space Hughes phenomena.

The main objective is to study the effectiveness of multi-view graph-based approach while applying soft classification schema. Given an image with training pixels seen from multi-views, including both labeled and unlabeled samples, multi-view learning graph intends to build a classifier by incorporating the complementary information from multi view perspectives. Currently, graph theory has been adopted for remotely sensed images processing. Lio et al. [19] propose a technique associating both feature fusion and decision for multi-sensor data classification. A general graph-embedding (GE) framework was proposed in [20]. In this framework, each algorithm is regarded as a un-directed weighted graph that incorporates ideal properties of the original data set. Yu et al. [21] investigate the relevance scores, which handled the classification process, among neighbor pixels with a hyper-graph learning schema. Our work is inspired and builds in a novel direction on the success of these previous approaches.

One of the prominent issues of remotely sensed images is the feature redundant aspect which is quite common with sensors covering wide areas. This can lead naturally to the challenging issue of overabundance affecting seriously the classifier accuracy. To overcome this problem, feature selection focuses on the election of a subset of the initial features space according to a selection criterion. It is an outstanding approach widely applied in pattern recognition. It allows the reduction of dimensionality by eliminating irrelevant and superfluous features, and thus allows to improve for applying algorithms, such as improving classification precision, boosting results readability, and reducing computational complexity. With reference to the choice of label information exploitation, feature selection algorithms can be categorized as supervised algorithms, unsupervised algorithms or semi-supervised algorithms [22]. From the outlook of selection design, feature selection approaches are chiefly declined into three families: filter, wrapper or embedded. The filter approach weigh features in an independent way without recourse to any algorithm. The wrapper approach involves a learning schema to extract and weigh the quality of input features. Finally, the embedded approach designs the feature selection process as an integral part of the algorithm and use the associated objective to lead searching for significant features. Conclusively, the reviewed approaches may either elect a subspace of the original space or return the weights of features evaluating their adequacy.

Another problem may arise when dealing with images, it concern the lack of labeled samples. This leads, inevitably, to a low accuracy particularly with a missed or incomplete ground truth. To overcome this problem, Shi et al. propose an hierarchical multi-view learning framework based on CNNs [23]. Aydav et al. use granular computing to improve classification [24]. The problem of missed labeled samples should be Incorporated in the learning process. If there is a great majority of works based on transfer learning, one trending approach is the active learning can offer a solution for these issues.

### III. PROPOSED APPROACH

The proposed approach is illustrated by Fig. 1. It begins with a first pre-processing step. Next, a feature extraction stage from different views is carried out. Secondly, a learning graph embedding approach is proposed. The learning process includes a features selection step which allows to eliminate redundant features.

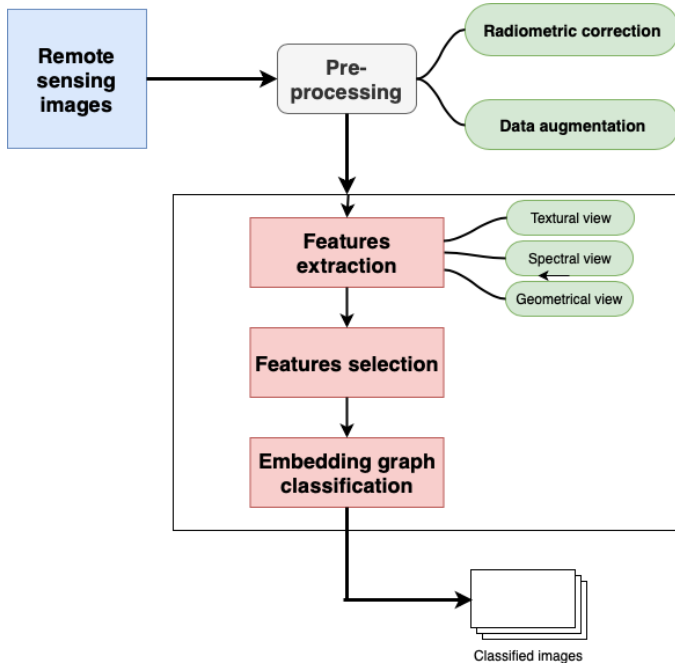


Fig. 1. Graphical Abstract of the Proposed Approach.

The first step of the proposed approach is the extraction of multi-view low-level visual features : spectral, textural, structural. The textural view is a combination of SIFT and 2D log Gabor texture features. The practical expression of this feature is given by equation 1.

$$G(f, \theta) = \exp \left\{ \frac{-[\log(f/f_0)]^2}{2[\log(\sigma_f/f_0)]^2} \right\} \exp \left\{ \frac{-(\theta - \theta_0)^2}{2\sigma_\theta^2} \right\} \quad (1)$$

The spectral view includes the concatenation of radiometric features, Grey Level Co-Occurrence Matrix (GLCM). The third view includes shape Hu's invariant moments (seven invariant forms to rotation, translation and scaling) [25]. This first 4 moments are illustrated by equation ???. The final target is to make a combination of them in the form of a compound-feature structure.

$$\begin{aligned} \phi_1 &= m_{20} + m_{02}, \\ \phi_2 &= (m_{20} - m_{02})^2 + 4m_{11}^2, \\ \phi_3 &= (m_{30} - 3m_{30}) + (3m_{21} - m_{03})^2 \end{aligned} \quad (2)$$

$$\text{where } m_{pq} = \sum_{x=0}^{M-1} \sum_{y=0}^{M-1} (x)^p \cdot (y)^q f(x, y).$$

The majority of related works try to exploit of the panoply of available features without paying attention to the dimensionality curve. A shortcoming which certainly affects the precision

of the learning model. We propose here an innovative feature selection strategy based on an embedded graph to extract efficient and suitable features from remote sensing data.

1) *Graph based modelling*: Each of extracting views, presented in Fig. 1, models a particular aspect of original data. In order to profit from the completeness of these views, a concatenation approach turns to be unavoidable. As discussed precendently, the concatenation of these features in a single vector will amplify the dimensionality problem and will affect the classification accuracy. In addition, the lack of labeled data complicates the classifier task. In order to overcome these challenges, we propose here to model this combination using a graph learning model. Let's make the following notations:

- N : Number of pixels ;
- M : Number of views ;
- C : the number of classes. So,  $X = \{x_1, x_2, \dots, x_N\}$  be a set of pixels seen from M views.

Hence, the proposed approach aims to model each of these view as a graph. For each graph, we set pixels as vertices, and specifies edges based on the similarity between samples. An edge between nodes  $i$  and  $j$  is drawn if  $x_i$  and  $x_j$  are "proximate". Edges may be weighted based on similarity scores [?]. Therefore, we construct M graphs each using a specific kind a feature.  $G^g$  denotes a  $K - NN$  graph build up on  $X$  using  $g^{th}$  feature. Accurately,  $G^g$  is designed by linking each two vertices  $x_i$  and  $x_j$  if one is with the  $k$  nearest neighbors of the other. We designate by  $W_g$  the edge affinity matrix of  $G^g$ . Each entry  $W_g(i, j)$  in  $W_g$  reflects the similarity between  $x_i$  and  $x_j$  according to the  $g^{th}$  features view. If the similarity is not null, there is an edge in  $G^g$  between  $x_i$  and  $x_j$ . Otherwise,  $W_g(i, j)$  is zero.

To compute  $W_g(i, j)$ , Gaussian kernel, a widely used measure of similarity between data instances, is used to compute edge weights as shown in Equation 3. It has shown to exceed the other distances for data classification [?].

$$W_{ij} = \exp\left(-\frac{d_A(x_i, x_j)}{2\sigma^2}\right) \quad (3)$$

where  $d_A(x_i, x_j)$  is the distance measure between instances  $x_i$  and  $x_j$ , and  $\sigma$  is the kernel bandwidth parameter. Owing to the high-dimensionality of the extracted features, the performance of the  $kNN$  rule classifies is imperatively related to the adopted metric. This choice can't be always optimal.

2) *Feature selection*: The significance of a feature can be assimilated to the following question: how much it respects the graph design. A legitimate criterion for selecting features is based on the minimization of the laplacian score of the  $g^{th}$  feature through the following equation:

$$L_r = \frac{\sum_{ij} (f_{ri} - f_{rj})^2 W_{ij}}{\text{var}(f_r)} \quad (4)$$

$$\text{where } f_r = [f_{r1}, f_{r2}, \dots, f_{rn}]^T$$

With the graph  $G = (V, E, W)$  constructed, we can presently achieve classification over the graph and assign labels to all remaining samples. Afterwards, the manifold ranking allows the adjusting process of the graph, the more similar



two samples, the more probably they have analogous labels. This process is called local smoothness. The labeled samples incrementally propagate the label relevance scores to unlabeled ones via graph edges until convergence. The final accomplishment of graph learning, called “global consistency”, is the consistency of the obtained given the initial label information [8].

Let  $D_g$  be the diagonal matrix of  $G^g$  where each component  $D_g(i, i)$  is specified as  $D_g(i, i) = \sum_{j=1}^n W_g(i, j)$ . In a semi-supervised context, the first  $m$  samples  $x_i (i = 1, 2, \dots, m)$  are labeled and the remaining other samples are unlabeled. Let's denote by  $L \in \mathbb{R}^{n \times c}$  be the relevance labeling matrix with  $L(i, j) = 1$ , if  $x_i$  is marked by label  $j$ , designated by  $L(x_i) = j (1 \leq j \leq c)$ , and 0 otherwise. Equivalently, let  $R_g \in \mathbb{R}^{n \times c}$  be the relevance score of unlabeled sample  $x_u$  affected to class  $j$  respecting the  $g$ th view. The final expression of optimal  $R_g$  is attained by minimizing the following objective function:

$$F(R_g) = \frac{1}{2} \left( \sum_{i,j=1}^n W_g(i, j) \left( \frac{1}{\sqrt{D_g(i, i)}} (R_g(i, \cdot) - L(i, \cdot)) \right)^2 \right) \quad (5)$$

$$- \frac{1}{\sqrt{D_g(j, j)}} (R_g(j, \cdot)) + \alpha_g \sum_{i=1}^n (R_g(i, \cdot) - L(i, \cdot))^2 \quad (6)$$

---

**Algorithm 1:** The proposed algorithm

---

**Input :**  $W_g^{[1]} (g = 1, 2, \dots, M), R_g^{[0]}, \alpha_g, \lambda, \varepsilon$   
(convergence threshold)

**Output:**  $R_{SSMF}^*$  : final label relevance matrix.

**for**  $g = 1, 2, \dots, M$  **do**

t=0  
compute  $W_g$

t=1,

**for**  $g = 1, 2, \dots, M$  **do**

$Z_g^{[t]} = Q_g^{[t]} \left( \frac{\sum_{j \neq g} R_{n,j}^{[t]}}{M-1} \right)$   
 $W_g^{[t+1]} = Z_g^{[t]} (Z_g^{[t]})^T + \lambda I$   
 $R_g^{[t+1]} = \alpha_g P_g^{[t+1]} + (1 - \alpha_g) L$   
 $L_r = \frac{\sum_{i,j} (f_{ri} - f_{rj})^2 W_{ij}}{\text{var}(f_r)}$

until  $c \leq \varepsilon$  /\* The change is smaller than a threshold  $\varepsilon$  \*/

**return** the converged relevance label matrix

---

#### IV. EXPERIMENTAL RESULTS

##### A. Data Sets

Experiments were conducted on two datasets: 1) UC Merced land use scenes, 2) Taif city aerial images. Those datasets, including a variety of spatial/textural patterns, boost the classification challenges.

1) *UC Merced dataset:* is expressed by 21 land-use classes selected from aerial imagery. Each set comprehends 100 images of 256x256 pixels for each of the 21 categories. This data set is delineated by Fig. 2.



Fig. 2. Images of UC MERCED Dataset.

2) *Taif region dataset:* For real case scenario, the studied area is Al-Taif city located in the south-eastern part of Makkah region. The centroid for the study area is at 32126'14.1828'' N and 4030'45.7704'' E. A series of Landsat images was used in this experiment were collected from the USGS library through the Glovis Viewer. This data set is delineated by Fig. 3.

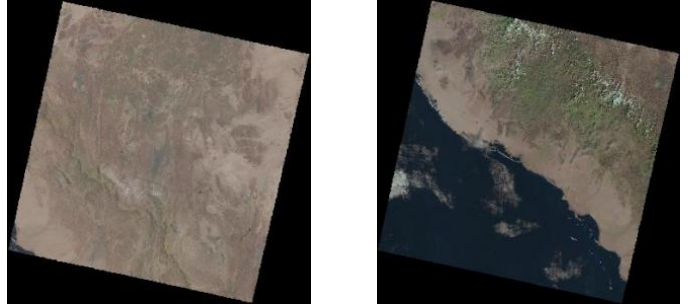


Fig. 3. Images of Taif Dataset.

##### B. Results

Fig. 4 and 5 illustrate the confusion matrix of the proposed approach for the two datasets. As noted, there is a few overlapping between some land-cover types. For example, some pixels belonging to the agriculture area are classified as baseballdiamond. This is, generally, acceptable according to the resemblance between them.

To allow a deeper assessment, we have compared the performance of the proposed approach against some conventional methods : adaptive nearest neighbor clustering (CAN) and LS-SVM. The efficiency of the proposed approach with different amounts of labeled training samples, Fig. 6 illustrates how the different methods reacts in the face of a changing number of labeled/unlabeled samples in terms of Ranking Loss and Average Precision. Regarding these outcomes, we notice that if the total precision increases in correlation with the number of labeled samples. Compared with other methods, our algorithm mostly accomplishes the best precision for different rates on all available datasets.

This proves that our algorithm may attain an advance efficiency given a fixed ratio of labeled training samples, and

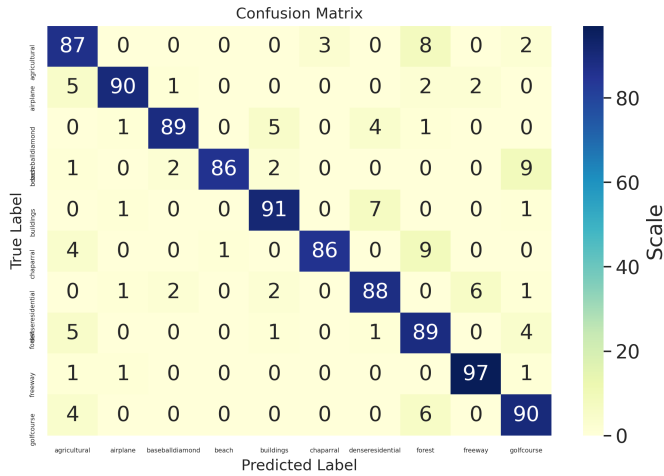


Fig. 4. Confusion Matrix of UC MERCEZ Dataset.

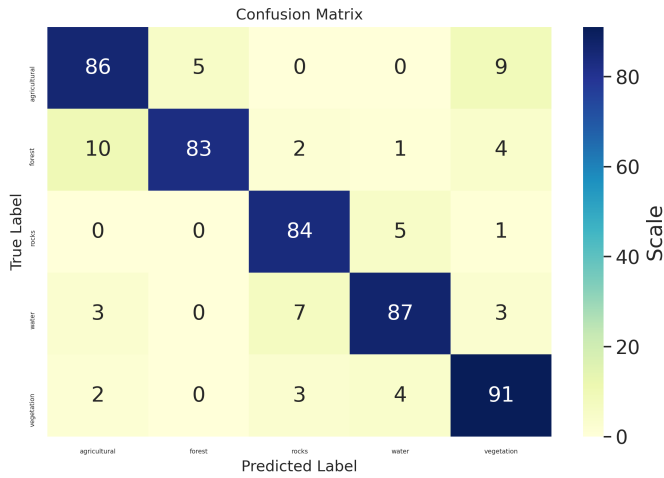


Fig. 5. Confusion Matrix of Taif Dataset.

certify the performance of the proposed methodology. Finally, to better assess the performance of the proposed algorithm, the overall precision (OA) and kappa coefficient (Kappa) are computed for all approaches and compared via Table I.

TABLE I. ACCURACY ASSESSMENT OF THE PROPOSED APPROACH

|                   | UC Merced dataset |       | Taif region dataset |       |
|-------------------|-------------------|-------|---------------------|-------|
|                   | OA                | KAPPA | OA                  | KAPPA |
| Proposed approach | 90.11             | 0.875 | 88.02               | 0.849 |
| CAN               | 88.75             | 0.812 | 85.97               | 0.795 |
| LS-SVM            | 89.64             | 0.844 | 87.74               | 0.819 |

The average processing time for the simulated images was 94s for the the Mac OS computer. It depends on the image and it is about  $O(N^2)$  complexity.

### V. DISCUSSIONS

The contribution of the proposed algorithm lies in establishing a multi-view graph. The results show that the proposed approach is persuasive in remotely sensed image classification.

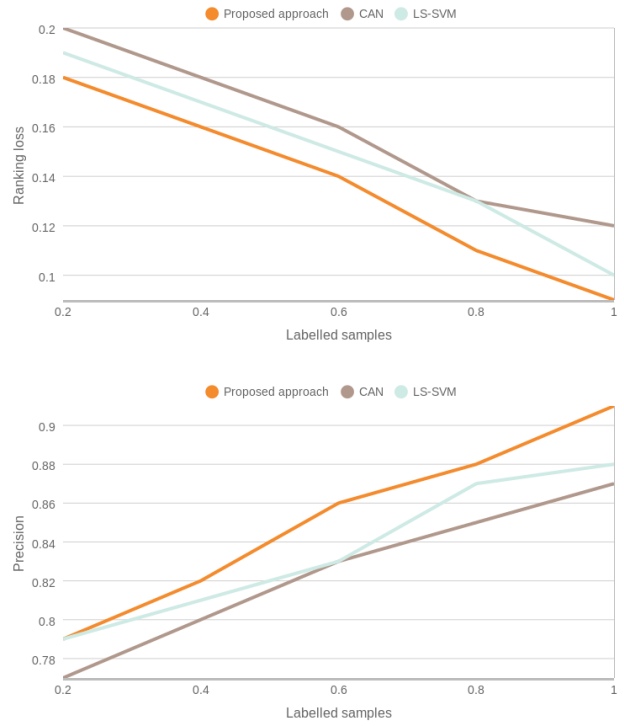


Fig. 6. Comparison of the Conventional Methods with Different Labeled Samples Ratios.

It significantly produces higher precision when compared to state of the art techniques. Hence, it is a conceivably an advantageous alternative when dealing with multi-view and feature selection scenarios.

We have also proposed an efficient multi-label embedding graph which allows a feasible resolution to multi-label ranking contrary to common approaches that adopts binary classifiers for unlabeled multi-view learning problem. This investigation enables us to apprehend the relationships between labels.

Despite the gratifying outcomes obtained by the proposed approach, further achievements need to be investigated in several aspects. First, our algorithm is developed according to a semi-supervised scenario. To expand applications areas, we are concerned with the proposition of a new version able to deal with more difficult entries such as completed unlabeled data. On the other hand, we project to propose a faster implementation of our approach using parallel computing. Finally, motivated by previous works, we hope to integrate big data and deep learning aspects to extend the number of views.

### VI. CONCLUSION

In this paper, we proposed a novel approach for remotely sensed image classification using based on multi-view classification and feature selection in a unified framework. This investigation allows a flexible integration of label information, a better handling of views discrepancy and a modeling of the non-linearity between the data samples. The improved discrimination rate shown through experimental results on

various datasets demonstrates the expressive contribution of each step in the proposed approach. Notably, the graphical modeling of nonlinear complex structure in multi-view features helped increase the recognition rate. Furthermore, the outcomes demonstrate also that our approach holds prevalence while maintaining a reasonable time complexity.

#### ACKNOWLEDGMENT

The authors would like to thank the Deanship of Scientific Research at Taif University for funding this work through the DAEM Research Support Program, Project no. (1-441-7). The authors extend their appreciation to Dr. I. Farah for his contribution and helpful advices.

#### REFERENCES

- [1] U. C. Benz, P. Hofmann, G. Willhauck, I. Lingenfelder, and M. Heynen, "Multi-resolution, object-oriented fuzzy analysis of remote sensing data for gis-ready information," *ISPRS Journal of Photogrammetry and Remote Sensing*, vol. 58, no. 3, pp. 239 – 258, 2004, integration of Geodata and Imagery for Automated Refinement and Update of Spatial Databases. [Online]. Available: <http://www.sciencedirect.com/science/article/pii/S0924271603000601>
- [2] U. Muhammad, W. Wang, and A. Hadid, "Feature fusion with deep supervision for remote-sensing image scene classification," in *2018 IEEE 30th International Conference on Tools with Artificial Intelligence (ICTAI)*, 2018, pp. 249–253.
- [3] M. Yang, C. Deng, and F. Nie, "Adaptive-weighting discriminative regression for multi-view classification," *Pattern Recognition*, vol. 88, pp. 236 – 245, 2019. [Online]. Available: <http://www.sciencedirect.com/science/article/pii/S0031320318304035>
- [4] H. Zeng, Q. Wang, and J. Liu, "Multi-feature fusion based on multi-view feature and 3d shape feature for non-rigid 3d model retrieval," *IEEE Access*, vol. PP, pp. 1–1, 03 2019.
- [5] J. Cai, J. Luo, S. Wang, and S. Yang, "Feature selection in machine learning: A new perspective," *Neurocomputing*, vol. 300, pp. 70 – 79, 2018. [Online]. Available: <http://www.sciencedirect.com/science/article/pii/S0925231218302911>
- [6] J. Zhao, X. Xie, X. Xu, and S. Sun, "Multi-view learning overview: Recent progress and new challenges," *Information Fusion*, vol. 38, pp. 43 – 54, 2017. [Online]. Available: <http://www.sciencedirect.com/science/article/pii/S1566253516302032>
- [7] Q. Wang, J. Lai, L. Claesen, Z. Yang, L. Lei, and W. Liu, "A novel feature representation: Aggregating convolution kernels for image retrieval," *Neural Networks*, vol. 130, pp. 1 – 10, 2020. [Online]. Available: <http://www.sciencedirect.com/science/article/pii/S0893608020302252>
- [8] Y. Wang, J. Pei, X. Lin, Q. Zhang, and W. Zhang, "An iterative fusion approach to graph-based semi-supervised learning from multiple views," in *Advances in Knowledge Discovery and Data Mining*, V. S. Tseng, T. B. Ho, Z.-H. Zhou, A. L. P. Chen, and H.-Y. Kao, Eds. Cham: Springer International Publishing, 2014, pp. 162–173.
- [9] R. Sharma, P. Garg, and R. Dwivedi, "Analysis of uncertainty ratio in classified imagery using independent indicator entropy," *The Egyptian Journal of Remote Sensing and Space Science*, vol. 23, no. 1, pp. 49 – 55, 2020. [Online]. Available: <http://www.sciencedirect.com/science/article/pii/S1110982317304209>
- [10] D. Niu, X. Zhao, X. Lin, and C. Zhang, "A novel image retrieval method based on multi-features fusion," *Signal Processing: Image Communication*, vol. 87, p. 115911, 2020. [Online]. Available: <http://www.sciencedirect.com/science/article/pii/S0923596520301107>
- [11] N. Bagri and P. Johari, "A comparative study on feature extraction using texture and shape for content based image retrieval," *International Journal of Advanced Science and Technology*, vol. 80, pp. 41–52, 07 2015.
- [12] R. Zhang, X. Tang, S. You, K. Duan, H. Xiang, and H. Luo, "A novel feature-level fusion framework using optical and sar remote sensing images for land use/land cover (lulc) classification in cloudy mountainous area," *Applied Sciences*, vol. 10, 04 2020.
- [13] H. Nweke, T. Wah, G. Mujtaba, U. Alo, and M. Al-Garadi, "Multi-sensor fusion based on multiple classifier systems for human activity identification," *Human-centric Computing and Information Sciences*, vol. 9, 12 2019.
- [14] X. Wu, H. Hui, M. Niu, L. Li, L. Wang, B. He, X. Yang, L. Li, H. Li, J. Tian, and Y. Zha, "Deep learning-based multi-view fusion model for screening 2019 novel coronavirus pneumonia: A multicentre study," *European Journal of Radiology*, vol. 128, p. 109041, 2020. [Online]. Available: <http://www.sciencedirect.com/science/article/pii/S0720048X20302308>
- [15] A. Alotaibi and M. Angelides, "A serious gaming approach to managing interference in ad hoc femtocell wireless networks," *Computer Communications*, vol. 134, 11 2018.
- [16] Q. Wei, J. Bioucas-Dias, N. Dobigeon, J.-Y. Tourneret, M. Chen, and S. Godsill, "Multi-band image fusion based on spectral unmixing," *IEEE Transactions on Geoscience and Remote Sensing*, vol. PP, 03 2016.
- [17] U. M. Khaire and R. Dhanalakshmi, "Stability of feature selection algorithm: A review," *Journal of King Saud University - Computer and Information Sciences*, 2019. [Online]. Available: <http://www.sciencedirect.com/science/article/pii/S1319157819304379>
- [18] Z. Tao, H. Liu, H. Fu, and Y. Fu, "Multi-view saliency-guided clustering for image cosegmentation," *IEEE Transactions on Image Processing*, vol. 28, no. 9, pp. 4634–4645, 2019.
- [19] W. Liao, R. Bellens, A. Pižurica, S. Gautama, and W. Philips, "Combining feature fusion and decision fusion for classification of hyperspectral and lidar data," in *2014 IEEE Geoscience and Remote Sensing Symposium*, 2014, pp. 1241–1244.
- [20] S. Yan, D. Xu, B. Zhang, H. Zhang, Q. Yang, and S. Lin, "Graph embedding and extensions: A general framework for dimensionality reduction," *IEEE Transactions on Pattern Analysis and Machine Intelligence*, vol. 29, no. 1, pp. 40–51, 2007.
- [21] Y. Wen, Y. Gao, S. Liu, Q. Cheng, and R. Ji, "Hyperspectral image classification with hypergraph modelling," 09 2012, pp. 34–37.
- [22] J. Miao and L. Niu, "A survey on feature selection," *Procedia Computer Science*, vol. 91, pp. 919 – 926, 2016, promoting Business Analytics and Quantitative Management of Technology: 4th International Conference on Information Technology and Quantitative Management (ITQM 2016). [Online]. Available: <http://www.sciencedirect.com/science/article/pii/S1877050916313047>
- [23] C. Shi, Z. Lv, X. Yang, P. Xu, and I. Bibi, "Hierarchical multi-view semi-supervised learning for very high-resolution remote sensing image classification," *Remote. Sens.*, vol. 12, no. 6, p. 1012, 2020. [Online]. Available: <https://doi.org/10.3390/rs12061012>
- [24] P. S. S. Ayday and S. Minz, "Granulation-based self-training for the semi-supervised classification of remote-sensing images," *Granular Computing*, vol. 5, pp. 309–327, 2019.
- [25] J. Žunić, K. Hirota, and P. L. Rosin, "A hu moment invariant as a shape circularity measure," *Pattern Recognition*, vol. 43, no. 1, pp. 47 – 57, 2010. [Online]. Available: <http://www.sciencedirect.com/science/article/pii/S0031320309002660>

# How Images Defects in Street Scenes Affect the Performance of Semantic Segmentation Algorithms

Hoda Imam<sup>1</sup>, Bassem A. Abdullah<sup>2</sup>, Hossam E. Abd El Munim<sup>\*3</sup>

Computer and Systems Engineering Department, Faculty of Engineering, Ain Shams University, Cairo, Egypt<sup>1,2,3</sup>  
Poolia IT Cloud, Stockholm, Sweden<sup>1</sup>

**Abstract**—Semantic segmentation methods are used in autonomous car development to label pixels of road images (e.g. street, building, pedestrian, car, and so on). DeepLabv3+ and PSPNet are two of the best performance semantic segmentation methods according to Cityscapes benchmark. Although these methods achieved a very high performance with clear road images, yet these two methods are not tested under severe imaging conditions. In this work, we provided new Cityscapes datasets with severe imaging conditions: foggy, rainy, blurred, and noisy datasets. We evaluated the performance of DeepLabv3+ and PSPNet using our datasets. Our work demonstrated that although these models have high performance with clear images, they show very weak performance among the different imaging challenges. We proved that the road semantic segmentation methods must be evaluated using different kinds of severe imaging conditions to ensure the robustness of these methods in autonomous driving.

**Keywords**—Semantic segmentation; deep learning; cityscapes; DeepLabv3+; PSPNet

## I. INTRODUCTION

Autonomous vehicles are vehicles that can move with little or no human interaction. It collects all the environment surrounding information to simulate human behavior in driving safely. Autonomous vehicles rely on sensors, actuators, driving algorithms, machine learning technologies, and powerful micro-controllers with GPUs to execute the self-driving software.

Self-driving software uses semantic segmentation algorithms that take road scene images as input and give a label to each pixel in the input images. These labels describe the object class that these pixels present (road, traffic light, vehicle, human, etc.). Fig. 1 shows an example of input and ground truth images used in semantic segmentation algorithms. Semantic segmentation is very powerful as it helps self-driving software with understanding scene images at the pixel level.

In recent years, after the emergence of convolutional neural networks (CNNs), segmentation made huge progress. Many semantic segmentation methodologies depending on CNN have been developed in [1-7]. These methodologies were trained and evaluated using large scale datasets [8-11].

These networks are designed and tested to work efficiently with clear images. Also, all the images in the large scale datasets [8-11] are clear images. Yet, semantic segmentation methodologies don't take into consideration the different types of defects in images coming from video cameras.

Defects in images could be a result of bad weather or electronic noise. These defects in images decrease the performance and the accuracy of semantic segmentation methodologies and thus lead to a wrong driving decision taken by the vehicle's self-driving system.

Overall, the state-of-the-art methods take into consideration only the performance of these methods on clear images, as these methods are limited by the existing datasets. These methods ignore the performance with unclear images. Semantic segmentation methods should take into consideration these challenges and handle these severe imaging conditions. Although certain works studied object detection methodologies with challenges as foggy [12], rainy [13, 14], blurred [15], and noisy [16-18] images, yet only a few works [12, 19] studied these challenges with semantic segmentation methodologies. Here, we are studying road semantic segmentation methodologies with different challenges.

In this work, we address different kinds of severe imaging conditions: fog, rain, blurring, and noise. We study the performance of semantic segmentation with these four imaging defects. As collecting real datasets with these conditions is very hard, we decided to use Cityscapes dataset [11] and introduce fog, rain, blurring, and noise on the clear images of the dataset.

Even that author in [12] addressed the performance of semantic segmentation methods [1, 2] with fog. These two methods have very low performance on the Cityscapes benchmark. The mIoU of these two methods is 73.6% and 67.1% respectively on Cityscapes test set.

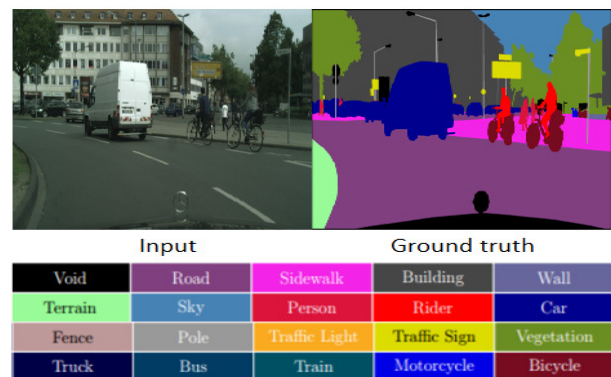


Fig. 1. Example of the Input Image used with Semantic Segmentation Methods and the Ground Truth Image that these Methods Seek to Achieve as an Output.

\*Corresponding Author

In this work, we are not only generating new evaluation datasets but also studying the performance of two powerful methods in semantic segmentation against imaging defects challenges. We study the performance of DeepLabv3+ and PSPNet [5, 4] which are rated as two of the top methods in semantic segmentation. DeepLabv3+ and PSPNet score mIoU of 82.1% and 81.2% respectively on Cityscapes test set.

This work is an expansion to our previous work [20], which studied the performance of semantic segmentation methods with fog and blur challenges. In this paper, we added rain and noise to the challenges used in the performance evaluation of semantic segmentation methods.

In summary, this work contributions are:

- (i) Addressing the performance degradation in semantic segmentation methods with severe imaging conditions.
- (ii) Creating rainy, foggy, blurred, and noisy datasets for evaluation purposes. We made use of an algorithm provided by [12] to add fog in Cityscapes dataset.
- (iii) Using our newly created datasets in performance evaluation of two top semantic segmentation methods (DeepLabv3+ and PSPNet).

This paper is organized as follows: Section 2 reviews shortly the methods of semantic segmentation used in performance measurement. Section 3 describes the challenging evaluation datasets. Section 4 shows the experiments and the performance evaluation results. Finally, Section 5 makes a brief conclusion.

## II. METHODS

In this section, we will describe briefly the semantic segmentation methods used in our methods performance search. DeepLabv3+ and PSPNet are two of the best-performing methods according to Cityscapes benchmark. These are two state-of-the-art road semantic segmentation methods used to label pixels of road images (e.g., street, building, pedestrian, car, and so on).

### A. DeebLabv3+

DeebLabv3+, the extension of DeebLabv3, is a very powerful semantic segmentation model invented by Google. DeebLabv3+ is mainly composed of two phases:

**Encoder:** In this phase, the model extracts the main features from the input image. It detects the presence of the objects and their location. DeepLabv3+ uses Atrous Spatial Pyramid Pooling (ASPP), which investigates convolutional features by applying atrous convolution at multiple scales.

**Decoder:** In this phase, the model refines the segmentation results along the object boundaries. It applies 1 x 1 convolutions on the low-level features and concatenates it with the upsampled encoded features. It then applies 3 x 3 convolutions and upsamples the features to output the prediction image with the same size of the input image.

DeebLabv3+ scored a performance of 89.0% using the test set of PASCAL VOC 2012 benchmark [10] and 82.1% using the test set of Cityscapes benchmark. Fig. 2 shows the network structure of DeepLabv3+.

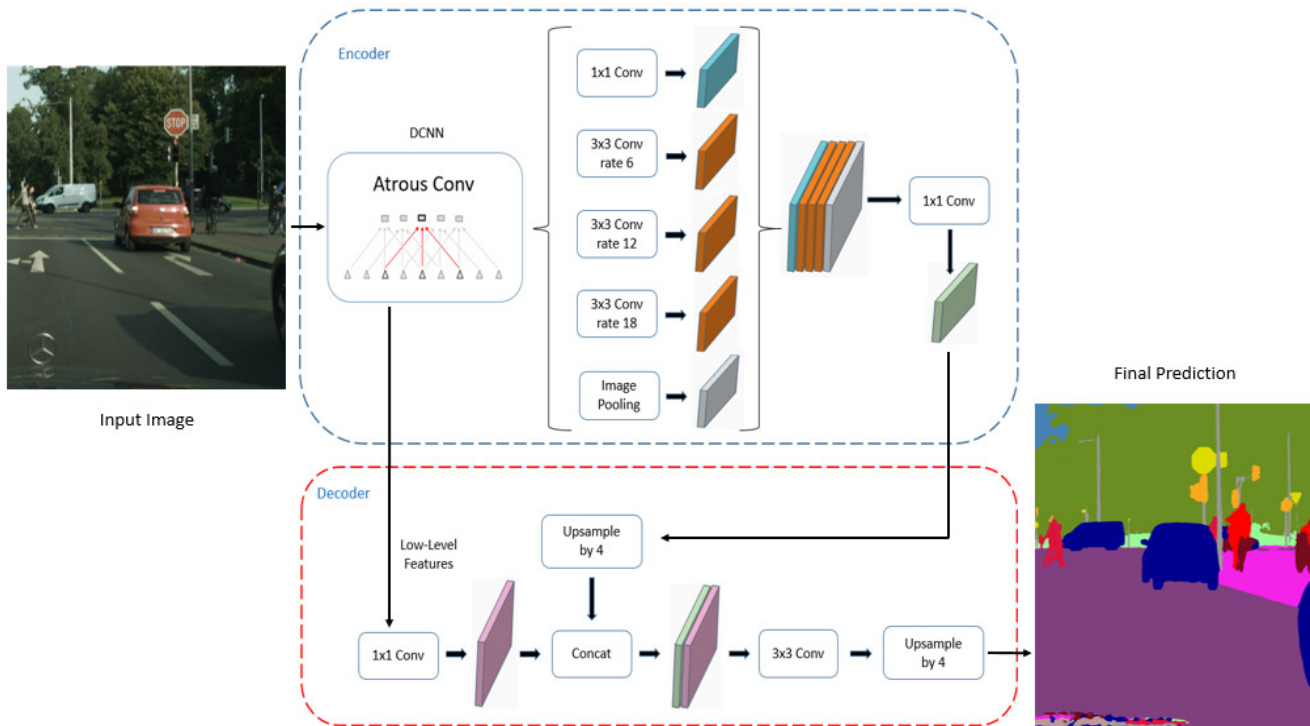


Fig. 2. DeebLabv3+ Method Structure Showing its different Phases. The Predicted Image is the Output of DeebLabv3+ Method using an Input Image from Cityscapes Clear Dataset.

### B. PSPNet

Pyramid Scene Parsing Network (PSPNet) is a semantic segmentation model developed to enhance learning the full context representation of the input scene. PSPNet is mainly composed of four phases:

- (i) Creating the feature map of the input image using CNN.
- (ii) Applying pyramid pooling mechanism. This pooling mechanism contains four pooling levels presented in a pyramid hierarchy that is proceeded with a 1x1 convolutional layer. Each pyramid level is responsible for analyzing different parts from the input image in different locations.
- (iii) Upsampling and concatenating the pyramid levels outputs to give an initial feature maps which contain the local and global information of the input image.
- (iv) Applying a convolutional layer to the feature maps to generate the prediction image.

PSPNet scored a performance of 85.4% using the test set of PASCAL VOC 2012 benchmark and 81.2% using the test set of Cityscapes benchmark. Fig. 3 shows the network structure of PSPNet.

### III. EVALUATION DATASET

In order to evaluate semantic segmentation methods, we chose to introduce fog, rain, blur, and noise to Cityscapes evaluation set which consists of clear images only. In this section, we will describe in details our proposed challenging datasets and examples from the datasets are shown in Fig. 4.

Due to the difficulty of collecting and annotating images for rainy weather, we choose to generate rain into clear weather images of Cityscapes dataset. In this work, we consider a rain image as a composition of a rain-free image and a rain layer. We formulate the rain image  $O(i,j)$  at pixel  $i,j$  as the following:

$$O(i, j) = I(i, j) + R(i, j) \quad (1)$$

where  $I(i,j)$  denotes the rain-free image and  $R(i,j)$  denotes the rain layer. The rain layer is created by the following processes:

#### Algorithm 1 Algorithm of adding rain to clear weather images

```

1: function ADDRRAIN($I(i, j), \alpha$) $\triangleright I(i, j)$ clear image, α
 rain density
 \triangleright create black layer with the same size of the Clear
 weather image $I(i, j)$
2: height, width $\leftarrow I(i, j).shape$
3: $B(i, j) \leftarrow zeros(height,width)$
 \triangleright Add Gaussian noise with standard deviation equals Rain
 density α
4: $N(i, j) \leftarrow B(i, j) +$ Gaussian noise with standard
 deviation α
 \triangleright Threshold the output to keep white pixels from (150 to
 255) only
5: $Z(i, j) \leftarrow threshold(N(i, j), 150, 255)$
 \triangleright Apply diagonal motion filter to the output with kernel
 size 50
6: $R(i, j) \leftarrow Z(i, j) * I50$
7: return $R(i, j)$ $\triangleright R(i, j)$ rainy image
8: end function

```

- (i) Creating a black layer  $B(i,j)$  with the size of the rain-free image.
- (ii) Adding Gaussian noise to the black layer. We used 1D Gaussian distribution. Its standard deviation  $\alpha$  determines the rain density.
- (iii) Applying motion blur filter to the black layer with the Gaussian noise to create the rain layer. We chose the rain motion to be diagonal. We convolved a 2D filter (50 x 50) across the image. As the direction of 1's across the filter grid gives the direction of the desired motion, we used an identity matrix as a motion blur

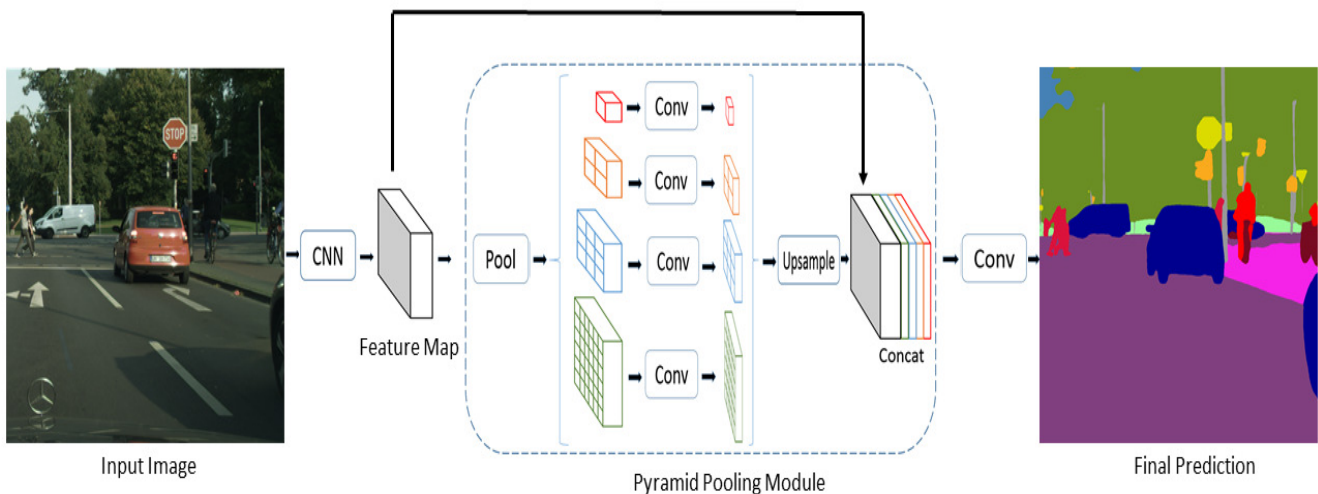


Fig. 3. PSPNet Method Structure Showing its different Phases. The Predicted Image is the Output of PSPNet Method using an Input Image from Cityscapes Clear Dataset.

filter.

Our rainy Cityscapes dataset images created are characterized by the parameter  $\alpha$  used to create the rain layer.  $\alpha$  determines the rain density. Rain density increases with an increase of  $\alpha$  parameter. We created four rainy datasets with  $\alpha$  of 15, 20, 25, and 30. Alg. 1 describes the procedures of adding rain to an input clear image.

The author in [12] developed an algorithm to add synthetic

fog to the clear weather images of Cityscapes dataset. We chose to use this algorithm to create our evaluation foggy dataset. In this dataset, fog density is defined by the visibility range of the image. We created four foggy datasets with visibility ranges of 600, 300, 150, and 75 meters.

In order to evaluate the performance of semantic segmentation methods, we blurred Cityscapes clear dataset. We convolved the clear images with a Gaussian 2D-kernel that has a standard deviation  $\gamma$ . The standard deviation  $\gamma$  of

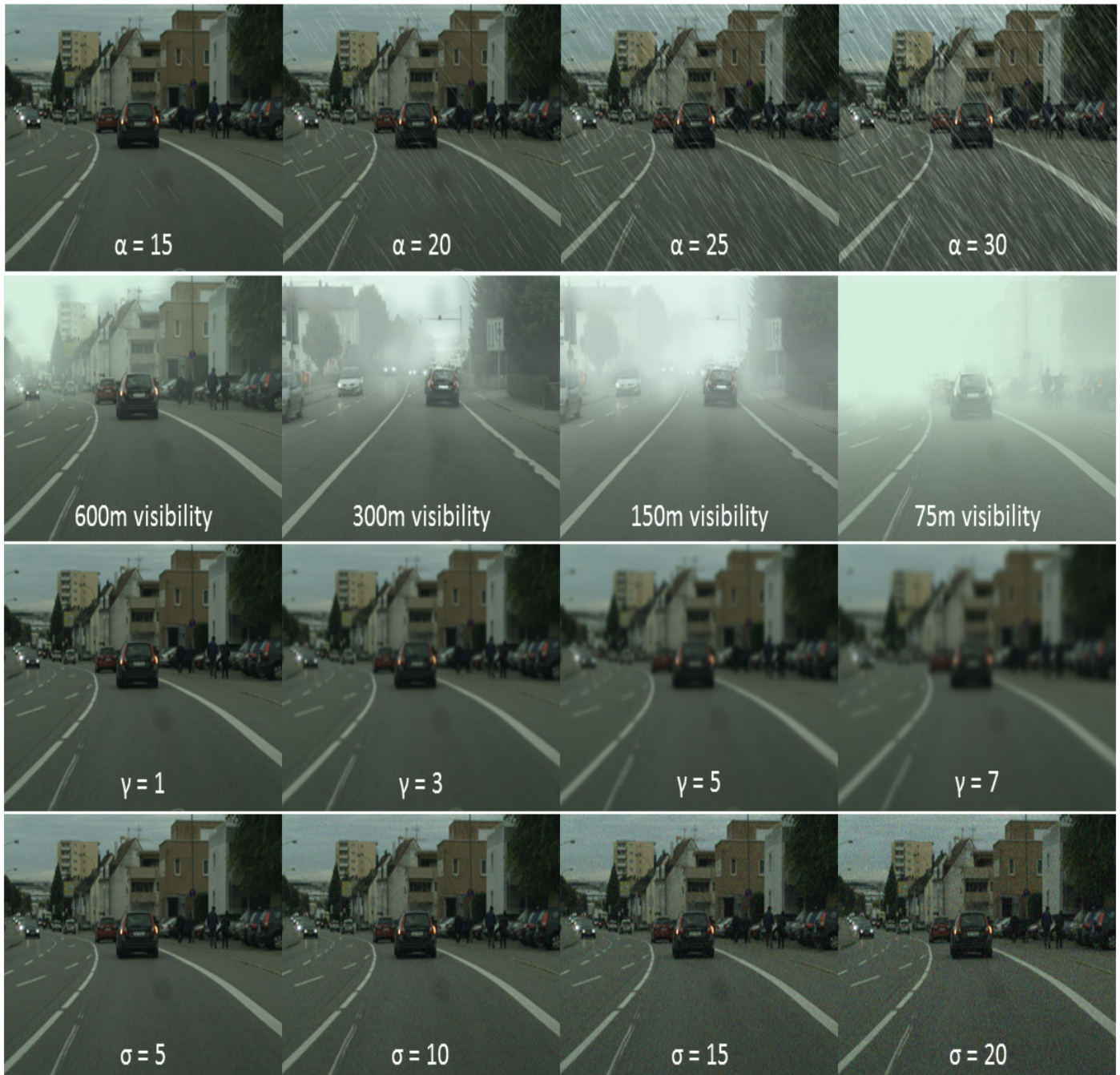


Fig. 4. The First Row shows Example Images from the Rainy Cityscapes with Varying Rain Density  $\alpha$ . The Second Row shows Example Images from the Foggy Cityscapes with Varying fog Density. The Third Row shows Example Images from the Blurred Cityscapes with Varying Blur Density  $\gamma$ . The Fourth Row shows Example Images from the Noisy Cityscapes with Varying Noise Density  $\sigma$ .

the Gaussian kernel represents the density of blurring. By increasing  $\gamma$  blurring density increases. We created four blurred datasets with  $\gamma$  of 1, 3, 5, and 7.

Noise is defined as aberrant pixels. This means that the pixels are not representing the color or the exposure of the scene correctly. Noise in images can make it impossible to determine the objects in the scene. To determine the performance of the semantic segmentation models with noisy images, we chose to add noise to the clear images from Cityscapes.

One kind of noise that occurs in all recorded images to a certain extent is Gaussian noise. This noise can be modeled with an independent, additive model, where the noise has a zero-mean Gaussian distribution and described by its standard deviation  $\sigma$ . We used the standard deviation  $\sigma$  of the Gaussian model to represent the noise density. As  $\sigma$  increases noise density increases. We created four noisy datasets with  $\sigma$  of 5, 10, 15, and 20.

#### IV. EXPERIMENTS

In this section, we evaluated the performance of DeepLabv3+ and PSPNet methods using foggy, rainy, blurred, and noisy datasets. We used intersection-over-union metric IoU to measure the methods' performance.

$$IoU = \frac{TP}{(TP + FP + FN)} \quad (2)$$

where TP is the true positive labeled pixels, FP is the false positive labeled pixels, and FN is the false negative. mIoU is the mean intersection-overunion of the whole evaluation set.

DeepLabv3+ and PSPNet score mIoU of 78.73% and 76.99% respectively on Cityscapes clear evaluation set. Our experiment evaluates the performance of these models throughout different density degrees of fog, rain, blur, and noise.

By comparing the performance of these two methods, we found that DeepLabv3+ performance overcomes PSPNet performance. Even that the two methods have approximately the same performance on clear Cityscapes dataset, DeepLabv3+ has a higher performance than PSPNet on foggy, rainy, blurred, and noisy Cityscapes datasets. The two methods showed a stable performance on light fog and rain, while the performance harshly degraded on excessive amounts of fog and rain. Also, the performance of the two models decreased at a high rate with low densities of blur or noise.

Although DeepLabv3+ shows a higher performance than PSPNet during the evaluation of different semantic segmentation challenges, our experiments show clearly that these two semantic segmentation methods don't show robust performance with foggy, rainy, blurred, and noisy images. We demonstrated that our challenging datasets killed the performance of both methods. Fig. 5 shows the mIoU of the two methods among the different density degrees of fog, rain, blur, and noise.

In order to have safe autonomous vehicles, systems on these vehicles should work efficiently in all the different weather conditions. Also, semantic segmentation methods in autonomous vehicles systems should show robustness against different types of noise in road images. Fig. 6, Fig. 7, Fig. 8, and Fig. 9 show some qualitative results examples of DeepLabv3+ and PSPNet with our challenging datasets.

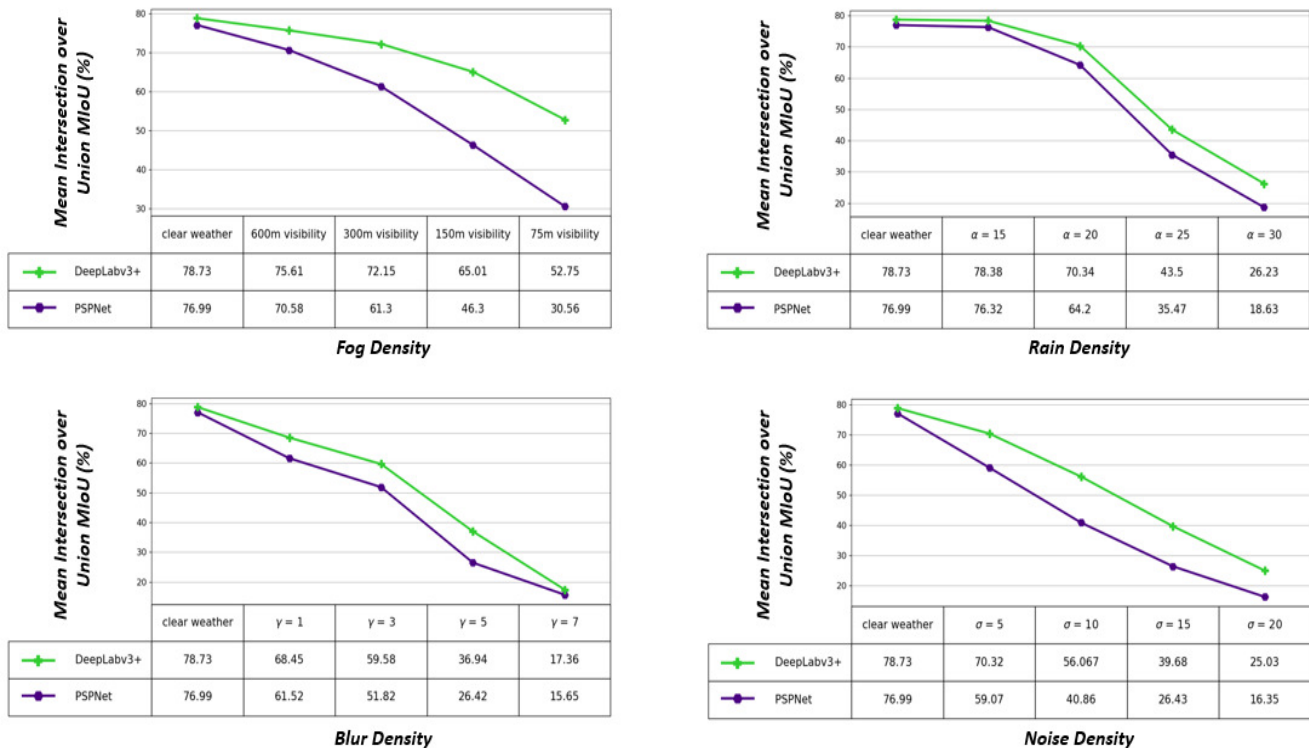


Fig. 5. Performance of DeepLabv3+ and PSPNet with Foggy, Rainy, Blurred, and Noisy Cityscapes Evaluation Datasets.



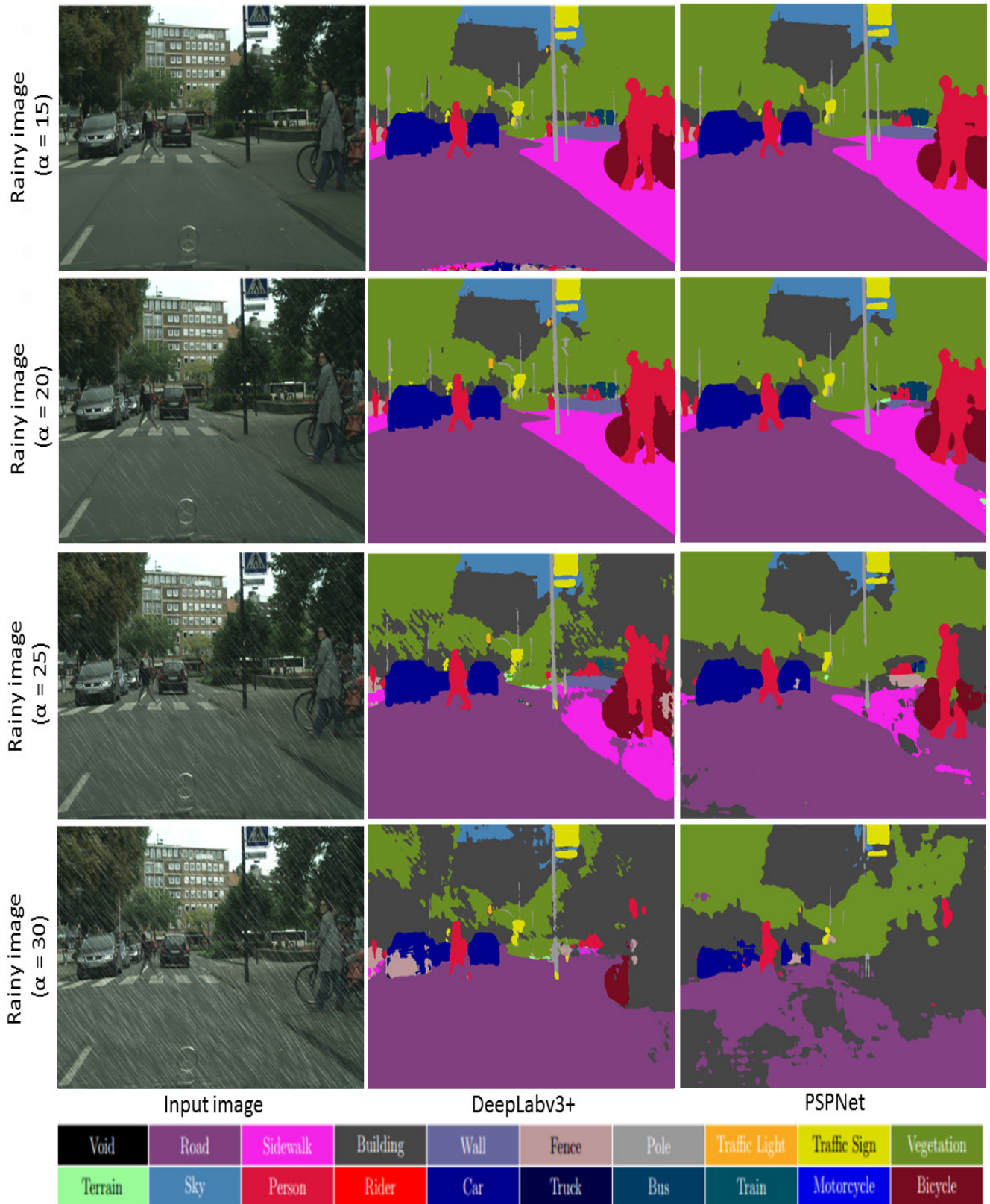


Fig. 6. Example of the Qualitative Results of DeepLabv3+ and PSPNet with Samples from the Rainy Dataset.

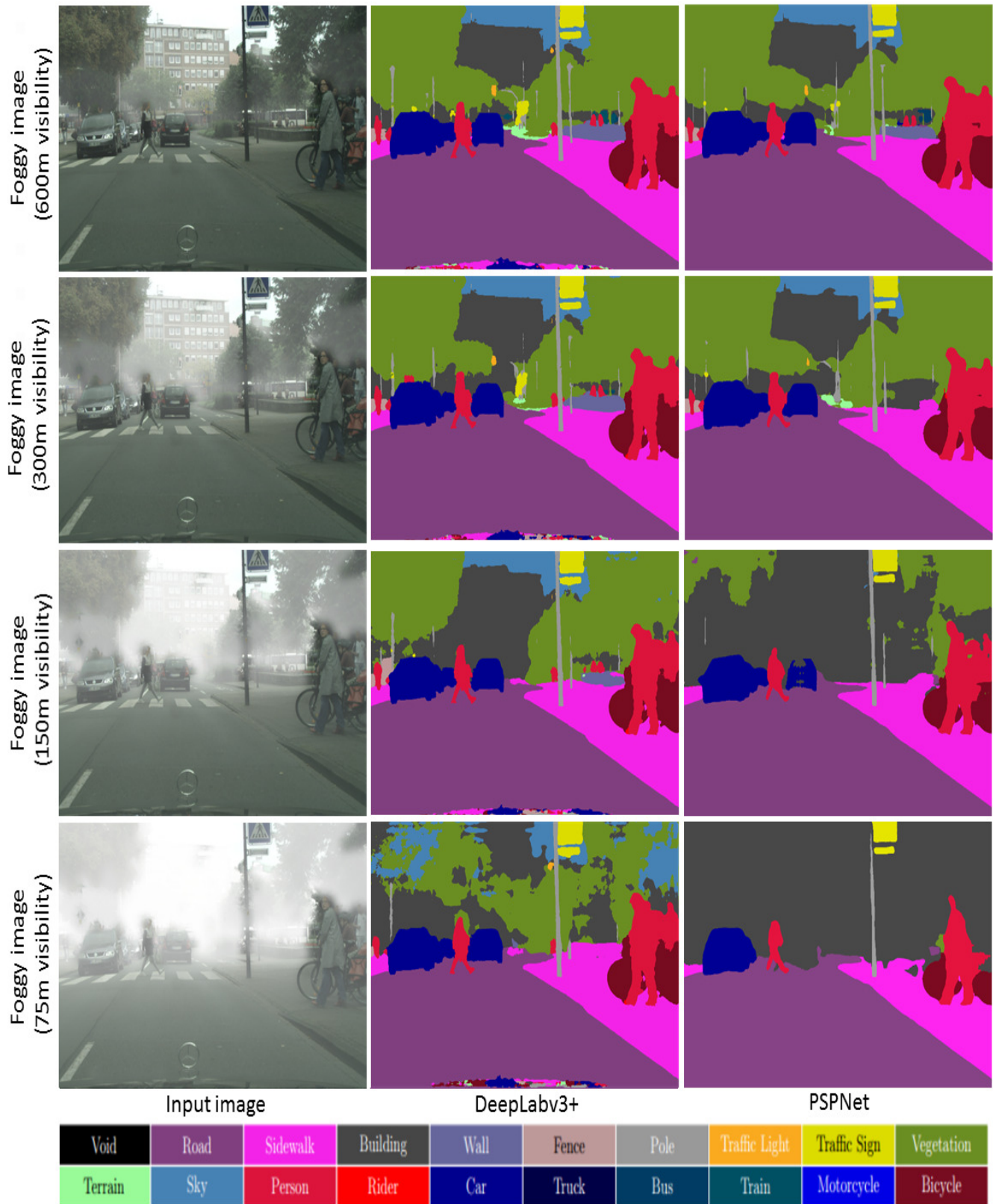


Fig. 7. Example of the Qualitative Results of DeepLabv3+ and PSPNet with Samples from the Foggy Dataset.

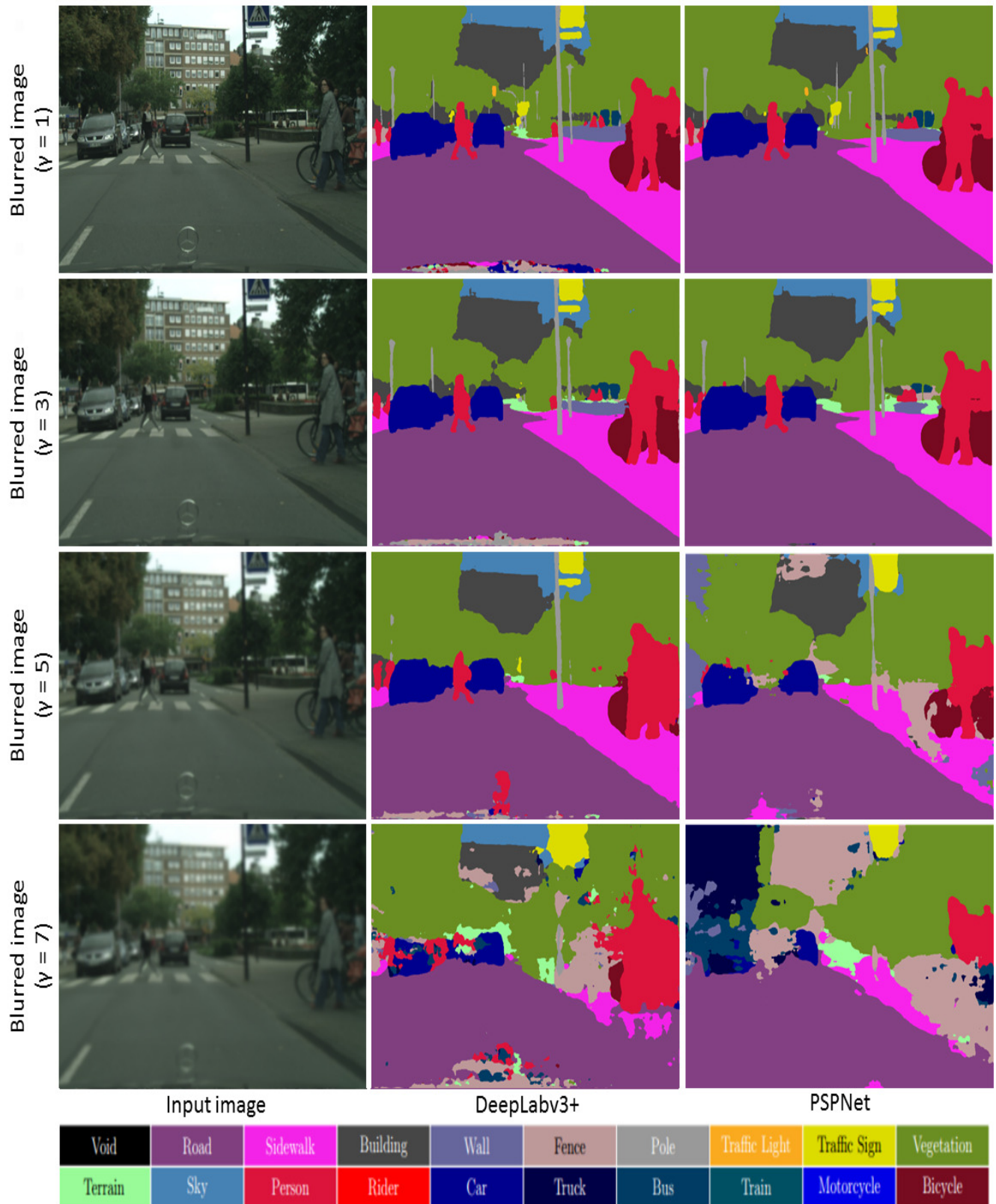


Fig. 8. Example of the Qualitative Results of DeepLabv3+ and PSPNet with Samples from the Blurred Dataset.

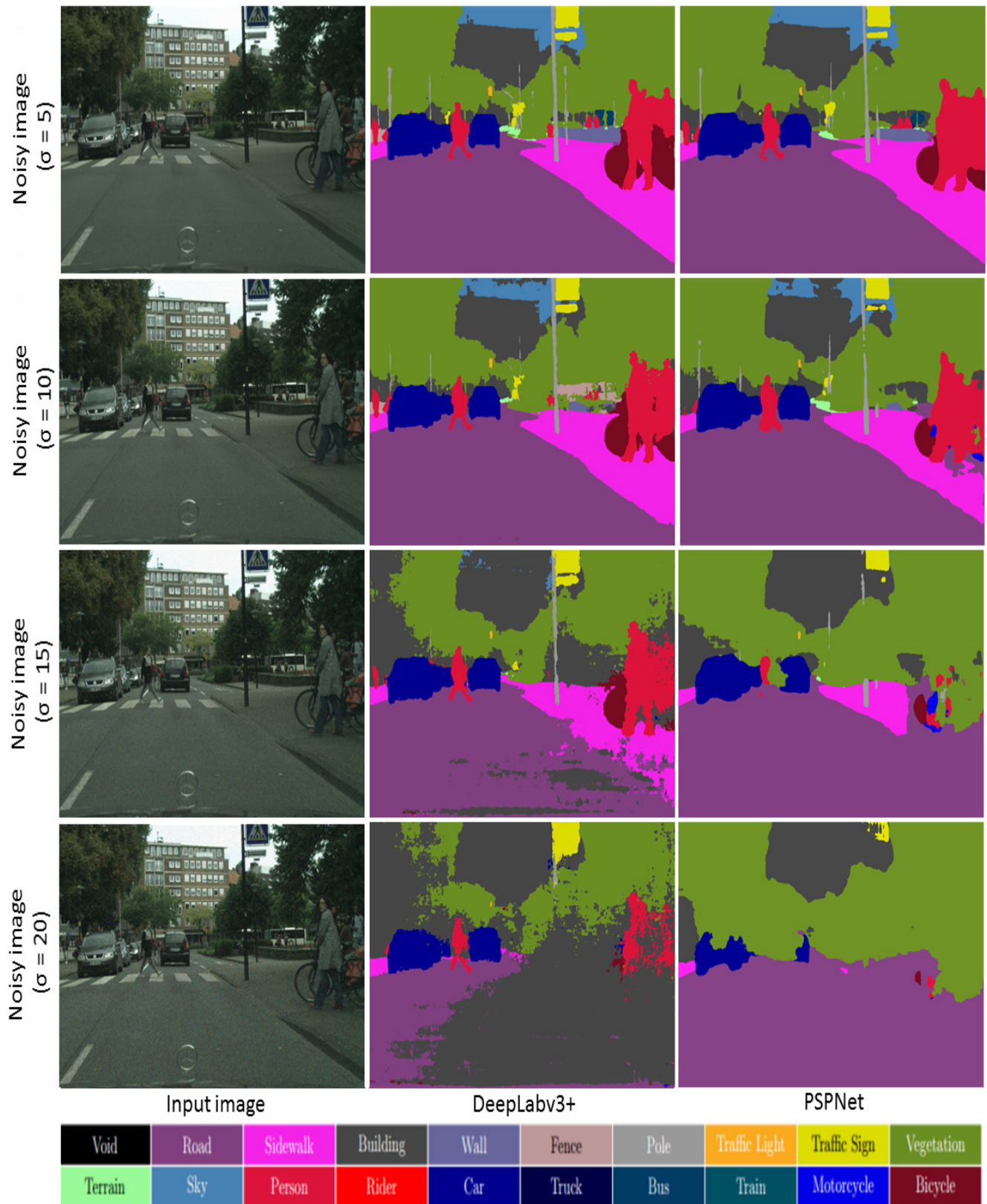


Fig. 9. Example of the Qualitative Results of DeepLabv3+ and PSPNet with Samples from the Noisy Dataset.

## V. CONCLUSION

In this paper, we studied the performance of state-of-the-art semantic segmentation methods with different severe imaging conditions and challenges. We used Cityscapes dataset which consists of clear images only to create new challenging datasets. We created foggy, rainy, blurred, and noisy Cityscapes datasets. We evaluated the performance of DeepLabv3+ and PSPNet methods using our new challenging datasets. We showed that although DeepLabv3+ and PSPNet have good performance with clear images, these two methods don't show a reliable performance with different challenging datasets.

Our created dataset can be used to boost the performance of semantic segmentation models. This could be done by fine-tuning these models during training using images from our datasets.

In this work, we prove that semantic segmentation methods must be evaluated with different kinds of severe imaging conditions to ensure the robustness of the methods and so the safety of autonomous vehicles.

## REFERENCES

- [1] F. Yu and V. Koltun, "Multi-scale context aggregation by dilated convolutions," *arXiv preprint arXiv:1511.07122*, 2015.
- [2] G. Lin, A. Milan, C. Shen, and I. D. Reid, "Refinenet: Multi-path refinement networks for high-resolution semantic segmentation," *CoRR*, abs/1611.06612, 2016.
- [3] L.-C. Chen, G. Papandreou, I. Kokkinos, K. Murphy, and A. L. Yuille, "Deeplab: Semantic image segmentation with deep convolutional nets, atrous convolution, and fully connected crfs," *IEEE transactions on pattern analysis and machine intelligence*, 40(4):834–848, 2017.
- [4] H. Zhao, J. Shi, X. Qi, X. Wang, and J. Jia, "Pyramid scene parsing network," In *Proceedings of the IEEE conference on computer vision and pattern recognition*, pages 2881–2890, 2017.
- [5] L.-C. Chen, Y. Zhu, G. Papandreou, F. Schroff, and H. Adam, "Encoder-decoder with atrous separable convolution for semantic image segmentation," In *Proceedings of the European conference on computer vision (ECCV)*, pages 801–818, 2018.
- [6] T. Takikawa, D. Acuna, V. Jampani, and S. Fidler, "Gated-scnn: Gated shape cnns for semantic segmentation," In *Proceedings of the IEEE International Conference on Computer Vision*, pages 5229–5238, 2019.
- [7] A. Tao, K. Sapra, and B. Catanzaro, "Hierarchical multi-scale attention for semantic segmentation," *arXiv preprint arXiv:2005.10821*, 2020.
- [8] A. Geiger, P. Lenz, and R. Urtasun, "Are we ready for autonomous driving? the kitti vision benchmark suite," In *2012 IEEE Conference on Computer Vision and Pattern Recognition*, pages 3354–3361, 2012.
- [9] O. Russakovsky, J. Deng, H. Su, J. Krause, S. Satheesh, S. Ma, Z. Huang, A. Karpathy, A. Khosla, M. Bernstein, et al, "Imagenet large scale visual recognition challenge," *International journal of computer vision*, 115(3):211–252, 2015.
- [10] M. Everingham, S. A. Eslami, L. Van Gool, C. K. Williams, J. Winn, and A. Zisserman, "The pascal visual object classes challenge: A retrospective," *International journal of computer vision*, 111(1):98–136, 2015.
- [11] M. Cordts, M. Omran, S. Ramos, T. Rehfeld, M. Enzweiler, R. Benenson, U. Franke, S. Roth, and B. Schiele, "The cityscapes dataset for semantic urban scene understanding," In *Proceedings of the IEEE conference on computer vision and pattern recognition*, pages 3213–3223, 2016.
- [12] C. Sakaridis, D. Dai, and L. Van Gool, "Semantic foggy scene understanding with synthetic data," *International Journal of Computer Vision*, 126(9):973–992, 2018.
- [13] K. Jeong and B. Song, "Image synthesis algorithm for road object detection in rainy weather," *IEIE Transactions on Smart Processing and Computing*, 7:342–349, 2018.
- [14] S. Hasirlioglu and A. Riener, "Challenges in object detection under rainy weather conditions," In *First International Conference on Intelligent Transport Systems*, pages 53–65, 2018.
- [15] H. Chiang, Y. Ge, and C. Wu, "Multiple object recognition with focusing and blurring," Technical report, technical report, Stanford Univ., [http://cs231n.stanford.edu/reports/2016/pdfs/259\\_Report.pdf](http://cs231n.stanford.edu/reports/2016/pdfs/259_Report.pdf), 2016.
- [16] P. Halkarnikar, H. Khandagle, S. Talbar, and P. Vasambekar, "Object detection under noisy condition," In *AIP Conference Proceedings*, pages 288–290, 2010.
- [17] S. Milyaev and I. Laptev, "Towards reliable object detection in noisy images," *Pattern Recognition and Image Analysis*, 27(4):713–722, 2017.
- [18] E. Medvedeva, "Moving object detection in noisy images," In *2019 8th Mediterranean Conference on Embedded Computing (MECO)*, pages 1–4, 2019.
- [19] S. Sharma, C. Goodin, M. Doude, C. Hudson, D. Carruth, B. Tang, and J. Ball, "Understanding how rain affects semantic segmentation algorithm performance," Technical report, technical report, SAE Technical Paper, 2020.
- [20] H. Imam, B. A. Abdullah, and H. E. A. El Munim, "Semantic segmentation under severe imaging conditions," In *2019 Digital Image Computing: Techniques and Applications (DICTA)*, pages 1–7. IEEE, 2019.

# Emotion Analysis of Arabic Tweets during COVID-19 Pandemic in Saudi Arabia

Huda Alhazmi<sup>1</sup>

College of Computer Science and Information System  
Umm AL-Qura University  
Makkah, Saudi Arabia

Manal Alharbi<sup>2</sup>

College of Computer Science and Information System  
Umm AL-Qura University  
Makkah, Saudi Arabia

**Abstract**—Social media has emerged as an effective platform to investigate people's opinion and feeling towards crisis situations. Along with Coronavirus crisis, range of different emotions reveal, including anger, sadness, fear, trust, and anticipation. In this paper, we investigate public's emotional responses associated with this pandemic using Twitter as platform to perform our analysis. We investigate how emotional perspective vary regarding lockdown ending in Saudi Arabia. We develop an emotion detection method to classify tweets into standard eight emotions. Furthermore, we present insights into the changes in the intensity of the emotions over time. Our finding shows that joy and anticipation are the most dominant among all emotions. While people express positive emotions, there are tones of fear, anger, and sadness revealed. Moreover, this research might help to better understand public behaviors to gain insight and make the proper decisions.

**Keywords**—Emotion analysis; Arabic tweets; COVID-19; Twitter; Lexicon-based

## I. INTRODUCTION

Coronavirus disease 2019 (COVID-19) is an illness assignable to a novel coronavirus that defined as severe acute respiratory syndrome coronavirus 2-SARS-CoV-2 [1]. It was first identified back to November 2019 at wholesale fish and seafood market, also known as wet markets in Wuhan City, Hubei Province, China. It was informed to World Health Organization (WHO), China country office on December 31, 2019. On 11 January 2020, WHO announced that Chinese authorities did not find a clear evidence of human-to-human transmission 2019-nCoV [2]. With the rapid increase of confirmed cases of COVID-19 on January 30, 2020, WHO stated the COVID-19 outbreak a global health emergency. Unfortunately, when WHO finally declared COVID-19 a global pandemic on March 11, 2020 [3], the number of confirmed cases has been growing exponentially and the novel coronavirus was spread across the world. In line with the precautionary measures that were taken by China to control the outbreak, WHO has recommended social distancing and self-quarantine [4]. China government locked down many affected cities and noticed that the infected cases started to decrease to zero-new-case in March 18, 2020. Many countries followed Chinese government procedures and forced lockdown for 21 days, which was the biggest isolation has ever occurred in the world [4]. The first case of coronavirus infection in Saudi Arabia announced by Ministry of Health (MOH) on March 2, 2020. Since then, Saudi Arabia took a firm precautionary and preventive measures in order to combat COVID-19 outbreak and limiting its spread among the citizens and residents across the country [5]. The economic,

psychological, and social impact of the full lockdown was very bad, and countries had to make the difficult decision of a gradual reopening [6], [7], [8], [9].

There is no doubt, nowadays social media platforms are considered as one of the best possible sources to analysis and detect human emotion [10],[11]. During the lockdown, and shortly after the early outbreak, social media platforms such as Twitter has become the source of information for many people on several subjects related to the COVID-19. This encouraged researchers to study and analysis people's reactions on Twitter about this global pandemic and its related implications [4], [12], [13], [14]. [4] The study analyzed positive and negative sentiment related to COVID19 tweets on twelve different countries between March 11 and March 31. Authors in [12] proposed a statistical analysis model on tweets during the February and March. They found that there was increasing in number of individual users tweeting about coronavirus, Covid-19, and Wuhan. In [13], the analysis shows that the Indian people felt positive to their governmental lockdown decision. [14] performed sentiment analysis on coronavirus tweets and study the evolution of fear over time.

Most of the research studied the crisis of COVID-19 through the outbreak. Moreover, emotions have also been studied, but with limited range. In this research, we present textual analysis of Arabic tweets to detect public emotions in Saudi Arabia of the lockdown ending phase. Our proposed method classifies and quantifies tweets according to eight emotions, namely: anticipation, anger, disgust, joy, fear, surprise, sadness, and trust. One of key contributions of this research is developing a system that can label and score Arabic text according to the standard emotions categories. Another key is analyzing the perception of Saudis' people towards COVID-19, and giving insight into their feeling and reactions. Our finding demonstrates that joy was the most dominated among the rest of emotional tones, while anticipation dominated later. Also, we gain insight into the changing of emotions intensity overtime.

The rest of this paper is organized as follows. Section 2 reviews related work and Section 3 introduces our dataset and preprocessing. In Section 4, we state our emotion detection method. Results and discussion presented in Section 5, followed by conclusion in Section 6

## II. RELATED WORK

People are sharing in social media like Twitter their thoughts which express their moods, emotions, and sentiments. Twitter is a fertile soil that helps researchers to analyze and understand individual's attitudes and behaviors. Tweets can be categorized into two types that convey information about users' mood state; personal tweets and sharing information. Extracting tweets for a given period can reflect changing in the state of general mood. It is much easier to understand moods through facial expression and gestures, voice's tones than written words [15]. Analyzing these written words have captured the attention for psychologists and social scientists [16], [17], [18]. Unlike sentiment analysis (SA) that classifies a text as positive, negative, or neutral, emotional analysis (EA) studies how to detect emotion conveyed in texts (e.g. sadness, happiness, optimism, etc.) [19]. EA can detect greater emotion than the eight-fundamental emotion [20]. The existing studies focused on sentiment analysis more than detecting emotion in text [19]. In the following section, we provide brief review of related work on EA.

Studies [21], [22] investigated and detected depressive disorders on Twitter's users. [21] Analyzed personal updates for 69 users has shown that signals for identifying the depression in individuals who using words related to negative emotion and anger in their tweets. [22] built a statistical classifier to estimate depression, and their model able to predict depression with an accuracy about 70%. In [15], authors studied the impact of major events such as social, economic on public mood, and used an extended version of profile of mood states namely a psychometric instrument to obtain six mood dimensions; tension, depression, anger, vigor, fatigue, confusion. [23] achieved 85% accuracy using a rules-based approach to classify a big data tweets into four classes of emotion. [24], [10] used lexical approach to detect emotion. Authors in [24] built a large lexicon for primitive emotion: joy, surprise, disgust, anger, sadness, and fear. However, they used a manually created training set, and their classifier was limited on news headlines. Whereas [10] built a lexicon of more than 200 moods. Researchers in [25] manually annotated emotions, and sentiments in a limited size sentence of news articles. The study [26] used unsupervised learning approach which convolutional neural network architecture in order to detect and identify emotion in Twitter messages. The authors of [27] classified emotion in social media text into six emotion (happiness, sadness, fear, anger, surprise and disgust) in two steps. First, they extracted emotion using natural language processing. Then, they used support vector machine (with training accuracy 91.7%) and J48 classifiers (with training accuracy 85.4%) of 900 tweets and created a large amount of words that described both emotion and word intensities.

There are many factors affect detecting and analyzing emotion in texts including spelling mistakes, using emoticons, and slang expression [28], [29]. Not to mention the difficulty of type of language used and its complexity such as Arabic language during the analyzing and preprocessing phase. Thus, there are not many studies on analyzing and detecting emotion in Arabic tweets. Authors in [30] proposed a model using Waikato environment for knowledge analysis that categorized Arabic tweets into four emotion sadness, joy, disgust, and anger. Their results achieved 80% accuracy. [31] applied a

binary classifier to detect Arabic irony tweets, and the results achieved 72.76% accuracy. The study [32] conducted ensemble learning methods that classified Arabic tweets into five emotions: sports, politics, culture, general topics, and technology. The results show that ensemble methods outperform other classification models such as decision tree model, Naïve Bayes, and sequential minimal model.

In fact, most of the work in Arabic tweets analysis consider sentiment analysis. However, our work performed emotion analysis on Arabic tweets to detect people emotion and identify changes in their moods.

## III. DATA COLLECTION AND PREPROCESSING

The study was started with data collecting, cleaning, and preparation process, which we explain in the following.

### A. Dataset Collection

The data were obtained by using Tweepy [33], which is a Python library for accessing the Twitter API. We collected Arabic tweets from July 1 to July 31 of 2020, applying multiple key words as shown in Table I to ensure a corpus covers COVID-19 crisis. We collect 1,828,229 Arabic tweets, then the dataset was filtered to focus on tweets belonging to Saudi Arabia, to result in 600640 tweets. These tweets reflect the discussion around the coronavirus after lockdown and quarantine end.

### B. Data Preprocessing

The collected tweets may contain lots of noisy and an uninformative data. Keeping these data make the analysis and the classifying complex and inaccurate. Therefore, we applied the following preprocessing steps to clean the raw text.

- Remove tweet features: features such as hashtags, mentions (@user), URLs, and retweet symbol (RT) do not have any impact on sentiment classification as reported in [34], [35]. We removed these unsentimental features in the tweet.
- Replace the repeated letters: users sometimes used a repetition of letter in the same word such as (خطيبين) to highlight some words or feeling. Removing these letters is very important to identify the word in classification process. We replaced the repeated letters with one letter.
- Remove Stop Words: stop words usually filtered out because they are considered as neutral polarity and are not useful to the polarity decision [36]. Arabic stop word such as (ليس، أن، على) removed using Python NLTK stop words.
- Remove repeated tweets: through extracting process for the tweets, API may return duplicate tweets. We removed them to avoid giving extra weight for specific tweets [37].
- Replace emoji with special tokens: Twitter users today often use emojis to express feeling, moods, and emotions [38]. Since our data contains emojis, we treat each emoji as token using the emojis sentiment lexicon from [39].

TABLE I. LIST OF ARABIC KEYWORDS THAT USED FOR DATA COLLECTING.

| NO. | Keywords      | English Translation of Arabic Keywords |
|-----|---------------|----------------------------------------|
| 1   | نعود بحذر     | Back carefully                         |
| 2   | فك الحظر      | Lockdown ending                        |
| 3   | جائحة         | Pandemic                               |
| 4   | كورونا        | Corona                                 |
| 5   | كوفيد         | Covid                                  |
| 6   | عزل صحي       | Sanitary isolation                     |
| 7   | حجر صحي       | Quarantine                             |
| 8   | احترازي       | Preventive measures                    |
| 9   | تباعد اجتماعي | Social distance                        |
| 10  | وزارة الصحة   | Ministry of Health in Saudi            |
| 11  | كمامات        | Masks                                  |
| 12  | كمامة         | Mask                                   |
| 13  | معقم          | Sterilizer                             |
| 14  | غسل اليدين    | Hand washing                           |
| 15  | قفاز          | Glove                                  |
| 16  | قفازات        | Gloves                                 |

#### IV. METHOD

In this research, we explored people emotions regarding coronavirus COVID-19 using tweets data. We developed emotion detection algorithm to classify Arabic tweets into eight emotion categories, namely: anger, fear, anticipation, trust, surprise, sadness, joy, and disgust as considered in NCR [40]. Also, we included the nonemotion sentiment neutral. We used NCR lexicon for Arabic language that includes the English words, the translation of the English words to Arabic language, the emotion for which the intensity score is provided, and emotion intensity score of the word. This lexicon contains 9922 words distributed over these emotions. Our emotion detection approach uses Natural Language Processing (NLP) to score and classify tweet according to the emotions exist in it. The proposed method is based on lexicon-based approach, which calculates the sentiment of a text using the polarity of the words or phrases in that text [41].

Our emotion detection algorithm uses the tweets after the preprocessing step. Programing codes are developed in Python for comprehensive analysis. This approach includes the following steps:

- Annotating the emotional words: First, we used the Natural Language Toolkit (NLTK) library in Python [42] to tokenize the tweets into tokens. Then, the tokens are checked against the words in the NCR lexicon. Through the matching process, the only tokens that are annotated as emotion word are considered. While, the named tokens that represent person, location, or time are considered not an emotion word. All the matched words with their associated emotion and wights are stored for scoring step.
- Scoring: Every stored word as weight and emotion category contribute in the scoring process. For each tweet, the emotional score for each category is calculated by summing over all weights associated with the words belongs to that category divided by the number

of the words for that emotion as demonstrated in (1), where  $\mathbf{E}$  represents the emotion category,  $\mathbf{j}=1,2,3,\dots,8$  is the category's number,  $\mathbf{Emoweigh}$  is the weight of the word, and  $\mathbf{nw}$  number of words in the tweet belongs to  $\mathbf{j}$  category.

$$EmoScore(E_j) = \frac{\sum_j Emoweight}{nw} \quad (1)$$

- The highest score among all categories is assigned to the tweet and classified with its emotion. Furthermore, the proportion score ProScore is calculated as shown in (2) to predict the percentage of each emotion in a tweet.

$$ProScore(E_j) = \frac{EmoScore(E_j)}{\sum_{i=1}^8 EmoScore(E_i)} \quad (2)$$

If there are no emotion words in the tweet, the scores of all emotion categories will be zero and the tweet will be classified as natural.

#### V. RESULTS AND DISCUSSION

This section deals with the visualizations and analysis of our finding regarding Coronavirus Tweets data.

A total of 600,640 tweets were analyzed. Table II shows the counts and percentage of the eight emotions. Our finding shows that the tweets demonstrated trend toward positive emotions with notable tone of joy and trust. While, the most notable negative emotions were fear and anger.

TABLE II. COUNTS AND PERCENTAGE OF THE EIGHT EMOTIONS.

| Emotions     | Counts | Percentage |
|--------------|--------|------------|
| Anger        | 50033  | 8.33%      |
| Anticipation | 89889  | 14.97%     |
| Disgust      | 26008  | 4.33%      |
| Fear         | 70771  | 11.78%     |
| Joy          | 95520  | 15.9%      |
| Sadness      | 18960  | 3.16%      |
| Surprise     | 1365   | 0.23%      |
| Trust        | 66456  | 11.06%     |
| Natural      | 181638 | 30.24%     |

Fig. 1 illustrates the counts of the emotional tones. The tone joy registers the highest percentage 15.9 %, followed by anticipation with percentage 14.97 %. Fear and trust show very close values which are 11.78 % and 11.06 %, respectively. The low percentage registered by anger, disgust, and sadness, where surprise has the lowest. The finding implies that people express their feeling of joy about lockdown ending, might they eager to back to the lives they had before. They might feel a huge relief because they can do what they miss over the past few months. The second highest value indicates that people try to express their anticipation feeling because they are uncertain about what the future holds and hard to predict the virus spread.



Moreover, after lockdown, people might be experiencing a range of emotions because new cases are registered daily

In our analysis, we also considered the comparison of each emotional tone relative to other tones. The ratio of emotional tone's count relative to the total counts for the other tones is calculated. The colored part of each bar in Fig. 2 is the proportional to the total of all parts. The analysis is done for each day of July, we observed that joy emotion was the most dominant among all emotions in the beginning and in the medial of the month, followed by anticipation. Whereas, the end of the month the anticipation emotion was dominate. The levels of fear were higher than anger as demonstrated in the figure.

In addition, we also investigate emotions over time, Table III reflects the daily scores for each emotion. we mapped people's emotions against time as displayed in Fig. 3. The emotional tones of anger, fear, and surprise increase over time and that reflects the people's feeling about the crisis's situation because the vaccine against the COVID-19 is not found yet. On the other hand, trust decreases might because the number of cases does not decrease as time goes. Joy is relatively constant over time, and that is understandable as people got back to their normal life. While anticipation, sadness, and disgust have steady curves during the time period.

In summary, this study giving insights for COVID-19 pandemic using Twitter data to explore public feeling. The study only considers tweets in Saudi Arabia. However, the method can be adopted to study crises or pandemic in the other cultures.

## VI. CONCLUSION

Public emotional responses are dynamic and might change during the crisis. People may experience different emotions at different stages of the crisis. During lockdown stage, there has been some analysis for people reacting toward the virus using social media. Moreover, most of research works have study Twitter data for sentiment analysis. Whereas a few studies focused on emotion analysis. In this research, we focused on emotion mining during lockdown ending stage. We analyzed emotions of Twitter posts during COVID-19 crisis in Saudi Arabia. We proposed an effective emotion classification method to explore textual data supported with necessary data visualizations. Our finding implies that joy dominated among other emotions at the beginning, but anticipation dominated later. Even though, people show positive emotions, they also express levels of negative emotions because of uncertainty of the information about the behavior of virus. In addition, interesting observation were noticed about the dynamic of the emotions over time. Thus, this study presented valuable informational and public emotional insights that could be used to understand and study the sociocultural system. It could be useful as well in developing strategies dealing with the dynamic of the emotions associated with the crisis. Our research regarding Covid-19 continue, we are developing a model to discover the frequent pattern in the tweet.

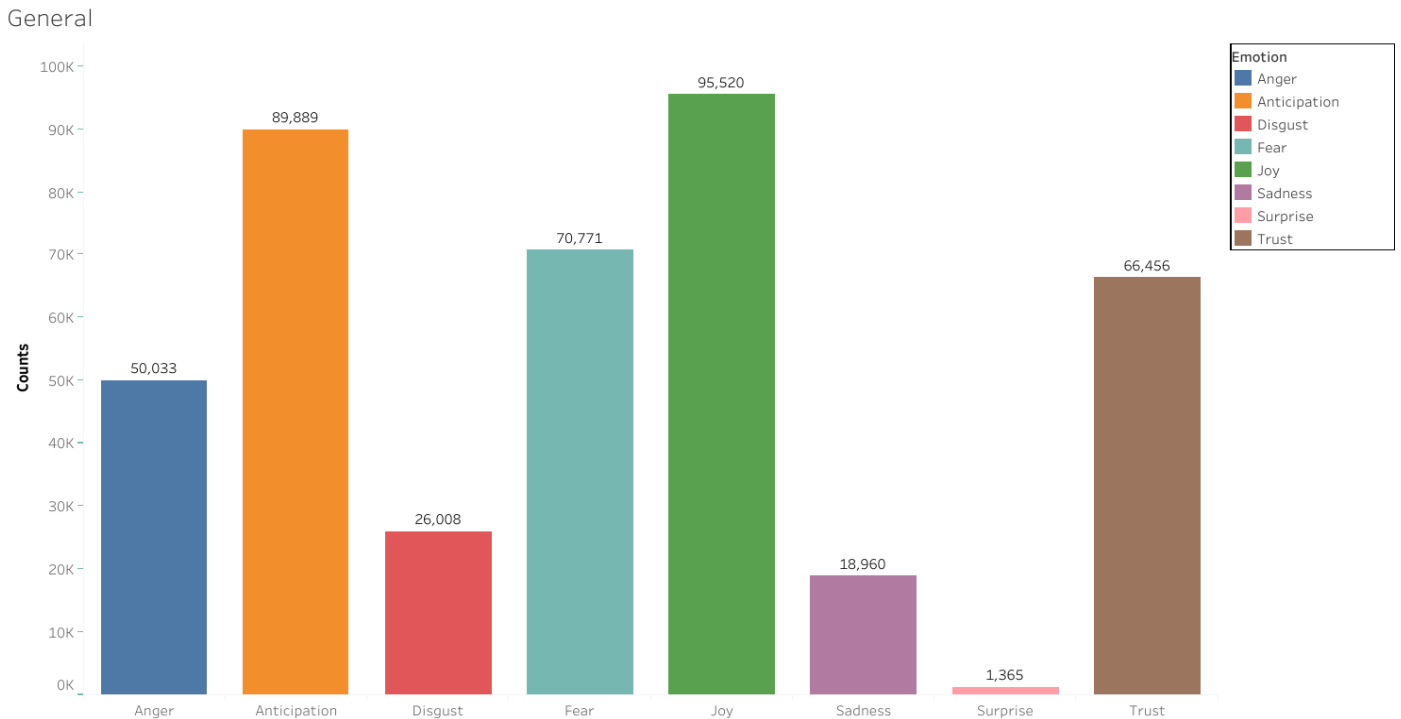


Fig. 1. Counts of all Emotions.

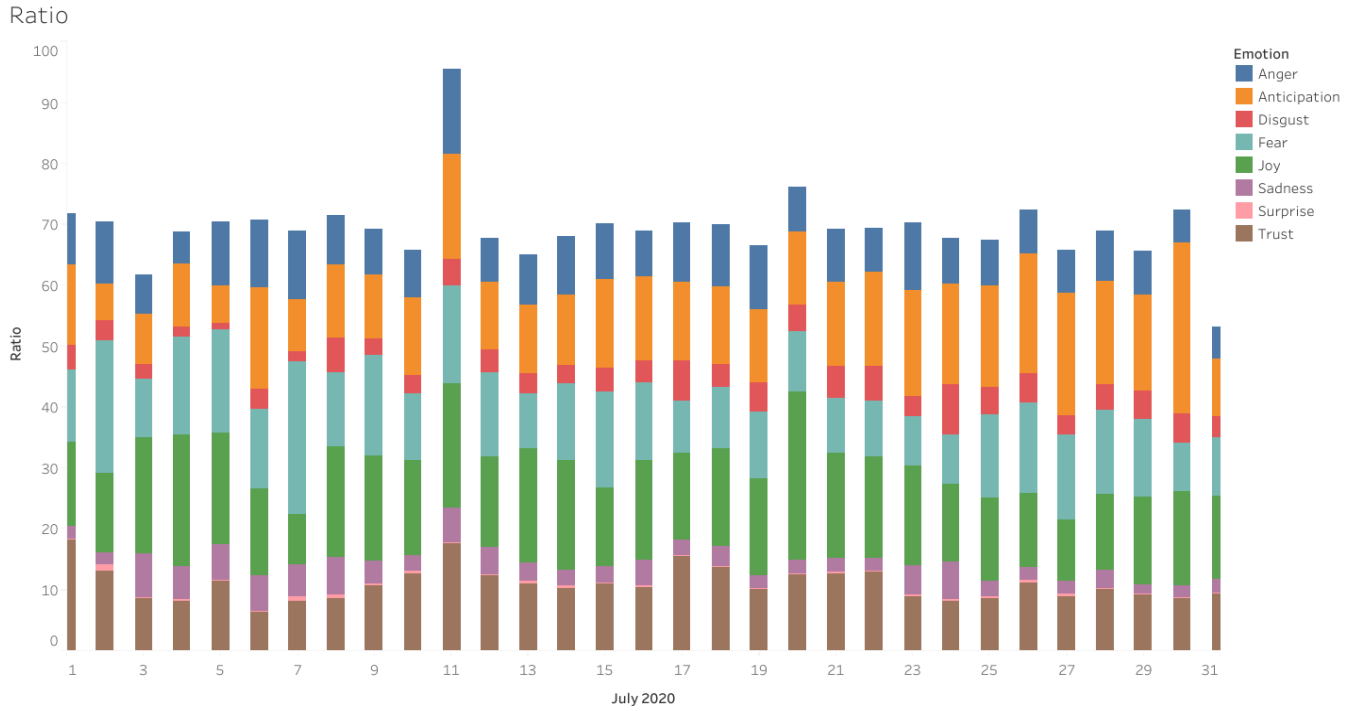


Fig. 2. The Ratio of Emotional Tone's Count Relative to the Total Counts.

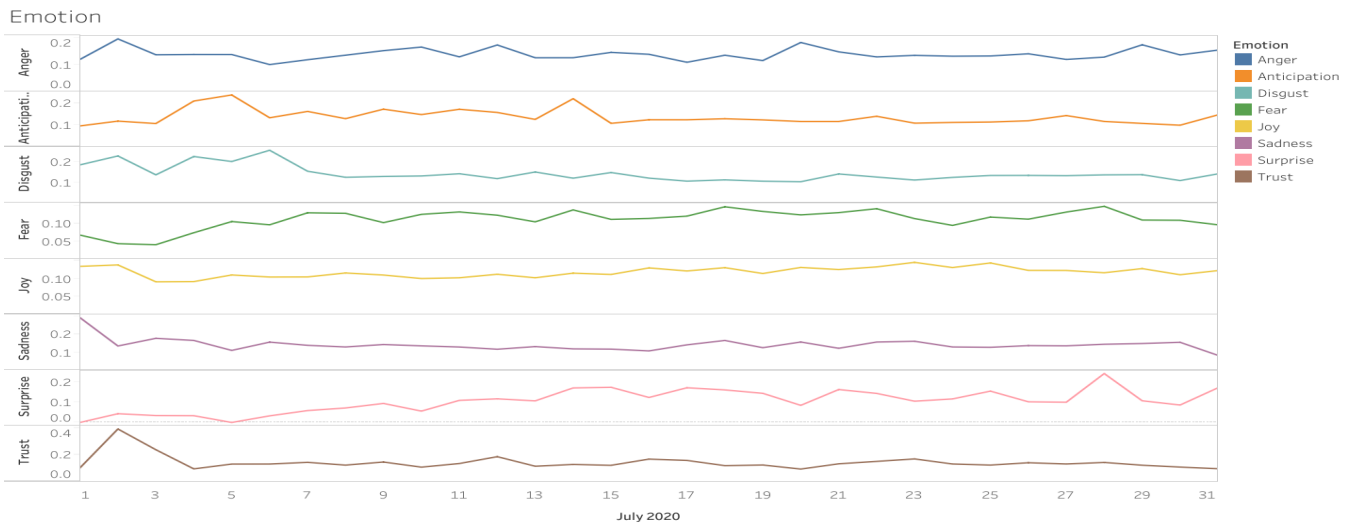


Fig. 3. The Distribution of Emotions' Scores over Time.

TABLE III. COUNTS AND PERCENTAGE OF THE EIGHT EMOTIONS.

| Date | Anger  | Anticipation | Disgust | Fear   | Joy    | Sadness | Surprise | Turst  |
|------|--------|--------------|---------|--------|--------|---------|----------|--------|
| 1    | 0.121  | 0.0962       | 0.1864  | 0.0686 | 0.1351 | 0.2942  | 0        | 0.1039 |
| 2    | 0.1979 | 0.1183       | 0.23    | 0.044  | 0.1392 | 0.1361  | 0.0436   | 0.3952 |
| 3    | 0.1384 | 0.1072       | 0.1376  | 0.041  | 0.0916 | 0.1789  | 0.0344   | 0.2398 |
| 4    | 0.1394 | 0.2104       | 0.2273  | 0.0753 | 0.0922 | 0.1671  | 0.0337   | 0.0962 |
| 5    | 0.1393 | 0.2382       | 0.2027  | 0.1073 | 0.1109 | 0.1114  | 0        | 0.1322 |
| 6    | 0.1016 | 0.1336       | 0.2578  | 0.098  | 0.1051 | 0.1577  | 0.0329   | 0.1325 |
| 7    | 0.1198 | 0.1627       | 0.1552  | 0.1323 | 0.1054 | 0.1398  | 0.0592   | 0.1451 |
| 8    | 0.1368 | 0.1295       | 0.1256  | 0.1309 | 0.1165 | 0.1306  | 0.0722   | 0.1243 |
| 9    | 0.1538 | 0.173        | 0.1298  | 0.1042 | 0.1107 | 0.1443  | 0.0948   | 0.1475 |
| 10   | 0.1673 | 0.1482       | 0.1321  | 0.1279 | 0.1008 | 0.1368  | 0.0565   | 0.1091 |
| 11   | 0.1306 | 0.1725       | 0.143   | 0.1348 | 0.103  | 0.1304  | 0.11     | 0.1362 |
| 12   | 0.1751 | 0.158        | 0.119   | 0.1255 | 0.1129 | 0.118   | 0.1177   | 0.1877 |
| 13   | 0.1272 | 0.1261       | 0.1515  | 0.1064 | 0.103  | 0.1327  | 0.1075   | 0.116  |
| 14   | 0.1273 | 0.2211       | 0.1213  | 0.1406 | 0.116  | 0.12    | 0.172    | 0.1294 |
| 15   | 0.1473 | 0.1081       | 0.1489  | 0.1135 | 0.1123 | 0.1186  | 0.1752   | 0.1228 |
| 16   | 0.1402 | 0.1245       | 0.1215  | 0.1162 | 0.1308 | 0.1086  | 0.1245   | 0.1695 |
| 17   | 0.1102 | 0.1244       | 0.1068  | 0.1228 | 0.1221 | 0.1425  | 0.1729   | 0.1596 |
| 18   | 0.1367 | 0.1292       | 0.1131  | 0.1495 | 0.1315 | 0.167   | 0.1621   | 0.1203 |
| 19   | 0.1166 | 0.1239       | 0.1065  | 0.1362 | 0.115  | 0.1266  | 0.1452   | 0.1252 |
| 20   | 0.1844 | 0.1165       | 0.1039  | 0.1264 | 0.1321 | 0.1583  | 0.0852   | 0.0948 |
| 21   | 0.1493 | 0.1165       | 0.1419  | 0.1328 | 0.1262 | 0.1233  | 0.164    | 0.1341 |
| 22   | 0.1304 | 0.1405       | 0.1268  | 0.144  | 0.1336 | 0.1582  | 0.1448   | 0.1523 |
| 23   | 0.1362 | 0.1089       | 0.1122  | 0.1158 | 0.1464 | 0.1625  | 0.1059   | 0.1709 |
| 24   | 0.1331 | 0.1122       | 0.1251  | 0.0963 | 0.1318 | 0.1306  | 0.1172   | 0.1327 |
| 25   | 0.1339 | 0.1141       | 0.1346  | 0.1201 | 0.1447 | 0.1287  | 0.1561   | 0.1246 |
| 26   | 0.1421 | 0.1198       | 0.1349  | 0.1141 | 0.1238 | 0.1383  | 0.1029   | 0.1422 |
| 27   | 0.1209 | 0.1437       | 0.1336  | 0.1344 | 0.1236 | 0.137   | 0.1008   | 0.1329 |
| 28   | 0.1296 | 0.1167       | 0.1375  | 0.1508 | 0.1171 | 0.1458  | 0.2437   | 0.1443 |
| 29   | 0.1758 | 0.1079       | 0.1384  | 0.1116 | 0.1289 | 0.1499  | 0.108    | 0.1236 |
| 30   | 0.1378 | 0.0995       | 0.1096  | 0.111  | 0.1115 | 0.1567  | 0.0868   | 0.1097 |
| 31   | 0.156  | 0.1471       | 0.1425  | 0.0979 | 0.1233 | 0.0837  | 0.1729   | 0.0973 |

REFERENCES

- [1] W. H. Organization. (2020) Naming the coronavirus disease (covid-19) and the virus that causes it. [Online]. Available: [https://www.who.int/emergencies/diseases/novel-coronavirus-2019/technical-guidance/naming-the-coronavirus-disease-\(covid-2019\)-and-the-virus-that-causes-it](https://www.who.int/emergencies/diseases/novel-coronavirus-2019/technical-guidance/naming-the-coronavirus-disease-(covid-2019)-and-the-virus-that-causes-it)
- [2] ——. (2020) Preliminary investigations conducted by the chinese authorities have found no clear evidence of human to human transmission of the novel coronavirus (2019-ncov) identified in wuhan, china. [Online]. Available: [twitter.com/WHO/status/1217043229427761152](https://twitter.com/WHO/status/1217043229427761152).
- [3] D. Cucinotta and M. Vanelli, "Who declares covid-19 a pandemic," *Acta Biomedica*, vol. 91, no. 1, jan 2020.
- [4] A. Dubey, "Twitter sentiment analysis during covid19 outbreak," *SSRN Electronic Journal*, 01 2020.
- [5] UNDP. (2020) Saudi arabia's ruthless fight against coronavirus. [Online]. Available: [https://www.sa.undp.org/content/saudi\\_arabia/en/home/library/saudi-arabia-s-ruthless-fight-against-coronavirus.html](https://www.sa.undp.org/content/saudi_arabia/en/home/library/saudi-arabia-s-ruthless-fight-against-coronavirus.html)
- [6] C. Huang, Y. Wang, X. Li, L. Ren, J. Zhao, Y. Hu, L. Zhang, G. Fan, J. Xu, X. Gu, Z. Cheng, T. Yu, J. Xia, Y. Wei, W. Wu, X. Xie, W. Yin, H. Li, M. Liu, and B. Cao, "Clinical features of patients infected with 2019 novel coronavirus in wuhan, china," *The Lancet*, vol. 395, pp. 157–160, 01 2020.
- [7] O. Mitjà, Àlex Arenas, X. Rodò, A. Tobias, J. Brew, and J. Benlloch, "Experts' request to the spanish government: move spain towards complete lockdown," *The Lancet*, vol. 395, p. 1193–1194, 03 2020.
- [8] S. Ghosal, R. Bhattacharyya, and M. Majumder, "Impact of complete lockdown on total infection and death rates: A hierarchical cluster analysis," *Diabetes & Metabolic Syndrome: Clinical Research & Reviews*, vol. 14, no. 4, pp. 707 – 711, 2020.
- [9] N. Fernandes, "Economic effects of coronavirus outbreak (covid-19) on the world economy," *SSRN Electronic Journal*, 2020.
- [10] M. D. Choudhury, S. Counts, and M. Gamon, "Not all moods are created equal! exploring human emotional states in social media," in *ICWSM*, 2012, pp. 66–73.
- [11] M. D. Choudhury and S. Counts, "The nature of emotional expression in social media : Measurement , inference and utility," in *Human Computer Interaction Consortium (HCIC)*, 2012.
- [12] N. K. Rajput, B. A. Grover, and V. K. Rathi, "Word frequency and sentiment analysis of twitter messages during coronavirus pandemic," *ArXiv*, vol. abs/2004.03925, 2020.
- [13] G. Barkur, Vibha, and G. Kamath, "Sentiment analysis of nationwide lockdown due to covid 19 outbreak: Evidence from india," *Asian Journal of Psychiatry*, vol. 51, p. 102089, 04 2020.
- [14] J. Samuel, G. G. M. N. Ali, M. M. Rahman, E. Esawi, and Y. Samuel, "Covid-19 public sentiment insights and machine learning for tweets classification," *Information*, vol. 11, no. 6, p. 314, Jun 2020. [Online]. Available: <http://dx.doi.org/10.3390/info11060314>
- [15] J. Bollen, A. Pepe, and H. Mao, "Modeling public mood and emotion: Twitter sentiment and socioeconomic phenomena," *international conference on weblogs and social media*, pp. 450–453, 2011.
- [16] E. Diener and M. E. P. Seligman, "Beyond money: toward an economy of well-being," *Psychological Science in the Public Interest*, vol. 5, p. 1–31, 2004.
- [17] E. Diener, *Assessing Well-Being: The Collected Works of Ed Diener*, 01 2009, vol. 39.
- [18] E. Diener, R. Lucas, and S. Oishi, "Subjective well-being: The science of happiness and life satisfaction," *Oxford Handbook of Positive Psychology*, 01 2002.
- [19] M. Hasan, E. A. Rundensteiner, and E. Agu, "Emotex: Detecting emotions in twitter messages," 2014.
- [20] O. Badarnah, M. Al-Ayyoub, N. Alhindawi, L. A. Tawalbeh, and Y. Jararweh, "Fine-grained emotion analysis of arabic tweets: A multi-target multi-label approach," 01 2018, pp. 340–345.
- [21] M. Park, C. Cha, and M. Cha, "Depressive moods of users portrayed in twitter," *Proceedings of the ACM SIGKDD Workshop On Healthcare Informatics (HI-KDD)2012*, pp. 1–8, 01 2012.
- [22] M. D. Choudhury, M. Gamon, S. Counts, and E. Horvitz, "Predicting depression via social media," in *ICWSM*, 07 2013, pp. 128–137.
- [23] S. Badugu and M. Suhasini, "Emotion detection on twitter data using knowledge base approach," *International Journal of Computer Applications*, vol. 162, pp. 28–33, 03 2017.
- [24] C. Strapparava and R. Mihalcea, "Learning to identify emotions in text," 01 2008, pp. 1556–1560.
- [25] J. Wiebe, T. Wilson, and C. Cardie, "Annotating expressions of opinions and emotions in language," *Language Resources and Evaluation (formerly Computers and the Humanities)*, vol. 39, pp. 164–210, 05 2005.
- [26] D. Stojanovski, G. Strezoski, G. Madjarov, and I. Dimitrovski, *Emotion Identification in Twitter Messages for Smart City Applications*, 01 2018, pp. 139–150.
- [27] B. Gaint, V. Syal, and S. Padgalwar, "Emotion detection and analysis on social media," pp. 78–89, 2019.
- [28] L. Wikarsa and S. Thahir, "A text mining application of emotion classifications of twitter's users using naïve bayes method," in *2015 1st International Conference on Wireless and Telematics (ICWT)*, 11 2015, pp. 1–6.
- [29] M. Abdullah, M. Almasawa, I. Makki, M. Alsolmi, and S. Mahrous, "Emotions extraction from arabic tweets," *International Journal of Computers and Applications*, pp. 1–15, 06 2018.
- [30] M. Al-Kabi, A. Gigieh, I. Alsmadi, H. Wahsheh, and M. Haidar, "Opinion mining and analysis for arabic language," *International Journal of Advanced Computer Science and Applications*, vol. 5, pp. 181–195, 05 2014.
- [31] J. Karoui, F. B. Zitoune, and V. Moriceau, "Soukhria: Towards an irony detection system for arabic in social media," *Procedia Computer Science*, vol. 117, pp. 161 – 168, 2017, arabic Computational Linguistics. [Online]. Available: <http://www.sciencedirect.com/science/article/pii/S1877050917321622>
- [32] H. M. Abdelaal, A. N. Elmahdy, A. A. Halawa, and H. A. Youness, "Improve the automatic classification accuracy for arabic tweets using ensemble methods," *Journal of Electrical Systems and Information Technology*, vol. 5, no. 3, pp. 363 – 370, 2018. [Online]. Available: <http://www.sciencedirect.com/science/article/pii/S2314717218300266>
- [33] J. Roesslein. (2020) Tweepy. [Online]. Available: <http://www.tweepy.org/>.
- [34] A. Pak and P. Paroubek, "Twitter as a corpus for sentiment analysis and opinion mining," in *In Proceedings of the Seventh Conference on International Language Resources and Evaluation*, vol. 10, 01 2010, pp. 1320–1326.
- [35] A. Mourad and K. Darwish, "Subjectivity and sentiment analysis of modern standard arabic and arabic microblogs," in *WASSA@NAACL-HLT*, 2013.
- [36] M. A.-A. and Safaa Bani essa and I. Alsmadi, "Lexicon-based sentiment analysis of arabic tweets," *International Journal of Social Network Mining (IJSNM)*, vol. X, pp. 0–0, 06 2014.
- [37] A. Go, R. Bhayani, and L. Huang, "Twitter sentiment classification using distant supervision," *Processing*, vol. 150, p. 1–12, 01 2009.
- [38] S. Wijeratne, L. Balasuriya, A. Sheth, and D. Doran, "Emojinet: An open service and api for emoji sense discovery," in *ICWSM*, 05 2017, pp. 437–446.
- [39] P. K. Novak, J. Smailovic, B. Sluban, and I. Mozetic, "Sentiment of emojis," *PloS one*, vol. 10, 09 2015.
- [40] S. Mohammad, "Word Affect Intensities," in *Proceedings of the Eleventh International Conference on Language Resources and Evaluation (LREC 2018)*. Miyazaki, Japan: European Language Resources Association (ELRA), May 7-12, 2018 2018.
- [41] P. Turney, "Thumbs up or thumbs down? Semantic orientation applied to unsupervised classification of reviews," *Computing Research Repository - CORR*, pp. 417–424, 12 2002.
- [42] Python. (2016) Python.org. [Online]. Available: <https://www.python.org/downloads/release/python-360/>

# HPSOGWO: A Hybrid Algorithm for Scientific Workflow Scheduling in Cloud Computing

Neeraj Arora<sup>1</sup>

School of Science and Technology  
Vardhman Mahaveer Open University  
Kota, Rajasthan, India 324010

Rohitash Kumar Banyal<sup>2</sup>

Department of Computer Science and Engineering  
Rajasthan Technical University  
Kota, Rajasthan, India 324010

**Abstract**—Virtualization is one of the key features of cloud computing, where the physical machines are virtually divided into several virtual machines in the cloud. The user's tasks are run on these virtual resources as per the requirements. When the user requests the services to the cloud, the user's tasks are allotted to the virtual resources depending on their needs. An efficient scheduling mechanism is required for optimizing the involved parameters. Scientific workflows deals with a large amount of data with dependency constraints and is used to simplify the applications in the diverse scientific domains. Scheduling the workflow in cloud computing is a well-known NP-hard problem. Deploying such data- and compute-intensive workflow on the cloud needs an efficient scheduling algorithm. In this paper, we have proposed a multi-objective model based hybrid algorithm (HPSOGWO), which combines the desirable characteristics of two well-known algorithms, particle swarm optimization (PSO), and grey wolf optimization (GWO). The results are analyzed under complex real-world scientific workflows such as Montage, CyberShake, Inspiral, and Sipt. We have considered the two essential parameters: total execution time and total execution cost while working in the cloud environment. The simulation results show that the proposed algorithm performs well compared to other state-of-the-art algorithms such as round-robin (RR), ant colony optimization (ACO), heterogeneous earliest time first (HEFT), and particle swarm optimization (PSO).

**Keywords**—Cloud computing; hybrid algorithms; metaheuristic algorithms; optimization; workflow scheduling

## I. INTRODUCTION

Cloud Computing is a buzzing word from decades in computer science as it offers advancements like hiding and abstraction of complexity, visualized resources, and efficient use of distributed resources. Few well-known cloud computing platforms are Amazon EC2, GoGrid, Google App Engine, Microsoft Azure, etc. [1] [2]. The services of cloud computing can be classified into Software as a Service (SaaS), Platform as a Service (PaaS), and Infrastructure as a Service (IaaS) [3].

The tasks are dependent on each other in the workflow. The workflow can be represented using Directed Acyclic Graph (DAG) [4], where the nodes in the DAG represent the tasks (T), and the edges (E) joining the nodes represent the dependency between the tasks. A sample workflow is shown in Fig. 1, containing eight tasks  $\{T_1, T_2, T_3, T_4, T_5, T_6, T_7, T_8\}$ . The tasks  $T_1$  and  $\{T_4, T_6, T_7, T_8\}$  are the entry and exit tasks, respectively. Each edge of the DAG shows the dependencies between the tasks. For example,  $T_2$  is executed after  $T_1$  which is shown by the paired set  $\{T_1, T_2\}$ . A scientific workflow is a specialized form of the workflow which is used in various

scientific domains like astrology, bio-informatics, gravitational waves, etc. [5].

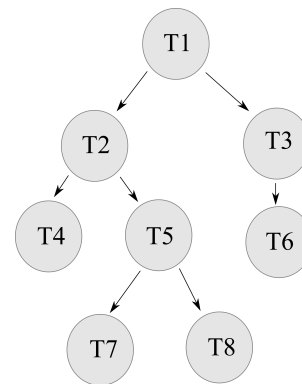


Fig. 1. Dependency of Tasks for Workflow Schedule.

Pegasus project published some of the realistic scientific workflows like Montage, CyberShake, Epigenomics, LIGO, and SIPHT [6] [7]. The structures of these workflows are shown in Fig. 2.

The workflow scheduling can be considered as a mapping function where several dependent tasks are mapped to several available virtual machines [9]. Suppose,  $m$  number of tasks maps to the  $n$  number of virtual machines; then,  $n^m$  combinations which are possible if the brute force algorithm is used. So, the workflow scheduling is a complex problem, and the solution is not found in polynomial time [10]. It is good to find a near-optimal solution to the workflow scheduling problem with a meta-heuristic algorithm.

Many meta-heuristic optimization algorithms have been used to solve workflow problems in cloud computing. Genetic Algorithm (GA) is used in workflow scheduling to minimize the makespan [11]. GA algorithm is robust and generates a high-quality search in polynomial time but takes a bit more time to find the solution. Pandey et al. [12] used Particle Swarm Optimization (PSO) to schedule workflow applications in a cloud computing environment. PSO is a fast optimization algorithm but has a problem such as earlier convergence and trapping in local optimal solution [13]. Grey Wolf Optimization (GWO) is the recent proposed meta-heuristic algorithm that mimics grey wolves' leadership hierarchy [14]. Khalil and Babamir [15] offered the extended version of Grey Wolf Optimizer for solving the workflow problem. GWO reduces the

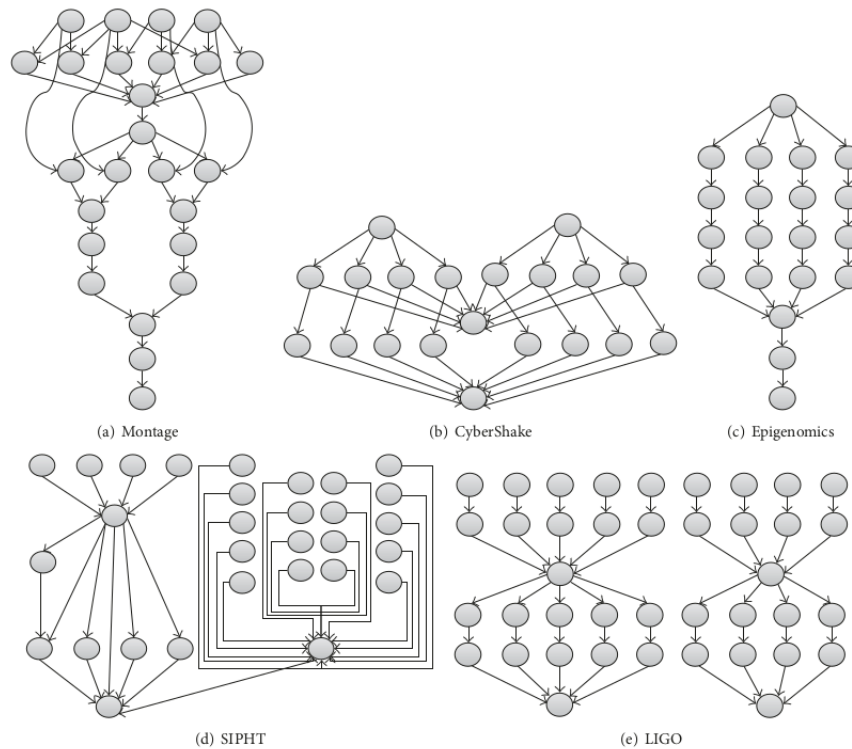


Fig. 2. Structures of Real-World Scientific Workflows [8].

probability of being trapped in the local optimal solution. By combining two or more algorithms considering their strengths, one can overcome the aforementioned issues of algorithms. In this paper, we proposed a hybrid algorithm combining Particle Swarm Optimization (PSO) and Grey Wolf Optimize (GWO), named HPSOGWO. The HPSOGWO is tested on the scientific workflow like montage, cybershake, inspiral, and siphT to optimize total execution cost and time. In the next section, we review some of the scheduling algorithms used in cloud computing.

## II. RELATED WORK

Workflow is more popular among the scientists in which a complex scientific process is modeled into small tasks [16]. These tasks can be executed on parallel and distributed computing like cloud computing. Workflow scheduling is a well-known NP-hard problem in cloud computing. Several list based heuristics have been proposed for task scheduling to optimize the performance of cloud computing like first come first serve (FCFS), round-robin (RR), shortest job first (SJF), minimum completion time (MCT), etc. The basic idea of list-based heuristics is to assign a priority to each task and allot to the available resources as per given preferences. The Heterogeneous Earliest Finish Time (HEFT) was designed for heterogeneous multiprocessor systems. Dubey et al. [17] proposed a modified version of HEFT, capable of reducing the makespan time compared to existing HEFT and Critical Path on a Processor (CPOP).

In the Min-Min algorithm, the minimum execution time task is mapped to the machine with minimum completion time [18]. A similar algorithm is Max-Min algorithm where

in the task with maximum execution time is assigned to the machine, which takes minimum completion time. The Min-Min and Max-Min are offline scheduling that work in batch mode, which means the tasks are not allocated to the resources as they enter [19]. Suffering from starvation is the drawback with Min-Min and Max-Min algorithms [20]. Besides, they consider only the time as a resource quality. The list-based heuristics concentrate only on the user perspectives; they are less focused on the resource quality parameters.

These aforementioned conventional heuristics algorithms are simple, easy to implement, and fast, but for further improvement in the quality of solution and to achieve the optimum results for complex problems like workflow scheduling, the meta-heuristic approaches can find the near-optimal solution [21]. In addition, the heuristic algorithms are problem-dependent techniques, whereas the meta-heuristic methods are problem-independent techniques. The meta-heuristic algorithms have been widely used due to its simplicity and strong searching power in less time and cost. Many of the meta-heuristics approaches were proposed for solving the workflow problem. Some of the standard algorithms are the Genetic Algorithm (GA), Ant Colony Optimization (ACO), Particle Swarm Optimization (PSO).

Dasgupta et al. [1] proposed a genetic-based algorithm used for task scheduling problem. The experiment results show better performance in terms of makespan when compared with First Come First Serve (FCFS), Round Robin (RR), and a local search algorithm Stochastic Hill Climbing (SHC). The GA algorithm was reported to be a time-consuming algorithm for reaching the optimum solutions [22].

Tawfeek et al. [23] used the Ant Colony Optimization (ACO) approach for task scheduling to minimize the makespan and found that ACO performed better than FCFS and RR. However, ACO is a very complex algorithm and takes a long time to get optimal results [24]. The dependency of tasks is not been considered.

Particle swarm optimization (PSO) is one of the popular meta-heuristic algorithms. It is simple to implement and has fast convergences. Despite its advantages, it gets trapped in local optimum for the complex problems[25].

Meta-heuristic algorithms are characterized by exploitation and exploration abilities [26]. Exploitation means that the algorithm is very successful in performing local searches. Exploring means that the algorithm is useful to find out the initial solution, which may be near to the global optimum. A good meta-heuristic algorithm balances the exploration and exploitation abilities. Particle Swarm Optimisation has high exploration ability but is low in exploitation ability. The grey wolf optimizer is proposed by Mirjalili et al. [14] and has a right balance between exploration and exploitation abilities.

A single meta-heuristic might not get the optimal solution and may stuck into the local optimal solution for complex problems like scientific workflow scheduling. It is a better approach to combine one or more meta-heuristic algorithms based on their best characteristics. In the last few decades, hybrid algorithms have become popular. Here, we discuss only those existing algorithms which are either hybrid with PSO or GWO. Manasrah and Ali [8] proposed a hybridization of the Genetic Algorithm and Particle Swarm Optimization (GA-PSO) algorithm. The hybrid GA-PSO algorithm reduces the total execution time compared with GA, PSO, and other algorithms. Another hybrid algorithm has been reported in [27], which was the hybrid version of the PSO and gravitation search algorithm (GSA). This hybrid algorithm performs well compared with some non-heuristics, PSO, and GSA algorithms in terms of cost. The hybridization of the Grey Wolf Optimization (GWO) and Genetic Algorithm (GA) was proposed by Bouzary and Frank [28] and they found that the proposed algorithm was superior than GWO and genetic algorithm (GA) cost wise. Khurana and Singh [29] have introduced a hybrid of flower pollination algorithm and GWO to reduce the cost and time and give efficient results compared to flower pollination with genetic algorithm.

Despite the advantages of the aforementioned hybrid algorithms, one might ask the motivation behind the proposed algorithm. The answer lies in the free lunch theorem [30]. The free lunch theorem specifies that the single algorithm is not fit for solving all the optimization problems. It might perform better for a particular optimization problem, but it may not perform well for the other optimization problems. There is no universal solution to optimization problems.

### III. BACKGROUND

In this section, we discuss the standard PSO and GWO algorithm used in the designing the proposed algorithm. The fitness function used in the proposed algorithm is also explained in this section.

#### A. Fitness Function

The fitness function described the targeted objectives to be optimized using the proposed scheduling algorithm [31]. There are two approaches to make a fitness function multi-objective: priori and posteriori [32]. In the priori approach, each involved objective is assigned a weight, as per their importance, to make a single-valued function, also known as fitness value. Whereas, the set of non-dominant solutions is found in the posteriori approach. Here, we follow the priori approach to design the fitness function. The fitness function is the composition of total execution cost (TEC) and total execution time (TET). Mathematically, the considered fitness function can be represented using the equation 1.

$$f(TET, TEC) = \alpha_1 \times TET + \alpha_2 \times TEC \quad (1)$$

where  $TET$  and  $TEC$  are the total execution time (makespan) and total execution cost respectively.  $\alpha_1$  and  $\alpha_2$  are the weight assigned for each objectives. Here, we consider similar weight to  $\alpha_1$  and  $\alpha_2$  that is 0.5. The complete description of total execution time (makespan) and total execution cost is explained in the following sub-sections:-

1) *Total execution time (makespan)*: The total execution time (makespan) is the maximum completion time taken by tasks in the workflow. In other words, makespan is the time required for finishing all the tasks allotted to different virtual machines [25]. Mathematically, the makespan of the workflow can be derived using equation 2.

$$TET_W = \max\{CT_i \mid i = 1, 2, \dots, m\} \quad (2)$$

where  $CT_i$  is the completion time of the task  $T_i$  in the workflow. The completion time is the total execution time of the tasks. In case tasks are dependent, then the waiting time of predecessor tasks is also considered. The completion time  $CT_i$  is depicted in equation 3.

$$CT_i = \begin{cases} ET_i & \text{iff } \text{pred}(T_i) = \emptyset \\ WK_i + ET_i & \text{iff } \text{pred}(T_i) \neq \emptyset \end{cases} \quad (3)$$

The waiting time of task  $T_i$  is the maximum completion time of all the predecessor tasks of workflow as shown in equation 4.

$$WK_i = \begin{cases} 0 & \text{iff } \text{pred}(T_i) = \emptyset \\ \max(CT_i) & \text{iff } \text{pred}(T_i) \neq \emptyset \end{cases} \quad (4)$$

$$ET_{i,j} = \frac{SZ_{Task}}{Num(PE_j) \times PE_{Unit}} \quad (5)$$

The execution time of the task  $T_i$  on virtual machine  $VM_j$  is calculated using equation 5, where  $SZ_{Task}$  is the size of task  $T_i$  in million instruction (MI),  $Num(PE_j)$  is the number of core assigned to the virtual machine  $VM_j$ ,  $PE_{Unit}$  is the size of each core in MIPS.

2) *Total execution cost*: The cost is a prominent objective to be optimized as cloud computing follows a pay-as-you-go billing scheme [33]. Major of the cloud service providers charges for some specific time interval based on the cloud services used. Cost in cloud computing involves execution cost, communication cost, and storage cost. The total execution cost of VM is the cost charged of VM per unit interval and the execution time of tasks on that VM. Mathematically, the total execution cost (TEC) of workflow  $W$  is shown in equation 6 [34].

$$TEC_W = \sum_{i \in W, i=1}^k \frac{ET_{i,j}}{\tau} \times CO_j : j \in VM_j \quad (6)$$

where  $CO_j$  is the cost of type- $i$  VM instance for a unit time in the cloud data center.  $\tau$  is the time period for which the resources are used by the user.  $ET_{i,j}$  is the execution time of task  $T_i$  by type- $j$  VM instance .

### B. Particle Swarm Algorithm

Kennelly and Eberhat proposed the Particle Swarm Optimization (PSO) technique in 1995 [35]. It is a meta-heuristic technique based on the social behavior of the swarm of birds or particles. Each particle represents a solution for the problem and searches the optimal solution in the problem space. The particle is characterized by its position and velocity. In every iteration, the position and velocity are updated and moves towards the optimal results. PSO consists of the following stages:-

1) *Evolve gbest and pbest of the Particles*: In Particle Swarm Optimisation, each particle represents a solution and in each generation of particle it produces the global best particle denoted by *gbest* and the personal best particle is denoted by *pbest*. The selection of *pbest* and *gbest* particles are determined by their fitness values.

2) *Update Position and Velocity*: Position and velocity of the particle are influenced by the personal best (*pbest*) and the global best particle (*gbest*).

$$V_i(t+1) = w.V_i(t) + C_1.r_1 * (pbest - x_i(t)) + C_2.r_2 * (gbest - x_i(t)) \quad (7)$$

Equation 7 represents the velocity of the  $i^{th}$  particle at the  $t$  iteration. The  $C_1$  and  $C_2$  are coefficient and  $w$  is the inertia weight. The initial values of the coefficient are given in Table II.  $r_1$  and  $r_2$  are the random numbers between 0 and 1.

$$x_i(t+1) = x_i(t) + V_i(t) \quad (8)$$

The position  $x$  of the  $i^{th}$  particle for  $t^{th}$  iteration is updated as the equation 8.

### C. Grey Wolf Algorithm

Mirjalili et al. [14] proposed Grey Wolf Optimization (GWO) technique which mimics the hunting behaviour and leadership hierarchy of grey wolf. According to the mathematical model of the GWO, there are four types of wolves that are alpha ( $\alpha$ ), beta ( $\beta$ ), delta ( $\delta$ ) and omega ( $\Omega$ ). Each

wolf represents a solution. The alpha wolf represents the best solution. The second best solution and the third best solutions are represented by beta and delta wolves respectively and all the other rest solutions are known as omega wolf. GWO algorithm is composed of steps shown in Sections III-C1, III-C2, and III-C3.

1) *Encircling prey*: The grey wolf encircle prey during the process and this can be mathematically modelled using the equations 9 and 10.

$$D = |C.X_p(t) - X(t)| \quad (9)$$

$$X(t+1) = X_p(t) - A.D \quad (10)$$

The position of the wolf is updated using equations 9 and 10 for the current iteration  $t$ , where  $X_p$  is the position of prey and  $X$  is the position of wolf.  $A$  and  $C$  are the coefficient vectors and calculated using equations 11 and 12 respectively.

$$A = 2a.r_1 - a \quad (11)$$

$$C = 2.r_2 \quad (12)$$

The values in the random numbers  $r_1$  and  $r_2$  in equations 11 and 12 are in the range from 0 to 1 and the value of variable  $a$  is linearly decrease from 2 to 0 and is calculated using equation 16

2) *Hunting*: The alpha wolf (best solution) guides the hunting process in GWO. Equations 13, 14 and 15 are used to update the position of the best search agents.

$$\begin{aligned} D_\alpha &= |C_1.X_\alpha - X(t)| \\ D_\beta &= |C_2.X_\beta - X(t)| \\ D_\delta &= |C_3.X_\delta - X(t)| \end{aligned} \quad (13)$$

$$\begin{aligned} X_1 &= X_\alpha - A_1.D_\alpha \\ X_2 &= X_\beta - A_2.D_\beta \\ X_3 &= X_\delta - A_3.D_\delta \end{aligned} \quad (14)$$

$$X(t+1) = \frac{(X_1 + X_2 + X_3)}{3} \quad (15)$$

In equation 14,  $X(t)$  is the position vector of grey wolf.  $X_1$ ,  $X_2$ , and  $X_3$  are position vectors of alpha, beta and delta wolves respectively.

3) *Attacking Prey*: The grey wolf attacks the prey until it stops moving. Mathematically, we decrease the value of  $a$  in each iteration. The controlling parameter  $a$  is defined in equation 16, where  $t$  is current iteration and  $N$  is the maximum number of iteration.

$$a = 2 \times \left(1 - \frac{t}{N}\right) \quad (16)$$



|    |    |    |    |    |    |    |    |
|----|----|----|----|----|----|----|----|
| T1 | T2 | T3 | T4 | T5 | T6 | T7 | T8 |
| 1  | 5  | 4  | 5  | 3  | 2  | 3  | 4  |

Solution 1

|    |    |    |    |    |    |    |    |
|----|----|----|----|----|----|----|----|
| T1 | T2 | T3 | T4 | T5 | T6 | T7 | T8 |
| 2  | 5  | 2  | 5  | 4  | 1  | 3  | 2  |

Solution 2

Fig. 3. Encoded Solution in Scheduling Problem.

#### IV. PROPOSED ALGORITHM

The complete description of the proposed algorithm is given in this section. The proposed algorithm, named HP-SOGWO, is the combination of Particle Swarm Optimization and Grey Wolf Optimization. The basic idea of the HPSOGWO algorithm is to run the PSO algorithm for the first half of the total iterations and the best solution generated by the PSO (*gbest*) is initialized to the alpha wolf ( $\alpha$ -wolf) and for the latter half of the total iterations run GWO algorithm. The best solution generated by the GWO is stored in alpha wolf and considered to be the best mapping of tasks and VMs. The complete algorithm is shown in Algorithm 1 and the major steps are shown in Fig. 5. The initial or range of the various parameters along with the explanation used in the proposed algorithm is shown in Table II.

##### A. Encoding the Scheduling Problem

The first step in applying the algorithm is to model the workflow scheduling problem. As discussed earlier, the scheduling problem is considered as a mapping between the user's tasks and virtual machines. The solution (particle and wolf) in the proposed algorithm can be represented using an array (or list). The array's index represents the tasks, and the value in the array represents the assigned VM. The similar encoding is used in [36] and it helps in the reduction of the complexity of the algorithm.

An example of the encoding of the solution is shown in Fig. 3. The array index represents the eight tasks (T1 to T8), and the value at each index represents a virtual machine or instance id. For Solution 1, the tasks T1 is allocated to VM1, T6 is assigned to VM2, T5 and T7 are assigned to VM3, T3 and T8 are allocated to VM4, and T2 and T4 are allocated to VM5. Similar is the case with Solution 2. This encoding does not deal with the precedence constraint of the workflow. For example, the tasks T1, T3, and T8 are assigned to VM2 which does not mean that T1 is executed first. In other words, it does not depicts the precedence among the tasks.

##### B. Initialize the Population

The HPSOGWO algorithm has a specific number of iterations; in our case, 500. The set of the solutions (particles) is known as the population. In the first iteration, the population is initialized with a random solution. The solution is improved with each iteration of the algorithm. A random initialization of population is illustrated in Fig. 4.

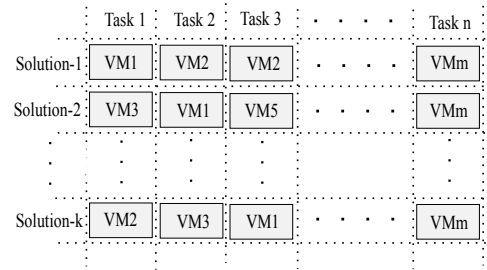


Fig. 4. Initializing the Population.

##### C. Evaluation of the Fitness Function

The algorithm begins with the calculation of execution time and assign these values into the execution time matrix as shown in equation 17. Each element value represent the execution time, for example  $ET_{1,1}$  is the execution time of task  $T_1$  on  $VM_1$ . The value of execution time in the matrix is calculated using equation 5.

$$ET - Mtx = \begin{matrix} & VM_1 & VM_2 & \dots & VM_m \\ \begin{matrix} T_1 \\ T_2 \\ \vdots \\ T_n \end{matrix} & \begin{pmatrix} ET_{1,1} & ET_{1,2} & \dots & ET_{1,m} \\ ET_{2,1} & ET_{2,2} & \dots & ET_{2,m} \\ \vdots & \vdots & \ddots & \vdots \\ ET_{n,1} & ET_{n,2} & \dots & ET_{n,m} \end{pmatrix} \end{matrix} \quad (17)$$

The dependency of the tasks in a workflow can be represented using task dependency matrix (TD-Mtx) as shown in equation 18. Each element in the matrix is either 1 or 0. Suppose the value of  $d_{1,2}$  is 1, then task  $T_2$  is executed after task  $T_1$ .

$$TD - Mtx = \begin{matrix} & T_1 & T_2 & \dots & T_n \\ \begin{matrix} T_1 \\ T_2 \\ \vdots \\ T_n \end{matrix} & \begin{pmatrix} d_{1,1} & d_{1,2} & \dots & d_{1,n} \\ d_{2,1} & d_{2,2} & \dots & d_{2,n} \\ \vdots & \vdots & \ddots & \vdots \\ d_{n,1} & d_{n,2} & \dots & d_{n,n} \end{pmatrix} \end{matrix} \quad (18)$$

The cost matrix stores the cost of execution for a unit time of each VM as depicted in equation 19.  $C_1, C_2, \dots, C_m$  are the unit execution costs of virtual machines  $VM_1, VM_2, \dots, VM_m$  respectively.

$$Cost - Mtx = (C_1 \quad C_2 \quad \dots \quad C_m) \quad (19)$$

According to these matrices, we evaluate total execution time and total execution cost and the fitness function of each solution as mentioned in Section III-A.

##### D. Applying PSO Algorithm

The PSO algorithm starts with random population, and run for  $n/2$  iterations, where  $n$  is the maximum iterations. PSO keeps track of the personal best (*pbest*) position and global best (*gbest*) position of the particle in each iteration. The updated position of the particles is influenced by *gbest* and *pbest* particle in each iteration to reach to the global best solution (*gbest*). The complete process is mentioned in Section III-B.

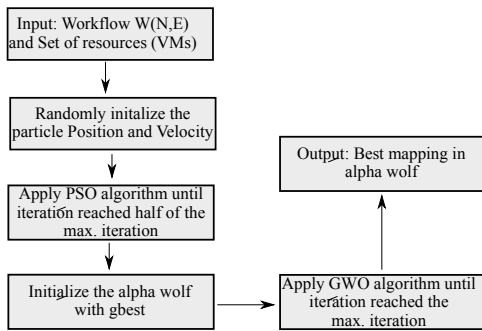


Fig. 5. Major Steps of the Proposed Algorithm.

### E. Applying GWO Algorithm

The best solution ( $\alpha$ -wolf) of GWO algorithm is initialized with the best solution ( $gbest$ ) obtained from the PSO algorithm. Then, we apply GWO algorithm for latter half of the iterations ( $n/2 + 1$  to  $n$ ) as mentioned in Section III-C. The  $\alpha$ -wolf leads all other wolves to the better solution in every iteration of GWO algorithm. After meeting the stopping criteria, the optimal solution is present in  $\alpha$ -wolf. And the tasks are assigned to the respective VM as suggested by the  $\alpha$ -wolf.

---

#### Algorithm 1 The Proposed Algorithm.

---

- 1: **Input:** Workflows  $W(N, E)$  and set of resources ( $VM_1, VM_2, \dots, VM_j$ )
  - 2: **Output:** Best solution in alpha wolf. (mapping of tasks in  $W$  with set of resources.)
  - 3: Set the number of particles equal to the total number of tasks.
  - 4: Randomly initialize the position and velocity of each particle.
  - 5: Calculate the fitness value of each particle according to equation 1.
  - 6: If the fitness value of the current particle is better than  $pbest$  particle, set the current particle as new  $pbest$ .
  - 7: After Steps 5 and 6 for all the particles, select the global best solution as  $gbest$ , among the  $pbest$  particle.
  - 8: For all particles, calculate velocity and update position as per equations 7 and 8.
  - 9: Repeat from the Step 5 until the iteration is reached to the half of maximum iterations.
  - 10: Set the number of wolves equal to the size of tasks.
  - 11: Initialize alpha wolf position as  $gbest$  and randomly initialize the other wolves position.
  - 12: Initialize  $A$ ,  $C$ , and  $a$  as per equations 11, 12, and 16, respectively.
  - 13: Calculate the fitness value of each wolf according to equation 1.
  - 14: Calculate alpha wolf, beta wolf and delta wolf according to fitness value.
  - 15: For all wolves, update position as per equations 15, 14, and 9.
  - 16: Update  $a$ ,  $A$  and  $C$ .
  - 17: Calculate the fitness value of all wolves.
  - 18: Repeat from the Step 14, until maximum iterations are reached.
- 

TABLE I. SIMULATION PARAMETERS

| Parameters          | Values      |
|---------------------|-------------|
| Number of tasks     | 25 to 1000  |
| Number of VMs       | 5           |
| MIPS                | 1000        |
| RAM                 | 512 MB      |
| Bandwidth           | 1000        |
| Number of Processor | 1           |
| VM Policy           | Time Shared |

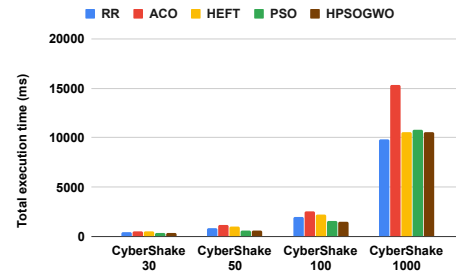


Fig. 6. Total Execution Time of Algorithms under CyberShake Workflow.

## V. PERFORMANCE EVALUATION

### A. Experimental Setup

The proposed algorithm (HPSOGWO) is executed under four scenarios to evaluate the total execution time and cost of the fitness function. The HPSOGWO algorithm is compared with the round-robin (RR) [37], ant colony optimization (ACO) [38], heterogeneous earliest time first (HEFT) [39], and particle swarm optimization (PSO) [12] algorithms. The four scenarios includes CyberShake, Montage, Inspiral, and Spith scientific workflows. These workflows are available with different tasks; for example, CyberShake is available with 30, 50, 100, and 1000 tasks. All experiment are carried out on a computer with Intel(R) Core i5-5200U CPU at 2.2.GHz, 4.00 GB of RAM, Windows 8 Pro 64-bit operating system. To simulate and evaluate the proposed algorithm's performance, we used the WorkflowSim-1.1 toolkit [40], which is an extension of CloudSim. Table I shows the simulation parameters used during the evaluation of the algorithm and Table II shows the initial values or the range of the values of different parameters used in the proposed algorithm.

### B. Simulation Results

In this section, we do the performance comparison of the proposed algorithm, HPSOGWO, with the RR, ACO, HEFT, and PSO algorithms. The performance is measured in terms of total execution time (TET) and total execution cost (TEC) with the increasing number of tasks in the ranges from 25 to 1000 under four well known workflows: CyberShake, Inspiral, Montage, and Spith. The maximum number of iterations were set to 500. Each scenario is executed 10 times and the average value of the result is considered. The simulation results are tabulated in Tables III, IV, and V.

1) *Performance evaluation under CyberShake workflow:*  
Fig. 6 shows the simulation results of the RR, ACO, HEFT,

TABLE II. PROPOSED ALGORITHM PARAMETERS.

| Parameters               | Values/Range | Explanation                                                                                                                         |
|--------------------------|--------------|-------------------------------------------------------------------------------------------------------------------------------------|
| Number of iterations     | 500          | The total number of runs of the algorithm.                                                                                          |
| <i>For PSO algorithm</i> |              |                                                                                                                                     |
| Particle Size            | 25           | The number of particles, each particle represent a solution.                                                                        |
| $C_1, C_2$               | 2            | They are the acceleration coefficients.                                                                                             |
| $w$                      | 0.1          | It is inertia weight.                                                                                                               |
| <i>For GWO algorithm</i> |              |                                                                                                                                     |
| Wolf Size                | 25           | The number of wolves, each wolf represent a solution.                                                                               |
| $a$                      | [2,0]        | It is descended from 2 to 0 during the algorithm iteration.                                                                         |
| $A$                      | $[-a, a]$    | Initially set to 0. It is used to model the convergence.<br>If $A > 1$ wolves diverge from prey if $A < 1$ wolves converge to prey. |
| $C$                      | [0,2]        | Initially set to 0. It is used to avoid falling into local optima.                                                                  |
| $D$                      | Any value    | It is mathematical model of surrounding the prey.                                                                                   |
| $r_1, r_2$               | [0,1]        | They are coefficients. The values are random in the range from 0 to 1.                                                              |

TABLE III. TOTAL EXECUTION TIME OF DIFFERENT SCENARIOS.

| Scenario        | RR        | ACO        | HEFT      | PSO       | HPSOGWO  |
|-----------------|-----------|------------|-----------|-----------|----------|
| CyberShake 30   | 441.72    | 545.845    | 519.05    | 344.457   | 336.62   |
| CyberShake 50   | 855.95    | 1150.6397  | 981.85    | 604.514   | 640.29   |
| CyberShake 100  | 1941.49   | 2570.846   | 2205.28   | 1547.124  | 1480.97  |
| CyberShake 1000 | 9842.98   | 15325.3909 | 10547.13  | 10765.049 | 10544.57 |
| Inspiral 30     | 2177.64   | 2110.17    | 3981.31   | 2119.124  | 1930.611 |
| Inspiral 50     | 3319.31   | 3718.62    | 3704.54   | 3123.322  | 2898.33  |
| Inspiral 100    | 4779.51   | 7327.449   | 6196.76   | 4957.428  | 4725.432 |
| Inspiral 1000   | 49640.257 | 60878.5568 | 54398.38  | 47443.998 | 47451.18 |
| Sipht 30        | 4413.64   | 5206.29    | 5534.87   | 4431.95   | 4454.72  |
| Sipht 60        | 8072.78   | 8942.873   | 10344.51  | 5943.129  | 5234.02  |
| Sipht 100       | 10184.85  | 10518.799  | 15417.59  | 7653.846  | 6502.37  |
| Sipht 1000      | 111822.22 | 119781.024 | 130992.15 | 89440.127 | 92791.18 |
| Montage 25      | 57.13     | 66.266     | 56.88     | 67.854    | 61.861   |
| Montage 50      | 132.23    | 139.977    | 130.35    | 135.604   | 137.631  |
| Montage 100     | 259.83    | 276.801    | 257.72    | 273.306   | 267.8    |
| Montage 1000    | 2559.28   | 2637.382   | 2559.35   | 2611.48   | 2635.56  |

TABLE IV. TOTAL EXECUTION COST OF DIFFERENT SCENARIOS.

| Scenario        | RR         | ACO         | HEFT      | PSO        | HPSOGWO    |
|-----------------|------------|-------------|-----------|------------|------------|
| CyberShake 30   | 1803.04    | 1497.941    | 1817.27   | 917.385    | 897.406    |
| CyberShake 50   | 3909.69    | 5053.1127   | 4180.39   | 2350.999   | 2218.277   |
| CyberShake 100  | 9172.47    | 11691.154   | 10498.68  | 6527.428   | 6461.2     |
| CyberShake 1000 | 48110.56   | 74273.85    | 51642.27  | 52036.77   | 50878.41   |
| Inspiral 30     | 9007.73    | 8984.759    | 15072.03  | 7029.795   | 7035.689   |
| Inspiral 50     | 14638.34   | 15092.29    | 15302.33  | 12525.773  | 12541.193  |
| Inspiral 100    | 22711.35   | 28375.691   | 24897.88  | 21497.265  | 21969.247  |
| Inspiral 1000   | 240473.418 | 243231.5666 | 266391.93 | 234635.922 | 233197.111 |
| Sipht 30        | 17704.2    | 19575.234   | 11077.42  | 8165.034   | 6727.67    |
| Sipht 60        | 36174.69   | 34359.755   | 30899.12  | 18551.321  | 18483.523  |
| Sipht 100       | 46959.56   | 41439.9     | 60947.59  | 30556.972  | 26477.83   |
| Sipht 1000      | 554868.95  | 585886.796  | 545244.42 | 438761.6   | 455008.262 |
| Montage 25      | 264.65     | 284.834     | 248.92    | 260.19     | 255.212    |
| Montage 50      | 628.34     | 636.823     | 570.58    | 584.654    | 572.457    |
| Montage 100     | 1248.27    | 1304.69     | 1143.3    | 1226.514   | 1192.534   |
| Montage 1000    | 12454.6    | 12605.791   | 11971.62  | 12304.51   | 12252.285  |

TABLE V. FITNESS VALUE OF DIFFERENT SCENARIOS.

| Scenario        | RR        | ACO        | HEFT      | PSO        | HPSOGWO   |
|-----------------|-----------|------------|-----------|------------|-----------|
| CyberShake 30   | 1122.38   | 1497.941   | 1168.16   | 630.926    | 617.01    |
| CyberShake 50   | 2382.82   | 3101.88    | 2581.12   | 1477.76    | 1429.282  |
| CyberShake 100  | 5556.98   | 7131       | 6351.98   | 4037.272   | 3971.086  |
| CyberShake 1000 | 28976.77  | 44799.6217 | 31094.7   | 31400.91   | 30711.49  |
| Inspiral 30     | 5592.685  | 5547.46    | 9526.67   | 4574.458   | 4483.157  |
| Inspiral 50     | 8978.825  | 9405.455   | 9503.44   | 7824.548   | 7719.768  |
| Inspiral 100    | 13745.43  | 17851.57   | 15547.32  | 13227.347  | 13347.343 |
| Inspiral 1000   | 145056.84 | 152055.06  | 160395.15 | 141039.96  | 140324.15 |
| Sipht 30        | 11058.92  | 12390.765  | 8306.14   | 6298.491   | 5591.192  |
| Sipht 60        | 22123.73  | 21651.315  | 20621.81  | 12247.225  | 11858.77  |
| Sipht 100       | 28572.2   | 25979.348  | 38182.59  | 19105.409  | 16490.1   |
| Sipht 1000      | 333345.59 | 352833.91  | 338118.29 | 264100.864 | 273899.72 |
| Montage 25      | 160.89    | 175.55     | 152.9     | 164.03     | 158.54    |
| Montage 50      | 380.285   | 388.4      | 350.47    | 360.132    | 355.044   |
| Montage 100     | 754.05    | 790.75     | 700.51    | 749.91     | 730.169   |
| Montage 1000    | 7506.94   | 7621.5865  | 7265.48   | 7457.99    | 7443.923  |

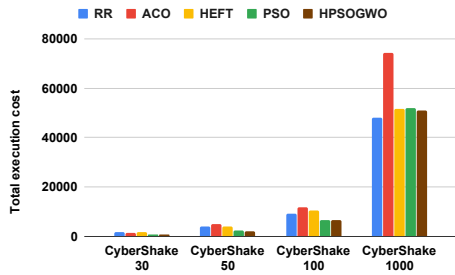


Fig. 7. Total Execution Cost of Algorithms under CyberShake Workflow.

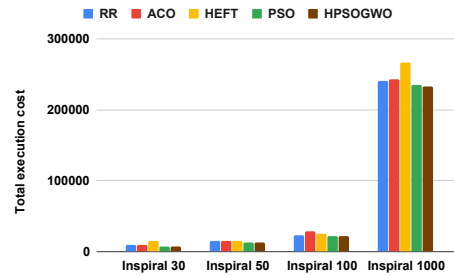


Fig. 9. Total Execution Cost of Algorithms under Inspiral Workflow.

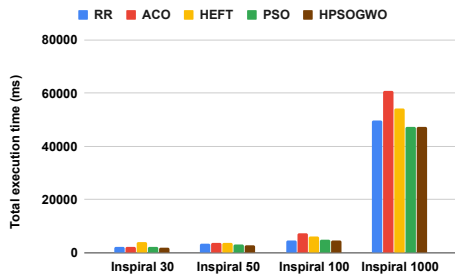


Fig. 8. Total Execution Time of Algorithms under Inspiral Workflow.

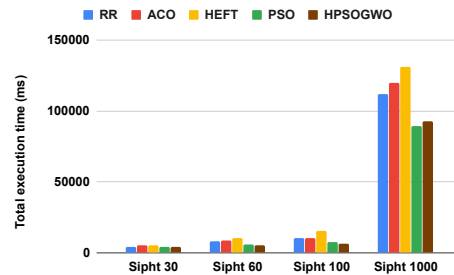


Fig. 10. Total Execution Time of Algorithms under Sipt Workflow.

PSO, and proposed algorithm (HPSOGWO) in term of total execution time (TET). The y-axis represents the total execution time, and the x-axis shows the number of tasks. For 30 tasks, the proposed algorithm decreases the TET by 2.33%, 54.19%, 62.16%, and 31.22% compared to PSO, HEFT, ACO, and RR, respectively. For 50 tasks, the proposed algorithm decreases the TET by 53.35%, 79.71%, and 33.68% compared to HEFT, ACO, and RR, respectively, but an increase of 5.59% in TET is noted compared to PSO. When the number of tasks are 100, the HPSOGWO reported 4.47%, 48.91%, 73.59%, 31.09% decrease in TET compared to PSO, HEFT, ACO, and RR, respectively. Similarly, for 1000 tasks, decrements of 2.09%, 0.02%, and 45.34% compared to PSO, HEFT, and ACO, respectively, but increase of 6.65% compared to RR was observed in TET.

Fig. 7 shows the total execution cost (TEC) of different algorithms under the CyberShake workflow with the increasing number of tasks. For 30 tasks, the HPSOGWO noted the decrease of 2.23%, 102.50%, 66.92%, and 100.92% in TEC compared to PSO, HEFT, ACO, and RR, respectively. While the TEC of HPSOGWO is decreased by 5.98%, 88.45%, 127.79%, and 76.25% compared to PSO, HEFT, ACO, and RR, respectively for 50 tasks. For 100 tasks, the TEC is decreased by 1.03%, 62.49%, 80.94%, and 41.96% compared to PSO, HEFT, ACO, and RR, respectively. The HPSOGWO algorithm lowers the TEC by 2.28%, 1.50%, 45.98%, and 5.44% compared to PSO, HEFT, ACO, and RR, respectively for 1000 tasks.

2) *Performance evaluation under Inspiral workflow:* Fig. 8 shows the performance of different algorithms in terms of total execution time with different number of tasks. The proposed algorithm performs well in almost all cases. The TET of the proposed algorithm is improved by 9.76%, 106.22%, 9.30%,

and 12.7% compared to PSO, HEFT, ACO, and RR, respectively, for 30 tasks. Similarly, it is improved by 7.76%, 27.82%, 28.30%, and 14.52% compared to PSO, HEFT, ACO, and RR, respectively, for 50 tasks. When the number of tasks are 100, the TEC improvement of HPSOGWO is 4.91%, 31.14%, 55.06%, and 1.14% compared to PSO, HEFT, ACO, and RR, respectively. The proposed algorithm's TEC is decreased by 14.64%, 28.29%, and 4.61% compared to HEFT, ACO, and RR, respectively for 1000 tasks. However, a slight increase in TET of 0.01% is observed compared to PSO for 1000 tasks.

As depicted in Fig. 9, there is an improvement in the TEC by 114.22%, 27.70%, and 28.03% in the HPSOGWO compared to HEFT, ACO, and RR respectively, while the deterioration of 0.08% in performance is reported compared to PSO, for 30 tasks. When there are 50 tasks, the proposed algorithm's performance is improved by 22.02%, 20.34%, and 16.72% compared to HEFT, ACO, and RR, respectively, while deterioration of 0.12% in performance is observed compared to PSO. For 100 tasks, the TEC of HPSOGWO is declined by 13.33%, 29.16%, and 3.38% compared to HEFT, ACO, and RR, respectively. Also, the performance of HPSOGWO is decreased by 2.15% compared to PSO. For 1000 tasks, the HPSOGWO outperformed compared to other compared algorithms. There is 0.62%, 14.23%, 4.30%, and 3.12% of improvement in TEC compared to PSO, HEFT, ACO, and RR, respectively.

3) *Performance evaluation under Sipt workflow:* Fig. 10 shows the total execution time of different algorithms under sipt workflow with a different number of tasks. The performance of the proposed algorithm for 30 tasks is better than that of HEFT and ACO, but compared to PSO and RR, it decreases a little. For 60 and 100 tasks, HPSOGWO performed well compared to other algorithms. For 1000 tasks, the performance

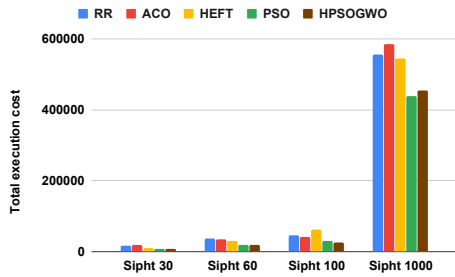


Fig. 11. Total Execution Cost of Algorithms under Sipt Workflow.

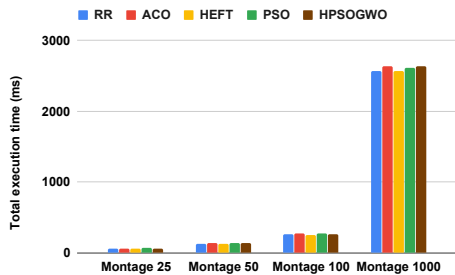


Fig. 12. Total Execution Time of Algorithms under Montage Workflow.

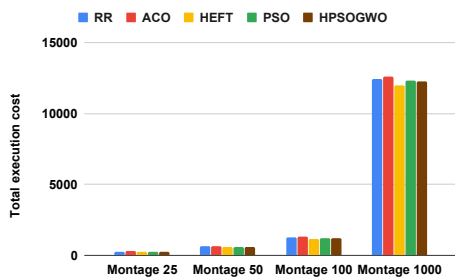


Fig. 13. Total Execution Cost of Algorithms under Montage Workflow.

is better than HEFT, ACO, and RR, but a slight increment of 3.61% in TET is observed compared to PSO.

The comparison among the total execution cost of different algorithms under sipht workflow is shown in Fig. 11. The proposed algorithm outperforms the other algorithms for all the cases with up to 190.97% of decrements in TEC. Except for 1000 tasks, an increment of 3.57% in TEC is observed in the proposed algorithm compared to the PSO algorithm.

4) *Performance evaluation under Montage workflow:* The performance in terms of total execution time and total execution cost with 25, 50, 100, and 1000 tasks under montage workflow are shown in Fig. 12 and Fig. 13 respectively. The proposed algorithm outperforms in all the cases compared to the ACO algorithm, with up to 7.12% reduction in TET. For 25 and 100 tasks, the declines of 9.69% and 2.06% are noticed in total execution time compared to PSO. While for other cases, the proposed algorithm did not perform well. The TEC is reduced for HPSOGWO compared to PSO, ACO, and RR. The HPSOGWO does not perform well compared to HEFT, with up to 4.13% of increment in TEC.

## VI. CONCLUSION

A novel hybrid meta-heuristic algorithm based on a multi-objective model called HPSOGWO is proposed in the present paper. The proposed algorithm is the hybrid version of Particle Swarm Optimisation (PSO) and Grey Wolf Optimisation (GWO) algorithms. The objectives of the proposed algorithm are to optimize the total execution cost and total execution time. The HPSOGWO algorithm is tested on the four scientific workflows: Montage, CyberShake, Inspiral, and Sipt with different number of tasks. The experimental results shows that the proposed algorithm reduces the total execution time and cost compared to PSO, HEFT, ACO, and RR algorithms. In future work, some other parameters like total energy consumption, load balancing, response time, etc. will be considered for the evaluation purpose. The other algorithms can be considered for making the new hybrid algorithm and evaluate under the same parameters.

## REFERENCES

- [1] K. Dasgupta, B. Mandal, P. Dutta, and S. Dam, "A Genetic Algorithm (GA) based Load Balancing Strategy for Cloud Computing," *Procedia Technology*, vol. 10, pp. 340–347, jan 2013. [Online]. Available: <https://www.sciencedirect.com/science/article/pii/S2212017313005318>
- [2] A. Mazrekaj, I. Shabani, and B. Sejdiu, "Pricing Schemes in Cloud Computing: An Overview," *International Journal of Advanced Computer Science and Applications*, vol. 7, no. 2, pp. 80–86, 2016.
- [3] G. Natesan and A. Chokkalingam, "Multi-Objective Task Scheduling Using Hybrid Whale Genetic Optimization Algorithm in Heterogeneous Computing Environment," *Wireless Personal Communications*, 2019.
- [4] R. Ferreira da Silva, H. Casanova, A. C. Orgerie, R. Tanaka, E. Deelman, and F. Suter, "Characterizing, Modeling, and Accurately Simulating Power and Energy Consumption of I/O-intensive Scientific Workflows," *Journal of Computational Science*, vol. 44, 2020.
- [5] G. Juve and E. Deelman, "Scientific Workflows in the Cloud," *Grids, Clouds and Virtualization*, pp. 71–91, 2011.
- [6] E. Deelman, G. Singh, M. H. Su, J. Blythe, Y. Gil, C. Kesselman, G. Mehta, K. Vahi, G. B. Berriman, J. Good, A. Laity, J. C. Jacob, and D. S. Katz, "Pegasus: A framework for mapping complex scientific workflows onto distributed systems," *Scientific Programming*, 2005.
- [7] G. Juve, A. Chervenak, E. Deelman, S. Bharathi, G. Mehta, and K. Vahi, "Characterizing and profiling scientific workflows," *Future Generation Computer Systems*, 2013.
- [8] A. M. Manasrah and H. B. Ali, "Workflow Scheduling Using Hybrid GA-PSO Algorithm in Cloud Computing," *Wireless Communications and Mobile Computing*, vol. 2018, 2018.
- [9] S. Saedi, R. Khorsand, S. Ghandi Bidgoli, and M. Ramezani, "Improved many-objective particle swarm optimization algorithm for scientific workflow scheduling in cloud computing," *Computers and Industrial Engineering*, vol. 147, no. June, p. 106649, 2020. [Online]. Available: <https://doi.org/10.1016/j.cie.2020.106649>
- [10] A. Kamalinia and A. Ghaffari, "Hybrid Task Scheduling Method for Cloud Computing by Genetic and DE Algorithms," *Wireless Personal Communications*, 2017.
- [11] J. Yu and R. Buyya, "A budget constrained scheduling of workflow applications on utility grids using genetic algorithms," *2006 Workshop on Workflows in Support of Large-Scale Science, WORKS '06*, 2006.
- [12] S. Pandey, L. Wu, S. M. Guru, and R. Buyya, "A particle swarm optimization-based heuristic for scheduling workflow applications in cloud computing environments," in *Proceedings - International Conference on Advanced Information Networking and Applications, AINA*, 2010.
- [13] M. Hosseini Shirvani, "A hybrid meta-heuristic algorithm for scientific workflow scheduling in heterogeneous distributed computing systems," *Engineering Applications of Artificial Intelligence*, vol. 90, no. September 2019, p. 103501, 2020. [Online]. Available: <https://doi.org/10.1016/j.engappai.2020.103501>

- [14] S. Mirjalili, S. M. Mirjalili, and A. Lewis, "Grey Wolf Optimizer," *Advances in Engineering Software*, 2014.
- [15] A. Khalili and S. M. Babamir, "Optimal scheduling workflows in cloud computing environment using Pareto-based Grey Wolf Optimizer," *Concurrency Computation*, vol. 29, no. 11, pp. 1–11, 2017.
- [16] L. Zhang, L. Zhou, and A. Salah, "Efficient scientific workflow scheduling for deadline-constrained parallel tasks in cloud computing environments," *Information Sciences*, vol. 531, pp. 31–46, 2020. [Online]. Available: <https://doi.org/10.1016/j.ins.2020.04.039>
- [17] K. Dubey, M. Kumar, and S. C. Sharma, "Modified HEFT Algorithm for Task Scheduling in Cloud Environment," *Procedia Computer Science*, vol. 125, pp. 725–732, 2018.
- [18] G. Patel, R. Mehta, and U. Bhoi, "Enhanced Load Balanced Min-min Algorithm for Static Meta Task Scheduling in Cloud Computing," in *Procedia Computer Science*, 2015.
- [19] R. Vijayalakshmi and V. Vasudevan, "Static batch mode heuristic algorithm for mapping independent tasks in computational grid," 2015.
- [20] M. M. Golchi, S. Saraeian, and M. Heydari, "A hybrid of firefly and improved particle swarm optimization algorithms for load balancing in cloud environments: Performance evaluation," *Computer Networks*, vol. 162, p. 106860, 2019. [Online]. Available: <https://doi.org/10.1016/j.comnet.2019.106860>
- [21] K. L. Eng, A. Muhammed, M. A. Mohamed, and S. Hasan, "A hybrid heuristic of Variable Neighbourhood Descent and Great Deluge algorithm for efficient task scheduling in Grid computing," *European Journal of Operational Research*, 2019.
- [22] Y. Ge and G. Wei, "GA-based task scheduler for the cloud computing systems," *Proceedings - 2010 International Conference on Web Information Systems and Mining, WISM 2010*, vol. 2, pp. 181–186, 2010.
- [23] M. Tawfeek, A. El-Sisi, A. Keshk, and F. Torkey, "Cloud task scheduling based on ant colony optimization," *International Arab Journal of Information Technology*, vol. 12, no. 2, pp. 129–137, 2015.
- [24] T. Deepa and D. Cheelu, "A Comparative Study of Static and Dynamic Computing," *2017 International Conference on Energy, Communication, Data Analytics and Soft Computing (ICECDS)*, pp. 3375–3378, 2017.
- [25] F. Ebadifard and S. M. Babamir, "A PSO-based task scheduling algorithm improved using a load-balancing technique for the cloud computing environment," *Concurrency Computation*, vol. 30, no. 12, pp. 1–16, 2018.
- [26] T. D. Braun, H. J. Siegel, N. Beck, L. L. Bölöni, M. Maheswaran, A. I. Reuther, J. P. Robertson, M. D. Theys, and B. Yao, "A Comparison of Eleven Static Heuristics for Mapping a Class of Independent Tasks onto Heterogeneous Distributed Computing Systems," *Journal of Parallel and Distributed Computing*, vol. 61, no. 4, pp. 810–837, 2001.
- [27] S. Mirzayi and V. Rafe, "A hybrid heuristic workflow scheduling algorithm for cloud computing environments," *Journal of Experimental and Theoretical Artificial Intelligence*, 2015.
- [28] H. Bouzary and F. Frank Chen, "A hybrid grey wolf optimizer algorithm with evolutionary operators for optimal QoS-aware service composition and optimal selection in cloud manufacturing," *International Journal of Advanced Manufacturing Technology*, 2019.
- [29] S. Khurana and R. Singh, "Workflow scheduling and reliability improvement by hybrid intelligence optimization approach with task ranking," *ICST Transactions on Scalable Information Systems*, 2018.
- [30] D. H. Wolpert and W. G. Macready, "No free lunch theorems for optimization," *IEEE Transactions on Evolutionary Computation*, vol. 1, no. 1, pp. 67–82, 1997.
- [31] F. Wu, Q. Wu, and Y. Tan, "Workflow scheduling in cloud: a survey," *Journal of Supercomputing*, 2015.
- [32] S. Mirjalili, S. Saremi, and S. Mohammad, "Multi-objective grey wolf optimizer : A novel algorithm for multi-criterion optimization," *Expert Systems With Applications*, vol. 47, pp. 106–119, 2016. [Online]. Available: <http://dx.doi.org/10.1016/j.eswa.2015.10.039>
- [33] A. Pasdar, Y. C. Lee, and K. Almi'ani, "Hybrid scheduling for scientific workflows on hybrid clouds," *Computer Networks*, vol. 181, no. August, p. 107438, 2020. [Online]. Available: <https://doi.org/10.1016/j.comnet.2020.107438>
- [34] M. Adhikari, T. Amgoth, and S. N. Srirama, "A survey on scheduling strategies for workflows in cloud environment and emerging trends," *ACM Computing Surveys*, vol. 52, no. 4, 2019.
- [35] J. Kennedy and R. Eberhart, "Particle Swarm Optimization, Proceedings of IEEE International Conference on Neural Networks Vol. IV: 1942–1948." 1995.
- [36] T. P. Pham and T. Fahringer, "Evolutionary Multi-objective Workflow Scheduling for Volatile Resources in the Cloud," *IEEE Transactions on Cloud Computing*, vol. 7161, no. c, pp. 1–12, 2020.
- [37] T. Ghafarian, B. Javadi, and R. Buyya, "Decentralised workflow scheduling in volunteer computing systems," *International Journal of Parallel, Emergent and Distributed Systems*, vol. 30, no. 5, pp. 343–365, 2015.
- [38] M. Tawfeek, A. El-Sisi, A. Keshk, and F. Torkey, "Cloud task scheduling based on ant colony optimization," *International Arab Journal of Information Technology*, 2015.
- [39] H. Topcuoglu, S. Hariri, and M. Y. Wu, "Performance-effective and low-complexity task scheduling for heterogeneous computing," *IEEE Transactions on Parallel and Distributed Systems*, vol. 13, no. 3, pp. 260–274, 2002.
- [40] W. Chen and E. Deelman, "WorkflowSim: A toolkit for simulating scientific workflows in distributed environments," in *2012 IEEE 8th International Conference on E-Science, e-Science 2012*, 2012.

# Evaluating the Effect of Multiple Filters in Automatic Language Identification without Lexical Knowledge

Guan-Lip Soon<sup>1</sup>

Hardware Building Block (HWBB)  
Motorola Solution (Malaysia) Sdn Bhd  
Penang, Malaysia

Nur-Hana Samsudin<sup>2</sup>

School of Computer Sciences  
Universiti Sains Malaysia,  
Penang, Malaysia

Dennis Lim<sup>3</sup>

PCR Software Architecture Group  
Motorola Solution (Malaysia) Sdn Bhd  
Penang, Malaysia

**Abstract**—The classical language identification architecture would require a collection of languages independent text and speech information for training by the system before it can identify the languages correctly. This paper also address language identification framework however with data has been downsized considerably from general language identification architecture. The system goal is to identify the type of language being spoken to the system based on a series of trained speech with sound file features and without any language text data or lexical knowledge of the spoken language. The system is also expected to be able to be deployed in mobile platform in future. This paper is specifically about measuring the performance optimisation of audio filters on a CNN model integration for the language identification system. There are several metric to gauge the performance identification system for a classification problem. Precision, recall and F1 Scores is presented for the performance evaluation with different combination of filters together with CNN model as the framework of the language identification system. The goal is not to get the best filter for noise, instead to identify the filter that is a good fit to develop language model with environmental noise for a robust language identification system. Our experiments manage to identify the best combination of filters to increase the accuracy of language identification using short speech. This resulting us to modify our pre-processing phase in the overall language identification system.

**Keywords**—Language identification; speech recognition; speech filters; minimal language data; minimal lexical information; optimal performance

## I. INTRODUCTION

Spoken language recognition system is the process of automatically determines the identity of a language spoken by a speech audio signal. The research on speech recognition has been started since 1930s progressing in the fifth generation of speech recognition starting from early 2000s to beyond 2020s [1]. Currently, the fifth generation focuses on key areas of improving recognition reliability, detecting and correcting linguistic irregularities and system robustness in detecting the speech against noise with the extension of machine learning model [1] that aligns to the objective of this paper.

Spoken language recognition is more challenging than text based language recognition because to date there is no single system that can offer a 100% error free recognition [2]. If we are to look at the human auditory perception towards a language, there are two categories identified in Zhao et al. [3]:

- (1) Pre-lexical information where human able to distinguish an unfamiliar language, and
- (2) Lexical semantic knowledge where human able to understand the semantic reasoning behind the words spoken.

A pre-lexical information can be referred to as how words are pronounced in individual terms, also known as phones, which also being applied in both speech recognition and text-to-speech system [4]. There are 6,909 languages in the whole world [5] with 200 to 300 different phones able to represent all available (recorded) languages [6]. We conducted the analysis of this paper with the assumption that all languages which is considered in the language identification system will have overlaps pre-lexical information, such as phones sounds, but at the same time they are unique enough to be distinguished from one language to another with the information from non-overlaps information as well. This idea is also supported by Muthusamy et al. [7] and Zissman [8] where their studies on human test subject confirm that pre-lexical information can be used to classify language. Experiments have also been carried out to ascertain the pre-lexical information able to perform language identification with lower error rate on human test subject [9], [10].

The challenge of this project as a whole is to employ automatic language identification (LID) through acoustic level feature accurately and to identify or classify the languages on an embedded device. The targeted device has also a set of predefined language settings which make the implementation of this idea is fitted into the device criteria. This paper focuses on evaluating the effect of multiple filters in order to find the most optimal filter to be used in the subsequent processes: feature extraction and post-processing towards a robust language identification system.

The acoustic level feature will be extracted through Mel-Frequency Cepstral Coefficient (MFCC) with filter-banks represent the cepstral coefficients across time. The feature will be further transform into frequency domain for better vector representation of each coefficient. The extracted speech feature will be further conditioned through cepstral mean and variance normalization (CMVN) to normalize the extracted phoneme acoustic feature, where background noise is expected. Basic frequency warping is applied to normalize the speech of difference voices that will improve accent and regional intonation differences. The conditioned features will be trained

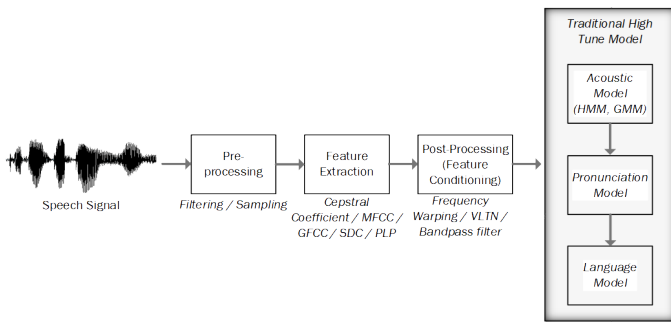


Fig. 1. A Conventional Speech Recognition System Pipeline Described by Schalkwyk [11].

on a Convolution Neural Networks (CNN) to classify the language. The evaluation metric will use standard classification evaluation metric.

Our intention of the implementation is also to break-away from conventional speech recognition system. Around 2014 researchers began using neural network to develop speech recognition system [11]. The conventional building block of speech recognition system comprises of an acoustic model that extrapolate audio speech to phonemes, a pronunciation model that connects the phonemes to form lexical words, and a language model that can be used to express semantically correct sentence [11]. Our motivation of cutting down the conventional layers of speech recognition system with the aid of neural network is to improve latency and processing requirement.

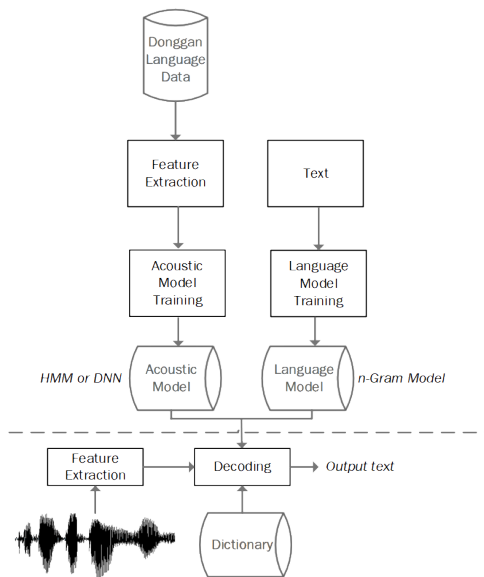


Fig. 2. A Conventional Speech Recognition System by Xu et al. [12].

Fig. 1 showed the traditional speech recognition system comprises of Acoustic Model, Pronunciation Model and Language Model. This is quite similar to Fig. 2 which is a general architecture of speech recognition system for Donggan province's language. This architecture is slightly different than the conventional speech recognition system without Deep Learning Model where it comprises an Acoustic Model and

Language Model that utilizes statistical model of GMM and HMM. Another relatable architecture is shown in Fig. 3 that uses machine learning model classifier through SVM and decision tree.

With the goal to simplify our language identification system, we reduce the implementation footprint based on these related architectures to construct a speech language identification system using neural network variation model.

This paper is organised into five parts. In Section II, we will give some overviews of relevant work in language identification in speech recognition system. This will be followed by Section III where we will highlight some relevant techniques related to the methodology implemented by others to build their language identification system. Section IV describes the proposed solution to carry out based on the literature, system architecture review and assessment techniques based on relevant works presented. To determine the applicability and performance of the different filters suggested, Section V will first show a complete pipeline of our language identification. Section VI finally shows the effect of filters to the performance of our language identification system by discussing how the evaluation are being carried out and followed by the effect of the different filters for preliminary language identification. We end our paper in Section VII with the improvement in affect of this study towards the modification on the filters combination towards a better language identification system.

## II. BACKGROUND STUDIES ON LANGUAGE IDENTIFICATION FRAMEWORK

This section will give an overview of relevant work in language identification in speech recognition system.

Duong and Duong [13] described acoustic audio technique to extract audio feature for voice pattern design. In this paper, the authors performed statistical model to conduct pattern recognition by using GMM, HMM and non-negative matrix factorization (NMF) on the extracted audio features. The main focus of Duong and Duong [13] as a relevant work was due to the input audio conditioning stage. There were two stages. During the first stage: pre-processing stage, Duong and Duong [13] extracted speech signal relevant frequency and frequency domain representation through Fourier Transform either using FFT, DCT or wavelet transform, all with filter. During the second stage, feature extraction using several relevant techniques like MFCC, Spectral Energy Peak (SEP) and Spectral Band Energy(SBE), Spectral Flatness Measure (SFM) and Spectral Centroid was observed. MFCC was the most preferred choice.

Mori et al. [15]'s paper was on spoken language identification closely related to the proposal of this paper which is a system without lexical knowledge. Their system able to detect six different languages. They were English, French, German, Dutch, Italian and Portuguese. All were from dataset derives from VoxForge. The feature extraction employed the MFCC alone and fed through a list of learning model and a statistical model. From the result of their paper, Neural Network (NN) performs better than Support Vector Machine (SVM) and GMM statistical model. Hence, this paper served as an important lesson for the endeavor of our project and justified that NN is best suited for the application of this project.



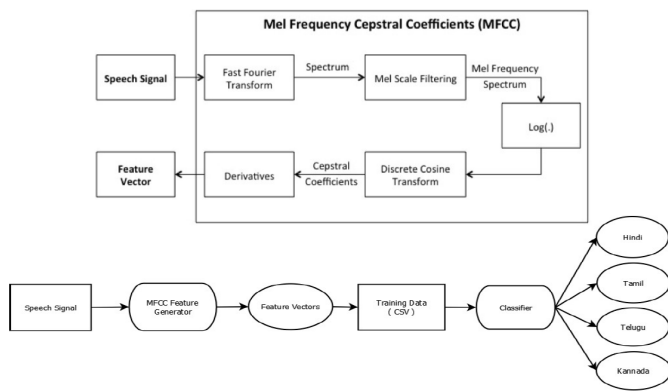


Fig. 3. An Example of Language Identification System Approach in Venkatesan et al. [14]. The Upper Portion show the Process of MFCC Extraction and the Bottom Portion shown how the Training Characterised the Speech Features into their Respective Languages

Vatin [16] worked on a language identification speech recognition system based on GMM. He discussed his effort during pre-conditioning of audio signal by using of filter to remove noise. Signal-to-Noise-Ratio (SNR) was introduced to measure the quality of desired audio signal against noise. In the case of our research, signal to noise ratio will highly dependent on device capability which is not the main objective. Some other technique employs for example Voice Activity Detector (VAD) to remove silence where users have a moment of silence before speech begins were also described in Vatin [16]. Other signal conditioning technique like RASTA filters were described to reduce vocal tract fluctuation from different speaker of the same language. The language identification system logic designed through fusing different GMM models was the focal research of his dissertation which is not the main focus of our research but will be very helpful to those developing non-dependent mobile device for language identification.

Van Segbroeck et al. [17] was an article on spoken language identification. The article is focused on computational cost consideration and recognition time requirement. The article showed the extracted audio feature had an impact on recognition performance. The identification of languages were modeled using GMM statistical model with each combined together as one large general speech models known as Universal Background Model. Van Segbroeck et al. [17] work concluded MFCC as the second fastest feature extraction method compared to FuSS (Fused Speech Stream) features. However, their approach required a very deliberate process where the utterance information would need to be transform into a low dimensional i-vector and then language classification methods will be applied. Should the focus of this research is not specific to the embedded device, FuSS could be a good alternative to explore into.

Aarti and Kopparapu [18] showed a language identification system that able to identify nine different Indian languages: Assamese, Bengali, Gujarati, Hindi, Marathi, Kannada, Malayalam, Tamil and Telugu through the use of Neural Network. A detailed high level diagram showed how the system comprised the process from pre-processing to feature extraction. There were using the common MFCC technique to perform feature

extraction that suggested the language detection is without lexical knowledge on the speech data.

Venkatesan et al. [14] showed a language identification system that able to identify 4 types of Indian language: Tamil, Kannada, Telugu, and Malayalam through the use of Machine learning like Decision Tree and Support Vector Machine (refer to Fig. 3). The result of Accuracy for SVM was around 76% and Decision Tree was around 73% with feature extraction which employed MFCC technique without lexical knowledge on the speech data.

In summary of the relevant works suggested MFCC and neural network may provide a better yielding detection performance of language with quick recognition time.

### III. REVIEW ON METHODOLOGIES USED IN LANGUAGE IDENTIFICATION SYSTEMS

This section highlighted some relevant techniques related to the methodology implemented by others to build their language identification system. This section provide a review on the proposed methods and also highlighting the component's focus for this paper and our future work.

#### A. Pre-Processing

This stage is where the input audio signal will be digitized for processing. The actual implementation of this project will be deployed on STMicroelectronics STM32 Nucleo-64 MCU Development Board NUCLEO-F446RE. In this pre-processing stage, every speech audio that is needed to be trained in the proposed project requires to achieve a certain level of speech quality consistency. The stages in pre-processing stage can be further breakdown on the following:

1) *Sampling rate or sampling frequency*: Sampling rate represent the time domain sample rate of an audio signal. The higher the sampling rates the better the signal representation of a the speech's sinusoid signal. However, it also means the larger the storage space required. The minimum sampling rate is dictated by Nyquist theorem, where a sample signal frequency denoted by  $f_{sample} = 2f_{source}$  which means the frequency of the sample must at least be twice of the signal frequency source [19]. But in speech recognition, quality recognition is a main focus, and there could be restriction of real time deployment for Voice over Internet Protocol (VoIP) where the sampling rate for VoIP usage is usually set to 16 kHz for decent speech quality [1].

2) *Filter*: Speech filter is functioned to extract speech signal by cutting off unnecessary polluting signal that is deemed undesirable such as noise. We can classify filters into four types: Low pass filter, bandpass filter, high pass filter and notch filter. For speech filtering, bandpass filter and low pass filter will be used where human audible range from 20Hz to 20kHz. The ranges of human generated phones can start from 31.5Hz to 16kHz range based on [1].

3) *Hamming Window*: Hamming window is a hypothetical signal frame used to cut or segment a short series of speech signal from the whole signal frame. It also provide to smooth discontinuities in speech signal [15], [1].

4) *Time domain to frequency domain transformation:* Speech signal is mostly represented using the time domain representation. However, in order to capture the most speech features in a speech recording, Discrete Fourier Transform (DFT) is used to represent the same time domain signal into frequency domain [20]. The conversion can be calculated through Fast Fourier Transform (FFT) [1] since FFT known to only consume lower computation resources during processing.

Another method known as Discrete Cosine Transform (DCT) offers an advantage of data compression capacity without capturing the full periodic amplitude of a speech signal. However, it will not be useful in multi-speech audio signal to segment of different speakers. Furthermore DCT compression will also omit non-linearity aspect of speech that usually present in real life [21]. Thus, DFT is able to reproduce the amplitude of the original speech signal. The expression of DCT is given in Vatin [16].

In summary between DFT, FFT, and DCT; DFT will be used during training stage of the dataset to reproduce the best possible representation of frequency domain to truly capture the speech signal as there are plans in future for the ability to detect main speaker's voice from background's speaker speech through amplitude or strength of the speech signal. FFT will be use for embedded device's end after prototype. Our pre-processing implement the stated pre-processing stage.

## B. Feature Extraction

Feature extraction is the process of finding feature representation from the speech audio for language identification. The focus techniques are primarily on acoustic phonemes feature extraction. A few important technique developed is highlighted.

1) *Mel-Frequency Cepstral Coefficients (MFCC):* MFCC is a widely used speech recognition feature extraction method. It exploits auditory principles, where filter banks perform mapping of auditory response [2]. The amount of filter banks reflect the coefficients in terms directly correlate to the power spectral envelop for each frame [16], [18]. In speech recognition system, there will be speaker to speaker variation audio imprinting accuracy feature which must not to be too accurate in feature extraction. Else, it will lead to miss-classification. Another reason it is widely used is due to the fact that speaker dependency can be greatly reduced in speech processing system [14].

MFCC can be referred to as Mel-Frequency Filter Bank (MFFB) without Discrete Fourier Transform (DCT). The use of DCT in learning model is due to highly correlated input data requires décor-relation usually require in machine learning model that does not perform well in highly correlated data. Without DCT only deep learning model able to handle highly correlated data present in the characteristic of speech signal [21].

2) *Perceptual Linear Prediction Coefficients (PLP):* is also based on frequency domain spectral plot. In Hermansky [22], it is introduced as a mean to offer computation efficiency to extract audio feature. It has one disadvantage due to susceptibility towards noise. The cepstral coefficients to reflect the acoustic phonemes are computed out by autoregressive

coefficient unlike MFCC designated by the filter banks set. Based on Van Segbroeck et al. [17], PLP is slower than MFCC.

3) *Gammatone Frequency Cepstral Coefficients (GFCC):* is based on auditory periphery model [23]. It uses Gammatone filterbank to generate a time sequence of Gammatone frequency. The Gammatone cepstral analysis is close to MFCC technique, where GFCC is transform into cepstrum through DCT [24]. GFCC shows greater detail of accuracy for speaker identification compared to MFCC. However, greater detail in accuracy means limitation of performance according to Van Segbroeck et al. [17].

4) *Mean-Hilbert Envelope Coefficients (MHEC):* is an extension of GFCC offers better noise immunity and distortion over MFCC according to Sadjadi and Hansen [25]. The recognition error rate has an average of 1.5% better than MFCC as observed on the result according to Sadjadi and Hansen [25].

5) *Fused Speech Stream (FSS):* FSS is a technique to combined different feature extractions technique to yield better recognition time known as feature fusion through Principle Component Analysis (PCA) according to Van Segbroeck et al. [17]. The feature will be trained on the extracting feature techniques. For fused speech stream, every input speech signal will have to go through the techniques before language model processing. Thus, implementation of this technique has to be carefully considered in computing restrictive environment. It may benefit during model training stage but not during implementation stage of model processing.

MFCC offers the fastest recognition time in terms of processing among the audio feature extraction techniques with descent feature integrity. Also, as explain in Fayek [21], without DCT in MFCC, only deep learning model able to handle highly correlated data using only the characteristic of speech signal.

## C. Post-Processing or Feature Conditioning

Post-processing is an augmentation technique to improve existing feature extraction method against noise, and the variation of speech. Feature conditioning must not be over-applied as it will impact the integrity of the feature that will compromise the accuracy in language identification. This paper will not be covering the post-processing stage. However, it is suffice to highlight CMVN, RASTA and VLTN are applied after feature extraction stage to condition and improve extracted features colluded by noise in our implementation.

## D. Model Stage

The modelling of our language identification system will be based on Convolution Neural Network (CNN) using the feature extracted from MFCC. CNN is chosen because it treats the frequency domain as an array image. CNN offers better discriminating effect on interfering noise if presents in the image array, which is not present in RNN where it is in time-series domain. Another reason CNN is more favourable in speech recognition over Deep Neural Network (DNN) is because DNN input is represented as vector resulting losing structural locality and susceptible in echo interference [26] as compared to CNN.

### E. Noise Cancelling and Noise Filtering Algorithm

Signal conditioning through filtering and noise cancellation are important to provide speech audio quality in an actual environment with actual noise colluded. The best quality on speech signal is always through the use of noise cancellation. Noise cancellation techniques usually require reference noise signal to provide close to silence noise cancellation effect. This type of noise cancellation is sometimes referred as Active Noise Cancellation (ANC) [27]. Thus, hardware implementation will be needing external mic source which can be difficult to implement in a software-only-implementation that are limited on the proposed language identification system.

Thus, Digital Signal Processing (DSP) filter will be used as a means of filtering noise both applies in training stage, testing stage and deployment stage. SNR or signal-to-noise ratio will be used as judging criteria of the filter.

Filtering is another way of noise filtration process with the ability of dampening noise but not total elimination of noise. There are two types of filters: Linear filter and non-linear filters. Linear filters will be used to chop-off and extract out specified band of frequencies to ease the Fourier transformation of the signal in subsequent feature extraction without considering the whole audio spectrum. Linear filters also help in certain none-speech related noise that can be filtered off to improve the human audible signal. However, the linear filters has a limitation in terms of audio signal which can be seen as poor filtering in non-additive noise like impulse noise or "salt and pepper" noise induced by the recording devices (hardware's internal circuitry switching) noise or sampling noise [28], [29]. Therefore, non-linear filters are also used to provide a solution against non-additive noise.

The four standards linear filters are usually used in signal processing based on the following [30], [31]:

- Butterworth Filter offers maximally flat response in passband with slower roll-off frequency during cut-off, can be improved by increasing poles or orders of the filter at the expense of computation power.
- Chebyshev Filter offers sharper roll-off than Butterworth filter at the same poles or orders therefore much efficient in transition band from passband to stopband. The sharpness of roll-off rate is placed second behind the Elliptic filter. One major disadvantage is high ripple response in pass band.
- Bessel/Thompson Filter has the flattest response but with poor roll-off rate compared to Butterworth filter and with slower magnitude response compared to Butterworth filter. It is much suitable for high-bandwidth signal filtering with flat response
- Elliptic Filter has the steepest roll-off at the same poles and orders compared to Chebyshev Filter but with both pass-band and stop-band with large ripples compared to Chebyshev filter

Hence, Butterworth filter will be selected for as the first stage filtering. A 6 poles configurations were chosen due to prevalent chosen number in the industry. The number of poles used dictates the implementation cost for both hardware and computational cost. However, the higher the poles (number)

offers sharper (and thus better) roll-off response to the target cut-off frequency.

Median filter works by replacing the median value of the neighbouring signal. The filtering window size is determined by the number of neighbours. Median filter does not work well with large filter size as it will cause the signal to lose its integrity resulting under-sampling effect in auditory quality which the sound will appear robotic or contain aliasing. A highly noisy signal will not be effective to be filtered by Median filter due to the filter reliance on neighbouring sampling quantized points [29].

Wiener filter is an algorithm gearing towards the ability to reduce noise with a reference noise signal to reconstruct back the signal as good as possible. It is possible to employ a randomized reference noise signal with designated power level in miliwatt region for example 0.2mW is good against impulse for non-additive noise especially in single channel microphone approach. Wiener Filter works by sensing noise present and estimate the amount of reference noise added to feedback to the system and reduce it. This approach is limited to non-additive noise and thus it is not a very efficient noise reduction algorithm.

## IV. PROPOSED SOLUTION

This section describes the proposed solution carried out based on the literature, system architecture review and assessment techniques and results based on relevant works presented. The focus of our study is to find a solution for a language identification system via speech interface with the best and direct approach and minimal language dependent lexical information so that it is feasible to be applied in an embedded device. As a start, we proposed the flow as shown in Fig. 4 which has a single pipeline model.

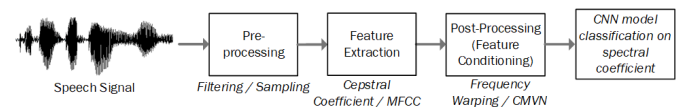


Fig. 4. The Initial Proposed Language Identification System.

The proposed language identification system architecture in Fig. 4 served as a guide towards a complete language identification system. In this paper, we are going to conduct exploratory analysis on the best possible pre-processing stage, specifically in filtering the speech signal in order to achieve the best performance system. The exploratory data analysis and evaluation is actually involved in all stages: pre-processing stage, feature extraction and post-processing stage to serve the same purpose.

Our pre-processing analysis consists of evaluating different filtering techniques. The combination of filters are to be tested by alternating and combining a selected filter or a series of filters which include: pre-emphasis signal conditioning, Butterworth High Pass Filter, Butterworth Band Pass Filter, Median Filter, Wiener Filter and three stage filters (combination of three filters: Butterworth, Median and Wiener filters). There are 10 permutations all together.

The following are the steps for our pre-processing stage:

- 1) Speech signal is framed at 25ms size..
- 2) The spectrogram representative in 10ms stride is prepared for the next phase (feature extraction).
- 3) nFFT=512, Full used would be 22050 where nFFT=552 for full spectrum based on Sampling Time/FilterBanks [32].
- 4) Filter Bank is set at 40. Too low of a filter banks will not capture the phoneme features from speech signal.
- 5) Apply permutation filters based on below:
  - a) Pre-emphasis conditioning
  - b) Butterworth Bandpass 275Hz to 7kHz
  - c) Median Filter
  - d) Wiener Filter

In short, the audio signal is captured in 3GP format as default codec. Then, it will be reconverted to MP3 before feeding to the feature extraction module in the standard PC. The feature extraction will further convert in raw *FLAC* format to perform further processing. It is suffice to highlight that the 3GP format is a standard issue of the device input where direct conversion to *FLAC* file is not recommended due to limited capacity of the device. The *FLAC* format was chosen over wave file format due to it size's capacity as well as lossless audio quality. Comparing *.wav* superior lossless quality and the concerns of memory size, *.flac* file was chosen due to its compressed lossless feature [33].

The different sets of filters are introduced due to their different filtering behaviour. Pre-emphasis filter is functioned to increase the frequency magnitude (within a frequency band) the magnitude of some (usually higher) frequencies with respect to the magnitude of other (usually lower) frequencies in order to improve the overall speech signal. Butterworth bandpass and highpass filter response with cut-off audible low frequency noise from 1Hz to 275Hz, and 7kHz and beyond to prevent down-modulated high frequency components. The Median filter is for removing sampling noises and white noise effectively, while Wiener offers noise reduction that can be used to remove or dampened noise in audible human speech range.

## V. IMPLEMENTATION

In order to show the effect of filters to the performance of our language identification system, a complete pipeline is needed. The following describes the process how the implementation is carried out.

This project is a classification problem in identifying the type of language based on the 'file name assigned' with the extracted cepstral coefficient that correlates the phoneme features of the specific spoken language in *FLAC* file format.

Although the focus is to minimise the lexical data, some information are required to classify the trained data to the correct language group. Thus, a proper naming convention and some info is required for all training and validation files.  $(language)_{(gender)}_{(recording\_ID)}_{(index)}$   $[(transformation)(index)]$  *.flac* is the representative wave file name.

The attributes comprise gender type and speaker ID. Each mp3 files is around 45 minutes long that can be broken into 10 seconds instances with differences in spoken speed, pitch

and noise, with 29 files each for German, English and Spanish. The cepstral feature will be varied in speed from 0.8 to 1.2 ratio with 1 as normal speed and pitch level varied from -200 to 200 ratio. The variation on the mp3 audio files will cater for different speeds and pitch level spoken by a variety of users.

The conditioning of the audio files starts by introducing noise files converted into *FLAC* format, normalize with a standard 16 bit and sampling rate mono before 10 second splits applies to all training files and test file as shown in Fig. 5. The original mp3 files, normalized files before split, and converted *FLAC* files before normalizations are removed to conserve space of the machine. The script will be carried out as task behind the task manager alleviating in speed up the CPU processes in the background. This phase still CPU intensive since no GPU intervention can be used when extracting and preparing the audio files.

Test File Conditioning

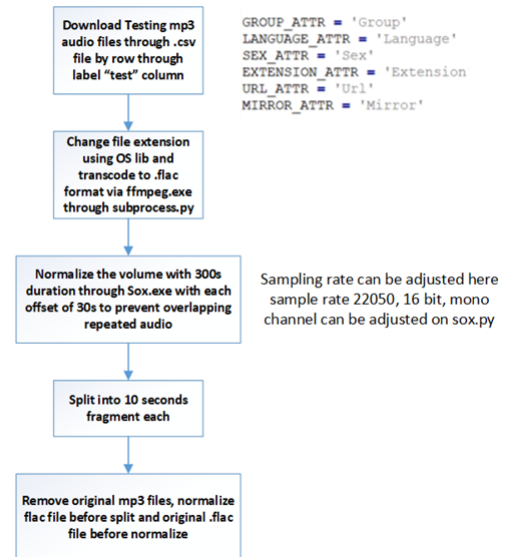


Fig. 5. The Steps for the Test Files Segmentation in every 10 Seconds Range

The expected outcome of this project is an application level prototype, with the embedded device user interface able to change its interfacing languages by speaking to the device. The expectation of the classifier performance for the initial prototype will be based on learning based related works as a benchmark [15] with an accuracy performance of 91% classifying between German and Italian using Neural Network alone, while [18] classifying 9 different Indian languages with accuracy performance around at most 44% with deep neural network (DNN).

The two prior work show a trend with a single model approach multi-class classification with large sets of language may impact overall performance. The maximum languages for the expected prototype will support four languages and minimum two languages to meet a highly accurate performance: >80%.

For this paper's implementation there are three languages for the filter evaluation model: German, English and Spanish. The methodology used for this project will focus primarily on

the optimization of pre-processing filters to improve the overall classification abilities of the deep learning model

## VI. EVALUATION AND RESULTS

For fundamental evaluation on speech recognition system, it can be evaluated based on accuracy on the amount of accurately classified language. But, to reveal more of a system performance, miss detection and false alarms can be used [34].

F1 metric is also a widely used metric for evaluating classification or decision making system [34]. More frequently use metric, like precision, computes the fraction of correctly labeled positive samples on the input and recall, is the fraction of correctly labeled samples among the positive samples [34]. In this paper, we will evaluate the accuracy of our language identification system by evaluating the performance using different version of filtering (and some combination) before the language identification process by this metric.

$$F_1 = \frac{2TP}{FN+FP+2TP} \text{ or } F_1 = \frac{2 \times \text{precision} \times \text{recall}}{\text{precision} + \text{recall}}$$

$$\text{Recall} = \frac{TP}{TP+FN}$$

$$\text{Precision} = \frac{TP}{TP+FP}$$

This research look for the performance of different filters permutations. The following section will be based on German, English and Spanish dataset as a fixed constant with different filters permutation. The dataset will be based on 67,860 entries with 5,220 validation entries, and 540 test entries. These are the representation of 180 test set for each language.

### A. Validation Set Performance

Using 5,220 validation entries, different filters permutation are implemented to observe the best model performance of default topology. The best feature extraction line up will be selected for further model optimization. Table I showed the precision, recall and F1 score from individual language in validation set.

There are 10 different permutation of filters' configuration applied in this observation as shown in Table I. No filter refers to the default filtering. Pre-emphasis refers to pre-emphasis for input frequency range most susceptible to noise. Butterworth refers to Butterworth Bandpass 275Hz (and lower) to 7kHz (and higher) to filter. Median and Wiener both are referring to Median filter and Wiener filter respectively. Median filter can remove sampling noise and white noise effectively while Wiener filter offers noise reduction that can be used to remove or dampened noise in audible human speech range. Default Wiener size is 3 but the observation is also carried out with different size with the assumption the algorithm can learn better fir on slightly broader spectrogram bandwidth visibility. The filters that is coming after that is a combination of a few filters mentioned above. 3 stage filters is referring to a combination of three mentioned filters: Butterworth filter, Median filter and Wiener filter size 5.

The different in size is necessary because when we combined Median filter and Wiener noise cancellation filter, the filter size of these two methods must not be the same because the filter magnitude is used to dampened the noise and thus compromising the auditory quality. To prevent such situation,

size 5 is selected for Wiener filter and size 3 is used for Median filter. The odd number sizing is used due to the Median filter averaging effect. The filter size on each averaging operation of the Median filter will degrade in terms of quantization and sampling rate of the quality of the signal to dampen off noise. Hence, filter size of Median filter is a cost trade off between signal quality and noise reduction. Thus, the higher the filter size, the lower the audio signal quality. This resulting Median filter size 5 cannot be used. Thus, Median filter of size 3 is still being used but for the Wiener filter, a higher filter size will need to be used to attain significant noise dampening effect after the Median filter is applied. Size 5 is minimal size used for Wiener because filter increment must be an odd number for convolutioning noise effect on the spectrogram.

The code of languages acronym are as follows: de is Deutsche or German Language, en is English (mix) and sp is Spanish.

TABLE I. PRECISION, RECALL AND F1 SCORE ON THE VALIDATION SET.

| Feature Permutation          | Validation Set = 5,220 entries |     |     |        |     |     |          |     |     |
|------------------------------|--------------------------------|-----|-----|--------|-----|-----|----------|-----|-----|
|                              | Precision                      |     |     | Recall |     |     | F1 Score |     |     |
|                              | de                             | en  | sp  | de     | en  | sp  | de       | en  | sp  |
| No filter                    | .94                            | .98 | .92 | .95    | .9  | .99 | .94      | .94 | .95 |
| Pre-emphasis                 | .96                            | .96 | .93 | .95    | .94 | .96 | .95      | .95 | .94 |
| Butterworth                  | .95                            | .97 | .94 | .95    | .94 | .97 | .95      | .95 | .95 |
| Median                       | .96                            | .94 | .95 | .94    | .96 | .94 | .95      | .95 | .94 |
| Wiener size 5                | .96                            | .97 | .94 | .96    | .94 | .97 | .96      | .96 | .95 |
| Wiener size 3                | .94                            | .96 | .94 | .96    | .93 | .96 | .95      | .95 | .95 |
| Butterworth + Median         | .95                            | .97 | .94 | .95    | .95 | .96 | .95      | .96 | .95 |
| Butterworth + Wiener 5       | .96                            | .97 | .93 | .95    | .94 | .97 | .95      | .95 | .95 |
| Butterworth + Wiener default | .94                            | .96 | .95 | .95    | .95 | .96 | .95      | .95 | .95 |
| 3 stage filters              | .96                            | .98 | .95 | .95    | .97 | .97 | .96      | .98 | .96 |

In summary, we can conclude the standard metric results on validation set to be as shown in Table II. Number of iteration column is referring to the value obtain after a routine check for recognizing overfitting or underfitting of data. Although the longer a network (in this case CNN) is trained, the better it performs on the training set, at some point, the network fits too well to the training data and loses its capability to generalize [35].

TABLE II. SUMMARY OF STANDARD METRIC RESULTS ON VALIDATION SET

| Feature of Permutation       | Standard Metric |                 |                    |                         |
|------------------------------|-----------------|-----------------|--------------------|-------------------------|
|                              | Accuracy        | No of Iteration | Average Confidence | Average Precision Score |
| No Filter                    | 0.9454          | 20              | 0.9699779          | 0.93                    |
| Pre-emphasis                 | 0.9477          | 14              | 0.959              | 0.92                    |
| Butterworth                  | 0.9498          | 24              | 0.9627879          | 0.96                    |
| Median                       | 0.947893        | 14              | 0.95913273         | 0.9                     |
| Wiener size 5                | 0.954           | 24              | 0.96213144         | 0.93                    |
| Wiener size 3                | 0.949234        | 22              | 0.95767            | 0.95                    |
| Butterworth + Median         | 0.9544          | 14              | 0.9646244          | 0.94                    |
| Butterworth + Wiener 5       | 0.95287         | 20              | 0.961755           | 0.97                    |
| Butterworth + Wiener default | 0.9521          | 19              | 0.96329778         | 0.96329778              |
| 3 stage filters              | 0.962835        | 23              | 0.97275305         | 0.98                    |

TABLE III. STATISTICAL HYPOTHESES GUIDELINES TO READ THE BINARIZED CONFUSION MATRIX. THE GRAYED AREA IS THE VALUES LISTED IN TABLE IV FOR DIFFERENT FILTERS AND LANGUAGES.

| Reality  | Study Finding  |                |
|----------|----------------|----------------|
|          | Negative       | Positive       |
| Negative | True Negative  | False Positive |
| Positive | False Negative | True Positive  |

B. Test Set Performance

This section will provide the evaluation obtained from test set for the three languages. Table IV shows the binarized confusion matrix for each language. To aid in reading the binarized confusion matrix table in Table IV, Table III will be the guide for reading Table IV. The language acronyms are similar to the validation set. In totally, each language will have 180 speech recordings test of the evaluated language and 360 other recordings belonging to the other two languages.

Table V shows the comparison of different filters confusion matrix on 540 entries test set. These are extracted from language specific binarized confusion matrix as shown in Table IV. From the confusion matrix, 3 stage filters yield the best performance. Individually, Deutsche entries classified with 7 false negatives with 0 false positives. English entries have 1 false negative and 4 false positives. Spanish entries have 4 false positives and 0 false negatives. However, Butterworth bandpass filter with Wiener size 5 alone yield better performance in Spanish language entries with 2 false positives and 0 false negatives.

From Table V the best performance on Confusion Matrix is still three stage filtering system comprises Butterworth Bandpass filter starting from 275Hz to 7 kHz, Median Filter and Wiener Filter. Among 180 test entries for German Language, there are four entries classified as English and three entries classified as Spanish. As for English, among 180 test entries, 1 is classified as Spanish. Spanish is perfectly classified for the 180 test entries.

The binarized confusion matrix in Table IV and the combinational confusion matrix in Table V can be summarised as Table VI. It shows the best performance is the three stage filters combination for each language for precision, recall and F1 score on the test set. However, Median filter performs worst in test set where the precision is less than 0.9 for English and recall is less than 0.9 for Deutsche.

VII. CONCLUSION

From the evaluation in the previous section, we have shown the best performance for filtering is the three stage filters combination where for each language’s precision, recall and F1 score on the test, the precision, recall and F1 score are consistently good as compared to other filters or combination filters. Thus, based on this evaluation, the three stage filters produces a better language identification system.

Based on our results, a minor modification on our pre-processing stage can improve the overall language identification accuracy. Thus, Fig. 4 is best to be modified into Fig. 6.

Based on the modified pre-processing, the research can further proceed into the next stages: feature extraction, post-processing towards the completion of the CNN model. In

TABLE IV. BINARIZED CONFUSION MATRIX ON INDIVIDUAL LANGUAGE TEST SET

|                                     |        |       |
|-------------------------------------|--------|-------|
| de                                  | en     | sp    |
| 360 0                               | 344 16 | 354 6 |
| 17 163                              | 4 174  | 1 179 |
| No filter                           |        |       |
| de                                  | en     | sp    |
| 359 1                               | 340 20 | 356 4 |
| 22 158                              | 3 177  | 0 180 |
| Default pre-emphasis                |        |       |
| de                                  | en     | sp    |
| 358 2                               | 353 7  | 357 3 |
| 8 172                               | 3 177  | 1 179 |
| Butterworth bandpass filter         |        |       |
| de                                  | en     | sp    |
| 355 5                               | 336 24 | 357 3 |
| 26 154                              | 2 178  | 4 176 |
| Median filter                       |        |       |
| de                                  | en     | sp    |
| 357 3                               | 350 10 | 357 3 |
| 10 170                              | 3 177  | 3 177 |
| Wiener filter size 3                |        |       |
| de                                  | en     | sp    |
| 357 3                               | 343 17 | 357 3 |
| 18 162                              | 2 178  | 3 177 |
| Wiener filter size 5                |        |       |
| de                                  | en     | sp    |
| 356 4                               | 346 14 | 357 3 |
| 14 166                              | 6 174  | 1 179 |
| Butterworth + Median filter         |        |       |
| de                                  | en     | sp    |
| 359 1                               | 350 10 | 357 3 |
| 9 171                               | 4 176  | 1 179 |
| Butterworth + Wiener default filter |        |       |
| de                                  | en     | sp    |
| 360 0                               | 353 7  | 358 2 |
| 8 172                               | 1 179  | 0 180 |
| Butterworth + Wiener filter size 5  |        |       |
| de                                  | en     | sp    |
| 360 0                               | 356 4  | 356 4 |
| 7 173                               | 1 179  | 0 180 |
| 3 stage filters                     |        |       |

TABLE V. COMPARISON OF DIFFERENT FILTERS FOR COMBINATIONAL CONFUSION MATRIX ON 540 ENTRIES TEST SET FROM THE BINARIZED CONFUSION MATRIX FOR INDIVIDUAL LANGUAGES.

|                              |     |     |     |
|------------------------------|-----|-----|-----|
|                              | de  | en  | sp  |
| de                           | 163 | 15  | 2   |
| en                           | 0   | 176 | 4   |
| sp                           | 0   | 1   | 179 |
| No filter                    |     |     |     |
|                              | de  | en  | sp  |
| de                           | 172 | 7   | 1   |
| en                           | 1   | 177 | 2   |
| sp                           | 1   | 0   | 179 |
| Butterworth                  |     |     |     |
|                              | de  | en  | sp  |
| de                           | 162 | 17  | 1   |
| en                           | 0   | 178 | 2   |
| sp                           | 3   | 0   | 177 |
| Wiener size 5                |     |     |     |
|                              | de  | en  | sp  |
| de                           | 166 | 13  | 1   |
| en                           | 4   | 174 | 2   |
| sp                           | 0   | 1   | 179 |
| Butterworth + Median         |     |     |     |
|                              | de  | en  | sp  |
| de                           | 172 | 7   | 1   |
| en                           | 0   | 179 | 1   |
| sp                           | 0   | 0   | 180 |
| Butterworth + Wiener 5       |     |     |     |
|                              | de  | en  | sp  |
| de                           | 158 | 20  | 2   |
| en                           | 1   | 177 | 2   |
| sp                           | 0   | 0   | 180 |
| Pre-emphasis                 |     |     |     |
|                              | de  | en  | sp  |
| de                           | 154 | 24  | 2   |
| en                           | 1   | 178 | 1   |
| sp                           | 4   | 0   | 176 |
| Median                       |     |     |     |
|                              | de  | en  | sp  |
| de                           | 170 | 9   | 1   |
| en                           | 1   | 177 | 2   |
| sp                           | 2   | 1   | 177 |
| Wiener default               |     |     |     |
|                              | de  | en  | sp  |
| de                           | 171 | 9   | 0   |
| en                           | 1   | 176 | 3   |
| sp                           | 0   | 1   | 179 |
| Butterworth + Wiener default |     |     |     |
|                              | de  | en  | sp  |
| de                           | 173 | 4   | 3   |
| en                           | 0   | 179 | 1   |
| sp                           | 0   | 0   | 180 |
| 3 Stage Filters              |     |     |     |

feature extraction, the fastest recognition time in terms of processing among the audio feature extraction techniques with descent feature integrity is looked for. Post-processing will complement the extracted features to improve existing signal feature extraction method against noise, and the variation of

TABLE VI. PRECISION, RECALL AND F1 SCORE FOR TEST SET AFTER EXTRACTING FROM CONFUSION MATRIX.

| Feature Permutations   | Test Set = 540 entries |     |     |        |     |     |          |     |     |
|------------------------|------------------------|-----|-----|--------|-----|-----|----------|-----|-----|
|                        | Precision              |     |     | Recall |     |     | F1 Score |     |     |
|                        | de                     | en  | sp  | de     | en  | sp  | de       | en  | sp  |
| No filter              | 1                      | .92 | .97 | .91    | .98 | .99 | .95      | .95 | .98 |
| Pre-emphasis           | .99                    | .9  | .98 | .88    | .98 | 1   | .93      | .94 | .99 |
| Butterworth            | .99                    | .96 | .98 | .96    | .98 | .99 | .97      | .97 | .97 |
| Median                 | .97                    | .88 | .98 | .86    | .99 | .98 | .91      | .93 | .98 |
| Wiener (size 5)        | .98                    | .91 | .98 | .9     | .99 | .98 | .94      | .95 | .98 |
| Wiener (default)       | .98                    | .95 | .98 | .94    | .95 | .98 | .96      | .96 | .98 |
| Butterworth + Median   | .98                    | .93 | .98 | .92    | .97 | .99 | .95      | .95 | .99 |
| Butterworth + Wiener 5 | 1                      | .96 | .99 | .96    | .99 | 1   | .98      | .98 | .99 |
| Butterworth + Wiener 3 | .99                    | .95 | .98 | .95    | .98 | .99 | .97      | .96 | .99 |
| 3 stages filters       | 1                      | .98 | .98 | .96    | .99 | 1   | .98      | .99 | .99 |

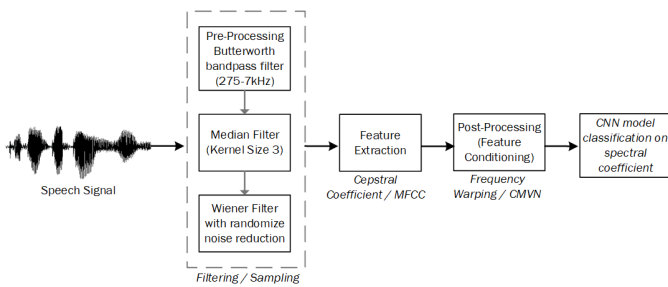


Fig. 6. Overall Modified Filtration within the Whole Architecture.

speech. It is hoped by having all the fined tune process will improve the language identification accuracy for a system without lexical knowledge.

ACKNOWLEDGMENT

The implementation on the dedicated device are copyrighted of ©2020 Motorola Solutions, Inc. All Rights Reserved. The authors would like to thank the insight of all experts - DSP techniques: Ondy Sukma, system level integration: Pang W. K, Sim Yew Tatt & Ondy Sukma, and Java related platform programming: Tan Chun Mun as well as special embedded level advice: Leong Kim Hong. This paper publication is funded by the Universiti Sains Malaysia's Short term grant no: 304/PKOMP/6315273.

REFERENCES

[1] J. Benesty, M. Sondhi, and Y. Huang, *Springer Handbook of Speech Processing*, ser. Springer Handbook of Speech Processing. Springer Berlin Heidelberg, 2007. [Online]. Available: <https://books.google.com.my/books?id=P-g3DwAAQBAJ>

[2] H. Li, B. Ma, and K. A. Lee, "Spoken language recognition: From fundamentals to practice," *Proceedings of the IEEE*, vol. 101, no. 5, pp. 1136–1159, May 2013.

[3] J. Zhao, H. Shu, L. Zhang, X. Wang, Q. Gong, and P. Li, "Cortical competition during language discrimination," *NeuroImage*, vol. 43, no. 3, pp. 624–633, nov 2008. [Online]. Available: <https://doi.org/10.1016%2Fj.neuroimage.2008.07.025>

[4] D. Jurafsky and J. H. Martin, *Speech and Language Processing: An Introduction to Natural Language Processing, Computational Linguistics, and Speech Recognition*, 1st ed. USA: Prentice Hall PTR, 2000.

[5] M. P. Lewis, *Ethnologue: Languages of the World*, 16th ed. Texas: SIL International.

[6] M. Ashby and J. Maidment, *Introducing Phonetic Science*. Cambridge University Press, mar 2005. [Online]. Available: <https://doi.org/10.1017%2F9780511808852>

[7] Y. K. Muthusamy, E. Barnard, and R. A. Cole, "Reviewing automatic language identification," *IEEE Signal Processing Magazine*, vol. 11, no. 4, pp. 33–41, 1994.

[8] M. Zissman, "Comparison of four approaches to automatic language identification of telephone speech," *IEEE Transactions on Speech and Audio Processing*, vol. 4, no. 1, p. 31, jan 1996. [Online]. Available: <https://doi.org/10.1109%2Ftsa.1996.481450>

[9] Y. K. Muthusamy, N. Jain, and R. A. Cole, "Perceptual benchmarks for automatic language identification," in *Proceedings of ICASSP '94. IEEE International Conference on Acoustics, Speech and Signal Processing*, vol. i, 1994, pp. I/333–I/336 vol.1.

[10] D. Van Leeuwen, M. Boer, and R. Orr, "A human benchmark for the nist language recognition evaluation 2005," January 2008.

[11] J. Schalkwyk, "An All-Neural On-Device Speech Recognizer," Internet, Google AI, 2019, accessed on March 2020. [Online]. Available: <https://ai.googleblog.com/2019/03/an-all-neural-on-device-speech.html>

[12] H. Xu, H. Yang, and Y. You, "Donggan speech recognition based on deep neural network," in *2019 IEEE 8th Joint International Information Technology and Artificial Intelligence Conference (ITAIC)*, 2019, pp. 354–358.

[13] N. Q. K. Duong and H. Duong, "A review of audio features and statistical models exploited for voice pattern design," *CoRR*, vol. abs/1502.06811, 2015. [Online]. Available: <http://arxiv.org/abs/1502.06811>

[14] H. Venkatesan, T. V. Venkatasubramanian, and J. Sangeetha, "Automatic language identification using machine learning techniques," in *2018 3rd International Conference on Communication and Electronics Systems (ICCES)*, 2018, pp. 583–588.

[15] J. D. Mori, M. Faizullah-Khan, C. Holt, and S. Pruisken, "Spoken language classification," 2012. [Online]. Available: <http://citeseerx.ist.psu.edu/viewdoc/download?doi=10.1.1.278.7614&rep=rep1&type=pdf>

[16] C. Vatin, "Automatic spoken language identification," Master's thesis, 2012.

[17] M. Van Segbroeck, R. Travadi, and S. S. Narayanan, "Rapid language identification," *IEEE/ACM Transactions on Audio, Speech, and Language Processing*, vol. 23, no. 7, pp. 1118–1129, 2015.

[18] B. Aarti and S. K. Koppurapu, "Spoken indian language classification using artificial neural network — an experimental study," in *2017 4th International Conference on Signal Processing and Integrated Networks (SPIN)*, 2017, pp. 424–430.

[19] E. Ayanoglu, "Data transmission when the sampling frequency exceeds the nyquist rate," *IEEE Communications Letters*, vol. 1, no. 6, pp. 157–159, 1997.

[20] E. W. Weisstein, *Fourier Transform*, 2020 (accessed July 30, 2020), <http://mathworld.wolfram.com/FourierTransform.html>.

[21] H. Fayek, *Speech Processing for Machine Learning: Filter banks, Mel-Frequency Cepstral Coefficients (MFCCs) and What's In-Between*, April 2016, <https://haythamfayek.com/2016/04/21/speech-processing-for-machine-learning.html>.

[22] H. Hermansky, "Perceptual linear predictive (PLP) analysis of speech," *The Journal of the Acoustical Society of America*, vol. 87, no. 4, pp. 1738–1752, apr 1990. [Online]. Available: <https://doi.org/10.1121%2F1.399423>

[23] R. D. Patterson, I. Nimmo-Smith, J. Holdsworth, and P. Rice, "An efficient auditory filterbank based on the gammatone function," in *IOC Speech Group on Auditory Modelling at RSRE*, vol. 2, no. 7, 1987.

[24] Y. Shao, S. Srinivasan, and D. Wang, "Incorporating auditory feature uncertainties in robust speaker identification," in *2007 IEEE International Conference on Acoustics, Speech and Signal Processing - ICASSP '07*, vol. 4, 2007, pp. IV–277–IV–280.

[25] S. O. Sadjadi and J. H. Hansen, "Mean hilbert envelope coefficients (MHEC) for robust speaker and language identification," *Speech Communication*, vol. 72, pp. 138–148, sep 2015. [Online]. Available: <https://doi.org/10.1016%2Fj.specom.2015.04.005>

[26] S. Park, Y. Jeong, and H. S. Kim, "Multiresolution cnn for reverberant speech recognition," in *2017 20th Conference of the Oriental Chapter of the International Coordinating Committee on Speech Databases and Speech I/O Systems and Assessment (O-COCOSDA)*, 2017, pp. 1–4.

[27] Say-Wei Foo, T. N. Senthilkumar, and C. Averty, "Active noise cancellation headset," in *2005 IEEE International Symposium on Circuits and Systems*, 2005, pp. 268–271 Vol. 1.

[28] G. George, R. M. Oommen, S. Shelly, S. S. Philipose, and A. M. Varghese, "A survey on various median filtering techniques for removal

- of impulse noise from digital image,” in *2018 Conference on Emerging Devices and Smart Systems (ICEDSS)*, 2018, pp. 235–238.
- [29] S. Vishaga and S. L. Das, “A survey on switching median filters for impulse noise removal,” in *2015 International Conference on Circuits, Power and Computing Technologies [ICCPCT-2015]*, 2015, pp. 1–6.
- [30] H. Zumbahlen and A. D. Inc., *Linear Circuit Design Handbook*. USA: Newnes, 2008.
- [31] Y. Sun, “ELE314 Linear Systems and Signals - Classic Filters,” Internet, The University of Rhode Island, 2018, accessed on March 2020. [Online]. Available: [https://www.ele.uri.edu/courses/ele314/handouts/YS06\\_Classicfilters.pdf](https://www.ele.uri.edu/courses/ele314/handouts/YS06_Classicfilters.pdf)
- [32] S. Adam, “Plotting & Cleaning - Deep Learning for Audio Classification p.3,” Youtube, 2018, accessed on March 2020. [Online]. Available: <https://youtu.be/mUXkj1BKk0>
- [33] W. Gordon, “What’s the Difference Between All These Audio Formats, and Which One Should I Use?” Liferhacker.com, 2012, accessed on January 2020. [Online]. Available: <https://liferhacker.com/what-s-the-difference-between-all-these-audio-formats-5927052>
- [34] D. Zhu, H. Li, B. Ma, and C. Lee, “Optimizing the performance of spoken language recognition with discriminative training,” *IEEE Transactions on Audio, Speech, and Language Processing*, vol. 16, no. 8, pp. 1642–1653, 2008.
- [35] R. Yamashita, M. Nishio, R. K. G. Do, and K. Togashi, “Convolutional neural networks: an overview and application in radiology,” *Insights into Imaging*, vol. 9, no. 4, pp. 611–629, jun 2018. [Online]. Available: <https://doi.org/10.1007%2Fs13244-018-0639-9>



# Classification of Common and Uncommon Tones by P300 Feature Extraction and Identification of Accurate P300 Wave by Machine Learning Algorithms

Rafia Akhter<sup>1</sup>

Electrical and Computer Engineering  
University of Georgia  
Athens, Georgia, USA

Kehinde Lawal<sup>2</sup>

Electrical and Computer Engineering  
University of Georgia  
Athens, Georgia, USA

Md. Tanvir Rahman<sup>3</sup>

Electrical and Electronic Engineering  
East Delta University  
Chittagong, Bangladesh

Shamim Ahmed Mazumder<sup>4</sup>

Electrical and Electronic Engineering  
Bangladesh University of Engineering Technology  
Dhaka, Bangladesh

**Abstract**—An event-related potential (ERP) is a measure of brain response to a specific sensory, cognitive, or motor event. One common ERP technique used in cognition research is the oddball paradigm where the brain's response to common and uncommon stimuli is compared. The neurologic response to the oddball paradigm produces a P300 ERP which is one of the major visual/auditory sensory ERP components. The purpose of this study to classify ERP responses to common and uncommon tones by extracting the P300 feature from ERP epochs and identify the accurate shape of the P300 wave. For recording ERP data, and OpenBCI system is used. P300 features are extracted using EEGLab which is a mathematical tool of MATLAB. Finally, various types of machine learning models are used for identifying the accurate shape of a P300 wave and then classifying common and uncommon auditory tones. For stimuli classification, all of the algorithms evaluated performed efficiently and built a consistent model with 93.75% to 99.1% evaluation accuracy. Also, for P300 shape detection, NN model showed the best performance with 94.95% accuracy. These findings have the potential to add useful machine learning-based methods to the clinical application of ERPs.

**Keywords**—Event Related Potential (ERP); classification ; P300; machine-learning; oddball-paradigm

## I. INTRODUCTION

Electroencephalography (EEG) is a non-invasive monitoring method that tracks and records the neural activities of the brain. The time-locked activities of EEG are known as Event-Related Potential (ERP) [1]. ERP research has provided significant insights into our understanding of many neurologic functions including cognition, affection, and clinical conditions such as schizophrenia [2]. ERP analysis can help to identify sleep disorders, changes in behavior, diagnose and monitor seizure disorders, and has even been used to evaluate brain activity after a severe head injury or before a heart or liver transplant surgeries [3]. A much-studied ERP component is the P300 that is formed as a component of recognition when

the brain responds to a series of stimuli that include a common (or frequent) stimulus and an uncommon (infrequent) stimulus. The P300 ERP is characterized by a large positive peak occurring at approximately 300 ms-600 ms after stimulus onsets and is found prominently over parietal region [4]. Besides, one of the major applications of ERP technology is based on using the P300 wave to implement a Brain-Computer Interface (BCI) that can incapacitate people by offering various ways of communicating with the external world. For example, P300 has been used to implement communication with devices, using mobile messages, playing games, and many more as described in [5, 6]. In our work, we have used auditory stimuli, which are also suitable for individuals who cannot receive or react to visual stimuli.

In this study, a passive paradigm has been used to stimulate P300. Here, subjects would only concentrate on the target stimuli without responses [7] and have to ignore common stimuli. Two audio stimuli with 1000Hz and 2000 Hz, were designed as the common and uncommon stimuli. The duration for any stimuli was 180 ms and the internal interval between two consecutive tones was 3500 ms (Figure 1). In this study, we will detect the target and non-target ERPs by oddball paradigm and will extract the features of component P300 (P3). For uncommon stimuli, ERP peak higher than common stimuli (Figure 2). The features are power (P), energy (E), mean of the amplitude, wavelength, and the number of events. Using these features we will classify the auditory stimuli by using a machine learning technique.

Classification of common and uncommon tones is an important step for using ERPs in the practical field of cognitive research. The typical signal classification includes filtering, artifact removal, extracting data epochs, and many other steps. All these steps make ERPs suitable for use by machine learning [8,9]. There are various types of machine learning algorithms that have been applied to the classification of ERPs. In our

study, six types of machine learning algorithms have been used for the classification of tones and identifying accurate P300 shape. They are Neural Networks (NNs), k- Nearest Neighbors algorithm (k-NN), Decision Tree algorithm (DT), Random Forest classifier (RF), Logistic Regression (LR), and Support Vector Machines (SVMs). All the models performed efficiently. For tone classification, the performance is between 93.75% and ,99.10% and RF performed with the most efficiency. Also, for “Accurate P300 plot “identification, NN performance is best with 94.95%. Therefore, this paper trains and tests different types of machine learning methods for the classification of common and uncommon tones by extracting the P300 feature from ERP epochs and then identify the accurate shape of the P300 wave.

The paper is organized as follows: In Section 2, there are literature reviews. In Section 3, a brief description of the data set and recording procedure. EEG signals pre-processing are described in Section 4. Machine learning implementation with tone classification and P300 plot identification are described in Sections 5 and 6. In Section 7, the Conclusion and suggested future work are provided.

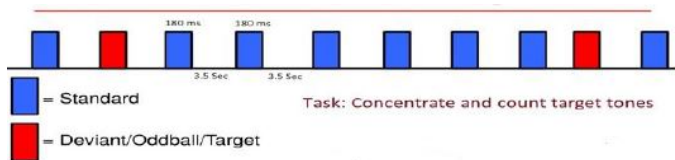


Fig. 1. Two Audio Stimuli Standard (1000Hz) in Blue and Target (2000 Hz) in Red Color. There were 20% Target and 80% Standard Stimuli. The Duration for the Stimuli was 180 ms while the Internal Interval between two Consecutive Tones were 3500 ms.

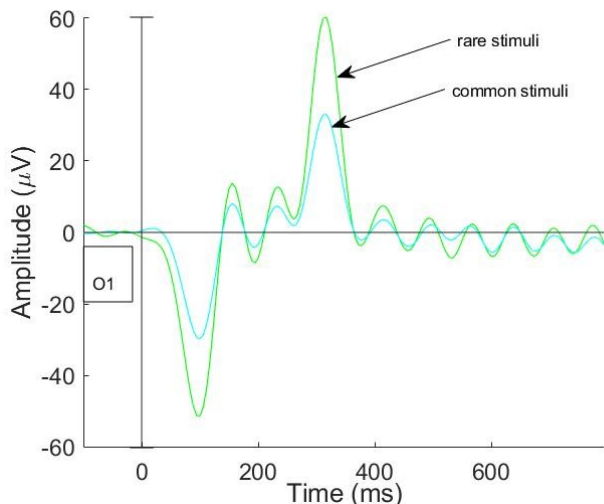


Fig. 2. EPR Plot for Rare (Uncommon) and Common Auditory Stimuli. P300 Peaks around 310 ms for both but Peak Amplitude is higher for Uncommon Stimuli.

## II. LITERATURE REVIEW

In [10], Amin classified EEG signals based on the pattern recognition approach. There they used classifiers such as K-nearest neighbors (KNN), Support Vector Machine (SVM),

Multi-layer Perceptron (MLP), and Naïve Bayes (NB). Outcomes yielded 99.11% accuracy via SVM classifier for coefficient approximations (A5) of low frequencies ranging from 0 to 3.90Hz. Accuracy rates for detailed coefficients were 98.57 and 98.39% for SVM and KNN, respectively; and for detailed coefficients (D5) deriving from the sub-band range (3.90–7.81Hz). Accuracy rates for MLP and NB classifiers were comparable at 97.11–89.63% and 91.60–81.07% for A5 and D5 coefficients, respectively. Besides, the proposed approach was also applied to the public dataset for the classification of two cognitive tasks and achieved comparable classification results, i.e., 93.33% accuracy with KNN.

In [11], Joshi classifies P300 using LSTM and deep learning. There, they proposed a neural network model based on Convolutional Long Short Term Memory (ConvLSTM) for single-trial P300 classification. Their proposed method outperforms previous CNN based approaches on raw EEG signals. The approaches were evaluated on publicly available data-set II of BCI competition III. Another dataset was recorded locally using audio beeps as stimuli to validate these approaches.

In [12], Cecotti presented a method for the detection of P300 waves. This model is based on a Convolutional Neural Network (CNN). The topology of the network is adapted to the detection of P300 waves in the time domain. Seven classifiers based on the CNN have proposed: four single classifiers with different features set and three multi classifiers. These models are tested and compared on the Data set II of the third BCI competition.

In [13], Alomari proposed an automated computer platform to classify Electroencephalography (EEG) signals associated with the left and right-hand movements using a hybrid system that uses advanced feature extraction techniques and machine learning algorithms. The datasets were inputted into two machine-learning algorithms: Neural Networks (NNs) and Support Vector Machines (SVMs). The research showed that the method of feature extraction holds some promise for the classification of various pairs of motor movements, which can be used in a BCI context to mentally control a computer or machine.

## III. METHODOLOGY

### A. Experimental Setup

The data set was collected from 28 subjects (both male and female) in an age group of 18 to 43 years. All participants had no history of neurological or psychiatric conditions and were healthy, with no hearing and visual impairment. The 8-channel EEG signals were recorded according to the international 10-20 system (excluding some electrodes) along the surface of the scalp in the OpenBCI GUI. The Ultracortex Mark IV headset (Fig. 4; Left) was used for recording brain activity. PIC24 microcontroller and macromedia board were used to generate tones. The program was coded in MPLAB X IDE in C language. GPIO pin 1 and 15 were used for detecting deviant and target stimuli. OpenBCI cyton board has 5 digital input-output (IO) pins to read from D11, D12, D13, D17, and D18. We connected D17 and D18 to detect the events from the microcontroller. There was a standard noise-free soundbox to hear the sound. In Fig. 3, the experimental setup for the experiment is shown.

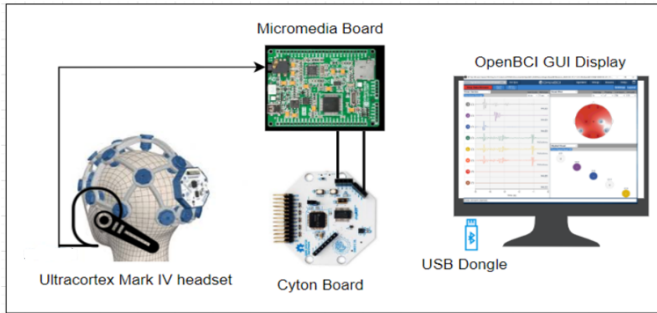


Fig. 3. Experimental Set up for Auditory Oddball Paradigm. Micromedia Board and Cyton Board are Connected for Stimuli Event Detection Automatically. Ultracortex Mark IV Headset is Connected to the OpenBCI GUI by the USB Dongle.

Subjects were seated in a comfortable chair and instructed to try to avoid fatigue. Also asked to keep the eyes closed and do minimal muscle movement during the recording. The subject heard a series of tones with two different pitch. One tone is known as “Frequent or non-target (1000Hz)” and the other is “Infrequent or target (2000Hz)”. The subject needs to concentrate on tones and mentally count the uncommon tones. After completion of one session, the subject relaxed for 5-10 mins and then again started the second session. The recording duration was for 3 to 4 minutes and each subject tested for 2-3 times. There were 6 to 12 targets and 24 to 50 non-target tones.

#### IV. EEG SIGNAL PROCESSING

##### A. Channel Used

OpenBCI cyton board has 8 channels for measuring brain EEG and by the use of a daisy board, it can be extended to 16 channels. For our auditory EEG experiment, we used 8 channels, cyton board. The channel names are Fp1, Fp2, C3, C4, P7, P8, O1, and O2. The position of the channel is shown on the head plot in Figure 4(Right). The reference and ground we used were two ears.

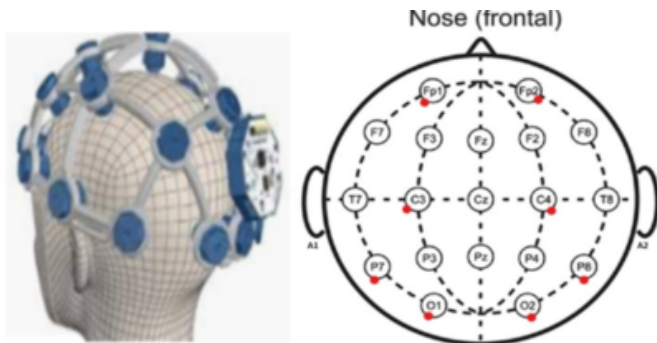


Fig. 4. Ultracortex Mark IV Headset (Cyton Board is Mounted on the Head Cap)(Left); EEG Testing Configuration for our Auditory EEG Experiment, we used 8 Channels: Fp1, Fp2, C3, C4, P7, P8, O1 and O2 and Two Ears are Reference and Ground)(Right).

##### B. Filtering

The EEG signals are very much affected by contamination, mainly bidirectional. It is very much noisy and un-stationary. For example, EEG recordings are contaminated as the results of eye movement and blinking (originating mostly from the frontal and lateral frontal areas) [14]. So, filtering the EEG signal is required to get rid of unnecessary information from the raw signal. The signals were sampled at 250 Hz. In MATLAB, there is an interactive toolbox, EEGLAB. EEGLAB was used to filter and all other offline calculations. We used a band-pass filter from 0.5 to 30 Hz for removing the DC effect and minimizing artifacts at epoch boundaries. We also applied a notch filter of 60 Hz.

##### C. Artifact Rejection and Epoch Extraction

For eye blinks and horizontal eye movements’ correction, independent component analysis (ICA) was conducted in offline by using EEGLAB. RUNICA routine was used for ICA. One to four eye blinks were marked per participants. Also, if the peak-to-peak voltage was greater than 400 mv then those trials were omitted in any channel.

The signals were sampled to 250 Hz in offline. After filtering and AR, the continuous EEG data were epoched by extracting data epochs computed with a 2000 ms. Epoch started 200ms before and 1.8 sec after the stimulus onset.

#### V. MACHINE LEARNING IMPLEMENTATION AND ANALYSIS FOR TONE-CLASSIFICATION

##### A. Features Extraction

As described in section three, data is recorded in CSV format and then by the use of MATLAB, feature vectors were calculated for each of the resulted in rare and frequent epochs. The EEG signals are in microvolt (uV) ranges and we extracted the mean of amplitude (uV), power (uW-microwatt), energy (nJ-nano Jule), wavelength (mV), and no of odd events. For each subject, there were 5 input feature vectors and two target matrix (rare and frequent tone). The constructed features were represented in a numerical format that is suitable for use with machine learning algorithms. Every column in the features matrices was normalized between 0 and 1.

##### B. Machine-Learning Algorithms

In this work, we classify our auditory data set with 6 types of machine learning algorithms. They are K-Nearest Neighbors algorithm (KNN), Neural Network (NN), Decision Tree algorithm(DT), Random Forest classifier(RF), Support Vector Machines (SVMs), and Logistic Regression(LR). A detailed description of these learning algorithms can be found in Jupyter notebooks also known as ipython notebooks were used for training and testing all kinds of machine learning classification models. A brief descriptions of models are given on the next page:

1) *Neural Network (NN)*: A sequence of an algorithm that is used to recognize the underlying relationship of a data process is known as a neural network. It can replicate the way the human brain operates. All the learning takes place in input, hidden, and active layers. There are countless weights(neurons) inside a hidden layer[15,16]. Every layer is connected through

an activation function, to estimate the performance of the learning phase, a loss function is used and for the improvement of learning, an optimizer is used (Fig. 5; left).

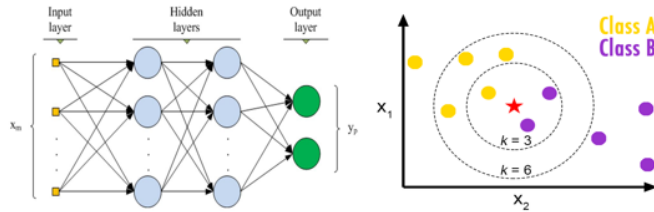


Fig. 5. Neural Network(left);k-Nearest Neighbors(right)

2) *K-Nearest Neighbors Algorithm (k-NN)*: The k-NN algorithm is a simple, supervised machine learning algorithm that can be used to solve both classification and regression problems. k-nearest neighbors have only one parameter – the number of neighbors (k) to be included in deciding on the majority-vote predicted classification. In Fig. 5 (right), the test sample (red star) should be classified either as to yellow circle or to purple circle. If  $k = 3$  it is assigned to Class B (as there are two purple circles) and if  $k = 6$  it is assigned to Class A (as there are four yellow circles)[17].

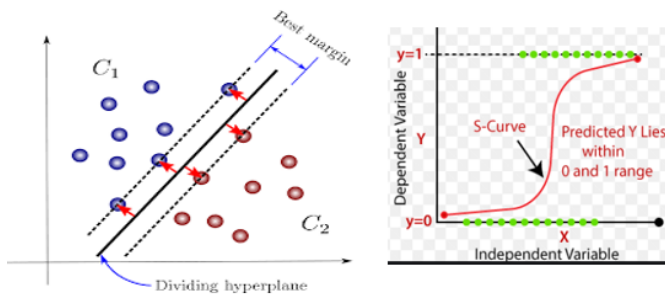


Fig. 6. Support Vector Machines (left);Logistic Regression (right)

3) *Support Vector Machines (SVMs)*: SVM is a method that fits the provided data, returns a “best fit” hyperplane that divides or categorizes the data. Then some features are feed to the classifier to see what the “predicted” class is. It is a supervised learning model (Fig. 6; left).  $M$  is a regularization parameter that controls the trade-off between achieving a low training error and a low testing error that is the ability to generalize the classifier to unseen data. In SVM, the hinge loss is a loss function used for training classifiers [18].

4) *Logistic Regression (LR)*: Logistic regression (LR) is a statistical model that uses a logistic function to model a binary dependent variable. In LR, a threshold value is specified and it at what value the data will be grouped in one class vs. other class (Fig. 6; right). It is best suited for binary classification but can be applied in the classification problem with more than two variables or groups [19].

5) *Random Forest (RF)*: Random forest is a supervised learning algorithm that is used for both classifications as well as regression. It is mostly used for classification problems. A random forest algorithm creates decision trees on data samples

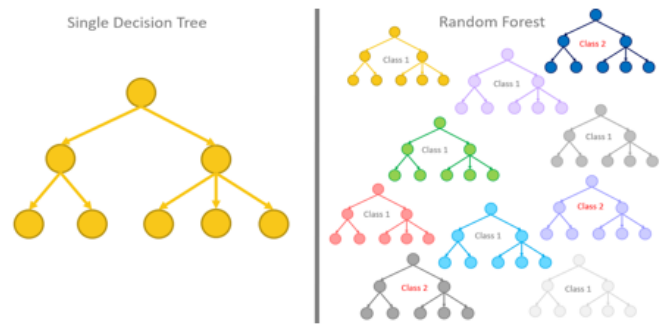


Fig. 7. Decision Tree (left); Random Forest Algorithm (right)

and then gets the prediction from each of them and finally selects the best solution utilizing voting (Fig. 7; right). It is an ensemble method that is better than a single decision tree because it reduces the over-fitting by averaging the result. The loss function is the Gini impurity. The training loss is often called the “objective function” as well. Validation loss. This is the function that we use to evaluate the performance of our trained model on unseen data[20].

6) *Decision Tree (DT)*: In the DT model, trees are used as a predictive model. It predicts the observation item and decides based on the item’s target values. In this model, leaves signify class, observation defines by branches and the tree models where the target variable can take a discrete set of values are called classification trees (Figure 7; left) [21].

### C. Performance Analysis

In NN, for the hidden layer, Relu ( Rectified linear unit) is used. The function gives a zero for all negative values. For defining the target, the softmax activation function is used. We have used “sparse-categorical cross-entropy” as a loss function. It can measure the dissimilarity between the distribution of observed class labels and the predicted probabilities of class membership. We have used “Adam” as an optimizer. The algorithm can handle sparse gradients on noisy problems. In k-NN and SVM, we have used the range of parameter  $k = (1,31)$  and in SVM, range= (1,100). For DT,  $sample\_split\_range=(2,30)$ . For all the algorithms, the data sample train and test ratio were 8:2.

1) *Performance Analysis of Random EEG and Auditory Stimuli*: In Table-I, the classification accuracy of random EEG (not auditory), auditory stimuli for common and uncommon tone is given. Here, we separated the random EEG from common and uncommon events. All the algorithms performed efficiently. Random Forest(RF) algorithms efficiency was 99.03% and other algorithms showed 97.91% except for Logistic Regression(LR). Overall, we can conclude that all the model was trained successfully and test accuracy was also remarkable.

2) *Performance Analysis of random EEG and auditory stimuli*: In Table II, the classification accuracy of auditory stimuli for common and uncommon tone is given. All the models performed with excellent accuracy, from 93.75% to

TABLE I. CLASSIFICATION ACCURACY OF RANDOM EEG, COMMON AND UNCOMMON AUDITORY STIMULI

| Algorithm                   | Classification accuracy (%) |
|-----------------------------|-----------------------------|
| K-Nearest Neighbors(k-NN)   | 97.91                       |
| Random Forest (RF)          | 99.03                       |
| Decision Tree(DT)           | 97.91                       |
| Support Vector Machine(SVM) | 97.91                       |
| Neural Networking(NN)       | 99.03                       |
| Logistic Regression(LR)     | 89.58                       |

99.1%. RF accuracy was maximum among all the methods. Overall, we can conclude that all the model was trained successfully and test accuracy was also remarkable.

TABLE II. CLASSIFICATION ACCURACY OF COMMON AND UNCOMMON AUDITORY STIMULI

| Algorithm                   | Classification accuracy (%) |
|-----------------------------|-----------------------------|
| K-Nearest Neighbors(k-NN)   | 93.75                       |
| Random Forest (RF)          | 99.10                       |
| Decision Tree(DT)           | 93.75                       |
| Support Vector Machine(SVM) | 93.75                       |
| Neural Networking(NN)       | 93.75                       |
| Logistic Regression(LR)     | 96.78                       |

#### D. ROC Curve and AOC

A ROC curve (receiver operating characteristic curve) is a graph which shows the performance of a classification model at all classification thresholds. This curve plots two parameters: True Positive Rate(TPR) on the y-axis & False Positive Rate(FPR) on the x-axis. As a baseline, a random classifier is expected to give points lying along the diagonal (FPR = TPR). The closer the curve comes to the 45-degree diagonal of the ROC space, the less accurate the test with the threshold values (0.5, 1, and 1).

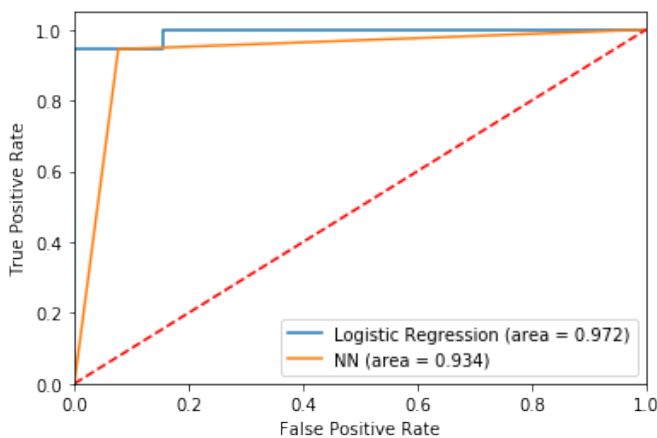


Fig. 8. ROC Curves of the LR and NN Classifiers for the Common and Uncommon Tones with AUC Values of 0.972 and 0.934, respectively.

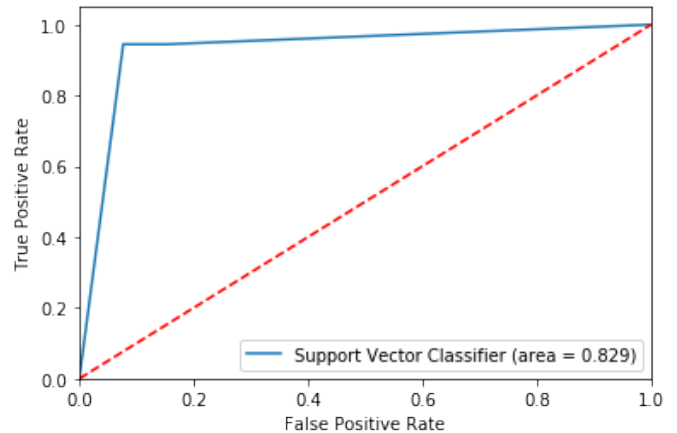
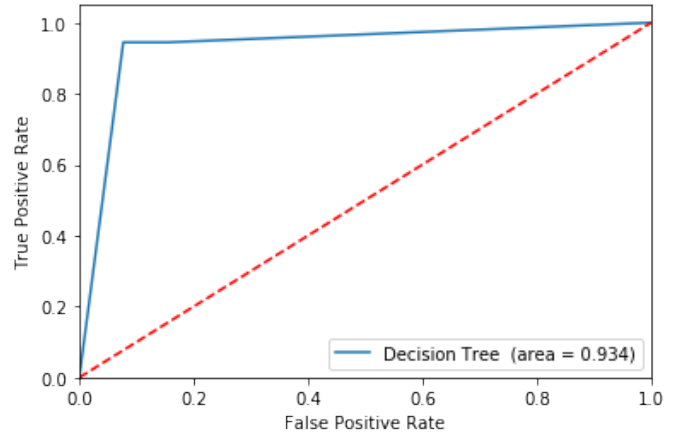
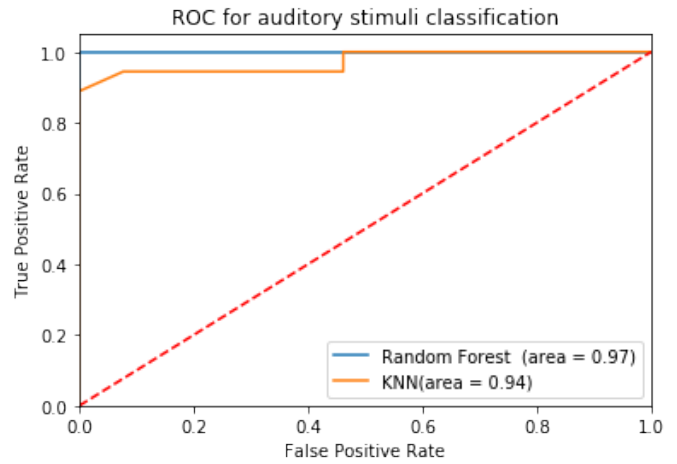


Fig. 9. ROC Curves of the RF,k-NN, DT and SV Classifiers for the Common and Uncommon Tones with AUC of 0.97,0.94, 0.934, and 0.829, respectively.

AUC stands for “Area under the ROC Curve”. That is, AUC measures the entire two-dimensional area underneath the entire ROC curve. In general, an AUC of 0.5 suggests no discrimination, 0.7 to 0.8 is considered acceptable, 0.8 to

0.9 is considered excellent, and more than 0.9 is considered outstanding [22,23].

Fig. 8 shows the ROC curves of the LR and NN classifier with area under the curve (AUC) values of 0.972 and 0.934. Fig. 9 shows the ROC curves of the RF and k-NN classifier(up) with AUC values of 0.972 and 0.94, DT classifiers (middle), and SV classifier (down) with AUC of 0.934 and 0.829 respectively for the common and uncommon tones. An area of 1 represents a perfect test; an area of 0.5 represents a random test. From the figures, it is clear that the performances of all of the methods of this study are outstanding except the SV classifier which is also excellent.

## VI. MACHINE LEARNING IMPLEMENTATION AND ANALYSIS FOR ACCURATE P300 PLOT IDENTIFICATION

After classifying common and uncommon stimuli from random EEG, we plot all P300 with filtered data and saved as an image format in .jpg. Here, our input features were images. We had around 2000 images among which 80% we used for training the model and the remaining 20% we used to test the image. Our aim was to identify that is the P300 is a good-shape (as in Fig. 10) P300 plot or not.

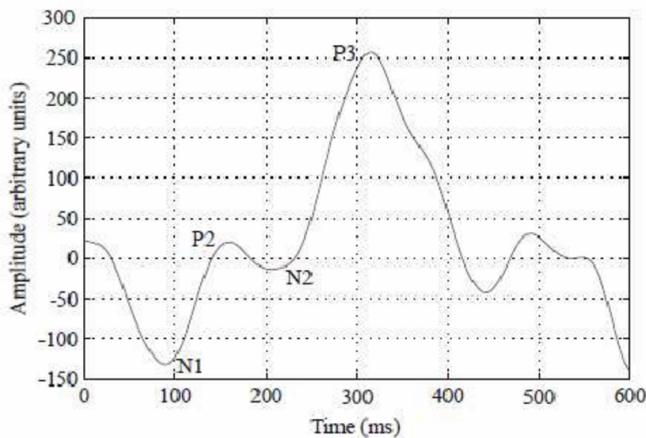


Fig. 10. ERP Plot with all its Most Common Underlying Components N1, P2, N2 and P3 (ERP Plot from Hoffman et al., 2008).

As described in Section I, the P300 response occurs at around 300ms in the oddball paradigm, regardless of the type of stimulus presented: visual, tactile, auditory, olfactory, gustatory, etc. Because of this general in-variance about stimulus type, the P300 component is understood to reflect a higher cognitive response to unexpected and/or cognitively salient stimuli. For detecting a good shape P300, we need to detect other components also, like N100 (N1), P200 (P2), N200 (N2), etc. Also, P300 (P3) must give a positive peak of around 300 ms.

We used EEGLab for plotting P300 which is a great tool for MATLAB. To extract the P300 plot, we need to create 6-8 files in EEGLab and then could draw the P300 plot. Then

for classification, we used Python Jupiter notebook. Which is very user friendly and the fastest procedure. We have grouped all the images in two-class, “P300” and “no-P300”. The plots which matched with Fig. 10 classified as “P300” and the remaining were classified as “no P300”.

### A. Performance Analysis

We train and tested image by the method of Neural Networks (NNs), K-Nearest Neighbors algorithm (KNN), Decision Tree algorithm (DT), Random Forest classifier (RF), and Support Vector Machines (SVMs). Amid all of the models, NN performed best with an evaluation accuracy of 94.95%. RF and DT also have good accuracy (83.94% and 76.78%). In Table III, the image classification accuracy percentage (%) is given.

TABLE III. CLASSIFICATION ACCURACY FOR IDENTIFYING P300 PLOT IS IN ACCURATE SHAPE

| Algorithm                   | Classification accuracy (%) |
|-----------------------------|-----------------------------|
| K-Nearest Neighbors(k-NN)   | 77.62                       |
| Random Forest (RF)          | 83.92                       |
| Decision Tree(DT)           | 76.78                       |
| Support Vector Machine(SVM) | 66.08                       |
| Neural Networking(NN)       | 94.95                       |

Fig. 11 shows the ROC curves of the DT, RF, k-NN, and SV and NN classifiers for the detection of “accurate P300 wave” with area under the curve (AUC) values of 0.75, 0.79, 0.72, 0.50, and 0.99 respectively. These results indicate that the NN (Neural Networking) method shows outstanding performance among all the methods. SV classifier performance is not satisfactory at all where the other three methods performances also satisfactory.

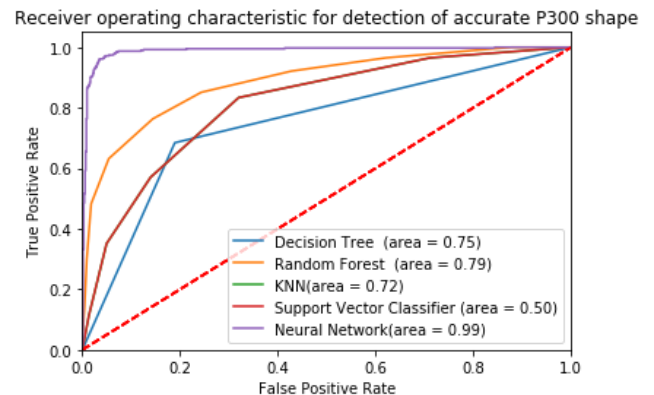


Fig. 11. Receiver Operating Characteristic for Detection of Accurate P300 Plot. (An AUC of 0.5 Suggests no Discrimination (i.e., Ability to Diagnose Patients with and without the Disease or Condition based on the Test), 0.7 to 0.8 is considered Acceptable, 0.8 to 0.9 is considered Excellent, and more than 0.9 is considered Outstanding.)

## VII. CONCLUSION

The study explores the classification of common and uncommon tones of RP signals for auditory stimuli and identification P300 wave in accurate shape based on P300 feature extraction. The study train and tested various types of machine learning. Our experiment has three phases. At first, we trained and test a model to separate auditory EEG signals from random EEGs [Table I]. All the models performed efficiently (89.58% - 99.03%). NN and DT showed a maximum accuracy of 99.03%. Then, classify common and uncommon tones [Table II]. There the classification accuracy was from 93.75% to 99.1%. Where LR showed 96.78% and RF showed 99.1%. Finally, identified the accurate P300 plots from distracted or non-P300 plots. The classification accuracy for all the models showed different accuracy. Among them, NN performed best with 94.95% and accuracy for RF 83.92%, DT 76.78%, k-NN 76.2%, and SVM with accuracy 66.08%. Overall, the audio-based P300 classification model showed outstanding performance and is comparable to today's foremost BCI research. Our experimental methods are simple but consistent and proved better performance for the research in neuroscience and machine learning.

In the future, classification experiments in virtual reality may study with external audio-visual distractions and may investigate their effect on various ERP components. It may show a huge contribution to ERP research.

## ACKNOWLEDGMENT

The authors would like to thank everyone.

## REFERENCES

- [1] Birbaumer, N. & Cohen, L. G., "Brain-computer interfaces: communication and restoration of movement in paralysis," *The Journal of Physiology* 579, 621–636, 2006.125633 (2007).
- [2] Ibáñez-Molina, Antonio J et al. "EEG Multiscale Complexity in Schizophrenia During Picture Naming." *Frontiers in physiology* vol. 9 1213. 7 Sep. 2018, DOI:10.3389/fphys.2018.01213
- [3] Pooja Kadambi, Joseph A. Lovelace, and Fred R. Beye, Jr," Audio Based Brain-Computer Interfacing for Neurological Assessment of Fatigue", *International IEEE/EMBS Conference on Neural Engineering* · November 2013 DOI: 10.1109/NER.2013.6695875
- [4] Kota Utsumi, Kouji Takano<sup>1</sup>, Yoji Okahara, Tetsuo Komori, Osamu Onodera Kenji Kansaku," Operation of a P300-based brain-computer interface in patients with Duchenne muscular dystrophy," *ScLeNuFIC REPOrTs* — (2018) 8:1753 — DOI:10.1038/s41598-018-20125
- [5] Vecchio, F.; Maatta, S. The use of auditory event-related potentials in Alzheimer's disease diagnosis. *Int. J. Alzheimer Dis.* 2011, 2011, 653173–10.
- [6] M. T. Giovanetti and F. R. Beye, "Physiological health assessment and hazard monitoring patch for firefighters," 2017 IEEE 60th International Midwest Symposium on Circuits and Systems (MWSCAS), Boston, MA, 2017, pp. 1168-1171, DOI: 10.1109/MWSCAS.2017.8053136.
- [7] Polich, J, "Updating P300: an integrative theory of P3a and P3b", *Clin. Neurophysiol.* 118, 2128–2148. doi: 10.1016/j.clinph.2007.04.019
- [8] O. Abdel-Hamid, L. Deng, and Yu, "Exploring convolutional neural network structures and optimization techniques for speech recognition," in *Proceedings of the 14th Annual Conference of the International Speech Communication Association, INTERSPEECH 2013*, pp. 3366–3370, fra, August 2013.
- [9] Craik A, He Y, Contreras-Vidal JL. Deep learning for electroencephalogram (EEG) classification tasks: a review. *J Neural Eng.* 2019 Jun;16(3):031001. DOI: 10.1088/1741-2552/ab0ab5. Epub 2019 Feb 26. PMID: 30808014.
- [10] Hafeez Ullah Amin\*, Wajid Mumtaz, Ahmad Rauf Subhani, Mohamad Naufal Mohamad Saad, and Aamir Saeed Malik," Classification of EEG Signals Based on Pattern Recognition Approach", *Frontiers in Computational Neuroscience*, November 2017 — Volume 11 — Article 103
- [11] Raviraj Joshi, Purvi Goel, Mriganka Sur, and Hema A. Murthy, "Single Trial P300 Classification Using Convolutional LSTM and Deep Learning Ensembles Method", *Springer Nature Switzerland AG* 2018, U. S. Tiwary (Ed.): IHCI 2018, LNCS 11278, pp. 3–15, 2018.
- [12] Hubert Cecotti and Axel Gra ser," Convolutional Neural Networks for P300 Detection with Application to Brain-Computer Interfaces", *IEEE TRANSACTIONS ON PATTERN ANALYSIS AND MACHINE INTELLIGENCE*, VOL. 33, NO. 3, MARCH 2011.
- [13] Mohammad H. Alomari, Aya Samaha, and Khaled AlKamha, " EEG Signals using Advanced Feature Extraction and Machine Learning", *International Journal of Advanced Computer Science and Applications*, Vol. 4, No. 6, 2013.
- [14] G. L. Wallstrom, R. E. Kass, A. Miller, J. F. Cohn, and N. A. Fox, "Automatic correction of ocular artifacts in the EEG: a comparison of regression-based and component-based methods," *International Journal of Psychophysiology*, vol. 53, no. 2, pp. 105–119, 2004.
- [15] Yan Qiu Chen, Robert I.Damper, M.S. Nixon," On neural-network implementations of k-nearest neighbor pattern classifiers", July 1997, *IEEE Transactions on Circuits and Systems I Fundamental Theory and Applications* 44(7):622– 629
- [16] Diederik P. Kingma, Jimmy Ba, "Adam: Method for Stochastic Optimization", Published as a conference paper at the 3rd International Conference for Learning Representations, San Diego, 2015.
- [17] Yun-Lei Cai, Duo Ji, Dongfeng Cai, "A KNN Research Paper Classification Method Based on Shared Nearest Neighbor", *Proceedings of NTCIR-8 Workshop Meeting*, June 15–18, 2010, Tokyo, Japan
- [18] Marco A. Wiering, Michiel H. van der Ree, M. Embrechts, Lambert Schomaker," The Neural Support Vector Machine", *The 25th Benelux Artificial Intelligence Conference (BNAIC)*, November 2013.
- [19] Hilbe, Joseph M., "Logistic Regression Models.", 2009, Chapman & Hall/CRC Press. ISBN 978-1-4200-7575-5.
- [20] James Bergstra, Yoshua Bengio," Random Search for Hyper-Parameter Optimization", *Journal of Machine Learning Research* 13 (2012) 281-305
- [21] Ishwar Sethi, "Entropy nets: From decision trees to neural networks", October 1990, *Proceedings of the IEEE* 78(10):1605 – 1613.
- [22] Matjaz Majnik, Zoran Bosni", "ROC Analysis of Classifiers in Machine Learning: Survey", Technical report MM-1/2011
- [23] Jayawant N. Mandrekar, "Receiver Operating Characteristic Curve in Diagnostic Test Assessment", *BIOSTATISTICS FOR CLINICIANS— VOLUME 5, ISSUE 9, P1315-1316, SEPTEMBER 01, 2010*

# A Perception Centered Self-Driving System without HD Maps

Alan Sun

School of Engineering  
Washington University in St. Louis  
St. Louis, Missouri 63130-4899

**Abstract**—Building a fully autonomous self-driving system has been discussed for more than 20 years yet remains unsolved. Previous systems have limited ability to scale. Their localization subsystem needs labor-intensive map recording for running in a new area, and the accuracy decreases after the changes occur in the environment. In this paper, a new localization method is proposed to solve the scalability problems, with a new method for detecting and making sense of diverse traffic lines. Like the way human drives, a self-driving system should not rely on an exact position to travel in most scenarios. As a result, without HD Maps, GPS or IMU, the proposed localization subsystem relies only on detecting driving-related features around (like lane lines, stop lines, and merging lane lines). For spotting and reasoning all these features, a new line detector is proposed and tested against multiple datasets.

**Keywords**—Self-driving; lane lines detection; traffic lines detection; visual localization; HD Maps

## I. INTRODUCTION

Ziegler's system [1] can drive full-autonomously over 100 kilometers without any interruptions in 2014. Despite these early achievements, the industry leaders are still struggling to pass the necessary tests according to [2]. It is critical to inspect why the current self-driving system is hard to implement and widely used. Current systems rely on HD Maps to produce centimeter-level accuracy of position. Readers are referred to [3] for more about typical system architecture. The big question is whether accurate positions necessary?

Human drivers make driving decisions based on what they see. They make sense of the environment around and decide when to turn or keep the current driving direction. They cannot mark the exact position of themselves on a map, but they know how to travel through a complicated intersection based on the knowledge of which way they should take. Likewise, a self-driving system without accurate locations should be a viable solution?

In this paper, a new perception centered self-driving system is proposed and discussed in two driving scenarios: the cruising scenario and the turning scenario. The cruising scenario is when the vehicle cruises on parallel lanes. The turning scenario is when the vehicle drives through free spaces (defined as the drivable area outside of lanes, like intersections or parking area).

The proposed system comes with several advantages in these two scenarios. Firstly, it does not rely on HD Maps. So it is easy to scale without recording new HD Maps.

Secondly, the proposed feature detection method is not based on any specialized end-to-end deep learning solutions. Hence it is easy to debug and visualize. Also, it does not need additional time-consuming training process for scaling. Lastly, it performs more robustly with a severely changed environment (like seasons, weather or lighting condition).

Just like the human drivers, the system only involves with related visual features (defined as traffic features, including traffic lines, traffic lights and traffic signs). The workflow of the detection and localization subsystem is shown in Fig. 1. In the cruising scenario, only the first step is needed, including 1.1 and 1.2. In the turning scenario, all four steps must be done. Note that the vehicle position from the localization subsystem is based on the rebuilt scene rather than a global map. The localization subsystem also projects the rebuilt scene onto a digital map (like Google Map) to provide navigation instructions while crossing free spaces. The navigation instruction leads the car to travel from one exit to the target entrance of the free space. The path planning system and control system also works on the rebuilt scene. Hence they are map unrelated.

The proposed system relies on traffic lines (including curbs) for tracking the vehicle's position. Hence, the lines detector is the priority. A general lines detector for understanding complicated traffic lines on the road is vital. The experiment covers several types of lines, including lane lines, stop lines, curbs, merging and splitting lines and intersections in a roundabout. For the popular lane lines detection problem, the proposed new traffic lines detector performs as good as other deep neural network supported approaches leveraging the prior knowledge of lines position and angles with easy erosion and clustering. This robust and straightforward method is then generalized and successfully detected other kinds of lines as well. After that, the process of localizing the position in the rebuilt scene will be discussed with examples and limitations. In that example, the system requires neither GPS signals nor IMU signals nor 3D HD Maps to locate the vehicle.

## II. RELATED WORK

What is a perception centered self-driving system? Most self-driving systems are relying on a map-based localization subsystem. They are categorized as localization centered systems because all other subsystems are working under the map space from the localization subsystem. The perception centered system uses a local scene, instead of a global map, as the working space for all other subsystems. Limited research have been done on this direction. One of the exceptions is [4]



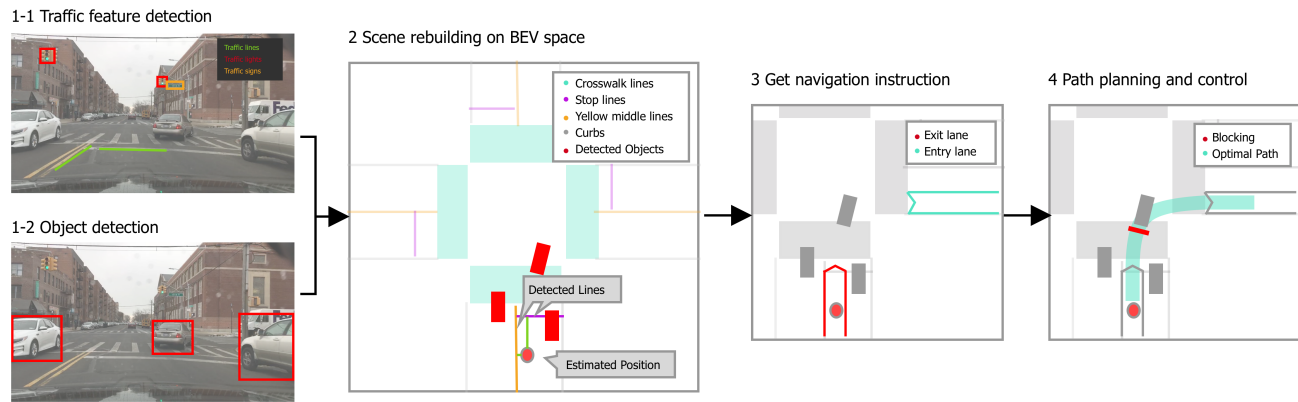


Fig. 1. The Workflow of the Proposed Perception Centered System.

by Bojarski from Nvidia. In this work, they tried to build an end-to-end system from camera images to control signals with the help of augmented learning. It is also map-unrelated. However, this system only works for minimal lane-keeping tasks in the cruising scenario. It is not compatible to work with other subsystems, and the scalability is not tested for more sophisticated roads or sensor settings.

#### A. Localization

For most localization centred systems, all decision making and path planning are based on a centimetre level localization accuracy from their localization subsystem. Using GPS, with the aid of IMU, is a popular solution and provides accuracy better than 20 centimetres with SLAM over an HD Map [5]. The problem of GPS is that the signals are not always available, and the result tends to drift accidentally. For quite a long time, SLAM is considered as the key to solving the localization problem for self-driving cars. The SLAM algorithm uses visual features stored in the HD Map to match features extracted from the live camera on the self-driving cars. Visual features are usually organized as bags of features (BoF) in the descriptor space. Without HD Maps or IMU, researchers can hardly reach the centimetres level accuracy like [6] and [7].

However, two problems of the SLAM based localization approach are tricky to solve. Firstly, the performance decreases once the environment changes. Light angle changes might cause different shadow shapes and season changes cause massive appearance changes on the trees and grass. These changes yield new visual features which cannot be matched with the recorded ones on the HD Map. This problem requires routine labour-intensive map recording once after the changes occur. Secondly, the localization result tends to drift after a long-range driving, and the error will accumulate with growing driven distance, as discussed in [5]. The intrinsic reason of these problems is that the original SLAM algorithm is designed for indoor localization problems where dramatic environment changes or long-distance moving is not considered. Hence these problems are hard to eliminate.

Recent researchers, like Ma [8], started to use as less visual features as possible for localization. Besides saving the storage

for the BoF of these features, using fewer features decrease the risk of being affected by the environment changes [9].

This trend brings the idea of using minimal features for localization. The LaneLoc system proposed by Schreiber [10] tried to use the exact appearance of lane markings for matching from pre-recorded maps. This approach could be seen as counting the number of dashed fragments the vehicle travelled to localize the car itself. This approach still has several limitations. Firstly, it will not work on a solid line situation and ends up with only relying on IMU without any visual aids. Secondly, the exact appearance will eventually change one day in the future. Think about the time when those dashed lines were repainted or worn out, which are both prevalent cases. Thirdly, the performance is very fragile. Slight turbulence, like occlusions or heavy shadows, will make the system omit one or more fragments and yield a steady error as a result. Lastly, the labelling process is both complicated and hard to finish accurately, as discussed by Schreiber in their paper. The proposed system solved these limitations by abstracting line features further to types and directions by the proposed lines detector.

#### B. Traffic Line Detection

The traffic line detection, or the lane detection which is a narrower problem, was the essence of many early driving assistant systems [11] like Lane Departure Warning System (LDWS) and Lane Keeping Assist System (LKAS). Many researchers, like Kim [12], used Convolutional Neural Network (CNN) to reduce noise and get the segmentation of the markings of those lines. Wang [13] used shape extracted from OpenStreetMap (OSM) as prior knowledge to help detect the lanes. Some problems remain for the CNN supported approaches.

Firstly, they still can not solve the long-tail challenging situations because CNNs heavily relies on the distribution of the training dataset. As a result, CNN generally works terribly in rare situations. Secondly, the segmentation result of the CNN approaches often cause blurry edges when it is not confident about the prediction. These blurry edges come with difficulty for the following algorithms when they try to form a line from these ambiguous pixels. Lastly, CNNs are

significantly dataset related. They tend to work well only on the dataset they have been trained on [14]. This limitation is because that different datasets and sensor settings tend to create distinctive patterns of noise in the images. For example, in the KITTI dataset [15], the same line marks show different appearances in different locations under the BEV space. Lines far from the camera shows clear artifacts caused by the BEV transformation. The self-driving related datasets are often covering just one type of the available camera settings. A vast and comprehensive dataset like MS-COCO [16] for the object detection task does not exist for now.

As a result, CNN was not used for lines detection in this paper. The proposed lines detector leverages the lines information from a topology map, similar to what Wang did in [13] from the OSM, as prior knowledge to help. The proposed lines detector separates different line types to boost the performance even more by using different lines detector for each type of lines (solid or dashed lines, straight or curved lines). It also used a sliding window to detect and connect traffic lines, similar to what Tsai did in [17]. The sliding window approach is proved to be both robust and easy to visualize for debugging.

### III. SYSTEM DESIGN

The overall workflow is shown in Fig. 1. In the cruising scenario, the detection subsystem will finish the part 1.1 and 1.2 to give the current lane number of the vehicle, and that is enough for generating a driving path and control signal without involving the localization system at all. However, the detection system needs to continuously detect the traffic features for the next traffic part (could be another lane ahead or a free space connected with an exit). The order of the series of traffic features are based on the topology map.

The topological map, being used as the descriptor space for matching with the digital map and the rebuilt scene, is the center and the relationship is shown in Fig. 2. The topology map should be drawn before the system can run on a new area. The topology map also provides lane information helping lines detection as prior knowledge and helps the vehicle to change to a preferred lane in advance. The topology map contains the following information:

- Lanes information: (1) the lines information on both sides (like straight yellow lines on the left and straight curb on the right), (2) ending information (like ends with a stop line or merges with other lanes on the left), (3) direction information (like starting direction, turning angle limitation for each window), (4) neighbour lanes used for lane changing while cruising, (5) connected entrance and exit numbers, (6) traffic rules metadata (like speed limits), (7) status (like normal, under maintenance or closed under specific time windows)
- Entrance and exit: (1) position, (2) direction, (3) the relationship (an N to N relationship) with each other.
- Free spaces: (1) detectable traffic features used for localization (including stop lines, crosswalk lines, traffic lights, traffic signs, lines of adjacent lanes) and their relative position in a real-world scale, (2) adjacent

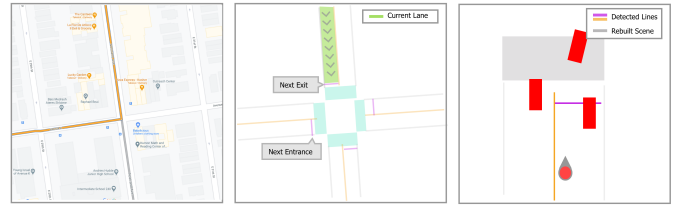


Fig. 2. The Left is a Digital Map used for Navigation, the Middle is the Topology Map, the Right is the Rebuilt Scene

entrance and exit numbers, (3) traffic rules (like speed limits), (4) status

#### A. Matching digital map with topology map for navigation

Each turning point on the digital map is used for finding a nearest entrance-exit pair which have the correlated directions. Define  $T = \{(\lambda_t, \phi_t), \alpha_t, \beta_t\}$  as the set of all turning points on the digital map, where  $\lambda_t$  and  $\phi_t$  is the latitude and longitude of turning point  $t$ ,  $\alpha_t$  is the direction before the turning and  $\beta_t$  is the direction after the turning.  $D_{in} = \{(\lambda_d, \phi_d), \beta_d\}$  and  $D_{out} = \{(\lambda_d, \phi_d), \alpha_d\}$  are the set of all entry points and all exit points. The score function  $f$  is the multiplication of  $g$  and  $h$ , as equation 1, where  $g$  is the Euclidean distance between two points and  $h$  is the difference of two angles, defined as  $g = \|d_{in}, t\| + \|d_{out}, t\|$  and  $h = |\alpha_t, \alpha_{in}| + |\beta_t, \beta_{out}|$ . The  $P = \{(d_{in}, d_{out})\}$  is the set of all legal pairs of entrance and exits. All legal pairs should connect with a same free space and follow the traffic law. For example, the exit on the end of a right turning lane cannot pair with the entrance ahead with the same direction. The optimal pair for a minimal  $f$  score is the matched result with the condition of  $(d_{in}^*, d_{out}^*) \in P$ . This method assumes the turning point on the digital map is the center point of the target exit and the target entrance.

$$f(d_{in}, d_{out}, t) = g(d_{in}, d_{out}, t) * h(d_{in}, d_{out}, t) \quad (1)$$

The data of  $P$  and  $D$  are manually initialized as part of the topology map. These data usually do not need to be changed unless the traffic features are changed. For example, an intersection was updated with an additional right changing lane or new construction on the road updated the lane changing rules temporarily. The maintenance of the topology map is easy and fast since the only parts need to be changed in the sets of  $P$  and  $D$  are the data of the lanes.

#### B. Matching Topology Map with Perception Scene for Localization

Lanes form two kinds of lane sets: driving lane sets and detectable lane sets. The driving lane sets provide information about lane changing behaviour and traffic laws, like speed limits. Two examples of driving lane sets are illustrated in Fig. 3. The vehicle can change to other lanes within the same driving lane set. The target lane and original lane information will be passed towards other following subsystems to act and finish the changing maneuver while lane changing.



Fig. 3. An Illustration of Lane Sets under Two different Situations Overlapping on a Satellite Map, the Left is on Highway Exit, the Right is a Complicated Lane Topology near a Roundabout, the Red and Green arrows Represent Entrances and Exits of those Lanes.

The detectable lane sets provide information about how to detect these lanes. Lanes with either the same travelling direction or opposite ones can be grouped into the same set. Each detectable lane sets has left and right line types, lane width (used as detection aid, but restrictions), dashed line intervals, suggested detection window size and other metadata which can be added at one's convenience. A detectable lane set must have at least two sides of lines information used for tracking lanes. The lane width follows the priority of (1) the width between two detected lines, (2) the width of other detected lanes within the same detectable lane sets, (3) equally divided width if two lines (probably are curbs) of the whole set are detected, (4) the default lane width of the detectable lane sets. For example:

- When there are two lanes travelling in opposite directions, and there is no middle line to separate these two lanes, if both sides are detected, the space in between will be divided by two for the width of each lane. If the vehicle only detected the right side (assume under right-hand driving condition), the lane width for the current lane is the default lane width of the lane set.
- When there are four lanes travelling in opposite directions by two groups of two lanes, the middle line is a solid line, and the line between two same direction lanes is a dashed line. The number one lane (counting from the right) is the space between the curb and the dashed line, and the number two lane is the space between the middle solid line and the dashed line. If the vehicle cannot detect the curb to get the lane width of lane number one, the width of number two will be used for the width of lane number one.

For the cruising driving scenario, there are two questions: (1) which lane set the self-driving cars are in (to prepare for the next exit) and (2) which is the ego lane from the lane set. For these two questions, the system relies on either initializing the lane number at the beginning of the currently running period or

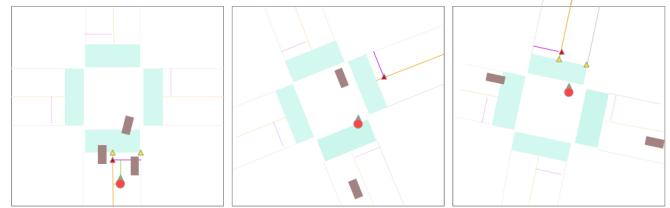


Fig. 4. How the Vehicle Locate itself using Lines Detection Results. The Yellow Triangle is a Weak Anchor and the Red Triangle is a Strong Anchor.

initializing the lane number after driving through a free space through a specific entrance. The detection system verifies and corrects the current lane set and lane number by matching detected types of lane lines with the ones from the topology map. The detection system provides four line detectors for each type of lines: (1) solid straight line, (2) solid curve, (3) dashed straight line, (4) dashed curve. In the remainder of this paper, curbs are considered as the same as traffic lines without further clearance.

The changes of the types of lane lines usually represent an end of the current lane. If is possible that there will be multiple types of lines in one side of a lane, the system uses the detector for the highest level type, because they are more complicated and can handle the task of detecting low-level types. These levels (one is the highest level and four is the lowest) are: (1) Dashed curves, (2) Solid curves, (3) Dashed straight lines, (4) Solid straight lines.

For the turning scenario, the detection subsystem only needs to detect one pair of non-parallel lines to form an anchor to rebuild the scene. For example, under the intersection scenario shown in Fig. 4, the middle lane line and the stop line are enough for a strong anchor to rebuild the scene based on the given relative position from the topology map. The target entrance on the right side can be predicted and used for path planning. Once the vehicle has driven into the free space passing the stop line which will no longer be detected, the stop line of the target lane will be detected and provide a strong anchor to follow up. The starting point of the target lane will form a weak anchor as additional clues for localization.

The detection of anchors might be effected by occlusions caused by other objects on the road. In other situations, there is a chance when the vehicle is crossing a large intersection, the vehicle will have no available anchor in sight in some area. The target lane direction and the current drivable area, as a backup, will aid the vehicle to finish the turning. The free space situation ends with positive detection of the next detectable lane set. If there are multiple lines parallel with each other nearby, the system assumes the detected one is the nearest one based on the current lane level position.

The system needs to be initialized at the beginning of each run based on GPS signals and the current driving direction from the gyroscope to tell the system which lane the vehicle is on. The GPS signal does not need to be centimetre-level accurate, and the detection subsystem will update the lane number, relying on counting the line numbers between the vehicle and the detected curbs.

This paper does not cover behaviour decision among crossing lanes because this can be considered as a separated and solved problem thanks to previous research like [1]. This behaviour decision includes behaviours, like yielding to vehicles coming out from other merging lanes. These rules are universal and consistent.

### C. General Lines Detector

The proposed lines detector in the detection subsystem can detect diverse types of lines. The code for lane lines detection for the KITTI dataset can be found on this repository. These types of lines were tested: (1) lane lines, (2) curbs, (3) stop lines, (4) merging or splitting points of two lines (pair of lines), (5) special lane lines or curbs (which are not parallel to the current ego lane). The lines detection problem was dissected by tracing back to the most significant visual feature of the lines, which is their long and narrow appearance. A sliding window was used to follow possible lines. All noise without this narrow feature was eliminated by applying these methods:

- **Region Restriction:** The detection subsystem leverage a given prior knowledge about the starting points to eliminate noise in unrelated regions. This knowledge comes from either previous lines detection results or predicted by the positive detection results of neighbour lines with given lane width from the topology map. For dashed lines, the sliding window moves at a step size of dash segment intervals given from the topology map to make sure optimal detecting position for each segment. The system tolerates minor errors for this interval distance. The more knowledge about the lines are available, the smaller window for detection can be used. A smaller region of interest gives better resilience for challenges, helps the segment normalize better and speeds up the lines detection process.
- **Special Convolution Kernel:** The system uses a special kernel, as shown in Fig. 5. This proposed kernel helps to produce a cleaner result in the Hough space for the next steps with less noise. Also, this kernel is more friendly for detecting curves, merging lines and splitting lines than the simple vertical kernel.
- **Directional Erosion:** The system uses a special directional erosion structuring element to erode noise which is not spanning through a specific direction ( $A \ominus B$ ,  $A$  is the pixels in the window and  $B$  is a 5 by 1 narrow structuring element), as illustrated in Fig. 6. The direction of the target lines is given from the topology map. In a sliding window, the line segment can be considered as a straight line. Sharp turning lines or circles will also be eroded into small segments which will be filtered out. Though there are some other more complicated ways to leverage the information of direction for lines detection [18], the directional erosion is the simplest and it works.
- **Types of Lines:** The system leverages prior knowledge of the types of the lines to get a better performance. For curves in each detection window, the turning angles are restricted to the thresholds, which is usually very small given from the topology map. For straight lines, a much narrower window for detection can be

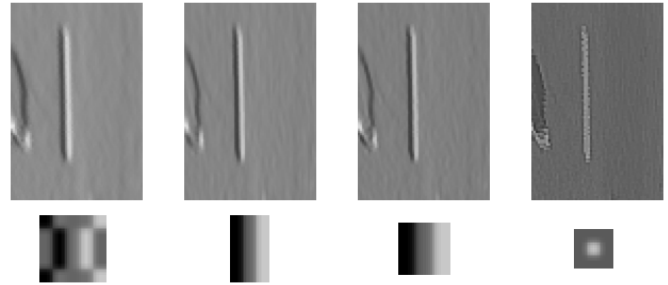


Fig. 5. Four Results for different Convolution Kernels. The First One is the Proposed One and the Last One is a Typical Square Edge Detection Kernel. The Result on the Left is more Smooth and Cleaner than the Ones on the Right in the Noisy Area.

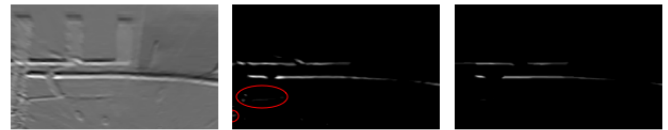


Fig. 6. Directional Erosion Eliminates Strong Noise in the Red Circles while Detecting Stop Lines.

used. For dashed lines, the marks which are too long or too short will be filtered out, as shown in Fig. 7. The topology map gives the length of segments of the dashed lines.

The proposed lines detector uses the Y channel from the YUV color channels since it was proved to perform better by Lin in [19]. The system works on the Bird-Eye-View (BEV) space since the prior knowledge of those lines can be leveraged without predicting the camera pose or estimating the vanishing point (VP) [20]. More about the homography transformation from the camera image to a BEV space with a given camera pose can be found in [21].

For the feature detection on the Hough space, a low-high-low kernel was widely used by [22], [23] and [24]. A new low-middle-high kernel was used and then mirrored to make the detection on the left and right side separately. So merging and splitting points and their directions (merging from / splitting to the left or the right) can be detected by comparing the lengths of these two lines detection results. For example, at the place a line is splitting to the right, the line detection from the right side will break coming with a shorter length of the line than the left side, as shown in Fig. 8. To separate splitting and merging, two additional windows will be created facing upwards and downwards. Positive result of lines in the upwards window means splitting and positive result in the downwards window means merging.

Lastly, the procedure for stop lines detection is as follows. After the detection of a window, if the line is broken in the upper end, two side windows will be created. A horizontal line detection, using horizontal convolution kernel and erosion structure, will be applied to detect the stop lines. If the result is positive, then this lane line is marked as finished, and no window will be created above.

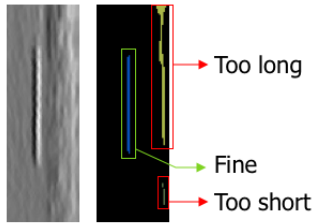


Fig. 7. An Example of how Length Information Helps to Filter Noise within a Single Window.

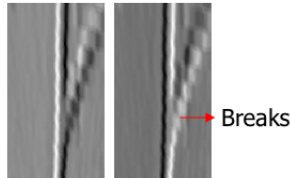


Fig. 8. Illustrate when Lines Splits, Left Side and Right Side Line Detection Result will not Agree with each other.

The overall process of lines detector is shown as follows:

- 1) Initialize the first window
- 2) Cut pixels in the window
- 3) Rotate the window
- 4) Commit Convolution
- 5) Cluster pixels
- 6) Form lines for all candidates
- 7) Filter and get the result for the current window
- 8) Slide the window up
- 9) If the window is not out of the image, go to step 2

For special lines which are not parallel to the current ego lines, an initial position for the sliding window to start will not be available to use. However, the system can still use the direction information from the topology map. Spotting the anchors from the target entrance while turning in free spaces is one of the situations which requires detecting special lines, as shown as in Fig. 4. The process is a little different, shown as follows:

- 1) Rotate the image
- 2) Commit Convolution
- 3) Commit Directional Erosion
- 4) Get valid pixel blocks
- 5) Form valid blocks into windows
- 6) Cut pixels into windows
  - a) For each window, cluster pixels
  - b) Form lines for all candidates
  - c) Filter short lines out
- 7) Connect and merge similar lines
- 8) Return the longest detection result

#### IV. RESULTS

The earlier part of this chapter shows the proposed general lines detector is robust to typical noise on the road, works well under different lighting conditions and detect multiple types of

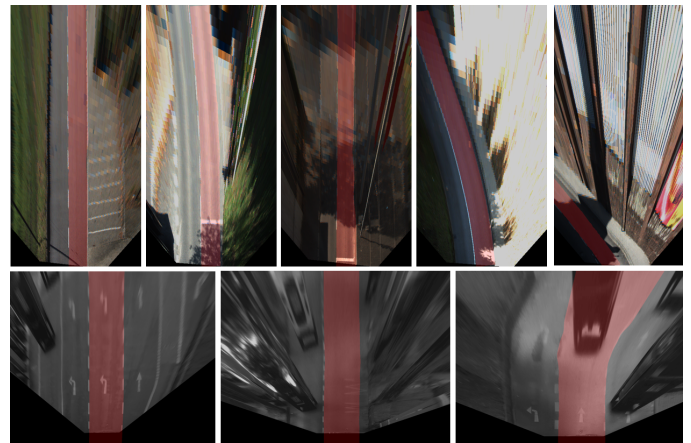


Fig. 9. The First Row is some of the Detection Results of KITTI-UM. The Second Row is some of the Detection Results of Cityscapes. The Red is the Converted Ego Lane based on Lines Detection.

lines. The later part of this chapter shows how the localization method helps the vehicle travels through an intersection in the turning scenario.

For lane lines detection, the method was tested on KITTI [15] and Cityscapes [25]. For general traffic lines detection, The proposed method was tested on the Berkeley deep drive (BDD 100k) [26], KITTI and a self-recorded video. These results of general lines detection cannot be compared to other methods due to lacking metrics. At last, the BDD 100k dataset and images from a self-recorded video are used for testing the localization method while passing free spaces.

##### A. Lane Lines Detection

The proposed lines detector, ECPrior (Erosion and Cluster with prior knowledge), perform as good as other deep neural network supporting approaches [27] [28] [29] [30] based on the KITTI behaviour evaluation [31] metric. The result is shown in Table I. Some of the detection results are shown in the first row of Fig. 9. The proposed detector does not include object detection; hence it will be affected by other cars close to the lines. A typical object detector can be added before to get a better result, like Satzoda did in [32]. The object detection is usually a separate module, and the same feature should not be implemented again in the lines detection module. The proposed lines detector works equally fine on Cityscape showing its scalability, as shown in the second row of Fig. 9, despite they have very different object aspect ratio from the aspect ratio of images from KITTI.

TABLE I. KITTI (UM LANE) LANE LINES DETECTION RESULT

| Method         | HR-30   | PRE-40  | F1-40   |
|----------------|---------|---------|---------|
| CyberMELD      | 97.55 % | 94.57 % | 89.66 % |
| RBNet          | 95.92 % | 95.56 % | 87.21 % |
| RoadNet3       | 95.57 % | 94.57 % | 83.72 % |
| ECPrior (Mine) | 93.96 % | 96.70 % | 91.86 % |
| Up-Conv-Poly   | 93.14 % | 90.11 % | 83.72 % |

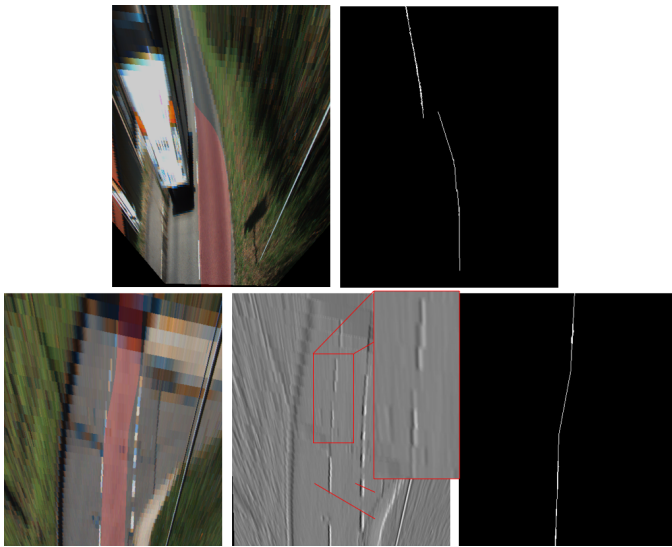


Fig. 10. Two Fail Cases in each Row: (1) the First Image is the Ego Lane Result and the Second is the Lines Detection Result of the Right Side Curb; (2) the Middle Image is the Gradient showing Clear Manifests and the Lines Detection Results shown in the Right Image.

The limitations of ECPrior are:

- Like all other methods, ECPrior relies on a stable and accurate BEV transformation. The transformation is hard to be accurate when the ground is not flat. Although the deep neural networks can learn to avoid this for a specific dataset, it is still hard to scale over different datasets. When it comes to non-flat surfaces, the width of a lane might shrink, as shown in the first fail case in Fig. 10. Dynamic adjustment of the window width can avoid windows from merging. ECPrior can tolerate minor distortion of the BEV transformation.
- Because ECPrior is for general cases, the input images should not have special manifests which would disturb the detector, as shown in the second fail case in Fig. 10. For KITTI, these manifests are mainly caused by the BEV transformation over low quality areas.

### B. General Lines Detection

ECPrior can solve the problem caused by shadows or short breaks for general lines detection. ECPrior is also proved to be robust with different lighting conditions. For stop lines, images from the BDD 100k was used for testing. The result is shown in Fig. 11. The upper case in that image is under a lightly snowing daylight environment, and the lower case in that image is in a night lighting environment. In both cases, ECPrior successfully detects the stop lines ahead.

ECPrior also detects special lines well. A self-recorded video was used for testing. An example in Fig. 12 shows the ability to detect special lines under a turning scenario travelling into a roundabout. In this situation, ECPrior needs to detect the rear inner side of the roundabout. The left side curb of the current lane and the inner side curb of the roundabout can then form a strong anchor used to rebuild the scene of the free space for localization.



Fig. 11. Stop Lines Detected Results on BDD 100K Dataset. Blue Pixels are the Detected Stop Line and Green Pixels are the Guiding Lane Line of that Stop Line.



Fig. 12. Detecting the Inner Side of the Roundabout is an Example of Detecting a Special Line with only its Direction Given. The Top 2 Results are shown as Red and Blue in the Last Image in the Red Box.

ECPrior uses intense erosion and threshold so that only a small portion of target lines will be detected at the pixel level. Hence the ECPrior detector is not a pixel-level detector. ECPrior, as an intact line detection module, provides lines detection result using regression for dash line segments and straight lines and using Spline for the others. ECPrior inevitably relies on an accurate BEV transformation to leverage the prior knowledge of the lines. Distortion due to camera behind the windshield or problematic camera settings also cause a narrower efficient area for general lines detection, at that situation only lines lie in the middle of the front can be detected. As an example, the detector failed to detect the left side of the inner curb due to distortion in Fig. 12.

### C. Localization

Based on these results from previous examples, strong and weak anchors can be established to locate the vehicle in the turning scenario. The proposed localization approach relies on neither GPS nor IMU for vehicles to travel through urban areas. The system provides a stable and accurate position based on the rebuilt scene for path planning and control subsystems in the turning scenario. For the cruising scenario, the detection system gives a lane level localization result (which lane the vehicle is on) which is enough for the following subsystems.

There are several limitations for using the naive approach of my proposed system for localization. Firstly, the proposed localization method relies on visual clues of specific traffic features. Heavy occlusion blocking most of the target traffic lines will affect the location result in some degree. In one situation, the vehicle was approaching the intersection with heavy traffic ahead, blocking most of the coming stop lines. The localization system did not spot anchors until when the vehicle was very close to the stop lines, producing a short

reaction time to stop for the following subsystems. In another situation, the vehicle was about to turn right into a small alley based on the navigation. Several parking vehicles blocked the view of the right side curb. Hence the detection subsystem did not detect the right turning feature for the alley and make the vehicle miss the target turning.

In the first situation, the behaviours of other vehicles can be exploited as an input for the localization subsystem, like the way Gao leveraged the position of other vehicles in [33]. For example, when the system detects a line of stopping vehicles, it can assume the position of the first stopping car is indicating the position of the stop line to form a prediction to extend the reaction time for the following subsystems. In the second situation, a more comprehensive drivable area analysis will show a right side road extension indicating the alley. Additionally, the localization subsystem is compatible with traffic lights, traffic signs and GPS as pieces of additional information to help.

## V. CONCLUSIONS

This paper proposes a new perception centered self-driving system and focuses on testing the proposed general lines detector, ECPrior, and the localization method on several urban cases. The proposed system design is a skeleton and a starting point with all potentials to work with additional modules to get better performance. For example, users can try to apply the method by Hillel in [34] to get rid of the lens flare to make the detection of ECPrior more robust when driving towards the sunshine. The potential is much more promising than other deep neural networks based detection methods. And diverse types of scenes rebuilding can be discussed in future works. Places like indoor parking area without GPS signals will heavily rely on the rebuilt scene to localize the vehicle. Hence they should be prioritized.

In the end, I appeal to the community to reconsider the necessity of using SIFT like visual features for localization, as well as the need for relying on deep neural networks for traffic lines detection in the context of self-driving.

## REFERENCES

- [1] J. Ziegler, P. Bender, M. Schreiber, H. Lategahn, T. Strauß, C. Stiller, T. Dang, U. Franke, N. Appenrodt, C. Keller, E. Kaus, R. Hertwich, C. Rabe, D. Pfeiffer, F. Lindner, F. Stein, F. Erbs, M. Enzweiler, C. Knoepfel, and E. Zeeb, "Making bertha drive—an autonomous journey on a historic route," *IEEE Intelligent Transportation Systems Magazine*, vol. 6, pp. 8–20, 10 2015.
- [2] DMV, "Autonomous vehicle disengagement reports," 2019, last accessed 15 August 2020. [Online]. Available: <https://www.dmv.ca.gov/portal/vehicle-industry-services/autonomous-vehicles/disengagement-reports>
- [3] S. Kuutti, S. Fallah, K. Katsaros, M. Dianati, F. McCullough, and A. Mouzakitis, "A survey of the state-of-the-art localization techniques and their potentials for autonomous vehicle applications," *IEEE Internet of Things Journal*, vol. 5, no. 2, pp. 829–846, 2018.
- [4] M. Bojarski, D. D. Testa, D. Dworakowski, B. Firner, B. Flepp, P. Goyal, L. D. Jackel, M. Monfort, U. Muller, J. Zhang, X. Zhang, J. Zhao, and K. Zieba, "End to end learning for self-driving cars," *CoRR*, vol. abs/1604.07316, 2016. [Online]. Available: <http://arxiv.org/abs/1604.07316>
- [5] G. Bresson, Z. Alsayed, L. Yu, and S. Glaser, "Simultaneous localization and mapping: A survey of current trends in autonomous driving," *IEEE Transactions on Intelligent Vehicles*, vol. 2, no. 3, pp. 194–220, 2017.
- [6] Yan Jiang, Feng Gao, and Guoyan Xu, "Computer vision-based multiple-lane detection on straight road and in a curve," in *2010 International Conference on Image Analysis and Signal Processing*, 2010, pp. 114–117.
- [7] T. Heidenreich, J. Spehr, and C. Stiller, "Laneslam – simultaneous pose and lane estimation using maps with lane-level accuracy," in *2015 IEEE 18th International Conference on Intelligent Transportation Systems*, 2015, pp. 2512–2517.
- [8] W.-C. Ma, R. Urtasun, I. Tartavull, I. A. Barsan, S. Wang, M. Bai, G. Mattyus, N. Homayounfar, S. K. Lakshmikanth, and A. Pokrovsky, "Exploiting sparse semantic hd maps for self-driving vehicle localization," *2019 IEEE/RSJ International Conference on Intelligent Robots and Systems (IROS)*, Nov 2019. [Online]. Available: <http://dx.doi.org/10.1109/IROS40897.2019.8968122>
- [9] C. Toft, E. Stenborg, L. Hammarstrand, L. Brynte, M. Pollefeys, T. Sattler, and F. Kahl, "Semantic match consistency for long-term visual localization," in *Proceedings of the European Conference on Computer Vision (ECCV)*, September 2018.
- [10] M. Schreiber, C. Knöppel, and U. Franke, "Laneloc: Lane marking based localization using highly accurate maps," in *2013 IEEE Intelligent Vehicles Symposium (IV)*, 2013, pp. 449–454.
- [11] Y. Son, E. S. Lee, and D. Kum, "Robust multi-lane detection and tracking using adaptive threshold and lane classification," *Mach. Vision Appl.*, vol. 30, no. 1, p. 111–124, Feb. 2019. [Online]. Available: <https://doi.org/10.1007/s00138-018-0977-0>
- [12] J. Kim and M. Lee, "Robust lane detection based on convolutional neural network and random sample consensus," 11 2014, pp. 454–461.
- [13] X. Wang, Y. Qian, C. Wang, and M. Yang, "Map-enhanced ego-lane detection in the missing feature scenarios," *IEEE Access*, vol. 8, p. 107958–107968, 2020. [Online]. Available: <http://dx.doi.org/10.1109/ACCESS.2020.3000777>
- [14] A. Borkar, M. Hayes, M. T. Smith, and S. Pankanti, "A layered approach to robust lane detection at night," in *2009 IEEE Workshop on Computational Intelligence in Vehicles and Vehicular Systems*, 2009, pp. 51–57.
- [15] A. Geiger, P. Lenz, and R. Urtasun, "Are we ready for autonomous driving? the kitti vision benchmark suite," in *2012 IEEE Conference on Computer Vision and Pattern Recognition*, 2012, pp. 3354–3361.
- [16] T.-Y. Lin, M. Maire, S. Belongie, J. Hays, P. Perona, D. Ramanan, P. Dollár, and C. L. Zitnick, "Microsoft coco: Common objects in context," *Lecture Notes in Computer Science*, p. 740–755, 2014. [Online]. Available: [http://dx.doi.org/10.1007/978-3-319-10602-1\\_48](http://dx.doi.org/10.1007/978-3-319-10602-1_48)
- [17] Luo-Wei Tsai, Jun-Wei Hsieh, Chi-Hung Chuang, and Kuo-Chin Fan, "Lane detection using directional random walks," in *2008 IEEE Intelligent Vehicles Symposium*, 2008, pp. 303–306.
- [18] A. S. Huang, D. Moore, M. Antone, E. Olson, and S. Teller, "Finding multiple lanes in urban road networks with vision and lidar," *Autonomous Robots*, vol. 26, no. 2, pp. 103–122, 2009. [Online]. Available: <https://doi.org/10.1007/s10514-009-9113-3>
- [19] Q. Lin, Y. Han, and H. Hahn, "Real-time lane departure detection based on extended edge-linking algorithm," in *2010 Second International Conference on Computer Research and Development*, 2010, pp. 725–730.
- [20] C. Lee and J. Moon, "Robust lane detection and tracking for real-time applications," *IEEE Transactions on Intelligent Transportation Systems*, vol. 19, no. 12, pp. 4043–4048, 2018.
- [21] Z. Kim, "Robust lane detection and tracking in challenging scenarios," *IEEE Transactions on Intelligent Transportation Systems*, vol. 9, no. 1, pp. 16–26, 2008.
- [22] M. Bertozzi and A. Broggi, "Gold: a parallel real-time stereo vision system for generic obstacle and lane detection," *IEEE Transactions on Image Processing*, vol. 7, no. 1, pp. 62–81, 1998.
- [23] R. Labayrade, J. Douret, J. Laneurit, and R. Chapuis, "A reliable and robust lane detection system based on the parallel use of three algorithms for driving safety assistance," *IEICE - Trans. Inf. Syst.*, vol. E89-D, no. 7, p. 2092–2100, Jul. 2006. [Online]. Available: <https://doi.org/10.1093/ietisy/e89-d.7.2092>
- [24] S. Wu, H. Chiang, J. Peng, C. Chen, B. Wu, and T. Lee, "The heterogeneous systems integration design and implementation for lane keeping on a vehicle," *IEEE Transactions on Intelligent Transportation Systems*, vol. 9, no. 2, pp. 246–263, 2008.

- [25] M. Cordts, M. Omran, S. Ramos, T. Rehfeld, M. Enzweiler, R. Benenson, U. Franke, S. Roth, and B. Schiele, "The cityscapes dataset for semantic urban scene understanding," *CoRR*, vol. abs/1604.01685, 2016. [Online]. Available: <http://arxiv.org/abs/1604.01685>
- [26] F. Yu, W. Xian, Y. Chen, F. Liu, M. Liao, V. Madhavan, and T. Darrell, "BDD100K: A diverse driving video database with scalable annotation tooling," *CoRR*, vol. abs/1805.04687, 2018. [Online]. Available: <http://arxiv.org/abs/1805.04687>
- [27] G. Oliveira, W. Burgard, and T. Brox, "Efficient deep methods for monocular road segmentation," in *IEEE/RSJ International Conference on Intelligent Robots and Systems (IROS 2016)*, 2016.
- [28] X. Wang, Y. Qian, C. Wang, and M. Yang, "Map-enhanced ego-lane detection in the missing feature scenarios," *arXiv preprint arXiv:2004.01101*, 2020.
- [29] Z. Chen and Z. Chen, "Rbnet: A deep neural network for unified road and road boundary detection," in *International Conference on Neural Information Processing*. Springer, 2017, pp. 677–687.
- [30] Y. Lyu, L. Bai, and X. Huang, "Road segmentation using cnn and distributed lstm," in *2019 IEEE International Symposium on Circuits and Systems (ISCAS)*. IEEE, 2019, pp. 1–5.
- [31] J. Fritsch, T. Kühnl, and A. Geiger, "A new performance measure and evaluation benchmark for road detection algorithms," in *16th International IEEE Conference on Intelligent Transportation Systems (ITSC 2013)*, 2013, pp. 1693–1700.
- [32] R. K. Sazoda and M. M. Trivedi, "Efficient lane and vehicle detection with integrated synergies (elvis)," in *2014 IEEE Conference on Computer Vision and Pattern Recognition Workshops*, 2014, pp. 708–713.
- [33] Tianshi Gao and H. Aghajan, "Self lane assignment using egocentric smart mobile camera for intelligent gps navigation," in *2009 IEEE Computer Society Conference on Computer Vision and Pattern Recognition Workshops*, 2009, pp. 57–62.
- [34] A. B. Hillel, R. Lerner, D. Levi, and G. Raz, "Recent progress in road and lane detection: a survey," *Machine vision and applications*, vol. 25, no. 3, pp. 727–745, 2014.



# Static vs. Dynamic Modelling of Acoustic Speech Features for Detection of Dementia

Muhammad Shehram Shah Syed<sup>1</sup>  
RMIT University, Australia

Zafi Sherhan Syed<sup>2</sup>  
Mehran University, Pakistan

Elena Pirogova<sup>3</sup>  
RMIT University, Australia

Margaret Lech<sup>4</sup>  
RMIT University, Australia

**Abstract**—Dementia is a chronic neurological disease that causes cognitive disabilities and significantly impacts daily activities of affected individuals. It is known that early detection of dementia can improve the quality of life of patients through a specialized care program. Recently, there has been a growing interest in speech-based screening of neurological diseases such as dementia. The focus is on continuous monitoring of changes in speech of dementia patients, aiming to identify the early onset of the disease which could facilitate development of preventative treatment care. In this work, we propose a dynamic (temporal) modeling of acoustic speech characteristics aiming at identifying the signs of dementia. The classification performance of the proposed framework is compared with a baseline static modeling of acoustic speech features. Experimental results show that the proposed dynamic approach outperforms the static method. It achieves the classification accuracy of 74.55% compared to 66.92% obtained using the static models.

**Keywords**—Dementia detection; speech classification; neural networks; recurrent neural networks

## I. INTRODUCTION

Dementia affects a large number of people worldwide. It is estimated that currently more than 50 million individuals suffer from this disease and the number is expected to grow to 75.63 million by the end of 2030 [1]. Dementia is an umbrella term for a set of progressive neurological diseases that lead to impairment or even complete loss of language, memory, thought processes, and problem-solving abilities which compromise the quality of living in affected individuals. There are various types of dementia. In Alzheimer's dementia, nerve cells connections and communication are impaired, eventually leading to nerve cells death and tissue loss throughout the brain. Over time, the brain shrinks dramatically, affecting nearly all its functions. Dementia can also be caused by prolonged suffering from high blood pressure as well as strokes, known as vascular dementia) [2], [3]. Alzheimer's disease disrupts both the way electrical charges travel within nerve cells and the activity of neurotransmitters, thus affecting functions of memory, movement, and thinking ability, which depend on the region of the brain being affected.

Traditional methods for diagnosis are based on neurophysiological tests [4], [5] and neuroimaging (MRI) [6]. However, in recent years there has been a growing focus on less invasive sensing technologies, in particular, speech-based diagnosis and monitoring of dementia [7]. This year, at the Interspeech 2020

conference, Alzheimer's Dementia Recognition through Spontaneous Speech (ADReSS) Challenge was organized which encouraged researchers to develop automated methods for detecting Alzheimer's dementia from speech recordings of patients [8].

This study is focused on developing a method for automated detection of dementia using the dataset provided as part of the ADReSS challenge. Here, we propose a framework based on temporal modelling of acoustic features and demonstrate its effectiveness for the task of identifying individuals with dementia. The performance of the temporal models is bench-marked against the static models which are based on functionals of descriptive statistics. The paper is organized as follows: In section II, we present a brief literature review, in section III we provide a summary of the ADReSS challenge dataset. In section IV we detail the methodology of the temporal modelling framework. Experimental results and discussion are provided in section V and section VI, summary and future outlook are presented in section VII.

## II. RELATED WORK

The ADReSS dataset, central to this study, is the baseline paper relevant to the ADReSS challenge by Luz et al. [8]. The dataset consists of speech recordings of subjects from two groups, healthy individuals and Alzheimer's dementia sufferers. For the classification baseline, Luz et al. computed four types of acoustic feature sets, (i) emobase [9], (ii) Computational Paralinguistics Challenge (ComParE) [10], (iii) Extended Geneva Minimalistic Acoustic Parameter Set (eGeMAPS) [11], and (iv) Multi-Resolution Cochleagram (MRCG) [12], to represent speech characteristics of subjects from the two groups. Here, the functionals based static modelling was used to generate a representation for speech recordings using the above mentioned acoustic feature sets. Results showed that ComParE provided the best classification performance amongst the four feature sets. In [13], Haider et al. investigated the feasibility of paralinguistic features for recognizing Alzheimer's dementia from recordings of spontaneous speech. Notably, while the authors used the same feature sets as [8], they found the eGeMAPS feature set to provide the best classification performance. This suggests that the efficacy of feature sets largely depends on the dataset itself.

Literature shows that it has been a common approach of using linguistic features for the task of recognizing dementia from speech. Fraser et al. [14] computed a large number of features to capture linguistic phenomena, such as grammar constituents, information content, part-of-speech, psycholinguistics, the richness of vocabulary, and the syntactic complexity of speech transcripts. In addition to these features, Fraser et al. also investigated the existence of acoustic abnormality using features derived from the Mel Frequency Cepstral Coefficients (MFCCs) [15] which provide information about the spectral characteristics of speech. Based on their investigation, it was reported that individuals with dementia have a semantically impoverished, syntactically and information deficient language, in addition to abnormal speech. Another notable research by Mirheidari et al. [16], the authors constructed a feature vector consisting of acoustic and linguistic features for the task at hand. In addition, they also computed conversational features that are tuned towards identifying individuals with memory disorders [17]. Their research findings suggest that conversational features provide the best classification performance when transcripts are annotated manually. However, when automated speech recognition was used, the classification accuracy significantly decreased from 96.70% to 76.70%. A decrease in accuracy was also observed for linguistic features with automatically generated transcripts. These results highlight the limitations of automated screening methods based on transcripts, especially when high-fidelity speech transcription is not possible, which can be the case for people suffering from diseases affecting their speaking capability. In the current work, therefore, we focus only on the audio modality.

### III. DATASET

To validate the proposed methodology, we used the dataset provided by the ADReSS challenge at Interspeech 2020. This is advantageous as our experiments can be reproduced by other researchers, since the dataset is available in the public domain. The dataset includes speech recordings from 144 subjects in total; one-half of those are individuals with dementia, whereas the other half are healthy individuals. The recordings have an average duration of 75.30 seconds, a standard deviation of 38.38 seconds, and a maximum duration of 268.48 seconds. Given the significant variation in the duration of speech recordings, we segment each recording into 10 seconds based on non-overlapping chunks for training classifiers on equal duration of speech. At the evaluation stage of the classifier, majority voting was conducted for classification performance analysis. This means that the class with higher probability was assigned to the input sample. A summary of dataset distribution is provided in Table I.

TABLE I. DISTRIBUTION OF SUBJECTS WITH DEMENTIA AND THOSE WHO ARE HEALTHY IN THE ADReSS DATASET

| Gender   | Label   |          |
|----------|---------|----------|
|          | Healthy | Dementia |
| Male     | 36      | 36       |
| Female   | 42      | 42       |
| $\Sigma$ | 72      | 72       |

### IV. METHODOLOGY

We hypothesize that temporal characteristics of speech acoustics can be useful for distinguishing between healthy and dementia individuals. The hypothesis is based on the fact that patients with dementia reveal a lack of speech fluency and exhibit other rhythmic issues (pause and forget, difficulty joining or following a conversation).

For this analysis, we started by computing low-level acoustic speech descriptors (LLDs) preserving the paralinguistic aspect of speech. The LLDs are extracted from speech waveforms segment by segment, thus preserving the temporal characteristics. We normalize the LLD features using standard scaling (z-scores), and then pass them to a recurrent sequence network for generating an embedding that preserves the temporal characteristics of speech. Finally, a fully connected dense classifier is applied to identify subjects with dementia and healthy. The functional block diagram of the proposed temporal modelling framework is shown in Fig. 1.

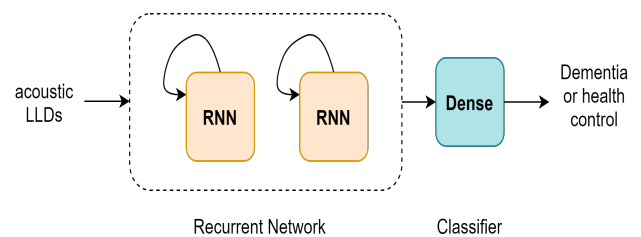


Fig. 1. Block Diagram of Temporal (Dynamic) Modelling of Speech Acoustic Features.

#### A. Audio Features for Speech Paralinguistics

The term speech paralinguistics refers to non-verbal and non-linguistic aspects of speech. As per Schuller et al. [18], paralinguistics are important facets of communication, when human-beings naturally communicate their underlying emotional states without explicitly describing them. It has been shown that audio (acoustic) features representing speech paralinguistics can also be used to screen individuals for various disorders, such as autism, bipolar disorder, depression, dementia, and Parkinson's disease (they can effectively characterize manifestations of mental and neurological disorders based on speech) [19], [20], [21], [13]. Here, we utilize three expert-knowledge based acoustic feature sets that are known to adequately represent characteristics of speech paralinguistics. These feature sets include the Interspeech 2010 Paralinguistics Challenge feature set (IS10-Paralinguistics) [22], the Interspeech 2013 Computational Paralinguistics Challenge (ComParE) feature set [18], and the Extended Geneva Minimalistic Acoustic Parameter Set (eGeMAPS) feature [11]. Given that these feature sets are well known, we refer the reader to [22], [18], [11] for further details on the feature sets.

#### B. Temporal Modeling of Acoustic Features

Recurrent neural networks (RNNs) are a special class of deep neural networks that can learn temporal characteristics from time-series data. In the context of this work, RNNs are used to model temporal variations in speech paralinguistics within utterances of subjects from the two groups. Although

there are various types of recurrent models, the two most popular structures include the Long-Short Term Memory and the Gated Recurrent Unit. Both of these provide various improvements over the legacy recurrent neural network structure (also known as *vanilla RNNs*) which has been difficult to train historically [23], [24]. This study makes use of four variations of the LSTM and one variation of the GRU for performing the temporal modeling.

1) *Long Short Term Memory (LSTM)*: The LSTM was invented by Hochreiter and Schmidhuber [25] aiming to alleviate the vanishing/exploding gradient problem of vanilla RNNs. An LSTM cell, shown in Fig. 2, consists of four interacting layers which include *forget gate*, *input gate*, *update layer*, and *output gate*. Each of these can be considered fully connected networks in their own right, and are therefore trainable. These layers enable the LSTM cell to learn temporal patterns by managing hidden state  $h_t$ , cell state  $C_t$ , and the output of LSTM cell  $y_t$ .

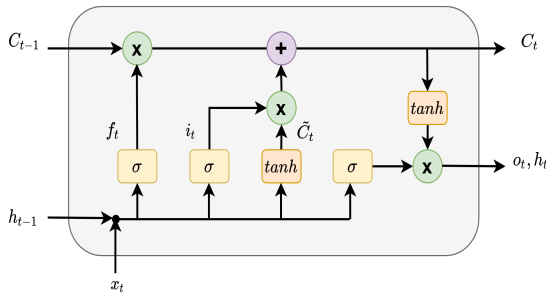


Fig. 2. Illustration of an LSTM Cell (Adopted from [26] ).

The first layer in an LSTM cell is the forget gate, which is responsible for identifying parts of the previous cell state ( $C_{t-1}$ ) that should be removed during the forthcoming update. If this is the first time step of the training process, the previous cell state is generated through random initialization. Next starts the process of updating the cell state with new information. Here, the input gate first identifies the location of values within the cell state which should be updated (and by how much). Then, a candidate vector of cell state values is prepared by passing the combination of input and hidden state through a *tanh* activation to squash their values between -1 and 1. Now, the cell state is updated by the summation of two products: (1) the output of forget gate and the cell state from the previous time-step ( $f_t * C_{t-1}$ ) and (2) the input gate output and the candidate cell state ( $i_t * \tilde{C}_t$ ). The output gate makes decisions about the parts of the cell state which should be produced as the output of the LSTM cell. Finally, the hidden state of the LSTM cell is updated for the next time-step by multiplying the cell output by the *tanh* squashed cell state. Mathematically, the process flow within the LSTM can be summarized as follows, with  $x_t$  representing the input  $N$ -dimensional acoustic features:

$$f_t = \sigma(W_f \cdot [h_{t-1}, x_t] + b_f)$$

$$i_t = \sigma(W_i \cdot [h_{t-1}, x_t] + b_i)$$

$$\tilde{C}_t = \sigma(W_c \cdot [h_{t-1}, x_t] + b_c)$$

$$C_t = f_t * C_{t-1} + i_t * \tilde{C}_t$$

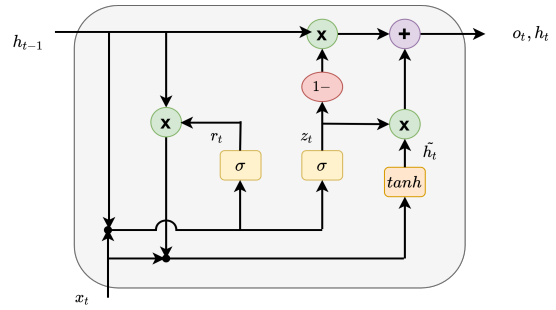


Fig. 3. Illustration of an GRU Cell (Adapted from [26] ).

$$o_t = \sigma(W_o \cdot [h_{t-1}, x_t] + b_o)$$

$$h_t = o_t * \tanh(C_t)$$

A bidirectional LSTM (BLSTM) is similar to an LSTM network, except that instead of the just processing the input in the forward direction for one LSTM cell, a BLSTM has another cell side by side which is fed the input in a reversed manner. By doing this, a BLSTM is able to learn from future occurrences in sequences, and is able to form more complex models than the simple LSTM. BLSTMs have been used in a variety of applications successfully (automatic speech recognition [27], voice conversion [28], etc.).

2) *Gated recurrent unit*: The GRU is a temporal sequence network proposed by Cho et al. [29] with a cell structure that is more simplified than LSTM's cell structure and also has a fewer number of parameters. The GRU cell, as shown in Fig. 2, achieves the reduced complexity by combining the functions of forget and input gates from the LSTM cell into a single update gate.

Mathematically, the process flow within the GRU cell can be summarized as:

$$z_t = \sigma(W_z \cdot [h_{t-1}, x_t] + b_z)$$

$$r_t = \sigma(W_r \cdot [h_{t-1}, x_t] + b_r)$$

$$h_t = (1 - z_t) * h_{t-1} + z_t * \tilde{h}_t$$

3) *Temporal models for recognizing dementia speech*: The process of determining a particular neural network architecture is usually a trial-and-error process based on cross-validation and guided by intuition. To overcome this, we investigate the efficacy of five temporal models to identify the best performing one for the task at hand. A summary of the structure of these models is provided in Table II.

TABLE II. A SUMMARY OF FIVE SEQUENCE MODELS USED FOR LEARNING TEMPORAL CHARACTERISTICS OF SPEECH

| Model ID | Model Summary                                                   |
|----------|-----------------------------------------------------------------|
| Model 1  | LSTM(N) + LSTM(2*N) + LSTM(N) + Dense(N) + Dense(2)             |
| Model 2  | GRU(N) + GRU(2*N) + GRU(N) + Dense(N) + Dense(2)                |
| Model 3  | BLSTM(N) + BLSTM(N) + Dense(N) + Dense(2)                       |
| Model 4  | LSTM(N) + LSTM(2*N) + LSTM(N) + Attention + Dense(N) + Dense(2) |
| Model 5  | BLSTM(N) + BLSTM(N) + Attention + Dense(N) + Dense(2)           |

The first model consists of the three-layer stacked LSTM with two dense layers, including the final layer which serves as the classifier. The first and last LSTM layer has recurrent units equal to the dimensionality ( $N$ ) of the input acoustic features. For example, since ComParE LLDs have a dimensionality of 65, therefore the first and last LSTM layers in Model 1 have 65 units. The middle layer is twice the size of the first and the last LSTM layers. We decided to use these settings assuming that a larger number of recurrent units may assist in learning complex temporal patterns from acoustic features. However, this is not straightforward, since the limited amount of training data may impact the learning ability of deeper LSTM models. Moreover, a dense layer was added to investigate whether the addition of a fully connected layer can aid in learning a more meaningful representation from the acoustic embedding learned by networks. Model 2 is identical to Model 1 except that it consists of GRU blocks rather than LSTM cells.

Model 3 is based on bi-directional LSTMs (BLSTM). It consists of two LSTM layers, each with the number of units equal to the dimensionality of the input acoustic LLDs and two dense layers. Here, we used smaller number of BLSTM layers, since BLSTMs naturally train two LSTMs, one in forward direction and the other - in reverse direction of the sequence.

Model 4 and Model 5 are similar to Model 1 and Model 3 except that an attention layer [30] is added to the networks. The attention layer takes into consideration the affect of long-term speech characteristics that may be learned by the LSTMs and have been found to improve the LSTM performance [31].

### C. Static Modelling of Acoustic Features

Whereas temporal models seek to learn a global representation for speech recordings by explicitly considering inter-frame changes, static modelling generates a global representation of speech through feature aggregation. The simplest method of static modelling is to compute functionals of descriptive statistics for acoustic features. While this method may appear trivial, it has often produced state-of-the-art classification performance for paralinguistics tasks [32], [33]. Further, we found static modelling of acoustic features to be useful in our previous research on recognition of perceived trustworthiness [?]. Therefore, we benchmark the classification performance of temporal models against the static models for the task of speech-based detection of dementia.

## V. EXPERIMENTS AND RESULTS

The classification experiments were conducted using the stratified 5-fold cross validation method. Stratification ensures that the distribution of labels in the training partition was matched by the distribution in test partition. The performance of temporal models was benchmarked against the static models using the same LLD feature sets under the same cross-validation settings. Two types of classifiers, the support vector machine classifier (SVC) and random forest classifier (RFC), are used for classification with default settings as given in the Scikit-learn toolkit [34]. The results are presented in Table III, where it can be seen the best performing model, ComParE-SVC, yields an accuracy of 66.92%.

TABLE III. SUMMARY OF CLASSIFICATION RESULTS FOR STATIC MODELS FOR IS10-PARALINGUISTICS, COMPAR E, AND eGEMAPS FEATURE SETS

| Feature set          | Accuracy (%) |              |
|----------------------|--------------|--------------|
|                      | SVC          | RF           |
| IS10-Paralinguistics | <b>61.92</b> | 58.85        |
| ComParE              | <b>66.92</b> | 61.92        |
| eGeMAPS              | 57.31        | <b>62.31</b> |

TABLE IV. SUMMARY OF CLASSIFICATION RESULTS FOR TEMPORAL MODELS USING IS10-PARALINGUISTICS FEATURE SET

| Model Name | Accuracy (%) |
|------------|--------------|
| Model 1    | 70.02        |
| Model 2    | 64.35        |
| Model 3    | 71.79        |
| Model 4    | 72.50        |
| Model 5    | <b>74.55</b> |

TABLE V. SUMMARY OF CLASSIFICATION RESULTS FOR TEMPORAL MODELS USING COMPAR E FEATURE SET

| Model Name | Accuracy (%) |
|------------|--------------|
| Model 1    | 64.87        |
| Model 2    | 60.02        |
| Model 3    | 67.14        |
| Model 4    | 65.34        |
| Model 5    | <b>69.60</b> |

TABLE VI. SUMMARY OF CLASSIFICATION RESULTS FOR TEMPORAL MODELS USING eGEMAPS FEATURE SET

| Model Name | Accuracy (%) |
|------------|--------------|
| Model 1    | 66.50        |
| Model 2    | 64.64        |
| Model 3    | 68.93        |
| Model 4    | 71.70        |
| Model 5    | <b>73.84</b> |

In Table IV, we summarize the classification performance of the static and temporal models for IS10-Paralinguistics acoustic features. As can be seen, the best performance for the static modelling of features is 61.92% whereas the best performing temporal model, Model 5 which uses BLSTM-Attention, achieves an accuracy of 74.55%, closely followed by Model 4 which is based on LSTM-Attention achieves an accuracy of 72.50%. While these results are preliminary, they indicate that attention mechanism can assist in improving the classification models.

The classification performance using ComParE feature set has been summarized in Table V. Here, the static modelling achieves the best performance with a classification accuracy of 62.31%. In contrast, best model amongst the temporal modelling approaches achieves an accuracy of 69.60%. Interestingly, the performance of the best sequence modelling result is significantly lower when compared to the result of the previous experiment. We suggest this is because the dimensionality of ComParE is much larger than that of IS10-Paralinguistic features (130 versus 76), and there are not enough examples in the dataset to adequately train temporal models with ComParE features.

Finally, Table VI shows the summary of classification performance for the static and temporal modelling using eGeMAPS features. As can be seen, the best performing model for the static features is eGeMAPS-RF which achieves an accuracy of 62.31%, whereas the best performing model amongst temporal models is Model 5 that provides an accuracy of 73.84%. The second placed temporal model, Model 4, achieves an accuracy of 71.70%. Both these results are more superior than the accuracy achieved through the static-modelling.

## VI. DISCUSSION

The results presented above lead to some interesting observations. Firstly, we note that the temporal models provide higher classification performance than the static models. A caveat to this is the performance of the temporal models with ComParE features which offer relatively smaller improvements than IS10-Paralinguistics and eGeMAPS feature set. We suggest this is due to the large dimensionality of ComParE LLDs – 130 for ComParE versus 76 for IS10-Paralinguistics and 23 for eGeMAPS LLDs, respectively. Another observation is that attention mechanism contributed to the consistently improved classification by the temporal models. We believe this is because attention mechanism assists the temporal models in focusing on time-dependent characteristics of acoustic LLDs that are unique for individuals with dementia.

Table VII summarizes the classification results of top-3 best performing models, where one can note that all of these models are based on the temporal modelling with attention mechanism, and two out of these make use of the IS10-Paralinguistic feature set. As can be seen, a significant improvement in classification accuracy is achieved when compared to the best performing statistic model (which achieved 66.92%).

TABLE VII. SUMMARY OF TOP-3 TEMPORAL MODELS

| Model   | Acoustic Feature     | Accuracy (%) |
|---------|----------------------|--------------|
| Model 5 | IS10-Paralinguistics | 74.55        |
| Model 5 | eGeMAPS              | 73.84        |
| Model 4 | IS10-Paralinguistics | 72.50        |

## VII. CONCLUSION

In this paper, we investigated the efficiency of the temporal modelling vs. static modeling of speech acoustics for detection of individuals with dementia. We benchmarked the proposed temporal models with the static models of acoustic features. Experimental results showed that the temporal modelling is a more effective approach for the intended classification task, revealing the best-case accuracy of 74.55% in a 5-fold cross-validation setup. This accuracy may not be sufficient to support a medical diagnosis; however it is sufficiently high to conduct a low-cost rapid screening for dementia that could be followed up by a professional assessment. The proposed acoustic speech classification could be used either alone or in combination with transcript analysis, questionnaires, and other standard screening techniques.

Our future work will investigate application of other deep learning models and integration of dynamic and static approaches into a combined decision-making system.

## REFERENCES

- [1] World Health Organization, "The Epidemiology and Impact of Dementia - Current State and Future Trends," Tech. Rep., 2018. [Online]. Available: <https://www.who.int/health-topics/dementia>
- [2] Stanford Healthcare, "Causes of Dementia," 2020. [Online]. Available: <https://stanfordhealthcare.org/medical-conditions/brain-and-nerve/dementia/causes.html>
- [3] Alzheimers Association, "What Is Dementia?" 2020. [Online]. Available: <https://www.alz.org/alzheimers-dementia/what-is-dementia>
- [4] K. Ritchie, I. Carriere, L. Su, J. T. O'Brien, S. Lovestone, K. Wells, and C. W. Ritchie, "The midlife cognitive profiles of adults at high risk of late-onset Alzheimer's disease: The PREVENT study," *Alzheimer's and Dementia*, vol. 13, no. 10, pp. 1089–1097, 2017.
- [5] M. Mortamais, J. A. Ash, J. Harrison, J. Kaye, J. Kramer, C. Randolph, C. Pose, B. Alcala, M. Ropacki, C. W. Ritchie, and K. Ritchie, "Detecting cognitive changes in preclinical Alzheimer's disease: A review of its feasibility," *Alzheimer's and Dementia*, vol. 13, no. 4, pp. 468–492, 2017.
- [6] C. Laske, H. R. Sohrabi, S. M. Frost, K. Lopez-De-Ipina, P. Garrard, M. Buscema, J. Dauwels, S. R. Soekadar, S. Mueller, C. Linnemann, S. A. Bridenbaugh, Y. Kanagasigam, R. N. Martins, and S. E. O'bryant, "Innovative diagnostic tools for early detection of Alzheimer's disease," *Alzheimer's and Dementia*, vol. 11, no. 5, pp. 561–578, 2015.
- [7] V. Boschi, E. Catricala, M. Consonni, C. Chesi, A. Moro, and S. F. Cappa, "Connected speech in neurodegenerative language disorders: A review," *Frontiers in Psychology*, vol. 8, pp. 1–21, 2017.
- [8] S. Luz, F. Haider, S. de la Fuente, D. Fromm, and B. MacWhinney, "Alzheimer's Dementia Recognition through Spontaneous Speech: The ADReSS Challenge," in *INTERSPEECH (to appear)*, 2020, pp. 1–5.
- [9] F. Eyben, F. Weninger, F. Gross, and B. Schuller, "Recent developments in openSMILE, the munich open-source multimedia feature extractor," in *ACM International Conference on Multimedia*, 2013, pp. 835–838.
- [10] B. Schuller, S. Steidl, A. Batliner, J. Hirschberg, J. K. Burgoon, A. Baird, A. Elkins, Y. Zhang, E. Coutinho, and K. Evanini, "The INTERSPEECH 2016 Computational Paralinguistics Challenge: Deception, Sincerity & Native Language," in *INTERSPEECH*, 2016, pp. 2001–2005.
- [11] F. Eyben, K. R. Scherer, B. W. Schuller, J. Sundberg, E. Andre, C. Busso, L. Y. Devillers, J. Epps, P. Laukka, S. S. Narayanan, and K. P. Truong, "The Geneva Minimalistic Acoustic Parameter Set (GeMAPS) for Voice Research and Affective Computing," *IEEE Transactions on Affective Computing*, vol. 7, no. 2, pp. 190–202, 2016.
- [12] J. Chen, Y. Wang, and D. Wang, "A feature study for classification-based speech separation at low signal-to-noise ratios," *IEEE/ACM Transactions on Audio Speech and Language Processing*, vol. 22, no. 12, pp. 1993–2002, 2014.
- [13] F. Haider, S. de la Fuente, and S. Luz, "An Assessment of Paralinguistic Acoustic Features for Detection of Alzheimer's Dementia in Spontaneous Speech," *IEEE Journal of Selected Topics in Signal Processing*, vol. 14, no. 2, pp. 272–281, 2019.
- [14] K. C. Fraser, J. A. Meltzer, and F. Rudzicz, "Linguistic features identify Alzheimer's disease in narrative speech," *Journal of Alzheimer's Disease*, vol. 49, no. 2, pp. 407–422, 2015.
- [15] D. Yu and L. Deng, *Automatic speech recognition*. Springer, 2016.
- [16] B. Mirheidari, D. Blackburn, T. Walker, M. Reuber, and H. Christensen, "Dementia detection using automatic analysis of conversations," *Computer Speech and Language*, vol. 53, pp. 65–79, 2019.
- [17] C. Eelsey, P. Drew, D. Jones, D. Blackburn, S. Wakefield, K. Harkness, A. Venneri, and M. Reuber, "Towards diagnostic conversational profiles of patients presenting with dementia or functional memory disorders to memory clinics," *Patient Education and Counseling*, vol. 98, no. 9, pp. 1071–1077, 2015.
- [18] B. Schuller, S. Steidl, A. Batliner, F. Burkhardt, L. Devillers, C. Muller, and S. Narayanan, "Paralinguistics in speech and language — State-of-the-art and the challenge," *Computer Speech and Language*, vol. 27, no. 1, pp. 4–39, 2013.
- [19] Z. S. Syed, K. Sidorov, and D. Marshall, "Depression Severity Prediction Based on Biomarkers of Psychomotor Retardation," in *ACM*

- International Workshop on Audio/Visual Emotion Challenge (AVEC)*, 2017, pp. 37–43.
- [20] —, “Automated Screening for Bipolar Disorder from Audio/Visual Modalities,” in *ACM International Workshop on Audio/Visual Emotion Challenge (AVEC)*, 2018, pp. 39–45.
- [21] S. Amiriparian, A. Baird, S. Julka, A. Alcorn, S. Ottl, S. Petrovic, E. Ainger, N. Cummins, and B. Schuller, “Recognition of Echolalic Autistic Child Vocalisations Utilising Convolutional Recurrent Neural Networks,” in *INTERSPEECH*, 2018, pp. 2334–2338.
- [22] S. Steidl, A. Batliner, F. Burkhardt, L. Devillers, M. Christian, S. Language, P. Group, D. Telekom, and A. G. Laboratories, “The INTERSPEECH 2010 Paralinguistic Challenge,” in *INTERSPEECH*, 2010, pp. 2794–2797.
- [23] Y. Bengio, P. Frasconi, and P. Simard, “Problem of learning long-term dependencies in recurrent networks,” in *IEEE International Conference on Neural Networks*, 1993, pp. 157–166.
- [24] Y. Bengio, P. Simard, and P. Frasconi, “Learning Long-Term Dependencies with Gradient Descent is Difficult,” *IEEE Transactions on Neural Networks*, vol. 5, no. 2, pp. 157–166, 1994.
- [25] S. Hochreiter and J. Schmidhuber, “Long Short-Term Memory,” *Neural Computation*, vol. 9, no. 8, pp. 1735–1780, 1997.
- [26] C. Olah, “Understanding LSTM Networks,” 2015. [Online]. Available: <https://colah.github.io/posts/2015-08-Understanding-LSTMs>
- [27] A. Zeyer, P. Doetsch, P. Voigtlaender, R. Schlüter, and H. Ney, “A comprehensive study of deep bidirectional lstm rnns for acoustic modeling in speech recognition,” in *2017 IEEE International Conference on Acoustics, Speech and Signal Processing (ICASSP)*. IEEE, 2017, pp. 2462–2466.
- [28] H. Ming, D. Huang, L. Xie, J. Wu, M. Dong, and H. Li, “Deep bidirectional lstm modeling of timbre and prosody for emotional voice conversion,” 2016.
- [29] K. Cho, B. van Merriënboer, C. Gulcehre, D. Bahdanau, F. Bougares, H. Schwenk, and Y. Bengio, “Learning Phrase Representations using RNN Encoder-Decoder for Statistical Machine Translation,” *arXiv:1406.1078*, pp. 1–15, 2014.
- [30] A. Vaswani, N. Shazeer, N. Parmar, J. Uszkoreit, L. Jones, A. N. Gomez, Ł. Kaiser, and I. Polosukhin, “Attention is all you need,” in *Advances in Neural Information Processing Systems*, 2017.
- [31] Y. Xie, R. Liang, Z. Liang, C. Huang, C. Zou, and B. Schuller, “Speech emotion classification using attention-based lstm,” *IEEE/ACM Transactions on Audio, Speech, and Language Processing*, vol. 27, no. 11, pp. 1675–1685, 2019.
- [32] B. Schuller, S. Steidl, A. Batliner, E. Bergelson, J. Krajewski, C. Janott, A. Amatuni, M. Casillas, A. Seidl, M. Soderstrom, A. S. Warlaumont, G. Hidalgo, S. Schnieder, C. Heiser, W. Hohenhorst, M. Herzog, M. Schmitt, K. Qian, Y. Zhang, G. Trigeorgis, P. Tzirakis, and S. Zafeiriou, “The INTERSPEECH 2017 Computational Paralinguistics Challenge: Addressee, Cold and Snoring,” in *INTERSPEECH*, 2017, pp. 1–5.
- [33] B. W. Schuller, S. Steidl, A. Batliner, P. B. Marschik, H. Baumeister, F. Dong, S. Hantke, F. Pokorny, E.-M. Rathner, K. D. Bartl-Pokorny, C. Einspieler, D. Zhang, A. Baird, S. Amiriparian, K. Qian, Z. Ren, M. Schmitt, P. Tzirakis, and S. Zafeiriou, “The INTERSPEECH 2018 Computational Paralinguistics Challenge: Atypical and Self-Assessed Affect, Crying and Heart Beats,” in *INTERSPEECH*, 2018, pp. 1–5.
- [34] F. Pedregosa, G. Varoquaux, A. Gramfort, V. Michel, B. Thirion, O. Grisel, M. Blondel, P. Prettenhofer, R. Weiss, V. Dubourg, J. Vanderplas, A. Passos, D. Cournapeau, M. Brucher, M. Perrot, and E. Duchesnay, “Scikit-learn: Machine Learning in Python,” *Journal of Machine Learning Research*, vol. 12, pp. 2825–2830, 2011.

# Multi-Objective Evolutionary Programming for Developing Recommender Systems based on Collaborative Filtering

Edward Hinojosa-Cardenas<sup>1</sup>  
Universidad Nacional de San Agustín  
de Arequipa, Peru

Edgar Sarmiento-Calisaya<sup>2</sup>  
Universidad Nacional de San Agustín  
de Arequipa, Peru

Cesar A. Martinez-Salinas<sup>3</sup>  
Universidad Nacional de San Agustín  
de Arequipa, Peru

Lehi Quincho-Mamani<sup>4</sup>  
Universidad Nacional de San Agustín  
de Arequipa, Peru

Jair F. Huaman-Canqui<sup>5</sup>  
Universidad Nacional de San Agustín  
de Arequipa, Peru

**Abstract**—In the era of internet, several online platforms offer many items to users. Users could spend a lot of time to find (or not) some items they are interested, sometimes, they will probably not find the desired items. An effective strategy to overcome this problem is a recommender system, one of the most popular applications of machine learning. Recommender systems select most appropriate items to a specific user based on previous information between items and users, and they are developed using different approaches. One of the most successful approach for developing recommender systems is collaborative filtering, which can filter out items that a user might like based on reactions of users with similar profiles. Often, traditional recommender systems only consider *precision* as evaluation metric of performance, however, others metrics (like recall, diversity, novelty, etc) are also important. Unfortunately, some metrics are conflicting, e.g., precision impacts negatively on other metrics. This paper presents a multi-objective evolutionary programming method for developing a recommender system, which is based on a new collaborative filtering technique, while maximizes the *recall* for a given *precision*. The new collaborative filtering technique uses three components for recommending an item to a user: 1) clustering of users; 2) a previous memory-based prediction; and 3) five decimal parameters (threshold average clustering, threshold penalty, threshold incentive, weight attached to average clustering and weight attached to *Pearson correlation*). The multi-objective evolutionary programming optimizes the clustering of users and the five decimal parameters, while, it searches maximizes both similarity precision and recall objectives. A comparison between the proposed method and a previous non-evolutionary method shows that the proposed method improves precision and recall metric on a benchmark database.

**Keywords**—Collaborative filtering; clustering; evolutionary programming; multi-objective; recommender systems

## I. INTRODUCTION

Huge amounts of user data are generated and collected every day on the web, given the explosive growth of information, users are often greeted with more than countless choices [1]. Recommender system is an effective tool for helping the user in cutting the time needs to find personalised movies, products, documents, friends, places, services, among others [2]. Also, a recommender system is one of the most important and new research area in machine learning [3].

The most commonly recommendation approaches [4] used to produce a list of items for a user are: content-based, collaborative filtering and hybrid approaches. Content-based filtering is based on the item to define the prediction, i.e., it uses features of the item to make a similar item recommendations. Collaborative filtering is one of the most prominent and popular approaches, It recommends similar items to similar users (similar users is based on past behavior, previous purchases, preferences, ratings of other products, average purchase amount, etc.). And, hybrid filtering combines the two filtering approaches.

Evolutionary computing (or evolutionary algorithm) is a research area within computer science, as the name suggests, it is a special flavour of computing, which draws inspiration from the process of natural evolution. The fundamental metaphor of evolutionary computing relates this powerful natural evolution to a particular style of problem solving - that of trial-and-error [5]. The main branches [6] of evolutionary computing are: Genetic Algorithm, Evolutionary Strategies, Differential Evolution, Genetic Programming and Evolutionary Programming. Evolutionary Programming (EP) is a computational optimization method to find global optimal solution for a given problem and, it is used in this paper. All of these branches have been used to resolve different trends in recommender systems research [7], among these trends, the use of evolutionary computing for optimizing weights of recommendation techniques/component and learning recommendation systems.

The performance of classical recommendation algorithms is usually evaluated by accuracy related metrics [8], like *precision* and *recall*. From the definitions, precision and recall are conflicting objectives because while recall tries to increase the number of tagged entries as much as possible or the fraction of relevant information that are retrieved, precision tries to increase the number of correctly tagged entries or the fraction of information retrieved that are relevant [9]. A common strategy for dealing with this problem is the evolutionary multi-objective optimization, which refers to the use of evolutionary algorithms to solve problems with two or more (often conflicting) objective functions [10].

The proposed method, named MOEP-CF, is based on

a Multi-Objective Evolutionary Programming for developing recommender systems, which uses a new Collaborative Filtering technique and, improves precision and recall objectives. The new collaborative filtering technique is based on three components to recommend an item to a user: 1) clustering of the users; 2) a previous memory-based prediction; and 3) five decimal parameters (threshold average clustering, threshold penalty, threshold incentive, weight attached to average clustering and weight attached to *Pearson correlation*). The optimization process is guided by a proposed new mutation operator with ten types of mutation and improves six components or sub components of the new collaborative filtering technique: 1) users assigned to each cluster; 2) threshold for penalty; 3) threshold for incentive; 4) threshold for average cluster ranking; 5) weight attached to average cluster ranking; and 6) weight attached to memory-based prediction. The MOEP-CF proposed method is based on a previous non multi-objective evolutionary method proposed in [11].

The main contributions of this work are summarized as follows:

- The new collaborative filtering technique based on three components.
- The use a multi-objective Evolutionary programming for developing recommender systems based on new collaborative filtering technique and improving precision and recall objectives.
- The new mutation operator with ten types of mutation to improve components or sub components of the new collaborative filtering technique.

The rest of the paper is structured as follows. Related work is presented in Section II. Section III defines collaborative filtering and gives an example of the clustering-based collaborative filtering algorithm used in this paper for recommendation process. Section IV presents a review of evolutionary programming and the multi-objective evolutionary programming algorithm used in the proposed method is presented. A detailed description of the proposed method is presented in Section V. Section VI shows experimental results and compares that results with the previous method, and presents advantages of the proposed method. Section VII concludes the work and presents future work.

## II. RELATED WORK

The proposed method in this paper is related to four broader research areas, namely CF approaches in recommender systems, clustering-based recommender systems, evolutionary computing in recommender systems and recommender systems that analyzed the performance metrics such as precision and recall.

### A. CF-Based Recommendation Approaches

Collaborative filtering, as one of the most successful recommendation techniques, has been widely studied and applied by various research institutions and industries. However, CF-based approach often suffers from several shortcomings [16] [17], such as data sparsity, cold start, and scalability issues, which seriously affect the efficiency of a recommender system

(RS). To overcome the mentioned problems, many data mining and machine learning techniques such as clustering [19] [22] [20] [21] and matrix factorization (Surveyed in [18]) are proposed to improve the performance of RS. Matrix factorization, one of the unsupervised learning methods, can play a role in reducing dimensionality and eventually alleviating the data sparsity [16].

Yang et al. [16] and Chen et al. [17] review and summarize the traditional CF-based approaches and techniques used in RS, classify and compare several typical CF algorithms as memory-based approaches and model-based approaches, and study some recent hybrid CF-based recommendation approaches and techniques, including the latest hybrid memory-based and model-based CF recommendation algorithms.

### B. Clustering-based Recommender Systems

There has been diverse research to enhance recommendation accuracy by means of clustering methods, such as [19] [22] [20] [21]. In [19], is presented an approach (D2P) to addresses the tradeoff between privacy and quality of recommendation, it can be applied to any collaborative recommender system. The main intuition behind D2P is to rely on a distance metric between items so that groups of similar items can be identified. As a result of grouping, the K most similar users based on the similarity measure were selected for recommendation. In [22], a k-means clustering-based recommendation algorithm is proposed, which addresses the scalability issues associated with traditional recommender systems. An issue with traditional k-means clustering algorithms is that they choose the initial k centroid randomly, which leads to inaccurate recommendations and increased cost for offline training of clusters. In [20], a fuzzy C-Means approach has been proposed for user-based collaborative filtering and its performance against different clustering approaches (including K-Means, self-organizing maps, and fuzzy C-Means) has been assessed. A collaborative filtering algorithm based on singular value decomposition (SVD) and fuzzy clustering was shown in [21]. It also reduces the dimensionality (scalability problem) and the search range of the neighbors.

### C. Evolutionary Computing in Recommender Systems

Evolutionary Computing (EC) can optimize and improve RS in the various applications. Horváth & de Carvalho [7] and Sadeghi & Asghari [23] provide comprehensive reviews of more relevant publications focusing on three relevant aspects: approaches in which EC are used to optimize weights of recommendation techniques or different component, approaches utilizing EC for clustering of items or users, and hybrid and other approaches. In [24] [25] [27] [26] [28], novel heterogeneous evolutionary clustering algorithms are presented.

In [24], a new genetic algorithm encoding is proposed as an alternative of k-means clustering. The initialization issue in the classical k-means is targeted by proposing a new formulation of the problem, to reduce the search space complexity affect as well as improving clustering quality.

In [25] [27] [26] [28], novel heterogeneous evolutionary clustering algorithms are presented. The goal of these algorithms is to gather users with similar interest into the same cluster and to help users find items that fit their personal tastes



best. Firstly, items and users are regarded as heterogeneous individuals in the network. According to the constructed network clustering model, states of users evolve over time. States of users would be stable after some period of iteration. In light of stable states of users, they are clustered into several groups. Liji et al. [27] compute the user attribute distances. In chen et al. [26], a dynamic evolutionary clustering algorithm based on time weight and latent attributes is proposed. Then, collaborative filtering is applied in each cluster to predict the ratings.

In [28], a novel collaborative filtering recommendation algorithm based on user correlation and evolutionary clustering is presented. Firstly, score matrix is pre-processed with normalization and dimension reduction. Based on these processed data, clustering principle is generated and dynamic evolutionary clustering is implemented. Secondly, the search for the nearest neighbors with highest similar interest is considered. A measurement about the relationship between users is proposed, called user correlation, which applies the satisfaction of users and the potential information.

In [29], a hybrid approach to increase the accuracy of recommendation of user-based collaborative filtering video recommender system is proposed. The proposed approach combines k-means clustering algorithm and two different evolutionary algorithms which are Accelerated Particle Swarm Optimization Algorithm (APSO) and Forest Optimization Algorithm (FOA).

#### D. Performance Analysis in terms of Accuracy (Precision and Recall)

Many evaluation metrics are available for recommendation systems and each has its own pros and cons, but a few works provide guidance on how to choose and evaluate the impacts among them. For example, Schröder et al. [30] describe accuracy related evaluation metrics and discuss their applicability for different types of recommender systems.

Classical recommender systems mainly focus on the accuracy related metrics. However, with the increase of the diversified demands of users, multiple metrics which may conflict with each other have to be considered in modern recommender systems, especially for the personalized recommender system. Lin et al. [31] present a multi-objective personalized recommendation algorithm using extreme point guided evolutionary computation (called MOEA-EPG). In MOEA-EPG, the accuracy, diversity, and novelty of recommendations are chosen as the three conflicting objectives, and the aim of that algorithm is to optimize the modeled MOP for personalized recommendation.

In the context of trade-offs among accuracy related metrics, specifically precision and recall, Karabadjji et al. [32] and Tran et al. [11] present methods to improve recommendation performance in terms of accuracy related metrics. Karabadjji et al. [32] propose an evolutionary multi-objective optimization-based recommendation system to pull up a group of profiles that maximizes both similarity with the active user and diversity between its members. The recommendation system will provide high performances in terms of both accuracy (precision, recall, f-measure) and diversity. Tran et al. [11] propose a new clustering-based CF (CBCF) method using

an incentivized/penalized user (IPU) model only with ratings given by users. The purpose of CBCF with the IPU model is to improve recommendation performance such as precision, recall, and F1 score by carefully exploiting different preferences among users, i.e, maximize the recall (or equivalently F1 score) for a given precision. In addition, performance on the precision and recall of other various recommender systems was analyzed in [33] [34] [35].

### III. COLLABORATIVE FILTERING

As one of the most successful approaches to building recommender systems, Collaborative Filtering (CF) uses the known preferences of a group of users to make recommendations or predictions of the unknown preferences for other users [12]. Three main categories of CF techniques are: memory-based, model-based, and hybrid (that combine the two before techniques).

Memory-based techniques use the entire or a sample of the user-item database to generate a prediction. Model-based techniques design and develop models that analyzes the training data to recognize complex patterns and then make intelligence predictions for test data. The proposed MOEP-CF method uses both a memory-based and a model-based technique.

The memory-based technique used by the proposed method is the Weighted Sum of Others' Ratings [13]. Predict rating of a particularity item  $i$  to a user  $a$  is calculated by the following equation:

$$\hat{r}_{a,i} = \bar{r}_a + \frac{\sum_{u \in U} (r_{u,i} - \bar{r}_u) \times w_{a,u}}{\sum_{u \in U} |w_{a,u}|} \quad (1)$$

where:

- $\hat{r}_{a,i}$ : Predict rating for the user  $a$  on the item  $i$
- $\bar{r}_a$ : Average rating for the user  $a$  on all other rated items
- $\bar{r}_u$ : Average rating for the user  $u$  on all other rated items
- $\sum_{u \in U}$ : The summations over all the users  $u \in U$  who have rated the item  $i$
- $w_{a,u}$ : Weight or *Pearson correlation* between the user  $a$  and the user  $u$ .

The *Pearson correlation* between the user  $a$  and user  $u$  is calculated by the following equation:

$$w_{a,u} = \frac{\sum_{i \in I} (r_{a,i} - \bar{r}_a) (r_{u,i} - \bar{r}_u)}{\sqrt{\sum_{i \in I} (r_{a,i} - \bar{r}_a)^2} \sqrt{\sum_{i \in I} (r_{u,i} - \bar{r}_u)^2}} \quad (2)$$

where:

- $w_{a,u}$ : Weight or *Pearson correlation* between the user  $a$  and the user  $u$
- $\bar{r}_a$ : Average rating of the co-rated items of the user  $a$
- $\bar{r}_u$ : Average rating of the co-rated items of the user  $u$

- $\sum_{i \in I}$ : The summations over all the items that both the users  $u$  and the user  $a$  have rated
- $w_{a,u}$ : Weight or *Pearson correlation* between the user  $a$  and the user  $u$ .

For illustration, Table I shows a rating matrix for 8 users and 5 items.

TABLE I. A SIMPLE EXAMPLE OF RATING MATRIX

|    | i1 | i2 | i3 | i4 | i5 |
|----|----|----|----|----|----|
| u1 | 4  | 4  | 1  |    | 5  |
| u2 | 2  | 5  |    | 3  | 1  |
| u3 | 3  | 1  | 5  |    | 1  |
| u4 | 5  | 2  | 2  | 3  | 1  |
| u5 | 1  | 4  | 3  | 5  | 5  |
| u6 | 1  |    | 2  |    | 2  |
| u7 | 3  | 4  | 2  | 4  | 3  |
| u8 | 3  | 5  |    | 1  | 5  |

Based on information available in Table I, it is possible to calculate the *Pearson correlation* between users and, predict rating between users and items. For instance,  $w_{1,5} = 0.28$  and  $w_{3,7} = -0.82$ ; and,  $\hat{r}_{1,4} = 3.18$  and  $\hat{r}_{8,3} = 2.72$ . Tables II and III show the *Pearson correlation* between users and predicted ratings for missed ratings, respectively.

TABLE II. *Pearson Correlation* OR WEIGHTS BETWEEN USERS

|    | u1    | u2    | u3    | u4    | u5    | u6    | u7    | u8    |
|----|-------|-------|-------|-------|-------|-------|-------|-------|
| u1 | 0.00  | -0.69 | -0.83 | 0.00  | 0.28  | -0.28 | 0.71  | 0.50  |
| u2 | -0.69 | 0.00  | -0.28 | -0.03 | 0.08  | -1.00 | 0.85  | 0.05  |
| u3 | -0.83 | -0.28 | 0.00  | 0.45  | -0.68 | -0.19 | -0.82 | -1.00 |
| u4 | 0.00  | -0.03 | 0.45  | 0.00  | -0.77 | -0.97 | 0.08  | -0.56 |
| u5 | 0.28  | 0.08  | -0.68 | -0.77 | 0.00  | 0.87  | 0.43  | 0.05  |
| u6 | -0.28 | -1.00 | -0.19 | -0.97 | 0.87  | 0.00  | -0.50 | 1.00  |
| u7 | 0.71  | 0.85  | -0.82 | 0.08  | 0.43  | -0.50 | 0.00  | -0.30 |
| u8 | 0.50  | 0.05  | -1.00 | -0.56 | 0.05  | 1.00  | -0.30 | 0.00  |

TABLE III. PREDICTED RATINGS

|    | i1 | i2   | i3   | i4   | i5 |
|----|----|------|------|------|----|
| u1 |    |      |      | 3.18 |    |
| u2 |    |      | 2.70 |      |    |
| u3 |    |      |      | 2.70 |    |
| u4 |    |      |      |      |    |
| u5 |    |      |      |      |    |
| u6 |    | 1.62 |      | 0.94 |    |
| u7 |    |      |      |      |    |
| u8 |    |      | 2.72 |      |    |

#### IV. MULTI-OBJECTIVE EVOLUTIONARY PROGRAMMING

Evolutionary Programming (EP) was proposed by Lawrence Fogel [14], it is based on natural evolution and it has been applied with success to many numerical and combinatorial optimization problems.

EP does not require the use of a specific form of representation (for example, real-valued or integer strings), allowing the user to select the most suitable representation for the problem at hand. That is an important feature used in this paper.

Whatever the choice of representation, EP uses an iterative improvement process whereby a parent population structures are perturbed using a suitably defined mutation operator, with a selection process taking place to see which structures survive

#### Algorithm 1: Evolutionary Programming Algorithm

```

RepresentationIndividuals();
t = 0;
Initialize($P_p(t)$);
Evaluate($P_p(t)$);
while isNotTerminated() do
 $P_o(t) = \text{Mutation}(P_p(t))$;
 Evaluate($P_o(t)$);
 $P_p(t + 1) = \text{Select}(P_p(t) \cup P_o(t))$;
 t = t + 1;
end

```

into the next iteration of the Algorithm [6]. An overview of the canonical EP algorithm is provided in Algorithm 1.

Multi-Objective Evolutionary Programming (MOEP) is an extended version of single objective EP. The MOEP algorithm with non-domination sorting can be described in Algorithm 2 and, it was proposed in [15]. The MOEP-CF method is based on MOEP.

#### Algorithm 2: Multi-Objective Evolutionary Programming

```

RepresentationIndividuals();
t = 0;
Initialize($P_p(t)$);
Evaluate($P_p(t)$);
while isNotTerminated() do
 $P_o(t) = \text{Mutation}(P_p(t))$;
 Evaluate($P_o(t)$);
 $P_m(t) = P_p(t) \cup P_o(t)$;
 IdentifyNonDominated($P_m(t)$);
 AssingFrontNumber($P_m(t)$);
 SortByFrontNumber($P_m(t)$);
 $P_p(t + 1) = \text{Select}(P_m(t))$;
 t = t + 1;
end

```

#### V. PROPOSED METHOD

The MOEP-CF proposed method is based on a method proposed in [11], and hybrids Collaborative Filtering (see Section III) and Multi-Objective Evolutionary Programming (see section IV). The MOEP-CF recommends or does not recommend a certain item  $i$  to a certain user  $a$  using a model-based technique based on three features: 1) Previous predicted ranking, 2) Clustering of the users, and 3) Five following parameters:

- $\gamma$ : threshold average clustering of item  $i$  in cluster  $c$
- $\alpha$ : threshold penalty
- $\beta$ : threshold incentive
- $\rho$ : weight attached to average clustering
- $\sigma$ : weight attached to *Pearson correlation*

To decide whether to recommend or not to recommend a certain item  $i$  to a certain user  $a$ , the proposed method follows the Algorithm 3.

**Algorithm 3:** Algorithm to Recommend or not Recommend the Item  $i$  to the User  $a$  (in the Cluster  $c$ )

```

if $\bar{C}_c^i \times \rho \geq \gamma$ then
 if $\hat{r}_{a,i} \times \sigma \geq \beta$ then
 Recommend item i to user a ;
 else
 Don't recommend item i to user a ;
 end
else
 if $\hat{r}_{a,i} \times \sigma \geq \alpha$ then
 Recommend item i to user a ;
 else
 Don't recommend item i to user a ;
 end
end

```

For illustration, Table IV shows the following features: three clusters and five parameters.

TABLE IV. EXAMPLES OF FEATURES FOR PROPOSED COLLABORATIVE FILTERING TECHNIQUE

| Features  | Value                     |
|-----------|---------------------------|
| Cluster 1 | $C_1 = \{u_1, u_4, u_7\}$ |
| Cluster 2 | $C_2 = \{u_2, u_6\}$      |
| Cluster 3 | $C_3 = \{u_3, u_5, u_8\}$ |
| $\gamma$  | 2.21                      |
| $\alpha$  | 0.51                      |
| $\beta$   | 0.99                      |
| $\rho$    | 0.94                      |
| $\sigma$  | 0.35                      |

Following the Algorithm 1 and the information provided in Table IV, it is possible to recommend the item 4 to the user 1; and don't recommend the item 3 to the user 8. A detail of that recommendations are explained in Algorithm 4 and 5, respectively.

**Algorithm 4:** Recommending the item 4 to the user 1 - Explanation

```

if $((3 + 4) \div 2 = 3.5) \times 0.94 \geq 2.21$ then
 if $3.18 \times 0.35 \geq 0.99$ then
 Recommend item 4 to user 1;
 else
 Don't recommend item 4 to user 1;
 end
else
 if $3.18 \times 0.34723 \geq 0.51$ then
 Recommend item 4 to user 1;
 else
 Don't recommend item 4 to user 1;
 end
end

```

**Algorithm 5:** Recommending (not) the item 3 to the user 8 - Explanation

```

if $((5 + 3) \div 2 = 4.0) \times 0.94 \geq 2.21$ then
 if $2.72 \times 0.35 \geq 0.99$ then
 Recommend item 3 to user 8;
 else
 Don't recommend item 3 to user 8;
 end
else
 if $2.72 \times 0.35 \geq 0.51$ then
 Recommend item 3 to user 8;
 else
 Don't recommend item 3 to user 8;
 end
end

```

In order to define features shown in the Table IV for maximizing the precision and recall metrics, the MOEP-CF proposed method follows the Algorithm 5. It is detailed in next subsections step by step.

#### A. Representation of Individuals

Each individual or solutions is encoded in a vector with two parts: the clusters part and the parameters part, such as depicted in Fig. 1.

The clusters part is an integer vector with  $|U|$  dimensions ( $U$  is the set of users); the dimension 1 contains the index of the cluster where user 1 belongs ( $iC_1$ ), the dimension 2 contains the index of the cluster where user 2 belongs ( $iC_2$ ), and so on.

The parameters part is a decimal vector with five dimensions; each dimension represents the parameters  $\gamma$ ,  $\alpha$ ,  $\beta$ ,  $\rho$  and  $\sigma$ , respectively.

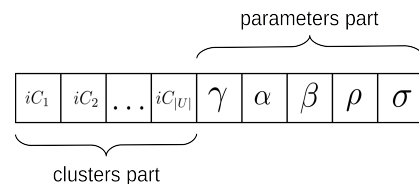


Fig. 1. Representation of Individuals.

Fig. ?? depicts a representation of features detailed in Table IV.

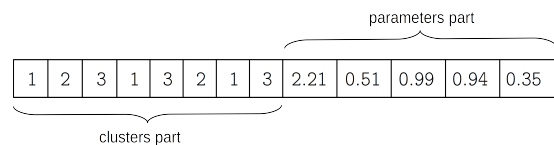


Fig. 2. Example of a Representation.

#### B. Initialize Parents Population

Initial population or parent population ( $P_p(t)$ ) of size  $sizeP$  are randomly generated. For the clusters part, each

dimensions contains a random integer between 1 and  $iC_{max}$  ( $iC_{max}$  represents the maximum number of clusters). For the parameters part,  $\gamma$ ,  $\alpha$  and  $\beta$  contains a random decimal between  $minRank$  and  $maxRank$ ;  $\rho$  and  $\sigma$  contains a random decimal between 0 and 1.

Values  $sizeP$ ,  $iC_{max}$ ,  $minRank$  and  $maxRank$  are a parameters of the proposed method.

### C. Evaluate Parent Population

The MOEP-CF proposed method uses training and test datasets. The test dataset contains some registers with ratings from users to items that are not in training dataset. For each individual in  $P_p(t)$ , it is calculated the precision and recall.

Based on training dataset, the Weighted Sum of Others' Ratings (see Section III) is used to define predicted ratings for the ratings in test dataset. Then, for each individual in  $P_p(t)$ , the Algorithm 1 is used to recommend or don't recommend an item to a user on test dataset. Finally, precision and recall are calculated based on the following equations:

$$precision = \frac{tp}{tp + fp} \quad (3)$$

$$precision = \frac{tp}{tp + fn} \quad (4)$$

$$tp = \sum_{v=0}^T [R_{v,u,i}^{test} \text{ and } r_{v,u,i}^{test} \geq \delta_{ref}] \quad (5)$$

$$fp = \sum_{v=0}^T [NR_{v,u,i}^{test} \text{ and } r_{v,u,i}^{test} < \delta_{ref}] \quad (6)$$

$$fn = \sum_{v=0}^T [NR_{v,u,i}^{test} \text{ and } r_{v,u,i}^{test} \geq \delta_{ref}] \quad (7)$$

where:

- $tp$ : true positive.
- $fp$ : false positive.
- $fn$ : false negative.
- $T$ : number of registers in test dataset.
- $R_{v,u,i}^{test}$ : Recommend the item  $i$  to user the  $u$  (in register  $v$ ) in test dataset following the Algorithm 1.
- $NR_{v,u,i}^{test}$ : Don't recommend the item  $i$  to user the  $u$  (in register  $v$ ) in test dataset following the Algorithm 1.
- $r_{v,u,i}^{test}$ : Rating of the user  $u$  on the item  $i$  (in register  $v$ ) in test dataset.
- $\delta_{ref}$ : Threshold value for determining whether a user is really satisfied with the recommended item. It is a parameter of the proposed method and generally set to 4.0 (or 8.0) in case of a five-point scale (or a ten-point scale).
- $[pred]$ : Evaluate to 1 if the predicate  $pred$  is true and 0 otherwise.

### D. Terminating Condition

The terminating condition of MOEP is the maximum number of iterations  $maxIter$ .

### E. Mutation

The mutation process is applied on each individual in  $P_p(t)$  to generate offspring population ( $P_o(t)$ ) and, it is one of the main contributions of the MOEP-CF proposed method. Each parent solution suffer a type of mutation (with a probability) to generate a offspring individual. Table V shows the ten probabilities and types of mutation using in the proposed method.

TABLE V. TYPES OF MUTATION

| Probability | Type of Mutation                                                                                             |
|-------------|--------------------------------------------------------------------------------------------------------------|
| 10%         | Changing randomly the cluster of the 10% of user, i.e., changing randomly 10% of dimensions in clusters part |
| 10%         | Changing randomly the cluster of the 20% of user, i.e., changing randomly 20% of dimensions in clusters part |
| 10%         | Changing randomly the cluster of the 30% of user, i.e., changing randomly 30% of dimensions in clusters part |
| 10%         | Changing randomly the cluster of the 40% of user, i.e., changing randomly 40% of dimensions in clusters part |
| 10%         | Changing randomly the cluster of the 50% of user, i.e., changing randomly 50% of dimensions in clusters part |
| 10%         | Changing the $\gamma$ parameter to a random value between $minRank$ and $maxRank$ values.                    |
| 10%         | Changing the $\alpha$ parameter to a random value between $minRank$ and $maxRank$ values.                    |
| 10%         | Changing the $\beta$ parameter to a random value between $minRank$ and $maxRank$ values.                     |
| 10%         | Changing the $\rho$ parameter to a random value between 0 and 1.                                             |
| 10%         | Changing the $\sigma$ parameter to a random value between 0 and 1.                                           |

### F. Evaluate Offspring Population

The process for calculating precision and recall of each individual in  $P_o(t)$  follows the same evaluation process explained in subsection V-C for  $P_p(t)$ . After that, the  $P_o(t)$  is merged to  $P_p(t)$  to generate a merged population ( $P_m(t)$ ).

### G. Identify Non-Dominated Solutions

A non-dominated solution is a solution that is not dominated by any other solution in  $P_m(t)$ . In the MOEP-CF proposed method, there is no other solution that performs better in precision and recall objective (or equal to one objective and better than another) than the non-dominated solution.

### H. Assign and Sort by Front Number

The no-dominated solutions in  $P_m(t)$ , identified in the previous step, are inserted in the Front 0. A new search for non-dominated solutions is carried out in the population  $P_m(t)$  without considering the solutions in the Front 0, the new non-dominated solutions found are inserted in the Front 1, and so on.

### I. Select the New Parent Population

The next parent population ( $P_p(t+1)$ ) is filled according to front ranking until the size of  $P_p(t+1)$  is equal to  $sizeP$ . If one front is taking partially, perform, for each solution, the sum

of Euclidean distance between the objectives of that solution and other solutions in order to diversify the solutions for next iterations. The greater sum of Euclidean distance are preferred.

Finally, the evolution process is repeated until a termination condition has been reached. The source code of the proposed MOEP-CF proposed method is available on github (username: Edward-Hinojosa-Cardenas, project: MOEP-CF).

## VI. EXPERIMENTAL RESULTS AND PERFORMANCE COMPARISON

In this section, the performance of the MOEP-CF proposed method is evaluated and compared with a similar previous method (non-evolutionary multi-objective method, named CBCF [11]). To show that MOEP-CF method performs better, it is applied on the MovieLens 100K dataset (collected by the GroupLens Research Project at the University of Minnesota). Table VI describes the dataset used in the evaluation. The proposed method is evaluated by 5 folds cross-validation.

TABLE VI. DESCRIPTION OF MOVIELENS 100K DATASET

| Feature              | Value                                                         |
|----------------------|---------------------------------------------------------------|
| Ratings or registers | 100 000 anonymous ratings (each user has at least 20 ratings) |
| Scale                | 5-star scale                                                  |
| Users                | 943                                                           |
| Movies               | 1682                                                          |

The parameters used in the MOEP-CF proposed method are outlined in Table VII.

TABLE VII. PARAMETERS OF THE MOEP-CF PROPOSED METHOD

| Parameter      | Value |
|----------------|-------|
| $sizeP$        | 50    |
| $C_{max}$      | 10    |
| $minRank$      | 1.0   |
| $maxRank$      | 5.0   |
| $maxRank$      | 5.0   |
| $\delta_{ref}$ | 4     |

Fig. ??, ??, ??, ?? and ?? show the results (non-dominated solutions in the last iteration for precision and recall objectives) of the MOEP-CF proposed method for each fold on the MovieLens 100K dataset.

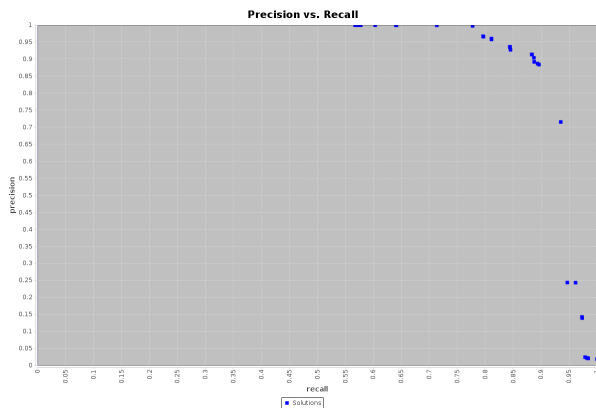


Fig. 3. Results for Two Objectives: Precision and Recall, on Fold 1 of the MovieLens 100K Dataset.

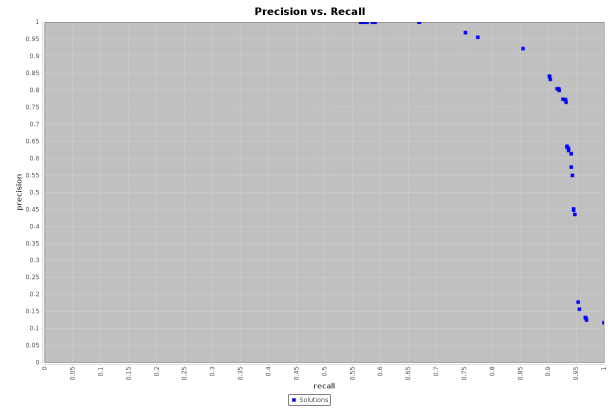


Fig. 4. Results for Two Objectives: Precision and Recall, on Fold 2 of the MovieLens 100K Dataset.

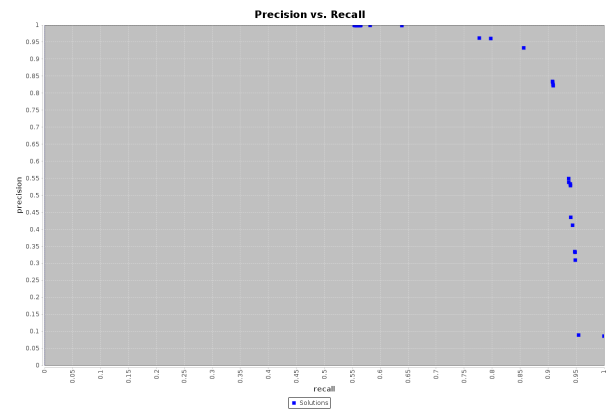


Fig. 5. Results for Two Objectives: Precision and Recall, on Fold 3 of the MovieLens 100K Dataset.

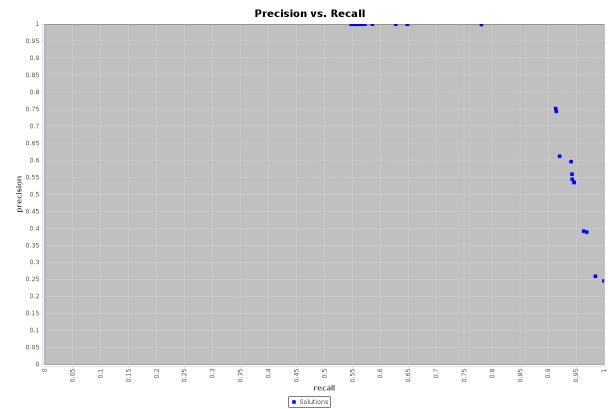


Fig. 6. Results for Two Objectives: Precision and Recall, on Fold 4 of the MovieLens 100K Dataset.

TABLE VIII. RESULTS OF THE MOEP-CF PROPOSED METHOD.

| Fold    | Gamma         | alpha         | beta          | rho           | sigma         | Precision     | Recall        | F1            |
|---------|---------------|---------------|---------------|---------------|---------------|---------------|---------------|---------------|
| Fold 1  | 0.5150        | 1.0714        | 1.1484        | 0.9375        | 0.2659        | 0.8838        | 0.9134        | 0.8984        |
| Fold 2  | 0.0576        | 4.0897        | 1.9213        | 0.6292        | 0.4712        | 0.8553        | 0.9220        | 0.8874        |
| Fold 3  | 0.2445        | 4.1708        | 1.8449        | 0.7097        | 0.4500        | 0.8566        | 0.9328        | 0.8930        |
| Fold 4  | 0.0576        | 4.0897        | 1.9213        | 0.6292        | 0.4712        | 0.8553        | 0.9220        | 0.8874        |
| Fold 5  | 0.4838        | 1.1868        | 0.9666        | 0.7030        | 0.2367        | 0.8654        | 0.9458        | 0.9038        |
| Average | <b>0.2717</b> | <b>2.9217</b> | <b>1.5605</b> | <b>0.7217</b> | <b>0.3790</b> | <b>0.8633</b> | <b>0.9272</b> | <b>0.8940</b> |

TABLE IX. COMPARING THE MOEP-CF METHOD WITH THE CBCF METHOD.

| Method  | Clustering                  | Gamma  | alpha  | beta   | rho    | sigma  | Precision     | Recall        | F1            |
|---------|-----------------------------|--------|--------|--------|--------|--------|---------------|---------------|---------------|
| CBCF    | 10 clusters (Fuzzy C-Means) | 3.3    | 3.7    | 2.9    | -      | -      | 0.6448        | 0.8730        | 0.7418        |
| MOEP-CF | 10 clusters                 | 0.2717 | 2.9217 | 1.5605 | 0.7217 | 0.3790 | <b>0.8633</b> | <b>0.9272</b> | <b>0.8940</b> |

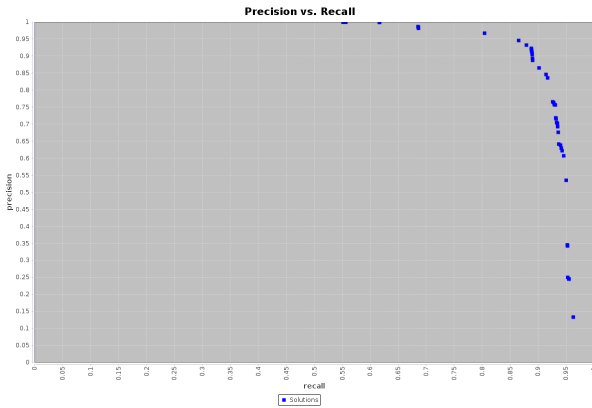


Fig. 7. Results for Two Objectives: Precision and Recall, on Fold 5 of the MovieLens 100K Dataset.

In order to assess the performance of the proposed method against the CBCF method [11]), we used the same dataset. Before of comparison, for each fold, the MOEP-CF method selects a random solution from non-dominated solutions in the last iteration. The average values for all selected solutions are shown in the Table VIII.

Table IX shows the clustering  $\gamma$ ,  $\alpha$  and  $\beta$  values and, the precision, recall and  $F1$  values obtained using the CBCF method. Next, it shows the number of cluster; the average of  $\alpha$ ,  $\beta$ ,  $\gamma$ ,  $\rho$  and  $\sigma$  optimized parameters; and, the average values of precision, recall and  $F1$  obtained in for that MOEP-CF proposed method.

The results show that the MOEP-CF method achieved better results than previous CBCF method on the three metrics mentioned above. The MOEP-CF method with a flexible clustering and two additional parameters (in comparison with the previous method), improves in 33.89%, 6.21% and 20.52% the precision, recall and  $F1$  metrics, respectively.

However, some *limitations* should be noted. First, the proposed method uses static probability values for each mutation which can influence the final result. Second, the proposed method doesn't consider important new metrics like novelty, diversity, stability and reliability in recommendation systems. Third, the parameters of the proposed method, showed in Table VII are defined empirically or experimentally.

## VII. CONCLUSION

Optimizing different objectives simultaneously is a well recognized problem in a recommender system setting. In this work, a multi-objective evolutionary programming method for developing recommender systems is proposed. It is based on a new collaborative filtering technique that achieves high precision and recall.

The main *contributions* of the proposed method are three: a new collaborative filtering technique; a multi-objective evolutionary programming for developing recommender systems improving precision and recall objectives, and, a new mutation operator with ten types of mutations.

*Future Work* includes: adding non-accuracy metrics like novelty, diversity, stability and reliability to multi-objective evolutionary optimization process; using other predicted ranking methods before multi-objective evolutionary optimization process; and, evaluating the proposed method taking as input other popular datasets.

## ACKNOWLEDGMENT

This work was supported by the Universidad Nacional de San Agustín de Arequipa under Project IBAIB-06-2019-UNSA.

## REFERENCES

- [1] Zhang, Shuai and Yao, Lina and Sun, Aixin and Tay, Yi "Dearning Based Recommender System: A Survey and New Perspectives," *ACM Computing Surveys*, vol. 1, no. 1, Feb. 2019.
- [2] Bushra Alhijawi and Yusef Kilani "The Recommender System: A Survey," *International Journal of Advanced Intelligence Paradigms*, vol. 5, no. 3, March 2020.
- [3] Mohamed, Marwa *et al.*, "Recommender Systems Challenges and Solutions Survey," *2019 International Conference on Innovative Trends in Computer Engineering (ITCE'2019)*, pp. 149–155, 2019.
- [4] R. Forsati *et al.*, "A fuzzy co-clustering approach for hybrid recommender systems," *International Journal of Hybrid Intelligent Systems*, vol. 10, no. 2, pp. 71–81, April 2013.
- [5] A.E. Eiben and J.E. Smith, "Introduction to Evolutionary Computing," in *Evolutionary Computing*, 2<sup>nd</sup> ed. Ed. Berlin, Germany: Springer-Verlag Berlin Heidelberg, 2015, pp. 13–16.
- [6] A. Brabazon, M. O'Neill and S. McGarraghy, "Natural Computing Algorithms," in *Natural Computing*, 1<sup>st</sup> ed. Ed. Berlin, Germany: Springer-Verlag Berlin Heidelberg, 2015, pp. 17–20.
- [7] Horváth, Tomáš and Carvalho, André C. "Evolutionary computing in recommender systems: a review of recent research," *Natural Computing: An International Journal*, vol. 16, no. 3, pp. 441–462, Sep. 2017.

- [8] L. Cui *et al.*, "A novel multi-objective evolutionary algorithm for recommendation systems," *Journal of Parallel and Distributed Computing*, vol. 103, pp. 53–63, 2017.
- [9] A. Ekbal, S. Saha, and C. S. Garbe, "Multiobjective Optimization Approach for Named Entity Recognition," in *PRICAI 2010: Trends in Artificial Intelligence*, 1<sup>st</sup> ed. Ed. Berlin, Germany: Springer, Berlin, Heidelberg, 2010, pp. 55–57.
- [10] C. A. Coello Coello, "Evolutionary multi-objective optimization: A historical view of the field," *Computational Intelligence Magazine, IEEE*, vol. 1, no. 1, pp. 28–36, 2006.
- [11] Cong Tran *et al.*, "Clustering-Based Collaborative Filtering Using an Incentivized/Penalized User Model," *IEEE Access*, vol. 7, pp. 62115–62125, 2019.
- [12] Su, Xiaoyuan and Khoshgoftaar, Taghi M. "A Survey of Collaborative Filtering Techniques," *Advances in Artificial Intelligence*, Jan. 2009.
- [13] P. Resnick *et al.*, "GroupLens: an open architecture for collaborative filtering of netnews," *Proceedings of the ACM Conference on Computer Supported Cooperative Work*, pp. 175–186, 1994.
- [14] L. Fogel "Autonomous Automata" *Industrial Research Magazine*, vol. 2, no. 2, pp. 14–19, Feb. 1962.
- [15] P. Venkatesh and K. Y. Lee "Multi-Objective Evolutionary Programming for Economic Emission Dispatch problem" *IEEE Power and Energy Society 2008 General Meeting: Conversion and Delivery of Electrical Energy in the 21st Century*, Aug. 2008.
- [16] Z. Yang *et al.* A survey of collaborative filtering-based recommender systems for mobile internet applications. *IEEE Access*, v. 4, p. 3273–3287, 2016.
- [17] R. Chen *et al.* A survey of collaborative filtering-based recommender systems: From traditional methods to hybrid methods based on social networks. *IEEE Access*, v. 6, p. 64301–64320, 2018.
- [18] D. Bokde, S. Girase and D. Mukhopadhyay, "Matrix factorization model in collaborative filtering algorithms: A survey", *Proc. Comput. Sci.*, vol. 49, pp. 136–146, Apr. 2015.
- [19] R. Guerraoui *et al.*, "D2P: distance-based differential privacy in recommenders," *J. Proc. VLDB Endowment*, vol. 8, no. 8, pp. 862–873, Apr. 2015.
- [20] H. Koochi and K. Kiani, "User based collaborative filtering using fuzzy c-means," *Measurement*, vol. 91, pp. 134–139, Sep. 2016.
- [21] J. Lin, X. H. Yan and B. Huang, "Collaborative filtering recommendation algorithm based on SVD and fuzzy clustering", *Comput. Syst. Appl.*, vol. 25, no. 11, pp. 156–163, 2016.
- [22] S. Zahra, M. A. Ghazanfar, A. Khalid, M. A. Azam, U. Naeem and A. Prugel-Bennett, "Novel centroid selection approaches for KMeans-clustering based recommender systems", *Inf. Sci.*, vol. 320, pp. 156–189, Nov. 2015.
- [23] M. Sadeghi and S. A. Asghari, Recommender systems based on evolutionary computing: a survey. *Journal of Software Engineering and Applications*, v. 10, n. 5, pp. 407–421, 2017.
- [24] C. Berbague, N. E. I. Karabadjji and H. Seridi, An evolutionary scheme for improving recommender system using clustering. In *IFIP International Conference on Computational Intelligence and Its Applications*, pp. 290–301, Springer, 2018.
- [25] J. Chen, H. Wang, and Z. Yan, "Evolutionary heterogeneous clustering for rating prediction based on user collaborative filtering," *Swarm and Evolutionary Comput.*, vol. 38, pp. 35–41, Feb. 2018.
- [26] J. Chen, L. Wei, and L. Zhang, "Dynamic evolutionary clustering approach based on time weight and latent attributes for collaborative filtering recommendation," *Chaos, Solitons & Fractals*, vol. 114, pp. 8–18, Sep. 2018.
- [27] U. Liji, Y. Chai, and J. Chen, "Improved personalized recommendation based on user attributes clustering and score matrix filling," *Comput. Standards & Interfaces*, vol. 57, pp. 59–67, Mar. 2018.
- [28] J. Chen, C. Zhao, and L. Chen, Collaborative filtering recommendation algorithm based on user correlation and evolutionary clustering. *Complex & Intelligent Systems*, v. 6, n. 1, pp. 147–156, 2020.
- [29] N. Tohidi and C. Dadkhah, Improving the performance of video Collaborative Filtering Recommender Systems using Optimization Algorithm. *International Journal of Nonlinear Analysis and Applications*, v. 11, n. 1, p. 283–295, 2020.
- [30] G. Schröder, M. Thiele and W. Lehner, Setting goals and choosing metrics for recommender system evaluations. In *UCERSTI2 workshop at the 5th ACM conference on recommender systems*, Chicago, USA, v. 23, p. 53, 2011.
- [31] Q. Lin *et al.*, Multiobjective personalized recommendation algorithm using extreme point guided evolutionary computation. *Complexity*, v. 2018, 2018.
- [32] N. E. I. Karabadjji *et al.*, Improving memory-based user collaborative filtering with evolutionary multi-objective optimization. *Expert Systems with Applications*, v. 98, p. 153–165, 2018.
- [33] Y. Wu *et al.* "Collaborative denoising auto-encoders for top-n recommender systems." *Proceedings of the Ninth ACM International Conference on Web Search and Data Mining*, 2016.
- [34] Y. Liu, J. Cheng, C. Yan, X. Wu, and F. Chen, "Research on the matthews correlation coefficients metrics of personalized recommendation algorithm evaluation," *Int. J. Hybrid Inf. Technol.*, vol. 8, no. 1, pp. 163–172, Jan. 2015.
- [35] D. Wu, G. Zhang, and J. Lu, "A fuzzy preference tree-based recommender system for personalized business-to-business E-services," *IEEE Trans. Fuzzy Syst.*, vol. 23, no. 1, pp. 29–43, Feb. 2015.

# Face Verification across Aging using Deep Learning with Histogram of Oriented Gradients

Areeg Mohammed Osman<sup>1</sup>  
Faculty of Science and Technology  
Sudan University of Science and Technology  
Khartoum, Sudan

Serestina Viriri<sup>2</sup>  
School of Maths, Statistics and Computer Science  
University of KwaZulu-Natal  
Durban, South Africa

**Abstract**—One of the complex procedures which affect man's face shape and texture is facial aging. These changes tend to deteriorate the efficacy of systems that automatically verify faces. It seems that CNN (also known as Convolutional Neural Networks) are thought to be one of the most common deep learning approaches where multiple layers are trained robustly while maintaining the minimum number of learned parameters to improve system performance. In this paper, a deeper model of convolutional neural network is fitted with Histogram of Oriented Gradients (HOG) descriptor to handle feature extraction and classification of two face images with the age gap is proposed. Furthermore, the model has been trained and tested in the MORPH and FG-NET datasets. Experiments on FG-NET achieve a state of the arts accuracy (reaching 100%) while results on MORPH dataset have significant improvements in accuracy of 99.85%.

**Keywords**—Facial aging; verify faces; Convolutional Neural Networks (CNN); Histogram of Oriented Gradients (HOG)

## I. INTRODUCTION

As age proceeds, face appearance is affected dramatically which is a phenomenon [1]. Despite the fact that age effects on face appearance have been studied for a while, novice work to reveal faces during age progress has been done. One of the most emergent issues is how to identify an invariant facial feature. In other words, the basic problem of this research is how to develop a scheme that represents and matches facial features and that is flexible to deal with different face aging changes. What is a suitable algorithm to extract invariant features is the one that improves performance throughout the system by boosting its accuracy. Moreover, a suitable algorithm stands out when compared with other systems that identify images of people as they age.

The effects of aging are normally seen on the face in the shape of subtle differences of both face shape and texture during maturity [2]. Overall, people with common ethnic groups or gender experience similar face features during their different ages. It is also the case that people who gain or lose weight across their ages tend to have analogous face aging features [3]. There are several causes that are thought to form constrains for face identification across age advancement.

There are several reasons that hinder facial identification through age advancement. One of them is due to changing facial biometrics, such as texture and shape that take place over the years. This seems to limit the development of a system that is able to adapt to these changes. This paper

will consider how a subject could be recognized despite age changes over the years and other significant variations caused by lighting, expressions, poses, resolutions, and backgrounds. Face verification in aging subjects is a challenging process, as human aging is non-uniform. Besides, extracting textural and shape features from the images is another challenge.

Some researchers study the effect of Local Binary Pattern (LBP) features [6,7] in face verification have achieved significant improvements. On the other hand, Histograms of Oriented Gradient (HOG) is a shape descriptor used to detect objects like cars and humans was chosen for its advanced results in facial recognition [3].

In this paper, deep convolutional neural network architecture is combined with HOG descriptor to extract features from facial images and classify them. Face verification is accommodated by calculating similarity distance using "Euclidean" distance.

The remaining parts of this paper are organized as follows: In Section 2, background and related works for face verification across age are introduced while methods and techniques for implementation are presented in Section 3. Subsequently, Section 4 consists of experimental results whereas the last section concludes the paper and gives future orientations.

## II. BACKGROUND AND RELATED WORK

A face verification system is defined as a complicated system that requires high system performance. Recently, many automatic systems have been using it for face verification. The most powerful technique is a deep learning approach which has been used to extract both textures and shape features from the face. The main issue, however, is how to build model architecture to improve system performance.

In the literature, both deep learning-based approaches and Convolutional Neural Network (CNN) has been used for face verification. CNN models differ in terms of layers' number, activation function, etc. Simone [4] conducted a research to investigate the task of long time gap face verification that deploys a DCNN through using a layer with injection feature that maximizes identification precision through spotting a scale of similarity for the external features. The method has been assessed in accordance with the LAG (Large Age Gap) database and proved to function better than other contemporary state-of-the-art systems.

The usage of CNN to recognize facial features for automatic face verification of themes that refer to various age,



ethnicity and gender groups has been tested by El Khyari and Wechsler [5]. As far as multiple demographic categories are concerned, the researchers concluded that face verification biometric performance was comparatively lower in black women themes (subjects) of 18 to 30 years old. Afterwards, the VGG-face convolutional neural network [6] was utilized for features mining through activation layers. Surprisingly enough, the distance of features between themes was equal to the distance between their relevant sets. Singleton and set similarity distances were both used in order to assess the performance of identification and verification.

Kasim and et al. [7] proposed a CNN model from scratch and compared it with two pre-trained methods AlexNet and GoogLeNet by implemented in Celebrity Face Recognition dataset. Their results concluded to that despite validation accuracy was 100% in both models; GoogLeNet was better compared to elapsed time.

Ling, Haibin, et al. [3] suggested using GOP (Gradient Orientation Pyramid) as a facial describer during age advancement. Subsequently, they compared it to other various methods such as gradient with magnitude, intensity difference, gradient orientation, Bayesian face, and surprisingly enough to a couple of other marketable face recognition products (Vendor A and Vendor B). The method could be considered simple if compared to its rivals and showed promising results. The suggested method was applied to passport verification operations and then validated on a couple of passport photo databases with long age gaps through the SVM classifier. Moreover, they studied how recognition performance varies with increasing time lapses between images resulting in saturation of the added age gaps if the gap is more than four years up to ten.

Facial aging has been investigated as a series of visco-elastic events by Pittenger and Shaw [8] face. They examined the importance of three human face growing parameters: shear, strain, and radial growth at the supposed age of faces and concluded to that the most influential factor that affected facial aging was the cardioidal strain transformations.

Biswas et al. [9] proposed a method based on the coherency of features drifts to being used in face verification across age progression. They noticed, depending on the shape and muscle structure of the individuals; there is a coherency among image features drifts. Therefore, they proposed a computational measure to calculate coherency and incoherency between two feature drifts maps. So, images belong of the same character, however, at different ages are constant. Contrary, incoherent images refer to various characters with dissimilar featuring drifts. In their work, the researchers assessed their method on children photographs that were captured at different ages through the FG-NET database (350 pairs) for a range of ages (1-18 years old) as well as an SIFT Feature extractor to extract drift landmarks. Their suggested approach performed superior to the other image difference and SVM classifiers.

Some models simulate the wrinkles process, for example Wu et al. [10] generated a 3D model to simulate wrinkles in plastic-visco-elastic processes. Furthermore, other variations have been included such as age, gender, expression, and facial hair, like Givens et al. [11] discussed three face recognition affected by these variations.

Park, Unsang, Yiying Tong, and Anil K. Jain [12] sug-

gested converting 2D age modeling into 3D age modeling via the points that show features on 2D portraits investigated by conventional Active Appearance Model (AAM) and then changing the 2D feature points into their equivalent 3D peers through the a reduced model (Morphable). The researchers also invented a model that deployed PCA to extract both texture's aging pattern and shapes aging patterns separately. Thereafter, simulated the aging process and tested the performance of the proposed structure through making a comparison between face recognition precision and with state-of-the-art matcher (FACEVACS).

### III. METHODOLOGY

The proposed Convolutional neural system is indicated in Fig. 1. Images preprocessing accomplished with data augmentation were the first system step. Then, a novel convolution neural network architecture is built from scratch to extract features and classify facial images. There are two databases that are relied upon in this system, which are MORPH dataset [13], and the FG-NET dataset [14]. Each contains sufficient face images. The proposed algorithm is given in algorithm 1.

---

#### Algorithm 1 Pseudo Code for the Proposed Methodology.

---

```
1: procedure
2: Training Dataset $T = \{x_i, y_i, \dots, z_i\}$
3: $i \leftarrow 1, 2, 3, \dots, m$
4: Test Dataset $S = \{x_j, y_j, \dots, z_j\}$
5: $j \leftarrow 1, 2, 3, \dots, n$
6: Class Labels $L = \{l_1, l_2, \dots, l_m\}$
7: Output: Predicted class label L for test image S
8: Training CNN with tarain dataset T, get training face classifier $f_T()$
9: Testing the test dataset S with CNN, get testing face classifier $g_S()$
10: Classify each image in S As
11: loop:
12: for $i=1$ to n
13: if $x_j \leftarrow T$ then
14: return L
15: End for.
16: close;
```

---

#### A. Image Preprocessing

Improving the model performance required pretreatment of the dataset. Additionally, Data Augmentation is used for preprocessing to prevent networks from over fitting by generalizing image features [15]. All input images are translated both horizontally and vertically in the range [-30, 30]. After that, images are rotated and measured against the size of the standard input layer (224×224). Finally, the processed images were introduced to the CCN network via RGB colour values.

#### B. Feature Extraction and Classification

1) *Deep Convolutional Neural Networks:* In recent years, there has been a great need to solve more complex problems in deep learning by going deeper and adding extra depth to the neural network to improve classification accuracy. However, adding more depth to the neural network results in network

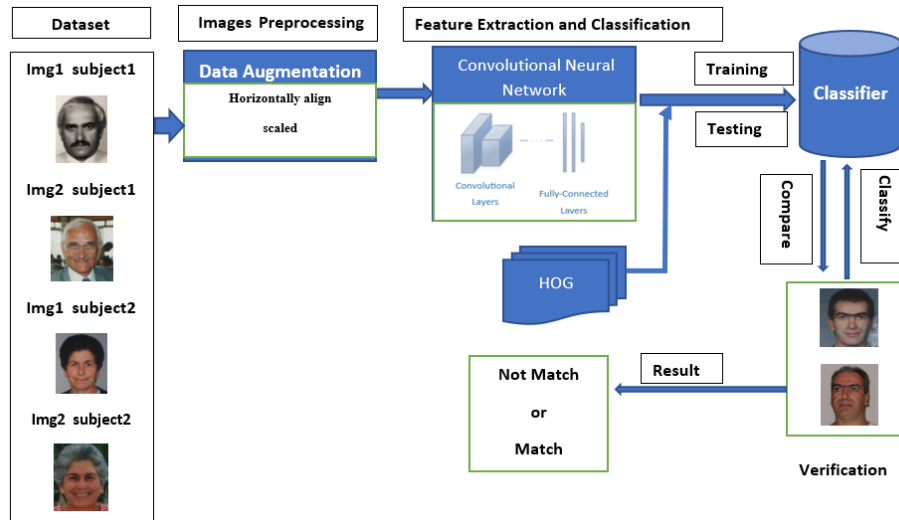


Fig. 1. HCNN:Proposed Deep Convolutional Neural Network with HOG Methodology.

complexity, at some points, could possibly degrade the system performance.

Our model consists of deep convolutional network architecture comprising five convolutional layers and one fully connected layer that is designed to accomplish the feature extraction and classification stage. CNN architecture consists of five convolutional layers, each one of them is followed by batch normalization, rectified linear unit (ReLU) as an activation layer, and a max-pooling layer. All these layers represent the feature extraction stage.

The input layer accepts a facial image of size  $224 \times 224$  with RGB color, which is passed to the first convolutional layer that has 8 filters with size  $3 \times 3$  pixel to detect general features in an image such as vertical and horizontal edges and textures. Furthermore, convolutional layers have several parameters including output size, filter size, stride, and filter numbers. On the other hand, the output features map from each convolutional layer is firstly normalized using batch normalization where ReLU function is used as an activation function to convert all negative values to zeros. In turn, the output of this layer is directed to the Max-pooling layer with stride value  $2 \times 2$  in order to reduce feature map size to a half.

In the classification stage, there is one fully connected layer which converts the feature map into a vector of 672 neurons for a classification task followed by a SoftMax layer, which has 672 neurons where each neuron represents class (subject). In addition to that, the loss function is cross entropy, which is calculated by this equation:

$$p_n = \frac{\exp(o_n)}{\sum_h \exp(o_h)} \quad (1)$$

The output is the predicted labels (classes) for each facial image and the reflects the probability for the predicted class. Table I contains more details about the CNN layers structure and the value of parameters. Fig. 2 shows the architecture.

Histogram Oriented Gradient (HOG) is a shape descriptor that is used to detect objects, e.g. cars, humans, etc. It was firstly introduced by Dalal and Triggs to detect humans [16]. The basic idea of their invention is that the shape of objects and the appearance inside images can be defined by the distribution of intensity gradients or edge directions. Therefore, there is a need to: divide images into cells, and for each cell create a histogram in order to describe the distribution of the directions. Then histograms are normalized and concatenated into vectors, which is calculated as follows [16]:

1. First compute Gradient with this equation.

$$g_x(x, y) = I(x + 1, y) - I(x - 1, Y) \quad (2)$$

$$g_y(x, y) = I(x, y + 1) - I(x, Y - 1) \quad (3)$$

2. Then Orientation  $\theta$  and magnitude  $m(x,y)$  are calculated as in the following formula.

$$m(x, y) = \sqrt{\delta x(x, y)^2 + \delta y(x, y)^2} \quad (4)$$

$$\theta(x, y) = \arctan \frac{\delta y(x, y)}{\delta x(x, y)} \quad (5)$$

3. Divide image Orientation and magnitude into cells so that the number of cells in rows and columns act as parameters to choose when implementing HOG.

4. Histogram of the orientations is computed for each block; then normalized by the formula below.

$$Hist_{norm} = \frac{Hist}{Hist + \varepsilon} \quad (6)$$

5. Concatenated Normalized Histograms into a Vector.

Local Binary Pattern (LBP) is a texture descriptor [17]. It works by dividing an image into multiple cells where each pixel in the center of the cell is compared to its eight neighbors, starting from the top-left direction. Beginning clockwise, if the

TABLE I. PROPOSED DEEP CONVOLUTIONAL NEURAL NETWORK ARCHITECTURE DETAILS.

| No. | Layer type            | Output size    | Filter Size | Stride | Number of Filters |
|-----|-----------------------|----------------|-------------|--------|-------------------|
| 1   | Image Input           | 224 × 224 × 3  | -           | -      | -                 |
| 2   | Convolution1          | 224 × 224 × 8  | 3 × 3       | 1 × 1  | 8                 |
| 3   | Batch Normalization1  | 224 × 224 × 8  | -           | -      | -                 |
| 4   | ReLU1                 | 224 × 224 × 8  | -           | -      | -                 |
| 5   | Max Pooling1          | 112 × 112 × 8  | -           | 2 × 2  | -                 |
| 6   | Convolution2          | 112 × 112 × 16 | 3 × 3       | 1 × 1  | 16                |
| 7   | Batch Normalization2  | 112 × 112 × 16 | -           | -      | -                 |
| 8   | ReLU2                 | 112 × 112 × 16 | -           | -      | -                 |
| 9   | Max Pooling2          | 56 × 56 × 16   | -           | 2 × 2  | -                 |
| 10  | Convolution3          | 56 × 56 × 32   | 3 × 3       | 1 × 1  | 32                |
| 11  | Batch Normalization3  | 56 × 56 × 32   | -           | -      | -                 |
| 12  | ReLU3                 | 56 × 56 × 32   | -           | -      | -                 |
| 13  | Max Pooling3          | 28 × 28 × 32   | -           | 2 × 2  | -                 |
| 14  | Convolution4          | 28 × 28 × 64   | 3 × 3       | 1 × 1  | 64                |
| 15  | Batch Normalization4  | 28 × 28 × 64   | -           | -      | -                 |
| 16  | ReLU4                 | 28 × 28 × 64   | -           | -      | -                 |
| 17  | Max Pooling4          | 14 × 14 × 64   | -           | 2 × 2  | -                 |
| 18  | Convolution5          | 14 × 14 × 128  | 3 × 3       | 1 × 1  | 128               |
| 19  | Batch Normalization5  | 14 × 14 × 128  | -           | -      | -                 |
| 20  | ReLU 5                | 14 × 14 × 128  | -           | -      | -                 |
| 21  | Fully Connected       | 1 × 1 × 672    | -           | -      | -                 |
| 22  | SoftMax               | 1 × 1 × 672    | -           | -      | -                 |
| 23  | Classification Output | -              | -           | -      | -                 |

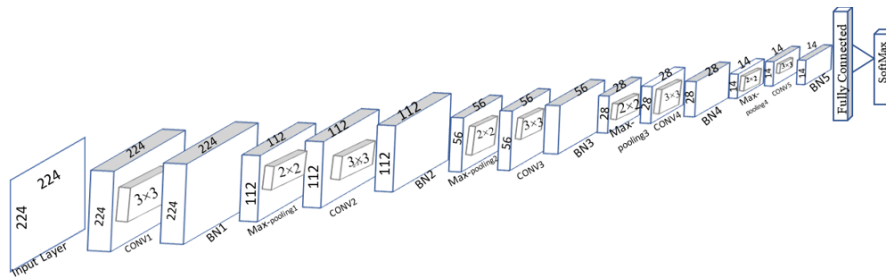


Fig. 2. Proposed Deep Convolutional Neural Network Architecture.

pixel in the center is larger than its neighbors, it is changed by zero and otherwise, it changes by one. After that, the decimal value of all binary numbers is calculated, resulting in LBP code which replaces the central pixel. To collect information over larger regions, you can select larger cell sizes. The LBP code for P neighbors situated on a circle of radius R is computed as follows [18]:

$$LBP_{P,R}(X, Y) = \sum_{p=0}^P S(g_p - g_c) 2^p \quad (7)$$

Where  $S(l)=1$  if  $l \geq 0$  and 0 otherwise.

### C. Classification

The adopted classifier in the previously mentioned methodology (fig. 1) is Support Vector Machine (SVM) [19]. Precisely, the study included a linear multi-class SVM in order to constitute subjects/classes. The Multi-class SVM technique is to use a one-versus-all classification approach to represent the output of the k-th SVM as in (8).

$$a_k(x) = W^T x \quad (8)$$

the forecast class is

$$\text{arg}_k(\text{max}) a_k(x) \quad (9)$$

1) *Performance Metrics*: Performance measures are established on the four digits obtained when running the classifier to test the dataset. These metrics are, false positives (FPs), true positives (TPs), true negatives (TNs), and false negatives (FNs). Thus, the system validation accuracy is calculated as follows [20]:

$$\text{Accuracy} = \frac{(TP + TN)}{(TP + TN + FP + FN)} \quad (10)$$

2) *Face verification*: The performance of facial verification across age method was evaluated using Euclidean distance [6], which measures the similarity between pairs of feature vectors. Given the two feature image vectors (a) and (b), the similarity distance is the Euclidean distance calculated in the following way:

$$d(a, b) = \| a - b \| \quad (11)$$

For two-image feature sets,  $A = \{a_1, \dots, a_N\}$  and  $B = \{b_1, \dots, b_N\}$ , the Minimum similarity distances between the two sets is defined as follows:

$$\text{MinimumDistance} = h_{\min}(A, B) = \min_{(a \in A \& b \in B)} d(a, b) \quad (12)$$

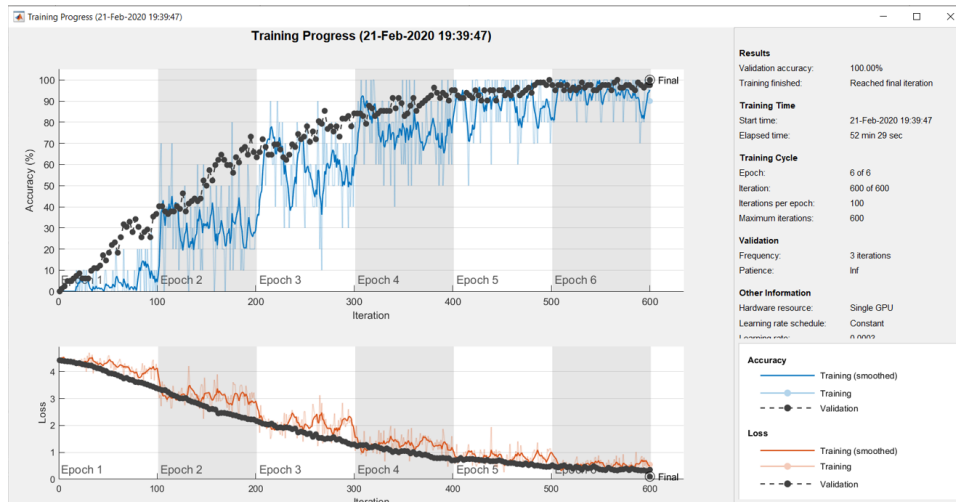


Fig. 3. Training and Testing Process of the Proposed Model.

TABLE II. TRAINING PARAMETERS.

| Initial Learn Rate | Dropout | No. of Epochs | Iterations |
|--------------------|---------|---------------|------------|
| 0.01               | —       | 70            | 1470       |

#### IV. EXPERIMENTS AND RESULTS

Various experiments were carried out in this section to assess the efficacy of the suggested face verification across age approach. Two publicly available datasets were used to demonstrate the anticipated methods.

##### A. Facial Dataset

In the current study, two datasets are used for training and testing; First, MORPH dataset, which is a standard benchmark dataset for face recognition [13]. Second, FG-NET dataset [14], which contains 1002 photos that show 82 characters, where multiple photos of the same character are considered to reflect variability in age, in addition to intrinsic variability, for instance, pose, illumination and expression.

The MORPH dataset comprises 4132 photos that show 672 characters which differ in terms of age. The images have been divided into classes; each class contains images of the same subjects at various ages with a maximum of 5 years' age difference. Moreover, the database was classified into a couple of categories: in the first, 80% of the data was picked arbitrary to train the CNN network, whereas the other 20% was utilized to examine it.

##### B. Model Implementation

The implementation is accomplished by a personal computer with Intel Core i7 processor 2.20 GHZ, include Nvidia GeforceGTX card with 4 GB and Matlab 2018 software.

Our experiment goal is to design a CNN model capable to verify two face images regardless of the age difference. After various experiments with different parameters value, researchers set initial learn rate to 0.1, L2 regularization to 1.0000000000000000e-04, with a gradient threshold method of 12 norm, validation frequency of 50, and finally to shuffle

every epoch. More details about training parameters for the pre-trained models are illustrated in Table II.

To make the model more general, the stochastic gradient descent with momentum (SGDM) optimizer was applied with a value of 0.9 [21], which is defined as follows:

$$\gamma = \gamma - \eta \cdot \Delta_{\gamma} J(\gamma; x^{(i)}; y^{(i)}) \quad (13)$$

Here, “ $\eta$ ” is defined as the learning rate and  $\Delta_{\gamma} J$  is the gradient of the loss term with respect to the weight vector  $\gamma$ .

The network in each restoration is validated by the system when training was applied. The fine-tuned CNN is used to classify the validated images and it is also the case in this stage of calculating the accuracy of classification.

The proposed system is evaluated based on two databases to predict face verification with an age difference. On the one hand, MORPH dataset contains 4132 images of 672 subjects that vary in age. On the other hand, the FG-NET dataset consists of 1002 images of 82 subjects within size 150x150 pixel. Images are converted to RGB color to match the CNN input layer. The process of training and testing is shown in Fig. 3, examples of classified images and their predicted labels in Fig. 4.

##### C. Experiments in FG-NET Dataset

The innovated model is examined and tested in FG-Net dataset, which included 1002 images of 82 subjects. It particularly contains different images of the same person at different ages. For evaluation, HOG descriptor with deep convolutional neural network reached a maximum accuracy of 100% that is the same when combining both LBP and HOG within the same CNN. From this result, it seems that HOG improves validation accuracy when compared to the minimum accuracy generated by LBP. FG-net database contained a limited number of images

which gave 100% accuracy. Usage was obtained and scored as in Table III.

#### D. Experiments in MORPH Dataset

The proposed model was evaluated in the MORPH dataset. when HOG is used as feature extraction, 29.61% accuracy is obtained, which is an improvement over LBP with a rate of 25.59%, combining deep convolutional neural network with LBP seems to give minimum accuracy than combining with both LBP and HOG. On the other hand, combining deep convolutional neural network architecture with HOG proved to give the highest accuracy value (99.85%). Despite the FG-NET dataset contains fewer images, it appears that there is no improvement in the accuracy of the MORPH dataset as shown in Table IV.

#### E. Performance Comparison of our Result with the State-of-the-Art Works

In Table V, improvements in accuracy over previous works can be seen. In the Morph dataset, combining HOG with deep convolutional neural network reaches 99.85% accuracy which is an improvements compared to results by [4] with layer injection. By comparing the proposed model with the results obtained by [7], we notice that despite obtaining 100% accuracy, but the model contains a limited number of layers and its depth is not sufficient to learn all features.

### V. CONCLUSION AND FUTURE WORK

The problem of facial image verification with an age difference as feature extraction and classification was outlined in this paper. The trained process was fine-tuned on MORPH and FG-NET publicly available datasets, HOG achieved much better results than LBP when combined with the deep convolutional neural network. Further analysis also showed that a state of the arts is achieved through fusion design of a CNN with more depth and efficiency to accommodate human's age and gender will be the action plan. Also, use pre-trained Models in deep learning is under consideration.

#### REFERENCES

- [1] N. Ramanathan, R. Chellappa, S. Biswas *et al.*, "Age progression in human faces: A survey," *Journal of Visual Languages and Computing*, vol. 15, pp. 3349–3361, 2009.
- [2] N. Ramanathan and R. Chellappa, "Modeling shape and textural variations in aging faces," in *2008 8th IEEE International Conference on Automatic Face & Gesture Recognition*. IEEE, 2008, pp. 1–8.
- [3] H. Ling, S. Soatto, N. Ramanathan, and D. W. Jacobs, "A study of face recognition as people age," in *2007 IEEE 11th International Conference on Computer Vision*. IEEE, 2007, pp. 1–8.
- [4] Y. Bengio, *Learning deep architectures for AI*. Now Publishers Inc, 2009.
- [5] H. El Khiyari and H. Wechsler, "Face verification subject to varying (age, ethnicity, and gender) demographics using deep learning," *Journal of Biometrics and Biostatistics*, vol. 7, no. 323, p. 11, 2016.
- [6] H. El Khiyari, H. Wechsler *et al.*, "Age invariant face recognition using convolutional neural networks and set distances," *Journal of Information Security*, vol. 8, no. 03, p. 174, 2017.
- [7] N. Kasim, N. Rahman, Z. Ibrahim, and N. N. A. Mangshor, "Celebrity face recognition using deep learning," *Indonesian Journal of Electrical Engineering and Computer Science*, vol. 12, no. 2, pp. 476–481, 2018.
- [8] J. B. Pittenger and R. E. Shaw, "Aging faces as viscal-elastic events: Implications for a theory of nonrigid shape perception," *Journal of Experimental Psychology: Human perception and performance*, vol. 1, no. 4, p. 374, 1975.
- [9] S. Biswas, G. Aggarwal, N. Ramanathan, and R. Chellappa, "A non-generative approach for face recognition across aging," in *2008 IEEE Second International Conference on Biometrics: Theory, Applications and Systems*. IEEE, 2008, pp. 1–6.
- [10] Y. Wu, N. M. Thalmann, and D. Thalmann, "A dynamic wrinkle model in facial animation and skin ageing," *The journal of visualization and computer animation*, vol. 6, no. 4, pp. 195–205, 1995.
- [11] G. Givens, J. R. Beveridge, B. A. Draper, P. Grother, and P. J. Phillips, "How features of the human face affect recognition: a statistical comparison of three face recognition algorithms," in *Proceedings of the 2004 IEEE Computer Society Conference on Computer Vision and Pattern Recognition, 2004. CVPR 2004.*, vol. 2. IEEE, 2004, pp. II–II.
- [12] U. Park, Y. Tong, and A. K. Jain, "Age-invariant face recognition," *IEEE transactions on pattern analysis and machine intelligence*, vol. 32, no. 5, pp. 947–954, 2010.
- [13] A. M. Albert and K. Ricanek Jr, "The morph database: investigating the effects of adult craniofacial aging on automated face-recognition technology," *Forensic Science Communications*, vol. 10, no. 2, 2008.
- [14] "FG-Net aging database," [http://http://www.sting.cycollege.ac.cy/\\_alanitis/fgnetaging/](http://http://www.sting.cycollege.ac.cy/_alanitis/fgnetaging/), accessed: 29 Marh 2020.
- [15] D. A. Van Dyk and X.-L. Meng, "The art of data augmentation," *Journal of Computational and Graphical Statistics*, vol. 10, no. 1, pp. 1–50, 2001.
- [16] N. Dalal and B. Triggs, "Histograms of oriented gradients for human detection," in *2005 IEEE computer society conference on computer vision and pattern recognition (CVPR'05)*, vol. 1. IEEE, 2005, pp. 886–893.
- [17] D. Huang, C. Shan, M. Ardabilian, Y. Wang, and L. Chen, "Local binary patterns and its application to facial image analysis: a survey," *IEEE Transactions on Systems, Man, and Cybernetics, Part C (Applications and Reviews)*, vol. 41, no. 6, pp. 765–781, 2011.
- [18] N. Bouadjenek, H. Nemmour, and Y. Chibani, "Writer's gender classification using hog and lbp features," in *International Conference on Electrical Engineering and Control Applications*. Springer, 2016, pp. 317–325.
- [19] V. Vapnik, *The nature of statistical learning theory*. Springer science & business media, 2013.
- [20] G. Levi and T. Hassner, "Age and gender classification using convolutional neural networks," in *Proceedings of the IEEE conference on computer vision and pattern recognition workshops*, 2015, pp. 34–42.
- [21] E. Dogo, O. Afolabi, N. Nwulu, B. Twala, and C. Aigbavboa, "A comparative analysis of gradient descent-based optimization algorithms on convolutional neural networks," in *2018 International Conference on Computational Techniques, Electronics and Mechanical Systems (CTEMS)*. IEEE, 2018, pp. 92–99.

TABLE III. RESULTS OF DIFFERENT METHODS ON FG-NET DATASET.

| Method            | Validation Accuracy |
|-------------------|---------------------|
| LBP               | 51.2%               |
| HOG               | 100%                |
| DCNN+LBP+HOG      | 100%                |
| DCNN+LBP          | 65.85%              |
| Proposed DCNN+HOG | 100%                |

TABLE IV. RESULTS OF DIFFERENT METHODS ON MORPH DATASET.

| Method            | Validation Accuracy |
|-------------------|---------------------|
| LBP               | 25.59%              |
| HOG               | 29.61%              |
| DCNN+LBP+HOG      | 61.75%              |
| DCNN+LBP          | 59.82%              |
| Proposed DCNN+HOG | 99.85%              |

TABLE V. PERFORMANCE COMPARISON OF RESULTS WITH THE STATE-OF-THE-ART WORKS.

| Approach                   | Dataset                     | Method                  | Accuracy   |
|----------------------------|-----------------------------|-------------------------|------------|
| Kasim and et al. [7]       | Celebrity FaceDataset       | CNN model               | 100%       |
| Ling, Haibin, et al. [3]   | FGnet Two passport datasets | GOP                     | —          |
| Bengio and Yoshua [4]      | LAG Dataset                 | Siamense DCNN Injection | 85.75%     |
| El Khiyari, H., et al. [5] | FG-NET                      | VGG-Face                | 0.16 (EER) |
| Proposed HDCNN model       | MORPH                       | DCNN model with HOG     | 99.85%     |
|                            | FG-NET                      |                         | 100%       |

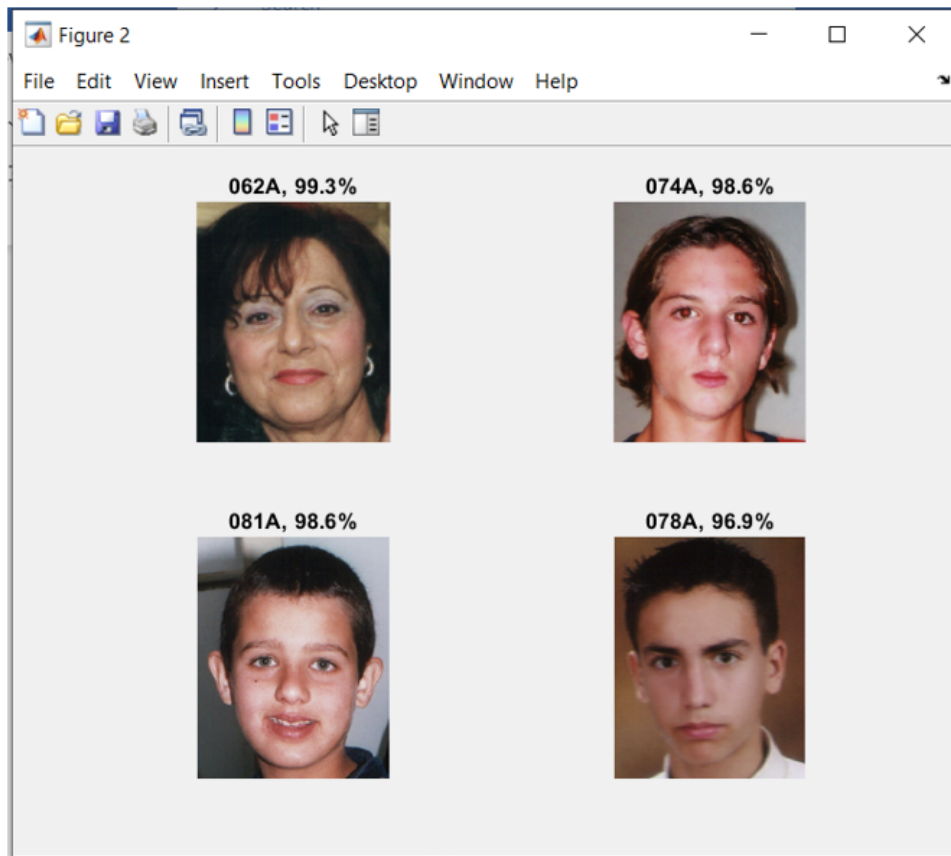


Fig. 4. Examples of Images and their Predicted Labels.

# Multi-Target Energy Disaggregation using Convolutional Neural Networks

Mohammed Ayub<sup>1</sup>, El-Sayed M. El-Alfy<sup>2</sup>  
College of Computer Sciences and Engineering,  
King Fahd University of Petroleum and Minerals,  
Dhahran 31261, Saudi Arabia

**Abstract**—Non-Intrusive Load Monitoring (NILM) has become popular for smart meters in recent years due to its low cost installation and maintenance. However, it requires efficient and robust machine learning models to disaggregate the respective electrical appliance energy from the mains. This study investigated NILM in the form of direct point-to-point multiple and single target regression models using convolutional neural networks. Two model architectures have been utilized and compared using five different metrics on two benchmarking datasets (ENERTALK and REDD). The experimental results showed that multi-target disaggregation setting is more complex than single-target disaggregation. For multi-target setting of ENERTALK dataset, the highest individual F1-score is 95.37% and the overall average F1-score is 75.00%. Better results were obtained for the multi-target setting of the other dataset with higher overall average F1-score of 83.32%. Additionally, the robustness and knowledge transfer capability of the models through cross-appliance and cross-domain disaggregation was demonstrated by training for a specific appliance on a specific data, and testing for a different appliance, house and dataset. The proposed models can also disaggregate simultaneous operating appliances with higher F1-scores.

**Keywords**—Energy disaggregation; smart meters; load monitoring; ENERTALK dataset; multi-target disaggregation; multi-target regression; NILM knowledge transfer

## I. INTRODUCTION

Using energy in an efficient manner has become one of the highest concerns for both utility and end-users nowadays, as the world is facing challenging problems including depletion of natural resources and emissions of environmentally hazardous gases. To be able to use electrical energy efficiently, first, both utility and consumers should know the amount of energy consumption of individual appliances. For this purpose, cost effective Non-Intrusive Load Monitoring (NILM) is considered a plausible alternative. NILM is a method that can deduce energy consumption of individual appliances from aggregated smart meter power data recorded at a single source. This process is based on software techniques and requires effective and efficient techniques for successful disaggregation. It can help understand consumer behavior and energy consumption of appliances, and hence provide feedback on how to save energy. According to [1], monitoring energy consumption can save up to 12% of electrical energy with positive impacts on natural resources and reduction of hazardous gas emission. Besides getting detailed insights of the energy usage, NILM is useful for better demand forecasting and tracing behavioral patterns of dwellers [2].

NILM can be realized using three major steps as shown in

Fig. 1: (1) Data acquisition which is the collection of data by installing hardware such as smart meters, (2) Feature extraction which is the derivation of features from the collected data, and (3) Learning and inferencing which is the deployment of models such as training machine learning to make prediction. NILM can be exploited for disaggregation using either classification or regression techniques. In classification methods, the detection or identification procedure is more sophisticated when unique signatures or fingerprints are needed to formulate for classification of appliances [3], [4]. In regression, the appliance's on/off state or classification is obtained by leveraging the disaggregation results based on the on-threshold value of an appliance [5].

There are a number of disaggregation studies that applied various machine learning techniques including Decision Trees (DT),  $K$ -Nearest Neighbors (KNN), Neural Networks (NN), Convolutional Neural Networks (CNN), Long Short Term Memory (LSTM), Denoising Auto Encoder (deAE), Sequence-to-sequence (seq2seq) and Sequence-to-point (seq2point) learning, Subtask Gated Network (SGU) and many others [6]–[13]. Sequence-to-sequence and sequence-to-point are recent NILM disaggregation paradigms that can predict direct energy consumption with promising results than the Hidden-Markov Model (HMM) and its variants. But in these techniques, choosing the receptive field (sliding window) is somewhat crucial as there are different types of appliances with the different activation cycles. Besides, there may be multiple predictions for a single time point in seq2seq which is redundant and calculation of mean is necessary for the final prediction. Considering all these points, this work formulates the disaggregation problem as a direct point to point regression problem on the motivation that it will retain the granularity of consumption information that will help the generalization capability and knowledge transfer in the disaggregation domain which is demonstrated in the experiment section. On the other hand, it will also reduce the burden of retaining contextual information and thereby releasing the computational and memory burden.

A disaggregation model can be trained either as a single-target [5], [14] or multi-target [15] regression problem, or as a single-label [2], [16]–[18], or multi-label [3], [7], [19]–[22] classification problem. Single- and multi-label classification and multi-class classification were explored in many works in the literature. To our best knowledge, multi-target regression models for disaggregation are still under-studied. As the principle application of NILM is to separate the individual consumption from aggregate reading, in real time scenario,

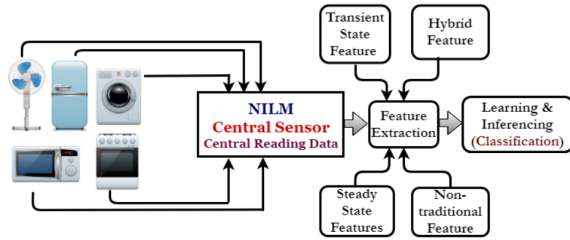


Fig. 1. Illustration of the Main Steps of Non-Intrusive Load Monitoring

direct disaggregation results are more preferable to the disaggregation results obtained after classification. Moreover, multi-target disaggregation models are more suitable on the reason that it can significantly reduce the training time by requiring low resources. Therefore, it is important to formulate NILM problem as a point-to-point multi-target regression model and compare its performance with single target regression models, especially for recent datasets such as ENERTALK. It is also emphasized that a multiple output classification or regression model poses challenges for disaggregation of multiple appliances of the same type [23], especially when the devices are multi-state devices and non-linear devices [24]. The works in [4], [25], [26] attempted the simultaneous detection of the load using different algorithms and features. However, their scopes were limited to classification of the load and there is still a need to explore this problem using regression models.

Keeping the above mentioned issues as main focus, this paper has the following contributions. Energy disaggregation is formulated as the direct point-to-point multi-target disaggregation learning that will help retain granular consumption meta information to foster generalization and knowledge transfer. The proposed multi-target disaggregation approach has highest individual and average F1-score of 95.37% and 75% respectively for ENERTALK dataset. For REDD dataset, the highest individual F1-score is 95.06% and overall average is 83.32%. For generalization, robustness and knowledge transferability of multiple and single target point-to-point disaggregation models, the highest F1-scores are 96.40% and 93.50% for single and multiple target, respectively. Furthermore, this study provides a base for NILM researchers to compare their results, especially for ENERTALK dataset which is a relatively recent dataset with large number of houses.

The remainder of this paper is organized as follows. Section II reviews related work and Section III describes the problem formulation and methodology. Section IV presents the details about experiments, results and discussions on ENERTALK and REDD. Finally, the paper summary and conclusions are presented in Section V.

## II. RELATED WORKS

Shin and his team [13] proposed Subtask Gated Network (SGN) for non-intrusive load monitoring in 2019. Their model used a classification subnetwork and a regression subnetwork and then the output of classification is gated with that of regression. A concise study of appliance features used for NILM is presented in [27] using Random Forest (RF) and Recursive Feature Elimination (RFE). Mengistu et al. [28] described

an online cloud-based NILM system using HMM and Mean-Shift Clustering (MSC) algorithm in an unsupervised fashion. Unlike previous works, the study in [29] investigated the data reduction strategy in aggregated power signals by applying non-uniform subsampling (NUS).

A Graph-based semi-supervised multi-label classification model based on active/inactive (on/off) state of appliance was proposed in [19] using three graph-based algorithms (i.e. Local and Global Consistency (LGC), Gaussian Fields and Harmonic Functions (GFHF), and Manifold Regularization (MR)). Another multi-label classification of appliances using Random k-labELsets (RAkEL) with Decision Tree (DT) was explored in [7]. However, it was observed that the low-power consumption appliances were not correctly identified. Kim and Lee [3] investigated multi-label classification using audio signal processing techniques: Spectrogram, Mel-Frequency Cepstral Coefficient (MFCC) and Mel-spectrogram. The spectrogram based feature is proved to have the promising results. Inspired by the success of CNN, the authors in [16] proposed a novel appliance identification method using CNN for feature extraction, and Adaptive Linear Programming Boosting (ALPBoost) for classification. An accuracy of 95.4% for single appliance identification and 91.8% for multiple appliance identification were achieved. In the literature, the voltage-current (V-I) trajectories were found powerful for formulating appliance signature. In [21] and [22], appliances were classified using V-I trajectory converted to grey-scale and color coded image, respectively. Though the models in [21] were able to successfully detect a large number of appliances, the washing machine, fan, fridge and air conditioner were not identified with better score. Reference [22] used AlexNet transfer learning methodology. The authors in [17] used wavelet coefficients for identification of four appliances using Decision Tree (DT) and Nearest Neighbor (NN) classifiers on the setting of semi-supervised learning.

Jiang et al. in their work [5] investigated the on/off detection of appliances and energy disaggregation using CNN, RNN and Wavenet that used fast sequence-to-point learning. Kaselimi et al. [30] exploited the multi-channel CNN based architecture to include multiple input features in sequence-to-sequence (seq2seq) learning. However, the energies of multi-state devices were not correctly estimated. Schirmer and his team [14], like in Kaselimi's work, proposed a two-state disaggregation model using DNN and temporal contextual information (TCI). The performance for single- and multi-state device without power peak and non-linear devices are relatively low. How different combination of statistical and electrical features influence the disaggregation of various device types were studied in [6]. The authors in [9] studied the energy disaggregation using CNN, LSTM and CNN+LSTM on REDD dataset. In [31], a causal 1-D convolutional neural network based power disaggregation system (Wave-nilm) was proposed and the model was tested on AMPds2 dataset. It is noticed that the use of reactive power (Q) as input feature increases performance. In [32], Markov model was used to relate activity chain to each occupant of a household and then the energy usage per appliance was calculated and again these power usages were grouped under certain appliance categories. Appliance recognition and thereby disaggregation of energy using high frequency spectrogram feature (Short Time Fourier Transform (STFT)) was conducted in [33]. The authors in



[15] used a composite deep LSTM (CD-LSTM) to study the disaggregation using multi-target setting. This is the only work that used multi-target disaggregation. However, their work was based on sequence-to-sequence paradigm which has the drawbacks mentioned in the introduction section.

### III. PROBLEM FORMULATION AND METHODOLOGY

The purpose of NILM is to deduce the individual appliance level power consumption from the total signal recorded through a smart meter. Inversely, the total aggregated energy of a residence can be estimated from all individuals' appliance consumption. This can be mathematically expressed as [24]:

$$p_t = \sum_{i=1}^n p_t^{(i)} + e_t \quad (1)$$

where  $p_t$  is the aggregated power consumption at time  $t$ ,  $p_t^{(i)}$  is the individual appliance power consumption at time  $t$ , and  $e_t$  is line loss or error of measurement at time  $t$ . Based on Eq. 1, the energy disaggregation problem is defined as the direct point to point estimation  $\hat{p}_t^{(i)}$  of the overall power  $p_t$ , where  $\hat{p}_t^{(i)}$  is the estimated  $i^{th}$  appliance energy at time  $t$ , given the ground truth consumption  $p_t^{(i)}$ . In exact terms, this estimation can be achieved either by formulating the disaggregation as a classification or regression problem.

In this work, as described in the introduction section, the NILM is formulated as a regression problem which can have significant advantages over classification problems. Classification requires deployment of various algorithms to identify various working states of the household devices. This can become more challenging when the devices with the different level of energy demand are operating simultaneously, requiring high sampling data to create unique signatures to differentiate one from the other devices. Moreover, keeping track of on/off timestamp, duration of on/off, and calculation of average load consumption during specific 'on' periods makes the algorithms more computationally burdened. In sequence-to-sequence and sequence-to-point learning, training the model for long sequences of input to cover activation cycle requires a relatively large memory due to the need to keep track of contextual information. This sometimes jeopardizes the system in a low-resource environment. On the other hand, a regression model does not require all these operations and per-appliance disaggregation value is obtained directly from the results of regression output layer. Additionally, regression model provides detailed information about energy usage at every time point which cannot be the case with classification model.

#### A. Multi-Target Disaggregation Problem

Let  $X = \{X_1, X_2, \dots, X_p\}$  and  $Y = \{Y_1, Y_2, \dots, Y_q\}$  be the two sets of input and target variables, respectively; each set with features derived from aggregate consumption and individual appliance ground truth consumption at specific time points (steps). The training dataset is defined as,

$$\mathbb{D} = \{(\mathbf{x}_1, \mathbf{y}_1), \dots, (\mathbf{x}_T, \mathbf{y}_T)\}, \quad (2)$$

where  $T$  is the total number of time steps. Then each instance of  $\mathbb{D}$  consists of input vector of  $p$  independent variables

(predictors) and output vector of  $q$  target variables at time  $t$ , which respectively, are defined as,

$$\mathbf{x}_t = (x_t^{(1)}, x_t^{(2)}, \dots, x_t^{(j)}, \dots, x_t^{(p)}), \quad (3)$$

and

$$\mathbf{y}_t = (y_t^{(1)}, y_t^{(2)}, \dots, y_t^{(i)}, \dots, y_t^{(q)}), \quad (4)$$

where  $j = 1, 2, \dots, p$ ,  $i = 1, 2, \dots, q$  and  $t = 1, 2, \dots, T$ .

Now, the task is to learn a multi-target disaggregation model  $\mathbb{M}$  from instances of  $\mathbb{D}$  such that a function  $f$  maps the vector  $\mathbf{x}$  consisting of  $p$  aggregate feature values to a vector  $\mathbf{y}$  consisting of  $q$  consumption values.

$$f : \mathbf{x} \mapsto \mathbf{y}, \quad (5)$$

where  $\mathbf{x} = (x^{(1)}, x^{(2)}, \dots, x^{(p)})$  and  $\mathbf{y} = (y^{(1)}, y^{(2)}, \dots, y^{(q)})$ . The trained model  $\mathbb{M}$  can be used to predict the power consumption of all included appliances denoted by  $\{\hat{\mathbf{y}}^{(T+1)}, \hat{\mathbf{y}}^{(T+2)}, \dots, \hat{\mathbf{y}}^{(T')}\}$  using the new input instances  $\{\mathbf{x}^{(T+1)}, \mathbf{x}^{(T+2)}, \dots, \mathbf{x}^{(T')}\}$ , i.e.,

$$\hat{\mathbf{y}}_{t'} = \mathbb{M}(\mathbf{x}_{t'}), t' = T + 1, T + 2, \dots, T' \quad (6)$$

For training loss, the Mean-Squared-Error (MSE) of single appliance disaggregation can be adopted for multiple devices as follows:

$$MSE = \frac{1}{q} \frac{1}{T} \sum_i \sum_t (y_t^{(i)} - \hat{y}_t^{(i)})^2 \quad (7)$$

Setting  $i = 1$  in Eq. (4) will transform a multi-target disaggregation problem to a single-target disaggregation problem.

#### B. CNN Multi-Target Regression Model

CNN was originally applied for image processing and computer vision where the input and each layer is multi-dimensional [34]. However, in this paper, NILM is formulated using 1-D CNN because the nature of data in load disaggregation is a uni-dimensional time series that keeps track of energy consumption of each appliance at a specific point. In line with this, every aggregate consumption feature at the specific time stamp is convolved with a kernel finding the relation between the features so that the part of aggregate consumption can be best mapped to the target appliance consumption value thereby finally producing optimum weights. Inspired by [35], two architectures of CNN are designed as follows. The first one will be referred to as CNN model-I (CNN1M), is built using two blocks of convolutional layers; the first block is followed with a max-pooling layer and the second block is followed with a global max-pooling layer. The first convolutional block consists of three convolutional layers, each with 64 filters of size 2 and the second block also has three convolutional layers but each with 128 filters of size 2. The global max-pooling layer acts as a bottleneck layer to branch each appliance as a separate output with a dense layer of 512 neurons and a final output layer with one neuron. Another deeper model called CNN model-II was designed that has one more convolutional block of three layers each with 32 filters of size 2 and all the other parameters are the same as CNN Model-I. For CNN model-II, two variants were used: one for single target (CNN2S) and the other for multi-target (CNN2M), where S stands for Single and M for

Multiple. For both architectures, the ‘stride’ and ‘learning rate’ are set to 1 and 0.001, respectively. Also, ‘ReLU’ is used as activation for all hidden layers and ‘linear’ is used as activation for all output layers. The architectures are shown in Fig. 2 and Fig. 3.

#### IV. EXPERIMENTAL WORK

For all experimental works, a machine with NVIDIA GEFORCE GPU model GTX 950 which has 4GB dedicated graphics and 16GB RAM was used. The implementation scripts were written using Python 3.7.3 and for CNN model, Keras which run on Tensorflow back-end was deployed. For all experiments, data normalization used was L2-norm implemented in scikit-learn preprocessing.normalize(). The sketch of overall workflow is given in Fig. 4.

##### A. Energy Disaggregation based Metrics

Five performance measures have been reported to evaluate the proposed models. In the following formulae,  $y_t^{(i)}$  represents the true energy consumed by appliance  $i$  at time point  $t$  and  $\hat{y}_t^{(i)}$  represents the disaggregated power of appliance  $i$  at time point  $t$ .

1) *Mean-Squared Error (MSE)*: MSE is defined as the average of the square of the difference between actual and predicted energy values as expressed by

$$MSE^{(i)} = \frac{1}{T} \sum_t (y_t^{(i)} - \hat{y}_t^{(i)})^2 \quad (8)$$

2) *Normalized Disaggregation Error (NDE)*: It is the ratio between the sum of squared difference of estimated (disaggregated) energy and true energy, and sum of square of actual energy, and then taking square root of it. It is a slight variation of the metric used in [36]. Its mathematical formula is

$$NDE^{(i)} = \sqrt{\frac{\sum_t (y_t^{(i)} - \hat{y}_t^{(i)})^2}{\sum_t (y_t^{(i)})^2}} \quad (9)$$

3) *Normalized Error in Assigned Power (NEAP)*: The sum of the absolute differences between the disaggregated power and the true energy consumption of appliance  $i$  in each time point  $t$ , divided by the total power consumption of appliance. In [37], the authors have shown that the error values greater than 1 is less representative towards the disaggregation performance and less explainable.

$$NEAP^{(i)} = \frac{\sum_t |y_t^{(i)} - \hat{y}_t^{(i)}|}{\sum_t y_t^{(i)}} \quad (10)$$

4) *Energy-based Precision ( $P^{(E)}$ )*: It can be mathematically expressed as [38]:

$$P_i^{(E)} = \frac{\sum_t \min(y_t^{(i)}, \hat{y}_t^{(i)})}{\sum_t \hat{y}_t^{(i)}} \quad (11)$$

5) *Energy-based Recall ( $R^{(E)}$ )*: It can be mathematically expressed as [38]:

$$R_i^{(E)} = \frac{\sum_t \min(y_t^{(i)}, \hat{y}_t^{(i)})}{\sum_t y_t^{(i)}} \quad (12)$$

6) *Energy-based F1-measure ( $F_1^{(E)}$ )*: It is a geometric mean between the precision and recall and can be mathematically expressed as:

$$F_1^{(E)} = 2 \frac{P^{(E)} R^{(E)}}{P^{(E)} + R^{(E)}} \quad (13)$$

where,

$$P^{(E)} = \frac{1}{m} \sum_{i=1}^m P_i^{(E)}, R^{(E)} = \frac{1}{m} \sum_{i=1}^m R_i^{(E)} \quad (14)$$

where  $m$  is the number of appliances. Equation (13) can be used to calculate the F1 score of individual appliance using Equation (11) and (12).

##### B. Datasets and Data Preparation

Two public datasets were deployed for experimenting the proposed models in this work. The first one is ENERTALK dataset [39] that has consumption data collected from 22 residences in Korea using 15Hz sampling rate for both individual and total (aggregate) consumption. One of the challenging and crucial aspects of energy disaggregation of this dataset is the alignment of target appliance and aggregate meter reading. Keeping this in mind, the daily consumption of all appliances including aggregate reading and daily consumption were concatenated in horizontal and vertical fashion where the data were resampled to one second. To handle missing data, one-step backward filling was used and the remaining missing values were subsequently removed. The other dataset is REDD [40] that has data collected from six residential buildings in USA. For this work, the low frequency data of six houses were used; where the mains consumption are sampled at 1Hz and all appliances are sampled at  $\frac{1}{3}$ Hz. These different sampling rates were aligned by using horizontal concatenation and downsampling to 3 seconds. Afterwards, the preprocessing with L2-norm was applied to the resultant dataframe of both datasets to normalize feature values.

The active power (P) and reactive power (Q) are the two original features available in ENERTALK dataset. Based on these two features, some other features were extracted based on power triangle shown in Fig. 5. For REDD dataset, only active power for two mains are available and are used as features.

Active Power (P),

$$P = V * I * \cos(\Phi) \quad (15)$$

where  $V$  is voltage,  $I$  is current and  $\Phi$  is the phase angle.

Reactive Power (Q),

$$Q = V * I * \sin(\Phi) \quad (16)$$

Apparent Power (S),

$$S = V * I, S^2 = P^2 + Q^2 \quad (17)$$

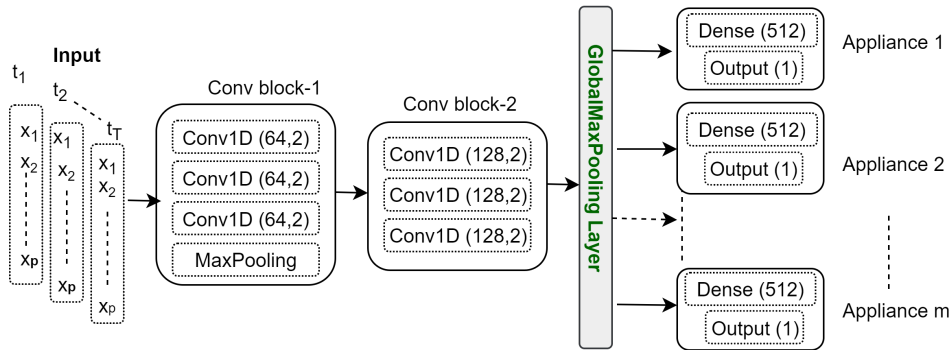


Fig. 2. Multi-Target CNN Model-I Architecture;  $x_1$  to  $x_p$  represent Energy Consumption (Features) at each time step  $t_1$  to  $t_T$ , where  $p$  is the Total Number of Features,  $T$  is the Total Number of Time Steps and  $m$  is the Total Number of Appliances

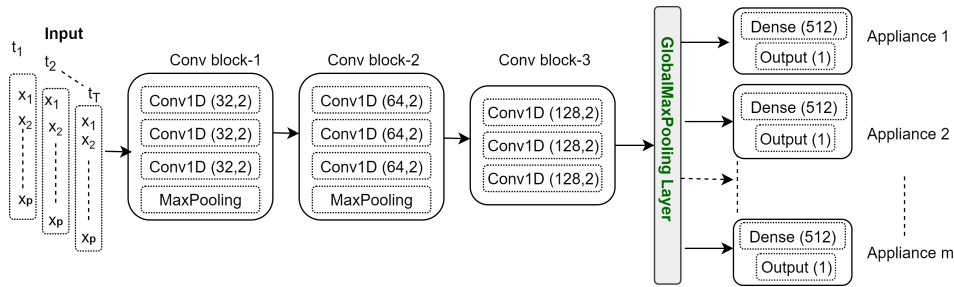


Fig. 3. Multi-Target CNN Model-II Architecture;  $x_1$  to  $x_n$  represent Energy Consumption (Features) at each Time Step  $t_1$  to  $t_T$ , where  $p$  is the Total Number of Features,  $T$  is the Total Number of Time Steps and  $m$  is the Total Number of Appliances

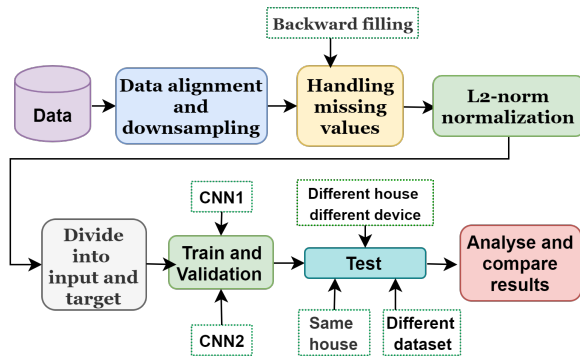


Fig. 4. Workflow Chart

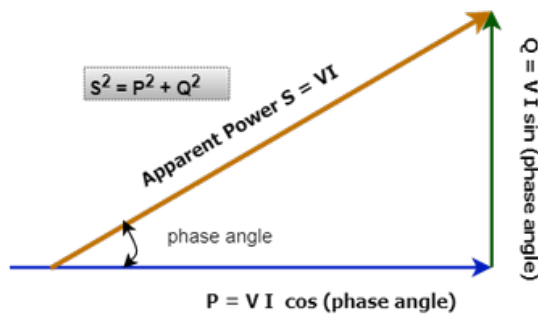


Fig. 5. Power Triangle

where  $P$ ,  $Q$ ,  $S$ ,  $V$  and  $I$  are as described earlier.

Power Factor (PF),

$$PF = \cos(\Phi) = \frac{P}{S} \quad (18)$$

where  $P$  and  $S$  are as described earlier.

Besides the above features, six additional features are extracted: (1) difference power between  $S$  and  $P$  ( $DP_{sp}$ ), (2) difference power between  $P$  and  $Q$  ( $DP_{pq}$ ), (3) difference power between  $S$  and  $Q$  ( $DP_{sq}$ ), (4) average of  $P$ ,  $Q$  and  $S$  ( $P_{avg}$ ), (5) sine of phase angle ( $Sin\_Ph$ ), and (6) tangent of phase angle ( $Tan\_Ph$ ), for ENERTALK dataset.

### C. Results for ENERTALK Dataset

For all the experiments with this dataset, 20% of the total data is kept for testing whereas the rest 80% is divided again in 80:20 ratio for training and validation. The batch size of 512 and number of epochs of 20 are used for training of the models with the loss function of total Mean Squared Error (MSE) for all appliances.

1) *Experiments on House00 Data:* These experiments used 24-days data of House00 that consists of the recording of seven appliances: TV, Washing Machine (WM), Rice Cooker (RC), Refrigerator (R), Water Purifier (WP), Microwave (MW) and Kimchi Fridge (KR). A total of 2073580 instances were generated after applying the horizontal and vertical concatenation. After all the data preparation steps were applied as explained earlier, 1983102 instances were available. This experiment used  $S$  and  $PF$  as features besides  $P$  and  $Q$ . From the scores shown in Table I, it is observed that the highest F1-score of

TABLE I. PERFORMANCE SCORES OF ENERGY DISAGGREGATION OF CNN MODEL-II FOR ENERTALK-HOUSE00 (S= SINGLE, M= MULTIPLE)

| Appliance   | NDE     | NEAP    | P       | R       | F1             |
|-------------|---------|---------|---------|---------|----------------|
| TV (S)      | 0.22661 | 0.38922 | 0.83034 | 0.98916 | 0.90282        |
| TV (M)      | 0.74338 | 1.05110 | 0.50121 | 0.41428 | <b>0.45362</b> |
| WM (S)      | 5.76306 | 6.33135 | 0.71930 | 0.75145 | 0.73503        |
| WM (M)      | 19.4733 | 15.8424 | 0.39069 | 0.50867 | 0.44194        |
| RC (S)      | 1.88011 | 1.96937 | 0.73848 | 0.91109 | 0.81576        |
| RC (M)      | 10.1996 | 4.40733 | 0.42545 | 0.45535 | 0.43989        |
| R(S)        | 0.15737 | 0.17893 | 0.93962 | 0.88391 | 0.91091        |
| R(M)        | 0.46575 | 0.49511 | 0.79155 | 0.70009 | 0.74302        |
| WP (S)      | 0.11281 | 0.13519 | 0.88762 | 0.99926 | <b>0.94014</b> |
| WP (M)      | 0.39986 | 0.35087 | 0.86114 | 0.78504 | <b>0.82133</b> |
| MW (S)      | 0.82996 | 1.02232 | 0.68390 | 0.78355 | 0.73034        |
| MW (M)      | 1.44944 | 1.21941 | 0.62349 | 0.70693 | 0.66259        |
| KR (S)      | 0.52759 | 0.64577 | 0.85249 | 0.89760 | 0.87446        |
| KR (M)      | 2.82818 | 2.00645 | 0.39634 | 0.31392 | 0.35035        |
| Average (S) | 1.35671 | 1.52459 | 0.80739 | 0.88800 | 0.84577        |
| Average (M) | 5.07993 | 3.62467 | 0.56998 | 0.55489 | 0.56234        |

82.13% and 94.01% are achieved by Water Purifier (WP) in multi- and single target, respectively. The lowest achiever for this set of experiment is Kimchi Fridge (KR) in multi-target setting with F1-score of 35%. In the multi-target disaggregation, WP has also the highest performance in terms of NDE and NEAP.

2) *Experiments on House12 Data:* With this data of House12, the CNN model-II was validated using multi-state, continuously varying (nonlinear) consumption and always-on devices. It consists of 4 months aggregate and appliance level consumption data for two WMs, TV, RC, KR and R. A total of ten features mentioned in Section IV-B from 8639267 data samples were used for multi- and single target regression. All the experiments results are shown in Table II. As seen from the table, the refrigerator has the highest F1-score of 95.37% and 99.34% in multi- and single target setting, respectively. Both actual and predicted energy consumption of the refrigerator for multi-target setting are shown in Fig. 6. These results confirm that the CNN model-II is robust enough to successfully disaggregate energy with higher F1-score. It is noteworthy that the model successfully disaggregates energy of two of the three multi-state devices with the acceptable F1-scores along with other devices except WM2. For the multi-target setting, WM2 has the lowest F1-score of 43.47%, and for the single-target setting, WM1 has the lowest disaggregation score of 32.47%. Furthermore, if we analyze the results in terms of precision and recall for the multi-target setting, it is seen that the refrigerator has the highest scores of 97.59% and 93.24%, respectively. WM2 has the worst NDE and NEAP scores in the multi-target disaggregation setting.

D. Results for REDD Dataset

This experiment was executed on the total of 1099738 data samples resulted from combination of House1, House2 and House3 data of the REDD dataset for four common kitchen appliances (three multi-state devices and one continuous consumption device) such as Microwave (MW), Refrigerator (R), Dishwasher (DW) and Washer Dryer (WD). The CNN model-I was trained with 20 epochs and batch size of 512. The CNN model-II was modified according to the features and data used, i.e. a filter size of 1 and 16 epochs were used. Moreover, the MaxPooling layer after the first convolutional block was

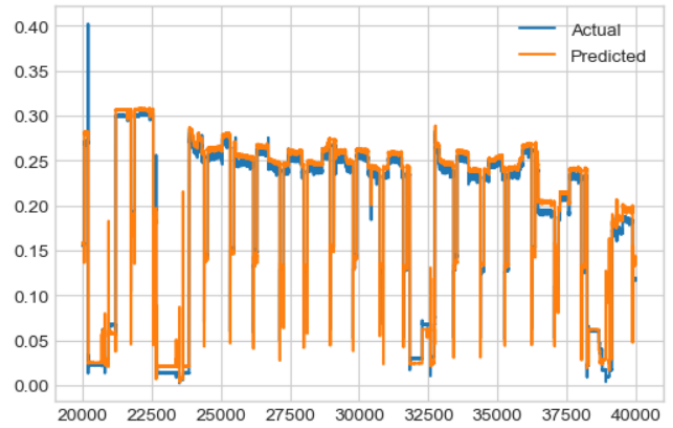


Fig. 6. Predicted Consumption of Refrigerator for Multi-Target CNN Model-II ((ENERTALK-House12)

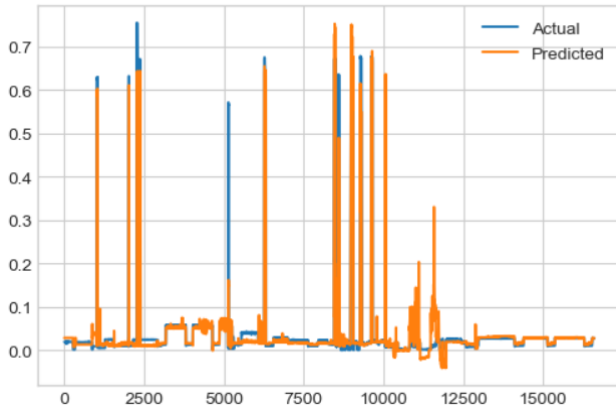
TABLE II. PERFORMANCE SCORES OF ENERGY DISAGGREGATION FOR CNN MODEL-II ON ENERTALK-HOUSE12. (S= SINGLE, M= MULTIPLE)

| Appliance   | NDE     | NEAP    | P       | R       | F1             |
|-------------|---------|---------|---------|---------|----------------|
| WM1 (S)     | 1.81104 | 2.12090 | 0.31159 | 0.33915 | 0.32479        |
| WM1 (M)     | 2.32865 | 1.84337 | 0.52510 | 0.74387 | 0.61563        |
| TV (S)      | 0.17689 | 0.31679 | 0.99975 | 0.71681 | 0.83496        |
| TV (M)      | 0.40574 | 0.38446 | 0.85595 | 0.77106 | <b>0.81129</b> |
| RC (S)      | 3.98337 | 4.85974 | 0.39227 | 0.97747 | 0.55987        |
| RC (M)      | 1.34695 | 0.83939 | 0.78732 | 0.74534 | 0.76576        |
| KR (S)      | 0.04056 | 0.06156 | 0.99173 | 0.96386 | 0.97760        |
| KR (M)      | 0.26382 | 0.24054 | 0.95253 | 0.84008 | 0.89278        |
| WM2 (S)     | 0.63658 | 0.66677 | 0.90117 | 0.77531 | 0.83351        |
| WM2 (M)     | 3.58233 | 2.33685 | 0.41711 | 0.45389 | 0.43472        |
| R (S)       | 0.01768 | 0.01294 | 0.99705 | 0.98971 | <b>0.99337</b> |
| R (M)       | 0.13047 | 0.09156 | 0.97591 | 0.93240 | <b>0.95366</b> |
| Average (S) | 1.11102 | 1.33978 | 0.76559 | 0.79372 | <b>0.77862</b> |
| Average (M) | 1.34299 | 0.95603 | 0.75232 | 0.74777 | 0.75004        |

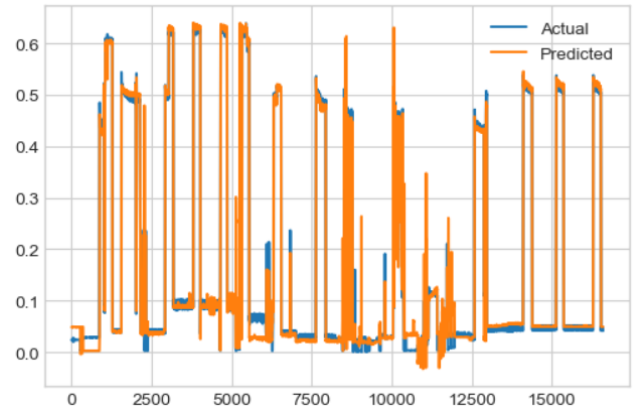
removed to train the model for the combined data of REDD dataset. For the testing set, 30% of the original data is reserved and the remaining 70% is used for training and validation with 70:30 split ratio. The scores of disaggregation using CNN model-I (CNN1M) and CNN model-II (CNN2M) models are shown in Table III and the predicted disaggregation of MW and R are shown in Fig. 7. As seen from the table, the highest F1-score is achieved by R using CNN-I model. It should be emphasized that all the multi-state devices are disaggregated with acceptable F1-scores above 75% and highest F1-score of 88.15%. Another point to be noted is that for all devices, CNN model-I outperformed CNN model-II, though CNN model-II has a deeper architecture. This supports that a relatively shallower architecture can effectively disaggregate the low-sampling consumption data (REDD dataset was sampled at 3s whereas ENERTALK was sampled at 1s).

E. Discussion and Analysis

1) *ENERTALK House00:* For the analysis of energy disaggregation performance of the appliances of this house, if multi-target setting is considered, it has the average F1-score of 56.23% and the individual highest F1-score 82.13% for WP which is also the highest in the single output setting. As for the scores of single output setting, it is seen that WP has the highest F1-score of 94% and MW has the lowest F1-score of 73.03%. The performance of other appliances according



(a) Actual Vs. Estimated Consumption of MW for Multi-Target CNN Model-I on Combined Data



(b) Actual Vs. Estimated Consumption of R for Multi-Target CNN Model-I on Combined Data

Fig. 7. Actual Vs. Estimated Consumption for CNN Model-I Multi-Target on Combined Data (REDD:House1+House2+House3)

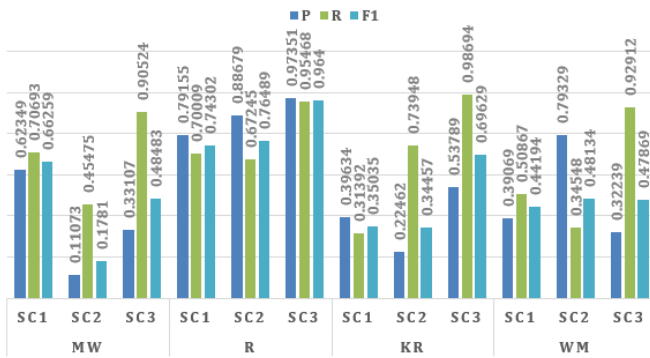


Fig. 8. Disaggregation Analysis of House00 (ENERTALK) Using the Models Trained on Different Appliance of Difference House of the Same Dataset and Same Appliance of Different Dataset. SC1, SC2 and SC3 stand for scenario 1, 2 and 3, respectively

TABLE III. PERFORMANCE SCORES OF CNN1M AND CNN2M ON REDD COMBINED DATA (REDD:HOUSE1+HOUSE2+HOUSE3)

| Appliance       | Model | P       | R       | F1             |
|-----------------|-------|---------|---------|----------------|
| MW              | CNN1M | 0.87503 | 0.88806 | <b>0.88150</b> |
|                 | CNN2M | 0.83395 | 0.82906 | 0.83150        |
| R               | CNN1M | 0.96422 | 0.93732 | <b>0.95058</b> |
|                 | CNN2M | 0.93352 | 0.94413 | 0.93880        |
| DW              | CNN1M | 0.79036 | 0.72423 | <b>0.75585</b> |
|                 | CNN2M | 0.62219 | 0.45417 | 0.52506        |
| WD              | CNN1M | 0.69692 | 0.78931 | <b>0.76309</b> |
|                 | CNN2M | 0.73521 | 0.64430 | 0.68676        |
| Average (CNN1M) |       | 0.83163 | 0.83473 | <b>0.83318</b> |
| Average (CNN2M) |       | 0.78122 | 0.71792 | 0.74824        |

to their F1-scores is 91.09%, 90.28%, 87.44%, 81.58% and 73.50% for R, TV, KR, RC and WM, respectively. In terms of all metrics scores, WP, R, TV, KR and MW have the highly acceptable disaggregation performance. WM and RC are not listed in this category because their respective NDE and NEAP have higher value even though they have better F1-score. Overall average performance F1-score is 84.58% which again confirms the robustness of point-to-point CNN model-II in single target setting for power disaggregation. For the

disaggregation performance of both setting, it is seen that the scores of multi-target model in this house are far lag behind those of the single target model (Table I).

2) *ENERTALK House12*: The main purpose of this experiment is to investigate how efficiently the CNN Model-II can disaggregate energy when there are simultaneously operating multiple mixed type of appliances. The experiment was conducted taking into consideration three multi-state devices (two WMs and one RC), one nonlinear device (TV) and two continuous consumption devices (R and KR). For this, the multi-target setting was considered and the results are shown in Table II. As seen from the table, the highest F1-score of 95.37% is for refrigerator and 75% is the average of all participating appliances. For the multi-state device (RC), F1-score is as high as 76.58%. This experiment also confirms that CNN mode-II can be used for future prototype for energy disaggregation of simultaneous operating of multiple multi-state devices. It should be also noted that our point-to-point multi-target CNN model can disaggregate the nonlinear device with F1-score of 81.13% in the presence of multiple multi-state devices which are also hard to disaggregate.

3) *Disaggregation Performance Across ENERTALK Houses*: For comparisons, please refer to Table I and Table II. It is seen that House00 has superior overall average performance than House12, for single target model. But in terms of multi-target setting, House12 has superior overall performance than House00. When compared the performance of appliances that are common (TV, KR, R, WM and RC) in all the two houses on the basis of appliance by appliance performance in single target setting, TV and RC have higher performance in House00 than House12, and WM1, KR and R have higher performance in House12 than House00. For multi-target setting, all appliances clearly outperform in House12 than House00. That is the reason that the overall performance of House12 is better than House00. Please note that the above analyses are based on F1-scores. To explore the differences, the data patterns of all appliances for all houses were analyzed. In that vein, we look into the data statistics in the houses and from the observation, it can generally be concluded that the usage patterns of individual appliance and

the duration of usage have an impact on the performance. This is based on the fact that the usage pattern and duration have the direct impact on the data distribution and range of data which in turn has remarkable influence on the performance. Neural network generally maps inputs to outputs based on certain mathematical operations, and penalizing the model for wrong mapping by adjusting the weights. This adjusting of weights become difficult for the model when data are sparsely distributed with most of the feature values with zero and some with very large values. This task becomes more difficult when the model has to extract small portion out from large values (blind-source separation) which is the case with the energy disaggregation. This point is particularly more applicable for the appliances that are less frequently used and disaggregation is done on event-less fashion. In addition, from the analyse of the average performance of multi-target regression models, it is observed that the highest F1-score of 75% is achieved by House12 and the lowest F1-score of 56.23% is achieved by House00. It is noteworthy that the reason of higher overall F1-score of House12. This may be due to the fact that when targets are correlated with one another, the multi-target produce better results. Again the correlation between the targets depend on data distribution which again is as mention above, depend on the usage pattern and duration. The study of correlation among the targets is beyond the scope this work. It is emphasized that in terms of NDE and NEAP also, the multi-target model in House12 performs better than both single and multi-target models in House00. Moreover, if we analyze the disaggregation performance of non-linear device (TV) in all two houses for multiple output regression model, the highest F1-score achieved is 81.13% for House12.

4) REDD Dataset: In combined data of House1, 2 and 3, the CNN1M has the highest individual F1-score of 95.06% with R and the overall average F1-score is 83.32%. In terms of individual scores CNN Model-I (CNN1M) has the best performance. This combined data experiment is further elaborated in IV-F.

#### F. Disaggregation Performance and Model Generalization

In general, according to our detail observation and analysis, the disaggregation performance of multi-target model is lower than single target model because in the single target setting, the weight is to adjust to multiple targets of different statistical differences using common features and parameter sharing. However, the multi-target models require less training resources and time than the single target model. On the other hand, the single target model can be customized for specific appliance but at the expense of extra training resources and time.

Generalization and robustness of single and multi-target disaggregation models are tested using CNN Model-II and CNN Model-I for ENERTALK and REDD dataset, respectively. To check the robustness of multi-target regression model, the model trained for four appliances (MW, R, DW, WD) on the combined data of House1+2+3 in REDD dataset was used to predict the energy of selected appliances of House 4, 5 and 6 of the same dataset. This is more challenging than the single output setting because there are ghost (unknown) appliance and miscellaneous outlet in House4 and House6. The scores and estimations are shown in Table IV, and Fig. 9.

TABLE IV. PERFORMANCE SCORES OF SELECTED APPLIANCES OF HOUSE4, 5 AND 6 DISAGGREGATED USING MODEL TRAINED ON HOUSE1+2+3 IN MULTIPLE OUTPUT SETTING (REDD)

| House   | Appliance     | P        | R              | F1             |
|---------|---------------|----------|----------------|----------------|
| House4  | DW            | 0.39813  | 0.10865        | 0.17072        |
|         | WD            | 0.43354  | 0.05639        | 0.09980        |
|         | Unknown       | 0.17495  | 0.22044        | 0.19508        |
|         | Miscellaneous | 0.30309  | 0.63820        | <b>0.41099</b> |
| House5  | MW            | 0.76739  | 0.55764        | 0.64591        |
|         | R             | 0.83057  | 0.66189        | <b>0.73670</b> |
|         | DW            | 0.89611  | 0.48298        | <b>0.62767</b> |
| House6  | WD            | -0.01229 | -0.55193       | -0.02406       |
|         | R             | 0.94380  | 0.92640        | <b>0.93503</b> |
|         | DW            | 0.10150  | 0.98172        | 0.18398        |
|         | WD            | 0.897518 | 0.64567        | <b>0.75104</b> |
|         | Electronics   | 0.16903  | 0.82885        | 0.28080        |
| Unknown | 0.52029       | 0.52725  | <b>0.52734</b> |                |

TABLE V. PERFORMANCE SCORES OF FOUR APPLIANCES OF HOUSE00 OF ENERTALK DISAGGREGATED USING CNN MODEL-I TRAINED ON COMBINED DATA OF REDD

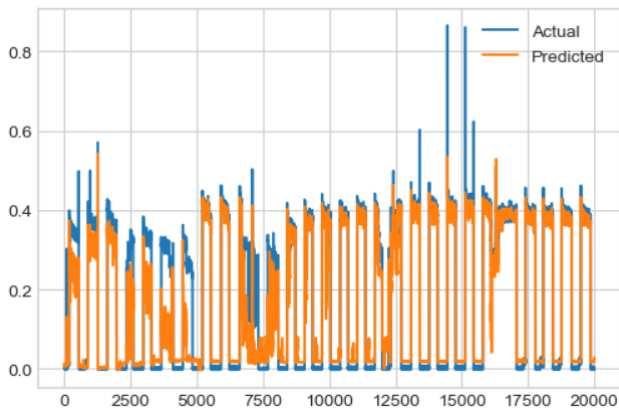
| Appliance | P       | R       | F1      |
|-----------|---------|---------|---------|
| KR        | 0.22462 | 0.73948 | 0.34457 |
| R         | 0.88679 | 0.67245 | 0.76489 |
| WM        | 0.79329 | 0.34548 | 0.48134 |
| MW        | 0.11073 | 0.45475 | 0.17810 |
| Average   | 0.50386 | 0.55304 | 0.52731 |

It is seen that the model can disaggregate the unknown and miscellaneous outlets with F1-score of 52.73% and 41.1%, respectively. Moreover, it can disaggregate the multi-state device (WD) and permanent consumer device (R) with F1-score of 75.1% and 93.50%, respectively. Next, the CNN Model-I trained using combined data of REDD was tested on House00 data of ENERTALK to verify cross-domain disaggregation of the model. The model was trained on dataset and tested on another dataset of of a different geographical location. The tested appliances are KR, R, WM and MW. From the scores given in Table V, it is clear that the energy of R can be disaggregated with the highest precision of 88.68% and the highest F1-score of 76.49%. But in terms of recall score, KR has the highest disaggregation performance score of 73.95%. It should be emphasized that KR and WM were disaggregated using R and WD of combined data as there was no KR and WM in REDD combined data. As overall average of the four appliances, the scores of all three metrics are above 50%.

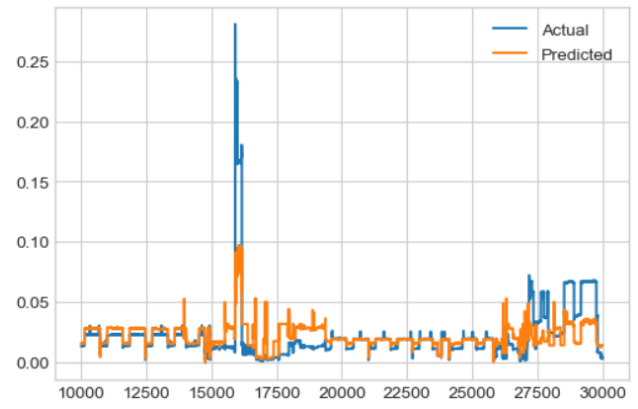
For single target regression, KR in House21 of ENERTALK dataset with total of 4215727 input instances is trained and the energy of all seven appliances (KR, R, TV, RC, WM, WP, MW) of House00 are disaggregated. In this scenario

TABLE VI. PERFORMANCE SCORES OF SEVEN APPLIANCES OF HOUSE00 DISAGGREGATED USING CNN MODEL-II TRAINED ON KR OF HOUSE21 IN SINGLE OUTPUT SETTING (ENERTALK)

| Appliance | P       | R       | F1             |
|-----------|---------|---------|----------------|
| KR        | 0.53789 | 0.98694 | 0.69629        |
| R         | 0.97351 | 0.95468 | <b>0.96400</b> |
| TV        | 0.84321 | 0.93860 | <b>0.88835</b> |
| RC        | 0.29038 | 0.96231 | 0.44614        |
| WM        | 0.32239 | 0.92912 | 0.47869        |
| WP        | 0.94289 | 0.97335 | 0.95788        |
| MW        | 0.33107 | 0.90524 | 0.48483        |
| Average   | 0.60591 | 0.95003 | <b>0.73990</b> |



(a) Energy of R of House6 Estimated by Multi-Target CNN Model-I Trained on House1+2+3



(b) Energy of MW of House5 Estimated by Multi-Target CNN Model-I Trained on House1+2+3

Fig. 9. Estimated Energy of Devices by the Model Trained on House1+2+3 (REDD)

of cross-appliance disaggregation, it is seen that the overall average F1-score is 73.99%. Cross-appliance disaggregation is using the model trained on one specific appliance for disaggregation of other different appliances. From Table VI, it is noticed that the model trained on KR of House21 data has successfully disaggregated energy of most of the appliances in House00, especially, nonlinear device TV with F1-score of 88.83% (see Table VI) and permanent consumer devices that have different operating states such as KR, R with F1-score of 69.63% and 96.40, respectively (see Table VI). But in terms of recall score, all seven devices have above 92% performance. This emphasizes that the direct point-to-point disaggregation models are powerful in learning granular information about consumption. Fig. 8 shows the disaggregation analysis of four selected appliances from House00 of ENERTALK. The scores are reported for three different scenarios: (1) The model trained and tested on House00 (CNN2M), (2) The model trained on REDD combined data (CNN1M) and tested on House00 (ENERTALK) and (3) The model trained on KR (CNN2S) of House21 (ENERTALK) and tested on House00 (ENERTALK). According to the scores in this figure, except MW, the other three appliances have higher disaggregation F1-scores in both scenario 2 and 3 than scenario 1. From previous analysis of generalization and robustness capability of single and multi-target point-to-point disaggregation, it can be emphasized that cross-appliance disaggregation and cross-domain disaggregation have very good performance.

## V. CONCLUSION

This work investigated the NILM problem in terms of training disaggregation algorithms in multiple and single target regression setting, i.e. energy disaggregation of simultaneously operating multiple devices of same types. We used ENERTALK dataset, which is the latest publicly available energy dataset containing records of 22 Korean Houses. We also used REDD dataset, which is the first released energy dataset. We deployed state-of-the-art deep learning algorithms based on CNN and evaluated the disaggregation performance using five energy-based performance metrics. In NILM, aligning the consumption of the target appliances with the aggregate

consumption is more challenging. To achieve this, for ENERTALK, we used vertical and horizontal concatenation of appliance and dates, with mean resampling of data in one second, and for REDD, we used horizontal concatenation. For the experiments, dataframe was divided into training, validation and testing sets. To reflect better generalization capability of the models, the actual prediction is made on the data that was not seen during the training. In ENERTALK, CNN model-II has the highest superior disaggregation performance with F1-score of 95.37% for individual appliance and 75.00% for overall average performance across the dataset for multi-target disaggregation model. Moreover, in ENERTALK, the proposed models can disaggregate the energy of non-linear devices with higher F1-score of 81.13% in multi-target model. The generalization and robustness of the models were also validated by training the model for one appliance and testing it for different appliances in different houses, which shows the knowledge transferability in NILM using the proposed direct point-to-point disaggregation models. As an overall conclusion, the proposed point-to-point regression models have demonstrated computational efficiency and disaggregation effectiveness with superior scores. As future work, other techniques such as energy disaggregation using wavelets can be explored.

## REFERENCES

- [1] K. Ehrhardt-Martinez, K. A. Donnelly, S. Laitner *et al.*, "Advanced metering initiatives and residential feedback programs: a meta-review for household electricity-saving opportunities," no. E105. American Council for an Energy-Efficient Economy Washington, DC (ACEEE), 2010, pp. 1–140.
- [2] M. A. Devlin and B. P. Hayes, "Non-intrusive load monitoring and classification of activities of daily living using residential smart meter data," *IEEE Transactions on Consumer Electronics*, vol. 65, no. 3, pp. 339–348, 2019.
- [3] J.-G. Kim and B. Lee, "Appliance classification by power signal analysis based on multi-feature combination multi-layer lstm," *Energies*, vol. 12, no. 14, pp. 2804(1–24), 2019.
- [4] A. Bouhouras, P. Gkaidatzis, K. Chatzivasvas, E. Panagiotou, N. Poulakis, and G. Christoforidis, "Load signature formulation for non-intrusive load monitoring based on current measurements," *Energies*, vol. 10, no. 4, pp. 538(1–21), 2017.

- [5] J. Jiang, Q. Kong, M. Plumbley, and N. Gilbert, "Deep learning based energy disaggregation and on/off detection of household appliances," *arXiv preprint arXiv:1908.00941*, 2019.
- [6] P. A. Schirmer and I. Mporas, "Statistical and electrical features evaluation for electrical appliances energy disaggregation," *Sustainability*, vol. 11, no. 11, pp. 3222(1–14), 2019.
- [7] B. Buddhahai, W. Wongseree, and P. Rakkwamsuk, "A non-intrusive load monitoring system using multi-label classification approach," *Sustainable Cities and Society*, vol. 39, pp. 621–630, 2018.
- [8] J. Kelly and W. Knottenbelt, "Neural nilm: Deep neural networks applied to energy disaggregation," in *Proceedings of the 2nd ACM International Conference on Embedded Systems for Energy-Efficient Built Environments*, 2015, pp. 55–64.
- [9] İ. H. Çavdar and V. Faryad, "New design of a supervised energy disaggregation model based on the deep neural network for a smart grid," *Energies*, vol. 12, no. 7, pp. 1217(1–18), 2019.
- [10] H. Rafiq, H. Zhang, H. Li, and M. K. Ochani, "Regularized lstm based deep learning model: First step towards real-time non-intrusive load monitoring," in *IEEE International Conference on Smart Energy Grid Engineering (SEGE)*, 2018, pp. 234–239.
- [11] M. D'Incecco, S. Squartini, and M. Zhong, "Transfer learning for non-intrusive load monitoring," *IEEE Transactions on Smart Grid*, 2019.
- [12] C. Zhang, M. Zhong, Z. Wang, N. Goddard, and C. Sutton, "Sequence-to-point learning with neural networks for non-intrusive load monitoring," in *Thirty-second AAAI conference on artificial intelligence*, 2018.
- [13] C. Shin, S. Joo, J. Yim, H. Lee, T. Moon, and W. Rhee, "Subtask gated networks for non-intrusive load monitoring," in *Proceedings of the AAAI Conference on Artificial Intelligence*, vol. 33, 2019, pp. 1150–1157.
- [14] P. A. Schirmer, I. Mporas, and A. Sheikh-Akbari, "Robust energy disaggregation using appliance-specific temporal contextual information," *EURASIP Journal on Advances in Signal Processing*, vol. 2020, no. 1, p. 3, 2020.
- [15] M. Xia, K. Wang, W. Song, C. Chen, Y. Li *et al.*, "Non-intrusive load disaggregation based on composite deep long short-term memory network," *Expert Systems with Applications*, vol. 160, p. 113669, 2020.
- [16] C. Min, G. Wen, Z. Yang, X. Li, and B. Li, "Non-intrusive load monitoring system based on convolution neural network and adaptive linear programming boosting," *Energies*, vol. 12, no. 15, pp. 2882(1–23), 2019.
- [17] J. M. Gillis and W. G. Morsi, "Non-intrusive load monitoring using semi-supervised machine learning and wavelet design," *IEEE Transactions on Smart Grid*, vol. 8, no. 6, pp. 2648–2655, 2016.
- [18] D. Jorde, T. Kriechbaumer, and H.-A. Jacobsen, "Electrical appliance classification using deep convolutional neural networks on high frequency current measurements," in *IEEE International Conference on Communications, Control, and Computing Technologies for Smart Grids (SmartGridComm)*, 2018, pp. 1–6.
- [19] D. Li and S. Dick, "Residential household non-intrusive load monitoring via graph-based multi-label semi-supervised learning," *IEEE Transactions on Smart Grid*, vol. 10, no. 4, pp. 4615–4627, 2018.
- [20] V. Singhal, J. Maggu, and A. Majumdar, "Simultaneous detection of multiple appliances from smart-meter measurements via multi-label consistent deep dictionary learning and deep transform learning," *IEEE Transactions on Smart Grid*, vol. 10, no. 3, pp. 2969–2978, 2018.
- [21] L. De Baets, J. Ruysinck, C. Develder, T. Dhaene, and D. Deschrijver, "Appliance classification using vi trajectories and convolutional neural networks," *Energy and Buildings*, vol. 158, pp. 32–36, 2018.
- [22] Y. Liu, X. Wang, and W. You, "Non-intrusive load monitoring by voltage-current trajectory enabled transfer learning," *IEEE Transactions on Smart Grid*, vol. 10, no. 5, pp. 5609–5619, 2018.
- [23] J. Kim, T.-T.-H. Le, and H. Kim, "Nonintrusive load monitoring based on advanced deep learning and novel signature," *Computational intelligence and neuroscience*, vol. 2017, 2017.
- [24] E. Aladesanmi and K. Folly, "Overview of non-intrusive load monitoring and identification techniques," *IFAC-PapersOnLine*, vol. 48, no. 30, pp. 415–420, 2015.
- [25] W. A. de Souza, F. D. Garcia, F. P. Marafão, L. C. P. da Silva, and M. G. Simões, "Load disaggregation using microscopic power features and pattern recognition," *Energies*, vol. 12, no. 14, pp. 2641(1–18), 2019.
- [26] P. Held, S. Mauch, A. Saleh, D. O. Abdeslam, and D. Benyoucef, "Frequency invariant transformation of periodic signals (fit-ps) for classification in nilm," *IEEE Transactions on Smart Grid*, vol. 10, no. 5, pp. 5556–5563, 2018.
- [27] N. Sadeghianpourhamami, J. Ruysinck, D. Deschrijver, T. Dhaene, and C. Develder, "Comprehensive feature selection for appliance classification in nilm," *Energy and Buildings*, vol. 151, pp. 98–106, 2017.
- [28] M. A. Mengistu, A. A. Girmay, C. Camarda, A. Acquaviva, and E. Patti, "A cloud-based on-line disaggregation algorithm for home appliance loads," *IEEE Transactions on Smart Grid*, vol. 10, no. 3, pp. 3430–3439, 2018.
- [29] M. Fagiani, R. Bonfigli, E. Principi, S. Squartini, and L. Mandolini, "A non-intrusive load monitoring algorithm based on non-uniform sampling of power data and deep neural networks," *Energies*, vol. 12, no. 7, pp. 1371(1–26), 2019.
- [30] M. Kaselimi, E. Protopapadakis, A. Voulodimos, N. Doulamis, and A. Doulamis, "Multi-channel recurrent convolutional neural networks for energy disaggregation," *IEEE Access*, vol. 7, pp. 81 047–81 056, 2019.
- [31] A. Harell, S. Makonin, and I. V. Bajić, "Wavenilm: A causal neural network for power disaggregation from the complex power signal," in *ICASSP 2019-2019 IEEE International Conference on Acoustics, Speech and Signal Processing (ICASSP)*. IEEE, 2019, pp. 8335–8339.
- [32] J. Holweger, M. Dorokhova, L. Bloch, C. Ballif, and N. Wyrsh, "Un-supervised algorithm for disaggregating low-sampling-rate electricity consumption of households," *Sustainable Energy, Grids and Networks*, vol. 19, p. 100244, 2019.
- [33] Q. Wu and F. Wang, "Concatenate convolutional neural networks for non-intrusive load monitoring across complex background," *Energies*, vol. 12, no. 8, pp. 1572(1–17), 2019.
- [34] Y. LeCun, Y. Bengio *et al.*, "Convolutional networks for images, speech, and time series," *The handbook of brain theory and neural networks*, vol. 3361, no. 10, p. 1995, 1995.
- [35] K. Simonyan and A. Zisserman, "Very deep convolutional networks for large-scale image recognition," *arXiv preprint arXiv:1409.1556*, 2014.
- [36] J. Z. Kolter and T. Jaakkola, "Approximate inference in additive factorial hmms with application to energy disaggregation," in *Artificial intelligence and statistics*, 2012, pp. 1472–1482.
- [37] E. T. Mayhorn, G. P. Sullivan, J. M. Petersen, R. S. Butner, and E. M. Johnson, "Load disaggregation technologies: real world and laboratory performance," Pacific Northwest National Lab.(PNNL), Richland, WA (United States), Tech. Rep., 2016.
- [38] R. Bonfigli and S. Squartini, *Machine Learning Approaches to Non-Intrusive Load Monitoring*. Springer, 2019.
- [39] C. Shin, E. Lee, J. Han, J. Yim, W. Rhee, and H. Lee, "The enertalk dataset, 15 hz electricity consumption data from 22 houses in korea," *Scientific data*, vol. 6, no. 1, pp. 1–13, 2019.
- [40] J. Z. Kolter and M. J. Johnson, "Redd: A public data set for energy disaggregation research," in *Workshop on data mining applications in sustainability (SIGKDD)*, San Diego, CA, vol. 25, no. Citeseer, 2011, pp. 59–62.



# Multi-Label Arabic Text Classification: An Overview

Nawal Aljedani<sup>1</sup>, Reem Alotaibi<sup>2</sup> and Mounira Taileb<sup>3</sup>

Faculty of Computing and Information Technology, King Abdulaziz University, Jeddah, Saudi Arabia

**Abstract**—There is a massive growth of text documents on the web. This led to the increasing need for methods that can organize and classify electronic documents (instances) automatically. Multi-label classification task is widely used in real-world problems and it has been applied on different applications. It assigns multiple labels for each document simultaneously. Few and insufficient research studies have investigated the multi-label text classification problem in the Arabic language. Therefore, this survey paper aims to present an extensive review of the existing multi-label classification methods and techniques that can deal with multi-label problem. Besides, we focus on Arabic language by covering the relevant applications of multi-label classification on the Arabic text, and identify the main challenges faced by these studies. Furthermore, this survey presents an experimental comparisons of different multi-label classification methods applied for the Arabic context and points out some baseline results. We found that further investigations are also needed to improve the multi-label classification task in the Arabic language, especially the hierarchical classification task.

**Keywords**—Machine learning; text classification; multi-label classification; Arabic natural language processing; hierarchical classification; Lexicon approach

## I. INTRODUCTION

With the emergence of unstructured data, social media mining, and a massive growth of text documents on the web, text classification (TC) has become an essential task that can be solved using machine learning. It is used for organizing a huge number of electronic documents (instances) efficiently [1]. In general, it can be formally defined as a supervised machine learning technique where a classification model is trained using a training data which consist of a set of instances and their associated labels (categories). In classification, the objective is to classify unseen instances using the trained model by assigning the appropriate labels to an unseen instance [2].

In the literature, two approaches are used for classification as shown in Fig.1; single-label classification, which is the traditional type of classification, it is concerned with assigning only one predefined label to each instance. In contrast, in multi-label classification (MLC), a set of predefined labels associated with the instance simultaneously [3]. Generally, it is usually inadequate to classify each instance under just one single label, because there are several labels that might be suitable to describe its content concurrently [4]. For example, a news article assigned with "education" label, may assigned with several labels simultaneously e.g., "social" and "technology".

MLC task is widely used in real-world problems and it has been applied on different applications like classification of digital libraries, electronic emails, electronic books, patents, and newspaper articles. Many studies have addressed the MLC problem in English language. However, regarding the Arabic language only limited and insufficient studies have been conducted in the MLC field [5].

Arabic language is "the native language of 380 million speakers" [6], and considered from the "six official languages of the United Nations" [7]. It has vast vocabulary and complex morphology [8]. Moreover, since online data in Arabic are increasing rapidly especially in the recent days. As a result, there is a need to develop an automatic text classification technique can organize and categorize such amount of electronic Arabic text documents efficiently. Arabic text classification task are well studied using traditional single label classification algorithms e.g., Naive Bayes (NB) [9], k-Nearest Neighbor (k-NN) [10], and Support Vector Machine (SVM) [11].

However, multi-label Arabic text classification is not well addressed. According to our performed review and the study conducted in [5], there are few researches have been conducted in this field on a small and non-publicly available datasets. Consequentially, MLC in the context of Arabic language is becoming a significant topic in the recent years and attracting attention of many researchers.

Therefore, the main contribution of this paper is to conduct an extensive review to get knowledge of the existing methods and techniques that can be applied to deal with MLC problems. It also contributes to organizing the sparse state-of-the-art MLC methods into a structured presentation. Besides, a set of common multi-label evaluation metrics used to evaluate MLC models have been presented. Furthermore, it focuses on the Arabic language by covering the existing studies that are applied in the Arabic context and identifies the main challenges faced by these studies. An experimental comparisons of several state-of-the-art MLC methods in the Arabic context are also provided.

A structured representation of different state-of-the-art MLC methods is provided in the text classification taxonomy shown in Fig. 1. According to this taxonomy, two approaches are used to solve MLC problems: lexicon approach which is based on creating a dictionary for each label that contains the list of all related words, or machine learning approach that relied on labelled instances. The two approaches are discussed in the following sections (see Section II and Section III).

The rest of the paper is organized as follows. Section II discusses MLC using lexicon approach. After that, Section III discusses MLC using machine learning approach. It also reports an extensive review of MLC methods by providing illustrative examples and discussing their advantages and limitations. The most common multi-label evaluation metrics are presented in Section IV. Then, Section V focuses on the Arabic language and presents a set of applications for multi-label Arabic text classification. It also identifies MLC techniques which have been applied in each application and briefly discusses some important challenges and remarks for future studies. An experimental comparisons of the state-of-the-art MLC methods for the Arabic text are conducted in

Section VI. Finally, Section VII concludes the paper.

## II. MLC USING LEXICON APPROACH

Lexicon-based classification as presented in [12] means that each instance is assigned to a label based on a classification rule which considers the count of words from lexicons of each label. Obviously, the basic rule is to predict the label that most of words in the instance are associated with its lexicon. Generally, lexicon-based approach has several advantages such as: it is intuitive, easy to use, simple, and makes the classification faster compared with labelled instances.

On the other hand, from machine learning perspective, lexicon-based classification suffers from some drawbacks. One of the most drawbacks is the lack of theoretical justification and it is not clear what conditions are required for it to work. Moreover, it assigns a similar weight for each word and this is not reasonable because some words are strongly predictive compared to others. In addition, the lexicon-based approach ignores multi-word phenomena, for example negation (e.g., not so good), and the lexicons might be incomplete.

MLC using machine learning approach which are trained on labelled instances, seem to outperform lexicon-based classification even without considering the multi-word phenomena. Lexicon-based classification is widely used in opinion mining and sentiment classification [12]. However, in some applications, it is used as a MLC approach [13].

## III. MLC USING MACHINE LEARNING APPROACH

Solving multi-label problem using machine learning approach can be divided as shown in Fig. 1 into flat and hierarchical classifications.

### A. Flat Classification

In the flat classification, the set of predefined labels are treated independently and classified in one level where they are not organized in a structure that defines the relationship among these labels [14] as shown in Fig. 2. The flat classification in multi-label problem divided into two techniques, which are problem transformation (PT) and algorithm adaptation technique.

PT can be defined as transformation of the multi-label problem into a set of single-label problems which are classified using classical (traditional) single-label classification algorithms. Whereas, algorithm adaptation are those methods that adapt single-label classification algorithms to deal directly with multi-label problem. It is worth mentioning that algorithm adaptation methods are algorithm-dependent and PT methods are algorithm-independent [2].

1) *Strategies based on PT Technique:* PT technique is considered as the simplest way to classify multi-label data because it simply transforms the data into single-label problems, then classical single-label classification algorithms are applied to perform the classification task. Basically, there are two straightforward PT techniques, either based on transformation to binary classification or transformation to multi-class classification.

The classification task in both techniques is based on single-label classifiers. But, concerning the multi-class classification, the similar set of labels are combined as a distinct class. Thus, every similar set of labels that found in the training dataset is considered a new class of a multi-class classification task [15]. The most common PT methods which are based on transformation to binary classification are described in the following.

**Binary Relevance (BR).** As presented in [2], a simple and straightforward method used to handle MLC task is BR method. Simply, it transforms a MLC problem into several single-label classification problems and predicts the instance relevance for each single-label independently by training a binary classifier one per label.

The instances of the original multi-label data are included in each single-label data and they are predicted with positive label if they have the existing label, otherwise, they are predicted with negative label. The classification of a new (unseen) multi-label problem using BR is performed by transforming it into  $n$  single-label problems (where  $n$  refers to number of labels). Consequently, the new instance will be labelled with a union of the positive labels predicted by the  $n$ -binary classifiers [15], as shown in Fig. 3.

BR presents several obvious advantages such as it is relatively fast and conceptually a simple method, it has a linear complexity related to the number of labels, so it has a low computational complexity. In addition, since it does not consider labels correlation, therefore it is possible to add or remove labels without having an effect on the rest of the BR model which makes it appropriate for a dynamic or evolving scenario and it can be easily parallelized.

However, BR has some drawbacks; it does not consider any label correlations and might reduce the predictive performance if such label dependency is present. Moreover, increasing the label dimensionality causes an increase in the number of trained binary classifiers. In addition, it suffers from sample imbalance problem that may occur when number of negative instances outperform the positive ones [2], [16].

**Classifier Chain (CC).** There are several methods that have been proposed to minimize the BR drawbacks. The most popular one is the CC method proposed in [17]. CC method is like BR method with small difference which is that, it resolves BR drawback by considering label correlations. Obviously, it transforms the MLC problem into a chain of binary classification problems where each subsequent binary classifier in the chain is extended with 0, 1 label predictions of all preceding classifiers, and these labels predictions are considered as future attributes for the next classifier. Chaining method passes the label information among the labels making the CC considering correlation in the label space. An example of CC method is presented in Fig. 4.

The main CC advantages are that it considers label dependency to obtain high predictive performance while maintaining a reasonable computational complexity of BR. It is straightforward to predict label from this chain by obtaining the label of one classifier and propagating it along the chain [17].

Furthermore, it has some drawbacks; since CC has chaining property it loses the opportunity of parallel implementation

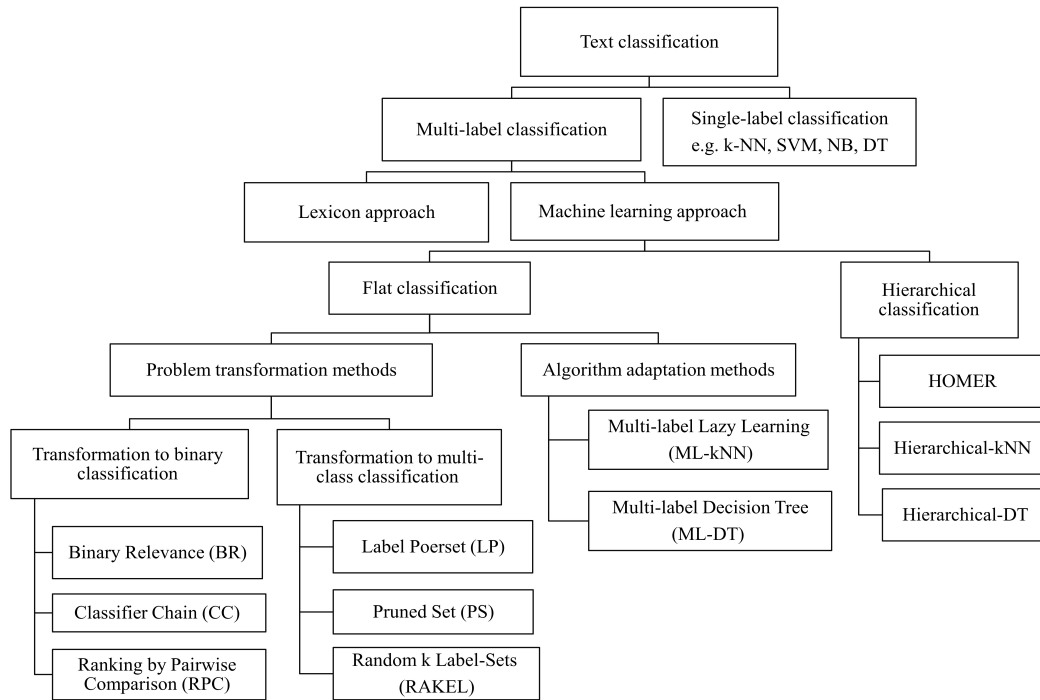


Fig. 1. Text Classification Taxonomy

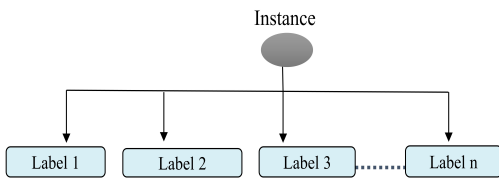


Fig. 2. Example of an Instance with Multi-Labels in the Flat Classification

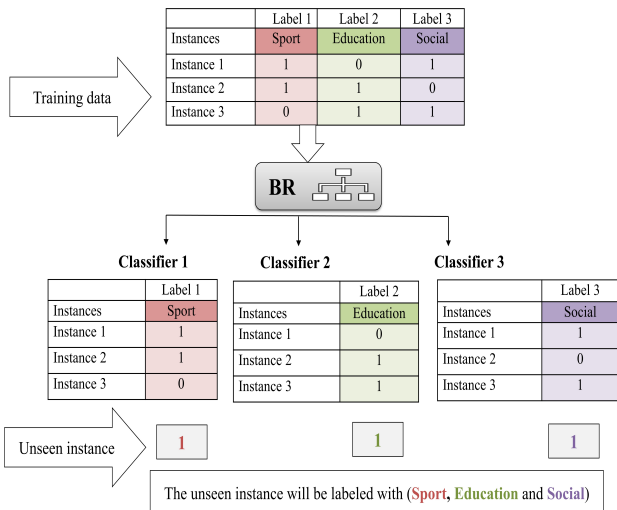


Fig. 3. Binary Relevance Method

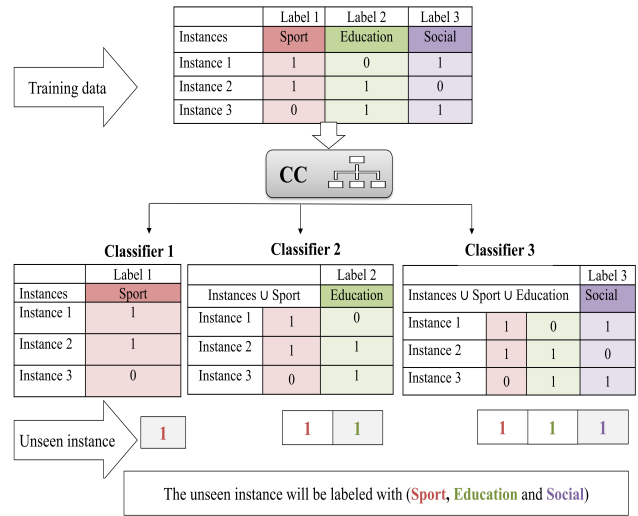


Fig. 4. Classifier Chain Method

[18]. In addition, the chaining property in CC also cause an error propagation at the classification time in case of a poor prediction from one or more of the preceding classifiers. This might affect the prediction of the following labels. Moreover, the poorly ordered of the chain can affect the prediction accuracy. Thus, an ensembles of CC method has been proposed to overcome this issue by training the CC classifiers with random order of chains [17].

**Ranking by Pairwise Comparison (RPC).** RPC proposed in [19] is another type of PT methods, it is considered as an extension of the original Pairwise Comparison (PC) method.

RPC is a sequence of two processes; in the first one, PC are trained with a given data. This means that the multi-label dataset with  $n$  labels is transformed into  $n(n-1)/2$  single-label binary classification problems, where for each pair of labels a binary classifier is used by covering all pairs of labels.

Each single binary classification problem involves the instances in the original multi-label problem, which are assigned to just one of the two labels but not both, as shown in Fig. 5. First, in the label prediction task of each classifier, the classifier performs a comparison between each pair of labels. For example, if it compares between label 1 and label 2, thus, the resulted predicted label, let us call it  $y$ , will be (0 or 1) according to Eq. (1).

$$y = \begin{cases} 1, & \text{Label1} \succ \text{Label2} \\ 0, & \text{Label2} \succ \text{Label1} \end{cases} \quad (1)$$

Then, in the second step, the predicted labels are ranked using a ranking procedure such as a generalization of voting strategy where all labels are ranked based on the evaluated sum of the weighted votes. To classify a new instance using RPC method, each binary classifier is invoked and voted to one of the two labels. After prediction of labels by all classifiers, the labels' ranking is obtained according to the sum of votes of each label.

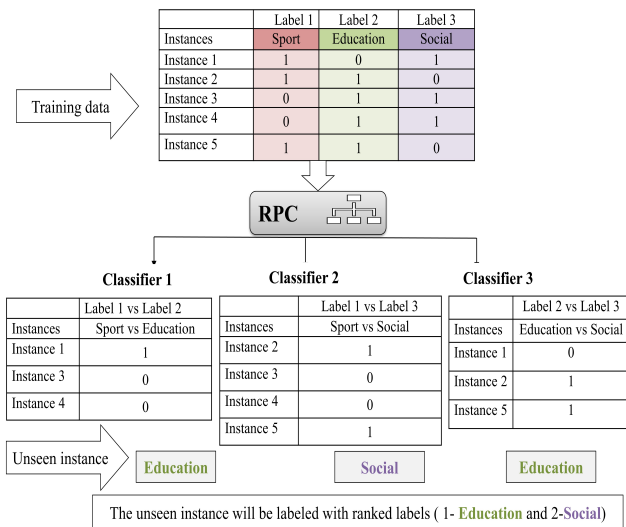


Fig. 5. Ranking by Pairwise Comparison Method

The main disadvantage of the RPC is the need to query all the generated classifiers at the classification time [2]. In addition, a quadratic complexity ( $n^2$ ) of RPC makes it very sensitive to the large number of labels and usually it is difficult to deal with large problems. However, more experiments showed that RPC is a competitive method in terms of accuracy and prediction quality. In addition, the extended version of the RPC uses the ensemble of pairwise classifiers to adapt to different loss functions on label ranking strategy without retraining the pairwise classifiers [19].

A summary of pros and cons of the above mentioned PT methods based on transformation to binary classification is presented in Table I. In the following we present the most common PT methods based on transformation to multi-class classification.

**Label Powerset (LP).** It is the most simple and standard method under this classification technique. It transforms the MLC problem into a multi-class classification problem, and considers each distinct label-set in the training data as a new class of a multi-class classification task [20]. To classify a new multi-label instance using LP, a multi-class classifier can be used to assign the most probable class from many new classes to this instance, which can then be reversible to the corresponding set of the initial labels. In the example shown in Fig. 6, the classifier will randomly predict a class for an unseen instance. Since there are two classes with 50% chance to be assigned to the unseen instance.

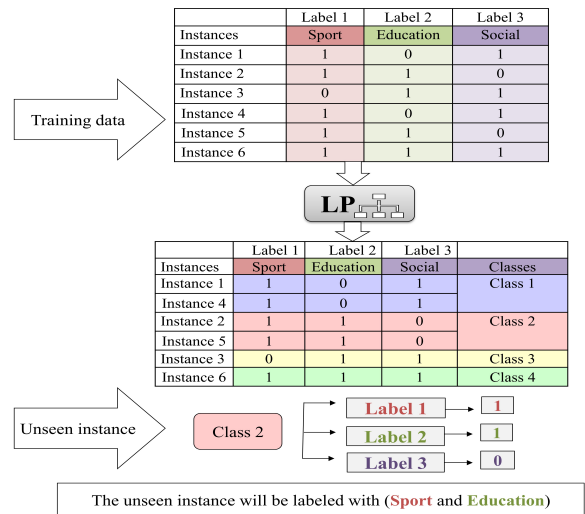


Fig. 6. Label Powerset Method

Although, LP has many advantages such as its simplicity, effectiveness, and consideration of correlations among labels in the training data. In contrast, it suffers from some drawbacks. The first problem is, it has a computational complexity increases exponentially with the number of labels and that is why LP quickly deteriorates for larger label-sets and makes the work of the classifier harder [15]. Consequently, LP is usually recommended just for datasets that have small number of distinct classes. On the other hand, since LP method can consider only the label-sets present in the training data, so it can not classify any unseen label-set. In addition, for many new classes, it is potential to have limited training instances due to the infrequent combinations of label-sets for those classes, so this lead to the class imbalance problem [2].

Two variants of LP method have been proposed, the first, is Pruned Set method proposed in [21], and the second proposed method is Random  $k$ -Labelsets [22].

**Pruned Set (PS).** The main idea of PS method is similar to LP, it extends the same paradigm of LP whereas trying to resolve the limitations related to LP complexity [21]. This is achieved by pruning away the label-sets with a frequency of occurrence less than a threshold defined by the user. Hence, it reduces the LP complexity by keeping just the label-set that are occurring more frequently by comparing it to the threshold.

TABLE I. PROS AND CONS OF PT METHODS BASED ON TRANSFORMATION TO BINARY CLASSIFICATION

| PT method | Pros                                                                                                                                                                                                                                                                                        | Cons                                                                                                                                                                                                                                                     |
|-----------|---------------------------------------------------------------------------------------------------------------------------------------------------------------------------------------------------------------------------------------------------------------------------------------------|----------------------------------------------------------------------------------------------------------------------------------------------------------------------------------------------------------------------------------------------------------|
| BR        | <ul style="list-style-type: none"> <li>• Relatively fast.</li> <li>• Conceptually simple.</li> <li>• Low computational complexity.</li> <li>• Appropriate for a dynamic scenario.</li> <li>• Can be easily parallelized.</li> <li>• Scale up linearly with the number of labels.</li> </ul> | <ul style="list-style-type: none"> <li>• Ignores labels correlations.</li> <li>• May reduce predictive performance.</li> <li>• An increase in the number of labels causes the increase in the number of binary classifiers.</li> </ul>                   |
| CC        | <ul style="list-style-type: none"> <li>• Considers labels dependencies.</li> <li>• Obtains high predictive performance.</li> <li>• Maintains acceptable computational complexity.</li> <li>• Straightforward to predict label from chain.</li> </ul>                                        | <ul style="list-style-type: none"> <li>• Loses the opportunity of parallel implementation.</li> <li>• Might cause an error propagation at the classification time.</li> <li>• Poorly ordered chain that might affect the accuracy prediction.</li> </ul> |
| RPC       | <ul style="list-style-type: none"> <li>• Provides high accuracy and prediction quality.</li> <li>• Does not require to retrain the pairwise classifiers if the label ranking method change.</li> </ul>                                                                                      | <ul style="list-style-type: none"> <li>• All generated binary classifiers are queried at the run-time.</li> <li>• Quadratic complexity.</li> <li>• Very sensitive to large number of labels.</li> </ul>                                                  |

An example is illustrated in Fig. 7 using PS method, it keeps only class 1 and class 2 because they have more frequent label-sets in the training data compared to the other classes and prunes away both of class 3 and class 4 represented in Fig. 6, because they occurred infrequently. However, it is similar to LP when taking into account only the distinct label-sets present in the training data. In addition, it suffers from class imbalance problem.

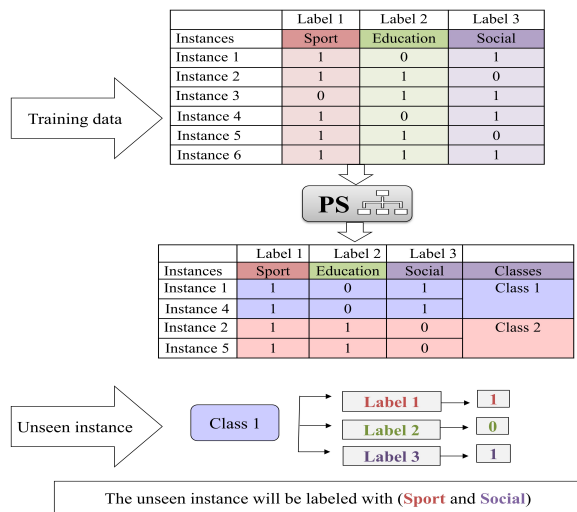


Fig. 7. Pruned Set Method

The classification of an unseen instance using PS method is illustrated with an example in Fig.7. It is similar to LP; a multi-class classifier is applied to randomly assign a probable class to this instance, which can be reversible to the corresponding set of the initial labels. Since there are two classes with 50% chance to be assigned to the unseen instance.

**Random  $k$ -Labelsets (RAKEL).** RAKEL method also has resolved LP problems by generating an ensembles of LP method by breaking the multi-label problem into  $r$  models or subsets [22]. Each subset is assigned with a random  $k$  label-sets

where  $k$  is a random number used to determine the size of each model. The label-sets in each model can be either disjoint or overlapping according to the strategy used to construct them.

To classify a new instance, RAKEL queries all models and obtains their average decision for each label. In addition, it makes the final prediction based on the value of the given threshold, so the final label prediction is positive when the average decision is greater than the threshold and negative otherwise.

Furthermore, it provides some advantages since it considers label correlation and overcomes LP limitation by increasing number of distinct label-sets and thus it provides more accurate label prediction and competitive performance. Nevertheless, it suffers from the increasing number of classifiers generated according to a  $k$  random number used to determine the size of each model. The pros and cons of the above mentioned PT methods based on transformation to multi-class classification are summarized in Table II.

## 2) Strategies based on Algorithm Adaptation Technique:

Overall, classical single-label classification algorithms can not deal directly with MLC problem. Consequently, algorithm adaptation technique has been developed to tackle MLC problem by extending and adapting single-label classification algorithm to be able to directly deal with MLC problem [23]. Almost most of classical single-label classifiers have been adapted to handle MLC problems directly [2].

For example, SVM algorithm has been adapted to Rank-SVM in [24], Neural Network algorithm has been customized as the baseline algorithm for a Back-Propagation Multi-Label Learning (BP-MLL) algorithm in [25]. Besides, a Multi-label Lazy Learning algorithm called ML-kNN proposed in [26] extended from the classical k-NN algorithm. In addition, Multi-Label Decision Tree algorithm (ML-DT) has been developed in [27], [28] by adapting the C4.5 decision tree algorithm. The most common algorithms in the algorithm adaptation context are detailed in the following paragraphs.

**Multi-Label Lazy Learning (ML-kNN).** MLC task consists of training a classification model using a specific algorithm to predict several labels for each unseen instance by analyzing labelled training instances. ML-kNN was proposed

TABLE II. PROS AND CONS OF PT METHODS BASED ON TRANSFORMATION TO MULTI-CLASS CLASSIFICATION

| PT method | Pros                                                                                                                                                                                                                                                               | Cons                                                                                                                                                                                                                                                   |
|-----------|--------------------------------------------------------------------------------------------------------------------------------------------------------------------------------------------------------------------------------------------------------------------|--------------------------------------------------------------------------------------------------------------------------------------------------------------------------------------------------------------------------------------------------------|
| LP        | <ul style="list-style-type: none"> <li>• Simple and effective.</li> <li>• Considers labels correlations.</li> <li>• Works well only when using datasets with a small number of classes.</li> </ul>                                                                 | <ul style="list-style-type: none"> <li>• Exponential increase of the computational complexity if the number of labels increases.</li> <li>• Class imbalance problem.</li> <li>• Can not classify any unseen label-set in the training data.</li> </ul> |
| PS        | <ul style="list-style-type: none"> <li>• Considers labels correlations.</li> <li>• Reduces LP complexity.</li> </ul>                                                                                                                                               | <ul style="list-style-type: none"> <li>• Class imbalance problem.</li> <li>• Can not classify any unseen label-set in the training data.</li> </ul>                                                                                                    |
| RAKEL     | <ul style="list-style-type: none"> <li>• Considers labels correlations.</li> <li>• Reduces LP complexity.</li> <li>• Provides more accurate label prediction.</li> <li>• Considers any unseen label-set even if it is not present in the training data.</li> </ul> | <ul style="list-style-type: none"> <li>• Increasing number of generated classifiers.</li> </ul>                                                                                                                                                        |

in [26], which is a MLC algorithm derived from the classical k-NN algorithm.

To predict the label-sets for a new instance using ML-kNN, the algorithm follows the same approach of the classical k-NN algorithm. First: the  $k$  nearest neighbors from the training instances are determined. Usually, "Euclidean distance" is used to compute the distance as well as similarity between instances to identify the  $k$  neighboring instances. The second step, which is the additional step in the ML-kNN algorithm focuses on label-sets aggregation of the  $k$  neighboring instances. It utilizes "Maximum A Posteriori (MAP) principle" to determine the more probable label-sets for the new instance by relying on prior and posterior probabilities for the frequency of each label in the  $k$  nearest neighbors. ML-kNN as well as can output an ordered list of ranking labels [3].

Finally, to validate the approach, the authors conducted some experiments on the three real world problems. The result showed that ML-kNN achieved better performance than some other MLC algorithms, e.g., Rank-SVM, Adtboost.Mh, and Boostexter.

**Multi-Label Decision Tree (ML-DT).** Regarding the DT algorithm, the C4.5 algorithm has been adapted in [27] to ML-DT algorithm to deal with MLC problem directly. The adaptation is accomplished by modifying the original entropy formula of C4.5 algorithm for solving MLC problems, where entropy is a metric of the amount of uncertainty in the dataset. The entropy formula was modified for multiple labels to compute the weighted sum of all entropies for each individual label in each subset as shown in Eq. (2).

$$Entropy = - \sum_{i=1}^n ((p(L_i) \log p(L_i)) + (q(L_i) \log q(L_i))) \quad (2)$$

Where;  $n$  = number of labels,  $p(L_i)$ = membership probability (relative frequency) of label  $L_i$  in a data subset,  $q(L_i) = 1 - p(L_i)$  = non-membership probability of label  $L_i$  in a data subset. Consequently, allowing ML-DT to handle multi-label problem means it should allow multiple labels for the leaf nodes in the tree. Besides, in case of generating rules in leaf nodes, these rules could output a set of labels.

The authors in [28], developed a multi-label decision tree

algorithm (LaCovaC) based on C4.5 that learns the labels relations and exploits them to improve the predictive performance.

### B. Hierarchical Multi-Label Classification

Hierarchical multi-label classification (HMC) is considered as an extension or variant of MLC where a hierarchy structure is used on the multi-label. In HMC, an instance is assigned with multiple labels concurrently and those labels are structured in a hierarchy [29]. Moreover, an instance should satisfy the hierarchy constraint, which means that if it belongs to some label  $L$  it automatically belongs to all super-labels of  $L$  [30].

There are many classification tasks in the real world that can be considered as HMC problems, where the predicted labels are classified as a hierarchy, typically as a tree-shaped or a directed a cyclic graph (DAG) [31]. However, according to a survey conducted in [32], most of the current researches are only concerned with the tree structured hierarchy as shown in Fig. 8. In general, HMC is considered as a more challenging task by nature compared to the flat classification [31]. A comparison between flat and hierarchical classification is illustrated in Table III.

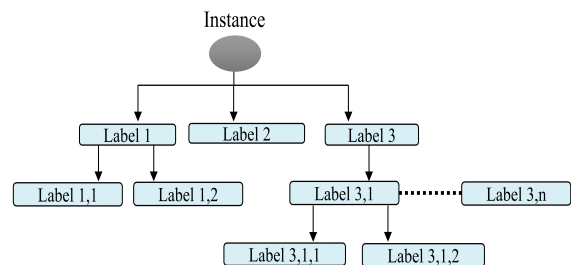


Fig. 8. Example of an Instance with Multi-Labels Classified using Hierarchical Multi-Label Classification; Labels are Structured in a Tree-Shaped Hierarchy

**1) Hierarchical Multi-Label Classification Algorithms:** Several algorithms have been proposed to deal with HMC problem such as: Hierarchy Of Multilabel classifiers algorithm (HOMER) [36], Hierarchical Decision Tree algorithm [37], Hierarchical k-NN algorithm [14], Incremental algorithm for hierarchical classification [38], Hierarchical-SVM [39], and

TABLE III. COMPARISON BETWEEN FLAT AND HIERARCHICAL CLASSIFICATION.

|                                                                             | Flat classification                                                                                                                                                                                                                                                                           | Hierarchical classification                                                                                                                                                                                                                                                           |
|-----------------------------------------------------------------------------|-----------------------------------------------------------------------------------------------------------------------------------------------------------------------------------------------------------------------------------------------------------------------------------------------|---------------------------------------------------------------------------------------------------------------------------------------------------------------------------------------------------------------------------------------------------------------------------------------|
| Basic concept                                                               | Classify labels in MLC problem as one level, where they are not organized as a structure that defines the relationship among these labels.                                                                                                                                                    | Imposing a hierarchy structure on MLC problem, where an instance belongs to many labels and the labels are structured in a hierarchy.                                                                                                                                                 |
| Properties                                                                  | <ul style="list-style-type: none"> <li>• Conceptually simple.</li> <li>• Ignoring the label hierarchy.</li> <li>• Difficult to handle a large number of labels.</li> <li>• Handle MLC task of unstructured documents.</li> <li>• Divided into PT and algorithm adaptation methods.</li> </ul> | <ul style="list-style-type: none"> <li>• More challenging approach.</li> <li>• Considering the label hierarchy.</li> <li>• Capable to handle a large number of labels.</li> <li>• Handle MLC task of structured documents.</li> <li>• Structured as tree or DAG hierarchy.</li> </ul> |
| Relevant studies conducted on Arabic text using machine learning algorithms | [33], [5], [34], [4].                                                                                                                                                                                                                                                                         | [35].                                                                                                                                                                                                                                                                                 |

HMC using Fully Associative Ensemble Learning [40]. We discuss some of them in the following paragraphs.

**Hierarchy Of Multilabel classifierS (HOMER).** HOMER algorithm is an effective hierarchical multi-label classifier, relies on divide-and-conquer approach [36]. This algorithm can efficiently handle a MLC problem with a large number of labels by constructing a tree-shaped hierarchy of simpler MLC problems. Then, each classifier can handle MLC problem with a small number of labels rather than handling a large label-set.

Labels distribution task in this algorithm is done using the top-down approach. That means the large label-sets should be distributed into  $k$  disjoint label-sets based on similarity, starting from parent to child nodes. This task is usually done using balanced clustering algorithm. However, in [36] the authors proposed a clustering algorithm for labels distribution called balanced  $k$ -means clustering algorithm.

Consequently, each node in the tree involves the union of meta-labels  $\mu$  of its children and the root node contains labels of all nodes in the tree. Besides, each internal node also has a multi-label classifier  $S$  to predict one or more meta-labels of its children. Figure 9 illustrates the tree hierarchy in HOMER for the classification task of multi-label problem with 9-labels  $\{L1, \dots, L9\}$ .

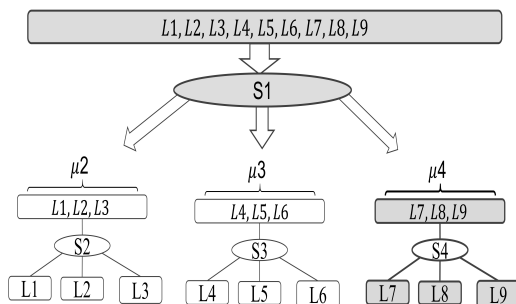


Fig. 9. Example of a Classification Task of Multi-Label Problem with 9 Labels using HOMER Algorithm

For multi-label classification task of an unseen instance  $e$ , HOMER starts from the root node then follows a top-down approach to forwards  $e$  to the most relevant multi-label classifier  $S$ . In the example of HOMER illustrated in Fig. 9,

the multi-label classifier  $S1$  at the root node will forward the instance  $e$  to the multi-label classifier  $S4$  only if  $\mu_4$  is among the predictions of  $S1$  classifier. Finally, by following a recursive process, the result of the final prediction labels will be a union of all predicted labels by the multi-label classifier that higher than the corresponding leaf(ves) nodes. Otherwise, if no labels are predicted, the algorithm returns an empty set.

The authors have conducted some experiments using HOMER algorithm by employing the BR as a multi-label classifier and NB as a base classifier. The results showed that, since HOMER relies on similarity-based distribution and employed BR and NB classifiers, this reduces the computational cost in both training and test phases and it improves the predictive performance as well.

**Hierarchical Multi-Label Classification using k-NN Algorithm.** The authors in [14] have proposed a new framework by extending the modified version of k-NN algorithm and proposed a new similarity measure to handle HMC task. The classical k-NN algorithm was modified to work with label representative instead of training instances. Where each label is represented by one instance constructed from all instances in the training data related to this label. This process is done by identifying the most important features of that label and combining the training instances accordingly. By using label representative, the classification time have been reduced because a new instance will be compared with just a portion of instances rather than all the training instances.

Several methods can be used to measure the instance similarity such as, cosine similarity, Jaccard, and dice. These measures calculate the similarity based on instance vector, where each vector consists of instance features along with their frequencies in the training instances. However, the proposed framework relies on a new proposed similarity measure named New Expected Information value  $I_{new}$ . It is calculated according to only the shared features between label representative and a test instance, this resulted to a smaller vector compared to the other similarity measures mentioned previously.

The authors have tested and evaluated the proposed framework by conducting an experiment using a test dataset. The results revealed that applying the proposed classifier with  $I_{new}$  similarity measure has reduced the classification time compared to the other similarity measures. Besides, precision and recall evaluation metrics showed that using  $I_{new}$  measure performed results close to the three similarity measures (cosine

similarity, Jaccard, and dice).

**Decision Tree for Hierarchical Multi-Label Classification.** The authors in [37] have investigated the suitability of the classical DT algorithm to HMC task. They have instantiated three decision tree algorithms: single-label classification (SC) algorithm, hierarchical single-label classification (HSC) algorithm, and hierarchical multi-label classification (HMC) algorithm. The three proposed algorithms are based on “predictive clustering trees (PCTs) framework” which represents the DT in a hierarchy of clusters.

SC approach tends to transform HMC task into a set of binary classification problems and applies DT algorithm for each label in the hierarchy. This algorithm is not efficient because it should run the DT algorithm  $n$  times based on the number of labels. In addition, it predicts each label separately and thus it is not automatically ensuring the hierarchy constraint. HSC overcomes the last SC drawback by imposing the hierarchy constraint. It adopts SC method and run DT algorithm for each edge in the hierarchy. In contrast, the third approach which is HMC aims to learn the single classification model by employing one DT algorithm to predict all hierarchical labels at once.

The authors have considered the label hierarchy as a tree then they have extended it toward a DAG structure. The three proposed algorithms have been evaluated by using 24 functional genomics datasets. The empirical evaluation showed the superiority of HMC in both of tree and DAG hierarchy structures. It has achieved better predictive performance that outperforms HSC and SC algorithms.

#### IV. MULTI-LABEL EVALUATION METRICS

MLC models are evaluated in terms of performance and accuracy using metrics that are commonly used in the MLC field [41]. The evaluation of MLC models is unlike the evaluation of single-label classification models. Thus, according to [2] several multi-label evaluation metrics have been proposed which are classified into two main approaches: example-based (instance-based) and label-based metrics. The first approach is computed for each test instance and then averaged over all test instances. Whereas, the second approach is computed for each label and then averaged over all labels.

##### A. Example-based Metrics

The most common example-based metrics that are used to evaluate MLC models are described in the following. Suppose that:  $m$  refers to the total number of instances in the test dataset,  $i$  indicates an instance in the test dataset (where  $1 \leq i \leq m$ ),  $n$  is the total number of labels,  $Z_i$  and  $Y_i$  refers to the predicted and actual labels, respectively.

- **Hamming loss** It calculates the average number of errors found in the instance-label pairs, averaged over all instances. The expression of this metric is shown in Eq. (3). Where the factor  $\frac{1}{n}$  is used to obtain the normalized value in [0,1] and  $\Delta$  defines the symmetric difference between predicted and actual labels.

$$Hamming\ loss = \frac{1}{m} \sum_{i=1}^m \frac{1}{n} |Z_i \Delta Y_i| \quad (3)$$

- **ML-accuracy.** It is known as multi-label accuracy or example-based accuracy. It computes the ratio of the labels predicted correctly over the total number of labels, as shown in Eq. (4).

$$ML - accuracy = \frac{1}{m} \sum_{i=1}^m \frac{|Z_i \cap Y_i|}{|Z_i \cup Y_i|} \quad (4)$$

- **Subset accuracy** [42]. It also called exact match ratio or classification accuracy. It is a very strict metric used to measure the ratio of predicted labels which exactly match their corresponding actual set of labels, as shown in Eq. (5). Where  $I(true) = 1$  and  $I(false) = 0$ .

$$Subset\ accuracy = \frac{1}{m} \sum_{i=1}^m I(Z_i = Y_i) \quad (5)$$

- **Precision.** This metric giving us the ratio of labels correctly classified of the predicted labels. The expression of this metric is shown in Eq. (6).

$$Precision = \frac{1}{m} \sum_{i=1}^m \frac{|Z_i \cap Y_i|}{|Z_i|} \quad (6)$$

- **Recall.** This metric is computed as shown in Eq. (7), computes the ratio of correctly predicted labels of the actual labels.

$$Recall = \frac{1}{m} \sum_{i=1}^m \frac{|Z_i \cap Y_i|}{|Y_i|} \quad (7)$$

- **F-Measure.** It is the harmonic mean between precision and recall. It is computed as shown in Eq. (8).

$$F - measure = \frac{1}{m} \sum_{i=1}^m \frac{2|Z_i \cap Y_i|}{|Z_i| + |Y_i|} \quad (8)$$

All example-based metrics described in this section indicate that the metric with the highest value has better performance, except Hamming loss metric, the lower value of Hamming loss indicates the better performance.

##### B. Label-based Metrics

The binary evaluation metrics (e.g., recall, precision, and F-measure) can be calculated for all labels based on two approaches of computing the average; either macro or micro averaged approaches. These metrics are widely used to measure the average for recall, precision, and F-measure. Let  $B$  a binary evaluation measure used to calculate these metrics, which computed based on the number of true positives (tp), false positives (fp), true negatives (tn), and false negatives (fn). The expressions of macro-averaged and micro-averaged metrics for  $B(tp, tn, fp, fn)$  are illustrated in Eq. (9) and Eq. (10), respectively.

$$B_{macro} = \frac{1}{n} \sum_{i=1}^n B(tp_i, fp_i, tn_i, fn_i) \quad (9)$$

$$B_{micro} = B \left( \sum_{i=1}^n tp_i, \sum_{i=1}^n fp_i, \sum_{i=1}^n tn_i, \sum_{i=1}^n fn_i \right) \quad (10)$$



## V. APPLICATIONS OF MLC METHODS IN ARABIC TEXT CLASSIFICATION

In this section we focus on Arabic language by presenting the relevant research studies which have been found in the literature that apply MLC methods in Arabic text classification.

### A. Lexicon Approach

The study conducted in [13] has proposed an Arabic multi-label text classification model based on lexicons. The authors of this study aimed to classify multi-label Arabic dataset using a combination of lexicons. They have collected 4,720 Arabic articles with 35 labels from the BBC news website. The collected datasets were divided into training and test datasets using 70/30 split. Then, the training data were exploited to construct the lexicons for each label. They implemented the term frequency (TF) method that automatically counts the term frequency of each label.

After that, they have built 35 lexicons for the 35 labels, there are some common terms found in the lexicons of several labels and this support the MLC and return multi-labels for those terms. Then, the lexicons are used by the classifier to predict the labels for a new instance. The label prediction is done by matching the terms of each label stored in the lexicons with the term vector of a given instance and classifying them according to the term frequency. Then, just the first five labels with the greatest count values are predicted.

Finally, they have evaluated their classification model using Hamming loss, ML-accuracy, subset accuracy, and the execution time. Several experiments have been performed and the results showed that the lexicon-based model achieved better performance in term of ML-accuracy compared with the corpus-based approach using MEKA tool<sup>1</sup>.

### B. PT Methods based on Binary Classification

Regarding transformation to binary classification method, a new model for MLC has been developed in [4] based on BR method. The main contribution of this study was to solve MLC problem for Arabic dataset by designing BR method based on different set of single label classifiers including SVM, NB, and k-NN. These base classifiers have been employed with BR, and evaluated using four approaches which are: the set of SVM classifiers, NB classifiers, k-NN classifiers, and various set of classifiers.

Besides, three feature selection methods have been investigated namely Chi-square, odd ratio, and mutual information to improve Arabic MLC performance. Obviously, this study aimed to incorporate feature selection method and classification algorithm efficiently to obtain a more accurate MLC task.

The developed model was trained using the standard corpus which is collected in [33], it contains 10,000 Arabic articles written in "modern standard Arabic language (MSA)", where those articles are assigned to five labels: Sports, Economy, Arts, Science, and Politics. In addition, three multi-label evaluation metrics were used to evaluate the given Arabic datasets which are average recall, average precision, and average F-measure.

After the evaluation process, the results showed that using BR which consists of various sets of machine learning classifiers (SVM, NB, k-NN) obtained the best results compared with the other evaluated methods. Moreover, the results showed the important effect of the feature selection method on the classification task. On the other hand, the main challenges faced by this study were the complex morphology of Arabic language, and the lack of a well-annotated publicly available Arabic datasets that covers more labels.

### C. PT Methods based on Multi-Class Classification

The study conducted in [33] aimed to handle the MLC problem of Arabic language based on transformation to multi-class classification approach using a set of single-label machine learning classifiers. The authors aimed to transform the MLC problem of Arabic data into several single-label classification problems by using MEKA tool to perform PT methods which are: LP, BR, and Ranking and Threshold-based method (RT). The main idea of RT is that, after transforming MLC problem into a set of single-label classification problems, it assigns each label to a copy of the instance. Then, the label that has a value greater than a particular threshold remains with this instance, otherwise it is discarded.

The standard single-label machine algorithms have been applied as a base classifier to predict each resulted single-label data are: SVM, k-NN, NB, and DT. Then, they train the problem transformation methods (LP, BR, and RT) using their own multi-label Arabic dataset. They faced the same problem of the previous studies which have been conducted on MLC for Arabic language, which is the lack of publicly available multi-label Arabic datasets. Therefore, they have built their standard corpus from BBC news website, which contains about 10,000 Arabic articles, where those articles assigned to five labels: Sports, Arts, Economy, Politics, and Science. In addition, they run several experiments on five versions of their datasets with different sizes ranging from 3,000 to 7,000 articles, to study the effect of the scaling up of the datasets on the considered methods.

Three multi-label metrics were used during the evaluation phase which are: Hamming loss, ML-accuracy, and subset accuracy. Consequently, after performing the evaluation process on the given datasets, the results showed that using SVM as a base classifier with LP method achieved the best result with 71% ML-accuracy. However, the ML-accuracy of some classifiers changed when scaling up the datasets, more experiments were needed to justify this abnormal behavior in this study.

### D. Algorithm Adaptation Technique

The study conducted in [34] focused on using algorithm adaptation technique to address MLC task on the Arabic news articles. Three multi-label classifiers were considered which are, Random Forest (RF) classifier, DT classifier, and the k-NN classifier (where  $k = 5$  (5NN)). They chose these classifiers due to their ability to support MLC in a natural way.

On the other hand, one of the main challenges faced by this study, as stated in [33], is the lack of publicly available and well-annotated multi-label Arabic dataset. Therefore, they

<sup>1</sup> <http://waikato.github.io/meka/>

have built their own crawler to collect the dataset which is used to train the considered multi-label classifiers.

The dataset consists of 10,997 articles obtained from the CNN Arabic news website and written in MSA. The articles have multiple labels e.g., Economics, Sports, Middle East, World, Science & Technology, and Miscellaneous. The considered classifiers were evaluated using several MLC metrics (Hamming loss, accuracy, micro-average F-measure, micro-average recall, and micro-average precision). After conducting some experiments, the evaluation results revealed that the DT classifier achieved better performance compared to the RF and 5NN classifiers.

Another recent study has been conducted in [5] addresses MLC in the Arabic language. The study investigated the MLC problem by conducting a vast evaluation comparison on the most common MLC algorithms including PT methods. It includes transformation to binary classification approaches such as BR, CC, and Calibrated Ranking by Pairwise Comparison (CRPC) [43]. Also, it covers PT methods which are based on transformation to multi-class classification such as LP. They trained these techniques using three base classifiers (SVM, kNN, and RF). Besides, four algorithms based on adaptation technique are also evaluated which are: ML-kNN, RFBoost [44], Instance-Based Learning by Logistic Regression Multi-label (IBLRML) [45], and Binary Relevance kNN (BRkNN) [46]. The algorithms were evaluated using the introduced multi-label Arabic dataset named "RTAnews", which is a new benchmark dataset consists of 23,837 Arabic news articles distributed over 40 multiple labels.

The comparison has been done to study the effectiveness of the new dataset on the MLC task. The experiments were evaluated using MLC evaluation metrics (macro-F-measure, macro-precision, macro-recall, micro-F-measure, micro-precision, micro-recall). The results showed that both RFBoost, and LP (with SVM base classifier) outperformed other MLC algorithms. Also, the performance of algorithm adaptation algorithms is faster than PT algorithms except for the LP algorithm.

### E. Hierarchical Multi-Label Classification

To address HMC problem in Arabic language, a hierarchical classification system has been constructed in [35] based on HOMER algorithm, to classify the received Islamic requests (fatwa) and send them to the most appropriate Muslim scholar. Since, each fatwa request has multi-labels organized in a tree hierarchy. Thus, for each incoming fatwa request, the proposed system can automatically route them to one or more appropriate labels associated with the relevant Muslim scholar, as shown in Fig. 10.

Before any classification task, the Arabic text (Islamic fatwa dataset) should go through several pre-processing and feature-selection phases to make the text appropriate for a classification task. Several methods can be used to do these tasks, for example, the authors found that using light stemmer (light 10) in the pre-processing phase and Chi-square method in the feature-selection phase are suitable for their data. They conducted the experiments and trained the HOMER classifier using the processed dataset that includes about 15,539 text instances where the instance is assigned to multiple labels

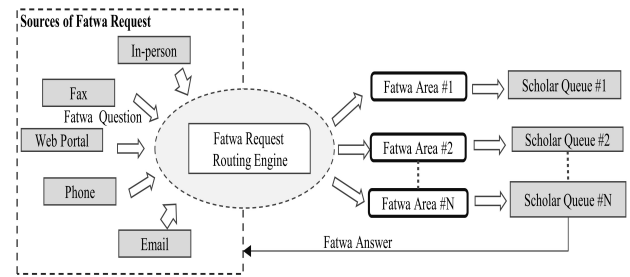


Fig. 10. Architecture of Fatwa Request System

organized in a tree-structured hierarchy consisting of 310 nodes (labels) in total.

They focused on comparing HOMER classifier against BR classifier (using NB base classifier). Several evaluation metrics were considered to evaluate the classification performance of the hierarchical multi-label classifier, which are Hamming loss, micro-averaged precision, micro-averaged F-measure, and micro-averaged recall. Finally, the results showed that using HOMER algorithm in the hierarchical classification of fatwa requests achieved more effective and efficient predictive performance compared to the BR classifier which relies on classifying each label independently.

Overall, we found that there are few researches conducted to tackle MLC problem in Arabic language compared to English [5]. The few research studies that addressed MLC problem for Arabic text in the literature are the aforementioned studies in this section [33], [5], [13], [34], [4], [35]. According to these studies we observed that feature selection method [4], dataset size [33], and pre-processing phase could have an important effect on the predictive performance of MLC model.

Table IV presents a summary of the relevant studies that applied MLC methods on the Arabic language. It shows the type of MLC methods and approaches that have been investigated in each application. Besides, it identifies the dataset size and the dataset source for each study.

The studies in this table are organized increasingly according to the publishing year. The main challenge has been mentioned by the authors of those studies which cause the limitation of the conducted studies on the MLC field in the Arabic context, is the lack of large enough and publicly available multi-label Arabic datasets. Besides, the vast vocabulary and complex morphology of the Arabic language. As a result, the study conducted in [5] addressed the lack of datasets by introducing a new benchmark dataset called "RTAnews". RTAnews dataset is a multi-label Arabic dataset which publicly available online in different formats including the format compatible with MEKA and MULAN multi-label learning tools. The RTAnews dataset obtained from "Russia Today Arabic news portal", and consists of 23,837 Arabic news articles distributed over 40 labels. Thus, this study led to promote evaluating of MLC methods and other supervised learning algorithms, by using the RTAnews dataset which is publicly available on its web page <sup>2</sup>.

<sup>2</sup> <https://data.mendeley.com/datasets/322pzsdxyw/1>

TABLE IV. SUMMARY OF THE RELEVANT STUDIES THAT APPLIED MLC METHODS ON THE ARABIC LANGUAGE

| Reference | Year | Multi-label classification |                           | Dataset size | Dataset source                                          |                             |
|-----------|------|----------------------------|---------------------------|--------------|---------------------------------------------------------|-----------------------------|
|           |      | Lexicon approach           | Machine learning approach |              |                                                         |                             |
|           |      |                            | Flat classification       |              |                                                         | Hierarchical classification |
| [35]      | 2015 |                            | ✓                         | 15,539       | Provided by the Egyptian Dar al-Ifta.                   |                             |
| [33]      | 2015 |                            | ✓                         | 10,000       | Collected from BBC news website.                        |                             |
| [4]       | 2016 |                            | ✓                         | 10,000       | Taken from the study conducted in [33].                 |                             |
| [13]      | 2016 | ✓                          |                           | 4,720        | Collected from BBC news website.                        |                             |
| [34]      | 2016 |                            | ✓                         | 10,997       | Obtained from the CNN Arabic news website.              |                             |
| [5]       | 2019 |                            | ✓                         | 23,837       | Collected from Russia Today Arabic news portal website. |                             |

Furthermore, according to Table IV it is noticeable that there are about four studies conducted on the flat multi-label classification using machine learning algorithms, and only one study conducted to address the hierarchical classification problem in Arabic. However, since hierarchical classification is becoming a very significant topic in the recent days and applied in different domains including text classification. Thus, there is a need to be well-investigated by the future studies.

## VI. EXPERIMENTAL COMPARISON OF MLC METHODS FOR ARABIC TEXT

In the previous sections, we presented an extensive review of the existing MLC methods and applications on Arabic text classification. It is interesting to evaluate the predictive performance of the state-of-the-art MLC methods introduced in this paper. The most common MLC methods have been evaluated involve four PT methods (BR, CC, LP, PS), one method based on algorithm adaptation technique (ML-kNN), and one hierarchical classification algorithm (HOMER).

The experiments performed using "RTAnews" dataset which was introduced in [5], and retrieved from its online web page. RTAnews is an imbalance dataset consists of 23,837 text instances distributed over 40 labels. It is available with a different set of features, 2000 feature is the selected dimension of the feature set used in the experiments. The summarization of the multi-label statistics of RTAnews dataset is illustrated in Table V.

TABLE V. RTANEWS DATASET STATISTICS

|                        |        |
|------------------------|--------|
| Number of instances    | 23,837 |
| Total number of labels | 40     |
| Number of features     | 2000   |
| Number of attributes   | 2040   |
| Number of label-sets   | 442    |

MULAN<sup>3</sup> is an open-source java library for multi-label learning used to conduct the experiments. The classification performance of MLC methods are measured concerning the three example-based metrics (Hamming loss, ML-accuracy, subset accuracy) and three label-based metrics (micro-averaged precision, micro-averaged recall, micro-averaged F-measure) which presented previously in Section IV.

To make the evaluation more reliable 10-folds cross-validation were applied. Two experiments have been per-

formed. The first experiment aims to investigate the performance of MLC methods (BR, CC, LP, PS, ML-kNN, and HOMER) on the predictive performance of the model. Noting that, all PT methods (BR, CC, LP, PS) evaluated using NB as a base classifier. HOMER algorithm was run using its default classifiers (BR and NB) and ML-kNN was evaluated by setting the number of  $k$  to 10. The second experiment aims to investigate the effect of three single-label base classifiers (NB, SVM, J48) on the performance of PT methods (BR, CC, LP, PS).

The results of the first experiment are presented in Table VI. We notice that the classification performance of all MLC methods in terms of Hamming loss, subset accuracy, micro-averaged precision, micro-averaged F-Measure, can be ranked according to the best performance achieved in the following order: ML-kNN, LP, PS, HOMER, CC, and BR. Whereas, concerning ML-accuracy, LP yielded the best results with 0.6219. Meanwhile, for micro-averaged recall, the best result was 0.8552 which obtained by the BR method.

Table VII presents the results of the second experiment. It is noticeable that the classification performance of PT methods might be affected by the single-label base classifier. Whenever the single-label base classifier changes, the performance of PT methods (BR, CC, LP, and PS) also change. Accordingly, we observe that, the SVM base classifier yielded the best results with all PT methods in terms of all evaluation metrics except micro-averaged recall. Whereas, concerning the micro-averaged recall, NB classifier with BR and CC methods obtained the best results. Note that in Table VII we used the abbreviation (e.g., BR-NB) to denote the multi-label classifier and the implemented base classifier.

Also, it is worth mentioning that the base classifier J48 obtained the second-best results with most of PT methods. Meanwhile, NB obtained the lowest results. Overall, we conclude that there are several factors affect the classification performance of MLC methods. For instance, PT methods might be affected by the base classifier. In contrast, algorithm adaptation techniques such as ML-kNN might be affected by the used parameters e.g.,  $k$ . Whereas, HOMER algorithm performance depends on the multi-label classifier, the base classifier, and the clustering algorithm [36].

## VII. CONCLUSION

Multi-label classification is an important research field and it has been increasingly required by many applications in various domains including text classification. In this paper, an

<sup>3</sup> <http://mulan.sourceforge.net/>

TABLE VI. EXPERIMENTAL COMPARISON AMONG MLC METHODS

| MLC method | Hamming loss         | ML-accuracy          | Subset accuracy      | Micro-averaged precision | Micro-averaged recall | Micro-averaged F-measure |
|------------|----------------------|----------------------|----------------------|--------------------------|-----------------------|--------------------------|
| BR         | 0.0549±0.0008        | 0.4293±0.0065        | 0.1948±0.0085        | 0.3288±0.0055            | <b>0.8552±0.0089</b>  | 0.4750±0.0065            |
| CC         | 0.0546±0.0008        | 0.4295±0.0065        | 0.1948±0.0085        | 0.3300±0.0055            | 0.8551±0.0088         | 0.4762±0.0064            |
| LP         | 0.0211±0.0006        | <b>0.6219±0.0113</b> | 0.5283±0.0119        | 0.6344±0.0133            | 0.6476±0.0088         | 0.6409±0.0103            |
| PS         | 0.0213±0.0007        | 0.6187±0.0110        | 0.5237±0.0119        | 0.6288±0.0139            | 0.6475±0.0090         | 0.6380±0.0105            |
| ML-kNN     | <b>0.0156±0.0004</b> | 0.6123±0.0081        | <b>0.5480±0.0091</b> | <b>0.8076±0.0052</b>     | 0.6075±0.0100         | <b>0.6933±0.0074</b>     |
| HOMER      | 0.0365±0.0008        | 0.5103±0.0075        | 0.3107±0.0089        | 0.4294±0.0078            | 0.7799±0.0059         | 0.5538±0.0062            |

TABLE VII. EXPERIMENTAL COMPARISON AMONG PT METHODS WITH DIFFERENT SINGLE-LABEL BASE CLASSIFIERS

| PT method                                            | Hamming loss         | ML-accuracy          | Subset accuracy      | Micro-averaged precision | Micro-averaged recall | Micro-averaged F-measure |
|------------------------------------------------------|----------------------|----------------------|----------------------|--------------------------|-----------------------|--------------------------|
| <b>BR method based on different base classifiers</b> |                      |                      |                      |                          |                       |                          |
| BR-NB                                                | 0.0549±0.0008        | 0.4293±0.0065        | 0.1948±0.0085        | 0.3288±0.0055            | <b>0.8552±0.0089</b>  | 0.4750±0.0065            |
| BR-J48                                               | 0.0178±0.0003        | 0.6076±0.0070        | 0.5078±0.0068        | 0.7125±0.0048            | 0.6502±0.0110         | 0.6799±0.0063            |
| BR-SVM                                               | <b>0.0163±0.0005</b> | <b>0.6632±0.0066</b> | <b>0.5561±0.0109</b> | <b>0.7269±0.0095</b>     | 0.7048±0.0058         | <b>0.7157±0.0063</b>     |
| <b>CC method based on different base classifiers</b> |                      |                      |                      |                          |                       |                          |
| CC-NB                                                | 0.0546±0.0008        | 0.4295±0.0065        | 0.1948±0.0085        | 0.3300±0.0055            | <b>0.8551±0.0088</b>  | 0.4762±0.0064            |
| CC-J48                                               | 0.0177±0.0003        | 0.6260±0.0060        | 0.5334±0.0068        | 0.7117±0.0057            | 0.6549±0.0092         | 0.6820±0.0053            |
| CC-SVM                                               | <b>0.0164±0.0005</b> | <b>0.6841±0.0089</b> | <b>0.5845±0.0124</b> | <b>0.7212±0.0091</b>     | 0.7096±0.0091         | <b>0.7153±0.0078</b>     |
| <b>LP method based on different base classifiers</b> |                      |                      |                      |                          |                       |                          |
| LP-NB                                                | 0.0211±0.0006        | 0.6219±0.0113        | 0.5283±0.0119        | 0.6344±0.0133            | 0.6476±0.0088         | 0.6409±0.0103            |
| LP-J48                                               | 0.0199±0.0006        | 0.6429±0.0084        | 0.5730±0.0091        | 0.6648±0.0107            | 0.6361±0.0092         | 0.6501±0.0093            |
| LP-SVM                                               | <b>0.0141±0.0004</b> | <b>0.7380±0.0075</b> | <b>0.6615±0.0117</b> | <b>0.7715±0.0052</b>     | <b>0.7295±0.0092</b>  | <b>0.7499±0.0068</b>     |
| <b>PS method based on different base classifiers</b> |                      |                      |                      |                          |                       |                          |
| PS-NB                                                | 0.0213±0.0007        | 0.6187±0.0110        | 0.5237±0.0119        | 0.6288±0.0139            | 0.6475±0.0090         | 0.6380±0.0105            |
| PS-J48                                               | 0.0198±0.0006        | 0.6427±0.0092        | 0.5725±0.0121        | 0.6665±0.0086            | 0.6355±0.0087         | 0.6506±0.0084            |
| PS-SVM                                               | <b>0.0142±0.0005</b> | <b>0.7369±0.0083</b> | <b>0.6605±0.0104</b> | <b>0.7695±0.0064</b>     | <b>0.7276±0.0107</b>  | <b>0.7480±0.0080</b>     |

extensive review has been conducted on the MLC methods by illustrating the concept of each method and discussing their advantages and limitations. In addition, it organized the sparse state-of-the-art MLC methods by providing a taxonomy which summarized different MLC methods and techniques that can deal with MLC problem. Besides, a set of common multi-label evaluation metrics used to evaluate MLC models have been presented. Furthermore, we focused on the Arabic language by discussing the existing applications of MLC methods in the Arabic context. It is noticeable that only a few research studies addressed the problem of MLC for the Arabic language which mainly focused on flat classification and neglected the hierarchical structure. We found that the main challenges faced by the those studies are the lack of large and publicly available multi-label Arabic datasets, and also the vast vocabulary and complex morphology of the Arabic language. Finally, the survey provided an experimental comparisons of different MLC methods in the Arabic context and points out some baseline results. However, further research is still needed to improve the multi-label classification task for the Arabic language, especially the hierarchical classification task. Additionally, there is a need to give more attention for preparation multi-label Arabic datasets in an appropriate representation for a multi-label classification task.

#### REFERENCES

- [1] M. Syiam, M. Tolba, Z. Fayed, M. Abdel-Wahab, S. Ghoniemy, and M. Habib, "An intelligent system for arabic text categorization," *International journal of cooperative information systems*, vol. 6, no. 1, pp. 1–19, 1 2006.
- [2] E. Gibaja and S. Ventura, "A tutorial on multilabel learning," *ACM Comput. Surv.*, vol. 47, no. 3, pp. 52:1–52:38, Apr. 2015. [Online]. Available: <http://doi.acm.org/10.1145/2716262>
- [3] G. Tsoumakas and I. Katakis, "Multi-label classification: An overview," *International Journal of Data Warehousing and Mining (IJDW)*, vol. 3, no. 3, pp. 1–13, 2007.
- [4] A. Y. Taha and S. Tiun, "Binary relevance (br) method classifier of multi-label classification for arabic text." *Journal of Theoretical & Applied Information Technology*, vol. 84, no. 3, 2016.
- [5] B. Al-Salemi, M. Ayob, G. Kendall, and S. A. M. Noah, "Multi-label arabic text categorization: A benchmark and baseline comparison of multi-label learning algorithms," *Information Processing & Management*, vol. 56, no. 1, pp. 212–227, 2019.
- [6] H. Mubarak and K. Darwish, "Using twitter to collect a multi-dialectal corpus of arabic," in *Proceedings of the EMNLP 2014 Workshop on Arabic Natural Language Processing (ANLP)*, 2014, pp. 1–7.
- [7] T. Eldos, "Arabic text data mining: a root-based hierarchical indexing model," *International Journal of Modelling and Simulation*, vol. 23, no. 3, pp. 158–166, 2003.
- [8] Y. Ahmed, J. Xiang, D. Zhao, M. A. A. Al-qaness, M. Elsayed abd el aziz, and D. Abdelghani, "A study of the effects of stemming strategies on arabic document classification," *IEEE Access*, vol. PP, pp. 1–1, 03 2019.
- [9] M. El Kourdi, A. Bensaid, and T.-e. Rachidi, "Automatic arabic document categorization based on the naïve bayes algorithm," in *proceedings of the Workshop on Computational Approaches to Arabic Script-based Languages*. Association for Computational Linguistics, 2004, pp. 51–58.
- [10] R. Al-Shalabi and R. Obeidat, "Improving knn arabic text classification with n-grams based document indexing," in *Proceedings of the Sixth*

- International Conference on Informatics and Systems, Cairo, Egypt, 2008, pp. 108–112.
- [11] G. Hassan, “Categorization arabic text using svm and knn algorithms,” *International Journal of Engineering and Technology*, pp. 906–909, 01 2018.
- [12] J. Eisenstein, “Unsupervised learning for lexicon-based classification,” *CoRR*, vol. abs/1611.06933, 2016. [Online]. Available: <http://arxiv.org/abs/1611.06933>
- [13] I. Hmeidi, M. Al-Ayyoub, N. A. Mahyoub, and M. A. Shehab, “A lexicon based approach for classifying arabic multi-labeled text,” *International Journal of Web Information Systems*, vol. 12, no. 4, pp. 504–532, 2016.
- [14] R. M. Duwairi and R. Al-Zubaidi, “A hierarchical k-nn classifier for textual data,” *Int. Arab J. Inf. Technol.*, vol. 8, no. 3, pp. 251–259, 2011.
- [15] A. Aldrees and A. Chikh, “Comparative evaluation of four multi-label classification algorithms in classifying learning objects,” *Computer Applications in Engineering Education*, vol. 24, no. 4, pp. 651–660, 2016.
- [16] O. Luaces, J. Díez, J. Barranquero, J. J. del Coz, and A. Bahamonde, “Binary relevance efficacy for multilabel classification,” *Progress in Artificial Intelligence*, vol. 1, no. 4, pp. 303–313, 2012.
- [17] J. Read, B. Pfahringer, G. Holmes, and E. Frank, “Classifier chains for multi-label classification,” *Machine learning*, vol. 85, no. 3, p. 333, 2011.
- [18] M.-L. Zhang and Z.-H. Zhou, “A review on multi-label learning algorithms,” *IEEE transactions on knowledge and data engineering*, vol. 26, no. 8, pp. 1819–1837, 2014.
- [19] E. Hüllermeier, J. Fürnkranz, W. Cheng, and K. Brinker, “Label ranking by learning pairwise preferences,” *Artificial Intelligence*, vol. 172, no. 16–17, pp. 1897–1916, 2008.
- [20] G. Tsoumakas and I. Vlahavas, “Random k-labelsets: An ensemble method for multilabel classification,” in *European conference on machine learning*. Springer, 2007, pp. 406–417.
- [21] J. Read, B. Pfahringer, and G. Holmes, “Multi-label classification using ensembles of pruned sets,” in *Data Mining, 2008. ICDM’08. Eighth IEEE International Conference on*. IEEE, 2008, pp. 995–1000.
- [22] G. Tsoumakas, I. Katakis, and I. Vlahavas, “Random k-labelsets for multilabel classification,” *IEEE Transactions on Knowledge and Data Engineering*, vol. 23, no. 7, pp. 1079–1089, 2010.
- [23] D. Stojanova, M. Ceci, D. Malerba, and S. Džeroski, “Learning hierarchical multi-label classification trees from network data,” in *International Conference on Discovery Science*. Springer, 2013, pp. 233–248.
- [24] A. Elisseeff and J. Weston, “A kernel method for multi-labelled classification,” in *Proceedings of the 14th International Conference on Neural Information Processing Systems: Natural and Synthetic*, ser. NIPS’01. Cambridge, MA, USA: MIT Press, 2001, pp. 681–687. [Online]. Available: <http://dl.acm.org/citation.cfm?id=2980539.2980628>
- [25] M.-L. Zhang and Z.-H. Zhou, “Multilabel neural networks with applications to functional genomics and text categorization,” *IEEE transactions on Knowledge and Data Engineering*, vol. 18, no. 10, pp. 1338–1351, 2006.
- [26] —, “MI-knn: A lazy learning approach to multi-label learning,” *Pattern recognition*, vol. 40, no. 7, pp. 2038–2048, 2007.
- [27] A. Clare and R. D. King, “Knowledge discovery in multi-label phenotype data,” in *European Conference on Principles of Data Mining and Knowledge Discovery*. Springer, 2001, pp. 42–53.
- [28] R. Al-Otaibi, M. Kull, and P. Flach, “Declaratively capturing local label correlations with multi-label trees,” in *Proceedings of the 22nd Biennial European Conference on Artificial Intelligence (ECAI2016), Including Prestigious Applications of Intelligent Systems (PAIS-2016)*, ser. Frontiers in Artificial Intelligence and Applications, G. A. Kaminka, M. Fox, P. Bouquet, E. Hüllermeier, V. Dignum, F. Dignum, and F. van Harmelen, Eds., vol. 285. IOS press, 29 August– 2 September 2016, pp. 1467 – 1475. [Online]. Available: <http://ebooks.iospress.com/volumearticle/44904>
- [29] F. Brucker, F. Benites, and E. Sapozhnikova, “Multi-label classification and extracting predicted class hierarchies,” *Pattern Recognition*, vol. 44, no. 3, pp. 724–738, 2011.
- [30] G. Madjarov, V. Vidulin, I. Dimitrovski, and D. Koccev, “Web genre classification via hierarchical multi-label classification,” in *International Conference on Intelligent Data Engineering and Automated Learning*. Springer, 2015, pp. 9–17.
- [31] C. N. Silla and A. A. Freitas, “A survey of hierarchical classification across different application domains,” *Data Mining and Knowledge Discovery*, vol. 22, no. 1-2, pp. 31–72, 2011.
- [32] W. Bi and J. T. Kwok, “Multi-label classification on tree-and dag-structured hierarchies,” in *Proceedings of the 28th International Conference on Machine Learning (ICML-11)*, 2011, pp. 17–24.
- [33] N. A. Ahmed, M. A. Shehab, M. Al-Ayyoub, and I. Hmeidi, “Scalable multi-label arabic text classification,” in *Information and Communication Systems (ICICS), 2015 6th International Conference on*. IEEE, 2015, pp. 212–217.
- [34] M. A. Shehab, O. Badarneh, M. Al-Ayyoub, and Y. Jararweh, “A supervised approach for multi-label classification of arabic news articles,” in *Computer Science and Information Technology (CSIT), 2016 7th International Conference on*. IEEE, 2016, pp. 1–6.
- [35] R. A. Zayed, M. F. A. Hady, and H. Hefny, “Islamic fatwa request routing via hierarchical multi-label arabic text categorization,” in *Arabic Computational Linguistics (ACLing), 2015 First International Conference on*. IEEE, 2015, pp. 145–151.
- [36] G. Tsoumakas, I. Katakis, and I. Vlahavas, “Effective and efficient multilabel classification in domains with large number of labels,” in *Proc. ECML/PKDD 2008 Workshop on Mining Multidimensional Data (MMD’08)*, vol. 21. sn, 2008, pp. 53–59.
- [37] C. Vens, J. Struyf, L. Schietgat, S. Džeroski, and H. Blockeel, “Decision trees for hierarchical multi-label classification,” *Machine learning*, vol. 73, no. 2, p. 185, 2008.
- [38] N. Cesa-Bianchi, C. Gentile, and L. Zaniboni, “Incremental algorithms for hierarchical classification,” *J. Mach. Learn. Res.*, vol. 7, pp. 31–54, Dec. 2006. [Online]. Available: <http://dl.acm.org/citation.cfm?id=1248547.1248549>
- [39] Y. Chen, M. M. Crawford, and J. Ghosh, “Integrating support vector machines in a hierarchical output space decomposition framework,” in *Geoscience and Remote Sensing Symposium, 2004. IGARSS’04. Proceedings. 2004 IEEE International*, vol. 2. IEEE, 2004, pp. 949–952.
- [40] L. Zhang, S. Shah, and I. Kakadiaris, “Hierarchical multi-label classification using fully associative ensemble learning,” *Pattern Recognition*, vol. 70, pp. 89–103, 2017.
- [41] G. Tsoumakas, I. Katakis, and I. Vlahavas, “Mining multi-label data,” in *Data mining and knowledge discovery handbook*. Springer, 2009, pp. 667–685.
- [42] S. Zhu, X. Ji, W. Xu, and Y. Gong, “Multi-labelled classification using maximum entropy method,” in *Proceedings of the 28th annual international ACM SIGIR conference on Research and development in information retrieval*. ACM, 2005, pp. 274–281.
- [43] J. Fürnkranz, E. Hüllermeier, E. L. Mencía, and K. Brinker, “Multilabel classification via calibrated label ranking,” *Machine learning*, vol. 73, no. 2, pp. 133–153, 2008.
- [44] R. E. Schapire and Y. Singer, “Improved boosting algorithms using confidence-rated predictions,” *Machine Learning*, vol. 37, no. 3, pp. 297–336, Dec 1999.
- [45] W. Cheng and E. Hüllermeier, “Combining instance-based learning and logistic regression for multilabel classification,” *Machine Learning*, vol. 76, no. 2, pp. 211–225, Sep 2009. [Online]. Available: <https://doi.org/10.1007/s10994-009-5127-5>
- [46] E. Spyromitros, G. Tsoumakas, and I. Vlahavas, “An empirical study of lazy multilabel classification algorithms,” in *Artificial Intelligence: Theories, Models and Applications*, J. Darzentas, G. A. Vouros, S. Votsinakis, and A. Arnellos, Eds. Berlin, Heidelberg: Springer Berlin Heidelberg, 2008, pp. 401–406.

# Census Estimation using Histogram Representation of 3D Surfaces: A Case Study Focusing on the Karak Region

Subhieh El-Salhi<sup>1</sup>

Department of Computer Information Systems  
The Hashemite University  
Zarqa, Jordan

Safaa Al-Haj Saleh<sup>2</sup>

Department of Software Engineering  
The Hashemite University  
Zarqa, Jordan

Frans Coenen<sup>3</sup>

Department of Computer Science  
University of Liverpool  
Liverpool, UK

**Abstract**—National and regional infrastructure planning is founded on the use of many factors, of which population size can be argued to be the most fundamental. Population size is typically acquired through a census. However, manual census collection is an expensive and resource intensive process; especially in regions that are poorly connected. Computer-aided population estimation, when done accurately, therefore offers significant benefit. This paper presents a comprehensive framework for estimating the population size of a region of interest by applying classification techniques to terrain data. Central to the proposed framework is a novel histogram representation technique designed to support the generation of appropriate and effective classifiers central to the operation of the framework. The presented work uses the Karak region, in Jordan, as a case study for population size estimation. The proposed framework and the representation technique have been evaluated using a variety of classification mechanisms and parameter settings. The reported evaluation of the proposed representation technique demonstrates that good results can be obtained with regard to estimate the population size.

**Keywords**—Histogram representation; Geographic Information System (GIS); population estimation; 3D surface; satellite images; data mining; classification technique; Karak region

## I. INTRODUCTION

Population size plays an essential role in a number of important governmental decision making strategies directed at the process of urban development. This is especially the case with respect to critical sectors, such as health, education, transport and urban services. Governments usually obtain population size data using a census [1]. This is typically collected in either a door-to-door manner or by requiring individuals to complete a form. Both entail considerable cost, particularly in areas which feature a poor communication infrastructure; form filling also assumes a high degree of literacy amongst the population of interest, not necessarily always the case. A solution is to adopt some form of population estimation mechanism. However, it is important that the estimation is as accurate as possible so as to best inform strategic planning and decision making activities.

In the past, population estimation was conducted using “Aerial Photography”; however in the modern day aerial photography has been replaced with satellite imagery. The advantages of using satellite imagery over methods involving aerial photography can be summarised as follows: (i) extensive

and regular coverage, (ii) time and cost efficiency, and (iii) accessibility to regions which would otherwise be difficult to access [2]. Satellite images provide a rich data source accurately depicting terrain features such as mountains, hills, valleys, plateaus, plains, deserts and, importantly, population centres of all kinds. The key challenge is then how best to extract population estimations from such imagery? In times gone-by, using aerial photography, this was done by visual inspection; an undesirable approach because of the resource required and the subjectivity involved. Using satellite imagery the process can be automated; the challenge is how best to implement this automation. In both cases the approach is particularly effective in rural areas, areas where traditional census collection is the most resource intensive.

The proposed solution to the population estimation from satellite imagery problem, presented in this paper, considers the problem in terms of a 3-D surface where the  $x$  and  $y$  coordinates are the  $x$ - $y$  coordinates of the centre point of each grid squares and the  $z$  coordinate is the number of dwellings (households) within the grid square (the value we wish to predict); the value at each 3-D location is then a terrain type. The idea is to represent individual locations in terms of their terrain type and neighbouring terrain types. The intuition is that population size, in a given region, is defined by terrain type. The basic idea is to use a machine learning approach whereby large-scale terrain image is input to a population estimation system. In more detail the input image is divided into a set of grid squares; with each grid square assigned a terrain type. A prediction model is then applied to predict the number of households in each grid square from which a population estimation can be obtained by multiplying the predicted number of households by an average household size. The challenge is the nature of the prediction model to be adopted, and how this model is to be generated. Most prediction (and classification) models take a feature vector as input. It is easy to see how this would work given tabular data, but not as clear given image data. How the image data should be represented so that a good prediction model is generated is therefore an issue. The proposed solution is to adopt a histogram-based technique, an idea founded on the concept of local binary patterns [3].

To train the prediction model a dataset encompassing the Karak region of Jordan was used together with the known location of households within the test region. The Karak region

was selected because it was considered to be a good exemplar region because of its geographical diversity.

The average household size data used in this case was obtained from a statistical study conducted by the Jordanian Department of Statistics [4], [5] and The United Nations [6]. The main contributions of the paper are:

- 1) A comprehensive framework to estimate (predict) population size (census) using terrain image data.
- 2) A novel technique to support the framework and represent the 3D surfaces depicted in 2D terrain image.

The rest of the paper is organised as follows. In Section II a brief overview of related work is presented. The characteristics of the selected dataset are described in Section III. In Section IV the proposed framework for census prediction is introduced followed by its usage in Section V. The evaluation of the proposed framework is reported in Section VI using a variety of parameters. Finally some conclusions are discussed in Section VII.

## II. OVERVIEW OF RELATED WORK

Automatic census estimation has recently emerged as a novel research area to overcome the drawbacks of traditional census collection approaches; namely the expensive of collecting the data, in terms of time and cost, especially in rural areas where the transportation infrastructure is typically insufficient. Generally speaking, automatic census estimation is inappropriate for inner city areas or commercial areas as it is difficult to distinguish between residential buildings and other types of building, and residential building shared by multiple families (such as tower blocks) and buildings occupied by a single family. Automatic census estimation is therefore most effective in rural areas where the main residential units are detached houses and the population is sparsely distributed [7], [8]; these are also the areas where traditional census data requires the greatest resource. There are a number of reports of research directed at census estimation founded on geographical features and labelled example data to produce a model that can then be used for census estimation purposes. The main challenge that most of the proposed census estimation techniques seek to address is how best to represent data extracted from GIS images so that classification techniques can be applied effectively. The need for a convenient representation arises from the fact that the extracted image data tends to be too large to be used in its raw form; so a representation is required that encapsulates the data in a reduced form.

The different data representation techniques presented in the literature include: colour histograms [7]–[10], local binary patterns [8]–[10] and graph based structures [9]–[12]. Colour histograms are used to represent the colour distribution in the image set. The X-axis of the histogram records “bin” identifiers, each bin representing a colour range; while the Y-axis represents the number of pixels falling into each bin. This representation offers computational simplicity and tolerance against changes such as rotation and scaling. Local Binary Patterns (LBPs) are essentially a texture representation technique that can be used more generally. The main idea of LBPs is to divide the examined image into cells and then compare the pixel values in each cell to each of its

eight neighbours; if the value is greater than neighbouring value a “0” is recorded, otherwise a “1” is recorded. The resulting eight binary digits are then formed into an eight-bit number representing the cell. This representation has been widely used as it is easy to generate and robust to illumination changes. Graph based techniques have been used to represent the structure images, a frequently used representation is the Quad-tree representation that has been frequently used in the context of census estimation applications. Given a collection of quad trees frequent sub-graph mining techniques have been applied to identify frequently occurring sub-graphs that can then be used subsequently to generate feature vectors.

In addition to satellite imagery, various other forms of image have been used for census estimation. These include various types of Geographic Information System (GIS) map [7]–[10], [12]–[15], 3D satellite images (which include a Z dimension with which to represent 3D surfaces) [11], Ikonos images (high-resolution satellite images) [16] and aerial images (images taken from aircraft or other forms of flying object) [17].

Given a suitable feature vector representation different classifiers can be applied so as to generate a census estimation model, these include: K-Nearest Neighbour, Decision Tree, Naive Bayes, Logistic Regression and Support Vector Machine. The  $k$ -Nearest Neighbor ( $k$ -NN) technique is a lazy classification model that classifies a previously unseen object according to the majority class associated with the  $k$  nearest neighbours to the object [18], a variety of similarity (distance) measures can be used such as: Euclidean distance, Manhattan distance and Mahalanob distance. A Decision Tree is a decision support structure based on a tree-like graph of decisions and their possible consequences. Each internal node represents a test on an attribute, each branch represents the output of the test and each leaf node represents a class label [18]. Naive Bayes is a simple probabilistic classifier that assumes that there are no dependencies amongst features [18]. Logistic Regression is a classification model where the dependent variable is categorical. It can be binomial, ordinal, or multinomial. The goal of this classifier is to find the best fitting model to describe the relationship between the dependent variable and the independent variables [19]. A Support Vector Machine (SVM) is a supervised, non-probabilistic, binary linear classifier. By representing the training data as points in a space the SVM operates by separating the points with a dimensional hyperplane that divides the two categories by a gap that is as wide as possible [19].

The presented previous work directed at automated census estimation has demonstrated that estimating census automatically has number of advantages, such as low cost and high speed of collection, compared to traditional census collection methods; although automatic estimation is less accurate than the real process of census collection. In the work presented by Reis et al. [13] a method for population estimation was developed based on demographic data extracted from satellite images where linear regression models were used to represent the extracted data. The developed method was evaluated using dataset representing districts of Belo Horizonte city in Brazil, the evaluation demonstrated that census results obtained using linear models were similar to these obtained using more complex models. Javed et al. [14] proposed a methodology for

population density estimation using texton-based classification. Satellite images were split up into blocks and then textons for each block were extracted using Leung Malik (LM) filter bank. Extracted textons (texture features) were then used as training features for a  $k$ -NN classifier. Different satellite images of cities in Pakistan were used to test the proposed methodology. In the work presented in [16] the authors proposed a methodology for population estimation using Ikonos images of a district in Khartoum city where two categories of population unit were considered: dwelling units and residential areas. The presented approach can be summarised as follows. Residential buildings were separated from non-residential building using a number of selected features such as shape, size, pattern and texture. After that, all residential buildings were represented as polygons, after which vector layers for the represented polygons were generated. Consequently, residential buildings were classified into one of the categories and areas belonging to the residential category identified. An estimated population for each residential category area was then derived and a total population estimation computed. Kurtz et al. [15] proposed a multi-resolution method to generate clusters for the purpose of mapping homogeneous patterns of urban elements. The proposed methodology worked by clustering two types of images representing the same scene, Medium Spatial Resolution (MSR) images and High Spatial Resolution (HSR) images, by combining a per-pixel-based analysis with region-based analysis. The use of HSR images, which have a finer resolution than a MSR images, enabled the detection of urban objects such as houses, gardens and roads and their construction material (for example houses with green roof tiles).

There have been a number reports where classification models have been used to label households according to family size so as to predict number of people living in a previously unseen household; the households are typically segmented individually and represented using some feature vector representation. For example Yu et al. [11] presented a technique for classifying households described in terms of 3D surface images using Vertex Unique Labelled Subgraphs (VULSs). A VULS is a sub graph within some larger graph that has a unique vertex labeling. A Backward Match Voting (BMV) algorithm was used for classifying the vertex labels. Several census estimation frameworks have been proposed by Dittakan et al., several that used a histogram representation [7], another that used a quad-tree representation [12] and a third that used LBPs [8]. Dittakan et al. produced a fourth framework that used a combination of representations colour histograms, LBPs and a graph-based representation [9].

It is worth mentioning that the histogram techniques proposed in the previous works were based on generating different "color histograms" -including red green blue, hue, saturation, value and gray scale- and Local Binary Patterns to represent segmented households to generate feature vectors that were used to build classification models. While in the presented work a terrain image is divided into grids; whereas for each grid a "histogram representation" of the terrain type associated with the neighbours of the grid is generated.

### III. CENSUS DATASET

As noted in the introduction to this paper the Karak region was selected as the case-study region with which to generate

the desired household prediction model. The Karak is rural region located at the southern part of Jordan (approximately 140 kilometres to the south of Amman) as shown in Fig. 1. The Karak governorate's topography is characterised by a diverse terrain of desert (in the eastern part), mountains (the Mo'ab heights in the western part) and agricultural areas (known as the Ghour and Semi-Ghour). The Karak governorate was selected with respect to the work presented in this paper because of the wide range of different types of geographical terrain that it covers, compared to other Jordanian governorates. It is also sparsely populated, it has lowest population density with respect to the other governorates in Jordan (90.6 inhabitants per square kilometer [20]) which means that it is particularly well suited to the application of population estimation using satellite imagery. This was also a region where the number of households was known; information required to for training the number of households prediction model and for evaluation purposes.



Fig. 1. The Karak Governorate in Jordan.

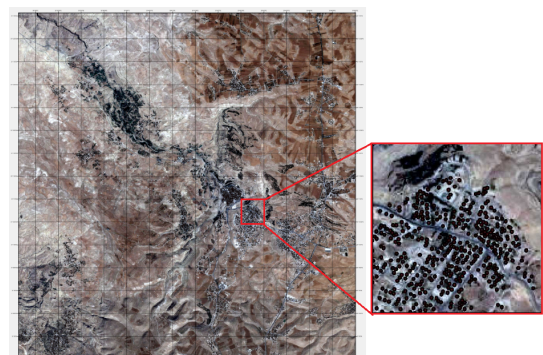


Fig. 2. Satellite Image of the Karak Region (Left-Hand Side) and Detailed showing Household Locations (Right-Hand Side).

Fig. 2 shows a 2D satellite image of the Karak test region with a grid superimposed. The example satellite image was released in April 2015 during the dry season and obtained from the Royal Jordanian Geographic Center (RJGC). The satellite



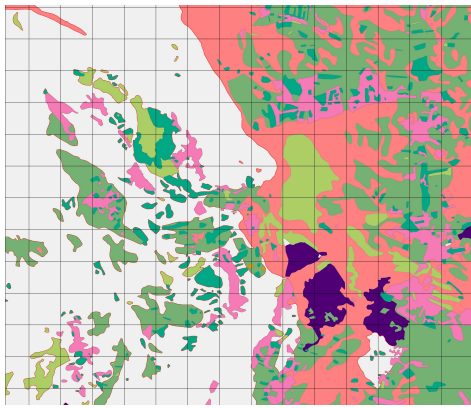


Fig. 3. Terrain Map for the Karak Region.

image comprises 42, 171, 195 pixels ( $6, 465 \times 6, 523$ ). It covers a region bounded by the parallels of latitude  $31^{\circ}12'05''$  N ( $31.201388$  N) and  $31^{\circ}25'00''$  N ( $31.416666$  N) and the meridians of longitude  $35^{\circ}62'0''$  E ( $36.034722$  E) and  $35^{\circ}75'00''$  E ( $36.250000$  E). The figure also includes a detail with households marked with black dots. The household location data was also provided by the RJGC.

Fig. 3 shows a terrain map corresponding to the same area covered by the satellite image given in Fig. 2. The Terrain map highlights eight terrain types were considered: (i) desert, (ii) rocky land, (iii) orchards, (iv) green house areas, (v) bushes cover, (vi) cultivated area, (vii) uncrowded urban areas and (viii) crowded urban areas (a more detailed description of each is given in Section IV-A). Each terrain type is identified by a unique colour and a corresponding numeric code ( $\{1, 2, \dots, 8\}$ ). Both the terrain image and the corresponding satellite image of houses' distribution are used as input to the proposed population estimation system.

#### IV. CENSUS ESTIMATION FRAMEWORK GENERATION

The generation of the proposed framework is presented in this section. The generation process comprises of the following phases (as shown in Fig. 4): (i) a Pre-processing, (ii) a Surface Representation, and (iii) a Classification. More detailed discussion concerning each phase in the following sections.

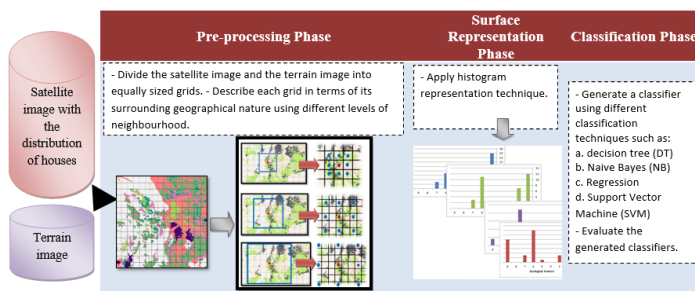


Fig. 4. The Histogram Representation Framework in the Context of Census Prediction.



Fig. 5. Detail of the Satellite Image, with House Locations Marked, Converted into a Binary Image.

##### A. Pre-Processing Phase: Grid Dataset Generation

The inputs to the pre-processing phase are: (i) a terrain image, and (ii) a corresponding satellite image of houses' distribution. Example satellite and terrain images of the Karak region were given in Fig. 2 and 3. The two images are divided into equally-sized grids and for each grid the dominant terrain type is extracted and then the grid is labelled with the number of houses located within it. In more detail:

- 1) Using the given house "coordinate" data each house location is marked on the satellite image.
- 2) The marked-up satellite image is then converted into binary image so that house locations appear as white dots while the rest of the image appears as a black region. Fig. 5 gives an example.
- 3) The terrain image and the corresponding marked-up binary satellite image are then divided into a set of equally-sized grids of size  $g$  pixels; for example if  $g = 50$  the grids will measure  $50 \times 50$  pixels. For the evaluation reported in Section VI a range of different values for  $g$  was experimented with. The generated grids are numbered sequentially row by row starting from the upper left corner and ending at the bottom right corner and thus the neighbours of each grid can be easily identified.
- 4) The grid squares in both images are then used to define a 3D surface where the z-dimension is the number of houses and the x and y dimensions are the x and y coordinates for the centre of each grid square. We can think of the surface as being a 3D lattice connecting grid square centres.
- 5) For each grid the dominant terrain type is extracted and then the grid is labelled with the number of houses located within it. The dominant geographic terrain type for each grid square is identified from the terrain image and is indicated by the dominant RGB colour in each grid. The number of houses in each grid is calculated by extracting the number of white dots for the grid in the associated binary image.
- 6) The number of surrounding neighbours of a given grid square is defined according to a neighbourhood distance parameter  $q$ . The maximum number of neighbouring grids is defined by  $(2q + 1)^2$ . For



generation a prediction value  $p$  needs to be added to the feature vector. The collection of feature vectors then forms the input data set  $D$  to the prediction model generation. Experiments were conducted, see Section VI, using five different prediction model learning techniques.

*Normalisation* and *discretisation* processes are two main preprocessing stages required to operate the functionality of the classification phase successfully and efficiently.

Normalisation is a preprocessing stage used to maintain all the attributes of different ranges (scales) in the dataset in the same range and to assure that all the attributes of the dataset are treated equally (in our case the attributes of the population size and the number of surrounding neighbours of each predefined geographical features are derived from different scales) [21], [22]. There are different techniques of Normalisation such as Min-Max Normalisation, Z-Score Normalisation and Decimal Point Normalisation. However, empirical results indicated that Min-Max Normalisation outperforms other normalisation techniques in terms of simplicity, computational time and accuracy. Thus, in this paper the reported experiments were conducted using Min-Max Normalisation technique.

Discretisation is the process of transforming the continuous attributes into nominal attributes in such a way that the real values are mapped into one of a predefined set of intervals [23]. Nominal data types are essential for some classification techniques to operate efficiently such as Decision Tree (C4.5) and Naive Bayes (NB) [24]. Equal Width Binning (EWB) and Equal Frequency Binning (EFB) are the most popular *unsupervised* techniques of discretisation. Equal Width Binning divides the continuous data into set of intervals of equal size while the Equal Frequency Binning divides the continuous data into set of intervals of equal number of values (further details about discretisation can be found in [25], [26]). However, earlier empirical experiments of the presented work indicated that there was no significant difference between using either of them, therefore EFB was adapted for the entire set of experiments in accordance with Min-Max Normalisation technique.

## V. CENSUS ESTIMATION FRAMEWORK USAGE

The census generation framework presented in the foregoing section, once trained, can then be used to predict the number of households in a given area. By multiplying this by the average number of inhabitants for a household. This will vary between geographic regions but the average number inhabitants for a Jordanian household, obtained from the Jordanian Department of Statistics (JDS), was 4.8 persons [4], [5]. Thus given a new region for which a population is to be estimated all that is required is a terrain map. This has to be segmented according to the same value of  $g$  used to train the system and feature vectors generated using the same value for  $q$  as originally used. Terrain maps are available for most geographic regions, the challenge will be converting these terrain maps so that they relate to the eight terrain types identified above. It may be possible to train a new model, using the process described in Section IV, but information concerning household locations would be required. An alternative is to automatically identify household locations. A mechanism for doing this was presented in [27], [28] with respect to a region

of Ethiopia where the standard roofing material was corrugated iron which was relatively easy to detect in satellite imagery.

## VI. EVALUATION

This section describes the results obtained from the evaluation of the proposed Census Estimation Framework. A sequence of experiments were conducted to evaluate the effectiveness of the Framework using the Karak region test data. Experiments were conducted using five different prediction model generation mechanism: (i)  $k$ -NN coupled with Dynamic Time Warping (DTW), (ii) Decision Tree (C4.5), (iii) Naive Bayes (NB), (iv) Logistic Regression and (v) Support Vector Machine (SVM). A range of values for  $g$  from 50 to 400 pixels increasing in steps of 50, and three of values for  $q$  from 1, 2 and 3, were used. The framework was implemented using MATLAB *R2013a*, the JAVA programming language and Waikato Environment for Knowledge Analysis (WEKA)<sup>1</sup>. The experiments were run using a 2.4 GHz Intel Core *i5* PC with 4 GB RAM and 64-bit operating system, running Windows 7 (SP1). The reported experiments were all conducted using real data obtained from RJGC for the Karak region where the total number of households is 9581. Ten fold Cross-Validation (TCV) (90% training set and 10% testing set) [29] was used throughout. The reported results are presented in terms of accuracy, Area Under the ROC Curve (AUC) and run time (in seconds). AUC and accuracy were selected as these are the most popular mechanisms used to assess the effectiveness of classifiers in machine learning and data mining research.

The objectives of the evaluation were:

- To identify the most appropriate prediction model generation mechanism to support the proposed Census Estimation Framework.
- To identify the most appropriate grid size with respect to the proposed histogram representation technique.
- To identify the most appropriate level of neighbourhood to be used (including whether a neighbourhood should be considered at all).
- To analyse the run time requirements for the proposed framework.

The results are presented in graph form in Fig. 10 to 15. Fig. 10 to 12 give AUC values, and Fig. 13 to 15 accuracy values. Each of the above objectives is discussed further, with respect to the reported results, in the following four sub-sections, sub-sections VI-A to VI-D, respectively.

### A. Prediction Model Generation Mechanism

From the results presented in Fig. 10 to 15 the following observations can be made with respect to the most appropriate prediction model generation mechanism. The  $k$ -NN technique achieved the “best” accuracy results among all classification techniques considered, on occasion reaching 1.00 (100%) regardless of the values of  $g$  and  $q$  used. However, accuracy does not take into account any “class bias”, whereas the AUC metric does; the  $k$ -NN technique did not perform well in terms of the AUC metric. Note that an AUC value of 0.5

<sup>1</sup><http://www.cs.waikato.ac.nz/ml/weka/>

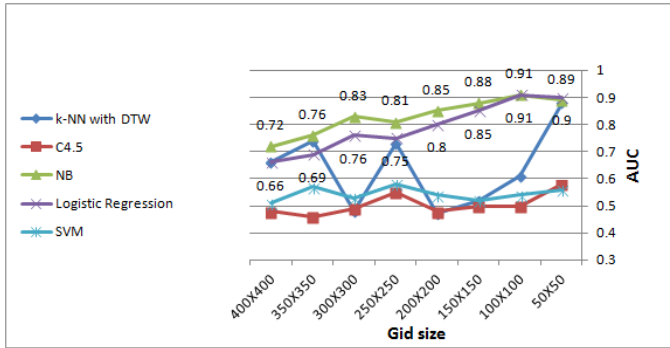


Fig. 10. The AUC Results  $q = 1$ .

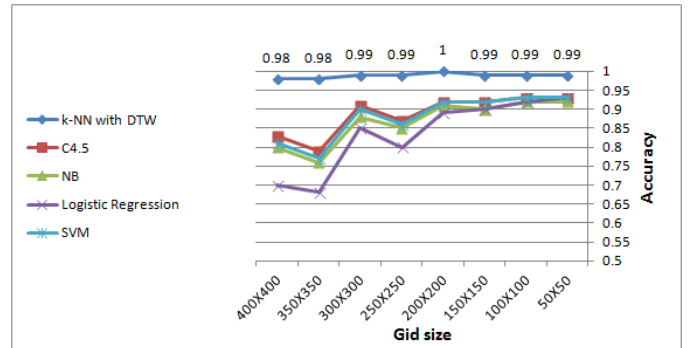


Fig. 14. The Accuracy Results  $q = 2$ .

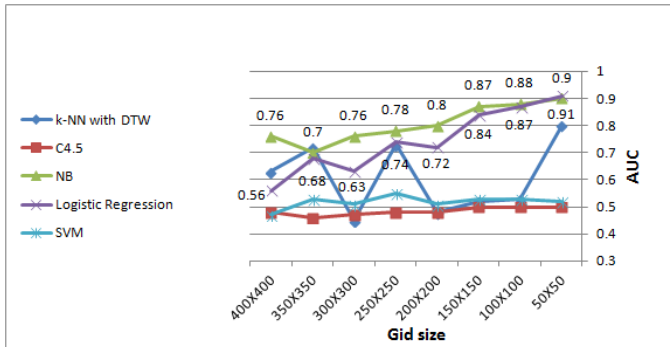


Fig. 11. The AUC Results  $q = 2$ .

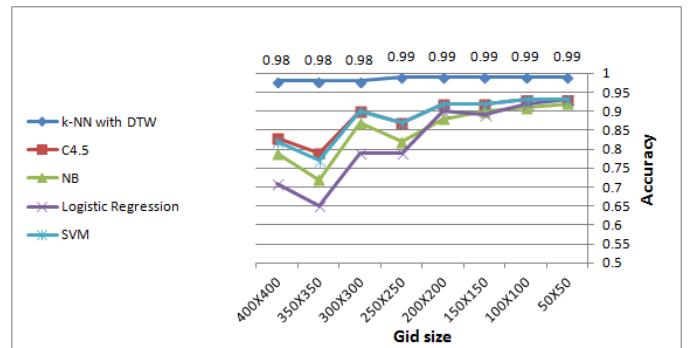


Fig. 15. The Accuracy Results  $q = 3$ .

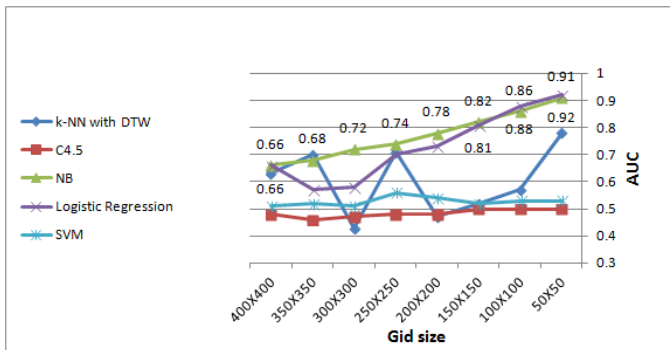


Fig. 12. The AUC Results  $q = 3$ .

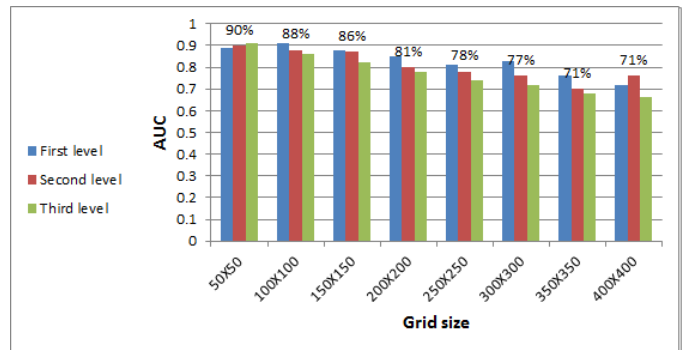


Fig. 16. The Average of the AUC Results of the NB Technique for the First, Second and Third Neighbourhood Levels using different Grid Sizes.

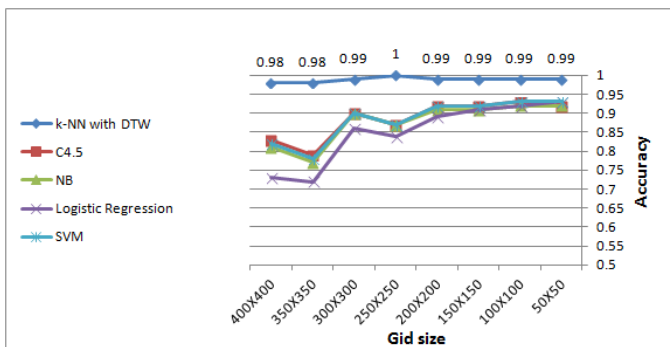


Fig. 13. The Accuracy  $q = 1$ .

is equivalent to a guess while anything less than 0.5 is worse than a guess; hence both  $k$ -NN and C4.5 can be dismissed. Out of the remainder Naive Bayes produced the best overall performance in terms of the AUC metric; a best AUC value of 0.91. Although Logistic Regression also produced good results, again a best AUC value of 0.91, it was concluded that Naive Bayes was the most appropriate prediction model. A more detailed review of the results obtained using Naive Bayes is given in Fig. 16.

### B. Grid Size

With reference to the results presented in Fig. 10 to 15 it can be seen that low grid sizes seem to be beneficial in the majority of cases; in the remainder of cases grid size

had little effect. In terms of the best performing prediction mechanism, Naive Bayes, grid size has a clear impact with best performance being recorded when  $g = 50$ . The likely reason for this is that larger grid sizes will cover a larger area of terrain which may not appropriate description with respect to the current grid square. Therefore it can be concluded that the grid size of  $g = 50$  ( $50 \times 50$ ) was the most appropriate.

C. The Analysis of Neighbourhood Levels

There is a degree of inter-operation between  $g$  and  $q$ , as  $g$  and  $q$  are increased the area “covered” will also increase. However, where  $g$  defines grid size  $q$  defines how many terrain descriptors are considered by the forecast model. Fig. 17 to Fig. 26 provide an alternative view of the results presented in Fig. 10 to 15 so as to highlight the effect of using different values for  $q$ . Inspection of Fig. 17 to Fig. 26 indicates that there is no significant difference between the three different values for  $q$  considered ( $q = 1, q = 2$  and  $q = 3$ ); although in terms of AUC and using the DT technique  $q = 1$  produced the best performance. Using Naive Bayes, the best performing forecast model as established in Sub-Section VI-A,  $q = 3$  produced best results but only in a very marginal manner. Therefore, it can be concluded that the first level of neighbourhood associated with smaller grid sizes is the “best” level of neighbourhood, it was conjectured that this was because the immediate neighbourhood of the current grid square gives a more accurate description of the nature of the current grid square.

An additional set of experiments was conducted with the neighbourhood distance set to zero,  $q = 0$ , using the Naive Bayes forecast model and  $g = 50$  (because this pairing had been shown to produce best results), and comparing the AUC values obtained with the values obtained previously using  $q = 1, q = 2$  and  $q = 3$ . The effect of using  $q = 0$  is that the neighbourhood of a given grid square is not considered, on the the terrain value in the current grid square. The results are summarised in Fig. 27. Inspection of the figure clearly indicates that inclusion of a neighbourhood in the forecast model is beneficial.

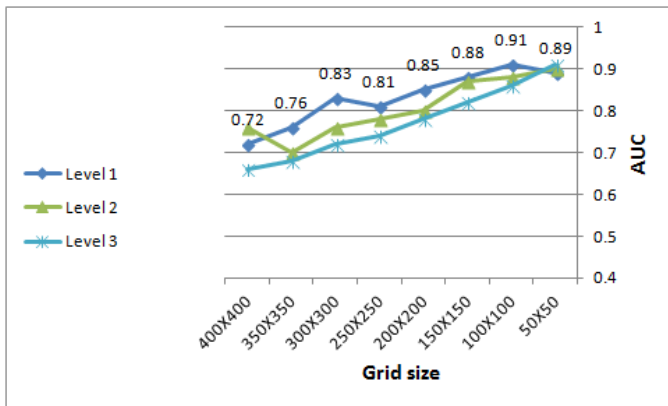


Fig. 17. The AUC Results of the Naive Bayes Technique using different Neighbourhood Distances ( $q$ ) and Grid Sizes ( $g$ ).

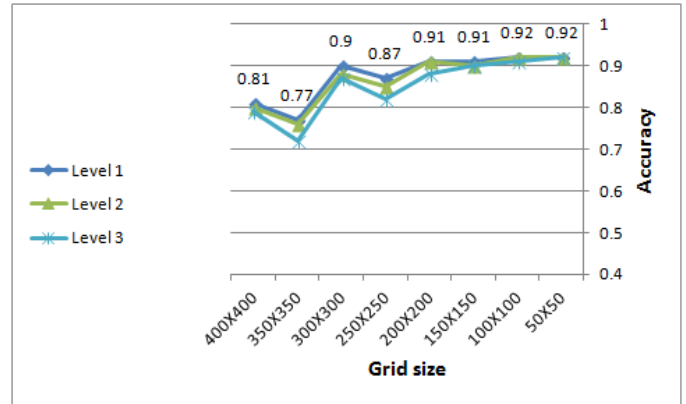


Fig. 18. The Accuracy Results of the NB Technique using different Neighbourhood Distances ( $q$ ) and Grid Sizes ( $g$ ).

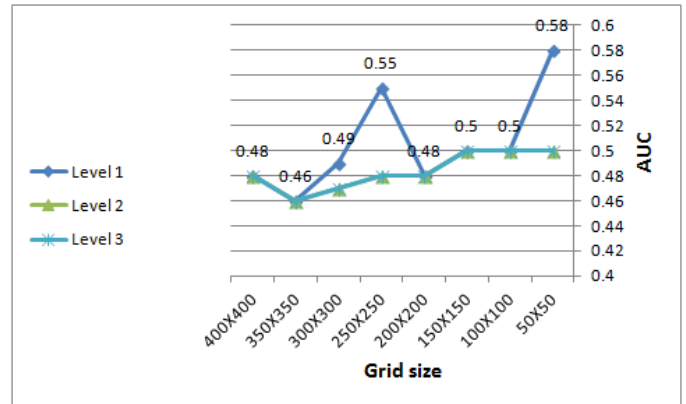


Fig. 19. The AUC Results of the DT Technique (C4.5) using different Neighbourhood Distances ( $q$ ) and Grid Sizes ( $g$ ).

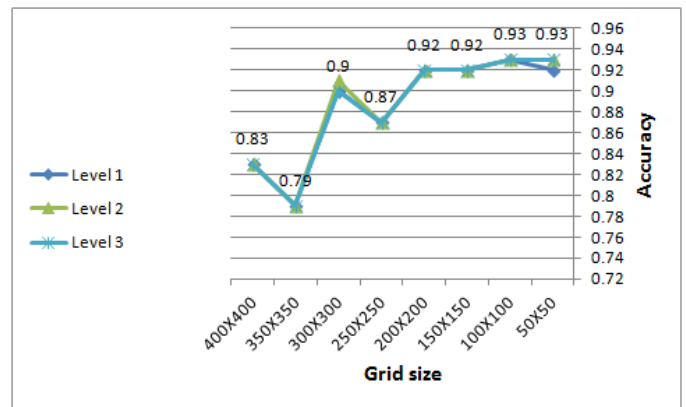


Fig. 20. The Accuracy Results of the DT Technique (C4.5) using different Neighbourhood Distances ( $q$ ) and Grid Sizes ( $g$ ).

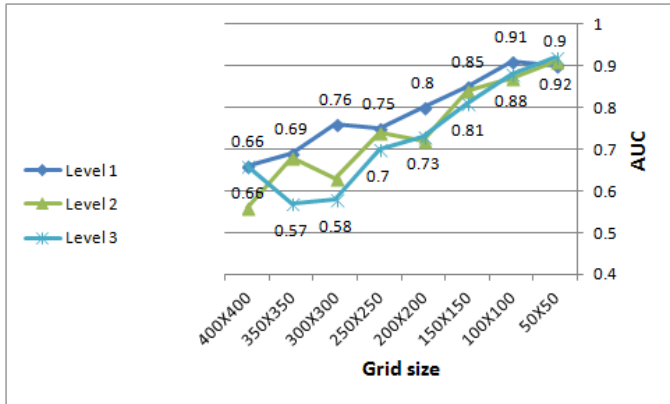


Fig. 21. The AUC Results of the Linear Regression Technique using different Neighbourhood Distances ( $q$ ) and Grid Sizes ( $g$ ).

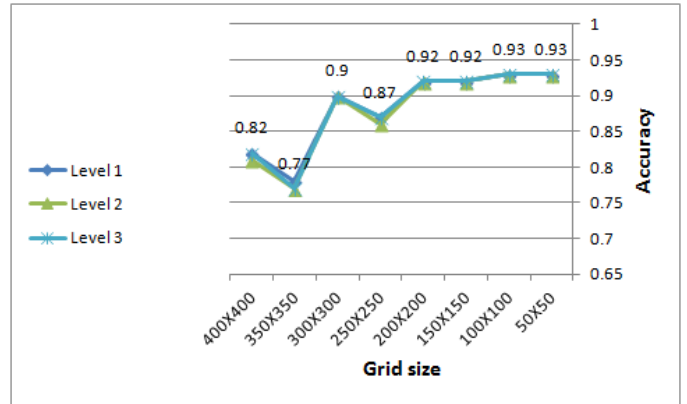


Fig. 24. The Accuracy Results of the SVM Technique using Neighbourhood Distances ( $q$ ) and Grid Sizes ( $g$ ).

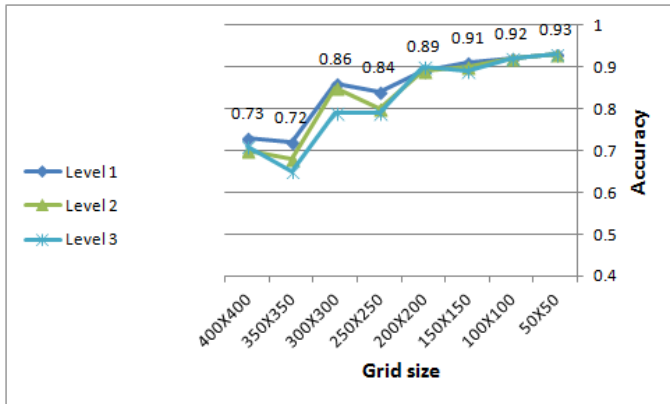


Fig. 22. The Accuracy Results of the Linear Regression Technique using different Neighbourhood Distances ( $q$ ) and Grid Sizes ( $g$ ).

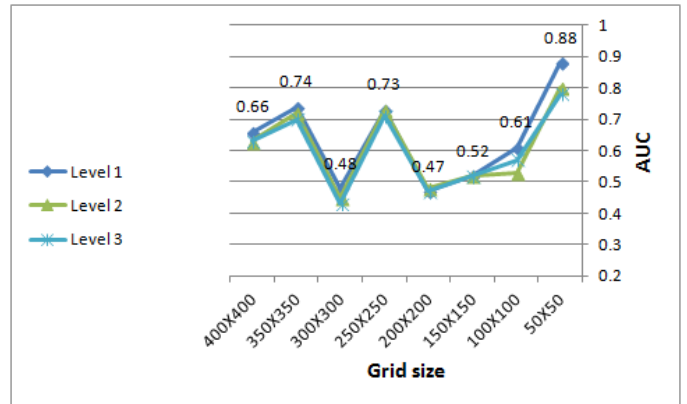


Fig. 25. The AUC Results of the  $k$ -NN Technique using different Neighbourhood Distances ( $q$ ) and Grid Sizes ( $g$ ).

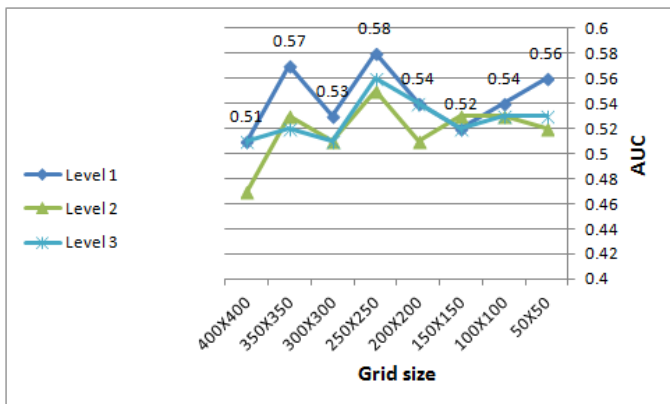


Fig. 23. The AUC Results of the SVM Technique using different Neighbourhood Distances ( $q$ ) and Grid Sizes ( $g$ ).

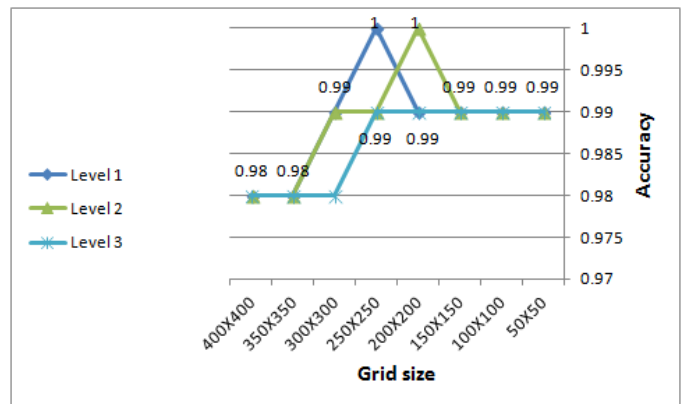


Fig. 26. The Accuracy Results of the  $k$ -NN Technique using different Neighbourhood Distances ( $q$ ) and Grid Sizes ( $g$ ).

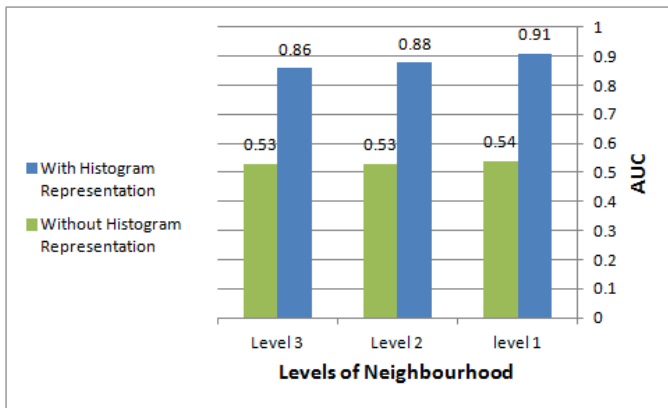


Fig. 27. The AUC Results Obtained, using Naive Bayes and  $g = 50$ , Comparing  $q = 0$  (No Neighbourhood) with Neighbourhood Distances of  $q = 1, q = 2$  and  $q = 3$ .

#### D. Run Time Analysis

Fig. 28 to 32 give the runtime recorded for each experiment. The run times are average runtime over ten folds of cross validation. As anticipated, as the value of  $g$  was increased the runtime decreased, this was because as  $g$  was increasing the number of grid squares in the test region decreased. This is illustrated in Table I. Further inspection of Fig. 28 to 32 indicates that the longest (worst) runtimes were recorded using Logistic Regression prediction models, and that the shortest (best) runtimes were recorded using Naive Bayes prediction models. The neighbourhood size tended to have little impact on the recorded runtime.

TABLE I. NUMBER OF GRID SQUARES OBTAINED USING DIFFERENT VALUES FOR  $g$  (GRID SIZE) WITH RESPECT TO THE KARAK TEST REGION

| $g$ (grid size) | $ D $ in terms of number of records (number of grid squares) |
|-----------------|--------------------------------------------------------------|
| 50              | 17030                                                        |
| 100             | 4290                                                         |
| 150             | 1936                                                         |
| 200             | 1089                                                         |
| 250             | 702                                                          |
| 300             | 484                                                          |
| 350             | 361                                                          |
| 400             | 289                                                          |

#### VII. CONCLUSION

This paper has presented a comprehensive Census Estimation Framework based on a novel *histogram representation technique*. The histogram technique incorporate with the framework to predict the population size based on the geographical nature of a given satellite image using data mining techniques, and more specifically classification techniques. The novelty of the histogram technique is the ability to capture the geographical nature of the local neighbourhood zone associated with the 3D surfaces of interest. The ultimate

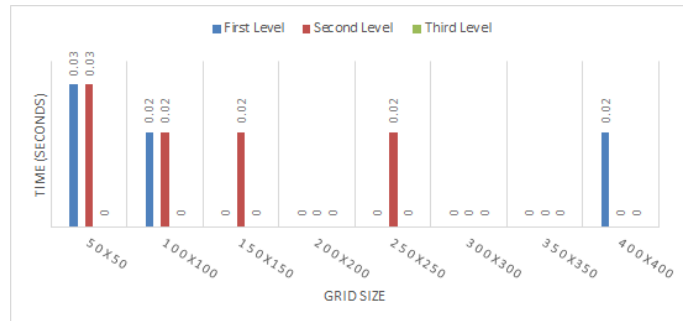


Fig. 28. The Run Time Analysis of NB Technique using different Grid Sizes ( $g$ ) and Neighbourhood Distances ( $q$ ).

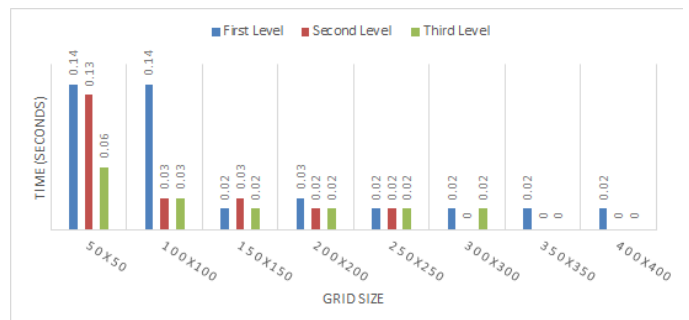


Fig. 29. The Run Time Analysis of DT Technique using different Grid Sizes ( $g$ ) and Neighbourhood Distances ( $q$ ).

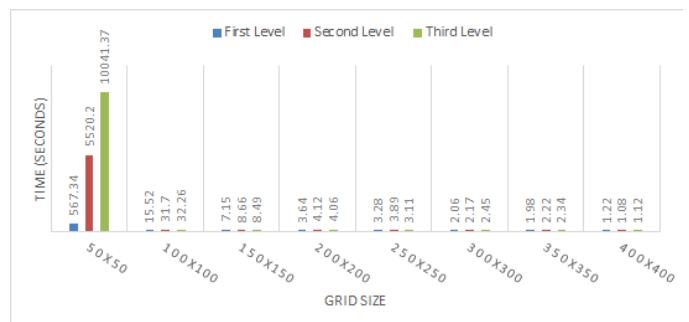


Fig. 30. The Run Time Analysis of Regression using different Grid Sizes ( $g$ ) and Neighbourhood Distances ( $q$ ).

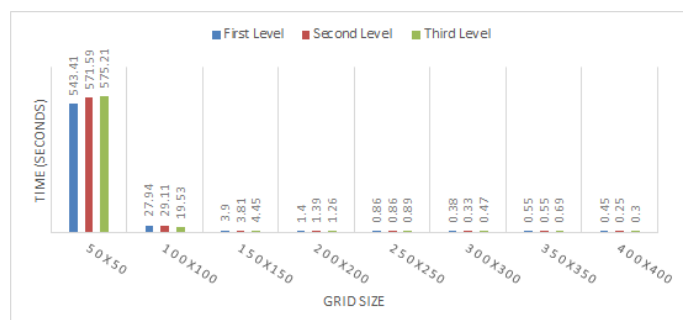


Fig. 31. The Run Time Analysis of SVM Technique using different Grid Sizes ( $g$ ) and Neighbourhood Distances ( $q$ ).

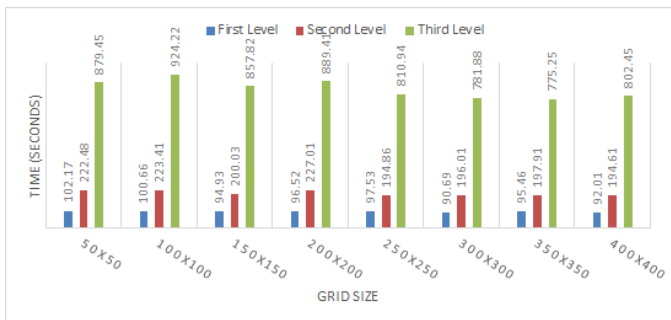


Fig. 32. The Run Time Analysis of  $k$ -NN with DTW Technique using different Grid Sizes ( $g$ ) and Neighbourhood Distances ( $g$ ).

goal of the Census Estimation Framework is to generate an accurate population predictor (classifier).

The major strength of the described framework is the ability of the proposed histogram representation to effectively encapsulate the characteristics and the features of the 3D surfaces so that they can support the classification phase while constructing the desired classifiers. The evidence of the effectiveness of the proposed framework is demonstrated by: (i) the classification results obtained using a real dataset of Karak city in Jordan and (ii) the run time analysis of the framework using different classification techniques.

The significant contributions of the work presented in this paper are discussed with respect to the theoretical and practical contributions. The theoretical contributions offered by the presented work can be listed as follows: (i) a novel 3D surface representation technique is proposed to express the local features effectively to support the process of classifier generation and thus the application of census prediction, (ii) a comparative study of the performance of different classification technique with respect to the 3D representation technique, and finally (iii) a significant analysis of the Census Estimation Framework performance when the 3D surface representation technique (histogram representation) is employed. However, the practical contributions offered by the work presented in this paper may be clearly seen in the application of the proposed framework to generate census prediction classifier using satellite images, given a previously unseen region on the satellite image, where by the foreseen population that is likely to be in a certain location can be predicted correctly. Consequently, the population prediction would guide the decision-making process of policy makers to (i) plan the future uninhabited regions easily, (ii) guide the resource allocation process effectively, and (iii) manage the development process carefully and this is of course with respect to the geographical distribution.

Some outstanding results were obtained as a consequence of a very comprehensive evaluation process (presented above) for employing the histogram representation in the framework. Naive Bayes technique along with the grid size of  $50 \times 50$  and using the first level of neighborhood succeeded to achieve the best overall results. Furthermore, the remarkable results give an indication that the histogram representation technique enhances the operation of the proposed framework.

In the context of future work, further investigations for

alternative representation mechanisms are needed. Moreover, additional experiments are required to determine the possibility to generating a generic classifier to predict the population using satellite images, not limited to the images obtained for regions in Jordan.

#### ACKNOWLEDGMENT

The authors would like to thank The Hashemite University for the continuous help and endless support. Authors also would like to acknowledge the Royal Jordanian Geographic Center (RJGC) for providing the data for this research. The comments and suggestions of the referees and editors are highly appreciated.

#### REFERENCES

- [1] J. Mennis and T. Hultgren, "Intelligent dasymetric mapping and its application to areal interpolation," *Cartography and Geographic Information Science*, vol. 33, no. 3, pp. 179–194, 2006.
- [2] C. Lo, "Automated population and dwelling unit estimation from high-resolution satellite images: a gis approach," *Remote Sensing*, vol. 16, no. 1, pp. 17–34, 1995.
- [3] D. Huang, C. Shan, M. Ardabilian, Y. Wang, and L. Chen, "Local binary patterns and its application to facial image analysis: A survey," *IEEE Transactions on Systems, Man, and Cybernetics, Part C (Applications and Reviews)*, vol. 41, no. 6, pp. 765–781, Nov 2011.
- [4] Department of Statistics, "Jordan in Figures 2016," <http://dosweb.dos.gov.jo/products/jordan-in-figures-2016/>, [Online; Accessed: July 12, 2018].
- [5] M. Ghazal, "Population stands at around 9.5 million, including 2.9 million guests," January 2016.
- [6] U. Nations, "Household size and composition around the world 2017." Data booklet, <http://www.un.org/en/development/desa/population/publications>, 2017.
- [7] K. Dittakan, F. Coenen, and R. Christley, "Towards the collection of census data from satellite imagery using data mining: A study with respect to the ethiopian hinterland." in *SGAI Conf.* Springer, 2012, pp. 405–418.
- [8] K. Dittakan, F. Coenen, and R. Christley, "Satellite image mining for census collection: a comparative study with respect to the ethiopian hinterland," in *International Workshop on Machine Learning and Data Mining in Pattern Recognition.* Springer, 2013, pp. 260–274.
- [9] K. Dittakan, F. Coenen, R. Christley, and M. Wardeh, "A comparative study of three image representations for population estimation mining using remote sensing imagery." in *ADMA (1)*, 2013, pp. 253–264.
- [10] F. Coenen, "Mining satellite images for census data collection: A study using the google static maps service." in *KDIR*, 2016, pp. 7–8.
- [11] W. Yu, F. Coenen, M. Zito, and K. Dittakan, "Classification of 3d surface data using the concept of vertex unique labelled subgraphs," in *Data Mining Workshop (ICDMW), 2014 IEEE International Conference on.* IEEE, 2014, pp. 47–54.
- [12] K. Dittakan, F. Coenen, R. Christley, and M. Wardeh, "Population estimation mining using satellite imagery," in *International Conference on Data Warehousing and Knowledge Discovery.* Springer, 2013, pp. 285–296.
- [13] I. A. Reis, V. L. Silva, and E. A. Reis, "Adjusting population estimates using satellite imagery and regression models," *Anais XV Simposio Brasileiro de Sensoriamento Remoto, SBSR*, pp. 830–837, 2011.
- [14] Y. Javed, M. M. Khan, and J. Chanussot, "Population density estimation using textons," in *Geoscience and Remote Sensing Symposium (IGARSS), 2012 IEEE International.* IEEE, 2012, pp. 2206–2209.
- [15] C. Kurtz, N. Passat, P. Gancarski, and A. Puissant, "Multi-resolution region-based clustering for urban analysis," *International Journal of Remote Sensing*, vol. 31, no. 22, pp. 5941–5973, 2010.
- [16] A. S. Alsalman and A. E. Ali, "Population estimation from high resolution satellite imagery: A case study from khartoum," *Emirates Journal for Engineering Research*, vol. 16, no. 1, pp. 63–69, 2011.



- [17] A. E. Ali, "Population estimation from aerial photographs: a case study from sudan," *Geography*, pp. 132–136, 1988.
- [18] A. Ashari, I. Paryudi, and A. M. Tjoa, "Performance comparison between naïve bayes, decision tree and k-nearest neighbor in searching alternative design in an energy simulation tool," *Int. J. Adv. Comput. Sci. Appl.*, vol. 4, no. 11, pp. 33–39, 2013.
- [19] N. Pochet and J. Suykens, "Support vector machines versus logistic regression: improving prospective performance in clinical decision-making," *Ultrasound in Obstetrics & Gynecology*, vol. 27, no. 6, pp. 607–608, 2006.
- [20] "Karak Governorate," [https://moi.gov.jo/EN/ListDetails/Governorates\\_and\\_Sectors/57/4](https://moi.gov.jo/EN/ListDetails/Governorates_and_Sectors/57/4), [Online; Accessed: October 18, 2020].
- [21] L. A. Shalabi and Z. Shaaban, "Normalization as a preprocessing engine for data mining and the approach of preference matrix," *2006 International Conference on Dependability of Computer Systems*, pp. 207–214, 2006.
- [22] S. G. K. Patro and K. Sahu, "Normalization: A preprocessing stage," *CoRR*, vol. abs/1503.06462, 2015.
- [23] U. M. Fayyad and K. B. Irani, "Multi-interval discretization of continuous-valued attributes for classification learning," in *IJCAI*, 1993, pp. 1022–1029.
- [24] M. K. Ismail and V. Ciesielski, "Design and application of hybrid intelligent systems," A. Abraham, M. Köppen, and K. Franke, Eds. Amsterdam, The Netherlands, The Netherlands: IOS Press, 2003, ch. An Empirical Investigation of the Impact of Discretization on Common Data Distributions, pp. 692–701.
- [25] J. Han, *Data Mining: Concepts and Techniques*. San Francisco, CA, USA: Morgan Kaufmann Publishers Inc., 2005.
- [26] I. H. Witten, E. Frank, and M. A. Hall, *Data Mining: Practical Machine Learning Tools and Techniques*, 3rd ed. San Francisco, CA, USA: Morgan Kaufmann Publishers Inc., 2011.
- [27] F. Coenen and K. Dittakan, "Image representation for image mining: A study focusing on mining satellite images for census data collection," in *International Joint Conference on Knowledge Discovery, Knowledge Engineering, and Knowledge Management*. Springer, 2016, pp. 3–27.
- [28] F. Coenen and K. Dittakan, "Image representation for image mining: A study focusing on mining satellite images for census data collection," in *Knowledge Discovery, Knowledge Engineering and Knowledge Management*. Cham: Springer International Publishing, 2019, pp. 3–27.
- [29] C. Schaffer, "Selecting a classification method by cross-validation," *Machine Learning*, vol. 13, no. 1, pp. 135–143, Oct 1993.

# Novel Control Scheme for Prosthetic Hands through Spatial Understanding

Yunan He<sup>1</sup>, Osamu Fukuda<sup>2</sup>, Nobuhiko Yamaguchi<sup>3</sup>, Hiroshi Okumura<sup>4</sup>, Kohei Arai<sup>5</sup>  
Computing Division, Graduate School of Science and Engineering, Saga University  
Saga 840-8502, Japan

**Abstract**—A novel control scheme for prosthetic hands through spatial understanding is proposed. The proposed control scheme features an imaging sensor and an inertial measurement unit (IMU) sensor, which makes prosthetic hands capable of visual and motion sensing. The imaging sensor captures the scene where the user is willing to grasp the object. The control system recognizes the target object, extracts its surface features and estimates its pose from the captured images. Then the spatial relationship is constructed between the hand and the target object. With the help of IMU sensors, the relationship can be tracked and kept wherever the prosthetic hand moves even the object is out of the view range of the camera. To interact with the user, this process is visualized using augmented reality (AR) technology. A test platform based on the proposed control scheme is developed and a case study is performed with the platform.

**Keywords**—Prosthetic hand; vision-inertial fusion; pose estimation; motion tracking; internal measurement unit; augmented reality; control scheme; spatial features

## I. INTRODUCTION

Humans grasping objects have two stages: they first glance at an object and instantly know what orientation, position and shape it is. Eyes then coordinate the hand to properly grasp the object. Inspired by the way that human grasps objects, many studies integrate cameras in the prosthetic hand control system [1], [2], [3], [4], [5], [6], [7], [8]. Such systems accept images as input and extract necessary information (e.g. Shape, orientation, position) for controlling prosthetic hands to adjust grasp postures. Vision-based control has developed rapidly in recent years due to the deep learning revolution in the field of computer vision [9]. State of the art deep learning algorithms can accurately detect object class and recognize object pose from a single image [10]. The information can be further used in planning a grasping movement. For example, Došen et al. [1] built a control system that uses an ultrasound distance sensor and an imaging sensor to locate the target object and estimate object size, so as to determine the grasp type and open size. Bando et al. [11] used a convolutional neural network (CNN<sup>1</sup>) to classify 20 classes of objects, the classification results help to select the grasp posture from a group of predefined postures. Shima et al. [12] takes advantage of object spatial information measured by depth sensor and classifies the objects in terms of their shapes. The shape of the object finally results in the grasp posture. In these studies, the grasp posture can be estimated but to successfully perform a grasp movement, the user needs to control the residual upper limb to orientate the prosthetic hand

in a proper position relative to the grasp target. Sometimes it has difficulties for users to do that.

If we look back to the way that humans grasp objects, it can be found that the vision-based control systems mentioned above only realize the first stage of grasping an object: recognizing object class, object position and object orientation. The orientation adjustment of the prosthetic hands still needs to be coordinated by human eyes. Since the control system has already integrated an imaging sensor, it is possible to use the imaging sensor instead of the human eyes to coordinate the prosthetic hand to grasp the objects. An intuitive method is to construct the spatial relationship between the prosthetic hand and the object using features from every image frame captured in a grasping session. The spatial relationship helps the prosthetic hand to adjust its orientation automatically. However, the algorithm complexity makes it hard to run in real time, especially when the grasp movement is relatively fast. In addition, the vision field of the imaging sensor will be very narrow at the end of the movement because the imaging sensor is usually fixed in the prosthetic hand, thus it will be difficult to extract the features.

Essentially, the camera-prosthesis coordination is to track the spatial relationship between the camera and the target object. Such a relationship guides the control system to adjust the orientation of the prosthetic hand. We introduce the combination of accelerometers and gyroscopes here to measure hand movement and further track the spatial relationship between the hand and target object. Compared to estimating the spatial relationship in every image frame, the spatial relationship tracked by accelerometers and gyroscopes costs extremely small computation resources and it is not restricted by the distance between the hand and the target object. The introduction of the accelerators and gyroscopes to the vision-based control system solves the camera-prosthesis coordination problem, which enables automatic orientation adjustment of prosthetic hand in reach-to-grasp movements.

The next section describes the proposed control system followed by some experiments. Then some discussions are described followed by conclusions with some additional discussions together with future research works.

## II. CONTROL SYSTEM

The overview of the proposed control system is illustrated in Fig. 1. The control system integrates three sensors

<sup>1</sup>[https://en.wikipedia.org/wiki/Convolutional\\_neural\\_network](https://en.wikipedia.org/wiki/Convolutional_neural_network)

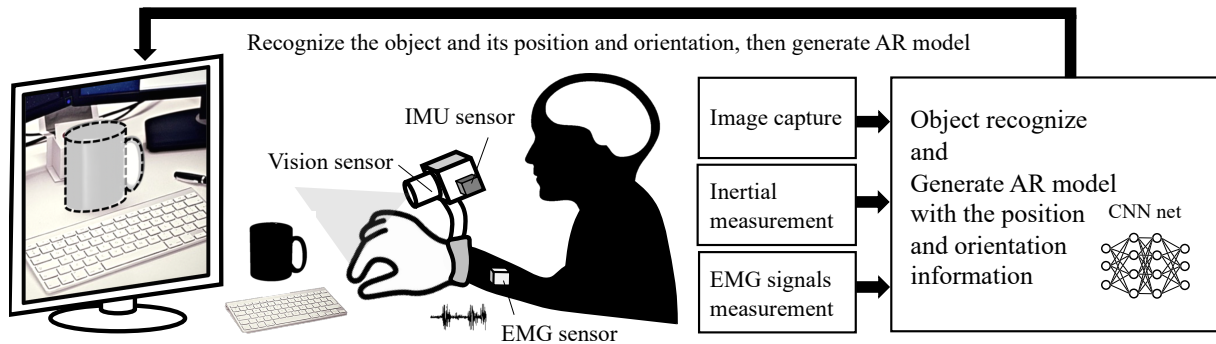


Fig. 1. System Overview.

(imaging sensor, IMU<sup>2</sup> sensor and EMG<sup>3</sup> sensor) to help collect information from the surrounding environment and the user. Imaging sensors help to recognize the target object and extract its pose information, IMU sensors help to track the extracted pose information, and EMG sensors are used to measure the EMG signals. The signals are further used to estimate the user intention that if the user is willing to start/quit/finish a grasp session [13]. The sensors work together to let the prosthetic hand be aware of the object pose. To visualize this information and let the user know if the pose is accurately extracted, we use augmented reality (AR) technology to generate a 3D object model and match the model with the object that resides in the real world. The generated graphics can be viewed through a display. It is better to use a head-mounted display to merge the generated graphics with human vision [14].

When a grasp session is triggered by the EMG signal to start, the camera glances at the scene where the user tries to grasp an object, and the prosthetic hand instantly knows what class the object belongs to, where the object stands/lies on and which orientation it is toward. The pose of the object can be continuously tracked and updated until a grasping session finishes. Its processing pipeline is shown in Fig. 2. The imaging sensor captures images of the surrounding environment and recognizes the target object in the scene. The system then retrieves the corresponding 3D features of the recognized object from the feature database and matches the features with the detected object to extract position and orientation. The system then generates a 3d graphical model and overlays the model with the detected object in the image to visualize the result of the pose estimation. The 3D model also provides the dimensions and shape information. Finally, the inertial sensors track the movement of the prosthetic hand and keep updating the extracted object pose. Since the position, orientation, and shape of the object are all known by the prosthetic hand, it is possible to control the prosthetic hand in a fine way. For example, finger-level control can be achieved.

Basically, the processing pipeline includes three main stages: object recognition, object matching and object tracking.

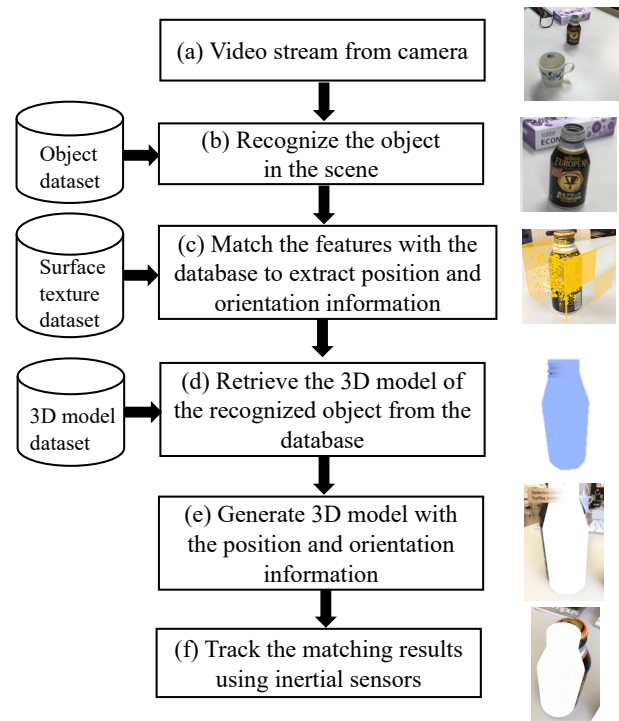


Fig. 2. Control Pipeline of the System.

Object recognition includes determining the grasp target object among several objects and cropping the target object from the original image for the convenience of feature matching. Object matching refers to matching the graphic 3D model with the real object in the image. It includes feature matching and pose estimation. Object tracking means the continuous tracking of the object pose without specifically estimating pose from every frame that camera captures. The three main stages are discussed sequentially in the following.

#### A. Object Recognition

Object recognition is a computer vision technique for identifying objects in images, outputting their categories and locations in an image. The state-of-the-art deep learning models can classify objects and regress their locations in a high degree of confidence [15]. In this study, object recognition is performed for two reasons. First, we want to

<sup>2</sup>[www.bwsensing.com/product-5.html](http://www.bwsensing.com/product-5.html)

<sup>3</sup><http://www.emgpickups.com/>

identify the categories of the objects so that the corresponding 3D graphical models and features can be successfully retrieved from the database. Second, the locations of the objects are expected to be used to crop the object image from the original image to have a pure surface texture for feature matching.

The control system uses YOLO<sup>4</sup> for object detection. YOLO is a real-time object detection system. On a GPU of Pascal Titan X<sup>5</sup> it processes images at 30 FPS and has a mAP (mean average precision) of 57.9% on COCO<sup>6</sup> which is a large-scale object detection dataset [10]. YOLO has some variations depending on the structure of the backbone and the regression/classification header. The main difference between these variations is that they have different number of convolutional layers. The selection of YOLO is to find a trade-off between accuracy and speed. In our study, the control system only needs to recognize the objects in one frame at the very beginning of a grasping session, so the detection speed is not the first thing to consider. We use the latest version of YOLO which has 53 convolutional layers in the backbone (feature extractor) to ensure the object recognition has an acceptable accuracy.

In the context of our study, a grasping session can only deal with one object. But in most cases, there is more than one object in camera view. It is necessary to determine the target among several objects. The control system follows a simple rule that the object which is closest to the center of the image is considered as the target object. This rule is also used in study [4]. Another thing that needs to be concerned is that sometimes the regression of the object location is not quite accurate, and some parts of the object may not be included in the cropped object image. It will have an effect on the feature matching. To avoid this, on the result of the location regression, we increase both the width and height size of the bounding box by 10%.

### B. Object Matching

Object matching refers to matching the graphic 3D model with the real object in the image. The first step is to find the transformation matrix between the camera coordinate system (CS) and the world CS using feature matching. The second step is to map the points of a 3D graphical model from the world CS to the image CS. They are discussed in the following.

1) *Find transformation matrix:* The transformation matrix is represented by a  $4 \times 4$  matrix. It contains rotation and translation information. With the transformation matrix, the relative position and orientation between the object and the camera is always known. So the transformation matrix step is the key to doing object matching. We use feature matching to calculate the transformation matrix.

Feature matching is a method that can find the corresponding points in the same object in two scenes. It detects object

surface texture features and compares them with pre-scanned object features (reference) to estimate the object position and orientation [16]. Given pre-scanned 3D feature points of an object,  $(P_1, P_2, P_3, P_4, \dots)$  and a bunch of detected 3D feature points of the same object,  $(P'_1, P'_2, P'_3, P'_4, \dots)$  but detected in run time. The correspondence can be found with matching features. The matching results are defined as  $(P_1, P'_1), (P_2, P'_2), (P_3, P'_3), \dots, (P_n, P'_n)$ . If we put the origin of the CS where pre-defined features points defined overlap with the origin of the camera CS and align their axis, the pre-scanned feature points will be represented in the camera CS. At the same time, the detected feature points (transformed points) are also in the camera CS. If the  $i$ -th pre-scanned feature point is defined as  $P_i = (P_{ix}, P_{iy}, P_{iz}, 1)^T$ , and its corresponding feature point detected in run time is  $P'_i = (P'_{ix}, P'_{iy}, P'_{iz}, 1)^T$ , the following equation shows their relationship.

$$\begin{bmatrix} P'_{ix} \\ P'_{iy} \\ P'_{iz} \\ 1 \end{bmatrix} = \begin{bmatrix} r_{00} & r_{01} & r_{02} & t_0 \\ r_{10} & r_{11} & r_{12} & t_1 \\ r_{20} & r_{21} & r_{22} & t_2 \\ 0 & 0 & 0 & 1 \end{bmatrix} \begin{bmatrix} P_{ix} \\ P_{iy} \\ P_{iz} \\ 1 \end{bmatrix} \quad (1)$$

Thus, the transformation matrix is calculated by substituting a list of matched feature points to Eq. 1.

2) *Project to the image frame:* The second step is to map the points of a 3D graphical model from the world CS to the image CS using the transformation matrix calculated from the first step and the camera projection matrix (can be calculated from the calibration process) for visualization. See Fig. 3. A camera projection matrix is a  $3 \times 4$  matrix which describes the mapping of a pinhole camera from 3D points in the world to 2D points in an image [17]. The visualization process uses Eq. 2 and Eq. 3 to project the 3D points to the 2D image frame. There are three CS involved: camera, image and world.

$$\begin{bmatrix} x_c \\ y_c \\ z_c \\ 1 \end{bmatrix} = \begin{bmatrix} r_{00} & r_{01} & r_{02} & t_0 \\ r_{10} & r_{11} & r_{12} & t_1 \\ r_{20} & r_{21} & r_{22} & t_2 \\ 0 & 0 & 0 & 1 \end{bmatrix} \begin{bmatrix} x_w \\ y_w \\ z_w \\ 1 \end{bmatrix} \quad (2)$$

$$\begin{bmatrix} \mu \\ \nu \\ 1 \end{bmatrix} = \begin{bmatrix} fk & 0 & \mu_0 & 0 \\ 0 & fk & \nu_0 & 0 \\ 0 & 0 & 1 & 0 \end{bmatrix} \begin{bmatrix} x_c \\ y_c \\ z_c \\ 1 \end{bmatrix} \quad (3)$$

### C. Object Tracking

After we got the transformation matrix, we know the spatial relationship between the object and the camera. The spatial relationship (transformation matrix) needs to be updated when the hand prosthesis moves. And the movement of the prosthetic hand is tracked by the combination of the accelerometer and gyroscope. No matter where the camera moves with the prosthetic hand, the position and orientation object are always known to the control system. But this tracking cannot be kept in a long term due to the sensor noise and drifting. Since the reach-to-grasp movement is usually happened in a short term, it guarantees the accuracy of the tracking to some extent. If the translation and the

<sup>4</sup><https://pjreddie.com/darknet/yolo/>

<sup>5</sup><https://www.nvidia.com/en-us/geforce/products/10series/titan-x-pascal/>

<sup>6</sup><https://cocodataset.org>

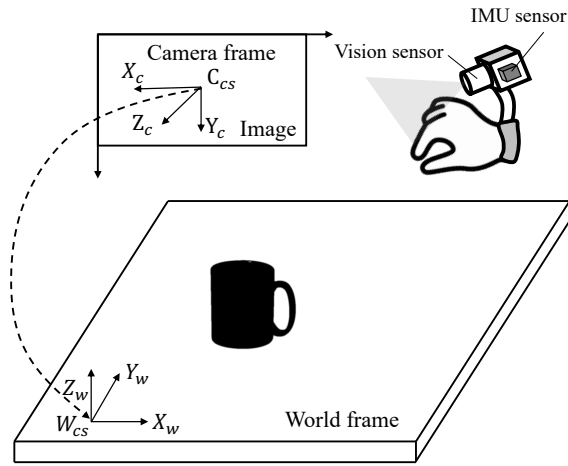


Fig. 3. Projection from world CS to camera CS

rotation of the camera can be tracked, we can update the transformation matrix using the translation and the rotation vector. The movement of the camera is represented by  $(\alpha, \beta, \gamma, T_x, T_y, T_z)$ , where  $\alpha, \beta, \gamma$  define the roll, pitch, and yaw respectively while  $T_x, T_y, T_z$  define the translation in three different axes.

The camera motion tracking has several ways, for example, visual odometry, visual-inertial odometry or IMU sensors. The easiest way is to use IMU sensors, which usually features an accelerometer and a gyroscope. An accelerometer measures acceleration forces while a gyroscope measures orientation or angular velocity. They each serve to offset the other's noise and drift errors to provide more complete and accurate movement tracking [18]. The movement of the camera is calculated by integrating the accelerations and angular velocity using Eq. 4 and Eq. 5. Due to the noise introduced by the IMU sensor, the tracking accuracy can be only acceptable in a short term.

$$pos(t) = \int_0^t \int_0^t (acc(\mu) - acc(0)) d^2\mu \quad (4)$$

$$ori(t) = \lim_{h \rightarrow 0} \prod_{i=1}^{\lfloor t/h \rfloor} \Delta rot_{mat}((i-1)h, ih) \quad (5)$$

where  $h$  is the length of the time interval between two subsequent sample,  $\Delta rot_{mat}$  is the rotation matrix in each sample. Putting the Eq. 4 and the Eq. 5 together give the final formula for the camera pose:

$$pose(t) = \int_0^t \int_0^t (ori(\mu)acc(\mu) - acc(0)) d^2\mu \quad (6)$$

### III. EXPERIMENTS

We evaluated the performance of the proposed control strategy from two aspects: object recognition and object matching/tracking.

#### A. Performance of the Object Recognition Model

The object detection model is trained from five common daily used objects: cup, bottle, spray bottle, ball and stapler. These five objects are selected because we use different postures to use/hold them. When the intersection over union (IoU) threshold is set to 0.5, the object detection network achieves 93.28% mAP. We used the trained object detection to detect a cup and a bottle on a table and then controlled the camera mounted on a prosthetic hand to perform a reach-to-object movement. The camera takes a bunch of images during the movement and these images are input to the object detection network. The detection results were reported. They are plotted in Fig. 4. As we can see from the figure, the detection accuracy in most of the reaching process is over 80%. The regressed locations included in detection results were further used to crop the object from the original pictures, which is shown in the right part of Fig. 4. The cropped image shows a better view of the surface pattern of the objects, which is good for feature detection and feature matching. But when the object is relatively far from the camera, the cropped object image is not clear enough. If the prosthetic hand detected more than one object in its view, the hand needs to determine which object is the grasp target. The simple rule is to find which object appears nearer to the center of the image.

#### B. Example of the Object Matching and Tracking

Most smartphones nowadays feature a camera as well as an IMU sensor. It is convenient to use the smartphone for a quick demonstration. In addition, the basic concept of the proposed method is very similar to an augmented reality (AR) application. The company of Apple and Google releases ARKit and ARCore<sup>7</sup> library for developers to develop AR applications, they can be used to verify the proposed method.

In the case of an iPhone, ARKit performs features matching for estimating the transformation matrix and uses visual-inertial odometry for tracking the camera movement [19]. The visual-inertial odometry method first uses the phone's camera to identify interesting feature points and tracks how those points move over time. With a combination of the movement of these points and readings from the phone's inertial sensors, both the position and orientation of the phone are determined as it moves through space.

To verify the proposed method, two 3D models: a bottle and a cup are created first based on two real objects. We want to estimate the transformation matrix between the camera coordinate system and the object local coordinate system using feature matching (see Fig. 5), then project the 3D models to the real world to make them positioned and orientated the same as the real object. The camera movement is tracked by the IMU sensors using the transformation matrix, and the transformation matrix is updated in every image frame to reconstruct the AR scene.

The demonstration is shown in Fig. 6. To show that the orientation is also recognized, we make the bottle lie on the top

<sup>7</sup><https://www.newgenapps.com/blog/arkit-vs-arcure-the-key-differences/>

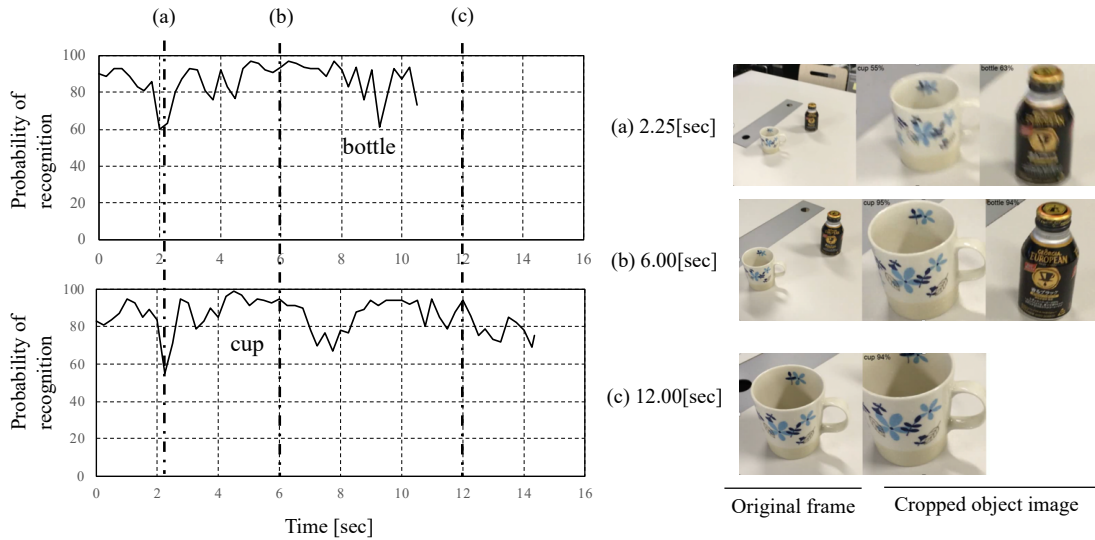


Fig. 4. Example of the Object Recognition.

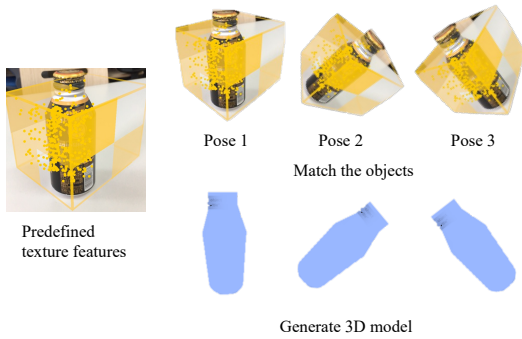


Fig. 5. Object Pose Estimation.

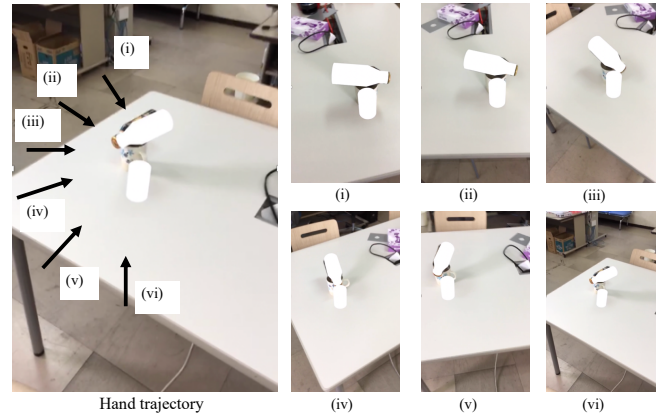


Fig. 6. Example of the Object Tracking.

of the cup. The white rigid body in the pictures is the 3D model created previously. After estimating the transformation matrix, the 3D models of the cup and the bottle are both projected to the 3D world scene to match their corresponding real objects. At the same time, the 3D world scene is again projected to a 2D image and shown in Fig. 6. We can find from the figure that the position and orientation of the cup and the bottle are both successfully estimated. Then, we try to change the view angle and move the camera farther from the object to make sure that the movement of the camera can be tracked. The scales and the perspective of the object are altered with the movement of the camera in the 2D image as the rendered 3D model exists in the real world, which proves that the hand is tracked properly.

#### IV. DISCUSSION

The experiment shows that it is possible to estimate the position and orientation of an object and track it in real-time using the sensor fusion. The transformation matrix represents the spatial relationship between the camera and the object. Estimating and tracking the transformation matrix is the key to constructing the spatial relationship. This relationship helps the prosthetic hands to comprehensively understand the

grasp scene and provides more evidence to control the hand prosthesis. It introduces many benefits. First, if we know the shape of an object as well as its 6D pose, the control can go in a very fine manner. Second, the timing to trigger a hand close movement in previous studies is usually determined by estimating the human intention from the EMG signals, but now it can be inferred from the transformation matrix since it represents the spatial relationship between the hand and the object. Third, the spatial awareness makes it possible for prosthetic hands to coordinate themselves.

However, during the test, we found that the orientation and position cannot be accurately estimated all the time. Some failure examples are shown in Fig. 7. The 3D model cannot perfectly match the real object in the AR scene. It may be caused for several reasons. But the drift from the IMU sensors is the biggest influencing factor. Drift is an ever-increasing difference between where the system thinks it is located and the actual location. Due to integration of a constant error in acceleration results in a linear error in velocity and a



Fig. 7. Some Tracking Failures.

quadratic error growth in position. It is hard to remove the drift completely, but we can make an effort to reduce the drift errors. Alternatively, we can use some markers with clear patterns to track the objects, like the ARuco markers used in AR applications [20]. But it is unrealistic to put markers around our living environment for detecting.

## V. CONCLUSION

This study introduces a new control scheme to control the vision-based hand prosthesis by combining the camera with the IMU sensor and present a demonstration to verify the proposed control. The proposed method controls the hand prosthesis based on the construction and tracking of spatial relationship between the hand and the object. The spatial relationship is represented by the transformation matrix, which provides more evidence for controlling a dexterous hand prosthesis. But as shown in the experiment, the spatial relationship cannot be perfectly constructed using the introduced method. In the future, we would like to introduce the deep learning technique to detect key points of the object and construct the transform matrix based on these points.

## ACKNOWLEDGMENT

This work was supported by JSPS KAKENHI Grant Number JP19K04296.

## REFERENCES

- [1] S. Došen, C. Cipriani, M. Kostić, M. Controzzi, M. C. Carrozza, and D. B. Popović, "Cognitive vision system for control of dexterous prosthetic hands: experimental evaluation," *Journal of neuroengineering and rehabilitation*, vol. 7, no. 1, p. 42, 2010.
- [2] G. Ghazaei, A. Alameer, P. Degenar, G. Morgan, and K. Nazarpour, "Deep learning-based artificial vision for grasp classification in myoelectric hands," *Journal of neural engineering*, vol. 14, no. 3, p. 036025, 2017.
- [3] M. Markovic, S. Dosen, C. Cipriani, D. Popovic, and D. Farina, "Stereovision and augmented reality for closed-loop control of grasping in hand prostheses," *Journal of neural engineering*, vol. 11, no. 4, p. 046001, 2014.
- [4] Y. He, R. Shima, O. Fukuda, N. Bu, N. Yamaguchi, and H. Okumura, "Development of distributed control system for vision-based myoelectric prosthetic hand," *IEEE Access*, vol. 7, pp. 54 542–54 549, 2019.
- [5] J. DeGol, A. Akhtar, B. Manja, and T. Bretl, "Automatic grasp selection using a camera in a hand prosthesis," in *2016 38th Annual International Conference of the IEEE Engineering in Medicine and Biology Society (EMBC)*. IEEE, 2016, pp. 431–434.
- [6] N. Bu, Y. Bando, O. Fukuda, and K. Okumura Hiroshi, Arai, "A semi-automatic control method for myoelectric prosthetic hand based on image information of objects," in *Proceedings of the 22nd International Symposium on Artificial Life and Robotics*, 2017, pp. 23–28.
- [7] M. Esponda and T. M. Howard, "Adaptive grasp control through multi-modal interactions for assistive prosthetic devices," *arXiv preprint arXiv:1810.07899*, 2018.
- [8] M. Markovic, S. Došen, D. Popovic, B. Graitmann, and D. Farina, "Sensor fusion and computer vision for context-aware control of a multi degree-of-freedom prosthesis," *Journal of neural engineering*, vol. 12, no. 6, p. 066022, 2015.
- [9] Y. LeCun, Y. Bengio, and G. Hinton, "Deep learning," *nature*, vol. 521, no. 7553, pp. 436–444, 2015.
- [10] J. Redmon and A. Farhadi, "Yolov3: An incremental improvement," *arXiv preprint arXiv:1804.02767*, 2018.
- [11] Y. Bando, N. Bu, O. Fukuda, and K. Okumura Hiroshi, Arai, "Object classification using a deep convolutional neural network and its application to myoelectric hand control," in *Proceedings of the 22nd International Symposium on Artificial Life and Robotics*, 2017, pp. 454–457.
- [12] R. Shima, Y. He, O. Fukuda, N. Bu, H. Okumura, and N. Yamaguchi, "Object shape classification using spatial information in myoelectric prosthetic control," *International Journal of Computer and Software Engineering*, vol. 3, 2018.
- [13] O. Fukuda, T. Tsuji, M. Kaneko, and A. Otsuka, "A human-assisting manipulator teleoperated by emg signals and arm motions," *IEEE transactions on robotics and automation*, vol. 19, no. 2, pp. 210–222, 2003.
- [14] A. Sanna and F. Manuri, "A survey on applications of augmented reality," *Advances in Computer Science: an International Journal*, vol. 5, no. 1, pp. 18–27, 2016.
- [15] J. Redmon, S. Divvala, R. Girshick, and A. Farhadi, "You only look once: Unified, real-time object detection," in *Proceedings of the IEEE conference on computer vision and pattern recognition*, 2016, pp. 779–788.
- [16] D. Wagner, G. Reitmayr, A. Mulloni, T. Drummond, and D. Schmalstieg, "Real-time detection and tracking for augmented reality on mobile phones," *IEEE transactions on visualization and computer graphics*, vol. 16, no. 3, pp. 355–368, 2009.
- [17] W. Fang, L. Zheng, H. Deng, and H. Zhang, "Real-time motion tracking for mobile augmented/virtual reality using adaptive visual-inertial fusion," *Sensors*, vol. 17, no. 5, p. 1037, 2017.
- [18] P. Neto, J. N. Pires, and A. P. Moreira, "3-d position estimation from inertial sensing: Minimizing the error from the process of double integration of accelerations," in *IECON 2013-39th Annual Conference of the IEEE Industrial Electronics Society*. IEEE, 2013, pp. 4026–4031.
- [19] U. Dilek and M. Erol, "Detecting position using arkit ii: generating position-time graphs in real-time and further information on limitations of arkit," *Physics Education*, vol. 53, no. 3, p. 035020, 2018.
- [20] F. Romero-Ramirez, R. Muñoz-Salinas, and R. Medina-Carnicer, "Speeded up detection of squared fiducial markers," *Image and Vision Computing*, vol. 76, 06 2018.

**AUTHORS' PROFILE**



**Yunan He** received the B.E. degree in mechanical engineering from Northeastern University, Shenyang, China, in 2013 and the M.E. degrees in mechanical engineering from Saga University, Saga, Japan, in 2017.

He is now a PhD student in the Department of Information Science in Saga University, Saga, Japan. His main research interests are in human-machine interface.



**Osamu Fukuda** received his B.E. degree in mechanical engineering from Kyushu Institute of Technology, Iizuka, Japan, in 1993 and the M.E. and Ph.D. degrees in information engineering from Hiroshima University, Higashi-Hiroshima, Japan, in 1997 and 2000, respectively.

From 1997 to 1999, he was a Research Fellow of the Japan Society for the Promotion of Science. He joined Mechanical Engineering Laboratory, Agency of Industrial Science and Technology, Ministry of International Trade and Industry, Japan, in 2000. Then, he was a member of National Institute of Advanced Industrial Science and Technology, Japan from 2001 to 2013. Since 2014, he has been a Professor of Graduate School of Science and Engineering at Saga University, Japan. Prof. Fukuda won the K. S. Fu Memorial Best Transactions Paper Award of the IEEE Robotics and Automation Society in 2003. His main research interests are in human interface and neural networks. Also, he is currently a guest researcher of National Institute of Advanced Industrial Science and Technology, Japan. Prof. Fukuda is a member of IEEE and the Society of Instrument and Control Engineers in Japan.



**Nobuhiko Yamaguchi** received the Ph.D. degree in intelligence and computer science from Nagoya Institute of Technology, Japan, in 2003.

He is currently an Associate Professor of Faculty of Science and Engineering at Saga University. His research interests include neural networks. He is a member of Japan Society for Fuzzy Theory and Intelligent Informatics.



**Hiroshi Okumura** received the B.E. and M.E. degrees from Hosei University, Tokyo, Japan, in 1988 and 1990, respectively, and the Ph.D. degree from Chiba University, Chiba, Japan, in 1993.

He is currently a full Professor of Graduate School of Science and Engineering at Saga University, Japan. His main research interests are in remote sensing and image processing. He is a member of the International Society for Optics and Photonics (SPIE), the Institute of Electronics, Information and Communication Engineers (IEICE) and the Society of Instrument and Control Engineers (SICE).



**Kohei Arai** received BS, MS and PhD degrees in 1972, 1974 and 1982, respectively. He was with The Institute for Industrial Science and Technology of the University of Tokyo from April 1974 to December 1978 also was with National Space Development Agency of Japan from January, 1979 to March, 1990. During from 1985 to 1987, he was with Canada Centre for Remote Sensing as a Post Doctoral Fellow of National Science and Engineering Research Council of Canada. He moved to Saga University as a Professor in Department of Information Science on April 1990. He was a councilor for the Aeronautics and Space related to the Technology Committee of the Ministry of Science and Technology during from 1998 to 2000. He was a councilor of Saga University for 2002 and 2003. He also was an executive councilor for the Remote Sensing Society of Japan for 2003 to 2005. He is an Adjunct Professor of University of Arizona, USA since 1998. He also is Vice Chairman of the Science Commission "A" of ICSU/COSPAR since 2008 then he is now award committee member of ICSU/COSPAR. He wrote 37 books and published 570 journal papers. He received 30 of awards including ICSU/COSPAR Vikram Sarabhai Medal in 2016, and Science award of Ministry of Mister of Education of Japan in 2015. He is now Editor-in-Chief of IJACSA and IJISA. <http://teagis.ip.is.saga-u.ac.jp/index.ht>.



# Deep Acoustic Embeddings for Identifying Parkinsonian Speech

Zafi Sherhan Syed<sup>1</sup>, Sajjad Ali Memon<sup>2</sup>, Abdul Latif Memon<sup>3</sup>  
Mehran University  
Pakistan

**Abstract**—Parkinson’s disease is a serious neurological impairment which adversely affects the quality of life in individuals. While there currently does not exist any cure for this disease, it is well known that early diagnosis can be used to improve the quality of life of affected individuals through various types of therapy. Speech based screening of Parkinson’s disease is an active area of research intending to offer a non-invasive and passive tool for clinicians to monitor changes in voice that arise due to Parkinson’s disease. Whereas traditional methods for speech based identification rely on domain-knowledge based hand-crafted features, in this paper, we investigate the efficacy of and propose the deep acoustic embeddings for identification of Parkinsonian speech. To this end, we conduct several experiments to benchmark deep acoustic embeddings against handcrafted features for differentiating between speech from individuals with Parkinson’s disease and those who are healthy. We report that deep acoustic embeddings consistently perform better than domain-knowledge features. We also report on the usefulness of decision-level fusion for improving the classification performance of a model trained on these embeddings.

**Keywords**—Affective computing; deep acoustic embeddings; Parkinson’s disease; social signal processing

## I. INTRODUCTION

Parkinson’s Disease (PD) is a progressive neurodegenerative disorder caused by decay of neurons in the area of the brain which controls body movements [1]. It manifests as muscle rigidity, slowness of body movement, compromised gait, and involuntary shaking amongst other symptoms. Individuals with Parkinson’s disease also suffer from vocal impairments such as impoverished speech prosody, hoarse voice quality, and imprecise articulation [2].

According to a handbook by the World Health Organization on public health challenges caused by neurological disorders [3], Parkinson’s disease contributes approximately 2% of the total global burden of diseases. In terms of disability-adjusted life year (DALY) score, a commonly used metric which quantifies the number of years lost due to ill-health, the burden of PD is on a rise, with the number of DALYs increasing from 1,617,000 in 2005 to 1,762,000 in 2015, and is expected to increase up to 2,015,000 by the year 2030. Parkinson’s disease does not currently have a cure and improving the quality-of-life of patients is of prime importance. According to Yousefi et al. [4], early detection can help improve the patients’ quality of life through physiotherapy, mental health counseling, and in some cases surgery. There also do not exist specific tests for diagnosis of Parkinson’s disease, therefore, patients are diagnosed by trained clinicians based on common signs and symptoms for the disease through physical and neurological examination as well as medical history [5]. It is common

to recommend brain imaging tests to patients for differential diagnosis in order to rule diseases than Parkinson’s [6], [7]. While brain imaging has indeed been a successful tool, it is invasive. Such tests also require patients to visit special facilities, which may not be convenient for the elderly.

Recently, there has been a growing interest in developing voice-based screening tools that can identify patients with Parkinson’s disease based on the characteristics of their voice alone. For example, Tsanas et al. [8] showed that speech-based tools can be used to recognize the progression of Parkinson’s in a telemonitoring setup. Traditional methods for speech based identification of Parkinson’s disease mostly rely on domain-knowledge based hand-crafted features [9], [10], [11], [12]. However, advances in the field of natural language processing have shown that embeddings from pre-trained deep neural networks often perform better than hand-crafted features. To this end, we investigate the efficacy of deep acoustic embeddings generated from pre-trained deep neural works for the task of automated identification of Parkinsonian speech. Whilst using domain-knowledge based features to create a baseline classification performance, we show that these embeddings can achieve a better classification performance than those hand-crafted features. Moreover, we also show that upstream training tasks for these embeddings are not a limiting factor for its downstream task of speech paralinguistics. Finally, we report that decision-level fusion is an effective method to improve the classification performance of machine learning models trained to identify Parkinsonian speech.

The rest of the paper is structured as follows: In Section II, we introduce the concept of deep acoustic embeddings for the task at hand and briefly describe the four deep neural models used in our work. In Section IV, we discuss the methodology followed for data-driven analysis. In Section V, we report the results of experiments and provide a discussion for each aspect of the experimentation. A conclusion of our work is provided in Section VI and supplementary data to support our work is provided as appendices.

## II. DEEP ACOUSTIC EMBEDDINGS

A major limitation of domain knowledge based hand-crafted features is that they are narrow in scope and often require subject expertise in order to be used in the correct context. For example, while Mel Frequency Cepstral Coefficients (MFCCs) is a popular acoustic feature for representing cepstral characteristics of audio signals, it is still represented by a relatively small number of coefficients as compared to say a Mel spectrogram, which offers a rich time-frequency representation of an audio signal. Deep neural network models

for applications based on audio modality are trained to learn useful features from Mel spectrogram representations of audio signals, similar to how deep learning based image classification models learn to recognize useful features from an image. In the case of audio, spectrograms serve as images. The word deep acoustic embeddings refer to features learned from deep neural networks that are trained for audio applications. These embeddings are typically extracted from the penultimate layer of the model meaning that these features are representative of the characteristics of audio signals that were used to train the models.

In our work, we experiment with embeddings generated from four deep neural networks which were optimized for applications based on audio modality. These are VGGish, YAMNet, openl3: Music, and openl3: Environment sounds.

### A. VGGish Embeddings

The VGGish is a deep convolutional neural network proposed by Hershey et al. [13] for large scale audio classification of Youtube videos based on their audio content. As the name suggests, VGGish is based on the famous VGGNet [14] which was once the state-of-art model for image classification and remains amongst performing models in computer vision. VGGish's network architecture consists of four blocks, each with convolutional kernels and maxpooling layers, which serve as a feature extractor. These are followed by two fully connected layers that serve as the classifier.

The VGGish was trained on an initial version of AudioSet corpus [15] consisting of more than 2 million video clips from Youtube which were manually annotated into 527 categories. Examples of these categories include male/female adult voice, infant babbles, animal sounds, and sounds produced by various types of machines. VGGish was envisaged as a model that can learn a meaningful representation of audio signals for these classification categories but in our recent work, we showed it to be useful for speech paralinguistic tasks such as identification of Alzheimer's dementia [16].

As with most deep neural networks that generate deep acoustic embeddings, the VGGish accepts spectrogram-based representation of audio clips. To begin, each audio clip is segmented into chunks of 1 second in duration and a Mel spectrogram is computed over short-time frame duration of 25ms and frame hop-duration of 10ms whilst using Mel frequency shaping filter with 96 bins. Our objective is to only compute deep acoustic embeddings from the VGGish model (and not to classify our dataset into 527 classes of the AudioSet corpus), we take the output from the model before the final classifier. With spectrograms as input, the VGGish model is therefore used as a feature extractor that produces 128-dimensional embeddings as its output. An illustration of this workflow is provided in Figure 1. We posit that these semantically relevant embeddings are useful for our downstream task of Parkinsonian speech classification. A pre-trained model for VGGish has been made available by Google for academic research <sup>1</sup> and we make use of this model in our work.

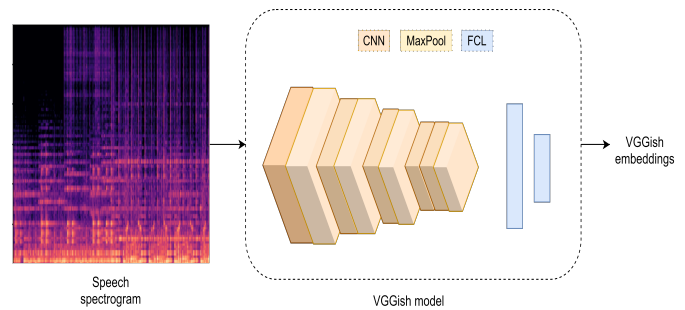


Fig. 1. Illustration of Feature Extractor for VGGish Embeddings

### B. YAMNet Embeddings

A major drawback of the VGGish model is that with more than 72 million parameters, it has high computational complexity. This inhibits the use of VGGish in most applications that are based on mobile embedded systems. The YAMNet model was developed by Ellis and Chowdhry <sup>2</sup>, as a computationally efficient model for classification of audio events for the AudioSet corpus. It is based on the MobileNet architecture proposed earlier by Howard et al. [17] that used depth-wise separable convolutional kernels to create lightweight models that can be used for mobile and embedded vision applications. As a result, the YAMNet model has 4.7 million parameters versus the 72 million required for VGGish.

The network architecture of YAMNet model consists of 14 blocks of convolutional layers where all except the first layer are based on depth-wise convolutional kernels. While there are no differences between VGGish and YAMNet models in terms of input spectrograms, there are some differences in terms of training data: the YAMNet is trained with the larger AudioSet corpus but it has a slightly smaller number of classes (521 versus 527 for VGGish) since some classes were removed from AudioSet corpus due to ethical considerations. Therefore, it is not possible to compare, in a fair manner, the classification performance of VGGish and YAMNet models on the AudioSet corpus. Nevertheless, we shall compare their classification for recognition of Parkinsonian speech through data-driven analysis and report results in Section V.

### C. openL3 Embeddings for Music and Environmental Sounds

In addition to deep acoustic embeddings generated from VGGish and YAMNet models, which are trained to recognize human voice amongst various other types of audio events, we also make use of embeddings generated from openl3 models [18] <sup>3</sup>, which are optimized to identify types of music and environmental sounds. Our motivation to use these embeddings is to investigate whether the upstream training task matters for downstream classification performance for deep acoustic embeddings. More specifically, we seek to answer whether embeddings from models trained to recognize music and environmental sounds can be used to recognize characteristics of speech paralinguistics which are present in Parkinsonian speech.

<sup>1</sup><https://github.com/tensorflow/models/tree/master/research/audioset/vggish>

<sup>2</sup><https://github.com/tensorflow/models/tree/master/research/audioset/YAMNet>

<sup>3</sup><https://github.com/marl/openl3>

The openl3 embeddings are based on the Look, Listen, and Learn (L3) concept which was proposed by Arandjelovic et al. [19] for training neural networks to learn meaningful audio representations in a self-supervised manner through audio-visual correspondence tasks. Their approach seeks to alleviate stringent requirements for manual annotation of training data. Cramer et al. [18] developed openl3 models as an extension to the work from [19] and investigated various network architecture choices, such as the choice between short-time-Fourier transform based spectrograms or Mel frequency scaled spectrograms and a different size for deep acoustic embeddings. It is important to mention here that the video recordings used to train openl3 models were also curated from within the AudioSet corpus, however, the scope of these models is much smaller than VGGish and YAMNet which seek to classify between all available classes in the AudioSet corpus. The network architecture for openl3 models consists of four blocks of convolutional layers which are used as feature extractors from spectrograms that are fed to the model as input. MaxPooling operation is performed to the output of feature extractor with an option to yield either an embedding of size 512 or an embedding of size 6144.

### III. DATASET

We make use of the GITA corpus of Parkinsonian speech in our experiments which was published by Orozco-Arroyave et al. [20] as part of work carried out at Applied Telecommunications Group (GITA) at Universidad de Antioquia, Colombia. The GITA corpus is one of the most prominent publicly available datasets on Parkinsonian speech. It consists of speech recordings from 100 native speakers of Spanish language amongst whom 50 subjects were diagnosed with Parkinson's disease as per the Unified Parkinson's Disease Rating Scale (UPDRS) scale [21]. These subjects were matched in terms of age and gender with their respective healthy counterparts. The GITA corpus consists of three main speaking tasks which vary in duration and phonetic content. The first speaking task is based on diadochokinetic non-words, short-duration utterances based on the pronunciation of words and phrases, and long duration utterances which require subjects to read out a section of text or monologue. A summary of statistics for time durations for each task is provided in Table I. For a more thorough description of the dataset such as the age and gender distribution of subjects, we refer the reader to [20].

### IV. METHODOLOGY

The process flow diagram for automated identification of Parkinsonian speech is illustrated in Fig. 2. Here, one starts with raw audio recordings from subjects that are preprocessed into a standard format used in audio signal processing (16 KHz sampling rate, mono-channel, and amplitude normalized between +/-1). The next step is to compute domain-knowledge features such as ComParE and eGeMAPS.

In order to compute deep acoustic embeddings such as VGGish, YAMNet, openl3:Music, and openl3:Environment Sounds, a Mel spectrogram based representation is generated for the recording and passed down to feature extractors based on these models (details of these models were provided in Section II). Since deep acoustic embeddings are computed over chunks of audio recordings, these embeddings need to

TABLE I. SUMMARY OF TIME-DURATION STATISTICS FOR EACH SPEAKING TASK IN THE GITA CORPUS

| Speaking Task  |            | Time Duration Statistics |       |        |
|----------------|------------|--------------------------|-------|--------|
| Category       | Task       | Min                      | Avg   | Range  |
| DDK            | ka         | 0.81                     | 2.76  | 8.02   |
|                | pa         | 0.76                     | 2.94  | 6.77   |
|                | pakata     | 1.39                     | 4.16  | 7.63   |
|                | pataka     | 1.39                     | 4.38  | 9.13   |
|                | petaka     | 1.10                     | 4.14  | 7.70   |
| Short-duration | ta         | 0.77                     | 2.92  | 8.36   |
|                | juan       | 1.81                     | 3.21  | 4.48   |
|                | laura      | 1.27                     | 2.18  | 2.65   |
|                | loslibros  | 1.84                     | 3.43  | 5.64   |
|                | luisa      | 2.21                     | 4.01  | 7.42   |
|                | micasa     | 1.20                     | 1.96  | 2.35   |
|                | omar       | 1.56                     | 2.65  | 3.38   |
|                | preocupado | 2.30                     | 4.32  | 6.16   |
|                | rosita     | 2.61                     | 4.36  | 5.58   |
|                | triste     | 1.74                     | 3.26  | 4.34   |
| Long-duration  | viste      | 4.81                     | 7.88  | 16.90  |
|                | readtext   | 10.35                    | 18.12 | 34.91  |
|                | monologue  | 14.10                    | 47.11 | 149.99 |

be summarized in order to generate a global representation for the audio recording. In this work, we use three functionals of descriptive statistics, namely, average, maximum, and range to pool a global feature vector for deep acoustic embeddings.

Finally, given the relatively small number of examples per speaking task (50 each for subjects with Parkinson's disease and those who are healthy), we conduct experimentation through leave-one-subject-out (LOSO) cross-validation. In each iteration, 99 examples are used to form the training set and the one remaining example is used for testing. Therefore, in total, the classification performance with each acoustic feature (domain-knowledge based as well as deep acoustic embeddings) is computed over 100 examples. We train a logistic regression classifier to differentiate between features from healthy and Parkinson's disease groups. Logistic regression has a hyper-parameter called *complexity* which needs to be optimized in order to tune its classification performance. To this end, we integrate hyper-parameter optimization within the LOSO cross-validation (we found this strategy to be successful in [16]) and optimize complexity over a logarithmically spaced grid between  $10^{-7}, 10^{-6}, \dots, 10^3$ .

In subsequent paragraphs, we provide details of domain-knowledge and deep acoustic embedding based features which are used in our experiments.

#### A. Domain-knowledge based Handcrafted Features

Evidence suggests that muscular dystrophy, where muscles shrink and weaken, due to Parkinson's disease causes aphasia, which leads to changes in paralinguistic characteristics of speech in terms of prosody, voice quality, and voice spectra [22], [23], [24], [25], [26]. Prosody is defined as the intonation or melodic contour speech and abnormal prosody is a recognized marker of individuals with Parkinson's disease [25]. Voice quality describes the degree of hoarseness, breathiness, or tenseness of voice [22]. It is known that muscular tightening causes glottis to function improperly which leads to poorer quality of voice for those with Parkinson's disease as compared to individuals who are healthy [11], therefore, acoustic features which quantify voice quality can be useful for the task of

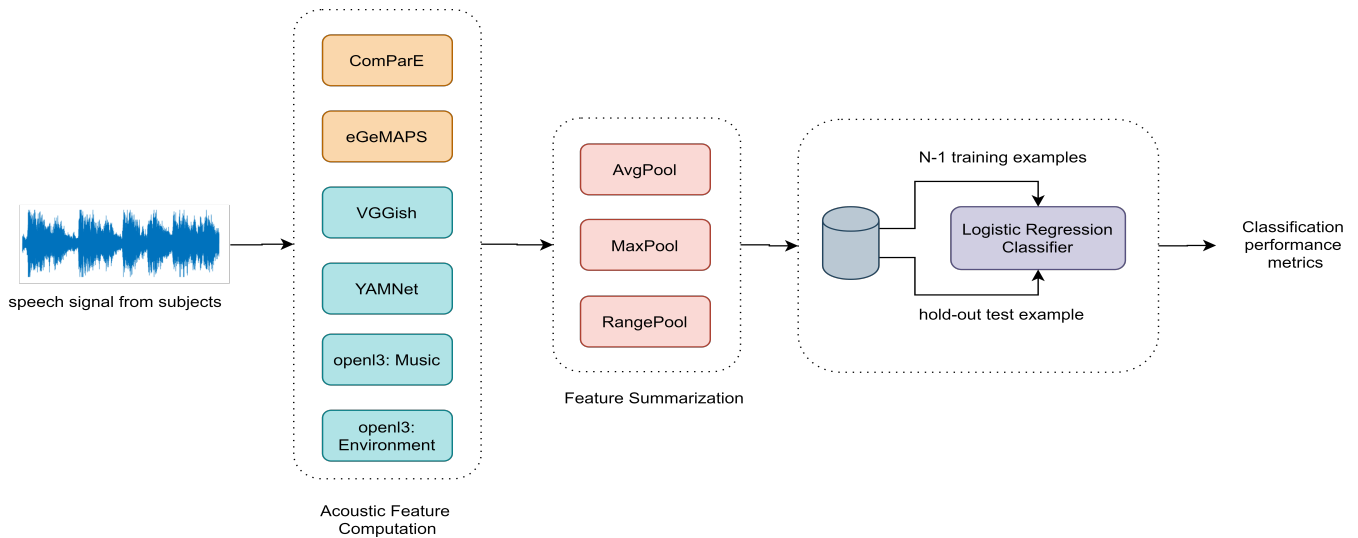


Fig. 2. Process Flow Diagram for Automated Identification of Parkinsonian Speech

identifying Parkinsonian speech. The final characteristic of voice that is popular in speech paralinguistics is voice spectra. It is reminded that spectral characteristics of voice are shaped by the movement of the vocal tract. One can surmise that this vocal tract becomes rigid due to muscular dystrophy therefore the speech of individuals with the disease will lack in spectral richness [26]. This suggests that spectral analysis of speech can be useful for the identification of Parkinsonian speech.

In order to represent these three paralinguistic characteristics of speech quantitatively, we shall compute acoustic features from two feature sets, (a) Computational Paralinguistics Challenge (ComParE) and (b) Extended Geneva Acoustic Minimalistic Feature Set (eGeMAPS) using the openSmile toolkit [27]. These feature sets are de facto standard in the field of social signal processing for quantification of characteristics of speech paralinguistics [28], [29].

The ComParE feature set consists of 65 acoustic low-level-descriptor (LLDs) amongst which 4 LLDs characterize voice energy, 6 features characterize voice quality, and 55 features represent voice spectra. It is used to develop baseline classification performance for the popular Interspeech Computational Paralinguistic Challenges and as a testament to its effectiveness, ComParE features have achieved better performance than deep learning methods as well [30]. The eGeMAPS feature set is considered as a lower-dimensional alternate to the ComParE feature set (88 vs 6373-dimensional feature vectors). eGeMAPS consists of 23 acoustic LLDs amongst which 13 features describe voice quality, 9 features describe voice spectra, and one acoustic feature is dedicated to voice energy. Further details of these features have been provided in Tables VII and VIII.

### B. Deep Acoustic Embeddings based Features

As mentioned earlier, we compute three types of pooling methods in order to summarize deep acoustic embedding features which are computed for short-duration chunks of audio recordings. Therefore, the pooling method is one of the hyper-parameters which needs to be optimized for deep

acoustic embeddings based features. Furthermore, there exist two further hyper-parameters for embeddings based on openl3 models. The first hyper-parameter amongst these determines whether a linear spectrogram or Mel spectrogram should be used as a representation of audio signal. The second hyper-parameter determines the dimensionality of openl3 embeddings with options of either a 512-dimensional embedding or a 6144-dimensional embeddings. Given the data-driven nature of machine learning, these hyper-parameters also need to be optimized using the cross-validation process.

## V. EXPERIMENTATION, RESULTS AND DISCUSSION

In this section, we summarize and report on results from experiments conducted to determine the efficacy of deep acoustic embeddings for a variety of speaking tasks, along with analysis into fusion and performance comparison of deep acoustic embeddings.

### A. Diadochokinesis Tasks

In Table II, we summarize results for experiments performed to identify individuals with Parkinson's disease based on six Diadochokinesis (DDK) tasks using two domain-knowledge based features (which serve as a baseline) and the four deep acoustic embeddings. Amongst the six tasks, one can note that `music_linear_512` embedding achieves the best classification performance thrice, i.e. for *ka*, *pakata*, and *pekata* utterances. This includes the overall best classification accuracy of 85.0% amongst the six DDK tasks and the highest average classification accuracy of 79.3% for the six tasks. One can also note that `environment_mel256_512` embedding offers a competitive performance, with best classification accuracy for *ka* utterance as well as an average classification accuracy of 78.0% compared to 79.3% of `music_linear_512` embedding. Meanwhile, VGGish and YAMNet embeddings, which are trained on audio recordings that also contain human voice perform worst for the DDK tasks amongst all deep acoustic embeddings.

TABLE II. CLASSIFICATION ACCURACY FOR VARIOUS ACOUSTIC FEATURES FOR SIX DIADOCHOKINESIS TASKS, ALONG WITH THE AVERAGE ACCURACY OVER ALL DIADOCHOKINESIS TASKS

| Feat                    | Diadochokinesic |             |             |             |             |             | Average     |
|-------------------------|-----------------|-------------|-------------|-------------|-------------|-------------|-------------|
|                         | pa              | ka          | ta          | pakata      | pekata      | pataka      |             |
| ComParE                 | 79.0            | 72.0        | <b>79.0</b> | 74.0        | 76.0        | 74.0        | 75.7        |
| eGeMAPS                 | 78.0            | 79.0        | 67.0        | 72.0        | 74.0        | 71.0        | 73.5        |
| VGGish                  | 65.7            | 66.3        | 67.0        | 71.0        | 65.0        | 70.0        | 67.5        |
| YAMNet                  | 66.0            | 73.0        | 76.0        | 69.0        | 68.0        | 71.0        | 70.5        |
| environment_linear_512  | 77.0            | 77.0        | 74.0        | 79.0        | 77.0        | 75.0        | 76.5        |
| environment_linear_6144 | 81.0            | 81.0        | 70.0        | 72.0        | 72.0        | 76.0        | 75.3        |
| environment_mel256_512  | <b>84.0</b>     | 77.0        | 74.0        | 79.0        | 79.0        | 75.0        | 78.0        |
| environment_mel256_6144 | 79.0            | 75.0        | 74.0        | 77.0        | 75.0        | <b>81.0</b> | 76.8        |
| music_linear_512        | 78.0            | <b>82.0</b> | 77.0        | <b>85.0</b> | <b>80.0</b> | 74.0        | <b>79.3</b> |
| music_linear_6144       | 74.0            | 81.0        | 68.0        | 77.0        | 75.0        | 73.0        | 74.7        |
| music_mel256_512        | 73.0            | 81.0        | 74.0        | 74.0        | 79.0        | 70.0        | 75.2        |
| music_mel256_6144       | 75.0            | 81.0        | 75.0        | 78.0        | 73.0        | 73.0        | 75.8        |

Another interesting observation from Table II is that environment\_mel256\_6144 embedding performs best for *pakata* utterance with a classification accuracy of 81.0%. In fact, the second placed acoustic feature is also based on environmental sounds, that is, environment\_linear\_6144 embedding which achieves an accuracy of 76.0%. This suggests that some characteristics of environmental sounds are also useful for identifying Parkinsonian speech based on *pakata* utterance.

Amongst domain-knowledge based features, ComParE offers competitive performance overall as evident from the average classification accuracy for all tasks. In fact, ComParE features even achieved best performance for the *ta* task. Overall, however, it is clear that deep acoustic embeddings are a better alternative to domain-knowledge based features if the objective is to maximize classification performance based on diadochokinesic speaking tasks.

### B. Short-Duration Utterance Tasks

The results of Parkinsonian speech classification based on short-duration utterances are summarized in Table III. On the basis of average classification computed for the ten utterances, one can note that environment\_mel256\_512 embedding achieves the best performance overall (77.3%), closely followed by music\_linear\_512 (76.5%). Here, environment\_mel256\_512 achieved top performances for most tasks (five out of ten), including *laura*, *luisa*, *micasa*, *preocupado*, *rosita*, and *viste* as well as the highest classification accuracy of 85.0%, that was achieved with *triste* utterance. The second placed acoustic features, music\_linear\_512, achieved top performances for *juan*, *loslibros*, and *omar* utterances.

Amongst the two domain-knowledge features, ComParE again performs much better than eGeMAPS – 74.6% average classification over the ten utterance tasks for ComParE versus 67.5% for eGeMAPS. Moreover, VGGish and YAMNet embeddings also perform poorly with an average classification accuracy of 70.7% and 69.1%, respectively.

### C. Long-Duration Utterance Tasks

The classification results for identification of Parkinsonian speech for *readtext* and *monologue* tasks are summarized in Table IV. A special characteristic of these tasks is that they

are of a relatively long duration as compared to *DDK* and *short utterance* tasks, therefore, more speech data is available per subject.

To begin, one can note that music\_linear\_512 embedding achieves the best classification performance overall, with top classification accuracy of 84.0% for the *readtext* task and a competitive 79.0% for the *monologue* task. The best performance for *monologue* task is achieved with environment\_linear\_512 feature but it lags behind other features for the reading task. As an example, consider environment\_mel256\_512, which achieves 79.0% and 78.0% for reading and monologue utterances to achieve a higher average accuracy than environment\_linear\_512. Furthermore, it is pertinent to mention here that environment\_mel256\_512 was also the best performing model for short-duration utterance tasks as well which shows that the embedding is consistent in its efficacy for the task at hand.

### D. Decision-Level Fusion

From Tables II–IV, one can note that embeddings from different upstream tasks achieve varying degrees of success at classification of Parkinsonian speech. For example, environment\_mel256\_512 and music\_linear\_512 are embeddings with different upstream tasks but yield top classification performance for a variety of speaking tasks. This suggests that machine learning models trained on these embeddings carry complimentary information which can be fused together in order to achieve improved classification accuracy. This is a well known premise of decision-level fusion [31] and we have had success at improving the quality of machine learning models using fusion in our previous works [32], [16].

To this end, we use two types of decision-level fusion, i.e. confidence based fusion and majority-vote based fusion for top three acoustic features for each speaking task. In confidence based fusion, the confidence scores of classifiers for predicting each class are averaged and judgement about class labels is made using the averaged confidence scores. Meanwhile, in majority-vote approach, each classifier makes its own judgement about class labels before a majority-vote is carried out to make final judgement about the class labels using information from all models. It must be mentioned here that due to data-driven nature of fusion process, one needs

TABLE III. CLASSIFICATION ACCURACY FOR VARIOUS ACOUSTIC FEATURES FOR TEN SHORT DURATION SPEECH UTTERANCE TASKS, ALONG WITH THE AVERAGE ACCURACY OVER ALL SHORT UTTERANCE TASKS

| Feat                    | Short Utterances |             |             |             |             |             |             |             |             |             | Average     |
|-------------------------|------------------|-------------|-------------|-------------|-------------|-------------|-------------|-------------|-------------|-------------|-------------|
|                         | juan             | laura       | loslibros   | luisa       | micasa      | omar        | preocupado  | rosita      | triste      | viste       |             |
| ComParE                 | 73.0             | 77.0        | 74.0        | 76.0        | 74.0        | 71.0        | 81.0        | 74.0        | 76.0        | 70.0        | 74.6        |
| eGeMAPS                 | 69.0             | 59.0        | 69.0        | 67.0        | 70.0        | 69.0        | 68.0        | 65.0        | 70.0        | 69.0        | 67.5        |
| VGGish                  | 72.0             | 70.0        | 67.0        | 67.0        | 69.0        | 73.0        | 76.0        | 69.0        | 76.0        | 68.0        | 70.7        |
| YAMNet                  | 69.0             | 66.0        | 70.0        | 71.0        | 66.0        | 74.0        | 70.0        | 67.0        | 69.0        | 69.0        | 69.1        |
| environment_linear_512  | 68.0             | 71.0        | 72.0        | 76.0        | 68.0        | 68.0        | 78.0        | 70.0        | <b>85.0</b> | 78.0        | 73.4        |
| environment_linear_6144 | 67.0             | 70.0        | <b>76.0</b> | 69.0        | 68.0        | 67.0        | 66.0        | 72.0        | 73.0        | 73.0        | 70.1        |
| environment_mel256_512  | 72.0             | <b>74.0</b> | <b>73.0</b> | <b>78.0</b> | <b>76.0</b> | 75.0        | <b>84.0</b> | <b>83.0</b> | 79.0        | <b>79.0</b> | <b>77.3</b> |
| environment_mel256_6144 | 68.0             | 71.0        | 73.0        | 74.0        | 72.0        | 73.0        | 76.0        | 74.0        | 79.0        | 77.0        | 73.7        |
| music_linear_512        | <b>78.0</b>      | 71.0        | <b>76.0</b> | 76.0        | 75.0        | <b>77.0</b> | 79.0        | 77.0        | 82.0        | 74.0        | 76.5        |
| music_linear_6144       | 68.0             | 71.0        | 75.0        | 72.0        | 71.0        | 74.0        | 70.0        | 71.0        | 75.0        | 70.0        | 71.7        |
| music_mel256_512        | 68.0             | 63.0        | 74.0        | 75.0        | 73.0        | 67.0        | 71.0        | 68.0        | 79.0        | 72.0        | 71.0        |
| music_mel256_6144       | 69.0             | 68.0        | 73.0        | 70.0        | 71.0        | 71.0        | 75.0        | 70.0        | 79.0        | 77.0        | 72.3        |

TABLE IV. CLASSIFICATION ACCURACY FOR VARIOUS ACOUSTIC FEATURES FOR TWO LONG DURATION SPEECH UTTERANCE TASKS, ALONG WITH THE AVERAGE ACCURACY OVER BOTH LONG UTTERANCE TASKS

| Feat                    | Long Utterances |             | Average     |
|-------------------------|-----------------|-------------|-------------|
|                         | readtext        | monologue   |             |
| ComParE                 | 69.0            | 72.0        | 70.5        |
| eGeMAPS                 | 72.0            | <b>80.0</b> | 76.0        |
| VGGish                  | 70.0            | 71.0        | 70.5        |
| YAMNet                  | 72.0            | 73.0        | 72.5        |
| environment_linear_512  | 74.0            | <b>81.0</b> | 77.5        |
| environment_linear_6144 | 79.0            | 76.0        | 77.5        |
| environment_mel256_512  | 79.0            | 78.0        | 78.5        |
| environment_mel256_6144 | 77.0            | 79.0        | 78.0        |
| music_linear_512        | <b>84.0</b>     | 79.0        | <b>81.5</b> |
| music_linear_6144       | 75.0            | 79.0        | 77.0        |
| music_mel256_512        | 79.0            | 77.0        | 78.0        |
| music_mel256_6144       | 76.0            | 80.0        | 78.0        |

TABLE V. SUMMARY OF CLASSIFICATION ACCURACY FOR EACH SPEAKING TASK BEFORE AND AFTER DECISION-LEVEL FUSION

| Speaking tasks | Best result (pre-fusion) | Decision-level Fusion |               |
|----------------|--------------------------|-----------------------|---------------|
|                |                          | Confidence            | Majority Vote |
| pa             | 84.0                     | 85.0                  | 88.0          |
| ka             | 82.0                     | 85.0                  | 81.0          |
| ta             | 79.0                     | 77.0                  | 80.0          |
| pakata         | 85.0                     | 84.0                  | 84.0          |
| pekata         | 80.0                     | 76.0                  | 80.0          |
| pataka         | 81.0                     | 81.0                  | 79.0          |
| juan           | 78.0                     | 78.0                  | 76.0          |
| laura          | 77.0                     | 72.0                  | 78.0          |
| loslibros      | 76.0                     | 71.0                  | 80.0          |
| luisa          | 78.0                     | 83.0                  | 80.0          |
| micasa         | 76.0                     | 72.0                  | 81.0          |
| omar           | 77.0                     | 77.0                  | 78.0          |
| preocupado     | 84.0                     | 86.0                  | 86.0          |
| rosita         | 83.0                     | 81.0                  | 85.0          |
| triste         | 85.0                     | 88.0                  | 89.0          |
| viste          | 79.0                     | 81.0                  | 84.0          |
| read text      | 84.0                     | 84.0                  | 82.0          |
| monologue      | 81.0                     | 84.0                  | 83.0          |

to experiment with both types of decision-level fusion and determine the one which is best suited for the task hand.

In Table V we summarize the results for experiments for decision-level fusion for top-3 performing models for each speaking task. Here, one can note that decision-level fusion, in most cases, improves the classification performance. The most notable examples are speaking tasks *pa* and *triste*

where classification accuracy was improved from 84.0% to 88.0% and 85.0% to 89.0%, respectively. There are also some cases where the classification accuracy after fusion actually decreases, for example, with speaking task *pakata* where pre-fusion accuracy of 85.0% decreases to 84.0%. We argue that fusion is still useful here since the slightly decreased accuracy is based on confidence of multiple models and it is more likely to be robust as compared to the accuracy achieved by a single model.

#### E. Performance Comparison of Deep Acoustic Embeddings

Finally, we compare the averaged classification accuracy over the eighteen speaking tasks which form the GITA corpus. A summary of results has been provided in Table VI where one can make out a ranking of deep acoustic embeddings based on their classification performance.

We note that `music_linear_512` embedding performs best with an accuracy of 78.0% and `environment_mel256_512` follows closely in second place with an accuracy of 77.7%. The third best performing embedding is `environment_linear_512` which achieves an accuracy of 74.9%. It is most interesting to note that acoustic embeddings which are trained to recognize types of music and environmental noise perform much better than VGGish and YAMNet embeddings, which are trained using data which also contains human voice. This suggests that the upstream task does not matter for downstream tasks whilst using deep acoustic embeddings. However, further testing over multiple datasets is required in order to reach a conclusion. For the sake of completeness, a summary of top-3 performing models including feature name as well as pooling method has been provided in Tables IX through XI for the three types of speaking tasks.

## VI. CONCLUSION

In this work, we investigated the usefulness of deep acoustic embeddings as effective representations of speech paralinguistics for the task of identifying Parkinsonian speech, benchmarking the classification performance of these embeddings against two popular domain-knowledge based hand-crafted feature sets. Our results show that deep acoustic embeddings are indeed useful for the task at hand and perform consistently better than hand-crafted features. We also report

TABLE VI. AVERAGE CLASSIFICATION ACCURACY COMPARISON OF VARIOUS DEEP ACOUSTIC EMBEDDINGS FOR EIGHTEEN UTTERANCE TASKS FOR IDENTIFYING PARKINSONIAN SPEECH

| Feat                    | Average Accuracy |
|-------------------------|------------------|
| VGGish                  | 69.6             |
| YAMNet                  | 69.9             |
| environment_linear_512  | 74.9             |
| environment_linear_6144 | 72.7             |
| environment_mel256_512  | 77.7             |
| environment_mel256_6144 | 75.2             |
| music_linear_512        | 78.0             |
| music_linear_6144       | 73.3             |
| music_mel256_512        | 73.2             |
| music_mel256_6144       | 74.1             |

that the upstream training task may not be a limiting factor for the classification performance in the downstream task. For example, models trained on music and environmental sound data performed much better than embeddings which were trained on data containing human voice. Finally, we showed that decision-level fusion is an effective method to improve the stability of machine learning models for identifying Parkinsonian speech.

#### REFERENCES

- [1] L. Marsili, G. Rizzo, and C. Colosimo, "Diagnostic criteria for Parkinson's disease: From James Parkinson to the concept of prodromal disease," *Frontiers in Neurology*, vol. 9, pp. 1–10, 2018.
- [2] P. Lieberman, E. Kako, J. Friedman, G. Tajchman, L. S. Feldman, and E. B. Jiminez, "Speech production, syntax comprehension, and cognitive deficits in Parkinson's disease," *Brain and Language*, vol. 43, no. 2, pp. 169–189, 1992.
- [3] World Health Organization, "Neurological Disorders: Public Health Challenges." [Online]. Available: [https://www.who.int/mental\\_{ }health/neurology/neurodiso/en](https://www.who.int/mental_{ }health/neurology/neurodiso/en)
- [4] B. Yousefi, V. Tadibi, A. Khoei, and A. Montazeri, "Exercise therapy, quality of life, and activities of daily living in patients with Parkinson disease: A small scale quasi-randomised trial," *Trials*, vol. 10, no. 67, pp. 1–7, 2009.
- [5] J. Massano and K. P. Bhatia, "Clinical approach to Parkinson's disease: Features, diagnosis, and principles of management," *Cold Spring Harbor Perspectives in Medicine*, vol. 2, no. 6, pp. 1–15, 2012.
- [6] U. Saeed, J. Compagnone, R. I. Aviv, A. P. Strafella, S. E. Black, A. E. Lang, and M. Masellis, "Imaging biomarkers in Parkinson's disease and Parkinsonian syndromes: Current and emerging concepts," *Translational Neurodegeneration*, vol. 6, no. 8, pp. 1–25, 2017.
- [7] S. G. Ryman and K. L. Poston, "MRI biomarkers of motor and non-motor symptoms in Parkinson's disease," *Parkinsonism and Related Disorders*, vol. 73, pp. 85–93, 2019.
- [8] A. Tsanas, M. A. Little, P. E. McSharry, and L. O. Ramig, "Accurate telemonitoring of parkinsons disease progression by noninvasive speech tests," *IEEE Transactions on Biomedical Engineering*, vol. 57, no. 4, pp. 884–893, 2010.
- [9] J. R. Orozco-Arroyave, F. Honig, J. D. Arias-Londono, J. F. Vargas-Bonilla, K. Daqrouq, S. Skodda, J. Ruzs, and E. Noth, "Automatic detection of Parkinson's disease in running speech spoken in three different languages," *The Journal of the Acoustical Society of America*, vol. 139, no. 1, pp. 481–500, 2016.
- [10] D. Sztaho, M. G. Tulics, K. Vicsi, and I. Valalik, "Automatic estimation of severity of Parkinson's disease based on speech rhythm related features," in *IEEE International Conference on Cognitive Infocommunications*, vol. 2018-Janua, 2017, pp. 11–16.
- [11] M. Cernak, J. R. Orozco-Arroyave, F. Rudzicz, H. Christensen, J. C. Vasquez-Correa, and E. Noth, "Characterisation of voice quality of Parkinson's disease using differential phonological posterior features," *Computer Speech and Language*, vol. 46, pp. 196–208, 2017.
- [12] L. Moro-Velazquez, J. A. Gomez-Garcia, J. I. Godino-Llorente, J. Vllalba, J. Ruzs, S. Shattuck-Hufnagel, and N. Dehak, "A forced gaussians based methodology for the differential evaluation of Parkinson's Disease by means of speech processing," *Biomedical Signal Processing and Control*, vol. 48, pp. 205–220, 2019.
- [13] S. Hershey, S. Chaudhuri, D. P. Ellis, J. F. Gemmeke, A. Jansen, R. C. Moore, M. Plakal, D. Platt, R. A. Saurous, B. Seybold, M. Slaney, R. J. Weiss, and K. Wilson, "CNN architectures for large-scale audio classification," in *IEEE International Conference on Acoustics, Speech and Signal Processing*, 2017, pp. 131–135.
- [14] K. Simonyan and A. Zisserman, "Very deep convolutional networks for large-scale image recognition," in *International Conference on Learning Representations*, 2015, pp. 1–14.
- [15] J. F. Gemmeke, D. P. Ellis, D. Freedman, A. Jansen, W. Lawrence, R. C. Moore, M. Plakal, and M. Ritter, "Audio Set: An ontology and human-labeled dataset for audio events," in *IEEE International Conference on Acoustics, Speech and Signal Processing*, 2017, pp. 776–780.
- [16] M. S. S. Syed, Z. S. Syed, M. Lech, and E. Pirogova, "Automated Screening for Alzheimer's Dementia through Spontaneous Speech," in *INTERSPEECH (to appear)*, 2020, pp. 1–5.
- [17] H. A. Andrew G. Howard, Menglong Zhu, Bo Chen, Dmitry Kalenichenko, Weijun Wang, Tobias Weyand, Marco Andreetto, "MobileNets: Efficient Convolutional Neural Networks for Mobile Vision Applications," *arXiv preprint arXiv:1704.04861*, pp. 1–9, 2017.
- [18] J. Cramer, H.-H. Wu, J. Salamon, and J. P. Bello, "Look, Listen, and Learn More: Design Choices for Deep Audio Embeddings," in *IEEE International Conference on Acoustics, Speech and Signal Processing*, 2019, pp. 1–5.
- [19] R. Arandjelovic and A. Zisserman, "Look, Listen and Learn," in *IEEE International Conference on Computer Vision*, 2017, pp. 609–617.
- [20] J. R. Orozco-Arroyave, J. D. Arias-Londono, J. F. Vargas-Bonilla, M. C. Gonzalez-Rativa, and E. Noth, "New Spanish speech corpus database for the analysis of people suffering from Parkinson's disease," in *International Conference on Language Resources and Evaluation*, 2014, pp. 342–347.
- [21] G. T. Stebbins and C. G. Goetz, "Factor structure of the Unified Parkinson's Disease Rating Scale: Motor Examination section," *Movement Disorders*, vol. 13, no. 4, pp. 633–636, 1998.
- [22] C. Gobl and A. N. Chasaide, "Acoustic characteristics of voice quality," *Speech Communication*, vol. 11, no. 4-5, pp. 481–490, 1992.
- [23] C. Dromey, L. O. Ramig, and A. B. Johnson, "Phonatory and articulatory changes associated with increased vocal intensity in Parkinson disease: A case study," *Journal of Speech and Hearing Research*, vol. 38, no. 4, pp. 751–764, 1995.
- [24] B. T. Harel, M. S. Cannizzaro, H. Cohen, N. Reilly, and P. J. Snyder, "Acoustic characteristics of Parkinsonian speech: A potential biomarker of early disease progression and treatment," *Journal of Neurolinguistics*, vol. 17, no. 6, pp. 439–453, 2004.
- [25] H. N. Jones, "Prosody in Parkinson's Disease," *Perspectives on Neurophysiology and Neurogenic Speech and Language*, vol. 1, no. 1, pp. 77–82, 2009.
- [26] L. K. Smith and A. M. Goberman, "Long-time average spectrum in individuals with Parkinson disease," *NeuroRehabilitation*, vol. 35, no. 1, pp. 77–88, 2014.
- [27] F. Eyben, M. Wollmer, and B. Schuller, "OpenSMILE - The Munich versatile and fast open-source audio feature extractor," in *ACM International Conference on Multimedia*, 2010, pp. 1459–1462.
- [28] F. Eyben, F. Weninger, F. Gross, and B. Schuller, "Recent developments in openSMILE, the munich open-source multimedia feature extractor," in *ACM International Conference on Multimedia*, 2013, pp. 835–838.
- [29] B. Schuller, F. Weninger, Y. Zhang, F. Ringeval, A. Batliner, S. Steidl, F. Eyben, E. Marchi, A. Vinciarelli, K. Scherer, M. Chetouani, and M. Mortillaro, "Affective and behavioural computing: Lessons learnt from the First Computational Paralinguistics Challenge," *Computer Speech and Language*, vol. 1, no. 1, pp. 1–25, 2018.
- [30] B. W. Schuller, S. Steidl, A. Batliner, P. B. Marschik, H. Baumeister, F. Dong, S. Hantke, F. Pokorny, E.-M. Rathner, K. D. Bartl-Pokorny, C. Einspieler, D. Zhang, A. Baird, S. Amiriparian, K. Qian, Z. Ren, M. Schmitt, P. Tzirakis, and S. Zafeiriou, "The INTERSPEECH 2018

Computational Paralinguistics Challenge: Atypical and Self-Assessed Affect, Crying and Heart Beats,” in *INTERSPEECH*, 2018, pp. 1–5.

- [31] T. Meng, X. Jing, Z. Yan, and W. Pedrycz, “A survey on machine learning for data fusion,” *Information Fusion*, vol. 57, no. 1, pp. 115–129, 2020.
- [32] Z. S. Syed, K. Sidorov, and D. Marshall, “Automated Screening for Bipolar Disorder from Audio/Visual Modalities,” in *ACM International Workshop on Audio/Visual Emotion Challenge (AVEC)*, 2018, pp. 39–45.

#### APPENDIX A: LIST OF ACOUSTIC FEATURES IN COMPARE AND EGEMAPS FEATURE SETS

TABLE VII. ACOUSTIC LOW-LEVEL DESCRIPTORS WHICH FORM THE COMPUTATIONAL PARALINGUISTICS CHALLENGE (COMPARE) FEATURE SET

| Energy related LLD                             | Group         |
|------------------------------------------------|---------------|
| Sum of auditory spectrum (loudness)            | Voice Spectra |
| Spectral LLDs                                  | Group         |
| Alpha ratio (50-1000 Hz, 1000-5000 Hz)         | Voice Spectra |
| Energy slope (0-500 Hz, 500-1500 Hz)           | Voice Spectra |
| Hammarberg index                               | Voice Spectra |
| MFCCs 1-4                                      | Voice Spectra |
| Spectral flux                                  | Voice Spectra |
| Voicing related LLDs                           | Group         |
| Fundamental frequency (linear and semitone)    | Prosodic      |
| Formants 1-2 (frequency, bandwidth, amplitude) | Voice Quality |
| Harmonic differences (H1-H2, H1-A3)            | Voice Quality |
| log. HNR, Jitter, and Shimmer                  | Voice Quality |

TABLE VIII. ACOUSTIC LOW-LEVEL DESCRIPTORS WHICH FORM THE EXTENDED GENEVA MINIMALISTIC ACOUSTIC PARAMETER SET (EGEMAPS) FEATURE SET

| Energy related LLD                                       | Group         |
|----------------------------------------------------------|---------------|
| Sum of auditory spectrum (loudness)                      | Voice Spectra |
| Sum of RASTA-filtered auditory spectrum (loudness)       | Voice Spectra |
| RMS energy and zero-crossing rate                        | Temporal      |
| Spectral LLDs                                            | Group         |
| RASTA-filtered audio spectrum bands 1-26                 | Voice Spectra |
| MFCCs 1-14                                               | Voice Spectra |
| Spectral energy 250-650 Hz, 1000-4000 Hz                 | Voice Spectra |
| Spectral roll-off at 0.25, 0.5, 0.75, and 0.9 percentage | Voice Spectra |
| Psychoacoustic sharpness, Harmonicity                    | Voice Spectra |
| Spectral variance, Spectral skewness, Spectral kurtosis  | Voice Spectra |
| Voicing related LLDs                                     | Group         |
| Fundamental frequency (SHS and Viterbi smoothing)        | Prosodic      |
| Probability of voicing                                   | Voice Quality |
| log. HNR, Jitter, and Shimmer                            | Voice Quality |

#### APPENDIX B: SUMMARY OF TOP-3 PERFORMING FEATURES (ALONG WITH THEIR POOLING METHOD) FOR DIADOCHOKINESIS, LONG, AND SHORT DURATION UTTERANCES

TABLE IX. SUMMARY OF TOP-3 PERFORMING FEATURES (ALONG WITH THEIR POOLING METHOD) FOR DIADOCHOKINESIS BASED SPEAKING TASKS

| Speaking task | Feature                 | Pooling | Accuracy |
|---------------|-------------------------|---------|----------|
| pa            | ComParE                 | x       | 79.0     |
|               | environment_linear_6144 | MaxPool | 81.0     |
|               | environment_mel256_512  | AvgPool | 84.0     |
| ka            | environment_mel256_6144 | AvgPool | 79.0     |
|               | environment_linear_6144 | AvgPool | 81.0     |
|               | music_linear_512        | AvgPool | 82.0     |
|               | music_linear_6144       | AvgPool | 81.0     |
|               | music_mel256_512        | MaxPool | 81.0     |
| ta            | music_mel256_6144       | AvgPool | 81.0     |
|               | ComParE                 | x       | 79.0     |
|               | YAMNet                  | MaxPool | 76.0     |
| pakata        | music_linear_512        | AvgPool | 77.0     |
|               | environment_linear_512  | MaxPool | 79.0     |
| pekata        | environment_mel256_512  | AvgPool | 79.0     |
|               | music_linear_512        | MaxPool | 85.0     |
|               | environment_mel256_512  | MaxPool | 79.0     |
| pataka        | music_linear_512        | AvgPool | 80.0     |
|               | music_mel256_512        | AvgPool | 79.0     |
|               | environment_linear_512  | AvgPool | 75.0     |
|               | environment_linear_6144 | AvgPool | 76.0     |
|               | environment_mel256_512  | AvgPool | 75.0     |
|               | environment_mel256_6144 | AvgPool | 81.0     |

TABLE X. SUMMARY OF TOP-3 PERFORMING FEATURES (ALONG WITH THEIR POOLING METHOD) FOR LONG DURATION UTTERANCE TASKS

| Speaking task | Feature                 | Pooling | Accuracy |
|---------------|-------------------------|---------|----------|
| readtext      | environment_mel256_512  | AvgPool | 79.0     |
|               | music_linear_512        | AvgPool | 84.0     |
|               | music_mel256_512        | AvgPool | 79.0     |
|               | environment_linear_6144 | AvgPool | 79.0     |
| monologue     | eGeMAPS                 | x       | 80.0     |
|               | environment_linear_512  | AvgPool | 81.0     |
|               | music_mel256_6144       | MaxPool | 80.0     |



TABLE XI. SUMMARY OF TOP-3 PERFORMING FEATURES (ALONG WITH THEIR POOLING METHOD) FOR SHORT DURATION UTTERANCE TASKS

| <i>Speaking task</i> | <i>Feature</i>          | <i>Pooling</i> | <i>Accuracy</i> |
|----------------------|-------------------------|----------------|-----------------|
| juan                 | ComParE                 | x              | 73.0            |
|                      | VGGish                  | AvgPool        | 72.0            |
|                      | environment_mel256_512  | AvgPool        | 72.0            |
|                      | music_linear_512        | MaxPool        | 78.0            |
| laura                | ComParE                 | x              | 77.0            |
|                      | environment_linear_512  | MaxPool        | 71.0            |
|                      | environment_mel256_512  | RangePool      | 74.0            |
|                      | environment_mel256_6144 | AvgPool        | 71.0            |
|                      | music_linear_512        | MaxPool        | 71.0            |
|                      | music_linear_6144       | AvgPool        | 71.0            |
| loslibros            | environment_linear_6144 | AvgPool        | 76.0            |
|                      | music_linear_512        | MaxPool        | 76.0            |
|                      | music_linear_6144       | AvgPool        | 75.0            |
| luisa                | ComParE                 | x              | 76.0            |
|                      | environment_linear_512  | AvgPool        | 76.0            |
|                      | environment_mel256_512  | AvgPool        | 78.0            |
| micasa               | music_linear_512        | AvgPool        | 76.0            |
|                      | ComParE                 | x              | 74.0            |
|                      | environment_mel256_512  | MaxPool        | 76.0            |
| omar                 | music_linear_512        | AvgPool        | 75.0            |
|                      | YAMNet                  | RangePool      | 74.0            |
|                      | environment_mel256_512  | AvgPool        | 75.0            |
| preocupado           | music_linear_512        | MaxPool        | 77.0            |
|                      | music_linear_6144       | AvgPool        | 74.0            |
|                      | ComParE                 | x              | 81.0            |
|                      | environment_mel256_512  | AvgPool        | 84.0            |
| rosita               | music_linear_512        | AvgPool        | 79.0            |
|                      | ComParE                 | x              | 74.0            |
|                      | environment_mel256_512  | AvgPool        | 83.0            |
| triste               | environment_mel256_6144 | MaxPool        | 74.0            |
|                      | music_linear_512        | MaxPool        | 77.0            |
|                      | environment_linear_512  | AvgPool        | 85.0            |
|                      | environment_mel256_512  | AvgPool        | 79.0            |
|                      | environment_mel256_6144 | MaxPool        | 79.0            |
|                      | music_linear_512        | AvgPool        | 82.0            |
| viste                | music_mel256_512        | AvgPool        | 79.0            |
|                      | music_mel256_6144       | AvgPool        | 79.0            |
|                      | environment_linear_512  | MaxPool        | 78.0            |
|                      | environment_mel256_512  | AvgPool        | 79.0            |
|                      | environment_mel256_6144 | MaxPool        | 77.0            |
|                      | music_mel256_6144       | MaxPool        | 77.0            |